Virginia B. Reef, D.V.M.

EQUINE DIAGNOSTIC ULTRASOUND

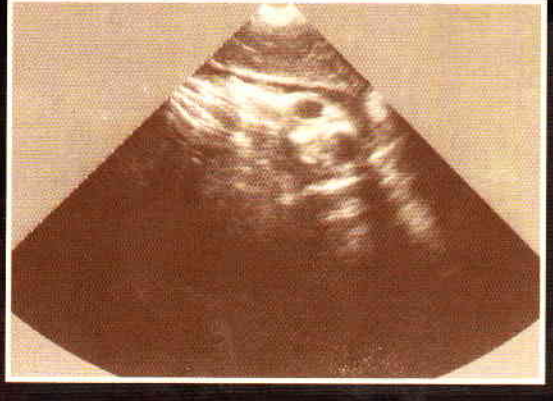

SAUNDERS

EQUINE
Diagnostic Ultrasound

Virginia B. Reef, D.V.M.

Professor of Medicine in the Widener Hospital
Director of Large Animal Cardiology and Diagnostic Ultrasonography
University of Pennsylvania
School of Veterinary Medicine
New Bolton Center
Kennett Square, Pennsylvania

W.B. SAUNDERS COMPANY

An Imprint of Elsevier Science
Philadelphia London New York St. Louis Sydney Toronto

Contents

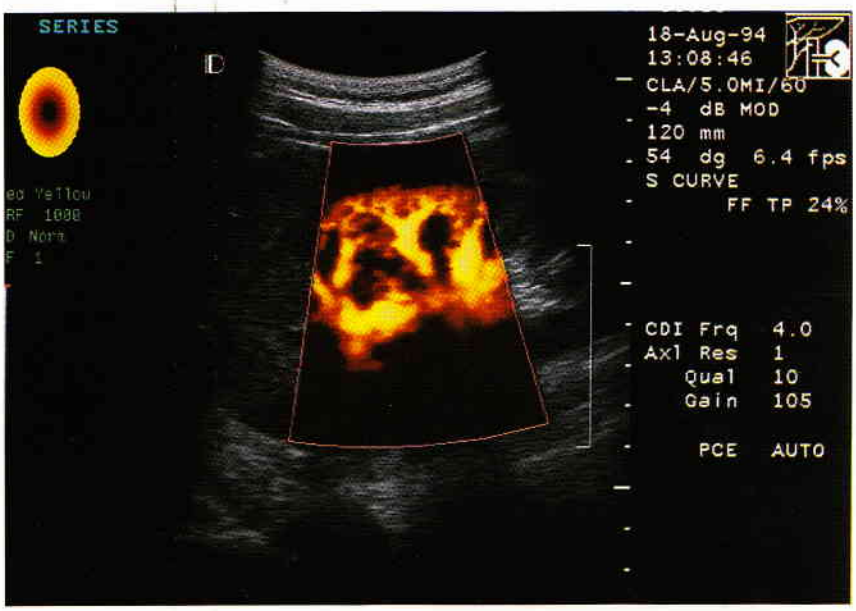

Color Figure 1–1

Power Doppler sonogram of an equine kidney. Notice the prominent renal blood supply visible with power Doppler ultrasonography, the branching of the renal vasculature into arcuate and interlobar arteries, and the arborization of the vessels in the renal cortex. This sonogram was obtained in the right fifteenth intercostal space with a wide-bandwidth curved linear-array transducer at a displayed depth of 13 cm. The right side of this sonogram is dorsal and the left side is ventral.

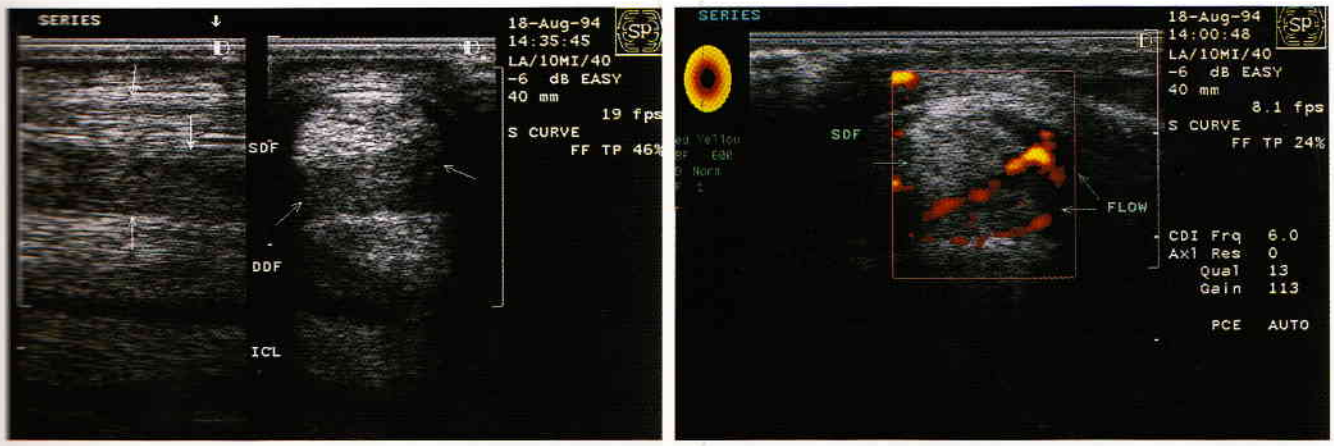

Color Figure 3–1

Sonograms of a healing area of injury in the proximal portion of the left fore superficial digital flexor tendon (SDF), obtained from a 12-year-old Holsteiner gelding imaged with traditional two-dimensional imaging and with power Doppler imaging. These sonograms were obtained at 5 cm distal to the point of the accessory carpal bone (zone 1A) with a wide-bandwidth 10.0-MHz linear-array transducer at a displayed depth of 4 cm. The right side of the transverse image is lateral and the left side is medial. The right side of the sagittal image is proximal and the left side is distal.

Left. The area of healing injury is imaged in the dorsal and lateral portion of the SDF (*arrows*) as a hypoechoic arrow lacking a normal fiber pattern. DDF, deep digital flexor tendon; ICL, inferior check ligament.

Right. Notice the large amount of low-velocity blood flow detected circumferentially around the edges of the lesion, depicted in color. This is consistent with significant blood vessel ingrowth to the area of tendon injury. A small amount of low-velocity flow (*color*) is also detected within the healing area.

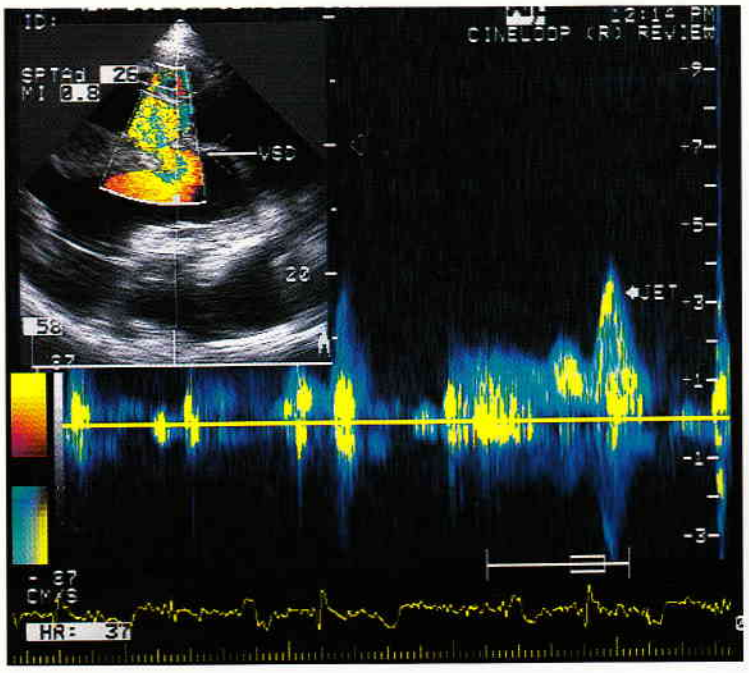

Color Figure 5–1

Long-axis color-flow echocardiogram and two-dimensional guided continuous-wave Doppler spectral tracing obtained from a 7-year-old Thoroughbred gelding with a membranous ventricular septal defect (VSD). The high-velocity turbulent color-flow jet (contained within the pie-shaped box) represents the shunt from the left ventricular outflow tract to the right ventricular inflow tract. Notice the flow convergence on the left ventricular side of the VSD. The outer edges of the color-flow jet are red and orange, with the jet color changing to yellow and then turquoise at the center, representing the highest velocity flow (the color-flow Doppler signal is aliased). The shunt direction is left to right because the blood flow is toward the transducer. Notice the spectral broadening of the blood flow in the continuous-wave Doppler spectral tracing, the high-velocity (approximately 4 m/sec) turbulent systolic jet (*short filled arrow*), the lower-velocity (approximately 2 m/sec) turbulent jet in mid to late diastole, and the blood flow direction (above the baseline), representing blood flow shunting from the left to the right ventricle through the VSD. This echocardiogram was obtained from the right cardiac window between the left ventricular outflow tract and mitral valve position with a 3.0/2.0-MHz phased-array transducer and a display depth of 27 cm. An electrocardiogram is superimposed for timing.

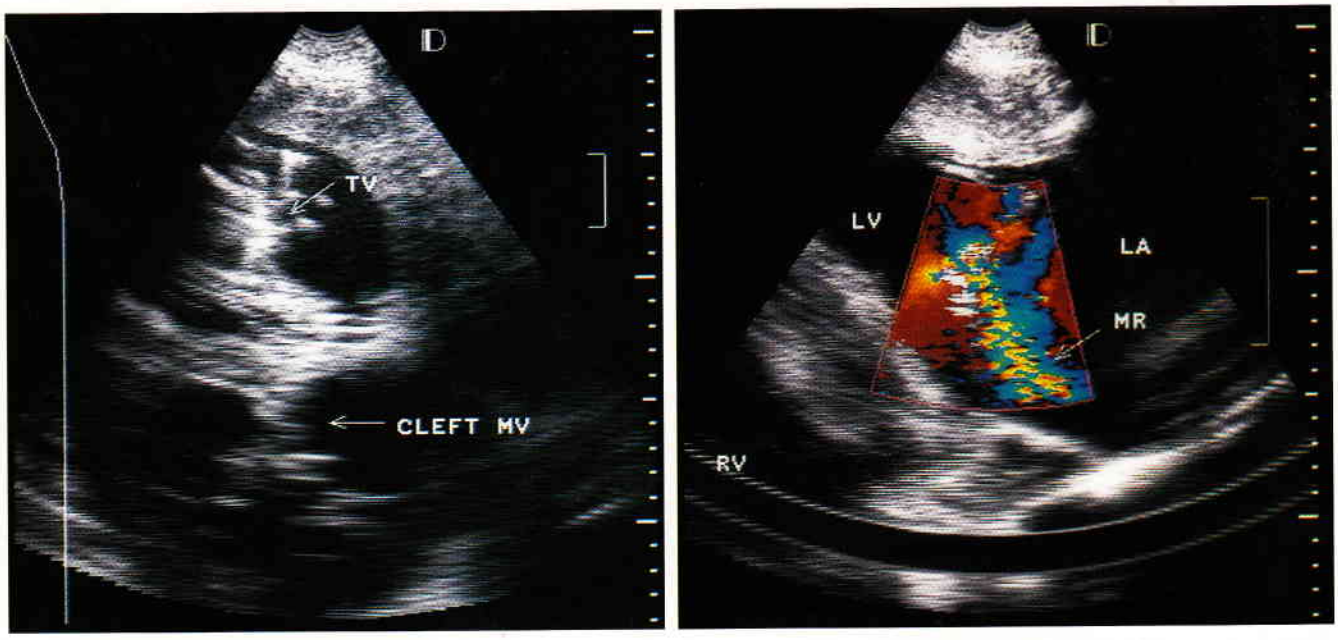

Color Figure 5–2

Echocardiograms of the mitral valve obtained from a yearling Thoroughbred colt with an endocardial cushion defect. These echocardiograms were obtained with a 2.25/2.0-MHz phased-array transducer and a 24-cm displayed depth.

Left, Short-axis echocardiogram obtained from the right cardiac window in the mitral valve position. The cleft in the septal leaflet of the mitral valve (*arrow*) splits the valve into cranial and caudal portions. TV, Tricuspid valve.

Right, Long-axis color-flow echocardiogram obtained from the left cardiac window in the mitral valve position. The blue to aqua jet of mitral regurgitation (MR) with the central aliased higher-velocity flow is associated with the cleft in the septal leaflet of the mitral valve. The jet extends axially along the free edge of the valve leaflet and along the interatrial septum. LA, Left atrium; LV, left ventricle; RV, right ventricle.

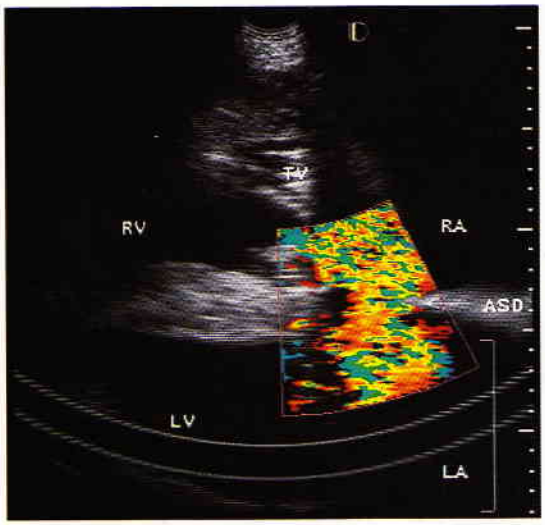

Color Figure 5–3

Long-axis color-flow Doppler echocardiogram obtained from a yearling Thoroughbred colt with an endocardial cushion defect (same colt as in Color Figure 5-2). The high-velocity turbulent color-flow jet (contained within the pie-shaped box) represents the shunt from left atrium (LA) to right atrium (RA) through the atrial part of the endocardial cushion defect (ASD) above fused atrioventricular valves. The outer edges of the color-flow jet are red and orange, with the jet color changing to yellow and then turquoise at the center, representing the highest-velocity flow (the color-flow Doppler signal is aliased). The shunt direction is left to right because the blood flow is toward the transducer. The echocardiogram was obtained from the right cardiac window in the four-chamber view with a 2.25/2.0-MHz phased-array transducer and a 24-cm displayed depth. TV, Tricuspid valve; RV, right ventricle; LV, left ventricle.

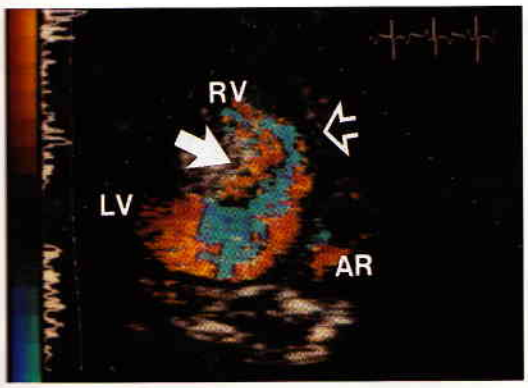

Color Figure 5–4

Color-flow echocardiogram obtained from a 6-week-old Thoroughbred filly (same foal as in Figure 5-26) with tricuspid atresia (*open arrow*). The orange jet goes from the left ventricle to the right ventricle through the large ventricular septal defect (*closed arrow*). The center of the jet is the higher-velocity flow represented by the aliased aqua signal. This echocardiogram was obtained from the right cardiac window in the left ventricular outflow tract position with a 2.5-MHz phased-array transducer and a displayed depth of 12 cm. An electrocardiogram is superimposed for timing. RV, Right ventricle; LV, left ventricle; AR, aortic root.

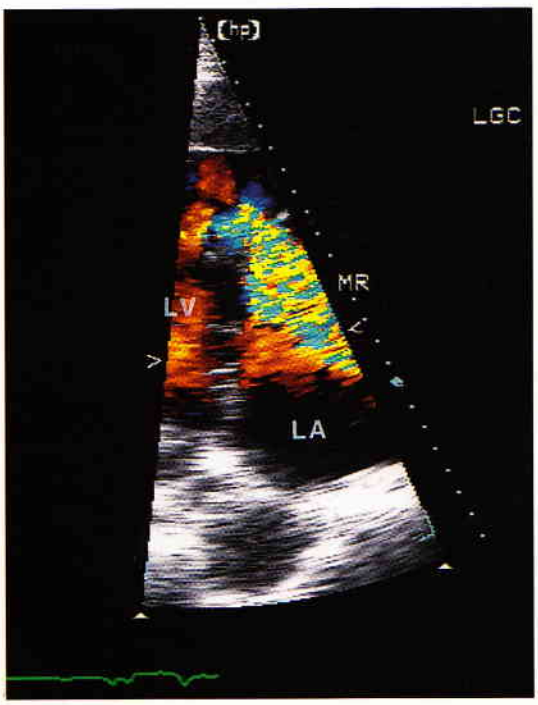

Color Figure 5–5

Long-axis color-flow echocardiogram obtained from a 19-year-old Thoroughbred gelding with mitral valve prolapse and mitral regurgitation. This horse had holosystolic crescendo murmurs, with the point of maximal intensity over the mitral and tricuspid valves, which had remained unchanged since 2 years of age. Mitral and tricuspid valve prolapse was diagnosed and mild cardiac enlargement was detected, which had remained unchanged since 6 years of age. The turquoise and yellow high-velocity turbulent jet of mitral regurgitation (MR) extends dorsally and axially into the left atrium in systole. This echocardiogram was obtained from the left cardiac window in the mitral valve position with a 2.5/2.0-MHz phased-array transducer. An electrocardiogram is superimposed for timing. LA, Left atrium; LV, left ventricle.

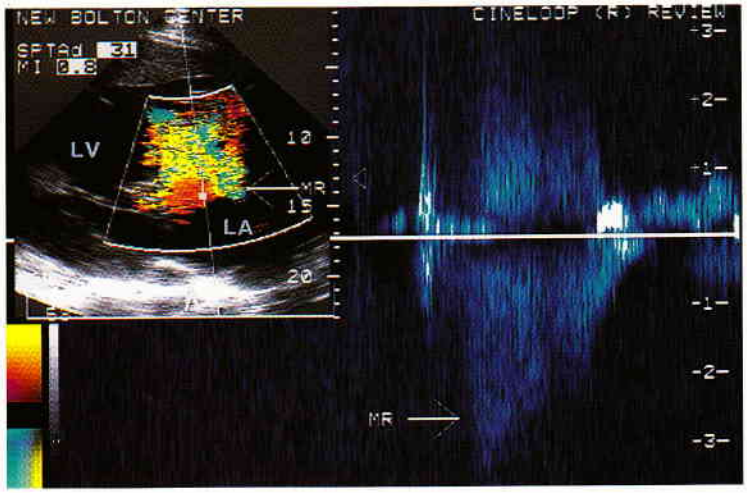

Color Figure 5–6

Long-axis color-flow Doppler echocardiogram and continuous-wave Doppler spectral tracing obtained from a 9-year-old Thoroughbred gelding with moderately severe mitral regurgitation. The high-velocity, turbulent, turquoise and yellow mitral regurgitation (MR) jet (contained within the pie-shaped box) sprays out in three directions from its origin, with the largest portion of the jet directed dorsally in the left atrium. The steep slope of the mitral regurgitation continuous-wave Doppler spectral tracing indicates rapidly increasing left atrial pressures during systole. The mitral regurgitation jet depicted in blue (MR) is detected below the baseline, as the orientation of the jet is away from the transducer into the left atrium. This echocardiogram was obtained from the left cardiac window in the mitral valve position with a 3.0/2.0-MHz phased-array transducer with a displayed depth of 23 cm. LA, Left atrium; LV, left ventricle.

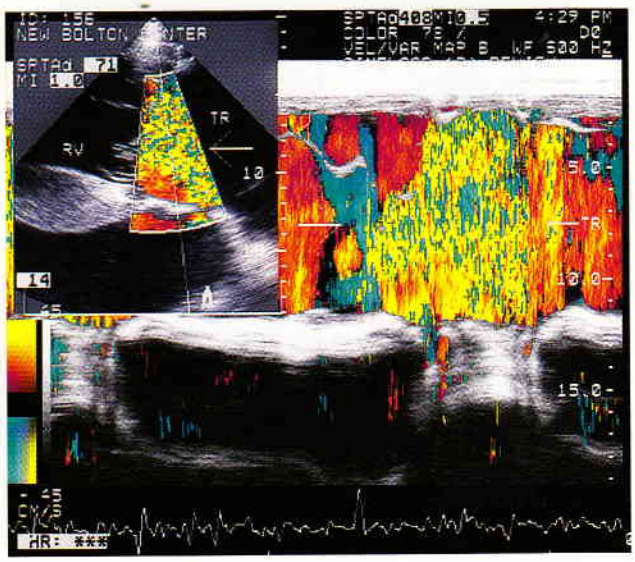

Color Figure 5–7

Long-axis color-flow Doppler echocardiogram (two-dimensional [2-D] and M-mode) obtained from a 9-year-old Thoroughbred gelding with severe tricuspid regurgitation (same horse as in Figures 5-44 and 5-46). The large turquoise and yellow regurgitant jet (*arrow*) of tricuspid regurgitation (TR) fills nearly the entire right atrium in systole on the 2-D color-flow echocardiogram (color-flow Doppler contained within the pie-shaped box on the 2-D echocardiogram). Notice the same jet of tricuspid regurgitation on the M-mode echocardiogram (*arrows*). The M-mode color-flow Doppler echocardiogram can be very useful for timing jets. The echocardiogram was obtained from the right cardiac window between the left ventricular outflow tract and the mitral valve position. An electrocardiogram is superimposed for timing. RV, Right ventricle.

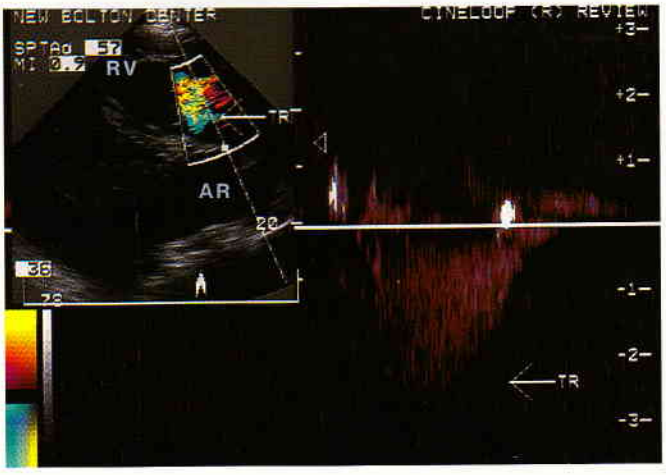

Color Figure 5–8

Long-axis color-flow Doppler and continuous-wave Doppler echocardiogram obtained from a 9-year-old Thoroughbred gelding with tricuspid prolapse and mild tricuspid regurgitation. The turquoise and yellow jet (*arrow*) of tricuspid regurgitation (TR) (color-flow Doppler is contained within the pie-shaped box) angles toward the aortic root (AR), occupying less than one third of the right atrium on the color-flow Doppler echocardiogram (*upper right*). The continuous-wave Doppler tracing of the tricuspid regurgitation (TR) jet (*arrow*) is below the baseline, as the tricuspid regurgitation jet is oriented away from the transducer. The peak velocity of the tricuspid regurgitation jet is only 2.8 m/sec, resulting in only a small pressure difference between the right atrium and the right ventricle. This echocardiogram was obtained from the right cardiac window in the left ventricular outflow tract position with a 3.0/2.0-MHz phased-array transducer and a displayed depth of 27 cm. An electrocardiogram is superimposed for timing. RV, Right ventricle.

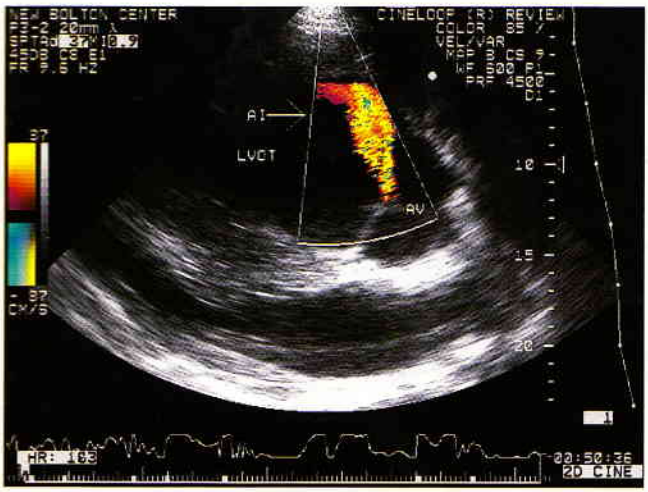

Color Figure 5–9

Long-axis color-flow echocardiogram obtained from a 9-year-old Quarter horse gelding with mild aortic regurgitation. The high-velocity turbulent jet (orange, yellow, and aqua) of aortic insufficiency (AI) originates at the aortic valve (AV) and angles toward the left ventricular free wall. The color-flow Doppler echocardiogram is contained within the pie-shaped box. This echocardiogram was obtained from the left cardiac window in the left ventricular outflow tract and aortic valve position with a 3.0/2.0-MHz phased-array transducer and a displayed depth of 24 cm. An electrocardiogram is superimposed for timing. LVOT, Left ventricular outflow tract.

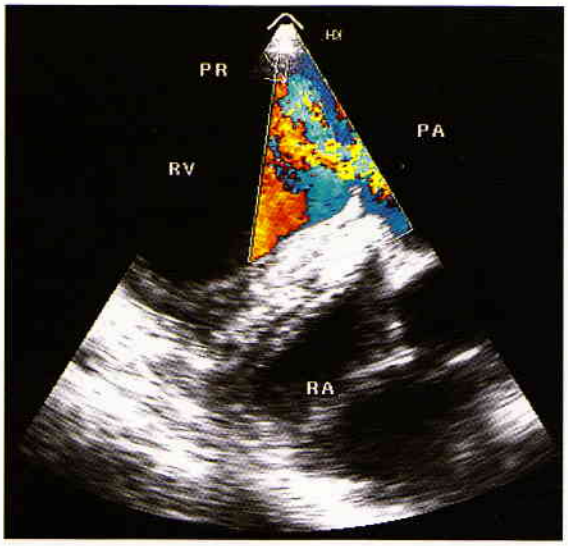

Color Figure 5–10

Long-axis color-flow echocardiogram obtained from a 5-year-old Thoroughbred-Percheron cross gelding with severe pulmonic (PR) and tricuspid regurgitation. The red to orange jet is deflected into the right ventricular outflow tract by the flail pulmonic valve leaflet, with a central aliased signal due to high-velocity flow (*arrow*). The jet area at its origin is large relative to the valve area, and proximal flow convergence is seen on the pulmonary artery side of the valve. This echocardiogram was obtained with a 3.0/2.0-MHz phased-array transducer and a displayed depth of 26.8 cm. PA, Pulmonary artery; RV, right ventricle; RA, right atrium.

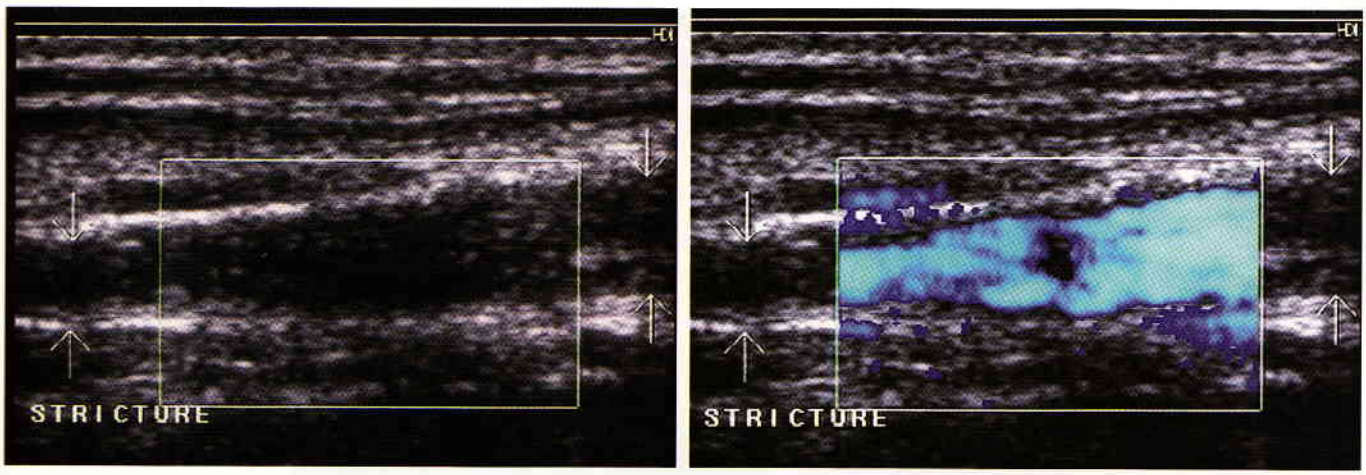

Color Figure 5–11

Sonogram and color angiogram of the left jugular vein obtained from an 11-year-old Dutch Warmblood gelding with chronic jugular vein thrombosis. The right sides of the sonogram and color angiogram are proximal and the left sides are distal. The left jugular vein narrows distally (*arrows*) at the point of a stricture in the jugular vein. The sonogram and color angiogram were obtained with a 10.0/5.0-MHz linear-array transducer and a displayed depth of 4 cm.

Left, The hypoechoic to echogenic echoes within the lumen of the left jugular vein are associated with thrombosis and scarring of the vessel. The irregular and thickened wall of the left jugular vein is associated with chronic jugular vein thrombosis. The rectangular area is the same view represented in the color-flow angiogram.

Right, The filling defects in the left jugular vein as the vein narrows proximal to the stricture are associated with thrombosis and scarring of the vessel. The rectangular area is the area of the color-flow angiogram and is the same area depicted in the sonogram. Note the anechoic filling defect in the center of the color-flow angiogram and the radiating areas of scarring and lesions along the wall of the vessel with very little flow (purple).

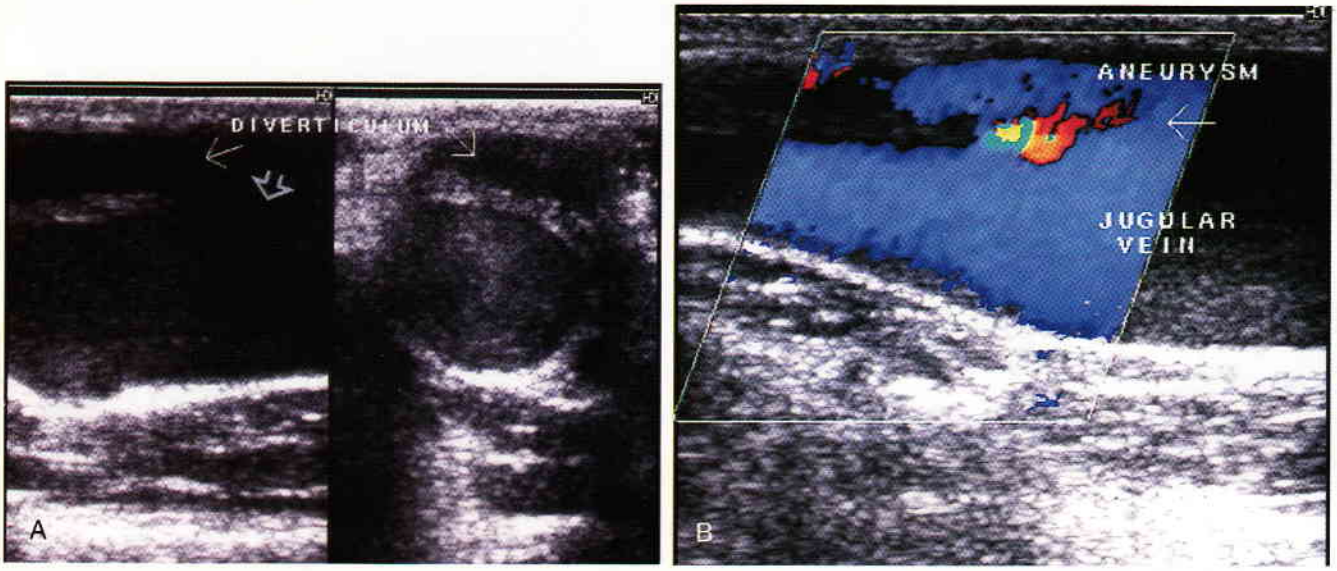

Color Figure 5–12

Sonograms of the right jugular vein from an 11-year-old Dutch Warmblood gelding with chronic jugular vein thrombosis and a diverticulum in the right jugular vein in the proximal cervical region (same horse as in Color Figure 5–11). These sonograms were obtained with a 10.0/5.0-MHz linear-array transducer and a displayed depth of 4 cm. The right side of the transverse (short-axis) image (*right image*) is dorsal and the left side is ventral. The right side of the sagittal (long-axis) image (*left image* and *B*) is proximal and the left side is distal.

A, The blood-filled blind sac or diverticulum (*arrows*) superficial to the right jugular vein communicates with the jugular vein through a break in the vessel wall (*open arrow*).

B, Color-flow sonogram demonstrating the high-velocity (aliased) flow (red, orange, yellow, and turquoise flow) through the narrow communications between the right jugular vein and the diverticulum (*arrow*).

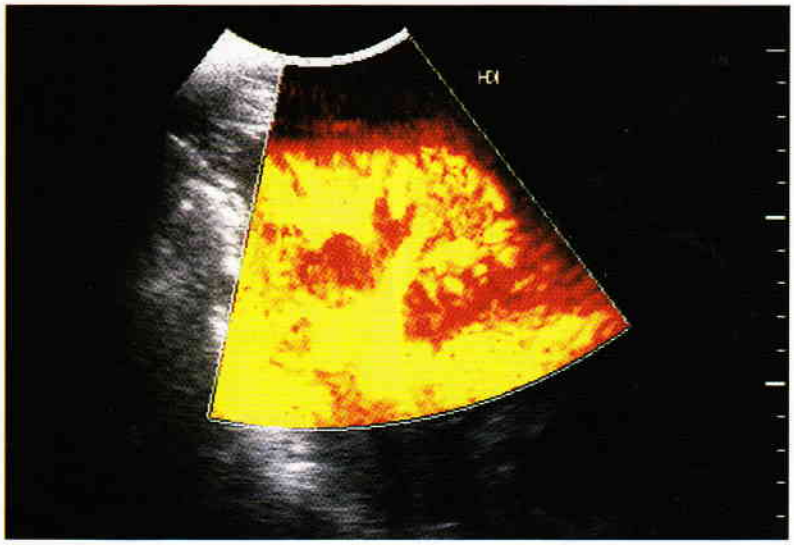

Color Figure 6–1

Power Doppler sonogram of the right kidney obtained from a 10-year-old Thoroughbred gelding. Notice the branching of the renal vasculature into arcuate and interlobar arteries and the arborization of the vessels in the renal cortex. This sonogram was obtained from the right sixteenth intercostal space with a wide-bandwidth 2.0 to 4.0-MHz curved linear-array transducer at a displayed depth of 19.9 cm. The right side of this sonogram is dorsal and the left side is ventral.

CHAPTER

1

Physics and Instrumentation

Ultrasonography is an active process that requires interaction between the veterinary sonologist, equine patient, ultrasound machine, and transducer to obtain optimal quality ultrasound images. The veterinary sonologist needs a thorough understanding of anatomy and of the behavior of ultrasound in tissues for accurate image interpretation. The ultrasonographic examination is an active process, and frequent instrument adjustments need to be made at the time of the ultrasonographic examination to improve image quality. Although a multitude of program presets are available on more sophisticated ultrasound machines, these settings are just a guide for obtaining the initial image. The image obtained should then be fine-tuned, using the instrument controls to obtain the highest quality images for interpretation. Standard scanning practices and image orientation can help simplify the image analysis and interpretation, but ultrasonography remains a dynamic scanning process that requires the active participation of a knowledgeable veterinary sonologist to obtain the most diagnostic information from the examination.

CREATING THE IMAGE

The ultrasound transducer generates a series of ultrasound pulses and ultrasound energy is transmitted into the horse. Echoes are reflected back to the transducer from different tissue interfaces within the patient, reflected ultrasound is received by the transducer, and this returning ultrasound energy is processed into electrical energy, creating an image. The origin of the reflected ultrasound energy and the strength of this ultrasound signal must be determined to create an accurate representation of the tissue scanned. The ultrasound reflections are processed by the ultrasound machine into a series of dots, which form the image displayed. The brightness of each dot corresponds to the amplitude of the returning echo, and the location of the dot corresponds to the anatomic location of the echo-generating structure.[1] A gray-scale image is produced by assigning a different shade of gray to the varying echo strengths. The location of the echo-generating structure is determined by knowing the direction of the pulse when it enters the horse and measuring the time it takes for its echo to return to the transducer. With the knowledge of the sound-propagation speed, the echo arrival time can be converted to the distance within the horse to the reflector that produced the echo.[1-7] A complete understanding of the physics of ultrasound and of the instrumentation is important to obtain the optimal ultrasonographic image.

PROPERTIES OF ULTRASOUND WAVES

Diagnostic ultrasound employs high-frequency sound waves (usually 2 to 10 megahertz [MHz], or millions of cycles per second), which are outside the range of human hearing.[1-7] These sound waves are described in terms of their frequency, period, wavelength, propagation speed, amplitude, and intensity. The sound source determines the frequency of the ultrasound emitted from the transducer, its amplitude, its intensity, and the period of the ultrasound wave. The medium or tissue through which the ultrasound is traveling determines the propagation speed of the ultrasound and, to some extent, the wavelength, which is also determined by the ultrasound source.

The frequency is the number of cycles or complete variations that the ultrasound beam goes through per unit time.[1] The positive portion of the cycle is the compression of the acoustic variable (ultrasound), and the negative portion of the cycle is its rarefaction. The period is the time it takes for one cycle to occur and is normally expressed in microseconds (μs).[1] The period decreases as the frequency of the ultrasound increases because more cycles are occurring per second and it takes less time (period) for each cycle to occur. The frequency of the ultrasound beam is expressed in terms of megahertz.[1-8] The higher the frequency of the ultrasound emitted, the shorter the wavelength. The wavelength is the distance that the ultrasound wave travels during one cycle and is commonly expressed in millimeters (mm). The shorter the wavelength, the higher the resolution of

the image. Frequency and wavelength are inversely related if the velocity of sound within the medium remains constant. Therefore, a higher-frequency transducer generates a shorter wavelength of ultrasound and an image with better resolution.[1-7]

$$\text{Velocity (m/sec)} = \text{frequency (cycles/sec)} \times \text{wavelength (m)}$$

High-frequency sound waves are attenuated more than low-frequency sound waves, limiting the depth of tissue to which the ultrasound beam can penetrate.[1] Therefore, increasing the resolution of the image by increasing the frequency of ultrasound used decreases the penetration of the ultrasound beam.

Propagation speed is the speed at which a wave moves through a medium.[1] The propagation speed divided by the frequency equals the wavelength.

$$\text{Wavelength (mm)} = \frac{\text{Propagation speed (mm/}\mu\text{s)}}{\text{Frequency (MHz)}}$$

The propagation speed is determined by the density and stiffness or hardness of a medium.[1] Density of the medium is the concentration of matter, or mass per unit volume. Stiffness is the resistance of a material or medium to compression. An increase in the stiffness of the medium results in an increase in the propagation speed, but an increase in the density of the medium results in a decrease in the propagation speed, if stiffness remains constant.[1] Differences in stiffness generally dominate the differences in density, resulting in higher-density structures usually having higher propagation speeds. Propagation speeds are generally highest in solid tissue, lower in fluid-filled structures, and lowest in air-filled structures because of the decreasing stiffness (Table 1-1).[1]

Pulses of ultrasound, not continuous ultrasound waves, are used to obtain most ultrasound images.[1-7] Electrical pulses are applied to the transducer to generate the ultrasound pulses. The pulse repetition frequency (PRF) is the number of pulses occurring per second and is measured in kilohertz (kHz). The pulse repetition period is the time from the beginning of one pulse to the beginning of the following pulse. As the PRF increases, the pulse repetition period decreases. The pulse duration is the length of time for one pulse to occur, which is equal to the pulse repetition period times the number of cycles in each pulse. Each pulse in sonography is usually between one and three cycles in length.[1] The spatial pulse length is the length of space over which a pulse occurs, and it increases with wavelength and the number of cycles within a pulse. Although propagation speeds are identical for pulsed- and continuous-wave ultrasound, frequency within the pulses is not the same as with continuous-wave ultrasound. A wide range of frequencies is present within an ultrasound pulse. The shorter the pulse of ultrasound, the greater the frequency range of ultrasound emitted and the broader or wider the bandwidth of the transducer.[1] The dominant (or center) frequency is close or equal to the frequency for continuous-wave ultrasound.

The amplitude of the ultrasound is the maximal variation of the ultrasound wave and is equal to the maximal value minus the normal (undisturbed) value.[1] The intensity of the ultrasound is the power of the ultrasound or the rate at which the ultrasound energy is transferred divided by the area over which the power is spread.[1] The intensity of the ultrasound is proportional to the amplitude of the ultrasound squared. Therefore, if the amplitude is doubled, the intensity is quadrupled. The amplitude and intensity of the ultrasound wave are decreased or attenuated as the ultrasound travels through tissue.

Table 1–1
Propagation Speed of Ultrasound in Tissue

Tissue	Propagation Speed (mm/μs)
Fat	1.44
Brain	1.51
Liver	1.56
Kidney	1.56
Muscle	1.57
Soft-tissue average	1.54

Adapted from Kremkau FW: Diagnostic Ultrasound: Principles and Instruments, 4th ed. Philadelphia, WB Saunders, 1993.

ULTRASOUND–TISSUE INTERACTIONS

Sound waves enter tissue and are reflected at tissue interfaces.[1-7] The strength of the reflected ultrasound wave depends upon the angle at which the ultrasound beam is directed and the acoustic impedance of the tissues through which the ultrasound beam travels. If the two tissues have the same acoustic impedance, no ultrasound is reflected and all the ultrasound is transmitted into the deeper tissues.

Acoustic Impedance

Ultrasound is transmitted into tissue and reflected from the interfaces between the tissues based upon the acoustic impedance of the adjacent tissues.[1-7] The acoustic impedance is the density of the tissue multiplied by the velocity at which sound travels through that tissue (propagation speed).

$$\text{Acoustic impedance (rayl)} = \text{velocity (m/sec)} \times \text{tissue density (kg/m}^2\text{)}$$

$$Z = vp$$

The acoustic impedance of tissue is determined by the density and stiffness of a medium.[1] Increases in either the density or the stiffness of the medium increase the acoustic impedance. Increases in the propagation speed also increase the acoustic impedance.

Only small differences in acoustic impedance occur between the various soft tissues and organs in the body, whereas large differences exist between the soft-tissue structures and bone or structures containing air (Table 1-2).[1-7] Bone has a very high acoustic impedance relative to that of soft tissue, whereas air has a very low acoustic impedance. The marked difference between the acoustic impedance of air and that of soft tissue causes nearly

Table 1–2
Acoustic Impedance of Tissue

Tissue	Acoustic Impedance*
Air	0.0004
Fat	1.38
Water (50° C)	1.54
Brain	1.58
Blood	1.61
Kidney	1.62
Liver	1.65
Muscle	1.70
Lens	1.84
Bone	7.8

*Acoustic impedance (Z) = x 10^6 kg/m^2 sec.
Adapted from Curry TS III, Dowdey JE, Murray RC Jr: Christensen's Physics of Diagnostic Radiology, 4th ed. Philadelphia, Lea & Febiger, 1990.

complete reflection of the ultrasound beam from the air-filled tissue back to the transducer, making air a nearly perfect reflector (Table 1-3). This high acoustic impedance mismatch results in the reflection of nearly all the ultrasound beam back to the transducer, leaving little or none of the ultrasound to penetrate deeper into the tissues. The result is the formation of an acoustic shadow (usually seen with bone) or a reverberation artifact caused by air at the tissue interface.[1-8]

Reflection, Refraction, Attenuation, Absorption, and Scatter

Ultrasound waves, like other sound waves, are reflected, refracted, scattered, attenuated, and absorbed. When the ultrasound beam is directed at a tissue interface with a perpendicular incidence, the ultrasound may be reflected, transmitted, or both.[1] The reflector is the medium boundary that produces a reflection, otherwise known as the reflecting surface. Reflection is the portion of ultrasound returned from a boundary of a medium. The ultrasound is reflected back to the transducer to be processed into an image. The transmitted ultrasound continues deeper into the tissues along the same path. The best ultrasound image is obtained by maximizing the reflected ultrasound and minimizing the refracted ultrasound

Table 1–3
Reflection of Ultrasound at Tissue Interfaces

Interface	Reflection (%)
Blood-brain	0.3
Kidney-liver	0.6
Blood-kidney	0.7
Liver-muscle	1.8
Blood-fat	7.9
Liver-fat	10.0
Muscle-fat	10.0
Muscle-bone	64.6
Brain-bone	66.1
Water-bone	68.4
Soft tissue-gas	99.0

Adapted from Hagen-Ansert SL: Textbook of Diagnostic Ultrasonography, 3rd ed. St. Louis, CV Mosby, 1989.

waves. Therefore, the ultrasound beam should be directed perpendicular to the structure(s) of interest, maximizing the portion of the ultrasound beam reflected back to the transducer to be processed by the scan converter into the ultrasound image. The intensity of the reflected and transmitted ultrasound depends upon the incident angle, incident intensity, and acoustic impedances of the tissues.

Refraction of the ultrasound beam occurs when the sound beam changes direction upon passing from one tissue or medium into another.[1] Refraction occurs when the angle of incidence is oblique. The incident angle and the reflected angle are always the same. When the incident angle is oblique, reflection may occur if the acoustic impedances are the same but propagation speeds are different and may not occur if acoustic impedances are different.[1]

Attenuation encompasses absorption, reflection, and scattering of the ultrasound beam. In general, approximately 0.5 dB of attenuation per centimeter of soft tissue occurs for each megahertz of frequency.[1] Attenuation of ultrasound in soft tissue increases as the frequency of the transducer increases. Attenuation is higher in lung and bone than in other soft tissues and does not depend on frequency in either of these tissues. Absorption of the ultrasound beam occurs when the energy of the sound beam is converted to heat and is a function of the frequency of the transducer and the tissue through which the ultrasound beam is traveling.

Specular reflectors are large, smooth, flat boundaries that reflect the ultrasound beam back to the transducer.[1] Specular reflection occurs if the tissue boundary is large relative to the wavelength of the ultrasound and if the boundary is smooth. The intensity of the reflected ultrasound from specular reflectors is highly angle dependent.

If the tissue boundary is small relative to the wavelength of ultrasound or the surface is rough, the ultrasound is diffused. Scatterers are objects or tissue that scatter the ultrasound beam because of their small size or surface roughness and represent most of the tissue in the body.[1] Scattering of the ultrasound beam is relatively independent of the incident angle. Cellular tissues or suspensions of components (such as blood) scatter or redirect the ultrasound in many directions. Sound that is scattered back in the direction from whence it came is called backscatter. The frequency of the ultrasound and the scatterer size determine the backscatter intensities. Backscatter intensities are normally less than specular reflection intensities but can be equal to the intensity of a boundary specular reflection. Backscatter intensities increase as frequency increases because the wavelength is smaller relative to the size of the scatterer. Thus, the tissue heterogeneity effectively increases as frequency increases. Scattering also results in the imaging of tissue boundaries that are not perpendicular to the ultrasound beam, such as the capsules of organs as well as the organ parenchyma.[1] Multiple scatterers are encountered by the ultrasound pulse, resulting in the generation of numerous echoes, which may reinforce one another or partially or totally cancel each other out, resulting in acoustic speckle. The acoustic speckle does not directly represent the scatterers but rather represents the interference echo pattern.

RESOLUTION

Three types of resolution are found in ultrasound imaging: detail, contrast, and temporal resolution.[1] Detail resolution is the ability to image two separate reflectors as two separate echoes. Detail resolution is determined by the axial and lateral resolution of the ultrasound pulses as they travel through tissue and the closeness of the two reflectors.[1] The contrast resolution (shades of gray) of the ultrasound system also influences the detail resolution (axial and lateral resolution). If the contrast resolution of the system is high, it can sense the dip in the combined amplitude of overlapping ultrasound pulses and resolve them.[1] The resolution of the imaging system, however, is normally not as good as the detail resolution of the transducers. Temporal resolution is the ability of a display to distinguish events that are closely spaced in time.[1] Temporal resolution improves with an increase in frame rate.

Lateral Resolution

Lateral resolution is the minimum distance between two reflectors located at the same depth, perpendicular to the direction of sound travel, such that when a beam is scanned across them, two separate echoes are produced.[1-7] Lateral resolution is equal to the diameter of the ultrasound beam in the scan plane. The primary method of improving lateral resolution is focusing the beam. The ability to distinguish two objects side by side, perpendicular to the long axis of the ultrasound beam (lateral resolution), is determined by the diameter of the ultrasound beam and the distance from the transducer as the ultrasound beam diverges in the near and far fields. Acceptable lateral resolution is usually found for several centimeters distance from the focal zone of the transducer.

Axial Resolution

Axial resolution is the minimum reflector separation required along the direction of ultrasound travel (scan line) to produce separate echoes.[1-7] The ability to distinguish two objects adjacent to one another along the long axis of the beam (axial resolution) is determined by the pulse length, which is determined by the frequency of the ultrasound transducer. Axial resolution is equal to half of the spatial pulse length emitted from the transducer. The spatial pulse length is the wavelength multiplied by the number of cycles in the pulse. Axial resolution is improved by decreasing the pulse length, increasing the cycles per pulse, or increasing the frequency of the transducer used. The axial resolution worsens at lower frequencies and deeper depths (Table 1-4). The axial resolution of most ultrasound systems is better than the lateral resolution.

Table 1–4
Axial Resolution (Two-Cycle Pulse) and Imaging Depth in Tissue

Frequency	Imaging Depth (cm)	Axial Resolution (mm)
2.0	30	0.77
3.5	17	0.44
5.0	12	0.31
7.5	8	0.20
10.0	6	0.15

Adapted from Kremkau FW: Diagnostic Ultrasound: Principles and Instruments, 4th ed. Philadelphia, WB Saunders, 1993.

INSTRUMENTATION

A wide range of ultrasonographic equipment is available today from small, portable, and inexpensive sector, linear, and curved (convex) linear-array systems to large, hospital-based ultrasound machines with color-flow Doppler and power Doppler capabilities and transesophageal and endoluminal imaging. The many different types of ultrasonographic transducers are designed with certain scanning needs in mind. Sector, linear, and curved linear-array transducers are most frequently used in equine practice. Annular-array and phased-array transducers are available with the more sophisticated ultrasonographic equipment, whereas the availability of transesophageal and endoluminal transducers is restricted at this time to the most expensive and technologically advanced machines. A thorough understanding of the equipment being used enables its user to obtain the best possible sonographic images.

Transducers

Ultrasound transducers are frequently referred to as probes or scan heads. At the hub of the transducer is a single or multiple piezoelectric (pressure-electric) crystal(s), which is deformed (excited) by an electrical current, emitting ultrasound.[1-7] A variety of different materials such as ceramic, quartz, polyvinylidene fluoride (PVDF), and others produce a voltage when deformed by an applied pressure and produce pressure when deformed by an applied voltage.[1] Therefore, ultrasound transducers convert electrical voltage into ultrasound energy and incident ultrasound back into electrical voltage.[1] The transducer consists of the piezoelectric element(s), damping and matching materials, and casing.[1] The damping material reduces the number of cycles per pulse and therefore reduces the pulse duration and spatial pulse length and results in improved axial resolution. This damping may also reduce the amplitude of the returning incident ultrasound and decrease the sensitivity of the system. A matching layer(s) is added to the surface of the ultrasound transducer that has an impedance intermediate between that of the piezoelectric element and the tissue to improve the transmission of ultrasound into the tissue. Similarly, an acoustic coupling gel must be applied between the transducer surface (footprint) and the skin surface to improve transmission of ultrasound into the tissues owing to the large difference in acoustic impedance between air and soft tissue.

Transducer Frequencies

A wide variety of transducer frequencies is currently available, ranging from low-frequency transducers im-

aging at 2.0 MHz to high-frequency transducers imaging at 10.0 MHz. Ultra-high-frequency transducers exist for specialty imaging. In endoluminal ultrasonography, transducer frequencies of 25 MHz and higher are currently being employed. In ophthalmologic and dermatologic scanning, frequencies of 25 to 100 MHz are used. The use of these ultra-high frequencies requires the purchase of special equipment and state-of-the-art, usually nonportable, imaging systems that are not in routine use in veterinary medicine at this time.

The selection of the appropriate transducer for an examination depends upon the structure being evaluated, the depth of that area from the transducer surface, and the acoustic properties of the intervening tissues.[9-12] Some transducers can be used transrectally, enabling the sonologist to place a transducer closer to the area of interest, minimizing the amount of intervening tissue through which the ultrasound beam travels to reach the area of interest. High-frequency transducers have excellent resolution but poor penetration capabilities. Low-frequency transducers can penetrate to depths of 30 to 40 cm but have less resolution. The best-quality sonographic examination is always obtained with the highest-frequency transducer that penetrates to the area being examined. Thus, a high-frequency transducer should be selected when examining a structure close to the skin surface, such as tendons, ligaments, umbilicus, jugular vein, eyes, pleura, epididymis, neonatal bladder, neonatal gastrointestinal viscera, or other structures immediately beneath the skin surface (Table 1-5). An intermediate-frequency transducer should be selected to examine structures 5 to 15 cm from the skin surface, such as the abdominal organs in foals; the liver, spleen, and, in some adult horses, the right kidney; the gastrointestinal viscera in foals and adults; uterus, ovaries, and testicles; and the lung and pleural cavity (Table 1-5). A lower-frequency transducer should be selected when imaging deeper structures such as the heart in the adult horse, the left kidney and spleen, the right kidney in fat adult horses, the lungs and pleural cavity in horses with extensive pleural and pulmonary disease, the cranial mediastinum, the pregnant uterus in late gestation, and large abdominal masses (Table 1-5).

The sonologist must select a transducer of a specific frequency to begin the examination. If better resolution is needed, a higher-frequency transducer is selected, whereas if penetration is inadequate, a lower-frequency transducer is selected. Many ultrasound transducers operate at a single frequency only; therefore, another transducer must be selected. With some equipment, multiple frequencies are available within the same transducer. With the newer wide-bandwidth transducers, each transducer emits a range of ultrasound frequencies around its center (or optimal) frequency (Fig. 1-1). Wide-bandwidth transducers are created by using short bursts of ultrasound, which result in a wide range of frequencies emitted.[3] Burst excitation is used selectively to operate the transducer at more than one frequency. If a higher-resolution image is needed, the higher frequencies emitted in the broad band can be selected, resulting in improved image quality (Fig. 1-1). This is done by emitting voltage bursts of the selected frequency contained within the wide-bandwidth transducer. Similarly, if more penetration is needed, the lower frequencies emitted in the broad band are selected, and the ultrasound beam can then penetrate further into the tissues being examined (Fig. 1-1). Although this ability enables the image to be fine-tuned in terms of resolution and penetration, the penetration of the lower frequencies and the resolution of the higher frequencies of the wide-bandwidth transducers are less than those of a transducer whose center frequency is the desired frequency. Some transducers are also designed with piezoelectric crystals of several different center frequencies within the transducer, enabling one transducer to be used for multiple purposes. However, the resolution of these transducers is poorer, and frame rate is slower because only some of the crystals are being used at any one time to obtain the image.

Table 1–5
Transducer Frequencies and Their Application in Equine Practice

Frequency (MHz)	Applications
10.0	Tendons (superficial digital flexor tendon), ligaments (collateral), bone, cornea, eye, jugular vein, other superficial vessels, internal umbilical remnants, external umbilicus, lymph nodes, glands, tongue
7.5/6.0	Tendons, ligaments, joints, tendon sheaths, bursae, muscle, bone, eye, jugular vein, other superficial vessels, internal umbilical remnants, external umbilicus, neonatal bladder, epididymis, testicles, penis, internal genitalia of the stallion, uteroplacental unit, transrectal aorta, transrectal iliac arteries, transrectal cranial mesenteric artery, gastrointestinal viscera, small abdominal masses, neonatal heart, neonatal kidneys, neonatal-weanling liver, neonatal-weanling spleen, lymph nodes, glands, tongue, pleura, and lung
5.0	Transrectal left kidney, transrectal uterus, transrectal ovaries, internal genitalia of the stallion, penis, testicles, adult liver, foal heart, foal left kidney, small to medium-sized abdominal mass, uterus and fetus in early to mid gestation, muscles, bone, lung, pleura, foal cranial mediastinum
3.5/3.0	Heart, left kidney, uterus and fetus in late gestation, large/fat adult spleen, large/fat adult liver, large/fat adult right kidney, large abdominal mass, cranial mediastinum, severe pleural/pulmonary disease, deep muscle, and bone
2.5	Heart, left kidney, uterus and fetus in late gestation, large/fat adult spleen, large/fat adult liver, large/fat adult right kidney, large abdominal mass, cranial mediastinum, severe pleural/pulmonary disease

Beam Profile

The beam diameter depends upon the wavelength and frequency of the ultrasound emitted, the transducer diameter, and the distance from the transducer.[1] The beam width in the scan plane and perpendicular to the scan plane is equal to the beam diameter for disk element transducers, cylindrical beams, and annular-array transducers, but not for linear-array transducers. For linear-array transducers the beam width in the scan plane determines the lateral resolution of the transducer, and the

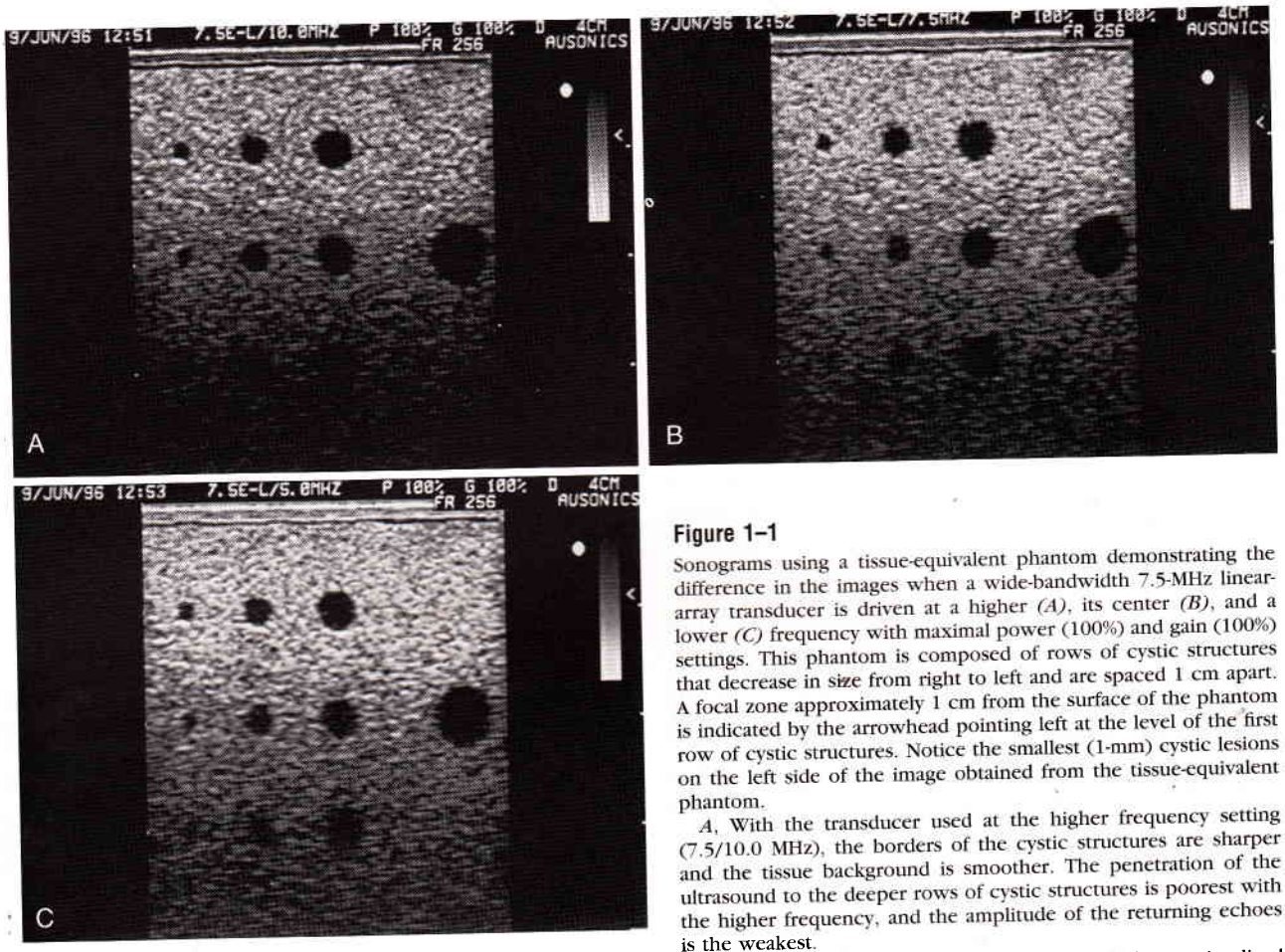

Figure 1–1

Sonograms using a tissue-equivalent phantom demonstrating the difference in the images when a wide-bandwidth 7.5-MHz linear-array transducer is driven at a higher *(A)*, its center *(B)*, and a lower *(C)* frequency with maximal power (100%) and gain (100%) settings. This phantom is composed of rows of cystic structures that decrease in size from right to left and are spaced 1 cm apart. A focal zone approximately 1 cm from the surface of the phantom is indicated by the arrowhead pointing left at the level of the first row of cystic structures. Notice the smallest (1-mm) cystic lesions on the left side of the image obtained from the tissue-equivalent phantom.

A, With the transducer used at the higher frequency setting (7.5/10.0 MHz), the borders of the cystic structures are sharper and the tissue background is smoother. The penetration of the ultrasound to the deeper rows of cystic structures is poorest with the higher frequency, and the amplitude of the returning echoes is the weakest.

B, With the transducer used at its center frequency (7.5/7.5 MHz), the 1-mm cystic structure at the second depth is better visualized than in *A* but not as easily imaged as in *C*. The graininess of the tissue background and the amplitude of the returning echoes are intermediate between the higher *(A)* and lower *(C)* frequency settings.

C, With the transducer used at the lower frequency setting (7.5/5.0 MHz), the borders of the cystic structures are less distinct and the tissue background is grainier. The penetration of the ultrasound to the deeper rows of cystic structures is best with the lower frequency, and the amplitude of the returning echoes is the strongest.

beam width in the plane perpendicular to the scan plane determines the extent of the section-thickness artifact (see Chapter 2). The near field of the beam, or the Fresnel zone, is the region extending one zone length out from the transducer element.[1] The near-field length increases proportionally with increasing frequency and with the square of the diameter.[1] The far field, or Fraunhofer zone, is the distance that lies beyond one near-zone length.[1] The diameter of the ultrasound pulse decreases in the near field and increases in the far field.

Focusing

Focusing the beam results in reduced beam diameter and improved lateral resolution.[1-7] Focusing of the beam can occur only in the near field of the ultrasound beam.[1] The wavelength, transducer size, and focal length determine the degree to which an ultrasound beam can be focused.[1] The focal zone of the ultrasound beam is the narrowest area of the ultrasound beam, where image quality is the best. The focal zone is fixed in sector-scanner transducers and cannot be changed by the operator but is, instead, predetermined by the manufacturer. With linear, curved (convex) linear, and phased- and annular-array transducers, the focal zone can be moved within the image, or additional focal zones can be added at different depths throughout the image, improving image quality (Fig. 1–2).

Steering

In more sophisticated systems, the ultrasound beam can be steered so that the scan plane can be manipulated around intervening structures such as ribs or bowel or the beam can be steered to improve the incident angle for Doppler flow studies (Fig. 1–3).

Transducer Types

Real-time images can be obtained electronically or mechanically. Mechanically the piezoelectric crystals are immersed in acoustic coupling fluid and are oscillated or rotated through a sweep at a rapid rate within the transducer housing. Electronic real-time scanning is performed

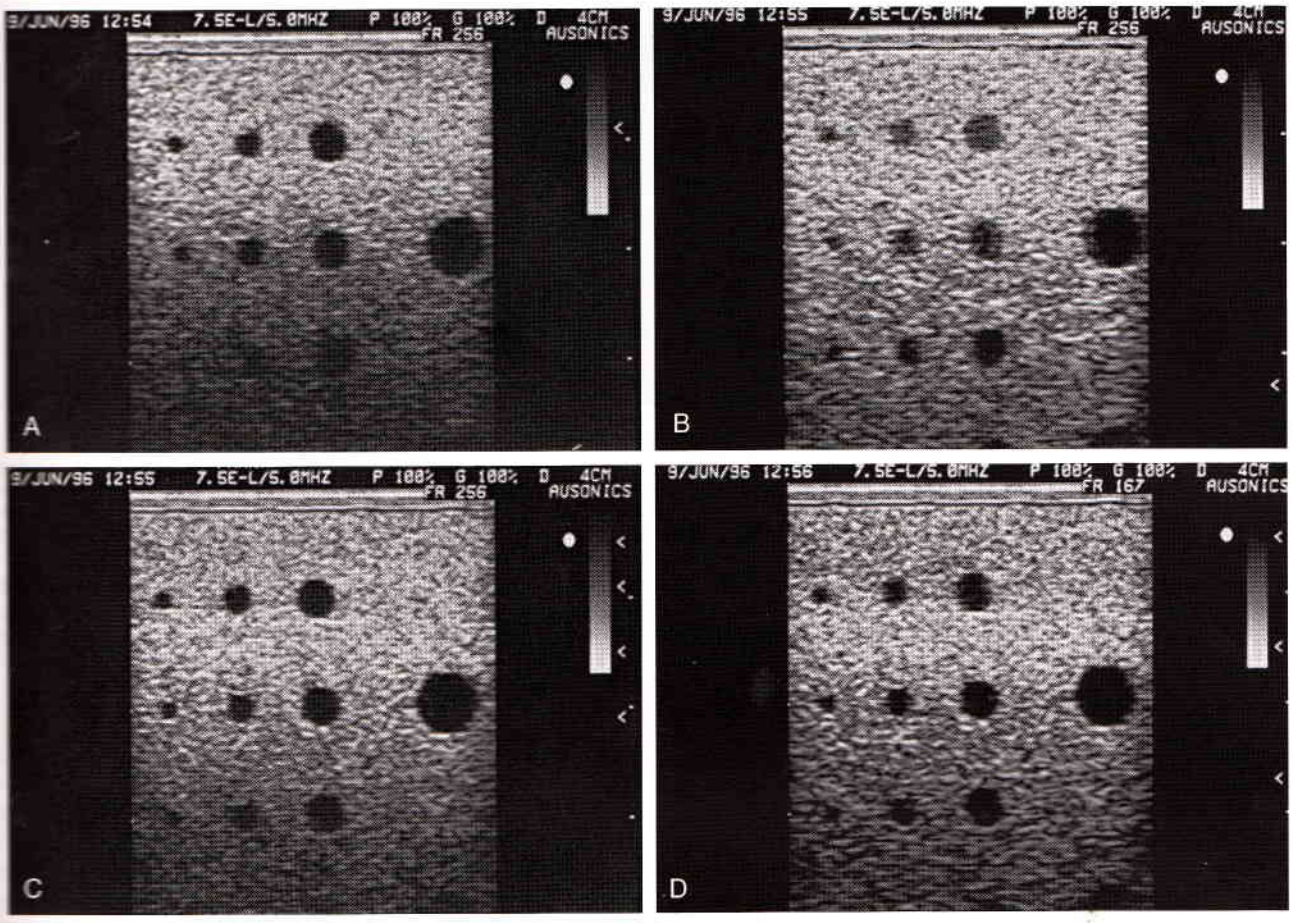

Figure 1–2

Sonograms using a tissue-equivalent phantom demonstrating the difference with one focal zone or multiple focal zones and moving the focal zones within the image. Notice the differences in the images when the wide-bandwidth 7.5/5.0-MHz linear-array transducer is focused close to the transducer surface at approximately 1 cm depth *(A)*, at 4 cm depth *(B)*, and when multiple (four) focal zones are used close to the transducer surface *(C)* and spread deeper into the phantom *(D)* with maximal power (100%) and gain (100%) settings. This phantom is composed of rows of cystic structures that decrease in size from right to left and are spaced 1 cm apart. The focal zone(s) is indicated by the arrowhead pointing left. Notice the smallest (1-mm) cystic lesions on the left side of the image obtained from the tissue-equivalent phantom.

A. With one focal zone at approximately 1 cm, the first row of cystic structures is very distinct, but the resolution of the cystic structures in the second row is poorer.

B. With one focal zone at approximately 4 cm, the third row of cystic structures appears most distinct, but the resolution of these structures is much poorer than in *A*, *C*, or *D*.

C. With four focal zones focused close together in the near field (in the first 2+ cm), the resolution of the three rows of cystic structures is best, but the first row is not quite as distinct as in *A*.

D. With four focal zones spread farther apart (in the first 4+ cm), the resolution of the second row of cystic structures is not as good as in *C* or *A*, but the third row is fairly distinct.

by electronically exciting arrays (or groups) of piezoelectric crystals rapidly through a predetermined sequence, depending upon the type of array.

Linear Array

Linear-array transducers were first used in equine practice for pregnancy diagnosis and are still the preferred transducer design for anyone in a practice doing primarily equine reproduction.[9–12] These transducers can also be used for evaluating the internal reproductive organs in the mare and stallion and for evaluating the external genitalia of the stallion. Linear-array transducers were then used by equine practitioners for the evaluation of tendon and ligament injuries. This use led to other musculoskeletal applications and the use of these transducers for the evaluation of small parts.

Linear-array transducers are solid-state transducers composed of a row of arrays of ultrasound crystals that are electronically fired in succession, forming a rectangular image (Fig. 1–4).[1–3, 9, 13, 14] The width of the image is approximately equal to the length of the array.[1] The greater the number of ultrasound crystals within the ultrasound transducer, the better the transducer's image quality. The number of crystals housed within a single linear transducer varies significantly between manufacturers, from 48 to 196 crystals. The best image quality is obtained with one wire (or channel) per crystal. In order to decrease cost, a series of up to five crystals is chan-

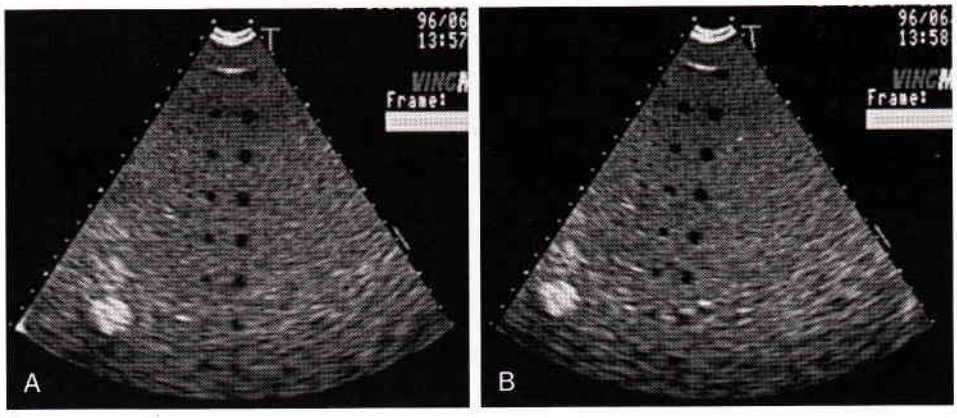

Figure 1–3

Sonograms using tissue-equivalent phantoms demonstrating the difference with beam steering on the portion of the tissue-equivalent phantom imaged. Notice the differences in the location of the echogenic circular structure in the lower left in the unsteered image *(A)* and when the beam is steered in the opposite direction *(B)*. These images were obtained with a 2.5-MHz wide-bandwidth annular-array transducer that was driven at a higher frequency. This phantom is composed of rows of cystic structures that decrease in size from right to left and are spaced 1 cm apart. The focal zone is indicated by the linear white marker to the right of the centimeter scale.

A, The cystic structures line up parallel with the center of the beam, and the echogenic circular structure is approximately 2 to 3 cm from the left side of the image.

B, The cystic structures now angle off to the left as the beam goes deeper into the phantom, and the echogenic circular structure is now near the left edge of the image.

neled to each wire using a multiplexer. A multiplexer is used in most portable ultrasound equipment. The size of the transducer connector is an indication of the number of channels because there is one pin in the connector for every channel. Therefore, the larger the transducer connector, the more channels contained within the transducer cord. With less than 32 channels, frame rate slows markedly when multiple focal zones are activated and focusing is less effective.

Linear-array transducers have less penetration for a particular ultrasound frequency than sector-scanner or annular-array transducers. However, the linear-array transducers can be electronically focused and have the ability to vary the depth of the focal zone or to have multiple focal zones, improving the image quality at a precise location(s) within the area being scanned. The receiving focus is also continuously changed (dynamic focusing). The linear-array transducers become larger as the frequency of the transducer decreases, resulting in the 3.0-MHz linear-array transducers having a very large footprint (contact area between the imaging surface of the transducer and the patient). This large footprint is a limiting factor in using linear-array transducers for thoracic and abdominal imaging in horses because the large footprint does not fit between the intercostal spaces and does not conform well to the shape of the abdomen or thorax.[9] The rectal linear transducer designed for equine reproduction is usually cigar- or pencil-shaped, with the beam emitted off line at a 90-degree angle, perpendicular to the long axis of the transducer (Fig. 1-5). Linear-array transducers are also designed with the beam emitted in line with the long axis of the transducer, making scanning superficial parts such as tendons and ligaments much easier. Transducer frequencies range from 3.0 to 7.5 MHz for most commercially available portable ultrasound equipment, although 10-MHz transducers are becoming more available.

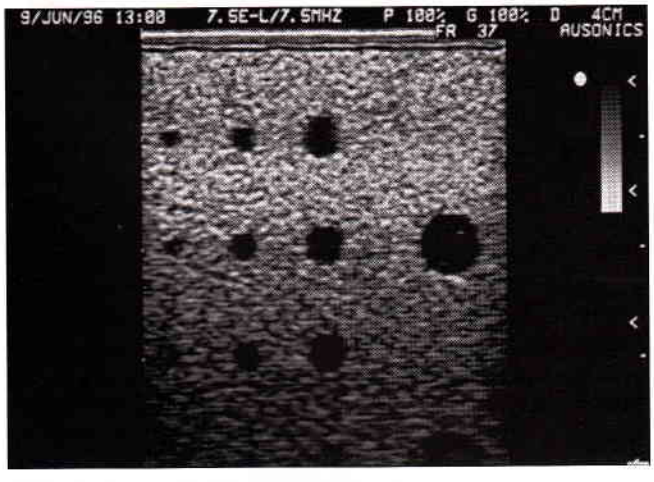

Figure 1–4

Sonogram using a tissue-equivalent phantom demonstrating the image obtained with a 7.5-MHz linear-array transducer. The multiple (four) focal zones spread deeper into the phantom with maximal power (100%) and gain (100%) settings. This phantom is composed of rows of cystic structures that decrease in size from right to left and are spaced 1 cm apart. The focal zones are indicated by the arrowheads pointing left. Notice the smallest (1-mm) cystic lesions on the left side of the image obtained from the tissue-equivalent phantom.

Curved (Convex) Linear Array

Curved linear-array transducers were developed initially for the ultrasonographic evaluation of pregnant women. Although the arrays of crystals are excited much like those of a standard linear-array transducer and the beam can be similarly electronically focused, the footprint of the standard linear-array transducer was curved (Fig. 1-6) to form a convex surface, yielding a curved pie-shaped

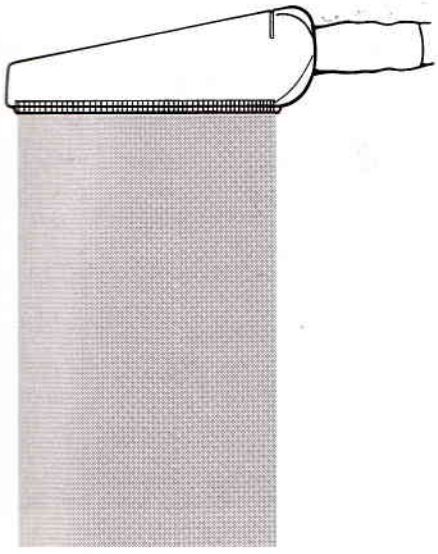

Figure 1–5

Diagram of a standard linear transrectal transducer with the beam emitted perpendicular to the long axis of the transducer. Notice the rectangular shape of the image obtained.

or sector-like) image (Fig. 1-7).[1-3, 14] With this modification, the imaging surface of the transducer conformed more to the abdomen, and a more complete image was obtained. The curved or convex linear-array transducer has a smaller footprint than the standard linear transducer but similar depth penetration. The larger, lower-frequency convex linear-array transducers (3.0 MHz) are used primarily for abdominal imaging but have limited applications in the adult horse owing to their penetration limitations (usually only 20 cm) and a footprint that is too large to fit in the intercostal spaces. The smaller, higher-frequency (6.0 to 10 MHz) convex (or microconvex) linear-array transducers have a wider application in equine practice and can be used for the sonographic evaluation of tendons and ligaments, other superficial musculoskeletal structures, the foal's abdomen (including gastrointestinal viscera, bladder, and umbilical remnants), small parts, and external genitalia of the stallion. This high-frequency microconvex transducer can also be used transrectally for the evaluation of the internal reproductive organs of the stallion and mare and for the evaluation of the aorta, iliac arteries, cranial mesenteric artery, palpable abdominal viscera, and abdominal masses. Transducer frequencies range from 3.0 to 10.0 MHz for most commercially available equipment, similar to those available with the standard linear-array transducer.

Sector Scanners

Sector-scanner transducers are widely used in equine practice because of their ability to penetrate farther into the tissue than linear-array or curved linear-array transducers of the same frequency.[9, 12, 13] Sector-scanner transducers are designed with one or more crystals that are mechanically oscillated or rotated to form a pie-shaped image (Figs. 1-8 and 1-9). The sector-scanner transducer has a small footprint that fits easily into the equine intercostal spaces. The small footprint and excellent penetration of the sector-scanner transducer (30 to 40 cm with the 2.5-MHz sector-scanner transducer) makes this transducer technology excellent for routine cardiac imaging in horses, as well as for deeper abdominal and thoracic imaging. Sector-scanner transducers have a fixed focal zone for each transducer, which cannot be electronically moved throughout the imaging field, limiting the optimal image quality to the fixed focal zone.[1-3] Only sequential, not simultaneous two-dimensional (2-D) real-time echocardiography, M-mode echocardiography, and pulsed and continuous-wave Doppler echocardiography can be obtained, in most instances with single-crystal technology, although split-crystal sector-scanner transducers are available which enable the echocardiographer to obtain simultaneous 2-D and continuous-wave Doppler echocardiograms.[15] Sector-scanner transducers usually have the beam in line with the long axis of the transducer, but offline transducers are available for transrectal ultrasonographic imaging in the horse. A few companies make high-frequency sector-scanner transducers with an acous-

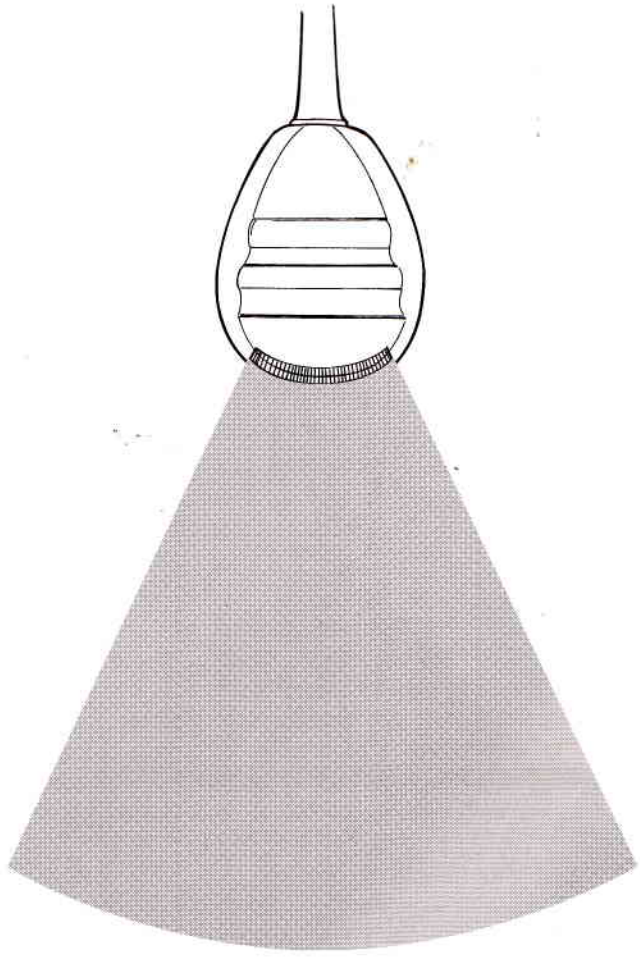

Figure 1–6

Diagram of a curved (convex) linear transducer with the beam emitted in line with the long axis of the transducer. Notice the sector-like shape of the image obtained.

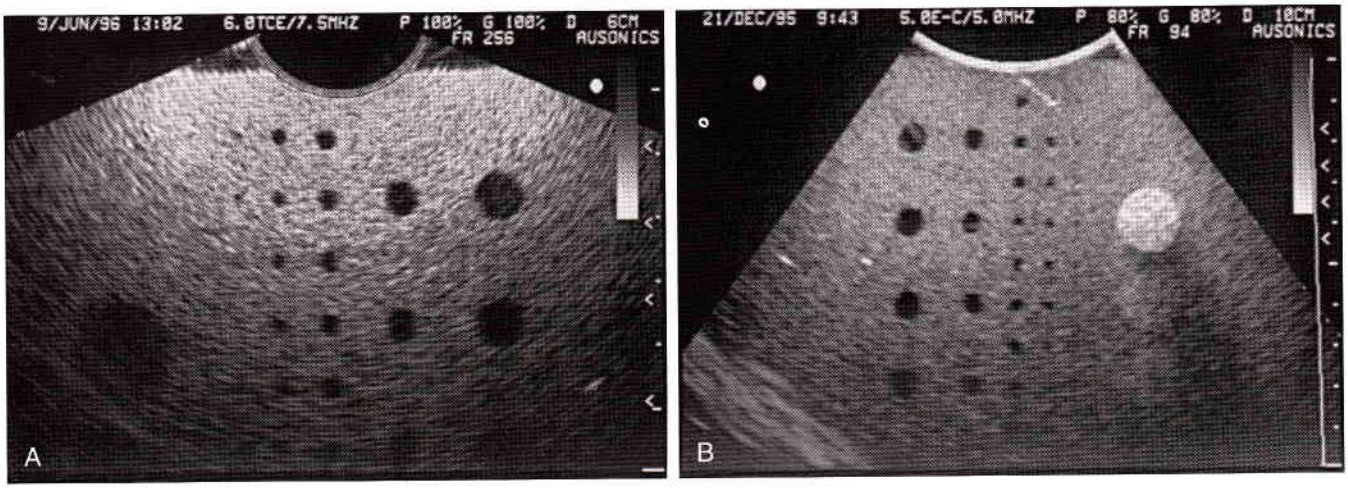

Figure 1–7

Sonograms using tissue-equivalent phantoms demonstrating the images obtained with a microconvex *(A)* and curved convex *(B)* linear transducer. Notice the curved top of the image (contact surface between the transducer and the phantom). The focal zones are indicated by the arrowheads pointing left.

A, Notice the wide field of view (150 degrees) with the microconvex transducer *(A)* compared with the standard convex transducer *(B)*. This is a wide-bandwidth 6.0-MHz transducer with four widely spaced focal zones.

B, Notice the standard width of the ultrasound image (90 degrees) and the increased penetration with the lower frequency convex transducer (5.0 MHz).

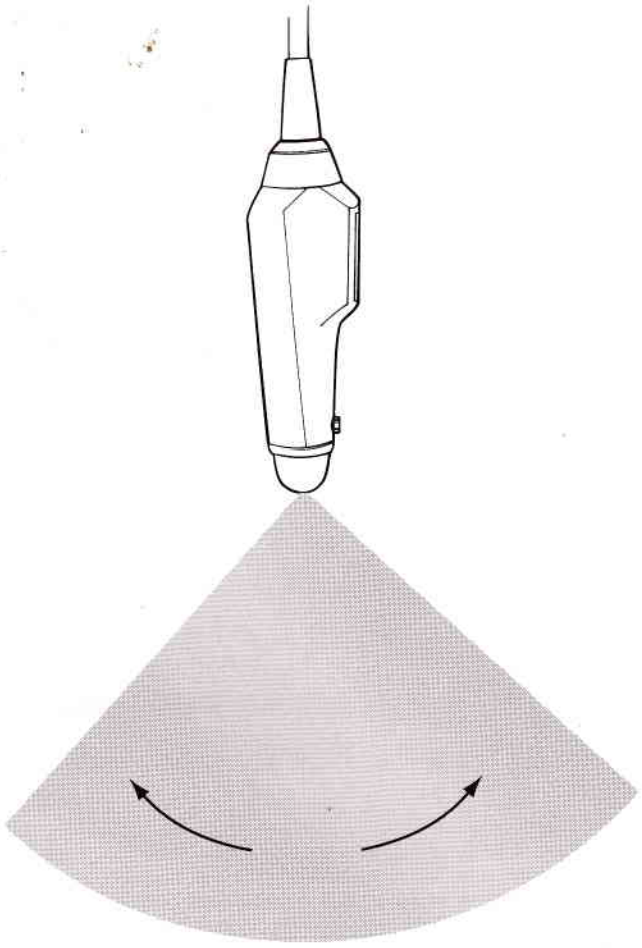

Figure 1–8

Diagram of a sector-scanner transducer with the beam emitted in line with the long axis of the transducer. Notice the pie-shaped 90-degree sector image obtained.

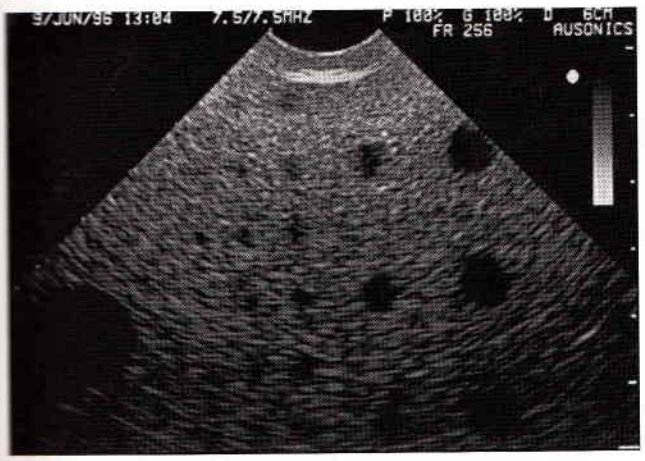

Figure 1–9

Sonogram using a tissue-equivalent phantom demonstrating the image obtained with a 7.5-MHz sector-scanner transducer. Notice the pie-shaped 90-degree sector image obtained. The penetration is better than with the 7.5-MHz linear transducer, but resolution of the cystic structures is poorer owing to the fixed focusing in the sector transducer (see Fig. 1-1B).

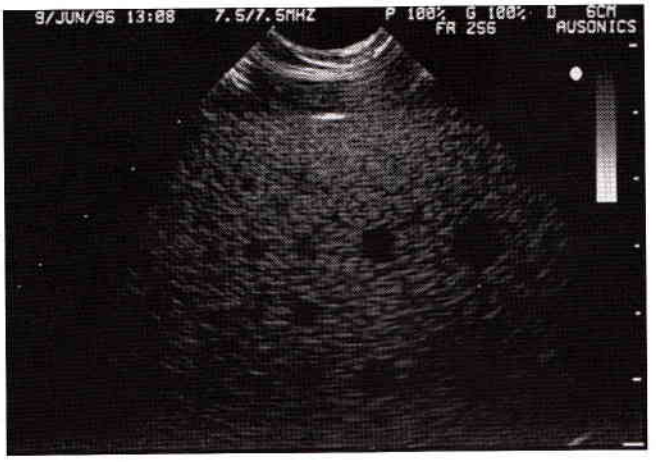

Figure 1–11

Sonogram obtained using a tissue-equivalent phantom demonstrating the image obtained with a 7.5-MHz sector-scanner transducer and a hand-held standoff pad using the same settings as in Figure 1-9. Notice the attenuation of the image that occurred with the use of the standoff pad but the improved resolution of the structures right below the surface of the tissue-equivalent phantom compared with Figure 1-9.

tically matched built-in fluid offset (Fig. 1-10), maximizing the image quality obtained with this transducer compared with that obtained using a hand-held standoff pad (Fig. 1-11).[16] The built-in fluid offset is also much easier to use than the hand-held standoff pad, freeing up one hand to change the equipment settings and to record the ultrasonographic findings. Transducer frequencies with most commercially available equipment range from 2.5 to 7.5 MHz.

Annular Array

Annular-array transducers are composed of multiple, ring-shaped crystals that are mechanically oscillated or rotated to form a pie-shaped image (Fig. 1-12).[1-3, 9] The more crystals housed within the annular-array transducer, the better its image quality. The image quality of annular-array transducers tends to be superior to that obtained with a sector scanner because of the multiple crystal technology present (Fig. 1-13). The beam profile is cone shaped because of the ring-shaped transducer elements, which reduce the beam width both in the scan plane

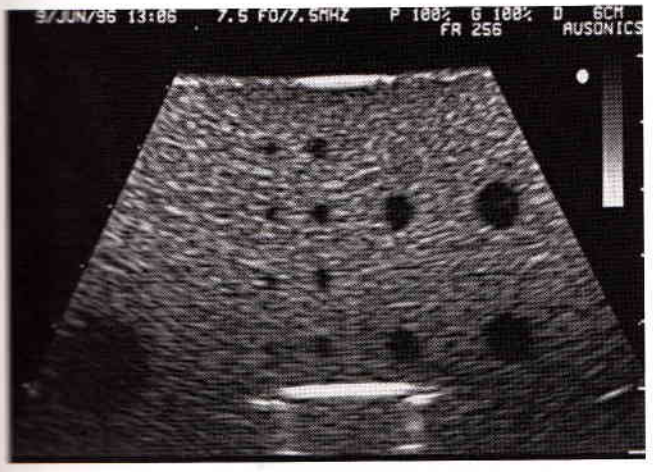

Figure 1–10

Sonogram using a tissue-equivalent phantom demonstrating the image obtained with a 7.5-MHz sector-scanner transducer containing an acoustically matched built-in fluid offset. Notice the improved resolution of the cystic structures compared with those in Figure 1-9, especially those structures close to the surface of the tissue-equivalent phantom.

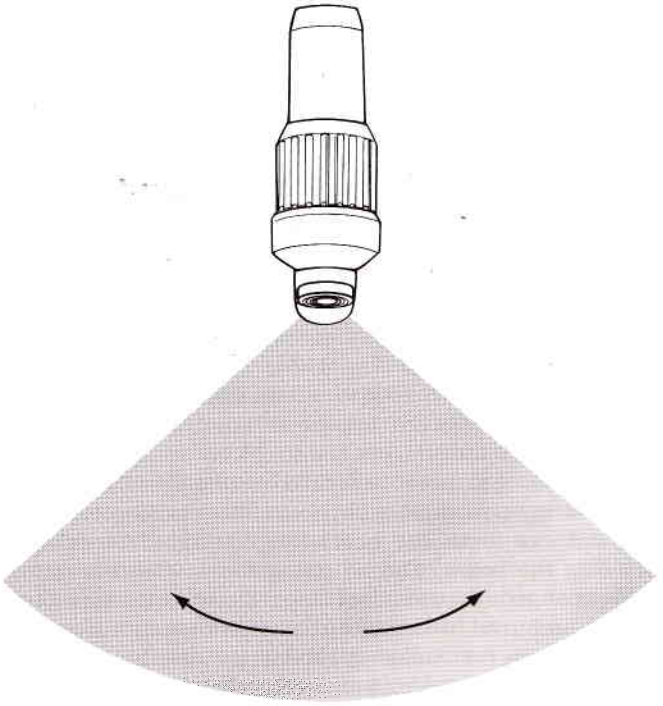

Figure 1–12

Diagram of an annular-array transducer with the beam emitted in line with the long axis of the transducer. Notice the pie-shaped image obtained.

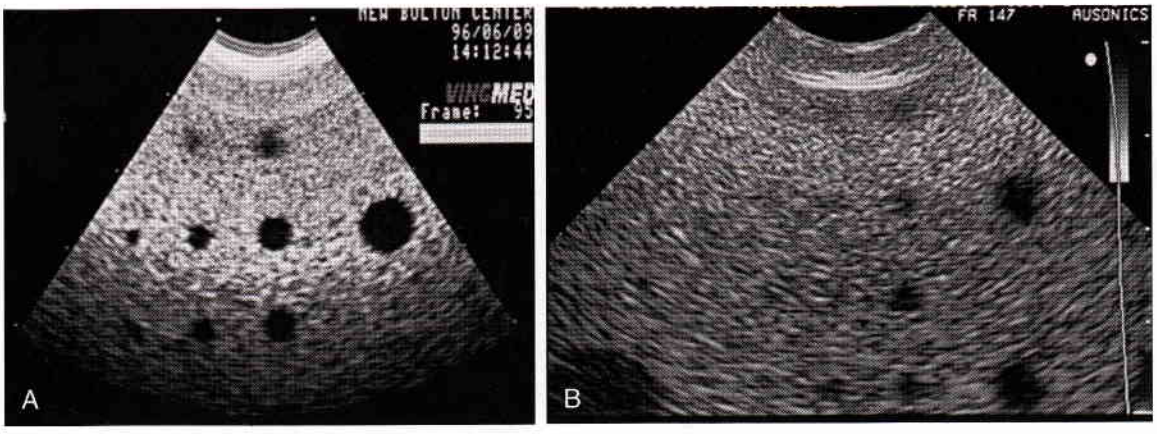

Figure 1–13

Sonograms obtained using a tissue-equivalent phantom demonstrating the image obtained with a 7.5-MHz annular-array transducer *(A)* and a sector-scanner transducer *(B)*. Notice the improvement in the resolution of the cystic structures with the annular-array transducer compared with the sector-scanner transducer.

and perpendicular to the scan plane. Annular-array transducers have variable focusing capabilities, improving the detail of the image in the area of interest. Dynamic focusing of the returning echoes is also possible. Sequential, not simultaneous 2-D, M-mode, pulsed-wave, continuous-wave, and color-flow Doppler echocardiography is obtained with annular-array technology.[15] Annular-array transducers have excellent penetration capabilities for each transducer frequency (30 cm for the 2.5-MHz transducer). Annular-array transducers also have small footprints, although their footprints tend to be slightly larger than the sector-scanner footprint for the same frequency transducer. The annular-array transducers also have a large range of transducer frequencies (7.5 to 2.5 MHz), similar to those available with the sector-scanner transducers, and are occasionally used for transesophageal imaging.

Phased Array

Phased-array transducers are composed of multiple crystals in a rectangular format that are electronically excited as a group with small time differences (phasing), which results in the sound pulse being sent out in a specific direction that is constantly changing and the formation of a pie-shaped image (Fig. 1-14).[1-3, 9, 13, 15] These transducers have a smaller footprint than linear-array or curved linear-array transducers, less penetration than annular or sector-scanner transducers (22 to 28 cm for the 2.5-MHz transducer), and poor near-field resolution (Fig. 1-15). Phased-array transducers have variable focusing capabilities and can focus the beam by phasing, electronically focusing the beam. The receiving focus is also continuously changed (dynamic focusing). Phased-array transducers are preferred by many cardiologists for echocardiography because two imaging modalities can be obtained simultaneously by using some of the ultrasound crystals for one imaging modality and the rest for the other.[15] Two-dimensional echocardiography can be obtained simultaneously with M-mode echocardiography, pulsed wave, continuous-wave, or color-flow Doppler echocardiography.[15] For this reason, phased-array technology is the primary transducer type used in transesophageal imaging transducers.[15] Transducer frequencies for most commercially available equipment range from 7.5 to 2.25 MHz.

Specialty Transducers

A wide variety of specialty transducers have been developed to meet particular scanning needs in both human (primarily) and veterinary medicine.

Transrectal Transducers. Transrectal ultrasound

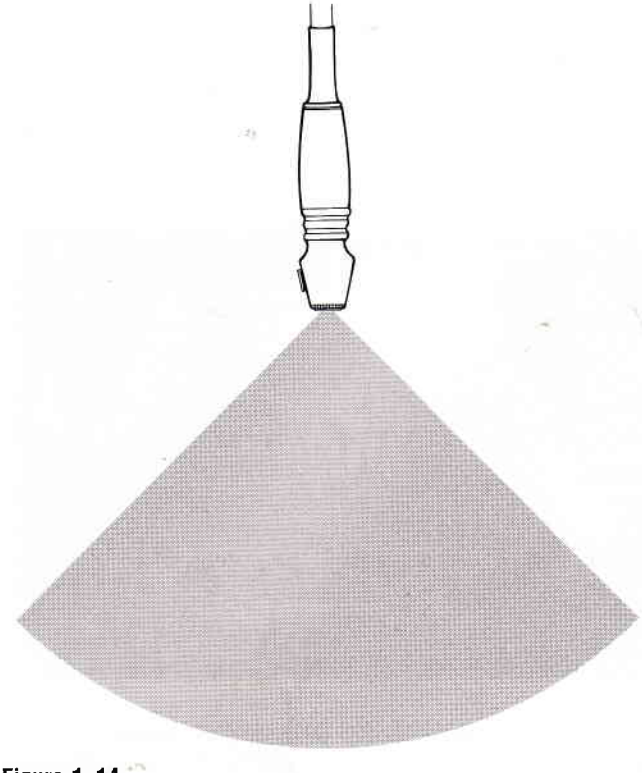

Figure 1–14

Diagram of a phased-array transducer with the beam emitted in line with the long axis of the transducer. Notice the pie-shaped image obtained.

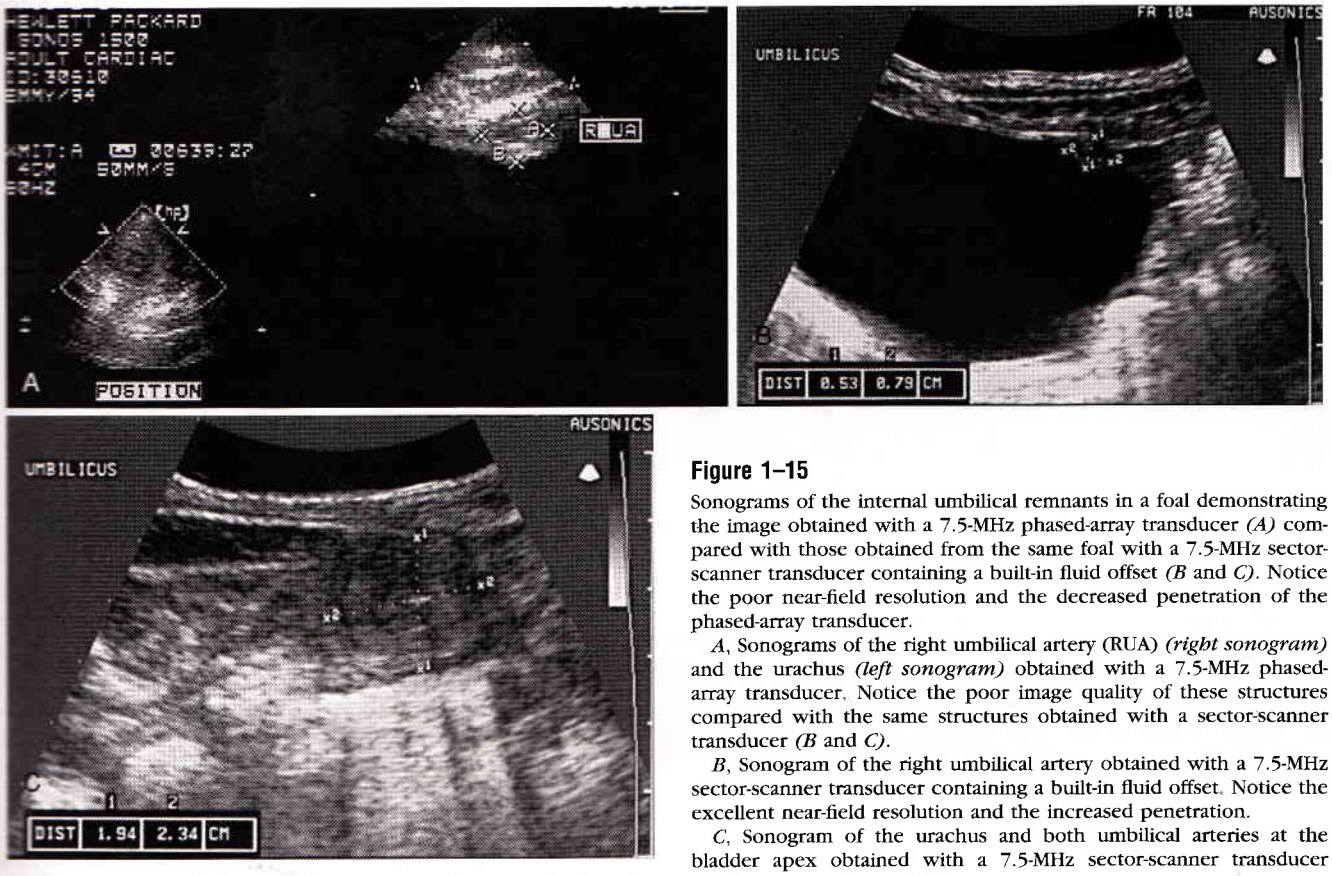

Figure 1–15

Sonograms of the internal umbilical remnants in a foal demonstrating the image obtained with a 7.5-MHz phased-array transducer *(A)* compared with those obtained from the same foal with a 7.5-MHz sector-scanner transducer containing a built-in fluid offset *(B* and *C)*. Notice the poor near-field resolution and the decreased penetration of the phased-array transducer.

A, Sonograms of the right umbilical artery (RUA) *(right sonogram)* and the urachus *(left sonogram)* obtained with a 7.5-MHz phased-array transducer. Notice the poor image quality of these structures compared with the same structures obtained with a sector-scanner transducer *(B* and *C)*.

B, Sonogram of the right umbilical artery obtained with a 7.5-MHz sector-scanner transducer containing a built-in fluid offset. Notice the excellent near-field resolution and the increased penetration.

C, Sonogram of the urachus and both umbilical arteries at the bladder apex obtained with a 7.5-MHz sector-scanner transducer containing a built-in fluid offset. Notice the excellent near-field resolution and the increased penetration.

transducers were one of the earliest transducer developments in veterinary medicine to allow the practitioner to safely take an ultrasound transducer into the rectum and scan the female reproductive tract.[9-12] These transducers were designed with a cigar or pencil shape, with a smooth covered exterior with no sharp protuberances, and with the beam originating at 90 degrees to the long axis of the transducer. These transducers were originally 5.0-MHz frequency, but 7.5-MHz transrectal transducers are now available for ultrasonographic evaluation of the female and male internal reproductive organs. These transducers are also useful for examining the aorta, iliac arteries, bladder, urethra, cranial mesenteric artery, perirectal masses, and portions of the gastrointestinal tract that can be palpated rectally. The disadvantage of these transducers is that the footprint of the transducer must be placed directly over the area to be examined and the depth of penetration of the image is usually limited.

Sector-scanner transducers were also designed for equine practice which could be safely taken into the rectum but were larger and less user friendly.[9] Transrectal sector-scanner transducers designed for use in equine reproduction have a beam that originates off line from the long axis of the transducer. The center of the sector sweep either is at 90 degrees to the long axis of the transducer or projects downward and forward 45 degrees from the transducer's long axis. The latter transducers have the advantage of being able to project the ultrasound beam in front of the footprint position to scan a structure in the more cranial abdomen, as long as the intervening tissues are not highly reflective. Sector scanners are also able to penetrate deeper into the tissues than linear scanners for the same frequency of transducer, giving a larger depth of field to examine large abdominal masses, the pregnant uterus, and other large structures.

Transrectal and transvaginal transducers are available for human ultrasonography. The transrectal transducers are biplane transducers, which result in the simultaneous acquisition of mutually perpendicular images (or images that are close to being mutually perpendicular). Similarly, transvaginal transducers are designed to image the uterus and pelvic structures through the vagina, enabling the use of higher-frequency transducers to obtain better resolution and improving access to structures that are either not visible or difficult to image from an abdominal window.

Transesophageal Transducers. Transesophageal transducers are medium- to high-frequency ultrasound transducers that are inserted into a gastroscope or endoscope and then passed into the esophagus and manipulated to image the heart, mediastinal structures, or cranial abdominal structures through the esophagus or stomach.[15] Transesophageal transducers can be single plane, biplane, or omniplane. Single-plane transesophageal transducers are less desirable because the ultrasound beam can be manipulated in only one scanning plane. With biplane transesophageal transducers, the ultrasound beam can be moved in two mutually perpendicular direc-

tions, and with omniplane transducers movement in all directions is possible. The use of transesophageal echocardiography has enabled the cardiologist to obtain much higher resolution images of a variety of cardiac structures and to obtain scan planes that were heretofore unavailable, optimizing evaluation of structures in the mediastinum and around the cardiac base, and of mitral, aortic, and pulmonic flows. Transesophageal echocardiography is being adapted for use in horses and has been valuable for monitoring cardiac function under general anesthesia.

Endoluminal Transducers. Endoluminal transducers are ultra-high-frequency ultrasound transducers that have been inserted into a variety of catheters so that imaging of small tubular structures can be obtained such as the coronary arteries and urethra.[9]

Intraoperative Transducers. High-frequency transducers of a wide variety of shapes have been designed for intraoperative use to aid the surgeon in localizing abnormalities within parenchymal organs or in areas of limited surgical visibility.[9]

Specialty Transducers. Ultra-high-frequency transducers (25 to 100 MHz) have been designed for evaluating very superficial structures such as the layers of the skin, the cornea, and the superficial structures within the eye. These transducers also require special ultrasonographic equipment.

The Pulser

The pulser produces the electric voltage that excites the piezoelectric crystal(s) and produces ultrasound pulses. To display the returning information in real time, it is necessary to use high pulse repetition frequency (PRF). All echoes from one pulse must be received before the next ultrasound pulse is emitted, a fact that requires a reduction in PRF and frame rate when imaging deeper tissues. The greater the voltage amplitude that the pulser produces, the greater the amplitude and intensity of the ultrasound pulses produced by the transducer.[1] The efficiency of the transducer also plays a role in the amplitude and intensity of the ultrasound pulses produced.

Instrument Controls

A variety of controls on the ultrasound machine enable the user to optimize the quality of the ultrasound image. The majority of these controls are preprocessing controls, controls that have to be adjusted before the image is frozen and can modulate the image only before it is stored in memory. Postprocessing functions are those controls that work once the image is frozen and the returning echoes are stored in memory. A knowledge of these settings and how to manipulate these controls is important to obtain the maximal performance from your ultrasound equipment.

Power

Power is the amount of energy or voltage delivered to the piezoelectric crystal or the amount of ultrasound energy emitted from the transducer.[1-7] Increasing the power increases the intensity of ultrasound energy delivered to the tissues. Therefore, a uniform increase in the amplitude of the returning echoes occurs when the power is increased. Power is usually expressed in decibels (dB) or as a percentage of the total output. The lowest power setting possible to penetrate to the area being examined is recommended to obtain optimal image quality. Higher-power settings result in more artifact (noise) than lower-power settings.

Gain

Amplification of the returning ultrasound, or echoes, reflected back to the transducer is accomplished by converting these smaller voltages received from the transducer to larger voltages that can be processed and stored. The gain is the ratio of output to input electrical power.[1-7] The gain control determines the amount of amplification accomplished in the receiver. Increasing the gain increases the amplitude of the reflected ultrasound. The gain controls should be used preferentially to amplify the returning echoes to obtain optimal image quality, rather than increasing the power (voltage) delivered to the piezoelectric crystal. With too little gain, the weak echoes are lost; with too much gain, image saturation occurs and differences in echo strength (contrast resolution) are lost. A decrease in the amplitude of the returning echoes as a result of low acoustic output can be compensated for by increasing the gain, with only a small reduction in imaging depth.

Time Gain Compensation

The amplitude of the ultrasound echoes returning from the deeper tissues (far field) is weaker than the amplitude of the ultrasound echoes returning from the superficial structures (near field). This difference in the amplitude of the ultrasound echoes returning from different depths occurs because ultrasound is absorbed, scattered, reflected, and refracted. Ultrasound energy is attenuated by all tissue to a greater or lesser extent, depending upon the type of tissue through which the ultrasound is passing. Attenuation of the ultrasound depends upon path length. Therefore, more ultrasound energy is lost on its way to deeper structures. Ultrasound energy is also refracted from different tissue interfaces. More ultrasound energy is refracted when the ultrasound beam must pass through multiple tissue interfaces before reaching the area of interest. This results in a further loss of ultrasound energy in the deeper tissues and less that can be reflected back to the receiver (the transducer).

Time gain compensation (TGC) is used to equalize the differences in received echo amplitude because of depth.[1-7] Similar reflectors (reflectors with equal reflection coefficients) have different echo amplitudes arriving at the transducer if their path lengths are different. Longer path lengths result in later arrival time for these echoes at the transducer (receiver). Thus, these echo amplitudes need to be adjusted so that similar reflectors

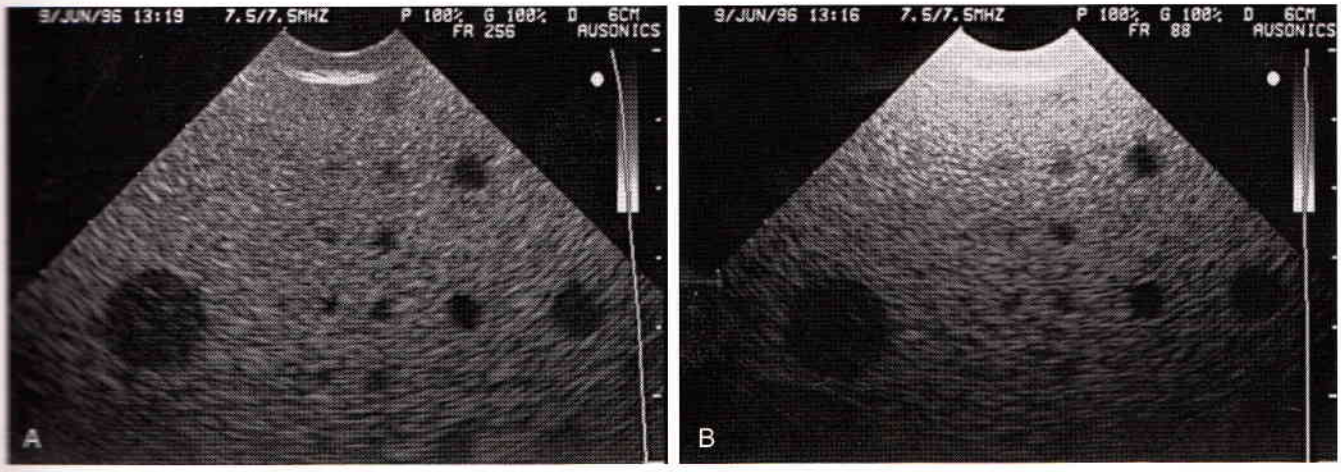

Figure 1–16

Sonograms obtained with a tissue-equivalent phantom demonstrating a gradually increasing time gain compensation (TGC) curve and the resultant smooth homogeneous brightness of the image *(A)* compared with the image with no TGC used *(B)*. These sonograms were obtained with a 7.5-MHz sector-scanner transducer and a displayed depth of 6 cm.

A. The smooth homogeneous image and the gradual slope indicated by the sloping DGC line on the right of the image are associated with properly applied TGC controls.

B. The excessive brightness in the near field of the image and the decreased echo amplitude in the far field of the image are associated with the lack of use of the TGC. The resultant image lacks homogeneous brightness.

are displayed as similar amplitude echoes (Fig. 1-16). Compensation results in these later returning echoes being amplified more than the echoes returning sooner from a shorter path length. This creates a homogeneous appearance of an individual organ or structure being examined in terms of the amplitude of the returning echoes.

The depth gain compensation (DGC) slope (Fig. 1-17) is the line displaying the rate of increase of gain (dB) with depth (cm).[1] This slope is adjusted during the ultrasound examination to achieve uniform brightness throughout the image. At greater depths, maximal brightness is often achieved, as maximal compensation for the ultrasound attenuation has occurred and no further compensation is possible; therefore the brightness of the image in the farthest portion of the field may begin to decrease (Fig. 1-18).

The gain controls may be very simple, with just a near and far (or overall) gain control, or more complex, with the ability to fine-tune the gain every few centimeters with TGC controls. If there are only near and far (overall) gain controls, the near gain should be set low to suppress the strong echoes returning from the reflectors in the near field and the far gain should be set higher to increase the amplitude of the echoes returning from farther away to obtain uniform brightness throughout the image. If a

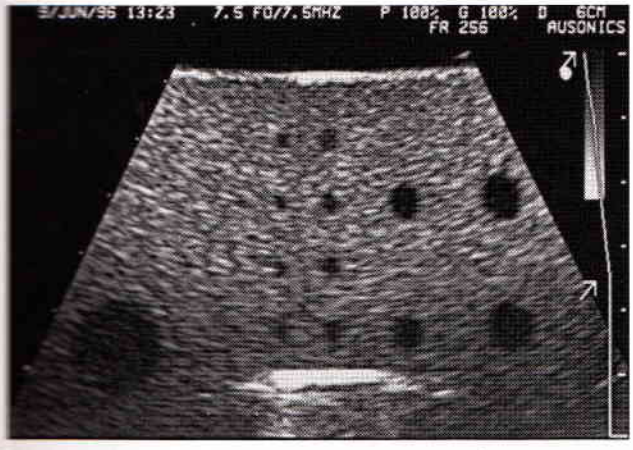

Figure 1–17

Sonogram obtained with a tissue-equivalent phantom demonstrating a gradually increasing time gain compensation (TGC) curve and the resultant smooth homogeneous brightness of the image. The arrows to the right point to the slope of the DGC curve that was used to obtain this image. This sonogram was obtained with a 7.5-MHz sector-scanner transducer containing a built-in fluid offset.

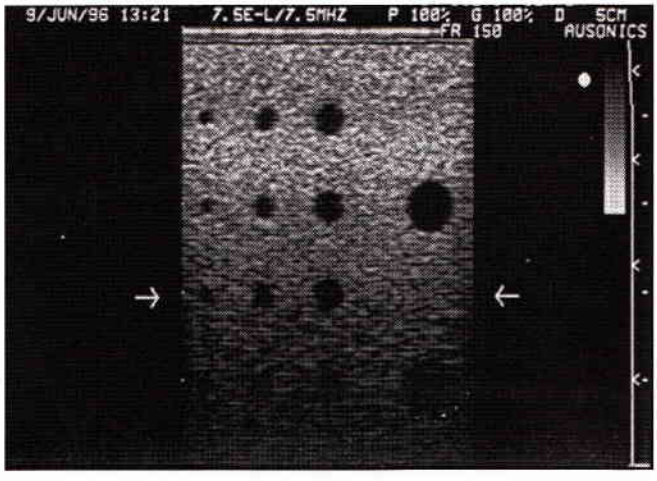

Figure 1–18

Sonogram using a tissue-equivalent phantom demonstrating the inability to increase the gain beyond 2 to 3 cm and the consequent reduction in image brightness at the second row of cystic structures, which becomes very pronounced at the level of the third row of cystic structures. This phantom is composed of rows of cystic structures decreasing in size from right to left and are spaced 1 cm apart. Four focal zones are indicated by the arrowheads pointing left.

slope delay and slope rate control are also present, the slope delay is set at the depth in the image where initial amplification of the echoes returning from deeper reflectors is desired. The slope rate control is set steep when a rapid increase in the echo amplification per centimeter depth is needed, whereas a more shallow slope results in a more gradual increase in the gain of the echoes returning from reflectors in the far field. If individual TGC controls are present, the brightness of the image can be adjusted every few centimeters to obtain a uniform brightness throughout the image. These controls enable the sonologist to maximally fine-tune the image brightness.

Dynamic Range

The dynamic range is the ratio of the largest to smallest amplitude that the system can process.[1] Amplifiers typically have a dynamic range of 100 to 130 dB; however, the human eye can perceive a dynamic range of only 20 dB.[1] Compression is the process of decreasing the difference between the smallest and largest amplitudes, thus amplifying the weaker voltages to a greater degree than the stronger ones. After compression, the dynamic range that usually remains is between 40 and 70 dB. The dynamic range adjusts the contrast of the echoes displayed (Fig. 1-19). Contrast resolution is the number of decibels of dynamic range covered by each gray shade and the average intensity difference between two echoes for them to be assigned to different shades in the system memory. Contrast resolution is improved by more gray shades.

Reject

Reject is a control that removes the low-amplitude (or weaker) signals from the displayed echoes.[1] The reject control removes these low-amplitude echoes by removing the same echo amplitude from all returning echoes relative to the baseline. This results in the reject control removing baseline (or noise) echoes, as well as slightly decreasing the amplitude of all information echoes by a similar amount. As the reject control is increased, more and more of the weaker information echoes are deleted, along with the noise echoes (Fig. 1-20). Thus, the reject control should be used sparingly to clean up the image, achieving a balance between removing the noise from the image and maintaining the weaker information echoes.

Scan Plane Angle

The angle of the scan plane with sector, annular, phased-array, or curved (convex) linear-array transducers can be variable and can range from 30 to 150 degrees or greater. In many situations, the scan-plane angle is fixed (usually 90 degrees) and narrower or wider angles are not possible. In more sophisticated equipment, changing the angle of the scan plane is possible (Fig. 1-21). The wider the scan plane, the slower the frame rate. Therefore, the ability to narrow the scan plane angle is helpful in some real-time imaging, particularly in cardiology, where maintaining a real-time frame rate is essential.

Magnification (Zoom)

Write magnification (write zoom) is a preprocessing function in which the image is magnified but the pixel size remains small. Write magnification is accomplished by writing a smaller portion of the image to be written into the entire memory, thus enlarging the image without enlarging the size of the pixels.[1] With read magnification (read zoom), the image is magnified after it is frozen or stored in memory (postprocessing function), resulting in magnification of the pixels (Fig. 1-22).[1] Read magnification makes the pixel nature of the image more obvious.

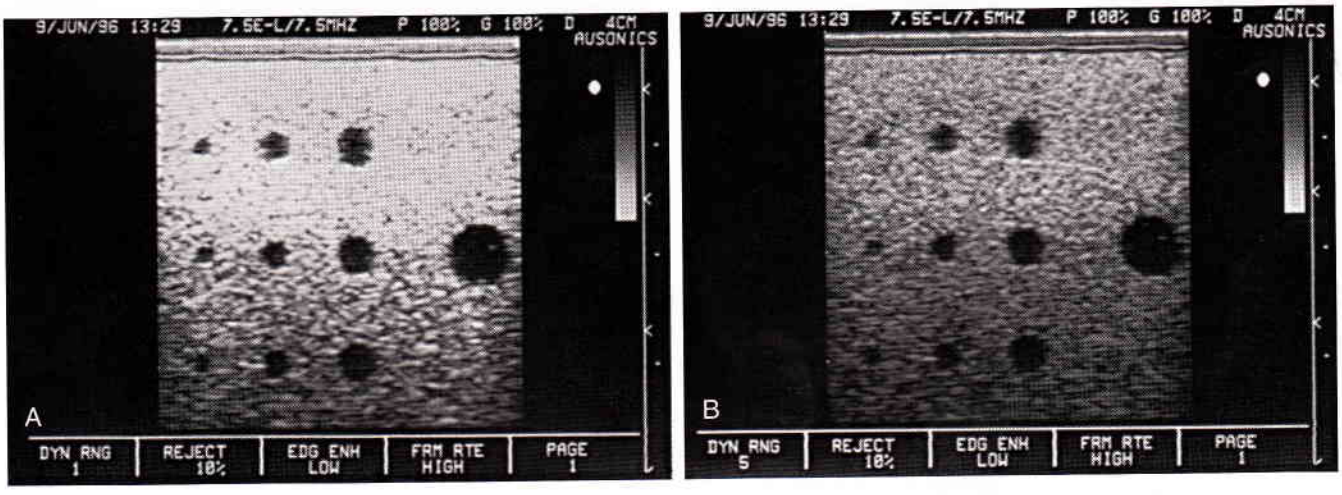

Figure 1–19

Sonograms using a tissue-equivalent phantom demonstrating the difference in the images with changes in dynamic range when a wide-bandwidth 7.5-MHz linear-array transducer is used with maximal power (100%) and gain (100%) settings. Notice the difference in the contrast of the image between the low (1) dynamic range setting *(A)* and the high (5) setting *(B)*. This phantom is composed of rows of cystic structures that decrease in size from right to left and are spaced 1 cm apart. Four focal zones are indicated by the arrowheads pointing left.

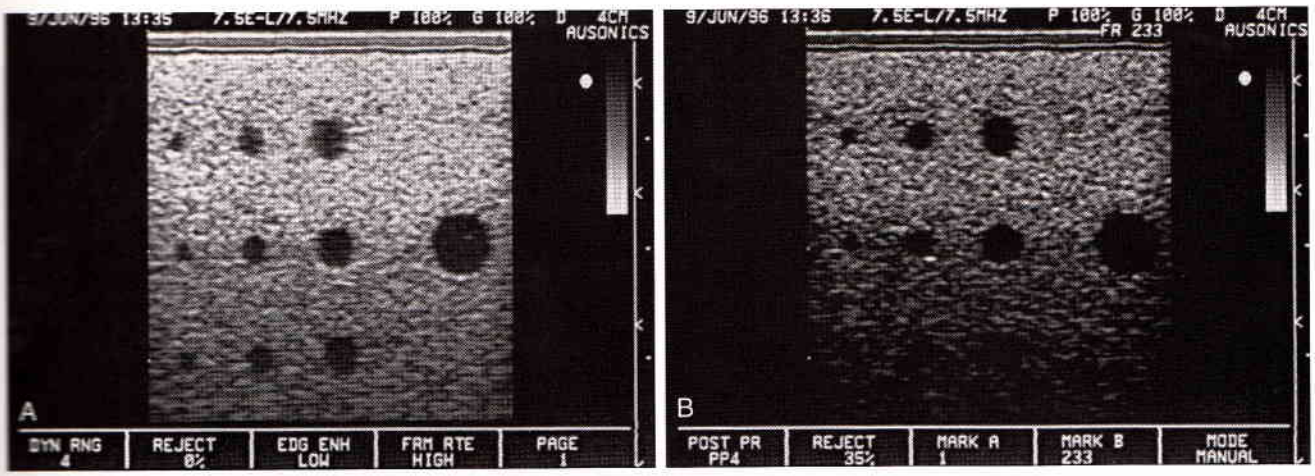

Figure 1–20

Sonograms using a tissue-equivalent phantom demonstrating the difference in the images with changes in reject when a wide-bandwidth 7.5-MHz linear-array transducer is used with maximal power (100%) and gain (100%) settings. Notice the difference in echo density of the image between the low (0%) reject setting *(A)* and the high (35%) setting *(B)*. The increased reject *(B)* carries less noise but also fewer information echoes. This phantom is composed of rows of cystic structures that decrease in size from right to left and are spaced 1 cm apart. Four focal zones are indicated by the arrowheads pointing left.

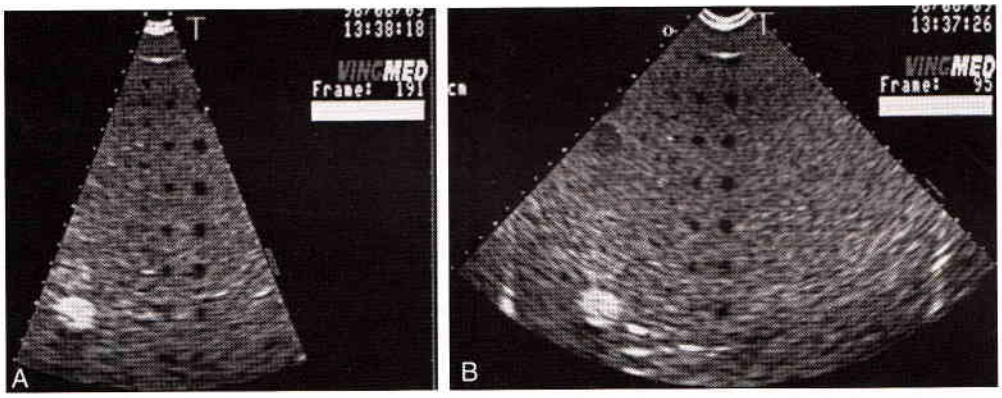

Figure 1–21

Sonograms using a tissue-equivalent phantom demonstrating the difference in the images with changes in scan-plane angle. These sonograms were obtained with a 2.5-MHz annular-array transducer. Notice the difference in the field of view between the narrow setting *(A)* and the wide setting *(B)*. With the increased scan-plane angle, a significant decrease in frame rate occurs. This phantom is composed of rows of cystic structures that decrease in size from right to left and are spaced 1 cm apart. The focal zone is indicated by the parallel lines along the right centimeter scale bar.

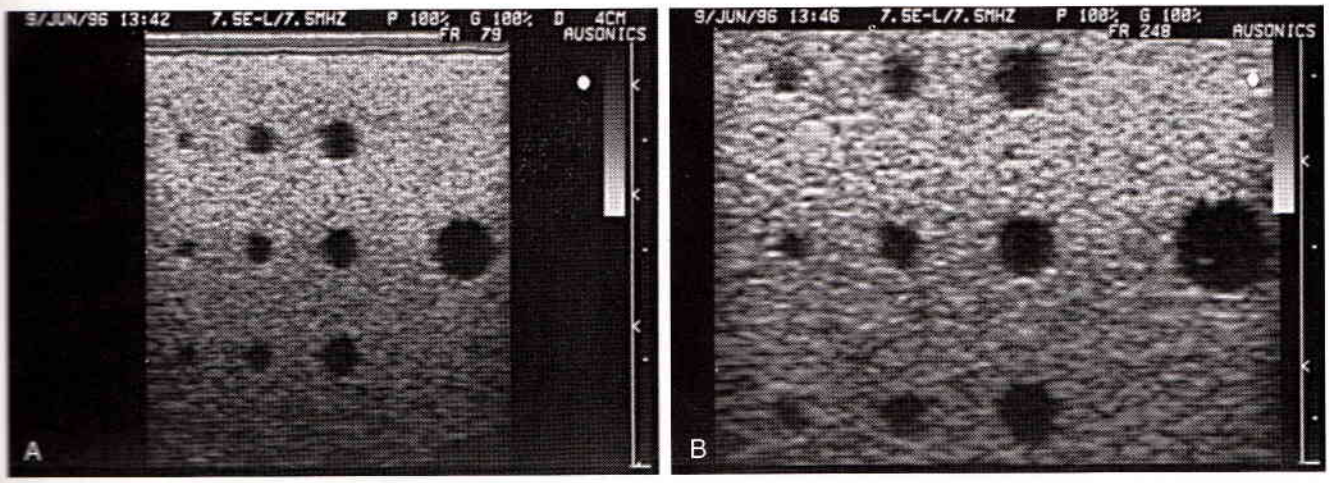

Figure 1–22

Sonograms using a tissue-equivalent phantom demonstrating the difference in the images without magnification *(A)* and when read magnification *(B)* is used. Notice the larger pixel size with the read magnification than without magnification. This phantom is composed of rows of cystic structures that decrease in size from right to left and are spaced 1 cm apart. Four focal zones are indicated by the arrowheads pointing left.

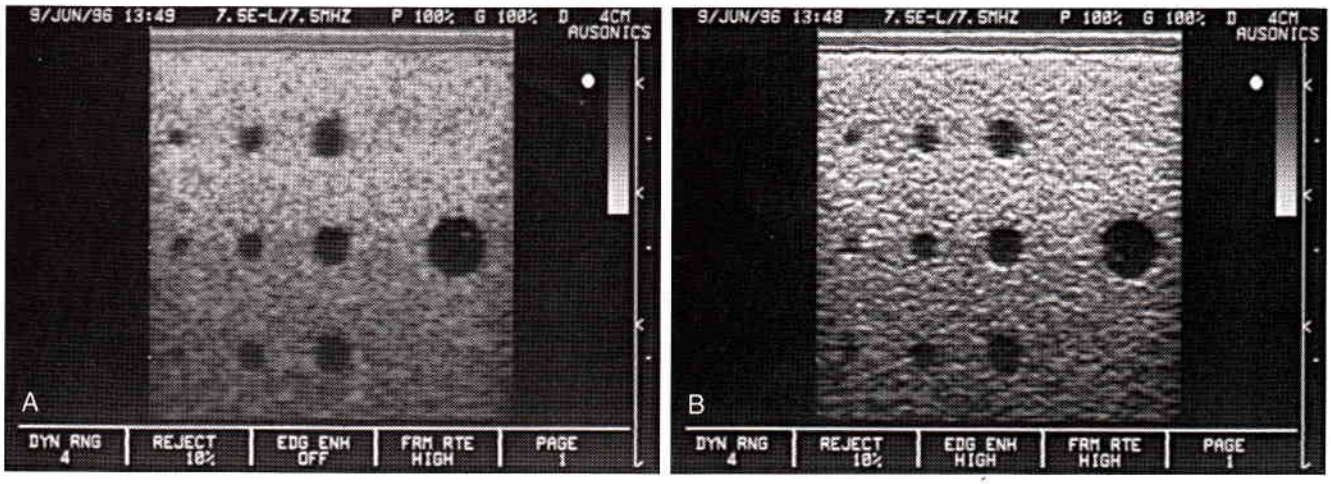

Figure 1–23

Sonograms using a tissue-equivalent phantom demonstrating the difference in the images with the use of edge enhancement when a wide-bandwidth 7.5-MHz linear-array transducer is used with maximal power (100%) and gain (100%) settings. Notice the difference in the sharpness of the image between the smooth image with no edge enhancement *(A)* and the sharp crisp image with high edge enhancement *(B)*. This phantom is composed of rows of cystic structures that decrease in size from right to left and are spaced 1 cm apart. Three focal zones are indicated by the arrowheads pointing left.

Edge Enhancement

This control sharpens the interface echoes and makes the edges of linear structures such as tendons and ligaments more distinct (Fig. 1-23).

Postprocessing

The postprocessing key is a method of changing the brightness of the image once the image has been stored in memory (Fig. 1-24). These curves may change the brightness of the image uniformly (linear curves) or preferentially assign more of the brightness range to certain portions of the stored image, which can improve the ability to differentiate between small echo strength differences stored in memory.[1] Changing the postprocessing curve reassigns the gray levels. Color (B color or color scale) may be used on some equipment to differentiate echo intensities, as the eye can differentiate more color tints than shades of gray, improving the contrast resolution of the system (Color Figure 1-1).

Image Storage

One frame of the image (freeze) or a series of images (cine loop) may be digitally stored in memory by the scan converter for analysis or review.

Gray Scale

The gray-scale capabilities of the ultrasound equipment are a very important part of the equipment selection process, as the amplitude of the returning echoes is

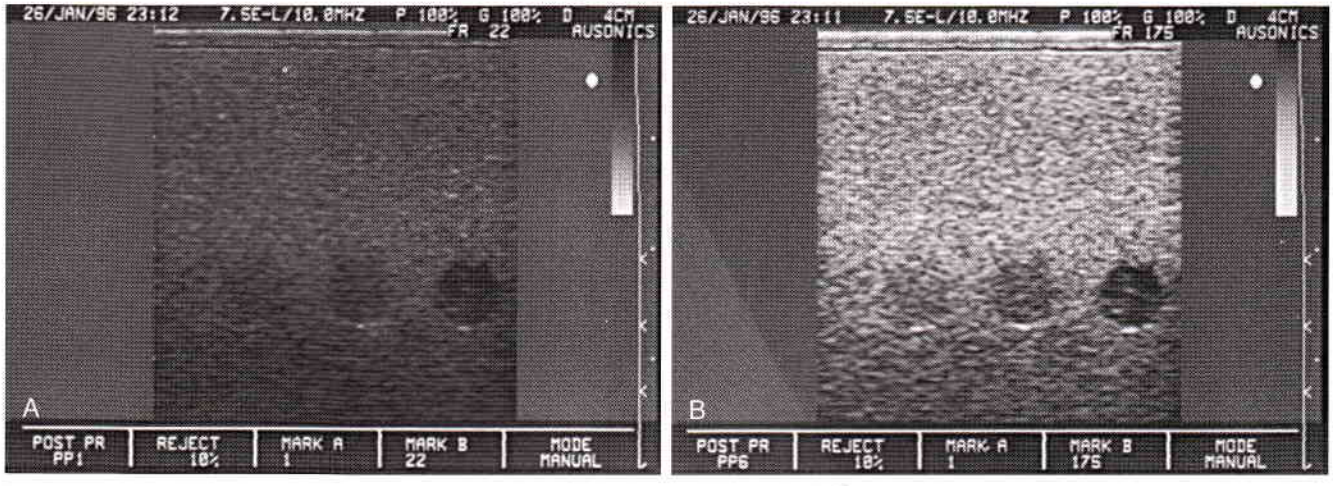

Figure 1–24

Sonograms obtained with a tissue-equivalent phantom demonstrating the difference in postprocessing curves with a 7.5-MHz linear-array transducer.
A, Postprocessing set at its lowest setting (1) yields a dark image with little contrast.
B, Postprocessing set at its highest setting (6) yields a brighter image with more contrast.

displayed in varying shades of gray. The number of gray shades is determined by the manufacturer and cannot be changed by the operator. In some ultrasound equipment, the number of gray shades changes with changes in the depth of penetration displayed. A lower gray scale is present when the depth of penetration is increased. The more shades of gray that are available to assign the varying reflected ultrasound waves, the better the tissue characterization of the image. The shades of gray available on different ultrasound machines ranges from 16 to 256.

MODES OF DISPLAY

A Mode

A mode refers to amplitude mode, where amplitude of the returning echo is displayed as a spike from a vertical baseline.[1-3, 5-7] The location of the echo reflector is represented by the depth of the spike from the top of the vertical baseline, and the strength of the returning echo is represented by the amplitude of the spike. A mode is used primarily for ophthalmologic applications to precisely locate a structure from the surface of the transducer.

B Mode

B mode, or brightness mode, is a 2-D display of the returning echoes; the amplitude of the returning echo stored in memory is converted to the brightness of a dot that represents that returning echo.[1-3, 5-7] The brighter the dot, the stronger the corresponding returning echo. The location of the dot corresponds to the location of the echo reflector within the tissue cross-section. The cross-section of the tissue within the scan plane is the area imaged with B mode. This cross-section may be obtained as a single frozen image (static B mode), or numerous frames can be acquired and displayed within one second (real time). Each frame is refreshed when the next echo pulse sweeps the cross-section. Frame-averaging occurs when a portion of the previous image is held in memory and the new image displayed is added to the portion of the image stored in memory. For static structures, frame averaging can add additional echoes and increase the line density, thus improving resolution of the image. Motion of the horse or the operator may introduce motion artifacts and thus decrease the resolution of the image obtained if frame averaging is used.

Frame Rate

The frame rate is the number of frames displayed per second while the ultrasound image is being obtained. The line density of the image is highest when a low frame rate is employed, yielding a higher-quality image. However, high frame rates are needed to resolve motion in real time, with the highest frame rates needed for structures that are moving very rapidly. In echocardiography, frame rates must be high because accurately resolving the motion of the moving heart is critical, and some detail in the image is sacrificed as a result.[15] In imaging static structures, however, such as tendons, ligaments, and abdominal organs, a low frame rate is ideal to obtain the highest-resolution image possible. Frame rate decreases when penetration is increased, when wider image angles are used, or when the number of focuses increases (Fig. 1-25).[1]

M Mode

M mode (time-motion mode) is a 1-D or "ice-pick" view of depth displayed against time. M mode is used in echocardiography to obtain high-resolution images of the cardiac structures moving over time.[1-3, 5-7, 15] The vertical axis is the depth of the structures from the transducer, and the horizontal axis is the time axis. The brightness of the dots sweeping across the image over time corresponds to the echo amplitude, and the location of the dots corresponds to the location of the echo reflector from the transducer (Fig. 1-26). M-mode echocardiogra-

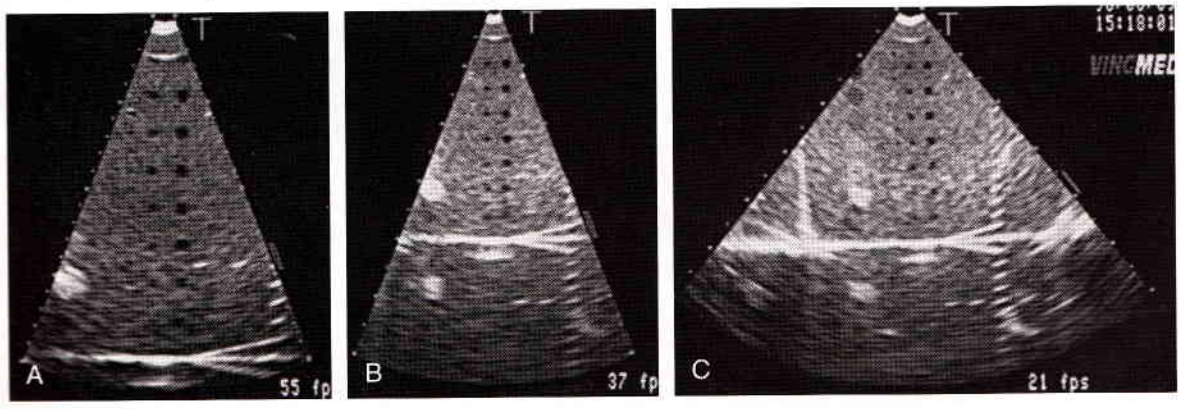

Figure 1-25

Sonograms using a tissue-equivalent phantom demonstrating the decrease in the frame rate from 55 frames/sec *(A)* to 37 frames/sec *(B)*, with an increase in depth from 20 cm *(A)* to 30 cm *(B)* and a further decrease in frame rate to 21 frames/sec (fps) with an increase in the scan-plane angle *(C)*.

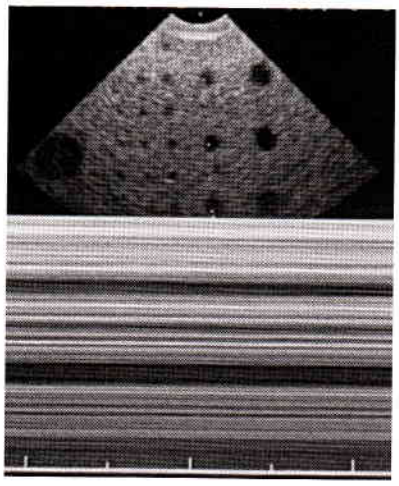

Figure 1–26

Sonogram using a tissue-equivalent phantom demonstrating the M mode display (a one-dimensional image of the phantom over time) along the plane of the cursor *(dotted line in the two-dimensional [2-D] image)*. The anechoic lines in the M mode correspond to the location of the cystic structures imaged on the 2-D image.

phy is used to obtain measurements of the cardiac chambers and myocardial wall thickness and to analyze valve motion and myocardial wall motion.

Three-Dimensional Ultrasound

Three-dimensional (3-D) reconstruction of ultrasound images is being performed in ultrasound laboratories across the country and is available commercially in some high-end ultrasound equipment using human algorithms to reconstruct the 3-D image. Although this technology is not available in portable ultrasound machines and algorithms have yet to be developed for 3-D reconstruction of most equine organs, research and development in this field are growing rapidly and 3-D reconstruction of equine organs will be possible in the future. Three-dimensional reconstruction of the equine superficial digital flexor tendon has already been performed successfully.[17]

DOPPLER ULTRASONOGRAPHY

Doppler ultrasonography relies on the ability to detect the Doppler shift as the ultrasound reflects off moving red blood cells.[1-3, 7, 9, 15, 18, 19] Christian Johann Doppler first described the Doppler shift, the change in frequency that occurs as a result of motion between the sound source (red blood cells) and the observer (transducer).[1] If the red blood cells are moving toward the transducer, the ultrasound is reflected back to the transducer at an increased frequency; if they are moving away, the ultrasound is reflected back at a decreased frequency. The magnitude of that frequency shift is determined by the velocity of blood flow, which can be calculated from the Doppler equation:

$$V = \frac{C\,(\pm\,\Delta f)}{2\,f_0 \cos\theta}$$

where V is the velocity of blood flow (m/sec), C is the speed of ultrasound in soft tissue (1540 m/sec), $\pm\,\Delta f$ is the Doppler frequency shift (Hz), f_0 is the transmitted frequency, and cos θ is the cosign function of the angle between the ultrasound beam and blood flow vector.

To obtain the best Doppler signal and measure accurate peak velocity, the ultrasound beam should be as parallel to blood flow as possible (< 20 degrees), as large errors occur in these calculations when the incident angle is large. In the horse, obtaining an incident angle in echocardiography of 20 degrees or less is possible with ventricular septal defects, difficult with tricuspid and pulmonic regurgitation, and usually impossible with mitral and aortic regurgitation. From the transesophageal window, incident angles of 20 degrees or less may be possible in horses with mitral and aortic regurgitation. When evaluating flow in peripheral vessels, it is also difficult to impossible to achieve an incident angle of 20 degrees or less when evaluating peripheral vessels close to the surface of the skin. An angle of 30 to 60 degrees is desirable in this setting but is also often difficult to achieve. Angle correction is available to correct for the inability to align the Doppler sample volume parallel to blood flow and is used primarily in peripheral vascular work.

Blood flow within the vascular system is normally undisturbed. Two types of blood flow exist within the vascular system, plug flow and laminar flow.[18] Plug flow refers to areas of flow where the speed of blood flow is essentially constant across the tube, such as that which occurs at the entrance to a vessel. Laminar flow develops further down the vessel. In laminar flow the central blood flow moves more rapidly than the fluid close to the vessel wall. Laminar flow is also known as parabolic flow. Disturbed blood flow occurs when the parallel stream lines that characterize normal flow are irregular but flow is still moving in a forward direction. Turbulent flow occurs when blood flow is chaotic and moving in all different directions with a net forward flow, such as is seen with an obstruction to flow (Fig. 1-27). The velocity of blood flow increases to pass the obstruction, and the turbulence is detected beyond the obstruction.

Venous flow is normally steady, whereas arterial flow is pulsatile. Although the flow velocity depends upon the interrogation angle, the difference between the peak systolic and end-diastolic values (pulsatility index) is independent of angle, making the pulsatility index a useful measurement in the description of flow characteristics of peripheral arteries.

Doppler Types

Pulsed Wave

With pulsed-wave Doppler ultrasonography, a pulse of ultrasound is sent out into the tissues to a certain predetermined depth, and the echoes returning from reflectors at that depth are received before the next ultrasound pulse is sent.[7, 9, 15, 18, 19] The PRF is the time between

ultrasound bursts and is determined by the distance from the transducer to the predetermined depth (sample volume or gate). The sample volume or gate is represented by a double hatched line perpendicular to the cursor (Fig. 1-28). The cursor indicates the line along which the ultrasound beam is directed, and the double hatched lines represent the precise location that is being interrogated for the Doppler shift. Thus, pulsed-wave Doppler ultrasound is "range gated," or the Doppler signal can be exactly located to its origin, the sample volume can be moved by the operator along the long axis of the cursor, and the cursor can be moved throughout the image. A large sample volume or gate should be used when initially searching for the Doppler signal desired, and, once localized, the sample volume should be decreased in length to decrease the signal-to-noise ratio.

The blood-flow velocities are displayed on a spectral Doppler tracing and the frequency shifts displayed.[15, 18, 19] The acoustic signal is an excellent guide to obtain the best possible spectral tracing and usually corresponds to the clearest signal with the highest pitch. The human ear is most accurate at determining normal and abnormal flow sounds and should be used as a guide, rather than looking at the spectral tracing, to localize areas of turbulent (abnormal) flow. Laminar blood flow produces a narrow line on the spectral tracing, indicating that the red blood cells are moving at similar velocities and in a similar direction over time (Fig. 1-29). When red blood cells are moving at different velocities and in different directions simultaneously, spectral broadening results

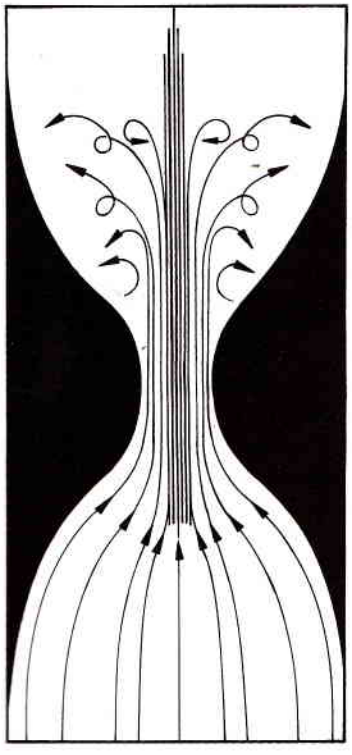

Figure 1–27

Diagram demonstrating the disruption of laminar blood flow by an obstruction to flow (narrowing), with the resultant turbulent blood flow.

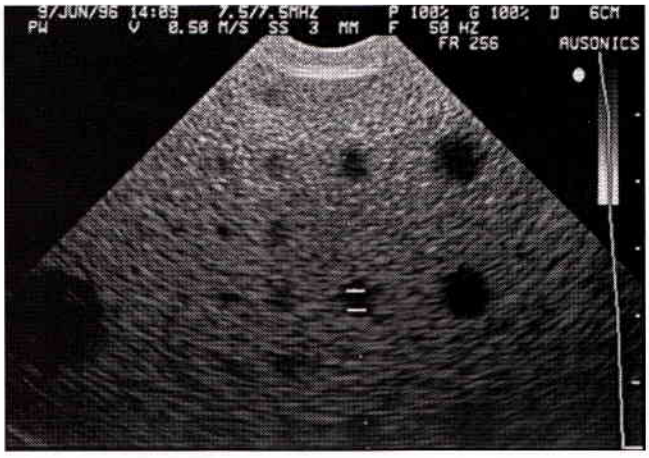

Figure 1–28

Sonogram using a tissue-equivalent phantom demonstrating the placement of the sample volume *(double parallel lines)* along the cursor. This sample volume represents the location of any flow disturbance detected when sampling this area with pulsed-wave Doppler ultrasonography. This can be very useful in determining whether a tubular, fluid-filled structure is a blood vessel, as flow should be detected within the vessel as long as the incident angle is less than 90 degrees (ideally 30 to 60 degrees).

(Fig. 1-29). This is depicted as a broadening of the previously narrow spectral tracing.

Owing to the length of time that must elapse between each ultrasound pulse, the ability to resolve high-velocity blood flow is severely limited. A maximal velocity (Nyquist limit) can be accurately determined for a given depth and frequency, which is one half the PRF.[15, 18, 19] If the Doppler shift exceeds the Nyquist limit, aliasing of the signal occurs. The aliased signal wraps around the baseline of the spectral Doppler and makes it appear as if blood flow is moving in two directions. Aliasing of the Doppler signal makes the interpretation of direction difficult, and maximal velocities cannot be accurately determined once the Nyquist limit has been exceeded. The lower the frequency of the transducer, the higher the velocity that can be recorded before aliasing of the signal occurs. High PRF Doppler has been used to try to overcome some of the aliasing that occurs with low PRF Doppler, but the multiple sample volumes used also introduce range ambiguity (Fig. 1-30).[18, 19] Multiple short pulses are transmitted during the time normally allotted to one pulse with low PRF Doppler, effectively increasing the Nyquist limit. High PRF Doppler can be used at shallow depths to measure high flow velocities because the echoes return quickly to the transducer. However, at greater depths, a slower pulse rate is needed to wait for the returning echoes, decreasing the maximal velocity that can be recorded and increasing the range ambiguity if all the echoes have not returned before the next pulse is sent. Precise localization of flow is also lost, as flow velocity information is sampled from multiple sites. If the multiple accessory sample volumes can be positioned in areas of no flow, the primary sample volume has depth discrimination. A lower-frequency transducer should be used if aliasing of the signal occurs.

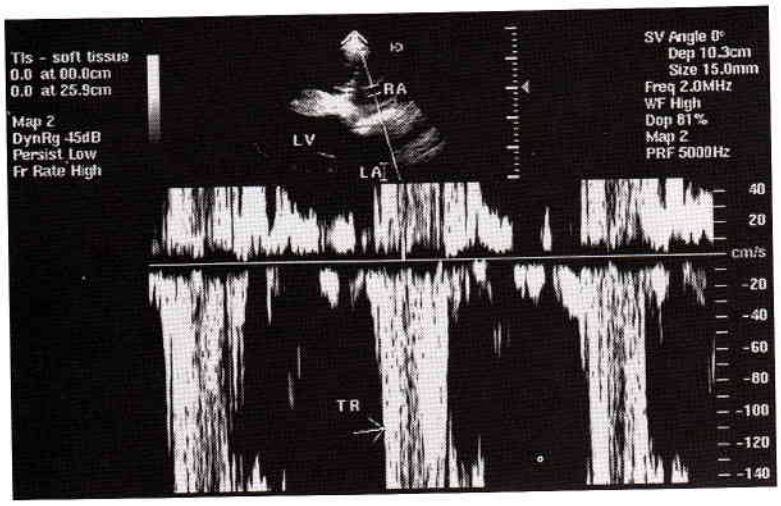

Figure 1–29

Echocardiogram (two-dimensional and pulsed-wave) of a horse with tricuspid regurgitation (TR). The laminar blood flow is the bright thick echogenic line above the baseline between the TR. The spectral broadening is identified by the broad white bands above and below the baseline, indicative of the turbulent, high-velocity blood flow associated with the TR *(arrow)*.

Continuous Wave

Continuous-wave Doppler ultrasound uses ultrasound that is continuously emitted from the transducer and continuously received by the transducer (see Chapter 5).[7, 15, 18, 19] Two piezoelectric elements located side by side are required for continuous-wave Doppler echocardiography; one element continuously emits the ultrasound while the other continuously receives the reflected echoes. In most portable systems, continuous-wave Doppler ultrasound is performed blind (with a nonimaging transducer). Combined imaging and continuous-wave Doppler transducers are available in some of the more sophisticated ultrasound systems by sharing crystals between the imaging and continuous-wave Doppler capabilities.

Continuous-wave Doppler ultrasound can be used to determine the direction of flow and can be used to resolve peak velocities of blood flow, even at very high flow velocities. Continuous-wave Doppler records Doppler shifts that occur along the entire beam axis and thus does not localize the site of abnormal (turbulent or high-velocity) flow (no range resolution).[7, 15, 18, 19]

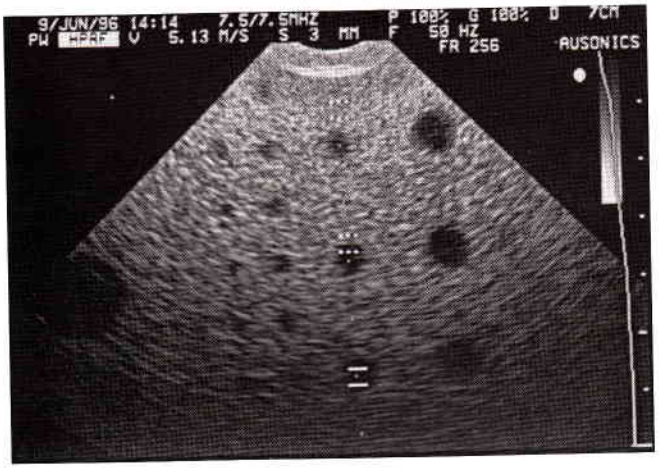

Figure 1–30

Sonogram obtained using a tissue-equivalent phantom demonstrating the multiple ghost sample volumes *(dotted parallel lines)* along the cursor, in addition to the main sample volume *(solid parallel lines)*, which occurs when high pulse repetition frequency (PRF) Doppler is used. The ghost sample volumes should be placed in areas of no flow, if possible, to preserve the range gating of pulsed-wave Doppler.

Color Flow

Color-flow Doppler ultrasound provides real-time 2-D blood flow information. Color-flow Doppler ultrasound is a form of pulsed-wave Doppler ultrasound in which the 2-D Doppler shift information is color coded and superimposed on a 2-D real-time ultrasound image (see Chapter 5).[7, 15, 18, 20, 21] With color-flow ultrasound, multiple gates or sample volumes are analyzed along multiple scan lines. Bursts of ultrasound pulses or a pulse train is emitted, and the PRF is determined by the time between the pulse trains. The Nyquist limits for color flow are typically very low (0.6 to 0.9 m/sec). These low Nyquist limits occur because the sampling opportunities are reduced, as each pulse must clear the field before another pulse can be sent, and because each line is interrogated more than once. Frame rates are also decreased owing to the time necessary to acquire this color-coded information. The color-flow image is a representation of the mean velocities that occur over the individual line-sampling periods, not the peak velocities.

Color is used to indicate the direction of blood flow, blood flow velocity, and turbulence of blood flow.[7, 15, 18, 20, 21] Red usually indicates a shift of blood flow toward the transducer, and blue indicates blood flow away from the transducer. Aliasing is common in color-flow ultrasound because of the low Nyquist limits. Aliasing is displayed as a color reversal where blue merges with red or vice versa without blood flow changing direction. The colors yellow, cyan, and white are also used to create a velocity and variance map. With the enhanced or velocity map, the higher velocities are displayed with brighter, more vivid colors. With the variance map, the differences between the blood flow velocities within a given sample volume are colored by adding a green color over the red and blue coloring, yielding colors from yellow to cyan. High-velocity turbulent blood flow is identified by its mosaic pattern and differentiated from aliased laminar flow. The color-flow map is used to identify areas of abnormal flow and locate pulsed-wave gates and continu-

ous-wave cursors to further characterize the flow disturbance identified. The color-flow display can also be superimposed over an M-mode echocardiographic image, yielding color M mode. Color-flow M-mode echocardiography can be helpful in the timing of regurgitant jets.

Power Doppler

Power Doppler is a color Doppler mode that displays an estimate of the total integrated Doppler power spectrum rather than an estimate of the mean frequency, resulting in increased sensitivity to low-flow states. Power Doppler is less angle dependent, has a better signal-to-noise ratio, and has no aliasing artifacts compared with color-flow Doppler mapping. Power Doppler is extremely useful in the evaluation of organ blood flow (Color Figure 1-2) and the evaluation of vascularity associated with neoplasia.

DOPPLER INSTRUMENT CONTROLS

Sample Volume Size, Baseline, Velocity, and Wall Filter

The size of the sample volume can be increased to find areas of abnormal flow and decreased to fine-tune the spectral display of the abnormal flow. The baseline of the spectral tracing can be moved up or down to preferentially display flow above or below the baseline. The velocity control allows the maximal velocity of flow displayed to increase or decrease to fill the display with the flow signal detected. The wall filter is a control that rejects the strong echoes from heart or wall motion that might otherwise overwhelm the weaker reflections from the red blood cells.

A basic understanding of the physics of ultrasound and the available instrumentation enables the equine practitioner to obtain the best possible images for interpretation.

References

1. Kremkau FW: Diagnostic Ultrasound: Principles and Instruments, 4th ed. Philadelphia, WB Saunders, 1993.
2. Curry TS III, Dowdey JE, Murray RC Jr: Christensen's Physics of Diagnostic Radiology, 4th ed. Philadelphia, Lea & Febiger, 1990.
3. Hagen-Ansert SL: Textbook of Diagnostic Ultrasonography, 3rd ed. St. Louis, CV Mosby, 1989.
4. Powis RL: Ultrasound science for the veterinarian. Vet Clin North Am [Equine Pract] 2:3-27, 1986.
5. Rantanen NW: Instrumentation and physical principles of ultrasound use. Proceedings of the 39th Annual Meeting of the American Association of Equine Practice, 1993, pp 3-4.
6. Rantanen NW, Ewing RL: Principles of ultrasound application in animals. Vet Radiol 22:196-203, 1981.
7. Nyland TG, Mattoon JS, Wisner ER: Physical principles, instrumentation, and safety of diagnostic ultrasound. *In* Nyland TG, Mattoon JS (eds): Veterinary Diagnostic Ultrasound. Philadelphia, WB Saunders, 1995.
8. Farrow CS: Ultratalk: Beginners guide to the language of ultrasound. Vet Radiol Ultrasound 33:31-32, 1992.
9. Reef VB: Advances in diagnostic ultrasonography. Vet Clin North Am [Equine Pract] 7:451-466, 1991.
10. Allen KA, Stone LR: Equine diagnostic ultrasonography: Equipment selection and use. Compend Contin Educ Pract Vet 12:1307-1311, 1990.
11. Rantanen NW: General considerations for ultrasound examinations. Vet Clin North Am [Equine Pract] 2:29-32, 1986.
12. Reef VB: The use of diagnostic ultrasound in the horse. Ultrasound Q 9:1-34, 1991.
13. Powis RL: The saga of the lingering transducer. J Equine Vet Sci 13:323-324, 1993.
14. Powis RL: At play in the transducer fields. J Equine Vet Sci 15:470-471, 1995.
15. Reef VB: Advances in echocardiography. Vet Clin North Am [Equine Pract] 7:435-450, 1991.
16. Biller DS, Myer W: Ultrasound scanning of superficial structures using an ultrasound standoff pad. Vet Radiol 29:138-142, 1988.
17. Wood AKW, Sehgal CM, Reef VB: Three-dimensional sonographic imaging of the equine superficial digital flexor tendon. Am J Vet Res 55:1505-1508, 1994.
18. Kremkau FW: Doppler Ultrasound: Principles and Instruments. Philadelphia, WB Saunders, 1990.
19. Hatle L, Angelsen B: Doppler Ultrasound in Cardiology: Physical Principles and Clinical Applications, 2nd ed. Philadelphia, Lea & Febiger, 1985.
20. Kisslo J, Adams DB, Belkin RN: Doppler Color Flow Imaging. New York, Churchill Livingstone, 1988.
21. Nanda NC: Textbook of Color Doppler Echocardiography. Philadelphia, Lea & Febiger, 1989.

CHAPTER

2

Artifacts

Artifacts occur routinely in ultrasound imaging, and their recognition is important in understanding and interpreting the image generated. Ultrasound waves, like other sound waves, are reflected, refracted, scattered, attenuated, and absorbed as they pass through different tissue interfaces. Artifacts can result from environmental factors, operational factors, or interactions between the patient and the ultrasound beam (Table 2-1).[1-3]

ELECTROMAGNETIC ARTIFACTS

Electromagnetic interference can occur with the simultaneous use of a wide variety of equipment such as clippers, fluorescent lights, other electrical equipment, and radiofrequency signals.[2-4] These artifacts usually occur as streaky lines that radiate throughout the image and are present with or without transducer-patient contact (Fig. 2-1). Turning off the offending equipment, if it can be determined what is causing the interference, or moving the equipment and patient to a different location should eliminate this problem.

Table 2-1
Classification of Ultrasound Artifacts

Environmental	Operator	Acoustic
Electromagnetic artifacts	Patient preparation	Resolution artifacts
Radiofrequency signals	Scanning technique	Axial resolution
Clippers	Gain settings	Lateral resolution
Fluorescent lights	Transducer frequency	Speckle
Electrical equipment		Section thickness
		Propagation path artifacts
		Reverberation
		Refraction
		Multipath
		Mirror image
		Side lobe
		Grating lobe
		Attenuation artifacts
		Shadowing
		Enhancement
		Edge shadowing
		Focal enhancement
		Miscellaneous artifacts
		Comet tail
		Ring down
		Speed error
		Range ambiguity

Adapted from Kremkau FW, Taylor KJW: Artifacts in ultrasound imaging. J Ultrasound Med 5:227-237, 1986; and Kirkberger RM: Imaging artifacts in diagnostic ultrasound—A review. Vet Radiol Ultrasound 36:297-306, 1995.

OPERATOR ARTIFACTS

Air on the surface of the skin reflects ultrasound, making it difficult or impossible to obtain an image. Clipping the hair from the skin surface or, if necessary, shaving the skin and applying copious amounts of acoustic coupling gel are needed to obtain the best possible image.[3, 5] Hair, scurf, or debris on the surface of the skin also reflects ultrasound, resulting in a poor-quality image or no im-

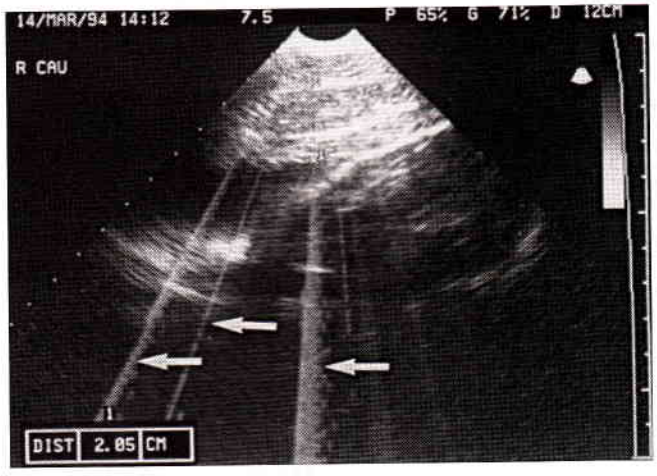

Figure 2-1
Electromagnetic artifacts are depicted radiating throughout the image of the uterus, fetal fluids, and fetus. These artifacts are seen as a series of bright bands of electrical noise radiating throughout the image *(arrows)*.

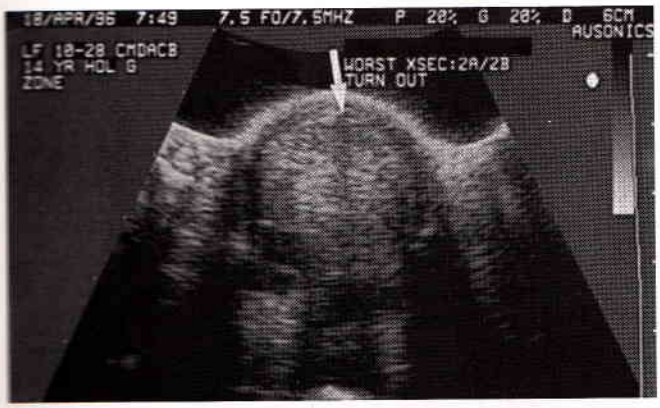

Figure 2–2

Poor patient preparation with residual hair or scurf on the skin resulted in this central area of image loss, which begins at the surface of the skin *(arrow)*. This poor image quality is seen as a vertical anechoic shadow from the skin surface throughout the central portion of the image, where the skin is covered by the surface debris.

age.[3, 5] Scurf from a blister is notorious for reflecting and scattering the ultrasound beam with little or no transmission of ultrasound to the deeper tissues beneath the skin surface (Fig. 2–2). Softening the scurf with warm-water compresses often aids in its removal. Cleaning the skin of any and all debris is also critical for optimal image quality. Dirt and other skin debris also act as reflectors of ultrasound, minimizing the amount of ultrasound available to enter the tissues and be reflected from the tissue interfaces.

The ultrasound transducer itself creates a near-field artifact produced by a series of vibrating points in the piezoelectric crystal. A small wavefront is produced by each point, and these wavefronts coalesce into a continuous wavefront at a certain distance from the transducer.[3, 6] This distance decreases with higher-frequency transducers. This near-field artifact can obscure visualization of structures in the near field (Fig. 2–3). Both built-in fluid offsets and hand-held standoff pads have been developed for use with high-frequency transducers when scanning superficial structures.[3, 7] These standoff pads move the near-field artifact into the standoff, permitting optimal visualization of near-field structures (Fig. 2–3). Built-in fluid offsets are acoustically matched to the transducer. Hand-held standoff pads are composed of synthetic polymer substances that have an acoustic impedance similar to that of soft tissue. A reverberation artifact is produced by the standoff, which is readily identified (Fig. 2–4).

Off-normal incidence artifacts are common operational artifacts that may result in erroneous diagnosis, particularly in equine tendon and ligament injuries. Off-normal incidence artifacts occur when the incident ultrasound beam is not perpendicular to the structures being interrogated. Off-normal incidence artifacts result in echo omission from a normal specular reflecting surface (Fig. 2–5).[3–5, 8] Repositioning the transducer so that it is perpendicular to the structures being examined eliminates off-normal incidence artifacts. Off-normal incidence artifacts can occasionally be helpful in distinguishing the border between two adjacent structures.

Artifacts can also be created by setting the near gain or power too high, minimizing the ability to see differences in adjacent tissues (Fig. 2–6).[3, 5] This error occurs most frequently when scanning in bright locations; therefore, if at all possible, the sonologist should work in shaded or darkened areas. If not, the sonologist should adjust the brightness and contrast settings in the equipment when scanning in bright locations, not the brightness and contrast settings on the monitor, and should avoid the use of excessive power and gain.[5] The sonologist can change the equipment's dynamic range or post-processing curve to compensate for the bright surround-

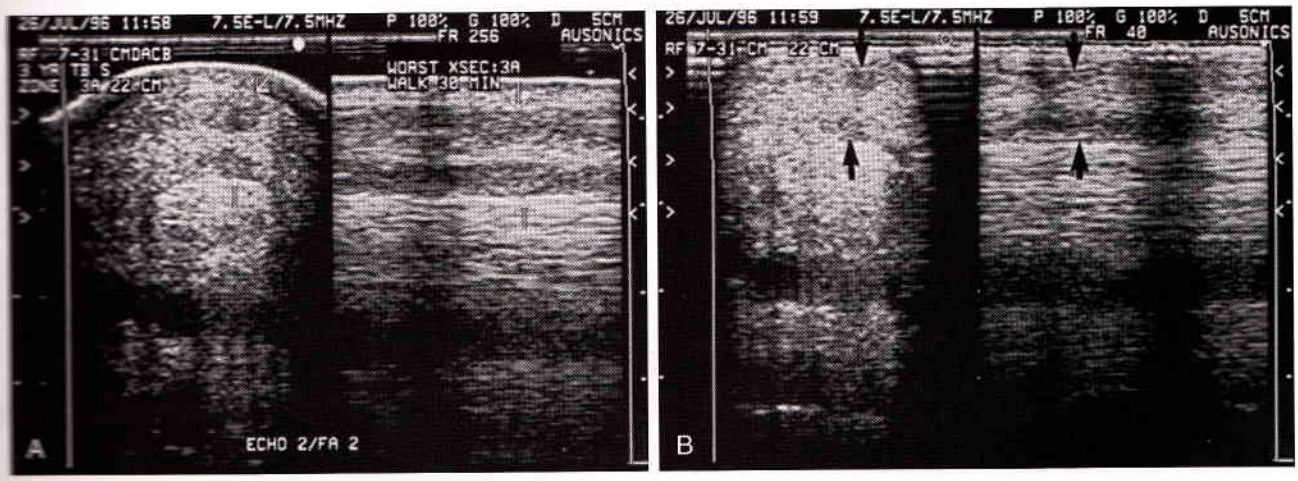

Figure 2–3

Sonograms of the flexor tendons and ligaments obtained with a 7.5-MHz linear-array transducer with *(A)* and without *(B)* a standoff pad. Notice the near-field artifact in the superficial portion of the superficial digital flexor tendon *(B)* and the excellent resolution of this area using a standoff pad *(A)*. The extent of the areas of fiber damage in the superficial digital flexor tendon *(arrows)* is much clearer in the image obtained with the standoff pad *(A)*. Both circular areas of damage are much better resolved in the transverse and sagittal images with the use of the standoff pad *(A)*, and the abnormal surrounding portion of the superficial digital flexor tendon is also clearer. The left images are the transverse view and the right images are the sagittal view. In both sagittal images the shadows are caused by poor contact between the skin and the transducer *(B)* or the skin and the standoff pad *(A)*.

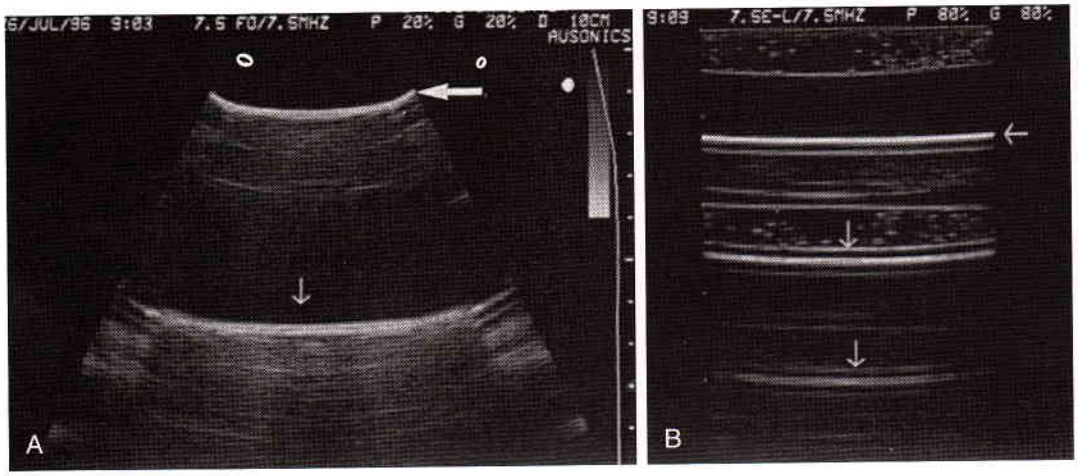

Figure 2–4

Sonogram of the reverberation artifact *(arrow)* produced by a built-in fluid offset *(A)* or hand-held standoff pad *(B)*. The vertical arrows point to the reverberation artifacts. The horizontal arrow in the image of the hand-held standoff pad *(B)* is pointing to the interface between the standoff pad and the skin. The anechoic layer above this interface is the standoff pad, and the anechoic layer above the standoff pad containing echogenic specks is the acoustic coupling gel with some air bubbles. This image is reproduced as a mirror image at the first vertical arrow. The horizontal arrow in the image of the built-in fluid offset *(A)* is pointing to the interface between the skin and the fluid offset.

ings. Using the highest contrast and brightness settings on the monitor rather than changing these settings in the ultrasound machine results in the monitor's burning out prematurely.

Frame-rate artifacts can be produced if the frame rate is too low to capture real-time movement. This can result in the appearance of an artifactual discontinuity within a structure which may be misinterpreted as a defect (Fig. 2–7). Frame rate should be increased if a questionable discontinuity appears within a structure and a low frame rate is being used to eliminate this artifact. Frame rate can be increased by decreasing the depth of display (if possible), decreasing the imaging angle, and decreasing the number of focal zones within the image (see Chapter 1).

Transducer selection is also critical to obtaining an optimal quality image. The transducer selected should be the highest frequency possible that will penetrate to the area under investigation. Lateral and axial resolution artifacts increase with lower-frequency transducers. The correct transducer type (sector, linear, convex linear, annular, or phased-array), footprint (the imaging surface of the transducer), and field of view should also be selected to maximize image quality. A thorough knowledge of your equipment and the physics of ultrasound (see Chapter 1) is important in obtaining optimal image quality and minimizing the production of artifacts.

ACOUSTIC ARTIFACTS

Acoustic artifacts result in the display of images that are added (not anatomically true), missing, or of improper

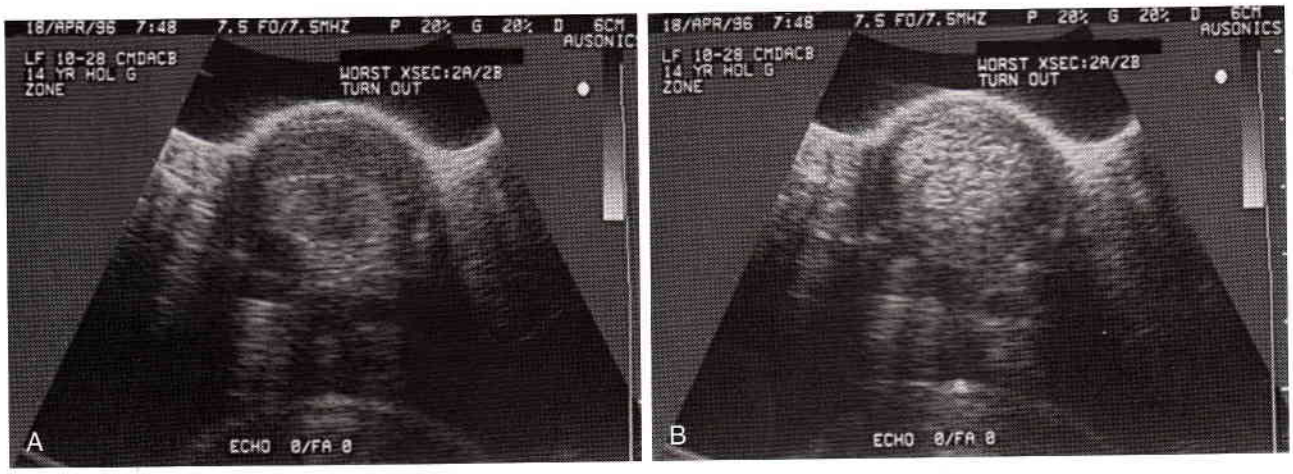

Figure 2–5

Sonograms of the left foreleg in the mid-metacarpal region demonstrating an off normal incidence artifact. The hypoechoic appearance of the superficial and deep digital flexor tendons *(A)* was created because the ultrasound beam was not perpendicular to these structures. The slightly heterogeneous appearance of the superficial digital flexor tendon *(B)* is associated with a previous injury to the superficial digital flexor tendon that is fairly well healed at this time.

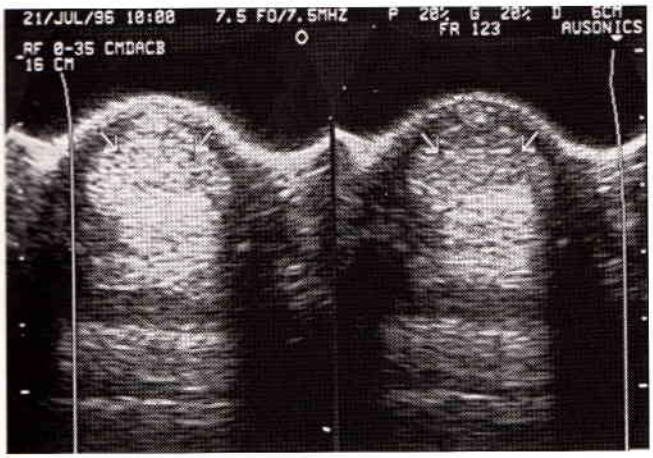

Figure 2–6

Sonograms of the flexor tendons and ligaments in the mid-metacarpal region of the right foreleg demonstrating the effect of excessive near-field gain *(left image)*. The arrows point to a healing core lesion within the superficial digital flexor tendon, with a small palmar hypoechoic area of newer damage that is not well visualized in the left image.

Table 2–2
The Etiology of Acoustic Artifacts

Artifact	Etiology
Axial resolution	Pulse length
Lateral resolution	Pulse width
Speckle	Interference
Section thickness	Pulse width
Reverberation	Reflection
Refraction	Refraction
Multipath	Reflection
Mirror image	Reflection
Side lobe	Side lobe
Grating lobe	Grating lobe
Shadowing	Attenuation
Enhancement	Low attenuation
Refraction shadowing	Refraction
Focal enhancement	Focusing
Comet tail	Reverberation
Ring down	Resonance
Speed error	Speed error
Range ambiguity	High pulse repetition frequency

Adapted from Kremkau FW, Taylor KJW: Artifacts in ultrasound imaging. J Ultrasound Med 5:227–237, 1986.

location, brightness, shape, or size (Table 2–2).[1] Acoustic artifacts result from assumptions that are made by the ultrasound manufacturers to display the returning echoes as an image. These assumptions include the round-trip travel time for ultrasound in biologic tissues, the direction of ultrasound travel, the location of the reflectors within the tissues, and the intensity of the returning ultrasound. The propagation speed of ultrasound through biologic tissues is assumed to be constant and to be equal to the velocity of ultrasound through soft tissue (1540 m/sec, or 13 microseconds [μs] per centimeter of depth).[1] The ultrasound energy is assumed to travel in straight lines, and the echoes that return are assumed to have originated from structures present along the long axis of the beam only. The intensity of the returning echoes is also assumed to be directly related to the scattering strength of the imaged objects. Acoustic artifacts can be broken down into resolution artifacts, propagation path artifacts, attenuation artifacts, and miscellaneous artifacts (see Table 2–1).[1]

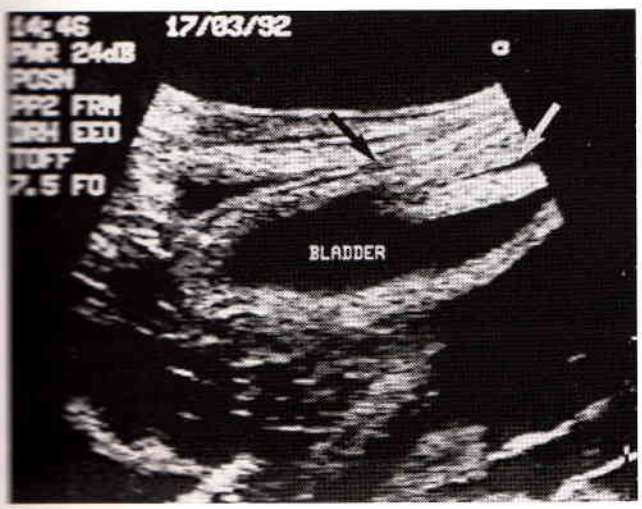

Figure 2–7

Sonogram obtained of the bladder from a neonatal foal suspected of having a ruptured bladder. The ventral surface of the bladder appears to be torn *(arrows)*, but this is an artifact created by a slow frame rate.

Resolution Artifacts

Spatial resolution artifacts are architectural and cause closely spaced structures to appear merged together and small structures to appear larger than they actually are.[1] Resolution artifacts include artifacts associated with axial and lateral resolution, speckle artifacts, and section-thickness artifacts.[1]

Axial Resolution Artifacts

Axial resolution varies primarily with the frequency of the transducer. Axial resolution worsens with a longer pulse length and with fewer cycles per pulse or when a lower-frequency transducer is used. Axial resolution artifacts cause two structures located along the long axis of the beam to appear on the ultrasound display as merging structures or as one structure or for one structure along the long axis of the beam to appear larger than it actually is.[1, 2, 9–13] Axial resolution is usually better than lateral resolution because pulse width is normally larger than pulse length.[1]

Lateral Resolution Artifacts

Lateral resolution varies with the depth of the structure being imaged from the transducer and the width of the ultrasound beam and is best in the focal zone of the transducer.[1, 2, 9–13] Lateral resolution artifact results in poor detail of the edges of structures perpendicular to the

long axis of the ultrasound beam. Structures smaller than the sound beam appear to be as wide as the sound beam (Fig. 2–8).[13] Lateral resolution artifact also causes structures located side by side, perpendicular to the long axis of the ultrasound beam, to be imaged as merging structures or as one structure or to appear singular and larger than they actually are.[1, 2, 9–13] Lateral resolution artifacts are most likely in the near and far fields and are most marked with lower-frequency sector-scanner transducers because these transducers usually have a larger crystal, resulting in a wider beam width, and have a fixed focal zone.

Speckle Artifacts

Acoustic speckle is best seen close to the transducer and is the granular echo texture observed which appears as parenchymal tissue texture.[1, 2] This apparent excellent resolution is not real, but instead is a resolution-degrading component that may obscure vital detail.[1, 2, 14, 15] Speckle artifacts are a lack of correlation between the actual and apparent resolution of an image.[1] Acoustic speckle artifacts are a form of acoustic noise and are caused by a convoluted returning wavefront with interference of returning scatterer echoes from the interrogated tissue volume.[1, 2, 14] This convoluted returning wavefront occurs secondary to the roughness of the reflector surface and the presence of complex intervening tissues with multiple interfaces and differing acoustic velocities.[14] The resolution of high- and low-contrast objects is limited by spatial resolution and acoustic speckle.[1] Speckle motion can be misleading, as it is not simply related to tissue motion and transducer motion.[1, 2, 15] Image-processing techniques have been developed to reduce speckle and improve resolution.[1]

Section-Thickness Artifacts

Section-, slice-, or beam-thickness artifacts create echoes on the display that are not really there within curved, fluid-filled structures such as anechoic vessels or ducts.[1–3, 12, 16] These echoes mimic dependent particulate material, which could be misinterpreted as thrombus, debris, or sludge. In the gallbladder of human beings and small animals, this is often referred to as "pseudosludge."[1–3, 16, 17] The artifact occurs where the curved, fluid-filled

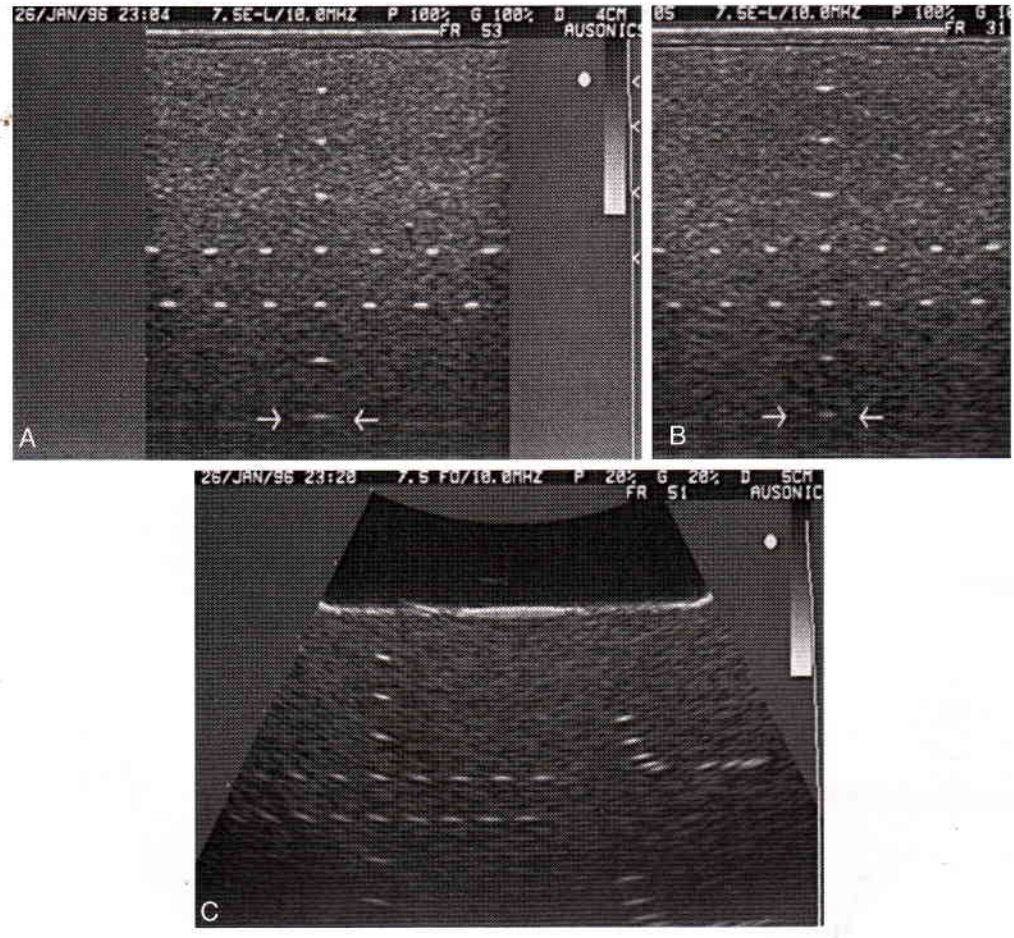

Figure 2–8

Sonograms obtained using a tissue-equivalent phantom demonstrating the improved lateral resolution within the focal zone of the ultrasound beam. Notice the crisp appearance of the echogenic dots when the multiple focal zones are in the near field of the image *(A)* and the lateral widening of these reflectors in the far field *(arrows)*. When the multiple focal zones are placed in the center and far field of the image *(B)*, the echogenic dots in the near field are wider (lateral beam-width artifact) than those in the center and far field *(arrows)*. Notice the superior resolution of the small echogenic reflectors obtained with the linear-array transducer using multiple focal zones *(A* and *B)* compared with the sector-scanner transducer *(C)*.

structure lies next to a more echogenic structure.[2] The section-thickness artifact occurs because the ultrasound beam has a finite thickness as it is transmitted through the patient. Echoes that are received originate from the center of the beam and from off axis and are compressed into a thin 2-D image.[1, 2, 16] Slice-thickness artifacts have a meniscus and margins that are not horizontal, and similar echoes may occur on the nondependent surface. The pseudosludge can be differentiated from true sediment because the pseudosludge interface is curved, whereas true sediment usually has a flat interface. The interface between a thrombus and the remaining blood within the vessel is often flat or has a convex, not concave, curved interface. Also, the pseudosludge interface remains perpendicular to the incident ultrasound beam, whereas the true sediment interface changes with changes in the patient's position.[2, 3, 16] Slice-thickness artifacts can be minimized by using higher-frequency transducers and imaging within the focal zone of the transducer.[2, 17]

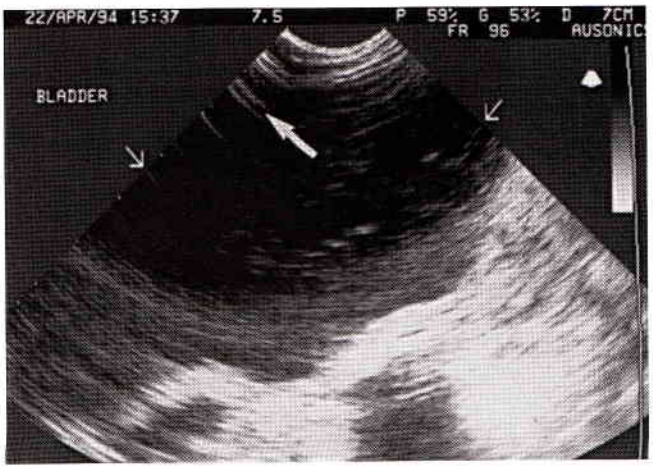

Figure 2–10

Sonogram of the urinary bladder in a foal demonstrating a contact artifact between the skin of the patient and the transducer on the left side of the image, creating the multiple curved echogenic reflections *(large arrow)*. This foal's bladder is filled with hypoechoic loculations and debris secondary to severe umbilical hemorrhage *(small arrows)*.

Propagation-Path Artifacts

Propagation-path artifacts are artifacts that occur because of the interaction of ultrasound with structures located along the path of the ultrasound beam. Propagation-path artifacts include reverberation, refraction, multipath, mirror-image, side-lobe, and grating-lobe artifacts.

Reverberation Artifacts

Multiple reflections or reverberations occur when two or more reflectors are encountered within the sound path or when a high-intensity returning ultrasound beam hits the transducer and is reflected back into the tissues a second time.[1, 2] These reflections may be sufficiently strong to be detected by the ultrasound instrument and displayed as spurious echoes within a viscus (Fig. 2-9). The ultrasound instrument assumes that the ultrasound beam has traveled once, for a longer distance, through the tissues and that this echo originated from a point twice as deep as the original reflector.[2] These reflections are placed behind the second real reflector at separation intervals equal to the distance between the first and second real reflectors.[1, 2] These reflections from the transducer back into the tissues can occur several times, resulting in multiple, evenly spaced reverberation echoes.[1, 2, 18] Each subsequent echo is weaker than the first echo, which is usually the transducer-skin interface. The contact artifact created by the presence of air between the skin surface and the transducer is a reverberation artifact (Fig. 2-10). The air reflects 99% of the ultrasound back to the transducer, and the ultrasound beam then bounces back and forth between the gas on the skin surface and the transducer. This reduction in echo amplitude is partially compensated for by the time gain compensation.[1, 2] Reverberation echoes can be external (transducer-skin interface) or internal (bone-soft tissue, gas-soft tissue, metal-soft tissue). Common internal reverberation artifacts include gas-filled bowel and gas-filled lung. This artifact is used in equine thoracic ultrasonography to identify normal, gas-filled lung (Fig. 2-11).[5, 19] Reverberation from metal objects is quite pronounced and makes metal easy to locate and identify because of the small metallic dimensions and high ultrasound speed.[2] Metal usually produces a series of closely spaced echoes or "comet-tail artifacts" (Fig. 2-12).[20–23]

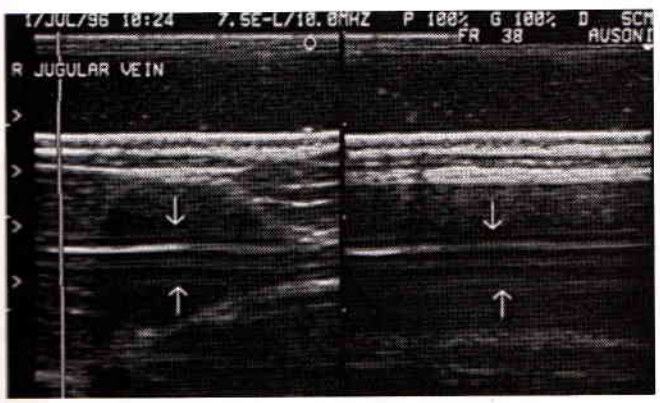

Figure 2–9

Sonogram obtained of the jugular vein using a linear transducer and a hand-held standoff pad. The echogenic linear artifact within the lumen of the jugular vein and surrounding soft tissues *(arrows)* is a reverberation artifact created by the standoff. The ultrasound beam reflects off the transducer-standoff interface and the standoff-skin interface and back again, creating this reflection. The left image is a transverse view and the right image is sagittal.

Refraction Artifacts

Refraction artifacts occur when the ultrasound beam changes direction as it crosses a tissue interface where a speed change occurs. The refraction artifact results in improper lateral positioning of the reflecting structure.[1, 10, 24] Refraction positioning artifacts are usually small and contribute primarily to loss of image quality.[1] Large errors in reflector positioning do not usually result from refrac-

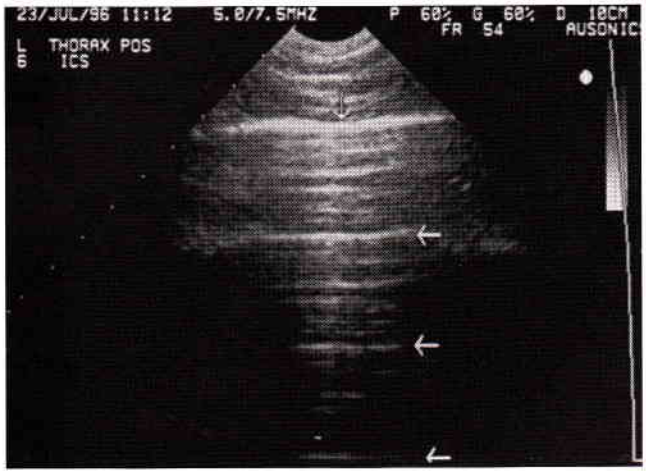

Figure 2–11

Sonogram of normal lung obtained from the right side of the thorax in the seventh intercostal space, demonstrating the visceral pleural surface of the lung *(vertical arrow)* and the multiple reflections occurring from this highly reflective interface *(horizontal arrows)*.

tion artifacts. However, refraction artifacts have occasionally been described in vivo and may result in a duplication of structures or a split-image artifact.[24, 25]

Multipath Artifacts

Multipath artifacts occur when the paths to and from a reflector are different.[1, 2] A small axial error in reflector positioning occurs from the longer path that the ultrasound takes to and from the reflector. The multipath artifact is an additional echo deep to the original echo because of the longer return path (Fig. 2-13).[2, 18] Multipath positioning errors are normally small and do not result in gross errors of structure location but rather contribute only to general image degradation.[1, 2]

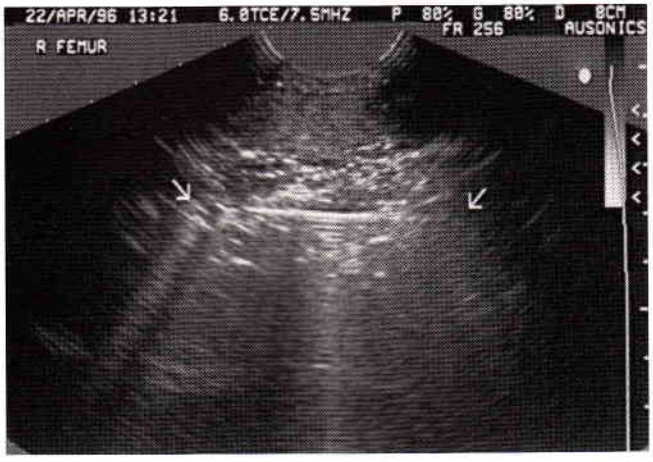

Figure 2–12

Sonogram of a surgical implant (plate) on the femur of a foal with a femoral fracture that was repaired with internal fixation. Notice the typical reverberation artifact associated with metal in the center of the plate. The plate is delineated by the two arrows. Superficial to the plate are myriad bright echogenic reflectors, which represent gas in the soft tissues overlying the plate and an infected surgical site.

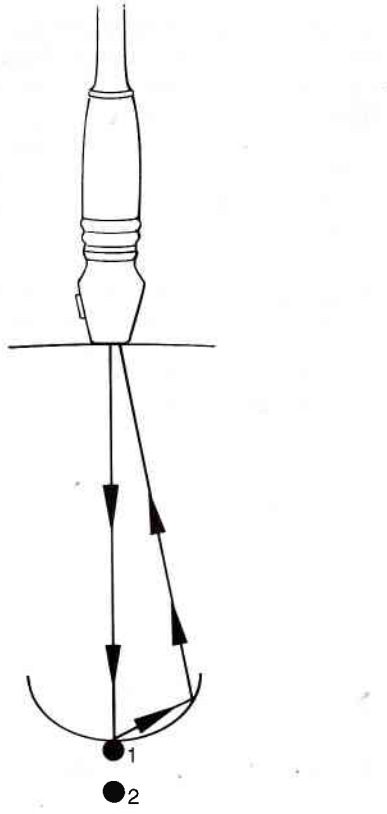

Figure 2–13

Diagram of the multipath artifact, which results in improper positioning of the reflector. Round-trip travel time increases when the ultrasound beam is reflected from two specular curved surfaces. The reflector displayed as the deeper structure (position 2) is actually located at position 1. (Adapted from Kirkberger RM: Imaging artifacts in diagnostic ultrasound—A review. Vet Radiol Ultrasound 36:297-306, 1995.)

Mirror-Image Artifacts

The mirror-image artifact occurs when ultrasound is reflected off a highly reflective curved interface like the diaphragm-lung interface (Fig. 2-14).[1-3, 12, 26] Ultrasound reflects off this interface after traveling through other tissue and then returns to the transducer after being reflected off another interface via the original highly reflective curved interface (Fig. 2-15). This results in the structure of interest being erroneously placed on the thoracic side of the diaphragm. The mirror-image artifact occurs because the instrument assumed that the ultrasound pulse and reflected echoes traveled in a straight line.[1-3, 12, 26] The increased round-trip ultrasound time results in the production of the mirror-image artifact. This delay in the echo return time occurs because of the multiple reflections. Awareness of this artifact and how it is produced is important to avoid the misdiagnosis of a diaphragmatic hernia.[2, 3] This artifact may also simulate pulmonary consolidation.[3] The mirror-image artifact may also occur at other highly reflective curved interfaces such as the pericardium-lung interface and from air-fluid levels within abscess cavities.[2, 12, 27]

Side-Lobe and Grating-Lobe Artifacts

Side-lobe and grating-lobe artifacts occur when structures not aligned with the ultrasound beam are laterally dis-

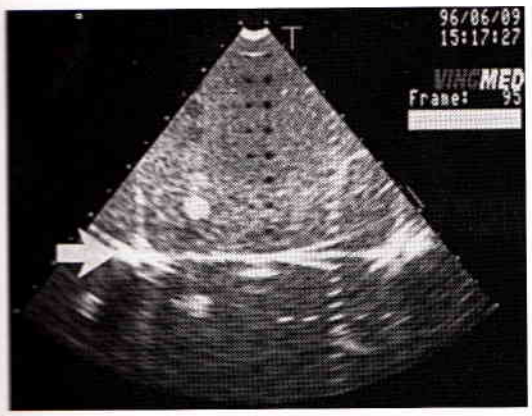

Figure 2–14

Sonogram using a tissue-equivalent phantom demonstrating a mirror-image artifact. The echogenic horizontal line near the bottom of the image is the bottom of the tissue-equivalent phantom *(arrow)*. Many of the reflectors within the tissue-equivalent phantom are displayed as if they were located deep to the bottom of the tissue-equivalent phantom, creating a mirror image.

placed.[1-3, 18, 28] Side-lobe artifacts occur in single-element transducers, whereas grating-lobe artifacts occur in multiple-element transducers.[1] These artifacts occur because the ultrasound beam is composed of a main lobe and multiple smaller secondary (side) lobes of varying intensities (Fig. 2–16). The side-lobe intensity is low, no more than one one-hundredth of the intensity of the main beam.[2, 28] This intensity is great enough, however, to produce echoes when imaging a highly reflective interface such as air or a highly curved, specularly reflecting surface such as the diaphragm or bladder. Both specular and diffuse side-lobe artifacts occur.[2] Highly reflective curved surfaces like the diaphragm are more likely to create specular side-lobe artifacts, whereas diffuse artifacts are more common from the highly reflective gas

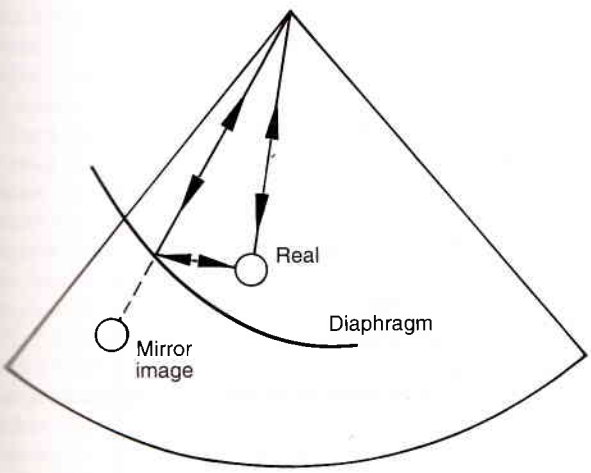

Figure 2–15

Diagram of the mirror-image artifact, which occurs when the incident ultrasound beam reflects off a highly reflective curved surface such as the diaphragm and then is reflected off another interface before returning to the transducer. The ultrasound equipment assumes that the ultrasound beam traveled in a straight line and therefore displays the reflector deep to the diaphragm because of the increased round-trip travel time. (Adapted from Kremkau FW: Diagnostic Ultrasound: Principles and Instruments, 4th ed. Philadelphia, WB Saunders, 1993, p 231.)

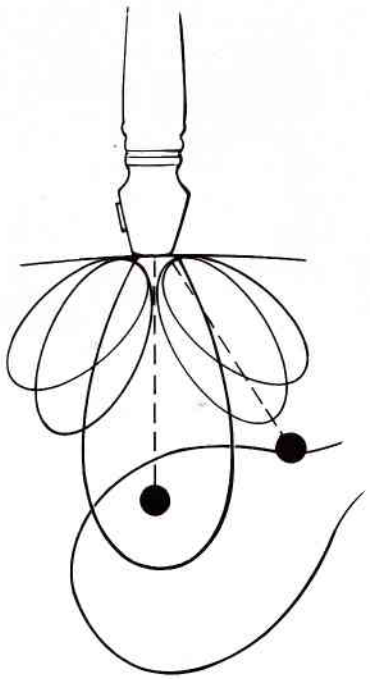

Figure 2–16

Diagram of side-lobe artifacts. The side lobes, or grating lobes, can produce a weak reflection from this secondary ultrasound beam. This reflector is placed at the proper distance from the transducer but at the incorrect location because the equipment assumes that these echoes originate along the axis of the primary ultrasound beam. (Adapted from Pennick DG: Imaging artifacts in ultrasound. *In* Nyland TG, Mattoon JS (eds): Veterinary Diagnostic Ultrasound. Philadelphia, WB Saunders, 1995, pp 19–29.)

interface. With side-lobe artifacts, echoes originating from side-lobe reflections are displayed along the path of the returning echoes from the main ultrasound beam, at the depth of the side-lobe reflector, in spite of their different origins.[2, 3] Side-lobe artifacts are best seen within anechoic structures because of their low intensity. Side-lobe echoes exhibit a threshold effect and disappear with lower instrument settings.[2, 3, 18]

Attenuation Artifacts

Attenuation is the reduction in the amplitude of the returning echoes from reflectors that lie deep to a highly reflecting or attenuating structure.[1] Attenuation artifacts include acoustic-shadowing, acoustic-enhancement, refraction, and focal-enhancement artifacts.

Acoustic-Shadowing Artifacts

Acoustic shadowing is a very useful artifact that occurs when ultrasound strikes a tissue of very high or low acoustic impedance relative to the soft tissue through which the ultrasound beam is traveling. This artifact has been used by many to determine the nature of the shadowing source.[1, 12, 29-33] The acoustic shadowing that occurs deep to calculi (high acoustic impedance) or gas (low acoustic impedance) was first described in 1980

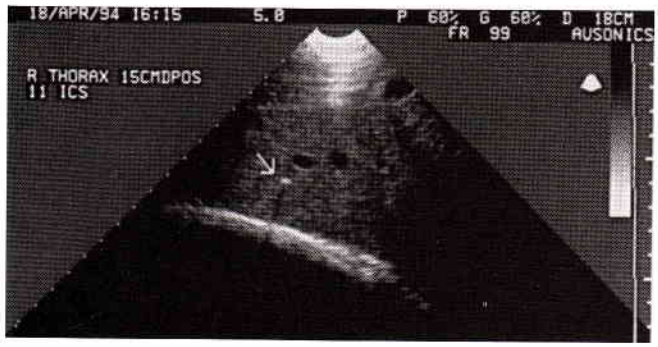

Figure 2–17

Sonogram of a small hepatolith *(arrow)* casting a clean acoustic shadow in the right side of the liver. The shadow from the hepatolith passes through the underlying colon.

and is commonly observed in routine ultrasonographic imaging.[30, 31]

Stones (Fig. 2-17), areas of calcification (Fig. 2-18), or bone (Fig. 2-19) usually create a clean shadow deep to the ultrasonic reflection owing to their high attenuation of the ultrasound beam.[31-32] A clean shadow is one with marked reduction in echo amplitude and few or no noise echoes. Bone, calcification, or stones usually create a clean shadow because most of the incident ultrasound is absorbed within the bony matrix and not reflected. Therefore, much less ultrasound energy is available for noise generation. Shadows similar in appearance are usually produced from all types of stones, regardless of their composition.[31, 34-36] Wood, glass, and suture material (Fig. 2-20) also usually produce clean shadows.[23, 33] Gas usually creates a dirty shadow deep to its ultrasonic reflection because gas is a nearly perfect reflector of ultrasound (Fig. 2-21).[30-32] Significant ultrasound energy is available to produce noise with a gas reflector because little of the ultrasound energy is absorbed. These noise echoes are produced by the multiple reflections that occur from the scatterers between the gas and the transducer and are displayed deep to the gas surface. Clean shadows can occasionally be detected from gas- or air-filled structures,[32, 37] and dirty shadows can occasionally occur with stones and wood.[20, 23, 38-41] Clean and dirty shadowing has also been reported from the same reflector.[20, 39, 41]

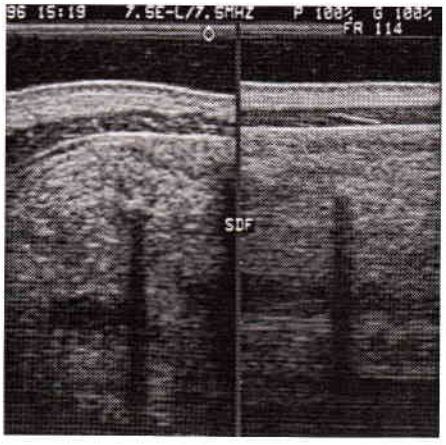

Figure 2–18

Sonogram of a small area of calcification within a repaired superficial digital flexor tendon which has a distinct, clean acoustic shadow. The left side of the image is the transverse view and the right side is sagittal.

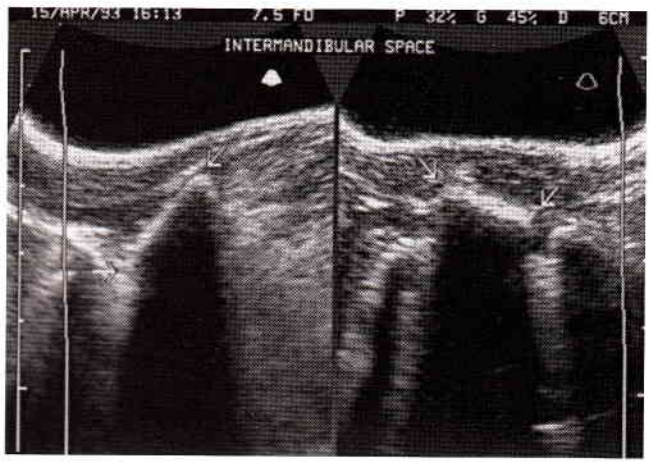

Figure 2–19

Sonogram of the intermandibular space in a foal demonstrating clean shadowing from the bony structures within the caudal aspect of the tongue *(arrows)*. The clean anechoic shadow originates from the bone. The left sonogram is the sagittal view, and the right image is the transverse view.

Although these properties are usually attributed to the composition of the shadowing object, a recent study demonstrated that the clean and dirty shadows are primarily related to the properties of the shadowing object's surface and not its composition.[31] Clean shadowing was most likely to be produced with a small radius of curvature of the shadowing object or when the surface of the shadowing object was rough because the backscattered ultrasound beam is spread and distorted after reflecting off the shadowing object.[31] The intensity of the returning ultrasound beam is markedly diminished because of the different reflections of the ultrasound backscatter from

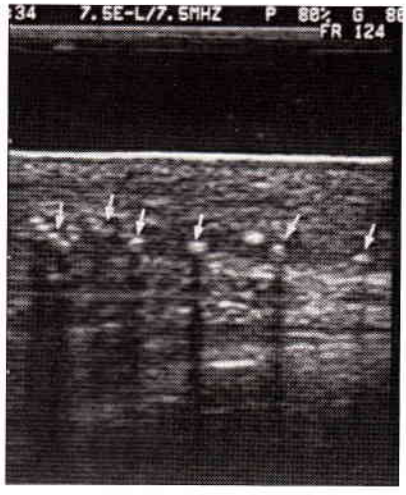

Figure 2–20

Sonogram of the ventral midline following abdominal surgery in a foal. The hyperechoic sutures *(arrows)* cast clean acoustic shadows through the deeper abdominal musculature. A small amount of hypoechoic fluid surrounds the suture material, indicating possible infection of the incision.

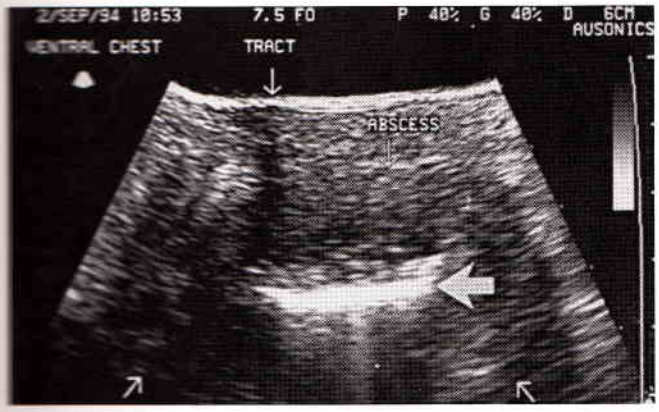

Figure 2–21

Sonogram obtained from a horse with a penetrating wound into the chest and a tract leading dorsally to an abscess. The abscess contains multiple small hyperechoic echoes consistent with gas bubbles within the relatively anechoic fluid and a hyperechoic dorsal gas cap. Notice the dirty shadow originating at the bright hyperechoic dorsal gas cap (large arrow).

the rough surface. This also markedly reduces the intensity of the multipath reflections. Phase incoherence is also produced from rough and curved surfaces, which produces a relatively incoherent returning ultrasound beam. The resultant phase cancellations and weaker signals that occur at the transducer surface result in the production of a clean acoustic shadow.[12, 42] Other authors have also previously suggested that surface properties and spatial geometry may alter the acoustic shadowing that occurs behind objects of high acoustic impedance.[30, 31, 34, 36, 44] With shadowing of objects that have a large radius of curvature relative to the beam width and a smooth surface, the reflected wave maintains its coherence and returns to the transducer via the ultrasound transmission path.[30] Secondary scattering from the surrounding tissues also reflects off the smooth surface, producing strong coherent multipath signals and visible echoes deep to the shadowing object. In spite of these findings, in most instances, the type of shadowing can be used, in conjunction with the location of the shadowing object, to assess the nature of the shadowing object. Care must be used, however, when shadowing objects are found in unusual locations, as the nature of the shadowing object cannot be definitively determined from the detection of a clean or dirty shadow.

Transducer frequency, focusing, stone position, stone size, stone orientation, power output, and receiver gain also determine whether or not shadowing occurs.[31, 34-36, 38, 45, 46] Distinct shadowing occurs only if the stone is greater than or equal to the beam width when the ultrasound beam reflects off the calculus.[2] Stones that are smaller than the width of the ultrasound beam either have no acoustic shadow (Fig. 2–22) or have backscattered echoes within the shadow, rendering the stone's margins indistinct.[2, 3, 30, 31, 38, 45, 47] Stones that are outside the focal zone may also have no shadow or may have indistinct margins owing to the presence of backscattered echoes within the shadow. The location of the shadowing object relative to the focal zone determines the amount of shadowing that occurs, because the amount of shadowing is related to the amount of the ultrasound beam's cross-sectional area that is attenuated.[1] The type of intervening tissue between the reflecting structure and the transducer may also affect shadowing if the intervening tissue affects the lateral and axial resolution of the sound beam.[2, 36] Shadowing may also occur from the edges of circular (round or oval) structures because part of the sound beam is refracted while the rest is reflected. Because the reflecting surface is not perpendicular to the ultrasound beam, the reflected ultrasound is not returned to the transducer, creating an acoustic shadow.

Acoustic-Enhancement Artifacts

Acoustic enhancement is the increase in the amplitude of the returning echoes from reflectors that lie deep to a weakly attenuating structure.[1, 2] The location of the weakly attenuating structure relative to the focus of the ultrasound beam determines the amount of acoustic enhancement that is observed. Acoustic enhancement occurs when ultrasound travels through a fluid-filled structure (Fig. 2–23) such as the urinary bladder, enhancing the far wall of the urinary bladder and the structures deep to it. Cystic structures can be readily differentiated from solid soft-tissue structures or hypoechoic structures because of the presence of this artifact. Optimal acoustic enhancement with small cystic or fluid-filled structures occurs when the structure lies within the focal zone of the transducer and high-frequency transducers are used.[2, 48]

Refraction Artifacts

Shadow artifacts are usually generated from the edge of a curved surface because part of the ultrasound beam is refracted off the curved edge of the structure and does not return to the transducer, diminishing the returning ultrasound beam's intensity (Fig. 2–24).[1, 2, 18] Shadow artifacts are displayed distal to the lateral margins of curved

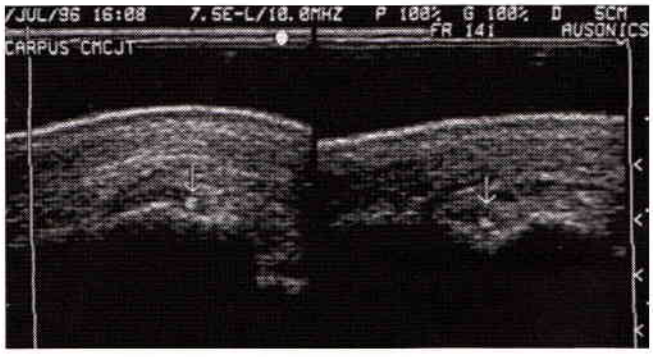

Figure 2–22

Small chip fracture *(arrows)* in the medial aspect of the carpal-metacarpal joint that does not cast an acoustic shadow. This fracture was not detected radiographically; it was found ultrasonographically when the specific view was taken that demonstrated this small fracture fragment. The right image is the sagittal view, and the left image is the transverse view.

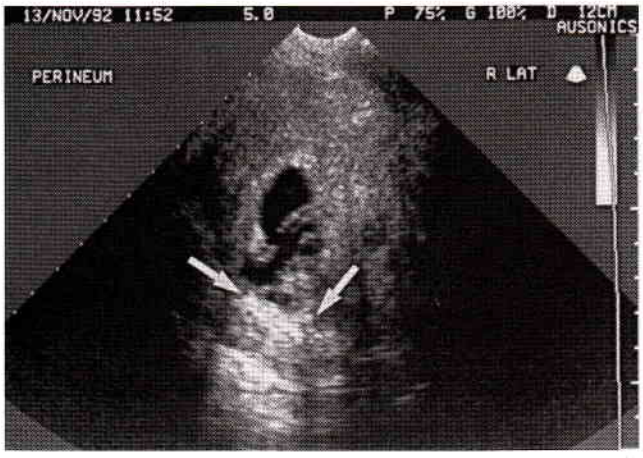

Figure 2–23

Sonogram of an abscess in the perineal region of a horse with marked acoustic enhancement of the far wall of the abscess *(arrows)*, confirming that the center of this mass is fluid filled.

or cystic structures (Fig. 2–25). The amount of reflection and refraction depends upon the angle at which the incident beam hits the curved structure. The change in the velocity of ultrasound passing through the curved structure and the surrounding tissue determines the amount and direction (converging or diverging) of the refraction.[2, 49] The resultant changes in the echo's size caused by the focusing and differential attenuation between the curved structure and surrounding tissue cause refraction of the ultrasound at the interface between the curved structure and the surrounding tissue, resulting in the edge shadowing.[2, 3, 49, 50] In a lower-velocity circular region, the reflected beam diverges while the refracted beam converges, because the region acts like a lens (see Fig. 2–24). In a higher-velocity region, the shape of the reflecting interface also causes the reflected beam to diverge. The refracted beam also diverges because of the variation in refracted angles across the beam. The edge shadows from divergent ultrasound beams tend to be wider and less distinct than those from convergent shadows.[2] Diverging refracted ultrasound beams result in slight displacement of the far wall of the curved structure toward the transducer, whereas converging refracted ultrasound beams have the opposite effect (see Fig. 2–24).[2, 50, 51] Sound concentration beyond the refracting structure occurs because of the converging refracted ultrasound beam and is known as retrolenticular afterglow.[2, 52] This afterglow is several centimeters deep to the reflecting structure and often must be specifically looked for to be recognized.[2, 52] Sector-scanner transducers have more prominent retrolenticular afterglow, which is most marked when the rounded structure is close to the transducer, whereas this effect is not reported for linear transducers.[2, 51]

Edge shadowing can be useful, as its presence indicates round to oval structures with different ultrasound velocities than those of the surrounding tissue.[2] This artifact is most helpful in identifying rounded structures with echogenicities similar to those of the surrounding tissue. Edge shadowing occurs commonly from vessel walls and can hinder the ability to image the suspensory ligament (Fig. 2–26). This artifact also commonly occurs from the edges of other rounded structures such as the bladder and kidney. Although this artifact commonly occurs from fluid-filled structures, other round structures such as tendons commonly have edge shadowing because of sound velocities higher than those in the surrounding soft tissues.[2] Divergence of the refracted ultrasound beam occurs in these cases, which results in the edge shadowing. Edge enhancement can also occur from refraction but is infrequently detected.[1]

Focal-Enhancement Artifacts

Focal-region enhancement can occur in the focal region of the transducer because of the higher ultrasound inten-

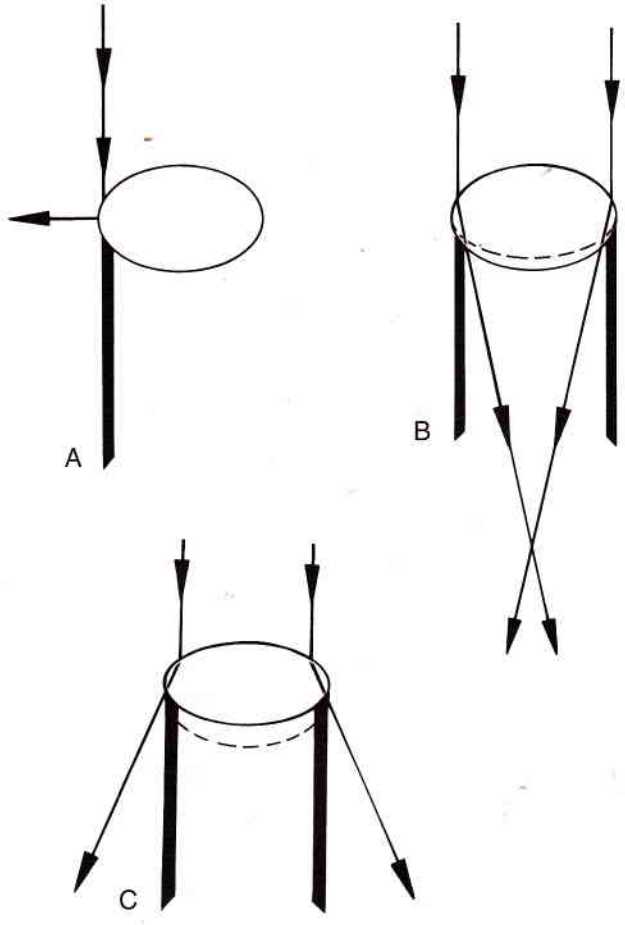

Figure 2–24

Diagram of the edge-shadowing artifact. Edge shadowing occurs when the incident ultrasound beam strikes a curved surface and is reflected *(A)*. When the curved structure has a lower tissue velocity than the surrounding tissue, the ultrasound beam is refracted toward the structure, resulting in displacement of the far wall of the structure slightly farther away from the transducer, producing a narrow acoustic shadow *(B)*. The retrolenticular afterglow is the increased ultrasound beam concentration that occurs in the deeper tissues. When the curved structure has a higher tissue velocity than the surrounding tissue, the ultrasound beam is refracted away from the structure, resulting in displacement of the far wall slightly toward the transducer and a slightly wider edge shadow *(B)*. (Adapted from Kirkberger RM: Imaging artifacts in diagnostic ultrasound—A review. Vet Radiol Ultrasound 36:297–306, 1995.)

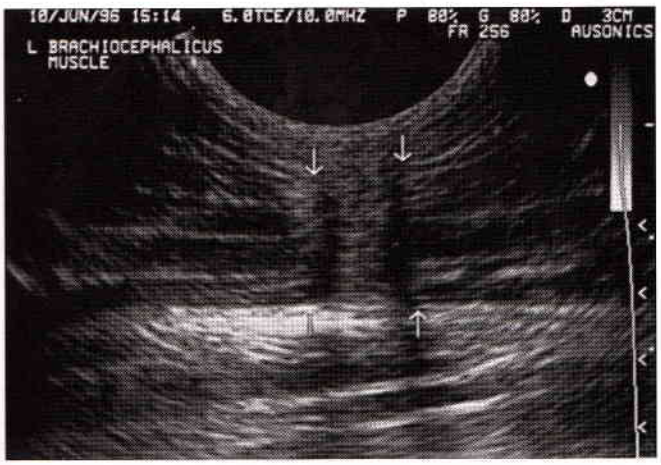

Figure 2–25

Sonogram of the brachiocephalic muscle in a horse demonstrating edge shadowing *(arrows)* from the edges of the hypoechoic scar tissue between the two portions of the muscle belly.

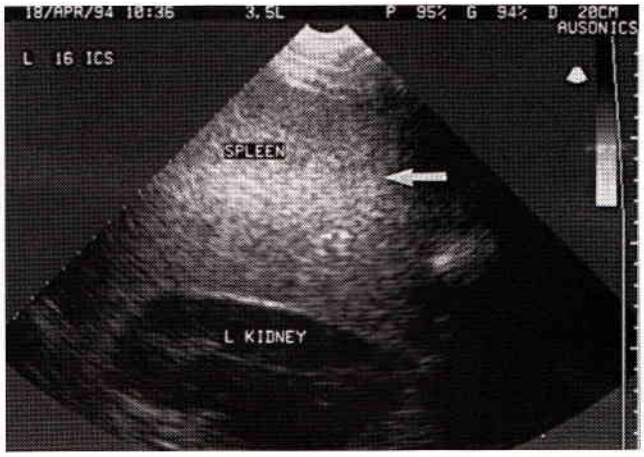

Figure 2–27

Sonogram of the spleen and left kidney obtained in the left sixteenth intercostal space demonstrating focal enhancement in the spleen. Notice the increased echogenicity of the splenic parenchyma within the focal zone of the transducer *(arrow)*.

sity present in this region (Fig. 2-27).[1] Apparent enhancement can also occur in other areas, which, upon closer inspection, is found to be due to other factors.

Miscellaneous Artifacts

Comet-Tail Artifacts

Comet-tail artifacts are a series of closely spaced reverberation artifacts and are commonly seen in the equine lung associated with small areas of peripheral irregularity (Fig. 2-28). The comet-tail artifact is a well-localized "enhancement" artifact.[1] The comet-tail artifact is caused by the creation of multiple reverberant reflections.[20] The greater the difference between the acoustic impedance of the reflecting structure and the surrounding tissues, the greater the number of reverberation echoes.[20] These echoes become more closely spaced as the reflecting object becomes smaller.[20] These echoes merge to create the comet-tail pattern when the echo bands are sufficiently close together and strong.[22] The comet-tail artifact is most intense when the reflecting object is perpendicular to the transducer, the interface between the object and its surroundings is flat, broad, and perpendicular, and the object is large.[20] When the reflecting object is located close to the transducer, the spacing between the fundamental echoes shortens but the spacing of the reverberant echoes arising from within the reflecting object does not change.[18] The comet-tail pattern is dense and more pronounced, with an increased number of interfaces of high acoustic impedance difference within the reflecting object.[20] The comet-tail artifact pattern is produced by reflectors with very high acoustic impedance relative to

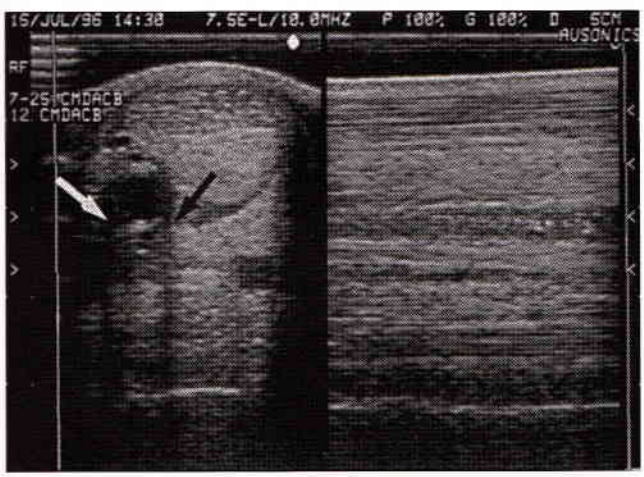

Figure 2–26

Sonogram of the metacarpal region in the right foreleg demonstrating edge shadowing from the median artery. The anechoic shadows *(arrows)* extend from the edges of the median artery through the deeper structures in the transverse *(left)* image. These shadows obliterate a portion of the medial edge of the inferior check ligament and the suspensory ligament. The right image is the corresponding sagittal image of these structures.

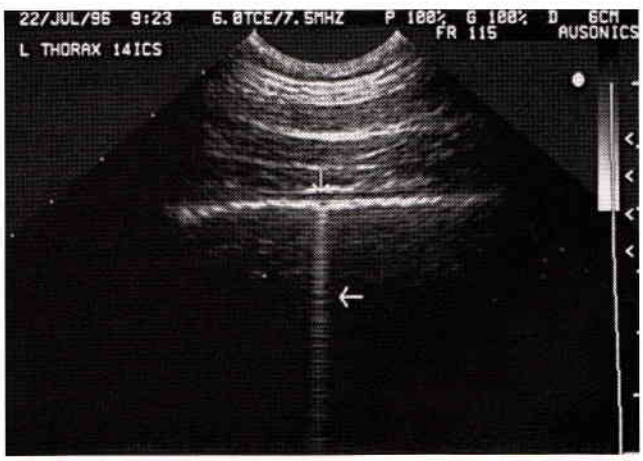

Figure 2–28

Sonogram of the left lung of a horse demonstrating a smooth visceral pleural surface and a single comet-tail artifact in the center of the image *(arrow)*.

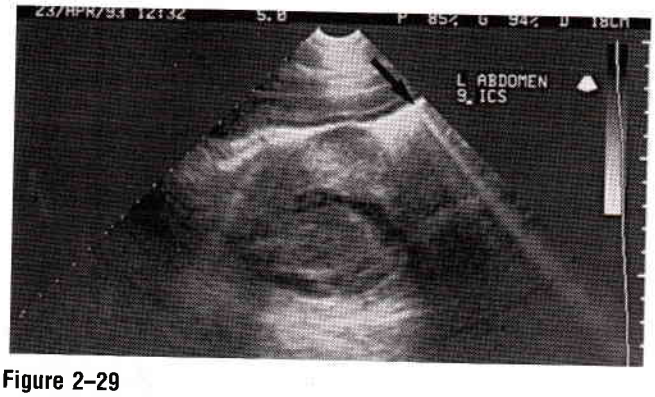

Figure 2–29

Sonogram of the stomach of a horse with gastric squamous cell carcinoma demonstrating a ring-down artifact from gas within the stomach *(arrow)*. Notice the continuous appearance of this gas artifact compared with the comet-tail artifact (see Fig. 2–28).

the surrounding soft tissues, such as metal foreign bodies or implants, and reflectors of very low acoustic impedance relative to the surrounding soft tissues, such as gas in the lung, gas bubbles, or bowel gas.[20–23]

Ring-Down Artifacts

The ring-down artifact may be produced by a resonance phenomenon associated with gas bubbles.[1] Ring-down artifacts reportedly originate from a bugle-shaped fluid collection trapped between two layers of gas bubbles.[2, 44] With the ring-down artifact there appears to be a continuous emission of sound from the origin of the artifact, resulting in a continuous artifact in which small, discrete echoes usually cannot be identified (Fig. 2–29).[44]

Propagation-Speed Error Artifacts

Propagation-speed error occurs when the assumed value for the propagation of ultrasound through tissue (1540 m/sec) is incorrect.[1–3, 53] This occurs because the average velocity of ultrasound through soft tissue (1540 m/sec) is used by manufacturers to calculate distance measurements in ultrasound equipment. Propagation-speed error occurs when the propagation speed that exists over the path the ultrasound travels is significantly greater or less than 1540 m/sec.[1–3, 53] The reflector is displayed closer to the transducer than it actually is if the propagation speed is greater because the calculated distance to the reflector is then too small. The reflector is displayed farther away from the transducer than it actually is if the propagation speed is less because the calculated distance to the reflector is then too great. In fat patients, for example, where the velocity of ultrasound is slower (1460 m/sec), deeper displacement of structures may occur secondary to the slower propagation of ultrasound through the fatty tissue. Both propagation-speed error and refraction can cause a structure to be displayed with an incorrect shape.[1]

Range-Ambiguity Artifacts

Range-ambiguity artifacts occur because the instrument assumes that all reflections are received before the next ultrasound pulse is produced.[1, 54] The maximum PRF is determined by the maximum depth that can be imaged unambiguously.[1] In real-time imaging the maximum depth imaged unambiguously (cm) multiplied by the frame rate (frames/second) and line density (lines/frame) cannot exceed 77,000.[1] If this number is exceeded, distant reflectors are displayed too close to the transducer. Range-ambiguity artifacts can be eliminated or minimized by selecting a higher-frequency transducer or decreasing the PRF.[2] Increasing the depth automatically reduces the PRF and also causes a reduction in frame rate.[12] This artifact has been reported in echocardiography and has been called "ring around" or "herbies" (Fig. 2–30).[1, 5] In the heart or another large fluid-filled viscus, this artifact creates a fluttering or flashing object within the fluid in real time and a blurred object when the image is frozen.[2, 5, 18]

Useful Artifacts

Acoustic shadowing and enhancement are both clinically useful artifacts. The presence of acoustic enhancement indicates a fluid-filled structure, whereas the presence of edge shadowing indicates different ultrasound tissue velocities in the circular or oval structure compared with the adjacent tissues.[2] Although the circular structure is most often fluid, this is not always the case. Although it is difficult to definitively determine the nature of the shadowing structure, careful evaluation of the type of acoustic shadow using properly focused transducers and multiple imaging planes and the identification of the origin of the shadowing structure help in accurate identification of the shadowing reflector.[2] Although echogenic structures with shadowing are most common, anechoic or hypoechoic structures with shadowing have been reported in human beings, as have echogenic structures

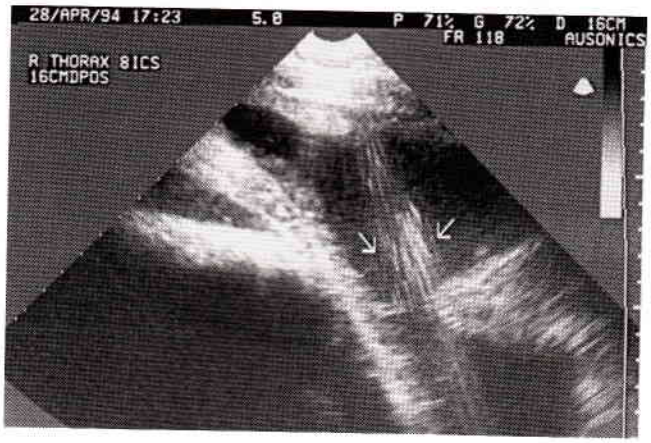

Figure 2–30

Sonogram obtained from a horse with pleuropneumonia and a large pleural effusion demonstrating a range-ambiguity artifact or "herbie" *(arrows)*.

Table 2–3
Sound Beam–Patient Interactions

Useful Artifacts	Confusing Artifacts
Shadowing	Axial resolution
Enhancement	Lateral resolution
Reflection/refraction	Slice thickness
Propagation-speed error	Range ambiguity
Edge shadowing	Reverberation
Comet tail	Comet tail
	Ring down
	Mirror image
	Multipath
	Ghosts
	Split image
	Speckle
	Side lobe
	Grating lobe

Adapted from Kirkberger RM: Imaging artifacts in diagnostic ultrasound—A review. Vet Radiol Ultrasound 36:297–306, 1995.

with acoustic enhancement.[1, 2] This seeming paradox occurs because absorption is the major contributor to tissue attenuation, with a minor contribution from scattering.[1, 2] Therefore, echogenicity (scattering level) and attenuation are not correlated.[2, 3]

Confusing Artifacts

Slice-thickness artifacts, range-ambiguity artifacts, and side-lobe artifacts can all result in artifactual echoes within anechoic structures.[2] Propagation-speed error, mirror-image artifacts, and side lobes can all result in reflectors within the body being located inaccurately, whereas range-ambiguity and multipath artifacts and the refractive effect of rounded structures cause less marked reflector displacement.[2]

Although some artifacts are useful and aid in image interpretation and diagnosis, many can cause confusion and error (Table 2-3). A thorough understanding of the types of artifacts that occur and how to deal with them when they are detected help sonologists avoid image interpretation pitfalls.[1] Multiple imaging planes, varying the patient position, changing the frequency of the transducer, and altering the gain settings may all help to minimize the effects of artifacts on the image.[2]

References

1. Kremkau FW, Taylor KJW: Artifacts in ultrasound imaging. J Ultrasound Med 5:227–237, 1986.
2. Kirkberger RM: Imaging artifacts in diagnostic ultrasound—A review. Vet Radiol Ultrasound 36:297–306, 1995.
3. Pennick DG: Imaging artifacts in ultrasound. *In* Nyland TG, Mattoon JS (eds): Veterinary Diagnostic Ultrasound. Philadelphia, WB Saunders, 1995, pp 19–29.
4. Park RD, Nyland TG, Lattimer JC, et al: B-mode gray-scale ultrasound: Imaging artifacts and interpretation principles. Vet Radiol 22:204–210, 1981.
5. Colby J: Artifacts and image quality in ultrasound. J Equine Vet Sci 5:295–297, 1985.
6. Pennick D, Cuvelliez S: Principes physiques et méthodes d'exploration échographie. Ann Med Vet 129:381–391, 1985.
7. Biller DS, Myer W: Ultrasound scanning of superficial structures using an ultrasound standoff pad. Vet Radiol 29:138–142, 1988.
8. Fornage BD: The hypoechoic normal tendon: A pitfall. J Ultrasound Med 6:19–22, 1987.
9. Nyland TG, Mattoon JS, Wisner ER: Physical principles, instrumentation, and safety of diagnostic ultrasound. *In* Nyland TG, Mattoon JS (eds): Veterinary Diagnostic Ultrasound. Philadelphia, WB Saunders, 1995, pp 3–18.
10. Powis RL: Ultrasound science for the veterinarian. Vet Clin North Am [Equine Pract] 2:3–27, 1986.
11. Rantanen NW: Instrumentation and physical principles of ultrasound use. Proceedings of the 39th Annual Meeting of the American Association of Equine Practice, 1993, pp 3–4.
12. Kremkau FW: Diagnostic Ultrasound: Principles and Instruments, 4th ed. Philadelphia, WB Saunders, 1993.
13. Rantanen NW, Ewing RL: Principles of ultrasound application in animals. Vet Radiol 22:196–203, 1981.
14. Abbott JG, Thurstone FL: Acoustic speckle: Theory and experimental analysis. Ultrasonic Imaging 1:303–324, 1979.
15. Morrison DC, McDicken WN, Smith DSA: A motion artifact in real-time ultrasound scanners. Ultrasound Med Biol 1:303–324, 1979.
16. Goldstein A, Madrazo BL: Slice-thickness artifacts in grey-scale ultrasound. J Clin Ultrasound 9:365–375, 1981.
17. Fiske CE, Filly RA: Pseudosludge. A spurious ultrasound appearance within the gallbladder. Radiology 144:631–632, 1982.
18. Laing FC: Commonly encountered artifacts in clinical ultrasound. Semin Ultrasound 4:27–43, 1983.
19. Rantanen NW: Ultrasound appearance of normal lung borders and adjacent viscera in the horse. Vet Radiol 22.217–219, 1981.
20. Ziskin MC, Thickman DI, Goldenberg NJ, et al: The comet tail artifact. J Ultrasound Med 1:1–7, 1982.
21. Thickman DI, Ziskin MC, Goldenberg NJ, Linder BE: Clinical manifestations of the comet tail artifact. J Ultrasound Med 2:225–230, 1983.
22. Wendell BA, Athey PA: Ultrasonic appearance of metallic foreign bodies in parenchymal organs. J Clin Ultrasound 9:133–135, 1981.
23. Shah ZR, Crass JR, Oravec DC, Bellon EM: Ultrasonographic detection of foreign bodies in soft tissues using turkey muscle as a model. Vet Radiol Ultrasound 33:94–100, 1992.
24. Buttery B, Davison G: The ghost artifact. J Ultrasound Med 3:49–52, 1984.
25. Sauerbrei EE: The split image artifact in pelvic ultrasonography. J Ultrasound Med 4:29–34, 1985.
26. Gardner FJ, Clark RN, Kozlowski R: A model of a hepatic mirror-image artifact. Med Ultrasound 4:19–21, 1980.
27. Golding RA, Li DKB, Cooperberg PL: Sonographic demonstration of air-fluid levels in abdominal abscesses. J Ultrasound Med 1:151–155, 1982.
28. Laing FC, Kurtz AB: The importance of ultrasonic side lobe artifacts. Radiology 145:763–768, 1982.
29. Saunders RC: Atlas of Ultrasonographic Artifacts and Variants, 2nd ed. St. Louis, Mosby-Year Book, 1992.
30. Sommer FG, Taylor KJW: Differentiation of acoustic shadowing due to calculi and gas collections. Radiology 135:399–403, 1983.
31. Rubin JM, Adler RS, Bude RO, et al: Clean and dirty shadowing at US: A reappraisal. Radiology 181:231–236, 1991.
32. Suramo I, Päivänsalo M, Vuoria P: Shadowing and reverberation artifacts in abdominal ultrasonography. Eur J Radiol 5:147–151, 1985.
33. Cartee RE, Rumph PF: Ultrasonographic detection of fistulous tracts and foreign objects in muscles of horses. J Am Vet Med Assoc 184:1127–1132, 1984.
34. Carroll BA: Gallstones: In vitro comparison of physical, radiographic and ultrasonic characteristics. AJR 131:223–226, 1978.
35. Filly RA, Moss AA, Way LW: In vitro investigation of gallstone shadowing with ultrasound tomography. J Clin Ultrasound 7:255–262, 1979.
36. Middleton WD, Dodds WJ, Lawson TL, Foley WD: Renal calculi: Sensitivity for detection with US. Radiology 167:239–244, 1988.
37. Chu JMG, Husband JE, Cosgrove DO, McCready VR: The B-scan ultrasonic appearances of gas in the biliary tree. Br J Radiol 51:728–730, 1978.
38. King W III, Kimme-Smith C, Winter J: Renal stone shadowing: An investigation of contributing factors. Radiology 154:191–196, 1985.

39. Rosenthal SJ, Cox GG, Wetzel LH, Batnitzky S: Pitfalls and differential diagnosis in biliary sonography. Radiographics 10:285–311, 1990.
40. Shapiro RS, Winsberg F: Comet-tail artifact from cholesterol crystals: Observations in the post lithotripsy gall bladder and an in vitro model. Radiology 177:153–156, 1990.
41. Suramo I, Pamilo M: Ultrasound examination of foreign bodies: An in vitro investigation. Acta Radiol 27:463–466, 1986.
42. Rubin JM, Adler RS, Fowlkes JB, Carson PL: Phase cancellation: A cause of acoustic shadowing at the edges of curved surfaces in B-mode ultrasound images. Ultrasound Med Biol 17:85–95, 1991.
43. Gonzalez L, MacIntyre WJ: Acoustic shadow formation by gallstones. Radiology 135:217–218, 1980.
44. Avruch L, Cooperberg P: The ring down artifact. J Ultrasound Med 4:21–28, 1985.
45. Taylor KJW, Jacobson P, Jaffee CC: Lack of an acoustic shadow on scans of gallstones: A possible artifact. Radiology 131:463–464, 1979.
46. Grossman M: Cholelithiasis and acoustic shadowing. J Clin Ultrasound 6:182–184, 1978.
47. Jaffee CC, Taylor KJW: The clinical impact of ultrasonic beam focusing patterns. Radiology 131:469–472, 1979.
48. Jaffee CC, Rosenfield AT, Sommer G, Taylor KJW: Technical factors influencing the imaging of small anechoic cysts by B-scan ultrasound. Radiology 135:429–433, 1980.
49. Sommer FG, Filly RA, Minton MJ: Acoustic shadowing due to refractive and reflective effects. Am J Roentgenol 132:973–977, 1979.
50. Robinson DE, Wilson LS, Kossoff G: Shadowing and enhancement in ultrasonic echograms by reflection and refraction. J Clin Ultrasound 9:181–188, 1981.
51. Ziskin MC, LaFollette PS, Blanthras K, Abraham V: Effect of scan format on refraction artifacts. Ultrasound Med Biol 16:183–191, 1990.
52. Ziskin MC, LaFollette PS, Radecki PD, Villafana T: The retrolenticular afterglow: An acoustic enhancement artifact. J Ultrasound Med 5:385–398, 1986.
53. Lamb CR, Boswood A: Ultrasound corner: An artifact resulting from propagation speed error. Vet Radiolol Ultrasound 36:549–550, 1995.
54. Goldstein A: Range ambiguities in real-time ultrasound. J Clin Ultrasound 9:83–90, 1981.

CHAPTER

3

Musculoskeletal Ultrasonography

One of the earlier applications of ultrasonography in horses was the diagnosis of flexor tendon and ligament injuries in the distal extremities.[1-17] The sonographic findings in the injured tendon or ligament were then compared to its gross and histopathologic appearance to characterize the tissue in the area of injury and correlate it with its sonographic appearance.[18-23] More recently, work has focused on the sonographic changes detected in horses during tendon and ligament healing.[24-39] Further studies on the usefulness of ultrasonography in the diagnosis and management of flexor tendon and ligament injuries continue.[40-58] As the usefulness of tendon and ligament ultrasonography has grown, sonographic evaluation of other tendinous and ligamentous structures has been undertaken.[59-75] Serial sonographic evaluations have been performed on horses in race training to evaluate the effects of training on the sonographic appearance of the superficial digital flexor tendon.[76, 77] More critical evaluation of tendon and ligament echogenicity has occurred but these techniques are not yet in widespread use.[78-80] Three-dimensional ultrasonographic imaging of normal and injured superficial digital flexor tendons is now possible in horses, although the software to perform the three-dimensional reconstruction is not present in any currently available ultrasonographic equipment.[81, 82]

Sonographic evaluation of the various tendon sheaths and bursae provides additional information about diseases involving these structures, along with evaluation of the contained tendons and ligaments.[59, 63, 66, 68, 70, 72, 74, 83-88] Musculoskeletal imaging has since progressed to evaluating muscular, synovial, and bony abnormalities.[89-108] The ultrasonographic evaluation of bone initially seemed to have little application because of the high acoustic impedance of bone relative to the surrounding soft tissue. However, its use in selected situations has been very rewarding and holds much promise.[92, 94, 95, 101-108] Although high-quality radiographs are still the ideal method for evaluation of bony structures, diagnostic ultrasound evaluation of bony structures has numerous applications in the horse.

EXAMINATION TECHNIQUE

Patient Preparation

The skin over the area to be examined should be surgically clipped with a No. 40 surgical clipper blade.[25, 47, 48, 109, 110] The skin should then be thoroughly cleaned prior to application of ultrasound coupling gel. The ultrasound gel should be applied to the entire area being examined and worked in well, following the direction of hair growth. A sterile couplant gel should be used if an aseptic examination is necessary. If clipping the hair off the skin is not possible, the leg can be soaked with water for 10 minutes. Either a 10-minute hosing of the area to be examined can be performed or a wet bandage can be applied. The topical application of isopropyl alcohol may also be used to obtain an image without clipping the hair; however, the optimal image will be obtained by clipping the area to be examined. Shaving the skin may be necessary or preferable in some situations to obtain optimal image quality.

Tendons and Ligaments

The skin over the entire palmar or plantar area of the leg should be surgically clipped from the base of the accessory carpal bone or point of the hock (tuber calcis) to the ergot to examine the flexor tendons and ligaments (Fig. 3-1). Both the medial and lateral branches of the suspensory ligament should be clipped from the lateral and medial sides of the limb, starting just above the suspensory bifurcation (at a point midway down the cannon bone) and continuing down to the insertion on the apex of both proximal sesamoid bones (see Fig. 3-1). The entire palmar or plantar, medial and lateral aspects of the pastern should be clipped from the ergot distally to the bulbs of the heels to examine the tendinous and ligamentous structures in the pastern (Fig. 3-2). The base of both proximal sesamoid bones must be included to

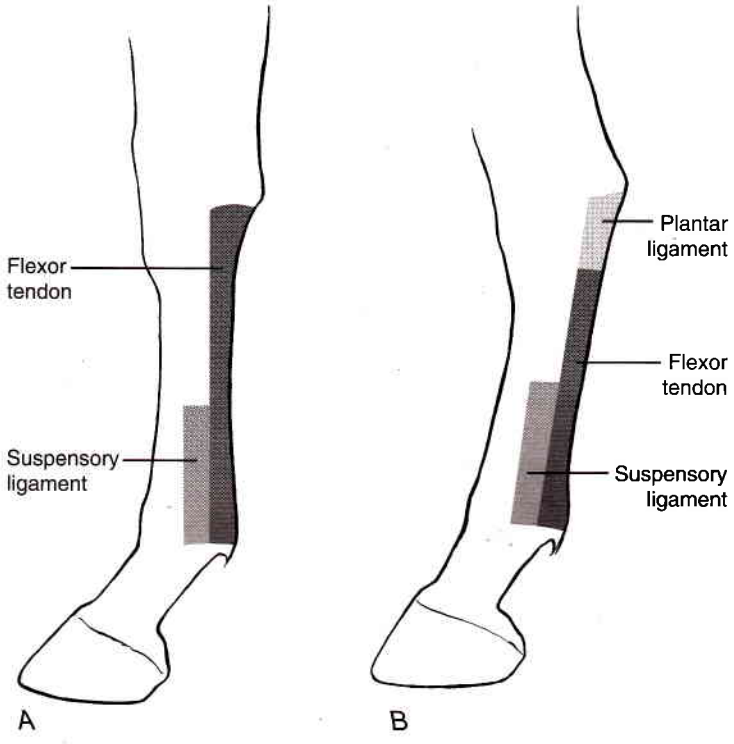

Figure 3–1

Diagrams of the areas to be surgically clipped along the palmar *(A)* or plantar *(B)* aspect of the limb. The broad darkened strip along the palmar or plantar aspect of the limb is the area to be surgically clipped for examination of the superficial digital flexor tendon (SDF), deep digital flexor tendon (DDF), inferior check ligament (ICL), body of the suspensory ligament (SL), and proximal portion of the digital sheath. The lighter strip along the distal lateral and medial aspects of the limbs is the area to be clipped for examination of the SL branches, the distal portion of the second and fourth metacarpal or metatarsal bones, the abaxial surfaces of the medial and lateral proximal sesamoid bones, and the medial and lateral compartments of the metacarpo- or metatarsophalangeal joint. The lightest strip along the plantar aspect of the hindlimb in the proximal-most portion of the limb *(B)* is the area to be surgically clipped for evaluation of the plantar ligament.

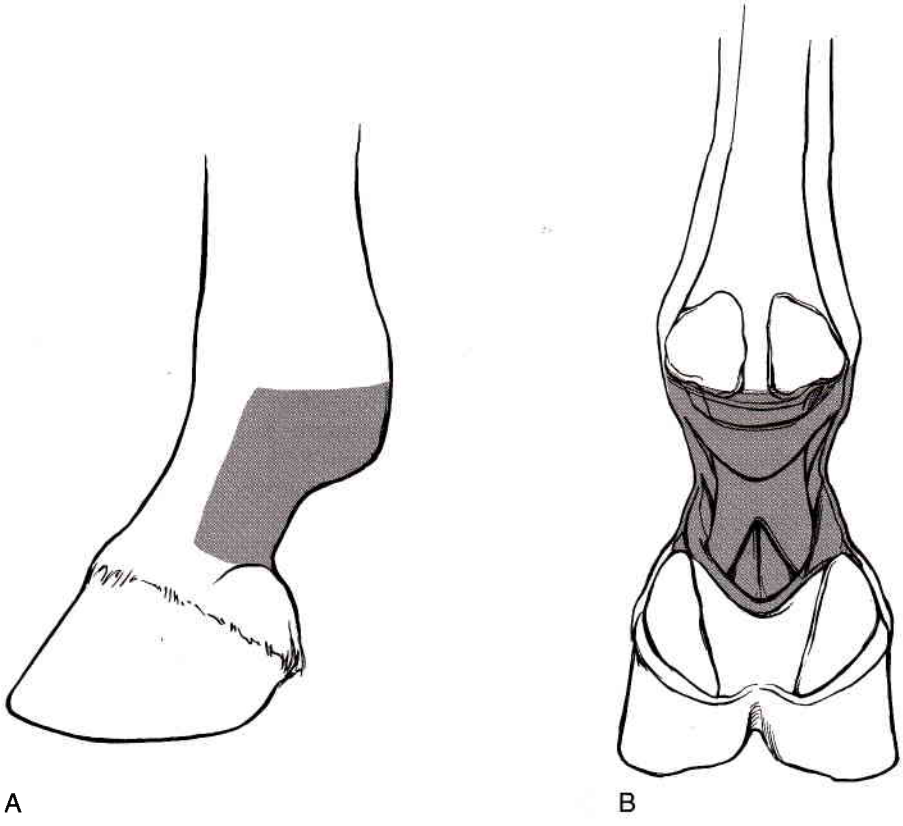

Figure 3–2

Diagrams of the areas to be surgically clipped along the medial and lateral aspect *(A)* and the palmar or plantar aspect of the pastern *(B)* for thorough evaluation of all the tendinous and ligamentous structures in the pastern.

image the origin of the distal sesamoidean ligaments (see Fig. 3-2). All the hair must be clipped, which is more difficult at the pastern, because the hair grows in a number of different directions. If all hair cannot be removed with a surgical clipper blade, the skin should be shaved over the area under investigation.

Tendon Sheaths and Bursae

The skin over the entire tendon sheath or bursa to be examined should be surgically clipped, including the entire length of the tendon associated with the sheath or the bursa. Lesions located in the portion of a tendon within a tendon sheath may extend proximal or distal to the tendon sheath. Thus, the entire length of the tendon should be examined, not just the portion contained within the tendon sheath. Similarly, lesions within a tendon may extend beyond the area of a bursa; therefore, the entire tendon overlying a bursa should be examined.

Nerves

The skin over the nerve of interest should be surgically clipped. Because the nerves are small structures that are difficult to image in the best of circumstances, proper patient preparation is critical. Shaving the skin may be necessary for optimal imaging.

Muscle, Bones, and Joints

The skin over the entire muscle, bone, or joint in question should be surgically clipped. To optimally evaluate the muscle in question, a rim of surrounding normal muscle should also be examined. To optimally evaluate the bone in question, the skin overlying the bone should be prepared from its proximal articulation to the distal articulation. The skin over the entire joint, including the synovial compartments and collateral ligaments, should be clipped for examination. A portion of the limb proximal and distal to the joint should be included. The entire affected area should be examined if diffuse swelling is present.

Anatomy

Flexor Tendons and Ligaments

The flexor tendons and ligaments in the metacarpal and metatarsal region are the most frequently imaged tendons and ligaments in horses. These tendons and ligaments should be scanned throughout their length. A thorough knowledge of the cross-sectional anatomy of the flexor tendons and ligaments (Fig. 3-3) is necessary to recognize subtle changes in their size and shape, early indications of injury to these structures.[111, 112]

Superficial Digital Flexor Tendon. The superficial digital flexor tendon in the forelimb originates from the humeral head of the superficial digital flexor muscle on the caudomedial aspect of the limb, approximately 6 to 10 cm proximal to the point of the accessory carpal bone.[111, 113] Its musculotendinous junction is located within the carpal canal. The accessory ligament of the superficial digital flexor tendon (superior check ligament) fuses with the superficial digital flexor tendon just proximal to the antebrachiocarpal joint.[111] The superficial digital flexor tendon extends along the palmar-most aspect of the metacarpal region, forming a ring (the manica flexoria) around the deep digital flexor tendon in the proximal pastern region and bifurcating into a medial and lateral branch that inserts onto the distal part of the first phalanx (P1) and the proximal part of the second phalanx (P2).[111, 113]

Both the superficial and deep digital flexor tendons are contained within the carpal sheath in the forelimb, whereas only the deep digital flexor tendon is contained within the tarsal sheath in the hindlimb. In the distal metacarpal region and proximal pastern, both the superficial and deep digital flexor tendons are contained within the digital sheath; whereas in the mid and distal pastern region, only the deep digital flexor tendon is surrounded by the digital sheath. In the hindlimb, the superficial digital flexor tendon originates from the musculotendinous junction in the proximal portion of the crus, widens and flattens to attach to the point of the tuber calcis, and extends distally along the plantar aspect of the metatarsus. It forms a ring around the deep digital flexor tendon in the proximal pastern and bifurcates to form a medial and lateral branch that inserts on distal P1 and proximal P2, as in the forelimb.

Deep Digital Flexor Tendon. The deep digital flexor tendon in the forelimb originates from the three heads of the deep digital flexor muscle in the distal region of the radius and extends distally dorsal to the superficial digital flexor tendon through the carpal canal and fetlock annular ligament region into the foot.[111, 113] The humeral head of the deep digital flexor has a strong tendon that appears about 8 to 10 cm proximal to the antebrachiocarpal joint but contains muscle fibers until the level of the joint where the ulnar and radial heads join the humeral head.[111] The accessory ligament of the deep digital flexor tendon (inferior check ligament) joins the deep digital flexor tendon in the mid to distal metacarpus, having originated from the palmar carpal ligaments. In the hind leg the deep digital flexor tendon originates from the union of the lateral digital flexor tendon and the medial digital flexor tendon. The lateral digital flexor tendon incorporates the tibialis caudalis tendon and passes over the sustentaculum tali in the plantar tarsal sheath. The medial digital flexor tendon passes over the proximal tubercle of the talus in its own sheath at the medial aspect of the talus to fuse with the lateral digital flexor tendon in the proximal metatarsus. The deep digital flexor tendon lies in a dorsal position relative to the superficial digital flexor tendon in the proximal metatarsal region. In the mid to distal metatarsal region, the deep digital flexor tendon is usually joined by a smaller accessory ligament of the deep digital flexor tendon. Its distal course is similar to that in the forelimb.

Inferior Check Ligament. The inferior check ligament or accessory ligament of the deep digital flexor

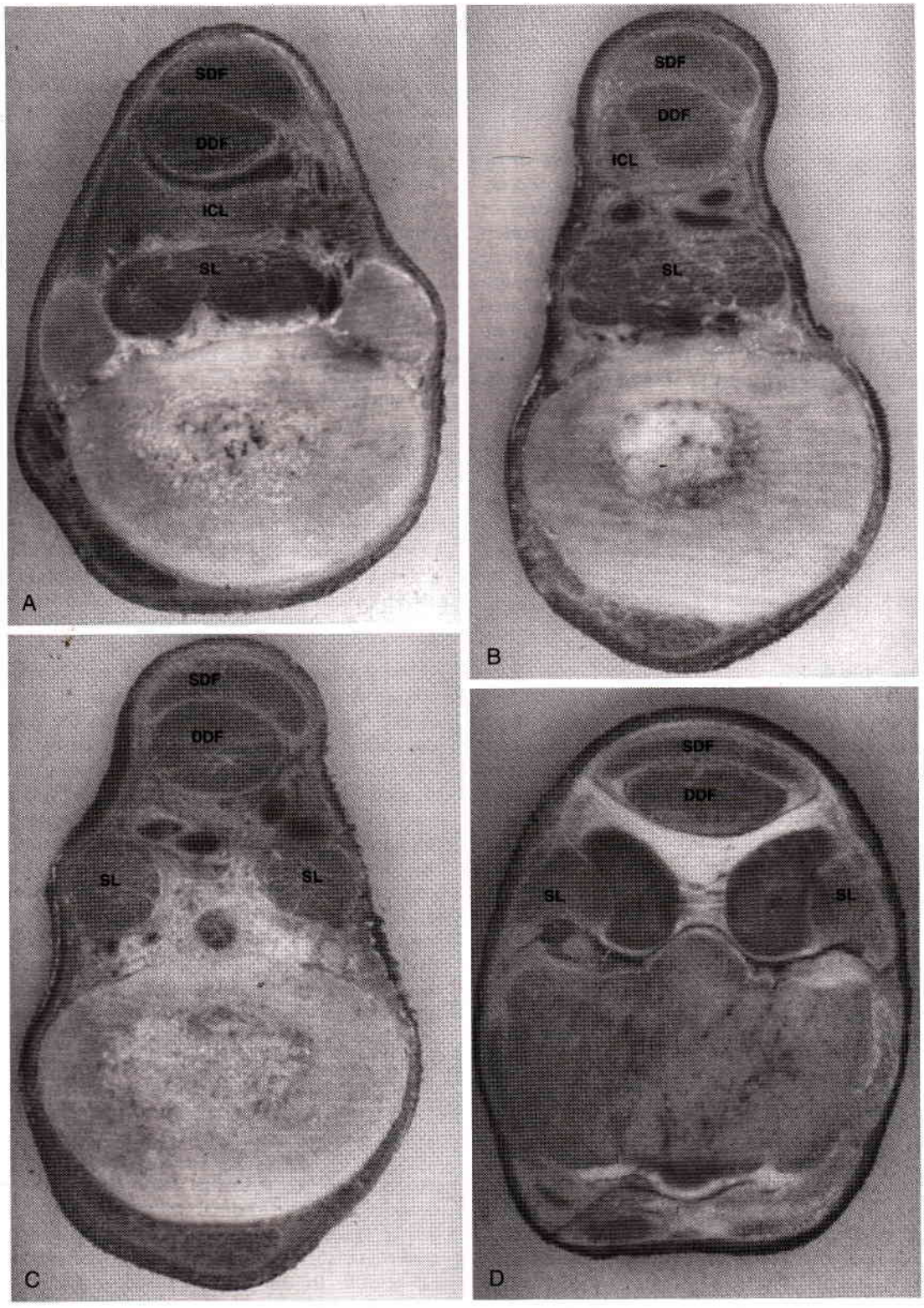

Figure 3–3 *See legend on opposite page*

tendon in the forelimb originates from the carpal retinaculum as a continuation of the palmar carpal ligament and inserts on the deep digital flexor tendon in the mid-metacarpal region.[111, 113] The accessory ligament of the deep digital flexor tendon may be missing in the hindlimb or is a small vestigial structure.

Suspensory Ligament. The suspensory ligament (third interosseous muscle) originates from the distal row of carpal or tarsal bones, the proximal palmar metacarpal or plantar metatarsal ridge, and the palmar carpal or tarsal ligament and extends distally between the second and fourth metacarpal or metatarsal bones to the junction between the mid and distal third of the metacarpus or metatarsus. It then bifurcates into two branches that insert on the abaxial surfaces of the proximal sesamoid bones.[111, 113] Small extensor branches are given off that insert on the dorsomedial and dorsolateral aspect of proximal P1. The origin of the suspensory ligament is bilobed in the forelimb and appears incompletely separated as it originates from the second and third carpal bones.[111] The suspensory ligament in the forelimb is approximately 20 to 25 cm long. The suspensory ligament in the hindlimb is trapezoid-shaped and measures approximately 25 to 30 cm in length. The suspensory ligament consists of striated muscle, fat, loose areolar connective tissue, connective tissue fibers, blood vessels, and nerves.[6]

Pastern. The cross-sectional anatomy of the tendons and ligaments in the pastern is even more confusing because the tendons and ligaments change shape and direction from their origin to insertion (Fig. 3-4).

Superficial Digital Flexor Tendon. The superficial digital flexor tendon forms a ring around the deep digital flexor tendon in the proximal pastern and then bifurcates to form medial and lateral branches that insert on the lateral and medial margins of the distal aspect of the first phalanx and the proximal aspect of the second phalanx. The branches of the superficial digital flexor tendon insert between the axial and abaxial palmar ligaments of the proximal interphalangeal joint onto the scutum medium (the fibrocartilage along the proximal border of P2).[59, 111]

Deep Digital Flexor Tendon. The deep digital flexor tendon lies immediately dorsal to the superficial digital flexor tendon in the proximal pastern region, palmar or plantar to the straight distal sesamoidean ligament, and is surrounded by the digital sheath throughout the length of the pastern. The distal digital annular ligament is adhered to the palmar or plantar surface of the distal portion of the deep digital flexor tendon.[111] The deep digital flexor tendon is molded to the navicular bone's contour as it extends palmar or plantar to the navicular bone. The deep digital flexor tendon extends distally into the foot to insert on the third phalanx.

Middle (Oblique) Distal Sesamoidean Ligament. In the proximal portion of the pastern, the origins of the middle distal sesamoidean ligament arise from the base of the medial and lateral proximal sesamoid bones and extend diagonally across the proximal aspect of the first phalanx to join each other near the junction of the proximal and middle third of the pastern. Here the branches of the middle distal sesamoidean ligament form one wide ligamentous band near the ligament's insertion on the palmar or plantar aspect of P1, beginning at the palmar or plantar aspect of proximal P1 and ending between the proximal insertion of the two axial palmar or plantar ligaments of the proximal interphalangeal joint near the junction of the middle and distal thirds of P1. The middle distal sesamoidean ligament is the most dorsal structure in the mid-pastern region.

Straight Distal Sesamoidean Ligament. Along the palmar or plantar aspect of the middle distal sesamoidean ligament lies the straight distal sesamoidean ligament in the mid-pastern region. In the distal portion of the pastern, the straight distal sesamoidean ligament is the most dorsal structure. It originates from the base of the proximal sesamoid bones, where it has a trapezoid shape, and extends distally to insert on the scutum medium onto proximal P2.

Cruciate Distal Sesamoidean Ligament. The cruciate distal sesamoidean ligaments form the palmar or plantar wall of the synovial recess of the distal palmar or plantar aspect of the metacarpal or metatarsal phalangeal joint. These ligaments insert on the axial aspect of the proximopalmar or proximoplantar tuberosity of P1.[111]

A thorough knowledge of the anatomy of the tendons and ligaments (origins and insertions and their relation-

Figure 3–3

Anatomy of the flexor tendons and ligaments in the metacarpal region of the horse. These figures are transverse cross-sections through the metacarpus of a normal horse, illustrating the interrelationships of the flexor tendons and ligaments. The right side of these cross-sections is medial and the left side is lateral.

A, The superficial digital flexor tendon (SDF), deep digital flexor tendon (DDF), inferior check ligament (ICL), and origin of the suspensory ligament (SL) in the metacarpal region at zone 1A are depicted. Notice the bilobed appearance of the SL origin in this zone and its more heterogeneous appearance with areas of muscle tissue contained within each lobe.

B, In the mid to distal metacarpal region (zone 2B), the SDF has flattened some in a dorsal to palmar direction and widened in a medial to lateral direction, the DDF is oval in shape, the ICL is inserting into the DDF at this level, and the SL body is beginning to bifurcate. Notice the widened, rectangular appearance of the SL body and its more heterogeneous appearance compared to the other tendinous and ligamentous structures.

C, In the distal metacarpal region in zone 3B, the SDF continues to flatten in a dorsal to palmar direction and widen in a medial to lateral direction. The DDF is somewhat rounder after being joined by the ICL. The SDF and DDF are surrounded by the digital sheath at this level. The SL branches are round at this level and must be imaged from the medial and lateral aspect of the limb because they are mostly out of the plane of the image from the palmar surface of the leg.

D, At the level of the metacarpophalangeal joint just proximal to the ergot in zone 3C, the SDF has a thin, flattened, slightly curved shape adjacent to the flattened, oval DDF. The SDF and DDF are surrounded by the digital sheath and the annular ligament is present at this level, although it is usually indistinguishable from the digital sheath. The SL branches are inserting on the abaxial surfaces of the proximal sesamoid bones and the intersesamoidean ligament is imaged along the axial margins of both proximal sesamoid bones. (From White NA II, Moore JN: Current Practice of Equine Surgery. Philadelphia, JB Lippincott, 1990, pp 426-427.)

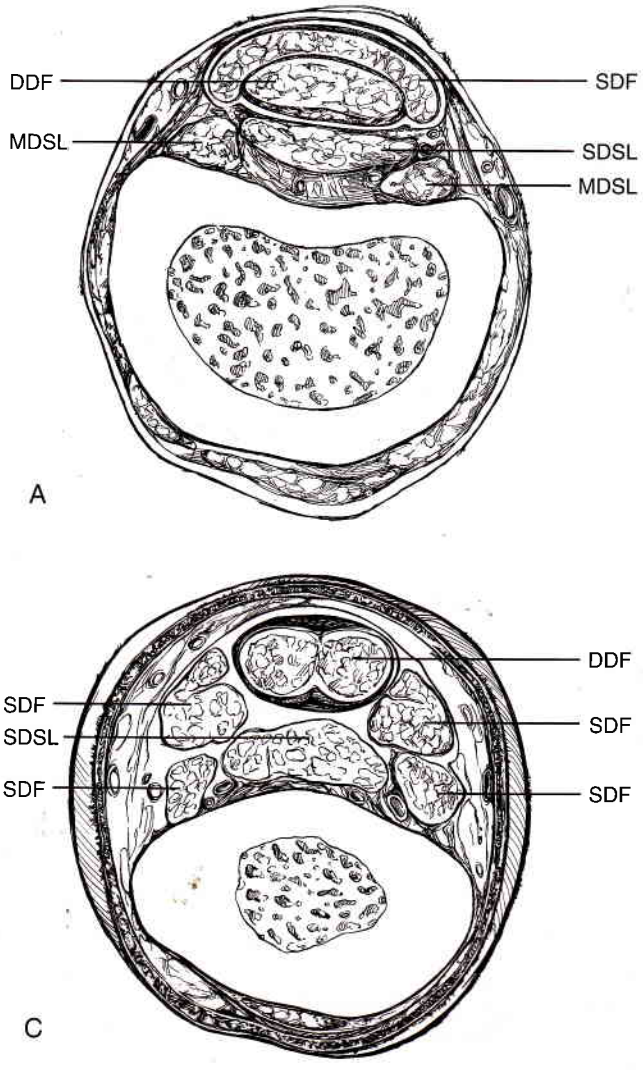

Figure 3–4

Anatomy of the tendons and ligaments in the pastern region of the horse. These figures are transverse cross-sections through the pastern of a normal horse, illustrating the interrelationships of the flexor tendons and distal sesamoidean ligaments.

A, Diagram of the proximal pastern obtained from a normal horse at zone P1A. Notice the thin superficial digital flexor tendon (SDF) arcing around the deep digital flexor tendon (DDF) and forming a thin ring at this level. The straight distal sesamoidean ligament (SDSL) is a broad-based structure near its origin. Notice the larger oval-shaped origins of the branches of the middle (oblique) distal sesamoidean ligaments (MDSL) as they originate from the base of the proximal sesamoid bones.

B, Diagram of the mid pastern obtained from a normal horse at zone P1B. Notice the branching of the SDF and the tear-shaped appearance of both SDF branches. Notice the bilobed appearance of the DDF within the digital sheath. The SDSL has become smaller and more oval in shape at this level. The two branches of the MDSL have joined and are inserting along the palmar aspect of the middle portion of the first phalanx (P1).

C, Diagram of the distal pastern obtained from a normal horse at zone P1C. Notice the insertions of the SDF branches along the medial and lateral aspects of the pastern. The DDF still has a somewhat bilobed appearance and is surrounded by the digital sheath. The SDSL is slightly broader as it approaches its insertion on the proximal portion of the second phalanx (P2).

ships to one another) and the related muscular, synovial, and bony structures is important to fully evaluate tendinous and ligamentous abnormalities.[111, 112]

Superior Check Ligament. The superior check ligament (accessory ligament or radial head of the superficial digital flexor tendon) attaches the musculotendinous junction of the superficial digital flexor tendon to the caudomedial surface of the distal radius. The superior check ligament is a strong fibrous band that arises from a ridge on the caudal surface of the radius near its medial border along the distal third of the radius.[111, 114] Medially, the superior check ligament is adjacent to the flexor carpi radialis tendon sheath.[111]

Annular Ligaments. The fetlock palmar/plantar annular ligament contains the superficial and deep digital flexor tendon and the digital sheath as they pass along the palmar or plantar aspect of the metacarpo- or metatarsophalangeal joint. The fetlock annular ligament attaches to the abaxial surfaces of the proximal sesamoid bones and extends transversely across the palmar or plantar aspect of the fetlock.[113] Its proximal-most extent is just proximal to the apex of the proximal sesamoid bones and its distal extent is the base of the proximal sesamoid bones.[60] The normal fetlock annular ligament is a thin structure in the normal horse, difficult to distinguish from the digital sheath with which it is intimately associated. The proximal digital annular ligament contains primarily the deep digital flexor tendon and digital sheath along the palmar or plantar aspect of the first phalanx. The proximal-most extent of the proximal digital annular ligament is the distal aspect of the proximal palmar aspect of P1 and the distal-most aspect is at the level of insertion of the middle (oblique) distal sesamoidean ligament. The proximal digital annular ligament has lateral and medial bands that originate on the middle of the borders of the proximal phalanx and insert distally on the palmar margin of the proximal end of the middle phalanx (P2) and its fibrocartilage.[111, 113]

Bicipital Tendon. The bicipital tendon originates from the supraglenoid tubercle of the scapula and inserts on the radial tuberosity, the medial collateral ligament of the elbow, forearm fascia, and the extensor carpi radialis tendon.[113] The bicipital tendon conforms to the shape of the intertuberal groove in the humerus with an isthmus connecting the larger lateral lobe with the smaller medial lobe. The isthmus of the bicipital tendon lies directly

cranial to the intermediate tubercle of the humerus. The lateral lobe rides over the greater tubercle of the humerus with the medial lobe riding over the lesser humeral tubercle. A tendinous band between the greater and lesser tubercles anchors the tendon in the intertuberal groove. The infraspinatus muscle inserts in the caudal eminence of the greater tubercle of the humerus from the lateral aspect of the shoulder.

Extensor Tendons

Extensor Carpi Radialis Tendon. The largest tendon on the dorsal aspect of the radius is the extensor carpi radialis tendon, which extends from the extensor carpi radialis muscle to the metacarpal tuberosity.[113] It is located on the dorsal midline of the carpus.

Common Digital Extensor Tendon. Lateral to the extensor carpi radialis tendon is the common digital extensor tendon, which may join the lateral digital extensor tendon via a branch or extend separately to the fetlock.[113] The long (common) digital extensor tendon is located on the craniolateral aspect of the distal radius and extends distally towards the midline in the proximal metacarpal region.

Extensor Carpi Obliquus Tendon. The extensor carpi obliquus extends from the proximal and lateral aspect of the distal radius in a distal and medial direction with its tendon running in the oblique groove of the distal radius and attaching to the proximal aspect of the second metacarpal bone.[113] The extensor retinaculum covers these tendons over the dorsal aspect of the carpus.

Lateral Digital Extensor Tendon. The lateral digital extensor tendon is the smallest extensor tendon and runs between the superficial (long) and deep (short) collateral ligaments along the lateral aspect of the carpus.[113]

Ulnaris Lateralis Tendon. The ulnaris lateralis has two tendons of insertion distally along the lateral aspect of the carpus. The short tendon inserts on the accessory carpal bone with the flexor carpi ulnaris. The long tendon inserts on the fourth metacarpal bone, originates in the proximal carpal region, and runs through a groove on the accessory carpal bone to its insertion.[113]

Gastrocnemius Tendon. The lateral and medial heads of the gastrocnemius muscle are superficial in location and unite to form the gastrocnemius tendon in the crus. The gastrocnemius tendon spirals around the superficial digital flexor tendon from lateral to dorsal and then inserts on the calcanean tuberosity. The common calcaneal tendon is a combination of the gastrocnemius and superficial digital flexor tendons and the axial and medial tarsal tendons with contributions from the biceps femoris, semitendinosus, gracilis, and soleus muscles.[65] The axial and medial tarsal tendons are also referred to as the deep tarsal tendons. The medial tarsal tendon inserts on the tendon of the gastrocnemius just proximal to its insertion. The axial tarsal tendon bifurcates distally and inserts on the os calcis with a larger medial than lateral branch.[65] The Achilles tendon is the combination of the gastrocnemius tendon and the soleus tendon only.[65] Along the caudal surface of the tibia, angling from lateral to medial, are the popliteus muscle and the three heads of the deep digital flexor muscle.

Plantar Ligament. The plantar ligament originates from the plantar aspect of the proximal and lateral extent of the tuber calcis and inserts on the fibular tarsal bone, fourth tarsal bone, and proximal extent of the fourth metatarsal bone.[113] The plantar ligament covers the lateral aspect of the plantar surface of the hock and is lateral to the deep digital flexor tendon along its distal margin.

Peroneus Tertius Tendon. The peroneus tertius tendon originates from the lateral aspect of the distal epicondyle of the femur along with the long digital extensor tendon, extends distally along the dorsal aspect of the tibia, and bifurcates over the dorsal aspect of the hock.[113] The peroneus tertius tendon inserts laterally on the calcaneus and fourth tarsal bone and medially on the third tarsal bone and third metatarsal bone.

Long Digital Extensor Tendon. The long digital extensor tendon originates from the extensor fossa of the femur in common with the origin of the peroneus tertius tendon and inserts on the extensor process of P3 and the dorsal surfaces of the proximal extremities of P1 and P2.[113]

Tibialis Cranialis and Cunean Tendon. The tibialis cranialis muscle lies deep to the peroneus tertius tendon and originates from the lateral condyle of the tibia and the lateral surface of the tibial tuberosity.[113] The insertion of the tibialis cranialis begins just proximal to the hock and bifurcates immediately distal to the peroneus tertius bifurcation. Several large blood vessels are present around this bifurcation. The tibialis cranialis tendon is surrounded by a sheath as it courses between the branches of the peroneus tertius tendon. The cunean tendon (the medial branch of the tibialis cranialis tendon) inserts on the first tarsal bone and the other tendon of insertion inserts on the proximal end of the third metatarsal bone.[113]

The Back. The nuchal ligament is that portion of the supraspinous ligament that is elastic and extends from the occipital bone to the withers. The remainder of the supraspinous ligament, which extends from the withers to the sacrum, is more fibrous. The supraspinous ligament inserts on the summits of the thoracic and lumbar spinous processes.[75, 113] Multiple tendons of insertion of the longissimus dorsi muscle contribute to the supraspinous ligament on each side, whereas ventrally it is directly continuous with the interspinal ligaments.[75] A bursa is present between the supraspinous ligament and the dorsal arch of the atlas.[75, 113] Another bursa may be present in some horses over the axis.[113] A bursa is also present between the ligamentum nuchae and the dorsal spinous processes at the withers, most commonly detected over the second thoracic spine.[113] Other bursae may occur over the highest thoracic spines. A variable amount of fat and connective tissue lies dorsal to the nuchal ligament in the cervical region extending as far caudally as the withers. A thick layer of subcutaneous fascia is continuous with the supraspinous ligament in the thoracic region. The dorsal spinous processes are connected by the interspinous ligaments that extend between the spines of adjacent vertebrae. The dorsal spinous processes have large cartilaginous caps in the cranial thoracic region (withers). The dorsal sacroiliac ligament originates from the left or right tuber sacrale and inserts onto the sacrum.[75, 113]

Tendon Sheaths and Bursae

Flexor Tendon Sheaths

Carpal Sheath. The carpal sheath is composed of two compartments in the metacarpal region: a dorsal and a palmar compartment, which communicate above the level of the accessory carpal bone.[115] The two compartments are separated by a fold of the visceral layer of the carpal sheath and the mesotendon.[115] The dorsal compartment extends along the dorsal aspect of the deep digital flexor tendon until the insertion of the inferior check ligament into the deep digital flexor tendon. The palmar compartment is located between the superficial and deep digital flexor tendons in the metacarpal region.

Tarsal Sheath. The tarsal sheath surrounds the deep digital flexor tendon and extends from approximately 6 cm proximal to the lateral malleolus of the tibia distally to the junction between the proximal and middle third of the metatarsus.[116] The proximal portion of the tarsal sheath is not surrounded by the deep tarsal fascia.[116]

Digital Sheath. The digital sheath begins near the junction of the middle to distal third of the metacarpus or metatarsus, surrounds the superficial and deep digital flexor tendons, and extends distally into the distal pastern, surrounding only the deep digital flexor tendon in the middle to distal region of the pastern.[61, 66] The digital sheath originates at the suspensory ligament bifurcation and extends distally through the fetlock annular ligament and the proximal and distal digital annular ligaments.[72, 115] The digital sheath is approximately 14 to 20 cm long.[8, 72, 115] The digital sheath has three recesses.[72, 111] Folding and sacculation of the digital sheath occur normally proximal to the fetlock annular ligament in the proximal recess of the digital sheath.[8] The collateral recesses are located on the lateral and medial aspectsof the pastern between the distal sesamoidean ligaments and the flexor tendons.[111] The distal recess extends between P2 and the dorsal aspect of the deep digital flexor tendon.[111] The digital sheath is adhered to the palmar or plantar aspect of the superficial digital flexor tendon in the palmar aspect of the fetlock and in the proximal pastern.[72, 111] The deep digital flexor tendon is attached to the digital sheath proximally along its medial and lateral margins by a mesotendon.[72, 113]

Extensor Tendon Sheaths

Extensor Carpi Radialis Tendon Sheath. The extensor carpi radialis tendon is surrounded by a synovial sheath over the dorsal aspect of the carpus. This synovial sheath extends from the distal aspect of the radius to the metacarpal tuberosity.[113]

Common Digital Extensor Tendon Sheath. The common digital extensor tendon and its branch are surrounded by a common synovial sheath over the dorsal aspect of the carpus that begins at the level of the distal radius and ends over the proximal aspect of the metacarpus.[113]

Extensor Carpi Obliquus Tendon Sheath. The tendon of the extensor carpi obliquus is covered by a synovial sheath over the dorsal aspect of the carpus between the extensor carpi radialis tendon and the medial collateral ligament and extends palmarly along most of its length.[87, 113]

Lateral Digital Extensor Tendon Sheath. The lateral digital extensor tendon is covered by a synovial sheath in the carpal region between the long and short collateral ligaments. This tendon joins the long digital extensor tendon just below the carpus.[113]

Ulnaris Lateralis Tendon Sheath. A synovial sheath covers the long tendon of the ulnaris lateralis muscle throughout its course from the proximal carpal region to its insertion on the proximal portion of the fourth metacarpal bone.[113]

Bursae

Bicipital Bursa. The bicipital bursa lies between the bicipital tendon and the intertuberal groove of the distal humerus.[113]

Navicular (Podotrochlear) Bursa. The navicular bursa lies between the navicular bone and the deep digital flexor tendon. It extends proximally along the deep digital flexor tendon for 1 to 1.5 cm proximal to the distal sesamoid bone and distally to the insertion of the deep digital flexor tendon onto P3.[111, 113]

Trochanteric Bursa. The trochanteric bursa lies between the accessory head of the middle gluteal muscle and the greater trochanter.[113]

Calcaneal Bursa. The calcaneal bursa lies between the superficial digital flexor tendon and the gastrocnemius tendon.[113]

Gastrocnemius Bursa. The gastrocnemius bursa is present in some horses and lies between the gastrocnemius tendon and the tuber calcis.[113]

Cunean Bursa. The cunean bursa lies between the cunean tendon and the underlying bone.[113]

Atlantal Bursa. The atlantal bursa lies between the nuchal ligament and the atlas.[113]

Supraspinous Bursa. The supraspinous bursa lies between the second thoracic vertebrae and the supraspinous ligament.[113]

Nerves

The anatomy of each nerve under examination should be known, along with its relationship to the surrounding structures, to locate the nerve for sonographic examination. The superficial nerves are very small and are located immediately under the skin surface. The palmar digital nerve lies immediately palmar or plantar to the palmar digital artery.

Muscle

The origins, insertions, shape, and size of each muscle should be known for thorough sonographic evaluation of suspected muscular abnormalities.

Bone

A thorough knowledge of the normal bony protuberances, the physes, the age of the horse at physeal closure, the locations of articular cartilage and joint capsules, the origins and insertions of the various tendons and ligaments, and the articulations between the various

bones is necessary for accurate sonographic evaluation of bony structures.

Joints

The locations of the joint capsule, synovial compartments, collateral ligaments, and articular cartilage are important aspects of the sonographic evaluation of a joint. The anatomy of these structures, as well as any associated periarticular structures such as surrounding tendons, ligaments, and muscles, must be known to thoroughly evaluate the joints of horses, because abnormalities may involve any of these structures.

Shoulder. The muscles and tendons of the shoulder are the stabilizers of this joint. The supraspinatus, infraspinatus, and teres minor muscles stablize the joint laterally; the subscapularis muscle is the medial stabilizer of the shoulder.[113] Cranially, the biceps brachii and the supraspinatus muscles stabilize the scapulohumeral joint; the triceps brachii is its caudal stabilizer.[113] The fibrous joint capsule is attached 1 to 2 cm distal to the articular margins of the scapulohumeral joint. Two elastic glenohumeral ligaments originate from the supraglenoid tubercle and insert on the tuberosities of the humerus, which also stabilize the shoulder joint.

Elbow. The short lateral collateral ligament originates from a depression on the lateral epicondyle of the humerus and inserts distally on the lateral tuberosity of the radius, just distal to the margin of the articular surface.[100, 113] The medial collateral ligament of the cubital joint originates proximal to an eminence on the medial epicondyle of the humerus and divides to insert in two parts on the radius.[100, 113] The longer branch of the insertion is more superficial and inserts on the medial border of the radius, just distal to the level of the interosseous space. The deeper shorter branch inserts onto the medial tuberosity of the radius.

Carpus. The extensor retinaculum is loose and covers the dorsal aspect of the carpal joints.[113] The palmar carpal ligament is thick and dense, is closely attached to the carpal bones, and forms the dorsal wall of the carpal canal.[100, 113] The lateral collateral ligament extends from the lateral (ulnar) styloid process distally to the fourth and third metacarpal bones.[100, 113] The lateral digital extensor tendon, surrounded by its synovial sheath, passes through a long and superficial collateral ligament and a short and deep lateral collateral ligament.[100, 113] The palmarolateral pouch of the antebrachial carpal joint is interposed between the long tendon of the ulnaris lateralis and the ulnar styloid process. The medial collateral ligament originates from the medial styloid process of the radius and inserts distally on the third and fourth metacarpal bones.[100, 113] The medial collateral ligament is stronger and wider distally than the lateral collateral ligament. Numerous short ligaments connect two or more adjacent carpal bones.[113] The accessory carpal bone is connected by three ligaments to the adjacent bones.[100, 113] The proximal ligament (accessorioulnar ligament) connects the lateral aspect of the accessory carpal bone to the distal lateral aspect of the radius. The middle (accessoriocarpoulnar) ligament connects the lateral aspect of the accessory carpal bone to the lateral aspect of the ulnar carpal bone. The distal ligament originates from the lateral aspect of the accessory carpal bone and inserts on the lateral aspect of the fourth carpal bone (accessoriooquartal ligament) and on the proximal end of the fourth metacarpal bone (accessoriometacarpal ligament). The joint capsule of the radiocarpal joint is the most voluminous, whereas the carpometacarpal joint is the most limited and closely attached to the bones.

Fetlock. Two layers of collateral ligaments of the metacarpo- or metatarsophalangeal joints exist.[100, 113] The long collateral ligament extends straight from the distal lateral or medial metacarpus or metatarsus to the proximal medial or lateral aspect of P1. The long (superficial) collateral ligament arises from the medial and lateral eminences of the distal metacarpus or metatarsus and inserts just distal to the center of the articular surface of P1.[100, 113] The short (deep) collateral ligament has an oblique orientation.[113] The short collateral ligament arises from the epicondylar fossa between the distal eminences and articular margin of the third metacarpal or metatarsal bones and extends in a distopalmar or distoplantar direction to insert on the abaxial surface of the proximal sesamoid bone and the palmar or plantar surface of P1.[100, 113] A dorsal compartment of the metacarpo- or metatarsophalangeal joint with a dorsal synovial reflection or plica and a medial and lateral compartment adjacent to the medial or lateral suspensory ligament branches and the distal medial or lateral metacarpus or metatarsus is present. A subtendinous bursa of the long digital extensor tendon is present over the dorsal aspect of the metacarpo- or metatarsophalangeal joint in normal horses.

Pastern. The collateral ligaments of the proximal interphalangeal joint originate from the medial and lateral eminences and adjacent depressions of distal P1 and insert on the medial and lateral eminences of proximal P2.[100, 113] Small medial, lateral, and dorsal compartments of the proximal interphalangeal joint are present. The collateral ligaments of the distal interphalangeal joint originate from the depressions on the medial and lateral aspects of the distal phalanx and insert on the abaxial depressions on the extensor process of P3 and on the dorsal aspects of the collateral cartilages.[100, 113] Small dorsal and palmar or plantar compartments are present in the distal interphalangeal joints.

Hip. The coxofemoral joint is formed by the articulation of the femoral head with the acetabulum and has a roomy joint capsule. Because it is a ball-and-socket joint, the femoral head is attached to the acetabulum by the round ligament of the femur. An accessory ligament of the femur, a strong band, passes through the acetabular notch from the symphysial tendon of the abdominal muscles to the head of the femur.[100, 113]

Stifle. The cruciate ligaments and meniscal ligaments are nonarticular and are separated from the articular spaces by the synovial membranes and surrounding connective tissue.[101] The menisci each have a proximal concave surface adapted to the femoral condyle and a distal surface that fits the tibial condyle. The menisci are attached to the tibia cranial and caudal to the tibial spine and to the caudal part of the intercondyloid fossa of the femur (lateral meniscus only) by the meniscal ligaments.

The medial collateral ligament originates from the proximal medial epicondyle of the femur and inserts on the margin of the medial condyle of the tibia.[100, 113] The lateral collateral ligament originates from a depression on the lateral epicondyle of the femur and inserts on the head of the fibula, covering the tendon of origin of the popliteus muscle.[100, 113] The cranial cruciate ligament originates from the lateral wall of the intercondyloid fossa and inserts on the central fossa on the tibial spine.[101, 113] The caudal cruciate ligament originates on the cranial part of the intercondyloid fossa of the femur and inserts on an eminence on the popliteal notch of the tibia.[101, 113]

The patellar ligaments originate on the patella and insert on the proximal tibia.[113] The lateral patellar ligament runs from the lateral part of the cranial surface of the patella to the craniolateral aspect of the tibial tuberosity. A strong tendon from the biceps femoris muscle and an aponeurotic insertion of the fascia lata join the lateral patellar ligament.[100] The middle patellar ligament originates from the cranial part of the apex of the patella and inserts on the distal part of a groove on the tuberosity of the tibia. The medial patellar ligament attaches proximally to the parapatellar fibrocartilage and inserts distally on the medial side of the groove on the tibial tuberosity. The proximal portion of the medial patellar ligament is the insertion of portions of the vastus medialis muscle, and its cranial margin is confluent with the common aponeurosis of the sartorius and gracilis muscles.[100] The lateral femoropatellar ligament runs from the lateral epicondyle of the femur just proximal to the lateral collateral ligament to the lateral border of the patella.[100, 113] The medial femoropatellar ligament arises proximal to the medial epicondyle and inserts on the parapatellar fibrocartilage.[100, 113]

Hock. The collateral ligaments here, as in the carpus, are multiple. The long medial collateral ligament originates on the caudomedial surface of the medial malleolus of the tibia and extends distally to its insertion on the distal tuberosity of the tibial tarsal bone, the medial surface of the small tarsal bones, and the proximal portion of the second and third metatarsal bones.[100, 113] The short collateral ligaments, of which three are located on the medial aspect of the tarsus, extend from their origin on the craniomedial aspect of the medial malleolus of the tibia plantarodistally under the long collateral ligament to their respective insertions.[100, 113] The flat superficial short medial collateral ligament inserts on the proximal and distal tuberosity of the tibial tarsal bone and the intervening ridge, with its plantarodistal attachment lying immediately adjacent to the attachment of the long collateral ligament. The insertion of the round middle short medial collateral ligament is the distomedial surface of the sustentaculum tali and the plantaromedial surface of the central tarsal bone. The insertion of the flat short deep medial collateral ligament is the tibial tarsal bone.

The long lateral collateral ligament originates from the lateral malleolus of the tibia, plantar to the lateral digital extensor tendon groove. At its plantar margin distally, its fibers blend with those of the long plantar ligament. The long collateral ligament inserts on the distolateral calcaneus, fourth tarsal bone, fourth metatarsal bone, and third metatarsal bone. The superficial short lateral collateral ligament originates with the short medial and deep lateral collateral ligaments from the lateral malleolus of the tibia and inserts on the calcaneus and talus just distal to the coracoid process. The middle short lateral collateral ligament inserts on the talus dorsal to the superficial ligament, whereas the deep short lateral collateral ligament inserts further dorsally on the talus, close to the lateral articular margins.[100, 113]

Three major compartments of the tarsocrural joint are present: dorsomedial, plantaromedial, and plantarolateral. The dorsomedial aspect of the tarsocrural joint capsule is the largest and is situated close to the underlying trochlear ridges. Only a small amount of synovial fluid is present within this joint in the normal horse. The proximal intertarsal joint lies between the talus and the calcaneus. The distal intertarsal joint is located between the central tarsal bone and the bones on either side, and the distal row of tarsal bones. The tarsometatarsal joint lies between the distal row of tarsal bones and the metatarsus.

Scanning Technique

Flexor Tendons and Ligaments

The initial scan of the flexor tendons and ligaments should be performed with a 7.5-MHz transducer containing a built-in fluid offset or using a hand-held standoff pad with a displayed depth of 4 to 6 cm.[12, 15, 25, 47–50, 117, 118] A 10.0-MHz transducer is ideal for imaging the more superficial tendons and ligaments as well as some of the smaller tendons and ligaments such as the extensor tendons and collateral ligaments. A displayed depth of 2 to 4 cm is all that is needed for most of these smaller tendons and ligaments. A 7.5-MHz transducer without a standoff pad can be used to image the deeper tendons and ligaments. If marked swelling of the limb is present, a standard 7.5-MHz transducer without a standoff pad and additional displayed depth may be needed to image the deeper tendons and ligaments. The smallest depth of field that can display all the flexor tendons and ligaments should be used for optimal image quality. A low frame rate, which gives a higher line density and superior resolution, should be used for scanning tendons and ligaments. In the sagittal scan plane, high-edge enhancement is preferable to help delineate the edges of the tendons and ligaments and their fiber alignment. The ultrasound examination should be performed with the horse weight bearing and standing squarely to distribute weight equally between both forelimbs or hindlimbs. The tendons and ligaments change in size, shape, and echogenicity when not loaded by full weight bearing.

From the palmar or plantar aspect of the limb, the transverse scan plane should display the medial side of the limb on the left-hand side of the screen and the lateral side of the limb on the right-hand side of the screen. The sagittal scan plane (proximal to distal scan plane) should display distal to the left-hand side of the screen and proximal to the right-hand side of the screen. The dorsal scan plane (proximal to distal scan plane from the right or left side of the limb) should display distal to

the left-hand side of the screen and proximal to the right-hand side of the screen.

The palmar or plantar surface of leg should be scanned from the point of the accessory carpal bone (ACB) or point of the hock (POH), respectively, to the ergot, with the transducer perpendicular to the long axis of the tendons and ligaments for the transverse or short-axis scan and parallel to their long axis for the sagittal or long-axis scan. For optimal image quality, the ultrasound beam must be angled so that it is perpendicular to the short or long axis of the tendon or ligament fibers being examined. At least two short-axis (transverse) and long-axis (sagittal) scans should be performed to critically examine each tendon or ligament in the limb, because the transducer orientation is slightly different for examination of the inferior check ligament and the suspensory ligament than for examination of the superficial and deep digital flexor tendons.

If the affected tendon or ligament is large or if the lesion or swelling bulges laterally or medially, scanning the tendon or ligament from the lateral or medial side is often necessary for accurate characterization of the full extent of the injury. The lateral and medial branches of the suspensory ligament must also be scanned from the lateral and medial side of the limb from the suspensory bifurcation to the insertion of the branch on the respective proximal sesamoid bone. The hind suspensory ligament is often difficult to completely image from the plantar approach with linear transducers because of limited contact between the linear transducer and the skin over the plantar aspect of the limb. A plantaromedial approach is often superior to the plantar approach because the skin surface in this area is flat and the transducer is closer to the suspensory ligament (Fig. 3-5).[56]

The surrounding bony and soft tissue structures should be critically evaluated sonographically while scanning the tendons and ligaments. The plantar aspect of the third metacarpal bone is more perpendicular to the ultrasound beam using the plantaromedial approach, making bony lesions in this area easier to detect.[56]

If the lesion in the tendon extends proximal to the carpus or hock or distal to the fetlock, these areas should also be thoroughly examined. Injuries to the superficial digital flexor tendon can extend distally to its insertions on distal P1 and proximal P2 and proximally to either the musculotendinous junction in the foreleg or to the plantar aspect of the hock or into the crus in the hind leg. Deep digital flexor tendon injuries often extend distally into the pastern, but less frequently extend proximally into the carpal canal or tarsal sheath. Injuries to the origin of the inferior check ligament or to the extensor branches of the suspensory ligament are rare but do occur. Therefore, extending the examination area proximally or distally is important if normal tendinous or ligamentous structures are still not detected.

Two methods are used to thoroughly examine the entire flexor tendons and ligaments: evaluating the tendon or ligament in its entirety from a reference point on the limb or dividing the tendons and ligaments into zones.[12, 15, 25, 47, 119] The reference point is usually the point of the accessory carpal bone, point of the hock, or point of the ergot; and the tendon or ligament is evaluated in

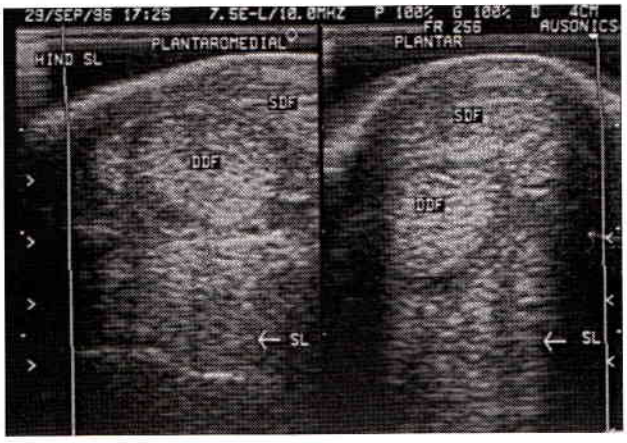

Figure 3–5

Sonograms of the normal proximal metatarsal region in the left hind leg of a 12-year-old Thoroughbred gelding. Notice the shadow through the origin of the suspensory ligament (SL) in zone 1B from the medial wall of the metatarsal artery in the plantar view *(right image)*. In the plantaromedial view *(left image)*, this shadow does not obscure visualization of the entire SL origin, although part of the superficial digital flexor tendon (SDF) is not visible. Notice also that at this level the deep digital flexor tendon (DDF) is located more medially in the limb. The echogenic tissue surrounding the DDF is part of the tarsal sheath, best visualized in the plantaromedial view. These transverse sonograms were obtained with a wide-bandwidth 7.5-MHz linear-array transducer operating at 10.0 MHz using a hand-held standoff pad at a displayed depth of 4 cm. The focal zones are placed in the far field at the depth of the SL. The right side of these transverse images is lateral and the left side is medial.

centimeters distal to this reference point.[25, 47, 119] With the zone method, the metacarpal region is divided into seven zones, four cm in length, beginning from the base of the accessory carpal bone and extending down to the ergot.[12, 15, 25, 47] The zones are 1A, 1B, 2A, 2B, 3A, 3B, and 3C. The metatarsal region has nine zones, also 4 cm in length, beginning from the base of the hock and extending distally to the ergot. These zones are 1A, 1B, 2A, 2B, 3A, 3B, 4A, 4B, and 4C.[12, 15, 25, 47]

The length of the injured or abnormal tendon or ligament should be measured in centimeters from the chosen reference point or the number of affected zones should be determined.[12, 15, 25, 47, 119] The length of the lesion should be measured from the proximal junction between normal and abnormal tendon or ligament to the beginning of normal-appearing tendon or ligament at the distalmost extent of the lesion.[25, 47, 119] The location of the largest lesion or other abnormal area in the tendon or ligament should be identified in centimeters from the reference point or by the zone in which it is located. The cross-sectional area of the lesion and the abnormal tendon or ligament at the maximal injury zone should be measured (Fig. 3-6). The percentage of tendon or ligament injured can then be calculated.

Tendon or ligament cross-sectional areas, lesion cross-sectional areas, tendon or ligament echogenicity, and fiber alignment should be graded in each of the zones throughout the length of the tendon or ligament to obtain an evaluation of the total tendon or ligament injury. If multiple lesions are identified, each lesion and tendon or ligament cross-sectional area at the worst injury point

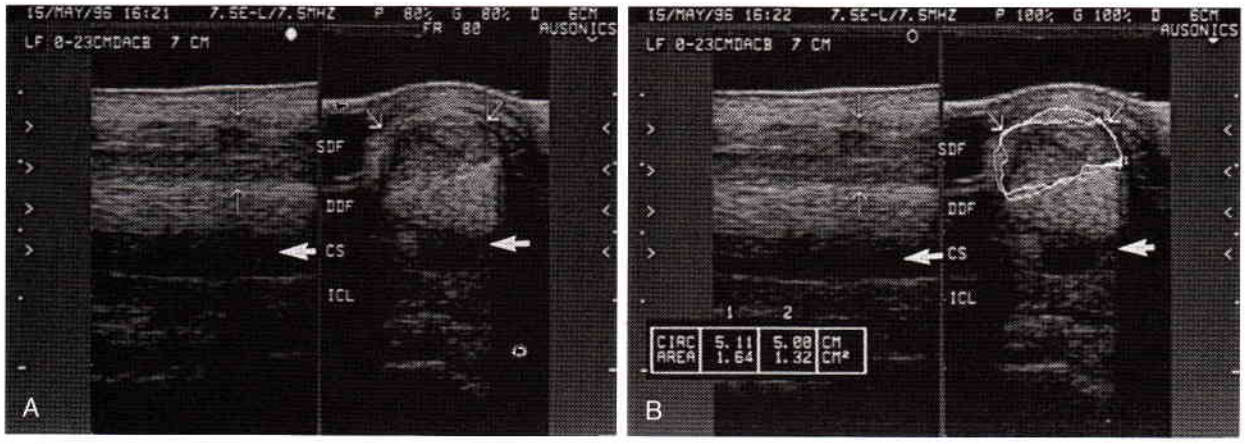

Figure 3–6

Sonograms of a new area of fiber tearing in the left fore superficial digital flexor tendon (SDF), obtained from a 22-year-old Quarter horse cross gelding. This large area of fiber tearing was imaged from 0 to 23 cm distal to the point of the accessory carpal bone and this image was obtained at 7 cm. These sonograms were obtained with a wide-bandwidth 7.5-MHz linear-array transducer operating at 7.5 MHz using a hand-held standoff pad at a displayed depth of 6 cm. The focal zones are placed in the near field of the images. The right side of the transverse image is lateral and the left side is medial. The right side of the sagittal image is proximal and the left is distal. DDF, deep digital flexor tendon; CS, carpal sheath; ICL, inferior check ligament.

A, Notice the large hypoechoic to anechoic core lesion *(arrows)* visualized in the transverse view *(right image)* involving 80% of the tendon's cross-sectional area at this level. Loss of fibers is complete within the lesion imaged in the sagittal view of the SDF *(left image)*. Notice also the anechoic fluid imaged within the carpal sheath *(wide arrows)*, which is normal for the proximal metacarpal region.

B, The cross-sectional area of the SDF at this level was 1.64 cm^2 (area 1) and the cross-sectional area of the lesion was 1.32 cm^2 (area 2), yielding an injury involving 80% of the tendon's cross-sectional area at this level.

should be measured. Measuring the lesion and the tendon or ligament in centimeters from a reference point and using cross-sectional area measurements rather than distance measurements are the most accurate techniques for the evaluation of tendon and ligament healing. The same place in the injured tendon or ligament can be precisely remeasured on follow-up examination, rather than reevaluating an area within each 4 cm zone.

Pastern. Three general regions are described in the pastern: proximal, mid, and distal (see Fig. 3-4). The tendons and ligaments in the pastern region are more difficult to examine sonographically because the tendons and ligaments are relatively small and are located in different scan planes, and because the contact area for successful imaging of these structures is relatively small. The ultrasound examination is often facilitated by extending the fetlock joint, thus maximizing the contact surface for placement of the ultrasound transducer. The bulbs of the heels may also present a problem in some horses, limiting the scanning window of the mid to distal pastern. The longer handle of some sector scanner transducers may also limit scanning in this area. This limitation can be overcome by standing the horse on a block. The tendons and ligaments in the pastern should be scanned with a 7.5-MHz or 10.0-MHz transducer containing a built-in fluid offset or used with a hand-held standoff pad at a displayed depth of 4 to 6 cm (usually 4 cm). A wide-bandwidth 6.0-MHz microconvex linear-array transducer is also very useful in scanning this region because it fits well into the space on the palmar or plantar aspect of the pastern and can be used at higher (up to 10.0-MHz) frequencies.

The pastern has been divided into four sonographic zones that correspond to proximal P1 (P1A), mid P1 (P1B), distal P1 (P1C), and proximal P2 (P2A).[59] A fifth zone over mid to distal P2 (P2B) has also been described.[66] Each tendon and ligament must be scanned individually from its origin to its insertion in both its long and short axes.

Superficial Digital Flexor Tendon. The superficial digital flexor tendon forms a thin ring around the deep digital flexor tendon at the ergot and in the proximal-most portion of the pastern and then bifurcates into medial and lateral branches. The branches of the superficial digital flexor tendon are easiest to follow in transverse section initially. At the bifurcation the branch has a teardrop appearance in short-axis cross-section and then enlarges and becomes more triangular at its insertion onto distal P1 and proximal P2. The insertions of the branches of the superficial digital flexor tendon are along the lateral- and medial-most aspects of the pastern, and the branches and their insertions cannot usually be imaged from the palmar or plantar scan plane. The transducer must be moved to the medial and lateral aspects of the pastern and centered over the superficial digital flexor tendon branch to obtain the best image of these structures.

Deep Digital Flexor Tendon. The deep digital flexor tendon and straight distal sesamoidean ligament can both be scanned completely from the palmar or plantar aspect of the limb in the pastern. The deep digital flexor tendon can be imaged from the ergot into the foot along the midline of the palmar or plantar aspect of the pastern. The deep digital flexor tendon lies palmar or plantar to the straight distal sesamoidean ligament and dorsal to the superficial digital flexor tendon, where it forms the ring in the proximal pastern. The fibers of the deep digital flexor tendon run at a slightly oblique angle. Therefore, optimal images of the deep digital flexor tendon require obliquing the transducer slightly dorsodistally. The portion of the deep digital flexor tendon that extends down

into the foot at the level of the navicular bone and navicular bursa is best visualized with a sector scanner or microconvex linear-array transducer, because the small footprint of these transducers enables the transducer to be positioned between the bulbs of the heel and angled distally into the foot following the deep digital flexor tendon.

Middle (Oblique) Distal Sesamoidean Ligament. The middle (oblique) distal sesamoidean ligament can be scanned from its origin at the base of the medial and lateral sesamoid bones to its insertion on the palmar or plantar aspect of mid to distal P1. The origin of the middle distal sesamoidean ligament cannot be identified from the palmar or plantar aspect of the limb. Rather, the origin of the medial or lateral branch of the oblique distal sesamoidean ligament is best found by placing the ultrasound transducer over the medial or lateral proximal sesamoid bone and scanning distally over the bone to its base. Immediately distal to the base of the proximal sesamoid bone is the origin of the middle distal sesamoidean ligament, best located initially in its transverse section as a large oval to round structure. This ligament is the most difficult to follow to its insertion because the ligament extends diagonally from the lateral or medial aspect of the proximal pastern to the midline in the mid-pastern region. Following the medial or lateral branch from its origin to its juncture with the opposing branch requires that the transducer be angled at approximately 45 degrees across the palmar or plantar aspect of the proximal pastern from the base of the proximal sesamoid bone to the midline of the first phalanx. A small, bony irregularity is commonly imaged at the insertion of the middle distal sesamoidean ligament on P1.

Straight Distal Sesamoidean Ligament. The straight distal sesamoidean ligament can be imaged from its origin or near its origin on the base of the proximal sesamoid bones to its insertion on the proximal palmar or plantar aspect of the second phalanx. The origin of the straight distal sesamoidean ligament is found by angling the transducer in a proximal and dorsal direction from the proximal-most aspect of the pastern just underneath the ergot to image the ligament and the base of the proximal sesamoid bones.

The limb may need to be held up off the ground with the carpus or hock flexed and the fetlock extended to examine the tendons and ligaments dynamically. Adhesions between the flexor tendons, ligaments, tendon sheaths, and surrounding soft tissues should be examined using repeated flexion and extension of the fetlock joint or other joints as indicated. If necessary, compare the tendon or ligament to the same structure on the opposite side of the same limb or in the opposite forelimb or hindlimb. Although the carpal/tarsal sheath or digital sheath are in specific areas of the limb, the entire sheath must be evaluated from proximal to distal, including entire scans of all tendons or ligaments that pass through the area of the sheath.

Superior Check Ligament. The normal superior check ligament can be successfully imaged from the medial side of the distal radius using a 6.0- or 7.5-MHz transducer and a displayed depth of 4 to 6 cm. A built-in fluid offset or hand-held standoff pad is usually not needed because of the ligament's deeper location. The tendon of the superficial digital flexor tendon is located and then its attachment to the distal radius via the superior check ligament can be identified. The attachment of the superior check ligament is easiest to find first in the transverse image, deep and slightly lateral to the superficial digital flexor tendon. The superior check ligament lies deep to the flexor carpi ulnaris muscle along the caudomedial aspect of the limb. If marked distention of the carpal sheath is present, a deeper displayed depth may be necessary to adequately image the superior check ligament.

Annular Ligament. Ultrasonographic examination of the annular ligaments should be performed with a high-frequency transducer, ideally a 10.0 MHz. A 7.5-MHz transducer suffices, although distinction between the annular ligament and the digital sheath, if it can be made, is more difficult. A hand-held standoff pad or built-in fluid offset should be used because these structures are within 2 mm of the skin surface in the normal horse and within 5 to 10 mm from the skin surface in most horses with annular ligament constriction or desmitis. The annular ligament should be scanned transversely from the lateral to medial side of the fetlock or pastern from its origin to its insertion, and it should be scanned in the sagittal plane. A displayed depth of only 2 to 4 cm is needed to image the annular ligament, but a deeper depth (4 to 6 cm) may be chosen, either to image the annular ligament in conjunction with the flexor tendons and ligaments or for use in horses with annular ligament desmitis or severe distention of the digital sheath.

Bicipital Tendon. The bicipital tendon should be scanned from its origin on the supraglenoid tubercle to its musculotendinous junction with a concurrent thorough evaluation of the bicipital bursa. The bicipital tendon is so large that accurately including the entire tendon in one transverse image is difficult to impossible with most transducers. Therefore, independent evaluation of each lobe is often performed. Evaluation of the biceps brachii muscle and other muscles of the shoulder girdle should also be performed in horses with lameness referable to the shoulder region or with swelling in the shoulder region. A 6.0- or 7.5-MHz transducer with or without a built-in fluid offset or hand-held standoff pad should be used. The displayed depth should be 6 cm in most adult horses, less in foals and young horses and more if extensive swelling is present in the shoulder region. The depth should be increased to evaluate the surrounding muscles of the shoulder girdle. The transverse image is easiest to obtain and should be used for orientation and initial identification of the abnormalities, followed by a sagittal scan of the region. The transducer is held transversely in the frontal plane with the lateral aspect of the shoulder displayed on the right-hand side of the image. A 5.0-MHz transducer may be needed for large horses or horses with extensive swelling in the shoulder region.

Extensor Tendons. The extensor tendons in the foreleg should all be imaged with a 7.5- or 10.0-MHz transducer containing a built-in fluid offset or used with a hand-held standoff pad at a displayed depth of 2 to 4 cm, because they are small and located immediately underneath the skin. If extensive soft tissue swelling or severe

tenosynovitis is present, the displayed depth may need to be increased to image the entire tendon within its sheath. Each of the extensor tendons (extensor carpi radialis, common digital extensor, extensor carpi obliquus, lateral digital extensor, and ulnaris lateralis) should be scanned from origin to insertion.

Gastrocnemius Tendon. The gastrocnemius tendon should be scanned with a 7.5-MHz transducer containing a built-in fluid offset or used with a hand-held standoff pad at a displayed depth of 4 to 6 cm. In most horses, a 10.0-MHz transducer may also be used to evaluate this area. The gastrocnemius tendon is easiest to identify immediately proximal to its insertion on the tuber calcis in the transverse or sagittal plane, and it can then be scanned proximally to its origin.

Plantar Ligament. The plantar ligament should be examined sonographically using a 7.5- or 10.0-MHz transducer containing a built-in fluid offset or used with a hand-held standoff pad at a displayed depth of 4 to 6 cm. If severe swelling of the plantar aspect of the hock is present, a built-in fluid offset or standoff pad is not necessary.

Peroneus Tertius Tendon, Long Digital Extensor Tendon, and Tibialis Cranialis and Cunean Tendon. The origin and insertion of the peroneus tertius tendon and the long digital extensor tendon and the insertion of the tibialis cranialis and the cunean tendon should be examined with a 7.5-MHz or 10.0-MHz transducer containing a built-in fluid offset or used with a hand-held standoff pad, because these structures are very close to the skin surface. Evaluation of the body of the peroneus tertius tendon in the mid tibia and tibialis cranialis muscle can be done with a 7.5-MHz transducer in most horses, but if swelling is severe in the mid-tibial region, a 5.0-MHz transducer may be indicated. The combined origin of the peroneus tertius and long digital extensor tendons is easiest to identify in the transverse plane, cranial to the lateral collateral ligament and caudal to the lateral patellar ligament. Initially, the peroneus tertius tendon is easiest to scan distally in the transverse plane; a sagittal scan follows. Similarly, identifying the tibialis cranialis and cunean tendon is also easiest initially in the transverse plane, using the adjacent structures for orientation.

The Back. The nuchal ligament is imaged with a 7.5-MHz transducer containing a built-in fluid offset or used with a hand-held standoff pad, unless significant swelling of the tissues is present in this location or the horse has a large crest of the neck. In these cases, a 5.0-MHz transducer may be needed. The supraspinous ligament, which extends from the withers to the sacrum, should be scanned with a 7.5- or 10.0-MHz transducer containing a built-in fluid offset or used with a hand-held standoff pad, because this ligament is immediately underneath the skin of the dorsal midline. A wide-bandwidth 6.0-MHz microconvex linear-array transducer may also be useful in scanning this region. The interspinous ligaments, cartilaginous caps of the dorsal spinous processes of the cranial thoracic vertebrae, and dorsal sacroiliac ligament can be imaged with a 7.5- or 10.0-MHz transducer containing a built-in fluid offset or used with a hand-held standoff pad or a wide-bandwidth 6.0-MHz microconvex linear-array transducer. The nuchal, supraspinous, interspinous, and dorsal sacroiliac ligaments should be imaged in transverse section across the midline of the dorsum and in sagittal section. The dorsal sacroiliac ligament should also be imaged in its short- and long-axis sections beginning at the tuber sacrale and extending across towards the midline on the sacrum.

Tendon Sheaths and Bursae

Flexor Tendon Sheaths. The carpal sheath, tarsal sheath, and digital sheaths should be evaluated sonographically with their respective tendons. The 7.5- or 10.0-MHz transducer containing a built-in fluid offset or used with a hand-held standoff pad and a displayed depth of 4 to 6 cm should be ideal for evaluating the flexor tendon sheaths in most horses, even those with marked distention of the digital sheath. A 6.0-MHz microconvex linear-array transducer may be helpful in examining the digital sheath in the pastern region in horses with marked digital sheath distention distally. In horses with marked swelling of the distal radius or crus and/or proximal metacarpus or metatarsus, a standoff pad is not needed. In some instances, a lower-frequency transducer (6.0- or 5.0-MHz) and additional displayed depth (6 to 10 cm or more) may be necessary to adequately image horses with marked carpal or tarsal sheath distention and associated soft tissue swelling.

Extensor Tendon Sheaths. The extensor tendon sheaths should be evaluated with their respective tendons. A high-frequency (7.5- or 10.0-MHz) transducer containing a built-in fluid offset or used with a hand-held standoff pad is usually necessary because of the sheaths' small size and close proximity to the skin surface. A displayed depth of 2 to 4 cm is usually all that is necessary to image these tendons and their sheaths. If marked swelling of the surrounding soft tissues is present or if a large effusion is within the extensor tendon sheath, a standoff pad or built-in fluid offset is not needed for the 7.5-MHz transducer and the displayed depth should be increased. In horses with severe swelling, a lower-frequency transducer (6.0 or 5.0 MHz) may be needed.

Bicipital Bursa. The bicipital bursa is evaluated between the bicipital tendon and the greater, lesser, and intermediate tubercles of the humerus using a 10.0-, 7.5-, or 6.0-MHz transducer. A standoff pad is usually not necessary for this evaluation because the bursa is deep to the tendon. The transverse image is easiest to obtain and should be used for orientation and initial identification of the abnormalities and followed by a sagittal scan of the region. If distention of the bicipital bursa is detected, the bursa distends around the sides of the bicipital tendon, making an evaluation of this area critical. The transducer is held transversely in the frontal plane with the lateral aspect of the shoulder displayed on the right-hand side of the image. A 5.0-MHz transducer may be needed for large horses or horses with extensive swelling in the shoulder region.

Navicular Bursa. Angling the transducer distally into the foot to evaluate the navicular bursa requires that the transducer have a curved footprint (sector scanner, annular-array, or microconvex linear-array transducer)

and a high-frequency (7.5- or 10.0-MHz) transducer. The displayed depth should be 4 to 6 cm. Standoff pads do not usually work well in this area because inadequate contact occurs between the standoff pad and the skin at the bulbs of the heel. To image the navicular bursa, the transducer must be angled distally into the foot along the palmar or plantar margin of the deep digital flexor tendon.[2] This is usually easiest to accomplish in the sagittal scan plane. The "T" ligaments or collateral sesamoidean ligaments (suspensory ligaments of the navicular bone) can also be imaged in some horses using this scanning technique.

Trochanteric Bursa. Sonographic examination of the trochanteric bursa requires a 7.5-, 6.0-, or 5.0-MHz transducer and a displayed depth of 4 to 8 cm or more, depending on the size of the horse being examined and the amount of local swelling in the area.

Calcaneal, Gastrocnemius, and Cunean Bursa. A 7.5- or 10.0-MHz transducer containing a built-in fluid offset or used with a hand-held standoff pad at a displayed depth of 4 to 6 cm (2 to 4 cm for the cunean bursa) yields excellent images of these bursae unless marked soft tissue swelling is present around these structures or severe distention occurs. If the bursitis is severe, the fluid offset or standoff pad is not necessary; and in some instances, a lower-frequency transducer may be needed (6.0- or 5.0-MHz) with a displayed depth of 6 to 10 cm.

Atlantal, Supraspinous, and Other Bursae in the Back. To image the bursae between the nuchal ligament and the atlas or axis or between the supraspinous ligament and the withers, a 5.0- or 6.0-MHz transducer may be needed with a displayed depth of 6 to 10 cm or more. The transducer frequency can usually be slightly higher (7.5-MHz) and the displayed depth slightly less (4 to 6 cm) in the poll region than in the withers, especially if local swelling is present in the region. With severe swelling in the poll or withers, displayed depths in excess of 10 cm may be needed.

Nerve

The nerve being examined is usually easiest to locate in its short axis in reference to the surrounding structures, particularly the adjacent blood vessels. The nerve should be scanned in its short axis and then, if possible, in its long axis. A very high frequency transducer should be used, ideally a 10.0-MHz transducer containing a built-in fluid offset or used with a hand-held standoff pad at a displayed depth of 2 to 4 cm. Slightly lower-frequency transducers and deeper displayed depths may be necessary for the evaluation of deeper nerves.

Muscle, Bone, and Joints

The examination should begin superficially with a high-frequency transducer (7.5-MHz) containing a built-in fluid offset or used with a hand-held standoff pad at a displayed depth of 4 to 6 cm to scan the most superficial muscle belly, bone, or joint capsule, synovium, and synovial fluid. The ultrasound examination should systematically progress to the deeper musculature, bone, or synovial compartments like the hip in the area under investigation, changing to lower frequency transducers and deeper displayed depths as needed. For optimal image quality, the selected depth setting should always be the least depth that displays the entire muscle, bone, or joint being examined.

The transverse scan-plane orientation obtained from the palmar, plantar, or ventral aspect of the head, limb, or body should be the right side on the left-hand side of the screen and the left side on the right-hand side of the screen. The transverse scan-plane orientation obtained from the dorsal aspect of the head, limb, or body should be the left side on the left-hand side of the screen and the right side on the right-hand side of the screen. The transverse scan-plane orientation obtained from the right side of the head, limb, or body should be dorsal to the left-hand side of the screen and palmar, plantar, or ventral to the right-hand side of the screen. The transverse scan-plane orientation obtained from the left side of the head, limb, or body should be palmar, plantar, or ventral to the left-hand side of the screen and dorsal to the right-hand side of the screen. The sagittal limb (proximal to distal scan plane from the palmar, plantar, dorsal, or ventral side of the limb) or sagittal body or head (cranial to caudal scan plane from the ventral or dorsal aspect of the head or body) scan-plane orientation should be proximal or cranial to the left-hand side of the screen and distal or caudal to the right-hand side of the screen. The dorsal limb (proximal to distal scan plane from the right or left side of the limb) or dorsal head or body (cranial to caudal scan plane from the right or left side of the head or body) scan-plane orientation should be proximal or cranial to the left-hand side of the screen and distal to the right-hand side of the screen. All structures under investigation should be examined in a short-axis (transverse) and long-axis (sagittal) plane. If necessary, scan the opposite muscle, bone, or joint to compare.

Draining Tracts

The examination of draining tracts should begin with the most superficial structures using high-frequency transducers containing built-in fluid offsets or used with hand-held standoff pads at displayed depths of 4 to 6 cm. The examination should progressively move deeper using lower frequency transducers and deeper displayed depths until the entire abnormality has been scanned to the border between normal/abnormal on all sides of the swelling or tract (see Chapter 11). If multiple tracts are present, all should be followed to their source (end). Draining tracts should end at a foreign body, fracture fragment, sequestrum, or bone (osteomyelitis). Always look for more than one cause of the drainage.

Joints

Joints are usually easiest to evaluate initially in a long-axis scan plane, using the proximal and distal extremities of the bones as landmarks to locate the joint capsule, syno-

vial compartments or normal joint spaces, the collateral ligaments, and other articular or periarticular structures. The joint capsule (if detectable), synovial compartments, articular cartilage, collateral ligaments, and other articular or periarticular structures should be examined.

Shoulder. The lateral aspect of the shoulder joint and scapula can be scanned with a 7.5-MHz transducer containing a built-in fluid offset or used with a hand-held standoff pad at a displayed depth of 4 to 6 cm. If marked swelling is present, a 7.5-MHz transducer without a standoff pad is needed. A microconvex 6.0-MHz linear-array transducer may be useful in examining this area in such cases. Rarely are a lower-frequency transducer (5.0-MHz) and increased displayed depth (6 to 10 cm) needed.

Elbow. The collateral ligaments of the elbow joint are easily scanned in their long axis, first by using a 7.5- or 10.0-MHz transducer containing a built-in fluid offset or used with a hand-held standoff pad. The collateral ligaments can then be scanned in their short axis. A displayed depth of 4 to 6 cm is ideal for most horses. If swelling in the elbow region is severe, the 7.5-MHz transducer without the standoff pad or a lower-frequency transducer (6.0- or 5.0-MHz) and a deeper displayed depth (6 to 10 cm) may be needed.

Carpus. The collateral ligaments of the carpus are numerous, and not all can be successfully imaged sonographically. However, those that can be assessed can be examined with a 7.5- or 10.0-MHz transducer containing a built-in fluid offset or used with a hand-held standoff pad at a displayed depth of 4 to 6 cm. With flexion of the carpus, the radiocarpal and intercarpal joints open up and more of the joint is accessible for sonographic imaging. The radiocarpal joint has a lateral outpouching between the ulnaris lateralis and the distal radius which is fluid-filled with radiocarpal joint distention. A 7.5-MHz transducer without a standoff or a 6.0-MHz microconvex-linear-array transducer at a displayed depth of 6 to 10 cm can be used in horses with extensive swelling of the carpus.

Fetlock and Pastern. The metacarpophalangeal and metatarsophalangeal joints and the proximal interphalangeal joint should be evaluated with a 7.5- or 10.0-MHz transducer containing a built-in fluid offset or used with a hand-held standoff pad. The medial and lateral collateral ligaments of the fetlock and pastern joints should be evaluated with the highest frequency transducer possible at a displayed depth of 2 to 4 cm, because they are normally very small. The collateral ligaments are easiest to examine by initially locating them in the sagittal scan plane and then evaluating them in the transverse plane. The dorsal aspect of the fetlock and pastern joints should also be examined.

The joint space and joint capsule are often easiest to locate in the sagittal scan plane, because the bony anatomy can be used for orientation before performing the transverse scan. The dorsal compartment of the metacarpo- or metatarsophalangeal joint should be evaluated in both the sagittal and transverse scan planes, evaluating the dorsal plica and the articular surfaces of the distal metacarpus and metatarsus and proximal P1. A displayed depth of 4 to 6 cm is often needed for examining the dorsal aspect of the fetlock joint.

Coffin Joint. Angling the transducer distally into the foot to evaluate the navicular bursa and the coffin joint requires a transducer with a curved footprint such as a sector scanner or annular-array or microconvex linear-array transducer. A high-frequency (7.5- or 10.0-MHz) transducer should be chosen. Standoff pads do not usually work well when examining the palmar or plantar aspect of the coffin joint because contact is inadequate between the footprint or contact surface of the transducer, the standoff pad, and the bulbs of the heel. The transducer must be angled distally into the foot along the palmar or plantar margin of the deep digital flexor tendon to image the palmar or plantar aspect of the coffin joint.[2] The dorsal compartment of the coffin joint can be imaged just proximal to the coronary band on the dorsal midline in horses with a coffin joint effusion. In these horses, a 7.5- or 10.0-MHz transducer containing a built-in fluid offset or used with a hand-held standoff pad is usually effective.

Hip. Sonographic evaluation of the coxofemoral joint usually requires a 7.5-, 6.0-, or 5.0-MHz transducer and a displayed depth of 6 to 10 cm to achieve the necessary penetration for evaluation of this region. The shaft of the ilium should be followed caudally in its long axis to the hip joint. The cranial, dorsal, and caudal margins of the hip joint should be evaluated. A transrectal examination of the pelvis should also be considered to further evaluate the pelvis and acetabular area. The remainder of the pelvis should be scanned from the tuber sacrale to the tuber coxae and from the tuber coxae to the tuber ischii from the external window. The shaft of the ilium, sacroiliac joint, and pubis should be scanned from the transrectal approach. A 7.5-, 6.0-, or 5.0-MHz transrectal transducer and a displayed depth of 4 to 6 cm are usually used unless marked internal swelling is present.

Stifle. The patellar ligaments are easily imaged with a 7.5- or 10.0-MHz transducer containing a built-in fluid offset or used with a hand-held standoff pad at a displayed depth of 4 to 6 cm. The patellar ligaments should be individually palpated and a transverse and longitudinal scan obtained from their origin to their insertion. The trochlear ridges can be imaged underneath the patellar ligaments or by flexing the joint and placing the transducer directly over the medial or lateral trochlear ridges.

The medial and lateral collateral ligaments and menisci are also easily imaged from the medial and lateral aspects of the femorotibial joint with a 7.5-MHz transducer containing a built-in fluid offset or used with a hand-held standoff pad. A 10.0-MHz transducer also gives excellent resolution of these structures, particularly those on the medial side, which are closer to the transducer. A displayed depth of 2 to 4 cm provides excellent resolution of the collateral ligaments, but a depth of 4 to 6 cm is usually needed to include the menisci. If extensive swelling of the stifle or a large femorotibial joint effusion is present, a 7.5-MHz transducer without a standoff pad or a 6.0-MHz microconvex linear-array transducer may be necessary to give excellent resolution of these structures. The medial and lateral collateral ligaments are located by palpating caudal to the medial and lateral patellar ligaments, respectively, and imaging directly over the ligaments once palpated. If swelling in this area is extensive,

the collateral ligaments can be located by finding the joint space between the distal femur and proximal tibia caudal to the medial or lateral patellar ligament and scanning caudally in the sagittal plane along the articular margins of the joint until the menisci and the collateral ligaments are identified. Between the lateral collateral ligament and the lateral patellar ligament is the tendon of origin of the peroneus tertius and the long digital extensor tendon, which can also be used as points of reference. The lateral collateral ligament crosses over the origin of the popliteus muscle. A bursa is present between the tendon or origin of the popliteus muscle and the lateral collateral ligament and between the lateral collateral ligament and the margin of the lateral condyle of the tibia, which is only a potential space in normal horses.

The medial meniscus is imaged between the medial patellar ligament and the medial collateral ligament, as well as underneath the medial collateral ligament. The medial compartment of the femorotibial joint is imaged just cranial to the medial collateral ligament. The lateral meniscus is imaged between the tendon of origin of the peroneus tertius and the long digital extensor tendon. Finding the medial and lateral meniscus in horses with extensive swelling of the stifle can be difficult but is usually less difficult than locating the collateral ligaments. The same technique for locating the menisci as for locating the collateral ligaments can be used in these horses.

The cranial aspect of the stifle can be successfully imaged with a 3.5- to 7.5-MHz transducer with a depth of field of 3 to 9 cm, depending on the size of the horse.[101] The cranial intercondylar space of the femorotibial joint is well visualized by flexing the stifle. This intercondylar space is well separated from the lateral and medial compartments of the joint by their synovial reflection along their axial margins. The cranial cruciate ligament is 1 to 2 cm in diameter and can be identified with sector scanner transducers in both its sagittal and transverse sections. The sagittal view of the cranial cruciate ligament is obtained by placing the transducer medial to the middle patellar ligament, 1 to 2 cm distal to the patella, and directing the beam in a caudal, lateral, and distal direction.[101] To orient the ultrasound beam perpendicular to the ligament fibers, the transducer should be rotated 20 to 25 degrees clockwise to its long axis in the left limb and counterclockwise in the right limb.[101] The cranial insertion of the cranial cruciate ligament is then located by following the lateral femoral condyle from lateral to medial until the lateral tibial eminence and the ligament fibers are imaged, then adjusting the transducer orientation as needed. The transverse view of the cranial cruciate ligament is obtained by placing the transducer just distal to the distal aspect of the patella and directing the beam distally until the proximal tibia is imaged. The proximal tibia is then scanned in a cranial to caudal direction until the tibial tubercles are imaged with the cranial cruciate ligament in between.

The femoral insertion of the caudal cruciate ligament is also best imaged with sector-scanner transducers.[101] The caudal cruciate ligament is best imaged with the transducer placed between the lateral and middle patellar ligaments, 2 to 3 cm proximal to their insertions on the tibial tuberosity, with the beam directed in a caudomedioproximal direction in the axial plane. The medial femoral condyle should be scanned in a medial to lateral direction until the intercondylar space is encountered, with its irregular bone surface and lack of articular cartilage. The caudal cruciate ligament is then imaged superficial to the bone surface.[101]

The cranial tibial meniscal ligaments can also be imaged in their longitudinal and transverse planes with the sector transducer placed on either side of the middle patellar ligament, 2 to 4 cm distal to the distal aspect of the patella.[101] To orient the beam perpendicular to the ligament fibers, the beam should be directed caudodistally and the transducer rotated laterally or medially, depending on the meniscal ligament being examined.

The large muscle mass overlying the caudal aspect of the stifle joint is the main limitation to adequately imaging the structures in the femorotibial joint from this window.[101] Depth of field to adequately image the structures within the stifle joint ranges from 6 to 14 cm, depending on the size of the horse. In most instances, a 3.5-MHz transducer is needed, but in some small ponies and foals, a good-quality image is obtained with a 5.0- or 7.5-MHz transducer. The examination in the sagittal plane is the easiest place to start, with the transducer placed 2 to 3 cm proximal to the skin fold created on the caudal stifle region by limb flexion. The cartilaginous surfaces of both femoral condyles are homogeneous in echogenicity and thickness with the overlying joint capsule visible as an interface between the cartilage and muscle mass.[101]

The popliteal tendon is imaged overlying the caudal aspect of the lateral meniscus and in the cartilage-covered groove in the lateral caudal aspect of the proximal tibia.[101] The musculotendinous junction and body of the superficial digital flexor muscle are imaged overlying the joint capsule proximally and the popliteus muscle distally. The popliteal vessels can be imaged overlying the joint capsule in the caudal groove of the tibia, in between the caudal cruciate ligament and the meniscofemoral ligament.[101] The short tibial insertion of the lateral meniscus can be imaged by scanning the lateral condyles from lateral to medial with the transducer in the axial plane, positioned approximately 3 to 5 cm proximal to the junction between the caudal thigh muscles and the crus muscles, with the transducer placed either lateral to or over the semitendinosus muscle. Angling the probe 30 degrees to the axial plane allows for visualization of the meniscofemoral ligament, which can be followed up to its insertion axial and proximal to the medial femoral condyle. The medial meniscus and condyles can be evaluated in a similar fashion, although the attachment of the meniscus on the tibial eminence is not adequately visualized.[101] The caudal cruciate can be imaged from this location by rotating the transducer 10 to 15 degrees clockwise to the axial plane in the right leg and the same amount counterclockwise in the left leg, and by tilting the transducer proximally, orienting the beam in a cranial and distal direction. The best images are obtained with the transducer placed over the semitendinosus muscle on the skin over the caudal midline or just medial to the midline, 3 to 5 cm proximal to the palpable distal extremity of the semimembranosus muscle.[101]

Hock. The ultrasonographic examination of the hock should be performed with a 7.5- or 10.0-MHz transducer containing a built-in fluid offset or used with a hand-held standoff pad at a displayed depth of 4 to 6 cm, because the collateral ligaments and joint capsule are located just underneath the skin. If marked soft tissue swelling or synovial distention is present, a lower-frequency transducer and increased depth may be indicated as previously described for other joints. Each collateral ligament should be scanned individually, and the three joint compartments (dorsomedial, plantaromedial, and plantarolateral) evaluated.

ULTRASONOGRAPHIC FINDINGS

Normal Structures

Tendons and Ligaments

The tendons and ligaments have characteristic sonographic appearances, sizes, and shapes which are the basis for diagnosing tendon or ligament injuries. To obtain optimal images of the tendons and ligaments, the ultrasound transducer must be held perpendicular to the long axis of the tendon or ligament fibers. The normal tendons and ligaments have a homogeneous echogenic appearance except for the suspensory ligament, which is also composed of muscle tissue, connective tissue, or fat.[121-123] Evaluating tendon and ligament echogenicity is usually somewhat subjective, and is dependent on both the equipment settings and the scanning technique of the operator. Objective assessments of tendon or ligament echogenicity can be obtained using mean gray-scale analysis if constant imaging parameters are used.[78-81] Off-normal incidence artifacts are easily created (see Chapter 2) when the ultrasound beam strikes the tendon or ligament at an angle other than 90 degrees to the tendon or ligament fibers, creating an artifactual hypoechoic appearance.[122, 123] Lack of weight bearing also creates a less echogenic appearance of the flexor tendons and ligaments.

Cross-sectional area measurements should be made of

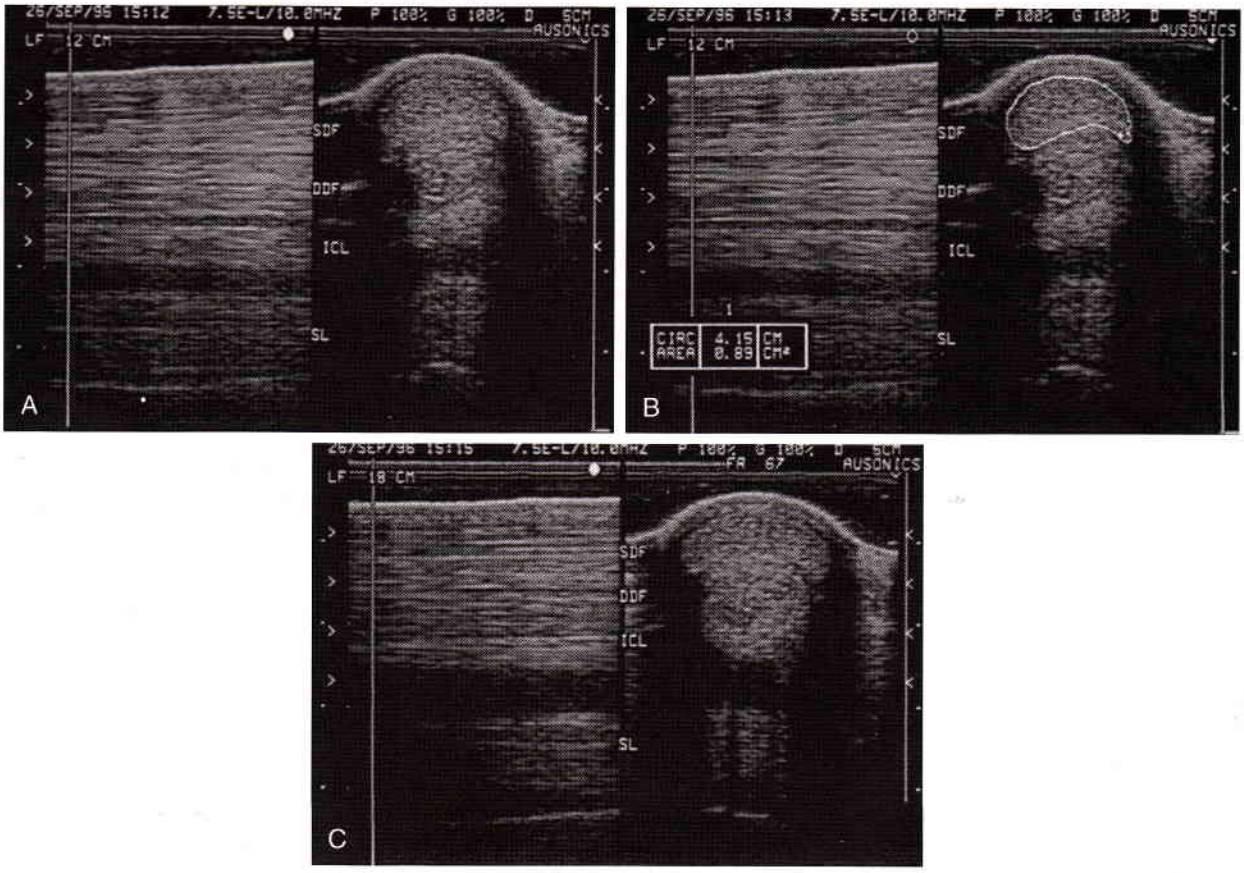

Figure 3–7

Sonograms of the normal flexor tendons and ligaments in the metacarpal region of the left foreleg of a 12-year-old Thoroughbred gelding. Notice that the superficial digital flexor tendon (SDF) and deep digital flexor tendons (DDF) are slightly less echogenic than the inferior check ligament (ICL). These sonograms were obtained with a wide-bandwidth 7.5-MHz linear-array transducer operating at 10.0 MHz using a hand-held standoff pad at a displayed depth of 5 cm. The focal zones are in the near field of the images. Notice the change in the size and shape of the tendons and ligaments as the scans progress distally. The left side of the transverse view *(right image)* is medial and the right side is lateral. The left side of the sagittal view *(left image)* is distal and the right side is proximal.

A, Sonogram of the proximal metacarpal region in zone 1B obtained 12 cm distal to the point of the accessory carpal bone.

B, Sonogram demonstrating the measurement of the cross-sectional area of the SDF in the proximal metacarpal region (0.89 cm^2) in zone 1B, obtained 12 cm distal to the point of the accessory carpal bone.

C, Sonogram of the mid-metacarpal region in zone 2B, obtained 18 cm distal to the point of the accessory carpal bone and demonstrating the flattening of the SDF in a dorsal to palmar direction and the ICL inserting onto the DDF.

the tendons and ligaments for the most accurate assessment of tendon or ligament size and to accurately monitor changes in these structures during the rehabilitation of horses with tendon or ligament injuries.[25, 33, 39, 47, 120] Width and thickness measurements should be made if tendon or ligament cross-sectional area cannot be determined. Considerable variation has been reported between the postmortem measurements of normal flexor tendons and ligaments and the sonographic measurements.[57] However, cross-sectional area measurement is a valid and accurate measurement technique.[120]

Superficial Digital Flexor Tendon—Metacarpus/Metatarsus. The normal superficial digital flexor tendon has a homogeneous and echogenic appearance and is usually slightly less echogenic than is the deep digital flexor tendon (Fig. 3-7).[7, 12, 25, 46, 78-81] However, the relative sonographic brightness of the superficial and deep digital flexor tendon are similar when gray-scale calibration procedures are used.[80] The superficial digital flexor tendon is significantly brighter proximally (7 cm distal to the accessory carpal bone) than in the middle (10, 15, and 20 cm) or distal (25 cm) tendon region. In the distal tendon region, the superficial digital flexor tendon has a similar relative brightness to that of the deep digital flexor tendon and the suspensory ligament branches.[80]

The superficial digital flexor tendon is composed of long parallel fiber bundles that appear as long white echoes in the sagittal or long-axis view and as a uniform distribution of pinpoint white echoes in the transverse or short-axis view (see Fig. 3-7). The superficial digital flexor tendon is nearly round in the proximal metacarpal region; becomes flattened in the distal metacarpal region, forming a ring around the deep digital flexor tendon in the proximal pastern region; then bifurcates into a medial and lateral branch, each of which inserts on the distal portion of the first phalanx and the proximal portion of the second phalanx.

The cross-sectional area of the superficial digital flexor tendons should be similar at the same level in the right and left forelimbs or right and left hindlimbs. In this author's experience, the cross-sectional area of the superficial digital flexor tendon in the metacarpal region should be less than 1.2 cm^2 in the forelimbs in normal Thoroughbred and Standardbred horses (see Fig. 3-7). More frequently, the superficial digital flexor tendon measures 0.8 to 1.0 cm^2 in Thoroughbreds and Standardbreds and 0.6 to 0.8 cm^2 in more fine-boned breeds such as Arabians. The mid-metacarpal region of the superficial digital flexor tendon has a smaller cross-sectional area than does the proximal (zones 1A or 1B) or distal (zones 3B and 3C) region. These measurements were obtained using built-in calibration packages contained in the ultrasound equipment.

Other investigators have reported similar tendon cross-sectional areas in racing Thoroughbreds in North America (Table 3-1).[77, 79, 120] Cross-sectional area measurements ranged from 1.01 cm^2 at 4 cm distal to the base of the accessory carpal bone (zone 1A) to 0.95 cm^2 at 12 cm (zone 2A) and 1.12 cm^2 at 24 cm distal to the base of the accessory carpal bone (zone 3B). These cross-sectional area measurement techniques were validated using ink-blot analysis.[120] The mean cross-sectional areas of the superficial digital flexor tendon for Thoroughbreds in Great Britain is reported to range from 1.35 ± 0.13 cm^2 in zone 1A, decreasing to 1.25 ± 0.18 cm^2 in zone 3A and increasing to 1.46 ± 0.15 cm^2 in zone 3C. These figures are significantly greater than those of the population of Thoroughbred racehorses in North America.[54] The mean cross-sectional areas of the superficial digital flexor tendons of Irish Draught crossbred horses did not differ significantly from that obtained in Thoroughbred racehorses in this study.[54] These values were substantiated by postmortem measurements using the same digitization technique of measuring tendon cross-sectional area. The discrepancy between these measurements and those made in Thoroughbreds racing in North America may relate to the calibration and digitization techniques used to measure the tendon cross-sectional area rather than the actual size of the horses' tendons.

Table 3-1
Mean SDFT and DDFT Cross-sectional Area in the Metacarpal Region*

Zone	Level (cm)	Cross-sectional Area (cm^2)	
		SDFT	*DDFT*
1A	4	1.01 ± 0.12	1.13 ± 0.18
2A	12	0.95 ± 0.14	1.01 ± 0.12
3B	24	1.12 ± 0.15	1.75 ± 0.29

*These data were obtained from 50 normal trained Thoroughbred racehorses in North America.

Abbreviations: SDFT, superficial digital flexor tendon; DDFT, deep digital flexor tendon.

Data from Gillis CL, Meagher DM, Cloninger A, Locatelli L: Ultrasound cross-sectional area and mean echogenicity of the superficial deep digital flexor tendon. *In* Proceedings of the 39th Annual Convention of the American Association of Equine Practitioners, 1993, pp 273-274; and Gillis C, Meagher DM, Cloninger A, et al: Ultrasonographic cross-sectional area and mean echogenicity of the superficial and deep digital flexor tendons in 50 trained Thoroughbred racehorses. Am J Vet Res 56:1265-1269, 1995.

The size and sonographic appearance of the superficial digital flexor tendon change in response to race training, with the cross-sectional area of the tendon enlarging somewhat (approximately 10%) and the echogenicity of the tendon decreasing slightly.[76, 77] The authors postulated that this decrease in tendon echogenicity seen in young horses in training may be caused by fascicle enlargement or by an increase in the number of less-mature collagen fibers per unit area within the tendon.[76] An inverse relationship between an increase in tendon cross-sectional area and a decrease in mean echogenicity was reported at each level in the tendon over time with training.[76, 77] However, the mean tendon cross-sectional area of these young Thoroughbreds in race training still did not exceed 1.2 cm^2.[76, 77]

In zone 1A, the superficial digital flexor tendon measures approximately 0.7 cm in a palmar-to-dorsal direction and 0.9 cm in a medial-to-lateral direction.[12, 25] The palmar-to-dorsal thickness of the superficial digital flexor tendon decreases as the tendon extends distally and measures 0.4 cm in zone 3B.[12, 25] The medial-to-lateral width of the superficial digital flexor tendon increases distally to 3 cm in zone 3B.[12, 25] In Anglo-Arabian-Andalusian crossbred horses, the palmar-to-dorsal thickness of the superficial digital flexor tendon ranged from 0.78 ± 0.03

cm at 2.5 cm distal to the accessory carpal bone to 0.63 ± 0.04 cm at 17.5 cm distal to the accessory carpal bone.[57] In these same crossbred horses, the medial-to-lateral width of the superficial digital flexor tendon measured from 1.66 ± 0.5 cm at 2.5 cm distal to the accessory carpal bone to 2.01 ± 0.05 cm at 17.5 cm distal to the accessory carpal bone. The palmar-to-dorsal measurements (0.53 ± 0.02) and lateral-to-medial measurements (2.39 ± 0.06 cm) obtained from Anglo-Arabian-Andalusian crossbred horses at 22.5 cm distal to the accessory carpal bone are similar to those obtained from Thoroughbred and Standardbred horses in zone 3B.[12, 57] This measurement (22.5 cm) is more likely in zone 3A than in zone 3B, if a more distal reference point on the accessory carpal bone was used, because these authors describe the bifurcation of the suspensory ligament as occurring 15 cm distal to the proximal aspect of the metacarpal bone. The suspensory bifurcation is normally found in zone 3A. A more proximal measurement results in a thicker palmar-to-dorsal measurement and a smaller medial-to-lateral measurement. Breed differences (Arabians have much smaller tendon cross-sectional areas) may also be significant. Measurements obtained more distally in the metacarpal region were not reported.

In the hindlimb, the superficial digital flexor tendon also has a homogeneous echogenic appearance with a parallel fiber pattern and is oval from its myotendinous junction to just proximal to the tuber calcis. It lies medial to the gastrocnemius tendon in the middle of the crus and then spirals caudal to the gastrocnemius tendon just proximal to the tuber calcis. At the point of the tuber calcis, the superficial digital flexor tendon fans out, becomes more crescent-shaped, and inserts on the proximal portion of the tuber calcis. The superficial digital flexor tendon narrows and flattens distal to the calcaneal tuber and becomes more semicircular in shape as it extends plantar to the plantar ligament.[93]

Deep Digital Flexor Tendon. The deep digital flexor tendon has a homogeneous echogenic appearance and usually appears more echogenic than does the superficial digital flexor tendon, but it may be isoechoic with the superficial digital flexor tendon (see Fig. 3-7).[7, 12, 25, 57] The deep digital flexor tendon has previously been described as less echogenic than the inferior check ligament. Recent work with a tissue equivalent phantom indicates that in the dorsal plane, the inferior check ligament is relatively less bright than is the deep digital flexor tendon, although this difference is not statistically significant.[80] In this same scan plane, the deep digital flexor tendon is slightly less bright than the superficial digital flexor tendon in the proximal tendon region (7 cm distal to the accessory carpal bone), but is slightly brighter than the superficial digital flexor tendon in the mid (10, 15, and 20 cm) and distal (25 and 30 cm) tendon regions. In the sagittal plane, the highest relative brightness is yielded by the suspensory ligament, followed by the inferior check ligament and deep and superficial digital flexor tendons.[80]

The deep digital flexor tendon also appears sonographically as long white echoes in the sagittal or long-axis view and a homogeneous distribution of pinpoint white echoes in the transverse or short-axis view. The deep digital flexor tendon is parallel to the superficial digital flexor tendon and is also nearly round in the proximal metacarpal region. It becomes oval in the distal metacarpal region and then has a bilobed appearance in the pastern region. In the distal metacarpal and pastern region, the deep digital flexor tendon is surrounded by the digital sheath, which often contains a small amount of fluid. Occasionally a dividing septum is imaged in the deep digital flexor tendon, a result of the three portions from the three separate muscular heads.[7]

The cross-sectional area of the deep digital flexor tendon has been reported in clinically normal Thoroughbred racehorses in North America (see Table 3-1) and ranges from 1.13 cm^2 at 4 cm distal to the base of the accessory carpal bone (zone 1 A) to 1.01 cm^2 at 12 cm and 1.75 cm^2 at 24 cm distal to the base of the accessory carpal bone (zone 3B).[79] No difference was found between the cross-sectional area measurements of the deep digital flexor tendon in either foreleg in this study. Tendon cross-sectional area measurements obtained from Thoroughbred racehorses in Great Britain were significantly larger than those reported in North America or those of this author's experience. In Great Britain, the cross-sectional area of the deep digital flexor tendon measured 1.29 cm^2 ± 0.15 cm^2 in zone 1A, 0.97 cm^2 ± 0.11 cm^2 in zone 1B, 1.83 cm^2 ± 0.22 cm^2 in zone 2A, 1.65 cm^2 ± 0.21 cm^2 in zone 3A, and 2.13 cm^2 ± 0.21 cm^2 in zone 3C.[54] Similar findings were obtained from Irish Draught crossbred horses in this study.[54] Differences in digitization and calibration techniques may account for these discrepancies, or a real size difference may exist between these tendons in the horses examined.

The deep digital flexor tendon reportedly measures 1.1 cm in a palmar-to-dorsal direction and 2.6 cm in a medial-to-lateral direction in zone 3B.[12] The palmar-to-dorsal thickness of the deep digital flexor tendon has been determined in Anglo-Arabian-Andalusian crossbred horses.[57] The dorsal-to-palmar thickness measured 1.0 ± 0.05 cm at 2.5 cm distal to the accessory carpal bone, 1.07 ± 0.05 at 17.5 cm distal to the accessory carpal bone, and 0.96 ± 0.05 cm at 22.5 cm distal to the accessory carpal bone. The medial-to-lateral width of the deep digital flexor tendon increased from 1.78 ± 0.05 at 2.5 cm distal to the accessory carpal bone to 1.89 ± 0.06 cm at 17.5 cm and to 2.10 ± 0.09 cm at 22.5 cm distal to the accessory carpal bone. Measurements obtained more distally were not reported.

In the tarsal region, the deep digital flexor tendon is oval to round and is located medial to the hock (Fig. 3-8). The deep digital flexor tendon remains somewhat medial in the proximal metatarsal region and only becomes parallel to the superficial digital flexor tendon in the mid-metatarsal region. Its insertion on the third phalanx cannot be imaged sonographically in either the forelimb or the hindlimb.

Inferior Check Ligament (Accessory Ligament of the Deep Digital Flexor Tendon). The inferior check ligament is rectangular at its origin from the carpal retinaculum and becomes crescent-shaped in the proximal metacarpal region, with the largest portion of the inferior check ligament located on the lateral aspect of the limb (see Fig. 3-7). The inferior check ligament retains this

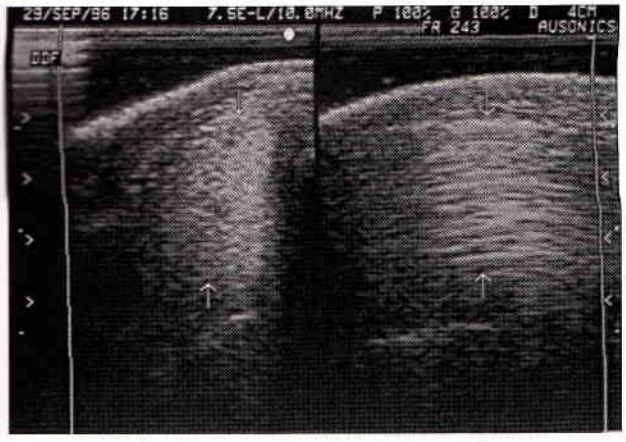

Figure 3–8

Sonograms of the normal deep digital flexor tendon (DDF) along the medial aspect of the hock in the left hindleg of a 12-year-old Thoroughbred gelding. Notice the large diameter of the DDF *(arrows)* near its origin. Due to its large size and curved structure at this location, the entire tendon cannot be imaged in the same scan plane at one time, creating a hypoechoic portion of the tendon that is artifactual. Notice the parallel fiber alignment of the DDF at this location. Although the tarsal sheath surrounds the DDF at this level, it is not usually imaged as a separate structure in normal horses. These sonograms were obtained with a 7.5-MHz wide-bandwidth linear-array transducer operating at 10.0 MHz using a hand-held standoff pad at a displayed depth of 4 cm. The focal zones are spread throughout the imaging field. The right side of the short-axis view *(left image)* is dorsal and the left side is plantar. The right side of the long-axis view *(right image)* is proximal and the left side is distal.

shape to its insertion on the deep digital flexor tendon in the mid-metacarpal to distal metacarpal region. The inferior check ligament runs in a slightly different plane from that of the superficial and deep digital flexor tendon, tilting slightly dorsal from the sagittal plane. In the hindlimb the inferior check ligament may be absent or is usually a small crescent-shaped structure, with its largest portion in the lateral aspect of the limb (Fig. 3-9). The inferior check ligament has a homogeneous echogenic appearance and may be the most echogenic structure in the proximal to mid-metacarpal region or the next most echogenic structure after the deep digital flexor tendon.[7, 12, 25, 44, 57, 80, 81] Forty percent of the horses in one study had an inferior check ligament that was less echogenic than the adjacent deep digital flexor tendon and suspensory ligament.[57] In studies of the relative brightness of the tendinous and ligamentous structures in the metacarpal region of normal horses, the inferior check ligament was slightly, but not significantly, less bright than the deep digital flexor tendon in the dorsal scan plane; it was significantly brighter than the deep digital flexor tendon in the sagittal images.[80] The echo pattern of the inferior check ligament is unchanged from that of the superficial and deep digital flexor tendons.

The palmar-to-dorsal thickness of the inferior check ligament has been reported at 2.5 cm and 7.5 cm distal to the accessory carpal bone in Anglo-Arabian-Andalusian crossbred horses, measuring 0.83 ± 0.03 cm and 0.69 ± 0.04 cm, respectively.[57] The lateral-to-medial width of the inferior check ligament at these levels is 1.97 ± 0.04 cm at 2.5 cm and 1.74 ± 0.04 cm at 7.5 cm distal to the accessory carpal bone. Other investigators have reported a palmar-to-dorsal thickness of 0.4 to 0.7 cm and a medial-to-lateral width of 1.4 to 1.6 cm in zone 1A.[12]

Suspensory Ligament. The suspensory ligament is rectangular at its origin from the proximal metacarpus and remains so until it bifurcates into a medial and lateral branch in the mid-metacarpal to distal metacarpal region (Fig. 3-10). In the hindlimb, however, the origin of the suspensory ligament is more trapezoid in shape (see Fig. 3-5). The hind suspensory ligament then becomes rectangular, as in the forelimb, and remains so until the bifurcation. Each branch of the suspensory ligament is oval just distal to the bifurcation and then becomes more trapezoid-shaped as it inserts onto the proximal sesamoid bones (Fig. 3-11). The suspensory ligament also has small medial and lateral extensor branches that insert on the fascia over the common digital extensor tendon on the dorsal aspect of the first phalanx.

The suspensory ligament origin and body are more heterogeneous than the other tendinous and ligamentous structures because they are composed of muscle tissue, connective tissue, and fat in addition to ligamentous fibers.[10, 25, 43, 58, 124] Differences occur in the amount of muscle tissue in the suspensory ligament body between different breeds and sexes of horses.[58, 111, 124] Standardbred horses have 40% more muscle in their suspensory ligament than do Thoroughbred horses.[124] Significantly more muscle is present in the hindlimb suspensory ligament than is present in the forelimb suspensory ligament in Standardbred, but not Thoroughbred, horses.[124] In Thoroughbred horses, a trend exists for more muscle content in the forelimb suspensory ligament.[124] The amount of muscle tissue in the body of the suspensory ligament varies from 2.1% to 11% between horses of the same breed.[58] The amount of muscle at the suspensory origin

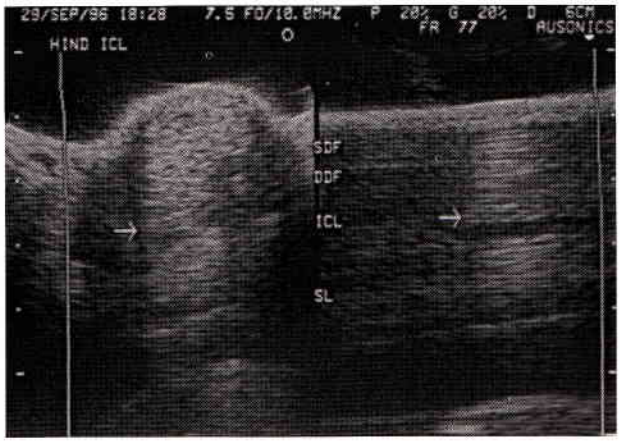

Figure 3–9

Sonogram of the normal flexor tendons and ligaments in the metatarsal region of the left hindleg of a 12-year-old Thoroughbred gelding. Notice the small remnant *(arrows)* of the inferior check ligament (ICL) that is dorsal to the deep digital flexor tendon (DDF). The tendons and ligaments are fairly uniform in echogenicity and have parallel fiber alignment. These sonograms were obtained in zone 2A with a wide-bandwidth 7.5-MHz sector scanner transducer containing a built-in fluid offset operating at 10.0 MHz at a displayed depth of 6 cm. The right side of the sagittal view *(right image)* is proximal and the left side is distal. The right side of the transverse view *(left image)* is lateral and the left is medial. SDF, superficial digital flexor tendon; SL, suspensory ligament.

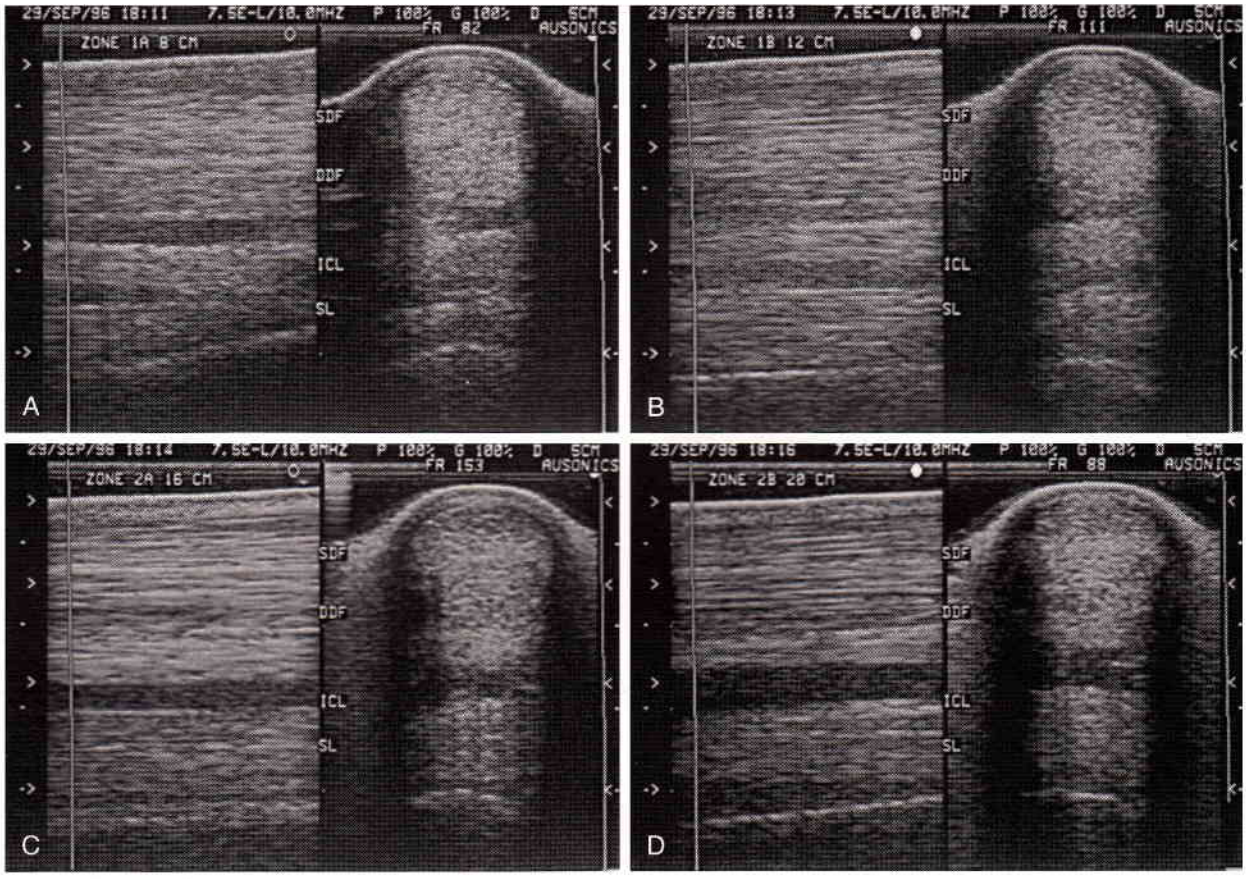

Figure 3–10

Sonograms of the normal flexor tendons and ligaments in the metacarpal region in the left foreleg of a 12-year-old Thoroughbred gelding (same horse as in Fig. 3–7). These sonograms were obtained with a wide-bandwidth 7.5-MHz linear-array transducer operating at 10.0 MHz using a hand-held standoff pad at a displayed depth of 5 cm. The focal zones are spread throughout the images. The right side of the transverse views *(right images)* is lateral and the left side is medial. The right side of the sagittal views *(left images)* is proximal and the left side is distal. SDF, superficial digital flexor tendon; DDF, deep digital flexor tendon; ICL, inferior check ligament; SL, suspensory ligament.

A, These sonograms were obtained 8 cm distal to the point of the accessory carpal bone (zone 1A). Notice the slightly hypoechoic SDF, the uniformly echogenic DDF, the artifactually hypoechoic ICL, and the hypoechoic dorsal border of the origin of the SL, the location of muscle fibers in many horses. Notice also the slight irregularity of the palmar metacarpal ridge and the normal space between the ICL and SL.

B, These sonograms were obtained 12 cm distal to the point of the accessory carpal bone (zone 1B). Notice the slightly hypoechoic SDF, the uniformly echogenic DDF, the more echogenic ICL, the slightly increased space between the ICL and SL, and the hypoechoic dorsal portion of the SL with its more rectangular shape.

C, These sonograms were obtained 16 cm distal to the point of the accessory carpal bone (zone 2A). Notice the slightly hypoechoic SDF, the uniformly echogenic DDF, the more echogenic ICL (now in a different scan plane), the slightly increased space between the ICL and SL, and the hypoechoic dorsal border of the SL with its more heterogeneous appearance and rectangular shape.

D, These sonograms were obtained 20 cm distal to the point of the accessory carpal bone (zone 2B). Notice the slightly hypoechoic SDF, the echogenic DDF with a hypoechoic dorsal border at the insertion of the ICL, the echogenic ICL, the slightly increased space between the ICL and SL, and the hypoechoic dorsal more uniform but still heterogeneous rectangular SL body. Notice the normal space between the ICL and SL.

and in the suspensory ligament body is similar in the contralateral limbs of the same horse.[124] Less muscle is present in Thoroughbred horses in training than in Thoroughbred horses of the same age that are not in training.[111, 124] Discrepancies occur in the literature about the differences, if any, in the amount of muscle tissue present in horses of different ages and in different stages of training.[58]

The unique composition of the suspensory ligament accounts for significant variability in the normal sonographic appearance of the suspensory ligament origin and body. Therefore, the hypoechoic areas seen in the normal suspensory ligament should be consistent in size, shape, and location between the right and left forelimbs or right and left hindlimbs.[124] The dorsal border of the proximal suspensory ligament body is poorly defined or hypoechoic in 9% of the limbs of clinically normal horses.[58] In 13% of clinically normal horses, a well or poorly defined central hypoechoic area is identified, whereas in 4%, the echogenicity of the suspensory ligament body is patchy.[58] The relative brightness of the suspensory ligament in the metacarpal region in the dorsal scan plane is less than that of the superficial digital flexor tendon in the proximal metacarpal region (7 cm distal to the accessory carpal bone) but greater than that of the superficial digital flexor tendon in the mid-metacarpal region (10, 15, and 20 cm). However, in the sagittal plane, the relative brightness of the suspensory ligament is greatest in the proximal and mid-metacarpal regions compared to that of the other tendinous and

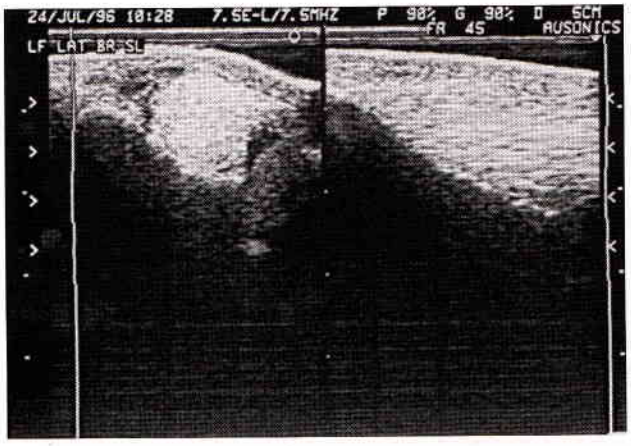

Figure 3–11

Sonograms of the normal lateral branch of the suspensory ligament, obtained from a 10-year-old Selle Français gelding. Notice the uniform echogenicity, the oval to trapezoid shape, and the parallel fiber pattern at the insertion of the suspensory branch on the lateral proximal sesamoid bone. These sonograms were obtained with a wide-bandwidth 7.5-MHz linear-array transducer operating at 7.5 MHz using a hand-held standoff pad at a displayed depth of 5 cm. The focal zones are in the near field of the images. The left side of the transverse view *(left image)* is palmar and the right side is dorsal. The left side of the sagittal view *(right image)* is distal and the right side is proximal.

ligamentous structures.[80] Although the suspensory ligament origin and body is heterogeneous and hypoechoic, the suspensory ligament branches are similar in echogenicity with the flexor tendons and have a similar sonographic texture or echo pattern. The relative brightness of the suspensory branches is similar to that of the superficial and deep digital flexor tendons in the distal metacarpal regions (25 and 30 cm distal to the accessory carpal bone).[71] The echogenicity of the suspensory ligament in the hindlimbs appears to be more consistent between horses than that in the forelimbs.

In this author's experience, the cross-sectional area of the normal suspensory ligament body in the forelimb of Thoroughbreds and Standardbreds ranges from 1.0 to 1.5 cm^2, with most horses having a cross-sectional area of the suspensory ligament body in the range of 1.0 to 1.2 cm^2. The cross-sectional area of the suspensory ligament body in the hindlimb is slightly larger, usually ranging from 1.2 to 1.75 cm^2, with most horses having a cross-sectional area of the hind suspensory ligament body of 1.2 to 1.5 cm^2. The cross-sectional area of the normal suspensory ligament branch is 0.6 to 0.8 cm^2 in the proximal portion of the branch in zone 3A and increases distally to 1.0 to 1.2 cm^2 at its insertion onto the abaxial surfaces of the proximal sesamoid bones (at the border between zones 3B and 3C). The medial branch of the suspensory ligament usually has a slightly larger cross-sectional area than does the lateral branch. The cross-sectional areas of the suspensory ligament origin, body, and branches range over a much wider spectrum than do those of the superficial digital flexor tendon, because of the marked changes in size of the suspensory ligament from its origin to its insertion. However, each portion of the suspensory ligament in the right and left forelimbs or right and left hindlimbs should have a similar cross-sectional area measurement at the same location in the limb.

Care must be taken in making these measurements, because delineating the medial and lateral borders of the suspensory ligament body can sometimes be difficult. This is due, in part, to the ligament's variable composition and to its location between the second and fourth metacarpal or metatarsal bones in the proximal to mid-metacarpal or metatarsal region.[46] In the forelimb, the suspensory ligament reportedly measures 0.8 to 0.9 cm in a palmar-to-dorsal direction and 1.7 to 1.9 cm in a medial-to-lateral direction in zone 1B.[12] In the distal third of the metacarpus, the suspensory branch measures 0.9 cm in a palmar-to-dorsal direction.[6] In Anglo-Arabian-Andalusian crossbred horses, the palmar-to-dorsal thickness measures 1.02 cm ± 0.03 cm at 2.5 cm distal to the accessory carpal bone, decreasing to 0.95 ± 0.02 cm at 17.5 cm and 0.93 ± 0.01 cm at 22.5 cm distal to the point of the accessory carpal bone.[57] In these same horses, the lateral-to-medial width decreased from 1.85 ± 0.01 at 2.5 cm to 1.05 ± 0.04 cm at 17.5 cm to 0.98 ± 0.02 cm at 22.5 cm distal to the accessory carpal bone.

Superficial Digital Flexor Tendon—Pastern. In the proximal pastern, the homogeneously echogenic superficial digital flexor tendon has a thin, half-moon shape in the transverse plane and lies immediately dorsal to the digital sheath, which is intimately associated with the fetlock annular ligament (Fig. 3-12). In normal horses,distinguishing the annular ligament from the digital sheath and the palmar or plantar border of the superficial digital flexor tendon is difficult. On sagittal sonograms the superficial digital flexor tendon has a triangular shape along the midline as its thickness decreases distally.[59] The body of the superficial digital flexor tendon ranges in thickness (palmar-to-dorsal) from 2 to 6 mm in the proximal pastern region and from 1 to 4 mm over the middle of P1.[59] The teardrop-shaped medial and lateral superficial digital flexor tendon branches in the middle pastern are similarly homogeneously echogenic with a parallel fiber pattern throughout their length (Fig. 3-13). The branches of the superficial digital flexor tendon become more triangular distally over the lateral and medial aspects of distal P1 and proximal P2. Although the superficial digital flexor tendon branches are uniformly echogenic here also and have a parallel fiber pattern, documenting this may be difficult in some horses, especially those with high heels and prominent collateral cartilages. These structures may preclude orienting the ultrasound beam perpendicular to the superficial digital flexor tendon branches and they may create a hypoechoic appearance due to an "off-normal" incidence artifact.

The cross-sectional area of the superficial digital flexor tendon branches ranges from 0.3 to 0.4 cm^2 in zone P1A to 0.4 to 0.6 cm^2 in zone P1B to 0.6 to 0.8 cm^2 just proximal to their insertion in zone P1C. A mean palmar-to-dorsal thickness of 3 ± 0 mm in zone P1A to 2 ± 0 in zone P1B to 10 ± 1.12 mm in zone P1C (distal P1) was reported by another investigator for the superficial digital flexor tendon, with a mean width (lateral-to-medial) of 33 ± 0.89 mm in zone P1A (proximal P1) and 31 ± 1.07 mm in zone P1B (mid P1).[66] Mean thickness of the superficial digital flexor tendon branches ranged from 0.2 ± 0 mm in zone P1B to 10 ± 1.01 mm in zone P1C in a palmar-to-dorsal direction and 6 ± 0.52 mm in

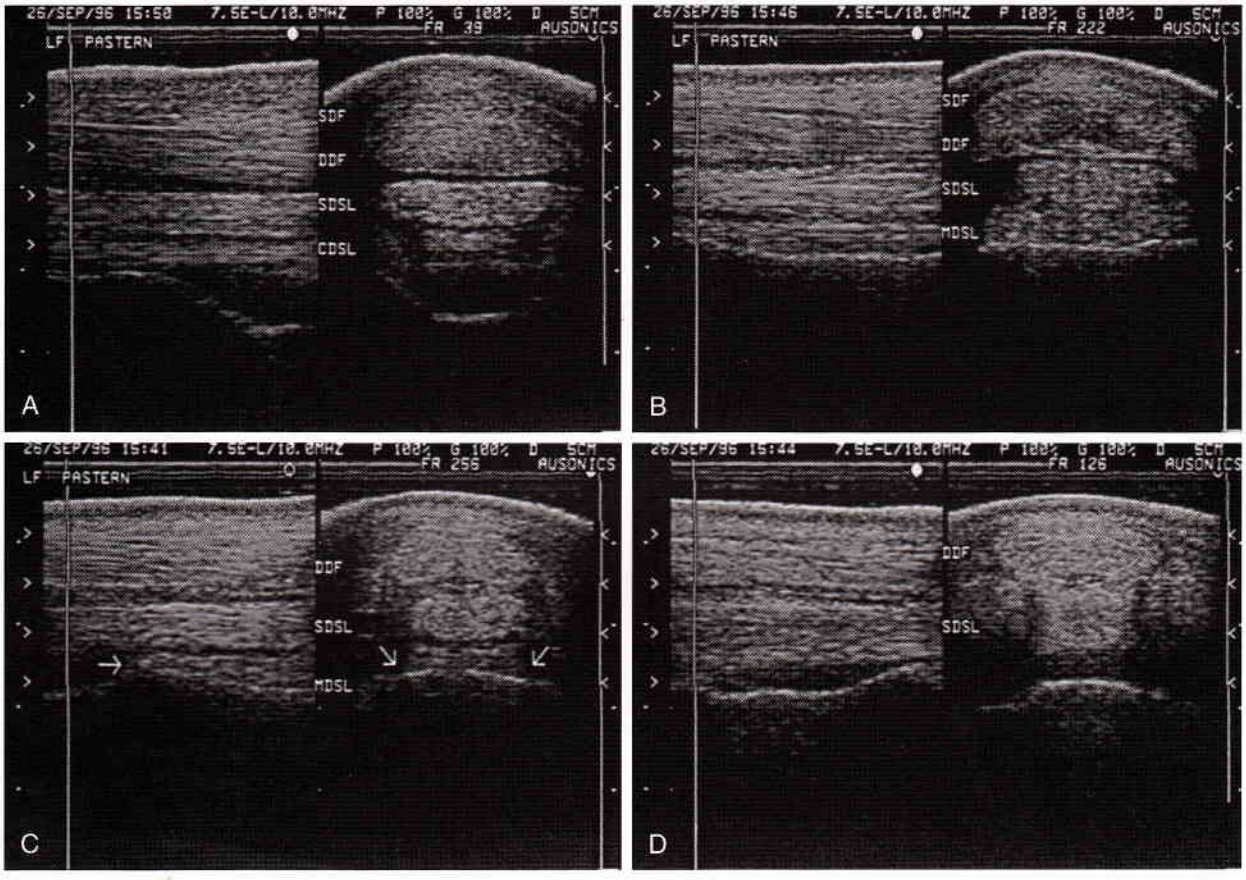

Figure 3–12

Sonograms of the normal tendons and ligaments in the pastern, obtained from a 12-year-old Thoroughbred gelding. These sonograms were obtained with a wide-bandwidth 7.5-MHz linear-array transducer operating at 10.0 MHz using a hand-held standoff pad at a displayed depth of 5 cm. The focal zones are in the near field of the images. The left side of the transverse views *(right images)* is medial and the right side is lateral. The left side of the sagittal views *(left images)* is distal and the right side is proximal.

A, Sonograms of the proximal-most portion of the pastern angling the transducer in a proximodorsal direction at zone P1A. Notice the thin curved superficial digital flexor tendon (SDF) along the palmar aspect of the leg, the oval deep digital flexor tendon (DDF) immediately dorsal to the SDF, and the broad trapezoid-shaped straight distal sesamoidean ligament (SDSL) dorsal to the DDF. Immediately dorsal to the SDSL is the cruciate distal sesamoidean ligaments (CDSL) which are imaged by angling the transducer in a proximodorsal direction. The edges of the branches of the middle (oblique) distal sesamoidean ligament (MDSL) are barely visible on the edge of the transverse sonogram. The thicker tissue palmar to the SDF is the subcutaneous tissue just distal to the ergot.

B, Sonograms of the proximal pastern obtained slightly distal to Fig. 3-12*A* at the level of zone P1A–P1B. Notice the ring that the SDF has formed around the bilobed DDF. The DDF is hypoechoic because it is in a different scan plane from the SDF (off-normal incidence artifact). The SDSL is oval at this level. The medial and lateral branches of the MDSL have just joined to form one rectangular ligament at this level.

C, Sonograms of the mid-pastern region at the level of zone P1B. Notice the bilobed appearance of the DDF and the insertion of the MDSL *(arrows)*. The horizontal arrow points to the insertion of the MDSL on the palmar aspect of mid P1 in the sagittal image and the obliqued arrows point to the same insertion viewed in the transverse image. The SDSL is more oval at this level.

D, Sonograms of the normal SDSL over distal P1 near its insertion onto proximal P2, dorsal to the DDF at the level of zone P1C. Notice the hypoechoic center at the insertion of the SDSL caused by the inability of the operator to angle the linear-array transducer perpendicular to the SDSL's fibers. The DDF still has somewhat of a bilobed appearance at this level. The distal portions of the branches of the SDF are visible on the edges of the transverse image.

zone P1B and 9 ± 1.01 in zone P1C in a medial-to-lateral direction.[66] The branches of the superficial digital flexor tendon reportedly range in thickness from 4 to 7 mm in the proximal pastern to 7 to 12 mm in the mid pastern and 13 to 20 mm over distal P1.[59]

Deep Digital Flexor Tendon—Pastern. The deep digital flexor tendon has an oval to bilobed appearance in the pastern. The two lobes of the deep digital flexor tendon in the pastern region should be symmetrical in size and shape (see Fig. 3-12). The fibers of the deep digital flexor tendon extend obliquely from a deeper to a more superficial position in the distal portion of the pastern. The deep digital flexor tendon is separated from the straight distal sesamoidean ligament by an anechoic space. The dorsal-to-palmar thickness and lateral-to-medial width of the deep digital flexor tendon decrease somewhat distally in the middle pastern and then increase again in the distal pastern.[59] Along the dorsal aspect of the deep digital flexor tendon in the middle pastern region is a synovial fold of the digital sheath, which is readily imaged and is surrounded by a small amount of the anechoic synovial fluid contained within the digital

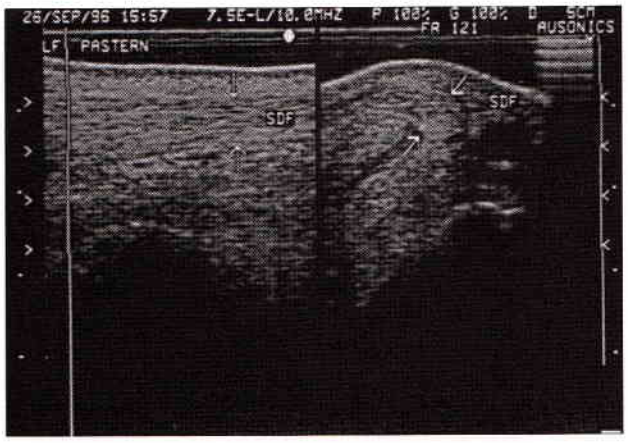

Figure 3–13

Sonograms of the normal lateral branch *(between the arrows)* of the superficial digital flexor tendon (SDF), obtained from a 12-year-old Thoroughbred gelding as the tendon branches and extends down the lateral aspect of the proximal to mid-pastern region. These sonograms were obtained with a wide-bandwidth 7.5-MHz linear-array transducer operating at 10.0 MHz using a hand-held standoff pad at a displayed depth of 5 cm. The focal zones are in the near field of the images. The left side of the transverse view *(right image)* is palmar and the right side is dorsal. The left side of the sagittal view *(left image)* is distal and the right side is proximal.

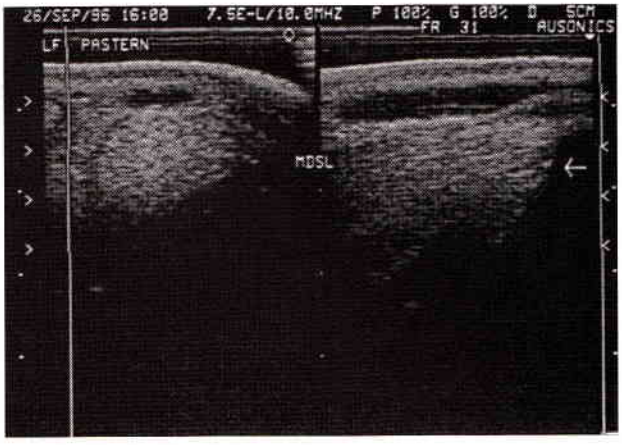

Figure 3–14

Sonograms of the normal lateral branch of the middle (oblique) distal sesamoidean ligament (MDSL), obtained from a 12-year-old Thoroughbred gelding. Notice the large homogeneously echogenic oval shape of the MDSL at its origin in the transverse view and its oblique path as it originates from the base of the lateral proximal sesamoid bone *(arrow)* and extends distally towards the midline of the first phalanx, seen in the sagittal view. These sonograms were obtained with a wide bandwidth 7.5-MHz linear-array transducer operating at 10.0 MHz using a hand-held standoff pad at a displayed depth of 5 cm. The focal zones are in the near field of the images. The left side of the transverse view *(left image)* is palmar and the right side is dorsal. The left side of the sagittal view *(right image)* is distal and the right side is proximal.

sheath. In the distal pastern region along proximal P2, the palmar aspect of the deep digital flexor tendon is adhered to the synovial membrane of the digital sheath.[59]

The deep digital flexor tendon reportedly measures 5 to 10 mm thick in a palmar-to-dorsal direction in the proximal pastern, slightly less in the middle pastern, and 7 to 12 mm in the distal pastern.[59] Its width in a lateral-to-medial direction ranges from 18 to 33 mm in the proximal pastern, from 15 to 23 mm in the middle pastern, and from 23 to 32 mm in the distal pastern.[59] A second investigator obtained palmar-to-dorsal measurements of 7 ± 2.05 mm in zone P1A, 5 ± 0.46 mm in zone P1B, and 6 ± 0.76 mm in zone P2B (mid to distal P2).[66] Its medial-to-lateral width ranges from 23 ± 0.89 mm in zone P1A to 18 ± 0.52 in zone P1B to 26 ± 1.6 mm in zone P2B.

Distal Sesamoidean Ligaments. The distal sesamoidean ligaments also have a similar echo pattern to that of the flexor tendons and appear homogeneously echogenic.

Middle (Oblique) Distal Sesamoidean Ligament. The middle or oblique distal sesamoidean ligament originates at the base of the sesamoid bones as two large round discrete branches (Fig. 3-14), which become somewhat oval in appearance (Fig. 3-15) and merge dorsal to the deep digital flexor tendon in the mid-pastern region into a broad rectangular band. This band inserts on the palmar or plantar aspect of the distal portion of the first phalanx (see Fig. 3-12). The middle distal sesamoidean ligament branches appear less echogenic because of their oblique orientation and properly aligning the transducer to eliminate the off-normal incidence artifact is difficult.

The branches are thicker in the medial-to-lateral direction proximally than they are just before their convergence. They measure 12 to 20 mm in a lateral-to-medial direction in the proximal pastern, 9 to 17 mm just before their convergence, and 0 to 9 mm (one side only) at the insertion of the ligament onto P1.[59] The palmar-to-dorsal thickness of the middle (oblique) distal sesamoidean ligament is 5 to 12 mm in the proximal pastern, 2 to 6 mm just proximal to branch convergence, and 0 to 3 cm at insertion onto P1.[59] Another investigator obtained medial-

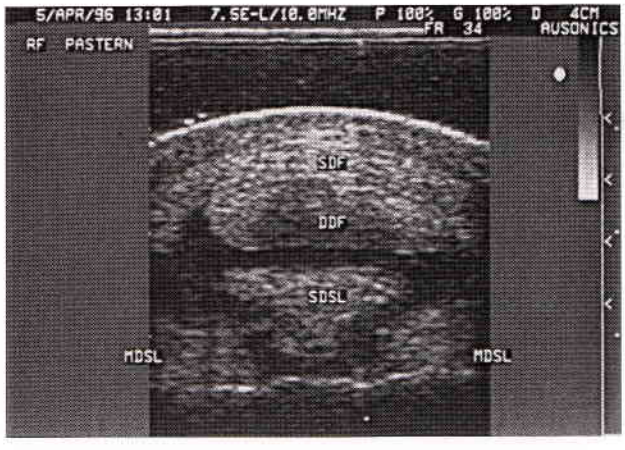

Figure 3–15

Sonogram of the proximal portion of the pastern at the level of zone P1A, obtained from a 7-year-old Thoroughbred gelding. Notice the triangular to trapezoid appearance of the straight distal sesamoidean ligament (SDSL) at its origin, the round to oval branches of the middle distal sesamoidean ligament (MDSL), the thin curved superficial digital flexor tendon (SDF), and the bilobed deep digital flexor tendon (DDF). The hypoechoic appearance of the DDF is artifactual, created by an off-normal incidence artifact. This sonogram was obtained with a wide-bandwidth 7.5-MHz linear-array transducer operating at 10.0 MHz using a hand-held standoff pad at a displayed depth of 4 cm. The focal zones are placed in the near field of the image. The right side of the transverse image is lateral and the left side is medial.

to-lateral width measurements of the middle (oblique) distal sesamoidean ligament in zone P1A of 14 ± 0.35 mm decreasing to 11 ± 1.38 mm in zone P1B just before insertion.[66] The palmar-to-dorsal thicknesses measured at these same zones are 5 ± 0.52 mm and 4 ± 0.75 mm, respectively.[66]

Straight Distal Sesamoidean Ligament. The straight distal sesamoidean ligament originates as a single trapezoid structure from the base of both sesamoid bones with a large concave palmar border (see Fig. 3-15). The straight distal sesamoidean ligament becomes a more oval-shaped structure and is palmar or plantar to the middle distal sesamoidean ligament in the mid-pastern region and dorsal to the deep digital flexor tendon. The straight distal sesamoidean ligament inserts on the proximal portion of the second phalanx (Figs. 3-12 and 3-16). The dorsal-to-palmar thickness of the straight distal sesamoidean ligament gradually increases as the medial-to-lateral width decreases. The straight distal sesamoidean ligament is very echogenic, with normal parallel fiber alignment throughout. The straight distal sesamoidean ligament often appears to have a hypoechoic center as it inserts onto the proximal portion of the second phalanx or P2 (see Fig. 3-12). This hypoechoic appearance disappears, however, when the ultrasound beam can be angled perpendicular to the ligamentous fibers at their insertion (see Fig. 3-16) in zone P2A.

The straight distal sesamoidean ligament measures 5 to 9 mm in palmar-to-dorsal thickness proximally, increasing slightly over distal P1 to 6 to 12 mm and then to 8 to 14 mm at the scutum medium.[59] The medial-to-lateral width of the straight distal sesamoidean ligament ranges from 17 to 30 mm in the proximal pastern region, decreases to 10 to 15 mm over distal P1, and then widens over the scutum medium to 45 to 65 mm. Another investigator found a mean medial-to-lateral width of the straight distal sesamoidean ligament of 20 ± 1.19 mm, 16 ± 1.89, and 14 ± 1.16 at zones P1A, P1B, and P1C, respectively.[66] The palmar-to-dorsal thickness of the straight distal sesamoidean ligament is 7 ± 0.71 mm, 8 ± 0.93 mm, 8 ± 0.92 mm, and 11 ± 2.1 mm in zones P1A, P1B, P1C, and P2A (proximal P2).[66]

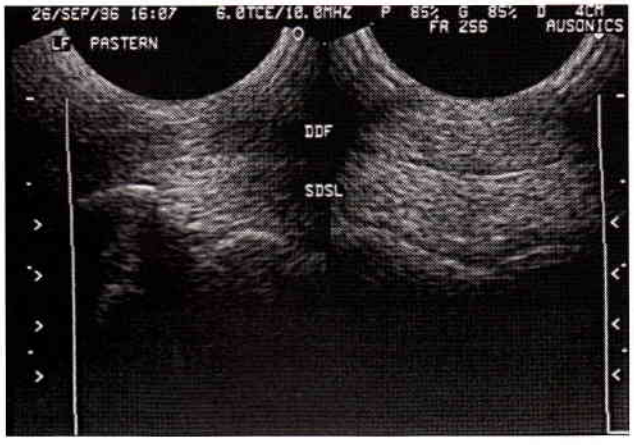

Figure 3–16

Sonograms of the normal insertion of the straight distal sesamoidean ligament (SDSL) at the level of zone P2, obtained from a 12-year-old Thoroughbred gelding. With a microconvex linear transducer, the insertion of the SDSL has an echogenic center in the sagittal view *(left image)* and the insertion of the SDSL onto the scutum median is visible in the transverse image *(right image)*. These sonograms were obtained with a wide-bandwidth 6.0-MHz microconvex linear-array transducer operating at 10.0 MHz at a displayed depth of 4 cm. The focal zones are in the far field of the images. The right side of the transverse image is lateral and the left side is medial. The right side of the sagittal image is lateral and the left side is distal.

Cruciate Distal Sesamoidean Ligaments. The cruciate distal sesamoidean ligaments are only imaged in the proximal-most portion of the pastern and measure 2 to 4 mm in a palmar-to-dorsal direction.[59]

Annular Ligaments. The normal fetlock annular ligament is a very thin structure in the normal horse and is difficult to distinguish from the digital sheath, with which it is intimately associated. In normal horses, the fetlock annular ligament measures 0 to 2 mm in thickness, including the overlying skin layer.[59, 60] Rarely can the fetlock annular ligament be imaged as a distinct structure.[60, 71] The fetlock annular ligament was visualized independent of the skin and tendon sheath in one large horse; the ligament measured 1 to 2 mm thick.[60] With the advent of higher-frequency transducers (10.0-MHz) for higher-resolution, near-field imaging, the annular ligament may become slightly easier to image independently but should still remain in close contact with the adjacent digital sheath.

The proximal digital annular ligament is also a very thin structure, difficult to distinguish from the underlying digital sheath or overlying skin. In normal Warmblood horses, the thickness of the proximal digital annular ligament and overlying skin combined is 2 mm.[69] A higher frequency transducer such as a 10.0-MHz may enable the delineation of the proximal digital annular ligament from the adjacent digital sheath and superficial digital flexor tendon to which it is closely attached.

Superior Check Ligament. The superior check ligament can be imaged arising from the distal radius as a band of parallel fibers that inserts on the superficial digital flexor tendon (Fig. 3-17). In the transverse plane, the superior check ligament has a somewhat triangular appearance. The superior check ligament has uniform echogenicity throughout its length.

Bicipital Tendon. The normal bicipital tendon has a homogeneous echogenic appearance with a parallel fiber pattern and is hyperechoic compared to the surrounding musculature (Fig. 3-18). The bicipital tendon is bilobed, with an isthmus connecting the two lobes. Artifactual hypoechoic areas may appear in a portion of the bicipital tendon because of the large size of the tendon, its curved contour, and the resultant difficulty in orienting the ultrasound transducer so that the beam is perpendicular to all the tendon fibers. Lesions should be identified in both the transverse and sagittal plane to be sure that a hypoechoic area is not artifactually induced. Deep to the bicipital tendon, a small anechoic space is imaged that represents the cartilage of the humerus and the synovial space.[70]

At its attachment to the supraglenoid tubercle, the bicipital tendon appears flat caudocranially and oval in shape, with the bilobed appearance visible over the cranial aspect of the shoulder. Distal to the point of the shoulder, the bicipital tendon again becomes oval and enlarges. The musculotendinous junction is imaged as a

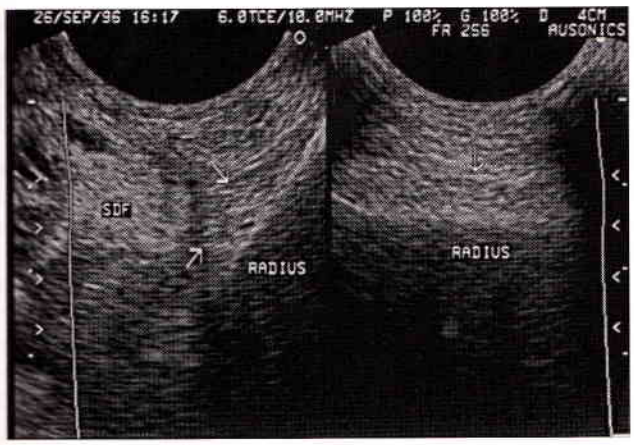

Figure 3–17

Sonograms of the normal superior check ligament along the distal medial aspect of the radius, obtained from a 12-year-old Thoroughbred gelding. Notice the triangular shape of the superior check ligament in short-axis section *(diagonal arrows)* adjacent to the superficial digital flexor tendon (SDF). The vertical arrow points to the superior check ligament in its long axis along the distal medial aspect of the radius. These sonograms were obtained with a wide-bandwidth 6.0-MHz convex linear-array transducer operating at 10.0 MHz at a displayed depth of 4 cm. The focal zones are in the middle of the images. The left side of the short-axis view *(left image)* is caudal and the right side is cranial. The left side of the long-axis view *(right image)* is distal and the right side is proximal.

heterogeneous area with echogenic tendon fibers interspersed between hypoechoic muscle and echogenic fascia. No significant differences between measurements of various portions of the bicipital tendon or bicipital bursa between forelimbs have been reported.[74] No association has been found between cranial and caudal tendon measurements and the horse's body weight, height at the point of the shoulder, height at the top of the withers, or girth circumference.[74] In this study of normal adult Quarter horses, the median cranial-to-caudal width (thickness) of the midsagittal portion (isthmus) of the bicipital tendon was 10 mm (range, 7 to 13.5 mm).[74] The median cranial-to-caudal width of the larger lateral lobe of the bicipital (thickness) tendon at its greatest dimension was 20.5 mm (range, 18 to 27.7 mm) and was 16 mm (range, 13 to 20.5 mm) for the smaller medial lobe.[74] In the sagittal plane, the median distance from the skin surface to the lateral lobe of the bicipital tendon was 14 mm (range, 8.5 to 19 mm), that to the midsagittal portion (isthmus) was 17 mm (range, 10.5 to 22 mm), and that to the medial lobe was 23 mm (range, 16.5 to 30 mm).[74]

Evaluation of the underlying cartilage and subchondral bone of the distal humerus should reveal a thin anechoic to hypoechoic layer immediately cranial to the hyperechoic subchondral bone, representing the cartilage. In the young horse, varying degrees of ossification of the intermediate tubercle result in scattered hyperechoic foci detected within the hypoechoic cartilage that represent early mineralization.[70] The hyperechoic echo from the subchondral bone of the humerus casts an acoustic shadow and, in the adult horse, should be a smooth bony-surface echo of even thickness. A small concavity in the subchondral contour of the intermediate tubercle was found in one clinically normal horse and may represent a normal variant.[70]

Extensor Tendons. All the extensor tendons have sonographic appearances similar to those of the flexor tendons, with a uniform echogenic appearance, parallel fiber alignment, and an oval-to-circular appearance in transverse section. The extensor tendons are each con-

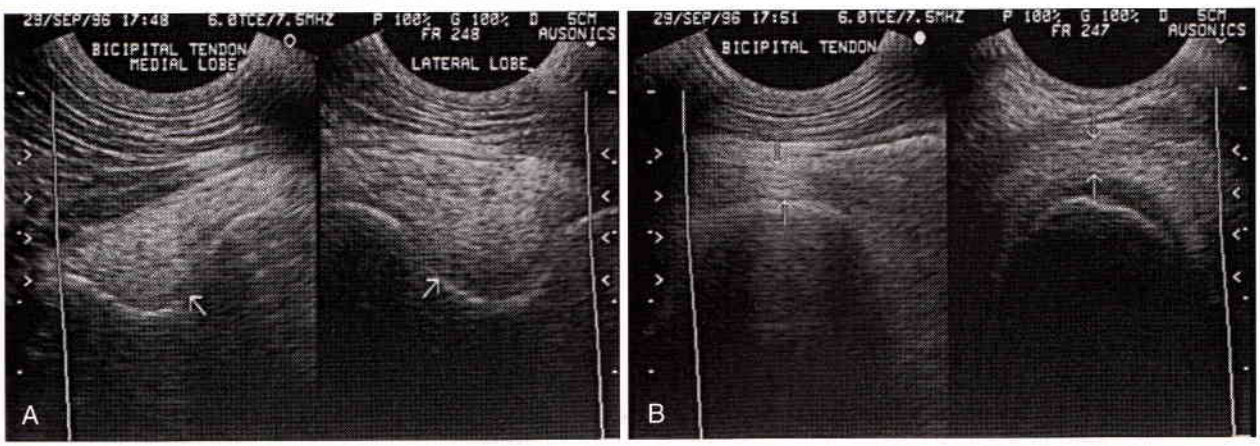

Figure 3–18

Sonograms of the normal bicipital tendon, obtained from a 12-year-old Thoroughbred gelding. These sonograms were obtained with a wide-bandwidth 6.0-MHz convex linear-array transducer operating at 7.5 MHz at a displayed depth of 5 cm. The focal zones are in the middle of the images. The right side of the transverse images is lateral and the left side is axial. The right side of the sagittal views *(left image in B)* is proximal and the left side is distal.

A, Notice the curved echogenic appearance of the medial *(left sonogram)* and lateral *(right sonogram)* lobes of the bicipital tendon *(arrows)* in the transverse views as it curves over the intermediate tubercle of the humerus. The bicipital tendon's large size and curved structure preclude its being imaged in its entirety in one scan plane. Artifactual hypoechoic areas are easily created within the bicipital tendon because the tendon does not all lie in the same scan plane. The overlying brachiocephalicus muscle has a normal striated appearance. The left side of the images is axial and the right side is lateral.

B, The isthmus of the bicipital tendon is much narrower but also very curved. The isthmus rides over the intermediate tubercle of the humerus. The right image is the transverse view and the left is the corresponding sagittal view.

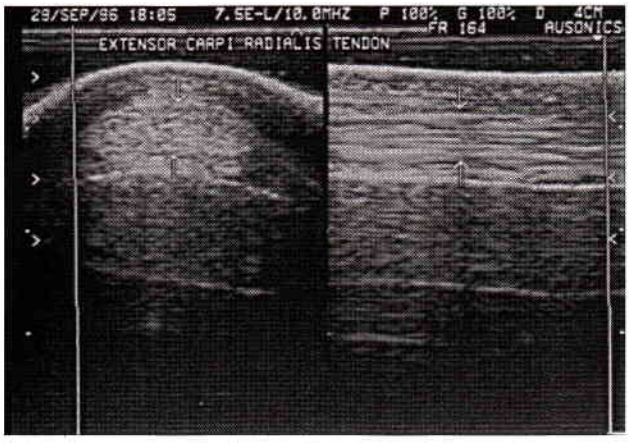

Figure 3–19

Sonograms of the normal extensor carpi radialis tendon over the dorsal aspect of the carpus, obtained from a 12-year-old Thoroughbred gelding. Notice the homogeneous echogenic appearance of the extensor carpi radialis tendon and the parallel fiber alignment *(arrows)*. No visible fluid is visualized within the extensor carpi radialis tendon sheath. The echogenic rim outside the arrows with the shorter linear echoes is the tendon sheath. These sonograms were obtained with a wide-bandwidth 7.5-MHz linear-array transducer operating at 10.0 MHz using a hand-held standoff pad at a displayed depth of 4 cm. The focal zones are in the near field of the images. The right side of the sagittal view *(right image)* is proximal and the left side is distal. The right side of the transverse view *(left image)* is lateral and the left side is medial.

tained within a separate tendon sheath over the dorsal aspect of the carpus and tarsus that contains little or no visible anechoic fluid in the normal horse (Fig. 3-19). The ultrasonographic appearance of the extensor carpi radialis tendon, common digital extensor tendon, extensor carpi obliquus tendon, lateral digital extensor tendon, and ulnaris lateralis tendon has been described.[87]

The extensor carpi radialis tendon originates as an oval-to-elliptical tendon containing residual muscle fibers proximally and flattens over the dorsal aspect of the carpus. The thickness of the extensor carpi radialis tendon in a dorsal-to-palmar direction was 6 to 7 mm with a medial-to-lateral width of 16 to 19 mm in normal horses in the proximal part of the distal radius. The thickness of the extensor carpi radialis tendon decreased to 4 to 6 mm in a dorsal-to-palmar direction, and the medial-to-lateral width increased to 19 to 21 mm over the distalmost aspect of the radius. The extensor carpi radialis tendon widens over the middle row of carpal bones to 23 to 26 mm and subsequently to 28 to 32 mm in a medial-to-lateral direction over the carpometacarpal joint.[87] The common digital extensor tendon originates as a triangular and then oval-shaped echogenic tendon. Proximally, the common digital extensor tendon is superimposed over the extensor carpi obliquus muscle, where it measures 4 to 5 mm thick in a dorsal-to-palmar direction and 16 to 18 mm wide in a medial-to-lateral direction.[87] The tendon flattens over the distal aspect of the radius and then becomes elliptical over the dorsal aspect of the carpus, becoming fusiform over the distal row of carpal bones and then elliptical again. The common digital extensor tendon measures 3 to 4 mm thick and 12 to 14 mm wide over the proximal metacarpus. The extensor carpi obliquus appears flat and measures 3 mm thick and 8 to 10 mm wide over the distal radius. It then becomes elliptical and narrows slightly.[87] The lateral digital extensor tendon is 3 to 4 mm thick and 9 to 10 mm wide over the lateral aspect of the radius and is difficult to identify through the two parts of the lateral collateral ligament.[87] The tendon of the ulnaris lateralis is round and measures 5 mm thick and 7 to 9 mm wide over the dorsal aspect of the carpus.[87] The tendon flattens out and narrows slightly towards its insertion.

Gastrocnemius Tendon. The gastrocnemius tendon is located in the distal aspect of the crus and winds laterally and cranially around the superficial digital flexor tendon in this region. In the distal aspect of the crus, the gastrocnemius tendon lies deep to the superficial digital flexor tendon and has a homogeneous echogenic appearance with uniform parallel fiber alignment (Fig. 3-20). In the middle of the crus, the two muscle bellies of the gastrocnemius muscle form a common tendon that surrounds the superficial digital flexor tendon at this level. The gastrocnemius tendon then extends along the lateral aspect of the crus from superficial to deep with the superficial digital flexor tendon extending from deep to superficial along the medial aspect of the crus. The calcaneal bursa is a potential space between the superficial digital flexor tendon and the gastrocnemius tendon and may be imaged as an anechoic space (Fig. 3-20). Some hypoechoic areas are usually detected within the gastrocnemius tendon at this level in the normal horse as it lies caudal or lateral to the superficial digital flexor tendon (see Fig. 3-20).[64] Some muscular tissue persists in this portion of the gastrocnemius tendon, which may account for its patchy echogenicity at this location, similar to that seen in the suspensory ligament.[64] Comparison with the opposite crus should be performed if questionable areas

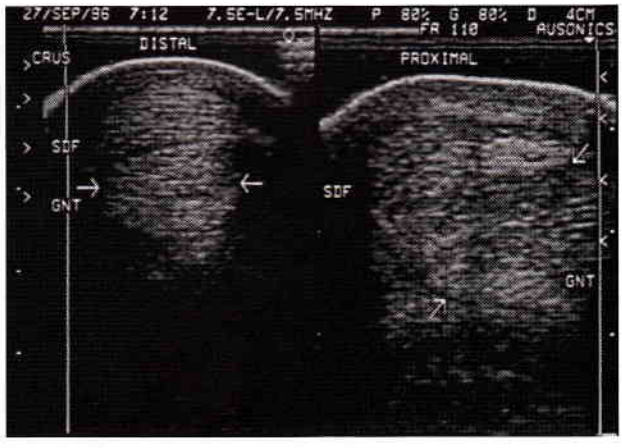

Figure 3–20

Transverse sonograms of the normal gastrocnemius tendon (GNT) and superficial digital flexor tendon (SDF), obtained from a 3-year-old Standardbred gelding. The right scan is in the proximal crus where the SDF is medial to the GNT. Notice the hypoechoic areas visible in the GNT *(diagonal arrows)*, representing areas of muscle present within the tendon at this level. The left scan is in the distal crus. At this level, the GNT *(horizontal arrows)* is relatively homogeneous, similar in echogenicity to the SDF. These sonograms were obtained with a wide-bandwidth 7.5-MHz linear-array transducer operating at 7.5 MHz using a hand-held standoff pad at a displayed depth of 4 cm. The focal zones are in the near field of the images. The left side of the images is medial and the right side is lateral.

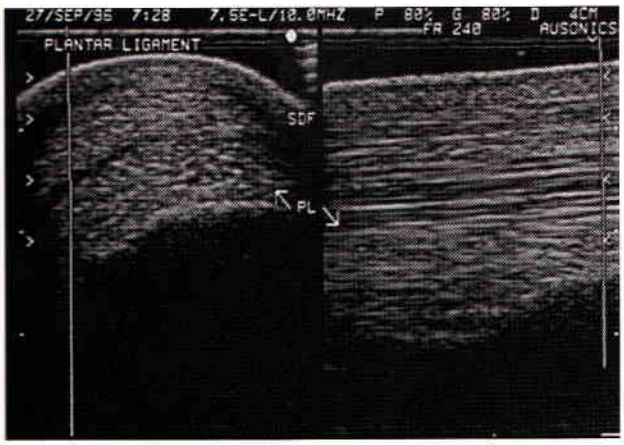

Figure 3–21

Sonograms of the normal superficial digital flexor tendon (SDF) and plantar ligament (PL) over the plantar aspect of the tarsus, obtained from a 3-year-old Standardbred gelding. Notice the flattened appearance of the SDF and PL near the origin of the PL. The SDF and PL are homogeneously echogenic with parallel fiber alignment. These sonograms were obtained with a wide-bandwidth 7.5-MHz linear-array transducer operating at 10.0 MHz using a hand-held standoff pad at a displayed depth of 4 cm. The focal zones are in the near field of the images. The left side of the transverse view *(left image)* is medial and the right side is lateral. The left side of the sagittal view *(right image)* is distal and the right side is proximal.

of injury within the gastrocnemius tendon in one hind limb are present. In the distal third of the crus, the gastrocnemius tendon and superficial digital flexor tendon both develop a uniform echogenic appearance and are nearly equal in size, with a clear interface between the two tendons detected ultrasonographically. The gastrocnemius tendon then becomes more rounded in appearance in transverse section and is nearly twice as thick as the superficial digital flexor tendon. Deep to the gastrocnemius tendon, the gastrocnemius bursa may be imaged, but it is only a potential space that does not normally contain synovial fluid. The gastrocnemius tendon is flat and crescent-shaped in short axis as it inserts on the proximal aspect of the calcaneal tuber covered by the flattened superficial digital flexor tendon.

Plantar Ligament. The plantar ligament is a short ligament along the plantar aspect of the tarsus that has a homogeneous echogenic appearance with a parallel fiber pattern (Fig. 3-21). The origin of the plantar ligament from the plantar aspect of the proximal extent of the tuber calcis is readily imaged as is its insertion on the fibular tarsal bone, fourth tarsal bone, and proximal extent of the fourth metatarsal bone. The plantar ligament has a rectangular appearance over the distal aspect of the calcaneus and the small tarsal bones and a somewhat triangular appearance near its insertion on the fourth metatarsal bone, where it is imaged lateral to the deep digital flexor tendon (Fig. 3-22).

Peroneus Tertius Tendon. The peroneus tertius tendon originates from the lateral aspect of the distal epicondyle of the femur with the long digital extensor tendon and appears as a thick echogenic semicircular structure in short-axis section with a homogeneous echogenic appearance and parallel fiber alignment (Fig. 3-23). The peroneus tertius tendon can be followed distally along the dorsal aspect of the tibia as an oval-to-circular homogeneous echogenic tendon with parallel fiber alignment (see Fig. 3-23). The peroneus tertius tendon bifurcates into two branches over the dorsal aspect of the hock. These branches insert on the tarsal bones and appear as much smaller oval-to-circular echogenic tendons, again with a parallel fiber pattern (see Fig. 3-23).

Cunean Tendon. The cunean tendon has a homogeneous echogenic appearance with a parallel fiber pattern (Fig. 3-24). The tendon has an oval shape in transverse section and is small, lying immediately underneath the skin over the dorsal aspect of the hock.

The Back. The supraspinous ligaments, interspinous ligaments, dorsal spinous processes, and dorsal sacroiliac ligament can all be evaluated ultrasonographically. At the withers, the nuchal ligament appears homogeneously echogenic and has a flat and broad shape in transverse section. The atlantal bursa, supraspinous bursa, and other bursae underneath the supraspinous ligament are only potential spaces and are not imaged in normal horses. In the mid-thoracic region, the supraspinous ligament becomes oval or circular in shape in transverse section (Fig. 3-25) and maintains this shape to its insertion on the sacrum. The supraspinous ligament is thinner at the dorsal-most aspects of the dorsal spinous processes and is more circular in shape in the interspinous spaces.[125] The supraspinous ligament is echogenic in its superficial part and hypoechoic deeper near the interspinous spaces. The fiber alignment is parallel throughout the superficial portion of the supraspinous ligament and oblique in the deeper portion.[75] The thick layer of subcutaneous fascia continuous with the supraspinous ligament

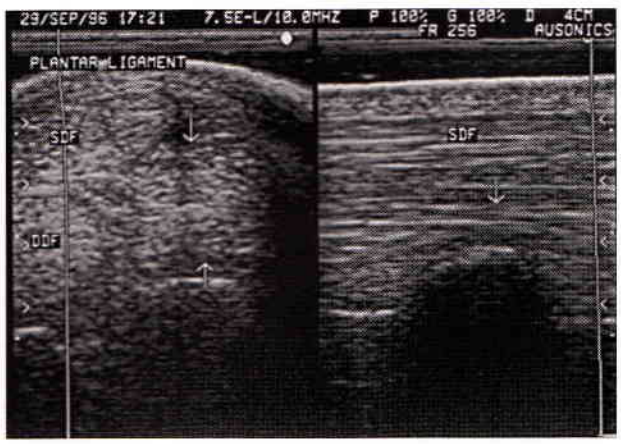

Figure 3–22

Sonograms of the normal superficial digital flexor tendon (SDF) and plantar ligament (PL) over the plantar aspect of the distal tarsus, obtained from a 12-year-old Thoroughbred gelding. Notice the parallel fiber alignment of the SDF and PL in the sagittal view *(right image)* and the homogeneous echogenic appearance of the SDF and PL in the transverse view *(left image)*. A portion of the deep digital flexor tendon (DDF) is imaged along the medial aspect of the PL in the transverse image. These sonograms were obtained with a wide-bandwidth 7.5-MHz linear-array transducer operating at 10.0 MHz using a hand-held standoff pad at a displayed depth of 4 cm. The focal zones are spread throughout the images. The left side of the transverse view is medial and the right side is lateral. The left side of the sagittal view is distal and the right side is proximal.

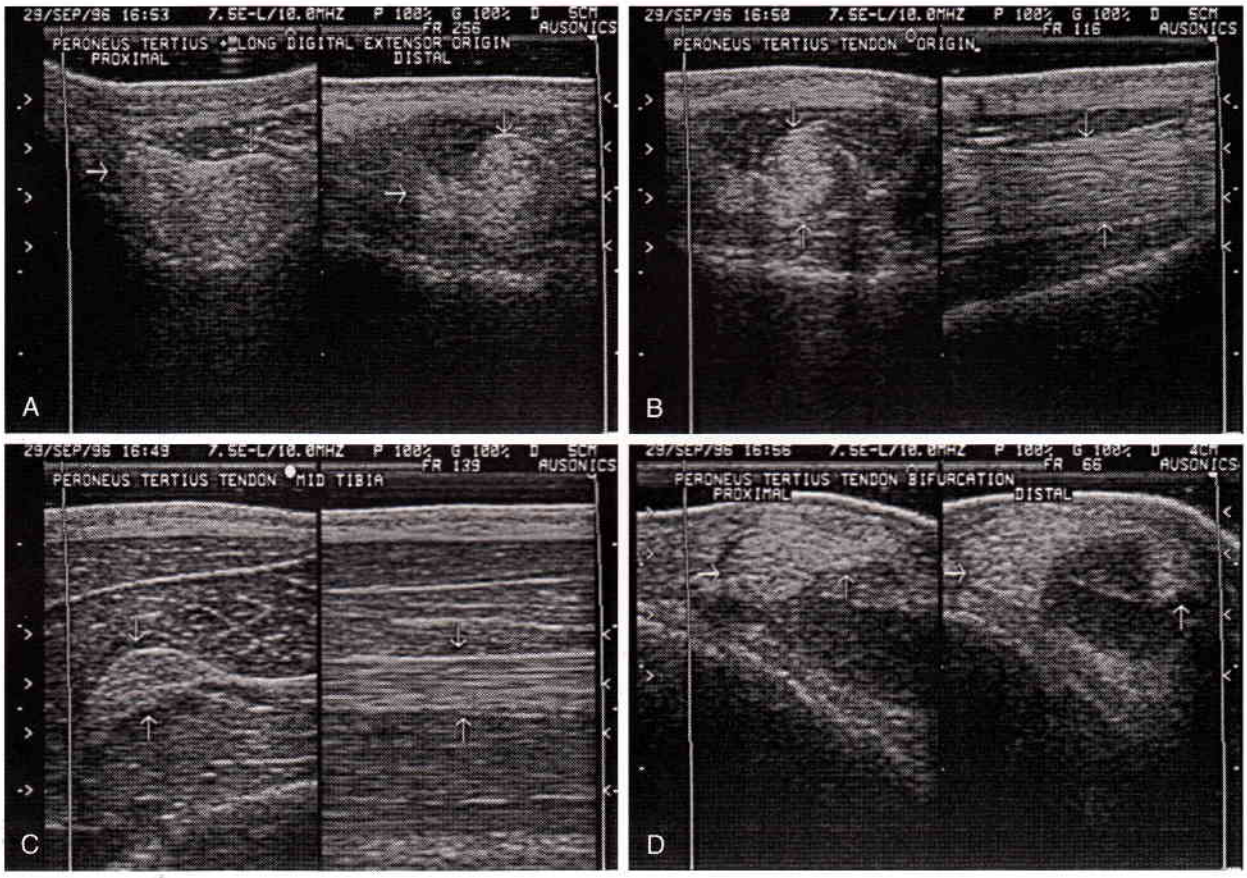

Figure 3–23

Sonograms of the normal peroneus tertius tendon from its origin to its insertion, obtained from a 12-year-old Thoroughbred gelding. Notice the surrounding hypoechoic speckled skeletal muscle most visible in *B* and *C*. These sonograms were obtained with a wide-bandwidth 7.5-MHz linear-array transducer operating at 10.0 MHz using a hand-held standoff pad. The right side of the transverse views is lateral and the left side is medial. The right side of the sagittal views is proximal and the left side is distal. The focal zones are in the near field except in *C*, where the focal zones have been moved deeper to center on the peroneus tertius tendon. The displayed depth is 5 cm except for the bifurcation *(D)* which is at a 4 cm displayed depth.

A, Origin of the peroneus tertius tendon and the long digital extensor tendon from the distolateral aspect of the femur. The horizontal arrow points to the long digital extensor tendon and the vertical arrow points to the peroneus tertius tendon. Both images are transverse with the left image being located slightly more proximally.

B, The peroneus tertius tendon *(arrows)* as it is separating from the long digital extensor tendon in the proximal tibia. Notice the homogeneous echogenic appearance and the parallel fiber pattern of the peroneus tertius tendon. The right image is sagittal and the left is transverse.

C, The peroneus tertius tendon surrounded by normal musculature in the mid tibia. Again notice its homogeneous echogenic appearance and the parallel fiber pattern. The right image is sagittal and the left is transverse.

D, The distal portion of the peroneus tertius tendon at its bifurcation. The left transverse image shows the tendon beginning to bifurcate. The right transverse image shows the area slightly more distal where the medial *(horizontal arrows)* and lateral *(vertical arrows)* branches of the peroneus tertius tendon are clearly visible.

in the thoracic region is also echogenic. The dorsal spinous processes have a pointed or beaked shape along their cranial margin with a more rounded caudal margin.[125] The dorsal margin of the dorsal spinous processes is smooth in the mid-thoracic region but is more irregular in the cranial thorax at the withers, where cartilaginous caps are common and irregular mineralization of these caps occurs even in older horses. Partially ossified osteochondral apophyseal nodules can be found in the first nine dorsal spinous processes at the withers, creating hyperechoic images.[75]

The interspinous ligaments have a homogeneous hypoechoic to echogenic appearance.[75, 125] In transverse section, the dorsal sacroiliac ligament is homogeneously echogenic and oval in shape and is located on either side of the midline between the tuber sacrale and the sacrum (Fig. 3-26). The sacroiliac joint is not visible ultrasonographically from the skin surface. However, a transrectal examination can be performed to image the ventral sacroiliac ligament, the ventral margins of the sacroiliac and lumbosacral joints, and the ventral intervertebral foramina.[75] The ventral sacroiliac ligament is located between the articular margins of the ilial wing and sacrum and is echogenic and smooth, with a thickness and width of approximately 5 mm.[75]

Tendon Sheaths and Bursae

Digital Sheath. The echogenicity of the digital sheath is reportedly slightly less than that of the adjacent tendons.[8] Little or no fluid is imaged within the digital sheath of clinically normal horses. The mesotendinous attach-

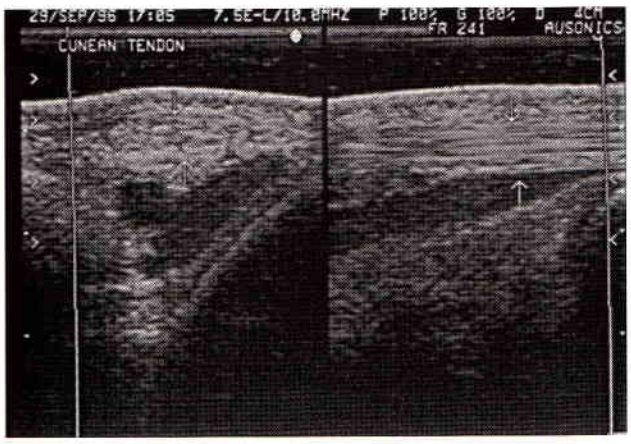

Figure 3–24

Sonograms of the normal cunean tendon over the dorsal aspect of the hock, obtained from a 12-year-old Thoroughbred gelding. Notice the homogeneous echogenic appearance and parallel fiber alignment of the cunean tendon *(arrows)*. These sonograms were obtained with a wide-bandwidth 7.5-MHz linear-array transducer operating at 10.0 MHz using a hand-held standoff pad at a displayed depth of 4 cm. The focal zones are in the near field of the images. The right side of the transverse view *(left image)* is lateral and the left side is medial. The right side of the sagittal view *(right image)* is proximal and the left side is distal.

ments of the deep digital flexor tendon to the digital sheath are not normally imaged. Clear anechoic fluid is imaged in clinically normal horses with small "windpuffs."

Carpal Sheath. Anechoic fluid is normally imaged within the carpal sheath in the proximal metacarpal region between the dorsal aspect of the deep digital flexor tendon and the inferior check ligament. The carpal sheath normally contains more fluid along its medial aspect, where it is not limited by the inferior check ligament.

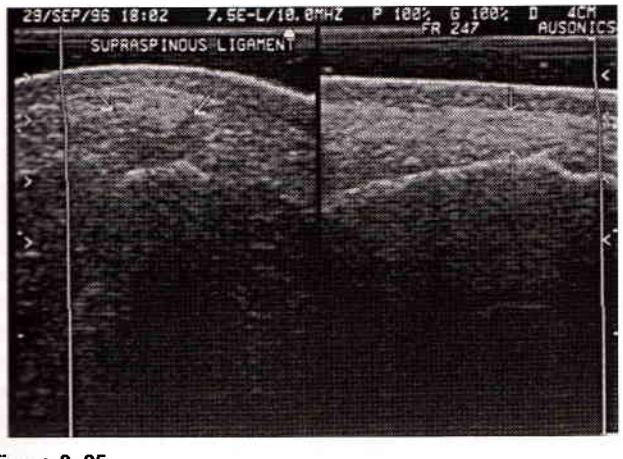

Figure 3–25

Sonograms of the normal supraspinous ligament in the thoracic region of a 12-year-old Thoroughbred gelding. Notice the homogeneous echogenic appearance of the supraspinous ligament *(arrows)*, its oval shape, and the parallel fiber pattern. These sonograms were obtained with a wide-bandwidth 7.5-MHz linear-array transducer operating at 10.0 MHz using a hand-held standoff pad at a displayed depth of 4 cm. The focal zones are in the near field of the images. The right side of the transverse view *(left image)* is left and the left side is right. The right side of the sagittal view *(right image)* is proximal and the left side is distal.

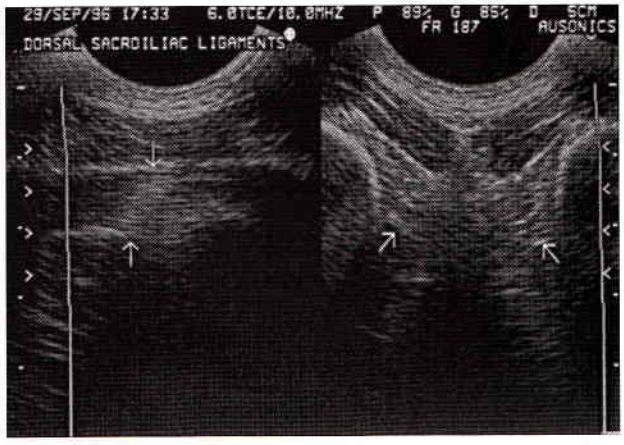

Figure 3–26

Sonograms of the normal dorsal sacroiliac ligament, obtained from a 12-year-old Thoroughbred gelding with a wide-bandwidth 6.0-MHz microconvex linear-array transducer operating at 10.0 MHz at a displayed depth of 6 cm. Notice that the dorsal sacroiliac ligaments have a slightly hypoechoic appearance in transverse section *(right image)*, but a parallel fiber pattern in sagittal section *(left image)*. The curved shape of this ligament precludes orienting the ultrasound beam perpendicular to its fibers, creating an artifactual hypoechoic appearance. The focal zones are in the middle of the images. The right side of the transverse image is the left side of the horse and the left side is the right side of the horse. The right side of the sagittal image is proximal and the left side is distal.

Tarsal Sheath. The tarsal sheath envelops the deep digital flexor tendon along the plantaromedial aspect of the tarsus and contains little visible fluid in the normal horse (see Fig. 3-8).[93] The tarsal sheath is an echogenic structure that is not usually distinguishable from the deep digital flexor tendon throughout its length. The tarsal sheath begins approximately 6 cm proximal to the medial malleolus and extends into the proximal quarter to third of the metatarsus.

Extensor Tendon Sheaths. The tendon sheaths of the extensor tendons over the dorsal aspect of the carpus have been thoroughly described.[87] Each extensor tendon is surrounded by a tendon sheath as it crosses the dorsal aspect of the carpus, and these can be imaged. A thin rim of fluid may occasionally be imaged within the sheath of the extensor carpi radialis tendon or long digital extensor tendon, but fluid is rarely imaged in the other extensor tendon sheaths in normal horses.

Bicipital Bursa. The bursa is a potential space between the bicipital tendon and the intertuberal groove of the distal humerus; in the normal horse, it does not contain visible fluid. The cranial-to-caudal width of the bicipital bursa measures 3 mm or less in normal Quarter horses.[74]

Navicular Bursa. The navicular bursa is the anechoic space bounded by the deep digital flexor tendon and the navicular bone. The collateral ligament of the navicular bone has a linear fiber pattern, but often appears hypoechoic in ultrasound images of this region because positioning the ultrasound beam perpendicular to the long axis of these fibers is usually not possible.

Trochanteric Bursa. The trochanteric bursa is only a potential space between the accessory head of the middle gluteal muscle and the greater trochanter. The bursa does not contain visible fluid in the normal horse.

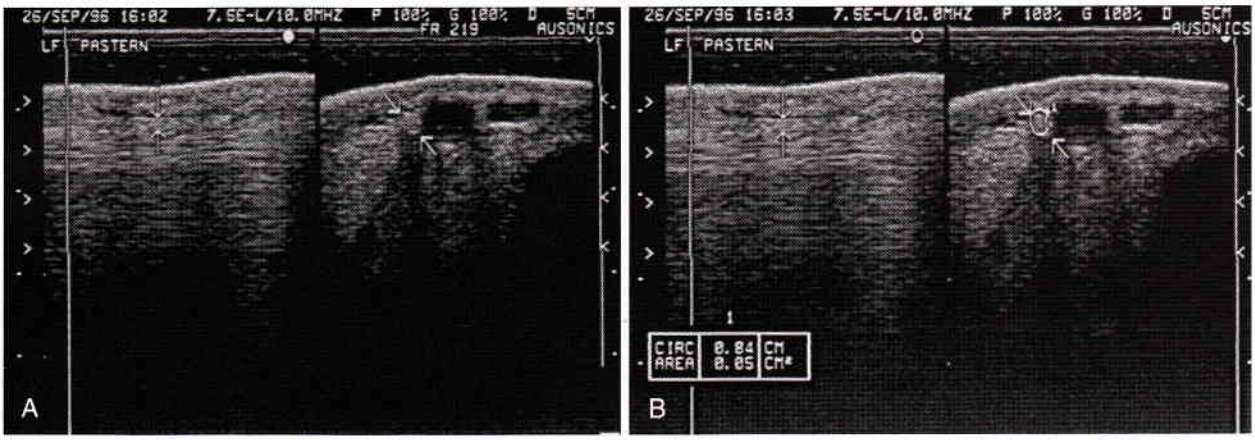

Figure 3–27

Sonograms of the normal posterior digital nerve along the proximal and lateral aspect of the pastern, obtained from a 12-year-old Thoroughbred gelding. These sonograms were obtained with a wide-bandwidth 7.5-MHz linear-array transducer operating at 10.0 MHz using a hand-held standoff pad at a displayed depth of 5 cm. The focal zones are in the near field of the images. The left side of the transverse views *(right images)* is palmar and the right side is dorsal. The left side of the sagittal views *(left images)* is distal and the right side is proximal.

A, Notice the small echogenic nerve *(arrows)*, which is slightly oval in transverse section immediately palmar to the posterior digital artery and dorsal to the superficial digital flexor tendon along the lateral aspect of the pastern. The posterior digital nerve has a somewhat coarser texture than the adjacent superficial digital flexor tendon when imaged in its long-axis section.

B, Sonogram demonstrating the measurement of the cross-sectional area of the normal posterior digital nerve *(arrows)*. This posterior digital nerve had a cross-sectional area of 0.05 cm^2.

Calcaneal and Gastrocnemius Bursa. The calcaneal bursa which extends from the mid-tibial level to the point of the hock, lies between the superficial digital flexor tendon and the gastrocnemius tendon. The calcaneal bursa is only a potential space in normal horses. The calcaneal bursa may be visible as a thin anechoic line between the superficial digital flexor tendon and the gastrocnemius tendon (see Fig. 3-20). A small gastrocnemius bursa also lies cranial to the insertion of the gastrocnemius tendon on the tuber calcis and may communicate with the more caudal calcaneal bursa between the gastrocnemius tendon and the superficial digital flexor tendon.[64] The gastrocnemius bursa may be imaged as a thin anechoic line adjacent to the cranial margin of the gastrocnemius tendon between the tendon and the underlying tuber calcis.

Tibialis Cranialis Tendon Sheath and Cunean Bursa. The sheath surrounding the tibialis cranialis tendon normally does not contain visible fluid. Therefore, this tendon sheath is not usually imaged as a distinctly separate echogenic structure (see Fig. 3-24). The cunean bursa is also a potential space deep to the flat elliptical cunean tendon. A small anechoic line may be imaged in the bursa of some horses between the cunean tendon and the underlying bone.

Atlantal and Supraspinous Bursa. The atlantal bursa is only a potential space between the ligamentum nuchae and the atlas and does not contain visible fluid in normal horses. Similarly, the supraspinous bursa is only a potential space and no visible fluid should be imaged in normal horses between the supraspinous ligament and the dorsal spinous processes of the second thoracic vertebrae.

Nerve

The normal nerve is echogenic and is difficult to distinguish from the surrounding tissues unless a machine with superior image quality is used. The digital nerves are easiest to recognize in the transverse plane by locating the digital vein and artery along the lateral or medial aspect of the limb. The digital nerve lies immediately palmar or plantar to the digital artery and immediately dorsal to the digital sheath and superficial and deep digital flexor tendons. The nerve normally is slightly more echogenic than the surrounding soft tissue and has an oval to circular appearance in transverse section. The normal digital nerve is very small, has a cross-sectional area of approximately 0.5 to 1.0 mm^2, and is 2 to 3 mm in thickness (Fig. 3-27).

Muscle

Normal muscle has a heterogeneous striated appearance with primarily hypoechoic muscle fibers interspersed with more echogenic fascia, connective tissue, and fat (Fig. 3-28). This gives skeletal muscle a "marbled" appearance in short-axis cross-section. Each muscle has a distinctive ultrasonographic appearance based on the amount of connective tissue present within the muscle belly. The normal triceps muscle appears similar between contralateral forelimbs with a wedge-shaped appearance in longitudinal section.[89] The muscle tissue appears hypoechoic with fine echoic lines representing interfascicular connective tissue. The fascial septum between the lateral and long heads of the triceps muscle is a definable hyperechoic line that appears as a double line in some scans.[89] The short linear echoes within the muscle bellies are parallel, their thickness and echogenicity varied, and they meet at a hyperechoic fascial line at 25 to 30 degrees.[89] In transverse sections, the triceps muscle has a speckled appearance. Anechoic areas are identified, usually near the fascial septum separating the long and lateral heads of the triceps muscles, in some scans. These anechoic

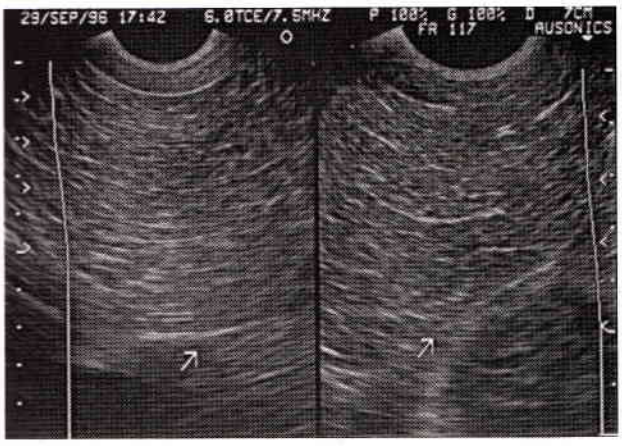

Figure 3–28

Sonograms of the normal semitendinosus and semimembranosus muscles in the left hindleg of a 12-year-old Thoroughbred gelding. Notice the hypoechoic musculature with echogenic linear echoes in the long-axis view of the muscle belly *(left image)* and the speckle pattern in the short-axis view *(right image)*. The fascia between the two adjacent muscle bellies is the more echogenic thicker linear echo *(arrows)*. These images were obtained with a wide-bandwidth 6.0-MHz microconvex linear-array transducer operating at 7.5 MHz at a displayed depth of 7 cm. The focal zones are in the near field *(left image)* and spread throughout the image *(right image)*. The right side of the short-axis view is lateral and the left side is medial. The right side of the long-axis view is proximal and the left side is distal.

areas are thought to represent loose connective tissue.[89] When the horse does not bear weight on the limb, the muscles consistently appear more echogenic.[89] This increased echogenicity appears to be the result of more closely packed muscle fasciculi.[89] Comparisons between muscle bellies in the contralateral limb should be performed if questionable areas of abnormality are detected ultrasonographically. Care must be taken in evaluating horses that are not bearing weight because the non-weight bearing muscle appears more echogenic, but the striated pattern should be preserved.

Bone

Normal cortical bone has a strong reflection, "bony surface echo," which is characteristic (Fig. 3-29). The physis in foals and young horses is a linear anechoic space between the metaphysis and the epiphysis of the bone and is oriented perpendicular to the bone's long axis (Fig. 3-30). A soft tissue layer normally overlies the bone in all areas except within a synovial structure, the only normal place where a fluid layer is immediately adjacent to the bony surface echo. The continuity of the bony surface echo may be disrupted by normal bony protuberances such as the greater trochanter. Careful scanning of these bony protuberances in two mutually perpendicular planes usually reveals that these structures are continuous with the bone in one or more planes and are not fractures. These structures should appear similar in the contralateral limb, confirming this normal discontinuity. The articular cartilage is normally anechoic (Fig. 3-31) with alarger amount of cartilage detected in foals because the bones ossify with development. The cartilage detected in foals that is in the process of ossification is more heterogeneous (Fig. 3-32) than is normal articular cartilage in the adult.

Joints

Joint fluid, if visible, should be anechoic. Synovial villi, if imaged, should appear as thin villous echogenic structures floating in the synovial fluid.

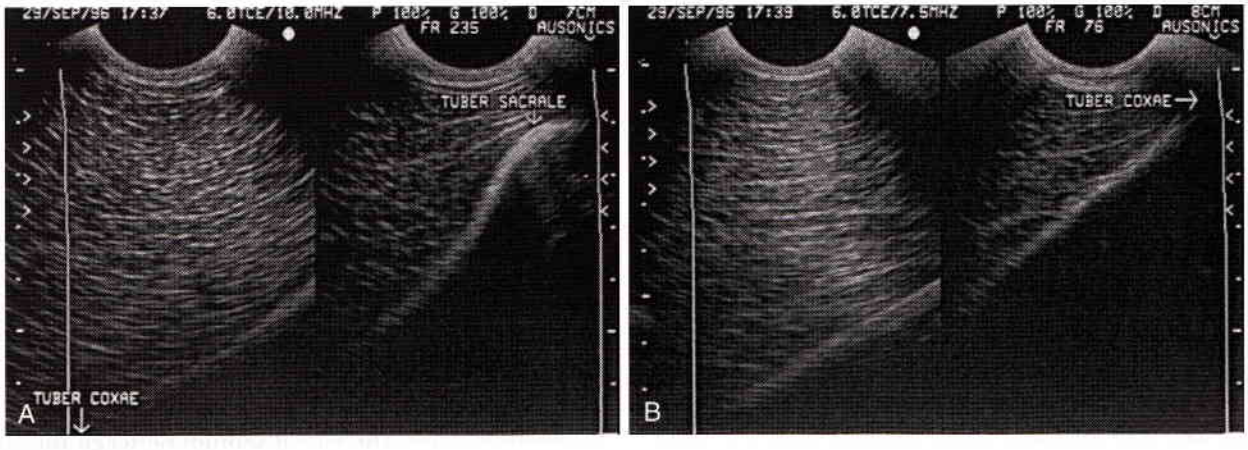

Figure 3–29

Sonograms of the normal gluteal muscles and underlying wing *(A)* and shaft *(B)* of the ilium, obtained from a 12-year-old Thoroughbred gelding. Notice the smooth contour of the bone and the strong bony surface echo. These sonograms were obtained with a wide-bandwidth 6.0-MHz microconvex linear-array transducer operating at 10.0 MHz *(A)* and 7.5 MHz *(B)* at a displayed depth of 7 cm *(A)* and 8 cm *(B)*. The focal zones are in the near field of the images.

A. The hyperechoic line extending from the tuber sacrale to the tuber coxae is the wing of the ilium scanned in its long axis. The right side of these sonograms is towards the tuber sacrale and the left side is towards the tuber coxae. The right sonogram was obtained at the edge of the tuber sacrale whereas the left sonogram was obtained close to the tuber coxae in the same scan plane.

B. The hyperechoic line extending from the tuber coxae distally is the shaft of the ilium. The right side of these sonograms is towards the tuber coxae and the left side is towards the acetabulum. The right sonogram was obtained at the edge of the tuber coxae and the left sonogram was obtained near the acetabulum in the same scan plane.

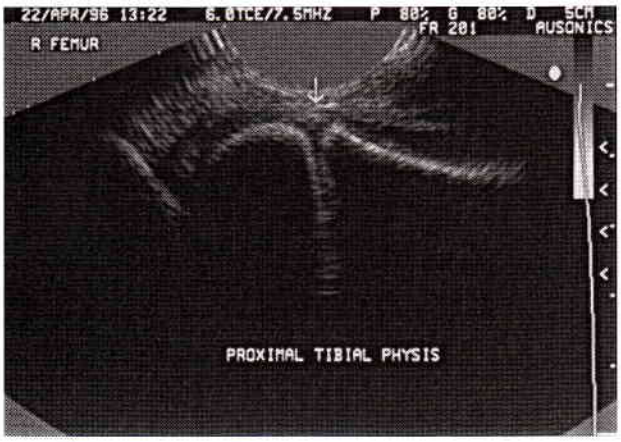

Figure 3–30

Sonogram of the normal proximal tibial physis, obtained from a 10-day-old Thoroughbred colt. Notice the anechoic physis *(arrow)* between the metaphysis and the diaphysis of the proximal tibia. The right side of this long-axis image is distal and the left side is proximal. The focal zones are in the near field of the image. This sonogram was obtained with a wide-bandwidth 6.0-MHz microconvex transducer operating at 7.5 MHz at a displayed depth of 5 cm.

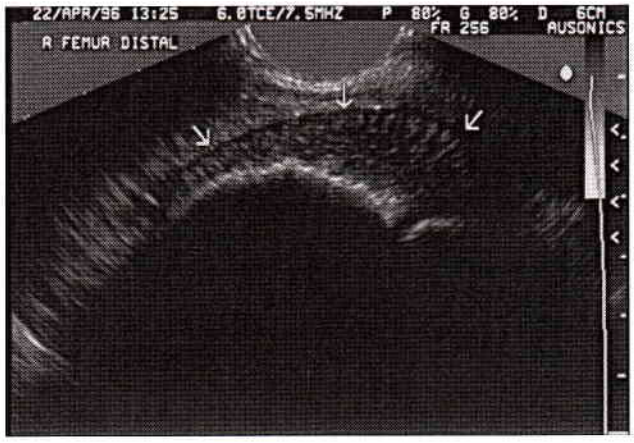

Figure 3–32

Sonogram of the cartilage of the normal lateral trochlear ridge of the femur, from a 10-day-old Thoroughbred colt. Notice the more heterogeneous appearance of the cartilage *(arrows)* and the large cartilage component of the distal femur present at this stage. The right side of this long-axis view is proximal and the left side is distal. This sonogram was obtained with a wide-bandwidth 6.0-MHz microconvex linear-array transducer operating at a frequency of 7.5 MHz at a displayed depth of 6 cm. The focal zones are in the near field of the image.

Shoulder. The musculature of the shoulder girdle should be thoroughly examined in horses with lameness in the shoulder region. These muscles should all have a normal muscle fiber pattern and normal speckled appearance. The contralateral shoulder can be used for comparison. The tendon of the biceps brachii should be followed to its insertion and the underlying bursa examined. Joint fluid is not usually imaged in the normal shoulder joint.

Elbow. The collateral ligaments of the elbow joint are readily imaged along the medial and lateral aspect of the cubital joint as homogeneously echogenic structures with parallel fiber alignment. They can be imaged from their origins on the lateral or medial epicondyle of the humerus to their insertions on the lateral tuberosity of the radius, just distal to the margin of the articular surface (lateral collateral ligament) (Fig. 3–33), or to the medial border of the radius, just distal to the level of the interosseous space, and the medial tuberosity of the radius (medial collateral ligament). Joint fluid is not normally imaged in the cubital joint.

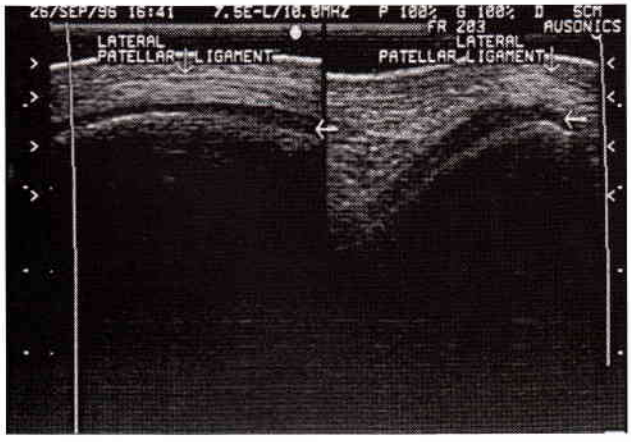

Figure 3–31

Sonograms of the normal articular cartilage over the lateral trochlear ridge of the femur in a 12-year-old Thoroughbred gelding. Notice the hypoechoic to nearly anechoic appearance of the articular cartilage *(horizontal arrows)* and a portion of the overlying echogenic lateral patellar ligament *(vertical arrows)*. These sonograms were obtained with a wide-bandwidth 7.5-MHz linear-array transducer operating at 10.0 MHz using a hand-held standoff pad at a displayed depth of 5 cm. The focal zones are in the near field of the images. The right sonogram is more proximal and lateral over the lateral trochlear ridge. Both sonograms are long-axis views with the left side of the long-axis view being distal and the right side proximal.

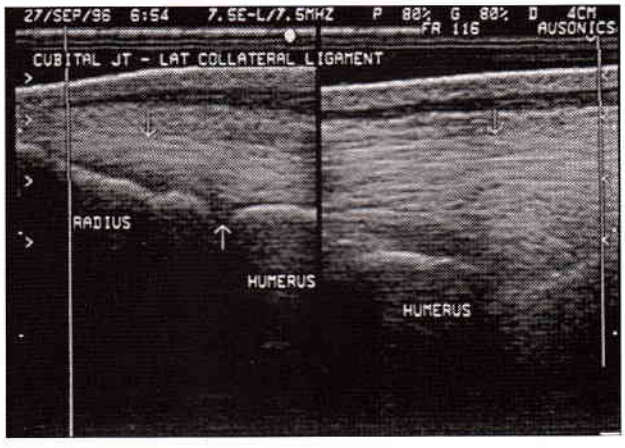

Figure 3–33

Sonograms of the normal lateral collateral ligament of the cubital joint, obtained from a 3-year-old Standardbred gelding. Notice the homogeneous echogenic appearance with a parallel fiber pattern throughout the lateral collateral ligament. Notice the broad origin *(right image)* and the narrower insertion distal to the lateral aspect of the radiohumeral joint *(left image)*. These sonograms are long-axis views obtained near the origin of the lateral collateral ligament from the humerus *(right image)* and at its insertion on the radius *(left image)*. These sonograms were obtained with a wide-bandwidth 7.5-MHz linear-array transducer operating at 7.5 MHz using a hand-held standoff pad at a displayed depth of 4 cm. The focal zones are in the near field of the images. The left sides of the images are distal and the right sides are proximal.

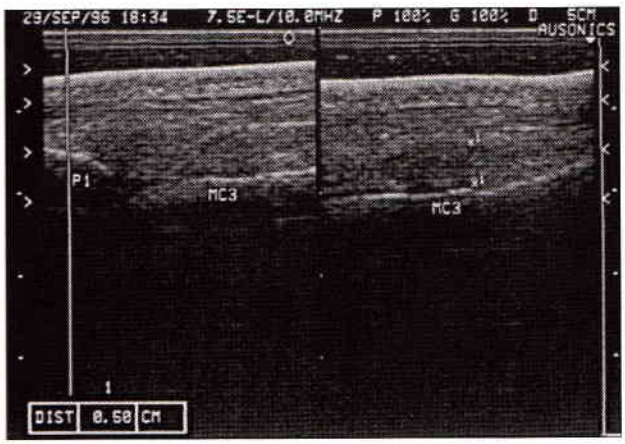

Figure 3–34

Sonograms of the normal dorsal reflection of the metacarpophalangeal joint, obtained from a 12-year-old Thoroughbred gelding. Notice the hypoechoic synovial fold in the dorsal recess of the metacarpophalangeal joint, which is 0.5 cm thick (x'), and the overlying extensor tendon. The joint capsule is not well visualized in this scan. The right image is more proximal at the dorsal reflection of the metacarpophalangeal joint, whereas the left image is more distal at the articulation between the distal metacarpus (MC3) and proximal P1. These sagittal sonograms were obtained with a wide-bandwidth 7.5-MHz linear-array transducer operating at 10.0 MHz using a hand-held standoff pad at a displayed depth of 5 cm. The focal zones are all in the near field. The right side of the sagittal sonograms is proximal and the left side is distal.

Carpus. The normal ultrasonographic appearance of the carpus has been described, focusing primarily on the sonographic appearance of the extensor tendons on the dorsal aspect of the carpus.[87] The lateral collateral ligament extends from the lateral (ulnar) styloid process distally to the fourth and third metacarpal bones. A long and superficial collateral ligament as well as a short and deep lateral collateral ligament are present, through which the lateral digital extensor tendon passes, surrounded by its synovial sheath. The lateral collateral ligament is approximately 5 mm thick and 27 to 29 mm wide, narrowing over the ulnar carpal bone to 19 to 21 mm wide with a slight increase in thickness.[87] At this level, the deep portion of the lateral collateral ligament extends dorsally whereas the superficial portion extends in a palmar direction. The lateral collateral ligament becomes wider (25 to 29 mm) and thicker (8 to 10 mm) over the fourth carpal bone and is crescent-shaped in transverse section as it expands to its insertion. The collateral ligaments have a homogeneous echogenic structure with a parallel fiber pattern. However, because the collateral ligaments are in different scan planes, the echogenicity of each one must be evaluated individually to prevent off-normal incidence artifacts. The fat areas in the antebrachiocarpal joint appear as two slightly less echogenic areas within the joint when compared to the more echogenic joint capsule.[87] The articular cartilage of the distal radius is detected as a smooth anechoic layer overlying the bone.[87] Fluid is not normally imaged in the dorsal aspect of the antebrachiocarpal and intercarpal joints.

Fetlock. Although the metacarpophalangeal joint was one of the first to be evaluated ultrasonographically in the horse, the initial description included only the sonographic findings in horses with proliferative synovitis and villonodular synovitis.[8, 90] The normal anatomy of this area has only recently been described.[96] Although the proximal synovial fold of the metacarpophalangeal joint was not clearly imaged in normal horses in this study, that has not been this author's experience. The normal proximal synovial fold of the metacarpo- or metatarsophalangeal joint should not exceed 5 mm in thickness (Fig. 3-34). Equipment with excellent resolution and high-frequency transducers, however, are necessary to successfully image these structures in the absence of excess synovial fluid.[96]

Both the long and short collateral ligaments of the fetlock joints have a parallel fiber pattern and should have a similar thickness and cross-sectional area between the lateral and medial aspects of the joint and in comparison to those in the contralateral forelimb or hindlimb (Fig. 3-35). The long collateral ligament is more easily imaged as it extends from the distal metacarpus or metatarsus to proximal P1 in the same plane. The short collateral ligament is more difficult to image due to its oblique orientation. It appears hypoechoic when viewed in the same image as the echogenic long collateral ligament. These collateral ligaments must be imaged independently because they lie in two different scan planes. The scan plane must be constantly changing when imaging both the short and long collateral ligaments to keep the ultrasound beam perpendicular to the fibers. The subtendinous bursa of the long digital extensor tendon is not normally imaged over the dorsal aspect of the metacarpo- or metatarsophalangeal joint in normal horses because this is just a potential space. A small amount of fluid is usually imaged in the volar pouches of the metacarpo- and metatarsophalangeal joints at the level of the distal portion of the branches of the suspensory ligament.

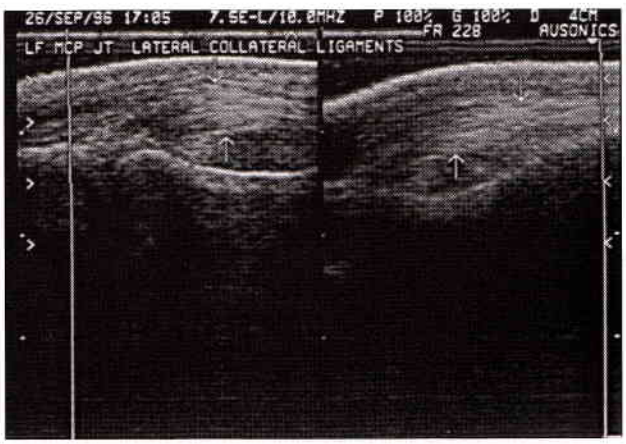

Figure 3–35

Sonograms of the normal lateral collateral ligaments of the metacarpophalangeal joint, obtained from a 12-year-old Thoroughbred gelding. Notice the outer longer ligament *(downward arrows)* and the shorter angled ligament *(upward arrows)*, which are rarely in the same scan plane at the same time. The sonogram on the right side of the image is proximal, along the distal lateral metacarpus; that on the left side is distal, along the distal lateral metacarpus and proximal P1. These sagittal sonograms were obtained with a wide-bandwidth 7.5-MHz linear-array transducer operating at 10.0 MHz using a hand-held standoff pad at a displayed depth of 4 cm. The focal zones are in the near field of the images. The left side of the sagittal views is distal and the right side is proximal.

Pastern. The collateral ligaments of the proximal interphalangeal joint can be imaged as homogeneously echogenic structures with a parallel fiber pattern from their origin on the distal aspect of P1 to their insertion on proximal to mid P2. Fluid is not normally imaged in the proximal interphalangeal joint. The distal interphalangeal joint was the first joint to be evaluated ultrasonographically in conjunction with ultrasonographic evaluation of the navicular bursa, navicular bone, and deep digital flexor tendon along the palmar aspect of the pastern.[2] The proximal palmar pouch of the distal interphalangeal joint is identified as a small anechoic fluid space palmar or plantar to the second phalanx. This outpouching of the distal interphalangeal joint is imaged dorsal to the collateral sesamoidean ligaments of the navicular bone and immediately proximal to the navicular bone.

The Pelvis and Hip. A smooth bony surface echo should be present along the dorsal aspect of the wing of the ilium from the tuber sacrale to the tuber coxae (see Fig. 3-29). The shaft of the ilium is slightly more irregular, but a strong bony surface echo should be produced from the ilial shaft. The greater trochanter of the femur and the outer portion of the acetabulum should also have a strong bony surface echo, although the deeper portions of the hip joint are not accessible for sonographic evaluation from the skin surface. The pelvis can also be imaged from a transrectal window and should produce a similar smooth bony surface echo.

Stifle. Several investigators have studied the ultrasonographic anatomy of the normal stifle in the standing horse, describing the patellar ligaments, collateral ligaments, menisci, and visible portions of the femoropatellar and femorotibial joints.[92, 94, 95, 101] Imaging the cruciate ligaments is much more difficult; the cooperative or sedated horse must stand with the stifle flexed, or else general anesthesia is required.[92, 101]

The middle, medial, and lateral patellar ligaments are homogeneously echogenic with a parallel fiber pattern and can be followed from their origin to their insertion (Fig. 3-36). The patellar ligaments appear oval in transverse section and lie immediately underneath the skin. The medial trochlear ridge appears wider than the lateral trochlear ridge with good visualization of the intertrochlear groove.[92] The articular cartilage of the trochlea is relatively anechoic between the hyperechoic subchondral bone and the echogenic soft tissue.[92] A large fat pad is imaged between the patellar ligaments and appears as somewhat heterogeneous echogenic soft tissue. Synovial fluid is not normally imaged in the femoropatellar joint.

The menisci are most easily recognized on sagittal scans as triangular echogenic structures with the apex of the triangle oriented towards the axial portion of the femorotibial joint (Fig. 3-37). The cranial lateral and cranial medial horns of the menisci are visible from between the lateral and middle patellar ligaments and between the medial and middle patellar ligaments in the standing horse. The cranial and caudal horns of the meniscus have a similar ultrasonographic appearance when imaged from the cranial and caudal aspects of the joint, respectively, with the joint flexed.

The cruciate ligaments appear similarly as homogeneously echogenic structures with a parallel fiber pattern, provided that the transducer can be positioned so that the ultrasound beam is perpendicular to the long axis of the ligamentous fibers. This is optimally obtained with a sector-scanner transducer.[101] Otherwise, the cruciate ligaments appear as hypoechoic ligamentous structures because of the off-normal incidence artifact, outlined by more echogenic fat. The cranial cruciate ligament appears somewhat oval in cross-section at its cranial insertion and rounder caudally. The femoral insertion of the caudal cruciate ligament is broad and flattened in a cranial to caudal direction.

The medial and lateral collateral ligaments of the femorotibial joint are readily imaged from their origins to their insertions. The medial collateral ligament originates from the medial epicondyle of the femur and is uniformly echogenic with a parallel fiber pattern. It inserts on a rough area distal to the margin of the medial condyle of the tibia (see Fig. 3-37). Cranial to the medial collateral ligament is a synovial outpouching of the medial femorotibial joint, which normally contains a small amount of fluid (Fig. 3-38). The lateral collateral ligament is slightly thicker and originates from the upper depression on the lateral epicondyle and inserts on the head of the fibula. The lateral collateral ligament covers the origin of the popliteus muscle. The bursa between the tendon of origin of the popliteus muscle and the lateral collateral ligament and between the lateral collateral ligament and the margin of the lateral condyle of the tibia is only a potential space and is not imaged in normal horses. Usually, little or no anechoic synovial fluid is imaged in the lateral compartment of the femorotibial joint (see Fig. 3-38). The combined origin of the long digital extensor muscle and the peroneus tertius tendon is cranial to the

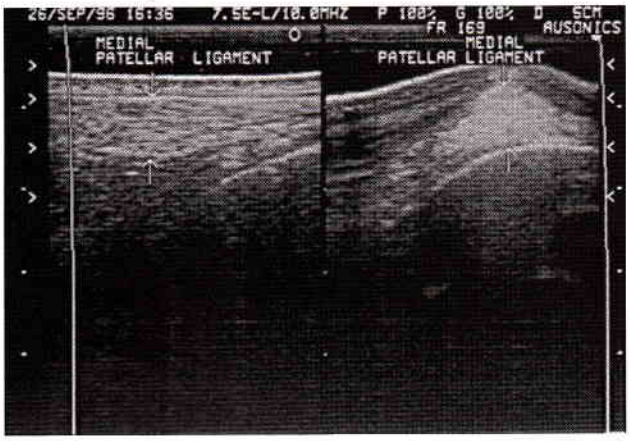

Figure 3–36

Sonograms of the normal medial patellar ligament, obtained from a 12-year-old Thoroughbred gelding. Notice the homogeneous echogenic appearance of the patellar ligament and its parallel fiber pattern. The medial patellar ligament is located between the arrows. These sonograms were obtained near the origin of the medial patellar ligament, with a wide-bandwidth 7.5-MHz linear-array transducer operating at 10.0 MHz using a hand-held standoff pad at a displayed depth of 5 cm. The focal zones are in the near field of the images. The left side of the short-axis view *(right image)* is caudal and the right side is cranial. The left side of the long-axis view *(left image)* is distal and the right side is proximal.

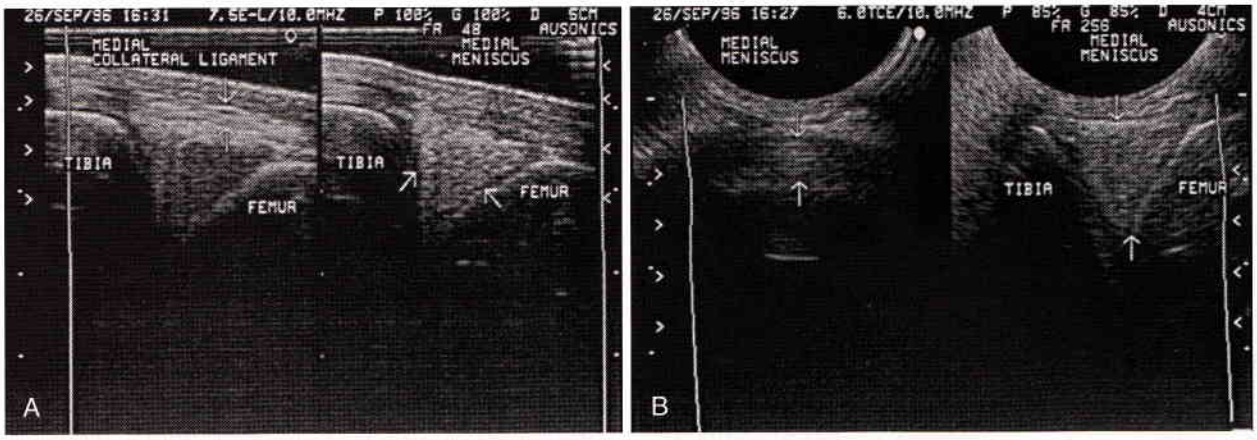

Figure 3–37

Sonograms of the normal medial collateral ligament of the femorotibial joint and the medial meniscus, obtained from a 12-year-old Thoroughbred gelding. These sonograms were obtained with a wide-bandwidth 7.5-MHz linear-array transducer using a hand-held standoff pad *(A)* or a 6.0-MHz microconvex-array transducer *(B)* operating at 10.0 MHz at a displayed depth of 5 cm *(A)* and 4 cm *(B)*. The focal zones are in the near field of the images. The left side of the short-axis view is caudal and the right side is cranial. The left side of the long-axis view is distal and the right side is proximal.

A, Notice the parallel fiber pattern of the medial collateral ligament *(vertical arrows)* and its homogeneous echogenic appearance in the left sonogram with a hypoechoic medial meniscus. The medial meniscus appears hypoechoic in the left sonogram because it is not in the same scan plane (off-normal incidence artifact). Notice the homogeneous and echogenic meniscus in the right sonogram *(diagonal arrows)* with a hypoechoic medial collateral ligament, again because of an off-normal incidence artifact. These are both long-axis sonograms.

B, Notice the disc shape to the medial meniscus *(arrows)* in its short-axis section *(left image)* with the more recognizable triangular appearance of the meniscus *(arrows)* in its long-axis section *(right image)*. The meniscus is located between the two vertical arrows in both images.

lateral collateral ligament and caudal to the lateral patellar ligament.

Hock. The ultrasonographic anatomy of a portion of the hock has been described, focusing on the medial collateral ligaments and the dorsomedial joint capsule of the tarsocrural joint.[93] The collateral ligaments here, as in the carpus, are multiple and may be difficult to separate sonographically if high-resolution imaging with high-frequency transducers is not possible. The long medial collateral ligament originates on the caudomedial surface of the medial malleolus of the tibia and extends distally to its insertion on the distal tuberosity of the tibial tarsal bone, the medial surface of the small tarsal bones, and the proximal portion of the second and third metatarsal bones (Fig. 3-39). The short collateral ligaments, three of which are on the medial aspect of the tarsus, extend from their origin on the craniomedial aspect of the medial malleolus of the tibia plantarodistally under the long collateral ligament to their respective insertions. The flat superficial short medial collateral ligament inserts on the proximal and distal tuberosity of the tibial tarsal bone and the intervening ridge, with its plantarodistal attachment lying immediately adjacent to the attachment of the long collateral ligament. The insertion of the round mid-

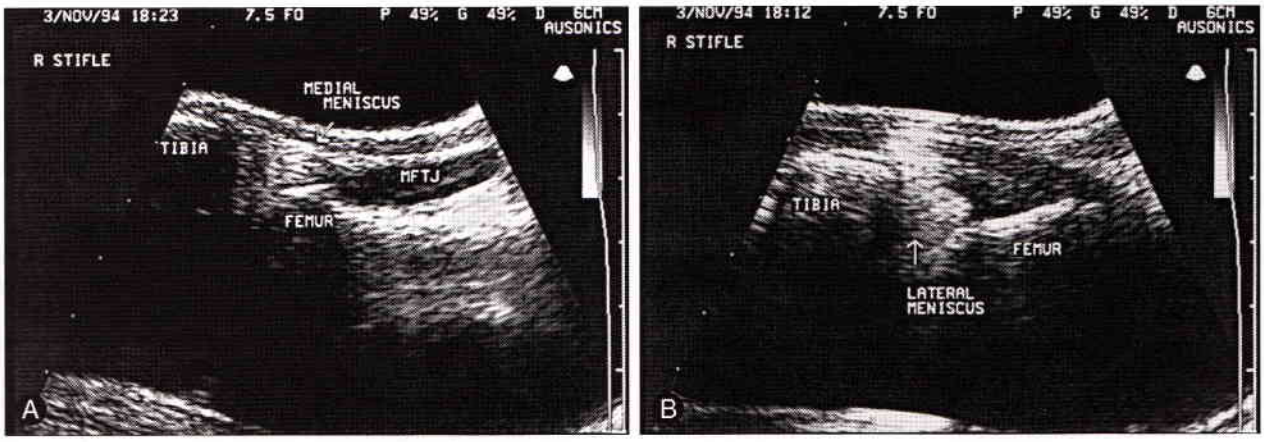

Figure 3–38

Sonograms of the normal medial *(A)* and lateral *(B)* compartments of the right femorotibial joint, obtained from a 17-year-old Quarter horse gelding. These are both long-axis sonograms, with the right side of the sonogram being proximal and the left side distal. Notice the larger outpouching and greater amount of synovial fluid in the medial femorotibial compartment compared with the lateral. The lateral collateral ligament is well-visualized over the lateral meniscus *(B)*, whereas only a portion of the medial meniscus is visualized in the image of the medial compartment of the femorotibial joint *(A)*. These sonograms were obtained with a 7.5-MHz sector-scanner transducer containing a built-in fluid offset at a displayed depth of 6 cm.

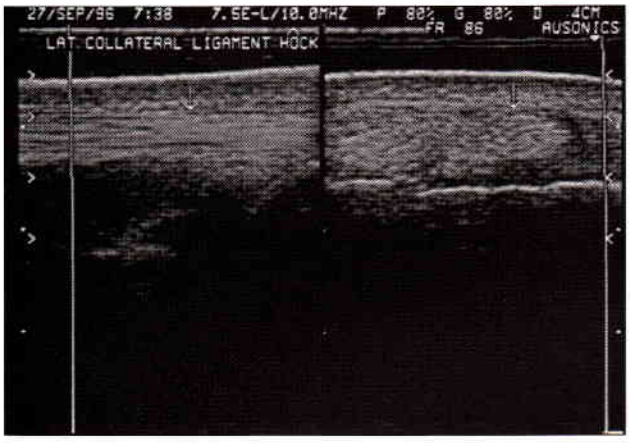

Figure 3–39

Sonograms of the normal long lateral collateral ligament *(arrows)* of the hock that reveal the homogeneous echogenic appearance and the parallel fiber pattern of the long collateral ligament. These sonograms were obtained from a 12-year-old Thoroughbred gelding with a wide-bandwidth 7.5-MHz linear-array transducer operating at 10.0 MHz using a hand-held standoff pad and a displayed depth of 4 cm. The focal zones are in the near field of the images. The left side of the short-axis view *(right image)* is caudal and the right side is cranial. The left side of the long-axis view *(left image)* is distal and the right side is proximal.

dle short medial collateral ligament is the distomedial surface of the sustentaculum tali and the plantaromedial surface of the central tarsal bone. The insertion of the flat short deep medial collateral ligament is the tibial tarsal bone.

The dorsomedial aspect of the tarsocrural joint capsule is situated close to the underlying trochlear ridges with minimal synovial fluid present that might help delineate this structure in the normal horse. The appearance of the inner surface of the medial compartment of the equine tarsocrural joint after the injection of 60 ml of physiologic saline has been described.[93] In this situation, the inner surface of the joint capsule is covered by short pointed villi that are most prominent in the middle region dorsal to the trochlear ridges of the tibial tarsal bone. The villi may appear to agglomerate proximally, dorsal to the distal end of the tibia, and may resemble a small villonodular mass, whereas distally the synovial villi are longer and have a more straggly appearance.[93]

Abnormal Structures

Tendon and Ligament Abnormalities

The most frequently injured structure in most types of performance horses is the superficial digital flexor tendon.[16, 19, 25] The superficial digital flexor tendon in the front leg is the most frequently injured tendon or ligament in Thoroughbred racehorses, National Hunt horses or other horses that race over fences, Standardbred racehorses, Arabian racehorses, horses that compete in combined training, and polo ponies. It is also a common injury in fox hunters and show jumpers. The swelling commonly seen along the plantar aspect of the hock, usually referred to by laymen as a "curb," most frequently represents superficial digital flexor tendon injury if it is the result of a tendinous or ligamentous injury.

The suspensory ligament is the second most frequently injured structure in performance horses, and injury to it occurs most frequently in Standardbred racehorses and dressage horses.[16, 19, 25] Suspensory ligament injuries also occur in Thoroughbred racehorses, National Hunt horses and other horses that race over fences, Arabian racehorses, Quarter horse racehorses, horses that compete in combined training, show jumpers, show hunters, fox hunters, polo ponies, reining and cutting horses, and endurance horses. Suspensory ligament injuries are part of the often catastrophic breakdown injury (traumatic disruption of the suspensory apparatus) that occurs in Thoroughbred flat racers. Although more common in the forelimb, suspensory ligament injuries also occur frequently in the hind limb, especially in Standardbred racehorses and dressage horses.

The inferior check ligament is the third most frequently injured tendon or ligament in the foreleg and is an extremely rare injury in the hindlimb because this structure is absent or is only a vestigial structure in the hindlimb of most horses.[16, 19, 25] Injuries to the inferior check ligament are often noticed after a horse has been turned out in the field, rather than during or after a competition, although both occur. Inferior check ligament injuries have been reported more frequently in ponies and older horses that have been used for jumping.[44, 53] The deep digital flexor tendon is the least frequently injured tendon or ligament in the foreleg of performance horses, but may be the second most common injury in the hind leg of horses, particularly upper-level show jumpers and dressage horses.[16, 19, 25]

The best indication of damage to a tendon or ligament is swelling of the affected structure, with less than 50% of horses showing lameness at the time the injury occurs or at the time of presentation to the veterinarian.[16, 25] Heat and sensitivity in the affected tendon or ligament are commonly detected. Although injury to the tendons and ligaments can occur without local swelling, heat, or sensitivity, a complete lameness examination with diagnostic nerve blocks should be performed initially if lameness is the only historical or presenting sign of injury. An ultrasonographic examination is only indicated in these horses after the lameness is localized and radiographic examination reveals no significant findings, because an ultrasonographic examination in these horses is less likely to yield abnormal findings.

A recent injury to the tendons or ligaments resulting in fiber disruption most frequently appears as an anechoic hole or "core" in the affected tendon or ligament. This core lesion can occur in any part of the tendon or ligament but occurs most frequently in the center of the affected tendon or ligament, especially the superficial digital flexor tendon and suspensory ligament. A more diffuse type of injury also occurs in which diffuse and often intermittent disruption of fibers is seen throughout the entire tendon or ligament, without a discrete area of fiber damage. The total cross-sectional area of the affected tendon or ligament may be enlarged with preservation of fiber alignment consistent with a tendinitis or desmitis. Knowledge of the normal tendon cross-sectional area at

each zone or comparison with the normal contralateral forelimb or hindlimb is useful in determining if a mild tendinitis or desmitis is present. Measurement of tendon or ligament cross-sectional area and the cross-sectional area of the injury allows for calculation of the percentage of tendon or ligament damage.[16] These calculations are essential for critical evaluation of tendon and ligament injuries and their response to treatment.[16]

The severity of tendon and ligament injuries has been characterized based on the echogenicity of the lesion into type 1 to 4 lesions.[15] Type 1 lesions are slightly less echogenic than normal and represent minimal disruption of the fiber pattern and minimal inflammatory cell infiltrate.[15] These lesions are most consistent with a tendinitis or desmitis with preservation of the normal fiber alignment. Type 2 lesions are half echogenic and half anechoic.[15] These lesions represent fiber disruption and local inflammation. Type 3 lesions are mostly anechoic and represent significant fiber tearing.[15] Type 4 lesions are completely anechoic and indicate total fiber tearing within the lesion and hematoma formation.[15] These injury types should be assigned to tendon and ligament injuries based on the sonographic findings in both the transverse and sagittal views. Organizing clot may appear isoechoic with normal tendon or ligament tissue and thus can be erroneously graded a type-1 injury. When imaged in the sagittal view, however, no fibers are present within the lesion—only organizing hemorrhage consistent with a type 4 lesion. Assessment of fiber alignment has also been used to grade the severity of tendon and ligament injuries.[38, 39] A fiber score of 0 is given when the fiber alignment in the "target zone" or injury area has 76% to 100% parallel fibers.[38, 39] When 51% to 75% of the "target zone" has parallel fiber alignment, a score of 1 is assigned. A fiber score of 2 refers to 26% to 50% parallel fiber alignment in the "target" zone and a fiber score of 3 refers to 0% to 25% parallel fibers within the lesion. In the beta-aminoproprionitrile fumarate (βAPN-F) trial, echogenicity scores of 0 to 3 were assigned similar to the fiber alignment scores. An echogenicity score of 0 represents normal tendon echogenicity. An echogenicity score of 1 represents a lesion that is mostly echogenic, a score of 2 a lesion that is 50% anechoic and 50% echogenic, and a score of 3 a lesion that is mostly anechoic.

As the tendon or ligament heals, its echogenicity increases and short linear echoes are detected in the affected tendon or ligament in the sagittal view. With continued tendon or ligament healing, longer linear echoes are often detected in the repairing area with improved alignment of these fibers. A decrease in the tendon or ligament cross-sectional area at the maximal injury zone and/or in the total cross-sectional area of the tendon or ligament is an indication of tendon or ligament healing and remodeling. A decrease in the amount of peritendinous or periligamentous swelling should occur. Complete resolution of this swelling may occur if all the inflammation has resolved in these tissues. The detection of echogenic peritendinous or periligamentous tissue is an indication of continued inflammation in the surrounding subcutaneous tissues that may progress to fibrosis with the development of adhesions between the tendons or ligaments and the adjacent soft tissue structures. The ideal tendon or ligament repair is one in which the lesion is no longer discretely visible sonographically because the area of injury has filled in with tissue that is isoechoic with that of the normal tendon or ligament, fiber alignment is normal (parallel) to near normal, and no evidence exists of peritendinous or periligamentous scarring.

The use of diagnostic ultrasound to monitor the rehabilitation of injured tendons and ligaments is relatively new. Much of this information has evolved from the frequent sonographic monitoring of horses with tendon and ligament injuries that were being treated in the recent clinical trials evaluating the efficacy of βAPN-F.[30, 38, 39, 126, 127] The majority of horses treated in these trials had injuries to the superficial digital flexor tendon, but injuries to the suspensory ligament, inferior check ligament, deep digital flexor tendon, and superficial digital flexor tendon in the pastern were also treated with βAPN-F and monitored sonographically. Horses were monitored ultrasonographically every month to 2 months with occasional exceptions until they had returned to their prior competition or had failed to do so. Total sonographic monitoring periods extended for 2 and one-half years or more whenever possible. Sonographic indications of tendon or ligament healing and remodeling were an increase in lesion echogenicity, an overall improvement in fiber alignment within the abnormal portion of the tendon or ligament, a decrease in the cross-sectional area of the lesion, and an overall decrease in the total cross-sectional area of the tendon or ligament. Peritendinous or periligamentous soft tissue swelling resolved in the majority of treated horses.

Superficial Digital Flexor Tendon Abnormalities. Swelling of the tendon is the most common clinical sign in horses with an injury of the superficial digital flexor tendon.[16, 25] Local heat and sensitivity are also commonly detected, both at the time the injury is first noticed and, to a somewhat lesser extent, at the time of referral to a veterinary hospital for sonographic examination.[16, 25] Lameness is not usually detected in most horses with injuries to the superficial digital flexor tendon, unless the injury to the tendon is severe. Lameness is more likely if the injury to the superficial digital flexor tendon involves the area of the tendon within the carpal canal or the branches of the superficial digital flexor tendon at the pastern. Sinking of the fetlock joint occurs with severe injuries to the superficial digital flexor tendon causing loss of support to the palmar aspect of the fetlock. Swelling over the plantar aspect of the hock, typically referred to as a "curb" by veterinarians and layman alike, is usually the result of an injury to the superficial digital flexor tendon in this region, rather than a plantar ligament desmitis, if a tendon or ligament injury has occurred. These swellings usually extend somewhat distal to the hock, but are not usually associated with tendinitis involving the superficial digital flexor tendon in the mid-metatarsal to distal metatarsal region. These areas of superficial digital flexor tendinitis usually cause more of a cosmetic problem than a functional problem.

The most minor injury to the superficial digital flexor tendon is a decreased echogenicity of the tendon with preservation of normal fiber alignment. The superficial digital flexor tendinitis can be mild (Fig. 3–40), with little

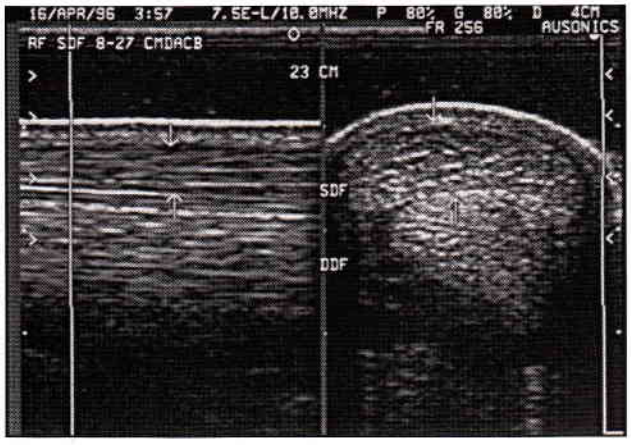

Figure 3–40

Sonograms of the right fore superficial digital flexor tendon, obtained from a 2-year-old Thoroughbred filly with mild filling that developed after a breeze. Notice the mild decrease in the echogenicity of the superficial digital flexor tendon (SDF), which was imaged from 8 to 27 cm distal to the point of the accessory carpal bone. The fiber pattern of the SDF is fairly well preserved but the fiber bundles are separated by anechoic fluid. The cross-sectional area of the SDF is mildly increased and measured 1.32 cm^2. This image was obtained at 23 cm distal to the point of the accessory carpal bone (zone 3A). These sonograms were obtained with a wide-bandwidth 7.5-MHz linear-array transducer operating at 10.0 MHz using a hand-held standoff pad at a displayed depth of 4 cm. The focal zones are in the near field of the images. The left side of the transverse view *(right image)* is medial and the right side is lateral. The left side of the sagittal view *(left image)* is distal and the right side is proximal. DDF, deep digital flexor tendon.

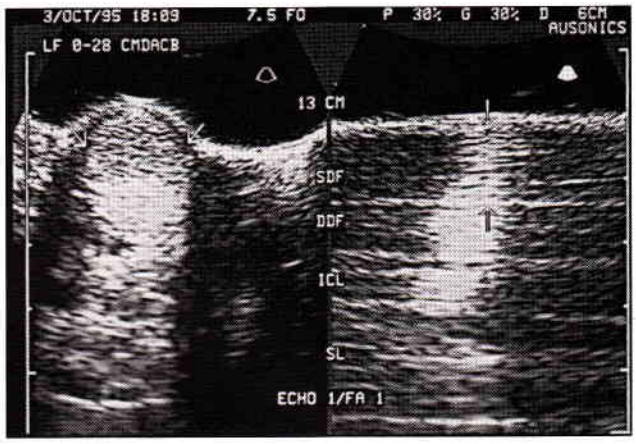

Figure 3–41

Sonograms of the left fore superficial digital flexor tendon (SDF), obtained from a 2-year-old Thoroughbred gelding with significant tendinitis in the left foreleg. Notice the hypoechoic appearance of the enlarged SDF and the separation of fiber bundles with some loss of their normal parallel alignment in the more superficial (palmar) portion of the tendon. The cross-sectional area of the SDF measured 1.75 cm^2 at the worst injury zone (13 cm distal to the point of the accessory carpal bone or at the border between zones 1B and 2A), which is at least 50% larger than normal. This diffuse tendinitis was present from 0 to 28 cm distal to the point of the accessory carpal bone. These sonograms were obtained with a 7.5-MHz sector-scanner transducer containing a built-in fluid offset at a displayed depth of 6 cm. The right side of the transverse view *(left image)* is lateral and the left side is medial. The right side of the sagittal view *(right image)* is proximal and the left side is distal. DDF, deep digital flexor tendon; ICL, inferior check ligament; SL, suspensory ligament.

or no enlargement of tendon cross-sectional area and only a mild decrease in tendon echogenicity. With more severe tendinitis, tendon cross-sectional area is significantly increased with little or no sonographic evidence of fiber disruption (Fig. 3–41). This increase in tendon cross-sectional area appears to occur with anechoic to hypoechoic separation of fibers, usually representing hemorrhage and/or serum or, more likely, an inflamma-

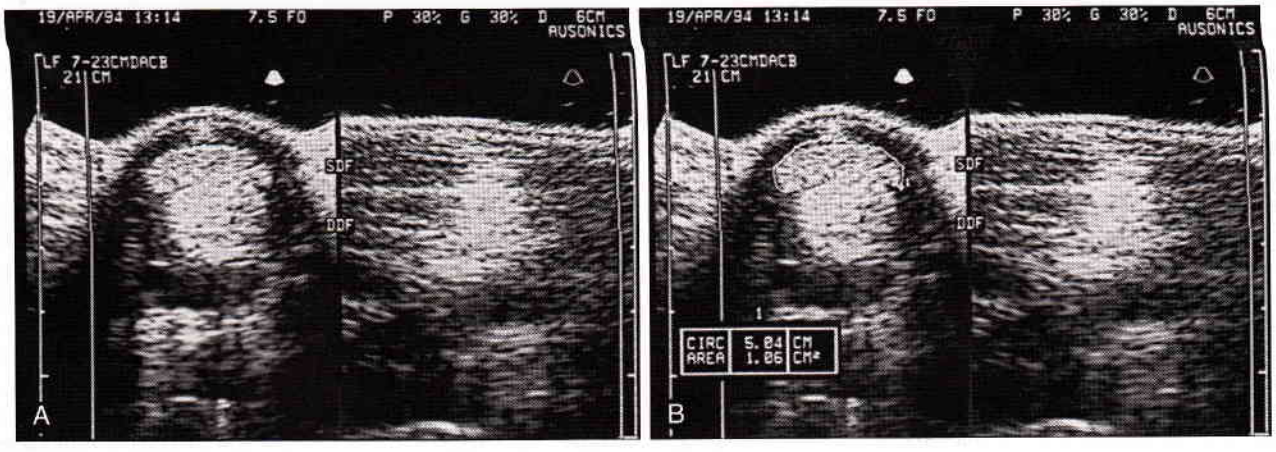

Figure 3–42

Sonograms of a significant peritendinitis, obtained from an 8-year-old Thoroughbred gelding with acute onset of marked soft tissue swelling in the left foreleg after a race. A mild tendinitis was visible from 7 to 23 cm distal to the point of the accessory carpal bone. These sonograms were obtained with a 7.5-MHz sector-scanner transducer containing a built-in fluid standoff at 21 cm distal to the point of the accessory carpal bone (the border between zones 2B and 3A) at a displayed depth of 6 cm. The left side of the transverse views *(left images)* is medial and the right side is lateral. The left side of the sagittal views *(right images)* is distal and the right side is proximal. DDF, deep digital flexor tendon.

A, Notice the large amount of anechoic fluid surrounding the left fore superficial digital flexor (SDF) tendon with a relatively normal-appearing SDF. A slight heterogeneity of the SDF occurs with small areas of slightly decreased echogenicity; but the SDF is normal in size and has a normal fiber pattern, indicating a mild SDF tendinitis associated with a severe peritendinitis.

B, The cross-sectional area of the SDF at the point of the largest swelling is 1.06 cm^2, normal for a horse of this size and comparable to that in the contralateral forelimb.

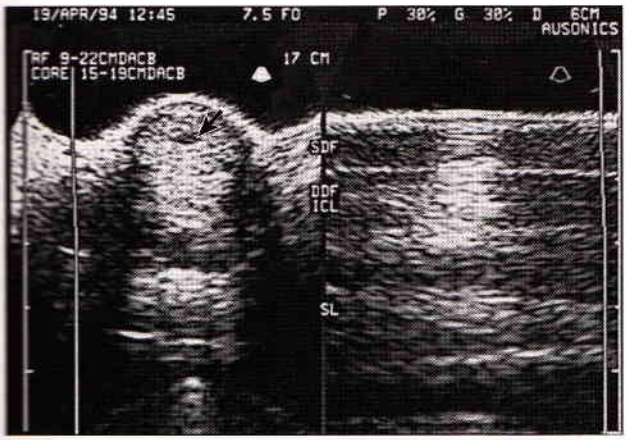

Figure 3–43

Sonograms of a very small acute central core lesion in the right fore superficial digital flexor tendon (SDF) of an 11-year-old Thoroughbred cross gelding competing in advanced-level combined training. Notice the small anechoic central core lesion *(arrow)* in the transverse view *(left image)* with loss of the normal fiber pattern imaged in the sagittal view *(right image)*. The tendon cross-sectional area at 17 cm (worst injury zone) distal to the point of the accessory carpal bone (border between zones 2A and 2B) is within normal limits (0.96 cm^2) with the largest percentage of injury to the tendon (this level) being 9.4%. A mild decrease in tendon echogenicity (tendinitis) was detected from 9 to 22 cm distal to the point of the accessory carpal bone, whereas the core lesion was only visible for 4 cm (15 to 19 cm). This sonogram was obtained with a 7.5-MHz sector-scanner transducer containing a built-in fluid offset at a displayed depth of 6 cm. The right side of the transverse view is lateral and the left side is medial. The right side of the sagittal view is proximal and the left side is distal. DDF, deep digital flexor tendon; ICL, inferior check ligament; SL, suspensory ligament.

tory cell infiltrate. This type of superficial digital flexor tendinitis can occur after blistering the leg, and, in some instances, tendon cross-sectional area remains increased and echogenicity decreased consistent with persistent active tendinitis. A peritendinous fluid accumulation with only mild tendinitis or no sonographic evidence of tendon fiber injury is consistent with a "bandage bow" (Fig. 3–42). In these horses, a large amount of peritendinous fluid accumulates around the superficial digital flexor tendon, causing a "peritendinitis" with a normal or near-normal superficial digital flexor tendon. Many horses with a "bandage bow" have sonographic evidence of a mild superficial digital flexor tendinitis. In young Thoroughbreds in race training, two of six horses developed clinical tendinitis in the left fore superficial digital flexor tendon at the location having the highest clinical frequency of tendinitis: the mid-metacarpal region (zones 2A, 2B, and 3A).[76, 77] One of these affected horses had a greater than average increase in tendon cross-sectional area and a greater than average decrease in mean echogenicity in the mid-metacarpal region associated with clinical superficial digital flexor tendinitis.[76, 77]

Injuries to the superficial digital flexor tendon in the foreleg are usually most severe in the mid-metacarpal region, in zone 2A, 2B, or 3A (Figs. 3–43 and 3–44). "Low bows," injuries to the superficial digital flexor tendon in the distal metacarpal region, are next most common (Fig. 3–45). These injuries often appear to be constricted by the annular ligament of the metacarpophalangeal joint. Low bows can extend down into the pastern and involve the distal portion of the superficial

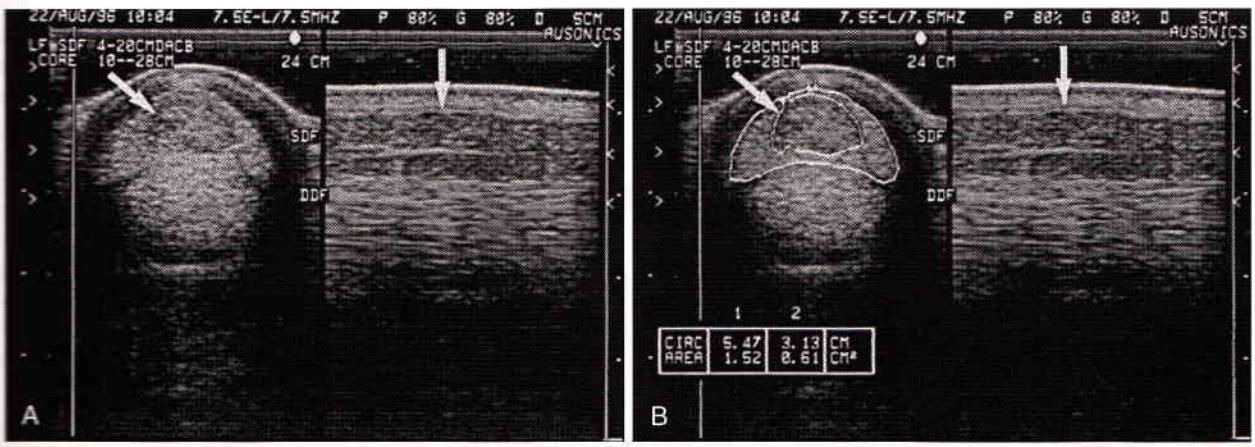

Figure 3–44

Sonograms of a large central core lesion *(large arrows)* in the superficial digital flexor tendon (SDF) of the left foreleg of a 3-year-old Thoroughbred filly. This hypoechoic core lesion was imaged from 10 to 28 cm distal to the point of the accessory carpal bone with a diffuse tendinitis imaged in the adjacent portion of the SDF from 4 to 20 cm. Peritendinous anechoic fluid is also imaged around the palmar, lateral, and medial borders of the SDF. These sonograms were obtained at 24 cm (zone 3A) with a wide-bandwidth 7.5-MHz linear-array transducer operating at 7.5 MHz using a hand-held standoff pad at a displayed depth of 5 cm. The focal zones are in the near field of the images. The right side of the transverse views *(left images)* is lateral and the left side is medial. The right side of the sagittal views *(right images)* is proximal and the left side is distal. DDF, deep digital flexor tendon.

A. Notice the enlarged SDF containing the central core lesion. Notice the echogenic appearance of most of the core lesion, which represents organizing clot, differentiated from normal to near normal tendon by the lack of fibers imaged in the sagittal view in the area of the echogenic core. The echogenic clot is surrounded by a hypoechoic rim, the outer edge of the core lesion.

B. The SDF is enlarged and the core lesion involves 40% of the tendon's cross-sectional area (0.61 cm^2/1.52 cm^2).

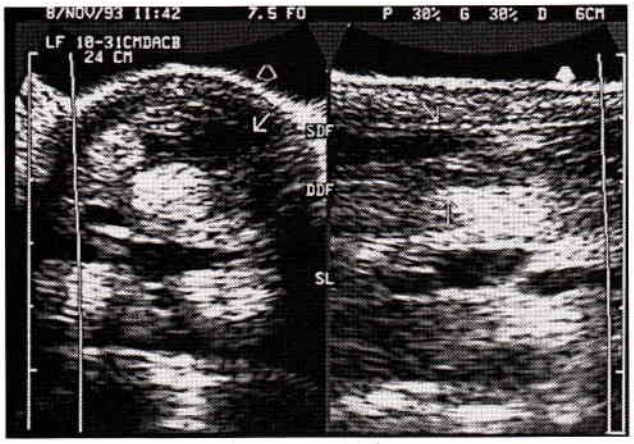

Figure 3–45

Sonograms of a 5-year-old Standardbred stallion with a severe "low bow" in the left fore superficial digital flexor tendon (SDF). Notice the discrete anechoic dorsal and lateral core lesion *(arrow)* surrounded by a hypoechoic area and the surrounding tendinitis in the transverse view *(left image)*. Notice in the sagittal view *(right image)* the lack of recognizable fibers *(arrows)* in all but the proximal palmar portion of the tendon. Peritendinous anechoic fluid is also imaged around the palmar, medial, and lateral borders of the SDF. This lesion was imaged from 10 to 31 cm distal to the point of the accessory carpal bone with the most severe injury in the distal tendon region at 24 cm (zone 3A). These sonograms were obtained with a 7.5-MHz sector-scanner transducer containing a built-in fluid offset at a displayed depth of 6 cm. The right side of the transverse view is lateral and the left side is medial. The right side of the sagittal view is proximal and the left side is distal. DDF, deep digital flexor tendon; SL, suspensory ligament.

digital flexor tendon and its branches (Fig. 3-46). Horses with injuries to the superficial digital flexor tendon that are detected in the distal metacarpal region should have the entire pastern scanned to evaluate the distal portion of the superficial digital flexor tendon and its branches for injury at these levels. Superficial digital flexor tendon injuries may also extend proximally into the carpal tunnel (canal) region and may begin at the musculotendinous junction of the superficial digital flexor tendon along the medial aspect of the distal radius (Fig. 3-47). These injuries are most common in jumpers, particularly those competing at the upper levels. Horses with injury to the superficial digital flexor tendon detected ultrasonographically in the most proximal portion of the metacarpal region (zone 1A) should have the superficial digital flexor tendon scanned proximally to the musculotendinous junction to evaluate this area for injury. Occasionally, affected horses may have involvement of the superficial digital flexor muscle and/or concurrent fasciitis or myositis. In the hind leg, the most common area of injury to the superficial digital flexor tendon is along the plantar aspect of the hock (Fig. 3-48), a common site for the curblike swelling; and in the proximal metatarsus, zones 1A, 1B, and 2A.

The most common superficial digital flexor tendon injury is a central core lesion (see Figs. 3-43 and 3-44), which appears as a central black hole in an otherwise echogenic tendon. These core injuries may be very small, with little enlargement of the tendon cross-sectional area at the site of the injury (see Fig. 3-43), or large, involving 40% or more of the tendon's cross-sectional area at the worst injury level (see Fig. 3-44). Lateral core lesions in the superficial digital flexor tendon are most common in Standardbred racehorses, but also occur in other types of competition horses (Fig. 3-49). The other horses that characteristically have an injury to the lateral portion of the superficial digital flexor tendon are the jumpers, with the area of fiber tearing involving primarily the lateral aspect of the superficial digital flexor tendon in the region of the carpal canal (see Fig. 3-47). Medial injuries to the superficial digital flexor tendon are more common than lateral injuries in most types of competition horses other than Standardbred racehorses (Fig. 3-50).

Before the use of ultrasonography, dorsal core lesions (Fig. 3-51) were often mistaken for injuries to the deep digital flexor tendon. The superficial digital flexor tendon, with injuries in the dorsal portion of the tendon, swells in a lateral to medial direction rather than bowing in the palmar direction as do most bowed tendons. This leads to swelling and sensitivity immediately adjacent to the palmar margin of the deep digital flexor tendon, mimicking a deep digital flexor tendon lesion.

Palmar lesions (Fig. 3-52) are the most likely injury to be caused by some type of external trauma, such as interference. Diffuse injuries (Fig. 3-53) to the superficial digital flexor tendons also occur and may be more difficult to diagnose if image quality is poor, because no discrete anechoic core lesion is evident. Splits in the superficial digital flexor tendon are also uncommon and appear similar to a longitudinal cut, or defect, in the tendon (Fig. 3-54).

The portion of the superficial digital flexor tendon around the discrete area of injury should be carefully evaluated for secondary injury or tendinitis (Fig. 3-55) adjacent to the discrete core lesion. Multiple areas of fiber tearing occur infrequently in horses with injuries to the superficial digital flexor tendon. With severe injuries to the superficial digital flexor tendon, the tendon swells around the medial and lateral margins of the deep digital flexor tendon. Large amounts of peritendinous soft tissue swelling are also common in horses with significant areas of fiber tearing in the superficial digital flexor tendon in the acute stage of the injury. Lacerations of the superficial digital flexor tendon may result in partial (Fig. 3-56) or complete (Fig. 3-57) disruption of the superficial digital flexor tendon. Complete ruptures of the superficial digital flexor tendon (Fig. 3-58) with loss of support to the metacarpophalangeal joint can also occur in horses in competition. Severe injury to the superficial digital flexor tendon should be recognized when the tendon has slipped to the medial aspect of the limb (Fig. 3-59).

Organized clot has an echogenicity similar to that of normal tendon or ligament fibers and can be mistakenly interpreted as normal or near-normal tendon if the sagittal view of the tendon is omitted. The differentiation between organized clot and normal tendon is easily made on the sagittal view, with the clot having an amorphous appearance, whereas the longitudinal fiber pattern is imaged in the normal tendon (Figs. 3-46, 3-58, and 3-60). A close association exists between the ultrasonographic and histopathologic appearance of lesions in horses with superficial digital flexor tendon injuries. Acute tears are characterized by a hypoechoic to anechoic region in the

Text continued on page 87

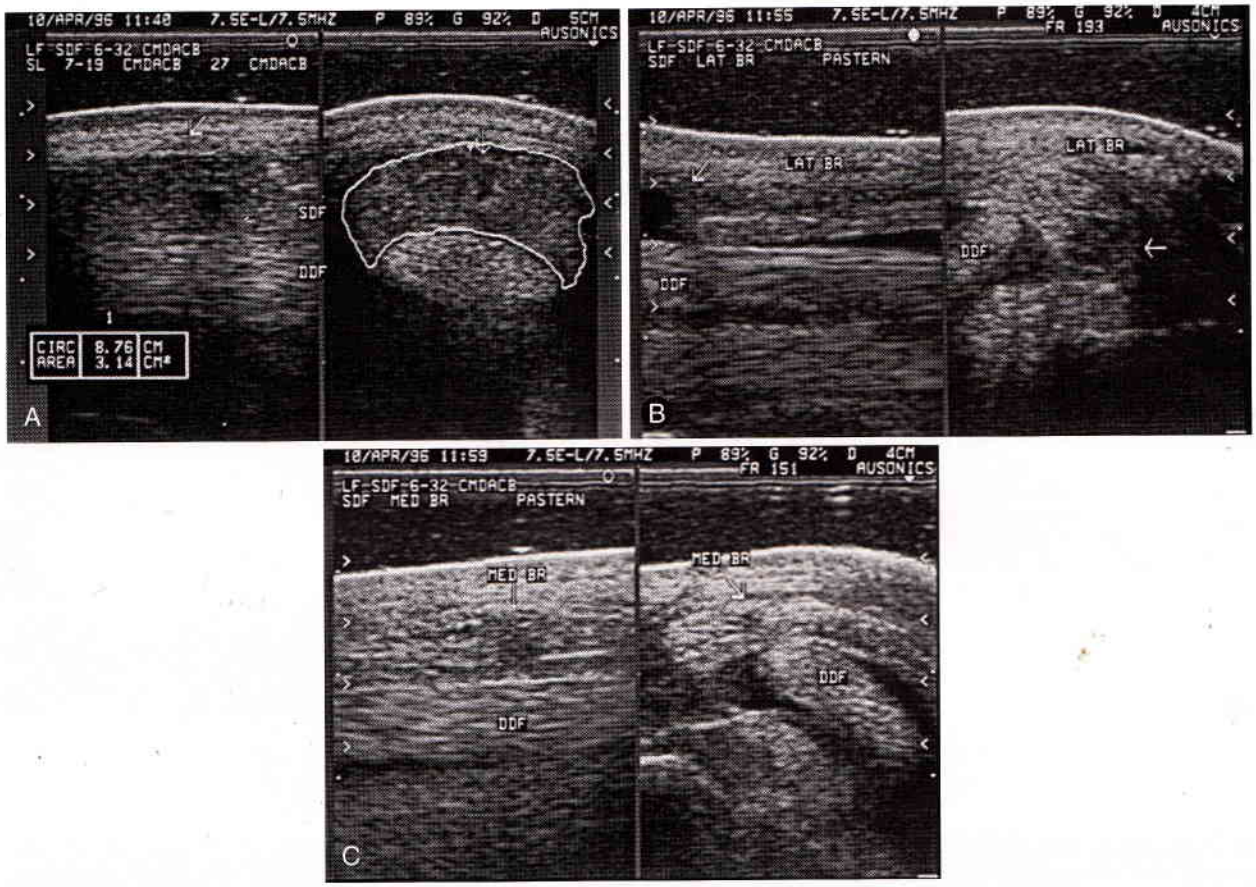

Figure 3–46

Sonograms of a rupture of the left fore superficial digital flexor tendon (SDF) that extends into the proximal pastern, obtained from a 5-year-old Standardbred stallion. These sonograms were obtained with a wide-bandwidth 7.5-MHz linear-array transducer operating at 7.5 MHz using a hand-held standoff pad at a displayed depth of 5 cm in the distal metacarpal region *(A)* and 4 cm in the pastern (*B* and *C*). The focal zones are in the near field of the images. The left side of the sagittal views *(left images)* is distal and the right side is proximal. DDF, deep digital flexor tendon.

A, This injury extended from 6 to 32 cm distal to the point of the accessory carpal bone in the metacarpal region. The worst injury zone in the distal metacarpal region was at 27 cm (zone 3B), where the tendon was enlarged to three times normal size (3.14 cm^2) and was very hypoechoic and completely lacking in tendon fibers. The left side of the transverse view *(right image)* is medial and the right side is lateral.

B, In the mid-pastern (zone P1B), the lateral branch of the SDF was completely ruptured. The free edge of the proximal portion of the lateral SDF branch *(arrow)* was imaged adjacent to anechoic fluid in the sagittal image *(left image)*. The hypoechoic dorsal margin *(horizontal arrow)* of the ruptured lateral SDF branch *(right image)* was the proximal extent of the area of fiber rupture. Notice that the teardrop shape of the lateral SDF branch is still preserved, although the cross-sectional area of the branch is enlarged *(right image)*. The left side of the transverse view *(right image)* is palmar and the right side is dorsal.

C, A small area of fiber damage is visible in the medial SDF branch in zone P1A as well, which appears as a small anechoic core *(diagonal arrow)* in the transverse view *(right image)* and as a split in the sagittal view *(vertical arrow)*. The left side of the transverse view *(right image)* is dorsal and the right side is palmar.

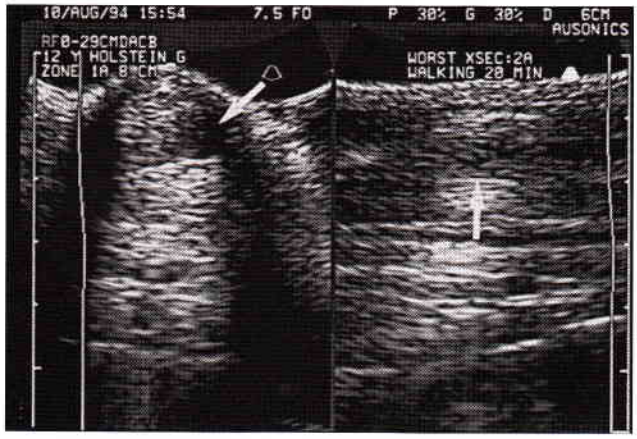

Figure 3–47

Sonograms of an area of fiber tearing in the proximal and lateral portion of the left fore superficial digital flexor tendon (SDF) of a 12-year-old Holsteiner gelding competing as a Grand Prix jumper. Notice the anechoic dorsal and lateral margin *(arrows)* of the proximal portion of the SDF. This lesion began at the musculotendinous junction and extended distally to 29 cm distal to the point of the accessory carpal bone. These sonograms were obtained at 8 cm (zone 1A) with a 7.5-MHz sector-scanner transducer containing a built-in fluid offset at a displayed depth of 6 cm. The right side of the transverse view *(left image)* is lateral and the left side is medial. The right side of the sagittal view *(right image)* is proximal and the left side is distal.

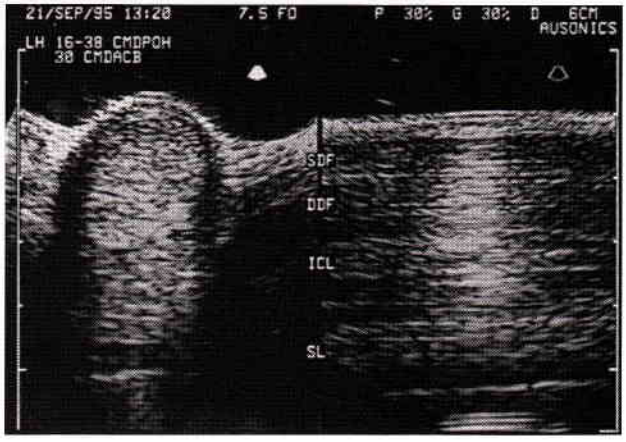

Figure 3–48

Sonograms of superficial digital flexor (SDF) tendinitis in the left hindleg of a 2-year-old Thoroughbred gelding. Notice the increased cross-sectional area of the SDF, the decrease in tendon echogenicity, and the slight separation of tendon fibers. The change in fiber alignment imaged on the sagittal view *(right image)* involves the plantar half of the SDF and corresponds to the hypoechoic area imaged in the transverse view *(left image)*. The SDF tendinitis was imaged from 16 to 38 cm distal to the point of the hock. These sonograms were obtained at 30 cm (zone 3A) with a 7.5-MHz sector-scanner transducer containing a built-in fluid offset at a displayed depth of 6 cm. The right side of the transverse view is lateral and the left side is medial. The right side of the sagittal view is proximal and the left side is distal. DDF, deep digital flexor tendon; ICL, inferior check ligament; SL, suspensory ligament.

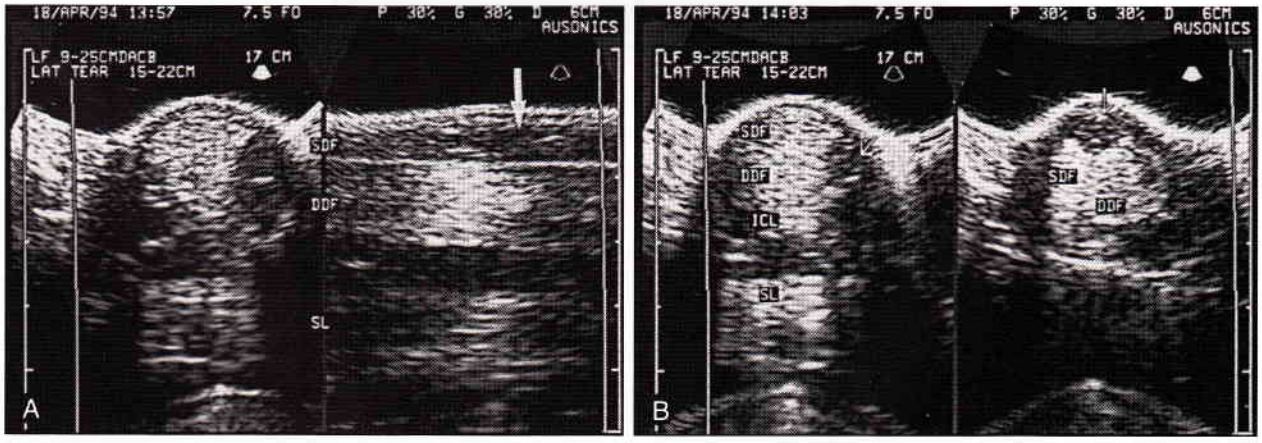

Figure 3–49

Sonograms of a discrete area of fiber tearing, obtained from a 5-year-old Arabian stallion with a lateral core lesion *(arrows)* in the left fore superficial digital flexor tendon (SDF). The lateral core lesion was imaged from 15 to 22 cm distal to the point of the accessory carpal bone. A mild tendinitis was visible in the SDF from 9 to 26 cm. These sonograms were obtained with a 7.5-MHz sector-scanner transducer containing a built-in fluid offset at a displayed depth of 6 cm. DDF, deep digital flexor tendon; ICL, inferior check ligament; SL, suspensory ligament.

A, Notice the anechoic lesion in the lateral aspect of the SDF in the transverse *(left)* and sagittal *(right)* images. The area of fiber disruption actually involved 38% of the tendon's cross-sectional area (0.47 cm^2/1.25 cm^2) at its largest point (17 cm—border between zones 2A and 2B). The right side of the transverse view is lateral and the left side is medial. The right side of the sagittal view is proximal and the left side is distal.

B, To better image the lateral area of fiber damage *(arrow)* seen in the standard palmar transverse image, the transducer was placed over the lateral aspect of the limb to yield a transverse view of the core lesion from the lateral side *(right image)*. The right side of the palmar transverse view *(left image)* is lateral and the left side is medial. The right side of the lateral transverse view *(right image)* is dorsal and the left side is palmar.

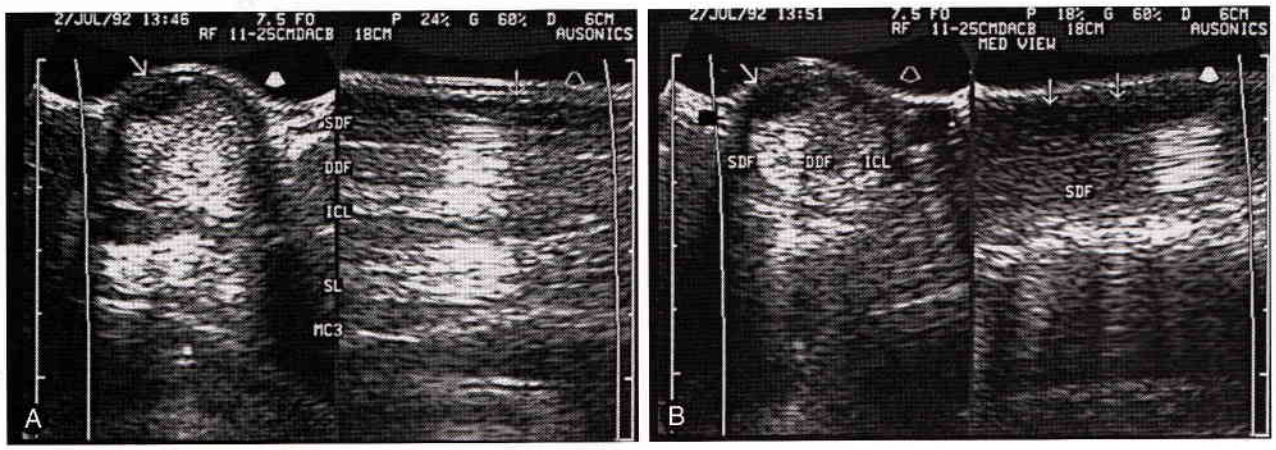

Figure 3–50

Sonogram of a palmar and medial area of fiber damage in the right fore superficial digital flexor tendon (SDF) of a 3-year-old Thoroughbred filly. The discrete area of fiber tearing *(arrows)* was imaged from 11 to 25 cm distal to the point of the accessory carpal bone and was most severe in zone 2B at 18 cm. Notice the significant decrease in tendon echogenicity in the adjacent tendon, lateral to the discrete area of fiber tearing associated with significant tendinitis. These sonograms were obtained with a 7.5-MHz sector-scanner transducer containing a built-in fluid standoff at a displayed depth of 6 cm. DDF, deep digital flexor tendon; ICL, inferior check ligament; SL, suspensory ligament; MC3, third metacarpal bone.

A, Notice the relatively small area of fiber damage appreciated in the palmar sagittal view with the transducer placed in the center of the tendon. The right side of the transverse view *(left image)* is lateral and the left side is medial. The right side of the sagittal view *(right image)* is proximal and the left side is distal.

B, With the transducer placed on the medial aspect of the limb, the area of fiber disruption appears much larger *(arrows)* because the sagittal scan is now through the largest area of fiber damage. The right side of the transverse view *(left image)* is dorsal and the left side is palmar. The right side of the sagittal view *(right image)* is proximal and the left side is distal.

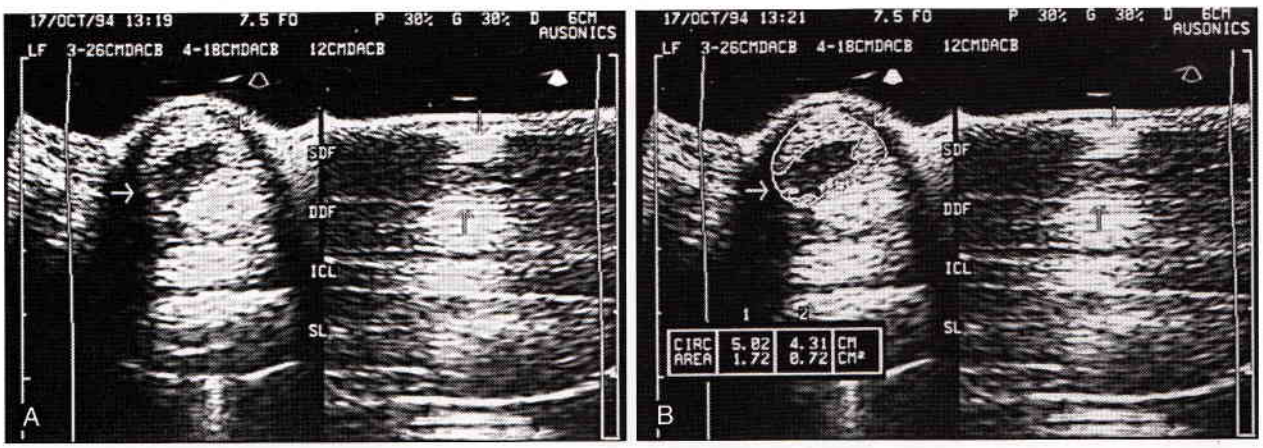

Figure 3–51

Sonograms of the left fore superficial digital flexor tendon (SDF) with a large dorsal and somewhat medial core lesion, obtained from a 3-year-old Thoroughbred gelding. The core lesion was imaged from 4 to 18 cm distal to the point of the accessory carpal bone with this lesion imaged at 12 cm (zone 1B). A mild diffuse tendinitis was imaged in the SDF from 3 to 26 cm distal to the point of the accessory carpal bone. These sonograms were obtained with a 7.5-MHz sector-scanner transducer containing a built-in fluid offset at a displayed depth of 6 cm. The right side of the transverse views *(left images)* is lateral and the left side is medial. The right side of the sagittal views *(right images)* is proximal and the left side is distal. DDF, deep digital flexor tendon; ICL, inferior check ligament; SL, suspensory ligament.

A, Notice the large anechoic core lesion *(arrows)* in the dorsal portion of the SDF and the normal palmar portion of the SDF. This tendon was swollen in a medial to lateral direction rather than creating a palmar bowing of the SDF. Notice the near-normal echogenicity of the surrounding tendon.

B, Notice that 42% of the tendon's cross-sectional area (0.72 cm^2/1.72 cm^2) is damaged at this point, the worst injury zone.

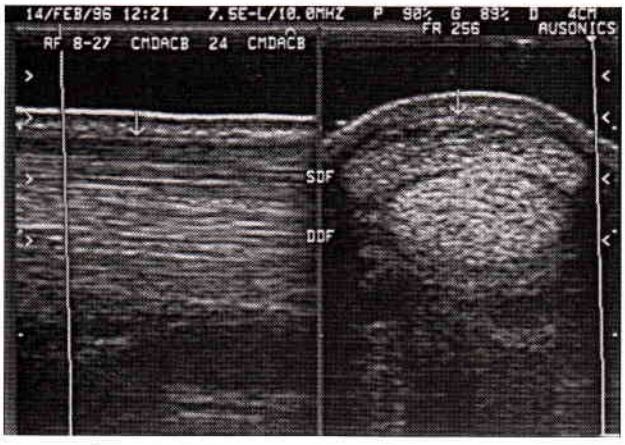

Figure 3–52

Sonograms of an area of damage on the palmar aspect of the right fore superficial digital flexor tendon (SDF) of an aged Thoroughbred polo pony mare. This area of hypoechogenicity and loss of the normal fiber pattern *(arrows)* extended from 8 to 27 cm distal to the point of the accessory carpal bone along the most superficial (palmar) portion of the tendon. The injury was worst in zone 3A at 24 cm, where the tendon cross-sectional area measured 1.11 cm^2 and the palmar hypoechoic area measured 0.51 cm^2. Superficial trauma to this region could possibly create this type of injury. These sonograms were obtained with a wide-bandwidth 7.5-MHz linear-array transducer operating at 10.0 MHz using a hand-held standoff pad at a displayed depth of 4 cm. The focal zones are in the near field of the images. The right side of the transverse view *(right image)* is lateral and the left side is medial. The right side of the sagittal view *(left image)* is proximal and the left side is distal. DDF, deep digital flexor tendon.

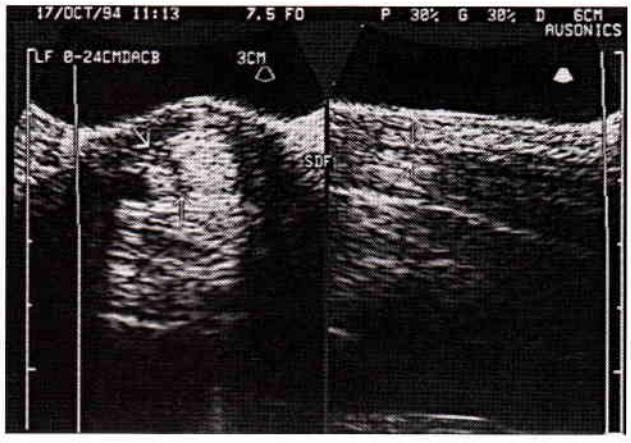

Figure 3–54

Sonograms of a linear area of fiber tearing or split in the left fore superficial digital flexor tendon (SDF) of a 17-year-old Thoroughbred/Quarter horse cross gelding. Notice the recent anechoic linear split *(arrows)* extending from palmar and medial to dorsal through the SDF in the transverse view *(left image)*. Notice the fiber disruption *(arrows)* in the sagittal view *(right image)* in the superficial portion of the SDF in this medial sagittal plane. This superficial digital flexor tendinitis was imaged from 0 to 24 cm distal to the point of the accessory carpal bone. This split in the SDF was best imaged at 3 cm, in the carpal canal region above zone 1A. These sonograms were obtained with a 7.5-MHz sector-scanner transducer containing a built-in fluid offset at a displayed depth of 6 cm. The right side of the transverse image is lateral and the left side is medial. The right side of the sagittal image is proximal and the left side is distal.

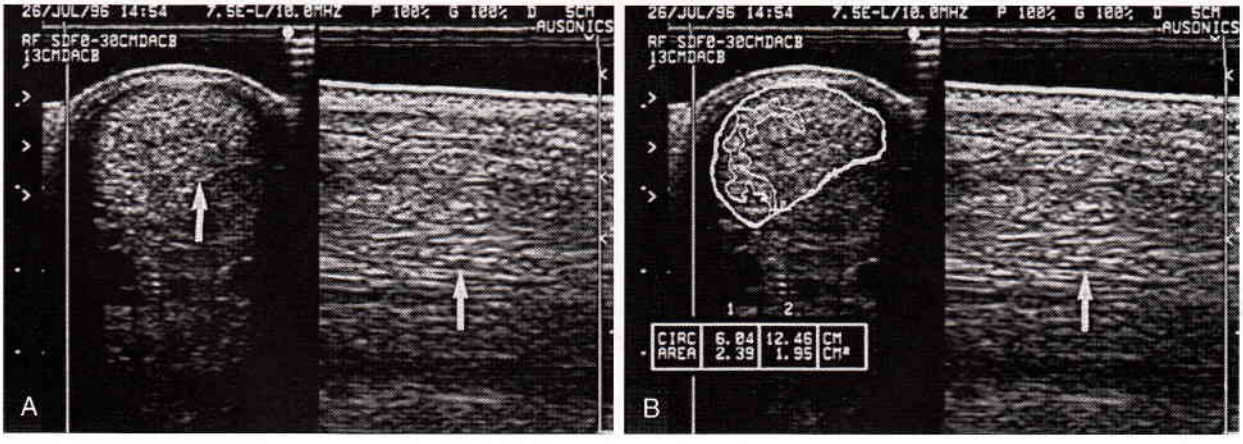

Figure 3–53

Sonograms of a severe diffuse superficial digital flexor (SDF) tendinitis in the right foreleg of a 3-year-old Thoroughbred gelding. Diffuse tendinitis was imaged from 0 to 30 cm distal to the point of the accessory carpal bone. These sonograms were obtained at 13 cm (the border between zones 1B and 2A) with a wide-bandwidth 7.5-MHz linear-array transducer operating at 10.0 MHz using a hand-held standoff pad at a displayed depth of 5 cm. The focal zones are in the near field of the images. The right side of the transverse views *(left images)* is lateral and the left side is medial. The right side of the sagittal views *(right images)* is proximal and the left side is distal.

A, Notice the enlarged cross-sectional area of the SDF in the transverse image and the loss of most of the normal fiber pattern in the sagittal image. The SDF is diffusely hypoechoic, particularly along the dorsal margin of the SDF *(arrows)*.

B, The SDF is more than twice normal size with a total cross-sectional area of 2.39 cm^2. The majority (81.6%) of the SDF (1.95 cm^2/2.39 cm^2) is affected with only a small more normal-appearing area imaged in the palmar and medial portion of the tendon.

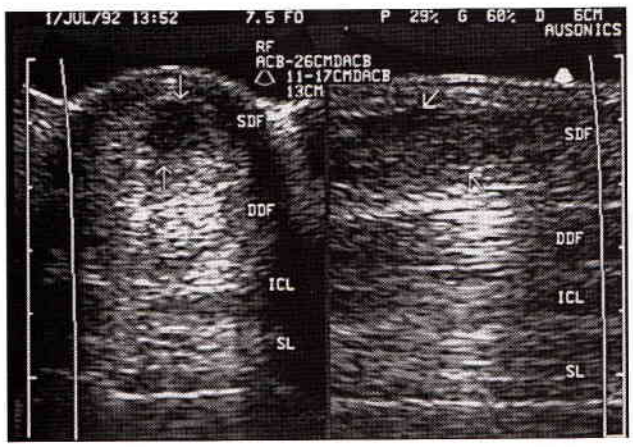

Figure 3–55

Sonograms of a discrete core lesion *(arrows)* in the right fore superficial digital flexor tendon (SDF) of a 5-year-old Thoroughbred gelding. Notice the large hypoechoic area surrounding the core lesion in the transverse view *(left image)* and the large area of fiber damage in the sagittal view *(right image)* consistent with a severe tendinitis in the portion of the SDF surrounding the anechoic core lesion. The amount of injury to the SDF is actually much more severe than just the area of the anechoic core lesion, and actually involves nearly the entire cross-sectional area of the SDF. The severe tendinitis was imaged from 0 to 26 cm distal to the point of the accessory carpal bone, whereas the discrete core lesion was only imaged from 11 to 17 cm. These sonograms were obtained at 13 cm (the border between zones 1B and 2A) with a 7.5-MHz sector-scanner transducer containing a built-in fluid offset at a displayed depth of 6 cm. The right side of the transverse view is lateral and the left side is medial. The right side of the sagittal view is proximal and the left side is distal. DDF, deep digital flexor tendon; ICL, inferior check ligament; SL, suspensory ligament.

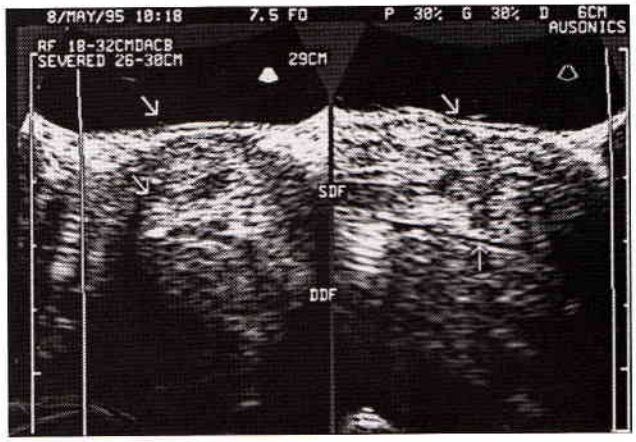

Figure 3–56

Sonograms obtained from a 7-year-old Thoroughbred mare with a partial laceration of the right fore superficial digital flexor tendon (SDF). Notice the anechoic linear echo *(angled arrow)* extending from the defect in the skin through the palmar surface of the tendon, nearly severing the tendon in this sagittal view *(right image)*. Notice the core lesion in the SDF and the laceration extending from the medial side of the SDF *(arrow)* into the core lesion in the transverse view *(left image)*. The laceration was detected from 26 to 30 cm distal to the point of the accessory carpal bone, and these images were obtained at 29 cm (the border between zones 3B and 3C). An associated tendinitis was detected from 18 to 32 cm distal to the point of the accessory carpal bone. These sonograms were obtained with a 7.5-MHz sector-scanner transducer containing a built-in fluid offset at a displayed depth of 6 cm. The right side of the transverse image is lateral and the left side is medial. The right side of the sagittal image is proximal and the left side is distal. DDF, deep digital flexor tendon.

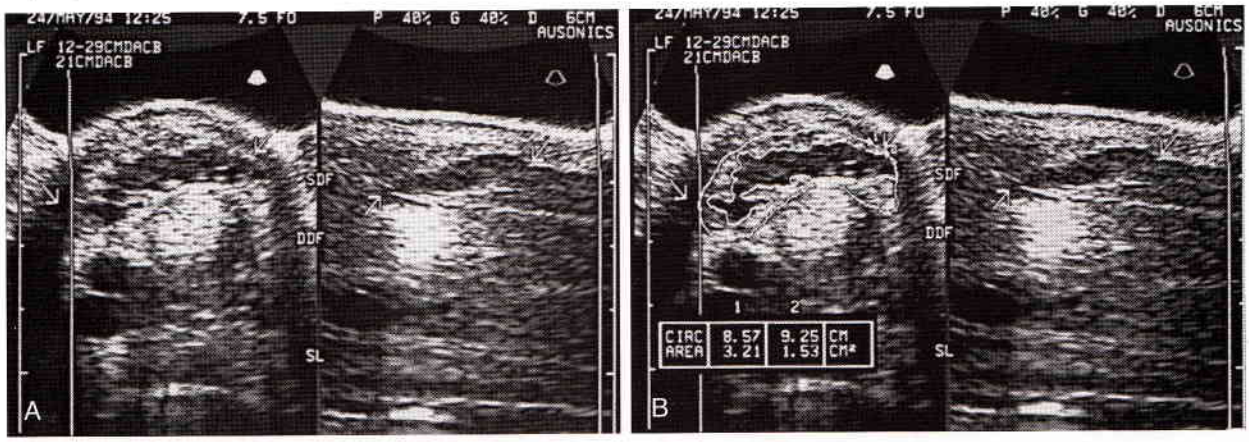

Figure 3–57

Sonograms obtained from a 3-year-old Thoroughbred gelding with a laceration of the entire left fore superficial digital flexor tendon (SDF) sustained 7 weeks earlier. The limb had been in a Kimsey splint since the injury occurred. A tendinitis associated with the SDF laceration was imaged from 12 to 29 cm distal to the point of the accessory carpal bone. These sonograms were obtained at 21 cm (the border between zones 2B and 3A) with a 7.5-MHz sector-scanner transducer containing a built-in fluid offset at a displayed depth of 6 cm. The right side of the sagittal views *(right images)* is proximal and the left side is distal. The right side of the transverse views *(left images)* is lateral and the left side is medial. DDF, deep digital flexor tendon; SL, suspensory ligament.

A, Notice the diagonal laceration through the SDF in a palmar to dorsal and proximal to distal direction *(arrows)* in the sagittal image. In the transverse image, notice the laceration extending from lateral to medial through the SDF in the transverse image.

B, The SDF was at least three times normal size and the laceration involved 48% of the tendon's cross-sectional area (1.53 cm^2/3.21 cm^2) at the point of worst injury (21 cm).

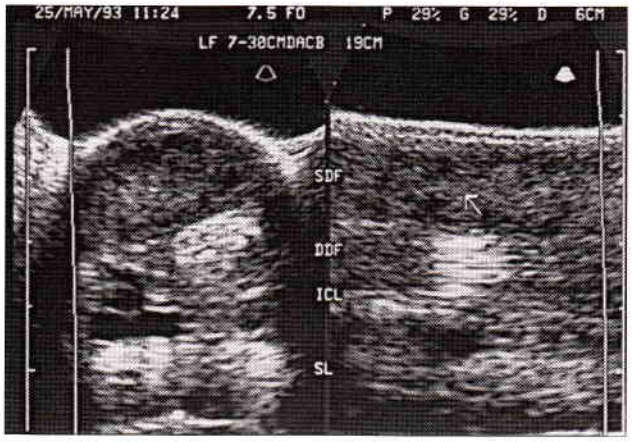

Figure 3–58

Sonograms of the left fore superficial digital flexor tendon (SDF), obtained from a 6-year-old Thoroughbred mare that had raced 3 weeks earlier and bowed the SDF tendon. Notice the complete rupture of the SDF *(arrow)* with no evidence of tendon fibers in the sagittal view *(right image)*. The hypoechoic material detected in the transverse *(left image)* and sagittal views most likely represents clot and early granulation tissue. This severe fiber disruption was imaged from 7 to 30 cm distal to the point of the accessory carpal bone. These sonograms were obtained at the cross-sectional area of worst injury (19 cm in zone 2B) with a 7.5-MHz sector-scanner transducer containing a built-in fluid offset at a displayed depth of 6 cm. The right side of the transverse image is lateral and the left side is medial. The right side of the sagittal image is proximal and the left side is distal. DDF, deep digital flexor tendon; ICL, inferior check ligament; SL, suspensory ligament.

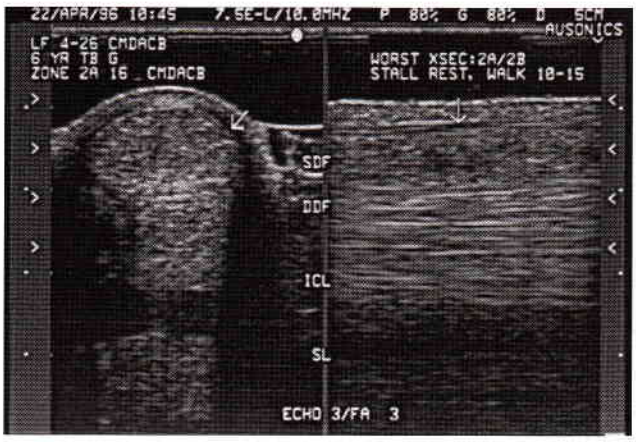

Figure 3–60

Sonograms of an organizing hematoma within a large area of injury to the left fore superficial digital flexor tendon (SDF), obtained from a 6-year-old Thoroughbred gelding. Notice the slight decrease in tendon echogenicity in the transverse view *(left image)*. A discrete area of fiber tearing is not detected in this view because the echogenicity of organizing clot is similar to that of normal tendon fibers. In the sagittal view *(right image)*, however, a large area of fiber disruption is imaged with only a small rim of more normal fibers in the palmar and dorsal portions of the tendon. If only the transverse view were obtained and the cross-sectional area of the SDF were not measured, the severity of this injury could be underestimated. This fiber tearing extended from 4 to 26 cm distal to the point of the accessory carpal bone. These sonograms were obtained at 16 cm in zone 2A with a wide-bandwidth 7.5-MHz linear-array transducer operating at 10.0 MHz using a hand-held standoff pad at a displayed depth of 5 cm. The focal zones are in the near field of the images. The right side of the transverse image is lateral and the left side is medial. The right side of the sagittal image is proximal and the left side is distal. DDF, deep digital flexor tendon; ICL, inferior check ligament; SL, suspensory ligament.

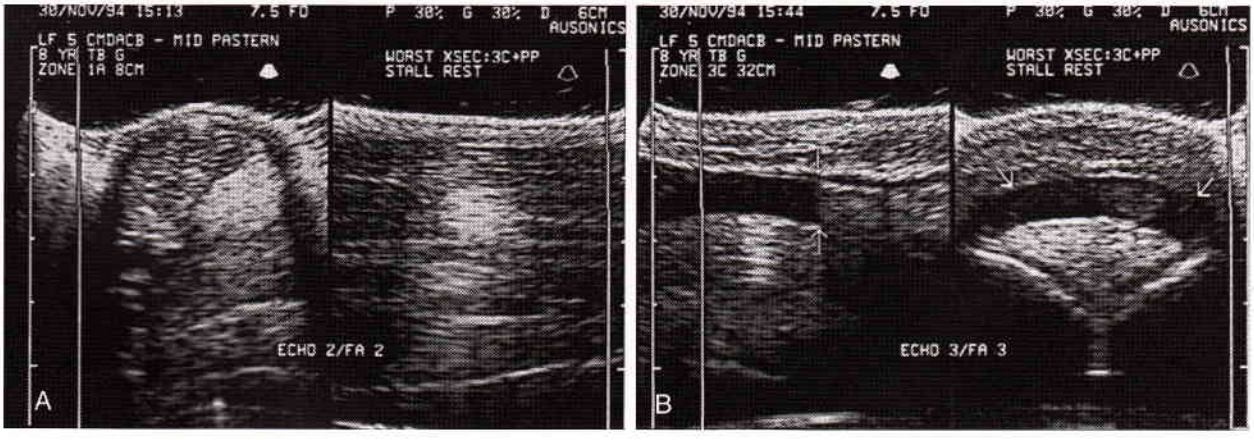

Figure 3–59

Sonograms of a left fore superficial digital flexor tendon (SDF) that has slipped to the medial aspect of the limb *(A)* because of rupture of the tendon in the more distal tendon region *(B)*, obtained from an 8-year-old Thoroughbred gelding. Damage to the SDF was imaged from 5 cm distal to the point of the accessory carpal bone to the level of the mid-pastern. These sonograms were obtained with a 7.5-MHz sector-scanner transducer containing a built-in fluid offset at a displayed depth of 6 cm. The right side of the transverse images is lateral and the left side is medial. The right side of the sagittal images is proximal and the left side is distal.

A, Notice that the SDF is running along the palmaromedial aspect of the deep digital flexor tendon, which has normal echogenicity. The SDF is enlarged and hypoechoic but still has some linear fibers present at this level (8 cm distal to the point of the accessory carpal bone in zone 1A) in the sagittal sonogram *(right image)*, but has slipped to the medial aspect of the limb in the transverse view *(left image)*.

B, Complete rupture of the SDF *(arrows)* in the annular ligament region at 32 cm in zone 3C with the hypoechoic end of a portion of the SDF visible in the sagittal view *(left image)* and just barely visible in the transverse view *(right image)*.

tendon that histologically is characterized by an area of hemorrhage, edema, and fibrinolysis with little cellular reaction.[18, 20, 22] Necrotic tendon fibers and early granulation tissue may also appear anechoic to slightly hypoechoic.[18, 22]

The average percentage of injury in the superficial digital flexor tendon in the mid 1980s was 40%,[16, 25] a number that has decreased as owners and trainers have become more aware that the number one clinical sign of tendon injury is swelling of the superficial digital flexor tendon. The average extent of a superficial digital flexor tendon injury at that time was approximately 14 cm in length. Smaller areas of fiber damage are now frequently detected, with most horses having initial injuries to the superficial digital flexor tendon of 25% or less. These tendon injuries are being treated before becoming more severe. Ultrasound examinations have revealed that most injuries to the superficial digital flexor tendon begin as small areas of fiber damage; these areas enlarge if the horse continues training and competing. Although some horses can compete successfully with small new areas of damage, this is rare at the upper levels of athletic competition. In most of these horses, additional injury occurs if the horse is continued in upper-level competition without giving the injured tendon adequate time to heal.

A severity rating has been described for the assessment of injuries to the superficial digital flexor tendon that may be used in formulating a prognosis for successful return to racing.[26] In this formula, the percentage of injury is calculated for each injury zone in the superficial digital flexor tendon and the lesion is typed as previously described on a scale of 1 to 4. The severity rating is the product of the percent injury in a given zone, the type rating, and a scaling factor, yielding a severity rating of 1 to 10. More recently, a 7-fold sonographic assessment of tendon injury has been proposed that yields a more thorough evaluation of the damage to the entire superficial digital flexor tendon.[38] These assessments developed from monitoring the healing response of tendon ultrasonographically in the intralesional βAPN-F study.[38] Seven sonographic parameters are evaluated:

1. MIZ-SA—The cross-sectional area of the tendon at the maximum injury zone (mm^2)
2. MIZ-HYP—The total lesion cross-sectional area in the maximum injury zone (mm^2)
3. MIZ-FAS—The fiber alignment at the maximum injury zone
4. T-SA—The sum of all the cross-sectional area measurements (cm^2) for all zones (for the superficial digital flexor tendon in the foreleg this involves seven zones)
5. T-HYP—The sum of all the lesion cross-sectional area measurements (mm^2)
6. T-FAS—The sum of all the fiber alignment scores at all levels
7. %T-HYP—The total percentage of hypoechoic fiber tracts (= T-SA-T-HYP)

The severity of the initial tendon injury is graded slight if the %T-HYP is 15% or less, moderate if the %T-HYP is 16% to 25%, and severe if the %T-HYP is more than 25%.

Lesions to the superficial digital flexor tendon are reported as one of five causes of a "curb-type" swelling along the plantar aspect of the hock. Subcutaneous edema, peritendinous fibrosis, plantar ligament desmitis, and deep digital flexor tendinitis (rare) also occur in this region.[15] A diffuse superficial digital flexor tendinitis is more common (see Fig. 3-48) than a core lesion in this location (Fig. 3-61). Lacerations of the hind superficial digital flexor tendon are also a common cause of tendon injury in the hindlimb.

As the superficial digital flexor tendon heals, the echogenicity of the lesion increases. Objective assessments of this increase in tendon and lesion echogenicity can be made using mean gray-scale analysis of the tendon images; these correlate with the histopathologic findings in

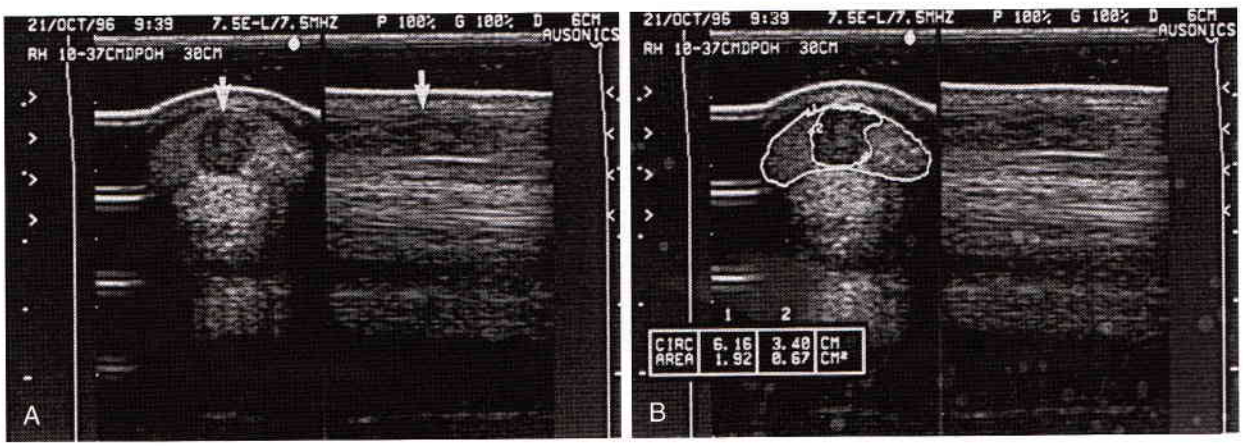

Figure 3–61

Sonograms of a large core lesion in the right hind superficial digital flexor tendon (SDF), obtained from a 5-year-old Thoroughbred gelding. These sonograms were obtained at the worst injury zone 30 cm distal to the point of the hock (zone 3A), but the lesion was visible from 10 to 37 cm distal to the point of the hock. A wide-bandwidth 7.5-MHz linear-array transducer was used operating at 7.5-MHz and using a hand-held standoff pad at a displayed depth of 6 cm. The right side of the transverse views *(left images)* is lateral and the left side is medial. The right side of the sagittal views *(right images)* is proximal and the left side is distal.

A, Notice the large area of fiber disruption in the center of the tendon and the lack of fibers in the sagittal view *(arrows).*

B, This lesion occupied 34.9% of the tendon's cross-sectional area at the worst injury zone (0.67 cm^2/1.92 cm^2).

the healing tendon.[21] Residual tendon fibrils may be imaged as bright echoes within an anechoic to hypoechoic lesion.[20] Initially the superficial digital flexor tendon fills in with amorphous echoes consistent with granulation tissue and inflammatory cells, followed by immature fibrous tissue (Fig. 3-62). At this time, during the early fibrosis phase of tendon healing, a loss of magnetic resonance imaging (MRI) signal intensity occurs while the sonographic appearance of the lesion is still quite sonolucent.[20] This loss of signal intensity on MRI images could be mistaken for significantly more tendon healing than is actually present; without evaluating the corresponding sonographic image, this impression could lead to returning the horse to rigorous work prematurely. Increased blood supply to the healing tendon can also be detected using power Doppler in horses (Color Figure 3-1). Short linear echoes are then detected within the lesion (Fig. 3-63), consistent with maturing fibrous tissue.[18, 20-22] The progressive increase in tendon echogenicity seen in the first 6 weeks after an acute reinjury to the superficial digital flexor tendon in one horse was attributed to the gradual reorientation of the bundles of tendon fibers along the lines of stress in the limb, an increase in the acoustic density of the tendon fiber bundles, and a decrease in the number of fibroblasts.[21] The reorienting fiber bundles now act as specular, rather than diffuse, reflectors, increasing the echogenicity and mean gray scale of the tendon. The increase in acoustic density is attributed to an increase in number of the intramolecular and intermolecular linkages in the collagen fibers.[21, 128]

The short linear echoes detected in the superficial digital flexor tendon are usually aligned randomly throughout the lesion, although with a controlled exercise program, time, and active tendon remodeling, these fibers do become more parallel (Fig. 3-64). The most common exception to this pattern of healing occurs in horses treated with intralesional βAPN-F. In these horses, parallel linear echoes (Fig. 3-65) are often detected very early in the healing phase of the injury (as early as 1 to 2 months after injection). Parallel linear echoes may also

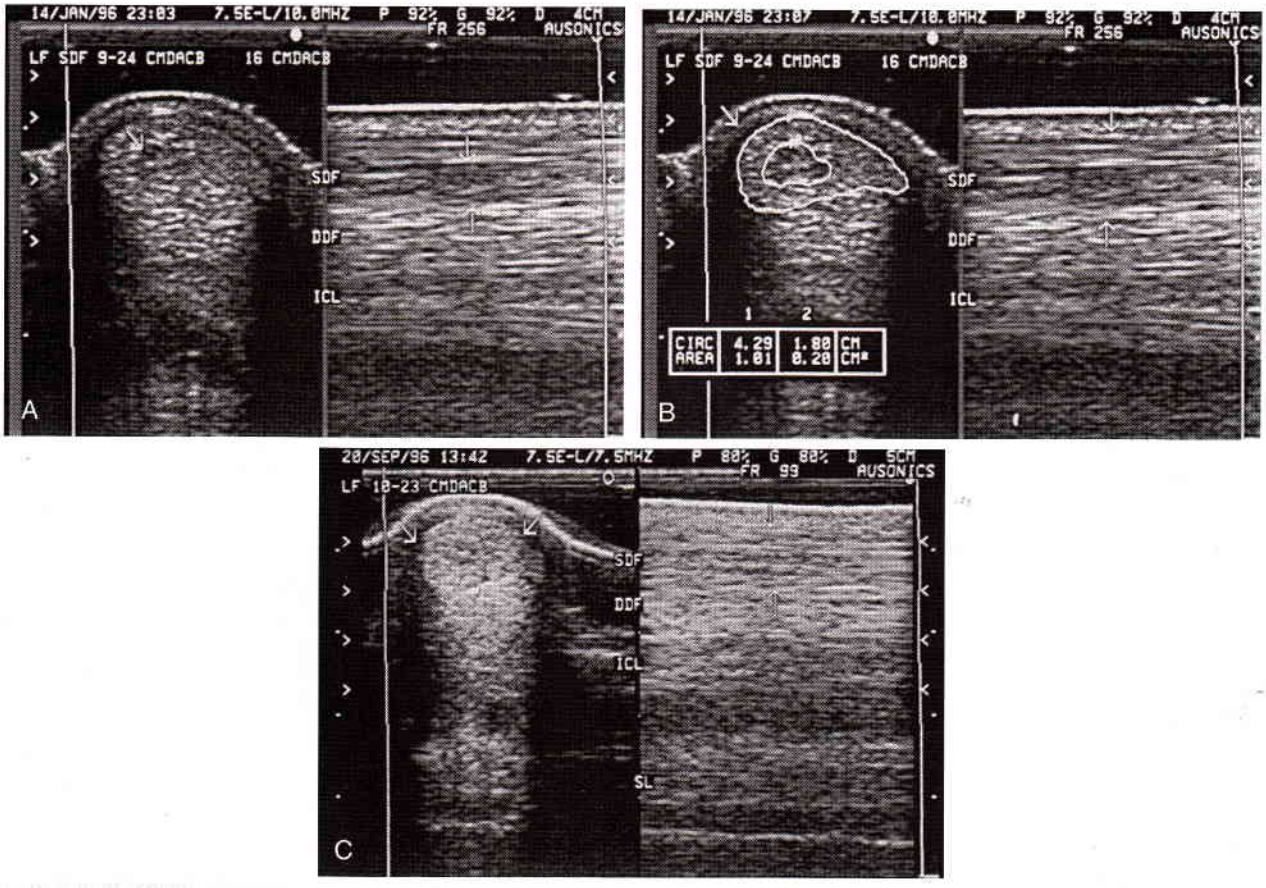

Figure 3-62

Sonograms of a healing area of injury in the left fore superficial digital flexor tendon (SDF) obtained from a 9-year-old Thoroughbred gelding. The core lesion extended from 9 to 24 cm distal to the point of the accessory carpal bone. These sonograms were obtained at 16 cm (zone 2A) with a wide-band width 7.5-MHz linear-array transducer operating at 10.0 MHz (*A* and *B*) and 7.5 MHz (*C*) and a hand-held standoff pad at a displayed depth of 4 cm (*A* and *B*) and 5 cm (*C*). The focal zones are in the near field of the images. The left side of the transverse view *(left images)* is medial and the right side is lateral. The left side of the sagittal view *(right images)* is distal and the right side is proximal. DDF, deep digital flexor tendon; ICL, inferior check ligament; SL, suspensory ligament.

A, Notice the hypoechoic to isoechoic central core lesion *(diagonal arrow)* in the transverse view *(left image)* and the amorphous echoes in the center of the lesion *(vertical arrow)* in the sagittal view, consistent with granulation tissue and immature fibrous tissue.

B, The original core lesion involved 20% of the cross-sectional area of the tendon (0.20 cm^2/1.02 cm^2) at the worst injury zone (16 cm).

C, Sonogram from the same horse 8 months later at the same level. Notice the improved echogenicity and fiber pattern, although the original area of injury is still barely visible as an echogenic center with a hypoechoic halo. The arrows delineate the borders of the superficial digital flexor tendon.

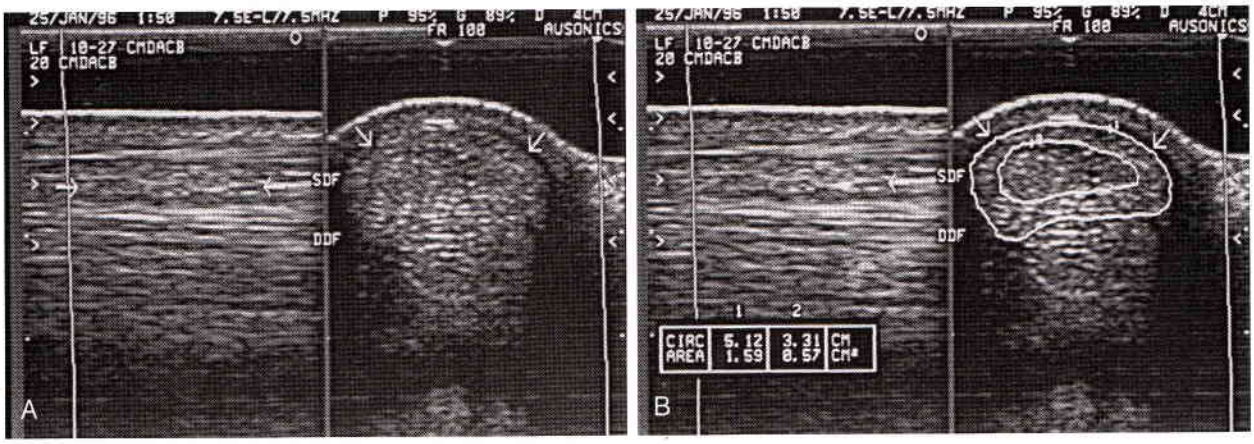

Figure 3–63

Sonograms of a repairing core lesion in the left fore superficial digital flexor tendon (SDF), obtained from a 6-year-old Thoroughbred gelding. This core lesion was imaged from 10 to 27 cm distal to the point of the accessory carpal bone. These sonograms were obtained at 20 cm (zone 2B) with a wide-bandwidth 7.5-MHz linear-array transducer operating at 7.5 MHz using a hand-held standoff pad at a displayed depth of 4 cm. The left side of the transverse views *(right images)* is medial and the right side is lateral. The left side of the sagittal views *(left images)* is distal and the right side is proximal. DDF, deep digital flexor tendon.

A, Notice the central core lesion, which is only slightly different in echogenicity than its surrounding (more normal) tendon in the transverse image, but which is clearly visible in the sagittal image as a hypoechoic area containing few linear echoes *(arrows)*. The echogenicity and pattern of fiber alignment in this lesion are most consistent with immature fibrous tissue, because few short linear echoes and rare long linear echoes are present within the lesion. This horse is ready for jogging exercise but not galloping or breezing.

B, The original extent of the injury can still be evaluated in this horse because the discrete area of fiber tearing is still imaged as subtly, but distinctly, separate from the surrounding more normal tendon. This core lesion involves 36% of the tendon's cross-sectional area (0.57 cm^2/1.59 cm^2).

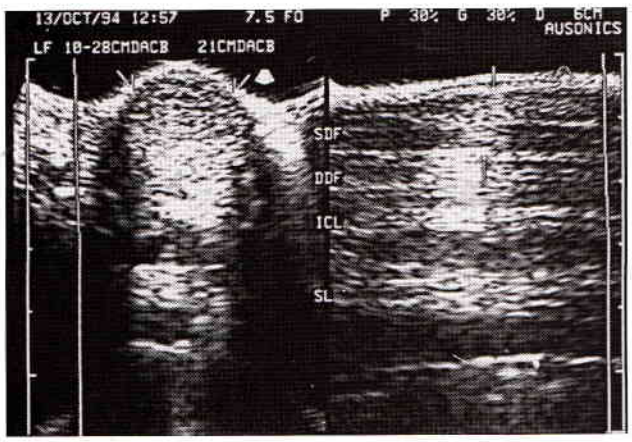

Figure 3–64

Sonograms of a healing superficial digital flexor (SDF) tendinitis in the left foreleg of a 7-year-old Thoroughbred gelding. The SDF tendinitis was imaged from 10 to 28 cm distal to the point of the accessory carpal bone. Notice the heterogeneous hypoechoic palmar and lateral portion of the SDF in the transverse view *(left image)* and the short linear echoes in the healing palmar portion of the SDF in the sagittal view *(right image)*. These sonograms were obtained at 21 cm (border between zones 2B and 3A) with a 7.5-MHz sector-scanner transducer containing a built-in fluid offset at a displayed depth of 6 cm. The right side of the transverse image is lateral and the left side is medial. The right side of the sagittal image is proximal and the left side is distal. DDF, deep digital flexor tendon; ICL, inferior check ligament; SL, suspensory ligament.

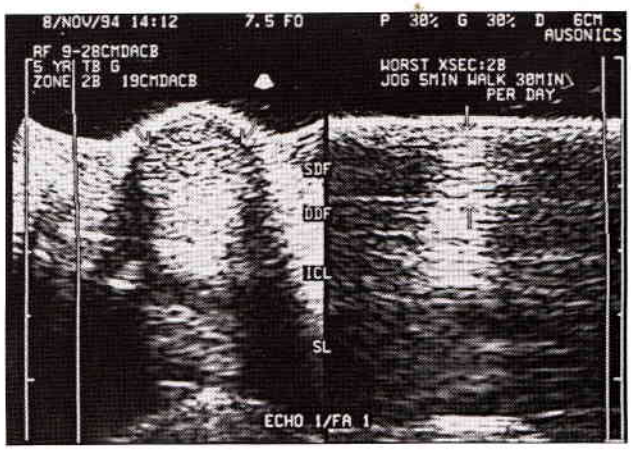

Figure 3–65

Sonograms obtained from a 5-year-old Thoroughbred gelding with a recent core lesion in the center of the right fore superficial digital flexor tendon (SDF). The injury had occurred 4 months earlier and the tendon was injected with βAPN-F 3 months before these sonograms were obtained. Notice the nearly normal echogenicity and fiber alignment in the SDF. The tendon was originally injured from 9 to 28 cm distal to the point of the accessory carpal bone and the worst injury zone was at 19 cm (zone 2B), involving 30% of the tendon's cross-sectional area. These sonograms were obtained with a 7.5-MHz sector-scanner transducer containing a built-in fluid offset at a displayed depth of 6 cm. The right side of the transverse view *(left image)* is lateral and the left side is medial. The right side of the sagittal view *(right image)* is proximal and the left side is distal. DDF, deep digital flexor tendon; ICL, inferior check ligament; SL, suspensory ligament.

be detected in horses with bowed tendons that are treated conservatively, but the incidence of parallel linear echoes is much lower in horses receiving treatments other than intralesional βAPN-F. These parallel linear echoes take many months to appear (Fig. 3-66) and the quality of repair varies tremendously (Figs. 3-67 and 3-68). In many horses treated conservatively, the original core lesion remains visible for years after the original injury occurs. Typically, these horses have an echogenic center where the core lesion has repaired with random scar tissue, a normal outer rim of tendon fibers that were not originally damaged, and a hypoechoic "halo" between the normal outer rim and the echogenic repaired core lesion (Fig. 3-69). Most horses with a healed injury to the superficial digital flexor tendon have enlarged tendon cross-sectional areas, persistent hypoechoic areas imaged in the superficial digital flexor tendon with a random pattern of fiber alignment, and a variable amount of peritendinous thickening imaged around the tendon or between the superficial and deep digital flexor tendons. Hyperechoic areas casting acoustic shadows consistent with areas of calcification are occasionally detected in old healed or healing tendon injuries (Fig. 3-70). Pinpoint hyperechoic foci were detected in the majority of horses with extensive scar formation within the superficial digital flexor tendon.[22] Unless extensive, this dystrophic calcification in the superficial digital flexor tendon is usually well tolerated by the equine athlete.

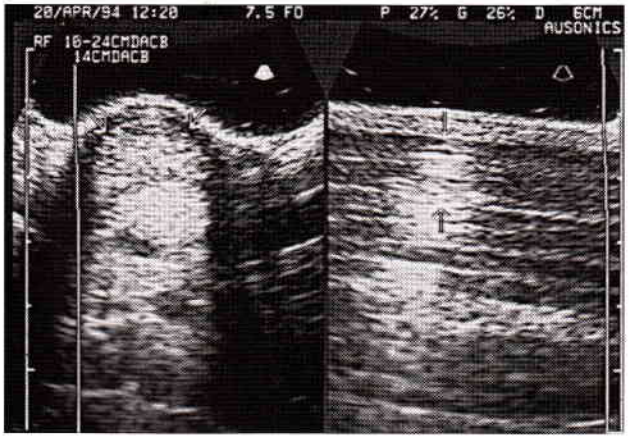

Figure 3–66

Sonograms of a chronic tendinitis in the right fore superficial digital flexor tendon (SDF), obtained from a 7-year-old Selle Français gelding. The area of SDF tendinitis extended from 10 to 24 cm distal to the point of the accessory carpal bone. At this level (14 cm or zone 2A), two different areas of previous injury can still be detected in the SDF. The more obvious area is the palmar portion of the SDF, which is still hypoechoic *(2 diagonal arrows point to this area in the transverse view, left image)* and lacks a normal fiber pattern in the sagittal view *(down arrow-right image)*. The less obvious area of previous injury is the more dorsal portion of the SDF, which has nearly normal echogenicity and still is somewhat heterogeneous, but has abnormal fiber alignment *(up arrow)* and is distinctly different in the sagittal view from the central (normal) portion of the SDF. Mild enlargement of the SDF occurs at this level with the tendon cross-sectional area measuring 1.5 cm^2. These sonograms were obtained with a 7.5-MHz sector-scanner transducer containing a built-in fluid offset at a displayed depth of 6 cm. The left side of the transverse image is medial and the right side is lateral. The left side of the sagittal image is distal and the right side is proximal.

Ideally, lesion and tendon echogenicity and fiber alignment should be normal with no detectable peritendinous scar, the lesion no longer discretely visible, and tendon cross-sectional area within the normal range before returning the horse to rigorous athletic competition. This quality of repair occurs only infrequently, prompting a continuous search for better treatments for tendon injuries to optimize tendon healing and the return of horses to their previous performance level.

The peritendinous area should be closely evaluated for the thickening of the subcutaneous tissues and the increased echogenicity of these tissues that indicate the formation of peritendinous scar tissue (see Fig. 3-68). The demarcation between the superficial digital flexor tendon and the adjacent deep digital flexor tendon should be closely evaluated because adhesions may develop between the adjacent flexor tendons. If tendinous or peritendinous adhesions are suspected, a dynamic ultrasound examination should be performed to determine if the superficial digital flexor tendon can glide normally by these adjacent tissues. The detection of hypoechoic to echogenic tissue surrounding the superficial digital flexor tendon correlates well with the detection of peritendinous fibrosis on histopathologic examination of the injured superficial digital flexor tendon and its surrounding peritendinous tissues.[18, 22]

As the tendon is loaded with gradually increasing exercise during tendon rehabilitation, tendon cross-sectional area should remain the same or decrease and tendon echogenicity and fiber alignment should similarly remain stable or improve on serial ultrasonographic examinations. The early studies of horses receiving intralesional βAPN-F and their placebo controls indicate that small variations in total tendon cross-sectional area occur as the tendon heals and remodels. These variations in tendon cross-sectional area that appear to be tolerated without reinjury are often in the range of 5% or less, with variations in tendon cross-sectional area for an individual zone of 5% to 10%. An increase in tendon cross-sectional area of more than 10% but less than 20% in a given zone or more than 5% but less than 10% for the total tendon cross-sectional area is an indication of tendon loading that may be excessive for the healing and remodeling that has occurred. The controlled exercise program should be maintained at the current level or slightly decreased (ideally) to prevent reinjury. An increase in tendon cross-sectional area of 20% or more in a given zone or 10% or more for the total tendon cross-sectional area is an indication of excessive loading and impending reinjury to the tendon. A decrease in the intensity of the controlled exercise is critical at this time. Maintenance of the same exercise level or increasing the training is gambling with a high probability of reinjury.

New areas of injury often occur adjacent to the old healed scar at the margin of the original tendon injury (Fig. 3-71). In the metacarpal region, the new area of fiber damage tends to occur proximal or distal to the old healed injury, rather than through the original area of injury. Several studies have shown that this junction is the weak link in the repair.[129]

Deep Digital Flexor Tendon Abnormalities. The deep digital flexor tendon is the most infrequently injured

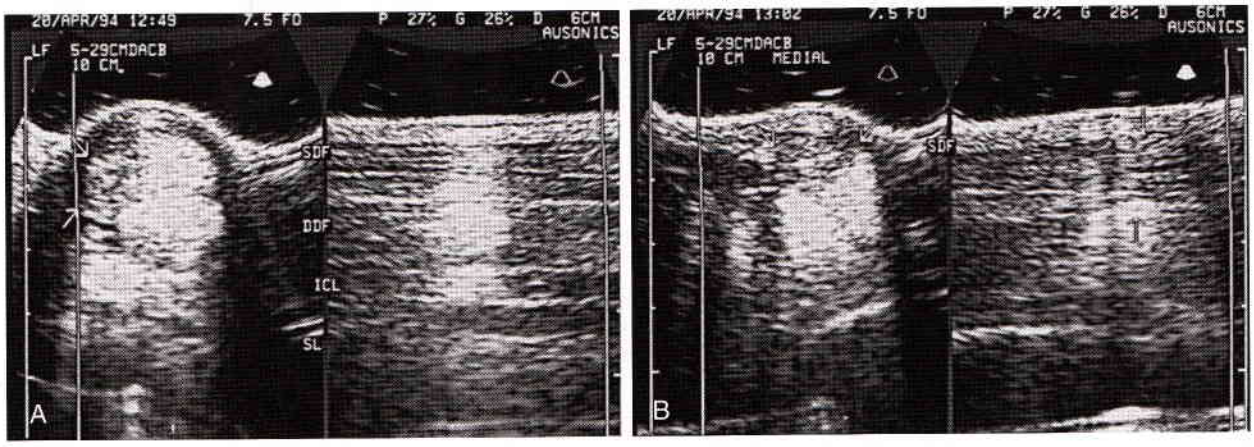

Figure 3–67

Sonograms of a chronic active left fore superficial digital flexor (SDF) tendinitis obtained from a 7-year-old Selle Français gelding (same horse as in Fig 3-66). This area of SDF damage was imaged from 5 to 29 cm distal to the point of the accessory carpal bone. These sonograms were obtained at 10 cm distal to the point of the accessory carpal bone (zone 1B) with a 7.5-MHz sector-scanner transducer containing a built-in fluid offset at a displayed depth of 6 cm. The left side of the transverse views *(left images)* is medial and the right side is lateral. The left side of the sagittal views *(right images)* is distal and the right side is proximal. DDF, deep digital flexor tendon; ICL, inferior check ligament; SL, suspensory ligament.

A, Notice the heterogeneous, somewhat hypoechoic medial side of the SDF *(arrows)* with a fairly good fiber pattern detected in the SDF from the palmar view. The superficial digital flexor tendon is enlarged and 47% of the tendon's cross-sectional area is affected at this level (0.96 cm^2/ 2.03 cm^2).

B, When this same area is scanned from the medial (swollen) side of the SDF, the hypoechoic areas within the damaged portion of the SDF are even more visible and the fiber pattern is not as good because the scan plane is now centered over the area of SDF injury.

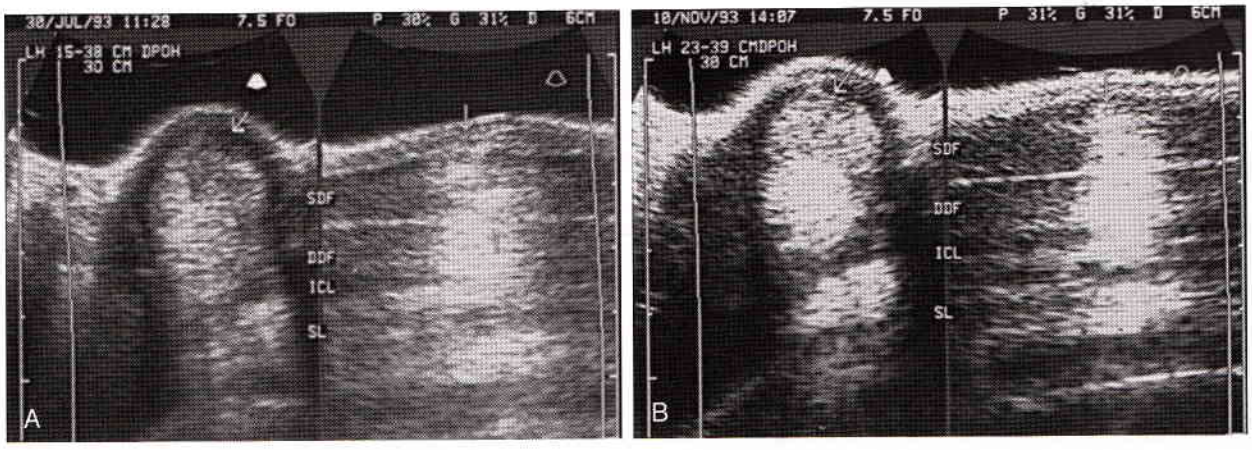

Figure 3–68

Sonograms of a healing area of injury to the superficial digital flexor tendon (SDF) in the left hind leg of a 13-year-old Warmblood mare. The superficial digital flexor tendinitis was imaged from 15 to 38 cm distal to the point of the hock. These sonograms were obtained at 30 cm distal to the point of the hock (zone 3A) with a 7.5-MHz sector-scanner transducer containing a built-in fluid offset at a displayed depth of 6 cm. The left side of the transverse views *(left images)* is medial and the right side is lateral. The left side of the sagittal views *(right images)* is distal and the right side is proximal.

A, Notice the hypoechoic central core lesion with the large area of peritendinous swelling centered over the plantarolateral aspect of the SDF. The core lesion involved 50% of the tendon's cross-sectional area at this level (1.03 cm^2/2.08 cm^2). Mild enlargement of the SDF and a somewhat random fiber pattern are present at this level.

B, Notice the improvement in lesion echogenicity within the SDF 3.5 months later, although the SDF still is heterogeneous. The size of the SDF has decreased slightly (1.74 cm^2 at the same level) and the fiber pattern is improved, although the most plantar aspect of the SDF still has a somewhat weak fiber pattern. The peritendinous soft tissue swelling still is present but has improved.

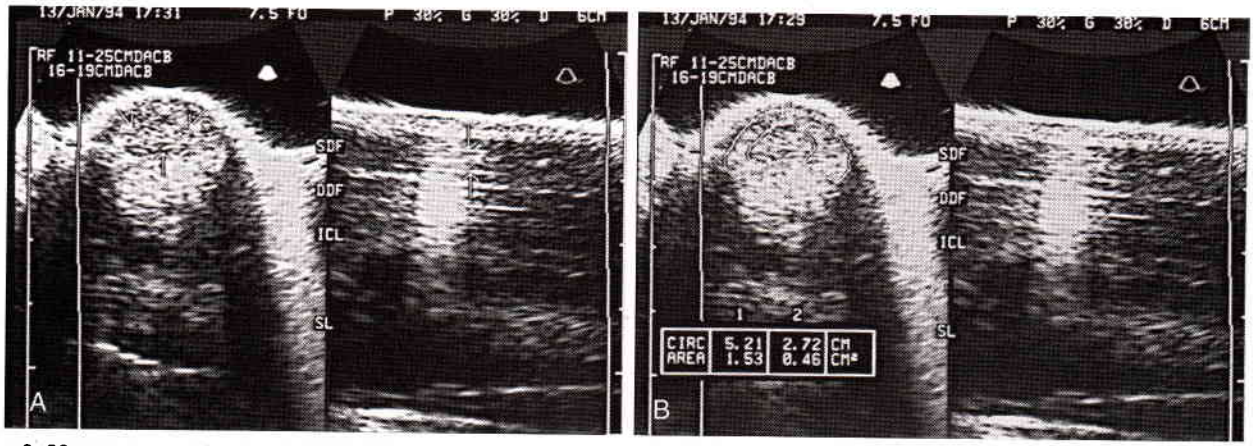

Figure 3–69

Sonograms of a healed "set" bowed right fore superficial digital flexor tendon (SDF), obtained from a 14-year-old Thoroughbred gelding. This horse has successfully competed for 2 years with this tendon (injury occurred 3 years earlier). Notice that the original core lesion is still visible *(arrows)* as a hypoechoic rim or halo between the original area of injury, now the repaired area, and the surrounding normal tendon. This is a very good-quality repair, although the SDF remains mildly enlarged (approximately 50% larger than normal). These sonograms were obtained with a 7.5-MHz sector-scanner transducer containing a built-in fluid offset at a displayed depth of 6 cm. The right side of the transverse views *(left images)* is lateral and the left side is medial. The right side of the sagittal views *(right images)* is proximal and the left side is distal. DDF, deep digital flexor tendon; ICL, inferior check ligament; SL, suspensory ligament.

A, Notice the original discrete core still sonographically detectable in the transverse view by the slightly hypoechoic rim between the normal and healed tendon *(arrows)* and the slight change in fiber alignment in the sagittal view *(arrows).*

B, The original core lesion involved 30% of the tendon's cross-sectional area at its largest point (0.46 cm^2/1.53 cm^2). It could still be imaged 3 years later from 16 to 19 cm distal to the accessory carpal bone with a more diffuse area of chronic inactive tendinitis detected from 11 to 25 cm distal to the accessory carpal bone.

tendon or ligament in the metacarpal region (Fig. 3-72). Deep digital flexor tendon injuries are often seen in horses with digital sheath effusions and are the most common injury in the hind metatarsal and pastern region

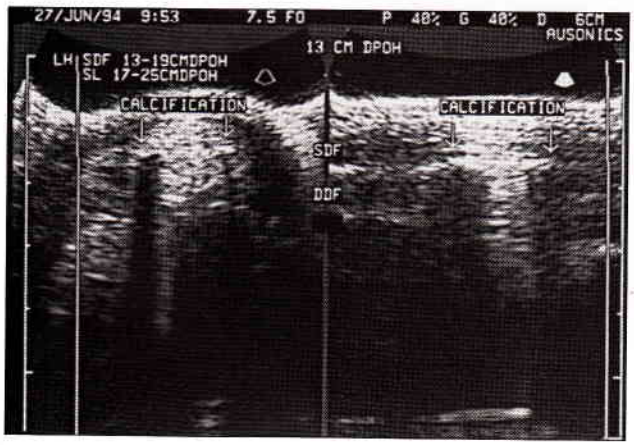

Figure 3–70

Sonograms of a chronic superficial digital flexor tendinitis with calcification in the left hind leg of a 5-year-old Standardbred stallion. Notice the hyperechoic areas casting acoustic shadows *(arrows)* in the middle of the superficial digital flexor tendon (SDF) on the sagittal view *(right image).* The areas of calcification are small in the transverse plane *(left image)* and are located in the lateral and medial portions of the SDF. No known history of intratendinous corticosteroid injections was reported for this horse. The chronic tendinitis was imaged from 13 to 19 cm distal to the point of the hock. This horse also had concurrent suspensory ligament desmitis, which is not visible in these images. These sonograms were obtained at 13 cm distal to the point of the hock (zone 1A) with a 7.5-MHz sector-scanner transducer containing a built-in fluid offset at a displayed depth of 6 cm. The left side of the transverse view is medial and the right side is lateral. The left side of the sagittal view is distal and the right side is proximal. DDF, deep digital flexor tendon.

of horses (Fig. 3-73). Deep digital flexor tendon injuries are the third most common injury in the fore pastern. In the metatarsal region, deep digital flexor tendon injuries are the second most common injury after injuries to the suspensory ligament, with the exception of "curb" swellings that extend into the metatarsal region and are usually associated with a superficial digital flexor tendinitis. Although deep digital flexor tendon injuries can occur in young horses during competition, they are much more common in older horses (≥ 10 years old) that compete in sports in which the hindlimb is loaded most in the stance phase of the stride (jumping and dressage). Many of these horses have histories of several years of chronic digital sheath tenosynovitis. In some horses, however, the digital sheath effusion is recent and occurs concurrent with the onset of the deep digital flexor tendinitis. Most horses with deep digital flexor tendinitis have a moderate to severe lameness present for a prolonged period of time. The digital sheath is usually very distended with a turgid feel; constriction of the digital sheath by the annular ligament is often evident. With rupture of the deep digital flexor tendon, the toe tips up on weight bearing and lameness is severe.

Sonographic findings in most older horses include hyperechoic areas within the deep digital flexor tendon, adjacent hypoechoic to anechoic areas of fiber tearing, thickening of the digital sheath, and moderate to severe distention of the digital sheath (Fig. 3-74). Most of the hyperechoic areas within the deep digital flexor tendon cast acoustic shadows to various degrees, consistent with dense mature scar tissue and calcification (Figs. 3-74 and 3-75). These hyperechoic areas are easily missed in the transverse plane because they are often scattered throughout the deep digital flexor tendon in a proximal to distal direction, with only small areas detected in each

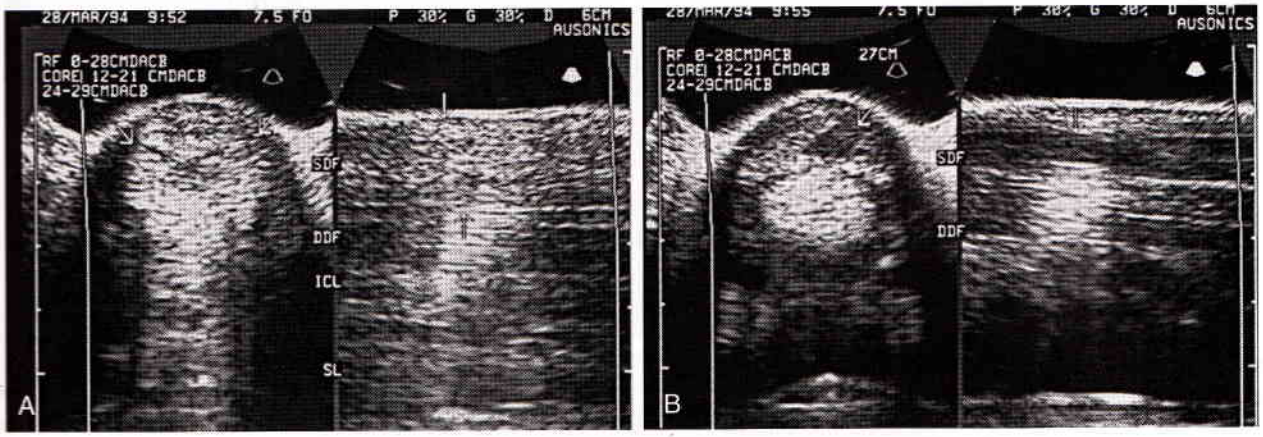

Figure 3–71

Sonograms of a poor-quality repair *(A)* of an injury to the right fore superficial digital flexor tendon (SDF) and its reinjury *(B)*, obtained from a 5-year-old Thoroughbred gelding. The new area of injury developed when the horse began galloping more than 2 years after the original injury. These sonograms were obtained with a 7.5-MHz sector-scanner transducer containing a built-in fluid offset at a displayed depth of 6 cm. The right side of the transverse views *(left images)* is lateral and the left side is medial. The right side of the sagittal views *(right images)* is proximal and the left side is distal. DDF, deep digital flexor tendon; ICL, inferior check ligament; SL, suspensory ligament.

A. Sonogram of the area of the previous injury where the original core lesion had been imaged from 12 to 21 cm distal to the point of the accessory carpal bone. Notice the marked enlargement of the SDF and its heterogeneous appearance with a very random pattern of fiber alignment *(arrows)*. This sonogram was obtained at 21 cm (border between zones 2B and 3A), where the hypoechoic area was 24% (0.57 cm^2/2.39 cm^2). This area had been stable sonographically for months.

B. Sonogram of the new area of fiber tearing *(arrows)* distal to the site of the previous injury 24 to 29 cm distal to the point of the accessory carpal bone. At its largest point at 27 cm (zone 3B), the tear involved 31% of the cross-sectional area of the SDF (0.49 cm^2/1.6 cm^2).

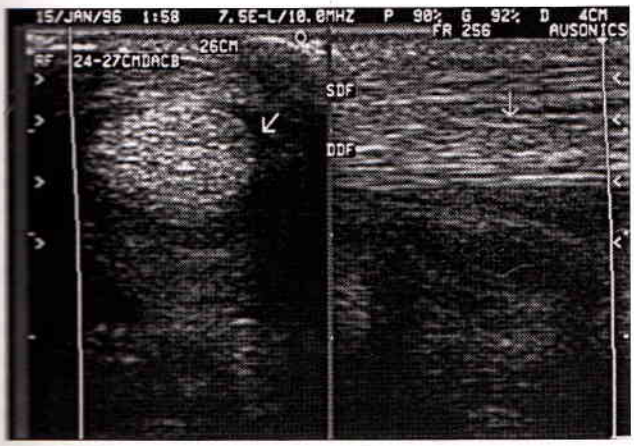

Figure 3–72

Sonograms of a small area of fiber damage in the lateral border of the deep digital flexor tendon (DDF) of the right foreleg of a 13-year-old Warmblood gelding which extended from 24 to 27 cm distal to the point of the accessory carpal bone. Notice the small hypoechoic lesion *(diagonal arrow)* in the lateral margin of the DDF in the transverse view *(left image)* and the mild enlargement of the lateral side of the DDF imaged at 26 cm (zone B). Notice the area of fiber disruption in the corresponding sagittal view *(right image)*. These sonograms were obtained with a wide-bandwidth 7.5-MHz linear-array transducer operating at 10.0 MHz at a displayed depth of 4 cm. The focal zones are positioned in the near field of the images. The right side of the transverse image is lateral and the left side is medial. The right side of the sagittal image is proximal and the left side is distal. SDF, superficial digital flexor tendon.

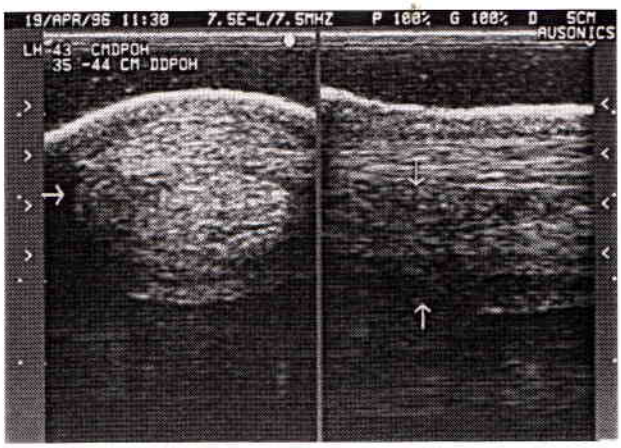

Figure 3–73

Sonograms of an recent area of fiber tearing in the left hind deep digital flexor tendon (DDF), obtained from an 8-year-old Thoroughbred gelding with a recent history of taking a bad step in a timber race. The horse presented with digital sheath effusion. Notice the discrete area of fiber damage involving the entire medial aspect of the DDF *(horizontal arrow)* in the transverse view *(left image)* and the complete absence of any tendon fibers *(vertical arrows)* when the medial parasagittal scan plane of the lesion *(right image)* was obtained. The area of tendon fiber disruption was imaged from 35 to 44 cm distal to the point of the hock, and these sonograms were obtained at 43 cm (zone 4C). The curved thick echogenic structure dorsal to the DDF is the digital sheath. These sonograms were obtained with a wide-bandwidth 7.5-MHz linear-array transducer operating at 7.5-MHz with a hand-held standoff pad at a displayed depth of 5 cm. The focal zones are positioned in the near field of the images. The right side of the transverse image is lateral and the left side is medial. The right side of the sagittal image is proximal and the left side is distal.

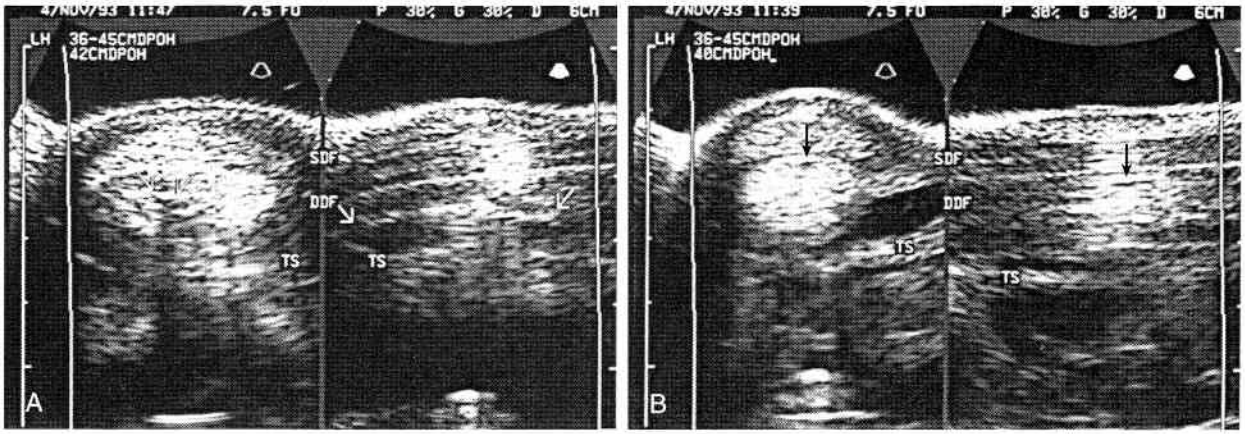

Figure 3–74

Sonograms of deep digital flexor (DDF) tendinitis with calcification and digital sheath tenosynovitis in the distal metatarsal region of the left hind leg, obtained from a 10-year-old Thoroughbred gelding. The deep digital flexor tendinitis extended from 36 to 45 cm distal to the point of the hock. These sonograms were obtained with a 7.5-MHz sector-scanner transducer containing a built-in fluid offset at a displayed depth of 6 cm. The right side of the transverse views *(left images)* is lateral and the left side is medial. The right side of the sagittal views *(right images)* is proximal and the left side is distal. SDF, superficial digital flexor tendon; TS, tendon sheath.

A, Sonogram of the areas of calcification *(arrows)* imaged as bright hyperechoic linear echoes casting weak to strong acoustic shadows. The areas of calcification are imaged in the central and medial portion of the DDF at 42 cm distal to the point of the hock in zone 4B. Hypoechoic areas and loss of the normal fiber pattern are detected in the plantar and medial portion of the DDF in both views.

B, Sonogram of chronic digital sheath tenosynovitis with thickening of the digital sheath and an anechoic effusion. A small area of fiber damage is detected in the plantar portion of the DDF as a hypoechoic lesion on the midline *(arrows)* at 40 cm distal to the point of the hock in zone 4A.

transverse scan plane. These hyperechoic areas are often easier to detect in a sagittal scan plane because more of these small hyperechoic echoes are within the same scan plane in the sagittal image. The hyperechoic lesions in the deep digital flexor tendon are most commonly located in the portion of the tendon found within the digital sheath and, more specifically, underneath or adjacent to the annular ligament.

The areas of fiber tearing in the deep digital flexor tendon usually extend proximally or distally from this area of calcification. Synovial proliferation is often present in addition to the effusion within the digital sheath. Fibrin and/or adhesions may also be visualized within the tendon sheath (see Fig. 3–75). Adhesions are often detected between the digital sheath and/or the superficial or deep digital flexor tendon and may be adjacent to the areas of deep digital flexor injury. Adhesions may appear very echogenic and somewhat rigid and may distort the shape of the deep digital flexor tendon or result in abnormal positioning of the tendon within the sheath. Thickening of the annular ligament associated with a concurrent annular ligament desmitis may also be detected in some horses (see Fig. 3–75).

Occasionally horses have hyperechoic areas casting acoustic shadows within the deep digital flexor tendon with no history of lameness and an acute effusion in the digital sheath (Fig. 3–76). More typically, however, the digital sheath tenosynovitis precedes the onset of lameness and deep digital flexor tendinitis by months or years. The pathophysiology of deep digital flexor tendinitis in the majority of horses is unknown. Probably, however, the existence of a chronic fibrinous digital sheath tenosynovitis predisposes the horse to developing this syndrome, particularly if it competes as a jumper or in dressage at the upper levels. The adhesions present within the digital sheath may cause abnormal loading of the deep digital flexor tendon when the horse is bearing weight, resulting in small areas of damage and fiber tearing. Poor perfusion of the deep digital flexor tendon in the region of the annular ligament in horses with chronic digital sheath tenosynovitis may also predispose this area to degenerative changes and subsequent calcification. Horses with chronic digital sheath tenosynovitis and lameness should be carefully scanned for deep digital flexor abnormalities, particularly if the horse is a jumper or dressage horse.

The deep digital flexor tendon is infrequently injured in young horses. A history of recent trauma to the limb, such as the horse being cast in the stall, slipping and falling, or sustaining a laceration is most common. Laceration of the deep digital flexor tendon also occurs, usually in conjunction with injury to the superficial digital flexor tendon. In these horses, a distinct demarcation at the site of the original injury is usually visible ultrasonographically in the deep digital flexor tendon. Previous surgeries that increase the risk of deep digital flexor tendinitis include an inferior check ligament desmotomy (in which inadvertent damage to the deep digital flexor tendon may have occurred) or a posterior digital neurectomy (after which deep digital flexor tendon disease often develops in the region of the navicular bursa and pastern).

Injuries to the deep digital flexor tendon usually occur without injury to other tendinous or ligamentous structures. The inferior check ligament, or accessory ligament of the deep digital flexor tendon, because of its close association with the deep digital flexor tendon, is most likely to be injured if more than one structure is injured in the metacarpal region. Complete rupture of the deep digital flexor tendon rarely occurs and may also involve damage to the inferior check ligament (Fig. 3–77).

Care must be taken not to mistake the normal insertion of the inferior check ligament on the dorsal aspect of the

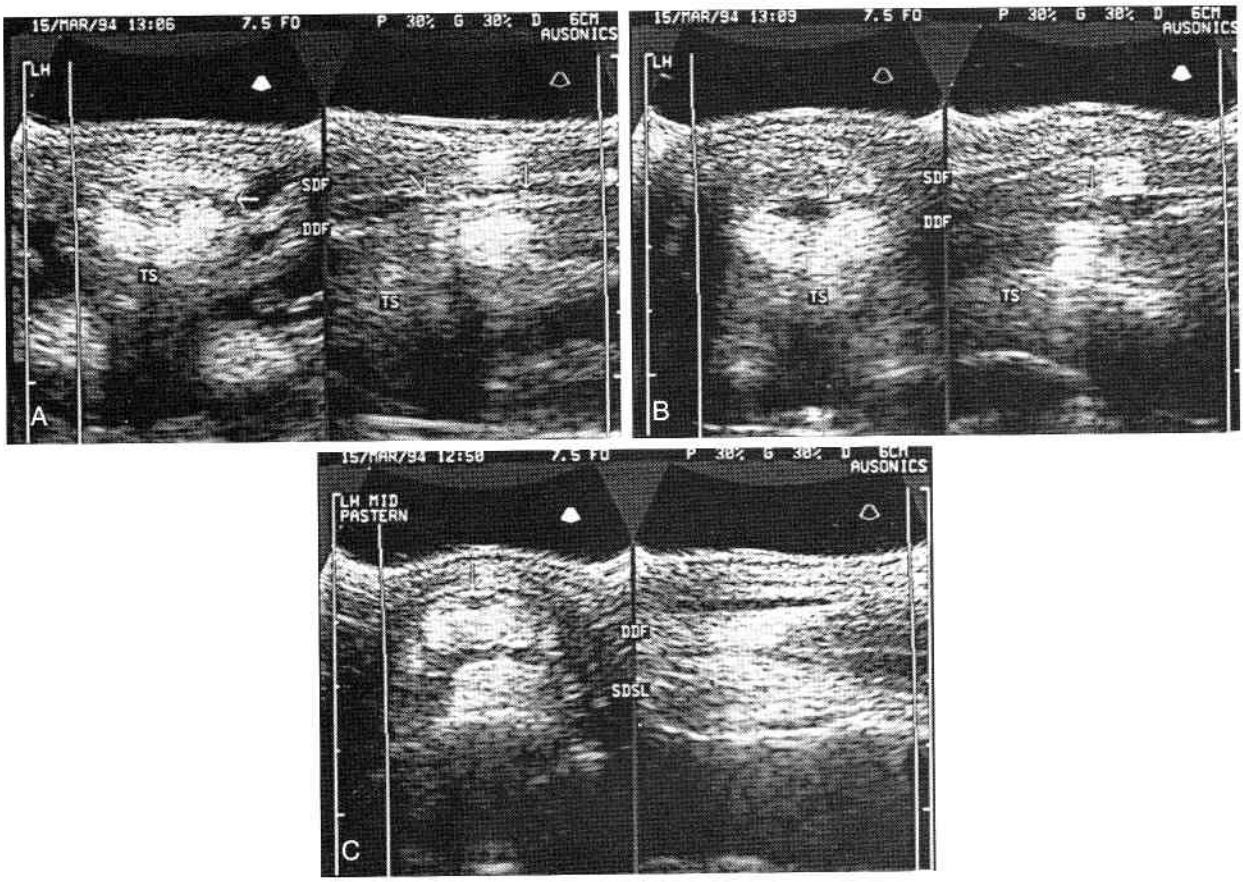

Figure 3–75

Sonograms of deep digital flexor (DDF) tendinitis with calcification within the DDF and a chronic tenosynovitis of the digital sheath in the left hind leg, obtained from an 11-year-old Thoroughbred mare. The area of deep digital flexor tendinitis extended from 30 cm distal to the point of the hock to the mid-pastern. These sonograms were obtained with a 7.5-MHz sector-scanner transducer containing a built-in fluid offset at a displayed depth of 6 cm. The right side of the transverse views *(left images)* is lateral and the left side is medial. The right side of the sagittal views *(right images)* is proximal and the left side is distal. SDF, superficial digital flexor tendon; TS, tendon sheath; SDSL, straight distal sesamoidean ligament.

A, Hyperechoic linear echoes are casting weak acoustic shadows, consistent with early calcification, in the central and somewhat medial and plantar portion of the DDF *(arrows)* extending down into the region of the fetlock annular ligament. The surrounding DDF is hypoechoic and lacks normal fiber alignment, consistent with DDF tendinitis. Hypoechoic material representing fibrin surrounds the dorsal aspect of the DDF. This sonogram was obtained at 40 cm distal to the point of the hock (zone 4B).

B, Sonogram of a large core lesion *(arrows)* in the DDF just distal to the area of calcification, involving the plantar and slightly medial aspect of the DDF. The annular ligament and digital sheath are thickened with a combined measurement of 6 mm. This sonogram was obtained at 43 cm distal to the point of the hock (zone 4C).

C, The core lesion in the DDF extends distally into the pastern and is still visible on the plantar surface of the tendon *(arrow)* in the mid-pastern region (zone P1C), although it is much smaller at this location. Hypoechoic material representing fibrin is imaged in the dorsal portion of the digital sheath.

deep digital flexor tendon for a lesion; this part of the ligament is typically hypoechoic because it inserts into the deep digital flexor tendon from a different scan plane. This insertion typically occurs at the level of the suspensory ligament bifurcation and at the proximal-most reflection of the digital sheath.

Inferior Check Ligament (Accessory Ligament of the Deep Digital Flexor Tendon) Desmitis. Injuries to the inferior check ligament in the foreleg occur more frequently than do deep digital flexor tendon injuries but are less common than injuries to the suspensory ligament or the superficial digital flexor tendon. Many horses with inferior check ligament desmitis develop clinical signs of injury after being turned out in a field. They show swelling, heat, and sensitivity in the affected area. Others develop clinical signs during pleasure riding or after a jumping competition.[44, 53] Inferior check ligament desmitis may also develop in young horses that have a history of an inferior check ligament desmotomy.

Desmitis of the accessory ligament of the deep digital flexor tendon is occasionally seen in horses after a major change in the angle of the foot, particularly in those horses with somewhat contracted tendons, "over at the knee" conformation, or club feet. Upright hoof conformation was detected in 19%[44] and 33%[53] of horses with inferior check ligament desmitis. In one study,[14] 7% of the horses had pigeon-toed conformation and 7% were over at the knee. The horses that were over at the knee also had superficial digital flexor tendinitis. Inferior check ligament injuries are reported to be more common in

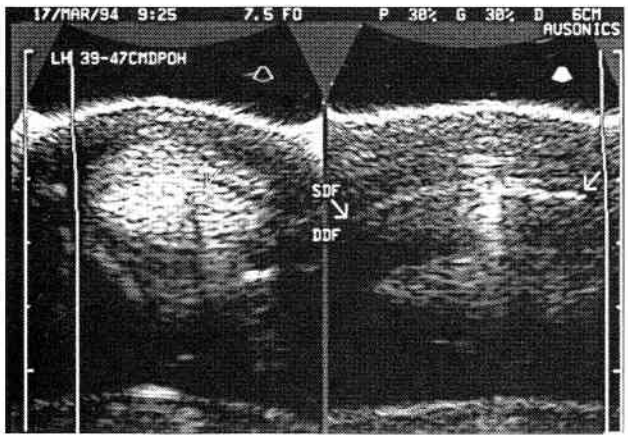

Figure 3–76

Sonograms of calcification in the deep digital flexor tendon (DDF) of the left hind leg of a 14-year-old Thoroughbred gelding. Digital sheath effusion was detected after a combined training competition. Calcification *(arrows)* was detected in the DDF from 39 to 47 cm distal to the point of the hock. In the sagittal view *(right image)* the calcification is seen as a hyperechoic line in the plantar portion of the DDF (between the two angled arrows), extending distally underneath the fetlock annular ligament. In the transverse view *(left image)*, the calcification is imaged as a small hyperechoic spot casting a strong acoustic shadow *(angled arrow)*. This sonogram was obtained at 45 cm (zone 4C) with a 7.5-MHz sector-scanner transducer containing a built-in fluid offset at a displayed depth of 6 cm. The right side of the transverse view is lateral and the left side is medial. The right side of the sagittal view is proximal and the left side is distal.

ponies and older horses.[44, 53] Inferior check ligament desmitis usually occurs in just one forelimb, although occasionally bilateral forelimb involvement or desmitis of both the forelimbs and hindlimbs occurs. Injuries to the hind inferior check ligament are extremely rare.

In most instances, the predominant swelling is lateral because the inferior check ligament runs lateral and dorsal to the deep digital flexor tendon. This swelling is fairly characteristic because it involves only the proximal two thirds of the metacarpus, often centered in the proximal to mid-metacarpal region. At the onset of the desmitis, most horses show local heat and sensitivity. Lameness is usually present initially but often resolves rapidly, although many horses are still lame at the time they are presented to a referral hospital (59%[44] and 56%[53]). Swelling of the inferior check ligament is nearly always present by the time of referral, whereas the local heat and sensitivity may have resolved. In some horses, the inferior check ligament is difficult to distinguish from the deep digital flexor tendon or, less frequently, from the superficial digital flexor tendon on palpation. Superficial digital flexor tendinitis may also be present in some horses with inferior check ligament desmitis. Concurrent superficial digital flexor tendinitis was reported in 19%[44] and 50%[53] of horses with inferior check ligament desmitis.

The most common sonographic finding is an enlarged cross-sectional area of the inferior check ligament with a diffuse desmitis (Fig. 3–78). This enlargement is usually in a palmar-to-dorsal direction as well as in a medial-to-lateral direction. The palmar-to-dorsal enlargement of the inferior check ligament often results in the dorsal aspect of the inferior check ligament touching the palmar portion of the suspensory ligament and, in severe cases, the dorsal portion of the superficial digital flexor tendon. If the inferior check ligament and suspensory ligament are touching anywhere throughout their length other than at the origin of the suspensory ligament, one of these two structures must be enlarged. The enlarged inferior check ligament also often wraps around the deep digital flexor tendon both medially and laterally, making distinguishing the border between these two structures difficult. Less commonly, loss of definition between the inferior check ligament and the superficial digital flexor tendon occurs because of the marked enlargement of the inferior check

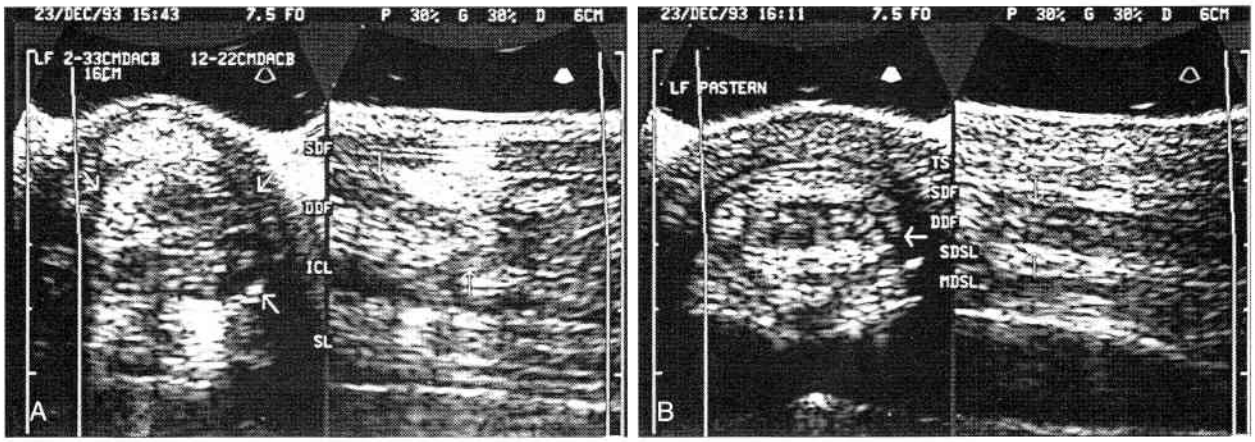

Figure 3–77

Sonograms of a severe rupture of the majority of the deep digital flexor tendon (DDF) and inferior check ligament (ICL) in the left foreleg, obtained from an 8-year-old Thoroughbred gelding. This severe DDF tendinitis extended from 2 to 33 cm distal to the point of the accessory carpal bone in the metacarpal region and distally into the pastern to the foot. These sonograms were obtained with a 7.5-MHz sector-scanner transducer with a built-in fluid offset at a displayed depth of 6 cm. The right side of the transverse views *(left images)* is lateral and the left side is medial. The right side of the sagittal views *(right images)* is proximal and the left side is distal. SDF, superficial digital flexor tendon; SL, suspensory ligament; TS, tendon sheath; SDSL, straight distal sesamoidean ligament; MDSL, middle distal sesamoidean ligament.

A, Notice the large anechoic lesion in the majority of the DDF and the entire ICL at 16 cm (zone 2A) in the transverse view. The sagittal sonogram is obtained over the medial aspect of the limb, where some near-normal fibers remain in the DDF and significant fiber disruption is imaged in the ICL. Some SL desmitis is also present.

B, Notice the large anechoic DDF with no normal DDF fibers imaged at this level *(arrows)* in zone P1 in either the transverse or sagittal views.

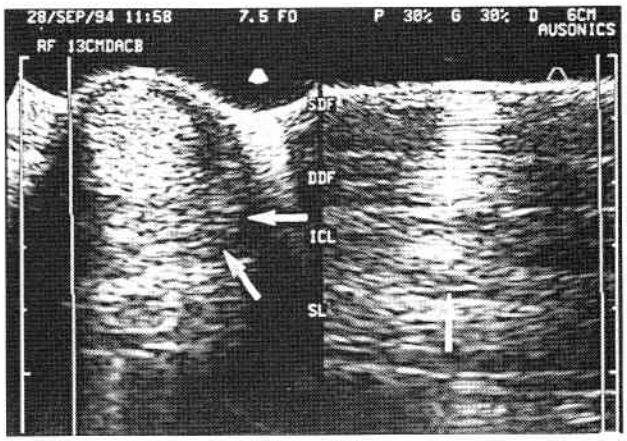

Figure 3–78

Sonograms of a diffuse inferior check ligament (ICL) desmitis in the right foreleg, obtained from a 9-year-old Cleveland Bay gelding. Notice the diffusely enlarged ICL *(arrows)*, best appreciated in the transverse view *(left image)*, with a slightly hypoechoic appearance and loss of some of the normal fiber pattern detected in the sagittal view *(right image)*. These sonograms were obtained at 13 cm distal to the point of the accessory carpal bone (at the border between zones 1B and 2A) with a 7.5-MHz sector-scanner transducer with a built-in fluid offset at a displayed depth of 6 cm. The right side of the transverse image is lateral and the left side is medial. The right side of the sagittal image is proximal and the left side is distal. SDF, superficial digital flexor tendon; DDF, deep digital flexor tendon; SL, suspensory ligament.

ligament. This loss of definition between two adjacent tendinous and ligamentous structures suggests adhesions. Occasionally, horses may sustain an injury to both the inferior check ligament and the deep digital flexor tendon simultaneously (see Fig. 3-77). These injuries are usually severe, although small focal hypoechoic areas have been reported in the dorsal aspect of the deep digital flexor tendon in horses with inferior check ligament desmitis.[44, 53]

The inferior check ligament is usually diffusely hypoechoic or heterogeneous, with large areas of fiber disruption in horses with diffuse desmitis. Although small discrete areas of fiber tearing (Fig. 3-79) are seen in horses with inferior check ligament desmitis, these are less common than either the larger core lesions (Fig. 3-80) or diffuse areas of damage. The most common area of injury is in the mid portion of the inferior check ligament in zones 1B and 2A. Injuries often extend distally into the insertion of the inferior check ligament into the deep digital flexor tendon. Less frequently, injuries are detected that begin at the origin of the inferior check ligament from the palmar carpal ligament. Complete rupture of the inferior check ligament is uncommon (Fig. 3-81) and the deep digital flexor tendon should be carefully evaluated in these horses.

As the inferior check ligament heals, its cross-sectional area decreases, its echogenicity returns toward normal, and short linear echoes are imaged within the repairing ligament (Fig. 3-82). In most cases, these linear echoes have a random pattern, but occasionally near-normal fiber alignment occurs. Periligamentous soft tissue thickening may become more echogenic, and periligamentous fibrosis with adhesions to surrounding structures may result (Fig. 3-83), particularly in horses with more severe injuries. Fibrous bundles joining the superficial and deep digital flexor tendons along their lateral and medial margins predispose the horse to the development of adhesions between the accessory ligament of the deep digital

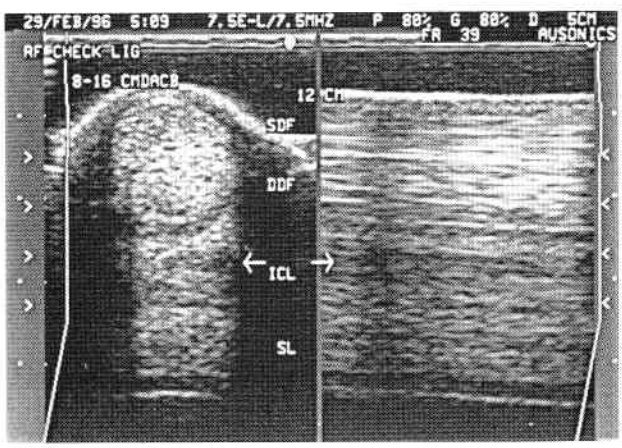

Figure 3–79

Sonograms of a small area of fiber tearing in the lateral portion of the right fore inferior check ligament (ICL), obtained from a 15-year-old Thoroughbred gelding. Notice the small linear hypoechoic defect *(arrows)* in the lateral portion of the ICL in the transverse view *(left image)*. The corresponding area of fiber disruption in the sagittal view *(right image)* is best imaged at 12 cm distal to the point of the accessory carpal bone (zone 1B). This area of fiber damage was detected from 8 to 16 cm distal to the point of the accessory carpal bone. These sonograms were obtained with a wide-bandwidth 7.5-MHz linear-array scanner transducer operating at 7.5-MHz with a hand-held standoff pad at a displayed depth of 5 cm. The right side of the transverse image is lateral and the left side is medial. The right side of the sagittal image is proximal and the left side is distal. SDF, superficial digital flexor tendon; DDF, deep digital flexor tendon; SL, suspensory ligament.

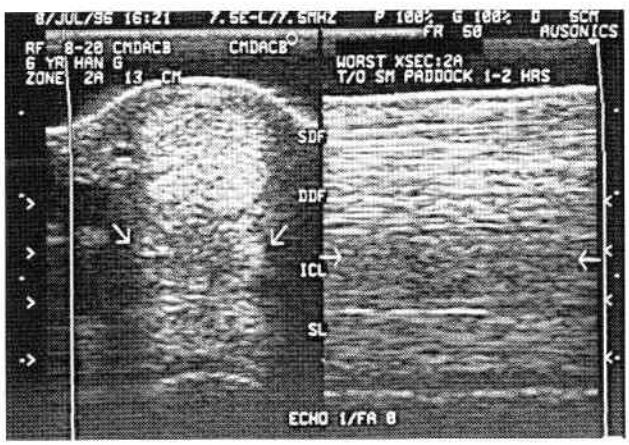

Figure 3–80

Sonograms of a large core lesion *(arrows)* in the right fore inferior check ligament (ICL), obtained from a 6-year-old Hanoverian gelding. Notice the large hypoechoic core lesion in the enlarged ICL in the transverse view *(left image)* and the fiber disruption imaged in the sagittal view *(right image)*. This core lesion was detected from 8 to 20 cm distal to the point of the accessory carpal bone. This sonogram was obtained at 13 cm distal to the point of the accessory carpal bone (at the border between zones 1B and 2A) with a wide-bandwidth 7.5-MHz linear-array transducer operating at 7.5 MHz with a hand-held standoff pad at a displayed depth of 5 cm. The focal zones are positioned in the middle to far field of the image. The right side of the transverse image is lateral and the left side is medial. The right side of the sagittal image is proximal and the left side is distal. SDF, superficial digital flexor tendon; DDF, deep digital flexor tendon; SL, suspensory ligament.

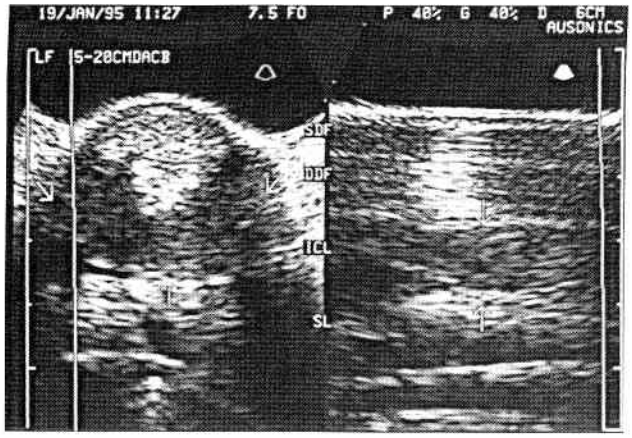

Figure 3–81

Sonograms of a ruptured inferior check ligament (ICL) in the left foreleg, obtained from a 17-year-old Thoroughbred gelding. Notice the complete absence of any fibers from the ICL *(arrows)* in either the transverse view *(left image)* or the sagittal view *(right image)*. This disruption of the ICL was evident for its entire length, from 5 to 20 cm distal to the point of the accessory carpal bone. These sonograms were obtained at 18 cm distal to the point of the accessory carpal bone (zone 2B) with a 7.5-MHz sector-scanner transducer containing a built-in fluid offset at a displayed depth of 6 cm. The right side of the transverse image is lateral and the left side is medial. The right side of the sagittal image is proximal and the left side is distal. SDF, superficial digital flexor tendon; DDF, deep digital flexor tendon; SL, suspensory ligament.

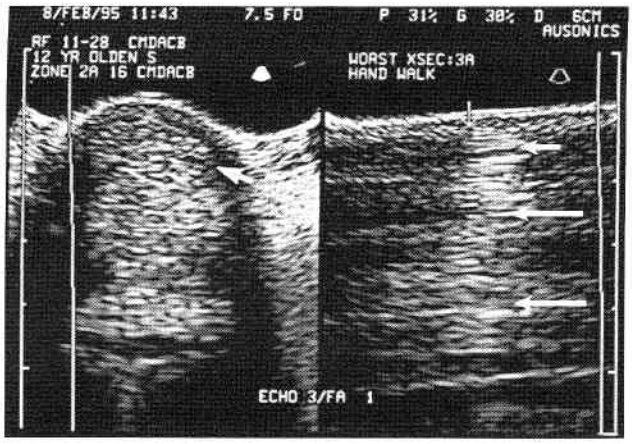

Figure 3–83

Sonograms of a diffuse inferior check ligament (ICL) desmitis with adhesions of the inferior check ligament to the adjacent superficial (SDF) and deep digital flexor tendons (DDF) and suspensory ligament (SL) in the right foreleg, obtained from a 12-year-old Oldenberg stallion at 16 cm distal to the point of the accessory carpal bone (zone 2A). Notice the difficulty in distinguishing the margins of the SDF and DDF from the ICL in the transverse view *(left image)* and the hypoechoic tissue representing fibrous tissue *(long arrows)* imaged in between the ICL and adjacent DDF and SL in the sagittal view *(right image)*. This horse also had a new superficial digital flexor tendinitis with a small area of fiber tearing *(short arrow)* that may have developed secondary to the chronic ICL desmitis with adhesions to the adjacent tendons and ligaments. These sonograms were obtained with a 7.5-MHz sector-scanner transducer with a built-in fluid offset at a displayed depth of 6 cm. The right side of the transverse sonogram is lateral and the left side is medial. The right side of the sagittal sonogram is proximal and the left side is distal.

flexor tendon and the superficial digital flexor tendon when these structures are injured.[111] Rarely, calcification is imaged in the inferior check ligament (Fig. 3–84).

A type of proliferative inferior check ligament desmitis has been recognized in which significant tendon and

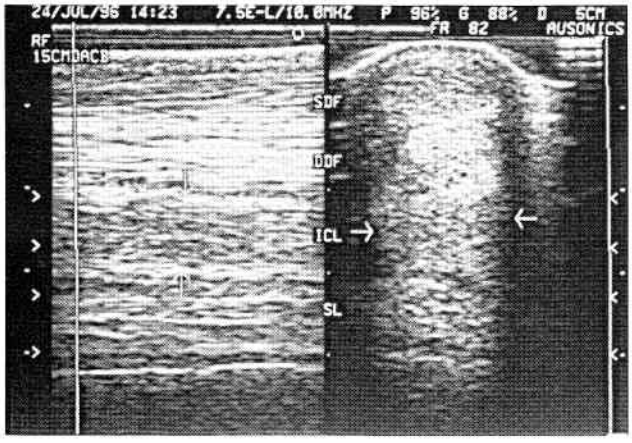

Figure 3–82

Sonograms of a healing desmitis *(arrows)* of the inferior check ligament in the right foreleg, obtained from a 14-year-old Thoroughbred cross gelding at 15 cm distal to the point of the accessory carpal bone (zone 2A). Notice the heterogeneous hypoechoic to echogenic appearance of the inferior check ligament (ICL) and the short and longer linear echoes in a somewhat random pattern repairing the area of injury. These sonograms were obtained with a wide-bandwidth 7.5-MHz linear-array transducer operating at 10.0 MHz with a hand-held standoff pad at a displayed depth of 5 cm. The focal zones are positioned in the far field of the images. The right side of the transverse view *(right image)* is lateral and the left side is medial. The right side of the sagittal view *(left image)* is proximal and the left side is distal. SDF, superficial digital flexor tendon; DDF, deep digital flexor tendon; SL, suspensory ligament.

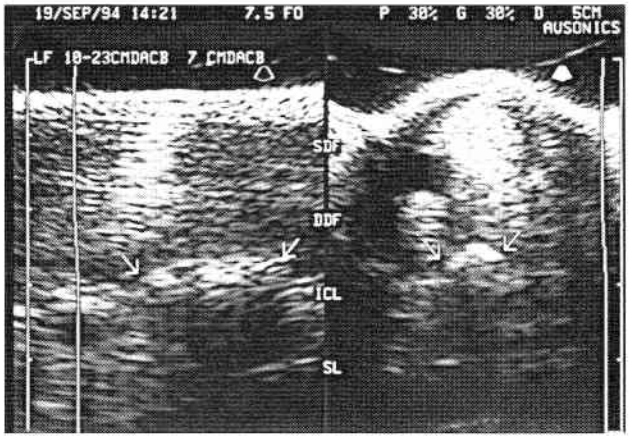

Figure 3–84

Sonograms of calcification in the left fore inferior check ligament (ICL), obtained from a 17-year-old Pinto gelding. Notice the hyperechoic echoes casting a strong acoustic shadow *(arrows)* through the majority of the ICL, most marked at 7 cm distal to the point of the accessory carpal bone (zone 1A). Heterogeneity of the ICL (hypoechoic, isoechoic, and hyperechoic areas) was imaged throughout the ligament from 10 to 23 cm distal to the point of the accessory carpal bone, consistent with a chronic desmitis. A small amount of the ICL can be visualized medial and to a lesser extent lateral to the areas of calcification in the transverse view *(right image)* and in the mid body in the sagittal view *(left image)*. These sonograms were obtained with a 7.5-MHz sector-scanner transducer with a built-in fluid offset at a displayed depth of 6 cm. The right side of the transverse image is lateral and the left side is medial. The right side of the sagittal images is proximal and the left side is distal. SDF, superficial digital flexor tendon; DDF, deep digital flexor tendon; SL, suspensory ligament.

ligament contracture develops, without an episode of acute inferior check ligament desmitis. These horses have diffuse thickening of the flexor bundle and are often presented for suspected suspensory ligament desmitis. Affected horses are usually unable to place the heel of the affected limb on the ground. Most horses with this severe proliferative inferior check ligament desmitis have been Quarter horses or Quarter horse crosses. Sonographic examination reveals a heterogeneous inferior check ligament that is markedly enlarged and often hyperechoic compared to normal tendinous and ligamentous tissue (Fig. 3-85). The borders of the inferior check ligament are difficult to distinguish from the adjacent deep digital flexor tendon and superficial digital flexor tendon. Many horses have concurrent injury in the superficial digital flexor tendon or, less frequently, in the deep digital flexor tendon. Concurrent suspensory ligament damage has not been detected in affected horses to date. These areas of tendon injury in the superficial digital flexor tendon are usually hypoechoic and in the early stages of tendon healing. Adhesions between these tendinous and ligamentous structures can be documented sonographically and have been confirmed at surgery and at postmortem examination of affected horses. Careful evaluation of the other limbs in affected horses usually reveals a similar, but less severe, proliferative inferior check ligament desmitis in two or more limbs.

In a good-quality sonographic repair, the inferior check ligament has normal to near-normal echogenicity and near-normal fiber alignment with only mild enlargement of the ligament cross-sectional area (Fig. 3-86). Recurrent inferior check ligament desmitis can occur, particularly in horses with a history of inferior check ligament desmotomy (Fig. 3-87). Inferior check ligament desmitis rarely occurs in other horses unless they are predisposed to this injury by conformational problems creating excessive lateral loading. As with other tendinous and ligamentous injuries, the new area of fiber disruption tends to occur adjacent to the original injury, extending proximally or distally (Fig. 3-88).

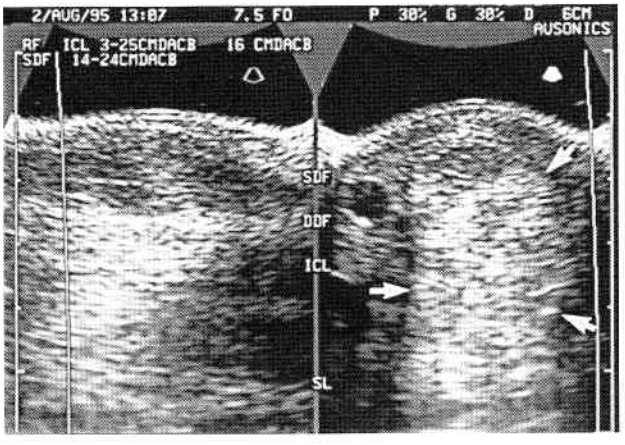

Figure 3–85

Sonograms of a chronic proliferative inferior check ligament (ICL) desmitis with an active superficial digital flexor (SDF) tendinitis, obtained from the right foreleg of a 17-year-old Hanoverian mare. Notice the markedly enlarged ICL *(arrows)* imaged from 3-25 cm distal to the point of the accessory carpal bone with its heterogeneous echogenicity enveloping the deep digital flexor tendon (DDF) and the lateral aspect of the SDF at 16 cm (zone 2A). The border between the ICL and the suspensory ligament (SL) is also difficult to distinguish. These structures all moved as a unit during a dynamic ultrasound examination. The SDF lacks a normal fiber pattern with a large hypoechoic lesion detected in the palmar aspect of the tendon which was imaged from 14-24 cm distal to the point of the accessory carpal bone. These sonograms were obtained with a 7.5-MHz sector-scanner transducer with a built-in fluid offset at a displayed depth of 6 cm. The right side of the transverse view *(right image)* is lateral and the left side is medial. The right side of the sagittal view *(left image)* is proximal and the left side is distal.

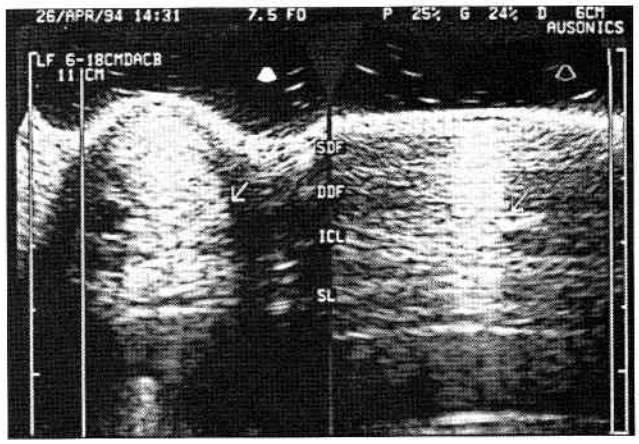

Figure 3–86

Sonograms of a healed inferior check ligament (ICL) desmitis secondary to an ICL desmotomy, obtained from the left foreleg of a 4-year-old Arabian filly. Notice the enlarged, somewhat heterogeneous appearance of the ICL in the transverse view *(left image)*, with the majority of the ligament having near-normal echogenicity, and the random pattern of fiber alignment in the sagittal view *(right image)*. The chronic inactive ICL was imaged from 6 to 18 cm distal to the point of the accessory carpal bone. These sonograms were obtained at 11 cm distal to the point of the accessory carpal bone (zone 1B) with a 7.5-MHz sector-scanner transducer with a built-in fluid offset at a displayed depth of 6 cm. The right side of the transverse image is lateral and the left side is medial. The right side of the sagittal image is proximal and the left side is distal. SDF, superficial digital flexor tendon; DDF, deep digital flexor tendon; SL, suspensory ligament.

Suspensory Ligament Desmitis. Injury to the suspensory ligament occurs in all breeds of horses, with injuries to the body and branches being more common than proximal suspensory ligament desmitis. Injuries to the suspensory ligament occur frequently in both the forelegs and hind legs. Standardbred racehorses and upper-level dressage horses have the highest incidence of suspensory ligament injuries in the hindlimb. In Thoroughbred racehorses, proximal suspensory desmitis and desmitis of the suspensory ligament branches are more common than desmitis in the body of the suspensory ligament.[58] Injuries to the suspensory ligament in the Thoroughbred racehorse can be catastrophic, associated with traumatic breakdown of the suspensory apparatus.

Local heat, swelling, and sensitivity of the suspensory ligament on palpation are characteristic of suspensory ligament desmitis. Distention of the medial palmar or plantar vein has also been reported in affected horses.[43, 52, 58] The local signs of heat, swelling, and sensitivity are more common with injuries to the body and/or branches of the suspensory ligament than with injuries at the origin of the suspensory ligament.[15, 43, 52, 58] Before the advent of diagnostic ultrasound, many horses diagnosed with inferior check ligament desmitis actually had injuries to the suspensory ligament. This was due, in part, to the type of swelling of the suspensory ligament when injured at

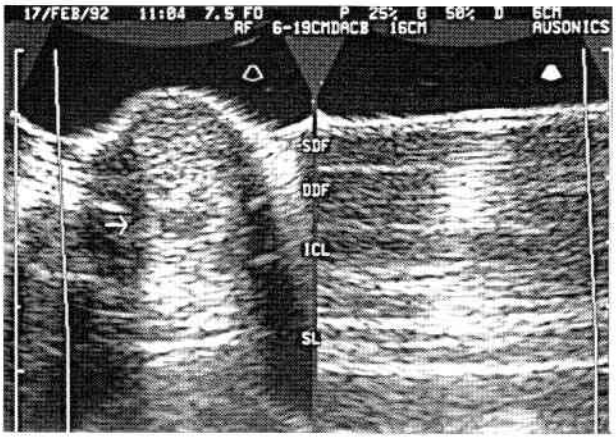

Figure 3–87

Sonograms of a recent injury to the right fore inferior check ligament (ICL), obtained from a 4-year-old Thoroughbred filly that had an inferior check ligament desmotomy performed on this leg at 6 months of age. Notice the hypoechoic palmar core lesion *(arrow)* in the inferior check ligament in the transverse view *(left image)* and the loss of the normal fiber pattern in the palmar portion of the ICL in the sagittal view *(right image)*. The fiber alignment in the more dorsal portion of the ICL adjacent to the new tear is abnormal, consistent with the prior healed surgical injury. The ICL is enlarged and is touching the adjacent suspensory ligament (SL) and deep digital flexor tendon (DDF). This lesion was imaged from 6–19 cm distal to the point of the accessory carpal bone. These sonograms were obtained at 16 cm (zone 2A) with a 7.5-MHz sector-scanner transducer containing a built-in fluid offset at a displayed depth of 6 cm. The right side of the transverse image is lateral and the left side is medial. The right side of the sagittal image is proximal and the left side is distal.

the origin and in the proximal portion of the suspensory ligament body. The primary swelling of the proximal portion of the suspensory ligament body is in a palmar or plantar direction. The injured portion cannot swell much in a dorsal direction due to the restriction caused by the overlying third metacarpal or metatarsal bone and, similarly, it cannot swell much in a medial to lateral direction because it is contained by the second and fourth metacarpal or metatarsal bones.

Desmitis of the suspensory ligament is also frequently associated with lameness. The lameness is usually exacerbated when the horse is trotted in a circle with the affected limb on the outside of the circle. Lameness localized to the proximal metacarpal region in horses with acute proximal suspensory ligament desmitis may be associated with local heat, swelling, and sensitivity. In more chronic lameness, these clinical signs are often absent.[43] Lameness, in the absence of detectable suspensory ligament swelling, is more common with proximal suspensory desmitis than with other tendinous or ligamentous injuries.[15] Lameness is likely to persist for longer periods of time in horses with desmitis involving the origin of the suspensory ligament, whereas those with mid-body suspensory ligament desmitis usually are sound in a period of several days or more.[15, 43, 52, 58] Lameness in horses with proximal suspensory ligament desmitis is often exacerbated by fetlock flexion in the affected forelimb or hindlimb and by hock flexion in horses with proximal suspensory ligament desmitis in the hindlimb.[43, 52, 58] Sinking of the fetlock joint may occur upon weight bearing, coupled with severe lameness if complete rupture of the suspensory ligament occurs.

The associated bony structures must be carefully evaluated in horses with suspensory ligament desmitis. Avulsion fractures of the origin of the suspensory ligament, fractures of the second and fourth metacarpal or metatarsal bones, periosteal proliferative change associated with the second or fourth metacarpal or metatarsal bones, apical or abaxial sesamoid fractures, or sesamoiditis may occur concurrently with suspensory ligament desmitis.

Mild injuries to the suspensory ligament body may be difficult to identify ultrasonographically because of the wide variation in its normal ultrasonographic appearance (Figs. 3-89 and 3-90), whereas mild areas of injury are easier to identify in the suspensory branches. Measurement of ligament cross-sectional area is helpful in identifying horses with mild suspensory ligament desmitis, in which only subtle decreases in overall echogenicity, but measurable increases in ligament cross-sectional area, may be detected. Hypoechoic areas in the suspensory ligament body should be bilaterally symmetrical if normal; comparison to the contralateral limb may be necessary to determine if a small area of injury is present. Injuries to the suspensory ligament may be discrete or diffuse. Splits are imaged most frequently in the suspensory ligament, although they are more common in the suspensory ligament branches than in the body (see Fig. 3-89). Core lesions are frequently seen in the suspensory ligament body and may be small (see Fig. 3-90) or large and located in the central (Fig. 3-91), medial (Fig. 3-92), lateral, dorsal (Fig. 3-93), or palmar (Fig. 3-94) portion of the suspensory ligament body. Cleft lesions (see Fig.

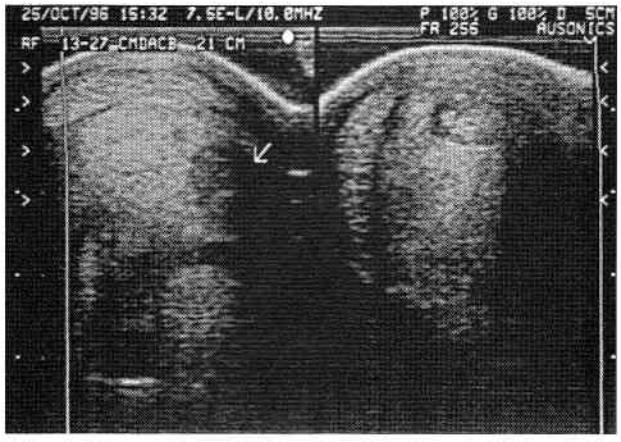

Figure 3–88

Sonograms of a large new area of fiber tearing adjacent to an old healed area of fiber injury in the right fore inferior check ligament (ICL) at its insertion into the deep digital flexor tendon (DDF), obtained from a 24-year-old Paint mare. Notice the new anechoic area of fiber injury *(diagonal arrow)*, which is in the lateral aspect of the ICL in the transverse view *(left image)* and is worst at 21 cm distal to the point of the accessory carpal bone (the border between zones 2B and 3A). Notice also in the lateral transverse view, which was obtained more proximally from the lateral aspect of the limb *(right image)*, a central echogenic scar surrounded by a small halo of anechoic to hypoechoic fluid. This was best imaged at 18 cm (zone 2B). The inferior check ligament appeared abnormal from 13 to 27 cm, with old desmitis in the proximal portion and the new desmitis in the distal portion. These sonograms were obtained with a wide-band width 7.5-MHz linear-array transducer operating at 10.0 MHz with use of a hand-held standoff pad at a displayed depth of 5 cm. The right side of the palmar transverse view is lateral and the left side is medial. The right side of the lateral transverse view is dorsal and the left side is palmar.

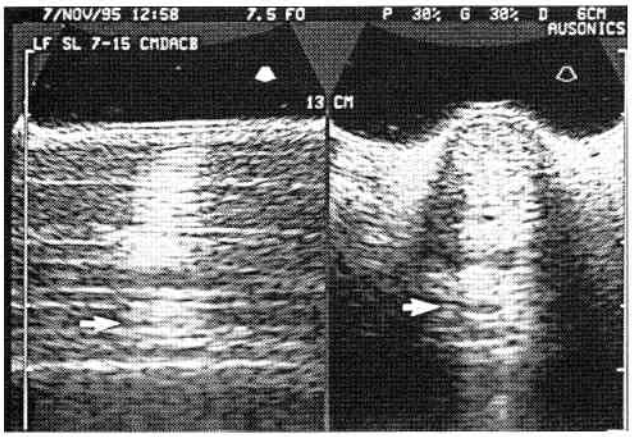

Figure 3–89

Sonograms of a very small area of recent fiber tearing in the left fore suspensory ligament (SL), obtained from an 11-year-old Thoroughbred gelding. Notice the small anechoic split lesion in the dorsal and medial aspect of the SL *(arrows)* imaged in the transverse view *(right image)* from 7 to 15 cm distal to the point of the accessory carpal bone. Notice the hypoechoic linear appearance of the lesion and the slight loss of fibers in the lesion in the sagittal view *(left image)* consistent with a recent area of injury. These sonograms were obtained at 13 cm (at the border between zones 1B and 2A) with a 7.5-MHz sector-scanner transducer containing a built-in fluid offset at a displayed depth of 6 cm. The right side of the transverse image is lateral and the left side is medial. The right side of the sagittal image is proximal and the left side is distal.

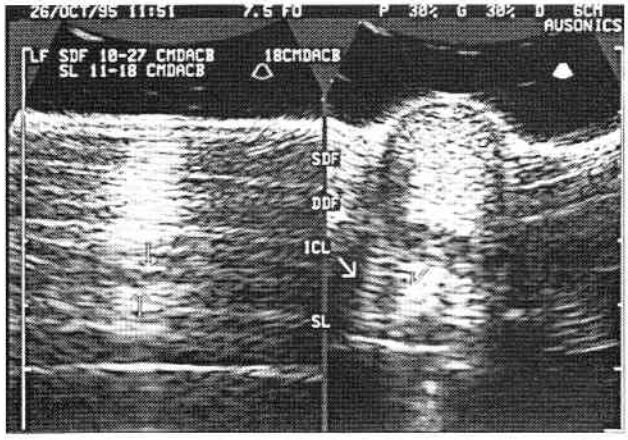

Figure 3–90

Sonograms of a small area of recent fiber tearing in the left fore suspensory ligament (SL), obtained from a 5-year-old Trakhener gelding. Notice the small anechoic core lesion in the medial aspect of the SL *(arrows)* imaged from 11 to 18 cm distal to the point of the accessory carpal bone. Notice the marked discrepancy in the size of the medial and lateral portions of the SL in the transverse view *(right image)* and the anechoic appearance of the lesion and the loss of fibers in the lesion in the sagittal view *(left image)*, consistent with a new area of injury. These sonograms were obtained at 18 cm (zone 2B) with a 7.5-MHz sector-scanner transducer containing a built-in fluid offset at a displayed depth of 6 cm. The right side of the transverse image is lateral and the left side is medial. The right side of the sagittal image is proximal and the left side is distal. SDF, superficial digital flexor tendon; DDF, deep digital flexor tendon; ICL, inferior check ligament.

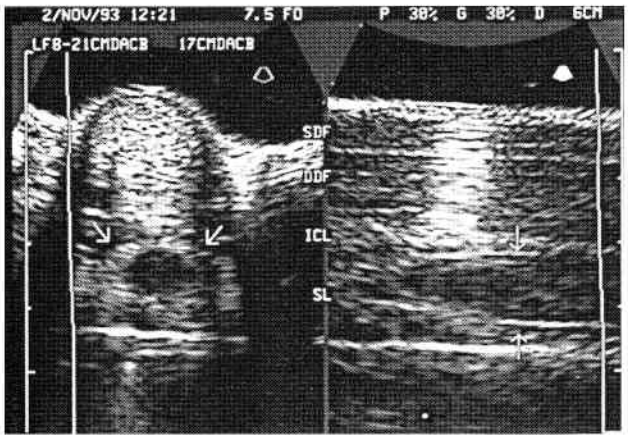

Figure 3–91

Sonograms of a large central core lesion *(arrows)* in the body of the left fore suspensory ligament (SL) of a 3-year-old Thoroughbred colt. Notice the enlarged SL body touching the adjacent inferior check ligament (ICL), the large anechoic core lesion in the center of the SL in the transverse view *(left image)* and the complete loss of fibers imaged in the sagittal view *(right image)*. This area of recent fiber tearing was imaged from 8 to 21 cm distal to the point of the accessory carpal bone. These sonograms were obtained at 17 cm (at the border between zones 2A and 2B) with a 7.5-MHz sector-scanner transducer containing a built-in fluid offset at a displayed depth of 6 cm. The right side of the transverse image is lateral and the left side is medial. The right side of the sagittal image is proximal and the left side is distal. SDF, superficial digital flexor tendon; DDF, deep digital flexor tendon.

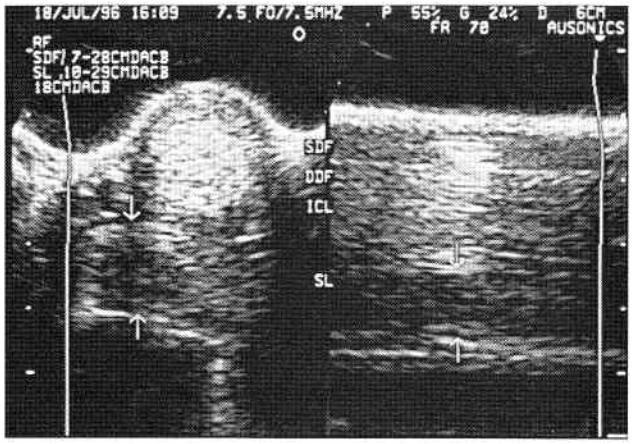

Figure 3–92

Sonograms of a large medial core lesion *(arrows)* in the distal portion of the right fore suspensory ligament (SL) body, obtained from a 4-year-old Thoroughbred stallion. The large anechoic area of fiber disruption and resultant hemorrhage is causing a very large swelling of the SL body to the medial side, detected in the transverse view *(left image)* and visible from 10 to 29 cm distal to the point of the accessory carpal bone. These sonograms were obtained at 18 cm distal to the point of the accessory carpal bone (zone 2B) with a wide-bandwidth 7.5-MHz sector-scanner transducer operating at 7.5 MHz containing a built-in fluid offset at a displayed depth of 6 cm. The right side of the transverse image is lateral and the left side is medial. The right side of the sagittal image *(right image)* is proximal and the left side is distal. SDF, superficial digital flexor tendon; DDF, deep digital flexor tendon; ICL, inferior check ligament.

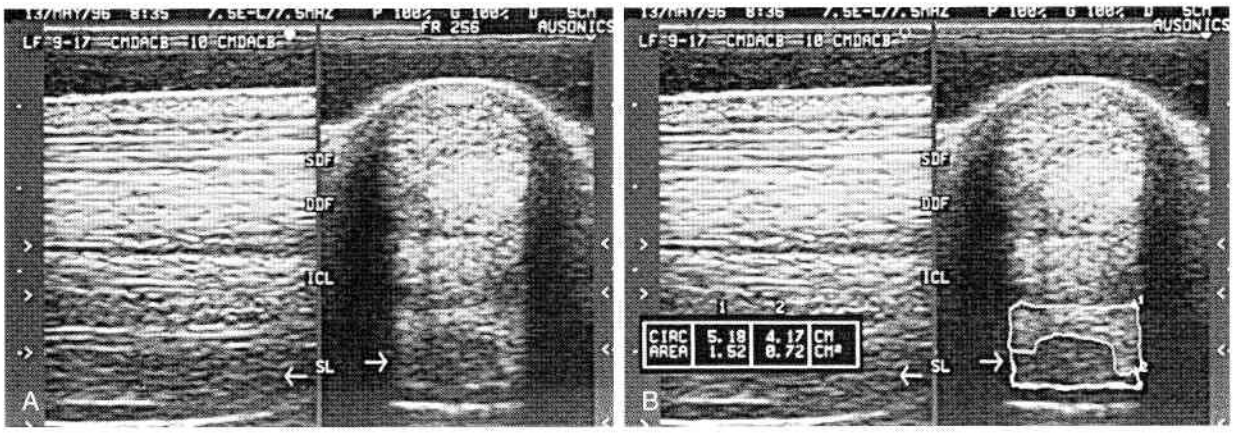

Figure 3–93

Sonograms of a large dorsal core lesion *(arrows)* in the body of the suspensory ligament (SL) in the left foreleg, obtained from an 11-year-old Warmblood stallion. This dorsal core lesion extended from 9 to 17 cm distal to the point of the accessory carpal bone. These sonograms were obtained at 10 cm (zone 1B) with a wide-bandwidth 7.5-MHz linear-array transducer operating at 7.5 MHz using a hand-held standoff pad at a displayed depth of 5 cm. The focal zones are positioned in the far field of the images. The right side of the transverse views *(right images)* is lateral and the left side is medial. The right side of the sagittal views *(left images)* is proximal and the left side is distal. SDF, superficial digital flexor tendon; DDF, deep digital flexor tendon; ICL, inferior check ligament.

A, Notice the large hypoechoic core lesion in the transverse view and the absence of normal fibers in the sagittal view.

B, Although the SL body is not greatly enlarged, the core lesion involves 47% of the cross-sectional area of the SL body at this level (0.72 cm^2/1.52 cm^2).

3-89) or a transverse split across the entire ligament occur in the suspensory ligament more frequently than in the other tendinous or ligamentous structures. Diffuse areas of fiber damage also occur in the suspensory ligament, as elsewhere. Periligamentous soft tissue swelling occurs frequently in horses with suspensory ligament injury. This periligamentous soft tissue swelling is often most marked around the injured suspensory ligament branches.

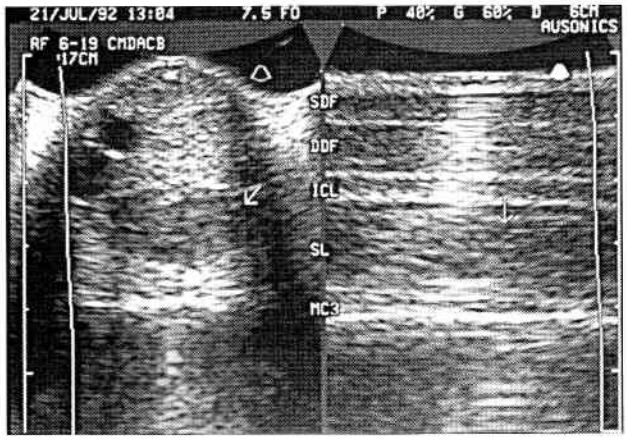

Figure 3–94

Sonograms of a large palmar lesion in the body of the right fore suspensory ligament (SL) obtained from a 3-year-old Standardbred colt. Notice the enlarged body of the SL touching the adjacent inferior check ligament (ICL), its hypoechoic palmar area of injury, and the lack of normal fibers in the lesion imaged from 6 to 19 cm distal to the point of the accessory carpal bone. The echogenicity and short echoes in the lesion suggest early repair with immature fibrous tissue and granulation tissue. These sonograms were obtained at 17 cm (at the border between zones 2A and 2B) with a 7.5-MHz sector-scanner transducer containing a built-in fluid offset at a displayed depth of 6 cm. The right side of the transverse view *(left image)* is lateral and the left side is medial. The right side of the sagittal view *(right image)* is proximal and the left side is distal. SDF, superficial digital flexor tendon; DDF, deep digital flexor tendon; MC 3, third metacarpal bone.

Injuries to the branches of the suspensory ligament occur frequently and are most common in the medial branch of the suspensory ligament. Core lesions are very common in the suspensory ligament branches (Figs. 3-95 through 97), as are splits through the branch (see Fig. 3-96). Although the core lesions are most common in the central portion of the suspensory ligament branch, these core lesions can occur axially or abaxially or along the dorsal or palmar/plantar portion of the branch (see Fig. 3-97). The split in the branch of the suspensory ligament usually occurs in the horizontal plane, perpendicular to the long axis of the suspensory ligament branch. Occasionally, splits through the branch of the suspensory ligament are longitudinal, parallel with the long axis of the ligamentous fibers (Fig. 3-96). These longitudinal splits in the suspensory ligament branches are more common in horses with sesamoid fractures. The split in the suspensory branch extends proximally from the fracture site.

Injuries to the hind suspensory ligament occur in both the body and the branch with nearly equal frequency. Discrete core lesions are common in the suspensory ligament body (Fig. 3-98), but diffuse injuries (Fig. 3-99) and splits also occur. Septic suspensory ligament desmitis and inferior check ligament desmitis are rare but have resulted in complete loss of the attachment between the origin of the suspensory ligament and the proximal metatarsus in one horse (Fig. 3-100).

In reports of horses with proximal suspensory ligament desmitis, one or more of the following ultrasonographic findings have been identified: enlargement, poor definition of the suspensory ligament margin (especially dorsally), a well-circumscribed central hypoechoic area

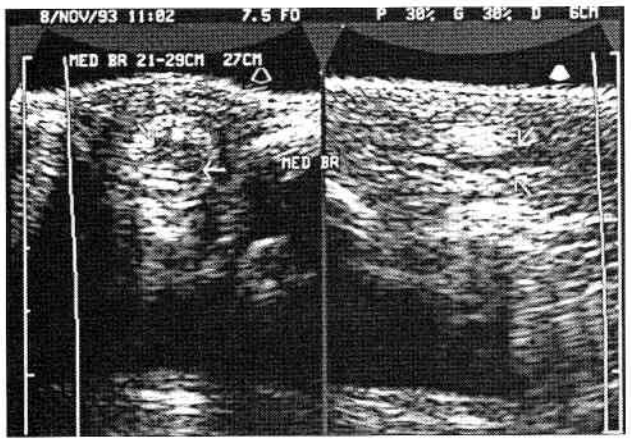

Figure 3–95

Sonograms of a discrete core lesion *(arrows)* in the medial branch of the suspensory ligament in the left foreleg, obtained from a 6-year-old Standardbred stallion. Notice the hypoechoic to anechoic core in the medial SL branch in the transverse view *(left image)* and the loss of normal fiber alignment in the sagittal view *(right image)* imaged throughout the entire medial branch. This core lesion was imaged from 21 to 29 cm distal to the point of the accessory carpal bone. These sonograms were obtained at 27 cm (zone 3B) with a 7.5-MHz sector-scanner transducer containing a built-in fluid offset at a displayed depth of 6 cm. The right side of the transverse image is dorsal and the left side is palmar. The right side of the sagittal image is proximal and the left side is distal.

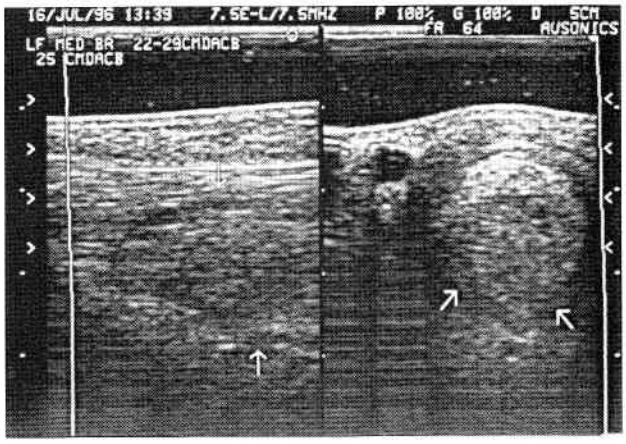

Figure 3–97

Sonograms of a large area of fiber damage *(arrows)* in the medial branch of the suspensory ligament (SL) in the left foreleg, obtained from a 4-year-old Thoroughbred filly. Notice the large hypoechoic defect in the SL branch in the transverse view *(right image)* and the abnormal fiber pattern in the sagittal view *(left image)* that extends distally to the insertion of the SL on the abaxial surface of the medial proximal sesamoid bone. This area of fiber tearing extended from 22 to 29 cm distal to the point of the accessory carpal bone. These sonograms were obtained at 25 cm (at the border between zones 3A and 3B) with a wide-bandwidth 7.5-MHz linear-array transducer operating at 7.5-MHz with a hand-held standoff pad at a displayed depth of 5 cm. The focal zones are positioned in the near field of the images. The right side of the transverse image is dorsal and the left side is palmar. The right side of the sagittal image is proximal and the left side is distal.

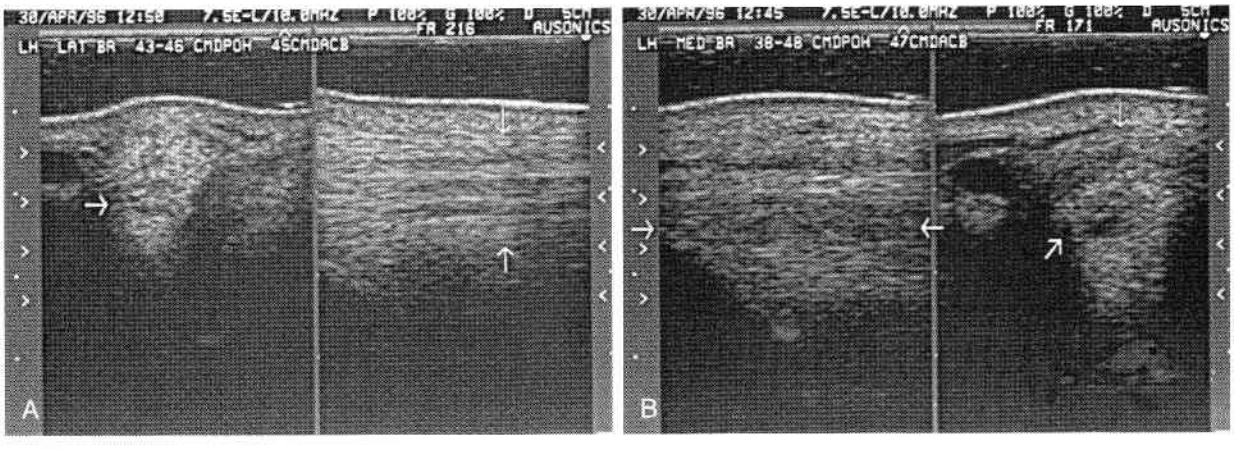

Figure 3–96

Sonograms of recent suspensory ligament (SL) desmitis in the left hindlimb, obtained from an 8-year-old Warmblood mare. The SL desmitis was imaged from 38 to 48 cm distal to the point of the hock. These sonograms were obtained with a wide-bandwidth 7.5-MHz linear-array transducer operating at 10.0 MHz with a hand-held standoff pad at a displayed depth of 5 cm. The focal zones are positioned in the near field of the images.

A, Notice the small linear areas of splitting along the length of the lateral SL branch, best imaged in the sagittal view *(right image)* and detected in the transverse view *(left image)* as small hypoechoic areas at 45 cm (zone 4C). The arrows are illustrating the borders of the lateral SL branch.

B, Notice the larger areas of fiber damage in the medial SL branch with two discrete anechoic areas surrounded by relatively hypoechoic areas, consistent with SL desmitis at 47 cm (zone 4C). The two areas of fiber injury are illustrated in the transverse view *(right image)* with two arrows. In the sagittal view *(left image),* only the large area of fiber damage is highlighted with an arrow.

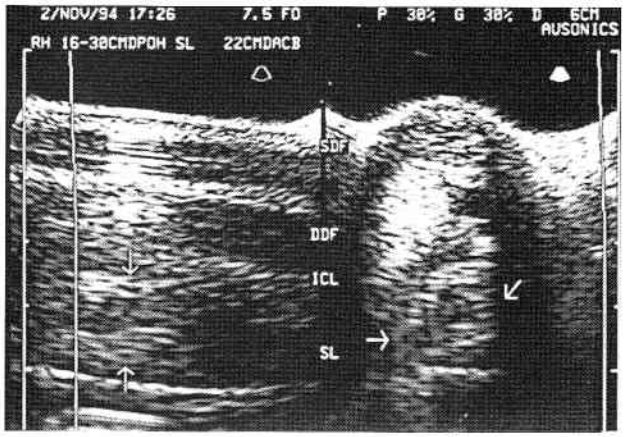

Figure 3–98

Sonograms of a core lesion in the origin of the suspensory ligament (SL) in the right hind leg of an 8-year-old Thoroughbred gelding. Notice the anechoic core lesion in the somewhat hypoechoic SL *(arrows)* that extended from 16 to 30 cm distal to the point of the hock. The anechoic core imaged in the transverse view *(right image)* with loss of normal fiber pattern in the sagittal view *(left image)* is consistent with a recent area of fiber tearing in the SL body. The surrounding hypoechoic areas in the dorsal, lateral, and medial portions of the SL body are consistent with desmitis in the adjacent portion of the SL body. These sonograms were obtained at 22 cm (zone 2A) with a 7.5-MHz sector-scanner transducer containing a built-in fluid offset at a displayed depth of 6 cm. The right side of the transverse image is lateral and the left side is medial. The right side of the sagittal image is proximal and the left side is distal. SDF, superficial digital flexor tendon; DDF, deep digital flexor tendon; ICL, inferior check ligament.

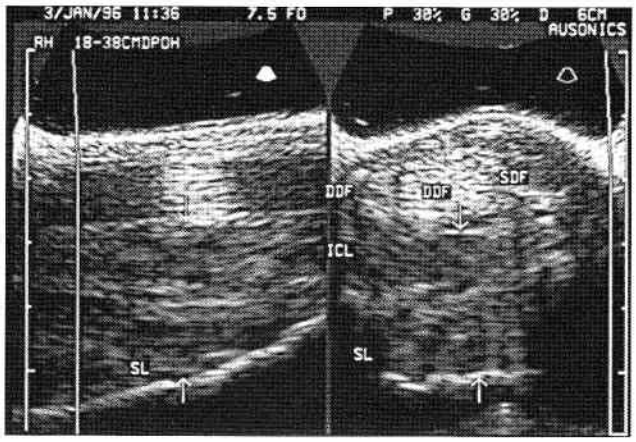

Figure 3–100

Sonograms of a septic suspensory ligament (SL) and inferior check ligament (ICL) desmitis resulting in SL and ICL rupture in the right hind leg, obtained from a 5-year-old Thoroughbred stallion. This septic desmitis developed after a severe cellulitis in the limb. Notice the complete absence of any ligamentous fibers imaged in either the transverse *(right image)* or sagittal *(left image)* views. The bony surface of the proximal metatarsus is also irregular and is covered with fluid, suggesting a septic osteitis or osteomyelitis. The plantar margin of the ICL is delineated by the downward arrows, and the dorsal margin of the SL is delineated by the upward arrows. These sonograms were obtained at 20 cm distal to the point of the hock (zone 1B) with a 7.5-MHz sector-scanner transducer containing a built-in fluid offset at a displayed depth of 6 cm. The right side of the transverse image is lateral and the left side is medial. The right side of the sagittal image is proximal and the left side is distal. SDF, superficial digital flexor tendon; DDF, deep digital flexor tendon.

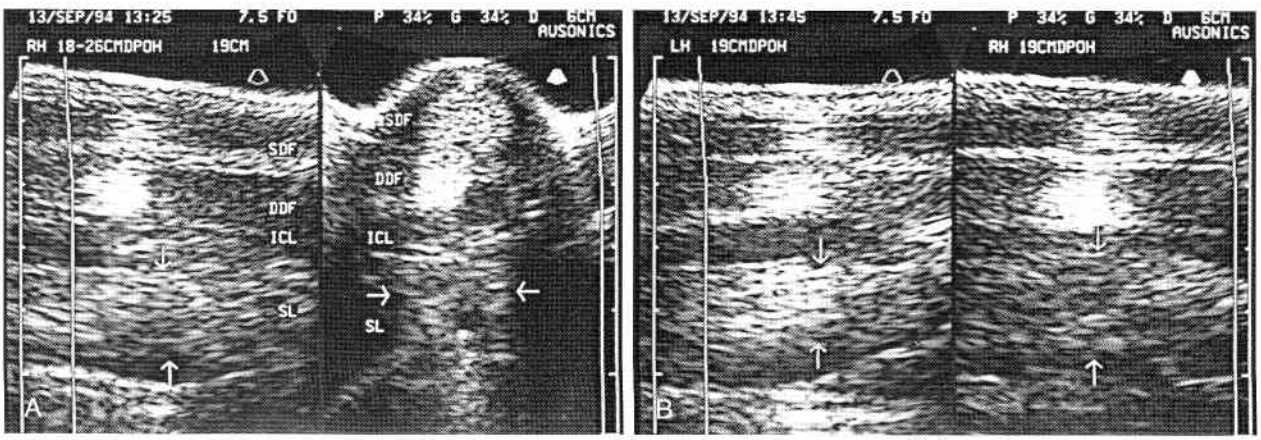

Figure 3–99

Sonograms of a more diffuse suspensory ligament (SL) desmitis *(arrows)* in the right hind leg, obtained from a 5-year-old Thoroughbred mare. This area of SL desmitis was imaged from 18 to 26 cm distal to the point of the hock. These sonograms were obtained at 19 cm (border between zones 1B and 2A) with a 7.5-MHz sector-scanner transducer containing a built-in fluid offset at a displayed depth of 6 cm. The right side of the transverse image is lateral and the left side is medial. The right side of the sagittal images is proximal and the left side is distal. SDF, superficial digital flexor tendon; DDF, deep digital flexor tendon; ICL, inferior check ligament.

A, Notice the diffuse hypoechoic lesion in the dorsal aspect of the SL body in the transverse *(right image)* and sagittal *(left image)* views.

B, The fiber pattern in the dorsal portion of the affected SL body is disrupted *(right image)* compared to that same area (19 cm) in the normal left hind leg *(left image).* The dorsal and plantar margins of the SL body are delineated by arrows in the normal and affected leg.

extending less than 1 to 4 cm in a proximal-to-distal direction, one or more poorly defined central or peripheral hypoechoic areas extending 1 to 3 cm in a proximal-to-distal direction, hyperechoic foci, an irregular plantar cortex of the third metatarsal bone (hindlimb), and/or a larger area of diffuse decrease in echogenicity.[43] Central circular hypoechoic areas were most common in the forelimb, occurring in 20 of 30 horses. In the hindlimbs, a diffuse decrease in suspensory ligament echogenicity was more common (8/11 horses), involving two thirds or more of the ligament's cross-sectional area and usually involving the dorsal portion of the suspensory ligament.

In another study, enlargement of the hind suspensory ligament was detected in 28.6% of 42 horses.[52] A diffuse decrease in echogenicity, particularly dorsally, was detected in 54.8% of horses with a diagnosis of proximal suspensory ligament desmitis in the hindlimb.[52] Focal central hypoechoic areas, poorly defined hypoechoic areas, or hyperechoic areas were detected in 6 horses each. Lesions extended less than 1 to 4 cm in length, except in one horse with a 7-cm lesion and one horse that also had desmitis of the suspensory ligament branches and periligamentous soft tissue thickening. A change in ultrasonographic appearance over time has also been used as evidence of a suspensory ligament lesion.[43, 52, 58]

The suspensory ligament origin along the proximal palmar/plantar aspect of the third metacarpal/metatarsal bone should be carefully evaluated for any associated avulsion fractures. Avulsion fractures should be detected ultrasonographically in two mutually perpendicular planes. However, irregularities of the palmar or plantar surface of the proximal third metacarpus or metatarsus, respectively, may suggest a bony lesion when distraction of the fracture fragment has not yet occurred. Follow-up sonographic examination in 2 to 3 weeks often reveals a distracted fragment. In a recent study, more avulsion fractures were detected with ultrasonography than with high-quality radiographs in horses that became sound with a high palmar or plantar nerve block.[130] All of these horses had areas of increased uptake seen in the area on nuclear scintigraphy but the intensity of this uptake was variable.

Bony abnormalities at the origin of the suspensory ligament are often associated with concurrent suspensory ligament desmitis (Fig. 3-101), although ligamentous injuries do not have to be present. A hairline sagittal fracture can also be detected at the origin of the suspensory ligament and should be confirmed radiographically. An anechoic break in the bony surface echo, detected in two mutually perpendicular planes, is consistent with a hairline fracture. A large bony plate at the suspensory ligament origin was associated with recurrent suspensory ligament desmitis in one horse (see Fig. 3-101). Avulsion fractures are often associated with some degree of suspensory ligament desmitis and are more common in the foreleg. The avulsion fractures can be single (Fig. 3-102) or multiple (Fig. 3-103) and are more frequently located on the medial aspect of the suspensory ligament origin. Avulsion fractures of the suspensory ligament origin are much less frequent in the hindlimb (Fig. 3-104). However, a high incidence of radiographic abnormalities of the proximal third metatarsal bone (compared to the third metacarpal bone) has been reported in horses with proximal suspensory desmitis.[43]

The insertions of the suspensory ligament branches on the abaxial surfaces of the proximal sesamoid bones should also be carefully evaluated, with particular attention to the bony surface echo of the proximal sesamoid bones and to the ligamentous echoes. The most common finding is an irregularity of the apical or abaxial bony

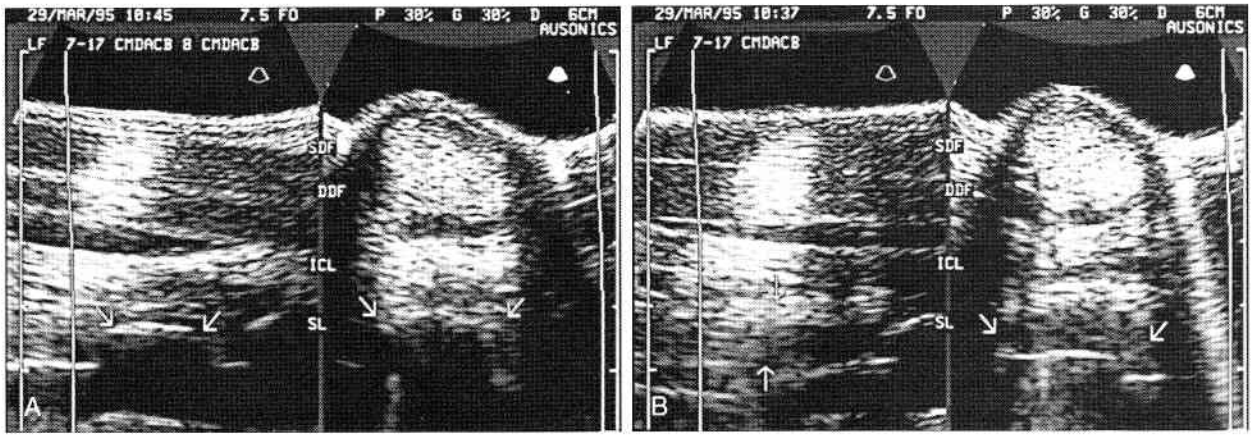

Figure 3–101

Sonograms of a large bony plate *(arrows)* at the origin of the suspensory ligament (SL) in the left foreleg, obtained from an 8-year-old Thoroughbred mare. These sonograms were obtained 8 cm (zone 1A) distal to the point of the accessory carpal bone *(A)* and 10 cm (zone 1B) distal to the point of the accessory carpal bone *(B)* with a 7.5-MHz sector-scanner transducer containing a built-in fluid offset at a displayed depth of 6 cm. The right side of the transverse views *(right images)* is lateral and the left side is medial. The right side of the sagittal views *(left images)* is proximal and the left side is distal. SDF, superficial digital flexor tendon; DDF, deep digital flexor tendon; ICL, inferior check ligament.

A, Notice the hyperechoic structure *(arrows)* casting a strong acoustic shadow from the palmar portion of the SL through the proximal metacarpus, consistent with a large piece of bone.

B, Distal to this large plate of bone, an enlarged, somewhat heterogeneous SL body is imaged that is thickened in a dorsal to palmar direction, lying adjacent to the ICL. The associated acute SL desmitis involved the dorsal aspect of the SL body and was imaged from 7 to 17 cm distal to the point of the accessory carpal bone *(arrows)*.

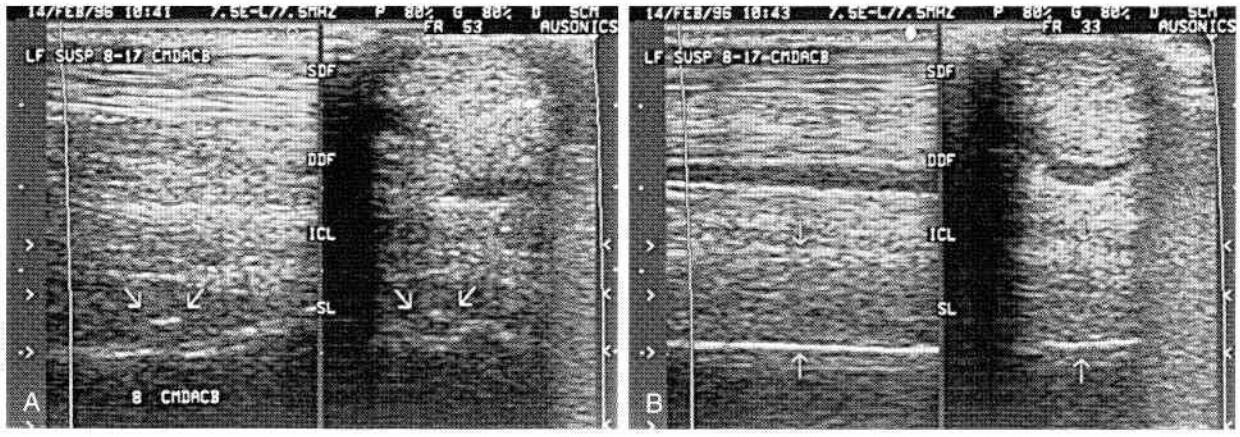

Figure 3–102

Sonograms of an avulsion fracture and a large area of associated suspensory ligament (SL) desmitis in the left foreleg, obtained from a 7-year-old Arabian stallion. The associated SL desmitis extended from 8 to 17 cm distal to the point of the accessory carpal bone. These sonograms were obtained at 8 cm (*A*, zone 1A) and 10 cm (*B*, zone 1B) with a wide-bandwidth 7.5-MHz linear-array transducer operating at 7.5-MHz at a displayed depth of 5 cm. The focal zones are positioned in the far field. The right side of the transverse views *(right images)* is lateral and the left side is medial. The right side of the sagittal views *(left images)* is proximal and the left side is distal. SDF, superficial digital flexor tendon; DDF, deep digital flexor tendon; ICL, inferior check ligament.

A, The hyperechoic structure visualized as a very narrow fragment *(arrows)* in the transverse view is longer in the sagittal view and is casting more of an acoustic shadow in this image. The fragment is originating from the proximal and medial aspect of the palmar metacarpus. The surrounding portion of the SL body at the origin is hypoechoic and completely lacks normal fibers.

B, The SL body is enlarged and is touching the ICL with a large area of fiber tearing imaged in the dorsal portion of the SL body just distal to the avulsion fracture. Notice that the hypoechoic dorsal portion of the SL body lacks normal fiber alignment but has a few short echoes, indicating early repair best seen in the sagittal view.

surfaces of the proximal sesamoid bones consistent with a diagnosis of sesamoiditis. Small avulsion fracture fragments may occur at the site of an area of fiber tearing (Fig. 3-105), or larger fragments may occur (Fig. 3-106). Large cystic lesions at the insertion of the suspensory ligament are frequently noticed in horses with significant sesamoiditis (see Fig. 3-106). Large apical or mid-body fractures are also readily imaged and the severity of the associated soft tissue injuries can be determined (Fig. 3-107).

"Blind splints" associated with periosteal proliferation from the axial aspect of the second or fourth metacarpal or metatarsal bone onto the palmar or plantar surface of the metacarpus or metatarsus may also contribute to suspensory ligament desmitis in some of these horses (see Fig. 3-103). The second and fourth metacarpal and metatarsal bones should be thoroughly examined, because periosteal proliferative change from the axial aspect of the medial or lateral (less common) splint bone on to the palmar or plantar surface of the metacarpus or metatarsus may cause a mild desmitis of the suspensory ligament or may be responsible for lameness that "blocks out" in the high suspensory region (Fig. 3-108). Abaxial deviation of the second and fourth metacarpal or metatarsal bones or "spreading" of the splint bones in the mid to distal metacarpal or metatarsal region is often detected and may predispose the horse to splint-bone fracture at a later date. Fractured splint bones are also frequently seen in horses with desmitis of the branches of the suspensory ligament (Fig. 3-109), particularly if the desmitis is severe and/or chronic.

The triad of the associated bony pathology (avulsion fractures of the origin of the suspensory ligament, abnormalities involving the proximal sesamoid bones and bony abnormalities involving the second or fourth metacarpal or metatarsal bones) should be evaluated ultrasonographically in horses with suspected suspensory ligament disease. The associated bony abnormalities are probably more frequently detected in Standardbred racehorses but may occur in all types of performance horses. These abnormalities may be initially detected sonographically, prompting further radiographic work evaluation.

With repair, the cross-sectional area of the suspensory ligament should decrease and improved echogenicity and fiber alignment should be detected (Fig. 3-110). In many horses, the improvement in echogenicity and fiber alignment is slow and the injured suspensory ligament may remain persistently hypoechoic for months. In some horses, the lesion never returns to normal or near-normal echogenicity. In contrast, in 75% of horses with no radiographic abnormalities in the proximal metacarpus or metatarsus and ultrasonographic findings consistent with proximal suspensory ligament desmitis, the ultrasonographic findings improve markedly, usually within 3 months.[43] Sonographic improvement was detected more rapidly in horses identified and treated for proximal suspensory ligament desmitis soon after the onset of lameness than it was in horses with a more chronic lameness.[43]

A poor-quality sonographic repair is more common with the suspensory ligament than with the other tendons and ligaments. Often, if the clinical situation warrants it, a gradual return to more rigorous work is indicated, coupled with frequent sonographic monitoring. A good-quality repair is a suspensory ligament that has returned to near-normal cross-sectional area with normal to near-normal echogenicity and normal to near-normal fiber alignment with little or no periligamentous soft tissue thickening (Fig. 3-111). Although the swelling

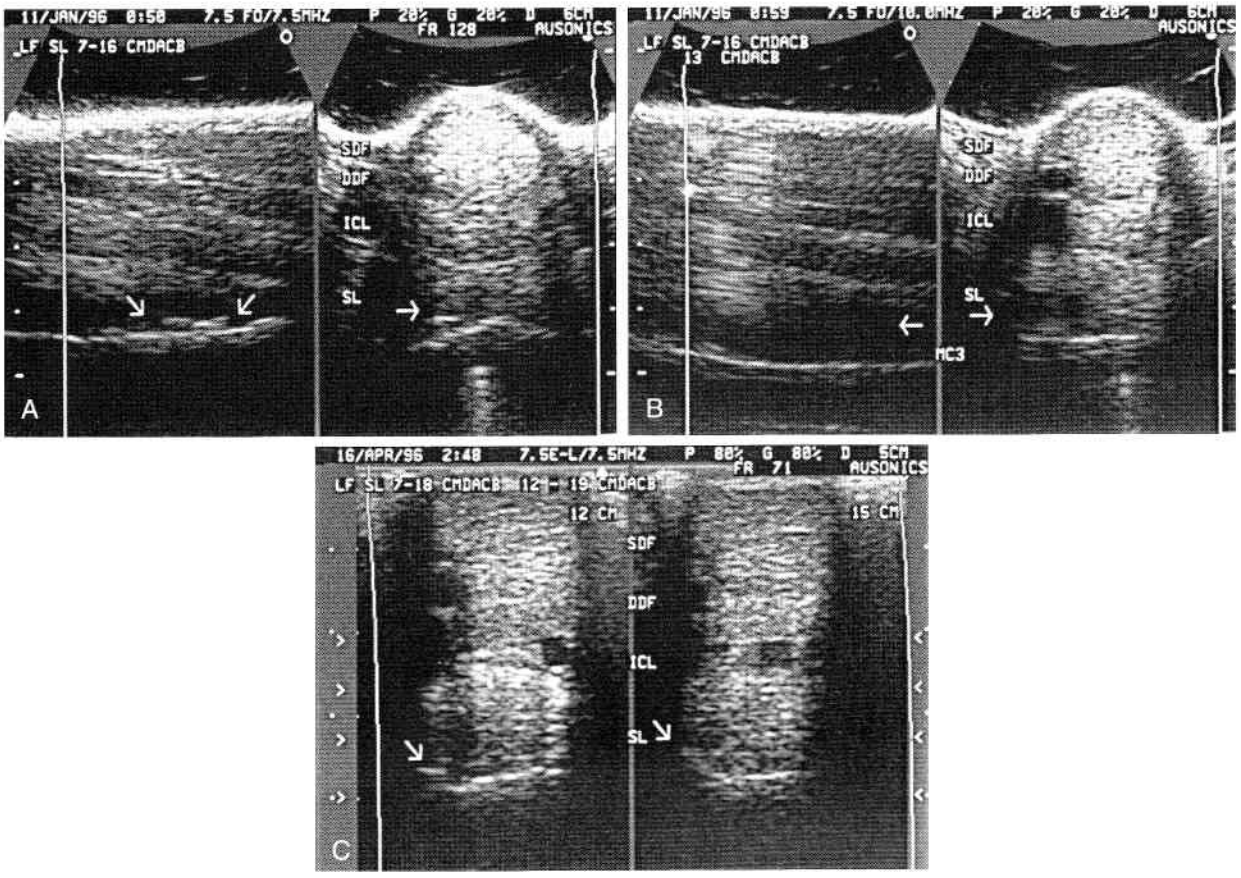

Figure 3–103

Sonograms of an avulsion fracture *(arrows)* with significant suspensory ligament (SL) desmitis in the left foreleg, obtained froma 3-year-old Thoroughbred gelding. The sonograms *A* and *B* were obtained with a wide-bandwidth 7.5-MHz sector-scanner transducer operating at 7.5 MHz *(A)* and 10.0 MHz *(B)* containing a built-in fluid offset at a displayed depth of 6 cm. The sonogram in *C* was obtained with a wide-bandwidth 7.5-MHz linear-array transducer operating at 7.5 MHz at a displayed depth of 5 cm. The focal zones are positioned in the far field. The right side of the transverse images is lateral and the left side is medial. The right side of the sagittal images is proximal and the left side is distal. SDF, superficial digital flexor tendon; DDF, deep digital flexor tendon; ICL, inferior check ligament; MC3, third metacarpal bone.

A, The avulsion fragment at 8 cm (zone 1A) is very medial in the transverse view *(right image)* and appears to be at least 1 cm in length and broken into 2 fragments in the sagittal view *(left image).*

B, A large area of fiber disruption is imaged in the dorsal and medial portion of the SL body, distal to the avulsion fragments at 13 cm (the border between zones 1B and 2A) seen in both the transverse view *(right image)* and sagittal view *(left image).*

C, Notice the bony proliferation *(arrows)* originating from the axial margin of the second metacarpal bone and extending axially over the palmar surface of the third metacarpal bone, which appears to be impinging on the medial border of the SL at 15 cm distal to the point of the accessory carpal bone (zone 2A–*right image*). The bony proliferation was imaged from 12 cm *(left image)* to 19 cm.

around the suspensory ligament body usually resolves, large amounts of echogenic swelling often persist at the suspensory bifurcation between the suspensory branches and around the suspensory ligament branches. The periligamentous fibrosis is often larger than the suspensory branches themselves. The reason for this proliferative fibroblastic response is unknown, although chronic inflammation in this area must be implicated. Calcification of the suspensory ligament does occur and is much more frequently detected in the branches than in the body. Calcification of the suspensory ligament branches is more common than that in the inferior check ligament or superficial digital flexor tendon and is usually associated with chronic recurring desmitis. This suspensory ligament calcification appears to be more common in Standardbred racehorses.

Tendon and Ligament Abnormalities—Pastern

In the fore pastern the superficial digital flexor tendon is the most frequently injured tendon or ligament and is injured in all types of performance horses.[16, 25, 59, 63, 67] This injury occurs frequently in event horses and steeplechasers, with a significant incidence in trotters.[71] However, in this author's experience, the injuries are also common in Thoroughbred flat racehorses. The middle (oblique) distal sesamoidean ligament is the second most common injury in the fore pastern, followed by injuries to the deep digital flexor tendon and straight distal sesamoidean ligament.[16, 25, 59, 63, 67] In the hindlimb, injuries to the deep digital flexor tendon are the most common injury in the pastern region with a low incidence of injuries to the other tendinous and ligamentous struc-

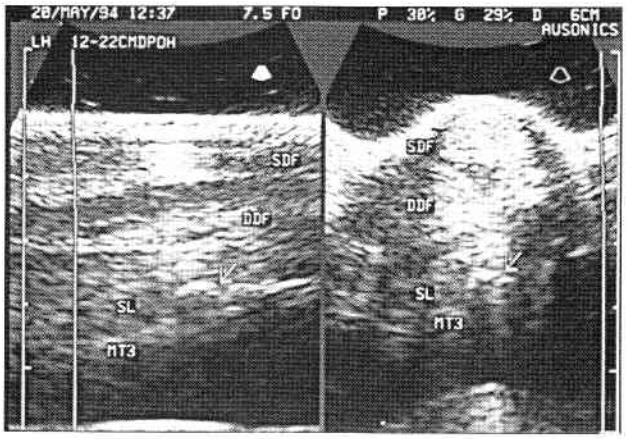

Figure 3–104

Sonograms of an avulsion fracture and associated suspensory ligament (SL) desmitis in the left hind leg of a 10-year-old Thoroughbred mare. Notice the avulsion fragment *(arrows)* distracted from the proximal metatarsus with a mild SL desmitis in the adjacent portion of the SL. The SL desmitis was imaged from 12 to 22 cm distal to the point of the hock. These sonograms were obtained at 15 cm (zone 1B) with a 7.5-MHz sector-scanner transducer containing a built-in fluid offset at a displayed depth of 6 cm. The right side of the transverse view *(right image)* is lateral and the left side is medial. The right side of the sagittal view *(left image)* is proximal and the left side is distal. SDF, superficial digital flexor tendon; DDF, deep digital flexor tendon, MT3, third metatarsal bone.

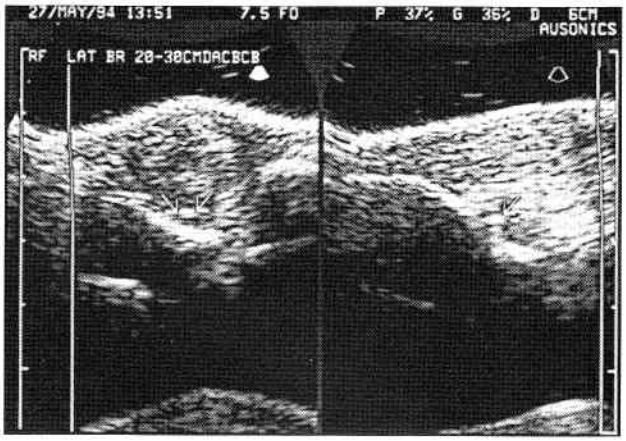

Figure 3–105

Sonograms of an avulsion fracture at the insertion of the lateral branch of the right fore suspensory ligament (SL) onto the apex of the lateral proximal sesamoid bone, obtained from an 8-year-old Thoroughbred mare. Notice the hyperechoic bony fragment *(arrows)* slightly distracted from the abaxial surface of the lateral proximal sesamoid bone. Notice the hypoechoic core lesion still visible in the transverse view *(left image)* with a heterogeneous echogenicity compatible with a chronic desmitis of the lateral SL branch. The hypoechoic appearance of the branch in this view is due to an off-incidence artifact because the ultrasound beam is perpendicular to the plane of the fracture fragment. Notice that the random fiber pattern in the sagittal view *(right image)* extends distally to the site of the avulsion fracture. The healing core lesion was imaged from 20 to 30 cm distal to the point of the accessory carpal bone. In the sagittal view, the repairing lesion appears more echogenic. These sonograms were obtained at 29 cm (at the border between zones 3B and 3C) with a 7.5-MHz sector-scanner transducer containing a built-in fluid offset at a displayed depth of 6 cm. The right side of the transverse image is dorsal and the left side is palmar. The right side of the sagittal image is proximal and the left side is distal.

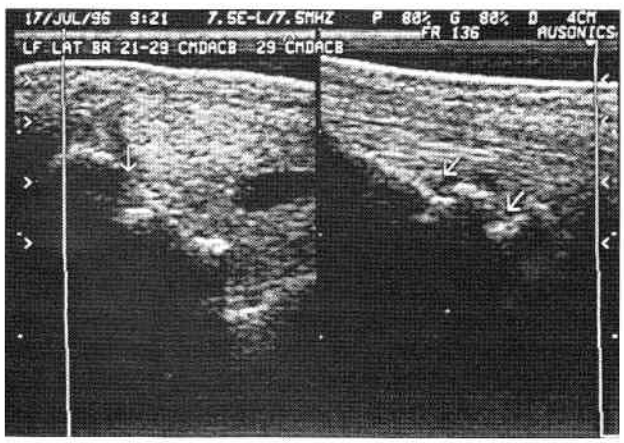

Figure 3–106

Sonograms of a cystic lesion and avulsion fracture involving the abaxial surface of the lateral proximal sesamoid bone in the left foreleg, obtained from a 7-year-old Thoroughbred gelding. Notice the scooped-out area in the abaxial surface of the lateral proximal sesamoid bone *(vertical arrow)* imaged in the transverse view *(left image)* and the hyperechoic fragment *(arrows)* distracted from the parent portion of the sesamoid bone in the sagittal view *(right image)*. The lateral suspensory ligament (SL) branch appears slightly heterogeneous with a small area of weak fiber pattern, consistent with an SL desmitis that was imaged from 21 to 29 cm distal to the point of the accessory carpal bone. These sonograms were obtained at 29 cm (at the border between zones 3B and 3C) with a wide-bandwidth 7.5-MHz linear-array transducer operating at 7.5 MHz using a hand-held standoff pad at a displayed depth of 4 cm. The right side of the transverse image is dorsal and the left side is palmar. The right side of the sagittal image is proximal and the left side is distal.

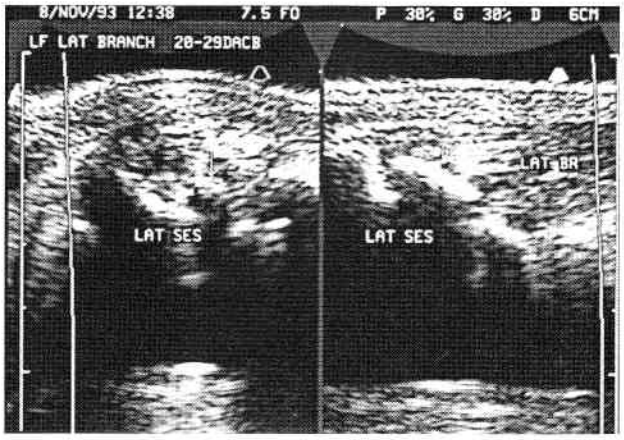

Figure 3–107

Sonograms of a large abaxial fracture and associated fiber tearing in the left fore lateral branch of the suspensory ligament (SL), obtained from a 2-year-old Standardbred filly. Notice the large hyperechoic fragment *(arrows)* distracted proximally from the parent portion of the lateral proximal sesamoid bone and the hypoechoic areas in the lateral branch surrounding the fracture in the transverse view *(left image)* and lateral and axial to it in the sagittal view *(right image)*, consistent with recent fiber tearing in the lateral SL branch. The area of fiber tearing was imaged from 20 to 29 cm distal to the point of the accessory carpal bone. These sonograms were obtained at 29 cm (at the border between zones 3B and 3C) with a 7.5-MHz sector-scanner transducer containing a built-in fluid offset at a displayed depth of 6 cm. The right side of the transverse image is dorsal and the left side is palmar. The right side of the sagittal image is proximal and the left side is distal.

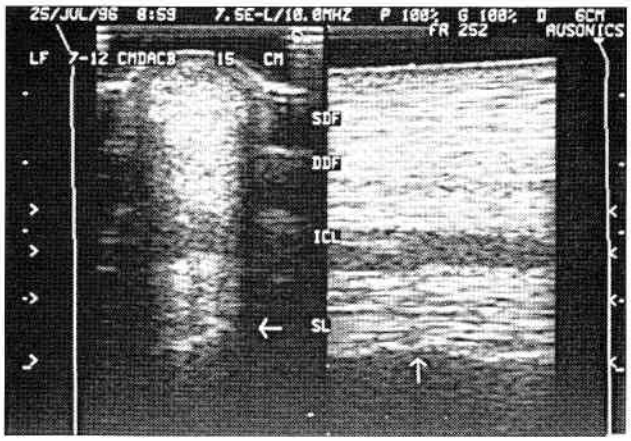

Figure 3–108

Sonograms of the left foreleg with bony proliferation along the palmar and lateral margin of the third metacarpal bone extending from the axial margin of the fourth metacarpal bone, obtained from a 10-year-old Thoroughbred mare. Notice the hyperechoic irregular bony surface echo extending in a palmar direction from the lateral splint bone *(horizontal arrow)* in the transverse view *(left image)*. In the sagittal view *(right image)*, the irregular bony proliferation appears to be impinging on the dorsal border of the suspensory ligament (SL). The SL has several small hypoechoic areas visible on transverse and sagittal view that could be consistent with mild desmitis, but no significant area of fiber tearing was imaged. The remaining tendinous and ligamentous structures appear relatively normal. The hypoechoic appearance of the palmar margin of the superficial digital flexor tendon (SDF) is an artifact, because the imaged is focused on the SL. These sonograms were obtained at 15 cm distal to the point of the accessory carpal bone (zone 2A) with a wide-bandwidth 7.5-MHz linear-array transducer operating at 10.0 MHz with a hand-held standoff pad at a displayed depth of 6 cm. The focal zones are positioned in the far field. The right side of the transverse image is lateral and the left side is medial. The right side of the sagittal images is proximal and the left side is distal. DDF, deep digital flexor tendon; ICL, inferior check ligament.

tures in this region.[16, 25, 59, 63, 67] In both the forelimb and hindlimb, injuries to the deep digital flexor tendon are often accompanied by digital sheath tenosynovitis.

Superficial Digital Flexor Tendon. Injury to the superficial digital flexor tendon in the pastern region often occurs in isolation, without an injury to the superficial digital flexor tendon in the metacarpal region. Some "low bows," injuries to the superficial digital flexor tendon in the distal metacarpal región, do extend through the region of the annular ligament into the proximal pastern region and, less frequently, also involve one or both branches of the superficial digital flexor tendon (see Fig. 3–46). In one study of injuries in the pastern region, the superficial digital flexor tendon was injured in 12 of 26 horses with tendon or ligament injuries in the pastern.[59]

The swelling associated with injuries to the superficial digital flexor tendon in this location is characteristic. The swelling is usually a longitudinal swelling that extends in a proximal-to-distal direction along the lateral and/or medial aspect of the pastern throughout its length, following the branch of the superficial digital flexor tendon. Focal heat and sensitivity usually accompany this swelling. Lameness at the onset of this injury is common. Lameness is more common with superficial digital flexor tendon injuries in the pastern than with "bows" in the metacarpal region. Lameness can occur initially in the absence of local swelling; it was present for up to 5 days in two horses before swelling developed.[71]

Lameness associated with a superficial digital flexor tendon injury in the pastern may persist longer (for 1 to 4 weeks) than that associated with injury in the metacarpal region.[71] Subluxation of the metacarpo- or metatarsophalangeal joint or the proximal interphalangeal joint can occur in horses with severe injury to or complete rupture of the superficial digital flexor tendon in the pastern. Severe dropping of the fetlock joint towards the ground with weight bearing may also occur with severe superficial digital flexor tendon injuries. Although this swelling in the pastern is commonly misdiagnosed as an injury to the XYZ ligaments, or distal sesamoidean ligaments, the characteristic location of the swelling should suggest that the injury is most likely in the superficial digital flexor tendon branches. Such injury should be confirmed ultrasonographically.

Core injuries to the superficial digital flexor tendon branches (Fig. 3–112) are the most common type of injury detected ultrasonographically, followed by complete ruptures or near-complete ruptures of the branches (Fig. 3–113). Diffuse injuries (Fig. 3–114) and splits also occur in this location. The medial branch of the superficial digital flexor tendon is more frequently injured than is the lateral branch, according to one study.[59] However, the number of affected horses studied was small (four horses sustained an injury to the medial branch, and in one horse, both branches were affected).[59] A hypoechoic lesion was detected in only one of these horses. A heterogeneous pattern of echogenicity and extensive thickening of the branch was the sonographic abnormality most frequently reported, a finding most common with chronic superficial digital flexor tendinitis.[59, 71] Injuries to the proximal and axial part of the tendon were slightly more common, but the majority of these horses (5 of 7 horses) had concurrent injuries to the superficial digital flexor tendon in the metacarpal region.[59] The total number of affected horses with injuries to the superficial digital flexor tendon at the pastern was small (7 of 12 horses) in this study. In this author's experience, the proximal and axial portion of the superficial digital flexor tendon is frequently injured in association with, rather than independent of, injuries to the superficial digital flexor tendon branches. Injuries to the proximal and axial portion of the superficial digital flexor tendon in the pastern occur most frequently in horses with tendon injuries in the metacarpal region that extend distally into the proximal pastern. Peritendinous soft tissue swelling is common with these injuries, and this swelling usually follows the anatomy of the superficial digital flexor tendon in this region. Avulsion fractures of the insertion of the superficial digital flexor tendon branch (Fig. 3–115) onto the distal aspect of P1 or the proximal aspect of P2 occur infrequently. They are usually found in horses with significant injuries to the superficial digital flexor tendon branch. An avulsion fracture of the insertion of the medial branch of the superficial digital flexor tendon onto proximal P2 was reported in 1 of 12 horses with injury of the superficial digital flexor tendon at the pastern.[59]

Sonographic findings with repair of the superficial digital flexor tendon should be similar to those described for

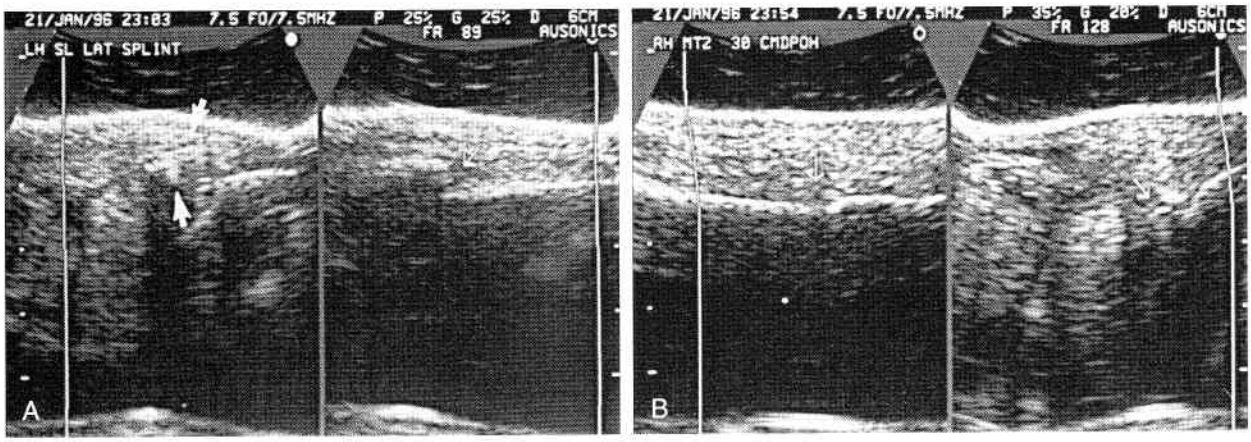

Figure 3–109

Sonograms of a fractured second and fourth metatarsal bones in the left hind leg, obtained from an 11-year-old Morgan mare at 30 cm distal to the point of the hock (zone 3A). These sonograms were obtained with a wide-bandwidth 7.5-MHz sector-scanner transducer operating at 7.5 MHz containing a built-in fluid offset at a displayed depth of 6 cm. The right side of the transverse images is dorsal and the left side is plantar. The right side of the sagittal images is proximal and the left side is distal.

A, Notice the hyperechoic linear echo *(thin arrow)* distracted away from the parent portion of the fourth metatarsal bone in the sagittal view *(right image),* casting an acoustic shadow consistent with a fracture fragment. The fracture fragment *(thick arrows)* is also seen in the transverse view *(left image).*

B, Notice the lucent line in the bony surface echo *(arrows)* best visualized in the sagittal view *(left image)* but also detected in the transverse view *(right image),* consistent with a hairline fracture of the second metatarsal bone.

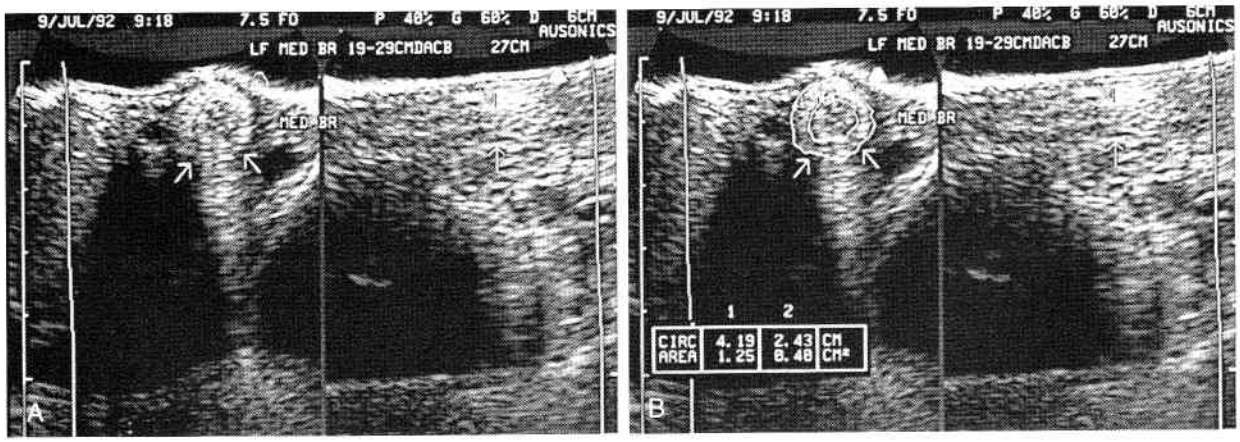

Figure 3–110

Sonograms of a healing core lesion in the medial branch of the suspensory ligament (SL) in the left foreleg, obtained from a 4-year-old Thoroughbred gelding. The healing area of SL desmitis was imaged from 19 to 29 cm distal to the point of the accessory carpal bone. These sonograms were obtained at 27 cm (zone 3B) with a 7.5-MHz sector-scanner transducer containing a built-in fluid offset at a displayed depth of 6 cm. The right side of the transverse views *(left images)* is dorsal and the left side is palmar. The right side of the sagittal views *(right images)* is proximal and the left side is distal.

A, Notice the heterogeneous slightly hypoechoic central core lesion *(arrows)* in the transverse view and the random pattern of fiber alignment *(arrows)* in the sagittal view. The echogenicity and fiber alignment in the core lesion is consistent with immature and maturing fibrous tissue.

B, The original central core lesion involved 32% of the cross-sectional area of the medial SL branch (0.40 cm^2/1.25 cm^2).

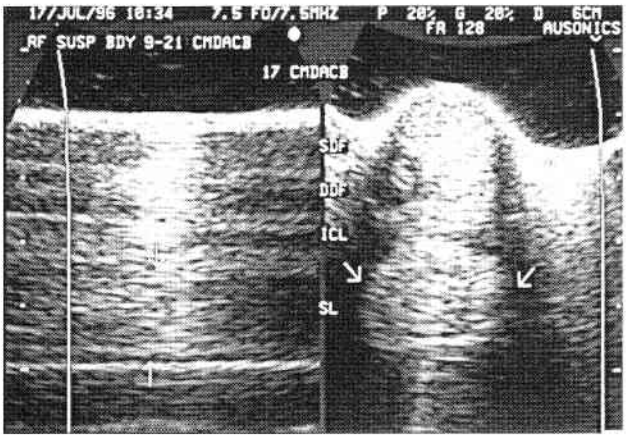

Figure 3–111

Sonograms of a large healing area of injury in the body of the suspensory ligament (SL) in the right foreleg, obtained from a 7-year-old Thoroughbred gelding. Notice the echogenic central and dorsal core lesion in the SL body, with a slightly more hypoechoic halo and a rim of more normal SL tissue along the palmar, medial, and lateral aspect of the SL *(arrows)* imaged in the transverse view *(right image)*. A random alignment of short and long linear echoes occurs in the repairing core imaged in the sagittal view *(left image)*. The original core lesion in the SL body extended from 9 to 21 cm distal to the accessory carpal bones. These sonograms were obtained at 17 cm (at the border between zones 2A and 2B) with a wide-bandwidth 7.5-MHz sector-scanner transducer operating at 7.5 MHz containing a built-in fluid offset at a displayed depth of 6 cm. The right side of the transverse image is lateral and the left side is medial. The right side of the sagittal image is proximal and the left side is distal. SDF, superficial digital flexor tendon; DDF, deep digital flexor tendon; ICL, inferior check ligament.

the metacarpal region. An increase in the echogenicity of the lesion and the subsequent appearance of short linear echoes occur with tendon healing (Fig. 3-116). Thickening of the superficial digital flexor tendon branch and the surrounding peritendinous tissues is likely to persist in most affected horses, although it is usually less than the initial swelling associated with the acute injury. A central echogenic scar surrounded by a hypoechoic "halo" may be detected in the superficial digital branch with a repaired core lesion. Peritendinous hypoechoic to echogenic tissue representing immature and maturing fibrous tissue is often imaged adjacent to the injured superficial digital flexor tendon branch. This tissue can result in adhesions between the branch and the surrounding tendinous and peritendinous structures. New areas of fiber disruption often occur adjacent to the previously repaired area (Fig. 3-117) or in association with adhesions to the surrounding tendinous or peritendinous structures.

Deep Digital Flexor Tendon. Injuries to the deep digital flexor tendon in the pastern occur in a variety of competition horses.[71] Lameness is often acute, severe, and persistent. As in the metacarpal or metatarsal region, deep digital flexor tendon injuries are usually associated with digital sheath tenosynovitis. Calcification is frequently found in the deep digital flexor tendon in the region of the fetlock annular ligament (see Figs. 3-75 and 3-76). Injury to the deep digital flexor tendon in the pastern region is often associated with injury to the metacarpal or metatarsal portion of the tendon (see Fig. 3-77), but can also occur without other deep digital flexor tendon disease. Injury to the deep digital flexor tendon in the distal pastern and foot is also commonly associated with navicular disease.

In some horses, the lameness is intermittent initially, with no local swelling and with clinical signs similar to those of navicular disease.[59] In these horses, the deep digital flexor tendinitis is usually in the distal pastern region in the area of the navicular bone, a difficult area to image sonographically. Enlargement of the deep digital flexor tendon in the pastern, focal or diffuse areas of decreased echogenicity within the tendon, and/or poor definitions of the margins of the tendon are usually associated with swelling in the region of the deep digital flexor tendon. Lesions reportedly extend less than 2 cm in a

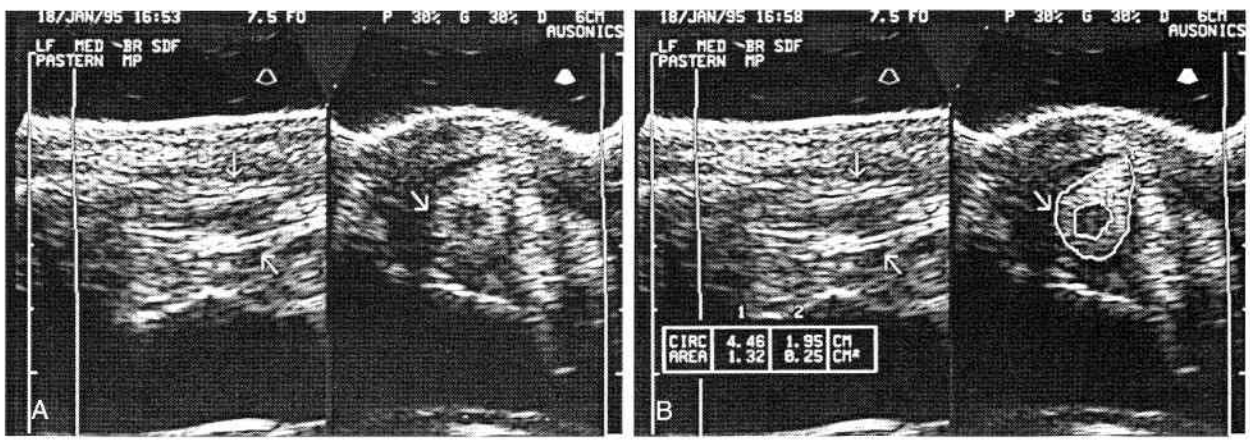

Figure 3–112

Sonograms of a discrete core lesion in the medial branch of the left fore superficial digital flexor tendon (SDF), obtained from a 5-year-old Thoroughbred gelding. These sonograms were obtained in zone P1B with a 7.5-MHz sector-scanner transducer containing a built-in fluid offset at a displayed depth of 6 cm. The left side of the transverse views *(right images)* is dorsal and the right side is palmar. The left side of the sagittal views *(left image)* is distal and the right side is proximal.

A, Notice the discrete anechoic central core *(arrow)* in the transverse view and the complete loss of fibers in the lesion *(arrows)* in the sagittal view.

B, This area of fiber tearing involved 19% of the medial SDF branch (0.25 cm^2/1.32 cm^2) at this level in the mid pastern.

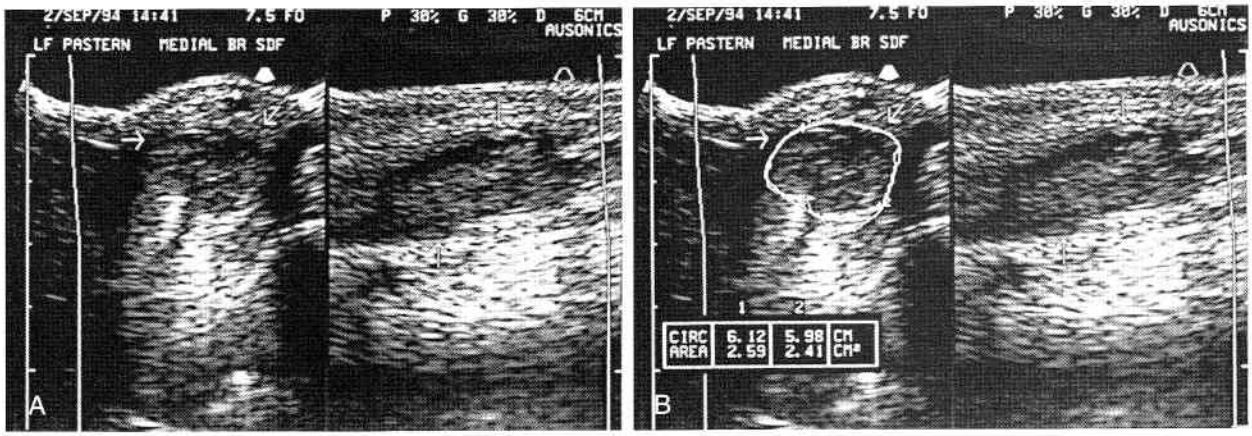

Figure 3–113

Sonograms of a large core lesion in the medial branch of the left fore superficial digital flexor tendon (SDF), obtained from a 4-year-old Thoroughbred stallion. These sonograms were obtained at the border between zones P1A and P1B with a 7.5-MHz sector-scanner transducer containing a built-in fluid offset at a displayed depth of 6 cm. The right side of the transverse views *(left images)* is dorsal and the left side is palmar. The right side of the sagittal views *(right images)* is proximal and the left side is distal.

A, Notice the large anechoic core lesion *(arrows)* involving nearly the entire cross-sectional area of the medial SDF branch.

B, This core lesion involved 93% of the cross-sectional area (2.41 cm^2/2.59 cm^2) of the medial SDF branch.

proximal-to-distal direction in these horses and some horses have associated digital sheath effusion. In this author's experience, lesions in the deep digital flexor tendon are usually more extensive: at least 4 to 6 cm in a proximal-to-distal direction, with areas of calcification in the deep digital flexor tendon extending for 6 to 8 cm.

Deep digital flexor tendon lesions in the pastern were found in five horses in one study with no mention of whether they appeared in the forelimb or hindlimb.[59] Three of these horses had an asymmetric deep digital flexor tendon that was thicker medially; hyperechoic areas consistent with calcification were detected within the tendon. Adhesions within the synovial sheath and cartilaginous metaplasia were detected in the deep digital flexor tendon of one of the horses on postmortem examination. A focal hypoechoic area was imaged in one horse with a concurrent digital sheath effusion. The lesion changed little over 6 months, but the horse was able to return to work. One horse had a complete rupture of the deep digital flexor tendon at the pastern, characterized by large hypoechoic areas within the tendon in the pastern and complete rupture in the fetlock.

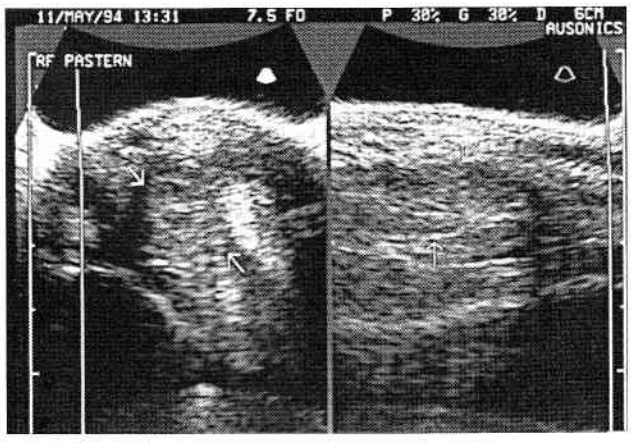

Figure 3–114

Sonograms of a more diffuse area of fiber tearing in the medial branch of the right fore superficial digital flexor tendon (SDF), obtained from a 5-year-old Thoroughbred gelding. Notice the diffusely enlarged and hypoechoic medial branch *(arrows),* with preservation of a few long linear echoes detected in the sagittal view *(right image).* These fibers are visible as the brighter echogenic short linear echoes in the medial SDF branch in the transverse view *(left image).* These sonograms were obtained in zone P1B with a 7.5-MHz sector-scanner transducer containing a built-in fluid offset at a displayed depth of 6 cm. The left side of the transverse view is dorsal and the right side is palmar. The left side of the sagittal view is distal and the right side is proximal.

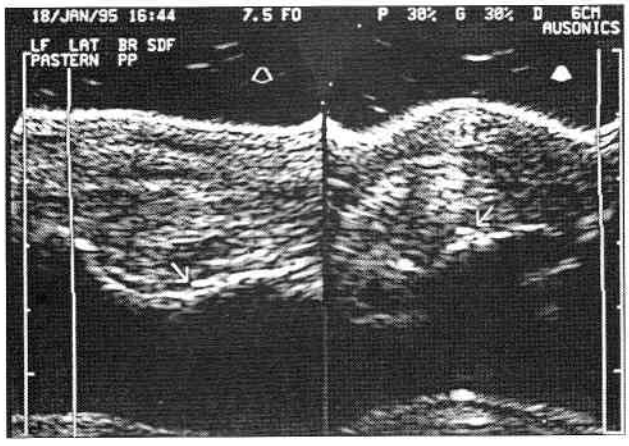

Figure 3–115

Sonograms of an avulsion fracture from the distal lateral portion of the first phalanx (P1) at the insertion of the lateral branch of the left fore superficial digital flexor tendon (SDF), obtained from a 5-year-old Thoroughbred gelding. Notice the small hyperechoic bony fragment *(arrows)* distracted slightly away from the parent portion of the underlying bone. An underlying irregular bony surface echo is adjacent to the avulsion fracture. The lateral SDF branch is heterogeneous, with hypoechoic areas and fiber disruption visible, and some random fiber alignment is detected in the sagittal view *(left image),* suggesting previous injury to this region. These sonograms were obtained at zone P1C with a 7.5-MHz sector-scanner transducer containing a built-in fluid offset at a displayed depth of 6 cm. The left side of the transverse view *(right image)* is palmar and the right side is dorsal. The left side of the sagittal images is distal and the right side is proximal.

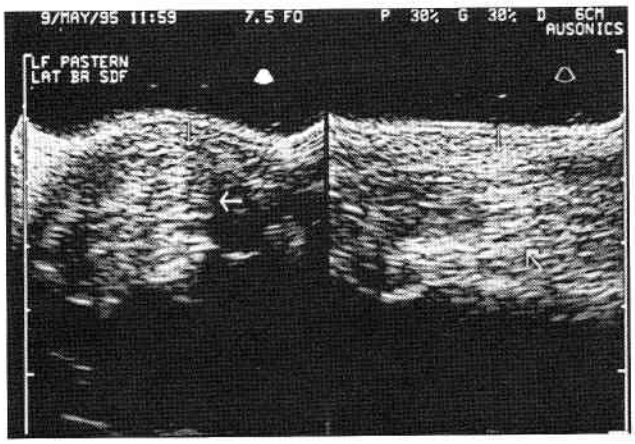

Figure 3–116

Sonograms of a healed core lesion in the lateral branch of the left fore superficial digital flexor tendon (SDF), obtained from a 10-year-old Thoroughbred gelding in zone PIB. Notice the slightly hyperechoic central core surrounded by a hypoechoic halo with a hypoechoic to isoechoic outer rim of SDF fibers. The entire lateral SDF branch *(arrows)* is somewhat heterogeneous with a somewhat random pattern of fiber alignment. These sonograms were obtained with a 7.5-MHz sector-scanner transducer containing a built-in fluid offset at a displayed depth of 6 cm. The left side of the transverse view *(left image)* is palmar and the right side is dorsal. The left side of the sagittal view *(right image)* is distal and the right side is proximal.

Distal Sesamoidean Ligament Desmitis

Middle (Oblique) Distal Sesamoidean Ligament Desmitis. Desmitis of the middle distal sesamoidean ligament is common and is seen in all types of performance horses. Swelling in the pastern associated with middle distal sesamoidean ligament desmitis is fairly characteristic because this ligament runs diagonally across the proximal to middle pastern. Most horses have local swelling, heat, pain, and sensitivity in the affected ligament and lameness in the affected leg. Subluxation of the metacarpo- or metatarsophalangeal joint or the proximal interphalangeal joint can occur in horses with complete rupture of the oblique (middle) distal sesamoidean ligament. A chronic ipsilateral suspensory ligament desmitis was reported in three horses with desmitis of the middle distal sesamoidean ligaments.[59]

Discrete core lesions (Fig. 3–118) are often seen in the medial and lateral branches of the middle distal sesamoidean ligament, although diffuse areas of fiber damage and splits also occur at this location. Injuries to the insertion of the middle distal sesamoidean ligament usually appear diffuse sonographically (Fig. 3–119). Periligamentous soft tissue thickening often surrounds the area of injury. The base of the sesamoids (origin of the middle distal sesamoidean ligaments) and the insertion of the ligament on the middle of P1 should be carefully evaluated for avulsion fractures. Avulsion fractures usually occur in association with fiber tearing in the distal sesamoidean ligaments. Avulsion fractures occur at the base of the sesamoids (Fig. 3–120) and at the insertion on mid P1 (Fig. 3–121) with seemingly equal frequency. Avulsion fractures remain visible for years after the original injury, long after the associated desmitis in the distal sesamoidean ligament has resolved (see Fig. 3–120). Irregularities of the bony surface echo at the insertion of the middle distal sesamoidean ligament onto the palmar or plantar (less common) aspect of mid P1 are frequently imaged in horses consistent with an insertional desmitis or enthesopathy. As the injury heals, the ligament's cross-sectional area usually decreases, the echogenicity of the

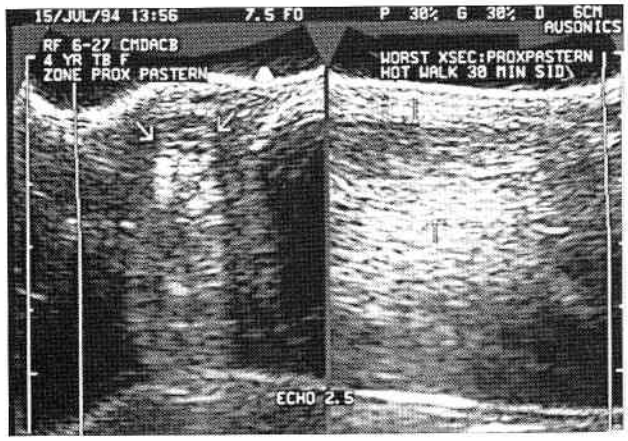

Figure 3–117

Sonograms of an area of reinjury to the medial branch of the right fore superficial digital flexor tendon (SDF), obtained from a 4-year-old Thoroughbred filly in zone P1A. Notice the echogenic axial portion of the medial SDF branch with a random fiber pattern *(up arrow)* in the sagittal view *(right image)* adjacent to the newer hypoechoic to anechoic area of fiber tearing *(down arrow)*. The old healed central core is visible in the transverse view *(left image)* as a central echogenic area surrounded by a hypoechoic halo, with a superficial hypoechoic to anechoic loculated area representing the new area of fiber tearing. The new area of injury occurred adjacent to the previously healed core lesion in the medial SDF branch. These sonograms were obtained with a 7.5-MHz sector-scanner transducer containing a built-in fluid offset with a displayed depth of 6 cm. The left side of the transverse image is palmar and the right side is dorsal. The left side of the sagittal image is distal and the right side is proximal.

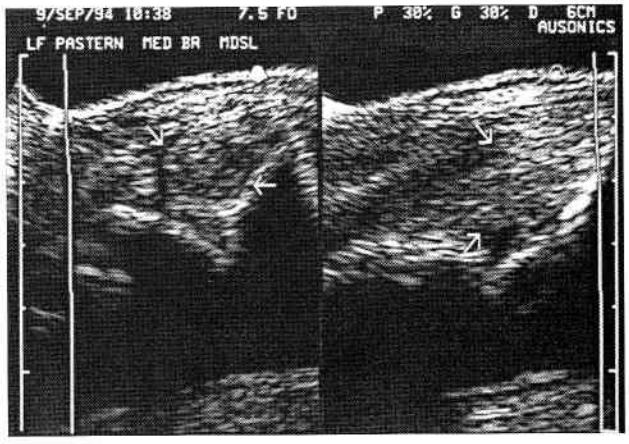

Figure 3–118

Sonograms of an acute core lesion in the medial branch of the middle distal sesamoidean ligament (MDSL) at its origin in zone P1A in the left foreleg, obtained from a 4-year-old Thoroughbred gelding. Notice the anechoic to hypoechoic axial core lesion *(arrows)* in the transverse view *(left image)* and the loss of the normal fiber pattern in the sagittal view *(right image)*. These sonograms were obtained with a 7.5-MHz sector-scanner transducer containing a built-in fluid offset at a displayed depth of 6 cm. The right side of the transverse image is dorsal and the left side is palmar. The right side of the sagittal image is proximal and the left side is distal.

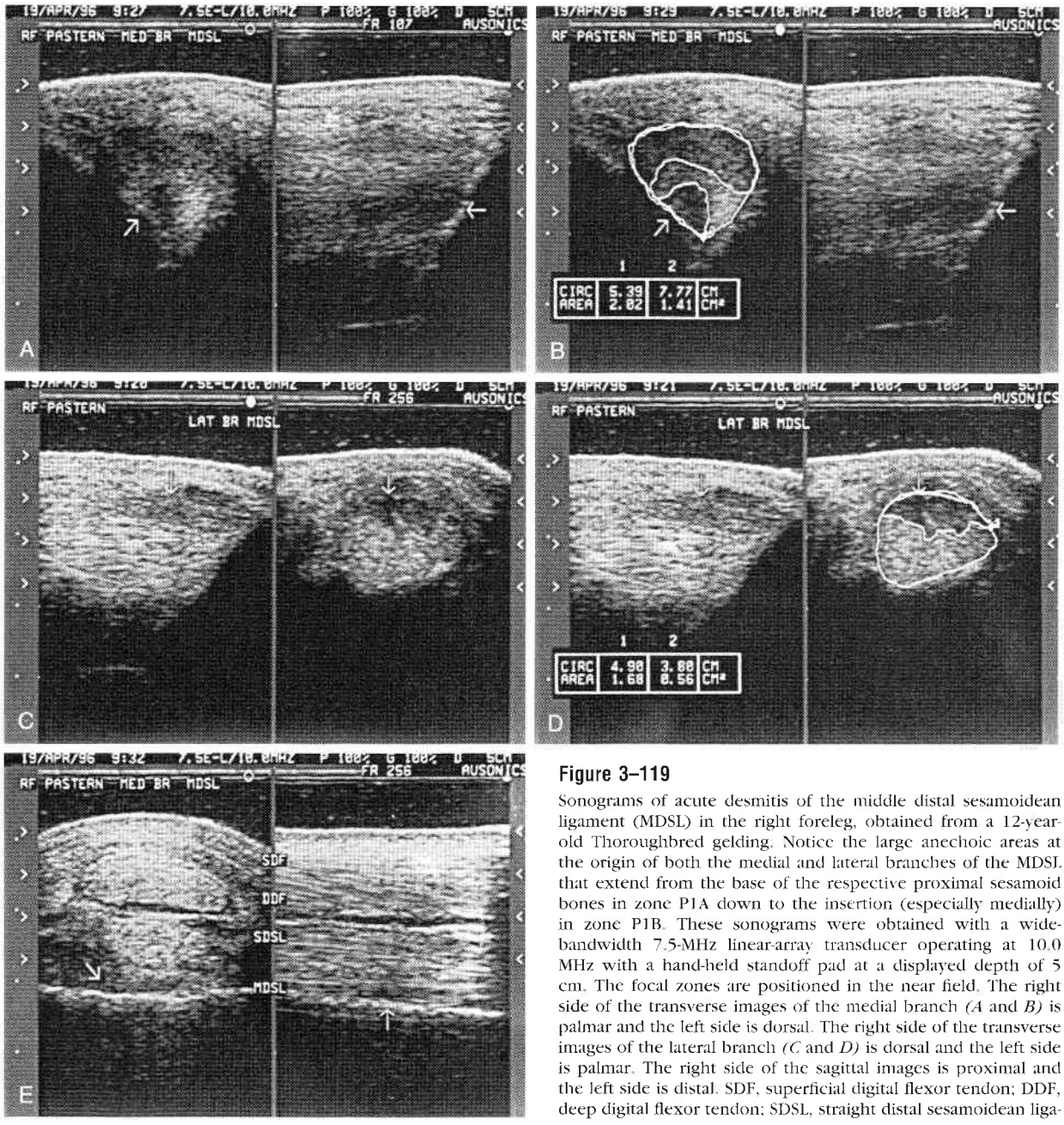

Figure 3–119

Sonograms of acute desmitis of the middle distal sesamoidean ligament (MDSL) in the right foreleg, obtained from a 12-year-old Thoroughbred gelding. Notice the large anechoic areas at the origin of both the medial and lateral branches of the MDSL that extend from the base of the respective proximal sesamoid bones in zone P1A down to the insertion (especially medially) in zone P1B. These sonograms were obtained with a wide-bandwidth 7.5-MHz linear-array transducer operating at 10.0 MHz with a hand-held standoff pad at a displayed depth of 5 cm. The focal zones are positioned in the near field. The right side of the transverse images of the medial branch *(A* and *B)* is palmar and the left side is dorsal. The right side of the transverse images of the lateral branch *(C* and *D)* is dorsal and the left side is palmar. The right side of the sagittal images is proximal and the left side is distal. SDF, superficial digital flexor tendon; DDF, deep digital flexor tendon; SDSL, straight distal sesamoidean ligament.

A, Sonograms obtained from the origin of the medial MDSL branch, which is more severely affected than the lateral branch. The branch is enlarged, and large anechoic areas representing fiber disruption and hemorrhage *(arrows)* are visible in both the transverse *(left image)* and sagittal *(right image)* views. A few intact fibers remain in this branch.

B, Sonograms of the same area of injury in the medial branch outlining the area of fiber disruption, which involves at least 70% of the branch's cross-sectional area (1.41 cm^2/2.02 cm^2) at its origin.

C, Sonograms obtained from the origin of the lateral branch, demonstrating a more discrete tear in the superficial portion of the lateral MDSL branch *(arrows).* This branch is also enlarged at the origin, but less so, with a discrete area of fiber damage adjacent to fibers that are more well preserved. The area of injury appears confined to the proximal portion of the lateral MDSL branch in the sagittal view *(left image)* and to the superficial portion of the branch in both the sagittal and transverse views *(right image).*

D, Sonograms of the same area of injury in the lateral MDSL branch, outlining the area of fiber disruption, which involves 33% of the branch's cross-sectional area (0.56 cm^2/1.68 cm^2) at its origin.

E, Sonograms of the insertion of the MDSL along mid P1 at zone P1B with an area of fiber tearing detected in the medial *(arrow)* and, to a lesser extent, lateral aspect of the MDSL at its insertion best imaged in the transverse view *(left image).* The damage to the central portion of the MDSL at its insertion *(up arrow)* is also imaged in the sagittal view *(right image).*

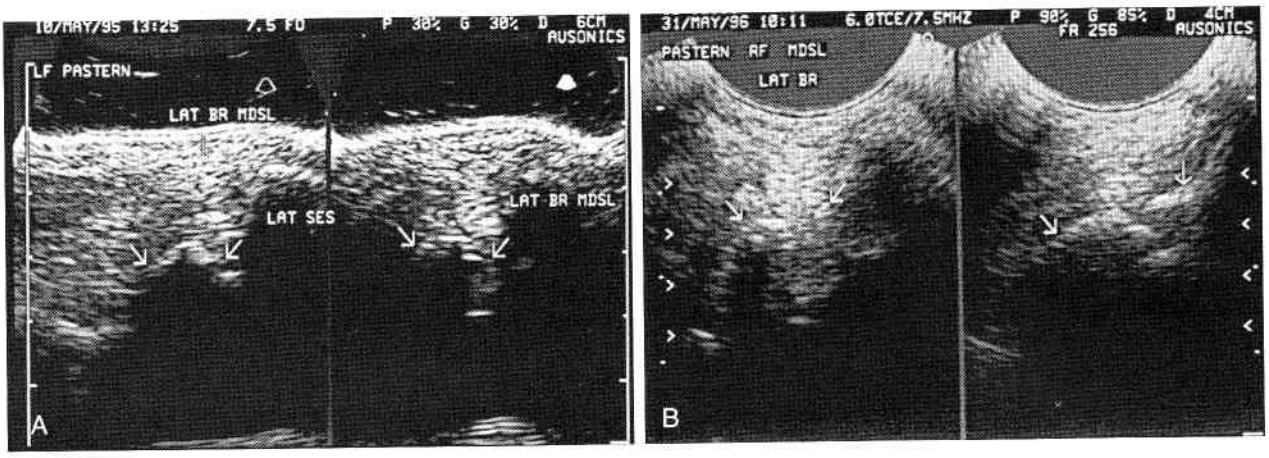

Figure 3–120

Sonograms of an avulsion fracture associated with the origin of the lateral branch of the middle distal sesamoidean ligament (MDSL) in the left foreleg, obtained from a 14-year-old Quarter horse gelding. Notice the hyperechoic structure casting an acoustic shadow at the base of the sesamoid and in the body of the lateral MDSL branch *(arrows)* in zone P1A that are associated with several fracture fragments in the transverse and sagittal views. The right side of the transverse images is dorsal and the left side is palmar. The right side of the sagittal images is proximal and the left side is distal.

A, The fibers of the MDSL are fairly hypoechoic and loss of the normal fiber pattern is associated with a healing injury to the MDSL. A small amount of periligamentous echogenic tissue is present, consistent with periligamentous inflammation and early fibrosis. This sonogram was obtained with a 7.5-MHz sector-scanner transducer containing a built-in fluid offset at a displayed depth of 6 cm. The left image is the sagittal view and the right image is the transverse view.

B, The fibers of the MDSL appear fairly echogenic 1 year later. However, a random fiber pattern is visible in the sagittal view *(right image)* consistent with a chronic MDSL desmitis involving the lateral branch, which does not appear active sonographically at this time. An increase in the amount of periligamentous echogenic thickening is present at this time, consistent with periligamentous fibrosis best seen in the transverse view *(left image)*. These sonograms were obtained with a wide-bandwidth microconvex 6.0-MHz linear-array transducer operating at 7.5 MHz at a displayed depth of 6 cm. The focal zones are positioned in the middle of the image.

lesion increases, and linear echoes are imaged in the area of previous fiber tearing (Fig. 3-122).

Distal sesamoidean ligament injuries involving the middle (oblique) distal sesamoidean ligament were found in the majority of horses in several studies.[59] The middle distal sesamoidean ligament was thickened and hypoechoic in five of seven horses in one study, with the medial branch being affected in 80% of these horses.[59] All of these injuries were in the forelimb. The injury to the lateral branch of the middle distal sesamoidean ligament was in the hindlimb.

Straight Distal Sesamoidean Ligament. Injuries to the straight distal sesamoidean ligament occur infrequently. These injuries are usually associated with lameness, but focal heat, swelling, and sensitivity are not always detected. Subluxation of the proximal interphalangeal joint can occur with these injuries. Care must be taken that off-normal incidence artifacts are not created at the insertion of the straight distal sesamoidean ligament on the proximal border of P2 as a result of difficulty in aligning the transducer perpendicular to the ligamentous fibers at that level (caused by the location of the horse's heels). A hypoechoic dropout is detected at this location by most ultrasound transducers because their shape precludes obtaining a 90-degree angle between the transducer and the ligament (see Fig. 3-12). If proper angulation of the transducer can be achieved, this off-normal incidence artifact is not imaged (see Fig. 3-16).

Small splits (see Fig. 3-122) or core lesions (Fig. 3-123) may be imaged in the straight distal sesamoidean liga-

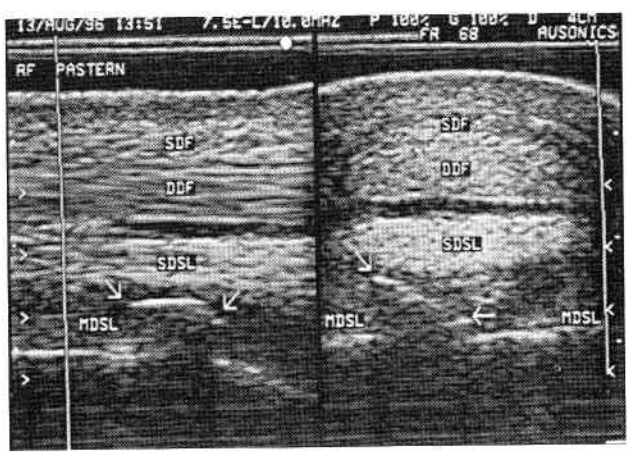

Figure 3–121

Sonograms of an avulsion fracture *(arrows)* of the insertion of the middle distal sesamoidean ligament (MDSL) in the right foreleg of a 12-year-old Warmblood stallion. The avulsion fracture is the hyperechoic linear structure casting a strong acoustic shadow *(arrows)*. This avulsion fracture is from the medial side of the mid pastern and is imaged distracted palmar and diagonally in the transverse view *(right image)*. The proximal and palmar distraction of the fragment is imaged in the sagittal view *(left image)*. This sonogram was obtained in zone P1B with a wide-bandwidth 7.5-MHz linear-array transducer operating at 10.0 MHz with a hand-held standoff pad and a displayed depth of 4 cm. The focal zones are positioned in the far field. The right side of the transverse image is lateral and the left side is medial. The right side of the sagittal image is proximal and the left side is distal. SDF, superficial digital flexor tendon; DDF, deep digital flexor tendon; SDSL, straight distal sesamoidean ligament.

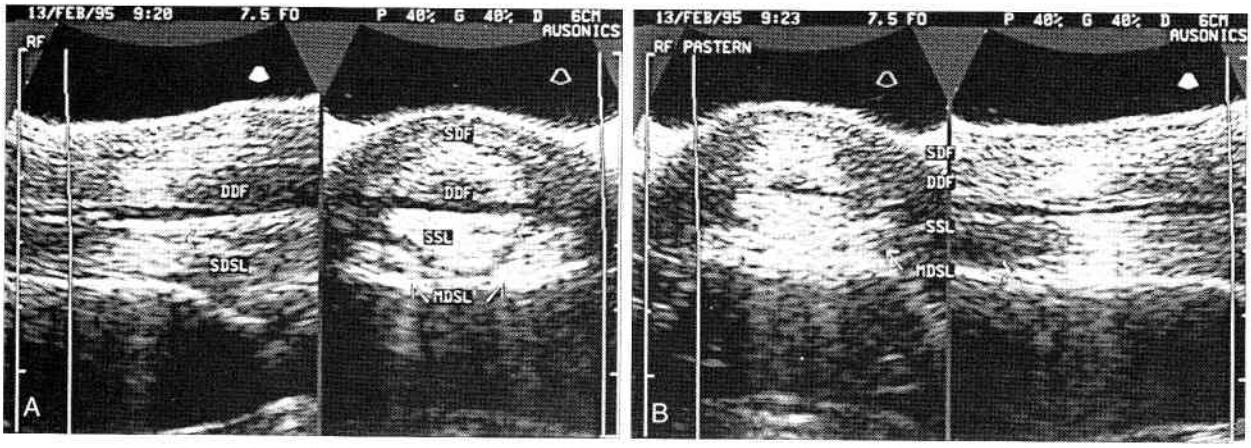

Figure 3–122

Sonograms of a desmitis in the straight distal sesamoidean ligament (SDSL) and the branches of the middle distal sesamoidean ligament (MDSL) in the right foreleg of an 11-year-old Thoroughbred gelding. These sonograms were obtained in zone P1B with a 7.5-MHz sector-scanner transducer containing a built-in fluid offset at a displayed depth of 6 cm. The right side of the transverse views is lateral and the left side is medial. The right side of the sagittal view is proximal and the left side is distal. SDF, superficial digital flexor tendon; DDF, deep digital flexor tendon.

A, Notice the hypoechoic linear split in the SDSL *(horizontal arrows)* that originates at its lateral margin and the slightly thicker lateral side of the SDSL in the transverse view *(right image)* and the fiber loss in the sagittal view *(left image).* The lateral branch of the MDSL is also significantly thicker than the medial branch, but it is fairly echogenic and has a random fiber pattern associated with a chronic inactive distal sesamoidean desmitis of the MDSL. There is a small newer area of fiber damage in the medial branch of the MDSL.

B, Slightly more distal, in zone P1B, the MDSL is thicker than normal at its insertion *(arrows)* and smooth irregularities of the bony surface echo of palmar P1 are present at the level of insertion of the MDSL. The lateral portion of the MDSL is thicker also at the insertion of the body of the MDSL, detected in the transverse view *(left image).* The fiber alignment of the central portion of the MDSL is near normal in the sagittal view *(right image).*

ment. Areas of periosteal proliferative change or avulsion fractures at the insertion of the straight distal sesamoidean ligament on proximal P2 may be seen in horses with desmitis of the straight distal sesamoidean ligament (Fig. 3–124). Insertional desmitis or enthesiopathy of the straight-distal sesamoidean ligament is less common than insertional desmitis involving the middle distal sesamoidean ligament. Avulsion fractures of the origin of the straight distal sesamoidean ligament occur less frequently than those associated with middle distal sesamoidean ligament desmitis. Nevertheless, the base of the sesamoids should be carefully imaged to check for avulsion fractures.

Injuries to the straight distal sesamoidean ligament were seen in only two of seven horses with distal sesamoidean ligament desmitis in one report.[59] The affected distal sesamoidean ligaments appeared thickened and slightly hypoechoic.

Cruciate Distal Sesamoidean Ligament Desmitis. Desmitis of the cruciate distal sesamoidean ligament is rare. It is difficult to diagnose ultrasonographically due to the location of these ligaments.

Intersesamoidean Ligament Desmitis. The intersesamoidean ligament is imaged from the palmar and plantar surfaces of the metacarpo- and metatarsophalangeal

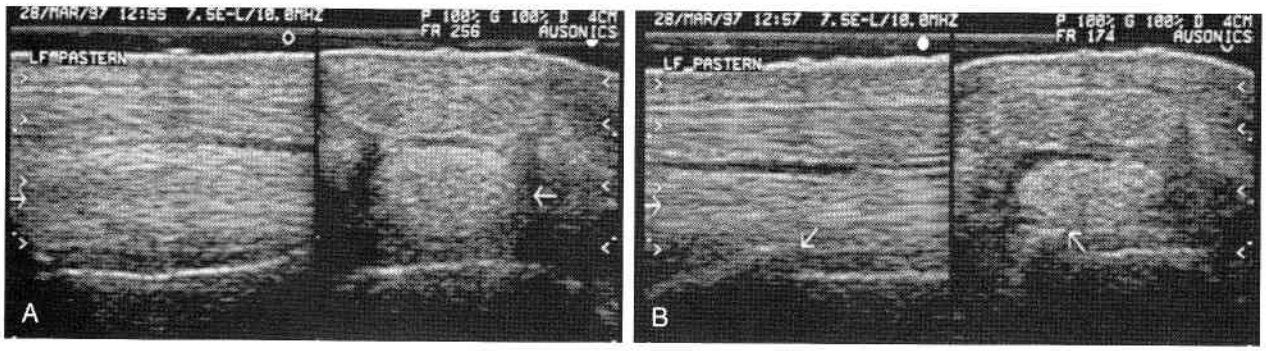

Figure 3–123

Sonograms of the pastern obtained from a 4-year-old Thoroughbred colt with straight distal sesamoidean ligament desmitis. These sonograms were obtained in zone P1C with a wide-bandwidth 7.5-MHz linear-array transducer operating at 10.0 MHz using a hand-held standoff pad at a displayed depth of 4 cm. The right side of the transverse views *(right images)* is lateral and the left side is medial. The right side of the sagittal views *(left images)* is proximal and the left side is distal.

A, Notice the enlargement of the straight distal sesamoidean ligament and the hypoechoic core lesion imaged in the center of the ligament *(arrows).* This decrease in the ligament's echogenicity and change in the fiber pattern is consistent with a chronic injury to the straight distal sesamoidean ligament. The deep digital flexor tendon is palmar to the straight distal sesamoidean ligament.

B, Immediately proximal to the area of distal sesamoidean ligament desmitis there is an area of bony proliferation from the palmaromedial aspect of the first phalanx *(arrows)* that appears to be impinging on the straight distal sesamoidean ligament and may be involved in the pathogenesis of this chronic injury.

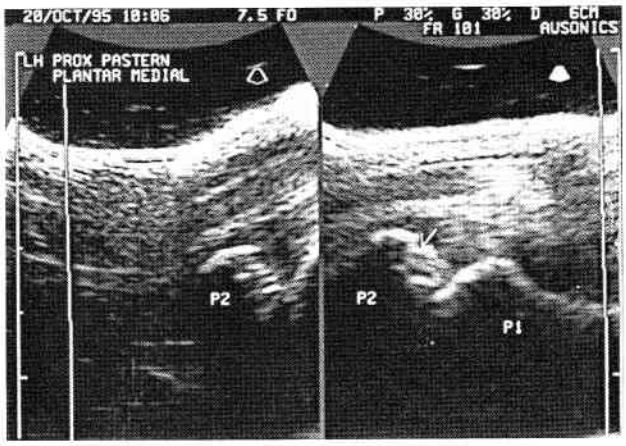

Figure 3–124

Sagittal sonograms of desmitis of the straight distal sesamoidean ligament (SDSL) in the left hind leg, obtained from a 2-year-old Thoroughbred colt. Notice the enthesophyte formation at its insertion onto the proximal portion of the second phalanx (P2). The bony surface echo of proximal P2 is irregular with a large lytic lesion *(arrow)* detected along the plantar margin. The SDSL is mildly enlarged and diffusely hypoechoic and has lost some of its normal fiber pattern. These sonograms were obtained in zone P2 with a 7.5-MHz sector-scanner transducer containing a built-in fluid offset at a displayed depth of 6 cm. The right side of the image is proximal and the left side is distal. P1, first phalanx.

joints, respectively. Injury to the intersesamoidean ligaments does occasionally occur, often with sesamoiditis of the adjacent areas in the sesamoid bones (Fig. 3-125). Careful examination of this area should be performed as part of the routine evaluation of the palmar metacarpal or plantar metatarsal regions.

Annular Ligament Desmitis. Annular ligament desmitis associated with fetlock annular ligament constriction is common in horses, but it usually occurs in conjunction with digital sheath tenosynovitis. Annular ligament desmitis is rarely primary, with local swelling, heat, and sensitivity present in the annular ligament only in the absence of digital sheath involvement. Annular ligament desmitis of the fetlock annular ligament has resulted in significant lameness when occurring primarily, with marked clinical signs of local inflammation. Primary annular ligament desmitis is associated with marked thickening of the annular ligament and anechoic or hypoechoic areas within the annular ligament (Fig. 3-126). More typically, fetlock annular ligament desmitis is concurrent with digital sheath tenosynovitis (Fig. 3-127).[59, 131, 132] A long history of chronic digital sheath tenosynovitis and chronic thickening of the annular ligament/digital sheath is common in affected horses.

Four different syndromes of equine fetlock annular ligament constriction have been described with use of ultrasonography.[60] Type-1 fetlock annular ligament constriction is the most common. It is characterized by thickening and distention of the digital sheath in conjunction with thickening of the annular ligament (Fig. 3-128).[59, 60] Affected horses had normal flexor tendons and a normal ratio of the thickness of the superficial digital flexor tendon to that of the deep digital flexor tendon (SDFT/DDFT ratio) of 0.4 to 0.6.[60] A prominent notch was usually present in these horses at the proximal-most extent of the fetlock annular ligament, because of distention of the digital sheath proximally.

Type-2 fetlock annular ligament desmitis is characterized by distention and thickening of the digital sheath

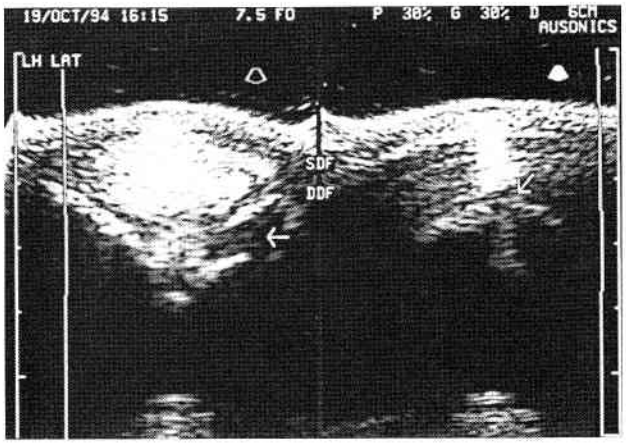

Figure 3–125

Sonograms of desmitis of the intersesamoidean ligaments and a lytic lesion along the axial border of the lateral proximal sesamoid bone in the left hind leg, consistent with osteomyelitis obtained from an 8-year-old Thoroughbred mare. Notice the large lytic lesion in the axial border of the lateral sesamoid bone *(horizontal arrow)* in the transverse view *(left image)*, which is also imaged as a lytic defect *(diagonal arrow)* in the sagittal view *(right image)*. Notice also the thickened heterogeneous appearance of the intersesamoidean ligament. These sonograms were obtained in the distal metatarsal region in zone 4C at 45 cm distal to the point of the hock with a 7.5-MHz sector-scanner transducer containing a built-in fluid offset at a displayed depth of 6 cm. The right side of the transverse image is lateral and left side is medial. The right side of the sagittal image is proximal and the left side is distal.

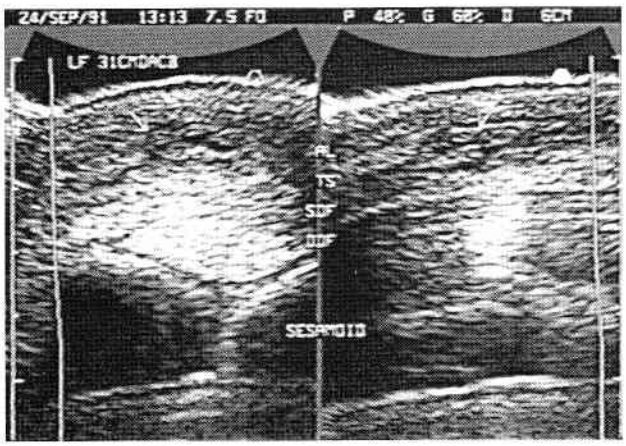

Figure 3–126

Sonograms of an acute annular ligament (AL) desmitis in the left foreleg, obtained from a 10-year-old Thoroughbred gelding. Notice the marked thickening of the fetlock annular ligament and the anechoic loculated fluid within the center of the annular ligament in zone 3C at 31 cm distal to the point of the accessory carpal bone. No sonographic evidence of digital sheath (TS) involvement exists. The superficial (SDF) and deep digital flexor tendons (DDF) are normal. These sonograms were obtained with a 7.5-MHz sector-scanner transducer containing a built-in fluid offset at a displayed depth of 6 cm. The right side of the transverse view *(left image)* is lateral and the left side is medial. The right side of the sagittal view *(right image)* is proximal and the left side is distal.

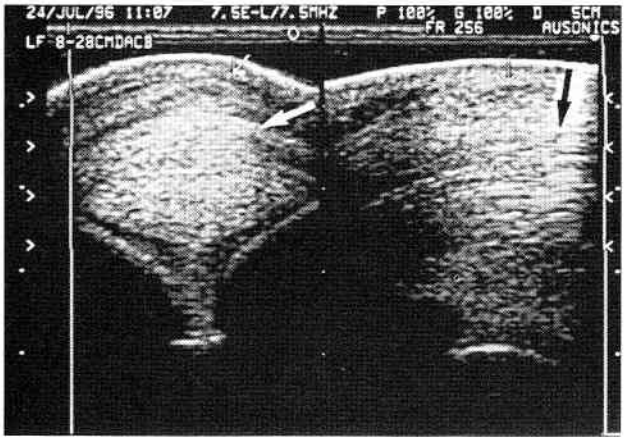

Figure 3–127

Sonograms of an annular ligament desmitis of the fetlock annular ligament in the left foreleg, obtained from a 10-year-old Thoroughbred gelding. Notice the thickening of the fetlock annular ligament and the focal decrease in echogenicity of the annular ligament along the midline *(thin arrows)*. The digital flexor tendon sheath also appears slightly thickened and is more echogenic than normal *(large arrows)*. The superficial and deep digital flexor tendons appear normal. These sonograms were obtained in zone 3C at 30 cm distal to the point of the accessory carpal bone with a wide-bandwidth 7.5-MHz linear-array transducer operating at 7.5-MHz using a hand-held standoff pad at a displayed depth of 5 cm. The focal zones are positioned in the near field. The right side of the transverse view *(left image)* is lateral and the left side is medial. The right side of the sagittal view *(right image)* is proximal and the left side is distal.

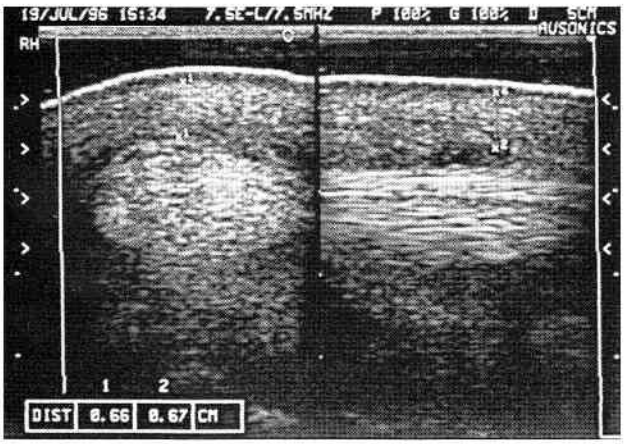

Figure 3–128

Sonograms of a digital sheath tenosynovitis and annular ligament desmitis in the right hindlimb, obtained from a 17-year-old Arabian stallion. Notice the thickened annular ligament and plantar-most portion of the digital sheath. Their combined thickness is 0.66 to 0.67 cm at 43 cm distal to the point of the hock. A small amount of fluid and some hypoechoic fibrin and loculations are detected within the digital sheath from 30–45 cm distal to the point of the hock. The superficial (SDF) and deep digital flexor (DDF) tendons are normal. The hypoechoic areas detected in both the SDF and DDF are artifactual and are not imaged in the sagittal view *(right image)*. These sonograms were obtained in zone 4C with a wide-bandwidth 7.5-MHz linear-array transducer operating at 7.5-MHz using a hand-held standoff pad at a displayed depth of 5 cm. The focal zones are positioned in the near field. The right side of the transverse view *(left image)* is lateral and the left side is medial. The right side of the sagittal view is proximal and the left side is distal.

and minimal nonspecific soft tissue thickening proximal to the annular ligament, making the palmar or plantar notch proximal to the annular ligament less obvious (Fig. 3-129).[60] In these horses, the flexor tendons were normal, with an SDFT/DDFT ratio of 0.6. The annular ligament was not thickened.[60]

Type-3 fetlock annular ligament constriction involves abnormalities in the superficial digital flexor tendon in conjunction with thickening of the annular ligament (Fig. 3-130).[60] Digital sheath distention may or may not be present. The lesions in the superficial digital flexor tendon vary from distinct hypoechoic lesions most prominent immediately dorsal to the annular ligament to irregular hypoechoic areas extending from proximal to the thickened annular ligament into the mid-metacarpal region. The SDFT/DDFT ratio in the three affected limbs was 1.4.[60] Both forms of type-3 fetlock annular ligament constriction have a notch detected at the annular ligament. The notch is associated with either the digital sheath effusion causing the bulge proximal to the annular ligament or the tendon itself bulging out in a palmar or plantar direction proximal to the annular ligament. The latter finding is common in those horses with superficial digital flexor tendinitis extending up into the mid-metacarpal region.

Type-4 fetlock annular ligament desmitis is the least common. In these horses, the constriction results from a thick layer of echoic subcutaneous tissue covering the palmar aspect of the distended digital sheath, extending proximally beyond the proximal limit of the digital sheath. The flexor tendons are normal (SDFT/DDFT ratio, 0.6). The thick layer of subcutaneous tissues prevents the

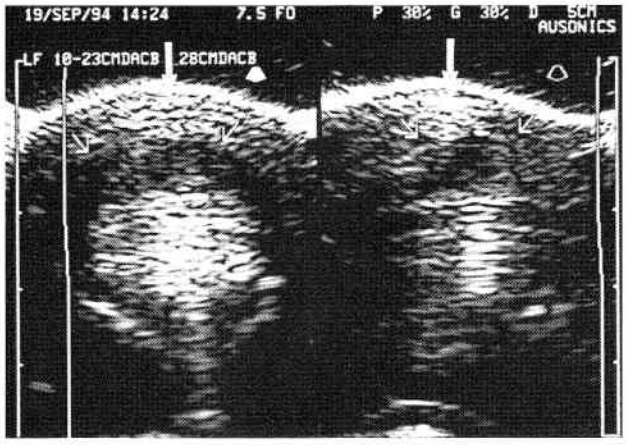

Figure 3–129

Sonograms of a digital sheath tenosynovitis with a normal annular ligament in the left foreleg obtained from a 7-year-old Pinto gelding. Notice the large anechoic to hypoechoic effusion in the digital sheath *(arrows)* over the palmar aspect of the superficial digital flexor tendon, with a thin normally echogenic annular ligament *(large arrow)*. These sonograms were obtained at 28 cm distal to the point of the accessory carpal bone in zone 3B with a 7.5-MHz sector-scanner transducer containing a built-in fluid offset at a displayed depth of 5 cm. The superficial digital flexor tendon (SDF) was normal in size but was slightly hypoechoic from 10 to 23 cm distal to the point of the accessory carpal bone, consistent with a mild superficial digital flexor tendinitis. The right side of the transverse view *(left image)* is lateral and the left side is medial. The right side of the sagittal view *(right image)* is proximal and the left side is distal.

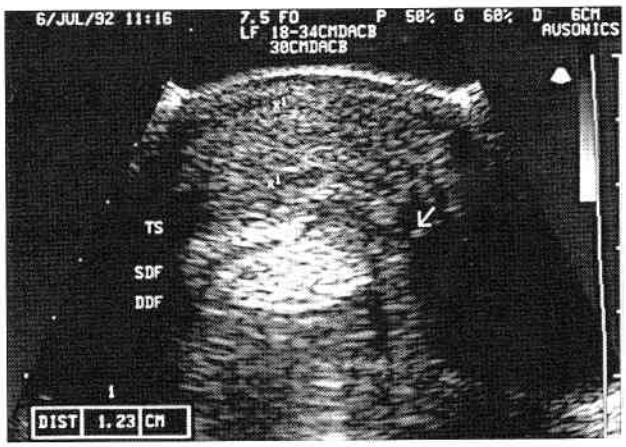

Figure 3–130

Sonogram of a severe annular ligament desmitis with a large lateral lesion in the superficial digital flexor tendon (SDF) of the left foreleg of an 8-year-old Thoroughbred gelding. Notice the markedly enlarged hypoechoic annular ligament that is difficult to distinguish separately from the digital sheath (TS), which measures at least 1.23 cm thick. A large anechoic split in the lateral portion of the SDF *(arrow)* results in a palmar and lateral bulging of the SDF at this site that is masked from palpation by the severe thickening of the annular ligament. This SDF tendinitis was imaged from 18 to 34 cm distal to the point of the accessory carpal bone. This sonogram was obtained at 30 cm (zone 3C) with a 7.5-MHz sector-scanner transducer containing a built-in fluid offset at a displayed depth of 6 cm. The right side of the transverse view is lateral and the left side is medial.

formation of a notch at the level of the fetlock annular ligament, preventing the bulging of the digital sheath. Although no lesions of the deep digital flexor tendon were reported in the study characterizing the types of annular ligament constriction, two horses in another study had deep digital flexor tendinitis and annular ligament desmitis. In both horses this was secondary to a septic digital sheath tenosynovitis.

Sonographic findings in horses with annular ligament desmitis include a marked thickening of the annular ligament with a decrease in the echogenicity of the annular ligament and marked periligamentous swelling. Palmar or plantar-to-dorsal measurements of the thickness of the annular ligament of 3 to 15 mm have been reported for horses with annular ligament desmitis.[59] The fiber pattern of the annular ligament is also disrupted (see Figs. 3-126 and 3-127). In horses with primary annular ligament desmitis, the digital sheath is normal. In several horses with primary annular ligament desmitis, digital sheath tenosynovitis developed within 4 to 8 weeks after the original injury to the annular ligament. In most horses, annular ligament desmitis develops simultaneously with digital sheath tenosynovitis (Fig. 3-131). As the acute annular ligament desmitis resolves, the hypoechoic to anechoic thickening of the ligament is replaced by a more echogenic thickening, consistent with chronic annular ligament desmitis.

Desmitis of the proximal digital annular ligament or constriction of the proximal digital annular ligament has been reported infrequently.[59, 69] Affected horses were chronically lame (moderate to severe lameness). The lameness did not improve with rest and worsened with exercise. The lameness did not respond to a palmar digital nerve block in the distal pastern region, but did improve markedly with either a base sesamoid block or intrasynovial anesthesia of the digital sheath. Distention of the palmar pouch of the digital sheath was present in each horse, in addition to subtle digital sheath distention proximal to the fetlock annular ligament. Marked thickening of the proximal digital annular ligament and skin, with distention of the digital sheath, was present in all horses. The combined structures measured 4 to 5 mm in thickness with only one horse having synovial proliferation visible within the digital sheath.[69]

Injuries to the superficial digital flexor tendon have also been reported in horses with constriction of the proximal palmar annular ligament (Fig. 3-132).[59] Proximal palmar annular ligament constriction may occur as a sequel to septic tenosynovitis of the digital sheath.[59]

Superior Check Ligament Desmitis. Injuries to the superior check ligament have been infrequently reported.[73, 86, 133] With the advent of diagnostic ultrasonography, more injuries to the superior check ligament (increased size, abnormal shape, decreased echogenicity, and areas of fiber tearing) may be diagnosed (Fig. 3-133). Injuries to the superior check ligament were reported in 32% of horses in which an ultrasound examination of the carpal canal was performed because of findings during lameness examination or diagnostic nerve blocks.[73] The injury was primarily diagnosed in high-performance horses; the majority were racehorses or sport horses. Thickening of the superior check ligament, decreased echogenicity, and alteration of the normal fiber pattern were found in these horses and in a previous study.[86] Injury to the superior check ligament was accompanied by injury to one or more structures in the carpal canal. The associated carpal canal injuries included effusion

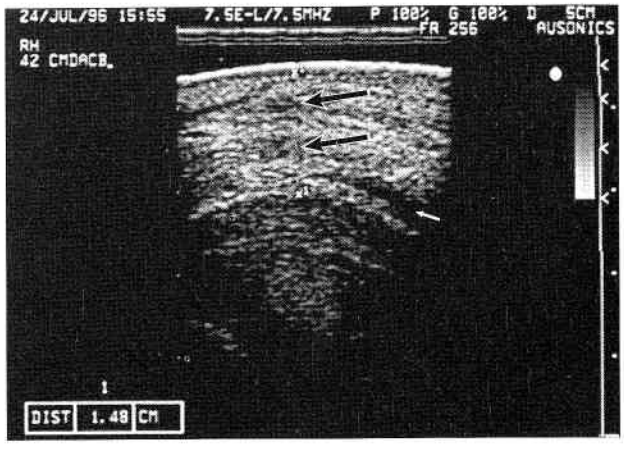

Figure 3–131

Sonogram of an acute annular ligament desmitis and digital sheath tenosynovitis in the right hindlimb, obtained from a 4-year-old Thoroughbred gelding at 42 cm distal to the point of the hock (zone 4B). Notice the marked thickening of these structures combined (1.48 cm) and the hypoechoic areas within the annular ligament (most plantar-*black arrow*) and the digital sheath (more dorsal-*black arrow*) in zone 4C. A small anechoic effusion is also present within the digital sheath *(white arrow)*. This sonogram was obtained with a wide-bandwidth 7.5-MHz linear-array transducer operating at 7.5 MHz using a hand-held standoff pad at a displayed depth of 5 cm. The focal zones are positioned in the near field. The right side of the transverse view is lateral and the left side is medial.

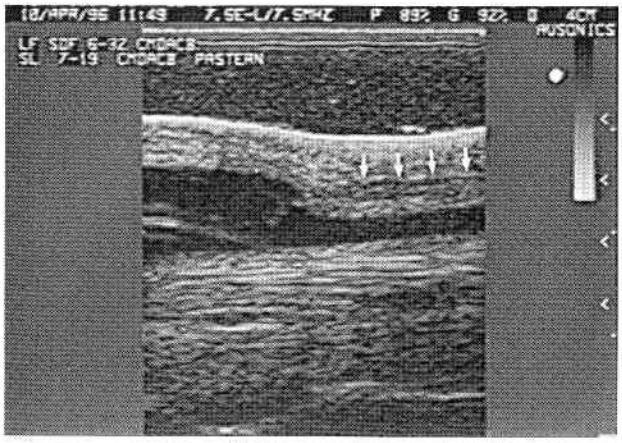

Figure 3–132

Sonogram of a desmitis involving the proximal digital annular ligament, obtained from a 5-year-old Standardbred stallion with concurrent superficial digital flexor tendinitis and suspensory ligament desmitis in the left foreleg. Notice the thickening of the proximal digital annular ligament *(arrows)*, the anechoic fluid containing hypoechoic fibrin within the digital sheath, and the distention of the digital sheath distal to the proximal digital annular ligament in zone P2. This sonogram was obtained with a wide-bandwidth 7.5-MHz linear-array transducer operating at 7.5 MHz using a hand-held standoff pad at a displayed depth of 4 cm. The focal zones are positioned in the near field. The right side of the sagittal view is proximal and the left side is distal.

within the carpal sheath, tendinitis of the superficial digital flexor tendon (see Fig. 3-133), distention or thickening of the retinaculum flexorum, tenosynovitis of the flexor carpi radialis tendon sheath, or proximal third interosseous muscle (suspensory ligament) injury. Horses with carpal sheath tenosynovitis or proximal tendinitis of the superficial digital flexor tendon, or those that "block out" in the proximal metacarpal region without having local radiographic or ultrasonographic abnormalities should be evaluated for injury to the superior check ligament.

Bicipital Tendinitis. Horses with bicipital tendinitis usually have lameness that varies in severity but is characterized by a shortened anterior phase of the stride. Hypoechoic to anechoic areas imaged within the tendon and loss of the normal fiber pattern have been diagnosed sonographically in several horses with tendinitis of the bicipital tendon.[70, 84, 88, 140] Bicipital tendinitis is usually seen in conjunction with bicipital bursitis and is covered in detail in that section.

Extensor Tendon Injuries. Extensor tendon injuries occur infrequently in horses and are usually trauma-related rather than performance-related. Tenosynovitis of the extensor tendon sheaths is much more common than injury to the extensor tendons themselves. Injuries to the extensor tendons in the forelimbs are most common over the dorsal aspect of the carpus. In the hindlimb, they are most common over the dorsal aspect of the metatarsus. Swelling of the affected tendon is the most common clinical sign, with local heat and sensitivity occurring less frequently. Lameness is uncommon unless extensor tendon rupture has occurred. Extensor tendon injuries rarely limit function unless the entire extensor tendon is severed. In these instances, the horse has difficulty advancing the limb during the anterior phase of the stride.

Tendinitis involving the extensor tendons appears similar ultrasonographically to that involving the flexor tendons. Most frequently, mild increases in tendon cross-sectional area are detected, with a decrease in tendon echogenicity, fluid separation of linear echoes, and no visible areas of fiber tearing (Fig. 3-134). Areas of fiber tearing are more often diffuse (Fig. 3-135), secondary to

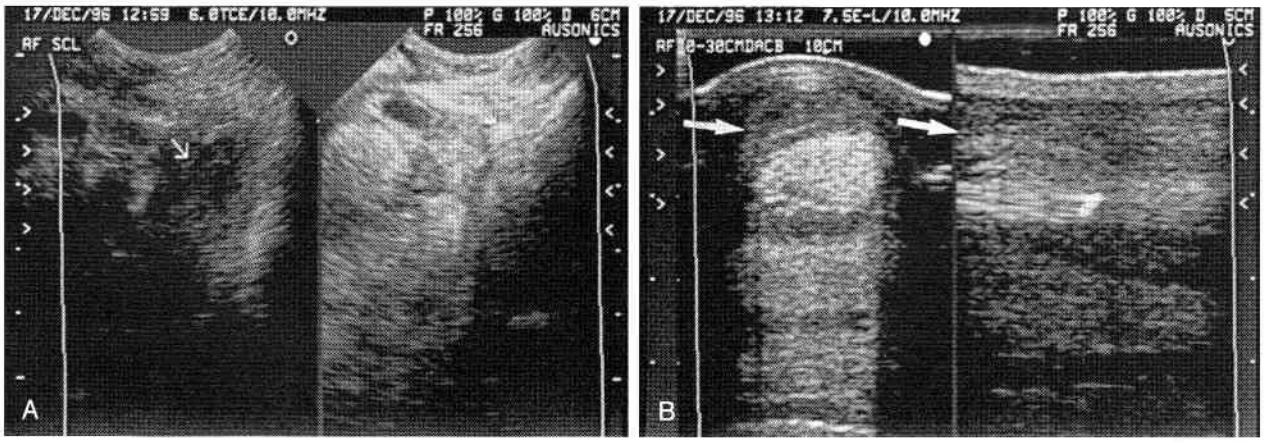

Figure 3–133

Sonograms of the superior check ligament and superficial digital flexor tendon obtained from a 15-year-old Thoroughbred gelding with a severe superficial digital flexor tendinitis and superior check ligament desmitis in the right foreleg. These sonograms were obtained with a wide-bandwidth 6.0-MHz microconvex linear-array transducer *(A)* or a wide-bandwidth 7.5-MHz linear-array transducer operating at 10.0 MHz using a hand-held standoff pad *(B)* at a displayed depth of 6 cm *(A)* and 5 cm *(B)*.

A, Transverse sonograms of the right fore superior check ligament *(left image)* compared to the normal superior check ligament in the left forelimb. The medial border of the superior check ligament is delineated with the arrow. Notice the anechoic lesion occupying most of the check ligament in its mid body which was continuous with a ruptured superficial digital flexor tendon at the musculotendinous junction that extended distally into the carpal canal and into the proximal metacarpal region. The right side of these sonograms is cranial and the left side is caudal.

B, The superficial digital flexor tendon *(arrows)* is completely hypoechoic in the transverse *(left image)* and sagittal veiws with no visible intact fibers in the sagittal view. The horse's fetlock dropped with weight-bearing due to the complete rupture of the superficial digital flexor tendon.

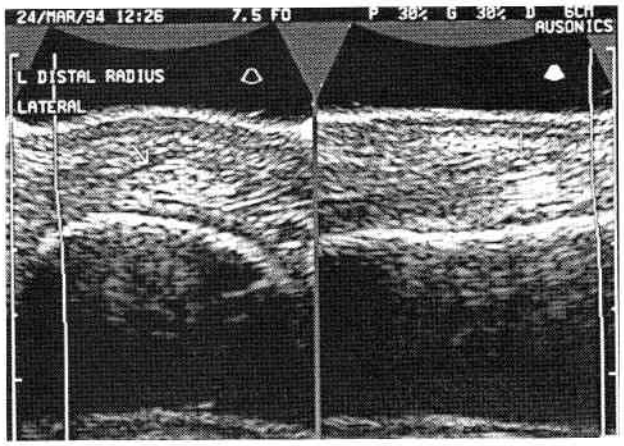

Figure 3–134

Sonograms of a mild tendinitis of the lateral digital extensor tendon in the left foreleg obtained from an 8-year-old Thoroughbred cross gelding. Notice the mild thickening of the lateral digital extensor tendon *(arrows)*, the somewhat heterogeneous hypoechoic appearance of the tendon, and the mild thickening of the surrounding tendon sheath. The amount of subcutaneous soft tissue swelling over the tendon is also increased. These sonograms were obtained with a 7.5-MHz sector-scanner transducer containing a built-in fluid offset at a displayed depth of 6 cm. The right side of the transverse view *(left image)* is lateral and the left side is medial. The right side of the sagittal view *(right image)* is proximal and the left side is distal.

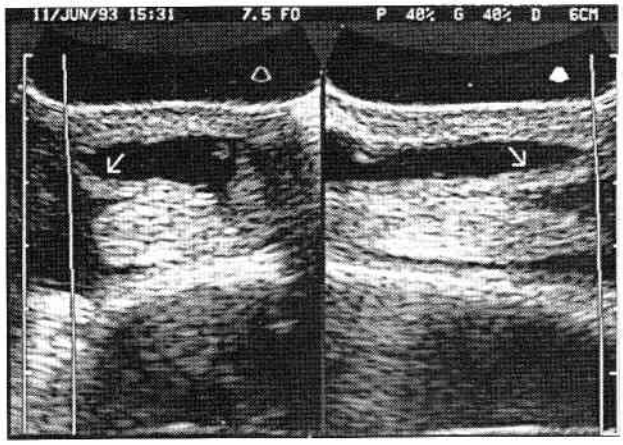

Figure 3–136

Sonograms of a moderate lateral digital extensor (LDE) tendinitis in the left foreleg, obtained from a 10-year-old Appaloosa gelding with an associated tenosynovitis of the extensor tendon sheath. The LDE tendon is enlarged, heterogeneous, and hypoechoic and has some disruption of its normal linear fiber pattern. The arrows point to a normal synovial reflection (attachment of the tendon to its sheath), although this attachment is thicker and more hypoechoic than normal. The effusion is anechoic but fibrinous; amorphous hypoechoic structures are imaged in the transverse view, representing fibrin clots *(arrows)*. These sonograms were obtained with a 7.5-MHz sector-scanner transducer containing a built-in fluid offset at a displayed depth of 6 cm. The right side of the transverse view *(left image)* is lateral and the left side is medial. The right side of the sagittal view *(right image)* is proximal and the left side is distal.

local trauma, rather than appearing as a discrete core lesion. Effusions are often present if the area of the tendon injured is contained within a tendon sheath (Fig. 3-136). Peritendinous soft tissue swelling is often marked because local trauma is the most common cause of these injuries. Complete ruptures of the extensor tendons do occur, most commonly in neonatal foals. Lacerations are a more common cause of extensor tendon disease; the severity of disease depends on the extent of the original laceration. Healing of extensor tendon injuries should follow a similar sonographic pattern to that of flexor tendon injuries.

Superficial Digital Flexor Tendon in the Crus. Injuries to the superficial digital flexor tendon are rare in this portion of the hindlimb. They occur most frequently with trauma to the crus. Areas of fiber disruption can be imaged in the superficial digital flexor tendon in the crus (Fig. 3-137), with or without injuries to the gastrocne-

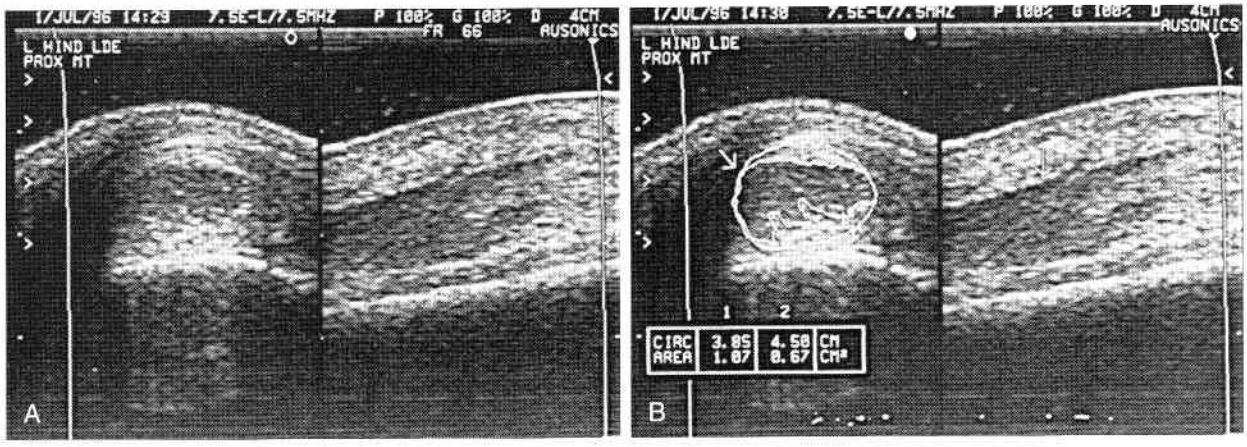

Figure 3–135

Sonograms of a severe tendinitis in the long digital extensor tendon (LDE) in the left hindleg, obtained from a 3-year-old Thoroughbred gelding in the proximal metatarsal region. These sonograms were obtained with a wide-bandwidth 7.5-MHz linear-array transducer operating at 7.5 MHz with a hand-held standoff pad at a displayed depth of 4 cm. The focal zones are positioned in the near field. The right side of the transverse views *(left images)* is lateral and the left side is medial. The right side of the sagittal views *(right images)* is proximal and the left side is distal.

A, Notice the marked enlargement of the LDE, the large hypoechoic lesion, and the complete loss of any fibers in the area of the lesion.

B, The area of fiber disruption involved 62.6% of the LDE at this level (0.67 cm^2/1.07 cm^2) and distally involved the entire cross-sectional area of the tendon.

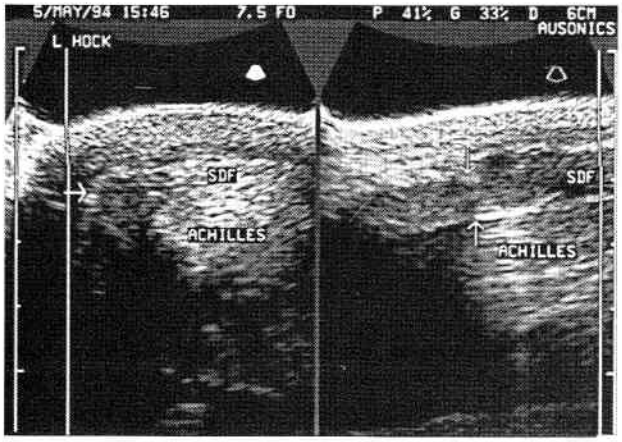

Figure 3–137

Sonograms of an area of fiber disruption in the medial portion of the superficial digital flexor tendon (SDF) in the distal aspect of the crus near the point of the hock in the left hind leg, obtained from a 12-year-old Standardbred gelding. Notice the large hypoechoic core lesion *(horizontal arrow)* in the medial aspect of the SDF in the transverse view *(left image)* and the complete loss of normal fibers in this region *(vertical arrows)* in the sagittal view *(right image)*. These sonograms were obtained with a 7.5-MHz sector scanner transducer containing a built-in fluid offset at a displayed depth of 6 cm. The right side of the transverse image is lateral and the left side is medial. The right side of the sagittal image is proximal and the left side is distal.

mius tendon. Rupture of the superficial digital flexor tendon from its attachment to the tuber calcis with lateral luxation of the tendon occurs infrequently but has been confirmed sonographically.

Gastrocnemius Tendinitis. Gastrocnemius tendinitis occurs infrequently in all types of performance horses. Clinical signs include swelling in the distal aspect of the crus, local heat and sensitivity, and lameness. A capped-hock appearance may also be present in some horses.[64] The lameness may range from mild to severe and consists of a shortened cranial phase of the stride and a lowered arc of foot flight.[64] In some affected horses, a reduced duration of weight bearing in the caudal phase of the stride is also present. Some affected horses are reluctant to place the heel of the foot on the ground when walking. Lameness is accentuated by flexion of the limb and improves with perineural analgesia of the tibial and fibular nerves or the tibial nerve alone.[64] Similar findings have been reported in horses with common calcaneal tendinitis.[65]

Sonographic findings include enlargement of the cross-sectional area of the gastrocnemius tendon, hypoechoic to anechoic areas within the gastrocnemius tendon, and loss of normal fiber alignment (Fig. 3-138). Diffuse areas of fiber damage have been detected in affected horses more frequently than have focal areas of injury to the gastrocnemius tendon (Fig. 3-139). In several horses, the margins of the gastrocnemius tendon were poorly defined.[64] In one horse, a concurrent focal decrease in echogenicity in the superficial digital flexor tendon was detected immediately distal to the tarsus. In the majority of horses, however, gastrocnemius tendinitis occurs without concurrent tendinous or ligamentous injury. The ultrasonographic diagnosis of tendinitis of the equine common calcaneal tendon has also been reported.[65] Calcaneal bursitis may be concurrent with gastrocnemius tendinitis (see Figs. 3-138 and 3-139) and has been documented sonographically in several horses.[64, 68] Rupture of the gastrocnemius tendon, although not reported sonographically, has been reported in horses and should be easily documented ultrasonographically.[134] Rupture of the gastrocnemius muscle has been reported in several foals with no report of concurrent gastrocnemius tendinitis.[135]

In humans, ultrasonography has been used successfully to document complete and partial rupture of the Achilles

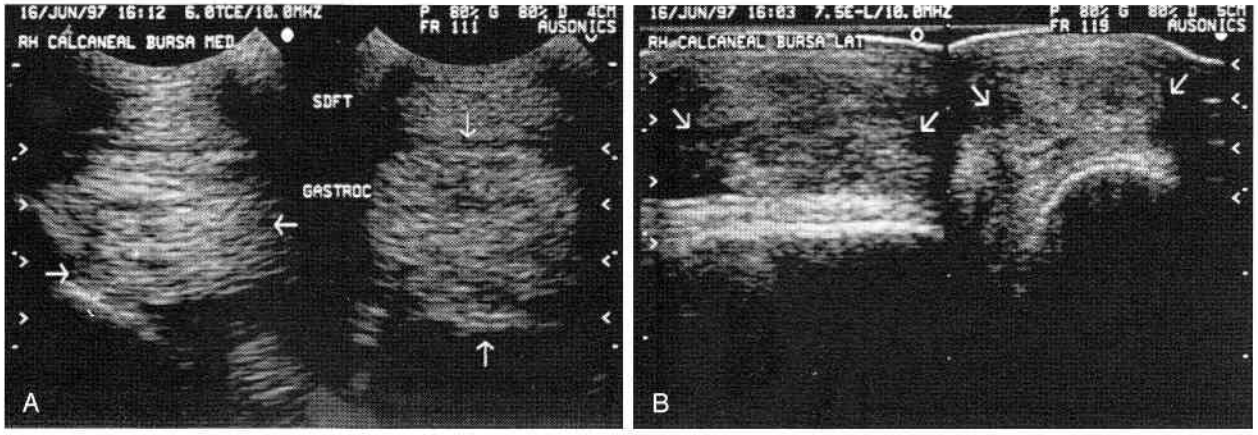

Figure 3–138

Sonograms of a gastrocnemius (gastroc) tendinitis and calcaneal bursitis in the right hind leg obtained from a yearling Arabian colt. These sonograms were obtained with a wide-bandwidth 6.0-MHz microconvex linear-array transducer *(A)* and a wide-bandwidth 7.5-MHz linear-array transducer *(B)* operating at 10.0 MHz using a hand-held standoff pad *(B)* at a displayed depth of 4 cm *(A)* and 5 cm *(B)*. The right side of the transverse views *(right images)* is lateral *(A)* and cranial *(B)* and the left side is medial *(A)* and caudal *(B)*. The right side of the sagittal views *(left images)* is proximal and the left side is distal.

A, There are several anechoic areas of fiber tearing with loss of the normal fiber alignment imaged within the gastrocnemius tendon *(arrows)* consistent with significant gastrocnemius tendinitis. The gastrocnemius tendon is enlarged. The overlying superficial digital flexor tendon (SDFT) is also mildly enlarged, slightly hypoechoic, and has some loss of the normal fiber pattern, consistent with a mild superficial digital flexor tendinitis.

B, The calcaneal bursa is distended along the lateral aspect of the crus and contains large amounts of hypoechoic fibrin *(arrows)*.

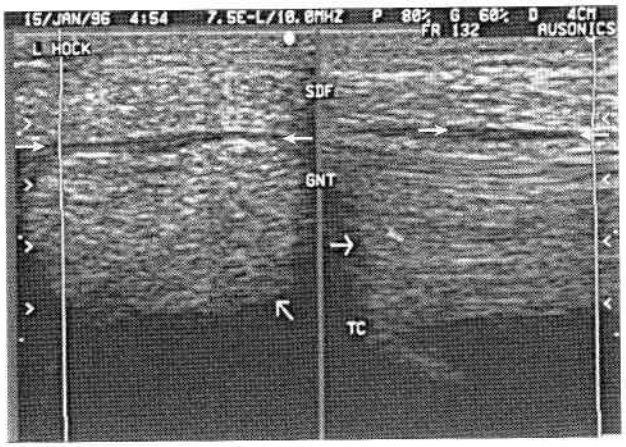

Figure 3–139

Sonograms of a gastrocnemius tendinitis in the left hindlimb, obtained from an 8-year-old Quarter horse gelding. Notice the enlargement of the gastrocnemius tendon (GNT), its heterogeneous hypoechoic appearance *(angled arrow)*, (best seen in the transverse view), and the mild fiber disruption *(horizontal arrow)* imaged in the sagittal view. The amount of anechoic fluid *(small arrows)* imaged in the calcaneal bursa is mildly increased consistent with a calcaneal bursitis. A larger quantity of fluid was imaged medial and lateral to the GNT. These sonograms were obtained with a wide-bandwidth 7.5-MHz linear-array transducer operating at 10.0 MHz using a hand-held standoff pad at a displayed depth of 4 cm. The right side of the transverse view *(left image)* is lateral and the left side is medial. The right side of the sagittal view *(right image)* is proximal and the left side is distal.

tendon.[136, 137] A sensitivity of 0.94 and a specificity of 1.00 with an overall accuracy of 0.95 for ultrasonographic diagnosis of Achilles tendinitis were found in one study of humans with partial rupture of the Achilles tendon.[137] In this study, the ultrasonographic findings were confirmed at surgery. In a few patients, histopathologic confirmation was also obtained from excised tendon material obtained at surgery. The sonographic findings consistent with a diagnosis of partial rupture of the Achilles tendon included discontinuity of tendon fibers, localized tendon swelling, and focal sonolucencies.[136, 137] Sonolucent thickening of the paratenon was detected in some patients at the level of the partial rupture. In this study, bursitis was also frequently found in patients with partial tears of the distal portion of the Achilles tendon. Ultrasonography has also been used successfully in humans to differentiate complete and partial rupture of the Achilles tendon, subachilles bursitis, and peritendinitis.[136]

As the tendon heals, its cross-sectional area should decrease, the echogenicity of the lesion should increase, and the fiber alignment should improve. However, little change was reported in the ultrasonographic appearance of gastrocnemius tendinitis in follow-up examinations of five affected horses performed 2 to 3 months after their initial sonographic examinations.[64] Sonographic examination at a later date would probably show improvement; the original areas of injury in three of these horses were severe. Sonographic evidence of tendon healing was detected in the horse with tendinitis of the common calcaneal tendon.[65]

Peroneus Tertius Tendinitis and Rupture. Peroneus tertius tendinitis and rupture of the peroneus tertius tendon occur in all types of performance horses. This injury results from hyperflexion of the hindlimb, such as may occur if the horse gets trapped in a bog and tries to propel itself out. The clinical signs of a rupture of the peroneus tertius tendon are dramatic. The affected horse is able to flex the stifle and extend the hock simultaneously. Swelling is characteristically detected in the peroneus tertius tendon, most frequently over the mid-tibial region but also over the dorsal aspect of the hock. Local heat and sensitivity may also be detected when the injury is acute. The horse's gait is abnormal.

Ultrasonographically, the peroneus tertius tendon has an enlarged cross-sectional area with decreased tendon echogenicity and separation of linear echoes when a tendinitis is present (Fig. 3-140) with tendon rupture. More commonly, large areas of the peroneus tertius tendon are hypoechoic to anechoic and completely lacking in tendon fibers, consistent with complete rupture (Fig. 3-141). Large segments of the peroneus tertius tendon are often damaged. Peritendinous soft tissue swelling is also usually detected after the acute injury. The mid-tibial portion of the peroneus tertius tendon is usually the area of most severe injury, but ruptures near or at the insertion (Fig. 3-142) or at the origin, in conjunction with avulsion fractures (Fig. 3-143), do occur. Avulsion fractures can occur without significant injury to the peroneus tertius tendon. More commonly, however, avulsion fractures at the origin of the peroneus tertius tendon are associated with a large area of tendon fiber disruption, beginning at the site of the avulsion (see Fig. 3-143).

In one report of peroneus tertius tendon rupture in the horse, the peroneus tertius tendon appeared markedly thinner than normal when scanned 3 months after injury.[68] Increased echogenicity of the adjacent cranial tibial and long digital extensor muscles was imaged, consistent with muscular fibrosis. The author of this report

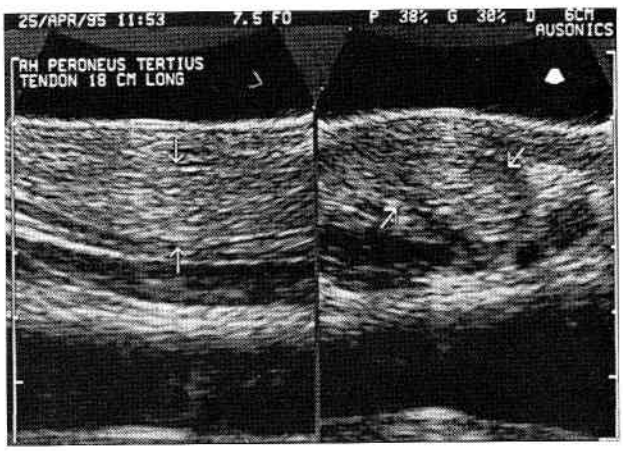

Figure 3–140

Sonograms of a severe peroneus tertius tendinitis with diffuse fiber injury to the entire cross-sectional area of the peroneus tertius tendon in the right hindlimb, obtained from a 4-year-old Tennessee Walking horse gelding. Notice the enlarged, hypoechoic peroneus tertius tendon and the loss of the normal fiber pattern *(arrows)*. These sonograms were obtained with a 7.5-MHz sector-scanner transducer containing a built-in fluid offset at a displayed depth of 6 cm. The right side of the transverse view *(right image)* is lateral and the left side is medial. The right side of the sagittal view *(left image)* is proximal and the left side is distal.

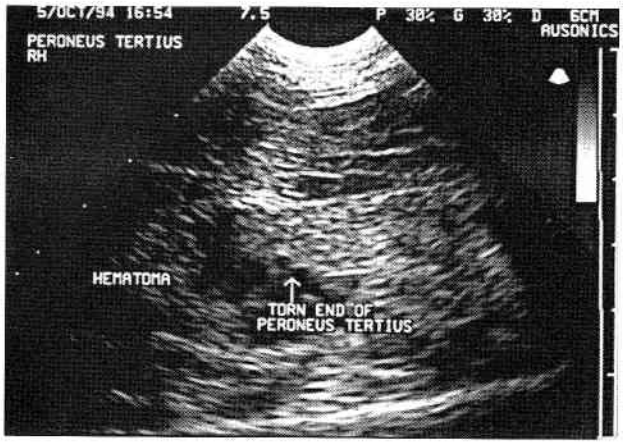

Figure 3–141

Sonogram of a ruptured peroneus tertius tendon in the right hindlimb, obtained from a 6-year-old Thoroughbred gelding. Notice the free proximal end of the peroneus tertius tendon *(arrow)* adjacent to a large anechoic and hypoechoic amorphous structure consistent with a hematoma. This sonogram was obtained with a 7.5-MHz sector-scanner transducer at a displayed depth of 6 cm. The right side of this sagittal sonogram is proximal and the left side is distal.

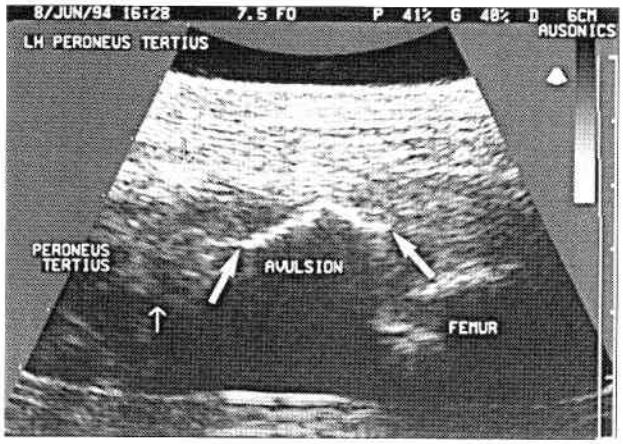

Figure 3–143

Sonogram of a ruptured peroneus tertius tendon associated with an avulsion fracture of the origin of the peroneus tertius tendon in the left hindlimb, obtained from a 5-year-old Thoroughbred gelding. Notice the large hyperechoic bone fragment distracted distally from the distal femur *(large arrows)* and the hypoechoic to anechoic appearance of the adjacent peroneus tertius tendon, completely lacking in any normal fibers *(small arrow)*. This sonogram was obtained with a 7.5-MHz sector-scanner transducer containing a built-in fluid offset at a displayed depth of 6 cm. The right side of this sagittal sonogram is proximal and the left side is distal.

suggested that recovery from rupture of the peroneus tertius tendon may occur, not from repair of the tendon itself, but rather from hypertrophy of the surrounding muscles.[68] This has not been the case in my experience. Sonographic repair of the peroneus tertius tendon occurs as in other tendons, with the area of injury initially filling in with hypoechoic tissue. This area of fiber injury then gradually becomes more echogenic and develops a random fiber pattern as the repair progresses. Occasionally, horses have areas of calcification detected in the peroneus tertius tendon that might predispose this tendon to reinjury (Fig. 3-144). Laceration of the peroneus tertius tendon can also occur with a laceration over the dorsal aspect of the hock or the dorsal aspect of the tibia.

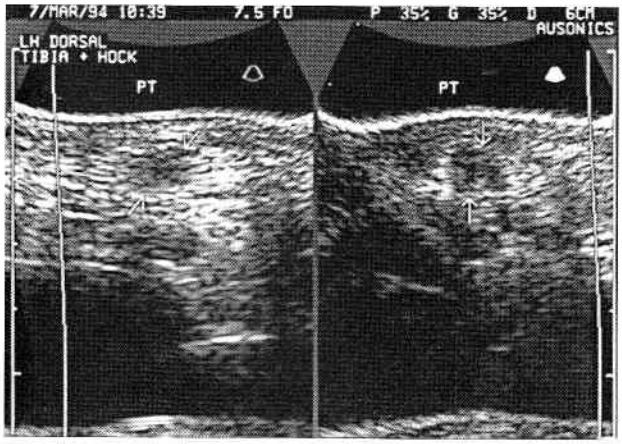

Figure 3–142

Sonograms of a ruptured peroneus tertius (PT) tendon near its insertion in the left hindlimb, obtained from an 18-year-old Thoroughbred cross mare. Notice the anechoic core lesion *(arrows)* in the medial branch of the peroneus tertius tendon as it extends over the dorsal aspect of the hock. These sonograms were obtained with a 7.5-MHz sector-scanner transducer containing a built-in fluid offset at a displayed depth of 6 cm. The right side of the transverse view *(right image)* is lateral and the left side is medial. The right side of the sagittal view *(left image)* is proximal and the left side is distal.

Tibialis Cranialis and Cunean Tendinitis. Tendinitis of the cranialis tibialis tendon (Fig. 3-145) or the cunean tendon is uncommonly recognized. These tendons are subject to local trauma as they cross the dorsal aspect of the hock and lacerations in this region are likely to result in tendon injury.

Plantar Ligament Desmitis. With the advent of ultrasonography, swellings in the curb region, although defined as plantar ligament desmitis, are rarely associated with damage to the plantar ligament. Decreased echogenicity of the plantar ligament and separation of the fiber bundles may be imaged in horses with plantar ligament desmitis (Fig. 3-146). Discrete areas of fiber injury or core lesions rarely occur in the plantar ligament (Fig. 3-147). Injuries to the superficial digital flexor tendon in this region are the most common tendinous or ligamentous cause for swelling along the plantar aspect of the hock (see Figs. 3-61 and 3-70). Soft tissue swelling, in the absence of injury to any of the tendinous or ligamentous structures, is also a common reason for swelling along the plantar aspect of the hock (Fig. 3-148). Calcification of the plantar ligament has been detected sonographically in one horse with a chronic plantar ligament desmitis (Fig. 3-149). Plantar ligament desmitis appeared as a small hypoechoic defect in the plantar ligament of a horse with subcutaneous thickening consistent with fibrosis in the plantar aspect of the tarsus.[68] A subcutaneous hematoma, which appeared as an encapsulated fluid-filled structure ultrasonographically, has occurred with swelling in the curb region.[68]

The Back. Ultrasonographic examination of the soft tissue and bony structures of the back should be only one part of a comprehensive examination of horses with

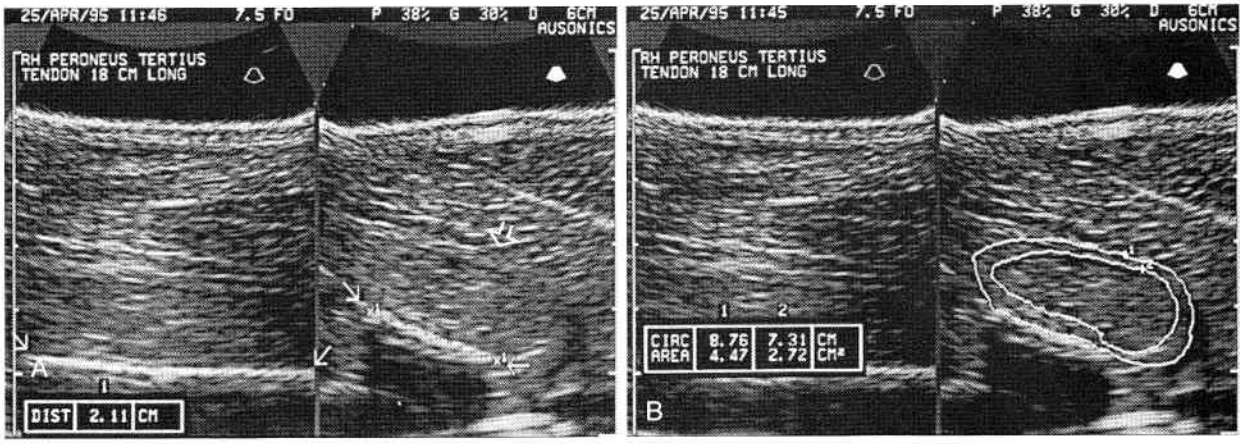

Figure 3–144

Sonograms of a ruptured peroneus tertius tendon with a large area of calcification along the caudal margin of the tendon in the right hindlimb, obtained from a 4-year-old Tennessee Walking horse gelding (same horse as in Fig. 3-140). These sonograms were obtained with a 7.5-MHz sector-scanner transducer containing a built-in fluid offset at a displayed depth of 6 cm. The right side of the transverse views *(right images)* is lateral and the left side is medial. The right side of the sagittal views *(left images)* is proximal and the left side is distal.

A, Notice the hyperechoic linear structure casting a strong acoustic shadow *(arrows)* that measures 2.11 cm in a lateral to medial direction and 18 cm long in a proximal to distal direction. Notice the enlarged hypoechoic peroneus tertius tendon lacking a normal fiber pattern cranial to the area of calcification *(open arrow)*.

B, The entire cross-sectional area of the peroneus tertius tendon measured 4.47 cm^2. A small rim of more normal, although hypoechoic, fibers are imaged surrounding the entire damaged portion of the tendon, yielding an injury of 60.85% (2.72 cm^2/4.47 cm^2) at this level.

back problems. Overriding dorsal spinous processes can be diagnosed ultrasonographically, but their clinical significance is questionable. Local anesthesia and/or nuclear scintigraphy should be used to further establish the significance of overriding dorsal spinous processes detected ultrasonographically.

Injuries to the supraspinous ligament can be detected ultrasonographically and appear as hypoechoic areas within the supraspinous ligament with disruption of the normal fiber pattern. Hypoechoic areas have been most frequently reported in the deep and intermediate portion of the supraspinous ligament.[75] Enlargement of the supraspinous ligament and local soft tissue swelling are more likely with an acute injury, whereas the absence of these findings with an area of abnormal echogenicity in the supraspinous ligament may suggest chronic degenerative change. Injuries to the supraspinous ligament have been reported most frequently in the lumbar region and are

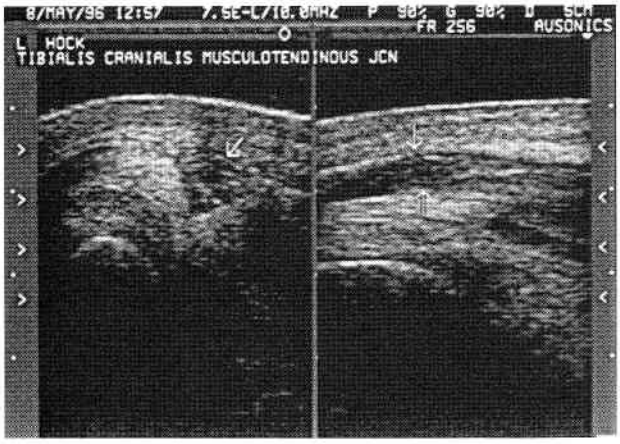

Figure 3–145

Sonograms of a ruptured tibialis cranialis tendon *(arrows)* at the musculotendinous junction in the left hind leg of a 6-year-old Thoroughbred gelding. Notice the anechoic tendon of the tibialis cranialis in the transverse view *(angled arrow)* adjacent to the medial branch of the normal peroneus tertius tendon. The tendon of the tibialis cranialis is mildly enlarged but is completely lacking in tendon fibers *(vertical arrows)* in the sagittal view. These sonograms were obtained with a wide-bandwidth 7.5-MHz linear-array transducer operating at 10.0 MHz with a hand-held standoff pad at a displayed depth of 5 cm. The focal zones are positioned in the near field. The right side of the transverse view *(left image)* is lateral and the left side is medial. The right side of the sagittal view *(right image)* is proximal and the left side is distal.

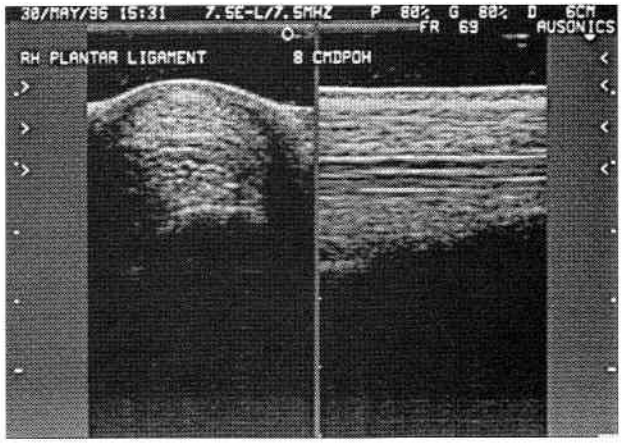

Figure 3–146

Sonograms of a mild plantar ligament desmitis in the right hindlimb, obtained from a 4-year-old Standardbred filly. Notice the hypoechoic heterogeneous appearance of the plantar ligament at 8 cm distal to the point of the hock and the slight fluid separation of fibers. These sonograms were obtained with a wide-bandwidth 7.5-MHz linear-array-transducer operating at 7.5 MHz with a hand-held standoff pad at a displayed depth of 6 cm. The focal zones are positioned in the near field. The right side of the transverse view *(left image)* is lateral and the left side is medial. The right side of the sagittal view *(right image)* is proximal and the left side is distal.

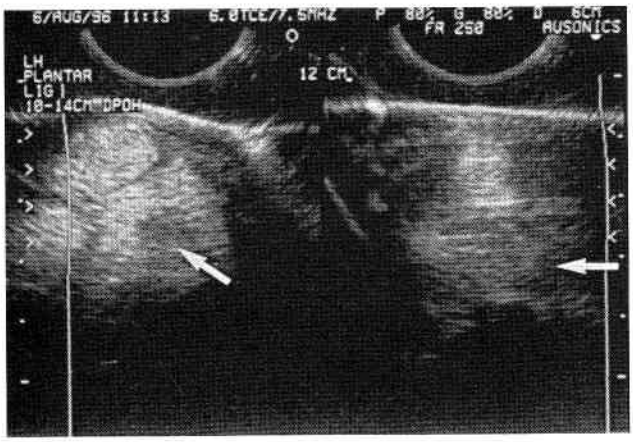

Figure 3–147

Sonograms of an acute plantar ligament desmitis obtained from a 13-year-old Thoroughbred gelding with swelling in the curb region from 10–14 cm distal to the point of the hock. There is a large hypoechoic core lesion in the dorsal portion of the plantar ligament near its insertion *(arrows)*. The superficial digital flexor tendon is plantar and medial to the plantar ligament and is imaged in both views. The deep digital flexor tendon is medial to the plantar ligament in the transverse view. These sonograms were obtained at 12 cm distal to the point of the hock with a wide-bandwidth 6.0-MHz microconvex linear-array transducer operating at 7.5 MHz using a hand-held standoff pad at a displayed depth of 6 cm. The right side of the transverse view *(left image)* is lateral and the left side is medial. The right side of the sagittal view *(right image)* is proximal and the left side is distal.

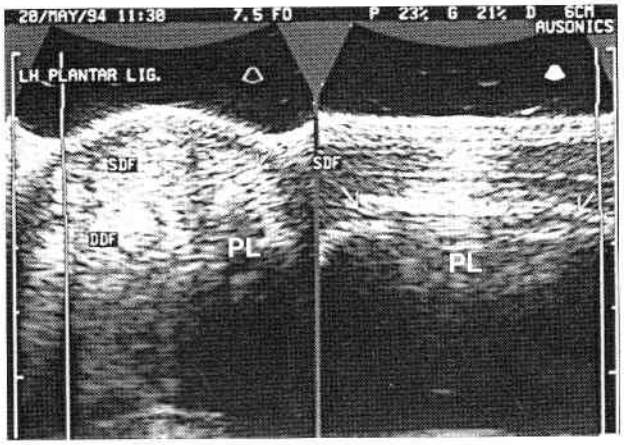

Figure 3–149

Sonograms of chronic plantar ligament desmitis with an area of calcification detected within the plantar ligament (PL) near its insertion in the left hindlimb, obtained from a 7-year-old Thoroughbred gelding. Notice the hyperechoic echoes *(arrows)* casting weak acoustic shadows in the body of the PL. The area of calcification is difficult to see in the transverse view *(left image)* because it is relatively small in this scan plane, but it is readily imaged in the sagittal view *(right image)*. These sonograms were obtained with a 7.5-MHz sector-scanner transducer containing a built-in fluid offset at a displayed depth of 6 cm. The right side of the transverse image is lateral and the left side is medial. The right side of the sagittal image is proximal and the left side is distal. SDF, superficial digital flexor tendon; DDF, deep digital flexor tendon.

associated with thickening of the ligament.[75] This thickening usually occurs at the level of, or at the caudal part of, the dorsal spinous processes.[75] Hyperechoic areas, with or without acoustic shadows, may be found at the dorsal limits of the interspinous spaces, consistent with a chronic desmopathy.[75]

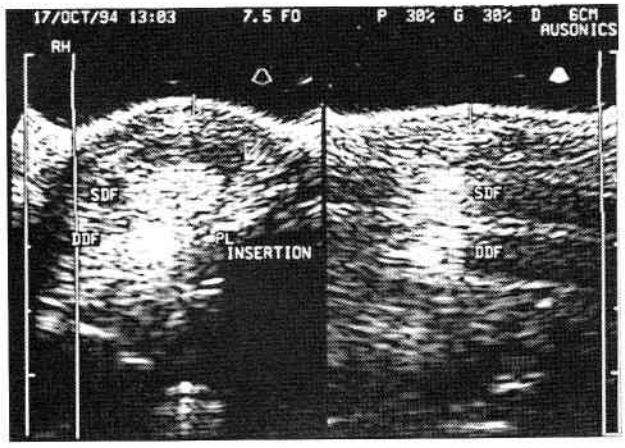

Figure 3–148

Sonograms of subcutaneous swelling over the plantar aspect of the right hock at the insertion of the plantar ligament (PL), obtained from a 3-year-old Standardbred filly. This swelling is often mistaken for a curb. Notice the hypoechoic fluid *(arrows)* over the plantar aspect of the superficial digital flexor tendon (SDF) extending over the plantar aspect of the tarsus. The SDF and deep digital flexor tendon (DDF) are normal. These sonograms were obtained with a 7.5-MHz sector-scanner transducer containing a built-in fluid offset at a displayed depth of 6 cm. The right side of the transverse view *(left image)* is lateral and the left side is medial. The right side of the sagittal view *(right image)* is proximal and the left side is distal.

Insertional desmopathy can be identified as bony irregularities at the supraspinous ligament insertion with changes in the ligament's echogenicity and fiber pattern.[75] Avulsion fractures of the insertion of the supraspinous ligament can also be identified as hyperechoic fragments distracted from the body of the dorsal spinous process. "False joints" may occur between dorsal spinous processes, and these may play a role in the back problems experienced by some horses (Fig. 3–150).[125] A large hyperechoic area casting a strong acoustic shadow was imaged in the nuchal portion of the supraspinous ligament in one older horse with bursitis in the region of the atlas (Fig. 3–151). Cartilaginous metaplasia was detected on postmortem examination of the supraspinous ligaments of two horses that had hypoechoic core lesions detected ultrasonographically.

Hypoechoic lesions may also be imaged in an enlarged sacroiliac ligament with loss of the normal fiber pattern. Although discrete hypoechoic areas have been imaged in the sacroiliac ligament, more diffuse hypoechoic enlargement of the dorsal sacroiliac ligament may be more common (Fig. 3–152). Enthesophyte formation may be present at the origin or insertion of the dorsal sacroiliac ligament (Fig. 3–153). Avulsion fractures from the tuber sacrale insertion have been imaged in a horse with desmitis of the dorsal sacroiliac ligament (see Fig. 3–152). These changes (enthesophyte formation and avulsion fractures) were more frequently observed at the tuber sacrale insertion than in the ligament itself.[75] Hyperechoic areas casting acoustic shadows have occasionally been imaged in the dorsal sacroiliac ligament, consistent with areas of calcification.[125] Ventral sacroiliac injuries were suspected when ventral periarticular remodeling of the

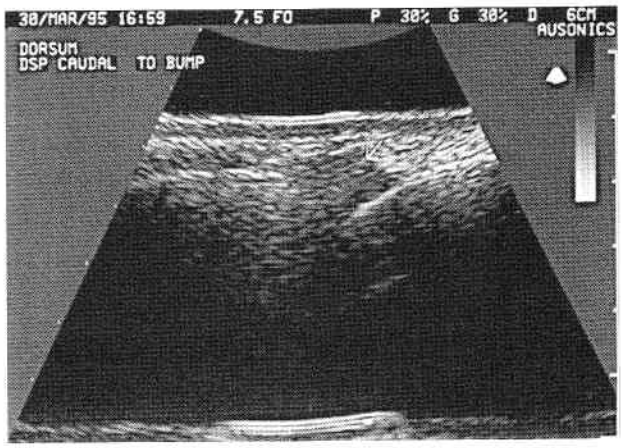

Figure 3–150

Sagittal sonograms of a desmitis of the supraspinous ligament and a "false joint" between the dorsal spinous processes, obtained from a 9-year-old Quarter horse mare. Notice the hypoechoic fluid bulging dorsally *(arrow)* between the two adjacent dorsal spinous processes, associated with the probable creation of a "false joint" between the two dorsal spinous processes. These sonograms were obtained with a 7.5-MHz sector-scanner transducer containing a built-in fluid offset at a displayed depth of 6 cm. The right side of the images is cranial and the left side is caudal.

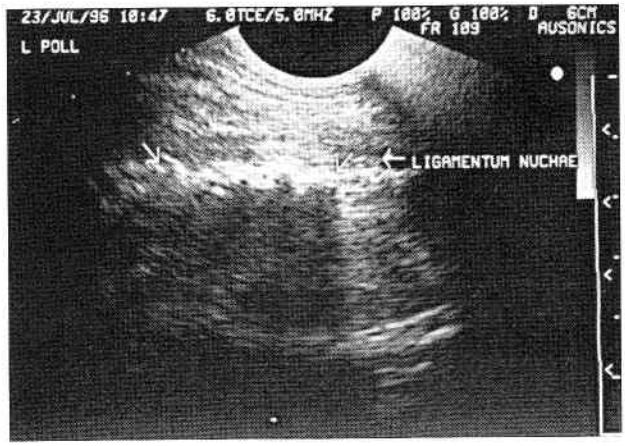

Figure 3–151

Sagittal sonogram of calcification within the dorsal portion of the ligamentum nuchae, obtained from a 30-year-old Appaloosa mare. Notice the thick irregular hyperechoic structure casting a strong acoustic shadow throughout the more dorsal portion of the ligamentum nuchae *(angled arrows)*. Some more normal fibers of the ligamentum nuchae can be imaged cranial to the ridge of calcification. This sonogram was obtained with a wide-bandwidth 6.0-MHz microconvex linear-array transducer operating at 5.0 MHz at a displayed depth of 6 cm. The focal zones are spread throughout the image. The right side of the image is cranial and the left side is caudal.

sacroiliac joint was observed when the relationship between the sacral wing and ilium was affected.

Careful sonographic evaluation of the back muscles may also yield abnormalities contributing to back soreness in horses. Diffuse areas of muscle swelling may be associated with myositis, but areas of muscle fiber tearing and hemorrhage can also occur in this region (Fig. 3-154).

Ultrasonographic Evaluation of Tenosynovitis and Bursitis

Most of the flexor and extensor tendons are surrounded by a tendon sheath in areas where they cross articulations. These tendon sheaths normally contain only small amounts of synovial fluid, and the amount varies from sheath to sheath. Horses with tenosynovitis usually have swelling of the affected tendon sheath, but local heat, sensitivity, and lameness are often lacking. If local heat, sensitivity, and lameness are severe, a septic process in the tendon sheath should be strongly considered. Similarly, the bursae are synovial structures between tendon or ligament and bone that normally contain only a minimal amount of synovial fluid. When the synovial bursa becomes inflamed, local swelling occurs with increased production of synovial fluid. Local heat, sensitivity, and lameness may or may not be present. If the clinical signs are severe, a septic bursitis must be considered. Sono-

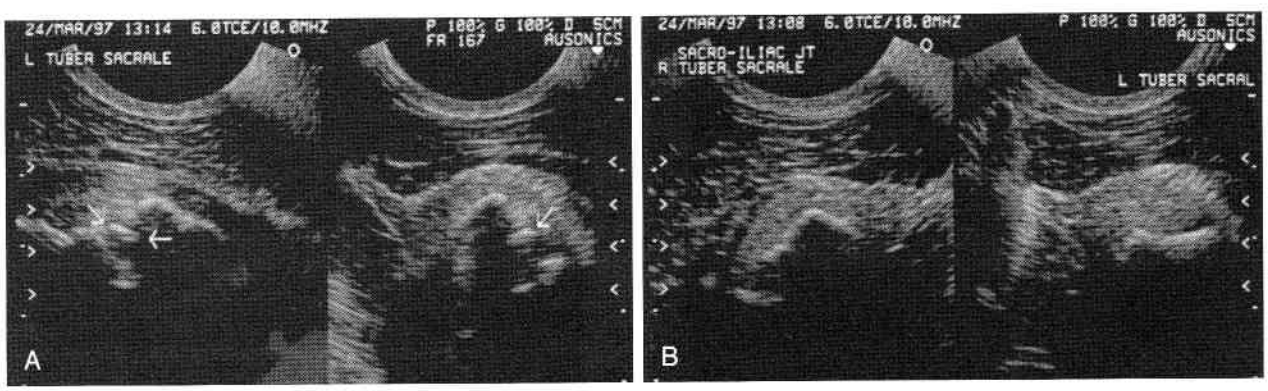

Figure 3–152

Sonograms of the sacroiliac joint obtained from a 5-year-old Thoroughbred gelding with a left sacroiliac luxation. These sonograms were obtained with a wide-bandwidth 6.0-MHz microconvex linear-array transducer operating at 10.0 MHz at a displayed depth of 5 cm.

A, There is an avulsion fracture fragment imaged associated with the insertion of the sacroiliac ligament on the tuber sacrale *(arrows)*. The sacroiliac ligament is slightly hypoechoic and is enlarged with slight fiber pattern disruption. The right side of the transverse view *(right image)* is to the left and the left side is toward the right side of the horse. The right side of the sagittal view *(left images)* is cranial and the left side is caudal.

B, The left sacroiliac ligament is markedly thicker than the right and is somewhat hypoechoic consistent with a chronic desmitis of the left sacroiliac ligament. The right side of the left tuber sacrale is to the left side of the horse and the right side of the right tuber sacrale is to the left side of the horse.

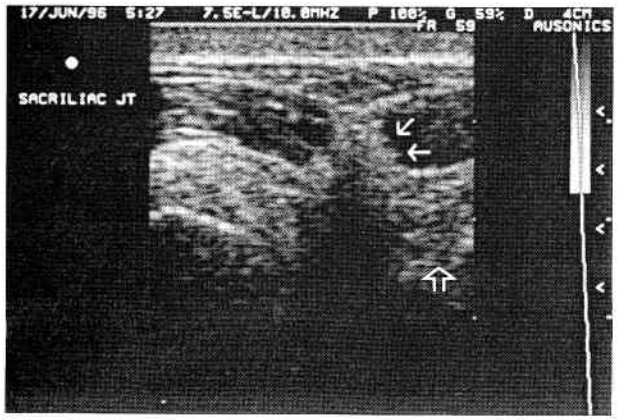

Figure 3–153

Transverse sonogram of a desmitis of the left sacroiliac ligament associated with a "hunter's bump," obtained from a 10-year-old Danish Warmblood gelding. Notice the thickened hypoechoic sacroiliac ligament *(open arrow)* and the enthesophyte formation *(small arrows)* along the left side of the tuber sacrale. This sonogram was obtained with a wide-bandwidth 7.5-MHz linear-array transducer operating at 10.0 MHz using a hand-held standoff pad at a displayed depth of 4 cm. The focal zones are positioned in the near field. The right side of the sonogram is the left side of the tuber sacrale and the left side is the right.

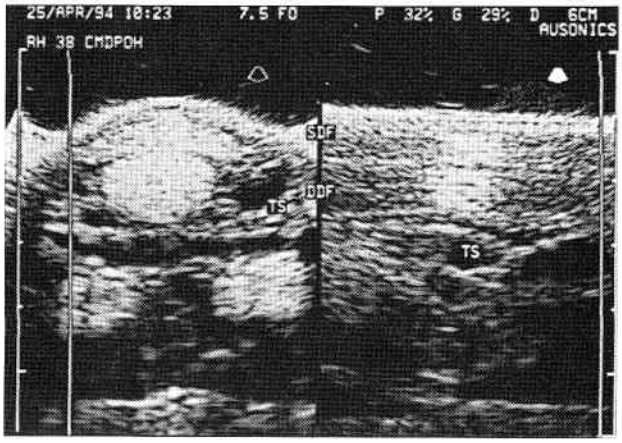

Figure 3–155

Sonograms of a digital sheath tenosynovitis in the right hindleg, obtained from a 9-year-old Thoroughbred gelding. Notice the mild to moderate distention of the digital sheath (TS) with anechoic fluid and fibrin in zone 4A at 38 cm distal to the point of the hock. The superficial (SDF) and deep digital flexor tendons (DDF) are normal. These sonograms were obtained with a 7.5-MHz sector-scanner transducer containing a built-in fluid offset at a displayed depth of 6 cm. The right side of the transverse view *(left image)* is lateral and the left side is medial. The right side of the sagittal view *(right image)* is proximal and the left side is distal.

graphic examination of the tendon sheath is useful in revealing effusion, synovial thickening, intrathecal adhesions, villonodular lesions, and calcification within the tendon sheath. It can also be used to differentiate a tenosynovitis from a perivaginal swelling.[42]

The mildest form of equine tenosynovitis or bursitis involves an increased amount of anechoic fluid visualized within the tendon sheath or bursa. This occurs most commonly in the digital sheath, causing "windpuffs" (Fig. 3-155). Normal mesotendinous attachments between the tendon and the sheath are imaged when an effusion is present; these should not be mistaken for adhesions within the tendon sheath. In the digital sheath, these normal attachments are imaged from the lateral and medial side of the deep digital flexor tendon above the fetlock joint (Figs. 3-155 and 3-156), and from the palmar or plantar aspect of the superficial digital flexor tendon in the region of the annular ligament. These attachments differ for each tendon sheath (see Fig. 3-136); therefore, a thorough understanding of the local anatomy is important to avoid a misinterpretation.

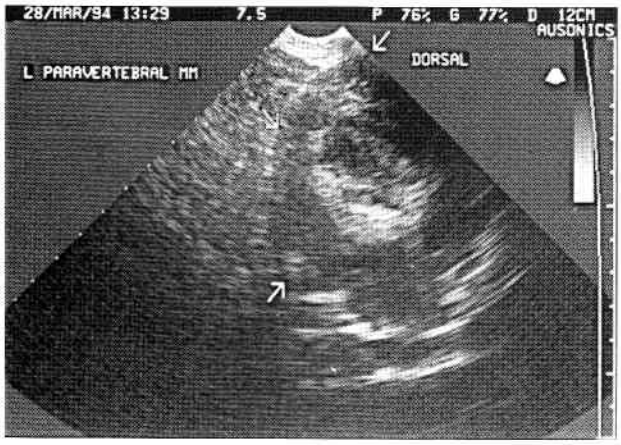

Figure 3–154

Transverse sonogram of a large hematoma in the left paravertebral muscles, obtained from an 18-year-old Thoroughbred mare. Notice the large area of muscle fiber disruption and internal fluid collection and loculation *(arrows)*. The unusual sonographic appearance of this mass (extensive muscle disruption and the appearance of a discrete complex mass) makes neoplasia a likely consideration. This area was confirmed histologically to represent a hematoma. This sonogram was obtained with a 7.5-MHz sector-scanner transducer at a displayed depth of 12 cm. The right side of this sonogram is dorsal.

Differentiating the tendon sheath from the annular ligament is difficult. In many instances, these two structures are evaluated together rather than separately. The tendon sheath itself may become thickened in horses with severe tenosynovitis (Figs. 3-156 and 3-157) and usually appears somewhat hypoechoic. The synovial lining of the tendon sheath or bursa may be thickened with more severe or chronic tenosynovitis or bursitis. Villonodular lesions (Fig. 3-158) are occasionally detected within the tendon sheath and may be a cause of lameness. Nodular masses detected with contrast radiography have been reported in the tarsal sheath.[116]

The fluid within the tendon sheath or bursa can be characterized ultrasonographically. An effusion that is clear and anechoic is most consistent with a nonseptic tenosynovitis or bursitis (Fig. 3-159). As the fluid becomes hypoechoic to echogenic, an increased cell count within the fluid and sepsis are likely (Fig. 3-160). The tendons contained within the tendon sheath should be carefully evaluated for any abnormalities, because septic tendinitis (Fig. 3-161) often occurs in horses with septic tenosynovitis, particularly that of the digital sheath. Horses with septic tendinitis usually have hypoechoic fluid within the tendon sheath and a hypoechoic, melting lesion in the affected tendon. Horses with acute septic

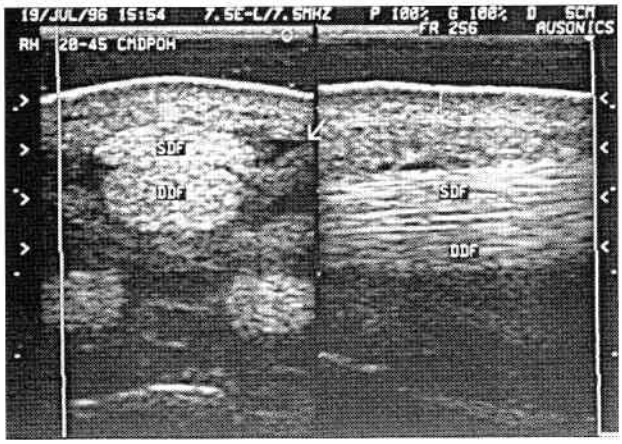

Figure 3–156

Sonograms of a chronic digital sheath tenosynovitis in the right hindlimb, obtained from an 18-year-old Arabian stallion. Notice the thickening of the digital sheath and the synovial lining *(vertical arrow)*, best visualized in the sagittal view *(right image)* along the plantar aspect of the superficial digital flexor tendon (SDF), and the thickening of the normal attachments between the tendon and the sheath *(diagonal arrow)* in the transverse view *(left image)* in zone 4A at 38 cm distal to the point of the hock. These normal attachments are also more hypoechoic than normal. A mild increase is present in the amount of fluid normally imaged within the digital sheath. These sonograms were obtained with a wide-bandwidth 7.5-MHz linear-array transducer operating at 7.5 MHz with a hand-held standoff pad at a displayed depth of 5 cm. The focal zones are positioned in the near field. The right side of the transverse image is lateral and the left side is medial. The right side of the sagittal image is proximal and the left side is distal. DDF, deep digital flexor tendon.

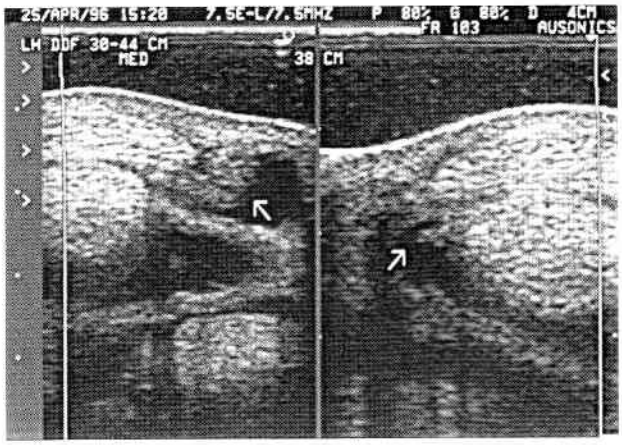

Figure 3–158

Transverse sonograms of a villonodular mass within the digital sheath in the left hind leg of an 18-year-old Warmblood mare. Notice the thickening of the tendon sheath surrounding the flexor tendons, the hypoechoic thickened synovial lining on the medial side of the superficial digital flexor tendon (SDF) *(diagonal arrow in the right image)* and the round villonodular lesion in the lateral aspect of the plantar and dorsal reflection of the digital sheath *(diagonal arrow in the left image)*. This horse also had a deep digital flexor (DDF) tendinitis imaged from 30 to 44 cm distal to the point of the hock. These sonograms were obtained in at 38 cm in zone 4A with a wide-bandwidth 7.5-MHz linear-array transducer operating at 7.5-MHz with a hand-held standoff pad at a displayed depth of 4 cm. The focal zones are positioned in the near field. The right side of the images is lateral and the left side is medial.

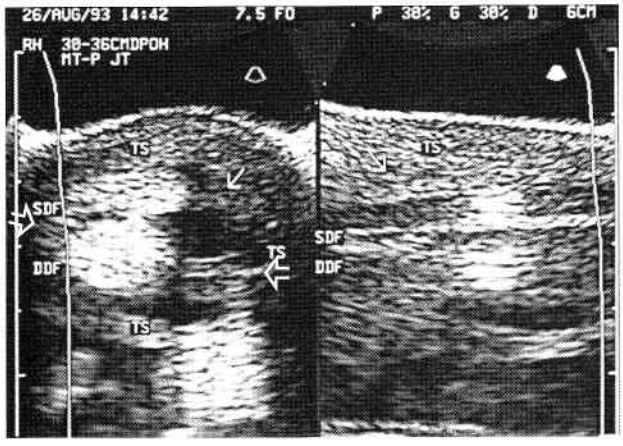

Figure 3–157

Sonograms of a chronic digital sheath tenosynovitis in the right hindlimb, obtained from an 11-year-old Dutch Warmblood gelding. Notice the thickening of the digital sheath (TS) surrounding the flexor tendons, the hypoechoic tissue extending from the tendon sheath to the lateral margin of the superficial digital flexor tendon (SDF) in the transverse view *(left image)*, which represents an adhesion between the SDF and the sheath *[diagonal arrow]*, the thickened normal attachment between the tendon and its sheath *(open arrow)*, and the increased amount of anechoic fluid within the tendon sheath. These sonograms were obtained in zone 4A at 38 cm distal to the point of the hock with a 7.5-MHz sector-scanner transducer containing a built-in fluid offset at a displayed depth of 6 cm. The right side of the transverse image is lateral and the left side is medial. The right side of the sagittal image *(right image)* is proximal and the left side is distal. DDF, deep digital flexor tendon.

tendinitis completely lack visible tendon fibers in the infected area of the tendon. Often, little or no enlargement of the affected tendon occurs, just an absence of tendon fibers in the affected portion of the tendon and replacement of these fibers with hypoechoic fluid. The

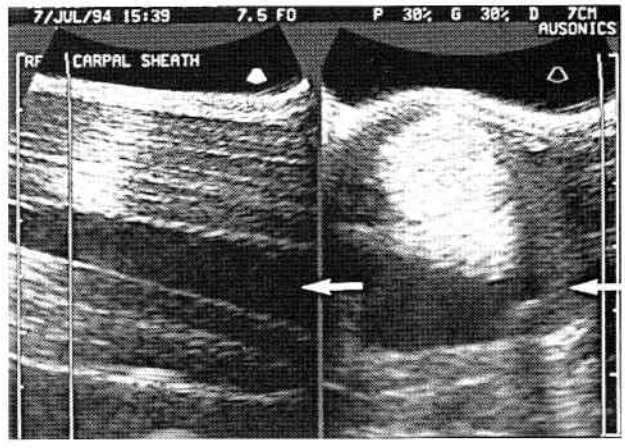

Figure 3–159

Sonograms of a carpal sheath tenosynovitis in the right foreleg, obtained from a 2-year-old Thoroughbred gelding. Notice the large amount of anechoic fluid in the carpal sheath between the deep digital flexor tendon and the inferior check ligament *(arrows)*. These sonograms were obtained in zone 1B at 10 cm distal to the point of the accessory carpal bone with a 7.5-MHz sector-scanner transducer containing a built-in fluid offset at a displayed depth of 7 cm. The right side of the transverse view *(right image)* is lateral and the left side is medial. The right side of the sagittal view *(left image)* is proximal and the left side is distal.

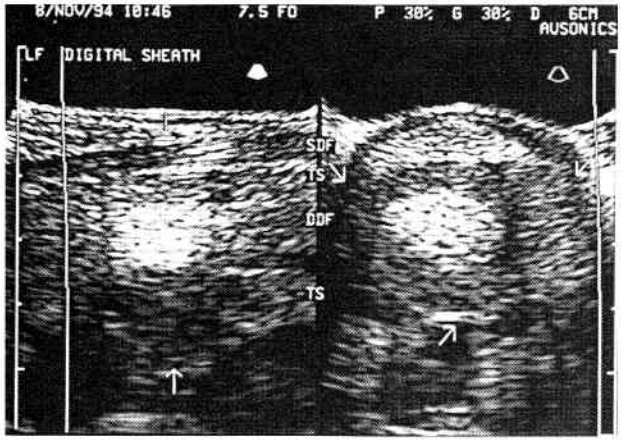

Figure 3–160

Sonograms of a septic digital sheath tenosynovitis in the left foreleg, obtained from a 4-year-old Thoroughbred gelding. Notice the marked distention *(arrows)* of the digital sheath (TS) with hypoechoic fluid in zone 3A at 23 cm distal to the point of the accessory carpal bone. The superficial (SDF) and deep digital flexor tendon (DDF) are normal. These sonograms were obtained with a 7.5-MHz sector-scanner transducer containing a built-in fluid offset at a displayed depth of 6 cm. The right side of the transverse view *(right image)* is lateral and the left side is medial. The right side of the sagittal view *(left image)* is proximal and the left side is distal.

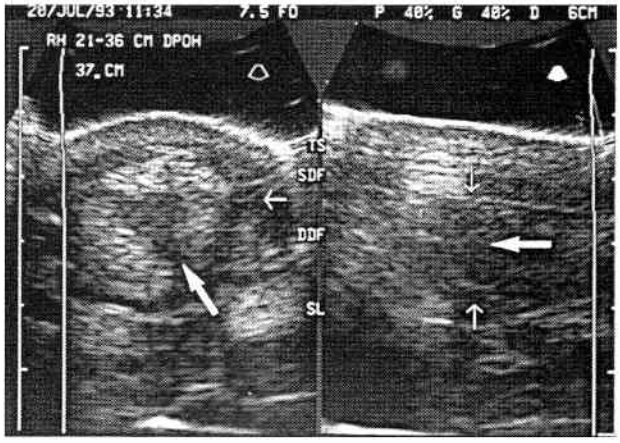

Figure 3–161

Sonograms of a septic digital sheath tenosynovitis and deep digital flexor (DDF) tendinitis in the right hindleg, obtained from an 11-year-old Tennessee Walking horse gelding. Notice the hypoechoic fluid surrounding the superficial digital flexor tendon (SDF) and DDF *(small arrows)*. Notice the enlarged DDF containing a large hypoechoic defect completely lacking in tendon fibers *(large arrow)* and the surrounding hypoechoic portion of the DDF. Mild thickening of the digital sheath (TS) is detected. These sonograms were obtained with a 7.5-MHz sector-scanner trapsducer containing a built-in fluid offset at a displayed depth of 6 cm. The right side of the transverse view *(left image)* is lateral and the left side is medial. The right side of the sagittal view *(right image)* is proximal and the left side is distal.

periphery of the tendon is most commonly affected, unless a penetrating wound has inoculated an area in the center of the tendon. However, the septic tendinitis usually progresses very quickly to involve other areas of the tendon. Care must be taken during the ultrasonographic examination to be certain that the purulent fluid is contained within the tendon sheath, because purulent fluid in close proximity to the tendon sheath may mimic a septic tenosynovitis (Fig. 3–162). Meticulous examination of the extent of the area of purulent fluid accumulation and the extent of the tendon sheath and its association with adjacent structures should prevent this inadvertent error.

Blood within the tendon sheath or bursa, if fresh, has an echogenic swirling pattern. Loculations develop as the blood organizes (Fig. 3–163). Fibrin within the synovial fluid is commonly seen with both nonseptic and septic tenosynovitis or bursitis and is an indication of active

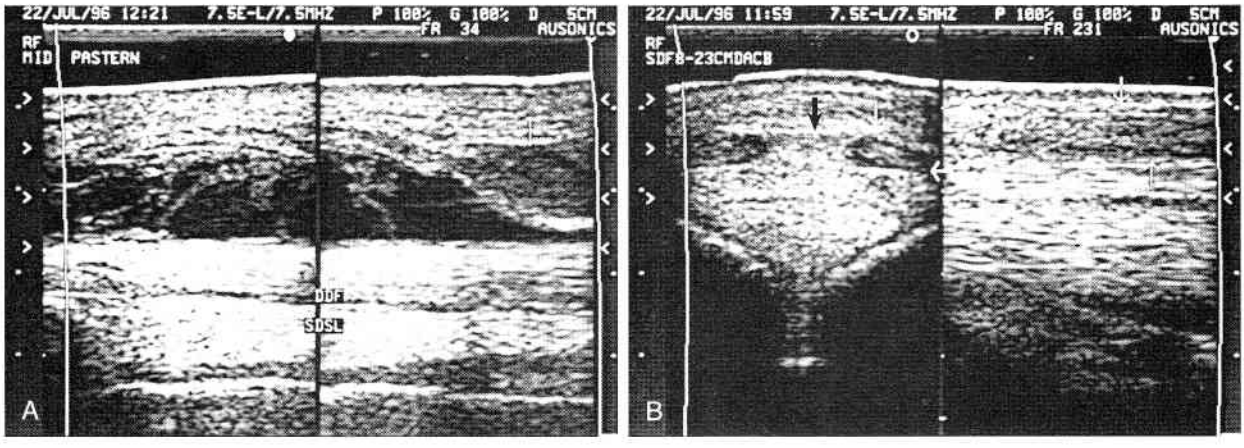

Figure 3–162

Sonograms of an abscess between the proximal digital annular ligament and the fetlock annular ligament that does not involve the digital sheath and a fibrinous digital sheath tenosynovitis in the right foreleg, obtained from a 3-year-old Standardbred colt. Significant soft tissue swelling is present palmar to the digital sheath. These sonograms were obtained with a wide-bandwidth 7.5-MHz-linear-array transducer operating at 7.5 MHz with a hand-held standoff pad at a displayed depth of 5 cm. The right side of the sagittal images is proximal and the left side is distal. The right sides of the transverse image is lateral and the left side is medial. DDF, deep digital flexor tendon; SDSL straight distal sesamoidean ligament.

A, Notice the loculated anechoic fluid within the digital sheath in these sagittal sonograms, consistent with an inflammatory fibrinous tenosynovitis, and the hypoechoic purulent fluid proximal to this loculated fluid and external to the digital sheath *(arrow)* in zone P1B.

B, Notice the fibrin within the distended digital sheath *(arrows)* in zone 3C and the thickened attachment between the SDF and the digital sheath *(black arrow)* in the transverse view *(left image)*, which is only visible with distention of the digital sheath.

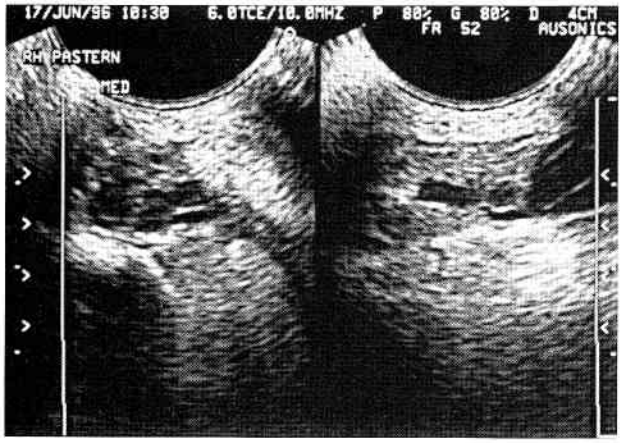

Figure 3–163

Sonograms of a chronic fibrinous digital sheath tenosynovitis in the right hind leg, obtained from an 8-year-old Oldenberg mare. Notice the thick layer of hypoechoic loculated material representing fibrin along the medial aspect of the digital sheath in the mid-pastern region, and the anechoic fluid adjacent to the thick fibrin layer. This sonographic appearance can be the result of hemorrhage into the sheath or severe chronic fibrinous inflammation within the digital sheath. These sonograms were obtained in zone P1C with a wide-bandwidth 6.0-MHz microconvex linear-array transducer operating at 10.0 MHz at a displayed depth of 4 cm. The focal zones are positioned in the middle of the image. The right side of the transverse view *(left image)* is plantar and the left side is dorsal. The right side of the sagittal view *(right image)* is proximal and the left side is distal.

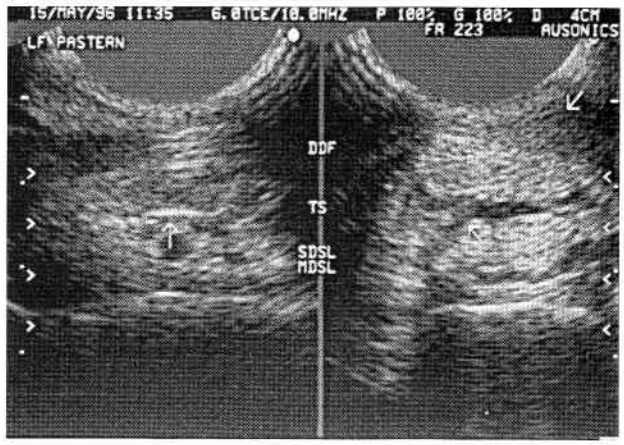

Figure 3–164

Sonograms of a chronic digital sheath tenosynovitis in the left foreleg, obtained from a 3-year-old Standardbred colt. Notice the hypoechoic to echogenic material surrounding the deep digital flexor tendon (DDF) consistent with organizing fibrin and fibrous tissue. This fibrous thickening of the digital sheath (TS) is displacing the DDF and straight distal sesamoidean ligament (SDSL) along their medial aspect and displacing the DDF along its palmar and lateral aspect, changing the plane of the DDF. These sonograms were obtained in zone P1B with a wide-bandwidth 6.0-MHz microconvex linear-array transducer operating at 10.0 MHz at a displayed depth of 4 cm. The focal zones are positioned in the center of the image. The right side of the transverse view *(right image)* is lateral and the left side is medial. The right side of the sagittal view *(left image)* is proximal and the left side is distal. MDSL, middle distal sesamoidean ligament.

inflammation within the tendon sheath (see Fig. 3-163) or bursa. Fibrin and loculations may also indicate sepsis in horses with anechoic fluid, especially in acute septic tenosynovitis. The fibrin within the inflamed tendon sheath may resolve with treatment or may organize and form fibrous attachments either between the tendons and the tendon sheath (see Fig. 3-157) or between the bursa and the tendon. These adhesions may result in abnormal alignment of the tendinous structures contained within the tendon sheath (Fig. 3-164). They may also lead to subsequent fiber tearing in the deep digital flexor tendon (most likely) or superficial digital flexor tendon (Fig. 3-165).

Tenosynovitis

Digital Sheath Tenosynovitis. Digital sheath tenosynovitis is often very mild with few clinical or sonographic signs other than an increased amount of synovial fluid contained within the digital sheath. This mild, chronic effusion in the digital sheath is usually idiopathic and is not associated with any tendinous and ligamentous abnormality. Of more concern is fibrinous digital sheath tenosynovitis (see Fig. 3-163), because the detection of filmy hypoechoic echoes within the digital sheath or loculations indicates the presence of fibrin and active inflammation within the digital sheath. Resolution of this inflammation and the disappearance of the fibrin within the digital sheath is the goal of therapy and patient management. These fibrinous loculations may mature and become fibrous adhesions between the superficial and deep digital flexor tendons (see Fig. 3-165) or between

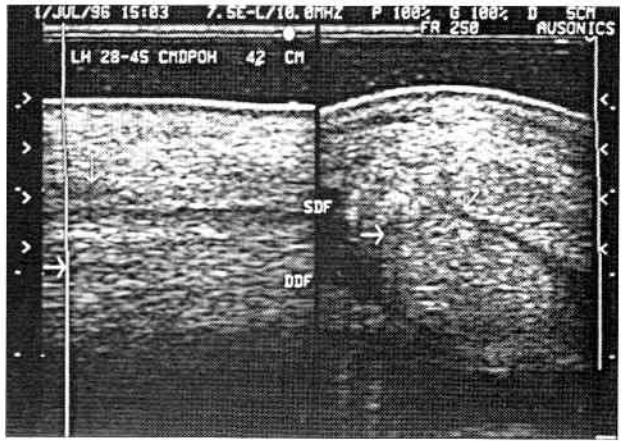

Figure 3–165

Sonograms of adhesions between the superficial (SDF) and deep digital flexor tendons (DDF) in the left hind leg, obtained from a 3-year-old Thoroughbred gelding. This horse had a chronic digital sheath tenosynovitis that was originally septic. Notice the adhesion *(arrows)* between the plantaromedial aspect of the DDF and the dorsomedial aspect of the SDF in the transverse view *(right image)*, distorting the shape of the two tendons. Both tendons are enlarged, hypoechoic, and lacking the normal fiber pattern. The SDF and DDF tendinitis was imaged from 28 to 45 cm distal to the point of the hock. These sonograms were obtained at 42 cm (zone 4B) with a wide-bandwidth 7.5-MHz linear-array transducer operating at 10.0 MHz with a hand-held standoff pad at a displayed depth of 5 cm. The focal zones are positioned in the near field. The right side of the transverse image is lateral and the left side is medial. The right side of the sagittal view *(left image)* is proximal and the left side is distal.

the flexor tendons and the tendon sheath (see Fig. 3-164). Chronic thickening of the synovial lining of the digital sheath also occurs in horses with chronic active digital sheath tenosynovitis. Fibrous proliferation is often imaged in these horses near the proximal and lateral reflection of the digital sheath (Fig. 3-166). This fibrous proliferation can become quite large and can result in the separation and subsequent malalignment of the flexor tendons. Hypoechoic to echogenic masses were identified sonographically in the distal recesses of the digital sheath in 3 of 17 horses.[59]

Carpal Sheath Tenosynovitis. Carpal sheath tenosynovitis is usually a performance-related injury and is one cause of carpal canal syndrome. Carpal sheath effusions may be mild and not associated with lameness. The more severe carpal sheath effusions, however, are usually associated with lameness at their onset. The majority of horses with carpal sheath effusion have an increased amount of anechoic fluid imaged within the tendon sheath, with no tendinous or ligamentous abnormalities (see Fig. 3-159). In horses with septic tenosynovitis, fibrin and loculations are usually present along with increased echogenicity of the synovial fluid. Fibrin and loculations may also be imaged within the carpal sheath (Fig. 3-167) and are often associated with hemorrhage into the carpal sheath secondary to a traumatic local injury. The distention of the carpal sheath can be relatively mild. It can also be massive, with large synovial outpouchings of the carpal sheath detected proximal to the carpal retinaculum, particularly on the lateral aspect of the limb (Fig. 3-168) and distal to the carpus along the medial aspect of the proximal to mid-metacarpal region.

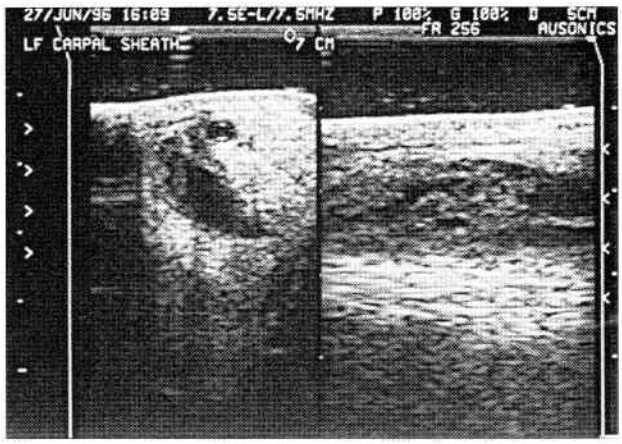

Figure 3–167

Sonograms of a fibrinous carpal sheath tenosynovitis in the left foreleg, obtained from a 3-year-old Thoroughbred colt. Notice the distended carpal sheath containing anechoic fluid and hypoechoic loculated fibrin. The largest distention of the carpal sheath in the proximal metacarpal region (7 cm distal to the point of the accessory carpal bone) is medial in zone 1A. These sonograms were obtained with a wide-bandwidth 7.5-MHz linear-array transducer operating at 7.5 MHz with a hand-held standoff pad at a displayed depth of 5 cm. The focal zones are positioned in the near field. The right side of the transverse view *(left image)* is lateral and the left side is medial. The right side of the sagittal view *(right image)* is proximal and the left side is distal.

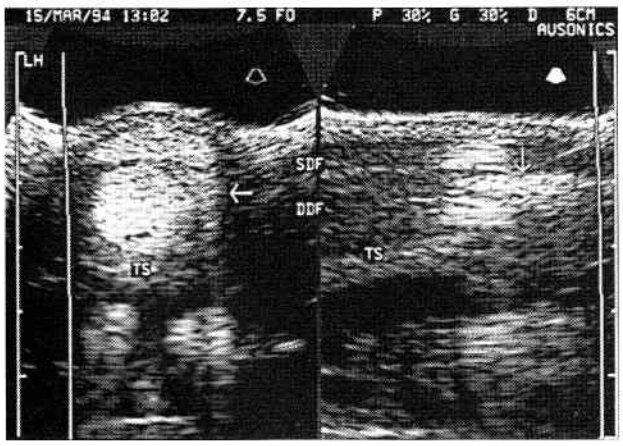

Figure 3–166

Sonograms of a chronic digital sheath tenosynovitis and deep digital flexor (DDF) tendinitis in the left hindlimb, obtained from an 11-year-old Thoroughbred mare. Notice the echogenic thickening *(arrows)* along the lateral aspect of the digital sheath (TS) separating the superficial digital flexor tendons (SDF) and DDF, representing an area of fibrous scar tissue. With dynamic real-time scanning, this area appeared adhered to the DDF. The DDF is enlarged and contains hypoechoic areas in the dorsal and plantar portions of the tendon. These sonograms were obtained near the dorsal-most reflection of the digital sheath in zone 3A at 30 cm distal to the point of the hock using a 7.5-MHz sector-scanner transducer containing a built-in fluid offset at a displayed depth of 6 cm. The right side of the transverse view *(left image)* is lateral and the left side is medial. The right side of the sagittal view *(right image)* is proximal and the left side is distal.

Thorough sonographic evaluation of all the structures contained within the carpal canal should be performed to determine if other tendinous, ligamentous, or bony disease is present. Large carpal sheath effusions can be associated with new or recent areas of fiber tearing in the superficial or deep digital flexor tendon. Equine carpal sheath tenosynovitis is more common with severe

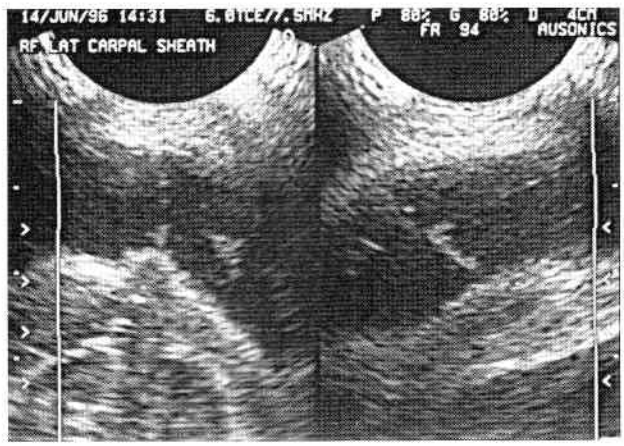

Figure 3–168

Sonograms of a severe, fibrinous carpal sheath tenosynovitis in the right foreleg, obtained from a 13-year-old Hanoverian mare. These sonograms were obtained proximal to the carpus along the lateral aspect of the distal radius. Notice the large anechoic fluid distention of the lateral compartment of the carpal sheath containing small amounts of hypoechoic fibrin. These sonograms were obtained with a wide-bandwidth 6.0-MHz microconvex linear-array transducer operating at 7.5 MHz at a displayed depth of 4 cm. The focal zones are positioned in the far field. The right side of the transverse view *(left image)* is cranial and the left side is caudal. The right side of the sagittal view *(right image)* is proximal and the left side is distal.

injury to the superficial digital flexor tendon within the carpal canal than with mild superficial digital flexor tendinitis. Large carpal sheath effusions may also be imaged in horses with bony proliferation along the physeal region of the distal radius (Fig. 3-169). Although many of these bony proliferative changes at the physeal region have been called osteochondromas, histopathologic examination of some affected horses has not confirmed this diagnosis. Large effusions in the carpal sheath can also be imaged with fractures of the accessory carpal bone. In these horses, the effusion is usually fibrinous, loculated, and hemorrhagic. Injuries to the superior check ligament may also be associated with effusions within the carpal sheath. Chronic thickening of the carpal sheath and its synovial lining may persist in some horses with carpal sheath tenosynovitis (Fig. 3-170) and may flare up periodically with increased effusion and fibrinous loculations.

Tarsal Sheath Tenosynovitis. Mild effusions are occasionally detected within the tarsal sheath (Fig. 3-171), as in the digital and carpal sheaths, that have little clinical significance. Fibrinous loculations (Fig. 3-172) and large effusions are more common in horses with tarsal sheath tenosynovitis than are benign small anechoic effusions. Tarsal sheath tenosynovitis is usually associated with a moderate to severe sudden-onset lameness.[116] Tenosynovitis of the tarsal sheath is often associated with trauma, although clinical signs appear occasionally after a race or competition.[116, 138] Changes in the underlying sustentaculum tali are frequently detected and consist of chip fractures, bony proliferation along the medial border, and both lytic and proliferative changes. Draining wounds from the medial aspect of the hock also occur in some affected horses.

Tarsal sheath rupture is one cause of a false thorough-

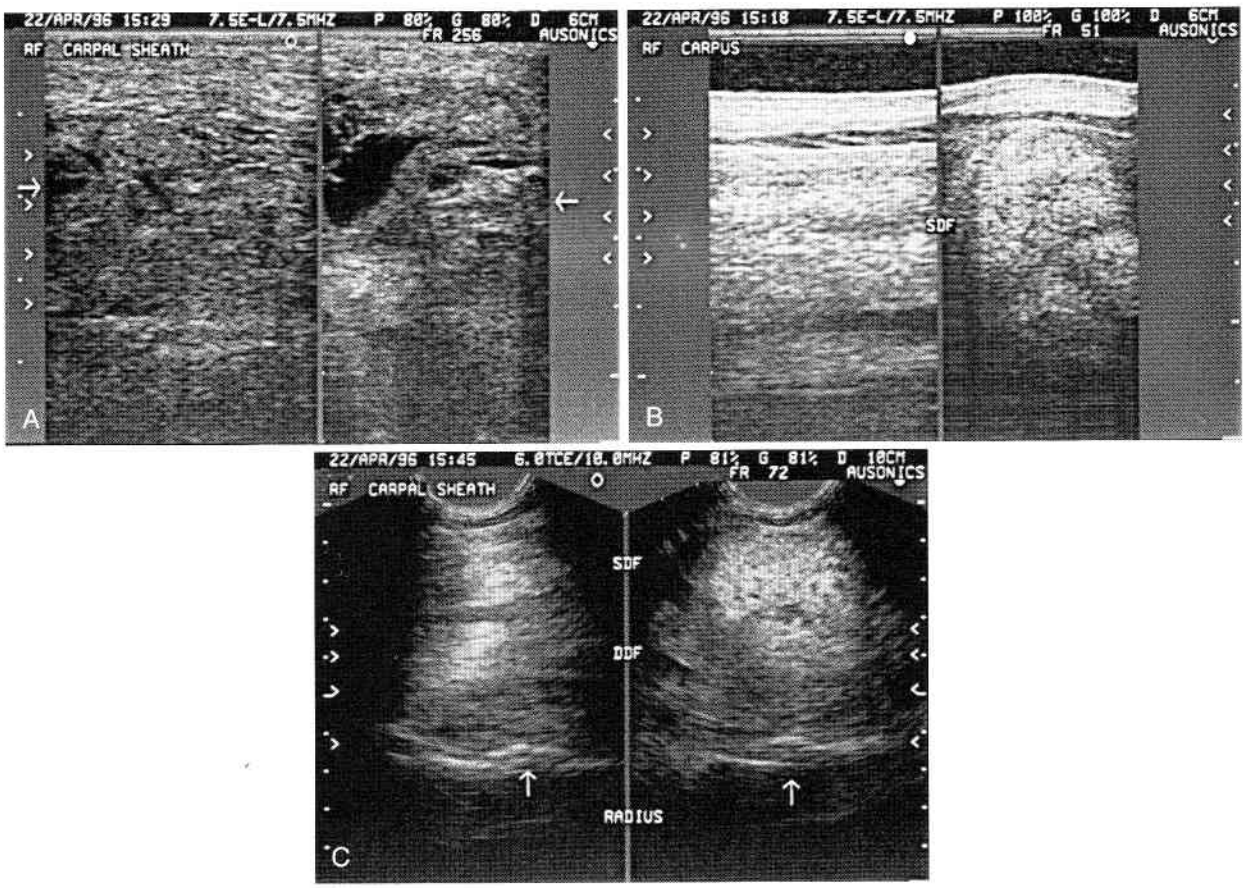

Figure 3–169

Sonograms of a severe carpal sheath tenosynovitis with chronic superficial digital flexor (SDF) tendinitis in the right foreleg, obtained from an 18-year-old Warmblood gelding. These sonograms were obtained by using a wide-bandwidth 7.5-MHz linear-array transducer operating at 7.5 MHz with a hand-held standoff pad at a displayed depth of 6 cm *(A* and *B)* and by using a 6.0-MHz microconvex linear-array transducer operating at 10.0 MHz at a displayed depth of 10 cm *(C)*. The focal zones are positioned in the near field *(A* and *B)* and in the far field *(C)*. The right side of the transverse image *(A)* is cranial and the left side is caudal; the right side of the transverse images *(B* and *C)* is lateral and the left side is medial. The right side of the sagittal images is proximal and the left side is distal. DDF, deep digital flexor tendon.

A, Notice the massive amount of fibrinous loculations within the carpal sheath in the sagittal view *(left image)* and the associated anechoic fluid in the transverse view *(right image)*. These fibrinous loculations could indicate previous hemorrhage into the carpal sheath or severe chronic inflammation. These images were obtained along the medial aspect of the distal radius.

B, Notice the enlarged, somewhat heterogeneous appearance of the SDF in the proximal metacarpal region at 5 cm distal to the point of the accessory carpal bone (zone 1A), consistent with a chronic, healing SDF tendinitis. This horse had a 2-year history of severe acute diffuse superficial digital flexor tendinitis with large areas of fiber tearing and severe carpal sheath tenosynovitis with bony proliferation along the distal radius. The left image is the sagittal view; right image is the transverse view.

C, Notice the bony proliferation along the distal aspect of the radius *(arrows)*, which appears to be impinging on the carpal canal in both the sagittal *(left image)* and transverse *(right image)* views.

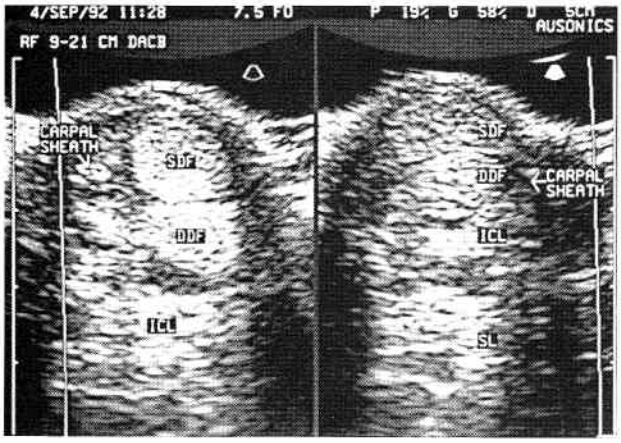

Figure 3–170

Transverse sonograms of a chronic carpal sheath tenosynovitis in the right foreleg, obtained from a 3-year-old Thoroughbred colt. Notice the thickening of the carpal sheath *(arrows)* with no significant effusion, which was imaged throughout the length of the carpal sheath. These sonograms were obtained in zones 1A *(left image)* at 8 cm distal to the point of the accessory carpal bone and 1B at 12 cm distal to the accessory carpal bone with a 7.5-MHz sector-scanner transducer containing a built-in fluid offset at a displayed depth of 5 cm. The right side of the images is lateral and the left side is medial. SDF, superficial digital flexor tendon; DDF, deep digital flexor tendon; ICL, inferior check ligament; SL, suspensory ligament.

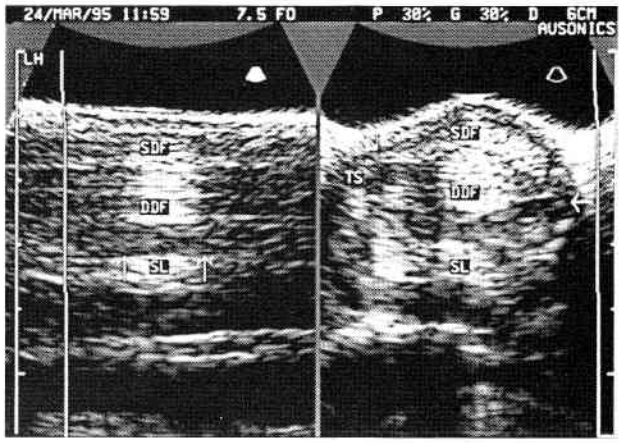

Figure 3–172

Sonograms of a chronic fibrinous tarsal sheath tenosynovitis in the right hindlimb, obtained from an 11-year-old Morgan mare at 24 cm distal to the point of the hock (zone 2B). Notice the hypoechoic to echogenic material representing organizing fibrin *(arrows)* contained within the tarsal sheath (TS) surrounding the deep digital flexor tendon (DDF). These sonograms were obtained with a 7.5-MHz sector-scanner transducer containing a built-in fluid offset at a displayed depth of 6 cm. The right side of the transverse view *(right image)* is lateral and the left side is medial. The right side of the sagittal view *(left image)* is proximal and the left side is distal. SDF, superficial digital flexor tendon; SL, suspensory ligament.

pin, the other being subcutaneous fluid swelling in the region of the tarsal sheath, usually a hematoma. Tarsal sheath rupture is usually diagnosed with contrast radiography, an invasive technique.[112, 139] Although communication between the tarsal sheath and the synovial ganglia should be detectable ultrasonographically with careful searching of the fluid-filled structures and the use of high-resolution ultrasound equipment, it could not be detected in one horse.[139] The tarsal sheath is at high risk of traumatic injury proximally because it protrudes proximally and medially to the deep fascia of the hock during extension.[116] Trauma to this region can result in tarsal sheath synovitis, rupture, or a hematoma in the subcutaneous tissues without tarsal sheath involvement.[116]

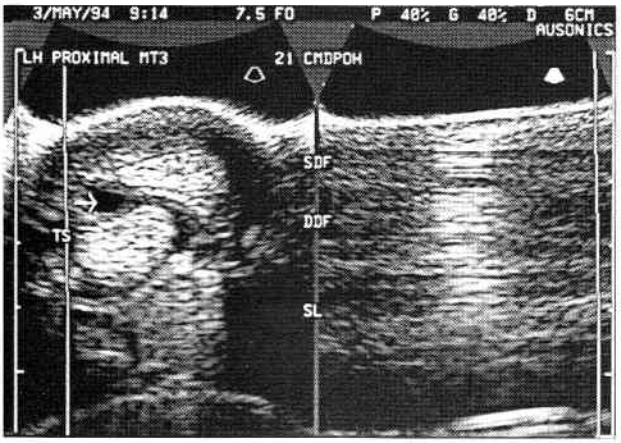

Figure 3–171

Sonograms of a tarsal sheath tenosynovitis in the left hindlimb, obtained from a 4-year-old Thoroughbred gelding at 21 cm distal to the point of the hock (zone 2A). Notice the anechoic effusion *(arrow)* within the tarsal sheath (TS) surrounding the deep digital flexor tendon (DDF). These sonograms were obtained with a 7.5-MHz sector-scanner transducer containing a built-in fluid offset at a displayed depth of 6 cm. The right side of the transverse view *(left image)* is lateral and the left side is medial. The right side of the sagittal view *(right image)* is proximal and the left side is distal. SDF, superficial digital flexor tendon; SL, suspensory ligament.

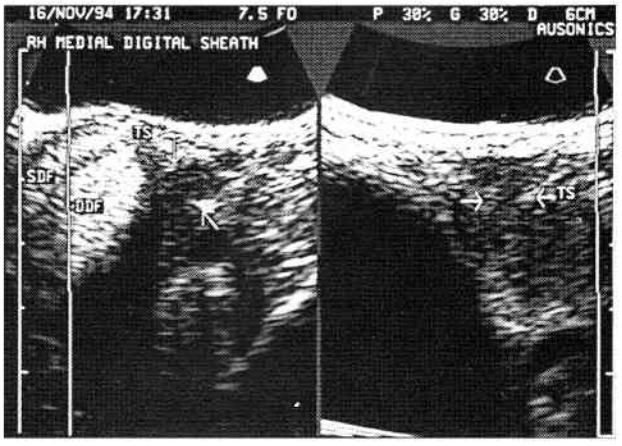

Figure 3–173

Sonograms of a synovial ganglion (fistula) in the medial aspect of the digital sheath (TS) in the right hind leg, obtained from an 8-year-old Thoroughbred gelding. Notice the small anechoic synovial outpouching along the medial and plantar aspect of the digital sheath, with a narrow neck at the site of the defect in the wall of the digital sheath *(between the arrows)*. These sonograms were obtained in zone 3B at 28 cm distal to the point of the accessory carpal bone with a 7.5-MHz sector-scanner transducer containing a built-in fluid offset at a displayed depth of 6 cm. The right side of the transverse view *(left image)* is dorsal and the left side is plantar. The right side of the sagittal view *(right image)* is proximal and the left side is distal. SDF, superficial digital flexor tendon; DDF, deep digital flexor tendon.

Synovial Ganglia and Tendon Sheath Rupture. Rupture of the tendon sheath occasionally occurs with the development of synovial ganglia. These synovial outpouchings can be very small and clinically insignificant (Fig. 3-173), or they may be quite large (Fig. 3-174) and involve a large portion of the tendon sheath. Synovial ganglia are most common in the digital sheath in the author's experience, but can occur in association with any of the tendon sheaths. Differentiation between a severe tenosynovitis and a ruptured tendon sheath is important, because different treatments may be indicated. Small anechoic to hypoechoic masses can occur in the wall of the tendon sheath and may be associated with a focal area of pain (Fig. 3-175). These areas usually resolve and are probably associated with local hemorrhage within the wall of the tendon sheath. Occasionally, these areas persist as blemishes that appear hypoechoic to echogenic but cause no functional problem.

Tenosynovitis of the Extensor Tendon Sheaths. Injuries to the extensor tendon sheaths over the dorsal aspect of the carpus are common, with development of a tenosynovitis of the affected tendon sheaths (Fig. 3-176). Associated injuries to the extensor tendons are uncommon. Most affected horses have a normal extensor tendon or only a mild tendinitis of the portion of the tendon contained within the sheath (mild decrease in tendon echogenicity and separation of fibers). Areas of fiber tearing do occur in the extensor tendons in horses with extensor tendon tenosynovitis, usually associated with local trauma (Fig. 3-177). Large hygromas may form in association with marked distention and/or rupture of the extensor tendon sheath. Hygromas are most common over the dorsal aspect of the carpus.

Penetrating Wounds into the Tendon Sheath. Penetrating wounds in the pastern, fetlock, and distal metacarpal or metatarsal region often involve the tendon sheath. The tract of the penetrating object can be followed from the defect in the skin or the scar into the deeper tissues. The tract usually appears as a linear or tubular hypoechoic path that extends from the skin sur-

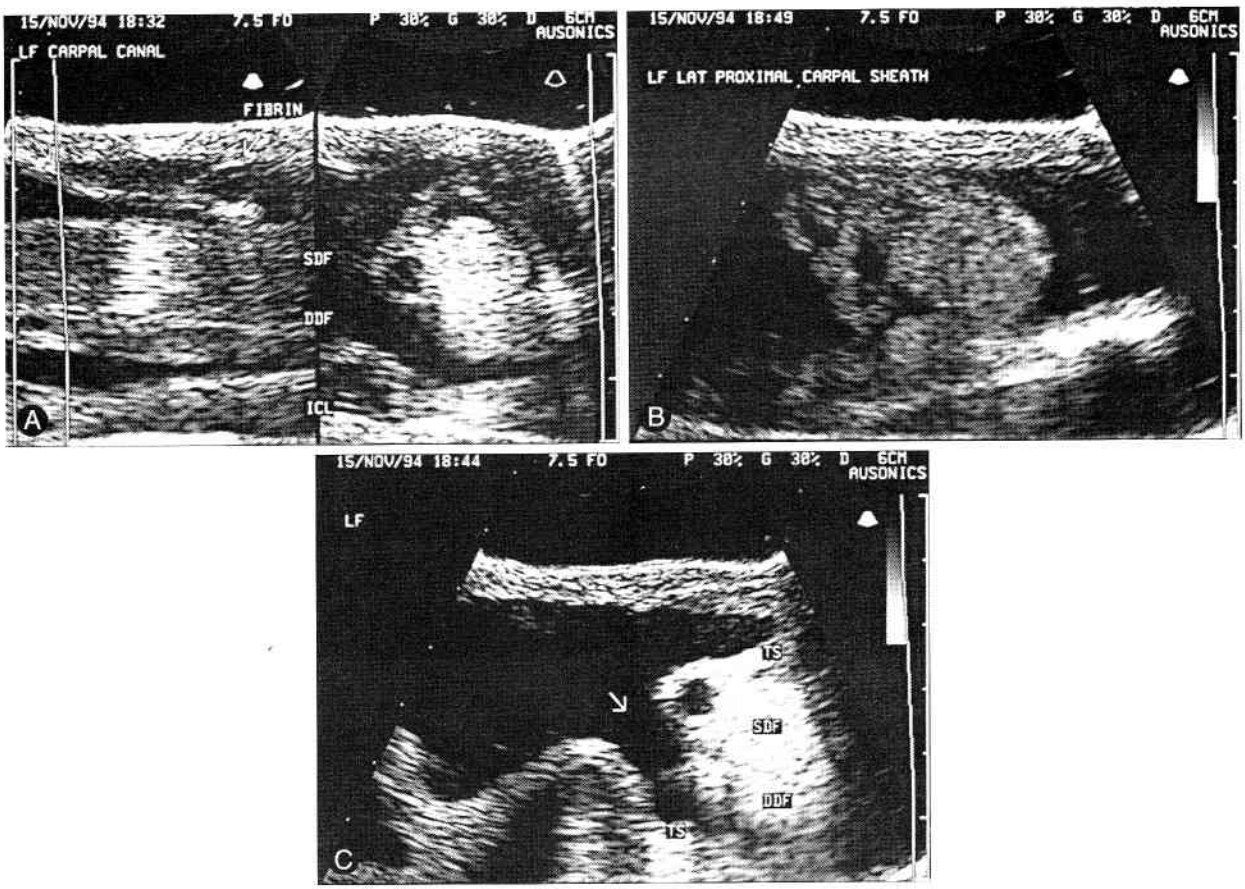

Figure 3–174

Sonograms of a ruptured carpal sheath in the left foreleg, obtained from a 3-year-old Thoroughbred colt. These sonograms were obtained with a 7.5-MHz sector-scanner transducer containing a built-in fluid offset at a displayed depth of 6 cm. The right side of the transverse images is lateral *(A)* or cranial *(C)* and the left side is medial *(A)* or caudal *(C)*. The right side of the sagittal images *(A* and *B)* is proximal and the left side is distal. SDF, superficial digital flexor tendon; DDF, deep digital flexor tendon; ICL, inferior check ligament.

A, Notice the large amount of anechoic fluid surrounding the SDF and DDF tendons with hypoechoic loculated fibrin in the transverse *(right image)* and sagittal *(left image)* views.

B, Notice the hypoechoic mass of loculations in the proximal and lateral portion of the carpal sheath, representing an organizing clot in this sagittal view.

C, Notice the defect in the wall of the carpal sheath *(arrow)* along the proximal and medial aspect of the carpal sheath in zone 1A and the large synovial outpouching containing anechoic fluid in this transverse view.

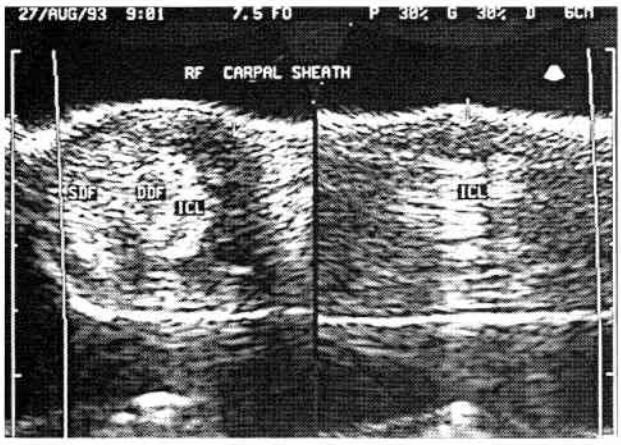

Figure 3–175

Sonograms of a small mass in the wall of the right carpal sheath along its lateral aspect, obtained from a 17-year-old Thoroughbred cross gelding with chronic superficial digital flexor (SDF) tendinitis. Notice the hypoechoic to anechoic oval mass in the wall of the carpal sheath, which does not communicate with other structures located at 15 cm distal to the point of the accessory carpal bone (zone 2A). This probably represents a traumatic injury that is repairing with granulation tissue and immature fibrous tissue. These sonograms were obtained with a 7.5-MHz sector-scanner transducer containing a built-in fluid offset at a displayed depth of 6 cm. The right side of the transverse view *(left image)* is dorsal and the left side is palmar. The right side of the sagittal view *(right image)* is proximal and the left side is distal. DDF, deep digital flexor tendon; ICL, inferior check ligament.

face into the subcutaneous tissues and then into the tendon sheath (Fig. 3–178), and occasionally into the tendon itself. The best technique to follow the tract to its origin is to scan the tract in its short axis, keeping the tract in the center of the image. The tract should be followed to its end, and if more than one tract is present,

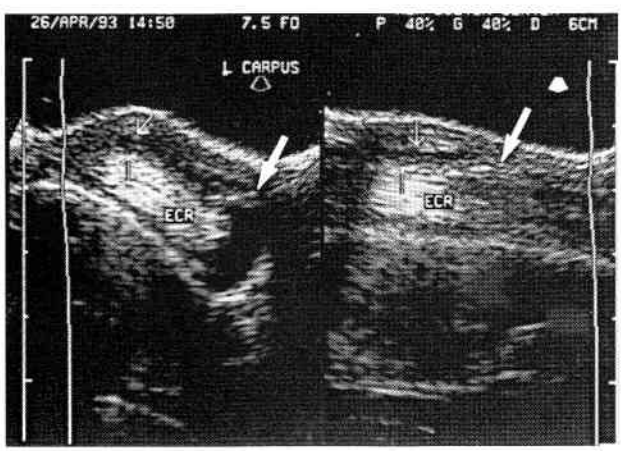

Figure 3–176

Sonograms of a tenosynovitis of the extensor carpi radialis (ECR) tendon sheath in the left foreleg, obtained from an 8-year-old Thoroughbred gelding. Notice the anechoic effusion in the tendon sheath with a small amount of fibrin *(small arrows)* and the normal attachment of the tendon to its sheath, which is thicker and more echogenic *(large arrows)*. The extensor carpi radialis tendon is normal. These sonograms were obtained with a 7.5-MHz sector-scanner transducer containing a built-in fluid offset at a displayed depth of 6 cm. The right side of the transverse view *(left image)* is lateral and the left side is medial. The right side of the sagittal view *(right image)* is proximal and the left side is distal.

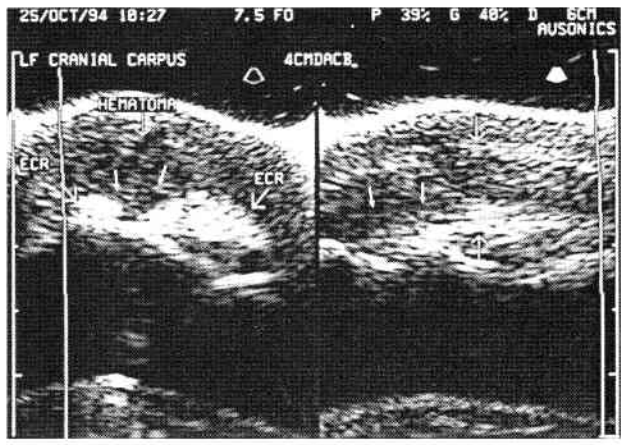

Figure 3–177

Sonograms of an area of fiber disruption and hemorrhage in the extensor carpi radialis tendon (ECR) with disruption of the tendon sheath *(down arrows)*, obtained from a 12-year-old Thoroughbred gelding. Notice the anechoic defect in the ECR *(small arrows)* and the hypoechoic loculated material adjacent to the defect, associated with organizing hemorrhage. These sonograms were obtained with a 7.5-MHz sector-scanner transducer containing a built-in fluid offset at a displayed depth of 6 cm. The right side of the transverse view *(left image)* is lateral and the left side is medial. The right side of the sagittal view *(right image)* is proximal and the left side is distal.

they should all be followed to their source. The tract may contain anechoic, hypoechoic, or echogenic fluid and may contain bright hyperechoic pinpoint echoes, consistent with gas. If the gas echoes are located only at or near the skin, these may be entering the tract from the air adjacent to the skin. If these gas echoes line the tract for its entire length or are uniformly dispersed throughout the fluid in the deeper tissues, or if a dorsal gas cap is detected, an anaerobic infection is likely.

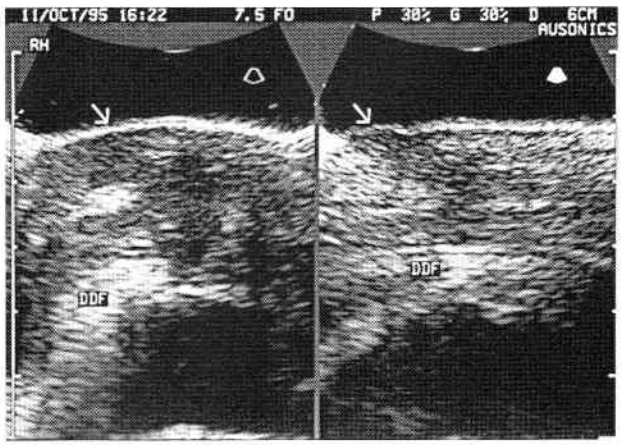

Figure 3–178

Sonograms of a penetrating injury into the tarsal sheath of the right hindleg, obtained from a 3-year-old Quarter horse filly. Notice the hypoechoic tract extending from the break in the skin surface *(arrows)* into the tarsal sheath. The deep digital flexor tendon (DDF) is surrounded by hypoechoic fluid, suggesting a septic tarsal sheath tenosynovitis. These sonograms were obtained along the medial aspect of the hock with a 7.5-MHz sector-scanner transducer containing a built-in fluid offset at a displayed depth of 6 cm. The right side of the transverse view *(left image)* is cranial and the left side is caudal. The right side of the sagittal view *(right image)* is proximal and the left side is distal.

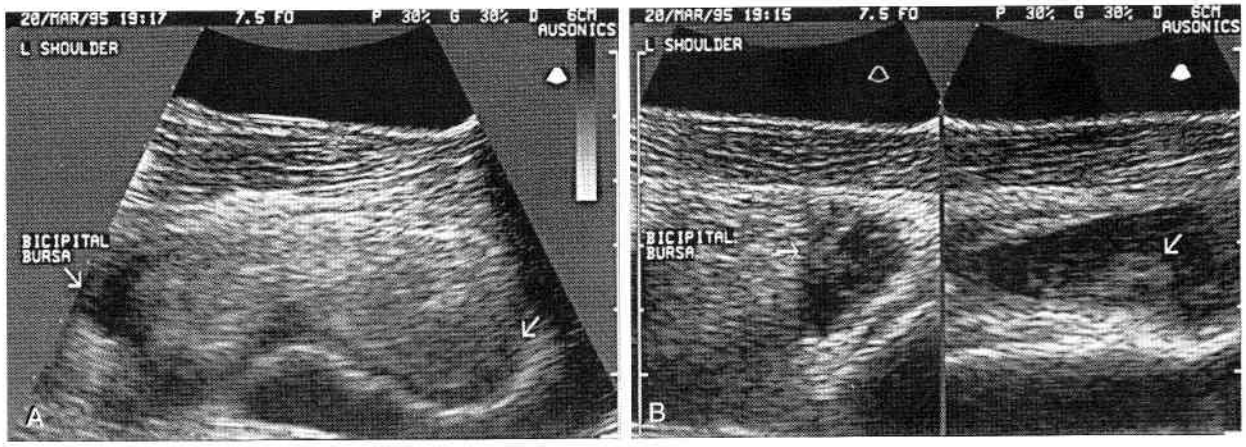

Figure 3–179

Sonograms of a septic bicipital bursitis in the left foreleg, obtained from a 3-year-old Standardbred gelding. These sonograms were obtained with a 7.5-MHz sector-scanner transducer containing a built-in fluid offset at a displayed depth of 6 cm. The right side of the sagittal view *(right image* in *B)* is proximal and the left side is distal. The right side of the transverse views *(A* and *left image* in *B)* is lateral and the left side is medial.

A, Transverse sonogram of the bicipital tendon and bicipital bursa *(arrows)*, illustrating hypoechoic effusion in the bicipital bursa with an echogenic mass (which probably represents clot) detected underneath the left diagonal arrow. The bicipital tendon is enlarged and somewhat heterogeneous with hypoechoic areas within, consistent with a diffuse tendinitis of the bicipital tendon.

B, Sonograms of the bicipital tendon and bursa illustrating marked distention of the bursa with a composite fluid and an enlarged hypoechoic appearance of the bicipital tendon. The hypoechoic material *(arrows)* within the bursa represents fibrin within the fluid.

Bursitis

Bicipital Tendinitis and Bursitis. Bicipital tendinitis and bursitis is an uncommon problem in horses, but it is a significant cause of lameness referable to the shoulder region. The horses usually show a shortened anterior phase to the stride and swelling, heat, and sensitivity in the region of the biceps tendon and bicipital bursa. Horses with mild bicipital bursitis may have only an increased amount of anechoic fluid in the bursa detected sonographically. However, sonographic findings in most horses with bicipital bursitis include an increased volume of hypoechoic fluid and fibrin and loculations within the bursa (Fig. 3-179). Thickening of the bicipital bursa and its synovial lining are often present, particularly in horses with long-standing bicipital bursitis. Adhesions can form between the bursa and the tendon, and these can be successfully imaged ultrasonographically (Fig. 3-180). The adhesions may limit function if they restrict movement of the biceps tendon and the shoulder. Hemorrhage, edema, and peritendinous thickening have been detected ultrasonographically in horses with bicipital bur-

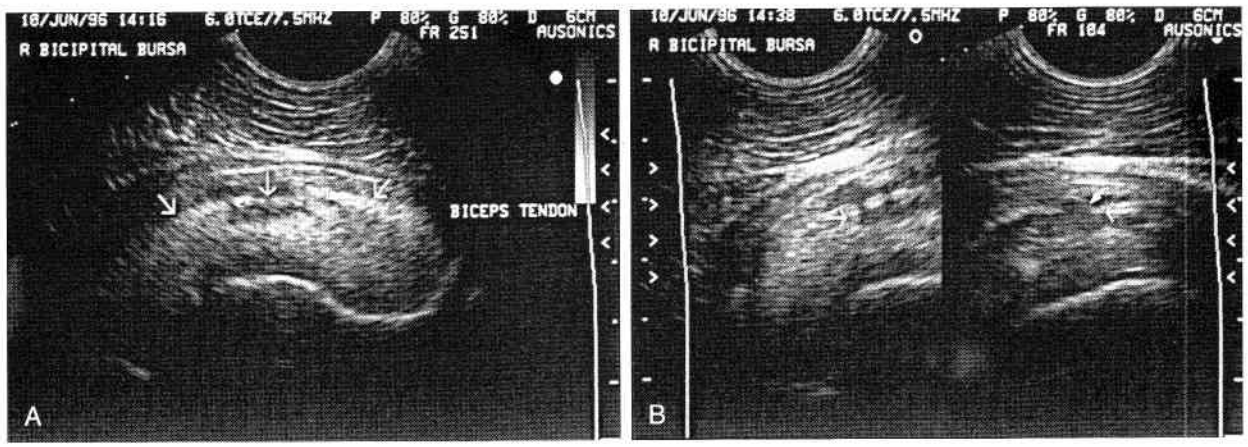

Figure 3–180

Sonograms of a bicipital tendinitis and chronic bicipital bursitis in the left foreleg, obtained from a 10-year-old Thoroughbred gelding. Notice the anechoic core lesion located over the intermediate tubercle of the humerus, the thickening of the bicipital bursa, and the adhesions between the bicipital tendon and the synovial lining of the bicipital bursa. These sonograms were obtained with a wide-bandwidth 6.0-MHz microconvex linear-array transducer operating at 7.5 MHz at a displayed depth of 6 cm. The right side of the sagittal view *(right image* in *B)* is proximal and the left side is distal. The right side of the transverse views *(A* and *left image* in *B)* is lateral and the left side is medial.

A, Transverse sonogram of the bicipital tendon with the arrows pointing to the cranial margin of the bicipital tendon. Notice the anechoic core lesion *(central arrow)* on the cranial margin of the tendon and the small increase in the amount of bursa fluid, which appears to be anechoic.

B, Anechoic defects are imaged in the cranial margin of the bicipital tendon in both the transverse view *(left image)* and the sagittal view *(right image)*. Notice the hypoechoic strand connecting the bicipital tendon with the synovial lining of the bicipital bursa in the sagittal scan *(small arrow)*. The synovial lining of the bicipital bursa is markedly thickened and measured 7.5 mm.

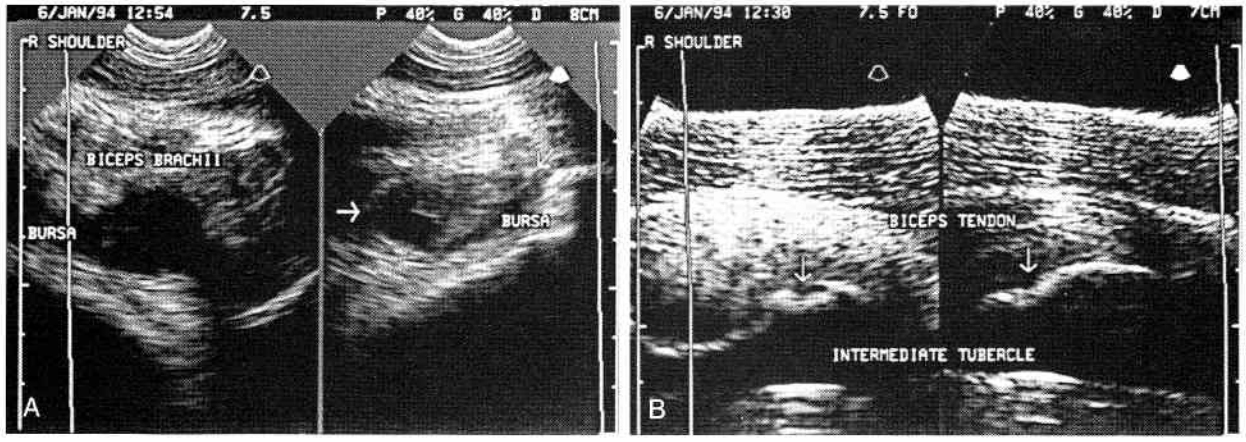

Figure 3–181

Sonograms of septic bicipital bursitis with osteomyelitis of the intermediate tubercle in the right foreleg, obtained from a 4-year-old Thoroughbred filly. These sonograms were obtained with a 7.5-MHz sector-scanner transducer *(A)* containing a built-in fluid offset *(B)* at a displayed depth of 8 cm *(A)* and 7 cm *(B)*. The right side of the sagittal images is proximal and the left side is distal. The right side of the transverse images is lateral and the left side is medial.

A, Sonograms of the bicipital bursa along the edge of the bicipital tendon, revealing hypoechoic composite fluid consistent with a septic bursitis and fibrin accumulation within the bursa. Loculated fibrin is imaged in the transverse view *(right image)* and a fibrin clot is imaged in the sagittal view *(left image)* in the bicipital bursa.

B, Sonograms of the bicipital tendon and intermediate tubercle of the humerus, illustrating the lytic lesion *(arrows)* detected most evident in the transverse view *(left image)*. The bicipital tendon has near-normal echogenicity and near-normal fiber alignment in the sagittal view *(right image)*, with only a slight decrease in tendon echogenicity detected consistent with a mild tendinitis. The overlying brachiocephalicus musculature looks normal.

sitis.[70, 84, 88, 140] In many horses with bicipital bursitis, the bicipital tendon is normal. However, hypoechoic to anechoic areas may be imaged within the bicipital tendon, consistent with areas of fiber tearing (see Fig. 3-180) and tendinitis. Tendinitis of the bicipital tendon with hypoechoic to anechoic areas imaged within the tendon and loss of the normal fiber pattern has been diagnosed sonographically in several horses.[70, 84, 88, 140]

The underlying bone should also be carefully examined ultrasonographically, because abnormalities in the intermediate tubercle of the humerus (Fig. 3-181) or other areas of the humerus (Fig. 3-182) may be detected in horses with septic bicipital bursitis. These may appear as lytic areas (see Figs. 3-181 and 3-182) in the underlying bony surface echo or proliferative areas, indicating bony involvement in the infection. Chip fractures originating from the lesser tubercle of the humerus were identified ultrasonographically in one horse with a concurrent bur-

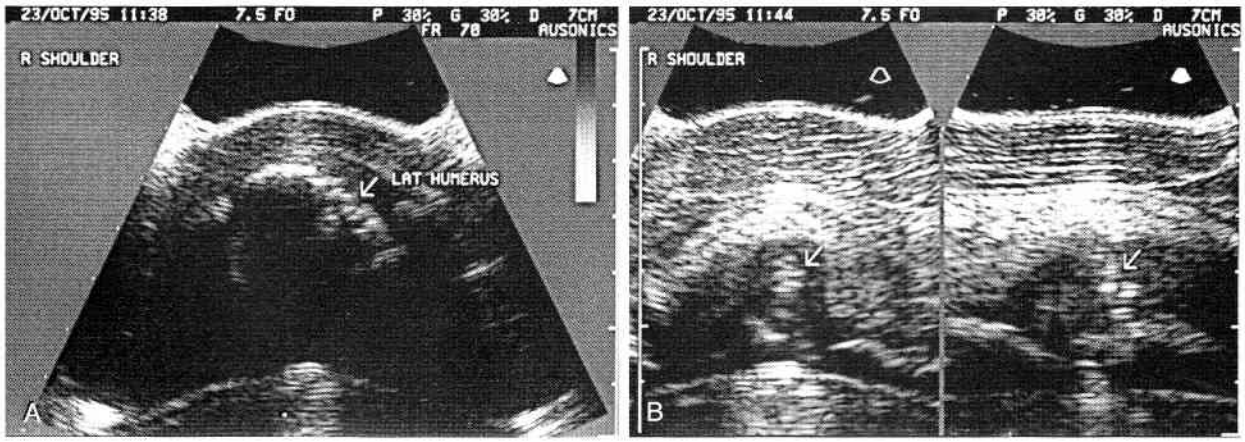

Figure 3–182

Sonograms of a septic bicipital bursa with osteomyelitis of the humerus, obtained from a 6-month-old Thoroughbred colt. These sonograms were obtained with a 7.5-MHz sector-scanner transducer containing a built-in fluid offset at a displayed depth of 7 cm. The right side of the sagittal views *(A* and *right image* in *B)* is proximal and the left side is distal. The right side of the transverse view *(left image* in *B)* is lateral and the left side is medial.

A, Notice irregular lytic bony surface echo *(arrow)* in the lateral humerus consistent with osteomyelitis in this sagittal view of the lateral humeral condyle.

B, Notice the irregular hyperechoic echoes in the intermediate tubercle of the humerus, which represent areas of mineralization in this youngster. A large cartilaginous cap can be seen normally in the humeral condyles and intermediate tubercle of the humerus in young foals; it gradually mineralizes.

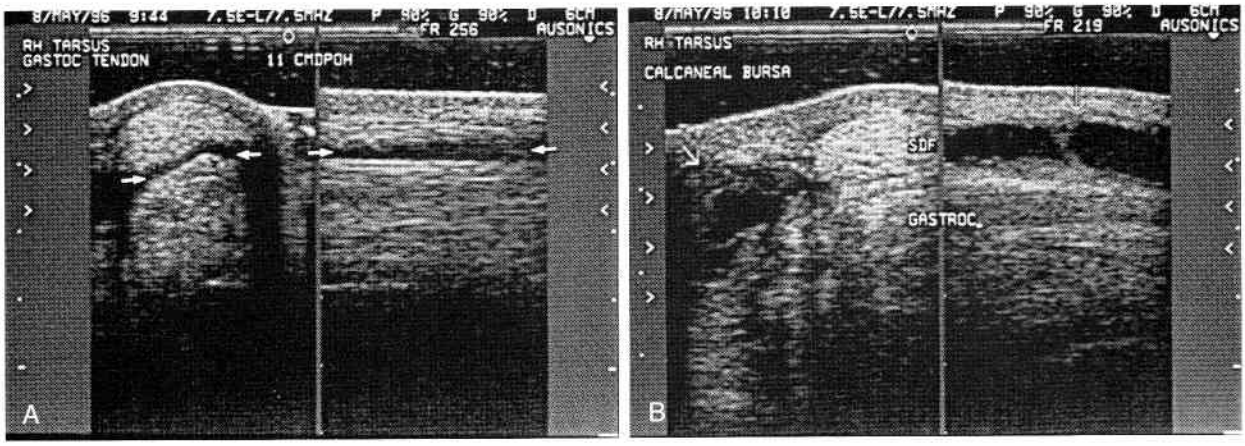

Figure 3–183

Sonograms of a nonseptic fibrinous calcaneal bursitis in the right hindlimb of a 7-year-old Thoroughbred mare. These sonograms were obtained with a wide-bandwidth 7.5-MHz linear-array transducer operating at 7.5-MHz using a hand-held standoff pad at a displayed depth of 6 cm. The focal zones are positioned in the near field of the image. The right side of the sagittal views *(right images)* is proximal and the left side is distal. The right side of the transverse views *(left images)* is lateral and the left side is medial.

A, Notice the anechoic fluid *(arrows)* between the more superficial digital flexor tendon and the deeper gastrocnemius tendon in the mid portion of the crus. The gastrocnemius tendon normally has a hypoechoic appearance at this level, 11 cm proximal to the point of the hock.

B, Notice the anechoic fluid-filled bursa with slight thickening of the synovial lining and fibrin crossing the bursa *(vertical down arrow)*. The fluid-filled bursa is bulging out between the superficial digital flexor tendon (SDF) and gastrocnemius tendon (gastroc) in the distal portion of the right crus.

sitis and bicipital tendinitis.[70] Extensive irregularities developed in the subchondral bone of this horse after surgical removal of the fracture fragments; a large fissure in the bicipital tendon and thickening of the peritendinous tissues with calcification also occurred, consistent with infection and osteomyelitis.[70]

Calcaneal Bursitis. Traumatic injuries to this area are common and result in hemorrhage into the bursa with a resultant loculated-fluid appearance. Inflammation of this bursa results in an anechoic to hypoechoic effusion within the bursa that is usually fibrinous. Loculations are usually detected within the synovial fluid (Fig. 3-183). Thickening of the synovial lining and of the bursa itself is frequently seen in horses with chronic bursitis in this region. Penetrating injuries to the calcaneal bursa are also common and may cause septic bursitis (Fig. 3-184). The sonographic findings previously reported in horses with calcaneal bursitis include fluid distention of the calcaneal bursa.[68] Chronic thickening of the bursa and adhesions of the tendons within the bursa (to each other or to the bursa) may be chronic sequelae of fibrinous bursitis (Fig. 3-185).

Gastrocnemius Bursitis. The equine gastrocnemius bursa may become distended with fluid without involvement of the calcaneal bursa, or both bursa may be involved with bursitis in the distal crus (Fig. 3-186). The bursitis may be traumatic or septic in origin.

Cunean Bursitis. The cunean bursa may become distended with anechoic to echogenic fluid in association with trauma or sepsis (Fig. 3-187). Tenotomy of the cunean tendon may also lead to thickening of the synovial lining and bursa, associated with fibrous scarring.

Supraspinous Bursitis. Fistulous withers is an inflammatory disease of the supraspinous bursa that is usually of long-standing duration. The inflammation and infection usually begin in the supraspinous bursa, with purulent fluid accumulating underneath the ligamentum nuchae.[141, 142] Trauma to the withers secondary to poorly fitting tack or a penetrating wound is another, less common cause of fistulous withers. *Brucella abortus* has traditionally been associated with fistulous withers, but many other organisms may also be responsible for this condition.

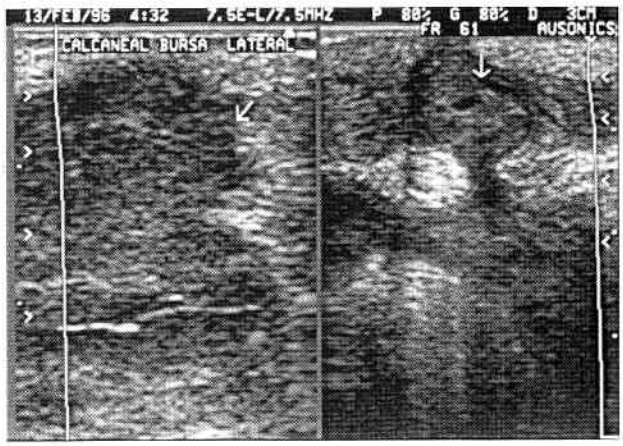

Figure 3–184

Sonograms of a septic calcaneal bursitis with rupture of the calcaneal bursa in the left hindleg, obtained from an 8-year-old Quarter horse gelding. Notice the communication of the bursa with the subcutaneous space *(arrow)* in the transverse view *(right image)* of the lateral aspect of the bursa at the site of the draining wound secondary to a previous penetrating wound. Notice the large amount of hypoechoic flocculent fluid in both the transverse view and the sagittal view *(left image)*. These sonograms were obtained with a wide-bandwidth 7.5-MHz linear-array transducer operating at 7.5-MHz at a displayed depth of 3 cm. The focal zones are positioned in the near field of the image. The right side of the transverse view *(right image)* is cranial and the left side is caudal. The right side of the sagittal view *(right image)* is proximal and the left side is distal.

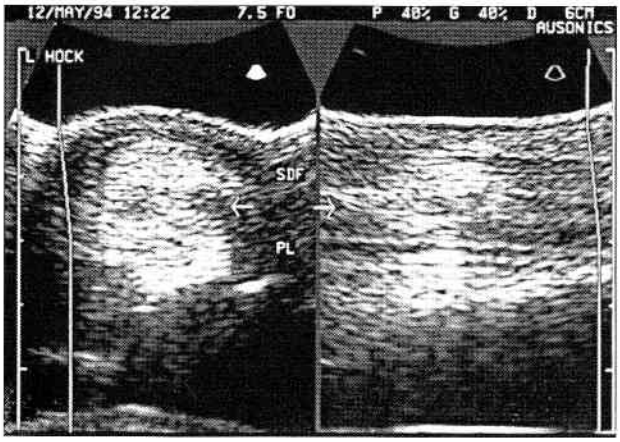

Figure 3–185

Sonograms of a chronic inactive calcaneal bursitis in the left hindlimb, obtained from a 9-year-old Shire gelding. Notice the hypoechoic and echogenic tissue between the superficial digital flexor tendon (SDF) and the plantar ligament (PL), consistent with synovial thickening and fibrosis of the calcaneal bursa. These sonograms were obtained with a 7.5-MHz sector-scanner transducer containing a built-in fluid offset at a displayed depth of 6 cm. The right side of the transverse view *(left image)* is lateral and the left side is medial. The right side of the sagittal view *(right image)* is proximal and the left side is distal.

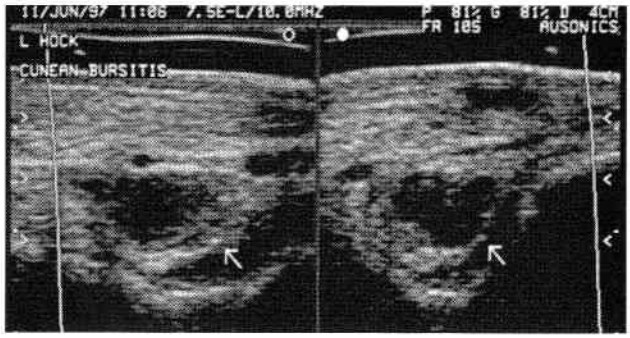

Figure 3–187

Sonograms of the dorsal aspect of the left hock obtained from an 8-year-old gelding with cunean bursitis. There is an anechoic collection of fluid *(arrows)* within the cunean bursa with hypoechoic strands representing fibrin consistent with a bursitis. This sonogram was obtained with a wide-bandwidth 7.5-MHz linear-array transducer operating at 10.0 MHz using a hand-held standoff pad at a displayed depth of 4 cm. The right side of the sagittal view *(left image)* is proximal and the left side is distal. The right side of the transverse view *(right image)* is lateral and the left side is medial.

Marked soft tissue swelling of the withers is usually present in affected horses, with local heat and swelling. Draining tracts are frequently present and, if detected, should be followed to their source, which is usually underlying bone (Fig. 3-188). Osteomyelitis of the dorsal spinous processes or transverse processes of the thoracic vertebrae is often present at the time of presentation (Fig. 3-189). Radiographic evidence of osteomyelitis was detected in 29% of horses with fistulous withers in one study.[143] Ultrasonography may reveal the extent of the infection; identify the number, location, and size of the fistulous tracts; and aid in the detection of foreign bodies, which are occasionally present in horses with osteomyelitis.[143] The presence and extent of bony involvement can be detected before lesions are seen radiographically (see Figs. 3-188 and 3-189), and any associated fracture fragments can be identified. Ultrasonography should be used to obtain a sample for culture and sensitivity testing. In many horses, the infection is located in the deeper tissues, requiring the use of a longer needle (spinal needle). Calcification of the surrounding soft tissues is not uncom-

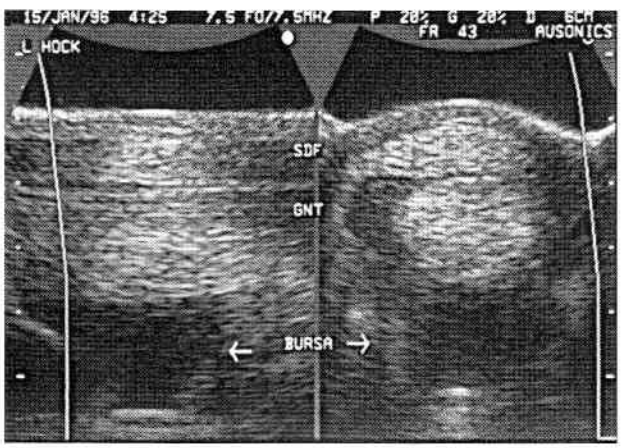

Figure 3–186

Sonograms of septic gastrocnemius bursitis *(arrows)*, obtained from an 8-year-old Quarter horse gelding. Notice the large amount of hypoechoic fluid dorsal to the gastrocnemius tendon (GNT) that extends around the sides of the tendon but is not between the GNT and the superficial digital flexor tendon (SDF). These sonograms were obtained with a wide-bandwith 7.5-MHz sector-scanner transducer operating at 7.5 MHz and containing a built-in fluid offset at a displayed depth of 6 cm. The right side of the sagittal view *(left image)* is proximal and the left side is distal. The right side of the transverse view *(right image)* is lateral and the left side is medial.

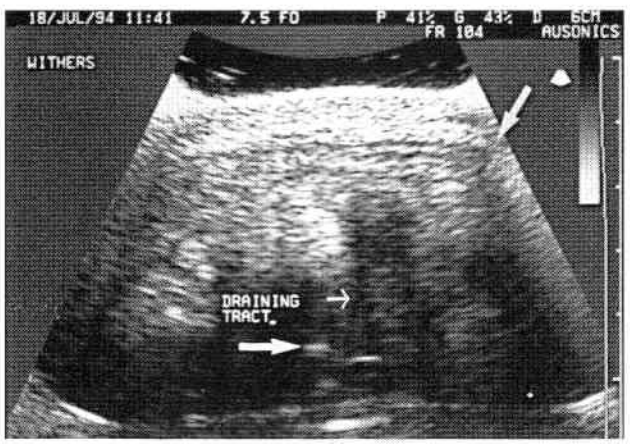

Figure 3–188

Sonogram of the withers obtained from a 16-year-old Thoroughbred Trakhener cross gelding with fistulous withers and a draining tract. There is a large amount of fluid overlying the dorsal spinous processes of the thoracic vertebrae. The fluid extends ventrally to the underlying bone and has resulted in a large fluid layer surrounding the dorsal spinous processes *(large arrow)*. A fluid tract is imaged extending from the dorsal spinous processes *(small arrow)* toward the skin *(diagonal arrow)*. The communication between the skin and the tract is not imaged in this sonogram but is just to the right of this image. This sonogram was obtained with a 7.5-MHz sector-scanner transducer containing a built-in fluid offset at a displayed depth of 6 cm. The right side of this sonogram is the left side of the withers and the left side of the image is to the right of the withers.

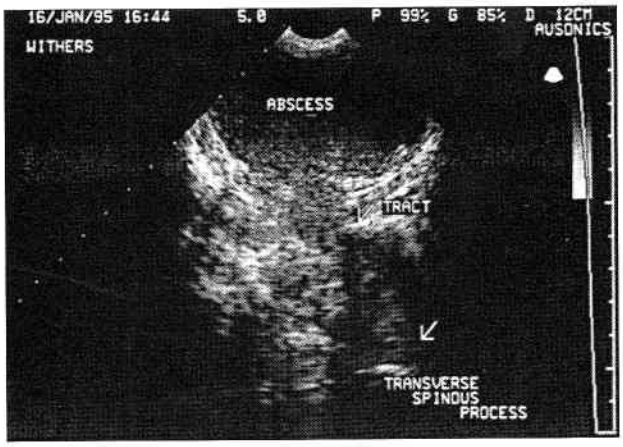

Figure 3–189

Sonogram of fistulous withers, obtained from an 8-year-old Appaloosa mare. Notice the hypoechoic fluid in the tract between the large subcutaneous abscess containing anechoic and hypoechoic fluid and the underlying right transverse processes of the thoracic vertebrae at the withers. This fluid layer overlying the bone extended from the third to the seventh thoracic transverse processes. This sonogram was obtained with a 5.0-MHz sector-scanner transducer at a displayed depth of 12 cm. The right side of this sonogram is towards the right side of the withers and the left side is towards the left side of the withers.

mon in horses with fistulous withers. On occasion, calcifications make following the purulent tracts to the underlying bone (dorsal spinous processes) difficult.[105] Many horses with fistulous withers have multiple tracts in the swollen tissue over the dorsal spinous processes, and each tract should be carefully followed deeper to its origin (necrotic tissues, infected bone, foreign body) to obtain an accurate appreciation of the extent of the infection (see Fig. 3-188). Infection of the supraspinous bursae and/or osteomyelitis of the dorsal spinous processes of the thoracic vertebrae in the region of the withers must be differentiated from more benign conditions of the withers.

Hematomas from poorly fitting tack or fractures of the dorsal spinous processes (Fig. 3-190) also occur and can be differentiated ultrasonographically. The classic anechoic loculated fluid of a hematoma should be detected in horses with traumatic injuries to the withers. A fluid layer adjacent to the underlying bone cannot be detected unless a recent fracture of the dorsal spinous processes has occurred. The fracture fragments in this situation are easy to identify ultrasonographically. Thus, differentiating traumatic injury from infection is relatively easy in the withers.

Atlantal Bursitis and Poll Evil. Bursitis of the atlantal bursa or the bursa over the axis (Fig. 3-191) is uncommon but can be identified ultrasonographically. Affected horses usually have swelling in the poll region, often with local heat and sensitivity. Sonographic examination usually reveals extensive soft tissue swelling in the region of the poll, with a localized or more widespread area of fluid accumulation. The fluid is usually hypoechoic and may be contained within the bursa in horses with bursitis (see Fig. 3-191). Alternatively, a fluid layer overlying the underlying bone consistent with osteomyelitis of the poll region (Fig. 3-192), with or without bursal involvement, may occur in horses with poll evil. Tracts may be found extending up to the skin surface in horses with poll evil (see Fig. 3-192). Calcification of the surrounding soft tissues is often present with long-standing disease.

Neuromas

Neuromas occur most frequently in the horse in association with posterior digital neurectomies. These painful enlargements of the nerve are usually associated with surgical transection of the nerve, but can also occur with

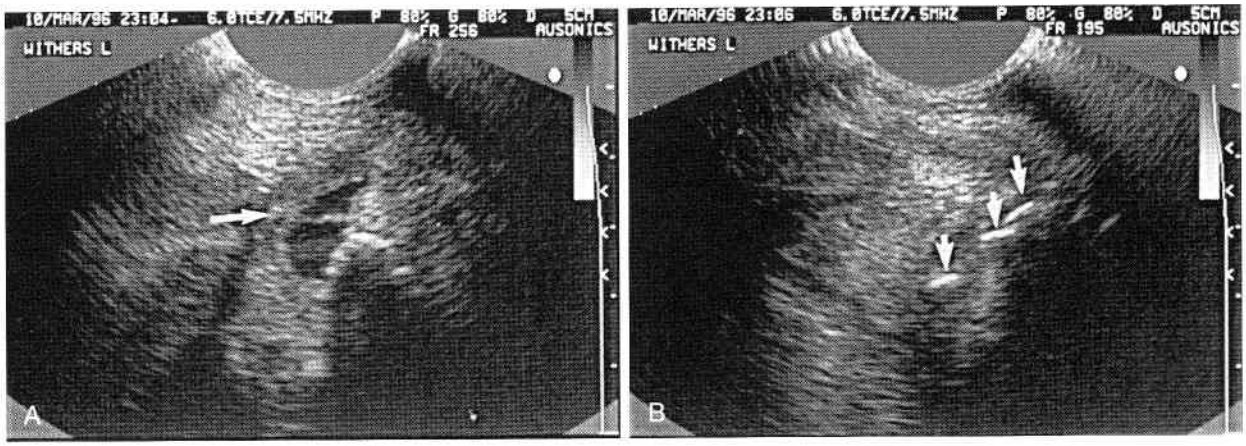

Figure 3–190

Sonograms of fractured dorsal spinous processes and a hematoma at the withers, obtained from an 11-year-old Thoroughbred gelding with a history of recent trauma to the withers. These sonograms were obtained with a wide-bandwidth 6.0-MHz microconvex linear-array transducer operating at 7.5 MHz at a displayed depth of 5 cm. The focal zones are in the near field of the images. The right side of these transverse views is the right side of the withers and the left side is the left side of the withers.

A, Notice the anechoic loculated fluid collection to the left of the dorsal spinous process *(arrow)*, consistent with a hematoma.

B, Notice the multiple hyperechoic structures casting acoustic shadows *(arrows)* in the region of the dorsal spinous process, consistent with fracture fragments immediately cranial to the hematoma.

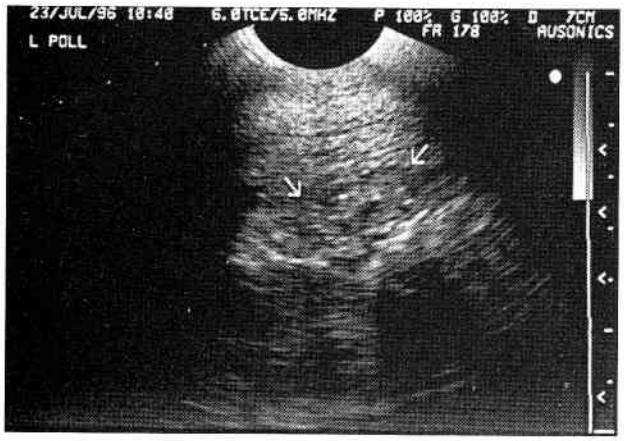

Figure 3–191

Sagittal sonogram of a septic bursitis within the caudal nuchal bursa, obtained from a 30-year-old Appaloosa mare (same horse as in Fig. 3-151). Notice the hypoechoic, somewhat oval swelling underneath the ligamentum nuchae just to the left and caudal to the poll. Several small hyperechoic echoes are within the bursa and may represent pinpoint areas of calcification or possible gas. The distal portion of the atlas is very irregular with evidence of lytic and proliferative changes, consistent with osteitis or osteomyelitis. This sonogram was obtained with a wide-bandwidth 6.0-MHz microconvex linear transducer operating at 5.0 MHz at a displayed depth of 7 cm. The right side of the image is cranial and the left side is caudal.

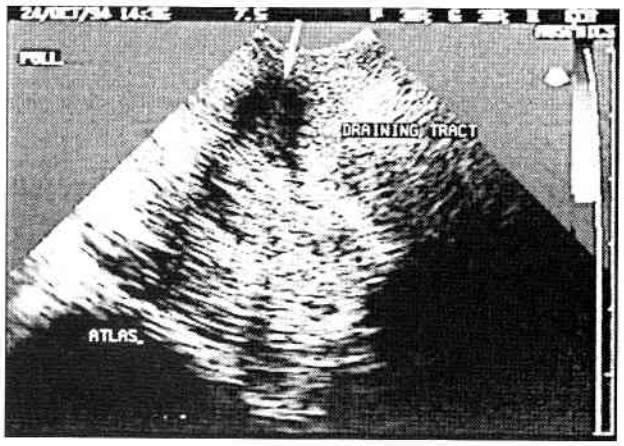

Figure 3–192

Sagittal sonogram of poll evil, obtained from a 26-year-old Quarter Horse cross gelding. Notice the large irregular anechoic tract extending down to the atlas *(arrow)* and the larger amount of soft tissue swelling surrounding the draining tract. This sonogram was obtained with a 7.5-MHz sector-scanner transducer at a displayed depth of 6 cm. The right side of the sagittal image is proximal and the left side is distal.

local trauma. The abnormal digital nerve is easier to locate than the normal digital nerve because it is larger and usually more hypoechoic (Fig. 3-193). Also, in most horses in which a posterior digital neurectomy has been performed, a soft tissue swelling is palpable at the site of the neurectomy. The neuroma imaged after a posterior digital neurectomy has a bulbous appearance with a large cross-sectional area, often greater than or equal to 0.2 cm^2 (see Fig. 3-193). The swollen nerve ending is usually hypoechoic and homogeneous, similar to findings in humans with neuromas.[144, 145] The echogenicity of the neuroma may be heterogeneous or homogeneous, depending on the surgical procedure used to perform the neurectomy and the surrounding perineuronal reaction (Fig. 3-194). Significant perineuronal soft tissue swelling is usually imaged around the neuroma. This perineuronal soft tissue swelling is hypoechoic to anechoic if acute inflammation surrounds the nerve or if infection is present within the neuroma (see Fig. 3-194). Echogenic perineuronal thickening is detected in some horses, consistent with fibrous scar tissue surrounding the neuroma (Fig. 3-195). In some instances, the more echogenic perineuronal scar can be differentiated from the relatively hypoechoic neuroma. In other horses, the neuroma is indistinguishable from the perineuronal scar tissue. The type of neurectomy performed can often be determined

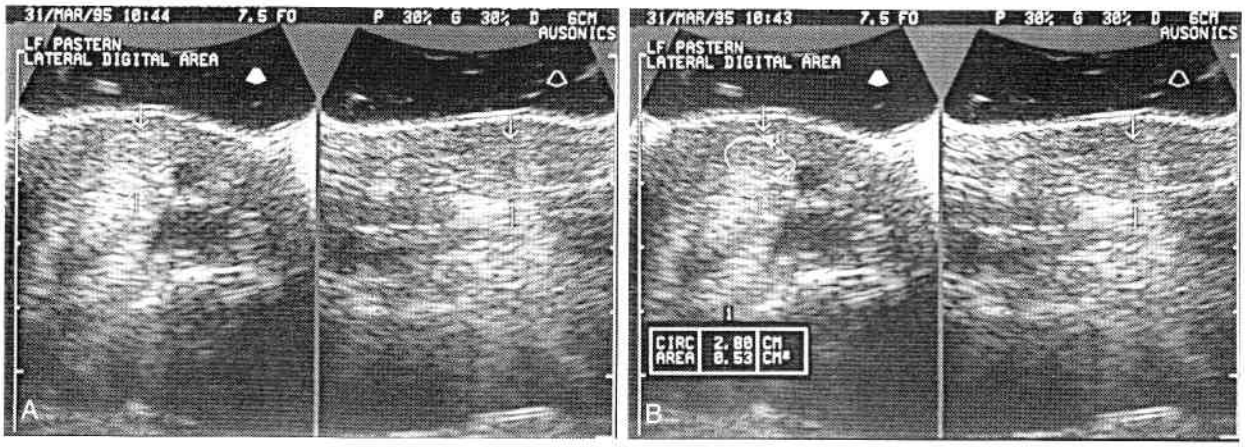

Figure 3–193

Sonograms of a neuroma in the lateral digital nerve of the left foreleg, obtained from a 15-year-old Warmblood gelding. A second posterior digital neurectomy had been performed 4 months earlier. The small anechoic circular structure to the right of the lateral digital nerve in the transverse view is the lateral digital artery. These sonograms were obtained with a 7.5-MHz sector-scanner transducer containing a built-in fluid offset at a displayed depth of 6 cm. The right side of the sagittal views *(right images)* is proximal and the left side is distal. The right side of the transverse views *(left images)* is dorsal and the left side is palmar.

A, Notice the enlarged bulbous hypoechoic end of the lateral digital nerve *(arrows)* with minimal perineuronal swelling.

B, The cross-sectional area of the neuroma is 0.53 cm^2, which is markedly enlarged.

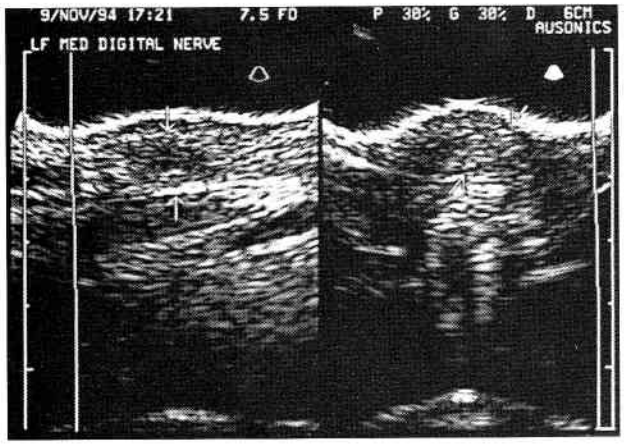

Figure 3–194

Sonograms of a neuroma in the medial digital nerve in the left foreleg, obtained from a 14-year-old Hanoverian gelding. A posterior digital neurectomy had been performed 4 months earlier. Notice the enlarged hypoechoic end of the medial digital nerve with an anechoic center imaged in the sagittal view *(arrows)* in the proximal pastern consistent with an infected neuroma. These sonograms were obtained with a 7.5-MHz sector-scanner transducer containing a built-in fluid offset at a displayed depth of 6 cm. The right side of the sagittal view *(left image)* is proximal and the left side is distal. The right side of the transverse view *(right image)* is dorsal and the left side is palmar.

if the transected end of the nerve was sutured or capped. Neuromas can also occur without surgical or traumatic transection of the nerve, but this is much less common. A hypoechoic homogeneous bulbous enlargement of the nerve is imaged in neuromas not involving transection of the nerve (Fig. 3-196).

The normal appearance of a posterior digital neurectomy site, if the surgery was successful and neuroma formation did not occur, is an echogenic distal nerve end with little enlargement and little perineuronal reaction (Fig. 3-197). The transected proximal end of the nerve should be imaged with no communication distally to nerve tissue.

Muscle

The most common abnormalities detected sonographically in equine muscle are areas of muscle fiber disruption and loculated anechoic fluid accumulation or hemorrhage (Fig. 3-198), associated with trauma to the underlying muscle. With complete muscle rupture, the free edge of the torn muscle is usually imaged floating in the surrounding fluid. Hypoechoic to echogenic clot may be imaged in the hemorrhagic fluid at the site of muscle fiber disruption (Fig. 3-199). Injuries to the muscles of the shoulder girdle (Fig. 3-200) and hindlimb (see Fig. 3-199) are most common. In humans, the detection of fluid-filled anechoic areas within the muscle or echogenic areas of clot correlates well with underlying muscle abnormality.[116] Ultrasound in the human athlete is now well accepted as an effective and accurate diagnostic method.[147, 148] The muscle(s) affected can be identified by carefully following the muscle bellies from their origin to their insertion.

Acute injuries to the lateral digital extensor muscle and biceps femoris muscle in the hindlimb of a horse and foal, respectively, have been detected sonographically.[68, 99] The muscle appeared swollen with loss of normal echogenicity. With aspiration, an intramuscular hematoma was confirmed. Ultrasonography of one foal with gastrocnemius rupture revealed a large cavernous fluid-filled area in the stifle region.[135] Ultrasonographic examination of one horse with incomplete rupture of the proximal caudal reciprocal apparatus from its origin on the femur revealed a large fluid-filled area along the proximal lateral tibia associated with fluid dissecting distally.[149] Necrosis

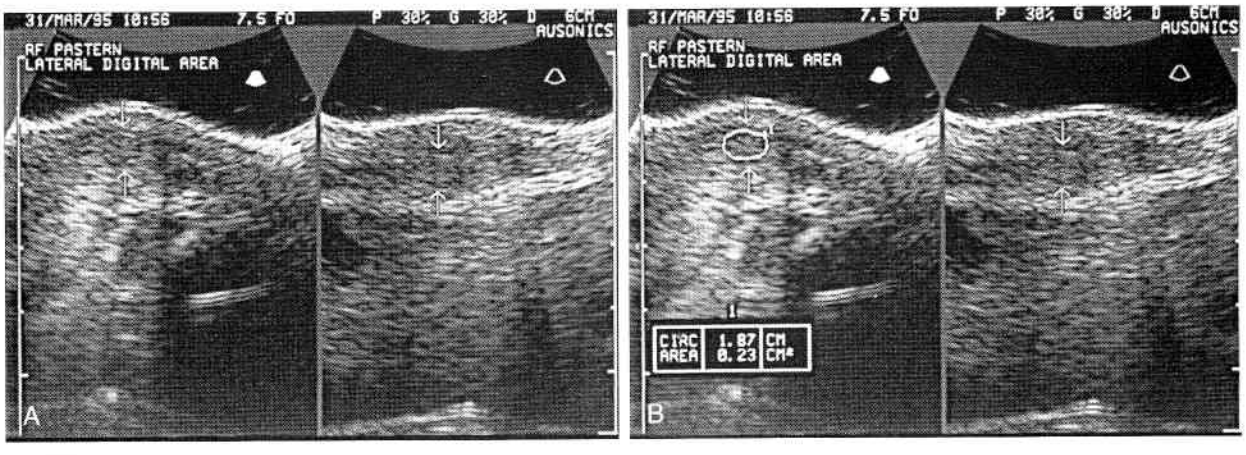

Figure 3–195

Sonograms of a neuroma in the lateral digital nerve of the right foreleg, obtained from a 15-year-old Warmblood gelding (same horse as in Fig. 3-193). A second posterior digital neurectomy had been performed 4 months earlier. These sonograms were obtained with a 7.5-MHz sector-scanner transducer containing a built-in fluid offset at a displayed depth of 6 cm. The right side of the sagittal views *(right images)* is proximal and the left side is distal. The right side of the transverse views *(left images)* is dorsal and the left side is palmar.

A, Notice the hypoechoic bulbous lateral digital nerve ending *(arrows)* surrounded by a slightly more echogenic rim of tissue, which probably represents perineuronal fibrosis (confirmed at surgery).

B, The cross-sectional area of the neuroma measured 0.23 cm^2 and would measure more than twice as much if the perineuronal fibrous tissue were included in the measurement.

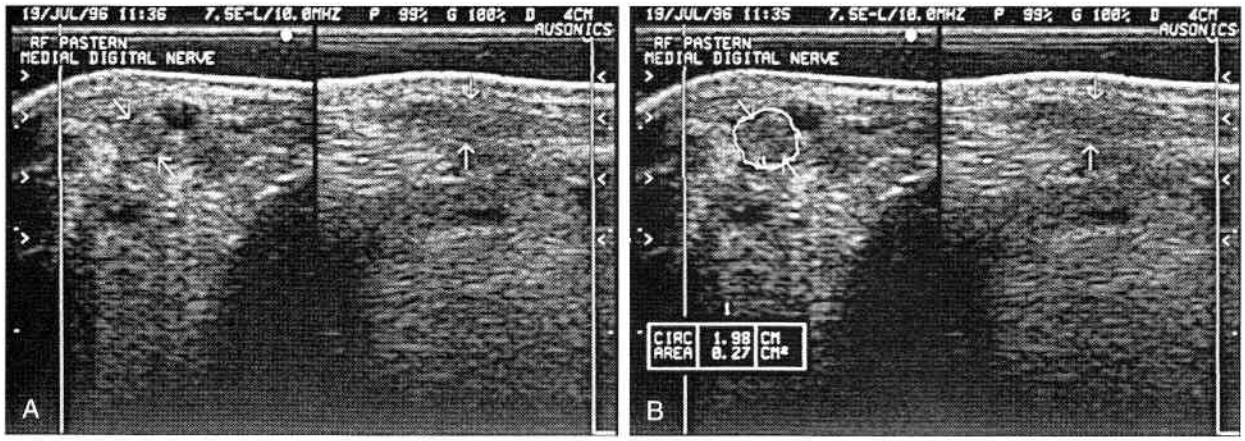

Figure 3–196

Sonograms of a neuroma *(arrows)* involving the medial digital nerve in the right foreleg, of a 3-year-old Thoroughbred filly. This filly had an intact medial digital nerve with a bulbous hypoechoic swelling in the nerve in the proximal pastern region. These sonograms were obtained with a wide-bandwidth 7.5-MHz linear-array transducer operating at 10.0 MHz with use of a hand-held standoff pad at a displayed depth of 4 cm. The right side of the transverse views *(left images)* is dorsal and the left side is palmar. The right side of the sagittal views *(right images)* is proximal and the left side is distal.

A, Notice the hypoechoic to anechoic bulging of the medial digital nerve *(arrows)*. In the sagittal view *(right image)* the more proximal portion of the nerve has a smaller, (but not normal) diameter, but is still hypoechoic. The diameter of the medial digital nerve in the distal portion (distal to the bulbous swelling) is normal and the echogenicity is normal (echogenic).

B, The cross-sectional area of the neuroma is large: 0.27 cm^2.

of the gastrocnemius muscle and surrounding semitendinosus, semimembranosus, vastus medialis, gracilis, and adductor muscles was also present in this foal at postmortem examination. Although gastrocnemius muscle rupture has been reported in the horse, its sonographic diagnosis has not been reported with acute injury.[135, 150] Partial rupture of the gastrocnemius muscle has been detected sonographically, however (Fig. 3–201). Large areas of muscle fiber tearing should be imaged in horses with gastrocnemius muscle rupture, as in horses with muscle fiber disruption of other muscle bellies.

Although complete disruptions of muscle bellies are usually associated with large hematomas and palpable abnormalities, partial ruptures are more difficult to diagnose. Ultrasonographic examination of the affected muscle can be extremely useful in the diagnosis of partial muscle ruptures, particularly in deeper areas where palpation is less helpful (Fig. 3–202). A loss of the normal striated pattern is detected, often with a jagged edge and increased echogenicity of the margins of the torn muscle. Partial ruptures in the muscle may be associated with defects in the muscle fascia, in addition to the partial

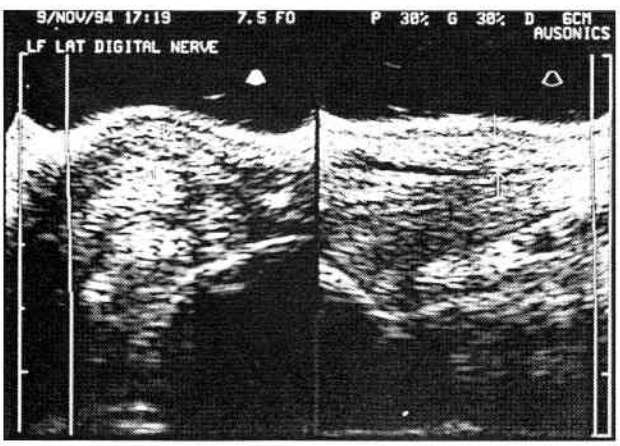

Figure 3–197

Sonograms of a transected lateral posterior digital nerve in the left foreleg of a 14-year-old Hanoverian gelding. Notice the small diameter of the echogenic remnant of the lateral digital nerve *(arrows)* and the minimal perineuronal soft tissue thickening. These sonograms were obtained with a 7.5-MHz sector-scanner transducer containing a built-in fluid offset at a displayed depth of 6 cm. The right side of the sagittal view *(right image)* is proximal and the left side is distal. The right side of the transverse view *(left image)* is dorsal and the left side is palmar.

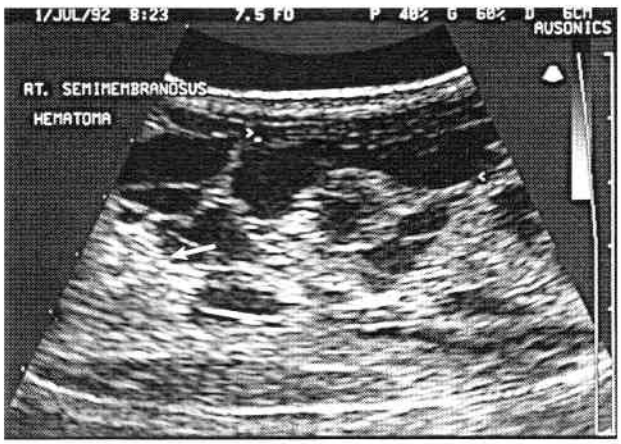

Figure 3–198

Sagittal sonogram of a large area of muscle fiber tearing and loculation in the right semimembranosus muscle of a 6-year-old Thoroughbred gelding. Notice the large, loculated, fluid-filled cavity and muscle fiber disruption in the semimembranosus muscle *(arrowheads)* with only a small amount of muscle tissue remaining *(arrow)*. This sonogram was obtained with a 7.5-MHz sector-scanner transducer containing a built-in fluid offset at a displayed depth of 6 cm. The right side of this image is proximal and the left side is distal.

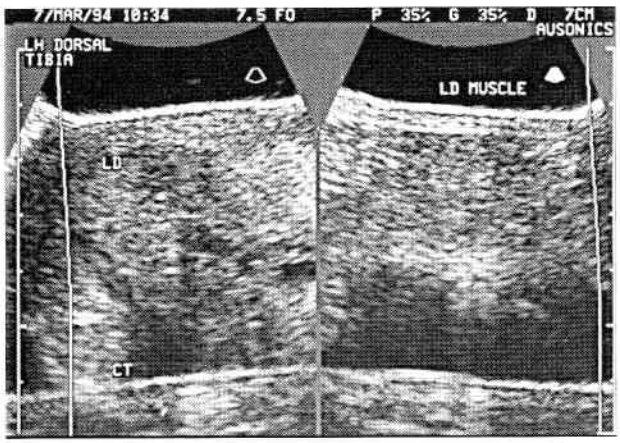

Figure 3–199

Sonograms of a large area of muscle fiber tearing involving the long digital (LD) extensor muscle and cranial tibial (CT) muscle in the left hind leg of a 10-year-old Thoroughbred cross mare. Notice the hypoechoic material filling the defect between the ruptured muscle; this represents organizing clot. These sonograms were obtained with a 7.5-MHz sector-scanner transducer containing a built-in fluid offset at a displayed depth of 7 cm. The right side of the sagittal view *(right image)* is proximal and the left side is distal. The right side of the transverse view *(left image)* is caudal and the left side is cranial.

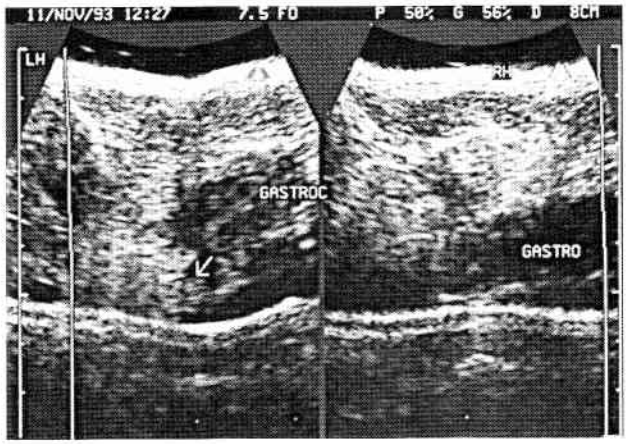

Figure 3–201

Transverse sonograms of an area of muscle tearing and fibrosis in the gastrocnemius muscle in the left hind limb of a 14-year-old Quarter Horse gelding. Notice the hypoechoic defect in the gastrocnemius muscle (gastroc) adjacent to an echogenic area in the muscle *(arrow)* in the left hind leg *(left image)*, compared to the same area in the right hind leg *(right image)*. This represents an area of recent muscle fiber injury adjacent to an older area of scarring. These sonograms were obtained with a 7.5-MHz sector-scanner transducer containing a built-in fluid offset at a displayed depth of 8 cm. The right side of the images is lateral and the left side is medial.

tear in the muscle belly (Fig. 3-203). Thickening and inflammation of muscle fascia, or fasciitis, has also been identified sonographically. The affected fascia was thickened and its echogenicity was initially decreased, although the fascial echogenicity in this horse increased as the fasciitis continued.

As the muscle tear repairs, the area fills in with granulation tissue that appears hypoechoic (Fig. 3-204). If the original sonogram revealed echogenic clot in the area of muscle rupture, this area will become less echogenic as the muscle heals.[151] In most horses, an anechoic loculated hematoma is detected; therefore, the echogenicity of the area of muscle rupture increases as this area heals with regenerating muscle fibers. Echogenic areas or areas of heterogeneous mixed echogenicity are associated with fibrous scarring in the muscle of human athletes.[146] Echogenic areas associated with the replacement of normal muscle with fibrous scar tissue are also commonly seen in horses and may be associated with gait abnormalities.

The most common places these areas of fibrotic myopathy are seen are the semitendinosus/semimembranosus muscles (Fig. 3-205) and the muscles surrounding the

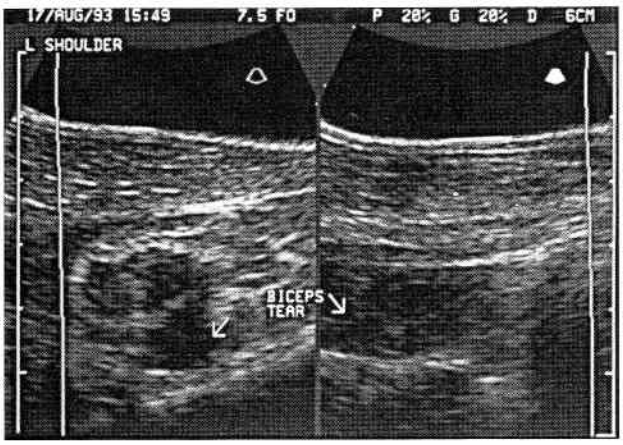

Figure 3–200

Sonograms of an area of muscle fiber tearing in the biceps brachii muscle *(arrows)* near its musculotendinous junction in the left foreleg, obtained from a 3-month-old Thoroughbred colt. Notice the defect in the muscle *(arrows)* that is filled with anechoic fluid and hypoechoic filmy echoes, representing fibrin. These sonograms were obtained with a 7.5-MHz sector-scanner transducer containing a built-in fluid offset and a displayed depth of 6 cm. The right side of the sagittal view *(right image)* is proximal and the left side is distal. The right side of the transverse view *(left image)* is lateral and the left side is medial.

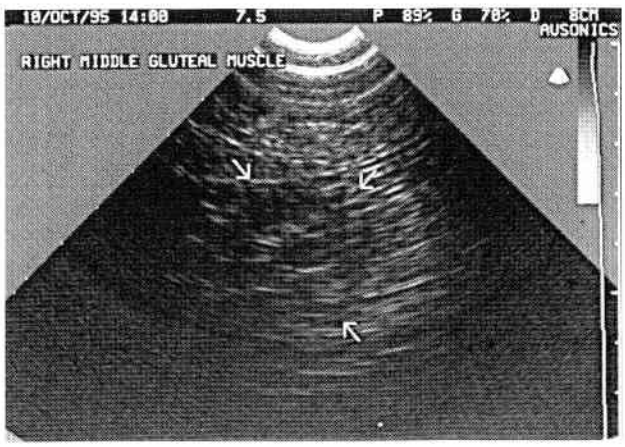

Figure 3–202

Sonogram of an area of tearing in the right middle gluteal muscle, obtained from an 8-year-old Thoroughbred gelding. Notice the anechoic loculated area in the middle gluteal muscle *(arrows)*. This sonogram was obtained with a 7.5-MHz sector-scanner transducer at a displayed depth of 8 cm. The right side of the image is cranial and the left side is caudal.

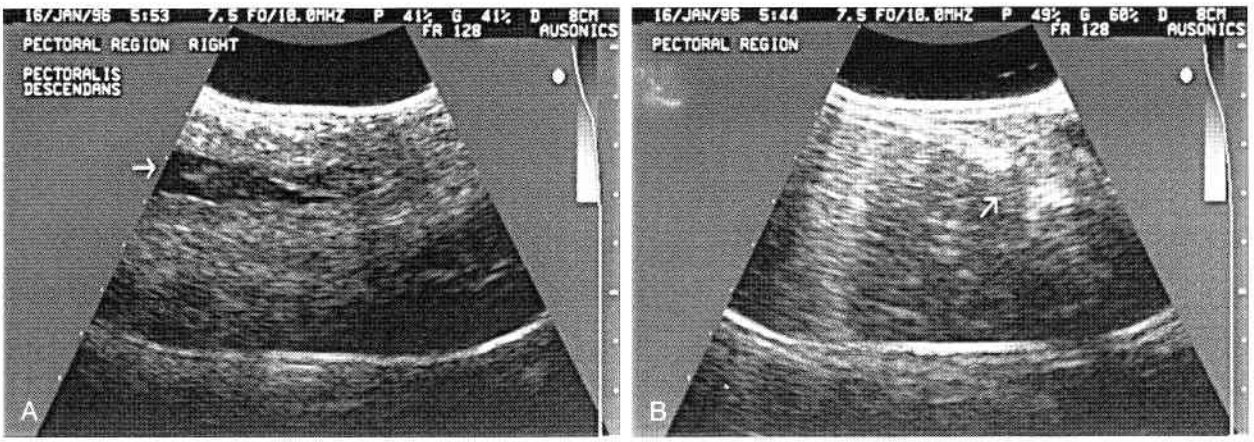

Figure 3–203

Sonograms of a muscle tear and fascial defect in the right pectoralis descendens muscle of a 2-year-old Quarter horse gelding. These long-axis sonograms were obtained with a wide-bandwidth 7.5-MHz sector-scanner transducer operating at 10.0 MHz with a built-in fluid standoff pad at a displayed depth of 8 cm. The right side of the sonograms is proximal and the left side is distal.

A, Notice the anechoic fluid containing hypoechoic fibrin in the muscle defect *(arrow)* and the loss of the normal muscle speckle pattern.

B, Notice the defect in the superficial muscle fascia and the associated area of muscle fiber disruption deep to the area of fascial rupture.

shoulder girdle (Fig. 3-206). Fibrotic myopathy has also been detected sonographically in the cranial tibial and long digital extensor muscles of a horse with a history of rupture of the peroneus tertius tendon.[68] Fibrous bands were detected ultrasonographically in the biceps femoris muscle of one horse with fibrotic myopathy.[152] Hyperechoic areas casting acoustic shadows can also be detected in muscle, associated with calcification. This has been reported in some horses with fibrotic myopathy (Fig. 3-207). Defects in the muscle belly may also be imaged in association with a fibrotic myopathy (Fig. 3-208).

Both fat and fibrosis can result in increased muscle echogenicity.[146, 151-154] Fat is a common cause of increased muscle echogenicity in children with neuromuscular disease.[153, 154] Although intramuscular lipomatosis usually results in echogenic muscle, hypoechoic muscle has been reported with severe lipomatosis.[155] In the one case report of a horse with an infiltrative lipoma, the lipoma appeared hypoechoic compared to the surrounding muscle, with an isoechogenic border between the tumor and the surrounding normal musculature.[156] Marked enlargement of the affected muscle bellies, with some loss of

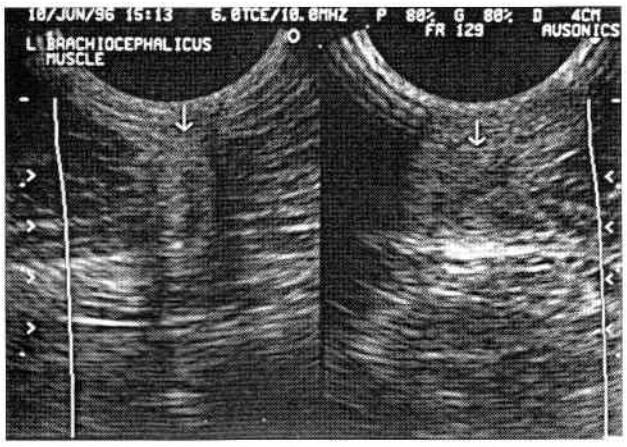

Figure 3–204

Sonograms of an area of repairing muscle injury in the brachiocephalicus muscle of the left foreleg of a 16-year-old Trakhener gelding. Notice the disruption in the normal longitudinal striations in the brachiocephalicus muscle *(down arrows)*, which has filled in with hypoechoic tissue. This hypoechoic tissue probably represents granulation tissue and early fibrous tissue. Shadow artifacts are created at the abrupt edge of the normal muscle and its junction with the area of repair. This sonogram was obtained with a wide-bandwidth 6.0-MHz microconvex linear-array transducer operating at 10.0 MHz with a displayed depth of 4 cm. The focal zones are positioned in the middle of the image. This is a long-axis view *(left image)* of the brachiocephalicus muscle with the right side of the sonogram being proximal and the left side distal. The corresponding transverse view *(right image)* displays lateral on the right side of the image and medial on the left.

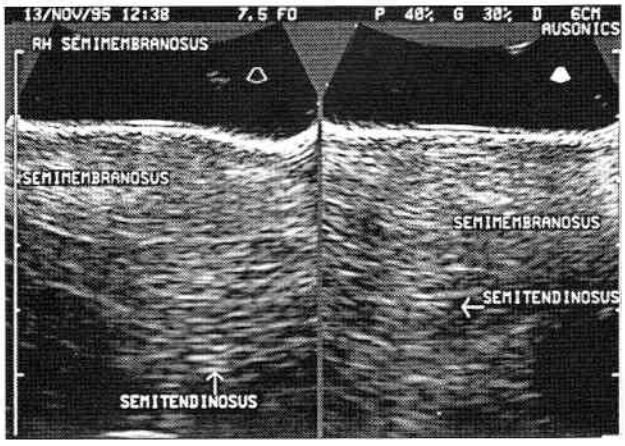

Figure 3–205

Sonograms of an area of fibrotic myopathy involving the semimembranosus and semitendinosus muscles in the right hind leg of a 15-year-old Thoroughbred Quarter horse cross gelding. Notice the focal echogenic areas in the semimembranosus and semitendinosus muscles *(arrows)* with the loss of some of the normal speckled muscle fiber pattern. These sonograms were obtained with a 7.5-MHz sector-scanner transducer containing a built-in fluid offset at a displayed depth of 6 cm. The right side of the sagittal view *(left image)* is proximal and the left side is distal. The right side of the transverse view *(right image)* is lateral and the left side is medial.

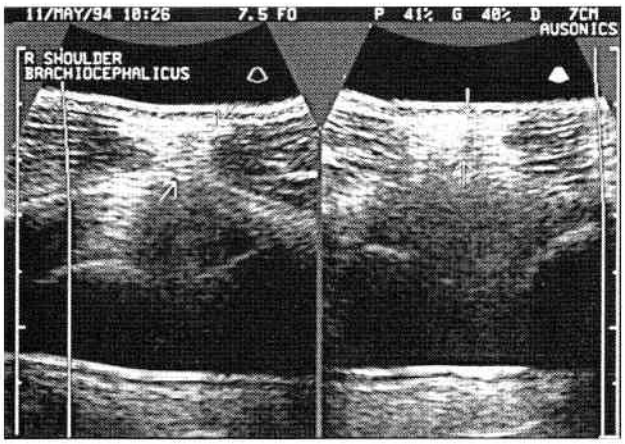

Figure 3–206

Sonograms of an area of fibrotic myopathy in the right brachiocephalicus muscle of a 3-year-old Standardbred colt. Notice the marked increase in echogenicity of the muscle, the contracture of the muscle at this location *(arrows)*, and the loss of the normal muscle speckle pattern. These sonograms were obtained with a 7.5-MHz sector-scanner transducer containing a built-in fluid offset at a displayed depth of 7 cm. The right side of the sagittal view *(right image)* is proximal and the left side is distal. The right side of the transverse view *(left image)* is lateral and the left side is medial.

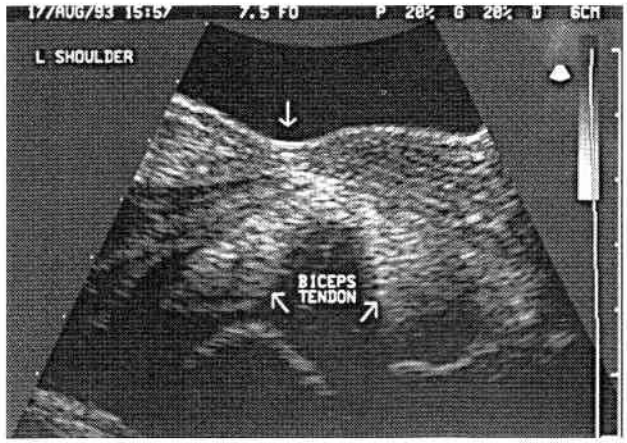

Figure 3–208

Transverse sonogram, obtained from a 3-month-old Thoroughbred cross colt with a ruptured brachiocephalicus muscle *(vertical arrow)* overlying the left bicipital tendon. Notice the defect in the muscle, with the abrupt discontinuation of muscle fibers in this area; little echogenic tissue is replacing the defect (minimal fibrosis) at this time. This sonogram was obtained with a 7.5-MHz sector-scanner transducer containing a built-in fluid offset at a displayed depth of 6 cm. The right side of the sonogram is lateral and the left side is medial.

the normal striated muscle pattern and a decrease in muscle echogenicity, was detected in one horse with steatitis (Fig. 3–209).

Sonographic findings with postanesthetic myopathy in horses consist of a loss of the normal muscle striations and an overall increase in muscle echogenicity.[89] A focal area of increased muscle echogenicity and loss of normal muscle striations correlated with a necrotic area in the muscle detected at postmortem examination in one horse that was humanely destroyed for other reasons.[89] Five other horses recovered from their postanesthetic myopathy. The affected triceps muscles returned to a normal ultrasonographic appearance in all but one horse, whose triceps muscle had focal hyperechoic regions persisting for at least 10 weeks after the postanesthetic myopathy.[89] Increased muscle echogenicity has also been reported in humans with chronic inflammatory myopathies.[157] Muscle edema, an important component of postanesthetic myopathy in horses, has been reported in humans to yield both decreased and increased muscle echogenicity.[157, 158]

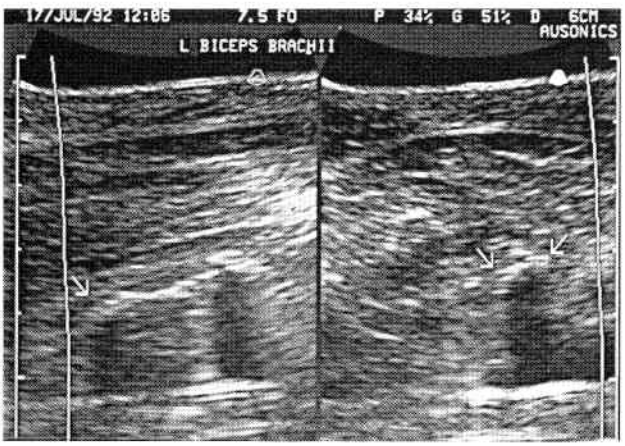

Figure 3–207

Sonograms of an area of calcifying myopathy of the biceps brachii muscle, obtained from a 3-year-old Thoroughbred colt. Notice the hyperechoic areas in the biceps brachii muscle casting strong acoustic shadows consistent with areas of calcification. Notice the disruption of some of the adjacent muscle, best visualized in the transverse view *(right image)*. These sonograms were obtained with a 7.5-MHz sector-scanner transducer containing a built-in fluid offset at a displayed depth of 6 cm. The right side of the sagittal view *(left image)* is proximal and the left side is distal. The right side of the transverse view is lateral and the left side is axial.

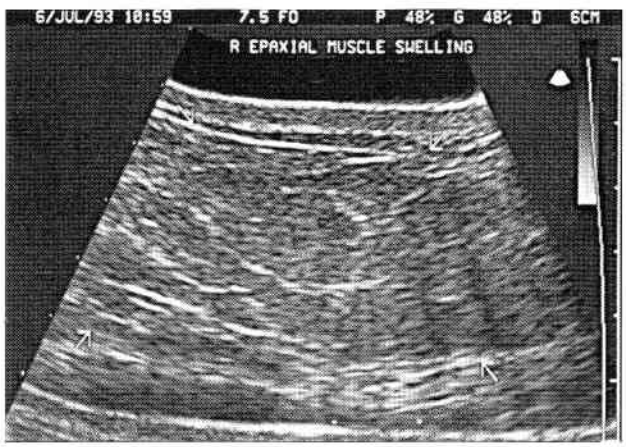

Figure 3–209

Transverse sonogram of the right epaxial muscles, obtained from a 14-year-old Arabian cross gelding with steatitis. Notice the replacement of some of the muscle tissue with homogeneous hypoechoic tissue, and the separation of the normal interfacial fascia. Biopsy of this swelling confirmed fatty replacement of muscle tissue consistent with steatitis. This sonogram was obtained with a 7.5-MHz sector-scanner transducer containing a built-in fluid offset at a displayed depth of 6 cm. The right side of the sonogram is axial and the left side is to the right side of the back.

Some of this apparent discrepancy in the echogenicity of edematous muscle may have to do with the severity of the inflammatory component that is usually present in diseases causing muscle edema. In humans with rhabdomyolysis, the muscle initially appears heterogeneous, with patchy areas of mixed echogenicity. As the disease becomes more chronic, these areas may become more hypoechoic and fluid-filled.[159, 160]

Loss of normal muscle architecture also occurs with a necrotizing myositis, often associated with bacterial infection. Abscesses in muscle bellies are frequently associated with disruption of the normal fiber pattern and replacement of this area with hypoechoic to echogenic fluid (Fig. 3-210).[161] Loculations may be detected in the abscess, especially if trauma was its underlying cause. Hyperechoic gas echoes casting typical shadows (reverberation artifacts or dirty shadows) indicate anaerobic infection (Fig. 3-211). Abscesses may be present in association with a foreign body. Foreign bodies are usually associated with fistulous tracts, which typically drain at the skin surface (Fig. 3-212). The draining tract should be followed back to its source and the origin of the drainage identified (see Chapter 11). The drainage associated with a fistulous tract usually originates at a foreign body or from necrotic bone or other necrotic tissue. Ultrasonography is extremely useful in the identification of foreign bodies, because many foreign bodies are not detectable radiographically.[42, 162] Foreign bodies usually cast a bright acoustic shadow with either a reverberation artifact or an acoustic shadow. Wood, steel wire, pencil graphite, rock, gravel, glass, and plastic all cast an acoustic shadow in turkey muscle, whereas BB pellets and nails created a comet-tail artifact.[163] Steel wire also created a reverberation artifact in addition to creating the comet-tail artifact, created by the BB pellet and the nail.[163] Hoof embedded in soft tissue also casts an acoustic shadow,

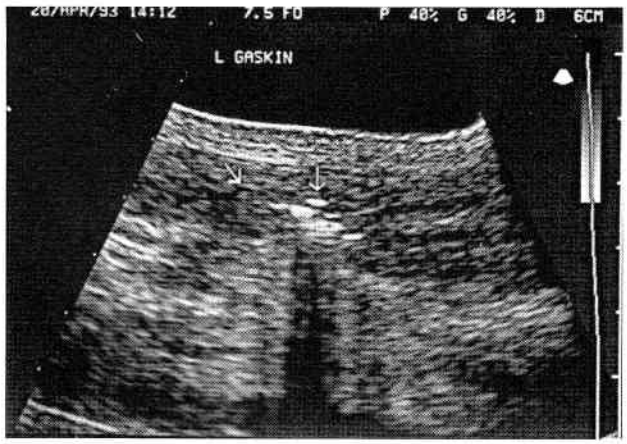

Figure 3–211

Sagittal sonogram of an area of muscle necrosis and anaerobic infection over the dorsal aspect of the left gaskin, obtained from a 9-year-old Thoroughbred gelding. Notice the complete loss of any normal muscle fibers in the injured muscle *(diagonal arrow)* with hyperechoic structures casting acoustic shadows consistent with gas *(vertical arrow)*. Anaerobes were cultured from this abscess in the necrotic muscle. This sonogram was obtained with a 7.5-MHz sector-scanner transducer containing a built-in fluid offset at a displayed depth of 6 cm. The right side of the sonogram is proximal and the left side is distal.

although its double-walled appearance can be detected sonographically.

A complex heterogeneous mass in the musculature is suggestive of an aggressive neoplasm, which is rare in horses (Fig. 3-213). Hemangiomas and hemangiosarcomas are the most common skeletal muscle tumors re-

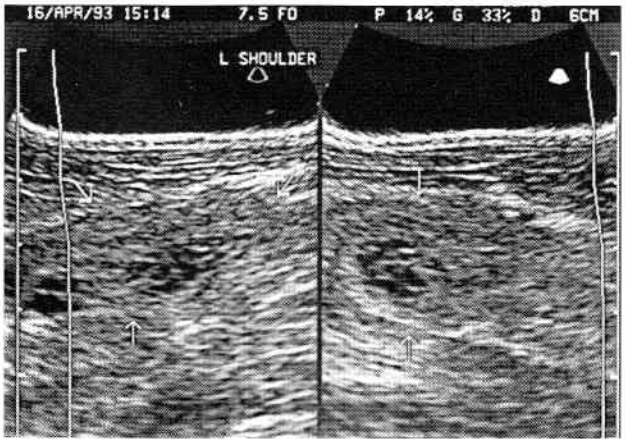

Figure 3–210

Sonograms of an area of muscle necrosis and abscess formation *(arrows)* in the scalenus muscle of the left foreleg, obtained from an 8-year-old Thoroughbred gelding. Notice the cavitation of the muscle with loss of the normal muscle fiber pattern. Anechoic loculated fluid is filling the muscle belly. These sonograms were obtained with a 7.5-MHz sector-scanner transducer containing a built-in fluid offset at a displayed depth of 6 cm. The right side of the long-axis view *(left image)* is proximal and the left side is distal. The right side of the short-axis view *(right image)* is cranial and the left side is caudal.

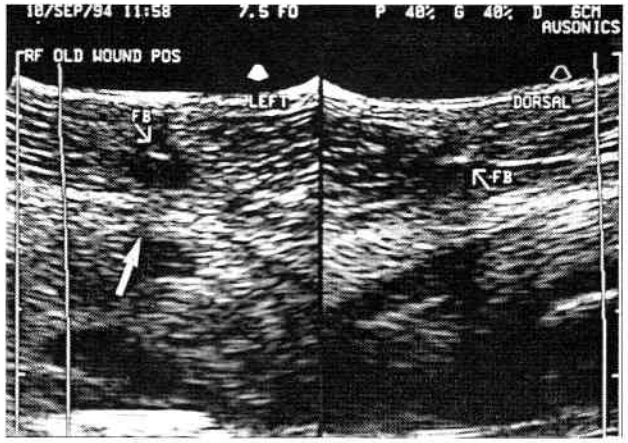

Figure 3–212

Sonograms of a small foreign body (FB) over the point of the right shoulder, obtained from a yearling Thoroughbred colt. Notice the small hyperechoic structure *(arrows)* surrounded by anechoic fluid and casting a weak acoustic shadow, consistent with a foreign body within the brachiocephalicus muscle. The foreign body, tract, and associated local infection did not involve the underlying bicipital tendon, best visualized in the sagittal view *(right image)*. However, the tract *(large arrow)* does appear to extend into the bicipital bursa, best visualized in the transverse view *(left image)* where an increased amount of fluid with a small amount of fibrin is present, consistent with a bicipital bursitis. These sonograms were obtained with a 7.5-MHz sector-scanner transducer containing a built-in fluid offset at a displayed depth of 6 cm. The right side of the short-axis image is the axial side of the shoulder. The right side of the long-axis image is proximal.

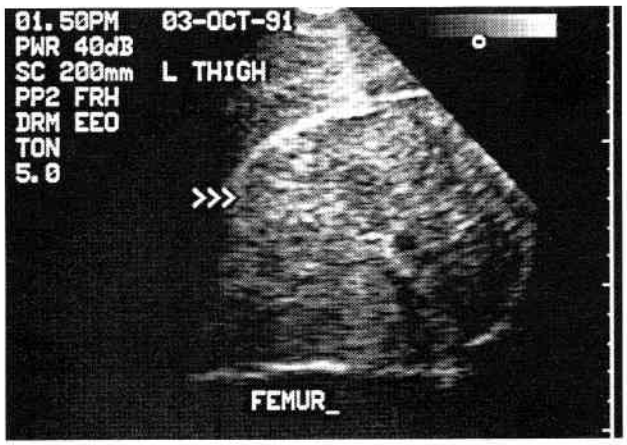

Figure 3–213

Sonogram of a rhabdomyosarcoma mass in the musculature of the caudomedial thigh in the left hind leg, obtained from a 21-year-old Thoroughbred mare. Notice the complex heterogeneous appearance of the mass *(arrowheads)*, completely disrupting the normal muscle fiber pattern and replacing the normal muscle. This complex appearance of the mass with hypoechoic to echogenic areas is consistent with a neoplasm. This sonogram was obtained with a 5.0-MHz sector-scanner transducer at a displayed depth of 20 cm. The right side of the sonogram is proximal and the left side is distal.

ported in horses. A large area of muscle fiber disruption is imaged in horses with skeletal muscle hemangiosarcoma (Fig. 3-214). The muscle fibers are replaced with anechoic loculated fluid and/or echogenic masses in horses with hemangiosarcoma. This tumor should always

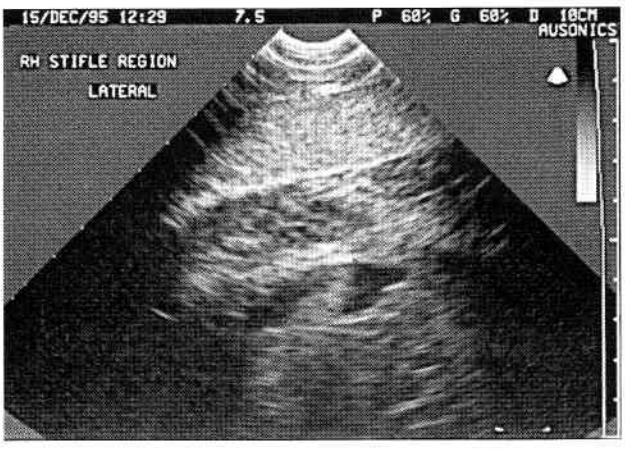

Figure 3–214

Sonogram of a hemangiosarcoma in the muscles of the lateral caudal and medial thigh and gaskin region in the right hind leg, obtained from a 2-year-old Thoroughbred gelding. Notice the complete disruption of the normal muscle architecture in the deeper musculature and the large anechoic fluid-filled areas within the muscle that contain hypoechoic fibrin. This disruption of the normal muscle architecture and replacement with fluid and fibrin is also seen in horses with muscle rupture. Differentiation between muscle rupture and a hemangioma or hemangiosarcoma is often difficult. In horses with primary muscle rupture, the free edge of the torn muscle is usually imaged adjacent to the hematoma. This free torn edge was lacking in this horse and all the caudal, lateral, and medial muscles of the thigh were involved, making a vascular neoplasm most likely. This sonogram was obtained with a 7.5-MHz sector-scanner transducer at a displayed depth of 10 cm. The right side of image is proximal and the left side is distal.

be on the differential diagnosis list of a horse with severe muscle fiber disruption. A vascular neoplasm should be suspected when the free edge of the torn muscle is not imaged and muscle fiber disruption is extensive. Echogenic masses replacing the normal muscle are frequently imaged in horses with hemangiosarcomas (see Chapter 11). Single or multiple arteriovenous fistulae may be detected in horses with hemangioma or hemangiosarcoma and, if detected, should put a vascular neoplasm first on the differential diagnosis list. A long bone or other large fracture should also be considered in horses with large areas of muscle fiber tearing and hemorrhage.

Bone

Ultrasonography can be extremely helpful in diagnosing fractures in areas that are not accessible or readily accessible to radiographic examination, such as the pelvis, femur, scapula, humerus, and areas of the head and spine. In these instances, the bone should be carefully scanned in at least two mutually perpendicular planes from all accessible windows. The contralateral limb or side of the skull should be scanned for comparison to be sure that normal bony discontinuities are not mistaken for fractures.

Fractures. The first report of this application of diagnostic ultrasound in the horse was for the diagnosis of pelvic fractures.[104] Prior to this application of ultrasonography, the diagnosis of pelvic fractures in horses was performed radiographically in the anesthetized horse. This procedure always carried an inherent risk of catastrophic fracture of the pelvis upon recovery from general anesthesia. The use of ultrasonography to diagnose pelvic fractures is now commonplace (Fig. 3-215).

Ultrasonography is often used in conjunction with nu-

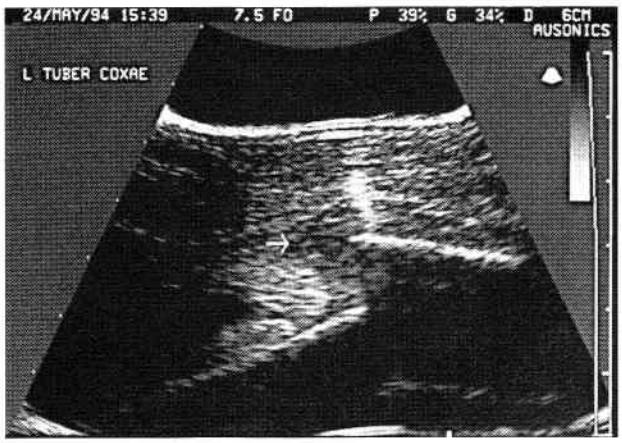

Figure 3–215

Sagittal sonogram of the iliac shaft and tuber coxae, obtained from a 5-day-old Thoroughbred cross colt. Notice the marked displacement of the two pieces of bone at the site of the ilial fracture and the hypoechoic fluid surrounding the fracture, consistent with hemorrhage *(arrow)*. Some disruption of the adjacent musculature is also present. This sonogram was obtained with a 7.5-MHz sector-scanner transducer containing a built-in fluid offset at a displayed depth of 6 cm. The right side of the sonogram is cranial (towards the tuber coxae) and the left side is caudal (towards the acetabulum).

clear scintigraphy in the horse with an acute onset of lameness consistent with a pelvic fracture.[105-107] Radiographs under general anesthesia are performed less frequently for horses with pelvic fracture and are usually reserved for horses in which the sonographic findings were negative or equivocal. Radiographic diagnosis of a pelvic fracture and other major long bone fractures in the adult horse must be performed at a referral hospital,[106] another limitation of the procedure. Shipping the horse with a suspected pelvic fracture or other long bone fractures carries with it the inherent danger of worsening the fracture. Sonographic examination of the pelvis and long bone fractures can be safely performed by the practitioner in the field.

The horse with pelvic fracture is usually acutely lame, but the lameness may resolve quickly if the fracture is nondisplaced or if only the wing of the ilium is involved. Unilateral hindlimb lameness was found in 97% of horses in one large study of equine pelvic fractures.[176] Significant relationships existed between presence of an iliac fracture and external pelvic asymmetry or the presence of a palpable swelling on rectal examination. Fractures involving the ventral aspect of the wing of the ilium that do not involve the dorsal iliac surface or nondisplaced fractures may not be detected ultrasonographically. Acetabular fractures are more difficult to diagnose because this area is anatomically complex and because not all of the acetabular area is available for sonographic examination. Distention of the hip joint may be appreciated in horses with an acetabular fracture. Anechoic areas with possible loculation may be imaged in the musculature surrounding the acetabulum or femur (Fig. 3-216) or adjacent to the fracture site along the ileal shaft or wing, raising the index of suspicion of a fracture. If the initial ultrasonographic examination is negative, a rectal ultrasonographic examination should be performed to rule out fractures detectable from this sonographic window. Nuclear scintigraphy should be performed in all horses for

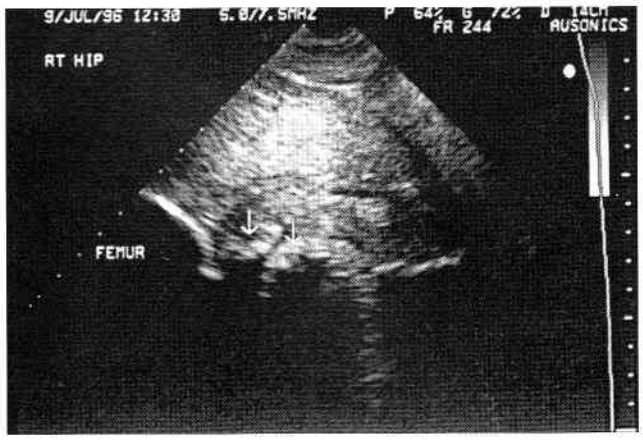

Figure 3–216

Sonogram of the fractured head of the femur and the right hip joint of a yearling Thoroughbred colt. Notice the multiple fracture fragments *(arrows)* adjacent to the head of the femur and the echogenic fluid (blood) within the hip joint. This sonogram was obtained with a wide-bandwidth 5.0-MHz sector-scanner transducer operating at 7.5 MHz at a displayed depth of 14 cm. The right side of this image is cranial and the left side is caudal.

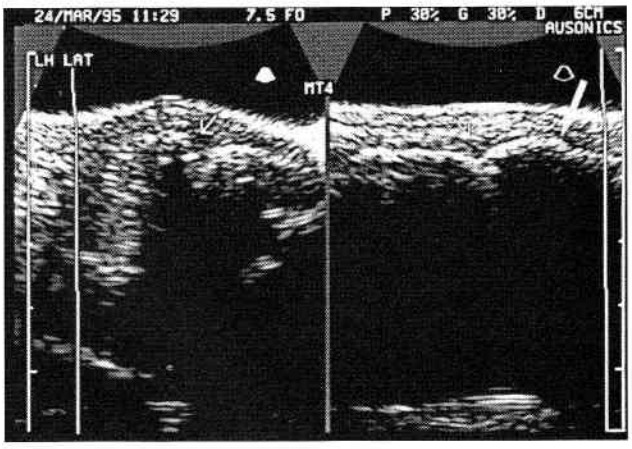

Figure 3–217

Sonograms of a hairline, minimally displaced fracture of the fourth metatarsal bone (MT4) in the left hind leg, obtained from an 11-year-old Morgan mare. Notice the defect in the bony surface echo at the site of the fracture *(arrows)* and the smooth bony proliferative change proximal to the site of the fracture *(large arrow)*, which represents an old lateral exostosis (splint). These sonograms were obtained with a 7.5-MHz sector-scanner transducer containing a built-in fluid offset and a displayed depth of 6 cm. The right side of the sagittal view *(right image)* is proximal and the left side is distal. The right side of the transverse view *(left image)* is dorsal and the left side is plantar.

which ultrasonographic examination for a pelvic fracture is negative if the clinician has a high index of suspicion that this is the correct diagnosis.

A fracture line is a hypoechoic to anechoic line through the cortical bone that allows the ultrasound beam to penetrate through the bone for a certain distance, imaging the fracture line. Thus, ultrasound can be useful in the diagnosis of a hairline or nondisplaced fracture (Fig. 3-217). Distraction of the fracture fragment from the parent portion of the bone is common and should be detected in two mutually perpendicular planes (Fig. 3-218).[104-107] Multiple fracture fragments are commonly detected ultrasonographically (see Fig. 3-216). In horses with extensive soft tissue swelling and a known fracture, ultrasonography can be used to characterize the type and severity of the soft tissue trauma (Fig. 3-219) and may aid in assessing the degree of comminution of the fracture (Fig. 3-220).[104] Ultrasound is also useful in horses with extensive soft tissue swelling and a suspected fracture in an area that is difficult to radiograph in the field or is inaccessible to radiographic examination (Fig. 3-221).

Ultrasonographic examination of a horse with a suspected fracture that cannot be located radiographically is often rewarding, resulting in the location of the fracture fragment and the subsequent positioning of the radiographic equipment and film to document the fracture radiographically (see Fig. 3-218). In many instances, the fracture fragment may be too small to be detected radiographically, or it may be located in an area from which it cannot be projected radiographically.

Osteitis and Osteomyelitis. Ultrasonography is particularly useful in the diagnosis of osteitis and osteomyelitis. Any bone can be affected, but septic osteitis/osteomy-

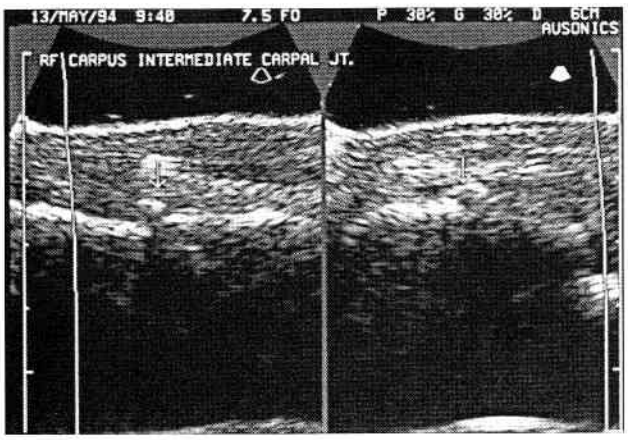

Figure 3–218

Sonograms of a small fracture fragment *(arrows)* from the intermediate carpal bone in the right foreleg, obtained from an 18-year-old crossbred gelding. This fracture was suspected but not located radiographically until sonographic localization of the fracture guided film placement. Notice the small hyperechoic structure (fracture fragment) distracted away from the parent portion of the intermediate carpal bone. These sonograms were obtained with a 7.5-MHz sector-scanner transducer containing a built-in fluid offset at a displayed depth of 6 cm. The right side of the long-axis view *(left image)* is proximal and the left side is distal. The right side of the short-axis view *(right image)* is lateral and the left side is medial.

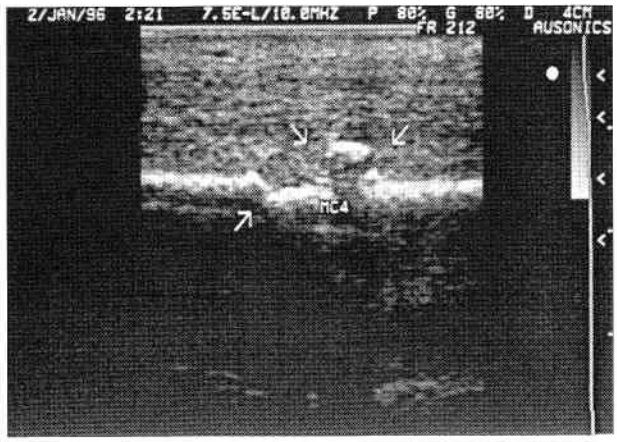

Figure 3–220

Sagittal sonogram of a comminuted fracture of the fourth metacarpal bone (MC4) in the right foreleg, obtained from a 5-year-old Thoroughbred gelding. Notice the fragment *(two angled-down arrows)* distracted from the parent portion of MC4 and the slightly displaced more-distal fracture *(up arrow)*. Notice the large amount of hypoechoic soft tissue swelling adjacent to the fractures. This sonogram was obtained with a wide-bandwidth 7.5-MHz linear-array transducer operating at 10.0 MHz at a displayed depth of 4 cm. The focal zones are positioned in the near field of the image. The right side of the sonogram is proximal and the left side is distal.

elitis in adult horses may be most common in the metacarpal and metatarsal bones.[103] A history of trauma is present for approximately 50% of horses with osteomyelitis.[103] The trauma may include a penetrating wound (Fig. 3-222) or an open wound at the site of a fracture. Osteomyelitis may also develop after elective surgery or fracture repair.[105] Clinical signs of local heat, pain, and swelling are usually detected in horses with osteomyelitis. Lameness and fever are frequently present. If purulent drainage is present, the hypoechoic tract can be followed to its source, the underlying infected bone. Bone fragments or sequestra are not uncommonly seen in horses with osteomyelitis.

The ultrasonographic finding consistent with a diagnosis of osteitis or osteomyelitis is a fluid layer immediately adjacent to the bone (Figs. 3-222 and 3-223).[103, 165, 166] The fluid layer overlying the bone may be anechoic to hypoechoic (see Fig. 3-222) or echogenic, or may contain hyperechoic echoes consistent with free gas (see Fig. 3-223). Culture of the fluid overlying the bone usually results in bacterial growth, except in a few horses

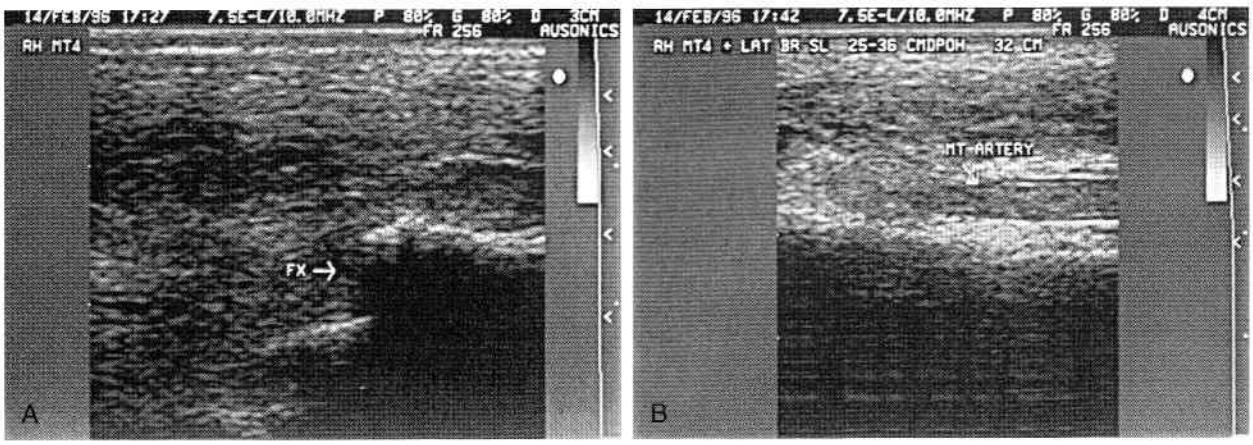

Figure 3–219

Sagittal sonograms of a fracture of the right fourth metatarsal bone (MT4) of an 11-year-old Thoroughbred gelding and the associated soft tissue structures. These sonograms were obtained with a wide-bandwidth 7.5-MHz linear-array transducer operating at 10.0 MHz at a displayed depth of 3 *(A)* and 4 *(B)* cm. The focal zones are positioned in the near field. The right side of the sonograms is proximal and the left side is distal.

A, Notice the marked distraction of the proximal portion of MT4 from the distal end of the bone (fx) and the large amount of hypoechoic to anechoic soft tissue swelling adjacent to the fracture, associated with hemorrhage at the fracture site.

B, Notice the severed great metatarsal artery adjacent to the fracture site, with the hypoechoic bulbous end of the artery associated with clot at the end of the torn artery. Adjacent to the disrupted artery is anechoic to hypoechoic fluid (blood) in the soft tissues.

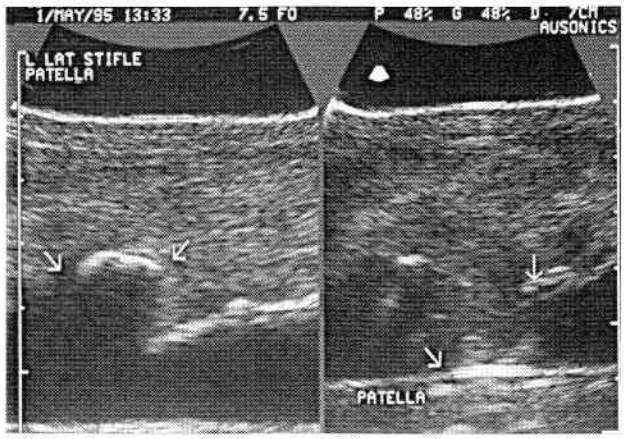

Figure 3–221

Sonograms of a fractured patella in the left hind leg, obtained from a 6-year-old Quarter horse mare. Notice the large fracture fragment *(arrows)* distracted from the parent portion of the patella in the sagittal view *(left image)*, the irregular surface of the patella *(arrows)* in the transverse view *(right image)* with visualization of another smaller fracture fragment, and the large amount of hypoechoic fluid around the patella, associated with peripatellar hemorrhage. These sonograms were obtained with a 7.5-MHz sector-scanner transducer containing a built-in fluid offset at a displayed depth of 7 cm. The right side of the long-axis view is proximal and the left side is distal. The right side of the short-axis view is cranial and the left side is caudal.

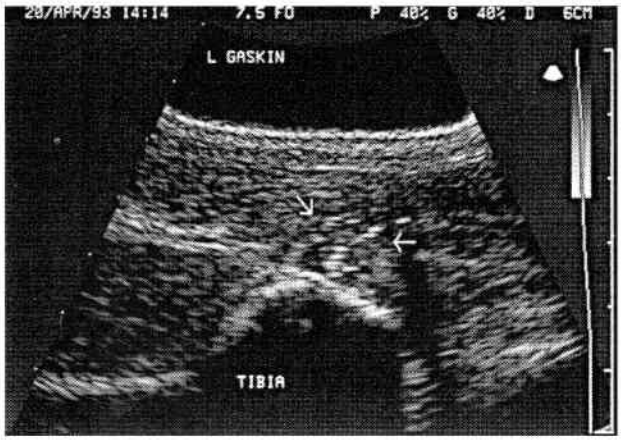

Figure 3–223

Sonogram of a localized area of osteitis/osteomyelitis over the lateral aspect of the mid tibia in the left hind leg, obtained from a 4-year-old Standardbred filly. Notice the hyperechoic echoes in the hypoechoic fluid consistent with free-gas echoes and an anaerobic infection. This sonogram was obtained with a 7.5-MHz sector-scanner transducer containing a built-in fluid offset at a displayed depth of 6 cm. The right side of the sonogram is cranial and the left side is caudal.

already treated with broad-spectrum antimicrobials.[103] This sonographic finding (fluid layer immediately adjacent to the bone) is pathognomonic for osteitis or osteomyelitis, except in synovial structures or in horses that have recently experienced trauma. Synovial fluid is not normally misdiagnosed as osteitis or osteomyelitis because the location of the joint is known and the presence of fluid within the joint is expected. In a horse with a recent history of trauma, hemorrhage might be located immediately adjacent to the bone if a fracture or subperiosteal hemorrhage is present. In the immediate postoperative period, fluid may be found immediately adjacent to the bone from hemorrhage at the time of surgery that has not yet been resorbed. These limitations are relatively minor, however, because a history of trauma is usually present or recent trauma is obvious in these cases.

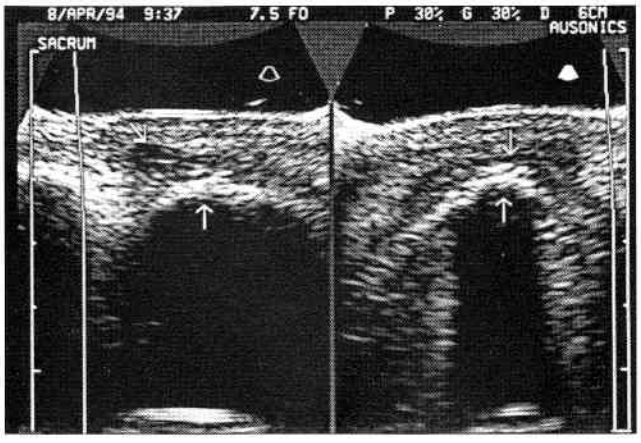

Figure 3–222

Sonograms of osteomyelitis of the sacrum, obtained from a 31-year-old Thoroughbred gelding after a bite wound to this area. Notice the hypoechoic fluid layer overlying the sacrum and the slightly irregular bony surface echo consistent with a diagnosis of osteomyelitis *(arrows)*. These sonograms were obtained with a 7.5-MHz sector-scanner transducer containing a built-in fluid offset at a displayed depth of 6 cm. The right side of the long-axis view *(left image)* is proximal and the left side is distal. The right side of the short-axis view *(right image)* is lateral and the left side is medial.

Radiographic evidence of osteitis or osteomyelitis, including characteristic lytic and proliferative changes, takes at least 10 to 14 days to appear. This is a critical period of time in which the infection can gain a significant foothold, making successful resolution of the infection more difficult. With ultrasonography, the quality of the bony surface echo can be evaluated. Marked thinning (Fig. 3-224) or thickening (Fig. 3-225) of the bony surface echo is abnormal and indicates bone lysis or cortical thickening, respectively. Periosteal lytic and proliferative changes can be detected ultrasonographically before they are visualized radiographically. Careful examination of the physis for fluid accumulation or cystic lesions should be performed in foals with suspected septic physitis so that the diagnosis can be made, cultures can be obtained under ultrasonographic guidance, and treatment can be initiated to bring the infection under control. Osteomyelitis was detected ultrasonographically in the majority of horses in which radiographic lesions of osteomyelitis were not detectable, enabling earlier diagnosis and treatment of the infection.[103]

Bony sequestra appear as hyperechoic to echogenic structures casting acoustic shadows of varying intensities. They are surrounded by hypoechoic to anechoic fluid and are located adjacent to bone (Fig. 3-226). Ultrasonography is extremely useful in the diagnosis of osteomyelitis in horses with surgical implants, because the lysis associated with the initial stage of fracture healing is difficult to differentiate radiographically from the lysis associated with bony infection (Fig. 3-227).

Radiographic evidence of osteomyelitis may not be

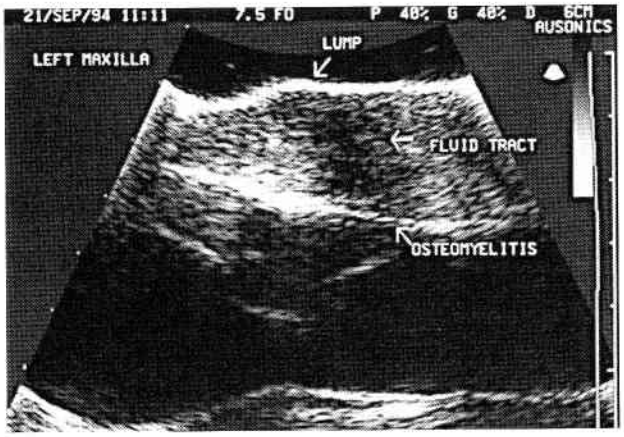

Figure 3–224

Sonogram of osteomyelitis of the left maxilla obtained from a 7-year-old Thoroughbred cross gelding. Notice the very thin, weak bony surface echo deep to the overlying fluid tract extending out to, but not through, the skin surface. This is an area of osteomyelitis with necrotic bone that crumbled at the time of surgery with minimal curettage. This sonogram was obtained with a 7.5-MHz sector-scanner transducer containing a built-in fluid offset at a displayed depth of 6 cm. The left side of the sonogram is rostral.

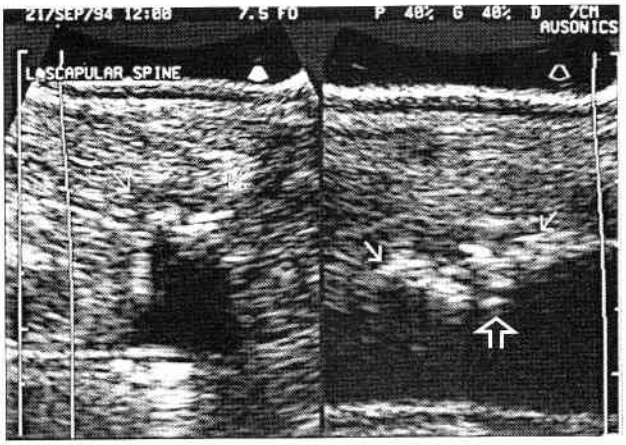

Figure 3–226

Sonograms of osteomyelitis of the left scapular spine with sequestrae at the area of most bony lysis, obtained from a 3-year-old Oldenberg filly. Notice the hyperechoic bony fragments *(arrows)* surrounded by hypoechoic fluid, consistent with sequestrae. Notice the large irregular bony surface echo with a scooped-out lytic area *(open arrow)*, best seen in the long-axis image of the scapular spine *(right image)*. These sonograms were obtained with a 7.5-MHz sector-scanner transducer containing a built-in fluid offset at a displayed depth of 7 cm. The right side of the long-axis view *(right image)* is proximal and the left side is distal. The right side of the short-axis view *(left image)* is cranial and the left side is caudal.

detected for 2 to 8 weeks in foals or horses with vertebral osteomyelitis.[108] Although nuclear scintigraphy[167] and computed tomography[168] can both be used to localize lesions in acute cases of vertebral osteomyelitis, ultrasonography can also be used to localize infections in the vertebrae and is most useful in foals or horses with an area of swelling near the vertebral column. Swelling of the cervical thoracic and lumbar regions has been reported in foals with vertebral osteomyelitis.[108, 169] Ultrasonographic examination of cervical swellings in two foals with vertebral osteomyelitis revealed large abscesses extending to the cervical vertebrae.[102, 103]

Osteomyelitis may occur associated with infection of a synovial sheath. Osteomyelitis of the sustentaculum tali has been reported in horses with tarsal sheath distention.[116, 138] Osteomyelitis of the axial surface of the proximal sesamoid bones (Fig. 3-228) has been reported in several horses with infected digital sheaths.[170] Two of

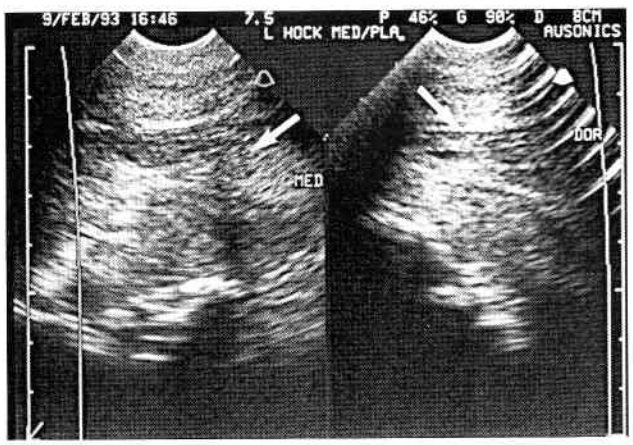

Figure 3–225

Sonograms of a chronic osteomyelitis of the sustentaculum tali of the left hindlimb, obtained from a 5-year-old Holsteiner mare. Notice the hypoechoic to anechoic fluid layer overlying the bone, tracking out towards the skin surface *(arrows)*. The extension of the tract to the skin surface is not imaged in this scan plane. The underlying bone is very irregular and thickened, with lytic and proliferative changes detected. The peritendinous tissues in this location were extremely thickened and echogenic, consistent with fibrosis of the surrounding soft tissues. These sonograms were obtained with a 7.5-MHz sector-scanner transducer at a displayed depth of 8 cm. The right side of the sagittal view *(right image)* is proximal and the left side is distal. The right side of the transverse view *(left image)* is dorsal and the left side is plantar.

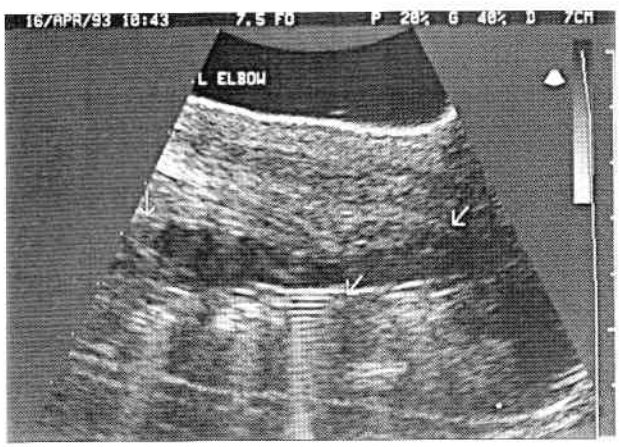

Figure 3–227

Sonogram of osteomyelitis of the left olecranon, obtained from a 3-year-old Arabian filly with a fractured olecranon repaired with a plate and screws. Notice the large hypoechoic fluid layer *(upper arrow)* overlying the plate (consistent with osteomyelitis) and the reverberation artifacts associated with the metallic implant *(lower arrow)*. Significant soft tissue swelling overlies the fracture repair. This sonogram was obtained with a 7.5-MHz sector-scanner transducer containing a built-in fluid offset at a displayed depth of 7 cm. The right side of the sonogram is proximal and the left side is distal.

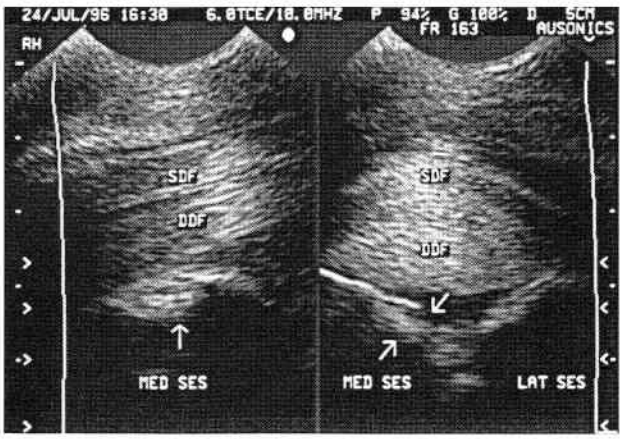

Figure 3–228

Sonograms of a focal area of osteomyelitis along the axial border of the medial proximal sesamoid bone in the right hind leg, obtained from a 3-year-old Thoroughbred gelding. Notice the large lytic defect in the axial margin of the medial proximal sesamoid bone *(arrows)* and the hypoechoic fluid in the digital sheath in the distal metatarsal region. These sonograms were obtained in zone 4C at 45 cm distal to the point of the hock with a wide-bandwidth 6.0-MHz microconvex linear-array transducer operating at 10.0 MHz at a displayed depth of 5 cm. The focal zones are positioned in the far field of the images. The right side of the sagittal view *(left image)* is proximal and the left side is distal. The right side of the transverse view *(right image)* is lateral and the left side is medial.

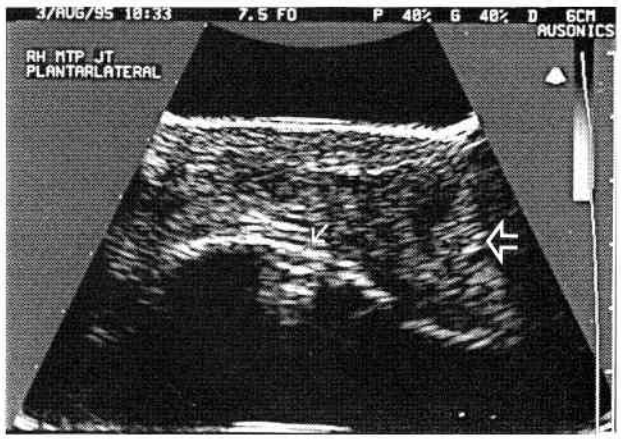

Figure 3–229

Sonogram of a focal area of osteomyelitis at the proximal physis of the first phalanx (P1) in the right hind leg, obtained from a 2-month-old Standardbred filly. Notice the abnormal bony surface echo and reverberation artifacts at the location of the cyst in the plantarolateral aspect of P1. Marked hypoechoic loculated fluid distention of the digital sheath *(open arrow)* is detected immediately adjacent to this area. This sonogram was obtained with a 7.5-MHz sector-scanner transducer containing a built-in fluid offset at a displayed depth of 6 cm. The right side of this sonogram is proximal and the left side is distal.

these horses also had septic synovitis of the fetlock joint. Lytic lesions along the axial border of the sesamoid bones should prompt careful sonographic evaluation of the intersesamoidean ligament, because intersesamoidean ligament desmitis has been reported in these horses. The osteomyelitis lesions appear as lytic areas along the axial margin of the proximal sesamoid bones. Cystic lesions also may be detected in this location (see Fig. 3-228). Cystic lesions along the abaxial surface of the proximal sesamoid bones also occur and may be associated with osteomyelitis or with chronic inflammation of the sesamoid bone at the insertion of the suspensory ligament. Cystic lesions associated with fluid along the bony surface or in an intra-articular location are often associated with osteomyelitis and can occur in any bone (Fig. 3-229) of horses or foals with osteitis and osteomyelitis.

Bone Cysts or Neoplasms. Other bony abnormalities such as a neoplasm or bone cyst are rare but can often be imaged ultrasonographically, at least in part, because of associated bone necrosis or complex composition of the tumor (Fig. 3-230). Neoplasms of the long bones are rare in horses, the most common being an osteoma.[171, 172] Osteosarcomas are rare and are localized to the bones of the axial skeleton.[172, 173] Neoplasms of the skull and mandible are more common in horses and may be of a wide variety of cell types with no particular characteristic features.[173, 174] Bone cysts are uncommon in horses and have been reported most frequently in the mandible.[175]

Joints

Evaluation of the amount and character of the synovial fluid and the synovium should be part of every sonographic examination of a synovial structure. Chronic nonseptic synovitis is most common in horses and usually is associated with anechoic synovial fluid and little or no fibrin within the joint. Synovial hyperplasia is often present in horses with chronic synovitis. Fibrinous loculations or fibrous adhesions may be detected in horses with chronic active synovitis associated with ongoing inflammation in the joint. Hypoechoic to echogenic synovial fluid is most likely septic, is usually present in large volumes, and is often associated with a large amount of fibrin within the joint. Synovial thickening is frequently present in horses with septic joints. Many of these horses

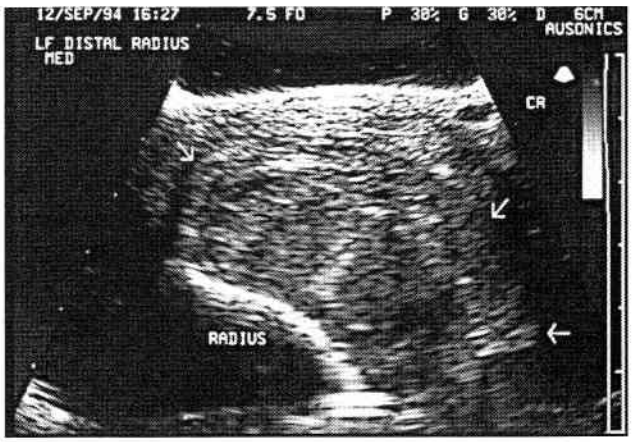

Figure 3–230

Sonogram of a large composite mass over the distal medial aspect of the left radius, obtained from a 14-year-old Thoroughbred mare. This mass was a fibrosarcoma and had resulted in some bony changes in the normal contour of the radius underneath the tumor. This sonogram was obtained with a 7.5-MHz sector-scanner transducer containing a built-in fluid offset at a displayed depth of 6 cm. The right side of the sonogram is cranial and the left side is caudal.

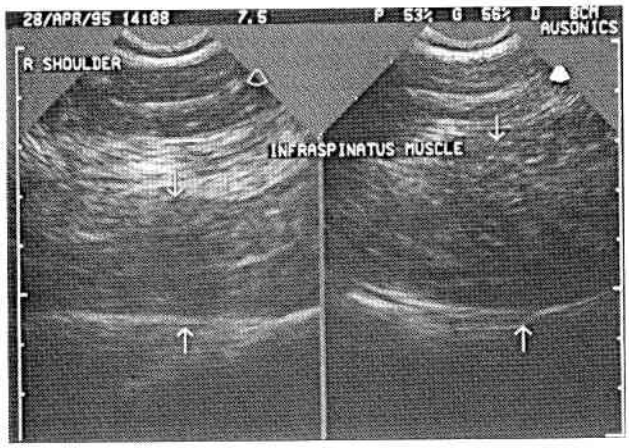

Figure 3–231

Sonograms of a large area of infraspinatus muscle injury in the right foreleg, obtained from a 17-year-old Thoroughbred mare. Notice the enlargement of the infraspinatus muscle and the absence of a normal speckled striated muscle fiber pattern associated with this injury. These sonograms were obtained with a 7.5-MHz sector-scanner transducer at a displayed depth of 8 cm. The right side of the long-axis view *(left image)* is proximal and the left side is distal. The right side of the short-axis view *(right image)* is cranial and the left side is caudal.

also have marked periarticular swelling. Hemorrhage may be detected in the joint and usually appears as echogenic swirling fluid within the joint. In horses with acute trauma, the joint capsule should be carefully evaluated for any discontinuity, because rupture of the joint capsule may have occurred.

Equine collateral ligament injuries occur more frequently than previously believed.[100, 176, 177] A thorough knowledge of anatomy coupled with a systematic examination of all the collateral ligaments of an affected joint is necessary to make this diagnosis. The collateral ligaments of some joints are very complicated. In some joints such as the carpus and tarsus, all the collateral ligaments cannot be imaged because of their intra-articular location. Injuries usually occur to either the lateral or medial collateral ligament rather than to both structures simultaneously. Collateral ligament injuries may be discrete areas of fiber tearing, but are more often diffuse lesions. Enlargement of the cross-sectional area of the collateral ligament is common with collateral ligament injury, as are a decrease in the ligament's echogenicity and loss of the normal parallel fiber pattern. Avulsion fractures of the origin or insertion of the collateral ligaments can occur in all joints, but are most common in the metatarsophalangeal joint and femorotibial joint.

Shoulder

Abnormalities of the shoulder joint are uncommon but have been detected sonographically. In foals, septic synovitis of the shoulder joint has been detected most frequently. In older horses, changes in the ultrasonographic appearance of the shoulder joint have been seen with chronic synovitis, including injury to the glenohumeral ligaments and calcification of the joint capsule and synovial lining. However, injuries to this joint are infrequent, are most likely to occur secondary to trauma, and more frequently involve the muscles of the shoulder girdle. Injuries to the infraspinatus and other surrounding shoulder muscles have been detected (Fig. 3-231). Injuries to the scapula, with rupture of the serratus ventralis muscle and displacement of the scapula from its normal position on the thoracic wall, have also been detected sonographically (Fig. 3-232).

Elbow

Abnormalities of the elbow joint other than septic arthritis are uncommon. Septic arthritis of the elbow joint is most common in foals but occasionally is seen in older horses in association with trauma (Fig. 3-233). Injuries to the elbow joint are possible, associated with the more common olecranon fracture. Collateral ligament injuries are uncommon and are most frequently associated with trauma. With trauma to the lateral aspect of the elbow joint, wounds may extend into the cubital joint and cause injury to the lateral collateral ligament (Fig. 3-234). Injuries to the collateral ligament usually result in an enlarged hypoechoic collateral ligament that lacks a normal fiber pattern. Avulsion fractures can occur associated with collateral ligament desmitis (see Fig. 3-234). These avulsion fractures may occur at the origin of the collateral ligament from the humeral epicondyle or at their insertion on the medial or lateral tuberosity of the radius. Fractures of the lateral tuberosity of the radius have been reported.[100, 176, 177]

Carpus

Numerous collateral ligaments are in the carpus between rows of carpal bones and in between the carpal bones, only some of which are visible ultrasonographically. In-

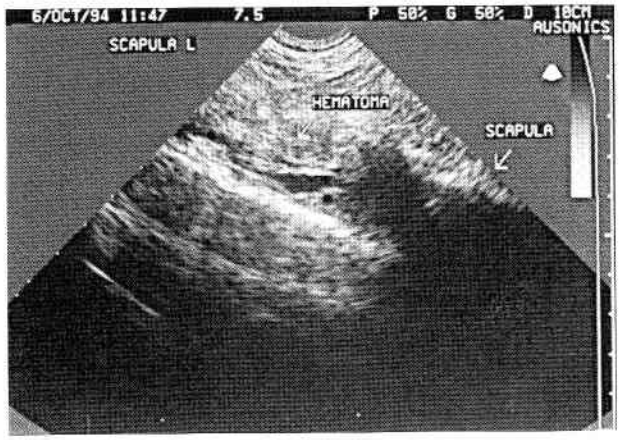

Figure 3–232

Sonogram of a ruptured serratus ventralis muscle with dissection of hemorrhage through the adjacent tissue planes and displacement of the scapula obtained from a 5-month-old Thoroughbred filly. Notice the loculated anechoic hematoma adjacent to the scapula. This sonogram was obtained with a 7.5-MHz sector-scanner transducer at a displayed depth of 10 cm. The right side of the sonogram is cranial and the left side is caudal.

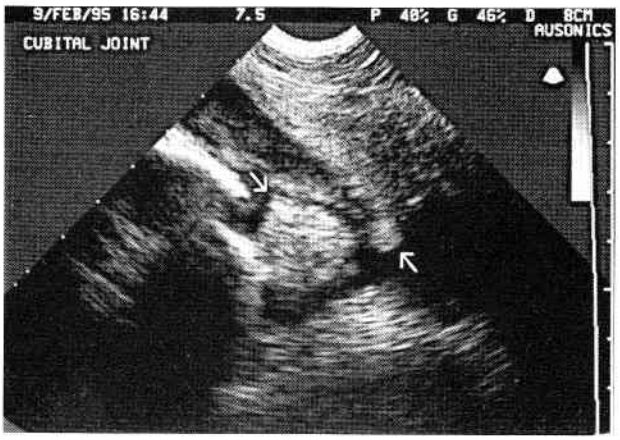

Figure 3–233

Sagittal sonogram of a septic cubital joint filled with hypoechoic fluid and hypoechoic to echogenic clot *(arrows)*, obtained from a 10-year-old Appaloosa gelding. Notice the marked distention of the joint. This sonogram was obtained with a 7.5-MHz sector-scanner transducer at a displayed depth of 8 cm. The right side of this long-axis image is proximal and the left side is distal.

juries to some of the collateral ligaments have been detected ultrasonographically. Avulsion fractures and rupture of the medial collateral ligament have been described.[100, 175, 176] Avulsion fractures or fractures resulting in damage to the intercarpal ligaments can often be imaged. Intra-articular fractures may be located sonographically when they are suspected, but have not been successfully imaged radiographically (see Fig. 3–218). Accurate localization of these fractures ultrasonographically can help to identify them radiographically by guiding positioning of the x-ray beam and cassette. Fracture of the accessory carpal bone usually involves one or more of the ligaments of the accessory carpal bone and is often associated with a large carpal sheath effusion.[175, 176] The cartilaginous surfaces of the distal radius and carpal bones should appear as thin anechoic lines.[87]

Ultrasonography can also be used to monitor the ossification of the cuboidal bones in the carpus, as has been reported for the tarsus.[97, 98] However, carpal bone ossification precedes tarsal bone ossification; thus, monitoring the ossification of the tarsal bones ultrasonographically is preferable.

Fetlock

Abnormalities occur more frequently in the metacarpophalangeal joint than in the metatarsophalangeal joint, with villonodular synovitis being the most common synovial abnormality detectable ultrasonographically.[90, 91, 96] A dorsal plica more than 4 mm thick is consistent with villonodular synovitis (Fig. 3–235). This thickening of the dorsal plica is usually homogeneous, hypoechoic, or echogenic,[90, 91, 96] and occurs in conjunction with generalized synovitis. Synovial thickening and anechoic fluid within the joint are usually imaged in horses with synovitis. Acute synovitis is often characterized by an anechoic joint effusion with fibrinous loculations, imaged within the synovial fluid (Fig. 3–236). Fracture fragments (usually from proximal P1) may also be imaged in these horses. Hypoechoic areas within the dorsal joint capsule were

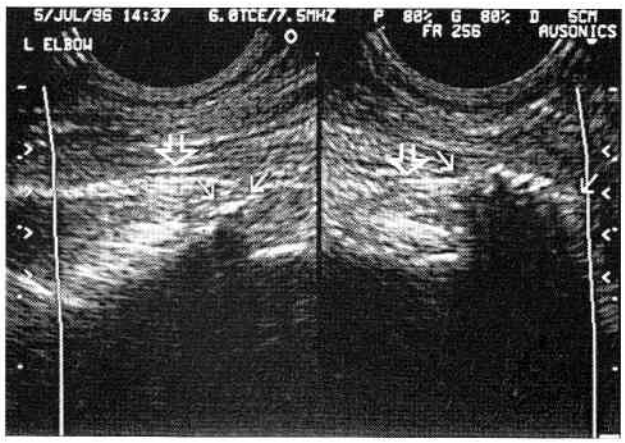

Figure 3–234

Sonograms of avulsion fractures at the origin of the lateral collateral ligament of the cubital joint, obtained from a 10-year-old Thoroughbred mare. Notice the hyperechoic bony fragments distracted away from the distal humerus *(arrows)* casting acoustic shadows. Notice the hypoechoic lateral (most superficial portion) of the lateral collateral ligament *(open arrows)*, which is lacking a normal fiber pattern, distal to the fracture fragments imaged in both the transverse view *(right image)* and sagittal view *(left image)*. Some swelling of the overlying soft tissue structures is present. These sonograms were obtained with a wide-bandwidth 6.0-MHz microconvex transducer operating at 7.5 MHz at a displayed depth of 5 cm. The right side of the transverse image is cranial and the left side is caudal. The right side of the sagittal images is proximal and the left side is distal.

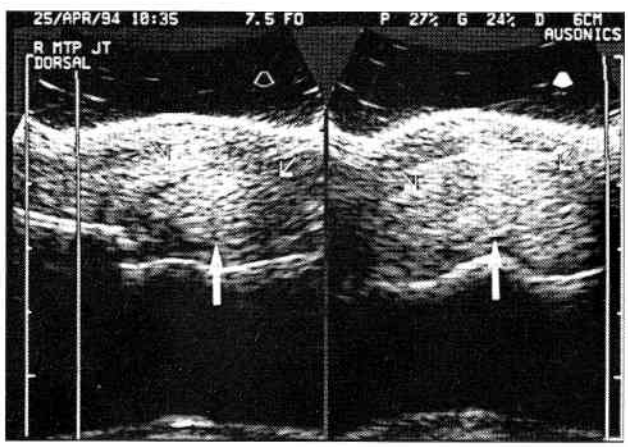

Figure 3–235

Sonograms of chronic proliferative synovitis in the dorsal reflection of the right metatarsophalangeal joint, obtained from a 9-year-old Thoroughbred gelding. Notice the marked thickening of the dorsal plica *(large arrow)* in the sagittal view *(left image)* measuring greater than 1 cm in thickness. Notice the slight thickening of the joint capsule *(arrows)*, which is also best delineated in the sagittal view. The prominent echogenic thickening of the dorsal plica *(large arrow)* is also very evident in the transverse view *(right image)* over the distal metatarsal ridge. These sonograms were obtained with a 7.5-MHz sector-scanner transducer containing a built-in fluid offset at a displayed depth of 6 cm. The right side of the sagittal image is proximal and the left side is distal. The right side of the transverse sonogram is lateral and the left side is medial.

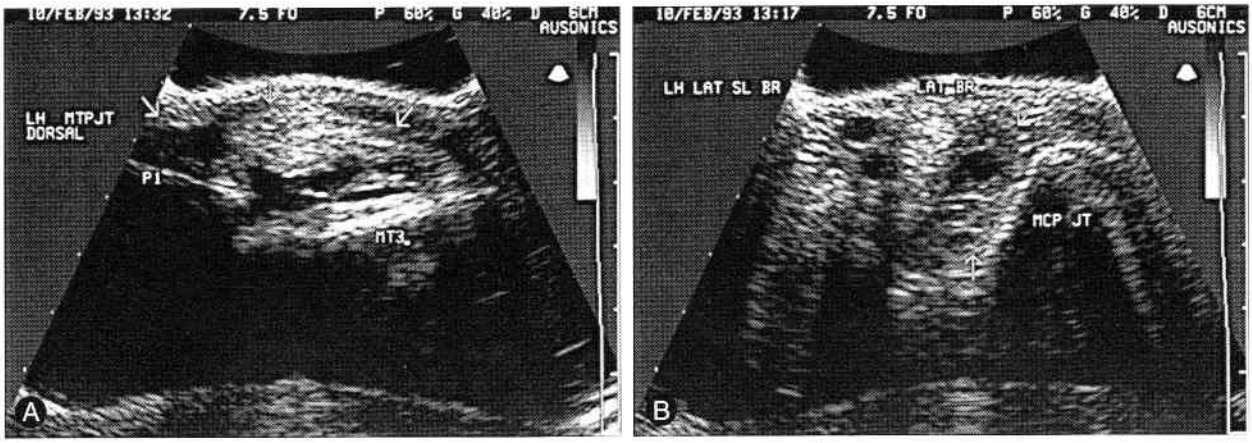

Figure 3–236

Sonograms of an acute fibrinous synovitis of the left metatarsophalangeal joint, obtained from a 3-year-old Thoroughbred filly. Notice the fibrinous loculations in both the dorsal *(A)* and lateral *(B)* compartments of the metatarsophalangeal joint and the moderate joint distention. These sonograms were obtained with a 7.5-MHz sector-scanner transducer containing a built-in fluid offset at a displayed depth of 6 cm. The right side of the sagittal view *(A)* is proximal and the left side is distal. The right side of the transverse view *(B)* is dorsal and the left side is plantar.

A, Notice the thickened joint capsule *(arrows)*, the thickened synovium, and the fibrinous loculations within the joint when imaged in the sagittal scan plane from its dorsal aspect.

B, The loculations present within the joint *(arrows)* are even more visible from the lateral aspect of the metatarsophalangeal joint and are most prominent cranial to the lateral branch of the suspensory ligament (lat br).

identified in 36% of horses with abnormal ultrasonographic findings in the fetlock joint and lameness referable to this region.[96] Chronic proliferative synovitis or synovial membrane thickening was present in 19% of these horses and in 52% of horses with hypoechoic areas detected sonographically within the dorsal joint capsule. Fracture fragments were seen in 12% of the horses in this study, and abnormal dorsal articular margins were detected sonographically in 17%. Calcification of the dorsal plica has been imaged in the form of small, hyperechoic structures casting acoustic shadows within the dorsal plica (Fig. 3-237). A bursitisis occasionally seen in the subtendinous bursa of the long digital extensor tendon and is more likely in horses with tendinitis of the long digital extensor tendon or periarticular swelling.

Septic arthritis is, unfortunately, a too-frequent occurrence in the metacarpo- or metatarsophalangeal joints. It has a sonographic appearance similar to that of septic joints elsewhere. Marked effusion with hypoechoic to echogenic joint fluid and a thickened synovium is consistent with sepsis (Fig. 3-238). Penetrating wounds into the metacarpo- or metatarsophalangeal joint can be identified ultrasonographically by following the hypoechoic tract associated with the skin wound into the joint through the joint capsule.

Collateral ligament desmitis in association with lameness that is localized to the fetlock joint region occurs more frequently than previously recognized. Most commonly, the areas of fiber damage to the collateral ligaments are diffuse, with loss of normal fiber pattern and decreases in ligament echogenicity. The ligament's cross-sectional area is enlarged in the area of injury (Fig. 3-239). Avulsion fractures may be detected in association with injuries to the collateral ligament; most frequently, in the author's experience, in the lateral collateral ligament of the metatarsophalangeal joint (Fig. 3-240). Avulsion fractures of the insertion of the collateral ligaments onto proximal P1 are reportedly most common.[100, 176] These avulsion fractures are often comminuted and displaced proximally.[100, 176] Collateral ligament desmitis, rupture, or insertional desmopathy (enthesopathy) was identified in 21% of horses with lameness localized to the fetlock region and abnormal ultrasonographic findings.[96] Remodeling of the medial or lateral articular margins was reported in 14% of these horses and bony nodules were

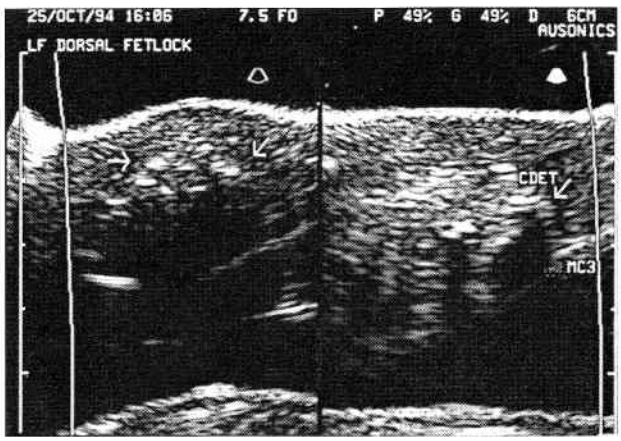

Figure 3–237

Sonograms of calcification in the left metacarpophalangeal joint capsule and dorsal synovial reflection, obtained from a 3-year-old Percheron filly. Notice the small bright hyperechoic areas *(arrows)* located within the joint capsule and dorsal synovial reflection that are casting acoustic shadows. The common digital extensor tendon (CDET) is imaged superficial to the calcification, although some of the calcification *(arrow)* appears to extend dorsally to the palmar margin of the tendon, best seen in the sagittal view *(right image)*. These sonograms were obtained with a 7.5-MHz sector-scanner transducer containing a built-in fluid offset at a displayed depth of 6 cm. The right side of the sagittal view is proximal and the left side is distal. The right side of the transverse view *(left image)* is lateral and the left side is medial. MC3, third metacarpal bone.

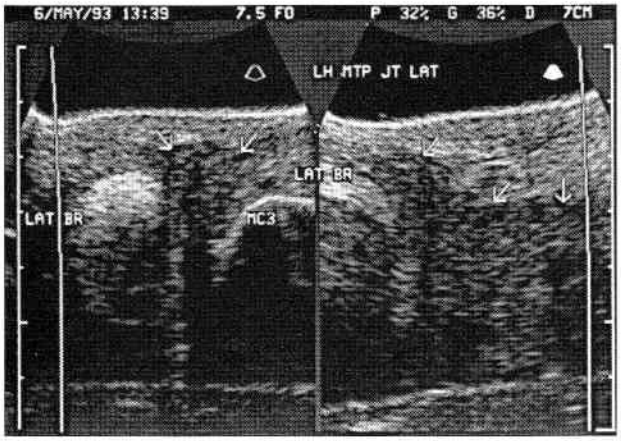

Figure 3–238

Sonograms of a septic metatarsophalangeal joint in the left hind leg, obtained from a 5-year-old Standardbred stallion. Notice the marked distention of the metatarsophalangeal joint, which is filled with hypoechoic fluid *(arrows)*. These sonograms were obtained with a 7.5-MHz sector-scanner transducer containing a built-in fluid offset at a displayed depth of 7 cm. The right side of the sagittal view *(right image)* is proximal and the left side is distal. The right side of the transverse view *(left image)* is dorsal and the left side is plantar.

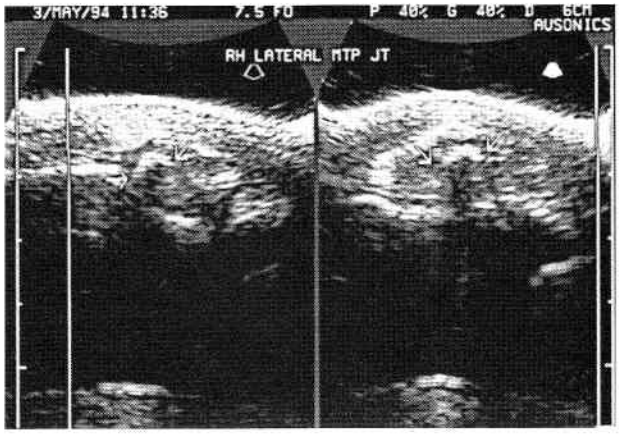

Figure 3–240

Sonograms of an avulsion fracture *(arrows)* from the proximal and lateral border of the first phalanx (P1) embedded in the synovium in the lateral compartment of the right metatarsophalangeal joint. Notice the curved hyperechoic fragment casting an acoustic shadow visible in two mutually perpendicular planes. In the transverse view *(right image)*, the fragment *(arrows)* is embedded in the superficial portion of the synovium and appears to be in the distal-most portion of the synovium when imaged in the sagittal scan *(left image)*. These sonograms were obtained with a 7.5-MHz sector-scanner transducer containing a built-in fluid offset at a displayed depth of 6 cm. The right side of the transverse image is dorsal and the left side is plantar. The right side of the sagittal image is proximal and the left side is distal.

detected in the collateral ligaments in 6%. Synovial fistulae occasionally occur associated with the metacarpo- or metatarsophalangeal joint; these can also be detected ultrasonographically. Sonographic evaluation of the fetlock joint is recommended in horses with swelling localized to the fetlock joint or periarticular structures, particularly in horses with lameness referable to this joint but without radiographic findings or in horses with suspected soft tissue injury (e.g., collateral ligament desmitis, villonodular synovitis).

Pastern

Abnormalities of the pastern and coffin joint occur less frequently, but collateral ligament injuries in these joints can occur (Fig. 3-241). In recent injuries, only the acute desmitis of the collateral ligaments may be imaged, with or without an associated avulsion fracture. In more

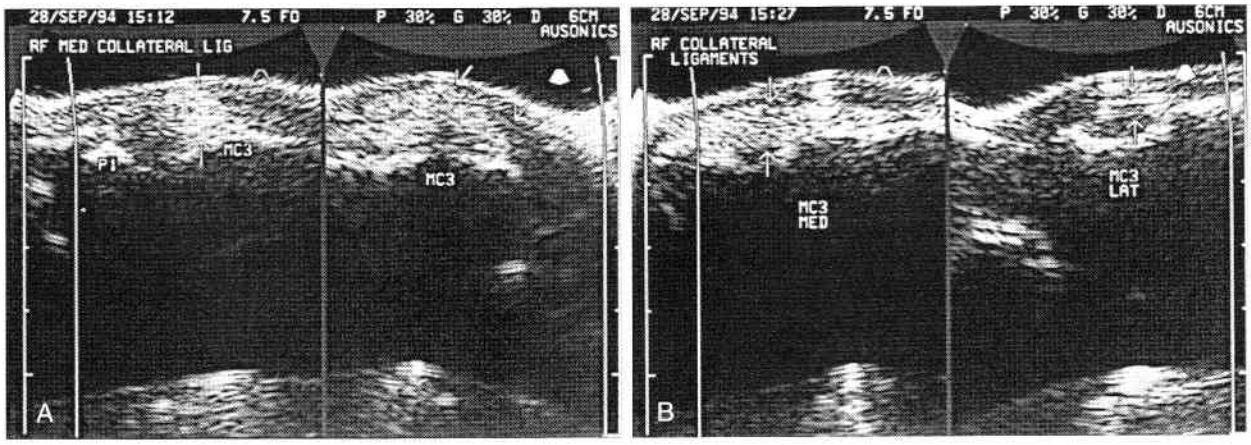

Figure 3–239

Sonograms of medial collateral ligament desmitis of the right metacarpophalangeal joint of a 5-month-old Thoroughbred colt. Notice the irregularities of the distal medial aspect of the third metacarpal bone near the origin of the medial collateral ligaments. These sonograms were obtained with a 7.5-MHz sector-scanner transducer containing a built-in fluid offset at a displayed depth of 6 cm. The right side of the sagittal views is proximal and the left side is distal. MC3, third metacarpal bone; P1, first phalanx.

A, Sagittal views of the enlarged heterogeneous medial collateral ligaments with a random fiber pattern evident which were obtained near their insertion *(left image)* and origin *(right image)*.

B, Sagittal views of the medial *(left image)* and lateral collateral ligaments *(right image)*, illustrating the marked size discrepancy and difference in fiber alignment between the normal long lateral collateral ligament and the injured long medial collateral ligament.

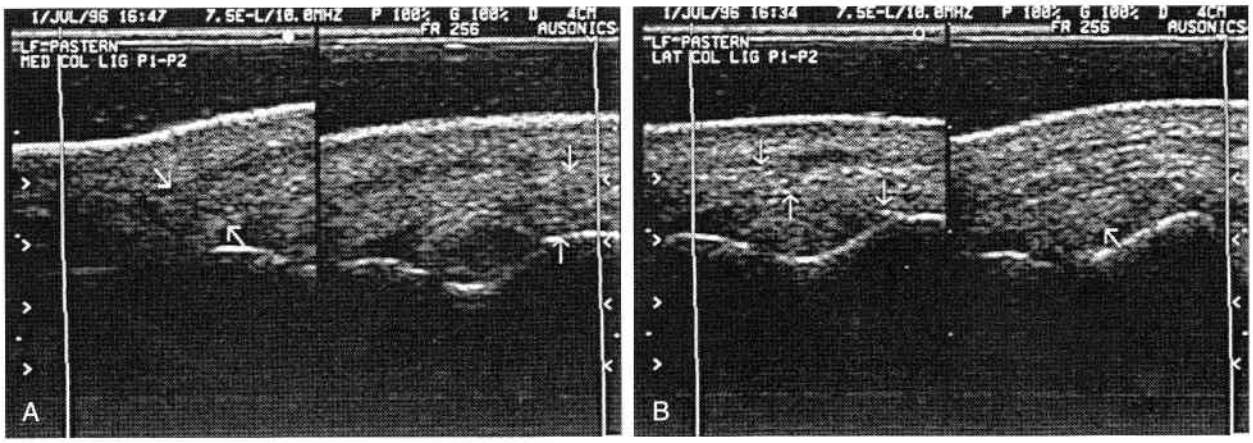

Figure 3–241

Sonograms of ruptured medial and lateral collateral ligaments of the proximal interphalangeal joint in the left foreleg that resulted in subluxation of the proximal interphalangeal joint of a 4-year-old Standardbred gelding. These sonograms were obtained with a wide-bandwidth 7.5-MHz linear-array transducer operating at 10.0 MHz using a hand-held standoff pad at a displayed depth of 4 cm. The right side of these sagittal images is proximal and the left side is distal.

A, Notice the complete loss of any recognizable fibers *(arrows)* in both sagittal views near the origin *(right image)* of the long medial collateral ligaments, the marked decrease in ligament echogenicity, and the marked enlargement of the ligaments' diameter. The insertion of the long medial collateral ligament onto proximal P2 *(left image)* is anechoic and nearly completely disrupted.

B, Notice the enlarged long lateral collateral ligament *(left image)* over the distal aspect of the first phalanx *(up and left down arrows)* and the enlarged hypoechoic short lateral collateral ligament *(diagonal arrow)* over the distal aspect of the first phalanx *(right image)*. Few fibers are visible remaining in either the long or short collateral ligament. A small avulsion fragment *(right down arrow)* is imaged near the origin of the long lateral collateral ligament in the left sagittal image.

chronic injuries, enthesophyte formation at the origin and the insertion of the collateral ligaments is usually detected in horses with collateral ligament desmitis. These areas of insertional damage become somewhat smoother as the collateral ligament injury heals and the desmitis becomes inactive.

Marked distention of the coffin joint is most frequently seen with sepsis (Figs. 3-242 and 3-243), although it may occur with degenerative joint disease. The joint fluid is usually hypoechoic to echogenic in horses with a septic coffin joint. Hyperechoic echoes representing free gas may also be detected, because many septic joints are the result of a penetrating wound through the foot. Penetrating wounds at the level of the coronary band can also result in coffin joint sepsis (see Fig. 3-243).

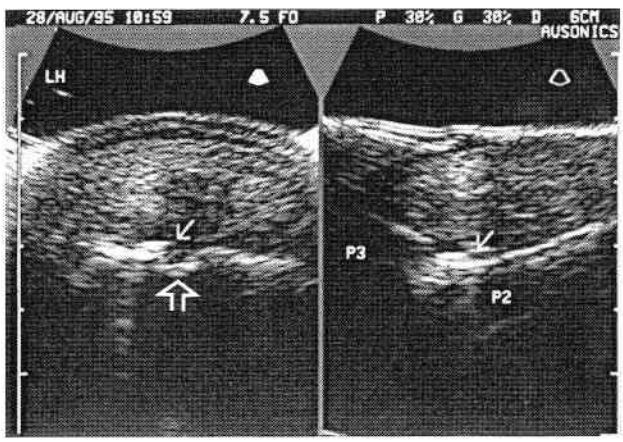

Figure 3–242

Sonograms of a distended left rear coffin joint with a small avulsion fracture *(arrows)* from the distal medial aspect of the second phalanx (P2), obtained from a 7-year-old Quarter horse gelding. Notice the small hyperechoic structure *(arrow in right image)* slightly distracted from the distal and medial aspect of the second phalanx (P2) and the small scooped-out area from which the fragment probably originated *(open arrow, left image)*. Notice the distention of the joint with hypoechoic fluid, the synovial thickening, and the thickened soft tissues consistent with a septic synovitis. These sonograms were obtained with a 7.5-MHz sector-scanner transducer containing a built-in fluid offset at a displayed depth of 6 cm. The right side of the transverse view *(left image)* is lateral and the right side is medial. The right side of the sagittal view *(right image)* is proximal and the left side is distal.

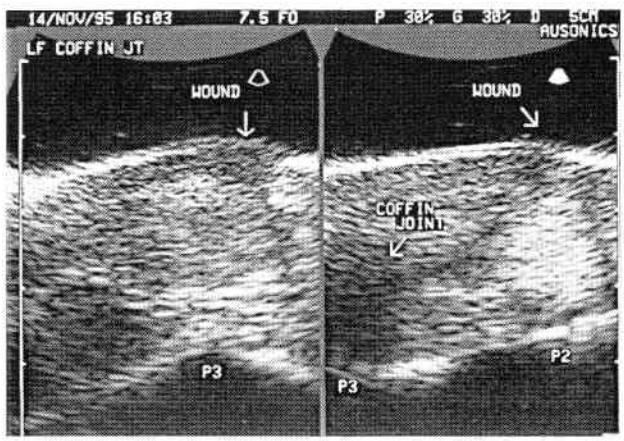

Figure 3–243

Sonograms of a wound penetrating into the coffin joint of the left foreleg and resulting in a septic synovitis, obtained from a 10-year-old Quarter horse gelding. Notice the hypoechoic tract extending from the skin through the joint capsule into the joint best visualized in the sagittal view and the increased amount of hypoechoic fluid within the joint. The periarticular structures are very swollen and echogenic. These sonograms were obtained with a 7.5-MHz sector-scanner transducer containing a built-in fluid offset at a displayed depth of 5 cm. The right side of the sagittal view *(right image)* is proximal and the left side is distal. The right side of the transverse view *(left image)* is lateral and the right side is medial.

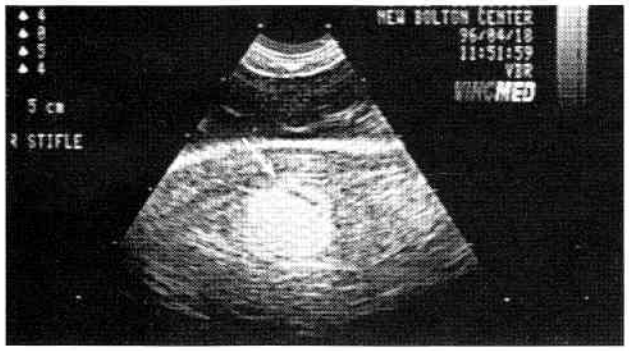

Figure 3–244

Sonogram of a small tear in the middle patellar ligament in the right hindleg, obtained from a 3-year-old Thoroughbred filly. Notice the linear anechoic area in the middle patellar ligament *(arrow)*. This area of fiber tearing was confirmed in the sagittal scan. Notice the homogeneous echogenic appearance of the majority of the middle patellar ligament. This sonogram was obtained with a wide-bandwidth 7.5-MHz annular-array transducer using a hand-held standoff pad at a displayed depth of 5 cm. The right side of this transverse sonogram is lateral and the left side is medial.

Hip

The hip joint is difficult to image successfully but can be imaged in part using lower-frequency transducers and an increased depth of field. Sepsis must always be considered in a foal with lameness referable to this joint, whereas trauma is a more common cause in older horses. Fractures of the acetabulum and femoral head may be associated with joint distention and hemorrhage in this region (see Fig. 3-216).[164]

Stifle

Soft tissue injury to the stifle in horses with hindlimb lameness occurs with similar frequency as bony injury, making ultrasonographic examination of the stifle region a worthwhile diagnostic technique.[95, 100, 176, 177] Abnormalities of the femoropatellar and femorotibial joint capsule, synovial lining, joint fluid, collateral ligaments, cruciate ligaments, femoropatellar ligaments, patellar ligaments, menisci, and adjacent cartilage and bone can be detected ultrasonographically. However, abnormalities of some of these structures, particularly the cruciate ligaments, menisci, joint cartilage, and bone, may be missed because this portion of the joint is less accessible or inaccessible for sonographic imaging. Sonographic examination of the stifle is well worth performing in horses with lameness localized to the stifle, periarticular swelling, and/or swelling of the femoropatellar or femorotibial joints. In most cases, ultrasonography is a valuable complementary diagnostic technique to radiography of the equine stifle.

Injury to the femoropatellar ligaments occurs most frequently with patellar fractures, which often involve the parapatellar fibrocartilage and insertion of the medial femoropatellar ligament.[100, 176] Injury to the patellar ligaments, in the absence of prior surgical intervention (patellar ligament desmotomy), is uncommon, but does occur occasionally. In most horses, spontaneous injury involves the middle patellar ligament; usually a discrete area of fiber tearing (core lesion) is present within this ligament (Fig. 3-244). However, injury to the other patellar ligaments has also been detected (Fig. 3-245). A defect at the origin of the middle patellar ligament was recognized sonographically in one severely lame horse.[176] Enthesophyte formation at the origin of the middle patellar ligament has been recognized, but may be unrelated to lameness.[176]

Far more common are injuries to the collateral ligaments of the femorotibial joint, with or without associated meniscal damage. Injuries to the medial collateral ligament may be associated with the triad of injuries commonly seen in the stifle: injury to the medial collateral ligament, medial meniscus, and cranial (anterior) cruciate ligament. However, injury to the medial collateral ligament and medial meniscus can occur without detectable injury to the cranial cruciate ligament. Injury to the medial collateral ligament and medial meniscus and an associated avulsion fracture at the insertion of the medial collateral ligament, without injury to the cranial cruciate ligament, have been detected ultrasonographically and confirmed at autopsy.[95] Injury to the medial meniscus with collapse and fragmentation of the meniscus, collapse of the medial femorotibial joint space, and hemarthrosis has also been detected ultrasonographically and confirmed at autopsy.[95] Injury of the cranial cruciate ligament is more common than that of the caudal cruciate ligament.

Injury to the collateral ligaments is usually associated with a diffuse area of fiber damage rather than a discrete core lesion (Fig. 3-246). Bony irregularities (enthesophyte formation) at the origin or insertion of the collateral ligaments are also frequently detected ultrasonographically (Figs. 3-246 and 3-247). These bony changes

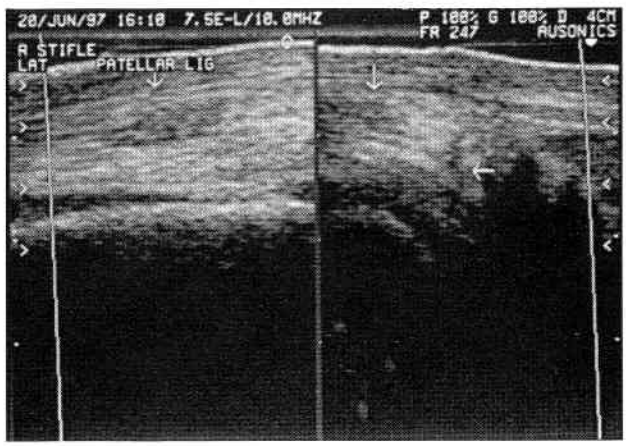

Figure 3–245

Sonograms of a lateral patellar ligament desmitis of the right stifle obtained from a 10-year-old Thoroughbred mare. Notice the hypoechoic lesion in the lateral patellar ligament, best imaged in the long-axis view *(left image)*. An area of swelling and fiber disruption is imaged under the vertical arrows in both the long-axis and short-axis *(right image)* views of the lateral patellar ligament. These sonograms were obtained with a wide-bandwidth 7.5-MHz linear-array transducer operating at 10.0 MHz using a hand-held standoff pad at a displayed depth of 4 cm. The right side of the short-axis view *(right image)* is cranial and the left side is caudal. The right side of the sagittal view *(left image)* is proximal and the left side is distal.

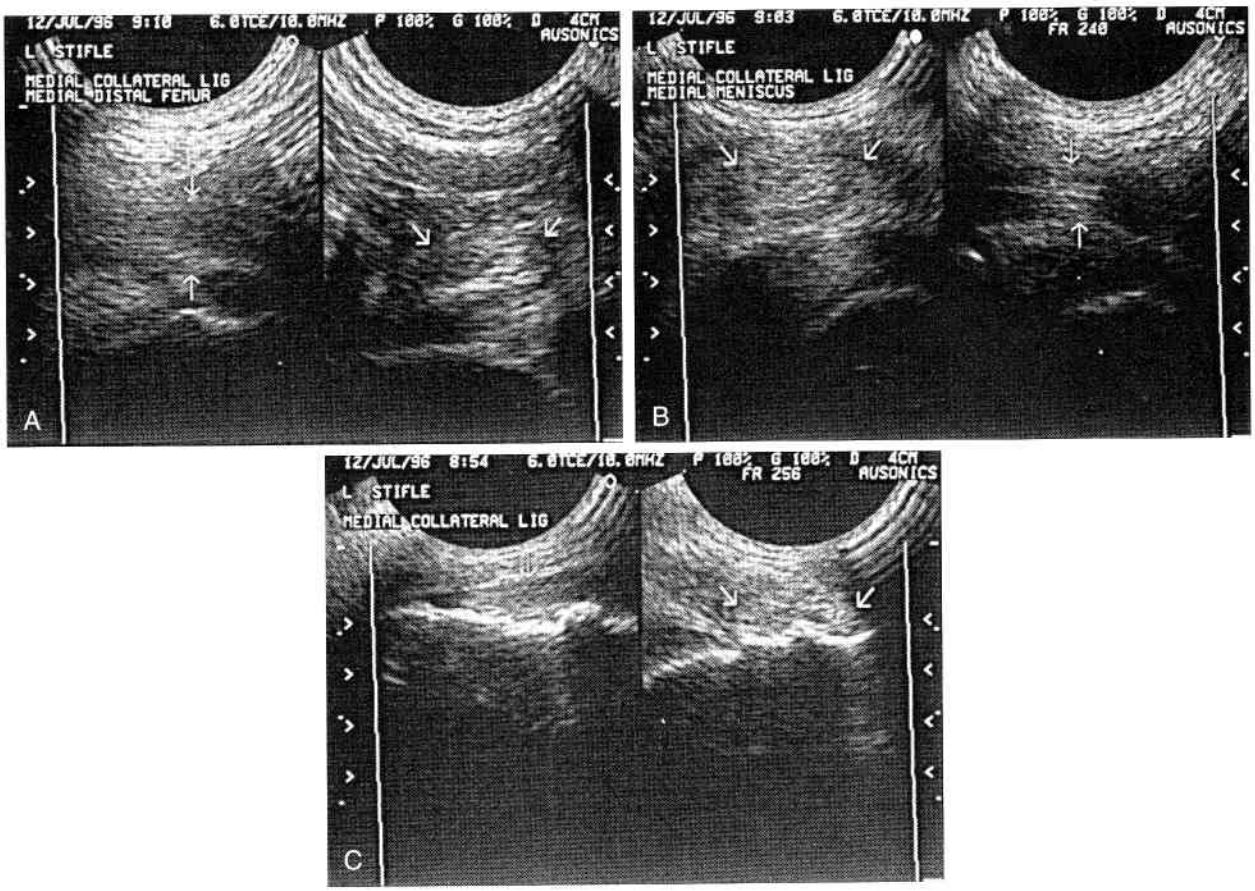

Figure 3–246

Sonograms of the medial femorotibial joint in the left hindlimb, obtained from a 12-year-old Appaloosa gelding with severe desmitis of the medial collateral ligament. The medial collateral ligament is markedly enlarged and hypoechoic from its origin to its insertion, with disruption of the majority of its fibers. Marked soft tissue swelling is present over the medial aspect of the femorotibial joint. These sonograms were obtained with a wide-bandwidth 6.0-MHz microconvex linear-array transducer operating at 10.0 MHz at a displayed depth of 4 cm. The focal zones are positioned in the middle of the image. The right side of the transverse images is cranial and the left side is caudal. The right side of the sagittal images is proximal and the left side is distal.

A, The medial collateral ligament is markedly enlarged and hypoechoic at its origin from the distal femur with a very heterogeneous appearance *(angled arrows)* in transverse section *(right image)* and few visible fibers *(vertical arrows)* in sagittal section *(left image)*.

B, The medial collateral ligament is still markedly enlarged in its mid body over the medial meniscus, with a slightly more homogeneous appearance *(angled arrows)* in transverse section *(left image)* and some visible fibers *(vertical arrows)* in sagittal section.

C, The medial collateral ligament is still enlarged and heterogeneous *(angled arrows)* in transverse section with no visible fibers *(vertical arrow)* in the sagittal section *(left image)*. Notice the marked bony irregularities along the insertion of the medial collateral ligament onto the proximal tibia.

are often very irregular in horses with a recent stifle injury, but they may become smooth and inactive in horses with healing of the collateral ligament desmitis, in the absence of meniscal injury. Avulsion fractures of the origin or insertion of the collateral ligaments can also be detected in association with a collateral ligament desmitis (Fig. 3-248).

Meniscal damage is detected when the meniscus shows change in its size, shape, echogenicity, or position relative to the femoral condyles and proximal tibia. Changes such as a decrease or increase in meniscal echogenicity or heterogeneous areas within the meniscus are relatively mild. Hyperechoic areas casting acoustic shadows indicate areas of calcification within the meniscus and more chronic meniscal damage (Fig. 3-249). Loss of the normal triangular meniscal shape in the sagittal image is indicative of meniscal tearing. If severe, extrusion of part of the meniscus from its normal position between the femoral condyles and proximal tibia can result (see Figs. 3-248 and 3-249). Comparison between the normal and affected side can be helpful in documenting collateral ligament and meniscal damage. Collapse of the joint space may also be appreciated in horses with meniscal damage. Femorotibial joint effusion often accompanies collateral ligament desmitis and meniscal injury, with a more severe synovitis (see Figs. 3-247 and 3-249) usually seen in horses with both collateral ligament and meniscal injury.

Cruciate ligament desmitis is uncommon, but similar changes in echogenicity, fiber alignment, and cross-sectional area of the cruciate ligaments occur with injury. Bony changes associated with the insertion of the cranial cruciate on the proximal tibia are detectable ultrasonographically (Fig. 3-250), but only with the stifle flexed. Avulsion fractures at the attachments of the cranial cruciate ligament have also been detected ultrasonographically.[42] These injuries often occur with medial collateral ligament and medial meniscal injury.

Bony irregularities on the femoral condyles may be

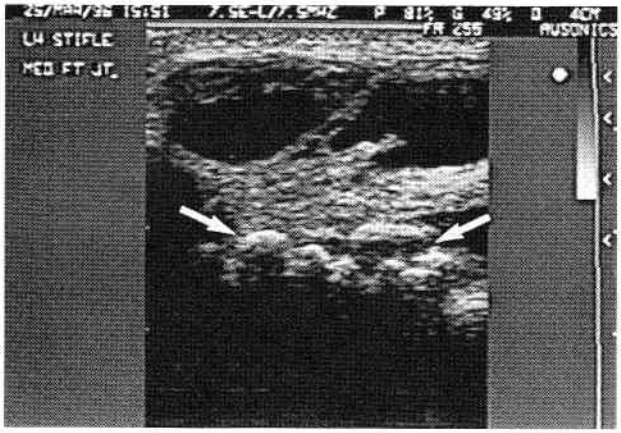

Figure 3–247

Sagittal sonogram of severe fibrinous synovitis of the medial femorotibial joint with severe periosteal proliferative and lytic changes along the medial aspect of the distal femur in the left hindlimb of a 5-year-old Standardbred stallion. Notice the hypoechoic fibrin crossing the femorotibial joint, the large anechoic effusion within the joint, and the large, slightly rounded bony irregularities along the medial aspect of the distal femur *(arrows)*. A severe medial collateral ligament desmitis was associated with these changes. This sonogram was obtained with a wide-bandwidth 7.5-MHz linear-array transducer operating at 7.5 MHz at a displayed depth of 4 cm. The focal zones are positioned in the near field. The right side of the sagittal image is proximal and the left side is distal.

detected in horses with severe degenerative joint disease or in association with osteochondrosis of the femoral condyles. Thinning of the articular cartilage of the femoral condyles, defects in the articular cartilage and underlying subchondral bone, and osteochondral or bony fragments are detectable in the portions of the femorotibial joint accessible to ultrasonographic examination. The accurate localization of bony fragments is possible ultrasonographically. The osteochondral fragments may not be free-floating within the joint, but may be attached to the synovial membrane.[95] Ultrasonographic examination has identified lesions in the articular cartilage and subchondral bone that were not detected radiographically.[92] Cartilaginous defects can be differentiated from defects in the subchondral bone, which may aid in the detection of small cartilaginous and subchondral lesions.[92] Ultrasonographic examination of the trochlear ridges has also corresponded well with findings at postmortem examination and on thin section radiographs of the femur.[92] However, radiographic examination of the stifle is more likely to reveal large subchondral bone cysts because many of these cysts are located in areas inaccessible to ultrasonographic examination.[178] Ultrasonographic findings may be consistent with a focal area of osteomyelitis in the subchondral bone, which has been described in one foal as an irregular hypoechoic to hyperechoic area deep to the cartilage-bone interface, with thickening of the overlying cartilage.[95] Communication between this focal area of osteomyelitis and the joint can be established ultrasonographically in most cases, unless the associated cartilaginous defect is small.[95] Ultrasonographic examination can also be used to assess the femoral condyles after surgery for osteochondritis dissecans (Fig. 3-251) and to assess the cause of postoperative periarticular swelling.

Periarticular swelling can be differentiated from joint distention, the character of the periarticular swelling can be determined, and communications between the periarticular swelling and the joint can be ruled out. Periarticular hematomas or abscesses may, in some horses, communicate with the joint, a determination that can be made

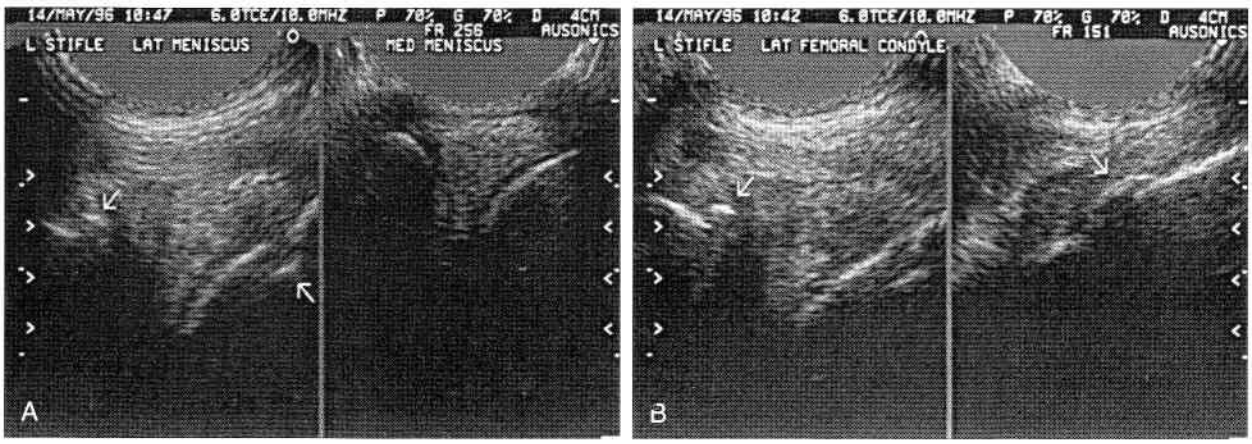

Figure 3–248

Sagittal sonograms of the lateral femorotibial joint in the left hindlimb, obtained from a 13-year-old Thoroughbred mare with damage to the lateral collateral ligament and lateral meniscus. These sonograms were obtained with a wide-bandwidth 6.0-MHz microconvex linear-array transducer operating at 10.0 MHz at a displayed depth of 4 cm. These focal zones are positioned in the middle of the image. The right side of the sonograms is proximal and the left side is distal.

A, Notice the marked enlargement and heterogeneity of the lateral meniscus compared to the medial meniscus, and the lateral meniscus protruding cranial to the cranial margins of the distal femur and proximal tibia. A large cystic lesion is seen in the subchondral bone of the distal femur along the lateral femoral condyle *(up arrow)* and an avulsion fracture of the proximal tibia *(down arrow)* is seen along the insertion of the lateral collateral ligament. The dorsal margin of the lateral meniscus appears hyperechoic and folded proximally adjacent to the cystic lesion in the subchondral bone.

B, Smooth periosteal proliferative change *(down arrow)* is also present along the distal femur adjacent to the cystic lesion in the more proximal view *(right image)*, whereas the avulsion fracture is clearly seen distracted from the proximal tibia in the more distal view *(left image)*. Again, the torn portion of the meniscus is imaged extending up towards the distal femur adjacent to the subchondral cystic lesion.

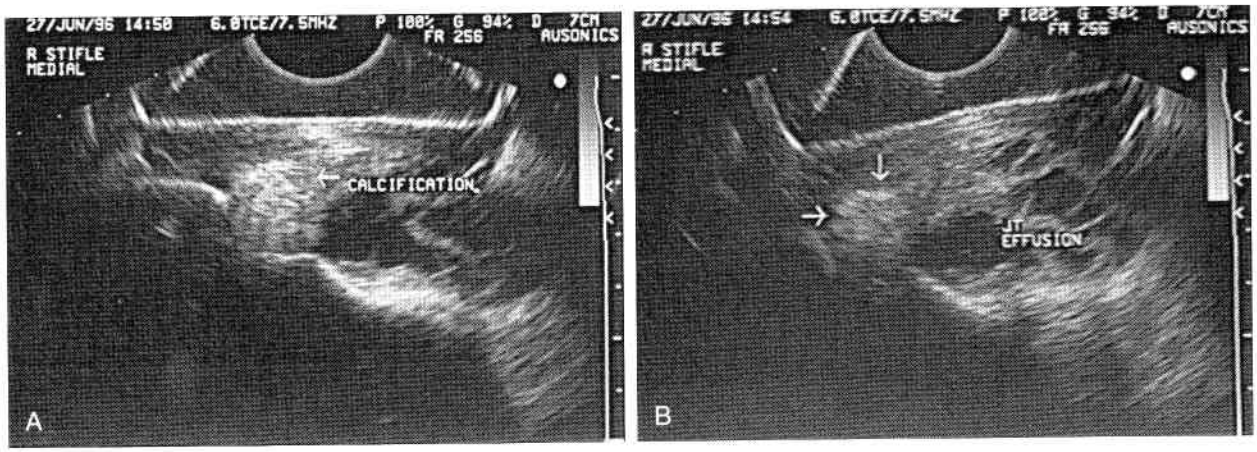

Figure 3–249

Sagittal sonograms of the medial femorotibial joint in the right hindlimb, obtained from a 13-year-old Thoroughbred gelding. These sonograms were obtained with a wide-bandwidth 6.0-MHz microconvex linear-array transducer operating at 7.5 MHz using a hand-held standoff pad at a displayed depth of 7 cm. These focal zones are positioned in the near field of the image. The right side of the sonograms is proximal and the left side is distal.

A, Notice the hyperechoic medial meniscus *(arrow)* extruded from its normal position between the distal femur and proximal tibia, consistent with a torn meniscus. The medial meniscus is enlarged, rounded in shape, and has hyperechoic areas within that cast small acoustic shadows consistent with areas of calcification. The medial collateral ligament is imaged superficial to the medial meniscus.

B, The medial compartment of the femorotibial joint has a large loculated effusion (jt effusion) consistent with chronic active synovitis. The meniscus is also visible in this more cranial sagittal sonogram protruding cranially from the cranial margins of the distal femur and proximal tibia *(arrows)*.

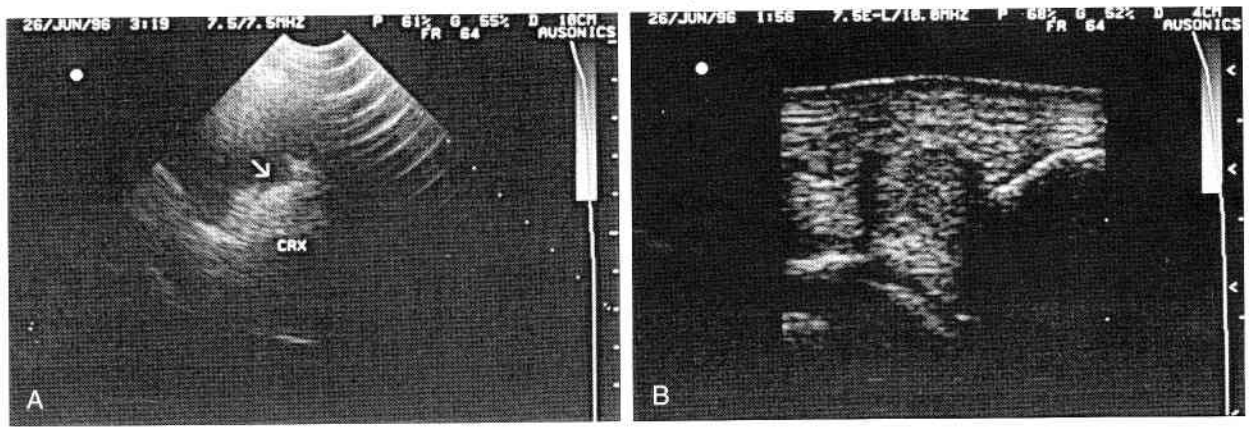

Figure 3–250

Sonograms of a torn cranial cruciate ligament and medial meniscus, obtained from an aged Thoroughbred cross gelding. These sonograms are courtesy of Dr. Ed Cauvin.

A, Notice the ragged appearance of the cranial cruciate ligament as it inserts on the proximal tibia. This horse had the classic triad of injuries including medial collateral ligament desmitis, a torn medial meniscus, and a torn cranial cruciate ligament. This sonogram was obtained with a wide-bandwidth 7.5-MHz sector-scanner transducer operating at 7.5 MHz at a displayed depth of 10 cm.

B, Notice the hypoechoic portion of the medial meniscus extruding from between the distal femur and proximal tibia, consistent with a meniscal tear. This sonogram was obtained with a wide-bandwidth 7.5-MHz linear-array transducer operating at 10.0 MHz with a hand-held standoff pad at a displayed depth of 4 cm. The right side of this sagittal view is distal and the left side is proximal.

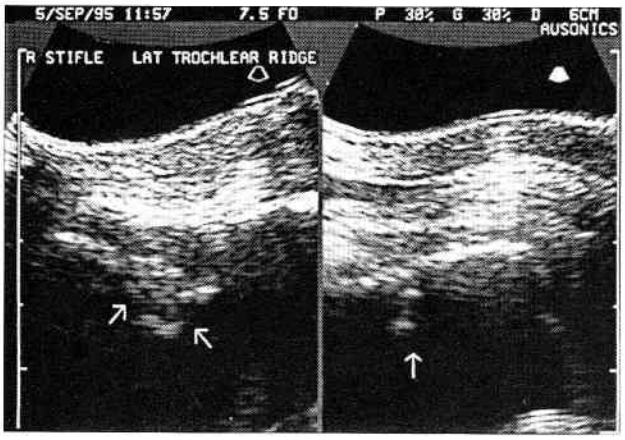

Figure 3–251

Sonograms of the lateral trochlear ridge after surgery for osteochondritis dissecans and curettage of the defects in the subchondral bone in the right hindlimb, obtained from a yearling Thoroughbred filly. Notice the large defect *(arrows)* in the lateral trochlear ridge of the femur in the transverse *(left image)* and sagittal *(right image)* views. These sonograms were obtained with a 7.5-MHz sector-scanner transducer containing a built-in fluid offset at a displayed depth of 6 cm. The right side of the transverse image is cranial and the left side is caudal. The right side of the sagittal image is proximal and the left side is distal.

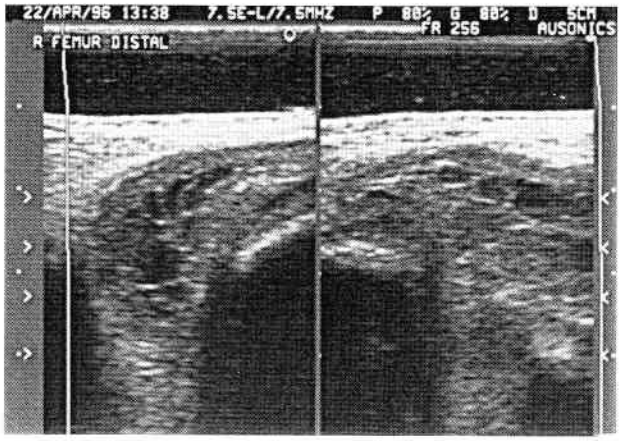

Figure 3–253

Sonograms of a septic femorotibial synovitis in the right hind leg, obtained from a 6-week-old Arabian colt. Notice the hypoechoic loculated fluid within the femorotibial joint, consistent with a severe, probably septic synovitis, confirmed with cytological evaluation and culture and sensitivity testing of a synovial fluid aspirate. These sonograms were obtained with a wide-bandwidth 7.5-MHz linear-array transducer operating at 7.5-MHz using a hand-held standoff pad at a displayed depth of 5 cm. The focal zones are in the middle of the image. The right side of the transverse view *(left image)* image is cranial and the left side is caudal. The right side of the sagittal view *(right image)* is proximal and the left side is distal.

ultrasonographically.[92, 95] Marked joint effusion is common in horses with traumatic injuries to the stifle, and rupture of the joint capsule can occur (Fig. 3-252). In acute injury, the hemorrhagic joint fluid can be recognized by its echogenic swirling pattern. Fibrin and loculations can be seen in the traumatized joint, but if the fluid is hypoechoic instead of anechoic and the swirling pattern of blood is missing, sepsis is most likely (Fig. 3-253).

Hock

Abnormalities of all the joints of the tarsus are frequently detected. Most of these abnormalities have to do with chronic synovitis of the tarsocrural, distal intertarsal, and tarsometatarsal joints. This is usually a nonseptic synovitis, a chronic "bog spavin" (Fig. 3-254). In horses with chronic nonseptic synovitis of the tarsocrural joint, an anechoic effusion is detected. However, septic hock joints are not uncommon, probably because of the frequency of intra-articular injections in these joints as a treatment for degenerative joint disease.

The joint fluid in horses with septic tarsocrural, distal intertarsal, or tarsometatarsal joints is usually hypoechoic

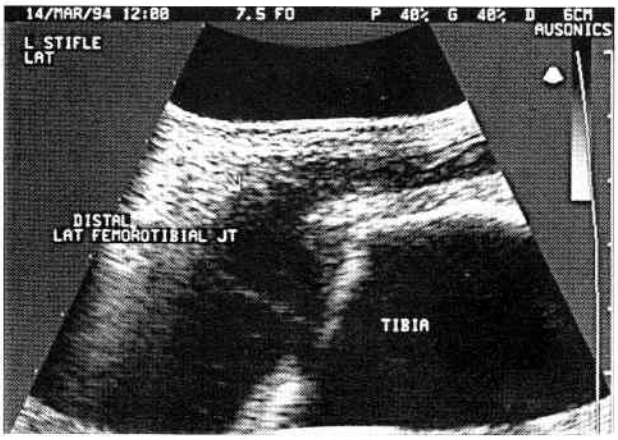

Figure 3–252

Sonograms of a ruptured lateral femorotibial joint compartment with a large anechoic fluid swelling extending around the lateral aspect of the tibia in the left hindlimb, obtained from a 1-month-old Thoroughbred colt. This sonogram was obtained with a 7.5-MHz sector-scanner transducer containing a built-in fluid offset at a displayed depth of 6 cm. The right side of the sonogram is cranial and the left side is caudal.

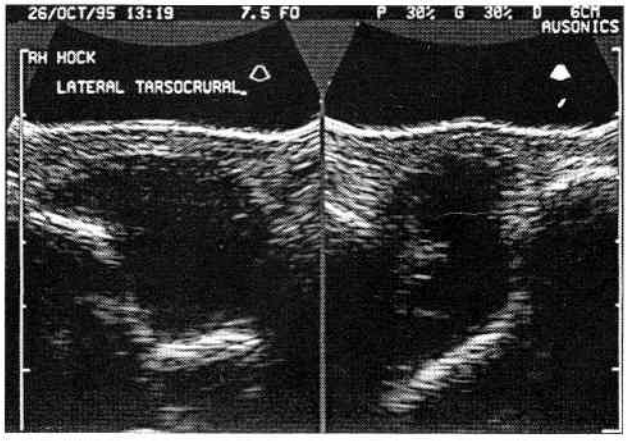

Figure 3–254

Sonograms of a severe nonseptic synovitis (bog spavin) in the right hock, obtained from a 3-year-old Quarter horse filly. Notice the large anechoic effusion in the lateral compartment of the tarsocrural joint in the right hindlimb. These sonograms were obtained with a 7.5-MHz sector-scanner transducer containing a built-in fluid offset at a displayed depth of 6 cm. The right side of the transverse view *(left image)* is cranial and the left side is caudal. The right side of the sagittal view *(right image)* is proximal and the left side is distal.

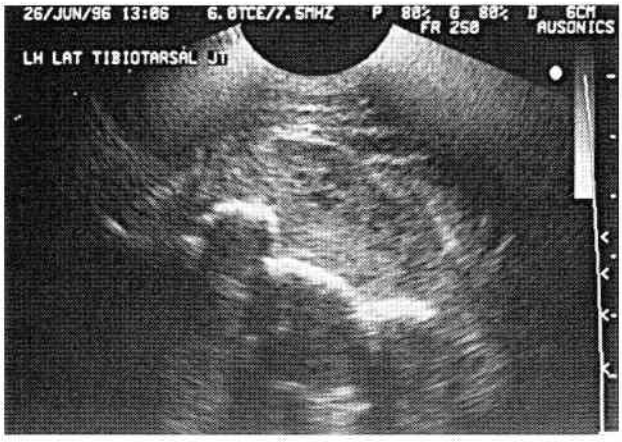

Figure 3–255

Sonograms of a septic loculated left tarsocrural synovitis obtained from a 5-year-old Thoroughbred gelding. Notice the marked distention of the lateral compartment of the tarsocrural joint with loculated hypoechoic fluid. This sonogram was obtained with a wide-bandwidth 6.0-MHz microconvex linear-array transducer operating at 7.5 MHz at a displayed depth of 6 cm. The right side of this sonogram is proximal and the left side is distal.

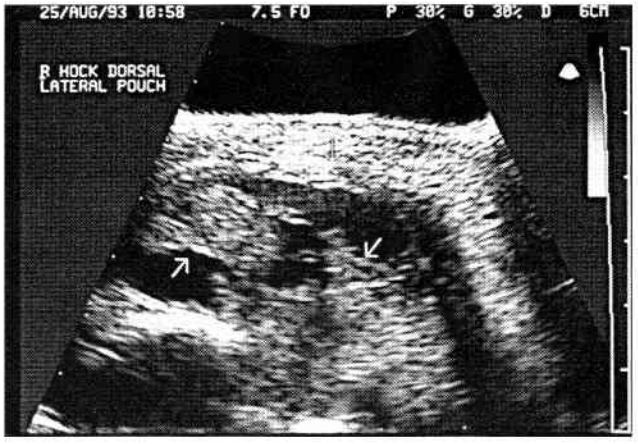

Figure 3–257

Sagittal sonogram of chronic fibrinous synovitis in a 7-year-old Thoroughbred gelding with chronic bog spavin of the right hind leg. Notice the hypoechoic to echogenic fibrin clots and loculations *(arrows)* within the lateral compartment of the tarsocrural joint. The joint fluid was anechoic and significant echogenic soft tissue swelling surrounded the tarsocrural joint, consistent with chronic periarticular inflammation. This sonogram was obtained with a 7.5-MHz sector-scanner transducer containing a built-in fluid offset at a displayed depth of 6 cm. The right side of the sagittal image is proximal and the left side is distal.

to echogenic (Fig. 3-255). Hyperechoic echoes casting reverberation artifacts or dirty shadows may be present, consistent with an anaerobic infection (Fig. 3-256). Fibrinous loculations may be detected in both septic and nonseptic synovitis. The synovial fluid in horses with nonseptic synovitis is anechoic (Fig. 3-257). Synovial thickening and hyperplasia may occur in both septic and nonseptic conditions, with synovial hyperplasia being most severe in horses with chronic synovitis (Fig. 3-258).

Severe capsular proliferation with loculation of the joint cavity in the medial aspect of the tibiotarsal joint has been detected sonographically in one horse after it was kicked.[93] Findings in this case, as in others, correlate well to those found on surgical intervention. Periarticular subcutaneous swelling is more common in horses with septic synovitis, but it may be detected in septic and nonseptic conditions. The joint should be carefully evaluated sonographically in horses with echogenic periarticular swelling, because a periarticular cellulitis may be present without a septic synovitis, and an arthrocentesis should be avoided in these situations. Hemorrhage associ-

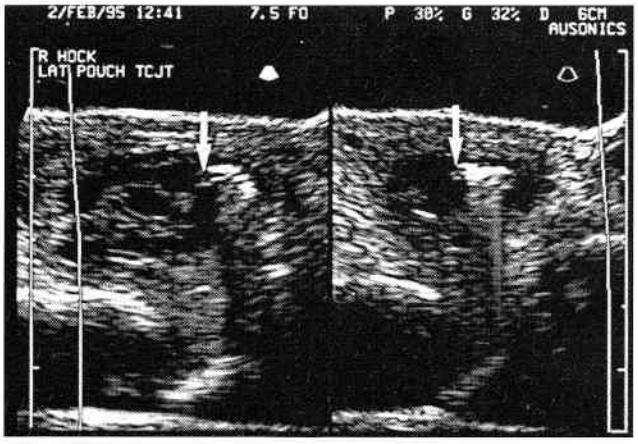

Figure 3–256

Sonograms of a septic loculated synovitis of the tarsocrural joint in the right hind leg, obtained from a 7-year-old Standardbred gelding. Notice the hyperechoic structures casting dirty acoustic shadows associated with free gas *(arrows)* in the dorsal portion of the lateral compartment of the tarsocrural joint. This sonogram was obtained with a 7.5-MHz sector-scanner transducer containing a built-in fluid offset and a displayed depth of 6 cm. The right side of the short-axis view *(right image)* is cranial and the left side is caudal. The right side of the long-axis view *(left image)* is proximal and the left side is distal.

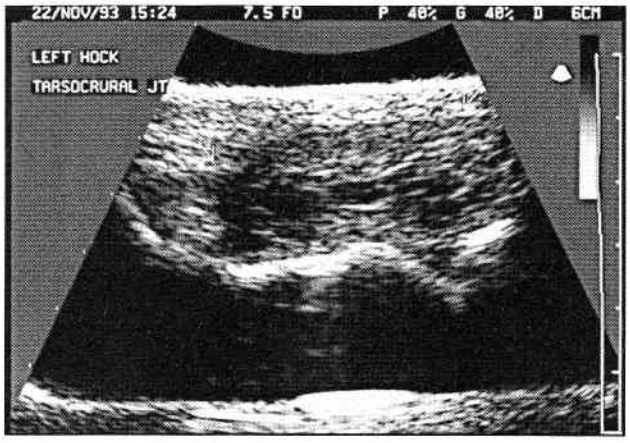

Figure 3–258

Sonogram of a chronic proliferative synovitis in the left tarsocrural joint, obtained from a 10-year-old Appaloosa gelding. Notice the marked thickening of the synovial lining of the lateral compartment of the tarsocrural joint, the hypoechoic appearance of the synovium, and the minimal amount of anechoic synovial fluid detected within the joint. This sonogram was obtained with a 7.5-MHz sector-scanner transducer containing a built-in fluid offset at a displayed depth of 6 cm. The right side of the sonogram is proximal and the left side is distal.

ated with trauma to the hock may also be detected, with both periarticular and intra-articular hemorrhage detectable sonographically. With acute bleeding, the fluid usually has an echogenic swirling pattern associated with the movement of red blood cells and other blood components. The joint capsule should be carefully evaluated in these horses, because rupture of the joint capsule, primarily that of the tarsocrural joint, has been detected in several affected horses (Fig. 3-259).

Collateral ligament injury in this joint appears less common than that in the fetlock or stifle joints. Similar to findings in other joints, collateral ligament desmitis is usually a diffuse injury to the lateral or medial collateral ligaments, rather than a discrete tear (Fig. 3-260). The ligament's cross-sectional area is increased, its echogenicity is decreased initially, and fiber alignment is disrupted. Enthesophyte formation at the origin or insertion of the collateral ligaments is common if the horse has collateral ligament desmitis (see Fig. 3-260). The bony surface echo is very rough, with a more acute desmitis associated with periosteal proliferative and lytic changes. A smoother, irregular bony surface echo is detected with a healed inactive collateral ligament desmitis. Medial collateral ligament desmitis was reported in one horse with injury to the short collateral ligaments. The injury appeared as two large, irregular hypoechoic defects in the mid body of these ligaments, with surrounding periarticular soft tissue swelling.[93]

The progress of tarsal bone ossification in foals with incompletely ossified cuboidal bones has been monitored ultrasonographically. This method appears reliable for assessing the ossification status of foals, because ossification of the carpal bones precedes that of the tarsal bones.[97, 98] The stages of ossification were graded I through IV in immature foals with incomplete ossification of the cuboidal bones by examining the distal dorsomedial aspect of the tarsus.[97, 98] The proximal part of the third metatarsal bone and the surface of the third and central tarsal bones are graded sonographically. Grade-I ossification is characterized by the detection of a curved line (representing the proximal metaphyseal part of the third metatarsal bone) and no visible bony surfaces of the third or central tarsal bones.[97, 98] The proximal epiphysis of the third metatarsal bone with an open physis may be visible in foals with grade-II ossification; or the proximal bony surface of the third metatarsal bone is imaged as a curved line.[97, 98] The third and central tarsal bones are partly visible in grade-II ossification and may appear malaligned. In grade-III ossification, the bony surfaces of the third and central tarsal bones are clearly visible, but are surrounded by thick cartilage.[97, 98] Some cartilage is visible on the dorsomedial bony surface of the third and/or central tarsal bones. The bony surfaces of the third carpal bone and central carpal bones are located further from the skin surface than is the proximal metatarsus. In grade-IV ossification, the bony surfaces of the third metatarsal bone, third tarsal bone, and central tarsal bone are aligned and are close to each other and close to the skin surface.[97, 98] The cartilage surrounding the bone may be quite thick in the early stages of cuboidal bone ossification. The cartilage may have echogenicity varying from hypoechoic to anechoic. The hypoechoic cartilage is more likely to be cartilage that later ossifies (precursor cartilage of bone), whereas the anechoic cartilage is imaged in the articular regions.[98] The proximal epiphysis of the third metatarsal bone changes more rapidly than do those of the small tarsal bones. The ossification pattern is irregular in immature foals and cartilaginous areas may be found radiographically in otherwise ossified bones.[98] Repeated ultrasonographic monitoring of the affected tarsi is better tolerated by foals than is radiographic monitoring; thus, ultrasonography may be a less stressful method of monitoring ossification.

Ultrasound examination of the bone can be used to diagnose bony abnormalities, confirm lesions detected with other physical examination or imaging modalities, evaluate the associated soft tissue damage or articular effusion, monitor fracture healing, and evaluate the response of the bone to treatment.

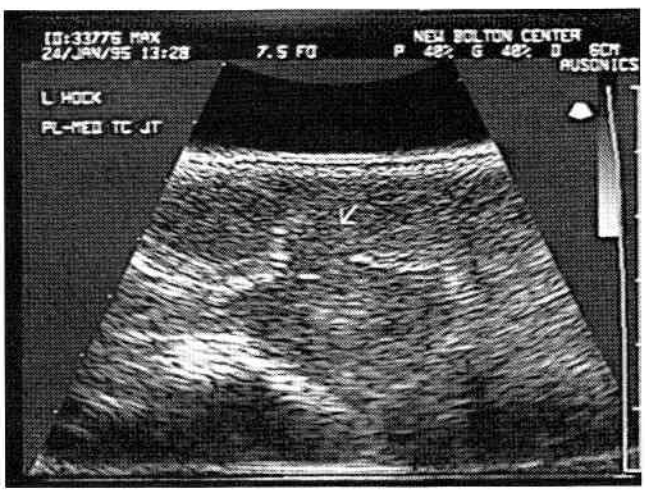

Figure 3–259

Sonogram of a rupture of the joint capsule of the left tarsocrural joint, obtained from a 6-year-old Thoroughbred gelding. Notice the defect in the plantar-medial (PL-MED) aspect of the tarsocrural joint capsule *(arrow)* and the hypoechoic fluid within the joint and in the surrounding soft tissues, consistent with recent hemorrhage. This sonogram was obtained with a 7.5-MHz sector-scanner transducer containing a built-in fluid offset at a displayed depth of 6 cm. The right side of the sonogram is proximal and the left side is distal.

PATIENT MANAGEMENT AND PROGNOSIS

Tendon and Ligament Injuries—Therapy

Initial treatment for injuries to the tendons or ligaments should be aggressive and should include cold water hosing or icing of the limb followed by a standing support bandage. Cold therapy should be used for 20 to 30 minutes several times daily, if possible, immediately after the injury and for several days thereafter. Local application of cold results in local vasoconstriction and slows the associated hemorrhage and release of inflammatory mediators in the injured tissues. Cold may also help dull pain associated with the injury.

Systemic nonsteroidal anti-inflammatory drugs such as phenylbutazone and/or flunixin meglumine are also indicated for an acute injury. The use of nonsteroidal anti-

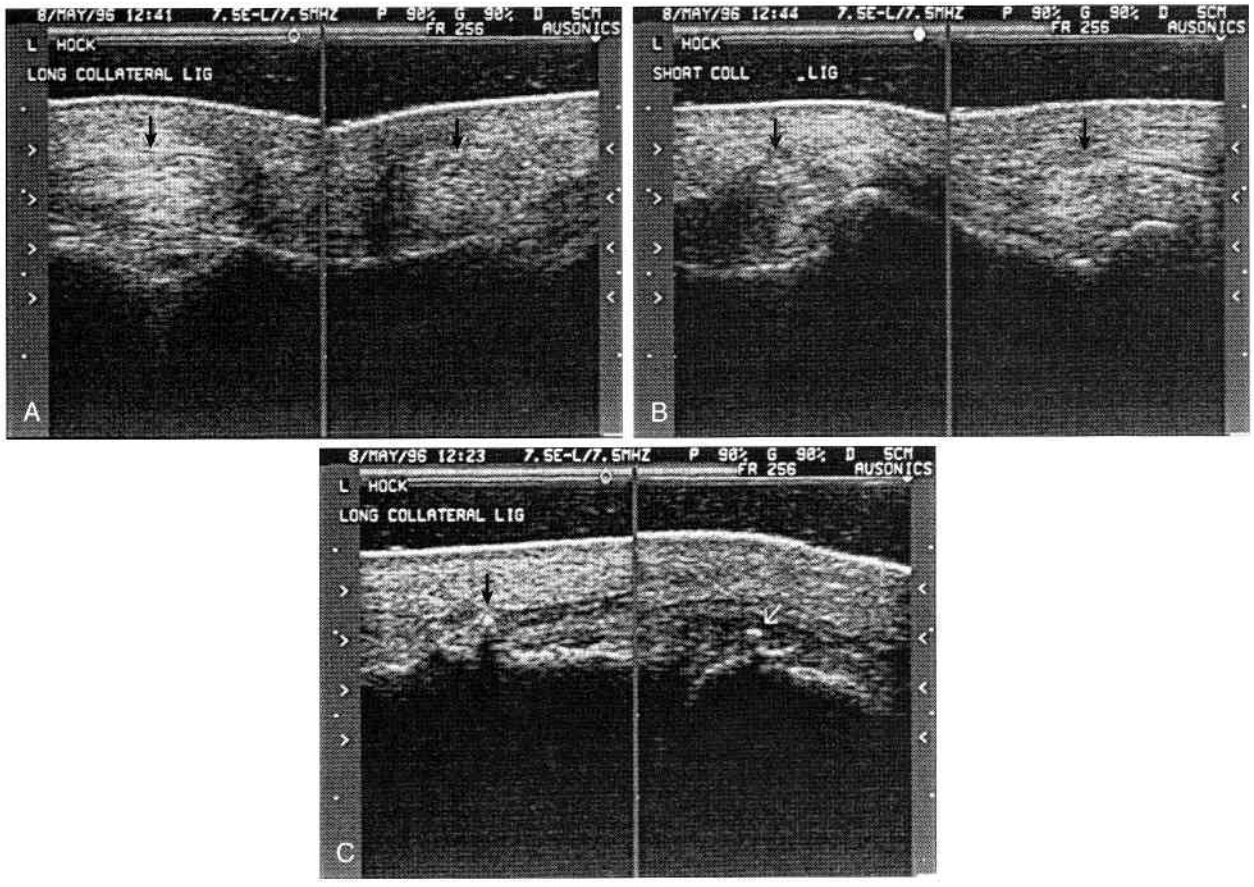

Figure 3–260

Sonograms of the long and short lateral collateral ligament of the hock joints, obtained from an 8-year-old Thoroughbred stallion. These sonograms were obtained with a wide-bandwidth 7.5-MHz linear-array transducer operating at 7.5 MHz using a hand-held standoff pad at a displayed depth of 5 cm. The focal zones are positioned in the near field. The right side of the transverse views is lateral and the left side is medial. The right side of the sagittal views is proximal and the left side is distal.

A, Sonograms of the short lateral collateral ligament obtained over the proximal portion of the hock, revealing the enlarged heterogeneous appearance of the short lateral collateral ligament *(ventral arrows)* in the sagittal *(right image)* and transverse *(left image)* views.

B, Sonograms of the long lateral collateral ligaments, obtained over the proximal portion of the hock and illustrating the marked enlargement of the long collateral ligament, its heterogeneity, and its loss of normal parallel fiber pattern *(vertical arrows)*. The sagittal *(left image)* view reveals the marked enlargement of this ligament, its heterogeneity, and its loss of normal fiber pattern. The transverse view *(right image)* reveals the marked enlargement and heterogeneity of the ligament affecting nearly all of the ligament's cross-sectional area at this level.

C, Marked bony irregularities along the insertion of the long lateral collateral ligament along the proximal lateral metatarsus, with the small avulsion fracture *(arrows)* detected in both sagittal *(left image)* and transverse *(right image)* views. Notice the marked disruption of ligamentous fibers in both views, with anechoic areas detected throughout the majority of the ligament.

inflammatory drugs helps to block the formation of prostaglandins and thromboxane in the injured tendinous and ligamentous tissues.[35] Corticosteroids are potent anti-inflammatory drugs that can decrease inflammation and adhesion formation, but they are also detrimental to tendon repair because of their ability to inhibit fibroplasia and collagen and glycosaminoglycan synthesis.[28] Systemic short-acting corticosteroids should be considered in the acute injury for their potent anti-inflammatory effects; they can be given by injection or orally. The use of oral Naquasone is preferred by some because of its combination of dexamethasone with the chlorthiazide diuretic.

Long-acting corticosteroids should be avoided because of their prolonged ability to inhibit fibroplasia and collagen and glycosaminoglycan synthesis. The intralesional injection of corticosteroids should be avoided because collagen fiber necrosis, fibrocyte death, and dystrophic calcification have been reported after injection of corticosteroids into normal tendon.[28, 35, 179] These changes in the tendon have resulted in a decrease in tendon strength for up to 1 year after the injection of corticosteroids into the tendon.[28]

Dimethyl sulfoxide (DMSO) is also of benefit in the treatment of acute tendon and ligament injuries because it is a potent anti-inflammatory agent and free-radical scavenger. DMSO also has vasodilatory properties that may be of benefit.[28] However, DMSO decreases the tensile strength of normal rat tail tendons up to 20% after 7 days of topical application.[28, 35, 180] Heparin has also been used in some horses with tendinitis, with anecdotal reports of success. However, no studies have confirmed any beneficial effect of heparin in tendinitis.[28, 35]

The initial exercise regimen for horses with a tendon or ligament injury should include stall rest with hand walking (Table 3-2). The amount of walking that should be performed depends in part on the severity of the

Table 3–2
Exercise Protocol for Tendon and Ligament Injuries*

Month 0–2
Stall rest and hand walk.
Walk 30 min/d first month, 45 min/d second month.

Month 3
Stall rest and hand walk 25–40 min/d, jog 5 min/d.

Month 4
Stall rest and hand walk 20–35 min/d, jog 10 min/d.

Month 5
Stall rest and hand walk 15–30 min/d, jog 15 min/d.
Turn out in small paddock, if quiet or tranquilized.

Month 6
Stall rest and hand walk 10–25 min/d, jog 20 min/d.
Turn out in small to medium paddock, if quiet or tranquilized.

Month 7
Week 1—Gallop 1 mile/d 2 times/wk, jog as before on alternate days.
Week 2—Gallop 1 mile/d 3 times/wk, jog as before on alternate days.
Weeks 3 & 4—Gallop 1 and a half miles/d 3 times/wk, jog as before on alternate days.

Month 8
Weeks 1 & 2—Gallop 2 miles/d 3 d/wk, jog as before on alternate days.
Weeks 3 & 4—Gallop 2 and a half miles/d 3 d/wk, jog as before on alternate days.

Month 9
Breeze 3/8ths—Continue to increase gallop speed and breeze length for next 8 weeks.

Month 11
Race.

*For moderate to severe injuries, the intervals would be prolonged with initial jogging delayed to 4–6 months. Other intervals may also need to be prolonged.

original injury. Horses with severe injuries to the tendons or ligaments with near-complete disruption of the affected tendinous or ligamentous structure should have complete stall rest with walking beginning only when support for the limb has returned.

The horse's foot should be trimmed so that it is balanced and level. Shoes with toe grabs and stickers should be removed. Significant hoof angle changes should be avoided whenever possible. The tendon or ligament should be allowed to heal with the limb in its normal position (angulation) to allow healing with the appropriate tendon or ligament length. Raising the heel of the foot actually increases the excursion of the superficial digital flexor tendon, because it inserts in the pastern on distal P1 and proximal P2. Lowering the heel of the foot straightens the fetlock and decreases the excursion of the superficial digital flexor tendon. Recent studies of ponies at a walk and trot were unable to demonstrate statistically significant changes in strain in the superficial digital flexor tendon when the heel was raised. However, most people agree that this is contraindicated in the treatment of injuries to the superficial digital flexor tendon.[181, 182]

Surgical Intervention

Tendon- or Ligament-Splitting Surgery. Tendon-splitting surgery is detrimental to tendon healing, unless the surgery is performed in the acutely injured tendon.[28, 128] The research to date suggests that if a discrete core lesion exists with an anechoic or hypoechoic core surrounded by normal or near-normal tendon fibers, surgical decompression of the lesion may be beneficial in the acute injury, decompressing this compartment within the tendon. A significant reduction in lesion size, tendon diameter, and lesion grade was detected within 8 to 12 days after surgery in horses with acutely to subacutely injured tendons that contained a core lesion.[28] Ideally, this surgery should be performed within the first 2 weeks after the development of the tendon or ligament injury.

Surgical decompression of this intratendinous or intraligamentous compartment may still be beneficial for 4 weeks after the injury, but the likelihood of improvement after surgery decreases the more time that passes between the onset of the injury and surgical intervention. The detection of a large anechoic core lesion in the tendon or ligament suggests that the surgery may still be beneficial, whereas the detection of a hypoechoic core indicates the presence of granulation tissue and immature fibrous tissue within the area of injury. Surgery is not indicated in these cases because a hematoma no longer exists, hence no compartment syndrome exists within the injured tendon or ligament to decompress. In some horses with severe injuries to the superficial digital flexor tendon, the tendon has been decompressed successfully with a 27-gauge needle as late as 5 or 6 weeks after injury. This occurs for less than 1% of tendon injuries, in this author's experience. Although surgical decompression of the core lesion ("tendon splitting") has only been studied in the superficial digital flexor tendon, this surgical procedure should be equally beneficial in acute core lesions in other injured tendons and ligaments.

Medical Treatment

Sodium Hyaluronate. Hyaluronate appears in the wound in high concentrations within the first 5 to 7 days of wound healing.[183, 184] Hyaluronate is thought to hydrate the extracellular matrix and thus promote cellular migration. Hyaluronate may also have a direct stimulatory effect on migrating repair cells.[28] The degradation of hyaluronate appears to promote cellular differentiation into collagen-producing cells and to stimulate angiogenesis. More rapid wound healing, decreased fibrosis, and enhancement of repair tissue maturation occur with the addition of high-molecular weight hyaluronic acid to a wound.[184] Hyaluronic acid has been used to treat tendinitis in horses and appears to decrease adhesion formation and promote tendon healing. A greater improvement was reported in treated tendons compared to untreated tendons when hyaluronic acid was injected in the surrounding peritendinous tissues in a collagenase-induced model of tendon injury.[24] Intrathecal injection of large amounts of hyaluronic acid in horses with a collagenase-induced tendon injury contained within the tendon sheath resulted in improvement in the histologic evidence of repair compared with controls at 8 weeks after injury.[185] However, the injection of sodium hyaluronate subcutaneously around the injured tendon resulted in no

significant differences between sodium hyaluronate-treated limbs and placebo-treated controls.[186] In fact, in this study trends existed towards less lameness in treated limbs, but better ultrasonographic evidence of tendon healing in control limbs. No significant biochemical or biomechanical differences between the two groups were found. However, significantly more inflammation was detected microscopically in treated tendons than in control tendons, and no difference was detected in the amount or severity of peritendinous adhesions.[186] Intralesional injection of sodium hyaluronate may be beneficial in horses with acute and chronic tendinitis.[186] No published studies document these findings, but an early, marked increase in small-diameter collagen fibrils and improved vascularization in treated versus untreated tendons have been reported in some preliminary European studies.[186]

Polysulfated Glycosaminoglycans. The glycosaminoglycan composition of the extracellular matrix may be important in collagen regulation and changes during tendon repair.[183] The polysulfated glycosaminoglycans (PSGAG) inhibit collagenase activity and macrophage activation.[32] The use of intralesional PSGAG has been reported in one horse that responded well clinically and ultrasonographically.[32] The original core lesion and total cross-sectional area of the tendon decreased in size and the original core lesion was no longer discretely visible in the transverse scan by 6 months after injury. Tendon echogenicity improved and was near normal at this time, although disruption of the normal fiber pattern was still visible in the sagittal scan. The volume of injected fluid should be limited to no more than 0.5 ml per site when performing intralesional tendon injections, to avoid abaxial spreading and tendon fibril disruption.[187] One study of National Hunt horses with tendinitis treated with intramuscular PSGAG revealed that fewer than 50% of horses were able to race, and recurrence rate was high among horses treated with PSGAG.[33]

Intralesional βAPN-F. Beta-aminoproprionitrile fumarate (βAPN-F) is a scar-remodeling drug that improves the quality of repair in horses with injuries to the superficial digital flexor tendon.[30, 38, 39, 126, 127] βAPN-F has also been used in other tendon and ligament injuries with similar success. Beta-aminoproprionitrile (βAPN) is found in the seeds of the wild sweet pea, *Lathyrus odoratus*. βAPN-F, administered in the early stages of scar formation, blocks the enzyme lysyl oxidase and thus blocks the formation of collagen cross-links in the area of repair. This brief interruption of collagen cross-linking allows for physiologically beneficial scar remodeling to occur.

βAPN-F is indicated in the treatment of a horse with significant injury to a tendon or ligament in which at least 20% or more of the tendon is damaged at its worst injury zone. The injury can be discrete or diffuse, as long as fiber tearing has occurred (imaged in the sagittal scan). A complete sonographic examination should be performed before beginning intralesional βAPN-F treatment with measurements of the tendon or ligament area and measurements of the lesion area being made in each zone. Fiber alignment and echogenicity should also be scored as previously described. Total tendon cross-sectional area and total lesion (injury) cross-sectional area should be calculated by summing all the lesion and tendon cross-sectional areas for the entire metacarpal or metatarsal region (Table 3-3). Total percentage of the tendon or ligament injured can then be calculated by dividing the total lesion cross-sectional area by the total tendon cross-sectional area.

$$\% \text{ Total Injury} = \frac{\text{Total Lesion Cross-Sectional Area}}{\text{Total Tendon/Ligament Cross-Sectional Area}}$$

After a sterile prep, βAPN-F is injected throughout the lesion with a 27-gauge 1¼-inch needle (shorter 25-gauge needles have also been used but may break more easily). The βAPN-F is injected from 1 cm proximal to 1 cm distal to the injury and into the area surrounding the discrete lesion if damage is also detected in the adjacent tendinous or ligamentous tissue. The injured area is injected every other day for a total of five treatments. Horses are then placed in a rigorous low-level controlled exercise program with frequent ultrasound monitoring (see Table 3-2). The treated horses begin walking 30 minutes per day for 4 weeks, then 45 minutes daily for another 4 weeks. All subsequent increases in the horse's exercise should be based on improvement in the sonographic findings.

The following exercise levels (EL) have been used successfully in horses treated with intralesional βAPN-F. Adjustments in the exercise level must be made based on the severity of the horse's original injury and the re-

Table 3–3
Calculation of Total Lesion and Tendon Cross-Sectional Area and Total % Injury

Zone	Lesion X-sec area (cm^2)	Tendon X-sec area (cm^2)	% Injury
1A	L @ 1A	T @ 1A	% @ 1A
1B	L @ 1B	T @ 1B	% @ 1B
2A	L @ 2A	T @ 2A	% @ 2A
2B	L @ 2B	T @ 2B	% @ 2B
3A	L @ 3A	T @ 3A	% @ 3A
3B	L @ 3B	T @ 3B	% @ 3B
3C (4A)	L @ 3C(4A)	T @ 3C(4A)	% @ 3C(4A)
(4B)	L @ 4B	T @ 4B	% @ 4B
(4C)	L @ 4C	T @ 4C	% @ 4C
Total	ΣL@1A + 1B + . . . 3C or ΣL@1A + 1B + . . . + 4C	ΣT@1A + 1B + . . . 3C or ΣT@1A + 1B + . . . + 4C	Σ%@1A + 1B + . . . 3C or Σ%@1A + 1B + . . . + 4C

Abbreviations: L, lesion; T, tendon; X-sec, cross-sectional; %, percentage; Σ, sum.

sponse of the individual horse to exercise loading. Horses with severe injuries to the tendons or ligaments should advance more slowly through this exercise protocol.

EL1—Walking in hand, or with a treadmill or mechanical walker

EL2—Jogging or ponying for no more than 5 to 10 minutes, or swimming; in the Standardbred, this is walking in the jog cart

EL3—Hacking at the walk, trot, and canter for 15 to 20 minutes 3 days per week, with walking and jogging on the other days for the Thoroughbred or show horse; one 6-minute jog mile 3 days/week for the Standardbred, with walking on alternate days

EL4—Limited free-choice paddock exercise

EL5—1 to 2 mile gallops for the Thoroughbred; normal "jog miles" for the Standardbred; normal ring work including low fences for the show horse

EL6—Normal galloping and slow breezes for the Thoroughbred racehorse; normal jogging and training slower than a 2:20 minute mile and normal hacking and practice jump rounds for the show horse

EL7—Maximal athletic competition, which is racing for the Thoroughbred and Standardbred and showing for the show horse

Alternative Therapies

Alternative therapies such as the therapeutic laser, the therapeutic ultrasound, and electromagnetic therapy have become increasingly popular among horse owners and veterinarians alike. Although these therapies are not a substitute for adequate time for tendon and ligament healing and a controlled exercise program for tendon and ligament rehabilitation, some beneficial effects have been reported. Controlled clinical studies demonstrating the efficacy of these treatments have not been performed in the horse, to date. The optimal time after injury to apply these alternative therapies, the method of their application, and their efficacy in the treatment of equine tendon and ligament injuries warrants further investigation.

Therapeutic Lasers. In one study of National Hunt horses, only 50% of horses treated with low-level laser or cold-laser therapy returned to training. Thirty percent returned to racing, with a 20% recurrence of tendinitis.[33] Conservatively treated horses did better, although this difference was not statistically significant. In another study with Standardbred racehorses, 66% successfully returned to racing after treatment for tendinitis with low-power laser therapy.[188] However, the prognosis for Standardbred racehorses is usually better, and these results are no better than those reported for Standardbreds managed conservatively.[16, 25]

Therapeutic Ultrasound. Therapeutic ultrasound may also be beneficial in tendon healing. Surgically split tendons that were treated with therapeutic ultrasound showed improved healing compared to those not treated with therapeutic ultrasound.[189]

Electromagnetic Therapy. The benefit of daily electromagnetic therapy in horses with tendon injuries is also questionable. With this therapy, repair tissue maturation and collagen type transformation were delayed and the vascularity of surgically created defects in the superficial digital flexor tendon was improved 8 and 12 weeks after surgery.[190] Another study using direct current stimulation also found no beneficial effects on equine tendon healing.[191]

Tendon and Ligament Injuries—Treatment and Prognosis

Superficial Digital Flexor Tendinitis

Prognosis. Treatments for injuries to the superficial digital flexor tendon are many and are as varied as the treating veterinarians. Most veterinarians agree, however, that a gradually increasing controlled exercise program maximizes the horse's chance of successfully returning to racing. Before the advent of ultrasonography, the prognosis for horses with bowed tendons was poor, with only 25% of horses returning successfully to racing. Several studies since that time, in which tendon injuries were documented ultrasonographically, have revealed that 55% to 60% of horses treated conservatively return successfully to racing. Thoroughbred horses racing on the flat had a 55% chance of racing successfully for three starts if only one tendon was injured. Only 25% of Thoroughbred horses were able to do so if both forelegs were bowed.[16] In contrast, 75% of Standardbred horses were able to return successfully to racing, and no difference occurred between horses with unilateral or bilateral injuries.[16] Similarly, no difference was noted between the success of horses with unilateral or bilateral bowed tendons among horses that race over fences or compete in combined training.

Others have also reported that Standardbred racehorses have a better prognosis than do Thoroughbred racehorses with superficial digital flexor tendon injuries.[15, 26] In another study, 64% of Thoroughbred racehorses that were rested and treated for superficial digital flexor tendinitis were able to complete two races without reinjury, whereas only 12% of Thoroughbreds who remained in training were able to do so.[15] One horse who remained in training had a mild (type-2) lesion involving only 15% of the tendon's total cross-sectional area. Most of the Thoroughbred racehorses that were successful when rested and treated for their superficial digital flexor tendinitis had damage to less than 25% of the tendon's total cross-sectional area.[15] Type-4 lesions involving greater than 25% of the tendon's total cross-sectional area carried a poor prognosis, and these horses were not successful. In contrast, 81% of Standardbred horses were able to complete two races without a recurrence of the superficial digital flexor tendinitis if they were rested and treated for the tendinitis, and 50% of Standardbred horses were able to continue racing in spite of the superficial digital flexor injury.[15] However, similar to the Thoroughbred racehorses, none of the Standardbred racehorses with type-4 lesions involving greater than 25% of the total

cross-sectional area of the tendon were able to compete successfully.

In a study using the severity rating of the superficial digital flexor tendon injury, an increased severity rating in Thoroughbred racehorses was associated with a drop in class.[26] Thoroughbred racehorses that were rested had a 64.3% chance of returning successfully to the races if they had a severity rating of 2.3 or less, and a 57.9% chance of returning successfully if they had a severity rating of greater than or equal to 3.9. Horses with a severity rating of less than 2.3 (small lesions) had an 83.3% chance of returning to a racing class equal to or above that attained prior to the injury, whereas horses with a severity rating of 3.9 (severe injury) and above had a 56.8% chance of returning to the same level of racing performance.[26] Of horses with a severity score of less than 2.3, 57.1% returned to an extended racing career (no evidence of reinjury and completed 12 or more starts), whereas only 31.6% of horses with a severity rating greater than or equal to 3.9 were able to return to an extended racing career. A drop in racing class also occurred with an increase in the severity rating.[26]

These authors also demonstrated that although 50% of Thoroughbred racehorses with a superficial digital flexor tendon injury may be able to complete four starts without rest, overall, only a 36.4% chance exists that a Thoroughbred racehorse with an injured superficial digital flexor tendon will be able to compete for an extended period of time.[26] Of Standardbred racehorses, 60% with aseverity rating of less than 2.3 were able to return successfully to the races and make seven starts if rested; 52.5% of horses with a severity rating greater than or equal to 3.9 were successful. All of the horses with severity ratings of less than 2.3 were able to race at the same or greater class than before sustaining the superficial digital flexor tendon injury, whereas only 71.5% of horses with a severity rating greater than or equal to 3.9 were able to do so.[26] With only palliative treatment, 66.7% of horses with a severity rating of 3.8 or less were able to return successfully to racing, whereas only 22.2% of those with a severity rating greater than or equal to 3.9 were able to do so.

A recent study used a more comprehensive sonographic evaluation of tendon injury and tendon healing.[38] Eighty percent of horses that had at least a 6-month break before returning to race training (EL5) and had received any of the conventional treatments for superficial digital flexor injuries (except βAPN-F) rebowed during their racing career. The majority of horses (57%) experienced a recurrence of the injury before racing, whereas 23% did race but still rebowed.[38] In contrast, the horses that received intralesional βAPN-F had better success. Although the majority of horses (55%) receiving βAPN-F rebowed during their entire racing career, only 24% bowed before returning to the races and only 31% experienced a reinjury of the tendon once they had returned to racing.[38]

When injury severity was evaluated, conservatively treated horses with a slight injury to the superficial digital flexor tendon who had spent at least 6 months out of race training before returning to EL5 had a 67% recurrence rate of the tendon injury during their entire racing career (22% rebowed before reaching EL7 and 44% after reaching EL7). In contrast, none of the horses with slight injuries that spent at least 6 months out of training before returning to EL5 and that had received βAPN-F rebowed before reaching EL7, and only 33% bowed after reaching EL7. Similar improvement occurred in the long-term success of βAPN-F–treated horses with moderate injuries, but not those with severe injuries.[38] Further studies are needed evaluating the long-term racing success of treated horses to determine the best treatment for a particular tendon injury and the most accurate prognosis that can be given based on the severity of the original injury and its subsequent healing. Horses in this study that had 4 to 7 unacceptable sonographic parameters (MIZ-SA, MIZ-HYP, MIZ-FAS, T-SA, T-HYP, T-FAS, %THYP) before beginning EL5 had a high recurrence of bowed tendons.[38] Delaying the start of EL5 until these parameters have improved should increase the chance of these horses returning successfully to the races.[38]

Surgical Intervention

Tendon-Splitting Surgery. This surgery is indicated in selected cases of superficial digital flexor tendon injury. The ideal candidates for tendon splitting surgery are horses that have a new (less than 2 weeks old), discrete core lesion in the superficial digital flexor tendon that has not already ruptured into the surrounding peritendinous tissues (Fig. 3-261). Studies in a collagenase-induced model of tendinitis demonstrated both ultrasonographic and histopathologic improvement after tendon-splitting surgery. Tendon and lesion cross-sectional area decreased in size and tendon echogenicity improved after tendon-splitting surgery. Earlier revascularization of the lesions was seen experimentally, along with a better-quality repair, at 4 and 8 weeks postsurgery.[27] An ultrasonographic study in clinical cases of tendinitis using ultrasound-guided tendon splitting revealed a 44% reduction in lesion size and a mean decrease in lesion grade of 0.9 by day 10 postsurgery.[29] The majority of horses (81%) treated with ultrasound-guided tendon puncture were able to return to performance, 68% at the same level.[29]

Horses with very small core lesions are not good candidates for this surgery, because damage to some of the remaining normal tendon fibers may occur. Furthermore, with a small area of injury, the creation of a compartment syndrome within the superficial digital flexor tendon is unlikely. This surgery is also contraindicated in horses with large core lesions involving greater than 75% of the superficial digital flexor tendon's cross-sectional area at the worst injury zone, because the surgery may result in additional damage to the few normal or near-normal fibers remaining. Surgery is also contraindicated in horses with complete or nearly complete rupture of the superficial digital flexor tendon, again because the surgery may result in additional fiber injury and loss of support to the fetlock joint. Previous histopathologic studies have also conclusively demonstrated that the surgery is detrimental to tendon healing unless the injury is acute.

In a recent study evaluating the long-term racing performance of horses treated with a wide variety of different regimens for superficial digital flexor tendon injuries, 74% of horses given at least 6 months of low-level controlled exercise before returning to EL5 and treated initially with tendon-splitting surgery (with or without supe-

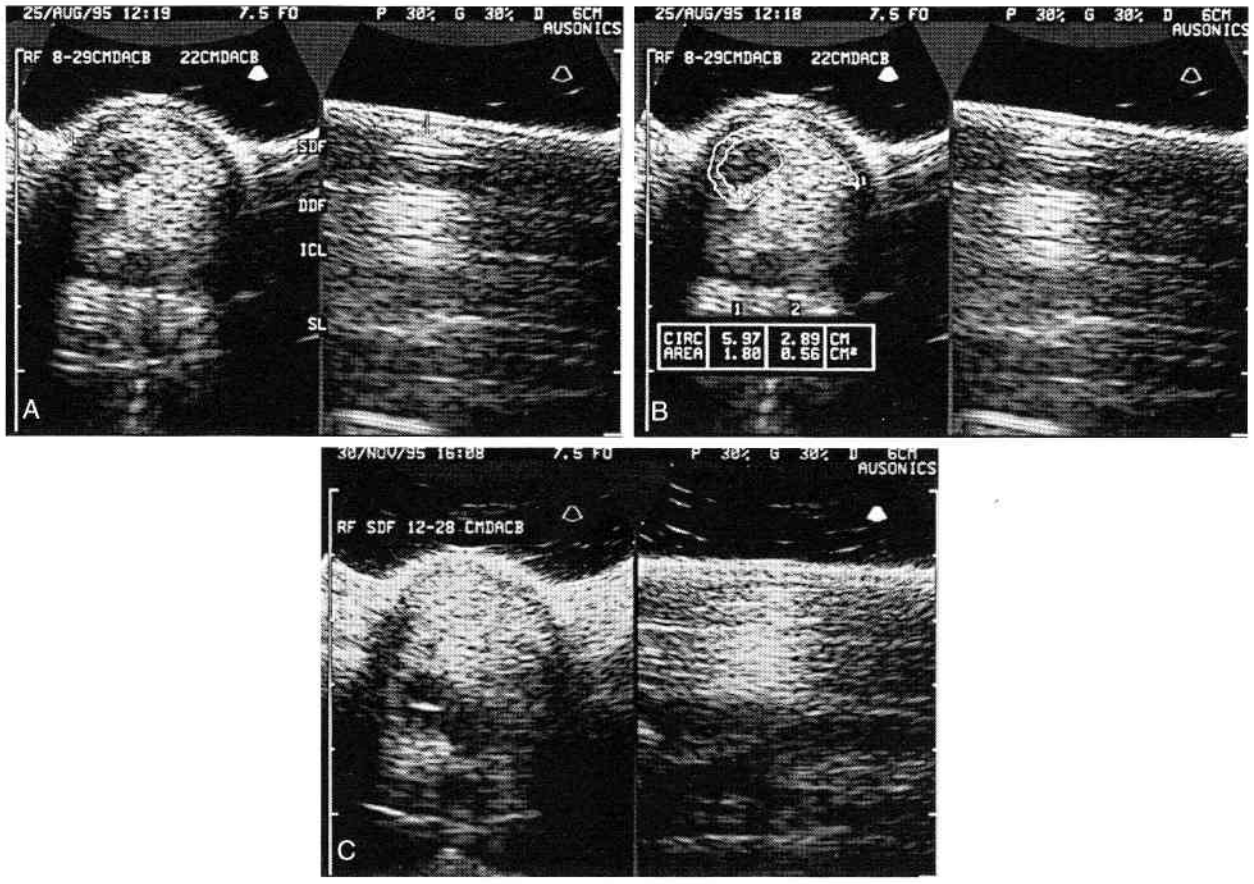

Figure 3–261

Sonograms of a fresh discrete core lesion in the medial portion of the right fore superficial digital flexor tendon (SDF) before *(A* and *B)* and after *(B)* surgically splitting the tendon, obtained from a 4-year-old Thoroughbred filly. Ten days after the injury occurred, these sonograms were performed with a 7.5-MHz sector-scanner transducer containing a built-in fluid offset at a displayed depth of 6 cm. The right side of the transverse views *(left images)* is lateral and the right side is medial. The right side of the sagittal views *(right images)* is proximal and the left side is distal. DDF, deep digital flexor tendon; ICL, inferior check ligament; SL, suspensory ligament.

A, Notice the discrete anechoic to hypoechoic core lesion in the medial aspect of the SDF *(arrows)* with complete loss of the normal fiber pattern. The original core lesion was detected from 8 to 29 cm distal to the point of the accessory carpal bone.

B, This lesion involved 31% of the SDF (0.56 cm^2/1.80 cm^2) at its largest point, 22 cm distal to the point of the accessory carpal bone (zone 3A).

C, Three months later, the SDF only appears abnormal from 12 to 28 cm distal to the point of the accessory carpal bone. The original core lesion is no longer visible, the tendon's cross-sectional area has decreased in size to 1.51 cm^2, and the lesion is repairing with a somewhat random fiber pattern. This sonogram was also obtained at 22 cm distal to the point of the accessory carpal bone.

rior check ligament desmotomy) rebowed during their racing career, 42% before reaching EL7, and 32% once they had reached EL7.[38] These long-term results were no better than those for any other surgical or external treatment.[38]

Superior Check Ligament Desmotomy. Superior check ligament desmotomy is often performed in conjunction with tendon-splitting surgery in horses with discrete core lesions, if the superior check ligament desmotomy surgery is performed soon after the injury to the superficial digital flexor tendon. Complete transection of the superior check ligament results in maximal lengthening of the superficial digital flexor musculotendinous unit and enables the superficial digital flexor muscle to assume a greater portion of the load.[28] The increased length may increase the elastic limit of the repaired tendon and partially counteract the loss of elasticity in the region of the fibrotic scar.[36] Success with this surgery has varied widely among investigators.[27, 36, 38, 192-195] Excellent surgical technique with complete transection of the superior check ligament is necessary for optimal long-term results (successful return to racing). This surgery has been successfully performed in both Thoroughbred and Standardbred horses with good return-to-racing results.[36, 192-195] Many of these horses also had the tendon-splitting surgery performed, making it difficult to accurately determine the successfulness of this surgical procedure alone.

Success with this procedure in Thoroughbred horses ranges from 25% for competing without reinjury for the entire racing career to greater than 70% for enabling at least five starts without reinjury.[38, 193] More than 90% of Thoroughbred horses with tendinitis were able to train and race after a superior check ligament desmotomy, with at least 66% starting at least five times.[193] More than 45% of the horses that raced maintained or increased their average earnings per start, and 86% raced in the same class as before the surgery.

Success in the racing Standardbred has also been good, with 69%[36] to more than 80%[195] returning successfully to racing for at least five starts (Fig. 3-262). Horses that had

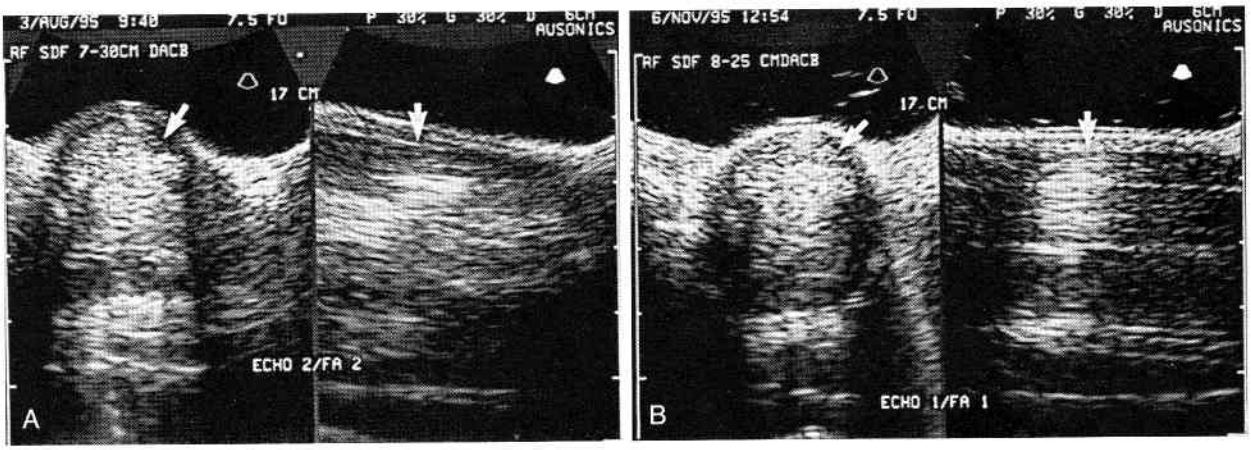

Figure 3–262

Sonograms of a small lateral tear in the periphery of the superficial digital flexor tendon (SDF) in the right foreleg, obtained before *(A)* and after *(B)* superior check ligament desmotomy performed in a 4-year-old Thoroughbred filly. These sonograms were obtained with a 7.5-MHz sector-scanner transducer containing a built-in fluid offset at a displayed depth of 6 cm. The right side of the transverse views *(left image)* is lateral and the left side is medial. The right side of the sagittal views *(left images)* is proximal and the left side is distal.

A, Notice the small anechoic defect *(arrows)* in the lateral portion of the SDF in the transverse view (0.20 cm^2/1.44 cm^2) and the adjacent hypoechoic areas and loss of normal fiber pattern in the lateral portion of the SDF in the sagittal view. The original tendinitis was imaged from 7 to 30 cm distal to the point of the accessory carpal bone, and these images were obtained at 17 cm (at the border between zones 2A and 2B).

B, Three months later, the discrete lateral tear *(arrows)* is difficult to visualize, but the entire palmar aspect of the SDF is hypoechoic and a weak fiber pattern is detected in the sagittal view. The SDF is unchanged in size at this time (0.43 cm^2/1.44 cm^2). The tendinitis is now imaged from 8 to 25 cm distal to the accessory carpal bone and these images were obtained at 17 cm.

not started before sustaining a superficial digital flexor tendon injury had significantly less earnings per horse or earnings per start than did those that had previously raced.[36] However, 58% to 64% of horses that had raced before surgery achieved faster lifetime marks after surgery than before, indicating that many Standardbreds can maintain or improve the quality of their racing performance after superior check ligament desmotomy surgery for treatment of superficial digital flexor tendinitis.[36, 195] The severity of the injuries was not critically evaluated in comparison to outcome in these studies.

One author reports that the size of the lesions detected ultrasonographically appears to decrease more rapidly in surgically treated than in conservatively treated horses, but no controlled studies document this.[36] A number of the Standardbred racehorses in which this surgery was performed had a high incidence of suspensory ligament injury when they returned to racing after surgery.[195] Recently, however, the long-term racing results of horses rested for at least 6 months before returning to EL5 and treated with superior check ligament desmotomy (with or without tendon-splitting surgery) were reported. Seventy-three percent showed recurrence of bowed tendons (60% rebowed prior to racing and 13% once they had successfully attained EL7).[38] These results were not different from the results for horses treated with other external or surgical methods.[38]

The superior check ligament is transected between its origin along the distal medial radius and its insertion on the muscle of the superficial digital flexor tendon. This allows the muscle to lengthen. It also hopefully reduces the incidence of recurrent injuries to the superficial digital flexor tendon by allowing the muscle to stretch more, reducing the lengthening of the superficial digital flexor tendon that must occur in the healed tendon. In a cadaver model, the metacarpophalangeal joint hyperextended an additional 15.8% and the muscle belly of the superficial digital flexor tendon elongated and moved distally after transection of the superior check ligament.[196] This additional lengthening, reported to be as much as 2.8 mm,[196] may allow the scarred, less elastic repair tissue to function with a lower incidence of reinjury. However, the strain on the superficial digital flexor tendon increased by 11.2% after transection of the accessory ligament of the superficial digital flexor tendon in this cadaver model.[196] This increased strain was attributed to the change in movement around the metacarpophalangeal joint and the increased length of the musculotendinous unit.[196]

Annular Ligament Desmotomy. Annular ligament desmotomy surgery is indicated in horses with an injury to the superficial digital flexor tendon in the distal tendon region when constriction of the tendon by the annular ligament has occurred. Cutting the annular ligament in affected horses may relieve the external constriction of the superficial digital flexor tendon at this level and allow for improved blood flow to the injured tendon, aiding in tendon repair.

Medical Treatment

Sodium Hyaluronate. The injection of intrathecal sodium hyaluronate is indicated in the treatment of horses with injuries to the superficial digital flexor tendon that are contained within the tendon sheath. To date, no published scientific data demonstrates a beneficial effect for intralesional or peritendinous injections of sodium hyaluronate in horses with naturally occurring injuries to the superficial digital flexor tendon.

Intralesional βAPN-F. Clinical trials using beta-aminoproprionitrile fumarate (βAPN-F) in horses with acute bowed tendons have demonstrated improved ten-

don healing.[30, 38, 39, 126, 127] The treated horses had large areas of damage to the superficial digital flexor tendon (Fig. 3-263). Treated tendons were at least 50% larger than normal or the cross-sectional area of the affected tendon was at least 1.5 cm^2. The lesion involved at least 25% of the tendon's cross-sectional area at its worst and extended over at least three of seven zones. Double-blind, placebo-controlled trials revealed statistically significant differences in tendon cross-sectional area, both at the maximal injury zone and of the total cross-sectional area of the injured tendon, when compared to placebo controls at 4 months after treatment.[126, 127] Statistically significant differences were also found in fiber alignment scores for the maximal injury zone and for the entire injured portion of the superficial digital flexor tendon. Double-blind, placebo-controlled trials have not previously been performed to evaluate the efficacy of other treatments for tendon and ligament injuries in the horse.

βAPN-F is indicated in the treatment of horses with significant injuries to the superficial digital flexor tendon in which at least 20% or more of the tendon is damaged at its worst injury zone. The injury can be discrete or diffuse, as long as fiber tearing has occurred (imaged in the sagittal scan). A complete sonographic examination should be performed before beginning intralesional βAPN-F treatment, with measurements of the tendon being made in each zone. Sonographic examination of the contralateral limb should also be performed because smaller injuries are frequently detected in this tendon.

Any increase in tendon cross-sectional area in βAPN-F-treated horses between examinations resulted in the horse remaining at the same exercise level for an additional 4 weeks, unless the increase in tendon cross-sectional area was greater than or equal to 20%, in a given zone or greater than or equal to 10% for the total tendon, in which case the amount of trotting exercise was decreased or discontinued altogether for the subsequent 4 weeks. Increases in tendon cross-sectional area of this magnitude indicated excessive tendon loading for the stage of tendon healing and increased the risk of reinjury.

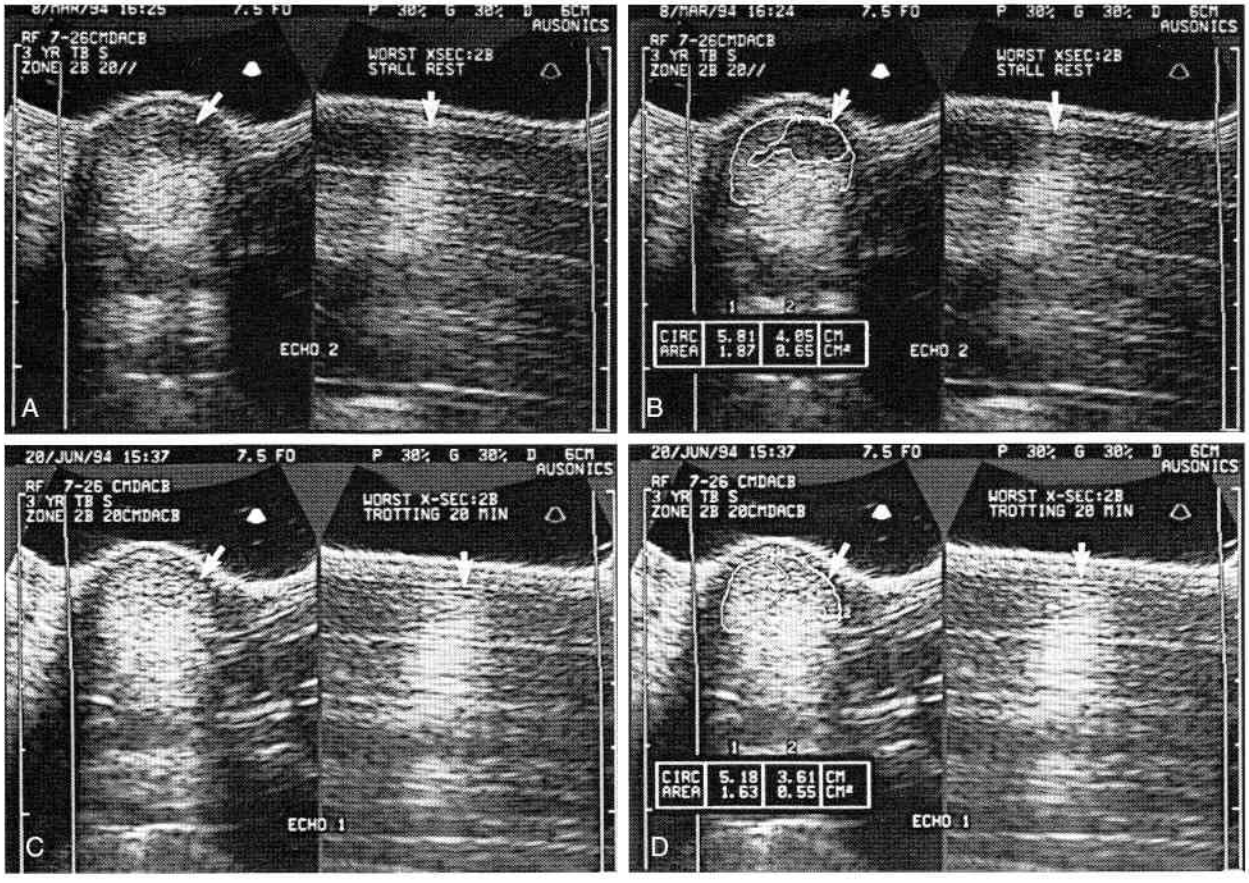

Figure 3-263

Sonograms of a large core lesion in the right fore superficial digital flexor tendon (SDF) treated with intralesional βAPN-F *(A* and *B)* 1 month after the injury occurred, obtained from a 3-year-old Thoroughbred colt. Follow-up sonograms were obtained 3 months later *(C* and *D)*. The original injury extended from 7 to 26 cm distal to the point of the accessory carpal bone. These sonograms were obtained with a 7.5-MHz sector-scanner transducer containing a built-in fluid offset at a displayed depth of 6 cm. The right side of the transverse views *(left images)* is lateral and the left side is medial. The right side of the sagittal views *(right images)* is proximal and the left side is distal.

A, Notice the large lateral anechoic to hypoechoic core lesion with the adjacent hypoechoic tendon and loss of normal fiber alignment.

B, The discrete area of fiber tearing (core lesion) involves 35% of the tendon's cross-sectional area (0.65 cm^2/1.87 cm^2) at its worst point (zone 2B at 20 cm).

C, Notice the good-quality fiber alignment and the filling in of the original core lesion, although a hypoechoic area still persists on the medial side.

D, The total tendon cross-sectional area has decreased significantly to 1.63 cm^2 and the horse is trotting 20 min/d. The original lesion area still measures 0.55 cm^2 for a percent injury of 34%.

Long-term follow-up data is still being obtained on these horses to evaluate their return to performance. However, initial studies indicate that a significantly higher percentage of βAPN-F–treated horses are able to return successfully to competition without recurrence of the injury, the ultimate goal of the treatment of equine athletes with tendon injuries.

Combined Medical and Surgical Treatment. The combination of both medical and surgical treatment for horses with superficial digital flexor tendon injuries may be the ideal treatment for allowing the horse to return to its previous performance level. The combination of treatments selected will depend, in part, on the type of lesion detected sonographically in the superficial digital flexor tendon. The surgical decompression of a fresh core lesion (ideally within the first 2 weeks after injury), accomplished with tendon splitting surgery, followed by injection of intralesional βAPN-F 2 to 4 weeks later, may provide the best-quality tendon repair. Superior check ligament desmotomy may be performed with tendon-splitting surgery (and often is) if the horse has a core lesion in the superficial digital flexor tendon and may also be coupled with the use of intralesional βAPN-F. Annular ligament desmotomy may also be performed in conjunction with the use of intralesional βAPN-F or with the injection of sodium hyaluronate into the tendon sheath if the injury to the superficial digital flexor tendon is contained within the tendon sheath.

Persistent hypoechoic areas and/or a large amount of random fiber alignment (see Fig. 3-71) indicate a poor quality repair and a more guarded prognosis, regardless of the treatment selected.[9] Horses with central echogenic to hyperechoic areas of scarring that are surrounded by a hypoechoic halo between the repaired and previously uninjured portion of the superficial digital flexor tendon should be returned to rigorous work slowly, because areas of reinjury are common adjacent to the central scar. In horses with intratendinous calcification in the superficial digital flexor tendon, however, no increase has been documented in the recurrence of injury. Injuries to the hind superficial digital flexor tendon in the plantar aspect of the hock, "pseudo-curb," usually become quiescent with a short period of local therapy and rest. The prognosis for horses with septic superficial digital flexor tendinitis is usually guarded to grave. The extensive tendon fiber damage that usually occurs in these horses and the adhesions that form between the tendinous and peritendinous structures usually result in persistent lameness and recurring tendon injuries, even if the septic tendinitis is resolved.

Deep Digital Flexor Tendinitis

Medical Treatment. Medical treatments for injuries to the deep digital flexor tendon are similar to those available for the superficial digital flexor tendon. The tendon should receive aggressive treatment for the acute injury as indicated above. Intralesional βAPN-F in horses with recent (1 to 3 months) areas of fiber tearing in the deep digital flexor tendon has also been beneficial and should have the same clinical results as with use in the superficial digital flexor tendon. Injection of large doses of hyaluronic acid into the tendon sheath is also indicated in horses with lesions in the deep digital flexor tendon that are contained within the digital sheath, because this has been shown, experimentally, to be beneficial.[185] The clinical impression regarding horses receiving this treatment is that intrathecal hyaluronic acid is helpful. Injection of corticosteroids into the tendon sheath should be avoided in horses with injuries to the deep digital flexor tendon, because this only delays tendon healing. The injection of intrathecal or intratendenous corticosteroids may also be associated with the development of calcification in the deep digital flexor tendon. Both medical and surgical treatment may be indicated in many horses with chronic digital sheath tenosynovitis and deep digital flexor tendinitis.[197] Intralesional βAPN-F and intrathecal hyaluronic acid should be considered in conjunction with annular ligament desmotomy if the injuries to the deep digital flexor tendon meet the above criteria.

Surgical Intervention. In most instances, deep digital flexor tendon injuries are not good candidates for tendon-splitting surgery because of their more focal nature and the presence of adjacent areas of calcification or mature scar tissue within the deep digital flexor tendon. Annular ligament desmotomy is indicated, however, in horses with (1) large areas of fiber tearing within the portion of the deep digital flexor tendon contained within the tendon sheath and (2) concurrent significant digital sheath tenosynovitis and/or annular ligament desmitis. Tenoscopy may also be considered in horses with chronic digital sheath tenosynovitis and adhesions within the digital sheath.[197] This surgery has variable results and may be more successful in horses with a more fibrinous tenosynovitis, rather than those with mature fibrous adhesions. Surgical intervention within the digital sheath often results in new inflammation and fibrin production within the digital sheath; a new cycle of fibrinous inflammation with subsequent organization into fibrous tissue is started.

Patient Management and Prognosis. Lay-up time for horses with deep digital flexor tendinitis is often very long, with 18 months to 2 years between time of diagnosis and return to competition in some high-performance horses. Lameness often persists for many months. Once sound, the horse should be returned to a program of gradually increasing exercise with frequent ultrasonographic monitoring. Until then, the horse should be walked daily to encourage parallel fiber alignment and minimize adhesion formation. In horses with chronic, severe, fibrous digital sheath tenosynovitis and adhesions within the digital sheath, noninvasive therapies such as therapeutic ultrasound should also be considered in an attempt to improve the range of motion of the fibrous tissue and adhesions.

The prognosis for affected horses is fair to poor, depending on the severity of the deep digital flexor tendinitis, the degree of calcification in the deep digital flexor tendon, and the presence of fibrous adhesions between the deep digital flexor tendon and the digital sheath and/or superficial digital flexor tendon. One study reported persistent visualization of lesions in the deep digital

flexor tendon, with variable improvement in soundness and a high incidence of recurrence of the injuries when the horse was returned to full work.[71]

Inferior Check Ligament Desmitis

Medical and Surgical Intervention. Aggressive medical treatment for acute inferior check ligament desmitis should be instituted as described above. The inferior check ligament can be injected with βAPN-F or the carpal sheath injected with hyaluronic acid, because both aid in the healing process. Similarly, splitting the inferior check ligament can also be considered in horses with an acute, discrete core lesion. The splitting of the inferior check ligament or the injection of intralesional βAPN-F or both should be considered in those horses for which a more cosmetic result is desirable. Both of these treatments should result in more of a decrease in the cross-sectional area of the inferior check ligament than would result if the ligament was conservatively treated. In most horses, however, the inferior check ligament injury heals and does not present a future performance problem, making these treatments less desirable for many owners. Most horses return to soundness quickly, within days to weeks after the injury occurred. Although swelling persists in the area of the injured check ligament, the horse can begin a controlled exercise program sooner and advance through the program more rapidly than can horses with other tendinous or ligamentous injuries. In one study, 44% of horses had resumed full work within 5 months.[44] Thickening of the inferior check ligament area usually persists to some degree in most horses that have experienced inferior check ligament desmitis, but it is usually only a cosmetic problem.

Prognosis. The prognosis for recovery of uncomplicated inferior check ligament desmitis is good to excellent. The majority of horses (75%) in one study returned to full work without a recurrence of the injury for at least 9 months (maximum 4 years).[44] Most horses are able to return successfully to their previous performance level more rapidly than those with other tendinous or ligamentous injuries. Inferior check ligament desmitis also carries a decreased likelihood of recurrence, unless the desmitis is associated with a previous inferior check ligament desmotomy, conformation abnormalities, or other tendinous or ligamentous injuries. Performance is not usually impaired in horses recovering from an uncomplicated injury to the inferior check ligament. In contrast to the author's experience and the findings in the first study,[44] a second study revealed that only 44% of horses returned to their prior level of performance without recurrence of the injury or development of a similar injury in the contralateral forelimb.[53] This study suggested that the difference between the two studies might result from differences in the severity of the inferior check ligament injuries.[53] Other possibilities might be the high percentage of concurrent superficial digital flexor tendinitis in the horses in the second study, the high incidence of suspected adhesions between the inferior check ligament and the superficial digital flexor tendon, and the different patient population (39%[53] ponies compared to 19%[44] ponies). A more guarded prognosis must be given for horses with concurrent superficial digital flexor tendinitis and adhesions to the superficial digital flexor tendon.[44] Although horses with small hypoechoic areas in the deep digital flexor tendon in conjunction with inferior check ligament desmitis have a similar prognosis to those with uncomplicated inferior check ligament desmitis,[44] a guarded to grave prognosis should be given for horses with severe deep digital flexor tendinitis and inferior check ligament desmitis.

Horses with a previous history of an inferior check ligament desmotomy, recurrent inferior check ligament desmitis, or over-at-the-knee or contracted flexor conformation should be treated more vigorously, with a longer period of controlled exercise before return to rigorous exercise. Horses with elevated heels, flexion of the metacarpo- or metatarsophalangeal joint, and a proliferative inferior check ligament desmitis with adhesions between the inferior check ligament and the superficial and deep digital flexor tendons should also be given a guarded to grave prognosis. Inferior check ligament desmotomy has been used with little success in this group of horses. Some success has been reported with this surgery in a few horses with superficial digital flexor tendinitis, inferior check ligament desmitis, and postural deformities at rest.[41, 44]

Inferior Check Ligament Desmotomy

Ultrasound-guided transection of the inferior check ligament (accessory ligament of the deep digital flexor muscle) has been used successfully in horses with flexural deformity of the distal interphalangeal joint and the metacarpophalangeal joint.[198] With this technique, a transverse ultrasound view from the lateral aspect of the limb is used to select the site for a small (1 to 1.5 cm) incision adjacent to the lateral edge of the inferior check ligament in the proximal metacarpal region. The surgical site should be proximal to the insertion of the inferior check ligament into the deep digital flexor tendon at a location where a hemostat can be placed between the inferior check ligament and deep digital flexor tendon and between the inferior check ligament and suspensory ligament to isolate the inferior check ligament from these two adjacent structures. A smaller surgical incision, less dissection of the paratenon, and the placement of only two or three sutures in the skin are advantages of this technique.[198] Accidental cutting of the deep digital flexor tendon is avoided with this technique, because the entire inferior check ligament is isolated ultrasonographically between the two curved hemostats and is pulled out of the incision. The technique reduced immediate postoperative wound morbidity.[198]

Suspensory Ligament Desmitis

Medical and Surgical Intervention. Aggressive medical treatment for acute suspensory ligament desmitis should be instituted as described earlier. The suspensory ligament can be injected with βAPN-F to aid ligament healing. Similarly, splitting the suspensory ligament can

also be considered in horses with an acute discrete core injury to the suspensory ligament. The splitting of the suspensory ligament or the injection of intralesional βAPN-F, or both, should be considered in horses in which a more cosmetic result is desirable. Both of these treatments should result in a smaller cross-sectional area of the suspensory ligament than would result from conservative treatment.

The horse with suspensory ligament desmitis should be stall rested with hand walking for at least 2 months, unless the desmitis is very mild. In one study, 86% of horses with proximal suspensory desmitis returned to work after box stall rest and controlled exercise for at least 2 months.[43, 58] Most horses received at least 3 to 6 months of this treatment regimen. The majority of these horses showed progressive improvement in the ultrasonographic appearance of the proximal suspensory ligament body.[43, 58] However, only 17% of horses with proximal suspensory desmitis in the hindlimb were able to return to full work. If the horse is lame, the period of stall rest with hand walking should extend until the horse has been sound for several weeks. A gradually increasing period of controlled exercise can be instituted at this time similar to that described for horses with tendon injuries. The advancements in the exercise program should occur when sonographic monitoring indicates improvement consistent with healing and remodeling of the ligament. In many horses, the degree of lameness appears to be disproportionate to the severity of the suspensory ligament injury. Careful evaluation of the surrounding structures such as the carpus, proximal metacarpus or metatarsus, second and fourth metacarpal or metatarsal bones, sesamoid bones, and metacarpo- or metatarsophalangeal joint should be performed to ensure that concurrent problems do not exist. The total convalescence of horses with proximal suspensory ligament desmitis and the speed of resolution of the lesions were proportional to the degree of lameness, according to one author.[58] The incidence of recurrence of proximal suspensory ligament desmitis in horses that have returned to full work for 1 year or more is low. For those in whom the lameness recurs, however, a guarded prognosis is warranted.[58]

Prognosis. The prognosis for horses with suspensory ligament injuries depends on the location and severity of the original injury, the presence of associated bony lesions, and the type of work that the horse performs. The percentage of the suspensory ligament's cross-sectional area that is damaged is associated with the likelihood of the horse returning successfully to racing and performing at its previous level. Thoroughbred horses racing on the flat have the poorest prognosis for a successful return to racing after a suspensory ligament injury; Standardbreds are more likely to return to racing successfully. The prognosis for suspensory ligament desmitis involving the body of the suspensory ligament is poorer than for that involving only the proximal suspensory ligament.[58] Both suspensory branch disease and suspensory body disease are high-risk problems in the Thoroughbred racehorse; they can result in catastrophic breakdown of the entire suspensory apparatus.[58] Suspensory ligament injuries can be chronic recurring problems, primarily in Standardbred racehorses and upper-level dressage horses but also in Thoroughbred racehorses (in which the problem is less common). Recurrences are also frequent in 3-day event horses compared to event horses competing at lower levels or in horse trials for 1 day only.[58] Horses with proximal suspensory ligament desmitis in the hindlimbs had a poorer prognosis than horses with proximal suspensory ligament desmitis in the forelimbs in one study.[58] In contrast, Standardbred horses with hindlimb suspensory desmitis can return successfully to racing.[17]

No significant difference occurred between the percentage of Thoroughbred (75%) or Standardbred (78%) horses with suspensory ligament desmitis that were able to return to racing and complete two starts without a recurrence of injury after the horses had been rested and treated for desmitis.[15] The majority (82%) of Standardbred horses that continued racing once the suspensory ligament injury was diagnosed, however, were also able to complete two races without a recurrence of the injury, whereas only 33% of Thoroughbred racehorses were able to do so.[15]

The Thoroughbred horses that were able to continue to race without rest and treatment for their suspensory ligament desmitis had small lesions that represented less than 25% of the ligament's total cross-sectional area.[15] Thoroughbred racehorses with large (less than 60%) type-4 lesions did not return to racing successfully even with adequate rest and treatment of the suspensory ligament desmitis. In this group of Thoroughbred racehorses, no difference was found between injuries to the suspensory ligament body or branches.

In Standardbred racehorses, lesions in the suspensory ligament body appeared to have a slightly better prognosis than did lesions in the suspensory ligament branches. Standardbred racehorses with type-3 or type-4 lesions involving greater than 40% of the ligament cross-sectional area were not successful if kept in training. Standardbred horses with Type-4 lesions involving greater than 60% of the ligament's cross-sectional area were not successful if rested and treated for desmitis.[15] Although most Standardbred racehorses are able to continue or return to racing, their performance level is usually reduced.[58]

Superficial Digital Flexor Tendinitis in the Pastern

Injuries to the superficial digital flexor tendon in the pastern must be given a more guarded prognosis than injuries to the superficial digital flexor tendon in the metacarpal region (see Fig. 3-117). Recurrences of superficial digital flexor tendon injuries are more common in the pastern, with both event horse and steeplechasers reported to have a high risk of recurrence of these lesions.[71] Intralesional βAPN-F has been used successfully in several horses with lesions of the superficial digital flexor tendon branches.

Deep Digital Flexor Tendinitis in the Pastern

Injuries to the deep digital flexor tendon in the pastern carry a guarded prognosis, as in the metacarpal or metatarsal region. Intrathecal sodium hyaluronate, coupled

with annular ligament desmotomy, should be considered for horses with areas of fiber tearing in the deep digital flexor tendon, digital sheath tenosynovitis, and annular ligament constriction. Intralesional βAPN-F may be indicated in horses with significant fiber damage in the deep digital flexor tendon in the pastern if the area is accessible for intratendinous injection. Horses with deep digital flexor tendinitis in the distal pastern region and/or navicular disease should be given a guarded to grave prognosis.

Distal Sesamoidean Ligament Desmitis

Treatment for acute injuries to the distal sesamoidean ligaments should include aggressive "cooling out" of these injuries. Stall rest and hand walking are indicated early on unless the injury is severe. Treatment with intralesional βAPN-F should be considered if intraligamentous injection of the drug is possible.

Prognosis for injuries to the middle and straight distal sesamoidean ligament must be guarded, unless the injury is relatively minor, because recurrent injuries are common in this location. Horses with small areas of fiber tearing at the origin or insertion with enthesopathy or small avulsion fractures have returned successfully to full athletic function. If the injuries are severe, the limb should be supported with a "heavy-duty" support wrap, a Robert Jones bandage, or a breakdown device such as a Kimsey splint. Arthrodesis is occasionally indicated with complete disruption of the distal sesamoidean ligaments and resultant loss of joint stability.

Annular Ligament Desmitis

If the horse has experienced primary annular ligament desmitis, treatment should include aggressive anti-inflammatory therapy, as for other tendinous and ligamentous injuries, in conjunction with a carefully controlled exercise program. Fetlock annular ligament desmotomy should be considered for horses in which the annular ligament constriction is identified as the cause of lameness and in which no severe fibrinous tenosynovitis with adhesions of the flexor tendons to the digital sheath exists. Some authors have found annular ligament desmotomy not to be worthwhile in horses with injury to the superficial digital flexor tendon and an annular ligament desmitis.[131] However, many surgeons have had good clinical response to this surgery, if adequate treatment of the superficial digital flexor tendon injury is also performed. A good response has also been reported in horses with deep digital flexor tendinitis.

Superior Check Ligament Desmitis

Local injection of the carpal sheath with hyaluronic acid and corticosteroids coupled with rest has allowed the majority of affected horses to return to their previous level of competition in 4 to 6 months.[73] Hyaluronic acid alone without corticosteroids should be considered in those horses with significant fiber damage in the superficial digital flexor tendon in addition to the superior check ligament desmitis.

Bicipital Tendinitis

The prognosis for horses with bicipital tendinitis is fair to poor for return to full athletic function. The prognosis depends on the severity of the initial tendon injury, the degree of associated bicipital bursitis, the adhesions that may be present between the bicipital tendon and the bursa, and the surrounding muscular abnormalities.

Extensor Tendinitis

Prognosis is usually good to excellent for horses with extensor tendinitis, unless complete rupture of the tendon has occurred. The horse usually remains sound and is able to extend the limb without difficulty, unless the tendon is severed. Horses with extensor tendon injuries should be treated aggressively for the tendon injury as indicated earlier and should undergo a hand-walking exercise program. A gradually increasing low-level controlled exercise program can begin 2 months after most injuries; if the tendon is completely ruptured, additional time is usually needed before the horse can extend the limb and begin the program. Although the formation of a peritendinous scar is common because of associated soft tissue trauma, this rarely limits the function of an extensor tendon. Persistent tenosynovitis of the injured tendon sheath with intratendinous adhesions is also common, but is rarely more than a cosmetic problem.

Gastrocnemius Tendinitis

The prognosis for horses with gastrocnemius tendinitis must be somewhat guarded until adequate time has passed to evaluate the horse's response to therapy. Initially, treatment should include aggressive cooling out of the injury as previously described, coupled with stall rest and hand walking. A gradually increasing program of low-level controlled exercise is ideal to return the horse to work, but should not begin until the horse is sound. Follow-up of five horses with gastrocnemius tendinitis revealed little improvement in soundness 2 to 3 months after the initial examination, but long-term follow-up was not available.[64] In a report of common calcaneal tendinitis, both horses returned successfully to their prior performance level after a prolonged period of box stall rest followed by gradually increasing amounts of controlled exercise.[65] The use of flexible carbon fiber implants in the gastrocnemius tendon of a foal in which the tendon was avulsed from its insertions has been reported.[133] The filly was slightly lame 15 months after surgery, but she had no other problems associated with the gastrocnemius tendon rupture or repair.

Peroneus Tertius Tendinitis or Rupture

The prognosis for horses with rupture of the peroneus tertius tendon is usually good, if the horse undergoes a

prolonged period of stall rest that enables tendon healing. Aggressive treatment of the acute injury is indicated as described earlier, but these horses need a period of stall rest which lasts until the hock and stifle can no longer be extended simultaneously. Most affected horses, if given an adequate period of stall rest, recover normal soundness and a normal gait. The tendon's cross-sectional area decreases, echogenicity improves, and linear echoes return within the tendon, although their orientation is likely to be random. The peritendinous soft tissue swelling usually resolves. Most horses have little, if any, peritendinous scar.

Patient Management of Tenosynovitis and Bursitis

Tenosynovitis. The prognosis for horses with nonseptic tenosynovitis is good to excellent. Treatment with anti-inflammatory drugs and rest is indicated for acute nonseptic tenosynovitis, with return to work delayed until the effusion resolves and does not return once treatment is discontinued. Intrathecal injection of corticosteroids and/or sodium hyaluronate is effective if coupled with rest. In horses with chronic nonseptic tenosynovitis, annular ligament desmotomy may be helpful in resolving the lameness associated with persistent distention of the tendon sheath. It may also enable the horse to return successfully to performance with persistent tenosynovitis. The results of annular ligament desmotomy are good if no tendon injury is present and if the tenosynovitis is not fibrous and restrictive.

The ultrasonographic examination should be used as a guide to locate the optimal site for obtaining a synovial fluid sample for culture and sensitivity testing, if a septic tenosynovitis is suspected. Sterile lavage of the infected tendon sheath should be performed (Fig. 3-264) and systemic broad-spectrum antimicrobials prescribed after obtaining a sample for culture and sensitivity testing. Periodic ultrasonographic examinations should be performed to monitor the treatment response of the tendon sheath and the associated tendons (Fig. 3-265). Debridement of the tendon sheath may be performed in horses with multiple fibrinous loculations or adhesions within the tendon sheath. The development of any hypoechoic to anechoic lesions within the tendon contained within the sheath should prompt more aggressive flushing and a possible change in the antimicrobial regimen. Hypoechoic or anechoic lesions in the tendons may also develop as a result of adhesions, indicating a poor prognosis (Fig. 3-266). In the end stage following successful resolution of septic tendinitis and tenosynovitis, a functional result may not be possible because of the severity of the tendinous damage that occurred and the resultant mass of scar tissue (Fig. 3-267).

Horses with tarsal sheath tenosynovitis and associated bony abnormalities of the sustentaculum tali have a poorer prognosis for soundness.[116, 158] Adhesions within the tarsal sheath are also more likely to result in soundness problems and in lesions within the deep digital flexor tendon, causing lameness.

Bursitis. A nonseptic bursitis in most locations usually carries a fairly good prognosis. Treatment of the bursitis should consist of anti-inflammatory drugs and rest. Septic bursitis carries a more guarded prognosis and should be treated aggressively with lavage (if possible) and antimicrobials (based on the results of culture and sensitivity testing).

Bicipital Bursitis. The prognosis for horses with bicipital bursitis is variable and depends on the presence or absence of sepsis, the amount of damage to the bicipital tendon, the adhesions that form within the bursa, and the presence and severity of any underlying bony abnormalities. Horses with bicipital bursitis with acute onset of swelling and lameness referable to the shoulder region,

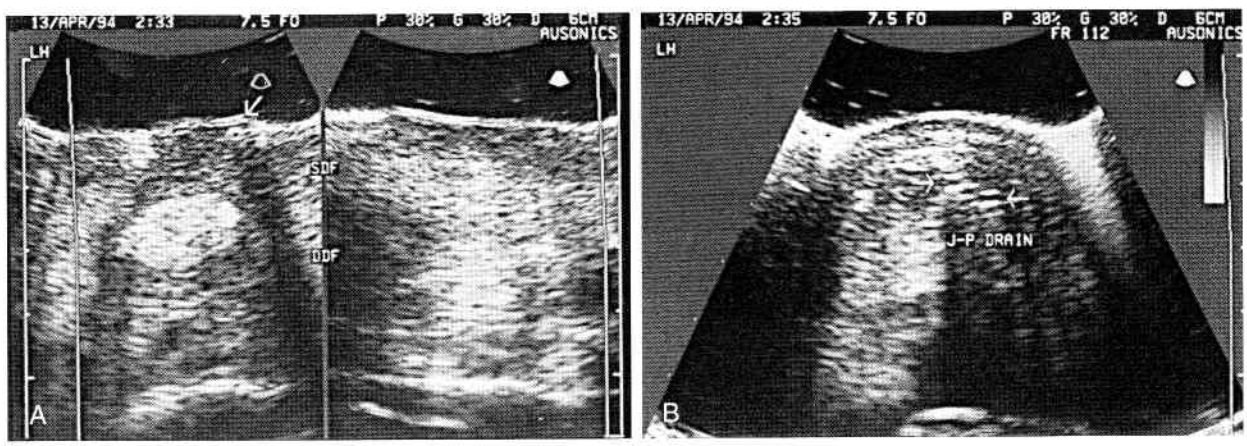

Figure 3-264

Sonograms of a septic digital sheath tenosynovitis with a septic superficial digital flexor (SDF) tendinitis in the left hindlimb that was treated with the instillation of a Jackson-Pratt (Baxter Healthcare Corporation, Deerfield, IL 60015) drain, obtained from a 5-year-old Arabian mare. These sonograms were obtained in zone 4B at 40 cm distal to the point of the hock with a 7.5-MHz sector-scanner transducer containing a built-in fluid offset at a displayed depth of 6 cm. DDF, deep digital flexor tendon.

A, Notice the defect in the skin and the shadow created by the edge of the drain exiting the skin *(arrow)*. Loss of the normal echogenicity of the lateral aspect of the SDF and random fiber alignment occur, consistent with septic tendinitis. The lateral aspect of the SDF is difficult to recognize, a common finding in septic tendinitis. The right side of the sagittal view *(right image)* is proximal and the left side is distal. The right side of the transverse view *(left image)* is lateral and the left side is medial.

B, Notice the hyperechoic interrupted echoes from the drain *(arrows)* within the digital sheath along the side of the DDF.

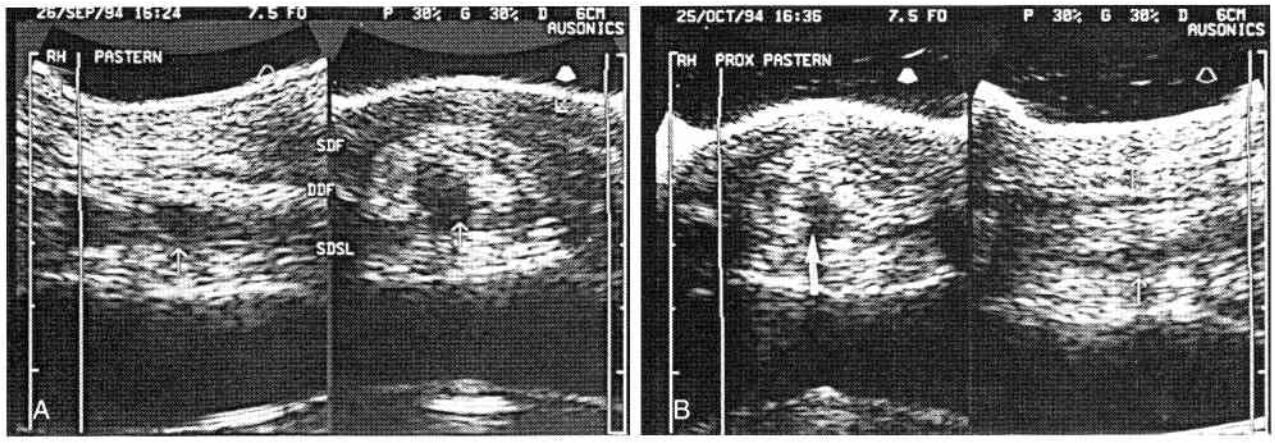

Figure 3–265

Sonograms of a septic tendinitis and digital sheath tenosynovitis in the right hind pastern, obtained from a 6-year-old Thoroughbred mare at the onset of *(A)* and after 1 month *(B)* of aggressive treatment. These sonograms were obtained in zone P1B with a 7.5-MHz sector-scanner transducer containing a built-in fluid offset at a displayed depth of 6 cm.

A, Notice the large anechoic defect *(arrow)* in the dorsal and medial aspect of the deep digital flexor tendon (DDF) visualized in both the transverse view *(right image)* and the sagittal view *(left image)*. The shape of the DDF is distorted and it appears adhered to the superficial digital flexor tendon (SDF) along its palmaromedial aspect, confirmed on a dynamic ultrasound scan. SDSL, straight distal sesamoidean ligament.

B, Notice the decrease in size of the defect in the dorsal and medial aspect of the DDF *(large arrow)*, best imaged in the transverse view *(left image)*, compared to the previous exam 1 month earlier. Some short linear echoes are detected within the DDF in the sagittal view *(left image)*, indicating early repair. This digital sheath had been aggressively lavaged and the horse had been receiving intravenous antimicrobials based on the results of culture and sensitivity testing of the synovial fluid obtained from the digital sheath at presentation. However, the SDF and DDF are now more difficult to distinguish from one another, suggesting more adhesions between the two tendons.

with no other abnormalities present, have the best prognosis. Aggressive lavage of the septic bicipital bursa and administration of appropriate antimicrobials (based on the results of culture and sensitivity testing of the fluid) can result in the horse returning successfully to racing. Arthroscopic debridement of fibrinous loculations and adhesions has been performed successfully in some horses with bicipital bursitis. Persistent lameness is more likely in horses with osteomyelitis, bicipital tendinitis, and adhesions between the bicipital bursa and the biceps tendon.

Fistulous Withers and Poll Evil. Horses with fistulous withers must be given a guarded to fair prognosis. Local drainage and lavage coupled with long-term antimi-

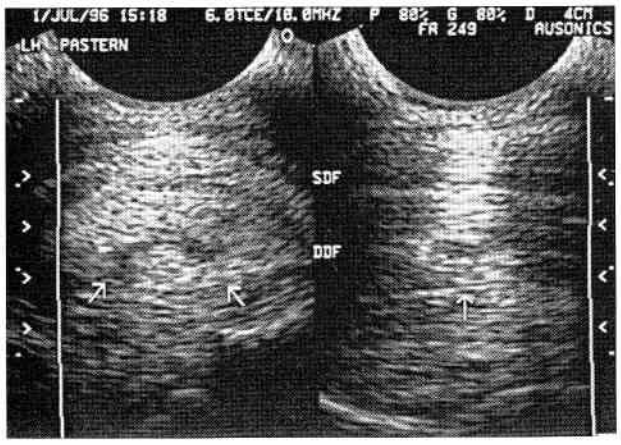

Figure 3–266

Sonograms of an area of fiber tearing in the deep digital flexor tendon (DDF) associated with a chronic (previously septic) digital sheath tenosynovitis and adhesions between the superficial (SDF) and deep digital flexor tendons at the level of the metatarsophalangeal joint (same horse as in Fig. 3–265). Notice the anechoic semi-circular defect *(arrows)* in the enlarged DDF with loss of the normal fiber pattern. These sonograms were obtained with a wide-bandwidth 6.0-MHz microconvex linear-array transducer operating at 10.0 MHz at a displayed depth of 4 cm. The right side of the transverse view *(left image)* is lateral and the left side is medial. The right side of the sagittal view *(right image)* is proximal and the left side is distal.

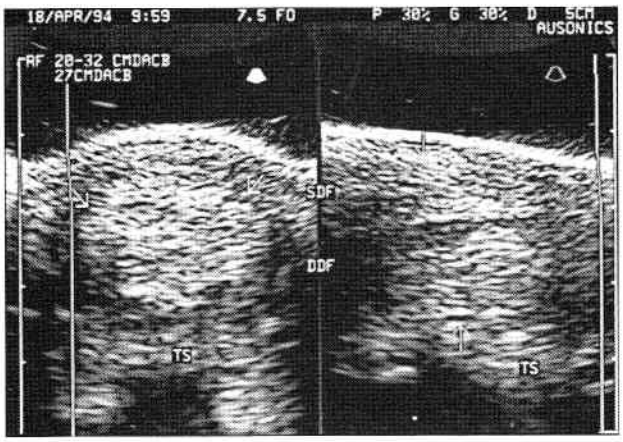

Figure 3–267

Sonograms of a chronic fibrous digital sheath tenosynovitis with adhesions between the flexor tendons and digital sheath secondary to a septic tenosynovitis, obtained from a 9-year-old Arabian cross gelding. Notice the heterogeneous echogenic to hyperechoic appearance of the superficial (SDF) and deep digital flexor (DDF) tendons, with inability to separate the two tendons sonographically from each other or from the digital sheath (TS). With dynamic scanning these structures all moved as one. These sonograms were obtained with a 7.5-MHz sector-scanner transducer containing a built-in fluid offset at a displayed depth of 5 cm. The right side of the transverse view *(left image)* is lateral and the left side is medial. The right side of the sagittal view *(right image)* is proximal and the left side is distal.

crobial therapy based on culture and sensitivity testing may be effective in horses with no foreign bodies or evidence of osteomyelitis. The fluid aspirated from the fistulous withers should be cultured for *Brucella abortus*.[143] The plate agglutination test is more sensitive and specific for antibody to *B. abortus*.[143] Horses that were exposed to cattle or other horses from the West are much more likely to have a positive culture for *B. abortus*.[141, 143] Surgical debridement of infected tissue, removal of foreign bodies, and curettage of the affected bone is indicated if osteomyelitis is present or if foreign bodies are detected. In one report, 59% of horses with fistulous withers treated surgically recovered; recurrence was reported in the other 41% (4 of 9 horses) of these horses.[141] The chance of a successful outcome with medical or surgical management is improved with early diagnosis, culture and sensitivity testing, and treatment with appropriate long-term antimicrobials. A similar prognosis can be given for horses with poll evil.

Horses with trauma to the withers from poorly fitting tack or fracture of the dorsal spinous processes in the withers have a better prognosis for resolution of the withers swelling and return to successful performance than do horses with fistulous withers. The horses should be given anti-inflammatory drugs and rest until the swelling in the withers has resolved. Careful refitting of the saddle may be necessary if the size and shape of the withers has changed.

Navicular Bursitis. Horses with navicular bursitis must be given a guarded to poor prognosis. Surgical debridement and drainage of this area may be indicated in horses with septic bursitis.

Patient Management of Neuromas

In horses that have undergone posterior digital neurectomies, ultrasonography can be very useful in identifying a neuroma and determining its extent. Sonographic monitoring can be used to monitor the horse's response to treatment or to decide at what level the nerve should be surgically resected to remove the neuroma in its entirety. In horses with intact nerves and neuromas that were detected ultrasonographically by this author, neuronal swelling and sensitivity has resolved with anti-inflammatory drugs and rest.

Patient Management of Muscular Abnormalities

Repeated ultrasonographic evaluation of injured muscle enables the clinician to make determinations about muscle healing that enable antimicrobial agents to be discontinued (Fig. 3-268), if infection was present, or to begin low-level exercise, if muscle repair has progressed to the appropriate point. A good prognosis can be given to most horses with muscle abscesses, unless the associated muscle fiber disruption is severe or the infection does not respond to appropriate antimicrobial therapy. Most horses with muscle rupture also have a good prognosis unless the muscle rupture is complete and catastrophic. Fibrotic myopathy may be a long-term sequelae in horses

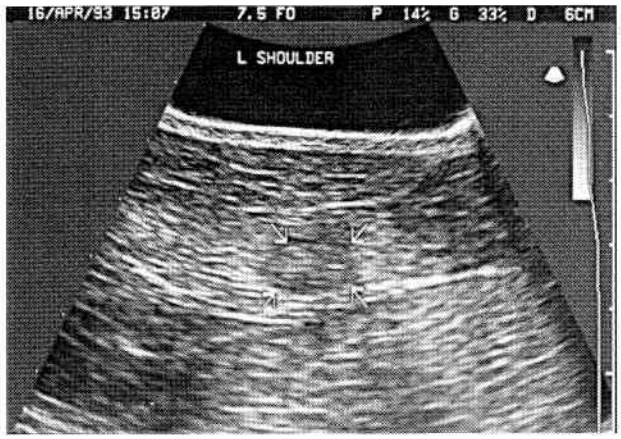

Figure 3–268

Sonogram of a resolving necrotic myositis and abscess in the left scalenus muscle of an 8-year-old Thoroughbred gelding. Notice the small hypoechoic core in the muscle belly *(arrows)*, which still has a slightly larger-than-normal contour. This sonogram was obtained with a 7.5-MHz sector-scanner transducer containing a built-in fluid offset at a displayed depth of 6 cm. The right side of the sonogram is proximal and the left side is distal.

with muscle abscess or muscle rupture. Ultrasound-guided muscle biopsy should be performed in horses in which a neoplasm is suspected or to confirm the type of cellular changes present in the muscle that are creating the abnormal sonographic appearance.

Patient Management of Bony Abnormalities

Fractures. The ultrasonographic detection of a fracture fragment in an area amenable to radiographic evaluation should prompt radiographic examination of the area using the sonographic information to determine the necessary views which will demonstrate the fracture. Horses with fractures should receive stall rest until ultrasonographic reexamination reveals bony remodeling adequate for the horse to begin a program of low-level gradually increasing exercise. Fractures of the wing of the ilium have a favorable prognosis, provided the sacroiliac joint is not affected. Stall rest for 3 to 4 months, usually in cross ties for the first 4 weeks to prevent the horse from lying down, is recommended. The affected horse can often be turned out 3 to 4 months after sustaining a pelvic fracture, if sonographic evidence exists of significant bony bridging and remodeling. Most horses with fractures of the wing of the ilium are ready to return to race training 6 months after the fracture occurred. The majority (77%) of horses in one large study of pelvic fractures had a positive outcome, although most of these horses were not returned to athletic function.[164] Acetabular fractures usually carry a poorer prognosis for maximal athletic function, although at least one horse has returned to racing after an acetabular fracture and several others have returned to athletic performance.[164] Periodic ultrasonographic examination can be used successfully to monitor fracture healing (Fig. 3-269).

Osteitis and Osteomyelitis. The detection of a fluid layer immediately adjacent to the bone that is not within

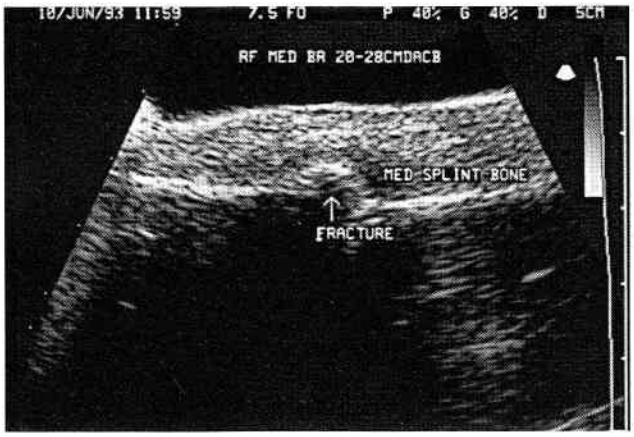

Figure 3–269

Sonogram of a healing fracture of the second metacarpal bone, obtained from a 6-year-old Arabian gelding. Notice the bridging of the fracture site and the persistence of some soft tissue swelling adjacent to the fracture site. This sonogram was obtained in zone 3A at 22 cm distal to the point of the accessory carpal bone with a 7.5-MHz sector-scanner transducer containing a built-in fluid offset at a displayed depth of 5 cm. The right side of the sonogram is proximal and the left side is distal.

a synovial structure should prompt an ultrasound-guided aspiration or biopsy. The sample should then be submitted for culture and sensitivity testing.[103] Broad-spectrum antimicrobial drugs can be instituted while awaiting the results of culture and sensitivity testing. The sonographic findings can be used to successfully drain an area or to determine the best approach for curettage or removal of a sequestrum. Curettage of the infected bone, coupled with broad-spectrum bacteriocidal antimicrobial therapy, should be performed whenever possible. A sample for culture and sensitivity testing can also be obtained at the time of surgery, if surgery is an option.

Surgical drainage and curettage of osteitis, osteomyelitis, and bone abscesses have a good prognosis if the organism causing the infection responds to long-term antimicrobial treatment.[103] Resolution of osteomyelitis occurred in 24 of 30 horses for which long-term follow-up was available after surgical debridement of the infected bone and/or long-term antibiotic therapy.[103] Three of the horses that did not recover died of complications unrelated to the osteomyelitis. For the resolution of the osteomyelitis to occur, removal of an infected implant may be necessary once fracture healing is adequate. Until implant removal can be performed, however, broad-spectrum antimicrobial therapy is indicated based on the results of culture and sensitivity testing. The prognosis for foals with osteomyelitis involving the vertebrae must be more guarded, because significant destruction of the vertebral body has often occurred by the time clinical signs are detected.[108]

In horses with suspected osteomyelitis of the proximal sesamoid bones, the digital sheath or fetlock joint should be aspirated and a sample submitted for culture and sensitivity testing if ultrasonographic, clinical, or radiographic findings are consistent with sepsis. If the digital sheath and fetlock joint appear normal, an ultrasound-guided aspirate of a cystic lesion on the surface of the sesamoid bone can also be performed to obtain a sample for culture and sensitivity testing.

Patient Management of Joint Abnormalities

Ultrasonography can be helpful in fine-tuning the prognosis for horses with joint abnormalities, determining where and if arthrocentesis is indicated and whether a fracture fragment is articular, or whether it is free floating or attached. The severity of the cartilaginous damage can be assessed in the visible portion of the joint, and the extent of involvement of the underlying subchondral bone determined. The radiographic detection of osteochondral fragments can be complemented by their ultrasonographic evaluation. The extent of the damage to the articular cartilage and subchondral bone can be further evaluated, osteochondral fragments can be precisely located, and small lesions that may not be visible radiographically can be detected ultrasonographically. Communication of a subchondral area of osteomyelitis with the joint can be detected ultrasonographically and carries a poorer prognosis than bony infections without articular involvement.[95]

The healing of collateral ligament injuries and the associated periosteal proliferative changes can be monitored sonographically (Fig. 3–270). The prognosis for return to full athletic function is guarded to poor for horses with injuries to the collateral ligaments of the carpus, coxofemoral joint, and cruciate ligaments. The best that can often be hoped for is salvage of these animals for breeding purposes. The prognosis for horses with injuries to the collateral ligaments of the cubital joint, metacarpo-

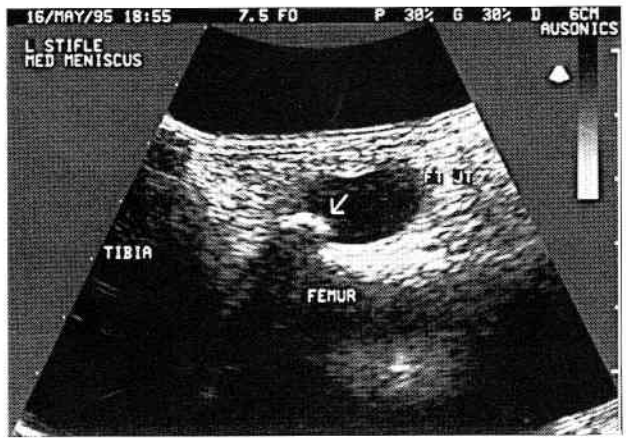

Figure 3–270

Sonogram of a small anechoic effusion in the medial compartment of the left femorotibial joint with a smooth area of periosteal proliferation *(arrow)* along the distal femur, obtained from a 13-year-old Holsteiner gelding. The bony proliferation along the distal femur is immediately proximal to the medial meniscus, part of which is imaged on the sonogram. The cranial margin of the medial meniscus is flush with the cranial margin of the distal femur and proximal tibia. The portion of the medial collateral ligament imaged over the medial meniscus is thicker than normal and has a random fiber pattern consistent with a chronic inactive collateral ligament desmitis. This sonogram was obtained with a 7.5-MHz sector-scanner transducer containing a built-in fluid offset at a displayed depth of 6 cm. The right side of the sagittal sonogram is proximal and the left side is distal.

or metatarsophalangeal joint, proximal interphalangeal joint, femorotibial joint, and tarsus is better, unless these injuries are severe and result in marked joint instability. If meniscal injury is detected, a partial meniscotomy can be considered in severely lame horses, mostly as a salvage procedure. This surgery has resulted in significant improvement in the severity of lameness in several horses with meniscal damage.

Injury to the cranial or caudal cruciate ligament can be diagnosed ultrasonographically, most likely with a high specificity and low sensitivity. The results of ultrasonographic evaluation can be used to formulate a more accurate prognosis and to guide the clinician as to the appropriateness of therapy and the likelihood of a good outcome with the available interventions.

References

1. Rantanen NW: The use of diagnostic ultrasound in limb disorders of the horse: A preliminary report. J Equine Vet Sci 2:62-63, 1982.
2. Hauser ML, Rantanen NW, Modransky PD: Ultrasound examination of distal interphalangeal joint, navicular bursa, navicular bone and deep digital tendon. J Equine Vet Sci 2:95-97, 1982.
3. Rantanen NW, Genovese RL, Gaines R: The use of diagnostic ultrasound to detect structural damage to the soft tissues of the extremities of horses. J Equine Vet Sci 3:134-135, 1983.
4. Hauser ML, Rantanen NW: Ultrasound appearance of the palmar metacarpal soft tissues of the horse. J Equine Vet Sci 3:19-22, 1983.
5. Rantanen NW: Assessing tenovaginitis. J Equine Vet Sci 4:171, 1984.
6. Hauser ML, Rantanen NW, Genovese RL: Suspensory desmitis: Diagnosis using real-time ultrasound imaging. J Equine Vet Sci 4:258-262, 1984.
7. Pharr JW, Nyland TG: Sonography of the equine palmar metacarpal soft tissues. Vet Radiol 25:265-273, 1984.
8. Spaulding K: Ultrasonic anatomy of the tendons and ligaments in the distal metacarpal-metatarsal region of the equine limb. Vet Radiol 25:155-166, 1984.
9. Rantanen NW, Hauser ML, Genovese RL: Superficial digital flexor tendonitis: Diagnosis using real-time ultrasound imaging. J Equine Vet Sci 5:115-119, 1985.
10. Hauser ML: Ultrasonographic appearance and correlative anatomy of the soft tissues of the distal extremities in the horse. Vet Clin North Am [Equine Pract] 2:127-144, 1986.
11. Genovese RL, Rantanen NW, Hauser ML, et al: Clinical application of diagnostic ultrasound to the equine limb. *In* Proceedings of the 31st Convention of the American Association of Equine Practitioners. pp 701-721, 1986.
12. Genovese RL, Rantanen NW, Hauser ML, et al: Diagnostic ultrasonography of equine limbs. Vet Clin North Am [Equine Pract] 2:145-226, 1986.
13. Henry GA, Patton CS, Goble DO: Ultrasonographic evaluation of iatrogenic injuries of the equine accessory (carpal check) ligament and superficial digital flexor tendon. Vet Radiol 27:132-140, 1986.
14. McClellan PD, Colby J: Ultrasonic structure of the pastern. J Equine Vet Sci 6:99-101, 1986.
15. Genovese RL, Rantanen NW, Hauser ML, et al: The use of ultrasonography in the diagnosis and management of injuries to the equine limb. Compend Contin Educ Pract Vet 9:945-957, 1987.
16. Reef VB, Martin BB, Elser A: Types of tendon and ligament injuries detected with diagnostic ultrasound: Description and follow up. *In* Proceedings of the 34th Annual Convention of the American Association of Equine Practitioners. 1988, pp 245-248.
17. Martin BB, Reef VB, Molesworth L: Ultrasonic evaluation of hindlimb desmitis in Standardbred racehorses. *In* Proceedings of the 35th Annual Convention of the American Association of Equine Practitioners. p 275, 1989.
18. Reef VB, Martin BB, Stebbins K: Comparison of ultrasonographic, gross and histologic appearance of tendon injuries in performance horses. *In* Proceedings of the 35th Annual Convention of the American Association of Equine Practitioners. p 279, 1989.
19. Denoix J, Mialot M, Levy I, et al: Etude anatomo-pathologique des lesions associees aux images echographiques abnormales des tendons et ligaments chez le cheval. Recueil de Medecine Veterinaire 166:45-55, 1990.
20. Crass JR, Genovese RL, Render JA, Bellon EM: Magnetic resonance, ultrasound and histopathologic correlation of acute and healing equine tendon injuries. Vet Radiol and Ultrasound 33:206-216, 1992.
21. Nicoll RG, Wood AKW, Rothwell TLW: Ultrasonographical and pathological studies of equine superficial digital flexor tendons: Initial observations, including tissue characterisation by analysis of image grey scale, in a Thoroughbred gelding. Equine Vet J 24:318-320, 1992.
22. Marr CM, McMillan I, Boyd JS, et al: Ultrasonographic and histopathological findings in equine superficial digital flexor tendon injury. Equine Vet J 25:23-29, 1993.
23. Spurlock GH, Spurlock SL, Parker GA: Ultrasonographic, gross and histologic evaluation of a tendinitis disease model in a horse. Vet Radiol 30:184-188, 1989.
24. Spurlock GH, Spurlock SL, Parker GA: Evaluation of Hylartin V therapy for induced tendonitis in the horse. Equine Vet Sci 9:242-246, 1989.
25. Reef VB: Ultrasonic diagnosis of tendon and ligament disease. *In* White NA, Moore JN (eds): Current Practice in Equine Surgery. Philadelphia, JB Lippincott, 1990, pp 425-435.
26. Genovese RL, Rantanen NW, Simpson BS, Simpson DM: Clinical experience with quantitative analysis of superficial digital flexor tendon injuries in Thoroughbred and Standardbred racehorses. Vet Clin North Am [Equine Pract] 6:129-145, 1990.
27. Henninger R, Bramlage L, Schneider R: Short-term effects of superior check ligament desmotomy and percutaneous tendon splitting as a treatment for acute tendinitis. *In* Proceedings of the 35th Annual Convention of the American Association of Equine Practitioners. 1990, pp 539-540.
28. Henninger R: Treatment of superficial digital flexor tendonitis in the horse. Equine Vet Educ 4:287-291, 1992.
29. Allen KA: Experience with ultrasound-guided tendon puncture or splitting. *In* Proceedings of the 38th Annual Convention of the American Association of Equine Practitioners. 1992, pp 273-277.
30. Genovese RL: Sonographic response to intralesional therapy with beta-aminopropionitrile fumarate for clinical tendon injuries in horses. *In* Proceedings of the 38th Annual Convention of the American Association of Equine Practitioners. 1992, pp 265-272.
31. Henninger RW, Bramlage LR, Bailey M, et al: Effects of tendon splitting on experimentally induced acute equine tendinitis. Vet Comp Orthopaedic Trauma 5:1-9, 1992.
32. Smith RKW: A case of superficial digital flexor tendinitis: Ultrasonographic examination and treatment with intralesional polysulphated glycosaminoglycans. Equine Vet Educ 4:280-285, 1992.
33. Marr CM, Love S, Boyd JS, McKellar Q: Factors affecting the clinical outcome of injuries to the superficial digital flexor tendon in National Hunt and point-to-point horses. Vet Rec 132:476-479, 1993.
34. Genovese RL: Prognosis of superficial flexor tendon and suspensory ligament injuries. *In* Proceedings of the 39th Annual Convention of the American Association of Equine Practitioners. 1993, pp 17-19.
35. Henninger R: Treatment of superficial digital flexor tendinitis. Vet Clinics N Am [Equine Pract] 10:409-424, 1994.
36. Hogan PA, Bramlage LR: Transection of the accessory ligament of the superficial digital flexor tendon for treatment of tendinitis: Long term results in 61 Standardbred racehorses (1985-1992). Equine Vet J 27:221-226, 1995.
37. Palmer SE, Genovese R, Lingo KL, et al: Practical management of superficial digital flexor tendinitis in the performance horse. Vet Clin North Am [Equine Pract] 10:425-481, 1994.
38. Genovese RL, Reef VB, Lingo KL, et al: Superficial digital flexor tendonitis: Long term sonographic and clinical study of racehorses. *In* Proceedings of the Dubai International Equine Symposium. 1996, pp 187-205.
39. Reef VB, Genovese RL, Byrd JW, et al: Treatment of superficial digital flexor tendon injuries with beta-aminoproprionitrile fumarate (βAPN-F): Sonographic evaluation of early tendon healing and

remodeling. *In* Proceedings of the Dubai International Equine Symposium. 1996, pp 423–430.
40. Dyson S: The use of ultrasonography for assessment of tendon damage. Equine Vet Educ 1:42, 1989.
41. Munroe G, Marr C: A case of flexural deformity of the metacarpophalangeal and distal interphalangeal joints in an adult horse. Equine Vet Educ 1:33–38, 1989.
42. Dik KJ: Ultrasonography in the diagnosis of equine lameness. Vet Annu 30:162–171, 1990.
43. Dyson S: Proximal suspensory desmitis: Clinical, ultrasonographic, and radiographic features. Equine Vet J 23:25–31, 1991.
44. Dyson S: Desmitis of the accessory ligament of the deep digital flexor tendon: 27 Cases (1986–1990). Equine Vet J 23:438–444, 1991.
45. Denoix J, Perrot P, Bousseau B, Scicluna C: Images echographiques des lesions du muscle interosseus III (ligament suspenseur du boulet). Pratique Vetérinaire Equine 23:23–33, 1991.
46. Steyn PF, McIlwraith CW, Rawcliff N: The use of ultrasonographic examination in conditions affecting the palmar metacarpal soft tissues of the equine limb. Equine Pract 13:8, 1991.
47. Reef VB: Evaluation of tendon and ligaments. *In* Robinson NE (ed): Current Therapy in Equine Medicine III. Philadelphia, WB Saunders, 1991, pp 796–798.
48. Reef VB: The use of diagnostic ultrasound in the horse. Ultrasound Quart 9:1–34, 1991.
49. Dyson S: Ultrasonographic examination of the metacarpal and metatarsal regions in the horse. Equine Vet Educ 4:139–144, 1992.
50. Marr CM: The differential diagnosis of soft tissue swelling of the palmar aspect of the metacarpal region. Equine Vet Educ 4:292–300, 1992.
51. Rantanen N: Proximal suspensory ligament injury. J Equine Vet Sci 13:443, 1993.
52. Dyson S: Proximal suspensory desmitis in the hindlimb: 42 cases. Br Vet J 150:279–291, 1994.
53. McDiarmid AM: Eighteen cases of desmitis of the accessory ligament of the deep digital flexor tendon. Equine Vet Educ 6:49–56, 1994.
54. Smith RKW, Jones R, Webbon PM: The cross-sectional areas of normal equine digital flexor tendons determined ultrasonographically. Equine Vet J 26:460–465, 1994.
55. Cowles RR, Johnson LD, Holloway PM: Proximal suspensory desmitis: A retrospective study. *In* Proceedings of the 40th Annual Convention of the American Association of Equine Practitioners. 1994, pp 183–185.
56. Denoix J, Farres D: Ultrasonographic imaging of the proximal third interosseous muscle in the pelvic limb using a plantaromedial approach. J Equine Vet Sci 15:346–350, 1995.
57. Cuesta I, Riber C, Pinedo M, et al: Ultrasonographic measurement of palmar metacarpal tendon and ligament structures in the horse. Vet Radiol Ultrasound 36:131–136, 1995.
58. Dyson SJ, Arthur RM, Palmer SE, Richardson D: Suspensory ligament desmitis. Vet Clin North Am [Equine Pract] 11:177–215, 1995.
59. Denoix J, Crevier N, Azevedo C: Ultrasound examination of the pastern in horses. *In* Proceedings of the 36th Annual Convention of the American Association of Equine Practitioners. 1991, pp 363–380.
60. Dik KJ: Ultrasonographic evaluation of fetlock annular ligament constriction in the horse. Equine Vet J 23:285–288, 1991.
61. Redding WR: Ultrasonic imaging of the structures of the digital sheath. Compend Contin Educ Pract Vet 13:1824–1832, 1991.
62. Van den Belt J, Keg PR: Ultrasonographic evaluation of fetlock annular ligament constriction in the horse. Equine Vet J 23:285–288, 1991.
63. Dyson S: Ultrasonographic examination of the pastern region. Equine Vet Educ 4:254–256, 1992.
64. Dyson SJ, Kidd L: Five cases of gastrocnemius tendinitis in the horse. Equine Vet J 24:351–356, 1992.
65. Proudman CJ: Common calcaneal tendonitis in a horse. Equine Vet Educ 4:277–279, 1992.
66. Redding WR: Evaluation of the equine digital flexor tendon sheath using diagnostic ultrasound and contrast radiography. Vet Radiol Ultrasound 34:42–48, 1993.
67. Redding WR: Sonographic exam of the digital flexor tendon sheath, distal flexor tendons, and soft tissues of the palmar pastern region. *In* Proceedings of the 39th Annual Convention of the American Association of Equine Practitioners. 1993, pp 11–16.
68. Dik KJ: Ultrasonography of the equine crus. Vet Radiol Ultrasound 34:28–34, 1993.
69. Dik KJ, Boroffka S, Stolk P: Ultrasonographic assessment of the proximal digital annular ligament in the equine forelimb. Equine Vet J 26:59–64, 1994.
70. Pugh CR, Johnson PJ, Crawley G, Finn ST: Ultrasonography of the equine bicipital tendon region. Vet Radiol Ultrasound 35:183–188, 1994.
71. Dyson S, Denoix J: Tendon, tendon sheath, and ligament injuries in the pastern. Vet Clin North Am [Equine Pract] 11:217–233, 1995.
72. Dik KJ, Dyson SJ, Vail TB: Aseptic tenosynovitis of the digital flexor tendon sheath, fetlock and pastern annular ligament constriction. Vet Clin North Am [Equine Pract] 11:151–162, 1995.
73. Denoix J, Guizien I, Perrot P, Bousseau B: Ultrasonographic diagnosis of spontaneous injuries of the accessory ligament of the superficial digital flexor tendon (proximal check ligament) in 23 horses. *In* Proceedings of the 41st Annual Convention of the American Association of Equine Practitioners. 1995, pp 142–143.
74. Crabill MR, Chaffin MK, Schmitz DG: Ultrasonographic morphology of the bicipital tendon and bursa in clinically normal Quarter horses. Am J Vet Res 56:5–10, 1995.
75. Denoix J: Ligament injuries of the axial skeleton in the horse: Supraspinal and sacroiliac desmopathies. *In* Proceedings of the Dubai International Equine Symposium. 1996, pp 273–286.
76. Gillis CL, Meagher DM, Pool RR, Stover SM: Comparison of clinical, ultrasonographic and histologic analyses of the response of equine superficial digital flexor tendons to race training. *In* Proceedings of the 38th Annual Convention of the American Association of Equine Practitioners. 1992, pp 279–280.
77. Gillis CL, Meagher DM, Pool RR, et al: Ultrasonographically detected changes in equine superficial digital flexor tendons during the first months of race training. Am J Vet Res 54:1797–1802, 1993.
78. Gillis CL, Meagher DM, Cloninger A, Locatelli L: Ultrasound cross-sectional area and mean echogenicity of the superficial and deep digital flexor tendon. *In* Proceedings of the 39th Annual Convention of the American Association of Equine Practitioners. 1993, pp 273–274.
79. Gillis C, Meagher DM, Cloninger A, et al: Ultrasonographic cross-sectional area and mean echogenicity of the superficial and deep digital flexor tendons in 50 trained Thoroughbred racehorses. Am J Vet Res 56:1265–1269, 1995.
80. Wood AKW, Sehgal CM, Polansky M: Sonographic brightness of the flexor tendons and ligaments in the metacarpal region of horses. Am J Vet Res 54:1969–1974, 1993.
81. Wood AKW, Polansky M, Kundel HL, et al: Equine tendon and ligament sonography: Current concepts and future directions. *In* Proceedings of the 38th Annual Convention of the American Association of Equine Practitioners. 1992, pp 253–264.
82. Wood AKW, Sehgal CM, Reef VB: Three-dimensional sonographic imaging of the equine superficial digital flexor tendon. Am J Vet Res 55:1505–1508, 1994.
83. Dik KJ: Radiographic and ultrasonographic imaging of soft tissue disorders of the equine carpus. Tijdschr Diergeneeskd 24:1168–1174, 1990.
84. Bohn A, Papageorges M, Grant BD: Ultrasonographic evaluation and surgical treatment of humeral osteitis and bicipital tenosynovitis in a horse. J Am Vet Med Assoc 201:305–306, 1992.
85. Grant BD, Peterson PR, Bohn A, et al: Diagnosis and surgical treatment of traumatic bicipital bursitis in the horses. *In* Proceedings of the 38th Annual Convention of the American Association of Equine Practitioners. 1992, pp 349–355.
86. Denoix J, Audigié F: Examen échographique du carpe du cheval: Lésions identifiées sur 45 cas cliniques. Pratique Vét Equine 25:193–203, 1993.
87. Tnibar M, Kaser-Hotz B, Auer JA: Ultrasonography of the dorsal and lateral aspects of the equine carpus: Techniques and normal appearance. Vet Radiol Ultrasound 34:413–425, 1993.
88. Grant BD: Diagnosis and treatment of bursitis. *In* Proceedings of the Dubai International Equine Symposium. 1996, pp 323–328.
89. Smith RKW, Dyson SJ, Head MJ, Butson RJ: Ultrasonography of the equine triceps muscle before and after general anaesthesia and in post anaesthetic myopathy. Equine Vet J 28:311–319, 1996.

90. Modransky PD, Rantanen NW, Hauser ML, Grant BD: Diagnostic ultrasound examination of the dorsal aspect of the equine metacarpophalangeal joint. Equine Vet Sci 3:56–58, 1983.
91. Steyn P, Schmitz D: The sonographic diagnosis of chronic proliferative synovitis in the metacarpophalangeal joints of a horse. Vet Radiol 30:125–127, 1989.
92. Pennick DG, Nyland TG, O'Brien TR, et al: Ultrasonography of the equine stifle. Vet Radiol 31:293–298, 1990.
93. Dik KJ: Ultrasonography of the equine tarsus. Vet Radiol Ultrasound 34:36–43, 1993.
94. Denoix J, Crevier N, Perrot P, Bousseau B: Ultrasound examination of the femorotibial joint in the horse. *In* Proceedings of the 40th Annual Convention of the American Association of Equine Practitioners. 1994, pp 57–58.
95. Dik KJ: Ultrasonography of the equine stifle. Equine Vet Educ 7:154–160, 1995.
96. Denoix J, Jacot S, Perrot P, Bousseau B: Ultrasonographic examination of the dorsal and abaxial aspects of the equine fetlock. *In* Proceedings of the 41st Annual Convention of the American Association of Equine Practitioners. 1995, pp 138–141.
97. Ruohoniemi M: Use of ultrasonography to evaluate the degree of ossification of the small tarsal bones in 10 foals. Equine Vet J 25:539–543, 1993.
98. Ruohoniemi M, Hildén L, Salo L, Tulamo RM: Monitoring the progression of tarsal ossification with ultrasonography and radiography in 3 immature foals. Vet Radiol Ultrasound 36:402–410, 1995.
99. Dik KJ, Leitch M: Soft tissue injuries of the tarsus. Vet Clin North Am [Equine Pract] 11:235–247, 1995.
100. Wright IM: Ligaments associated with joints. Vet Clin North Am [Equine Pract] 11:249–291, 1995.
101. Cauvin ERJ, Munroe GA, Boyd JS, Paterson C: Ultrasonographic examination of the femorotibial articulation in horses: Imaging of the cranial and caudal aspects. Equine Vet J 28:285–296, 1996.
102. Richardson DW: Eikenella corrodens osteomyelitis of the axis in a foal. J Am Vet Med Assoc 188:298–299, 1986.
103. Reef VB, Reimer J, Reid CF: Ultrasonographic findings in horses with osteomyelitis. *In* Proceedings of the 37th Annual Convention of the American Association of Equine Practitioners. 1991, pp 381–391.
104. Reef VB: Diagnosis of pelvic fractures using ultrasonography (abstract). Vet Radiol 33:33, 1992.
105. Pilsworth RC, Holmes MA, Shepherd M: An improved method for the scintigraphic detection of acute bone damage to the equine pelvis by probe point counting. Vet Rec 113:490–495, 1993.
106. Shepherd MC, Pilsworth RC: The use of ultrasound in the diagnosis of pelvic fractures. Equine Vet Educ 6:223–227, 1994.
107. Pilsworth RC, Shepherd MC, Herinckx BMB, Holmes MA: Fracture of the wing of the ilium, adjacent to the sacroiliac joint, in Thoroughbred racehorses. Equine Vet J 26:94–99, 1994.
108. Giguère S, Lavoie JP: *Rhodococcus equi* vertebral osteomyelitis in 3 Quarter Horse colts. Equine Vet J 26:74–77, 1994.
109. Rantanen NW: General considerations for ultrasound examinations. Vet Clin North Am [Equine Pract] 2:29–32, 1986.
110. Rantanen NW: Principles of ultrasonographic examination of tendons and ligaments. *In* Proceedings of the 39th Annual Convention of the American Association of Equine Practitioners. 1993, pp 9–10.
111. Denoix J: Functional anatomy of tendons and ligaments in the distal limbs (manus and pes). Vet Clin North Am [Equine Pract] 10:273–322, 1994.
112. Denoix J: Diagnostic techniques for identification and documentation of tendon and ligament injuries. Vet Clin North Am [Equine Pract] 10:365–407, 1994.
113. Getty R: Sission and Grossman's The Anatomy of the Domestic Animals. Philadelphia, WB Saunders, 1975.
114. Jann HW, Beroza GA, Fackelman GE: Surgical anatomy for desmotomy of the accessory ligament of the superficial digital flexor tendon in horses. Vet Surg 15:378–382, 1986.
115. Hago BED, Vaughan LC: Use of contrast radiography in the investigation of tenosynovitis and bursitis in horses. Equine Vet J 18:375–382, 1986.
116. Dik KJ, Merkens HW: Unilateral distention of the tarsal sheath in the horse: A report of 11 cases. Equine Vet J 19:307–313, 1987.
117. Allen KA, Stone LR: Equine diagnostic ultrasonography: Equipment selection and use. Compend Contin Educ Pract Vet 12:1307–1311, 1990.
118. Biller DS, Myer W: Ultrasound scanning of superficial structures using an ultrasound standoff pad. Vet Radiol 29:138–142, 1988.
119. Pugh CR: A simple method to document the location of ultrasonographically detected tendon lesions. Vet Radiol Ultrasound 34:211–212, 1993.
120. Gillis C, Sharkey N, Stover S, et al: Ultrasonography as a method to determine tendon cross-sectional area. Am J Vet Res 56:1270–1274, 1995.
121. Crass JR, van de Vegte GL, Harkavy LA: Tendon echogencity: Ex vivo study. Radiology 167:499–501, 1988.
122. Neuwirth L, Selcer B, Mahaffey M: Equine tendon ultrasonography: Common artefacts. Equine Vet Educ 3:149–152, 1991.
123. Fornage BD: The hypoechoic normal tendon: a pitfall. J Ultrasound Med 6:19–22, 1987.
124. Wilson DA, Baker GJ, Pijanowsky GJ, Boero MJ, Badertscher RR: Composition and morphologic features of the interosseous muscle in Standardbreds and Thoroughbreds. Am J Vet Res 52:133–139, 1991.
125. Marr CM: Personal communication, 1996.
126. Reef VB, Genovese RL, Byrd JW, et al: Treatment of bowed tendons with intralesional βAPN-F: Results of the dose ranging trial. Am J Vet Res, submitted 1997.
127. Reef VB, Genovese RL, Byrd JW, et al: Treatment of bowed tendons with intralesional βAPN-F: Results of the dose confirmation trial. Am J Vet Res, submitted 1997.
128. Silver IA, Brown PM, Goodship AE: A clinical and experimental study of tendon injury, healing and treatment in the horse. Equine Vet J 1:5–32, 1983.
129. Crevier N, Collobert C, Denoix JM, et al: Mechanical consequences of equine superficial digital flexor tendon in relation to its histological structure. *In* Proceedings of the 41st Annual Convention of the American Association of Equine Practitioners. 1995, pp 144–145.
130. Walsh BA, Ross MW, Reef VB, Reid CF: Positive scintigraphic findings in the equine proximal metacarpus and metatarsus: A comparison with clinical, radiographic and ultrasonographic findings. Vet Radiol Ultrasound, submitted 1997.
131. Gerring EL, Webbon PM: Fetlock annular ligament desmotomy: A report of 24 cases. Equine Vet J 16:113–116, 1984.
132. Verschooten F, Picavet TM: Desmitis of the fetlock annular ligament in the horse. Equine Vet J 18:138–142, 1986.
133. Lingard TR: Strain of the superior check ligament. J Am Vet Med Assoc 148:364–366, 1966.
134. Valdez H, Coy C, Swanson T: Flexible carbon fibre for repair of gastrocnemius and superficial digital flexor tendons in a heifer and gastrocnemius tendon in a foal. J Am Vet Med Assoc 181:154–157, 1982.
135. Sprinkle F, Swerczeck T, Crowe M: Gastrocnemius muscle rupture and haemorrhage in foals: Nine cases. Equine Pract 7:10–17, 1985.
136. Laine HR, Harjula ALJ, Peltokallio P: Ultrasonography as a differential diagnostic aid in achillodynia. J Ultrasound Med 6:351–362, 1987.
137. Kälebo P, Allenmark C, Peterson L, Swärd L: Diagnostic value of ultrasonography in partial ruptures of the Achilles tendon. Am J Sports Med 20:378–381, 1992.
138. Edwards GB: Changes in the sustentaculum tali associated with distention of the tarsal sheath (thoroughpin). Equine Vet J 10:97–102, 1978.
139. Whitton RC, Kannegieter NJ: Tarsal sheath rupture in a horse. Aust Equine Vet 13:50–52, 1995.
140. Adams SB, Blevins WE: Shoulder lameness in horses—part I. Compend Contin Educ Pract Vet 11:64–70, 1989.
141. Gaughan EM, Fubini SI, Dietze A: Fistulous withers in horses: 14 cases (1978–1987). J Am Vet Med Assoc 193:964–966, 1988.
142. Rashmir-Raven A, Gaughan EM, Modransky P, et al: Fistulous withers. Compend Contin Educ Pract Vet 12:1633–1641, 1990.
143. Cohen ND, Carter GK, McMullan WC: Fistulous withers in horses: 24 cases (1984–1990). J Am Vet Med Assoc 201:121–124, 1992.
144. Fornage BD: Peripheral nerves of the extremities: Imaging with US. Radiology 167:179–182, 1988.
145. Fornage BD: Sonography of the peripheral nerves of the extremities. Radiologia Medica 85(5 suppl.1):162–167, 1993.
146. Fornage BD, Touche DH, Segal P, Rifkin MD: Ultrasonography in

the evaluation of muscular trauma. J Ultrasound Med 2:549–554, 1983.
147. Fornage B, Touche D, Raguet M, et al: Accidents musculaires du sportif. Nouv Presse Med 11:571–575, 1982.
148. Laine H, Harjula A, Peltokallio P: Experience with real-time sonography in muscle injuries. Scand J Sports Sci 7:45–49, 1985.
149. Shoemaker RS, Martin GS, Hillman DJ, et al: Disruption of the caudal component of the reciprocal apparatus in two horses. J Am Vet Med Assoc 198:120–122, 1991.
150. Pascoe R: Death due to rupture of the origin of the gastrocnemius muscles in a filly. Aust Vet J 51:107, 1975.
151. Lehto M, Alanen A: Healing of a muscle trauma: Correlation of sonographical and histopathological findings in an experimental study in rats. J Ultrasound Med 6:425–429, 1987.
152. Valentine BA, Rouselle SD, Sams AE, Edwards RB: Denervation atrophy in three horses with fibrotic myopathy. J Am Assoc Vet Med 205:332–336, 1994.
153. Heckmatt JZ, Peir N, Dubowitz V: Real time ultrasound imaging of muscles. Muscle Nerve 11:56–65, 1988.
154. Lamminen A, Jääskeläinen J, Rapola J, Suramo I: High-frequency ultrasonography of skeletal muscle in children with neuromuscular disease. J Ultrasound Med 7:505–509, 1988.
155. Reimers K, Reimers CD, Wagner S, et al: Skeletal muscle sonography: A correlative study of echogenicity and morphology. J Ultrasound Med 2:73–77, 1993.
156. Lepage OM, Laverty S, Drolet R, Lavoie JP: Infiltrative lipoma in a Quarter horse. Cornell Vet 83:57–60, 1993.
157. Reimers CD, Fleckenstein JL, Witt TN, et al: Muscular ultrasound in idiopathic inflammatory myopathies of adults. J Neurol Sci 116:82–92, 1993.
158. van Holsbeck M, Introcaso M: Musculoskeletal ultrasonography. Radiol Clin North Am 30:907–925, 1992.
159. Kaplan GN: Ultrasonic appearance of rhabdomyolysis. Am J Radiol 134:375–377, 1980.
160. Fornage BD, Nérot C: Sonographic diagnosis of rhabdomyolysis. J Clin Ultrasound 14:389–392, 1986.
161. Love NE, Nickels F: Ultrasonographic diagnosis of a deep muscle abscess in a horse. Vet Radiol Ultrasound 34:207–209, 1993.
162. Cartee RE, Rumph PF: Ultrasonographic detection of fistulous tracts and foreign objects in the muscles of horses. J Am Vet Med Assoc 184:1127–1132, 1984.
163. Shah ZD, Crass JR, Oravec DC, Bellon EM: Ultrasonographic detection of foreign bodies in soft tissues using turkey muscle as a model. Vet Radiol Ultrasound 33:94–100, 1992.
164. Rutkowski JA, Richardson DW: A retrospective study of 100 pelvic fractures in horses. Equine Vet J 21:256–259, 1989.
165. Abiri NN, Kirpekar M, Ablow RC: Osteomyelitis: Detection with ultrasound: Work in progress. Radiology 169:795–797, 1988.
166. Abiri MM, Kirpekar M, Ablow RC: Osteomyelitis: Detection with ultrasound. Radiology 172:509–511, 1989.
167. Markel MD, Madigan JE, Lichtensteiger CA, et al: Vertebral body osteomyelitis in the horse. J Am Vet Med Assoc 188:632–634, 1986.
168. Markel MD, Ryan AM, Madigan JE: Vertebral and costal osteomyelitis in a foal. Compend Cont Educ Pract Vet 10:856–861, 1988.
169. Olchowy TWJ: Vertebral body osteomyelitis due to *Rhodococcus equi* in two Arabian foals. Equine Vet J 26:79–82, 1994.
170. Wisner ER, O'Brien TR, Pool RR, et al: Osteomyelitis of the axial border of the proximal sesamoid bones in seven horses. Equine Vet J 23:383–389, 1991.
171. Held JP, Patton CS, Shires M: Solitary osteochondroma of the radius of three horses. J Am Vet Med Assoc 193:563–564, 1988.
172. Gibbs C: Radiological signs of bone infection and neoplasia. Equine Vet Educ 6:103–110, 1994.
173. Livesey MA, Wilkie IW: Focal and multifocal osteosarcomas in two foals. Equine Vet J 18:407–410, 1986.
174. Gibbs C, Lane JG: Radiographic examination of the facial nasal and paranasal sinus regions of the horse, II: Radiological findings. Equine Vet J 19:474–482, 1987.
175. Jackman BR, Baxter GM: Treatment of a mandibular bone cyst by use of a corticocancellous bone graft in a horse. J Am Vet Med Assoc 201:892–894, 1992.
176. Wright I: Ligaments associated with joints. *In* Proceedings of the 1st Dubai International Equine Symposium 1996, pp 241–272.
177. Stashak TS: Lameness. *In* Stashak TS (ed): Adam's Lameness in Horses, 4th ed. Philadelphia, Lea and Febiger, 1987, pp 486–785.
178. Jeffcott LB, Kold SE: Clinical and radiographic aspects of stifle bone cysts in the horse. Equine Vet J 12:40–46, 1982.
179. Pool RR, Wheat JD, Ferraro GL: Corticosteroid therapy in common joint and tendon injuries of the horse, Part II: Effects on tendons. *In* Proceedings of the 26th Annual Convention of the American Association of Equine Practitioners. 1980, pp 407–410.
180. Albrechtsen SJ, Harvey JS: Dimethyl sulfoxide: Biomechanical effects on tendons. Am J Sports Med 10:177–179, 1982.
181. Reimersma DJ, Van Den Bogert AJ, Jansen MO, Schamhardt HC: Influence of shoeing on ground reaction forces and tendon strains in the forelimbs of ponies. Equine Vet J 28:126–132, 1996.
182. Reimersma DJ, Van Den Bogert AJ, Jansen MO, Schamhardt HC: Tendon strain in the forelimbs as a function of gait and ground characteristics and in vitro limb loading in ponies. Equine Vet J 28:133–138, 1996.
183. Alexander SA, Donoff RB: The glycosaminoglycans of open wounds. J Surg Res 29:422–429, 1980.
184. Amiel D, Ishizue K, Billings E, et al: Hyaluronan in flexor tendon repair. J Hand Surg 14A:837–843, 1989.
185. Gaughan EM, Nixon AJ, Krook LP, et al: Effects of sodium hyaluronate on tendon healing and adhesion formation in horses. Am J Vet Res 52:764–773, 1991.
186. Foland JW, Trotter GW, Powers BE, et al: Effect of sodium hyaluronate in collagenase-induced superficial digital flexor tendinitis in horses. Am J Vet Res 53:2371–2376, 1992.
187. van den Belt AJM, Keg PR, Dik KJ: The correlation between the dose and the distribution of intratendinous fluid injections in the flexor tendon of the horse [abstract]. Vet Radiol Ultrasound 33:120, 1992.
188. McKibbin LS, Paraschak DM: A study of the effects of lasering on chronic bowed tendons at Wheatley Hall Farm Limited, Canada, January 1983. Lasers Surg Med 3:55–59, 1983.
189. Morcos MB, Aswad A: Histologic studies of the effects of ultrasonic therapy on surgically split flexor tendons. Equine Vet J 10:267–269, 1978.
190. Watkins JP, Auer JA, Morgan SJ, et al: Healing of surgically created defects in the equine superficial digital flexor tendon: Effects of pulsing electromagnetic field therapy on collagen-type transformation and tissue morphologic reorganization. Am J Vet Res 46:2097–2103, 1985.
191. Norrie RD: A preliminary report on the regenerative healing in equine tendon. Am J Vet Res 36:1523–1524, 1975.
192. Bramlage LR: Superior check desmotomy as a treatment for superficial digital flexor tendinitis: Initial report. *In* Proceedings of the 32nd Annual Convention of the American Association of Equine Practitioners. 1986, pp 365–369.
193. Bramlage LR, Rantanen NW, Genovese RL, Page LE: Long-term effects of surgical treatment of superficial digital flexor tendinitis by superior check ligament desmotomy. *In* Proceedings of the 34th Annual Convention of the American Association of Equine Practitioners. pp 655–656, 1988.
194. Bramlage LR: Superior check ligament desmotomy as a treatment for superficial digital flexor tendinitis: Follow-up results. Proceedings of the Veterinary Orthopedic Society 15:10, 1988.
195. Hawkins J, Ross MW: Transection of the accessory ligament of the superficial digital flexor muscle for the treatment of superficial digital flexor tendinitis in Standardbreds: 40 cases (1988–1992). J Am Vet Med Assoc 206:674–678, 1995.
196. Shoemaker RS, Bertone AL, Mohammad LN, Arms SW: Desmotomy of the accessory ligament of the superficial digital flexor muscle in equine cadaver limbs. Vet Surg 20:245–252, 1991.
197. Nixon AJ: Tenosynovitis: Diagnosis, treatment and prognosis. *In* Proceedings of the 1st Dubai International Equine Symposium. 1996, pp 329–336.
198. White NA: Ultrasound-guided transection of the accessory ligament of the deep digital flexor muscle (distal check ligament desmotomy) in horses. Vet Surg 24:373–378, 1995.

CHAPTER

4

Thoracic Ultrasonography: Noncardiac Imaging

Ultrasonographic evaluation of the thorax is commonly performed in horses.[1-7] Thoracic ultrasonography yields information about the lung and pleural cavity heretofore unavailable to the veterinarian (Table 4-1).[1-10] Consolidation, pleuropneumonia, abscesses, granulomas, tumors, penetrating thoracic wounds, and diaphragmatic hernias have all been detected ultrasonographically in the lung or pleural cavity of horses.[1-8, 10, 11] Thoracic radiographs were the standard imaging modality of the lower respiratory tract and remain very useful, particularly in horses with interstitial pneumonia, pulmonary edema, chronic obstructive pulmonary disease (COPD), exercise-induced pulmonary hemorrhage (EIPH), penetrating thoracic wounds, blunt thoracic trauma, diaphragmatic hernia, and suspected metastatic neoplasia or diffuse granulomatous disease (Table 4-1).[1, 3, 5, 6, 12-21] Thoracic radiography has several disadvantages, however (Table 4-2).[2, 3, 5, 6, 12, 22] Only lateral thoracic radiographs can be obtained in adult horses, requiring four overlapping film placements.[2, 3, 12, 14, 20, 23, 24] The typical portable x-ray machine used in equine practice cannot be used to obtain good-quality lateral thoracic radiographs in the adult horse. Instead, a large machine with high milliamperage and kilovolt peak is needed, something that is usually available only at referral centers.[3, 5, 6, 12, 14, 23, 24] The mediastinum, right apical lung lobe, and lung overlying the cardiac silhouette cannot be critically evaluated owing to the difficulty of penetrating the cranial ventral portion of the thorax radiographically and the superimposition of the heart and lung.[16, 23] Small pleural effusions are easily missed radiographically but are detectable ultrasonographically.[1-6, 13, 17, 19] Neither pleural fluid nor pulmonary parenchyma can be characterized in horses with pleural effusion.[2, 3, 5, 6, 13, 17] Many of the causes of inflammatory lung disease in horses have similar radiographic patterns, making a definitive diagnosis with radiography nearly impossible.[12, 13, 16] It is also difficult to determine which side of the horse's thorax is affected with pleural effusion, consolidation, or abscesses, although obtaining both right and left lateral radiographs helps in making this determination.[2, 3, 20, 24] Exposure of personnel to radiation is always a concern.[2, 3, 20, 23-28]

Table 4-1
Preferred Imaging Modality for Diagnosis of Equine Thoracic Diseases

Radiography	Ultrasonography
Interstitial pneumonia (viral)	Pleuropneumonia
Pulmonary edema	Superficial pulmonary abscess
Chronic obstructive pulmonary disease (COPD)	Necrotizing pneumonia
	Bronchopleural fistula/abscess
Exercise-induced pulmonary hemorrhage (EIPH)	Multifocal granulomas/neoplasia
	Cranial mediastinal abscess
Deep pulmonary abscess	Cranial mediastinal neoplasia
Diffuse granulomatous disease	Diaphragmatic hernia
Diffuse neoplasia	Pneumothorax
Diaphragmatic hernia	Pulmonary fibrosis
Pneumothorax	Penetrating thoracic wound
Pulmonary fibrosis	Blunt thoracic trauma
Penetrating thoracic wound	
Blunt thoracic trauma	

In contrast, no known safety problems exist for the sonographer performing thoracic ultrasonography.[19, 29] Almost the entire thorax can be evaluated ultrasonographically, including the cranial mediastinal region.[2, 3, 6, 8] The lung overlying the heart and the most ventral portion of the right apical lung lobe can be evaluated. Two mutually perpendicular views can be obtained by scanning the thorax in both transverse (dorsal to ventral imaging plane, dividing the thorax into cranial and caudal portions) and dorsal (cranial to caudal imaging plane obtained from the right or left side of the thorax, dividing the thorax into dorsal and ventral portions) planes. The side(s) of the thorax affected, as well as the precise locations of lesions, can be determined in most horses because the involved lung segment is usually pleurally based. Exceptions are lesions located in the axial portion of the lung with no peripheral lung involvement, or a hernia in the axial portion of the diaphragm with no gastrointestinal viscera against the thoracic wall or displacing the lung dorsally.[1-3, 5, 6, 22, 30, 31] The character of pleural fluid can be determined ultrasonographically, as can the type and severity of underlying pulmonary parenchymal disease in individuals with pleural effu-

Table 4–2
Thoracic Radiography and Ultrasonography: Advantages and Disadvantages

Radiography Disadvantages	Ultrasonography Advantages
Only lateral view obtainable in adults	Localize lesion
Large machine with high kilovolt peak and milliamperage	Portable equipment, relatively inexpensive
Superimposition of heart and lung	Delineate lesions in cranial ventral area
Small pleural effusion missed	Detect pleural effusions of any size
Unable to characterize pleural fluid	Determine character of pleural fluid
Difficult to characterize pulmonary lesions	Identify pulmonary lesion and severity
Difficult to determine affected side	Affected area determined
Radiation exposure of personnel	No equine or human hazard
Fluoroscopy for lesion biopsy	Guided biopsy easily performed
Similar patterns for many diseases	

sion.[1–7, 25, 28, 30, 31] A portable machine that obtains high-quality images is available for performing these examinations in the field.[3, 5, 6, 27, 28] Aspirates or biopsies of small masses (0.5 cm) or small fluid collections can be safely performed using ultrasonographic guidance.[3, 25–27, 32–36] However, normal lung or nonspecific, subtle abnormalities of the visceral pleural surface may be all that is detected ultrasonographically in horses with interstitial pneumonia, a deep pulmonary abscess, pulmonary edema, COPD, EIPH, or neoplastic or diffuse granulomatous disease.[1–3, 5, 6] Thoracic radiographs are indicated in these horses to further characterize the severity of their pulmonary disease because lesions that do not involve the periphery of the lung cannot be imaged ultrasonographically.

EXAMINATION TECHNIQUE

Patient Preparation

Ideally, the hair over the portion of the thorax under examination should be surgically clipped with a No. 40 blade.[1, 3, 6, 9, 17, 19] The skin should be thoroughly cleaned prior to the application of ultrasonographic coupling gel.[3, 6, 19] Shaving the skin is usually not necessary unless a good-quality image cannot be otherwise obtained. In horses with very fine hair coats, the hair and skin can be thoroughly cleaned, coupling gel applied in the direction of hair growth, and an adequate image obtained to determine if any abnormalities exist.[1, 3, 6] However, the best image quality is obtained with the hair surgically clipped. The size of the clipped area should initially be based upon the auscultatory findings and enlarged as needed to include all the abnormal lung and pleura (Fig. 4-1).[2, 3, 6] If no abnormal lung sounds are heard, the entire thorax can be scanned through the hair or the clipped area determined by the probable location of the suspected underlying disease process (i.e., EIPH—caudodorsal lung field; pneumonia—cranial and caudoventral lung field; pulmonary edema—perihilar lung region; COPD—perihilar, cranial, and caudoventral lung field; lymphosar-

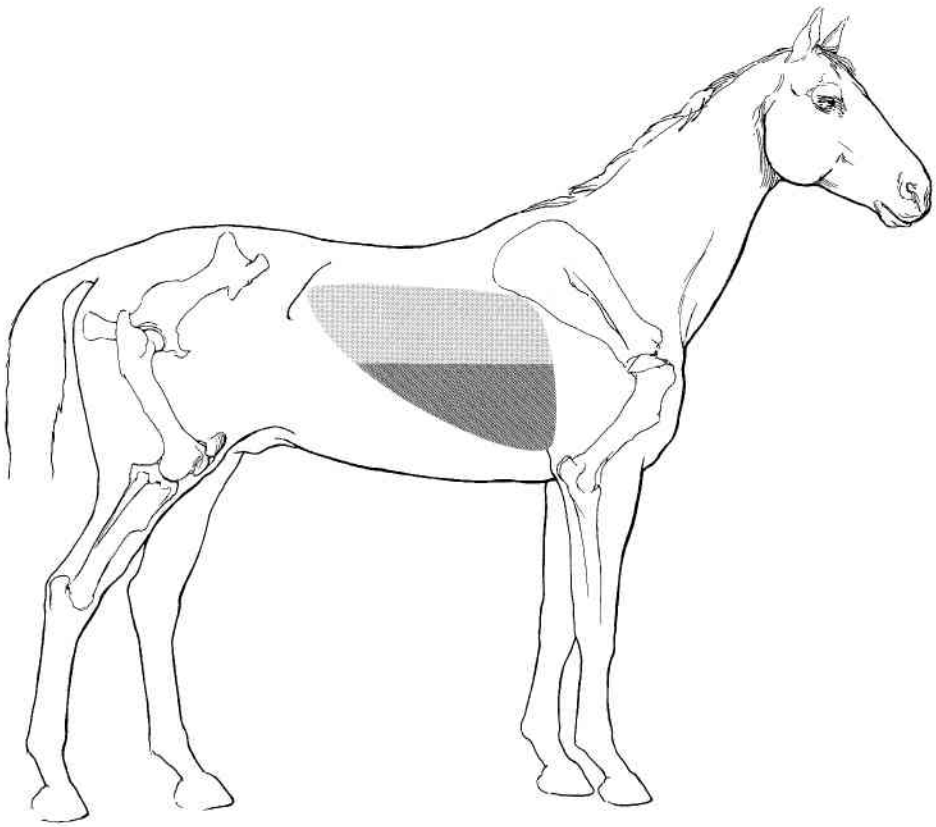

Figure 4–1
Diagram of area to be clipped for noncardiac thoracic ultrasonography. The darker shaded area located ventrally should be clipped if the only abnormal lung sounds auscultated are located ventrally. The upper and lower portions of the thorax should be clipped if abnormal lung sounds are also detected dorsally.

coma—cranial mediastinum; metastatic neoplasia or diffuse granulomatous disease—entire lung field; abscess—cranial and caudoventral lung field). Additional clipping should be performed to further characterize the pulmonary or pleural abnormalities initially imaged.

Anatomy

In a normal horse, lung can be imaged on both sides of the thorax from just below the dorsal musculature to where the lung crosses the diaphragm.[1, 3, 37] The ventral border of the lung field is usually a sloping line that is level with the tuber coxae in the seventeenth intercostal space (ICS), the tuber ischii in the fifteenth ICS, the dorsal to ventral middle of the thorax in the thirteenth ICS, the point of the shoulder in the eleventh ICS, and the point of the elbow in the ninth ICS. The line then continues forward to the point of the elbow in the fifth ICS. Lung can be imaged in the fifth to sixteenth or seventeenth ICS on both sides of the thorax. Lung can also be imaged in the fourth ICS on both sides, and the right apical lung tip can be imaged in the right third ICS.

Scanning Technique

The initial scanning of the thorax in adult horses should be performed with a 5.0-MHz transducer and a depth setting of 10 to 15 cm.[3, 5, 6, 38] If superficial pulmonary or pleural lesions are detected, a standard 7.5-MHz transducer or one containing a built-in fluid standoff yields superior images.[32, 33] In these instances, the depth setting should be decreased to display 4 to 12 cm. These transducers should also be used for the initial examination in a neonatal or weanling foal. If extensive pulmonary or pleural disease is detected in an adult horse, or the horse is obese, a lower-frequency transducer (3.5 or 2.5 MHz) or an increased displayed depth (25 to 30 cm in adult horses with severe pleural or pulmonary disease) may be needed to penetrate and successfully image the abnormality in its entirety.[3, 5, 6] A sector-scanner transducer is ideal because the footprint of the transducer is small and fits well in the small ICS of the horse.[1, 3, 6, 39] Straight or curved linear-array transducers may be used but have several significant limitations; only a fixed depth of 10 cm can be displayed with some machines when using a 5.0-MHz transducer, and much of the transducer footprint is not in contact with the skin in the ICS, yielding a limited field of view.[3, 6, 39] The newer microconvex linear-array transducers have a smaller footprint and variable displayed depth, overcoming these limitations. Phased-array transducers also have a larger footprint, but the displayed depth can be tailored to the individual examination.

The lung is scanned in the third (right side of the thorax only unless the heart is displaced caudally by a space-occupying mass in the cranial mediastinum) through the seventeenth ICS. Care must be taken to center the transducer in the ICS so that acoustic shadowing from the rib does not prevent visualization of the lung and pleura.[1, 3, 6] The lung should be scanned initially in a transverse plane (dorsal to ventral scan plane orientation, dividing the thorax into cranial and caudal portions), starting from the dorsalmost lung or from normal lung dorsal to the area of abnormality, extending ventrally into the abnormal areas and to the diaphragm.[1, 3, 6] When scanning from the left side of the thorax (left transverse), the image should be displayed with the left side of the thorax at the top of the image, dorsal on the right side of the screen and ventral on the left side. The right transverse image (scanning from the right side of the thorax) should display the right side of the thorax at the top of the image, dorsal on the right side of the screen, and ventral on the left. The scan should be carefully labeled with the extent of the abnormalities imaged by listing the ICS being scanned and the most dorsal point at which the first pulmonary or pleural lesions are detected.[3, 29] This can easily be done using the point of the shoulder as a reference line and measuring the distance in centimeters dorsal or, rarely, ventral to this imaginary line. The scan should continue in this imaging plane until the diaphragm and adjacent abdominal structures ventral to the diaphragm are visualized. The scan should proceed slowly in a dorsal to ventral direction so that an entire respiratory cycle is imaged before moving ventrally to a different area.[3, 6] Many subtle pulmonary and pleural abnormalities are detected only during exhalation, with respiratory movement or the lack of movement of the lung against the parietal pleura during deep inspiration. Each ICS should be scanned in this fashion until all the abnormalities within the thorax have been imaged in the transverse plane and normal lung and pleura (if present) have been imaged cranial and caudal to the abnormal area(s). To scan the lung in the fourth ICS, the transducer must be placed as high up within the axilla as possible. The right apical lung lobe and cranial mediastinum are imaged by placing the transducer in the right third ICS just above the level of the point of the elbow and angling the transducer cranially across the thorax toward the point of the left shoulder (Fig. 4-2).[3, 6] This imaging window is very narrow, and the scan plane orientation must be oblique to fit between the ribs and yet remain in the axilla. This area may also be scanned while one foreleg is held forward and off the ground, but this often is less well tolerated by the horse.[6, 40]

Scanning each ICS in a dorsal plane (cranial to caudal scan plane orientation dividing the thorax into dorsal and ventral portions) should also be performed to further characterize any abnormalities detected on the initial examination.[3, 29] In the dorsal imaging plane, the right or left side of the thorax should be displayed at the top of the image, cranial on the left side of the screen, and caudal on the right side.[41] Rib artifacts are commonly seen in this scan plane as the cranial and caudal edges of the scan plane intersect the ribs, causing acoustic shadowing. This scan should also proceed slowly to evaluate the lung and pleura during inhalation and exhalation to be certain that surfaces glide past one another and that the pulmonary parenchyma beneath the ribs is also visualized. The relationship of any abnormalities in the cranial and caudal mediastinum to the heart can be more accurately determined in this imaging plane. Both imaging planes are needed to completely characterize pleural and pulmonary abnormalities. However, if time is short, the transverse scans are the quickest to perform

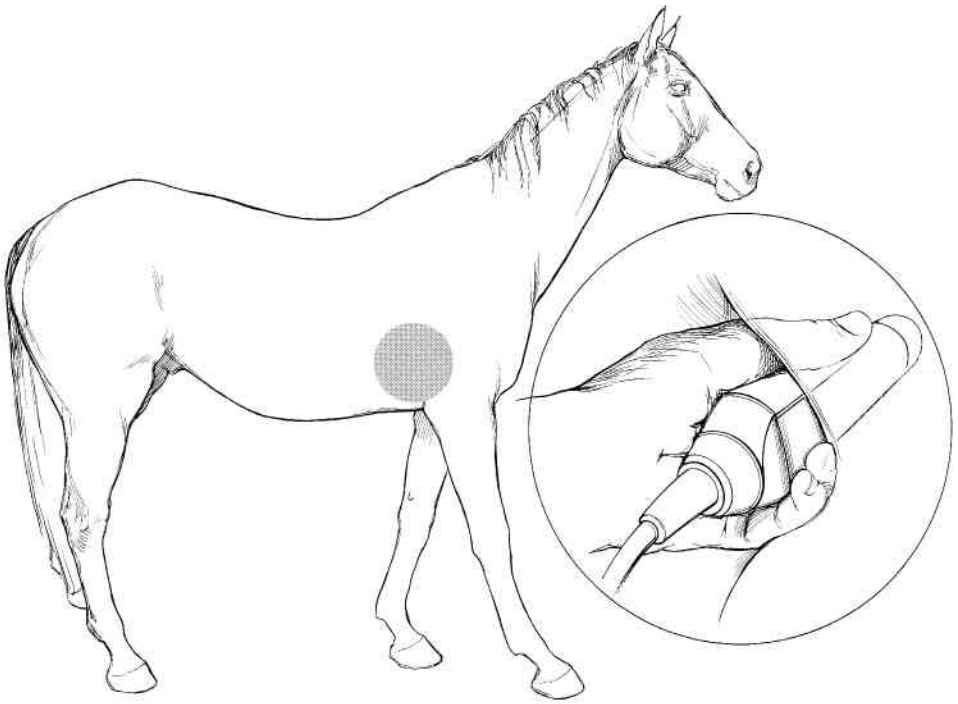

Figure 4–2
Diagram of limb position and transducer position for imaging the right apical lung and cranial mediastinum. The right forelimb is advanced as far forward as is comfortable for the horse, and the transducer is placed in the third intercostal space and angled toward the point of the opposite shoulder.

and yield the best images with the least amount of rib artifact.

ULTRASONOGRAPHIC FINDINGS

Normal Structures

Lung and Pleura

A large difference exists between the acoustic impedance of air and soft tissue, resulting in air being a nearly perfect reflector of ultrasound. Therefore, the normal visceral pleural edge of the lung appears as a straight hyperechoic line with characteristic equidistant reverberation air artifacts indicating normal aeration of the pulmonary periphery (Fig. 4-3).[1, 3, 5, 6, 9, 17, 19, 22, 28, 33, 37, 41-44] Watching the lung as the horse breathes, the visceral pleural edge of the lung is imaged gliding ventrally across the diaphragm with inhalation and dorsally with exhalation—"the gliding sign."[3, 6, 17, 44] Thus, the hyperechogenic band of the visceral pleural reflection has a characteristic inspiratory lowering and expiratory rising.[22, 28, 33] These back-and-forth movements synchronous with respiration are seen in all normal individuals but may be difficult to appreciate in horses with apnea or shallow respiratory movements.[3, 28] The gliding sign should always be sought in thoracic ultrasonography.[3, 22, 33] If these normal respiratory movements of the visceral pleural edge of the lung are not seen, the horse should be made to take deep breaths during the sonographic examination, either by holding off the horse's air or, preferably, by using a rebreathing bag.[3] In most normal horses no pleural fluid is visualized. However, small accumulations (up to 3.5 cm) of anechoic pleural fluid in the most ventral portions of the thorax have been detected in clinically normal horses.[1, 3, 6, 44] The diaphragm is curvilinear and appears thick and muscular in the more ventral locations and thin and tendinous dorsally and caudally.[1, 3] Liver (right side and cranioventrally on left side) and spleen (left side) are normally imaged ventral to the diaphragm unless the horse is older and has atrophy of the right liver lobe.[1, 3, 37] In these instances, large bowel echoes are imaged ventral to the diaphragm.[1, 3, 37] The intercostal muscles (usually 3 to 5 cm thick, thicker dorsally) are imaged superficial to the

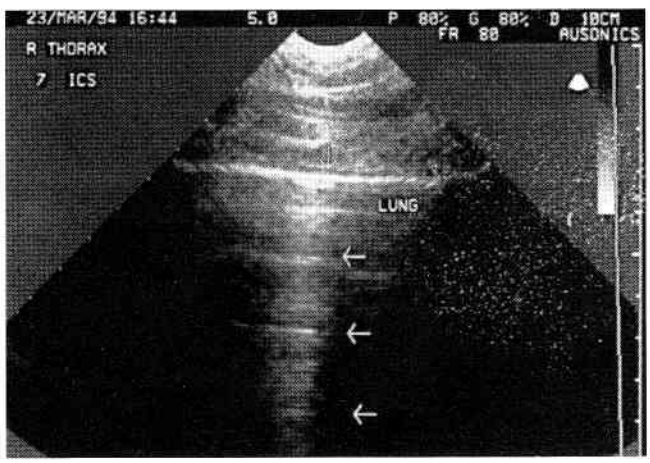

Figure 4–3
Sonogram of the right side of the thorax in the seventh intercostal space obtained from a 3-year-old Thoroughbred gelding with normal lung. The hyperechoic line represents the aerated visceral pleural surface of the lung *(vertical arrow)*, and the characteristic equidistant reverberation echoes *(horizontal arrows)*, indicate normally aerated lung. This sonogram was performed with a 5.0-MHz sector-scanner transducer and a 10-cm displayed depth. The right side of the sonogram is dorsal and the left side is ventral.

underlying lung and have the characteristic striated appearance of skeletal muscle.[5, 37] Rib artifacts are seen at the level of the deeper intercostal musculature, casting acoustic shadows (Fig. 4-4).[5, 37, 41]

Mediastinum

The lung covers the cranial and caudal mediastinum in most horses, although a hypoechoic soft-tissue mass (thymus) may be visualized in young horses in the cranial mediastinum ventral and medial to the right apical lung lobe and cranial to the heart. Fatty tissue may also be imaged in this area and around the heart, most commonly detected in ponies and fat horses. Fat is usually slightly more heterogeneous and echogenic (Fig. 4-5) than thymus and continues caudally around the heart into the caudal mediastinum.[41] The cranial mediastinum can be imaged only from the right third ICS in normal horses, as the heart is in contact with the thoracic wall in the left third ICS.[5]

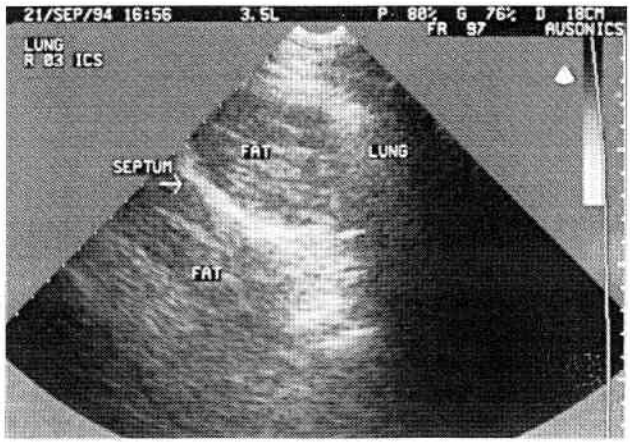

Figure 4-5

Sonogram of the right side of the thorax in the third intercostal space obtained from a 13-year-old Warmblood mare with fat in the cranial mediastinum. Notice the heterogeneous appearance of the fat on either side of the echogenic mediastinal septum and the hyperechoic ventral tip of the right apical lung. This sonogram was obtained with a 3.5-MHz sector-scanner transducer and an 18-cm displayed depth. The right side of this sonogram is dorsal and the left side is ventral.

Pleural Abnormalities

Pleural Effusion

The most common pleural abnormality found in horses is pleural effusion (Fig. 4-6), represented ultrasonographically as an anechoic space between the lung (visceral pleura), thoracic wall (parietal pleura), diaphragm, and heart.[3-6, 17, 19] The criteria for a fluid-containing space include that it be relatively free of echoes; have a sharp margin adjacent to the diaphragm, lung, and mediastinum; demonstrate acoustic enhancement deep to the lesion (increased transmission of ultrasound occurs through fluid); change shape with respiration; and may contain septa or strands floating within.[35, 42] Pleural effusions in horses in the United States are most frequently associated with pneumonia or lung abscesses, whereas in the United Kingdom the primary thoracic pathology is usually neoplasia, particularly mediastinal lymphosarcoma.[1, 3-8, 18, 45-52] Other neoplasms have been associated with pleural effusions in horses, including mesothelioma, gastric squamous cell carcinoma, and other carcino-

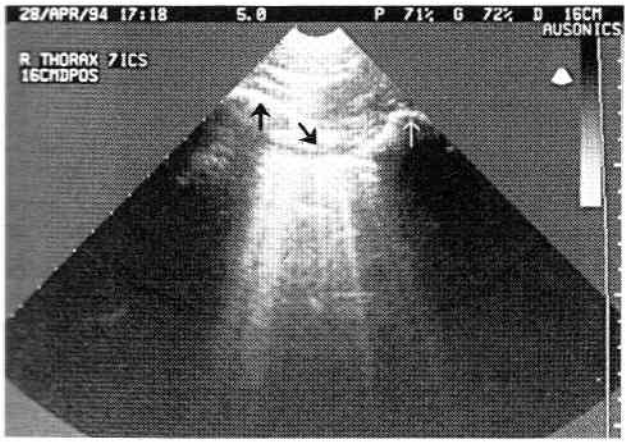

Figure 4-4

Sonogram of the right side of the thorax in the seventh intercostal space obtained from a 4-year-old Thoroughbred stallion. This sonogram was obtained 16 cm dorsal to a line level with the point of the shoulder. The hyperechoic echoes *(vertical arrows)* from the ribs cast strong acoustic shadows. The visceral pleural surface of the lung is relatively smooth but has radiating comet-tail artifacts compatible with small areas of fluid accumulation in the peripheral alveoli. These comet-tail artifacts were imaged up to 16 cm dorsal to a line level with the point of the shoulder. The slanted arrow points to the parietal pleura. This sonogram was obtained with a 5.0-MHz sector-scanner transducer and a 16-cm displayed depth. The right side of the sonogram is caudal and the left side is cranial.

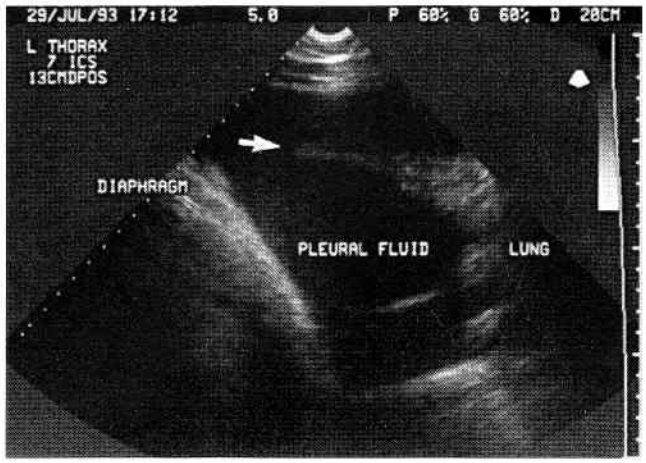

Figure 4-6

Sonogram of the left side of the thorax in the seventh intercostal space obtained from a 2-year-old Thoroughbred filly with pleuritis. Notice the anechoic pleural fluid in the ventral portion of the thorax and the compressed hypoechoic (atelectatic) ventral tip of the lung *(arrow)* floating in the pleural fluid. The pleural fluid extended dorsally 13 cm above a line level with the point of the shoulder. This sonogram was performed with a 5.0-MHz sector-scanner transducer and a 20-cm displayed depth. The right side of the sonogram is dorsal and the left side is ventral.

mas.[8, 19, 46, 53-59] Penetrating thoracic wounds or other thoracic trauma may also be the cause of pleural effusions in horses.[18, 49, 51, 60, 62] Chylothorax has also been reported in one foal associated with a congenital diaphragmatic defect.[63] Pleural effusions in horses may also be associated with primary or idiopathic pleuritis, pulmonary granulomas, coccidioidomycosis, nocardiosis, equine infectious anemia, pulmonary embolism, diaphragmatic hernias, esophageal rupture, congestive heart failure, pericarditis, enteric conditions, viral infections, abdominal inflammation, and post-surgical interventions.[2, 3, 47, 49, 51, 64-67]

Thoracocentesis performed where pleural effusion is detected ultrasonographically usually results in the successful aspiration of fluid from the thorax.[1, 3-6, 8-10, 17, 19, 21, 25, 26, 35, 45, 46, 68, 71] This fluid is usually found in the most ventral portion of the thorax and causes compression of normal healthy lung parenchyma (compression atelectasis), retraction of the lung toward the pulmonary hilus, and a ventral lung tip that floats in the surrounding fluid (Figs. 4-6 to 4-8).[1-6, 8, 9, 17, 19, 45] The larger the effusion, the greater the amount of compression atelectasis and lung retraction that occurs. Care should be taken in selecting a site for thoracocentesis, as large pleural effusions may cause displacement of the diaphragm caudally and ventrally. Selecting the lowest possible site for thoracocentesis could result in performing an abdominocentesis as well as a thoracocentesis, leaving a hole in the diaphragm and, possibly, the subsequent development of septic peritonitis. The thoracocentesis should be performed several centimeters above the normal ventralmost margin of the thorax in the first interspace caudal to the heart, where nonloculated pleural fluid or the largest pocket of loculated fluid is imaged (usually the seventh ICS). Monitoring the success of pleural fluid drainage is also easily performed ultrasonographically.[1, 3, 21, 70] Ultrasonographic examination of the thorax also prevents unnecessary thoracocentesis in individuals without pleural effusion or with very small or loculated effusions unlikely to result in successful sample collection.[25, 26]

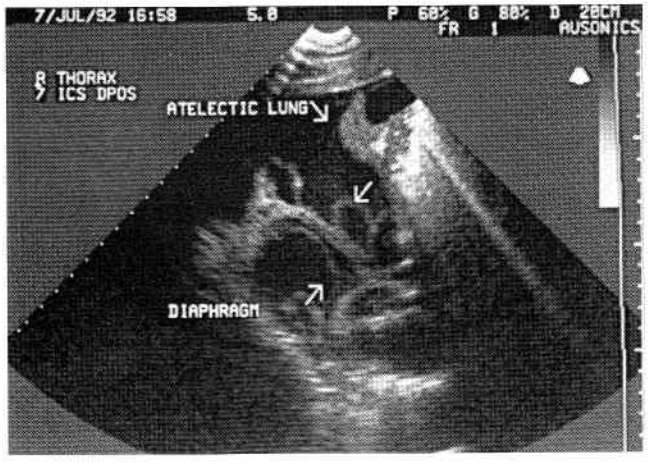

Figure 4–7

Sonogram of the right side of the thorax in the seventh intercostal space obtained from a 4-year-old Thoroughbred filly with pleuropneumonia. Notice the anechoic pleural fluid in the ventral portion of the right side of the thorax and the compressed hypoechoic (atelectatic) ventral tip of the lung *(arrow)*, floating in the pleural fluid. The pleural fluid extended dorsally to a line level with the point of the shoulder. Notice the membranous structures (pericardial diaphragmatic ligament) attached to the diaphragm floating in the ventral portion of the thorax *(arrows)*. This sonogram was performed with a 5.0-MHz sector-scanner transducer and a 20-cm displayed depth. The right side of the sonogram is dorsal and the left side is ventral.

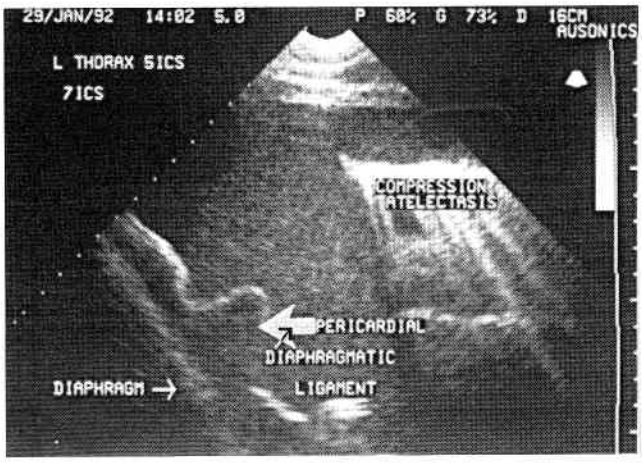

Figure 4–8

Sonogram of the left side of the thorax in the seventh intercostal space obtained from a 4-year-old Thoroughbred gelding with pleuropneumonia. Notice the pericardial-diaphragmatic ligament *(large arrow)* floating in the pleural fluid. Compression atelectasis is seen at the ventral lung tip, which is also floating in the echogenic (highly cellular) pleural fluid. The pleural effusion extended dorsally 15 cm above a line level with the point of the shoulder. This sonogram was obtained with a 5.0-MHz sector-scanner transducer and a 16-cm displayed depth. The right side of the sonogram is dorsal and the left side is ventral.

With pleural effusions the pericardial-diaphragmatic ligament, a normal pleural reflection of the parietal pleura over the diaphragm and heart, is imaged as a thick membrane floating in pleural fluid (Figs. 4-7 and 4-8).[2, 3, 5, 6, 44] This membrane is easily mistaken by the novice ultrasonographer for fibrin but is, in reality, a normal structure, imageable in the ventral thorax of every horse with pleural effusion, regardless of cause. This membrane runs from the thoracic side of the diaphragm over the heart and appears as a 3- to 6-mm-thick, undulating sheet of homogeneous tissue. Similarly, scanning in the cranial mediastinum in horses with pleural effusion usually reveals hypoechoic fluid with dorsal displacement of the lung. A thick echogenic band of tissue is imageable dividing the mediastinum into right and left sides (Fig. 4-9; see also Fig. 4-5). Small nodular densities (lymph nodes) are often visualized in this band of tissue.

The amount of pleural fluid in the thorax can be roughly estimated by the fluid level and the amount of pulmonary parenchymal consolidation or abscesses present.[3, 5] In horses with pleuropneumonia, less than 1 liter of fluid was recovered from each side by thoracocentesis when the only pleural fluid imaged was around the cranioventral tip of the lung. A pleural fluid line level with the point of the shoulder corresponds to the recovery of 1 to 5 liters of pleural fluid per side, whereas 4 to 10 liters were recovered by thoracocentesis in horses with a pleural fluid line extending above the point of the shoulder.[3, 5] In two of these horses, extensive loculations and adhesions limited the amount of pleural fluid recovered.[5]

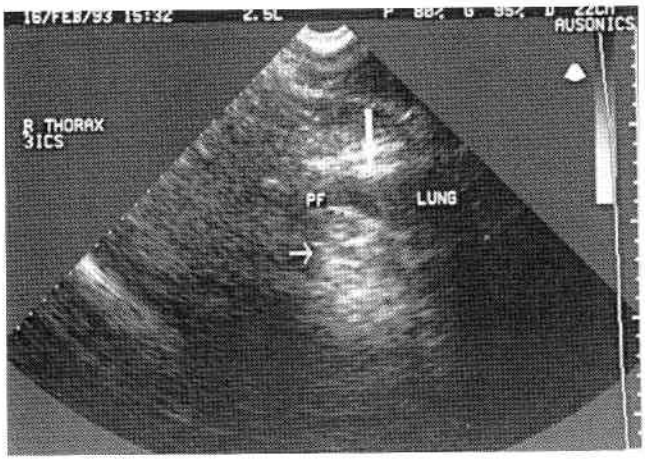

Figure 4–9

Sonogram of the right side of the cranial mediastinum in the third intercostal space obtained from a 3-year-old Thoroughbred filly with persistent unilateral thumps. Notice the aerated ventral lung tip *(large vertical arrow)*, the small (normal) amount of anechoic pleural fluid (PF), and the hypoechoic to echogenic thick mediastinal septum dividing the cranial mediastinum *(small horizontal arrow)*. The ventral portion of the mediastinal septum is normally thicker than the dorsal part but appeared slightly thickened in this filly. This sonogram was performed with a 2.5-MHz sector-scanner transducer and a 22-cm displayed depth. The right side of the sonogram is dorsal and the left side is ventral.

Pleural Fluid Character

The sonographic pattern of pleural effusions includes anechoic, complex nonseptated, and complex septated fluid.[26, 35] Composite fluids are complex and more echogenic than normal, containing fibrin, cellular debris, a higher cell count and total protein concentration, and gas.[1-6, 9, 26, 35, 69] Anechoic fluid represents a transudate or modified transudate with a relatively low cell count and total protein concentration (see Figs. 4-6 and 4-7).[3, 9, 26, 35] A change in shape of the fluid collection within the thorax and movement of echogenic septae detected within pleural fluid in human beings are associated with lower-viscosity fluid and a high likelihood of fluid recovery on thoracocentesis.[72] Increased echogenicity of the fluid indicates an increased cell count or total protein concentration (Fig. 4-10; see also Fig. 4-8).[2, 3, 6, 7, 9, 35, 44] Complex echogenic septated fluid detected ultrasonographically in human beings is consistent with inspissated fluid and a difficult or nonproductive thoracocentesis.[26] Blood within the pleural cavity (hemothorax) or within any body cavity often has a hypoechoic to echogenic swirling pattern (Fig. 4-11), may be septated, and can usually be differentiated from a more purulent exudate by the latter's more homogeneous echogenic appearance and the tendency for layering to occur with pyothorax.[6, 9, 28, 73, 74] Hemangiosarcoma should always be considered in the differential diagnosis of hemothorax because this is one of the more common thoracic neoplasms in horses.[73] Clotting may be imaged in pleural fluid as soft, echogenic masses (Fig. 4-11).[9, 74] The cells and cellular debris in pyothorax are more echogenic, heavier, and in the most ventral location whereas the less cellular fluid or gas cap is detected dorsally. Similarly, esophageal rupture results in a pyothorax and pneumothorax (Fig. 4-12) with ingesta layered in the most ventral portion of the thoracic cavity. Free gas within the fluid (polymicrobullous fluid) is imaged as small, very bright hyperechoic echoes, with more free gas echoes imaged dorsally in the pleural fluid (Fig. 4-13; see also Figs. 4-10 and 4-12).[2-4, 6, 7, 28] The echoes from the microbubbles are usually pinpoint and linear, appearing somewhat larger and less linear in the deeper pleural fluid because of the deterioration in lateral resolution of these echoes with increasing depth.[28, 41] Polymicrobullous fluid is caused by the mixing of air or gas microbubbles and pleural fluid.[3, 7] The microbubble echoes move rapidly and spontaneously in various directions, depending upon respiratory, cardiac, and the horse's body movements.[3, 7, 28] The free gas echoes often adhere to the fibrinous pleural surfaces and may be detected there initially without being mixed into the pleural fluid (Fig. 4-13).[3] Free gas echoes may also be compartmentalized in only one portion of the thorax when initially imaged (Fig. 4-13) but usually spread rapidly to all portions of the thorax.[3, 7] Free gas echoes are usually caused by an anaerobic infection within the pleural cavity.[2-4, 6, 7, 18, 50] Although the lack of free gas echoes on the thoracic sonogram does not exclude the possibility of an anaerobic infection, their detection is a sensitive indicator of anaerobic infection.[7] Free gas echoes were detected in the pleural or abscess fluid of 74% of horses with confirmed anaerobic pneumonia.[7] Free gas echoes were also detected in the pleural fluid of 20% of horses with pleuropneumonia and in 50% of horses with ultrasonographic evidence of concurrent pulmonary parenchymal necrosis; these horses all had confirmed anaerobic pleuropneumonia.[4] Occasionally free gas echoes can be introduced into the pleural cavity from a thoracocentesis or indwelling

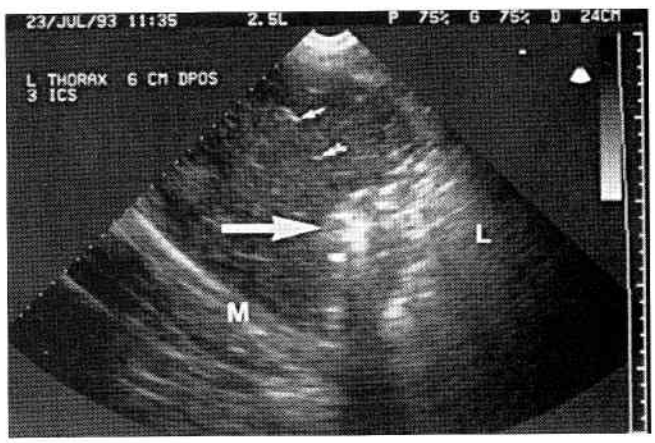

Figure 4–10

Sonogram of the left side of the thorax in the third intercostal space obtained from a 4-year-old Thoroughbred colt with aerobic and anaerobic pleuropneumonia. Notice the composite nature of the fluid in the ventral portion of the thorax with echogenic fluid and hyperechoic free gas echoes *(small arrows)*. The fluid line extended dorsally 6 cm above a line level with the point of the shoulder. Notice the rounded hypoechoic ventral tip of the left apical lung with free gas echoes within, compatible with severe consolidation and probable anaerobic pneumonia *(large arrow)*. The large clump of hyperechoic gas echoes in the consolidated lung is probably residual air trapped in a larger airway. This sonogram was performed with a 2.5 MHz sector-scanner transducer and a 24-cm displayed depth. The right side of the sonogram is dorsal and the left side is ventral. L, Aerated lung; M, mediastinal septum.

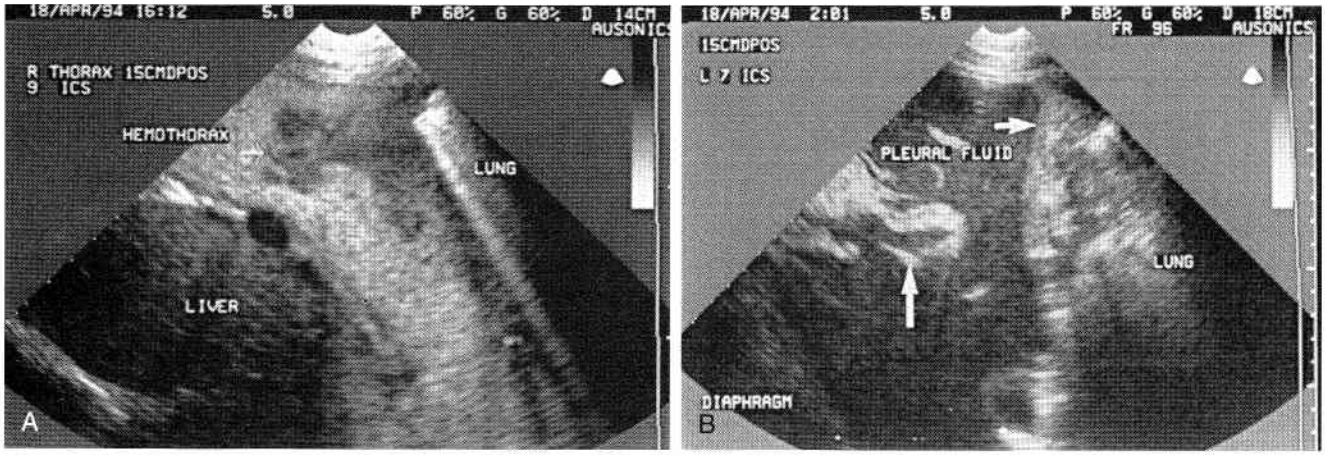

Figure 4–11

Sonograms of the thorax from a 10-year-old Arabian mare with hemothorax. The hemothorax extended dorsally 15 cm above a line level with the point of the shoulder. These sonograms were obtained with a 5.0-MHz sector-scanner transducer and 14-cm *(A)* and 18-cm *(B)* displayed depths. The right sides of the sonograms are dorsal and the left sides are ventral.

A, Sonogram of the right side of the thorax obtained in the ninth intercostal space. Notice the swirling pattern *(arrow)* and varying echogenicities within the fluid, typical of a hemothorax.

B, Sonogram of the left side of the thorax obtained in the seventh intercostal space. Notice the echogenic masses *(long vertical arrow)* or clots floating in the echogenic fluid (hemothorax) and the hypoechoic area of lung *(short horizontal arrow)*. The hypoechoic area of lung was an area of pulmonary congestion and atelectasis.

chest tube, but this air is usually rapidly reabsorbed and does not persist in the pleural fluid unless air is continually leaking into the thorax from an open chest tube or an anaerobic infection is present in the thoracic cavity.[7]

Fibrin has a filmy to filamentous or frondlike appearance and is usually hypoechoic. Fibrin is deposited in layers (Fig. 4–14) or in weblike filamentous strands on the parietal and visceral pleural surfaces (Fig. 4–15).[1-6, 17, 44] Fibrin was detected ultrasonographically in 23% of horses with pleuropneumonia.[4] The detection of a thick layer of fibrin on the pleural surface or "pleural peel" in human beings with refractory empyema (not responding to chest tube drainage) often prompts a thoracotomy and decortication.[21, 75] Decortication includes complete evacuation of the pleural peel, stripping of the visceral pleura, and debridement of the parietal pleura.[21, 75] Loculations (Fig. 4–16) between the parietal and visceral pleural

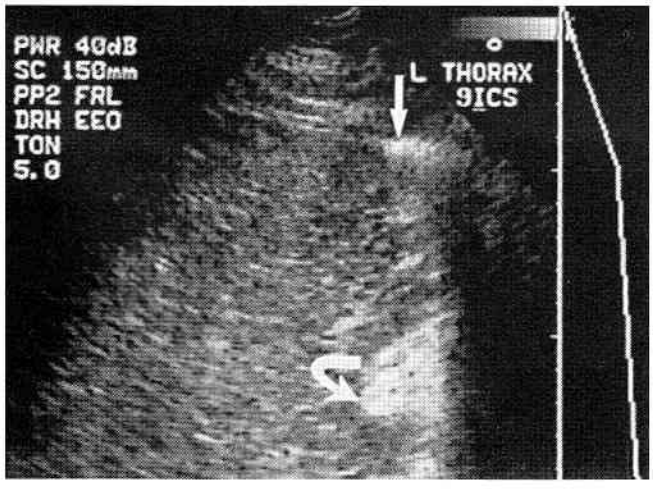

Figure 4–12

Sonogram of the left side of the thorax in the ninth intercostal space obtained from a 17-year-old Thoroughbred-Quarter horse cross gelding with an intrathoracic esophageal rupture. Notice the echogenic fluid containing small gas echoes, the dorsal free gas associated with a pneumothorax *(vertical arrow)*, and the ventral lung tip floating in the fluid *(curved arrow)*, mostly hidden by the pneumothorax. The pleural fluid extended dorsally 18 cm above a line level with the point of the shoulder. The free gas moved ventrally during inspiration, masking the underlying lung and creating the "curtain" sign. This sonogram was obtained with a 5.0-MHz sector-scanner transducer and a displayed depth of 15 cm. The right side of the sonogram is dorsal and the left side is ventral.

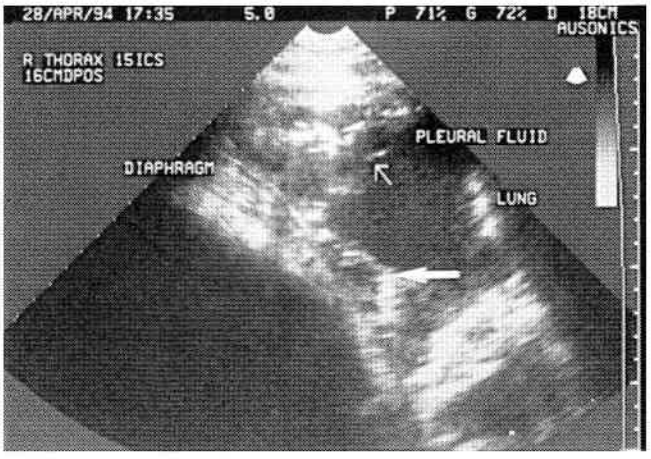

Figure 4–13

Sonogram of the right side of the thorax in the fifteenth intercostal space obtained from a 4-year-old Thoroughbred stallion with anaerobic pleuropneumonia. Notice the free gas echoes *(small arrow)* trapped in the fibrin and beneath the pericardial-diaphragmatic ligament along the diaphragm *(large arrow)*. The pleural fluid line extended dorsally 16 cm above a line level with the point of the shoulder. This sonogram was obtained with a 5.0-MHz solar-scanner transducer and an 18-cm displayed depth. The right side of the sonogram is dorsal and the left side is ventral.

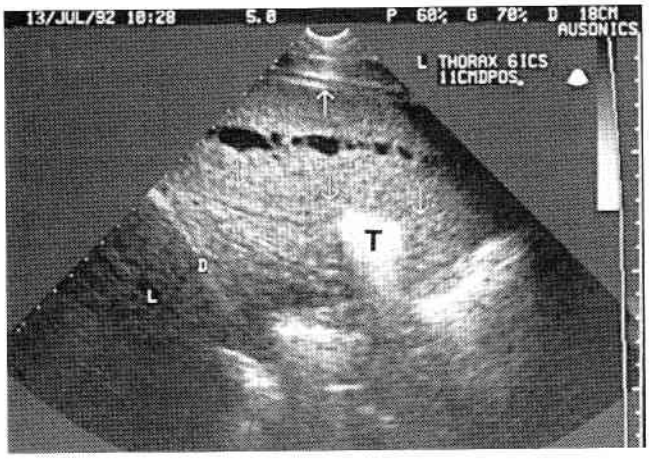

Figure 4–14

Sonogram of the left side of the thorax in the sixth intercostal space obtained from a 4-year-old Thoroughbred filly with pleuropneumonia. Notice the thick layer of fibrin on the parietal *(up arrow)* and visceral *(down arrows)* pleural surfaces. The fibrin and fluid extended dorsally 11 cm above a line level with the point of the shoulder. Notice the hypoechoic hepatized (liver-like) ventral lung, with fluid bronchograms immediately adjacent to the diaphragm (D) and liver (L). The bright hyperechoic areas are areas of the lung that were still aerated or contained trapped air (T). This sonogram was performed with a 5.0-MHz sector-scanner transducer and an 18-cm displayed depth. The right side of the sonogram is dorsal and the left side is ventral.

surfaces of the lung, diaphragm, pericardium, and inner thoracic wall limit pleural fluid drainage.[1-3, 5, 6, 17, 44] Loculations were detected ultrasonographically in 10% of horses with pleuropneumonia and in 56.5% of horses with fibrinous pleuropneumonia.[4] The presence of loculated or septated pleural fluid correlates with exudative pleural fluid chemistries in human beings.[26, 35, 69, 74, 76] Loculation is a valuable marker for the progression of a

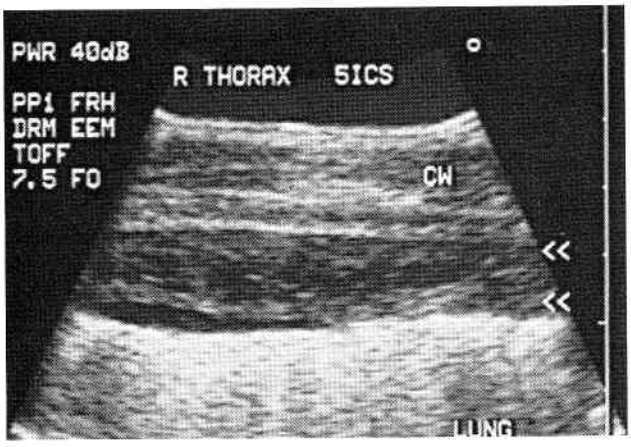

Figure 4–15

Sonogram of the right side of the thorax in the fifth intercostal space obtained from a 3-year-old Thoroughbred filly with postoperative pleuropneumonia. Notice the weblike lacy network of fibrin between the parietal and visceral pleural surfaces of the lung *(arrowheads)*, which was detected throughout the entire right side of the thorax. This sonogram was performed with a 7.5-MHz sector-scanner transducer containing a built-in fluid standoff and a 7.5-cm displayed depth. The right side of the sonogram is dorsal and the left side is ventral. CW, Chest wall.

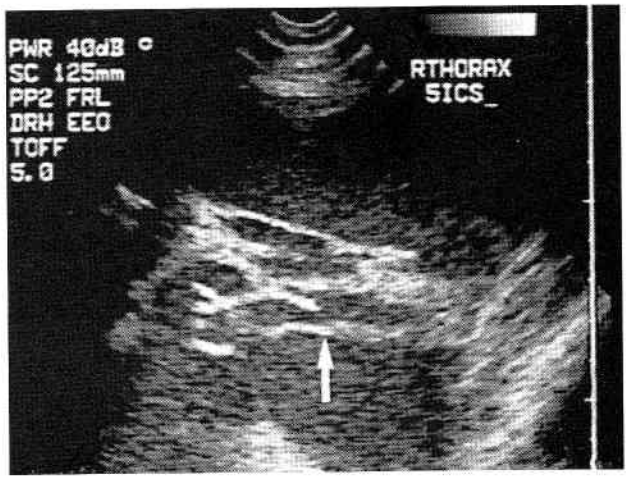

Figure 4–16

Sonogram of the right side of the thorax in the fifth intercostal space obtained from a 5-year-old Thoroughbred stallion with fibrinous pleuropneumonia. Notice the thick fibrin loculations *(arrow)* in the echogenic pleural fluid. The pleural fluid line extended dorsally 12 cm above a line level with the point of the shoulder. This sonogram was obtained with a 5.0-MHz sector-scanner transducer and a displayed depth of 12.5 cm. The right side of the sonogram is dorsal and the left side is ventral.

parapneumonic effusion from the exudative to the fibrinopurulent stage.[76] Fibrin is most commonly detected in association with pleuropneumonia but has been detected in horses with thoracic neoplasia.[5, 44, 46] As these fibrin strands become more organized and fibrous, they become more rigid and echogenic, often distorting the structures to which they are attached during one phase of respiration and possibly restricting pulmonary mechanics.[1, 3, 6, 21, 75] The detection of these mature adhesions (Fig. 4-17) indicates a chronic pleuritis of at least several weeks' duration.[5, 17, 44] Fibrin strands may also be imaged in the cranial mediastinum between the thoracic wall and the mediastinal division (Fig. 4-18), pericardium, or right apical lung lobe. This fibrin may eventually organize in the cranial mediastinum and wall this area off from the rest of the thorax, resulting in a cranial mediastinal abscess.[2, 40]

Pneumothorax

A gas-fluid interface is detected in individuals with hydropneumothorax (pleural effusion and pneumothorax).[2, 3, 6, 28] This pneumothorax is usually caused by a bronchopleural fistula, which occurs in horses with severe pulmonary parenchymal necrosis.[2-7] The dorsal gas (pneumothorax) has the characteristic reverberation artifact caused by the large difference in acoustic impedance between gas and soft tissue or fluid.[2, 3, 5, 37, 43] The gas-fluid interface can be imaged moving simultaneously in a dorsal to ventral direction with respiration, the "curtain sign," reproducing the movements of the diaphragm (Fig. 4-19; see also Fig. 4-12).[2, 3, 28] The dorsal air echo moves ventrally during inspiration, similar to the lowering of a curtain, gradually masking the underlying structures.[28] The curtain sign is best visualized on the transverse intercostal scan obtained just below the air-fluid level.[28] At this level, only pleural fluid is imaged during exhalation; however, during inhala-

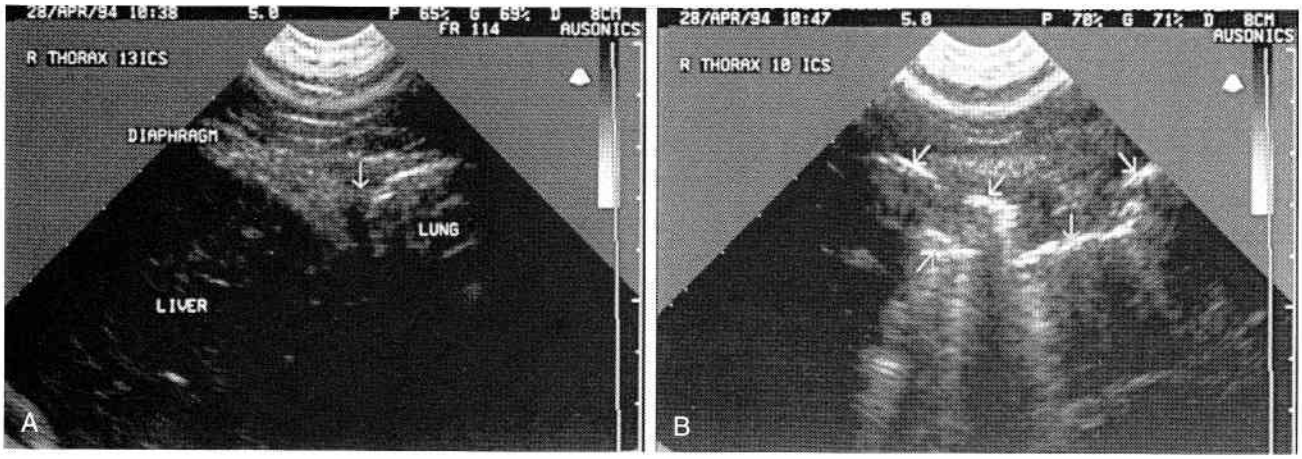

Figure 4–17

Sonograms of the right side of the thorax obtained from a 7-year-old Thoroughbred gelding. This horse had severe pleuropneumonia 6 years earlier, which had been treated with a thoracotomy to provide adequate pleural drainage. The right sides of these sonograms are dorsal and the left sides are ventral.

A, The ventral lung is adhered *(arrow)* to the diaphragm in all interspaces. Adhesions between the parietal and visceral pleural surfaces extended dorsally 25 cm above a line level with the point of the shoulder in this side of the thorax. This sonogram was obtained with a 5.0-MHz sector-scanner transducer and a displayed depth of 8 cm in the thirteenth intercostal space.

B, An area of pleural thickening is imaged along the parietal pleura in the dorsal portion of the right tenth intercostal space (ICS). The lung surface *(downward arrows)* is irregular and radiates comet-tail artifacts from the visceral pleural surface. These irregularities in the visceral pleura are caused by scarring of the pulmonary periphery and visceral pleura from the previous pleuropneumonia. An area of hypoechoic lung *(upward arrow)* represents an area of parenchymal scarring. The lung moves only slightly over the parietal pleural scar in real time with a very short, jerky motion, compatible with pleural adhesions. The scar along the parietal pleura extended from the eleventh ICS cranially and ventrally to the fourth ICS, the site of the previous thoracotomy. This sonogram was obtained with a 5.0-MHz sector-scanner transducer and a displayed depth of 8 cm in the right tenth ICS.

tion the air echoes of the pneumothorax with their characteristic reverberation artifacts progressively invade the image from a dorsal direction, replacing the pleural fluid. The curtain sign is best visualized with pleural effusion and parenchymal consolidation, or atelectasis.[7] The lung echo changes position relative to the pleural fluid, whereas the dorsal free gas echo moves with pleural fluid movement and respiration. The lung is imaged floating in the pleural fluid retracted toward the pulmonary hilus (see Figs. 4-12 and 4-19).[2, 3, 6] The extent of underlying pulmonary disease is evaluated ultrasonographically from the ventral pleural fluid acoustic window. Without looking deep into the thorax, the underlying consolidated or

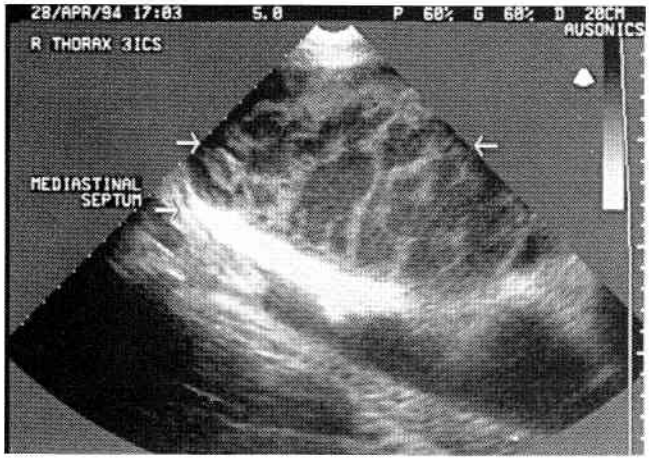

Figure 4–18

Sonogram of loculated pleural fluid *(arrows)* in the right side of the thorax in the third intercostal space obtained from a 4-year-old Thoroughbred stallion with pleuropneumonia. Notice the mediastinal septum dividing the right and left sides of the cranial mediastinum. This sonogram was obtained with a 5.0-MHz sector-scanner transducer and a 20-cm displayed depth. The right side of the sonogram is dorsal and the left side is ventral.

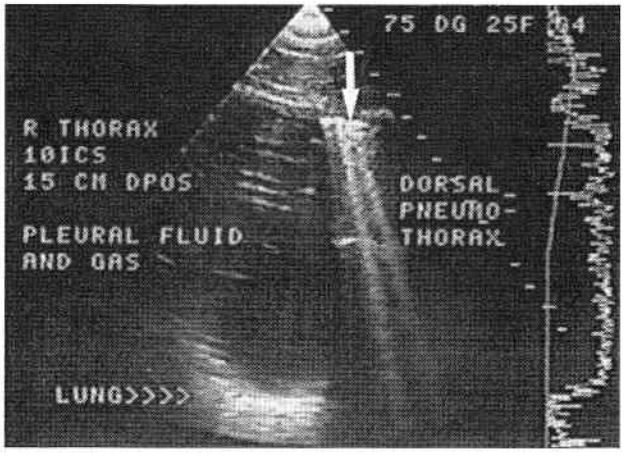

Figure 4–19

Sonogram of the right side of the thorax in the tenth intercostal space obtained from a 2-year-old Thoroughbred colt with anaerobic pleuropneumonia. Notice the gas-fluid interface against the parietal pleura *(vertical arrow)*, which demonstrated the "curtain sign" in real time. This free gas prevents visualization of the pulmonary parenchyma. The atelectatic ventral lung tip *(arrowheads)* is visualized approximately 10 cm deep to the parietal pleura floating in the pleural fluid. The gas-fluid interface was detected 15 cm dorsal to a line level with the point of the shoulder. This sonogram was obtained with a 5.0-MHz sector-scanner transducer and a displayed depth of 17 cm. The right side of the sonogram is dorsal and the left side is ventral.

atelectatic lung could be missed and the dorsal pneumothorax might be mistaken for lung.[2, 5] With hydropneumothorax, the lung is not imaged adjacent to the parietal pleura because it is surrounded by fluid and gas. Normal underlying lung is compressible and appears collapsed, whereas consolidated lung is not compressible and appears wedge shaped; both, however, are surrounded by fluid ventrally.[1-6] The echotexture of the pleural effusion in horses with hydropneumothorax is usually anechoic but may be polymicrobullous with gaseous effusions or echogenic with hemothorax.[2, 6, 7, 28]

A pneumothorax without pleural effusion is more difficult to detect ultrasonographically because gas free in the pleural cavity and air within the lung have the characteristic hyperechoic reflection and reverberation artifacts with periodicity.[1, 2, 6, 28, 77, 78] The small, discrete hypoechoic irregularities with comet-tail artifacts seen in the visceral pleural surface of horses with nonspecific or subtle pulmonary disease such as EIPH, COPD, or scarring from previous respiratory disease are absent at the site of the pneumothorax.[1, 3, 77-80] To detect dorsal pneumothorax in horses without pleural effusion, the scan should begin at the most dorsal aspect of the thorax and continue ventrally, looking for a break in the characteristic reverberation air artifact (Fig. 4-20).[1, 3, 6] A soft tissue-density echo may be detected at the site of pulmonary atelectasis between the dorsal free gas echo and the ventral air echo from aerated lung.[6] The echoes from the dorsal pneumothorax and pulmonary atelectasis move relative to one another with respiration (the dorsal free gas echoes move ventrally, covering the pulmonary atelectasis with inhalation), whereas the interfaces between the pulmonary atelectasis and the normally aerated lung move together. The gliding sign is absent at the site of the pneumothorax because the normal respiratory excursions of the visceral pleura are hidden from view by the pneumothorax.[1, 3, 28, 77-79] The amount of dorsal lung compression (pulmonary atelectasis) detected in horses with pneumothorax is determined by the size of the pneumothorax. Severe pneumothorax and compression atelectasis are most likely in horses with a penetrating thoracic wound or subcutaneous emphysema dissecting into the mediastinum and pleural cavity. The amount of pulmonary collapse in horses with pneumothorax cannot be accurately determined ultrasonographically, only estimated, because the compression atelectasis adjacent to the thoracic wall is an inadequate imaging window.[28]

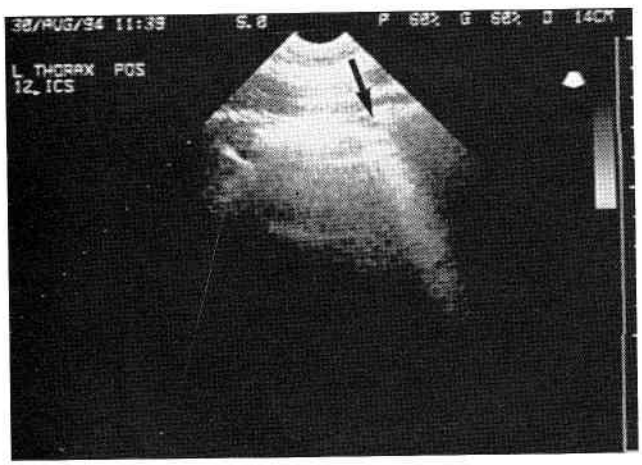

Figure 4–20

Sonogram of the left side of the thorax in the twelfth intercostal space obtained from a 2-year-old Thoroughbred filly with a pneumothorax from a penetrating chest wound. Notice the break in the characteristic air artifact *(arrow)* and the comet-tail artifact at the junction of the dorsal pneumothorax and ventral aerated lung. The lung hidden from view by the pneumothorax is atelectatic. The pneumothorax begins at a line level with the point of the shoulder. This sonogram was obtained with a 5.0-MHz sector-scanner transducer and a displayed depth of 14 cm. The right side of the sonogram is dorsal and the left side is ventral.

Noneffusive Pleuritis

A dry pleuritis is more difficult to detect ultrasonographically because no fluid separates parietal and visceral pleural surfaces. Careful examination of the interface between the parietal and visceral pleural surfaces should be performed during inspiration and expiration, evaluating movement of the visceral pleural lung surface relative to the parietal pleural surface of the thoracic wall and diaphragm. The lung surface should glide smoothly across the parietal pleura, moving outward during inhalation and inward during exhalation, without sticky or jerky movement: the gliding sign.[3, 22] If movement of the lung across the parietal pleural surfaces is rough or erratic, a dry pleuritis is probably present. Absence of any movement between these surfaces during respiration is also an indication of a dry pleuritis or adhesions between parietal and visceral pleural surfaces but is occasionally seen in normal horses taking very shallow breaths.[1, 3, 4] Therefore, if the gliding sign is absent, the horse should be forced to take a series of deep breaths (ideally by breathing into a rebreathing bag) to thoroughly evaluate the pleural surfaces and their movement relative to one another.

Pleural Thickening

Pleural thickening (Fig. 4-21) can be accurately differentiated from pleural effusion.[3, 5, 25] Pleural thickening is most frequently imaged in horses with effusive pleuritis but has also been reported in one horse with mesothelioma and in one horse with lymphosarcoma.[1, 3, 5, 19, 44] Horses with thickening of the parietal pleura should be scanned carefully with a higher-frequency transducer (7.5 MHz) to screen for subpleural masses or hematomas.[1, 4] Although both occur infrequently in horses, anechoic subpleural masses that may contain septations and echogenic areas of internal clot formation (hematomas)[71] may be detected in horses with thoracic trauma or vascular neoplasms such as hemangiomas or hemangiosarcomas. Subpleural masses of soft-tissue echogenicity are most likely metastatic neoplastic masses and should be biopsied under ultrasonographic guidance.[32, 55] Masses involving the chest wall and parietal pleura can be differentiated from superficial pulmonary masses invading the parietal pleura by careful examination of the margins of the mass and their movement with respiration. In most human beings with chest wall tumors, the margin be-

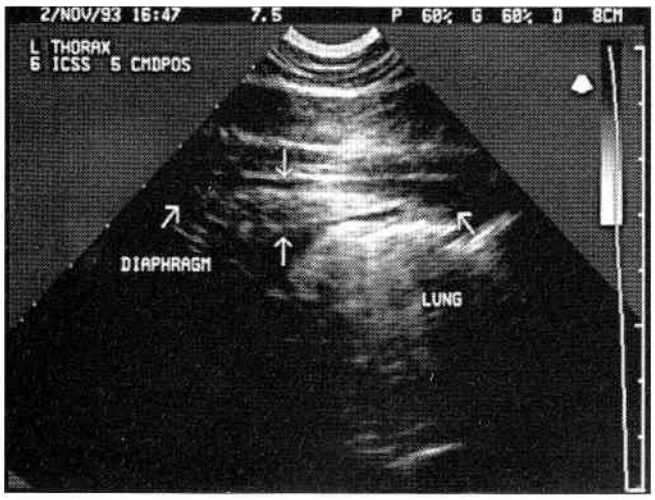

Figure 4–21

Sonogram of the left side of the thorax in the sixth intercostal space obtained from a 2-year-old Standardbred colt with pleural thickening 1 year after treatment for pleuropneumonia. Notice the fibrosis along the parietal pleural surface of the chest wall *(arrows)*, which extended dorsally 5 cm above a line level with the point of the shoulder. The irregularities in the visceral pleural surface of the lung and the radiating comet-tail artifacts are associated with the previous pleuropneumonia. The lung was imaged gliding past this area of pleural thickening in real time. This colt did return successfully to racing. This sonogram was performed with a 7.5-MHz sector-scanner transducer and an 8-cm displayed depth. The right side of the sonogram is dorsal and the left side is ventral.

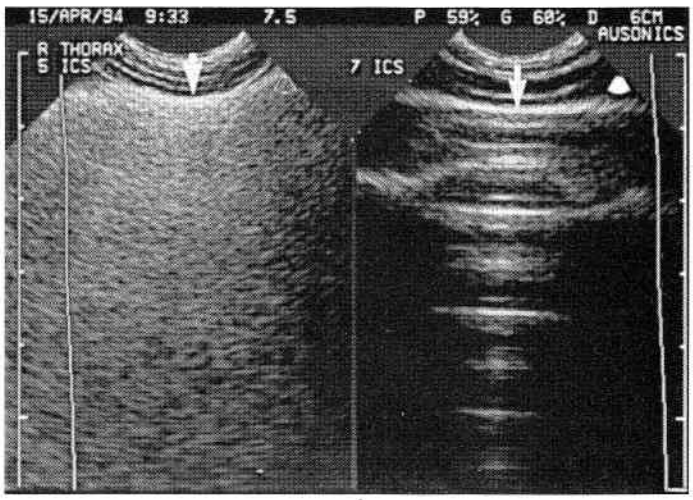

Figure 4–22

Sonogram of right side of the thorax in the fifth *(left image)* and seventh *(right image)* intercostal spaces obtained from a 2-day-old Thoroughbred colt with neonatal respiratory distress syndrome. Notice the normal air echo at the lung periphery *(arrow)* in the right image and the abnormal air echo *(arrow)* in the left image. This latter appearance is associated with small accumulations of fluid in the peripheral alveoli or interstitium or both. These sonograms were obtained along a line level with the point of the shoulder with a 7.5-MHz sector-scanner transducer and a displayed depth of 6 cm. The right sides of these sonograms are dorsal and the left sides are ventral.

tween tumor and lung is curved, smooth, and continuous, and the mass moves synchronously with the chest wall.[32] Lung tumors that involve the parietal pleura or chest wall usually have irregular margins, disrupt the visceral and parietal pleural surface, and do not move during respiration.[32]

Pulmonary Abnormalities

Compression Atelectasis

Compression atelectasis occurs whenever the lung parenchyma is collapsed by fluid (see Figs. 4-6 to 4-8), air (see Figs. 4-12, 4-19, and 4-20), or viscera (in horses with diaphragmatic hernia) occupying space normally containing lung.[1-6, 19] The compressed lung is collapsed, and smaller airways are no longer aerated, leaving this portion of lung hypoechoic (echogenicity of soft tissue).[3, 6, 9, 17, 45] The atelectatic lung is retracted toward the hilus (see Figs. 4-6 to 4-8, 4-12, and 4-19). Linear air echoes may be imaged in larger airways and appear crowded together as they converge toward the root of the lung.[31] The acoustic shadowing and reverberation artifacts from air within the large bronchi may be very prominent in individuals with compression atelectasis, probably as a result of crowding of the larger bronchi as they converge toward the root of the lung.[31] If the lung is easily compressed by the surrounding fluid, air, or viscera within the thorax, it is probably normal. Normal lung is also lighter than fluid and floats on top of and within pleural fluid.[2-6]

Consolidation

The replacement of alveolar air with fluid in lung adjacent to the thoracic wall creates an acoustic window detectable ultrasonographically.[2-6, 22, 33] The affected area of lung is hypoechoic and/or lacks the normal air echo at the surface (Fig. 4-22).[1-6, 17] The earliest sign of consolidation may be dimpling or an irregularity of the visceral pleural surface of the lung, a nonspecific change caused by nonuniform aeration of the lung periphery (Fig. 4-23).[1, 3, 4, 33] Comet-tail artifacts radiate from these nonaerated areas, created by small accumulations of exudate, blood, mucus, edema fluid, or tumor cells or by scarring secondary to a

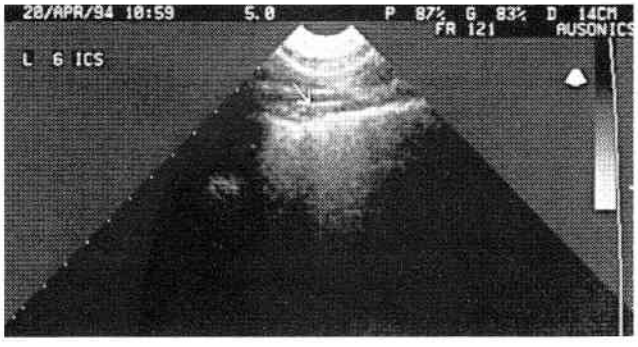

Figure 4–23

Sonogram of the left side of the thorax in the sixth intercostal space obtained from an 8-year-old Oldenberg mare with septic bronchitis. Notice the small area of dimpling of the visceral pleural surface *(arrow)* and the ray (comet-tail) artifacts originating from the ventral tip of the lung. This sonogram was performed with a 5.0-MHz sector-scanner transducer and a 14-cm displayed depth. The right side of the sonogram is dorsal and the left side is ventral.

previous bout of pneumonia or pleuritis. These changes can be detected in horses with pneumonia, pleuritis, pulmonary hemorrhage, pulmonary edema, COPD or bronchitis, granulomatous or neoplastic disease, or scarring from previous pleuropneumonia. In horses with pneumonia, hypoechoic areas representing pulmonary parenchymal consolidation appear, surrounded by normally aerated portions of lung. These small superficial hypoechoic areas are homogeneous, consistent with "superficial fluid alveolograms."[3, 4, 6, 22] These interruptions of the normal, highly reflective pleuropulmonary surface are detected in most individuals with pulmonary consolidation.[22] These areas of pulmonary parenchymal consolidation usually have an irregular margin with hyperechoic artifacts deep to the lesion which mimic acoustic enhancement.[22, 43] Small consolidated areas may be imaged only during exhalation because the lesion moves beneath the adjacent rib or inhaled air entering the surrounding airways and alveoli intervenes, reflecting the ultrasound beam and preventing their visualization (Fig. 4-24).[3, 4] Therefore, it is critical that each area of the lung be examined carefully during both inhalation and exhalation so that smaller areas of consolidation and areas that are not at the visceral pleural surface but are slightly deeper can be detected ultrasonographically. Because pneumonia is a dynamic process, air in the superficial alveoli can be detected ultrasonographically early in the course of the disease or during resolution of the pneumonia.[68]

The ultrasonographic diagnosis of pulmonary parenchymal consolidation is based upon the detection of hypoechoic pulmonary parenchyma and visualization of one or more of the lung's anatomic features: sonographic air bronchograms, sonographic fluid bronchograms, pulmonary vessels, or scattered echogenic foci due to residual air in consolidated lung parenchyma.[2-6, 22, 30, 31, 68] The detection of these anatomic structures in hypoechoic lung is crucial for the differentiation of severe pulmonary consolidation from pleural effusion, pulmonary parenchymal necrosis, or a pulmonary abscess.[2-6, 31, 68] Although earlier studies in human beings suggested that it was not always possible to differentiate pleural effusion from pulmonary consolidation, improved equipment, higher-frequency transducers with better resolution, and improved sonographer skill suggest that pleural effusion can be reliably differentiated from pulmonary consolidation.[2-7, 31, 68] Sonographic air bronchograms are imaged as distinctive hyperechoic linear air echoes in hypoechoic lung (Fig. 4-25). The interface between air within bronchi, bronchial walls, and the surrounding fluid-filled pulmonary parenchyma produces strong hyperechoic linear reflections.[31, 68] These hyperechoic linear echoes correspond to the traditional air bronchograms detected on thoracic radiographs.[27, 30, 31, 68] These hyperechoic linear echoes of sonographic air bronchograms are best imaged when the scan plane is parallel to the long axis of the bronchi. Scattered echoes of varying length are imaged when different scan planes are used and air bronchograms are being sliced obliquely.[31] These strongly echogenic branching lines of the air-filled bronchi converge toward the root of the lung, becoming larger as they merge.[3, 4, 22, 31, 68] Acoustic shadowing and reverberation artifacts are imaged in association with the larger proximal bronchi.[31] These artifacts are more prominent when a large object with a flat surface is imaged perpendicular to the ultrasound beam.[31] The presence of the hyperechoic linear echoes, associated artifacts, and their lack of pulsations differentiates them from anechoic pulmonary vessels.[31]

The normal respiratory movements of the lung against the pleura should be evaluated in all horses with suspected pleural or pulmonary disease. The gliding sign

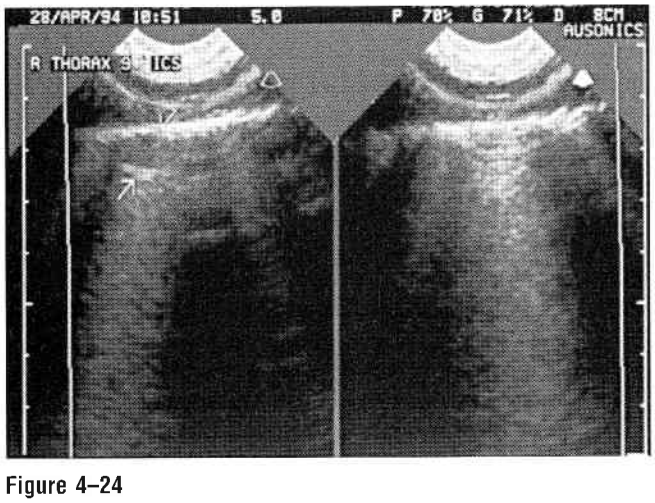

Figure 4–24

Sonograms of the right side of the thorax in the ninth intercostal space obtained from a 7-year-old Thoroughbred gelding with a previous history of pleuropneumonia. The small hypoechoic area of lung *(arrows)* is visible during exhalation *(left image)* but is poorly visualized during inhalation *(right image)*. The visceral pleural surface of the lung is irregular and radiates comet-tail artifacts. These sonograms were obtained 10 cm above a line level with the point of the shoulder, with a 5.0-MHz sector-scanner transducer and an 8-cm displayed depth. The right sides of these sonograms are dorsal and the left sides are ventral.

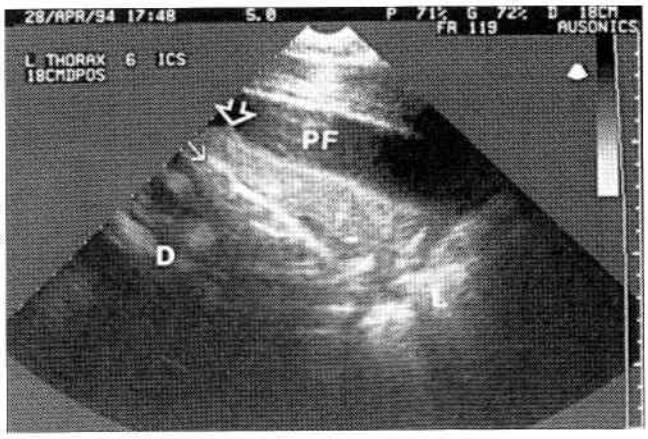

Figure 4–25

Sonogram of the left side of the thorax in the sixth intercostal space in a 4-year-old Thoroughbred stallion demonstrating an air bronchogram *(arrow)* in a ventral area of parenchymal consolidation. A small amount of fibrin *(open arrow)* is imaged on the visceral pleural surface of the lung. The consolidated lung and hypoechoic pleural effusion extended dorsally 18 cm above a line level with the point of the shoulder. The echogenic lung (L) with comet-tail artifacts on the right side of the image is more normally aerated lung. This sonogram was obtained with a 5.0-MHz sector-scanner transducer and an 18-cm displayed depth. The right side of the image is dorsal and the left side is ventral. D, Diaphragm; PF, pleural fluid.

is detectable sonographically in most individuals with pneumonia and consolidation. The absence of the gliding sign in horses usually indicates a concomitant dry pleuritis. Phrenic nerve paralysis has been proposed as the cause of the absence of the gliding sign in human beings with consolidation and inflammatory lung disease.[22] This is an unlikely cause of the lack of respiratory movement in horses.

Sonographic fluid bronchograms are nonpulsatile, anechoic tubular structures that also converge toward the root of the lung, becoming larger as they converge (Fig. 4-26).[1, 3, 22, 30, 68] In contrast to air bronchograms, fluid bronchograms are detectable only sonographically, not radiographically.[22] Although the diameter of sonographic fluid bronchograms normally decreases toward the superficial fluid alveologram, an increase in its diameter toward the periphery suggests pulmonary consolidation with fluid bronchiectasis (Fig. 4-27).[22] Sonographic fluid bronchograms can be differentiated from pulmonary vessels, which are pulsatile, tubular structures that also enlarge as they converge toward the root of the lung.[22, 30, 68] Pulsed-wave or color-flow Doppler imaging can be used to detect flow in these vessels if a pulse is not detected. However, distinguishing between a fluid bronchogram and pulmonary vessel is usually not necessary, as visualization of either or both structures is associated with pulmonary consolidation.[3-5, 22, 30, 68] Nonlinear scattered echogenic to hyperechoic foci visible in multiple scanning planes in areas of consolidation represent residual trapped air.[6, 22, 68]

The consolidation is usually located cranioventrally, with the right lung more frequently and more severely affected.[1, 3, 5] Often, if the ultrasound examination is performed very early in the course of the disease and the pneumonia is severe, it appears less extensive. This "tip-of-the-iceberg" impression occurs because air-filled alveoli, and small and larger airways are reflecting ultrasound, preventing its transmission to the deeper affected portions of lung (Fig. 4-28). Occasional glimpses deeper into abnormal pulmonary parenchyma are an indication of a

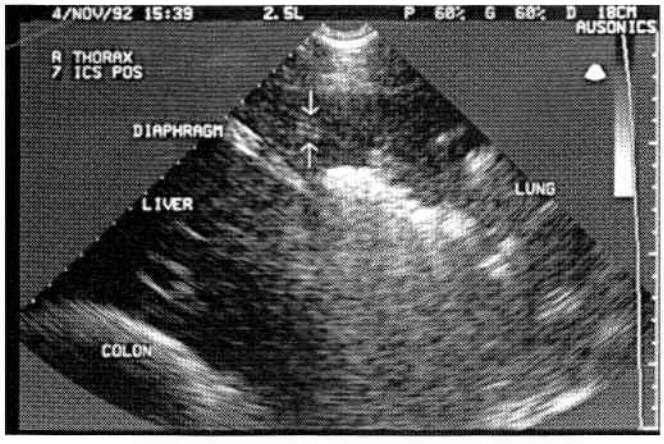

Figure 4–26

Sonogram of the right side of the thorax in the seventh intercostal space obtained from a 20-year-old Thoroughbred gelding with pneumonia. Notice the fluid bronchogram *(arrows)* adjacent to a pulmonary vessel in the ventral hepatized (liver-like) lung. The fluid bronchogram has the more echogenic walls and is the deeper of the two fluid-filled tubular structures. The echogenicity and texture of the hepatized lung are very similar to those of the underlying liver. The consolidation extended dorsally to a line level with the point of the shoulder. This sonogram was performed with a 2.5-MHz sector-scanner transducer and an 18-cm displayed depth. The right side of the sonogram is dorsal and the left side is ventral.

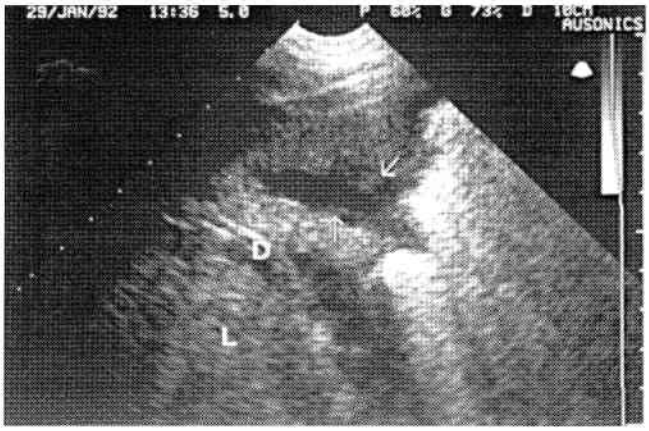

Figure 4–27

Sonogram of the right side of the thorax in the seventh intercostal space obtained from a 4-year-old Thoroughbred gelding with pleuropneumonia. The enlarging fluid bronchogram *(arrows)* is consistent with bronchiectasis in the hepatized right ventral lung, which was detected along a line level with the point of the shoulder. The more echogenic lung is the more normally aerated lung. A small anechoic pleural effusion surrounds this portion of lung. D, Diaphragm; L, liver. This sonogram was obtained with a 5.0-MHz sector-scanner transducer and a 10-cm displayed depth. The right side of this sonogram is dorsal and the left side is ventral.

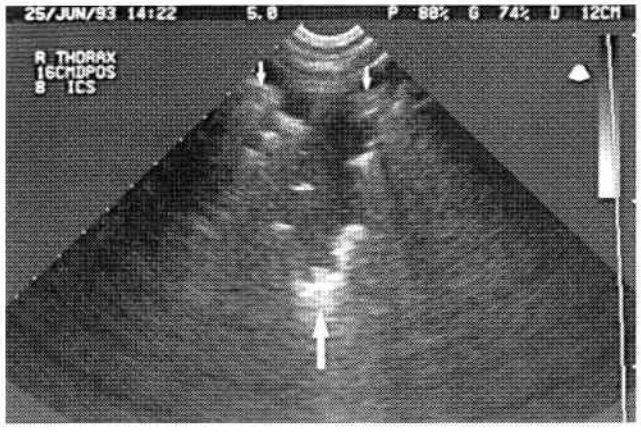

Figure 4–28

Sonogram of the right side of the thorax in the eighth intercostal space from a 2-year-old Standardbred colt with acute severe pneumonia. Notice the hypoechoic lung parenchyma at the visceral pleural surface *(small arrows)*, with a larger hypoechoic area extending deep into the lung parenchyma *(large arrow)* detected 16 cm dorsal to a line level with the point of the shoulder. This glimpse of deeper hypoechoic pulmonary parenchyma, imaging larger areas of consolidation, suggests that the consolidation is more severe than it appears sonographically. This occurs in acute severe pneumonia when air is still trapped out in the periphery and in larger airways before the entire area becomes hepatized. These sonograms often become worse, with larger hypoechoic areas of consolidation imaged, before they improve. This sonogram was performed with a 5.0-MHz sector-scanner transducer and a 12-cm displayed depth. The right side of the sonogram is dorsal and the left side is ventral.

severe pneumonia, likely to appear worse ultrasonographically before improving. This occurs because air is initially trapped in the peripheral alveoli and smaller airways before the entire affected area is filled with exudate. These small hypoechoic tip-of-the-iceberg areas tend to coalesce into larger areas of consolidation as the disease process continues.

A large area of consolidated lung is usually wedge shaped, poorly defined, and hypoechoic (Fig. 4–29).[1-6, 31] The echogenicity of consolidated lung is hypoechoic compared with normal aerated lung and is usually hypoechoic relative to the spleen and liver. Consolidated lung usually has an echogenicity between that of normal liver and pleural fluid transudate.[31] Large areas of consolidation often appear heterogeneous (anechoic, hypoechoic, and hyperechoic) sonographically (Fig. 4–30; see also Figs. 4–10, 4–14, and 4–25 to 4–29).[2-5, 22] The anechoic areas represent fluid-filled or necrotic areas; hypoechoic areas are the typical consolidated areas containing fluid bronchograms; and hyperechoic areas represent air bronchograms.[3, 6] Hepatization of lung parenchyma occurs with severe consolidation, resulting in an ultrasonographic appearance similar to that of liver (see Figs. 4–14 and 4–26).[1-4, 6, 9, 42] In severely hepatized lung, air echoes are lacking in all affected lung, including larger airways, and the branching pattern of pulmonary vessels and bronchi is seen.[2-4, 6, 22, 68] These echoes initially resemble those from the liver but are found above, rather than below, the diaphragm. The sonographic fluid bronchogram is recognizable as a fluid-filled nonpulsatile linear structure that enlarges toward the root of the lung, associated with branching of the bronchial tree (Fig. 4–30). Multiple small hyperechoic gas echoes in a severely consolidated or hepatized lung are suggestive of an anaerobic pneumonia (Fig. 4–31; see also Fig. 4–29). A rounded or bulging area of consolidation suggests severe consolidation, often progressing to pulmonary necrosis or abscess formation.[2-4, 6] A gelatinous-appearing lung occurs with parenchymal necrosis; the affected lung is usually hypoechoic and bulging, although collapse of this area may follow (Fig. 4–32). These bulging areas of parenchymal necrosis may split, an infrequent ultrasonographic finding that has

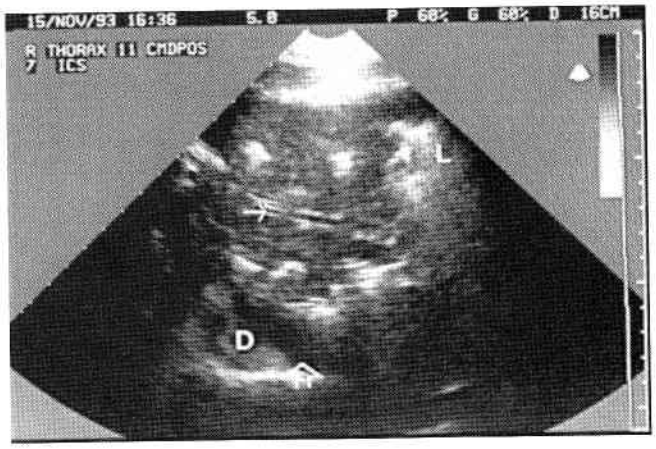

Figure 4–30

Sonogram of the right side of the thorax in the seventh intercostal space obtained from a 3-year-old Standardbred gelding with pleuropneumonia. Notice the liver-like appearance of the wedge-shaped area of lung, with fluid bronchograms *(small arrow)* that extended dorsally 11 cm above a line level with the point of the shoulder. The bright hyperechoic areas represent air trapped in larger bronchi. A small pleural effusion *(open arrow)* is not compressing the lung because the lung is severely consolidated. This sonogram was performed with a 5.0-MHz sector-scanner transducer and a displayed depth of 16 cm. The right side of the sonogram is dorsal and the left side is ventral. L, Aerated lung; D, diaphragm.

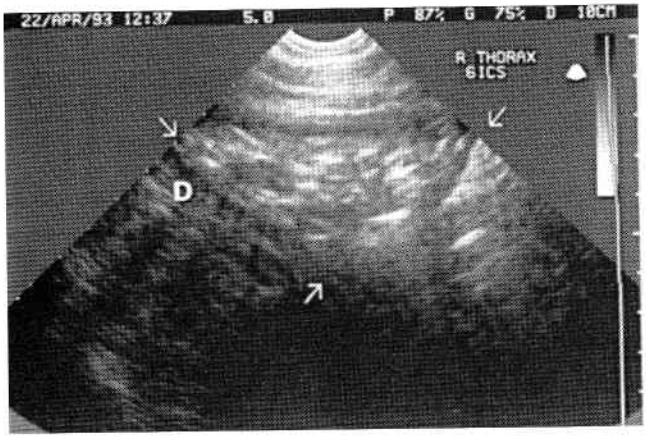

Figure 4–29

Sonogram of the right side of the thorax in the sixth intercostal space obtained from a 4-year-old Thoroughbred gelding with anaerobic pneumonia. Notice the wedge-shaped hypoechoic lung *(arrows)* with multiple hyperechoic gas echoes within the parenchyma and small airways that extended dorsally to a line level with the point of the shoulder. This scattered distribution of hyperechoic gas echoes in severely consolidated lung is often detected in horses with anaerobic pneumonia. The lung adheres to the parietal pleura and diaphragm (D). This sonogram was performed with a 5.0-MHz sector-scanner transducer and a 10-cm displayed depth. The right side of the sonogram is dorsal and the left side is ventral.

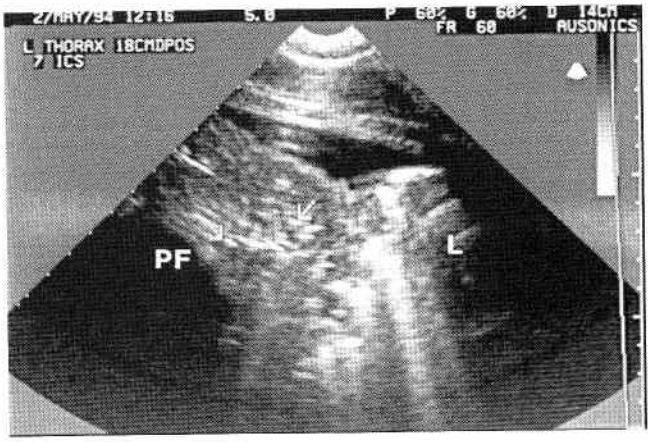

Figure 4–31

Sonogram of the left side of the thorax in the seventh intercostal space obtained from a 4-year-old Thoroughbred stallion with anaerobic pleuropneumonia. The multiple small hyperechoic "air" echoes *(arrows)* in the otherwise hepatized pulmonary parenchyma are consistent with anaerobic pneumonia. This abnormal pulmonary parenchyma and surrounding pleural fluid (PF) extended dorsally 18 cm above a line level with the point of the shoulder. This sonogram was obtained with a 5.0-MHz sector-scanner transducer and a 14-cm displayed depth. The right side of the sonogram is dorsal and the left side is ventral. L, Aerated lung.

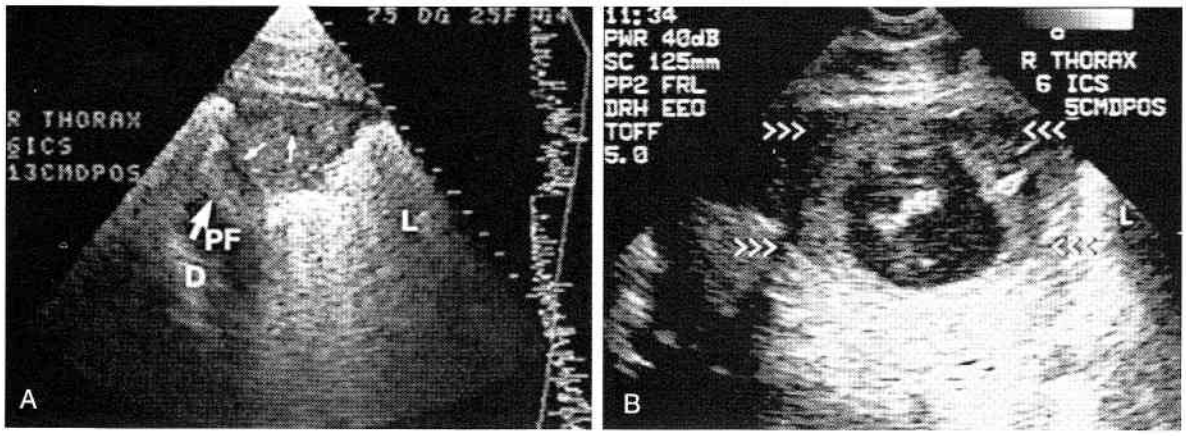

Figure 4–32

Sonograms of the right side of the thorax in the sixth intercostal space obtained from a 5-year-old Thoroughbred stallion with pleuropneumonia. These sonograms were both obtained with a 5.0-MHz sector-scanner transducer and a displayed depth of 17 cm *(A)* and 12.5 cm *(B)*. The right sides of the sonograms are dorsal and the left sides are ventral.

A, The bulging ventral lung tip *(large arrow)* is consistent with a necrotizing pneumonia and the cavitation of the pulmonary parenchyma *(small arrows)*. A small amount of gas is still present in the ventral tip of the lung. A small anechoic pleural effusion (PF) is also present. Abnormal pulmonary parenchyma was imaged dorsally to a line 13 cm above the level of the point of the shoulder. L, Aerated lung; D, diaphragm.

B, The cavitated area in the ventral tip of the lung is now an abscess *(arrowheads)*. This sonogram was obtained 11 days after the one in *A*. At this time abnormal pulmonary parenchyma was imaged dorsally to a line 5 cm above the point of the shoulder.

been detected only in horses with severe acute necrotizing pneumonia. These necrotic areas then either cavitate and form an abscess (Fig. 4-32) or rupture into the pleural space, creating a bronchopleural fistula (Fig. 4-33).[3] In severe acute necrotizing pneumonia, these changes can occur over a relatively short period of time (24 to 72 hours).

Bronchopleural Fistula/Abscess

A bronchopleural fistula is diagnosed ultrasonographically when the visceral pleural edge of the lung is no longer present, a cavitation is imaged involving the visceral edge of the lung and hyperechoic air echoes, and hypoechoic fluid echoes can be imaged in real time moving from the gelatinous area of pulmonary necrosis into the pleural space (Fig. 4-33).[2-5] This results in a pneumothorax, as a bronchus communicates with the pleural space. The pneumothorax may occur with or without a concomitant pleural effusion. A gas-fluid interface makes the bronchopleural fistula easier to diagnose. The gas and exudate from the lung can be imaged in real time mixing with the pleural fluid because the gas-fluid interface is usually dorsal to the necrotic area in the lung.

Horses with bronchopleural fistulas, if they survive, usually develop a large bronchopleural abscess surrounding the site of the bronchopleural fistula (Fig. 4-34).[2-4, 6] These abscesses can persist for years in some horses, causing chronic cough, mucopurulent nasal discharge, and weight loss. Bronchopleural abscesses can be drained percutaneously, an indwelling chest tube placed, and surgical drainage of the abscess performed under ultrasonographic guidance. Surgical drainage of the bronchopleural abscess via a rib resection can be performed relatively safely in the standing horse if the abscess is located in an area where a rib resection can be safely performed. A rib resection and surgical drainage of the abscess can also be performed under general anesthesia, if indicated. Indications for performing a rib resection under general anesthesia are the location of the abscess; lack of complete circumferential adhesions between the abscess, lung, and chest wall; and temperament of the horse. Surgical resection of the bronchopleural abscess with attempted surgical closure of the communicating bronchus has also been performed successfully in horses under general anesthesia.[3, 4, 6] A rib resection and surgical drainage or surgical resection of the bronchopleural abscess under general anesthesia should not be performed in lateral recumbency, but rather with the horse positioned as close to the standing position as possible. The use of the standing position prevents or minimizes the possibility of aspiration pneumonia developing in the unaffected (down) lung, a likely possibility in horses that have surgery performed in lateral recumbency, because of the bronchial communication with the abscess.

Pulmonary Abscess

Abscesses are identified ultrasonographically in the lung by their cavitated appearance and the absence of any normal pulmonary structures (vessels or bronchi) detected within (Fig. 4-35).[2-6, 17, 81, 82] An anechoic area lacking air or fluid bronchograms with acoustic enhancement of the wall or lung deep to the hypoechoic area is the initial sonographic appearance of an abscess.[2, 3, 5, 6, 22, 43] Pulmonary hematomas, although rare, may also appear as anechoic cavitary lesions with acoustic enhancement deep to the hematoma.[74] Internal echoes (loculations or echogenic clots) may be present within these lesions as the hematoma starts to organize. Abscesses may be encapsu-

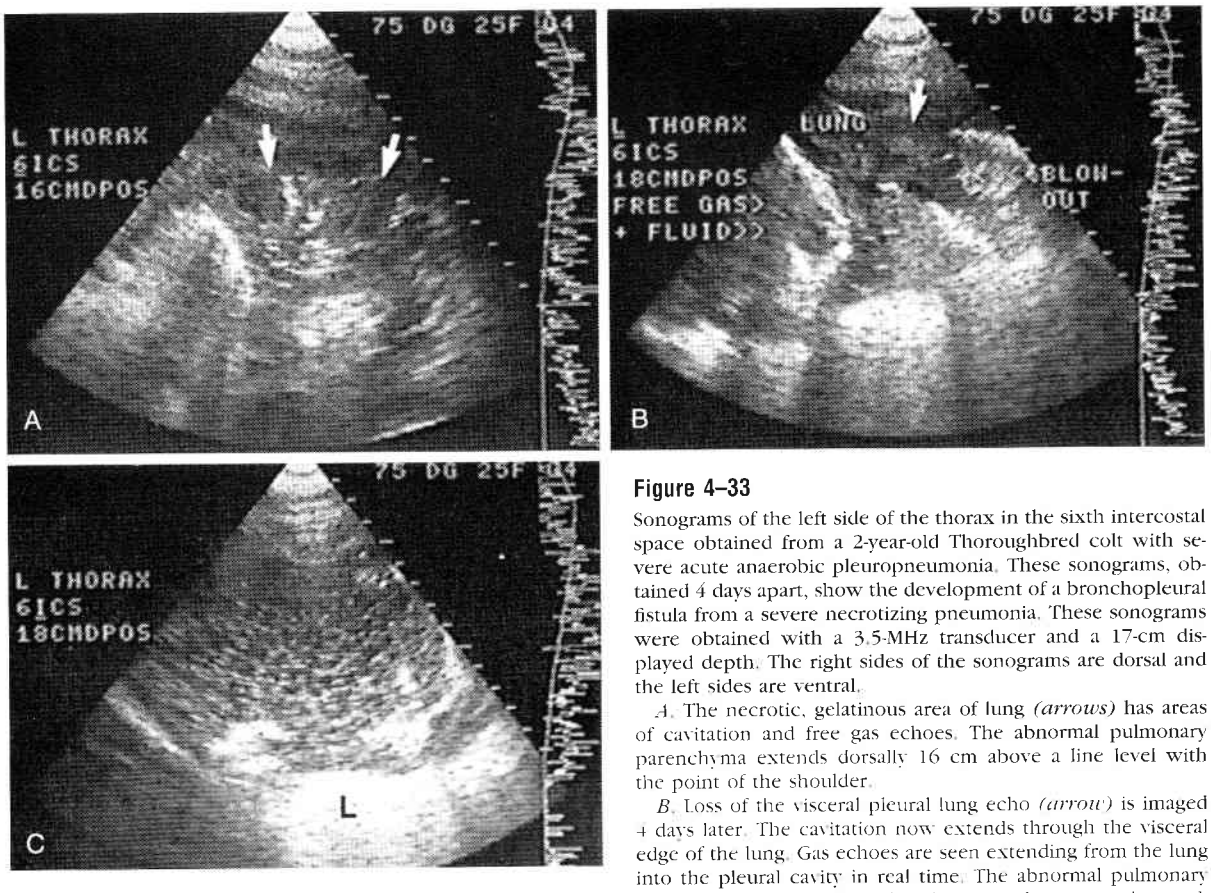

Figure 4–33

Sonograms of the left side of the thorax in the sixth intercostal space obtained from a 2-year-old Thoroughbred colt with severe acute anaerobic pleuropneumonia. These sonograms, obtained 4 days apart, show the development of a bronchopleural fistula from a severe necrotizing pneumonia. These sonograms were obtained with a 3.5-MHz transducer and a 17-cm displayed depth. The right sides of the sonograms are dorsal and the left sides are ventral.

A, The necrotic, gelatinous area of lung *(arrows)* has areas of cavitation and free gas echoes. The abnormal pulmonary parenchyma extends dorsally 16 cm above a line level with the point of the shoulder.

B, Loss of the visceral pleural lung echo *(arrow)* is imaged 4 days later. The cavitation now extends through the visceral edge of the lung. Gas echoes are seen extending from the lung into the pleural cavity in real time. The abnormal pulmonary parenchyma was visible dorsally 18 cm above a line level with the point of the shoulder, and a dorsal pneumothorax was detected.

C, Polymicrobullous (gaseous) fluid is detected 4 days later in the pleural fluid just dorsal to the site of the bronchopleural fistula. L, Aerated lung.

lated with an echogenic fibrous capsule (Fig. 4-36) but are more frequently imaged without any ultrasonographic evidence of encapsulation (Fig. 4-37).[3-6, 17, 81, 82] As the abscess forms, the parenchyma may begin to cavitate while retaining part of a bronchus within (Fig. 4-38). The circumference of the abscess may be imaged expanding slightly during inspiration in human beings, whereas lung adjacent to echogenic, complex pleural fluid moves in association with respiratory movement.[26, 83] The material contained within the abscess may vary from anechoic to hyperechoic, depending upon the type of exudate present. Loculations or compartmentalization of the abscess may be present.[1, 3-6, 17, 81] Most abscesses are more hypoechoic than the surrounding pulmonary parenchyma but may appear more echogenic if thick purulent or caseous exudate is present (see Fig. 4-36). Hyperechoic free gas echoes may be imaged mixed in with the exudate, again suggesting the presence of anaerobic organisms (see Fig. 4-36).[3, 4, 7] The free gas within an abscess usually appears more stationary than when imaged free within the pleural fluid.[7] The material within the abscess tends to be layered, with the heaviest, most echogenic debris in the most ventral portion of the abscess, followed by more hypoechoic fluid in the center and the hyperechoic gas echoes in the most dorsal portion of the abscess. The detection of a dorsal gas cap within the abscess is indicative of a bronchial communication and probable anaerobic infection (Fig. 4-39; see also Fig. 4-34).[3, 4, 6, 9, 26]

Most abscesses are visible ultrasonographically because they are located in the cranial and ventral lung and usually involve the pulmonary periphery.[2, 3, 5-7, 17, 30, 82] Abscesses, like parenchymal consolidation, are more common in the horse's right lung.[4] In some instances, abscesses may be detected ultrasonographically but not radiographically. This is most likely if they are located in portions of the lung overlying the heart base or abdomen (Fig. 4-40).[3, 5] Conversely, if an abscess is located in the more axial portion of lung and does not involve the periphery, it may not be detected ultrasonographically but may be imaged radiographically.[2, 3, 5, 6, 82] This latter situation occurs infrequently and is most likely in foals with *Rhodococcus equi* abscesses. These abscesses are usually multifocal in distribution and often involve the more axial portions of the lung and hilar lymph nodes.[82] However, in foals with multiple *Rhodococcus equi* abscesses, many do involve the pulmonary periphery and therefore are detectable ultrasonographically (Fig. 4-41). These foals should be treated until the abscesses are no longer imageable, either ultrasonographically or radiographically. Pleural abscesses are rare without pulmonary involvement, but their ultrasonographic appearance has been described as thick-walled structures surrounded by pleural fluid.[17]

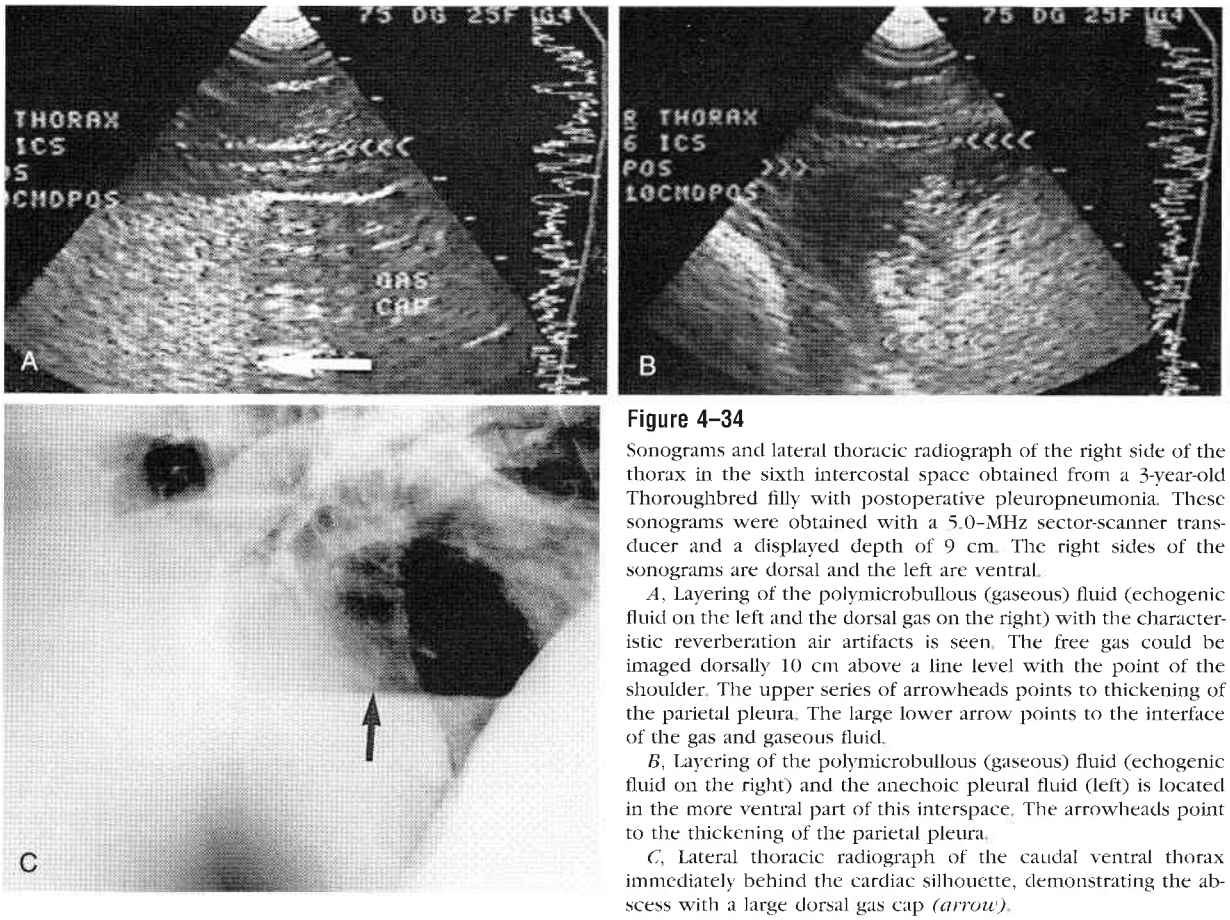

Figure 4–34

Sonograms and lateral thoracic radiograph of the right side of the thorax in the sixth intercostal space obtained from a 3-year-old Thoroughbred filly with postoperative pleuropneumonia. These sonograms were obtained with a 5.0-MHz sector-scanner transducer and a displayed depth of 9 cm. The right sides of the sonograms are dorsal and the left are ventral.

A, Layering of the polymicrobullous (gaseous) fluid (echogenic fluid on the left and the dorsal gas on the right) with the characteristic reverberation air artifacts is seen. The free gas could be imaged dorsally 10 cm above a line level with the point of the shoulder. The upper series of arrowheads points to thickening of the parietal pleura. The large lower arrow points to the interface of the gas and gaseous fluid.

B, Layering of the polymicrobullous (gaseous) fluid (echogenic fluid on the right) and the anechoic pleural fluid (left) is located in the more ventral part of this interspace. The arrowheads point to the thickening of the parietal pleura.

C, Lateral thoracic radiograph of the caudal ventral thorax immediately behind the cardiac silhouette, demonstrating the abscess with a large dorsal gas cap *(arrow)*.

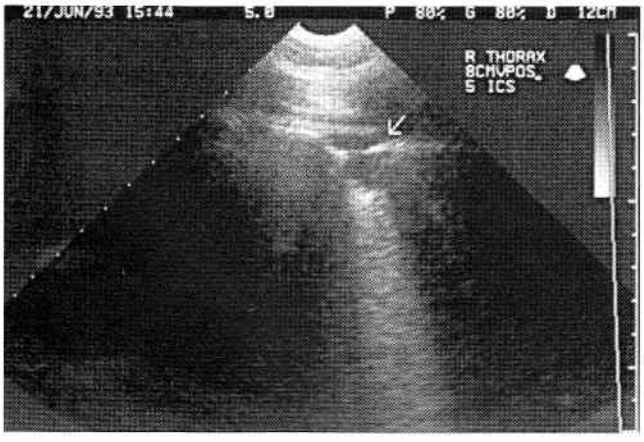

Figure 4–35

Sonogram of the right side of the thorax in the fifth intercostal space obtained from a 3-year-old Standardbred filly with a small pulmonary abscess and pneumonia. The small hypoechoic circular area in the ventral lung with acoustic enhancement of the far wall indicating a fluid-filled center is consistent with a small abscess *(arrow)*. This abscess was detected 5 cm ventral to a line level with the point of the shoulder. This sonogram was performed with a 5.0-MHz sector-scanner transducer and a 12-cm displayed depth. The right side of the sonogram is dorsal and the left side is ventral.

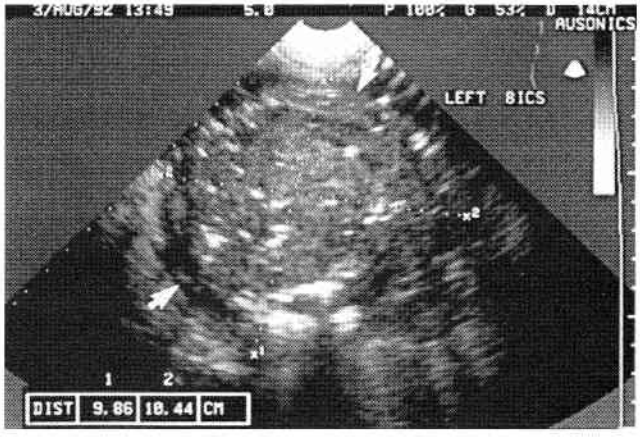

Figure 4–36

Sonogram of the left side of the thorax in the eighth intercostal space obtained from a 3.5-month-old Arabian filly with pneumonia and pulmonary abscesses. The thick echogenic capsule *(arrows)* surrounding the pulmonary abscess and the multiple hyperechoic free gas echoes within it are consistent with anaerobic infection. The abscess is surrounded by hypoechoic consolidated lung and was detected 10 cm dorsal to a line level with the point of the shoulder. The cursors measure the dimensions of the abscess. This sonogram was performed with a 5.0-MHz sector-scanner transducer and a 14-cm displayed depth. The right side of the sonogram is dorsal and the left side is ventral.

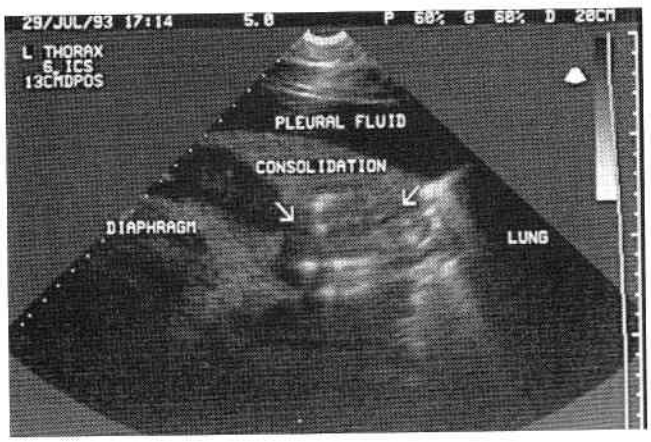

Figure 4–37

Sonogram of the left side of the thorax in the sixth intercostal space obtained from a 2-year-old Thoroughbred filly with pleuropneumonia and pulmonary abscesses. The cavitated area of the abscess *(arrows)* contains varying echogenicities within the hypoechoic consolidated lung. This ventral lung is compressed slightly by the surrounding anechoic pleural fluid, indicating less severe consolidation. The pleural fluid extends dorsally 13 cm above a line level with the point of the shoulder. The more dorsal lung has a normal visceral pleural air echo. This sonogram was performed with a 5.0-MHz sector-scanner transducer and a 20-cm displayed depth. The right side of the sonogram is dorsal and the left side is ventral.

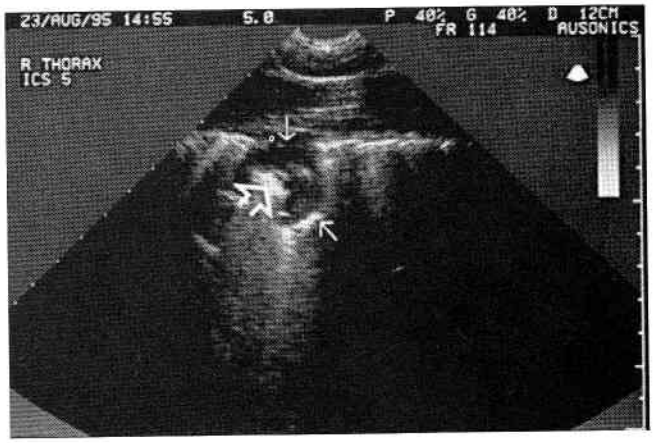

Figure 4–38

Sonogram of the right side of the thorax in the fifth intercostal space obtained from a 4-year-old Thoroughbred colt with pleuropneumonia. The small area of cavitation *(arrows)* in the pulmonary parenchyma was detected along a line level with the point of the shoulder. A large linear air echo is detected within the cavitation *(open arrow)* from a remaining intact bronchus. Four days earlier this lung had been severely hepatized in this area. This sonogram was performed with a 5.0-MHz sector-scanner transducer and a 12-cm displayed depth. The right side of this sonogram is dorsal and the left side is ventral.

Pulmonary Neoplasia/Granulomatous Disease/Pulmonary Fibrosis

The detection of small multifocal hypoechoic to echogenic masses distributed randomly throughout the lung is consistent with granulomatous disease (Fig. 4–42) or metastatic neoplasia (Fig. 4–43) and, rarely, with primary pulmonary neoplasia or pulmonary fibrosis (Fig. 4–44).[2, 3, 6, 9, 84-86] These soft-tissue masses are usually small and diffusely scattered throughout the lung field.[85-88] The margins of neoplastic or granulomatous masses are usually smooth, but irregular masses may be detected in some individuals.[34] In human beings, masses with irregular margins and heterogeneous echogenicity are most frequently inflammatory granulomatous lesions.[34] Interruption of the visceral pleural echo is common, and acoustic enhancement may be detected deep to these masses.[33, 34, 43, 86] In horses with suspected diffuse granulomatous disease or metastatic neoplasia, the entire lung field should be scanned carefully during both inspiration and expiration.

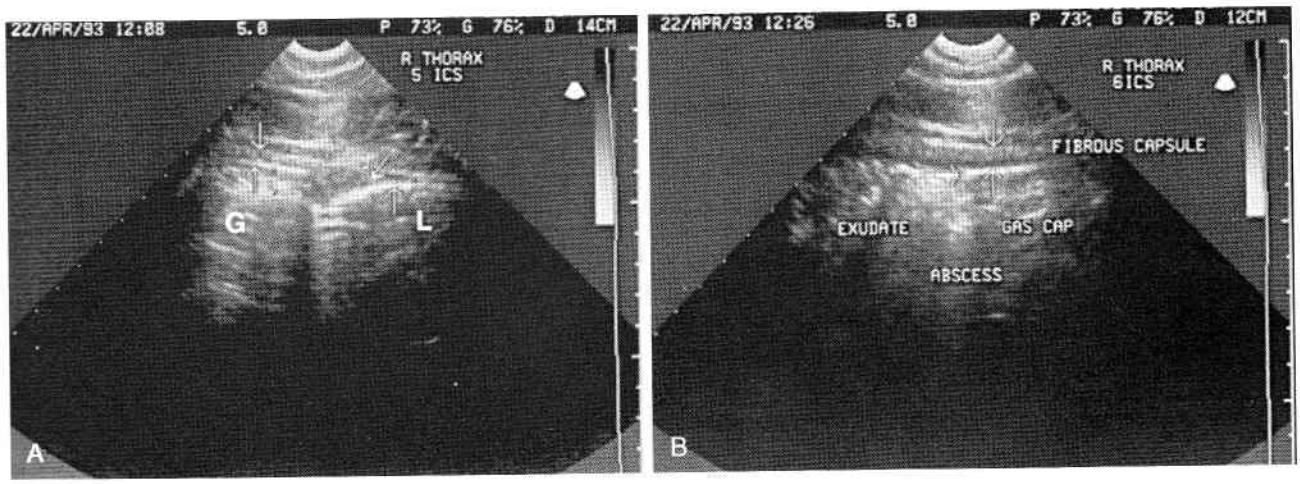

Figure 4–39

Sonogram of the right side of the thorax in the fifth *(A)* and sixth *(B)* intercostal spaces from a 4-year-old Thoroughbred gelding with a large pulmonary abscess and pneumonia in the lung overlying the heart. These sonograms were performed with a 5.0-MHz sector-scanner transducer and 14-cm *(A)* and 12-cm *(B)* displayed depths. The right sides of these sonograms are dorsal and the left sides are ventral.

A. This sonogram illustrates the border between the normal lung (L) dorsally and the dorsal portion of the abscess containing a dorsal gas cap (G). The two arrows on the right point to the visceral pleural edge of the lung *(tilted arrow)* and the normal air echo from the lung *(vertical arrow)*. The two arrows on the left point to the abscess capsule, beneath which are gas echoes from the dorsal gas cap within this abscess.

B. This sonogram was obtained slightly more ventrally and caudally, illustrating the border *(horizontal arrow)* between the exudate within the abscess and the dorsal gas cap. The fibrous capsule is delineated by the two vertical arrows. This abscess could easily be missed owing to the large dorsal gas cap, which could be mistaken for more normal lung.

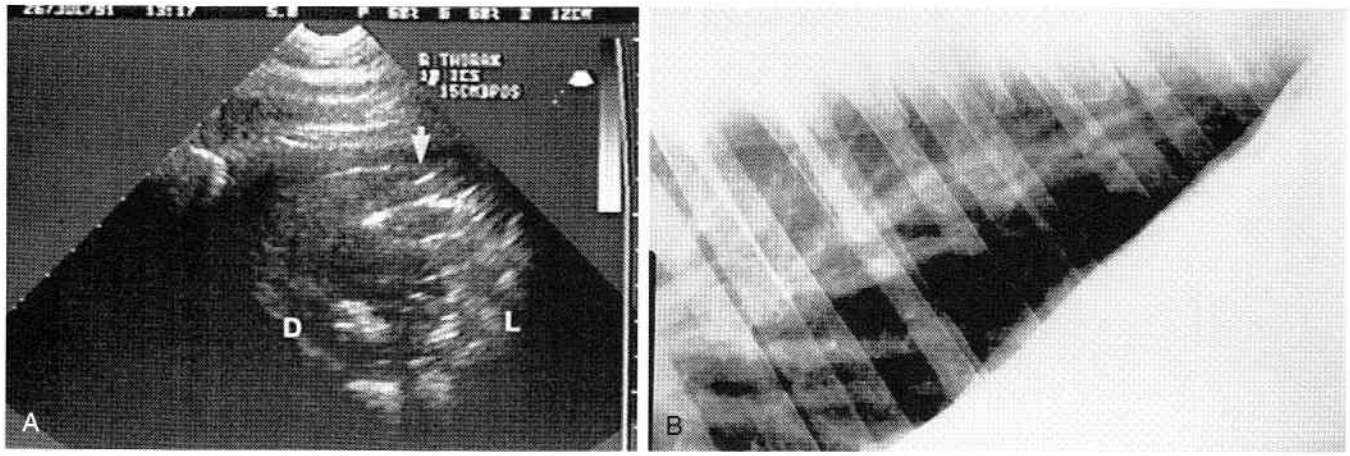

Figure 4–40

Sonogram *(A)* and lateral thoracic radiograph *(B)* obtained from a 3-year-old Thoroughbred filly with a pulmonary abscess.

A, Sonogram of the right side of the thorax in the eleventh intercostal space demonstrating a large pulmonary abscess with a dorsal gas cap and ventral hypoechoic fluid. The arrow points to the border between the dorsal gas cap and the ventral fluid. The dorsalmost extent of this abscess was detected 16 cm above a line level with the point of the shoulder and extended ventrally to the diaphragm (D). This sonogram was obtained with a 5.0-MHz sector-scanner and a displayed depth of 12 cm. L, Aerated lung.

B, Lateral thoracic radiograph obtained on the same day as *A*. The abscess, located in the midthorax, is not detected radiographically.

Many small masses close to the visceral pleural surface of the lung are imaged most successfully during one phase of respiration, usually exhalation.[33, 36] With inhalation small masses may move beneath an adjacent rib or be obscured by air entering superficial alveoli. Although thoracic radiographs may provide a more complete evaluation of the entire lung field in affected horses, precise localization of affected areas of lung is not possible radiographically. Accurate localization of peripheral masses as small as 0.5 cm in diameter can be achieved ultrasonographically, and ultrasound-guided aspirates or biopsies of lung masses are performed for cytologic and histopathologic characterization with high sensitivity and specificity.[3, 6, 9, 27, 31, 36, 79, 81, 84, 86, 89] The size of the nodule is unrelated to the likelihood of obtaining a successful aspirate or biopsy and to the complication rate from the procedure.[36]

The majority of neoplastic pulmonary masses are homogeneous and hypoechoic compared with the surrounding normal lung, but may be isoechoic or have heterogeneous echogenicity.[6, 9, 36, 79, 84] Neoplastic masses can usually be differentiated from parenchymal consolida-

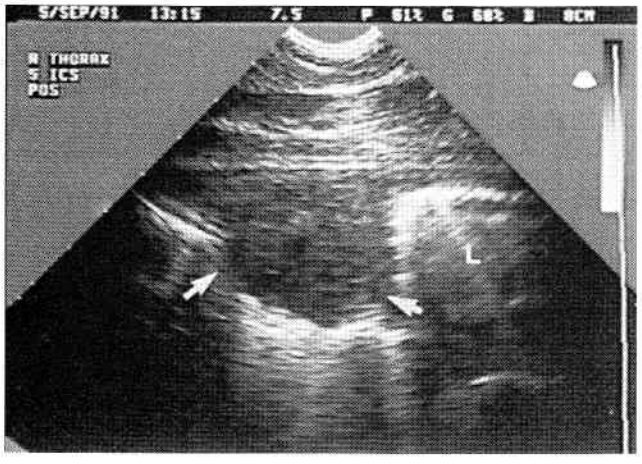

Figure 4–41

Sonogram of the right side of the thorax in the fifth intercostal space obtained from a 6-month-old Thoroughbred colt with *Rhodococcus equi* pneumonia and pulmonary abscesses. Notice the circular hypoechoic abscess *(arrows)* in the periphery of the lung (L) lacking pulmonary vessels and bronchi. This sonogram was obtained along a line level with the point of the shoulder with a 7.5-MHz sector-scanner transducer and an 8-cm displayed depth. The right side of the sonogram is dorsal and the left is ventral.

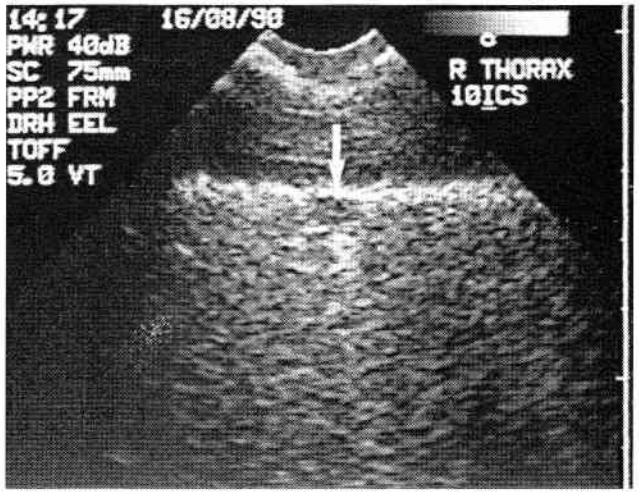

Figure 4–42

Sonogram of the right side of the thorax in the tenth intercostal space obtained from a 16-year-old Thoroughbred gelding with diffuse granulomatous disease. The hypoechoic area of lung in the pulmonary periphery *(arrow)* lacks normal pulmonary architecture. Similar masses were scattered throughout both lung fields. An ultrasound-guided lung biopsy revealed granulomatous disease. This sonogram was obtained with a 5.0-MHz sector-scanner transducer and a 7.5-cm displayed depth. The right side of this sonogram is dorsal and the left side is ventral.

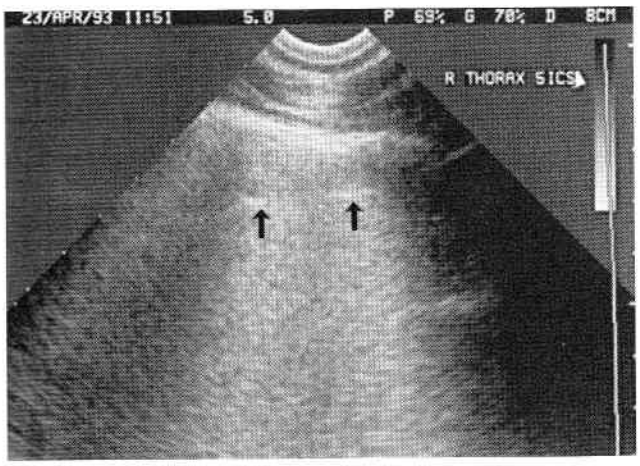

Figure 4–43

Sonogram of right side of the thorax in the fifth intercostal space obtained from a 15-year-old Thoroughbred gelding with gastric squamous cell carcinoma. These barely visible hypoechoic areas near the pulmonary periphery *(arrows)* represent metastatic pulmonary infiltrates and are typical of the subtle changes seen with diffuse granulomatous or metastatic neoplasia in the lung. Similar findings were scattered throughout both sides of the thorax. This sonogram was performed with a 5.0 MHz sector-scanner transducer and an 8-cm displayed depth. The right side of the sonogram is dorsal and the left side is ventral.

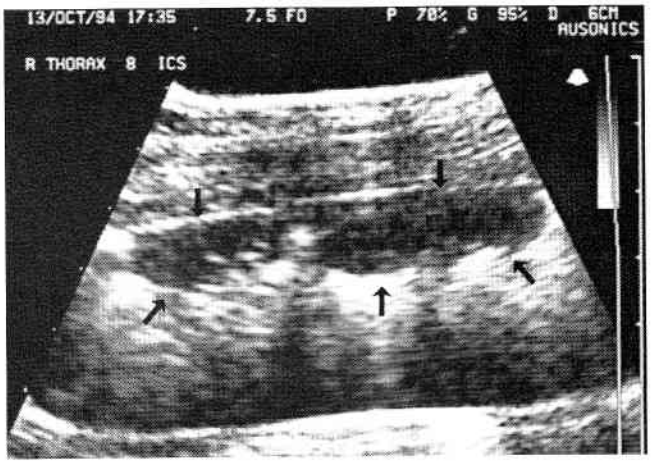

Figure 4–44

Sonogram of the right side of the thorax in the eighth intercostal space obtained from a 19-year-old Thoroughbred gelding with chronic interstitial pneumonia and pulmonary fibrosis. The irregular hypoechoic soft-tissue-density masses *(arrows)* involve the periphery of the lung. These areas were scattered throughout the pulmonary parenchyma. The diagnosis was confirmed with multiple ultrasound-guided lung biopsies. This sonogram was obtained with a 7.5-MHz sector-scanner transducer and a 6-cm displayed depth. The right side of the sonogram is dorsal and the left side is ventral.

tion by the absence of bronchial and normal vascular structures within the masses.[6, 9, 30, 86] Cystic necrotic areas or areas of dystrophic calcification casting acoustic shadows may be imaged within neoplastic masses.[9, 90, 91] Larger neoplastic (Figs. 4–45 and 4–46) or granulomatous pulmonary masses are uncommon but are occasionally imaged ultrasonographically.[2, 3, 90] A large cystic lesion was imaged ultrasonographically in one horse with bronchogenic squamous cell carcinoma, although histopathologic evaluation of lung specimens from three sites in this horse revealed only an interstitial pneumonia. However, it was unclear whether ultrasound-guided biopsies of the lung lesion were obtained in this horse.[90] A large pulmonary plasma cell granuloma (inflammatory pseudotumor), granular cell myoblastoma, and bronchial adenocarcinoma have been reported in horses, which probably could have been imaged ultrasonographically and an ultrasound-guided aspirate and biopsy obtained.[92–94] A myoblastoma has been imaged ultrasonographically in a 9-year-old Thoroughbred mare (Fig. 4–46). The mass was hypoechoic, relatively homogeneous, and very vascular, with cavitated areas filled with hypoechoic fluid. The

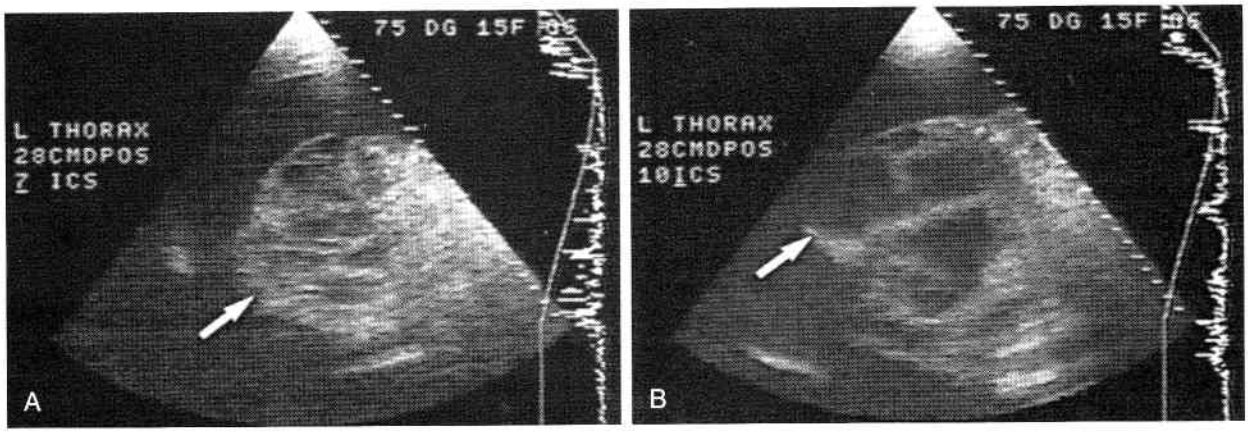

Figure 4–45

Sonograms of the left side of the thorax obtained from a 7-year-old Standardbred gelding with hemangiosarcoma in the lung. This mass extended over five intercostal spaces (ICS). The pleural fluid line extended dorsally 28 cm above a line level with the point of the shoulder. These sonograms were obtained with a 5.0-MHz sector-scanner transducer and a 25-cm displayed depth. The right sides of the sonograms are dorsal and the left sides are ventral.

A, Sonogram of the left side of the thorax in the seventh ICS showing a large loculated mass *(arrow)* in the ventral portion of the lung containing some soft-tissue areas and many fluid spaces.

B, Sonogram of the left side of the thorax in the tenth ICS demonstrating the large cavitary, loculated-fluid nature of the mass *(arrow)* in the more caudal ICS.

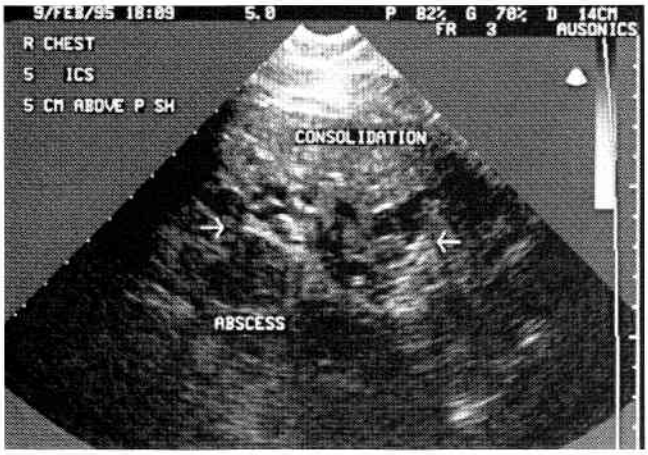

Figure 4–46

Sonogram of the right side of the thorax in the fifth intercostal space obtained from a 9-year-old Thoroughbred mare with a granular cell myoblastoma. The irregular complex vascular pattern of the hypoechoic mass *(arrows)* with the nearly anechoic cavitated abscess deep to the vascular mass is located 5 cm dorsal to a line level with the point of the shoulder. This sonogram was obtained with a 5.0 MHz sector-scanner transducer and a 14-cm displayed depth. The right side of this sonogram is dorsal and the left side is ventral.

affected area appeared similar to consolidated lung but had disruption of normal pulmonary architecture and excessive vascularity. Diffuse granulomatous disease and metastatic neoplasia are uncommon in horses, but both occur more frequently than primary pulmonary neoplasia.[57, 84-88, 90, 94-96] Pulmonary fibrosis associated with chronic interstitial pneumonia is rare in horses but has been detected sonographically. Pulmonary fibrosis appears as irregular hypoechoic coalescing soft-tissue masses lacking the normal pulmonary architecture (see Fig. 4-44). The masses are both pleurally based and located deeper within the pulmonary parenchyma. Ultrasound-guided lung biopsy is indicated in these cases to definitively diagnose the cause of these masses. Pleural masses may also be imaged with primary or metastatic neoplasia and are best visualized with a concurrent pleural effusion.[9]

Secondary hypertrophic osteopathy (HO) has been reported in horses with granulomatous and neoplastic (primary and metastatic) pulmonary disease as well as in horses with chronic pneumonia or pulmonary abscesses, pulmonary infarction, pleural adhesions, and lung laceration.[18, 81, 90, 92, 93, 97-103] Thoracic abscesses and granulomas are most common in horses with HO.[81, 97, 102, 103] Secondary HO is usually associated with a space-occupying chronic lesion in the thoracic cavity of affected horses.[81, 90, 92, 93, 97, 102, 103] Therefore, the thorax should be carefully evaluated ultrasonographically in horses presenting with signs of HO, and ultrasound-guided lung biopsies or aspirates should be obtained when indicated to accurately diagnose the underlying pulmonary pathology.[81] In many of the horses diagnosed with HO prior to the advent of ultrasonography, ultrasonographic examination of the thorax would have imaged the lesion or lesions and enabled ultrasound-guided biopsies or aspirates to be obtained.[92, 97, 102, 103]

Cranial Mediastinal Abnormalities

Pleural Effusion/Cranial Mediastinal Abscess

Pleural fluid accumulation is the most common abnormality detected ultrasonographically in the cranial mediastinum (Fig. 4-47). As previously described, the membrane dividing the right and left sides of the cranial mediastinum is easily imaged in horses with pleural effusion (see Fig. 4-18). The character and amount of fluid on each side of the mediastinum can be assessed and are often quite different, suggesting the presence of a complete mediastinum in these individuals. If a large amount of fluid is present in the cranial mediastinum, the heart is pushed caudally one or two ICS. In these horses, the cranial mediastinum is also easily imageable from the left side of the thorax using the same ICS and scan plane that would be used on the right side of the thorax. With chronic complex effusions, the fluid in the cranial mediastinum may wall off and become encapsulated as an abscess (Fig. 4-48), occasionally causing signs of cranial vena caval obstruction.[40] This may easily be misinterpreted as congestive heart failure if a thorough physical examination is not performed. The ultrasonographic examination of the thorax, heart, and cranial mediastinum is important in differentiating these diagnoses. Cranial mediastinal masses are either loculated and fluid filled or are thick-walled masses filled with echogenic inspissated material that displaces the lung dorsally.[1, 6, 40] Drainage of the cranial mediastinal loculated mass or abscess has been attempted in the standing horse but was unsatisfactory.[40] Catheter drainage of cranial mediastinal abscesses under general anesthesia using ultrasonographic guidance has been successfully performed.[40] Mediastinal masses or accumulations of pleural fluid may compress the heart and compromise its function, but more commonly they dis-

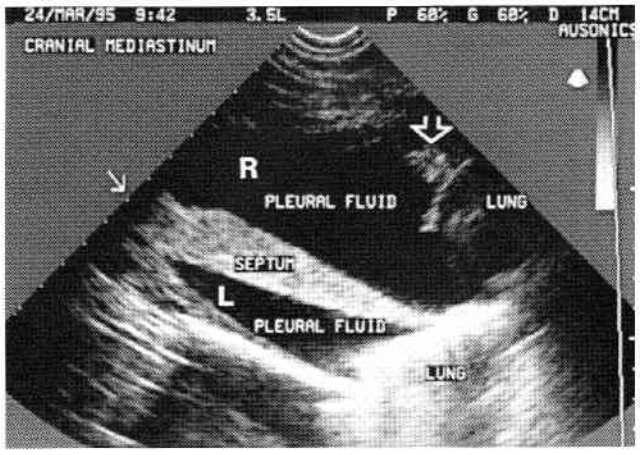

Figure 4–47

Sonogram of the right side of the thorax obtained in the third ICS from a 3-year-old Standardbred colt with pleuropneumonia. Notice the anechoic pleural fluid on both sides of the mediastinal septum *(arrow)*, the hypoechoic cranial ventral tip of the right apical lung with a fibrin tag on its visceral pleural surface *(open arrow)*, and the nearly normally aerated left ventral lung tip. This sonogram was obtained with a 3.5-MHz sector-scanner transducer and a 14-cm displayed depth. The right side of the sonogram is dorsal and the left side is ventral. L, Left side; R, right side.

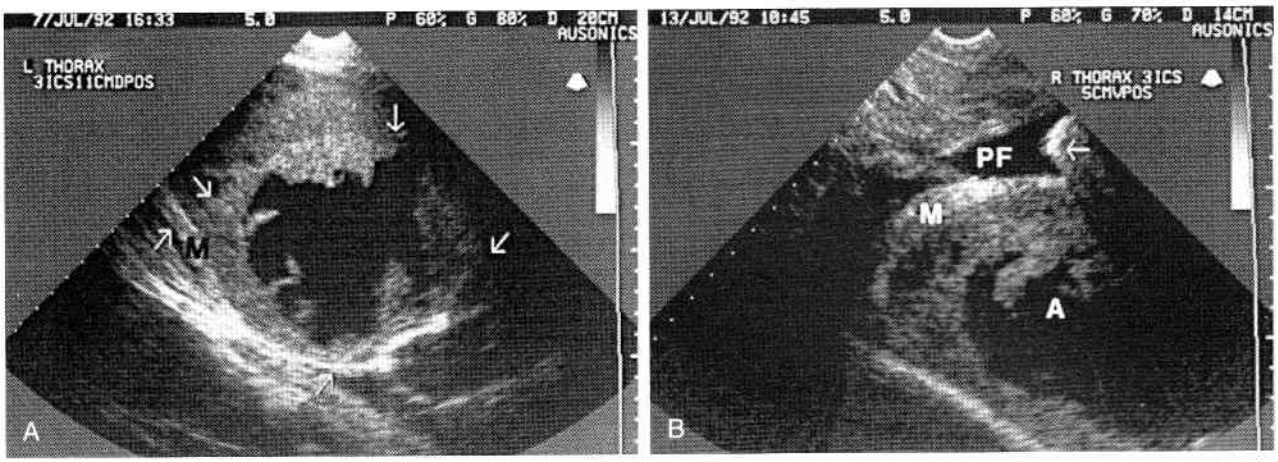

Figure 4–48

Sonograms of an abscess forming in the left side of the cranial mediastinum in a 4-year-old Thoroughbred filly with chronic pleuropneumonia. These sonograms were performed with a 5.0-MHz sector-scanner transducer and 20-cm *(A)* and 14-cm *(B)* displayed depths. The right sides of these sonograms are dorsal and the left sides are ventral.

A, Sonogram obtained from the left side of the thorax in the third intercostal space (ICS). The organizing fibrin surrounding the pleural fluid *(arrows)* is forming an abscess. M, Mediastinal septum.

B, Sonogram performed from the right side of the thorax in the third ICS, demonstrating a small amount of pleural fluid (PF) in the right side of the cranial mediastinum with a slightly rounded but aerated ventral lung tip *(arrow)* and the abscess (A) forming in the left side of the cranial mediastinum. M, Mediastinal septum.

place the heart within the thorax.[6, 8, 19, 40] In these horses the cranial cardiac vascular structures may be imaged.[40]

Cranial Mediastinal Neoplasia

Soft-tissue masses may be imaged in the cranial mediastinum and are most common in horses with thoracic lymphosarcoma, although they may be detected in horses with mesothelioma or hemangiosarcoma.[2, 3, 8, 55, 73, 88, 104] Lymphosarcoma masses in the cranial mediastinum are usually associated with large pleural effusions, making these large soft-tissue masses easier to image.[2, 3, 8, 9, 19, 49, 55, 104–106] These masses usually occupy the entire cranial mediastinum, obliterating the normal thick membranous division imaged in horses with pleural effusion (Fig. 4–49). The mass usually displaces the right apical lung lobe dorsally and the heart caudally, and therefore can be imaged from either side of the thorax in the third ICS. In most horses, only one large mass can be imaged, which may have a homogeneous or heterogeneous ultrasonographic appearance.[2, 3, 8] This mass may be imaged extending dorsally and cranially toward the thoracic inlet and up the neck with cervical lymph node involvement.

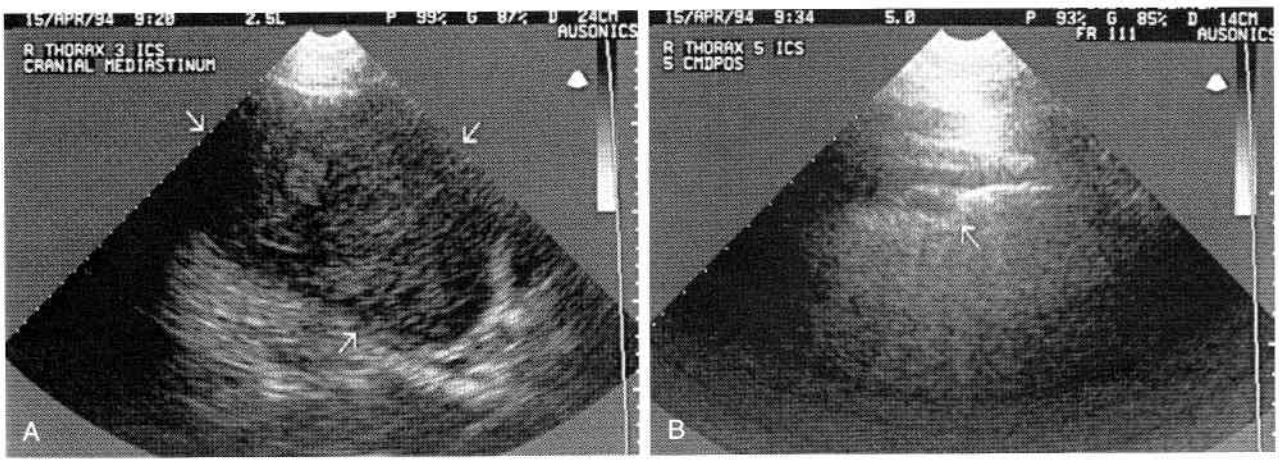

Figure 4–49

Sonograms of the right side of the thorax in the third *(A)* and fifth *(B)* intercostal spaces obtained from a 6-year-old crossbred mare with cranial mediastinal lymphosarcoma. The right sides of these sonograms are dorsal and the left sides are ventral.

A, Notice the relatively homogeneous appearance of the soft-tissue mass *(arrows)* occupying the entire cranial mediastinum. This sonogram was obtained with a 2.5-MHz sector-scanner transducer and a 24-cm displayed depth.

B, The small oval hypoechoic area in the periphery of the right lung *(arrow)* was detected 5 cm dorsal to a line level with the point of the shoulder. The hypoechoic area is homogeneous and is soft tissue and not fluid filled, as no acoustic enhancement of the far wall is seen. This is an area of metastatic lymphosarcoma. This sonogram was obtained with a 5.0-MHz sector-scanner transducer and a 14-cm displayed depth.

In these horses, the cranial mediastinal mass can also be imaged from the thoracic inlet. Occasionally, free (mobile) soft-tissue (tumor) masses are imaged in the pleural fluid moving with respiration and cardiac movement (Fig. 4-50). The pleural fluid in horses with thoracic lymphosarcoma is usually relatively hypoechoic with a low total protein content (<2.5 gm/dl), low total cell count (<32,000 cells/μl), and very large volume, often 20 to 50 liters.[8, 18, 49] Complex fluid with fibrin layers, loculation, or free gas is not usually imaged in horses with thoracic lymphosarcoma.[8] Occasionally a large cranial mediastinal lymphosarcoma mass is imaged in horses without pleural effusion.[8] These masses are more difficult to detect because the lung and heart are not displaced as much, making less of the mass visible ultrasonographically. These masses must also be differentiated from fat around the heart present in normal horses. Careful characterization of the tissue in the cranial mediastinum and its relationship to surrounding structures can help the ultrasonographer distinguish the normal fat surrounding the heart from a cranial mediastinal mass. Normal pericardial and intrathoracic fat should not displace the heart significantly and should be found behind the heart in the caudal mediastinum as well as in the cranial mediastinum. Secondary hyperparathyroidism with mineralization of the heart and great vessels has been reported in several horses with lymphosarcoma and hypercalcemia.[104] Lymphosarcomatous infiltration of the heart has also been reported in horses with cranial mediastinal lymphosarcoma.[88] Therefore, an echocardiogram should be performed on any horse with hypercalcemia and a suspected diagnosis of lymphosarcoma, in addition to thoracic or abdominal ultrasonography.

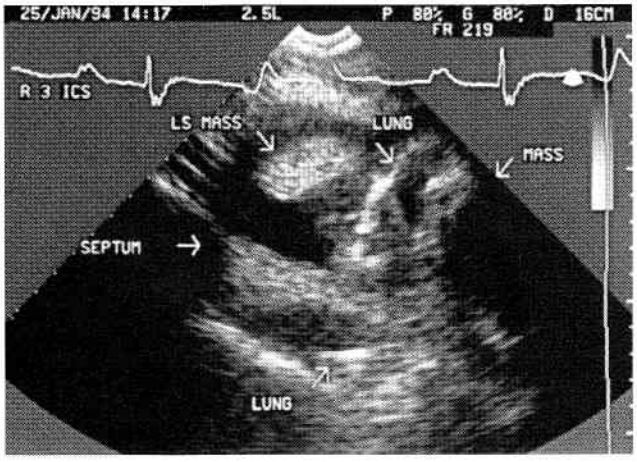

Figure 4–50

Sonogram of a free lymphosarcoma mass in the cranial mediastinum of a 17-year-old Appaloosa gelding with generalized lymphosarcoma. An arrow points to the lymphosarcoma mass and a larger cranial mediastinal mass just visualized through a hypoechoic area of lung. The mediastinal septum is visualized as a hypoechoic longitudinal structure dividing the left side of the thorax, which contains a small amount of pleural fluid and aerated lung, from the right side of the thorax, containing the free tumor mass and the larger cranial mediastinal mass. This sonogram was obtained from the right side of the thorax in the third intercostal space with a 2.5-MHz sector-scanner transducer and a 16-cm displayed depth. The right side of the thorax is dorsal and the left side is ventral.

Caudal Mediastinal Abnormalities

Pleural effusion is the most common ultrasonographic abnormality in the caudal mediastinum. The thick membranous division between the right and left sides of the thorax is more difficult to image because it is located much farther from the thoracic wall than in the cranial mediastinum, owing to the increased width of the thoracic cavity caudal to the heart. Therefore, a lower-frequency transducer and larger depth of field must be selected to image this area ultrasonographically. Both sides of the caudal thorax cannot be imaged ultrasonographically from one thoracic window in adult horses owing to depth limitations but can be imaged successfully in smaller foals. Abscesses involving the caudal mediastinum, diaphragm, thoracic wall, and lung are more common than cranial mediastinal abscesses and often have a communicating bronchus.[5] Caudal mediastinal abscesses that do not extend out to or involve the thoracic wall are unusual but do occur and may not involve pulmonary parenchyma.[5] Soft-tissue masses in the caudal mediastinum are rare but could be detected ultrasonographically if present in the ventral portion of the caudal mediastinum. A cholangiocellular carcinoma was reported invading the dorsal portion of the caudal mediastinum in a horse, and only pleural fluid was detected ultrasonographically.[58]

Diaphragmatic Hernias

Diaphragmatic hernias are likely to result in viscera occupying a portion of the caudal mediastinum or caudal thorax. A diaphragmatic hernia can be diagnosed ultrasonographically when viscera are imaged in the thoracic cavity immediately adjacent to the lung or floating within pleural fluid without the diaphragm separating the thoracic and abdominal viscera (Fig. 4-51).[5, 6, 9-11, 25] When pleural effusion is present, more of the diaphragm and adjacent abdominal viscera can be imaged.[11, 19] The size of the rent in the diaphragm can be crudely estimated by determining the number of interspaces in which the diaphragm is missing between the thoracic and abdominal viscera and the length of that defect in a dorsal-to-ventral direction. Care must be taken to examine the entire thorax extending past the normal ventral borders so that hernia size is not overestimated. This is possible when a small or central rent in the diaphragm is present but the herniated abdominal viscera have spread out along the thoracic wall and are immediately adjacent to the lung. In these instances, lung may be found in the dorsal portion of the thorax adjacent to herniated abdominal viscera, with the diaphragm imaged ventral to the herniated abdominal viscera and other abdominal viscera imaged ventral to the diaphragm. Although a series of overlapping thoracic radiographs is the optimal method of diagnosing a diaphragmatic hernia, hernia size is often difficult to assess radiographically, and the type of herniated viscera cannot always be correctly determined. Also, the hernia may be missed radiographically if located in the ventral portion of the diaphragm in horses with large pleural effusions.[9, 11] The torn diaphragmatic crus may

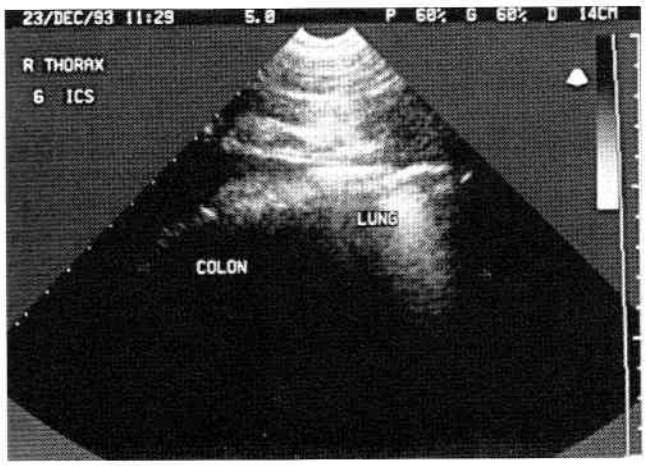

Figure 4–51

Sonogram of the right side of the thorax in the sixth intercostal space obtained from an 18-year-old Thoroughbred mare with a diaphragmatic hernia. The lung immediately overlies the colon without intervening diaphragm separating the thorax and abdomen. This sonogram was performed with a 5.0-MHz sector-scanner transducer and a 14-cm displayed depth. The right side of the sonogram is dorsal and the left side is ventral.

be imaged ultrasonographically in some individuals with diaphragmatic rupture.[9] Ultrasonographic visualization of the herniated viscera should enable correct identification of the viscera within the thorax, although all the herniated viscera may not be imaged and identified.[11] The viability of the herniated viscera can be determined ultrasonographically by assessing its wall thickness, distention, and motility, information that cannot be obtained radiographically (see Chapters 6 and 7 on Abdominal Ultrasonography).[11] In some instances, the ability to determine viability of the imageable herniated bowel may improve the horse's prognosis for a successful surgical outcome and prompt the owner to select surgical intervention. A diaphragmatic hernia or diaphragmatic diverticulum should not be ruled out if a normal thoracic sonogram is obtained, however, because the defect may involve the central portion of the diaphragm and herniated viscera may not be adjacent to the thoracic wall.[3, 107] Thoracic radiographs should always be performed if a diaphragmatic hernia is suspected and cannot be visualized ultrasonoraphically.[3, 6] However, in most instances the horse must be transported to a referral facility to obtain adequate thoracic radiographs to make the diagnosis, whereas the ultrasonographic examination can be performed in the field. A diaphragmatic diverticulum has been imaged ultrasonographically in one horse. A complete echocardiographic examination should also be performed if a diaphragmatic hernia is suspected, as a peritoneal-pericardial hernia has been reported in a horse.[108]

PATIENT MANAGEMENT AND PROGNOSIS

The thoracic ultrasound examination can be used to help form a more accurate prognosis for survival and select appropriate treatment at the horse's initial presentation, as well as to monitor response to therapy.[1-4] Thoracic ultrasonography can also be used as a screening test in the preoperative situation, looking for areas of consolidation, abscesses, and pleuritis which were not suspected on the basis of a thorough physical examination and hematology. If pulmonary or pleural abnormalities are found in the preoperative situation, appropriate antimicrobial therapy can be instituted and elective surgeries postponed until the ultrasonographic abnormality has resolved, reducing the incidence of postoperative pleuropneumonia. Survival of horses with pleuropneumonia is more likely if pleural fluid, fibrin, loculations, free gas echoes, and parenchymal necrosis are not detected on the initial ultrasonographic examination.[2-4] Survival rates of horses with anaerobic pleuropneumonia vary from 32 to 41%, with few horses successfully returning to their prior performance level.[3, 4, 7, 50] If free gas echoes are detected in pleural fluid, a guarded to grave prognosis should be given, and broad-spectrum antimicrobial therapy, including coverage effective against anaerobic microorganisms (metronidazole), should be initiated immediately, before results of culture and sensitivity testing are available. The detection of parenchymal necrosis also warrants a grave to guarded prognosis initially, as only 30% of horses with parenchymal necrosis survived in one study. Also, 50% of horses with parenchymal necrosis had free gas echoes detected in their pleural fluid (anaerobic pleuropneumonia), and 30% had pulmonary abscesses.[4] Horses with parenchymal necrosis should also be treated aggressively with broad-spectrum antimicrobials covering an anaerobic spectrum. The cost-effectiveness of treatment must be considered because horses with anaerobic pleuropneumonia or parenchymal necrosis are likely to require a longer period of antimicrobial treatment and are unlikely to return to their prior performance level if they survive. The ultrasonographic detection of fibrinous pleuropneumonia, with or without loculations, also warrants a guarded prognosis initially and the initiation of broad-spectrum antimicrobial therapy after obtaining a transtracheal fluid and pleural fluid aspirates for culture and sensitivity testing.[1-4] The survival of horses with fibrinous pleuropneumonia and loculated fibrinous pleuropneumonia is 52% and 40%, respectively, with a better chance of affected horses returning to their prior performance level. The number of treatment days was longer for horses with pleuropneumonia when pleural fluid, fibrin, loculations, free gas echoes, pulmonary parenchymal necrosis, or abscesses were detected ultrasonographically at initial examination.[3, 4] Human beings with loculated effusions have larger effusions, longer hospitalizations, and more frequent tube thoracostomies than those with nonloculated effusions. They are also more likely toundergo sclerosis and decortication procedures or to die from sepsis than those patients with nonloculated effusions.[75, 76]

Initial treatment duration can be estimated from the initial ultrasonographic findings and their severity. A horse with anechoic pleural effusion and compression atelectasis, a small (<5 cm) abscess, or a small (<5 cm) area of parenchymal consolidation may need only 2 to 4 weeks of appropriate antimicrobial therapy before antimicrobials can be discontinued, if subsequent clinical and ultrasonographic findings indicate a response to therapy.

Slightly larger areas of consolidation (5 to 10 cm) may resolve with 1 to 2 months of appropriate antimicrobial therapy. Severe consolidation usually results in treatment durations of 2 to 6 months or longer, depending upon the severity of the pneumonia. Abscesses usually also require treatment durations of 2 to 6 months or longer, depending upon their size, number, and degree of encapsulation. Treatment duration for horses with complex septated pleuropneumonia, anaerobic pleuropneumonia, and necrotizing pneumonia is also long, usually 2 to 6 months or longer.[4] These initial guidelines can be used to formulate a therapeutic plan for treatment duration, which will be subsequently modified by the clinical and ultrasonographic response of the horse to therapy. The initial antimicrobial therapy is empirical, based upon the common pathogens in the area and the pathogens most likely to be responsible for the ultrasonographic findings. Antimicrobial therapy should ultimately be based upon culture and sensitivity testing of transtracheal or pleural fluid aspirates, whichever is indicated.

Follow-up ultrasonographic examinations should be based upon the severity of the underlying pulmonary and pleural disease and the horse's clinical signs. If significant quantities of pleural effusion are detected, an ultrasonographically guided thoracocentesis should be performed to obtain a sample for cytologic examination, culture, and sensitivity testing. Repeat ultrasonographic examinations should be performed every several days (or daily, if indicated) if thoracic auscultation and percussion indicate fluid accumulation. Once pleural fluid ceases to accumulate (or in horses without pleuritis), the frequency of repeat ultrasonographic examinations can be based upon the severity of the parenchymal disease and its response to therapy (every 3 to 10 days initially unless pneumonia is very severe). Ideally, antimicrobials should be continued until the consolidation or abscess has resolved ultrasonographically and is replaced by aerated lung. When this is not practical, the decision to discontinue therapy is based upon the response of the horse to therapy. The horse should be re-examined ultrasonographically 1 to 2 weeks after discontinuing antimicrobials to ensure continued improvement in the ultrasonographic appearance of the lung and pleural cavity. The horse should be periodically re-examined (every 4 to 8 weeks) until the lung and pleural cavity return to normal before returning the horse to training. Occasionally, small adhesions or areas of pulmonary nonaeration and scarring persist in horses who have recovered from pleuropneumonia, but this is the exception rather than the rule. If horses are put back into training before the lung or pleural cavity has returned to normal, periodic ultrasonographic re-examinations are indicated to be certain that the pulmonary or pleural disease is not worsening with the stress of training. The return of horses with pleuropneumonia to their prior performance level is also related to the absence of free gas echoes and parenchymal necrosis on the initial ultrasonographic examination.[4] Horses with pleural effusion, fibrin, compression atelectasis, consolidation, and abscesses are likely to return to their prior performance level.

Ultrasonographic examination of the equine thorax is useful for the diagnosis of a plethora of noncardiac thoracic diseases, fine-tuning the prognosis based upon the ultrasonographic findings, performing ultrasound-guided aspirations or biopsies, and monitoring the response of the horse to therapy.[1-4, 6] The initial ultrasonographic examination can be based upon the findings from a thorough auscultatory examination performed in a quiet area with a rebreathing bag. As most of the auscultatory abnormalities involve the superficial pulmonary parenchyma and pleura (approximately 10 cm), any abnormal sounds detected suggest disease of the pleura or superficial lung. Ultrasonographic examination of these areas usually reveals abnormal findings. However, if the examination is being used as a screening test, as in the preoperative or prepurchase situation or when scanning the thorax for diffuse granulomatous disease or neoplasia, the entire accessible lung field should be thoroughly evaluated.

References

1. Rantanen NW: Diseases of the thorax. Vet Clin North Am [Equine Pract] 2:49-66, 1986.
2. Reef VB: The use of diagnostic ultrasound in the horse. Ultrasound Q 9:1-34, 1991.
3. Reef VB: Ultrasonographic evaluation. *In* Beech J (ed): Equine Respiratory Disorders. Philadelphia, Lea & Febiger, 1991, pp 61-88.
4. Reef VB: Outcome and return to performance in horses with pleuropneumonia evaluated ultrasonographically. Proceedings of the 8th Annual American College of Veterinary Internal Medicine Forum, 1990, pp 573-575.
5. Reef VB, Boy M, Reid C, et al: Evaluation of horses and cattle with thoracic disease: Comparison between diagnostic ultrasonography and radiography: 56 cases (1984-1985). J Am Vet Med Assoc 198:2112-2118, 1991.
6. Reimer JM: Diagnostic ultrasonography of the equine thorax. Compend Contin Educ Pract Vet 12:1321-1327, 1990.
7. Reimer JM, Reef VB, Spencer PA: Ultrasonography as a diagnostic aid in horses with anaerobic bacterial pleuropneumonia and/or pulmonary abscessation: 27 cases (1984-1986). J Am Vet Med Assoc 194:278-282, 1989.
8. Garber JL, Reef VB, Reimer JM: Ultrasonographic findings in horses with mediastinal lymphosarcoma: 13 cases (1984-1992). J Am Vet Med Assoc 205:1432-1436, 1994.
9. Stowater JL, Lamb CR: Ultrasonography of noncardiac thoracic diseases in small animals. J Am Vet Med Assoc 195:514-520, 1989.
10. Byars TD, Halley J: Uses of ultrasound in equine internal medicine. Vet Clin North Am [Equine Pract] 2:253-258, 1986.
11. Hartzband LE, Kerr DV, Morris EA: Ultrasonographic diagnosis of diaphragmatic rupture in a horse. Vet Radiol 31:42-44, 1990.
12. Farrow CS: Equine thoracic radiology. J Am Vet Med Assoc 179:776-781, 1981.
13. Farrow CS: Radiological aspects of inflammatory lung disease in the horse. Vet Radiol 22:107-114, 1981.
14. Farrow CS: Radiography of the equine thorax: Anatomy and technic. Vet Radiol 22:62-68, 1981.
15. Kangstrom L-E: The radiological diagnosis of equine pneumonia. J Am Vet Radiol Soc 9:80-88, 1968.
16. King GK: Equine thoracic radiography. Part II. Radiographic patterns of equine pulmonary and pleural diseases using air-gap rare-earth radiography. Compend Contin Educ Pract Vet 3:S283-S287, 1981.
17. Mackey VS: Equine pleuropneumonia: Radiology-diagnostic ultrasound-pleuroscopy. Proceedings of the 29th Annual American Association of Equine Practitioners, 1983, pp 75-80.
18. Mair TS, Lane JG: Pneumonia, lung abscesses and pleuritis in adult horses: A review of 51 cases. Equine Vet J 21:175-180, 1989.
19. Rantanen NW, Gage L, Paradis MR: Ultrasonography as a diagnostic aid in pleural effusion of horses. Vet Radiol 22:211-216, 1981.
20. Sanderson GN, O'Callaghan MW: Radiographic anatomy of the

equine thorax as a basis for radiological interpretation. N Z Vet J 31:127–130, 1983.
21. Silverman SG, Mueller PR, Saini S, et al: Thoracic empyema: Management with image-guided catheter drainage. Radiology 169:5–9, 1988.
22. Targhetta R, Chavagneux R, Bourgeois J-M, et al: Sonographic approach to diagnosing pulmonary consolidation. J Ultrasound Med 11:667–672, 1992.
23. King GK, Martens RJ, McCall VH: Equine thoracic radiography. Part I. Air-gap rare-earth radiography of the normal equine thorax. Compend Contin Educ Pract Vet 3:S278–S281, 1981.
24. Feeney DA, Gordon BJ, Johnston GR, et al: A 200 centimeter focal-spot-film distance (FFD) technique for equine thoracic radiography. Vet Radiol 23:13–19, 1982.
25. Glazier CM, Leithiser RE, Williamson SL, et al: Extracardiac chest ultrasonography in infants and children: Radiographic and clinical implications. J Pediatr 114:540–544, 1989.
26. Hirsh JH, Rogers JV, Mack LA: Real-time sonography of pleural opacities. Am J Roentgenol 136:297–301, 1981.
27. Ikezoe J, Morimoto S, Arisawa J, et al: Percutaneous biopsy of thoracic lesions: Value of sonography for needle guidance. Am J Roentgenol 154:1181–1185, 1990.
28. Targhetta R, Bourgeois JM, Chavagneux R, et al: Ultrasonographic approach to diagnosing hydropneumothorax. Chest 101:931–934, 1992.
29. Rantanen NW, Ewing RL: Principles of ultrasound application in animals. Vet Radiol 22:196–203, 1981.
30. Dorne HL: Differentiation of pulmonary parenchymal consolidation from pleural disease using the sonographic fluid bronchogram. Radiology 158:41–42, 1986.
31. Weinberg B, Diakoumatis EE, Kass EG, et al: The air bronchogram: Sonographic demonstration. Am J Roentgenol 147:593–595, 1986.
32. Saito T, Kobayashi H, Kitamura S: Ultrasonographic approach to diagnosing chest wall tumors. Chest 94:1271–1275, 1988.
33. Sugama Y, Tamaki S, Kitamura S, et al: Ultrasonographic evaluation of pleural and chest wall invasion of lung cancer. Chest 93:275–279, 1988.
34. Yang PC, Luh KT, Sheu JC, et al: Peripheral pulmonary lesions: Ultrasonography and ultrasonically guided aspiration biopsy. Radiology 155:451–456, 1985.
35. Yang P-C, Sheu J-C, Luh K-T, et al: Clinical application of real-time ultrasonography in pleural and subpleural lesions. J Formosan Med Assoc 83:646–657, 1984.
36. Yuan A, Yang P-C, Chang D-B, et al: Ultrasound-guided aspiration biopsy of small peripheral pulmonary nodules. Chest 101:926–930, 1992.
37. Rantanen NW: Ultrasound appearance of normal lung borders and adjacent viscera in the horse. Vet Radiol 22:217–219, 1981.
38. Allen KA, Stone LR: Equine diagnostic ultrasonography: Equipment selection and use. Compend Contin Educ Pract Vet 12:1307–1311, 1990.
39. Reef VB: Advances in diagnostic ultrasonography. Vet Clinics North Am [Equine Pract] 7:451–466, 1991.
40. Byars TD, Dainis CM, Seltzer KL, et al: Cranial thoracic masses in the horse: A sequel to pleuropneumonia. Equine Vet J 23:22–24, 1991.
41. Park RD, Nyland TG, Lattimer JC, et al: B-mode gray-scale ultrasound: Imaging artifacts and interpretation principles. Vet Radiol 22:204–210, 1981.
42. Hirsh JH, Carter SJ, Chikos PM, et al: Ultrasonic evaluation of radiographic opacities of the chest. Am J Roentgenol 130:1153–1156, 1978.
43. Kremkau FW, Taylor KJW: Artifacts in ultrasound imaging. J Ultrasound Med 5:227–237, 1986.
44. Mair TS, Sweeney CR: The investigations of pleural effusions in the horse. Equine Vet Educ 4:70–74, 1992.
45. Hoffman AM, Baird JD, Kloeze HJ, et al: *Mycoplasma felis* pleuritis in two show-jumper horses. Cornell Vet 82:155–162, 1992.
46. Mair TS, Hillyer MH, Brown PJ: Mesothelioma of the pleural cavity in a horse: Diagnostic features. Equine Vet Educ 4:59–61, 1992.
47. Raphel CF, Beech J: Pleuritis secondary to pneumonia or lung abscessation in 90 horses. J Am Vet Med Assoc 181:808–810, 1982.
48. Schott HC, Mansmann RA: Thoracic drainage in horses. Compend Contin Educ Pract Vet 12:251–261, 1990.
49. Smith BP: Pleuritis and pleural effusion in the horse: A study of 37 cases. J Am Vet Med Assoc 170:208–211, 1977.
50. Sweeney CR, Divers TJ, Bensen CE: Anaerobic bacteria in 21 horses with pleuropneumonia. J Am Vet Med Assoc 187:721–724, 1985.
51. Sweeney CR: Causes of pleural effusion in the horse. Equine Vet Educ 4:75–77, 1992.
52. Thatcher CD, Roussel AJ, Chickering WR, et al: Pleural effusion with thoracic lymphosarcoma in a mare. Compend Cont Educ Pract Vet 7:S726–S730, 1985.
53. Foreman JH, Weidner JP, Hargis A: Pleural effusion secondary to thoracic metastatic mammary adenocarcinoma in a mare. J Am Vet Med Assoc 197:1193–1195, 1990.
54. Kramer JW, Nickels FA, Bell T: Cytology of diffuse mesothelioma in the thorax of a horse. Equine Vet J 8:81–83, 1976.
55. Morris DD, Acland HM, Hodge TG: Pleural effusion secondary to metastasis of an ovarian adenocarcinoma in a horse. J Am Vet Med Assoc 187:272–274, 1985.
56. Rossier Y, Sweeney CR, Heyer G, et al: Pleuroscopic diagnosis of disseminated hemangiosarcoma in a horse. J Am Vet Med Assoc 196:1939–1940, 1990.
57. Sweeney CR, Gillette DM: Thoracic neoplasia in equids: 35 cases (1967–1987). J Am Vet Med Assoc 195:374–377, 1989.
58. Mueller POE, Morris DD, Carmichael KP, et al: Antemortem diagnosis of cholangiocellular carcinoma in a horse. J Am Vet Med Assoc 201:899–901, 1992.
59. Wrigley RH, Gay CC, Lording P, et al: Pleural effusion associated with squamous cell carcinoma of stomach of a horse. Equine Vet J 13:99–102, 1981.
60. Bradfield T: Traumatic pericarditis in a horse. Southwestern Vet 23:145–146, 1970.
61. Burbidge HM: Penetrating thoracic wound in a Hackney mare. Equine Vet J 14:94–95, 1982.
62. Fenno CH: Severe equine pleuritis due to wire penetration. Vet Med Small Anim Clin 70:458–461, 1975.
63. Mair TS, Pearson H, Waterman AE, et al: Chylothorax associated with a congenital diaphragmatic defect in a foal. Equine Vet J 20:304–306, 1988.
64. Bernard W, Reef VB, Clark ES, et al: Pericarditis in horses: Six cases (1982–1986). J Am Vet Med Assoc 196:468–471, 1990.
65. Deem DA, Harrington DD: *Nocardia brasiliensis* in a horse with pneumonia and pleuritis. Cornell Vet 70:321–328, 1980.
66. DeMartini JC, Riddle WE: Disseminated coccidioidomycosis in two horses and a pony. J Am Assoc Vet Med 155:149–156, 1969.
67. Zeimer EL, Pappagianis D, Madigan JE, et al: Coccidioidomycosis in horses: 15 cases (1975–1984). J Am Vet Med Assoc 201:910–916, 1992.
68. Acunas B, Celik L, Acunas A: Chest sonography: Differentiation of pulmonary consolidation from pleural disease. Acta Radiol 30:273–275, 1989.
69. Ichikawa Y, Mitutake Y, Hayashi S, et al: The observation of pleural opacities by B mode ultrasonogram. Kurume Med J 32:141–146, 1985.
70. O'Moore PV, Mueller PR, Simeone JF, et al: Sonographic guidance in diagnostic and therapeutic interventions in the pleural space. Am J Roentgenol 149:1–5, 1987.
71. Reinhold C, Illescas FF, Atri M, et al: Treatment of pleural effusions and pneumothorax with catheters placed percutaneously under imaging guidance. Am J Roentgenol 152:1189–1191, 1989.
72. Marks WM, Filly RA, Callen PW: Real-time evaluation of pleural lesions: New observations regarding the probability of obtaining free fluid. Radiology 142:163–164, 1982.
73. Freestone JF, Williams MM, Norwood G: Thoracic haemangiosarcoma in a 3-year-old horse. Aust Vet J 67:269–270, 1990.
74. Martinez OC, Serrano BV, Romero RR: Real-time ultrasound evaluation of tuberculous pleural effusions. J Clin Ultrasound 17:407–410, 1989.
75. Muskett A, Burton NA, Karwande SV, et al: Management of refractory empyema with early decortication. Am J Surg 156:529–532, 1988.
76. Himelman RB, Callen PW: The prognostic value of loculations in parapneumonic pleural effusions. Chest 90:852–856, 1986.
77. Targhetta R, Bourgeois J-M, Chavagneux R, et al: Ultrasonic signs of pneumothorax: Preliminary work. J Clin Ultrasound 21:245–250, 1993.
78. Wernecke K, Galaski M, Peters PE, et al: Pneumothorax: Evaluation by ultrasound preliminary results. J Thorac Imaging 2:76–78, 1987.

79. Targhetta R, Bourgeois JM, Chavagneux R, et al: Diagnosis of pneumothorax by ultrasound immediately after ultrasonically guided aspiration biopsy. Chest 101:855-856, 1992.
80. Ziskin MC, Thickman DI, Goldenberg NJ, et al: The comet tail artifact. J Ultrasound Med 1:1-9, 1982.
81. Chaffin MK, Ruoff WW, Schmitz DG, et al: Regression of hypertrophic osteopathy in a filly following successful management of an intrathoracic abscess. Equine Vet J 22:62-65, 1990.
82. Reef VB: Equine pediatric ultrasonography. Compend Contin Educ Pract Vet 13:1277-1285, 1991.
83. Simeone JF, Mueller PR, van Sonnenberg E: The uses of diagnostic ultrasound in the thorax. Clin Chest Med 5:281-290, 1984.
84. Anderson JD, Leonard JM, Zeliff JA, et al: Primary pulmonary neoplasm in a horse. J Am Vet Med Assoc 201:1399-1401, 1992.
85. Schultze AE, Sonea I, Bell TG: Primary malignant pulmonary neoplasia in two horses. J Am Vet Med Assoc 193:477-480, 1988.
86. Woods PR, Farrar WP, Chaffin MK, et al: Metastatic renal adenocarcinoma in a mule. Cornell Vet 83:67-75, 1993.
87. Anzai T, Kamada M, Kanemaru T, et al: Isolation of *Mycobacterium avium* complex from a Thoroughbred racehorse with fatal pneumonia. Bull Equine Res Inst 26:73-77, 1989.
88. Van den Hoven R, Franken P: Clinical aspect of lymphosarcoma in the horse: A clinical report of 16 cases. Equine Vet J 15:49-53, 1983.
89. Kapoor R, Saha MM: Sonographic evaluation of chest masses in children. Australas Radiol 35:223-236, 1991.
90. Lavoie JP, Carlson GP, George L: Hypertrophic osteopathy in three horses and a pony. J Am Vet Med Assoc 201:1900-1904, 1992.
91. Rosenberg HK: The complementary roles of ultrasound and plain film radiography in differentiating pediatric chest abnormalities. Radiographics 6:427-445, 1986.
92. Alexander JE, Keown GH, Palotay JL: Granular cell myoblastoma with hypertrophic pulmonary osteoarthropathy in a mare. J Am Vet Med Assoc 146:703-708, 1965.
93. Slocombe RF, Miller CL, MacLean AA: Pulmonary plasma cell granuloma (inflammatory pseudotumor) in a horse. Equine Vet J 24:492-493, 1992.
94. Uphoff CS, Lyncoln JA: A primary pulmonary tumor in a horse. Equine Pract 9:19-20, 1987.
95. Dill SG, Moise NS, Meschter CL: Cardiac failure in a stallion secondary to metastasis of an anaplastic pulmonary carcinoma. Equine Vet J 18:414-417, 1986.
96. Murphy JR, Breeze RG, McPherson EA: Myxoma of the equine respiratory tract. Mod Vet Pract 59:529-532, 1978.
97. Goodbary RF, Hage TJ: Hypertrophic pulmonary osteoarthropathy in a horse—A case report. J Am Vet Med Assoc 137:602-605, 1960.
98. Holmes JR: A case of hypertrophic pulmonary osteoarthropathy in a mare. Vet Rec 73:333-335, 1961.
99. Kersjes AW, Van de Watering CC, Kalsbeek HC: Hypertrophic pulmonary osteoarthropathy (Marie-Bamberger disease) in a horse. Neth J Vet Sci 1:55-68, 1968.
100. Leach MW, Pool RR: Hypertrophic osteopathy in a Shetland pony attributable to pulmonary squamous cell carcinoma metastases. Equine Vet J 24:247-249, 1992.
101. McClintock SA, Hutchins DR: Hypertrophic osteopathy in a stallion with minimal thoracic pathology. Aust Vet Pract 11:115-120, 1981.
102. Messer NT, Powers BE, Snyder SP: Hypertrophic osteopathy associated with pulmonary infarction in a horse. Compend Contin Educ Pract Vet 5:S636-S641, 1983.
103. Wright JJ, Reinertson E, Tennant B: Hypertrophic pulmonary osteodystrophy in the horse: A report of two cases. J Equine Med Surg 3:230-236, 1979.
104. Mair TS, Hillyer MH: Clinical features of lymphosarcoma in the horse: 77 cases. Equine Vet Educ 4:108-113, 1991.
105. Mair TS, Lane JG, Lucke VM: Clinicopathological features of lymphosarcoma involving the thoracic cavity in the horse. Equine Vet J 17:428-433, 1985.
106. Schalm OW: Lymphosarcoma in the horse. Equine Pract 3:23-27, 1981.
107. Proudman CJ, Edwards GB: Diaphragmatic diverticulum (hernia) in a horse. Equine Vet J 24:244-246, 1992.
108. Orsini JA, Koch C, Stewart B: Peritoneal pericardial hernia in a horse. J Am Vet Med Assoc 179:907-910, 1981.

CHAPTER

5

Cardiovascular Ultrasonography

ECHOCARDIOGRAPHY

The first application of echocardiography in horses was the development of M-mode echocardiography in the mid-1970s.[1] The use of M-mode echocardiography expanded to include normal cardiac dimensions in foals, ponies, and different breeds of horses and the diagnosis of a wide variety of cardiac diseases.[2-19] M-mode echocardiography was also used to assess cardiac size and function in the equine athlete, work that is still going on today.[20-24] The development of two-dimensional (2-D) real-time echocardiography in horses occurred in the 1980s and has continued to expand.[25-75] The ability to assess blood flow direction was first accomplished with contrast echocardiography, initially using M-mode and subsequently 2-D technology, prior to the development and widespread use of Doppler echocardiography.[12, 76] The ability to assess blood flow velocity, turbulence, and direction was subsequently developed in horses in the late 1980s and early 1990s with the use of pulsed-wave, continuous-wave, and color-flow Doppler echocardiography.[31, 33, 36, 38, 48, 49, 63, 64, 72, 75, 77-85]

Echocardiographic examinations are important in horses because physiologic flow murmurs are commonly auscultated and may be difficult to distinguish from murmurs of valvular regurgitation.[8, 33, 83, 86-94] Also, abnormal cardiac function can be detected echocardiographically in horses without significant murmurs. Echocardiography should be part of a complete work-up in animals presenting for poor performance[8, 24, 33, 69-72] because normal cardiac function is crucial for superior athletic performance.

Echocardiographic Technology

Two-Dimensional Real-Time Echocardiography

The 2-D echocardiogram is the template from which all other echocardiographic examinations are performed.[8, 9, 81] Cardiac anatomy is readily identifiable, making 2-D echocardiography easy to understand. The cardiac images obtained are frequently updated and appear as if they are moving in real time.[7-9, 81] These images have depth (y-axis) and width but no significant thickness.[7] The best echocardiographic images are obtained with the ultrasound beam perpendicular to the structures being evaluated, maximizing the ultrasound reflected back to the transducer. Although an infinite number of imaging planes can be obtained, long- and short-axis images of the heart are standard.[7-9, 25, 26, 31, 81, 95] Therefore, a thorough knowledge of cardiac anatomy is essential for accurately obtaining and interpreting the echocardiogram.

M-Mode Echocardiography

The M-mode (motion mode) echocardiogram is a one-dimensional ("ice-pick") representation of the cardiac structures moving over time (x-axis).[7-9, 81] The depth of the cardiac structures from the transducer are depicted on the y-axis and a simultaneous electrocardiogram (ECG) is recorded for timing. M-mode echocardiography is used to obtain measurements of the right ventricle, left atrial appendage, mitral valve, left ventricle, and aorta; to evaluate cardiac and valve motion; and to time cardiac events more accurately.[8, 9, 81] M-mode echocardiography has a very high sampling rate compared with 2-D echocardiography and is therefore superior for characterizing rapidly moving structures and for precisely timing events occurring during the cardiac cycle.[8, 9, 81]

Doppler Echocardiography

Doppler echocardiography is a noninvasive means of evaluating blood flow within the heart and great vessels. It has several forms—pulsed-wave, continuous-wave, and color-flow—which are useful and complement one another.[8, 10, 81, 82] In contrast to 2-D and M-mode echocardiography, low-frequency transducers produce the best Doppler signals, and the optimal imaging planes are as parallel to blood flow as possible.[8, 81, 82]

Pulsed-Wave Doppler Echocardiography. With pulsed-wave Doppler, a pulse of ultrasound is transmitted from the transducer to a predetermined depth (sample volume), and the reflected ultrasound waves are received by the transducer before another pulse of ultrasound is sent.[8, 81, 82] The time between the transmitted ultrasound bursts, the pulse repetition frequency (PRF), is determined by the location of the sample volume.[81] Pulsed-wave Doppler echocardiography is combined with 2-D echocardiography to allow the echocardiographer to place the sample volume in a specific area within the heart.[8, 10, 81, 82] Pulsed-wave Doppler echocardiography is used to localize flow accurately to a specific area (range gated) within the heart or great vessels but cannot resolve peak velocities associated with fast blood flow.[8, 10, 81, 82] Aliasing of the Doppler signal occurs when the Doppler shift exceeds one-half the PRF (Nyquist limit), making the determination of direction and peak velocity difficult or impossible.[8, 10, 81, 82] High-PRF Doppler is a method of increasing the Nyquist limit by two-, three-, or four-fold and thereby increasing the velocity of blood flow that can be detected before the signal aliases. This is accomplished by inserting two, three, or four sample volumes or gates along the cursor. However, high-PRF Doppler also introduces range ambiguity because the Doppler signal and spectral tracing now reflect blood flow at several sites along the axis of the ultrasound beam.

Continuous-Wave Doppler Echocardiography. Continuous-wave Doppler echocardiography is used to accurately determine the peak flow velocity in situations of high-velocity blood flow.[8, 81, 82] Two ultrasound crystals are located side by side in the transducer, one that continuously emits ultrasound and the other that continuously receives the reflected ultrasound waves.[8, 81, 82] Continuous-wave Doppler echocardiography accurately records high-velocity flow but does not have range resolution because flow is detected along the entire axis of the ultrasound beam.[8, 81, 82] The angle between the ultrasound beam and the blood flow should be as close to 0 degrees as possible (less than 20 degrees) to obtain accurate measurements of maximal velocities.[8, 81, 82] Continuous-wave Doppler echocardiography can be blind (no 2-D echocardiographic guidance) or guided by 2-D echocardiography in the new phased- and annular-array units by sharing the multiple element crystals.[8, 81]

Color-Flow Doppler Echocardiography. Color-flow Doppler echocardiography is a form of pulsed-wave Doppler echocardiography in which a color picture of blood flow is superimposed upon an M-mode or 2-D echocardiographic image.[8, 81, 82] In color-flow Doppler echocardiography there are numerous sample volumes, each of which is color coded to display the blood flow associated with that sample volume. Blood flow velocity, direction, and turbulence are all displayed with different color-flow maps.[8, 81, 82] Blood flow toward the transducer is normally coded in red and flow away from the transducer in blue.[8, 81, 82] The higher the velocity of blood flow, the lighter the shade of red or blue in most instances. Aliasing occurs at lower velocities than with pulsed-wave Doppler because the Nyquist limit is lower.[81] Thus, aliasing can occur with some normal flow velocities in horses. In color-flow Doppler the aliased signal is displayed as a color reversal, where red merges with blue or blue with red, although the direction of blood flow has not changed.[8, 81, 82] With turbulent blood flow (variance map), green is coded over the red or blue colors, yielding colors from yellow or orange to cyan.[81, 82] A mosaic pattern is produced in areas of high-velocity turbulent blood flow.[8, 81] Color M-mode and spectral Doppler can be used to accurately time cardiac events.[81-83] Newer technology using amplitude information from the color Doppler signal is becoming available which allows for visualization of flow in small vessels and areas of low-velocity blood flow.

Contrast Echocardiography

Contrast echocardiography involves the creation of microbubbles in the circulation using a variety of injectable agents or the patient's own blood.[12, 34, 76] Injected agents used for contrast echocardiography include 5% dextrose solution, 0.9% NaCl solution, indocyanine dye, and carbon dioxide, usually mixed with some of the patient's blood. The area containing the microbubbles is opacified because of the large difference in acoustic impedance between the microbubbles and the surrounding blood, causing most of the ultrasound to be reflected back to the transducer.[12, 34, 76] The path of blood flow through the heart can then be traced by following the path of echo contrast. The microbubbles are normally cleared in the microvasculature of the lung and do not pass from the right side to the left side of the circulation unless a right-to-left shunt is present or a left-sided injection has been made.[12, 34, 76] Newer contrast agents are being developed which will pass through the microcirculation of the lungs but have not yet been used in horses.

Transesophageal Echocardiography

Transesophageal echocardiography (TEE) can be performed in foals with standard TEE transducers or in horses with a lower-frequency ultrasound crystal (3.5 MHz) in a longer fiberoptic endoscope (2 to 3 m). This new window (the esophagus) from which the heart can be imaged provides superior visualization of the great vessels and intracardiac structures in human beings than those obtained from the standard transthoracic approach.[81, 96] TEE transducers are monoplane, biplane, or omniplane. The omniplane and biplane transducers are preferable for obtaining the most imaging planes.

Examination Technique

Patient Preparation

The cardiac window is the right fourth intercostal space (ICS) and left third, fourth, and fifth ICS midway between a line level with the point of the elbow and the point of the shoulder (Fig. 5-1).[1-6, 8-10, 25, 26, 31, 33] For best image

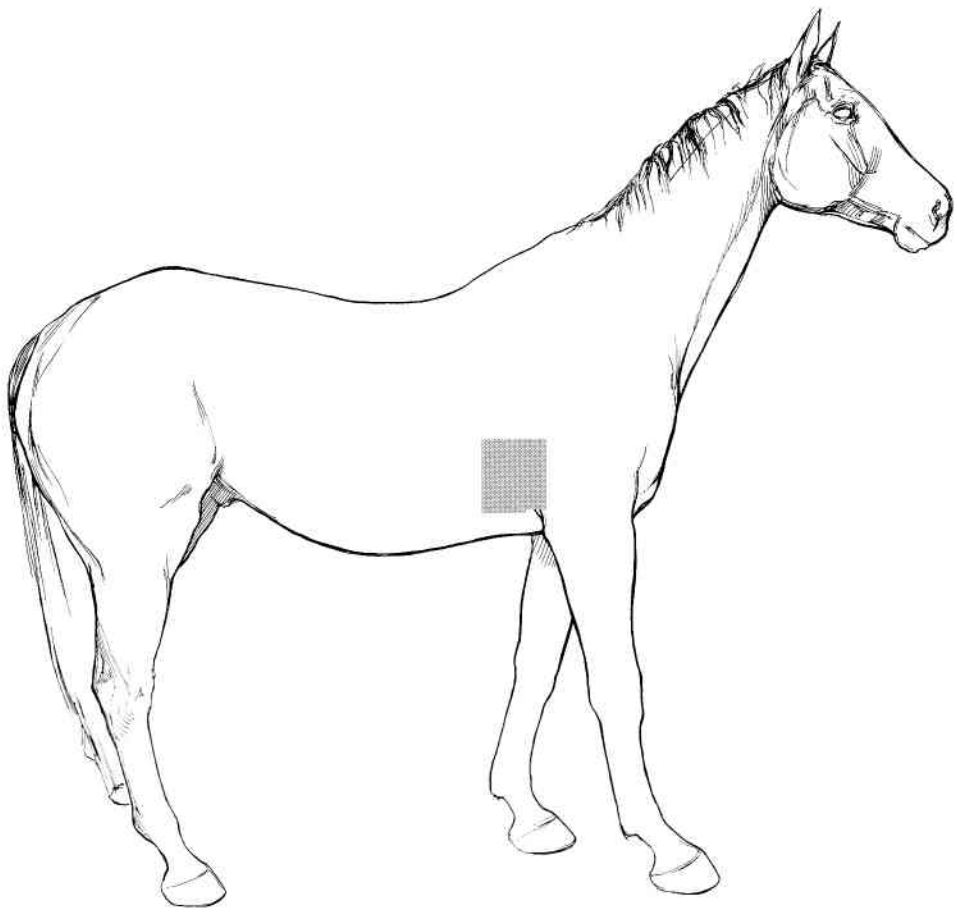

Figure 5–1

The right cardiac window is represented by the shaded area in the right axillary region of the horse. The transducer should be placed in the fourth intercostal space in the center of the cardiac window. Notice the position of the right foreleg for optimal imaging from the right cardiac window. The right foreleg should be positioned forward of the left foreleg so that the horse can stand comfortably during the echocardiogram.

quality, the area over the heart on both sides of the thorax in the third to fifth ICS should be clipped free of hair between a line level with the point of the shoulder and a line level with the point of the elbow, using a No. 40 surgical clipper blade.[8, 9, 25, 31] The caudal aspect of the triceps muscle should be included in the prepared area and the skin cleaned before ultrasonic coupling gel is applied. This area of the thorax is relatively hairless and can often be scanned without clipping the hair off the skin.[8, 9] If the horse is being scanned without clipping, the skin should be thoroughly cleaned and ultrasonic coupling gel applied in the direction of hair growth. The right forelimb should be positioned slightly forward of the left forelimb to facilitate scanning in the right cardiac window (Fig. 5-1).[1, 4, 5, 9]

Anatomy

The horse's heart is positioned in the thorax in a right cranial-to-left caudal orientation. The right ventricular outflow tract is located most cranially in the thorax, with the left ventricle, mitral valve, and left atrium most caudal (Fig. 5-2). The mitral valve is immediately adjacent to the thorax in the left fifth ICS. The aortic valve and left ventricular outflow tract are located in the fourth ICS, and the right ventricular outflow tract and pulmonic valve are immediately adjacent to the left chest wall in the third ICS. The tricuspid valve, right atrium, and right ventricle are centered in the right fourth ICS, and the right ventricular outflow tract is also imaged in the right third ICS (Fig. 5-2).

Scanning Technique

The entire heart should be imaged from one cardiac window so that the echocardiographer can best appreciate relative sizes of the cardiac chambers and vessels and their relationship to one another and to the cardiac valves.[81] Normal adult horse hearts are completely displayed using a depth setting of 26 to 30 cm.[8, 9, 33] Most, but not all, hearts in horses with cardiomegaly can be displayed with a 30-cm depth setting. Therefore, the initial echocardiographic examination should be performed with a 2.5-MHz transducer and 26- to 30-cm displayed depth from the right cardiac window in an adult horse.[8, 9, 33] In large weanlings, yearlings, or small, thin adult horses, a 3.5-MHz transducer and a 20- to 26-cm displayed depth are indicated.[8, 9, 33] A 5.0-MHz transducer and 14- to 20-cm displayed depth are indicated for performing echocardiograms on most equine neonates and small weanlings.[8, 33] A 7.5-MHz transducer and a displayed depth of 10 to 12 cm is indicated for scanning the hearts of most miniature horses and small pony foals. The highest transducer frequency that images the entire heart and the smallest depth setting that includes all imageable cardiac structures, but little of the surrounding struc-

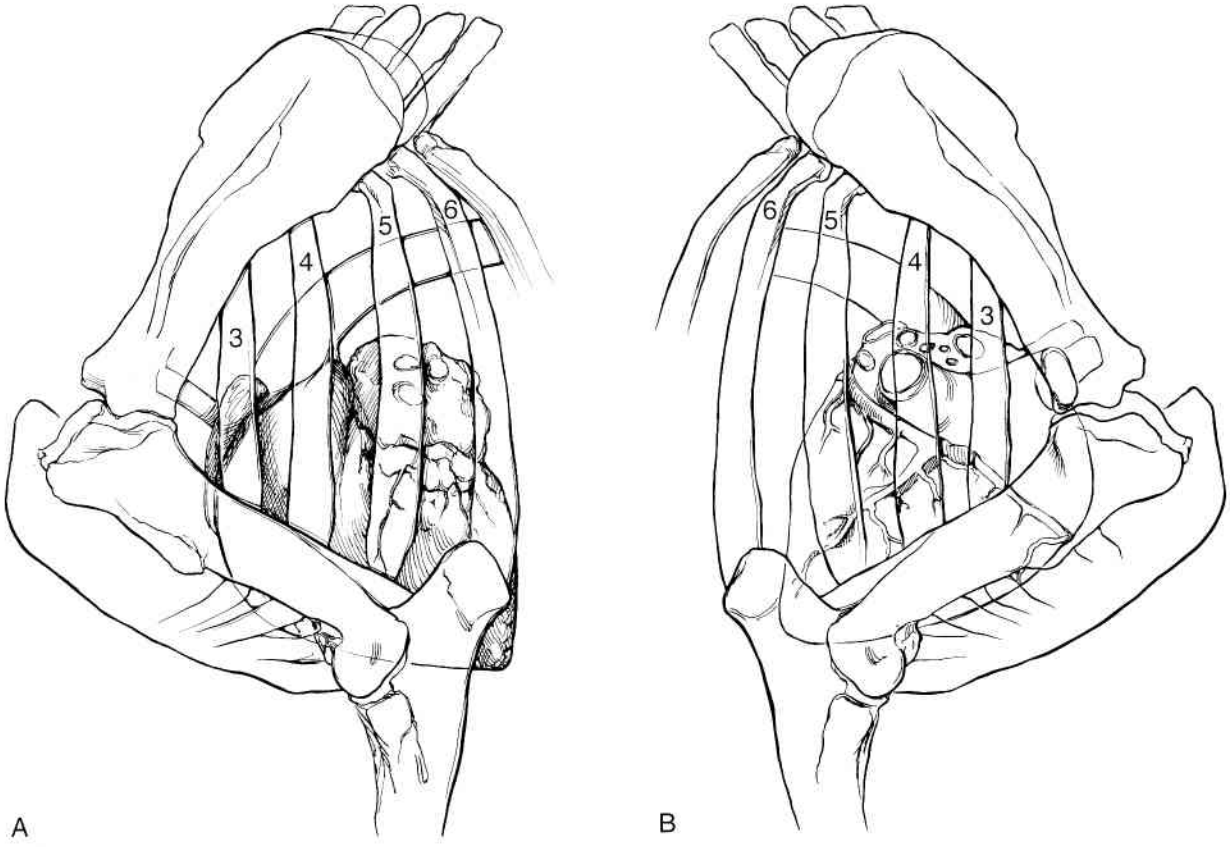

Figure 5–2

The position of the heart in the horse's thorax. *A*, View from the left side of the horse. *B*, View from the right side of the horse.

tures, should be selected for optimal image quality. Simultaneous ECG should be used in conjunction with echocardiography for timing the cardiac events.[1, 2, 4, 6–9, 31, 81] A rhythm strip is adequate for timing purpose, and the base-apex lead is usually the best tolerated by the horse during the echocardiographic examination.

A sector-scanner transducer is ideal for most practitioners performing echocardiography because the small transducer footprint is maneuverable in the small ICS of the horse and it has up to 30 cm penetration.[8, 9, 31, 81] A linear or curved linear transducer is not desirable for echocardiography because there is poor contact between the transducer footprint and the skin in the small intercostal space and the depth of penetration is limited with the lowest-frequency transducer, the 3.0 MHz.[8, 9, 31] Sequential 2-D, M-mode, pulsed-, and continuous-wave Doppler echocardiography are possible with sector technology, whereas two simultaneous images (2-D, M-mode, pulsed-wave, continuous-wave, 2-D color-flow, and M-mode color-flow) can be displayed with phased- and annular-array technology.[8, 9, 81] Phased- or annular-array technology is superior for performing Doppler echocardiographic examinations, as color-flow echocardiography can be used to rapidly localize abnormal blood flow within the heart and great vessels and to partially quantitate the severity of valvular regurgitation, shunts, and stenosis in horses.[8, 33, 81, 82] TEE can also be performed in horses with specially made transducers using annular-array or phased-array technology.[33]

The 2-D echocardiogram should first be performed from the right cardiac window to image the heart in its entirety, assess its function, and evaluate the relationships between the various cardiac structures.[8, 81] Both long-axis (sagittal) and short-axis (transverse or coronal) images should be obtained.[7–9] The M-mode echocardiogram should then be performed from the short-axis view using the criteria accepted by the American Society of Echocardiography.[9] A 2-D echocardiogram should then be obtained from the left cardiac window in all horses in which left-sided murmurs were detected, the heart could not be completely displayed from the right cardiac window, or any other clinical or echocardiographic findings prompted further evaluation from the left cardiac window.[8, 9] The scan plane orientation should display dorsal and cranial structures to the right side of the screen and ventral and caudal structures to the left side of the screen for the corresponding long-axis (dorsal to ventral) and short-axis (cranial to caudal) views, as described by the Echocardiography Committee of the Specialty of Cardiology in the American College of Veterinary Internal Medicine.[8, 95] The structures nearest the transducer should be displayed at the top of the echocardiographic image and the structures farthest away at the bottom of the image.[6, 25, 95]

Right Parasternal Views. Begin scanning in the long-axis scan plane with the transducer in the right cardiac window (fourth ICS) about midway between a line level with the point of the shoulder and a line level with the

point of the elbow with the horse's right leg positioned slightly forward (see Fig. 5-1). With the scan plane marker dorsal and slightly cranial (1 o'clock), angle the transducer toward the left third ICS for the most cranial view of the right inflow and outflow tracts (Fig. 5-3).[8] This right inflow and outflow tract view includes the right atrium, tricuspid valve, right ventricular inflow tract, right ventricular outflow tract (RVOT), pulmonic valve, pulmonary artery, and aorta (Fig. 5-3). Keeping the transducer in the same scan plane orientation and same position on the chest wall, angle the transducer straight across the chest toward the left fourth ICS to record

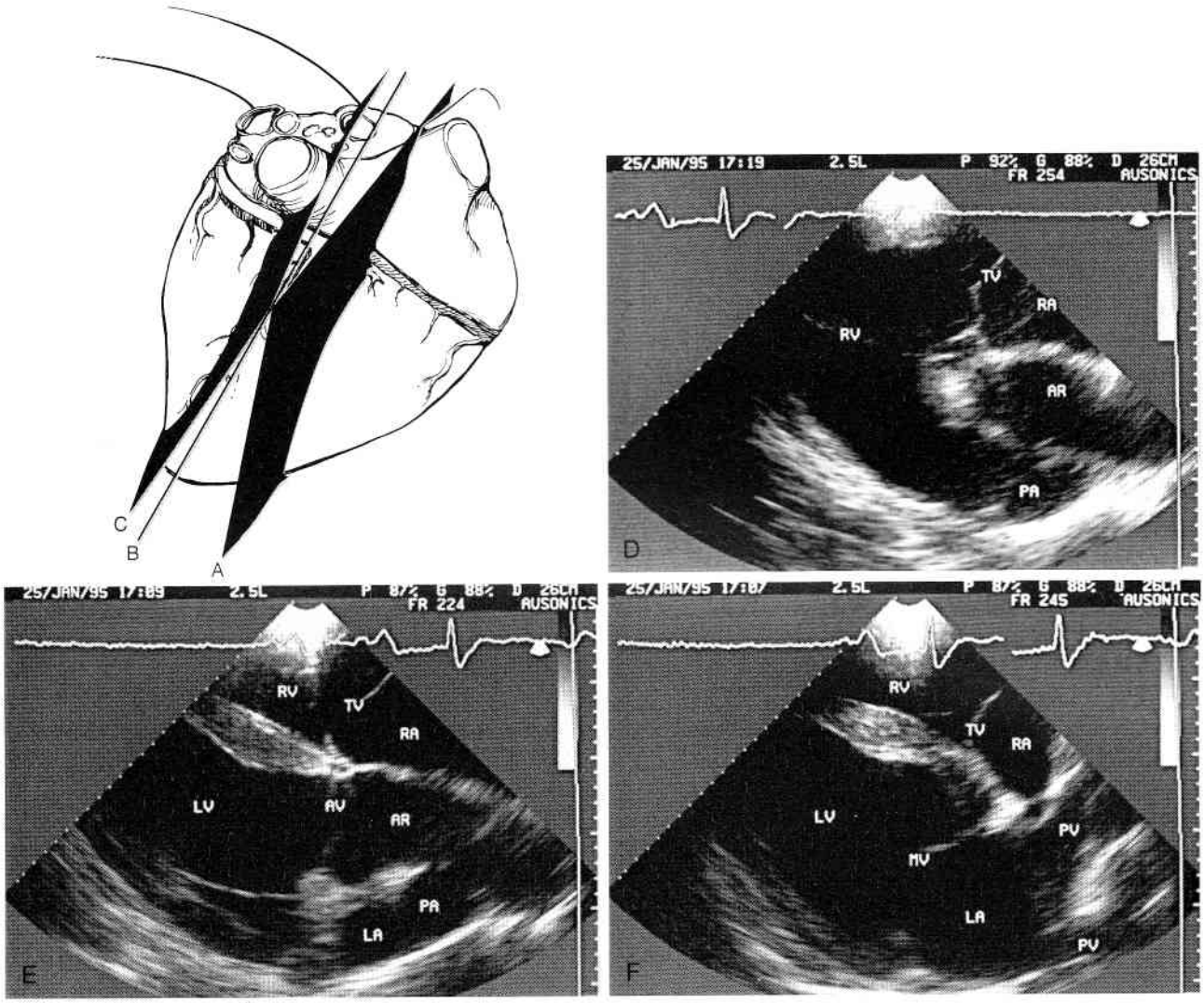

Figure 5–3

Scan planes and corresponding echocardiograms of the long-axis views obtained from the right cardiac window.

A, Scan plane of the long-axis view of the right ventricular inflow and outflow tracts obtained from the right cardiac window. Notice the cranial orientation of the scan plane. The transducer points toward the left third intercostal space to obtain the corresponding echocardiogram *(D).*

B, Scan plane of the long-axis view of the left ventricular outflow tract obtained from the right cardiac window. The scan plane is oriented perpendicular to the heart and chest wall. The transducer points directly across the thorax toward the left fourth intercostal space to obtain the corresponding echocardiogram *(E).*

C, Scan plane of the long-axis four-chamber view obtained from the right cardiac window. Notice the caudal orientation of the scan plane. The transducer points toward the left fifth intercostal space to obtain the corresponding echocardiogram *(F).*

D, Long-axis echocardiogram of the right ventricular inflow and outflow tracts obtained from a normal 9-year-old Thoroughbred mare. This echocardiogram was obtained from the right cardiac window in the right ventricular outflow tract position (same position as in *A*) with a 2.5-MHz sector-scanner transducer at a displayed depth of 26 cm. An electrocardiogram is superimposed for timing. RA, Right atrium; TV, tricuspid valve; RV, right ventricle; PA, pulmonary artery; AR, aortic root.

E, Long-axis echocardiogram of the left ventricular outflow tract obtained from a normal 9-year-old Thoroughbred mare (same horse as in *D*). This echocardiogram was obtained from the right cardiac window in the left ventricular outflow tract position (same position as in *B*) with a 2.5-MHz sector-scanner transducer at a displayed depth of 26 cm. An electrocardiogram is superimposed for timing. RA, Right atrium; TV, tricuspid valve; RV, right ventricle; LV, left ventricle; AV, aortic valve; LA, left atrium; PA, pulmonary artery; AR, aortic root.

F, Long-axis echocardiogram of the four-chamber view obtained from a normal 9-year-old Thoroughbred mare (same horse as in *D* and *E*). This echocardiogram was obtained from the right cardiac window in the left ventricular and mitral valve position (same position as in *C*) with a 2.5-MHz sector-scanner transducer at a displayed depth of 26 cm. An electrocardiogram is superimposed for timing. RA, Right atrium; TV, tricuspid valve; RV, right ventricle; LV, left ventricle; MV, mitral valve; LA, left atrium; PV, pulmonary veins.

views of the left ventricular outflow tract (Figs. 5-3 and 5-4).[8, 25] The right atrium, tricuspid valve, right ventricle, interventricular septum, left ventricular outflow tract (LVOT), aortic valve, aortic root, left atrial appendage, and part of the pulmonary artery are visualized in the long-axis view of the LVOT (Figs. 5-3 and 5-4). To visualize the entire ascending aorta, the transducer may need to be rotated slightly more clockwise.[8, 9] Keeping the transducer in the same scan plane orientation and position on the chest wall, angle caudally toward the left fifth ICS to record the parasternal long-axis four-chamber view of the heart (see Fig. 5-3).[8, 25] This view includes the right atrium, tricuspid valve, right ventricle, interventricular septum, left atrium, mitral valve, left ventricle, and left ventricular free wall (see Fig. 5-3). Rotate the transducer 90 degrees so that the scan plane marker is cranial and slightly ventral (4 o'clock) to obtain the short-axis views of the same structures (Fig. 5-5).[8, 25] Begin aiming slightly ventrally to include the cardiac apex and papillary muscles, aim straight across to visualize the chordae tendineae and mitral valve, and continue dorsally to include the aortic valve in short-axis cross-section (Fig. 5-5).[8, 25, 83] For all views, slight changes in transducer placement, angulation, or rotation may be necessary to acquire a true long- or short-axis view.

M-Mode Echocardiography. The M-mode echocardiographic images should be obtained from the short-axis views with the cursor placed across their widest part, as perpendicular to the structures being examined as possible while bisecting these structures.[8, 9] For the most accurate representation, the M-mode echocardiographic measurements are made from the leading endocardial edge of the near side to the leading endocardial edge of the far side of the structure being measured.[2, 8, 9] These measurements should be performed routinely to determine if any cardiac enlargement exists. To obtain an M-mode echocardiogram of the aortic valve, the cursor is placed through the center of the aortic valve leaflets in the short-axis view of the aorta (Fig. 5-6).[8-10] In this view the tricuspid valve, aortic root containing aortic valve leaflets, and left atrial appendage are imaged (Fig. 5-6). Standard measurements include the diameters of the aortic root and left atrial appendage and the ejection time. The aortic root diameter is measured at end-diastole at the onset of the Q-wave of the ECG, and the left atrial appendage is measured in systole at its widest internal diameter.[2, 4, 8-10] The diameter of the aortic root is between 8 and 9 cm in most horses and should always measure larger than the diameter of the left atrial appendage in normal horses (Table 5-1).[1, 2, 7, 8] The left atrial-to-aortic ratio is 0.8 in adult horses but is slightly greater in foals.[2, 4, 7] A left atrial appendage diameter equal to or greater than the diameter of the aortic root is a specific but not very sensitive indication of left atrial enlargement. The ejection time is measured from the opening to the closing of the aortic valve leaflets.[2, 4, 8] The ejection time in a normal horse at rest usually measures between 0.400 and 0.500 seconds. The mitral valve M-mode echocardiogram is obtained by placing the M-mode cursor through the mitral valve in a short-axis view, as perpendicular as possible to the septum and left ventricular free wall (Fig. 5-7). In this view the right ventricle, interventricular septum, septal leaflet of the mitral valve, free wall leaflet of the mitral valve, and left ventricular free wall are imaged (Fig. 5-7). The distance from the septum to the maximum opening (E point) of the mitral valve (SEP) is an indication of the size of the LVOT and is normally 1 cm or less. The SEP is obtained by measuring from the interventricular septum to the peak opening of the mitral valve in early diastole.[2, 4, 8] The measurements of ventricular chamber size and septal and left ventricular free wall thickness are made from the left ventricular view. The M-mode cursor is placed through the left ventricle between the papillary muscles just below the mitral valve, as perpendicular as possible to the interventricular septum and left ventricular free wall (Fig. 5-8). Measurements obtained from this view include the septal and left ventricular free wall thickness at end-diastole and peak systole, right and left ventricular internal diameter (chamber size) at end-diastole and peak systole, and fractional shortening (Fig. 5-8). The diameters of the right ventricle, septum, left ventricle, and left ventricular free wall at end-diastole are measured at the onset of the Q-wave on the ECG, and at peak systole are measured at the peak downward deflection of the septum.[2, 4, 8-10] In adult horses, the normal left ventricular internal diameter at end-diastole ranges from 9 to 13 cm when measured from the right parasternal window (Table 5-1).[1, 2, 7, 8] The fractional shortening (FS), an index of cardiac contractility, is calculated by subtracting the left ventricular internal diameter at peak systole ($LVID_s$) from the left ventricular internal diameter at end-diastole ($LVID_d$), dividing this number by the left ventricular inter-

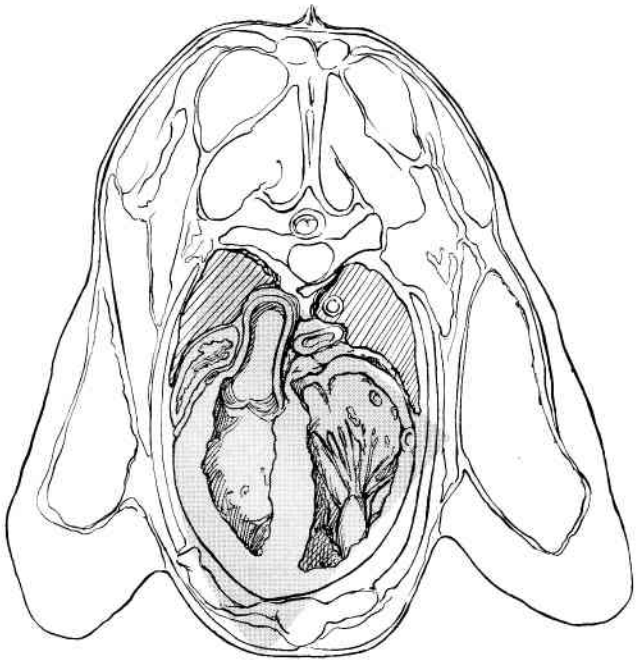

Figure 5–4

Cross-section through the thorax of the horse at the fourth intercostal space (ICS) illustrating the scan plane *(shaded area)* used to obtain the long-axis view of the left ventricular outflow tract from the right cardiac window. The point of the scan plane represents the location of the transducer footprint in the fourth ICS in the right axillary region beneath the triceps muscle.

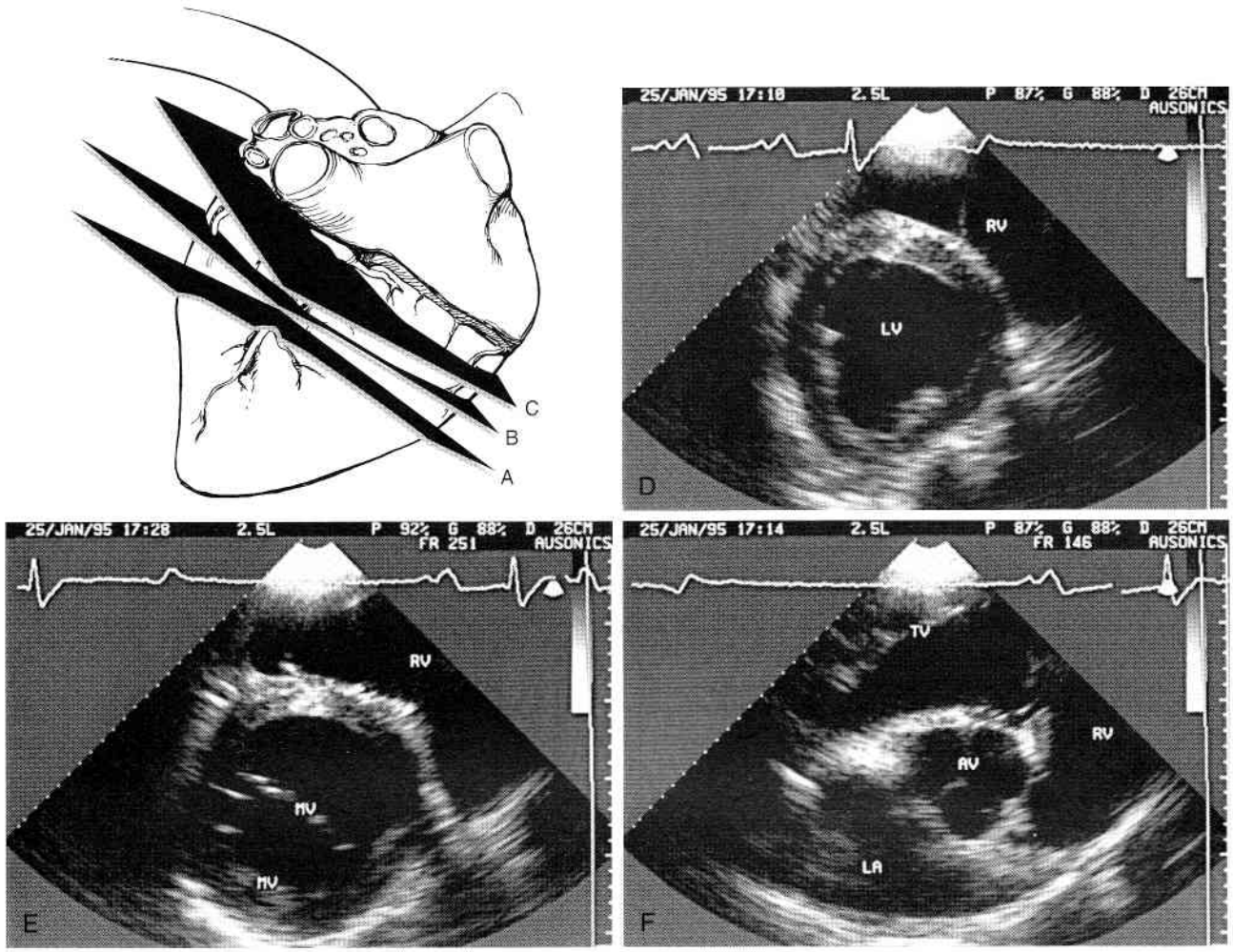

Figure 5–5

Scan planes and corresponding echocardiograms of the short-axis views obtained from the right cardiac window.

A, Scan plane of the short-axis view of the left ventricle obtained from the right cardiac window. Notice the caudal and ventral orientation of the scan plane. The transducer points toward the left fifth intercostal space and is angled slightly ventrally.

B, Scan plane of the short-axis view of the mitral valve obtained from the right cardiac window. Notice the caudal orientation of the scan plane. The transducer points toward the left fifth intercostal space and is oriented perpendicular to the heart and chest wall.

C, Scan plane of the short-axis view of the aortic valve obtained form the right cardiac window. Notice the dorsal orientation of the scan plane. The transducer points directly across the thorax toward the left fourth intercostal space with a slight clockwise rotation.

D, Short-axis echocardiogram of the left ventricle obtained from a normal 9-year-old Thoroughbred mare (same horse as in Figure 5–3). This echocardiogram was obtained from the right cardiac window in the left ventricular position (same position as in *A*) with a 2.5-MHz sector-scanner transducer at a displayed depth of 26 cm. An electrocardiogram is superimposed for timing. RV, Right ventricle; LV, left ventricle.

E, Short-axis echocardiogram of the mitral valve obtained from a normal 9-year-old Thoroughbred mare (same horse as in Figure 5–3 and in *D*). This echocardiogram was obtained from the right cardiac window in the mitral valve position (same position as in *B*) with a 2.5-MHz sector-scanner transducer at a displayed depth of 26 cm. An electrocardiogram is superimposed for timing. RV, Right ventricle; MV, mitral valve.

F, Short-axis echocardiogram of the aortic valve position obtained from a normal 9-year-old Thoroughbred mare (same horse as in Figure 5–3, and in *D* and *E*). This echocardiogram was obtained from the right cardiac window in the aortic valve position (same position as in *C*) with a 2.5-MHz sector-scanner transducer at a displayed depth of 26 cm. An electrocardiogram is superimposed for timing. TV, Tricuspid valve; RV, right ventricle; AV, aortic valve; LA, left atrium.

nal diameter at end-diastole ($LVID_d$) and then multiplying this number by 100 to get a percentage.[1, 2, 4, 8–10]

$$FS\ (\%) = \frac{LVID_d - LVID_s}{LVID_d} \times 100$$

Left Parasternal Views. The examination should continue from the left side of the horse if left ventricular or left atrial enlargement is present; mitral, pulmonic, or aortic insufficiency is suspected; or all of the structures of the left heart cannot be visualized adequately from the right side.[7–11, 14] The horse's leg should be positioned slightly forward and the transducer placed in the ICS space about halfway between a line level with the point of the shoulder and the point of the elbow. The short- and long-axis views of the right ventricular inflow and outflow tracts are obtained in the third ICS with the transducer aimed straight across the chest and the scan plane marker facing cranially (Fig. 5–9). The right atrium, tricuspid valve, right ventricle, pulmonic valve, pulmo-

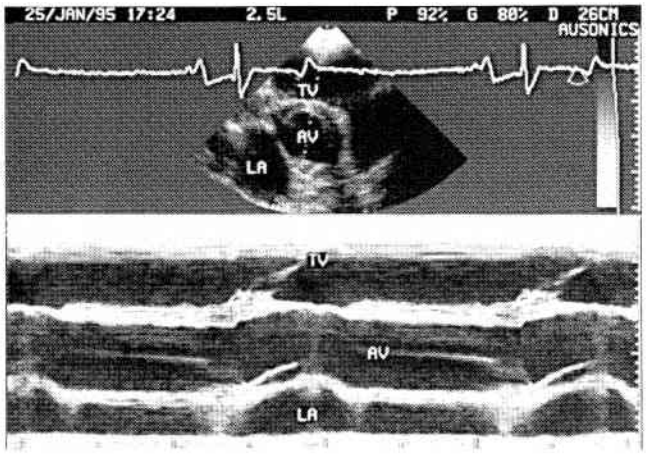

Figure 5–6

Short-axis echocardiogram and corresponding M-mode echocardiogram of the aortic valve position obtained from a normal 9-year-old Thoroughbred mare (same horse as in Figures 5–3 and 5–5). The cursor *(dotted line)* placement through the aortic valve to obtain the M-mode echocardiogram is demonstrated in the short-axis echocardiogram. These echocardiograms were obtained from the right cardiac window in the aortic valve position (same position as in Figure 5–5*C* and *F*) with a 2.5-MHz sector-scanner transducer at a displayed depth of 26 cm. An electrocardiogram is superimposed for timing. TV, Tricuspid valve; AV, aortic valve; LA, left atrium.

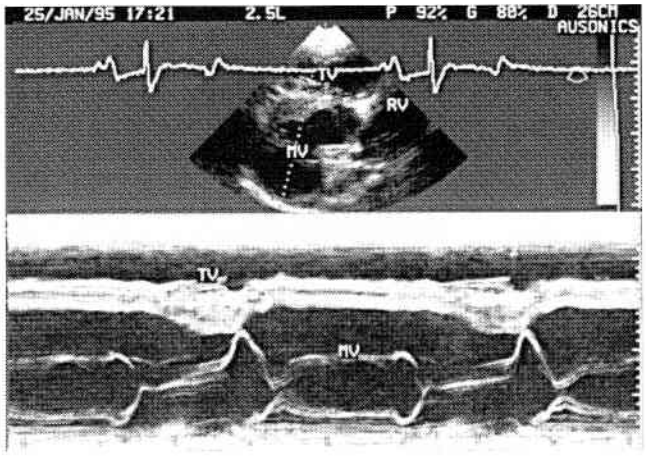

Figure 5–7

Short-axis echocardiogram and corresponding M-mode echocardiogram of the mitral valve position obtained from a normal 9-year-old Thoroughbred mare (same horse as in Figures 5–3, 5–5, and 5–6). The cursor *(dotted line)* placement through the mitral valve to obtain the M-mode echocardiogram is demonstrated in the short-axis echocardiogram. These echocardiograms were obtained from the right cardiac window in the mitral valve position (same position as in Figure 5–5*B* and *E*) with a 2.5-MHz sector-scanner transducer at a displayed depth of 26 cm. An electrocardiogram is superimposed for timing. TV, Tricuspid valve; MV, mitral valve; RV, right ventricle.

nary artery, and aorta are imaged in this view (Fig. 5–9).[8] The long-axis LVOT view can be imaged with the scan plane marker facing dorsally and slightly cranially in the fourth ICS (Fig. 5–9).[8] The long-axis two-chamber view of the left atrium, mitral valve, and left ventricle can be imaged with the same scan plane orientation in the fifth ICS or with the transducer angled slightly caudally (Fig. 5–9).[8] The internal diameter of the left atrium at its widest point parallel to the mitral valve should not exceed 13.5 cm in normal Thoroughbreds and Standardbreds and 14 cm in larger horses.[14] Short-axis images of all these structures can be performed by rotating the

Table 5–1
Normal Echocardiographic Measurements in the Horse

Measurements Obtained from the Right Cardiac Window		Mean (cm)	SD
RV_d	(Right ventricular internal diameter at end-diastole)	3.83*	0.91*
		3.86†	0.63†
RV_s	(Right ventricular internal diameter at peak systole)	2.71*	1.00*
$LVID_d$	(Left ventricular internal diameter at end-diastole)	11.90*	0.71*
		11.06†	1.34†
		9.3‡, §	0.3‡, §
$LVID_s$	(Left ventricular internal diameter at peak systole)	7.35*	0.72*
		6.11†	0.90†
		5.7‡, §	0.23‡, §
FS	(Fractional shortening)	38.76*	4.59*
		44.1†	6.4†
		38.6‡, §	1.6‡, §
LV_d	(Left ventricular free wall thickness at end-diastole)	2.39*	0.26*
		2.92†	0.49†
LV_s	(Left ventricular free wall thickness at peak systole)	3.96*	0.93*
		4.45†	0.59†
IVS_d	(Interventricular septal thickness at end-diastole)	3.02*	0.39*
		3.06†	0.6†
IVS_s	(Interventricular septal thickness at peak systole)	4.55*	0.55*
		4.81†	0.70†
AR_d	(Diameter of the aortic root at end-diastole)	8.50*	0.51*
		7.31†	0.83†
		7.7‡, §	0.16‡, §

*Data obtained from 26 Thoroughbred horses with a mean weight of 517 kg.
†Data obtained from 100 horses weighing 445.23 ± 86.86 kg.
‡Data obtained from 25 normal horses weighing approximately 300 kg.
§All values in this reference reported as ± SEM.

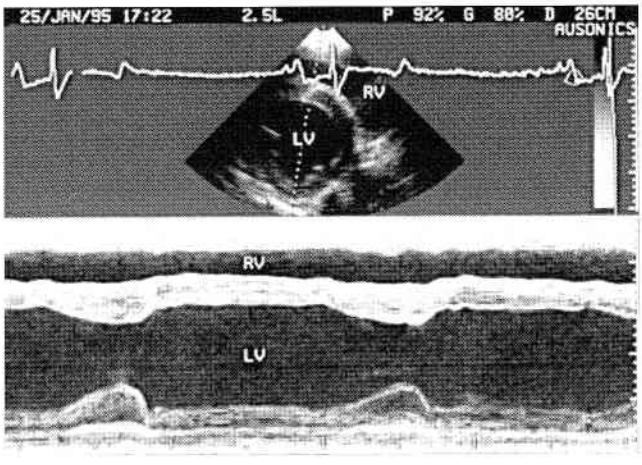

Figure 5–8

Short-axis echocardiogram and corresponding M-mode echocardiogram of the left ventricular position obtained from a normal 9-year-old Thoroughbred mare (same horse as in Figures 5–3 and 5–5 to 5–7). The cursor *(dotted line)* placement through the left ventricle to obtain the M-mode echocardiogram is demonstrated in the short-axis echocardiogram. These echocardiograms were obtained from the right cardiac window in the left ventricular position (same position as in Figure 5–5*A* and *D*) with a 2.5-MHz sector-scanner transducer at a displayed depth of 26 cm. An electrocardiogram is superimposed for timing. RV, Right ventricle; LV, left ventricle.

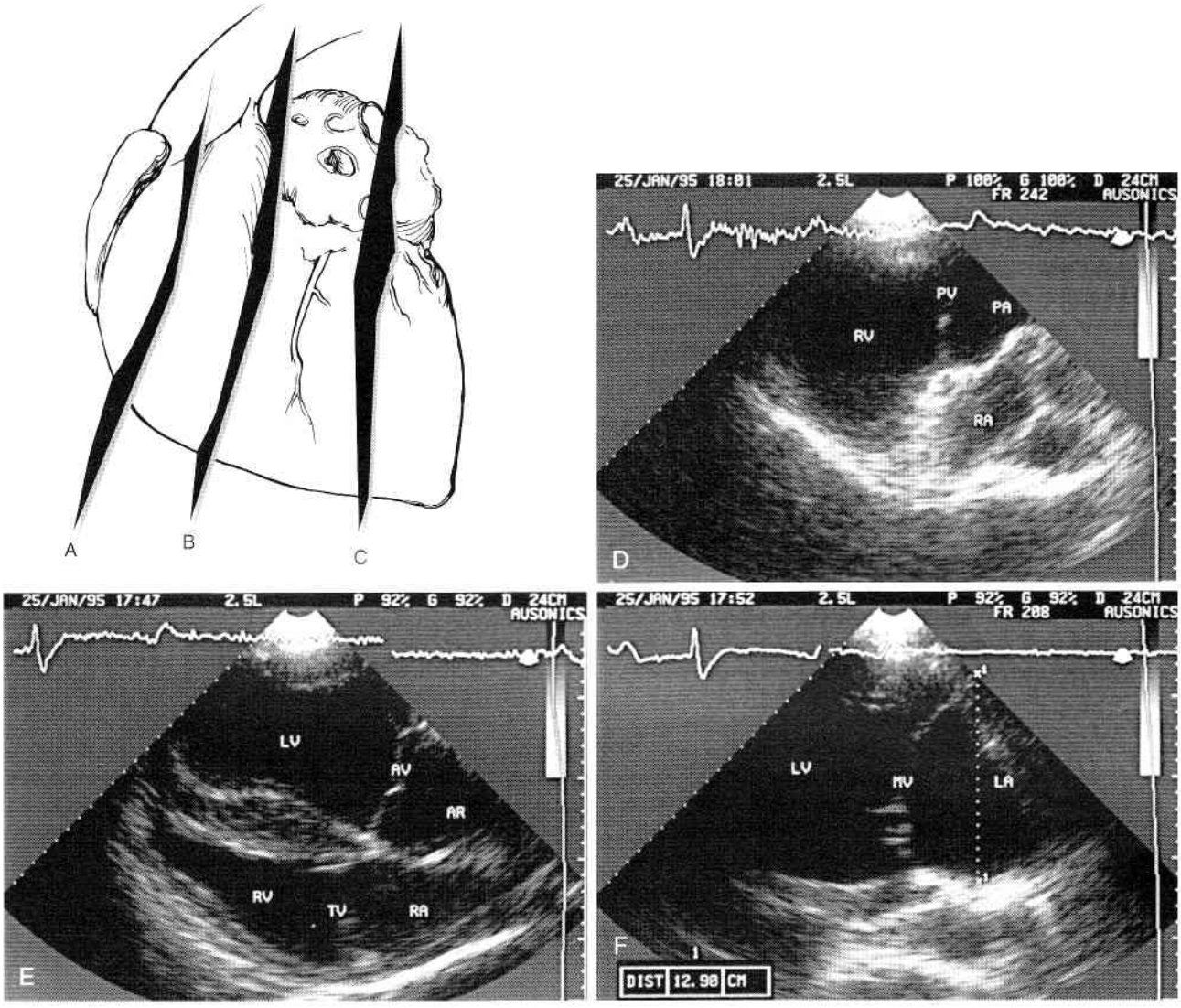

Figure 5–9

scan planes and corresponding echocardiograms of the long-axis views obtained from the left cardiac window.

A. Scan plane of the long-axis view of the right ventricular outflow tract obtained from the left cardiac window. Notice the scan plane oriented perpendicular to the heart and chest wall and the slight clockwise rotation of the scan plane. The transducer points directly across the thorax toward the right third intercostal space.

B. Scan plane of the long-axis view of the left ventricular outflow tract obtained from the left cardiac window. Notice the scan plane oriented perpendicular to the heart and chest wall and the slight counterclockwise rotation of the scan plane. The transducer points directly across the thorax toward the right fourth intercostal space.

C. Scan plane of the long-axis view of the left ventricle and mitral valve obtained from the left cardiac window. The scan plane is oriented perpendicular to the heart and chest wall.

D. Long-axis echocardiogram of the right ventricular outflow tract obtained from a normal 9-year-old Thoroughbred mare (same horse as in Figures 5–3 and 5–5 to 5–8). This echocardiogram was obtained from the left cardiac window in the right ventricular outflow tract position (same position as in *A*) with a 2.5-MHz sector-scanner transducer at a displayed depth of 24 cm. An electrocardiogram is superimposed for timing. RA, Right atrium; RV, right ventricle; PV, pulmonic valve; PA, pulmonary artery.

E. Long-axis echocardiogram of the left ventricular outflow tract obtained from a normal 9-year-old Thoroughbred mare (same horse as in Figures 5–3 and 5–5 to 5–8 and in *D*). This echocardiogram was obtained from the left cardiac window in the left ventricular outflow tract position (same position as in *B*) with a 2.5-MHz sector-scanner transducer at a displayed depth of 24 cm. An electrocardiogram is superimposed for timing. LV, Left ventricle; AV, aortic valve; AR, aortic root; RA, right atrium; TV, tricuspid valve; RV, right ventricle.

F. Long-axis echocardiogram of the mitral valve obtained from a normal 9-year-old Thoroughbred mare (same horse as in Figures 5–3 and 5–5 to 5–8 and in *D* and *E*). This echocardiogram was obtained from the left cardiac window in the mitral valve position (same position as in *C*) with a 2.5-MHz sector-scanner transducer at a displayed depth of 24 cm. A maximal diameter of the left atrium (12.9 cm) is displayed between the two cursors. An electrocardiogram is superimposed for timing. LV, Left ventricle; MV, mitral valve; LA, left atrium.

transducer counterclockwise 90 degrees from the corresponding long-axis image. An M-mode echocardiogram can be performed at the chordal level from a left parasternal short-axis view of the left ventricle if the measurement cannot be obtained from the right parasternal short-axis view.

Doppler. The pulsed-wave Doppler flow profiles have been described in clinically normal Standardbred horses.[77] Laminar blood flow was detected throughout the heart and great vessels. Peak flow velocity in the right ventricular inflow and outflow tracts, pulmonary artery, left ventricular inflow and outflow tracts, and ascending aorta was less than 1.5 m/sec.[77] Results in other breeds of horses have been similar.[84, 85]

A cardiac Doppler examination should be performed in any horse with a holosystolic or pansystolic murmur grade 3/6 or higher, a holodiastolic murmur grade 1/6 or higher, or a continuous murmur grade 1/6 or higher.[64] The examination should begin with pulsed-wave Doppler or color-flow Doppler echocardiography. The entire valve or shunt area being examined should be interrogated by placing the sample volume at the valve or shunt and moving farther away from the area in question until abnormal blood flow is no longer imaged or heard, mapping the total area of abnormal flow.

The tricuspid valve, right atrium, interatrial septum, and interventricular septum should be examined from the right parasternal window. If tricuspid regurgitation is suspected, interrogate the tricuspid valve and right atrium in all three right parasternal long-axis views (the right inflow/outflow tract view, LVOT view, and four-chamber view). Most tricuspid regurgitation jets are detected in the LVOT view, with the jet emanating from the tricuspid valve and flowing toward the ascending aorta.[64, 72, 78, 80, 83] The interatrial septum, especially around the area of the foramen ovale, should be carefully evaluated for any shunt at the atrial level. Ventricular septal defects (VSD) in horses are most commonly found in the inflow portion of the interventricular septum (membranous septum), just beneath the septal leaflet of the tricuspid valve and the aortic valve, and are usually best imaged from the right parasternal window.[9, 15, 33, 35-38, 72] The right ventricle and RVOT should be interrogated beginning at the defect and extending into the right ventricle or RVOT. If no defect is seen and a VSD is suspected, interrogate the entire septum. The maximal velocity of shunt flow through the defect should then be measured with continuous-wave Doppler echocardiography to determine the hemodynamic significance of the shunt in horses without LVOT obstruction.[33, 36, 38, 64, 72, 82] Using the formula $4\ v^2$, where v is the maximal velocity of flow through the shunt, the pressure difference between the two ventricles can be calculated (modified Bernoulli equation). This can then be used to estimate right ventricular systolic pressure in horses with a VSD defect by subtracting $4\ v^2$ from the systolic blood pressure.

Abnormalities associated with the pulmonic and aortic valves should be interrogated from both right and left parasternal windows; one window is usually optimal depending upon the size of the horse, the direction of the regurgitant or stenotic jet, and the degree of cardiac enlargement.[64, 79, 80] Interrogate the RVOT from the right parasternal short- and long-axis views and the left parasternal short-axis view beginning at the right ventricular side of the valve and moving back into the RVOT. Interrogate the pulmonary artery from the right parasternal views if close enough to successfully examine the main pulmonary artery; otherwise only the left parasternal window can be used for Doppler evaluation of the pulmonary artery. The LVOT is usually most successfully interrogated in horses with aortic regurgitation from the left cardiac window because the jet is most frequently coming toward the left ventricular free wall.[64, 79, 80, 83] However, this area should be examined from the right parasternal window because some horses have regurgitant jets that angle toward the interventricular septum and are best detected in this view. In many horses, however, the regurgitant jet is nearly perpendicular to the ultrasound beam from this window. Interrogation of the LVOT should begin at the aortic valve and extend apically into the LVOT. Doppler evaluation of the ascending aorta may also be performed from the right or left parasternal windows.[10, 77, 83] The left parasternal window is preferable if a good signal can be obtained because the ultrasound beam is more parallel to blood flow. However, this area is sometimes difficult to image from the left parasternal window.

The mitral valve and left atrium should be interrogated from the left parasternal view in all horses with a holosystolic or pansystolic murmur grade 3/6 or higher, with its point of maximal intensity over the mitral or aortic valve area, beginning at the mitral valve and extending dorsally to the left atrial side of the mitral valve and out to the base of the left atrium.[64, 72, 83] Any other shunts or jets caused by obstruction to flow should be interrogated in the same fashion by beginning at the suspected area of abnormality and fanning out from there to detect the size and shape of the high-velocity turbulent flow.

Echocardiographic Findings

Normal Structures

The vena cava, right atrium, right ventricle, pulmonary artery, pulmonary veins, left atrium, and left ventricle are all identified echocardiographically using a segmental approach to cardiac anatomy.[38] The cranial and caudal venae cavae deliver blood to the right atrium. The foramen ovale is imaged as two flaps of tissue in the center of the atrial septum and is easily imaged in normal neonatal foals. This area becomes more difficult to visualize and less flaplike in older horses. The right ventricle has a trabeculated endocardial surface, moderator band, chordae tendineae inserting into the interventricular septum, infundibular muscle band, triangular cavity, and a tricuspid atrioventricular valve with a relatively apical insertion.[25, 26, 38] The pulmonary artery bifurcates into the right and left pulmonary arteries. The main pulmonary artery is more cranial than the aorta, but the pulmonary artery bifurcation is caudal to the aortic arch. The pulmonary artery bifurcation can normally be imaged in neonates and older foals and can occasionally be imaged in normal adult horses (Fig. 5-10).[38] Two pulmonary veins

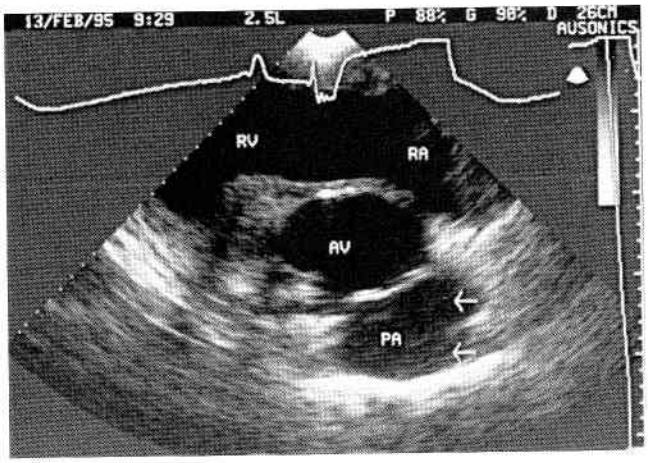

Figure 5–10

Long-axis echocardiogram of the bifurcation of the main pulmonary artery (PA) obtained from a 3-year-old Standardbred colt. Notice the branching of the main pulmonary artery into right and left pulmonary arteries *(arrows)*. This echocardiogram was obtained from the right cardiac window in the right ventricular outflow tract position, angling dorsally and rotating the transducer slightly counterclockwise. This echocardiogram was obtained with a 2.5-MHz sector-scanner transducer at a displayed depth of 26 cm. An electrocardiogram is superimposed for timing. RA, Right atrium; RV, right ventricle; AV, aortic valve.

are usually imaged entering the left atrium, which is caudal and to the left of the right atrium. In the right parasternal four-chamber view, the left atrium appears slightly larger than the right atrium.[25] The left ventricle has an ellipsoid cavity with a smooth endocardial surface, two papillary muscles, and a bicuspid (two major leaflets) atrioventricular (mitral) valve with a slightly more basilar insertion.[25, 26, 38] The aorta is centrally located, caudal and to the right of the main pulmonary artery, and can be followed echocardiographically out to the aortic arch. The right and left coronary arteries arise from the right and left coronary cusps of the aortic valve. The right coronary cusp of the aortic valve is adjacent to the right ventricle and RVOT, the left coronary cusp is adjacent to the main pulmonary artery, and the noncoronary cusp is next to the tricuspid valve.

The atrioventricular valves normally have a biphasic pattern of motion during diastole, with the valves opening maximally in early diastole, drifting toward each other at the end of rapid ventricular filling, drifting open somewhat, and then opening again in association with atrial systole. The atrioventricular valves then close at the onset of ventricular systole. At the end of isovolumetric ventricular contraction, the semilunar valves open and remain open throughout the ejection period (ejection time). The pre-ejection period is the time from the closure of the atrioventricular valves to the opening of the semilunar valves. During ventricular ejection, the interventricular septum and left ventricular free wall should thicken and move toward each other, shortening approximately 30 to 40%.

Congenital Cardiac Disease

Congenital cardiac disease should be suspected in all neonatal and older foals with a holosystolic or pansystolic murmur grade 3/6 or higher, a holodiastolic murmur grade 1/6 or higher, or a continuous murmur grade 1/6 or higher which persists more than 96 hours after birth.[15] Two-dimensional real-time echocardiography is superior to cardiac catheterization in human neonates and in horses for correct anatomic diagnosis of congenital malformations.[14, 15, 38, 97–99] A thorough understanding of cardiac anatomy is essential for the correct diagnosis of congenital cardiac defects, as these echocardiographic examinations can often be quite challenging.[38, 98, 99] There are a myriad of possible relationships between cardiac structures that may be present; the echocardiographer must therefore identify all cardiac structures.

Ventricular Septal Defect. VSD is the most common congenital disorder in horses.[7, 9, 11, 14, 15, 33–38, 64, 72, 91, 100] The characteristic murmur is a grade 3/6 or higher, harsh, band-shaped pansystolic murmur with the point of maximal intensity in the right third to fourth ICS.[15, 36–38, 64, 72, 100] Most horses with VSD have a palpable precordial thrill over the right cardiac silhouette. An ejection murmur (crescendo-decrescendo) with its point of maximal intensity over the pulmonic valve area is usually detected, which is one grade softer, unless the defect is located in the right ventricular outlet portion of the interventricular septum.[36] A complete echocardiogram should be performed on all foals or horses in which a VSD is suspected. This examination should begin with a thorough 2-D echocardiogram followed by a standard M-mode echocardiogram. The heart should be carefully examined for any other concurrent cardiac abnormalities. The cardiac chambers should be carefully evaluated to determine the degree of volume overload caused by the VSD, and left ventricular function should be critically assessed. Pulsed-wave and color-flow Doppler should be used to further characterize flow abnormalities when the 2-D echocardiogram or clinical examination indicates an abnormality. Finally, continuous-wave Doppler echocardiography should be used to determine the pressure gradient between the two ventricles.

Two-dimensional echocardiography, combined with Doppler echocardiography, is the technique of choice for diagnosing VSD in large animals.[7, 9, 15, 33, 35–38, 64, 82] VSD is most common in the right ventricular inlet and membranous portion of the interventricular septum but has also been detected in horses in the outflow and muscular portions of the interventricular septum.[9, 14, 15, 33, 36, 38, 64] The membranous portion of the interventricular septum extends from the commissure between the right and noncoronary aortic valve cusps to the inlet and outlet portions of the muscular septum.[38] Inlet or membranous VSD is most frequently imaged beneath the septal leaflet of the tricuspid valve and the noncoronary or right coronary cusp of the aortic valve (Fig. 5–11).[9, 33, 36, 38, 64] Therefore, most VSD are best imaged in the right parasternal LVOT long-axis view and may not be imaged in alternative views, particularly if the defect is 2.5 cm or less in diameter, the size of most VSD in horses.[9, 33, 36, 38, 64] The inflow or membranous defect can be imaged in the right parasternal short-axis plane using an imaging plane that transects the interventricular septum immediately ventral to the aortic valve leaflets. The size of the VSD should be measured in two mutually perpendicular planes across

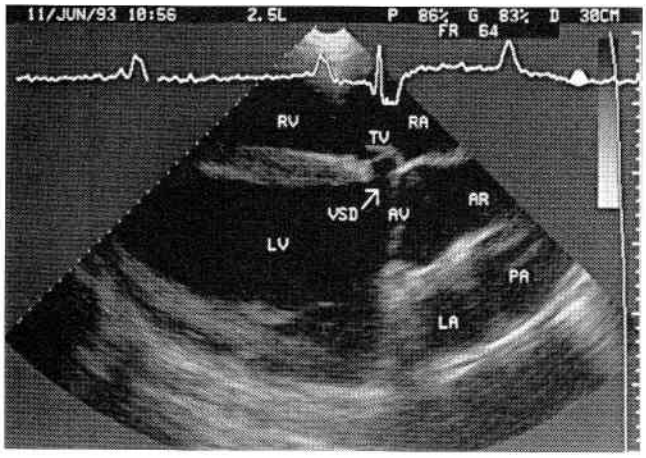

Figure 5–11

Long-axis echocardiogram of an inflow or membranous ventricular septal defect (VSD) obtained from a 2-year-old Standardbred colt. The septal dropout *(arrow)* in the membranous portion of the interventricular septum is just ventral to the aortic valve (AV) and the septal leaflet of the tricuspid valve (TV). A small chorda tendinea extends from the septal leaflet of the tricuspid valve to the right side of the interventricular septum. This echocardiogram was obtained from the right cardiac window in the left ventricular outflow tract position with a 2.5-MHz sector-scanner transducer at a displayed depth of 30 cm. An electrocardiogram is superimposed for timing. RA, Right atrium; RV, right ventricle; LV, left ventricle; LA, left atrium; AR, aortic root; PA, pulmonary artery.

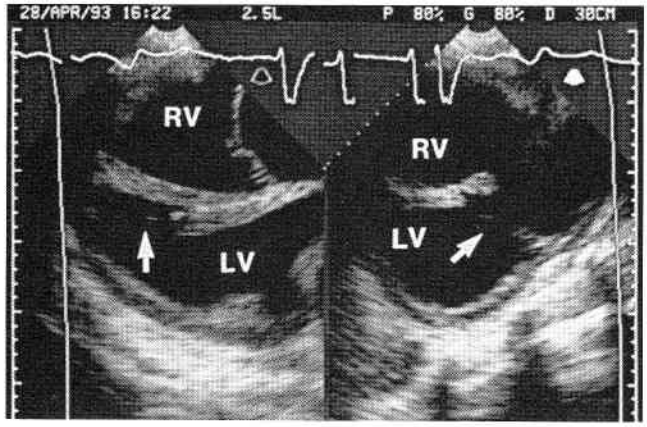

Figure 5–13

Echocardiograms obtained from a 5-year-old Pony of the Americas (POA) mare with a large muscular ventricular septal defect (VSD) *(arrows)* located in the outflow portion of the interventricular septum. This mare presented with congestive heart failure and atrial fibrillation. The echocardiogram on the left side is a long-axis view obtained between the left and right ventricular outflow tract views, showing the large VSD located in the outflow portion of the interventricular septum *(arrow)* and a large thick moderator band in the large right ventricle. The echocardiogram on the right side is a short-axis view of the right ventricular outflow tract, demonstrating the large VSD in the outlet portion of the interventricular septum *(arrow)* and the large right ventricle. These echocardiograms were obtained from the right cardiac window with a 2.5-MHz sector-scanner transducer at a displayed depth of 30 cm. An electrocardiogram is superimposed for timing. RV, Right ventricle; LV, left ventricle.

the defect's largest diameter to obtain an estimate of the defect's size, information that is critical in formulating a prognosis for the usefulness of the affected horse (Fig. 5–12).[9, 33, 35, 36, 38, 64] The actual size of the VSD may be less than actually measured because the margins of the defect are often irregular and because of poor lateral resolution of the defect's edges.[38] VSD in the muscular and outflow portions of the interventricular septum is more difficult to detect but can often be found with a careful search of the interventricular septum.[36, 101, 102] The outflow tract VSD is usually best imaged in the right parasternal short-axis view of the RVOT (Fig. 5–13). Mus-

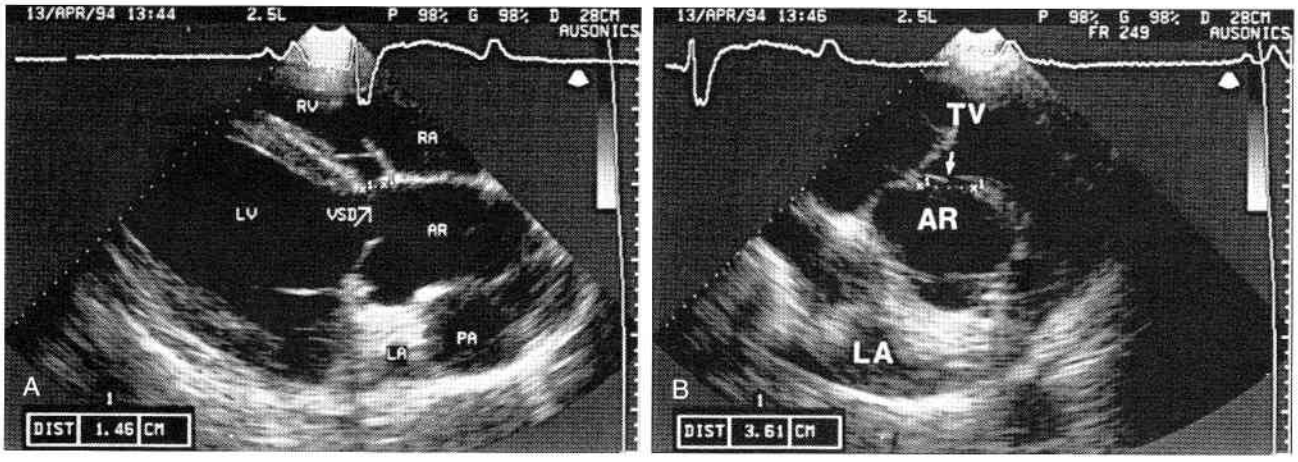

Figure 5–12

Echocardiograms from an 8-year-old Arabian gelding with a membranous ventricular septal defect (VSD). These echocardiograms were obtained from the right cardiac window with a 2.5-MHz sector-scanner transducer at a 28-cm displayed depth. An electrocardiogram is superimposed for timing.

A, Long-axis echocardiogram of the left ventricular outflow tract demonstrating the VSD *(arrow)* and its maximal long-axis diameter (1.46 cm) between the interventricular septum and the right side of the aortic root. RA, Right atrium; RV, right ventricle; LV, left ventricle; LA, left atrium; AR, aortic root; PA, pulmonary artery.

B, Short-axis echocardiogram of the root of the aorta demonstrating the VSD *(arrow)* and its maximal short-axis diameter (3.61 cm) between the cranial and caudal margins of the septal defect. TV, Tricuspid valve; AR, aortic root; LA, left atrium.

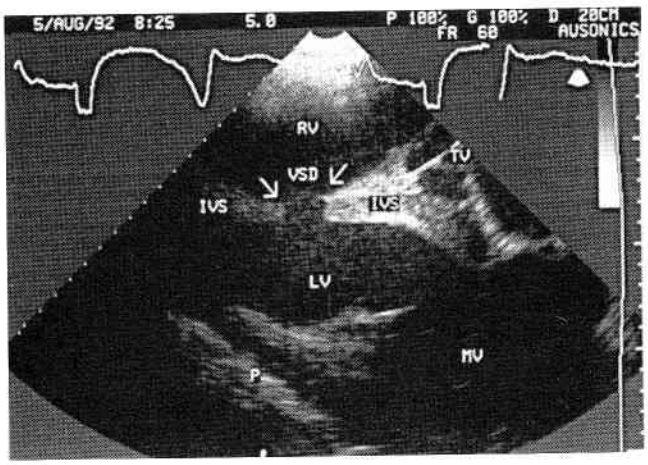

Figure 5–14

Long-axis echocardiogram obtained from a yearling Arabian filly with a muscular ventricular septal defect (VSD). The VSD *(arrows)* is in the muscular portion of the interventricular septum (IVS). This echocardiogram was obtained from the right cardiac window in the mitral valve position with a 5.0-MHz sector-scanner transducer at a displayed depth of 20 cm. An electrocardiogram is superimposed for timing. TV, Tricuspid valve; RV, right ventricle; LV, left ventricle; MV, mitral valve; P, pericardium.

cular VSD can be located anywhere in the ventricular septum, and thus the interventricular septum must be carefully scanned in all imaging planes to detect this defect (Fig. 5–14).[36, 38, 101, 102] One of the aortic valve cusps (usually the noncoronary or, less frequently, the right coronary cusp) may prolapse into the VSD, making the defect more difficult to detect for the novice echocardiographer and frequently resulting in mild aortic regurgitation (Fig. 5–15).[36, 38, 60, 64, 103] This aortic valve prolapse occurs because of a lack of support of the right side of the aortic root, more likely in human beings with a large VSD located in the outlet portion of the interventricular septum, immediately beneath the aortic root.[36, 38, 104] If aortic valve prolapse is present, the associated regurgitation is usually small.[36, 60, 81, 103] Thickened, distorted, and furled aortic cusps resulted in aortic regurgitation in one horse with a VSD.[103] A flail aortic leaflet and severe aortic regurgitation have been reported in one horse with a large VSD.[36, 64] Care should be taken to measure the diameter of the VSD from the actual margins of the defect and not from the edge of the aortic valve cusp, which may be prolapsing into the defect and making the defect appear smaller than it actually is. Left atrial and left ventricular enlargement and volume overload are usually detected in horses with a VSD (Fig. 5–16). Right ventricular enlargement and volume overload are usually detected only in horses with a larger perimembranous VSD or a large defect located in the muscular portion of the interventricular septum (Fig. 5–17). Pulmonary artery dilatation is infrequently detected in horses with VSD and may be detected in horses with increased volume of blood flow through the pulmonary artery (horses with a large VSD and right ventricular volume overload) or in horses with concurrent pulmonary hypertension (Fig. 5–17).

VSD has also been diagnosed successfully using M-mode echocardiographic techniques in large animals.[7, 11, 14, 15, 35] Drop-out of the right side of the aortic root is usually detected with M-mode echocardiography during part of the cardiac cycle (usually during systole) in horses with an inflow or membranous VSD (Fig. 5–18). High-frequency vibrations of the septal leaflet of the tricuspid valve may also be detected in horses with a membranous VSD (Fig. 5–18). Finding the site of a muscular VSD is

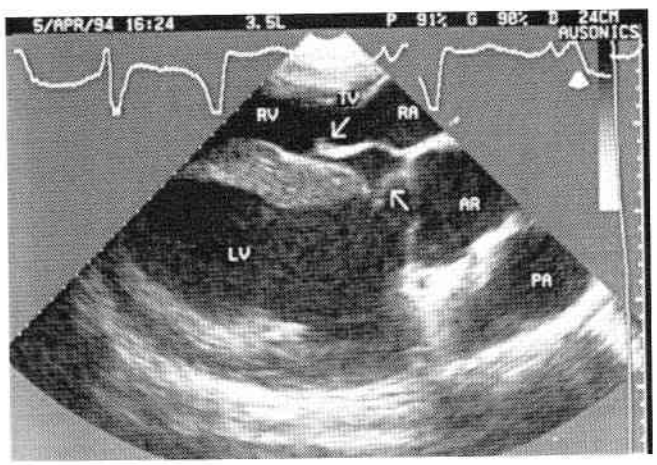

Figure 5–15

Long-axis echocardiogram of a membranous ventricular septal defect obtained from a yearling Standardbred colt demonstrating prolapse of the noncoronary cusp of the aortic valve into the septal defect *(up arrow)*. Notice the elongated and thickened septal leaflet *(down arrow)* of the tricuspid valve (TV). This echocardiogram was obtained from the right cardiac window in the left ventricular outflow tract position with a 3.5-MHz sector-scanner transducer at a displayed depth of 24 cm. An electrocardiogram is superimposed for timing. RA, Right atrium; RV, right ventricle; LV, left ventricle; AR, aortic root; PA, pulmonary artery.

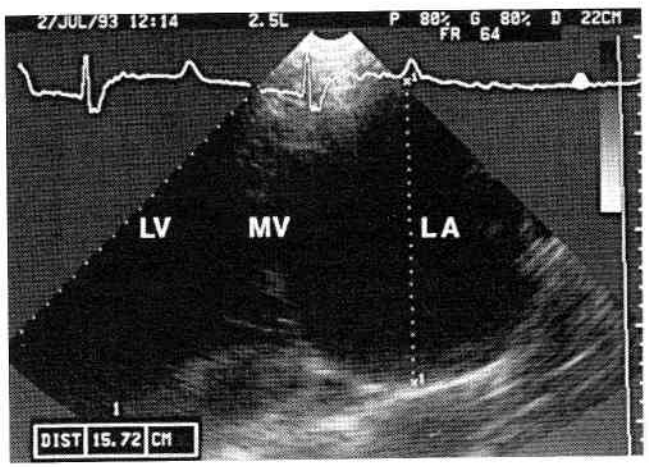

Figure 5–16

Long-axis echocardiogram of the left atrium and left ventricle obtained from a 2-year-old Standardbred colt with a membranous ventricular septal defect (same colt as in Figure 5–11). The enlarged left atrium measures 15.72 cm in diameter. This echocardiogram was obtained from the left cardiac window in the mitral valve position with a 2.5-MHz sector-scanner transducer at a displayed depth of 22 cm. An electrocardiogram is superimposed for timing. LA, Left atrium; MV, mitral valve; LV, left ventricle.

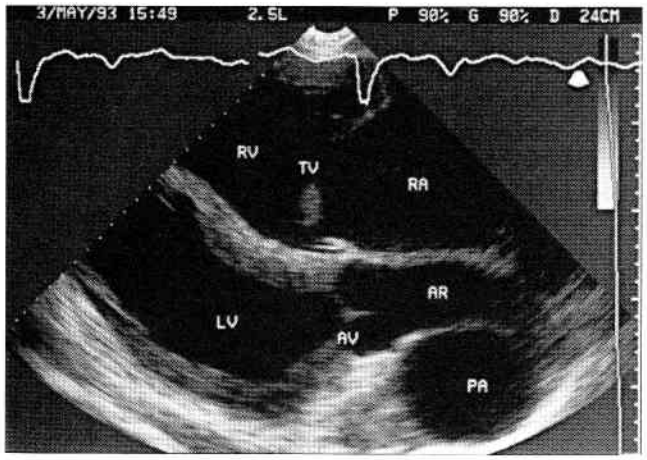

Figure 5–17

Long-axis echocardiogram obtained from a 5-year-old Pony of the Americas mare with a large muscular outflow tract ventricular septal defect, atrial fibrillation, and biventricular failure (same mare as in Figure 5–13). Notice the enlarged right atrium (RA) and right ventricle (RV), dilated pulmonary artery (PA), smaller-than-normal aortic root (AR), and thickened septal leaflet of the tricuspid valve (TV). This echocardiogram was obtained from the right cardiac window in the left ventricular outflow tract position with a 2.5-MHz sector-scanner transducer at a 24-cm displayed depth. An electrocardiogram is superimposed for timing. LV, Left ventricle; AV, aortic valve.

difficult with M-mode echocardiography, and a careful search of the septum must be performed with 2-D echocardiography.

Contrast echocardiography has been used in large animals with suspected VSD to confirm the shunting of blood through the ventricular septum.[7, 12, 14, 33-35, 76] Injection of contrast agents into the jugular vein or right ventricle results in opacification of the right ventricle with microbubbles, and a negative contrast jet may be seen in the right ventricle from the shunt through the VSD.[33, 34] Passage of contrast material into the left ventricle may also be seen in diastole with left-to-right VSD.[35] Although a VSD in a large animal is usually easily visualized with careful scanning of the interventricular septum using 2-D echocardiography, a smaller VSD may be missed owing to its small size or variable location in the interventricular septum.[100]

Pulsed, color-flow, and continuous-wave forms of Doppler echocardiography are used to identify a VSD and its location, determine shunt direction and the associated pressure gradient, and map shunt flow and any associated regurgitation.[33, 35, 36, 58, 64, 72, 81, 82, 104-107] With Doppler echocardiography, a harsh sound is heard throughout systole. This sound is displayed on the pulsed-wave Doppler spectral tracing as an aliased systolic signal with spectral broadening (Fig. 5–19). The spectral tracing obtained with continuous-wave Doppler echocardiography is a high-velocity systolic envelope present above the baseline when the examination is performed from the right parasternal window in a horse with a left-to-right shunt (Fig. 5–20). From the same cardiac window in the horse with a left-to-right shunt, a red jet is imaged coming through the defect into the right ventricle (toward the transducer) with color-flow Doppler echocardiography.[38] Color reversal (aliasing) and a mosaic pattern are detected in association with high-velocity (aliased), turbulent (mosaic) flow in the center of the jet (Color Figure 5–1).[38] The com-

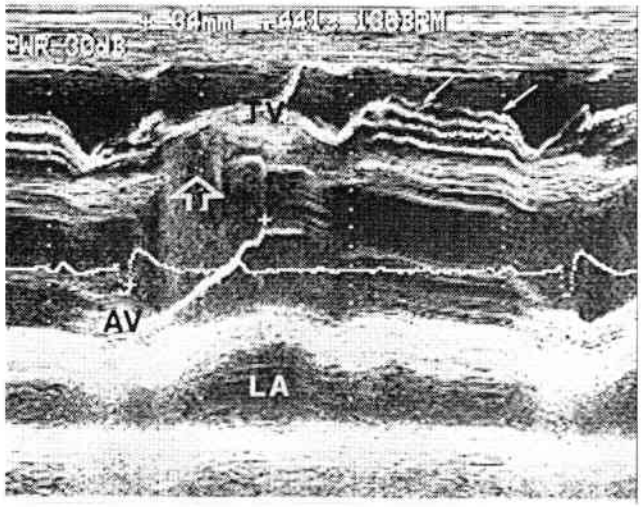

Figure 5–18

M-mode echocardiogram obtained from a 9-year-old Standardbred stallion with a membranous ventricular septal defect (VSD). Notice the dropout of the aortic root at the site of the VSD *(open arrow)* and the high-frequency vibrations of the septal leaflet of the tricuspid valve during diastole *(arrows)*, caused by turbulence from the shunt. The cursors are measuring the aortic ejection time of 0.441 sec (normal). This echocardiogram was obtained from the right cardiac window in the left ventricular outflow tract position with a 2.5-MHz transducer at a 27.5-cm displayed depth. An electrocardiogram is superimposed for timing. TV, Tricuspid valve; AV, aortic valve; LA, left atrium.

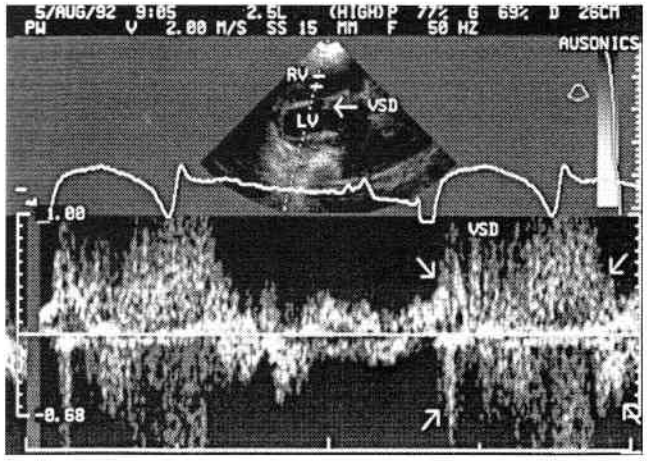

Figure 5–19

Long-axis echocardiogram and pulsed-wave Doppler spectral tracing of the high-velocity turbulent blood flow shunting through the muscular ventricular septal defect (VSD) in a yearling Arabian filly (same filly as in Figure 5–14). The sample volume (two parallel lines) is positioned on the right ventricular side of the VSD *(arrow)*. Notice the aliased signal (flow depicted above and below the baseline) and the spectral broadening during systole *(arrows)* in the pulsed-wave Doppler spectral tracing. This echocardiogram and spectral tracing were obtained from the right cardiac window in the mitral valve position with a 2.5-MHz sector-scanner transducer, which emits ultrasound pulses (pulsed-wave Doppler) at a frequency of 2.0 MHz at a displayed depth of 26 cm. An electrocardiogram is superimposed for timing. RV, Right ventricle; LV, left ventricle.

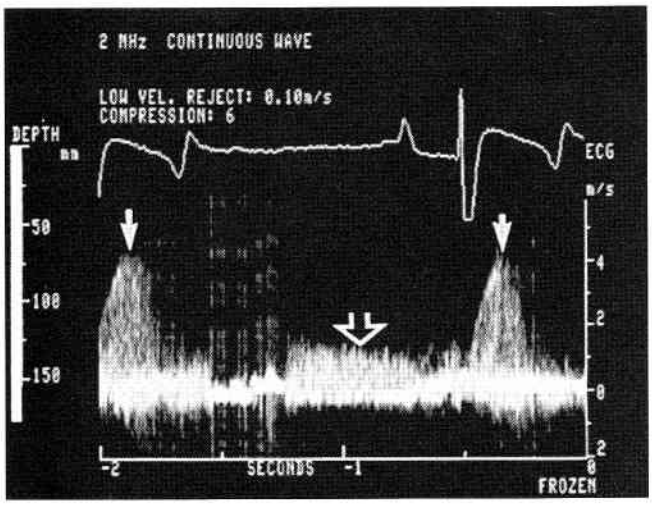

Figure 5–20

Continuous-wave Doppler spectral tracing of the high-velocity turbulent blood flow through the membranous ventricular septal defect in a 2-year-old Standardbred colt (same colt as in Figures 5-11 and 5-16). Notice the spectral broadening in systole *(closed arrows)* and diastole *(open arrow)* and the peak flow velocity of approximately 4 m/sec in systole and 1.5 m/sec in diastole. This continuous-wave Doppler spectral tracing was obtained from the right cardiac window with a stand-alone 2.0-MHz continuous-wave Doppler (Pedoff) transducer, angling the transducer toward the left ventricular outflow tract. An electrocardiogram is superimposed for timing.

bined use of 2-D and Doppler echocardiography has a high sensitivity and specificity for the detection of isolated perimembranous VSD in human beings and horses.[36, 105-108] Color-flow Doppler echocardiography has a higher sensitivity than 2-D echocardiography coupled with pulsed- or continuous-wave Doppler echocardiography for the diagnosis of multiple VSD.[109] Interventricular pressure gradients should be noninvasively estimated with continuous-wave Doppler echocardiography and are indicative of the hemodynamic significance of the VSD in human beings and horses.[33, 36, 38, 81, 82, 105, 107, 108] This noninvasive estimate of the interventricular pressure gradient is valid if there is no right or left ventricular outflow tract obstruction. A peak shunt velocity *(v)* through the VSD of 4 m/sec or more measured with continuous-wave Doppler echocardiography is indicative of a restrictive VSD and a defect of lesser hemodynamic significance.[33, 36, 38, 81, 82, 105] Measuring systolic arterial blood pressure (SAP) directly or indirectly through coccygeal arterial Doppler measurements allows the echocardiographer to estimate right ventricular pressure (RVP) in horses with a VSD using the following formula:[33, 36, 38, 81, 82, 97, 105]

$$RVP = SAP - 4v^2$$

There may be no flow through the VSD if ventricular pressures are equal, or flow reversal (from right to left) may be detected if right ventricular pressure exceeds left ventricular pressure, a situation that occurs with severe pulmonary hypertension. Right-to-left shunts are rare in horses with VSD.[33] Analysis of the flow convergence region on the left ventricular side of the defect is also an indication of the hemodynamic significance of the VSD (Color Figure 5-1).[110]

Patient Management and Prognosis. Ventricular septal defects are the most likely congenital defects to be diagnosed as an incidental finding and may be detected in horses performing up to their owner's or trainer's expectations.[15, 33, 35, 36, 38, 64, 76, 100, 103, 111] VSD can also be the cause of exercise intolerance in horses with large (>2.5 cm diameter) defects.[15, 33, 35-38, 64, 100, 103, 112, 113] Horses with complex congenital cardiac defects are usually poor doers, have exercise intolerance or poor performance, and have shortened life expectancy.[11, 15, 33, 36, 38, 39, 64, 114] Prognosis for horses with a VSD is based upon the number, location, and size of VSD, interventricular pressure gradient, shunt direction, degree of left ventricular volume overload, left ventricular function, and presence or absence of concomitant aortic prolapse, aortic regurgitation, and its severity.[33, 36, 38, 64] Horses with a perimembranous VSD of 2.5 cm or less, with a peak shunt velocity greater than 4 m/sec and little or no aortic prolapse or aortic regurgitation, have a good prognosis and may even be able to compete successfully as racehorses.[33, 35, 36, 38, 64, 111] Horses with a larger muscular or multiple VSD are more likely to have performance problems or a shortened life expectancy. Horses with VSD greater than 2.5 cm but less than 3.5 cm and shunt velocities of 3 m/sec or more but less than 4 m/sec usually do not have normal exercise tolerance but may be useful pleasure horses.[15, 36, 38, 64, 103, 112, 113] Most horses with VSD greater than 3.5 cm in diameter or shunt velocities less than 3 m/sec have a shortened life expectancy and develop congestive heart failure.[15, 35-38, 64, 100]

Ventricular Septal Defect with Pulmonic Stenosis. Ventricular septal defects have been infrequently reported in conjunction with pulmonic stenosis and/or a hypoplastic pulmonary artery. Affected foals have a grade 4/6 or higher, band-shaped pansystolic murmur with the point of maximal intensity in the pulmonic valve or tricuspid valve area. Murmurs may also be of equal intensity in the tricuspid and pulmonic valve areas. Both membranous and muscular locations for the VSD have been reported. A hypoplastic pulmonary artery has been detected by the author in two foals with VSD, one with a defect in the muscular portion of the interventricular septum and a bicuspid pulmonic valve and one with a membranous VSD (Fig. 5-21).

Patient Management and Prognosis. Prognosis for affected foals depends upon the size and location of the VSD and the severity of the RVOT obstruction. The foals with severe RVOT obstruction and large and/or muscular VSD are likely to grow poorly and have exercise intolerance within the first year of life.

Atrial Septal Defect. Atrial septal defects (ASD) occur infrequently in horses as isolated congenital defects and are more common as part of a complex congenital cardiac disorder.[15, 38, 72, 115-118] Affected individuals usually have a holosystolic murmur with the point of maximal intensity over the pulmonic valve or heart base. Right atrial, right ventricular, and usually left atrial enlargement are detected echocardiographically (Fig. 5-22) as well as dilatation of the pulmonary artery.[38, 72, 119] Paradoxical septal motion, an echocardiographic sign of right ventric-

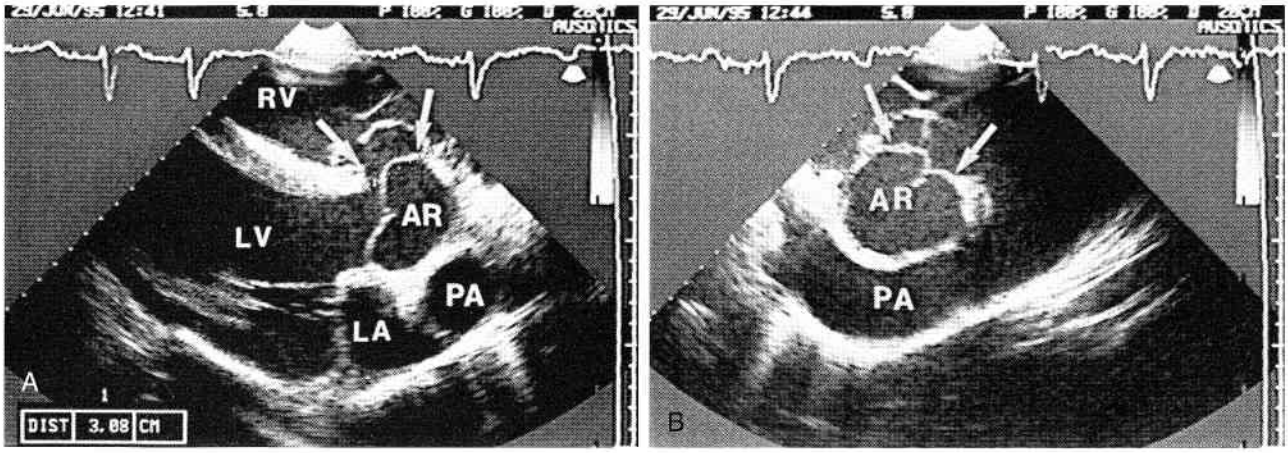

Figure 5–21

Echocardiograms obtained from a 4-month-old Thoroughbred colt with a membranous ventricular septal defect (VSD) and pulmonary artery hypoplasia. Notice the size discrepancy between the aortic root (AR) and the pulmonary artery (PA). These echocardiograms were obtained with a 5.0-MHz sector-scanner transducer at a displayed depth of 20 cm. An electrocardiogram is superimposed for timing.

A, Long-axis view of the VSD *(arrows)* located in the membranous portion of the interventricular septum, beneath the septal leaflet of the tricuspid valve, measuring 3.08 cm in this plane. LV, Left ventricle; LA, left atrium; RV, right ventricle.

B, Short-axis view of the aortic root demonstrating the large membranous VSD beneath the right coronary and noncoronary leaflets of the aortic valve *(arrows).*

ular volume overload, is also detected.[38, 119] An increased area under the tricuspid valve, compared with the area under the mitral valve, has been imaged in diastole in human beings with ASD. Some people also have abnormal interventricular septal motion in early diastole.[38, 119] Drop-out of the atrial septal echoes is detected in the portion of the atrial septum associated with the defect: at the most basilar portion of the atrial septum with sinus venosus defects, in the area of the foramen ovale with atrial secundum defects, and in the ventral portion of the atrial septum, immediately adjacent to the ventricular septum, with atrial primum defects.[38, 119] Persistently patent foramen ovale is imaged in the center of the atrial septum (Fig. 5–23). Anatomic closure of the foramen ovale should be present by 9 weeks after birth.[90] Drop-out of the atrial septum can occur in normal hearts, particularly in the area of the foramen ovale, so identification of the defect in two mutually perpendicular views is important for the 2-D echocardiographic diagnosis of ASD.[38] The drop-out that can occur in normal hearts is a

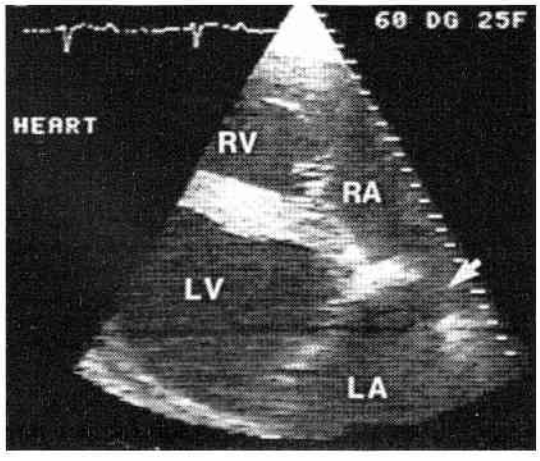

Figure 5–22

Long-axis echocardiogram obtained from a 4-year-old Appaloosa gelding with an atrial septal defect (ASD). Notice the defect *(arrow)* in the upper portion of the interatrial septum (sinus venosus ASD). Contrast and color-flow Doppler echocardiography demonstrated a left-to-right shunt at this level. The large left atrium (LA), right atrium (RA), and right ventricle (RV) are consistent with an atrial septal defect. This echocardiogram was obtained from the right cardiac window in the four-chamber position, angling dorsally to see the base of the atria with a 2.25-MHz sector-scanner transducer at a displayed depth of 25 cm. An electrocardiogram is superimposed for timing. LV, Left ventricle.

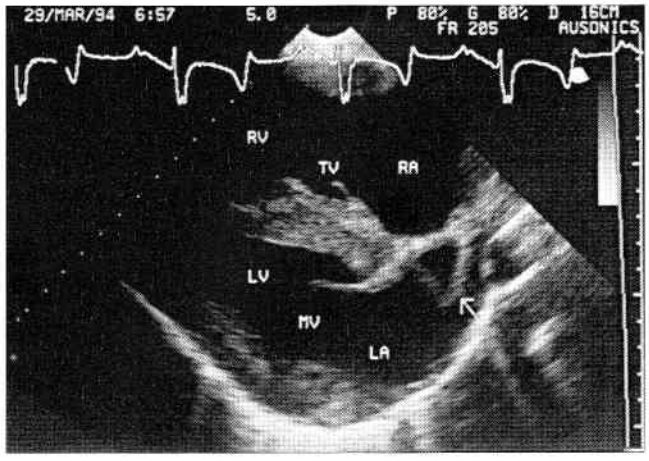

Figure 5–23

Echocardiogram obtained from a 6-day-old Standardbred colt with pulmonary hypertension and a foramen ovale *(arrow)* bulging into the left atrium (LA) owing to increased right atrial (RA) pressures. A small amount of blood was detected shunting from right to left at the atrial level through the foramen ovale with contrast echocardiography. This long-axis four-chamber view was obtained from the right cardiac window with a 5.0-MHz sector-scanner transducer at a displayed depth of 16 cm. An electrocardiogram is superimposed for timing. TV, Tricuspid valve; RV, right ventricle; LV, left ventricle; MV, mitral valve.

gradual thinning of the atrial septum in the area of the foramen ovale, whereas the drop-out associated with an ASD is usually associated with the T sign. The T sign is a bright echo that is imaged perpendicular to the defect at the site of the echo drop-out.[38, 119]

Doppler or contrast echocardiographic confirmation of the shunt should be performed. Contrast echocardiography is very sensitive for the detection of ASD and should be performed whenever an ASD is suspected.[38, 119] With a peripheral venous injection (jugular vein), a negative contrast jet should be detected coming through the atrial septum (left-to-right shunt).[38] Occasionally in horses and human beings with left-to-right shunts, a small amount of positive contrast shunts through the ASD or patent foramen ovale into the left atrium in individuals with normal pulmonary arterial pressures.[38, 119] A small amount of right-to-left shunting also occurs with the Valsalva maneuver.[38, 119] A large amount of positive contrast is imaged in the left atrium and, subsequently, the left ventricle in horses and human beings with right-to-left shunts and in individuals with pulmonary hypertension.[38, 119] A low-velocity jet through the atrial septum into the right atrium, increased tricuspid valve velocity, and increased pulmonary artery velocity are detected with Doppler echocardiography. The largest flow through the ASD is present during systole, with smaller amounts in early and late diastole.[38, 120] Flow through the ASD also varies with respiration.[38, 120] The color-flow map reveals a reddish orange jet traversing the interatrial septum when the horse is scanned from the right parasternal window and the shunt is from left to right.

Patient Management and Prognosis. If the shunt through the ASD is small, the horse may have no apparent compromise. Most ASD are associated with complex congenital cardiac disorders and therefore have a guarded to grave prognosis. Smaller ASD may be well tolerated, and an ASD has been detected echocardiographically in one horse with atrial fibrillation.[72, 121]

Patent Ductus Arteriosus. This congenital cardiac anomaly is also rare as an isolated congenital cardiac defect in horses and is most frequently seen in individuals with complex congenital cardiac disorders.[7, 11, 15, 33, 38, 44, 72, 115, 116, 122–125] The ductus arteriosus is functionally closed in normal foals 16 hours after birth.[126] A patent ductus arteriosus (PDA) results in a continuous machinery murmur that is loudest in the pulmonic valve area.[15, 72, 123, 124] Visualization of the ductus arteriosus is difficult in equine neonates, and it is often not possible to image the ductus arteriosus in foals or adults owing to the presence of overlying lung.[38, 44, 72] The ductus can sometimes be imaged from the right or left parasternal window in the most cranial position with careful scanning of the aorta and pulmonary artery in the area of the ductus arteriosus (Fig. 5-24).[44] An enlarged, volume-overloaded left atrium and left ventricle and a dilated aorta and pulmonary artery should be detected with echocardiography if a significant shunt occurs through the ductus arteriosus.[38, 72] In most individuals, continuous high-velocity flow is detected with Doppler echocardiography traversing the ductus arteriosus from aorta to pulmonary artery, unless severe pulmonary hypertension exists.[38, 44, 72, 105, 119, 120] The ductal flow is most easily detected by examination of the main

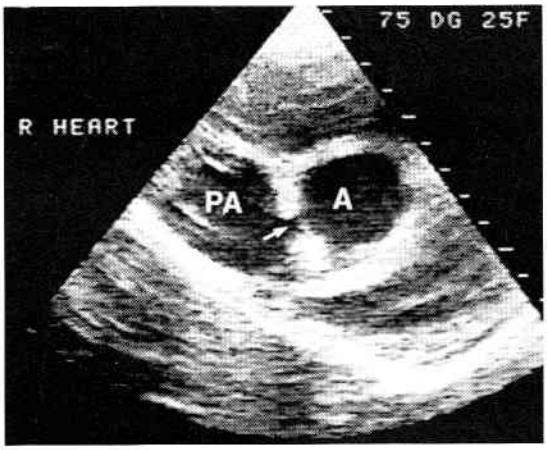

Figure 5–24

Echocardiogram obtained from a 5-day-old Thoroughbred colt with a patent ductus arteriosus. Notice the communication *(arrow)* between the main pulmonary artery (PA) and the ascending aorta (A). Pulsed-wave, continuous-wave, and color-flow Doppler echocardiography demonstrated continuous flow from the aorta into the pulmonary artery. This echocardiogram was obtained from the right cardiac window, angling dorsally from the right ventricular outflow tract position with a 3.5-MHz sector-scanner transducer at a displayed depth of 14 cm.

pulmonary artery from the left cardiac window.[72] Continuous or pandiastolic flow is associated with normal pulmonary arterial pressure and a small PDA.[38, 105, 119, 120] Color-flow Doppler echocardiography has been useful in detecting the shunt associated with PDA in horses and provides a rapid and sensitive detection of PDA in human beings.[38, 119] From the right parasternal window, flow through the left-to-right PDA is depicted as bluish green, whereas from the left parasternal window the shunt flow is reddish orange.[38]

Patient Management and Prognosis. A guarded prognosis must be given for foals with a PDA when detected as an isolated defect.[15, 122, 123, 125] PDA is occasionally detected in neonatal foals for longer than 96 hours after birth, most frequently in premature foals or foals with pulmonary hypertension associated with pneumonia.[72] The PDA often closes later once the pulmonary disease has been successfully treated and the pulmonary hypertension resolves. Foals diagnosed with a PDA and other congenital cardiac defects warrant a guarded to grave prognosis, as these complex congenital defects are associated with a shortened life expectancy.[11, 15, 44, 72, 114]

Complete Atrioventricular Canal Defect. Endocardial cushion defect or complete absence of the atrioventricular canal is a rare defect in horses.[38, 40, 72] A loud grade 4/6 or higher, harsh pansystolic band-shaped murmur of equal intensity is present over both sides of the cardiac silhouette. Echocardiographic findings in affected foals include a large primum ASD, a large membranous and perimembranous VSD, and abnormalities of the atrioventricular valves (Color Figure 5-2).[38, 40, 72] Fusion of the atrioventricular valves or cleft valve leaflets may be detected. Blood flow from left to right atrium and left to right ventricle can be demonstrated with contrast and color-flow echocardiography (Color Figure 5-3).[38, 40, 72] Mitral and tricuspid regurgitation are also frequently present.

Patient Management and Prognosis. Prognosis for affected foals is guarded to grave and depends on the obstruction, if any, to right ventricular outflow.[40, 72] The majority of affected foals have a life expectancy of 1 year or less.

Tetralogy of Fallot. Tetralogy of Fallot is one of the more common complex congenital cardiac defects in horses.[7, 11, 15, 33, 38, 41, 72, 90, 116, 117, 127-129] Affected foals have a loud grade 3/6 or higher holosystolic or pansystolic ejection murmur with its point of maximal intensity in the pulmonic valve area.[15, 41, 72, 90] A slightly softer, coarse, band-shaped pansystolic murmur is also auscultated over the tricuspid valve area. The defects associated with tetralogy of Fallot (VSD, overriding aorta, RVOT obstruction, and right ventricular hypertrophy) are easily detectable echocardiographically (Fig. 5-25).[12, 15, 38, 41, 72] The VSD is located in the perimembranous portion of the interventricular septum. The subaortic VSD and the overriding aorta are best imaged in the long-axis view of the left ventricular outflow tract.[38] The severity and type of RVOT obstruction are best determined from the RVOT views. Most affected horses have a hypoplastic pulmonic valve and pulmonary artery rather than a discrete valvular, subvalvular, or supravalvular obstruction.[72] A high-velocity turbulent jet is imaged in the main pulmonary artery above the RVOT obstruction with Doppler echocardiography.[38] This jet may be best detected from the left parasternal window in larger individuals but often can be imaged from both cardiac windows. Little flow may be detected across the VSD if right ventricular pressure is high; however, with color-flow Doppler echocardiography, flow is coded in blue leaving the right ventricle and shunting out the aorta through the VSD.[38] Contrast echocardiography also demonstrates this shunt nicely with a peripheral venous injection. Opacification of the right ventricle is followed by simultaneous opacification of the left ventricle, aorta, and pulmonary artery.[12, 15, 38, 72]

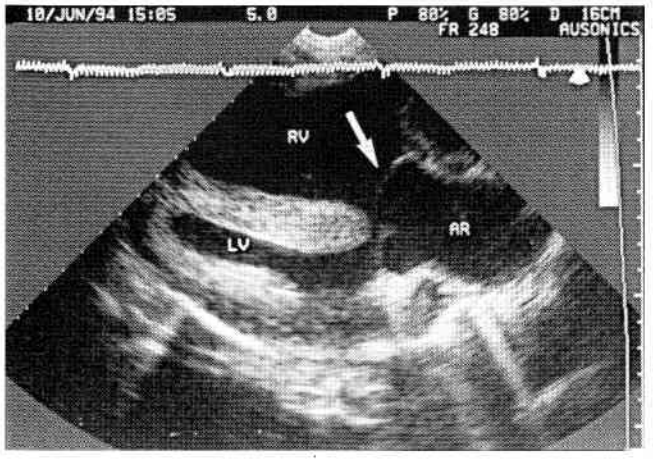

Figure 5-25

Echocardiogram obtained from a 1-week-old Arabian-Thoroughbred cross filly with tetralogy of Fallot. Long-axis view of the left ventricular outflow tract demonstrates the large ventricular septal defect *(arrow)*, the overriding aorta (AR), and right ventricular dilatation and hypertrophy. This echocardiogram was obtained with a 5.0-MHz sector-scanner transducer at a displayed depth of 16 cm. An electrocardiogram is superimposed for timing. RV, Right ventricle; LV, left ventricle.

Patient Management and Prognosis. The size of the VSD and the severity of the RVOT obstruction determine the hemodynamic significance of this congenital cardiac defect.[15, 72, 90] Prognosis for survival is guarded to grave, with the majority of foals humanely destroyed in the first year of life.[15, 33, 41, 72, 127-129] The oldest reported horse diagnosed with tetralogy of Fallot was 3 years old.[41]

Pulmonary Atresia. Pulmonary atresia, also known as pseudotruncus arteriosus, is another complex congenital cardiac defect that has been reported primarily in Arabian foals.[11, 38, 72, 114] Affected foals have a loud grade 4/6 or higher, holosystolic or pansystolic murmur usually equally loud over both sides of the cardiac silhouette, or a continuous murmur may be auscultated.[11, 114] This malformation is the most severe form of tetralogy of Fallot, as RVOT obstruction is complete because the pulmonic valve and pulmonary artery are atretic.[38, 72, 114] The aorta is markedly dilated and overrides the ventricular septum and the large subaortic VSD. The right and left pulmonary arteries originate from the PDA, or bronchial arteries are responsible for pulmonary blood flow.[38, 72, 114] The large VSD, overriding aorta, and right ventricular hypertrophy are easily imaged echocardiographically. Echocardiographic diagnosis of pulmonic valve and pulmonary artery atresia is more difficult; however, color-flow Doppler and/or contrast echocardiography should detect any flow from the RVOT into the pulmonary artery through the pulmonic valve, differentiating pulmonary atresia from tetralogy of Fallot with severe RVOT obstruction.[38]

Patient Management and Prognosis. These foals usually have a guarded to grave prognosis because they have a complete right-to-left shunt.[11, 72] The more pulmonary blood flow present, the longer the foal is likely to live.[72]

Persistent Truncus Arteriosus. A loud grade 4/6 or higher, holosystolic or pansystolic murmur has been reported in foals with persistent truncus arteriosus.[130, 131] A persistent truncus arteriosus is easily confused echocardiographically and pathologically with a pseudotruncus arteriosus or pulmonary atresia if careful attention is not paid to cardiac anatomy.[72, 114] In a persistent truncus arteriosus there is no aorticopulmonary septum because the truncus arteriosus failed to divide. One large vessel communicates with both ventricles through a large subaortic VSD (Fig. 5-26).[72, 114, 129-131] One or more pulmonary arteries arise directly from the truncus arteriosus, or pulmonary blood flow is supplied solely through the bronchial circulation. The large VSD, large great vessel (truncus arteriosus), and right ventricular hypertrophy are easily detected with echocardiography.[130, 131] The absence of the main pulmonary artery is suspected echocardiographically by the inability to image this vessel or to detect blood flow through it with color-flow Doppler or contrast echocardiography. However, it is difficult to differentiate the foal with pulmonary atresia from the one with a true truncus arteriosus echocardiographically.[130, 131] It is also difficult to image the anatomy of the pulmonary vessels as they branch off the truncus arteriosus, owing to the presence of overlying lung.

Patient Management and Prognosis. These foals also must be given a guarded to grave prognosis, as they

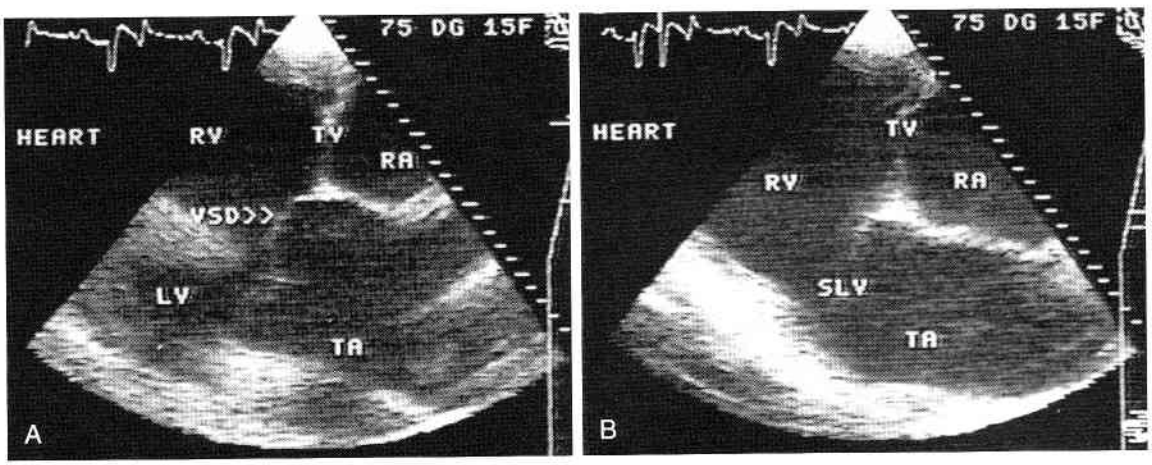

Figure 5–26

Long-axis echocardiograms obtained from a yearling Arabian gelding with a truncus arteriosus. Notice the large single vessel communicating with the outflow tracts of both ventricles. These echocardiograms were obtained from the right cardiac window with a 2.25-MHz sector-scanner transducer at a displayed depth of 25 cm. An electrocardiogram is superimposed for timing.

A, Long-axis echocardiogram of the left ventricular outflow tract view demonstrating the ventricular septal defect (VSD) *(arrowheads)* and the large single vessel, the truncus arteriosus (TA), overriding the interventricular septum and communicating with both right (RV) and left (LV) ventricles. TV, Tricuspid valve; RA, right atrium.

B, Long-axis echocardiogram of the right ventricular outflow tract demonstrating the same large vessel, the truncus arteriosus (TA), communicating with the right ventricle (RV). RA, Right atrium; TV, tricuspid valve; SLV, semilunar valve.

have a complete right-to-left shunt.[11, 72, 114, 117, 129, 130] The amount of pulmonary blood flow determines how severe their clinical signs are and how long the affected individual survives.

Tricuspid Atresia. Tricuspid atresia is one of the more frequently reported complex congenital cardiac defects in foals.[11, 15, 38, 39, 72, 116, 132–137] Harsh grade 4/6 or higher holosystolic or pansystolic band-shaped or crescendo-decrescendo murmurs, loudest over the left heart base or, in some foals, equally loud over the left heart base and tricuspid valve area, have been described.[11, 15, 39, 72, 116, 132, 133, 137] Echocardiographically, a thick band of muscular echoes is detected in the area of the right atrioventricular valve with absent tricuspid valve leaflets, a large VSD, and a patent foramen ovale or ASD (Fig. 5-27).[11, 15, 38, 39] The right ventricle is diminutive, and the right atrium is enlarged and thickened. The left atrium, mitral valve annulus, and left ventricle are also enlarged. Contrast or color-flow echocardiography can be used to trace the path of blood flow through the heart (Color Figure 5-4).[15, 38, 39] The blood flows from the right atrium, through the patent foramen ovale or ASD into the left atrium, through the mitral valve into the left ventricle.[15, 38, 39] Simultaneous filling of the right ventricle and aorta then occurs.

Patient Management and Prognosis. Prognosis for affected foals is grave, and few foals live past weaning age.[11, 15, 39, 72, 116, 132, 133, 137]

Transposition of the Great Vessels. Transposition of the great vessels is another complex congenital cardiac anomaly that occurs infrequently in horses.[15, 38, 138] Transposition of the great vessels may be complete or partial and usually occurs in conjunction with other cardiac defects such as pulmonic stenosis.[138–141] The echocardiographic diagnosis of complete transposition of the great vessels requires careful evaluation of the anatomy and orientation of the vessel leaving each ventricle. The aorta is imaged arising from the right ventricle, cranially, and to the right of the pulmonary artery, arising from the left ventricle.[38] One or more shunts are necessary for the foal to survive, and these can usually be imaged echocardiographically as well as with pulsed-wave and color-flow Doppler echocardiography.[38]

Patient Management and Prognosis. These foals must be given a guarded to grave prognosis, and few foals survive beyond weaning age.

Other Congenital Cardiac Defects. Several other congenital cardiac defects have been described in foals,

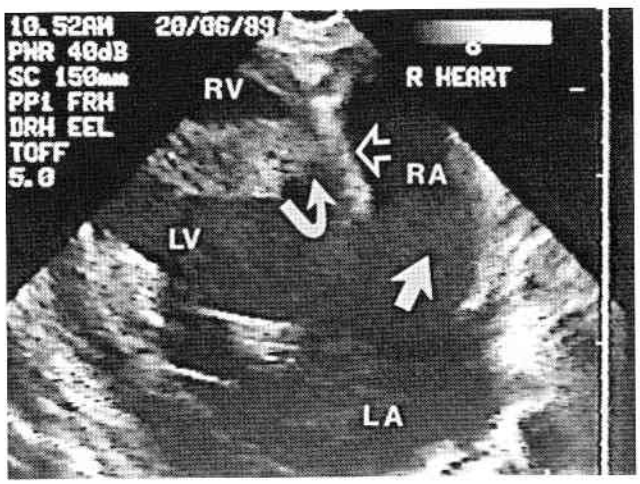

Figure 5–27

Long-axis echocardiogram of a 6-week-old Thoroughbred filly with tricuspid atresia. Notice the thick muscular band *(open arrow)* where the tricuspid valve should be, the right atrium (RA), the large atrial septal defect *(straight arrow)*, the large left atrium (LA), the ventricular septal defect *(curved arrow)*, the hypoplastic right ventricle (RV), and the larger left ventricle (LV). This echocardiogram was obtained from the right cardiac window in the four-chamber view with a 5.0-MHz sector-scanner transducer at a displayed depth of 15 cm.

most of them complex.[142-147] Abnormalities of the semilunar valves resulting in aortic or pulmonic stenosis are rare congenital cardiac defects in horses and occur more frequently (pulmonic stenosis) in conjunction with other cardiac defects.[11, 15, 138, 145-147] Aortic insufficiency has also been reported as a congenital lesion in one horse.[148] Most of the complex cardiac defects can be delineated echocardiographically with a careful evaluation of cardiac anatomy and a segmental approach to the echocardiographic examination (Fig. 5-28).[38] Doppler and contrast echocardiographic evaluation are useful to trace the path of blood flow in these affected hearts and to help determine the significance of the abnormalities detected.[38]

Acquired Valvular Heart Disease

Physiologic flow murmurs are often difficult to distinguish from murmurs associated with valvular insufficiency.[7, 55, 64, 72, 78, 79, 93, 94] Valvular regurgitation is common in horses, ranges from clinically insignificant to severe, and may result in the development of congestive heart failure.[7, 8, 15, 14, 30, 33, 34, 47-64, 72, 74, 78, 79, 81-83, 91, 93, 94, 111, 121, 148] Valvular stenosis (congenital or acquired) is rare and has most frequently been reported in association with bacterial endocarditis in horses.[7, 15, 33, 43, 54, 59, 64, 72, 82, 93, 116, 122, 147] Mitral and tricuspid regurgitation murmurs are the most common causes of systolic murmurs associated with underlying cardiac disease in horses.[7, 33, 64, 72, 78, 81, 91, 94, 121, 149] Murmurs of mitral and tricuspid regurgitation are usually harsh, band shaped, grade 3/6 or higher, holosystolic or pansystolic, with their point of maximal intensity at the atrioventricular valve area.[78, 88, 90, 93, 149-151] Mitral and tricuspid valve prolapse usually produces crescendo mid to late systolic murmurs, whereas horses with ruptured chordae tendineae tend to have harmonic, musical, or honking murmurs.[14, 93] Holodiastolic murmurs indicative of aortic insufficiency are loudest in the aortic valve area, are usually decrescendo or musical, and can be any intensity.[13, 60-62, 64, 79, 80, 93, 152-155] Pulmonic insufficiency is a rare clinical finding, most common in horses with left-sided congestive heart failure and pulmonary hypertension, although trivial pulmonic regurgitation is commonly detected with Doppler echocardiography.[49, 63, 64, 79, 80, 93] Holodiastolic murmurs of mitral or tricuspid stenosis are extremely rare in horses.[64, 72, 82, 88, 93] Prior to the use of echocardiography in horses, the diagnosis of valvular heart disease and its severity was based upon the location, quality, and intensity of the murmur auscultated and the clinical signs exhibited by the horse.[86-88, 90, 93, 94] A complete echocardiographic examination (M-mode, 2-D real-time, and Doppler) provides an objective assessment of the existence and severity of the horse's valvular regurgitation.[7-9, 15, 33, 47-56, 59-64, 72, 81-83, 94]

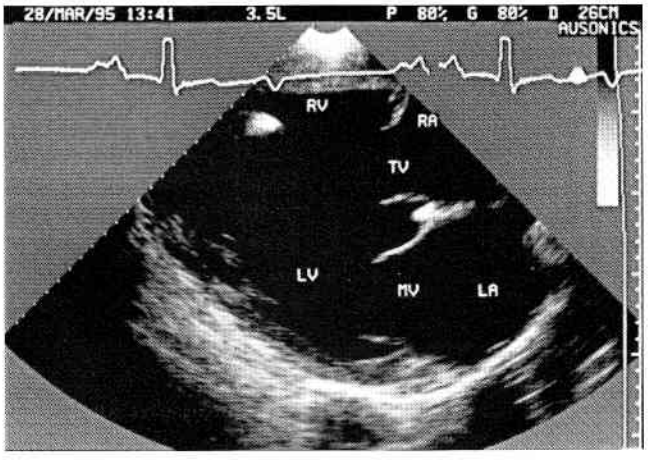

Figure 5-28

Long-axis echocardiogram obtained from a 3-year-old Appaloosa filly with a common ventricle. Both atrioventricular valves communicate with a single ventricle. No ventricular septum is present. This echocardiogram was obtained from the right cardiac window in the four-chamber view with a 3.5-MHz sector-scanner transducer at a displayed depth of 26 cm. An electrocardiogram is superimposed for timing. RV, Right side of the common ventricle; LV, left side of the common ventricle; RA, right atrium; TV, tricuspid valve; LA, left atrium; MV, mitral valve.

Mitral Regurgitation. Mitral regurgitation is the valvular insufficiency most likely to be associated with poor performance or clinical signs of left- or right-sided heart failure because significant mitral regurgitation leads to pulmonary hypertension.[7, 33, 47-50, 64, 72, 78, 81, 86, 93, 121, 149, 150, 156] Left atrioventricular valvular insufficiency usually progresses more rapidly because the left side of the heart is the systemic side of the circulation. Abnormalities of the mitral valve leaflets and/or chordal apparatus may be detected echocardiographically, or the horse may have mitral regurgitation and a structurally normal valve. The normal equine mitral valve is composed of two primary leaflets, the septal and caudal (free wall or parietal) leaflets, a variable number of accessory leaflets, and a variable distribution of chordae tendineae between the two papillary muscles.[157] The septal leaflet is the largest leaflet, followed by the smaller caudal (parietal or free wall) leaflet and the even smaller accessory cusps. Proper coaptation of the mitral valve leaflets depends upon normal function of the mitral valve leaflets, chordae tendineae, papillary muscles, and associated ventricular myocardium.

The mitral valve abnormalities that have been detected echocardiographically in horses with mitral regurgitation include congenital abnormalities (Fig. 5-29) of the mitral valve (rare), valvular thickening (degenerative), prolapse, ruptured chordae tendineae, noninfective valvulitis, vegetative endocarditis, and stretching of the mitral valve annulus with an anatomically normal valve (primary myocardial disease).[7, 14, 33, 47-49, 64, 72, 74, 121] Prolapse and thickening of the mitral valve leaflets are the most common changes detected echocardiographically in horses with mitral regurgitation.[7, 14, 33, 47-49, 64, 72, 121] In horses with mitral valve prolapse, the entire mitral valve leaflet, or a portion thereof, is imaged bulging backward into the left atrium (Fig. 5-30).[14] This dorsal displacement of the mitral valve usually happens during mid to late systole and is usually best imaged when examining the mitral valve from the left cardiac window in the parasternal long-axis view. Mitral valve prolapse is less frequently detected from the right parasternal long-axis view of the mitral valve. M-mode echocardiographic diagnosis of mitral valve prolapse has been described in horses[14] but is much easier to diagnose with 2-D echocardiography. The pro-

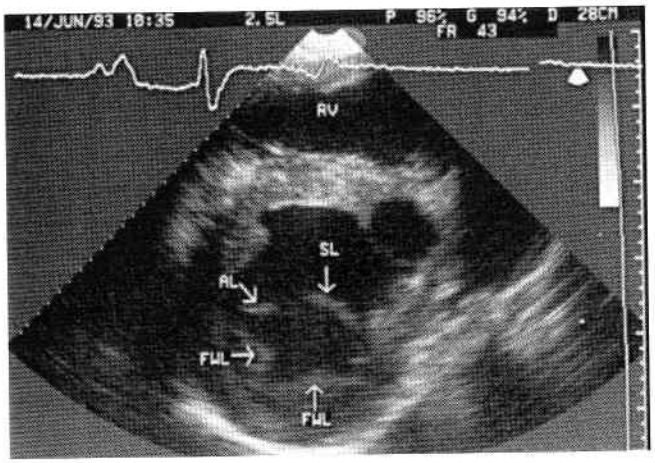

Figure 5–29

Short-axis echocardiogram of a cleft mitral valve obtained from a 10-year-old Thoroughbred gelding. Notice the two portions of the free wall leaflet (FWL), the septal leaflet (SL), and one of the accessory leaflets (AL) of the mitral valve. Only a small amount of mitral regurgitation was detected with pulsed-wave Doppler echocardiography at the site of the cleft in the FWL. This echocardiogram was obtained from the right cardiac window in the mitral valve position with a 2.5-MHz sector-scanner transducer at a 28-cm displayed depth. An electrocardiogram is superimposed for timing. RV, Right ventricle.

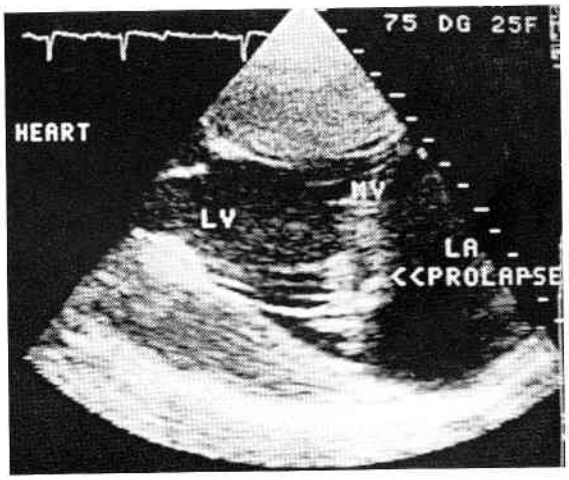

Figure 5–31

Long-axis echocardiogram obtained from a 4-month-old Morgan colt with mitral valve prolapse and severe mitral regurgitation. Notice the marked thickening of the mitral valve (MV) leaflets and the chordal apparatus and the bulging of the septal leaflet of the mitral valve into the enlarged left atrium (LA) during systole (prolapse). This echocardiogram was obtained from the left cardiac window in the mitral valve position with a 5.0-MHz sector-scanner transducer at a displayed depth of 17 cm. An electrocardiogram is superimposed for timing. LV, Left ventricle.

lapsing mitral valve may also be thickened and have redundant leaflets or elongated chordae tendineae (Fig. 5-31), findings that are frequently reported in human beings with mitral valve prolapse.[158] A ruptured chorda tendinea can also cause mitral valve prolapse, and therefore all horses with significant mitral valve prolapse should be carefully scanned for a possible ruptured chorda tendinea or flail mitral valve leaflet (Fig. 5-32).[47-49, 72, 158, 159]

Degenerative changes of the mitral valve leaflets or a noninfective valvulitis results in thickening of the leaflets, most easily detected with 2-D echocardiography. Horses with noninfective valvulitis usually have slightly hypoechoic to echogenic valvular thickening, whereas those with degenerative valve disease usually have echogenic to hyperechoic thickening of the valve leaflets, often with other echocardiographic abnormalities of the valve or valve apparatus. An irregular free edge of the valve leaflet with nodular or ridgelike thickenings or other deformation of the free edge of the cusps and, less frequently, thickening of the chordal apparatus is also detectable with 2-D echocardiography. Degenerative changes of the mitral valve leaflets are the most frequently detected postmortem finding in older horses and can be detected in the absence of mitral regurgitation.[90, 121, 149, 156, 160-162]

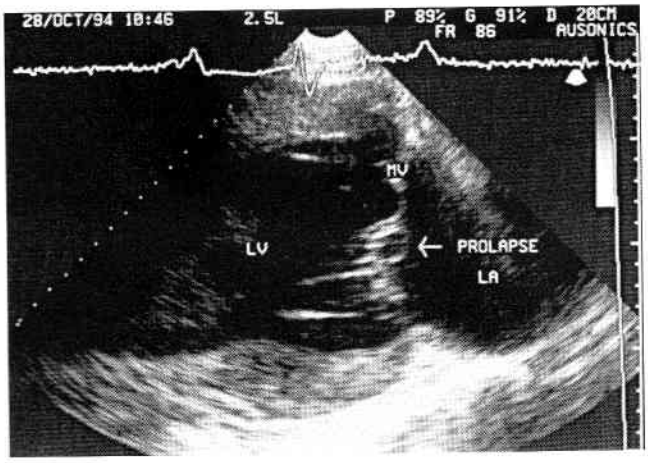

Figure 5–30

Long-axis echocardiogram of a prolapsing portion of the mitral valve from a 17-year-old Quarter Horse gelding. The free edge of the mitral valve leaflet (MV) bulges backward into the left atrium (LA) or prolapses (*arrow*). This echocardiogram was obtained from the left cardiac window in the mitral valve position with a 2.5-MHz sector-scanner transducer at a 20-cm displayed depth. An electrocardiogram is superimposed for timing. LV, Left ventricle.

Ruptured chordae tendineae and flail valve leaflets occur less frequently in horses.[47-49, 64, 72, 150, 163] The echocardiographic detection of a mobile linear echo everting into the left atrium in systole is diagnostic of a ruptured chorda tendinea (Fig. 5-33).[47-49, 72] The entire chorda tendinea may be imaged everting into the left atrium with a whiplike action if the chordal rupture involves one of the longer chordae tendineae ruptured at or near its papillary muscle insertion. The ruptured chorda tendinea moves either with the valve leaflet or with the subvalvular apparatus, depending on the site of chordal rupture.[158] Echocardiographic findings indicative of a septal chordal rupture include systolic mitral valve flutter, chaotic diastolic leaflet flutter, increased septal leaflet excursion with rapid leaflet opening, and a lack of coaptation of mitral valve leaflets in systole.[47, 158] Most frequently, however, a short chorda tendinea associated with a caudal or accessory cusp chordal rupture (Fig. 5-33) or a contracted chorda tendinea is imaged everting into the left atrium, or a flail valve leaflet (Fig. 5-34) is detected in horses with ruptured mitral chordae tendineae.[47-49, 64, 72] The asynchronous movement of a valve leaflet, or

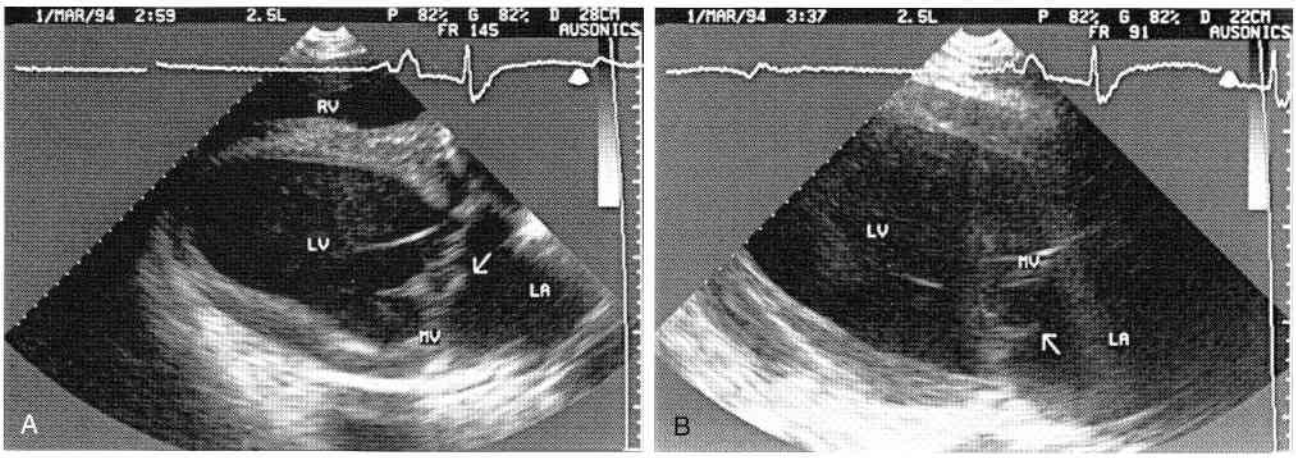

Figure 5–32

Long-axis echocardiograms of a flail mitral valve leaflet associated with a ruptured chorda tendinea obtained from a 4-year-old Thoroughbred filly. An electrocardiogram is superimposed for timing.

A, The accessory leaflet of the mitral valve (MV) prolapses *(arrow)* into the left atrium (LA), but a flail leaflet could not be detected from this cardiac window. This echocardiogram was obtained from the right cardiac window in the mitral valve position with a 2.5-MHz transducer at a displayed depth of 28 cm. RV, Right ventricle; LV, left ventricle.

B, The flail accessory leaflet of the mitral valve (MV) flips backward *(arrow)* but does not evert into the left atrium (LA) during systole. This echocardiogram was obtained from the left cardiac window in the mitral valve position with a 2.5-MHz sector-scanner transducer at a 22-cm displayed depth. LV, Left ventricle.

any portion thereof, in any phase of the cardiac cycle is indicative of a flail valve leaflet.[47, 164] The valve leaflet can often be imaged flipping from left atrium to left ventricle.[158] A prolapsed valve leaflet, the flail chorda tendinea and/or paradoxical mitral valve motion may be imaged echocardiographically with a rupture of a free wall or accessory leaflet chorda tendinea.[47] Ruptured chordae tendineae and flail valve leaflets most frequently involve the accessory cusps in horses.[47, 48, 64, 72, 150] Degenerative changes associated with degenerative valve disease may be the most common cause of chordal rupture in horses, as it is in human beings, but endocarditis, myocardial necrosis of the papillary muscles, and surrounding left ventricle and idiopathic chordal rupture have been reported as causes of ruptured mitral valve chordae tendineae in horses.[47–49] Most flail valve leaflets or ruptured chordae tendineae are best visualized from the left parasternal window in the two-chamber view of the mitral valve, scanning caudally and dorsally. The entire mitral valve apparatus should be thoroughly scanned from both parasternal windows and in all planes to detect ruptured chordae tendineae and flail mitral valve leaflets.[48, 49, 64, 72]

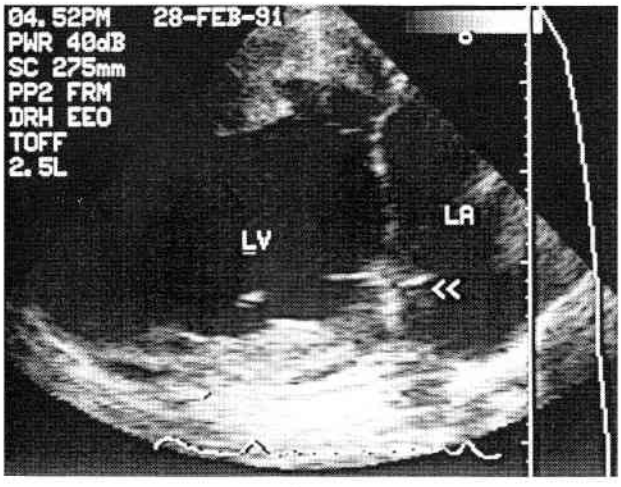

Figure 5–33

Long-axis echocardiogram obtained from an 11-year-old Standardbred stallion with a ruptured chorda tendinea of the accessory leaflet of the mitral valve. The linear echo *(arrowheads)* of the chorda tendinea everts into the left atrium (LA) in systole. This echocardiogram was obtained from the left cardiac window in the mitral valve position with a 2.5-MHz sector-scanner transducer at a displayed depth of 27.5 cm. An electrocardiogram is superimposed for timing. LV, Left ventricle.

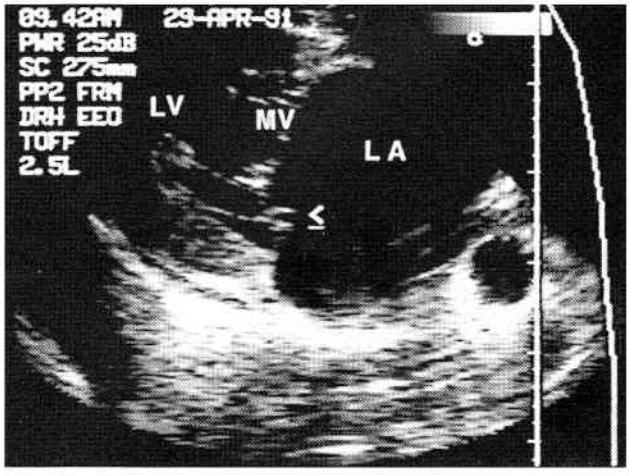

Figure 5–34

Long-axis echocardiogram obtained from a 3-year-old Standardbred filly with a flail accessory mitral valve leaflet associated with a ruptured chorda tendinea. Notice the flail accessory leaflet *(arrowhead)* in the left atrium (LA) during systole and the enlarged, rounded, and turgid appearance of the left atrium. This echocardiogram was obtained from the left cardiac window in the mitral valve position with a 2.5-MHz sector-scanner transducer at a displayed depth of 27.5 cm. LV, Left ventricle; MV, mitral valve.

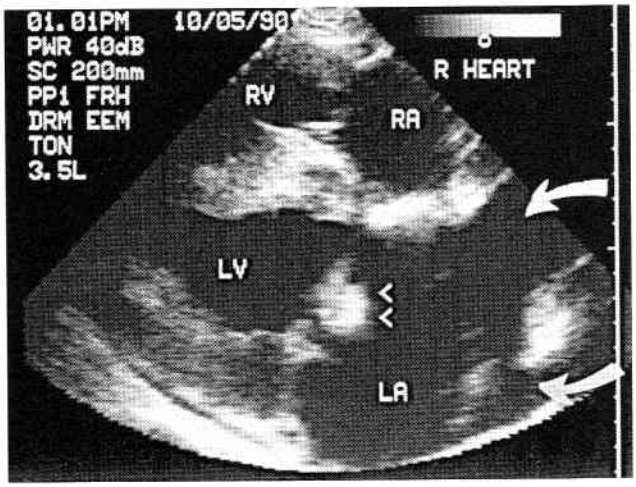

Figure 5–35

Long-axis echocardiogram obtained from a 5-month-old Hanoverian filly with bacterial endocarditis. Notice the large echogenic mass on the septal leaflet of the mitral valve *(arrowheads),* the isoechoic mass on the free wall leaflet, and the thickening of the septal and free wall leaflets of the mitral valve. Significant left atrial (LA) enlargement and marked distention of the pulmonary veins *(curved arrows)* are associated with severe mitral regurgitation. This echocardiogram was obtained from the right cardiac window in the mitral valve position with a 3.5-MHz sector-scanner transducer at a displayed depth of 20 cm. RA, Right atrium; RV, right ventricle; LV, left ventricle.

The mitral valve is one of the common sites of bacterial endocarditis in horses, but endocarditis lesions occur infrequently in horses.[47, 49-51, 64, 72, 165, 166] Two-dimensional echocardiography is superior to M-mode echocardiography for the diagnosis of bacterial endocarditis because all four valve leaflets and most of the endocardial surfaces of the heart can be carefully imaged. TEE is superior for the detection of small endocarditis lesions that cannot be imaged with routine transthoracic echocardiography in human beings and may become available at large equine referral centers in the future.[81, 96, 167, 168] Endocarditis lesions can range from a slight thickening of the valve leaflet to large vegetative masses on the valve leaflet, subvalvular structures, and mural endocardium.[7, 33, 47, 49-51, 64, 72] The vegetative masses are usually echogenic to hyperechoic with irregular margins and move with the affected valve leaflet (Fig. 5-35).[7, 33, 47, 49-51, 64, 72] The detection of mural vegetative masses without involvement of the valve leaflets is rare in horses with bacterial endocarditis.[47, 49-51] Ruptured chordae tendineae can occur secondary to involvement of the chordal apparatus with the bacterial infection and the subsequent weakening of these structures.[47, 72] The irregular vegetative masses usually become rounder and smoother if the horse is responding to treatment.[33, 50, 51, 64, 72] Often, however, the mitral regurgitation becomes more severe because of severe damage to the valve that occurred from the infection and secondary to scarring of the leaflets.[50, 72]

Mitral regurgitation can be clinically insignificant or mild, resulting in little or no left atrial and left ventricular enlargement.[64, 72] Rounding of the left ventricular apex, dilatation of the left atrium (>13.5 cm in the left parasternal two-chamber view) and left ventricle, thinning of the left ventricular free wall and interventricular septum, and an increased shortening fraction (left ventricular volume overload) are detected echocardiographically in horses with clinically significant mitral regurgitation and normal myocardial function.[7, 33, 47-51, 64, 72] The left ventricular internal dimension at end-diastole ranges from approximately 12 to 20 cm in horses with congestive heart failure and mitral regurgitation.[49, 64] A left atrium significantly larger than the right atrium or a left atrial appendage in systole equal to or larger than the diameter of the aortic root indicates left atrial enlargement (Fig. 5-36).

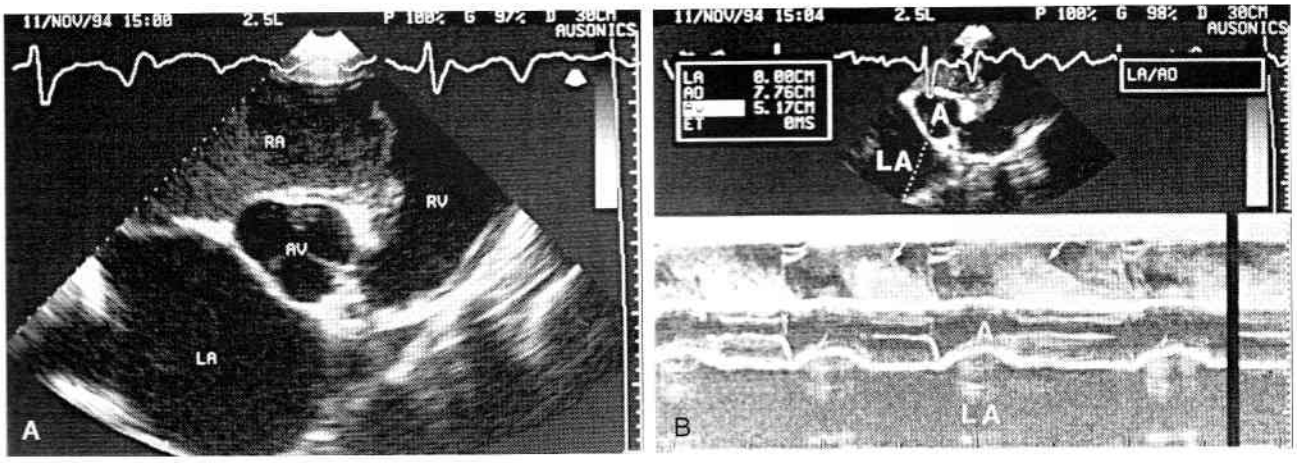

Figure 5–36

Echocardiograms obtained from a 13-year-old Thoroughbred gelding with acute-onset atrial fibrillation and left-sided congestive heart failure secondary to a ruptured mitral chorda tendinea. Echocardiograms are obtained from the right cardiac window in the aortic root position with a 2.5-MHz sector-scanner transducer at a displayed depth of 30 cm. An electrocardiogram is superimposed for timing.

A, Short-axis echocardiogram demonstrating the very large left atrium (LA) and the spontaneous contrast (increased echoes or smoke) associated with low-flow states in the right atrium (RA). RV, Right ventricle; AV, aortic valve.

B, M-mode echocardiogram from the same position as Figure 5-6 showing the placement of the M-mode cursor through the left atrial appendage (LA). Notice the spontaneous contrast *(arrows)* in the right atrium at the tricuspid valve and the enlarged left atrial appendage (larger than the diameter of the aortic root). A, Aortic valve.

However, these estimations of left atrial enlargement are not as sensitive as the measurement of left atrial diameter made in the left parasternal two-chamber view, which is more likely to detect mild left atrial enlargement (Fig. 5-37).[64] Horses with mitral regurgitation and congestive heart failure have left atrial diameters ranging from 16 to 23 cm, depending upon the cause, initial severity, and speed of progression of the mitral regurgitation.[49, 64] With acute-onset severe mitral regurgitation, such as that which occurs with the rupture of a major chorda tendinea of the mitral valve, the left atrium has less time to stretch, and signs of congestive heart failure may appear with a left atrial diameter of 16 cm. The left atrium may also appear rounded and turgid with severe, hemodynamically significant mitral regurgitation (Fig. 5-38).[49, 64, 72] Bulging of the interatrial septum toward the right atrium is another indication of significantly increased left atrial pressures (Fig. 5-39). A normal or decreased fractional shortening in a horse with severe mitral regurgitation indicates concurrent left ventricular dysfunction (Fig. 5-40).[7, 49, 64, 72, 93] Dilatation of the pulmonary artery is an echocardiographic indication of hemodynamically severe mitral regurgitation and pulmonary hypertension (Fig. 5-41).[7, 47, 49, 50, 64, 72] The severity of mitral regurgitation can also be demonstrated with contrast echocardiography, but an injection of echo contrast material must be made into the left ventricle.[12, 34, 76]

The severity of mitral regurgitation can be estimated from evaluation of the size of the regurgitant jet area detected with pulsed-wave and color-flow Doppler echocardiography (Color Figure 5-5).[33, 48, 64, 72, 78, 80-83, 169-171] The regurgitant jet has a characteristic mosaic appearance with color-flow Doppler echocardiography, as the regurgitant jet contains turbulent, high-velocity blood flow.[81, 158, 169, 170] Proximal flow convergence (speeding up of blood flow as it approaches the regurgitant orifice) has been detected in human beings with severe mitral regurgitation and has been seen in some horses. A regurgitant jet detected only immediately dorsal to the valve leaflets is usually clinically insignificant, whereas one that occupies two thirds or more of the left atrial cavity is indicative of severe mitral regurgitation.[33, 78, 80, 104] A regurgitant jet area of one third of the left atrial cavity or less indicates mild mitral regurgitation, whereas a regurgitant jet area of one third to two thirds of the left atrial cavity is compatible with moderate mitral regurgitation.

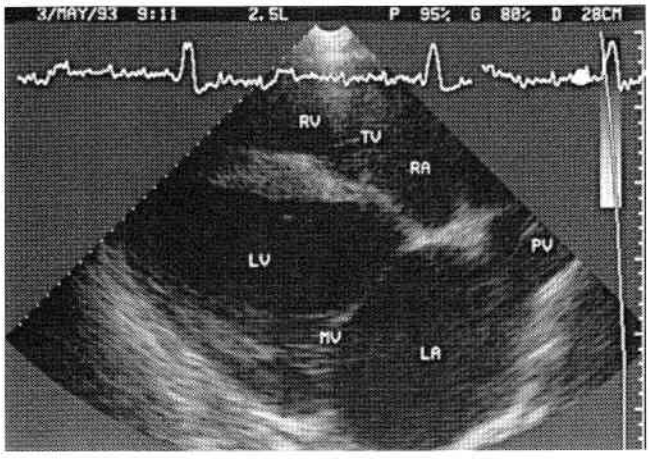

Figure 5–38

Long-axis echocardiogram obtained from an 18-year-old Arabian mare with atrial fibrillation, severe mitral regurgitation, and biventricular failure. Notice the round, turgid-appearing left atrium (LA) and enlarged pulmonary vein (PV). Right atrial (RA), right ventricular (RV), and left ventricular (LV) enlargement is also present. This echocardiogram was obtained from the right cardiac window in the four-chamber position with a 2.5-MHz sector-scanner transducer at a displayed depth of 28 cm. An electrocardiogram is superimposed for timing. TV, Tricuspid valve; MV, mitral valve.

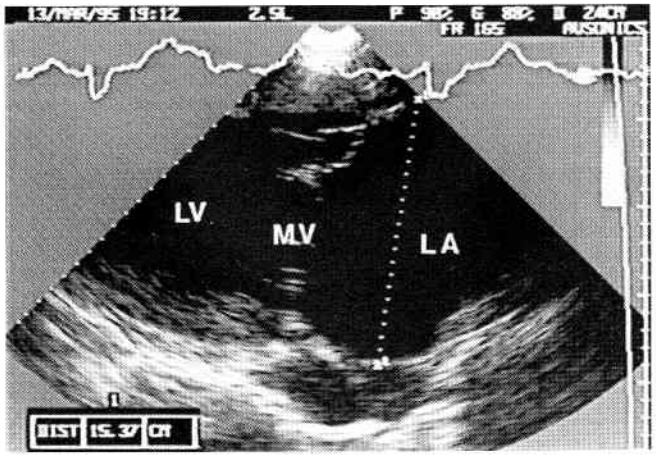

Figure 5–37

Long-axis echocardiogram obtained from a 3-year-old Thoroughbred gelding with atrial fibrillation, mitral valve prolapse, a small ruptured chorda tendinea of an accessory mitral valve leaflet, and mild left atrial enlargement. The left atrium (LA) has a maximal diameter of 15.37 cm. This echocardiogram was obtained from the left cardiac window in the mitral valve position with a 2.5-MHz sector-scanner transducer at a displayed depth of 24 cm. LV, Left ventricle; MV, mitral valve.

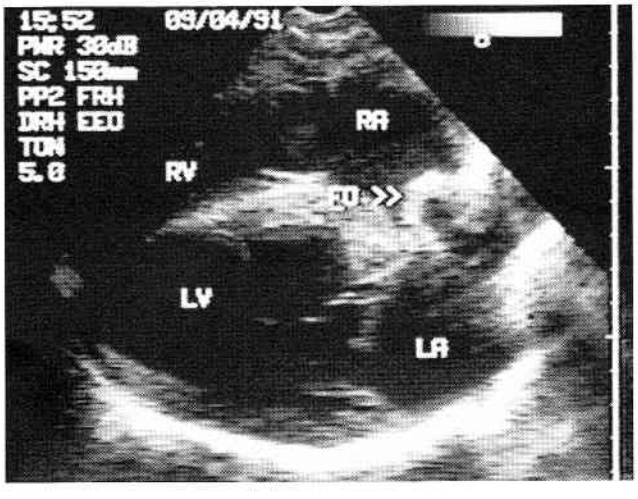

Figure 5–39

Long-axis two-dimensional echocardiogram obtained from a 1-week-old Standardbred filly with moderate mitral, pulmonic, and tricuspid regurgitation. Notice the herniation of the foramen ovale (FO) into the right atrium (RA), indicating elevated left atrial pressures. This filly presented with severe tachycardia and tachypnea shortly after birth. This echocardiogram was obtained with a 5.0-MHz sector-scanner transducer at a displayed depth of 15 cm. RV, Right ventricle; LV, left ventricle; LA, left atrium.

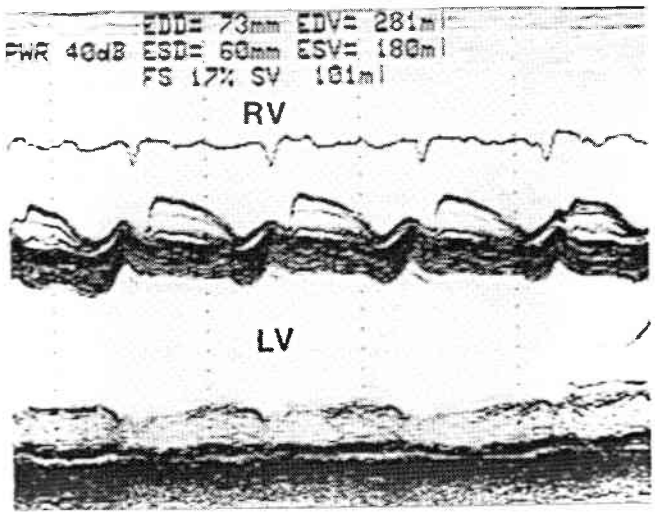

Figure 5–40

M-mode echocardiogram obtained from a 6-month-old Standardbred filly with cardiomyopathy of unknown cause and severe mitral, pulmonic, and tricuspid regurgitation. The poor interventricular septal and left ventricular free wall motion with minimal systolic thickening of the myocardium results in a fractional shortening (FS) of 17%. The right ventricle (RV) is also markedly enlarged secondary to the left-sided heart failure, pulmonary hypertension, and pulmonic and tricuspid regurgitation. The slight variation in the R-R intervals and baseline fibrillation waves is consistent with a diagnosis of atrial fibrillation. This echocardiogram was obtained from the right cardiac window in the left ventricular position with a 2.5-MHz sector-scanner transducer at a displayed depth of 27.5 cm. An electrocardiogram is superimposed for timing. LV, Left ventricle.

The size of the color-flow jet area has been shown to be accurate in the semiquantitation of the severity of mitral regurgitation in human beings.[158, 169, 170] One exception is when mitral regurgitation jets hug the left atrial wall rather than spraying out into the left atrial cavity, making the jet area appear small and the regurgitation less significant than it actually is.[169] Another exception occurs when the angle between the regurgitant jet and the ultrasound beam is almost perpendicular, making it difficult for accurate assignment of color to the regurgitant flow.[64, 80, 81] In these horses, the auditory Doppler signal can usually be detected even when a good color-flow map or spectral tracing cannot be obtained.[64, 80, 81] If the regurgitant jet is exactly perpendicular to the ultrasound beam, the jet cannot be detected.[105] The echocardiographer must keep in mind that the spatial distribution of the regurgitant jet is influenced by the pressure and volume of the receiving chamber, as well as by the size and configuration of the regurgitant orifice, the timing of the regurgitation (Fig. 5-42), loading conditions, heart rate, rhythm, and the orientation of the jet to the ultrasound beam.[170, 171] With these limitations in mind, pulsed and color-flow Doppler echocardiography can be successfully used to partially quantitate the severity of the regurgitant jet.[64, 78, 80, 81, 104, 105, 158, 169-171]

The intensity of the Doppler signal of mitral regurgitation increases and the velocity of mitral inflow increases as mitral regurgitation becomes more severe.[104, 169] Reverse systolic flow has been reported in the pulmonary veins of human beings with severe (4+) mitral regurgitation.[104, 169, 170] A steep slope (rapid decrease in jet velocity) of the continuous-wave Doppler spectral tracing of the mitral regurgitation jet occurs with severe mitral regurgitation and rapidly increasing systolic left atrial pressures (Color Figure 5-6). Estimations of pressure differences between the left atrium and ventricle must be made with care because the ultrasound beam needs to be positioned parallel to the regurgitant jet (±20 degrees) for these

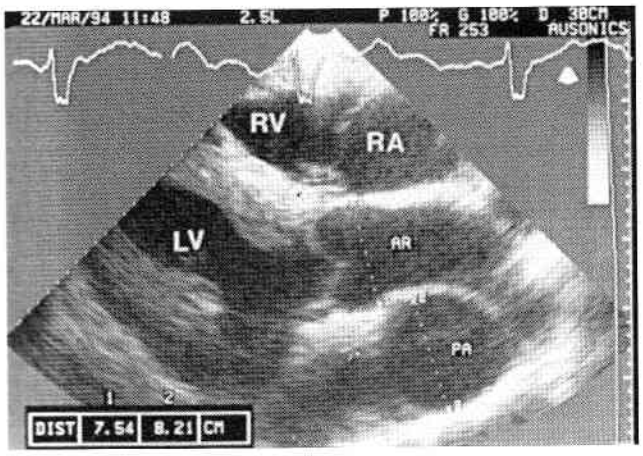

Figure 5–41

Long-axis echocardiogram obtained from a 20-year-old Thoroughbred gelding with severe mitral regurgitation and left-sided congestive heart failure. Compare the diameter of the aortic root (AR) and pulmonary artery (PA). The enlarged pulmonary artery (8.21 cm) is consistent with pulmonary hypertension. This echocardiogram was obtained from the right cardiac window in the left ventricular outflow tract position with a 2.5-MHz sector-scanner transducer at a displayed depth of 30 cm. An electrocardiogram is superimposed for timing. LV, Left ventricle; RV, right ventricle; RA, right atrium.

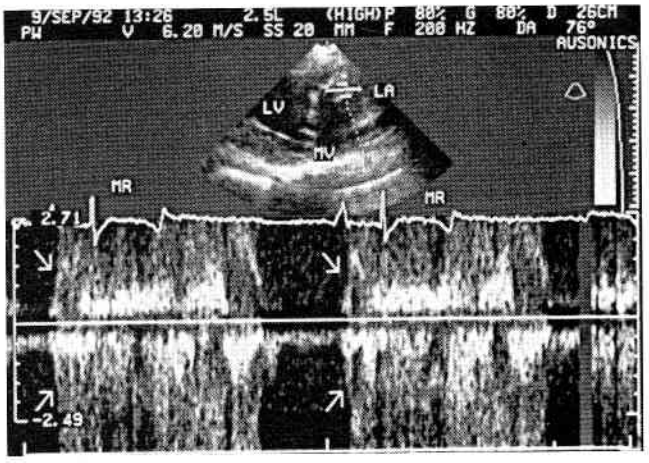

Figure 5–42

Long-axis echocardiogram and pulsed-wave Doppler spectral tracing obtained from a 7-year-old Hanoverian gelding with moderate mitral regurgitation (MR). The sample volume (two parallel lines perpendicular to the cursor) is positioned on the left atrial (LA) side of the mitral valve (MV). Notice the spectral broadening and aliasing of the mitral regurgitation jet on the spectral tracing and the presystolic onset *(arrows)* of the mitral regurgitation. This echocardiogram was obtained from the left cardiac window in the mitral valve position with a 2.5-MHz sector-scanner transducer, which emits ultrasound pulses (pulsed-wave Doppler) at a frequency of 2.0 MHz at a displayed depth of 26 cm. An electrocardiogram is superimposed for timing. LV, Left ventricle.

measurements to be accurate.[33, 64, 72, 78, 80, 81, 105, 169] Most often in horses, the angles for interrogation of the left atrium and mitral valve with Doppler echocardiography are far from ideal.[64, 72, 78, 80, 81] Often the mitral valve is perpendicular to the ultrasound beam from the left parasternal window. Alternative transverse imaging planes must be used to optimize the angle between the regurgitant jet and the ultrasound beam to obtain the best Doppler study.[10, 64, 72, 78, 80, 81] Jets of mitral regurgitation can be found in a wide variety of imaging planes. There is no one consistent jet direction in horses with mitral regurgitation, such as typically is seen in horses with tricuspid regurgitation.[64, 72, 83] Jets of mitral regurgitation may be located far from the skin surface in some horses with severe mitral regurgitation and marked left atrial enlargement. The regurgitant jet may not be able to be completely mapped because the depth of the regurgitant jet from the skin surface exceeds the Doppler penetration capabilities of the ultrasound equipment.[33, 64, 78, 80]

Patient Management and Prognosis. Patient factors and echocardiographic findings must be considered together when formulating a prognosis for life and performance in horses with mitral regurgitation. The age of the horse at the onset of mitral regurgitation, the clinical signs and the speed of their progression, and the performance expected currently and in the future are the most important patient factors to consider.[64, 72] Clinical signs associated with mitral regurgitation include exercise intolerance, increased respiratory rate and effort at rest, prolonged recovery to resting respiratory rate after exercise, and coughing.[47-49, 64, 72, 121, 149, 150, 156, 163] Atrial fibrillation is also common in horses with moderate to severe mitral regurgitation.[47, 48, 51, 72, 74, 121, 149] Acute signs of left-sided congestive heart failure, including severe respiratory distress and fulminant pulmonary edema, are unusual unless acute severe mitral regurgitation is present.[47-49, 72, 149, 150, 156, 163] With more longstanding mitral regurgitation, signs of right-sided heart failure are frequently seen, including ventral edema, generalized venous distention, and jugular pulses.[47-49, 72, 149] The changes detected on the mitral valve leaflets, the degree of left atrial and/or left ventricular enlargement, the severity of the resultant left ventricular volume overload, the presence and severity of myocardial dysfunction, the size of the regurgitant jet relative to left atrial size, the detection of proximal flow convergence, and the slope of the continuous-wave Doppler spectral tracing of mitral regurgitation are the echocardiographic factors that are helpful in determining the horse's prognosis.[33, 64, 72, 81]

Mitral regurgitation is the valvular insufficiency most likely to affect a horse's performance because significant mitral regurgitation leads to increases in left atrial pressure, pulmonary hypertension, and pulmonary edema.[7, 33, 47-50, 64, 72, 78, 81, 86, 93, 121, 149, 150, 156] Horses with mitral valve prolapse or degenerative mitral valve disease, clinically insignificant or mild mitral regurgitation, no significant left atrial or left ventricular enlargement, and normal myocardial function have a good to excellent prognosis for life and performance. The mitral regurgitation is likely to remain unchanged or progress slowly throughout the life of the horse. Mitral valve prolapse and mild mitral regurgitation, the severity of which has not changed echocardiographically in 13 years, has been documented in one horse.[64] Horses with a ruptured chorda tendinea may have minimal mitral regurgitation if only a small chorda tendinea is involved. These horses also have a good prognosis if there is only mild left atrial and left ventricular enlargement and normal myocardial function. The mitral regurgitation in horses with degenerative valve disease, moderate mitral regurgitation, moderate enlargement of the left atrium and left ventricle, and normal myocardial function will probably progress slowly over a period of several years unless atrial fibrillation or a ruptured chorda tendinea occurs. These horses should have a useful performance life for several years but should have annual cardiac examinations, including echocardiography. These examinations can be used to determine more accurately when the horse's exercise level should be restricted or the horse is no longer safe to ride.

If the regurgitant jet area is larger than expected for the degree of left atrial enlargement, a recent onset of mitral regurgitation should be suspected. Horses with severe mitral regurgitation detected with Doppler echocardiography and only mild to moderate left atrial and left ventricular enlargement are likely to deteriorate more rapidly and should be examined more frequently. These horses should be given a more guarded prognosis. Horses with a major ruptured chorda tendinea, flail mitral valve leaflet, or bacterial endocarditis must be given a guarded to poor prognosis, as rapid deterioration is likely.[47-50, 64, 72, 149, 150, 156, 163] Severe mitral regurgitation with Doppler echocardiography, proximal flow convergence, a steep slope of the continuous-wave Doppler spectral tracing of mitral regurgitation, a round turgid left atrium, marked left atrial and left ventricular enlargement, and decreased left ventricular function are indications of hemodynamically significant mitral regurgitation and a guarded to poor prognosis. Once the mitral regurgitation becomes hemodynamically significant, it is likely to affect performance, particularly for more rigorous types of athletic endeavor. Horses with pulmonary artery dilatation should be given a guarded to grave prognosis and should not be used for performance because of the risk of pulmonary artery rupture and sudden death.[47, 48, 50, 64, 72, 125]

Treatment for congestive heart failure (digoxin, furosemide, and vasodilators) should be administered to horses with severe mitral regurgitation and congestive heart failure. Angiotensin-converting enzyme (ACE) inhibitors should be considered in horses with moderate to severe mitral regurgitation, as these drugs have been shown to improve left ventricular performance, may prolong the time to valve replacement in human beings with moderate to severe mitral regurgitation, and may be similarly effective in horses.[172]

Tricuspid Regurgitation. Tricuspid regurgitation occurs frequently in horses but is rarely associated with poor performance or other clinical signs unless the tricuspid regurgitation is severe or other significant concurrent cardiac disease is present.[14, 19, 33, 47, 49, 55, 64, 72, 74, 80, 94, 111, 121, 149, 150, 156, 173] The degree of tricuspid regurgitation is minimal to moderate in most horses and usually does not change or slowly worsens over a period of years.[64] Severe tricuspid insufficiency is rarely a primary cause of congestive heart failure and death but occurs most frequently

in horses with severe mitral regurgitation and/or left ventricular dysfunction and chronic pulmonary hypertension.[7, 33, 49, 64, 72, 93] Horses with severe tricuspid regurgitation may develop atrial fibrillation, generalized venous distention, systolic jugular pulsations, peripheral edema, pleural effusion, hepatic congestion, and, rarely, ascites.[19, 55, 64, 72, 93]

The tricuspid valve abnormalities that have been detected echocardiographically in horses with tricuspid regurgitation include valvular thickening (degenerative or inflammatory), valvulitis, prolapse, ruptured chordae tendineae, vegetative endocarditis, and stretching of the tricuspid valve annulus with an anatomically normal valve (usually secondary to severe pulmonary hypertension).[7, 14, 30, 33, 34, 47, 49, 55-57, 64, 72, 94] Most horses with tricuspid regurgitation have no valvular abnormalities detected echocardiographically, or one or more of the tricuspid valve leaflets is thickened or prolapsing.[7, 34, 47, 49, 64, 72, 94] With tricuspid valve prolapse a portion of the tricuspid valve leaflet (most common) or the entire leaflet is imaged bulging backward into the right atrium during mid to late systole (Fig. 5-43).[64, 158] Tricuspid valve prolapse is usually best imaged with 2-D echocardiography when examining the tricuspid valve from the right cardiac window in the parasternal long-axis view of the LVOT, although it may be detected in the other long-axis planes. A ruptured chorda tendinea can also cause tricuspid valve prolapse. Therefore, all horses with significant tricuspid valve prolapse should be carefully scanned for a possible ruptured chorda tendinea.[7, 19, 56, 64, 72]

Thickening of the tricuspid valve leaflets may be associated with primary degenerative changes of the valve leaflets, a noninfective valvulitis, bacterial endocarditis, or secondary to regurgitation from dilatation of the tricuspid valve annulus secondary to chronic pulmonary hypertension. Degenerative changes of the tricuspid valve leaflets

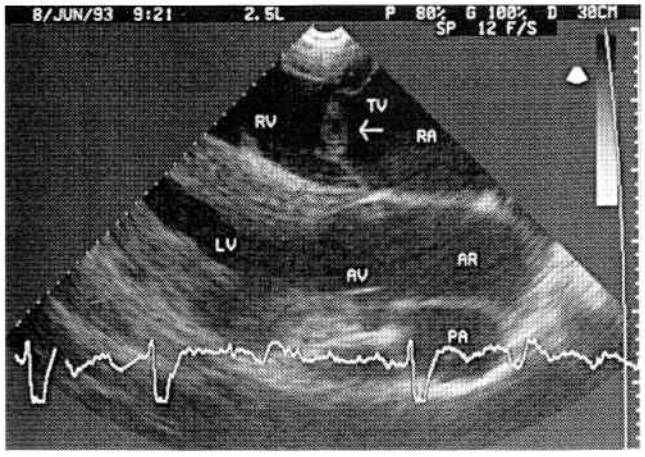

Figure 5-43

Long-axis echocardiogram obtained from a 4-year-old Thoroughbred gelding with refractory atrial fibrillation and moderate tricuspid regurgitation. Notice the prolapse *(arrow)* of a portion of the tricuspid valve (TV) in systole. This echocardiogram was obtained from the right cardiac window in the left ventricular outflow tract position with a 2.5-MHz sector-scanner transducer at a displayed depth of 30 cm. An electrocardiogram is superimposed for timing. RA, Right atrium; RV, right ventricle; AR, aortic root; AV, aortic valve; LV, left ventricle; PA, pulmonary artery.

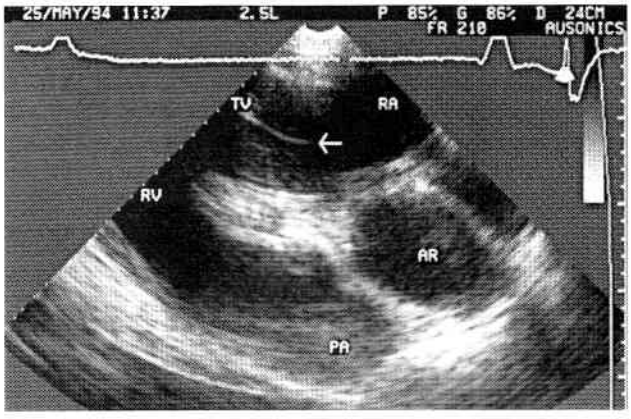

Figure 5-44

Long-axis echocardiogram obtained from a 2-year-old Standardbred colt with clinically insignificant tricuspid regurgitation and a ruptured chorda tendinea. The long linear echo of the ruptured chorda tendinea *(arrow)* everts into the right atrium (RA), originating from the tricuspid valve (TV). This echocardiogram was obtained from the right cardiac window in the right ventricular outflow tract position with a 2.5-MHz sector-scanner transducer at a displayed depth of 24 cm. An electrocardiogram is superimposed for timing. AR, Aortic root; PA, pulmonary artery; RV, right ventricle.

are less commonly detected echocardiographically than changes of the mitral valve leaflets and are infrequently detected at postmortem examination.[34, 64, 72, 161-163] Degenerative valve disease and endocarditis are the most common causes of tricuspid chordal rupture in horses.[56, 64, 72, 161] The entire tricuspid valve apparatus should be thoroughly scanned in all planes to detect ruptured chordae tendineae and flail valve leaflets.[7, 56, 64, 72] The echocardiographic detection of a mobile linear echo that moves with the valve leaflet or the subvalvular apparatus, everting into the right atrium in systole, is diagnostic of a ruptured chorda tendinea (Fig. 5-44).[56, 64, 72] Ruptured chordae tendineae and flail tricuspid valve leaflets are rare in horses (Fig. 5-45).[56, 64, 72, 161] A tricuspid leaflet or portion thereof that moves asynchronously or chaotically from right atrium to right ventricle during any phase of the cardiac cycle is consistent with a flail valve leaflet.[7, 64, 72]

The tricuspid valve is a common site of bacterial endocarditis in horses with septic jugular vein thrombophlebitis.[14, 56] Bacterial endocarditis has been diagnosed echocardiographically in horses with both M-mode and 2-D echocardiography (superior).[7, 14, 30, 33, 56, 57, 64, 72, 173] TEE, once it becomes more readily available at large equine referral centers, should be superior for the detection of small endocarditis lesions on the right atrioventricular valve as well as the left, which cannot be imaged with routine transthoracic echocardiography.[81, 96, 167, 168] Slight thickening of the valve leaflet and chordal apparatus, owing to large irregular vegetative masses on the valve leaflet, with atrial thrombi and a lenticular abscess of the tricuspid valve leaflet, has been described in horses with tricuspid valve endocarditis.[7, 14, 33, 55-57, 64, 72, 173] The irregular vegetative masses usually become rounder and smoother if the horse is responding to treatment (Fig. 5-46).[56] Although the regurgitation usually becomes more severe secondary to leaflet scarring caused by the

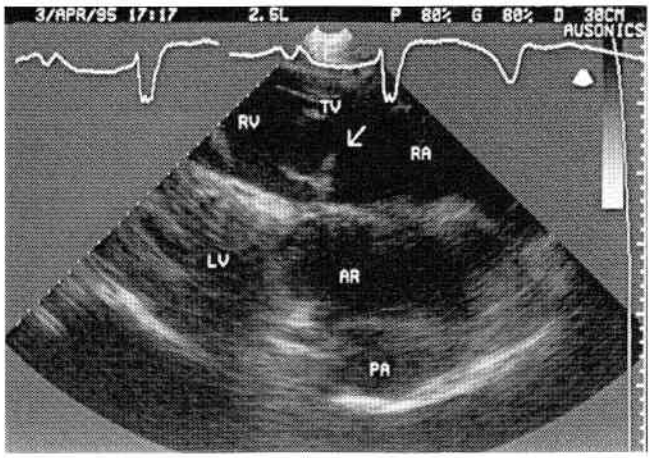

Figure 5–45

Long-axis echocardiogram obtained from a 9-year-old Thoroughbred gelding with severe tricuspid regurgitation. The flail *(arrow)* cranial leaflet of the tricuspid valve (TV) everts into the large right atrium (RA) and right ventricle (RV). This echocardiogram was obtained from the right cardiac window between the right and left ventricular outflow tract positions with a 2.5-MHz sector-scanner transducer at a displayed depth of 30 cm. An electrocardiogram is superimposed for timing. PA, Pulmonary artery; LV, left ventricle; AR, aortic root.

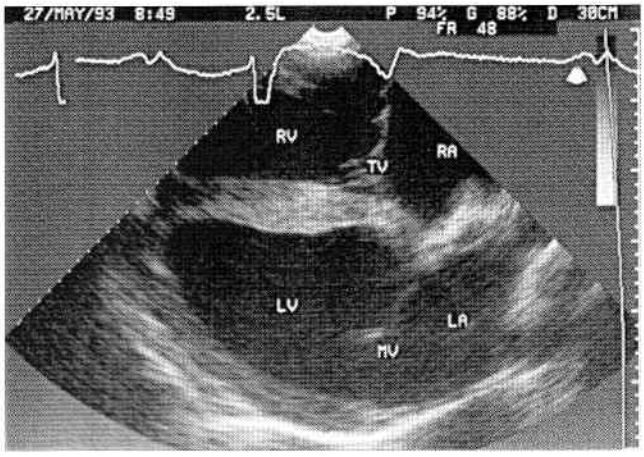

Figure 5–47

Long-axis echocardiogram obtained from a 9-year-old Thoroughbred gelding with severe tricuspid regurgitation (same horse as in Figure 5–45). Notice the markedly enlarged right atrium (RA) and right ventricle (RV). This echocardiogram was obtained from the right cardiac window in the mitral valve position with a 2.5-MHz sector-scanner transducer at a displayed depth of 30 cm. An electrocardiogram is superimposed for timing. TV, Tricuspid valve; LA, left atrium; MV, mitral valve; LV, left ventricle.

infection, even if a bacteriologic cure is achieved, the valvular insufficiency is much better tolerated than when the mitral valve is involved.

Right atrial and right ventricular volume overload occurs in moderate to severe tricuspid regurgitation (Fig. 5–47).[7, 33, 64, 72] The determination of right atrial enlargement is made by comparing right and left atrial size in the right parasternal four-chamber view. The normal right atrium should appear slightly smaller than the left.[8, 25, 64]

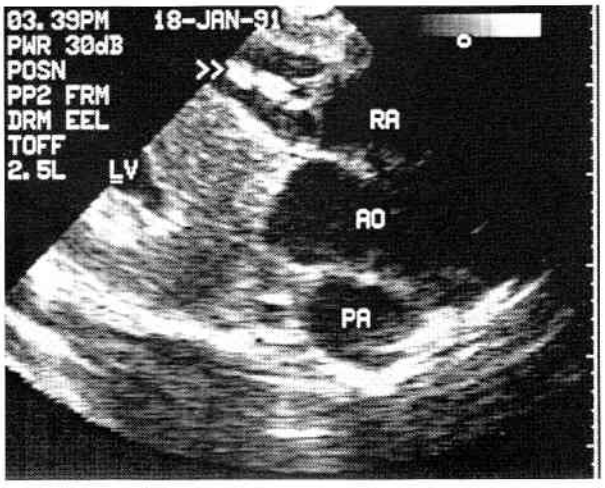

Figure 5–46

Long-axis echocardiogram obtained from a 10-year-old Thoroughbred mare with a previous history of septic jugular vein thrombophlebitis and bacterial endocarditis on the chordae tendineae of the tricuspid valve. Notice the healed lesions *(arrowheads)* on the tricuspid chordae tendineae. This echocardiogram was obtained from the right cardiac window between the right and left ventricular outflow tract views, where the healed endocarditis lesions were best demonstrated. This echocardiogram was obtained with a 2.5-MHz sector-scanner transducer at a displayed depth of 27.5 cm. RA, Right atrium; LV, left ventricle; AO, aorta; PA, pulmonary artery.

The right ventricle is normally approximately one third the size of the left ventricle in this view. Normal measurements for the right ventricular internal diameter at end-diastole have been reported for this view using M-mode and 2-D echocardiography (see Table 5-1).[1, 7, 8, 26] Bulging of the interatrial septum into the left atrium indicates significantly increased right atrial pressures (see Fig. 5–23). Movement of the interventricular septum toward the right ventricle in systole, rather than toward the left (paradoxical septal motion), is detected with moderate to severe right ventricular volume overload.[7, 64, 72] Lack of coaptation of the tricuspid valve leaflets may also be detected. However, this must be interpreted with care, as the echocardiogram is a 2-D slice through a 3-D heart, and this image could possibly be created if a true long- or short-axis imaging plane is not obtained.[7]

The extent of the regurgitant jet can be determined with pulsed-wave or color-flow Doppler flow mapping from the right cardiac window (Color Figure 5-7).[78, 80, 82] The best angles for interrogation of the regurgitant jet are usually obtained from horses with tricuspid regurgitation because the angle between the regurgitant jet and the ultrasound beam is small.[77, 78, 80] The majority of horses with tricuspid regurgitation have a regurgitant jet that is oriented toward the aortic root (Color Figure 5-8). Indications of severe tricuspid regurgitation include a regurgitant jet that occupies two thirds or more of the right atrial chamber, reverse systolic flow in the hepatic veins, proximal flow convergence, and an intense Doppler signal.[64, 72, 78, 80, 104, 105, 158, 174] Contrast echocardiography is also useful to document the to-and-fro movement of blood across the tricuspid annulus.[12, 34, 64, 72, 76] Continuous-wave Doppler (Color Figure 5-8) echocardiographic estimation of the pressure difference between right atrium and ventricle can be performed by adding 10 to 15 mm Hg (the estimated right atrial pressure) to 4 v^2 in horses with severe tricuspid regurgitation.[64, 72, 105, 158] A

slow rate of rise of the regurgitant jet velocity (gradual slope) is an indication of right ventricular failure.[105]

Patient Management and Prognosis. Patient factors (horse's age, clinical signs, rapidity of their onset, performance level) and echocardiographic findings must be considered together when formulating a prognosis for life and performance in horses with tricuspid regurgitation, just as with mitral regurgitation.[64, 72] Clinical signs associated with tricuspid regurgitation include exercise intolerance, ventral edema, jugular pulsations, and generalized venous distention.[47, 49, 55, 64, 72, 91, 121, 149, 150, 156] Atrial fibrillation is also common in horses with moderate to severe tricuspid regurgitation.[64, 72, 74, 91, 121, 149] The changes detected on the tricuspid valve leaflets, the degree of right atrial and/or ventricular enlargement, the severity of the resultant right ventricular volume overload, the presence and severity of paradoxical septal motion and myocardial dysfunction, the size of the regurgitant jet relative to right atrial size, the detection of proximal flow convergence, and the slope of the continuous-wave Doppler spectral tracing of tricuspid regurgitation are the echocardiographic factors that are helpful in determining the horse's prognosis.[55, 64, 72, 81]

Primary tricuspid regurgitation is unlikely to affect a horse's performance unless it is severe[19, 49, 55, 64, 72, 93, 121] because the pressure difference between the right atrium and ventricle is relatively small, and significant tricuspid regurgitation leads to increases in vena caval and hepatic venous pressures which are relatively well tolerated. Horses with tricuspid valve prolapse or degenerative tricuspid valve disease, clinically insignificant to moderate tricuspid regurgitation, minimal to moderate right atrial and ventricular enlargement, and normal myocardial function have an excellent prognosis for life and performance. The tricuspid regurgitation is likely to remain unchanged or progress slowly throughout the life of the horse. Tricuspid and mitral valve prolapse and mild tricuspid and mitral regurgitation, the severity of which has not changed echocardiographically in 13 years, has been documented in one horse.[64] Horses with a ruptured chorda tendinea may have minimal tricuspid regurgitation if only a small chorda tendinea is involved.[56] These horses also have a good prognosis if there is only minimal to mild right atrial and ventricular enlargement and normal myocardial function. If the regurgitant jet area is larger than expected for the degree of right atrial enlargement, a recent onset of tricuspid regurgitation should be suspected, prompting a re-examination in 6 to 12 months, especially if severe tricuspid regurgitation is detected with Doppler echocardiography. These horses should be given a more guarded prognosis. Horses with a major ruptured chorda tendinea, flail tricuspid valve leaflet, bacterial endocarditis, or pulmonary hypertension from severe left-sided heart disease must be given a guarded to poor prognosis, as more rapid deterioration is likely.[19, 47, 49, 55, 57, 64, 72, 91, 149, 150, 156] The detection of severe tricuspid regurgitation with Doppler echocardiography, proximal flow convergence, a steep slope of the continuous-wave Doppler spectral tracing of tricuspid regurgitation, a round turgid right atrium, bulging of the interatrial septum into the left atrium, marked right atrial and ventricular enlargement, and decreased right and/or left ventricular function are indications of hemodynamically significant tricuspid regurgitation and a guarded to poor prognosis.[64, 72] Once tricuspid regurgitation is severe, it is likely to affect performance, particularly for the most rigorous types of athletic endeavor. However, the progression to congestive heart failure and death in horses with severe primary tricuspid regurgitation, without bacterial endocarditis, is extremely slow compared with that in horses with severe mitral regurgitation. One horse with a completely flail tricuspid valve leaflet and severe tricuspid regurgitation has remained unchanged for 8 years.[64]

Aortic Regurgitation. Aortic regurgitation is usually a disease of older horses (>10 years) secondary to the development of degenerative valve disease.[60, 64, 72, 152, 154] Congenital aortic regurgitation is rare in horses.[60, 148] Both bicuspid or quadracuspid valve leaflets have been infrequently detected in horses causing aortic stenosis and/or aortic regurgitation.[60, 72] An indication of the severity of the aortic regurgitation can be obtained from the arterial pulse quality.[60, 64, 72] Bounding arterial pulses are an indication of significant left ventricular volume overload and moderate or severe aortic regurgitation.[60, 64, 72] Aortic regurgitation is usually mild to moderate when the murmur is first detected, often in a prepurchase, insurance, or routine examination. Aortic regurgitation usually progresses slowly and rarely causes poor performance or the development of congestive heart failure.[33, 64]

Thickening of the aortic valve cusps, particularly focal thickening of the left coronary cusp, is the most common finding in aortic regurgitation in older horses (Fig. 5-48).[60-62, 64, 72, 152] This thickening often appears as an echogenic thickening parallel to the free edge of the valve leaflets and corresponds to the parallel fibrous band lesions described in postmortem studies of horses with aortic regurgitation.[152, 154, 161] Nodular thickenings of the aortic valve cusps are less frequently detected, either

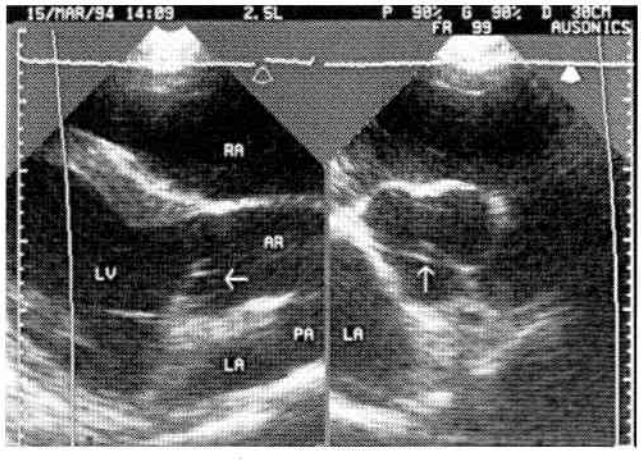

Figure 5–48

Long- and short-axis echocardiograms obtained from a 23-year-old Quarter Horse gelding with mild aortic regurgitation. The linear echo *(arrows)* in the left coronary cusp of the aortic valve is near the free edge of the leaflet. These echocardiograms were obtained from the right cardiac window in the left ventricular outflow tract (long-axis image) and aortic valve (short-axis image) positions with a 2.5-MHz sector-scanner transducer at a displayed depth of 30 cm. An electrocardiogram is superimposed for timing. RA, Right atrium; LV, left ventricle; AR, aortic root; LA, left atrium; PA, pulmonary artery.

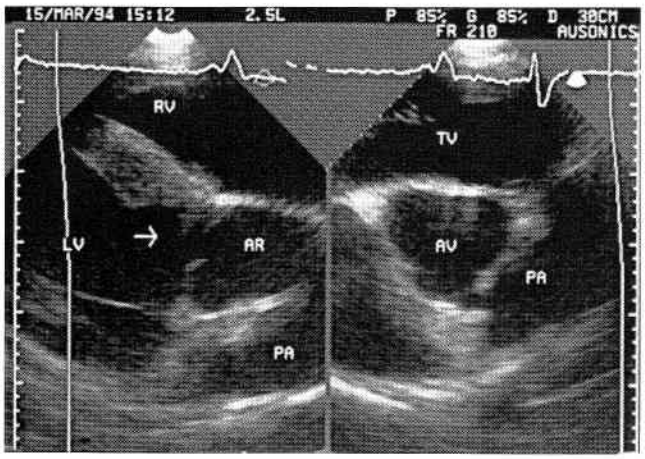

Figure 5–49

Long- and short-axis echocardiograms obtained from a 20-year-old Thoroughbred gelding with mild aortic regurgitation. Notice the prolapse *(arrow)* of the noncoronary cusp of the aortic valve (AV) into the left ventricular (LV) outflow tract in diastole. These echocardiograms were obtained from the right cardiac window in the left ventricular outflow tract (long-axis image) and aortic valve (short-axis image) positions with a 2.5-MHz sector-scanner transducer at a displayed depth of 30 cm. An electrocardiogram is superimposed for timing. RV, Right ventricle; AR, aortic root; PA, pulmonary artery; TV, tricuspid valve.

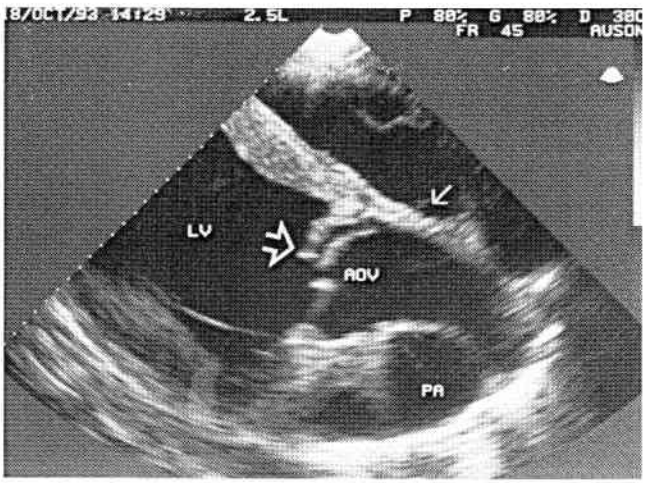

Figure 5–50

Long-axis echocardiogram obtained from a 12-year-old Thoroughbred mare with bacterial endocarditis involving the aortic valve (AOV). Notice the thickening of the three aortic cusps, the echogenic nodular density at the free edge of the left and noncoronary cusps, the prolapse *(open arrow)* of the noncoronary cusp into the left ventricular (LV) outflow tract, and the thickening of the aortic wall along the right side of the aorta *(arrow)* consistent with the development of an aortic root abscess. This echocardiogram was obtained with a 2.5-MHz sector-scanner transducer at a displayed depth of 30 cm. PA, Pulmonary artery. (The author would like to thank Drs. Ietje Leenderjerske and Georg Wiesenecker for their assistance in obtaining this echocardiogram.)

echocardiographically or at postmortem examination. Prolapse of the aortic valve leaflets is commonly imaged, usually involving the right coronary or noncoronary cusp (Fig. 5-49). Vegetative endocarditis lesions, although uncommon, frequently involve the aortic valve (Fig. 5-50).[13, 52, 60, 64, 72, 166, 173] Fenestrations of the aortic valve cusps (Fig. 5-51), small tears in the free edge of the aortic cusps (Fig. 5-52), or flail aortic leaflets may be less frequently imaged.[152, 175] Diastolic fluttering of the aortic valve cusp may be detected echocardiographically (Fig. 5-53) with both M-mode and 2-D echocardiography, caused by fenestrated, torn, or ruptured aortic valve cusps or associated with a vegetative endocarditis lesion.[7, 13, 60, 62, 104, 158] A fenestrated, torn, or flail leaflet or bacterial endocarditis (less likely) should be suspected in all horses with musical harmonic holodiastolic decrescendo murmurs (Fig. 5-54). Aortic regurgitation com-

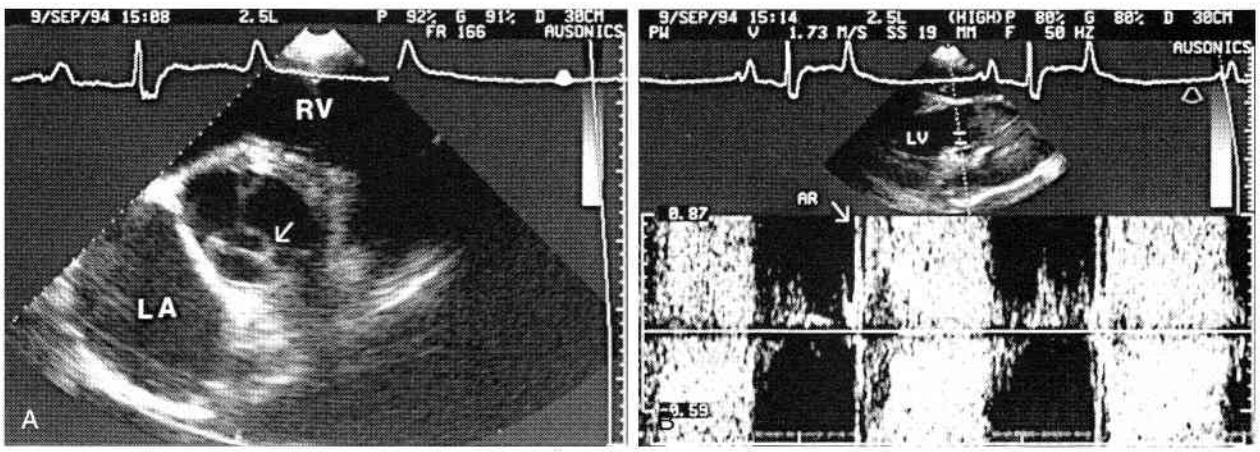

Figure 5–51

Echocardiograms obtained from a 14-year-old Thoroughbred gelding with moderate aortic regurgitation. These echocardiograms were obtained from the right cardiac window in the left ventricular outflow tract position with a 2.5 MHz sector-scanner transducer, which emits ultrasound pulses (pulsed-wave Doppler) at a frequency of 2.0-MHz at a displayed depth of 30 cm. An electrocardiogram is superimposed for timing.

A, Notice the fenestration in the left aortic cusp (arrow points to the free edge of the aortic cusp) in the short-axis echocardiogram. LA, Left atrium; RV, right ventricle.

B, The origin of the aortic regurgitation (AR) jet *(arrow)* is the fenestrated portion of the left coronary cusp of the aortic valve. The pulsed-wave Doppler sample volume (two parallel lines along the cursor on the two-dimensional echocardiogram) is positioned just below the left aortic cusp at the origin of the aortic regurgitation jet. The aliasing of the aortic regurgitation jet throughout most of diastole on the spectral tracing indicates the presence of a high-velocity turbulent jet. LV, Left ventricle.

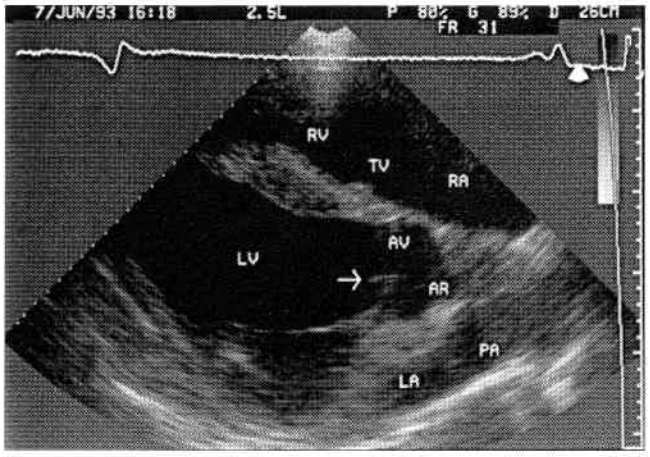

Figure 5–52

Long-axis echocardiogram obtained from a 7-year-old Arabian stallion with mild aortic regurgitation. The flail portion *(arrow)* of the left coronary cusp of the aortic valve (AV) everts into the left ventricular (LV) outflow tract during diastole. This echocardiogram was obtained from the right cardiac window in the left ventricular outflow tract position with a 2.5-MHz sector-scanner transducer at a displayed depth of 26 cm. An electrocardiogram is superimposed for timing. RA, Right atrium; TV, tricuspid valve; RV, right ventricle; AR, aortic root; PA, pulmonary artery; LA, left atrium.

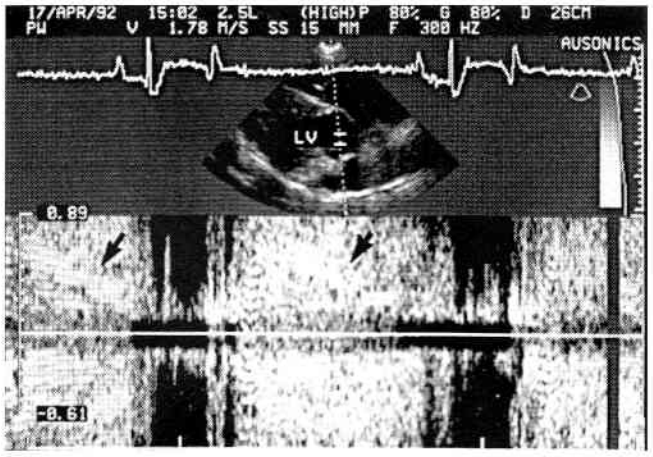

Figure 5–54

Two-dimensional (2-D) echocardiogram and pulsed-wave Doppler spectral tracing obtained from a 7-year-old Arabian stallion with a torn free edge of the left coronary cusp of the aortic valve and mild aortic regurgitation (same horse as in Figure 5-52). The pulsed-wave Doppler sample volume (two parallel lines along the cursor on the 2-D echocardiogram) is positioned on the left ventricular side of the aortic valve. Notice the harmonic *(black arrows)* on the spectral tracing of the aortic regurgitation jet and the aliasing of the pulsed-wave Doppler signal associated with high-velocity turbulent flow. This is produced by the turbulent blood moving near or at one frequency and is usually associated with vibration of a portion of a valve leaflet or a chorda tendinea. These echocardiograms were obtained from the right cardiac window in the left ventricular outflow tract position with a 2.5-MHz sector-scanner transducer, which emits ultrasound pulses (pulsed-wave Doppler) at a frequency of 2.0 MHz at a displayed depth of 26 cm. An electrocardiogram is superimposed for timing.

monly causes high-frequency vibrations on the septal leaflet of the mitral valve during diastole; these were noticed in all 23 horses in one study (Fig. 5-55).[14, 80] These high-frequency vibrations are caused by turbulence in the LVOT associated with the aortic regurgitation jet and are usually best imaged with M-mode echocardiography.[7, 60-62, 64, 72, 104] High-frequency vibrations can also be imaged on the interventricular septum, caused by the

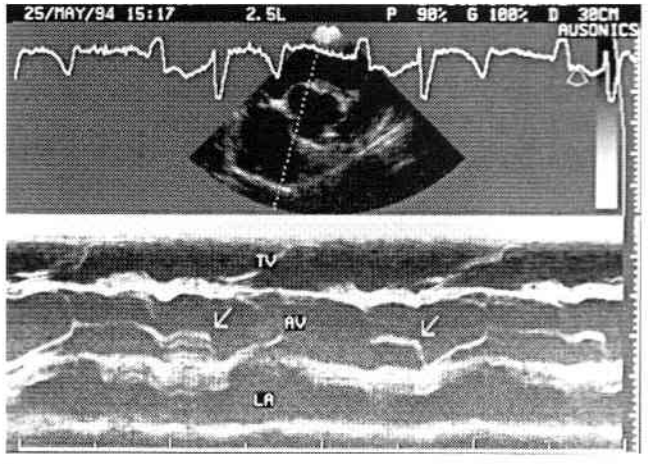

Figure 5–53

M-mode and two-dimensional (2-D) echocardiograms of the aortic valve obtained from a 15-year-old Thoroughbred mare with mild aortic regurgitation. High-frequency vibrations *(arrows)* are seen on the left coronary cusp of the aortic valve (AV) in late diastole in the M-mode echocardiogram. The short-axis 2-D echocardiogram shows the position of the M-mode cursor used to obtain the M-mode echocardiogram. This horse had a small tear in the left aortic cusp and some nodular thickening of the valve leaflet. These echocardiograms were obtained from the right cardiac window in the aortic valve position with a 2.5-MHz sector-scanner transducer at a displayed depth of 30 cm. An electrocardiogram is superimposed for timing. TV, Tricuspid valve; LA, left atrium.

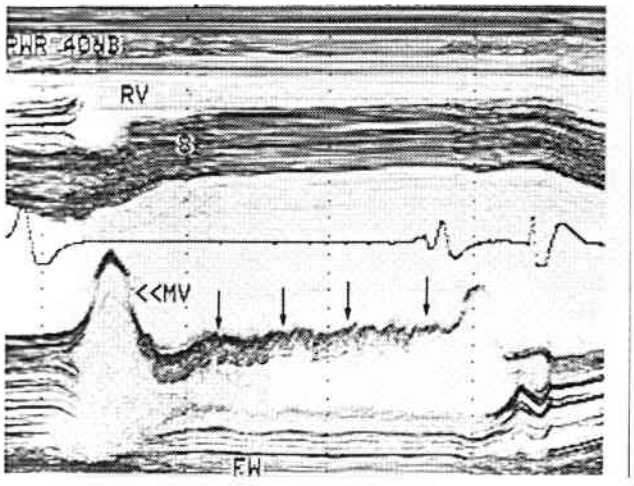

Figure 5–55

M-mode echocardiogram of the mitral valve obtained from a 3-year-old Standardbred stallion with moderate aortic regurgitation. The high-frequency vibrations *(arrows)* on the septal leaflet of the mitral valve (MV) in diastole are associated with turbulence in the left ventricular outflow tract from the aortic regurgitation jet. The septal-to-E-point (SEP) distance was enlarged at 1.6 cm, indicating dilatation of the left ventricular outflow tract. This echocardiogram was obtained from the right cardiac window in the mitral valve position with a 2.5-MHz sector-scanner transducer at a displayed depth of 27.5 cm. An electrocardiogram is superimposed for timing. RV, Right ventricle; S, interventricular septum; FW, left ventricular free wall.

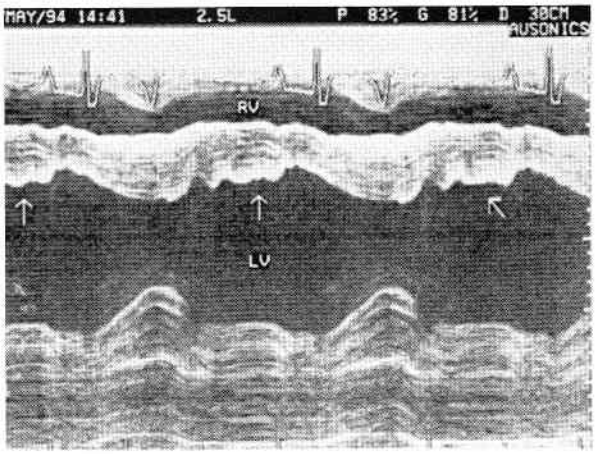

Figure 5–56

M-mode echocardiogram obtained from a 20-year-old crossbred gelding with mild aortic regurgitation. The high-frequency vibrations along the interventricular septum during mid to late diastole are associated with the aortic regurgitation jet hitting this portion of the interventricular septum. The aortic regurgitation jet originated from a fenestrated area in the left coronary cusp with a jet that angled toward the interventricular septum instead of the septal mitral valve leaflet. This echocardiogram was obtained from the right cardiac window in the left ventricular position with a 2.5-MHz sector-scanner transducer at a displayed depth of 30 cm. An electrocardiogram was superimposed for timing. RV, Right ventricle; LV, left ventricle.

regurgitant jet impinging on the interventricular septum, although these occur much less frequently (Fig. 5-56).[60]

Significant aortic regurgitation results in left ventricular enlargement (as high as 23.5 cm), an increased shortening fraction (as high as 60%), and thinning of the left ventricular free wall and, to a lesser extent, the interventricular septum (Fig. 5-57).[7, 55, 60-62, 64, 72] Hyperdynamic interventricular septal motion and left ventricular free wall motion are frequently detected in horses with significant aortic regurgitation and normal myocardial function.[7, 60, 64, 72] Increased SEP separation is a common finding in horses with aortic regurgitation[7, 60-62, 72] but did not correlate with the severity of the aortic regurgitation in horses (Fig. 5-58).[60] Early systolic closure of the mitral valve, an indication of severe aortic regurgitation in human beings, also did not correlate with severity of the aortic regurgitation in horses but is detected in some horses with aortic regurgitation.[60] Aortic root dilatation (>9 cm) is a common echocardiographic finding in horses with aortic regurgitation, usually detected in horses with longstanding, moderate to severe aortic regurgitation (Fig. 5-59).[60, 64] This dilatation of the aortic root does not predispose horses to aortic root rupture, unless there is a pre-existing aneurysm of the right sinus of Valsalva.[19, 45, 46, 60, 64, 72, 75] Enlargement of the aortic root is also frequently associated with aortic regurgitation in human beings.[158] Aortic root abscess has been reported as an infrequent sequela to aortic valve endocarditis in horses (see Fig. 5-50).[13] Left atrial enlargement is common in horses as aortic regurgitation becomes more severe, although significant mitral regurgitation from stretching of the mitral annulus does not usually develop until late in the course of the disease, when the aortic regurgitation and left ventricular enlargement are severe.

The best angle for interrogation of the aortic regurgitant jet is usually obtained from the left parasternal window because the angle of interrogation is usually more acute (the ultrasound beam and the regurgitant jet are more parallel).[64, 80] However, the size of the heart and the direction of the jet determine where the best flow map of the regurgitant jet can be obtained. Therefore, flow mapping should be performed from both cardiac windows.[64, 80, 82] Determining the size and extent of the regurgitant jet with flow mapping is a semiquantitative

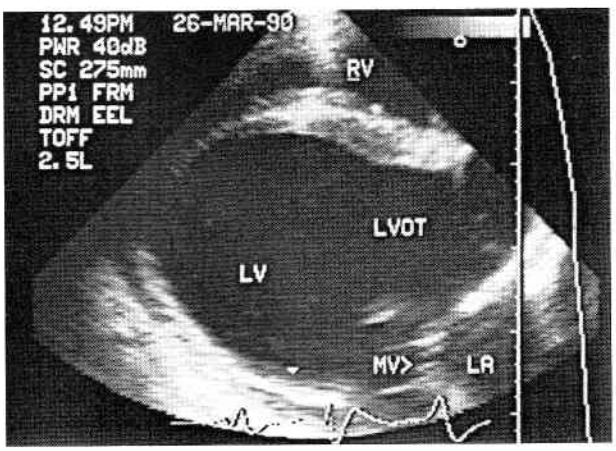

Figure 5–57

Long-axis echocardiogram obtained from a 3-year-old Standardbred colt with moderate to severe aortic regurgitation. The marked rounding and dilatation of the left ventricle (LV) and the smaller-than-normal right ventricle (RV) are consistent with a significant left ventricular volume overload. This echocardiogram was obtained from the right cardiac window in the four-chamber view with a 2.5-MHz sector-scanner transducer at a displayed depth of 27.5 cm. An electrocardiogram is superimposed for timing. LVOT, Left ventricular outflow tract; MV, mitral valve; LA, left atrium.

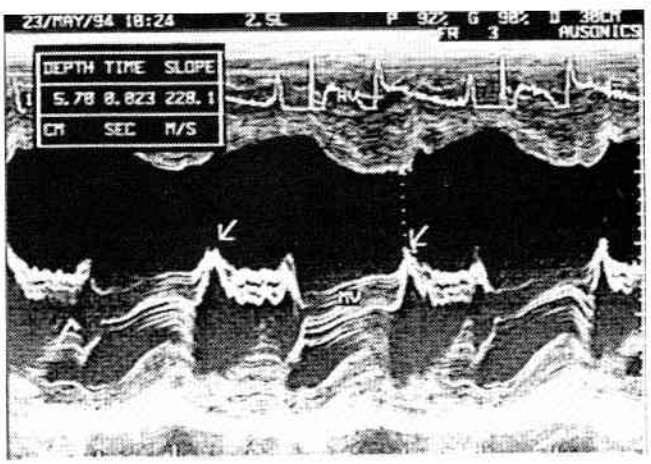

Figure 5–58

M-mode echocardiogram obtained from a 17-year-old Arabian stallion with severe aortic regurgitation. Notice the markedly increased septal-to-E-point (SEP) separation (5.78 cm) and the high frequency vibrations *(arrows)* on the septal leaflet of the mitral valve (MV). This echocardiogram was obtained from the right cardiac window in the mitral valve position with a 2.5-MHz sector-scanner transducer at a displayed depth of 30 cm. An electrocardiogram is superimposed for timing. RV, Right ventricle.

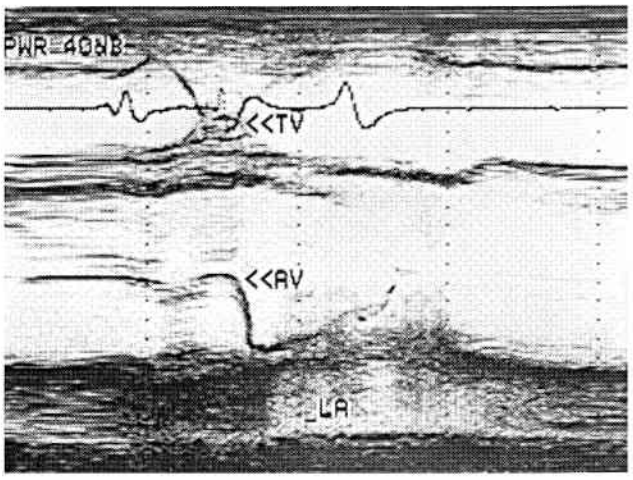

Figure 5–59

M-mode echocardiogram obtained from a 3-year-old Standardbred colt with moderate aortic regurgitation (same horse as in Figure 5-55). Notice the large diameter of the aortic root (9.6 cm). This echocardiogram was obtained from the right cardiac window in the aortic root position with a 2.5-MHz sector-scanner transducer at a displayed depth of 27.5 cm. An electrocardiogram is superimposed for timing. TV, Tricuspid valve; AV, aortic valve; LA, left atrium.

method of assessing the severity of aortic regurgitation. Severe aortic regurgitation is present when the regurgitant jet extends beyond the septal leaflet of the mitral valve, occupying two thirds or more of the LVOT.[64, 79, 80, 158] The area of the regurgitant jet as its origin, compared with the area of the LVOT at its origin, is a more sensitive indicator of the severity of the aortic regurgitation in human beings and also appears to be a sensitive indicator in horses (Color Figure 5-9).[158, 176] An elevated or short pressure half-time is another accurate indicator of severe aortic regurgitation.[64, 104, 105, 158, 176, 177] The pressure half-time is the time it takes for the velocity of the aortic regurgitation jet (determined with continuous-wave Doppler echocardiography) to decrease by half (Fig. 5-60). A steep slope (elevated pressure half-time) indicates a rapid increase in left ventricular pressure during diastole owing to severe aortic regurgitation. Reverse diastolic flow in the aorta is also detected in human beings and horses with severe aortic regurgitation.[61, 104, 158, 177] As the aortic regurgitation becomes more severe, the Doppler signal becomes more intense and proximal flow acceleration is more likely to be detected.[64, 104, 105, 158, 177] Horses with severe aortic regurgitation should also be examined for late diastolic mitral regurgitation, an indication of marked left ventricular end-diastolic pressure elevation.[177]

Patient Management and Prognosis. Once again, the echocardiographic findings and patient factors (horse's age, clinical signs, rapidity of their onset, performance level) must be combined to determine the significance of the aortic regurgitation for life and future performance.[64, 72] Clinical signs are not usually detected in horses with aortic regurgitation and normal myocardial function; instead these murmurs are usually detected during routine examinations. Atrial fibrillation may develop in horses with moderate to severe aortic regurgitation associated with significant left atrial enlargement, with or without concurrent mitral regurgitation.[60, 62, 64, 72, 148] The changes detected on the aortic valve leaflets, the degree of left ventricular and aortic root enlargement, the severity of the resultant left ventricular volume overload, the presence of left atrial enlargement, the left ventricular function, the size of the regurgitant jet area at the origin relative to the area of the LVOT, the size of the regurgitant jet relative to the size of the LVOT, the detection of proximal flow convergence and/or late diastolic mitral regurgitation, and the pressure half-time are echocardiographic factors that are helpful in determining the horse's prognosis.[33, 60, 64, 72, 158, 176, 177]

Aortic regurgitation is usually very well tolerated by horses with normal left ventricular function, in the absence of mitral regurgitation.[60, 64] Horses and human beings with moderate to severe aortic regurgitation and normal left ventricular function can exercise as well as normal individuals and the regurgitation usually progresses slowly over many years.[178] These horses can compete successfully as grade 1 stakes winners, as Grand Prix show jumpers or dressage horses, or in other types of rigorous athletic competition. With severe aortic regurgitation and normal myocardial function there is a reduction in the severity of the aortic regurgitation during exercise as a result of the decreased length of diastole.[178] Aortic regurgitation is well tolerated because it causes a pure left ventricular volume overload (increased stretch), which the normal left ventricle responds to by increasing myocardial contractility (Starling's law). Horses with aortic valve prolapse or degenerative aortic valve disease, clinically insignificant to moderate aortic regurgitation, minimal to moderate left ventricular and aortic root en-

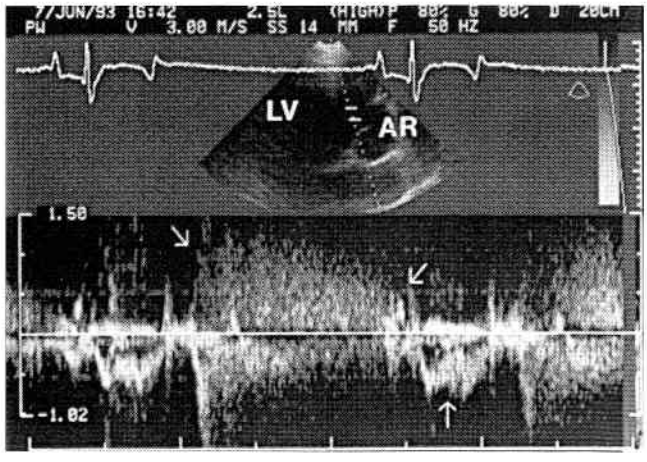

Figure 5–60

Long-axis two-dimensional and pulsed-wave Doppler echocardiogram obtained from a 7-year-old Arabian stallion with mild aortic regurgitation (same horse as in Figures 5-52 and 5-54). The gradually decreasing slope of the pulsed-wave Doppler spectral tracing *(two upper angled arrows)* indicates a small pressure difference between the two chambers and mild aortic regurgitation. The up arrow points to normal left ventricular outflow. The sample volume (two parallel lines along the cursor) is placed in the left ventricular outflow tract just beneath the aortic valve. This echocardiogram was obtained from the left cardiac window in the left ventricular outflow tract position with a 2.5-MHz sector-scanner transducer, which emits ultrasound pulses (pulsed-wave Doppler) at a frequency of 2.0 MHz at a displayed depth of 20 cm. LV, Left ventricle; AR, aortic root.

largement, normal myocardial function, and a jet area consistent with the degree of left ventricular enlargement have an excellent prognosis for life and performance. The aortic regurgitation is likely to progress slowly throughout the life of the horse. Annual examinations should be performed on these horses to determine the progression of the aortic regurgitation. Horses with fenestrations, small tears of the free edge of the valve leaflet, flail valve leaflets, and bacterial endocarditis should initially be given a more guarded prognosis, as these valvular insufficiencies could progress more rapidly. These horses often have a loud harmonic musical murmur associated with the vibration of the free edge of the valve leaflet or endocarditis lesion vibrating at one harmonic frequency. Occasionally, however, the torn edge may repair (scar) and the regurgitation or murmur almost disappears.

Even most horses with severe aortic regurgitation and severe left ventricular dilatation may continue to perform successfully for 2.5 to 3 years, if they have normal myocardial function, before developing signs of congestive heart failure and/or sudden death.[64] Ventricular arrhythmias may develop secondary to decreased myocardial perfusion associated with severe aortic regurgitation. A continuous 24-hour Holter electrocardiogram and exercising electrocardiogram (obtained with radiotelemetry) should be performed in horses with ventricular extrasystoles and aortic regurgitation to determine the frequency and severity of these arrhythmias. Once significant mitral regurgitation develops secondary to dilatation of the mitral annulus or a ruptured mitral chorda tendinea, these horses deteriorate rapidly and develop severe pulmonary hypertension and signs of left-sided heart failure.[62, 64] Therefore, horses with severe aortic regurgitation should be re-examined every 6 months to closely monitor the worsening of the aortic regurgitation and the safety aspects of continued use of the horse for athletic performance. The use of ACE inhibitors should also be considered in horses with moderate to severe aortic regurgitation, as these drugs have been shown in human beings to reverse left ventricular dilatation, decrease left ventricular mass and left ventricular hypertrophy, and probably delay the time to valve replacement in these patients.[172] These drugs should be similarly efficacious in horses.

If the regurgitant jet area is larger than expected for the degree of left ventricular enlargement, a recent onset of aortic regurgitation should be suspected, also prompting a re-examination in 6 months, especially if severe aortic regurgitation is detected with Doppler echocardiography. The detection of severe aortic regurgitation with Doppler echocardiography, proximal flow convergence, a short (elevated) pressure half-time, round turgid left ventricle with decreased wall thickness, marked left atrial and ventricular enlargement, enlargement of the aortic root, and decreased left ventricular function are indications of hemodynamically significant aortic regurgitation and a guarded to poor prognosis.[64, 72]

Pulmonic Regurgitation. Primary pulmonic regurgitation is rare and has been reported in one horse with pulmonic valve rupture and in a few horses with bacterial endocarditis.[59, 63, 166] Pulmonic regurgitation is common in horses with congestive heart failure and pulmonary hypertension but is rarely detected clinically. Bicuspid and quadracuspid valves can occur but are rare, causing both valvular stenosis and regurgitation (Fig. 5-61). Echocardiographic findings in horses with moderate to severe pulmonic regurgitation include abnormalities of the pulmonic valve leaflets, pulmonary artery dilatation, right ventricular dilatation, right ventricular volume overload, and paradoxical septal motion (Fig. 5-62).[7, 63, 64, 72] Flow mapping of the right ventricular outflow tract from either the right or left parasternal window can be used to partially quantify the severity of the pulmonic regurgitation (Color Figure 5-10).[79, 80] The best angle for Doppler interrogation of a pulmonic regurgitation jet is from the right cardiac window, but, in some horses, depth limitations may preclude the use of this window.[8] Small amounts of clinically insignificant pulmonic regurgitation are frequently detected with color-flow Doppler echocardiography in normal horses.

Similar Doppler echocardiographic findings as is found with aortic regurgitation indicate increasing severity of pulmonic regurgitation. The large cross-sectional area of the jet at its origin relative to the cross-sectional area of the RVOT at its origin is a sensitive indication of severe pulmonic regurgitation.[64, 174] Reverse diastolic flow in the pulmonary artery and a regurgitant jet that occupies more than two thirds of the RVOT are compatible with severe pulmonic regurgitation.[64, 81, 104] The intensity of the Doppler signal also increases as the regurgitation becomes more severe.[81, 104] The slope of the continuous-wave Doppler velocity spectral tracing of the pulmonic regurgitation jet becomes steeper as the pulmonic regurgitation becomes more severe, and a rapid equalization of right ventricular and pulmonary artery diastolic pressures occurs.[105] The detection of late diastolic tricuspid regurgitation also indicates severe pulmonic regurgitation and rising right ventricular end-diastolic pressures in human beings.[174]

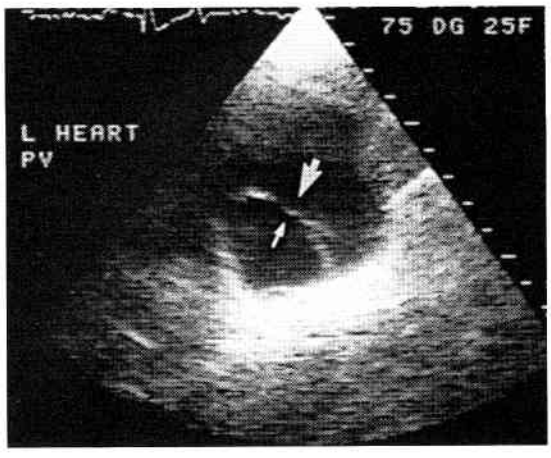

Figure 5–61

Short-axis echocardiogram obtained from a 4-year-old Thoroughbred gelding with mild pulmonic stenosis and pulmonic regurgitation associated with a bicuspid pulmonic valve. Notice the two pulmonic valve leaflets, one small *(small arrow)* and a larger leaflet, probably representing two fused leaflets *(larger arrow)*. This echocardiogram was obtained from the left cardiac window in the pulmonic valve position with a 2.25-MHz sector-scanner transducer at a displayed depth of 14 cm. An electrocardiogram is superimposed for timing.

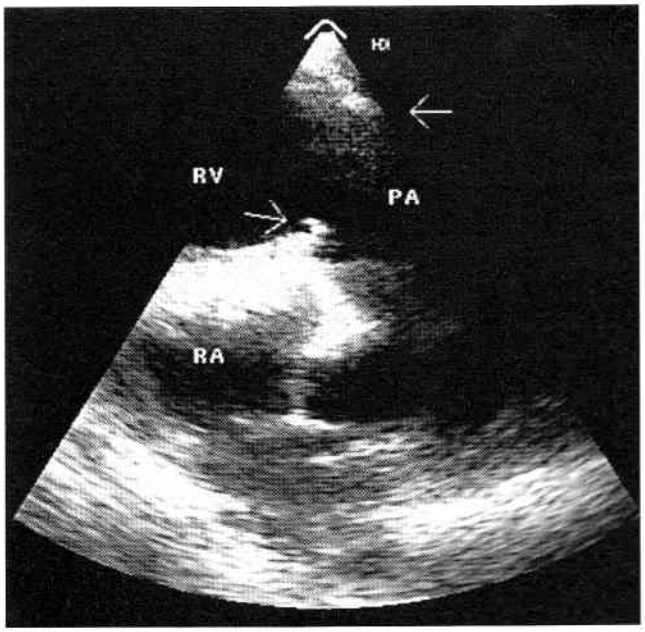

Figure 5–62

Long-axis two-dimensional echocardiogram obtained from a 5-year-old Thoroughbred-Percheron cross gelding with severe pulmonic and tricuspid regurgitation. Notice the two pulmonic valve leaflets moving in different directions during systole. The upper leaflet (*right arrow*) opens normally, whereas the lower leaflet (*left arrow*) is flail and everts into the right ventricular outflow tract. This echocardiogram was obtained from the left cardiac window in the pulmonic valve position with a 3.0/2.0-MHz phased-array transducer at a displayed depth of 26.8 cm. PA, Pulmonary artery; RV, right ventricle; RA, right atrium.

Patient Management and Prognosis. Horses with pulmonic regurgitation must be given a guarded to grave prognosis, as this valvular insufficiency is usually secondary to severe pulmonary hypertension and left-sided heart disease. Other reported causes of pulmonic regurgitation, flail pulmonic valve cusps, and vegetative endocarditis also carry with them a guarded to grave prognosis.

Myocardial Disease

Myocardial disease is more common in horses than previously reported and has a multitude of causes.[33, 47–49, 64, 69–72, 90, 91, 149, 150, 156, 162, 173, 179–212] Toxins (heavy metals, ionophore antibiotics), drugs, nutritional imbalances (vitamin E and selenium), hypoxia, ischemia, infarcts, bacteria, viruses, parasites, trauma, neoplasia, and concurrent infections (bacterial endocarditis, pericarditis) can all cause myocardial disease. The first indication of myocardial disease may be clinical signs of poor performance, exercise intolerance, collapse, or sudden death, or it may be an incidental finding.[33, 49, 69–72, 93] Cardiac auscultation may be normal or cardiac arrhythmias, usually premature beats or atrial fibrillation, or murmurs of valvular regurgitation may be detected. Some arrhythmias associated with myocardial disease, such as multifocal ventricular tachycardia, are life threatening. Clinical signs of low-output heart failure can be seen in horses with severe myocardial dysfunction, with or without concurrent cardiac dysrhythmias. Resting heart rates in horses with myocardial disease may be normal or elevated, but affected animals usually have elevated exercising heart rates and prolonged heart rate recovery after exercise.

An echocardiographic examination should be part of the complete cardiac evaluation in the horse with suspected myocardial disease. Premature atrial and ventricular beats can occur in the absence of structural heart disease, particularly secondary to sepsis, toxemia, hypoxia, and electrolyte, metabolic, or autonomic imbalances. Frequent atrial or ventricular extrasystoles, sustained atrial or ventricular tachycardia, or multifocal arrhythmias are usually indicative of primary myocardial disease.[69, 70, 72, 90, 91, 179–186] Echocardiographic examinations in these horses may be normal, other than the abnormalities in valve and wall motion associated with the particular dysrhythmia. In some horses, however, areas of abnormal myocardial echogenicity or wall motion abnormalities, such as areas of focal or global hypokinesis, dyskinesis, or akinesis may be detected.[7, 16, 33, 69, 70, 72, 74, 179, 181, 182, 188]

Myocarditis/Cardiomyopathy. The echocardiogram from horses with myocarditis is usually normal, except for the abnormal opening and premature closure of the atrioventricular and semilunar valves, which occur with both atrial and ventricular premature depolarizations (Fig. 5-63). Ejection time may be shortened or absent altogether, particularly with very early ventricular premature depolarizations (Fig. 5-63). Abnormalities of interventricular septal motion may also be detected with ventricular premature depolarizations (Fig. 5-64). Some horses with atrial or ventricular premature depolarizations or atrial fibrillation may also have low-normal to low shortening fractions with focal or global hypokinesis or dyskinesis (Fig. 5-65).[69, 70, 72] A low-normal or low shortening fraction (24% or higher) has been reported in horses with atrial fibrillation, which returns to normal with conversion to sinus rhythm. The return of the shortening fraction to normal with conversion to sinus rhythm suggests that, in these horses, the low shortening fraction is secondary to the arrhythmia and not to primary myocardial disease.[74] Shortening fractions less than 24% in horses with atrial fibrillation are, however, suggestive of concurrent myocardial dysfunction. Postexercise echocardiography may also be useful in detecting horses with borderline myocardial function at rest but with abnormalities in left ventricular function immediately following exercise (Fig. 5-66).[33, 69, 72] The normal myocardium (left ventricle and interventricular septum) should thicken significantly, more during systole in the immediate postexercise period than at rest, and this improvement in myocardial contractility should occur globally. The detection of global or segmental areas of myocardial hypokinesis, dyskinesis, or akinesis is indicative of underlying myocardial disease and may reflect exercise-induced myocardial ischemia or hypoxia or pre-existing myocardial disease or myocarditis.[33, 69, 72] Severe myocardial necrosis occurs infrequently in horses with myocarditis and is usually associated with multifocal ventricular arrhythmias and acute onset of congestive heart failure. Marked myocardial dysfunction is detected echocardiographically in these horses with large

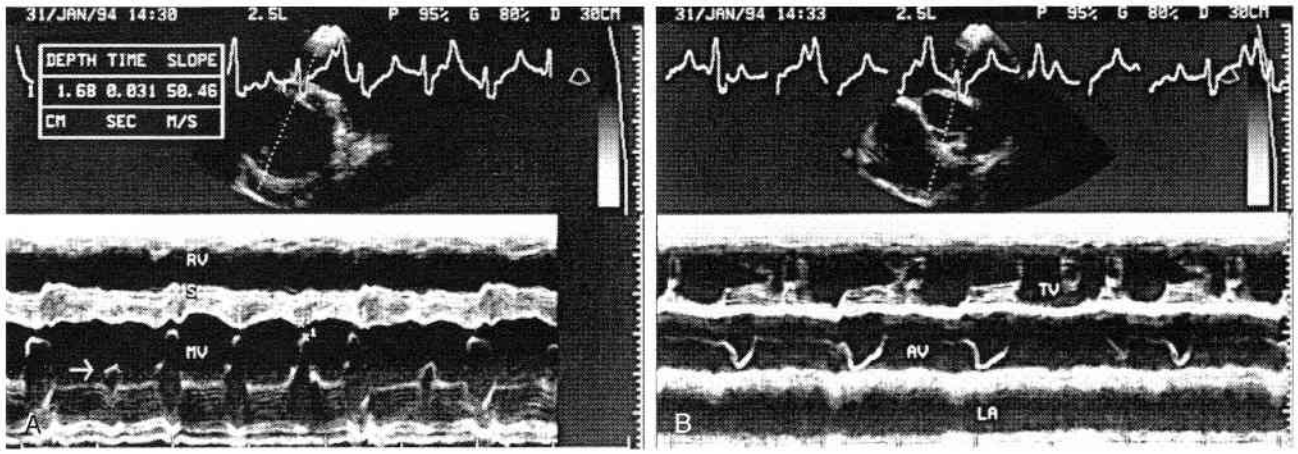

Figure 5–63

Two-dimensional (2-D) and M-mode echocardiograms obtained from a 12-year-old Thoroughbred gelding with myocarditis and unifocal ventricular tachycardia. These echocardiograms were obtained from the right cardiac window with a 2.5-MHz sector-scanner transducer at a displayed depth of 30 cm. The M-mode echocardiograms were obtained from the cursor position illustrated on the 2-D echocardiograms. An electrocardiogram is superimposed for timing.

A, Short-axis 2-D *(top)* and M-mode *(bottom)* echocardiograms of the mitral valve (MV). The minimal opening and early closure of the mitral valve are most marked at the arrow and the large septal-to-E-point (SEP) separation of 1.68 cm. RV, Right ventricle; S, interventricular septum.

B, Short-axis 2-D *(top)* and M-mode *(bottom)* echocardiograms of the aortic valve (AV). The M-mode echocardiogram was obtained from the cursor position illustrated in the 2-D echocardiogram. Notice the infrequent openings of the aortic valve leaflets (five) with many ventricular depolarizations (five) unable to generate a left ventricular pressure great enough to exceed aortic pressure and open the aortic leaflets. The amount of opening of the aortic leaflets varies, and the ejection times vary. TV, Tricuspid valve; LA, left atrium.

segmental areas or global myocardial dyskinesis (Fig. 5-67).

Areas of abnormal myocardial echogenicity are infrequently detected in horses (Fig. 5-68).[69, 70, 72, 179] These areas are typically more echogenic than normal, usually representing areas of myocardial fibrosis.[179] Although these areas of increased myocardial echogenicity can be associated with an inflammatory cell infiltrate, calcification (Fig. 5-68), and/or myocardial necrosis, fibrosis secondary to a prior myocardial insult is more likely (Fig. 5-69) and contracture of the scarred area may even be detectable echocardiographically. Areas of increased myocardial echogenicity were commonly detected in horses that sustained significant or life-threatening myocardial injury when accidentally exposed to monensin.[71] Infiltration of the myocardium with neoplastic cells must also be considered when areas of abnormal myocardial echogenicity are detected, but myocardial neoplasia is

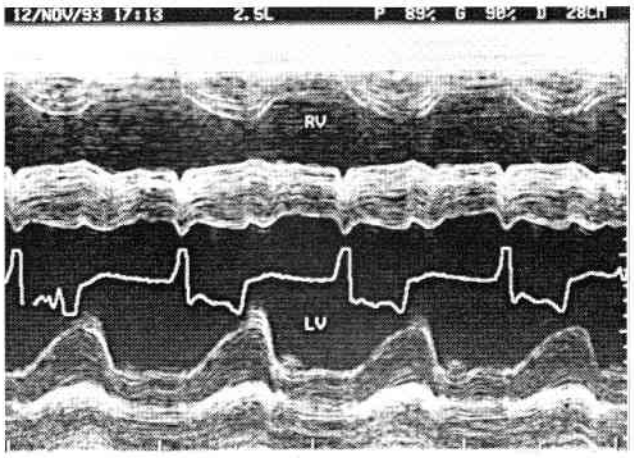

Figure 5–64

M-mode echocardiogram from a 4-year-old Standardbred gelding with an idioventricular rhythm. The abnormal septal motion is associated with the abnormal ventricular activation and the atrioventricular dissociation. This echocardiogram was obtained at the ventricular position from the right cardiac window with a 2.5-MHz sector-scanner transducer at a displayed depth of 28 cm. An electrocardiogram is superimposed for timing. RV, Right ventricle; LV, left ventricle.

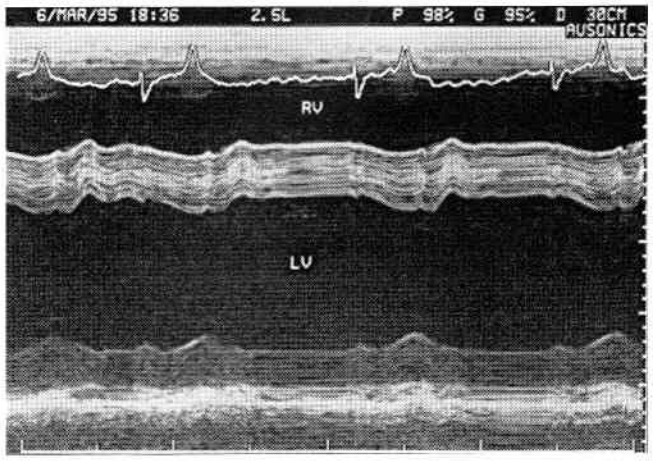

Figure 5–65

M-mode echocardiogram obtained from a 2-year-old Standardbred colt with atrial fibrillation and significant left ventricular dysfunction. The minimal thickening of the left ventricular free wall and interventricular septum in systole results in a shortening fraction of 16 to 20%. The R-R intervals are irregular and baseline fibrillation waves are present, characteristic of atrial fibrillation. This echocardiogram was obtained at the ventricular position from the right cardiac window with a 2.5-MHz sector-scanner transducer at a displayed depth of 30 cm. RV, Right ventricle; LV, left ventricle.

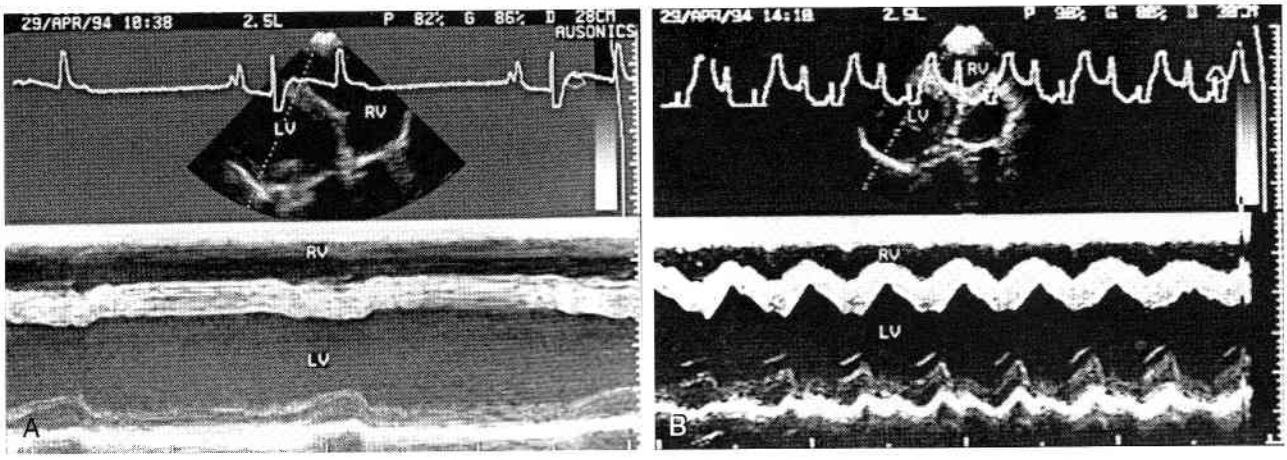

Figure 5–66

Short-axis two-dimensional and M-mode echocardiograms obtained from a 3-year-old Standardbred colt with poor racing performance. These echocardiograms were obtained from the right cardiac window in the left ventricular position with a 2.5-MHz sector-scanner transducer at a displayed depth of 28 cm (resting) or 30 cm (postexercise). An electrocardiogram is superimposed for timing. RV, Right ventricle; LV, left ventricle.

A, Notice the normal resting heart rate (30 beats/minute) and the normal thickening of the left ventricular free wall and interventricular septum (shortening fraction = 30%) in the resting echocardiogram.

B, Notice the elevated heart rate (120 beats/minute) and the swinging pattern of interventricular septal and left ventricular free wall motion with little thickening of the left ventricular free wall or interventricular septum (shortening fraction = 30 to 35%) in the echocardiogram obtained immediately after exercise. RV, Right ventricle; LV, left ventricle.

uncommon in horses. Lymphosarcoma and hemangiosarcoma may most commonly infiltrate the myocardium in the horse, but other tumors such as lipomas, pulmonary carcinomas, and other neoplasms may also metastasize to the heart.[70, 190, 191, 199–201] Areas of abnormal myocardial echogenicity may also occur secondary to penetrating foreign bodies (most likely wood), intracardiac punctures from intracardiac injections or broken intravenous catheters (Fig. 5–70), or a pericardial or myocardial abscess (rare).[75, 202]

Dilated cardiomyopathy occurs in the horse and is often probably a sequela to myocarditis.[72] In most cases the cause of the dilated cardiomyopathy is unknown, as endomyocardial biopsies are not commonly performed in horses. A dilated left ventricular chamber with thinning of the interventricular septum and left ventricular free wall and decreased shortening fraction are common echocardiographic findings.[7, 33, 49, 69, 70, 72, 93, 121] The left

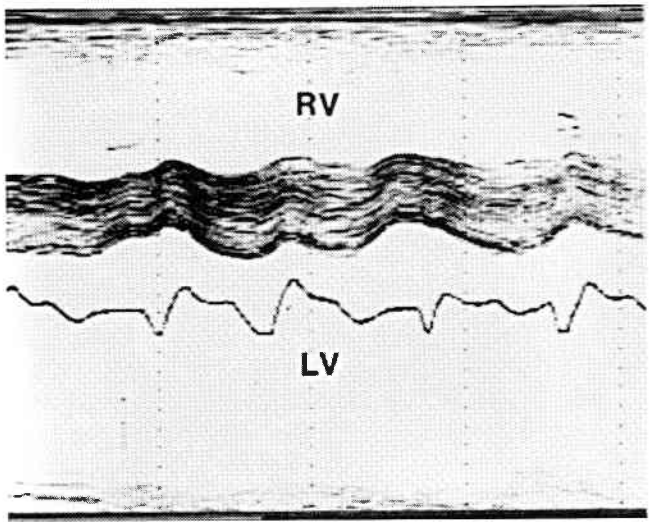

Figure 5–67

M-mode echocardiogram obtained from a 10-year-old Thoroughbred cross gelding with acute onset of multifocal ventricular tachycardia and left-sided congestive heart failure. The gelding died within hours after this echocardiogram was made. Severe widespread myocardial necrosis was detected at postmortem examination. Notice the severe depression of left ventricular function with little or no left ventricular free wall thickening and some thickening of the interventricular septum. This echocardiogram was obtained from the right cardiac window in the left ventricular position with a 2.5-MHz sector-scanner transducer at a displayed depth of 27.5 cm. An electrocardiogram is superimposed for timing. RV, Right ventricle; LV, left ventricle.

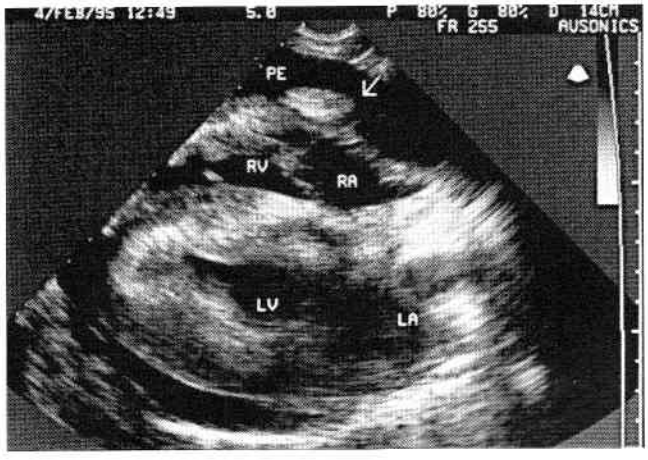

Figure 5–68

Two-dimensional echocardiogram obtained from a 6-month-old burro with myocardial calcification of unknown cause and pericardial effusion. Notice the multifocal areas of increased myocardial echogenicity, the anechoic pericardial effusion (PE), and the mild right atrial (RA) collapse. The arrow points to echogenic tissue in the coronary groove, which represented fat with calcification. This echocardiogram was obtained from the right cardiac window in the four-chamber view with a 5.0-MHz sector-scanner transducer at a displayed depth of 14 cm. RV, Right ventricle; LV, left ventricle; LA, left atrium.

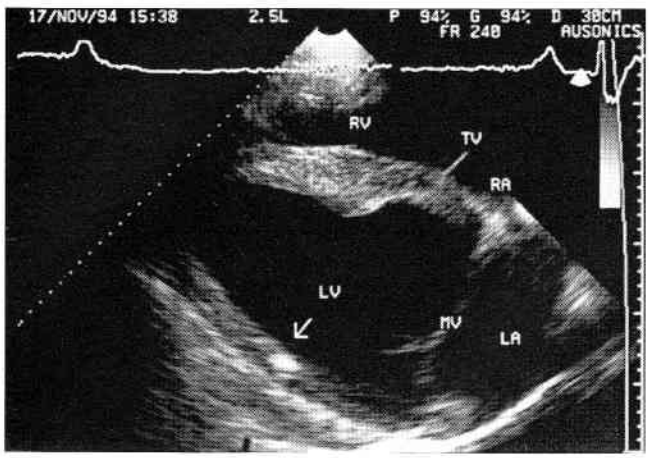

Figure 5–69

Echocardiogram obtained from a 9-year-old Oldenburg stallion with a history of acute collapse and hemopericardium 7 months earlier. The echogenic area in the left ventricular free wall *(arrow)* represents an area of myocardial scarring. This echocardiogram was obtained from the right cardiac window in the mitral valve position with a 2.5-MHz sector-scanner transducer at a displayed depth of 30 cm. An electrocardiogram is superimposed for timing. RA, Right atrium; TV, tricuspid valve; RV, right ventricle; LV, left ventricle; MV, mitral valve; LA, left atrium.

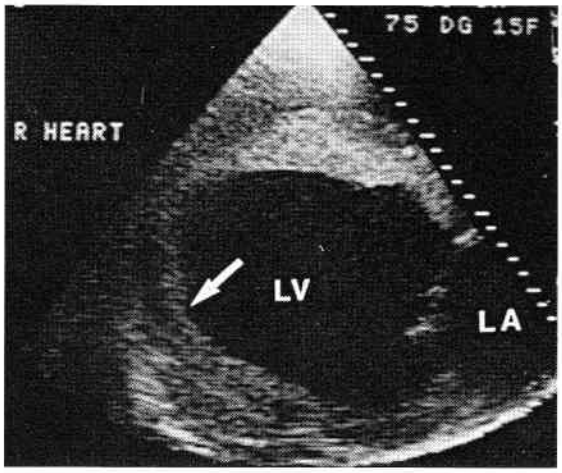

Figure 5–71

Long-axis echocardiogram obtained from a 2-year-old Arabian gelding with cardiomyopathy of unknown cause. This colt had been lethargic since birth and presented for severe exercise intolerance and persistent tachycardia after mild trotting exercise. Notice the rounded appearance of the left ventricle and the small left atrium. This gelding had marked hypokinesis of the interventricular septum and left ventricular free wall with an akinetic area near the left ventricular apex *(arrow)* where the ventricle had a squared appearance. This colt did not have any valvular regurgitation at presentation. This echocardiogram was obtained from the right cardiac window in the four-chamber position with a 2.25-MHz sector-scanner transducer at a displayed depth of 25 cm. LA, Left atrium; LV, left ventricle.

ventricular internal diameter is increased at both end-diastole and end-systole. Segmental wall motion abnormalities may also be detected (Fig. 5-71). Spontaneous contrast (smoke) may be imaged in the left atrium, left ventricle, and aorta associated with the low-flow state.[69, 70, 72] The aortic root diameter may be smaller than normal with a shortened ejection time and little or no movement of the aortic root, associated with low cardiac output.[7, 49, 69, 70, 72, 93] Little systolic separation of the aortic or pulmonic valve leaflets also occurs in horses with low cardiac output.[7] The pulmonary artery may be dilated secondary to pulmonary hypertension created by the severe left ventricular dysfunction.[7, 49, 70, 72, 93] The separation between the maximal opening of the septal leaflet of the mitral valve and the interventricular septum (E point to septal separation) is increased and mitral EF slope may be decreased.[7, 69] Delayed systolic closure of the atrioventricular valves may also occur in horses with left ventricular failure.[7] Valve leaflets are usually normal but may be thickened in horses with marked cardiac enlargement and valvular regurgitation secondary to dilatation of the atrioventricular valve annulus.[70] Right-sided cardiac enlargement may develop secondary to the left-sided failure. These severely affected horses usually have marked mitral, pulmonic, and tricuspid regurgitation.[70] Right ventricular cardiomyopathy has also been seen in horses but is rare (Fig. 5-72). Affected horses have marked dilatation of the right ventricle with thinning of the right ventricular free wall and abnormalities of right ventricular free wall and interventricular septal motion. Marked tricuspid regurgitation and right atrial enlargement occur secondary to the severe right ventricular myocardial dysfunction.

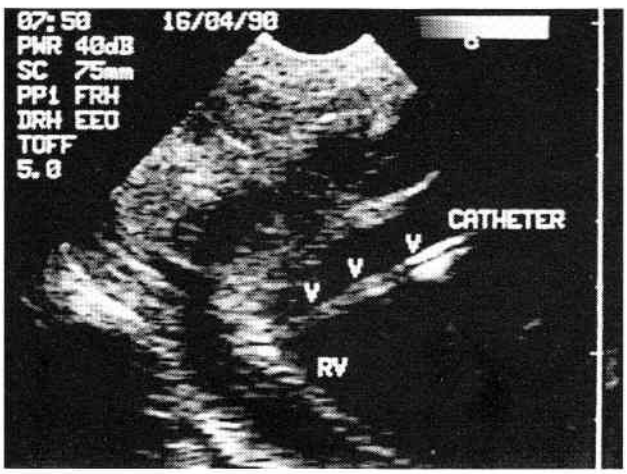

Figure 5–70

Echocardiogram obtained from a 3-week-old Thoroughbred colt with a broken intravenous catheter stuck in the right ventricular free wall *(arrowheads)* at the apex of the right ventricle (RV). A small pericardial effusion is present. This echocardiogram was obtained from the right cardiac window between the right ventricular and left ventricular outflow tract positions, angling ventrally toward the right ventricular apex, with a 5.0-MHz sector-scanner transducer at a displayed depth of 7.5 cm.

Ionophore Toxicity. Monensin toxicosis causes marked changes in myocardial function which are detectable echocardiographically.[69-72] In acute monensin toxicosis the cardiac chambers may be normal size; however, there is a marked decrease in myocardial contractility with minimal thickening of the left ventricular free wall and interventricular septum and shortening fractions as low as 7% (Fig. 5-73).[69-72] Areas of myocardial dyskinesis are imaged, particularly in the interventricular septum, and/or paradoxical septal motion is detected (Fig. 5-74). Marked amounts of spontaneous contrast may be imaged

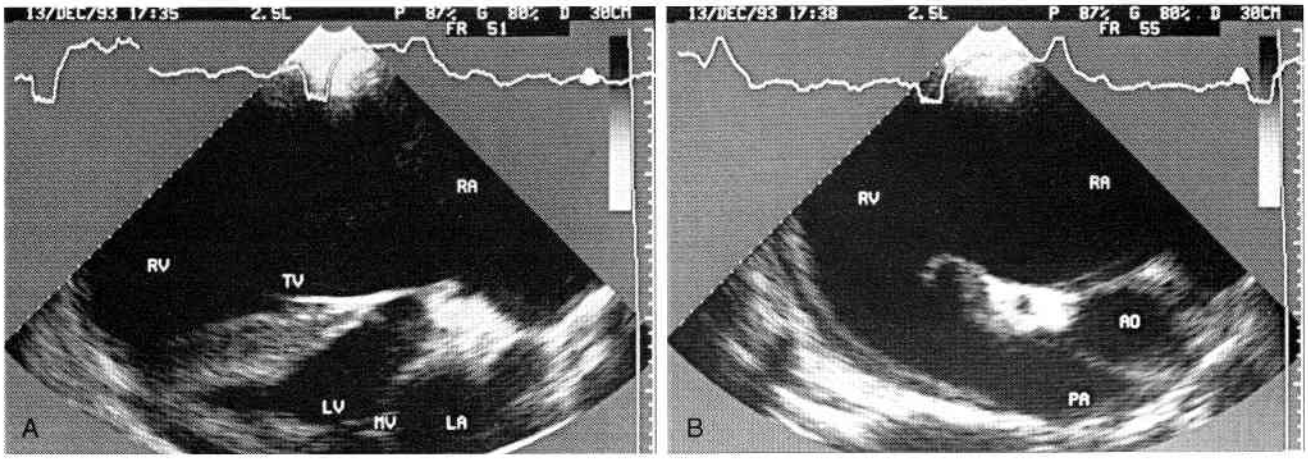

Figure 5–72

Long-axis two-dimensional echocardiograms obtained from a 2-year-old Standardbred colt with right ventricular cardiomyopathy, massive tricuspid regurgitation, and atrial fibrillation. These echocardiograms were obtained from the right cardiac window with a 2.5-MHz sector-scanner transducer at a displayed depth of 30 cm. An electrocardiogram is superimposed for timing.

A, Four-chamber view demonstrating massive right atrial (RA) and right ventricular (RV) enlargement with normal tricuspid valve (TV) leaflets. Notice the very small left atrium (LA) and left ventricle (LV). MV, Mitral valve.

B, Right ventricular outflow tract view demonstrating a smaller-than-normal pulmonary artery (PA) due to the severe right ventricular failure and low cardiac output from the right ventricle. Notice the massive right atrium (RA) and right ventricle (RV) and smaller-than-normal aorta (AO).

in the left atrium, left ventricle (Fig. 5-75), and aorta as well as on the right side of the heart.[69-72] A flat aortic root with no systolic aortic root movement and premature closure of the aortic valve may also be detected in horses with severe myocardial injury associated with acute monensin toxicosis (Fig. 5-76).[70-72] Areas of increased myocardial echogenicity were frequently detected in horses with acute monensin toxicosis.[71] Similar findings to those seen in horses with dilated cardiomyopathy were detected in horses that survived an exposure to monensin with the development of left ventricular dilatation and thinning of the left ventricular free wall and interventricular septum and shortening fractions of 20 to 30%. Atrioventricular valvular insufficiency may develop in horses with marked ventricular dilatation.

Patient Management and Prognosis. The findings

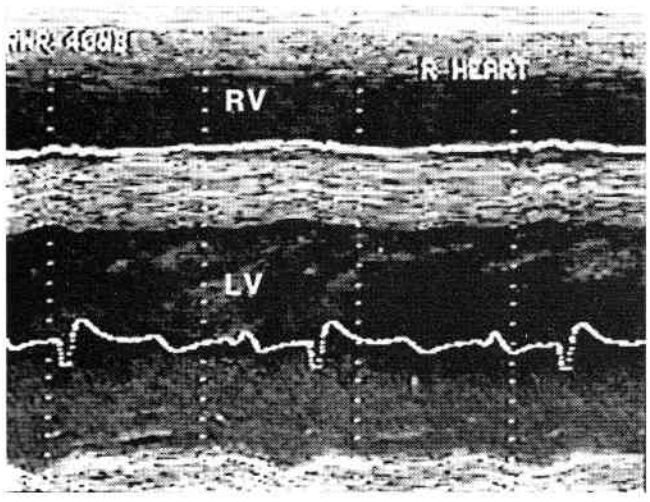

Figure 5–73

M-mode echocardiogram obtained from a 4-year-old Thoroughbred gelding with acute monensin toxicosis and severe myocardial dysfunction. The lack of thickening of the interventricular septum and left ventricular free wall in systole and the lack of cardiac motion resulted in a shortening fraction of 7%. This horse died within 24 hours after this echocardiogram was made. This echocardiogram was obtained from the right cardiac window in the left ventricular position with a 2.5-MHz sector-scanner transducer at a displayed depth of 27.5 cm. An electrocardiogram is superimposed for timing. RV, Right ventricle; LV, left ventricle.

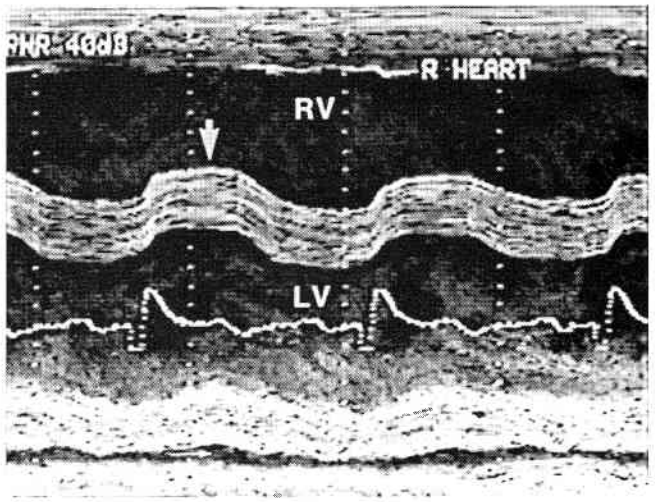

Figure 5–74

M-mode echocardiogram obtained from a yearling Thoroughbred filly with acute monensin toxicosis and severe myocardial dysfunction. Notice the minimal thickening of the left ventricular free wall and interventricular septum and the paradoxical motion of the interventricular septum *(vertical arrow).* Notice also the enlarged right ventricle and small pericardial effusion *(horizontal arrow).* This horse died within 24 hours after this echocardiogram was made. This echocardiogram was obtained from the right cardiac window in the left ventricular position with a 2.5-MHz sector-scanner transducer at a displayed depth of 27.5 cm. An electrocardiogram is superimposed for timing. RV, Right ventricle; LV, left ventricle.

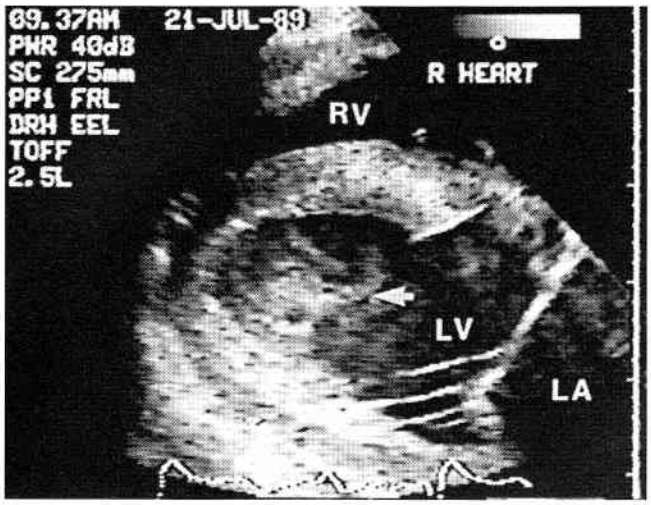

Figure 5–75

A long-axis two-dimensional echocardiogram obtained from a 4-year-old Thoroughbred gelding with monensin toxicosis (same horse as in Figure 5–73). Notice the large amounts of spontaneous contrast in the left ventricle *(arrow)* and the mild left atrial (LA) enlargement. This gelding died within 24 hours after this echocardiogram was made. This echocardiogram was obtained from the right cardiac window in the four-chamber view with a 2.5-MHz sector-scanner transducer at a displayed depth of 27.5 cm. An electrocardiogram is superimposed for timing. RV, Right ventricle; LV, left ventricle.

on the echocardiogram in horses with myocarditis or cardiomyopathy can be very useful in formulating a prognosis.[69, 70, 72] The horses with cardiac arrhythmias and normal myocardial function, except for those valvular or wall motion abnormalities associated with the dysrhythmia, have an excellent prognosis for return to performance and normal life expectancy as long as the arrhythmia resolves with rest and/or antiarrhythmic or corticosteroid therapy.[69, 70, 72] The horses with severe left ventricular dysfunction and low cardiac output states must be given a guarded to grave prognosis for life, as these horses usually have irreversible myocardial injury.[69, 70, 72]

The echocardiogram is an excellent predictor of outcome in horses with exposure to monensin and probably with exposure to other ionophores.[70-72] Shortening fraction was the best predictor of outcome in horses with monensin toxicosis during a recent outbreak.[70] Horses with shortening fractions less than 20% have a grave prognosis for life and should be stall rested with minimal stimulation. These horses are likely to die of low-output heart failure. Horses with shortening fractions of 20 to 30% are likely to survive and be useful as breeding animals but may be "cardiac cripples" that are able to perform only low-level physical activity. Some of these horses may recover and have normal myocardial function if the injury to the myocardium is mild. In another report of horses inadvertently exposed to monensin, exercise intolerance, congestive heart failure, and arrhythmias, primarily atrial fibrillation, developed months after the initial exposure to monensin.[207] These horses were not examined echocardiographically at the time monensin exposure was diagnosed and probably represent this intermediate group of affected horses, which should be identifiable on the initial echocardiographic examination with shortening fractions of 20 to 30%. Occasionally horses may develop cardiac arrhythmias several months following ionophore exposure, secondary to focal areas of myocardial injury and scarring that were not initially evident.[70] Therefore, cardiac rhythm and myocardial function should be re-evaluated periodically (every 4 to 6 months) in the first year following ionophore exposure. A normal echocardiogram in horses recently exposed to monensin is a good prognostic indicator. However, these horses should also be stall rested with minimal stimulation for at least several weeks (minimum 4 weeks) following exposure.[69-72] Normal resting and postexercise echocardiograms in horses exposed to monensin several months earlier were associated with an excellent prognosis for returning to previous performance.

Pericardial Disease

Pericardial disease is uncommon in horses and, until recently, affected horses were given an extremely poor prognosis.[17, 18, 65-68, 70, 72, 213-220] The cause of pericarditis in horses is usually either septic or idiopathic, but pericarditis can also occur associated with a viral infection, neoplasia, a penetrating wound, or a foreign body.[17, 18, 33, 65-68, 70, 72, 213-220] Pericardial hernias have also been reported but are rare.[70, 72, 221] The clinical signs of pericarditis include colic, generalized venous distention, jugular pulsations, ventral edema, anorexia, depression, fever, and weight loss.[14, 17, 18, 65-68, 70, 72, 213-220] Cardiac auscultation usually reveals tachycardia, muffled heart sounds, and/or pericardial friction rubs and absent lung sounds in the ventral

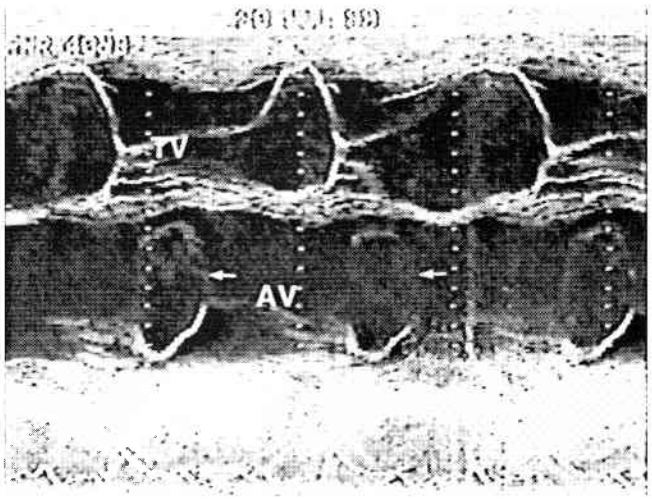

Figure 5–76

M-mode echocardiogram obtained from a 4-year-old Thoroughbred gelding with acute monensin toxicosis (same horse as in Figures 5–73 and 5–75). Notice the shortened aortic ejection time *(arrows)* and the small amount of spontaneous contrast present between the aortic leaflets. The aortic valve (AV) closes more than 150 msec prior to the opening of the tricuspid valve (TV). This gelding was in sinus rhythm and died within 24 hours after this echocardiogram was made. This echocardiogram was obtained from the right cardiac window in the aortic valve position with a 2.5-MHz sector-scanner transducer at a displayed depth of 27.5 cm. An electrocardiogram is superimposed for timing.

portion of the thorax. Echocardiography is extremely useful in diagnosing pericardial effusion, characterizing the type of effusion, determining where to perform a pericardiocentesis, and monitoring the response to therapy.[14, 17, 18, 33, 65-68, 70, 72]

Pericarditis. The echocardiogram is extremely useful in differentiating pericardial and pleural effusion.[7, 17, 18, 33, 65-68, 70, 72] Pleural effusion is usually also present in horses with pericarditis and may displace the heart caudally when present in the cranial mediastinum in large amounts. With pericardial effusion fluid is imaged between the pericardium and epicardium.[7, 14, 17, 18, 65-68, 70, 72] With small pericardial effusions, the epicardium and pericardium separate only in systole.[18] Sheets of fibrin, fibrin strands, and loculations are frequently detected between the epicardial and pericardial surfaces, as fibrinous pericarditis is common in horses (Fig. 5-77). Swirling echogenic fluid in the pericardial sac is most consistent with hemorrhage and clot (Fig. 5-78), whereas a clear anechoic effusion is most consistent with a transudate associated with congestive heart failure.[70] A composite or more echogenic fluid with fibrin is typical of septic or traumatic pericarditis. Hyperechoic free gas echoes are rarely imaged in horses with pericarditis and, if detected, a penetrating wound or traumatic pericarditis should be suspected. The most reliable sign of pericardial effusion is collapse of the right atrium (Fig. 5-79) and, with larger effusions, right ventricular diastolic collapse, indicators of hemodynamically significant pericardial effusions and cardiac tamponade.[18, 65, 70, 72] In most horses with pericardial effusion, fluid is imaged around both ventricles, but little fluid is imaged around the left atrium because the pericardium adheres tightly to the left atrium (Fig. 5-79).[70] Fluid may also be imaged between the descending aorta and the left ventricular free wall with pericardial effusions in some individuals.[70] The left ventricle is smaller than normal with significant pericardial effusions, and normal left ventricular free wall and pericardial motion is lost. The motion of the interventricular septum may be increased or paradoxical with larger pericardial effusions.[7, 18, 70, 72] Excessive cardiac motion occurs and often corresponds to the electrical alternans detected electrocardiographically.[18] Respiratory variations in right ventricular filling may be detected in horses with large pericardial effusions and cardiac tamponade.[7, 18, 70, 72] Early echocardiographic signs of cardiac tamponade include right atrial systolic collapse, an inspiratory increase in right ventricular chamber dimension (two or more times the dimension during expiration), and an inspiratory decrease in left ventricular chamber dimension.[70] As the pericardial tamponade becomes more hemodynamically significant, the right atrial systolic inversion is prolonged and compression of the right ventricular free wall occurs. Compression of the RVOT is detected initially because this area collapses first with increasing intrapericardial pressure.[70] In horses with chronic pericarditis, the fibrin in the pericardial space may become thicker and more echogenic as it begins to organize into fibrous tissue.[18, 66, 67] Constrictive and restrictive pericarditis, although uncommon in horses, can be diagnosed echocardiographically.[7, 67, 72] With constrictive pericarditis there is restriction of left ventricular filling in late diastole and flattening of the visceral pericardial side of the left ventricular myocardium.[70] An atrial systolic notch and early diastolic notch may be detected in the interventricular septum.[67, 70] A leftward movement of the atrial and ventricular septum has also been reported.[70] Thickening of the visceral pericardium and epicardium is usually detected.

Pericardial Abscess/Neoplasia. Pericardial masses

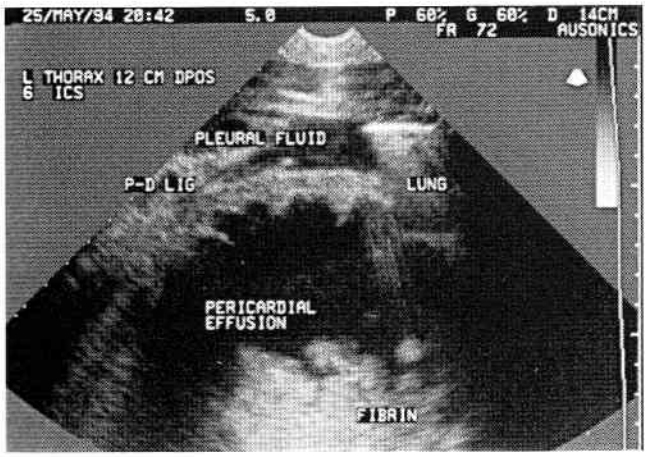

Figure 5-77

Long-axis echocardiogram obtained from a 12-year-old Thoroughbred mare with septic pericarditis. Notice the fibrin on the epicardial surface of the heart and on the parietal pericardium. A small pleural effusion and an aerated ventral tip of the lung are visible. This echocardiogram was obtained from the left cardiac window in the sixth intercostal space, evaluating the caudal border of the left ventricle and the caudal aspect of the pericardial sac. This echocardiogram was obtained with a 5.0-MHz sector-scanner transducer at a displayed depth of 14 cm. P-D LIG, Pericardial-diaphragmatic ligament.

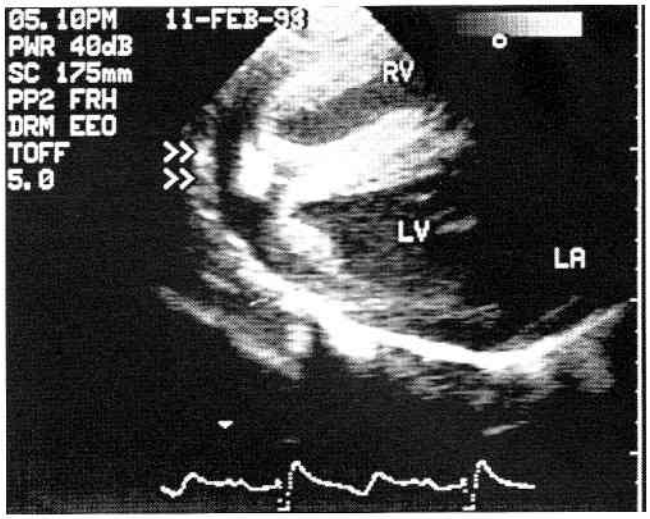

Figure 5-78

Long-axis two-dimensional echocardiogram obtained from a 1-day-old Standardbred filly that had received an intracardiac injection of epinephrine at birth. Notice the echogenic clot *(arrowheads)* at the right ventricular (RV) apex, with the tag of fibrin extending to the left ventricular (LV) side of the interventricular septum and the small localized pericardial effusion. This four-chamber view was obtained from the right cardiac window, angling ventrally to image the cardiac apex with a 5.0-MHz sector-scanner transducer at a displayed depth of 17.5 cm. An electrocardiogram is superimposed for timing. LA, Left atrium.

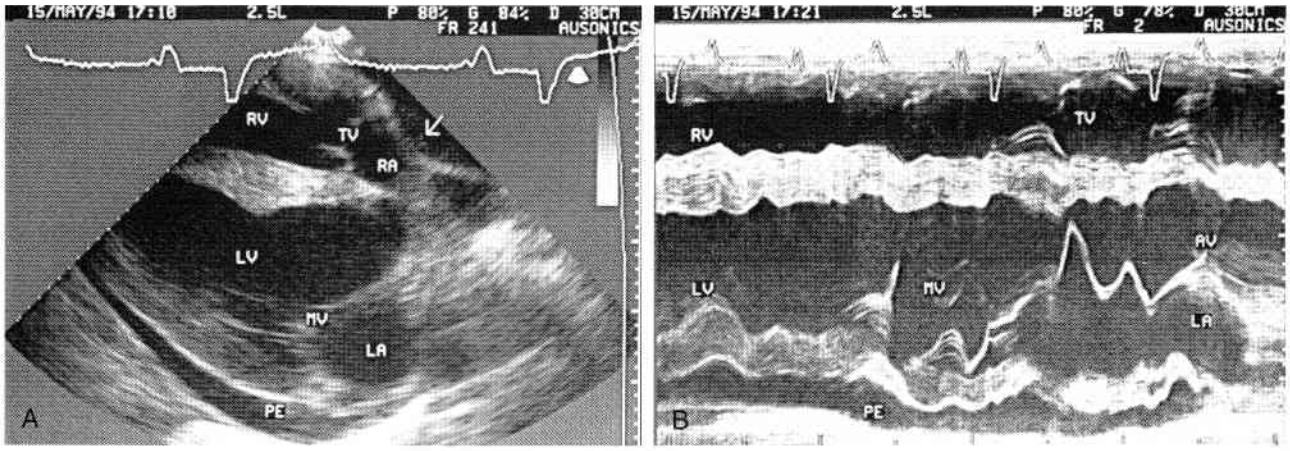

Figure 5–79

Echocardiograms obtained from a 2-year-old Standardbred filly with pericardial effusion (PE). These echocardiograms were obtained from the right cardiac window with a 2.5-MHz sector-scanner transducer at a displayed depth of 30 cm. An electrocardiogram is superimposed for timing.

A, Long-axis two-dimensional echocardiogram obtained from the right cardiac window in the mitral valve position. Notice the anechoic pericardial effusion (PE), the right atrial (RA) collapse *(arrow),* and the small amount of pericardial fluid surrounding the left atrium (LA). TV, Tricuspid valve; RV, right ventricle; LV, left ventricle; MV, mitral valve.

B, M-mode echocardiogram showing a sweep from the left ventricle (LV) to left atrium (LA), demonstrating the decrease in the pericardial effusion (PE) surrounding the left atrium. RV, Right ventricle; TV, tricuspid valve; MV, mitral valve; AV, aortic valve.

are infrequently detected in horses and are usually associated with pericardial abscesses or neoplasia.[33, 70, 72] Pericardial abscesses are rare in horses but have been imaged in one horse with myocardial involvement (Fig. 5-80).[70] More frequently, cranial mediastinal abscesses mimic the clinical signs of pericarditis by causing cranial vena caval obstruction.[70] These abscesses usually occur secondary to chronic pleuropneumonia.[222] The cranial mediastinal abscesses may displace the heart caudally and involve the parietal pericardium but do not usually cause pericarditis. Cranial mediastinal abscesses can be imaged ultrasonographically and differentiated from pericardial effusions or abscesses.[222] Cranial mediastinal abscesses displace the heart caudally and frequently impinge on right atrial and/or right ventricular filling (see Chapter 4). Foreign bodies rarely occur in the equine pericardium but have been occasionally reported in horses and could possibly be imaged if located in an area routinely examined echo-

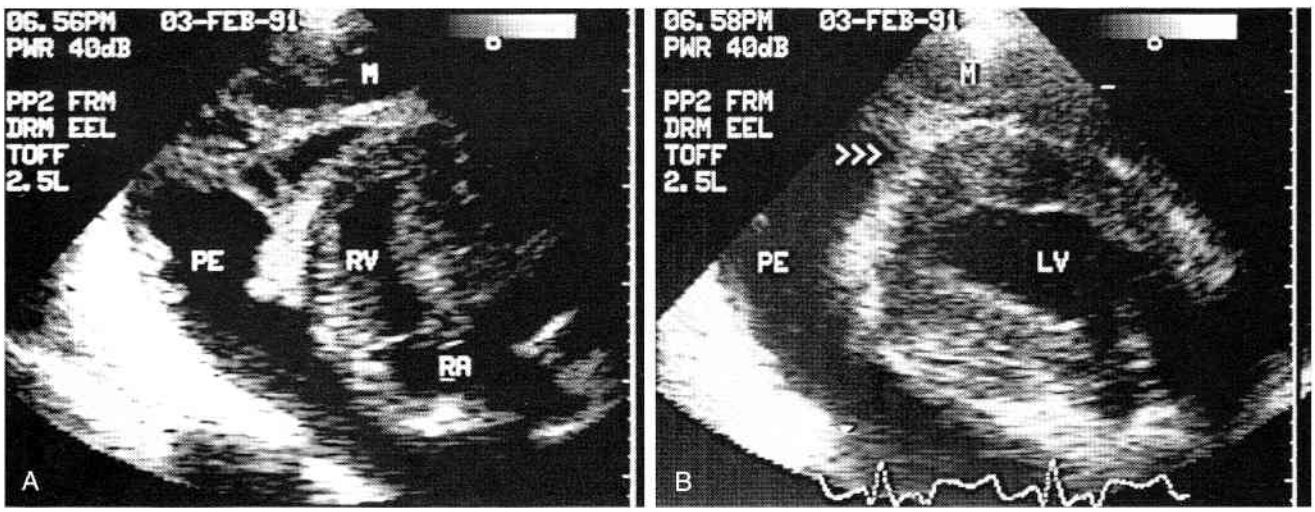

Figure 5–80

Echocardiograms obtained from a 3-year-old Thoroughbred filly with a pericardial abscess and pericarditis. These echocardiograms were obtained from the left cardiac window with a 2.5-MHz sector-scanner transducer at a displayed depth of 27.5 cm.

A, Long-axis echocardiogram of the right ventricular outflow tract demonstrating the fibrinous adhesions of the mass (M) to the epicardium of the right ventricle (RV). The fluid within the mass is anechoic to echogenic, most consistent with an abscess. PE, Pericardial effusion; RA, right atrium.

B, Long-axis echocardiogram of the left ventricle (LV) at the mitral valve position demonstrating fibrous adhesions *(arrowheads)* to the left ventricular epicardium and distortion of the shape of the left ventricle due to the scarring associated with these adhesions. Increased echogenicity of the myocardium is present at the site of the adhesions between the abscess (M) and the epicardium, suggesting myocardial involvement. An electrocardiogram is superimposed for timing. PE, Pericardial effusion.

cardiographically.[70, 72] Pericardial tumors are uncommonly detected in horses (Fig. 5-81). Mesotheliomas, one of the most common pericardial tumors in horses, have been detected echocardiographically.[70] Pericardial effusion is usually detected in horses with mesotheliomas in association with epicardial and pericardial masses, but pericardial mesotheliomas occasionally occur in horses without pericardial effusion.[70, 223, 224]

Patient Management and Prognosis. The optimal site for placement of a catheter for pericardiocentesis should be determined echocardiographically.[7, 18, 33, 65, 66, 68, 70, 72] The amount and type of pericardial fluid present help determine if an indwelling catheter can be placed for pericardial drainage and lavage or whether only a sample for cytology, culture, and sensitivity testing can be obtained. Such a sample should be obtained whenever possible unless only a small pericardial effusion is detected.[17, 18, 65-68, 70, 72] If possible, a large-bore Argyle chest tube should be placed in the pericardial sac under ultrasonographic guidance for repeated drainage, lavage of the pericardial sac with sterile isotonic fluids, and direct instillation of antimicrobials into the pericardial sac.[18, 33, 65, 68, 70, 72] This aggressive therapy has been successful in all horses with pericarditis and large pericardial effusions treated at New Bolton Center since 1986. The twice-daily or daily drainage and lavage should be continued until only small amounts of pericardial fluid are imaged echocardiographically and less than 1 liter of fluid is consistently obtained at the time of initial pericardial drainage. Follow-up echocardiograms performed on horses with pericarditis approximately 1 month after discontinuing the indwelling drainage and lavage reveal little or no echocardiographic evidence of the previous pericarditis.[65, 68] The use of indwelling chest tubes in the pericardial sac, coupled with aggressive drainage, lavage, direct instillation of antimicrobials into the pericardial sac, and the systemic administration of broad-spectrum antimicrobials with or without corticosteroids, has markedly improved the prognosis for horses with fibrinous pericarditis and has decreased the incidence of constrictive pericarditis.[18, 33, 65, 68, 70] Broad-spectrum bactericidal antimicrobials should be administered until the septic pericarditis has resolved or the results of the cytology, culture, and sensitivity testing of the pericardial fluid indicate an idiopathic (nonseptic) pericarditis.[18, 65, 68, 70, 72] Corticosteroids have been shown to be useful in horses with fibrinous pericarditis when no evidence of pericardial sepsis is present.[17, 65, 70, 72] Horses with pericardial abscesses or neoplasia should be given a guarded to grave prognosis for life.[70, 72]

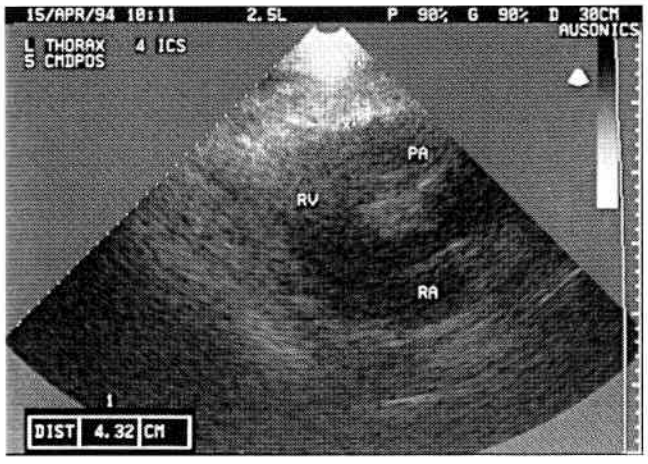

Figure 5-81

Long-axis two-dimensional echocardiogram obtained from a 6-year-old Standardbred mare with cranial mediastinal lymphosarcoma. The heart was extremely difficult to image owing to the infiltration of the pericardium with neoplastic lymphocytes, resulting in a markedly thickened (4.32 cm) heterogeneous pericardial sac and cardiac compression. This long-axis view of the pulmonary artery was obtained from the left cardiac window with a 2.5-MHz sector-scanner at a displayed depth of 30 cm. PA, Pulmonary artery; RV, right ventricle; RA, right atrium.

VASCULAR DISEASES

Echocardiography is useful in the diagnosis of abnormalities of the aortic root and pulmonary artery, particularly aneurysms of the sinus of Valsalva, aortic root rupture, and aortic and pulmonary artery dilatation.[7, 19, 33, 45, 46, 49, 72, 75] Diagnostic ultrasound is similarly useful in the diagnosis of peripheral vascular abnormalities, particularly aortoiliac thrombosis, cranial mesenteric arteritis, and jugular vein thrombophlebitis and monitoring response to treatment if indicated.[33, 72, 225-233]

Examination Technique

Patient Preparation

The horse should be prepared for an echocardiographic examination if the ascending aorta and/or main pulmonary artery or pulmonary artery branches are to be examined. If the terminal portion of the aorta, iliac arteries, cranial mesenteric and its branches, renal artery, middle uterine artery, or any other abdominal artery accessible to transrectal examination is to be evaluated, the rectum should be thoroughly emptied. The horse should be restrained in stocks or in a stall with minimal distractions. The horse should be quiet and relaxed and should be tranquilized if necessary, particularly if one is examining vessels deep within the abdomen. The hair over the peripheral vessels to be examined should be removed with a No. 40 surgical clipper blade, the skin cleaned, and coupling gel applied (Fig. 5-82).

Anatomy

The vessel being examined should be scanned in its entirety if accessible to the examiner. The branches of the affected vessel should also be examined, if possible, to determine the extent of the vascular abnormality. A quick review of the vascular anatomy in question is helpful in clarifying suspected abnormalities. In most peripheral vessels, a comparison can be made to the contralateral vessel if abnormalities are suspected. A thorough knowledge of normal vascular anatomy is important in

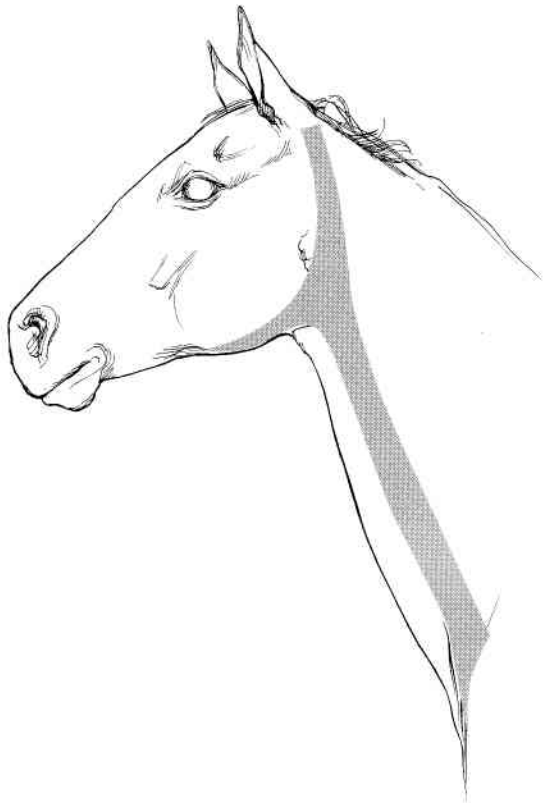

Figure 5–82

Diagram of the left skin that should be surgically clipped overlying the jugular, lingual facial, and external maxillary veins *(shaded area)* in the left side of the horse's neck to perform the ultrasonographic examination.

performing a thorough vascular ultrasonographic examination.

Scanning Technique

The technique for scanning the ascending aorta and pulmonary artery has been described. The intra-abdominal and intrapelvic vessels to be examined should be palpated first and then the appropriate transducer introduced to the rectum for sonographic examination (Fig. 5-83). A 7.5- 6.0- or 5.0-MHz transrectal transducer should be used to evaluate these vessels during rectal examination. Either linear-array, microconvex linear-array, or sector-scanner transducers can be used for these examinations. Depending upon the vessel being scanned, the size of the horse, and the sonographer's arm, a linear-array, microconvex linear-array, or sector scanner may be preferable. To scan the aorta and iliac arteries, a transducer must be used which emits the ultrasound beam at an angle to the long axis of the transducer, preferably 90 degrees. Other transducers that emit the beam at an angle less than 90 degrees can be used but are less user friendly. The linear transducer produces a sagittal or long-axis image of the aorta and a transverse or short-axis image of the iliac arteries and cranial mesenteric or renal arteries, if the latter two vessels can be reached by the examiner. A 90-degree sector-scanner transducer produces a transverse image of the aorta and a long-axis image of the iliac, cranial mesenteric, and renal arteries. With a 150-degree microconvex linear-array transducer, short- and long-axis images of the aorta, iliac arteries, and cranial mesenteric or renal arteries are obtainable because the transducer is small enough to maneuver transrectally and has a wide field of view. With transducer configurations in which the ultrasound beam is emitted at 90 degrees to its long axis, the transducer must be placed over the artery in question. With an end-fire transducer (ultrasound beam is parallel to the transducer's long axis) or a transducer that emits a beam at less than 90 degrees, the transducer can be pointed toward the artery being examined and imaged, if there is no intervening gas-filled bowel. For imaging superficial vessels, the transducer should be placed directly over the vein being examined. For vessels just beneath the skin, a 7.5- or 10-MHz transducer should be used with a built-in or hand-held stand-off. For deeper vessels, a lower-frequency transducer may be needed. The highest frequency transducer that can successfully obtain a high-quality image of the vessel being examined should be used. It may be necessary to change transducers when examining deeper vessels if they move significantly in relationship to the skin surface. The superficial veins should be occluded to distend the vessel while scanning because the vein collapses with transducer pressure. It is easiest if an assistant performs the Valsalva maneuver while the sonographer performs the ultrasonographic examination of the jugular vein.

Ultrasonographic and Echocardiographic Findings

Normal Findings

The veins are easily recognized by their thin echogenic wall, which is easily compressible unless contained within tissues that cannot be compressed. The veins have valves that are readily imaged when carefully scanning the venous system. Doppler evaluation of venous flow reveals continuous low-velocity flow throughout the veins. In contrast, the arteries are thicker-walled vessels that lack valves and contain laminar pulsatile flow when interrogated with Doppler ultrasound.

Abnormal Findings

Sinus of Valsalva Aneurysm and Aortic Root Rupture. Sinus of Valsalva aneurysms are congenital anomalies that occur in horses but are not associated with aortic root rupture until later in life.[19, 45, 46, 72, 75] Most horses with sinus of Valsalva aneurysms that rupture are male and at least 10 years old, although at least one horse was 9 years old when the sinus of Valsalva aneurysm ruptured. These aneurysms are caused by congenital defects in the media of the wall of the aorta which are located in the right sinus of Valsalva. At least one horse has been diagnosed at an early age (3 years) with an unruptured sinus of Valsalva aneurysm.[45] This defect is detectable echocardiographically long before the rupture of the si-

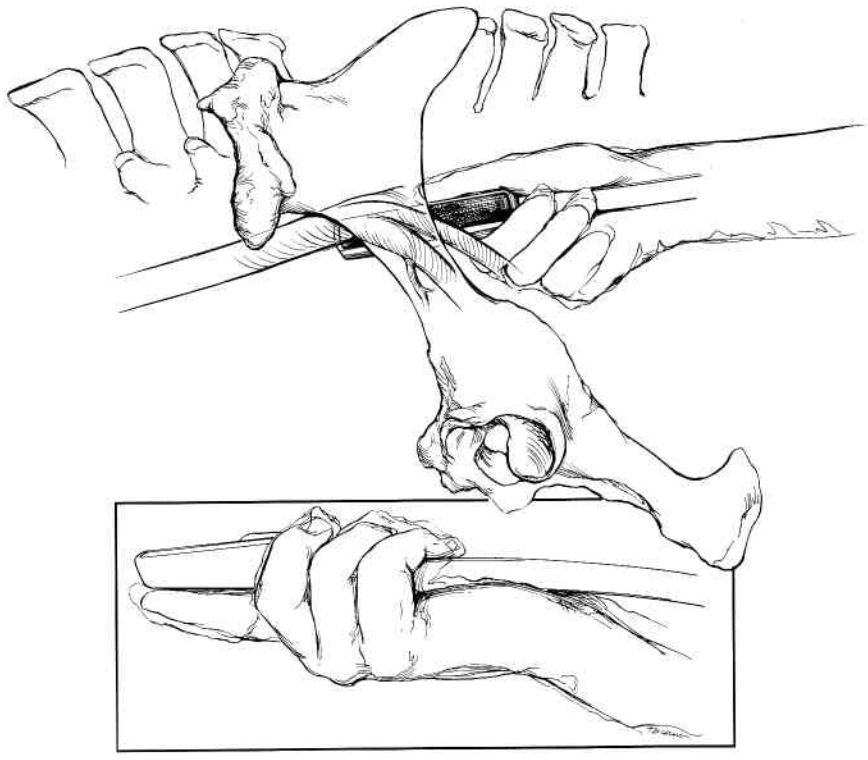

Figure 5–83

Diagram of the aorta and left internal and external iliac arteries within the horse's pelvis. The examiner is shown scanning the left side of the aortic quadrifurcation (left internal and external iliac arteries). The inset illustrates the transducer position to scan the aorta from its ventral aspect.

nus of Valsalva aneurysm occurs. A ruptured sinus of Valsalva aneurysm should be considered in the differential diagnosis for a stallion or gelding 10 years old or more with tachycardia and colic without any detectable primary gastrointestinal problem.[75]

An intact sinus of Valsalva aneurysm in horses appears echocardiographically as a thin membrane at the right coronary sinus of Valsalva, continuous with the right wall of the aortic root, that bulges into the right atrium, right ventricle, or tricuspid valve (Fig. 5-84).[45] When the aortic sinus of Valsalva aneurysm ruptures into the heart, an aortic cardiac fistula results.[19, 46, 72, 75] The aneurysm can rupture into the right atrium or right ventricle or through the tricuspid valve or dissect down into the interventricular septum (Fig. 5-85). The thin dilated portion of the right aortic wall, a portion of the ruptured aneurysm, is usually imaged fluttering in the right atrium or right ventricle as blood shunts from the aorta into the right atrium or ventricle. Abnormalities of the tricuspid valve leaflets, such as a ruptured chorda tendinea, may also be imaged, depending upon the site of the rupture into the right heart.[19] If blood is dissecting down the interventricular septum, an anechoic fluid space is imaged between the endocardium and the myocardium which originates from the right sinus of Valsalva.[46, 75] These subendocardial fluid tracts should be followed to their distalmost extent. The subendocardial dissections can subsequently rupture into the right or left ventricle, secondary to the constant pressure from the aortic cardiac fistula pushing the dissection. The rupture of a sinus of Valsalva aneurysm usually causes a severe right atrial and right ventricular volume overload. A left ventricular volume overload is possible if the ruptured aneurysm also communicates with the left ventricle through a subendocardial dissection. Doppler echocardiography can be used to detect the high-velocity turbulent blood flow associated with the aortic cardiac fistula, which is easiest to detect with color-flow Doppler echocardiography.[46, 75] Contrast echocardiography also demonstrates the shunt associated with the aortic-cardiac fistula as a negative contrast jet in the right atrium or ventricle with a peripheral venous injection of microbubbles (Fig. 5-86).[75] The size of the

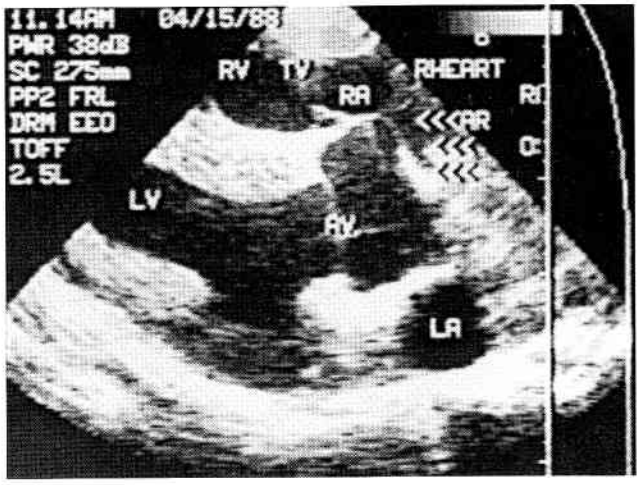

Figure 5–84

Long-axis echocardiogram obtained from a 3-year-old Thoroughbred gelding with an intact sinus of Valsalva aneurysm *(arrowheads)*. The thin membrane in the right wall of the aortic root (AR) at the right sinus of Valsalva bulges into the right atrium (RA) just above the tricuspid valve (TV). This echocardiogram was obtained from the right cardiac window in the left ventricular outflow tract position with a 2.5-MHz sector-scanner transducer at a displayed depth of 27.5 cm. RV, Right ventricle; LV, left ventricle; AV, aortic valve; LA, left atrium.

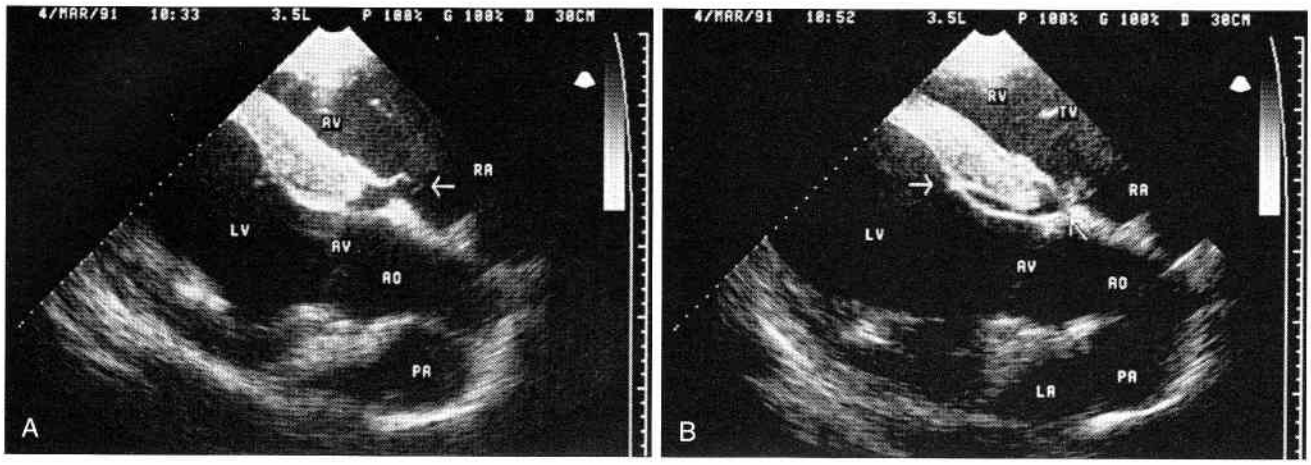

Figure 5–85

Long-axis two-dimensional echocardiogram obtained from an 11-year-old Standardbred gelding with a ruptured sinus of Valsalva aneurysm. These echocardiograms were obtained with a 3.5-MHz sector-scanner transducer at a displayed depth of 30 cm.

A, Long-axis view of the left ventricular outflow tract obtained from the right cardiac window. Notice the ragged edge of the ruptured sinus of Valsalva aneurysm *(arrow)* in the right atrium (RA). In real time this portion of the ruptured aneurysm was imaged moving in the right atrium with shunt flow and atrial filling. RV, Right ventricle; LV, left ventricle; AV, aortic valve; AO, aorta; PA, pulmonary artery.

B, Long-axis view of the left ventricular outflow tract obtained from the right cardiac window. This view was obtained slightly caudal to the view in *A.* The anechoic fluid (blood) dissects subendocardially toward the cardiac apex on both the right and left sides of the interventricular septum. Notice the vibrating ragged edge of the ruptured sinus of Valsalva aneurysm *(right arrow)* in the right atrium (RA) and the break in the left ventricular endocardium *(left arrow),* which resulted in rupture of a mitral chorda tendinea and marked left ventricular volume overload. TV, Tricuspid valve; RV, right ventricle; LV, left ventricle; AV, aortic valve; AO, aorta; PA, pulmonary artery; LA, left atrium.

aortic cardiac shunt and its hemodynamic significance should be determined, if possible, at the time the rupture is diagnosed.

Aortic root rupture at the right sinus of Valsalva can also occur without a pre-existing aneurysm.[19, 45, 46, 72, 75, 254] The echocardiographic findings are similar to those detected in horses with a ruptured sinus of Valsalva aneurysm, if the rupture occurs within the heart, except that no thin billowing membrane representing the ruptured aneurysm is detected fluttering in the right side of the heart.[75] Instead, a defect is imaged in the wall of the aorta at the right sinus of Valsalva, with no other pre-existing abnormalities of the aortic wall (Fig. 5-87). The rupture creates an aortic-cardiac fistula with a communi-

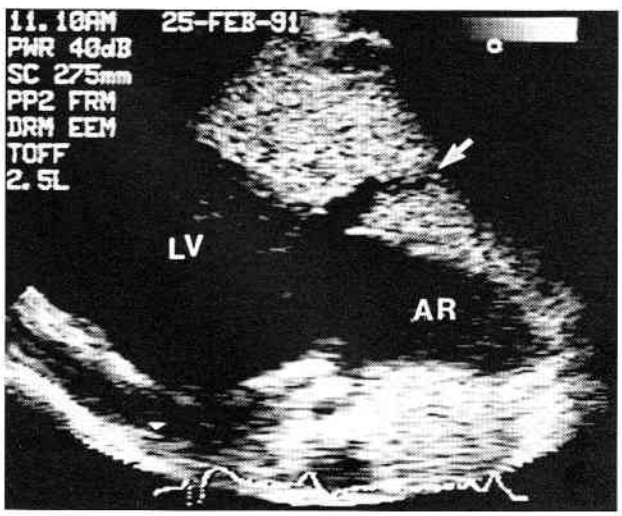

Figure 5–86

Contrast echocardiogram obtained from an 11-year-old Standardbred gelding with a ruptured sinus of Valsalva aneurysm (same horse as in Figure 5-85). The negative-contrast jet *(arrow)* enters the right atrium from the right sinus of Valsalva. This echocardiogram was obtained from the right cardiac window in the left ventricular outflow tract position with a 2.5-MHz sector-scanner transducer at a displayed depth of 27.5 cm. LV, Left ventricle; AR, aortic root.

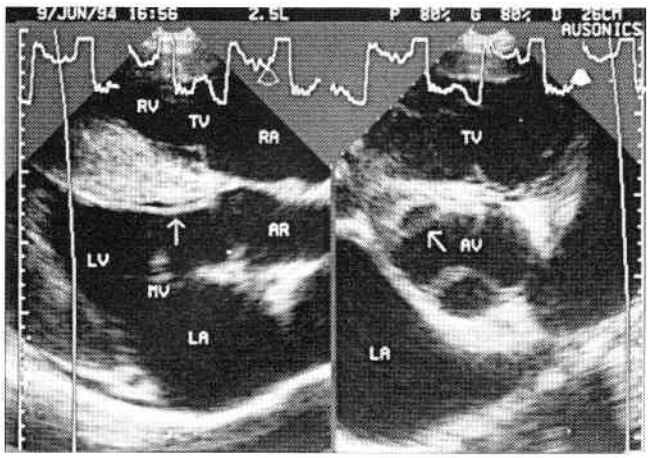

Figure 5–87

Echocardiograms of a ruptured aorta in a 10-year-old Standardbred gelding with subendocardial dissection. The subendocardial dissection originates at the aorta, probably at the right coronary leaflet, and dissects around the aorta behind the noncoronary leaflet *(arrow)* of the aortic valve (AV) in the short-axis view of the aorta *(right image).* The subendocardial dissection extends apically along the left side of the interventricular septum *(arrow)* as seen in the long-axis view of the left ventricular outflow tract *(left image).* These echocardiograms were obtained with a 2.5-MHz sector-scanner transducer at a displayed depth of 26 cm. RA, Right atrium; TV, tricuspid valve; RV, right ventricle; LV, left ventricle; MV, mitral valve; LA, left atrium; AR, aortic root.

cation between the right sinus of Valsalva and the right atrium or right ventricle. Right atrial and right ventricular volume overload may be detected, and abnormalities of the tricuspid valve leaflets can occur. Dissection of the blood into the interventricular septum has also been reported in horses with aortic root rupture.[75, 234]

Patient Management and Prognosis. The rupture of a sinus of Valsalva aneurysm or the aortic root is life threatening, and the only horses that have survived with a chronic aortic-cardiac fistula have had a rupture with dissection of blood into the interventricular septum.[46, 75, 234] There is one report of a stallion with aortic root rupture in which the aortic rupture dissected into the interventricular septum from the right sinus of Valsalva and was detected as an incidental finding at postmortem examination.[234] In most horses in which a ruptured sinus of Valsalva aneurysm or a rupture of the aortic root at the right sinus of Valsalva is diagnosed before death, the prognosis is guarded to grave. Most affected horses have lived less than 6 months following the time of probable rupture, with only a rare horse alive after 1 year.[19, 46, 75, 234] Ventricular tachycardia is common at the time of the rupture and is usually unifocal and responsive to antiarrhythmic therapy.[46, 75] The size of the aortic-cardiac fistula and the chambers that are affected by the development of this acquired shunt (the hemodynamic significance of the shunt) is crucial to formulating a prognosis for survival. The affected animals should not be used for performance, as the risk of sudden death and possible human injury is high.

Aortic Aneurysms and/or Rupture (Thoracic or Abdominal). Intrathoracic and intra-abdominal aortic aneurysms occur infrequently in horses and are rarely diagnosed before death. Intrathoracic aortic aneurysms have been associated with right-sided congestive heart failure in horses.[235-238] Rupture of intrathoracic aortic aneurysms in horses has been associated with collapse, recumbency, cardiovascular collapse, and sudden death.[235-237] Aneurysms of the ascending aorta, like aneurysms of the sinus of Valsalva, should be detectable echocardiographically because this portion of the aorta is routinely imaged in a standard transthoracic echocardiogram.[235, 236] The antemortem diagnosis of intrathoracic aortic aneurysms involving the aortic arch and descending aorta in horses could probably be made with TEE because the majority of the thoracic aorta should be visible with a transesophageal transducer long enough to reach the equine stomach. Intrathoracic and intra-abdominal aortic ruptures occur infrequently in horses and are usually associated with sudden death.[238] Massive hemorrhage into the thoracic or abdominal cavity or into surrounding musculature from other major vessels can also cause sudden death in horses.[191, 238-240] Hemothorax and/or hemoperitoneum can occur in horses with rupture of smaller aneurysms in the thoracic and/or abdominal cavity (Fig. 5-88).

Cranial Mesenteric Arteritis/Aneurysm. Intra-abdominal aneurysms are most commonly reported in the cranial mesenteric artery and its branches and the terminal portion of the aorta and iliac arteries.[225-232] Ultrasonographic evaluation of the cranial mesenteric artery can be performed in horses in which verminous arteritis is suspected to look for aneurysmal dilatations of the vessel

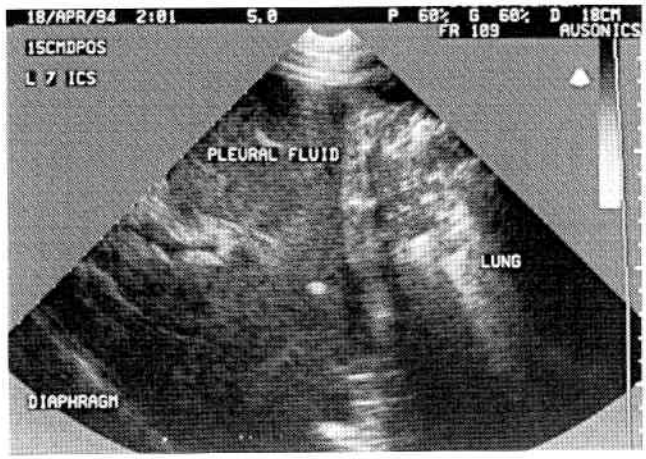

Figure 5-88

Sonogram of the left side of the thorax obtained from a 6-year-old Arabian mare with a hemothorax secondary to a ruptured thoracic aortic aneurysm. The swirling fluid in the thorax is consistent with blood and the echogenic material in the ventral portion of the thorax represents clot. The ventral portion of the lung is relatively hypoechoic. The atelectatic ventral lung tip is actually folded back upon itself as it floats on the fluid owing to the dense nature of the bloody fluid. This sonogram was obtained in the seventh intercostal space on a line 15 cm dorsal to a line level with the point of the shoulder with a 5.0-MHz sector-scanner transducer at a displayed depth of 18 cm. Dorsal is to the right of the sonogram and ventral is to the left.

and/or intraluminal plaque or thrombus.[230-232] The cranial mesenteric artery should be scanned with a 6.0 or 7.5 MHz transducer in an adequately sedated horse. Aneurysmal dilatation, thickening of the vessel wall, increased or variable echogenicity of the vessel wall, an irregular luminal surface, and intraluminal thrombi have been successfully imaged ultrasonographically in horses with verminous arteritis.[230-232] Increased echogenicity of the luminal side of the cranial mesenteric artery has been detected in horses with no other ultrasonographic abnormalities and was associated with histopathologic evidence of verminous arteritis.[232] Ultrasonography has a high specificity (86%) for detecting abnormal cranial mesenteric arteries in horses with verminous arteritis and a high sensitivity (90%) for detecting normal cranial mesenteric arteries.[231] Ultrasonography would be useful in monitoring response to therapy of horses with verminous arteritis.

Aortoiliac Thrombosis/Aneurysms. Ultrasonography has also been very useful in the diagnosis of aortoiliac thrombosis and in monitoring the response of affected horses to treatment.[225-229] Thickening of the wall of the terminal portion of the aorta and/or iliac arteries, aneurysmal dilatation of the terminal portion of the aorta, and the presence of thrombus and/or plaque of variable echogenicities within the terminal portion of the aorta and iliac arteries have been detected ultrasonographically (Fig. 5-89).[225-229] The echogenicity of the mass in the terminal portion of the aorta and iliac arteries can be used to help differentiate between an immature or organized thrombus and plaque within the vessel wall and lumen. The immature thrombus appears homogeneous and hypoechoic to anechoic, whereas the organized thrombus is more echogenic and may be heterogeneous in appearance, particularly if areas of fibrosis and calcification are

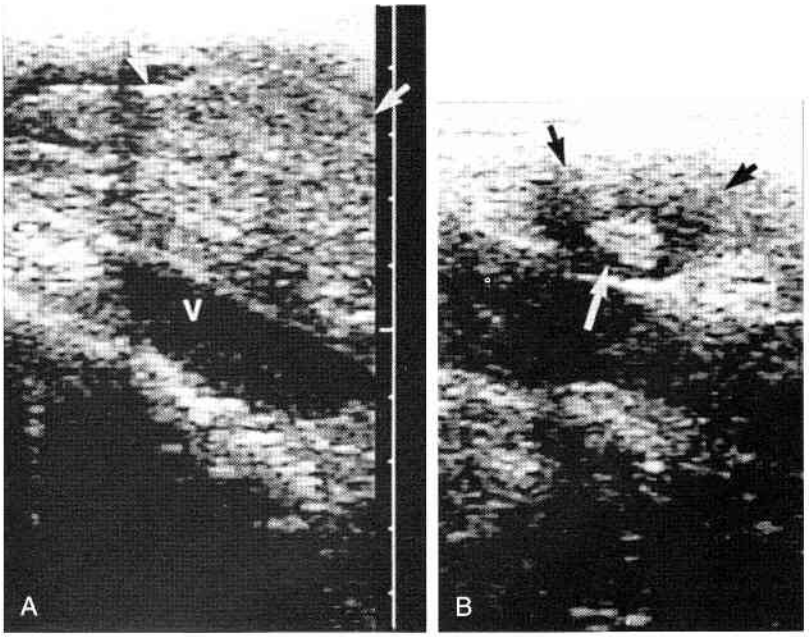

Figure 5–89

Sonograms obtained from a 6-year-old Standardbred stallion with aortoiliac thrombosis. These sonograms were obtained transrectally with a 5.0-MHz linear-array transducer at a displayed depth of 10 cm. Cranial is to the right of the sonogram and caudal is to the left.

A, The large heterogeneous mass originating from the dorsal wall of the aorta obstructs aortic blood flow *(arrows)*. This mass occupied 90% of the terminal portion of the aorta. The common iliac vein (V) is normal.

B, The more homogeneous thrombus *(white arrow)* floats in the internal iliac artery *(black arrows)*. This thrombus originated from the thrombotic mass in the terminal portion of the aorta.

present within the thrombus. The vessel wall can usually be distinguished from the immature thrombus because the wall of the aorta and/or iliac arteries is more echogenic. As the thrombus becomes more fibrotic, differentiation between the thrombus and the vessel wall becomes increasingly more difficult. Plaque along the vessel wall is usually echogenic to hyperechoic, with acoustic shadowing if calcification is present. Thickening of the arterial wall is common in more chronic cases with areas of fibrosis and calcification. The degree of vessel occlusion

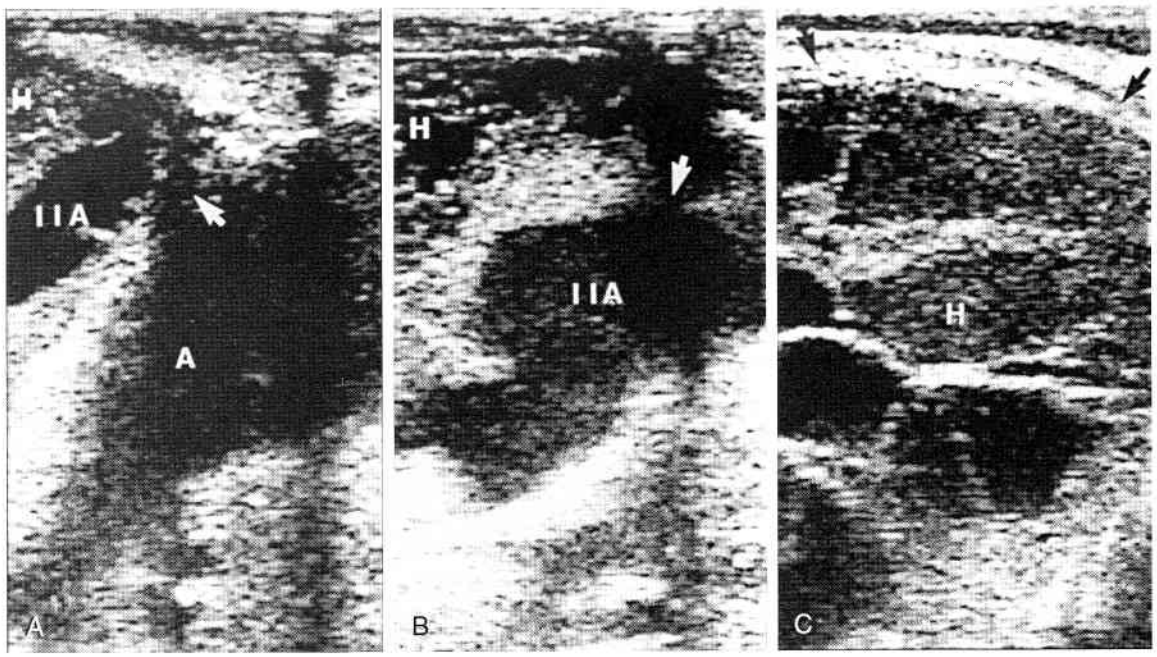

Figure 5–90

Sonogram obtained from a 9-year-old Thoroughbred mare with an aortic and right internal iliac artery fistula and a large perirectal hematoma. In real time, blood was imaged flowing from the terminal portion of the aorta and right internal iliac artery into the surrounding hematoma. These sonograms were obtained transrectally with a 5.0-MHz linear transducer at a displayed depth of 10 cm. Cranial is to the right of these sonograms and caudal is to the left.

A, The terminal portion of the aorta (A) communicates *(arrow)* with the large perirectal hematoma (H), with blood dissecting around the right internal iliac artery (IIA).

B, Notice the large communication *(arrow)* between the internal iliac artery (IIA) and the large perirectal hematoma (H).

C, The large loculated fluid spaces *(arrows)* in the perirectal tissues surrounding the terminal portion of the aorta and right internal iliac artery are consistent with a portion of the large perirectal hematoma (H).

by the thrombus and/or plaque and its extent can be determined and monitored during the course of treatment.

The cause of aortoiliac thrombosis is unknown, although aberrant strongylus migration and trauma to the vascular endothelium from turbulent blood flow at the aortic quadrifurcation have been most frequently proposed.[241, 242] Indwelling catheters, cardiac defects, and septicemia have also been implicated as causes of aortoiliac thrombosis in horses.[243] Aortic aneurysms are frequently associated with the presence of aortoiliac thrombosis.[226-229, 244] Aortic and iliac aneurysms and fistulae can occur without aortoiliac thrombosis, primarily from trauma such as may be experienced by the mare during parturition (Fig. 5-90). Aneurysms of the aortic quadrifurcation and iliac arteries resulting in an arterioureteral fistula have been reported in a 5-month-old Quarter horse-Percheron cross colt and have been imaged ultrasonographically in a 7-month-old Standardbred filly.[244] In the Standardbred filly seen by the author, the aneurysm of the left internal iliac artery and hydronephrosis and hydroureter of the left kidney were imaged ultrasonographically, but the obstruction of the left ureter by the aneurysm was not detected (Fig. 5-91). The cause of these arterioureteral fistulae was unknown. Extravascular compression of the terminal portion of the aorta and iliac arteries can occur secondary to large intrapelvic masses and may mimic the clinical signs of aortoiliac thrombosis (Fig. 5-92).

Patient Management and Prognosis. Aortoiliac thrombosis usually has a guarded prognosis because the thrombus in the terminal portion of the aorta and iliac arteries is usually very organized by the time the diagnosis is made, containing fibrous tissue and occasionally areas of calcification. Successful treatment of aortoiliac thrombosis has been reported, and treatment is most successful when the horse is treated aggressively soon after the onset of clinical signs.

Other Arterial Aneurysms, Fistulae, and Thrombosis. Aneurysms of other vessels occur infrequently in horses, although rupture of other major arteries, particularly the middle uterine artery, is more frequently reported.[239, 240, 245] An enlarging carotid arterial aneurysm was seen by the author in a horse with esophageal rupture secondary to a kick in the cervical region (Fig. 5-93).

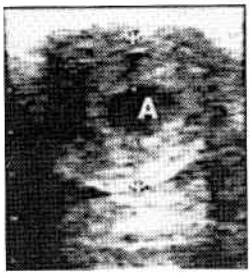

Figure 5-91

Sonogram obtained from an 8-month-old Standardbred filly revealed an aneurysm (A) associated with the terminal portion of the aorta. The thick walled aneurysm measured 28 mm in diameter. This aneurysm communicated with and obstructed the left ureter, resulting in hydronephrosis and hydroureter. This sonogram was obtained transrectally with a 5.0-MHz linear-array transducer at a displayed depth of 10 cm. Cranial is to the left of the sonogram and caudal is to the right.

Figure 5-92

Sonogram obtained from a 20-year-old Thoroughbred gelding with an acute onset of lameness and edema in the right flank and right rear leg. The right external iliac artery is compressed by a large homogeneous mass *(arrows)* that extended around the right side of the aorta and surrounded the right external iliac artery. The mass extended cranially up to the cranial mesenteric artery. An ultrasound-guided biopsy revealed the mass to be lymphosarcoma. This sonogram was obtained with the 5.0-MHz linear-array transducer at a displayed depth of 10 cm. The right side of the sonogram is cranial and the left side is caudal.

Arterial venous fistulae have also been detected in horses, both naturally occurring and surgically created, but are rare (Fig. 5-94). A vascular tumor should always be considered in the differential diagnosis of a horse with an arteriovenous fistula, particularly if detected in a large vascular plexus. Thrombosis of arteries other than the aortic quadrifurcation and iliac arteries is uncommon and probably occurs most frequently secondary to arterial catheterization or aberrant parasite migration. Coronary artery thrombosis has been infrequently reported as a cause of sudden death in horses.[195, 240] A routine echocardiographic examination may have detected the coronary artery thrombosis in three affected horses, as the thrombosis involved the origin of the left or right coronary artery. These coronary thrombi were verminous lesions, and the incidence of these lesions appears to have decreased with the introduction of newer anthelmintics. However, the coronary ostia and the proximal portion of the coronary arteries should be carefully scanned as part of a routine echocardiographic examination.

Pulmonary Arterial Disease and Pulmonary Artery Rupture. Abnormalities of the main pulmonary artery or left and/or right pulmonary arteries are uncommon, whether congenital or acquired.[49, 50, 236, 237, 239, 245] Murmurs of pulmonic stenosis have been seen in horses secondary to a cranial mediastinal abscess (Fig. 5-95) or tumor compressing the main pulmonary artery.[72] This

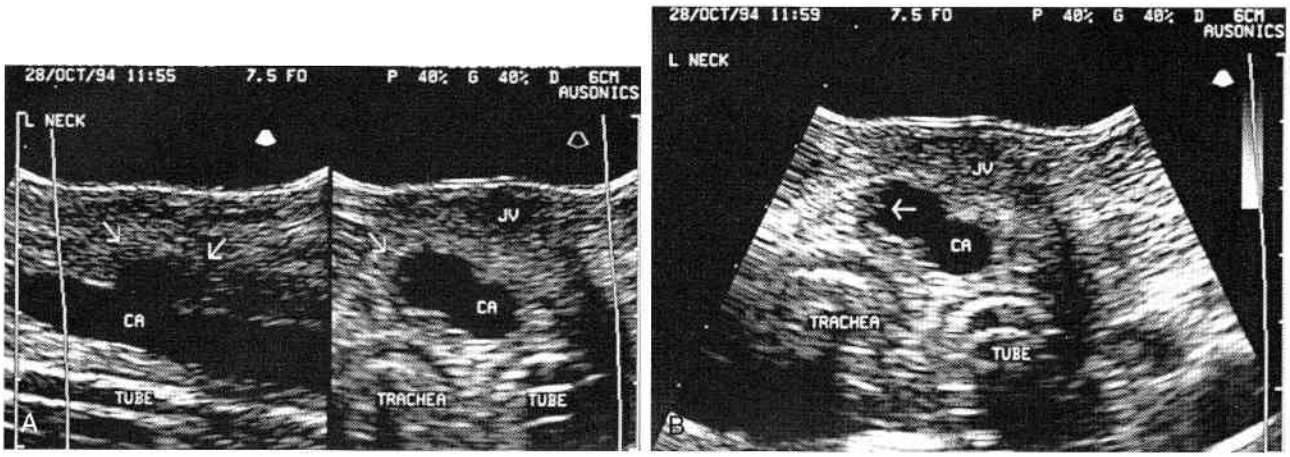

Figure 5–93

Sonograms obtained from a 19-year-old Quarter Horse gelding with an aneurysm of the left carotid artery (CA) following a kick to the left side of the neck, resulting in esophageal rupture 1 month earlier. The small thrombosed left jugular vein (JV) is visible in the short-axis images. These sonograms were obtained with a 7.5-MHz sector-scanner transducer containing a built-in fluid offset at a displayed depth of 6 cm.

A, The aneurysm *(arrows)* of the left carotid artery is seen in both the long-axis *(left image)* and short-axis *(right image)* views. The ballooning of the carotid artery progressed rapidly until the aneurysm was larger than the diameter of the left carotid artery *(right image).* The right side of the long-axis image is proximal and the left side is distal. The right side of the short-axis image is dorsal and the left side is ventral.

B, A small amount of hypoechoic material within the aneurysm *(arrow)* represents part of a thrombus. The right side of the sonogram is dorsal and the left side is ventral.

acquired supravalvular pulmonic stenosis is rare in horses. Aneurysms of the pulmonary artery have not been reported in horses, although post-stenotic pulmonary artery dilatation has been detected echocardiographically in horses with RVOT obstruction. Pulmonary artery rupture has been reported but is usually a fatal event secondary to severe mitral regurgitation and left-sided heart failure.[49, 50] The author has seen one horse survive a pulmonary artery tear only to die from pulmonary artery rupture 1 month later. This horse was seen prior to the availability of 2-D echocardiography. A defect in the wall of the main pulmonary artery should be detectable with echocardiography, as long as the affected portion of the pulmonary artery can be successfully imaged. The most common cause of pulmonary artery rupture in horses is pulmonary hypertension from left-sided heart failure, present in the horse that survived an initial small pulmonary artery tear. Dilatation of the pulmonary artery can occur from either pulmonary hypertension (more common) or increased flow through the pulmonary artery.

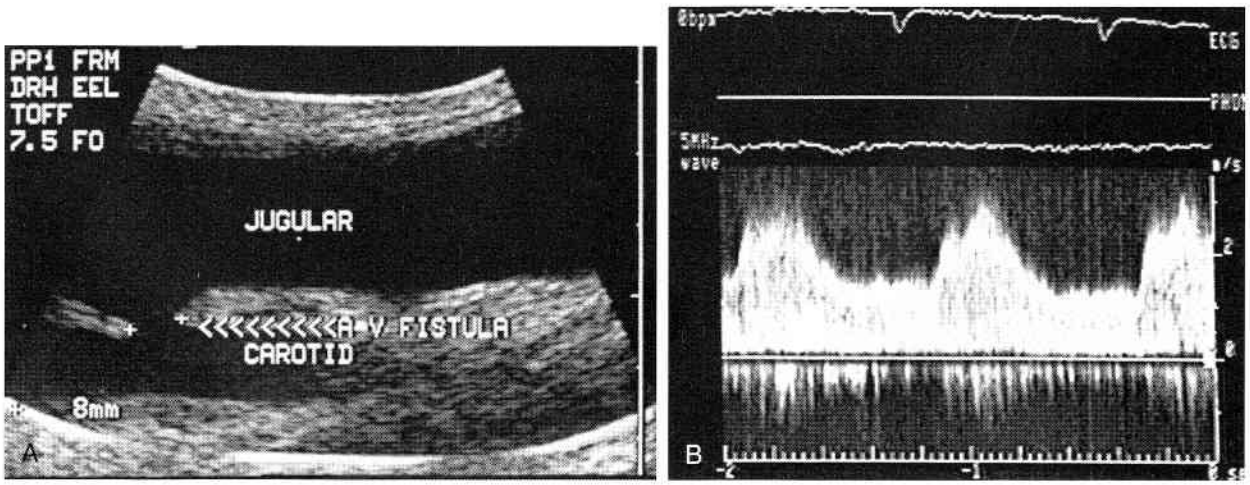

Figure 5–94

Sonogram and continuous-wave Doppler spectral tracing obtained from a 9-year-old Hanoverian gelding with an arteriovenous fistula between the right jugular vein and the right carotid artery. This horse had severe scarring of the right jugular vein, which led to its removal and replacement with a venograft. The arteriovenous fistula was surgically created to prevent thrombosis of the venograft.

A, Sagittal (long-axis) sonogram of the right jugular vein and carotid artery demonstrating a surgically created arteriovenous fistula *(arrowheads)* 8 mm in diameter. This sonogram was obtained with a 7.5-MHz sector-scanner transducer containing a built-in fluid offset at a displayed depth of 6 cm. The right side of this sonogram is proximal and the left side is distal.

B, Continuous-wave Doppler spectral tracing of blood flow through the arteriovenous fistula demonstrating high-velocity flow of approximately 3 m/sec in systole and 1.4 m/sec in diastole. This spectral tracing was obtained with a stand-alone 5.0-MHz continuous-wave Doppler transducer.

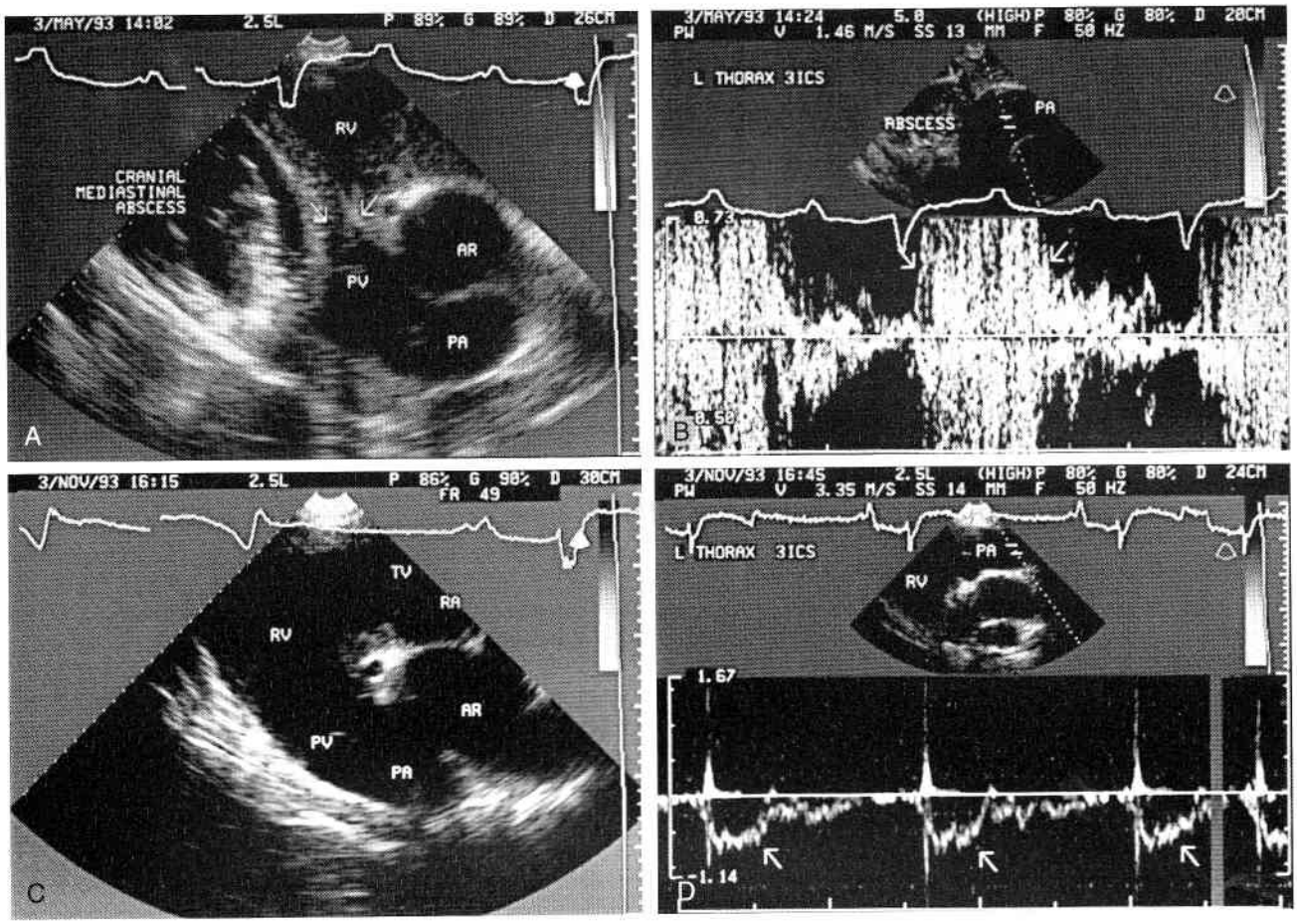

Figure 5–95

Two-dimensional and pulsed-wave Doppler echocardiograms obtained from a 4-year-old Thoroughbred gelding with a cranial mediastinal abscess causing right ventricular outflow tract obstruction. These echocardiograms were obtained with a 2.5 MHz sector-scanner transducer, which emits ultrasound pulses (pulsed-wave Doppler) at a frequency of 2.0-MHz. An electrocardiogram is superimposed for timing.

A, Long-axis view of the right ventricular outflow tract obtained from the right cardiac window at a displayed depth of 26 cm. A large gas- and fluid-filled cranial mediastinal abscess obstructs right ventricular outflow. The right ventricular outflow tract *(arrows)* is severely narrowed just below the pulmonic valve (PV). RV, Right ventricle; PA, pulmonary artery; AR, aortic root.

B, Pulsed-wave Doppler spectral tracing of blood flow in the long-axis view of the pulmonary artery (PA) obtained from the left cardiac window at a displayed depth of 20 cm. The spectral broadening of the aliased signal in systole *(arrows)* is consistent with a murmur of pulmonic stenosis.

C, Long-axis view of the right ventricular outflow tract from the right cardiac window at a displayed depth of 30 cm. This echocardiogram was obtained 6 months later after drainage of the abscess under general anesthesia and long-term antimicrobial therapy. No evidence of right ventricular outflow tract obstruction is seen. RV, Right ventricle; PV, pulmonic valve; PA, pulmonary artery; AR, aortic root; RA, right atrium; TV, tricuspid valve.

D, Pulsed-wave Doppler spectral tracing of blood flow in the long-axis view of the pulmonary artery (PA) obtained from the left cardiac window at a displayed depth of 24 cm. Notice the normal flow in the pulmonary artery with no evidence of pulmonic stenosis. The arrows point to the normal blood flow out the pulmonary artery in systole. The echocardiogram was obtained 6 months later after drainage of the abscess under general anesthesia and long-term antimicrobial therapy. The murmur of pulmonic stenosis had disappeared. RV, Right ventricle.

The detection of a dilated pulmonary artery is most frequently an echocardiographic sign of elevated pulmonary arterial pressures and possible impending pulmonary artery rupture and is a grave prognostic indicator.[49]

Venous Thrombosis and Thrombophlebitis. The most common site for venous thrombosis in the horse is the jugular vein, usually secondary to intravenous injections or catheterizations, although thrombosis and thrombophlebitis occur in the absence of pre-existing vascular trauma.[233, 246, 247] The proximal and mid-cervical portions of the jugular vein and the external maxillary vein are most frequently affected in horses with jugular vein thrombophlebitis, with less frequent involvement of the jugular vein immediately proximal to the thoracic inlet and the linguofacial vein.[233] Perivasculitis, a swelling of the soft tissue surrounding the vein, frequently occurs in horses with jugular vein thrombophlebitis.[233] This perivascular swelling may be anechoic to hyperechoic, depending on the type of perivascular inflammation. Thrombosis and thrombophlebitis can easily be distinguished ultrasonographically from a perivasculitis. Any thickening of the vessel wall or hypoechoic to echogenic mass within the lumen is diagnostic of thrombophlebitis. The wall of the vein is usually thickened, although a fibrin catheter sleeve or intraluminal thrombus may be imaged with little or no thickening of the vein wall (Fig. 5-96).[233, 246] A fibrin sleeve is a thin hypoechoic to echogenic fibrin envelope that surrounds the catheter and is attached to the endothelium at the site of catheter insertion. This can be detected surrounding the catheter or in

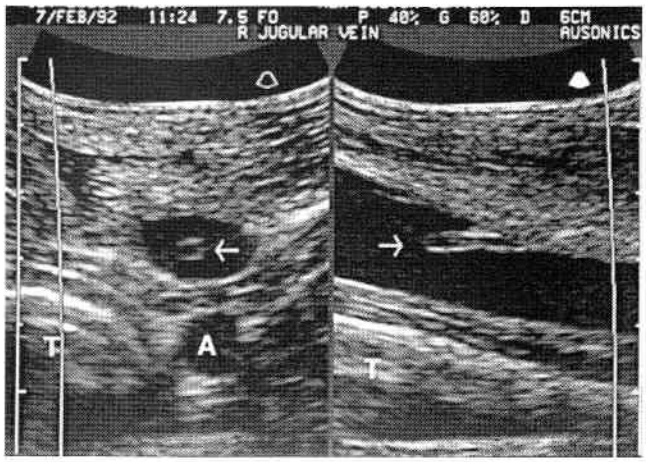

Figure 5–96

Sonograms obtained from a 3-year-old Quarter Horse gelding with a fibrin sleeve detected in the right jugular vein following intravenous catheterization. The echogenic fibrin sleeve *(arrows)* floats in the venous return (short-axis image) and is attached to the most superficial wall of the jugular vein at the site of the intravenous catheterization (long-axis image). The marked amount of hypoechoic to anechoic perivascular swelling is associated with a perivasculitis and probable infection of the surrounding soft-tissue structures. These sonograms were obtained with a 7.5-MHz sector-scanner transducer containing a built-in fluid offset at a displayed depth of 6 cm. The right side of the short-axis sonogram *(left image)* is dorsal and the left side is ventral. The right side of the long-axis sonogram *(right image)* is proximal and the left side is distal. T, Trachea; A, carotid artery.

situ in the vein when the intravenous catheter is removed. The typical appearance of a venous thrombus is a mass of low- to medium-amplitude echoes within the venous lumen attached to the endothelium (Fig. 5-97).[233] The thrombus may partially or completely occlude the lumen of the vein, resulting in venous distention and sludging of the venous blood proximal to the thrombus. Occasionally the thrombus is more anechoic and difficult to distinguish from venous blood. Pulsed-wave and color-flow Doppler echocardiography can be used to distinguish anechoic thrombus from blood. Swelling, heat, and sensitivity of the affected vein are associated with the ultrasonographic detection of a cavitating thrombus.[233] A heterogeneous thrombus with anechoic to hypoechoic areas representing fluid and/or necrosis is a cavitating thrombus and is indicative of a septic thrombophlebitis (Fig. 5-98).[233] In most horses a single anechoic or hypoechoic cavitating area is imaged in the center of an echogenic thrombus. The cavitation is usually located at the site of previous catheterization if an intravenous catheter had been inserted into the jugular vein (Fig. 5-99).

Patient Management and Prognosis. Local treatment of the thrombophlebitis is indicated in horses with homogeneous thrombi in the affected vein and/or perivascular swelling. Systemic anti-inflammatory therapy is also indicated if the affected vessel is extremely warm, swollen, and painful. Cavitation within the center of the thrombus should prompt a sterile aspirate of the cavitated area for cytology and culture and sensitivity testing using ultrasonographic guidance.[233] The aspirate obtained is usually serosanguinous and dark. The detection of pinpoint hyperechoic echoes is indicative of free gas and an anaerobic infection.[233] Rarely hypoechoic flocculent material can be imaged throughout the length of the thrombus, contained within a large long cavitation.[233] In these horses the aspirate from the jugular vein is usually purulent. Ultrasonography is very useful in differentiating a septic from nonseptic thrombophlebitis and in monitoring the response of the affected vein to appropriate antimicrobial treatment. If culture and sensitivity results

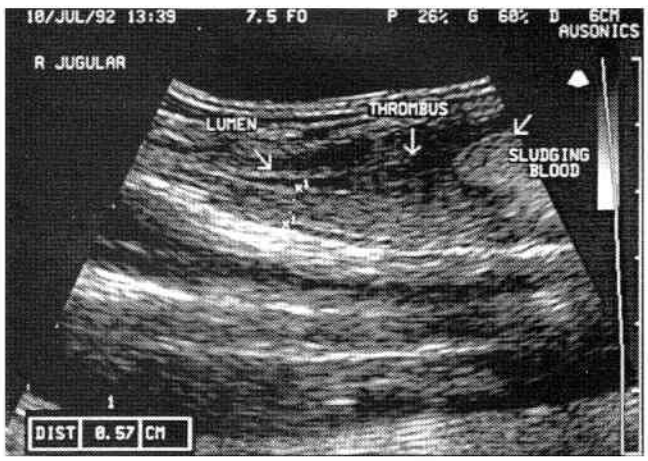

Figure 5–97

Sagittal sonogram of the right jugular vein obtained from a 4-year-old Thoroughbred filly with jugular vein thrombophlebitis and occlusion of the right jugular vein with thrombus. The relatively homogeneous hypoechoic thrombus occludes the jugular vein, and the echogenic blood swirls at the proximal edge of the thrombus. The walls of the jugular vein are markedly thickened (0.57 cm), and the lumen is narrowed at the site of the marked thickening of the vessel wall. This sonogram was obtained with a 7.5-MHz sector-scanner transducer containing a built-in fluid offset at a displayed depth of 6 cm. Proximal is to the right of the sonogram and distal is to the left.

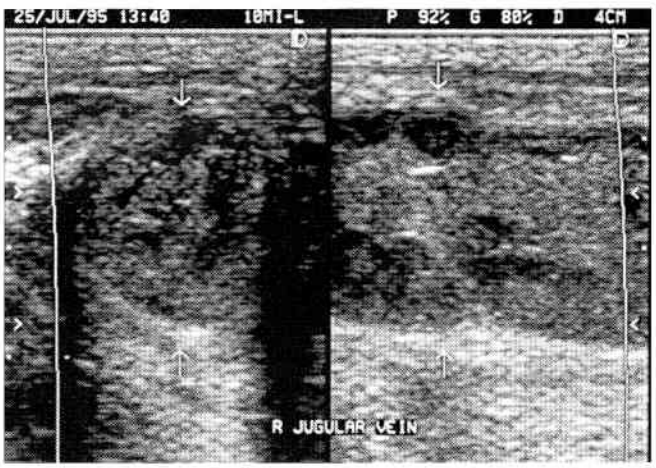

Figure 5–98

Sonograms of right jugular vein obtained from a 5-year-old Standardbred stallion with septic jugular vein thrombophlebitis *(arrows)*. The wall of the jugular vein is slightly thickened. The thrombus is heterogeneous with anechoic cavitated areas consistent with a septic thrombophlebitis. These sonograms were obtained with a 7.5-MHz sector-scanner transducer containing a built-in fluid offset at a displayed depth of 4 cm. The right side of the short-axis view *(left image)* is dorsal and the left side is ventral. The right side of the long-axis view *(right image)* is proximal and the left is distal.

are negative, broad-spectrum, bactericidal antimicrobial drugs should be used, as a mixed infection is common.[233] Antimicrobials should be continued until all clinical signs of sepsis resolve and the thrombus has a more homogeneous, noncavitated appearance.

Recanalization of the thrombosed vessel frequently occurs as the thrombophlebitis resolves. The vessel usually begins to recanalize along one side of the thrombus as the thrombus begins to reorganize.[233] In most horses the thrombus gradually decreases in size, and more flow passes through the affected vessel. In some horses with thrombophlebitis, the vessel returns to normal, whereas in others narrowing or stricture of the vessel may occur, often secondary to a severe septic thrombophlebitis (Color Figure 5-11). The affected vessel may not recanalize in horses with complete occlusion of the vein with thrombus, particularly with severe thrombophlebitis, perivasculitis, and infection. In these horses the thrombus becomes smaller and more organized, and an echogenic mass fills the affected vessel. Occasionally weblike masses of fibrous tissue fill the jugular vein secondary to a severe thrombophlebitis and impair normal venous drainage (Fig. 5-100). A venous graft may be necessary in horses with problems from impaired venous drainage. A jugular vein graft has been successfully performed in a horse (see Fig. 5-94) with impaired venous drainage due to the presence of weblike masses of fibrous tissue in the jugular vein secondary to severe thrombophlebitis 1 year earlier. Venous aneurysms (Color Figure 5-12) also occur in horses but are uncommon and may be clinically insignificant.

Ultrasonography should be performed on horses with suspected peripheral vascular disease, and the aortic root, coronary arteries, and pulmonary artery should be examined echocardiographically if these vascular abnormalities are suspected. Echocardiographic examination of the aorta and pulmonary artery can detect abnormalities (aneurysm and dilatation) when no other clinical or auscultatory signs of cardiovascular disease are present. Similarly, abnormalities of the aorta, iliac arteries, and other vessels can be detected ultrasonographically when palpation of these vessels is normal or questionable. Most importantly, the ultrasonographic and/or echocardiographic findings can help the veterinarian make an accurate diagnosis, formulate a prognosis for the vascular abnormality present, and monitor the response of affected vessels to treatment, improving the quality of patient care.

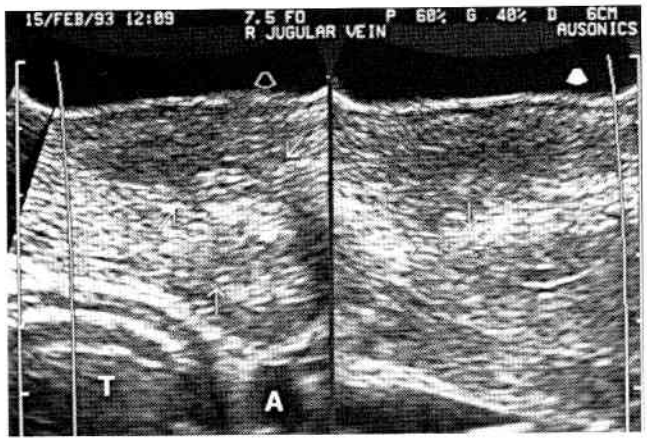

Figure 5–99

Sonograms of the right jugular vein obtained from a 5-year-old Standardbred gelding with septic jugular vein thrombophlebitis, a perivascular abscess, and a draining tract from the jugular vein, and subcutaneous abscess to the skin surface. The heterogeneous appearance of the thrombus and the tracts extending out into the subcutaneous tissues *(arrow)* from the thrombus are best seen in the transverse (short-axis) view *(left image)* of the right jugular vein. The tract from the jugular vein to the subcutaneous abscess is also demonstrated *(arrows)* in the sagittal (long-axis) view of the jugular vein *(right image)*. The trachea (T) is recognized by its echogenic rings and next to it is the carotid artery (A). These sonograms were obtained with a 7.5-MHz sector-scanner transducer containing a built-in fluid offset at a displayed depth of 6 cm. The right side of the short-axis image is dorsal and the left side is ventral. The right side of the long-axis image is proximal and the left side is distal.

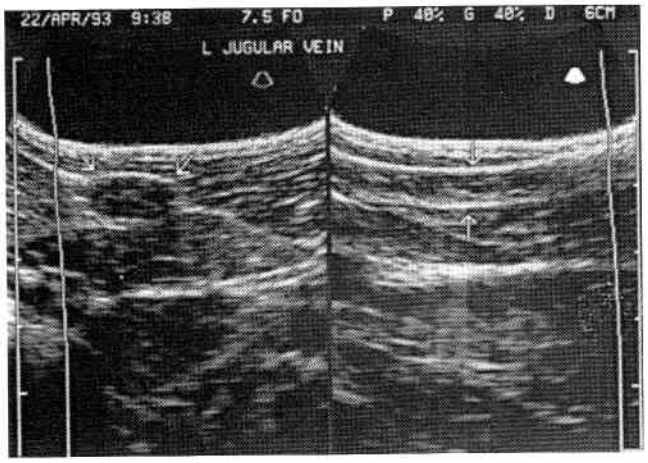

Figure 5–100

Sonograms of the left jugular vein obtained from a 4-year-old Thoroughbred stallion with a narrowed, scarred jugular vein. Notice the lacy echogenic webs crisscrossing the jugular vein *(arrows)* and the narrow diameter of the vessel. The echogenic webs represent strands of fibrous scar tissue crisscrossing the vein and are one possible sequela to jugular vein thrombophlebitis. These sonograms were obtained with a 7.5-MHz sector-scanner transducer containing a built-in fluid offset at a displayed depth of 6 cm. The right side of the transverse (short-axis) image *(left image)* is dorsal and the left side is ventral. The right side of the sagittal (long-axis) image *(right image)* is proximal and the left side is distal.

References

1. Pipers FS, Hamlin RL: Echocardiography in the horse. J Am Vet Med Assoc 170:815-819, 1977.
2. Lescure F, Tamzali Y: Valeurs de référence en échocardiographie T M chez le cheval de sport. Revue Med Vet 135:405-418, 1984.
3. Lombard CW, Evans M, Martin L, et al: Blood pressure, electrocardiogram and echocardiogram measurements in the growing pony foal. Equine Vet J 16:342-347, 1984.
4. Stewart JH, Rose RJ, Barko AM: Echocardiography in foals from birth to three months old. Equine Vet J 16:332-341, 1984.
5. Yamaga Y, Kimehiko T: Diagnostic ultrasound imaging in domestic animals: Two-dimensional and M-mode echocardiography. Jpn J Vet Sci 46:493-503, 1984.
6. O'Callaghan MW: Comparison of echocardiographic and autopsy measurements of cardiac dimensions in the horse. Equine Vet J 17:361-368, 1985.
7. Bonagura JD, Herring DS, Welker F: Echocardiography. Vet Clin North Am [Equine Pract] 1:311-333, 1985.
8. Reef VB: Echocardiographic examination in the horse: The basics. Compend Contin Educ Pract Vet 12:1312-1320, 1990.

9. Long KJ: Two-dimensional and M-mode echocardiography. Equine Vet Educ 4:303–310, 1992.
10. Long KJ, Bonagura JD, Darke PG: Standardised imaging technique for guided M-mode and Doppler echocardiography in the horse. Equine Vet J 24:226–235, 1992.
11. Bayly WM, Reed SM, Leathers CW, et al: Multiple congenital heart anomalies in five Arabian foals. J Am Vet Med Assoc 181:684–689, 1982.
12. Bonagura JD, Pipers FS: Diagnosis of cardiac lesions by contrast echocardiography. J Am Vet Med Assoc 182:396–402, 1983.
13. Bonagura JD, Pipers FS: Echocardiographic features of aortic valve endocarditis in a dog, a cow, and a horse. J Am Vet Med Assoc 182:595–599, 1983.
14. Pipers FS, Hamlin RL, Reef V: Echocardiographic detection of cardiovascular lesions in the horse. J Equine Med Surg 3:68–77, 1979.
15. Reef VB: Cardiovascular disease in the equine neonate. Vet Clin North Am [Equine Pract] 1:117–129, 1985.
16. Wingfield WE, Miller CW, Voss JL, et al: Echocardiography in assessing mitral valve motion in 3 horses with atrial fibrillation. Equine Vet J 12:181–184, 1980.
17. Freestone JF, Thomas WP, Carlson GP, et al: Idiopathic effusive pericarditis with tamponade in the horse. Equine Vet J 19:38–42, 1987.
18. Reef VB, Gentile DG, Freeman DE: Successful treatment of pericarditis in a horse. J Am Vet Med Assoc 185:94–98, 1984.
19. Roby KA, Reef VB, Shaw DP, Sweeney CR: Rupture of an aortic sinus aneurysm in a 15-year-old broodmare. J Am Vet Med Assoc 189:305–308, 1986.
20. Bertone JJ, Paull KS, Wingfield WE, et al: M-mode echocardiographs of endurance horses in the recovery phase of long-distance competition. Am J Vet Res 48:1708–1712, 1987.
21. Paull KS, Wingfield WE, Bertone JJ, et al: Echocardiographic changes with endurance training. *In* Gillespie JR, Robinson NE (eds): Equine Exercise Physiology 2. Davis, International Conference on Equine Exercise Physiology Publications, 1987, pp 34–40.
22. Leadon D, McAllister H, Osborne M: Electrocardiographic and echocardiographic measurements of cardiac parameters in Thoroughbred yearlings and their relationship to performance [Abstract]. Proceedings of the 3rd International Conference on Equine Exercise Physiology Publications, 1990, p 18.
23. McNie J, Mason K, Watkins K, et al: Echocardiograph evaluation of training associated cardiac change [Abstract]. Proceedings of the 3rd International Conference on Equine Exercise Physiology Publications, 1990, p 19.
24. Kuramoto K, Shiraishi A, Nakanishi Y, et al: Application of echocardiography for assessing left ventricular function of Thoroughbred horses at resting stage. Bull Equine Res Inst 26:23–30, 1989.
25. Carlsten J: Two-dimensional real-time echocardiography in the horse. Vet Radiol 28:76–87, 1987.
26. Voros K, Holmes JR, Gibbs C: Anatomical validation of two-dimensional echocardiography in the horse. Equine Vet J 22:392–397, 1990.
27. Voros K, Holmes JR, Gibbs C: Left ventricular volume determination in the horse by two-dimensional echocardiography: An in vitro study. Equine Vet J 22:398–402, 1990.
28. Voros K, Holmes JR, Gibbs C: Measurement of cardiac dimensions with two-dimensional echocardiography in the living horse. Equine Vet J 23:461–465, 1991.
29. Stadler P, D'Agostino U, Deegen E: Real-time, two-dimensional echocardiography in horses. Pferdeheilkunde 4:161–174, 1988.
30. Rantanen NW: Diseases of the heart. Vet Clin North Am [Equine Pract] 2:33–47, 1986.
31. McGladdery AJ, Marr CM: Echocardiography for the practitioner. Equine Vet Educ 2:11–14, 1990.
32. Pipers FS: Applications of diagnostic ultrasound in veterinary medicine. Equine Vet J 14:341–344, 1982.
33. Reef VB: The use of diagnostic ultrasound in the horse. Ultrasound Q 9:1–34, 1991.
34. Carlsten J, Kvart C, Nilsfors L: Two-dimensional contrast echocardiography in horses with valvular insufficiencies and septal defects. Imaging of the equine heart: An angiocardiographic and echocardiographic investigation. Ph.D. Thesis Carlsten J University of Uppsala, 1986.
35. Pipers FS, Reef V, Wilson J: Echocardiographic detection of ventricular septal defects in large animals. J Am Vet Med Assoc 187:810–816, 1985.
36. Reef VB: Echocardiographic evaluation of ventricular septal defects in horses. Equine Vet J Suppl 19:86–95, 1995.
37. Seahorn TL, Hormanski CE: Ventricular septal defect and atrial fibrillation in an adult horse: A case report. J Equine Vet Sci 13:36–38, 1993.
38. Reef VB: Echocardiographic findings in horses with congenital cardiac disease. Compend Contin Educ Pract Vet 13:109–117, 1991.
39. Reef VB, Mann PC, Orsini PG: Echocardiographic detection of tricuspid atresia in two foals. J Am Vet Med Assoc 191:225–228, 1987.
40. Ecke P, Malik R, Kannegieter NJ: Common atrioventricular canal in a foal. N Z Vet J 39:97–98, 1991.
41. Cargile J, Lombard C, Wilson JH, Buergelt CD: Tetralogy of Fallot and segmental uterine aplasia in a three-year-old Morgan filly. Cornell Vet 81:411–418, 1991.
42. Chaffin MK, Miller MW, Morris EL: Double outlet right ventricle and other associated congenital cardiac anomalies in an American Miniature Horse foal. Equine Vet J 24:402–406, 1992.
43. Hinchcliff KW, Adams WM: Critical pulmonary stenosis in a newborn foal. Equine Vet J 23:318–320, 1991.
44. Reimer JM, Marr CM, Reef VB, Saik JE: Aortic origin of the right pulmonary artery and patent ductus arteriosus in a pony foal with pulmonary hypertension and right-sided failure. J Am Vet Med Assoc 25:466–468, 1992.
45. Reef VB, Klump S, Maxson AD, et al: Echocardiographic detection of an intact aneurysm in a horse. J Am Vet Med Assoc 197:752–755, 1990.
46. Lester GD, Lombard CW, Ackerman N: Echocardiographic detection of a dissecting aortic root aneurysm in a Thoroughbred stallion. Vet Radiol Ultrasound 33:202–205, 1992.
47. Reef VB: Mitral valvular insufficiency associated with ruptured chordae tendineae in three foals. J Am Vet Med Assoc 191:329–331, 1987.
48. Marr CM, Pirie HM, Northridge DB: Confirmation by Doppler echocardiography of valvular regurgitation in a horse with a ruptured chorda tendinea of the mitral valve. Vet Rec 127:376–379, 1990.
49. Reef VB, Bain FT, Spencer PA: Severe mitral insufficiency in horses: Clinical, echocardiographic, and pathologic findings. Equine Vet J, in press.
50. Dedrick P, Reef VB, Sweeney RW, et al: Treatment of bacterial endocarditis in a horse. J Am Vet Med Assoc 193:339–342, 1988.
51. Collatos C, Clark ES, Reef VB, et al: Atrial fibrillation, cardiomegaly, left atrial mass and *Rhodococcus equi* septic osteoarthritis in a Thoroughbred colt. J Am Vet Med Assoc 197:1039–1042, 1990.
52. Ball MA, Weldon AD: Vegetative endocarditis in an Appaloosa gelding. Cornell Vet 82:301–309, 1992.
53. Hillyer MH, Mair TS, Holmes JR: Treatment of bacterial endocarditis in a Shire mare. Equine Vet Educ 2:5–7, 1990.
54. Hatfield CE, Rebhun WC, Dietze AE: Endocarditis and optic neuritis in a Quarter horse mare. Compend Contin Educ Pract Vet 9:451–454, 1987.
55. Hines MT, Heidel JR, Barbee DD: Bacterial endocarditis with thrombus formation and abscessation in a horse. Vet Radiol Ultrasound 34:47–51, 1993.
56. Reef VB, Reimer JM, Rubin J: The case of the day. J Ultrasound Med 10:590–592, 1991.
57. Rantanen NW, Byars TD, Hauser ML, et al: Spontaneous contrast and mass lesions in the hearts of race horses: Ultrasound diagnosis-preliminary data. J Equine Vet Sci 4:220–223, 1984.
58. Mahoney C, Rantanen NW, DeMichael JA, Kincaid B: Spontaneous echocardiographic contrast in the Thoroughbred: High prevalence in racehorses and a characteristic abnormality in bleeders. Equine Vet J 24:129–133, 1992.
59. Nilsfors L, Lombard CW: Diagnosis of pulmonic valve endocarditis in a horse. Equine Vet J 23:479–482, 1991.
60. Reef VB, Spencer P: Echocardiographic evaluation of equine aortic insufficiency. Am J Vet Res 48:904–909, 1987.
61. Clark ES, Reef VB, Sweeney C, et al: Aortic valve insufficiency in a one-year-old colt. J Am Vet Med Assoc 191:841–844, 1987.
62. Shaftoe S, McGuirk SM: Valvular insufficiency in a horse with atrial fibrillation. Compend Contin Educ Pract Vet 9:203–209, 1987.

63. Reimer JM, Reef VB, Sommer M: Echocardiographic detection of pulmonic valve rupture in a horse with right-sided failure. J Am Vet Med Assoc 198:880–882, 1991.
64. Reef VB: Heart murmurs in horses: Determining their significance with echocardiography. Equine Vet J Suppl 19:71–80, 1995.
65. Robinson JA, Marr CM, Reef VB, Sweeney RW: Idiopathic, aseptic, effusive, fibrinous, nonconstrictive pericarditis with tamponade in a Standardbred filly. J Am Vet Med Assoc 201:1593–1598, 1992.
66. Voros K, Felkai C, Szilagyi Z, Papp A: Two-dimensional echocardiographically guided pericardiocentesis in a horse with traumatic pericarditis. J Am Vet Med Assoc 198:1953–1956, 1991.
67. Hardy J, Robertson JT, Reed SM: Constrictive pericarditis in a mare: Attempted treatment by partial pericardiectomy. Equine Vet J 24:151–154, 1992.
68. Bernard W, Reef VB, Clark ES, et al: Pericarditis in horses: Six cases (1982–1986). J Am Vet Med Assoc 196:468–471, 1990.
69. Reef VB: Myocardial disease. *In* Robinson NE (ed): Current Therapy in Equine Medicine III. Philadelphia, WB Saunders, 1991, pp 393–395.
70. Reef VB: Pericardial and myocardial diseases. *In* Koblick CN, Ames TR, Geor RJ, Trent AM: The Horse: Diseases and Clinical Management. New York, Churchill-Livingstone, 1993, pp 185–197.
71. Reef VB: A monensin outbreak in horses in the eastern United States: Pathogenesis, clinical signs and epidemiology. Proceedings of the 8th Annual Veterinary Medicine Forum 8:619–622, 1990.
72. Bonagura JD, Reef VB: Cardiovascular diseases of the horse. *In* Reed S, Bayly W (eds): Equine Internal Medicine. Philadelphia, WB Saunders, 1997.
73. Lees MJ, Read RA, Klein KT, et al: Surgical retrieval of a broken jugular catheter from the right ventricle of a foal. Equine Vet J 21:384–387, 1989.
74. Marr CM, Reef VB, Reimer JM, et al: An echocardiographic study of atrial fibrillation in horses before and after treatment with quinidine sulfate. J Vet Int Med 9:336–340, 1995.
75. Marr CM, Reef VB, Brazil T, et al: Clinical and echocardiographic findings in horses with aortic root rupture. Vet Radiol Ultrasound, in press.
76. Kvart C, Carlsten J, Jeffcott LB, et al: Diagnostic value of contrast echocardiography in the horse. Equine Vet J 17:357–360, 1985.
77. Reef VB, Lalezari K, De Boo J, et al: Pulsed-wave Doppler evaluation of intracardiac blood flow in 30 clinically normal Standardbred horses. Am J Vet Res 50:75–83, 1989.
78. Reef VB: Pulsed and continuous wave Doppler echocardiographic evaluation of mitral and tricuspid insufficiency in horses. Proceedings of the 6th Annual Veterinary Medicine Forum 6:385–387, 1988.
79. Reef VB: Pulsed and continuous wave Doppler echocardiographic evaluation of aortic and pulmonic insufficiency in horses. Proceedings of the 6th Annual Veterinary Medicine Forum 6:388–390, 1988.
80. Reef VB: Color flow Doppler mapping of horses with valvular insufficiency. Proceedings of the 8th Annual Veterinary Medicine Forum 8:483–485, 1990.
81. Reef VB: Advances in echocardiography. Vet Clinics North Am [Equine Pract] 7:435–450, 1991.
82. Long K: Doppler echocardiography in the horse. Equine Vet Educ 2:15–17, 1990.
83. Long KJ: Doppler echocardiography—Clinical applications. Equine Vet Educ 5:161–166, 1993.
84. Stadler P, Weinberger T, Deegen E: Echokardiographische Messungen im gepulsten Dopplerverfahren (PW) beim gesunden Warmblutpferd. J Vet Med 40:757–778, 1993.
85. Blissitt KJ, Bonagura, JD: Pulsed wave Doppler echocardiography in normal horses. Equine Vet J Suppl 19:38–46, 1995.
86. Holmes JR: The equine heart. Problems and difficulties in assessing cardiac function on clinical examination. Equine Vet J 1:10–24, 1968.
87. Detweiler DK, Patterson DF: The cardiovascular system. *In* Catcott ES, Smithcors JF (eds): Equine Medicine and Surgery, 2nd ed. Santa Barbara, CA, American Veterinary Publications, 1972, pp 277–347.
88. Glendinning SA: Significance of clinical abnormalities of the heart in soundness. Equine Vet J 4:21–30, 1972.
89. Holmes JR: Prognosis of equine cardiac conditions. Equine Vet J 9:181–182, 1977.
90. Fregin GF: The cardiovascular system. *In* Mansmann RA, McAllister ES, Pratt PW (eds): Equine Medicine and Surgery, 3rd ed. Santa Barbara, CA, American Veterinary Publications, 1982, pp 645–704.
91. Bonagura JD: Equine heart disease, an overview. Vet Clin North Am [Equine Pract] 1:267–274, 1985.
92. Reef VB: Evaluation of the equine cardiovascular system. Vet Clin North Am [Equine Pract] 1:275–288, 1985.
93. Bonagura JD: Clinical evaluation and management of heart disease. Equine Vet Educ 2:31–37, 1990.
94. Patteson MW, Cripps PJ: A survey of cardiac auscultatory findings in horses. Equine Vet J 25:409–415, 1993.
95. Thomas WP, Gaber CE, Jacobs GJ, et al: Recommendations for standards in transthoracic two-dimensional echocardiography in the dog and cat. J Vet Int Med 7:247–252, 1993.
96. Nanda NC, Pinheiro L, Sanyal RS, Storey O: Transesophageal biplane echocardiographic imaging: Technique, planes, and clinical usefulness. Echocardiography 7:771–788, 1990.
97. Rice MJ, Seward JB, Hagler DJ, et al: Impact of 2-dimensional echocardiography on the management of distressed newborns in whom cardiac disease is suspected. Am J Cardiol 51:288–292, 1983.
98. Armstrong WF: Congenital heart disease. *In* Feigenbaum H (ed): Echocardiography, 4th ed. Philadelphia, Lea & Febiger, 1986, pp 365–461.
99. Gutgesell HP, Hutha JC, Latson LA, et al: Accuracy of two-dimensional echocardiography in the diagnosis of congenital heart disease. Am J Cardiol 55:514–518, 1985.
100. Lombard CW, Scarratt WK, Buergelt CD: Ventricular septal defects in the horse. J Am Vet Med Assoc 183:562–565, 1983.
101. Bierman FZ, Fellows K, Williams RG: Prospective identification of ventricular septal defects in infancy using subxiphoid two-dimensional echocardiography. Circulation 62:807–817, 1980.
102. Sutherland GA, Goodman MJ, Smallhorn JF, et al: Ventricular septal defects: Two-dimensional echocardiography and morphological correlation. Br Heart J 47:316–328, 1982.
103. Glazier DB, Farrelly BT, O'Connor J: Ventricular septal defect in a 7-year-old gelding. J Am Vet Med Assoc 167:49–50, 1975.
104. Feigenbaum H (ed): Echocardiography, 4th ed. Philadelphia, Lea & Febiger, 1986.
105. Hatle L, Angelsen B: Doppler Ultrasound in Cardiology: Physical Principles and Clinical Applications, 2nd ed. Philadelphia, Lea & Febiger, 1985.
106. Stevensen JG, Kawabori I, Dooley TK, et al: Diagnosis of ventricular septal defect by pulsed Doppler echocardiography: Sensitivity, specificity and limitations. Circulation 58:322–326, 1978.
107. Reeder GS, Currie PJ, Hagler DJ, et al: Use of Doppler techniques (continuous-wave, pulsed-wave, and color flow imaging) in the noninvasive hemodynamic assessment of congenital heart disease. Mayo Clin Proc 61:725–744, 1986.
108. Murphy DJ, Ludomirsky A, Huhta JC: Continuous wave Doppler in children with ventricular septal defect: Noninvasive estimation of interventricular pressure gradient. Am J Cardiol 57:428–432, 1985.
109. Ludomirsky A, Huhta JC, Vick GW, et al: Color Doppler detection of multiple ventricular septal defects. Circulation 74:1317–1322, 1986.
110. Weyman AE: Principles and Practice of Echocardiography. Philadelphia, Lea & Febiger, 1994.
111. Muyelle E, DeRoose P, Oyaert W, Van Der Hende C: An interventricular septal defect and a tricuspid valve insufficiency in a trotter mare. Equine Vet J 6:174–176, 1974.
112. Critchley KL: The importance of blood gas measurement in the diagnosis of an interventricular septal defect in a horse: A case report. Equine Vet J 8:128–129, 1976.
113. Knauer KW, McMullan WC, Clark DR: Diagnosis of an interventricular septal defect. Veterinary Medicine/Small Animal Clinician 68:75–78, 1973.
114. Vitums A, Bayly WM: Pulmonary atresia with dextroposition of the aorta and ventricular septal defect in three Arabian foals. Vet Pathol 19:160–168, 1982.
115. Crowe MW, Swerczek TW: Equine congenital defects. Am J Vet Res 46:353–358, 1985.
116. Rooney JR, Franks WC: Congenital cardiac anomalies in horses. Path Vet 1:454–464, 1964.
117. Physick-Sheard PW, Maxie MG, Palmer NC, Gaul G: Atrial septal defect of the persistent ostium primum type with hypoplastic

right ventricle in a Welsh pony foal. Can J Comp Med 49:429-433, 1985.
118. Wilson AP: Persistent foramen ovale in a foal. Vet Med 38:491-492, 1943.
119. Armstrong WF: Congenital heart disease. *In* Feigenbaum H (ed): Echocardiography, 4th ed. Philadelphia, Lea & Febiger, 1986, pp 365-461.
120. Moise NS: Doppler echocardiographic evaluation of congenital cardiac disease: An introduction. J Vet Int Med 3:195-207, 1989.
121. Reef VB, Levitan CW, Spencer PA: Factors affecting prognosis and conversion in equine atrial fibrillation. J Vet Int Med 2:1-6, 1988.
122. Glazier DB: Congestive heart failure and congenital cardiac defects in horses. Equine Pract 8(9):20-23, 1986.
123. Glazier DB, Farrelly BT, Neylon JF: Patent ductus arteriosus in an eight-month-old foal. Irish Vet J 28:12-13, 1974.
124. Carmichael JA, Buergelt CD, Lord PF, et al: Diagnosis of patent ductus arteriosus in a horse. J Am Vet Med Assoc 158:767-775, 1971.
125. Buergelt CD, Carmichael JA, Tashjian RJ, Das KM: Spontaneous rupture of the left pulmonary artery in a horse with patent ductus arteriosus. J Am Vet Med Assoc 157:313-320. 1970.
126. Scott EA, Kneller SK, Witherspoon DM: Closure of ductus arteriosus determined by cardiac catheterization and angiography in newborn foals. Am J Vet Res 36:1021-1023, 1975.
127. Prickett ME, Reeves JT, Zent WW: Tetralogy of Fallot in a Thoroughbred foal. J Am Vet Med Assoc 162:552-555, 1973.
128. Reynolds DJ, Nicholl TK: Tetralogy of Fallot and cranial mesenteric arteritis in a foal. Equine Vet J 10:185-187, 1978.
129. Greene HJ, Wray DD, Greenway JA: Two equine congenital cardiac anomalies. Irish Vet J 29:115-117, 1975.
130. Steyn PF, Holland P, Hoffman J: The angiocardiographic diagnosis of a persistent truncus arteriosus in a foal. Tydskr S Afr Vet Ver 60:106-108, 1989.
131. Sojka JE: Persistent truncus arteriosus in a foal. Equine Pract 9:19-26, 1987.
132. Button C, Gross DR, Allert JA, Kitzman JV: Tricuspid atresia in a foal. J Am Vet Med Assoc 172:825-830, 1978.
133. Gumbrell RC: Atresia of the tricuspid valve in a foal. N Z Vet J 18:253-255, 1970.
134. Hadlow WJ, Ward JK: Atresia of the right atrioventricular orifice in an Arabian foal. Vet Pathol 17:622-637, 1980.
135. Van der Linde-Sipman JS, van der Ingh TS: Tricuspid atresia in a foal and a lamb. Zentralbl Veterinarmed [A] 26:239-242, 1979.
136. Van Nie CJ, van der Kamp JS: Atresie van het ostium atrioventriculare dextrum (tricuspidalis) ij een te vroeg geboren veulen. Tijdschr Diergeneeskd 104:411-416, 1979.
137. Wilson RB, Haffner JC: Right atrioventricular atresia and ventricular septal defect in a foal. Cornell Vet 77:187-191, 1987.
138. McClure JJ, Gaber CE, Watters JW, Qualls CW: Complete transposition of the great arteries with ventricular septal defect and pulmonary stenosis in a Thoroughbred foal. Equine Vet J 15:377, 1983.
139. Vitums A: Origin of the aorta and pulmonary trunk from the right ventricle in a horse. Pathol Vet 7:482-491, 1970.
140. Vitums A, Grant BD, Stone EC, et al: Transposition of the aorta and atresia of the pulmonary trunk in a horse. Cornell Vet 63:41-57, 1973.
141. Zamora CS, Vitums A, Nyrop KA, Sande RD: Atresia of the right atrioventricular orifice with complete transposition of the great arteries in a horse. Anat Histol Embryol 18:177, 1989.
142. Zamora CS, Vitums A, Foreman JH, et al: Common ventricle with separate pulmonary outflow chamber in a horse. J Am Vet Med Assoc 186:1210-1213, 1985.
143. Tadmor A, Fischel R, Tov AS: A condition resembling hypoplastic left heart syndrome in a foal. Equine Vet J 15:175, 1983.
144. Musselman EE, Loquidice RJ: Hypoplastic left ventricular syndrome in a foal. J Am Vet Med Assoc 185:542-543, 1984.
145. Hinchcliff KW, Adams WM: Critical pulmonary stenosis in a newborn foal. Equine Vet J 23:318-320, 1991.
146. Critchley KL: An interventricular septal defect, pulmonary stenosis and bicuspid pulmonary valve in a Welsh pony foal. Equine Vet J 8:176-178, 1976.
147. King JM, Flint TJ, Anderson WI: Incomplete subaortic stenotic rings in domestic animals—a newly described congenital anomaly. Cornell Vet 78:263-271, 1988.
148. Gross DR, Clark DR, McDonald DR, et al: Congestive heart failure associated with congenital aortic insufficiency in a horse. Southwest Vet 30:27-33, 1977.
149. Miller PJ, Holmes JR: Observations on seven cases of mitral insufficiency in the horse. Equine Vet J 17:181-190, 1985.
150. Holmes JR, Miller PJ: Three cases of ruptured mitral valve chordae in the horse. Equine Vet J 16:125-135, 1984.
151. Holmes JR, Else RW: Cardiac pathology in the horse. (3) Clinical correlations. Equine Vet J 4:195-203, 1972.
152. Bishop SP, Cole CR, Smetzer DL: Functional and morphologic pathology of equine aortic insufficiency. Pathol Vet 3:137-158, 1966.
153. Deegen E, Lieske R, Schoon H: Klinische und kardiologische untersuchungsbefunde bei 3 deckhengsten mit aortenklappeninsuffizienz. Tierarztl Prax 8:211-222, 1980.
154. Smetzer DL, Bishop S, Smith RC: Diastolic murmur of equine aortic insufficiency. Am Heart J 72:489-497, 1966.
155. Sporri H: Two clinical types of aortic insufficiency in horses. Ann NY Acad Sci 127:358-363, 1965.
156. Brumbaugh GW, Thomas WP, Hodge TG: Medical management of congestive heart failure in a horse. J Am Vet Med Assoc 180:878-883, 1982.
157. Miller PJ, Holmes JR: Observations on structure and function of the equine mitral valve. Equine Vet J 16:457-460, 1984.
158. Olsen LJ, Tajik AJ: Echocardiographic evaluation of valvular heart disease. *In* Marcus ML, Schelbert HR, Skorton DJ, Wolf GL (eds): Cardiac Imaging. A Companion to Braunwald's Heart Disease. Philadelphia, WB Saunders, 1991, pp 419-448.
159. Grenadier E, Alpan G, Keidar S, Palant A: The prevalence of ruptured chordae tendineae in the mitral valve prolapse syndrome. Am Heart J 105:603-610, 1983.
160. Else RW, Holmes JR: Pathological changes in atrial fibrillation in the horse. Equine Vet J 3:56-64, 1971.
161. Else RW, Holmes JR: Cardiac pathology in the horse. (1) Gross pathology. Equine Vet J 4:1-8, 1972.
162. Else RW, Holmes JR: Cardiac pathology in the horse. (2) Microscopic pathology. Equine Vet J 4:57-62, 1972.
163. Brown CM, Bell TG, Paradis M-R, Breeze RG: Rupture of mitral chordae tendineae in two horses. J Am Vet Med Assoc 182:281-283, 1983.
164. Avgeropoulou CC, Rahko PS, Patel AK: Reliability of M-mode, two-dimensional and Doppler echocardiography in diagnosing a flail mitral valve leaflet. J Am Soc Echo 1:433-445, 1988.
165. Roussel AJ, Kasari TR: Bacterial endocarditis in large animals. Part II. Incidence, causes, clinical signs and pathologic findings. Compend Cont Educ Pract Vet 11:769-773, 1989.
166. Buergelt CD, Cooley AJ, Hines SA, Pipers FS: Endocarditis in 6 horses. Vet Pathol 22:333-337, 1985.
167. Nanda NC, Pinheiro L, Sanyal RS, Storey O: Transesophageal biplane echocardiographic imaging: Technique, planes, and clinical usefulness. Echocardiography 7:771-788, 1990.
168. Klodas E, Edwards WD, Khandheria B: Use of transesophageal echocardiography for improving the detection of valvular vegetations in subacute bacterial endocarditis. J Am Soc Echo 2:386-389, 1989.
169. Gatewood RP, Helmcke FR, Nanda NC: Conventional and color Doppler assessment of mitral regurgitation. *In* Nanda NC (ed): Textbook of Color Doppler Echocardiography. Philadelphia, Lea & Febiger, 1989, pp 141-150.
170. Kisslo J, Adams DB, Belkin RN: Doppler Color Flow Imaging. New York, Churchill-Livingstone, 1988.
171. Maciel BC, Moises VA, Shandas R, et al: Effects of pressure and volume of the receiving chamber on the spatial distribution of regurgitant jets as imaged by color Doppler flow mapping. An in vitro study. Circulation 83:605-613, 1991.
172. Schon HR: Hemodynamic and morphologic changes after long-term angiotensin converting enzyme inhibition in patients with chronic valvular regurgitation. J Hyperten 12 (suppl 4):S95-S104, 1994.
173. Roby KAW, Reef VB: ECG of the month. J Am Vet Med Assoc 188:570-571, 1986.
174. Cooper J, Fan P-H, Chopra HK, Nanda N: Conventional and color Doppler assessment of right-side valvular regurgitation. *In* Nanda NC (ed): Textbook of Color Doppler Echocardiography. Philadelphia, Lea & Febiger, 1989, pp 160-167.
175. Mahaffey LW: Fenestration of the aortic and pulmonary semilunar valves in the horse. Vet Rec 70:415-420, 1958.

176. Perry GJ, Nanda NC: Conventional and color Doppler assessment of aortic regurgitation. *In* Nanda NC (ed): Textbook of Color Doppler Echocardiography. Philadelphia, Lea & Febiger, 1989, pp 151-159.
177. Grayburn PA, Handshoe R, Smith MD, et al: Quantitative assessment of the hemodynamic consequences of aortic regurgitation by means of continuous wave Doppler recordings. J Am Coll Cardiol 10:137-141, 1987.
178. Thompson R, Ross I, Leslie P, Easthope R: Haemodynamic adaptation to exercise in asymptomatic patients with severe aortic regurgitation. Cardiovasc Res 19:212-218, 1985.
179. Traub-Dargatz JL, Schlipf JW, Boon J, et al: Ventricular tachycardia and myocardial dysfunction in a horse. J Am Vet Med Assoc 205:1569-1573, 1994.
180. Machida N, Nakamura T, Kiryu K, et al: Cardiopathological observation on a case of persistent ventricular tachycardia in a pony mare. J Vet Med Sci 54:1213-1216, 1992.
181. Reimer JM, Reef VB, Sweeney RW: Ventricular arrhythmias in the horse: Twenty-one cases (1984-1989). J Am Vet Med Assoc 201:1237-1243, 1992.
182. Marr CM, Reef VB: ECG of the month. J Am Vet Med Assoc 198:1533-1534, 1991.
183. Kiryu K, Kaneko M, Mori S, et al: Cardiopathological observation on a case of paroxysmal ventricular tachycardia in a Thoroughbred colt: Formal pathogenesis. Exp Rep Equine Health Lab 12:74-88, 1975.
184. Senta T, Kubo K, Kiryu K, et al: A case report on ventricular paroxysmal tachycardia (permanent type) in a Thoroughbred colt. Exp Rep Equine Health Lab 8:61-71, 1971.
185. MacDonald MH, Reef VB: ECG of the month. J Am Vet Med Assoc 190:1280-1281, 1987.
186. Fregin GF: Acquired cardiovascular diseases affecting exercise performance—Diagnosis, therapy and prognosis. J S Afr Vet Assoc 45:269-270, 1974.
187. Fisher EW, Pirie HM, Andrew H: Clinical-pathological correlation of an equine cardiac arrhythmia. Vet Rec 86:499-502, 1970.
188. Reef VB, Clark ES, Oliver JA, et al: Implantation of a permanent transvenous pacing catheter in a horse with complete heart block and syncope. J Am Vet Med Assoc 189:449-452, 1986.
189. Kiryu I, Nakamura T, Kaneko M, et al: Cardiopathology of sudden death in the race horse. Heart Vessels, Suppl 2:40, 1987.
190. Schiff P, Knottenbelt DC: Sudden death in an 11 year old Thoroughbred stallion. Equine Vet Educ 2:8-10, 1990.
191. Pascoe RR, O'Sullivan BM: Sudden death in a Thoroughbred stallion. Equine Vet J 12:211-212, 1980.
192. Cranley JJ, McCullagh KG: Ischaemic myocardial fibrosis and aortic strongylosis in the horse. Equine Vet J 13:35-42, 1981.
193. Gelberg HB, Zachary JF, Everitt JI, et al: Sudden death in training and racing Thoroughbred horses. J Am Vet Med Assoc 187:1354-1356, 1985.
194. Marcus LC, Ross JN: Microscopic lesions in the hearts of aged horses and mules. Pathol Vet 4:162-185, 1967.
195. Hughes PE, Howard EB: Endocardial fibroelastosis as a cause of sudden death in the horse. Equine Pract 6:23-26, 1984.
196. Cronin MTL, Leader GH: Coronary occlusion in a thoroughbred colt. Vet Rec 64:8, 1952.
197. Dudan F, Rossi GL, Luginbuhl H: Cardiovascular study of the horse: Relationships between vascular and tissue lesions in the myocardium. 2. Schweiz Arch Tierheilkd 126:527-538, 1984.
198. Dudan F, Rossi GL, Luginbuhl H: Cardiovascular study in the horse: Relationship between vascular and myocardial lesions. 3. Schweiz Arch Tierheilkd 127:319-338, 1985.
199. Volckart VW, Loeffler K: Atrioventrikulare herzblockbildungen bei einem pferd mit lymphosarkomen in der milz. Dtsch Tierarztl Wochenschrift 78:446-449, 1971.
200. Dill SG, Moise NS, Meschter CL: Cardiac failure in a stallion secondary to metastasis of an anaplastic pulmonary carcinoma. Equine Vet J 18:414-417, 1986.
201. Baker D, Kreeger J: Infiltrative lipoma in the heart of a horse. Cornell Vet 77:258-262, 1987.
202. Hoskinson JJ, Wooten P, Evans R: Nonsurgical removal of a catheter embolus from the heart of a foal. J Am Vet Med Assoc 199:233-235, 1991.
203. Whitlock RH, White NA, Rowland GN, et al: Monensin toxicosis in horses: Clinical manifestations. Proceedings of the 24th Annual Convention of the American Association of Equine Practitioners 24:473-486, 1978.
204. Beck BE, Harries WN: The diagnosis of monensin toxicosis: A report on outbreaks in horses, cattle and chickens. Proceedings of the 22nd Annual Meeting of the American Association of Veterinary Laboratory Diagnosis, 1979, pp 269-282.
205. Amend JF, Nichelson RL, King RS, et al: Equine monensin toxicosis: Useful antemortem and post-mortem clinical pathologic tests. Proceedings of the 32nd Annual Convention of the American Association of Equine Practitioners 32:361-371, 1985.
206. Amend JF, Mallon FM, Wren WB, Ramos AS: Equine monensin toxicosis: Some experimental clinicopathological observations. Compend Contin Educ Pract Vet 11:S173-183, 1980.
207. Muyelle E, Vandenhende C, Oyaert W, et al: Delayed monensin sodium toxicity in horses. Equine Vet J 13:107-108, 1981.
208. Doonan GR, Brown CM, Mullaney TP, et al: Monensin poisoning in horses—An international incident. Can Vet J 30:165-169, 1989.
209. Boemo CM, Tucker JC, Huntington PJ, et al: Monensin toxicity in horses: An outbreak resulting in the deaths of ten horses. Aust Vet J 9:103-107, 1991.
210. Hanson LJ, Eisenbies HG, Givens SV: Toxic effects of lasalocid in horses. Am J Vet Res 42:456-461, 1981.
211. van Amstel SR, Guthrie AJ: Salinomycin poisoning in horses: Case report. Proceedings of the 31st Annual Convention of the American Association of Equine Practitioners 31:373-382, 1985.
212. Rollinson J, Taylor FGR, Chesney J: Salinomycin poisoning in horses. Vet Rec 121:126-128, 1987.
213. Dill SG, Simoncini DC, Bolton GR, et al: Fibrinous pericarditis in the horse. J Am Vet Med Assoc 180:266-271, 1982.
214. Wagner PC, Miller RA, Merritt F, et al: Constrictive pericarditis in the horse. J Equine Med Surg 1:242-247, 1977.
215. Bertone JJ, Dill SG: Traumatic gastropericarditis in a horse. J Am Vet Med Assoc 187:742-743, 1985.
216. Bradfield T: Traumatic pericarditis in a horse. Southwest Vet 23:145-146, 1970.
217. Foss RR: Effusive-constrictive pericarditis: Diagnosis and pathology. Vet Med 80:89-97, 1985.
218. Rainey JW: A specific arthritis with pericarditis affecting young horses in Tasmania. Aust Vet J 20:204-206, 1944.
219. Ryan AF, Rainey JW: A specific arthritis with pericarditis affecting horses in Tasmania. Aust Vet J 21:146-148, 1945.
220. Stevens G, Fincher MG: Pericarditis. Cornell Vet 28:254-256, 1938.
221. Orsini JA, Koch C, Stewart B: Peritoneopericardial hernia in a horse. J Am Vet Med Assoc 179:907-910, 1981.
222. Byars TD, Dainis CM, Seltzer KL, et al: Cranial thoracic masses in the horse: A sequel to pleuropneumonia. Equine Vet J 23:22-24, 1991.
223. Carnine BL, Schneider G, Cook JE, Leipold HW: Pericardial mesothelioma in a horse. Vet Pathol 14:513-515, 1977.
224. Wallace SS, Jayo MJ, DeBowes RM, et al: Mesothelioma in a horse. Compend Contin Educ Pract Vet 9:210-216, 1987.
225. Tithof PK, Rebhun WC, Dietze AE: Ultrasonographic diagnosis of aorto-iliac thrombosis. Cornell Vet 75:540-544, 1985.
226. Reef VB, Roby KAW, Richardson DW, et al: Use of ultrasonography for the detection of aortic-iliac thrombosis in horses. J Am Vet Med Assoc 190:286-288, 1987.
227. McDonnell SM, Love CC, Martin BB, et al: Two cases of ejaculatory failure associated with aortic-iliac thrombosis in stallions. J Am Vet Med Assoc 200:954-956, 1992.
228. Edwards GB, Allen WE: Aorto-iliac thrombosis in two horses: Clinical course of the disease and use of real-time ultrasonography to confirm the diagnosis. Equine Vet J 20:384-387, 1988.
229. Barrelet A: Aorto-iliac thrombosis in a breeding stallion and an eventer mare. Equine Vet Educ 5:86-89, 1993.
230. Wallace KC, Selcer BA, Becht J: Techniques for transrectal ultrasonography of the cranial mesenteric artery of the horse. Am J Vet Res 50:1695-1698, 1989.
231. Wallace KC, Selcer BA, Tyler DE, et al: Transrectal ultrasonography of the cranial mesenteric artery of the horse. Am J Vet Res 50:1699-1703, 1989.
232. Wallace KC, Selcer BA, Tyler DE, et al: In vitro ultrasonographic appearance of the normal and verminous equine aorta, cranial mesenteric artery, and its branches. Am J Vet Res 50:1774-1778, 1989.

233. Gardner SY, Reef VB, Spencer PA: Ultrasonographic evaluation of 46 horses with jugular vein thrombophlebitis: 1985-1988. J Am Vet Med Assoc 199:370-373, 1991.
234. Rooney JR, Prickett ME, Crowe MW: Aortic ring rupture in stallions. Pathol Vet 4:268-274, 1967.
235. Derksen FJ, Reed SM, Hall CC: Aneurysm of the aortic arch and brachial trunk in a horse. J Am Vet Med Assoc 179:692-694, 1981.
236. Holmes JR, Rezakhani A, Else RW: Rupture of a dissecting aortic aneurysm into the left pulmonary artery in a horse. Equine Vet J 5:65-70, 1973.
237. van der Linde-Sipman JS, Kroneman J, Meulenaar H, Vos JH: Necrosis and rupture of the aorta and pulmonary trunk in four horses. Vet Pathol 22:51-53, 1985.
238. Baker JR, Ellis CE: A survey of post mortem findings in 480 horses 1958 to 1980: (1) Causes of death. Equine Vet J 13:43-46, 1981.
239. Brown CM, Kaneene JB, Taylor RF: Sudden and unexpected death in horses and ponies: An analysis of 200 cases. Equine Vet J 20:99-103, 1988.
240. Platt H: Sudden and unexpected death in horses; a review of 69 cases. Br Vet J 138:417-429, 1982.
241. Azzie MAJ: Aortic/iliac thrombosis of Thoroughbred horses. Equine Vet J 1:113-116, 1969.
242. Maxie MG, Physick-Sheard PW: Aortic-iliac thrombosis in horses. Vet Pathol 22:238-249, 1985.
243. Spier S: Arterial thrombosis as the cause of lameness in a foal. J Am Vet Assoc 187:164-165, 1985.
244. Latimer FG, Magnus R, Duncan RB: Ateriioureteral fistula in a colt. Equine Vet J 23:483-484, 1991.
245. Buergelt CD, Carmichael JA, Tashjian RJ, Das KM: Spontaneous rupture of the left pulmonary artery in a horse with patent ductus arteriosus. J Am Vet Med Assoc 157:313-320, 1970.
246. Spurlock SL, Spurlock GH, Parker G, et al: Long-term jugular vein catheterization in horses. J Am Vet Med Assoc 196:425-431, 1990.
247. Spurlock SL, Spurlock GH: Risk factors of catheter-related complications. Compend Contin Educ Pract Vet 12:241-248, 1990.

CHAPTER

6

Adult Abdominal Ultrasonography

Prior to the application of ultrasonography to the evaluation of diseases of the equine abdomen, evaluation of the horse with abdominal disease was limited primarily to rectal examination, peritoneal fluid cytology and culture, clinical chemistry, and hematology. Radiographic examination of the adult equine abdomen is extremely limited because of the low yield of the procedure, the need to have equipment with high maS and kVp, and the radiation exposure to personnel. Only a lateral abdominal radiograph can be obtained in adult horses, although these films lack good detail of the abdominal viscera. Abdominal radiography is performed primarily in adult horses with suspected enterolithiasis. The enterolith can usually be successfully imaged radiographically when it is not detectable with other diagnostic techniques.[1]

Sonographic examination of the adult abdomen has become an important part of the diagnostic armamentarium in the evaluation of horses with suspected abdominal disease. The use of diagnostic ultrasound in the evaluation of the equine abdomen began with sonographic evaluation of the liver and kidneys. Evaluation of the gastrointestinal viscera with ultrasonography developed later, once sonologists overcame their initial hesitation over its application in the evaluation of a gas-filled structure. The information obtained from an abdominal sonographic examination is often not obtainable from other diagnostic procedures, and the information obtained can often lead the clinician to the correct diagnosis.[2-6]

EXAMINATION TECHNIQUE

Patient Preparation

For ultrasonographic examination of the adult abdomen, the entire ventral abdomen from the xiphoid caudally to the inguinal region should be surgically clipped with a No. 40 clipper blade.[2] The lateral sides of the abdomen and paralumbar fossa should also be included ventral to a diagonal line from the tuber coxae to the elbow, ventral to the ventral most border of the lung. The ventral aspect of the lung extends along a diagonal line running from the seventeenth intercostal space at the level of the tuber coxae, the fifteenth intercostal space level with the tuber ischii, the thirteenth intercostal space level with the middle of the thorax (in a dorsal to ventral direction), the eleventh intercostal space level with the point of the shoulder, and the ninth intercostal space level with the point of the elbow. In some horses the urinary bladder can be examined from the caudal ventral abdomen just in front of the pubis if the bladder is distended with urine. The skin in this area is usually relatively hair free, and clipping is rarely required. If the urinary bladder is not imageable from this window, a transrectal approach is required. To examine the right kidney, the skin should be clipped with a No. 40 surgical clipper blade from the right fourteenth to the seventeenth intercostal space or cranial edge of the paralumbar fossa between a line parallel to the dorsal and ventral most aspects of the right tuber coxae (Fig. 6-1). The left kidney is located further caudally and ventrally in the abdomen. Therefore, the clipped area should extend from the left sixteenth intercostal space to the caudal edge of the paralumbar fossa between a line parallel with the tuber coxae and the tuber ischii (Fig. 6-1). To examine the right side of the liver, the skin over the right side of the abdomen should be clipped with a No. 40 surgical clipper blade from the sixth through the sixteenth intercostal space along the previously described diagonal line from the tuber coxae to the elbow (Fig. 6-2). The skin over the left paralumbar fossa should be surgically clipped for ultrasonographic examination of the spleen extending cranially to the eighth intercostal space (Fig. 6-3). The clipped area should extend cranially to the sixth intercostal space to include the left lobe of the liver (see Fig. 6-2). The dorsal margin of the clipped area should extend to the ventral aspect of the left lung for examination of both the spleen and the left side of the liver.

The stomach can be examined by clipping the hair off the skin over the left side of the abdomen in the eighth to thirteenth intercostal spaces. The stomach is frequently imaged at the level of the point of the shoulder in the eleventh to thirteenth intercostal spaces,[7] although it can be imaged both cranial and caudal to this if distended or displaced. The duodenum can be examined by clipping (with a No. 40 surgical clipper blade) a 20-cm-long strip

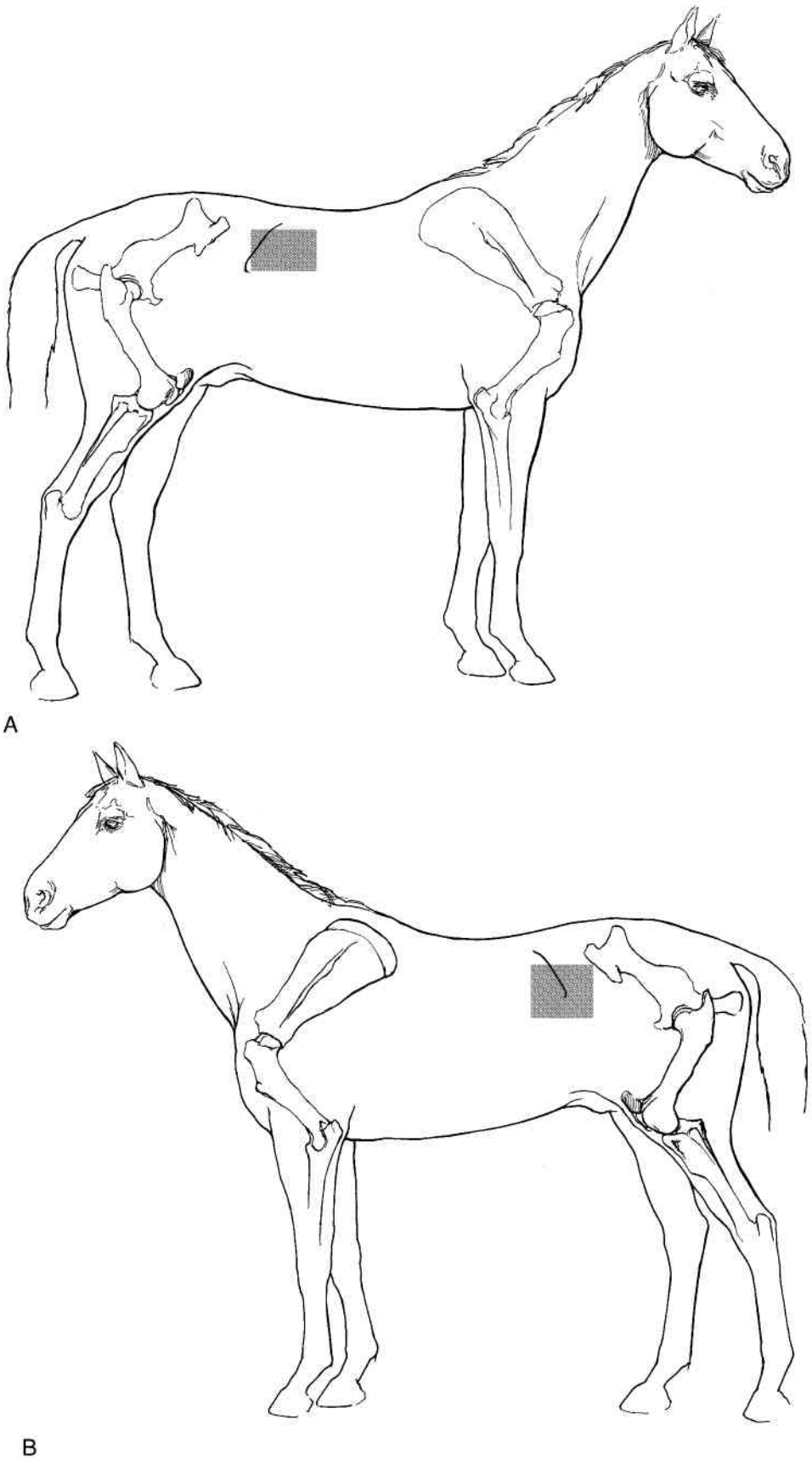

Figure 6–1

Diagram of the area to clip to image both kidneys in a horse. *A*, The shaded area represents the clipped area over the right kidney and the curved black line represents the last rib. *B*, The shaded area represents the clipped area over the spleen and left kidney and the curved black line represents the last rib.

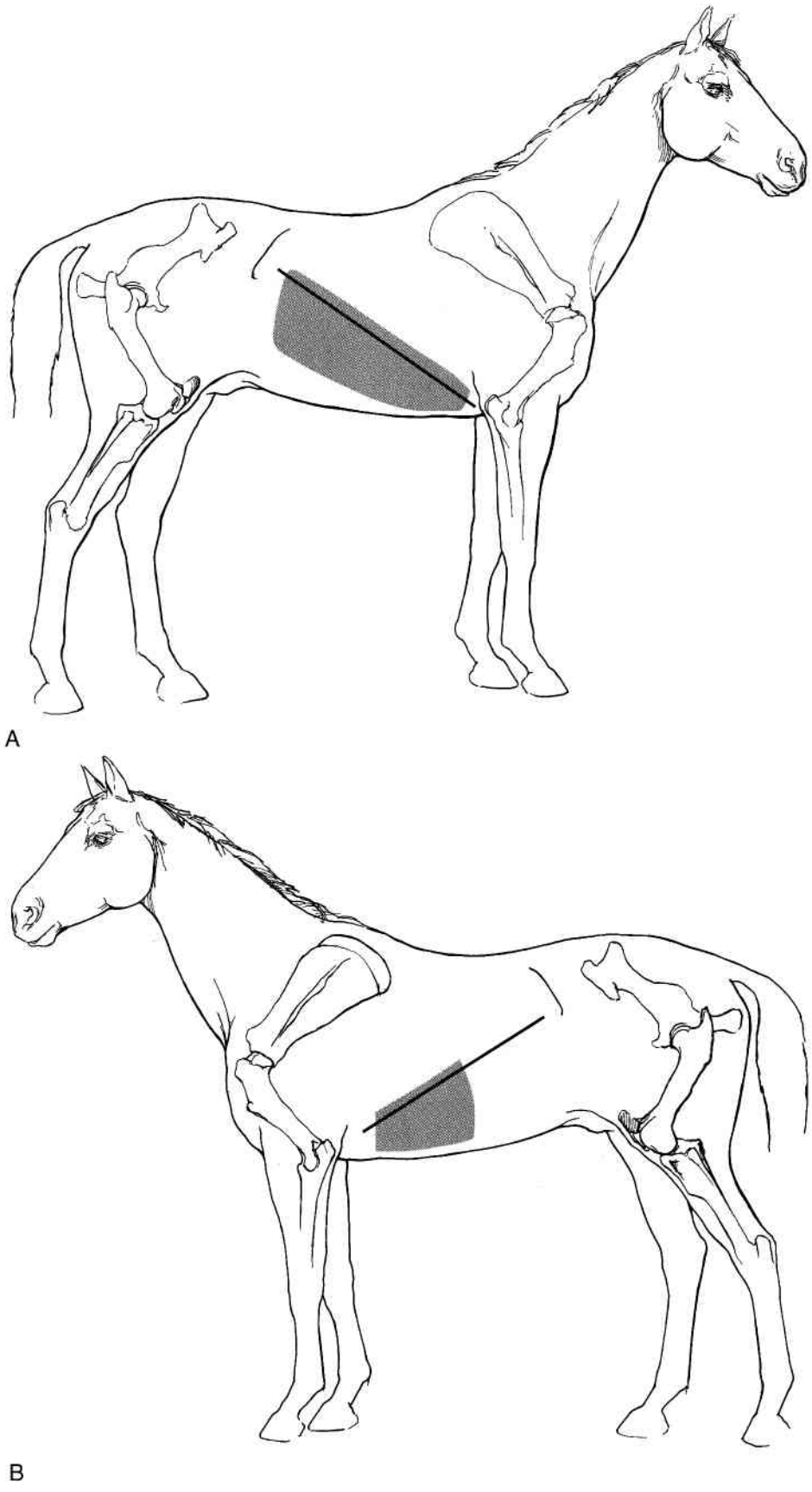

Figure 6–2

Diagram of the area to clip to image the liver below the ventral lung field in a horse. *A*, The shaded area represents the clipped area over the right side of the liver, and the diagonal black line represents the ventral border of the lung field. *B*. The shaded area represents the clipped area over the left side of the liver, and the diagonal black line represents the ventral border of the lung field.

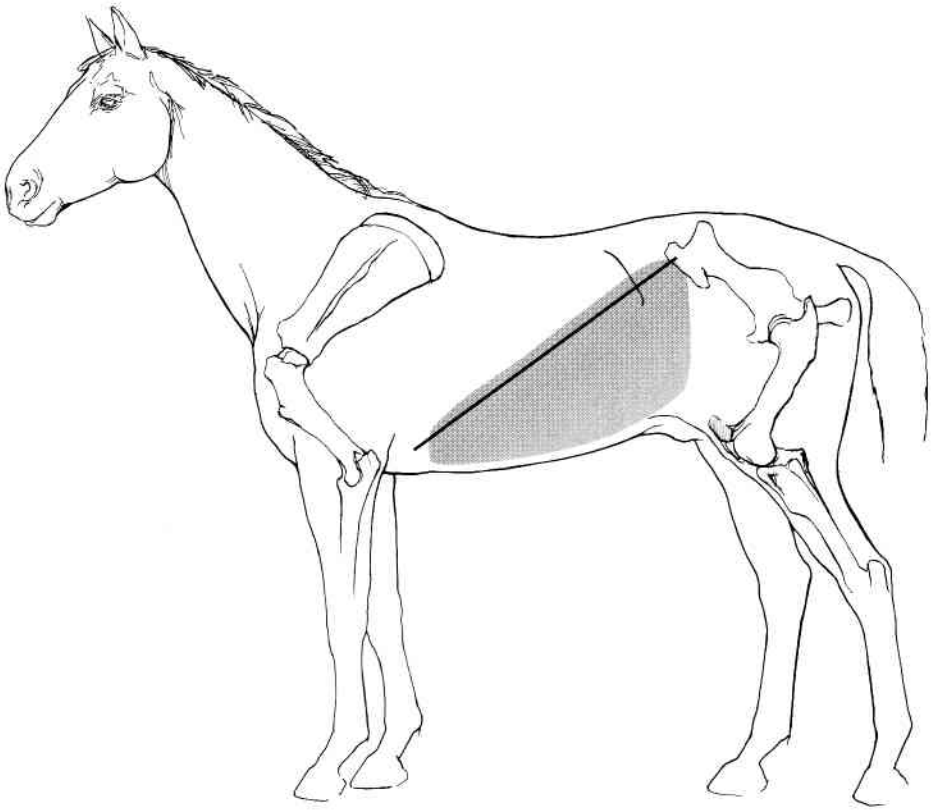

Figure 6–3
Diagram of the area to clip to image the spleen in a horse. The shaded area represents the area to be clipped for the spleen, and the diagonal black line represents the ventral border of the lung field.

from the skin overlying the right eighth intercostal space to the paralumbar fossa. This clipped area should extend 5 cm ventral to a line joining the right olecranon and tuber sacrale (Fig. 6-2).[8]

Anatomy

Urinary Bladder

The urinary bladder is located in the caudal most portion of the abdomen at the pelvic brim and has both an intrapelvic and an abdominal location, depending upon the amount of urine contained within it. When the urinary bladder is full, it extends cranially and ventrally, displacing the large colon. The urinary bladder joins the pelvic urethra at the trigone, which is located in the pelvic canal. The bladder is suspended in the abdominal cavity by its round ligaments, remnants of the umbilical arteries. The wall of the bladder is muscular and stretches, becoming thinner when the bladder is full.

Kidneys

The right kidney is located more cranially in the abdomen and can usually be found in the retroperitoneal space just beneath the abdominal wall and immediately ventral to the transverse processes between the fourteenth and seventeenth intercostal spaces at the level of the tuber coxae.[2, 4, 9-13] The cranial pole of the right kidney sits in the renal fossa of the liver and lies deep to the diaphragm at the sixteenth intercostal space in most horses (range, fourteenth to seventeenth intercostal space).[11] The caudal extremity of the right kidney is located at the seventeenth intercostal space to the first lumbar vertebra.[11] The duodenum courses ventrally around the caudal pole of the right kidney, and the cecum is imaged ventral and caudal to the right kidney and the duodenum. The right kidney has a triangular curvilinear or heart shape with a prominent hilar notch.[11] This kidney measures approximately 15 to 18 cm wide, 13 to 15 cm long, and 5 cm thick.[11] The left kidney is located further caudally and ventrally in the abdomen (Fig. 6-4) and is usually found in the seventeenth intercostal space and the paralumbar fossa between a line parallel to the tuber coxae and the tuber ischii.[2, 4, 9-13] The cranial extremity of the left kidney is usually at the level of the seventeenth rib (range, sixteenth to eighteenth) but may lie caudal to the last rib in some normal horses.[11] The left renal hilus is at the level of the caudal extremity of the right kidney.[11] The caudal extremity of the left kidney is at the level of the first to third lumbar vertebrae.[11] The left kidney has more of a bean shape and is longer and narrower than the right kidney. The left kidney is 15 to 18 cm long, 11 to 15 cm wide, and 5 to 6 cm thick. The left kidney lies medial to the spleen in the left caudal abdomen. The caudal vena cava and aorta lie medial to the left and right kidney along the ventral aspect of the dorsal midline.

The kidney in the horse has a distinct cortex and medulla, but in the center of the kidney fusion of the renal papillae forms the renal crest, a crescent-shaped projection into the renal pelvis.[11] The papillary ducts of the center of the kidney open onto the renal crest,

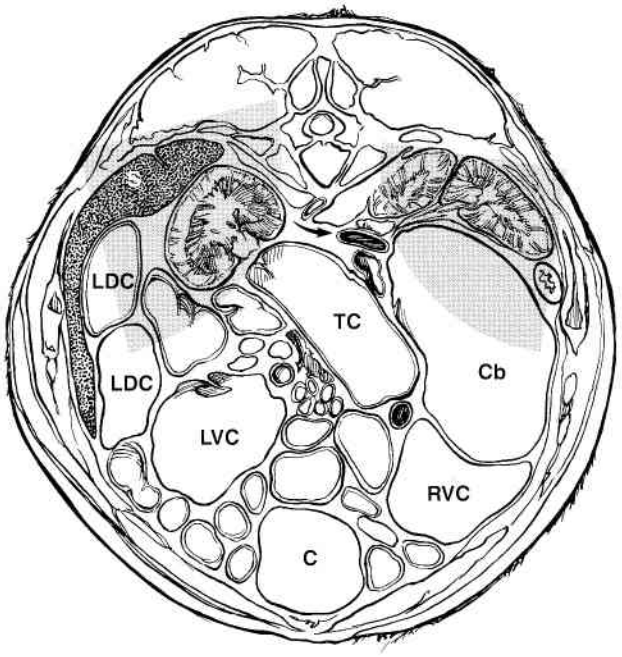

Figure 6–4

Cross-section of the equine abdomen illustrating the scan planes to evaluate the right and left kidneys, the nephrosplenic space, and the caudal pole of the spleen at the level of the seventeenth thoracic vertebra. The shaded areas represent the scan planes to examine the left and right kidneys. The arrow points to the duodenum. S = spleen, Cb = cecal base, C = cecal body, RVC = right ventral colon, TC = transverse colon, LDC = left dorsal colon, LVC = left ventral colon.

whereas those from the extremities of the kidney open into the terminal recesses, which then drain into the renal pelvis.[11]

Liver

The right lobe of the liver extends from the sixth or seventh intercostal space to the fourteenth or fifteenth intercostal space. The left lobe of the liver is smaller and usually extends from the sixth to the ninth intercostal spaces.[2, 4, 12, 14] The liver is immediately adjacent to and caudal to the diaphragm. The right dorsal colon is deep to the liver on the right side of the abdomen with the duodenum between the right dorsal colon and liver in the cranial to mid portion of the abdomen (Fig. 6-5). The right kidney is caudal and lateral to the caudate process of the right lobe of the liver. On the left side of the abdomen the cranial pole of the spleen is located medial to the liver, usually in the eighth to ninth intercostal space. Atrophy of the right liver lobe occurs in older horses.

Spleen

The spleen is variable in size but usually extends along the left abdominal wall from the eighth or ninth intercostal space to the seventeenth intercostal space or paralumbar fossa.[2, 12] The spleen is immediately adjacent to the diaphragm and left body wall in the mid and caudal abdomen (Figs. 6-4 and 6-5) and medial to the liver in the left cranial abdomen. The cranial pole of the spleen can occasionally be found lateral to the liver or in the right cranioventral abdomen in a small percentage of normal horses. The left dorsal colon is located medial to the spleen. Ventral to the spleen is the left dorsal and/or left ventral colon.

Gastrointestinal Viscera

The horse's stomach is located medial to the spleen along the left abdominal wall from the eighth or ninth to the twelfth or thirteenth intercostal space. In most horses the stomach is adjacent to the spleen for three intercostal spaces only (ninth to eleventh, in the author's experience). The stomach is adjacent to the spleen at the level of the splenic vein.[4] There is a consistent relationship between the greater curvature of the stomach, the spleen, and the gastrosplenic vein, enabling the sonologist to accurately identify the stomach.[7] The duodenum is imaged around the ventral and caudal aspects of the right lobe of the liver and the caudal pole of the right kidney (see Fig. 6-4). The duodenum is located between the liver and the right dorsal colon from the pylorus (located in the proximal to mid portion of the right side of the abdomen) to the mid to caudal abdomen (see Fig. 6-5).[4] The right dorsal colon is adjacent to the duodenum from the fifteenth intercostal space cranially. The duode-

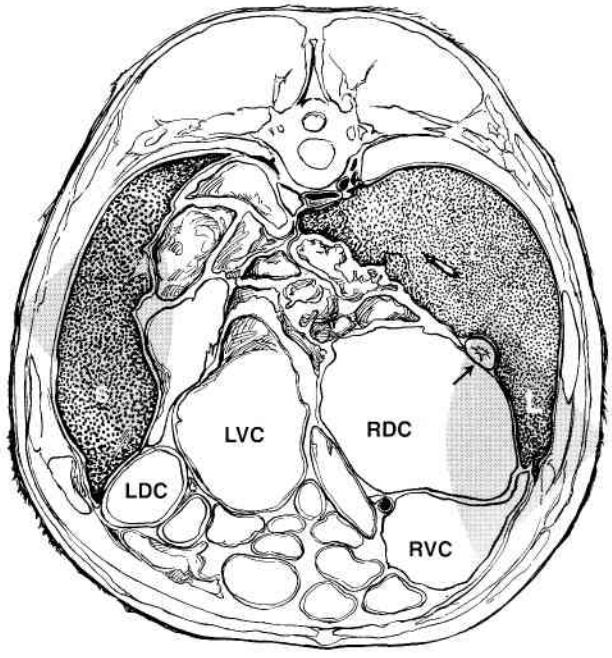

Figure 6–5

Cross-section of the equine abdomen illustrating the scan planes to evaluate the liver (L) and spleen (S) at the junction of the thirteenth and fourteenth thoracic vertebrae. The shaded areas represent a scan plane to examine the spleen on the left side of the abdomen and a scan plane to examine the liver, duodenum (*arrow*), and right dorsal (RDC) and ventral (RVC) colon. LDC = left dorsal colon, LVC = left ventral colon.

num then courses caudodorsally to the caudal pole of the right kidney and lies between the liver and the cecum.[4] The distance of the duodenum from the body wall depends upon the thickness of the interposed liver.[8] The pancreas is located caudal to the stomach and duodenum, mostly to the right of midline. The left caudal border of the pancreas lies between the saccus cecus of the stomach and the cranial border of the left kidney. The right caudal border of the pancreas is adjacent to the ventral surface of the right kidney and the right adrenal gland. The large intestine is in contact with the ventral abdominal wall throughout the abdomen of the adult horse. The diameter of the right dorsal colon is 30 to 50 cm, with a rapid reduction of diameter in the transverse colon.[15] The small colon is located dorsal to the urinary bladder in the left caudodorsal quadrant of the abdomen.[15] The small colon is suspended from the dorsal midline by the mesocolon and has a diameter of 7 to 10 cm.[15] The proximal small colon is connected to the distal duodenum by the duodenocolic fold. The small colon is sacculated and has a mesenteric and antimesenteric band.

Scanning Technique

The examination of the urinary bladder and gastrointestinal viscera should begin with a 7.5-MHz sector-scanner or linear-array transducer or a 6.0-MHz microconvex linear-array transducer and a displayed depth of 4 to 8 cm.[16] A 5.0-MHz transducer should then be used to further evaluate these structures if the urinary bladder has not been examined in its entirely[16] and to thoroughly evaluate all the imageable gastrointestinal viscera. The highest frequency transducer that penetrates to the area under investigation should be selected, and the smallest depth of field necessary should be displayed.

The dorsal (cranial to caudal scan plane from the right or left side of the abdomen) scan-plane orientation should display the cranial aspect of the abdomen on the right side of the screen and the caudal aspect on the left. The sagittal (cranial to caudal scan plane from the ventral aspect of the abdomen) scan plane should be displayed with the cranial aspect of the abdomen on the right side of the screen and the caudal aspect on the left. The left transverse scan plane orientation should display the ventral aspect of the abdomen on the left side of the screen and the dorsal aspect on the right. The ventral transverse scan plane orientation should display the right side of the abdomen on the left side of the screen and the left side of the abdomen on the right. The right transverse scan plane orientation should display the dorsal aspect of the abdomen on the right side of the screen and the ventral aspect on the left.

Urinary Bladder

The ultrasonographic evaluation of the horse's urinary bladder should include a thorough transrectal evaluation. The transrectal examination usually requires either a 6.0-MHz microconvex linear-array transducer or a 5.0-MHz linear-array or sector-scanner transducer to image the bladder in its entirety. A transverse, sagittal, or combination of both scan planes can be obtained, depending upon the type of transducer used. A transcutaneous examination from the ventral abdominal window can be performed if the urinary bladder can be successfully imaged from this window. The weight of the urine in the full bladder may displace the gas-filled large colon, resulting in the bladder being positioned against the floor of the ventral abdomen just cranial to the pelvic brim. A 5.0- or 3.5-MHz linear-array or sector-scanner transducer or 6.0-MHz microconvex linear-array transducer is often necessary to image the entire bladder from this window because of the bladder distention. The urinary bladder should be scanned in transverse and sagittal scan planes from the ventral abdomen, carefully evaluating the bladder apex, bladder wall, and retroperitoneal area.[2, 16, 17] The echogenicity of the urine within the bladder should be assessed, and the bladder should be carefully imaged for calculi or other abnormal contents. Sonographic evaluation of the urethra should also be performed if urethral obstruction is suspected or urinary calculi are detected. The entire penile, perineal, and pelvic urethra should be examined sonographically from a transcutaneous and transrectal window as indicated by the portion of the urethra being examined. The urethra is best examined with a 7.5- or 10.0-MHz transducer in both its short- and long-axis planes. Transrectal examination of the pelvic urethra can be done in both imaging planes with some transducers such as a 6.0-MHz microconvex or small 7.5-MHz linear-array transducer, but only one scan plane can be obtained with large transrectal linear 5.0-MHz transducers. The transducer should be used at the highest frequency possible because the urethra is very close to the transducer and optimal image quality is desired. The ureters and the ureteral openings into the urinary bladder are not normally visible sonographically from the abdominal window but may occasionally be imaged from the transrectal window using a high-frequency transducer.

Kidneys

Ultrasonographic evaluation of the horse's kidneys can be performed from the left and right body wall. The right kidney should be scanned from the right side of the abdomen in the fourteenth to seventeenth intercostal spaces using a 3.5- or 5.0-MHz transducer.[2, 13, 18] The left kidney should be scanned from the left side of the abdomen in the seventeenth intercostal space and paralumbar fossa using a 2.5- or 3.5-MHz transducer.[2, 13, 18] The kidneys should be scanned in the dorsal scan plane (from the dorsolateral abdomen) and in the transverse scan plane (two mutually perpendicular planes). Images from the sagittal and transverse oblique planes of both kidneys should also be obtained from the transcutaneous window.[11] In an in vivo study of seven horses, sonographic images of the right kidney were obtained in the sagittal, transverse, and transverse oblique planes in all horses, with the transducers positioned in the fifteenth, sixteenth, or seventeenth intercostal spaces, but images in the dorsal plane were obtained in only three horses.[11] Sonographic images of the left kidney were able to be

obtained in all horses from the left sixteenth or seventeenth intercostal spaces and the paralumbar fossa in all scan planes. Dorsal and sagittal images were obtained in all horses with transrectal scanning of the left kidney.[11]

Liver

Only a portion of the liver can be imaged sonographically in the horse, the portion ventral to the ventralmost margins of the lungs. The entire imageable part of the liver should be evaluated ultrasonographically along the right side of the abdomen from the sixth to the fifteenth intercostal spaces and along the left side of the cranial ventral abdomen from the sixth to the ninth intercostal spaces.[2, 14] The liver should be scanned in two mutually perpendicular planes (dorsal and transverse).

Spleen

The spleen is found along the left side of the abdomen adjacent to the body wall from the eighth or ninth intercostal spaces (cranial pole) to the seventeenth intercostal space or paralumbar fossa (tail or caudal pole of the spleen).[2] The spleen is found dorsally in the caudal abdomen, lateral to the left kidney. The spleen is located more ventrally in the left cranial ventral abdomen and is found across the midline in the right cranial ventral abdomen in a small percentage of normal horses. The spleen should be scanned in the dorsal and transverse scan planes as well as in the sagittal and parasagittal scan planes, location of the spleen permitting.

Gastrointestinal Viscera

The ultrasonographic examination of the gastrointestinal viscera should be performed from the most ventral portion of the abdomen and therefore is easiest to perform in the standing horse. The right and left sides of the abdomen should also be thoroughly evaluated. If the horse is recumbent, the gastrointestinal viscera should be scanned from the ventralmost portion of the abdomen as well as from the remaining accessible abdominal windows. The stomach is located medial to the spleen in the cranial and mid portion of the left side of the abdomen. The fundus of the stomach is located at the level of the splenic vein.[4] The duodenum is imageable medial to the ventral and caudal aspect of the right lobe of the liver coursing caudodorsally around the caudal pole of the right kidney (see Figs. 6-4 and 6-5). The duodenum can be imaged from the right eleventh intercostal space to the cranial aspect of the paralumbar fossa along a line from the right olecranon to the tuber sacrale or slightly dorsal to this line.[8] The duodenum is consistently imaged between the fourteenth and seventeenth intercostal spaces just ventral to the right kidney and dorsal to dorsolateral to the large bowel (cecal base).[8] Jejunum is not usually imageable in the adult horse owing to the interposed large colon. The large colon is normally visible throughout the majority of the abdomen along both body walls and along the ventral abdomen. The cecum is imaged along the right body wall in the dorsal and caudal portions of the abdomen. The small colon dorsal to the urinary bladder can be imaged from the ventral abdomen if the bladder is full and adjacent to the ventral abdominal wall. The urinary bladder can then be used as an acoustic window to image the small colon. Transrectally the small colon can be imaged, primarily in the left caudodorsal quadrant, dorsal to the pelvic flexure. The root of the mesentery and cranial mesenteric artery can be imaged on the midline between the right and left kidneys, with the duodenum coursing caudal to the root of the mesentery from the caudal pole of the right kidney. The base of the cecum can be imaged in the right dorsal quadrant, with the right dorsal colon immediately ventral to the cecal base. Jejunum can occasionally be imaged in the center of the abdomen near the root of the mesentery.

ULTRASONOGRAPHIC FINDINGS

Normal Structures

The abdomen should always be examined from the ventral most location, in addition to the left and right sides of the abdomen, unless the abdominal organs (liver, kidneys, or spleen) are being imaged. The gas present in the gastrointestinal viscera rises dorsally and is less likely to interfere with the examination if the scan is performed from the most ventral location. The abnormal gastrointestinal viscera are heavy and fall to the ventral portion of the abdomen, making their detection most likely if the scan is performed from the most ventral location.

Urinary Bladder

The urinary bladder is usually obscured from view by gas in the interposed large bowel.[2, 4] The urinary bladder is imaged in the caudal most portion of the ventral abdomen and may be imaged in adult horses when filled with urine, displacing the large colon (Fig. 6-6). The urinary bladder can be examined from the transrectal window in all horses large enough to receive a rectal examination. The urinary bladder is round to oval in transverse section and oval in sagittal section. Slightly biconcave lateral walls are detected in the full urinary bladder because the round ligaments of the bladder suspend the bladder from its lateral aspects. The urinary bladder usually contains echogenic urine in the adult horse.[2] This is the result of the normal crystalluria (calcium carbonate) and mucus in the urine of the adult horse. However, the echogenicity of the contents of the urinary bladder varies among normal horses from anechoic to hyperechoic particles, with a homogeneous pattern similar to that of the spleen.[19] The contents of the urinary bladder can be seen to swirl during a real-time examination, and this helps to define the boundaries between the urinary bladder wall and its contents.[19] The urinary bladder should always maintain a round to oval shape, whether empty or full. In sagittal section the urinary bladder should be rounder at the apex than toward the trigone region. The urinary bladder

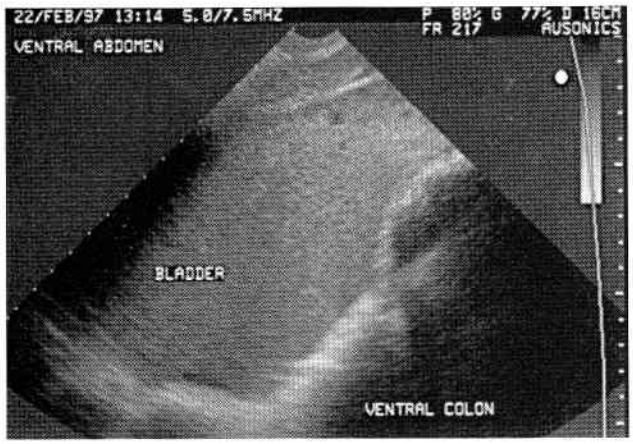

Figure 6–6

Sonogram of a urinary bladder obtained from a 2-year-old Quarter horse filly. Notice the echogenic nature of the urine associated with the high concentration of calcium carbonate crystals and mucus in equine urine. The slight inhomogeneities within the echogenic fluid are caused by the urine swirling within the bladder. The sacculated hyperechoic structures adjacent to the urinary bladder are from the overlying ventral colon. This sonogram was obtained from the ventral abdomen just cranial to the pelvic brim with a wide-bandwidth 5.0-MHz sector-scanner transducer operating at 7.5 MHz at a displayed depth of 16 cm. The right side of the sonogram is caudal and the left side is cranial.

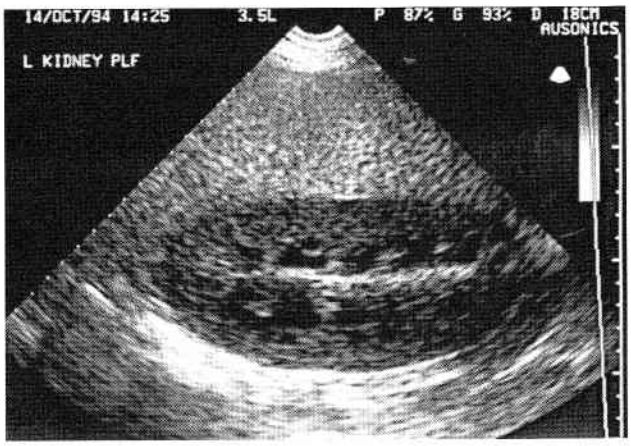

Figure 6–7

Sonogram of the left kidney obtained from a 15-year-old Arabian mare in the scan plane illustrated in Fig. 6-4. Notice the hypoechoic appearance of the left kidney relative to the adjacent, more echogenic spleen. The renal pelvis is echogenic, and the adjacent renal calyces are anechoic. This sonogram was obtained from the paralumbar fossa with a 3.5-MHz sector-scanner transducer at a displayed depth of 18 cm. The right side of this sonogram is dorsal and the left side is ventral.

may appear somewhat irregular when the bladder is catheterized or when it is compressed by surrounding structures. Evaluation of the urinary bladder is ideally performed when the bladder is full to minimize error in image interpretation. The wall of the urinary bladder is hypoechoic to echogenic, and its thickness varies with the amount of bladder distention (normally from 3 to 6 mm). The mucosa and muscular wall of the urinary bladder are not separable sonographically. The urinary bladder can be found anywhere from just cranial to the pubis when empty or cranial to the external umbilical remnant, if the bladder is very distended. The ureters are not normally imaged from a transrectal window. The pelvic urethra can be followed along the pelvis and is best delineated with a 7.5- or 10.0-MHz linear-array transducer or a 6.0-MHz microconvex linear-array transducer. The urethra is easiest to visualize when filled with fluid after urination and was detected in stallions and geldings in only one study when examining these structures with a 5.0-MHz transducer.[19]

Kidneys

High-quality images from the left kidney are difficult to obtain from a transcutaneous window owing to the depth of the left kidney from the skin surface and the attenuation of the ultrasound beam by the overlying spleen. Routinely only the most echogenic structures of the left kidney (renal pelvis and interlobar vessels) are imaged from this window (Fig. 6-7). Images containing greater anatomic detail are obtainable of the right kidney from the transcutaneous window (Fig. 6-8) and the left kidney from a transrectal window. The renal capsule is not distinctly imaged as a discrete structure in vivo, although it appears as an echogenic structure surrounding the kidney in vitro.[11] The renal cortex is hypoechoic compared with the surrounding tissues and is composed of fine homogeneous echoes with a slightly mottled appearance, measuring approximately 1 to 2 cm in thickness.[9, 13] The adjacent medulla is less echogenic than the renal cortex.[4, 9-11, 13] In the cranial and caudal extremities of each kidney, acoustic anisotropy was observed between the renal cortex and medulla, resulting in the cortex and medulla in these areas appearing more echogenic than in the center of the kidney.[11] The renal pelvis is normally very echogenic owing to the presence of intrapelvic fat and fibrous tissue. The renal pelvis appears as an echogenic pair of diverging lines leading to the crescent-shaped renal crest

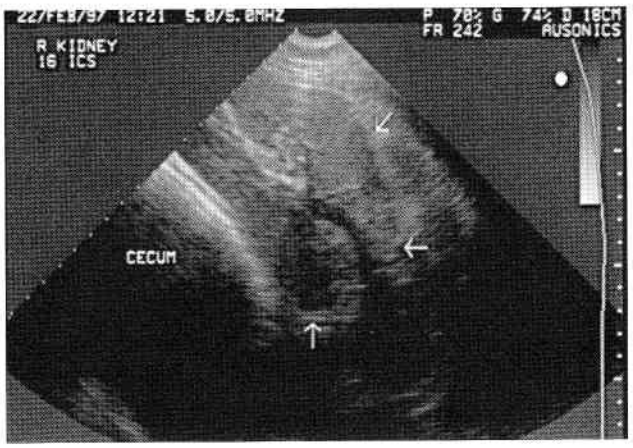

Figure 6–8

Sonogram of the right kidney (*arrows*) obtained from a 2-year-old Thoroughbred colt. The anechoic tubular structure leaving the right kidney is the ureter. The hyperechoic curvilinear structure adjacent to the right kidney is the cecum. This sonogram was obtained from the right sixteenth intercostal space with a wide-bandwidth 5.0-MHz sector-scanner transducer operating at 5.0 MHz at a displayed depth of 18 cm. The right side of this sonogram is cranial and the left side is caudal.

in the lateral half of the kidney in the transverse plane and as a pair of parallel echogenic lines separated by the moderately echogenic line of the renal crest in the sagittal plane.[11] The terminal recesses appear as moderately echogenic lines in the medulla of the cranial and caudal extremities of each kidney, measuring 1 to 3 mm in diameter.[11] The proximal portion of the right ureter appears as a strongly echogenic circular structure in sagittal images and as an elliptical structure in transverse oblique images.[11] The proximal portion of the left ureter can not be differentiated sonographically from the other peripelvic structures in sonograms of the left kidney obtained from the transcutaneous window. Irregular echogenic lines in the medulla are the interlobar vessels of the kidney.[11] The arcuate arteries may be imaged at the corticomedullary junction as small echogenic points measuring about 1 mm in diameter.[11] The renal vessels can usually be imaged at the hilus of the kidney. The renal artery and/or branches of the renal artery are imaged cranial to the renal vein.[11] The renal vein is located cranial to the proximal portion of the ureter.[11] Power Doppler ultrasound can be used to image the renal vasculature, including the arcuate and interlobar arteries (Color Figures 1-1 and 6-1). Power Doppler ultrasound is used to detect the lower-velocity blood flow present in the smaller vessels of the normal kidney and to image the small arteries arborizing the renal cortex. With topographic Doppler maps, the renal vasculature is also well demonstrated and a sample volume in the renal vasculature produces a spectral display of the flow velocities within the renal

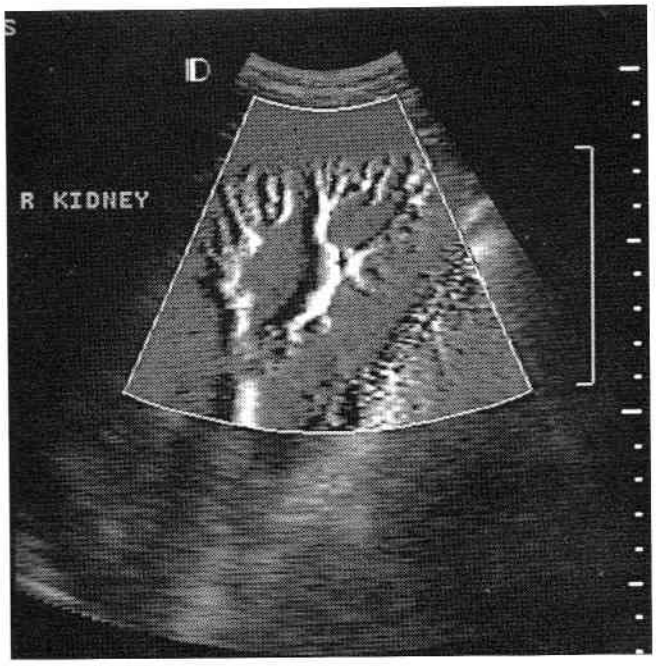

Figure 6–9

Power Doppler sonograms of the right kidney obtained from a 10-year-old Thoroughbred gelding displaying the renal vasculature in a topographical map. Notice the branching of the renal artery into arcuate and interlobar arteries. These sonograms in this and Figure 6-10 were obtained from the right sixteenth intercostal space with a wide-bandwidth 3.5-MHz curved linear-array transducer at a displayed depth of 17 cm.

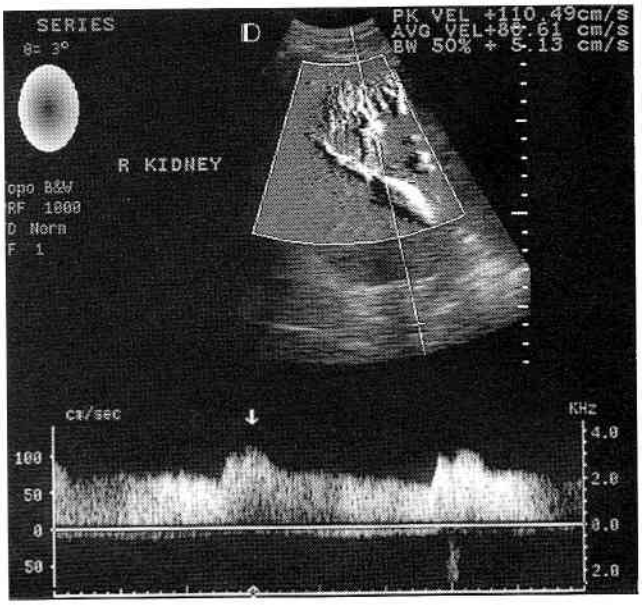

Figure 6–10

A power Doppler sonogram of a different part of the kidney with the pulsed-wave Doppler sampling blood flow in one of the arcuate arteries. Notice the pulsatile flow depicted in the spectral Doppler tracing, with the increased velocity of blood flow during systole (*arrow*).

vessels (Figs. 6-9 and 6-10). With transrectal ultrasonography, branches of the renal arteries can be imaged in the medullary and pelvic areas of the kidney, deep to the renal cortex, as anechoic pulsatile vessels 2 to 3 mm in diameter.

The caudal vena cava and aorta may be imaged axial to the left and right kidneys along the ventral aspect of the dorsal midline. The parenchyma of the kidney (renal cortex and medulla) should be the most anechoic of the abdominal organs when they are sonographically compared (kidney < liver < spleen).[2, 4] However, in many normal horses the kidney may appear isoechoic with the liver. The ureters are not normally imaged from the abdominal windows, with the exception of the proximal most portion of the right ureter.[2, 4, 11, 13] The adrenal glands are also not usually detected sonographically along the cranial and medial margin of both kidneys. Although the medial border of the right kidney is in close proximity to the pancreas, portal vein, and some of the mesenteric and visceral vessels, they are not usually visible sonographically from the right abdominal window because of their size and the depth of these structures from the skin surface.[9] During inspiration the lung often obscures the cranial pole of the right kidney from the right lateral abdominal window. Gas in the left dorsal colon may obscure visualization of the caudal pole of the left kidney from the left lateral abdominal window. Occasionally the caudal pole of the left kidney lies adjacent to the left body wall rather than in its more common position, medial to the spleen.

Liver

The liver is recognizable by its branching vasculature with the portal and hepatic veins (Fig. 6-11).[12] The walls

of the portal veins are more echogenic than those of the hepatic veins, similar to the situation in humans and dogs.[3, 12, 20] This is because the portal veins are surrounded by connective tissue, whereas little or no connective tissue surrounds the hepatic veins.[20] The blood in the hepatic veins may appear anechoic, or small moving echoes may be imaged as the ultrasound beam reflects off the moving cells and other blood components. The hepatic veins can be traced to their junction with the caudal vena cava if the caudal vena cava can be successfully imaged. The caudal vena cava is rarely imageable in adult horses. The liver parenchyma is homogeneous and of medium echogenicity (Fig. 6-11). The bile ducts are not normally visible sonographically.[14] Normally 4 to 8 cm of hepatic parenchyma is visible in the young horse when the liver is imaged from the lateral sides of the abdomen. Estimations of hepatic size are relative and are based on the amount of liver tissue imaged ventral to the lung margin. The size of the thoracic cavity, the volume of the colonic contents, and the presence of fluid or masses within the thoracic or abdominal cavity all influence the amount of hepatic parenchyma visible ventral to the ventral lung margins. The ventral margin of the liver should appear sharp throughout both liver lobes. In older horses atrophy of the right lobe of the liver is common. The amount of hepatic parenchyma imaged below the ventral margin of the right lung decreases with age so that little or none of the right liver lobe is imaged in the right side of the abdomen of normal older horses.

Spleen

The spleen is the most homogeneous and echogenic of the abdominal organs (Fig. 6-12 and see Fig. 6-7).[2, 4]

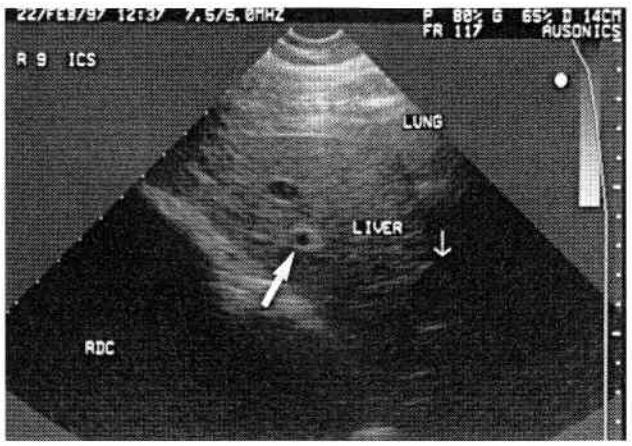

Figure 6–11

Sonogram of the liver obtained from a 2-year-old Thoroughbred colt. The hepatic and portal veins are the small linear to tubular structures contained within the parenchyma of the liver. The portal veins have the thicker, more echogenic walls (*large arrow*), whereas the walls of the hepatic veins are thinner and less echogenic. The right dorsal colon (RDC) is medial to the right lobe of the liver. The down arrow points to the large portal vein before it branches in the liver. The ventral most tip of the lung is imaged covering the liver on the right side of the image. This sonogram was obtained from the right ninth intercostal space with a wide-bandwidth 7.5-MHz sector-scanner transducer operating at 5.0 MHz at a displayed depth of 14 cm. The right side of this sonogram is dorsal and the left side is ventral.

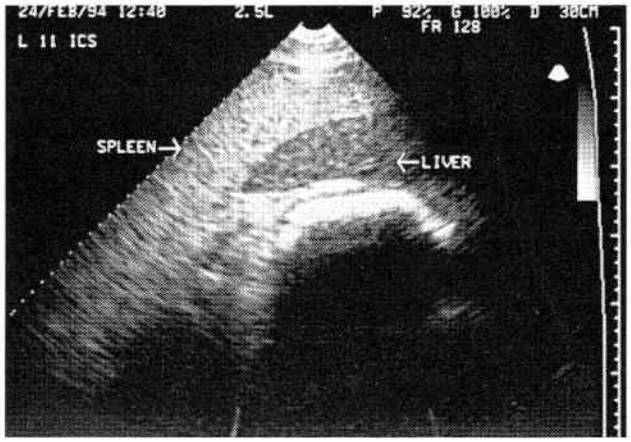

Figure 6–12

Sonogram of the left side of the ventral abdomen obtained from a 24-year-old Thoroughbred mare. The spleen is more echogenic and homogeneous in appearance than the adjacent liver, which is located medial to the spleen. The hyperechoic curvilinear structure adjacent to the liver is the left ventral colon. This sonogram was obtained with a 2.5-MHz sector-scanner transducer at a displayed depth of 30 cm. The right side of this sonogram is dorsal and the left side is ventral.

Compared with the liver, the spleen has few visible vessels. Transrectally the spleen also appears homogeneously echogenic with a paucity of blood vessels.[19] The spleen has a hyperechoic capsule with parenchyma that is moderately echogenic and appears to have a finely mottled pattern when imaged from the transrectal window.[19] The size of the spleen can be quite variable in the normal horse but usually runs along the majority of the left body wall up to the eight or ninth intercostal space. The thickness of the caudal pole of the spleen when imaged from the transrectal window has been reported to be 5 to 8 cm, tapering caudally to a thin edge.[19] The spleen should be found lateral to the left kidney and stomach but medial to the left lobe of the liver. In some horses the spleen may be found lateral to the left lobe of the liver (Fig. 6-12) along the ventral midline (Fig. 6-13) or on the right side of the cranial ventral abdomen (Fig. 6-14). The splenic vein is easily recognized as an anechoic tubular structure located along the medial aspect of the spleen around the tenth intercostal space.[4] The splenic vein is a reliable landmark for the location of the gastric fundus, medial to the spleen (Fig. 6-15). The dorsal border of all but the caudal pole of the spleen is usually obscured from view by the overlying lung.

Gastrointestinal Viscera

Ultrasonographic evaluation of the gastrointestinal tract has continued to gain favor as an alternative, noninvasive imaging modality in humans and small and large animals, in all of whom the normal sonographic appearance of the stomach and intestinal tract has been described.[8, 21-30] Although no difference in thickness of the intestinal wall was detected between dogs of various ages, differences were detected between dogs of different breeds, with the larger breed dogs having thicker gastric walls.[21] A

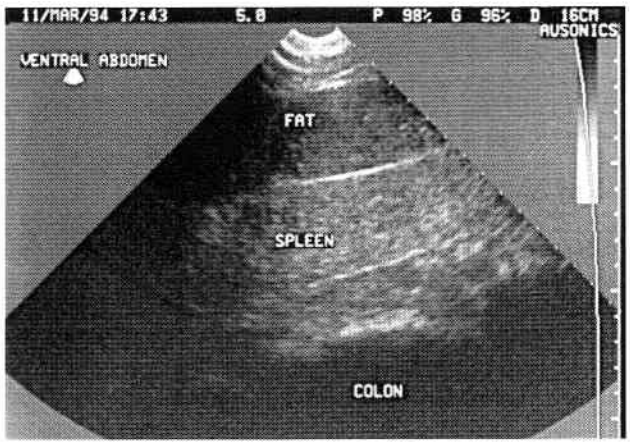

Figure 6–13

Sonogram of the ventral abdomen obtained from a 7-year-old Quarter horse cross gelding demonstrating a large retroperitoneal layer of abdominal fat ventral to the spleen. The retroperitoneal fat has relatively homogeneous echogenicity in this horse and is approximately 3.5 cm thick. The shadowing on the left side of the sonogram is from the distal end of the rib. This sonogram was obtained from the cranioventral abdomen to the left of midline with a 5.0-MHz sector-scanner transducer at a displayed depth of 16 cm. The right side of this sonogram is toward the midline, and the left side is toward the left side of the abdomen.

difference in thickness of 2 mm has been reported in humans between the distended and nondistended bowel wall.[21, 31] The administration of water via nasogastric tube to distend the stomach with fluid improves visualization of the gastric mucosa and portions of the gastrointestinal tract in the cranial abdomen if the stomach can be used as an acoustic window. The administration of water via a stomach tube at a dose of 15 ml/kg, after withdrawing any free air, is reportedly beneficial for sonographic evaluation of the upper segments of the gastrointestinal tract in the dog.[22] Fasting is also reportedly helpful in examining the intestinal tract of the dog,[22] but its usefulness in the examination of the equine patient has not been demonstrated.

The equine stomach is recognized by its large semicircular curvilinear echo medial to the spleen at the level of the splenic vein and caudal to the liver (Fig. 6–15). The wall thickness of the stomach can range up to 7.5 mm in the adult horse. The stomach echo may be hyperechoic with acoustic shadowing owing to the gas present along its inner mucosal surface (gas pattern), echogenic without acoustic shadowing owing to mucus adjacent to the gastric mucosa (mucous pattern), or anechoic owing to fluid adjacent to the gastric mucosa (fluid pattern).[21, 22, 28] The gastric serosa and subserosa are more hyperechoic in human beings because relatively more fibrous connective tissue is present within these layers. Solid feed material is rarely imaged in the horse's stomach. The gas echo along the mucosal surface of the stomach usually prevents visualization of the other gastric contents.

The small intestine has a characteristic sonographic appearance and is easily differentiated from large bowel. Peristaltic activity in the equine small intestine is described as rhythmic contractions causing a change in lumen size or as motion of two opposing serosal surfaces.[3] The duodenum and jejunum have thin walls that rarely exceed 3 mm in thickness, whereas the ileum is slightly thicker (4 to 5 mm). The duodenum normally has a fairly fluidly ingesta that moves through the lumen in a pulsatile fashion. The duodenum often appears fairly collapsed until a wave of ingesta moves through the lumen (Fig. 6–16). The duodenum can be found along the caudal and medial margin of the right lobe of the liver in the cranial to mid portion of the right side of the

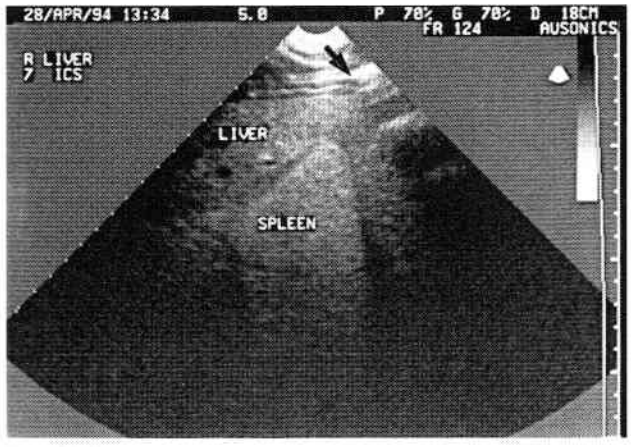

Figure 6–14

Sonogram of the right cranioventral abdomen obtained from a 4-year-old Thoroughbred gelding demonstrating the cranial pole of the spleen adjacent to the right lobe of the liver. The echogenicity of the cranial pole of the spleen and the liver are similar in this view, with the spleen appearing only slightly more echogenic. The liver is recognized by the small vessels imaged within the hepatic parenchyma. The hyperechoic structure casting a reverberation artifact (*arrow*) is the right ventral lung. This sonogram was obtained with a 5.0-MHz sector-scanner transducer at a displayed depth of 18 cm. The right side of this sonogram is dorsal and the left side is ventral.

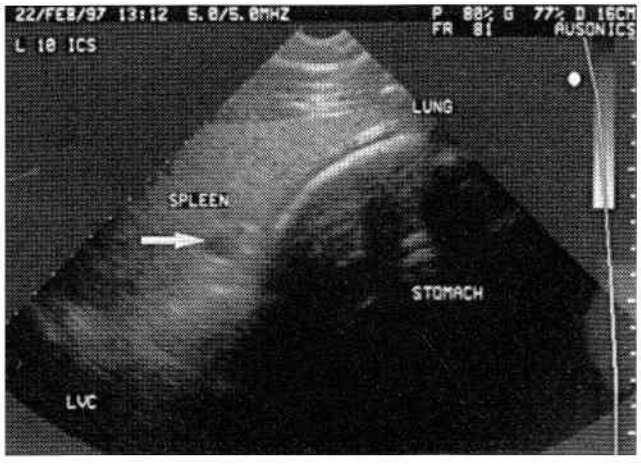

Figure 6–15

Sonogram of the stomach adjacent to the splenic vein obtained from a 2-year-old Quarter horse filly. The stomach is recognized by its large hyperechoic curvilinear appearance, lack of sacculations, and location adjacent to the splenic vein (*arrow*). The spleen appears homogeneously echogenic. The ventral tip of the left lung is just visible on the far right side of the sonogram. Medial to the spleen is the left ventral colon (LVC). This sonogram was obtained from the left tenth intercostal space with a wide-bandwidth 5.0-MHz sector-scanner transducer operating at a frequency of 5.0 MHz at a displayed depth of 16 cm. The right side of this sonogram is dorsal and the left side is ventral.

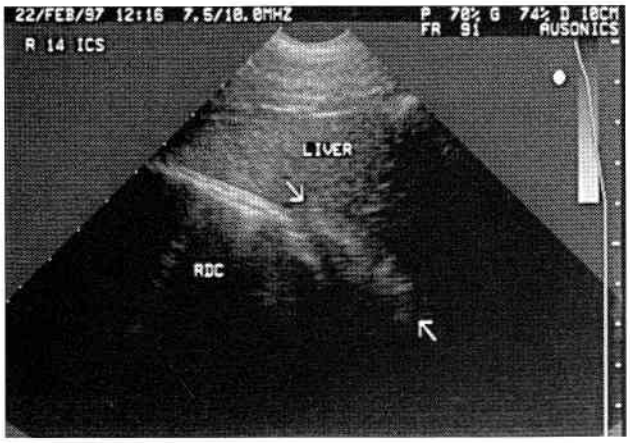

Figure 6–16

Sonogram of the duodenum medial to the right lobe of the liver obtained from a 2-year-old Thoroughbred colt in the scan plane illustrated in Fig. 6-5. The duodenum (*arrows*) is recognized by its oval shape, with a hyperechoic center and relatively hypoechoic wall. The duodenum is collapsed in this image, but ingesta can be imaged moving through the duodenum with periodic duodenal contractions. The right dorsal colon (RDC) is medial to the liver and duodenum at this location. The hyperechoic structure at the upper right edge of the sonogram casting a clean acoustic shadow is the edge of the rib. This sonogram was obtained in the right fourteenth intercostal space with a wide-bandwidth 7.5-MHz sector-scanner transducer operating at a frequency of 10.0 MHz at a displayed depth of 10 cm. The right side of this sonogram is dorsal and the left side is ventral.

abdomen. The duodenum can be followed caudodorsally around the caudal pole of the right kidney, where it lies lateral to the base of the cecum. In starved horses (fasted for 36 hours) the nondistended duodenum was not continuously imaged because of excessive large bowel distention and movement.[8] The lung and the more medial location of the duodenum interfere with its detection in the more cranial portions of the equine abdomen.

The duodenum normally appears flattened, except when a wave of ingesta passes through it, giving the duodenum an oval to round shape. A completely round duodenum with a centralized star shape was reportedly imaged during circular contraction phases.[8] This sonographic appearance was created by the mucosal invaginations of the duodenum. Circular distentions of the duodenum were rarely imaged owing to the compressive effects of the adjacent large bowel. The diameter of the duodenum during the circular contraction phase did not exceed 16.2 ± 4 mm for normal adult horses fed concentrate or hay rations or for starved horses.[8] The number of circular contractions ranged between 2.2 ± 1.2 and 2.5 ± 1.1 per minute for the concentrate and hay groups, respectively, to 0.4 ± 0.5 per minute for the starved horses.[8] The duodenal diameters during the distention phase did not exceed 33 ± 6.6 mm for normal adult horses fed concentrate or hay or for starved horses. The distention phase varied from 0.5 to 5 seconds. The number of duodenal distentions varied from 2.6 ± 1.4 and 2.8 ± 1.0 per minute in the concentrate and hay-fed horses to 0.9 ± 0.2 per minute in the starved horses. Although the differences between fed and starved horses were not significantly different when comparing the number of duodenal distentions and contractions, in three starved horses the duodenum could not be consistently visualized. However, when the duodenum was well visualized there were markedly fewer contractions and distentions in the starved horses than in the fed groups of horses.[8] Contractions of the duodenum appear to decrease when no ingesta is present. The movement of ingesta was aboral in the majority of horses studied.[8]

The jejunum is not normally imaged but if detected is usually rounder and contains a more fluid-filled ingesta than that present in the duodenum. The normal small intestine usually contains only a small amount of luminal contents. Periodic waves of ingesta are imaged rhythmically traversing the intestinal lumen.[3] Small intestine can occasionally be imaged transrectally in normal horses and appears as a small tubular structure approximately 2 cm in diameter with thin, hypoechoic walls and heterogeneously echogenic fluid in the lumen.[19] The ileum, if imaged, has a thicker muscular layer and a similar appearance of the contained ingesta. The large colon and cecum are recognized by their larger size and sacculated appearance (Fig. 6-17) and have a similar wall thickness to the jejunum. The large bowel is usually hyperechoic along its mucosal surface owing to the gas contained within; therefore, the ingesta is not normally imaged. The small colon is smaller in size (7 to 10 cm in diameter) but has a sacculated appearance similar to that of the large bowel and usually has a hyperechoic mucosal surface. Formed fecal balls may be imaged in the small colon as echogenic luminal masses. The small colon is located in the left caudodorsal abdominal quadrant.[15] Only a small amount of peritoneal fluid or none at all is imaged in the abdomen of the normal horse.

Five layers of the bowel wall may be imaged if a high-frequency transducer with excellent resolution is used. These layers are not normally imaged with transcutaneous ultrasound in horses with normal intestine. However, the five layers of the bowel wall may be imaged with a high-frequency transducer used transrectally or in thin, sonolucent patients. The ability to image these various

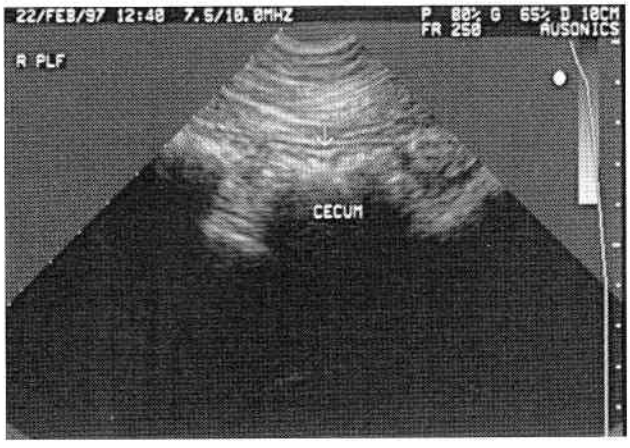

Figure 6–17

Sonogram of the cecum obtained from a 2-year-old Thoroughbred colt. Notice the sacculated appearance of the wall of the cecum (*arrow*) against the right abdominal wall. This sonogram was obtained in the right paralumbar fossa with a 7.5-MHz sector-scanner transducer operating at a frequency of 10.0 MHz at a displayed depth of 10 cm. The right side of this sonogram is dorsal and the left side is ventral.

layers of the bowel depends upon the echogenicity of the luminal contents and the surrounding structures. The layers include a hyperechoic outer serosal surface, a hypoechoic muscularis, a hyperechoic submucosa, a hypoechoic mucosa, and an inner hyperechoic mucosal surface.[8, 29] In the normal equine duodenum, each layer is 1 mm or less in thickness, with a total wall thickness of 3 to 4 mm.[8] The mucosa, submucosa, and muscularis are most readily imaged in normal equine duodenum.[8] Similar layers have been imaged in the intestinal walls of dogs and humans.[21, 22, 28] In normal distended duodenum in the adult horse, the mucosal folds disappear and the wall thickness decreases to 2 mm.[8] Similarly, in humans the wall thickness normally decreases with bowel distention.[32] In the ileum, an additional thinner hyperechoic line is visible in the center of the muscular layer and corresponds to the connective tissue separating the longitudinal and circular muscular layers.[29] The mucosal surface is hyperechoic owing to the multiple reflectors caused by the folding of the epithelial lining[26] and the trapping of gas on the mucosal surface.[29] The more tightly packed the mucosal folds are, the higher the echogenicity of the mucosal surface of the intestine. With high-frequency ultrasound in humans, it has been demonstrated that the interface between the submucosa and muscularis is echogenic, but the submucosa itself, composed of numerous blood vessels and loose connective tissue, is hypoechoic.[26] The muscularis is hypoechoic throughout the gastrointestinal tract in humans.[26] In normal bowel these layers are differentiated only with high-frequency (20 MHz) endoluminal ultrasound and are not routinely imaged with transcutaneous ultrasound.[26] The different layers of the intestinal wall are, however, usually visualized in patients (human, equine, or canine) with inflamed, edematous, or congested bowel or with hypoproteinemia.

Several patterns (mucus, fluid, and gas) have been described in the bowel of humans, dogs, and horses.[8, 27, 33] These patterns depend upon the type of intraluminal contents in the bowel. The mucous pattern is seen when the imaged bowel has a hyperechoic lumen without distal acoustic shadowing. This sonographic appearance is created by mucus and trapped gas along the mucosal surface of the empty and collapsed bowel. The fluid pattern occurs when the imaged bowel has sonolucent intraluminal contents. The detection of echogenic intraluminal contents with distal acoustic shadowing is typical of the gas pattern. The gas pattern may consist of high- or low-intensity reverberation artifacts, creating clean or dirty acoustic shadows, or have a more mottled appearance. In the equine duodenum, the mucous phase was most frequently imaged in horses fed hay or concentrate, during the static phase, changing to a gas pattern with low-intensity dirty shadowing during duodenal distention.[8] In starved horses the duodenal content during distention was primarily a fluid pattern with a few echogenic flecks imaged within the fluid. This pattern was replaced by a mucous pattern in these horses when imaged over longer periods of time. The gas pattern was rarely imaged in the equine duodenum.[8] The large bowel and cecum typically had a gas pattern in the fed horses but a fluid pattern containing multiple echogenic specks, and occasional free gas caps were imaged in the right dorsal colon and, less frequently, the cecum in starved horses.[8] Although the gas pattern, when detected in the equine bowel, may obscure lesions in the medial wall of the bowel, peristaltic activity and the resultant changing of the bowel patterns should enable imaging of this area over time in the majority of horses.

Abnormal Findings

The most important aspect of diagnosing abdominal pathology in the horse is a thorough understanding of ultrasonographic anatomy. The relationship of the gastrointestinal viscera, abdominal organs, and vessels to one another is critically important in arriving at a correct diagnosis or list of differential diagnoses. If a mass or an unknown structure is detected in the abdomen, the ultrasonographic evaluation of this structure should be performed in a systematic fashion. The origin, size, shape, vascularity, and sonographic character of the mass or structure should be determined, along with its relationship to contiguous organs, blood vessels, and other structures in a reproducible fashion. This information can then be used to evaluate the progression of the disease and the efficacy of treatment selected.

Abnormalities of the Urinary Bladder and Urethra

Sonographic examination of the urinary bladder should be performed in horses with clinical signs of lower urinary tract disease (hematuria, pyuria, dysuria, and stranguria), in horses in which the urinary bladder is difficult to catheterize, and in horses with hydroureter and hydronephrosis. Ultrasound can also be used to verify the correct placement of a Foley catheter within the bladder in horses requiring long-term urinary bladder catheterization. The Foley catheter appears as an echogenic double-walled tubular structure with an anechoic fluid-filled balloon. The distended urinary bladder can also serve as a window for sonographic examination of the structures in the ventral portion of the caudal abdomen immediately cranial to the pelvis from a transrectal window. In the adult horse it is rare for the distended urinary bladder to serve as a window for sonographic examination of the structures in the dorsal portion of the caudal abdomen using a ventral transcutaneous window because of the depth limitations and the inability to consistently image the bladder from this window.

Cystitis/Atonic Bladder. Cystitis is an uncommon problem in horses that causes dysuria, stranguria, and pollakiuria. Urinary scalding is frequently present in affected mares. Diffuse thickening of the bladder wall is the most common sonographic abnormality detected in affected horses.[2] Focal bladder wall thickening and irregularity of the wall of the urinary bladder may be detected occasionally in affected horses (Fig. 6-18). The urine imaged is usually echogenic to hyperechoic. Layering of the urine may occur with severe pyuria because the cellular debris settles to the more ventral aspects of the urinary bladder. Fibrin strands may also be imaged in the

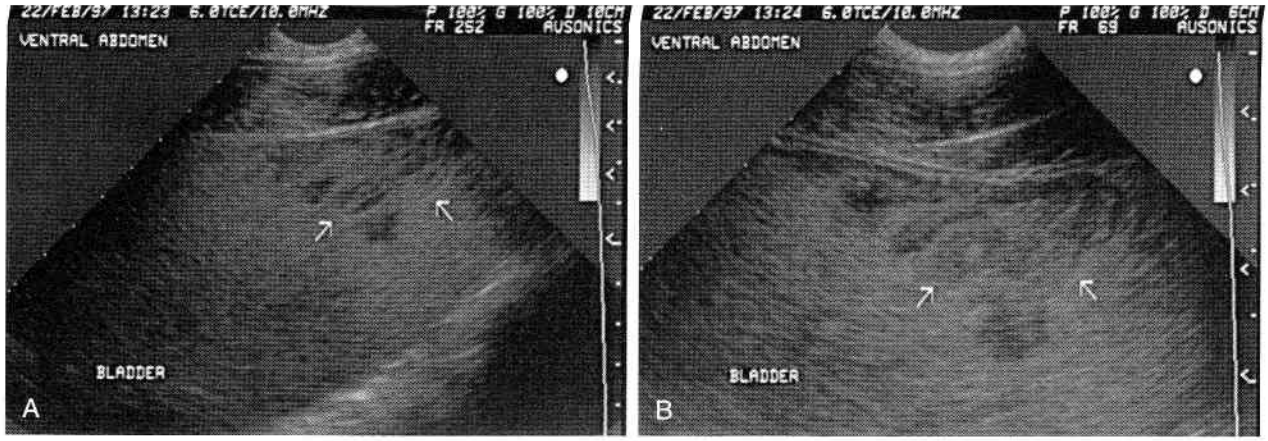

Figure 6–18

Sonograms of the bladder obtained from a 2-year-old Quarter horse filly with hematuria. Notice the echogenic urine surrounding the hypoechoic mucosal folds (*arrows*) protruding into the lumen from ventral aspect of the urinary bladder. These sonograms were obtained from the ventral abdomen just cranial to the brim of the pelvis with a wide-bandwidth 6.0-MHz microconvex linear-array transducer operating at a frequency of 10.0 MHz at a displayed depth of 10 (*A*) and 6 (*B*) cm. The right side of these sonograms is caudal and the left side is cranial. *A*, The caudal aspect of the urinary bladder with the dorsal wall of the urinary bladder and overlying large colon visible. *B*, The displayed depth is decreased to enlarge the image of the abnormal mucosal folds detected in the ventral wall of the urinary bladder.

bladder in a horse with severe cystitis. One stallion with chronic cystitis and a history of dribbling urine had a markedly thickened bladder wall detected sonographically. These sonographic findings correlated with a moderate infiltration of lymphocytes, plasma cells, and neutrophils in the wall of the urinary bladder at postmortem examination.[34]

Bladder atony is common with some neurologic diseases in the horse and may be associated with urinary incontinence. Cauda equina neuritis; equine herpes virus-1 myeloencephalitis; the sorghum ataxia-cystitis complex; and traumatic, inflammatory, or neoplastic diseases of the spinal cord or peripheral nerves can cause urinary bladder paralysis.[35] Urinary bladder paralysis has also been reported in some horses in the absence of other neurologic signs.[35, 36] Large amounts of sabulous material have been reported in the urinary bladder of horses with bladder atony.[2, 35, 36] In these horses the sabulous calculous material was semisolid sedimented sludge composed of calcium carbonate. Sonographic appearance of the urinary bladder in horses with bladder atony usually reveals a markedly distended urinary bladder with echogenic urine and hyperechoic sludge accumulating ventrally in the bladder (Fig. 6-19).[2] The wall of the urinary bladder is usually normal in these horses unless a concurrent cystitis is present.

Cystic Calculi. Urinary tract calculi are most commonly found in the urinary bladder and are less frequently detected in the urethra, ureter, or kidney. In one large study of 68 horses with urolithiasis, 47 horses had cystic calculi, 11 horses had urethral calculi, 15 horses had renal calculi, and 2 horses had ureteral calculi.[37] The calculi were in more than one location in 6 horses. In 2 horses they were present in the urethra and the bladder, in 1 horse in the bladder and both kidneys, and in 1 horse in the bladder, both ureters, and both kidneys. These horses ranged in age from 7 months to 27 years with a mean age of 10.2 ± 6.5 years.

The majority of horses with cystic calculi are male.[36–40] Most horses present with hematuria that is often exercise induced, tenesmus, and altered micturition (pollakiuria, incontinence, and dysuria).[36–42] Colic, reluctance to exercise, penile protrusion, and hindquarter stiffness have also been reported.[36, 38–40, 43] Urine culture may be positive in affected horses and should be performed, although the cause of the cystitis has often been thought to be traumatic.[40] However, cultures of the centers of the calculi were positive in 19 of 30 horses with uroliths, although only 2 horses had positive urine cultures. Both of these positive cultures were from horses with cystic calculi.[37] Urinalysis revealed proteinuria in all horses with cystic calculi. Hematuria and pyuria were most common in horses with calculi in the lower urinary tract.[37] Rectal

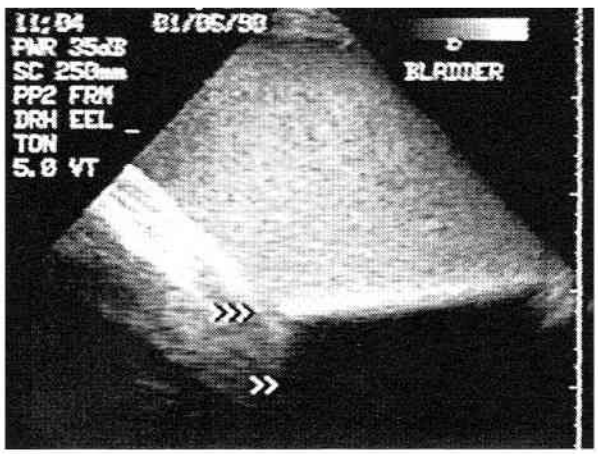

Figure 6–19

Sonogram of the urinary bladder obtained from a 10-year-old Warmblood gelding with bladder atony and sabulous calculi (*triple arrowhead*). The ventral aspect of the urinary bladder is filled with hyperechoic sludgy material casting a strong acoustic shadow (*double arrowhead*), consistent with sabulous calculi. This sonogram was obtained from a transrectal window with a 5.0-MHz sector-scanner transducer with an off-line beam orientation at a displayed depth of 25 cm. The right side of this sonogram is cranial and the left side is caudal.

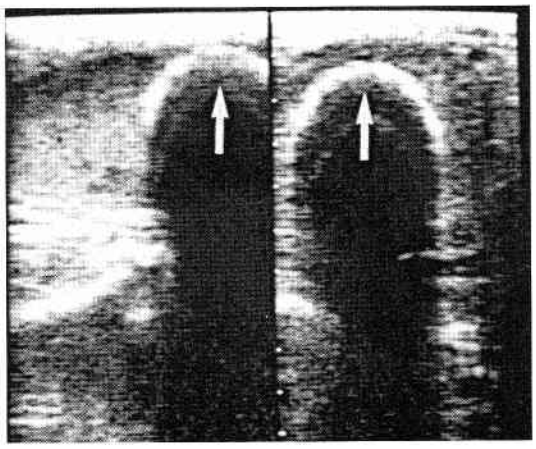

Figure 6–20

Sonogram of the urinary bladder obtained from a 16-year-old Thoroughbred gelding with a cystic calculus. The cystic calculus is the bright hyperechoic curved structure (*arrows*) casting the strong acoustic shadow surrounded by echogenic urine. The left image was obtained near the trigone region of the urinary bladder, demonstrating the calculus embedded in the mucosa and the narrowing of the bladder neck in the trigone region. The right image was obtained slightly more cranially, centered over the cystic calculus. The urine surrounding the calculus is echogenic, which is normal in adult horses. These sonograms were obtained with a 5.0-MHz linear-array transducer at a displayed depth of 12 cm. The right side of these sonograms is cranial and the left side is caudal.

palpation of the urinary bladder reveals a hard mass attached to the bladder wall or freely moveable within the lumen. The calculi embedded in the mucosa of the urinary bladder are usually firmly attached in the trigone region and therefore are usually in an intrapelvic location. The entire bladder and pelvic urethra should be carefully palpated and examined sonographically in horses with clinical signs suggestive of urolithiasis so that the calculi located in the trigone region or urethra are not accidentally missed.

Cystic calculi are easy to image with transrectal ultrasonography. The calculi are large hyperechoic structures casting a strong acoustic shadow. The acoustic shadow begins at the near side of the calculus and extends through the deeper structures (Fig. 6–20). In most horses only one large cystic calculus is present, usually 5 cm or greater in diameter. The urinary bladder wall often appears thickened. With an experienced sonographer and transrectal placement of the ultrasound transducer over all aspects of the urinary bladder, including the trigone region, cystic calculi should not be missed sonographically. The transrectal ultrasonographic detection of cystic calculi have been reported.[2, 19, 41, 42, 44] In one horse, multiple smaller uroliths were imaged in addition to the large cystic calculus, and the bladder wall was thickened.[41] In another horse a thickened urinary bladder wall, a large (10 cm) calculus, and dilated (2 cm) ureters were imaged with transrectal ultrasonography.[42] The cystic calculus is usually located in the trigone region of the urinary bladder and has a rough, somewhat irregular surface typical of the calcium carbonate calculus. These calculi are often embedded in the urinary bladder mucosa and fill the entire bladder lumen in the trigone region. Freely moveable calcium carbonate calculi have also been reported.[35, 41] The calcium oxalate calculus is usually free in the urinary bladder and is usually found in the ventral most portion of the urinary bladder at the apex, surrounded by urine. Urate calculi have also been reported and are more brittle than calcium phosphate calculi.[45] The urate calculi are also firmly attached to the urinary bladder mucosa, similar to the calcium carbonate calculi. Hyperechoic sandy debris is often also imaged in the ventral most portion of the urinary bladder in affected horses. Sonographic examination of the bladder yields information about the urinary bladder wall and the presence of other smaller calculi or sandy debris, in addition to confirming the diagnosis made usually on rectal examination.

Marked ureteral distention (Fig. 6–21) and moderate hydronephrosis were detected sonographically in one horse with a large cystic calculus. This combination of sonographic findings in a horse with a cystic calculus has been previously reported.[42] Ureteral distention was reported in one pony with a cystic calculus that was not completely obstructing urine flow.[44] Although primary renal disease is uncommon in horses with cystic calculi, hydronephrosis, nephrolithiasis, and a renal abscess have been reported in horses with cystic calculi.[36, 37, 40] Urethral calculi have also been reported in horses with cystic calculi and have led to uroperitoneum and a ruptured bladder in two horses.[37] In this study 9% of horses had calculi in multiple locations.[37] Therefore, a complete sonographic examination of the entire urinary tract is indicated in a horse with cystic calculi to determine if other urinary tract structures are involved.

Urethral Calculi. Horses with urethral calculi usually present with a history of colic and straining to urinate.[37, 42, 46–49] Percutaneous palpation of the urethral calculus is usually possible and has been successful in locating the calculus in the majority of horses.[37, 46] In 8 male horses with urethral obstruction, the urethral calculi were identi-

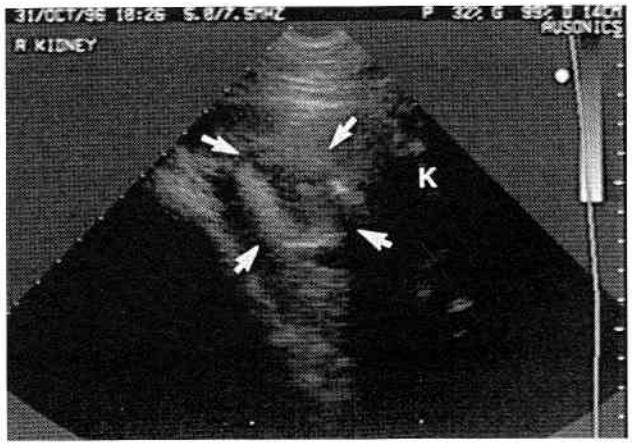

Figure 6–21

Sonogram of a distended right ureter obtained from a 10-year-old Warmblood gelding with a cystic calculus. Notice the enlarged ureter (*arrows*) containing hyperechoic debris adjacent to the right kidney (K). This sonogram was obtained from the right seventeenth intercostal space with a wide-bandwidth 5.0-MHz sector-scanner transducer operating at 7.5 MHz at a displayed depth of 14 cm. The right side of this sonogram is dorsal and the left side is ventral.

fied on direct percutaneous palpation in 5 horses, with passage of the urinary catheter in 2 horses, and at the time of urethroscopy in 1 horse.[37] Proteinuria was present in all horses with urethral calculi. Microscopic hematuria and pyuria were most common in horses with calculi in the lower urinary tract.[37] Cellular or proteinaceous debris secondary to infection is the most likely cause of urethral calculus formation. A ruptured urinary bladder is more likely in horses with urethral calculi and urethral obstruction than with calculi in other portions of the urinary tract. Uroperitoneum and urinary bladder rupture secondary to urethral obstruction have been reported in male horses with urethral obstruction.[37, 46, 48, 49] In one report of horses with urethral calculi, 4 of 5 horses died and had a necrotic and/or ruptured bladder detected at postmortem examination.[46] In a more recent report, 4 of 11 horses with urethral calculi had a ruptured bladder secondary to urethral obstruction.[37]

Sonographic examination of the perineal and intrapelvic portions of the urethra was recommended for horses with suspected urethral obstruction as early as 1986.[3] The typical sonographic appearance of a urethral calculus is a hyperechoic concretion casting an acoustic shadow wedged in the lumen of the urethra. Fluid distention is detected proximal to the urolith. A urolith was imaged causing obstruction of the penile urethra in a yearling 10 months after laproscopic repair of a ruptured bladder.[50] Staples had been used to close the defect in the urinary bladder and may have been the nidus for calculus formation. Videoendoscopic examination of the urinary bladder revealed ulceration in the region of the staple line. Ultrasonographic examination of the upper and lower urinary tract is useful in identifying the location of urinary calculi in horses with urolithiasis.[37] One urethral calculus was imaged transrectally in one horse, but transcutaneous examination of the penile and perineal urethra was not performed in any of the affected horses.

Urinary calculi must be 3 to 4 mm in diameter to be routinely detected sonographically in sheep.[51] The urethral calculi obstructing horses are usually much larger because the diameter of their urethra is larger. In male sheep and goats with urethral obstruction, sonographic examination has confirmed the obstruction, localized the site of the obstruction, and characterized the associated abnormalities of the urinary bladder, ureters, and kidneys.[51, 52] Associated abnormalities of the urinary tract in sheep and goats with urethral obstruction included ureteral rupture and bladder rupture, resulting in uroperitoneum[51] and urethral rupture.[52] A complete sonographic evaluation of the entire urinary tract is indicated in horses with urolithiasis to investigate possible sites of calculus formation and/or infection, to assess the integrity of the urethra, bladder, ureters, and kidneys, and to look for hydroureter and hydronephrosis that may develop secondary to the urethral obstruction or to calculi elsewhere in the urinary tract.

Ruptured Bladder and Uroperitoneum. Ruptured bladder and uroperitoneum are rare in the adult horse, reported most frequently in the postpartum mare.[3, 53-56] Foaling injuries can also result in prolapse or eversion of the urinary bladder.[53, 57, 58] Urethral obstruction in males associated with a urethral calculus (more common) or a hematoma of the corpus spongiosum (rare) can also lead to urinary bladder rupture.[37, 46, 48, 59] Rupture through the scar at the site of a previously repaired tear in the neonatal urinary bladder has also been reported.[60] The rapid identification of the horse with a ruptured bladder and uroperitoneum can be performed ultrasonographically and the site located for surgical repair.[2, 16] Although the injection of new methylene blue, fluorescein, or azosulfamide into the urinary bladder and subsequent retrieval of peritoneal fluid containing dye can be used to confirm the diagnosis of uroperitoneum, this technique is time consuming and does not localize the defect for subsequent surgical repair.[16]

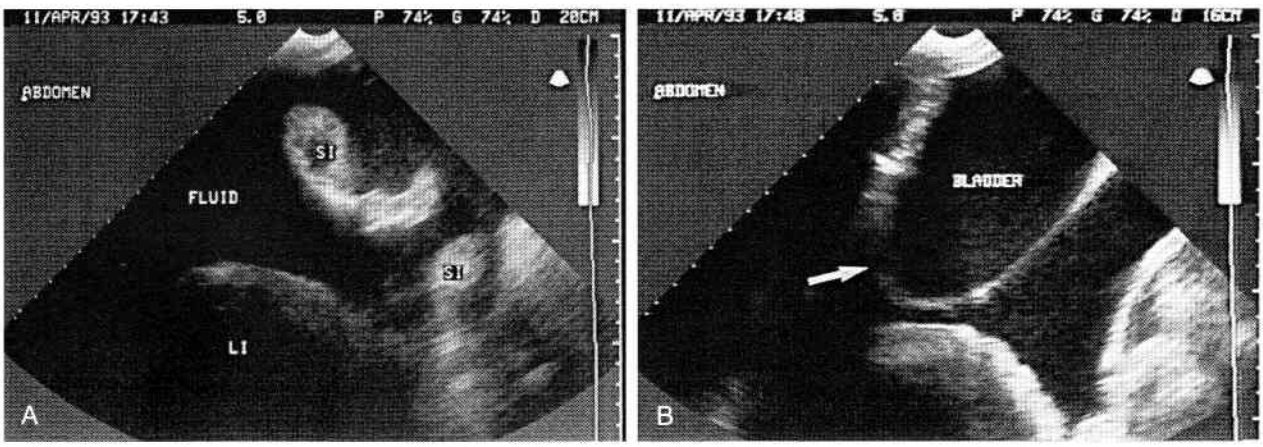

Figure 6–22

Sonogram of the abdomen (*A*) and urinary bladder (*B*) obtained from a 12-year-old recently postpartum Thoroughbred mare with uroperitoneum. These sonograms were obtained from the ventral abdominal window (*A*) and right paralumbar fossa (*B*) with a 5.0-MHz sector-scanner transducer at a displayed depth of 20 cm (*A*) and 16 cm (*B*). *A*, A large amount of anechoic fluid is present in the peritoneal cavity, and the jejunum (SI) and large intestine (LI) are floating in the fluid. The small intestine is recognized as jejunum because of its long mesentery. The right side of this sonogram is cranial and the left side is caudal. *B*, The bladder is imaged along the right body wall floating in the anechoic fluid within the peritoneal cavity. The actual defect in the ventral portion of the apex of the bladder is not clearly imaged from this view but is suggested by the thickened ventral wall of the bladder with loss of the bladder margins (*arrow*). The two echogenic thickenings in the wall of the bladder represent the remnants of the umbilical arteries. The right side of this sonogram is dorsal and the left side is ventral.

The horses with uroperitoneum are usually depressed and lethargic with a progressively distending abdomen.[16, 46, 48, 53, 54, 56, 60] Affected horses typically have pollakiuria, with small amounts of urine produced frequently.[16, 53, 54, 60] Many horses have ileus, decreased fecal production, and abdominal pain.[53, 54, 56, 60] Ballotment of the abdomen may reveal a fluid wave.[53-55, 60] The urinary bladder is often not palpable on rectal examination.[60]

The urinary bladder or ureter may be ruptured. Uroperitoneum is most commonly associated with a defect in the wall of the urinary bladder.[2, 16, 53, 54, 56] Ureteral defects are rare unless associated with ureteral calculi.[16] Horses with uroperitoneum are usually hyponatremic, hypochloremic, hyperkalemic, azotemic, and hyperosmolar, and have a metabolic acidosis.[53, 61] A peritoneal fluid creatinine that is more than twice the serum creatinine is considered diagnostic for ruptured bladder.[48, 49, 53-56, 60, 61] Cytologic evaluation of the peritoneal fluid may reveal a secondary peritonitis and sepsis, a secondary complication in affected horses.[37, 46, 53, 61] A secondary peritonitis associated with bladder rupture is more common in adult horses than in neonates, possibly owing to the increased likelihood of urinary tract infection in the adult horse with ruptured bladder.[49] Peritonitis has also been reported in one horse with a necrotic urinary bladder without uroperitoneum.[58]

With uroperitoneum the peritoneal cavity is filled with fluid and the gastrointestinal viscera are imaged floating in and on top of the fluid (Fig. 6-22).[2, 3, 16] The peritoneal fluid may become hypoechoic and contain strands of fibrin if a secondary peritonitis develops[2, 3, 16] or may have increased echogenicity associated with a concurrent cystitis. The urinary bladder is also imaged floating within the fluid (Fig. 6-22). If the urinary bladder is ruptured, the bladder usually appears collapsed, flaccid, and folded upon itself and containing little or no fluid.[2, 16] The defect itself may not be directly imaged during the sonographic examination.[2, 3, 16] In some affected horses, fluid may be imaged passing through the rent in the bladder wall from a partially filled urinary bladder into the peritoneal cavity (Fig. 6-23).[2, 3, 16] The collapsed and folded appearance of the urinary bladder should not be mistaken for a recently voided or empty bladder, which is small and contracted but does not appear folded upon itself. A diverticulum in the urinary bladder was detected 18 months following conservative treatment of uroperitoneum in a horse with a necrotic bladder, secondary to a urethral obstruction.[49] The urethra should be evaluated sonographically if urethral obstruction is suspected as the cause of the uroperitoneum.

The most difficult defect to diagnose sonographically is the ureteral defect because the ureters are not normally visible throughout their length. These horses have a normal fluid-filled urinary bladder with a large amount of free fluid in the peritoneal cavity.[16, 62, 63] Sonographic evaluation of the kidneys should be performed because retroperitoneal fluid (urine) may be imaged surrounding the kidney in horses with a ruptured ureter.[16, 62, 63]

Bladder Neoplasia. Neoplasia of the urinary bladder is uncommon in the horse, squamous cell carcinoma being the most commonly reported tumor.[64] Transitional cell carcinomas, lymphosarcoma, and a fibromatous polyp have also been reported.[64-66] Affected horses are usually over 10 years of age, but bladder neoplasia has been reported in a horse as young as 3 years old.[64] Clinical signs of stranguria, pollakiuria, hematuria (including the passage of clotted blood with urination), weight loss, and depression have been reported in affected horses.[64, 66] Proteinuria, hematuria, leukocyturia, and a moderate nonregenerative anemia are usually detected in horses with bladder neoplasia. In one review of horses with bladder neoplasia, only two of six had positive urine cultures, and one horse had neoplastic cells detected on cytologic analysis of the urine.[64] The urine sediment and peritoneal fluid of a horse with lymphosarcoma involving the urinary bladder contained neoplastic lymphocytes.[66] Rectal palpation reveals a fleshy mass within the urinary bladder or a thickened wall of the urinary bladder. Additional abdominal masses were palpated rectally in two of six horses in one review.[64] Extension of bladder tumors in horses appears to be primarily from direct invasion of the adjacent structures. Cystoscopic examination of the urinary bladder revealed the corrugated thickened mucosa with localized ulceration in the horse with lymphosarcoma, necrotic mucosa with multiple fibrin tags and blood clots in one mare with transitional cell carcinoma, and the presence of the tumor in five of six horses with bladder neoplasia of other causes.[64-66] A biopsy in four of the five horses was diagnostic of neoplasia.[64] Hydronephrosis, hydroureter, and pyelonephritis may be observed

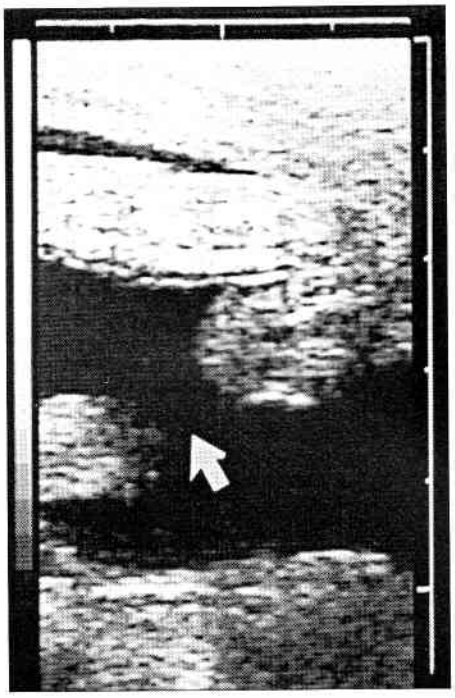

Figure 6-23

Sonogram of the defect in the ventral wall of the bladder (*arrow*) obtained transrectally in a 12-year-old Thoroughbred mare (same horse as in Fig. 6-22) with uroperitoneum. The defect was located in the ventral portion of the bladder near the bladder apex. In real time, fluid was imaged moving through this defect into the peritoneal cavity. This sonogram was obtained with a 5.0-MHz linear-array transducer at a displayed depth of 10 cm. The right side of the sonogram is cranial and the left side is caudal.

when the tumor masses obstruct the ureter or urethra.[64, 66] Three of six horses with bladder neoplasia had pyelonephritis at postmortem examination.[64] Two of six horses had hydronephrosis, and one of these two horses also had pyelonephritis.[64] One horse with pyelonephritis also had a necrotizing cystitis detected at postmortem examination.

A squamous cell carcinoma of the urinary bladder was detected sonographically in one horse (Fig. 6-24). The mass was irregular in shape, had a heterogeneous appearance with composite echogenicities, and involved both the dorsal and ventral walls of the urinary bladder. Portions of the bladder appeared sonographically normal. As with squamous cell carcinomas elsewhere, metastases were seen in this horse. Sonographic examination of a horse with a transitional cell carcinoma revealed an irregular mass protruding into the bladder lumen with a composite pattern of echogenicity. An abrupt demarcation between the affected and unaffected portions of the urinary bladder was seen. Metastases to the abdominal organs are common in horses with transitional call carcinomas of the urinary bladder. Sonographic evaluation of the right side of the abdomen with static B-mode ultrasound in the horse with transitional cell carcinoma revealed a 4- to 6-cm mass medial to the right kidney and multiple masses on the diaphragmatic surface on both sides of the abdomen, consistent with tumor metastases.[65] A transrectal examination of the pelvic mass was not possible with this ultrasound technology, and thus the pelvic mass was not imaged. Metastases to the peritoneum, serosal surfaces of the abdominal organs, and omentum and a large composite abdominal effusion have been described in one horse with transitional cell carcinoma.[4]

Sonographic examination of the pelvic canal in the horse with lymphosarcoma revealed a homogeneous soft-tissue density mass with thickening of the walls of the urinary bladder and vagina.[66] Distention of the right ureter, enlargement of the right kidney, loss of the normal renal architecture, and increased lobulation were also detected sonographically. The left kidney was normal ultrasonographically. Postmortem examination revealed a large neoplastic pelvic mass that infiltrated the bladder, vagina, uterus, and broad ligament and enlargement of the right kidney and right ureter secondary to chronic ureteral obstruction from the neoplasm.

Ultrasound examination of the urinary bladder via the transrectal window has been successful in identifying the neoplastic bladder mass in several horses (Fig. 6-24). The neoplastic bladder mass usually appears as a composite mass or masses protruding into the lumen of the bladder,[2] although involvement of the urinary bladder from direct extension of the tumor from adjacent structures can occur, as seen in the horse with lymphosarcoma involving the urinary bladder. Sonographic examination of the urinary bladder in horses with suspected urinary bladder neoplasia can determine the presence, location, and extent of involvement of the urinary bladder. Sonographic examination of the urethra should be performed routinely in all horses with urinary bladder masses to determine if urethral involvement is present. Sonographic examination of both kidneys and the ureters (if visible) should be performed to determine if hydroureter, hydronephrosis, and/or pyelonephritis is present secondary to lower urinary tract obstruction. The abdominal and pelvic structures surrounding the urethra, urinary bladder, ureters, and kidneys should also be examined sonographically for extension of the tumor into the surrounding structures or tumor metastases.

Sonographic examination of the urinary bladder in dogs with transitional cell carcinoma revealed the tumor in all affected dogs, most frequently in the trigone region or dorsal wall of the bladder.[67] In most affected dogs the transition between the tumor mass and the normal bladder mucosa was abrupt. The echogenicity of the tumor mass was usually complex and hypoechoic or isoechoic compared with the bladder wall, although hyperechoic masses were also detected. Hydronephrosis and hydroureter were detected sonographically in the dogs (20%) with ureteral obstruction secondary to the bladder mass. The size of the bladder lesion influences the rate of sonographic detection of the mass. In dogs, lesions 3 mm or greater can be detected with a moderately distended urinary bladder.[67] In humans, the sonographic detection rate is 95% for tumors larger than 2 cm, 83% for tumors larger than 1 cm, and 33% for tumors less than 0.5 cm.[68]

Blood clots may mimic the sonographic appearance of a bladder tumor but should move with palpation of the urinary bladder.[67] Humans with cystitis usually show a gradual transition from normal to edematous mucosa, the mucosal surface of the bladder is usually smoother, and the wall of the urinary bladder is less echogenic than in those with urinary bladder neoplasia.[69] The detection of a pedunculated mass is most consistent with a diagnosis of polypoid cystitis,[67] a rare finding in horses. A suture reaction from previous surgery on the urinary bladder may mimic a tumor of the urinary bladder, a problem reported in humans.[70]

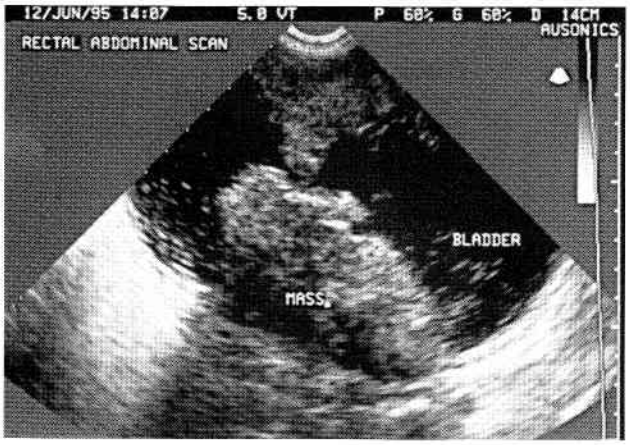

Figure 6-24

Sonogram of the bladder obtained from a 24-year-old Standardbred stallion with a squamous cell carcinoma (mass) of the urinary bladder. The bladder mass has a hyperechoic heterogeneous appearance with irregular margins. Portions of the bladder wall are unaffected, but the tumor involves both the dorsal and ventral walls of the bladder. This sonogram was obtained from the transrectal window with a 5.0-MHz sector-scanner transducer with an off-line beam orientation at a displayed depth of 14 cm. The right side of the sonogram is the left side of the urinary bladder.

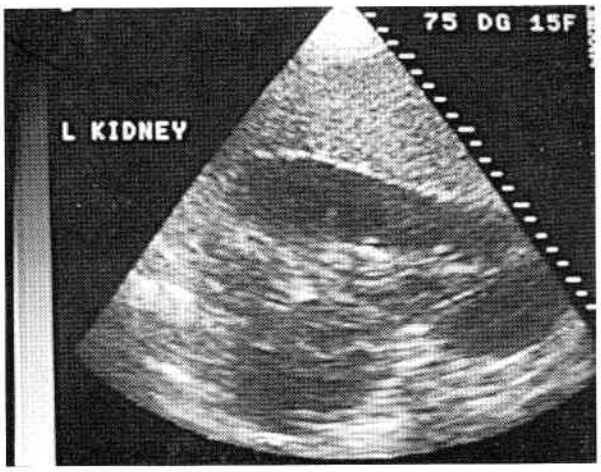

Figure 6–25

Sonogram of the left kidney obtained from a 4-year-old Thoroughbred stallion with acute renal failure. The left kidney is enlarged, measuring 15.1 cm wide by 19.5 cm long and appears fairly anechoic, consistent with acute renal failure. This sonogram was obtained from the left seventeenth intercostal space with a 5.0-MHz sector-scanner transducer at a displayed depth of 25 cm. The right side of this sonogram is cranial and the left side is caudal.

Abnormalities of the Kidneys

Renal Disease. Renal disease is more common in adult horses than previously thought. Changes in the size, shape, architecture, and echogenicity of the kidneys can be detected ultrasonographically. In a study of 239 human patients with renal insufficiency, ultrasonography provided definitive information as to the cause of the renal failure in approximately one third of the patients and was abnormal in another third of the patients but did not provide a definitive diagnosis for the cause of the renal insufficiency.[71] Kidneys that appear less echogenic than normal are consistent with renal edema (Fig. 6–25). Kidneys that appear more echogenic than normal are consistent with a cellular infiltrate in the renal parenchyma and medical renal disease (Fig. 6–26).[2, 4] This increase in parenchymal echogenicity may be diffuse or multifocal. To increase the specificity of the comparison of renal echogenicity with that of the adjacent liver in horses with suspected renal disease, the kidney should appear more echogenic than the adjacent liver, assuming that the liver is normal. Using this criterion in humans increased the specificity for the detection of renal disease to 96%, up from 58% when renal echogenicity greater than or equal to hepatic echogenicity was used.[72] The sensitivity of renal echogenicity greater than hepatic echogenicity was only 20%, however, down from 62% when renal echogenicity greater than or equal to hepatic echogenicity was used. No correlation has been reported in humans between the nature and severity of glomerular lesions detected on renal biopsy and the sonographic findings.[73] The sonographic clarity of the corticomedullary junction in these patients also did not correlate with any one histopathologic finding. However, a relationship was found between the nature and severity of interstitial changes seen on renal biopsy and the echointensity of the renal cortex.[73] Minimal increases in cortical echogenicity were produced with focal interstitial disease, a moderate increase in cortical echogenicity was produced by diffuse scarring, and the most intense increase in cortical echogenicity was detected in patients with active interstitial changes.[73]

Acute Renal Failure. Acute renal failure can be caused by a wide variety of toxic, drug, and septic causes, in addition to hemoglobin, myoglobin, and immune-mediated diseases. Hemodynamic causes of acute renal failure in horses have also been documented.[74] In acute renal failure the kidneys usually feel enlarged and soft on rectal palpation.[74]

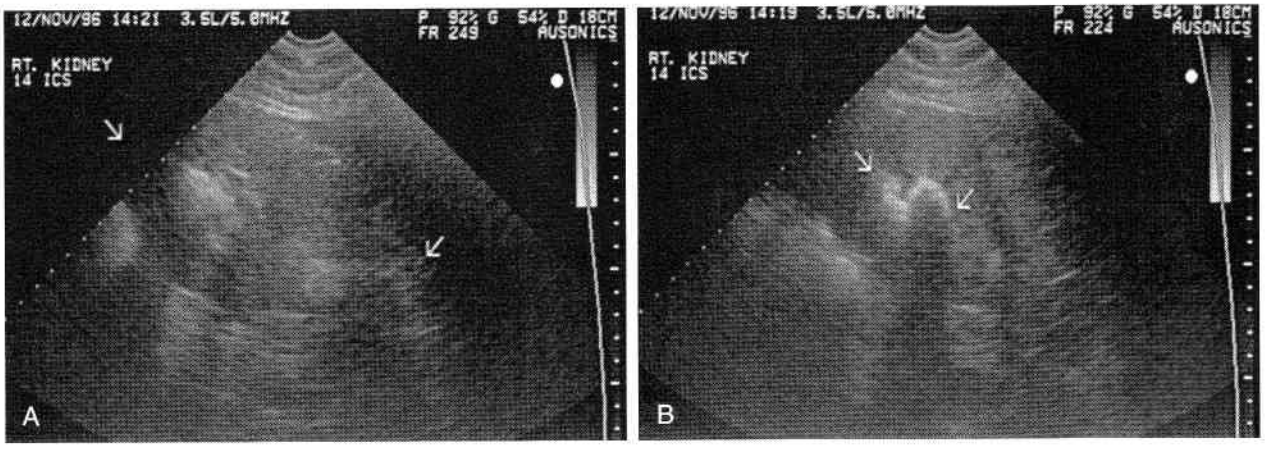

Figure 6–26

Sonograms of the right kidney obtained from a yearling Warmblood gelding with azotemia. Both kidneys were markedly decreased in size, irregular, and very echogenic and had loss of the normal corticomedullary distinction. These sonograms were obtained from the right fourteenth intercostal space with a wide-bandwidth 3.5-MHz sector-scanner transducer operating at 5.0 MHz at a displayed depth of 18 cm. *A*, The lack of distinction between the cortex and medulla is evident with some central areas of increased echogenicity in the renal pelvis, casting an acoustic shadow from the far side of this echogenic material, most consistent with debris in the renal pelvis. The arrows delineate the dorsal and ventral margins of the right kidney. The right side of this sonogram is dorsal and the left side is ventral. *B*, The indistinct corticomedullary junction is also seen in this transverse oblique image, which is oriented slightly more cranially. A hyperechoic structure in the renal pelvis casts an acoustic shadow from the near side of this structure, consistent with a calculus (*arrows*). The right side of this sonogram is dorsal and the left side is ventral.

Sonographic examination of the kidneys usually reveals bilateral renal enlargement, with the renal parenchyma appearing less echogenic than normal (see Fig. 6-25), although kidneys of normal size and echogenicity have been reported in horses with acute renal failure.[2, 9, 13, 17] Bilateral renal enlargement was detected sonographically in one horse with acute renal failure.[74] The cortex of the kidney may be thicker than normal in horses with acute renal failure.[9] Doppler ultrasound evaluation of renal arterial blood flow revealed an absence of blood flow in late diastole or throughout diastole in children with acute renal failure.[75] The diastolic blood flow reappeared in these children with recovery. To the author's knowledge, renal arterial blood flow has not been evaluated in adult horses with acute renal failure. Ultrasonographic examination of the kidneys in horses with acute renal failure is helpful in assessing the gross renal changes that have occurred.[74] Occasionally, with oliguric or anuric renal failure, perirenal edema is detected (Fig. 6-27).[2, 9, 76] Perirenal edema has been described as a homogeneous hypoechoic band peripheral to the renal cortex.[76] A ruptured ureter or kidney should also be considered in horses with perirenal fluid accumulation (Fig. 6-28), prompting sonographic examination of the ventral abdomen for the presence of excess fluid (uroperitoneum).

Increases in renal echogencity are often seen in horses with renal insufficiency (Fig. 6-29). The mechanism of an increase in renal parenchymal echogenicity is not well understood in humans and may occur with all types of cellular infiltration (including fibrosis), changes in renal perfusion, or changes in the interstitial fluid in relation to cellular fluid.[77] Increases in renal cortical echogenicity have been reported in humans with global sclerosis, focal tubular atrophy, hyaline casts, and focal leukocyte infiltration.[78] Numerous glomerulonephropathies (Fig. 6-29), tubular abnormalities, and interstitial diseases (Fig. 6-30) may also cause increased renal echogenicity.[73] Antigen-antibody complex deposition and glomerulonephritis were found in a large number of horses at postmortem examination, although only one of these horses had chronic renal failure.[79] Focal glomerulosclerosis-like disease may also produce increased renal parenchymal echogenicity. Focal glomerulosclerosis-like disease with nephrotic syndrome has been reported in one horse.[80]

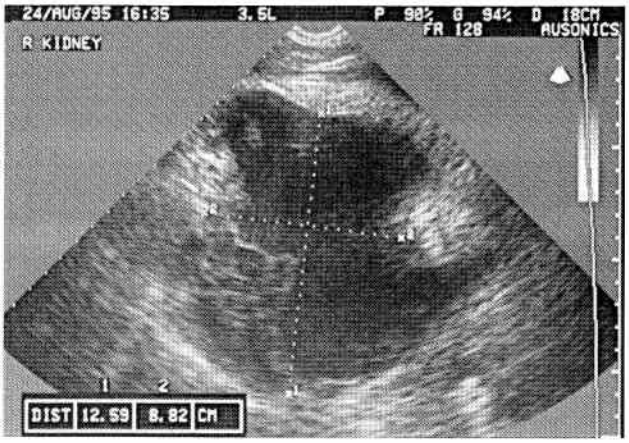

Figure 6–28

Sonogram of the perirenal space caudal to the right kidney obtained from a 5-year-old Thoroughbred mare with a large pool of retroperitoneal fluid associated with a ruptured ureter. The fluid cavity appears relatively anechoic with some hypoechoic fibrinous loculations and measures at least 12.59 by 8.82 cm in diameter. This sonogram was obtained from the right paralumbar fossa with a 3.5-MHz sector-scanner transducer at a displayed depth of 18 cm. The right side of this sonogram is dorsal and the left side is ventral.

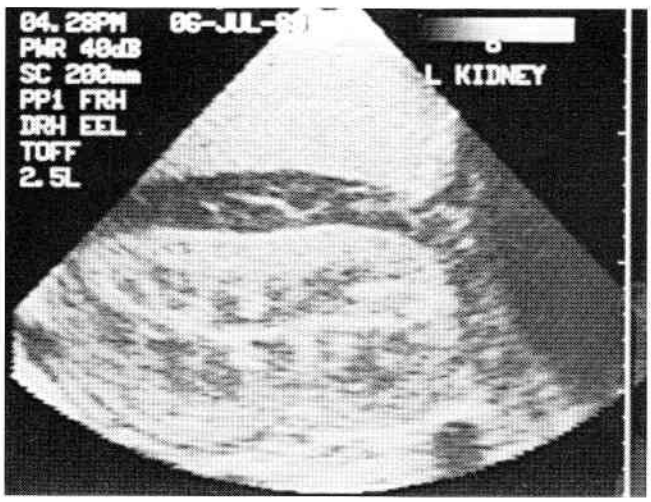

Figure 6–27

Sonogram of the left kidney with perirenal edema obtained from a 5-year-old Arabian stallion with acute renal failure. The loculated hypoechoic fluid surrounding the left kidney is most evident between the left kidney and the spleen. The left kidney is more echogenic than normal, with the renal cortex appearing only slightly less echogenic than the adjacent spleen. The left kidney appeared enlarged in this small horse, measuring approximately 18 cm in length with the width of the caudal pole measuring 8 cm. This sonogram was obtained in the left paralumbar fossa with a 2.5-MHz sector-scanner transducer at a displayed depth of 20 cm. The right side of this sonogram is caudal and the left side is cranial.

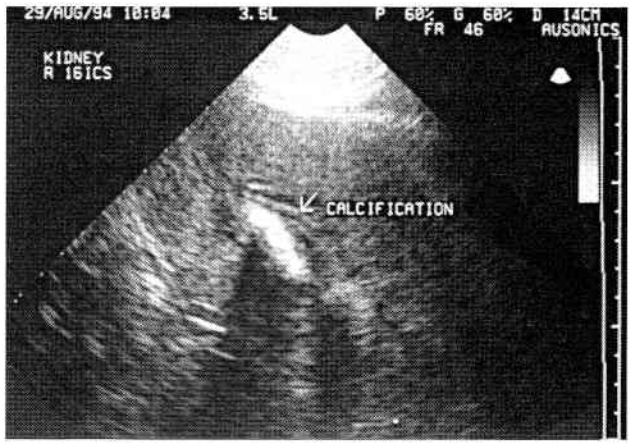

Figure 6–29

Sonogram of the right kidney obtained from an 11-year-old pony gelding with chronic glomerulonephritis. Both the renal cortex and medulla are more echogenic than normal, and the corticomedullary junction is difficult to distinguish. A hyperechoic structure casts a strong acoustic shadow from the far side of the structure, most consistent with a more proteinaceous calculus. This sonogram was obtained from the right sixteenth intercostal space with a 3.5-MHz sector-scanner transducer at a displayed depth of 14 cm. The right side of this sonogram is dorsal and the left side is ventral.

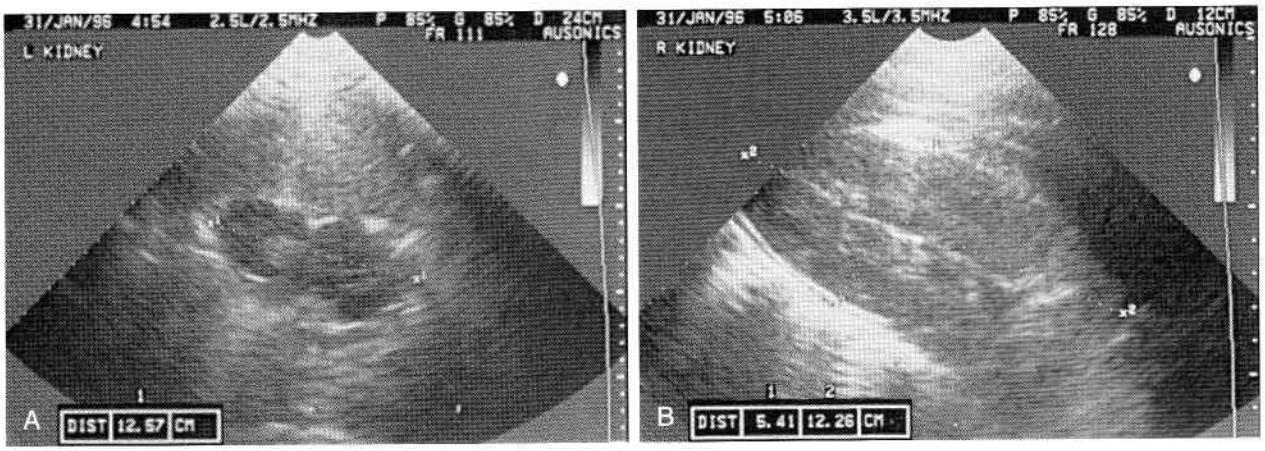

Figure 6–30

Sonograms of the right and left kidneys obtained from a 2-year-old Quarter horse colt in chronic renal failure. Both kidneys are small and more echogenic than normal, and the left kidney has a slightly irregular surface. The histopathologic diagnosis was severe tubulointerstitial nephritis and glomerulonephritis. The right side of these sonograms is cranial and the left side is caudal. *A*, The left kidney is very small, measuring 12.57 cm long with the width of the caudal pole measuring 4.8 cm. The surface of the left kidney is also somewhat irregular. This sonogram was obtained with a wide-bandwidth 2.5-MHz sector-scanner transducer operating at 2.5 MHz at a displayed depth of 24 cm. *B*, The right kidney is approximately 12.26 cm long, with the width of the caudal pole measuring 5.41 cm. This sonogram was obtained with a wide-bandwidth 3.5-MHz sector-scanner transducer operating at 3.5 MHz at a displayed depth of 12 cm.

Other focal abnormalities have been detected in the cortex and medulla of the kidney of azotemic horses, resulting in focal areas of increased echogenicity and slight bulging of the surface of the kidney, but histopathologic correlation with the sonographic appearance of the kidney has not been established (Fig. 6-31). Amyloid deposition may also result in an enlarged echogenic kidney with increased echogenicity of the renal cortex. However, amyloid is more likely to be deposited in the liver and spleen of affected horses and less likely to be found in the kidneys.[81] Renal amyloidosis has been reported primarily in horses used for the production of antiserum but has also been reported secondary to chronic infection.[81]

The iatrogenic administration of a variety of drugs may be toxic to the renal tubules and also results in increased renal parenchymal echogenicity. Of particular concern are the aminoglycoside antibiotics. Gentamicin toxic nephropathy has been described in horses with disseminated bacterial infection.[82] Cephalosporin, erythromycin, rifampin, and sulfonamide can also cause increased renal parenchymal echogenicity in children and probably in the horse. Mercury toxicity has caused acute tubular necrosis and renal failure secondary to the application of a mercuric blister on a horse's legs.[83] Vitamin K_3 has also been shown to cause acute tubular nephrosis and renal failure in horses at the dosage recommended by the manufacturer and has been removed from the market.[84] Analgesic nephropathy in humans has been characterized by the detection of calcified renal papillae surrounding the central sinus in a garland pattern.[85] Renal papillary necrosis in humans has also been described sonographically as the detection of fluid-filled spaces corresponding in distribution to the renal pyramids.[86] However, in many humans with renal papillary necrosis, an intense elliptical echogenic focus associated with acoustic shadowing is detected, thought to be caused by ischemic necrosis and fibrofatty degeneration of pyramidal tissue or early nonhomogeneous calcification.[87] Phenylbutazone has also been shown to cause similar histopathologic lesions of the renal medullary crest in horses.[88, 89] Gritty, firm necrotic sequestered tips of the renal crest and granular debris were found at postmortem examination in the renal calyces of horses treated with phenylbutazone.[88] Pelvic calculi often resulted from the sequestration of these mineralized necrotic renal crests in these horses. Increased echogenicity of the renal papilla and echogenic debris in the renal pelvis have been detected in horses with renal papillary necrosis (Fig. 6-32). Septic, toxic, and ischemic insults and pigmenturia may result in acute tubular nephrosis, with chronic interstitial nephritis and fibrosis developing as chronic sequelae to these insults.[90]

An echogenic line in the outer zone of the renal me-

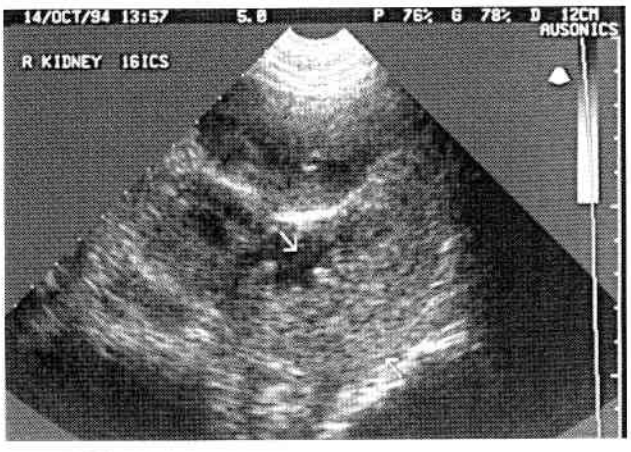

Figure 6–31

Sonogram of the right kidney obtained from a 15-year-old Arabian mare with azotemia. Notice the thickened cortex and medulla in the medial side of the kidney (*arrows*). This sonogram was obtained from the right sixteenth intercostal space with a 5.0-MHz sector-scanner transducer at a displayed depth of 12 cm. The right side of this sonogram is dorsal and the left side is ventral.

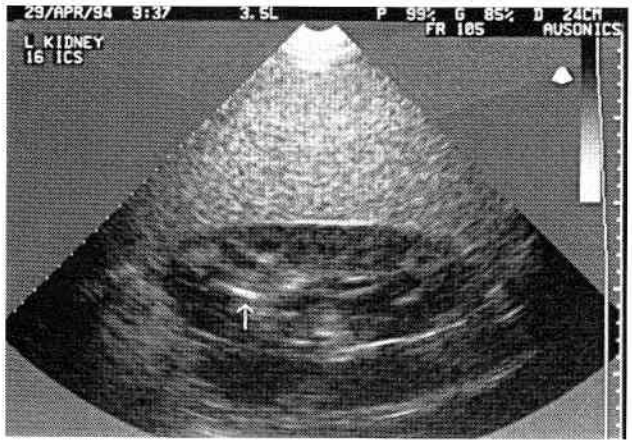

Figure 6–32

Sonogram of the left kidney obtained from a 3-year-old Thoroughbred gelding. The left kidney appeared fairly normal sonographically except for a small hyperechoic area in the caudal aspect of the left kidney that may represent hyperechoic debris associated with calcification of the medullary crest and sloughing of these cells into the renal pelvis. This sonogram was obtained from the left paralumbar fossa with a 3.5-MHz sector-scanner transducer at a displayed depth of 24 cm. The right side of this sonogram is cranial and the left side is caudal.

dulla, paralleling the corticomedullary junction, is known as the medullary rim sign (Fig. 6–33).[91] The medullary rim sign is an indication of primary renal disease but is not specific for the disease or the patient's prognosis.[91, 92] The medullary rim sign has been imaged in dogs and cats with hypercalcemic nephropathy, chronic interstitial nephritis, and acute tubular necrosis associated with idiopathic causes or ethylene glycol toxicity (oxalate nephropathy).[91, 93, 94] In five of six small animals, the medullary rim sign was associated with the deposition of mineral, primarily in the outer zone of the medulla.[91] Oxalate nephropathy may also cause increased renal parenchymal echogenicity in the horse and may result in the appearance of the medullary rim sign, seen in small animals with this disease. Oxalate nephropathy in horses may occur secondary to the ingestion of oxalate-producing fungi in corn silage or ethylene glycol.[95] Oxalate nephropathy may also occur secondary to underlying renal disease.[96] The outer zone of the renal medulla is the most likely to show signs of early renal tubular damage because this is the most metabolically active region relative to the amount of oxygen delivered.[91] Subsequent dystrophic calcification may occur in these regions of tubular necrosis and result in the appearance of the renal medullary rim sign.[91] The medullary rim sign has been imaged in several horses with renal disease, but histopathologic correlation with the sonographic appearance was not possible in these cases (Fig. 6–33). One horse with multicentric lymphosarcoma had a hyperechoic medullary rim, which may be consistent with hypercalcemic nephropathy (Fig. 6–34). The "halo" sign (a hypoechoic rim at the corticomedullary junction) has been described in small animals with ethylene glycol toxicity and may represent the more normal medulla between the cortex and the echogenic medullary rim.[91]

Chronic Renal Failure. The most common causes of chronic renal disease in the horse are chronic interstitial nephritis and fibrosis, glomerulonephritis, and pyelonephritis.[13, 90, 97–99] Chronic glomerulonephritis is the most common cause of chronic renal failure in horses documented in the literature.[90, 96–99] Chronic renal failure may develop in horses surviving acute vitamin K_3 toxicosis. In one horse with chronic renal failure associated with vita-

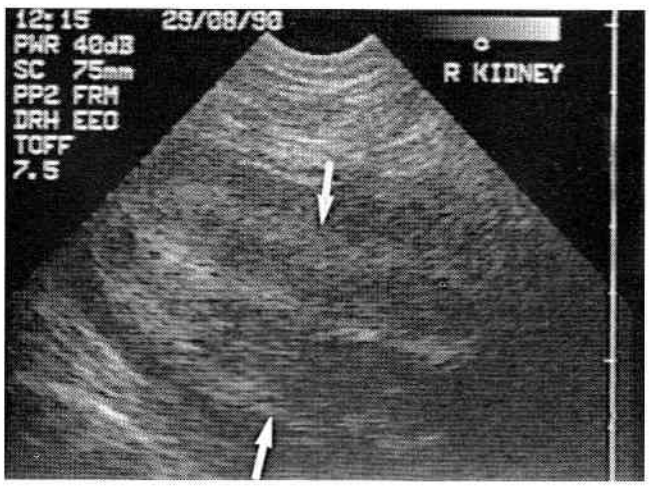

Figure 6–33

Sonogram of the right kidney with the medullary rim sign obtained from a 2-year-old miniature horse filly. Notice the outer rim of the medulla, similar in echogenicity to that of the renal pelvis (*arrows*). Both kidneys had a similar sonographic appearance. This filly had hemoperitoneum associated with a ruptured ovarian hematoma and severe anemia. A renal biopsy was declined, and the cause of this sonographic appearance of the kidneys was not determined. This sonogram was obtained in the right fifteenth intercostal space with a 7.5-MHz sector-scanner transducer at a displayed depth of 7.5 cm. The right side of the sonogram is dorsal and the left side is ventral.

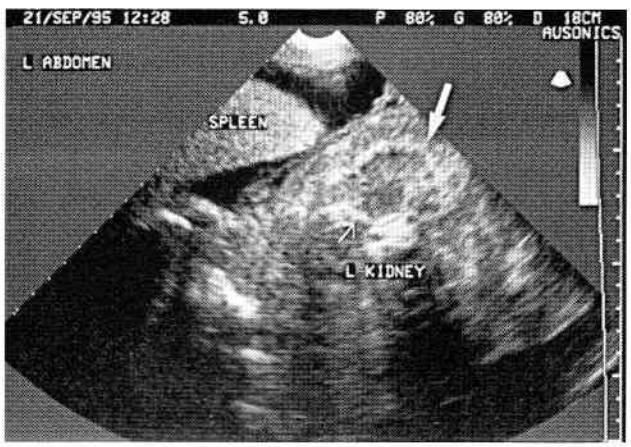

Figure 6–34

Sonogram of the left kidney obtained from a 5-year-old Standardbred gelding with multicentric lymphosarcoma. The outer edge of the medulla is hyperechoic (medullary rim sign), and hyperechoic material in the renal pelvis casts an acoustic shadow from the far side of the hyperechoic structure, consistent with calcified proteinaceous debris in the renal pelvis. The edge of the medulla is delineated by the small arrow, and a large arrow points to the medullary rim sign. This horse also has a large peritoneal effusion. This sonogram was obtained from the left paralumbar fossa with a 5.0-MHz sector-scanner transducer at a displayed depth of 18 cm. The right side of this sonogram is dorsal and the left side is ventral.

min K_3 toxicosis, the kidneys were one-third normal size 20 months later and had severe interstitial fibrosis.[84]

Presenting signs in horses with chronic renal disease include weight loss, decreased appetite, polyuria, dysuria, and lethargy or poor performance.[37, 90, 97, 100] Abdominal pain, a common complaint in humans with nephrolithiasis, is not commonly reported in horses with nephrolithiasis. However, colic was reported in 40% of horses with nephrolithiasis in one study.[37] In two of these horses the pain may have been associated with the presence of renal calculi. In one horse the renal calculus was associated with a renal abscess and peritonitis, and in the other horse bilateral renal calculi were thought to be the cause of chronic abdominal pain. Azotemia and isosthenuria are common in affected horses.[100] Hypercalcemia is frequently detected in horses with chronic renal failure and was present in 50% of horses with obstructive nephrolithiasis and ureterolithiasis.[100] Bacterial nephritis is not usually associated with ureterolithiasis and/or nephrolithiasis.[100] Pyelonephritis has been reported in a few horses with nephrolithiasis and ureterolithiasis.[90, 101, 102]

Rectal palpation is usually helpful in horses with chronic renal disease because the kidneys are usually smaller than normal and irregular.[2, 90, 100] Enlargement of the kidney may be detected if obstructive nephrolithiasis is present in the left kidney. However, the majority (80%) of horses with obstructive nephrolithiasis and ureterolithiasis had smaller than normal kidneys, despite the ureteral and/or renal obstruction.[100] Rectal palpation of the right kidney is usually not possible, even with marked hydronephrosis. In horses with ureterolithiasis, the stone may be palpated in the obstructed ureter or a dilated ureter may be palpated.[100, 103] Most ureteral stones palpated per rectum are located just cranial to the brim of the pelvis.[100] However, a ureteral stone has been palpated as far cranially as 12 cm cranial to the pelvic inlet.[103]

Information about the proximal ureter, renal pelvis, kidney, and perirenal tissues that cannot be obtained from rectal examination can be obtained sonographically. Chronic renal disease in horses is characterized by increased parenchymal echogenicity and a smaller than normal kidney with an irregular contour (see Figs. 6-26, 6-29, and 6-30). This increase in parenchymal echogenicity associated with fibrosis has been reported in both transrectal and transcutaneous images of affected kidneys.[2, 4, 10, 19] Poor differentiation of the internal architecture, particularly between the cortex and the medulla, has been detected in adult horses with chronic renal disease.[9] Often small hyperechoic echoes casting faint acoustic shadows, associated with sandy mineral debris, are imaged in the renal pelvis (Fig. 6-35). Movement of the hyperechoic material in the renal pelvis in real time is an indication of the presence of sandy or silt-like debris in the renal pelvis. Sand-like material may also be present in the renal pelvis in horses with renal calculi and chronic renal disease.[19] Renal calculi are frequently imaged in both kidneys in horses with chronic renal disease. The renal parenchyma is usually increased in echogenicity associated with renal fibrosis,[100] although an inflammatory cell infiltrate may also account for some of the increased renal echogenicity.

Nephrolithiasis. A hyperechoic structure casting an acoustic shadow through the deeper tissues is characteristic of a nephrolith (Fig. 6-36; see also Fig. 6-26). The more calcified nephrolith usually has an acoustic shadow that originates from the near surface of the calculus, whereas one with a more proteinaceous component has an acoustic shadow that originates from the deeper side of the nephrolith (see Figs. 6-29 and 6-34). These pro-

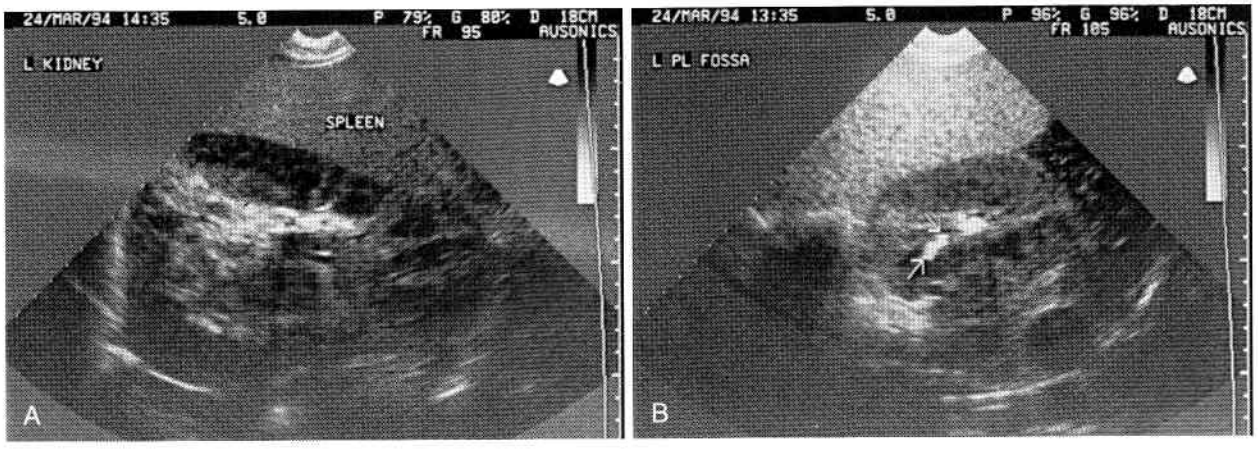

Figure 6–35

Sonograms of the left kidney obtained from a yearling Thoroughbred gelding with enlarged kidneys and echogenic debris in the renal pelvis. The long axis of the left kidney measured 16.34 cm, and the caudal pole measured 6.95 cm in diameter. Both measurements were thought to be large for this yearling. The echogenicity of the kidney is slightly greater than normal, but less than that of the adjacent spleen. Echogenic debris (*A*) is seen in the renal pelvis, some of which is hyperechoic and casts weak acoustic shadows associated with mineralized debris (*B*), possibly associated with previous renal papillary necrosis. Both kidneys had this debris imaged in the renal pelvis, and the renal parenchyma, particularly the cortex, was more echogenic than normal. An ultrasound-guided renal biopsy revealed chronic interstitial nephritis and fibrosis. These sonograms were obtained from the left paralumbar fossa with a 5.0-MHz sector-scanner transducer at a displayed depth of 18 cm. *A*, Sonogram of the left kidney demonstrating the hypoechoic to echogenic material in the renal pelvis. The right side of this sonogram is cranial and the left side is caudal. *B*, Sonogram of the left kidney demonstrating the hyperechoic debris (*arrows*) casting faint acoustic shadows within the collecting system of the kidney, consistent with small concretions. The right side of this sonogram is dorsal and the left side is ventral.

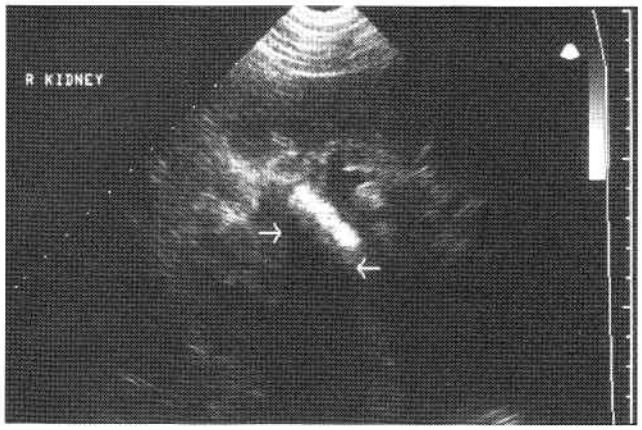

Figure 6–36

Sonogram of the right kidney obtained from an 8-year-old Thoroughbred gelding with a nephrolith and no other clinical or clinocopathologic evidence of renal disease. The nephrolith was found incidentally during a routine examination. The nephrolith is large, located in the renal pelvis, is hyperechoic and casts a large acoustic shadow (*arrows*). This sonogram was obtained from the right sixteenth intercostal space with a 5.0-MHz sector-scanner transducer at a displayed depth of 16 cm. The right side of this sonogram is dorsal and the left side is ventral.

teinaceous calculi are very fragile and often crumble when removed. Unilateral renal calculi have been found in horses as an incidental finding on postmortem examination.[37] Bilateral nephroliths and ureteroliths were reported in one mare that was clinically normal until ureteral obstruction occurred.[104] Although calculi can occasionally be found as an incidental finding in an otherwise normal horse (Fig. 6-36), underlying renal disease should always be suspected in horses with nephrolithiasis.

Both transrectal and transabdominal detection of renal calculi has been reported.[4, 19, 90, 100, 105] The obstructing calculus may be located transrectally if it is not found via the transcutaneous sonographic examination of the kidney. The image obtained transrectally of the left kidney is usually superior to that obtained through the left paralumbar fossa and caudal intercostal spaces and may be useful in more clearly characterizing ureteral and renal calculi and the parenchymal abnormalities.

Hydronephrosis and Hydroureter. One or both kidneys may be obstructed by a nephrolith, creating hydronephrosis. Ureterolithiasis and/or nephrolithiasis is commonly detected in horses with hydroureter and/or hydronephrosis, and these horses usually have chronic renal disease.[4, 9, 19, 101, 105, 106] The sonographic detection of hydroureter (Fig. 6-37) and/or hydronephrosis (Fig. 6-38) and a hyperechoic structure in the ureter and/or renal pelvis casting an acoustic shadow (ureterolith and/or nephrolith) are consistent with a diagnosis of urinary tract obstruction associated with ureterolithiasis and/or nephrolithiasis.[2, 3, 105] Dilatation of the renal pelvis is usually marked in horses with hydronephrosis. The renal cortex is usually very thin and may even be difficult to recognize in some horses with severe hydronephrosis. The hydronephrotic kidney often has an irregular contour because hydronephrosis in the adult horse is usually associated with chronic renal disease and nephrolithiasis. Ureteral calculi should be suspected if bilateral ureteral distention and hydronephrosis are imaged.[42] Dilated renal calyces were imaged in all kidneys with ureteral or renal pelvic obstruction in one group of horses with obstructive nephrolithiasis and ureterolithiasis.[100] The dilated renal calyces may have a cystic appearance on sonographic examination of the affected kidney.[105] Dilated renal recesses, dilated ureters, and bilateral ureteroliths were detected sonographically in one filly with bilateral ureterolithiasis and nephrolithiasis.[103] In this filly the right renal corticomedullary junction lacked definition and was felt sonographically to be more abnormal; however, this

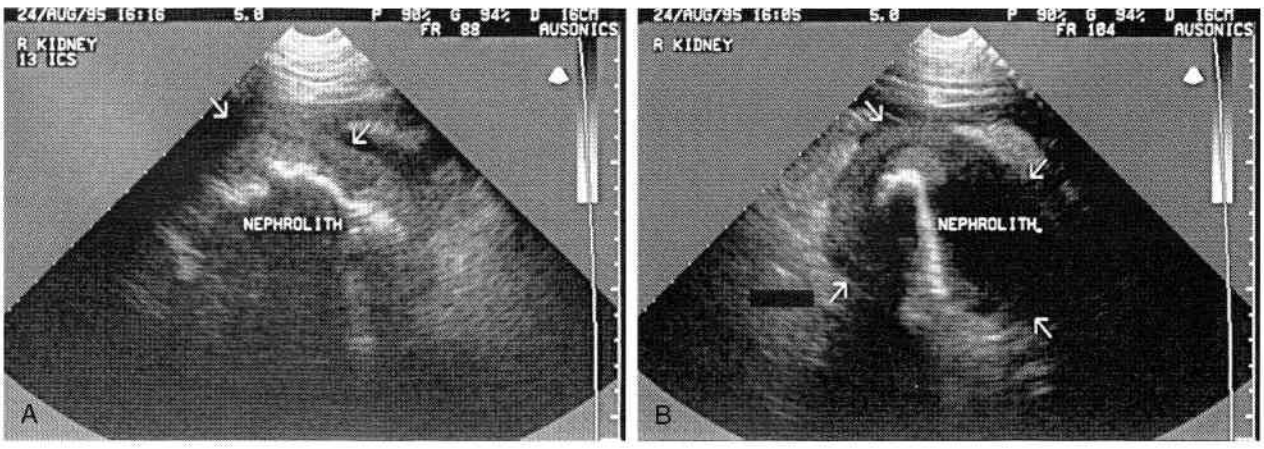

Figure 6–37

Sonograms of the right ureter obtained from a 5-year-old Thoroughbred mare with hydronephrosis, nephrolithiasis, and a ruptured ureter (same horse as in Fig. 6-28). The right ureter is filled with a large nephrolith or ureterolith that casts a strong acoustic shadow from the near side of the calculus. The ureter is thickened and dilated to approximately 9 cm in diameter. These sonograms were obtained in the right thirteenth intercostal space with a 5.0-MHz sector-scanner transducer at a displayed depth of 16 cm. *A*, Sonogram of the right ureter demonstrating the length of the uretorolith (nephrolith). A small amount of anechoic perirenal fluid is imaged around its cranial aspect. The arrows delineate the lateral margin of the right ureter. The right side of this sonogram is cranial and the left side is caudal. *B*, Sonogram of the right ureter demonstrating the fluid in the ureter adjacent to the obstructing nephrolith. The arrows delineate the borders of the right ureter. The right side of this sonogram is dorsal and the left side is ventral.

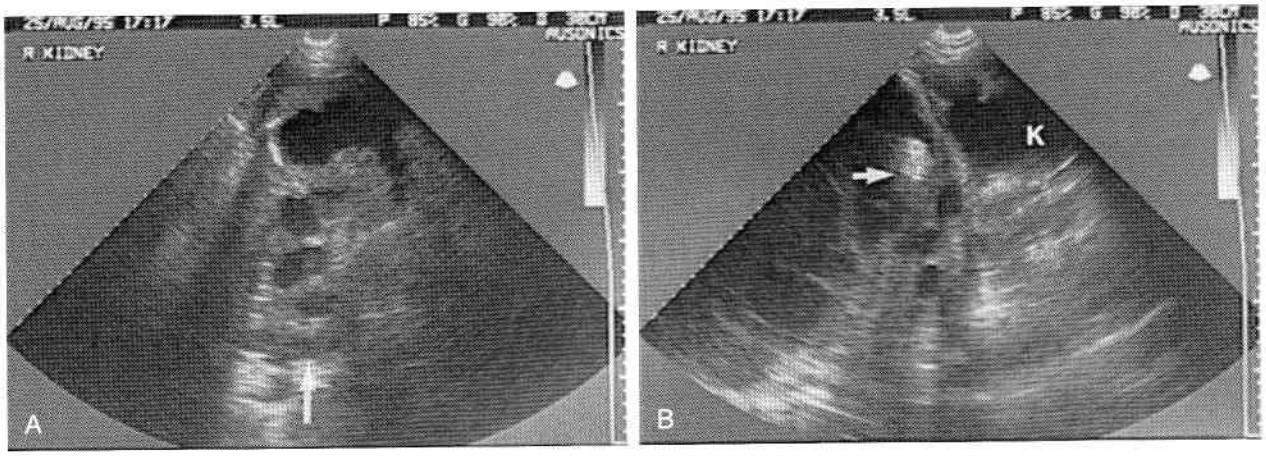

Figure 6–38

Sonograms of the right kidney and retroperitoneal space obtained from a 5-year-old Thoroughbred mare with hydronephrosis, nephrolithiasis, and ureteral rupture (same horse as in Figs. 6–28 and 6–37). These sonograms were obtained from the right paralumbar fossa with a 3.5-MHz sector-scanner transducer at a displayed depth of 30 cm. The right side of these sonograms is cranial and the left side is caudal. *A*, Sonogram of the caudal pole of the right kidney demonstrating the cystic hydronephrotic nature of this kidney. The arrow marks the medial border of the right kidney. *B*, Sonogram of the large retroperitoneal fluid accumulation associated with the ureteral rupture. A hyperechoic structure casts an acoustic shadow consistent with a proteinaceous calculus in the retroperitoneal fluid (*arrow*). The hydronephrotic caudal pole of the right kidney (K) is adjacent to this retroperitoneal fluid accumulation.

distinction did not reveal the more functional of the affected kidneys. Most horses with obstructive ureterolithiasis and/or nephrolithiasis have calculi imaged in both kidneys, although only one horse presented with bilateral renal obstruction.[100, 106] One or both poles of the kidney may be tightly packed with nodular calculi in horses with nephrolithiasis.[107]

Perirenal fluid accumulation may be detected with renal rupture or retroperitoneal rupture of the ureter (see Fig. 6–28). Rupture of the kidney has been reported in one horse with a renal calculus.[37] Perirenal fluid accumulation surrounding a severely hydronephrotic right kidney was imaged in one cow with suspected renal rupture.[108] Rupture of the kidney was confirmed at the time of unilateral nephrectomy.

Hydronephrosis of a single pole of the kidney or portion thereof is occasionally imaged in horses with nephrolithiasis (Figs. 6–39 and 6–40). Large renal masses associated with the kidney have been detected in several broodmares as incidental findings.[9] Sonographic examination of the kidney in these affected mares has revealed hydronephrosis of a portion of the kidney associated with nephrolithiasis. Rupture of these fluid-filled masses has been reported during foaling, creating a life-threatening situation.[9] In most horses with hydroureter the dilated ureter measures 2.5 to 3.0 cm in diameter and has a thick wall. The hydroureter is often easier to image transrectally because a higher-frequency transducer is used and the transducer can be positioned directly over the dilated ureter. Sonographic detection of hydronephrosis and hydroureter in horses was reported as early as 1986.[9] Large fluid-filled masses associated with hydroureter have been detected in broodmares with fever and weight loss (Fig. 6–41). These saccular distentions of the ureter are predisposed to infection. Percutaneous renal ultrasonography should be performed on both kidneys in horses with obstructive nephrolithiasis or ureterolithiasis to determine the presence and number of nephroliths or ureteroliths; size, echogenicity, and architecture of the kidneys; and the presence of renal pelvis or proximal ureteral obstruction.[106] Bladder and pelvic urethral ultrasonography should also be performed to rule out calculi in this location and to determine the cause of the hydronephrosis.

Pyelectasia. Fluid distention of the renal pelvis or pyelectasia can occur iatrogenically secondary to aggressive intravenous fluid replacement therapy.[109, 110] Pyelectasia should be diagnosed when pelvic distention occurs

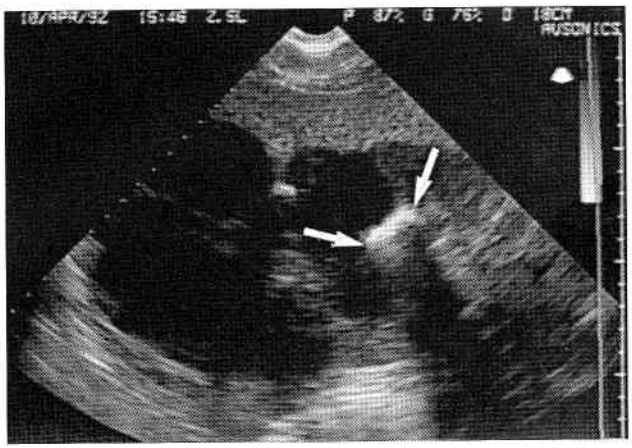

Figure 6–39

Sonogram of the left kidney obtained from a 20-year-old Thoroughbred mare with partial hydronephrosis of the left kidney. A large anechoic fluid-filled area involves the entire caudal pole and the hilar portion of the cranial pole of the left kidney, measuring 16 by 18 cm in diameter. No visible renal parenchyma surrounds the hydronephrotic portion of the caudal pole, and minimal renal parenchyma is imaged in the hilar part of the cranial pole of the left kidney. A large hyperechoic structure casting an acoustic shadow is consistent with a nephrolith obstructing the renal pelvis in the cranial pole and causing the hydronephrosis (*arrows*). This sonogram was obtained with a 2.5-MHz sector-scanner transducer at a displayed depth of 18 cm. The right side of this sonogram is cranial and the left side is caudal.

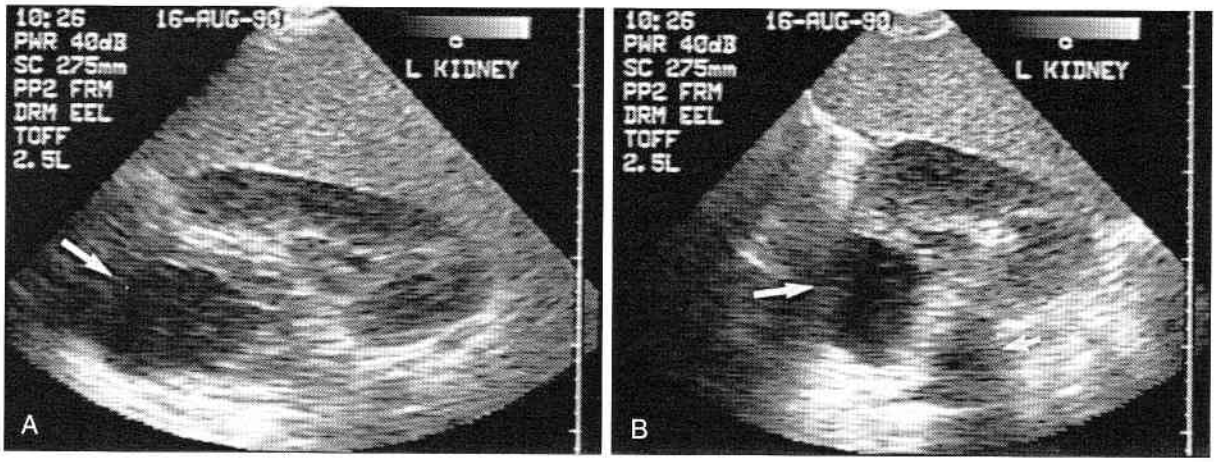

Figure 6–40

Sonograms of the left kidney obtained from a 10-year-old Thoroughbred mare with hydronephrosis involving a portion of the caudal pole of the left kidney. A large anechoic fluid-filled structure involves part of the caudal pole, with marked thinning of the renal parenchyma in this region. These sonograms were obtained from the left paralumbar fossa with a 2.5-MHz sector-scanner transducer at a displayed depth of 27.5 cm. *A*, Sagittal sonogram of the left kidney demonstrating the area of hydronephrosis in the caudal pole (*arrow*). The right side of this sonogram is cranial and the left side is caudal. *B*, Transverse oblique sonogram of the left kidney demonstrating the area of hydronephrosis in the caudal pole (*large arrow*). Notice the dilated ureter leaving the area of the renal pelvis containing slightly more echogenic fluid (*small arrow*). The right side of this sonogram is dorsal and the left side is ventral.

in the absence of obstruction of the ureter or renal pelvis.[109] Hydronephrosis should be reserved for distention of the renal pelvis and calyces with urine as a result of ureteral obstruction with accompanying atrophy of the renal pelvis.[109] The renal pelvis should be enlarged with a decreased amount of renal parenchyma present.[3] Sonographically detectable pyelectasia was diagnosed in 17 of 23 humans following ingestion of 56 ounces of fluid and was bilateral in 14 of these patients.[111] Other authors have suggested further sonographic division of dilatation of the renal pelvis into four categories.[110] Functional distention of the renal pelvis is of short duration with no retention of urine; this type of distention occurs with intravenous fluid administration. Distention of the renal pelvis with stasis refers to prolonged distention of the renal pelvis with retention of urine but preservation of the parenchymal structure of the kidney. Distention of the renal pelvis with stasis may occur with pyelonephritis (without obstruction). Mild hydronephrosis is distention of the renal pelvis with narrowing of the renal parenchyma, but the renal parenchyma is still discernible. Advanced hydronephrosis is marked distention of the renal pelvis with no more than a thin rim of homogeneous renal parenchyma remaining.

Congenital Renal Disease. Congenital renal abnormalities are rare in horses, but renal cysts, renal ectopia,

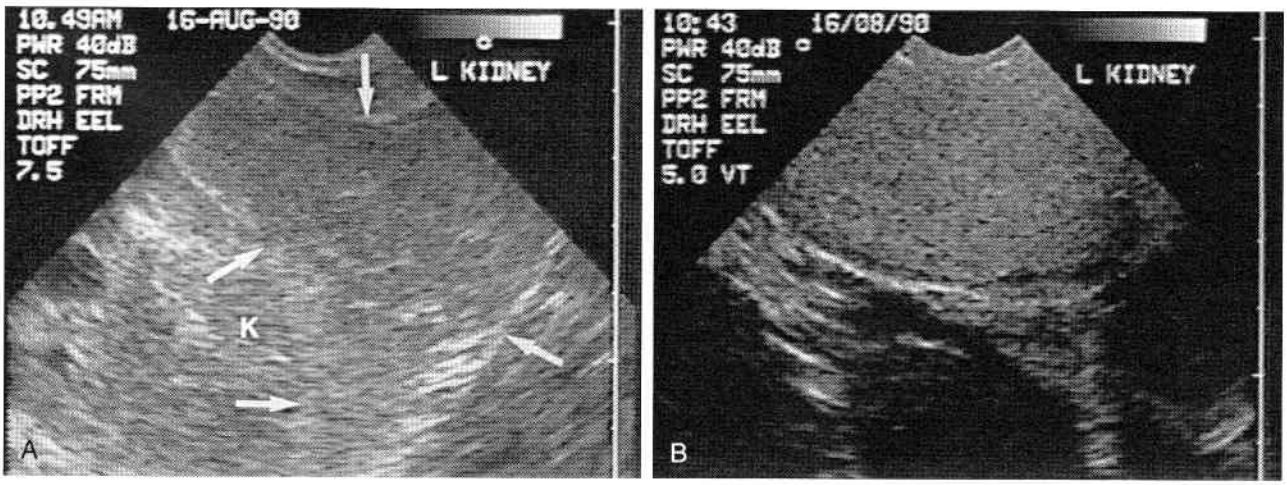

Figure 6–41

Sonogram of the dilated ureter containing echogenic urine at the kidney (*A*) and slightly further caudally in the abdomen (*B*) obtained from a 10-year-old Thoroughbred mare with hydronephrosis involving a portion of the caudal pole of the left kidney (same horse as in Fig. 6–40). These sonograms were obtained from the transrectal window with a 5.0-MHz sector-scanner transducer with an off-line beam orientation at a displayed depth of 7.5 cm. *A*, Large dilated diverticulum of the left ureter adjacent to the hilus of the left kidney (K), with echogenic urine swirling in this cavity in real time. The right side of this sonogram is toward the midline of the abdomen and the left side is toward the left. *B*, Large dilated left ureter caudal to the caudal pole of the left kidney filled with echogenic urine. The right side of this sonogram is cranial and the left side is caudal.

renal hypoplasia, and renal agenesis are all possible findings. A dysplastic, multicystic kidney should be considered in horses with multiple renal cysts intermixed with echogenic stroma. Bilateral polycystic kidneys have been reported in the adult horse.[112, 113] Sonographic examination of the kidneys in one horse revealed multiple 2- to 15-cm thin-walled cystic structures in both kidneys. The parenchyma of the left kidney was markedly abnormal, with only a small rim of hypoechoic parenchyma imaged. The right kidney was only mildly distorted with a hyperechoic renal parenchyma. Ultrasound-guided renal biopsy confirmed the presence of chronic renal disease (severe tubular sclerosis), and the cysts were sonographically drained from the right kidney, again with ultrasonographic guidance. The kidneys in the other horse with polycystic kidneys were grossly enlarged (up to 35 cm long and weighing 12 kg each) and filled with small, thin-walled cysts up to 1.5 cm in diameter. Sonographic examination of these kidneys would have revealed the polycystic renal parenchyma if ultrasound examination of the kidneys had been performed. A large single renal cyst has been imaged in one pole of the kidney of a horse that may have been associated with chronic renal disease, although small single cysts can be an incidental finding.[13]

Bilateral renal hypoplasia has been reported in four young horses, three of which were 9 months, 1 year, and 3 years old.[114] These three horses were thin, stunted, depressed, and lethargic for a month prior to presentation. Azotemia and isosthenuria were found in these horses at presentation. Ultrasonographic examination of the kidneys transrectally and percutaneously revealed the yearling to have small, irregularly shaped kidneys. The renal medulla and renal pelvis appeared smaller than normal in both kidneys. Severe medullary hypoplasia and moderate thinning of the renal cortex were detected in all horses at postmortem examination. Glomerular degeneration, tubular degeneration, interstitial fibrosis, and interstitial inflammation occurred in the older horses secondary to the renal hypoplasia.

Renal agenesis should be considered in those horses in which only one kidney can be found in the normal or an ectopic location. The author has imaged one horse with agenesis of the right kidney and a hypertrophic left kidney. These findings were subsequently confirmed on laparoscopic examination. In humans with renal agenesis, the remaining kidney hypertrophies over time.[77] The adrenal gland, if present, appears larger than normal and fills in the space along with the spleen and colon on the left side of the abdomen. The cecum would be expected to fill this space on the right side of the abdomen in the horse, along with the liver. If one kidney is absent on sonographic examination, and not just obscured from view by gas-filled large bowel, renal agenesis should be considered. The possibility that the horse had a previous unilateral nephrectomy should also be investigated.

Pyelonephritis. Pyelonephritis occurs infrequently in horses but is also more common than previously thought. Pyelonephritis may occur secondary to an ascending infection with urolithiasis, trauma, or neurologic disease of the urinary tract.[90, 99, 102] Pyelonephritis has also been reported in a horse secondary to a wooden foreign body embedded in the urinary bladder[115] and to fibrosarcomas obstructing the urethra at its vaginal opening.[116] Sonographic examination of the urinary bladder in this horse should have revealed the embedded foreign body as a hyperechoic linear structure casting a strong acoustic shadow. However, a sonographic examination of the bladder was not performed in this horse. Renal calculi are more likely to form in horses with pyelonephritis because the purulent debris serves as a nidus for stone formation. Both ureteral and urethral calculi and obstruction have been seen in horses with pyelonephritis. Calculi are frequently found in the renal pelvis or ureter at postmortem examination in affected horses.[90, 101, 102]

The sonographic finding most suggestive of pyelonephritis in horses is the detection of a large amount of echogenic to hyperechoic debris in the renal pelvis (Fig. 6-42). The hyperechoic debris may cast an acoustic shadow, associated with the formation of renal concretions (calculi). Gross renal enlargement is often present. The renal pelvis and renal calyces are often dilated, and normal renal architecture is often lost. Ureteral dilatation is also frequently detected in horses with pyelonephritis. A grossly dilated renal cortex and a hyperechoic renal pelvis with an irregular contour were detected ultrasonographically in one horse with pyelonephritis.[115] Hydronephrosis, ureterolithiasis, nephrolithiasis, and perirenal urine were imaged sonographically in one cow with pyelonephritis.[117]

Renal or Perirenal Abscess. A renal or perirenal abscess is rare in horses but should also be considered in the differential diagnosis of a renal or perirenal mass. A renal abscess involving one or both kidneys was reported in 3 of 25 horses with abdominal abscesses.[118] A renal abscess was detected in one horse with a large nephrolith in the renal pelvis 5 months after surgical removal of a cystic calculus.[36] Multiple renal abscesses have been reported in one horse with pyelonephritis.[102] One abscess measured 9 by 7 cm and would have been readily imaged sonographically. In one horse with multiple *Corynebacterium pseudotuberculosis* abscesses, both kidneys were 1.5 times normal size and contained numerous 2.5- to 5-cm abscesses, primarily in the renal cortex. These abscesses were filled with thick, purulent exudate[119] and would have been detectable sonographically. The sonographic appearance of a renal or perirenal abscess is that of a hypoechoic to echogenic fluid-filled cavity within (renal) or adjacent to (perirenal) the kidney. Hyperechoic structures casting acoustic shadows may also be detected in horses with renal abscesses associated with nephrolithiasis.

Renal or Perirenal Hematoma. A renal or perirenal hematoma is rare in adult horses and most frequently occurs secondary to abdominal trauma or a renal biopsy (Fig. 6-43). The kidney may feel enlarged on rectal examination. A double linear echo may be detected in horses with a subcapsular hematoma. The outer linear echo represents the renal capsule, and the inner linear echo represents the outer surface of the renal cortex. The renal or perirenal hematoma is usually anechoic and often contain loculations. Amorphous echogenic material may be detected in the subcapsular or perirenal space associated with organizing clot. The renal capsular echoes may

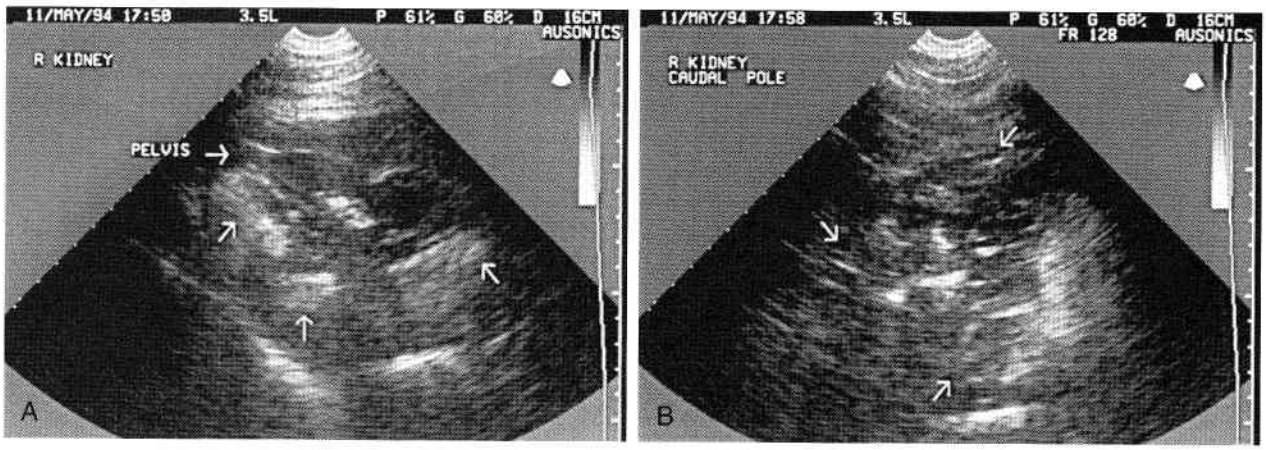

Figure 6–42

Sonograms of the right kidney obtained from the right fifteenth (*A*) and sixteenth (*B*) intercostal spaces in a 5-year-old Dutch Warmblood gelding with pyelonephritis. This horse originally presented with a urethral calculus and urinary tract obstruction, prompting this sonographic examination. These sonograms were obtained with a 3.5-MHz sector-scanner transducer at a displayed depth of 16 cm. The right side of these sonograms is cranial and the left side is caudal. *A*, The renal pelvis is dilated (*horizontal arrow*) and contains large amounts of echogenic to hyperechoic debris (*arrows*), some of which casts faint acoustic shadows consistent with renal calculus formation. Notice the thin rim of cortex remaining adjacent to the right body wall secondary to the hydronephrosis. *B*, A large amount of hypoechoic to hyperechoic debris is contained within a somewhat circular structure approximately 10 cm in diameter (*arrows*) in the region of the caudal pole of the right kidney. This accumulation of urinary debris is contained within the proximal ureter, not the caudal pole of the kidney, a finding subsequently confirmed at surgery. This structure is most likely the ureter because the caudal pole of the right kidney is still recognizable in the fifteenth intercostal space.

be indistinct. A blotchy renal parenchymal echogenicity may be detected with renal contusion. A renal or perirenal hematoma should be considered in a horse with a perirenal and/or renal mass, particularly in one with a history of abdominal trauma or a renal biopsy. Clear anechoic fluid in the retroperitoneal space around the kidney suggests a ruptured renal pelvis, calyx, or ureter.

Renal Granuloma. Parasitic renal granulomas have been reported in horses with *Halicephalobus deletrix* infection.[120–124] The horses with renal granulomas have had marked hematuria, with passage of frank blood and blood clots. Neurologic disease and mandibular involvement may also be present in affected horses. Large homogeneous soft-tissue masses, similar in echogenicity to the renal cortex or slightly more echogenic, are imaged within the renal parenchyma, disrupting the renal architecture and distorting the shape of the kidney (Fig. 6-44). The sonographic findings in one horse with renal granulomas associated with *H. deletrix* infection have been reported.[124] In this horse an echogenic oval structure was detected in the renal pelvis consistent with a large blood clot, in addition to the large homogeneous soft-tissue mass disrupting the renal parenchyma and bulging from the surface of the kidney.

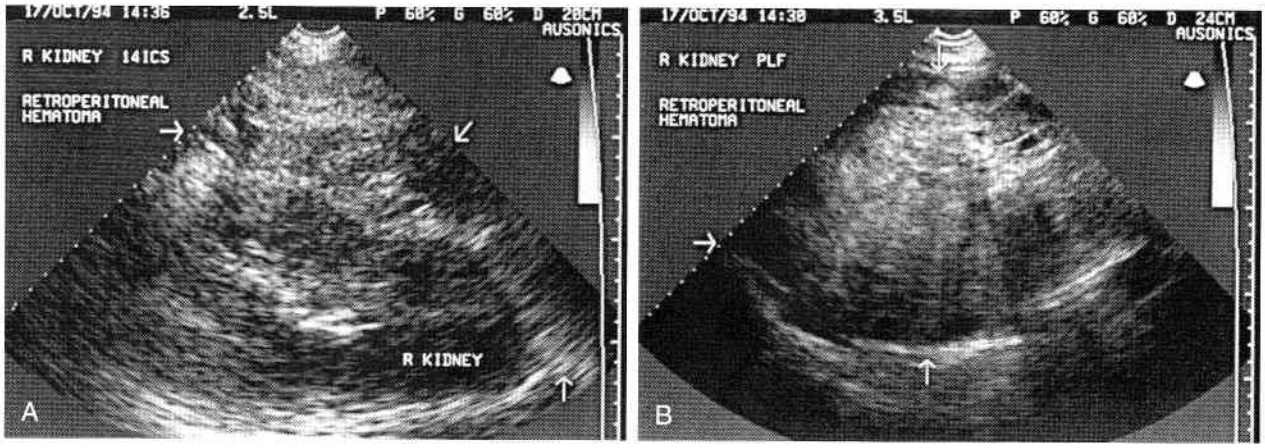

Figure 6–43

Sonograms of the right kidney (*A*) and retroperitoneal space (*B*) obtained from a 15-year-old Arabian mare with a large perirenal hematoma secondary to a renal biopsy (same mare as in Fig. 6-31). These sonograms were obtained from the right fourteenth intercostal space (*A*) and right paralumbar fossa (*B*) with a 2.5-MHz (*A*) and 3.5-MHz (*B*) sector-scanner transducer at a displayed depth of 20 cm (*A*) and 24 cm (*B*). The right side of these sonograms is cranial and the left side is caudal. *A*, Hypoechoic fluid and fibrin are imaged in the retroperitoneal space surrounding the right kidney (*arrows*). The hypoechoic to echogenic material in the retroperitoneal space represents immature fibrin clot. *B*, The retroperitoneal hematoma (*arrows*) extends caudally into the paralumbar fossa from the fourteenth intercostal space and measures approximately 14 cm thick. The large amount of hypoechoic to echogenic material in the hematoma represents an organizing clot.

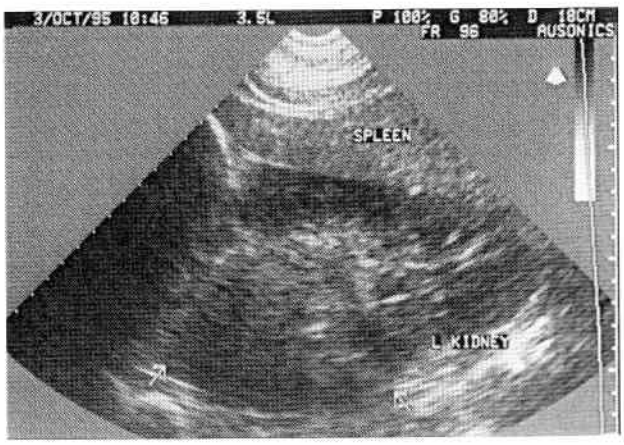

Figure 6–44

Sonogram of the left kidney obtained from an 18-year-old Shire mare with renal granulomas associated with *Halicephalobus deletrix* infection. A large, relatively homogeneous mass (*arrows*) disrupts the renal architecture in the caudal pole of the left kidney. The mass is slightly more echogenic than the normal renal parenchyma but slightly less echogenic than the spleen. The remainder of the left kidney has a normal sonographic appearance and is hypoechoic relative to the adjacent spleen. This sonogram was obtained from the left seventeenth intercostal space with a 3.5-MHz sector-scanner transducer at a displayed depth of 18 cm. The right side of this sonogram is cranial and the left side is caudal.

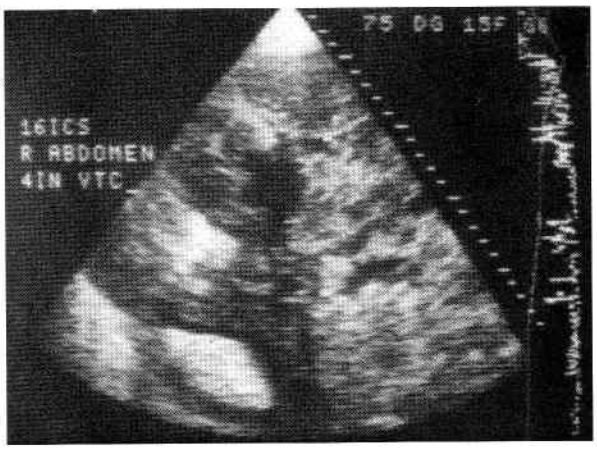

Figure 6–45

Sonogram of the right kidney obtained from an 11-year-old Standardbred mare with a renal adenocarcinoma. The kidney is markedly enlarged and unrecognizable, with its normal architecture destroyed by the tumor. Hyperechoic, echogenic, hypoechoic, and anechoic areas are seen within this large mass. This sonogram was obtained in the right sixteenth intercostal space with a 2.5-MHz sector-scanner transducer at a displayed depth of 25 cm. The right side of this sonogram is cranial and the left side is caudal.

Renal Neoplasia. Renal adenocarcinoma and lymphosarcoma are the most common tumors found in the equine kidney, with renal adenocarcinoma being the most common primary renal tumor. However, the incidence of these tumors is low.[125] Horses between 4 and 18 years old have been reported with renal adenocarcinoma.[126–129] The most common presenting clinical sign in horses with renal adenocarcinoma is hematuria. Weight loss, ascites, anorexia, colic, back pain, polydipsia, and polyuria have also been reported.[125, 127, 129, 130] I have seen one Standardbred racehorse with renal adenocarcinoma that presented with exercise intolerance and grunting at the end of the mile, only able to pace a mile in 2:20. Rectal examination may reveal an enlarged left kidney or a palpable mass associated with the left kidney, if the left kidney is affected.[125, 129] Otherwise, the rectal examination and clinical examination of the urinary tract may be nonremarkable because the right kidney is not normally palpable. However, several affected horses and one mule have had marked enlargement of the right kidney associated with complete destruction of the right kidney by the neoplasm.[126, 127, 131] A large mass palpable rectally in the right dorsal quadrant of the abdomen in several of these horses was the neoplastic right kidney.[125–127] The primary renal masses are often 25 to 30 cm in diameter, although renal masses as small as 6 cm and as large as 75 cm have been reported.[125–127, 130, 131] Although this tumor is most frequently unilateral, metastases to the other kidney have occurred in at least one horse.[127] The tumor grows by expansion and frequently metastasizes to the liver and lung following invasion of the renal vein. Rapid deterioration usually occurs once clinical signs are present.[125, 131] In the horse with exercise intolerance, the tumor spread into the caudal vena cava from the right renal vein and metastasized to the liver and lungs. A transitional cell carcinoma originating from the renal pelvis of the left kidney was reported in one horse.[132] A large sublumbar mass was palpable in this horse, obliterating the left kidney, but the bladder was normal.

Sonographic examination of the affected kidney in a horse with renal adenocarcinoma reveals a large mass disrupting all (Fig. 6-45) or a portion of the renal parenchyma (Fig. 6-46). Some horses show no evidence of recognizable renal tissue, only this large heterogeneous

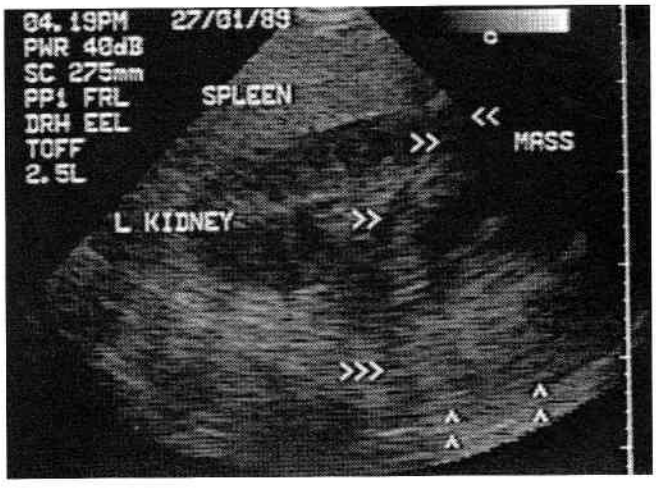

Figure 6–46

Sonogram of the left kidney obtained from a 25-year-old Connemara gelding with a renal adenocarcinoma involving the caudal pole. Notice the composite heterogeneous mass (*arrowheads*) in the caudal pole of the left kidney and the relatively normal sonographic appearance of the cranial pole. The mass contained hyperechoic, isoechoic, and anechoic areas relative to the normal portion of the left kidney. This gelding presented with hematuria. This sonogram was obtained from the left paralumbar fossa with a 2.5-MHz sector-scanner transducer at a displayed depth of 27.5 cm. The right side of this sonogram is caudal and the left side is cranial.

mass in the area where the kidney should be. The echogenicity of the renal adenocarcinoma is complex compared with renal lymphosarcoma.[2] A large mass of mixed echogenicity replaced the caudal pole of the left kidney in one horse with a renal papillary adenocarcinoma[2] and in one horse with a renal tubular cell carcinoma that extended caudally to the pelvic brim.[129] Multiple hyperechoic foci were detected in the renal tubular carcinoma with an edge shadow artifact that was produced at the border between the normal and abnormal part of the kidney. The other kidney appeared sonographically normal in both horses. In one mule with renal adenocarcinoma a 5-cm sphere-shaped locule of anechoic fluid containing an irregular pedunculated mass with a mixed pattern of echogenicity was detected within a large complex mass that had completely replaced the right kidney.[131] A renal adenoma has been detected sonographically in a 2-year-old horse presented for hematuria. The mass was 3 cm in diameter, was located within the renal pelvis, and had well-defined but irregular borders and a complex pattern of echogenicity. Numerous small anechoic circular areas were detected within the mass, surrounded by a hyperechoic border casting an acoustic shadow.[10] A mucous adenoma in the renal pelvis has been reported as an incidental finding on postmortem examination in one horse.[125] Sonographic examination of the horse with transitional cell carcinoma originating in the left renal pelvis would probably have revealed a large composite mass involving and surrounding the left kidney, renal vessels, and abdominal aorta. Pulmonary metastases were present in this horse.

Horses with lymphosarcoma usually have discrete homogeneous masses in the renal parenchyma which are slightly hypoechoic to nearly isoechoic compared with the normal renal cortex (Fig. 6-47). The remainder of the kidney may appear normal. In humans renal lymphoma is usually imaged as a hypoechoic to anechoic mass. Moderate transmission of ultrasound through the mass is due to the homogeneous cellular composition of the tumor, with few tissue interfaces of differing acoustic impedance.[133, 134] A similar sonographic appearance for renal lymphoma has also been described in the dog.[135] However, in one horse with lymphosarcoma, the left kidney was homogeneously echogenic throughout, similar to the pattern of normal spleen, although the kidney was twice normal size.[19] The normal renal architecture had been totally disrupted, and both the renal medulla and pelvis were infiltrated with neoplastic cells. The detection of renal masses in horses with lymphosarcoma is usually an incidental finding in a horse with multicentric lymphosarcoma rather than the cause of renal disease or failure.

In humans with renal carcinomas, ultrasound had excellent diagnostic accuracy in tumor detection unless the tumors were smaller than 2 cm.[136] Similarly, ultrasound has been successful in the identification of renal tumors in small animals.[135] Although a sonographic diagnosis of the tumor type cannot be made with accuracy in other species,[135] the two most common tumors of the equine kidney have very different sonographic appearances. In spite of this, however, a definitive diagnosis of renal neoplasia, the type of neoplasm, and the degree of malignancy depend upon histopathologic evaluation of the renal mass.

Perirenal Masses. The perirenal soft tissues should be carefully examined sonographically for any soft tissue masses that may also be neoplastic. Masses surrounding the right kidney and aorta have been imaged in horses with lymphosarcoma and metastatic melanoma. Perirenal and periaortic masses associated with lymphosarcoma can have a composite or homogeneous sonographic ap-

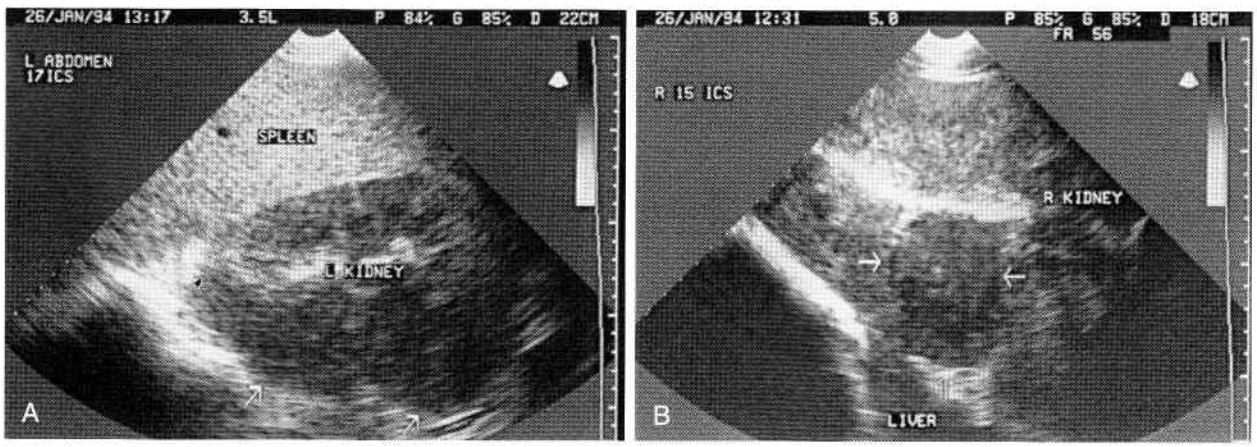

Figure 6-47

Sonograms of both kidneys obtained from an 18-year-old Appaloosa gelding with multicentric lymphosarcoma. These sonograms were obtained from the left seventeenth intercostal space with a 3.5-MHz sector-scanner transducer (*A*) and from the right fifteenth intercostal space with a 5.0-MHz (*B*) sector-scanner transducer at a displayed depth of 22 cm (*A*) and 18 cm (*B*). The right side of these sonograms is dorsal and the left side is ventral. *A*, The architecture of the left kidney is disrupted by two homogeneous masses (*arrows*) near the hilus of the left kidney. These masses involve both the cortex and the medulla and are consistent with lymphosarcoma (confirmed at postmortem examination). These masses are slightly hypoechoic compared with the adjacent renal parenchyma. The adjacent splenic parenchyma appears fairly homogeneous in its sonographic appearance but has a somewhat rounded dorsal border. With higher-frequency ultrasound examination of the spleen, however, the heterogeneous nature of the splenic parenchyma became evident (see Fig. 6-72). *B*, The architecture of the right kidney is disrupted by the homogeneous mass (*arrows*) invading both the cortex and the medulla (primarily the medulla). This soft tissue-density mass is relatively homogeneous, isoechoic with the renal medulla, and consistent with lymphosarcoma (confirmed at postmortem examination).

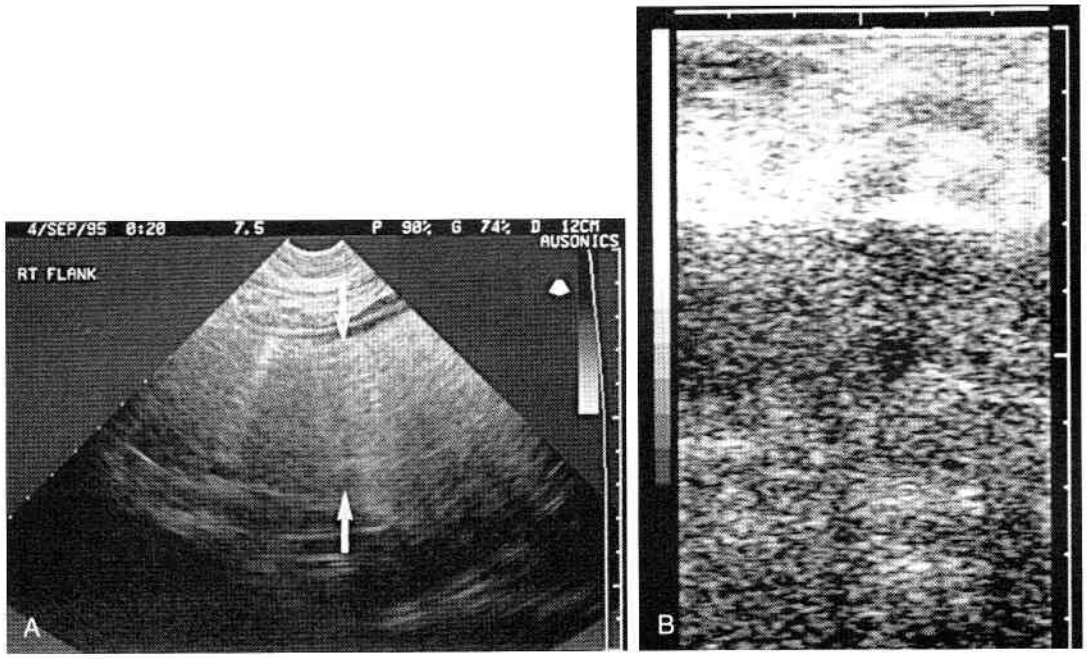

Figure 6–48

Sonograms of the right side of the abdomen obtained from a 20-year-old Quarter horse gelding with lymphosarcoma. This horse had a large sublumbar mass extending from the right flank to the caudal pole of the right kidney along the right and ventral side of the aorta. *A*, The sublumbar mass appears as a slightly heterogeneous echogenic mass approximately 5 cm thick immediately ventral to the sublumbar musculature (*arrows*). This sonogram was obtained from the right paralumbar fossa with a 3.5-MHz sector-scanner transducer at a displayed depth of 12 cm. The right side of this sonogram is cranial and the left side is caudal. *B*, The sublumbar mass appears slightly more heterogeneous in this view but cannot be displayed in its entirety owing to its large size in the caudalmost portion of the abdomen. This sonogram was obtained with a 5.0-MHz linear-array transducer from the transrectal window. The top of this sonogram is the ventral aspect of the right sublumbar region, the right side is cranial, and the left side is caudal.

pearance (Fig. 6–48). In one report of a horse with lymphosarcoma, the periaortic masses had a complex pattern of echogenicity. Composite or homogeneous masses surrounding the kidney and aorta have been imaged in horses with metastatic melanoma (Fig. 6–49). A large composite mass compressing the right kidney was imaged in one horse with a sarcoma (Fig. 6–50).

Adrenal Gland Neoplasia. Both pheochromocytomas and adrenocortical carcinomas have been reported in horses with perirenal masses.[137–140] In a mare with adrenocortical adenoma,[140] a stallion with adrenocortical carcinoma,[138] and a gelding with pheochromocytoma,[141] a large firm mass was palpable in the left sublumbar region that could have been examined sonographically from the transrectal window if the equipment had been available. In two horses with functional pheochromocytomas, a large retroperitoneal blood clot (30 cm in one horse)[139] surrounded the right kidney. A smaller 8 × 6 × 4 cm[139] or 6 cm[137] cystic tumor mass was found near the renal hilus. Sonographic examination of the right kidney should have revealed the large retroperitoneal blood clot, although the neoplastic adrenal gland probably would have been difficult to distinguish from the large hematoma. In another horse with a functional pheochromocytoma, no palpable perirenal or sublumbar mass was present. At postmortem examination a large, 10- to 12-cm mass in the caudal pole of the right adrenal gland was found. This mass should have been detectable adjacent to the cranial pole of the right kidney in the renal fossa of the liver if ultrasonography had been available. The other abdominal organs and peritoneum should be carefully scanned for evidence of additional tumors or tumor metastases. Widespread metastases (liver, spleen, and lung) and peritonitis were reported in the stallion with

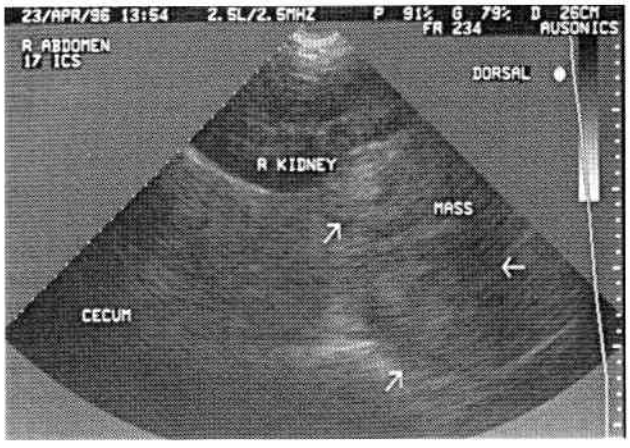

Figure 6–49

Sonogram of the right side of the abdomen obtained from a 17-year-old Oldenberg gelding with metastatic melanoma. Notice the large perirenal mass (*arrows*) dorsal to the right kidney that extended cranially to the right lobe of the liver. The mass is hypoechoic but is slightly more echogenic than the adjacent kidney, has a heterogeneous appearance, and is much larger than the right kidney. This sonogram was obtained from the right seventeeth intercostal space with a wide-bandwidth 2.5-MHz sector-scanner transducer operating at 2.5 MHz at a displayed depth of 26 cm.

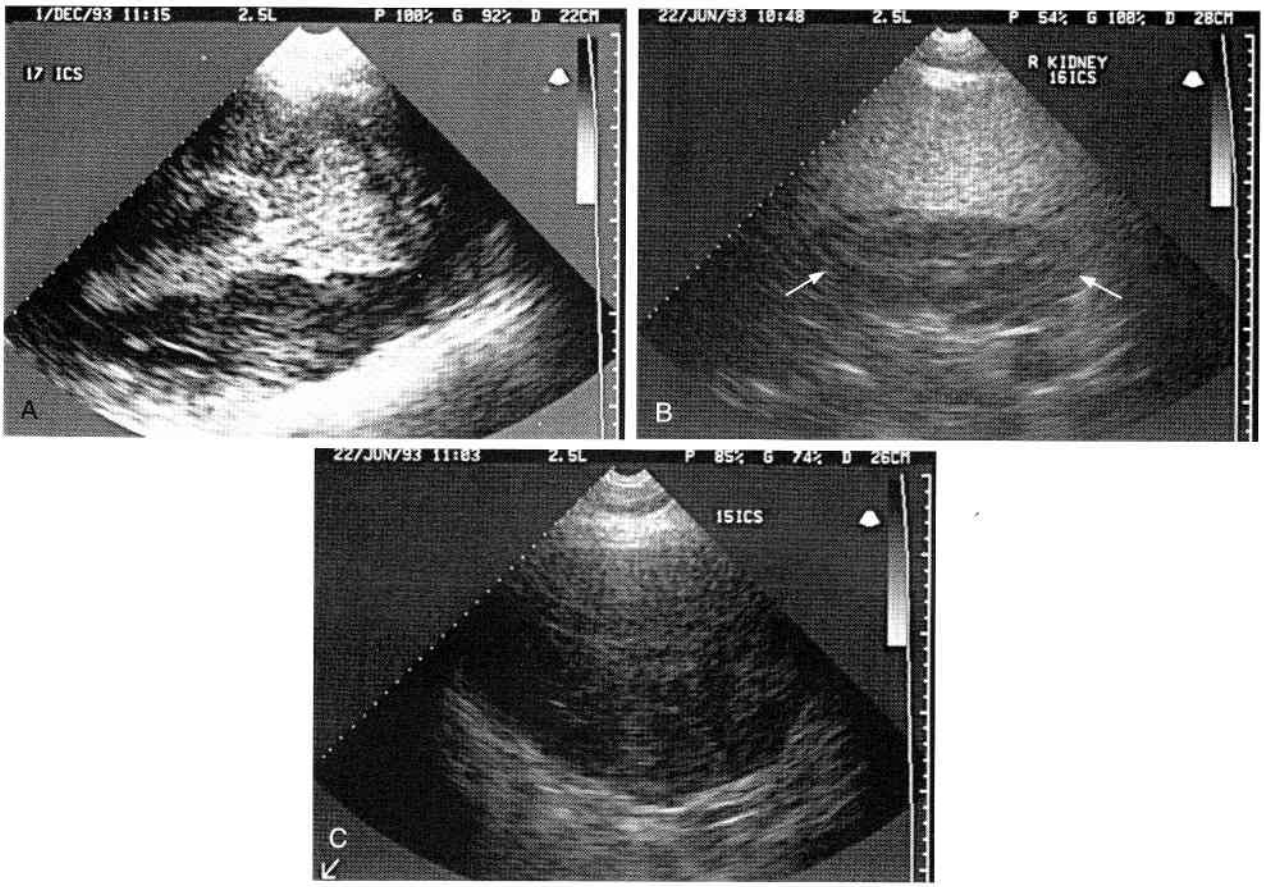

Figure 6–50

Sonograms of the right kidney and perirenal area obtained from a 3-year-old Arabian gelding presenting with hematuria. These sonograms were obtained from the right seventeenth (*A*), sixteenth (*B*), and fifteenth (*C*) intercostal spaces with a 2.5-MHz sector-scanner transducer at a displayed depth of 22 cm (*A*), 28 cm (*B*), and 26 cm (*C*). The right side of these sonograms is dorsal and the left side is ventral. *A*, The mass had a very heterogeneous appearance, with central hyperechoic areas surrounded by heterogeneous tissue of varying echogenicities. *B*, The right kidney was very small and compressed (*arrows*) by a large composite perirenal mass. The heterogeneous portion of this mass is medial to the right kidney and appears to involve the right kidney at the hilus. At postmortem examination, the right kidney was completely compressed and surrounded by a sarcoma that had invaded the right kidney at the hilus. *C*, This large, relatively homogeneous portion of the mass was located along the craniolateral margin of the mass between the liver and right kidney and appeared less echogenic than the adjacent liver or renal cortex. It measured 16.2 by 21.7 cm in diameter.

adrenocortical carcinoma.[138] Other organ involvement is common in horses with lymphosarcoma and renal adenocarcinoma, particularly hepatic involvement.

An ultrasound-guided renal biopsy should be performed if renal neoplasia is suspected. Radiographic and/or sonographic examination of the lungs should be performed to determine the presence of pulmonary metastases, which are most likely in horses with renal adenocarcinoma. An ultrasound-guided biopsy of one of the pulmonary masses can be safely performed in most horses. A blind, ultrasound-localized biopsy yielded neoplastic cells consistent with a renal adenocarcinoma in the horse with exercise intolerance. Hepatic ultrasonography should also be performed in horses with suspected renal neoplasia because hepatic metastases are common in horses with renal adenocarcinoma and liver involvement is common in horses with lymphosarcoma.

Abnormalities of the Liver

Infectious liver disease occurs in adult horses, most frequently in the form of cholangiohepatitis.[142–156] Viral hepatitis may occur in horses associated with the administration of products containing equine serum (Theiler's disease). Theiler's disease is usually reported following the administration of tetanus antitoxin in adult horses, particularly in post-foaling mares.[157, 158] Plants, toxins, and drugs can cause acute hepatocellular necrosis and subsequent fibrosis.[159–169] Excessive amounts of lipid can accumulate in the liver of horses, also causing hepatocellular necrosis.[169–171] Hepatic congestion, most frequently imaged in horses with congestive heart failure, is characterized by an enlarged liver of decreased echogenicity with prominent hepatic vasculature. Most of the disease processes affecting the liver in the horse are associated with diffuse hepatic disease. Focal cavitated areas may be seen in horses with hydatid cysts, polycystic liver disease, abscesses, or neoplasia.[172–174] Polycystic liver disease and hepatic abscesses are rare findings in adult horses.[174] Primary hepatic neoplasia is uncommon in horses, but the liver is often a site of tumor metastases and neoplastic infiltration in horses with multicentric lymphosarcoma.

Sonographic evaluation of the liver in horses with diffuse liver disease should include an assessment of parame-

ters routinely evaluated in humans: parenchymal echogenicity, the visibility of the portal and hepatic veins, the depth of penetration of the ultrasound beam, the images from the edge of the liver and from the liver surface, and the liver-kidney contrast.[175, 176] All these findings analyzed together help differentiate between hepatic cirrhosis/fibrosis and fatty liver and between patients with acute hepatitis and those with normal livers.[176] Although hepatic ultrasonography is extremely useful, its major limitation is that only a small portion of the liver can be routinely imaged in the adult horse because most of the liver is covered by aerated lung or large colon. The ultrasonographic diagnosis of liver disease, especially if it is diffuse, should be substantiated by a liver biopsy obtained from a representative area of the liver, and histopathologic examination of the tissue.

Acute Hepatitis and Hepatocellular Necrosis. Acute hepatitis results in widespread hepatocellular necrosis.[158] Hepatocellular necrosis has been reported in horses associated with migrating strongyle larvae or moldy hay.[169] Acute aflatoxicosis and pyrrolizidine alkaloid toxicosis also cause hepatocellular necrosis in horses.[165-167] The major target organ of aflatoxin in all species is the liver.[167] The effect on the hepatic parenchyma is centrilobular fatty change, hepatic cell necrosis, bile stasis, and periportal fibrosis. At low doses the periportal fibrosis is more severe and is accompanied by bile duct proliferation. In horses with acute Theiler's disease or idiopathic acute hepatic disease, decreased parenchymal echogenicity and collapse of the hepatic parenchyma resulting in a smaller than normal liver have been identified sonographically. Toxic insults resulting in hepatocellular necrosis may also occur and result in decreased echogenicity and collapse of the hepatic parenchyma.[2] A few horses with hepatocellular necrosis have enlarged livers with multifocal irregular areas of decreased echogenicity (Fig. 6-51). In humans with acute hepatitis, an overall decrease in hepatic echogenicity occurs, with accentuated brightness and more visible portal vein walls.[177] As the hepatitis becomes chronic, the overall echogenicity of the liver increases and the brightness and visibility of portal vein walls decrease.[177]

Iron toxicity has been reported in adult horses as well as in equine neonates and results in marked periportal bile ductule proliferation and cholestatic hepatopathy.[159-164] Hepatic necrosis has been reported in one horse that died acutely with severe hepatic necrosis after ingestion of an iron-containing vitamin supplement.[159] Although the hepatic sonogram performed in the one horse that survived iron toxicity was normal, subsequent liver biopsy revealed focal areas of moderately severe hepatocellular necrosis with a surrounding lymphocytic infiltrate, bile ductule proliferation with cholestasis, and periportal inflammatory cell infiltrate.[159] The sonogram was performed at admission, and the biopsy was obtained 5 days later. A repeat hepatic sonogram at that time may have revealed parenchymal abnormalities in the liver. Sonographic evaluation of the liver in foals with iron toxicity did reveal a heterogeneous appearance of the hepatic parenchyma with loss of the normal hepatic architecture.

Suppurative Hepatitis. Suppurative hepatitis is rarely reported in adult horses. Small multifocal areas of increased echogenicity scattered throughout the hepatic parenchyma have been imaged in horses with multifocal suppurative hepatitis.[2] A very enlarged liver with multiple bulging areas along its capsular surface, in addition to rounded ventral margins, was detected in several horses with suppurative hepatitis (Fig. 6-52). Multifocal heterogeneous hyperechoic areas, small hyperechoic areas casting acoustic shadows consistent with hepatoliths or calcification, irregular hypoechoic areas, and some hypoechoic material in the biliary tree have been imaged throughout the liver in these horses, with small areas of more normal-appearing hepatic parenchyma (see Color Fig. 1-1). A more diffuse increase in parenchymal echogenicity is indicative of a diffuse inflammatory cell infiltrate.[2] Severe hepatitis is one cause of the "bright liver" in humans.[178] Hepatomegaly is frequently detected in horses with inflammatory liver disease. Some loss of the normal hepatic architecture may be imaged with a severe diffuse or multifocal hepatitis with parenchyma of normal or decreased echogenicity.

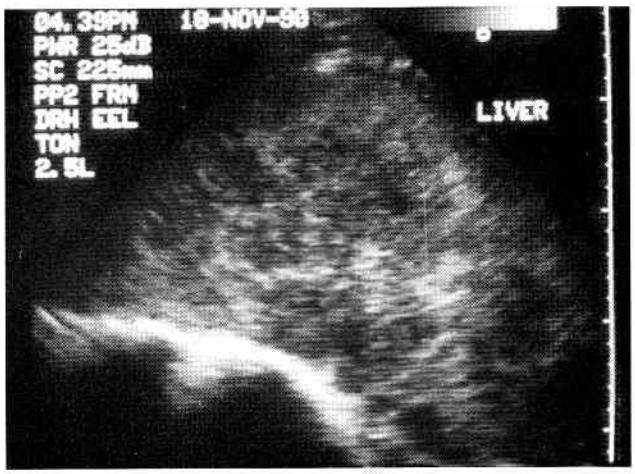

Figure 6-51

Sonogram of the right lobe of the liver obtained from a 15-year-old Appaloosa gelding with severe hepatocellular necrosis. The liver is markedly enlarged and heterogeneous, with multifocal areas of decreased echogenicity scattered throughout the liver. This sonographic appearance is very suggestive of hepatic neoplasia but was not confirmed at postmortem examination; only hepatocellular necrosis was detected. This sonogram was obtained from the right fourteenth intercostal space with a 2.5-MHz sector-scanner transducer at a displayed depth of 22.5 cm. The right side of this sonogram is dorsal and the left side is ventral.

Chronic Hepatic Fibrosis/Chronic Liver Disease. Hepatic fibrosis is another common cause of increased parenchymal echogenicity. Most horses with hepatic fibrosis have a smaller than normal liver, associated with chronic liver disease. However, horses with severe hepatic fibrosis have been imaged with hepatomegaly and echogenic hepatic parenchyma.[14] Hepatic cirrhosis, as a result of ragwort toxicity, has been reported in a group of horses.[169, 179] The liver in these horses was characterized by fibrosis of the periportal, central, and hepatic vein areas, megalocytosis, and bile duct proliferation. Megalocytic hepatopathy is most frequently found in horses after the chronic ingestion of plant[s] of the genus

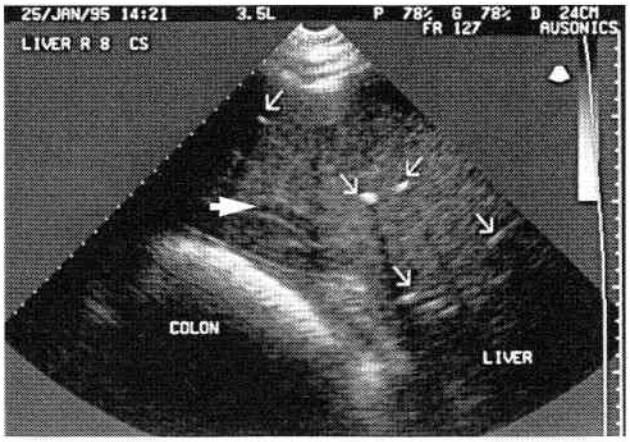

Figure 6–52

Sonogram of the right lobe of the liver obtained from a 22-year-old Quarter horse cross gelding with suppurative hepatitis. The liver is markedly enlarged with rounded borders. Notice the heterogeneous echogenicities within the liver, with hyperechoic areas casting acoustic shadows consistent with hepatolithiasis or areas of calcification (*three upper arrows*), areas of increased echogenicity (*lowest two arrows*), distention of the bile ducts with hypoechoic material (*large arrow*), and areas of decreased echogenicity. Normal parenchymal and vascular detail is lost. This sonogram was obtained from the right eighth intercostal space with a 3.5-MHz sector-scanner transducer at a displayed depth of 24 cm. The right side of this sonogram is dorsal and the left side is ventral.

Crotalaria, containing pyrrolizidine alkaloids, although acute pyrrolizidine alkaloid toxicosis does occur in horses that ingest large quantities of the plant over a short period of time.[168] The liver in affected horses and ponies is usually small and firm.[165, 166] In most horses with chronic liver disease, the initial cause of the hepatic injury leading to severe fibrosis is unknown. Hepatic cirrhosis and portal tract fibrosis are two additional causes of a bright liver in humans with liver disease.[178]

Cholangiohepatitis. Cholangiohepatitis occurs more frequently than suppurative hepatitis, usually in older horses with a history of fever of unknown origin, colic, icterus, and weight loss.[2, 17, 152] The majority of affected horses are 9 years of age or older.[142–147, 150, 152, 153] Hepatic encephalopathy and photosensitization have been less frequently reported.[152] Cholelithiasis has also caused duodenal obstruction in one horse.[151] The liver may be palpated rectally in some horses with marked hepatomegaly. A neutrophilic leukocytosis, hyperproteinemia, and hyperfibrinogenemia may be present.[142] Liver enzymes, especially those associated with the biliary tract (gamma-glutamyl transferase and alkaline phosphatase), serum bile acids, and bilirubin (total and direct) are usually elevated.[142, 153] Biliary reflux may be the cause of the cholangiohepatitis in many horses.[153] Enteric bacteria and vegetable matter have been found in one cholelith, suggesting a retrograde source of infection from the duodenum.[153]

Hepatic enlargement has been detected sonographically, at the time of surgical exploration of the abdomen or at postmortem examination, in the majority of horses with cholelithiasis reported in the literature.[142–145, 152, 154] The liver is usually markedly enlarged and often extends ventral to the costochondral junction of the ribs on the right side of the abdomen from the sixth through the fifteenth intercostal spaces.[152] Enlargement of the left lobe of the liver is less frequently detected and was appreciated in three of eight horses in one study.[152] However, the author has seen two older horses with severe longstanding cholangiohepatitis and hepatic fibrosis with small echogenic (fibrotic) livers at the time of initial ultrasonographic examination and smaller-than-normal and fibrotic livers at postmortem examination.

Increased echogenicity of the hepatic parenchyma may also be detected in horses with cholangiohepatitis (Fig. 6–53).[2] The increased echogenicity of the hepatic parenchyma is associated with a cellular infiltrate in the liver, most likely a combination of fibrosis and an inflammatory cell infiltrate (Fig. 6–54). Occasionally these sonographic findings are lacking in horses with acute cholangiohepatitis.[148] Biliary, portal, and interlobular fibrosis are common in horses with chronic cholangiohepatitis, detected sonographically as increased echogenicity of these areas and thickening of the bile ducts (Fig. 6–54), as is a neutrophil and mononuclear cell infiltrate. Neutrophilic and mononuclear cell infiltrate and hepatocyte necrosis are frequently detected.[142–144, 146, 147] Hepatocellular necrosis was detected in four of seven horses, two of which had suppurative cholangitis. Bacteria were cultured from liver tissue in four of seven horses with cholelithiasis, and in one horse gram-negative bacteria were detected on Gram's stain of the hepatic tissue but were not isolated on culture.[152] Periportal and intralobular fibrosis was detected histopathologically from all horses with cholelithiasis in one large study.[152] The degree of hepatic fibrosis may depend somewhat on the duration and degree of biliary obstruction and the severity of the associated cholangiohepatitis. Ultrasound-guided biopsy is im-

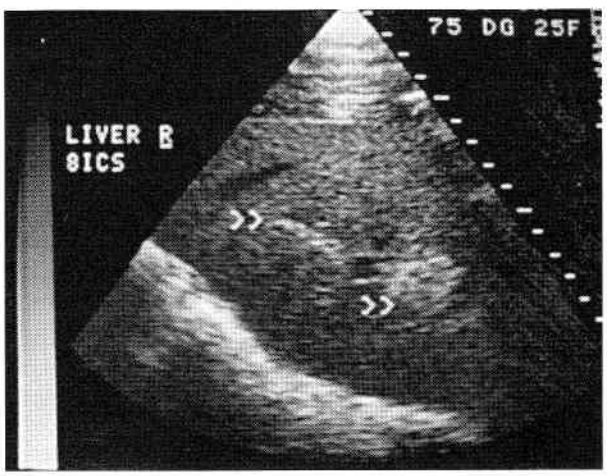

Figure 6–53

Sonogram of the right lobe of the liver obtained from a 10-year-old Quarter horse gelding with cholangiohepatitis. The liver is enlarged with irregular margins and rounded ventral borders. The parenchyma is more echogenic than normal with slightly heterogeneous echogenicity. Detail of the hepatic vasculature is poor. Echogenic material (*arrowheads*) fills the bile ducts, consistent with biliary sludge. This sonogram was obtained from the right eighth intercostal space with a 3.5-MHz sector-scanner transducer at a displayed depth of 17 cm. The right side of this sonogram is dorsal and the left side is ventral.

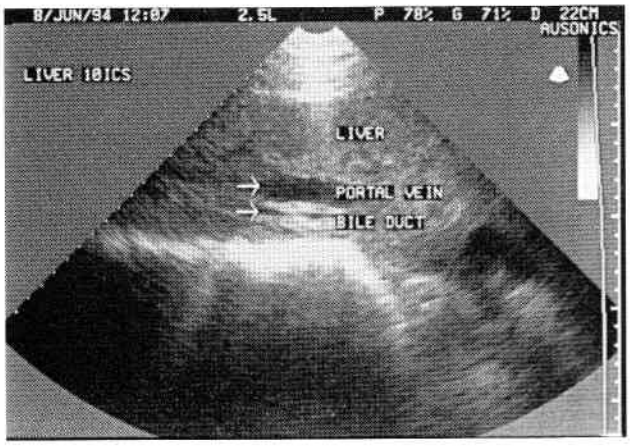

Figure 6–54

Sonogram of the right lobe of the liver obtained from a 5-year-old Arabian gelding with marked thickening of the bile duct and mild biliary distention (*lower arrow*). Notice the severe thickening of the walls of the bile duct as it parallels the portal vein (*upper arrow*). Detail of most of the hepatic vasculature is poor. The parenchyma of the liver is more echogenic than normal, with an increase in the parenchymal echogenicity in the periportal areas. The liver is enlarged and has rounded ventral margins. This sonogram was obtained in the right tenth intercostal space with a 2.5-MHz sector-scanner transducer at a displayed depth of 22 cm. The right side of this sonogram is dorsal and the left side is ventral.

portant to document the severity of the underlying liver disease. Histologic examination frequently shows increased connective tissue in the bile ducts and portal area and between the liver lobules.[142-147] Hepatic cirrhosis has been reported in one horse with cholelithiasis.[147]

Cholelithiasis. Mild to marked distention of the biliary tree is usually detected sonographically in horses with biliary obstruction associated with hepatolithiasis and cholangiohepatitis (Fig. 6–55).[144, 145, 150, 152, 154] The biliary distention becomes more severe in the caudal dorsal portions of the liver, the areas usually farthest away from the obstruction. In one study, all affected horses had distended bile ducts detected in the right lobe of the liver, whereas only 50% had these findings in the left liver lobe.[152] The parallel channel sign, caused by dilatation of the interhepatic biliary radicals adjacent to the portal vein, was detected in 50% of affected horses. The parallel channel sign is detected when the distended intrahepatic bile duct is imaged alongside the portal vein (Fig. 6–56; see also Fig. 6–54). Although the intrahepatic bile ducts were previously thought to have a constant relationship to the portal veins in humans, recent work has demonstrated no consistent relationship between the intrahepatic bile ducts and the corresponding portal veins.[180] It is likely that this is also the situation in horses, as both relationships (cranial and caudal to the portal veins) have been imaged in the horse. Bile duct proliferation and bile stasis are commonly detected histopathologically in horses with cholelithiasis.[142, 144-147, 152] Cholelithiasis should be suspected in all horses with bile duct dilatation, although the obstructing stone is not usually imaged.

Although a single stone may obstruct the common bile duct, most horses have multiple hepatoliths present within the biliary tree. The hepatolith completely or partially obstructing the common bile duct is often quite large (≥ 8 cm in diameter) but is usually inaccessible sonographically. However, the multitude of other hepatoliths scattered throughout the liver are usually easily imaged. As many as 50 small (2 to 15 mm) hepatoliths have been found in the intrahepatic ducts of horses with cholelithiasis by one investigator,[142] and up to 1000 concretions were reported by another investigator in the liver of a horse with cholelithiasis.[146] A single cholelith was detected obstructing the duodenum in one horse

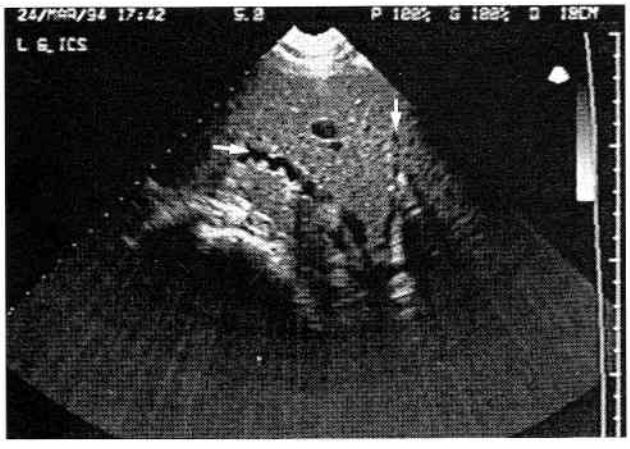

Figure 6–55

Sonogram of the left lobe of the liver obtained from a 6-year-old Thoroughbred mare with cholangiohepatitis. The bile ducts are dilated with a tortuous appearance and contain some echogenic debris within the lumen (*arrows*). The lining of the bile duct is irregular. The liver is enlarged and slightly hyperechoic, with rounded ventral margins. This sonogram was obtained in the left sixth intercostal space with a 5.0-MHz sector-scanner transducer at a displayed depth of 18 cm. The right side of this sonogram is dorsal and the left side is ventral.

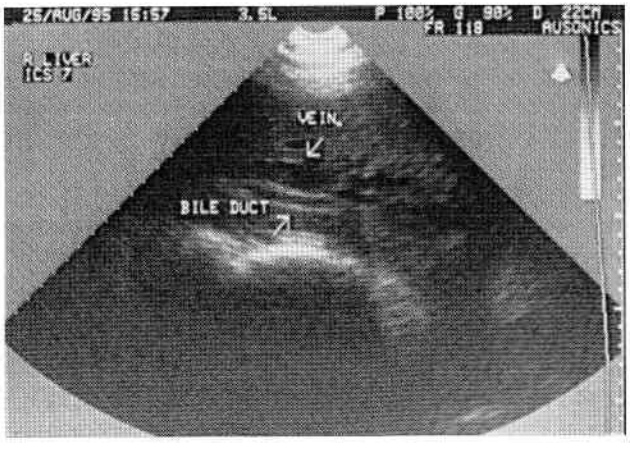

Figure 6–56

Sonogram of the right lobe of the liver obtained from a 7-year-old Thoroughbred gelding with cholangiohepatitis. The bile duct is mildly distended, and the walls of the bile duct are slightly thickened as it parallels the portal vein (parallel channel sign). The liver is enlarged and rounded. This sonogram was obtained in the right seventh intercostal space with a 3.5-MHz sector-scanner transducer at a displayed depth of 22 cm. The right side of this sonogram is dorsal and the left side is ventral.

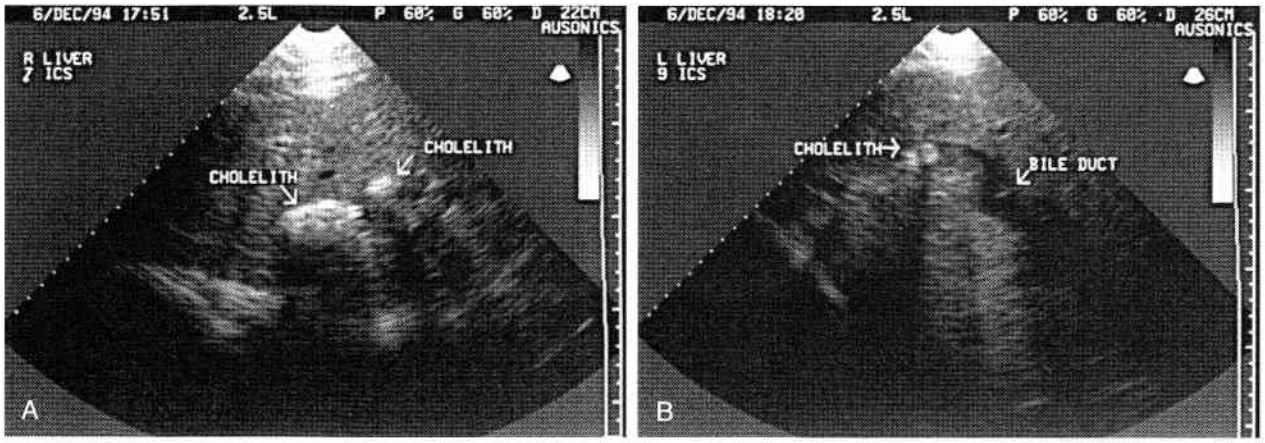

Figure 6–57

Sonograms of the liver obtained from both sides of the abdomen in an 8-year-old Thoroughbred mare with cholangiohepatitis, hepatolithiasis, and biliary distention. The liver parenchyma is homogeneously increased in echogenicity, and the liver is enlarged with rounded ventral borders and irregular margins. The vascular detail is poor. These sonograms were obtained from the right seventh (*A*) and left ninth (*B*) intercostal spaces with a 2.5-MHz sector-scanner transducer at a displayed depth of 22 cm (*A*) and 26 cm (*B*). *A*, Notice the large hyperechoic structures (*arrows*) casting acoustic shadows in the liver consistent with hepatoliths (cholehiths). These hepatoliths probably have a large proteinaceous component because the majority of the hepatolith is imaged prior to its casting an acoustic shadow. If the hepatolith were more calcified, the shadow would arise from the near surface of the calculus. The right side of this sonogram is cranial and the left side is caudal. *B*, Notice the smaller, more circular hepatoliths (cholehiths) casting an acoustic shadow (*horizontal arrow*) slightly farther caudally in the liver and the biliary distention (*angled arrow*), with some hypoechoic sludging material (biliary sludge) imaged within the bile duct, in addition to the hepatoliths. The right side of this sonogram is dorsal and the left side is ventral.

with seven 1- to 2-cm cholehiths present within the stomach and a few small cholehiths in the pancreatic duct.[151]

Cholehiths were imaged sonographically in 75% of horses with cholelithiasis in one study.[152] Multiple cholehiths were imaged in all but one of these horses, and in that horse, multiple cholehiths were suspected because of the marked biliary distention detected and the lack of complete biliary obstruction by the one detected cholelith. Multiple cholehiths were detected in all but one of the seven horses that had a postmortem examination performed, and in that horse the single obstructing cholelith was not detected sonographically.[152] The cholehiths detected sonographically were most frequently imaged in the cranioventral portion of the right lobe of the liver, primarily in the sixth to eight intercostal spaces.[2, 152] The entire liver, especially the cranioventral portion, should be carefully scanned for cholehiths in all horses with biliary distention because the stones tend to accumulate ventrally.

Hepatoliths usually appear as hyperechoic structures within the biliary tree casting variable acoustic shadows through the deeper tissues (Fig. 6–57). In some horses the cholehiths do not cast any acoustic shadow (Fig. 6–58). Strong acoustic shadows were detected from the cholelith in 50% of affected horses, in 33% of horses the acoustic shadows cast were faint, and in the remaining horse the cholehiths imaged did not cast any acoustic shadow.[152] These imaged cholehiths measured between 2 mm and 12 cm sonographically and between 3 mm and 12 cm at postmortem examination. Both shadowing (Fig. 6–57) and nonshadowing (Fig. 6–58) cholehiths have been imaged in horses with cholelithiasis.[2, 3, 14, 145, 150, 154] Large hyperechoic structures casting distinct acoustic shadows have been imaged in a horse with hepatolithiasis and biliary obstruction.[145] In this report, a large echogenic region casting an acoustic shadow was imaged in the liver with dilated hepatic ducts lateral to the portal vein.[145] The large hyperechoic structure casting an acoustic shadow imaged prior to surgery was no longer detectable following surgical removal of three large and multiple small cholehiths. The biliary distention and hepatomegaly persisted in this horse.

Hepatoliths are stones that are present within the intra-

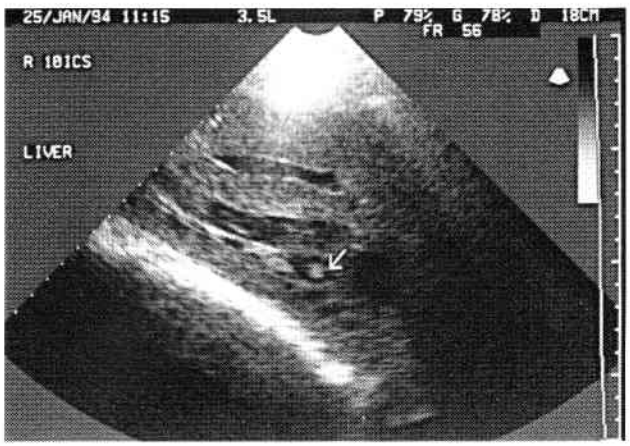

Figure 6–58

Sonogram of the right lobe of the liver obtained from an 11-year-old Standardbred mare with cholangiohepatitis and cholelithiasis. Numerous small round to oval echogenic hepatoliths in the mildly distended bile duct parallel the portal vein (parallel channel sign). Although the bile duct contains many small hepatoliths, none casts an acoustic shadow. The liver is enlarged with a rounded border, and the echogenicity of the parenchyma is increased. This sonogram was obtained from the right tenth intercostal space with a 3.5-MHz sector-scanner transducer at a displayed depth of 18 cm. The right side of this sonogram is dorsal and the left side is ventral.

hepatic ducts above the right and left hepatic ducts. Choledocholeliths are calculi located within the common bile duct or the hepatic duct. Choleliths can be variable in composition and can be firm or friable. Ascarid eggs have been found in the center of intrahepatic stones in a horse and were postulated to be the nidus for calculus formation.[155] A foreign body (wooden stick) was thought to be the nidus for calculus formation in one horse with choledocholithiasis.[154] Although hepatoliths can occasionally be detected at postmortem examination in horses with no antemortem signs of hepatic disease, underlying hepatic disease should always be suspected in horses in which hepatoliths are found. Hepatoliths are occasionally imaged as an incidental finding in horses with no clinical or clinical laboratory evidence of liver disease (Fig. 6-59). These horses were having thoracic or abdominal ultrasound examinations performed for another reason when the hepatoliths were discovered. Evaluation of liver enzymes in these horses revealed no abnormalities, although one horse with pleuropneumonia developed suppurative hepatitis 1 year after the detection of hepatolithiasis (Fig. 6-60).

Hepatoliths in horses have variable composition but usually contain bile pigments, bile acids, and protein.[142, 145] Cholesterol, choleic acid esters, and carboxylic acid esters were reported in the analysis of some of the biliary calculi obtained from horses.[142, 147] Calcium has also been reported in equine hepatoliths.[142] In 66% of stones analyzed from one study of horses with cholelithiasis, the stones were composed primarily of calcium bilirubinate.[152] Calcium phosphate was the predominant component in one horse, and sodium taurodeoxychoate was the principal component in another. All stones analyzed contained bile pigments at a percentage of 20% or less. Cholesterol was detected in five of six horses but was 10% or less of the total content of the choleliths. In one horse with an obstructing cholelith, the stone was 25% cholesterol and 75% calcium bilirubinate.[151] No correlation between the composition of the stones and their mineral content has been found in horses with cholelithiasis.[142] No association has been found between the chemical composition of the cholelith and its shadowing properties in the horse.[152] In humans with cholelithiasis, cholesterol-containing stones usually cast a reverberation or comet-tail artifact owing to the large amount of cholesterol within the stone. In horses, however, the percentage of cholesterol contained within the stones usually does not exceed 10%, not enough cholesterol to produce the reverberation artifact. The acoustic shadow is more likely to be related to the relationship between the cholelith and the ultrasound beam. Choleliths with a flat surface facing the ultrasound beam cast the strongest acoustic shadow. This clean acoustic shadow is produced because a large amount of the ultrasound is absorbed within the cholelith.

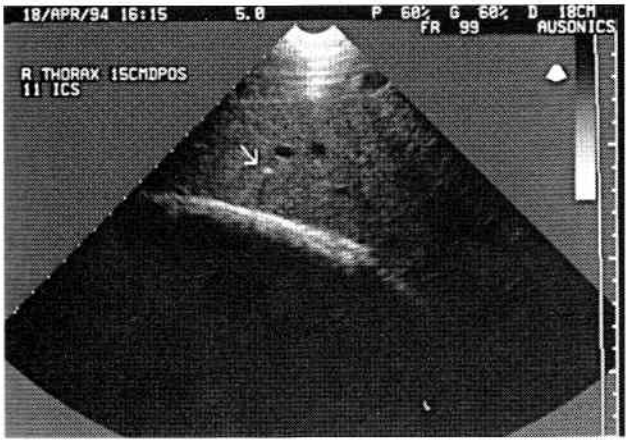

Figure 6–59

Sonogram of a small hepatolith obtained from a 10-year-old Arabian mare. This hepatolith was imaged as an incidental finding during a sonographic examination of the thoracic cavity. The hepatolith is very small and hyperechoic and casts a strong acoustic shadow (*arrow*). This sonogram was obtained from the right eleventh intercostal space with a 5.0-MHz sector-scanner transducer at a displayed depth of 18 cm. The right side of this sonogram is dorsal and the left side is ventral.

Most horses with cholelithiasis have chronic liver disease. Chronic liver disease results in increased parenchymal echogenicity, a more lobular contour of the liver surface, and decreased overall size of the liver. In one study, all horses with cholelithiasis had increased hepatic parenchymal echogenicity.[152] The echogenicity of the liver was equal to that of the spleen in seven of eight horses. The increased parenchymal echogenicity is usually present diffusely throughout the liver. Focal areas of increased parenchymal echogenicity have been detected, however, in horses with cholelithiasis.[152] Hypoechoic material may be imaged in the bile ducts of some affected horses (see Fig. 6-53). Thickening of the walls of the bile ducts may also be detected and may be more evident than the biliary sludge or biliary distention (see Fig. 6-54). The combination of an enlarged liver, increased parenchymal echogenicity, mild biliary distention with or without biliary sludge, and biliary wall thickening is consistent with a diagnosis of cholangiohepatitis.[2, 144, 145, 150, 152] Sonographic examination of the liver in affected horses can be used to select a site for an ultrasound-guided liver biopsy.

Hepatic Lipidosis. Hepatic lipidosis has been seen in horses with pituitary adenomas, hyperlipemia, and aflatoxicosis.[167, 169-171] Hyperlipemia can be primary or secondary and occurs most frequently in ponies, donkeys, and miniature horses.[171, 181] Lipid accumulation in the liver occurs with prolonged increases in serum triglyceride concentrations, as well as in the kidney, myocardium, and skeletal muscle, impairing the function of these organs.[171] With marked hepatic lipidosis the liver becomes friable, and hepatic rupture and death can occur.[181]

Sonographic examination of the liver of horses with pituitary adenomas and hepatic lipidosis has revealed generalized hepatomegaly and a diffuse increase in parenchymal echogenicity, with some loss of the normal hepatic architecture (Fig. 6-61).[2] The increased echogenicity of the liver parenchyma in horses with hepatic lipidosis is due to the relatively low acoustic impedance of fat relative to soft tissue. This increased parenchymal echogenicity, vascular blurring, blurring of the liver margins, and deep attenuation have been reported in humans and cattle with fatty infiltration of the liver.[175, 176, 178, 182] Fatty infiltration of the liver is also one of the causes of "bright liver" in humans.[178] In humans the accuracy of

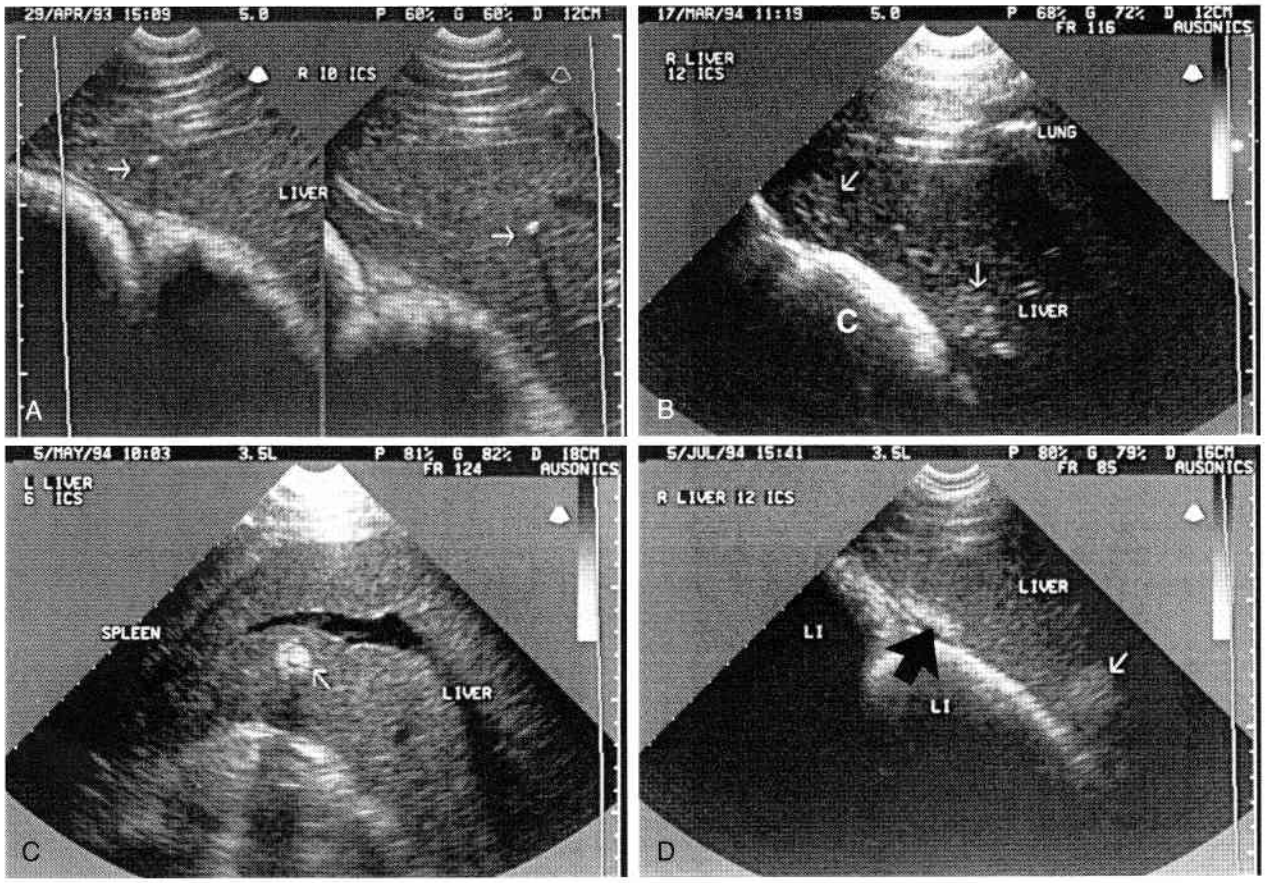

Figure 6–60

Sonograms of the liver obtained from both sides of the abdomen in a 4-year-old Thoroughbred stallion with suppurative hepatitis. The right side of these sonograms is dorsal and the left side is ventral. *A*, Sonograms obtained from the right tenth intercostal space demonstrating small incidental hepatoliths (*arrows*). These hepatoliths were discovered during a thoracic ultrasound examination for pleuropneumonia 11 months before the horse developed suppurative hepatitis. Notice the sharp ventral border of the right lobe of the liver in the left image. The right image is more dorsal and the left is more ventral in the right tenth intercostal space. These sonograms were obtained with a 5.0-MHz sector-scanner transducer at a displayed depth of 12 cm. *B*, Sonogram obtained from the right twelfth intercostal space 11 months later when the horse presented with acute signs of sepsis and liver disease. Notice the multifocal areas of increased echogenicity with a slightly heterogeneous appearance *(arrows)* and the slight bulging of the medial surface of the liver adjacent to the echo from the large colon (C). An ultrasound-guided biopsy revealed a suppurative hepatitis. This sonogram was obtained with a 5.0-MHz sector-scanner transducer at a displayed depth of 12 cm. *C*, Sonogram of a small hepatic abscess (*arrow*) in the left lobe of the liver obtained 7 weeks later. The abscess has a cavitated echogenic center, and the left lobe of the liver is enlarged and somewhat rounded. This sonogram was obtained from the left sixth intercostal space with a 3.5-MHz sector-scanner transducer at a displayed depth of 18 cm. *D*, Sonogram of the right lobe of the liver in the twelfth intercostal space (same as in *B*) demonstrating the multifocal areas of increased parenchymal echogenicity (*arrows*). These areas are more homogeneous and echogenic than 4 months earlier and no longer cause bulging of the surface of the liver. The one adjacent to the large intestine (LI) is very echogenic (*black arrow*) and represents an area of hepatic fibrosis. The liver remains enlarged, with loss of the normal parenchymal detail. This sonogram was obtained with a 3.5-MHz sector-scanner transducer at a displayed depth of 16 cm.

sonographic detection of fatty liver increases as the fatty infiltration becomes more severe, with an accuracy of 90% in patients with severe fatty infiltration.[183] In cattle, the sensitivity and specificity of increased parenchymal echogenicity and deep attenuation of the ultrasound were excellent for severe fatty infiltration.[184] However, the sensitivity of the hyperechoic liver pattern, deep attenuation of the ultrasound beam, or a combination of the two assessments was poor overall, with attenuation of the ultrasound beam having the most sensitivity for detection of fatty infiltrate. Liver-kidney contrast has also been used successfully in humans to diagnose fatty infiltration of the liver because fatty change rarely occurs in the human kidney.[185] In contrast, fatty infiltration of the kidney was seen in more than half the cattle with fatty infiltration of the liver. Liver-kidney contrast was useful in the cows with severe fatty infiltration of the liver only when deposition of fat in the liver was greater than in the renal cortex.[186]

Granulomatous Liver Disease. An increase in parenchymal echogenicity was imaged in several horses with diffuse granulomatous disease (Fig. 6-62). The increase in parenchymal echogenicity is slightly heterogeneous in most horses, with a more multifocal miliary distribution seen in one horse (Fig. 6-63). The liver has been markedly enlarged in all horses with slightly irregular and rounded margins. The majority of the hepatic and portal veins were not detectable. One horse had blurring of the hepatic veins and loss of the normal hepatic architecture.[2]

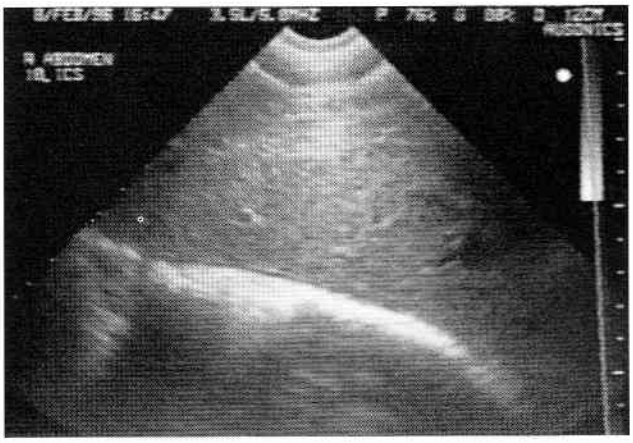

Figure 6–61

Sonogram of the liver obtained from a 22-year-old Appaloosa gelding with a pituitary adenoma and hepatic lipidosis. Notice the large amount of the liver imaged in the 10th intercostal space and the increased echogenicity of the hepatic parenchyma with poor architectural detail. The ventral margin of the right and left sides of the liver extended ventral to the costochondral junction. This sonogram was obtained with a wide-bandwidth 3.5-MHz sector scanner transducer operating at 5.0 MHz at a displayed depth of 12 cm. The right side of this sonogram is dorsal and the left side is ventral.

Hepatic Amyloidosis. Amyloidosis has also been reported in horses, resulting in hepatic lipidosis.[169] A horse with hepatic amyloidosis has been examined by the author and found to have a larger amount of hepatic parenchyma imageable than normal, increased parenchymal echogenicity and poor detail of the vascular markings. Hepatic amyloidosis in cattle was characterized by a bright echo pattern, with increased parenchymal echogenicity and blurring of the hepatic margins.[182]

Hepatic Abscess. Liver abscesses can result from septicemia and the development of suppurative hepatitis,

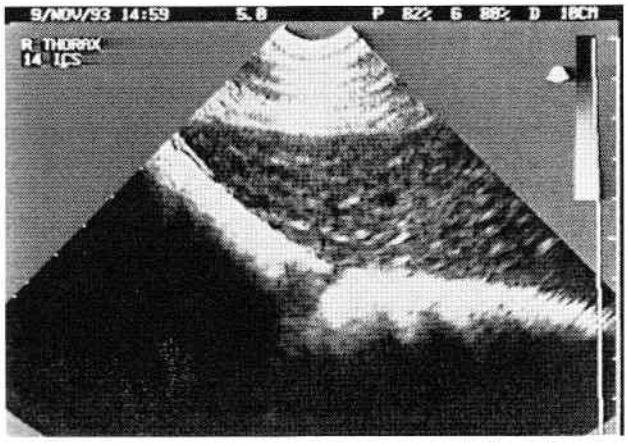

Figure 6–62

Sonogram of the right lobe of the liver obtained from a 20-year-old Appaloosa mare with liver disease. Notice the heterogeneous appearance of the right lobe of the liver, which is enlarged and extends ventrally nearly to the costochondral junction. The ventral tip of the right lobe of the liver is slightly rounded. Evidence of granulomatous infiltrate and nodular regeneration was seen on biopsy. This sonogram was obtained from the right fourteenth intercostal space with a 5.0-MHz sector-scanner transducer at a displayed depth of 10 cm. The right side of the sonogram is dorsal and the left side is ventral.

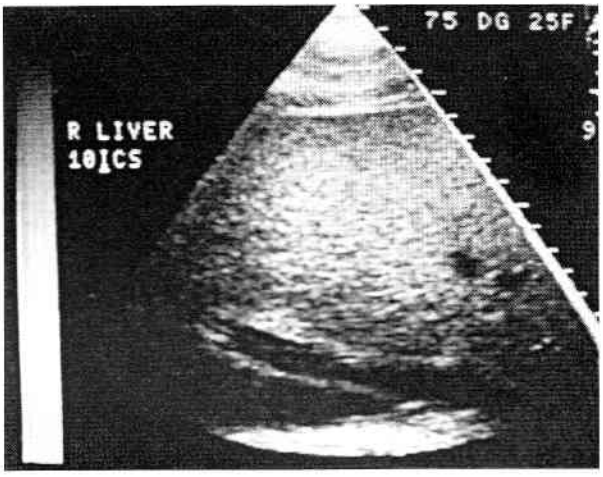

Figure 6–63

Sonogram of the right lobe of the liver obtained from an 18-year-old Paint gelding with diffuse granulomatous disease. The liver is markedly enlarged with rounded borders. The parenchyma of the liver is markedly increased in echogenicity, with loss of the normal small vascular detail. Irregular areas of the liver with poorly defined margins appear extremely bright. A liver biopsy revealed numerous pyogranulomas scattered throughout the hepatic parenchyma. No etiologic agent was identified. This sonogram was obtained from the right tenth intercostal space with a 3.5-MHz sector-scanner transducer at a displayed depth of 17 cm. The right side of this sonogram is dorsal and the left side is ventral.

from direct spread from an infected area, or from a penetrating wound to the abdomen and the liver. Ten of 15 horses with abdominal abscesses had abscesses detected in the liver in one large study,[5] whereas only 2 of 25 horses had liver abscesses in another large study.[118] A liver abscess associated with *Escherichia coli* was detected at postmortem examination in one horse with cholelithiasis and hepatic cirrhosis.[147]

Liver abscesses are usually poorly marginated and hypoechoic when scanned early in the course of the disease (Fig. 6-64) and become better defined, encircled by more echogenic inflammatory tissue, as the abscess progresses (see Fig. 6-60). Liver abscesses can also appear as discrete focal areas of increased echogenicity within the hepatic parenchyma.[14] Liver abscesses are described by one investigator as denser fluid-filled structures located subcapsularly or intraparenchymally that may occasionally be compartmentalized.[3] Hepatic abscesses have been imaged ultrasonographically in cattle inoculated with *Fusobacterium necrophorum* and in calves with umbilical vein infection.[187, 188] Initially, hyperechoic foci were imaged that corresponded to necrotic foci. These spherical hyperechoic areas were imaged as early as 3 days after inoculation of the liver with *F. necrophorum*.[187] By day 8 the adjacent hyperechoic areas had coalesced to form one larger abscess characterized by a hyperechoic capsule enclosing anechoic fluid and hyperechoic material determined at necropsy to represent purulent material and inspissated debris.[187] In other affected cattle, hyperechoic areas surrounded by a hypoechoic halo were subsequently imaged and corresponded to necrotic tissue surrounded by granulation tissue.[188] The central hyperechoic area changed to hypoechoic in some cows, with a subsequent capsule and scar of the abscess that was

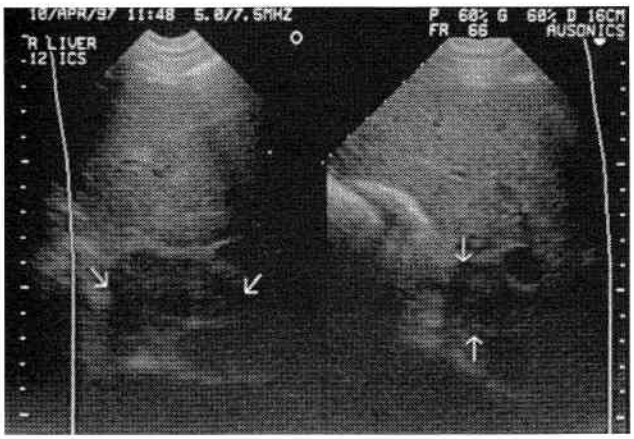

Figure 6–64

Sonograms of the liver obtained from a yearling Tennessee Walker gelding with a hepatic abscess. The poorly defined hypoechoic oval structure adjacent to the caudal vena cava and portal vein is the hepatic abscess (*arrows*). The parenchyma of the liver has multifocal areas of increased echogenicity, with a somewhat heterogeneous appearance. A necrotizing hepatitis was diagnosed on histopathologic examination of the hepatic parenchyma and several gram negative organisms grew from a culture of the peritoneal fluid. These sonograms were obtained with a wide-bandwidth 5.0-MHz sector scanner transducer operating at 7.5 MHz at a displayed depth of 16 cm. The right side of the right image is dorsal and the left side is ventral. The right side of the left image is cranial and the left side is caudal.

isoechoic or remained hypoechoic once the abscesses resolved.[188]

Cystic Liver Disease. Equine hydatidosis has been reported primarily in Great Britain, where it reached epidemic proportions in the mid-1970s.[173, 174] Affected horses were of all ages and rarely exhibited clinical signs. Multiple hydatid cysts were detected throughout the liver in affected horses and could be imaged sonographically if routine screening was done. Routine sonographic screening of the liver in sheep and goat herds has been successful in detecting occult hydatidosis in Africa.[189] In humans with hydatid disease of the liver, a single spherical cyst, a flattened spherical cystic area, a cyst within a cyst, and a complex cyst mass have been detected sonographically. The detection of daughter cysts within the complex internal echoes is diagnostic of hydatid cyst disease.[190, 191]

Hepatic cysts can be located in the hepatic parenchyma or subcapsularly.[3] Multiple hepatic cysts were detected sonographically in one horse with thoracic granular cell tumor and hypertrophic osteopathy.[172] Cavitary fluid-filled cystic structures ranging in size from 5 to 20 cm in diameter were imaged throughout the right lobe of the liver of this horse. Normal hepatic tissue was imaged merging with the cystic structures. The liver was enlarged, extending caudally to the level of the paralumbar fossa, and displaced the right kidney 20 cm caudally. Liver enzymes (gamma-glutamyl transpeptidase and alkaline phosphatase) and total bilirubin were elevated in this horse and the serum albumin was decreased. Postmortem examination of this mare revealed multilocular hepatic cysts and severe chronic suppurative cholangiohepatitis.

Hepatic Neoplasia. Neoplastic infiltration of the liver occurs most frequently with lymphosarcoma, reported in 41% of horses with lymphosarcoma.[192] Elevated liver enzymes (gamma-glutamyl transferase, L-iditol dehydrogenase, aspartate transaminase, alkaline phosphatase) have been reported in horses with hepatic lymphosarcoma, although the primary presenting complaints in these horses were weight loss, anorexia, and lethargy.[193]

Hepatic lymphosarcoma usually results in a diffuse increase in the echogenicity of the liver, with loss of the normal parenchymal architecture associated with the diffuse cellular infiltrate (Fig. 6-65). Horses with hepatic lymphosarcoma have hepatomegaly, and the ventral margins of the liver are rounded (Fig. 6-66). The liver may often extend ventrally to the level of the costochondral junctions on the right side of the abdomen. In one horse with lymphocytic lymphosarcoma, diffuse infiltration of the liver with neoplastic cells was detected.[193] The liver reportedly had a homogeneous, slightly hyperechoic pattern with no architectural distortion detected sonographically. In horses with hepatic enlargement and a noticeable alteration in parenchymal texture, a diffuse neoplastic infiltrate such as lymphosarcoma should be suspected.[14] Discrete masses in an otherwise normal liver have been reported occasionally in horses with lymphosarcoma. In one report of three horses with lymphosarcoma, the two horses with multicentric lymphoblastic lymphosarcoma had nodules in the spleen and liver.[193] In only one of these horses was the neoplastic mass in the liver imaged sonographically. This mass had a complex pattern of echogenicity and appeared as a spherical, well-marginated hypoechoic mass (11 × 13 cm) with hyperechoic reflections from within. In the other horse the neoplastic nodules in the liver were small (1 to 6 mm) and located deep within the liver.

In humans with hepatic lymphoma, hypoechoic or

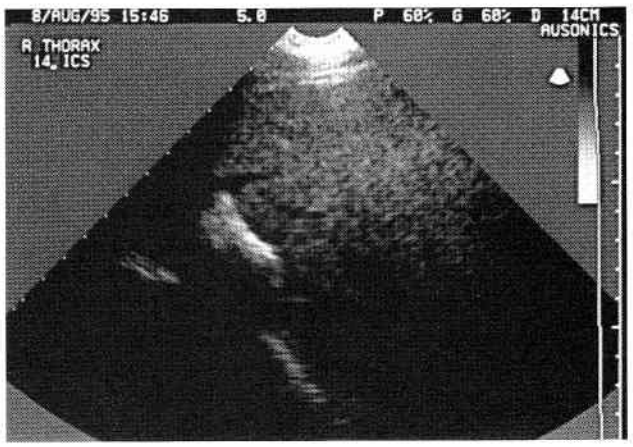

Figure 6–65

Sonogram of the right lobe of the liver obtained from a 16-year-old Thoroughbred gelding with multicentric lymphosarcoma. The right lobe of the liver is markedly enlarged, with loss of the normal vascular detail, marked rounding of the liver margins, and loss of the normal hepatic architecture. The echogenicity of the liver is normal to slightly increased. The ultrasound is rapidly attenuated in the deeper portions of the liver by the density of the hepatic tissue. This sonogram was obtained from the right side of the abdomen in the fourteenth intercostal space with a 5.0-MHz sector-scanner transducer at a displayed depth of 14 cm. The right side of this sonogram is dorsal and the left side is ventral.

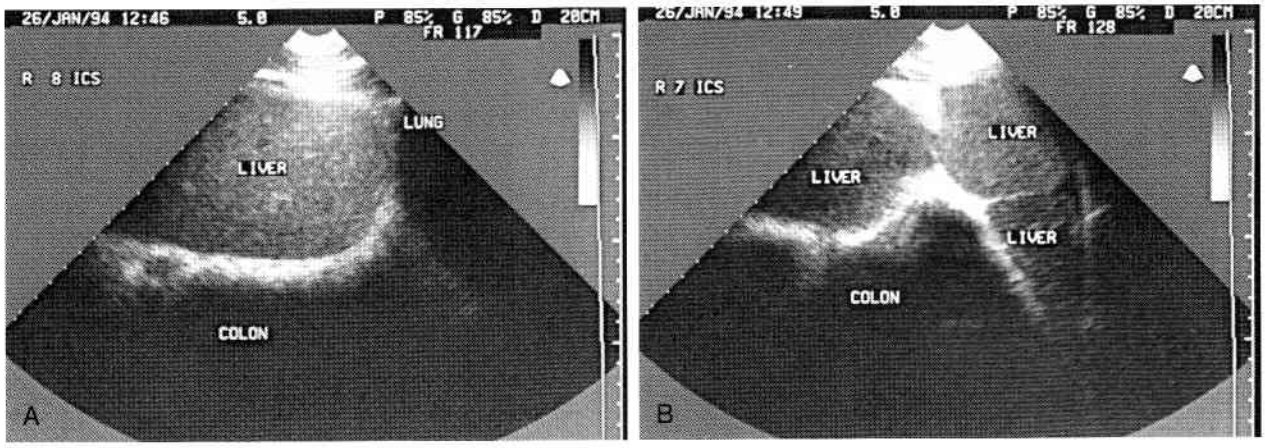

Figure 6–66

Sonograms of the right side of the liver obtained from an 18-year-old Appaloosa gelding with multicentric lymphosarcoma (same horse as in Fig. 6-47). The liver was markedly enlarged and extended ventrally beyond the costochondral junctions. Notice the relatively homogeneous appearance of the liver, the loss of vascular detail, and the loss of the normal hepatic architecture. The hyperechoic sacculated adjacent structure represents the large colon, most likely the right ventral colon. These sonograms were obtained with a 5.0-MHz sector-scanner transducer at a displayed depth of 20 cm. The right side of these sonograms is dorsal and the left side is ventral. *A*, The ventral border of the right lobe of the liver is markedly rounded, and the hepatic veins are almost imperceptible. This sonogram was obtained in the eighth intercostal space at the ventral most margin of the right lobe of the liver. *B*, The ventral border of the liver is multilobulated with markedly rounded ventral borders and complete loss of parenchymal detail. This multilobulated sonographic appearance is abnormal. This sonogram was obtained in the seventh intercostal space at the ventral most margin of the liver.

diffuse disease was detected in both Hodgkin and non-Hodgkin lymphoma, whereas target and echogenic lesions were detected only in the non-Hodgkin lymphoma.[194] Three ultrasonic patterns of canine hepatic lymphosarcoma have been described by one investigator.[195] The liver has either a normal parenchymal appearance or only a slight reduction in echogenicity in dogs with diffuse infiltration. Anechoic or hypoechoic, poorly marginated lesions or round echodensities surrounded by areas of sonolucency have been described.[195] In another study, the dogs with hepatic lymphosarcoma had diffuse, mildly hyperechoic livers or multifocal hypoechoic masses within the liver.[196]

Complex masses containing a composite of echogenicities are most common in horses with more aggressive neoplasms and have been imaged in horses with cholangiocarcinomas and hepatocellular carcinomas (Fig. 6-67).[197] Hepatocellular carcinomas in humans are thought to begin as small hypoechoic masses that later become isoechoic and then inhomogeneous and hyperechoic as they enlarge.[198] These tumors occur infrequently in horses. One horse with hepatocellular carcinoma had marked erythrocytosis.[197] The liver in this horse was markedly enlarged at postmortem examination, with severe destruction of the hepatic parenchyma by one large multilobulated 30-cm mass and 20 to 30 similar masses of 5 cm or less. The largest mass ruptured through the capsule of the liver and resulted in hemoperitoneum, the cause of death in this filly.[197] These tumor masses should have produced a composite sonographic appearance of the liver with complete loss of the normal architecture. In dogs, carcinomas in the liver usually have a focal or multifocal hyperechoic or mixed pattern of echogenicity.[196] A malignant hepatoblastoma has also been reported in a horse presenting with pleural effusion.[199] This horse had a markedly enlarged right liver lobe that displaced the stomach caudodorsally. A 45-cm round primary tumor mass and multiple 1- to 10-cm nodules were scattered throughout the rest of the liver. The largest mass contained cavitated areas on gross examination, which would have produced anechoic areas in the composite sonographic appearance of the large tumor mass in the liver.[199] An hepatic adenoma was imaged intraoperatively by the author in a yearling Morgan colt with hepatic encephalopathy. This tumor was characterized by irregularly shaped masses of homogeneous sonographic appearance that were nearly isoechoic with the normal hepatic parenchyma but completely disrupted the normal hepatic architecture (Fig. 6-68). The left lobe of the liver in this yearling was small, and images of the left lobe of the liver (affected lobe) could not be obtained from the transcutaneous window prior to surgery. In one yearling with hepatomegaly and nodules in the hepatic parenchyma that were slightly more echogenic than the surrounding tissue, a primary liver tumor of unknown type was diagnosed.[14] Increased peritoneal fluid is often detected in horses with advanced primary hepatic neoplasia as well as with severe metastatic neoplasia.

Multifocal masses scattered throughout the hepatic parenchyma are consistent with metastatic neoplasia and have been detected sonographically in one mule with renal adenocarcinoma.[131] In this mule the masses were of variable size and shape and were homogeneously hypoechoic relative to the surrounding normal hepatic parenchyma, invading the majority of the liver.[131] Significant elevations of gamma-glutamyl transpeptidase were detected in this mule. An ultrasound-guided liver biopsy revealed hepatic neoplasia, although the initial tentative diagnosis was hepatocellular carcinoma. Numerous metastases to the liver have been reported in horses with renal adenocarcinoma.[125, 127, 130, 169] Hepatic metastases were detected sonographically in two horses with intesti-

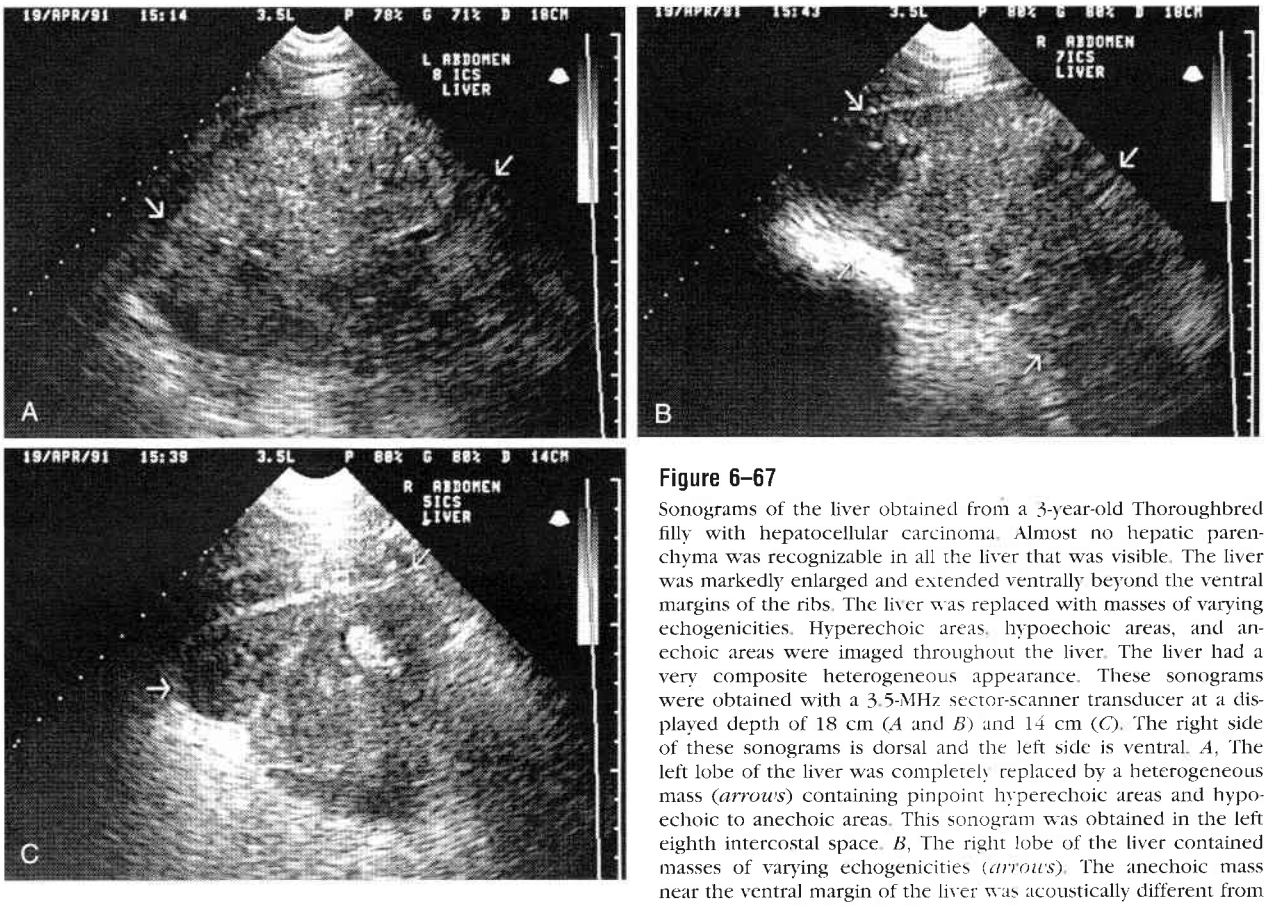

Figure 6–67

Sonograms of the liver obtained from a 3-year-old Thoroughbred filly with hepatocellular carcinoma. Almost no hepatic parenchyma was recognizable in all the liver that was visible. The liver was markedly enlarged and extended ventrally beyond the ventral margins of the ribs. The liver was replaced with masses of varying echogenicities. Hyperechoic areas, hypoechoic areas, and anechoic areas were imaged throughout the liver. The liver had a very composite heterogeneous appearance. These sonograms were obtained with a 3.5-MHz sector-scanner transducer at a displayed depth of 18 cm (*A* and *B*) and 14 cm (*C*). The right side of these sonograms is dorsal and the left side is ventral. *A*, The left lobe of the liver was completely replaced by a heterogeneous mass (*arrows*) containing pinpoint hyperechoic areas and hypoechoic to anechoic areas. This sonogram was obtained in the left eighth intercostal space. *B*, The right lobe of the liver contained masses of varying echogenicities (*arrows*). The anechoic mass near the ventral margin of the liver was acoustically different from the intervening liver. Dorsally a large composite mass was mostly hypoechoic compared with the remaining hepatic parenchyma. This sonogram was obtained in the right seventh intercostal space. *C*, The cranioventral margin of the right lobe of the liver had the appearance of a butterfly wing (*arrows*) and was heterogeneous, completely lacking in hepatic vascular detail or visible hepatic architecture, and contained an oval hyperechoic area. This sonogram was obtained in the fifth intercostal space.

nal adenocarcinoma.[4, 65] These appeared as numerous circumscribed lesions that were hypoechoic compared with the normal hepatic parenchyma with static B-mode ultrasonography.[65] Metastases to the liver have been imaged in one horse with squamous cell carcinoma of the urinary bladder (Fig. 6-69). Hepatic involvement is frequently detected in horses with metastatic melanoma.[6, 65] Homogeneous circular masses of decreased echogenicity were imaged in the liver of one pony with multiple hepatic melanomas.[6] The masses in the liver associated with metastatic melanoma usually appear homogeneous and somewhat circular sonographically (Fig. 6-70). In humans with metastases of a malignant melanoma to the liver, three types of sonographic appearance are seen. The metastases are either homogeneously hypoechoic and lack a "halo" sign (hypoechoic border around a center of varying echogenicities), hypoechoic metastases and metastases with "halo" signs, or metastases with "halo" signs and isoechoic metastases.[200] The positive and negative predictive value for hepatic ultrasonography in humans for the diagnosis of malignant liver lesions is 97% and 96%, respectively.[201]

Hepatic Lobe Torsion. Hepatic lobe torsion has been reported in the horse, resulting in septic peritonitis and a mass located between the stomach and the right lobe of the liver.[202] The left lobe of the liver was involved and was found to be congested and necrotic when surgically removed. Although it is unlikely that this mass could have been imaged prior to surgery, intraoperative ultrasonography could have been used to image the mass and further characterize it prior to resection. The detection of large dilated and congested portal veins and sinusoids, distended bile ducts, and multifocal areas of necrosis would result in a complex sonographic appearance with multiple areas of cavitation. Although rare, hepatic lobe torsion should be considered in the differential diagnosis of a composite hepatic mass involving only one lobe of the liver.

Other Liver Disease. Congenital vascular shunts, rare in horses, may also occur, resulting in hepatic encephalopathy (see Chapter 7).[2, 203] Hepatic venous enlargement in conjunction with decreased parenchymal echogenicity and hepatomegaly is consistent with passive congestion of the liver and right heart failure. Trauma to the liver from a blow to the abdomen may result in an hepatic fracture, hematoma, and/or hemoperitoneum. The hematoma usually appears as anechoic loculated fluid with echogenic or hyperechoic areas within, representing organizing clot. The blood in the peritoneal cavity also usually appears echogenic. The liver in horses is fairly well protected, however, by the ribs, and rib fractures are more likely than hepatic trauma.

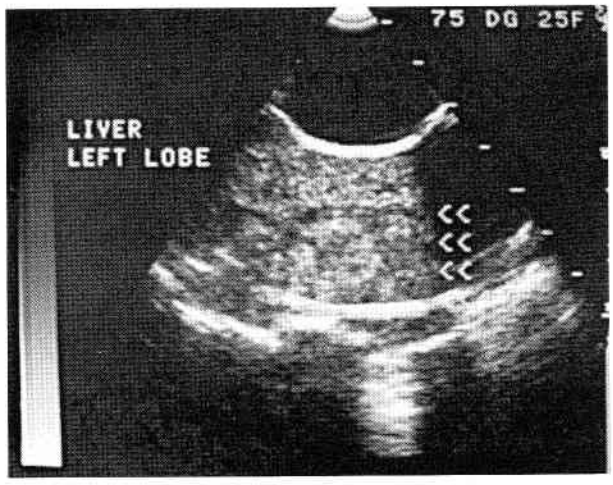

Figure 6–68

Sonogram of the left lobe of the liver obtained from a yearling Morgan colt with hepatic encephalopathy. The left lobe of the liver could not be imaged from the left side of the abdomen and was imaged intraoperatively during an exploratory celiotomy to look for evidence of a portacaval shunt. The left lobe of the liver had multiple masses scattered throughout this lobe, disrupting the normal hepatic parenchyma. The masses were heterogeneous with a complex pattern of echogenicity and appeared to have a swirling pattern within (*arrowheads*). Multiple small hyperechoic areas casting small acoustic shadows were imaged, consistent with areas of calcification. The echogenicity of the liver was increased overall, and the liver was smaller than normal. The right lobe of the liver was unaffected. The left lobe of the liver was removed, and a diagnosis of hepatoma was obtained on histopathologic examination of the tissue. This sonogram was obtained with a 7.5-MHz sector-scanner transducer containing a built-in fluid offset. The right side of this sonogram is cranial and the left side is caudal.

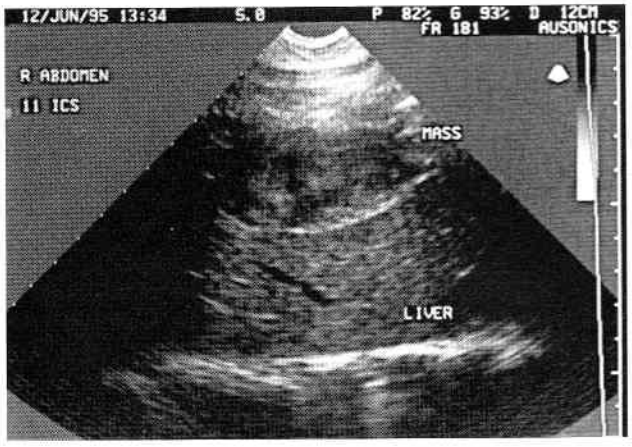

Figure 6–69

Sonogram of the liver obtained from a 24-year-old Standardbred stallion with squamous cell carcinoma of the urinary bladder that had metastasized to the capsular surface of the liver (same horse as in Fig. 6-24). Notice the composite appearance of the mass, well delineated from the remaining hepatic parenchyma. The right dorsal colon is medial to the liver. This sonogram was obtained in the right eleventh intercostal space with a 5.0-MHz sector-scanner transducer at a displayed depth of 12 cm. The right side of this sonogram is cranial and the left side is caudal.

Abnormalities of the Spleen

Splenic Neoplasia. Splenic abnormalities are most common in horses with abdominal neoplasia.[2, 192, 204-207] Lymphosarcoma is the most common splenic neoplasm

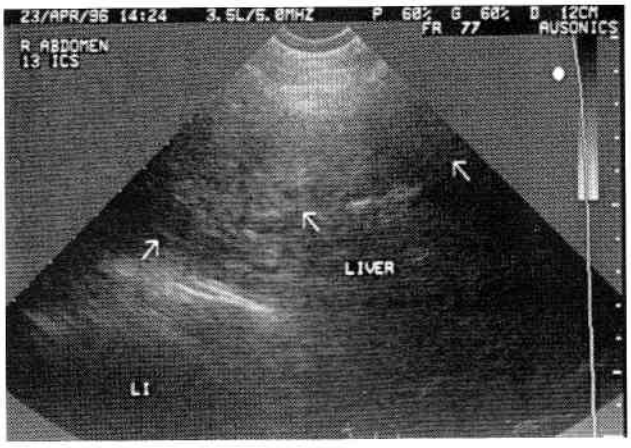

Figure 6–70

Sonogram of the right lobe of the liver obtained from a 17-year-old Oldenberg gelding with metastatic melanoma. A mass (*arrows*) in the right lobe of the liver replaces the normal hepatic parenchyma with hypoechoic heterogeneous tissue, which is slightly more echogenic than the normal hepatic parenchyma. This mass appeared to be confluent with a large sublumbar and perirenal mass on the right side of the abdomen. The metastatic melanoma covered the entire peritoneal surfaces and involved the right lobe of the liver.

in the horse, but other tumors can metastasize to the spleen. Splenic involvement has been reported in 37% of horses with lymphosarcoma.[192] Weight loss, anorexia, lethargy, and fever are common in horses with splenic lymphosarcoma. Splenic lymphosarcoma usually results in marked enlargement of the spleen, with masses bulging from the surface of the spleen adjacent to areas of more normal splenic parenchyma. In most affected horses the majority of the spleen is affected, with little normal splenic parenchyma remaining. The spleen may exceed 25 cm in thickness and extend from the left paralumbar fossa into the cranial most portion of the left abdomen, across the ventral midline. The cranial pole of the spleen in horses with marked splenic enlargement can often be imaged in the right cranial ventral portion of the abdomen.

Splenic masses may be well marginated or irregular in shape. These masses are usually sonographically complex and contain anechoic to hyperechoic areas (Fig. 6-71), often with acoustic shadowing associated with calcification.[2] In several horses with splenic lymphosarcoma, the splenic masses were hypoechoic, with interspersed normoechoic and hyperechoic reflections.[19, 193] In one horse the neoplastic spleen was described as containing irregularly shaped hyperechoic nodules with anechoic areas interspersed between the hyperechoic areas.[204] A miliary multifocal distribution of lymphosarcoma masses (Fig. 6-72) or a diffuse neoplastic infiltrate (Fig. 6-73) is uncommon in horses with lymphosarcoma. Generalized infiltration of the spleen was reported in one horse in addition to the detection of multiple small masses scattered throughout the splenic parenchyma.[65] The mass detected sonographically in this horse was described as echolucent, medial to the spleen and adjacent to the gastric wall.[65] This mass encompassed the aorta, renal arteries, cranial mesenteric arteries, and portions of the pancreas and kidneys. A hypoechoic splenic nodule has been detected sonographically in three horses with

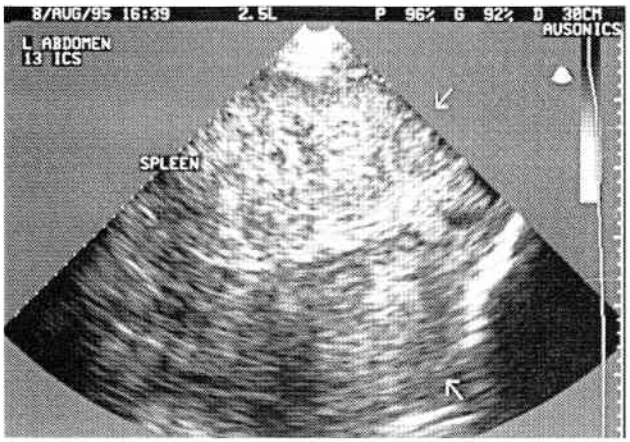

Figure 6–71

Sonogram of the spleen obtained from a 16-year-old Thoroughbred gelding with multicentric lymphosarcoma. The spleen has a very large hyperechoic mass with a complex sonographic appearance completely disrupting the normal splenic architecture (*arrows*). The mass caused marked splenic enlargement and an irregular capsular surface. Only a small amount of normal splenic parenchyma could be located sonographically. This sonogram was obtained from the left thirteenth intercostal space with a 2.5-MHz sector-scanner transducer at a displayed depth of 30 cm. The right side of this sonogram is dorsal and the left side is ventral.

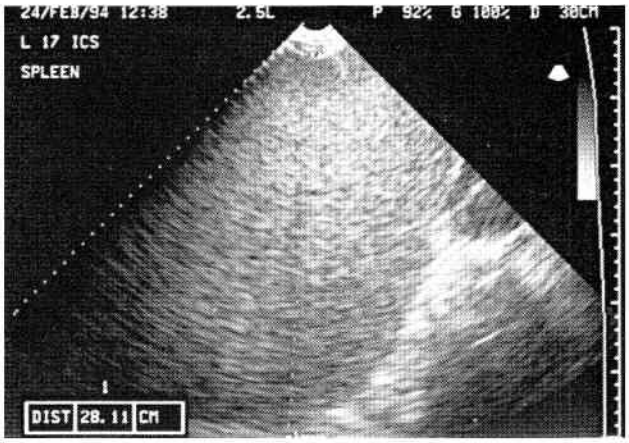

Figure 6–73

Sonogram of a markedly enlarged spleen obtained from a 24-year-old Thoroughbred mare with splenic lymphosarcoma. The spleen measures 28.11 cm thick at this location and has a bulging rounded appearance. The splenic parenchyma is slightly heterogeneous, and the normal architecture of the spleen in not visible. This sonogram was obtained from the seventeenth intercostal space with a 2.5-MHz sector-scanner transducer at a displayed depth of 30 cm. The right side of this sonogram is dorsal and the left side is ventral.

lymphosarcoma.[193, 208] Both complete replacement of the normal spleen with a composite echogenicity as well as multiple irregular to circular complex masses adjacent to areas of normal spleen have been reported in horses with splenic lymphosarcoma.[19, 204] Transrectal sonographic examination of the splenic masses reveals similar sonographic findings if the caudal pole of the spleen is involved, but image quality is usually superior. Transrectal imaging of caudal pole of the spleen in one horse with lymphosarcoma revealed a splenic mass with a complex pattern of echogenicity. Ascites has also been reported in horses with splenic and hepatic lymphosarcoma.[193]

Hypoechoic nodules have also been imaged in horses with metastatic melanoma (Fig. 6–74). In most horses with metastatic melanoma in the spleen, the masses are small and homogeneous, but larger masses have been detected in a horse with malignant melanoma.[65] The sonographic appearance of splenic metastases in a horse with malignant melanoma has been described as multiple masses 6 to 12 cm in diameter located throughout the

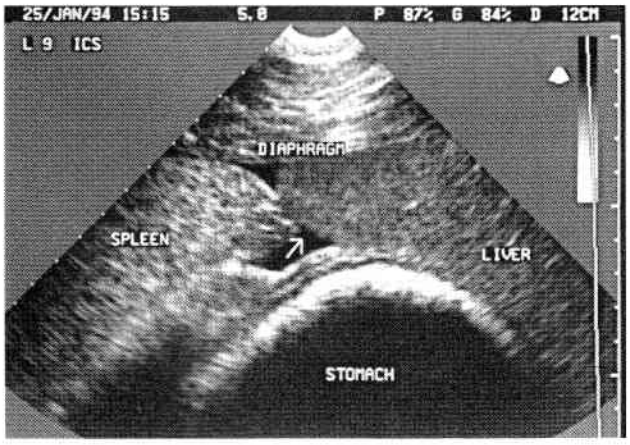

Figure 6–72

Sonogram of the spleen, liver, and stomach obtained from an 18-year-old Appaloosa gelding with generalized lymphosarcoma (same horse as in Fig. 6–47). The spleen has a very heterogeneous sonographic appearance associated with a miliary multifocal distribution of neoplastic lymphocytes. A mass of similar echogenicity extends from the splenic border to the adjacent stomach wall in the region of the gastric lymph node but does not appear to invade the gastric lumen. The gastric lymph node was also infiltrated with neoplastic lymphocytes. The liver is enlarged and has a rounded ventral border (*arrow*) with loss of the normal hepatic architecture and vascular detail consistent with neoplastic infiltration of the liver. This sonogram was obtained from the left ninth intercostal space with a 5.0-MHz sector-scanner transducer at a displayed depth of 12 cm. The right side of this sonogram is dorsal and the left side is ventral.

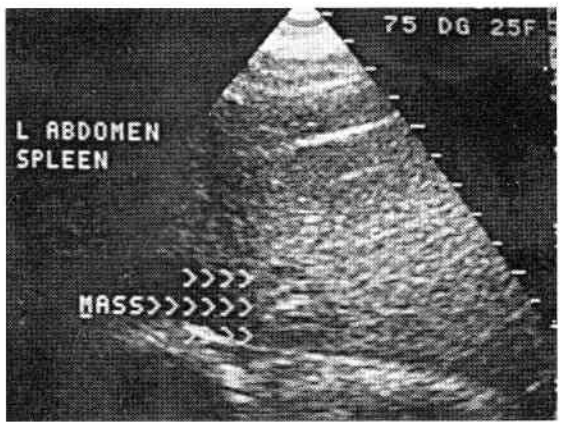

Figure 6–74

Sonogram of the spleen obtained from a gray 12-year-old Thoroughbred gelding with perirectal melanoma. The horse presented with chronic colic, prompting an abdominal ultrasound examination. A small heterogeneous mass was found in the spleen that replaced the normal splenic architecture but did not disrupt the surface of the spleen. A splenic melanoma was suspected, but the owner declined a biopsy of this mass.

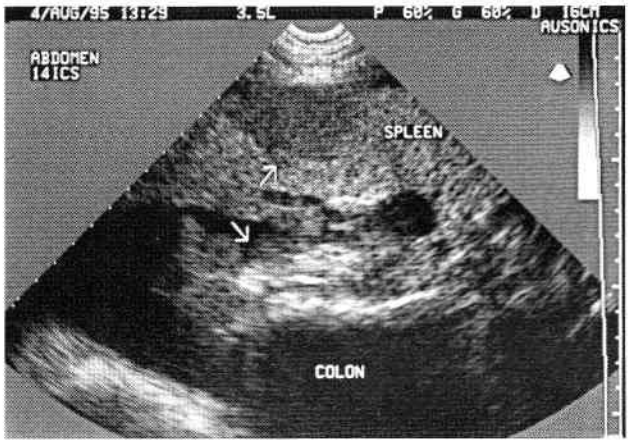

Figure 6–75

Sonogram of the spleen obtained from an 18-year-old half-Arabian gelding with gastric squamous cell carcinoma. The homogeneous, hypoechoic, somewhat circular mass in the spleen that replaces the normal splenic parenchyma (*up arrow*) is a metastasis of the gastric squamous cell carcinoma. The spleen also appears adhered to the large colon along the medial surface of the spleen immediately caudal to the stomach at the splenic vein. The mesentery of the large colon appears thickened and more echogenic than normal (*down arrow*), and a hypoechoic mass appears to be attached to the mesentery immediately to the left of the down arrow. The large anechoic circular structure is the splenic vein. This sonogram was obtained from the left fourteenth intercostal space with a 3.5-MHz sector-scanner transducer at a displayed depth of 16 cm. The right side of this sonogram is dorsal and the left side is ventral.

spleen.[6, 65] These masses appeared homogeneous and hypoechoic relative to the echogenicity of the spleen. Metastatic nodules have been detected sonographically in the spleen in horses with gastric squamous cell carcinoma (Fig. 6–75).[6] These nodules have most typically appeared as hypoechoic, somewhat circular nodules. In horses with splenic neoplasia, a peritoneal effusion, usually serosanguinous, may be present. With peritoneal effusion, the abdominal organs are imaged floating within the peritoneal fluid.

Splenic Hematoma. Splenic hematomas are rare in horses but have been seen in several horses with abdominal trauma as well as in horses with no history of abdominal injury. The mass may be detected as a swelling or mass in the spleen on rectal palpation if the caudal pole or tail of the spleen is involved. The hematoma may appear as a loculated anechoic mass within otherwise normal splenic parenchyma (Fig. 6–76) or may contain echogenic to hyperechoic masses, representing clot formation within the hematoma (Fig. 6–77). If the hematoma is recent, hypoechoic loculated areas may be imaged in the hematoma associated with the recent bleeding into the splenic parenchyma (Fig. 6–78). The remaining spleen in these horses should be smaller than normal, associated with splenic contraction. The organized echogenic clots imaged within the spleen are usually imaged in horses with splenic hematomas that occurred weeks to several months earlier. The size of the unaffected portion of the spleen in these horses is usually returning toward normal. The anechoic loculated hematomas also represent more longstanding injuries to the spleen. The amount of normal splenic parenchyma in horses with splenic hematomas older than 3 to 4 months is usually within normal limits.

In one horse with a splenic hematoma, a large abdominal mass was imaged containing multiple fluid-filled areas surrounded by a thick echogenic wall that adhered to the left flank.[209] The fluid within the mass was homogeneous and of low echogenicity, consistent with a splenic hematoma. An aspirate of the fluid consisted primarily of

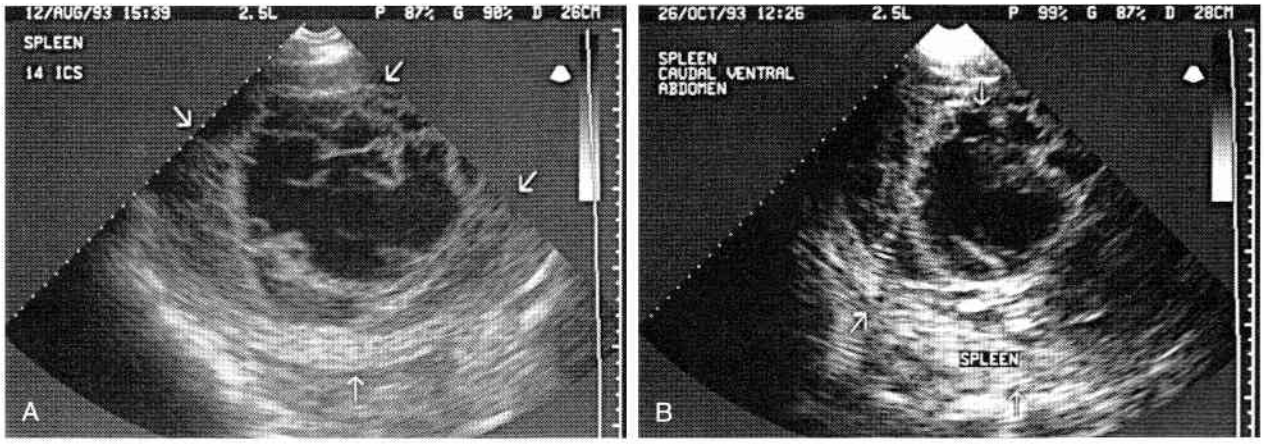

Figure 6–76

Sonograms of the spleen obtained from a 16-year-old Quarter horse gelding with a splenic hematoma. The hematoma was first diagnosed 1 year after the horse experienced severe abdominal trauma from a kick to the abdomen. Cytologic evaluation of an aspirate from the mass (*A*) revealed a hematoma. The right side of these sonograms is dorsal and the left side is ventral. *A*, The intraparenchymal hematoma (*angled arrows*) has a similar sonographic appearance to that of hematomas elsewhere, with many fibrinous loculations within an anechoic fluid-filled cavity. The hematoma appears to be encapsulated and surrounded by a rim of slightly more echogenic tissue (*up arrow*) representing more normal splenic parenchyma. This sonogram was obtained in the left fourteenth intercostal space with a 2.5-MHz sector-scanner transducer at a displayed depth of 26 cm. *B*, The sonographic appearance and size of this hematoma changed little in 3 months. The hematoma continues to contain a large amount of anechoic fluid and fibrinous loculations (*angled and down arrows*), surrounded by a rim of normal spleen (*up arrow*). This sonogram was obtained from the ventral abdomen in the region of the fourteenth intercostal space with a 2.5-MHz sector-scanner transducer at a displayed depth of 28 cm.

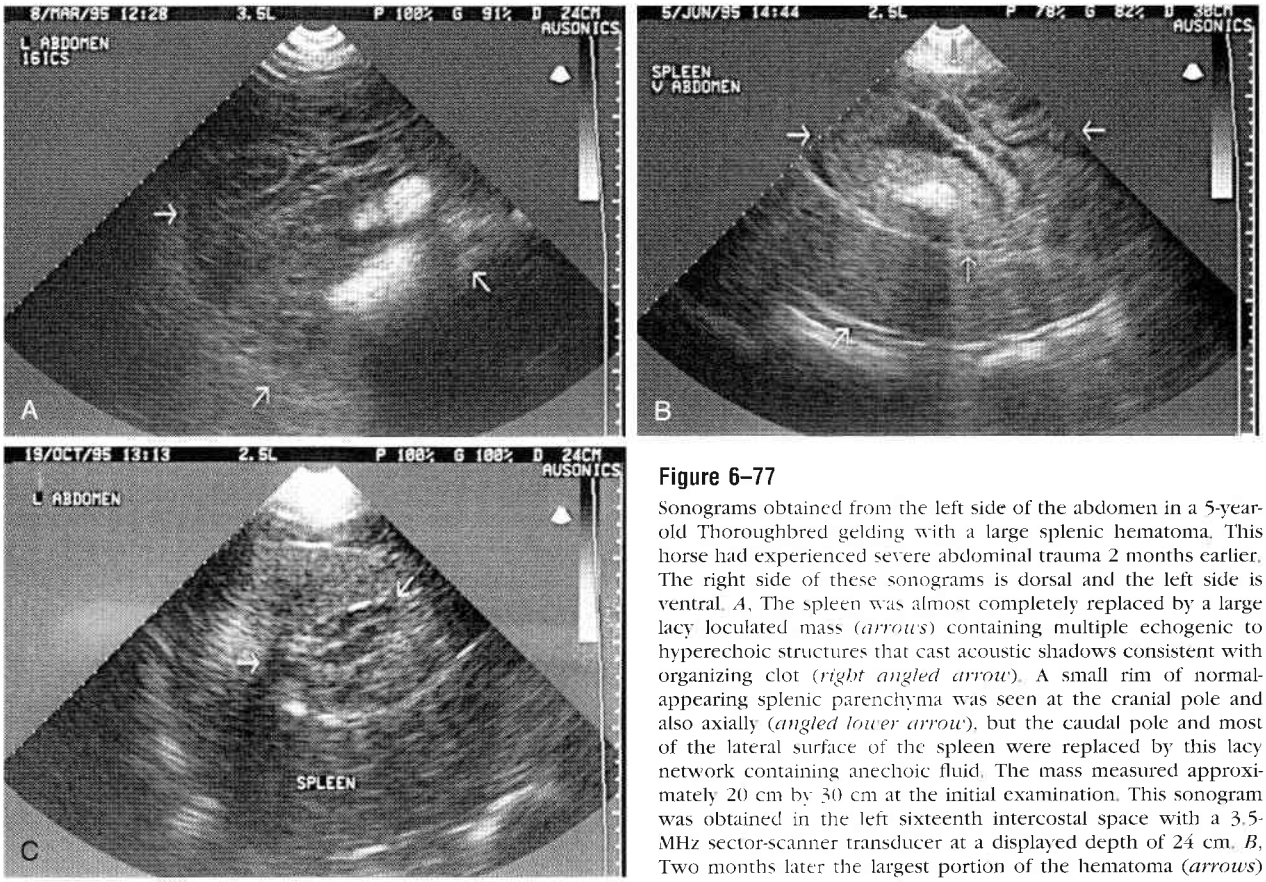

Figure 6–77

Sonograms obtained from the left side of the abdomen in a 5-year-old Thoroughbred gelding with a large splenic hematoma. This horse had experienced severe abdominal trauma 2 months earlier. The right side of these sonograms is dorsal and the left side is ventral. *A*, The spleen was almost completely replaced by a large lacy loculated mass (*arrows*) containing multiple echogenic to hyperechoic structures that cast acoustic shadows consistent with organizing clot (*right angled arrow*). A small rim of normal-appearing splenic parenchyma was seen at the cranial pole and also axially (*angled lower arrow*), but the caudal pole and most of the lateral surface of the spleen were replaced by this lacy network containing anechoic fluid. The mass measured approximately 20 cm by 30 cm at the initial examination. This sonogram was obtained in the left sixteenth intercostal space with a 3.5-MHz sector-scanner transducer at a displayed depth of 24 cm. *B*, Two months later the largest portion of the hematoma (*arrows*) was best imaged from the left ventral abdomen. By this time the mass had decreased in size significantly, measuring approximately 10 cm by 20 cm. Fewer hyperechoic masses casting acoustic shadows (clots) were detected at this time. A slightly larger axial rim of normal-appearing spleen (*lower angled arrow*) was present. This sonogram was obtained along the left ventral abdomen in the region of the sixteenth intercostal space with a 2.5-MHz sector-scanner transducer at a displayed depth of 30 cm. *C*, The hematoma continued to decrease significantly in size, and 7½ months after the initial sonographic examination only this small anechoic loculated area (*arrows*) was detectable in the spleen, most visible in the sixteenth intercostal space. The previously imaged hyperechoic masses within the hematoma casting the acoustic shadows (clots) were no longer present. An echogenic band of tissue detected in the splenic parenchyma in the area of the resolving hematoma probably represents fibrous scar tissue. An acoustic shadow is cast from the border between the resolving hematoma and the more normal splenic parenchyma. This sonogram was obtained from the left sixteenth intercostal space with a 2.5-MHz sector-scanner transducer at a displayed depth of 24 cm.

hemolyzed red blood cells, also consistent with a splenic hematoma. Drainage of this hematoma was performed via a flank laparotomy and instillation of a large-bore indwelling catheter. Follow-up sonographic evaluation of the mass revealed an initial marked reduction in size of the splenic hematoma 7 days postoperatively. Another horse had a large 10- to 15-cm subcapsular hematoma that extended over most of the parietal surface of the spleen.[210] The hematoma had numerous fibrin septa and homogeneous hypoechoic to anechoic fluid. A discrete 5-cm circular lesion containing hypoechoic to anechoic fluid was imaged within the splenic parenchyma in the caudal pole of the spleen. This circular fluid-filled cavity became hyperechoic and cast an acoustic shadow from the far side of the hyperechoic material within 10 days of the initial sonographic examination.

Echogenic, lucent, or mixed patterns of echogenicity have been reported in humans with intraparenchymal and perisplenic collections of blood.[77] A double linear interface of the outline of the spleen is consistent with a subcapsular collection of blood.[77] The outer linear echo represents the capsule of the spleen, and the inner linear echo originates from the outer surface of the splenic parenchyma. Transrectal examination of the spleen may be helpful if the caudal pole of the spleen is involved. A higher-frequency transducer may be used transrectally, resulting in better image quality and improving the ability to differentiate sonographically between a hematoma, abscess, and neoplasia. Hemoperitoneum may occur in association with the splenic hematoma (Fig. 6–78) or may indicate splenic rupture. The actual defect in the capsule of the spleen is difficult to find owing to the marked splenic contraction and hematoma formation. The detection of both hemoperitoneum and a splenic hematoma strongly suggests splenic rupture. Splenic rupture has been reported in the horse but is rare and may occur in conjunction with splenic hematoma.[211–213] Focal lymphoid necrosis has been detected histopathologically in horses with splenic rupture and no history of trauma.[211]

Splenic Abscess. Other splenic abnormalities such as splenitis and splenic abscesses are rare in horses. A horse with severe necrotizing splenitis of unknown cause was

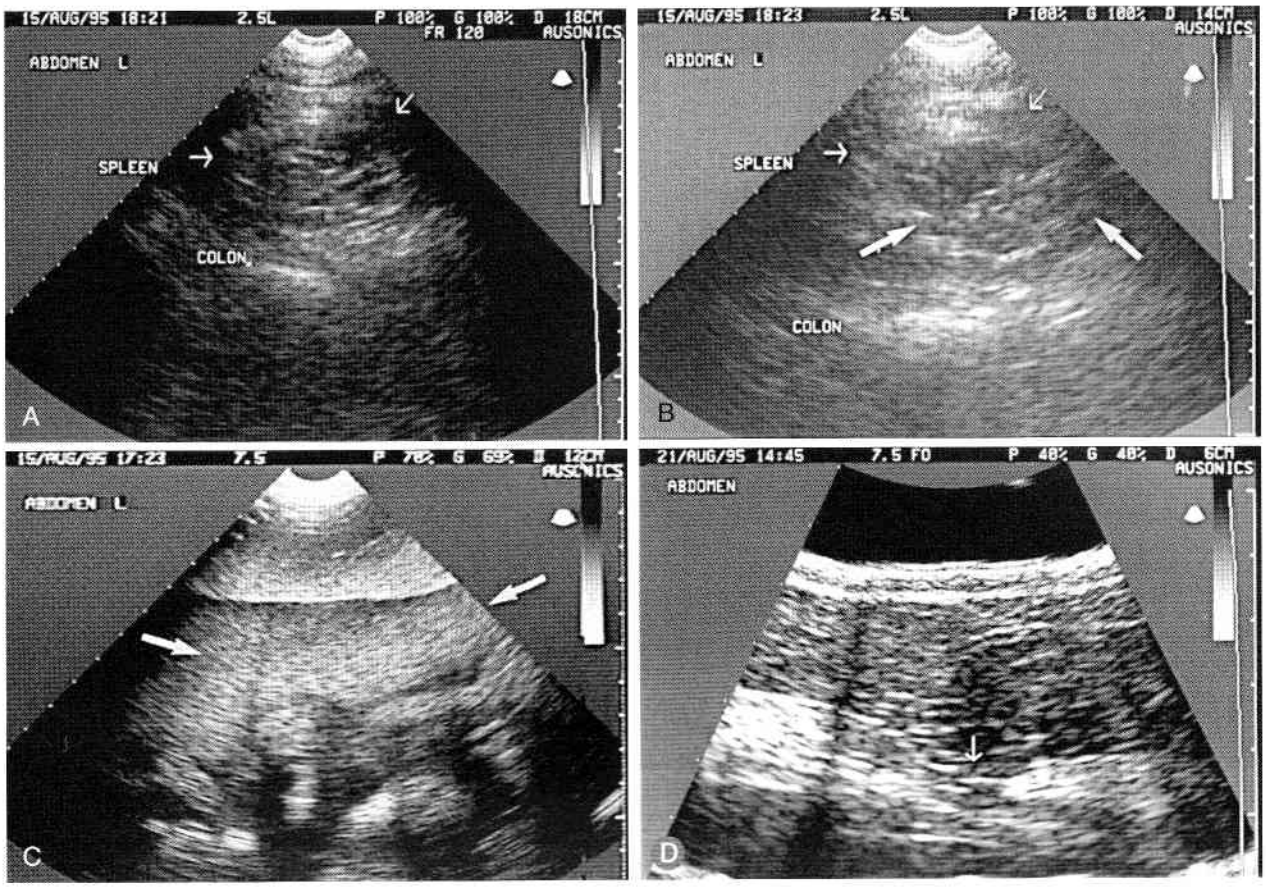

Figure 6–78

Sonograms of the abdomen obtained from a 6-year-old miniature horse mare with severe, life-threatening hemoperitoneum and anemia (packed cell volume = 10%) and splenic trauma. The spleen was extremely small and contracted. These sonograms were obtained with a 2.5-MHz sector-scanner transducer (*A* and *B*), a 7.5-MHz sector-scanner transducer (*C*), and a 7.5-MHz sector-scanner transducer containing a built-in fluid offset (*D*) at a displayed depth of 18 cm (*A*), 14 cm (*B*), 12 cm (*C*), and 6 cm (*D*). *A*, The arrows delineate two of the borders of the splenic hematoma adjacent to the area of suspected splenic rupture. The hematoma is loculated and contains only a small amount of anechoic fluid, compared with the hematomas depicted in Figures 6–76 and 6–77. This sonogram was obtained in the left sixteenth intercostal space. The right side of this sonogram is dorsal and the left side is ventral. *B*, The spleen is extremely difficult to visualize in the seventeenth intercostal space, with poor definition of its margins and a hypoechoic to anechoic area within (*small arrows*). Several areas along the visceral (medial) side of the spleen in which the splenic capsule could not be defined suggest possible sites of rupture (*large arrows*). This sonogram was obtained in the left seventeenth intercostal space. The right side of this sonogram is dorsal and the left side is ventral. *C*, The large amount of echogenic fluid swirling in the abdominal cavity is the hemoperitoneum (*arrows*). Loops of jejunum, which appear echogenic and circular with their long echogenic mesentery, are imaged floating on the bloody fluid surrounded by more anechoic fluid. The right side of the sonogram is the left side of the horse's abdomen. *D*, Sonogram of the abdominal wall obtained 6 days later, demonstrating a hypoechoic area of muscle disruption with disruption of the deeper internal abdominal oblique muscle (*arrow*) below the eighteenth rib, evidence of external trauma that resulted in the splenic rupture and hematoma. The right side of this sonogram is dorsal and the left side is ventral.

reported with a markedly enlarged, necrotic spleen.[215] Three of 15 horses with abdominal abscesses were found to have splenic abscesses in one large study,[5] and in another 2 of 25 horses had splenic abscesses.[118] A foreign body (wire) was found in 2 of 4 horses with splenitis and splenic abscesses at postmortem examination, with tracts leading to the adjacent large intestine.[215] In each of these horses, the splenic abscess was at least 10 cm in diameter. Most splenic abscesses were associated with adhesions between the spleen, stomach, and adjacent large intestine.[215] A splenic abscess has been imaged sonographically by the author in a horse with a penetrating abdominal wound. In another horse the splenic abscess appeared as a hyperechoic capsule surrounding an area in which the normal splenic architecture had been replaced by areas of reduced echogenicity.[6] In the horse with the splenic hematoma that was surgically drained, a splenic abscess caused its demise.[209] The abscess was located in the cranial portion of the spleen underlying the ribs, an area that reportedly could not be imaged sonographically.

Other Splenic Abnormalities. Splenomegaly is difficult to diagnose definitively in horses because of the wide range of normal sizes for the equine spleen. Splenomegaly is due to either neoplasia, infarction, infection, or extramedullary hematopoiesis. Marked splenomegaly was imaged in one horse with splenic congestion and a mural and intramural jejunal hematoma (Fig. 6–79). Splenomegaly has been reported in two horses.[216, 217] In one horse the splenomegaly was thought to be primary, associated with splenic congestion;[216] in the other horse it was associated with a splenic infarct.[217] Splenomegaly has been associated with equine infectious anemia, immune-mediated hemolytic anemias, salmonellosis, and neoplasia

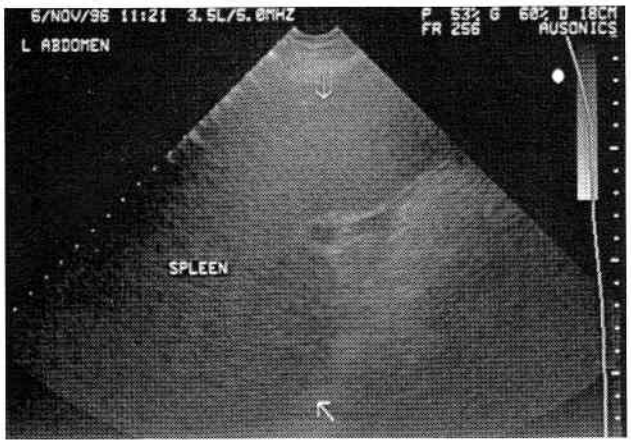

Figure 6–79

Sonogram of the spleen obtained from a 38-year-old Quarter horse mare with marked splenomegaly associated with splenic congestion. The spleen is markedly enlarged, with rounded borders and bulging of the capsular surface of the spleen. The mare was very fat, decreasing the image quality significantly. This sonogram was obtained from the left fourteenth intercostal space with a wide-bandwidth 3.5-MHz sector-scanner transducer operating at 5.0 MHz at a displayed depth of 18 cm. The right side of the sonogram is dorsal and the left side is ventral.

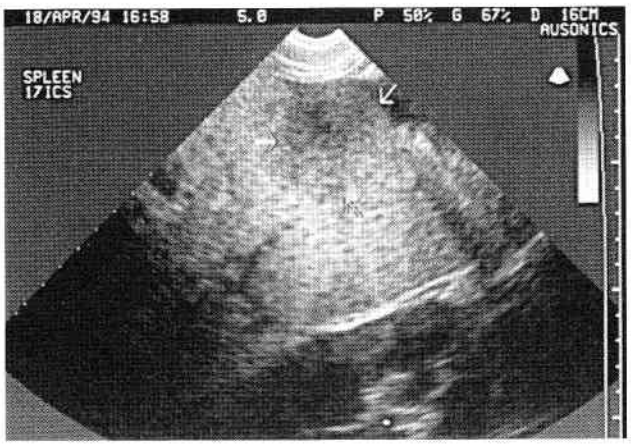

Figure 6–80

Sonogram of the spleen obtained from a 10-year-old Arabian mare with hemothorax. The hypoechoic mass delineated by the arrows bulges from the surface of the spleen and appears almost cavitated in the center. The spleen has a somewhat irregular appearance surrounding this mass but elsewhere had a normal sonographic appearance. This area was suspicious for a neoplasm but was diagnosed as a regenerative splenic nodule on histopathologic examination. This sonogram was obtained from the left seventeenth intercostal space with a 5.0-MHz sector-scanner transducer at a displayed depth of 16 cm. The right side of this sonogram is dorsal and the left side is ventral.

in horses.[211] Humans with splenomegaly are also prone to splenic infarction.[218] Splenic infarction in humans has been associated with disseminated intravascular coagulopathy, left-sided bacterial endocarditis, dilated cardiomyopathy, atrial fibrillation, generalized vasculitis, and other vascular diseases.[218] Splenic necrosis and infarction in dogs have been described as an area of the spleen containing a coarse "lacy" heteroechoic or hypoechoic pattern diffusely involving a portion or all of the spleen but not deforming the normal contour of the spleen.[218, 219] This sonographic appearance could be confused with that of splenic hematoma. Focal hypoechoic or isoechoic well-marginated areas that deform the surface of the spleen have also been described in humans and in the dog with splenic infarction.[218, 219] A third pattern in dogs of focal ventral enlargement with retention of normal shape of the spleen has been reported.[218] These lesions in humans usually rapidly become more echogenic and have a densely hyperechoic appearance when the infarct has resolved or healed.

Regenerative splenic nodules were detected sonographically by the author in a horse with hemothorax. The regenerative nodules were hypoechoic, with a more anechoic center, and bulged from the capsular surface of the spleen (Fig. 6-80). Occasionally focal hyperechoic areas are imaged in the spleen as incidental findings, usually casting an acoustic shadow associated with a small area of dense fibrous scar tissue or calcification (Fig. 6-81). These areas may represent an area of scarring from a previous infarct, hematoma, or possible parasite migration. Multiple hypoechoic nodules have been imaged in one horse with systemic granulomatous disease with involvement of the liver, lung, and spleen (Fig. 6-82). Noncaseous granulomatous inflammation in humans has been reported to have a uniformly low splenic sonodensity.[220]

Pancreatic Neoplasia. A portion of a pancreatic adenocarcinoma was imaged as a large encapsulated mass in the region of the left kidney in one horse[221] and as an irregularly shaped mass adjacent to the left kidney in another horse.[222] Rectal examination in both horses revealed the large mass surrounding the left kidney, with multiple smaller masses in the center of the abdomen[221] or adjacent to the left kidney and spleen.[222] Splenomegaly was detected sonographically and rectally in one horse,

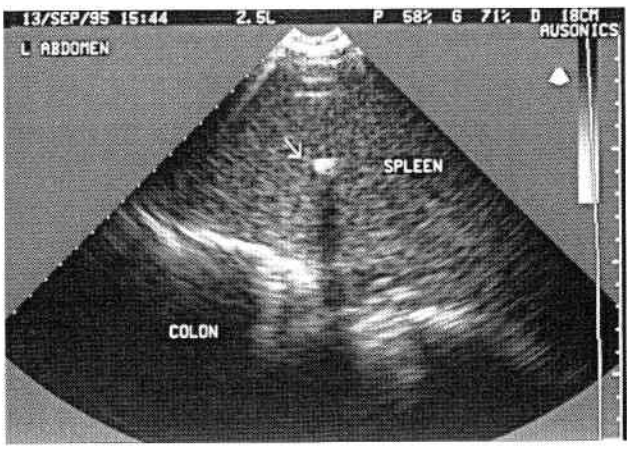

Figure 6–81

Sonogram of the spleen obtained from a 4-year-old Thoroughbred colt with anterior enteritis. Notice the hyperechoic structure (*arrow*) casting an acoustic shadow in the otherwise normal-appearing splenic parenchyma. This probably represents an area of dense fibrous scar tissue, as the thickness of the hyperechoic structure is displayed superficial to the acoustic shadow. With an area of calcification, the acoustic shadow should originate at the most superficial part of the hyperechoic structure. This sonogram was obtained from the left fourteenth intercostal space with a 2.5-MHz sector-scanner transducer at a displayed depth of 18 cm. The right side of this sonogram is dorsal and the left side is ventral.

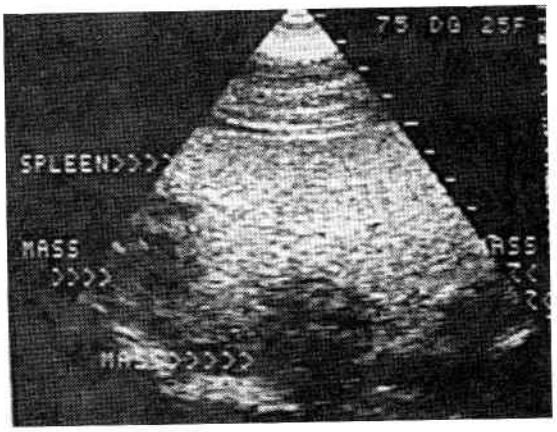

Figure 6–82

Sonogram of the spleen obtained from an 18-year-old Paint gelding with diffuse granulomatous disease and splenomegaly (same horse as in Fig. 6–63). Multiple circular and irregular hypoechoic masses are scattered throughout the periphery of the spleen. These granulomas bulge somewhat from the surface of the spleen and locally disrupt the splenic architecture. This sonogram was obtained in the left fourteenth intercostal space with a 3.5-MHz sector-scanner transducer at a displayed depth of 14 cm. The right side of this sonogram is dorsal and the left side is ventral.

but no discrete masses were imaged in the spleen of this horse.[222] Metastases were present throughout the abdominal cavity in both horses, particularly along the serosal surfaces of the stomach, spleen, small colon, liver, diaphragm, omentum, and mesenteric lymph nodes. The mare with pancreatic adenocarcinoma presented for hematuria and weight loss, and blood was seen on cystoscopic examination emanating from the left ureter.[221] At necropsy, extensive neoplastic infiltration of the left kidney was reported and was the likely cause of the hematuria. The other horse presented for failure to thrive and depression.[222]

More typically, however, the pancreatic adenocarcinoma occludes the common bile duct and causes cholestasis and severe liver dysfunction.[223, 224] In one donkey with pancreatic adenocarcinoma, metastases were present throughout the mesentery, on the diaphragm, and on the serosal surface of the colon, cecum, and stomach. A large mass was detected in the right lobe of the liver that histopathologically was most consistent with metaplasia to squamous cell carcinoma.[223] The multiple tumor metastases and liver mass should have been detectable ultrasonographically if imaging of this donkey's abdomen had been possible. In two horses with pancreatic adenocarcinoma, diffuse lymphocytic infiltration of the small intestine was also present (in one horse the large colon was similarly affected).[224]

In humans with extrapancreatic pancreatic carcinoma, the primary tumor masses have low-amplitude echoes, the involved lymph nodes have mildly enlarged ovoid masses of moderate echogenicity, and the liver metastases tend to be small and hypoechoic.[225] The extrapancreatic pancreatic carcinoma occurs when biliary obstruction, hepatic metastases, regional lymph node involvement, splenic enlargement, and ascites are present, similar to what has been reported in the majority of affected horses.

Pancreatitis. Antemortem sonographic description of pancreatitis has not been made in the horse, because pancreatitis is rarely diagnosed. However, a large heterogeneous mass was imaged in one horse medial to the right kidney and right lobe of the liver (Fig. 6–83). The mass was also imaged medial to the cranial pole of the left kidney. The mass had a composite echogenicity with a large semicircular area superimposed on the mass, casting a discrete acoustic shadow consistent with superimposed gas-filled small intestine. At postmortem examination this area represented a markedly enlarged pancreas with severe necrotizing pancreatitis. Pancreatitis has been reported in horses with cholelithiasis.[146, 151]

Gastrointestinal Diseases

Sonographic evaluation of the gastrointestinal tract is extremely valuable in the evaluation of horses with colic or suspected gastrointestinal disease.[2, 17, 226–228] The entire abdomen can be evaluated and the sonographic information used to help make the decision between medical and surgical colic.[2, 17] Scanning the abdomen from the most ventral location is critical to successfully making this determination, in addition to examining the left and right sides of the abdomen. The affected fluid-filled intestine falls to the most ventral location and is readily visible if scanned from the most ventral portion of the abdomen. Abnormal small intestine may be missed, however, if scanned from the lateral or dorsal portion of the abdomen because the interposed gas-filled bowel prevents visualization of the affected intestine. In one study of 226 horses that presented for colic and had abdominal ultrasonography performed, significant differences were seen between the three areas in the abdomen in which small intestine was identified sonographically.[229] Enlarged or edematous small intestine was identified more frequently in the ventral portion of the abdomen than in the right or left paralumbar fossa regions. Abdominal ultrasonography correctly identified the presence of distended or edematous small intestine in all horses with a primary small intestinal lesion; only 50% of these cases were detected on rectal examination.[229] Abdominal sonography helped to distinguish clinically between large and small intestinal disease, although the specific small intestinal lesion was not identified sonographically.[229] Large colon only was detected sonographically in 152 horses; none of these horses had primary small intestinal disease.[229]

The preponderance of large intestinal disease over small intestinal disease in the adult horse limits somewhat the usefulness of abdominal sonography in the adult horse compared with the foal. An increase in the diameter of the small intestine, increased thickness of the small intestinal wall, and absent motility detected on abdominal ultrasonography are indications that an exploratory celiotomy should be performed because primary small intestinal disease is likely.[229] Most intussusceptions can be diagnosed sonographically if the entire abdomen is examined. Diseases of the cecum are more likely to be imaged from the right paralumbar fossa or the right caudal abdomen ventral to the costochondral junction. Sonographic diag-

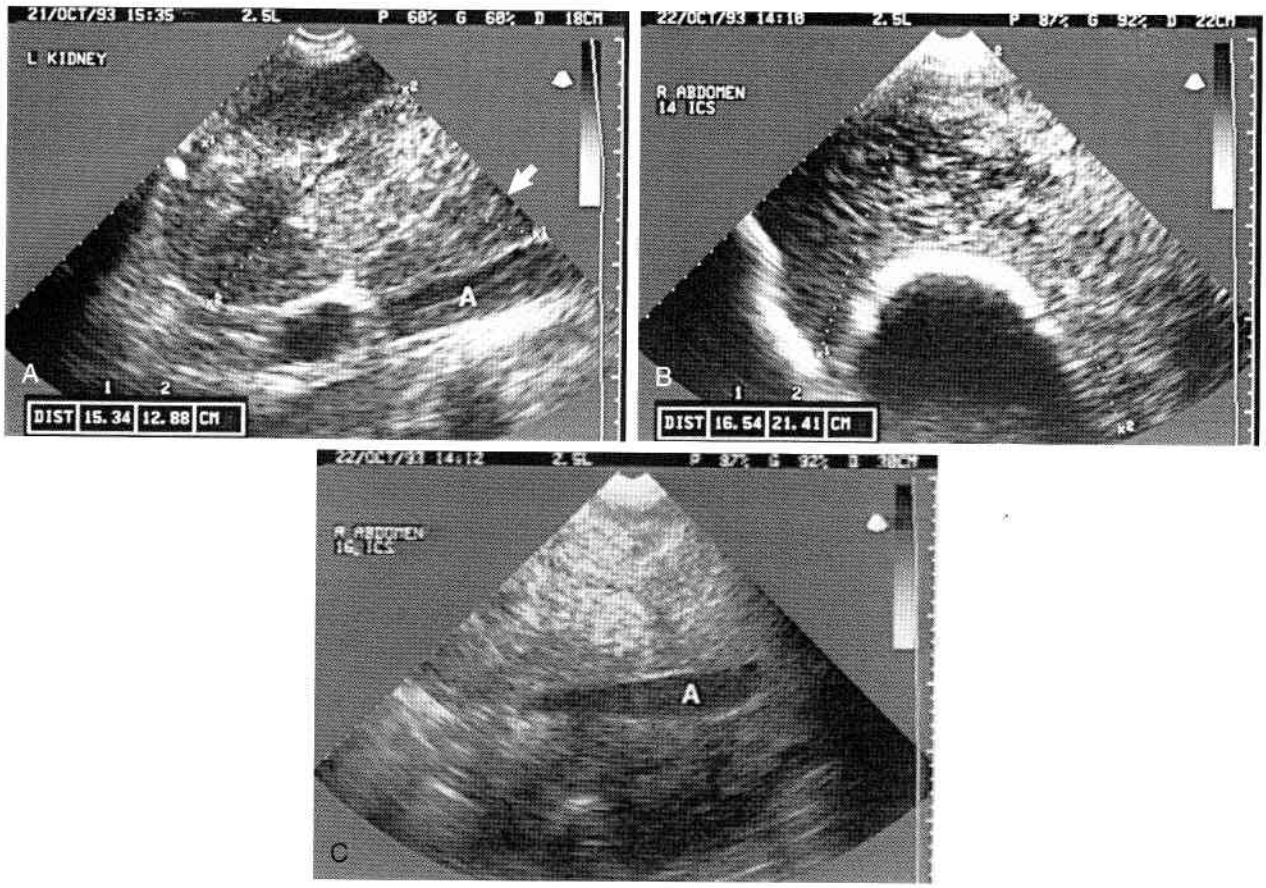

Figure 6–83

Sonograms of the abdomen obtained from a 21-year-old Paint gelding with a large abdominal mass palpated medial to the left kidney. Postmortem examination revealed this to be an enlarged necrotic pancreas with severe necrosis and fibrosis. These sonograms were obtained from the left paralumbar fossa (*A*), the right fourteenth intercostal space (*B*), and the right sixteenth intercostal space (*C*) with a 2.5-MHz sector-scanner transducer at a displayed depth of 18 cm (*A*), 22 cm (*B*), and 30 cm (*C*). *A*, The left kidney appears somewhat hyperechoic with poor anatomic detail. A hypoechoic nodular mass lateral to the left side of the aorta (*A*) and medial to the right side of the left kidney (*arrow*) enlarges toward the cranial pole. The right side of this sonogram is cranial and the left side is caudal. *B*, The right dorsal abdomen in the sublumbar region is filled with a large heterogeneous mass containing composite echogenicities with a large semicircular hyperechoic structure superimposed on the mass, which represents gas in the mucosal side of the adherent small intestine. The right side of this sonogram is dorsal and the left side is ventral. *C*, A large heterogeneous mass of composite echogenicity is imaged surrounding the aorta (*A*) and is pushing the right kidney caudally. The right side of this sonogram is cranial and the left side is caudal.

nosis of displacement of the large colon can be made, particularly in horses with nephrosplenic ligament entrapment.[230] However, care must be taken to evaluate the location of all abdominal viscera in a horse with suspected intestinal displacement because enlargement or atrophy of one organ or viscus can result in malpositioning of other normal structures.

Ultrasonographic evaluation of the peritoneal cavity is also useful to determine if peritoneal fluid can be obtained on abdominal paracentesis. The likelihood of obtaining peritoneal fluid from an abdominal paracentesis is small if no peritoneal fluid is imageable, and the risk of iatrogenically lacerating the intestine or performing an enterocentesis is high, particularly in a horse with marked abdominal distention.[231]

Intussusception. Horses presenting with a jejunal intussusception usually have more acute abdominal pain, whereas horses with an intussusception involving the ileum, large colon, cecum, and small colon often have a more chronic history of abdominal pain.

Jejunal-Jejunal Intussusception. Although jejunal-jejunal intussusceptions are usually thought to be more common in foals, jejunal intussusceptions do occur in adult horses.[232] Nine of 11 horses in one study had signs of acute abdominal discomfort for 5 to 16 hours prior to presentation at a referral hospital, and 2 horses had signs for 2.5 and 5 days, with initial signs of mild pain that became increasingly more severe.[232] Horses ranged in age from 2 to 24 years, with a mean age of 10.5 years.[232] Small intestinal distention was palpable rectally in all horses in which the results of the rectal examination were recorded and was detected via abdominal radiography in 1 miniature horse.[232] In 1 horse the jejunal intussusception was palpable rectally in the dorsal right quadrant as a mass. The intussusception was more frequently found in the middle of the jejunum but was also found in the proximal and distal third of the jejunum in some horses at the time of surgery. The intussusception involved 0.4 to 9.1 meters (mean 3.4 meters) of the jejunum. A luminal or intramural mass was found associ-

ated with the intussusception in 5 of 11 horses. These intraluminal or intramural masses were leiomyomas (3 horses), granuloma (1 horse), and intestinal carcinoid (1 horse).[232] Leiomyomas have been reported associated with jejunal intussusceptions, as have granulomas and papillomas.[233-235]

Sonographic examination of the abdomen from the most ventral location should reveal the jejunal intussusception in most horses because the thickened, fluid-filled bowel is heavy and falls to the floor of the ventral abdomen with the long jejunal mesentery. Transrectal sonographic examination of the intestinal mass, if palpable per rectum, should also reveal the characteristic sonographic appearance of an intussusception. Transrectal imaging of the jejunal-jejunal intussusception is most likely if the caudal portion of the jejunum is involved. The first report of the use of ultrasonography in the diagnosis of gastrointestinal disease was the diagnosis of small intestinal intussusceptions in foals (see Chapter 7).[226] The detection of a characteristic "target" or "bull's-eye" sign is obtained by scanning through the apex of the intussusception where the intussusceptum is surrounded by fluid and the intussuscipiens, similar to the appearance previously described in humans.[2, 226, 227, 236, 237] This ultrasonographic appearance is created by the difference in acoustic impedance between the thick-walled, congested, edematous inner intussusceptum and outer intussuscipiens and the interposed fluid layer.[226] Invaginated mesenteric fat or mesenteric lymph nodes may also create this sonographic appearance. The intussusception can have myriad different sonographic appearances, depending upon the portion of the intussusception being imaged.[226, 236-240] The intussusception may appear as two concentric rings with a central circular area or echogenic core representing the inner lumen of the intussusceptum, the "multiple ring" sign.[226, 237, 238] This appearance occurs where the walls of the intussusceptum and intussuscipiens are less edematous.[226] Occasionally fibrin may be imaged between the inner intussusceptum and the outer intussuscipiens. Fluid distention of the more proximal small intestine is detected, usually with normal or nearly normal wall thickness and little or no peristaltic activity.[226]

Ileal-Ileal Intussusception. Ileal-ileal intussusceptions have been reported in horses 3 years old or younger, with the majority of affected horses being weanlings and yearlings.[241] The intussusception is often associated with chronic intermittent low-grade abdominal pain, usually of several days' or weeks' duration. The cause of the intussusception is unknown, with a large tapeworm burden possibly playing a role in some, but not all, horses.[241-243] Distended small intestine was palpable in all horses in which a rectal examination could be performed. The intussusception is typically located 6 to 12 cm from the ileocecal junction and is about 6 cm in length, although in some horses the intussusception was more proximal, approximately 20 cm from the ileocecal junction.[241] Ileal-ileal intussusceptions can be diagnosed sonographically transrectally if the affected portion of the bowel can be imaged (Fig. 6-84). Sonographic detection of the ileal-ileal intussusception has also been performed from the flank in affected youngsters. The typical sonographic appearance described for jejunal intussusceptions should be detected.

Ileocecal Intussusception. Ileocecal intussusceptions have been reported in young horses ranging in age from 8 to 26 months, with a mean age of 14 months.[244] Affected horses usually have a history of chronic, usually intermittent, abdominal pain of several days' to weeks' duration (5 days to more than 3 weeks) and usually have normal vital signs at presentation, passing small amounts of feces.[244] *Anoplocephala perfoliata* infection with a tapeworm burden at the leading edge of the intussuscep-

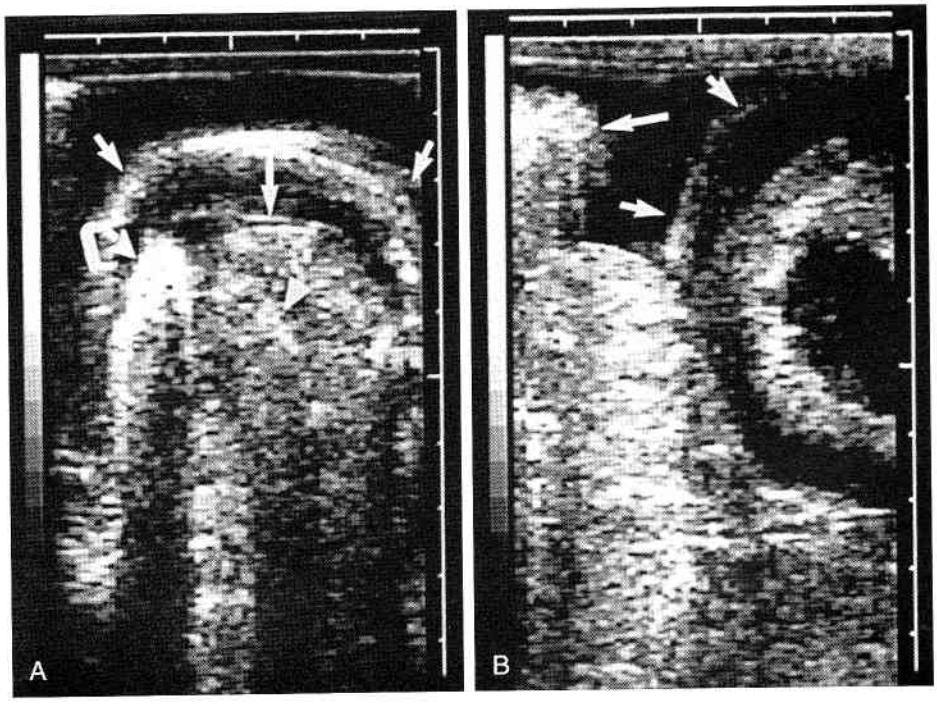

Figure 6-84

Sonograms of the abdomen obtained from a 5-year-old Welsh pony gelding with an ileoileal intussusception. This intussusception most likely involves the ileum because the affected bowel is small and circular in appearance, consistent with a portion of the small intestine, and five layers are imaged within the compromised bowel wall. These sonograms were obtained transrectally with a 5.0-MHz linear-array transducer at a displayed depth of 10 cm. *A*, The outer rim of bowel (*short arrows*) is thickened (approximately 1.5 cm), and the inner loop of bowel is heterogeneous in appearance, with loss of the normal mural layers (*long arrow*). A small gas shadow is present from the small lumen of the intussusceptum (*arrowhead*), and a large gas shadow is generated between the intussusceptum and intussuscipiens (*curved arrow*). *B*, The wall of the ileum (*short arrows*) is markedly thickened (up to 2 cm thick) adjacent to some fluid- and gas-filled intestine (*long arrow*). The compromised portion of ileum has a large hypoechoic subserosal layer.

tion has also been implicated in ileocecal intussusceptions in horses.[243] Small intestinal dilatation and/or thickening was palpable in all horses in which a rectal examination could be performed.[244] A 2- to 10-cm length of ileum was intussuscepted into the cecum in affected horses.[244]

Ileocecal intussusceptions can be imaged ultrasonographically from the right flank area and/or transrectally in youngsters large enough to have a rectal examination performed. The ultrasonographic appearance of an ileocecal intussusception is a larger sacculated outer segment of bowel (the cecum) and an thicker inner bowel wall (ileum). The sacculations are usually present in the affected portion of the cecum unless the bowel wall is markedly thickened and the cecum is markedly distended, making the sacculations more difficult to recognize sonographically. Hypertrophy and marked dilatation of the distal jejunum have also been reported in equine youngsters with ileocecal intussusception and may be detected ultrasonographically.[244] Ileocecal intussusceptions are common in dogs, and the "multiple ring" sign has been detected in affected dogs.[22] An "hourglass" or "fused target-like" pattern has also been described in children with an ileocecal intussusception as the intussusception is imaged simultaneously within the colon.[245] Other terms such as "hayfork," "trident," and "sausage" have been used to describe the longitudinal view of an intussusception.[22, 245-249] "Doughnut" and "pseudokidney" have also been used to describe the transverse view of an intussusception but are not specific for an intussusception.[22, 248, 249]

Cecocecal or Cecocolic Intussusception. Horses with cecocolic or cecocecal intussusception are usually young.[243, 250, 251] A mean age of 2.4 years and an age range of 7 months to 8 years was reported in a group of horses with cecocolic intussusception.[250] A history of mild to moderate abdominal pain of several days' duration and chronic wasting are common in horses with cecocecal or cecocolic intussusception.[250, 252, 253] Acute severe colic with unrelenting pain has also been reported.[250] Tapeworms, particularly *A. perfoliata*, have frequently been associated with cecocolic intussusceptions, although their role in causing the intussusception remains unclear.[243, 250-252] Cecal wall abscesses, deworming with organophosphate compounds, vascular compromise by *Strongylus vulgaris* and *Eimeria leukarti* infection, and parasympathomimetic drugs have all been associated with cecocolic intussusception.[250] The lack of identification of the cecum on rectal examination has been noted in horses with cecocolic intussusception but is not specific for this problem.[250, 252] Other abnormal rectal findings include pain in the right dorsal abdominal quadrant, a mass in the right dorsal quadrant, large colon distention, edema in the large colon, a possible large colon impaction, and small intestinal distention.[250] In only one horse was the cecocolic intussusception palpated on rectal examination.[250]

Although findings on rectal palpation are often inconclusive,[250, 252, 253] the sonographic identification of the target or bull's-eye sign is diagnostic of an intussusception. Cecocecal and cecocolic intussusceptions can be identified by their characteristic appearance and their location within the abdomen. The outer intussuscipiens has a somewhat sacculated appearance and is separated from the thick-walled, congested, edematous inner intussusceptum by the interposed fluid layer. The cecocecal intussusception is found in the right ventral abdomen because the apex of the cecum is invaginated into the cecal base (Fig. 6-85). The cecocolic intussusception is located in the upper right quadrant because the entire cecum is invaginated into the right dorsal colon. The intussusception and adjacent large bowel lumen should be carefully scanned for any evidence of the tapeworm segments. It is unlikely, however, that these small proglottid segments can be detected within the intussusception owing to the marked thickening of the bowel wall, with only a small amount of fluid between the intussusceptum and the intussuscipiens.

Small Intestinal Volvulus. Acute severe abdominal pain with rapid deterioration and cardiovascular collapse is consistent with a small intestinal volvulus. Large amounts of nasogastric reflux are usually obtained during gastric decompression. If turgid, fluid-filled, amotile small intestine with thicker than normal walls is imaged, a small intestinal volvulus should be suspected (see Chapter 7).[2, 17] A similar sonographic appearance is detected shortly after the volvulus occurs, but jejunal wall thickness may still be normal or nearly normal as the congestion and edema of the bowel wall are developing.

Other Small Intestinal Obstruction/Displacement. Other surgical diseases of the small intestine can also be diagnosed ultrasonographically in horses presenting with abdominal pain. With a mechanical obstruction, dilated proximal loops of intestine and collapsed distal intestinal loops can both be imaged, although the cause of the mechanical obstruction may not be visible.[2] Little or no peristaltic activity of the affected portion of small intestine can be imaged. In horses with primary small intestinal strangulation or obstruction, transcutaneous abdominal ultrasonography should reveal small intestinal distention, wall thickening, and ileus, suggesting primary small intestinal disease. Transrectal sonography in horses with small intestinal distention should also reveal similar sonographic findings. Fluid distention of the intestine proximal to a mural or intraluminal obstruction facilitates being able to image the area of abnormality.[2] Distended small intestine with increased wall thickness and absent peristalsis detected sonographically had a sensitivity, specificity, and positive and negative predictive values of 100% for small intestinal strangulation obstructions.[229]

Congenital abnormalities such as Meckel's diverticulum or a mesodiverticular band may cause small intestinal obstruction with thickened, turgid, fluid-filled, amotile small intestine imaged proximal to and in the area of the obstruction. Pedunculated lipomas are a common cause of small intestinal strangulation/obstruction in older horses.[254, 255] In 17 horses with intestinal obstruction associated with pedunculated lipomas, small intestinal distention was palpated on rectal examination in 13 horses, a displaced large colon in 7 horses, and a large colon impaction in 2 horses.[254] The pedunculated lipoma was not palpable in any affected horses. The ileum or jejunum was strangulated in 15 horses and the small colon in 1 horse, and the jejunum was obstructed in 1 horse. The

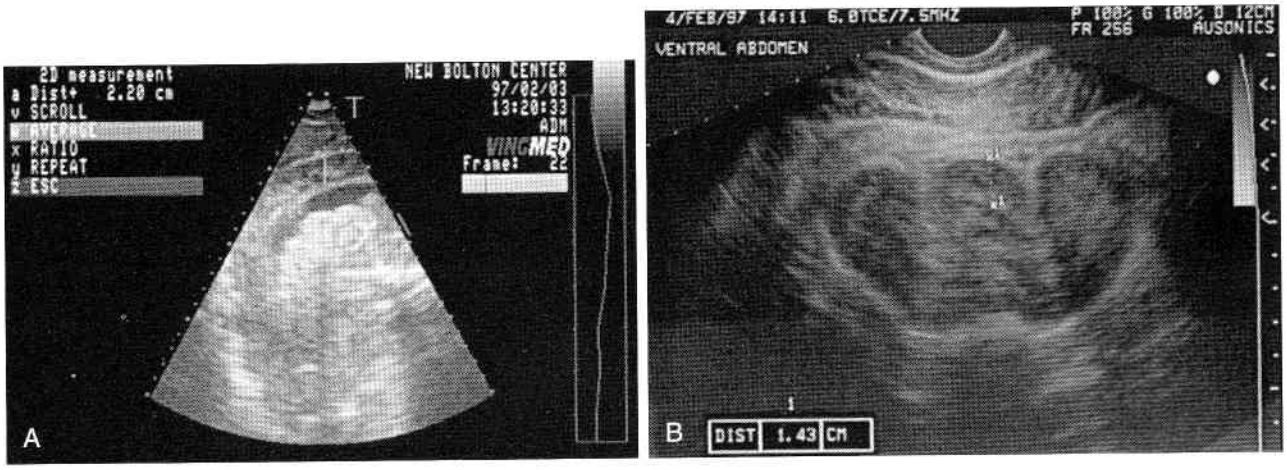

Figure 6–85

Sonograms obtained from a yearling Thoroughbred filly with a cecocolic intussusception. The intussusception was imaged in the right caudoventral abdomen behind the costochondral junction for a length of approximately 12 cm. *A*, The outer wall of the intussusception (the intussuscipiens) has a slightly sacculated appearance and is markedly thickened, measuring 2.20 cm. A small amount of fluid is imaged surrounding the intussusceptum, which appears hyperechoic. This sonogram was obtained with a 5.0-MHz annular-array transducer at a displayed depth of 20 cm. The right side of the sonogram is dorsal and the left side is ventral. *B*, Sonogram of the intussusception, demonstrating the sacculated nature of the cecum containing the intussusception. The outer wall of the intussusception (the intussuscipiens) measured 1.43 cm thick. This sonogram was obtained with a 6.0-MHz microconvex linear-array transducer at a displayed depth of 12 cm. The right side of the sonogram is cranial and the left side is caudal.

length of resected intestine varied from 0.15 to 7.2 meters, with the smallest resection in the horse with the lipoma strangulating the small colon.[254] The pedunculated lipoma causing the obstruction is unlikely to be imaged ultrasonographically owing to its location in the mesentery. However, the distended, thickened, amotile small intestine indicative of a strangulation/obstruction should be detected ultrasonographically, prompting surgical intervention.

Mural masses or thickening may be detected sonographically in the adult, most frequently associated with lymphosarcoma. Echogenic eccentric thickenings of the bowel wall have been reported in children with intramural hematomas secondary to trauma and should be considered in horses in which abdominal trauma is a possibility.[256, 257] These intramural hematomas should rapidly improve on follow-up sonograms. Intramural hematomas have been imaged in the small intestine of one horse with lymphosarcoma and mesenteric bleeding (Fig. 6–86). Intraluminal hemorrhage may result in brightly echogenic fibrin clots swirling within the intestinal lumen[258] or in an intraluminal hematoma. Abscesses or granulomas in the intestinal wall occur infrequently in the adult horse.[2, 17, 235] Enteric pythiosis has been described as a cause of jejunal obstruction in the horse.[259, 260, 261] Enteric pythiosis has also been associated with intramural and mural masses ranging in size from 0.2 mm to 6 cm. A nodular 3 cm × 4 cm × 5 cm intramural mass was detected at surgery in the jejunum of one horse with chronic eosinophilic enteritis attributed to *Pythium* species.[262] Intestinal fibrosis and partial small intestinal obstruction were diagnosed in seven horses and ponies.[263] The extent of the fibrosis ranged from the entire small intestine (jejunum to cecum) to involvement of just the jejunum. All animals had multiple thickened areas of the small intestine palpated at the time of rectal examination, and one pony had a markedly distended stomach palpated as a large abdominal mass in the left cranial portion of the abdomen. Transrectal sonographic examination of the palpable masses was performed in four affected horses and ponies. The intestinal wall appeared more defined than usual and thickened (5 mm), with a fluid-filled lumen.[263] Transcutaneous sonographic examination of the abdomen should also have revealed the extensive pathology in the small intestine. Severe fibrosis with arteriolar lesions and some smooth muscle hypertrophy was detected in these horses at necropsy.[263] Similar findings

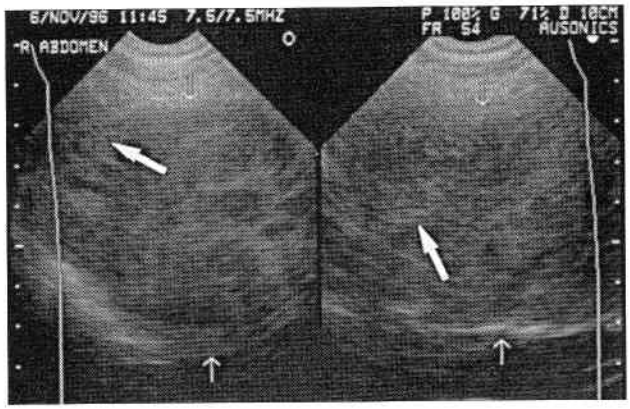

Figure 6–86

Sonogram of a mural and intraluminal hematoma in the jejunum of a 38-year-old Quarter horse mare (same horse as in Fig. 6–79). The small arrows point to the intraluminal mass, which has a hypoechoic, somewhat heterogeneous appearance with small areas of cavitation imaged within. The large arrows point to the mural portion of the mass. The right image is the transverse image of this loop of intestine, and the left image is the long-axis image. These sonograms were obtained from the right side of the abdomen just ventral to the costochondral junction below the thirteenth intercostal space with a wide-bandwidth 7.5-MHz sector-scanner transducer operating at 7.5 MHz at a displayed depth of 10 cm.

were detected in three other horses but involved only 3 to 6 meters of the jejunum.[264]

Idiopathic muscular hypertrophy of the ileum has been described in adult horses with histories of chronic mild intermittent colic, chronic weight loss, and partial anorexia, usually for several months prior to presentation.[265] In some horses the thickened ileum was palpable on rectal examination and felt rigid. The thickened ileum is usually palpated in the right dorsal quadrant of the abdomen, near the cecal base.[265] Multiple loops of distended small intestine are also frequently detected in affected horses on rectal examination, even if the thickened ileum is not palpable.[265] Ileal hypertrophy may be detected sonographically as a thickening of the muscular layer of the ileum, with fluid distention of the more proximal small intestine. The affected ileum is usually 15 to 25 mm thick at the caudal aspect of the ileum, tapering toward normal thickness cranially in most horses.[265] Both the circular and longitudinal layers are affected. Herniation of the mucosa through the muscularis may be detected, forming small outpouchings of the serosa in the majority of horses with idiopathic muscular hypertrophy.[265] Although involvement of the ileum alone is most common, a few horses have idiopathic muscular hypertrophy of only the jejunum, whereas others have several segments of small intestine affected.[265] Affected length of the ileum and affected small intestine range from 0.2 to 21.3 meters, with a median length of 1 meter of affected bowel.[265] Narrowing of the lumen of the affected ileum or small intestine is occasionally seen in affected horses.[265] Ileal impaction can occur in the portions of ileum in which the luminal diameter is narrowed.[265] Ileal hypertrophy can result in ileal rupture and diffuse peritonitis in some horses.[265] Diagnosis of ileal hypertrophy is often difficult and requires histopathologic examination of the wall of the affected small intestine. Transrectal ultrasonography in horses with palpable abdominal masses in the right dorsal quadrant near the cecal base has been helpful in determining that the thickening of the affected ileum and/or small intestine is confined primarily to the muscular layer, with no intussusception. Transcutaneous sonographic examination of the abdomen, particularly the right dorsal quadrant, may also reveal the affected portion of the ileum or small intestine.

Nephrosplenic Ligament Entrapment. The diagnosis of a renosplenic entrapment should be confirmed before a rolling procedure is performed to correct the entrapment.[266, 267] The left dorsal and ventral colon migrate dorsally between the spleen and the left abdominal wall and subsequently become entrapped over the nephrosplenic ligament.[266] The large colon is often found entrapped over the nephrosplenic ligament on rectal examination, confirming the diagnosis of nephrosplenic ligament entrapment. In one large study, entrapment of the large colon over the nephrosplenic ligament was detected on rectal examination in 61% of horses.[266] However, in many instances a definitive diagnosis cannot be made upon rectal examination because of severe abdominal tympany, or the size of the patient may preclude obtaining a diagnosis with rectal examination.[266] Nephrosplenic entrapment was not confirmed at surgery or at necropsy in 15% of horses in one study.[267]

Nephrosplenic ligament entrapment has a characteristic ultrasonographic appearance.[4, 230] This results in a rapid ultrasonographic diagnosis, and the findings during the ultrasound examination can be used in conjunction with the rectal examination findings to confirm the correction of the nephrosplenic ligament entrapment. Nephrosplenic ligament entrapment was correctly diagnosed sonographically in 88% of horses with this displacement, whereas a definitive diagnosis was able to made on rectal examination in only 32%.[230] Ultrasonographic diagnosis of nephrosplenic ligament entrapment has two critical components: the lack of visualization of the left kidney and a straight (horizontal) dorsal border of the spleen in the paralumbar fossa extending cranially from the more caudal interspaces (Fig. 6-87).[230] The straight dorsal border of the spleen is caused by the dorsal displacement of the colon over the nephrosplenic ligament. The gas in the entrapped large colon prevents the visualization of the underlying dorsal border of the spleen and creates the straight horizontal appearance of the dorsal splenic border. The most dorsal border of the spleen that can be imaged is also ventrally displaced by the entrapped large colon.[230] Left dorsal displacement of the large colon was not diagnosed sonographically in five horses in one study because the entrapped large colon was not filled with gas (Fig. 6-88) and/or there was little ventral displacement of the dorsal border of the spleen.[230] Knowledge of these variations of the sonographic findings in horses with nephrosplenic ligament entrapment and the experience of the sonologist minimize false-negative sonographic findings. The entrapped colon is usually very hypomotile or completely lacking in peristaltic activity. Care must be taken not to overdiagnose a nephrosplenic ligament entrapment when the left kidney is obscured from view by colonic gas. A recent rectal examination often obscures visualization of the left kidney but

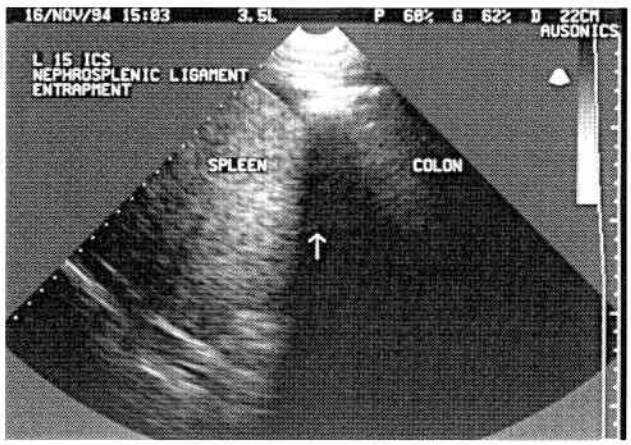

Figure 6-87

Sonogram of the spleen and left colon obtained from a 2-year-old Standardbred colt with a nephrosplenic ligament entrapment. The dorsal border of the spleen is obscured from view and appears horizontal owing to the gas trapped in the overlying colon. The gas-filled colon casts a strong acoustic shadow and obliterates the kidney from view in the more caudal interspaces. This sonogram was obtained in the left fifteenth intercostal space with a 3.5-MHz sector-scanner transducer at a displayed depth of 22 cm. The right side of this sonogram is dorsal and the left side is ventral.

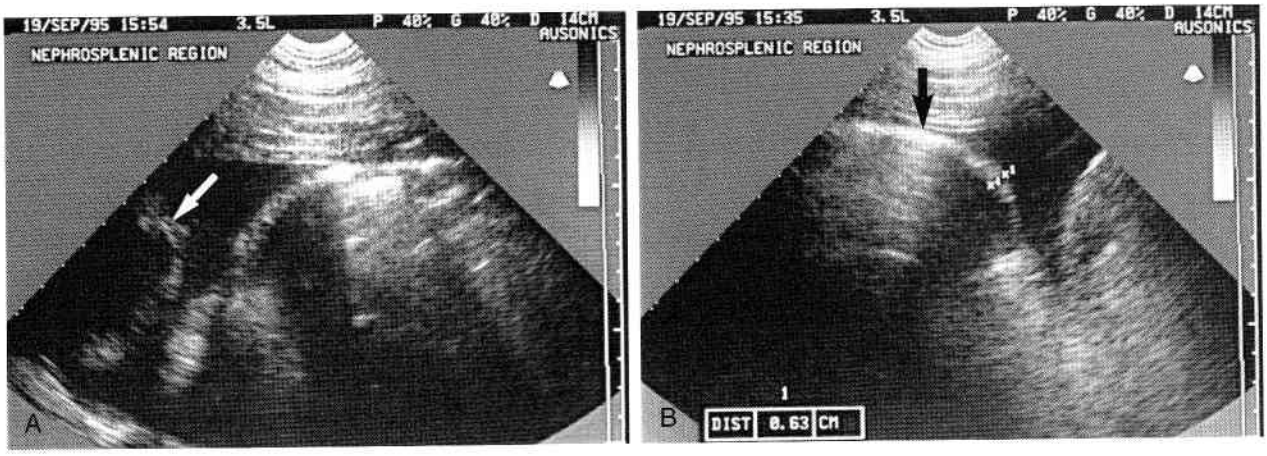

Figure 6–88

Sonograms of a left dorsal displacement of the large colon obtained from an 8-year-old Thoroughbred gelding. A fluid- and gas-filled large colon is displaced in the area of the nephrosplenic ligament, preventing visualization of the left kidney. The sharp dorsal border of the spleen found in horses with nephrosplenic ligament entrapment is not imaged. The spleen was imaged medial to the fluid- and gas-distended large colon consistent with a lateral displacement of the large colon. An increased amount of peritoneal fluid is present in the peritoneal cavity. These sonograms were obtained from the left sixteenth intercostal space (*A*) and seventeenth intercostal space (*B*) with a 3.5-MHz sector-scanner transducer at a displayed depth of 14 cm. The right side of these sonograms is dorsal and the left side is ventral. *A*, A gas-fluid interface (*small arrow*) in the displaced large colon with fluid distention of the adjacent small intestine (*large arrow*). In real time the large and small intestine had minimal peristaltic activity. *B*, The wall of the large colon is slightly thickened (6.3 mm). Two large gas- (*black arrow*) and fluid-filled (*open arrow*) portions of the large colon are imaged in this view.

does not create the straight horizontal dorsal border of the spleen. The left kidney can be imaged occasionally in horses with nephrosplenic ligament displacement if little or no gas is present in the entrapped colon. The type of ingesta trapped in the large colon in horses with a nephrosplenic ligament entrapment can occasionally be determined when very fluid ingesta is present within the entrapped large colon. In these horses, ingesta, fluid, and gas can often be imaged in the entrapped large colon and may have a layered appearance (Fig. 6–88).

Large Colon Disease. Large colon disease is common in the adult horse, in contrast to the foal, in which small intestinal disease is more common. Many adult horses with colic have a gas-filled, distended large colon occupying the majority of the abdomen, making diagnosis of a surgical lesion difficult to impossible.[2] Differentiation of a spasmodic colic from a large colon displacement or volvulus is difficult ultrasonographically. Diagnosing a surgical lesion in the large colon of the adult horse depends upon the recognition of malpositioning of the large colon or other parts of the gastrointestinal tract or abdominal viscera (Fig. 6–89), the detection of a mural or intraluminal mass, or the detection of thickened colonic wall lacking peristaltic activity. Abnormal positioning of the large colon is difficult to diagnose ultrasonographically, with the exception of a nephrosplenic ligament displacement,[230] cecal impaction, and cecal intussusception. Diagnosis of lateral displacement of the large colon is possible sonographically when the entire spleen is obscured from view by gas-filled large bowel.[230]

In many instances a distended, gas-filled large bowel viscus with normal wall thickness, adjacent to the body wall, is all that can be imaged. The large colon or cecal distention may resolve with medical therapy alone, or surgery may be indicated. Therefore, if only gas-distended large bowel with normal wall thickness is imaged and a surgical lesion is not detected sonographically, a repeat rectal and sonographic examination should be performed if the horse remains colicky. Fluid- and ingesta-filled large colon or cecum with normal to nearly normal wall thickness may also be imaged in colicky horses and may respond to medical therapy.

Large Colon and Cecal Impactions. Impactions of the large colon and cecum are frequently associated with mild persistent colic or intermittent colic. The intermittent colic is probably associated with transient periods of obstruction. Impactions can also be imaged in the large colon and cecum as a hyperechoic intraluminal structure casting a strong acoustic shadow (Fig. 6–90). Gas, fluid, and ingesta layers can be imaged in some horses with cecal impaction or obstruction (Fig. 6–91). Impactions can be imaged sonographically only when the impacted portion of the large colon or cecum is adjacent to the body wall or fluid is interposed between the affected portion of the intestine and the body wall. Fluid distention of the more proximal small intestine may be detected in horses with large colon or cecal impactions (Fig. 6–90). The wall thickness of the distended small intestine is usually normal to nearly normal, although the distended small intestine usually lacks peristaltic activity.

Sand impactions can also be detected ultrasonographically by imaging the ventral portion of the horse's abdomen. The large colon appears flattened against the ventral body wall with loss of the normal sacculations (Fig. 6–92). Little peristaltic movement of the large colon is detected because it is weighted to the floor of the abdomen by the accumulation of sand. The large colon looks like it adheres to the ventral abdomen owing to the lack of motility between these two structures. Evaluation of the more dorsal portions of the large colon reveals normal sacculations and motility. The sand grains on the mucosal surface of the large intestine look like small,

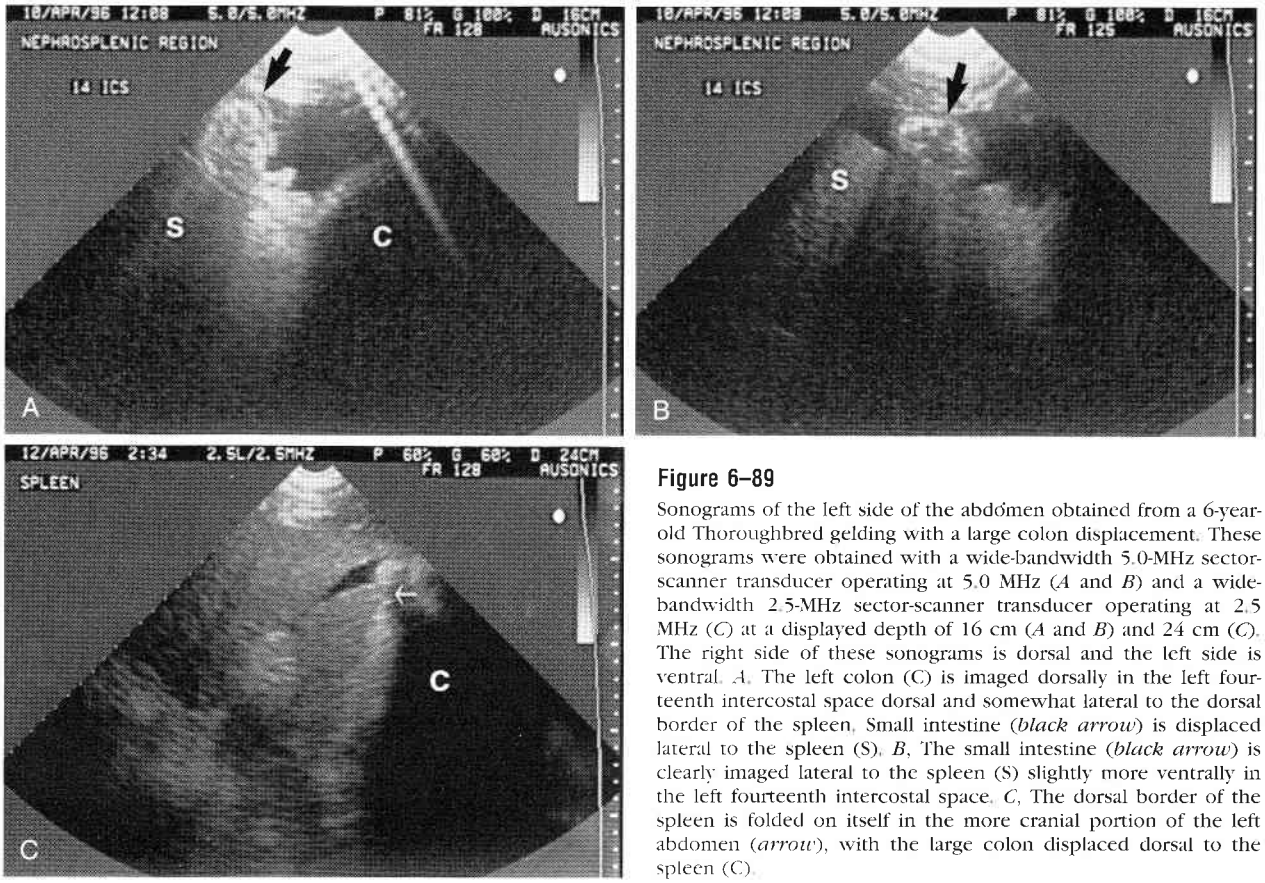

Figure 6–89

Sonograms of the left side of the abdomen obtained from a 6-year-old Thoroughbred gelding with a large colon displacement. These sonograms were obtained with a wide-bandwidth 5.0-MHz sector-scanner transducer operating at 5.0 MHz (*A* and *B*) and a wide-bandwidth 2.5-MHz sector-scanner transducer operating at 2.5 MHz (*C*) at a displayed depth of 16 cm (*A* and *B*) and 24 cm (*C*). The right side of these sonograms is dorsal and the left side is ventral. *A*, The left colon (C) is imaged dorsally in the left fourteenth intercostal space dorsal and somewhat lateral to the dorsal border of the spleen. Small intestine (*black arrow*) is displaced lateral to the spleen (S). *B*, The small intestine (*black arrow*) is clearly imaged lateral to the spleen (S) slightly more ventrally in the left fourteenth intercostal space. *C*, The dorsal border of the spleen is folded on itself in the more cranial portion of the left abdomen (*arrow*), with the large colon displaced dorsal to the spleen (C).

pinpoint, hyperechoic structures casting small acoustic shadows in varying directions, depending upon the angle of the ultrasound beam.

Enterolithiasis. Horses with enteroliths usually have recurrent mild abdominal pain, anorexia, gaseous distention, and minimal gastrointestinal motility.[268] The history of mild colic varies in affected horses from 12 hours to 6 weeks' duration.[268, 269] Enterolithiasis involving the right dorsal colon, transverse colon, ventral colon, and small colon has been described.[1, 268, 269] In one large study of 141 horses, 59 horses had enteroliths in the right dorsal colon. Enteroliths were found in the transverse colon in 28 horses, in the small colon in 24 horses, and in the ventral colon in 1 horse, with 12 horses having enteroliths detected at multiple sites.[1] Although most enteroliths are not palpable on rectal examination, enteroliths in the right dorsal colon and small colon are detectable on rectal examination.[268, 269]

Enteroliths are usually single and spherical but can be multiple and tetrahedral.[268] The enterolith is usually smooth and thus should be imaged as a smooth circular or tetrahedral hyperechoic intraluminal structure casting a large acoustic shadow. Enteroliths are therefore difficult to image sonographically owing to their characteristic location in the proximal small colon, transverse colon, or diaphragmatic flexure, areas inaccessible to ultrasono-

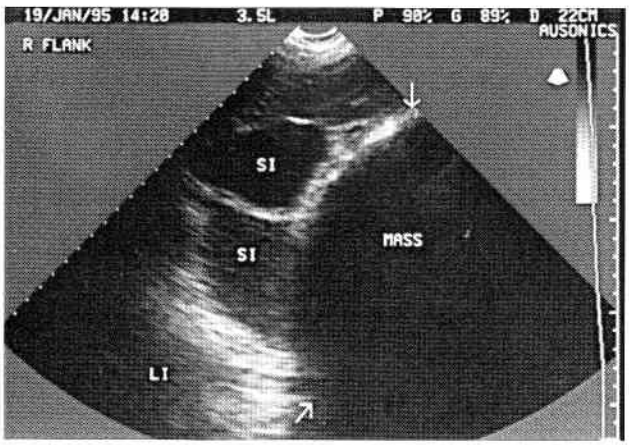

Figure 6–90

Sonogram of a cecal impaction obtained from a 22-year-old Thoroughbred gelding. The large circular hyperechoic mass in the large colon (*arrows*) casts an acoustic shadow consistent with a dense material or an enterolith. This mass extended from the right flank ventral to the costochondral junction at the level of the thirteenth intercostal space caudally into the paralumbar fossa and was greater than 20 cm in diameter. The large colon in the area of the impaction had a complete ileus. Notice the lack of sacculations in the affected portion of the large colon compared with the sacculations imaged in the adjacent large intestine (LI). The adjacent small intestine (SI) is fluid filled and hypomotile, with normal wall thickness. This sonogram was obtained from the right paralumbar fossa with a 3.5-MHz sector-scanner transducer at a displayed depth of 22 cm. The right side of the sonogram is dorsal and the left side is ventral.

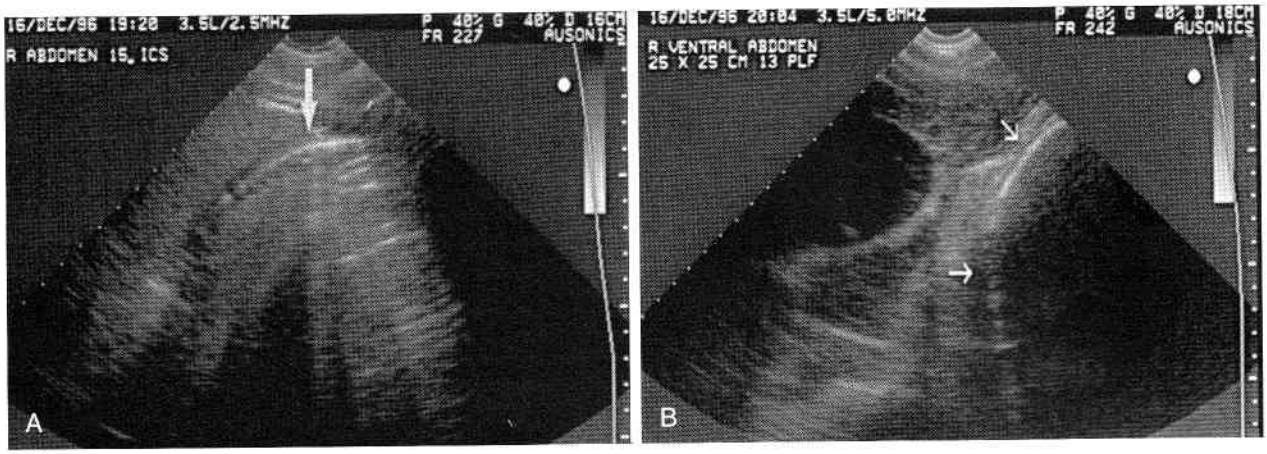

Figure 6–91

Sonograms of the right side of the caudal abdomen obtained from a 15-year-old Warmblood gelding with a cecal impaction. A large 25 by 25 cm mass was imaged extending from the right thirteenth intercostal space to the paralumbar fossa. These sonograms were obtained from the right fifteenth intercostal space (*A*) and the ventral aspect of the right paralumbar fossa (*B*) with a wide-bandwidth 3.5-MHz sector-scanner transducer operating at 2.5 MHz (*A*) and 5.0 MHz (*B*) at a displayed depth of 16 (*A*) and 18 (*B*) cm. The right side of these sonograms is dorsal and the left side is ventral. *A*, The mass was circular. A dorsal gas cap and echogenic fluid and ingesta were imaged ventrally in the more cranial portion of the abdomen. The arrow points to the gas-fluid interface. *B*, The mass cast a complete acoustic shadow ventrally and caudally from the mucosal surface of the large colon (*arrows*) consistent with impacted ingesta. Distended small intestine (SI) is imaged adjacent to this impaction.

graphic examination. The medium-sized enteroliths tend to lodge in the transverse colon and the larger enteroliths in the right dorsal colon or diaphragmatic flexure.[268, 269] Radiographic examination of the abdomen is preferable to ultrasonographic examination in horses in which enterolithiasis is suspected.[1] Cases with only large colon enteroliths were correctly identified 83.2% of the time, whereas small colon enteroliths were identified only 41.6% of the time.[1]

Large Colon and Cecal Obstruction. Obstruction of the large colon with fecaliths or trichophytobezoars has been reported in horses and ponies, particularly miniature horses.[270–272] Mild colic is a common presenting sign, along with progressive abdominal distention. Fecaliths are composed of inspissated fibrous fecal material and can reach 8 to 12 cm in diameter and 15 to 20 cm in length.[273] Trichophytobezoars are combinations of animal hair, plant fiber, and magnesium ammonium phosphate. Phytoconglobates are ball-shaped concretions of undigested food and foreign particulate matter.[15] Impaction of the right dorsal colon, transverse colon, and small colon with synthetic fencing material has been reported.[274] A firm mass was felt on rectal examination in three horses with distended loops of small or large intestine and in two other horses with fibrous foreign body impaction.[274] Ultrasonographic visualization of the impaction (Figs. 6-90 and 6-91), fecalith, or trichophytobezoar depends upon the amount of gas distention of the surrounding intestine and the location of the obstruction in the large colon (whether a sonographic window exists to image this area). If a mass is palpable rectally, transrectal sonographic examination of the mass should be rewarding. The fecalith and trichophytobezoar usually have a somewhat irregular surface with many acoustic interfaces and should have an irregular hyperechoic to composite sonographic appearance in the lumen of the bowel. The fecalith and trichophytobezoar cast acoustic shadows, but the shadows are likely to be dirty and irregular.

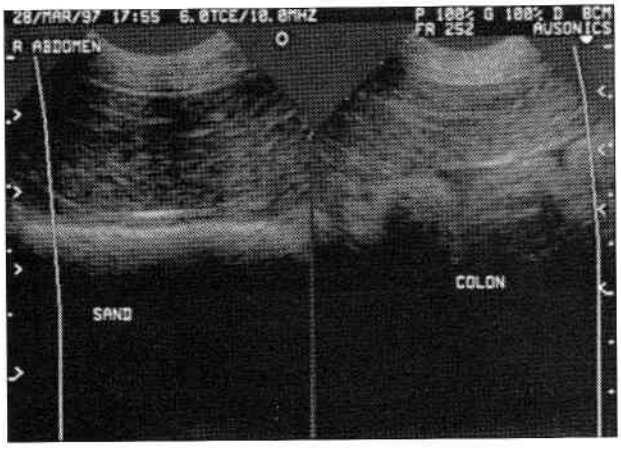

Figure 6–92

Sonograms of the colon obtained from a 4-year-old miniature horse filly with a sand impaction. The left image is of the right ventral colon, which is loaded with sand and has lost its normal sacculations against the ventral portion of the abdomen. In real time, peristaltic movement of this portion of the bowel was difficult to appreciate. The right image is of the left ventral colon that has normal sacculations and peristalsis against the ventral abdominal wall. These sonograms were obtained with a wide-bandwidth 6.0-MHz microconvex linear array transducer operating at 10.0 MHz at a displayed depth of 8 cm. The right side of these sonograms is cranial and the left side is caudal.

Small Colon Impaction/Obstruction. Horses with small colon disease typically have a history of mild colic and normal to nearly normal hydration.[15, 274, 275] Horses with small colon disease pass little or no manure and gradually deteriorate, with progressive distention of the more proximal large colon.[275, 276] Small colon impaction is the most common disorder of the small colon.[15] Impaction of the small colon with fecaliths, phytobezoars, trichobezoars, phytoconglobates, foreign bodies, and enteroliths has been described. Enteroliths have been fre-

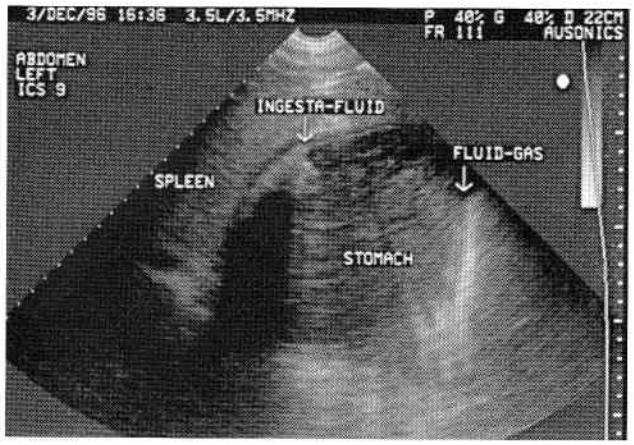

Figure 6–93

Sonogram of the stomach obtained from a 15-year-old Thoroughbred gelding with gastric reflux. The stomach is filled with fluid, gas, and some ingesta. Notice the fluid-gas and ingesta-fluid interfaces in the stomach. The dorsal gas cap casts a dirty shadow with the characteristic gas artifact, and the ventral ingesta casts a clean shadow, consistent with dense ingesta. The distention of the stomach is mild to moderate but not severe, measuring 12.25 cm in diameter. This sonogram was obtained from the left ninth intercostal space with a wide-bandwidth 3.5-MHz sector-scanner transducer operating at 3.5 MHz at a displayed depth of 22 cm. The right side of this sonogram is dorsal and the left side is ventral.

quently reported in the proximal portion of the small colon.[1, 276] Impaction of the proximal small colon and adjacent right dorsal colon with rubber tire fencing, synthetic nylon fencing, rope, rag, and twine has been reported.[15, 274, 275] Horses with small colon impaction associated with the ingestion of rubber fencing are all 3 years of age or younger.[274] In 3 of 6 horses and 3 of 10 horses with small colon impactions associated with a foreign body, the mass could be palpated rectally.[274, 275]

Lipomas can occur in the mesocolon and mesorectum in aged horses because these structures contain large amounts of fat that predisposes to lipoma formation.[15] Lipomas can result in strangulating obstruction of the small colon.[15] Obstruction of the small colon by intramural or submucosal hematomas has also been described in several horses.[277, 278] This occurred secondary to ulceration and a dissecting cellulitis in one horse and to iatrogenic rectal trauma in another.[277] In the other five horses, no cause of the hematoma was found. Communication of the hematoma with the bowel lumen was not present in four of the six horses. An abdominal mass was palpated in one of these horses. Transrectal ultrasonographic examination of the mass or transcutaneous examination of the caudal abdomen might have revealed a mural mass in these horses.

Small colon impactions are most readily diagnosed sonographically with a transrectal ultrasonographic examination of the affected small colon. In miniature horses, the small colon impaction may be diagnosed sonographically by examining the caudal abdomen through the paralumbar fossa. A full urinary bladder can also be used as a sonographic window for visualization of the small colon. The impaction is usually imaged as a hyperechoic intraluminal structure casting an acoustic shadow. Little or no peristaltic activity is seen surrounding the impaction, and the normal sacculations of the small colon are difficult to image. Fecaliths have been successfully imaged in the small colon from the flank area in young miniature horses. They appear as echogenic to hyperechoic masses that cast an acoustic shadow, similar to gastric trichobezoars in children.[279-281] Enteroliths in the small colon may be successfully imaged transrectally if the mass is palpable. However, this is often not the case owing to their frequent location in the proximal portion of the small colon.

Gastric Distention, Ulceration, and Impaction. Ultrasonographic evaluation of the stomach should be a part of the sonographic evaluation of the abdomen in all horses with suspected gastritis or gastric neoplasia. Marked gastric distention can be readily detected and the luminal contents determined.[2] Distention of the stomach with anechoic to hypoechoic fluid is detected with small intestinal obstructions and ileus (Fig. 6-93). Gastric and duodenal distention is often detected in horses with anterior enteritis. A thicker than normal gastric wall may occur with gastritis or edema in the stomach wall (Figs. 6-94 and 6-95). Thickening of the gastric wall has been reported in human beings and dogs with gastric ulcers and may be detectable in affected horses.[21, 282-284] The visualization of an ulcer crater has also been described in both humans and dogs with gastric ulcers but has not been described in affected horses to the author's knowledge.[21, 283-285] Ulceration of both the squamous and glandular portions of the stomach has been described in horses, with gastric ulcers occurring more frequently in the nonglandular portion of the stomach. Perforated gastric ulcers located at the margo plicatus or near the pylorus have been reported to cause peritonitis and death. Perforated gastric ulcers have been detected ultrasonographically in children as a inflammatory mass surrounding a portion of the stomach, creating an ultrasonic

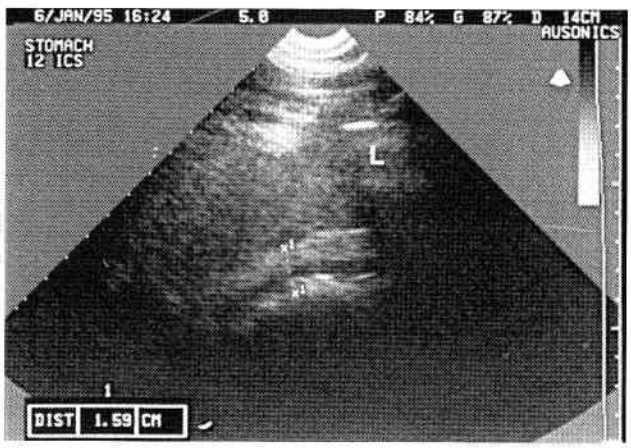

Figure 6–94

Sonogram of the stomach obtained from a 27-year-old Thoroughbred gelding. Notice the thickened stomach wall (1.59 cm) medial to the spleen, which was determined to represent edema on postmortem examination. The ventral most tip of the lung (L) is imaged on the right side of the image. This sonogram was obtained from the left twelfth intercostal space with a 5.0-MHz sector-scanner transducer at a displayed depth of 14 cm. The right side of this sonogram is dorsal and the left side is ventral.

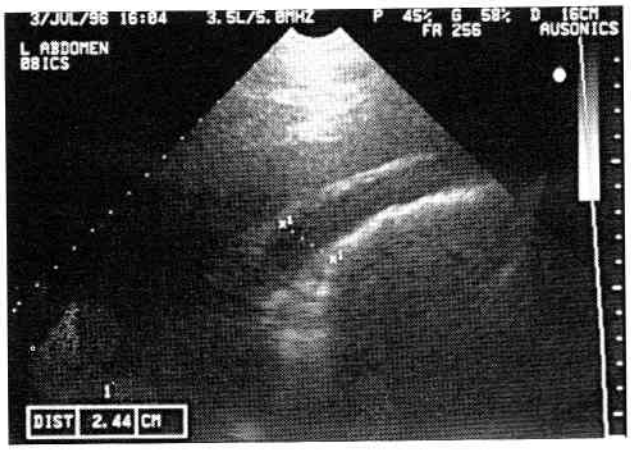

Figure 6–95

Sonogram of the stomach obtained in the left eighth intercostal space from a 15-year-old Morgan mare with fever of unknown origin. Notice the marked thickening of the gastric wall (at least 2.44 cm). The mural thickening is homogeneous and may reflect edema or a diffuse cellular infiltrate in this region. This sonogram was obtained with a wide-bandwidth 3.5-MHz sector-scanner transducer operating at a frequency of 5.0 MHz at a displayed depth of 16 cm. The right side of this sonogram is dorsal and the left side is ventral.

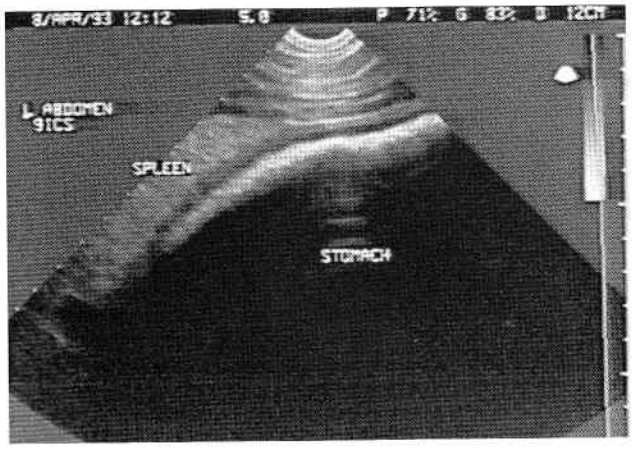

Figure 6–96

Sonogram of severe gastric distention obtained from a 19-year-old Thoroughbred gelding. The stomach is markedly distended, having lost some of its curved semicircular shape owing to the marked distention. The stomach is recognized by its somewhat semicircular shape and its location adjacent to the splenic vein. The stomach was imaged over six intercostal spaces on the left side of the abdomen. This sonogram was obtained from the left ninth intercostal space with a 5.0-MHz sector-scanner transducer at a displayed depth of 12 cm. The right side of this sonogram is dorsal and the left side is ventral.

"doughnut."[77, 286] Thickening of the wall of the stomach has been imaged in one horse with suspected gastritis, but a definitive diagnosis was not obtained (Fig. 6–95). Gastroscopic examination of this horse revealed minimal gastric ulcerations. Marked distention of the stomach may be imaged occasionally in horses with little or no visible gastric fluid.

Gastric emptying problems may be identified sonographically on repeat examinations if large amounts of ingesta persist unchanged in the stomach in a fasted, anoretic, or refluxing horse (Fig. 6–96). Gastric impactions have been imaged in several older horses presenting for weight loss and anorexia. The sonographic appearance of a gastric impaction is a markedly enlarged gastric echo extending over five or more intercostal spaces on the left side of the abdomen (Fig. 6–96). The stomach is usually slightly less circular than normal, with hyperechoic material casting an acoustic shadow in the lumen of the stomach. In one horse the enlarged stomach was also imaged for several intercostal spaces on the right side of the horse's abdomen (Fig. 6–97). Emphysematous gastritis has also been reported in a horse associated with *Clostridium perfringens*.[287] A localized gas-filled stomach wall was detected at necropsy. Along the greater curva-

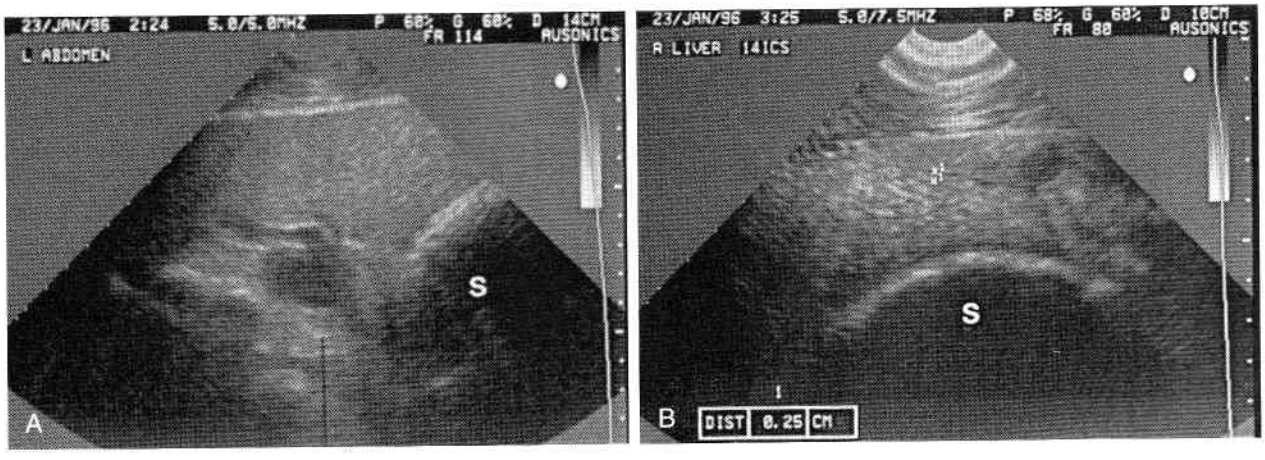

Figure 6–97

Sonograms obtained from a 19-year-old Quarter horse gelding with marked gastric distention and a gastric impaction. The stomach was imaged over seven intercostal spaces on the left side and three on the right side. Thickened mesentery was imaged surrounding the stomach containing enlarged vessels. These sonograms were obtained from the left (*A*) and right (*B*) fourteenth intercostal space with a wide-bandwidth 5.0-MHz sector-scanner transducer operating at 5.0 MHz (*A*) and 7.5 MHz (*B*) at a displayed depth of 14 cm (*A*) and 10 cm (*B*). The right side of these sonograms is dorsal and the left side is ventral. *A*, Sonogram of the stomach adjacent to the splenic vein obtained from the left side of the abdomen in the fourteenth intercostal space. The stomach was imaged over seven intercostal spaces on the left. *B*, Sonogram of the stomach with some thickened omentum between the stomach and the adjacent liver. The cursors measure the space between the liver and the omentum. The stomach was imaged for three intercostal spaces on the right.

ture of the stomach were extensive areas of full-thickness necrosis involving 30% of the wall of the stomach, and the stomach was tightly adherent to the spleen and liver, with excessive peritoneal fluid and fibrin. This area is accessible for percutaneous sonographic examination. Sonographic examination of the stomach for size and contents may help determine the underlying abnormality and help prevent gastric rupture.[288]

Gastric Neoplasia. Gastric squamous cell carcinoma is the most common gastric tumor in the horse and is the most common primary gastrointestinal neoplasm.[289] Gastric squamous cell carcinomas represent 3% to 4% of all equine squamous cell carcinomas.[289] A leiomyoma and several adenocarcinomas of the glandular portion of the stomach have also been reported.[290, 291] The tumor usually occurs in middle-aged to older horses presenting with weight loss, anorexia, and anemia.[4, 289, 290, 292] Abnormal chewing and swallowing behavior and dysphagia have also been reported.[289, 292] The mass appeared to originate in the esophageal portion of the stomach in four reported cases[289] and at the cardia in five horses.[292] Passage of the nasogastric tube or gastroscope may be difficult owing to the involvement of the cardia.[292] Rectal examination revealed palpable abdominal masses in four of five horses in one study[292] and in three of six horses in another study.[289] Large peritoneal effusions were present in many affected horses.[292] Peritoneal fluid analysis revealed neoplastic cells in the majority of horses.[5, 292] However, the absence of neoplastic cells does not rule out gastric squamous cell carcinoma. At postmortem examination the tumors ranged from 13 to 25 cm in diameter[290] and weighed from a few grams to 1 kg.[292] Involvement of the greater curvature of the stomach that extends through the serosa to the adjacent diaphragm and liver is common in affected horses.[290, 292] Multiple metastatic masses are detected throughout the peritoneal cavity, located in the omentum, liver, and spleen and on the parietal peritoneum and kidney.[289, 290, 292] Adhesions between the stomach, liver, and spleen were commonly detected in horses with gastric squamous cell carcinoma.[289, 292] Metastases to the thoracic cavity are also common.[289, 290]

Sonographic examination of the stomach in horses with gastric squamous cell carcinoma reveals a large mural gastric mass in the left side of the abdomen associ-

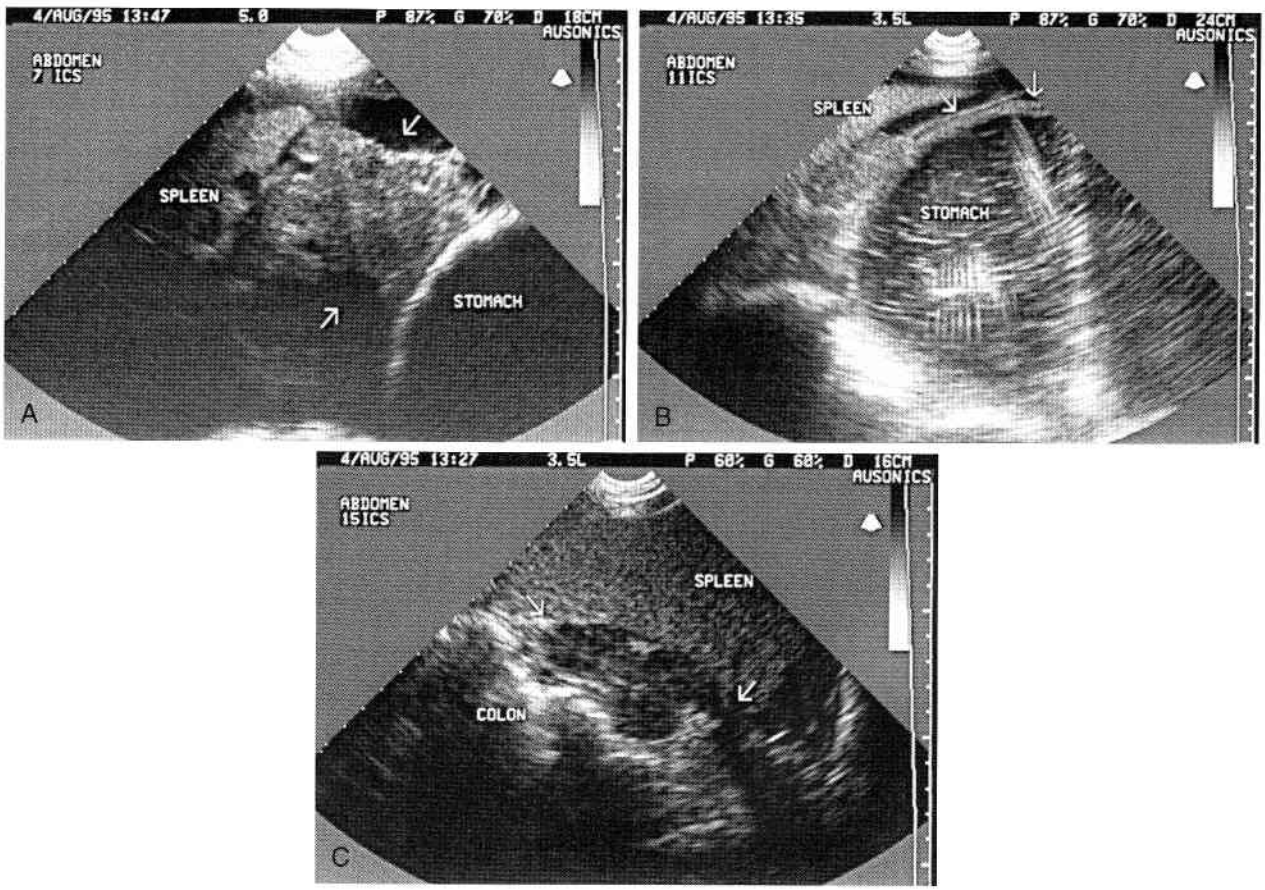

Figure 6–98

Sonograms of the stomach obtained from an 18-year-old half-Arabian gelding with gastric squamous cell carcinoma. The irregular heterogeneous composite mass is imaged proliferating from the greater curvature of the stomach and adhering to the spleen (*A*, *B*, and *C*) and the large colon (*C*). The mass extended from the sixth through the fifteenth intercostal spaces. These sonograms were obtained from the left seventh (*A*), eleventh (*B*), and fifteenth (*C*) intercostal spaces with a 5.0-MHz sector-scanner transducer (*A*) and a 3.5-MHz sector-scanner transducer (*B* and *C*) at a displayed depth of 18 cm (*A*), 24 cm (*B*), and 16 cm (*C*). The right side of these sonograms is dorsal and the left side is ventral. *A*, The large heterogeneous mass with composite echogenicities protrudes from the serosal side of the stomach (*arrows*) and is adherent to the adjacent spleen. *B*, A more normal portion of the gastric wall is imaged (*arrows*) adjacent to the gastric mass, which still is adherent to the spleen at this level. The stomach shows marked fluid and gas distention. *C*, The caudal aspect of the gastric squamous cell carcinoma is adherent to the large colon and spleen (*arrows*).

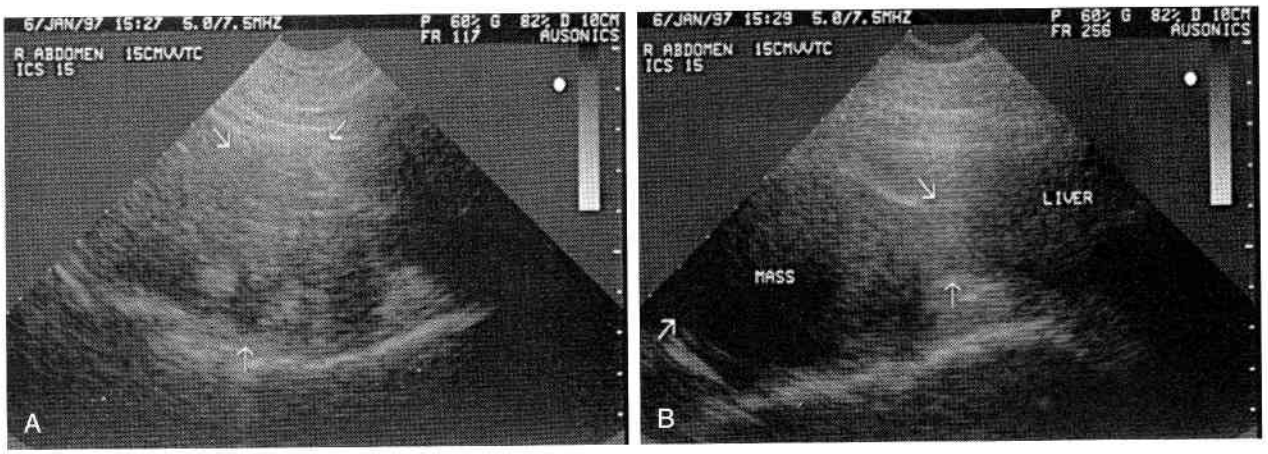

Figure 6–99

Sonograms of a large mass in the right side of the abdomen adjacent to the liver in a 13-year-old Morgan gelding with gastric squamous cell carcinoma. The mass was imaged only on the right side of the abdomen adjacent and caudal to the right lobe of the liver. These sonograms were obtained from the right fifteenth intercostal space 15 cm ventral to the ventral border of the tuber coxae with a wide-bandwidth 5.0-MHz sector-scanner transducer operating at 7.5 MHz at a displayed depth of 10 cm. The right side of these sonograms is dorsal and the left side is ventral. *A*, The mass (*arrows*) contains heterogeneous echogenicities and appears adjacent to the large intestine (*up arrow*). *B*, The mass (*left arrow*) appears adherent to the liver by a stalk of tissue of similar echogenicity (*two right arrows*).

ated with the greater curvature in nearly all affected horses (Fig. 6–98). In one horse, however, the neoplastic mass imaged was associated with the medial side of the right liver lobe and the cardia (Fig. 6–99). The mural mass is usually heterogeneous with a complex pattern of echogenicity and is usually greater than 10 cm in diameter by the time the horse presents with clinical signs (Fig. 6–100).[2] In some horses, marked tumor necrosis occurs and secondary abscessation may occur (Fig. 6–100). An echolucent mass superficial to the stomach gas echo has

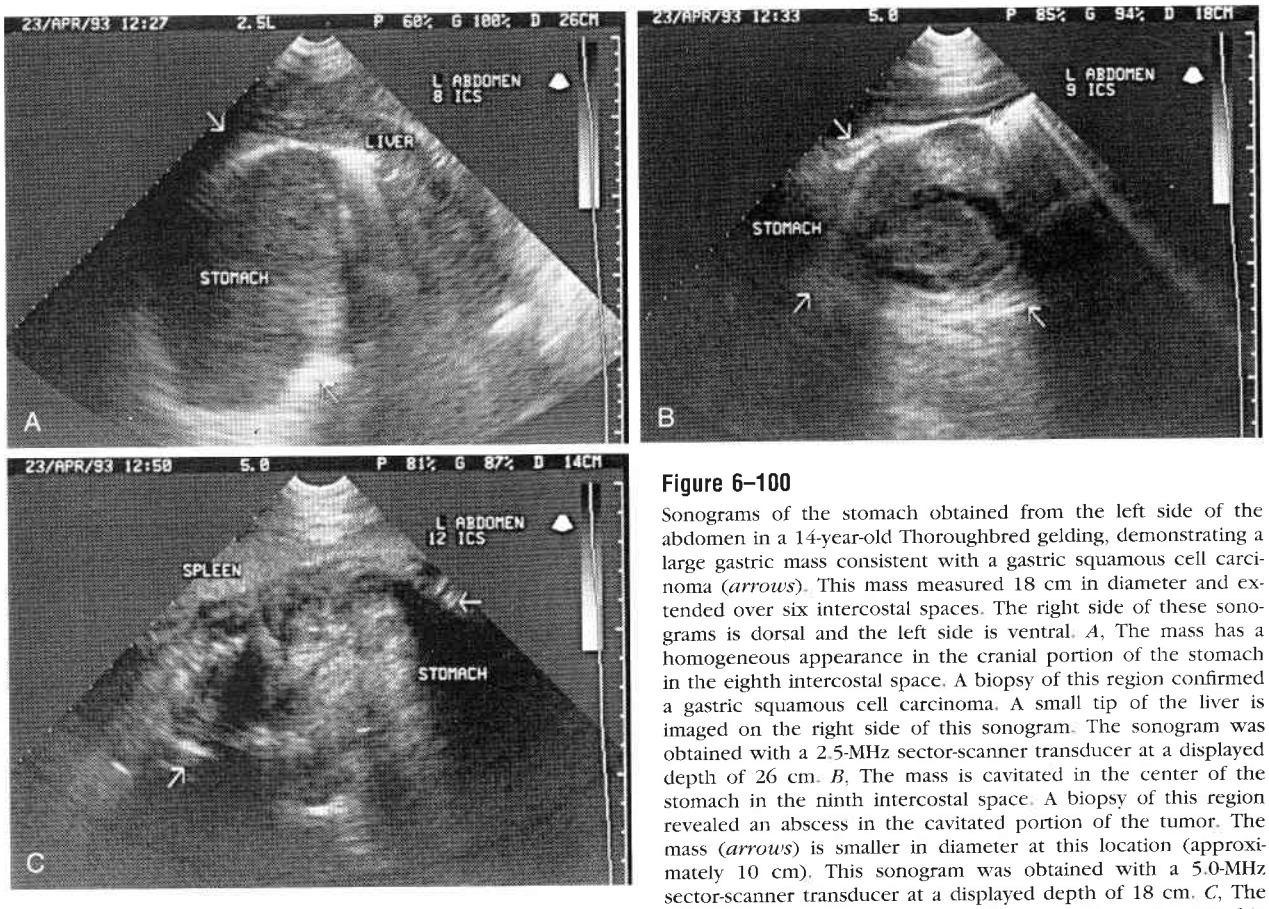

Figure 6–100

Sonograms of the stomach obtained from the left side of the abdomen in a 14-year-old Thoroughbred gelding, demonstrating a large gastric mass consistent with a gastric squamous cell carcinoma (*arrows*). This mass measured 18 cm in diameter and extended over six intercostal spaces. The right side of these sonograms is dorsal and the left side is ventral. *A*, The mass has a homogeneous appearance in the cranial portion of the stomach in the eighth intercostal space. A biopsy of this region confirmed a gastric squamous cell carcinoma. A small tip of the liver is imaged on the right side of this sonogram. The sonogram was obtained with a 2.5-MHz sector-scanner transducer at a displayed depth of 26 cm. *B*, The mass is cavitated in the center of the stomach in the ninth intercostal space. A biopsy of this region revealed an abscess in the cavitated portion of the tumor. The mass (*arrows*) is smaller in diameter at this location (approximately 10 cm). This sonogram was obtained with a 5.0-MHz sector-scanner transducer at a displayed depth of 18 cm. *C*, The caudal aspect of the gastric squamous cell carcinoma is adherent to the adjacent spleen and has a much more heterogeneous sonographic appearance (*arrows*). The diameter of the mass is smaller in the twelfth intercostal space (approximately 6 cm). This sonogram was obtained with a 5.0-MHz sector-scanner transducer at a displayed depth of 14 cm.

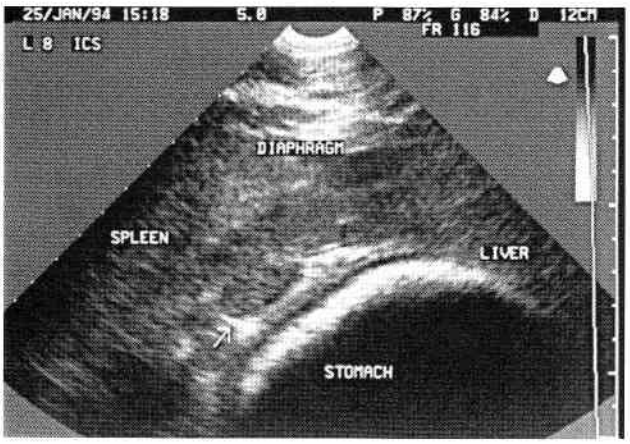

Figure 6–101

Sonogram of the left eighth intercostal space obtained from an 18-year-old Appaloosa gelding with generalized lymphosarcoma (same horse as in Figs. 6-47, 6-66, and 6-72). The gastric lymph node is enlarged, with a homogeneous sonographic appearance consistent with a diffuse cellular infiltrate. The wall of the stomach is slightly thickened (1 cm) but is otherwise nonremarkable. The adjacent liver appears enlarged with a rounded ventral border and loss of the normal parenchymal detail. The adjacent spleen appears slightly heterogeneous. This sonogram was obtained with a 5.0-MHz sector-scanner transducer at a displayed depth of 12 cm. The right side of the sonogram is dorsal and the left side is ventral.

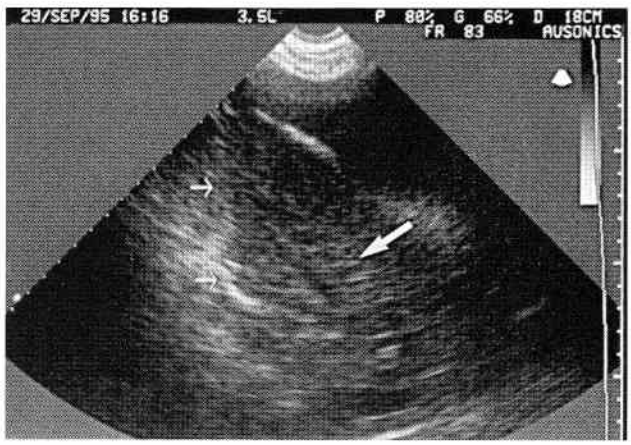

Figure 6–103

Sonogram of the right side of the abdomen obtained from an 11-year-old Thoroughbred gelding with marked duodenal thickening secondary to torsion of the left liver lobe. The smaller arrows point to the edge of the cecum, adjacent to the more hypoechoic duodenum. The larger arrow points to the junction between the duodenum and the adjacent liver-kidney border at the renal fossa of the liver. The duodenal lumen contains only a very small amount of anechoic fluid. This sonogram was obtained from the right fifteenth intercostal space with a 3.5-MHz sector-scanner transducer at a displayed depth of 18 cm. The right side of this sonogram is dorsal and the left side is ventral.

been described for horses with gastric squamous cell carcinoma.[4] A homogeneous mass was imaged with static B-mode ultrasound between the gastric lumen and spleen in one horse with gastric squamous cell carcinoma.[65] In one report the gastric wall was markedly thickened (at least 6 to 8 cm) but was diffusely hypoechoic.[6] Increased thickening of the gastric wall and abnormal echogenicity of the wall are consistent with gastric squamous cell carcinoma.[6] However, other causes of gastric wall thickening should also be considered.

The squamous cell carcinoma may invade the adjacent spleen and liver, or adhesions may develop between the stomach and adjacent abdominal viscera. Metastases to the serosal surfaces of the omentum, intestines, liver, spleen, and peritoneum have been detected ultrasonographically, appearing as a slight roughening of the serosal surface or masses several centimeters in size.[4] Metastatic nodules on the splenic capsule have also been detected sonographically in a horse with gastric squamous cell carcinoma.[6] Enlargement of the gastric lymph nodes may be imaged in horses with abdominal neoplasia with a normal to nearly normal appearance of the adjacent stomach wall. Homogeneous enlargement of the

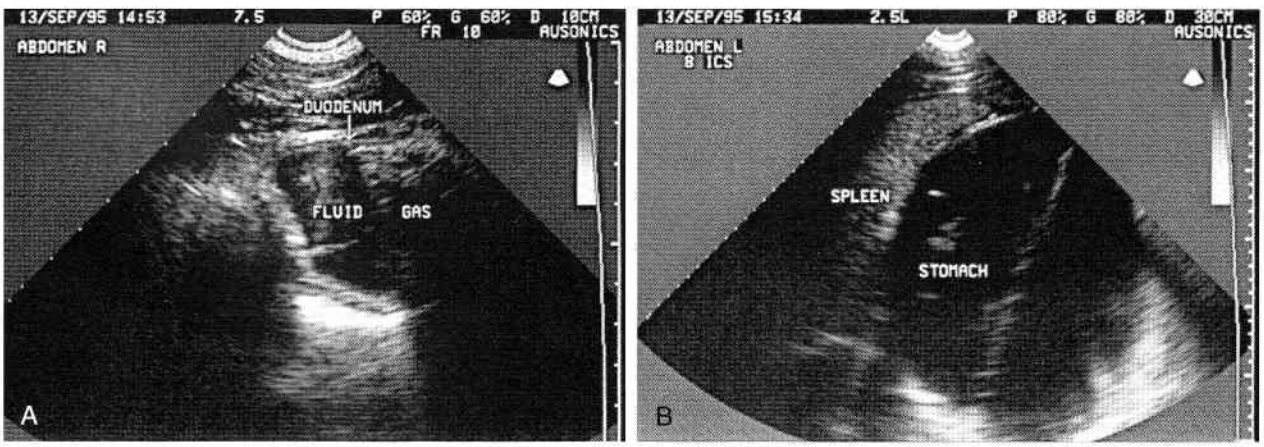

Figure 6–102

Sonogram of the duodenum (*A*) and stomach (*B*) obtained from the right fifteenth intercostal space (*A*) and the left eighth intercostal space (*B*) in a 4-year-old Thoroughbred gelding with anterior enteritis. These sonograms were obtained with a 7.5-MHz (*A*) and 2.5-MHz (*B*) sector-scanner transducer at a displayed depth of 10 cm (*A*) and 30 cm (*B*). The right side of these sonograms is dorsal and the left side is ventral. *A*, The duodenum is distended with gas and fluid and a gas-fluid interface is detected (*arrow*). The wall of the duodenum is slightly thickened (4 to 5 mm). *B*, The stomach is markedly distended with fluid and measures 25 cm in diameter. The dorsal border of the spleen is imaged to the left of (ventral to) the distended stomach.

gastric lymph nodes has been imaged in one horse with generalized lymphosarcoma (Fig. 6-101). Neoplastic peritoneal effusions are often present in horses with gastric squamous cell carcinoma, as well as in horses with other forms of abdominal neoplasia (see Fig. 6-98). A composite fluid has been described in the peritoneal cavity in horses with gastric squamous cell carcinoma.[4]

Duodenitis/Enteritis. Duodenitis can have a wide variety of sonographic appearances but is usually characterized by fluid-filled hypomotile bowel.[2,17] The wall thickness of the affected intestine may be normal to near normal (Fig. 6-102) or increased (Fig. 6-103).[2] The intestinal wall thickening is usually relatively symmetric and extensive and may also appear edematous (more hypoechoic than normal), particularly in horses with severe inflammatory bowel disease.[2] Inflammatory bowel disease may affect any portion of the intestinal tract from the duodenum to the small colon. In horses with anterior enteritis, the wall of the duodenum may have normal thickness with a large fluid- or fluid and gas-distended lumen; fluid or fluid and gas distention of the duodenum may be detected with a thickened duodenal wall (Fig. 6-102), or the duodenal wall may be thickened and hypoechoic with a compromised lumen (Fig. 6-104). Mucosal irregularities may be imaged in horses with severe anterior enteritis/duodenitis. Gastric distention is also detected in horses with anterior enteritis (see Fig. 6-102).

Fluid-filled hypermotile intestine is most frequently imaged in horses with enteritis involving the small and/or large intestine (Fig. 6-105), in contrast to the hypomotile intestine usually detected in horses with anterior enteritis. Thickening of the intestinal wall (Figs. 6-106 and 6-107) and mucosal irregularities (Fig. 6-107) are frequently detected if the enteritis is severe. Shreds of mucosa may be imaged sloughing into the bowel lumen in horses with enteritis.[2] Small hyperechoic echoes representing gas have been imaged along the mucosal surface

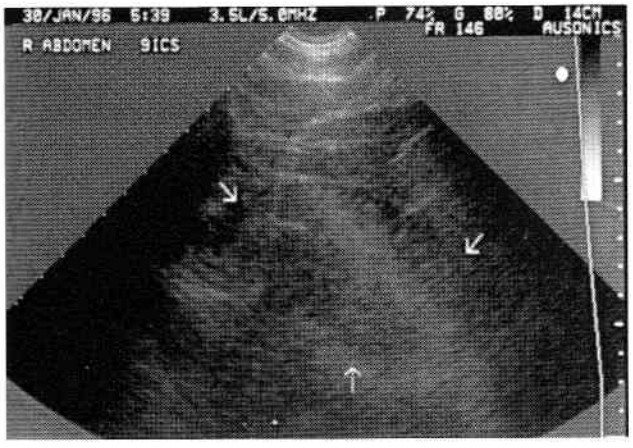

Figure 6–104

Sonogram obtained from a 10-year-old Thoroughbred mare with severe duodenitis. The duodenum is markedly thickened (*arrows*), with the walls obstructing the lumen of the bowel. No ingesta was seen to move through this area. This sonogram was obtained from the right ninth intercostal space with a wide-bandwidth 3.5-MHz sector-scanner transducer operating at 5.0 MHz at a displayed depth of 14 cm. The right side of this sonogram is dorsal and the left side is ventral.

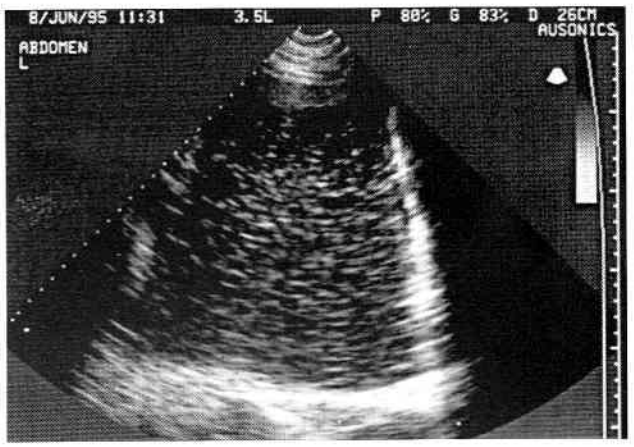

Figure 6–105

Sonogram of the left dorsal colon obtained from a 2-year-old Standardbred filly with enteritis. Note the large amount of fluid ingesta in the lumen of the large colon. The wall thickness is only slightly increased, however. This sonogram was obtained from the left paralumbar fossa with a 3.5-MHz sector-scanner transducer at a displayed depth of 26 cm. The right side of this sonogram is dorsal and the left side is ventral.

or in the wall of horses with clostridial enteritis (Fig. 6-108). Bowel wall gas in humans is considered highly suggestive, if not diagnostic, of intestinal necrosis.[293] The "bright ring" appearance is caused by the bright gas echoes in the intestinal wall surrounding the fluid-filled intestinal lumen. Tiny gas bubbles ("effervescent bowel") have also been reported in humans with necrotic bowel rising from the dependent surface of the intestine.[293] Clostridial enteritis should be a primary differential diagnosis for horses with gas echoes imaged in the bowel wall or along the mucosal surface. Clostridial enteritis or another necrotizing enteritis should also be considered when a diphtheritic membrane is imaged sloughing into the bowel lumen. Peritonitis may also be detected concurrently with clostridial enteritis. Therefore, the peritoneal cavity should also be carefully examined ultrasonographically for abnormal fluid or adhesions in horses with enteritis.

Thickening of the bowel wall may be detected in

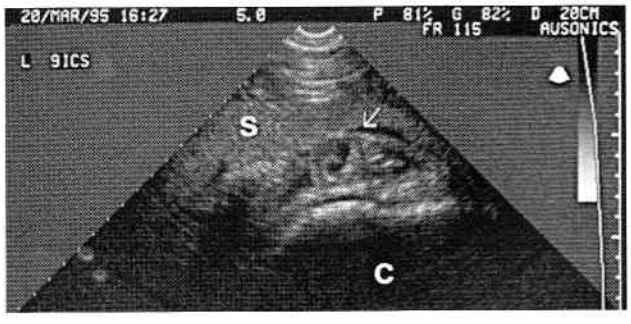

Figure 6–106

Sonogram of the left side of the abdomen obtained from an 8-year-old Thoroughbred gelding with enteritis. The small intestine is slightly thickened (*arrow*) and is imaged between the spleen (S) and the large colon (C). This sonogram was obtained from the left ninth intercostal space with a 5.0-MHz sector-scanner transducer at a displayed depth of 20 cm. The right side of this sonogram is dorsal and the left side is ventral.

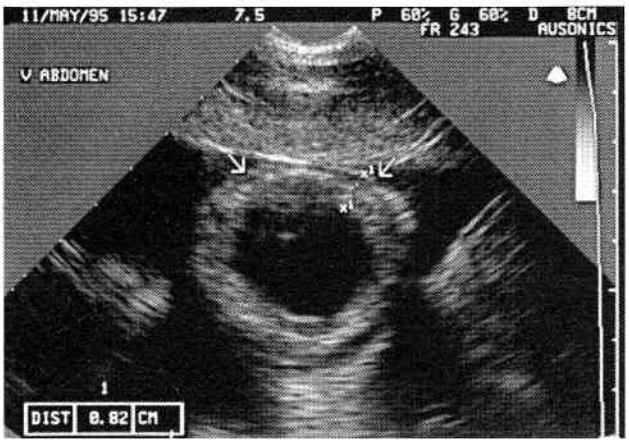

Figure 6–107

Sonogram of the ventral abdomen obtained from a 16-year-old Standardbred mare with enteritis. The jejunum is markedly thickened (0.82 mm) and filled with anechoic fluid and has a turgid, doughnut-like appearance. An excess amount of anechoic fluid is imaged in the peritoneal cavity, but this heavily compromised small intestine is not floating in the fluid. This sonogram was obtained from the ventral abdomen in the area of the umbilicus with a 7.5-MHz sector-scanner transducer at a displayed depth of 8 cm. The right side of this sonogram is cranial and the left side is caudal.

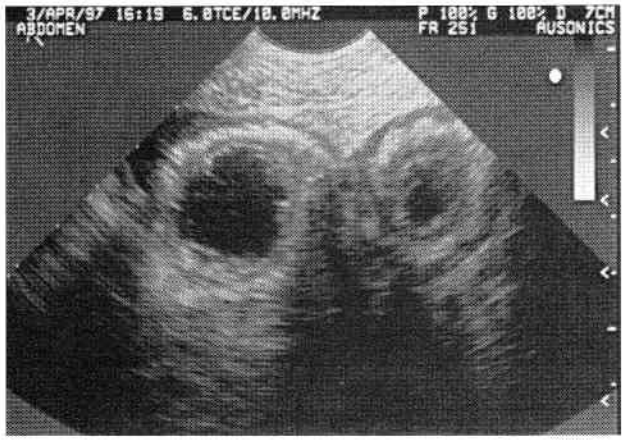

Figure 6–108

Sonogram of the ventral abdomen obtained from a yearling Standardbred colt with Clostridial enteritis. The wall of the jejunum is markedly thickened, measuring over 1 cm in some areas, and the mucosa has pinpoint hyperechoic echoes within, consistent with the "effervescent" bowel seen in individuals with Clostridial enteritis. The layers of the bowel wall are readily distinguished in this yearling due to edema associated with severe hypoproteinemia. The jejunum is moderately distended with anechoic fluid and in real time there was little peristaltic activity detected. This sonogram was obtained with a wide-bandwidth 6.0-MHz microconvex linear array transducer operating at 10.0 MHz at a displayed depth of 7 cm. The right side of this sonogram is cranial and the left side is caudal.

horses with granulomatous enteritis. The small intestine is usually affected, primarily the jejunum and ileum, but all parts of the intestine may be affected.[294–297] Nodules associated primarily with the serosal surface of the intestine and mucosal thickening are the most consistent findings. Wall thickness of the affected small intestine of up to 5 cm has been reported in affected horses.[296] Histopathologically and sonographically, the lesions may be difficult to distinguish from lymphosarcoma in affected horses. Mesenteric lymph node enlargement is frequently present, with the lymph nodes often measuring four times normal size or greater, also common in horses with intestinal lymphosarcoma. Mesenteric lymphadenopathy is occasionally detected in horses with other intestinal diseases (Fig. 6-109). Hepatic granulomas were also reported in horses with granulomatous enteritis and ranged from small multifocal granulomatous infiltrates to large masses.[297] Discrete intestinal granulomas have been identified in several horses associated with cryptococcal organisms or have had an unknown origin.[232, 235] A horse with jejunal obstruction caused by a *Pythium insidiosum* granuloma has also been described. This horse had a large (19.2 × 10 cm) mass associated with the jejunal wall, which resulted in jejunal stenosis and partial jejunal

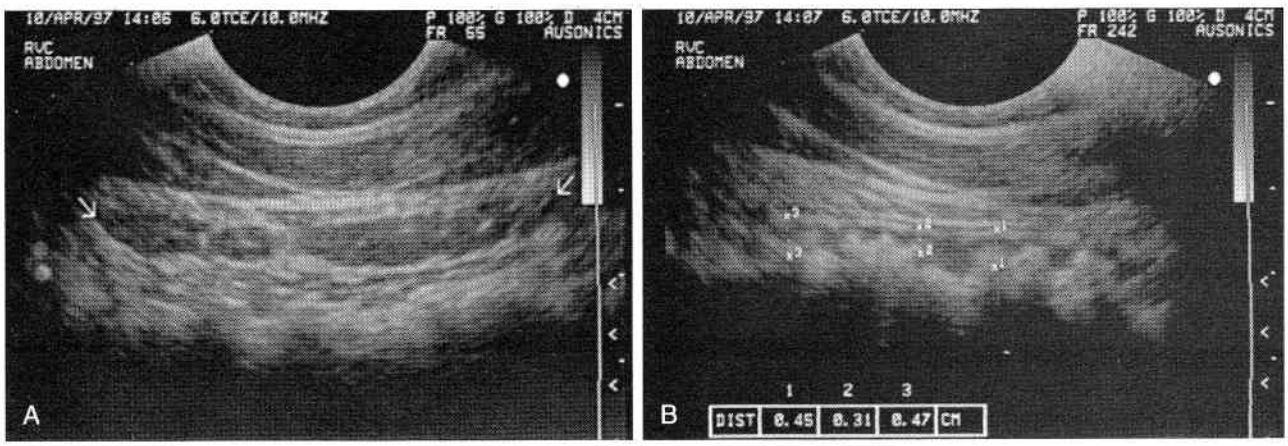

Figure 6–109

Sonograms of the right ventral colon obtained from a yearling Thoroughbred colt with colic and hypoproteinemia. These sonograms were obtained with a wide-bandwidth 6.0-MHz microconvex linear array transducer operating at 10.0 MHz at a displayed depth of 4 cm. The right side of these sonograms is cranial and the left side is caudal. *A*, There is significant lymphadenopathy (*arrows*) detected in the mesentery of the right ventral colon. The colonic lymph nodes are enlarged and uniformly hypoechoic with a swollen appearance. *B*, The wall of the right ventral colon appears corrugated, with the thickening of the colon wall involving primarily the mucosal surface. The thickness of the wall of the right ventral colon was mildly increased, ranging from 3.1 to 4.7 mm in thickness, and was slightly thicker in other areas of the right ventral colon.

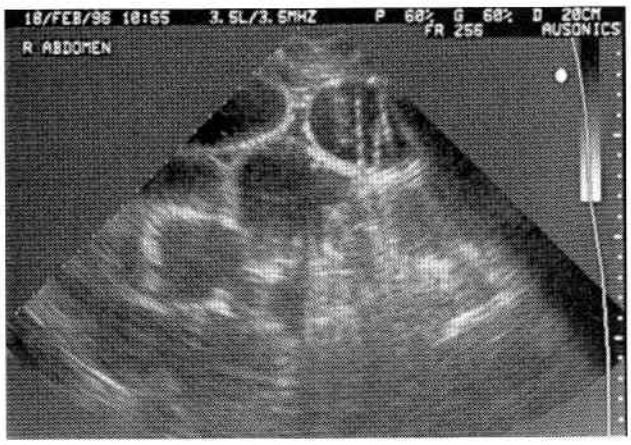

Figure 6–110

Sonogram of the right side of the abdomen obtained from a yearling Thoroughbred filly with ileus. Notice the distended loops of small intestine, which were hypomotile to amotile when viewed in real time. The thickness of the small intestinal wall is normal to nearly normal. This sonogram was obtained from the right paralumbar fossa with a wide-bandwidth 3.5-MHz sector-scanner transducer operating at 3.5 MHz at a displayed depth of 20 cm. The right side of this sonogram is dorsal and the left side is ventral.

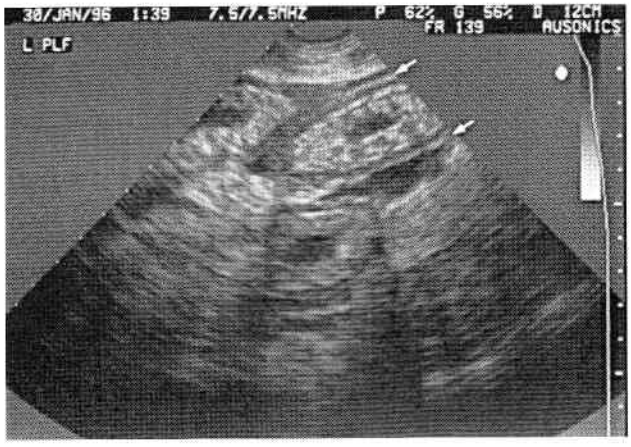

Figure 6–112

Sonogram of the jejunum obtained from a yearling Thoroughbred colt with peritonitis and an abdominal abscess. The walls of the small intestine are markedly thickened (> 1 cm), with five layers of the bowel wall clearly visible. The outer serosal surface is hyperechoic (*arrows*), with a hypoechoic muscularis, hyperechoic submucosa, and markedly thickened mucosa with a mucosal surface of varying echogenicities. This sonogram was obtained from the left paralumbar fossa with a wide-bandwidth 7.5-MHz sector-scanner transducer operating at 7.5 MHz at a displayed depth of 12 cm. The right side of this sonogram is dorsal and the left side is ventral.

obstruction.[259] Other reports of obstruction associated with enteric pythiosis have been published.[260]

Ileus. Ileus is a mechanical or adynamic obstruction of the bowel that may be primary or may occur secondary to mechanical obstruction, abdominal surgery, peritonitis, and other less common conditions.[4] Mechanical ileus in horses is caused by intussusceptions, volvulus, mural masses, trichophytobezoars, impactions, and other lesions causing mechanical obstruction. Functional ileus is most frequently seen in horses following abdominal surgery or anesthesia.

Horses with ileus usually have little or no visible peristaltic activity. The diameter of the bowel is normal or increased, but the intestinal wall thickness is usually normal (Fig. 6–110). In some horses with ileus, depending upon the cause, the wall thickness may be increased, and other intestinal or peritoneal fluid abnormalities may be detected (Figs. 6–111 and 6–112). The luminal contents of the affected bowel are usually static, or some random motion of the ingesta is observed. Contractions of the

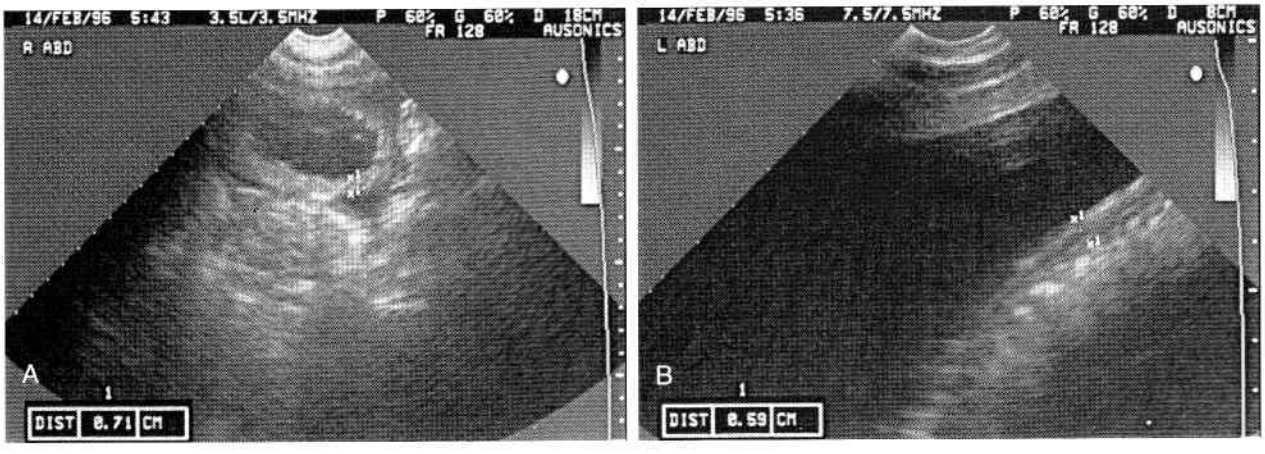

Figure 6–111

Sonograms of the abdominal cavity obtained from a yearling Thoroughbred filly with severe enteritis and peritonitis. These sonograms were obtained from the right (*A*) and left (*B*) sides of the abdomen with a wide-bandwidth 3.5-MHz sector-scanner transducer operating at its center frequency (3.5 MHz) at a displayed depth of 18 cm (*A*) and a 7.5-MHz sector-scanner transducer operating at its center frequency (7.5 MHz) at a displayed depth of 8 cm (*B*). *A*, Marked thickening of the jejunal wall is detected (0.71 mm), with irregularities of the mucosal surface detected. Distention of the loops of jejunum with anechoic to hyperechoic fluid is seen, depending upon the peristaltic activity at the time. This sonogram was obtained in the right paralumbar fossa. The right side of this sonogram is dorsal and the left side is ventral. *B*, Sonogram of the excess peritoneal fluid detected, which is anechoic and lacks visible fibrin. The wall of the left ventral colon is markedly thickened (> 0.59 mm; 0.59 cm = the serosal, muscularis, and submucosa layers), and the layers of the bowel wall are visible. The outer serosal layer is hyperechoic, followed by a hypoechoic muscularis, a more echogenic submucosa, a hyperechoic mucosa, and less echogenic mucosal surface. This sonogram was obtained from the ventral aspect of the left paralumbar fossa. The right side of this sonogram is dorsal and the left side is ventral.

affected intestine and propulsion of the luminal contents are absent. In ileus involving the small intestine, a composite fluid is frequently imaged in the lumen of the intestine for a prolonged period of time. No significant narrowing of the lumen is detected in association with contraction of the bowel.[4] In children with ileus, the bowel loses its multifaceted appearance and is imaged as discrete tubular structures.[256] Children with adynamic or functional ileus (nonobstructive) have distended small bowel with normal to somewhat increased peristaltic activity, whereas those with dynamic or mechanical ileus (obstructive) have more intestinal distention and variable peristaltic activity, ranging from none to increased.[256] In small animals, mechanical ileus tends to produce segmental dilatation, whereas functional ileus is usually associated with generalized intestinal distention.[22] In both functional and mechanical ileus in small animals, gastrointestinal motility appears decreased throughout the bowel.[22] The same findings appear to be true in horses.

Small intestinal distention with segmental ileus may be imaged in some adult horses with colic (Figs. 6-113 and 6-114) and may be associated with small or large intestinal displacement. If the wall thickness of the affected portion of small intestine is normal and no obstruction is detected, the colic may resolve with medical treatment. Layering of the ingesta may occur with prolonged ileus (Fig. 6-115). If the bowel appears turgid, surgical intervention should be considered or frequent sonographic monitoring performed to evaluate wall thickness. Thickening of the wall with severe ileus suggests vascular compromise to the intestine and a surgical lesion.

Neoplastic Infiltration of the Bowel Wall. Lymphosarcoma is the most common neoplastic infiltrate in the intestinal wall. Thickening of the wall of the small intestine has been imaged in horses with lymphosarcoma. The wall thickening is usually echogenic, and distinguishing the layer or layers affected is difficult. Thickening of the bowel wall is a nonspecific finding and can occur with other disease processes. An intestinal adenosarcoma has been reported in two horses but was not imaged sonographically;[5, 65] only the hepatic and diaphragmatic metastases and the ascites were detected sonographically.[65] An intestinal myxosarcoma has also been reported in a horse that was not imaged sonographically. A 25-cm mass was palpable, however, in the right caudodorsal abdomen and could have been imaged sonographically from the

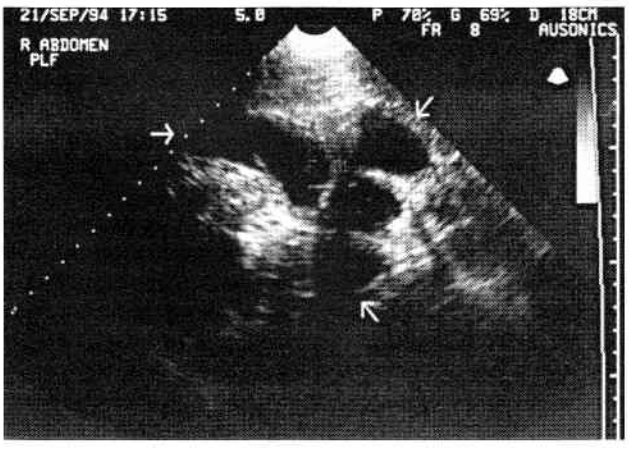

Figure 6–113

Sonogram of the distended small intestine (*arrows*) obtained in the right paralumbar fossa from a 10-year-old Thoroughbred gelding with colic. The affected portions of small intestine are fluid filled and hypomotile, with normal wall thickness. Only large bowel (cecal) echoes should be imaged in the right paralumbar fossa. This sonogram was obtained with a 5.0-MHz sector-scanner transducer at a displayed depth of 18 cm. The right side of this sonogram is dorsal and the left side is ventral.

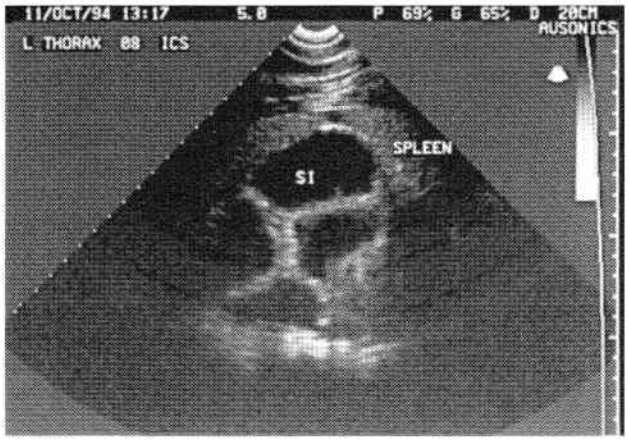

Figure 6–114

Sonogram of the left side of the abdomen obtained from a 3-year-old Standardbred filly with chronic colic. Notice the distended small intestine (jejunum) detected in the left cranioventral abdomen between the liver and spleen and deeper large colon, which has a slightly increased wall thickness. The jejunum (SI) is distended with anechoic fluid but does not appear turgid because the shape of these distended loops is somewhat irregular. This sonogram was obtained from the right eighth intercostal space with a 5.0-MHz sector-scanner transducer at a displayed depth of 20 cm. The right side of this sonogram is dorsal and the left side is ventral.

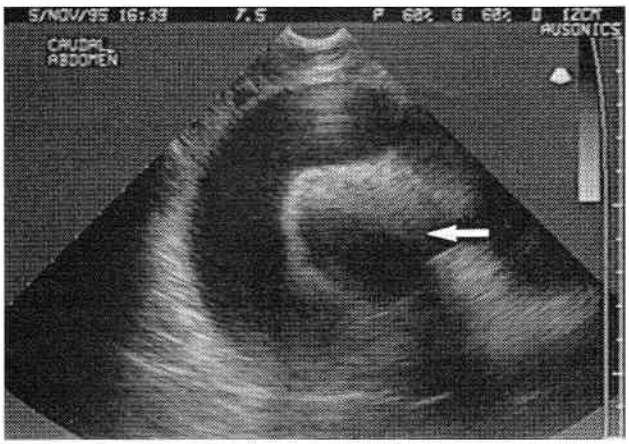

Figure 6–115

Sonogram of the caudal ventral abdomen obtained from a 10-year-old Thoroughbred mare with colic and a possible small intestinal obstruction and ileus. This sonogram demonstrates marked distention of the jejunum, with mild thickening of the intestinal wall and little peristalsis, as evidenced by the settling of the intraluminal contents in the central loop of jejunum (*arrow*). The wall thickness of the small intestine is normal, but the bowel is extremely distended and turgid. This sonogram was obtained from the ventral abdomen with a 7.5-MHz sector-scanner transducer at a displayed depth of 12 cm. The right side of this sonogram is cranial and the left side is caudal.

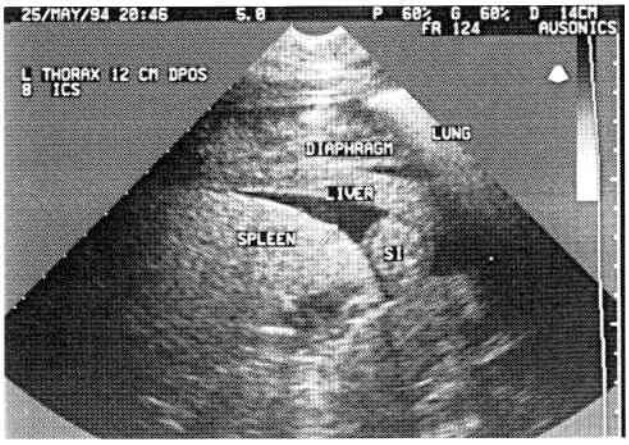

Figure 6–116

Sonogram of the abdomen obtained from a 9-year-old Standardbred mare with ascites secondary to pericarditis. A small amount of anechoic fluid is present in the peritoneal cavity with no fibrin detected. The fluid is most evident between the liver and spleen (*arrow*) and surrounding the small intestine (SI). The wall of the small intestine is normal thickness (< 3 mm), but the small intestine contains hyperechoic fluid that was hypermotile in real time, associated with an enteritis that was also present and preceded the pericarditis. The liver is only slightly less echogenic than the spleen but has a small amount of peritoneal fluid on both its diaphragmatic and visceral surfaces. This sonogram was obtained from the left twelfth intercostal space at a level 12 cm dorsal to the level of the point of the shoulder at a displayed depth of 14 cm. The right side of the sonogram is dorsal and the left side is ventral.

transrectal window and probably from the right flank. The mass was gelatinous with large areas of fibrous tissue, was located in the cecal base, and probably would have had a composite appearance sonographically. Intestinal carcinoids are slowly growing malignant neoplasms that can occur throughout the intestine, develop as submucosal masses, and have been associated with jejunal intussusception.[232, 298] Carcinoids can range in diameter up to 6 cm but are usually 1.5 cm or less.[298] This tumor can become a large polypoid growth attached to the underlying muscularis layer and can invade surrounding tissues. Leiomyomas are benign tumors of the smooth muscle layer of the intestine that can appear as intramural or luminal masses.[232] Leiomyomas have been reported in the jejunum,[232, 234, 299] where they may be associated with jejunal intussusception[234] and in the rectum and small colon.[15] Benign polyps can also occur in the rectum and the colon.[15]

Diseases of the Peritoneal Cavity. Diagnostic ultrasound is useful in determining the amount of peritoneal fluid, characterizing the type of fluid present, and detecting masses in the peritoneal cavity. Clear anechoic fluid is typical of ascites, occasionally detected in horses with congestive heart failure (Fig. 6-116). Hemoperitoneum is commonly detected in horses following trauma (Figs. 6-117 and 6-118; see also Fig. 6-78) and may also occur with rupture of vessels within the peritoneal cavity associated with a wide variety of causes (Fig. 6-119). Organ rupture can also result in life-threatening bleeding into the peritoneal cavity.

Peritonitis. Intestinal laceration, peritonitis, and abdominal wall cellulitis can occur as complications of abdominal paracentesis in the horse.[231] The risk in performing this diagnostic procedure is minimal (4 serious complications in 850 samples),[231] but it is probably increased in horses with marked abdominal distention. In one study evaluating the cytologic findings with abdominoparacentesis, no complications occurred in more than 100 collections, with four or five horses having experienced an intestinal puncture with no ill effects.[300] Sonographic examination of the peritoneal cavity can determine if fluid can be obtained on abdominocentesis, minimizing the risk of this diagnostic procedure. If the marked abdominal distention is due to severe distention of the gastrointestinal viscera and no free peritoneal fluid is detected sonographically, an abdominal paracentesis is unlikely to yield fluid and the risk of bowel laceration is significant if a needle is used to perform the diagnostic procedure.

Peritonitis is usually associated with fever, colic, ileus, and diarrhea.[301-304] Weight loss has also been reported as a common presenting sign.[301, 303, 304] In the postoperative abdominal patient, peritonitis may be seen with incisional infection. In many horses the cause of the peritonitis is unknown. Parasite migration has been implicated as a possible inciting cause in the development of peritonitis.[301] Physical examination findings and the analysis of the peritoneal fluid sample were the most valuable tools for diagnosing intestinal rupture in one study of horses with peritonitis.[302] However, abdominal ultrasonography was not used as a diagnostic aid in this study.

Sonographic examination of the abdomen can be useful in diagnosing peritonitis and in determining the character and volume of peritoneal fluid.[2] Fibrin tags (Fig. 6-120), fibrin coating the serosal surfaces, fibrinous loculations (Fig. 6-121), and cellular debris in the peritoneal fluid can be determined in the portions of the abdominal

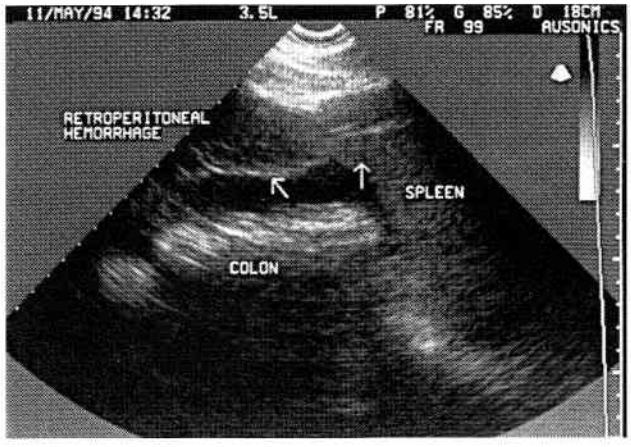

Figure 6–117

Sonogram of the ventral abdomen obtained from a 4-year-old Paint filly with severe anemia. A large amount of hypoechoic fluid, representing blood, is seen in the retroperitoneal space, bulging primarily into the right side of the peritoneal cavity (*angled arrow*). The ventral tip of the spleen (*up arrow*) is positioned right on the midline. The large colon is floating in a small but increased amount of relatively anechoic fluid in the peritoneal cavity. This sonogram was obtained from the ventral midline with a 3.5-MHz sector-scanner transducer at a displayed depth of 18 cm. The right side of this sonogram is the left side of the abdomen.

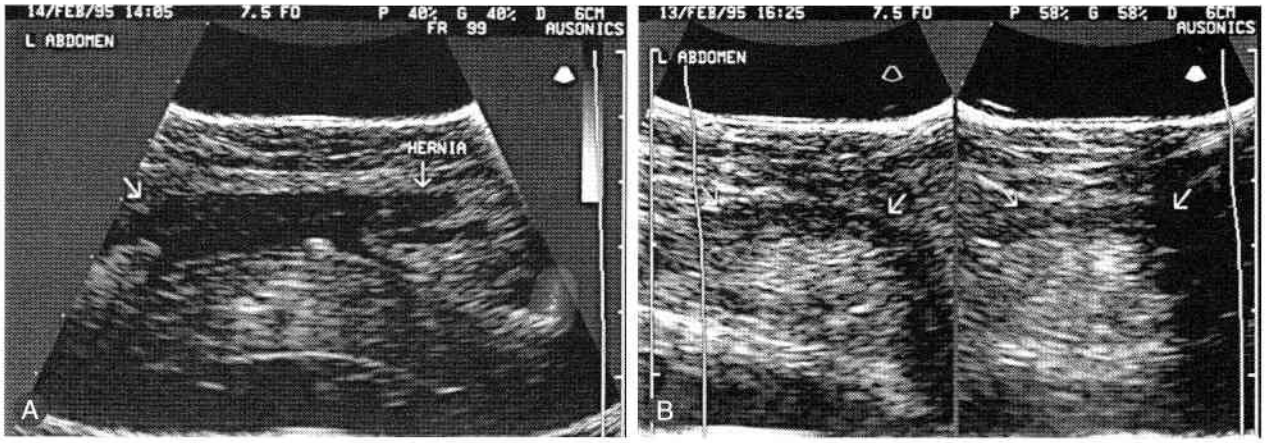

Figure 6–118

Sonograms of the abdominal wall and abdomen obtained from a 21-year-old Thoroughbred mare with a partial-thickness ventral abdominal hernia and small intestinal entrapment. These sonograms were obtained from the left ventral abdomen with a 7.5-MHz sector-scanner transducer containing a built-in fluid offset at a displayed depth of 6 cm. *A*, The hernia in the abdominal musculature is clearly imaged as an area of muscle fiber disruption (*arrows*) in the ventral abdominal musculature, involving the internal abdominal oblique and transversus abdominis muscles. *B*, A piece of jejunum (*arrows*) is trapped in the hernia between two muscle layers and contains hyperechoic ingesta with little evidence of peristaltic activity or propulsive movements of the ingesta from this entrapped portion of the jejunum. The wall of the jejunum is hypoechoic and thickened, measuring between 5 and 12 mm thick. The left image is a long-axis section through the entrapped piece of jejunum, and the right image is a short-axis section through the affected loops of jejunum.

cavity accessible to sonographic examination.[2] Fibrin may also be free floating or attached to roughened serosal surfaces.[3] Adhesions between the serosal surfaces of the bowel and the peritoneum can also be determined in these areas.[2] Intestinal loops that are fixed in location and do not move independently of the body wall or adjacent bowel with peristaltic activity suggest adhesions (Fig. 6-122).[4] The difference between fibrinous and fibrous adhesions can often be determined sonographically, with fibrous adhesions having a worse prognosis. The detection of large fibrin strands on the serosal surfaces indicates an unfavorable prognosis in horses with peritoneal effusions.[4] Large particulate matter and free gas can be imaged in the peritoneal cavity in horses with intestinal rupture.[2] Composite fluid was seen in a foal with peritoneal effusion, consistent with a ruptured viscus.[4] In one report of horses with peritonitis, two of three horses had excess quantities of peritoneal fluid and adhesions identified ultrasonographically; in one of these horses the peritoneal fluid was hyperechoic.[304] The horse

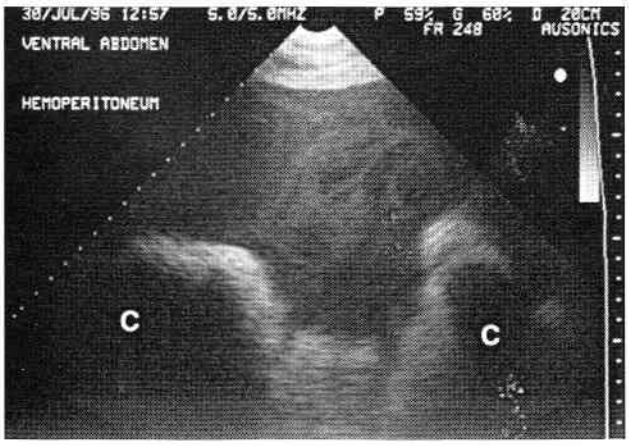

Figure 6–119

Sonogram of the ventral abdomen obtained from a 4-year-old miniature horse filly with hemoperitoneum. Notice the echogenic swirling fluid in the peritoneal cavity with the large colon (C) floating on the dense, bloody fluid. The swirling appearance is created by the movement of the blood components in the peritoneal cavity with peristalsis and respiratory movement. This sonogram was obtained with a wide-bandwidth 5.0-MHz sector-scanner transducer operating at 5.0 MHz at a displayed depth of 20 cm. The right side of this sonogram is cranial and the left side is caudal.

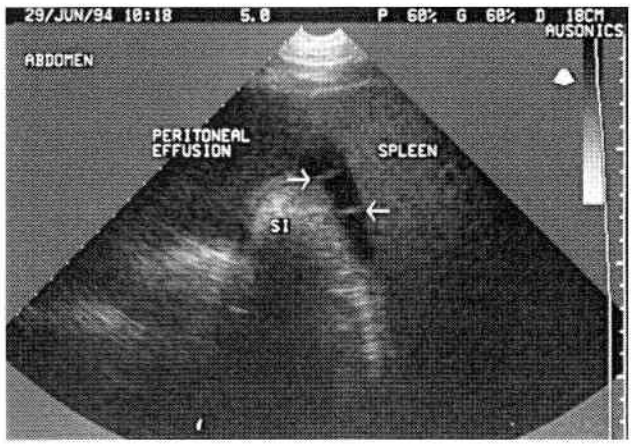

Figure 6–120

Sonogram of the abdomen obtained from an 11-year-old Hanoverian mare with peritonitis. An increased amount of cloudy peritoneal fluid and small fibrin strands are imaged between the spleen and jejunum (SI) along the ventral midline (*arrows*). This sonogram was obtained with a 5.0-MHz sector-scanner transducer at a displayed depth of 18 cm. The right side of the sonogram is the left side of the horse's abdominal cavity.

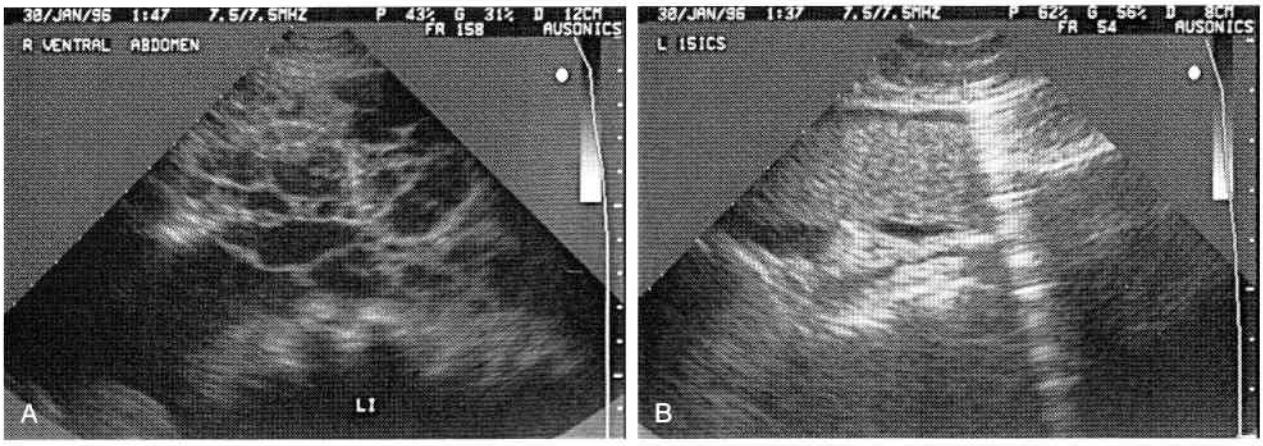

Figure 6–121

Sonograms of the abdomen obtained from the left fifteenth intercostal space in a yearling Thoroughbred colt with an abdominal abscess, peritonitis (*A*), and pneumoperitoneum (*B*). These sonograms were obtained with a wide-bandwidth 7.5-MHz sector-scanner transducer operating at 7.5 MHz at a displayed depth of 12 cm (*A*) and 8 cm (*B*). *A*, Severe fibrinous peritonitis with loculated strands of fibrin floating in the relatively anechoic fluid is imaged. The fibrin strands are attached to the overlying large intestine (LI). Fibrin also adhered to the adjacent small intestine (not shown). This sonogram was obtained cranial to the abdominal abscess. The right side of this sonogram is cranial and the left side is caudal. *B*, A distinct gas-fluid interface (*arrow*) is seen at the border between the pneumoperitoneum and peritoneal fluid. The curtain sign associated with free air within a body cavity was clearly visible in real time. Notice the hyperechoic free gas echo in the dorsal portion of the abdomen with its characteristic equidistant reverberation artifacts consistent with air. The free gas obliterates the dorsal border of the spleen and the underlying gastrointestinal viscera. The right side of this sonogram is dorsal and the left side is ventral.

with the hyperechoic peritoneal fluid had a 3-cm perforated ulcer in the cecum that was the cause of the peritonitis, and it did not survive. The other horse had no sonographic abnormalities detected and survived, as did the other horse with peritoneal effusion and adhesions.

Abdominal Abscess. Abdominal abscesses may occur in the abdominal organs or may be associated with the mesenteric root, gastrointestinal tract, or abdominal wall. The cause of abdominal abscesses includes septicemia, penetrating abdominal wounds, and intestinal perforation. Intestinal perforation associated with colonic perforation, foreign bodies, or parasite impactions has been reported in the horse.[305, 306] Clinical signs in affected horses often include depression, anorexia, fever, colic, diarrhea, stranguria, and weight loss.[5, 118, 307–309] A mass is frequently identified in horses on rectal palpation of the abdomen and was detected in 64% of horses with abdominal abscesses in one large study.[118] The majority of these horses have abscesses in and around the root of the mesentery (17 horses), with 3 abscesses involving one or both kidneys, 2 splenic abscesses, 2 hepatic abscesses, and one horse with an abscess involving the uterus.[118] In another large study of 15 horses, abdominal abscesses involving the liver were most common (10 horses), followed by abscesses in the mesenteric lymph nodes (4 horses), splenic abscesses (3 horses), abscesses of the caudoventral portion of the abdomen (3 horses), and abdominal wall abscesses (2 horses), and in 1 horse the entire abdomen was diffusely involved.[5] One third of these horses had multiple organ involvement. In four horses with very large palpable abdominal masses, the jejunum and mesentery were involved in the abdominal abscess in 3 horses and the cecum and mesentery in the fourth horse.[307, 309] In another horse the abdominal abscess was palpated on the left lateral and ventral floor of the pelvis and adhered to the pelvic flexure.[306] Abdominal paracentesis supported the diagnosis of abdominal abscess in 92.8% of 14 horses in one study.[118] An exudate was found in the peritoneal fluid of the 2 horses with large mesenteric abscesses involving the jejunum[309] and in 1 horse with a large intrapelvic abscess.[306] Bacteria were often seen in Gram-stained cytologic preparations of the peritoneal fluid but were infrequently cultured from the fluid. Organisms most frequently cultured from

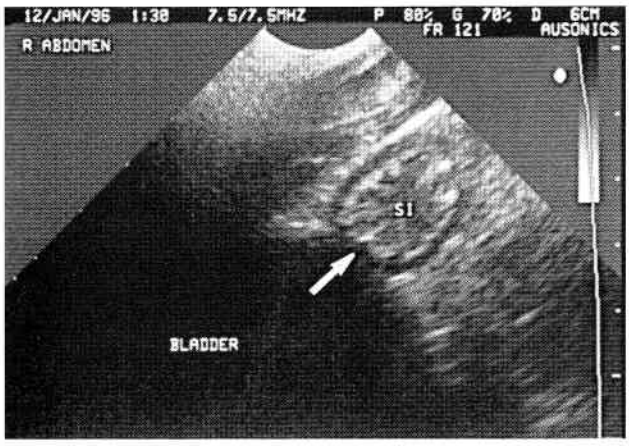

Figure 6–122

Sonogram obtained from a 2-year-old Standardbred mare with colic. An adhesion of the small intestine (SI) to the cranial and ventral wall of the bladder is seen (*arrow*). In real time the small intestine did not glide over the surface of the bladder but adhered to it. This mare had a history of previous colic surgery. This sonogram was obtained with a wide-bandwidth 7.5-MHz sector-scanner transducer operating at 7.5 MHz at a displayed depth of 6 cm. The right side of this sonogram is cranial and the left side is caudal.

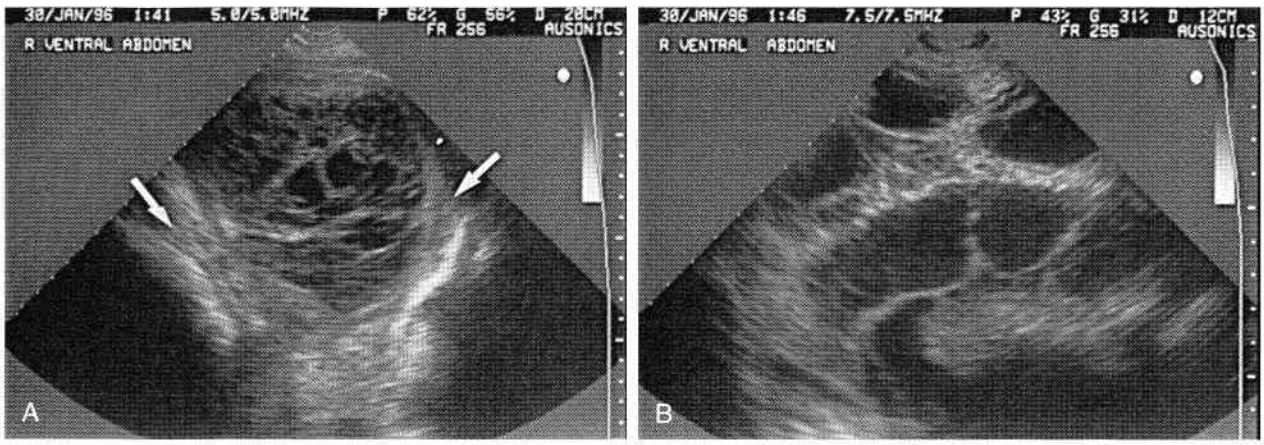

Figure 6–123

Sonograms of the right ventral abdomen in a yearling Thoroughbred colt with an abdominal abscess (same colt as in Fig. 6–121). These sonograms were obtained with a wide-bandwidth 5.0-MHz sector-scanner transducer operating at 5.0 MHz at a displayed depth of 20 cm (*A*) and a wide-bandwidth 7.5-MHz sector-scanner transducer operating at 7.5 MHz at a displayed depth of 12 cm (*B*). The right side of these sonograms is cranial and the left side is caudal. *A*, The abdominal abscess is multiloculated and adheres to the adjacent large colon (*arrows*). The abscess measured 13.5 cm by 15 cm. *B*, The abscess appears to contain relatively anechoic fluid and fibrin with several thick-walled cavities within. This sonogram is of the cranial and ventral portion of the abscess.

the abdominal abscess include *Streptococcus equi*, *S. zooepidemicus*, and *Corynebacterium pseudotuberculosis*.[118, 119, 309, 310] In another large study the peritoneal fluid was classified as an exudate in 12 of 15 horses with abdominal abscesses; however, bacteria were identified cytologically in only 3 of these horses.[5] Scintigraphy has also been used to identify an abdominal abscess in a horse.[311] Indium-111–labeled leukocyte scans compare favorably in human beings with ultrasonography in the sensitivity and overall accuracy of detecting abdominal abscesses.[311] In this horse, the abscess was thought to have originated in the mesenteric lymph nodes, with adhesions of adjacent small intestine to the abscess.

Sonographic examination of a palpable abdominal mass is helpful in differentiating an abdominal abscess from neoplasia in most cases. Abdominal abscesses often have a loculated appearance (Figs. 6–123 to 6–125) and may involve a portion of the intestinal wall (Figs. 6–124 and 6–125). Air-fluid interfaces have been demonstrated sonographically in horses with abdominal abscesses (Figs. 6–126 and 6–127). The air in an abdominal abscess often causes an intense acoustic shadow with reverberation artifacts typical of gas. An echogenic line may be demonstrated in the abdominal abscess at the air-fluid interface (Fig. 6–127).[312] Abdominal abscesses had a multiloculated sonographic appearance in two weanlings, with one of these also having more echogenic masses with central, slightly less echogenic areas.[313, 314] In one horse with an intrapelvic abscess the mass had a uniform echogenic appearance with a few small anechoic areas within and impinged on the cranial aspect of the bladder.[306] A large spherical mass involving the mesentery and small intestine was imaged in two horses with a large abdominal abscess.[309] In one horse with an abdominal abscess the mass appeared solid sonographically, but only a 5.0-MHz transducer was used transrectally and penetration of the mass was inadequate.[308] At surgery, the mass was found to be an abscess with a 10-cm-thick capsule that had adhesions to the left kidney, small colon, and jejunum.

Perirectal/Perivaginal Abscesses. Perirectal abscesses probably occur in most horses in association with rectal perforation. Perivaginal abscesses are also common in mares in association with trauma at parturition (most common) or breeding. Common presenting signs in

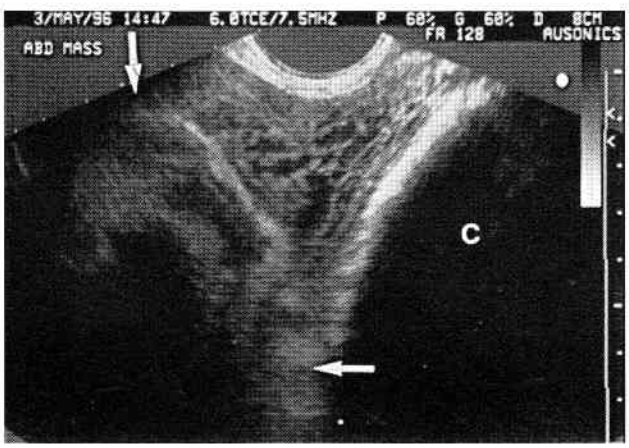

Figure 6–124

Transrectal sonogram obtained from a 9-year-old Thoroughbred mare with an abdominal abscess (*arrows*). The mass was associated with the cecum (C) and contained loculated anechoic to hypoechoic fluid. This sonogram was obtained with a wide-bandwidth 6.0-MHz microconvex linear-array transducer operating at 7.5 MHz at a displayed depth of 8 cm. The right side of this sonogram is to the right of the abdomen and the left side is to the left.

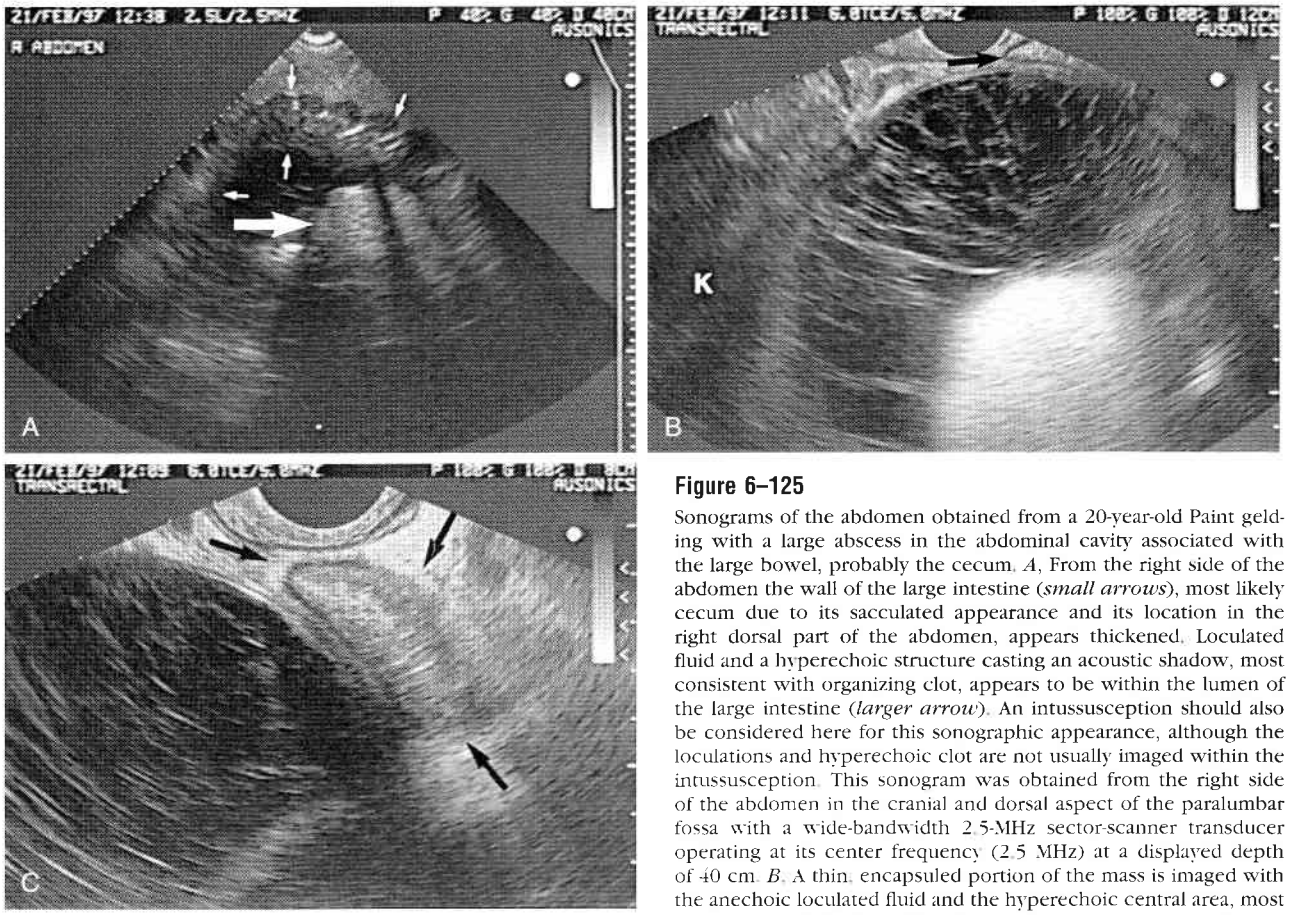

Figure 6–125

Sonograms of the abdomen obtained from a 20-year-old Paint gelding with a large abscess in the abdominal cavity associated with the large bowel, probably the cecum. *A*, From the right side of the abdomen the wall of the large intestine (*small arrows*), most likely cecum due to its sacculated appearance and its location in the right dorsal part of the abdomen, appears thickened. Loculated fluid and a hyperechoic structure casting an acoustic shadow, most consistent with organizing clot, appears to be within the lumen of the large intestine (*larger arrow*). An intussusception should also be considered here for this sonographic appearance, although the loculations and hyperechoic clot are not usually imaged within the intussusception. This sonogram was obtained from the right side of the abdomen in the cranial and dorsal aspect of the paralumbar fossa with a wide-bandwidth 2.5-MHz sector-scanner transducer operating at its center frequency (2.5 MHz) at a displayed depth of 40 cm. *B*, A thin, encapsuled portion of the mass is imaged with the anechoic loculated fluid and the hyperechoic central area, most consistent with an organizing clot. Small intestine appears adherent to the capsular surface of the mass (*arrow*). This sonogram was obtained from a transrectal window using a wide-bandwidth 6.0-MHz convex linear-array transducer operating at 5.0 MHz at a displayed depth of 12 cm. The right side of the sonogram is toward the right side of the abdomen, with the caudal pole of the left kidney (K) imaged on the left side of the sonogram. *C*, Small intestine (*arrows*) is adherent to the capsule of the mass with slightly thicker than normal walls but normal peristaltic activity detected in real time. This sonogram is also obtained from the transrectal window with a wide-bandwidth 6.0-MHz microconvex linear-array transducer operating at 5.0 MHz with a displayed depth of 8 cm. The right side of the sonogram is the right side of the abdomen.

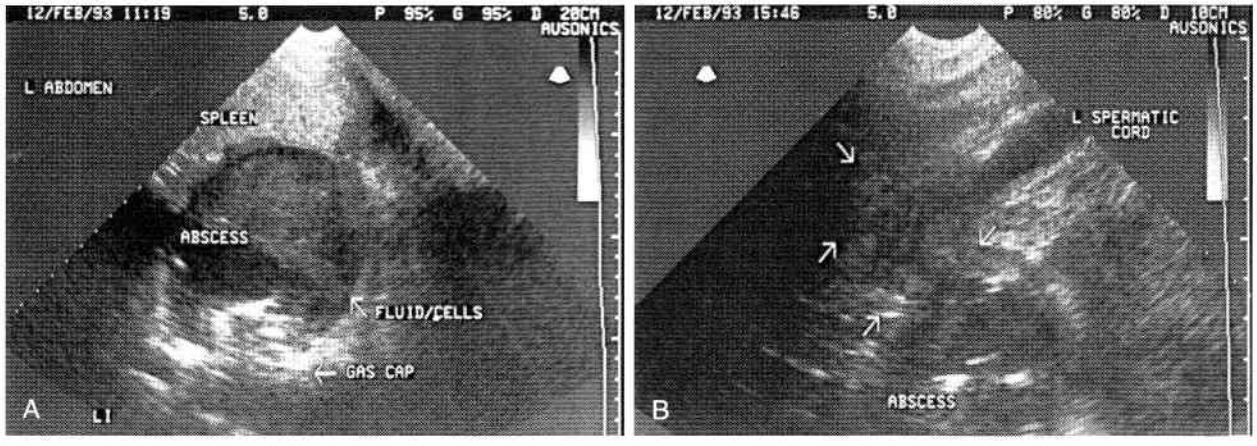

Figure 6–126

Sonograms of a large abdominal abscess extending from the inguinal region in a 3-year-old Standardbred stallion that presented with scrotal swelling and fever. These sonograms were obtained with a 5.0-MHz sector-scanner transducer at a displayed depth of 20 cm (*A*) and 10 cm (*B*). *A*, The large abdominal abscess is clearly imaged dorsal and to the left of the spleen, adjacent to the left internal inguinal ring. The abscess is layered with a more echogenic ventral portion, a more anechoic center, and a hyperechoic dorsal portion associated with a dorsal gas cap. The abscess measured 11.48 cm by 9.35 cm. In real time the adjacent large intestine (LI) appeared adherent to the dorsal border of the abscess. This sonogram was obtained from the left ventral abdomen just cranial to the left external inguinal ring. The right side of this sonogram is the left side of the abdomen and the left side is toward the midline of the abdomen. *B*, The abdominal abscess communicates dorsally with a fluid tract in the left inguinal canal adjacent to the left spermatic cord (*arrows*). The tract is imaged extending from the external inguinal ring through the internal inguinal ring into the abdominal abscess. This sonogram was obtained from the region of the left external inguinal ring. The right side of the sonogram is ventral and the left side is dorsal.

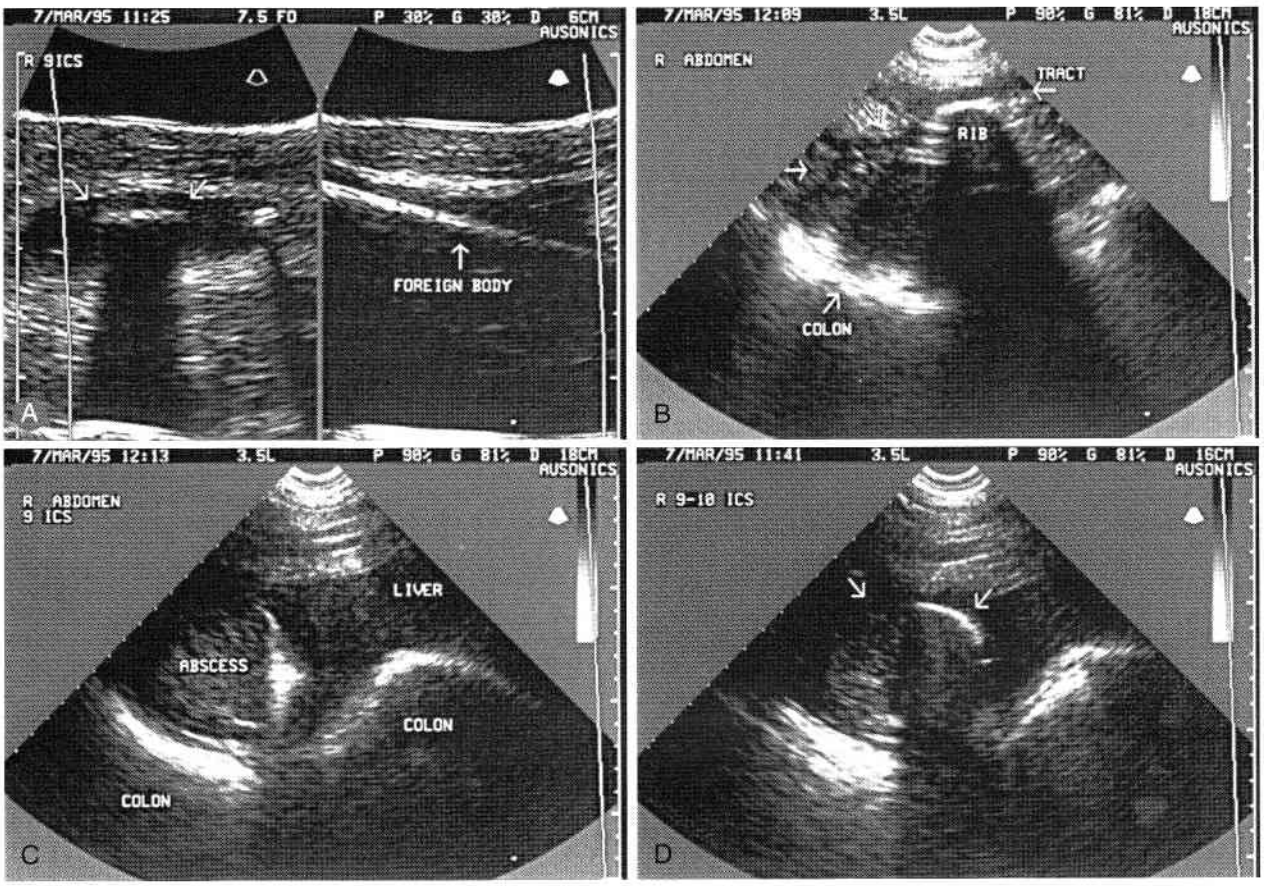

Figure 6–127

Sonograms of the right side of the abdomen and abdominal wall obtained from a 7-year-old Thoroughbred gelding with a draining tract from the right side of the abdomen. Sonographic examination of the draining tract revealed a hyperechoic structure casting a strong acoustic shadow surrounded by fluid consistent with a foreign body (most likely wood) in the abdominal musculature extending into the peritoneal cavity. These sonograms were obtained from the right ninth and tenth intercostal spaces with a 7.5-MHz sector-scanner transducer containing a built-in fluid offset (*A*) and a 3.5-MHz sector-scanner transducer (*B*, *C*, and *D*) at a displayed depth of 6 cm (*A*), 18 cm (*B* and *C*) and 16 cm (*D*). *A*, The hyperechoic linear structure casting a strong acoustic shadow is a long foreign body (piece of wood) surrounded by fluid, with a smaller additional wood fragment imaged on the right side of the transverse (*left*) image. These foreign bodies are embedded in the intercostal musculature, and the larger one extends through the intercostal musculature into the abdominal cavity. The right side of the transverse (*left*) image is dorsal and the left side is ventral. The right side of the long-axis image of the foreign body is cranial and the left side is caudal. *B*, A hypoechoic tract (*arrows*) adjacent to the foreign body is imaged crossing caudal to the ninth rib and penetrating through the intercostal muscles into the peritoneal cavity. Composite fluid (mostly hypoechoic) is imaged at the site of foreign-body penetration. The right side of this sonogram is cranial and the left side is caudal. *C*, Sonogram of the peritoneal cavity in the ninth intercostal space illustrating the discrete abscess containing echogenic fluid, the hypoechoic fluid between the abscess and the liver associated with a localized area of peritonitis, and the large colon adherent to the abscess and the ventral most tip of the right liver lobe at this location. The right side of this sonogram is dorsal and the left side is ventral. *D*, Immediately caudal to the initial visualization of the abdominal abscess a gas-fluid interface is detected within the discrete abscess, suggesting anaerobic infection. The hyperechoic curvilinear border from the right side of the abscess represents the dorsal gas cap, which is casting a slightly dirty acoustic shadow (*arrows*). This sonogram was obtained between the ninth and tenth intercostal spaces. The right side of this sonogram is dorsal and the left side is ventral.

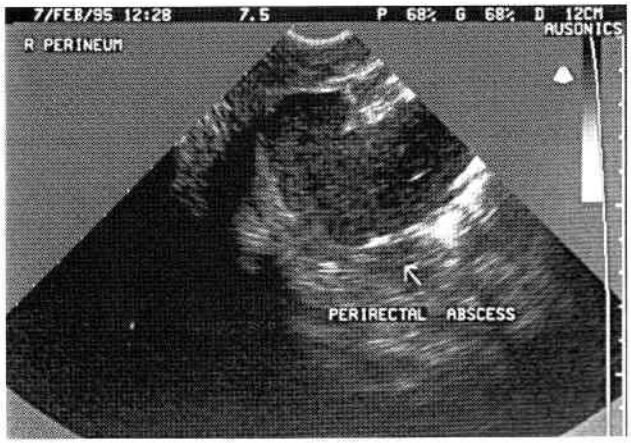

Figure 6–128

Sonogram of the right perineum obtained from a 3-year-old Thoroughbred colt with a perirectal abscess. The abscess contained hypoechoic cellular-appearing fluid (*arrow*) and was drained percutaneously using ultrasonographic guidance. This sonogram was obtained from the right side of the perineum, adjacent to the anus, with a 7.5-MHz sector-scanner transducer at a displayed depth of 12 cm. The right side of this sonogram is dorsal and the left side is ventral.

horses with perirectal abscesses include tenesmus, colic, fever, depression, and anorexia. Weight loss may also be present in some affected horses.

Perirectal abscesses are easily detected sonographically and often have hyperechoic echoes that cast dirty acoustic shadows consistent with free gas. The fluid contained within the perirectal abscesses is usually hypoechoic to echogenic (Fig. 6–128) and fibrinous loculations are frequently imaged. These abscesses are frequently encapsulated by a thick echogenic fibrous capsule.

Abdominal Neoplasia. Rectal examination of a horse with abdominal neoplasia often reveals a palpable abdominal mass or masses. Sonographic evaluation of the abdominal mass should be thorough and determine the organ of origin of the mass, if possible, and its relationship to adjacent organs and vessels (Table 6–1). The size and type or character of the abdominal mass (abscess, hematoma, or neoplasia) should be determined (see Figs. 6–48 and 6–49). Involvement of the mesenteric and abdominal lymph nodes often occurs in horses with abdominal neoplasia, and metastases to these lymph nodes are common. The entire abdomen should be thoroughly examined sonographically for evidence of metastases to other organs or to the peritoneum.

Table 6–1
Findings Obtained from Ultrasonographic Examination of an Abdominal Mass

The organ of origin of the mass
The size of the mass
The character of the mass
The relationship of the mass to the contiguous organs and blood vessels
The presence of lymphadenopathy or metastases
The vascularity of the mass

From Teele RL, Share JC (eds): Ultrasonography of Infants and Children. Philadelphia, WB Saunders, 1991.

Primary neoplasia involving only the mesenteric and abdominal lymph nodes is less common because multicentric lymphosarcoma usually involves the abdominal organs as well.[315] A large 20-cm malignant lymphoma was palpated rectally, at postmortem examination it was found to involve the right dorsal and ventral colon.[316] A similar mass was present between the left dorsal and ventral colon, replacing the mesenteric lymph nodes. Both masses had ulcerated into the ventral colon. Transrectal evaluation of the palpable mass should have revealed the nature of the mass and the involvement of the colon if ultrasound equipment had been available. Sonographic examination of enlarged palpable lymph nodes should be performed transrectally to determine the extent of lymph node involvement.

Cytologic evaluation of fluid obtained on abdominoparacentesis often yields an exudate (56% of 25 horses in one study), but neoplastic cells are detected less frequently in the peritoneal fluid (44% of these same horses).[5] A mean number of 1.45 cytologic examinations of peritoneal fluid samples was needed in horses with abdominal neoplasia to identify the neoplastic cells.[5] However, in 9 horses only one peritoneal fluid sample was required to obtain a definitive diagnosis, whereas in 2 other horses, three and four samples were examined before a definitive diagnosis of neoplasia was made. Lymphosarcoma (6 of 12 horses) and squamous cell carcinoma of the stomach (5 of 9 horses) were the tumors detected on cytologic examination of the peritoneal fluid, whereas none of the 4 horses with adenocarcinoma were diagnosed by peritoneal fluid cytology.[5]

Metastases to the peritoneum are common in horses with abdominal neoplasia (Fig. 6–129). Sonographic detection of peritoneal masses has been reported in horses with gastric squamous cell carcinoma.[6] The metastatic

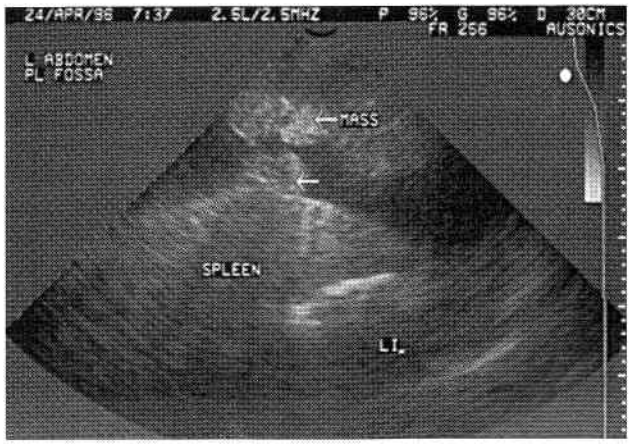

Figure 6–129

Sonogram of the peritoneal cavity obtained from a 17-year-old Oldenberg gelding with metastatic melanoma (same horse as in Figs. 6–49 and 6–70). Multiple small to large irregular composite masses (*arrows*) line the peritoneum and the capsular surfaces of the abdominal organs. The mass on the capsular surface of the spleen creates an artifact due to the absorption of sound by the mass and the enhancement of the splenic parenchyma that occurred on either side from the effusion in the peritoneal cavity. This sonogram was obtained from the left paralumbar fossa with a wide-bandwidth 2.5-MHz sector-scanner transducer operating at 2.5 MHz at a displayed depth of 30 cm. The right side of this sonogram is dorsal and the left side is ventral.

nodule detected sonographically in the horse with gastric squamous cell carcinoma was hypoechoic and homogeneous. Mesotheliomas have been detected sonographically as multiple small hypoechoic to echogenic masses scattered throughout the peritoneal cavity, lining the peritoneum and the serosal surfaces of the abdominal viscera. Large abdominal effusions are common in horses with mesotheliomas. The peritoneal fluid makes the visualization of the small peritoneal and serosal masses easier because the structures are separated and delineated by the peritoneal fluid.

PATIENT MANAGEMENT AND PROGNOSIS

Disorders of the Urinary Bladder

Cystitis

The presence of cystitis should be confirmed with culture and sensitivity testing of an aseptically obtained urine sample. Treatment of cystitis should be based on the results of culture and sensitivity testing, selecting an antimicrobial that is concentrated in the urine, such as trimethoprim-sulfamethoxazole.

Bladder Paralysis

Treatment of the underlying neurologic disease, if present and treatment is available, is recommended for horses with bladder paralysis. The treatment for upper motor neuron and lower motor neuron bladder dysfunction differs, and thus the cause of the bladder paralysis must be determined for selection of the appropriate treatment for urinary incontinence associated with neurologic disease. Bladder catheterization and lavage have been recommended for treatment of horses with bladder paralysis and sabulous urolithiasis. The long-term prognosis for these horses is guarded to poor, with most horses being humanely destroyed within 14 months of diagnosis.[35, 36]

Cystic Calculi

The removal of cystic calculi can be successfully performed in the mare via gradual urethral dilatation and removal of the calculus or with urethral sphincterotomy.[317] The removal of cystic calculi in the gelding or stallion can be performed with a laparocystotomy, laparocystidotomy, or perineal (subischial) urethrotomy. Good long-term results are achieved in most cases with manual removal of the calculus in its entirety from the bladder or by crushing the calculus and removing the fragments.[36, 37, 40, 41, 318, 319] Electrohydraulic lithotripsy has been used successfully for the treatment of cystic calculi in three horses.[44, 45] Other surgical approaches have also been described but are used less frequently.[36, 40]

Recurrence of clinical signs of urolithiasis was seen in 41% of horses in one study in which long-term follow-up information was available.[37] The recurrence of cystic calculi after perineal urethrostomy was 46% in one study, slightly higher than the overall recurrence rate.[37] The advantages of electrohydraulic lithotripsy include minimal tissue trauma, especially with calculi embedded in the bladder mucosa; direct visualization of the calculus is possible; and the risks associated with laparocystotomy are avoided.[44, 45] In horses in which a perineal urethrotomy has been performed and the calculus has been crushed and subsequently removed, sonographic re-examination of the bladder can be helpful in determining the amount of residual debris that remains either free in the bladder or attached to the bladder mucosa. These residual fragments of the calculus could serve as a nidus for subsequent calculus formation.[40, 319]

Complications occurred in 19% of horses undergoing a perineal urethrostomy for removal of a cystic calculus, all thought to have occurred secondary to urethral trauma from the calculus.[37] The complications included a rectal tear, perforation of the pelvic urethra, orchitis, peritonitis, and tenesmus. Other reported complications include a urethral diverticulum near the surgery site in a horse with urethral obstruction,[47] dysuria,[36] and fibrosis and a stricture at the surgery site.[46] Sonographic re-examination of the urethra can also be performed if subsequent problems with urination develop and urethral stricture is suspected.

Acidification of the urine has been recommended to prevent recurrence of urolithiasis in horses.[40] However, the efficacy of the most frequently recommended treatment, ammonium chloride, is questionable. There is one report of a horse with recurrent cystic calculi treated successfully with ammonium sulfate.[320] Ascorbic acid has been suggested to be a better urinary acidifier in the horse.[321] However, the efficacy of these treatments in the prevention of equine urolithiasis has yet to be proven, and these urinary acidifiers are either not very palatable (ammonium chloride and ammonium sulfate) or must be given via nasogastric intubation.[322] Additional work is needed, however, to determine if urinary acidification is of benefit in horses with urolithiasis. Salting the horse's food to increase water consumption increases the frequency and volume of urination and helps prevent urine stasis. Antibiotics that are concentrated in the urine and effective against pathogens cultured from the urine should be used if bacterial cystitis is present.

Urethral Calculi

The location of obstruction of the urethra by a calculus can be determined sonographically and the appropriate surgical approach selected. A perineal urethrotomy is commonly performed in the male to remove the urethral calculus.[49] However, a urethrotomy at the site of the obstruction was performed successfully in one 3-month-old colt[48] and in three adult horses with urethral obstruction.[37] No complications were observed with the urethrotomy in the three adult horses. In two horses the urethral calculi were removed through the external urethral orifice.[37] In one of these horses, the urethral calculus recurred on two occasions, and a urethral diverticulum was identified in the distal portion of the urethra after the third calculus removal. A urethral diverticulum

also developed in one stallion with urethral obstruction corrected by a perineal urethrostomy.[47] Treatment for the possible prevention of urethral calculi should be similar to that described for cystic calculi.

Rupture of the Urinary Bladder

Cystoscopy with a flexible fiberoptic endoscope is useful in documenting the extent of the bladder rupture and evaluating the mucosal surface of the urinary bladder.[49, 56] Rupture of the urinary bladder in the adult horse can be surgically repaired in mares by everting the bladder through the urethra or by an intravesicular approach with the surgeon's hand and instruments in the bladder lumen via the urethra.[53, 57] Urethral sphincterotomy has been reported for the repair of tears involving the neck of the bladder and the ventral bladder wall.[54, 55, 59] Transient loss of urethral sphincter function may occur postsurgically, and a stricture may also develop at the urethral sphincter.[55] Caudal midline and paramedian laparotomy has been used to repair tears in the apex of the urinary bladder in adult horses.[56, 60] There is one report of conservative (nonsurgical) management of uroperitoneum in a horse with bladder wall necrosis secondary to an obstructive urethral calculus.[49] However, surgical repair of a ruptured bladder is recommended in the adult horse if the tear can be identified owing to the high incidence of peritonitis in horses with uroperitoneum and the probable continued leakage of urine into the peritoneal cavity.[49]

Sonographic evaluation of the surgical repair can also be performed if the horse is experiencing problems postoperatively. Defects in the repaired wall of the urinary bladder or adhesions between the urinary bladder and surrounding structures may be detected. Some leakage of urine through the bladder wall is possible when the surgical line appears intact sonographically but is usually minimal.

Neoplasia of the Urinary Bladder

Horses with urinary bladder neoplasia must be given a poor prognosis because these tumors are usually relentlessly progressive.[64] Topical 5-fluorouracil or triethylenethiophosphoramide and/or surgical resection may be helpful if the bladder tumor is diagnosed early and treated aggressively.[64]

Renal Diseases

Acute Renal Failure

The best prognosis for the treatment of acute renal failure is in horses with vasomotor nephropathy and some of the nephrotoxic and pigment nephropathies. Correction of electrolyte, fluid, and acid-base abnormalities is the usual focus of treatment for horses with acute renal disease. In acute renal failure, once systemic blood pressure is restored, intravenous dobutamine and furosemide are recommended for horses with oliguric renal failure. Systemic blood pressure should be monitored during this treatment. In nonoliguric renal failure fluid diuresis is recommended until the serum creatinine returns to normal or nearly normal.

Chronic Renal Failure

Glomerulonephritis may respond to treatment with corticosteroids, especially if treated early.[74, 99] However, in many horses the administration of corticosteroids has been of limited benefit in slowing the progression of the disease. Plasma transfusions and/or diuretics may be used in horses with severe hypoproteinemia and edema for short-term control of the edema. Free-choice water and sodium chloride should be provided unless edema is present.[90] In horses with chronic renal failure and weight loss, there should be a gradual increase in the amount of carbohydrates and fat in the diet. Protein should be limited, and switching from alfalfa hay to a high-quality grass hay may be helpful in some horses, particularly those with hypercalcemia. The prognosis for long-term survival for horses with chronic renal failure is guarded to grave in most instances.

Nephrolithiasis and Ureterolithiasis

Resolution of a left ureteral stone was accomplished in a 3-year-old Thoroughbred colt with electrohydraulic lithotripsy.[322] The only abnormalities found on transcutaneous ultrasound examination of the kidneys were that both corticomedullary junctions appeared indistinct and the right kidney appeared more hyperechoic than the left. A biopsy of the right kidney revealed chronic interstitial nephritis and marked interstitial medullary fibrosis. In spite of the poor prognosis suggested by the biopsy of the right kidney, the horse returned successfully to racing and his azotemia resolved.[322] Successful removal of a ureterolith has also been described in a mare using two different surgical techniques.[45] The mare was clinically normal following the removal of each urolith. Multiple nephroliths were found in both kidneys at subsequent postmortem examination of this mare. However, in another filly, removal of the calculi via a ureterotomy incision did not result in improved renal function.[103] Percutaneous nephrostomy was performed with ultrasonographic guidance in this horse for short-term management of ureterolithiasis and renal dysfunction.[103] Sonographic re-examination of this kidney after placement of the percutaneous nephrostomy revealed a decrease in the mineralization in the right renal pelvis. The placement and guidance of the indwelling nephrostomy tube required surgical skill and ultrasonographic interpretation to accurately direct the cannula into the renal pelvis. Sonographic evaluation of both kidneys should be performed prior to surgical removal of an obstructing ureterolith or nephrolith to determine if multiple nephroliths are present in one or both kidneys, increasing the probability of the obstruction recurring. Unilateral nephrectomy has also been performed as a treatment for hematuria associated with nephrolithiasis in a colt.[323]

Pyelonephritis

Treatment with appropriate antibiotics based on culture and sensitivity testing of the urine should be instituted. Antibiotics should be selected that are concentrated in the urine and effective in the pH of the patient's urine.[90] Trimethoprim-sulfamethoxazole is often a good first-line treatment in many horses with pyelonephritis. Chronic unilateral pyelonephritis with severe destruction of the affected kidney may be best managed with unilateral nephrectomy if the other kidney is functioning normally.[90] Unilateral nephrectomy has been successfully performed in one adult horse with severe unilateral pyelonephritis, nephrolithiasis, and ureteral obstruction (see Fig. 6-42).

Renal Abscess/Hematoma

Renal abscess in the horse may be treated by unilateral nephrectomy if only one kidney is affected. Percutaneous drainage of a renal or perirenal abscess associated with the right kidney may be considered using ultrasonographic guidance if the abscess was confined to the retroperitoneal space. Treatment for a renal hematoma usually involves supportive care until the hematoma has resolved on its own.

Renal Granuloma

A biopsy should be obtained from the kidney or other involved tissues such as the mandibular region to confirm the diagnosis of *H. deletrix* infection. Anthelmintic treatment has been recommended for the treatment of this infection. However, successful treatment of *H. deletrix* has not been reported.[124] In two cases reported in the literature, neurologic signs developed after anthelmintic treatment.[122, 124]

Renal Neoplasia

A biopsy of the kidney or affected perirenal tissues should be obtained to confirm the diagnosis of renal neoplasia. The prognosis of horses with renal neoplasia is guarded to poor, with survival times usually very short after diagnosis. In one horse with a large (22 × 33 cm) renal tubular cell carcinoma, the mare was still alive and in foal 1 year after diagnosis and was reportedly doing well.[129] Unilateral nephrectomy may be considered in horses with a discrete renal tumor and no evidence of metastases.

Renal Biopsy

Prior to the development of two dimensional real-time ultrasonography, renal biopsies were performed blindly through the left flank with an assistant immobilizing the left kidney per rectum.[324-326] This technique enabled the clinician to obtain a biopsy of the left kidney only. Damage to the left kidney, renal vessels, or spleen was possible owing to the blind technique, and an inadequate sample could be obtained. Therefore, it is important to adequately immobilize the left kidney and not to pass the needle through the entire kidney to prevent possible damage to the renal vessels.[326] A large perirenal hematoma was reported in one horse prior to the advent of ultrasound-guided or ultrasound-localized renal biopsies.[325] Even using ultrasound-guided or ultrasound localization techniques for obtaining a renal biopsy, significant hemorrhage can result. This hemorrhage is usually associated with laceration of an accessory vessel, which is occasionally found in the caudal pole of the equine kidney.[90] Therefore, the caudal pole of the kidney should be avoided. When taking a sample of the lateral border of the kidney, macroscopic hematuria was detected in one of six horses after biopsy, and microscopic hematuria was detected in four of these horses.[327] Microscopic hemorrhage has commonly been reported in horses within the first 36 hours of the renal biopsy prior to the advent of ultrasound-guided or ultrasound-localized techniques.[325, 326] Perirenal hemorrhage around the biopsied kidney was detected in five of six horses at postmortem examination.[327] Hemoperitoneum may occur if the peritoneal cavity has been inadvertently penetrated.[325] A biopsy of the left kidney often requires penetration of the spleen with the biopsy needle owing to its location medial to the caudal pole of the spleen. Two of three horses that had a biopsy of the left kidney performed using ultrasound guidanace or ultrasound localization had the spleen penetrated by the biopsy needle.[327] Therefore, a renal biopsy should be performed only in horses in which it is likely that the results will change the treatment or prognosis.[90] A clotting profile should be obtained in every horse prior to performing a renal biopsy because of the risk of significant hemorrhage.[325-327] A packed cell volume measurement should also be obtained prior to performing a renal biopsy to have as a baseline in monitoring the horse for postbiopsy hemorrhage.[327]

In seven normal horses, the capsule of the right kidney was located 3.16 ± 0.63 cm from the skin and the capsule of the left kidney was imaged 7.27 ± 2.43 cm from the skin surface, depending upon the thickness and location of the spleen.[327] The costodiaphragmatic pleural recess located dorsal to the cranial pole of the right kidney should be avoided when performing a renal biopsy, if possible, to prevent accidental penetration of the pleural space. The renal fossa of the liver should be avoided adjacent to the cranial pole of the right kidney. The lateral angle of the right kidney is where the cranial and caudal parts of the lateral border of the kidney meet and is the most ventral aspect of the kidney immediately adjacent to the right body wall.[327] The kidney widens significantly dorsal to this angle, resulting in ample renal tissue for biopsy at a level 2 to 3 cm dorsal to the lateral angle. The preferred site for obtaining a biopsy sample from the horse's right kidney is close to the lateral border while imaging the kidney transversely.[327] In normal horses in this study this site was located in the seventeenth intercostal space. The biopsy needle should be directed perpendicular to the body wall. This technique was confirmed to be safe and accurate when the renal biopsy

of the right kidney was obtained from the seventeenth intercostal space.[327]

Both ultrasound-guided biopsies and blind biopsies following ultrasound localization can be performed. The blind biopsy technique requires only one operator and no specialized biopsy equipment.[327] If bilateral renal disease is present, the right kidney should be chosen for biopsy, as this kidney is retroperitoneal and adjacent to the right body wall. An ultrasound-guided biopsy should be performed if the kidney contains a focal lesion, in order to maximize the likelihood of obtaining a tissue sample from the area of interest. With the increased distance of the left kidney from the lateral body wall, slight bending of the biopsy needle may occur, resulting in the needle disappearing from the biopsy guide path during the procedure and requiring repetition of the procedure if the needle cannot be localized. Using an ultrasound-guided biopsy procedure, the biopsy needle tip is imaged as a hyperechoic structure, often with a double-walled appearance. The size of the needle tip echo depends upon the diameter of the biopsy needle, the direction the bevel of the needle is pointing, and the incident angle of the needle replacement relative to the direction of the ultrasound beam.[328] As the biopsy needle passes into the deeper tissues, the tip of the needle becomes more difficult to detect owing to attenuation of the ultrasound beam. Enhanced sonographic visualization of the biopsy needle results from using a needle with a roughened or scored tip.[328] These biopsy needles are now commercially available and make the needle easier to detect sonographically. The presence of side holes and an intraluminal guide wire or stylet also enhance visualization of the needle tip.[328] Automated ultrasound-guided biopsy instruments are also commercially available and have been shown in dogs to result in larger and higher-quality biopsy samples when the liver or left kidney is sampled using the automated techniques than when performing a manual ultrasound-guided biopsy.[329] The automated technique also requires only one operator to perform the biopsy successfully. Trauma to the organ should be reduced because the sample obtained should be of good quality, and thus only one sample should be necessary in most cases.

The hair on the skin over the kidney to be biopsied should be clipped with a No. 40 surgical clipper blade or shaved and ultrasound coupling gel applied to locate the kidney and the site to undergo biopsy. If a blind biopsy is to be performed, the distance from the skin to the renal capsule and the optimal needle angle should be determined.[327] Adequate restraint is needed, and sedation may be necessary, particularly for biopsy of the left kidney.[325] The skin should then be surgically prepared and aseptic technique used to infiltrate the skin and subcutaneous tissues with local anesthetic. A small stab incision should then be made through the skin. If a blind biopsy technique is being used, the sterile biopsy needle should then be directed aseptically along the predetermined path and the biopsy sample obtained at the predetermined depth. If an ultrasound-guided biopsy is being performed, the transducer should be placed in a sterile sleeve containing ultrasound coupling gel. A sterile biopsy guide should be attached to the transducer and the biopsy needle introduced into the biopsy guide. Sterile ultrasound coupling gel is applied to the skin, and the sterile transducer is placed on the skin. The biopsy site should be located and placed in the path of the biopsy guide markers on the ultrasound screen. The biopsy needle is then advanced to the renal capsule, where the biopsy sample is obtained by advancing the obturator through the renal parenchyma and holding the outer cannula still. The outer cannula is then advanced over the specimen, and the entire biopsy needle and tissue sample are withdrawn. With some biopsy needles the manufacturer may recommend passing the entire needle into the tissue to be sampled, retracting the outer cannula without moving the obturator, and then quickly advancing the cannula over the obturator and the biopsy needle when the specimen is withdrawn. The ultrasound-guided biopsy can also be performed freehand, although this technique is more difficult than using the manufacturer's biopsy guide. The biopsy may be repeated if an adequate sample was not obtained but should be performed at a slightly different location, if possible. The needle should be not be redirected once the renal capsule has been penetrated but rather should be repositioned before advancing the needle to the kidney. The tract of the biopsy needle was imaged as a hyperechoic line through the renal parenchyma and was detected for 48 hours after the biopsy was performed.[327]

Perirenal and Periaortic Masses

The prognosis for the perirenal mass depends upon the type of mass (hematoma, abscess, neoplasia). An ultrasound-guided aspiration of a perirenal mass can be performed if access to the mass is relatively straightforward. Cytologic examination of the fluid obtained and culture and sensitivity testing of the fluid should be performed. An ultrasound-guided biopsy should be attempted if the mass appears to have a soft-tissue density. The prognosis for horses with perirenal and periaortic neoplastic masses is usually poor to grave, and the tumors are usually quite invasive and extensive by the time the diagnosis is made.

Adrenal Neoplasia

Horses with pheochromocytomas have a very grave prognosis, with most horses living only hours to days after the onset of clinical signs. Horses with nonfunctional tumors of the adrenal glands may also have a guarded to grave prognosis if the tumor is very invasive by the time the diagnosis is made. Adrenal gland adenomas are occasionally detected as incidental findings on postmortem examination.

Liver Disease

Acute and Chronic Hepatic Failure

The best prognosis for horses with liver failure is in horses with acute hepatitis or cholangiohepatitis and in those without chronic hepatic fibrosis. A liver biopsy is

helpful in determining the type of underlying liver disease and in formulating a prognosis. The treatment of horses with acute liver failure is primarily supportive and is directed at correcting any acid-base and electrolyte abnormalities. The horse should be treated with intravenous dextrose if hypoglycemia is present. Intravenous dextrose may also be helpful to decrease the hepatic workload. Signs of hepatic encephalopathy should be controlled if present, and treatment should be directed at decreasing the blood ammonia concentrations. Dietary management in animals that are eating should include meeting the animal's energy and protein requirements. Branched-chain amino acids should be used as much as possible. Corticosteroids can be considered in horses with chronic active hepatitis if bacterial infection has been ruled out. No successful treatment for pyrrolizidine alkaloid toxicity in horses is available. Death in affected horses is usually within 1 to 2 weeks after the onset of clinical signs.

Suppurative Hepatitis

Suppurative hepatitis has been treated successfully in one horse. Long-term antimicrobial treatment and supportive care were required, and this horse continues to have persistent elevations in liver enzymes but is clinically normal. Sonographic examination of this horse's liver reveals it to be of normal size with irregular margins. Discrete echogenic to hyperechoic areas are seen in the parenchyma, some of which are casting faint acoustic shadows from the deeper margins of the hyperechoic area consistent with severe fibrosis.

Cholelithiasis and Cholangiohepatitis

The detection of biliary distention, biliary sludge, hepatoliths, or increased echogenicity of the hepatic parenchyma should prompt an ultrasound-guided biopsy in these horses. Biopsy samples should be submitted for histopathologic evaluation and culture and sensitivity testing in the hope of isolating the causative agents. In the absence of a positive culture, trimethoprim-sulfamethoxazole and ceftiofur are good first-line drugs for the treatment of cholangiohepatitis in horses. The majority of horses have an infection associated with organisms that are sensitive to these antimicrobials. *Salmonella, Escherichia coli, Citrobacter* species, and *Aeromonas* species have been isolated from the liver of horses with cholangiohepatitis and cholelithiasis.[152, 153] Antimicrobial treatment should be prolonged, at least 4 to 8 weeks or more, and ideally should continue until the clinical signs have resolved and liver enzymes have returned to normal or nearly normal. Repeat sonograms may be helpful in determining the response to treatment. Liver size and echogenicity should gradually return toward normal, and biliary distention, if present, should improve. In horses with chronic liver disease and severe hepatic fibrosis, the liver enzymes may return toward normal but are likely to remain elevated. Medical management of these horses should include low-protein, high-carbohydrate diets.[154] Prognosis in affected horses should be guarded initially until the results of the biopsy are known and the response of the horse to therapy can be evaluated. Horses with severe hepatic fibrosis, severe biliary distention, and obstruction or presenting with hepatic encephalopathy must be given an extremely guarded prognosis. Cholangiocarcinoma developed in one horse with septic cholangiohepatitis, metastasized to the metacarpophalangeal joint, and was the cause of the horse's demise.[156] The authors speculated that the chronic biliary tract inflammation documented in this horse led successively to metaplasia, dysplasia, and neoplastic transformation.[156] The initial sonographic appearance of the liver in this horse was normal, followed by the development of multiple hyperechoic foci, one of which cast an acoustic shadow suggestive of choleliths. However, choleliths were not found on postmortem examination.

Biliary obstruction most frequently results in the death of the horse.[143, 145-147, 150] Horses reported in the literature presenting with hepatic encephalopathy also either have been humanely destroyed or have died.[142, 147] However, hepatoliths are occasionally detected as an incidental finding in horses with no clinical signs of hepatic disease (see Figs. 6-59 and 6-60).[150]

Obstructing choleliths that can be crushed by digital manipulation should be fragmented and manipulated into the duodenum (choledocholithotripsy). In one study all three horses with an obstructing stone were treated surgically with cholelithotripsy, and the obstructing stone was successfully crushed.[153] However, two of the horses were euthanized because of hepatoencephalopathy. Although the obstructing cholelith usually feels hard, it can usually be crushed with continued digital manipulation.[153] A sterile needle, intravenous tubing, and saline can be used to flush the fragments of the cholelith into the duodenum if the obstructing calculus can be crushed.[143] Most obstructing stones are oval to circular in shape and have often incorporated the underlying biliary duct mucosa.[143-146] Surgical removal of an obstructing stone can be performed via choledochotomy and has been successfully performed in a few horses. However, choledochotomy should be avoided if possible because the surgical exposure of the common bile duct is limited in the horse, multiple choleliths are usually the rule, and choleperitoneum is a severe complication of choledochotomy.[144, 145, 153] Medical dissolution of choleliths is not a viable option in the horse owing to the large expense of treatment, the length of time that it takes to dissolve the cholelith with treatment, and the low percentage of cholesterol in equine choleliths, making this treatment less likely to be successful.[153]

Hepatic Lipidosis

The treatment for horses with hepatic lipidosis should be directed at the underlying disease. If the liver appears markedly enlarged with a sonographic appearance consistent with fatty liver and the clinical signs and history are consistent with this diagnosis, a liver biopsy may not be indicated because of the risk of hepatic rupture. Fluid therapy, nutritional support, and supportive care are indicated in addition to the treatment of the underlying con-

dition for horses and ponies with hyperlipemia.[171] Treatment of secondary hyperlipemia in miniature horses and donkeys had a better prognosis than treatment of primary hyperlipemia in ponies.[171] If a pituitary tumor is the underlying disease, treatment should also be aimed at this endocrine disease with fluid therapy, nutritional support, and other supportive care as needed.

Granulomatous Liver Disease and Hepatic Amyloidosis

The diagnosis of granulomatous liver disease or hepatic amyloidosis is made on histopathologic examination of tissue obtained from a liver biopsy. If the liver changes seen sonographically are not diffuse, the biopsy should be ultrasound guided, sampling an area of parenchymal abnormality. An agent responsible for granulomatous liver disease has not been reported, but the tissues should be examined for acid-fast organisms. Prognosis for horses with hepatic granulomatous disease or amyloidosis is guarded to grave.

Cystic Liver Disease

Treatment of hydatid cyst disease in horses should be aimed at prevention rather than treatment owing to the potential public health hazards.[173] Dogs should not be fed raw meat because dogs are the definitive host for *Echinococcus granulosus*.

Hepatic Neoplasia

The prognosis for horses with hepatic neoplasia is guarded to poor, with most horses surviving only weeks to months following the diagnosis. Rupture of the tumor and severe hemoperitoneum have occurred in several horses with primary liver tumors.

Hepatic Lobe Torsion

If hepatic lobe torsion is diagnosed prior to surgical intervention, resection of the affected liver lobe can be performed and has been done successfully in one horse.[202]

Liver Biopsy

In the majority of horses with liver disease, the liver is diffusely affected and a liver biopsy accurately reflects hepatic disease, although not necessarily the underlying cause of the liver disease.[169] The liver biopsy is also a good reflection of the findings at necropsy in horses with liver disease.[168, 169] However, in two horses with hepatic metastases the blind liver biopsies were normal,[169] suggesting that an ultrasound-guided biopsy should be performed in horses with suspected hepatic neoplasia, selecting sonographically abnormal areas of the liver for biopsy.

Blind liver biopsies can be performed through the right abdomen or right lung in the midthoracic region. The biopsy sample is obtained from the right twelfth to fourteenth intercostal space just below a line drawn from the tuber coxae to the point of the shoulder or from the right tenth or eleventh intercostal space just beneath a line drawn from the point of the hip to the point of the shoulder.[326, 330, 331] Complications that can result from the blind liver biopsy include accidental perforation of the bowel and peritonitis, bile peritonitis, pneumothorax, and hemorrhage.[326] Significant hemorrhage occurred in only 1 of 27 horses following a blind liver biopsy. Although serious hemorrhage is an infrequent complication of a liver biopsy, a clotting profile should be performed on all patients prior to a liver biopsy. Delayed coagulations times should be considered an increased risk for hemorrhage following liver biopsy.[168] Bile peritonitis has been reported in two cats following ultrasound-guided liver biopsy and accidental puncture of the bile duct.[332] Both cats had significant hepatic lipidosis. Although bile peritonitis is rare, it is a potential complication of liver biopsy in the horse.

Both ultrasound-guided liver biopsies and blind biopsies following ultrasound localization can be performed. The blind biopsy technique requires only one operator and no specialized biopsy equipment. If both lobes of the liver are involved, the right lobe usually provides the operator with more imageable hepatic parenchyma to select a site for biopsy than does the left lobe of the liver, unless atrophy of the right liver lobe is present. If the horse is older and significant atrophy of the right lobe of the liver is present, hepatic parenchyma is usually imageable in the left cranioventral abdomen and a biopsy sample can be taken there if the liver disease is diffuse. An ultrasound-guided biopsy should be performed if a focal lesion is present in the liver to maximize the likelihood of obtaining a tissue sample from the area of interest. Using an ultrasound-guided biopsy procedure, the biopsy needle tip is imaged as a hyperechoic structure, often with a double-walled appearance. Enhanced sonographic visualization of the biopsy needle results from using a biopsy needle with a roughened or scored tip.[328] These biopsy needles are now commercially available and make the needle easier to detect sonographically. Automated ultrasound-guided biopsy instruments are also commercially available and have been shown in dogs to result in larger and higher-quality biopsy samples with the automated techniques than with a manual ultrasound-guided biopsy.[329] The automated technique also requires only one operator to perform the biopsy successfully. Trauma to the organ should be reduced because the sample obtained should be of good quality, and thus only one sample should be necessary in most cases. If a completely blind liver biopsy is performed, the biopsy needles should be advanced in a caudad and ventrad direction through the intercostal muscles and should be advanced through the thoracic cavity on expiration to prevent puncturing the lung.[326] The needle is advanced to the diaphragm, where it can be seen to move with each respiration. The biopsy needle is then advanced through the diaphragm and the capsule of the liver, and a sample is collected as previously described.

The hair on the skin over the part of the liver to be biopsied should be clipped with a No. 40 surgical clipper blade or shaved and ultrasound coupling gel applied to locate the liver and the biopsy site. If a blind ultrasound-localized biopsy is to be performed, the distance from the skin to the liver capsule and the optimal needle angle should be determined. Adequate restraint is needed, and sedation may be necessary. The skin should then be surgically prepared and aseptic technique used to infiltrate the skin and subcutaneous tissues with local anesthetic. A small stab incision should then be made through the skin. If a blind ultrasound-localized biopsy technique is used, the sterile biopsy needle should then be directed aseptically along the predetermined path and the biopsy sample obtained at the predetermined depth. If an ultrasound-guided biopsy is being performed, the transducer should be placed in a sterile sleeve containing ultrasound coupling gel. A sterile biopsy guide should be attached to the transducer and the biopsy needle introduced into the biopsy guide. Sterile ultrasound coupling gel is applied to the skin, and the sterile transducer is placed on the skin. The biopsy site should be located and placed in the path of the biopsy guide markers on the ultrasound screen. The biopsy needle is then advanced to the liver capsule, where the biopsy sample is obtained by advancing the obturator through the hepatic parenchyma and holding the outer cannula still. The outer cannula is then advanced over the specimen, and the entire biopsy needle and tissue sample are withdrawn. With some biopsy needles the manufacturer may recommend passing the entire biopsy needle into the tissue to be sampled, retracting the outer cannula without moving the obturator, and then quickly advancing the cannula over the obturator and withdrawing the biopsy needle with the specimen.[526] The ultrasound-guided biopsy can also be performed freehand, although this technique is usually more difficult for the novice than using the manufacturer's biopsy guide. The needle tip may be easier to visualize, however, because the needle can be placed more perpendicular to the ultrasound beam. The biopsy may be repeated if an adequate sample was not obtained but should be performed at a slightly different location, if possible. The needle should be not be redirected once the liver capsule has been penetrated but rather should be repositioned before advancing the needle to the liver.

Splenic Diseases

Splenic Neoplasia

Splenic neoplasia has a varied prognosis depending upon the neoplasm involved. Melanomas can metastasize to the spleen and cause no clinical problems. Lymphosarcoma or metastatic neoplasms are likely to markedly shorten life expectancy, with a rapid clinical deterioration of the patient.

Splenic Hematoma/Rupture

Stall rest with periodic ultrasonographic monitoring is recommended for most horses with splenic hematoma. Stall rest is important in these horses owing to the risk of rupture of the hematoma and fatal intra-abdominal hemorrhage. The author has seen four horses with splenic hematoma that were treated conservatively and have done well (see Figs. 6-76 and 6-77), as well as one horse with splenic rupture involving the periphery of the spleen that survived the massive intra-abdominal hemorrhage with aggressive supportive care (see Fig. 6-78). One horse reported in the literature was treated conservatively for a splenic hematoma after initial stabilization of the mare and was doing well 1 year later.[210] Ultrasonographically, the hematoma continued to organize, and 5 months after the original examination the parietal capsule of the spleen appeared irregularly thickened.[210] Some areas appeared hyperechoic and cast acoustic shadows. No further change was seen in the lesion within the splenic parenchyma.

A fine-needle aspirate of the splenic mass may be considered to confirm the diagnosis, but it carries with it a risk of iatrogenically creating a splenic abscess. Successful drainage of a splenic hematoma has been described using a large-bore chest tube in a horse with the hematoma adhering to the left body wall. In that horse the splenic hematoma was no longer detectable sonographically 15 months later. Although splenectomy is a possibility, the cost and risk of splenectomy are considerable.[209, 210, 216] Splenectomy has been successfully performed in one horse with primary splenomegaly but is a complicated procedure.[216, 353] In most horses, however, splenic rupture is a fatal event.[211-214] Splenic infarction has a poor prognosis in dogs and is usually a reflection of other severe underlying systemic disease, and probably carries a similar prognosis in horses.[218]

Splenic Abscess

Long-term systemic antimicrobial therapy can be attempted if the splenic abscess is small and can be facilitated if an aspirate can safely be obtained (ultrasound-guided) for culture and sensitivity testing without contaminating the peritoneal cavity. Splenic abscesses can be drained with percutaneous catheterization if the abscess adheres to the left body wall. Splenectomy is another possible treatment for a horse with splenic abscesses, but the splenectomy is an expensive and somewhat risky surgery.

Pancreatic Adenocarcinoma

The prognosis for horses with pancreatic adenocarcinoma is guarded to poor, with most horses surviving only days to weeks after presentation to a referral hospital for evaluation. However, these horses often have a history of chronic weight loss of several months' duration. An ultrasound-guided biopsy of the mass should be obtained, if possible. An ultrasound-guided biopsy of the mass in one horse with pancreatic adenocarcinoma yielded normal renal tissue in one biopsy and no abnormal cells.[221] In another horse with pancreatic adenocarcinoma, a diagnostic specimen was not retrieved.[222]

Pancreatitis

Treatment for pancreatitis in the horse is symptomatic, with large volumes of intravenous fluid needed and analgesics for control of abdominal pain. Frequent nasogastric decompression may be necessary. Calcium supplementation may be indicated if hypocalcemia is a problem. Broad-spectrum antibiotics should be administered for possible bacterial infection.

Gastrointestinal Diseases

The sonographic examination helps determine if medical or surgical intervention is indicated. Most horses require supportive therapy with intravenous fluids and analgesics for control of pain if surgery is not indicated.

Intussusception

Partial jejunal resection and jejunojejunal anastomosis are usually required in horses with jejunal-jejunal intussusception because manual reduction of the intussusception is usually not successful.[232] Also 45% of horses with jejunal-jejunal intussusception had intraluminal or mural masses requiring surgical resection. Ileal resection and jejunocecal or ileocecal anastomosis may be required in horses with an ileal intussusception if the intussusception cannot be manually reduced. An ileal side-to-side anastomosis has also been performed successfully in horses with ileal intussusception.[241] In horses with ileocecal intussusception, an end-to-side or side-to-side ileocecostomy was successful in the majority of horses.[244] Manual reduction of the cecocolic intussusception and partial typhlectomy have been successfully performed in horses with cecocolic intussusception.[250] Partial or complete cecal bypass is indicated in horses with a nonreducible cecocolic intussusception. A partial typhlectomy is often indicated, and if there is ileal involvement, an ileocolostomy may be required.[252] Manual reduction of the cecocecal intussusception and partial typhlectomy have also been performed successfully in horses with cecocecal intussusception.[243-251]

Small Intestinal Volvulus/Obstruction

Surgical correction of a small intestinal volvulus is indicated, followed by evaluation of the viability of the small intestine after the volvulus has been corrected. The prognosis for affected horses is guarded to poor unless surgical intervention occurs soon after the onset of clinical signs. Surgical resection and anastomosis or surgical bypass of the lesion is indicated, depending upon the type of obstruction encountered. Surgical resection of strangulated jejunum in horses with obstruction and strangulation caused by pedunculated lipomas followed by anastomosis has a good prognosis in affected horses, with a short-term survival rate (discharge from the hospital) of 78.6%.[254] End-to-end jejunojejunostomy, end-to-end jejunoileal anastomosis, and end-to-side jejunocecostomies were performed on affected horses depending on the lesions present. The long-term survival rate of horses with intestinal strangulation/obstruction caused by pedunculated lipomas treated surgically was 50%.[254] Surgical resection of affected jejunum has been performed successfully in three horses with intestinal fibrosis.[264] However, in five horses and two ponies with small intestinal fibrosis and partial obstruction, the length of the affected small intestine was so extensive that surgical resection was not possible.[263]

Nephrosplenic Ligament Entrapment

Both surgical and nonsurgical correction for nephrosplenic ligament entrapment is possible. The success with nonsurgical correction varies from 50%[267] to 79%.[266] The likelihood of successful nonsurgical management decreases with increasing duration of clinical signs associated with nephrosplenic ligament entrapment.[266] Advantages of nonsurgical correction include less anesthesia time and no risk for the complications of abdominal surgery. However, the diagnosis of nephrosplenic ligament entrapment should be confirmed before attempting nonsurgical correction, and other concurrent abdominal lesions are possible. Horses with moderate to severe distention of the large colon may not respond as well to nonsurgical correction.[266] Correction of the nephrosplenic ligament entrapment can be confirmed sonographically during the rolling procedure and minimizes the need for repeated rectal examinations to confirm the position of the large colon. Sonographic examination while the horse is hoisted upside down by its feet should be confirmed with the horse in right lateral recumbency.[230] Both the normal dorsal splenic border and the left kidney should be clearly imaged after correction of the nephrosplenic ligament entrapment (Fig. 6-130). This should be performed as soon as possible after rolling the horse and returning the horse to right lateral recumbency because the colon is still usually lateral to the spleen. Converting the displacement from a nephrosplenic ligament entrapment to a lateral displacement while the horse is still recumbent is enough to correct the nephrosplenic ligament entrapment. If, after rolling a horse with a nephrosplenic ligament entrapment or treating the horse with phenylephrine and exercise, a portion of the left kidney is imaged but the entire dorsal border of the spleen is not imaged, some of the large colon is still trapped in the nephrosplenic space. If the large colon is still trapped in the nephrosplenic space in dorsal or right lateral recumbency, further manipulation of the area over the left caudal rib cage or an additional rolling maneuver should be performed. Surgical correction is indicated if the large colon displacement is not successfully corrected after the horse has been rolled two or three times.[230] An additional lesion requiring surgery may be present in a small number of horses with nephrosplenic ligament entrapment and should be considered in horses with unrelenting pain.

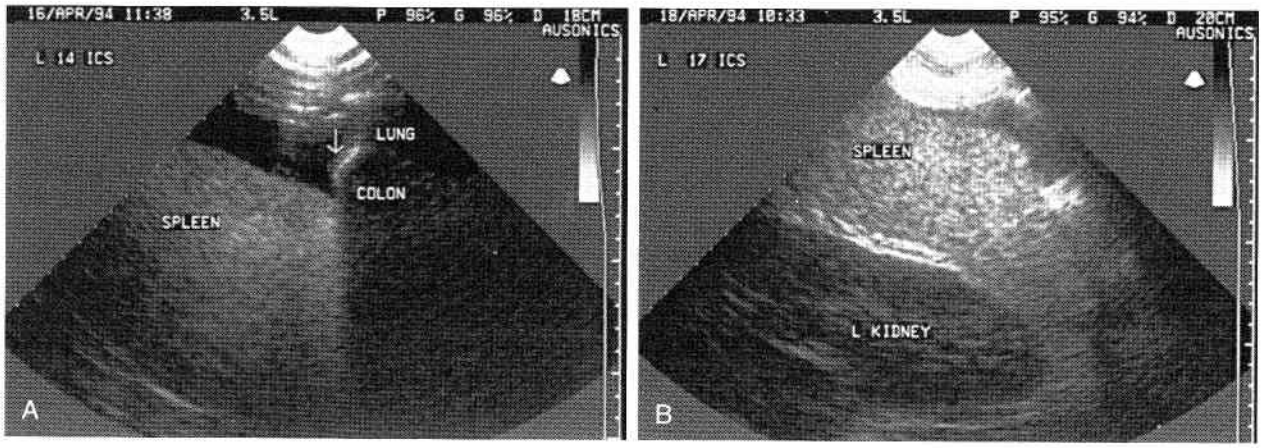

Figure 6–130

Sonograms of the left colon obtained from the left fourteenth (*A*) and seventeenth (*B*) intercostal spaces in a 5-year-old Thoroughbred gelding with a nephrosplenic ligament entrapment before (*A*) and after (*B*) correction by rolling the horse. These sonograms were obtained with a 3.5-MHz sector-scanner transducer at a displayed depth of 18 (*A*) and 20 (*B*) cm. The right side of these sonograms is dorsal and the left side is ventral. *A*, Notice the sharp dorsal border of the spleen (*arrow*) created by the colon entrapped in the neprosplenic space. The dorsal border of the spleen is not visible, and the hyperechoic structure casts a clean shadow (left colon) that creates this sharp dorsal border. This sonographic appearance was detected from the paralumbar fossa to the twelfth intercostal space. *B*, The dorsal border of the spleen and the left kidney are now clearly imaged, consistent with correction of the nephrosplenic ligament entrapment. A normal sonographic appearance was detected for the dorsal border of the spleen in the more cranial interspaces.

Large Colon Displacement

Lateral displacement of the large colon has an excellent prognosis, with resolution of the clinical signs with medical therapy alone occurring in 75% of horses.[230] The remaining horse in this study had a concurrent sand impaction that was evaluated surgically. Other large colon displacements often require surgical intervention for correction of the displacement.

Large Colon/Cecal Impaction

Medical therapy for large colon and cecal impactions is often effective if the treatment is aggressive. Oral fluids and laxatives may be administered if there is no gastric reflux. Large quantities of intravenous fluids are often helpful in relieving the impaction. For sand impactions *Psyllium hydrophilia* mucilloid, which binds with the sand and lubricates the impaction, is recommended. Mild analgesics may be needed in horses with impactions to control pain until the impaction is relieved. Surgical treatment of the large colon or cecal impaction should be performed in any horse with suspected fibrous foreign body impaction, unrelenting abdominal pain, a large colon displacement, increased thickening of the intestinal wall detected on repeated sonographic examination, deteriorating clinical status, or deterioration in the peritoneal fluid parameters.

Enterolithiasis

Surgical treatment is indicated for horses with enterolithiasis to remove the obstructing foreign body. Although horses occasionally pass small enteroliths in their feces, the majority of enteroliths need to be surgically removed before the intestine at the site of the obstruction becomes devitalized and intestinal rupture becomes likely.

Small Colon Impaction/Obstruction

Small colon impaction may be treated medically with success. Enemas may be helpful in relieving the obstruction but should not be administered under pressure. If medical treatment is not successful, surgical relief of the impaction with an enterotomy may be necessary. Horses with enteroliths or fibrous foreign bodies obstructing the small colon require an enterotomy and removal of the obstructing foreign body or enterolith. The prognosis for affected horses is good as long as the obstructed colon is not severely devitalized at the time of surgery and bowel rupture or contamination of the peritoneal cavity does not occur with the enterotomy.[268, 269, 274, 275] Small colon obstruction usually carries a good prognosis if the lesion is resectable.[278] Horses with intramural or submucosal hematoma obstructing the small colon have a good prognosis if the bowel is not ruptured and the horse is metabolically in good shape.[277, 278]

Gastric Distention/Gastritis/Gastric Impaction

The detection of marked gastric distention sonographically should prompt immediate nasogastric intubation and decompression to prevent the possibility of gastric rupture.[288] The underlying cause of the marked gastric distention should be investigated. Horses with suspected or confirmed areas of gastric ulceration should be examined with a gastroscope to evaluate the extent of the ulceration. Protectants and H_2 antagonists are commonly used in the treatment of gastric ulcers if the ulcers are severe enough to warrant treatment.

Gastric impaction has been reported as a primary cause of colic in horses and has also been associated with pyrrolizidine alkaloid toxicosis in ponies and grass sickness in horses. Treatment for idiopathic gastric impaction includes oral fluids by nasogastric intubation or injection into the stomach at the time of surgery and large volumes of intravenous fluids.

Gastric Neoplasia

Horses with gastric squamous cell carcinoma have a guarded to grave prognosis, with a short survival time after diagnosis. The neoplasia is usually fairly advanced by this time, and metastases are common.

Duodenitis/Enteritis

Treatment of affected horses is supportive, with gastric decompression performed regularly, if needed. Intravenous fluid therapy and correction of electrolyte imbalances should be part of the treatment of any horse with severe duodenitis or gastritis.

Granulomatous Enteritis

If granulomatous enteritis is suspected, a rectal mucosal or intestinal biopsy is indicated to confirm the cause of the intestinal malabsorption. Corticosteroid treatment has been advocated for horses with granulomatous enteritis. In general, horses with granulomatous enteritis have a poor prognosis for survival.

Ileus

Nasogastric decompression is important for horses with ileus involving the more proximal portions of the gastrointestinal tract. Correction of electrolyte imbalances is important, and intravenous fluid therapy is also indicated. Nonsteroidal anti-inflammatory drugs are often helpful in treating horses with ileus, and prokinetic drugs can be considered. Drugs that impair normal gastrointestinal motility, such as the alpha-2 agonists, should be avoided or used as infrequently as possible in small doses.

Neoplastic Infiltration of the Bowel Wall

Diagnosis of neoplastic infiltration of the bowel wall must be made with a biopsy of the affected portion of intestine or resection of the affected area followed by histopathologic examination of the resected tissue. If the affected area is focal, as in horses with leiomyomas, the prognosis is good with resection and anastomosis. If the intestine is extensively infiltrated, the prognosis for survival is grave.

Diseases of the Peritoneal Cavity

Ascites/Hemoperitoneum

The horse with ascites should be thoroughly examined to determine the underlying cause of the peritoneal effusion. If hemoperitoneum is detected, the entire abdomen should be carefully examined sonographically to see if the cause of the hemoperitoneum can be determined. The horse should be treated with aggressive intravenous fluid support if there has been significant blood loss into the peritoneal cavity. In some cases a blood transfusion may be indicated. If splenic rupture or rupture of another organ has occurred, surgical resection of the injured organ may be possible.

Peritonitis

Once peritonitis is diagnosed, a peritoneal fluid sample should be obtained for culture and sensitivity testing. Positive culture results were obtained from 59.7%,[302] 26.7%,[303] and 14.3%[304] of horses in three separate studies. The prognosis for horses with peritonitis is poor in most studies, with prognosis depending upon whether horses with intestinal rupture or postoperative colic are included in the data analysis. Prognosis for horses with intestinal rupture is grave, with all horses with intestinal rupture dying in three large studies of horses with peritonitis.[302-304] In one study of 67 horses with peritonitis, the overall survival rate was 40.3%.[302] When only horses with postoperative peritonitis were evaluated, the survival rate was 44%, and for horses without intestinal rupture or abdominal surgery the survival rate was 57.1%. Eighty-one per cent of horses with positive culture results from the peritoneal fluid sample had polymicrobial infections that had a negative effect on survival.[302] In two other studies of horses with peritonitis without obvious intestinal rupture or abdominal surgery, the survival rate was 57.1%[304] and 70%.[303] In a group of horses with peritonitis associated with *Actinobacillus equuli* infection, survival was 100%, with subsequent deaths unrelated to the peritonitis.[334] Adhesions associated with peritonitis may also negatively affect the prognosis. In the horses with postoperative peritonitis, 57.1% had fibrous adhesions detected at necropsy examination.[302]

Broad-spectrum antimicrobial coverage is indicated in the treatment of peritonitis, with anaerobic coverage (metronidazole) included until the results of culture and sensitivity testing of the peritoneal fluid are available and the selection of antimicrobials can be narrowed based upon the sensitivity patterns of the organisms cultured.

Ultrasonographic examination of the abdomen in the post-surgery patient can be helpful in determining if peritonitis is the cause of postoperative fever or abdominal discomfort. Large quantities of echogenic fluid, with or without fibrin (Fig. 6-131), localized peritonitis with adhesions of the abdominal viscera to the incision (Fig. 6-132), or adhesions of the abdominal viscera to the peritoneum or to other viscera without significant fluid accumulation (Fig. 6-133) can all be imaged in the postoperative patient with peritonitis. Collections of locu-

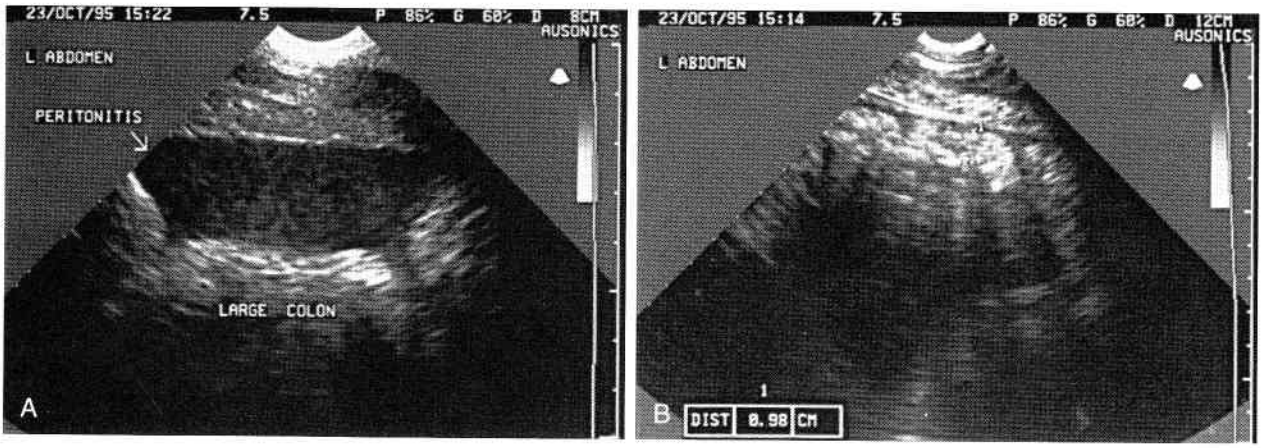

Figure 6–131

Sonograms of the peritoneal cavity obtained from a yearling Throughbred colt following a ventral midline celiotomy. The colt developed fever and diarrhea 1 week after surgery, prompting this sonographic examination. These sonograms were obtained along the left side of the ventral abdomen with a 7.5-MHz sector-scanner transducer at a displayed depth of 8 cm (*A*) and 12 cm (*B*). The right side of these sonograms is cranial and the left side is caudal. *A*, An accumulation of hypoechoic cloudy fluid (*arrow*) is seen adjacent to a thickened wall of the left ventral colon. *B*, The wall of the left ventral colon is markedly thickened and echogenic, measuring in excess of 0.98 cm.

lated peritoneal fluid are not routinely seen in humans by the seventh postoperative day and support a diagnosis of peritonitis or abdominal abscess formation.[335] Peritoneal fluid collections were absent in 96% of asymptomatic patients undergoing abdominal sonography on the seventh postoperative day following abdominal surgery.

Abdominal Abscess

Treatment with large doses of penicillin for an extended period of time is indicated in horses with abdominal abscesses because the majority of affected horses have abscesses caused by infection with *Streptococcus equi*, *S. zooepidemicus*, and *Corynebacterium pseudotuberculosis*.[118] Treatment with broad-spectrum antimicrobials is initially recommended until the results of culture and sensitivity testing of the peritoneal fluid are available. If organisms are not grown on culture but are seen on Gram-stained preparations of the peritoneal fluid, these findings can be used as a guide in the selection of appropriate antimicrobials. Many abscesses in the peritoneal cavity are not discretely walled off from surrounding structures but involve many different structures within the abdomen and are not amenable to surgical resection.[118] Periodic sonographic examinations of the abscess can be used to monitor its response to antimicrobial therapy and as an aid to determine the time to discontinue antimicrobial therapy.

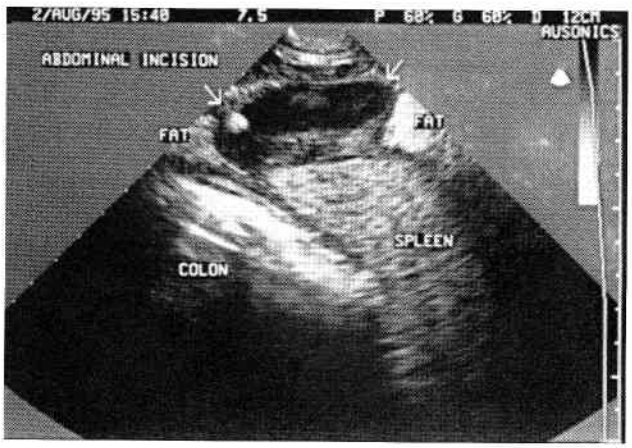

Figure 6–132

Sonogram of the ventral abdomen obtained from a 7-year-old Warmblood gelding several days following a ventral midline celiotomy. The horse had developed a fever and diarrhea postoperatively. A 5- to 6-cm defect (*arrows*) is imaged in the retroperitoneal fat containing anechoic fluid and hypoechoic fibrin. Adhesions between the retroperitoneal fat, spleen, and large colon are consistent with a localized area of peritonitis. This sonogram was obtained along the ventral midline celiotomy incision with a 7.5-MHz sector-scanner transducer at a displayed depth of 12 cm. The right side of this sonogram is the left side of the horse's abdomen, and the left side is the horse's right side.

Resection of the entire abscess, if possible, may be the treatment of choice in some horses with abdominal abscesses.[308] Care must be taken with surgical resection of abdominal abscesses so that peritoneal contamination does not occur. Marsupialization of the abdominal abscess has been used in two horses with large abdominal abscesses, with one of the horses doing well long term.[309] This surgery is recommended for treatment of focal well-encapsulated abscesses located close to the ventral abdominal wall in which no adhesions are present.[309] Percutaneous drainage of the abscess with a large-bore catheter should also be considered if the abscess adheres to the body wall without intervening organs or tissues (Fig. 6–134). Resolution of the abscess can then be followed with sonographic monitoring. If adhesions are present, a surgical bypass procedure should also be considered.[307, 309] Follow-up ultrasonography of a filly with abdominal abscesses was used to monitor her response to surgical drainage and antimicrobial therapy.

Perirectal/Perivaginal Abscess

Surgical drainage of perirectal or perivaginal abscess through the perineum or vagina, respectively, can be

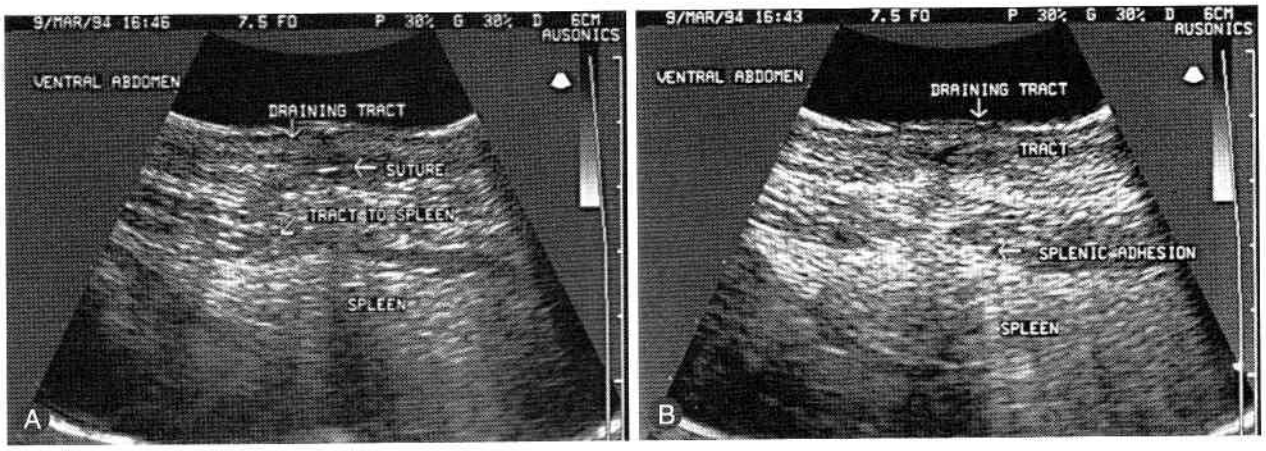

Figure 6–133

Sonograms of the ventral abdomen obtained from a 23-year-old Arabian mare several days following a ventral midline celiotomy. The mare developed purulent drainage from the incision at several sites and was febrile. A hypoechoic tract is imaged extending dorsally to the abdominal cavity along the original incision line. The tract appears to enter the peritoneal cavity and stop at the spleen. Hypoechoic fluid and fibrin are imaged between the spleen and the peritoneum, which are adherent at this location. These sonograms were obtained with a 7.5-MHz sector-scanner transducer containing a built-in fluid offset at a displayed depth of 6 cm. The right side of these sonograms is to the left side of the mare's abdomen. *A*, The anechoic area at the skin surface is associated with an infected suture (*horizontal arrow*), which is creating a foreign body reaction and is surrounded by fluid. The hypoechoic fluid tract, however, extends deeper than this suture through the full thickness of the abdominal incision and into the peritoneal cavity (*angled arrow*), stopping at the spleen. The spleen appears to contain the sepsis locally, creating an area of localized peritonitis with the adhesions to the ventral peritoneum along the incision. *B*, A fairly echogenic adhesion is seen between the spleen and the incision (*horizontal arrow*) cranial to the draining tract, which suggests a maturing adhesion secondary to the local infection in this area. A portion of the hypoechoic purulent tract is imaged (*down arrow*), and hypoechoic material is imaged between the spleen and the peritoneum.

safely performed under ultrasonographic guidance. This treatment should be combined with broad-spectrum antimicrobial therapy until treatment can be initiated based on culture and sensitivity testing. Metronidazole should be included if hyperechoic gas echoes are detected within the abscess. The prognosis for affected horses is usually good with ultrasound-guided drainage, appropriate antimicrobial treatment, and periodic sonographic monitoring of the abscess. Lavage of the abscess should be performed only if the abscess is walled off from the peritoneal cavity and adjacent retroperitoneal structures.

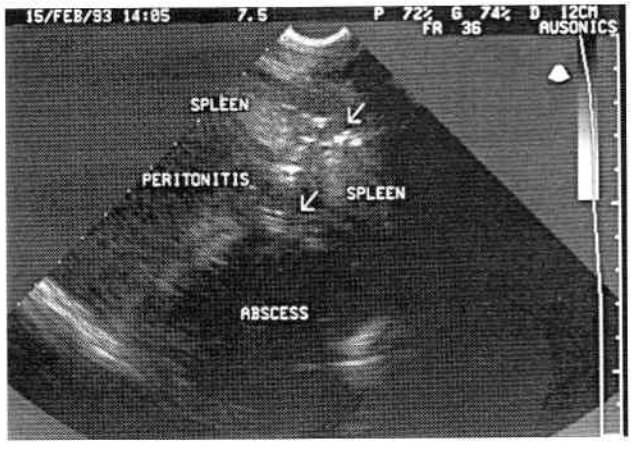

Figure 6–134

Sonogram of left ventral abdomen in a 3-year-old Standardbred stallion obtained 6 days following percutaneous catheterization and drainage of the abscess with a large-bore chest tube without sonographic guidance (same horse as in Fig. 6-126). The path of the percutaneous drainage tube is clearly visible in the abdominal cavity (*arrows*) as it tracts through the spleen and then into the abscess, highlighted by the presence of hyperechoic gas echoes along the tract. The abscess is smaller, and the ventral cellular layer is no longer imaged within the abscess; however, a large amount of hypoechoic peritoneal fluid is detected adjacent to the abscess, consistent with peritonitis. This sonogram was obtained with a 7.5-MHz sector-scanner transducer at a displayed depth of 12 cm. The right side of this sonogram is dorsal and the left side is ventral.

Abdominal Neoplasia

Horses with abdominal neoplasia have a guarded to grave prognosis, with surgical resection a possibility if the tumor is localized and metastases are not detected, an unusual occurrence in most horses by the time abdominal neoplasia is diagnosed. Using an autogenous vaccine and cimetidine, treatment of metastatic melanoma in the abdomen has been tried in horses. Success has been limited in cases seen by the author because the tumor was very advanced by the time treatment was initiated.

References

1. Yarborough TB, Langer DL, Snyder JR, et al: Abdominal radiography for diagnosis of enterolithiasis in horses: 141 cases (1990-1992). J Am Vet Med Assoc 205:592-595, 1994.
2. Reef VB: The use of diagnostic ultrasound in the horse. Ultrasound Q 9:1-34, 1991.
3. Byars TD, Halley J: Uses of ultrasound in equine internal medicine. Vet Clin North Am [Equine Pract] 2:253-258, 1986.
4. Rantanen NW: Diseases of the abdomen. Vet Clin North Am [Equine Pract] 2:67-88, 1986.
5. Zicker SC, Wilson WD, Medearis I: Differentiation between intra-abdominal neoplasms and abscess in horses, using clinical and laboratory data. J Am Vet Med Assoc 196:1130-1134, 1990.
6. Hillyer MH: The use of ultrasonography in the diagnosis of abdominal tumors in the horse. Equine Vet Educ 6:273-278, 1994.

7. Cannon JH, Andrews A: Ultrasound of the equine stomach. Proceedings of the 41st Annual American Association of Equine Practitioners 41:38-39, 1995.
8. Kirkberger RM, van den Berg JS, Gottschalk RD, Guthrie AJ: Duodenal ultrasonography in the normal adult horse. Vet Radiol Ultrasound 36:50-56, 1995.
9. Rantanen NW: Diseases of the kidneys. Vet Clin North Am [Equine Pract] 2:89-103, 1986.
10. Penninck DG, Eisenberg HM, Teuscher EE, Vrins A: Equine renal ultrasonography: Normal and abnormal. Vet Radiol 3:81-84, 1986.
11. Hoffman KL, Wood AKW, McCarthy PH: Sonographic-anatomic correlation and imaging protocol for the kidneys of horses. Am J Vet Res 56:1403-1412, 1995.
12. Yamaga Y, Too K: Diagnostic ultrasound imaging in domestic animals: Fundamental studies on abdominal organs and fetuses. Jpn J Vet Sci 46:203-212, 1984.
13. Kiper ML, Traub-Dargatz JL, Wrigley RH: Renal ultrasonography in horses. Compend Contin Educ Pract Vet 12:993-1000, 1990.
14. Rantanen NW: Diseases of the liver. Vet Clin North Am [Equine Pract] 2:104-114, 1986.
15. Keller SD, Horney KD: Diseases of the equine small colon. Compend Contin Educ Pract Vet 7:S113-S120, 1985.
16. Reef VB: Sonographic diagnosis of uroperitoneum in foals and horses. Proceedings of the 13th Annual Veterinary Medical Forum 13:582-584, 1995.
17. Reef VB: Evaluation of abdominal disorders in horses using ultrasonography. Proceedings of the 17th Annual Veterinary Surgical Forum 17:141-143, 1989.
18. Rantanen NW: Renal ultrasound in the horse. Equine Vet Educ 2:135-136, 1990.
19. Schmidt AR: Transrectal ultrasonography of the caudal portion of the abdominal and pelvic cavities in horses. J Am Vet Med Assoc 194:365-371, 1989.
20. Wu J-X, Carlisle CH: Ultrasonographic examination of the canine liver based on recognition of hepatic and portal veins. Vet Radiol Ultrasound 36:234-239, 1995.
21. Penninck DG, Nyland TG, Fischer PE, Kerr LY: Ultrasonography of the normal canine gastrointestinal tract. Vet Radiol 30:272-276, 1989.
22. Penninck DG: Ultrasonography of the gastrointestinal tract. *In* Nyland TG, Mattoon JS (eds): Veterinary Diagnostic Ultrasound. Philadelphia, WB Saunders, 1995, pp 125-140.
23. Fleischer AC, Dowling AD, Weinstein ML, James AE Jr: Sonographic patterns of distended, fluid-filled bowel. Radiology 133: 681-685, 1979.
24. Stringer DA, Daneman A, Brunelle F, et al: Sonography of the normal and abnormal stomach (excluding hypertrophic pyloric stenosis) in children. J Ultrasound Med 5:183-188, 1986.
25. Miller JH, Kemberling C: Ultrasound scanning of the gastrointestinal tract in children: Subject review. Radiology 152:671-677, 1984.
26. Pozniak MA, Scanlan KA, Yandow D, Mulligan G: Current status of small-bowel ultrasound. Radiology 30:254-265, 1990.
27. Fleischer AC, Muhletaler CA, James AE Jr: Sonographic patterns arising from normal and abnormal bowels. Radiol Clin North Am 18:145-159, 1980.
28. Kimmey MB, Silverstein FE, Waggitt RC, et al: Cross-sectional imaging method: A system to compare ultrasound, computed tomography and magnetic resonance with histologic findings. Invest Radiol 22:227-231, 1987.
29. Worth LT: Ultrasonography of the normal equine small intestine [abstract]. Vet Radiol Ultrasound 36:355, 1995.
30. Braun U, Mermier O: Ultrasonographic examination of the small intestine of cows. Vet Rec 136:239-244, 1995.
31. Fleischer AC, Muhletaler CA, James AE Jr: Sonographic assessment of the bowel wall. Am J Radiol 136:887-891, 1981.
32. Bolondi L, Caletti G, Casanova P, et al: Problems and variations in the interpretation of the ultrasound feature of the normal upper and lower GI tract wall. Scand J Gastroenterol Suppl 123:16-26, 1986.
33. Dubbins PA: The gastrointestinal tract. Clin Diagn Ultrasound 23:195-230, 1988.
34. Held JP, McCracken MD, Toal R, Latimer F: Epididymal swelling attributable to generalized lymphosarcoma in a stallion. J Am Vet Med Assoc 201:1913-1915, 1992.
35. Holt PE, Mair TS: Ten cases of bladder paralysis associated with sabulous urolithiasis in horses. Vet Rec 127:108-110, 1990.
36. Holt PE, Pearson H: Urolithiasis in the horse—a review of 13 cases. Equine Vet J 16:31-34, 1984.
37. Laverty S, Pascoe JR, Ling GV, et al: Urolithiasis in 68 horses. Vet Surg 21:56-62, 1992.
38. Lowe JE: Surgical removal of equine uroliths via the laparocystomy approach. J Am Vet Med Assoc 139:345-348, 1961.
39. Mair TS, McCaig J: Cystic calculus in a horse. Equine Vet J 15:173-174, 1983.
40. DeBowes RM, Nyrop KA, Boulton CH: Cystic calculi in the horse. Compend Contin Educ Pract Vet 6:S235-S273, 1984.
41. Kaneps AJ, Shires GMH, Watrous BJ: Cystic calculi in two horses. J Am Vet Med Assoc 187:737-739, 1985.
42. Laing JA, Raisis AL, Rawlinson RJ, Small AC: Chronic renal failure and urolithiasis in a 2 year-old colt. Australian Vet J 69:199-200, 1992.
43. Wright JG, Neal PA: Laparo-cystotomy for urinary calculus in a gelding. Vet Rec 72:301-303, 1960.
44. Eustace RA, Hunt JM: Electrohydraulic lithotripsy for the treatment of cystic calculus in two geldings. Equine Vet J 20:221-223, 1988.
45. MacHarg MA, Foerner JJ, Phillips TN, et al: Electrohydraulic lithotripsy for treatment of a cystic calculus in a mare. Vet Surg 14:325-327, 1985.
46. Trotter GW, Bennett DG, Behm RJ: Urethral calculi in five horses. Vet Surg 10:159-162, 1981.
47. Dyke TM, Maclean AA: Urethral obstruction in a stallion with possible synchronous diaphragmatic flutter. Vet Rec 121:425-426, 1987.
48. Vacek JR, Macharg MA, Phillips TN, et al: Struvite urethral calculus in a three-month-old Thoroughbred colt. Cornell Vet 82:275-279, 1992.
49. Gibson KT, Trotter GW, Gustafson SB: Conservative management of uroperitoneum in a gelding. J Am Vet Med Assoc 200:162-164, 1992.
50. Edwards RB, Ducharme NG, Hackett RP: Laparoscopic repair of a bladder rupture in a foal. Vet Surg 24:60-63, 1995.
51. Braun U, Schefer U, Föhn J: Urinary tract ultrasonography in normal rams and rams with obstructive urolithiasis. Can Vet J 33:654-659, 1992.
52. Haven ML, Bowman KF, Engelbert TA, Bilkslager AT: Surgical management of urolithiasis in small ruminants. Cornell Vet 83:47-55, 1993.
53. Jones PA, Sertich PL, Johnston JK: Uroperitoneum associated with a ruptured urinary bladder in a post partum mare. Aust Vet J 74:354-357, 1996.
54. Behr MJ, Hackett RP, Bentinck-Smith J, et al: Metabolic abnormalities associated with rupture of the urinary bladder in neonatal foals. J Am Vet Med Assoc 178:263-266, 1981.
55. White KK: Urethral sphincterotomy as an approach to repair of rupture of the urinary bladder in the mare: A case report. J Equine Med Surg 1:250-253, 1977.
56. Nyrop KA, DeBowes RM, Cox JH, Coffman JR: Rupture of the urinary bladder in two postparturient mares. Compend Contin Educ Pract Vet 6:S510-S513, 1984.
57. Tulleners EP, Richardson DW, Reid BV: Vaginal evisceration of the small intestine in three mares. J Am Vet Med Assoc 186:385-387, 1985.
58. Squire KRE, Adams SB, Conley R: Postpartum partial cystectomy through the vagina in a mare with everted partially necrotic bladder. J Am Vet Med Assoc 200:1111-1113, 1992.
59. Firth EC: Dissecting hematoma of corpus spongiosum and urinary bladder rupture in a stallion. J Am Vet Med Assoc 169:800-801, 1976.
60. Pankowski RL, Fubini SL: Urinary bladder rupture in a two-year-old horse: Sequel to a surgically repaired neonatal injury. J Am Vet Med Assoc 191:560-562, 1987.
61. Genetzky RM, Hagemoser WA: Physical and clinical pathological findings associated with experimentally induced rupture of the equine urinary bladder. Can Vet J 26:391-395, 1985.
62. Divers TJ, Byars D, Spirito M: Correction of bilateral ureteral defects in a foal. J Am Vet Med Assoc 192:384-386, 1988.
63. Robertson JT, Spurlock GH, Bramlage LL, Landry SL: Repair of ureteral defect in a foal. J Am Vet Med Assoc 183:799-800, 1983.
64. Fischer AT Jr, Spier S, Carlson GP, Hackett RP: Neoplasia of the

equine urinary bladder as a cause of hematuria. J Am Vet Med Assoc 186:1294-1296, 1985.
65. Traub JL, Bayly WM, Reed SM, et al: Intraabdominal neoplasia as a cause of chronic weight loss in the horse. Compend Contin Educ Pract Vet 5:S526-S534, 1983.
66. Sweeney RW, Hamir AN, Fisher RR: Lymphosarcoma with urinary bladder infiltration in a horse. J Am Vet Med Assoc 199:1177-1178, 1991.
67. Léveillé R, Biller DS, Partington BP, Miyabayashi T: Sonographic investigation of transitional cell carcinoma of the urinary bladder in small animals. Vet Radiol Ultrasound 33:103-107, 1992.
68. Itzchak Y, Singer D, Fischelovitch Y: Ultrasonographic assessment of bladder tumors. I. Tumor detection. J Urol 126:31-33, 1981.
69. Abu-Yosef MM, Narayana AS, Franken EA, Brown RC: Urinary bladder tumors studied by cystosonography. Part I. Detection. Radiology 153:223-226, 1984.
70. Dershaw DD, Scher HI: Serial transabdominal sonography of bladder cancer. AJR 150:1055-1059, 1988.
71. Chang VH, Cunningham JJ: Efficacy of sonography as a screening method in renal insufficiency. J Clin Ultrasound 13:415-417, 1985.
72. Platt JF, Rubin JM, Bowerman RA, Marn CS: The inability to detect kidney disease on the basis of echogenicity. AJR 151:317-319, 1988.
73. Rosenfield AT, Siegel NJ: Renal parenchymal disease: Histopathologic-sonographic correlation. AJR 137:793-798, 1981.
74. Divers TJ, Whitlock RH, Byars TD, et al: Acute renal failure in six horses resulting from haemodynamic causes. Equine Vet J 19:178-184, 1987.
75. Wong SN, Lo RNS, Yu ECL: Renal blood flow pattern by noninvasive Doppler ultrasound in normal children and acute renal failure patients. J Ultrasound Med 8:135-141, 1989.
76. Bayly WM, Elfers RS, Ligett HD, et al: A reproducible means of studying acute renal failure in the horse. Cornell Vet 76:287-298, 1986.
77. Teele RL, Share JC (eds): Ultrasonography of Infants and Children. Philadelphia, WB Saunders, 1991.
78. Hricak H, Cruz C, Romanski R, et al: Renal parenchymal disease: Sonographic-histologic correlation. Radiology 144:141-147, 1982.
79. Banks KL, Henson JB: Immunologically mediated glomerulitis of horses. II. Antiglomerular basement membrane antibody and other mechanisms of spontaneous disease. Lab Invest 26:708-715, 1972.
80. Wimberly HC, Antonovych TT, Lewis RM: Focal glomerulosclerosis-like disease with nephrotic syndrome in a horse. Vet Pathol 18:692-694, 1981.
81. Jakob W: Spontaneous amyloidosis of mammals. Vet Pathol 8:292-306, 1971.
82. Riviere JE, Traver DS, Coppoc GL: Gentamicin toxic nephropathy in horses with disseminated bacterial infection. J Am Vet Med Assoc 180:648-651, 1982.
83. Markel MD, Dyer RM, Hattle AL: Acute renal failure associated with application of a mercuric blister in a horse. J Am Vet Med Assoc 185:92-94, 1984.
84. Rebhun WC, Tennant BC, Dill SG, King JM: Vitamin K_3 renal toxicosis in the horse. J Am Vet Med Assoc 184:1237-1239, 1984.
85. Weber M, Braun B, Köhler H: Ultrasonic findings in analgesic nephropathy. Nephron 39:216-222, 1985.
86. Hoffman JC, Schnur MJ, Koenigsberg M: Demonstration of renal papillary necrosis by sonography. Radiology 145:785-787, 1982.
87. Braden GL, Kozinn FE, Hampf FE Jr, et al: Ultrasound diagnosis of early renal papillary necrosis. J Ultrasound Med 10:401-403, 1991.
88. Read WK: Renal medullary crest necrosis associated with phenylbutazone therapy in horses. Vet Pathol 20:662-669, 1983.
89. Gunson DE: Renal papillary necrosis in horses. J Am Vet Med Assoc 182:263-266, 1983.
90. Divers TJ: Chronic renal failure in horses. Compend Contin Educ Pract Vet 5:S310-S317, 1983.
91. Biller DS, Bradley GA, Partington BP: Renal medullary rim sign: Ultrasonographic evidence of renal disease. Vet Radiol Ultrasound 33:286-290, 1992.
92. Paivansalo MJ, Kallioinen MJ, Merikanto JS, Jalovaara PK: Hyperechogenic "rings" in the periphery of renal medullary pyramids as a sign of renal disease. J Clin Ultrasound 19:283-287, 1991.
93. Barr FJ, Patteson MW, Lucke VM, Gibbs C: Hypercalcemic nephropathy in three dogs: Sonographic appearance. Vet Radiol 30:169-173, 1987.
94. Adams WH, Toal RL, Breider MA: Ultrasonographic findings in dogs and cats with oxalate nephrosis attributed to ethylene glycol intoxication: 15 cases (1984-1988). J Am Vet Med Assoc 199:492-496, 1991.
95. Andrews FJ: Oxalate nephropathy in a horse. J Am Vet Med Assoc 159:49-51, 1979.
96. Roberts MC, Seiler RJ: Renal failure in a horse with chronic glomerulonephritis and renal oxalosis. J Equine Med Surg 3:278-283, 1979.
97. Tennant B, Bettleheim P, Kaneko JJ: Paradoxic hypercalcemia and hypophosphatemia associated with chronic renal failure in horses. J Am Vet Med Assoc 180:630-634, 1982.
98. Brobst DF, Lee HA, Spencer GR: Hypercalcemia and hypophosphatemia in a mare with renal insufficiency. J Am Vet Med Assoc 173:1370-1372, 1978.
99. Koterba AM, Coffman JR: Acute and chronic renal disease in the horse. Compend Contin Educ Pract Vet 3:S461-S470, 1981.
100. Ehnen SJ, Divers TJ, Gillette D, Reef VB: Obstructive nephrolithiasis and ureterolithiasis associated with chronic renal failure in horses: Eight cases (1981-1987). J Am Vet Med Assoc 197:249-253, 1990.
101. Hope WD, Wilson JH, Hager DA, et al: Chronic renal failure associated with bilateral nephroliths and ureteroliths in a two-year-old Thoroughbred colt. Equine Vet J 21:228-231, 1989.
102. Held JP, Wright B, Henton JE: Pyelonephritis associated with renal failure in a horse. J Am Vet Med Assoc 189:688-689, 1986.
103. Byars TD, Simpson JS, Divers TJ, et al: Percutaneous nephrostomy in short-term management of ureterolithiasis and renal dysfunction in a filly. J Am Vet Med Assoc 195:499-501, 1989.
104. Marcharg MA, Foerner JJ, Phillips TN, Barclay WP: Two methods for the treatment of ureterolithiasis in a mare. Vet Surg 13:95-98, 1984.
105. Hillyer MH, Mair TS, Lucke VM: Bilateral renal calculi in an adult horse. Equine Vet Educ 2:117-120, 1990.
106. Divers TJ: Nephrolithiasis and ureterolithiasis in horses and their association with renal disease and failure. Equine Vet J 21:161-162, 1989.
107. Jackson OF: Renal calculi in a horse. Vet Rec 91:7-9, 1972.
108. Harrison GD, Biller DS, Wilson DG, Castleman WL: Ultrasonographic diagnosis of hydronephrosis in a cow. Vet Radiol Ultrasound 33:49-51, 1992.
109. Pugh CR, Schelling CG, Moreau RE, Golden D: Iatrogenic renal pyelectasia in the dog. Vet Radiol Ultrasound 35:50-51, 1994.
110. Felakai CS, Vörös K, Fenyves B: Lesions of the renal pelvis and proximal ureter in various nephro-urological conditions: An ultrasonographic study. Vet Radiol Ultrasound 36:397-401, 1995.
111. Morin ME, Baker DA: The influence of hydration and bladder distention on the sonographic diagnosis of hydronephrosis. J Clin Ultrasound 7:192-194, 1979.
112. Ramsey G, Rothwell TLW, Gibson KT, et al: Polycystic kidney in an adult horse. Equine Vet J 19:243-244, 1987.
113. Bertone JJ, Traub-Dargatz JL, Fettman MJ, et al: Monitoring the progression of renal failure in a horse with polycystic kidney disease: Use of the reciprocal of serum creatinine concentration and sodium sulfanilate clearance half time. J Am Vet Med Assoc 191:565-568, 1987.
114. Andrews FM, Rosol TJ, Kohn CW, et al: Bilateral renal hypoplasia in four young horses. J Am Vet Med Assoc 189:209-212, 1986.
115. Hamlen H: Pyelonephritis in a mature gelding with an unusual urinary bladder foreign body: A case report. J Equine Vet Sci 13:159-162, 1993.
116. Sloet van Oldruitenborgh-Oosterbaan MM, Kalsbeek HC: Uteropyelonephritis in a Freisan mare. Vet Rec 122:609-610, 1988.
117. Divers TJ, Reef VB, Roby KA: Nephrolithiasis resulting in intermittent ureteral obstruction in a cow. Cornell Vet 79:143-149, 1989.
118. Rumbaugh GE, Smith BP, Carlson GP: Internal abdominal abscesses in the horse: A study of 25 cases. J Am Vet Med Assoc 172:302-309, 1978.
119. Hughes JP, Biberstein EL, Richards WPC: Two cases of generalized *Corynebacterium pseudotuberculosis* infection in mares. Cornell Vet 52:51-62, 1962.
120. Blunden AS, Khalil LF, Webbon PM: *Halicephalobus deletrix* infection in a horse. Equine Vet J 19:255-260, 1987.
121. Rubin HC, Woodward JC: Equine infections with *Micronema deletrix*. J Am Vet Med Assoc 165:256-258, 1974.

122. Keg PR, Mirck MH, Dik KJ, Vos JH: *Micronema deletrix* infection in a Shetland pony stallion. Equine Vet J 16:471–475, 1984.
123. Alstad AD, Berg JE, Samuel C: Disseminated *Micronema deletrix* infection in the horse. J Am Vet Med Assoc 174:264–266, 1979.
124. Ruggles AJ, Beech J, Gilette DE, et al: Disseminated *Halicephalobus deletrix* infection in a horse. J Am Vet Med Assoc 203:550–552, 1993.
125. Haschek WM, King JM, Tennant BC: Primary renal cell carcinoma in two horses. J Am Vet Med Assoc 179:992–994, 1981.
126. Owen RR, Haywood S, Kelly DF: Clinical course of renal adenocarcinoma associated with hypercupraemia in a horse. Vet Rec 119:291–294, 1986.
127. Berggren PC: Renal adenocarcinoma in a horse. J Am Vet Med Assoc 176:1252–1253, 1980.
128. West HJ, Kelly DF, Ritchie HE: Renal carcinomatosis in a horse: A case report. Equine Vet J 19:548–551, 1987.
129. Ramirez S, Seahorn TL: Ultrasonography as an aid in the diagnosis of renal cell carcinoma in a horse. Vet Radiol Ultrasound 37:383–386, 1996.
130. Brown PJ, Holt PE: Primary renal cell carcinoma in four horses. Equine Vet J 17:473–477, 1985.
131. Woods PR, Farrar WP, Chaffin MK, Carter GK: Metastatic renal adenocarcinoma in a mule. Cornell Vet 83:67–75, 1993.
132. Servantie J, Magnol JP, Regnier A, Lescure F: Carcinoma of the renal pelvis with bony metaplasia in a horse. Equine Vet J 18:236–238, 1986.
133. Kaude JV, Lacy GD: Ultrasonography in renal lymphoma. J Clin Ultrasound 6:321–323, 1978.
134. Kaude JV, Joyce PH: Evaluation of abdominal lymphoma by ultrasound. Gastrointest Radiol 5:249–254, 1980.
135. Konde LJ, Wrigley RH, Park RD, Lebel JL: Sonographic appearance of renal neoplasia in the dog. Vet Radiol 26:74–81, 1985.
136. Plainfosse MC, Delecoeullerie G, Vital JL, et al: 165 renal carcinomas: Accuracy of imaging for diagnosis and spread—cost efficiency. Eur J Radiol 3:132–137, 1983.
137. Yovich JV, Ducharme NG: Ruptured pheochromocytoma in a mare with colic. J Am Vet Med Assoc 183:462–464, 1983.
138. Fix AS, Miller LD: Equine adrenocortical carcinoma with hypercalcemia. Vet Pathol 24:190–192, 1987.
139. Duckett WM, Snyder JR, Harkema JR, Carlson GP: Functional pheochromocytoma in a horse. Compend Contin Educ Pract Vet 9:1118–1121, 1987.
140. Van der Kolk JH, Mars MH, van der Gaag I: Adrenocortical carcinoma in a 12-year-old mare. Vet Rec 134:113–115, 1994.
141. Gelberg H, Cockerbell GL, Minor RR: A light and electron microscopic study of a normal adrenal medulla and a pheochromocytoma from a horse. Vet Pathol 16:395–404, 1979.
142. Scarratt WK, Saunders GK: Cholelithiasis and biliary obstruction in a horse. Compend Contin Educ Pract Vet 7:S428–S431, 1985.
143. Tulleners EP, Becht JL, Richardson DW, Divers TJ: Choledocholithotripsy in a mare. J Am Vet Med Assoc 186:1317–1319, 1985.
144. Roussel AJ, Becht JL, Adams SB: Choledocholithiasis in a horse. Cornell Vet 74:166–171, 1984.
145. Traub JL, Grant BD, Rantanen NW, et al: Surgical removal of cholelithes in a horse. J Am Vet Med Assoc 182:714–716, 1983.
146. Van der Luer RJT, Kroneman J: Three cases of cholelithiasis and biliary fibrosis in the horse. Equine Vet J 14:251–253, 1982.
147. McDole MG: Cholelithiasis in a horse. Equine Pract 2:37–40, 1980.
148. Schulz KS, Simmons TR, Johnson R: Primary cholangiohepatitis in a horse. Cornell Vet 80:35–40, 1990.
149. Holland PS, Schmitz DG, Read WK: Hepatolithiasis in an Arabian mare. Equine Vet J 23:229–232, 1991.
150. Traub JL, Rantanen N, Reed S, Schecter L: Cholelithiasis in four horses. J Am Vet Med Assoc 181:59–62, 1982.
151. Laverty S, Pascoe JR, Williams JW, Funk KA: Cholelith causing duodenal obstruction in a horse. J Am Vet Med Assoc 201:751–752, 1992.
152. Reef VB, Johnston JK, Divers TJ, et al: Ultrasonographic findings in horses with cholelithiasis: Eight cases (1985–1987). J Am Vet Med Assoc 196:1836–1840, 1990.
153. Johnston JK, Divers TJ, Reef VB, et al: Cholelithiasis in horses: Ten cases (1982–1986). J Am Vet Med Assoc 194:405–409, 1989.
154. Gerros TC, McGuirk SM, Biller DS, et al: Choledocholithiasis attributable to a foreign body in a horse. J Am Vet Med Assoc 202:301–303, 1993.
155. Kataria RS, Verma GP: Intrahepatic stones in a horse. Indian Vet J 44:1025–1029, 1967.
156. Durando MM, MacKay RJ, Staller GS, et al: Septic cholangiohepatitis and cholangiocarcinoma in a horse. J Am Vet Med Assoc 206:1018–1021, 1995.
157. Messer NT, Johnson PJ: Idiopathic acute hepatic disease in horses: 12 cases (1982–1992). J Am Vet Med Assoc 204:1934–1937, 1994.
158. Robinson M, Gopinath C, Hughes DL: Histopathology of acute hepatitis in the horse. J Comp Pathol 85:111–118, 1985.
159. Edens LM, Robertson JL, Feldman: Cholestatic hepatopathy, thrombocytopenia and lymphopenia associated with iron toxicity in a Thoroughbred gelding. Equine Vet J 25:81–84, 1993.
160. Divers TJ, Warner A, Vaala WE, et al: Toxic hepatic failure in newborn foals. J Am Vet Med Assoc 12:1407–1413, 1983.
161. Divers TJ, Sweeney R, Acland HM, et al: Hepatic failure in a three-day-old foal. Compend Contin Educ Pract Vet 5:S252–S258, 1983.
162. Acland HA, Mann PC, Robertson JL, et al: Toxic hepatopathy in neonatal foals. Vet Pathol 21:3–9, 1984.
163. Mullaney TP, Brown CM: Iron toxicity in neonatal foals. Equine Vet J 20:119–124, 1988.
164. Mullaney TP, Brown CM, Taylor RF: Hepatic failure in foals associated with oral administration of a digestive inoculant. Am Assoc Vet Lab Diagnost 20:211–220, 1983.
165. Garrett BJ, Holtan DW, Cheeke PR, et al: Effects of dietary supplementation with butylated hydroxyanisole, cysteine, and vitamin B on tansy ragwort (*Senecio jacobea*) toxicosis in ponies. Am J Vet Res 45:459–464, 1984.
166. Mendel VE, Witt MR, Gitschell BS, et al: Pyrrolizidine alkaloid-induced liver disease in horses: An early diagnosis. J Am Vet Res 49:572–578, 1988.
167. Cysewski SJ, Pier AC, Baetz AL, Cheville NF: Experimental equine alfatoxicosis. Toxicol Appl Pharmacol 65:354–365, 1982.
168. Tennant BC, Evans CD, Schwartz LW, et al: Equine hepatic insufficiency. Vet Clin North Am 3:279–289, 1973.
169. West HJ: Clinical and pathological studies in horses with hepatic disease. Equine Vet J 28:146–156, 1996.
170. Schotman AJH, Wagenaar G: Hyperlipaemia in ponies. Zbl Vet Med Assoc 16:1–7, 1969.
171. Rush Moore B, Abood SK, Hinchcliff HW: Hyperlipemia in 9 miniature horses and miniature donkeys. J Vet Intern Med 8:376–381, 1994.
172. Godber LM, Brown CM, Mullaney TP: Polycystic hepatic disease, thoracic granular cell tumor and secondary hypertrophic osteopathy in a horse. Cornell Vet 83:227–235, 1993.
173. Thompson RCA, Smyth JD: Equine hydatidosis: A review of the current status in Great Britain and the results of an epidemiological survey. Vet Parasitol 1:107–127, 1975.
174. Dixon JB, Baker-Smith JK, Greatorex JC: The incidence of hydatid cysts in Great Britain. Vet Rec 93:255, 1973.
175. Arima K, Watanabe S, Hirabayashi S, et al: Sonographic diagnosis of diffuse chronic liver disease. Comparison with peritoneoscopic findings. Proc Jpn Soc Ultrasonic Med 505–506, 1990.
176. Gosnik BB, Lemon SK, Scheible W, Leopold GR: Accuracy of ultrasonography in diagnosis of hepatocellular disease. Am J Roentgenol 133:19–23, 1979.
177. Kurtz AB, Rubin CS, Cooper HS, et al: Ultrasound findings in hepatitis. Radiology 136:717–723, 1980.
178. Joseph AEA, Dewbury KC, Mcguire PG: Ultrasound in the detection of chronic liver diseases (the "bright liver"). Br J Radiol 52:184–188, 1979.
179. Giles CJ: Outbreak of ragwort (*Senecio jacobaea*) poisoning in horses. Equine Vet J 15:248–250, 1983.
180. Lim JH, Ryu N, Ko YT, Lee DH: Anatomic relationship of intrahepatic bile ducts to portal veins. J Ultrasound Med 9:137–143, 1990.
181. Gay CC, Sullivan ND, Wilkinson JS, et al: Hyperlipaemia in ponies. Austr Vet J 54:459–462, 1978.
182. Acorda JA, Yamada H, Ghamsari SM: Ultrasonographic features of diffuse hepatocellular disorders in dairy cattle. Vet Radiol Ultrasound 35:196–200, 1994.
183. Foster KJ, Dewbury KC, Griffith AH, Wright R: The accuracy of ultrasound in the detection of fatty infiltration of the liver. Br J Radiol 53:440–442, 1979.
184. Acorda JA, Yamada H, Ghamsari SM: Evaluation of fatty infiltration of the liver in dairy cattle through digital analysis of hepatic ultrasonograms. Vet Radiol Ultrasound 35:120–123, 1994.

185. Sumino Y, Yoshida N, Ishii M, et al: Echographic diagnosis of liver disease. Proc Jpn Soc Ultrasonic Med 45-46, 1985.
186. Acorda JA, Yamada H, Ghamsari SM: Ultrasonography of fatty infiltration of the liver in dairy cattle using kidney-liver contrast. Vet Radiol Ultrasound 35:400-404, 1994.
187. Lechtenberg KF, Nagaraja TG: Hepatic ultrasonography and blood changes in cattle with experimentally induced hepatic abscesses. Am J Vet Res 52:801-809, 1991.
188. Itabishi T, Yamamoto R, Satoh M: Ultrasonogram of hepatic abscess in cattle inoculated with *Fusobacterium necrophorum*. Jpn J Vet Sci 49:585-592, 1987.
189. Maxson AD, Wachira TM, Zevhle EE, et al: The use of ultrasound to study the prevalence of hydatid cysts in the right lung and liver of sheep and goats in Turkana, Kenya. Int J Parasitol 26:1335-1338, 1996.
190. Esfahani F, Rooholamini SA, Vessal K: Ultrasonography of hepatic hydatid cysts: New diagnostic signs. J Ultrasound Med 7:443-450, 1988.
191. Hussain S: Diagnostic criteria of hydatid cyst disease on hepatic sonography. J Ultrasound Med 4:603-607, 1985.
192. Neufeld JL: Lymphosarcoma in the horse: A review. Can Vet J 14:129-135, 1973.
193. Chaffin MK, Schmitz DG, Brumbaugh GW, Hall DG: Ultrasonographic characteristics of splenic and hepatic lymphosarcoma in three horses. J Am Vet Med Assoc 201:743-747, 1992.
194. Geraldi S, Bernardino ME, Jing B, Green B: Ultrasonic patterns of hepatic lymphoma. Radiology 136:427-431, 1980.
195. Nyland TG: Ultrasonic patterns of canine hepatic lymphosarcoma. Vet Radiol 25:167, 1984.
196. Whiteley MB, Feeney DA, Whiteley LO, Hardy RM: Ultrasonographic appearance of primary and metastatic canine hepatic tumors: A review of 48 cases. J Ultrasound Med 8:621-630, 1989.
197. Roby KA, Beech JA, Bloom JC, et al: Hepatocellular carcinoma associated with erythrocytosis and hypoglycemia in a yearling filly. J Am Vet Med Assoc 196:465-467, 1990.
198. Sheu J-C, Chen D-S, Sung J-L, et al: Hepatocellular carcinoma: US evolution in the early stage. Radiology 155:463-467, 1985.
199. Prater PE, Patton CS, Held JP: Pleural effusion resulting from malignant hepatoblastoma in a horse. J Am Vet Med Assoc 3:383-385, 1989.
200. Holm J, Jacobsen B: Accuracy of dynamic ultrasonography in the diagnosis of malignant liver lesions. J Ultrasound Med 5:1-4, 1986.
201. Stutte H, Müller PH, d'Hoedt B, Stroebel W: Ultrasonographic diagnosis of melanoma metastases in liver, gallbladder, and spleen. J Ultrasound Med 8:541-547, 1989.
202. Turner TA, Brown CA, Wilson JH, et al: Hepatic lobe torsion as a cause of colic in a horse. Vet Surg 22:301-304, 1993.
203. Buonanno AM, Carson G, Kantrowitz B: Clinical and diagnostic features of portosystemic shunt in a foal. J Am Vet Med Assoc 192:387-389, 1988.
204. Marr CM, Love S, Pirie HM: Clinical, ultrasonographic and pathologic findings in a horse with splenic lymphosarcoma and pseudohyperparathyroidism. Equine Vet J 21:221-226, 1989.
205. Neufeld JL: Lymphosarcoma in a mare and review of cases at the Ontario Veterinary College. Can Vet J 14:149-153, 1973.
206. Browning AP: Splenic lymphosarcoma in a stallion associated with an acute abdominal crisis. Vet Rec 119:178-179, 1986.
207. Nyack B, Padmore CL, Dunn D, et al: Splenic lymphosarcoma in a horse. Mod Vet Pract 65:269-272, 1984.
208. Hance SR, Shiroma JT, Bertone JJ: Ultrasonographic diagnosis. Vet Radiol Ultrasound 33:101-102, 1992.
209. Spier S, Carlson GP, Nyland TG, et al: Splenic hematoma and abscess as a cause of chronic weight loss in a horse. J Am Vet Med Assoc 189:557-559, 1986.
210. McGorum BC, Young LE, Milne EM: Nonfatal subcapsular haematoma in a horse. Equine Vet J 28:166-168, 1996.
211. Steiner JV: Splenic rupture in a horse. Equine Pract 3:37-38, 1981.
212. Finnocchio EJ: Splenic rupture in a horse. Vet Med/Small Anim Clin 66:233, 1971.
213. Dyke TM, Friends SCE: Ruptured splenic haematoma in a mare. Equine Vet J 20:138-140, 1988.
214. Zhao Q: A case of haematoma and rupture of the spleen in a mule. Chin J Vet Med 8:27, 1982.
215. Swan RA: Splenitis in horses. Aust Vet J 44:459-461, 1968.
216. Varra DL, Nelson AW: Primary splenomegaly in a horse. J Am Vet Med Assoc 168:608-609, 1967.
217. Scott EA, Trapp AL, Derksen FJ, et al: Splenomegaly and splenic infarction in a Standardbred colt. Equine Pract 73:1549-1556, 1978.
218. Hardie EM, Vaden SL, Spaulding K, Malarkey DE: Splenic infarction in 16 dogs: A retrospective study. J Vet Intern Med 9:141-148, 1995.
219. Schelling CS, Wortman JA, Saunders HM: Ultrasonic detection of splenic necrosis in the dog. Vet Radiol 29:227-233, 1988.
220. Mittelstaedt CA, Partain CL: Ultrasonic-pathologic classification of splenic abnormalities: Gray scale patterns. Radiology 134:697-705, 1980.
221. Carrick JB, Morris DD, Harmon BG, Fawzi M: Hematuria and weight loss in a mare with pancreatic adenocarcinoma. Cornell Vet 82:91-97, 1992.
222. Furr MO, Robertson JR: Two cases of equine pancreatic disease and a review of the literature. Equine Vet Educ 4:55-58, 1992.
223. Kerr ON, Pearson GR, Rice DA: Pancreatic adenocarcinoma in a donkey. Equine Vet J 14:338-339, 1982.
224. Church S, West HJ, Baker JR: Two cases of pancreatic adenocarcinoma in horses. Equine Vet J 19:77-79, 1987.
225. Shawker TH, Garra BS, Hill MC, et al: The spectrum of sonographic findings in pancreatic carcinoma. J Ultrasound Med 5:169-177, 1986.
226. Bernard WV, Reef VB, Reimer JM, et al: Ultrasonographic diagnosis of small-intestinal intussusception in three foals. J Am Vet Med Assoc 194:395-397, 1989.
227. McGladdery AJ: Ultrasonography as an aid to the diagnosis of equine colic. Equine Vet Educ 4:248-251, 1992.
228. Klohnen A, Vachon A, Fischer AT: Diagnostic ultrasonography of the equine acute abdomen. Proceedings of the 41st Annual American Association of Equine Practitioners 41:187-188, 1995.
229. Klohnen A, Vachon AM, Fischer AT: Use of diagnostic ultrasonography in horses with signs of acute abdominal pain. J Am Vet Med Assoc 209:1597-1601, 1996.
230. Santschi EM, Slone DE, Frank WM: Use of ultrasound in horses for diagnosis of left dorsal displacement of the large colon and monitoring its nonsurgical correction. Vet Surg 22:281-284, 1993.
231. Tulleners EP: Complications of abdominocentesis in the horse. J Am Vet Med Assoc 182:232-234, 1983.
232. Gift LJ, Gaughan EM, DeBowes RM, et al: Jejunal intussusception in adult horses: 11 cases (1981-1991). J Am Vet Med Assoc 202:110-112, 1993.
233. Edwards GB: Surgical management of intussusception in the horse. Equine Vet J 18:313-321, 1986.
234. Collier MA, Trent AM: Jejunal intussusception associated with leiomyoma in an aged horse. J Am Vet Med Assoc 182:819-821, 1983.
235. Boulton CH, Williamson L: Cryptococcal granuloma associated with jejunal intussusception in a horse. Equine Vet J 16:548-551, 1984.
236. Montali C, Croce F, De Pra L, Solbiati L: Intussusception of the bowel: A new sonographic pattern. Br J Radiol 56:621-623, 1983.
237. Seibert JJ, Williamson SL, Golladay ES, et al: The distended gasless abdomen: A fertile field for ultrasound. J Ultrasound Med 5:301-308, 1986.
238. Holt S, Samuel E: Multiple concentric ring sign in the ultrasonographic diagnosis of intussusception. Gastrointest Radiol 3:307-309, 1978.
239. Pracros JP, Tran-Minh VA, Morin de Finfe CH, et al: Acute intestinal intussusception in children: Contribution of ultrasonography (145 cases). Ann Radiol 30:525-530, 1987.
240. Shanbhogue RL, Hussain SM, Meradji M, et al: Ultrasonography is accurate enough for the diagnosis of intussusception. J Pediatr Surg 29:324-328, 1994.
241. Greet TRC: Ileal intussusception in 16 young Thoroughbreds. Equine Vet J 24:81-83, 1992.
242. Edwards GB: Obstruction of the ileum in the horse: A report of twenty seven clinical cases. Equine Vet J 13:158-166, 1981.
243. Barclay WP, Phillips TN, Foerner JJ: Intussusception associated with *Anoplocephala perfoliata* infection in five horses. J Am Vet Med Assoc 180:752-753, 1982.
244. Hackett MS, Hackett RP: Chronic ileocecal intussusception in horses. Cornell Vet 79:353-361, 1989.
245. Bowerman RA, Silver TM, Jaffee MH: Real-time ultrasound diagnosis of intussusception in children. Radiology 143:527-529, 1982.

246. Seibert JJ, Williamson SL, Golladay ES, et al: The distended gasless abdomen: A fertile field for ultrasound. J Ultrasound Med 5:301-308, 1986.
247. Alessi V, Salerno G: The "hayfork" sign in the ultrasonic diagnosis of intussusception. Gastrointest Radiol 10:177-179, 1985.
248. Swischuk LE, Hayden CK, Boulden T: Intussusception: Indications for ultrasonography and an explanation for the doughnut and pseudokidney signs. Pediatr Radiol 15:388-391, 1985.
249. Verbanck JJ, Rutgeerts LJ, Douterlunge PH, et al: Sonographic pathologic correlation in intussusception of the bowel. J Clin Ultrasound 14:393-397, 1986.
250. Gaughan EM, Hackett RP: Cecocolic intussusception in horses: 11 cases (1979-1989). J Am Vet Med Assoc 197:1373-1375, 1990.
251. Owen RR, Jaggar DW, Quan-Taylor R: Cecal intussusception in horses and the significance of *Anoplocephala perfoliata*. Vet Rec 124:34-47, 1989.
252. Ward JL, Fubini SL: Partial typhlectomy and ileocolostomy for treatment of nonreducible cecocolic intussusception in a horse. J Am Vet Med Assoc 205:325-328, 1994.
253. Foerner JJ: Diseases of the large intestine: Differential diagnosis and surgical management. Vet Clin North Am (Large Animal Pract) 4:129-146, 1982.
254. Bilkslager AT, Bowman KF, Haven ML, et al: Pedunculated lipomas as a cause of intestinal obstruction in horses: 17 cases (1983-1990). J Am Vet Med Assoc 201:1249-1252, 1992.
255. Edwards GB, Proudman CJ: An analysis of 75 cases of intestinal obstruction caused by pedunculated lipomas. Equine Vet J 26:18-21, 1994.
256. Miller JH, Kemberling CR: Ultrasound scanning of the gastrointestinal tract in children: Subject review. Radiology 152:671-677, 1984.
257. Hernanz-Schulman M, Genieser NB, Ambrosino M: Sonographic diagnosis of intramural duodenal hematoma. J Ultrasound Med 8:273-276, 1989.
258. Pozniak MA, Scanlan KA, Yandow D, Mulligan G: Current status of small-bowel ultrasound. Radiologe 30:254-265, 1990.
259. Purcell KL, Johnson PJ, Kreeger JM, Wilson DA: Obstruction caused by a *Pythium insidiosum* granuloma in a mare. J Am Vet Med Assoc 205:337-339, 1994.
260. Allison N, Gillis JP: Enteric pythiosis in a horse. J Am Vet Med Assoc 196:462-464, 1990.
261. Brown CC, Roberts ED: Intestinal pythiosis in a horse. Aust Vet J 65:88-89, 1988.
262. Morton LD, Morton DG, Baker GJ, Geldberg HB: Chronic eosinophilic enteritis attributed to *Pythium* sp in a horse. Vet Pathol 28:542-544, 1991.
263. Traub-Dargatz JL, Schultheiss PC, Kiper ML, et al: Intestinal fibrosis with partial obstruction in five horses and two ponies. J Am Vet Med Assoc 201:603-607, 1992.
264. Barclay WP, McCracken RJ, Phillips TN, et al: Chronic nongranulomatous arteritis in seven horses. J Am Vet Med Assoc 190:684-686, 1987.
265. Chaffin MK, Fuenteabla IC, Shoemaker J, et al: Idiopathic muscular hypertrophy of the equine small intestine: 11 cases (1980-1991). Equine Vet J 24:372-378, 1992.
266. Baird AN, Cohen ND, Taylor TS, et al: Renosplenic entrapment of the large colon in horses: 57 cases (1983-1988). J Am Vet Med Assoc 198:1423-1426, 1991.
267. Sivula NJ: Renosplenic entrapment of the large colon in horses: 33 cases (1984-1989). J Am Vet Med Assoc 199:244-246, 1991.
268. Blue MG: Enteroliths in horses—a retrospective study of 30 cases. Equine Vet J 11:76-84, 1979.
269. Ferraro GL, Evans DR, Trunk DA, Roberts TT: Medical and surgical management of enteroliths in equidae. J Am Vet Med Assoc 162:208-210, 1973.
270. Yvorchuk-St. Jean KE, DeBowes RM, Gift LJ, et al: Trichophytobezoar as a cause of transverse colon obstruction in a foal. Cornell Vet 83:169-175, 1993.
271. McClure JT, Kobluk C, Voller K, et al: Fecalith impaction in four miniature foals. J Am Vet Med Assoc 200:205-207, 1992.
272. Kristoffersen J: Ileus hos ponyføl forårsaget af håransamling i colon tenue. Dansk Vet Tidsskr 68:640, 1985.
273. Tennant B: Intestinal obstruction in the horse—some aspects of differential diagnosis in equine colic. Proceedings of the 27th Annual Meeting of the American Association of Equine Practitioners 27:426-439, 1975.
274. Boles CL, Kohn CW: Fibrous foreign body impaction colic in young horses. J Am Vet Med Assoc 171:193-195, 1977.
275. Gay CC, Spiers VC, Christie BA, et al: Foreign body obstruction of the small colon in six horses. Equine Vet J 11:60-62, 1979.
276. Blue MG, Wittkopp RW: Clinical and structural features of equine enteroliths. J Am Vet Med Assoc 179:79-82, 1981.
277. Speirs VC, vanVeenendaal C, Christie BA, et al: Obstruction of the small colon by intramural haematoma in three horses. Australian Vet J 57:88-90, 1981.
278. Pearson H, Waterman AE: Submucosal haematoma as a cause of obstruction of the small colon in the horse: A review of four cases. Equine Vet J 18:340-341, 1986.
279. Newman B, Girdany BR: Gastric trichobezoars—sonographic and computed tomographic appearance. Pediatr Radiol 20:526-527, 1990.
280. McCracken S, Jongeward R, Silver TM, et al: Gastric trichobezoar: Sonographic findings. Radiology 161:121-124, 1986.
281. Malpani A, Ramani SK, Wolverson MK: Role of sonography in trichobezoars. J Ultrasound Med 7:661-663, 1988.
282. Lorentzen T, Nolsøe CP, Khattar SC, et al: Gastric and duodenal wall thickening on abdominal ultrasonography. Positive predictive value. J Ultrasound Med 12:633-637, 1993.
283. Tomooka Y, Onitsuka H, Goya T, et al: Ultrasonography of benign gastric ulcers. J Ultrasound Med 8:513-517, 1989.
284. Rosenberg ER, Morgan CL, Trought WS, et al: The ultrasonic recognition of a gastric ulcer. Br J Radiol 56:365-366, 1983.
285. Ranschaert E, Rigauts H: Confined gastric perforation: Ultrasound and computed tomographic diagnosis. Abdom Imaging 18:318-319, 1993.
286. Teele RL: A dozen ultrasonographic donuts. Mt. Sinai J Med 51:528-534, 1984.
287. Weldon AD, Rowland PH, Rebhun WC: Emphysematous gastritis in a horse. Cornell Vet 81:51-58, 1991.
288. Todhunter RJ, Erb HN, Roth L: Gastric rupture in horses: A review of 54 cases. Equine Vet J 18:288-293, 1986.
289. Tennant B, Keirn DR, White KK, et al: Six cases of squamous cell carcinoma of the stomach of the horse. Equine Vet J 14:238-243, 1982.
290. Meagher DM, Wheat JD, Tennant BC, Osburn BI: Squamous cell carcinoma of the equine stomach. J Am Vet Med Assoc 164:81-84, 1974.
291. Cotchin E: Tumors of farm animals: A survey of tumors examined at the Royal Veterinary College, London during 1950-1960. Vet Rec 72:816-822, 1960.
292. Olsen SN: Squamous cell carcinoma of the equine stomach: A report of 5 cases. Vet Rec 131:170-173, 1992.
293. Bloom RA, Craciun E, Lebensart PD, et al: The ultrasound appearances of intramural bowel gas: The bright ring appearance and the effervescent bowel. A report of 3 cases. Br J Radiol 65:585-588, 1992.
294. Bester RC, Coetzer JAW: A chronic wasting syndrome in a horses associated with granulomatous enteritis. J S Afr Vet Ass 49:351-353, 1978.
295. Cimprich RE: Equine granulomatous enteritis. Vet Pathol 11:535-547, 1974.
296. Merritt AM, Cimprich RE, Beech J: Granulomatous enteritis in nine horses. J Am Vet Med Assoc 169:603-609, 1976.
297. Sweeney RW, Sweeney CR, Saik J: Chronic granulomatous bowel disease in three sibling horses. J Am Vet Med Assoc 188:1192-1194, 1989.
298. Orsini JA, Orsini PG, Sepsey L, et al: Intestinal carcinoid in a mare: Consideration for chronic colic in horses. J Am Vet Med Assoc 193:87-88, 1988.
299. Ramey DW, Reinerston EL: Strangulating lipoma and small intestinal leiomyoma in a horse: A case report. Equine Vet Sci 4:88-89, 1984.
300. Bach LG, Ricketts SW: Paracentesis as an aid to the diagnosis of abdominal disease in the horse. Equine Vet J 6:116-121, 1974.
301. Coffman JR, Tritschler LG: Exudative peritonitis in two horses. J Am Vet Med Assoc 160:871-872, 1972.
302. Hawkins JF, Bowman KF, Roberts MC, Cowen P: Peritonitis in horses: 67 cases (1985-1990). J Am Vet Med Assoc 203:284-288, 1993.
303. Dyson S: Review of 30 cases of peritonitis in the horse. Equine Vet J 15:25-30, 1983.

304. Mair TS, Hillyer MH, Taylor FGR: Peritonitis in adult horses: A review of 21 cases. Vet Rec 126:567–570, 1990.
305. Dipietro JA, Boero M, Ely RW: Abdominal abscess associated with *Parascaris equorum* infection in a foal. J Am Vet Med Assoc 9:991–992, 1983.
306. Toeske K, Lofstedt J, Miller L, Horney B: Dysuria and stranguria associated with colonic ulceration and abdominal abscess in a horse. Can Vet J 33:809–811, 1992.
307. Taylor TS, Martin MT, McMullan EC: Bypass surgery for intestinal occluding abscesses in the equine: A report of two cases. Vet Surg 10:136–138, 1981.
308. Skidell J: Resection of an intra-abdominal abscess in the horse using a stapling technique. Equine Vet Educ 8:140–142, 1996.
309. Prades M, Peyton L, Pattio N, Langlois J: Surgical treatment of an abdominal abscess by marsupialization in the horse: A report of two cases. Equine Vet J 21:459–461, 1989.
310. Hughes JP, Biberstein EL: Chronic equine abscesses associated with *Corynebacterium pseudotuberculosis*. J Am Vet Med Assoc 135:559–562, 1959.
311. Koblick PD, Lofstedt J, Jakowski RM, Johnson KL: Use of ^{111}In labelled autologous leukocytes to image an abdominal abscess in a horse. J Am Vet Med Assoc 186:1319–1322, 1985.
312. Golding RH, Li DK, Cooperberg PL: Sonographic demonstration of air-fluid levels in abdominal abscess. J Ultrasound Med 1:151–155, 1982.
313. Hanselaer JR, Nyland TG: Chyloabdomen and ultrasonographic detection of an intra-abdominal abscess in a foal. J Am Vet Med Assoc 183:1465–1467, 1983.
314. Reef VB, Jones PA, Beech J, et al: Diagnostic dilemma. Compend Contin Educ Pract Vet 15:92–95, 1993.
315. Esplin DG, Taylor JL: Hypercalcemia in a horse with lymphosarcoma. J Am Vet Med Assoc 170:180–182, 1977.
316. Conboy HS, Powers RD: Equine malignant lymphoma. J Am Vet Med Assoc 159:53–54, 1971.
317. Firth EC: Urethral sphincterotomy for delivery of vesical calculus in the mare: A case report. Equine Vet J 8:99–100, 1976.
318. Wright JG, Neal PA: Laparocystotomy for urinary calculus in a gelding. Vet Rec 72:301–303, 1960.
319. Lowe JE: Surgical removal of equine uroliths via the laparocystomy approach. J Am Vet Med Assoc 139:345–348, 1961.
320. Remillard RL, Modransky PD, Welker FH, et al: Dietary management of cystic calculi in a horse. J Equine Vet Sci 12:359–363, 1992.
321. Wood T, Weckman TJ, Henry PA, et al: Equine urine pH: Normal population distributions and methods of acidification. Equine Vet J 22:118–121, 1990.
322. Rodger LD, Carlson GP, Moran ME, et al: Resolution of left ureteral stone using electrohydraulic lithotripsy in a Thoroughbred colt. J Vet Intern Med 9:280–282, 1995.
323. Juzwiak JS, Bain FT, Slone DE, et al: Unilateral nephrectomy for treatment of chronic hematuria due to nephrolithiasis in a colt. Can Vet J 29:931–933, 1988.
324. Osborne CA, Fahning ML, Schultz RH, Perman V: Percutaneous renal biopsy in the cow and the horse. J Am Vet Med Assoc 153:563–570, 1968.
325. Bayly WM, Paradis MR, Reed SM: Equine renal biopsy: Indications, technic, interpretation and complications. Modern Vet Pract 61:763–768, 1990.
326. Modransky PD: Ultrasound-guided renal and hepatic biopsy techniques. Vet Clin North Am (Equine Pract) 2:115–125, 1986.
327. Barratt-Boyes SM, Spensley MS, Nyland TG, Olander HJ: Ultrasound localization and guidance for renal biopsy in the horse. Vet Radiol 32:121–126, 1991.
328. Allen JK, Kramer RW: Enhanced sonographic visualization of biopsy needles. Vet Radiol Ultrasound 34:359–360, 1993.
329. Hoppe FE, Hager DA, Poulos PW, et al: A comparison of manual and automatic ultrasound-guided biopsy techniques. Vet Radiol Ultrasound 27:99–101, 1986.
330. Gibbons WJ: Equine liver biopsy technique. Mod Vet Pract 45:72–74, 1980.
331. Pearson EG, Craig AM: The diagnosis of liver disease in equine and food animals. Mod Vet Pract 61:233–237, 1980.
332. Léveillé R, Partington BP, Biller DS; Miyabayashi T: Complications after ultrasound-guided biopsy of abdominal structures in dogs and cats: 246 cases (1984–1991). J Am Vet Med Assoc 203:413–415, 1993.
333. Rigg DL, Reinertson EL, Buttrick ML: A technique for elective splenectomy of equidae using a transthoracic approach. Vet Surg 16:389–391, 1987.
334. Golland LC, Hodgson DR, Hodgson JL, et al: Peritonitis associated with *Actinobacillus equuli* in horses: 15 cases (1982–1992). J Am Vet Med Assoc 205:340–343, 1994.
335. Gold JP, Canizaro P, Kazam E, et al: The reliability of the results of ultrasound detection of fluid collections in the early postoperative period. Surg Gynecol Obstet 161:5–8, 1985.

CHAPTER

7

Pediatric Abdominal Ultrasonography

Ultrasonography was first used in the equine neonate for the diagnosis of internal umbilical remnant infections and has since been used for the diagnosis of a wide variety of foal diseases.[1-31] Abdominal ultrasonography has developed increasing importance as a diagnostic technique because it is noninvasive and is usually well tolerated by the neonatal or older foal. Abnormalities of the equine neonate—in particular, infection of the internal umbilical remnant structures, uroperitoneum and gastrointestinal disorders—lend themselves readily to ultrasonographic investigation.[1-6, 8-26, 28, 29, 31] Ultrasonographic evaluation of the abdominal organs is extremely useful in foals, as other diagnostic techniques are often not applicable owing to the large size of the equine abdomen.[8-12, 14-16, 19, 30-33] The smaller size of the foal abdomen, the close proximity of many imageable structures (internal umbilical remnants, bladder, gastrointestinal viscera, abdominal organs), and the higher incidence of small intestinal diseases, compared with the adult horse, make the foal an ideal patient for abdominal ultrasonography.

EXAMINATION TECHNIQUE

Patient Preparation

For ultrasonographic examination of the foal abdomen, the entire ventral abdomen from the xiphoid caudally to the inguinal region should be surgically clipped with a No. 40 clipper blade (Fig. 7-1).[9-14] The lateral sides of the abdomen and paralumbar fossa ventral to a diagonal line from the tuber coxae to the elbow should also be included. For ultrasonographic examination of the internal umbilical remnants and/or bladder, the ventral abdomen should be surgically clipped from the xiphoid to the pubis for a width of approximately 4 cm (Fig. 7-1).[1-3, 5, 8, 10, 26] The entire area around and including the external umbilical remnant should be surgically clipped if the internal and/or external umbilical structures are to be evaluated. The clipping of the ventral abdomen is not well liked, but most foals tolerate the clipping without sedation. The use of warm water for washing the abdomen prior to the application of warm ultrasound coupling gel is better tolerated by the foal.

Anatomy

Umbilical Remnants and Bladder

The internal umbilical remnant structures are small and located very close to the skin surface (Fig. 7-2).[2, 3, 5, 7, 9, 10] The umbilical vein transports blood from the placenta to the fetal liver. The umbilical vein runs along the midline to the liver and becomes the round ligament of the liver, part of the falciform ligament.[1, 2, 5, 34] The umbilical arteries transport blood from the internal iliac arteries of the fetus to the placenta and become the round ligaments of the bladder, suspending the bladder in the peritoneal cavity.[1, 2, 5, 34] The urachus transports urine from the fetal bladder to the allantoic cavity. After birth the urachus retracts and becomes the median ligament of the bladder.[5, 34] The urachus normally closes throughout its length after birth, leaving a round to oval bladder apex. The bladder is adjacent to the ventral abdominal wall for 4 to 8 weeks after birth, following which the large colon is interspersed between the bladder and the ventral abdominal wall.[1-3, 9, 10] The trigone region of the bladder is located just caudal to the pelvic brim and is continuous with the pelvic urethra. The ureters enter the dorsal lateral region of the bladder near the bladder neck.

Kidneys

The right kidney is located more cranially in the abdomen and can usually be found in the retroperitoneal space just beneath the abdominal wall and immediately ventral to the transverse processes between the fourteenth and sixteenth intercostal spaces (ICS) at the level of the tuber coxae.[9-12, 19, 35-38] The cranial pole of the right kidney sits in the renal fossa of the liver and lies deep to the dia-

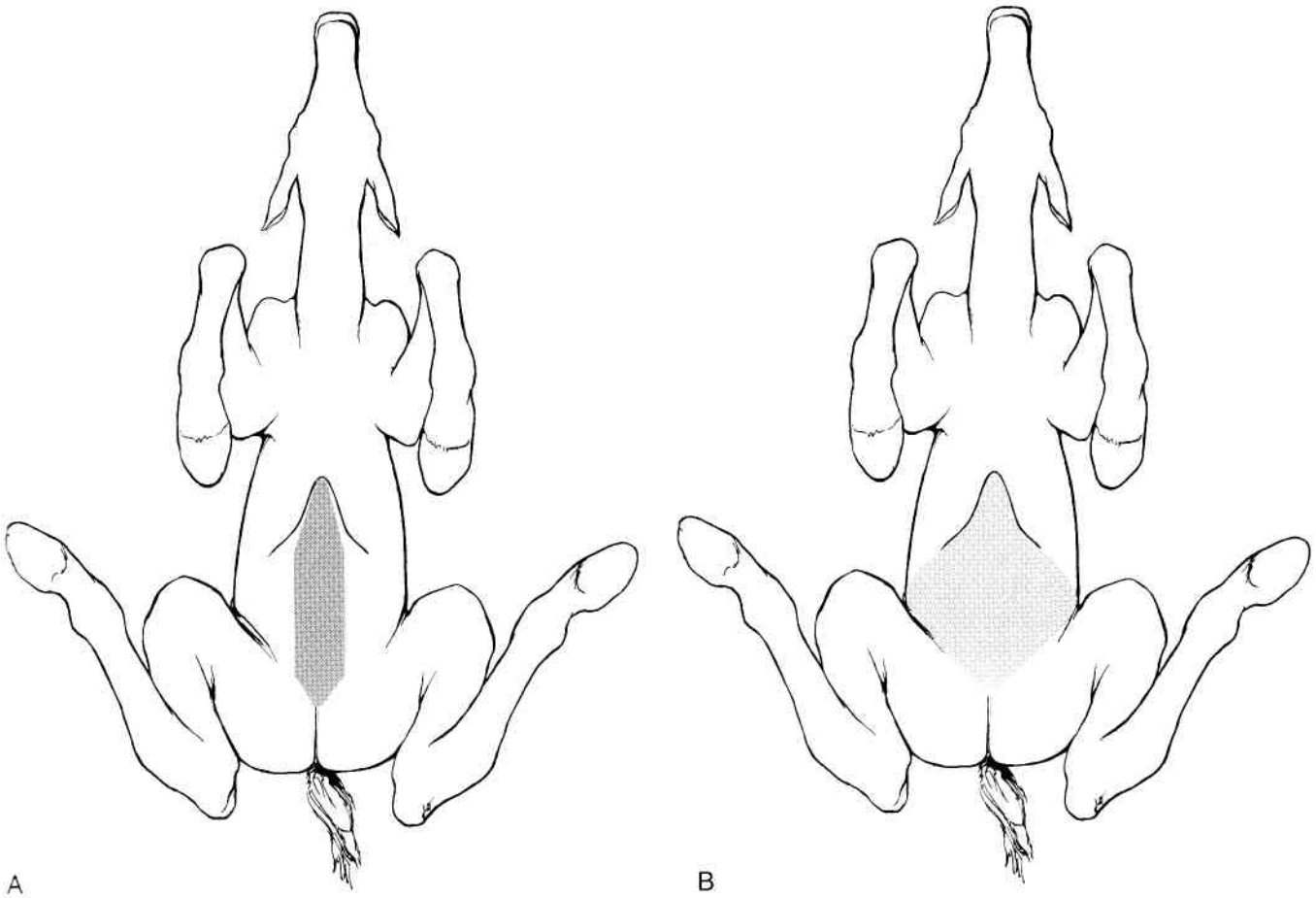

Figure 7–1

Diagram of the clipped area on the foal's ventral abdomen for an *(A)* umbilical or bladder or *(B)* general abdominal ultrasonographic examination. *A*. The darker shaded area represents the area that should be clipped to examine the internal umbilical remnants and the bladder. *B*. The lighter shaded area represents the additional area that should be clipped to examine the entire ventral abdomen of the foal.

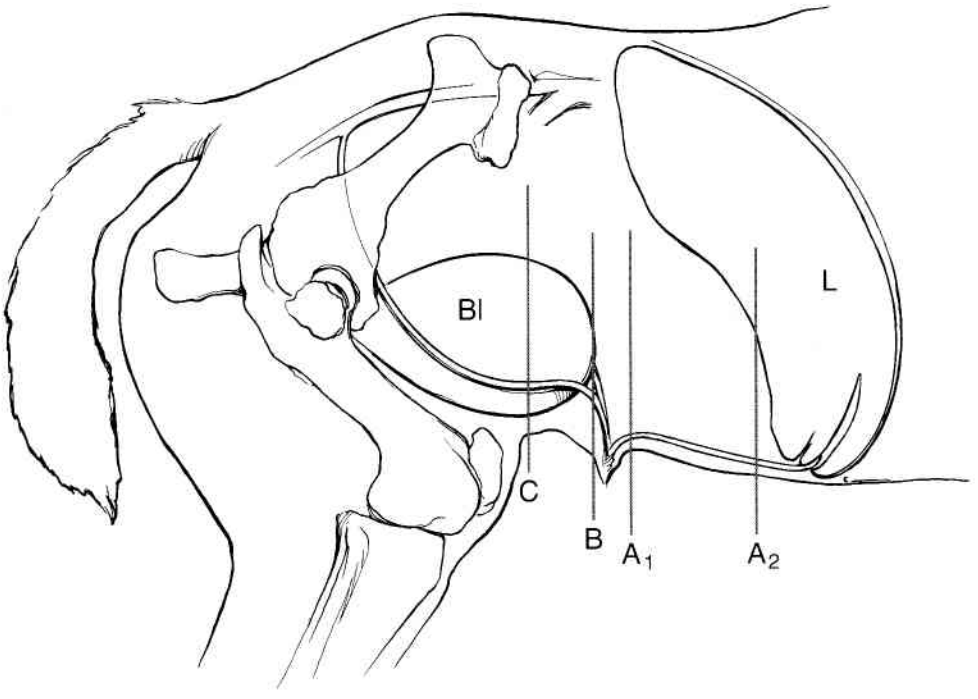

Figure 7–2

Diagram of the location of the normal internal umbilical remnants in a neonatal foal. The cranial line represents the scan plane through which the umbilical vein is measured cranial to the external umbilical remnant (A_1) and caudal to the liver (A_2). The middle line (B) represents the scan plane through which the umbilical arteries and the urachus are measured at the apex of the bladder (Bl). The caudal line (C) represents the scan plane through which the umbilical arteries are measured alongside the bladder. L, Liver.

phragm. The duodenum courses ventrally around the caudal pole of the right kidney, and the cecum is imaged ventral and caudal to the right kidney and the duodenum. The left kidney is located farther caudally and ventrally in the abdomen and is usually found in the seventeenth ICS and the paralumbar fossa between a line parallel to the tuber coxae and the tuber ischii.[9-12, 19, 35-38] The left kidney lies medial to the spleen in the left caudal abdomen. The caudal vena cava and aorta lie medial to the left and right kidneys along the ventral aspect of the dorsal midline.

Liver

The liver extends from the sixth or seventh ICS on the right side of the abdomen to the fourteenth or fifteenth ICS; the left lobe of the liver is smaller and usually extends from the sixth to the ninth ICS ventral to the lung field.[9-12, 19, 37] The liver is immediately adjacent to and caudal to the diaphragm. The right dorsal colon is deep to the liver on the right side of the abdomen, with the duodenum between the right dorsal colon and liver in the cranial to mid portion of the abdomen. The right kidney is caudal and lateral to the caudate process of the right lobe of the liver. On the left side of the abdomen, the spleen is located medial to the liver beginning at approximately the eighth ICS. The neonatal foal liver is usually in contact with the cranial ventral abdomen for the first 4 to 8 weeks of life.[9-12]

Spleen

The spleen is variable in size but usually extends along the left abdominal wall from the eighth or ninth ICS to the seventeenth ICS or paralumbar fossa.[9-12, 37] The spleen is immediately adjacent to the diaphragm and left body wall in the mid and caudal abdomen and medial to the liver in the left cranial abdomen. The cranial pole of the spleen can occasionally be found lateral to the liver or in the right cranioventral abdomen in a small percentage of normal foals. The left dorsal colon is located medial to the spleen. Ventral to the spleen is the left dorsal and/or left ventral colon.

Gastrointestinal Viscera

The foal's stomach is located medial to the spleen along the left abdominal wall from the eighth or ninth to the twelfth or thirteenth ICS and is often in contact with the cranial ventral abdomen in the neonate, but not in the adult horse.[10, 39] The stomach is adjacent to the spleen at the level of the splenic vein.[19] The duodenum is imaged around the ventral and caudal aspects of the right lobe of the liver and the caudal pole of the right kidney. The duodenum is located between the liver and the right dorsal colon from the pylorus (located in the proximal to mid portion of the right side of the abdomen) to the mid to caudal abdomen.[19, 39] The duodenum then courses caudodorsally to the caudal pole of the right kidney and lies between the liver and the cecum.[19] Small intestine (jejunum) is often in contact with the ventral abdominal wall at the foal's midline or slightly to the left of midline in the umbilical region, whereas large colon is in contact with the remainder of the ventral abdomen in the foal. Small colon can be found dorsal to the urinary bladder.

Scanning Technique

The examination of the internal umbilical remnants, bladder, and gastrointestinal viscera should begin with a 7.5-10.0-MHz transducer containing a built-in fluid offset or using a hand-held standoff pad and a displayed depth of 4 to 6 cm.[1-6, 10, 12, 14, 26] A standard 7.5-MHz transducer should then be used to further evaluate these structures if there is massive enlargement of the internal umbilical remnants, a large umbilical hernia, or the bladder has not been examined in its entirety.[10, 26] A standard 7.5-MHz transducer or a wide bandwidth 6.0-MHz microconvex linear array transducer, followed by a 5.0-MHz transducer, should be used to thoroughly evaluate all the imageable gastrointestinal viscera for optimal image quality.[10, 14] The highest-frequency transducer that penetrates to the area under investigation should be selected and the smallest depth of field necessary should be displayed.

The dorsal (cranial to caudal scan plane from the right or left side of the abdomen) scan-plane orientation should display the cranial aspect of the abdomen on the right side of the screen and the caudal aspect of the abdomen on the left side of the screen. The sagittal (cranial to caudal scan plane from the ventral aspect to the abdomen) scan plane should be displayed with the cranial aspect of the abdomen on the right side of the screen and the caudal aspect of the abdomen on the left side of the screen. The left transverse scan-plane orientation should display the ventral aspect of the abdomen on the left side of the screen and the dorsal aspect on the right side. The ventral transverse scan-plane orientation should display the right side of the abdomen on the left side of the screen and the left side of the abdomen on the right side of the screen. The right transverse scan-plane orientation should display the dorsal aspect of the abdomen on the right side of the screen and the ventral aspect of the abdomen on the left side of the screen.

The foal is usually examined unsedated, but sedation may be used to make an intractable foal more manageable. The ultrasonographic examination of the umbilicus is most easily performed in the awake, standing foal when the internal umbilical remnants are lying on the ventral midline.[2, 10] The internal umbilical remnants are most easily found in this location by the novice ultrasonographer. In the recumbent foal, the umbilical arteries and urachus, and to a lesser extent the umbilical vein, fall away from the midline toward the most ventral portion of the abdomen. This position makes them more difficult to find and follow sonographically owing to the remnants' small size in the normal foal. The ultrasonographic examination of the bladder is most easily performed in the standing foal because the weight of the urine within the bladder positions the bladder against the floor of the ventral abdomen and displaces gas-filled large bowel, par-

particularly in older foals. The bladder falls ventrally, away from the midline, in the recumbent foal but is relatively easy to locate because of its size and shape.

The ultrasonographic examination of the gastrointestinal viscera must be done from the most ventral portion of the abdomen and therefore is also most easily performed in the standing foal.[10, 14, 15] If the foal is recumbent, the gastrointestinal viscera should be scanned from the ventralmost portion of the abdomen. This requires propping the foal's thorax and pelvis up with a pillow, mattress, or something similar so that the transducer can be maneuvered beneath the foal while the foal is recumbent.

Umbilical Remnants

The ultrasonographic examination of the umbilicus should include a complete sonographic evaluation of the internal and external umbilical remnants. The external umbilical remnant should be scanned in its entirety and any enlarged structures identified. The umbilical vein should be scanned in the transverse plane from its caudal extent in the external umbilical remnant up to the liver.[2, 3, 5] Measurements of the diameter of the umbilical vein should be made immediately cranial to the external remnant and just caudal to the liver (Fig. 7-2), as well as anywhere enlargement or other abnormalities of the umbilical vein are detected.[2-6] The umbilical vein can also be scanned in the sagittal scan plane, but the vessel is much more difficult to follow in this scan plane. The umbilical arteries and the urachus should be scanned in the transverse plane from their cranial extent in the external umbilical remnant to the bladder apex.[2, 3, 5] The umbilical arteries and the urachus should be measured together just cranial to the apex of the bladder (Fig. 7-2).[2, 3, 5, 6] Both horizontal and vertical diameters should be obtained. The urachus should also be examined in the sagittal scan plane looking for a urachal diverticulum or patent urachus. The umbilical arteries should also be followed individually along the lateral sides of the bladder as far caudally as possible.[2, 3, 5] Measurements of the diameter of the umbilical arteries should be made along the lateral aspects of the bladder as close to the iliac arteries as possible (Fig. 7-2).[2, 3, 6] The adjacent structures (bladder, liver, and surrounding gastrointestinal viscera) should also be carefully examined while scanning the internal umbilical remnants.

Urinary Bladder

The ultrasonographic evaluation of the foal's bladder should include a thorough evaluation of the urachus. The bladder should be scanned in transverse and sagittal scan planes from the ventral abdomen, carefully evaluating the bladder apex, bladder wall, urachus, and retroperitoneal area, especially around the umbilicus.[8-12, 26] The echogenicity of the urine within the bladder should be assessed and the bladder should be carefully imaged for calculi or other abnormal contents. Sonographic evaluation of the urethra should also be performed if urethral obstruction is suspected. The ureters and the ureteral openings into the bladder are not normally visible sonographically.

Kidneys

Ultrasonographic evaluation of the foal's kidneys can be performed from the left and right body walls, as in adult horses, and, in many neonates, from the ventral abdominal window as well. The right kidney should be scanned from the right side of the abdomen in the fourteenth to sixteenth ICS using a 7.5-MHz or 6.0-transducer in neonates. A 5.0-MHz transducer may be needed in older foals.[9-12, 36] The left kidney should be scanned from the left side of the abdomen in the seventeenth ICS and paralumbar fossa using a 7.5-, 6.0-, or 5.0-MHz transducer in neonates and a 5.0- or 3.5-MHz transducer in older foals.[9-12, 36] The same transducer may be used to examine the kidneys from the ventral abdominal window at, or caudal to, the umbilicus in the neonatal foal. The kidneys should be scanned in the dorsal scan plane (from the dorsolateral abdomen) and in the transverse scan plane (two mutually perpendicular planes). In neonates, the kidneys can also be scanned from the parasagittal scan plane (from the ventral abdomen).

Liver

Only a portion of the liver can be imaged sonographically in the horse, but more is visible in the foal than in the adult. The entire imageable part of the liver should be evaluated ultrasonographically ventral to the ventralmost extent of the lung along the right side of the abdomen from the sixth to the fifteenth ICS and along the left side of the cranial ventral abdomen from the sixth to the ninth ICS.[9-12] The cranial ventral portion of the abdomen should also be examined ultrasonographically, particularly in neonatal foals, as the liver can also be evaluated from this window (caudal to the xiphoid) for the first 4 to 8 weeks of life. A 7.5-10.0-MHz transducer will produce optimal images of the neonatal liver. A 5.0-6.0-MHz transducer may be needed in older foals to image all the hepatic parenchyma. The liver should be scanned in two mutually perpendicular planes (dorsal and transverse). In neonatal foals, the liver should also be scanned in the sagittal and parasagittal scan planes.

Spleen

The spleen is found along the left side of the abdomen adjacent to the body wall from the eighth or ninth ICS (cranial pole) to the seventeenth ICS or paralumbar fossa (tail or caudal pole of the spleen).[9, 10] The spleen is found more dorsally in the caudal abdomen, lateral to the left kidney. The spleen is located more ventrally and is occasionally found across the midline in the right cranial ventral abdomen in a small percentage of normal foals. A 7.5-10.0-MHz transducer should be selected in neonatal foals whereas a 5.0-6.0-MHz transducer may be needed to image the entire spleen in older foals. The spleen

should be scanned in the dorsal and transverse scan planes as well as in the sagittal and parasagittal scan planes, location of the spleen permitting.

Gastrointestinal Viscera

The stomach is located medial to the spleen in the cranial and mid portions of the left side of the abdomen. The fundus of the stomach is located at the level of the splenic vein.[19] The stomach is also easily imaged in the neonatal foal immediately caudal to the liver along the floor of the cranial ventral abdomen.[10, 11, 14] The duodenum is imageable medial to the ventral and caudal aspect of the right lobe of the liver coursing caudodorsally around the caudal pole of the right kidney. In the neonate, the jejunum is usually imaged from the ventral abdominal window in the region of the umbilicus or slightly caudal to the umbilicus. Jejunum may not be visible in the older foal owing to the interposed large colon. The ileum is rarely imaged in the normal foal. The large colon is normally visible throughout the majority of the abdomen along both body walls and along the ventral abdomen, with the cecum being imaged in the dorsal and caudal portions of the right side of the abdomen. The small colon dorsal to the bladder can be imaged by using the bladder as an acoustic window and scanning through the bladder from the ventral abdominal window. The initial survey of the gastrointestinal tract should be performed with a 7.5–10.0-MHz transducer to critically evaluate the layers of the intestinal wall. A lower frequency transducer can then be used if penetration to the deeper portions of the gastrointestinal tract is possible.

ULTRASONOGRAPHIC FINDINGS

Normal Structures

The abdomen should always be examined from the ventralmost location unless the abdominal organs (liver, kidneys, or spleen) are being imaged.[10] The gas present in the gastrointestinal viscera rises dorsally and is less likely to interfere with the examination if the scan is performed from the most ventral location.[10] The abnormal gastrointestinal viscera are heavy and fall to the ventral portion of the abdomen, making their detection most likely if the scan is performed from the most ventral location.

Umbilical Remnants

The external umbilical remnant contains the umbilical vein, both umbilical arteries, and the urachus, which are recognizable for several days after parturition (Fig. 7-3). These structures within the external umbilical remnant normally atrophy after birth, and the external umbilical remnant subsequently detaches from the skin of the ventral abdomen. The internal umbilical remnant structures also atrophy after birth and become normal ligaments within the abdominal cavity.[1, 2, 5] The umbilical vein is a small oval or elliptical vessel with a thin echogenic wall

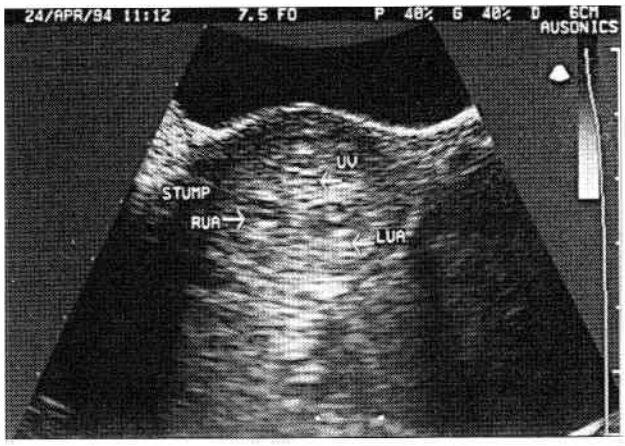

Figure 7–3

Sonogram of a normal external umbilical remnant obtained from a 5-day-old Thoroughbred cross colt. Notice the thicker-walled umbilical arteries and the thinner-walled umbilical vein (UV) in the external umbilical remnant. The urachus is located in the potential space between the right (RUA) and left (LUA) umbilical arteries. This is a transverse image of the external umbilical remnant obtained ventral to the abdomen. This sonogram was obtained with a 7.5-MHz sector-scanner transducer containing a built-in fluid offset and a displayed depth of 6 cm.

and an anechoic center (Fig. 7-4).[2, 5] The umbilical vein (lumen and vessel wall) usually measures 10 mm in diameter or less throughout its length from just cranial to the external umbilical remnant to its entrance into the liver (Table 7-1).[1, 2, 5, 9–12] The umbilical vein tends to be slightly larger just cranial to the external umbilical remnant as well as at its entrance into the liver. The horizontal diameter of the umbilical vein is usually slightly larger than its

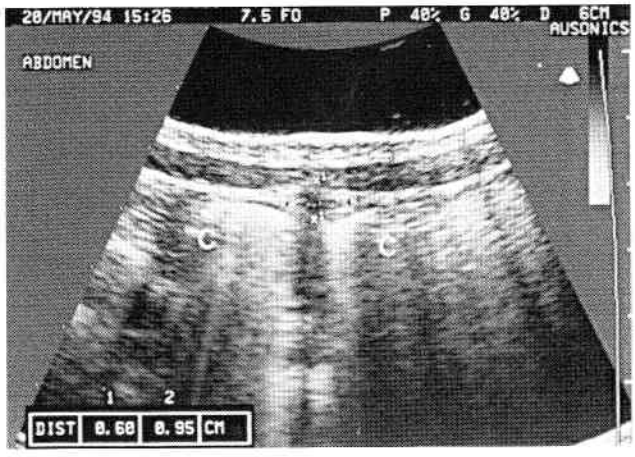

Figure 7–4

Sonogram of a normal umbilical vein obtained from a 2-day-old Thoroughbred filly. The umbilical vein measured 0.60 (x^1) by 0.95 cm (x^2) in diameter. Notice the thin echogenic wall and the small anechoic fluid center of the umbilical vein. Notice also the thin hypoechoic abdominal musculature ventral to the umbilical vein and the hyperechoic gas-filled large colon (C) against the abdominal wall. This sonogram was obtained just cranial to the external umbilical remnants at the level of the cranial scan plane (see Figure 7-2 at A_1). The right side of the sonogram is the left side of the foal's abdomen, and the top of the sonogram is ventral. This sonogram was obtained with a 7.5-MHz sector-scanner transducer containing a built-in fluid offset and a displayed depth of 6 cm.

Table 7–1
Measurements of Normal Internal Umbilical Remnant Structures

Structure	Mean ± SD*	Range
Umbilical vein†	6.1 ± 2.0 mm	3–11 mm
Umbilical vein‡	5.2 ± 1.9 mm	2–9 mm
Umbilical vein§	6.0 ± 1.9 mm	3–10 mm
Umbilical artery	8.5 ± 2.1 mm	5–14 mm
Umbilical arteries and urachus	17.5 ± 3.7 mm	12–24 mm

*SD, Standard deviation from the mean.
†Just cranial to the external umbilical remnant (see Figure 7-2 at A_1).
‡Midway between the external umbilical remnant and the liver.
§Just caudal to the liver (see Figure 7-2 at A_2).

vertical diameter. The umbilical arteries are small round vessels that are thicker walled than the umbilical vein and usually contain an echogenic center that represents clot (Fig. 7-5).[2, 5] The umbilical arteries contain sludging blood immediately after birth, and their pulsations can often be detected for up to 24 hours after birth. The umbilical artery (lumen and vessel wall) alongside the bladder usually measures slightly larger than the umbilical vein because of the thicker arterial wall. The normal umbilical artery measures 12 mm in diameter or less.[2, 5, 9-12] The combined horizontal measurement of both umbilical arteries at the apex of the bladder with the urachus in between is normally 25 mm or less. The vertical measurement should be similar to that of the umbilical arteries alongside the bladder because the diameter of the umbilical arteries does not change from the umbilicus to the bladder.[2, 5, 9-12] The urachus is only a potential space

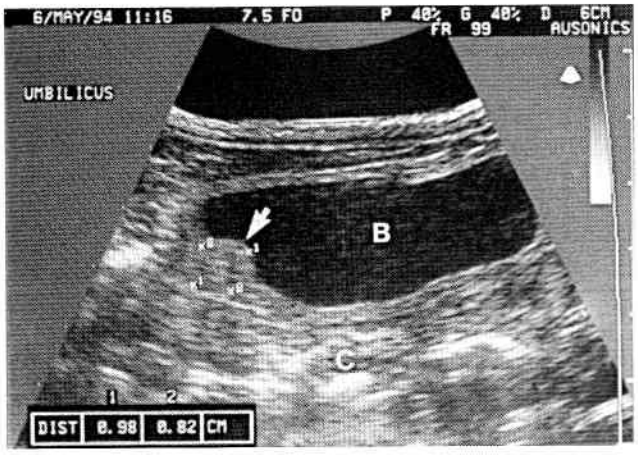

Figure 7–5
Sonogram of a normal right umbilical artery along the lateral aspect of the bladder obtained from a 12-day-old Thoroughbred filly. The umbilical artery measured 0.98 (x^1) by 0.82 (x^2) cm in diameter along the right side of the bladder. Notice the hypoechoic wall of the right umbilical artery and the slightly more echogenic (nearly isoechoic) central clot in the lumen of the umbilical artery. The umbilical artery normally indents the bladder wall (*arrow*). Notice the thin hypoechoic abdominal musculature and the hyperechoic gas-filled large colon (C) against the bladder. This sonogram was obtained caudal to the external umbilical remnants at the level of the caudal scan plane (see Figure 7-2 at C). The right side of the sonogram is the left side of the foal's abdomen, and the top of the sonogram is ventral. This sonogram was obtained with a 7.5-MHz sector-scanner transducer containing a built-in fluid offset and a displayed depth of 6 cm.

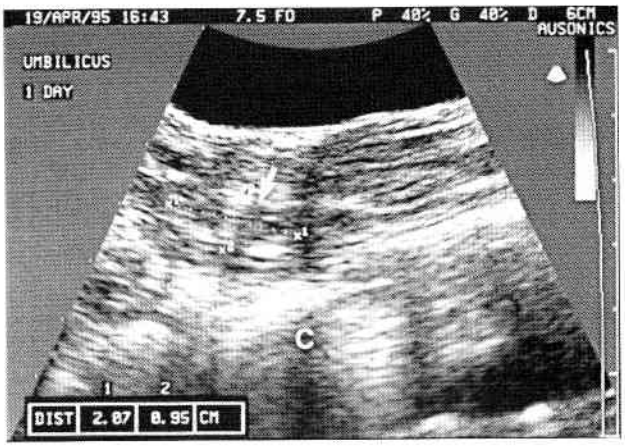

Figure 7–6
Sonogram of the normal umbilical arteries and urachus at the apex of the bladder obtained from a 1-day-old Thoroughbred colt. Notice the thick muscular walls of the umbilical arteries with the potential space of the urachus in between (*arrow*). The umbilical arteries with the urachus in between measured 2.07 (x^1) by 0.95 (x^2) in diameter. The left umbilical artery is located to the left of the right x^1 cursor, and the right umbilical artery is located to the right of the left x^1 cursor. This sonogram was obtained just caudal to the external umbilical remnant at the level of the middle scan plane (see Figure 7-2 at B). The hyperechoic gas-filled large colon (C) presses against the abdominal wall. The right side of the sonogram is the left side of the foal's abdomen, and the top of the sonogram is ventral. This sonogram was obtained with a 7.5-MHz sector-scanner transducer containing a built-in fluid offset and a displayed depth of 6 cm.

in normal foals and contains no fluid in the normal equine neonate. The umbilical arteries and urachus are visible in nearly all foals for the first 4 weeks of life (Fig. 7-6) and usually become obscured from view by gas-filled large colon between 4 and 8 weeks of age.[1, 2, 5, 9, 12]

Urinary Bladder

The urinary bladder is normally visible from the ventral abdomen in the neonatal foal for the first 4 to 8 weeks and then is usually obscured from view by gas in the interposed large bowel.[1, 2, 9, 10, 12, 19] The bladder is imaged in the caudalmost portion of the ventral abdomen and may be imaged in older foals when filled with urine, displacing the large colon. The bladder is round to oval in transverse section and oval in sagittal section and contains anechoic urine in the foal (Fig. 7-7).[10, 12] The bladder should always maintain a round to oval shape, whether empty or full. The bladder may appear somewhat irregular when it is catheterized (Fig. 7-8) or compressed by surrounding structures. In sagittal section the neonatal foal bladder should be rounder at the apex than toward the trigone region. The bladder wall is hypoechoic, and its thickness varies with the amount of bladder distention (Fig. 7-8). The bladder can be found anywhere from just cranial to the pubis when little urine is contained within it, to cranial to the external umbilical remnant if the bladder is very distended. The urachus should be closed off from the bladder apex, which should have a round to oval cranial border.

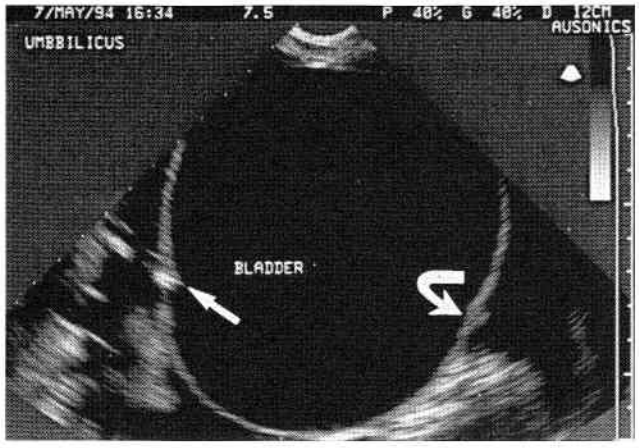

Figure 7–7

Sonogram of the normal distended bladder obtained from a 1-month-old Thoroughbred colt. Notice the anechoic fluid contained within the bladder and the oval to rounded appearance of the bladder. The small echogenic structure along the lateral aspect of the bladder (*straight arrow*) is the right umbilical artery. The left umbilical artery is smaller and more difficult to visualize (*curved arrow*). This sonogram was obtained caudal to the external umbilical remnant along the ventral body wall (see Figure 7–2 at C). The right side of this sonogram is the left side of the foal's abdomen, and the top is ventral. This sonogram was obtained with a 7.5-MHz sector-scanner transducer and a displayed depth of 12 cm.

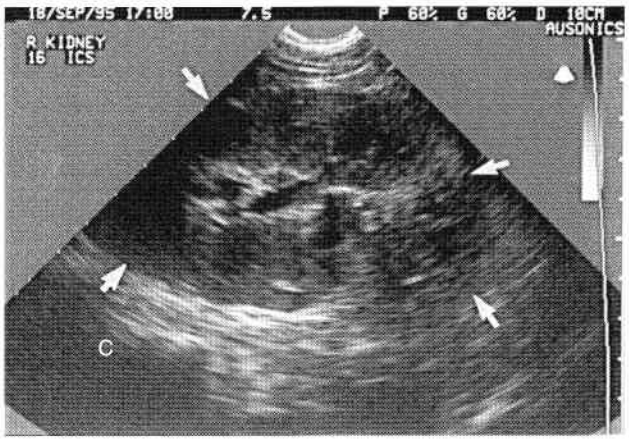

Figure 7–9

Sonogram of a normal right kidney (*arrows*) obtained from a 2-month-old Arabian colt in the right sixteenth intercostal space. Notice the anechoic renal calyces, the echogenic renal pelvis, and the hypoechoic renal cortex. The hyperechoic echoes deep to the right kidney are from the gas-lined mucosal surface of the adjacent cecum (C). The right side of the sonogram is dorsal, and the left side is ventral. This sonogram was obtained with a 7.5-MHz sector-scanner transducer and a displayed depth of 10 cm.

Kidneys

The renal pelvis is normally very echogenic owing to the presence of intrapelvic fat and fibrous tissue. The renal cortex is hypoechoic compared with the surrounding tissues and is composed of fine homogeneous echoes. The adjacent medulla is less echogenic than the renal cortex (Fig. 7–9).[19, 35–38, 40] The renal vessels can usually be imaged at the hilus of the kidney. The caudal vena cava and aorta may be imaged medial to the left and right kidneys along the ventral aspect of the dorsal midline. The parenchyma of the foal kidney (renal cortex and medulla) should be the most anechoic of the abdominal organs when they are sonographically compared (kidney < liver < spleen).[9, 10, 12, 19] The ureters are not normally imaged from the abdominal windows.[19, 33, 40] The adrenal glands are also not usually detected sonographically along the cranial and medial margin of both kidneys. Although the medial border of the right kidney is in close proximity to the pancreas, portal vein, and some of the mesenteric and visceral vessels, they are not usually visible sonographically from the lateral abdominal window because of their small size and the depth of these structures from the skin surface.[33] The lung often obscures the cranial pole of the right kidney during inspiration from the right lateral abdominal window. Gas in the left dorsal colon may obscure visualization of the caudal pole of the left kidney from the left lateral abdominal window. Occasionally the caudal pole of the left kidney is adjacent to the left body wall, rather than lying in its more common position, medial to the spleen.

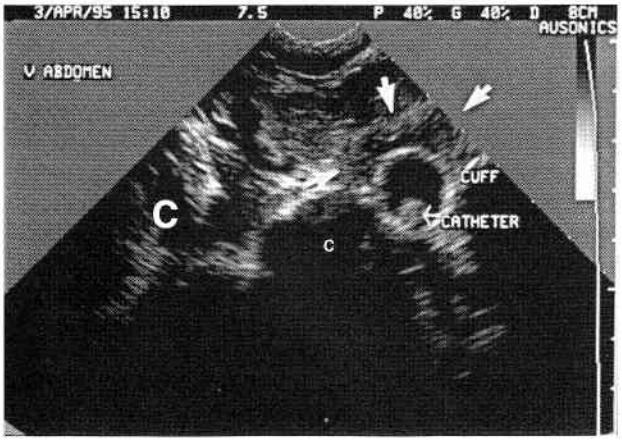

Figure 7–8

Transverse sonogram of a collapsed bladder containing a Foley catheter obtained from a 2-month-old Thoroughbred colt with anuria. The Foley catheter (*thin arrow*) with the distended cuff is contained within a nearly empty bladder (*thicker arrows*). The surrounding hyperechoic echoes are from the gas-lined mucosal surface of the adjacent large colon (C). The right side of the sonogram is the left side of the foal's abdomen, and the top is ventral. This sonogram was obtained with a 7.5-MHz sector-scanner transducer and a displayed depth of 8 cm.

Liver

The liver is recognizable by its branching vasculature with the large portal vein and small hepatic veins (Fig. 7–10).[12, 37] The walls of the portal veins are more echogenic than those of the hepatic veins, similar to their appearance in human beings and dogs.[16, 32, 37, 41] This is because the portal veins are surrounded by connective tissue, whereas little or no connective tissue surrounds the hepatic veins.[41] The blood in the hepatic veins may appear anechoic, or small moving echoes may be imaged as the ultrasound beam reflects off the moving cells and other blood components. The hepatic veins can be traced

to their junction with the caudal vena cava if the latter can be successfully imaged. The caudal vena cava may be visible in neonatal foals but is rarely imageable in older foals. The liver parenchyma is homogeneous and of medium echogenicity. The bile ducts are not normally visible sonographically.[32] Normally 4 to 8 cm of hepatic parenchyma is visible in the foal when the liver is imaged from the lateral abdomen.[12] Estimations of hepatic size are relative and are based on the amount of liver tissue imaged ventral to the lung margin. The size of the thoracic cavity, the volume of the colonic contents, and the presence of fluid or masses within the thoracic or abdominal cavity all influence the amount of hepatic parenchyma visible ventral to the ventral lung margins. The ventral margin of the liver should appear sharp throughout both liver lobes. In the neonatal foal, hepatic size can also be estimated from the amount of hepatic parenchyma imaged in the cranioventral abdomen from the ventral abdominal window. In some foals there is a small amount of large colon (diaphragmatic flexure) between the diaphragm and liver in the most cranial portion of the ventral abdomen.

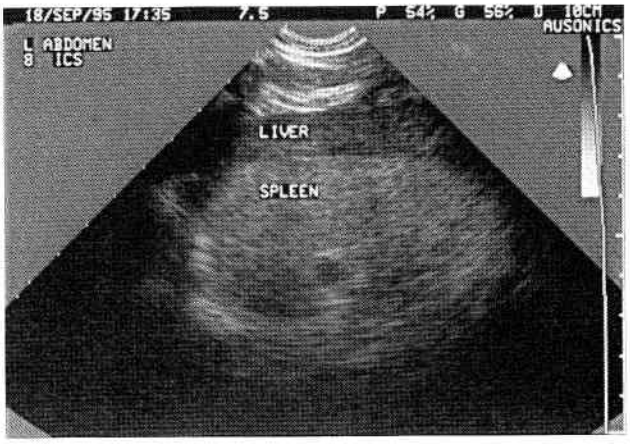

Figure 7–11

Sonogram of a normal spleen adjacent to the left lobe of the liver obtained from a 2-month-old Arabian colt (same colt as in Figures 7-9 and 7-10) in the left eighth intercostal space. Notice the homogeneous echogenic texture of the spleen adjacent to the more hypoechoic liver. The right side of the sonogram is dorsal, and the left side is ventral. This sonogram was obtained with a 7.5-MHz sector-scanner transducer and a displayed depth of 10 cm.

Spleen

The spleen is the most homogeneous and echogenic of the abdominal organs (Fig. 7-11).[9, 10, 19] Compared with the liver, the spleen has a paucity of visible vessels. The size of the spleen can be quite variable in the normal foal but usually runs along the majority of the left body wall up to the eighth or ninth ICS. The spleen should be found lateral to the left kidney and stomach but medial to the left lobe of the liver. In some foals the spleen may be found along the ventral midline or on the right side of the cranial ventral abdomen. The splenic vein is easily recognized as an anechoic tubular structure located along the medial aspect of the spleen around the tenth ICS.[19] The splenic vein is a reliable landmark for the location of the gastric fundus medial to the spleen. The dorsal border of all but the caudal pole of the spleen is usually obscured from view by the overlying lung.

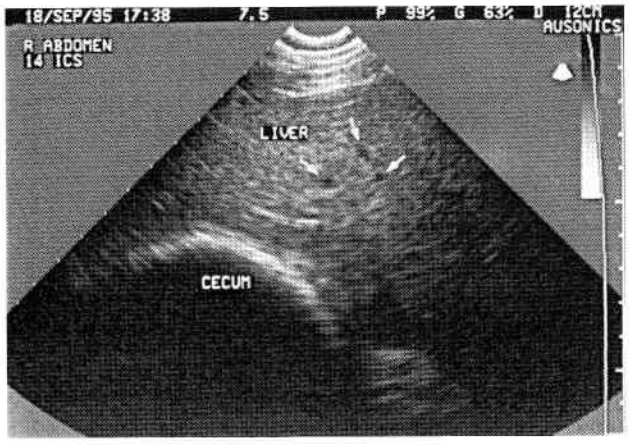

Figure 7–10

Sonogram of a portion of the right lobe of the liver (normal) obtained from a 2-month-old Arabian colt (same colt as in Figure 7-9) from the right fourteenth intercostal space. Notice the homogenous echo texture and the hepatic veins (*arrows*) throughout the liver parenchyma. Deep to the liver is the wall of the cecum, with its characteristic hyperechoic gas-lined mucosal surface. The right side of the sonogram is dorsal, and the left side is ventral. This sonogram was obtained with a 7.5-MHz sector-scanner transducer and a displayed depth of 12 cm.

Gastrointestinal Viscera

Ultrasonographic evaluation of the gastrointestinal tract has continued to gain favor as an alternative, noninvasive imaging modality in human beings and small and large animals. The normal sonographic appearance of the stomach and intestinal tract has been described in human beings and small and large animals.[42-51] Although no difference in thickness of the intestinal wall was detected between dogs of various ages, differences were detected between dogs of different breeds, with the larger-breed dogs having thicker gastric walls.[42] A difference in thickness of 2 mm has been reported in human beings between the distended and nondistended bowel wall.[44, 52] The administration of water via nasogastric tube to distend the stomach with fluid improves visualization of the gastric mucosa and portions of the gastrointestinal tract in the cranial abdomen, if the stomach can be used as an acoustic window. The administration of water via a stomach tube at a dose of 15 ml/kg, after withdrawing any free air, is reportedly beneficial for sonographic evaluation of the upper segments of the gastrointestinal tract in the dog.[43] Fasting is also reportedly helpful in examining the intestinal tract of the dog,[43] but its usefulness in the examination of the equine patient has not been demonstrated.

The equine stomach is recognized by its large semicircular curvilinear echo medial to the spleen at the level of the splenic vein and caudal to the liver. The wall thickness of the stomach can range up to 7.5 mm in the adult equine and is usually thinner in the foal. The stom-

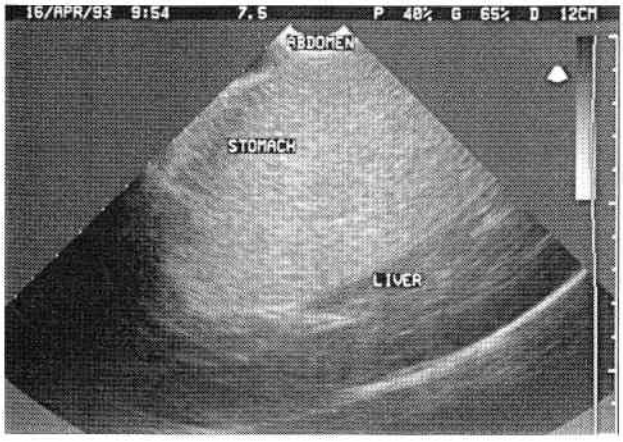

Figure 7–12

Sonogram of the stomach viewed from the ventral abdomen in a 5-day-old Thoroughbred colt. Notice the echogenic appearance of the milk within the stomach and the sharp margin of the adjacent liver. The right side of this sonogram is cranial, and the top is ventral. This sonogram was obtained with a 7.5-MHz sector-scanner transducer and a displayed depth of 12 cm.

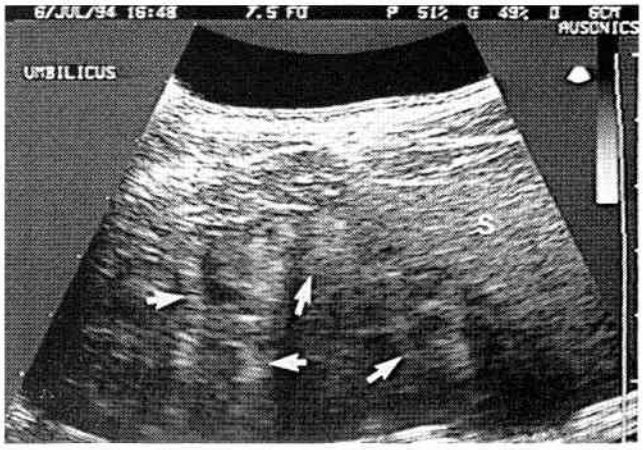

Figure 7–13

Sonogram of normal jejunum obtained from a 3-month-old Thoroughbred filly. The small hypoechoic loops of jejunum (*arrows*) are in various stages of contraction, with hypoechoic to anechoic luminal contents. The spleen (S) is next to the ventral abdominal wall on the left side of the abdomen. The right side of this sonogram is the left side of the foal's abdomen, and the top is ventral. This sonogram was obtained with a 7.5-MHz sector-scanner transducer containing a built-in fluid offset and a displayed depth of 6 cm.

ach echo may be hyperechoic with acoustic shadowing owing to the gas present along its inner mucosal surface (gas pattern), echogenic without acoustic shadowing owing to mucus adjacent to the gastric or intestinal mucosa (mucous pattern), or anechoic owing to fluid adjacent to the gastric mucosa (fluid pattern).[42, 45] The gastric serosa and subserosa are more hyperechoic in human beings because relatively more fibrous connective tissue is present within these layers. Milk appears echogenic sonographically (Fig. 7-12), whereas solid feed material is rarely imaged. The gas echo along the mucosal surface of the stomach usually prevents visualization of the other gastric contents in the older foal.

The small intestine has a characteristic sonographic appearance and is easily differentiated from large bowel, which is visible throughout the majority of the foal's abdomen. The duodenum and jejunum have thin walls that rarely exceed 3 mm in thickness, whereas the ileum is slightly thicker (4 to 5 mm). The duodenum normally has a fairly fluid ingesta that moves through the lumen in a pulsatile fashion. The duodenum often appears fairly collapsed until a wave of ingesta moves through the lumen. The duodenum can be found along the caudal and medial margins of the right lobe of the liver in the cranial to mid portion of the right side of the abdomen. The duodenum can be followed caudodorsally around the caudal pole of the right kidney, where it lies lateral to the base of the cecum. The jejunum is usually rounder in its sonographic appearance, with more hypoechoic ingesta (Fig. 7-13). The normal small intestine usually contains only a small amount of luminal contents. Periodic waves of ingesta are imaged rhythmically traversing the intestinal lumen.[14, 16] The ileum, if imaged, has a thicker muscular layer and a similar appearance of the contained ingesta. The large colon is recognized by its larger size and sacculated appearance and has a similar wall thickness to the jejunum (Fig. 7-14). The large bowel is usually hyperechoic along its mucosal surface owing to the gas contained within, and the ingesta is therefore not normally imaged. The small colon is smaller in size but has a sacculated appearance similar to that of the large bowel and usually has a hyperechoic mucosal surface. Formed fecal balls may be imaged in the small colon as echogenic luminal masses. Only a small amount of peritoneal fluid or none at all is imaged in the abdomen of the normal foal.

Five layers of the bowel wall may be imaged if a high-frequency transducer with excellent resolution is used. However, these layers are not normally imaged with trans-

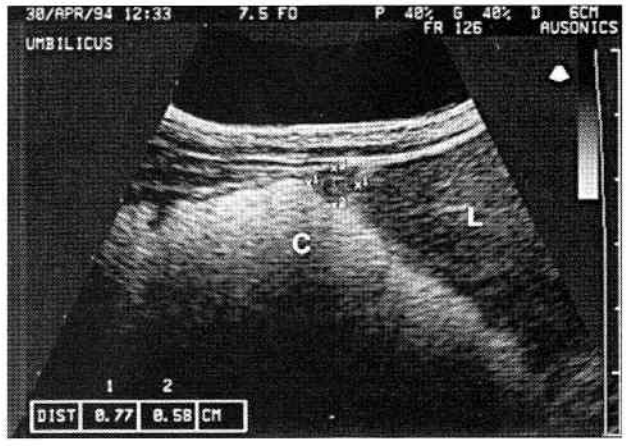

Figure 7–14

Sonogram of normal large colon (C) obtained from a 6-day-old Thoroughbred filly. The hyperechoic echoes are associated with gas on the mucosal surface of the large bowel (C). Notice the sacculated appearance of the large bowel adjacent to the ventral abdomen and liver (L) in the cranial ventral abdomen. The normal umbilical vein is immediately ventral to the large colon and measures 0.77 (x^1) by 0.58 (x^2) cm in diameter. The right side of this sonogram is the left side of the foal's abdomen, and the top is ventral. This sonogram was obtained with a 7.5-MHz sector-scanner transducer containing a built-in fluid offset and a displayed depth of 6 cm.

cutaneous ultrasound in foals with normal intestine. These layers are a hyperechoic outer serosal surface, a hypoechoic muscularis, hyperechoic submucosa, hypoechoic mucosa, and an inner hyperechoic mucosal surface.[50] Similar layers have been imaged in the intestinal walls of dogs and human beings.[42, 43, 49] In the ileum, an additional thinner hyperechoic line is visible in the center of the muscular layer and corresponds to the connective tissue separating the longitudinal and circular muscular layers.[50] The mucosal surface is hyperechoic owing to the multiple reflectors caused by the folding of the epithelial lining,[47] and the adherence of gas to the mucosal surface. The more tightly packed the mucosal folds are, the higher the echogenicity of the mucosal surface of the intestine. With high-frequency ultrasound in human beings, it has been demonstrated that the interface between the submucosa and muscularis is echogenic, but the submucosa itself, composed of numerous blood vessels and loose connective tissue, is hypoechoic.[47] The muscularis is hypoechoic throughout the gastrointestinal tract in human beings.[47] In normal bowel these layers are differentiated only with high-frequency (20-MHz) endoluminal ultrasound and are not routinely imaged with transcutaneous ultrasound.[47] The different layers of the intestinal wall are, however, usually visualized in patients (human, equine, or canine) with inflamed, edematous, or congested bowel or in patients with hypoproteinemia.

Abnormal Findings

The most important aspect of diagnosing abdominal pathology in the foal is a thorough understanding of ultrasonographic anatomy. The relationship of the gastrointestinal viscera, abdominal organs, and vessels to one another is critically important in arriving at a correct diagnosis or list of differential diagnoses. If a mass or an unknown structure is detected in the foal's abdomen, the ultrasonographic evaluation of this structure should be performed in a systematic way. The origin, size, shape, vascularity, and sonographic character of the mass or structure should be determined, along with its relationship to contiguous organs, blood vessels, and other structures, in a reproducible fashion.[53] This information can then be used to evaluate the progression of the disease and the efficacy of the treatment selected.

Umbilical Remnant Abnormalities

Infected Umbilical Remnants. Infection of the internal umbilical remnant structures, with or without involvement of the external remnant of the umbilicus, is a common problem in neonatal foals and calves.[1-6, 9, 10, 54] Affected foals are usually 1 to 5 weeks old.[2, 3, 5, 8-11] A history of patent urachus or an external umbilical remnant infection may be present, but the majority of foals with infected internal umbilical remnants have neither history.[3, 10] Clinical signs vary from an incidental finding in an otherwise normal foal to fever, depression, and anorexia in a foal that is not growing well. The foal frequently has other concurrent problems such as neonatal septicemia, septic physitis or arthritis, or pneumonia.[1-3, 6, 8-10] Clinicopathologic abnormalities usually include a neutrophilic leukocytosis and hyperfibrinogenemia.[6, 9-11] A low serum IgG may be detected in foals with failure of passive transfer, a common history in affected foals. The majority of foals referred for sonographic examination are referred because of septicemia, another infection (usually septic arthritis), an unexplained persistent neutrophilic leukocytosis or hyperfibrinogenemia, fever of unknown origin, or palpable abnormalities of the external umbilical remnant.[6, 8, 11]

The diagnosis of an infected external umbilical remnant can be made clinically if purulent material drains from the external umbilicus or if heat, swelling, and sensitivity are palpable locally. Sonographically, an external umbilical remnant infection is characterized by an enlarged, thickened external umbilical remnant filled with hypoechoic to echogenic fluid (Fig. 7-15). Hyperechoic echoes representing gas may be detected. The hyperechoic gas echoes are indicative of an anaerobic infection unless a gas-filled tract can be imaged extending from the skin surface into the umbilical remnant.

The diagnosis of infected internal umbilical remnants is best made ultrasonographically. Enlargement of the internal umbilical remnants usually indicates infection.[1-12] Infection of the urachus and umbilical arteries is most common, with infrequent involvement of the umbilical vein.[3, 5] The infected umbilical vein is enlarged (>10 mm) and usually contains hypoechoic to echogenic material within the lumen of the vein (Fig. 7-16), although the purulent material occasionally appears anechoic.[3, 5, 8, 11] Hyperechoic gas echoes may be detected, indicating an anaerobic infection.[3, 5, 6, 9-12] The wall of the umbilical vein may become thickened, more likely with longstanding umbilical vein infection (Fig. 7-16). The infected umbili-

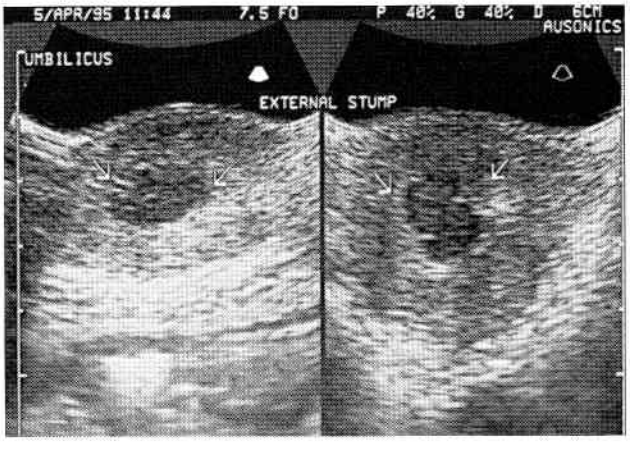

Figure 7–15

Sonograms of an abscessed external umbilical remnant obtained from a 6-week-old Thoroughbred colt. The large hypoechoic abscessed area (*arrows*) is imaged within the echogenic thick-walled external umbilical remnant. The left image is a transverse view, and the right image is a sagittal view of the external umbilical remnant. The right side of the transverse image is the left side of the foal's abdomen and the top is the ventral aspect of the external remnant. The right side of the sagittal image is cranial and the top is ventral. These sonograms were obtained with a 7.5-MHz sector-scanner transducer containing a built-in fluid offset and a displayed depth of 6 cm.

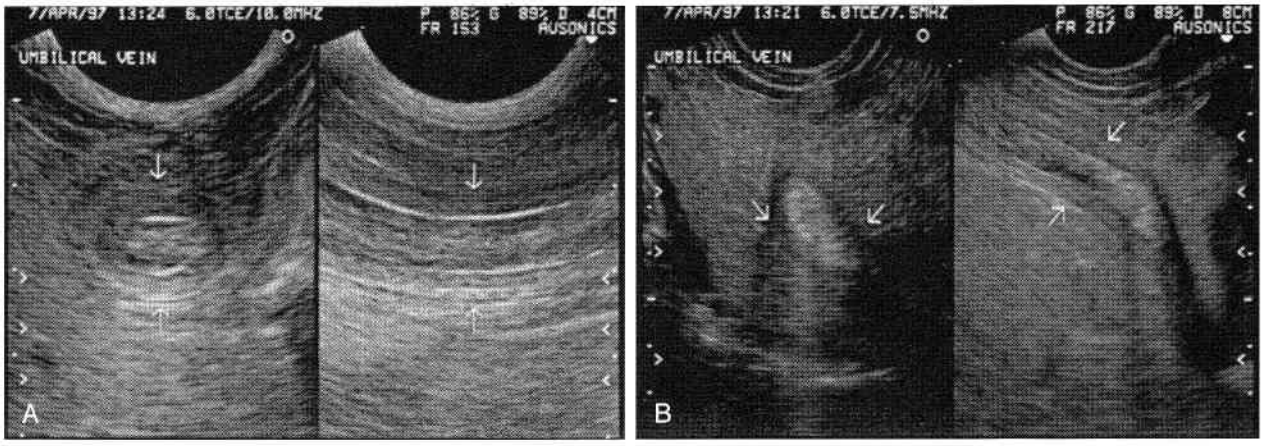

Figure 7–16

Sonograms of the umbilical vein from a 14-day-old Thoroughbred filly with omphalophlebitis. Notice the marked enlargement of the umbilical vein with the thickened walls *(arrows)* and the echogenic fluid within the lumen of the umbilical vein. Both left images are the transverse views and the right images are the sagittal views of the infected umbilical vein. The right side of the transverse views is the left side of the foal's abdomen and the top is ventral. The right side of the sagittal view is cranial. These sonograms were obtained with a wide-bandwidth 6.0-MHz microconvex linear-array transducer operating at 10.0 MHz *(A)* and 7.5 MHz *(B)* and a displayed depth of 4 cm *(A)* and 8 cm *(B)*.

A, These sonograms were obtained just cranial to the external umbilical remnant at A_1 in Figure 7–2. The arrows delineate the outer wall of the enlarged umbilical vein. The walls of the umbilical vein are thickened and the endothelial side of the vessel wall is hyperechoic. The lumen of the umbilical vein is primarily echogenic.

B, These sonograms were obtained at the liver in the cranial abdomen cranial to A_2 in Figure 7–2. The enlarged thick walled umbilical vein filled with echogenic fluid is present at the liver consistent with an ascending omphalophlebitis.

cal vein is usually largest at or near the external umbilical remnant and is smaller in diameter cranially. The majority of umbilical vein infections do not extend into the liver, and the umbilical vein returns to a normal sonographic appearance caudal to its entrance into the liver. If the umbilical vein infection extends cranially into the liver, hepatic abscesses or suppurative hepatitis is likely.[5] The liver should be carefully and thoroughly examined sonographically in these foals. An infected umbilical artery is enlarged (>13 mm) and usually has a swollen, thickened, isoechogenic or hypoechoic arterial wall (Fig. 7-17).[3, 5, 8, 11] Swelling of the surrounding tissues is occasionally detected. The lumen of the infected umbilical artery is usually distended with hypoechoic or anechoic fluid; however, echogenic or hyperechoic fluid is occasionally detected in infected arteries (Fig. 7–18).[3, 5, 9–12] The infected umbilical arteries are usually largest in diameter just caudal to the external umbilical remnant or at the apex of the bladder and become more normal along the lateral sides of the bladder. The urachus, when infected,

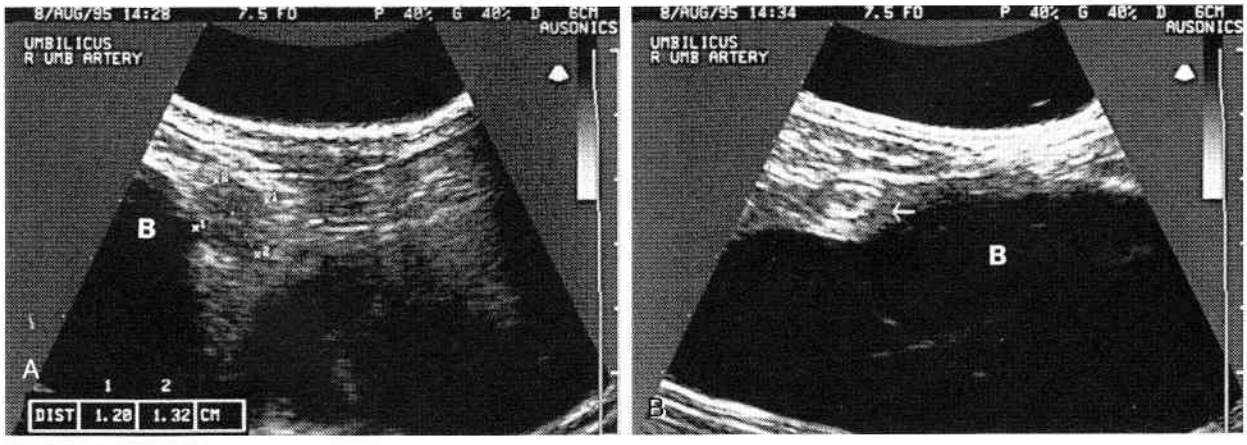

Figure 7–17

Sonograms of the umbilical arteries obtained from a 18-day-old Appaloosa filly with omphaloarteritis. The right side of these sonograms is the left side of the foal's abdomen and the top is ventral. These sonograms were obtained with a 7.5-MHz sector-scanner transducer containing a built-in fluid offset and a displayed depth of 6 cm. B, Bladder.

A, The thickened left umbilical artery with the swollen hypoechoic vessel wall and the hypoechoic fluid center is consistent with omphaloarteritis. The distinction between the wall and lumen of the vessel is poor. The left umbilical artery was enlarged and measured 1.2 (x^1) by 1.32 (x^2) cm in diameter along the left side of the bladder.

B, The slightly smaller right umbilical artery (*arrow*) with an echogenic wall but an abnormal hypoechoic fluid-filled center is consistent with mild omphaloarteritis along the right side of the bladder.

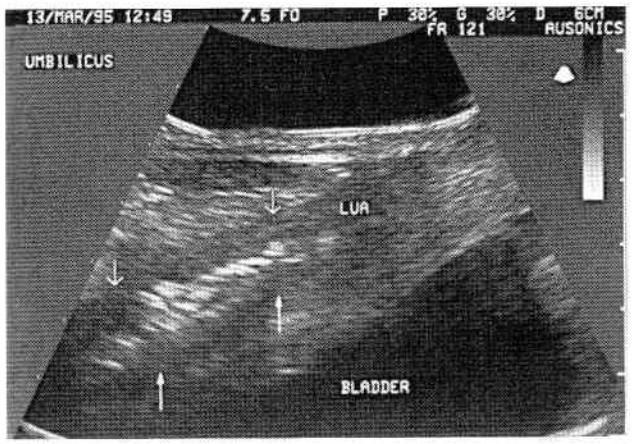

Figure 7–18

Sonogram of the left umbilical artery (LUA) obtained from a 1-month-old Thoroughbred colt with omphaloarteritis. The marked enlargement of the left umbilical artery (*arrows*) and the hyperechoic echoes within the lumen of the left umbilical artery which cast faint acoustic shadows are consistent with free gas and a probable anaerobic infection. The left umbilical artery is imaged in its long axis coursing alongside the bladder. The right side of this sonogram is cranial, and the top is ventral. This sonogram was obtained with a 7.5-MHz sector-scanner transducer containing a built-in fluid offset and a displayed depth of 6 cm.

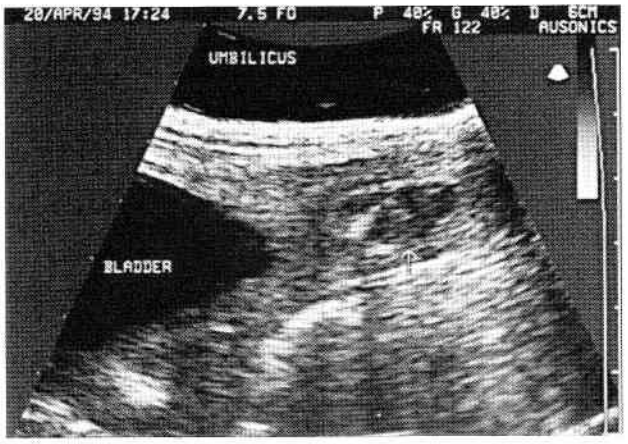

Figure 7–20

Sonogram of the urachus and apex of the bladder obtained from a 3-week-old Standardbred filly. The cavitated fluid-filled urachus with loculations (*arrow*) is consistent with urachitis. The urachus is walled off from the bladder apex and no longer communicates with the bladder. The right side of this sonogram is cranial, and the top is ventral. This sonogram was obtained with a 7.5-MHz sector-scanner transducer containing a built-in fluid offset and a displayed depth of 6 cm.

is also swollen and filled with fluid and/or cellular debris (Fig. 7-19).[3, 5, 9-12] The fluid within the infected urachus may be anechoic, hypoechoic, or echogenic (Fig. 7-20).[10] Hyperechoic gas echoes may also be detected in the urachus (Fig. 7-21) and indicate a concurrent anaerobic infection.[10] The maximal distention of the urachus may be at the bladder apex, midway between the bladder and the external umbilical remnant, or just caudal to the external umbilical remnant. A combined measurement for the urachus and both umbilical arteries at the apex of the bladder greater than 25 mm is consistent with infection.[3, 5, 8, 11] Occasionally, in more longstanding umbilical vein or urachal infections, the infection becomes walled off and appears as an encapsulated abscess (Fig. 7-21). Multiple internal umbilical structures are often infected in affected foals.[1, 3, 5, 9-12] Ultrasonographic detection of enlarged fluid-filled internal umbilical remnants is an accurate indication of infected internal umbilical remnants.[3, 4]

The surrounding structures should also be carefully

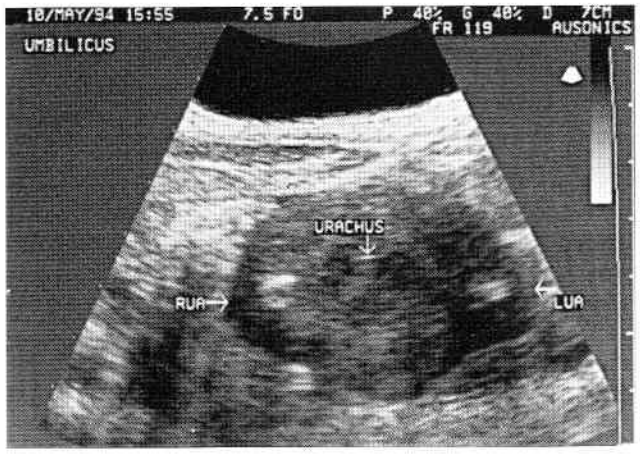

Figure 7–19

Sonogram of the urachus and both umbilical arteries obtained from a 1-month-old Thoroughbred cross colt with urachitis. Notice the marked enlargement of the urachus containing hypoechoic fluid (*down arrow*). The walls of the urachus are thickened and bulging around the left (LUA) and right (RUA) umbilical arteries. The walls of the umbilical arteries are also swollen and hypoechoic. The right side of this sonogram is the left side of the foal's abdomen, and the top is ventral. This sonogram was obtained with a 7.5-MHz sector-scanner transducer containing a built-in fluid offset and a displayed depth of 7 cm.

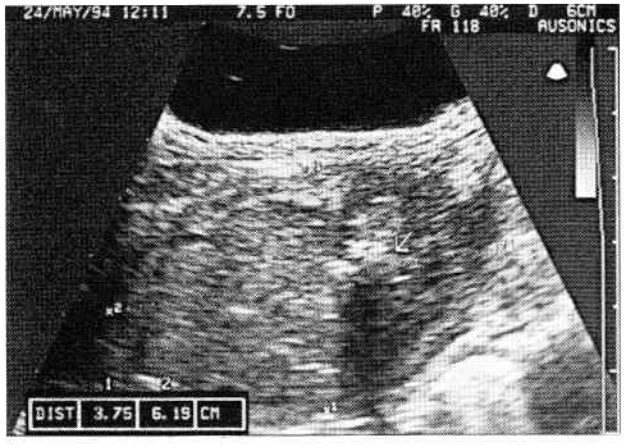

Figure 7–21

Sonogram of the urachus and both umbilical arteries obtained from a 1-month-old Thoroughbred colt with an infected urachus. The urachus is markedly enlarged, measuring 3.75 cm (x^1) in thickness by 6.19 (x^2) in length. The hyperechoic echoes (*arrow*) within the hypoechoic to echogenic fluid represent free gas and probable anaerobic infection. The urachus is thick walled and appears encapsulated. The right side of this sonogram is cranial, and the top is ventral. This sonogram was obtained with a 7.5-MHz sector-scanner transducer containing a built-in fluid offset and a displayed depth of 6 cm.

evaluated, as the infection may also involve the adjacent tissues.[26] Localized peritonitis with adhesions of gastrointestinal viscera and spleen to the infected urachus (Fig. 7-22) and involvement of the bladder wall have been detected (Fig. 7-23).[26, 55] If the bladder wall is involved in the infection, the foal is at increased risk for the development of uroperitoneum.[23, 55] Abnormalities within the bladder may also occur in foals with infected umbilical remnants. A concurrent cystitis is most commonly detected in foals with urachitis. Increased echogenicity of the urine contained within the bladder is consistent with an increased cell count and probable infection, as foal urine is normally anechoic.[5] Cellular debris may be imaged extending from the urachus into the ventral portion of the bladder (Fig. 7-24) in a small number of foals with urachitis. Although internal umbilical remnant infections are usually only detected in foals less than 8 weeks old, occasionally older foals present with a history of an acute onset of abdominal swelling and fever.[3, 4] These foals may also have a neutrophilic leukocytosis and a hyperfibrinogenemia. Sonographic evaluation of the abdomen in these foals reveals ventral edema, cellulitis (Fig. 7-25), a subcutaneous abscess, and large thick-walled infected internal umbilical remnants, similar to the findings in older calves.[4, 54] The oldest horse reported with infected internal umbilical remnants was 16 months old.[4]

Umbilical Remnant Hemorrhage. Enlargement of the internal umbilical vessels occurs occasionally with extensive hemorrhage from the umbilical cord at parturition. Marked swelling of the internal umbilical vessels, large fibrin clots within the vessels, or loculated hemorrhage in the immediate perivascular tissues may be detected in these foals.[5] Occasionally a ruptured umbilical artery or vein may be imaged in association with a large area of vascular and perivascular hemorrhage (Fig. 7-26) and/or a large fibrin clot (Fig. 7-27). Examination of the

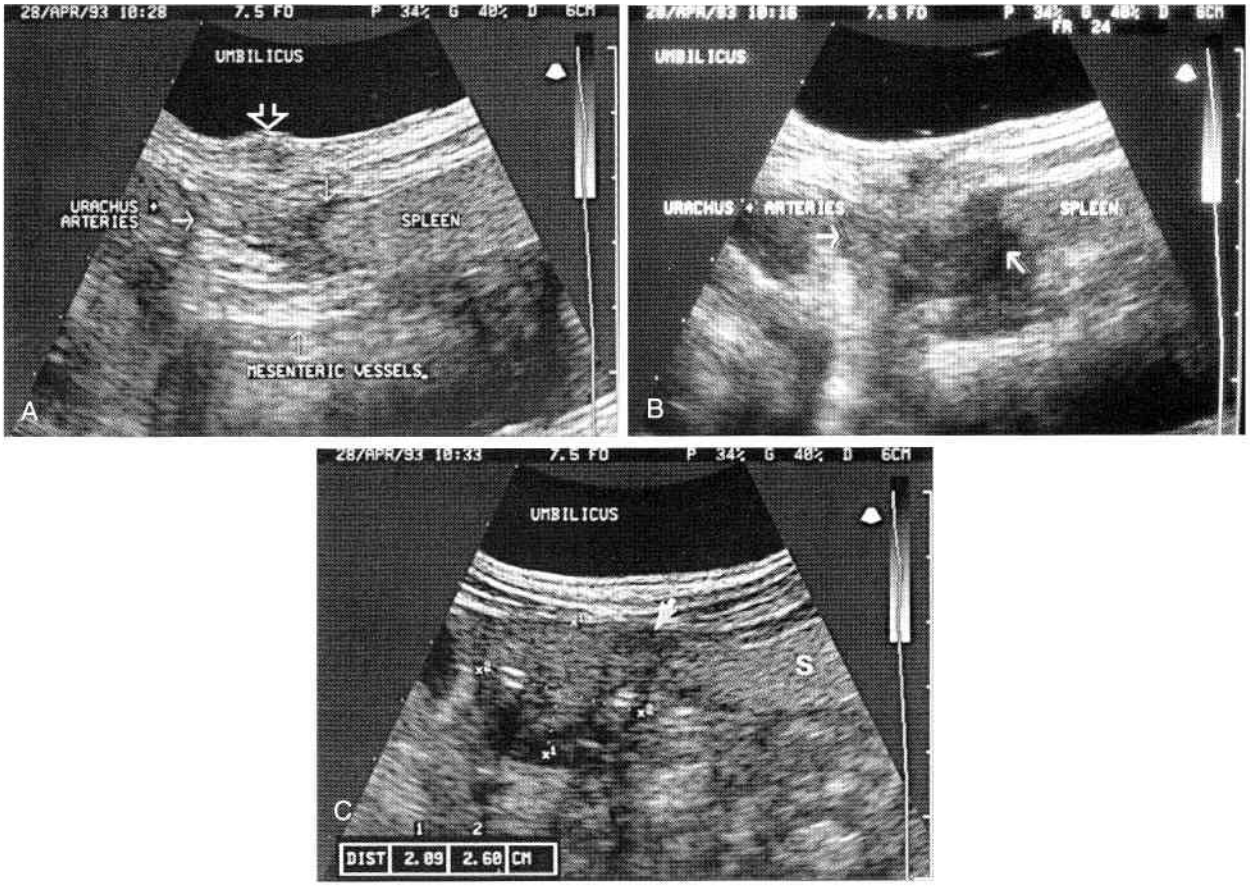

Figure 7-22

Sonograms of the caudal ventral abdomen obtained from a 5-week-old Standardbred colt with localized peritonitis associated with urachitis. The right side of these sonograms is the left side of the foal's abdomen, and the top is ventral. These sonograms were obtained with a 7.5-MHz sector-scanner transducer containing a built-in fluid offset and a displayed depth of 6 cm.

A, Notice the small amount of hypoechoic peritoneal fluid (*vertical down arrow*) between the rounded tip of the spleen, the mesenteric vessels of the large colon, and the caudal internal umbilical remnants (urachus and umbilical arteries). This sonogram was obtained at the level of the external umbilical remnant (*open arrow*).

B, Sonogram of the localized area of peritonitis (*diagonal arrow*) between the tip of the spleen, the large colon (C), and the caudal internal umbilical remnants (urachus and umbilical arteries). This was the largest area of hypoechoic fluid and fibrin accumulation and was located slightly caudal to the view in *A*.

C, Sonogram of the umbilical arteries and the urachus at the apex of the bladder. The large hypoechoic fluid-filled urachus is consistent with urachitis. The umbilical arteries with the urachus in between measured 2.09 (x^1) by 2.60 (x^2) cm in diameter. The defect in the urachus adjacent to the spleen (*arrow*) is the probable cause of the localized peritonitis. The double echogenic lines represent the inner walls of the umbilical arteries. S, Spleen.

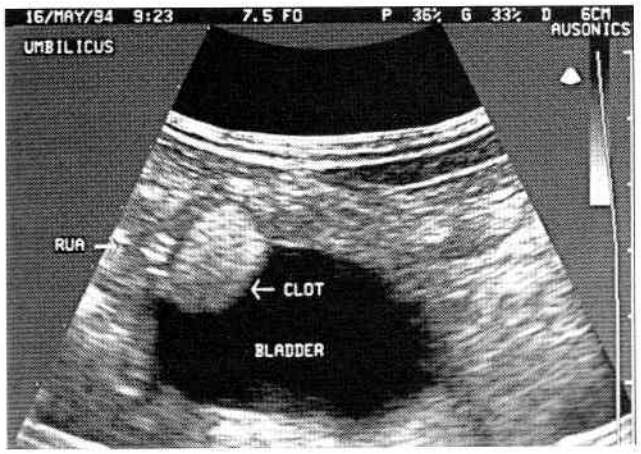

Figure 7–23

Sonogram of the bladder and right umbilical artery obtained from a 3-week-old Thoroughbred filly with an omphaloarteritis of the right umbilical artery. The enlarged right umbilical artery (RUA) with the large echogenic clot along the wall of the right umbilical artery involves the right bladder wall. This omphaloarteritis was not responding to broad-spectrum antimicrobial therapy, and the infection was progressing to involve the bladder wall. Surgical resection of this infected tissue was performed. The right side of this sonogram is the left side of the foal's abdomen, and the top is ventral. This sonogram was obtained with a 7.5-MHz sector-scanner transducer containing a built-in fluid offset and a displayed depth of 6 cm.

bladder is also indicated in foals with a history of bleeding from the umbilicus at birth. Large echogenic masses representing blood clots or lacy webs of loculated fibrin have been imaged in the bladder of several septicemic foals with histories of excessive bleeding from the umbilical cord (Fig. 7-28).[11, 12] Organisms cultured from the urinary bladder were the same as those cultured from the blood in affected foals.[11, 12] Fibrin clots have also been detected ultrasonographically in the bladder and urachus of foals with urachitis.

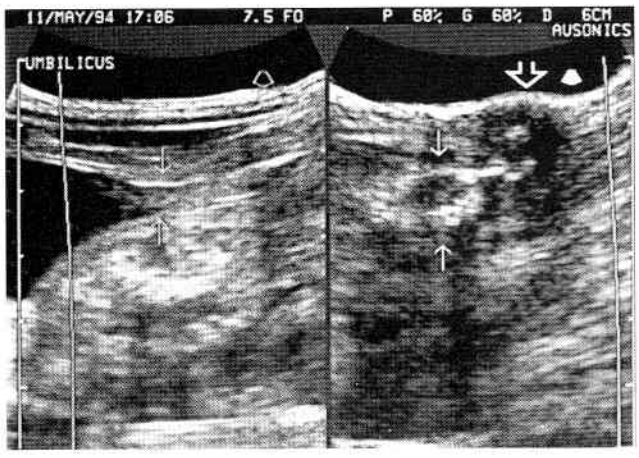

Figure 7–24

Sonograms of the urachus and apex of the bladder obtained from a 2-week-old Thoroughbred filly with omphaloarteritis and urachitis. The hypoechoic cellular debris (*arrows*) extends into the bladder from the urachus in the left sagittal image. The hypoechoic fluid pocket within the urachus in the right sagittal image with the hyperechoic echoes along the inner wall of the urachus (*arrows*) is consistent with an anaerobic urachitis. The left sagittal image was obtained at the level of the apex of the bladder, whereas the right sagittal image was obtained just caudal to the external umbilical remnant (*open arrow*). The right side of these sonograms is cranial, and the top is ventral. These sonograms were obtained with a 7.5-MHz sector-scanner transducer containing a built-in fluid offset and a displayed depth of 6 cm.

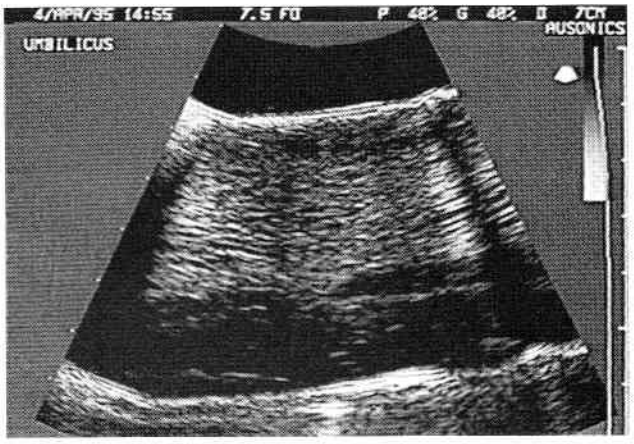

Figure 7–25

Sonogram of the ventral abdomen obtained from a 6-month-old Thoroughbred filly with ventral abdominal swelling. The thick layer of finely loculated fluid and the increased echogenicity of the subcutaneous tissues are consistent with a cellulitis of the ventral abdomen. This filly also had urachitis. The right side of this sonogram is the left side of the foal's abdomen. This sonogram was obtained with a 7.5-MHz sector-scanner transducer containing a built-in fluid offset and a displayed depth of 7 cm.

Patent Urachus and Urachal Diverticulum. Noninfectious urachal abnormalities, such as patent urachus and urachal diverticulum, have a characteristic ultrasonographic appearance that can be easily differentiated from urachitis. A patent urachus is a urachus containing a small amount of anechoic fluid that is continuous with the

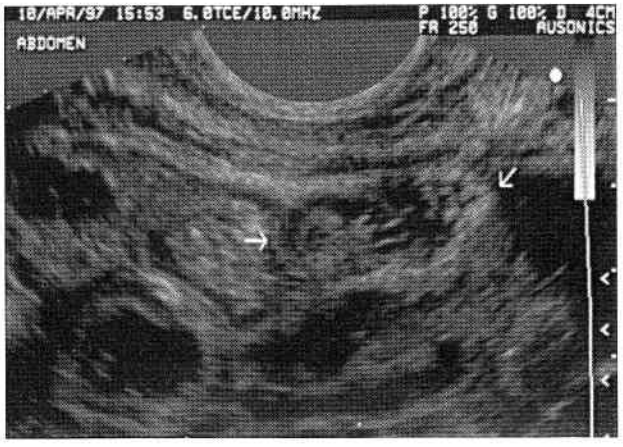

Figure 7–26

Sonogram of the umbilical arteries immediately caudal to the external umbilical remnant obtained from a 2-day-old Thoroughbred colt with a ruptured left umbilical artery and extensive hemorrhage from the umbilicus at birth. The horizontal arrow points to the intact right umbilical artery imaged at B in Figure 7-2. The diagonal arrow points to an anechoic loculated fluid space where the left umbilical artery should be. Further caudally along the left side of the bladder, the left umbilical artery was recognized. The right side of this sonogram is the left side of the foal's abdomen and the top is ventral. This sonogram was obtained with a wide-bandwidth 6.0-MHz microconvex linear-array transducer operating at 10.0 MHz and a displayed depth of 4 cm.

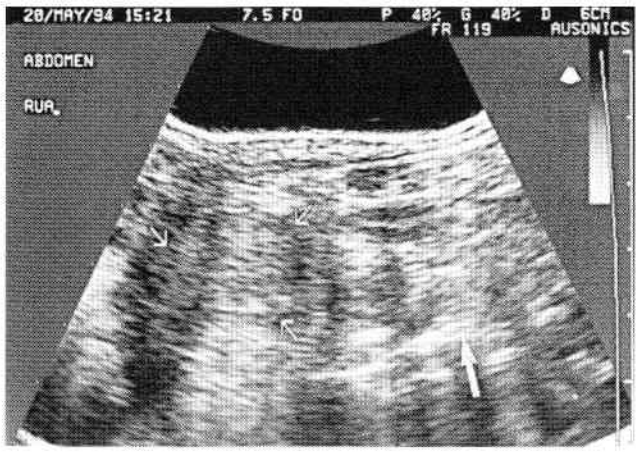

Figure 7–27

Sonogram obtained of the umbilical arteries and urachus near the apex of the bladder (see Figure 7-2 at B) obtained from a 2-day-old Thoroughbred filly with extensive hemorrhage from the umbilicus at birth. An echogenic clot *(thin arrows)* is visible where the right umbilical artery should be. The right umbilical artery could not be identified, only the large clot and surrounding perivascular hemorrhage, consistent with a ruptured right umbilical artery. The left umbilical artery is barely recognizable *(large arrow)*. The right side of this sonogram is the left side of the foal's abdomen, and the top is ventral. This sonogram was obtained with a 7.5-MHz sector-scanner transducer containing a built-in fluid offset and a displayed depth of 6 cm.

bladder apex (Fig. 7-29).[5, 8-12] Care must be taken in making this diagnosis sonographically because the small amount of fluid within the urachus can easily be displaced by the pressure of the transducer against the abdominal wall. Therefore, scanning the urachus with gentle pressure is indicated, when a patent urachus is suspected, to minimize compression of the walls of the urachus and subsequent fluid displacement. A fluid-filled caudal urachus continuous with the bladder apex, but not with the external umbilicus, is consistent with a

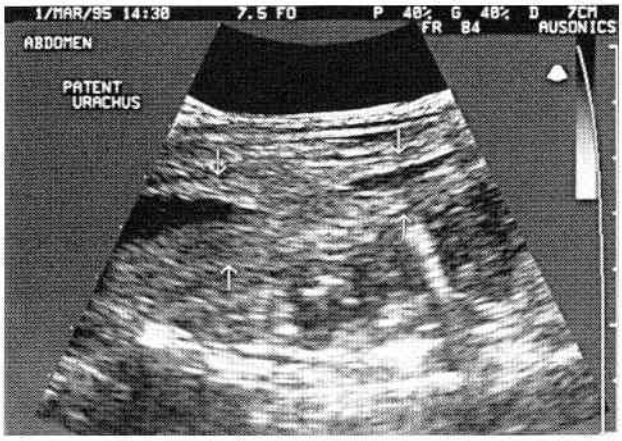

Figure 7–29

Sonogram of a patent urachus obtained from a 12-day-old Thoroughbred colt. Notice the thick wall of the urachus and the anechoic fluid contained within the urachus *(arrows)*. This anechoic urine could be followed from the bladder to the external umbilical remnant. The right side of this sonogram is cranial, and the top is ventral. This sonogram was obtained with a 7.5-MHz sector-scanner transducer containing a built-in fluid offset and a displayed depth of 7 cm.

urachal diverticulum (Fig. 7-30).[8-12] The urachal diverticulum and patent urachus are often most easily visualized in the sagittal image because the connection with the bladder and more cranial aspects of the urachus can be visualized in the same scan plane.

Uroperitoneum and Abnormalities of the Bladder

The rapid identification of the foal with a ruptured bladder and uroperitoneum is another useful application of diagnostic ultrasound. Ultrasonography of the urinary bladder and urachus is a quick and noninvasive method

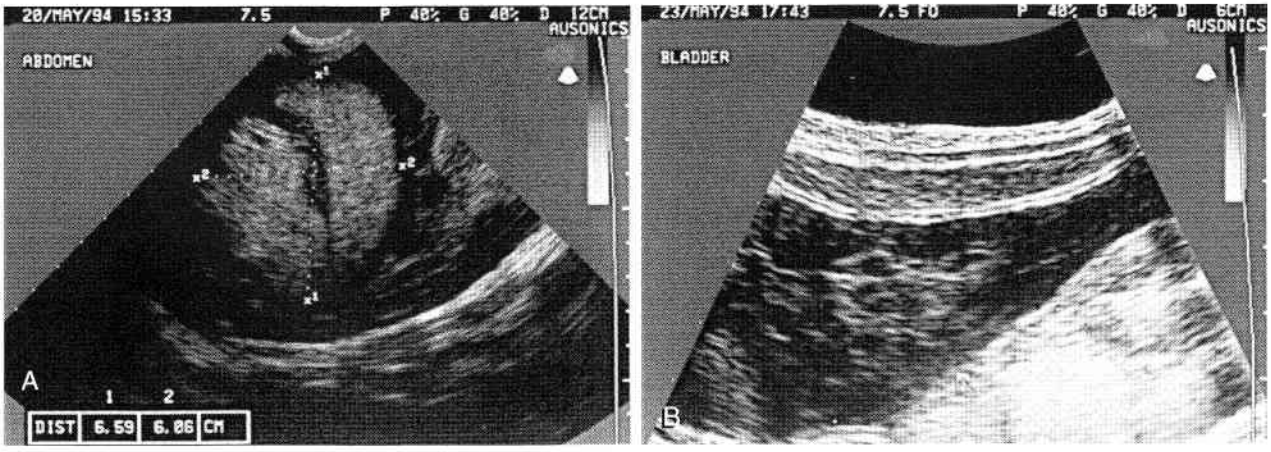

Figure 7–28

Sonograms of the bladder obtained from a Thoroughbred filly with extensive hemorrhage from the umbilicus at birth and a ruptured right umbilical artery (same filly as in Figure 7-27). The right side of these sonograms is cranial, and the top is ventral.

A, The large echogenic clot within the bladder measures at least 6.59 (x^1) by 6.06 (x^2) cm in diameter. This sonogram was obtained the same day as the image of the ruptured right umbilical artery in Figure 7-26. This sonogram was obtained with a 7.5-MHz sector-scanner transducer and a displayed depth of 12 cm.

B, Lacy loculations appear within the bladder *(arrow)* as the hemorrhage begins to resolve. This sonogram was obtained 3 days later with a 7.5-MHz sector-scanner transducer containing a built-in fluid offset and a displayed depth of 6 cm. The bladder contained much less urine at this time.

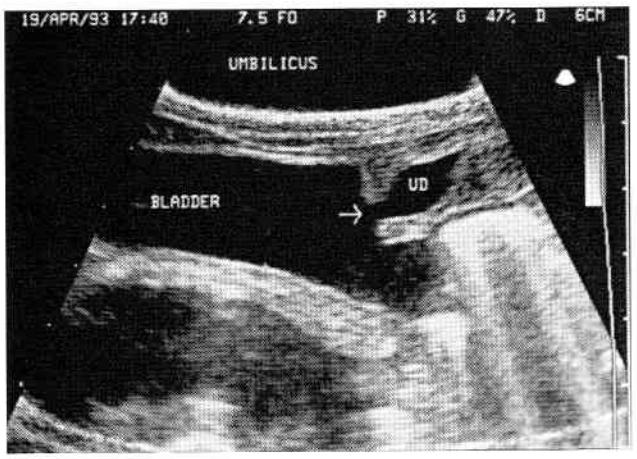

Figure 7–30

Sonogram of a urachal diverticulum obtained from a 9-day-old Thoroughbred filly. Notice the anechoic fluid in the bladder, the urachal diverticulum (UD), and the narrowed neck of the urachal diverticulum at the apex of the bladder (*arrow*). The right side of this sonogram is cranial, and the top is ventral. This sonogram was obtained with a 7.5-MHz sector-scanner transducer containing a built-in fluid offset and a displayed depth of 6 cm.

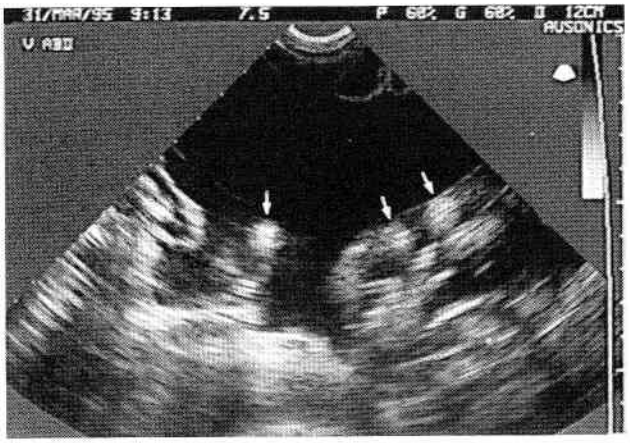

Figure 7–31

Sonogram of the ventral abdomen obtained from a 1-day-old Thoroughbred filly with uroperitoneum. Notice the large volume of anechoic fluid and the gastrointestinal viscera floating in the fluid. Multiple loops of jejunum (*arrows*) are recognizable by their long mesentery, round appearance in short-axis cross-section, and the small diameter of the bowel. The right side of the sonogram is the left side of the foal's abdomen, and the top is ventral. This sonogram was obtained with a 7.5-MHz sector-scanner transducer and a displayed depth of 12 cm.

of confirming the diagnosis of uroperitoneum and locating the site of the defect for surgical repair.[9–11, 14, 22, 26] A variety of diagnostic techniques can be used to confirm the diagnosis, including injection of a nontoxic dye such as new methylene blue, fluorescein, or azosulfamide into the bladder and subsequent retrieval of peritoneal fluid containing dye, positive-contrast cystography, and excretory urography, but all of these techniques are invasive and time consuming.[26]

The reported incidence of urinary bladder rupture in neonatal foals is 0.2 to 2.5%.[56] Affected foals are usually males, less than 1 week old and have a history of straining to urinate or dribbling small amounts of urine.[10, 11, 14, 23, 26, 29, 56–64] Foals with uroperitoneum become depressed and lethargic with a progressively distending abdomen.[10, 11, 14, 23, 26, 29, 55–61, 63, 64] The bladder, urachus, or ureter may be ruptured, or a congenital defect may be present. Uroperitoneum is most commonly associated with a defect in the wall of the bladder.[9, 11, 14, 22, 23, 29, 56, 59–62] Ureteral defects are rare in foals.[11, 14, 61] Urachal defects occurred with nearly equal frequency to ruptured bladders in hospitalized foals in one study.[23] Affected foals had a high incidence of co-existing gastrointestinal disease and bacterial or fungal infection.[23, 62] Older foals (approximately 1 month old) may also develop uroperitoneum, usually secondary to an infectious or necrotic focus in the bladder or a urinary tract obstruction, usually urethral.[14, 26, 56] These foals have often been chronically ill or septicemic. Foals with uroperitoneum are usually hyponatremic, hypochloremic, hyperkalemic, azotemic, and hyperosmolar and have a metabolic acidosis.[10, 23, 26, 56, 59–62] A peritoneal fluid creatinine that is more than twice the serum creatinine is considered diagnostic for ruptured bladder.[23, 26, 29, 56, 59–61] Cytologic evaluation of the peritoneal fluid may reveal peritonitis and sepsis, a secondary complication in affected foals.

With uroperitoneum, the peritoneal cavity is filled with fluid and the gastrointestinal viscera are imaged floating in and on top of the fluid (Fig. 7-31).[8, 9, 11, 12, 14, 16, 22, 23, 26, 29] The peritoneal fluid may become hypoechoic and contain strands of fibrin if a secondary peritonitis develops (Fig. 7-32)[9, 14, 16, 26] or have increased echogenicity associated with a concurrent cystitis.[23] The urinary bladder is also imaged floating within the fluid suspended by the umbilical arteries (Fig. 7-33). If the urinary bladder is ruptured, the bladder usually appears collapsed, flaccid, and folded upon itself, containing little or no fluid (Fig. 7-33).[8, 9, 11, 12, 14, 22, 23, 26] Although the defect is usually in the dorsal wall of the bladder, the defect itself may not be directly imaged during the sonographic examination

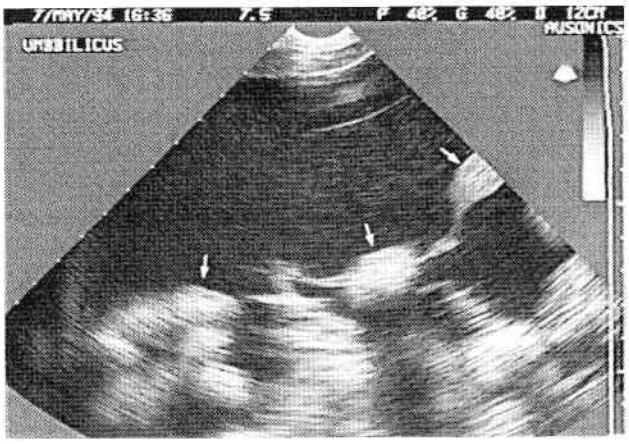

Figure 7–32

Sonogram of the ventral abdomen obtained from a 3.5-week-old Thoroughbred colt with uroperitoneum associated with a ruptured ureter. The hypoechoic fluid in the ventral abdomen is consistent with a secondary chemical peritonitis, and the jejunum (*arrows*) is floating in this fluid. The right side of this sonogram is the left side of the foal's abdomen, and the top is ventral. This sonogram was obtained with a 7.5-MHz sector-scanner transducer and a displayed depth of 12 cm.

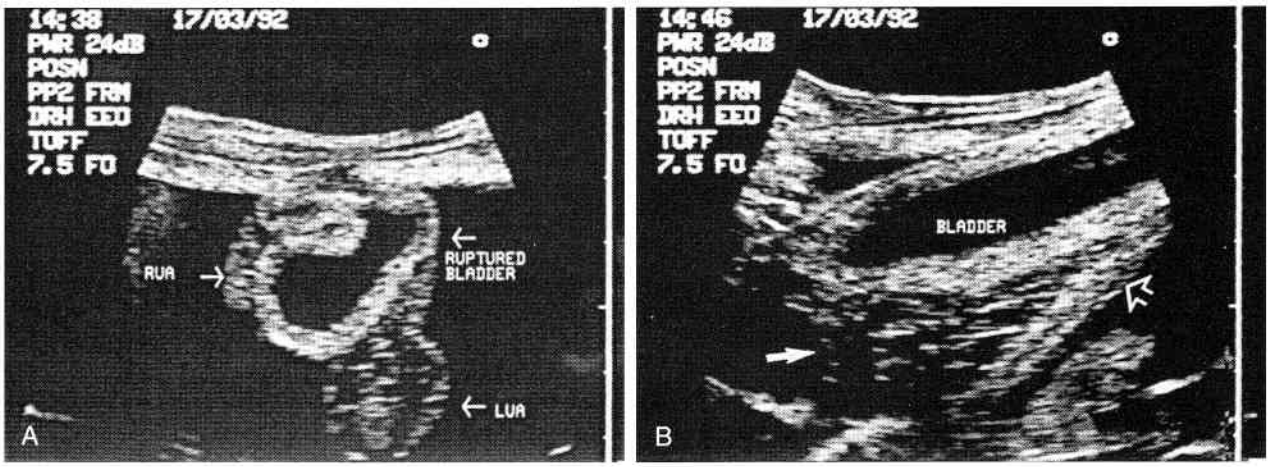

Figure 7–33

Sonograms of a ruptured bladder obtained from a 4-day-old Thoroughbred filly with uroperitoneum and a ruptured bladder. Notice the small amount of urine within the bladder and the large amount of anechoic fluid within the peritoneal cavity. These sonograms were obtained with a 7.5-MHz sector-scanner transducer containing a built-in fluid offset and a displayed depth of 7.5 cm.

A, Notice the collapsed and folded appearance of the bladder (*arrow*) and the fluid dissecting out (*arrow*) along the left umbilical artery (LUA). The bladder is suspended in the abdominal cavity by the right (RUA) and left (LUA) umbilical arteries (*arrows*), which will atrophy and become the round ligaments of the bladder. The right side of the sonogram is the left side of the foal's abdomen, and the top is ventral.

B, The collapsed bladder with the fluid (*solid arrow*) dissecting out along the left dorsal aspect of the bladder along the left umbilical artery (*open arrow*). The dissection of this fluid (probably urine) suggests a tear along the left dorsal wall of the bladder. The right side of this sonogram is cranial, and the top is ventral.

because of the folding of the bladder wall.[9, 10, 14, 26] If fluid is imaged dissecting along one of the umbilical arteries, a defect in this location should be suspected (Fig. 7-33). In some affected foals, fluid may be imaged passing through the rent in the bladder wall from a partially filled bladder into the peritoneal cavity (Fig. 7-34).[9, 11, 14, 26] The collapsed and folded appearance of the bladder should not be mistaken for a recently voided or empty bladder, which is small and contracted but does not appear folded upon itself (Fig. 7-35). Marked distention of the gastrointestinal viscera may indent the bladder wall (Fig. 7-36) but does not cause the bladder to develop a folded appearance, such as is seen with a ruptured bladder. In foals with renal failure, urine production can be assessed by sonographically monitoring the accumulation of urine in the bladder.

With a urachal defect, fluid is imaged dissecting around the urachus in the retroperitoneal and/or subcutaneous space (Figs. 7-37 and 7-38).[8-12, 14, 24, 26] Again, the actual defect in the urachal wall may be difficult to appreciate sonographically, but the dissection of urine into the sur-

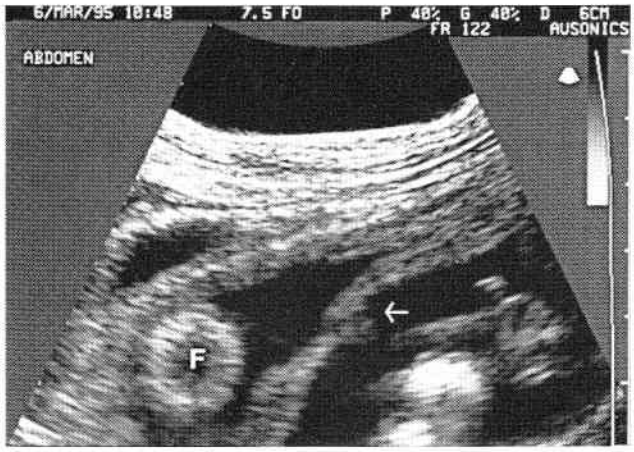

Figure 7–34

Sonogram of a ruptured bladder obtained from a 2-day-old Standardbred filly delivered by cesarean section. Notice the rent in the dorsal bladder wall (*arrow*) and the Foley catheter with the distended balloon (F) in place in the bladder lumen. Fluid was imaged in real time passing through the rent in the bladder wall. Excess anechoic fluid was detected in the peritoneal cavity. The jejunum is imaged floating in the excess abdominal fluid. The right side of this sonogram is cranial, and the top is ventral. This sonogram was obtained with a 7.5-MHz sector-scanner transducer containing a built-in fluid offset and a displayed depth of 6 cm.

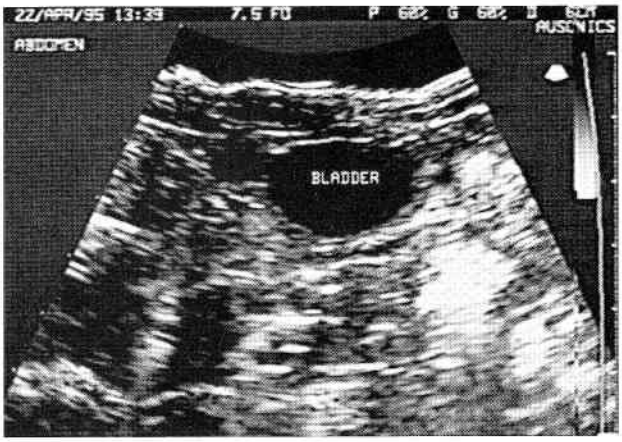

Figure 7–35

Sonogram of the ventral abdomen obtained from a 2-day-old Thoroughbred colt. The small intact bladder is surrounded by gas- and ingesta-filled large and small bowel. This is a typical appearance for a recently voided bladder. The right side of this sonogram is the left side of the foal's abdomen, and the top is ventral. This sonogram was obtained with a 7.5-MHz sector-scanner transducer containing a built-in fluid offset and a displayed depth of 6 cm.

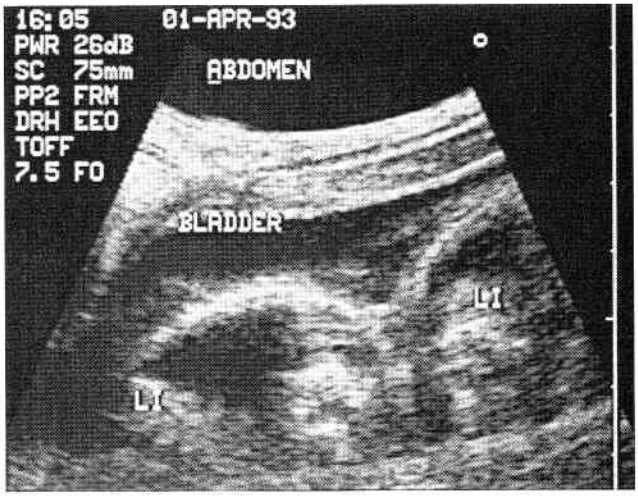

Figure 7–36

Sonogram of the caudal ventral abdomen obtained from a 4-day-old Thoroughbred filly with spasmodic colic. The marked gaseous distention of the large colon (LI) indents the foal's bladder. The right side of this sonogram is cranial, and the top is ventral. This sonogram was obtained with a 7.5-MHz sector-scanner transducer containing a built-in fluid offset and a displayed depth of 7.5 cm.

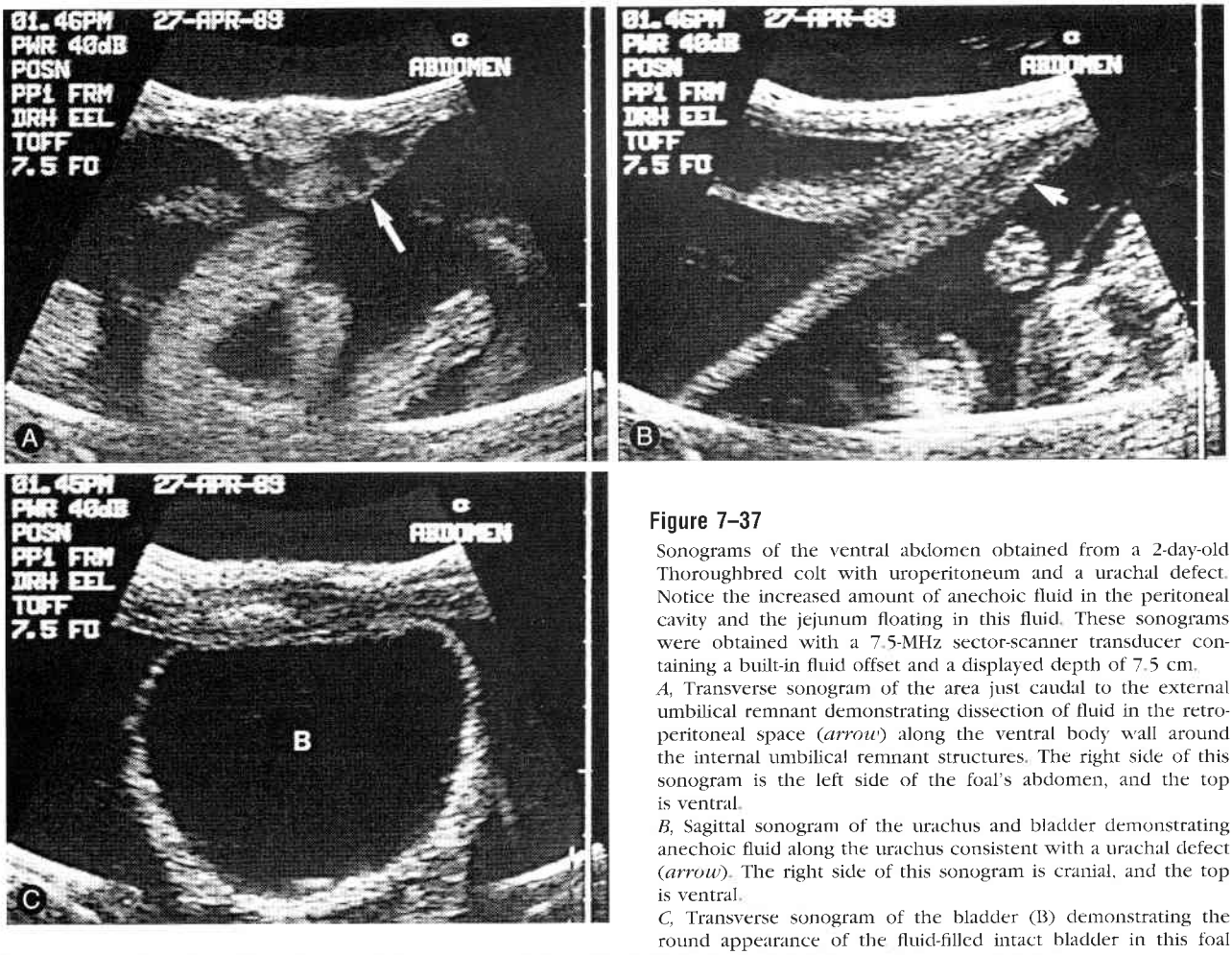

Figure 7–37

Sonograms of the ventral abdomen obtained from a 2-day-old Thoroughbred colt with uroperitoneum and a urachal defect. Notice the increased amount of anechoic fluid in the peritoneal cavity and the jejunum floating in this fluid. These sonograms were obtained with a 7.5-MHz sector-scanner transducer containing a built-in fluid offset and a displayed depth of 7.5 cm.

A, Transverse sonogram of the area just caudal to the external umbilical remnant demonstrating dissection of fluid in the retroperitoneal space (*arrow*) along the ventral body wall around the internal umbilical remnant structures. The right side of this sonogram is the left side of the foal's abdomen, and the top is ventral.

B, Sagittal sonogram of the urachus and bladder demonstrating anechoic fluid along the urachus consistent with a urachal defect (*arrow*). The right side of this sonogram is cranial, and the top is ventral.

C, Transverse sonogram of the bladder (B) demonstrating the round appearance of the fluid-filled intact bladder in this foal with a ruptured urachus. The right side of this sonogram is the left side of the foal's abdomen, and the top is ventral.

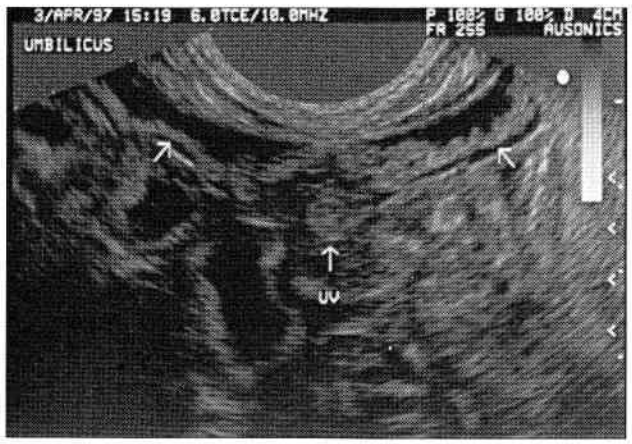

Figure 7–38

Sonogram of the umbilical vein and retroperitoneal space obtained from a 7-day-old Thoroughbred foal with a urachal leak and elevated creatinine. There is a large amount of anechoic fluid dissecting out in the retroperitoneal space *(arrows)* and around the umbilical vein (UV) with only a small increase in the amount of free fluid in the abdomen. This fluid was traced caudally to a defect in the urachus adjacent to a localized area of urachitis. This foal was treated medically and monitored sonographically and the retroperitoneal fluid resolved and the plasma creatinine returned to normal. The right side of this sonogram is the left side of the foal's abdomen. This sonogram was obtained with a wide-bandwidth 6.0-MHz microconvex linear-array transducer operating at 10.0 MHz and a displayed depth of 4 cm.

rounding tissues is detectable. In foals with a urachal defect, the bladder is usually round and filled with urine (Fig. 7-37) because the defect is often small and urine is slowly leaking into the peritoneal cavity.[9, 11, 14, 26] The most difficult defect to diagnose sonographically is the ureteral defect because the ureters are not normally visible. Foals with a ureteral defect have normal urachal remnants and a normal fluid-filled bladder with a large amount of free fluid in the peritoneal cavity.[11, 12, 14, 25, 26, 59] Sonographic evaluation of the kidneys should be performed because retroperitoneal fluid (urine) may be imaged surrounding the kidney in some foals with a ruptured ureter.[12, 25, 26, 59]

In older foals with a necrotizing cystitis, a thickened bladder wall is imaged (Fig. 7-39).[12] Abnormalities of bladder wall echogenicity (usually increased) are often detected in these foals in association with inflammatory cell infiltrate and necrosis.[12, 14, 26] Gas echoes have been imaged in the wall of the bladder in one foal with a necrotizing cystitis and uroperitoneum.[12, 26] A discrete defect in the bladder wall may or may not be visualized. Many of these foals may have adhesions between the bladder and the surrounding gastrointestinal viscera (Fig. 7-39).[26] Fibrin and echogenic fluid may be imaged in the peritoneal cavity owing to the associated peritonitis.

The urethra should be evaluated sonographically if urethral obstruction is suspected as the cause of the uroperitoneum. The typical sonographic appearance of a urethral calculus is a hyperechoic concretion casting an acoustic shadow wedged in the lumen of the urethra with fluid distention proximal to the urolith. Urethral calculi have been reported in older foals with uroperitoneum and have been seen in foals admitted to our hospital with uroperitoneum.[65] Cellular or proteinaceous debris secondary to infection is the most likely cause for the formation of these calculi in foals with urethral obstruction. A complete sonographic evaluation of the entire urinary tract is indicated in these foals to investigate possible sites of calculus formation and/or infection. A urolith has also been reported to cause obstruction of the penile urethra in a yearling 10 months after laparoscopic repair of a ruptured bladder.[66] In this foal, staples had been used to close the defect in the bladder and may have been the nidus for calculi formation, as videoendoscopic examination of the bladder revealed ulceration in the region of the staple line. The urolith was imaged sonographically in the penile urethra in this yearling. Urethral obstruction without uroperitoneum has also been reported in a 3-month-old colt.[23] In one large study of urolithiasis, horses as young as 7 months were affected, although the sites of the uroliths in these youngsters were not reported.[67] Ultrasonographic examination of the upper and lower urinary tract was useful in identifying the location of urinary calculi.

Sonographic evaluation of the surgical repair can also be performed if the foal is experiencing problems postoperatively (Figs. 7-40 and 7-41). Defects in the repaired bladder wall or adhesions between the bladder and surrounding structures may be detected. Some leakage of urine through the bladder wall is possible when the surgical line appears intact sonographically, but is usually minimal.

Abnormalities of the Abdominal Organs

Renal Disease. Renal disease is probably the most common organ disease in young foals because many neonatal foals experience peripartum asphyxia and hypoxic renal injury. Sonographic evaluation of the kidneys in these foals may reveal no abnormalities or a slight de-

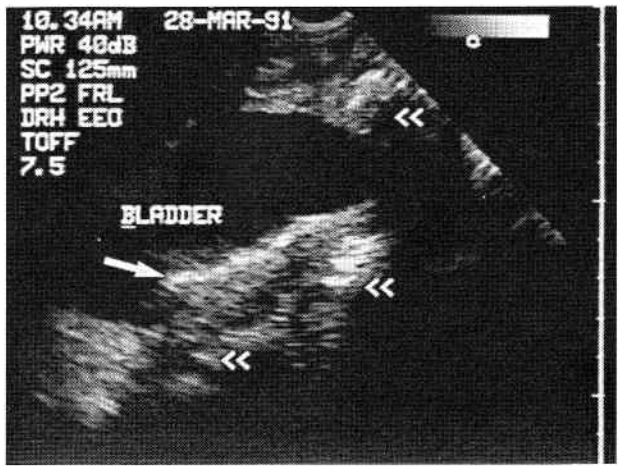

Figure 7–39

Sonogram of the bladder obtained from a 1-month-old Thoroughbred colt with necrotizing cystitis and adhesions between bladder and large colon *(arrowheads)*. Notice the marked thickening of the dorsal bladder wall and irregular mucosal surface of the bladder *(arrow)*. This colt had an emphysematous cystitis. The right side of the sonogram is cranial, and the top is ventral. This sonogram was obtained with a 7.5-MHz sector-scanner transducer and a displayed depth of 12.5 cm.

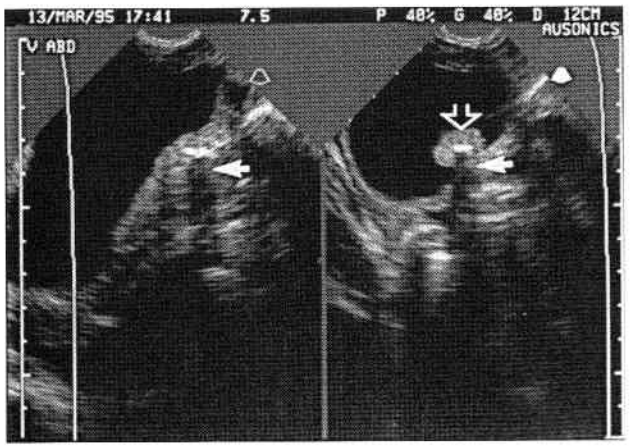

Figure 7–40

Sonograms of the bladder following surgical repair of a ruptured bladder in a 9-day-old Standardbred filly (same filly as in Figure 7–34). The bladder had been repaired 7 days earlier. Notice the invaginated bladder mucosa (*open arrow*) and the hyperechoic suture material in the dorsal bladder wall casting an acoustic shadow (*arrows*). This filly had abdominal distention and an increased amount of peritoneal fluid, but the bladder incision appeared intact. Clinicopathologic and cytologic evaluation of the peritoneal fluid revealed a modified transudate and no evidence of urine contamination. This excess peritoneal fluid gradually resolved. The sonogram on the left is a sagittal view, and the sonogram on the right is a transverse view of the bladder. The right side of the sagittal view is cranial and the top is ventral. The right side of the transverse view is the left side of the foal's abdomen. These sonograms were obtained with a 7.5-MHz sector-scanner transducer and a displayed depth of 12 cm.

crease in parenchymal echogenicity. In other affected foals the kidneys are enlarged and less echogenic than normal, consistent with acute renal failure.[8–12, 16, 33] Doppler ultrasound evaluation of renal arterial blood flow revealed an absence of blood flow in late diastole or throughout diastole in children with acute renal failure.[68] The diastolic blood flow re-appeared in these children with recovery. Renal arterial blood flow has not been evaluated in foals with acute renal failure, to the author's knowledge. Occasionally, with oliguric or anuric renal failure in foals, perirenal edema is detected.[10, 33] A ruptured ureter should also be considered in foals with perirenal fluid accumulation, prompting sonographic examination of the ventral abdomen for the presence of excess fluid (uroperitoneum).

Kidneys that appear more echogenic than normal are consistent with a cellular infiltrate in the renal parenchyma and medical renal disease (Fig. 7–42).[9–12, 33] This increase in parenchymal echogenicity may be diffuse or multifocal. In young foals, an infectious cause must be considered because embolic nephritis has been seen in colostrum-deprived septicemic foals.[69] The mechanism of an increase in renal parenchymal echogenicity is not well understood in human beings and may occur with all types of cellular infiltration (including fibrosis), changes in renal perfusion, or changes in the interstitial fluid in relation to cellular fluid.[53] In one large study of newborn human infants, increased renal echogenicity was detected in infants with low birth weight, deteriorating medical status, increasing blood urea nitrogen and creatinine, and prematurity. Prematurity was the most important factor related to the increased renal cortical echogenicity in infants and appears to be a normal finding that gradually progresses to an isodense pattern.[70] Medullary nephrocalcinosis has been seen in low-birth-weight babies who have received furosemide for several days (at least 10 days).[53] The medulla has a variably increased echogenicity in the affected babies, with a normal-appearing renal cortex. Numerous glomerulopathies, tubular abnormalities, and interstitial diseases also cause increased renal echogenicity in children.[53] The iatrogenic administration

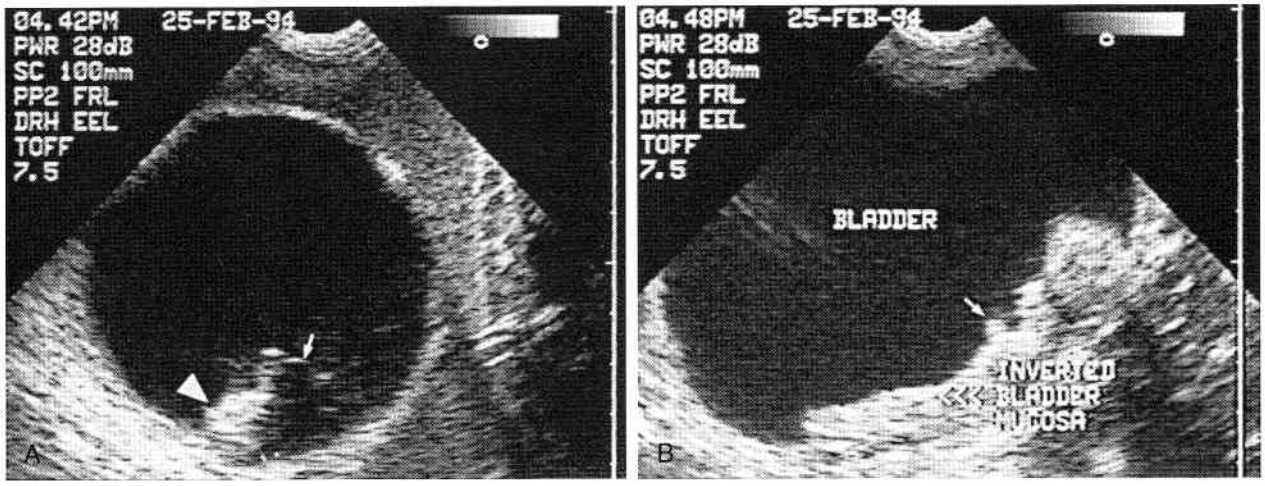

Figure 7–41

Sonograms of the bladder following surgical repair of a ruptured bladder in a 7-day-old Standardbred colt. The bladder had been repaired 2 days earlier. Notice the inverted bladder mucosa (*arrowheads*) in the dorsal wall of the bladder and the fibrin tags (*arrows*) attached to the inverted mucosa. These sonograms were obtained with a 7.5-MHz sector-scanner transducer and a displayed depth of 10 cm.

A, Transverse view of the bladder filled with anechoic urine. Notice the echogenic fluid in the peritoneal cavity surrounding the bladder associated with a chemical peritonitis in this foal. The right side of this sonogram is the left side of the foal's abdomen.

B, Sagittal view of the bladder demonstrating the repair in the dorsal bladder wall (*arrowheads*). The right side of this sonogram is cranial, and the left side is caudal.

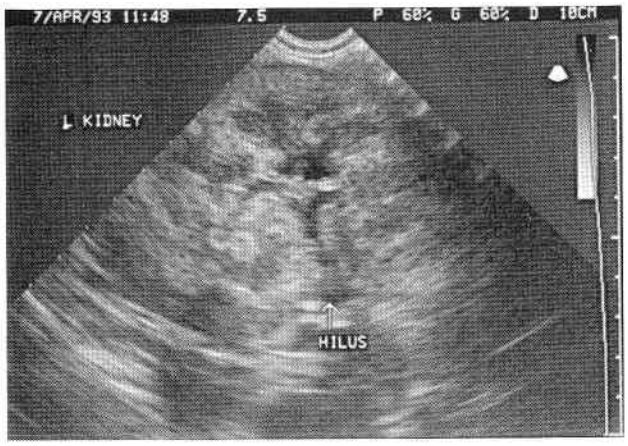

Figure 7–42

Sonogram of the left kidney obtained from a 12-day-old Standardbred colt with oliguric renal failure. Notice the marked increase in the echogenicity of the renal parenchyma. The renal cortex is relatively hypoechoic, with an echogenic corticomedullary junction and medulla. The right side of this sonogram is cranial, and the left is caudal. This sonogram was obtained in the left paralumbar fossa with a 7.5-MHz sector-scanner transducer and a displayed depth of 10 cm.

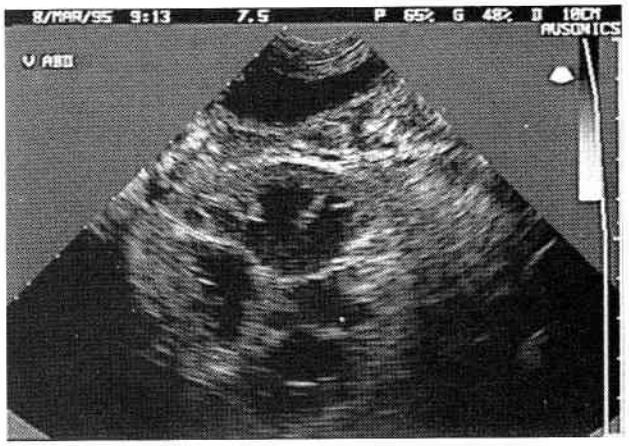

Figure 7–43

Sonogram of the right kidney obtained from a 5-day-old Standardbred filly with hydronephrosis. Notice the dilatation of the renal pelvis and renal calyces with the small rim of normal renal parenchyma remaining. The right side of this sonogram is the left side of the foal's abdomen, and the top is ventral. This sonogram was obtained from the ventral abdomen with a 7.5-MHz sector-scanner transducer and a displayed depth of 10 cm.

of a variety of drugs used in the treatment of septicemic foals may also result in increased renal parenchymal echogenicity. Of particular concern are the aminoglycosides, which may be toxic to the renal tubules. Cephalosporins, erythromycin, rifampin, and sulfonamides can also result in increased renal parenchymal echogenicity in children and probably in the foal.[53] Increased echogenicity of the renal papilla and echogenic debris in the renal pelvis may be detected in foals with renal papillary necrosis.[10] In human beings with renal papillary necrosis, the intense elliptical echogenic foci associated with acoustic shadowing are thought to be caused by ischemic necrosis and fibrofatty degeneration of pyramidal tissue but may also be caused by early nonhomogeneous calcification.[71] Phenylbutazone has also been shown to cause similar histopathologic lesions of the renal medullary crest in horses.[72]

Hydronephrosis and/or hydroureter may be detected in foals with urinary tract obstruction (Fig. 7-43).[12, 21] In foals, the hydronephrotic kidney usually has a smooth contour. If a hydronephrotic kidney is detected, the bladder, ureter, other kidney, and structures adjacent to the urinary tract should be carefully examined sonographically to determine the cause of the hydronephrosis. Renal pyelectasia (fluid distention of the renal pelvis or ureter in the absence of ureteral obstruction or obstruction of the renal pelvis) should be diagnosed in foals with fluid distention of the ureter and/or renal pelvis and no evidence of renal atrophy (Fig. 7-44). Renal pyelectasia usually occurs secondary to large volumes of intravenous

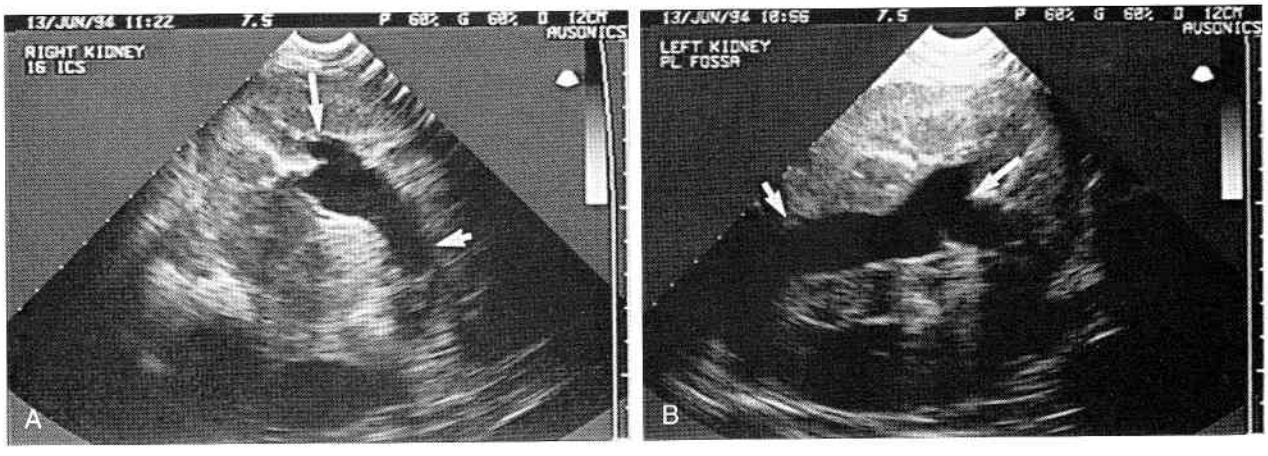

Figure 7–44

Sonograms of both kidneys obtained from a 2-day-old Thoroughbred colt with hydroureter and dilatation of the renal pelvis. Notice the marked dilatation of the renal pelvis (*large arrow*) and the large fluid-filled ureter (*small arrow*) exiting the renal pelvis in both the right (*A*) and left (*B*) kidneys. The sonogram of the right kidney was obtained in the right 16th intercostal space while that of the left kidney was obtained in the left paralumbar fossa. The right side of both sonograms is cranial. These sonograms were obtained with a 7.5-MHz sector-scanner transducer and a displayed depth of 12 cm.

fluids. A dilated renal pelvis and ureter associated with both kidneys have been detected in one foal with bilateral ectopic ureters and in several foals with an arterioureteral fistula.[27, 55] Dilated ureters may not be detected, however, if there is no obstruction to the drainage of urine into the vagina. Hematuria was reported in the weanlings with an arterioureteral fistula,[27, 55] and a palpable mass was detected on rectal examination in the aortic quadrifurcation, which was sonographically consistent with an aneurysm.[27] Congenital renal abnormalities are rare in horses, but renal cysts, renal ectopia, renal hypoplasia, and renal agenesis are all possible findings. A dysplastic multicystic kidney should be considered in foals with multiple renal cysts intermixed with echogenic stroma because these are the sonographic findings in children with dysplastic multicystic kidneys.[73] Depending upon the location of the atresia, a dilated renal pelvis may be detected connected to dilated renal calyces (cysts) in human infants with multicystic renal dysplasia.[53] The polycystic kidney usually appears lobular in human infants, whereas the hydronephrotic kidney usually has a smooth contour.[53] Renal agenesis should be considered in those foals in which only one kidney can be found in the normal or an ectopic location. In human beings with renal agenesis, the remaining kidney hypertrophies over time.[53] The adrenal gland, if present, appears larger than normal and fills in the space along with the spleen and colon on the left side of the abdomen.[53] The cecum, along with the liver, would be expected to fill this space on the right side of the abdomen in the foal.

Trauma to the kidneys from a kick or being stepped on by the mare may also occur, resulting in a renal or perirenal hematoma or hemoperitoneum. In children, perinephric blood tends to accumulate around the area of the renal laceration, which appears as a linear echogenicity when the ultrasound beam is perpendicular to the crack.[53] A double linear interface may be detected in a child with a subcapsular hematoma if the beam is directed perpendicular to the renal border; otherwise, the renal capsular echoes may appear fuzzy.[53] A blotchy echogenicity to the renal parenchyma is detected in children with renal contusion.[53] Clear fluid in the retroperitoneal space around the kidney suggests a ruptured renal pelvis, calyx, or ureter.

Hepatic Disease. Liver disease does occur in foals and usually has an inflammatory cause. *Actinobacillus* and other bacterial infections have been identified in foals with suppurative hepatitis. Hepatitis has also been reported in colostrum-deprived septicemic foals.[69] A diffuse or multifocal suppurative hepatitis occurs most commonly, with occasional foals developing a suppurative cholangiohepatitis or hepatocellular necrosis. Small areas of increased echogenicity scattered throughout the hepatic parenchyma have been imaged in foals with multifocal suppurative hepatitis (Fig. 7-45).[8, 10-12] Hepatomegaly may be detected in foals with inflammatory liver disease. A more diffuse increase in parenchymal echogenicity is indicative of a diffuse inflammatory cell infiltrate.[9, 11, 12] Tyzzer's disease should be suspected in foals with acute hepatic failure, enlarged livers, and a diffuse increase in parenchymal echogenicity.[12] Tyzzer's disease was also suspected in one foal with marked hepatomegaly and an

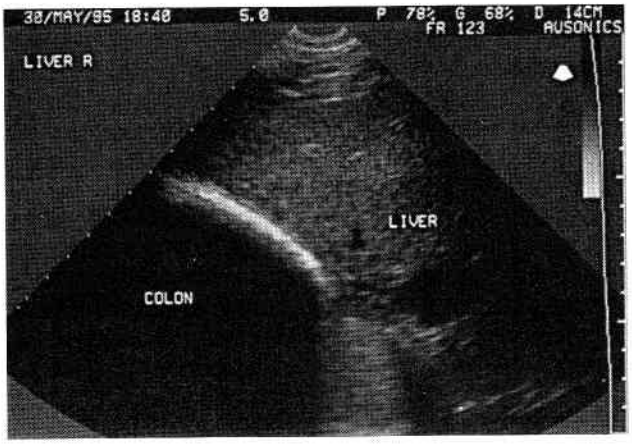

Figure 7–45

Sonogram of the liver obtained from a 7-week-old Thoroughbred colt with small multifocal areas of increased echogenicity detected throughout the liver. Notice the small scattered areas of increased echogenicity in the right lobe of the liver consistent with suppurative hepatitis. The right side of the sonogram is dorsal, and the left side is ventral. This sonogram was obtained in the right thirteenth intercostal space with a 5.0-MHz sector-scanner transducer and a displayed depth of 14 cm.

increased vascular pattern.[30] Some loss of the normal hepatic architecture may be imaged with a severe diffuse or multifocal hepatitis with parenchyma of normal or decreased echogenicity. Cavitated areas may be seen associated with liver abscesses, a rare finding in foals. The abscesses are usually poorly marginated and hypoechoic when scanned early in the course of the disease and become better defined, encircled by more echogenic inflammatory tissue, as the abscess progresses. Liver abscesses can result from septicemia and the development of suppurative hepatitis or by direct spread from an infected umbilical vein. The portal vein should be carefully scanned for a possible septic thrombus, which has been detected in calves with hepatic abscesses, but not in foals to the author's knowledge.

Cholangiohepatitis occurs less frequently than suppurative hepatitis but has been reported in foals with duodenitis and duodenal stricture.[8, 10-12, 14, 74-76] Biliary reflux may be the cause of the cholangiohepatitis.[74-76] Thickening of the bile ducts with echogenic material imaged within the biliary tree (Fig. 7-46) is indicative of a cholangiohepatitis.[9-12, 14] Increased echogenicity of the surrounding hepatic parenchyma may also be detected in foals with cholangiohepatitis.[9, 12, 14] Distention of the biliary tree may be detected sonographically in foals with biliary obstruction secondary to duodenal stricture and cholangiohepatitis.[8-12, 14, 74-76] Chronic liver disease may result in increased parenchymal echogenicity, with a more lobular contour of the liver surface and decreased overall size of the liver. Toxic insults resulting in hepatocellular necrosis may also occur in young foals. Decreased echogenicity and collapse of the hepatic parenchyma may be detected in foals with toxic hepatopathy or hepatocellular necrosis.[9, 10, 12, 77] Marked hepatic lucency has also been detected in children who suffered severe asphyxia.[53]

Congenital vascular shunts, rare in foals, may also occur, resulting in hepatic encephalopathy.[10, 11, 78] Ultrasonographic evaluation of the liver with Doppler evaluation

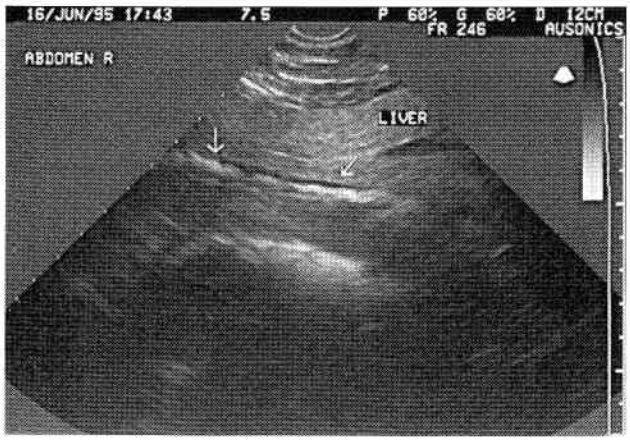

Figure 7–46

Sonogram of the liver obtained from a 6-week-old Thoroughbred filly with cholangiohepatitis. The prominent distended bile ducts are filled with echogenic material (*arrows*) representing biliary sludge. The right side of the sonogram is dorsal, and the left side is ventral. This sonogram was obtained in the right eleventh intercostal space with a 7.5-MHz sector-scanner transducer and a displayed depth of 12 cm.

of liver blood flow may aid in diagnosing portosystemic shunts in affected foals. A patent ductus venosus was detected sonographically in a calf with hepatic encephalopathy, and portosystemic shunts have been diagnosed ultrasonographically in young dogs.[79-82] Other vascular anomalies may also be detected, but their accurate diagnosis requires a thorough knowledge of the hepatic vascular anatomy. Portal vein thrombosis and arteriovenous anomaly were reported in a young Thoroughbred gelding with hepatic encephalopathy.[83] Hepatic venous enlargement in conjunction with decreased parenchymal echogenicity and hepatomegaly is consistent with passive congestion of the liver and right heart failure. Trauma to the foal's liver from a blow to the abdomen may result in a hepatic hematoma and/or hemoperitoneum (Fig. 7-47). Clotting blood in the peritoneal cavity usually appears echogenic. Hematomas associated with liver lacerations in children can be hypoechogenic or hyperechogenic. Subcapsular collections of blood may be detected in children with liver trauma. The liver in foals is fairly well protected, however, by the ribs, and rib fractures are more likely than hepatic trauma.

Splenic Disease. Splenic abnormalities occur infrequently in foals.[10] Trauma to the spleen resulting in a splenic hematoma and/or hemoperitoneum may occur following a kick to the foal's abdomen or being stepped on by the mare. In children, a double linear interface of the outline of the spleen is consistent with a subcapsular collection of blood.[53] Intraparenchymal and perisplenic collections of blood may be echogenic or lucent or have a mixed pattern of echogenicity in children.[53, 84] The spleen may also be involved in areas of localized peritonitis associated with internal umbilical remnant infections (see Fig. 7-22). Splenic abscesses, however, are rare in foals.

Gastrointestinal Diseases

Sonographic evaluation of the gastrointestinal tract is extremely valuable in the evaluation of foals with colic or suspected gastrointestinal disease.[8-16, 20] The entire abdomen can be evaluated and the sonographic information used to help make the decision between a medical and surgical colic.[8-12, 14, 15] Scanning the foal from the most ventral portion of the abdomen is critical to successfully making this determination. The affected fluid-filled intestine usually falls to the most ventral location and is readily visible if scanned from the most ventral portion of the abdomen. Abnormal intestine may be missed, however, if scanned from the lateral or dorsal portion of the abdomen because the interposed gas-filled bowel prevents visualization of the affected intestine. The preponderance of small intestinal diseases in the equine neonate also facilitates sonographic diagnosis. Ultrasonographic evaluation of the peritoneal cavity is also useful to determine if peritoneal fluid can be obtained on abdominal paracentesis. The liklihood of obtaining peritoneal fluid from an abdominal paracentesis is small if no imageable peritoneal fluid is present, and the risk of iatrogenically lacerating the intestine or performing an enterocentesis is high, particularly in a foal with marked abdominal distention.[85] An abdominal paracentesis is usually not indicated in these foals.

Intussusception. The first report of the use of ultrasonography in the diagnosis of gastrointestinal disease in foals was the diagnosis of small intestinal intussusceptions (Fig. 7-48).[13] The detection of a characteristic "target" or "bull's-eye" sign is obtained by scanning through the apex of the intussusception where the intussusceptum is surrounded by fluid and the intussuscipiens. The image thus obtained is similar in appearance to that previously described in humans.[8-15, 20, 86, 87] This ultrasonographic appearance is created by the difference in acoustic impedance between the thick-walled, congested, edematous inner intussusceptum and outer intussusci-

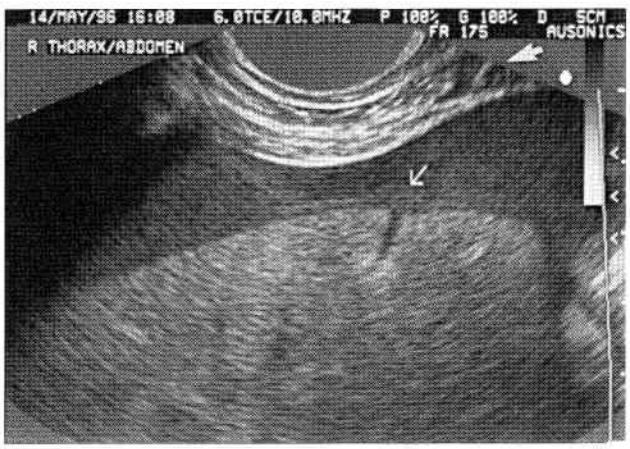

Figure 7–47

Sonogram of the right side of the abdomen obtained from a 2-month-old Thoroughbred colt with hemoperitoneum and a fractured liver. Sonographic examination of the abdomen revealed a large quantity of echogenic swirling fluid with the largest accumulation of blood and fibrin in the right cranial abdomen. There was a defect in the liver parenchyma detected *(arrow)* and swelling in the overlying intercostal muscles *(large arrow)* associated with trauma to the right side of the ventral thorax and cranial abdomen. The right side of this sonogram is dorsal and the left side is ventral. This sonogram was obtained with a wide-bandwidth 6.0-MHz microconvex linear-array transducer operating at 10.0 MHz and a displayed depth of 5 cm.

piens and the interposed fluid layer.[11-13] Invaginated mesenteric fat or mesenteric lymph nodes may also create this sonographic appearance. The intussusception can have myriad different sonographic appearances, depending upon the portion of the intussusception being imaged.[10, 13, 14, 86-90] The intussusception may appear as two concentric rings, with a central circular area or echogenic core representing the inner lumen of the intussusceptum, the "multiple-ring" sign.[11-14, 87, 88] This appearance occurs where the walls of the intussusceptum and intussuscipiens are less edematous.[11-14] Occasionally fibrin may be imaged between the inner intussusceptum and the outer intussuscipiens (Fig. 7-49). Fluid distention of the more proximal small intestine is detected, usually with normal or nearly normal wall thickness and little or no peristaltic activity.[10-12, 14] The differentiation between one or multiple intussusceptions may not be possible, but the presence of the intussusception is readily diagnosed sonographically.

Although jejunojejunal intussusceptions are most common in foals, ileal-ileal and ileocecal intussusceptions have been reported in weanlings and yearlings.[91] Affected youngsters usually have a history of chronic, usually intermittent, abdominal pain of several days' to weeks' duration and normal vital signs at presentation.[91] Ileal-ileal and ileocecal intussusceptions can be imaged ultrasonographically from the right flank area and/or transrectally in those youngsters large enough to safely undergo a rectal examination. The ultrasonographic appearance of an ileal-ileal intussusception and a jejunojejunal intussusception is similar. With the ileocecal intussusception, the outer segment of bowel (the cecum) is larger and sacculated (although the sacculations are not easily imaged in the affected portion of the cecum), and the wall of the inner segment of bowel (the ileum) is normally thicker. Hypertrophy and marked dilatation of the distal jejunum

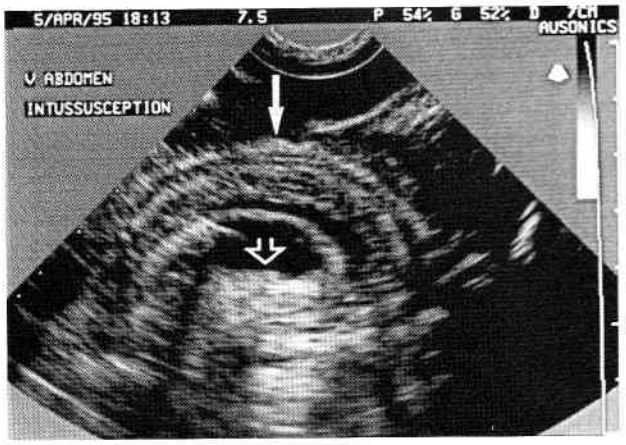

Figure 7-48

Sonogram of the ventral abdomen obtained from a 3-day-old Thoroughbred colt with an intussusception. Notice the characteristic target or "bull's-eye" sign of the intussusception. The "bull's-eye" sign is created by the edematous outer intussuscipiens (*solid arrow*), a fluid layer between the outer intussuscipiens and the inner intussusceptum, and the more echogenic inner intussusceptum (*open arrow*). The right side of this sonogram is the left side of the foal's abdomen, and the top is ventral. This sonogram was obtained with a 7.5-MHz sector-scanner transducer and a displayed depth of 7 cm.

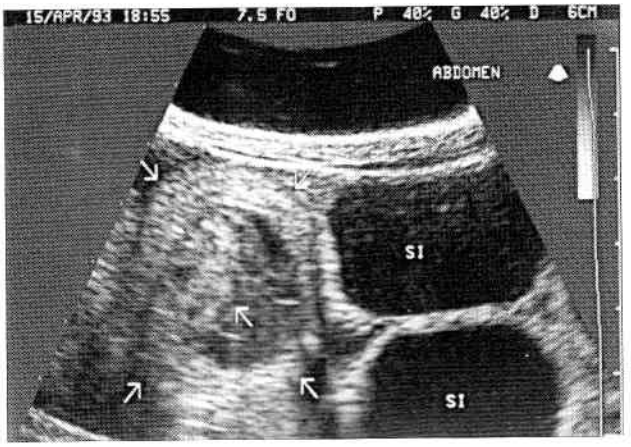

Figure 7-49

Sonogram of the ventral abdomen obtained from a 5-day-old Thoroughbred colt with an intussusception. Notice the fibrin between the thick outer intussuscipiens (*outer arrows*) and the inner intussusceptum (*inner arrow*). The fibrin is loculated and hypoechoic. The distended amotile loops of jejunum (SI) are proximal to the intussusception. The right side of this sonogram is the left side of the foal's abdomen, and the top is ventral. This sonogram was obtained with a 7.5-MHz sector-scanner transducer containing a built-in fluid offset and a displayed depth of 6 cm.

have also been reported in equine youngsters with ileocecal intussusception and may be detected ultrasonographically.[91] Ileocecal intussusceptions are most common in dogs, and the "multiple-ring" sign has been detected in affected dogs.[43] An "hourglass" or "fused target-like" pattern has also been described in children with an ileocecal intussusception as the intussusception is imaged simultaneously within the colon.[92] Other terms such as "hayfork," "trident," and "sausage" have been used to describe the longitudinal view of an intussusception.[42, 87, 92-95] "Donut" and "pseudokidney" have also been used to describe the transverse view of an intussusception but are not specific for an intussusception.[42, 94, 96]

Small Intestinal Volvulus. If turgid, fluid-filled, amotile small intestine with thicker than normal walls is imaged, a small intestinal volvulus should be suspected (Fig. 7-50).[8-12, 14] A similar sonographic appearance is detected shortly after the volvulus occurs, but jejunal wall thickness may still be normal or nearly normal as the congestion and edema of the bowel wall are developing. Rotation around the mesenteric vessels may be visible at the mesenteric root. In children, the detection of duodenal obstruction with the duodenum twisting around the superior mesenteric artery, an abnormal relationship of the superior mesenteric artery and vein (the vein is detected at the left ventral side of the artery), and a hyperdynamic pulse in the superior mesenteric artery as a solitary vessel in the center of the volvulated bowel are sonographic indications of midgut volvulus.[87, 97-100] Volvulus secondary to adhesions has also been described sonographically in children with the involved loop having the appearance of a U on longitudinal section and a C or coffee bean in transverse section.[101]

Other Small Intestinal Obstruction. Other surgical diseases of the small intestine can also be diagnosed ultrasonographically. With a mechanical obstruction, di-

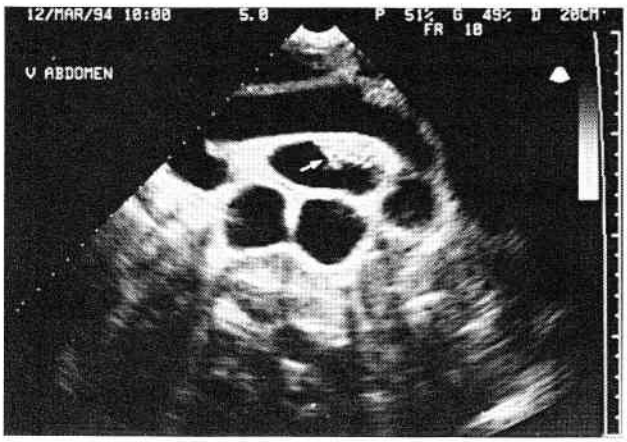

Figure 7–50

Sonogram of the abdomen obtained from a 3-week-old Thoroughbred colt with a small intestinal volvulus. The turgid distended loops of jejunum wrap around each other in a circular pattern. The loops of jejunum are filled with anechoic fluid with only a small amount of ingesta detected (*arrow*). The wall of the jejunum is only slightly thicker than normal at this time. The right side of the sonogram is the left side of the foal's abdomen, and the top is ventral. This sonogram was obtained with a 5.0-MHz sector-scanner transducer and a displayed depth of 20 cm.

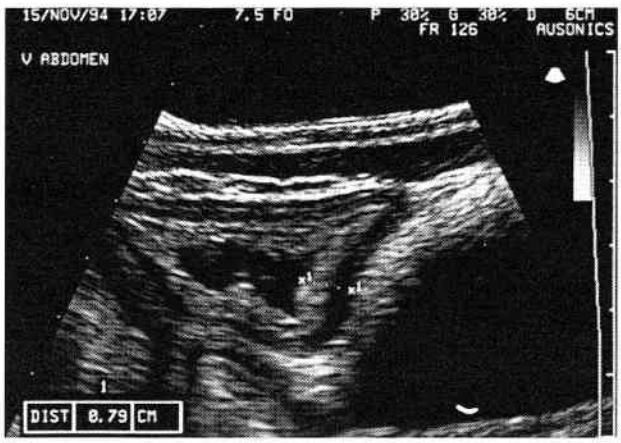

Figure 7–52

Sonogram of the abdomen obtained from a 7-month-old Thoroughbred filly with ileal hypertrophy. Notice the thickening of the wall of the ileum (0.79 cm) and the fluid contents of the intestine. The ileum does not, however, have a turgid appearance. The right side of the sonogram is the left side of the foal's abdomen, and the top is ventral. This sonogram was obtained with a 7.5-MHz sector-scanner transducer containing a built-in offset and a displayed depth of 6 cm.

lated proximal loops of intestine and collapsed distal intestinal loops can both be imaged, although the cause of the mechanical obstruction may not be visible.[9-12, 14] Congenital abnormalities such as Meckel's diverticulum and other embryologic remnants may cause small intestinal obstruction with thickened, turgid, fluid-filled, amotile small intestine imaged proximal to and in the area of the obstruction. Mural masses may be detected sonographically in the equine neonate (Fig. 7–51) and often occur, associated with hypoxic bowel syndrome, in foals that experienced peripartum asphyxia. Masses within the intestinal wall are most likely to occur in foals with abscesses or infection in the intestinal wall and appear to involve primarily the small intestine.[8, 9, 13] Fluid distention of the more proximal small intestine, with little or no peristaltic activity, is also detected sonographically. Thickening of the small intestinal wall immediately proximal to the mural mass has been detected with a corrugated appearance to the bowel wall (Fig. 7–51). Mural thickening of the ileum has been seen in older foals with ileal hypertrophy (Fig. 7–52). Echogenic eccentric thickenings of the bowel wall have been reported in

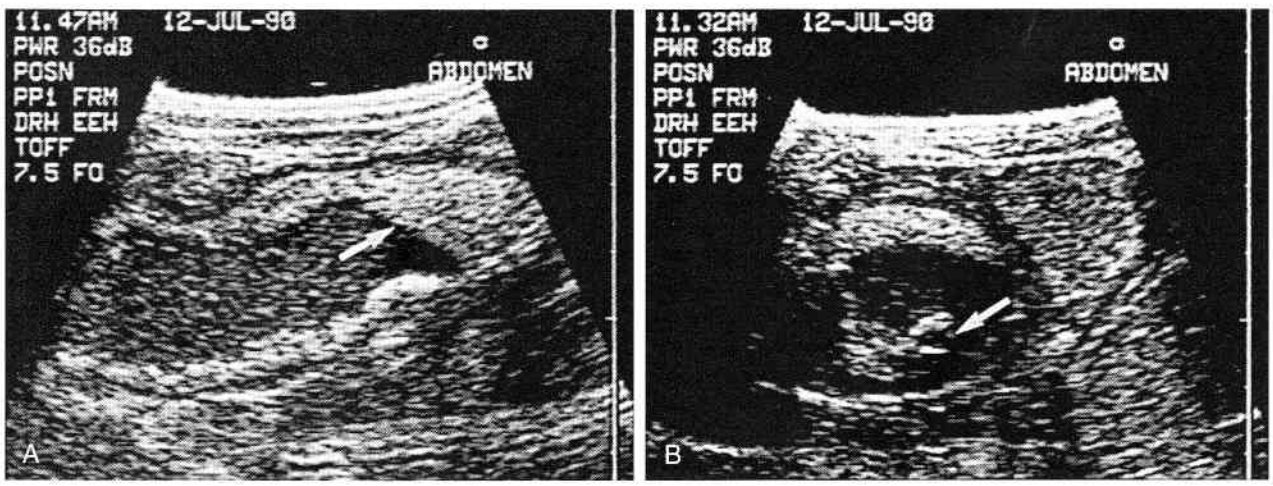

Figure 7–51

Sonograms of the ventral abdomen obtained from a 1-month-old Arabian colt with a small intestinal obstruction. These sonograms were obtained with a 7.5-MHz sector-scanner transducer containing a built-in fluid offset and a displayed depth of 7.5 cm.

A, Notice the large echogenic mural mass (*arrow*) obstructing the jejunum and the distention of the jejunum immediately proximal to the mass. The right side of this sonogram is cranial and the top is ventral.

B, Notice the echogenic mural thickening, the hypoechoic mural thickening, and the small echogenic circular structure (*arrow*), which was the mucosal surface of the bowel. The lumen of the jejunum had been reduced to approximately 2 mm here at the site of the most severe obstruction. The hypoechoic wall of the jejunum was filled with multifocal abscesses. The right side of this sonogram is the left side of the foal's abdomen, and the top is ventral.

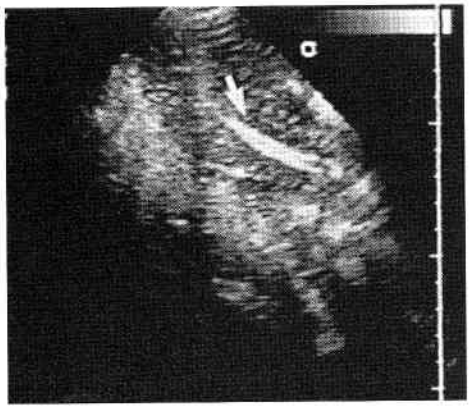

Figure 7–53

Sonogram of the abdomen obtained from a 5-month-old Paint colt with an ascarid impaction. The thick echogenic ascarid worm (*arrow*) is surrounded by fluid in the small intestine. The right side of this sonogram is the left side of the foal's abdomen, and the top is ventral. This sonogram was obtained with a 5.0-MHz sector-scanner transducer and a displayed depth of 20 cm.

children with intramural hematomas secondary to trauma and should be considered in foals in which abdominal trauma is a possibility.[101, 102] These intramural hematomas should rapidly improve on follow-up sonograms. Intraluminal hemorrhage may result in brightly echogenic fibrin clots swirling within the intestinal lumen.[47] Intraluminal blood clots were imaged in the jejunum of one foal that presented with a history of colic and tarry feces. This foal also had a jejunojejunal intussusception detected sonographically. The cathartic effect of blood within the intestinal lumen causes hypersecretion and hypermotility of the blood-containing intestinal loops in human beings and may cause similar changes in foals. Changes in intestinal motility are one postulated reason for the development of an intussusception in foals. Intraluminal masses may also be detected in both large and small intestines. Fluid distention of the intestine proximal to the obstruction makes visualization of the intraluminal mass easier.[9-12] Ileal masses associated with masses of paralyzed ascarid worms have been imaged sonographically in older foals that have recently been dewormed and have an ascarid impaction (Fig. 7-53).[8, 11, 12, 14]

Large Intestinal (Large and Small Colon) Obstruction. Obstruction of the large and small colon with fecaliths or trichophytobezoars has been reported in foals.[103-105] Although fecaliths have been reported in foals as young as 19 days, fecaliths have been more frequently reported in slightly older miniature horses and ponies.[104] The fecaliths reported in miniature horse foals were 4 to 6 cm in diameter.[104] Few reported cases of trichophytobezoars in foals exist in the veterinary literature. Ultrasonographic visualization of the fecalith or trichophytobezoar depends upon the amount of gas distention of the surrounding intestine and the location of the obstruction in the large or small colon (whether a sonographic window exists to image this area). Fecaliths have been successfully imaged in the small colon from the flank area in young miniature horses. They appear as echogenic to hyperechoic masses that cast an acoustic shadow, similar to gastric trichobezoars in children.[106-108]

Meconium Impactions. Meconium impactions have been accurately diagnosed with retrograde contrast radiography in foals.[109] However, meconium impactions are easier to diagnose sonographically with less risk to the foal. Meconium impactions are most frequently detected dorsal to the bladder in the terminal portion of the small colon, with fluid distention of the more proximal small colon (Fig. 7-54).[9-12, 14] The meconium in the small colon is usually very echogenic and has a ball or log-like shape (Fig. 7-54). Meconium can also be imaged in the large colon, where it may have a more variable ultrasonographic appearance. Meconium in the large colon can

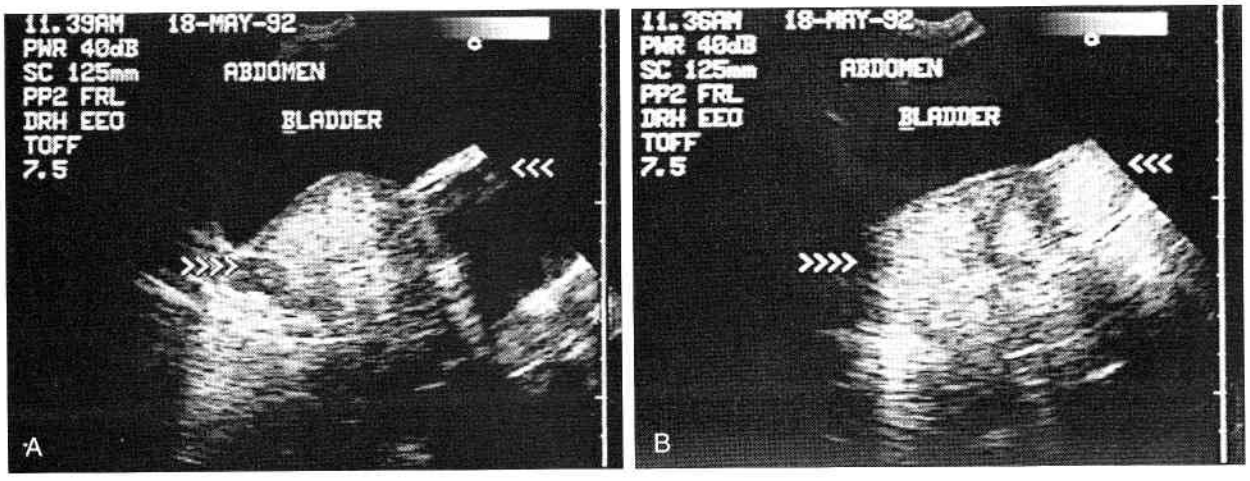

Figure 7–54

Sonograms of the caudal ventral abdomen obtained from a 2-day-old Thoroughbred colt with a meconium impaction. The right side of these sonograms is cranial, and the top is ventral. These sonograms were obtained with a 7.5-MHz sector-scanner transducer and a displayed depth of 12.5 cm.

A, Notice the echogenic meconium in the small colon (*left arrowheads*) dorsal to the bladder, with the fluid-distended small colon (*right arrowheads*) immediately cranial to the impacted meconium.

B, The echogenic meconium in the small colon (*arrowheads*) is dorsal to the bladder. This sonogram was obtained slightly more caudal than the view in *A*.

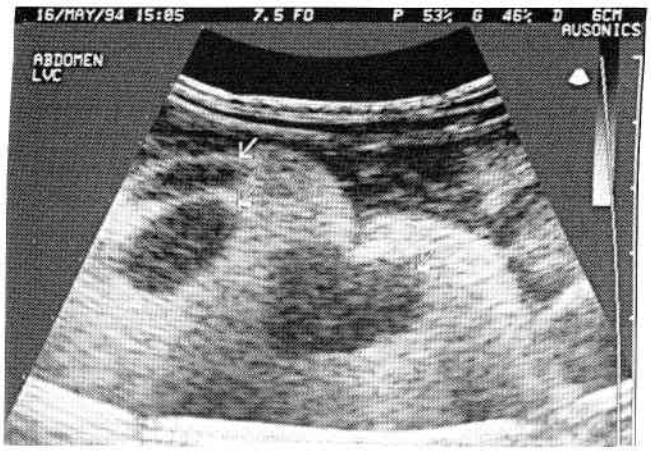

Figure 7–55

Sonogram of meconium in the large colon obtained from a 2-day-old Thoroughbred colt with a meconium impaction. The hypoechoic meconium (*arrows*) is surrounded by echogenic fluid in the large colon. Notice the small amount of free peritoneal fluid present within the abdominal cavity. The right side of this sonogram is cranial, and the top is ventral. This sonogram was obtained with a 7.5-MHz sector-scanner transducer containing a built-in fluid offset and a displayed depth of 6 cm.

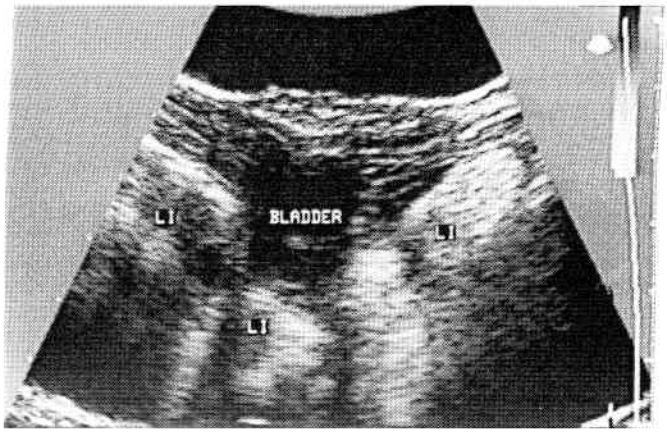

Figure 7–57

Sonogram of gas-filled large colon obtained from a 6-day-old Thoroughbred colt with abdominal distention and colic. The gas-filled large intestine (LI) compresses the bladder in the caudal ventral abdomen. The right side of this sonogram is the left side of the foal's abdomen, and the top is ventral. This sonogram was obtained with a 7.5-MHz sector-scanner transducer containing a built-in fluid offset and a displayed depth of 6 cm.

appear as large hypoechoic (Fig. 7–55) or echogenic (Fig. 7–56) masses and is often surrounded by fluid. The retained meconium may have a variety of shapes within the large colon.

Atresia Coli. Atresia coli may be imaged if the blind end of the proximal segment is located in an area with a good acoustic window. Gas and fluid distention are detected in the proximal segment with normal wall thickness.[12] Visualization of the empty caudal segment may be possible using the bladder as an acoustic window. Otherwise, the large gaseous distention of the proximal segment may prevent visualization of the blind empty caudal segment.

Large Colon Disease. Many foals with colic have gas-filled, distended large colon occupying the majority of the abdomen, without a surgical lesion (Fig. 7–57).[8–12, 14] In most foals with gas-distended large bowel, the distention resolves with medical therapy alone and surgery is not indicated. Fluid- and ingesta-filled large intestine may also be imaged in colicky foals and respond similarly to medical therapy (Fig. 7–58). Abnormal positioning of the large bowel viscera in the foal, although uncommon, is difficult to diagnose ultrasonographically unless there is thickening and congestion or edema of the bowel wall. In these foals, all that can be imaged is the gas-filled mucosal surface of the large bowel adjacent to the body wall. Imaging gastrointestinal viscera deeper in the abdo-

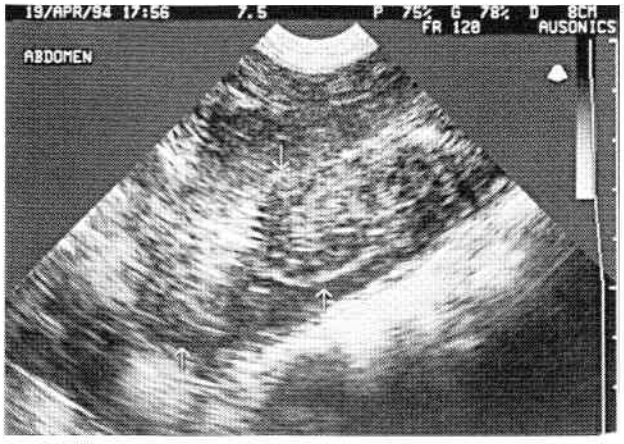

Figure 7–56

Sonogram of meconium in the large colon obtained from a 2-day-old Thoroughbred colt with a meconium impaction. The echogenic meconium (*arrows*) in the large colon is surrounded by hypoechoic fluid. The right side of this sonogram is cranial, and the top is ventral. This sonogram was obtained with a 7.5-MHz sector-scanner transducer and a displayed depth of 8 cm.

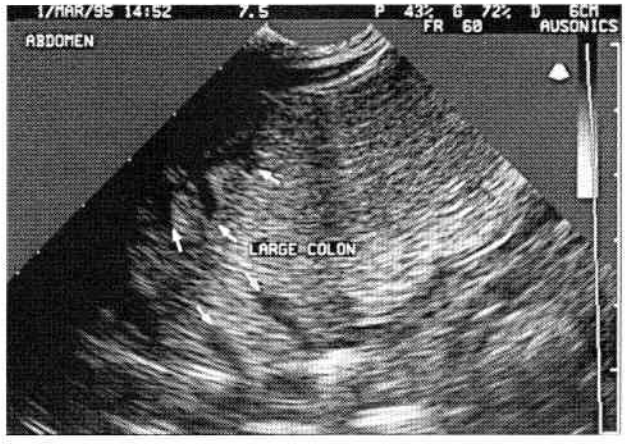

Figure 7–58

Sonogram of ingesta-filled large bowel obtained from a 12-day-old Thoroughbred colt with abdominal distention and colic. Notice the ingesta-filled large colon and the normal sacculations (*arrows*) of the large colon delineated by the echogenic ingesta. The right side of this sonogram is cranial, and the top is ventral. This sonogram was obtained with a 7.5-MHz sector-scanner transducer and a displayed depth of 6 cm.

men is not possible because the ultrasound is reflected by the gas at the mucosal surface of the large bowel.[11] Therefore, if only gas-distended large bowel is imaged, a definite surgical lesion is not detected sonographically, and the foal remains colicky, a repeat sonographic examination should be performed. A large colon torsion or displacement, although uncommon in foals, should still be considered in the differential diagnosis of a foal with unrelenting abdominal pain and gaseous distention of the large bowel.

Gastric Distention/Gastric Ulceration. Ultrasonographic evaluation of the stomach should be a part of the sonographic evaluation of the abdomen in all foals with suspected abdominal disease. Marked gastric distention can readily be detected and the luminal contents determined.[9-12, 14] Distention of the stomach with anechoic to hypoechoic fluid is detected with small intestinal obstructions (Fig. 7-59). Gastric and duodenal distention is often detected in foals with gastric ulcer syndrome.[19] Thickening of the gastric wall has been reported in human beings and dogs with gastric ulcers and may be detectable in affected foals.[42, 110-113] The visualization of an ulcer crater has also been described in both human beings and dogs with gastric ulcers.[42, 111, 112, 114] Ulceration of both the squamous and glandular portions of the stomach has been described in foals with gastric ulcers, occurring more frequently in the nonglandular portion of the stomach.[74-76, 115, 116] Perforated gastric ulcers located at the margo plicatus or near the pylorus have been reported in foals, causing peritonitis and death.[115, 116] Perforated gastric ulcers have been detected ultrasonographically in children as an inflammatory mass surrounding a portion of the stomach, creating an ultrasonic "doughnut."[53, 96] Gaseous distention of the stomach may be imaged occasionally in foals with little or no visible gastric fluid (Fig. 7-60). Gastric emptying problems may be identified sonographically if large amounts of ingesta persist unchanged in the stomach in a fasted or refluxing foal on repeat examinations (Fig. 7-61). Lactobezoars and trichobezoars have been detected sonographically in children in the stomach, but trichobezoars are more common in the small colon in foals.[103-106, 117] Lactobezoars in human beings have a bright irregular surface and cast a strong acoustic shadow typical of a foreign body.

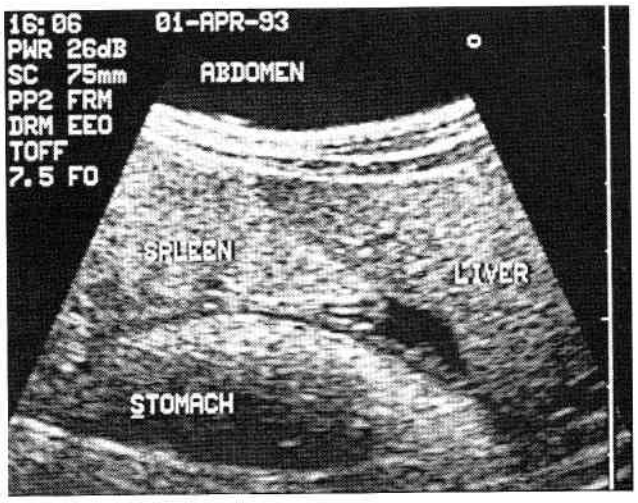

Figure 7-60

Sonogram of the stomach obtained from a 4-day-old Thoroughbred filly with colic. The large semicircular gas-filled stomach is deep to the echogenic spleen and the more hypoechoic liver. Large amounts of gas were obtained from nasogastric decompression. Notice the small amount of anechoic peritoneal fluid between the liver, spleen, and stomach. The right side of this sonogram is dorsal, and the left side is ventral. This sonogram was obtained in the left eighth intercostal space with a 7.5-MHz sector-scanner transducer containing a built-in fluid offset and a displayed depth of 7.5 cm.

Enteritis/Duodenitis. Enteritis can have a wide variety of sonographic appearances but is usually characterized by fluid-filled hypermotile bowel.[8-12, 14, 15] The wall thickness of the affected intestine may be normal or increased (Figs. 7-62 and 7-63). The intestinal wall thick-

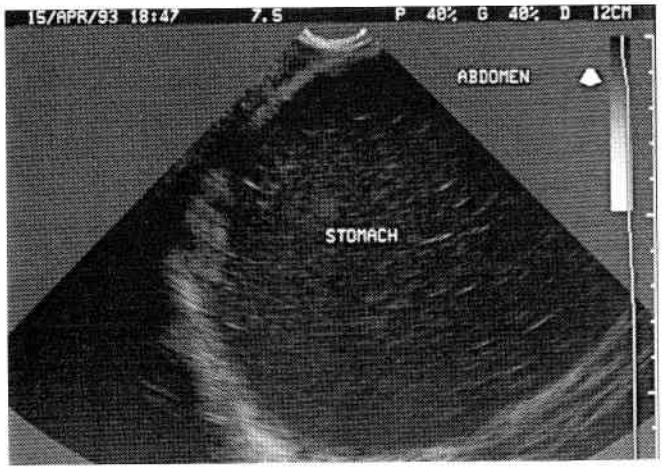

Figure 7-59

Sonogram of gastric distention obtained from a 5-day-old Thoroughbred colt. The hypoechoic fluid-filled stomach occupies most of the cranial abdomen. The right side of this sonogram is cranial, and the top is ventral. This sonogram was obtained with a 7.5-MHz sector-scanner transducer and a displayed depth of 12 cm.

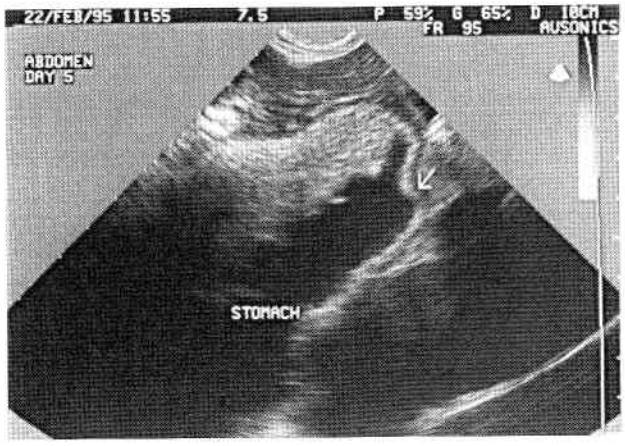

Figure 7-61

Sonogram of the stomach obtained from a 12-day-old Thoroughbred colt with delayed gastric emptying. Notice the layering between the anechoic (*arrow*) and echogenic fluid in the stomach. The right side of this sonogram is the left side of the foal's abdomen, and the top is ventral. This sonogram was obtained with a 7.5-MHz sector-scanner transducer and a displayed depth of 10 cm.

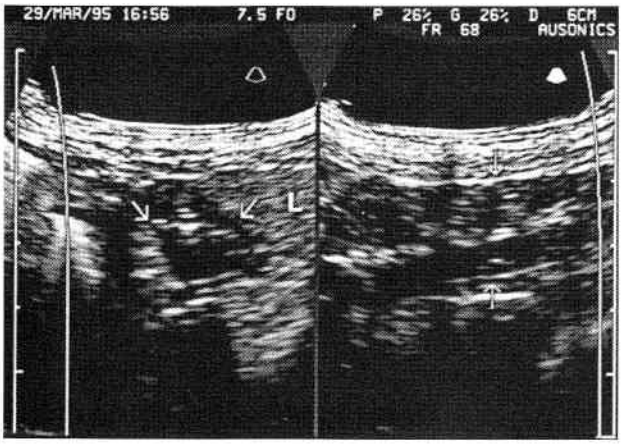

Figure 7–62

Sonogram of the duodenum obtained from a 2-day-old American Saddlebred filly with duodenitis. Notice the thickened, nearly anechoic wall of the duodenum (*arrows*) with the gas-lined mucosal surface adjacent to the liver (L). The left sonogram is a transverse image, and the right sonogram is a sagittal image of the duodenum adjacent to the right lobe of the liver. The right side of the transverse image is dorsal and the top is the right abdominal wall. The right side of the sagittal image is cranial. These sonograms were obtained with a 7.5-MHz sector-scanner transducer containing a built-in fluid offset and a displayed depth of 6 cm.

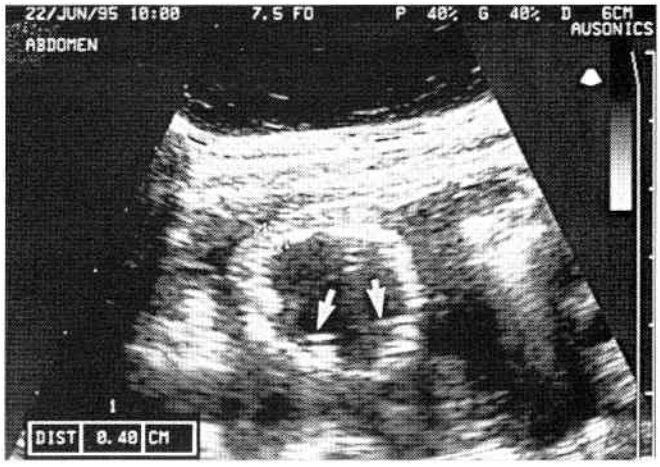

Figure 7–64

Sonogram of the ventral abdomen obtained from a 1-month-old Standardbred colt with enteritis. Notice the fluid-distended loop of small intestine with the thickened wall (0.40 cm), the irregular gas-lined mucosal surface, and the shreds of mucosa (*arrows*) floating in the intraluminal fluid. The right side of the sonogram is the left side of the foal's abdomen, and the top is ventral. This sonogram was obtained with a 7.5-MHz sector-scanner transducer containing a built-in fluid offset and a displayed depth of 6 cm.

ening is usually relatively symmetric and extensive and may also appear edematous (more hypoechoic than normal), particularly in foals with severe inflammatory bowel disease.[9–12, 14, 15] Inflammatory bowel disease may affect any portion of the intestinal tract from the duodenum to the small colon. In foals with duodenitis, the wall of the duodenum may be of normal thickness with a large fluid-distended lumen or the duodenal wall may be thickened and hypoechoic with a compromised lumen. Gastric distention is also detected in foals with duodenitis and duodenal obstruction.[74–76] Shreds of mucosa may be imaged sloughing into the bowel lumen in foals with duodenitis or enteritis (Fig. 7-64).[9, 10, 12, 14, 15] In some neonatal foals with duodenitis or clostridial enteritis, pinpoint gas echoes have been imaged in the wall of the affected intestine or lining the mucosal surface (Fig. 7-65).[12] These areas of mural and mucosal abnormalities may later develop mural masses similar to those seen in foals with hypoxic bowel syndrome, associated with periparturient asphyxia syndrome (Fig. 7-66). Bowel wall gas in human beings is considered highly suggestive, if not diagnostic, for intestinal necrosis.[118] The "bright ring" appearance is caused by the bright gas echoes in the intestinal wall surrounding the fluid-filled intestinal lumen. Tiny gas bubbles ("effervescent bowel") have also been reported in human beings with necrotic bowel rising from the dependent surface of the intestine.[118] Clostridial enteritis should be a primary differential diagnosis for foals with gas echoes imaged in the bowel wall or along the mucosal surface and in foals with hemorrhagic enteritis.[119, 120] Clostridial enteritis or another necrotizing enteritis should also be considered when a diphtheritic membrane is imaged sloughing into the bowel lumen.[119–122] Peritonitis has been reported in conjunction with enteritis in a foal with *Clostridium septicum* septicemia, in foals with clostridial enteritis, and in foals with duodenitis and duodenal stricture.[74–76, 119, 120] Therefore, the peritoneal cavity should also be carefully examined ultrasonographically for abnormal fluid or adhesions in foals with enteritis or duodenitis.

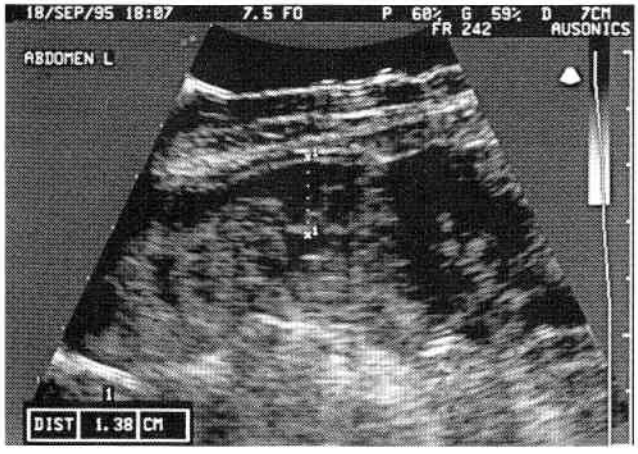

Figure 7–63

Sonogram of the left ventral abdomen obtained from a 3-month-old Thoroughbred colt with erythromycin-induced enterocolitis. The marked thickening of the small intestine (1.38 cm) with hypoechoic to anechoic fluid is consistent with edema. The right side of this sonogram is cranial, and the left side is caudal. This sonogram was obtained with a 7.5-MHz sector-scanner transducer containing a built-in fluid offset and a displayed depth of 7 cm.

Ileus. Foals with ileus usually have little or no visible peristaltic activity. The diameter of the bowel is increased, but the intestinal wall thickness is usually normal. In some foals with ileus, depending upon the cause, the wall thickness may be increased, and other intestinal or peritoneal fluid abnormalities may be detected. The

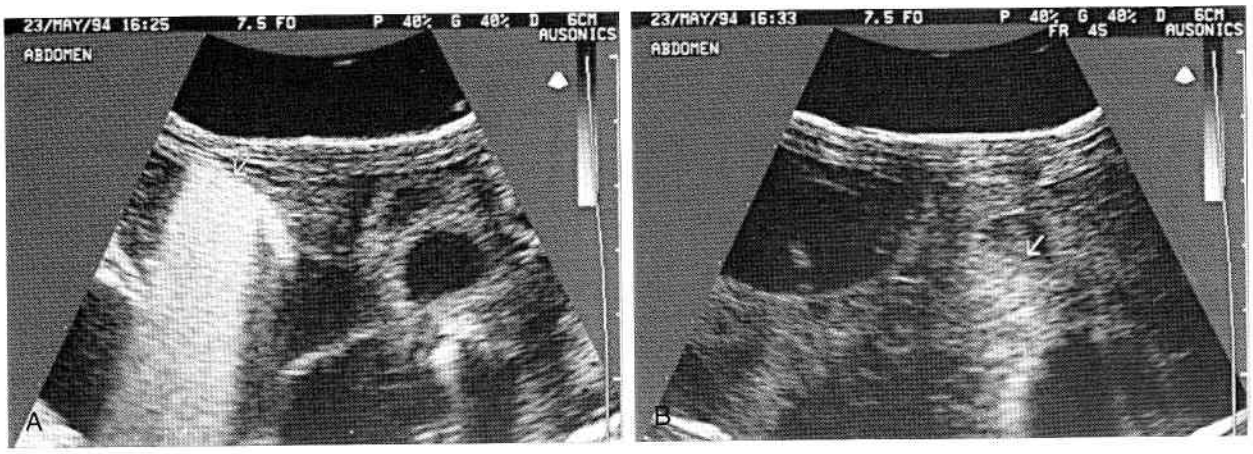

Figure 7–65

Sonograms of the ventral abdomen obtained from a 6-day-old premature Thoroughbred filly with periparturient asphyxia syndrome. The right side of the sonograms is the left side of the foal's abdomen, and the top is ventral. These sonograms were obtained with a 7.5-MHz sector-scanner transducer containing a built-in fluid offset and a displayed depth of 6 cm.

A, The hyperechoic echoes in the wall of the small bowel (*arrow*) are consistent with gas in the bowel wall.

B, The asymmetric thickening of the wall of the small intestine results in a mural mass (*arrow*) that obstructs the jejunum. The distended fluid-filled jejunum to the left of the segment contains the mural thickening and mural mass.

luminal contents of the affected bowel are usually static, or some random motion of the ingesta may be observed in foals with ileus. Contractions of the affected intestine and propulsion of the luminal contents are absent. In children with ileus, the bowel loses its multifaceted appearance and is imaged as discrete tubular structures.[101] Children with adynamic or functional ileus (nonobstructive) have distended small bowel with normal to somewhat increased peristaltic activity, whereas those with dynamic or mechanical ileus (obstructive) have more intestinal distention and variable peristaltic activity, ranging from none to increased.[101] In small animals, mechanical ileus tends to produce segmental dilatation, whereas functional ileus is usually associated with generalized intestinal distention.[45] In both functional and mechanical ileus in small animals, gastrointestinal motility appears decreased throughout the bowel.[45] The same findings appear to be true in foals. Mechanical ileus in foals is caused by intussusceptions, volvulus, obstructive embryonic remnants, mural masses, trichophytobezoars, meconium, or ascarid impactions or other lesions causing mechanical obstruction. Functional ileus in foals is most frequently associated with hypoxic bowel injury or follows abdominal surgery or anesthesia.

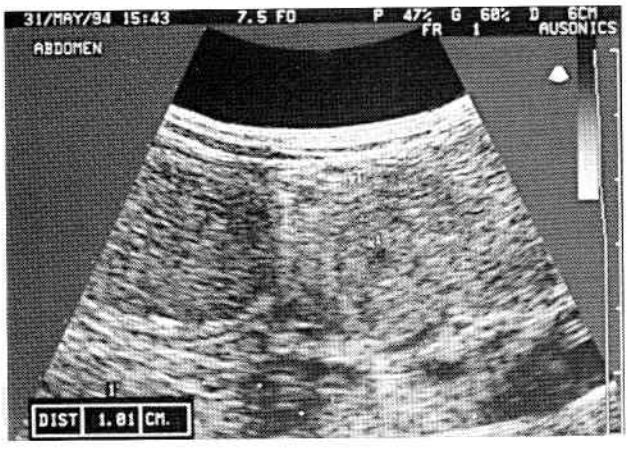

Figure 7–66

Sonogram of the ventral abdomen obtained from a 2-week-old Thoroughbred filly with hypoxic bowel syndrome. The marked thickening of the wall of the small intestine (1.01 cm) caused small intestinal obstruction. Notice the ingesta-filled distended loops of jejunum to the left of the obstructed loop of jejunum. The right side of the sonogram is the left side of the foal's abdomen, and the top is ventral. This sonogram was obtained with a 7.5-MHz sector-scanner transducer containing a built-in fluid offset and a displayed depth of 6 cm.

Abdominal Abscess

Diagnostic ultrasound is also useful for detecting abdominal abscesses, particularly those associated with *Rhodococcus equi* or *Streptococcus equi.* Large multiloculated mesenteric masses are often imaged at or near the ventral abdominal wall (Fig. 7-67).[12, 17, 31] Although multiloculated masses are more typically imaged with abdominal abscesses, more homogeneous unilocular masses have also been detected with abdominal abscesses in foals.[17] The more echogenic the material contained within the abdominal mass, the thicker and more caseated the purulent fluid is likely to be. The large size and weight of the abdominal abscess displace it toward the most ventral part of the abdomen. Abnormal peritoneal fluid (quantity and/or character) may also be detected in foals with abdominal abscesses.

Ascites/Peritonitis

Ultrasonography is the noninvasive study of choice for the diagnosis and evaluation of peritoneal fluid.[123] The quantity and character of the peritoneal fluid should also be evaluated sonographically. In an experimental porcine model, as little as 60 ml of fluid injected into the perito-

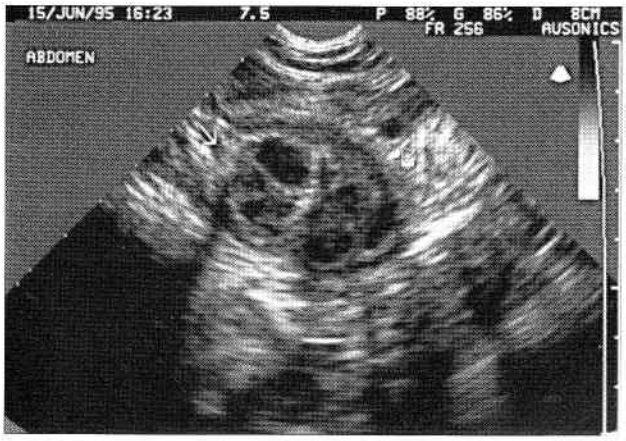

Figure 7–67

Sonogram obtained from a 2-month-old Thoroughbred filly with an abdominal abscess. The abscess (*arrows*), which is lying against the floor of the ventral abdomen, has a multiloculated appearance. This sonographic appearance is typical for *Rhodococcus equi* abscesses. The right side of this sonogram is the left side of the foal's abdomen, and the top is ventral. This sonogram was obtained with a 7.5-MHz sector-scanner transducer and a displayed depth of 8 cm.

neal cavity resulted in free-floating bowel imaged sonographically.[124] Smaller quantities of fluid were detectable sonographically in the peritoneal cavity, depending upon the pig's position. Peritoneal fluid can be sonographically classified into anechoic fluid, homogeneously echogenic, or echogenic and septated.[123] Peritoneal fluid becomes more echogenic as the cellularity of the fluid increases. The peritoneal cavity should be carefully evaluated for adhesions between the gastrointestinal viscera, internal organs, and parietal peritoneum (Fig. 7-68).[9-12, 14, 16, 19, 125] The transducer should be held still in one position and the bowel carefully examined to be sure that the segments of intestine move independently of one another, the adjacent abdominal organs, and the peritoneum.[126] Adhesions may be present in a foal with normal sonographic findings because the serosal surface of much of the intestine is not accessible sonographically.

The peritoneal fluid may be anechoic, hypoechoic, or echogenic or have a composite appearance. Anechoic fluid most frequently represents a transudate, although a modified transudate or, less likely, an exudate is possible, depending upon the size and number of the reflectors (primarily cells). The transudate may be secondary to congestive heart failure, pericarditis, hypoproteinemia, or uroperitoneum. Peritoneal fluid that is homogeneously echogenic or echogenic and septated is usually an exudate.[123] Complex peritoneal fluid may be chylous, hemorrhagic, inflammatory, or neoplastic. In equine neonates inflammatory ascites is most common. Localized peritonitis, although less common than generalized peritonitis, is occasionally detected in some foals (Fig. 7-69). Fever, anorexia, and weight loss are common presenting signs in foals with peritonitis. Colic and diarrhea have also been reported in foals with peritonitis.[127] A homogeneous swirling pattern in the peritoneal fluid is consistent with a hemoperitoneum. A chylous effusion has been reported in a foal in association with a lymphatic leak and an abdominal abscess.[17] Sonographically the chylous effusion should appear as a homogeneous echogenic effusion.[53] A ruptured viscus (Fig. 7-70) should be suspected if a composite fluid with large particulate matter, variable-sized echogenic material, fibrin, and/or free gas echoes is imaged within the peritoneal fluid.[9-12, 14, 15, 19, 20] Composite fluid with a fibrinous peritonitis has been detected in foals with ruptured gastric ulcers, as well as with other sites of intestinal rupture.[9-12, 14, 15, 19, 20, 127]

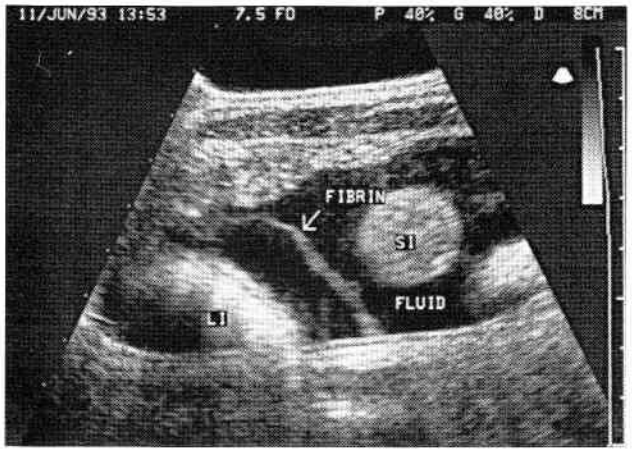

Figure 7–68

Sonogram of the ventral abdomen obtained from an 11-month-old Thoroughbred filly with peritonitis. Notice the hypoechoic peritoneal fluid and the shaggy appearance of the serosal surface of the jejunum and colon (LI). Echogenic strands (*arrow*) are seen between the visceral peritoneal surfaces. The right side of this sonogram is the left side of the foal's abdomen, and the top is ventral. This sonogram was obtained with a 7.5-MHz sector-scanner transducer and a displayed depth of 8 cm. SI, Small intestine.

Hernias

Umbilical Hernias. The majority of umbilical hernias in foals are small (<2.5 cm in diameter) and easily

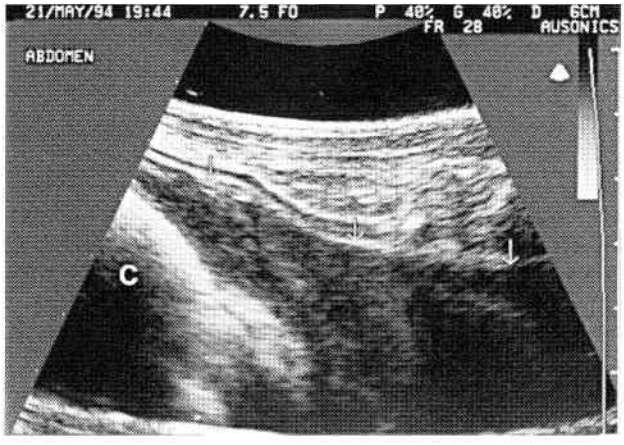

Figure 7–69

Sonogram of hypoechoic peritoneal fluid walled off in the cranial portion of the abdomen obtained from a 1-month-old Standardbred colt with peritonitis. Notice the hypoechoic fluid (*arrows*) between the large colon (C) and the ventral abdominal wall. The right side of this sonogram is cranial, and the top is ventral. This sonogram was obtained with a 7.5-MHz sector-scanner transducer containing a built-in fluid offset and a displayed depth of 6 cm.

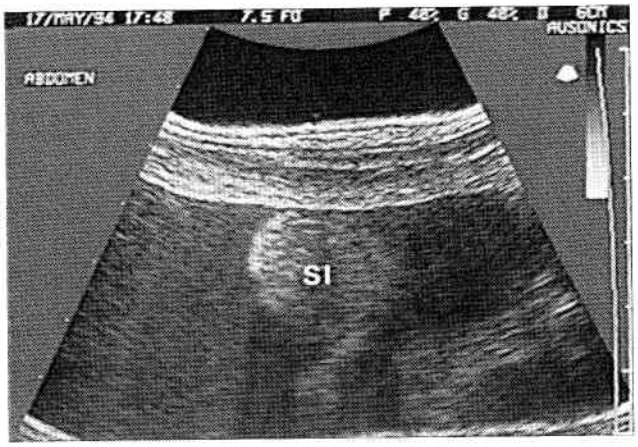

Figure 7–70

Sonogram of the ventral abdomen obtained from a 6-week-old Standardbred colt with a ruptured viscus. The echogenic peritoneal fluid surrounding the loop of ingesta-filled small intestine (SI) lies on the floor of the ventral abdomen. Large fibrin tags were imaged in the more cranial portions of the abdomen. The right side of the sonogram is the left side of the foal's abdomen, and the top is ventral. This sonogram was obtained with a 7.5-MHz sector-scanner transducer containing a built-in fluid offset and a displayed depth of 6 cm.

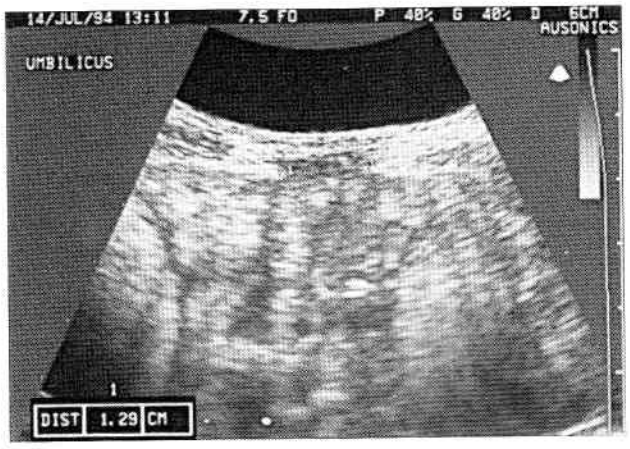

Figure 7–71

Sonogram obtained from a 2-month-old Thoroughbred filly with a small uncomplicated umbilical hernia. Notice the small defect in the abdominal musculature between the two x^1 cursors. The hernia measured 1.29 cm in the transverse plane, was easily reduced by the pressure of the transducer, and contained only peritoneal fluid. Notice the normal small and large bowel echoes in the abdominal cavity. The right side of this sonogram is the left side of the foal's abdomen, and the top is ventral. This sonogram was obtained with a 7.5-MHz sector-scanner transducer containing a built-in fluid offset and a displayed depth of 6 cm.

reducible.[28, 128-130] The hernial sac usually contains peritoneal fluid and possibly omentum. Intestine, if present in the hernial sac, is usually ileum or jejunum and only infrequently becomes strangulated within the hernial sac.[28, 128, 131] Omentum, ventral colon, and cecum have also been found incarcerated in the umbilical hernia.[131] Umbilical hernias are easily scanned to determine their contents (fluid, omentum, or intestine), size, and the presence of internal umbilical remnant or subcutaneous infection.[5-9, 12, 14, 28] Characterizing the size of the hernia aids the surgeon preoperatively in the selection of the type of hernial closure necessary.[9-11, 14, 28] The simple umbilical hernia appears as a defect in the ventral body wall at the umbilicus (Fig. 7-71) with a diameter that can be measured in its sagittal and transverse planes. The complicated umbilical hernia (a hernia with internal or external umbilical infection) has an infection of the internal or external umbilical remnants or the adjacent subcutaneous structures that complicates the surgical procedure for hernial closure.[28] If draining tracts are detected in association with an umbilical hernia (Fig. 7-72), careful sonographic evaluation should be performed to determine the source of the drainage (subcutaneous abscess, internal umbilical remnant infection, or leaking bowel incarcerated within the hernia). If an umbilical abscess is adjacent to the umbilical hernia, another fluid-filled sac is detected in the subcutaneous space adjacent to, but not communicating with, the hernial sac (Figs. 7-72 and 7-73). These foals should be carefully scanned to eliminate the possibility of a concurrent internal umbilical remnant infection, which would alter the surgical approach to hernial repair. A nonreducible umbilical hernia can occur with omentum, small intestine (usually ileum—see Fig 7-73), ventral colon, or cecum strangulated or incarcerated in the hernial sac.[28, 131] Omentum has a heterogeneous hypoechoic to echogenic appearance created by the fat contained within the omentum. Omentum may appear solid or cavitated when strangulated within the hernia, depending upon the amount of tissue necrosis and cellular infiltrate in the strangulated tissues. The strangulated ileum or jejunum appears similar to compromised small intestine previously described in other types of surgical obstructions. The wall of the ileum or jejunum appears thickened and hypomotile or amotile (more likely), with a turgid appearance to the portion of the small intestine strangulated within the hernia (see Fig. 7-74).[9-11] In the foals in which large intestine was

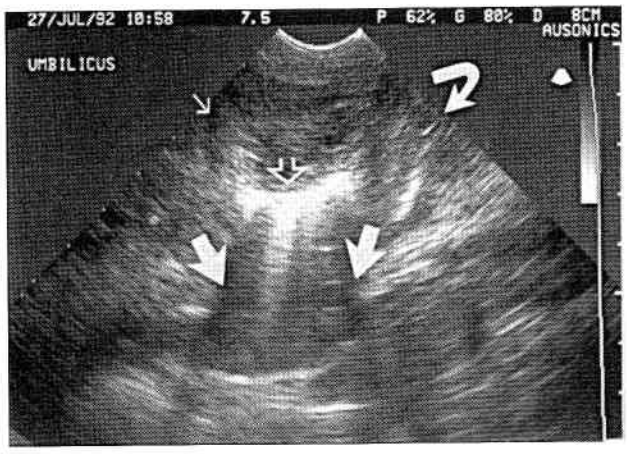

Figure 7–72

Sonogram obtained from a 3-month-old Thoroughbred filly with an umbilical hernia, an umbilical abscess, and a draining tract. Notice the large defect in the abdominal wall (*large arrows*), the loculated subcutaneous abscess (*small arrow*), and the gas-filled tract along the cranial margin of the abscess and hernia (*curved arrow*) extending from the abscess toward the abdominal cavity (enterocutaneous fistula). Notice also the hyperechoic gas echoes in the dorsalmost portion of the umbilical abscess (*open arrow*), obscuring adequate visualization of the hernial sac and its contents. The right side of this sonogram is cranial, and the top is ventral. This sonogram was obtained with a 7.5-MHz sector-scanner transducer and a displayed depth of 8 cm.

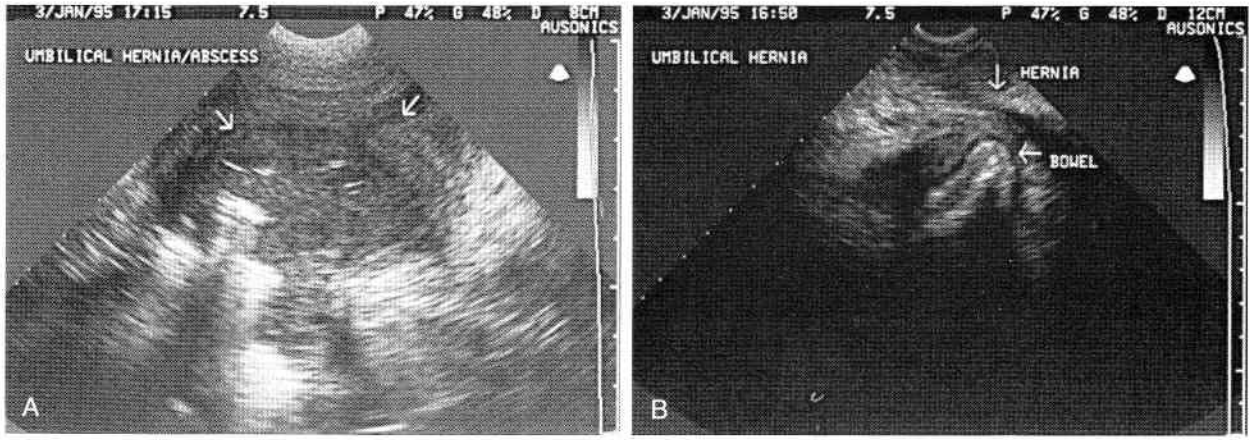

Figure 7–73

Sonograms of the umbilicus and ventral abdomen obtained from a 9-month-old Quarter horse colt with an umbilical hernia. Thickened edematous soft tissues are located immediately ventral to the umbilical abscess and hernial sac. The right side of these sonograms is cranial, and the top is ventral. These sonograms were obtained with a 7.5-MHz sector-scanner transducer and a displayed depth of 8 *(A)* and 12 *(B)* cm.

A, Sonogram of the umbilical swelling demonstrating the large umbilical abscess (*arrows*) associated with the umbilical hernia. The umbilical abscess was located in the soft tissues to the left of the umbilical hernia and contained hypoechoic fluid with hyperechoic echoes consistent with free gas and a probable anaerobic infection.

B, Sonogram of the thickened ileum trapped within the hernia. The wall of this loop of ileum measured 0.67 to 0.92 cm in thickness. Notice the marked thickening of the soft tissue structures surrounding the umbilical hernia.

found incarcerated in the umbilical hernia, only a portion of the circumference of the ventral colon or cecum was incarcerated within the umbilical hernia. This devitalized portion of the large intestine should be imaged as an outpouching of the ventral colon or cecum with thickened edematous, amotile intestinal walls. Foals with intestinal incarceration within the umbilical hernia usually have a history of colic associated with increased swelling, firmness, and sensitivity in the hernial sac prior to admission.[28, 131]

Diaphragmatic Hernias. Displacement of the gastrointestinal viscera into the thoracic cavity through a diaphragmatic hernia can usually be diagnosed by scanning the affected side of the thorax and cranial abdomen (see Chapter 4).[12, 132] In most instances the rent in the diaphragm can be directly imaged because displacement of the overlying lung by the herniated viscera occurs. The type and amount of abdominal viscera herniated into the thoracic cavity can be determined, as well as the viability of the herniated bowel (Fig. 7–75).[12, 132] The ultrasonographic examination can be used to determine if resection of incarcerated bowel is necessary and if a mesh implant is needed to repair the diaphragmatic de-

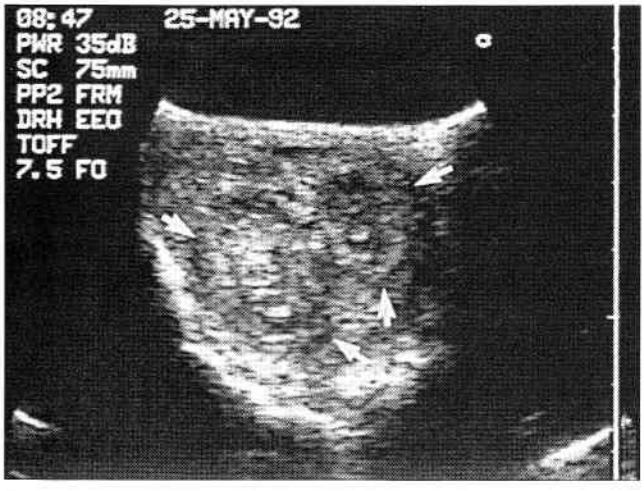

Figure 7–74

Sonogram obtained from a 3-day-old Thoroughbred colt with an umbilical hernia. The ileum is incarcerated in the umbilical hernia. One loop of ileum, which is imaged in two sections, is trapped within the umbilical hernia with thickened edematous walls (*arrows*). These loops of intestine were hypomotile in real time and not reducible. This is a transverse view through the hernial sac. The right side of the sonogram is the left side of the hernial sac. This sonogram was obtained with a 7.5-MHz sector-scanner transducer containing a built-in fluid offset and a displayed depth of 7.5 cm.

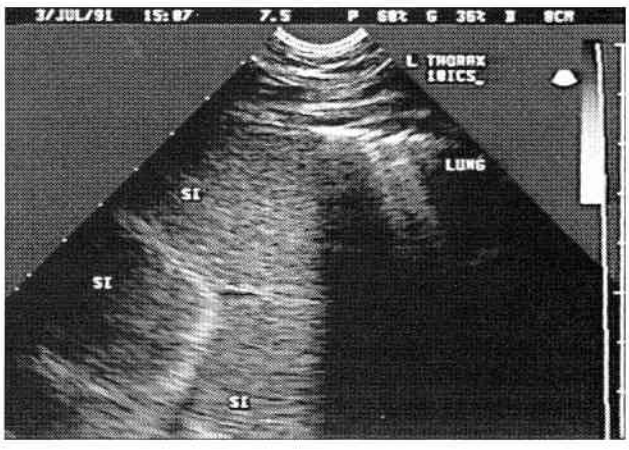

Figure 7–75

Sonogram of the left side of the thorax obtained in the tenth intercostal space from a 1-month-old Standardbred filly with a diaphragmatic hernia. The fluid-distended small intestine (SI) is immediately adjacent to the ventral lung with no diaphragm separating them. Although the small intestine is turgid and amotile, the wall thickness of the herniated small intestine is still normal to nearly normal. This sonogram was obtained with a 7.5-MHz sector-scanner transducer and a displayed depth of 8 cm. The right sides of the sonograms are dorsal, and the left sides are ventral.

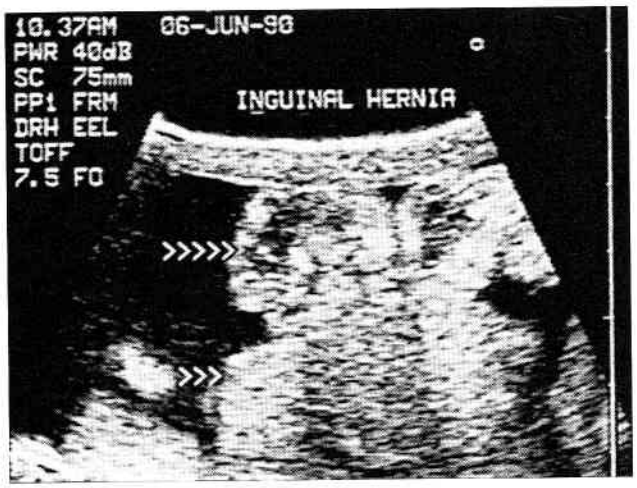

Figure 7–76

Sonogram obtained from a 1-week-old Standardbred colt with a bilateral inguinal hernia that was easily reducible. Notice the excess fluid contained within the scrotum, the normal testicle (*three arrowheads*), and the adjacent jejunum with normal peristalsis (*five arrowheads*). The central hypoechoic area in the testicle is created by the shadowing from the superimposed jejunum and is not a real change in the echogenicity of the testicle. The right side of this sonogram is dorsal, and the left is ventral. This sonogram was obtained with a 7.5-MHz sector-scanner transducer containing a built-in fluid offset and a displayed depth of 7.5 cm.

fect. Diaphragmatic hernias are most frequently associated with colic, although with large hernias, respiratory distress may be the primary presenting sign in affected foals.[132-136] The severity of clinical signs depends upon which portion of the gastrointestinal tract has herniated into the thoracic cavity, the degree of obstruction of the herniated bowel, and the amount of herniated viscera. A history of trauma is common in foals and horses with diaphragmatic hernias, although congenital diaphragmatic hernias do occur.[133, 136-138] Diaphragmatic hernias should be considered in foals with other congenital defects and have been reported in foals with a ventricular septal defect,[133] chylothorax, and a defect in the thoracic duct,[137] scoliosis, and arthrogryposis.[136]

Inguinal and Abdominal Wall Hernias. Ultrasonography can also be used in colts with inguinal hernias to characterize the viability of the incarcerated bowel, as well as to further describe the hernia.[9-12, 14] Jejunum is usually detected in the inguinal hernia (Fig. 7-76). The long jejunal mesentery enables this portion of the intestine to herniate through the inguinal ring into the scrotum. Abdominal wall abnormalities can also be identified sonographically in foals with abdominal wall hernias secondary to abdominal wall trauma.

PATIENT MANAGEMENT AND PROGNOSIS

Umbilical Abnormalities

Umbilical Remnant Infection

Management of foals with diagnosed external and/or internal umbilical infections may be medical or surgical. Medical treatment is recommended for all foals with external umbilical remnant infection and normal internal umbilical remnants.[1-12] Medical treatment of internal umbilical remnant infections is recommended in all foals that are clinically stable when the problem is initially diagnosed.[3, 6, 9-12] Initial treatment should include broad-spectrum antibiotic coverage.[1, 3-12] Blood cultures are indicated in neonatal foals to determine if there is a concurrent septicemia. A sample should be obtained for culture and sensitivity testing from any concurrent infection (e.g., septic arthritis, pneumonia, draining external umbilical remnant), as these infections are usually caused by one or more of the organisms present in the internal umbilical remnant infection.[3, 11] Surgical intervention is recommended when the foal has been treated aggressively medically without improvement, when septic arthritis or another concurrent infection which may be secondary to spread of the umbilical remnant infection is detected, or if another elective surgery is planned (e.g., periosteal stripping).[3, 9-12] Surgical intervention is also recommended if there are multiple internal remnants affected or an individual affected internal umbilical remnant structure is more than twice normal size.[3, 9-12] The internal umbilical remnants removed surgically should be submitted for culture and sensitivity testing. Multiple organisms are usually recovered from infected internal umbilical remnants.[3, 11, 12] If other concurrent infections exist, the causative agents are usually also found in the infected internal umbilical remnants.[3, 11, 12] Therefore, it is important to submit samples for culture and sensitivity testing from all infected areas and to use broad-spectrum antimicrobial coverage until the results of the cultures and sensitivity testing are known. Marsupialization of an infected umbilical vein should be considered in foals in which the infection extends up to or into the liver, precluding complete resection of the infected tissue.[7]

Foals with external and/or internal umbilical remnant infections usually have a good prognosis if the infection is treated aggressively with broad-spectrum antibiotics and the foals are closely monitored clinically and ultrasonographically, unless there is involvement of the umbilical vein up to or including the liver.[3, 6, 11, 12] Such an infection of the umbilical vein carries a poorer prognosis because the infection is more likely to spread and surgical resection or drainage is difficult or impossible without some contamination of the peritoneal cavity.[3, 5, 12] If broad-spectrum antimicrobial treatment for internal umbilical remnant infection is selected, follow-up ultrasonographic examination should be performed in 3 to 5 days. Sonographic improvement is usually detectable in this time if the appropriate antimicrobials have been selected (Fig. 7-77).[3, 5, 6, 10-12] The majority of foals with internal umbilical remnant infection improve following a course of broad-spectrum antimicrobial therapy. If the affected internal umbilical remnant is enlarging, antimicrobial therapy should be changed or surgical intervention considered to prevent worsening of the infection and possible seeding of other organs, especially joints.[3, 6, 11] Surgical removal of necrotic or severely infected urachal or umbilical artery remnants is indicated to remove the source of sepsis and to prevent the development of uroperitoneum.

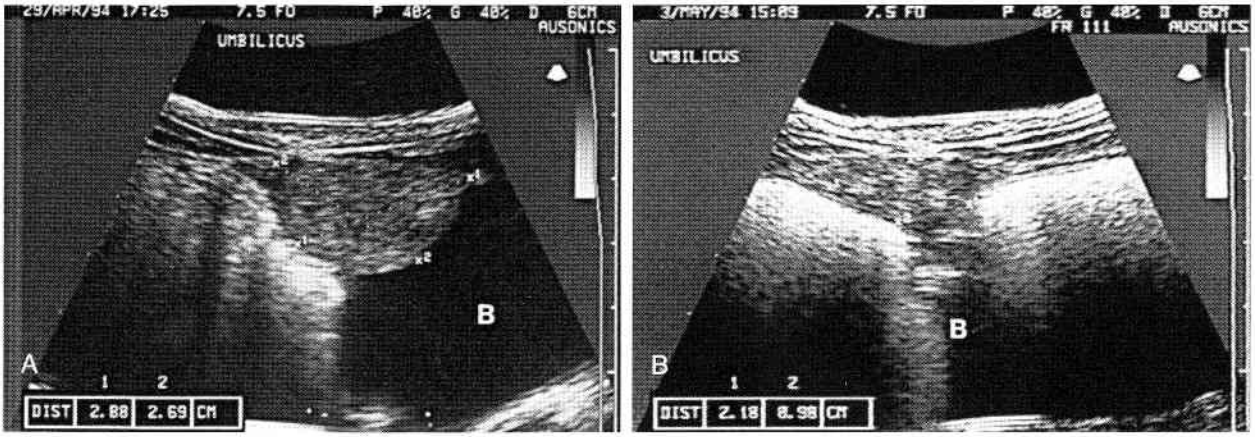

Figure 7–77

Sonograms obtained from a 1-week-old Quarter horse filly with urachitis. The hyperechoic mucosal surface of the large colon is imaged adjacent to the urachus and umbilical arteries. The right side of these sonograms is the left side of the foal's abdomen, and the top is ventral. These sonograms were obtained with a 7.5-MHz sector-scanner transducer containing a built-in fluid offset and a displayed depth of 6 cm.

A, Initial sonogram of the urachus and both umbilical arteries at the apex of the bladder (B), demonstrating an enlarged urachus filled with hypoechoic fluid measuring 2.88 (x^1) by 2.69 (x^2) cm.

B, Sonogram of the urachus and both umbilical arteries at the apex of the bladder obtained 4 days later after the foal had been placed on broad-spectrum antimicrobials. Notice the significant decrease in the size of the urachus, particularly in the dorsal-to-ventral scan plane. The urachus and both umbilical arteries measured 2.18 (x^1) by 0.98 (x^2) cm at the apex of the bladder. Only a small amount of echogenic debris was imaged in the urachus at this time. This foal was successfully treated with medical therapy.

Umbilical Remnant Hemorrhage

Foals with excessive hemorrhage from the umbilical vessels at birth and perivascular or intravesicular hematomas should be placed on broad-spectrum antimicrobials prophylactically because septicemia and infection of these internal umbilical remnants are common sequelae. Frequent ultrasonographic monitoring of the resolution of the perivascular and intravesicular hematomas should be performed.[5, 12] Surgical intervention may be necessary to remove a large intravesicular clot if it is not resorbed because the clot is a nidus for infection. Concurrent cystitis and septicemia may occur.[11] Frequent ultrasonographic monitoring is also indicated in foals with patent urachus to evaluate the internal umbilical remnants for the development of a urachitis or omphaloarteritis, which should be aggressively treated with broad-spectrum antimicrobials.[5] Similarly, frequent ultrasonographic monitoring is indicated in foals with a urachal diverticulum, as the urachal diverticulum may also be a potential area for infection resulting in a localized urachitis or cystitis.

Patent Urachus

Cautery of the patent urachus results in closure of the patent urachus in the majority of foals.[61] Overzealous cautery is discouraged because tissue necrosis and infection may result. Surgical resection of the patent urachus is indicated in foals in which cautery fails to result in closure or infection is a complicating factor.[61]

Uroperitoneum and Abnormalities of the Bladder

Surgery is indicated for correction of a defect in the urinary tract after appropriate stabilization of the foal. There is one case report of successful medical treatment of a ruptured bladder, but this should be considered in foals only when surgical repair is not an option.[62] Intravenous fluid replacement therapy is critical prior to surgical intervention and should consist of NaCl-containing fluids with no KCl added.[26, 56, 59-61] Intravenous dextrose, insulin, and sodium bicarbonate are usually needed to help correct the hyperkalemia.[26, 59-61] The excess peritoneal fluid should be slowly drained before surgery while the foal is being stabilized.[26, 29, 56, 59-61] Correction of the electrolyte disturbances prior to general anesthesia is important because these foals are prone to the development of life-threatening cardiac arrhythmias (complete atrioventricular block, ventricular tachycardia) under general anesthesia.[56, 60] Suture lines should be tested prior to abdominal closure by distending the bladder with normal saline, as 25% of the repairs leaked in one report.[29, 56, 60] The long-term prognosis is usually good for foals with uncomplicated urinary bladder or urachal rupture, with more than 66% surviving to weanling age.[23, 26, 29, 56, 59-61] Foals with ureteral defects and necrotizing cystitis have a poorer prognosis (33% survival).[26] Resection of the affected bladder wall must be performed in foals with a necrotic emphysematous cystitis, and the resected bladder wall should be submitted for culture and sensitivity testing and histopathologic evaluation. Often there is little normal bladder tissue remaining in affected foals. Breakdown of the surgical incision, peritonitis, and gastrointestinal adhesions with the subsequent development of colic are the most common postoperative complications.[26] Ultrasonographic evaluation of the abdomen should be performed postoperatively in foals experiencing postoperative complications (fever, abdominal distention, straining to urinate, colic), as peritonitis, adhesions (Figs. 7-78 and 7-79), ileus, or abnormalities of the bladder wall (Fig. 7-80) may be diagnosed and

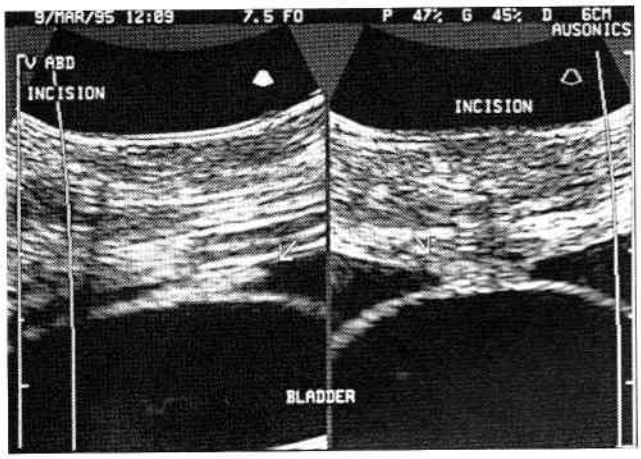

Figure 7–78

Sonograms of the ventral abdomen obtained from a 5-day-old Standardbred filly. This filly had a ruptured bladder that had been repaired 3 days earlier. This sonogram shows a fibrinous adhesion between the bladder apex and the incision (*arrows*). The sonogram on the left is a sagittal view, and the sonogram on the right is a transverse view of the ventral abdominal wall and ventral bladder wall. Notice the hypoechoic to echogenic tissue between the apex of the bladder and the ventral abdominal wall at the site of the incision (*arrows*). Excess anechoic peritoneal fluid is present in the abdominal cavity. The right side of the sagittal image is cranial and the top is ventral. The right side of the transverse image is the left side of the foal's abdomen. These sonograms were obtained with a 7.5-MHz sector-scanner transducer containing a built-in fluid offset and a displayed depth of 6 cm.

appropriate treatment selected (surgical or nonsurgical).[22]

Disease of the Abdominal Organs

Sonographic evaluation of the abdominal organs may help the clinician diagnose the disease process and its severity, but a definitive diagnosis must be made histopathologi-

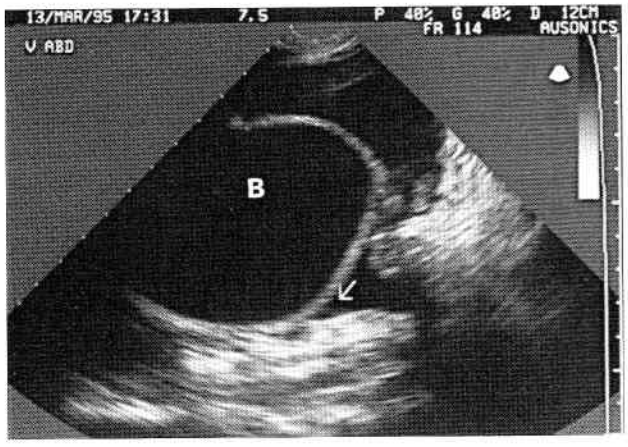

Figure 7–79

Sonogram of the caudal ventral abdomen obtained from a 9-day-old Standardbred filly that had a ruptured bladder repaired 7 days earlier. Notice the increased amount of anechoic fluid present in the peritoneal cavity and the adhesion (*arrow*) of the large colon to the dorsal wall of the bladder (B). The right side of this sonogram is cranial, and the top is ventral. This sonogram was obtained with a 7.5-MHz sector-scanner transducer and a displayed depth of 12 cm.

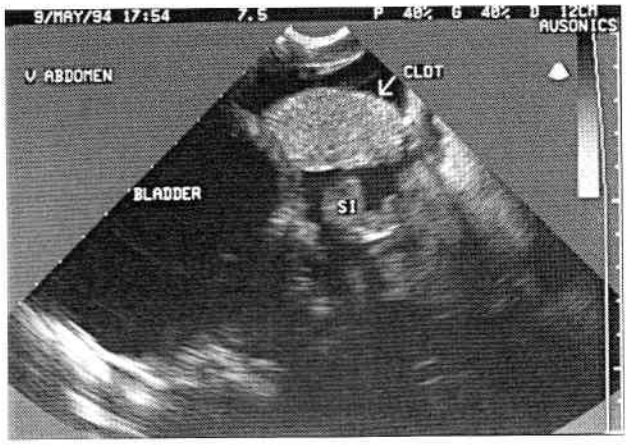

Figure 7–80

Sonogram of the bladder obtained from a 1-month-old Thoroughbred colt following resection of the urachus and umbilical arteries several days earlier. A large echogenic clot (*arrow*) is adhered to the bladder wall at the site of the urachal resection. Notice the increased amount of peritoneal fluid and the jejunum (SI) floating in the excess fluid. The right side of this sonogram is cranial and the top is ventral. This sonogram was obtained with a 7.5-MHz sector-scanner transducer and a displayed depth of 12 cm.

cally. Ultrasound-guided biopsies can be obtained from all the abdominal organs for histopathologic evaluation and culture and sensitivity testing when indicated (see Chapter 6).[11, 14, 15, 139, 140] Blood cultures should also be obtained from foals in which septicemia is likely. Broad-spectrum antibiotics should be started after obtaining samples for culture and sensitivity testing because neonatal foals are likely to deteriorate rapidly if treatment is not instituted immediately. Antimicrobial selection should be based on the most likely organism to cause the clinical disease. Repeat sonographic examinations may be useful in monitoring the clinical course in affected foals, and they demonstrated reduction in liver size and vascularity in one foal successfully treated for suspected Tyzzer's disease.[30] Ultrasonography has been used intraoperatively in a calf with a patent ductus venosus to evaluate the blood flow through the portosystemic shunt.[79] Doppler ultrasound confirmed the successful closure of the shunt at the time of surgery and postoperatively in this calf. Ultrasonography has also been used intraoperatively to guide the surgeon ligating the ductus venosus in a dog.[81]

Gastrointestinal Diseases

The decision about whether or not to operate can be made quickly following an abdominal ultrasonographic examination in a colicky foal, without waiting for the results of an abdominal paracentesis. In fact, an abdominal paracentesis may be contraindicated in foals with marked abdominal distention and no imageable peritoneal fluid because of the risk of intestinal laceration.[85] Although many intussusceptions (95.5%) have been successfully reduced in children using hydrostatic pressure and ultrasonographic guidance without surgical intervention, this has not been performed in foals or small animals to the author's knowledge.[141, 142] The different location of

most intussusceptions in foals (jejunojejunal) may make this procedure less successful than in children, in whom ileocecal intussusceptions are more common. Surgical intervention is indicated when an intussusception or other strangulated obstructed intestine is imaged sonographically. Surgical intervention is usually indicated when an ascarid intraluminal mass or fecalith is detected. Although repeated enemas may help the foal to pass a fecalith or meconium impaction, surgical intervention and the removal of the fecalith via an enterotomy are often necessary.[104] Injection of the fecalith or meconium impaction with a solution of saline and dioctyl sodium succinate via an abdominal celiotomy may result in the foal being able to excrete the impacted fecal material normally, without an enterotomy. Nasogastric intubation is indicated when marked gastric distention is imaged, either fluid or gas (less likely), to decompress the foal's abdomen and minimize the possibility of gastric rupture.[8, 9, 11, 13] Medical therapy is indicated initially for foals with gas-, fluid-, or ingesta-filled bowel when the wall thickness of the bowel is normal to nearly normal. If fluid-filled hypermotile gastrointestinal viscera are imaged, the foal should be moved to an isolation area in preparation for the development of diarrhea, if not already present, to minimize the spread of infectious disease.

Abdominal Abscess/Peritonitis

If a large abdominal abscess is detected sonographically, the foal should be carefully screened for *Rhodococcus equi* and *Streptococcus equi.* Serum should be obtained for an enzyme-linked immunosorbent assay or agar gel immunodiffusion test for *Rhodococcus equi* and a peritoneal tap obtained, if peritoneal fluid was visible sonographically, for cytology and culture and sensitivity testing. The lungs should be carefully evaluated for any evidence of concurrent pulmonary disease. Thoracic radiographs should be obtained, if possible, and a transtracheal aspirate performed for cytology and culture and sensitivity testing, if the auscultatory findings or thoracic radiographs are abnormal. The foal should be treated for *Rhodococcus equi* infection with erythromycin and rifampin until the results of the culture and sensitivity testing are available. Follow-up ultrasonographic examinations should be performed every month, or more frequently if desired, to monitor the regression of the abscess. Surgical exploration of the abdomen and resection or drainage of the abscess should also be considered in foals that are good surgical candidates. The best surgical candidates are foals with a discrete abdominal abscess with no evidence of adhesions between the abscess and the surrounding intestine or abdominal viscera and no detectable pulmonary disease. Resolution of abdominal abscesses caused by *Streptococcus equi* has been reported in a foal with a combination of surgical drainage and antibiotics. Follow-up sonographic examinations revealed a resolution of the abdominal abscesses.[17]

Ultrasonography is more sensitive than radiography for detecting small quantities of peritoneal fluid in small animals and should be similarly sensitive in large animals.[143] If no peritoneal fluid is imaged ultrasonographically, the likelihood of obtaining a sample of peritoneal fluid for cytologic evaluation and culture and sensitivity testing is extremely low. If excess peritoneal fluid is detected sonographically, the peritoneal fluid should be further characterized by cytologic evaluation and culture and sensitivity testing. If more than one type of peritoneal fluid is imaged or the fluid is loculated, an ultrasound-guided sample of the fluid in question can be obtained.[123] If uroperitoneum is suspected and the bladder and urachus appear normal sonographically, creatinine and K^+ measurements should be obtained on the peritoneal fluid and compared with those values in the serum. Treatment for most foals with peritonitis is initially broad-spectrum antimicrobial therapy until the results of culture and sensitivity testing become available. Bacterial infections should be suspected as the most likely cause of the peritonitis in foals, even with a negative culture of the peritoneal fluid.[127] Peritoneal lavage should be considered in those foals with large quantities of fibrin in the peritoneal cavity, although the effectiveness of peritoneal lavage and drainage still remains in question. Surgical exploration may be indicated occasionally in some foals to determine the source of the peritonitis and repair the defect, if possible. The gastrointestinal viscera and abdominal organs should be carefully evaluated to determine if the cause of the peritonitis can be found. Intestinal parasites have been associated with abdominal abscesses and peritonitis in foals. In the absence of other identifiable causes, intestinal parasites probably play an important role in the pathogenesis of peritonitis in foals.[127] Aggressive deworming should, therefore, be considered in foals in which parasitism can be documented, those with a poor or absent deworming history, and those in which the cause of the peritonitis is undetermined. Diarrhea is a poor prognostic sign in foals and horses with peritonitis. All the foals and horses presenting with diarrhea and peritonitis were destroyed in one study.[127] Humane destruction must be considered for foals with a ruptured gastrointestinal viscus.

Hernias

Small umbilical hernias that are easily reducible and do not contain omentum or intestine may be repaired by nonsurgical techniques after returning any contained omentum or intestine to the abdominal cavity.[128, 130] Hernias that are selected for nonsurgical repair should be reducible, 5 cm long or less, and free from any history or evidence of infection.[128] Larger simple umbilical hernias or complicated umbilical hernias should be surgically corrected.[28, 128-131] Care must be taken to remove the subcutaneous, external umbilical remnant abscess and/or infected internal umbilical remnants without contaminating the surgery site in foals in which the umbilical hernias are complicated by infection. Although the prevalence of intestinal incarceration and subsequent strangulation is low in foals with umbilical hernias, the persistence of the umbilical hernia after conservative management appears to increase the likelihood for incarceration and strangulation to develop.[128, 131] Most foals with intestinal incarceration and strangulation are older than 6 months

when the problem develops, with a mean age of affected individuals of 11.5 months in one study.[151] With enterocutaneous fistulae, loss of large volumes of intestinal fluids may occur, resulting in severe electrolyte imbalances and emaciation.[28, 151] In these foals resection of the involved bowel is recommended, followed by an enteroenterostomy.[28] With large umbilical, diaphragmatic, or abdominal wall hernias, mesh may be needed to close the defect. An appropriate-sized piece of mesh should be sterilized and ready, if needed, based upon the preoperative estimation of hernial size. Ultrasonographic evaluation of the hernial closure is useful in foals that are experiencing postoperative problems following hernia repair. The hernial closure, abdominal viscera, intestinal motility, and peritoneal fluid can all be examined ultrasonographically. Closure of abdominal wall hernias should be postponed until a fibrous ring has formed around the hernial edges for optimal surgical results.

Inguinal hernias usually correct themselves within the first few days of life. Bandaging of the affected area in a figure-eight pattern is successful in foals with large amounts of viscera herniated into the scrotum, as long as the hernia is reducible.[61] Surgical resection is indicated only in those rare cases in which the hernia is not reducible or strangulated bowel is present.[61]

References

1. Reef VB: Abnormalities of the neonatal umbilicus detected by ultrasound. Proceedings of the 32nd Annual American Association of Equine Practitioners 1986:32, 157-162.
2. Reef VB, Collatos CA: Ultrasonography of umbilical structures in clinically normal foals. Am J Vet Res 49:2143-2146, 1988.
3. Reef VB, Collatos, CA, Spencer PA, et al: Clinical, ultrasonographic and surgical findings in foals with umbilical remnant infections. J Am Vet Med Assoc 195:69-72, 1989.
4. Collatos CA, Reef VB, Richardson DW: Umbilical cord remnant abscess in a yearling colt. J Am Vet Med Assoc 195:1252-1254, 1989.
5. Pennick DG, Reef V: L'echographie des structures ombilicales chez le poulain. Pract Vet Equine 23:5-10,1991.
6. Reimer JM: Ultrasonography of umbilical remnant infections in foals. Proceedings of the 39th Annual American Association of Equine Practitioners 1993:39, 247-248.
7. Edwards, RB, Fubini SL: A one-stage marsupialization procedure for management of infected umbilical vein remnants in calves and foals. Vet Surg 24:32-35, 1995.
8. Reef VB: Evaluation of abdominal disorders in horses using ultrasonography. Proceedings of the 17th Annual Veterinary Surgery Forum 1989:17, 141-143.
9. Reef VB: The use of diagnostic ultrasound in the horse. Ultrasound Q 9:1-34, 1991.
10. Reef VB: Equine pediatric ultrasonography. Compend Contin Educ Pract Vet 13:1277-1285, 1991.
11. Reef VB: Ultrasonographic evaluation and diagnosis of foal diseases. In Robinson NE (ed): Current Therapy in Equine Medicine III. Philadelphia, WB Saunders, 1991, pp 417-421.
12. Reef VB: Diagnostic ultrasonography of the foal's abdomen. In McKinnon AO, Voss JL (eds): Philadelphia, Lea & Febiger, 1993, pp 1088-1094.
13. Bernard WV, Reef VB, Reimer JM, et al: Ultrasonographic diagnosis of small-intestinal intussusception in three foals. J Am Vet Med Assoc 194:395-397, 1989.
14. Reef VB: Ultrasonographic evaluation of the acute abdomen in the foal. Proceedings of the 10th Annual Veterinary Medicine Forum 1992:10, 424-426.
15. Reimer JM. Sonographic evaluation of gastrointestinal diseases in foals. Proceedings of the 39th Annual American Association of Equine Practitioners 39;245-246, 1993.
16. Byars TD, Halley J: Uses of ultrasound in equine internal medicine. Vet Clin North Am [Equine Pract] 2:253-258, 1986.
17. Hanselaer JR, Nyland TG: Chyloabdomen and ultrasonographic detection of an intra-abdominal abscess in a foal. J Am Vet Med Assoc 183:1465-1467, 1983.
18. Foreman JH, Reed SM, Rantanen NW, et al: Congenital internal hydrocephalus in a quarter horse foal. J Equine Vet Sci 3:154-164, 1983.
19. Rantanen NW. Diseases of the abdomen. Vet Clin North Am [Equine Pract] 2:67-88, 1986.
20. McGladdery AJ: Ultrasonography as an aid to the diagnosis of equine colic. Equine Vet Educ 4:248-251, 1992.
21. Bilkslager AT, Green EM, MacFadden KE, et al: Excretory urography and ultrasonography in the diagnosis of bilateral ectopic ureters in a foal. Vet Radiol Ultrasound 33:41-47, 1992.
22. Bathe AP: Urinary tract disruption in neonatal foals. Equine Vet Educ 6:83-84, 1994.
23. Adams R, Koterba AM, Cudd TC, Baker WA: Exploratory celiotomy for suspected urinary tract disruption in neonatal foals. A review of 18 cases. Equine Vet J 20:13-17, 1988.
24. Lees MJ, Easley KJ, Sutherland RJ, et al: Subcutaneous rupture of the urachus, its diagnosis and surgical management in three foals. Equine Vet J 21:462-464, 1989.
25. Divers TJ, Byars D, Spirito M: Correction of bilateral ureteral defects in a foal. J Am Vet Med Assoc 192:384-386, 1988.
26. Reef VB: Sonographic diagnosis of uroperitoneum in foals and horses. Proceedings of the 13th Annual Veterinary Medicine Forum 13:582-584, 1995.
27. Latimer FG, Magnus R, Duncan RB: Arterioureteral fistula in a colt. Equine Vet J 23:483-484, 1991.
28. Freeman DE, Orsini JA, Harrison IW, et al: Complications of umbilical hernias in horses: 13 cases (1972-1986). J Am Vet Med Assoc 192:804-807, 1988.
29. Van Pelt RJ: Correction of rupture of the urinary bladder in a foal. Equine Vet Educ 6:80-82, 1994.
30. Peek SF, Byars TD, Rueve E: Neonatal hepatic failure in a Thoroughbred foal: Successful treatment of a case of presumptive Tyzzer's disease. Equine Vet Educ 6:307-309, 1994.
31. Reef VB, Jones PA, Beech J, et al: Diagnostic dilemma. Compend Contin Educ Pract Vet 15:92-95, 1993.
32. Rantanen NW: Diseases of the liver. Vet Clin North Am [Equine Pract] 2:104-114, 1986.
33. Rantanen NW: Diseases of the kidneys. Vet Clin North Am [Equine Pract] 2:89-103, 1986.
34. Witwell KE: Morphology and pathology of the equine umbilical cord. J Reprod Fert (Suppl) 23:599-603, 1975.
35. Pennick DG, Eisenberg HM, Teuscher EE, et al: Equine renal ultrasonography: Normal and abnormal. Vet Radiol 27:81-84, 1986.
36. Rantanen NW: Renal ultrasound in the horse. Equine Vet Educ 2:135-136, 1990.
37. Yamaga Y, Too K: Diagnostic ultrasound imaging in domestic animals: Fundamental studies on abdominal organs and fetuses. Jpn J Vet Sci 46:203-212, 1984.
38. Hoffman KL, Wood AKW, McCarthy PH: Sonographic-anatomic correlation and imaging protocol for the kidneys of horses. Am J Vet Res 56:1403-1412, 1995.
39. Campbell ML, Ackerman N, Peyton LC: Radiographic gastrointestinal anatomy of the foal. Vet Radiol 25:194-204, 1984.
40. Kiper ML, Traub-Dargatz JL, Wrigley RH: Renal ultrasonography in horses. Compend Contin Educ Pract Vet 12:993-1000, 1990.
41. Wu J-X, Carlisle CH: Ultrasonographic examination of the canine liver based on recognition of hepatic and portal veins. Vet Radiol Ultrasound 36:234-239, 1995.
42. Pennick DG, Nyland TG, Fisher PE, et al: Ultrasonography of the normal canine gastrointestinal tract. Vet Radiol 30:272-276, 1989.
43. Pennick DG: Ultrasonography of the gastrointestinal tract. In Nyland TG, Mattoon JS (eds): Veterinary Diagnostic Ultrasound. Philadelphia, WB Saunders, 1995, pp 125-140.
44. Fleischer AC, Dowling AD, Weinstein ML, James AE Jr: Sonographic patterns of distended, fluid-filled bowel. Radiology 133:681-685, 1979.
45. Stringer DA, Daneman A, Brunelle F, et al: Sonography of the

normal and abnormal stomach (excluding hypertrophic pyloric stenosis) in children. J Ultrasound Med 5:183–188, 1986.
46. Miller JH, Kemberling C: Ultrasound scanning of the gastrointestinal tract in children: Subject review. Radiology 152:671–677, 1984.
47. Pozniak MA, Scanlan KA, Yandow D, Mulligan G: Current status of small-bowel ultrasound. Radiologe 30:254–265, 1990.
48. Fleischer AC, Muhletaler CA, James AE Jr: Sonographic patterns arising from normal and abnormal bowels. Radiol Clin North Am 18:145–159, 1980.
49. Kimmey MB, Silverstein FE, Waggitt RC, et al: Cross-sectional imaging method: A system to compare ultrasound, computed tomography and magnetic resonance with histologic findings. Invest Radiol 22:227–231, 1987.
50. Worth LT: Ultrasonography of the normal equine small intestine [abstract]. Vet Radiol Ultrasound 36:355, 1995.
51. Braun U, Mermier O: Ultrasonographic examination of the small intestine of cows. Vet Rec 136:239–244, 1995.
52. Fleischer AC, Muhletaler CA, James AE Jr: Sonographic assessment of the bowel wall. Am J Radiol 136:887–891, 1981.
53. Teele RL, Share JC (eds): Ultrasonography of Infants and Children Philadelphia, WB Saunders, 1991.
54. Staller GS, Tulleners EP, Reef VB, Spencer PA: Concordance of ultrasonographic and physical findings in cattle with an umbilical mass or suspected to have infection of the umbilical cord remnants: 32 cases (1987–1989) J Am Vet Med Assoc 206:77–82, 1995.
55. Pascoe RR: Complications following a ruptured bladder in a 60-day-old foal. Austr Vet J 52:473–475, 1976.
56. Hackett RP: Rupture of the urinary bladder in neonatal foals. Compend Contin Educ Pract Vet 6:488–491, 1984.
57. Stickle RL, Wilcock BP, Huseman JL: Multiple ureteral defects in a Belgian foal. Veterinary Medicine/Small Animal Clinician 70:819–822, 1975.
58. Behr MJ, Hackett RP, Bentinck-Smith J, et al: Metabolic abnormalities associated with rupture of the urinary bladder in neonatal foals. J Am Vet Med Assoc 178:263–266, 1981.
59. Robertson JT, Spurlock GH, Bramlage LL, Landry SL: Repair of ureteral defect in a foal. J Am Vet Med Assoc 183:799–800, 1983.
60. Richardson DW, Kohn CW: Uroperitoneum in the foal. J Am Vet Med Assoc 182:267–270, 1983.
61. Richardson DW: Urogenital problems in the neonatal foal. Vet Clin North Am [Equine Pract] 1:179–188, 1985.
62. Lavoie J-P, Harnagal SH: Nonsurgical management of ruptured urinary bladder in a critically ill foal. J Am Vet Med Assoc 192:1577–1580, 1988.
63. Rooney JR: Rupture of the urinary bladder in the foal. Vet Pathol 8:445–451, 1971.
64. Pascoe RR: Repair of a defect in the bladder of a foal. Austr Vet J 47:343–344, 1971.
65. Vacek JR, Macharg MA, Phillips TN, et al: Struvite urethral calculus in a three-month-old Thoroughbred colt. Cornell Vet 82:275–279, 1992.
66. Edwards RB, Ducharme NG, Hackett RP: Laproscopic repair of a bladder rupture in a foal. Vet Surg 24:60–63, 1995.
67. Laverty S, Pascoe JR, Ling GV, et al: Urolithiasis in 68 horses. Vet Surg 21:56–62, 1992.
68. Wong SN, Lo RNS, Yu ECL: Renal blood flow pattern by noninvasive Doppler ultrasound in normal children and acute renal failure patients. J Ultrasound Med 8:135–141, 1989.
69. Robinson JA, Allen GK, Green EM, et al: A prospective study of septicaemia in colostrum-deprived foals. Equine Vet J 25:214–219, 1993.
70. Cramer BC, Jequier S, de Chadarevian JP: Factors associated with renal parenchymal echogenicity in the newborn. J Ultrasound Med 5:633–638, 1986.
71. Braden GL, Kozinn FE, Hampf FE Jr, et al: Ultrasound diagnosis of early renal papillary necrosis. J Ultrasound Med 10:401–403, 1991.
72. Read WK: Renal medullary crest necrosis associated with phenylbutazone therapy in horses. Vet Pathol 20:662–669, 1983.
73. Griscom NT, Vawter GF, Fellers FX: Pelvinfundibular atresia: The usual form of multicystic kidney: 44 unilateral and two bilateral cases. Semin Roentgenol 10:125–131, 1975.
74. Orsini JA, Donawick WJ: Surgical treatment of gastroduodenal obstructions in foals. Vet Surg 15:205–213, 1986.
75. Acland HM, Gunson DE, Gilette DM: Ulcerative duodenitis in foals. Vet Pathol 20:653–661, 1983.
76. Campbell-Thompson ML, Brown MP, Slone DE, et al: Gastroenterostomy for treatment of gastroduodenal ulcer disease in 14 foals. J Am Vet Med Assoc 188:840–844, 1986.
77. Divers TJ, Warner A, Vaala WE, et al: Toxic hepatic failure in newborn foals. J Am Vet Med Assoc 12:1407–1413, 1983.
78. Buonanno AM, Carson G, Kantrowitz B: Clinical and diagnostic features of portosystemic shunt in a foal. J Am Vet Med Assoc 192:387–389, 1988.
79. Reimer JM, Donawick WJ, Reef VB, et al: Diagnosis and surgical correction of patent ductus venosus in a calf. J Am Vet Med Assoc 193:1539–1541, 1988.
80. Wrigley RH, Konde LJ, Park RD: Ultrasonographic diagnosis of portacaval shunts in young dogs. J Am Vet Med Assoc 191:421–424, 1987.
81. Wrigley RH, Macy DW, Wykes PM: Ligation of ductus venosus in a dog using ultrasonographic guidance. J Am Vet Med Assoc 183:1461–1464, 1983.
82. Holt DE, Schelling CG, Saunders HM, Orscher RJ: Correlation of ultrasonographic findings with surgical, portographic, and necropsy findings: 63 cases (1987–1993). J Am Vet Med Assoc 207:1190–1193, 1995.
83. Beech J, Dubielzig R, Bester R: Portal vein anomaly and hepatic encephalopathy in a horse. J Am Vet Med Assoc 170:164–166, 1977.
84. Hanson JA, Pennick DG: Ultrasonographic evaluation of a traumatic splenic hematoma and literature review. Vet Radiol Ultrasound 35:463–466, 1994.
85. Tulleners EP: Complications of abdominocentesis in the horse. J Am Vet Med Assoc 182:232–234, 1983.
86. Montali C, Croce F, De Pra L, Solbiati L: Intussusception of the bowel: A new sonographic pattern. Br J Radiol 56:621–623, 1983.
87. Seibert JJ, Williamson SL, Golladay ES, et al: The distended gasless abdomen: A fertile field for ultrasound. J Ultrasound Med 5:301–308, 1986.
88. Holt S, Samuel E: Multiple concentric ring sign in the ultrasonographic diagnosis of intussusception. Gastrointest Radiol 3:307–309, 1978.
89. Pracros JP, Tran-Minh VA, Morin de Finfe CH, et al: Acute intestinal intussusception in children: Contribution of ultrasonography (145 cases). Ann Radiol 30:525–530, 1987.
90. Shanbhogue RL, Hussain SM, Meradji M, et al: Ultrasonography is accurate enough for the diagnosis of intussusception. J Pediatr Surg 29:324–328, 1994.
91. Hackett MS, Hackett RP: Chronic ileocecal intussusception in horses. Cornell Vet 79:353–361, 1989.
92. Bowerman RA, Silver TM, Jaffee MH: Real-time ultrasound diagnosis of intussusception in children. Radiology 143:527–529, 1982.
93. Alessi V, Salerno G: The "hayfork" sign in the ultrasonic diagnosis of intussusception. Gastrointest Radiol 10:177–179, 1985.
94. Swischuk LE, Hayden CK, Boulden T: Intussusception: Indications for ultrasonography and an explanation for the doughnut and pseudokidney signs. Pediatr Radiol 15:388–391, 1985.
95. Verbanck JJ, Rutgeerts LJ, Douterlunge PH, et al: Sonographic pathologic correlation in intussusception of the bowel. J Clin Ultrasound 14:393–397, 1986.
96. Teele RL: A dozen ultrasonographic donuts. Mt. Sinai J Med 51:528–534, 1984.
97. Dufour D, Delaet MH, Dassonville M, et al: Midgut malrotation, the reliability of sonographic diagnosis. Pediatr Radiol 22:21–23, 1992.
98. Smet MH, Marchal G, Ceulemans R, Eggermont E: The solitary hyperdynamic pulsating superior mesenteric artery: An additional dynamic sonographic feature of midgut volvulus. Pediatr Radiol 21:156–157, 1991.
99. Gaines PA, Saunders AJS, Drake D: Midgut malrotation diagnosed by ultrasound. Clin Radiol 38:51–53, 1987.
100. Hayden CKJ, Boulden TF, Swischuk LE, Lobe TE: Sonographic demonstration of duodenal obstruction with midgut volvulus. AJR 143:9–10, 1984.
101. Miller JH, Kemberling CR: Ultrasound scanning of the gastrointestinal tract in children: Subject review. Radiology 152:671–677, 1984.
102. Hernanz-Schulman M, Genieser NB, Ambrosino M: Sonographic diagnosis of intramural duodenal hematoma. J Ultrasound Med 8:273–276, 1989.
103. Yvorchuk-St. Jean KE, DeBowes RM, Gift LJ, et al: Trichophyto-

bezoar as a cause of transverse colon obstruction in a foal. Cornell Vet 83:169-175, 1993.
104. McClure JT, Kobluk C, Voller K, et al: Fecalith impaction in four miniature foals. J Am Vet Med Assoc 200:205-207, 1992.
105. Kristoffersen J: Ileus hos ponyføl forårsaget af håransamling i colon tenue. Dansk Vet Tidsskr 68:640, 1985.
106. Newman B, Girdany BR: Gastric trichobezoars—Sonographic and computed tomographic appearance. Pediatr Radiol 20:526-527, 1990.
107. McCracken S, Jongeward R, Silver TM, et al: Gastric trichobezoar: Sonographic findings. Radiology 161:121-124, 1986.
108. Malpani A, Ramani SK, Wolverson MK: Role of sonography in trichobezoars. J Ultrasound Med 7:661-663, 1988.
109. Fischer AT, Yarbrough TY: Retrograde contrast radiography of the distal portions of the intestinal tract in foals. J Am Vet Med Assoc 207:734-737, 1995.
110. Lorentzen T, Nolsøe CP, Khattar SC, et al: Gastric and duodenal wall thickening on abdominal ultrasonography. Positive predictive value. J Ultrasound Med 12:633-637, 1993.
111. Tomooka Y, Onitsuka H, Goya T, et al: Ultrasonography of benign gastric ulcers. J Ultrasound Med 8:513-517, 1989.
112. Rosenberg ER, Morgan CL, Trought WS, et al: The ultrasonic recognition of a gastric ulcer. Br J Radiol 56:365-366, 1983.
113. Hayden CK Jr, Swischuk LE, Rytting GE: Gastric ulcer disease in infants: US findings. Radiology 164:131-134, 1987.
114. Ranschaert E, Rigauts H: Confined gastric perforation: Ultrasound and computed tomographic diagnosis. Abdom Imaging 18:318-319, 1993.
115. Rooney JR: Gastric ulceration in foals. Pathol Vet 1:497-503, 1964.
116. Valdez H: Perforating gastrointestinal ulcers in three foals. Equine Pract 1:44-47, 1979.
117. Niak DR, Bolia A, Boon AW: Demonstration of a lactobezoar by ultrasound. Br J Radiol 60:506-507, 1987.
118. Bloom RA, Craciun E, Lebensart PD, et al: The ultrasound appearances of intramural bowel gas: The bright ring appearance and the effervescent bowel. A report of 3 cases. Br J Radiol 65:585-588, 1992.
119. Jones SL, Wilson WD: *Clostridium septicum* septicemia in a neonatal foal with hemorrhagic enteritis. Cornell Vet 83:143-151, 1993.
120. Jones RL, Adney WS, Alexander AF, et al: Hemorrhagic necrotizing enterocolitis associated with *Clostridium difficile* infection in four foals. J Am Vet Med Assoc 193:76-79, 1988.
121. Pearsson EG, Hedstrom OR, Sonn R, Wedam J: Hemorrhagic enteritis caused by *Clostridium perfringens* type C in a foal. J Am Vet Med Assoc 188:1309-1310, 1986.
122. Howard-Martin M, Morton RJ, Qualls CW Jr, McAllister CG: *Clostridium perfringens* type C enterotoxemia in a newborn foal. J Am Vet Med Assoc 189:564-565, 1986.
123. Spaulding KA: Sonographic evaluation of peritoneal effusion in small animals. Vet Radiol Ultrasound 34:427-431, 1993.
124. Dinkel E, Lehnart R, Tröger J, et al: Sonographic evidence of intraperitoneal fluid: An experimental study and its clinical implications. Pediatr Radiol 14:299-303, 1984.
125. Mair TS, Hillyer MH, Taylor GR: Peritonitis in adult horses: A review of 21 cases. Vet Rec 126:567-570, 1990.
126. Kolecki RV, Golub RM, Sigel B, et al: Accuracy of viscera slide detection of abdominal wall adhesions by ultrasound. Surg Endosc 8:871-874, 1994.
127. Dyson S: Review of 30 cases of peritonitis in the horse. Equine Vet J 15:25-30, 1983.
128. Fretz PB, Hamilton GF, Barber SM, Ferguson JG: Management of umbilical hernias in cattle and horses. J Am Vet Med Assoc 183:550-552, 1983.
129. Peyton LC: Surgical correction of equine umbilical hernias. Veterinary Medicine/Small Animal Clinician 76:1212-1215, 1981.
130. Greenwood RES, Dugdale DJ: Treatment of umbilical hernias in foals with Elastrator rings. Equine Vet Educ 5:113-115, 1993.
131. Markel MD, Pascoe JR, Sams AE: Strangulated umbilical hernias in horses: 13 cases (1974-1985) J Am Vet Med Assoc 190:692-694, 1987.
132. Hartzband LE, Kerr DV, Morris EA: Ultrasonographic diagnosis of diaphragmatic rupture in a horse. Vet Radiol 31:42-44, 1990.
133. Johnson JW, DeBowes RM, Cox JH, Leipold HW: Diaphragmatic hernia with a concurrent cardiac defect in an Arabian foal. Equine Vet Sci 4:225-226, 1984.
134. Mitchell G: Unilateral diaphragmatic aplasia in a thoroughbred foal. Aust Vet J 56:610-611, 1980.
135. Speirs VC, Reynolds WT: Successful repair of a diaphragmatic hernia in a foal. Equine Vet J 8:170-172, 1976.
136. Firth EC: Diaphragmatic hernia in horses. Cornell Vet 66:353-361, 1976.
137. Mair TS, Pearson H, Waterman AE, et al: Chylothorax associated with a congenital diaphragmatic defect in a foal. Equine Vet J 20:304-306, 1988.
138. Wyn-Jones G, Baker JR: A probable congenital diaphragmatic defect in an adult pony. Vet Rec 105:251-252, 1979.
139. Modransky PD: Ultrasound-guided renal and hepatic biopsy techniques. Vet Clin North Am [Equine Pract] 2:115-126, 1986.
140. Barratt-Boyes SM, Spensley MS, Nyland TG, Olander HJ: Ultrasound localization and guidance for renal biopsy in the horse. Vet Radiol 32:121-126, 1991.
141. Wang GD, Liu SJ: Enema reduction of intussusception by hydrostatic pressure under ultrasonographic guidance. A report of 377 cases. J Pediatr Surg 23:814-818, 1988.
142. Choi SO, Park WH, Woo SK: Ultrasound-guided water enema: An alternative method of nonoperative treatment for childhood intussusception. J Pediatr Surg 29:498-500, 1994.
143. Henley RK, Hager DA, Ackerman N: A comparison of two-dimensional ultrasonography and radiography for the detection of small amounts of free peritoneal fluid in the dog. Vet Radiol Ultrasound 30:121-124, 1989.

VetBooks.ir

CHAPTER

8

Ultrasonography of the Genital Tract of the Mare

Patricia L. Sertich, MS, VMD

Ultrasonography was initially used in equine reproduction to diagnose early pregnancy.[1] An embryonic vesicle can be detected ultrasonographically as early as 9 to 10 days after ovulation. Assessment of the conceptus and monitoring of the fetus throughout gestation are possible, as well as early detection of twin pregnancy.[2–4] Ultrasonography allows for a more objective evaluation of the postpartum genital tract so that appropriate therapy can be instituted if needed and sound decisions can be made for rebreeding.[5, 6] Thorough evaluation of ovarian status and uterine character, including diagnosis of abnormalities, can be obtained ultrasonographically.[7–11] Accurate determination of ovulation can be made by the characteristic changes that occur in the ovary in association with the luteinization.[12, 13]

EXAMINATION TECHNIQUE

Patient and Equipment Preparation

The mare should be restrained to allow for safe and thorough examination by palpation and ultrasonography per rectum. Care should be taken to avoid damage to the equipment. This can be accomplished by placing the mare in stocks. Most brood mares do not require additional restraint, but anxious or fractious mares may warrant use of a nose twitch or chemical restraint. Xylazine (0.6 mg/kg) and acepromazine (0.02 mg/kg)* intravenously may help relax the nonpregnant mare so that the procedure can be performed safely for both mare and operator. Stocks can be designed with a small enclosure in front of the mare to contain her foal. Alternatively, the mare's hindquarters may be backed out through an open stall door such that her hind feet are in the aisle and her body is parallel to the stall divider. The stall method is useful for a mare with a foal by her side. The ultrasound equipment can then be placed on the latched side of the door. It is advantageous to be proficient in palpating with either hand so that, depending on the location of the electrical outlet, the ultrasound machine can be positioned on the side opposite the examination hand to permit ease of screen viewing.

The mare's tail can be wrapped and tied to the side to keep it clean and prevent tail hairs from irritating the rectum. If large numbers of mares are to be examined, one may elect to not wrap the tail and simply have an assistant hold the tail to the side. The mare's rectum should be emptied of feces and a thorough genital examination performed to determine the location and character of the genital organs. When ultrasonography was first introduced for genital examination, practitioners were concerned that competence in palpation would no longer be necessary. This is not true because a complete ultrasound examination requires thorough palpation per rectum.

Anatomy

The mare ovary is kidney bean–shaped with a prominent depression, the ovulation fossa, on the ventral concave border. Average size is 5 × 3 × 3 cm, but considerable variation exists owing to follicular activity and stage of reproductive cycle. The mare ovary is unusual in that the medullary or vascular zone is superficial and the cortical zone, which contains the follicles (parenchyma), is in the interior of the gland. The parenchyma reaches the surface of the ovary only at the ovulation fossa, which is where normal ovulation occurs. A corpus luteum can be imaged ultrasonographically but cannot readily be detected by palpation because an ovulation papilla is not present on the surface of the ovary.

The oviduct is a tortuous tube, supported by the mesosalpinx, that transfers the ovum from the ovary to the uterus. It is composed of three parts: the infundibulum, which is nearest the ovary and covers the ovulation fossa during ovulation; the ampulla, which is the site of fertilization; and the isthmus, which is nearest the uterus and enters the uterus by a small projection into the uterine lumen, the oviduct papilla.

*Plumb DC: Central Nervous System Drugs in Veterinary Drug Handbook. White Bear Lake, MN, Pharma Vet Publishing, 1991, p 58.

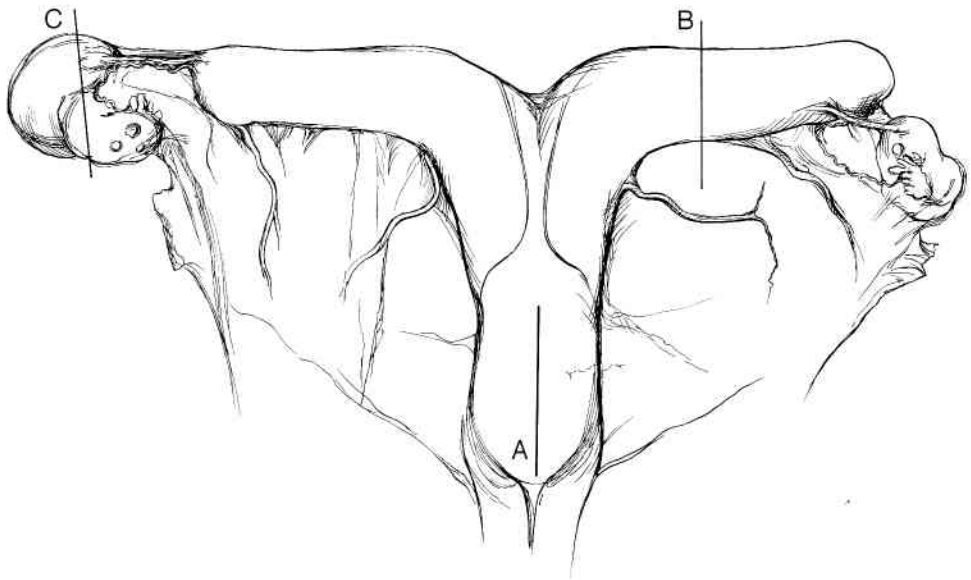

Figure 8–1

Diagram of typical linear array transducer orientations (*black lines*) over the genital tract during examination per rectum. When the transducer is over the cervix and uterine body (A), a longitudinal image is produced. The uterine horn is generally seen in short-axis cross-section (B), which allows assessment of the endometrial folds. Sections through the ovary show follicles and corpora lutea cut in different planes (C).

The mare's cervix is muscular and contains longitudinal folds. It can be dilated manually at most stages of the estrous cycle. Its shape and degree of closure vary with the stage of the estrous cycle and endocrine status of the mare. The cervix forms the third barrier for the uterus against external contaminants.

The suspended in situ uterus is "Y" shaped. It consists of two uterine horns and a single uterine body. The intercornual ligament is not prominent. The lumen is usually obliterated and exists as a potential space. Prominent longitudinal endometrial folds project into the lumen. The uterus consists of the endometrium, the myometrium (an inner circular muscle layer and outer longitudinal muscle layer), and the perimetrium or serosal surface.

The vagina extends from the cervix to a point just cranial to the urethral orifice. The caudal limit is marked by a transverse fold (hymen). The vagina exists as a collapsed potential space. The transverse fold forms the second barrier for the uterus against external contaminants.

The broad ligament is a large ligamentous sheet that attaches the abdominal portion of the reproductive tract to the abdominal and pelvic walls. It also carries blood, lymphatic vessels, and nerves to the ovaries, oviducts, uterus, and cervix. The broad ligament contains a large amount of smooth muscle that is continuous with the outer longitudinal muscular layer of the uterus and oviduct. The broad ligament is attached to the dorsal body wall at the level of the third lumbar vertebra to the fourth sacral vertebra. Although the reproductive organs are suspended in the abdominal cavity, they actually lie on the intestinal viscera or intermingle with them.[14]

Scanning Technique

Examinations of the nongravid and early pregnant genital tract are performed per rectum, typically with a 5-MHz linear-array transducer.[15] A 7.5-MHz or 10-MHz linear-array transducer may be used per rectum when needed for greater detail of areas less than 4 to 8 cm from the transducer. With experience and practice, a 5.0-MHz sector-scanner transducer can be used successfully per rectum. For transcutaneous evaluation of late-gestation mares, a 2.5- (ideal), 3.0-, or 3.5-MHz sector-scanner transducer is recommended for evaluation of the fetus, whereas a 7.5- or 5.0-MHz sector-scanner transducer or 6.0 microconvex linear-array transducer is ideal for evaluation of the placenta and uteroplacental unit.[16–21] A 3.0- or 3.5-MHz linear-array or convex linear-array transducer may also be used to evaluate the fetus but has less penetration than the sector-scanner or annular-array transducer, although it has a larger footprint. Similarly, a 7.5- or 5.0-MHz sector, linear-array or convex linear-array transducer may be used to evaluate the placenta and uteroplacental continuity.

A plastic examination sleeve should be placed over the examiner's arm and water-soluble lubricant applied liberally to the arm. It is desirable to cover the ultrasound transducer with a plastic sleeve to facilitate clean-up of the equipment and prevent damage to the transducer. The rectum should be emptied of feces and the transducer introduced into the rectum. The transducer should not be forced into position because one can easily pass it through the rectal wall and into the peritoneal cavity. After examination, the mare's perineum should be rinsed or wiped clean of lubricant and feces.

For ultrasonographic evaluation of the genital tract, one should place the transducer over the genital organs. The uterine horns are seen in transverse cross-section and the body in sagittal (longitudinal) section (Fig. 8–1). One must be careful to evaluate the entire uterus from one side to the other (left ovary to left horn to body to right horn to right ovary). Particularly with early-preg-

Figure 8–2

Ovarian follicle. A typical ovarian follicle is round and anechoic and is bordered by homogeneously dense ovarian stroma. This sonogram was obtained transrectally with a 5.0-MHz linear-array transducer at a displayed depth of 12 cm. The right side of the sonogram is cranial and the left side is caudal.

nancy examination, one should be sure to view the uterine body and cervical area.

ULTRASONOGRAPHIC FINDINGS

Ovaries and Oviducts

The interovulatory interval in the mare is 21 days.[22] Estrus (4 to 9 days in length) occurs during the follicular phase of the estrous cycle.[23] Although several follicles may be present on the ovaries, normally only one or two follicles mature to a diameter of 35 mm or more (Figs. 8-2 and 8-3) and ovulate.[24] Follicles are viewed ultrasonographically as anechoic round structures with an echogenic follicular wall less than 2 mm thick. The ovarian parenchyma is moderately echogenic and homogeneous in character. Preovulatory follicles may be imaged projecting toward the ovulation fossa (Fig. 8-4).[25] Follicular growth and ovulation can be accurately assessed ultrasonographically. Ovulation in the mare is unique among domestic farm animals in that all ovulations occur through an ovulation fossa as opposed to through the surface of the ovary.[23, 26] Therefore, the surface of the ovary remains smooth even during the luteal phase of the cycle. Although there usually is a change in consistency of the follicle and some transient increased sensitivity of the ovary, it may be difficult to accurately determine when ovulation occurred by direct palpation of the ovary per rectum. Ovulation may be indicated by a collapse of the follicle, the walls of which thicken as luteinization occurs.[27] The resulting corpus luteum is within the ovary and does not protrude from the surface, thereby making direct palpation of the corpus luteum difficult. Substantial hemorrhage may occur into the follicle with the development of a corpus hemorrhagicum (Fig. 8-5), which is imaged ultrasonographically as an increase in echogenicity at the site of the ovulating follicle.[12, 15] The pattern of increase in echogenicity may be homogeneous (Fig. 8-6) or lacy in appearance, as in an echogenic network.[10]

Breeding farms that are intensely managed should employ ultrasonography during estrus to assess follicular activity, time breedings, and efficiently limit the number of breedings or inseminations. In an embryo transfer program, accurate determination that ovulation has occurred allows for proper timing of embryo recovery from the uterus and selection of an optimal recipient for the recovered embryo.[28]

The normal oviduct is not visible with a 5.0-MHz transducer but may be seen with a 7.5-MHz transducer (Fig. 8-7).

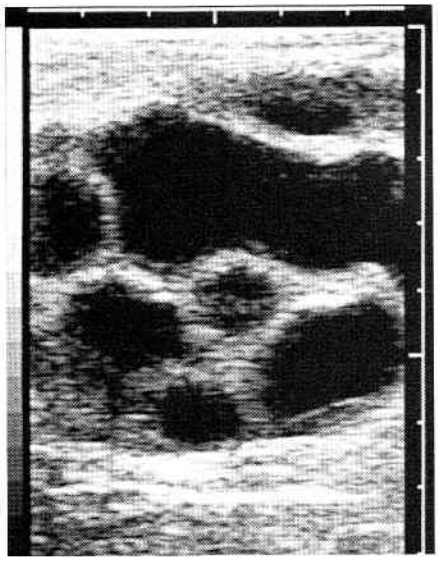

Figure 8–3

Normal transitional ovary with numerous follicles. It is normal for a mare to have a large ovary containing numerous anechoic follicles (>20 mm) during the transitional breeding season. Notice the hyperechoic follicular walls separating the follicles. This sonogram was obtained transrectally with a 5.0-MHz linear-array transducer at a displayed depth of 10 cm. The right side of the sonogram is cranial and the left side is caudal.

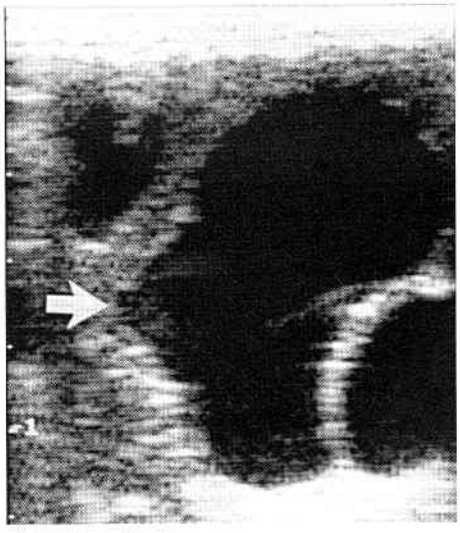

Figure 8–4

Preovulatory follicle. A large anechoic preovulatory follicle can be imaged projecting toward the ovulation fossa (*arrow*). This sonogram was obtained transrectally with a 5.0-MHz linear-array transducer at a displayed depth of 6 cm. The right side of the sonogram is cranial and the left side is caudal.

Figure 8–5

Corpus hemorrhagicum less than 12 hours old. It is more echogenic than a follicle and is bordered by the hyperechoic developing luteal tissue. This sonogram was obtained transrectally with a 5.0-MHz linear-array transducer at a displayed depth of 10 cm. The right side of the sonogram is cranial and the left side is caudal.

Cervix, Uterus, and Vagina

The diestrous or pregnant cervix is imaged in longitudinal section and is outlined by horizontal echogenic parallel lines on ultrasonographic examination.[29] During estrus the cervix becomes more hypoechoic and may be difficult to differentiate from the adjacent structures. Although lacerations and adhesions are most readily identified by direct palpation, hematomas and cysts may be imaged ultrasonographically.

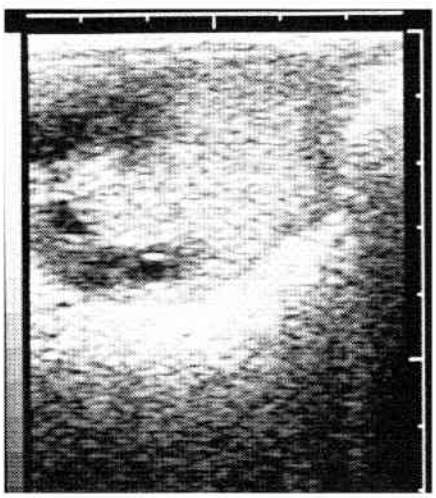

Figure 8–6

A 2-day-old homogeneously echogenic corpus luteum. This same luteal structure (as in Figure 8–5) would now be classified as a more densely hyperechoic corpus luteum 48 hours old. This sonogram was obtained transrectally with a 5.0-MHz linear-array transducer at a displayed depth of 10 cm. The right side of the sonogram is cranial and the left side is caudal.

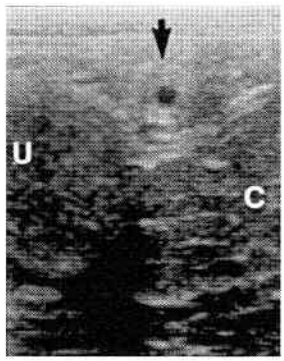

Figure 8–7

Normal equine oviduct (*arrow*) adjacent to the right uterine horn (u) and cecum (c). This sonogram was obtained transrectally with a 7.5-MHz linear-array transducer at a displayed depth of 6 cm. The right side of the sonogram is cranial and the left side is caudal.

The mare's uterus is shaped with the uterine horns perpendicular to the body of the uterus. In situ, it assumes a "Y" shape as it is suspended in the pelvic canal and abdomen by the broad ligament, which is attached dorsally to the sublumbar and sacral region.[30] Thorough systematic examination of the entire uterus should be made. Because the linear-array transducer is positioned longitudinally in the rectum, the uterine body is usually imaged longitudinally and the uterine horns are imaged transversely so that a short-axis cross-section of the horn is seen on the screen (see Fig. 8–1). If the transducer is short enough, it may be possible to position it at a right angle to the body and horn and produce a short-axis cross-section of the body and a longitudinal section of the uterine horn. Measurements obtained ultrasonographically permit determination of the size of the uterine horns.

The character of the uterus changes during the estrous cycle. The uterus has several endometrial folds that increase the surface area of the endometrium. During estrus, these endometrial folds become edematous, which gives a characteristic "cut pie" appearance, seen on ultrasonography as alternating echogenic and anechoic lines projecting into the lumen of the uterine horn (Fig. 8–8).[9] In most mares, the edematous appearance of the endometrial folds decreases in late estrus before ovulation occurs. After ovulation and development of the corpus luteum, the uterus comes under the influence of progesterone. Uterine tone increases and the endometrial folds are no longer edematous. During diestrus, the uterus is homogeneous in echogenicity, and the endometrial folds are not well defined.

Pregnancy

Real-time ultrasonographic reproductive examinations in the mare were first reported in 1980.[1] Prior to the use of ultrasonography, pregnancy could not be consistently detected in mares until 28 days after ovulation, when a bulge in the uterine horn caused by the enlarging conceptus could be palpated per rectum.[2, 31] Because the mare's interovulatory interval is 21 days,[22] veterinarians and

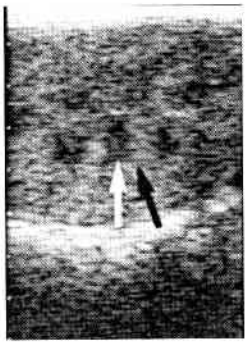

Figure 8–8

Edematous endometrial folds typical of uterine edema are seen during estrus as alternating hypoechoic (*white arrow*) and hyperechoic (*black arrow*) areas projecting toward the lumen of the uterine horn. This sonogram was obtained transrectally with a 5.0-MHz linear-array transducer at a displayed depth of 12 cm. The right side of the sonogram is cranial and the left side is caudal.

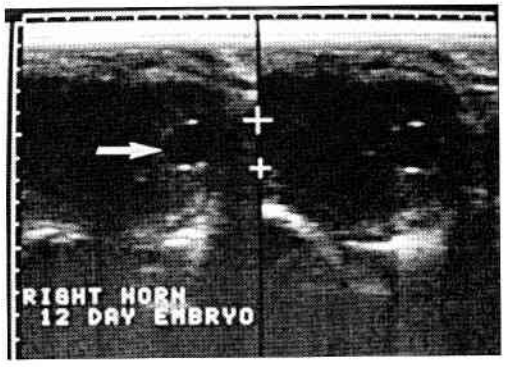

Figure 8–9

Twelve-day equine conceptus (*arrow*). Notice the characteristic specular reflections (*white bars*) dorsal and ventral to the anechoic vesicle. The white cursors (+) are positioned to measure the diameter of this conceptus. The right half of the screen is the same image without markings. These sonograms were obtained transrectally with a 5.0-MHz linear-array transducer at a displayed depth of 20 cm. The right sides of these sonograms are cranial and the left sides are caudal.

breeding farm managers desired a method to detect pregnancy before 21 days so that nonpregnant mares could be rebred as soon as possible. The accessible position of the mare genital tract per rectum and the relatively large spherical shape of the equine conceptus readily allows for ultrasonographic evaluation of early equine pregnancy as early as 9 to 11 days after ovulation.[2, 7] Early equine studies reported a greater than 90% accuracy after 14 days.[1, 32] The equine conceptus is unique among domestic farm animals in that it is mobile from day 6 after ovulation, when it enters the uterus, until day 16, when it lodges at the base of one uterine horn.[2, 33] It remains spherical in shape throughout early pregnancy. Intensive management of brood mares may include an ultrasonographic examination of the genital tract for pregnancy between 14 and 19 days and again at 30 to 42 days. Early pregnancy detection allows for the detection and management of twins and for timely rebreeding of open mares.

Equine fetal membranes develop in a pattern that permits accurate estimation of stage of gestation by ultrasonography until 45 days after ovulation. With a 5.0-MHz transducer, the yolk sac may first be seen as a spherical anechoic embryonic vesicle in the uterus at 9 to 10 days, when it is 4 mm in diameter. The early conceptus (yolk sac) has a bright white (echogenic) line on the dorsal and sometimes the ventral aspect of its image caused by specular reflections (Figs. 8–9 to 8–11). This characteristic can be helpful in differentiating an embryo from some uterine cysts (Fig. 8–12). From day 10 to 16, the motile round anechoic conceptus is observable in the uterine lumen. Between days 9 and 16, the embryo can be imaged as it moves throughout the lumen of the uterine horns as well as into the uterine body until it lodges in the base of one of the uterine horns on day 16.[33] The conceptus frequently has a characteristic triangular or "guitar pick" shape on days 17 to 21. At day 21, the embryo proper of the conceptus can be seen as a small echogenic mass in the ventral aspect of the yolk sac (Fig. 8–13). At 25 days, the heartbeat is seen as a fluttering movement within the echogenic mass of the embryo proper, and the allantoic cavity begins to develop ventral to the embryo proper from an outpouching of the hindgut. As the anechoic allantoic cavity enlarges ventrally, the dorsally located anechoic yolk sac comprises a decreasing portion of the conceptus. These two compartments are separated by the allantois, which is seen as an echogenic line. The position of the allantois and relative size of the fetal fluid cavities are characteristic for the stage of gestation between days 25 and 45. At 30 days, the allantois divides the conceptus in half so that the size of the dorsal yolk sac is nearly the same as the size of the ventral allantoic cavity (Fig. 8–14). At 42 days, the yolk sac is barely discernible (Fig. 8–15). The visible anechoic fluid cavity is the allantoic cavity, and the fetus hangs in dorsal recumbency from the dorsal wall of the uterus by its umbilical cord. The size of the conceptus increases linearly from day 11 to 16 (3.4 mm/day), reaches a plateau of size increase between day 18 and 26, and then continues to increase in size at a linear rate of 1.8 mm/day from day 28 to 48.[1, 2]

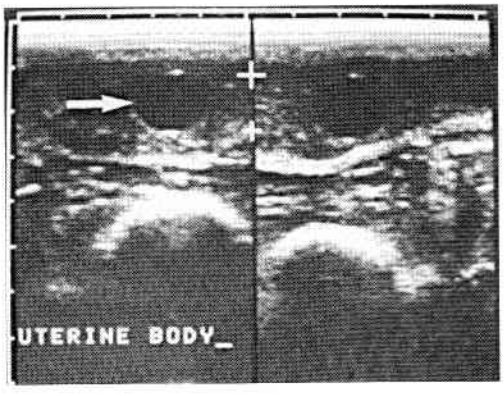

Figure 8–10

Thirteen-day equine conceptus. Notice the characteristic specular reflections (*white bars*) dorsal and ventral to the anechoic vesicle. The white cursors (+) are positioned to measure the diameter of this conceptus. The right half of the screen is the same image without markings. These sonograms were obtained transrectally with a 5.0-MHz linear-array transducer at a displayed depth of 10 cm. The right sides of these sonograms are cranial and the left sides are caudal.

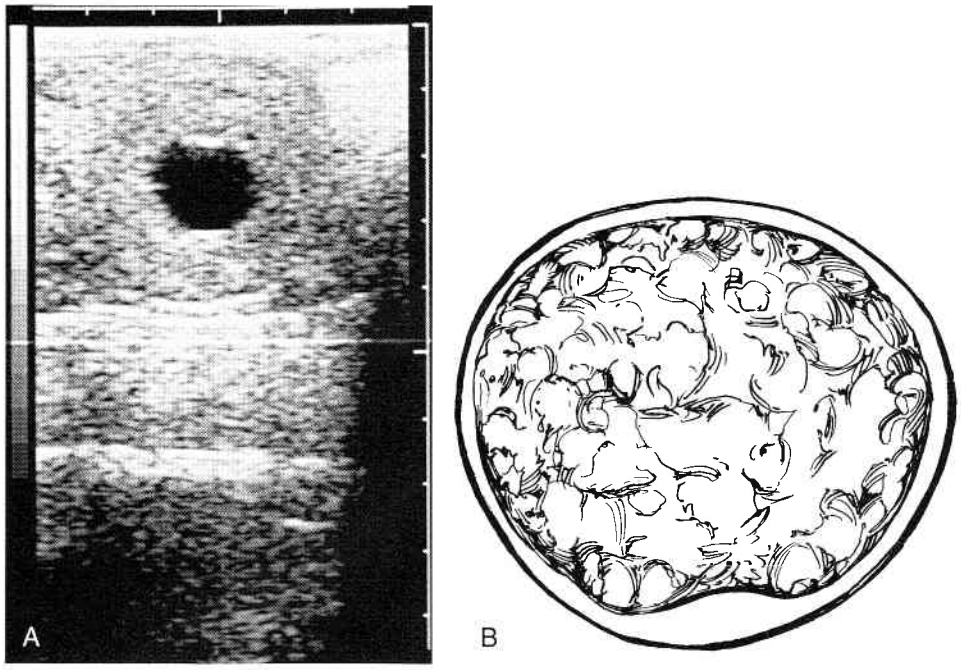

Figure 8–11

A, Fifteen-day equine conceptus. Notice the characteristic specular reflections (*white bars*) dorsal and ventral to the anechoic embryonic vesicle. Notice also the homogeneous uterine tissue surrounding the centrally located embryo. This sonogram was obtained transrectally with a 5.0-MHz linear-array transducer at a displayed depth of 10 cm. The right side of the sonogram is cranial and the left side is caudal. *B*, Sketch of the 15-day conceptus.

Twins

Ultrasonography has allowed for the early detection and subsequent management of twins. In the horse, twin embryos are dizygotic[34] and result from double ovulations. Double ovulations and twinning rate may be affected by age,[35, 36] breed,[34, 35, 37] and reproductive status.[37-39] Double ovulation rate was higher in older than in younger mares,[35] and older mares had a high rate of twin births.[36] Incidence of double ovulations was lower in ponies than in draft mares and Thoroughbreds (15 to 25%).[35] Double ovulation and twinning rates in Arabians and Standardbreds would be considered intermediate in frequency.[36] Foaling mares bred in the postpartum period have been reported to have a reduced double ovulation and twinning rate.[37, 38]

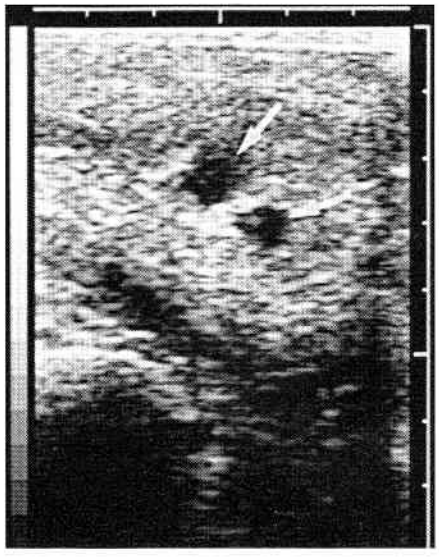

Figure 8–12

Two small endometrial cysts (*arrows*). The characteristic specular reflections typically seen in young embryos are not always present when imaging uterine cysts. This sonogram was obtained transrectally with a 5.0-MHz linear-array transducer at a displayed depth of 10 cm. The right side of the sonogram is cranial and the left side is caudal.

In the mare, if one twin is not resorbed and does not undergo natural reduction to a singleton early in gestation, twin pregnancies usually result in abortion or the birth of nonviable foals; only rarely are two healthy, productive offspring produced.[34] Delivery of two foals also places the mare at great risk for trauma and damage to the reproductive tract that can even result in death of the mare. These complications are serious enough that, before ultrasonography was available for routine use in diagnosing twins, on some farms a mare with two preovulatory follicles may not have been bred for fear of producing twins.[39]

Between days 10 and 16, twin concepti may appear as two separate anechoic round structures that move throughout the uterine lumen. The concepti may be the same size after synchronous ovulations or of different sizes due to asynchronous double ovulations (Fig. 8–16).[4] After day 16, one conceptus may lodge at the base of each of the uterine horns (bilateral fixation) and give an appearance similar to that of a singleton conceptus. They may also lodge adjacent to each other in one uterine horn (unilateral fixation), in which case their appearance is that of a larger than expected bilobed anechoic structure that may be divided by a thin membrane. This division may be difficult to image because it consists of only the adjacent two-layered trophoblasts of each embryo (Figs. 8–17 and 8–18). Such twin concepti can be easily mistaken for one embryo lodged next to an endometrial cyst(s). In order to differentiate, sequential scans may be necessary to follow the growth and development of each conceptus. The embryo proper and its own beating heart should be observed in each vesicle. It is common for the

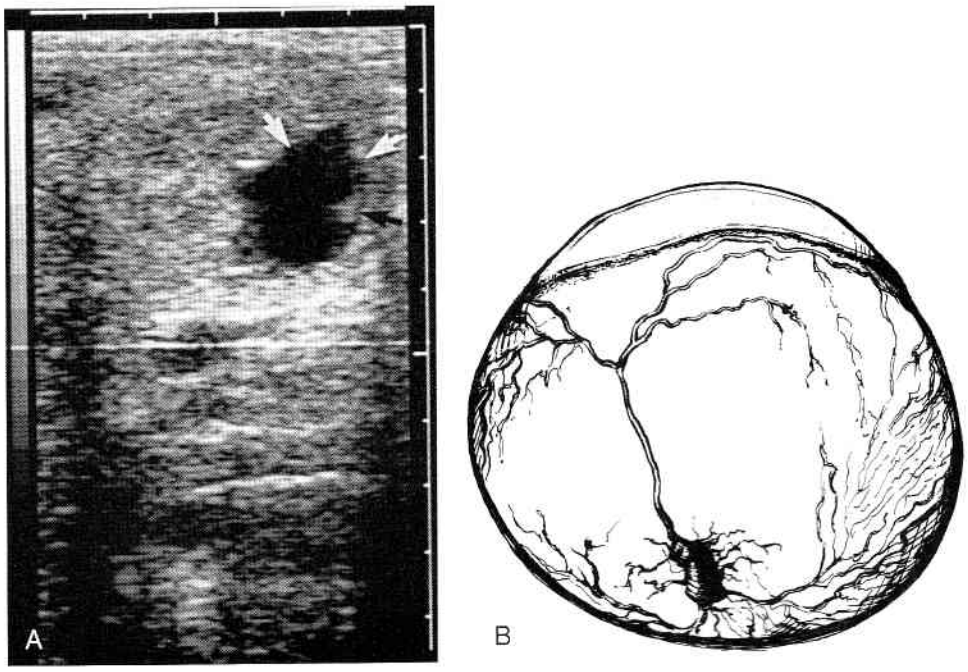

Figure 8–13

A, The "guitar pick" shape characteristic of a 17- to 21-day embryo. At 21 days, the embryo proper (*black arrow*) is first seen in the conceptus. The orientation of this vesicle is not typical, as the embryo proper is at the 3 o'clock position rather than ventral. The dorsal uterine wall (*white arrows*) is thought to be causing the shape of the conceptus. This sonogram was obtained transrectally with a 5.0-MHz linear-array transducer at a displayed depth of 10 cm. The right side of the sonogram is cranial and the left side is caudal. *B,* Sketch of a 21-day conceptus in normal orientation.

orientation of surviving twin concepti to be distorted such that the developing allantoic cavity is not ventral to the regressing yolk sac (see Fig. 8-13).[4] After 65 days of gestation, it becomes increasingly difficult to accurately diagnose twins by transrectal ultrasonography because the concepti are too large for each to be completely imaged with a 5.0-MHz transducer. After 70 to 80 days, transabdominal ultrasonography with a 2.5- or 3.5-MHz sector-scanner transducer may permit detection of two fetuses, each with its own beating heart. It is difficult to be absolutely certain that twins are not present at this stage of gestation; accurate diagnosis requires a patient and skillful ultrasound operator, cooperation of the dam, and fortunate location of the fetuses.

Currently, there are three options in managing a mare that is diagnosed with twins during the first month of gestation. One option is to not intervene and hope that one conceptus is eliminated naturally.[14] A second option is to terminate the pregnancy using prostaglandin to cause luteolysis. The mare can then be rebred at the ensuing estrus. The third option is manual rupture of one conceptus. The efficacy of this procedure has been documented.[3, 40] When performed before 30 days' gestation, manual rupture has approximately a 90% success

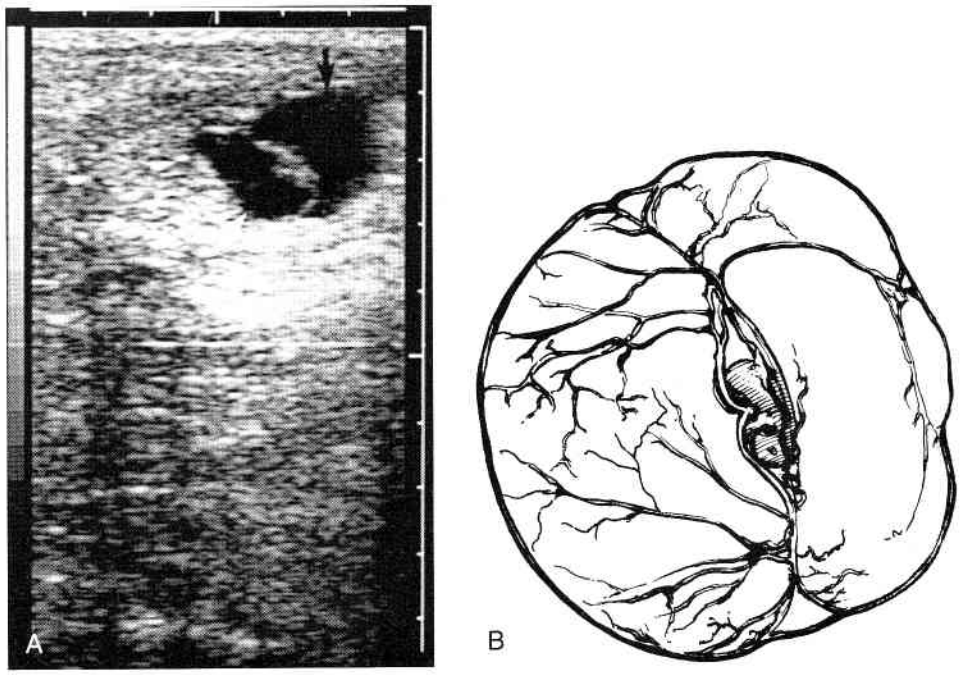

Figure 8–14

A, At day 28, the ventral developing allantoic cavity (*white arrow*) is nearly equal in size to the regressing yolk sac (*black arrow*). This sonogram was obtained transrectally with a 5.0-MHz linear-array transducer at a displayed depth of 10 cm. The right side of the sonogram is cranial and the left side is caudal. *B,* Sketch of a 28-day conceptus.

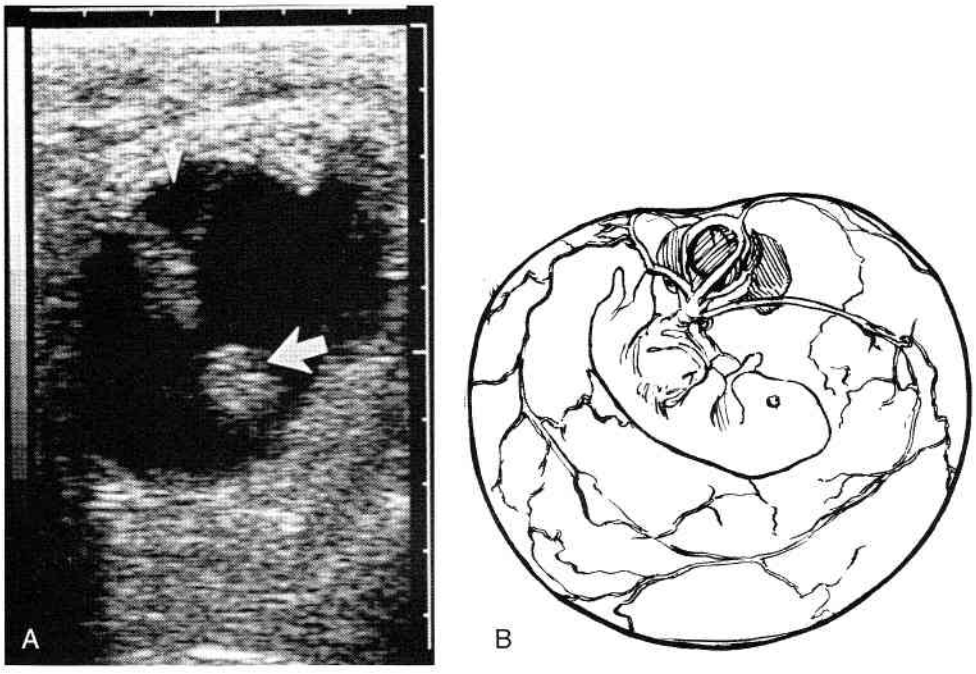

Figure 8–15

A, At 42 days, the yolk sac (*small arrow*) is barely discernible and the fetus (*large arrow*) hangs in ventral position from the dorsal wall of the uterus by the umbilical cord. This sonogram was obtained transrectally with a 5.0-MHz linear-array transducer at a displayed depth of 10 cm. The right side of the sonogram is cranial and the left side is caudal. *B*, Sketch of a 42-day fetus.

rate in yielding a live foal.[41, 42] Methods of twin reduction using manual rupture depend upon whether the embryo is mobile or has undergone fixation and whether fixation is unilateral or bilateral.[43] If fixation has not occurred, reduction is performed by identifying one embryo in the uterine horn, grasping the uterine horn caudal to the embryo to be ruptured but cranial to the embryo to remain, and moderately compressing the uterus between the thumb and finger as the hand is moved toward the tip of the horn. Collapse (rupture) of the vesicle may be felt as the fingers move over it.[44] Care should be taken not to move the vesicle into the uterine body because it is more difficult to rupture in this position. Repeated ultrasonographic evaluations may be necessary to confirm successful reduction to a singleton pregnancy.

If fixation has occurred, one embryo can be ruptured by direct compression of the conceptus with thumb and fingers. If unilateral twins are present, direct compression over the edge of one embryo using the transducer allows visualization of damage to that embryo (Fig. 8-19). Manipulations should be kept to a minimum so that only

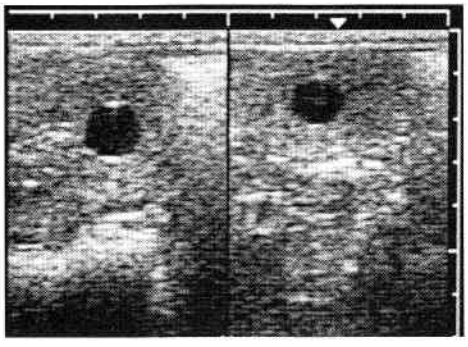

Figure 8–16

Bilateral twin equine embryos produced from asynchronous double ovulations. Notice central location of embryos in homogeneous, moderate hyperechoic uterine horn and white specular reflections. These sonograms were obtained transrectally with a 5.0-MHz linear-array transducer at a displayed depth of 15 cm. The right sides of these sonograms are cranial and the left side are caudal.

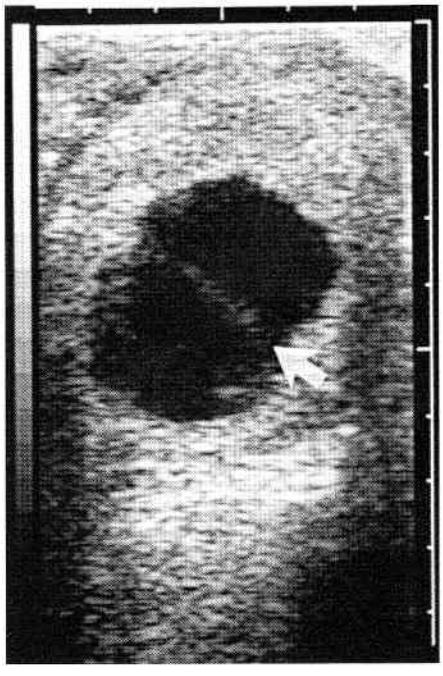

Figure 8–17

Unilaterally fixed 18-day equine twins separated by their trophoblasts (*arrow*). Care must be taken to slowly image these structures so as not to overlook the twins. Compare this figure with Figure 8-14*A*. If breeding date was unknown, 18-day twins could easily be confused with a 28- to 30-day singleton. Only one heartbeat would be present in a singleton. This sonogram was obtained transrectally with a 5.0-MHz linear-array transducer at a displayed depth of 10 cm. The right side of the sonogram is cranial and the left side is caudal.

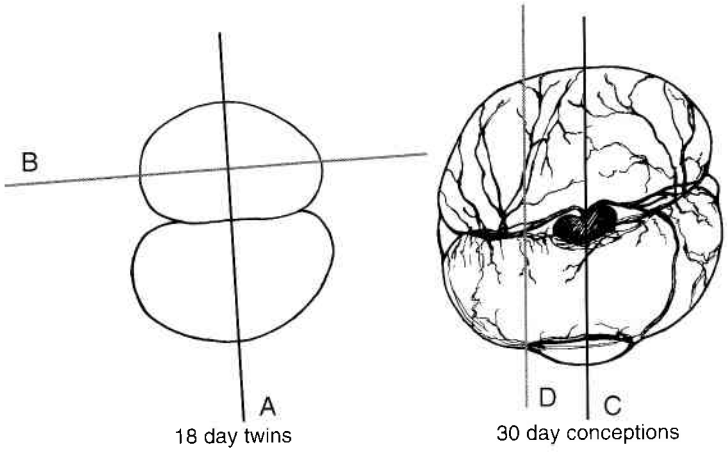

Figure 8–18

The conceptus should always be carefully evaluated, and one should try to see as many planes of view as possible. On the left side are unilaterally fixed twins. The transducer should be positioned as indicated by the vertical line (A) so that both embryos are imaged simultaneously. Positioning of the transducer as indicated by the horizontal line (B) allows imaging of only one embryo. A 30-day singleton is on the right side. The transducer should be positioned over the embryo proper, as indicated by the line on the right (C), so that one beating heart may be imaged. Positioning the transducer as indicated by the line on the left (D) may lead to an incorrect diagnosis of twins. Compare these drawings to the sonograms in Figures 8-14 and 8-17.

one embryo appears to become irregular in its outline or slightly hyperechoic (Fig. 8-20). Manipulation until one embryo has completely collapsed may cause lethal damage to the adjacent twin.

With these reduction methods, the examiner must be experienced in palpation and ultrasonography per rectum and have a strong understanding of embryo and uterine anatomy coupled with patience during the procedure. Repeated imaging of the conceptus during the procedure helps monitor progress. All mares should be re-examined 1 to 4 days after reduction to assess success; additional attempts at reduction can be made if two embryos are still present. Pregnancy should be evaluated again at 30 to 42 days' gestation. Although prostaglandin $F\text{-}2_{alpha}$ increases during manual twin reduction, administration of progesterone or antiprostaglandins does not enhance survival of the remaining twin.[41] Attempts at manual reduction of a twin pregnancy after 30 days usually result in loss of both fetuses.

The decision as to when to use ultrasonography per rectum to examine mares after breeding for the management of twins depends on a number of factors.[43]

Days 11 to 12—The embryonic vesicle (6 to 9 mm) is difficult to rupture manually because it is small and turgid. If double ovulation was asynchronous, the second vesicle may be too small to image at this time.

Days 13 to 15—The embryonic vesicle (12 to 18 mm) is mobile, and one vesicle can be ruptured while it is not in close proximity to its twin. If embryos are adjacent when first examined, periodic examinations can be performed until they are separated. Most embryos from asynchronous double ovulations are large enough to image.

Days 17 to 19—Bilaterally fixed twins are easy to rupture. Unilaterally fixed twins may be difficult to image as two separate vesicles, and manual rupture of one may cause damage to the second. Examination at this time allows identification of nonpregnant mares so that they can be rebred before their 21-day ovulation. Mares with uterine fluid may be examined for endometritis and therapy initiated promptly.

Days 21 to 25—Embryos can be more readily differenti-

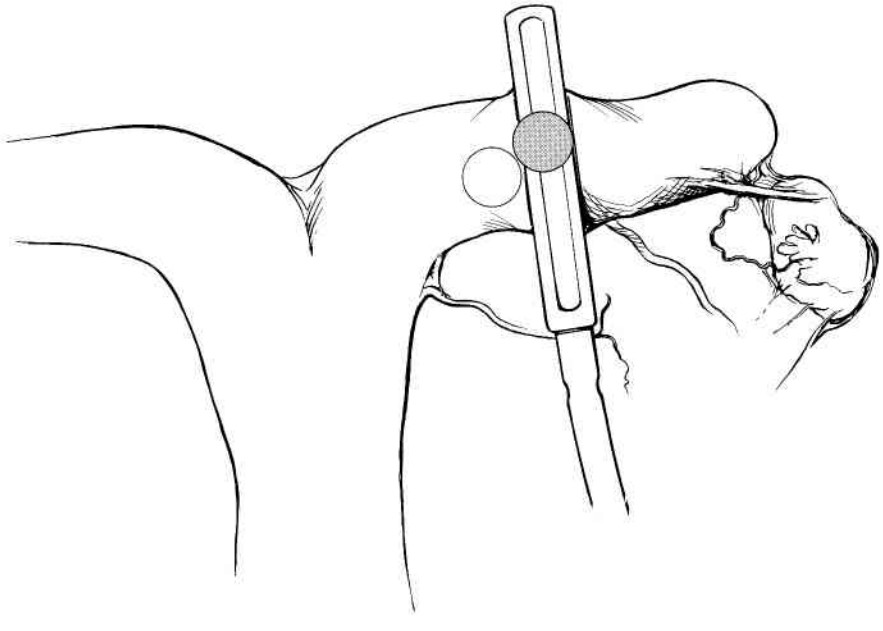

Figure 8–19

Diagram of transducer position over one unilaterally fixed twin. Direct compression of the edge of one embryo (shaded conceptus) using the transducer allows visualization of damage to one embryo.

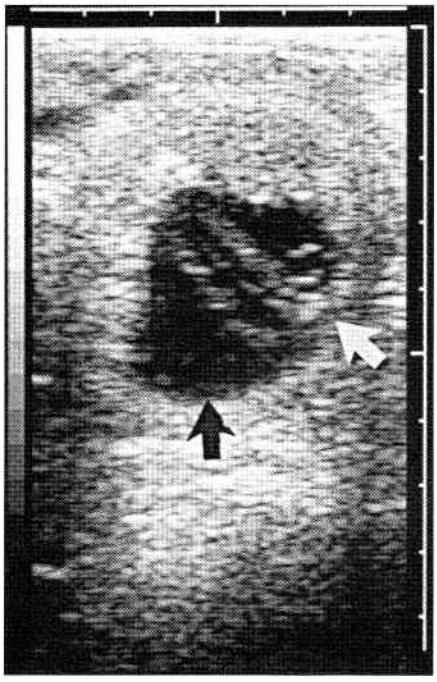

Figure 8–20

Twin embryos after manual reduction of one twin. When unilateral twins are present, reduction is more likely to be successful if one embryo (*white arrow*) is manipulated only until it shows signs of damage (increased echogenicity, irregular outline, undulating trophoblast), rather than attempting to completely rupture it. The surviving embryo (*black arrow*) should be examined in 1 to 2 days and then periodically throughout pregnancy. This sonogram was obtained transrectally with a 5.0-MHz linear-array transducer at a displayed depth of 10 cm. The right side of the sonogram is cranial and the left side is caudal.

ated from endometrial cysts because of the development of the embryo proper, the allantoic cavity, and the heartbeat in the embryonic vesicle. Bilaterally fixed twins may be readily corrected, but manual rupture of one unilaterally fixed twin may cause damage to its adjacent twin. Nonpregnant mares have just missed an opportunity to be rebred.

After 30 days—Correction of twins, whether unilateral or bilateral, becomes less successful by manual rupture.

Fetal Sexing

The sex of an equine fetus can be determined ultrasonographically between days 59 and 68 of gestation.[45] The genital tubercle is imaged as a hyperechogenic bilobulated structure 2 mm in diameter, with each lobe elongated and oval shaped. The genital tubercle is located close to the umbilical cord in males and under the tail in females (Fig. 8-21). Prior to day 53, the male cannot be differentiated from the female because the genital tubercle is located between the hindlegs of both sexes. After day 68, it may not be possible to view the entire fetus for adequate determination of genital tubercle location. Successful determination of fetal sex using ultrasonography requires proper timing of examination, a skilled examiner, high-quality ultrasound equipment, subdued external light, and adequate restraint and cooperation of the mare.

Late Gestation

Although much of the conceptus and uterus is positioned too cranial for transrectal evaluation after 4 months of gestation, the caudal portion of the genital tract can still provide useful information regarding the status of the pregnancy (Fig. 8-22). The chorion is intimate with the uterus and forms a solid homogeneous unit that typically has only a slightly echogenic interface. The normal uteroplacental unit thickness just cranial to the cervix ranges

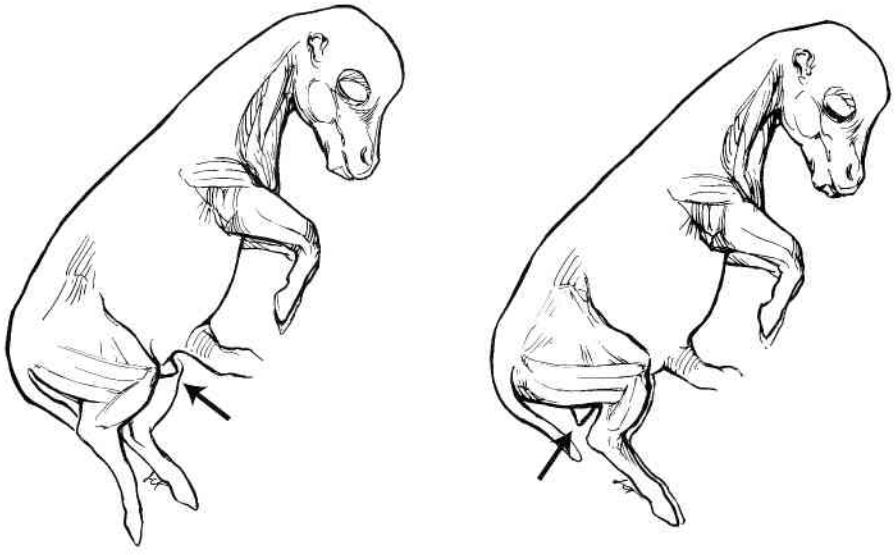

Figure 8–21

The genital tubercle of the male fetus is located in close proximity to the umbilicus. In the female, the genital tubercle is closer to the tail.

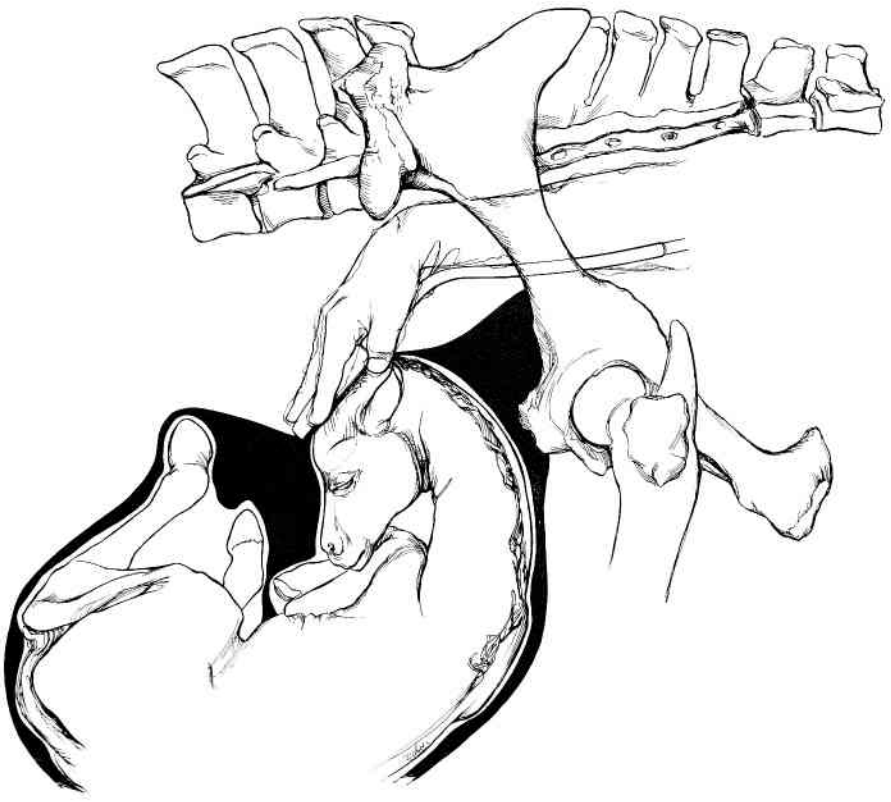

Figure 8–22

Although a large portion of the conceptus is not within view, valuable information can be gained by using transrectal ultrasonography to evaluate the late-gestation uterus. The black fluid surrounding the fetus represents the allantoic fluid while the white fluid immediately adjacent to the fetus represents the amniotic fluid.

in thickness from 7 to 13 mm, with a uterine wall thickness of 2 to 7 mm. A large blood vessel (0.5 to 1.0 cm in diameter) is often imaged just ventral and cranial to the cervix (Fig. 8-23). This may be mistakenly diagnosed as placenta separation. Careful imaging of this anechoic structure in cross-section may be helpful in arriving at a correct interpretation.

The larger allantoic fluid cavity is separated from the smaller amniotic fluid cavity by the filamentous, echogenic amnion, which is intimately associated with the fetus (Fig. 8-24). The largest pockets of amnionic fluid are seen mostly between flexed fetal appendages. The depth of the allantoic fluid can be quite variable depending on the position of the fetus within the uterus. The fetal fluids are anechoic in early gestation, but during the last few months of gestation the echogenicity of the allantoic fluids increases, and echogenic particles may be stirred by fetal movement. Amniotic fluid tends to be anechoic, but echogenicity may increase and particles appear to swirl owing to fetal activity. Fortuitous imaging of the fetal orbit indicates that the fetus is in anterior presentation, although not seeing the orbit does not necessarily mean that the fetus is in posterior position.

After 70 to 80 days, transcutaneous scanning of the gravid uterus is possible, and evaluation can be made of fetal heart rate, fetal movements, character of the amniotic and allantoic fluids, and fetal membranes. Measurement of the orbit (Fig. 8-25), aortic root, and intercostal spaces (Fig. 8-26) can be helpful in estimation of fetal age.[16, 46] Heart rate can be evaluated. Rates inappropriate for the gestational age of the fetus or arrhythmias may indicate fetal stress.[19] Subjective assessment of fetal activity can be made (see Chapter 9).[20] Normal activity patterns are being established in the horse.[20]

Ovarian Abnormalities

In making a tentative diagnosis of the condition of the ovary, it is important not only to carefully evaluate its ultrasonographic appearance, but to palpate the ovary in question for character, consistency, and ovulation fossa; to evaluate the contralateral ovary for activity, size, and shape; and to assess the mare's reproductive status and behavior.

Ovarian Hematoma

Ovarian hematomas can occur in cycling mares after ovulation. It is thought that an excessive amount of follicular fluid is present at the site of evacuation and interferes with blood clotting, resulting in a hematoma.[47] These hematomas usually resolve spontaneously over time and cause no further problem. The mare continues to cycle normally. Occasionally, a calcified area may persist in the ovarian stroma that, depending on its size and location, may possibly interfere with future ovulations. The ovarian hematoma initially appears as a large (up to 10 cm) homogeneous echogenic structure on the ovary (Fig. 8-27). Over time, the structure may appear loculated owing to the organization of the fibrin clot inside the hematoma. The ovary is palpably enlarged and round, but, unlike with a granulosa cell tumor, the ovulation

Figure 8–23

A large blood vessel (*arrow*) can typically be imaged just ventral and cranial to the cervix. This structure should not be mistakenly diagnosed as placental separation. This sonogram was obtained transrectally with a 5.0-MHz linear-array transducer at a displayed depth of 10 cm. The right side of the sonogram is cranial and the left side is caudal.

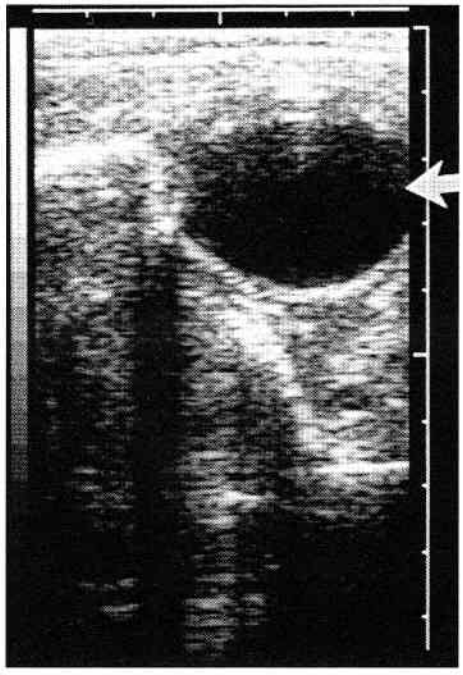

Figure 8–25

Anechoic orbit (*arrow*) of a late-gestation equine fetus, imaged per rectum, indicates that the fetus is in anterior presentation. This sonogram was obtained transrectally with a 5.0-MHz linear-array transducer at a displayed depth of 10 cm. The right side of the sonogram is cranial and the left side is caudal.

fossa is usually palpable. The opposite ovary should feel normal and have normal follicular activity for the stage of the estrous cycle. The size of the ovary with a hematoma should decrease over time, usually within 1 to 2 months. Hemorrhage is usually confined to the ovary. The author knows of one mare that experienced recurrent colic associated with estrus that seemed to be caused by ovarian hemorrhage into the peritoneal cavity and subsequent peritoneal irritation. Recurrent colic ceased when the mare was ovariectomized.

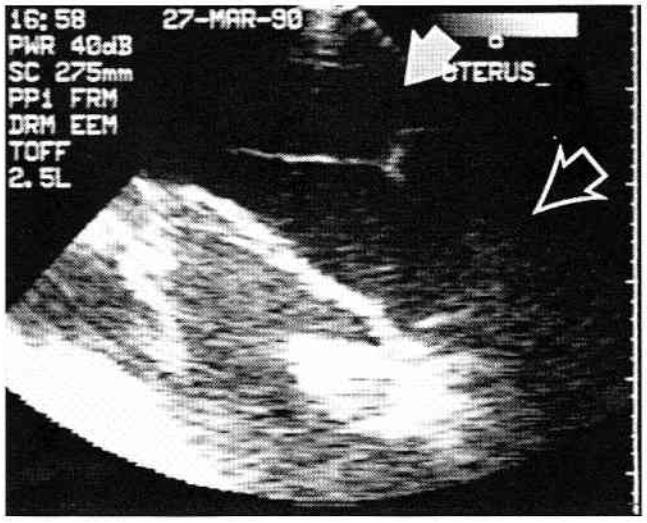

Figure 8–24

Allantoic cavity (*closed arrow*) separated from amniotic cavity (*open arrow*) by the filamentous amnion. This sonogram was obtained with a 2.5-MHz sector-scanner transducer from the ventral abdominal window at a displayed depth of 27.5 cm. The right side of the sonogram is cranial and the left side is caudal.

Ovarian Cysts

Cystic ovarian disease as it occurs in cattle does not occur in mares. Occasionally, a remnant of the mesonephric duct, an epoophoron cyst, may be present in the ovarian capsule. Parovarian cysts may be present in the fimbria or the mesovarium and originate from the remnant of the mesonephric or paramesonephric ducts.[30] These cysts are not usually palpable but can be seen on ultrasonographic examination as round, anechoic, fluid-filled structures that are intimately associated with the ovary. They can be differentiated from follicles by repeated observations of the same structure with little change in size and location. Parovarian and epoophoron cysts do not interfere with normal cyclicity.

Anovulatory Follicles

Occasionally, follicles fail to ovulate and may luteinize without release of an egg. An anovulatory follicle may have a persistent echogenically lacy appearance (Fig. 8-28) or a thick echogenic rim (Fig. 8-29) surrounding the anechoic center of the follicle. Ginther[47] has reported the presence of echogenic floating specks being observed

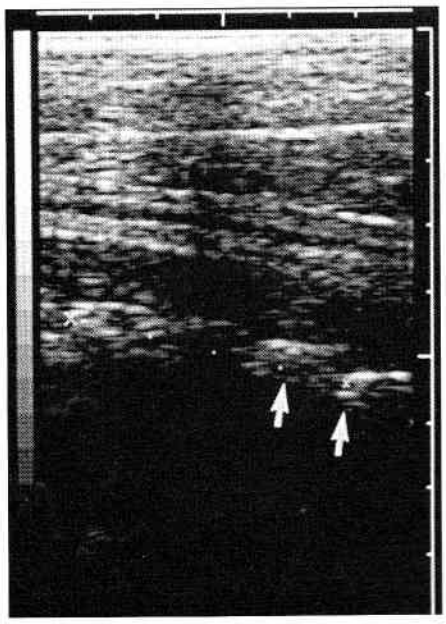

Figure 8–26

Intercostal spaces can be measured between the fetal ribs (*arrow*). This sonogram was obtained transrectally with a 5.0-MHz linear-array transducer at a displayed depth of 10 cm. The right side of the sonogram is cranial and the left side is caudal.

upon ovarian ballottement for 1 to 2 days. The contents of the anovulatory hemorrhagic follicles then become gel-like and quiver upon ballottement on the third day of observation, after which they become firm (Fig. 8-30).

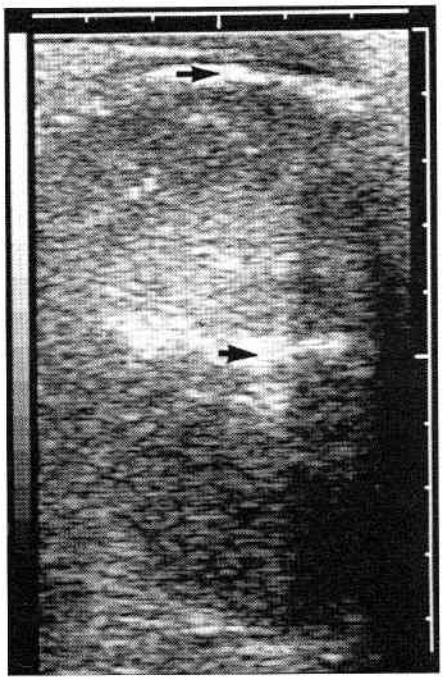

Figure 8–27

An ovarian hematoma initially may be a large homogeneous echogenic structure. Dorsal and ventral limits of the hematoma are designated by arrows. This sonogram was obtained transrectally with a 5.0-MHz linear-array transducer at a displayed depth of 10 cm. The right side of the sonogram is cranial and the left side is caudal.

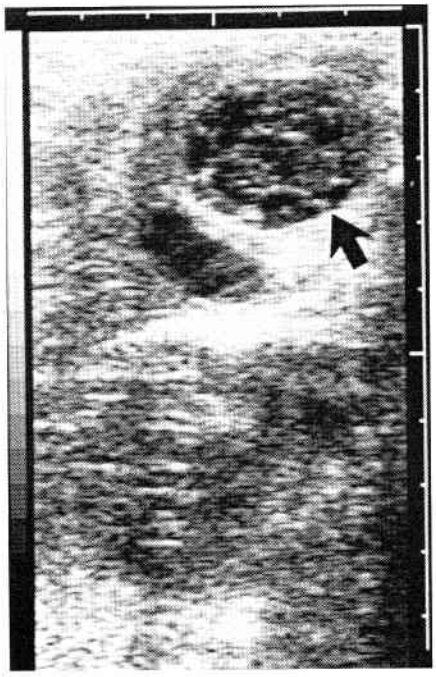

Figure 8–28

The lacy pattern (*arrow*) sometimes seen with an anovulatory follicle. This lacy appearance may be seen transiently after a follicle ovulates normally. Notice the hyperechoic rim of tissue surrounding the structure. This sonogram was obtained transrectally with a 5.0-MHz linear-array transducer at a displayed depth of 10 cm. The right side of the sonogram is cranial and the left side is caudal.

Granulosa Cell Tumor

The most common ovarian tumor in the mare is the granulosa cell tumor.[48] Clinically, the mare has an enlarged ovary with no palpable ovulation fossa. The contralateral ovary is usually small and inactive and appears as a small (<4 cm) homogeneous, moderately echogenic structure with only a few less-than-10-mm anechoic follicles.[49] The atrophied condition of the contralateral ovary is hypothesized to be due to production of inhibin by the tumor.[50] Approximately half of the mares with a granulosa cell tumor have elevated plasma testosterone concentrations, and some display stallion-like behavior. Ultrasonographic examination of the enlarged ovary reveals it to be one of three types, depending on the character of the tumor. Typically, the tumor is multicystic. These cysts are of various sizes and shapes and are filled with clear yellow fluid. Cysts may be separated by dense echogenic ovarian stoma. On ultrasonographic examination, this type of granulosa cell tumor may look like a transitional ovary that contains numerous anechoic follicles less than 25 mm in size (Fig. 8-31) but can be differentiated from a normal ovary because the granulosa cell tumor does not have a palpable ovulation fossa. Occasionally, a granulosa cell tumor is uniloculated. These masses are composed of one large thick-walled (2 to 3 mm) cyst filled with clear yellow anechoic fluid. They may be quite large in diameter and can be significantly reduced in size by aspiration of the fluid to facili-

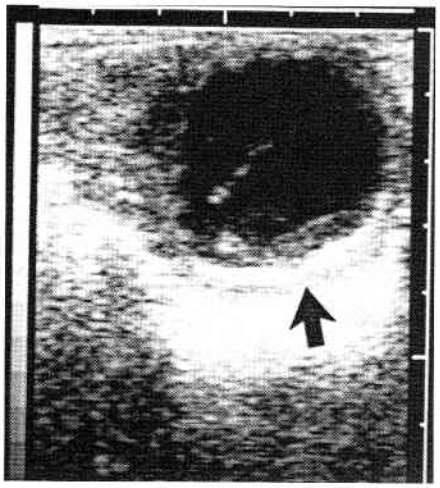

Figure 8–29

Persistent thick rim (*arrow*) of luteal tissue in an anovulatory follicle. Ballottement of the structure would reveal its gel-like consistency. This sonogram was obtained transrectally with a 5.0-MHz linear-array transducer at a displayed depth of 10 cm. The right side of the sonogram is cranial and the left side is caudal.

tate removal during surgery. The least common appearance of a granulosa cell tumor is that of a solid mass with no cystic structures. These granulosa cell tumors are hyperechoic and dense and may be homogeneous or heterogeneous. The contralateral ovary is small in diameter and has no or a few small follicles present (Fig. 8–32).[30]

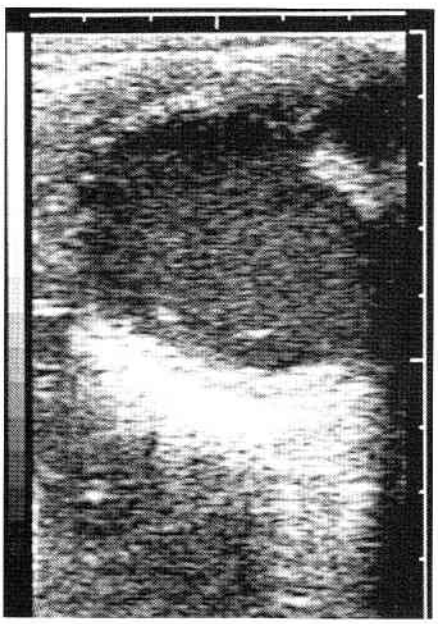

Figure 8–30

A gradual increase in echogenicity of an anovulatory follicle occurs over several days. This sonogram was obtained transrectally with a 5.0-MHz linear-array transducer at a displayed depth of 10 cm. The right side of the sonogram is cranial and the left side is caudal.

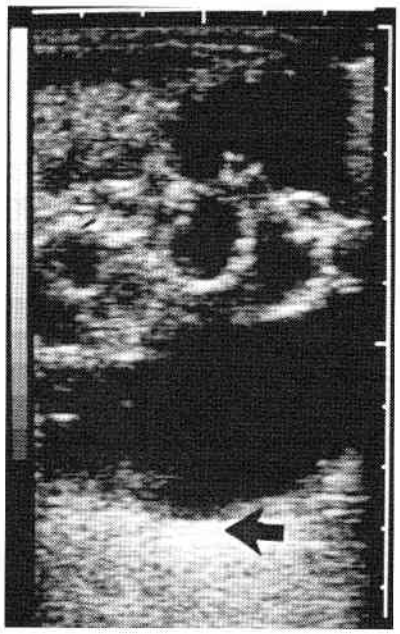

Figure 8–31

Granulosa-cell tumor in the mare, typically composed of numerous anechoic cystic structures on the ovary. All of the tissue above the arrow is abnormal. This sonogram was obtained transrectally with a 5.0-MHz linear-array transducer at a displayed depth of 10 cm. The right side of the sonogram is cranial and the left side is caudal.

Cystadenoma

Cystadenomas are an uncommon ovarian tumor in the mare. They have numerous anechoic cystic spaces and may secrete testosterone. Hinrichs and Freeman[51] reported that the cystic areas are regular in size and smoothly spherical compared with a granulosa cell tumor. In attempting to clinically differentiate a cystadenoma from a granulosa cell tumor, the presence of an ovulation fossa on the affected ovary and a functional contralateral

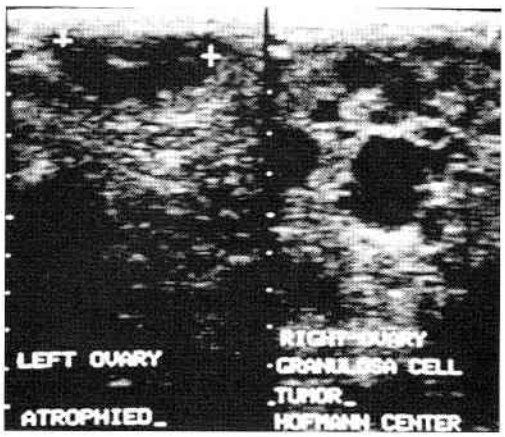

Figure 8–32

Contralateral ovary of a mare with granulosa-cell tumor is atrophied and inactive, whereas the ovary containing the tumor is enlarged and multicystic. Cursors (+) designate limits of the atrophied contralateral ovary. These sonograms were obtained transrectally with a 5.0-MHz linear-array transducer at a displayed depth of 12 cm. The right sides of these sonograms are cranial and the left sides are caudal.

Figure 8–33

Organized clots (*arrow*) in a hematoma in the uterine wall may appear quite echogenic. This sonogram was obtained transrectally with a 5.0-MHz linear-array transducer at a displayed depth of 12 cm. The right side of the sonogram is cranial and the left side is caudal.

ovary may be more helpful than the tumor's ultrasonographic appearance. Definitive diagnosis requires histologic evaluation of the mass.

Teratoma

Another uncommon ovarian tumor in the mare is the teratoma. It may be solid or cystic and may contain many different tissue types that can include bone, cartilage, hair, skin, muscle, fat, and teeth.[30] Its ultrasonographic appearance, accordingly, reflects the different tissues present, imaged as structures of various echogenicities with acoustic shadowing from the bone or teeth within the mass.[52] The contralateral ovary has normal function and follicular activity for the stage of the reproductive cycle.

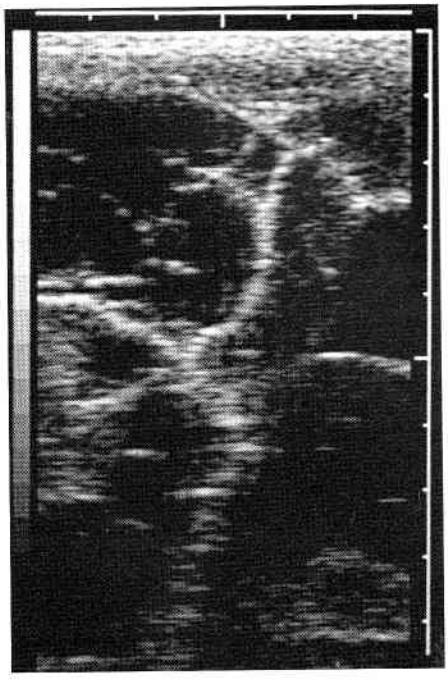

Figure 8–34

This hematoma in the broad ligament 4 days after foaling had numerous anechoic loculated spaces. This sonogram was obtained transrectally with a 5.0-MHz linear-array transducer at a displayed depth of 10 cm. The right side of the sonogram is cranial and the left side is caudal.

Uterine Hematoma

Hematomas may occur in the uterine wall or broad ligament after parturition and typically have loculated anechoic fluid-filled cavities within a large hyperechoic mass in the uterine wall or broad ligament (Figs. 8-33 and 8-34). These may also be associated with blood in the uterine lumen and even fatal hemorrhage due to a periparturiently ruptured uterine artery. This blood may initially be homogeneous and moderately echogenic and may swirl if hemorrhage is active. Eventually the blood clots and forms loculated hyperechoic spaces surrounding anechoic areas.

Numerous round, prominent, anechoic blood vessels are typically present in the broad ligament after a normal parturition (Fig. 8-35). These decrease in size within a few days.

Uterine Fluid

Free fluid is not normally seen in the uterine lumen during diestrus. Accumulations of uterine fluid can be assessed by their echogenicity and the diameter of the

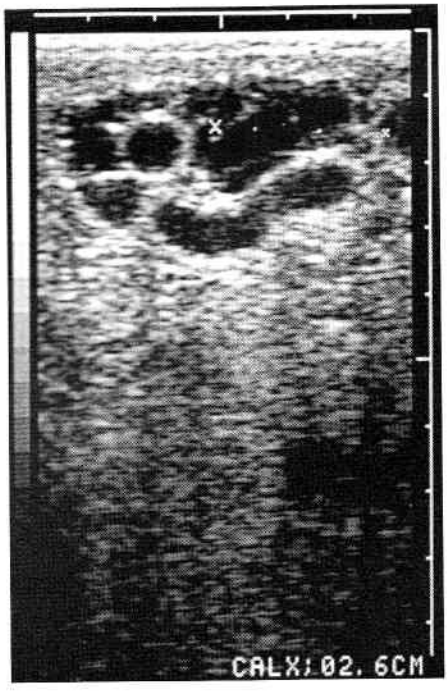

Figure 8–35

Transverse cross-section and longitudinal section of anechoic enlarged blood vessels seen in the broad ligament after parturition. This sonogram was obtained transrectally with a 5.0-MHz linear-array transducer at a displayed depth of 10 cm. The right side of the sonogram is cranial and the left side is caudal.

distended uterine lumen (Fig. 8-36). Purulent tenacious debris is hyperechoic in mares with pyometra. Ultrasonography can be particularly useful in monitoring uterine involution after parturition. One can assess the size and character of the uterus and any uterine contents and develop a therpeutic plan accordingly.

Antibiotic or saline uterine infusions have a regular pattern of horizontal reflections that are typical of a solution. Clear nonechogenic fluid in the uterus is usually associated with a conceptus (see Figs. 8-9 to 8-11) or a uterine cyst within the endometrium (see Fig. 8-12).

Uterine Cysts

The clinical significance of endometrial cysts is not well understood. In the past, uterine cysts were diagnosed by direct palpation, visualization by hysteroscopy, or direct visualization of the excised uterus. Many uterine cysts are too small or diffuse in character to be detected clinically by these means. Cysts are detected much more frequently using ultrasonography. Cysts have a rounded anechoic appearance in the uterus. Their position relative to the uterine wall may be determined by infusing the uterus with sterile saline and then repeating the examination (Fig. 8-37). A cyst may be pedunculated and hang in the uterine lumen, be on the surface of the endometrium, or be located deep within the endometrium. It is thought that if the cyst is pedunculated and obstructs the uterine lumen, it can decrease fertility by interfering with early embryo mobility and maternal recognition of pregnancy.

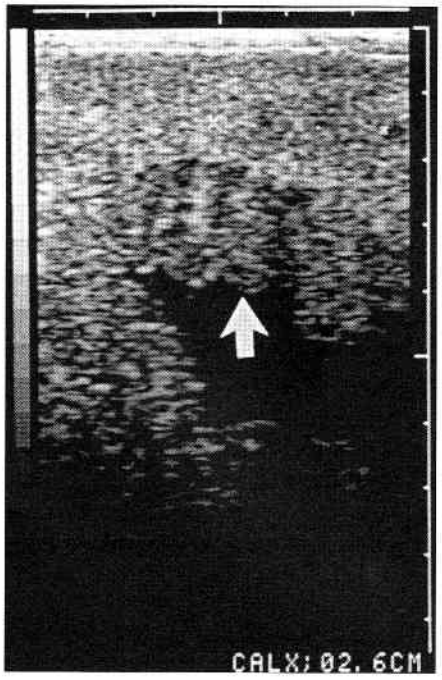

Figure 8-36

Anechoic fluid accumulation in a uterus 5 days after parturition. Notice the edematous endometrial folds (*arrow*) of the uterus. This sonogram was obtained transrectally with a 5.0-MHz linear-array transducer at a displayed depth of 10 cm. The right side of the sonogram is cranial and the left side is caudal.

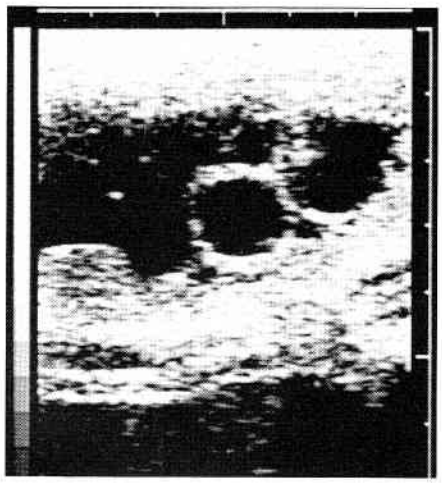

Figure 8-37

The position of uterine cysts in the uterus may be outlined more clearly by infusing saline into the uterine lumen. This sonogram was obtained transrectally with a 5.0-MHz linear-array transducer at a displayed depth of 10 cm. The right side of the sonogram is cranial and the left side is caudal.

Pedunculated cysts can be easily removed transcervically using a uterine biopsy forceps. Cysts that are deep in the endometrium may hamper endometrial gland function. In early pregnancy (<44 days), embryo loss was greater in mares with cysts (24%) than in those without cysts (6%).[53] Pregnancy rates at day 40 tended to be lower in mares with severe uterine cysts.[54] Removal of cysts may improve fertility in some cases, but the presence of endometrial cysts may not adversely affect the establishment or maintenance of pregnancy in other mares.[55]

Mummified Fetus and Retained Fetal Membranes

A mummified fetus (Fig. 8-38) or retained fetal membranes (Fig. 8-39) may be imaged in the uterus of a barren mare. The fetus has areas of different degrees of echogenicity that expand the surrounding uterus. Retained fetal membranes may appear as a thin layer of speckled hyperechoic material in the uterine lumen. The amount and character of fluid associated with the membranes are quite variable and can range from none to large amounts of slightly to very hyperechoic fluid. Uterine lavage with several liters of sterile saline may help dislodge and remove a mummified fetus or tags of retained fetal membranes.

Oviduct Abnormalities

Hydrosalpinx

This condition is rare in the mare. The ultrasonographic appearance of hydrosalpinx is that of a structure in the position of the ovary having numerous anechoic cystic spaces due to the short-axis cross-sectional view of the distended, tortuous oviduct (Fig. 8-40). The cystic spaces may be mistaken for follicles during ultrasound examina-

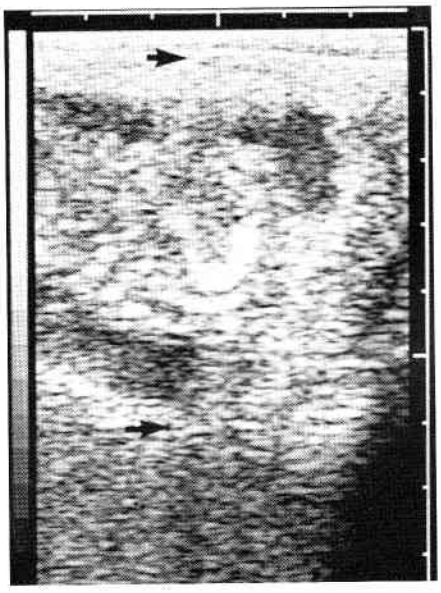

Figure 8–38

Hyperechoic reflections of a mummified fetus in a barren mare. The uterine wall was enlarged owing to the mass in the lumen. Arrows indicate the outline of the uterus. This sonogram was obtained transrectally with a 5.0-MHz linear-array transducer at a displayed depth of 10 cm. The right side of the sonogram is cranial and the left side is caudal.

tion because their size can change during the reproductive cycle. The change in size of the cystic spaces is due to changes in the amount of fluid in the oviduct during the reproductive cycle. If the condition is unilateral, removal of the ipsilateral ovary may allow the mare to cycle continuously from the normal side.

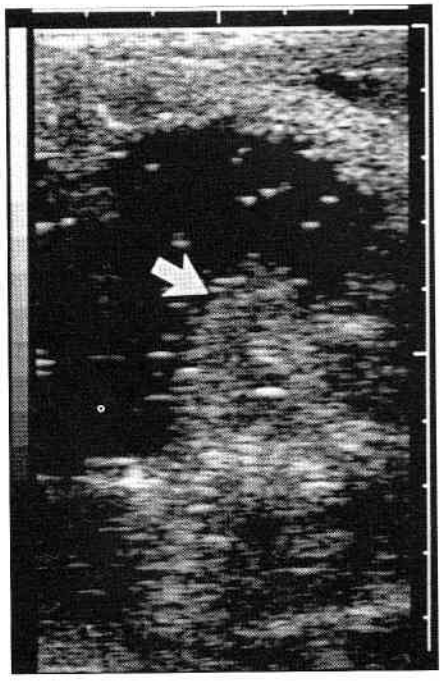

Figure 8–39

Speckled, slightly hyperechoic fluid accumulation associated with a mass in the uterus that was found to be retained fetal membranes (*arrow*). This sonogram was obtained transrectally with a 5.0-MHz linear-array transducer at a displayed depth of 10 cm. The right side of the sonogram is cranial and the left side is caudal.

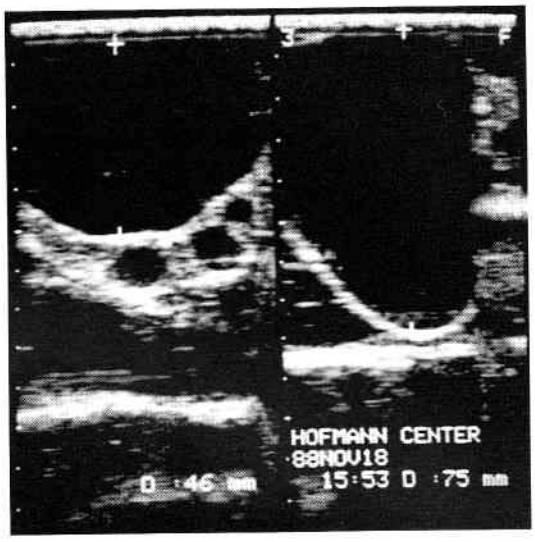

Figure 8–40

The convoluted distended oviduct seen with hydrosalpinx in the mare can be confused with follicles on the ovary. The fluid within the oviduct is anechoic. This sonogram was obtained transrectally with a 5.0-MHz linear-array transducer at a displayed depth of 10 cm. The right side of the sonogram is cranial and the left side is caudal.

Vaginal Abnormalities

Varicose Blood Vessels

Varicose blood vessels may be seen in the vagina and transverse fold of late pregnant mares and are a common cause of bloody vulvar discharge in late gestation. The vagina is normally quite homogeneous and moderately echogenic in character when imaged ultrasonographically. A varicosity is imaged as a round, short-axis (cross-section) anechoic structure in the vaginal tissue. Direct confirmation of a varicose vessel requires a vaginal speculum examination.

Vaginal Hematoma

Hematomas in the wall of the vagina caused by trauma of the foal passing through the birth canal may be seen after delivery in the mare (Fig. 8-41). Their appearance is that of multiloculated hyperechoic fibrin clots separated by anechoic serum. Vaginal hematomas usually resolve spontaneously. Attempts to drain or aspirate fluid from a hematoma may result in formation of an abscess.

Urovagina

Urine in the vagina (urovagina) can be seen ultrasonographically. One should observe the bladder and the location of the neck and note any accumulations of echogenic fluid caudal to the cervix (Fig. 8-42). To support a diag-

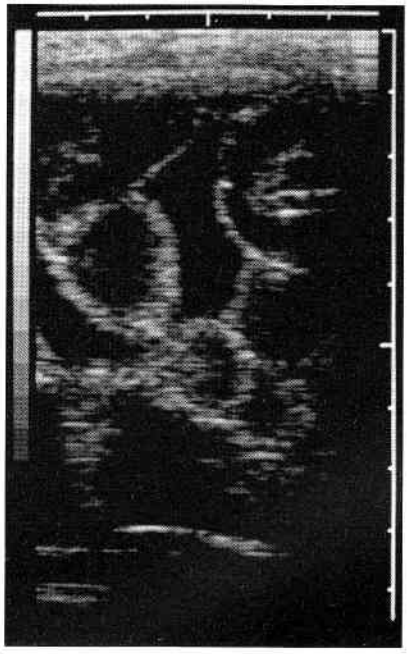

Figure 8–41

A postpartum vaginal hematoma may appear similar to hematomas in other body parts. Hematomas consist of multiloculated hyperechoic fibrin clots separated by anechoic serum. This sonogram was obtained transrectally with a 5.0-MHz linear-array transducer at a displayed depth of 10 cm. The right side of the sonogram is cranial and the left side is caudal.

nosis of urovagina made by ultrasonography, one must directly observe urine in the vagina by speculum examination or an abnormal voiding pattern of urine. Urometra may also be present in mares that are pooling urine in the vagina (Fig. 8–43). Surgery may be performed to correct urovagina.

Persistent Hymen

A persistent hymen may be diagnosed by direct visualization of the nonpatent transverse fold. Clinically a filly may

Figure 8–42

The neck of the bladder (*arrow*) normally is just ventral to the vestibular vaginal ring. This sonogram was obtained transrectally with a 5.0-MHz linear-array transducer at a displayed depth of 12 cm. The right side of the sonogram is cranial and the left side is caudal.

Figure 8–43

Urometra. Accumulation of urine (*arrow*), seen as mottled hyperechoic material inside a uterine horn in a mare that was pooling urine in her vagina. This sonogram was obtained transrectally with a 5.0-MHz linear-array transducer at a displayed depth of 12 cm. The right side of the sonogram is cranial and the left side is caudal.

be reported to have a white spherical mass at the vulvar lips when she lies down. Ultrasonography may show the accumulation of slightly echogenic fluid in the vagina and the resulting hydrometra (Figs. 8–44 and 8–45). The condition is easily resolved by manual rupture of the hymen. The transverse fold should not be completely surgically excised because it plays a role in protecting the uterus from external contamination.

High-Risk Pregnancy

The caudal portion of the pregnant uterus can be evaluated during late gestation by transrectal ultrasonography. Abnormalities of the placenta, such as placentitis and separation of the placenta, may be suspected by changes seen ultrasonographically (Figs. 8–46 to 8–48). Chronic ascending placentitis may be imaged as a thickened hyperechoic chorioallantois with areas of demarcation be-

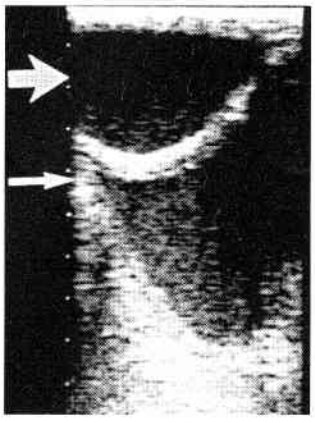

Figure 8–44

Persistent hymen. Notice the accumulation of fluid (*large arrow*) in the vagina dorsal and cranial to the neck of the bladder (*small arrow*). This sonogram was obtained transrectally with a 5.0-MHz linear-array transducer at a displayed depth of 12 cm. The right side of the sonogram is cranial and the left side is caudal.

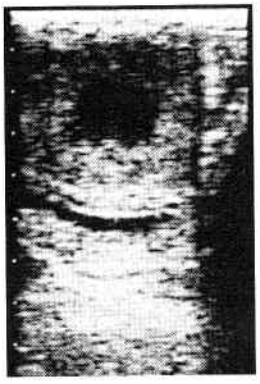

Figure 8–45

Hydrometra due to a persistent hymen in an 18-month-old filly. Anechoic fluid is present in the center of the hyperechoic uterine wall. This sonogram was obtained transrectally with a 5.0-MHz linear-array transducer at a displayed depth of 12 cm. The right side of the sonogram is cranial and the left side is caudal.

tween the uterine wall and fetal membranes. These mares may be at risk of the placenta not rupturing normally at the end of first-stage labor. Premature separation of the chorioallantois may occur during expulsion of the fetus. The foal may exhibit clinical signs caused by hypoxia during the delivery (i.e., periparturient asphyxia syndrome). Placentitis may be controlled by systemic antibiotics in the mare. A mare with placentitis requires close observation and assistance during parturition to ensure timely delivery of the fetus.

The evaluation of advanced pregnancy and fetal monitoring is an emerging area under investigation (see Chapter 9). Data collection to determine the range of normal findings will help clinicians assess pregnancies at risk. Procedures used in monitoring human pregnancies need

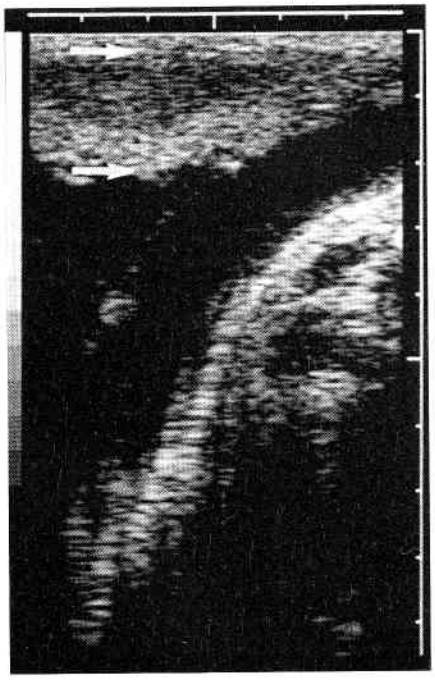

Figure 8–46

Uteroplacental unit (*area between arrows*) in the body of the uterus appears thickened (*arrow*). The chorion was later diagnosed to have placentitis. This sonogram was obtained transrectally with a 5.0-MHz linear-array transducer at a displayed depth of 10 cm. The right side of the sonogram is cranial and the left side is caudal.

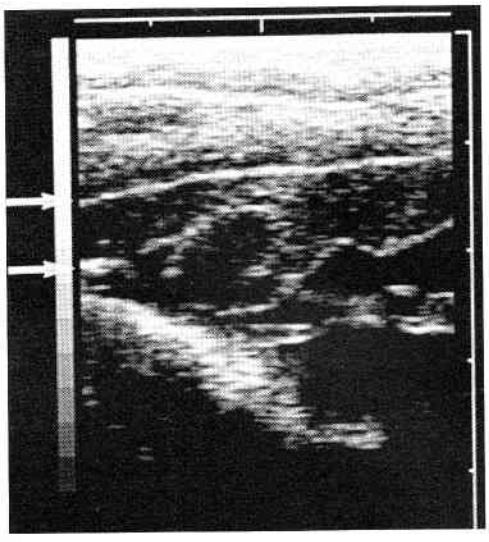

Figure 8–47

Hyperechoic outline of chorioallantois (*area between white arrows*) in the body of the uterus that prematurely separated at parturition and was diagnosed as chronic placentitis. This sonogram was obtained transrectally with a 5.0-MHz linear-array transducer at a displayed depth of 6 cm. The right side of the sonogram is cranial and the left side is caudal.

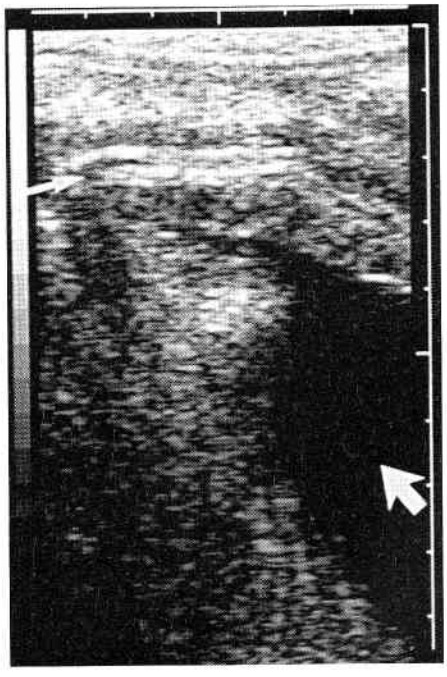

Figure 8–48

Chorioallantois of a mare that had premature separation of chorion at parturition. Notice the hyperechoic line (*small arrow*) demarcating the chorioallantois from the uterine wall. Allantoic fluid (*large arrow*) is cranial to the cervix. This sonogram was obtained transrectally with a 5.0-MHz linear-array transducer at a displayed depth of 10 cm. The right side of the sonogram is cranial and the left side is caudal.

to be applied to the mare to help veterinarians increase their understanding of fetal development and placental well-being.

References

1. Palmer E, Draincourt M: Use of ultrasonic echography in equine gynecology. Theriogenology 13:203-216, 1980.
2. Ginther OJ: Fixation and orientation of the early equine conceptus. Theriogenology 19:613-623, 1983.
3. Simpson DJ, Greenwood RES, Ricketts SW, et al: Use of ultrasound echography for early diagnosis of single and twin pregnancy in the mare. J Reprod Fertil Suppl 32:431-439, 1982.
4. Ginther OJ: Mobility of twin embryonic vesicles in mares. Theriogenology 22:83-95, 1984.
5. McKinnon AO, Squires EL, Harrison LA, et al: Ultrasonographic studies on the reproductive tract of mares after parturition: Effect of involution and uterine fluid on pregnancy rates in mares with normal and delayed first postpartum ovulatory cycles. J Am Vet Med Assoc 192:350-353, 1988.
6. Sertich PL, Watson ED: Plasma concentrations of 13,14-dihydro-15-ketoprostaglandin F-2_{alpha} in mares during uterine involution. J Am Vet Med Assoc 201:434-440, 1992.
7. McKinnon AO, Squires EL, Voss JL: Ultrasonic evaluation of the mare's reproductive tract, Part I. Compend Contin Educ Pract Vet 9:336-345, 1987.
8. McKinnon AO, Squires EL, Voss JL: Ultrasonic evaluation of the mare's reproductive tract, Part II. Compend Contin Educ Pract Vet 9:472-480, 1987.
9. Hayes KEN, Pierson RA, Scraba ST, Ginther OJ: Effects of estrous cycle and season on ultrasonic uterine anatomy in mares. Theriogenology 24:465-477, 1985.
10. Townson DH, Ginther OJ: The development of fluid-filled luteal glands in mares. Anim Reprod Sci 17:155-163, 1988.
11. Townson DH, Ginther OJ: Ultrasonic characterization of follicular evacuation during ovulation and fate of the discharged follicular fluid in mares. Anim Reprod 20:131-141, 1989.
12. Ginther OJ, Pierson RA: Ultrasonic anatomy of equine ovaries. Theriogenology 21:471-483, 1984.
13. Pierson RA, Ginther OJ: Ultrasonic evaluation of the corpus luteum of the mare. Theriogenology 23:795-806, 1985.
14. Ginther OJ: Reproductive Biology of the Mare. Cross Plains, WI, Equiservices, 1992, pp 1-36, 550-554.
15. Ginther OJ, Pierson RA: Ultrasonic evaluation of the reproductive tract of the mare: Principles, equipment, and techniques. J Equine Vet Sci 3:195-201, 1983.
16. Adams-Brendemuehl C, Pipers FS: Antepartum evaluations of the equine fetus. J Reprod Fertil Suppl 35:565-573, 1987.
17. Adams-Brendemuehl C: Fetal assessment. *In* Koterba AM, Drummond WH, Kosch PC (eds): Equine Clinical Neonatology. Philadelphia, Lea & Febiger, 1990, pp 16-33.
18. Pipers FS, Adams-Brendemeuhl CS: Techniques and applications of transabdominal ultrasonography in the pregnant mare. J Am Vet Med Assoc 185:766-771, 1984.
19. Reef VB, Vaala WE, Worth LT, et al: Transabdominal ultrasonographic assessment of fetal well-being during late gestation: A preliminary report on the development of an equine biophysical profile. Equine Vet J 28:200-208, 1996.
20. Reef VB, Vaala WE, Worth LT, et al: Ultrasonographic evaluation of the fetus and intrauterine environment in healthy mares during late gestation. Vet Radiol Ultrasound 36:533-541, 1995.
21. Allen KA, Stone LR: Equine diagnostic ultrasonography: Equipment selection and use. Compend Contin Educ Pract Vet 12:1307-1311, 1990.
22. Ginther OJ, Pierson RA: Regular and irregular characteristics of ovulation and the interovulatory interval in mares. J Equine Vet Sci 9:4-12, 1989.
23. Ginther OJ: Reproductive Biology of the Mare: Basic and Applied Aspects. Cross Plains, WI, Equiservices, 1979, p 413.
24. Ginther OJ: Ultrasonic imaging of equine ovarian follicles and corpora lutea. Vet Clin North Am: Equine Pract 4:197-213, 1988.
25. Hinrichs K: Ultrasonographic assessments of ovarian abnormalities. Proceedings of the 36th Annual Convention of the American Association of Equine Practitioners, 1990, vol 36, pp 31-40.
26. Bergin WC, Shipley WD: Genital health in the mare. I. Observations concerning the ovulation fossa. Vet Med/Small Anim Clin 63:362-365, 1968.
27. Ginther OJ: Ultrasonic Imaging and Reproductive Events in the Mare. Cross Plains, WI, Equiservices, 1986.
28. Sertich PL: Transcervical embryo transfer in performance mares. J Am Vet Med Assoc 195:940-944, 1989.
29. Day WE, Evans JW, Vogelsang MM, Westhusin ME: Characterization of the cervix in cycling mares using ultrasound. Biol Reprod Mono I, Eq Repro VI:519-526, 1995.
30. Roberts SJ: Veterinary Obstetrics and Genital Diseases. Woodstock, VT, Theriogenology, 1986, p 9.
31. Zemjanis R: Pregnancy diagnosis in the mare. J Am Vet Med Assoc 139:543-547, 1961.
32. Rantanen N, Forbeck R, DuMond S: Early pregnancy diagnosis in the mare using transrectal ultrasound scanning techniques: A preliminary report. Equine Vet Sci 2:27-29, 1982.
33. Ginther OJ: Mobility of the early equine conceptus. Theriogenology 19:603-611, 1983.
34. Jeffcott LB, Whitwell K: Twinning as a cause of foetal and neonatal loss in the Thoroughbred mare. J Comp Pathol 83:91-106, 1973.
35. Henry M, Coryn M, Vandeplassche M: Multiple ovulation in the mare. Zentralbl Veterinarned 29:170-184, 1982.
36. Deskur S: Twinning in Thoroughbred mares in Poland. Theriogenology 23:711-718, 1985.
37. Ginther OJ: Twinning in mares: A review of recent studies. J Equine Vet Sci 2:127-135, 1982.
38. Ginther OJ, Douglas RH: The outcome of twin pregnancies in mares. Theriogenology 18:237-244, 1982.
39. Ginther OJ, Douglas RH, Lawrence JR: Twinning in mares: A survey of veterinarians and analysis of theriogenology records. Theriogenology 18:333-347, 1982.
40. Roberts CJ: Termination of twin gestation by blastocyst crush in the broodmare. J Reprod Fertil Suppl 32:447-449, 1982.
41. Pascoe DR, Pascoe RR, Hughes JP, et al: Comparison of two techniques and three hormone therapies for management of twin conceptuses by manual embryonic reduction. J Reprod Fertil Suppl 35:701-702, 1987.
42. Bowman T: Ultrasonic diagnosis and management of early twins in the mare. Proceedings of the Annual Convention of the American Association of Equine Practitioners, Las Vegas, NV, 1986, vol 32, pp 35-43.
43. Ginther OJ: Twin equine embryos. Proceedings of the Annual Meeting of the Society for Theriogenology, Coeur d'Alene, Idaho, 1989, pp 143-152.
44. Ginther OJ: The twinning problem: From breeding to day 16. Proceedings of the Annual Convention of the American Association of Equine Practitioners, Las Vegas, NV, 1983, pp 11-26.
45. Curran S, Ginther OJ: Ultrasonic diagnosis of equine fetal sex by location of the genital tubercle. Equine Vet Sci 9(2):77-83, 1989.
46. Kaehn W: Pferdefetus. *In* Atlas und Lehrbuch der Ultraschalldiagnostik. Hannover, Germany, Schlutersche Verlagsanstalt und Druckerei, 1991, pp 64-67.
47. Ginther OJ: Ultrasonic Imaging and Animal Reproduction: Horses. Book 2. Cross Plains, WI, Equiservices, 1995, p 31.
48. Norris HJ, Taylor HB, Garner FM: Equine ovarian granulosa tumours. Vet Rec 82:419-420, 1968.
49. Jubb KVK, Kennedy PC, Palmer N: The female genital system. *In* Pathology of Domestic Animals, 3rd ed. San Diego, Academic Press, 1985, vol 3, pp 318-323.
50. Piquette GN, Sertich PL, Kenney RM, et al: Equine granulosa-theca cell tumors express inhibin alpha- and $beta_A$-subunit messenger ribonucleic acids and proteins. Biol Reprod 43:1050-1057, 1990.
51. Hinrichs K, Freeman D: Granulosa cell tumor. *In* White NA, Moore JN (eds): Current Practice of Equine Surgery. Philadelphia, JB Lippincott, 1990, pp 711-716.
52. Panciera RJ, Slusher SA, Hayes KEN: Ovarian teratoma and granulosa cell tumor in two mares. Cornell Vet 81:43-49, 1991.
53. Chevalier-Clement F: Pregnancy loss in the mare. Anim Reprod Sci 20:231-244, 1989.
54. Adams GP, Kastelic JP, Bergfelt DR, Ginther OJ: Effect of uterine inflammation and ultrasonographically-detected uterine pathology on fertility in the mare. J Reprod Fertil, Suppl 35:445-454, 1987.
55. Eilts BE, Scholl DT, Paccamonti DL, Causey R, Klimczak JC, Corley JR: Prevalence of endometrial cysts and their effect on fertility. Biol Reprod Mono I, Eq Repro VI:527-532, 1995.

CHAPTER 9

Fetal Ultrasonography

Ultrasonography has been widely used for early pregnancy diagnosis in brood mares and was one of the earliest applications of ultrasonography in horses.[1-31] Ultrasonographic pregnancy diagnosis involves transrectal uterine scanning in early gestation (as early as 10 to 14 days) and identifying the embryonic vesicle. Ultrasonographic visualization of two embryonic vesicles enabled the equine theriogenologist to detect twins and subsequently develop techniques for early embryonic reduction of one twin fetus.[9, 10, 16, 17, 25, 26] In utero fetal determination of sex was then developed using high-resolution transrectal ultrasound in the first trimester of pregnancy (59 to 68 days) but requires an experienced veterinary ultrasonologist specializing in theriogenology to achieve a high degree of accuracy in determining the sex of equine fetuses.[32]

Transcutaneous fetal monitoring from the ventral abdominal window is a relatively new application of diagnostic ultrasonography in brood mares.[25, 33-37] As in human medicine, transcutaneous fetal monitoring is useful in the management of high-risk pregnancies and, in particular, for evaluating fetal well-being during all stages of gestation, especially late in the last trimester.[25, 33, 34, 36-50] Another application of transcutaneous fetal monitoring is embryo reduction in mares with twin fetuses that were either not evaluated, missed, or not successfully reduced in early gestation.[51, 52] This procedure involves the use of transcutaneous fetal scanning early in the second trimester, locating both fetuses ultrasonographically and injecting KCl into the heart or thorax (less desirable) of the smaller or less viable fetus until cardiac motion stops.[51, 52] Transcutaneous ultrasonographic monitoring to assess fetal well-being in the mare has shown great promise in the evaluation of high-risk pregnancies.[25, 33, 34, 37] Work on the development of an equine fetal biophysiologic profile is ongoing with the hope that more accurate assessments of the equine fetus in late gestation may enable the equine perinatologist to intervene when indicators of fetal distress are present.[37] Possible interventions include trying to maintain pregnancy; treatment of the underlying problem(s), inducing parturition; performing a cesarean section; and preparation for the care of a high-risk neonate, resulting, it is hoped, in an improved outcome.[25, 37]

EXAMINATION TECHNIQUE

Patient Preparation

The hair over the ventral abdomen must be surgically clipped with a No. 40 blade.[25, 33-37, 51] The size of the clipped area should initially be based upon the stage of gestation and enlarged as needed to include the entire uterus and fetus (Fig. 9-1).[25, 33-37] The area in front of the mammary gland is clipped cranially to the umbilicus and laterally to the stifles or flank folds in the first trimester of pregnancy. As pregnancy advances, the clipped area is extended cranially and laterally to correspond with the increasing gestational age of the fetus. The clipped area should extend to the xiphoid and include the lateral sides of the abdomen (the latter is especially important in mares with large plaques of ventral edema) in late gestation. The lateral sides of the abdomen should be clipped ventral to a line extending from stifle to elbow. The skin should be thoroughly cleaned with soap and water to remove any dirt or debris from its surface prior to the application of ultrasonographic coupling gel.[25, 33-37] Although hair removal prior to scanning may not be necessary in horses with very fine hair coats, this rarely works on the ventral abdomen of brood mares. If attempted, the hair and skin must be thoroughly cleaned and copious amounts of coupling gel applied in the direction of hair growth to obtain any kind of an image. This approach is most likely to be successful in very early pregnancy when the entire fetus is still located in the dam's caudal abdomen, cranial to the mammary gland, because this area is relatively hairless. However, the best image quality is obtained with the hair surgically clipped from the skin and the skin thoroughly cleaned.

Anatomy

In the normal pregnant mare, the fetus can be imaged from the ventral abdomen, just in front of the mare's

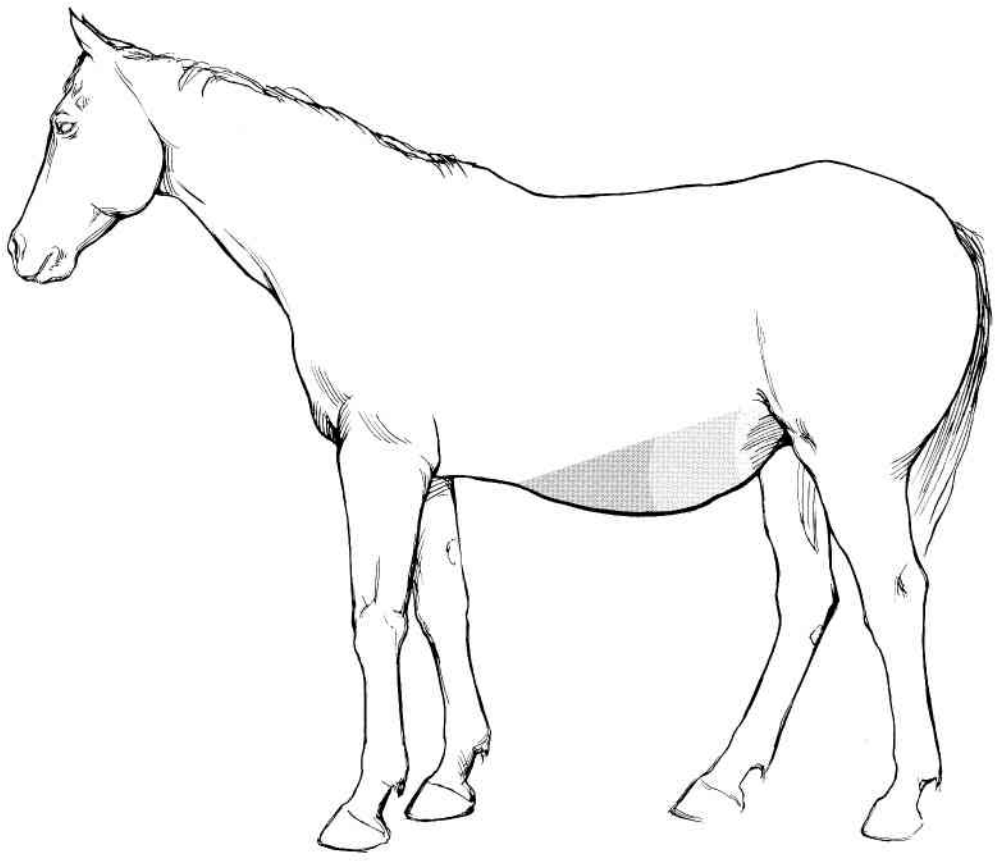

Figure 9–1

Diagram of the ventral abdomen in a pregnant mare in late gestation. The shaded areas represent the areas to be surgically clipped. The caudal most area (area with the lightest shading) represents the area to be clipped in the first trimester, the caudal and mid (area with intermediate shading) areas are to be clipped in the second trimester, and the cranial (area with the darkest shading), mid, and caudal areas are to be clipped in late gestation (last trimester).

mammary gland, from approximately 70 days of gestation until term.[25, 33-37] In late pregnancy the uterus and fetus usually extend along the ventral abdomen from pubis to xiphoid, more on one side than the other (Fig. 9-2). The fetal and nonfetal horns can be differentiated ultrasonographically by the visualization of the uterine folds and associated chorioallantois in the cranial tip of the nonfetal horn (Fig. 9-3).[25, 33-37] The chorioallantois is intimately associated with the placenta and uterus and cannot always be distinguished as a separate structure. The majority of the intrauterine fluids are allantoic, with a much smaller amount of amniotic fluid detected surrounding the equine fetus.[25, 33-37] The amnion is imaged as a thin membrane surrounding the fetus, which is in intimate contact with the fetus over much of its body. The amnion is best visualized around the fetus as it surrounds the neck, shoulder, thorax, and foreleg, with the largest pocket of amniotic fluid usually visualized beneath the foreleg near the thorax (Fig. 9-4).[25, 33-37] Fetal orientation is random in early gestation, but by the ninth month of pregnancy the fetus should be positioned for normal parturition in a cranial (anterior) presentation.[37]

Scanning Technique

The initial scanning of the pregnant uterus and equine fetus should be performed with a 2.5- (preferable) or 3.5-MHz transducer and a depth setting of 20 to 30 cm (preferable).[25, 33-37, 53] If the mare is in the first trimester of pregnancy, a 3.5- or 5.0-MHz transducer may be ideal because the uterus and fetus are still relatively small and the added penetration obtained with a 2.5-MHz transducer is not needed.[25, 33-37, 51, 53] In these instances, the depth setting should be decreased to display 10 to 20 cm. These transducers should also be used for the initial examination in a pony or miniature horse. For high-resolution images of the uteroplacental unit, a 5.0-, 6.0-, 7.5- (preferable), or 10.0-MHz transducer should be selected with a displayed depth of 4 to 10 cm.[34, 36, 37] The transducer and displayed depth selected depend upon the size of the broodmare, the thickness of the mare's ventral abdomen, the amount of ventral edema present (if any), and placental thickness. A wide-bandwidth 6.0-MHz microconvex linear-array transducer operating at a higher frequency (10.0 MHz) obtains excellent images of the utero-placental unit in most mares. The highest-frequency transducer that penetrates to the depth needed to image the entire fetus and placenta, respectively, with optimal resolution should be selected. A linear-array transducer would be ideal because of the larger transducer footprint, providing a larger window from which to assess the fetus. However, the limited depth of penetration of the 3.5-MHz (usually only 20 cm) or 5.0-MHz (usually only 10 cm) linear-array transducer limits the usefulness of a linear system in the pregnant mare in late gestation.[53, 54] The sector-scanner transducer is best because the 2.5-MHz transducer can penetrate to depths of 30 cm or more, enabling the veterinary ultrasonologist to image the fetus more completely (see Fig. 9-2).[25, 33-37, 51]

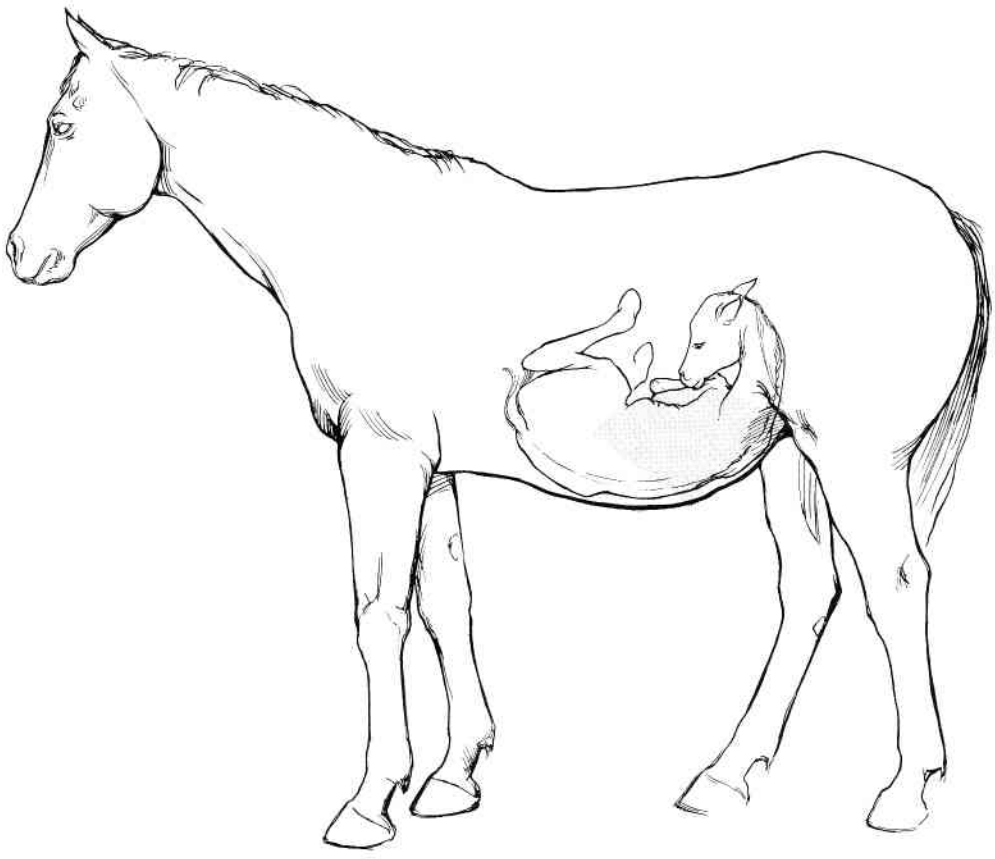

Figure 9–2

Diagram of the fetus in the uterus of a pregnant mare in late gestation. Notice the position and presentation of the fetus. The fetus should be in a cranial (anterior) presentation lying on its back or side. The shaded sector represents the sagittal scan plane used to examine the fetal thorax. This is the most frequent location of the fetus and this scan plane in late gestation.

Similar penetration can also be achieved with an annular-array transducer. Phased-array transducers have a larger footprint than sector-scanner transucers but a smaller footprint than most linear or curved linear-array transducers, and the displayed depth can be tailored to the individual examination; however, there is usually a limitation of 24 cm (occasionally 28 cm) displayed depth with a 2.5-MHz transducer.

The uterus and fetus are scanned from the ventral abdomen beginning just cranial to the mare's mammary gland and moving cranially to locate the fetal thorax and

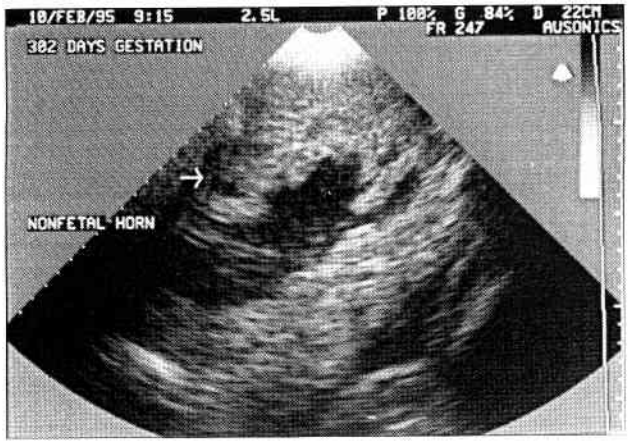

Figure 9–3

Sonogram of the nonfetal horn *(arrow)* obtained from a 15-year-old American Saddlebred mare at 302 days of gestation. Notice the uteroplacental folding that is normally present in the tip of the nonfetal horn. This sonogram was obtained with a 2.5-MHz sector-scanner transducer at a displayed depth of 22 cm. The mare's ventral abdomen is at the top of the sonogram.

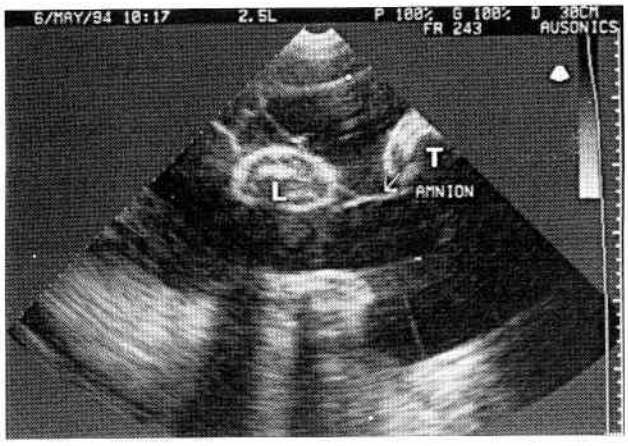

Figure 9–4

Sonogram demonstrating the amnion *(arrow)* surrounding the fetal forelimb (L) obtained from an 8-year-old Thoroughbred mare at 309 days of gestation. Notice the thin amniotic membrane surrounding the fetal forearm (radius and ulna) and fetal thorax (T). This fetus is in a cranial (anterior) presentation, with the fetal thorax to the right of the sonogram. This sonogram was obtained with a 2.5-MHz sector-scanner transducer at a displayed depth of 30 cm. The mare's ventral abdomen is at the top of the sonogram.

abdomen. The fetus should be scanned initially in a sagittal plane (cranial to caudal scan-plane orientation dividing the abdomen into right and left portions), as this scan plane is most useful to obtain fetal orientation (see Fig. 9-2). The sagittal (cranial to caudal scan plane from the ventral midline) and dorsal (cranial to caudal scan plane from the right and left sides of the abdomen) scan-plane orientation should display cranial on the right side of the screen and caudal on the left side of the screen. The mare's uterus should be thoroughly scanned in two mutually perpendicular scan planes—sagittal and transverse (dorsal to ventral or left to right scan-plane orientation dividing the abdomen into cranial and caudal portions—starting in front of the udder and scanning cranially to the xiphoid in multiple parasagittal planes, and then scanning from left to right sides of the abdomen in multiple transverse planes from the udder to the xiphoid to ascertain that only one fetus is present.[25, 36] When scanning is done from the left side of the abdomen (left transverse), the image should be displayed with the left side of the abdomen at the top of the image, dorsal on the right side of the screen, and ventral on the left side. The ventral transverse image (scanning from the ventral abdomen) should display the ventral abdomen on the top of the image, the left side of the abdomen on the right side of the screen, and the right side of the abdomen on the left side of the image. The right transverse image (scanning from the right side of the abdomen) should display the right side of the abdomen at the top of the image, dorsal on the right side of the screen, and ventral on the left.

Each examination should include the number of fetuses, the fetal horn, the presentation of each fetus (if more than one is present), fetal activity, fetal tone, fetal aortic diameter, fetal thoracic diameter, fetal heart rate (resting, exercising, and postexercise) and rhythm, fetal breathing movements, maximal vertical depth of amniotic and allantoic fluid, quality of amniotic and allantoic fluid, uteroplacental thickness, and any fetal, placental, or uterine abnormalities detected.[25, 33-37] The fetal heart is located in the fetal thorax, measurements of fetal heart rate are obtained, and cardiac rhythm is evaluated. Multiple measurements of fetal heart rate and assessments of fetal heart rhythm are made throughout the examination, during a minimum 30-minute period, with at least three resting measurements and three measurements after periods of activity.[25, 33-37] If possible, exercising heart rates (heart rates during periods of activity) should also be obtained.[37] The fetal heart rate and rhythm are evaluated accurately with M-mode echocardiography. An M-mode fetal echocardiogram should be obtained using two-dimensional echocardiographic guidance. Fetal heart rhythm is evaluated and heart rate calculated by measuring the time interval between two identical portions of the cardiac cycle, using a built-in cardiac calculations package (Fig. 9-5).[36, 37] Measurements of exercising heart rate in the equine fetus are meaningful but are difficult to obtain ultrasonographically. The diameter of the aorta (long axis) is measured in the thorax as close to the heart as possible from leading edge to leading edge of the aortic wall (Fig. 9-6).[36, 37] Maternal weight is important to obtain, as the mare's weight is used to estimate fetal aortic diameter and fetal size.[36, 37] The fetal thorax, diaphragm, and abdomen are evaluated continuously for at least 30 seconds for the presence and pattern of fetal breathing movements (Figs. 9-7 and 9-8).[36, 37] Fetal breathing movements are present when movement of the diaphragm and/or ribs is imaged without any movement of the fetus. Care must be taken not to mistake breathing

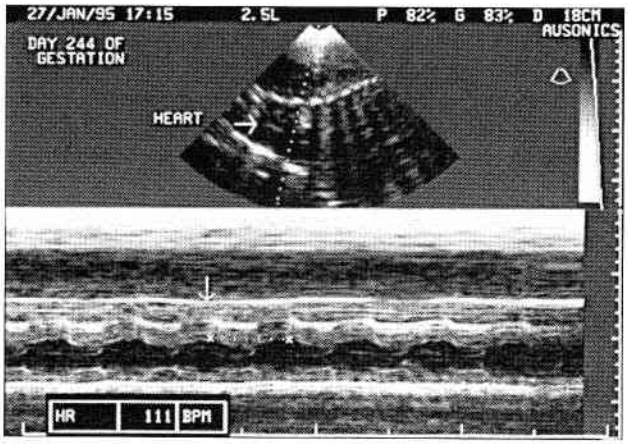

Figure 9–5

Sonogram demonstrating the technique of measuring fetal heart rate with M-mode echocardiography obtained from a pregnant 9-year-old Thoroughbred mare at 244 days of gestation. Notice the M-mode cursor *(dotted line)* transecting the fetal heart *(arrow)*. The corresponding fetal M-mode echocardiogram was obtained from this cursor position. The two cursors (x) are positioned on the fetal interventricular septum at end-diastole and are used to calculate a fetal heart rate of 111 beats/minute. This fetus is in a cranial (anterior) presentation, with the neck of the fetus on the left side of the sonogram. This sonogram and corresponding M-mode fetal echocardiogram were obtained with a 2.5-MHz sector-scanner transducer at a displayed depth of 18 cm. The mare's ventral abdomen is at the top of the sonogram.

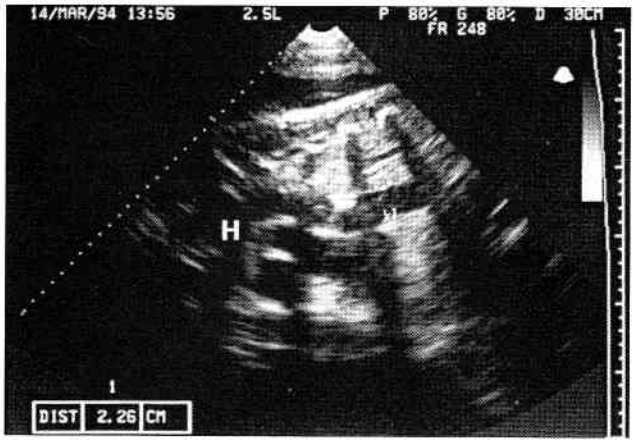

Figure 9–6

Sonogram of the fetal aorta obtained from a 12-year-old Thoroughbred mare at 333 days of gestation. The cursors (x^1) on the fetal aorta are placed as close to the heart (H) as possible without measuring the aorta at the aortic root. The cursors measure the aorta from the leading edge of the near side of the aorta to the leading edge of the far side of the aortic wall. The diameter of the fetal aorta is 2.26 cm. Notice the rib shadows interrupting the image of the intrathoracic structures. This fetus is in a cranial (anterior) presentation, with the fetal neck on the left side of the sonogram. This sonogram was obtained with a 2.5-MHz sector-scanner transducer at a displayed depth of 30 cm. The mare's ventral abdomen is at the top of the sonogram.

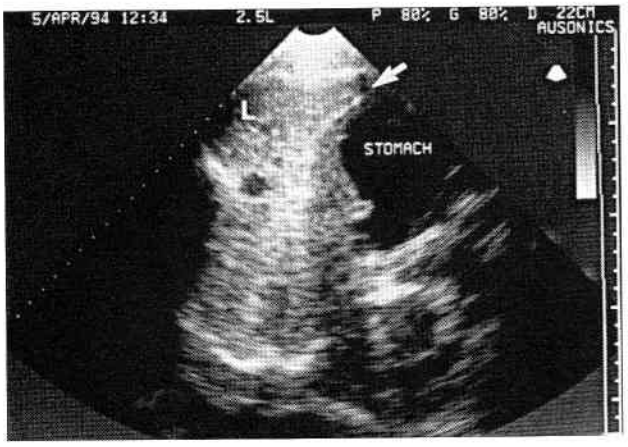

Figure 9–7

Sonogram of the fetal thorax and abdomen obtained from a 5-year-old Thoroughbred mare at 297 days of gestation. The curvilinear echo *(arrow)* of the diaphragm divides the more echogenic lung (L) from the hypoechoic liver and anechoic fluid-filled stomach. This fetus is in a cranial (anterior) presentation, with the fetal thorax to the left of the sonogram and the fetal abdomen to the right. This sonogram was obtained with a 2.5-MHz sector-scanner transducer at a displayed depth of 22 cm. The mare's ventral abdomen is at the top of the sonogram.

movements of the mare for fetal breathing movements. The maximal fetal thoracic diameter is measured from the spine to the sternum over the caudal part of the thorax, if the entire thorax can be imaged successfully (Fig. 9-8).[36, 37] Other measurements of fetal parts can be made to estimate fetal size, including fetal biparietal and orbital diameters.

Fetal activity is graded on a 0 to 3 scale, with 0 representing no movement detected throughout the entire examination and 3 representing a very active fetus, with few or no quiet periods detected (active ≥66% of the examination time).[36, 37] Fetal activity is graded 1 if only a small amount of movement is detected (active ≤33% of the examination time) and 2 if the fetus is fairly active throughout the examination (active >33 to <66% of the examination time). Fetal movements include extension or flexion of a limb and partial to 360-degree rotations around the fetal long axis. Fetal tone is absent if the fetus appears flaccid and present if the fetus flexes and extends the limbs, torso, or neck.[36, 37]

The depth of both allantoic and amniotic fluid should be measured at their deepest point, using the amniotic membrane to divide the two fluid cavities (Fig. 9-9).[36, 37] These fluids are measured at four quadrants relative to the fetus in the mare: right cranial, right caudal, left cranial, and left caudal. These measurements should be made as perpendicular to the uteroplacental surface as possible. The overall quality of the allantoic fluid and amniotic fluid is assessed throughout the uterus using a scale of 0 to 3, with 0 representing no particles visualized and 3 representing very echogenic fluid with numerous particles visualized continuously throughout the scan (Fig. 9-10).[36, 37] The fetal fluids are graded 1 if only a small amount of echogenic debris is detected and 2 if a moderate amount of echogenic debris is imaged. Uteroplacental thickness is measured in the same four quadrants at the thickest area (Fig. 9-11). Any thickened areas of the uteroplacental unit, areas of placental separation, fluid accumulation, or disruption of the uteroplacental unit should be differentiated from normal placental or uterine vessels (Fig. 9-12) and measured and the extent of these abnormalities critically assessed. Fetal anatomy should be carefully evaluated for any abnormalities. An ultrasound-guided aspiration (amniocentesis or allanto-

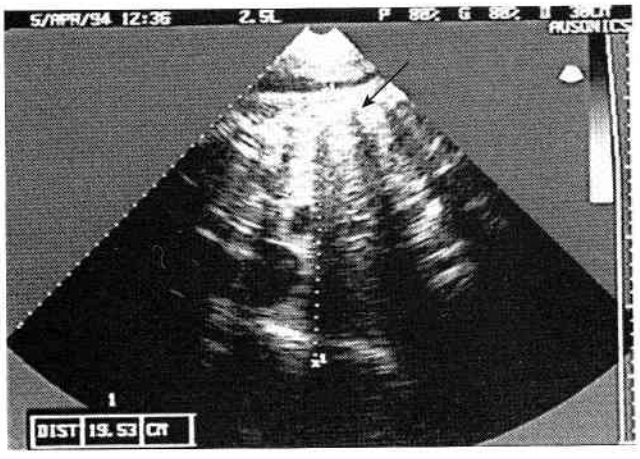

Figure 9–8

Sonogram of the fetal thorax obtained from a 5-year-old Thoroughbred mare at 297 days of gestation (same mare as in Figure 9-7). The placement of the cursors (x^1) on the fetal back over the thoracic spine and over the fetal sternum result in a maximal thoracic diameter of 19.53 cm. This fetus is in a cranial (anterior) presentation with the fetal thorax on the left side of the sonogram and the fetal abdomen on the right divided by the diaphragm *(arrow)*. This sonogram was obtained with a 2.5-MHz sector-scanner transducer at a displayed depth of 30 cm. The mare's ventral abdomen is at the top of the sonogram.

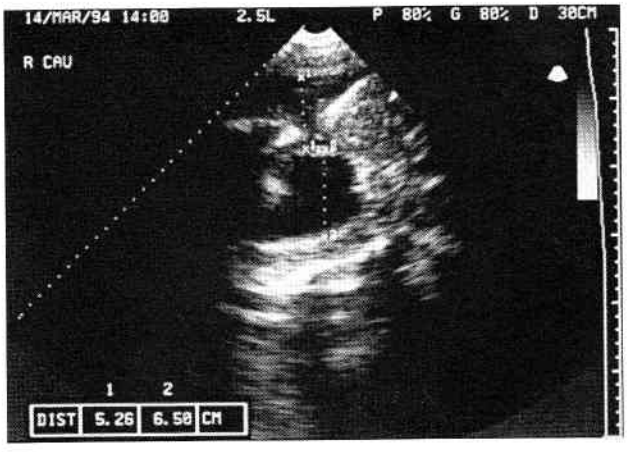

Figure 9–9

Sonogram of the fetal fluids obtained from a 12-year-old Thoroughbred mare at 333 days of gestation (same mare as in Figure 9-6). The cursors (x) measure the maximal vertical fluid pocket depth of allantoic fluid (x^1) and amniotic fluid (x^2). The cursors measuring the maximal allantoic fluid pocket depth (5.26 cm) are placed on the chorioallantois at its junction with the allantoic fluid (x^1) and the amnion (x^1). The cursors measuring the maximal amniotic fluid pocket depth (6.50 cm) are placed on the amnion (x^2) and the fetus (x^2). This fetal fluid measurement was obtained at the junction of the fetal forearm and neck. This fetus is in a cranial (anterior) presentation, and the fetal neck is to the left side of the sonogram. This sonogram was obtained with a 2.5-MHz sector-scanner transducer at a displayed depth of 30 cm. The mare's ventral abdomen is at the top of the sonogram.

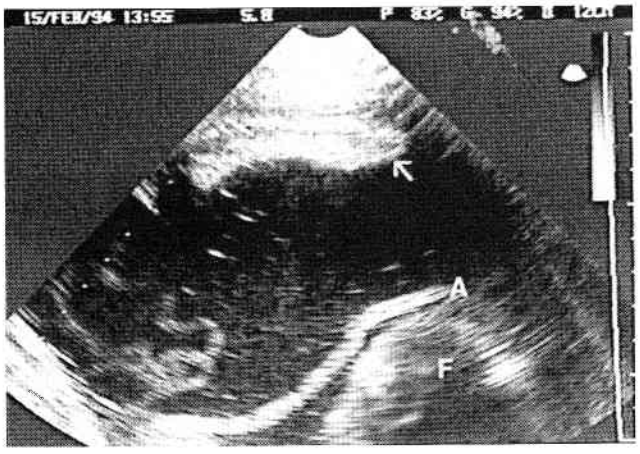

Figure 9–10

Sonogram of allantoic fluid obtained from an aged Thoroughbred mare at 328 days of gestation. Notice the numerous echogenic particles floating throughout the grade 3 allantoic fluid and the thickened uteroplacental unit *(arrow)*. The amnion (A) is thickened surrounding the fetus (F). This sonogram was obtained with a 5.0-MHz sector-scanner transducer at a displayed depth of 12 cm. The mare's ventral abdomen is at the top of the sonogram.

centesis) can be performed, when indicated, for cytology, culture, and sensitivity testing.

ULTRASONOGRAPHIC FINDINGS

Normal Structures

The uteroplacental unit appears as a two-part structure with a slightly more echogenic outer layer (uterus) and more sonolucent inner layer (allantochorion), with a total maximal thickness of the uteroplacental unit (see Fig. 9-11) that ranges from 1.15 ± 0.24 to 1.38 ± 0.23 cm in the fetal horn (Table 9-1).[33, 34, 36] The uteroplacental contact should be carefully evaluated for any fluid-filled spaces, which may indicate disruption of uteroplacental contact. Small areas of uteroplacental separation were seen in a few (8%) normal mares that delivered normal foals and may represent survival umbilical structures or other normal avillous areas.[36, 55] Five areas of the chorioallantois are normally devoid of microvilli and are potentially separate from the uterus: the cervical star, base of the umbilicus, openings to the oviducts, endometrial cups, and placental folds, which tend to occur over the larger allantoic vessels.[55] The uterine folds are visualized at the tip of the nonfetal horn, where the total uteroplacental thickness is greater owing to the infolding of the placenta over the uterine folds (see Fig. 9-3).

The allantoic and amniotic fluids are anechoic until late gestation, when increased particulate matter associated with sloughing cells, proteinaceous debris, and meconium (allantoic fluid) is visualized in normal pregnancies. Echogenic particles are more likely to be imaged in the allantoic fluid, often swirling after vigorous fetal movement, and have been imaged as early as 44 days prior to gestation in normal mares.[33, 36] Increased echogenic particles in both the amniotic and allantoic fluid may be detected in late gestation mares following transport. Smaller debris in equine allantoic fluid may be associated with mucoproteins, calcium phosphate, and other mineral deposits.[33] Hippomanes are frequently visualized in the allantoic fluid during late gestation. Hippomanes appear ultrasonographically as oval hypoechoic free-floating masses with echogenic centers associated with calcification of the proteinaceous debris (Fig. 9-13). The hippomanes are usually detected along the ventral aspect of

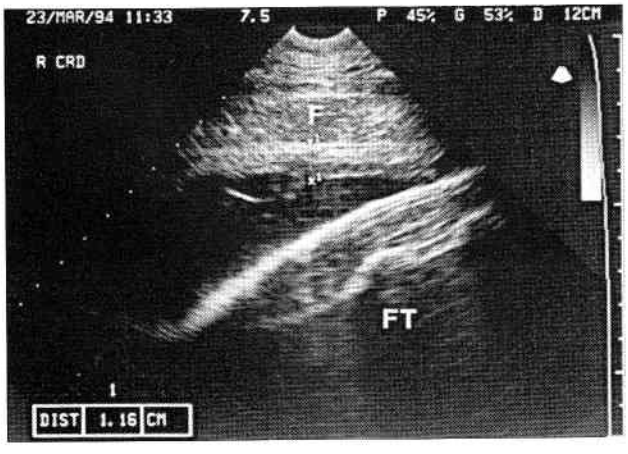

Figure 9–11

Sonogram of the uteroplacental unit obtained from a 16-year-old Thoroughbred mare at 326 days of gestation. The slightly more echogenic uterus is adjacent to the mare's ventral abdomen, and the slightly more hypoechoic chorioallantois is immediately adjacent to the anechoic allantoic fluid. The cursors (x^1) are measuring the thickness of the uteroplacental unit (1.16 cm). The fetal thorax (FT) is visualized on the lower right side of the sonogram. The slightly heterogeneous hypoechoic layer of the mare's ventral abdomen immediately adjacent to the uterus is a layer of intra-abdominal fat (F). This sonogram was obtained with a 7.5-MHz sector-scanner transducer at a displayed depth of 12 cm. The mare's ventral abdomen is at the top of the sonogram.

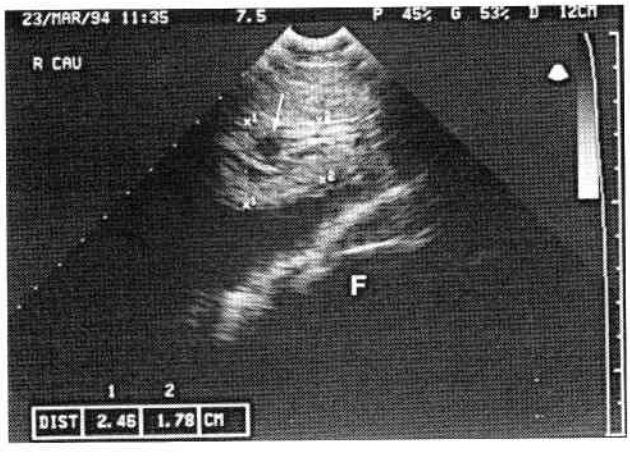

Figure 9–12

Sonogram of the uteroplacental unit obtained from a 16-year-old Thoroughbred mare at 326 days of gestation (same mare as in Figure 9-11). The uterine blood vessel *(arrow)* makes the uteroplacental unit measure thicker than normal (x^1 = 2.46 cm). This blood vessel should not be mistaken for an area of placental separation. This sonogram was obtained with a 7.5-MHz sector-scanner transducer at a displayed depth of 12 cm. The mare's ventral abdomen is at the top of the sonogram. F, Fetus.

Table 9–1
Normal Fetal and Maternal Measurements in Late Gestation

Fetal or Maternal Measurement	Mean ± SD*	Range
Fetal heart rate (HR)		
Low HR < 330 days (bpm)	70.1 ± 6.8	61–85
Low HR > 329 days (bpm)	66.4 ± 8.7	52–81
High HR (bpm)	92.9 ± 11.0	56–118
HR range (bpm)	16.7 ± 10.0	1–40
Mean HR (bpm)	74.6 ± 7.4	53.8–87.8
Aortic diameter		
Ascending aorta (mm)	22.8 ± 2.2	18–27
Thoracic width		
At diaphragm (cm)	18.4 ± 1.2	16.2–21.3
Fetal breathing		
Presence and rhythm	Present and rhythmic	
Fetal activity		
(0–3)	1.6 ± 0.6	1–3
Fetal tone		
Presence	Present	
Fetal fluids		
Allantoic fluid		
Maximal depth (cm)	13.4 ± 4.4	5.5–22.7
Quality (0–3)	1.41 ± 0.7	0–3
Amniotic fluid		
Maximal depth (cm)	7.9 ± 3.5	2–14.3
Quality (0–3)	1.6 ± 0.6	1–3
Uteroplacental thickness		
Maximal thickness (mm)	11.5 ± 2.4	6–16
Minimal thickness (mm)	7.1 ± 1.6	4–11
Uteroplacental contact		
Vessels	Small uterine and placental vessels imaged	
Continuity	Rare small areas of discontinuity	

*SD, Standard deviation.

the uterus and move around the uterus secondary to fetal movement.

The amnion closely adheres to the fetus in most areas, with the largest pocket of amniotic fluid present around the junction of the foreleg and neck with the thorax (see Figs. 9-4 and 9-9). This site is normally most productive for obtaining amniotic fluid for cytologic examination or culture and sensitivity testing using ultrasonographic guidance. An allantoic fluid sample can also be safely obtained at this location. The amounts of amniotic and allantoic fluids that surround the fetus are important indicators of fetal well-being. The quantities of fetal fluids present are the result of an equilibrium between the fluids that are produced, primarily in the fetal kidney and lung, and those removed by swallowing.[43] These maximal vertical fluid pocket depths vary from 0 cm of amniotic and/or allantoic fluid around the fetal rump to a maximum of 7.9 ± 3.5 cm for amniotic and 13.4 ± 4.4 cm for allantoic fluid (Table 9-1).[36]

The uterus should be thoroughly scanned to be sure that only a single fetus is present. The fetus may be detected in any position within the uterus but is usually found in a cranial (anterior) presentation, dorsopubic position.[33, 36, 37, 56, 57] After the ninth month, the fetus is usually positioned within the uterus as if for delivery and rarely changes position within the uterus from this time onward. The fetal head is infrequently imaged from the floor of the ventral abdomen (Fig. 9-14) unless the scan

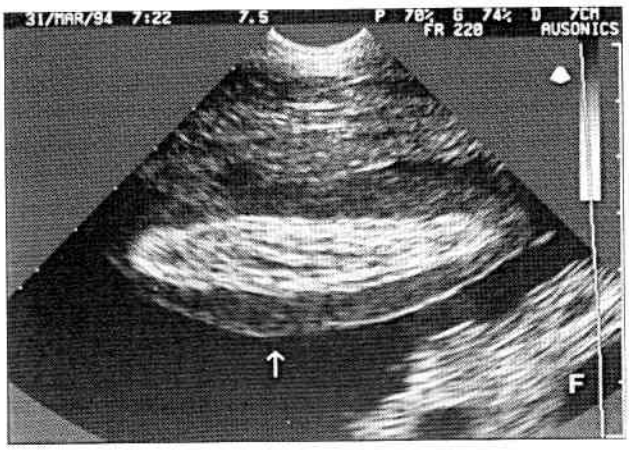

Figure 9–13
Sonogram of a hippomane *(arrow)* obtained from a 12-year-old Thoroughbred mare at 350 days of gestation (same mare as in Figure 9-6 and 9-9). Notice the central echogenic area of the hippomane and the outer hypoechoic region. The hippomane is resting on the chorioallantois surrounded by allantoic fluid. A portion of the fetus (F) is visible on the right lower edge of the image. This sonogram was obtained with a 7.5-MHz sector-scanner transducer at a displayed depth of 7 cm. The mare's ventral abdomen is at the top of the sonogram.

is done early in gestation. In late gestation, the fetal head is usually positioned near the mare's pelvis and is best scanned transrectally, if measurements of orbital diameters are needed, unless the head can be imaged from the transcutaneous approach.[18] The detection of the fetal head along the mare's caudal ventral abdomen in late gestation should alert the clinician to the possibility of a dystocia. The fetal neck is also usually imaged from the ventral abdomen and from the transrectal approach. The fetal thorax is a triangular structure containing the fetal

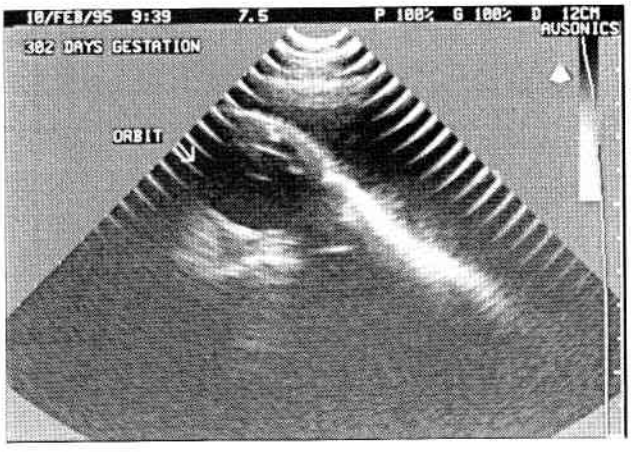

Figure 9–14
Sonogram of the fetal head and orbit *(arrow)* obtained from a 15-year-old American Saddlebred mare at 302 days of gestation (same mare as in Figure 9-3). The thin echogenic line represents the anterior and posterior capsule of the lens. This fetus was in a cranial (anterior) presentation, lying on its left side with the head positioned in front of the udder on the left side of the mare's abdomen. This sonogram was obtained with a 7.5-MHz sector-scanner transducer at a displayed depth of 12 cm. The mare's ventral abdomen is at the top of the sonogram. The concentric echogenic lines present on both sides of the sonogram are artifacts from poor skin contact.

heart at the cranial and narrowest aspect of the thorax, with lungs, diaphragm, and liver visualized within a cranial to caudal direction. Acoustic shadowing is detected from the vertebral bodies and from the ribs, making identification of the thorax easier (see Figs. 9-6 and 9-8). However, the rib shadows or shadowing from any of the bony skeleton may make visualization of the fetal heart in a particular scan plane difficult and force the examiner to change scan-plane orientation or to wait for fetal movement. In the cranial abdomen the liver and stomach are easily visualized with fluid normally detected in the fetal stomach (see Fig. 9-7). The spleen, both kidneys, and bladder are usually also visible ultrasonographically in their normal anatomic position. The umbilical cord is not usually imaged from the mare's ventral abdomen owing to its dorsal attachment. Occasionally the umbilical cord is imaged from the abdominal window (Fig. 9-15), usually when the fetus is lying on its side or in a twin pregnancy. The limbs are visible in multiple different positions and different scan planes and are rarely imaged in their entirety in one scan plane.

The fetal thorax is an important area of the fetus to locate for determination of fetal heart rate (at rest and during and after exercise), cardiac rhythm, aortic diameter, and fetal breathing. These assessments are important indicators of fetal well-being (heart rate, rhythm, and breathing movements) and fetal size (aortic diameter). Four chambers and two great vessels should be recognized in the fetal heart, with a heartbeat detectable from 25 days on. The normal anatomic relationship of the cardiac valves, chambers, and great vessels should be present. The normal fetal cardiac rhythm is sinus and should be evaluated at rest and during and after activity.[36, 37, 58, 59] Fetal heart rates are related to gestational age and fetal activity. The lowest resting heart rate of the equine fetus decreases as gestational age increases.[5, 60-64] A baseline mean resting fetal heart rate of 75 ± 7[36] or 76 ± 8 beats/minute[64] has been found in two studies of normal fetuses from mares in late gestation using fetal echocardiography (Table 9-1). Similar fetal heart rates have been found in studies using fetal electrocardiography.[60, 63, 65-67] Slightly higher heart rates have been found in Percheron[7] and pony fetuses in late gestation with fetal electrocardiography.[60, 63] Fetal movement normally results in heart rate accelerations, which can be detected with fetal electrocardiography,[60] transcutaneous Doppler fetal heart rate monitoring from the ventral abdominal window,[5, 33] and fetal echocardiography.[36, 37] The rapid motion of the normal fetus makes it difficult to obtain a fetal heart rate measurement without the use of M-mode echocardiography, as the fetus is rarely still for 10 to 15 seconds while the thorax is being imaged. Transcutaneous Doppler fetal heart rate monitoring is superior because fetal heart rates can be recorded along with fetal movement. However, many of these systems designed for humans are difficult to adapt to the large abdominal size of the pregnant mare. Cardiac accelerations of 25 to 40 beats/minute for approximately 30 seconds in duration have been reported in association with fetal movement using transcutaneous Doppler fetal heart rate monitoring.[5, 34] These cardiac accelerations occur frequently (average of 10 cardiac accelerations in 10 minutes) and rarely (5%) occur without fetal motion. Cardiac accelerations in response to fetal activity are an indication of fetal well-being in humans and horses.[33, 68, 69] With transcutaneous fetal ultrasonography, a mean heart rate range of 15 ± 10 beats/minute was found between resting and postexercise heart rates,[36] whereas physiologic variations in fetal heart rates of 7 to 15 beats/minute were reported with transcutaneous Doppler fetal heart rate monitoring.[33] Exaggerated fetal heart rate responses have been observed with transcutaneous Doppler fetal heart rate monitoring[4, 33] and fetal electrocardiography[62] 2 to 3 days prior to parturition.

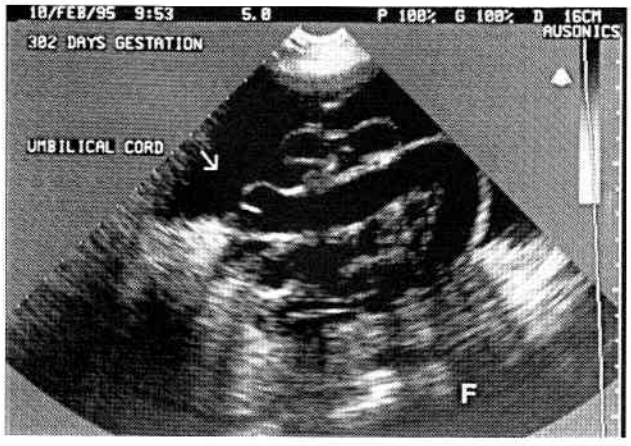

Figure 9–15

Sonogram of the umbilical cord obtained from a 15-year-old American Saddlebred mare at 302 days of gestation (same mare as in Figures 9-3 and 9-14). The anechoic umbilical vessels *(arrow)* are coiled ventral to the fetus (F). This fetus was in a cranial (anterior) presentation lying on its left side. This sonogram was obtained with a 5.0-MHz sector-scanner transducer and a displayed depth of 16 cm. The mare's ventral abdomen is at the top of the sonogram.

Normal equine fetuses are very active during the scan and are rarely quiet or imaged in the same place for longer than 5 minutes at one time. Ultrasound studies of the equine fetus have shown that the equine fetus has an average of nine simple, singular movements in 10 minutes beginning in the fifth month of gestation. These simple, singular movements decrease in frequency during the last quarter of gestation, when complex fetal movements become more common, averaging 20 per hour in the 330-day fetus.[4] Complex movements occur less regularly than simple movements. Most dormant periods in the late-gestation equine fetus are 10 minutes or less but occasionally last 30 to 60 minutes or longer. The equine fetus should have normal muscular tone during these dormant periods and should not appear flaccid.[36] Therefore, long periods of fetal inactivity during transcutaneous fetal ultrasonography should prompt re-examination, as the equine fetus appears to spend less time sleeping or resting than does the human fetus.

The fetal lungs are not aerated and resemble liver, with the normal branching of the pulmonary vasculature visible. The diaphragm should be identified between the fetal lung and liver, and regular thoracic excursions and diaphragmatic movements (normal breathing movements) should be detected in all late-gestation fetuses. The rib cage can also be detected expanding with respira-

tory movements.[20, 36] The gestational age when rhythmic breathing movements normally begin has not yet been determined for the equine fetus.

Fetal aortic diameter is correlated with neonatal foal weight[33, 34, 36, 37] and maternal weight.[36] Maternal weight can be used to accurately predict fetal aortic diameter and therefore estimate fetal weight and maturity.[33, 36] Fetal aortic diameter can be predicted from the regression equation (Y = 0.00912*X + 12.46), where Y = predicted fetal aortic diameter (mm) and X = pregnant mare's weight in pounds.[37] The maximal thoracic diameter is also an indication of fetal size. The normal maximal thoracic diameter of a late-gestation foal is 18.4 ± 1.2 cm (Table 9-1).[37] Foal girth measurements and hip height have also been correlated with fetal aortic diameter measurements.[34] Fetal size that is normal for gestational age is one indication of normal intrauterine conditions.[33, 34, 36, 37]

Twins

The detection of twin fetuses is abnormal and usually results in the abortion or premature birth of one or both fetuses in mid to late gestation. Rarely are twin foals born alive at term and, if they are, they are often small and dysmature. With rare exception, the detection of twin pregnancies can be successfully performed by the experienced ultrasonologist at all stages of pregnancy. In early pregnancy the detection of twin embryonic vesicles can be readily performed transrectally (see Chapter 8). If twin pregnancies could not be successfully eliminated transrectally early in gestation, twin elimination can be performed transcutaneously by injection of KCl into the heart of the smaller and less active twin (Fig. 9-16).[51, 52] Twin elimination by the intracardiac injection of KCl has been performed from 66 to 168 days of gestation.[51] This procedure, performed by an experienced veterinary ultrasonologist, results in 40–50% of mares carrying a single healthy foal to term if performed at or after 115 days; the remaining mares usually abort both fetuses. Part of the selection for this procedure involves ultrasonographically assessing fetal well-being by evaluating fetal size, movement, heart rate, and cardiac rhythm to choose the larger and more active fetus as the designated survivor and injecting the smaller, less active twin.[25, 51, 52] The selection of the site for twin elimination should be performed after adequate sedation of the mare. The sedation also quiets the fetuses and results in the fetuses sliding cranially in the abdomen into a more accessible position. A surgical preparation is performed at the abdominal site selected for twin elimination (usually cranial to the mare's flank fold) after a local block is performed. An 18- or 20-gauge disposable 6-inch spinal needle is used for piercing the thorax of the fetus selected for elimination. This procedure is usually best performed under ultrasonographic guidance with a biopsy guide (Fig. 9-17), but a free-hand ultrasound-guided thoracic puncture can also be performed by the experienced ultrasonologist. The needle is guided through the abdominal and uterine wall of the mare, and then the fetal thorax is penetrated with a quick, sharp advancement of the needle. After a flashback of blood is obtained, an intracardiac injection of approximately 4 ml of sterile KCl (2 mEq/ml) is administered within the heart. If the heart cannot be successfully punctured, a slightly larger volume of KCl can be administered intrathoracically. A rapid slowing of the heart rate and arrhythmias are detected with a successful intracardiac puncture. Complete cessation of cardiac motion should be determined in the twin selected for elimination (Fig. 9-17) before terminating the procedure and confirmed at follow-up examination of the surviving twin. After successful twin elimination, the opposite twin should be re-evaluated for evidence of fetal distress (Fig. 9-16). Flunixin meglumine and progesterone should be

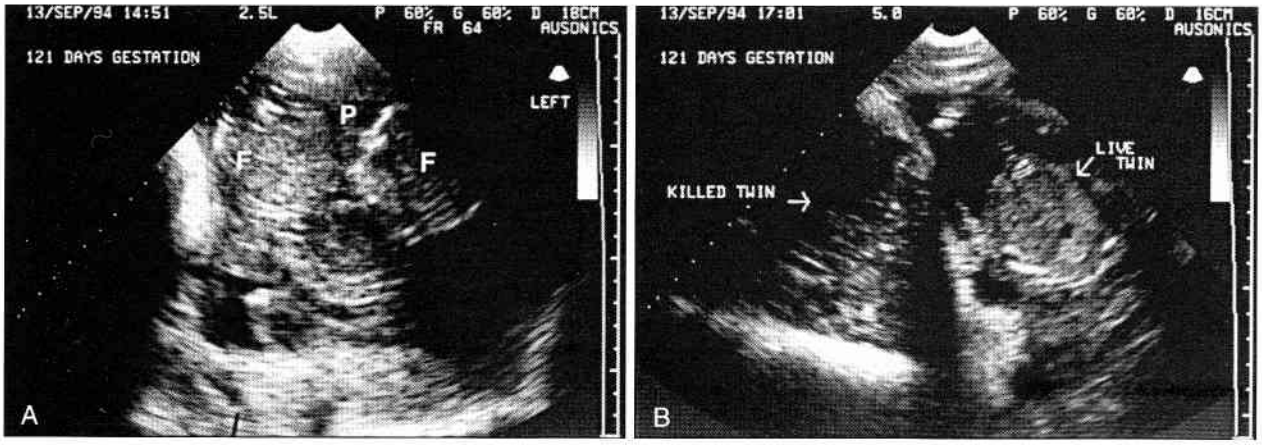

Figure 9–16

Sonograms of twins obtained from a 22-year-old Thoroughbred mare at 121 days gestation.

A, The two fetuses (F) are divided by the adjoining placentas (P). The left fetus was slightly smaller and less active, had a lower heart rate, and therefore was selected for elimination. This sonogram was obtained with a 2.5-MHz sector-scanner transducer at a displayed depth of 18 cm. The mare's ventral abdomen is at the top of the sonogram.

B, An intrathoracic injection of 8 mEq of KCl was administered to the left fetus, resulting in fetal demise. At the time of death the fetal fluids surrounding the left fetus became echogenic and flocculent, associated with the probable expulsion of urine and meconium into the fluids surrounding the fetus. The right twin remained active and surrounded by anechoic fetal fluids. This sonogram was obtained with a 5.0-MHz sector-scanner transducer at a displayed depth of 16 cm.

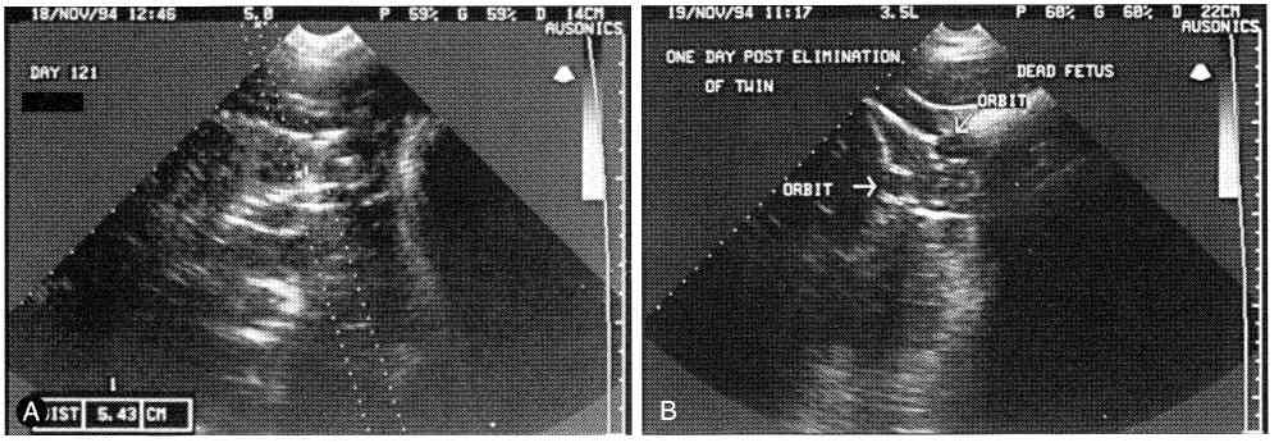

Figure 9–17

Sonograms of one of a pair of twin fetuses obtained from a 13-year-old Arabian mare at day 121 of gestation. These sonograms were obtained with a 5.0-MHz (*A*) and 3.5-MHz (*B*) sector-scanner transducer and a displayed depth of 14 cm (*A*) and 22 cm (*B*).

A, This twin fetus was selected for elimination because it was smaller than the surviving twin. The biopsy guide markers (2 parallel dotted lines) are centered over the fetal heart on this sonogram. The fetal heart was 5.43 cm (x') from the mare's ventral abdomen. The spinal needle was then aseptically advanced through the biopsy guide into the fetal heart after a local block and sterile preparation of the ventral abdomen had been performed.

B, This sonogram of the dead twin was obtained one day after elimination of this twin by an intracardiac injection of KCl. The head of the fetus is clearly visible and was folded over the fetal body.

administered immediately following this procedure and for several days or more thereafter.

Twins may also be detected later in gestation when the twin elimination procedure is no longer an option. Often these mares present at 7 to 8 months of gestation because their abdomens are larger than normal for this stage of gestation or they are bagging up and/or lactating. A thorough evaluation of the uterus at this stage may reveal two live fetuses or one (Fig. 9–18) or two (less likely) dead fetuses (Fig. 9–19). The dead fetus often appears folded on itself (Figs. 9–18 and 9–19). The approximate size of each fetus should be determined and the fetuses evaluated for indications of fetal distress. The intrauterine environment should also be carefully evaluated, and follow-up transabdominal ultrasonographic examinations are usually indicated to monitor fetal well-being. Areas of placental thickening and placental separation have developed during late gestation in mares in which one twin died at 7 to 9 months (Fig. 9–20). Orientation of both fetuses is important to determine because one fetus is often in a caudal (posterior) presentation. Dystocia is possible with this presentation, although the malpresented fetus is usually small and may be delivered without incident. As these are high-risk pregnancies, transporting the mare to a facility equipped to handle high-risk neonates should be considered.

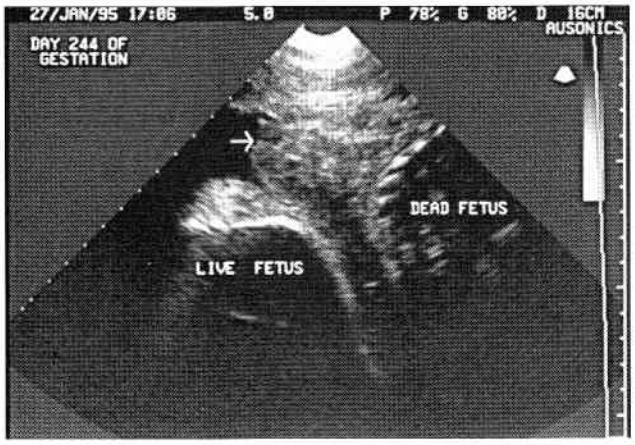

Figure 9–18

Sonogram of twins obtained from a 9-year-old Thoroughbred mare at 244 days of gestation (same mare as in Figure 9–5). The dead fetus is surrounded by very echogenic fetal fluids *(arrow)*, and the live fetus is surrounded by anechoic fluid. The live fetus was small for gestational age but had a relatively normal heart rate and no other indications of fetal distress. The dead fetus was much smaller than the surviving twin and was folded on itself, with the head and neck overlying the thorax. This sonogram was obtained with a 5.0-MHz sector-scanner transducer at a displayed depth of 16 cm. The mare's ventral abdomen is at the top of the sonogram.

Fetal Abnormalities

Aortic diameter is an accurate predictor of fetal size in normal pregnancies[33, 34, 36] and has been shown to be a sensitive indicator of fetuses that are small for gestational age in high-risk pregnancies.[37] A smaller-than-predicted aortic diameter (< predicted − 4 (SE) [= 5.038]) indicates the presence of twins (Fig. 9–21) or a small or growth-retarded fetus (Fig. 9–22). Smaller-than-predicted fetal size is an indication of the birth of a small-for-gestational-age, growth-retarded, or dysmature foal(s).[31, 37] A small-for-gestational-age foal may be produced whenever intrauterine conditions are unfavorable for a prolonged period of time.[37] Maximal fetal thoracic diameter is also significantly correlated with fetal aortic diameter and neonatal foal weight in high-risk pregnancies (Fig. 9–23).[37] Although measurements of fetal aortic diameter and maximal thoracic diameter are frequently used to predict small-for-gestational-age equine fetuses in high-risk pregnancies, these measurements would also be use-

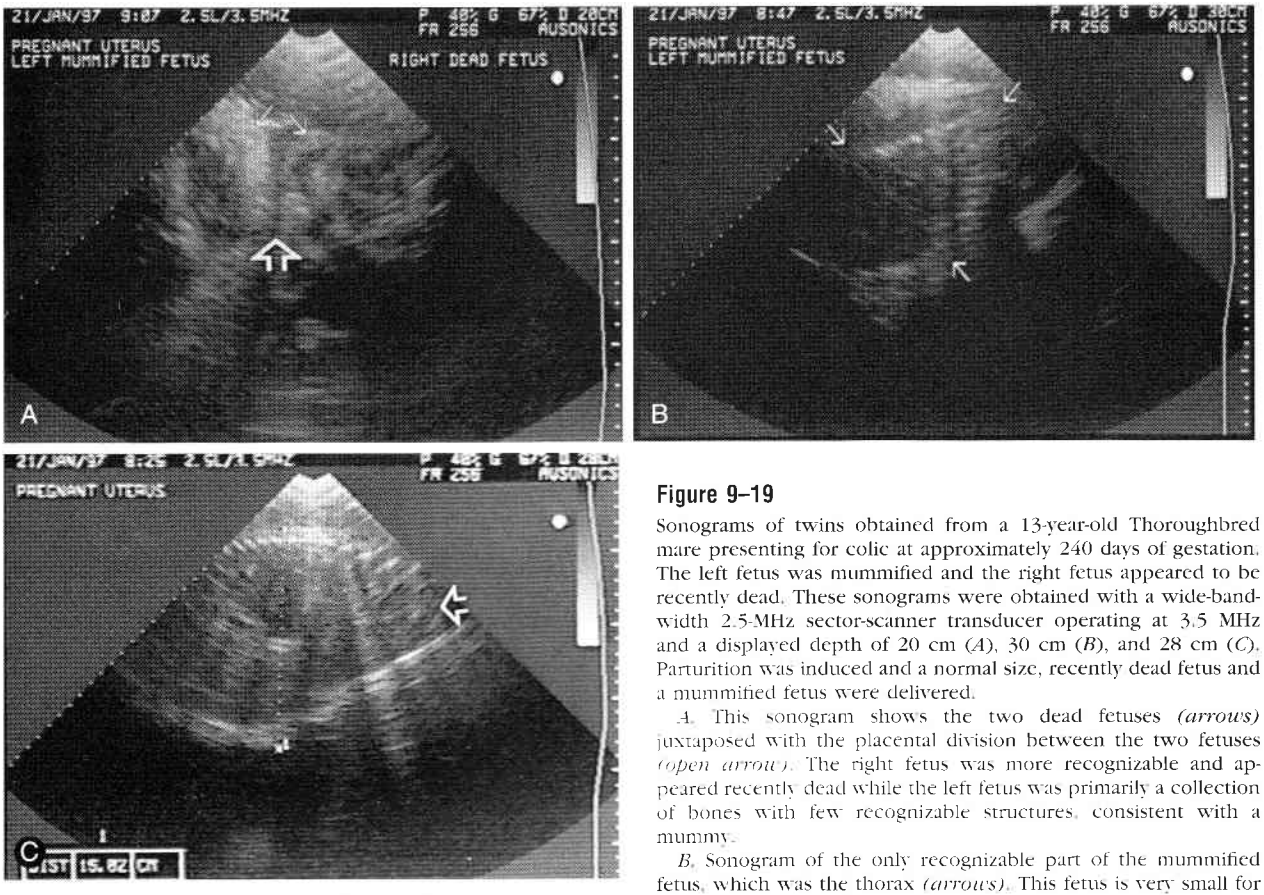

Figure 9–19

Sonograms of twins obtained from a 13-year-old Thoroughbred mare presenting for colic at approximately 240 days of gestation. The left fetus was mummified and the right fetus appeared to be recently dead. These sonograms were obtained with a wide-bandwidth 2.5-MHz sector-scanner transducer operating at 3.5 MHz and a displayed depth of 20 cm (*A*), 30 cm (*B*), and 28 cm (*C*). Parturition was induced and a normal size, recently dead fetus and a mummified fetus were delivered.

A, This sonogram shows the two dead fetuses *(arrows)* juxtaposed with the placental division between the two fetuses *(open arrow)*. The right fetus was more recognizable and appeared recently dead while the left fetus was primarily a collection of bones with few recognizable structures, consistent with a mummy.

B, Sonogram of the only recognizable part of the mummified fetus, which was the thorax *(arrows)*. This fetus is very small for a gestational age of approximately 240 days. None of the remaining portions of the mummified fetus had identifiable anatomic structures.

C, Sonogram of the recently dead fetus demonstrating the thorax (right side) and abdomen (left side). The cardiac structures *(open arrow)* are barely recognizable in the cranial portion of the thorax of the right (recently dead) fetus. This fetus is in a caudal (posterior) presentation and is nearly normal size for its gestational age.

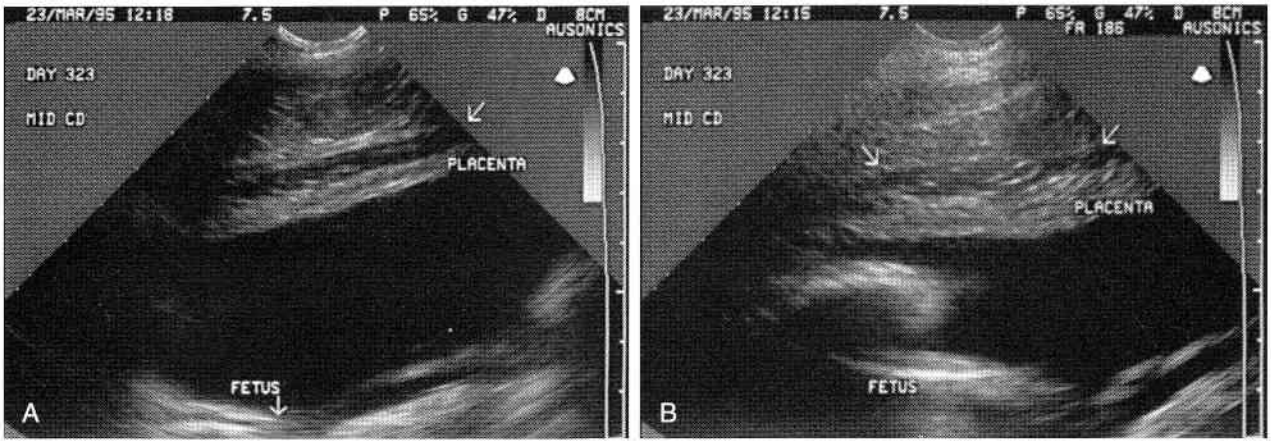

Figure 9–20

Sonograms of the uteroplacental unit obtained from a 13-year-old Thoroughbred mare (same mare as in Figures 9-5 and 9-18) with twins (one twin had died at approximately 244 days). The mare is now at 323 days of gestation and has developed areas of uteroplacental separation *(A)* and thickening of the uteroplacental unit *(B)*, although the fetus is active and shows no signs of fetal distress other than being small for its gestational age. These sonograms were obtained with a 7.5-MHz sector-scanner transducer operating at 10.0 MHz and a displayed depth of 8 cm. The mare was again placed on broad-spectrum antimicrobials and progesterone and maintained the pregnancy until term; however, the live twin, which was very small and weak, did not survive.

A, The anechoic area of uteroplacental separation *(arrow)* is new since the sonogram one month earlier but is localized to the mid portion of the caudal abdomen.

B, Thickening of the chorioallantois is developing in and around the areas of uteroplacental separation *(arrows)*, and the entire uteroplacental unit now exceeds 1.8 cm in thickness.

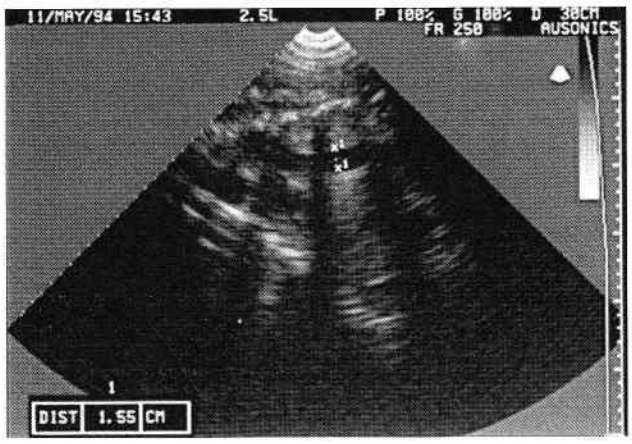

Figure 9–21

Sonogram of a smaller-than-predicted fetal aorta from a twin fetus obtained from an 8-year-old Thoroughbred mare at 314 days of gestation. This twin was the smaller of the two, with a fetal aortic diameter of 1.55 cm. This fetus is in a cranial (anterior) presentation, with the fetal thorax on the left of the sonogram and the fetal abdomen on the right. This sonogram was obtained with a 2.5-MHz sector-scanner transducer at a displayed depth of 30 cm. The mare's ventral abdomen is at the top of the sonogram.

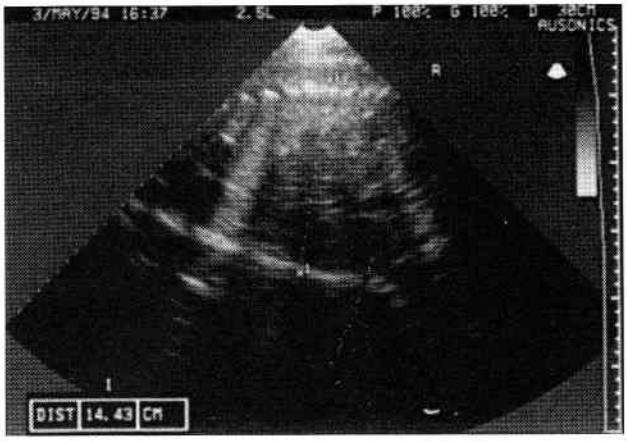

Figure 9–23

Sonogram of a small fetal thorax from the twin fetus in Figure 9-21 obtained from an 8-year-old Thoroughbred mare at 306 days of gestation. Notice the small thoracic diameter of 14.43 cm. This twin was the smaller of the two fetuses. This fetus is in a cranial (anterior) presentation, with the fetal thorax on the left side of the sonogram and the fetal abdomen on the right. This sonogram was obtained with a 2.5-MHz sector-scanner transducer at a displayed depth of 30 cm. The mare's ventral abdomen is at the top of the sonogram.

ful in predicting an unusually large fetus, (< predicted + 4 (SE) [= 5.038]), which might result in a dystocia.

Fetal heart rate and rhythm abnormalities are indications of fetal distress. Significant bradycardia (Fig. 9-24) and lack of normal heart rate variations suggest CNS depression, usually due to hypoxia. Normal heart rate variations occur in response to fetal activity and environmental changes. Heart rate varies with gestational age and normally slows as the fetus nears term. Fetal heart rates obtained with transcutaneous ultrasonography averaged 70 beats/minute in fetuses less than 330 days' gestational age and 66 beats/minute in fetuses 330 days and older (Table 9-1).[36] Significant bradycardia has been associated with a poor outcome in pregnant mares at all stages of gestation.[33, 34, 37, 51, 60] The actual heart rate below which the ultrasonologist should be concerned about fetal well-being varies with the gestational age of the fetus, dropping as the fetus approaches term. Heart rates less than 57 beats/minute are considered abnormal in a late-term fetus if the fetus is less than 330 days' gesta-

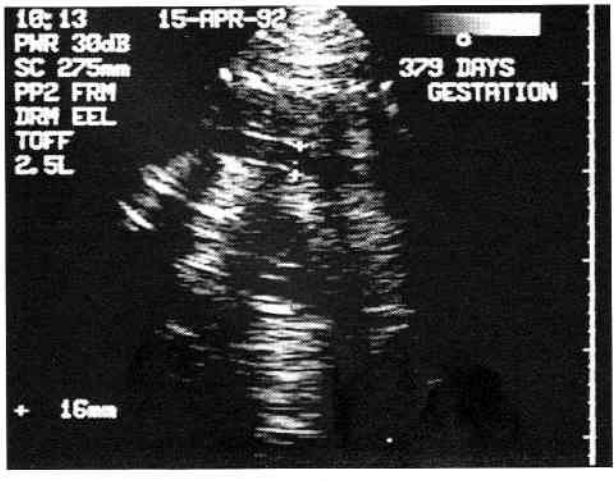

Figure 9–22

Sonogram of a smaller-than-predicted fetal aorta from a fetus with intrauterine growth retardation obtained from a 13-year-old Thoroughbred mare with a prolonged gestation at 379 days of gestation. Notice the small fetal aortic diameter of 1.6 cm. This fetus is in a cranial (anterior) presentation, with the fetal thorax on the left side of the sonogram and the fetal abdomen on the right. This sonogram was obtained with a 2.5-MHz sector-scanner transducer at a displayed depth of 27.5 cm. The mare's ventral abdomen is at the top of the sonogram.

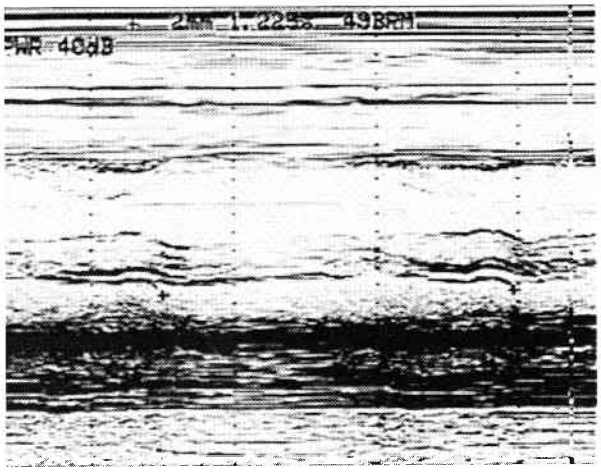

Figure 9–24

M-mode echocardiogram of the fetal heart obtained from a 20-year-old Standardbred mare at 341 days of gestation. The mare had colic surgery for repair of a ruptured branch of the middle uterine artery 2 months earlier. The cursors are positioned at the same place in the cardiac cycle on the right side of the interventricular septum to measure instantaneous heart rate. Notice the very slow fetal heart rate of 49 beats/minute. This fetus was born 4 days after this sonogram was obtained. The foal was weak and dysmature and took a long time to suckle. This M-mode echocardiogram was obtained with a 2.5-MHz sector-scanner transducer at a displayed depth of 27.5 cm. The mare's ventral abdomen is at the top of the sonogram.

Table 9–2
Equine Biophysical Profile

Fetal or Maternal Measurement	Normal (2)	Abnormal (0)
Fetal heart rate (HR) and rhythm		
Rhythm	Regular (sinus)	Irregular or abnormal
Lowest resting HR < 330 days gestation (bpm)	57	< 57
Lowest resting HR > 329 days gestation (bpm)	50	< 50
High (postactivity) HR (bpm)	104	> 104
HR range (bpm)	1.1–38.4	> 38.4
Fetal aortic diameter		
Y = 0.00912*X + 12.46	Y + 4*SE(5.038)	> or < Y ± 4*SE(5.038)
Fetal activity		
(0–3)	1–3	0
Fetal fluids		
Maximal allantoic fluid depth (cm)	4.7–22.1	< 4.7 or > 22.1
Maximal amniotic fluid depth (cm)	0.8–14.9	< 0.8 or > 14.9
Uteroplacental thickness (mm)	7–20	< 7 or > 20
Uteroplacental contact		
Areas of discontinuity	None or small	Large

Y = predicted aortic diameter; X = pregnant mare's weight in lbs;
* = multiplied by; SE = standard error.

tional age, and less than 50 beats/minute if the fetus is greater than 329 days' gestational age (Table 9-2).[37] Fetal bradycardia may be the most reliable indicator of impending fetal demise.[37, 51, 60] The absence or disappearance of a fetal heart beat associated with fetal death has been detected with fetal electrocardiography and transcutaneous ultrasonography.[51, 62] Transcutaneous ultrasonography is useful in the identification of a dead fetus, as the fetus has no cardiac activity (Fig. 9-25; see also Fig. 9-18).[37] Postactivity (high) heart rates greater than 104 beats/minute are also an indication of fetal distress in the late-term fetus. Marked elevations of fetal heart rate (Fig. 9-26) or a high heart rate range indicates fetal stress and has been documented in several fetuses that were aborted or born dead and during parturition.[37, 58, 60] Cardiac arrhythmias are another indication of fetal distress. Abnormalities of fetal cardiac rhythm have been detected with fetal echocardiography and have been associated with a negative outcome (Fig. 9-27).[33] Arrhythmias have also been reported with fetal electrocardiography immediately prior to, during, and after parturition.[37, 60, 62] The absence of fetal breathing movements in the late-gestation fetus is also an indication of fetal distress and a

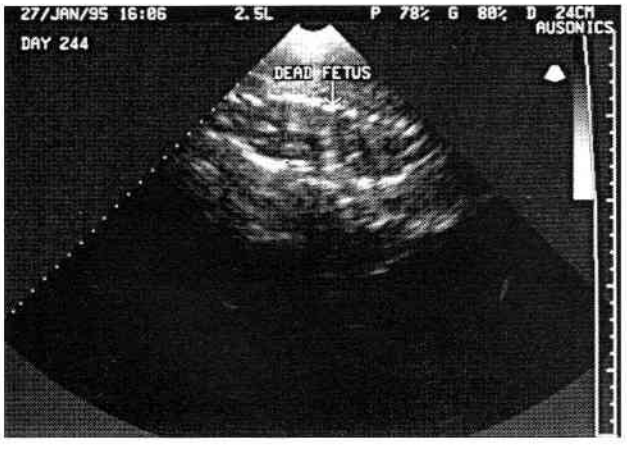

Figure 9–25
Sonogram of a dead fetus obtained from a 9-year-old Thoroughbred mare at 244 days gestation (same mare as in Figures 9-5 and 9-18). The very small fetus lacked any cardiac motion or movement during the examination. The fetal thorax is to the right side of the sonogram, and the abdomen to the left. This fetus was in a caudal (posterior) presentation. This sonogram was obtained with a 2.5-MHz sector-scanner transducer at a displayed depth of 24 cm. The mare's ventral abdomen is at the top of the sonogram.

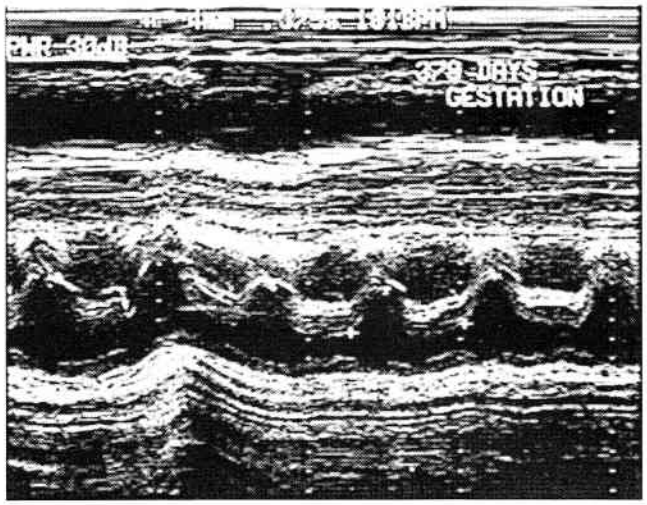

Figure 9–26
M-mode echocardiogram of the fetal heart obtained from a 13-year-old Thoroughbred mare with a prolonged gestation of 379 days (same mare as in Figure 9-22). The fetus had intrauterine growth retardation, and the foal was very small for its gestational age at birth. Notice the rapid heart rate of 161 beats/minute, with a fairly regular rhythm obtained during slight fetal movement. This sonogram was obtained with a 2.5-MHz sector-scanner transducer at a displayed depth of 27.5 cm. The mare's ventral abdomen is at the top of the sonogram.

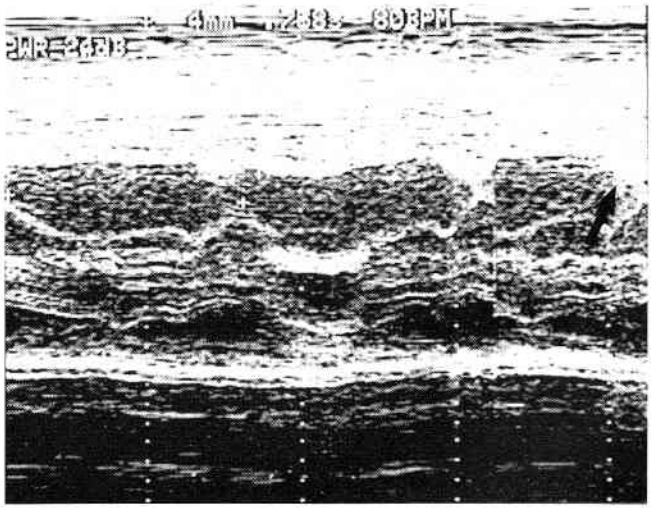

Figure 9–27
M-mode echocardiogram of the fetal heart obtained from an 18-year-old Standardbred mare at 312 days of gestation. Notice the irregular fetal heart rhythm, with a beat detected earlier than normal *(arrow)*. The fetal heart rate preceding the premature beat was regular at 80 beats/minute. This echocardiogram was obtained with a 2.5-MHz sector-scanner transducer and a displayed depth of 27.5 cm. The mare's ventral abdomen is at the top of the sonogram.

sensitive indicator of acute hypoxia in the human fetus.[37] Absence of fetal breathing has been associated with a negative outcome in equine fetuses.[37]

The lack of fetal movement and the absence of fetal tone are also indicators of fetal distress, central nervous system depression, and advancing hypoxia and have been associated with a negative outcome.[33-35, 37] The lack of fetal movement and absence of fetal tone indicate impending fetal demise, but a depressed, distressed, or sleeping fetus may also be quiet and immobile. Therefore, observation of the beating fetal heart is critical for determining fetal viability. The dormant periods in late-gestation equine fetuses are usually less than 10 minutes in duration, but 30- to 60-minute or longer dormant periods have been reported.[4] In my experience, the normal equine fetus is usually active throughout the majority of the transcutaneous ultrasonographic examination. It is often difficult to obtain a fetal heart rate with M-mode echocardiography owing to the continual movement of the fetus during the examination. Therefore, any prolonged period of fetal inactivity should prompt an ultrasonographic re-examination.

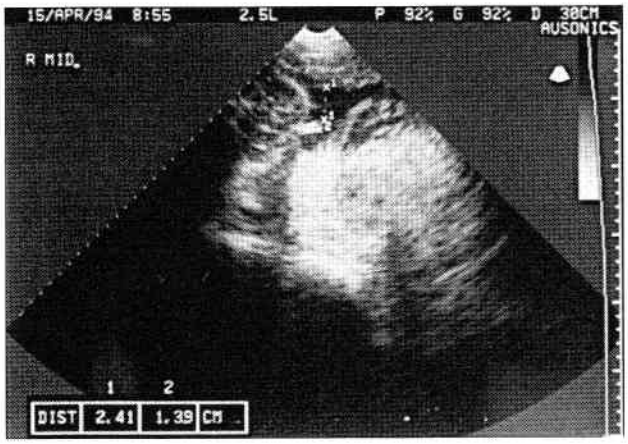

Figure 9–28

Sonogram of the fetal fluids obtained from an 8-year-old Appaloosa mare at 304 days of gestation. Notice the decreased maximal vertical fluid depth (x^1) of allantoic fluid (2.41 cm) between the fetal forearm and thorax, the only site at which any amniotic or allantoic fluid was imaged. The maximal vertical fluid depth (x^2) of amniotic fluid was 1.39 cm. This fetus was in a cranial (anterior) presentation, with the fetal forearm on the left side of the sonogram and the fetal thorax on the right. This sonogram was obtained with a 2.5-MHz sector-scanner transducer at a displayed depth of 30 cm. The mare's ventral abdomen is at the top of the sonogram.

Uterine and Placental Abnormalities

Abnormal quantities of allantoic or amniotic fluid are indications of fetal or maternal problems. Decreased fetal fluid quantity usually occurs from decreased fetal urine production in the human fetus and is a good indicator of hypoxia experienced chronically by the fetus.[43] Decreased fetal fluid quantity can also occur from the rupture of placental membranes.[37] Fluid quantities should be considered decreased if the maximal vertical amniotic fluid depth is less than 0.8 cm and the maximal vertical allantoic fluid depth is less than 4.7 cm (Table 9-2).[36, 37] Decreased fetal fluid quantities are an indication of fetal distress and are associated with a negative outcome in human beings and horses (Fig. 9-28).[37] Problems with fetal blood flow can occur as a result of umbilical cord compression when the lack of fetal fluids is severe. Folding of the fetal membranes and umbilical cord against the fetus is an indication of a severe lack of fetal fluids (Fig. 9-29). In human beings, intrauterine growth retardation and a poor perinatal outcome are associated with decreased amniotic fluid quantities and chronic hypoxia.[38, 40, 44] The majority of equine fetuses with decreased allantoic and/or amniotic fluid quantities are abnormal at birth.[37] Increased fetal fluid volumes are also abnormal (Fig. 9-30) and have been associated with a negative outcome in human beings and in two mares with hydrops amnii.[34, 39, 70] Both equine fetuses with hydrops amnii had severe bradycardia for their stage of gestation.[34, 70] Fetal fluid quantities should be considered increased if the maximal vertical amniotic fluid depth exceeds 14.9 cm or the maximal vertical allantoic fluid depth exceeds 22.1 cm (Table 9-2).

The quality of the allantoic and amniotic fluids is important to evaluate. Increased echogenicity of the fetal fluids (grade 3) has been associated with a negative outcome (Fig. 9-30).[33, 34, 37] The early detection of echogenic particles in the amniotic or allantoic fluid is an indicator of fetal distress in human and equine fetuses.[33, 34, 71, 72] The early increase in fetal fluid echogenicity may be associated with meconium, infection (inflammatory cellular debris), or blood.[33, 34, 37, 71, 72] The earlier in gestation that echogenic particles are detected, the more significant (abnormal) the finding, as fetal fluids normally increase in echogenicity in late gestation. The increased echogenicity of fetal fluids in late-gestation pregnancies may not be significantly related to outcome.[37] However, increased fetal fluid echogenicity (grade 3) detected ear-

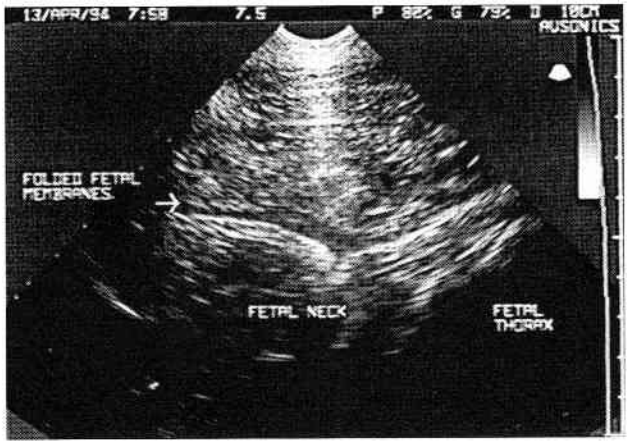

Figure 9–29

Sonogram of the fetal membranes obtained from the 8-year-old Appaloosa mare in Figure 9-28 at 302 days of gestation. The severe folding of all the fetal membranes was a result of the severe lack of fetal fluids. This fetus was in a cranial (anterior) presentation, with the fetal neck on the left side of the sonogram and the fetal thorax on the right. This sonogram was obtained with a 7.5-MHz sector-scanner transducer at a displayed depth of 10 cm. The mare's ventral abdomen is at the top of the sonogram.

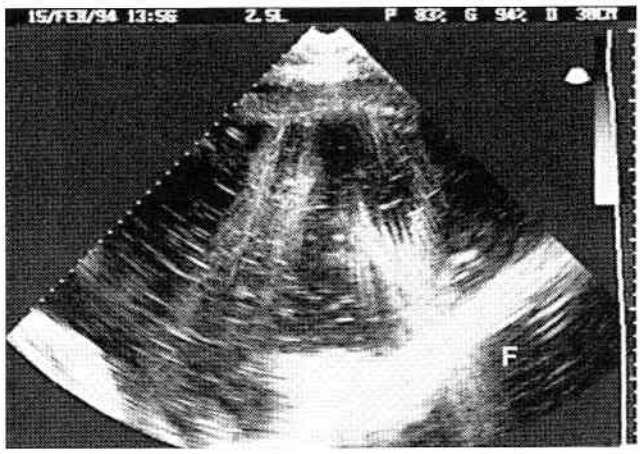

Figure 9–30

Sonogram of an excessive amount of echogenic (grade 3) allantoic fluid obtained from an aged Thoroughbred mare at 328 days of gestation (same mare as in Figure 9-10). Notice the large number of echogenic particles in the allantoic fluid and the excessive amount of allantoic fluid. The maximal allantoic fluid depth measured 23.5 cm. The vertical diagonal echogenic lines crossing the allantoic fluid and the fetus (F) are artifacts. This sonogram was obtained with a 2.5-MHz sector-scanner transducer at a displayed depth of 30 cm. The mare's ventral abdomen is at the top of the sonogram.

lier in gestation or late in gestation, coupled with other abnormal ultrasonographic findings, should be considered an indication of fetal distress (Fig. 9-31).

Increased thickness of the uteroplacental unit in the fetal horn has been associated with a negative outcome and placental abnormalities such as placentitis, placental edema, and premature placental separation.[33, 37] A uteroplacental thickness greater than 2.0 cm in late-gestation equine pregnancies (Fig. 9-32) is considered abnormal and is an indication of placentitis or other placental abnormalities (Table 9-2).[33, 34, 37] A decrease in the echogenicity of the chorioallantois coupled with an increase in its thickness is consistent with placental edema and placentitis (Fig. 9-33). Anechoic areas imaged in the chorioallantois represent fluid spaces, which often appear cystic (Fig. 9-33). Placental calcification in mares (Fig. 9-34) has been associated with the abortion of fetuses and with the delivery of one septic foal with peripartum asphyxia syndrome (Fig. 9-35).[33, 34, 37] Thickening of the amnion is less frequently detected but is also an indication of placentitis or placental edema (Fig. 9-36). Areas of calcification are also infrequently detected in the amnion in mares with a thicker than normal amnion. A "ribbon candy" appearance to the uteroplacental unit in the fetal horn is an indication of premature placental separation and placentitis and usually progresses to more extensive disruption in uteroplacental contact (Fig. 9-37). Any large disruptions in the uteroplacental unit should be carefully monitored with follow-up ultrasonographic examinations, as extensive disruption in the integrity of the uterine and placental contact has been associated with premature placental separation and a negative outcome (Fig. 9-38).[37] Hemorrhage between the uterus and the placenta has been detected in one mare with a uterine tear secondary to a uterine torsion (Fig. 9-39).[37] The foal delivered had peripartum asphyxia syndrome and was septic.[37] An ascending placentitis resulted in marked (7.6 cm) uteroplacental separation in one mare (Fig. 9-40). Heterogeneous fluid separated the chorioallantois from the uterus consistent with exudate and gas. The detection of a thickened uteroplacental unit and/or extensive disruptions in uteroplacental contact has, in every case, proved to be a sensitive and specific finding of an impending negative outcome.[33, 34, 37] The significance of a thinner than normal (less than 0.7 cm) uteroplacental unit is unclear, as 33% of foals delivered to mares with thinner than normal uteroplacental units were abnormal at birth.[37]

Sonographic examination of the ventral abdominal muscles should be carefully performed during the placental evaluation so that defects in the abdominal wall can be detected sonographically in clinically normal mares (Fig. 9-41), before large ventral hernias develop. Defects

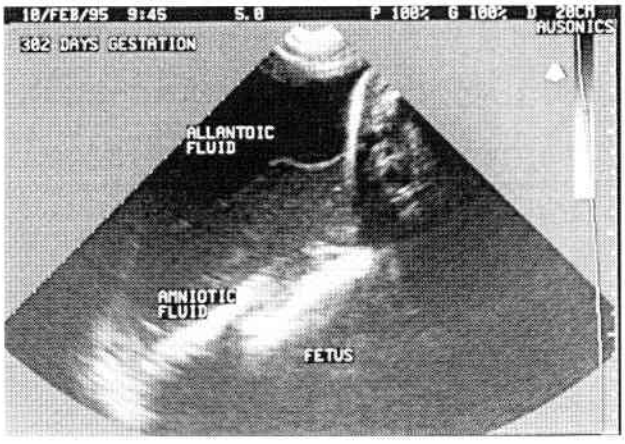

Figure 9–31

Sonogram of echogenic amniotic fluid (grade 3) obtained from a 15-year-old American Saddlebred mare at day 302 of gestation (same mare as in Figures 9-3, 9-14, and 9-15). Notice the cloudy echogenic amniotic fluid and the anechoic allantoic fluid. This sonogram was obtained with a 5.0-MHz sector-scanner transducer at a displayed depth of 20 cm. The mare's ventral abdomen is at the top of the sonogram.

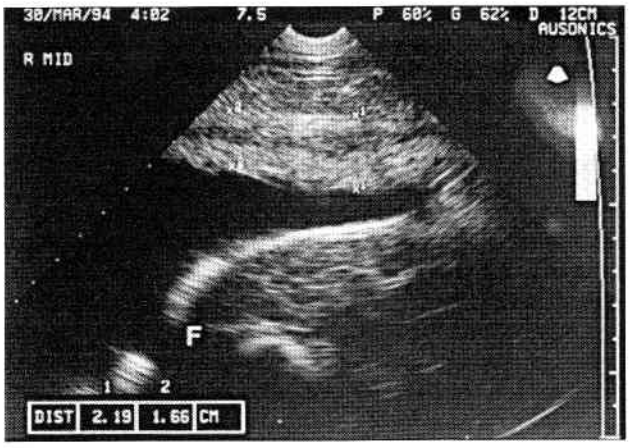

Figure 9–32

Sonogram of the uteroplacental unit obtained from a 16-year-old Thoroughbred mare at 333 days of gestation (same mare as in Figures 9-11 and 9-12). The thickened uteroplacental unit varies from 1.66 (x^2) to 2.19 (x^1) cm. This sonogram was obtained with a 7.5-MHz sector-scanner transducer at a displayed depth of 12 cm. The mare's ventral abdomen is at the top of the sonogram. F, Fetus.

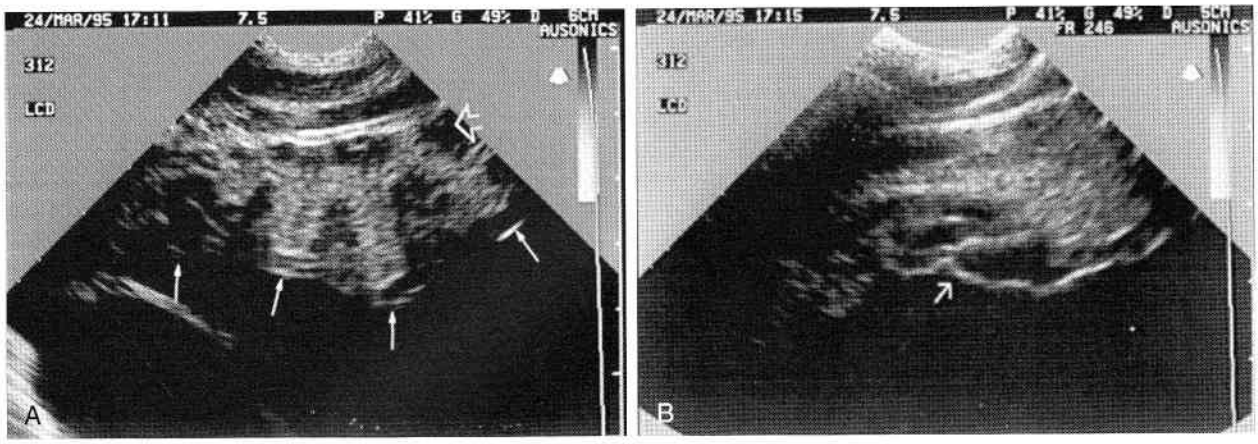

Figure 9–33

Sonograms of uteroplacental unit obtained from a 10-year-old Thoroughbred mare with placentitis and placental edema. These sonograms were obtained with a 7.5-MHz sector-scanner transducer at a displayed depth of 6 cm (*A*) and 5 cm (*B*).

A, The uterus is hyperechoic compared to the adjacent hypoechoic to echogenic chorioallantois. The chorioallantois *(arrows)* is markedly folded with finger-like projections surrounded by more hypoechoic to anechoic fluid and separation is developing between the uterus and the chorioallantois *(open arrow)*.

B, There are numerous anechoic fluid spaces, some of which appear cyst-like, in the edge of the chorioallantois *(arrow)*.

in the ventrolateral wall of the abdomen are most common in pregnant mares and occur more frequently than ruptures of the prepubic tendon.[73-75] Mares with large ventral abdominal hernias or prepubic tendon ruptures present with ventral abdominal swelling.[73-75] With prepubic tendon rupture there is a loss of the proper alignment between the pelvis and the spine, and the mare may have abdominal pain.[75]

BIOPHYSIOLOGIC PROFILE

Work is ongoing concerning the development of a biophysiologic profile for the equine fetus in late gestation (298 days until term). Six variables have been used in the preliminary development of an equine biophysiologic profile that were related to outcome (Table 9-2).[37] These variables are heart rate (lowest, highest, and heart rate range), fetal movement or activity level, fetal aortic diameter, maximal fetal fluid depths (allantoic or amniotic), uteroplacental thickness, and uteroplacental contact.[37] A score of 2 is assigned to each variable if it falls within the normal range and 0 if it falls outside this predetermined range.[37] In a preliminary retrospective study developing the biophysiologic profile, a score of 8 or less was an assurance of an abnormal outcome (dead foal, dysmature foal, or a foal with sepsis or periparturient

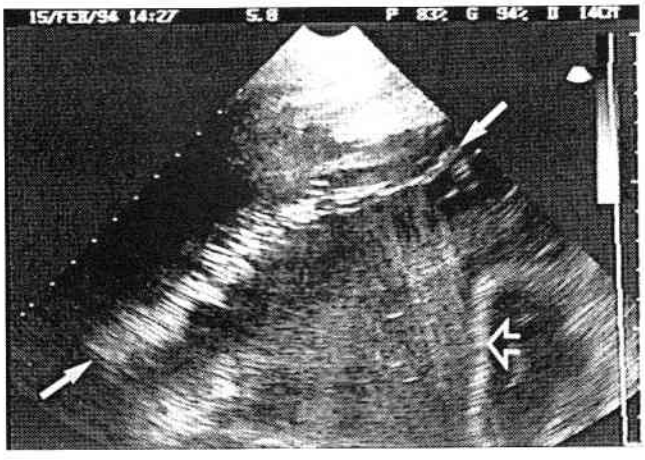

Figure 9–34

Sonogram of hyperechoic areas within the chorioallantois obtained from an aged Thoroughbred mare at 328 days of gestation (same mare as in Figures 9-10 and 9-30). Notice the thick hyperechoic echoes in the chorioallantois suggesting early calcification of the fetal membranes *(arrows)*, the echogenic allantoic fluid, and the thick amniotic membrane *(open arrow)*. This sonogram was obtained with a 5.0-MHz sector-scanner transducer at a displayed depth of 14 cm. The mare's ventral abdomen is at the top of the sonogram.

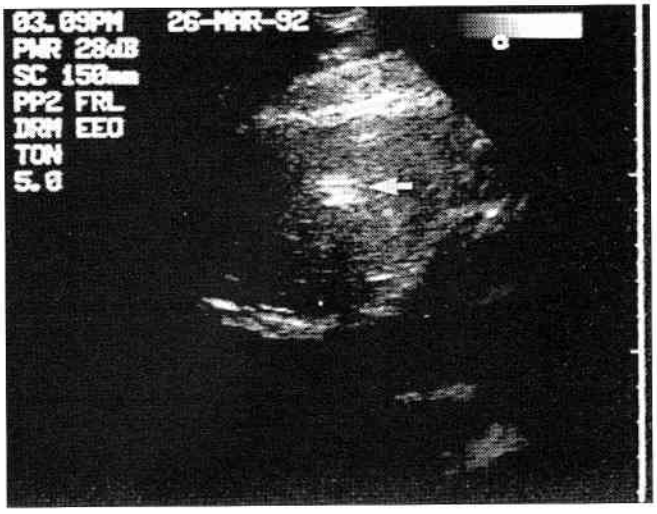

Figure 9–35

Sonogram of hyperechoic areas *(arrow)* within the chorioallantois obtained from a 5-year-old Thoroughbred mare at 327 days of gestation. Notice the marked thickening of the uteroplacental unit (approximately 6 cm) and the hyperechoic tissue casting a faint acoustic shadow consistent with early calcification. This sonogram was obtained with a 2.5-MHz sector-scanner transducer at a displayed depth of 15 cm. The mare's ventral abdomen is at the top of the sonogram.

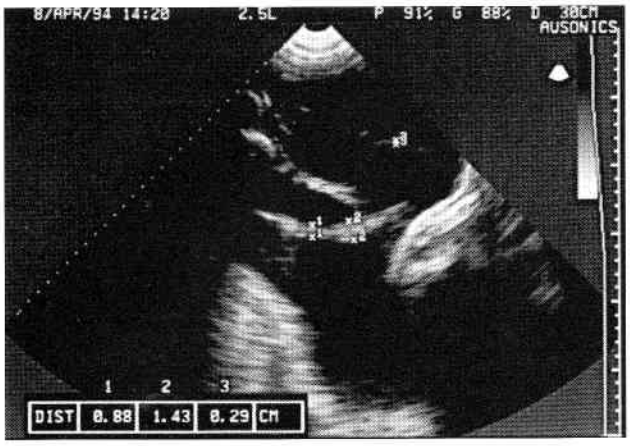

Figure 9–36

Sonogram of thickened amniotic membranes obtained from a 14-year-old Thoroughbred mare at 354 days of gestation. Notice the multiple reflections of the amnion, which measures up to 1.43 cm (x^2) in thickness. This sonogram was obtained with a 2.5-MHz sector-scanner transducer and a displayed depth of 30 cm. The mare's abdomen is at the top of the sonogram.

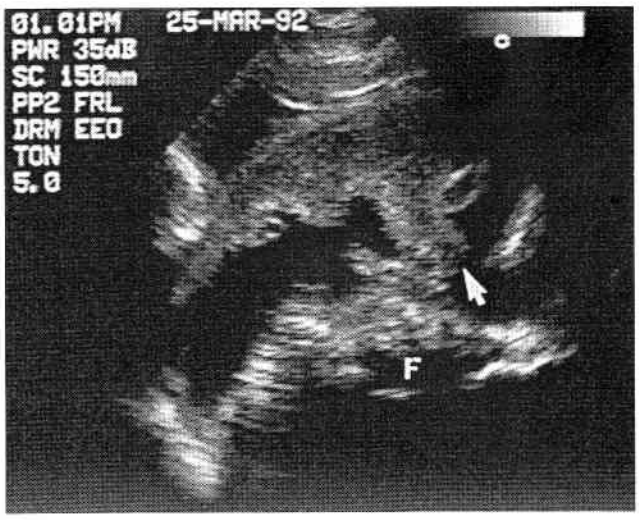

Figure 9–38

Sonogram of large areas of disruption of the uteroplacental unit *(arrow)* obtained from a 5-year-old Thoroughbred mare at 326 days of gestation (same mare as in Figure 9–35). The large areas of fluid separation and the folding of the chorioallantois make the uteroplacental unit vary markedly in thickness, measuring in excess of 6 cm. This sonogram was obtained with a 5.0-MHz sector-scanner transducer at a displayed depth of 15 cm. The mare's ventral abdomen is at the top of the sonogram. F, Fetus.

asphyxia syndrome [PAS]).[37] However, a perfect score was not an assurance of a positive outcome.[37] Several mares experienced premature placental separation or a dystocia at the time of foaling, abnormalities that could not have been predicted from the earlier sonographic examination, as these problems were not present at that time. Similarly, in a previous study attempting to develop a biophysiologic profile, 22% of foals born to mares with perfect scores were born dead or delivered prematurely and died.[33, 34] In this earlier study, 6 of the 17 pregnancies included in the development of the biophysiologic profile were examined at an earlier stage of gestation than their control (normal) population. There were only two pregnancies at a gestational age equivalent to their control population that were predicted to be abnormal based on the biophysiologic profile (one bradycardic fetus and a pair of twins—one dead and one bradycardic).[33] The variables used to develop their biophysiologic profile included fetal size, fetal heart rate (heart rate <60 beats/minute), fetal movement, uteroplacental thickness (>2.0 cm), qualitative allantoic fluid appearance, and allantoic fluid volume estimation.[33, 34] Allantoic fluid volume estimations (mean = 1.9 ± 0.9 cm) were made from a fixed position on the fetal thorax just caudal to the shoulder

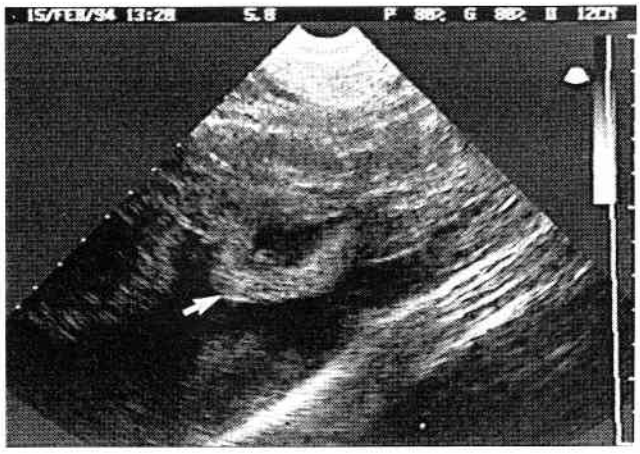

Figure 9–37

Sonogram of a uteroplacental unit with a "ribbon candy" appearance obtained from an 18-year-old Standardbred mare at 334 days of gestation. Notice disruption in uteroplacental contact and the folding of the chorioallantois that occurred *(arrow)* associated with the placental separation and placentitis. This sonogram was obtained with a 5.0-MHz sector-scanner transducer at a displayed depth of 12 cm. The mare's abdomen is at the top of the sonogram.

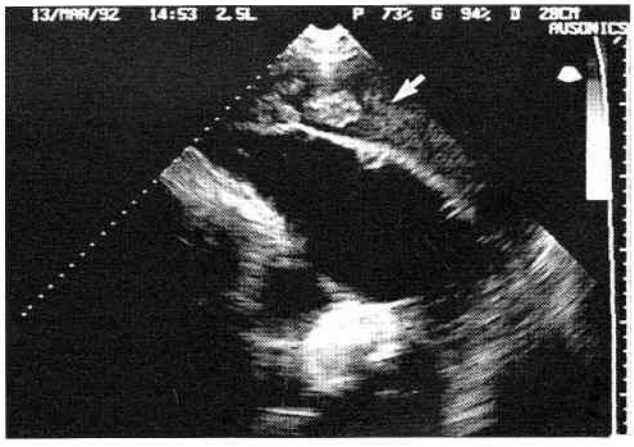

Figure 9–39

Sonogram of intrauterine hemorrhage in a 10-year-old Thoroughbred mare with a uterine tear and a ruptured middle uterine artery at 338 days of gestation. The echogenic clot and swirling echogenic fluid between the uterus and the chorioallantois *(arrow)* are consistent with blood. This sonogram was obtained with a 2.5-MHz sector-scanner transducer at a displayed depth of 28 cm. The mare's ventral abdomen is at the top of the sonogram. F, Fetus.

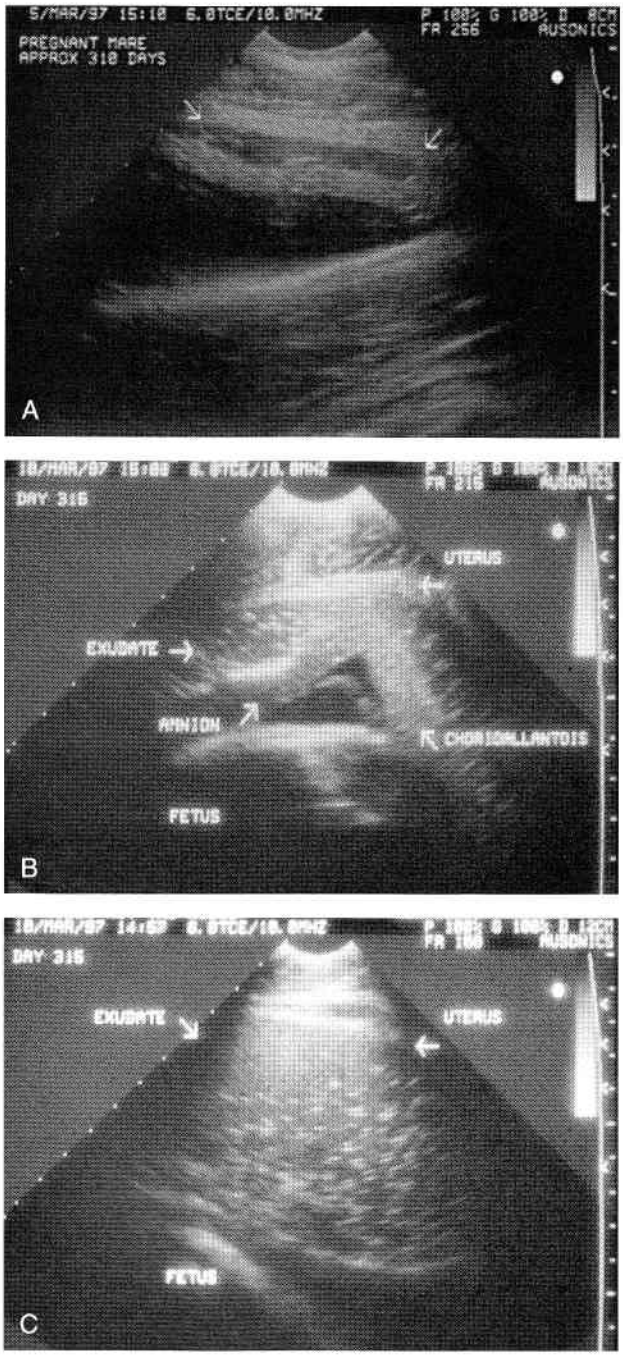

Figure 9–40

Sonograms of the uterus and chorioallantois obtained from a 7-year-old Thoroughbred mare with ascending placentitis. These sonograms were obtained at 310 days (*A*) and 315 days (*B* and *C*) with a wide-bandwidth 6.0-MHz microconvex linear-array transducer operating at 10.0 MHz and a displayed depth of 8 cm (*A*), 10 cm (*B*), and 12 cm (*C*).

A, Small areas of hypoechoic fluid were imaged separating the uterus and the chorioallantois in the right caudal portion of the uterus from the transcutaneous window, although larger areas of heterogeneous fluid were imaged transrectally at this time between the chorioallantois and the uterus. The fetus showed no signs of distress at this time.

B, Large areas of separation of the uterus from the chorioallantois were imaged with thickening of the chorioallantois. Hyperechoic pinpoint echoes representing free gas were imaged throughout the area of separation consistent with a probable anaerobic infection.

C, The areas of separation between the chorioallantois and uterus were largest in the right and left caudal abdomen with the uteroplacental unit measuring up to 7.6 cm. There heterogeneous echogenic fluid containing the hyperechoic free gas echoes was imaged throughout the areas of uteroplacental separation.

to the allantochorion.[33] The major differences between the previously developed and more recently developed biophysiologic profiles are the equations used to estimate fetal size, the abnormalities of fetal heart rate evaluated, the method used to estimate allantoic fluid volume, the addition of an estimate of amniotic fluid volume, the addition of evidence of disruptions in uteroplacental contact, the deletion of qualitative allantoic fluid appearance, and the gestational ages of the fetuses. The regression equation used to predict fetal size in their pregnancies was not useful in the pregnancies that we examined.[36]

The biophysiologic profile needs to be tested prospectively in a large population of mares to determine its value, as has been done in human beings.[37] Additional variables such as fetal breathing movements and fetal tone need to be assessed critically in a prospective fashion to see if they improve the sensitivity and specificity of the equine biophysiologic profile.[37] Fetal arrhythmias should be included as part of the abnormalities associated with the fetal heart (rate and rhythm).[37] More normal pregnant mares need to be evaluated in late gestation to provide a larger normal data base. Fetal and maternal measurements need to made throughout gestation, as many of the variables measured change throughout gestation. High-risk mares and fetuses evaluated earlier in gestation (prior to 298 days) need a comparable control population. Fetal heart rate should be higher, fetal aortic and thoracic diameter smaller, fetal fluids clearer, and

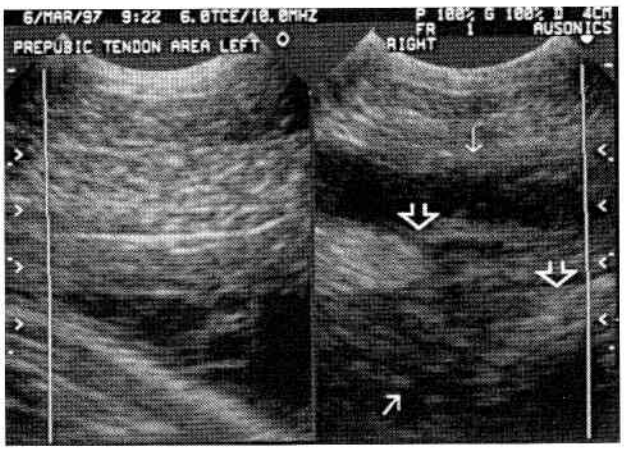

Figure 9–41

Sonograms of the ventral abdominal wall obtained from a 23-year-old Thoroughbred mare with tearing of the ventral lateral abdominal wall at 310 days of gestation. This mare was being scanned because of a history of placentitis for the 2 previous years. This defect *(down arrow)* in the mare's ventral lateral body wall was detected at the time of the placental examination. An area of separation was imaged in the retroperitoneal fat *(open arrows)* and inner abdominal muscle layer (transverse abdominis muscle) on the right side of the abdomen that was not present in the same area on the left. The peritoneum is still intact over the area of abdominal muscle rupture. The mare was treated with a belly bandage and 10 days later the area of muscle rupture was healing. The mare foaled uneventfully approximately 30 days later. This sonogram was obtained with a wide-bandwidth 6.0-MHz microconvex linear-array transducer operating at 10.0 MHz and a displayed depth of 5 cm.

estimated fetal fluid quantities less than in late gestation (298 days or greater).[33–37] Fetal breathing movements are absent in early gestation, but the time of onset of fetal breathing movements in the equine fetus is unknown. Patterns of fetal movement also change as parturition approaches. Only with large-scale testing of the equine biophysiologic profile can its sensitivity and specificity be improved. The information about fetal well-being and the fetal environment in high-risk pregnancies can then be used to evaluate treatment options and the success of various interventions.

PATIENT MANAGEMENT

Follow-up sonographic examinations should be performed in any pregnancies in which fetal or maternal abnormalities are detected. The fetus goes through normal sleep-wake cycles that may affect fetal heart rate at rest, heart rate responsiveness, and fetal activity. However, heart rates outside the previously described normal ranges or cardiac arrhythmias are indications of acute hypoxia and fetal distress. Absence of fetal breathing may be a more sensitive or equally sensitive indicator of acute hypoxia in the equine fetus. The persistent lack of fetal activity and the lack of fetal tone are more advanced indicators of fetal hypoxia and fetal distress. Abnormal estimated quantities of amniotic or allantoic fluid are indicators of chronic longstanding hypoxia and severe fetal distress and are associated with the birth of a dead or abnormal foal. Increased echogenicity of these fluids is an indicator of fetal distress early in pregnancy, may also be significant in late gestation, and is associated with an abnormal outcome in early to mid gestation. The detection of a small-for-gestational-age fetus should prompt a careful search for twins. If twins are not found, intrauterine growth retardation should be expected. Any or all of these fetal abnormalities should prompt sonographic re-evaluation and/or transportation to a facility equipped to deal with high-risk neonates. Depending upon the degree of fetal distress and the suspected cause or if twins are detected, the use of flunixin meglumine, progesterone, isoxsuprine, and/or broad-spectrum antimicrobials may be indicated in an attempt to maintain the pregnancy. If fetal distress is severe, induction of parturition or a cesarean section may be warranted.

Significant thickening of the uteroplacental unit is indicative of placentitis and should prompt treatment with broad-spectrum antimicrobials, progesterone, and other medications as indicated, such as intravenous dimethyl sulfoxide and/or isoxsuprine. Significant thickening of the uteroplacental unit and disruptions of uteroplacental contact should be closely monitored sonographically (see Fig. 9-40). If enlarging or extensive areas of placental disruption are detected, induction of parturition or a cesarean section are indicated if the gestational age of the fetus warrants a chance at survival.

If an unusually large aortic diameter is detected compared with the predicted aortic diameter, the mare should be foaled at a facility where immediate intervention is possible (assisted delivery and/or caesarean section) if a dystocia occurs. The foaling should also be attended or the mare foaled at a facility where immediate intervention is possible if the foal is repeatedly found to be in an abnormal presentation, also increasing the risk for a dystocia.

Treatment for ventral abdominal hernias should begin with a large, snug belly bandage to support the abdominal viscera and prevent further tearing of the ventral abdominal muscles. This has been used successfully in a mare with a small ventrolateral hernia, before the development of clinical signs (Fig. 9-41). This mare subsequently foaled uneventfully and follow-up sonographic examinations revealed healing of the ventral abdominal hernia.

A thorough understanding of normal fetal and maternal structures, their function and variation with gestational age, and activity help veterinary ultrasonologists, theriogenologists, and neonatologists assess the high-risk pregnancy and identify the high-risk neonate. Once they are identified, repeated ultrasonographic monitoring can help evaluate when treatment is indicated, the response to treatment, and when parturition should be induced or a cesarean section performed, improving mare, fetal, and foal morbidity and mortality.

References

1. Allen WE, Goddard PJ: Serial investigations of early pregnancy in pony mares using real-time ultrasound scanning. Equine Vet J 16:509–514, 1984.
2. Bain AM, Howey WP: Ovulation and transuterine migration of the conceptus in Thoroughbred mares. J Reprod Fert Suppl 23:541–544, 1975.

3. Chevalier F, Palmer E: Ultrasonic echography in the mare. J Reprod Fert Suppl 32:423-430, 1982.
4. Fraser AF, Hastie H, Callicot RB, et al: An exploratory ultrasonic study on quantitative foetal kinesis in the horse. Appl Anim Ethol 1:395-404, 1975.
5. Fraser AF, Keith NW, Hastie H: Summarized observations on the ultrasonic detection of pregnancy and foetal life in the mare. Vet Rec 92:20-21, 1973.
6. Ginther OJ: Mobility of the early equine conceptus. Theriogenology 19:603-611, 1983.
7. Ginther OJ: Fixation and orientation of the early equine conceptus. Theriogenology 19:613-623, 1983.
8. Ginther OJ: Intrauterine movement of the early conceptus in barren and postpartum mares. Theriogenology 21:633-644, 1984.
9. Ginther OJ: Mobility of twin embryonic vesicles in mares. Theriogenology 22:83-95, 1984.
10. Ginther OJ: Postfixation embryo reduction in unilateral and bilateral twins in mares. Theriogenology 22:213-223, 1984.
11. Ginther OJ: Ultrasonic evaluation of the reproductive tract of the mare: The single embryo. J Equine Vet Sci 4:75-81, 1984.
12. Ginther OJ: Embryonic loss in mares: Incidence and ultrasonic morphology. Theriogenology 24:73-86, 1985.
13. Ginther OJ: Embryonic loss in mares: Pregnancy rate, length of interovulatory interval, and progesterone concentrations associated with loss during days 11 to 15. Theriogenology 24:409-417, 1985.
14. Ginther OJ: Dynamic physical interactions between the equine embryo and uterus. Equine Vet J (Suppl) 3:41-47, 1985.
15. Ginther OJ: Ultrasonic Imaging and Reproduction Events in the Mare. Cross Plains, WI, Equiservices, 1986.
16. Ginther OJ: Twin embryos in mares. I: From ovulation to fixation. Equine Vet J 21:166-170, 1989.
17. Ginther OJ: Twin embryos in mares. II: Post fixation embryo reduction. Equine Vet J 21:171-174, 1989.
18. Kahn W, Leidl W: Differentiation of uterine pathology and normal early gestation in the mare with ultrasound scanning. Vlaams Diergeneeskundig Tijdschrift 53:170-179, 1984.
19. Leith GS, Ginther OJ: Characterization of intrauterine mobility of the early conceptus. Theriogenology 22:401-408, 1984.
20. O'Grady JP, Yeager CH, Findleton L, et al: In utero visualization of the fetal horse by ultrasonic scanning. Equine Pract 3:45-49, 1981.
21. Palmer E, Draincourt MA: Use of ultrasonic echocardiography in equine gynecology. Theriogenology 13:203-216, 1980.
22. Pierson RA, Kastelic JP, Ginther OJ: Basic principles and techniques in transrectal ultrasonography in horses and cattle. Theriogenology 29:3-20, 1988.
23. Pipers FS: Applications of diagnostic ultrasound in veterinary medicine. Equine Vet J 14:341-344, 1982.
24. Rantanen NW, Torbeck RL, DuMond SS: Early pregnancy diagnosis in the mare using transrectal ultrasound scanning techniques: A preliminary report. J Equine Vet Sci 2:27-29, 1982.
25. Reef VB: The use of diagnostic ultrasound in the horse. Ultrasound Q 9:1-34, 1991.
26. Simpson DJ, Greenwood RES, Ricketts SW, et al: Use of ultrasound echography for early diagnosis of single and twin pregnancy in the mare. J Reprod Fert Suppl 32:431-439, 1982.
27. Squires EL, McKinnon AO, Shideler RK: Use of ultrasonography in reproductive management of mares. Theriogenology 29:55-70, 1988.
28. Taverne MAM: The use of linear-array real-time echography in veterinary obstetrics and gynaecology. Tijdschr Diergeneested 109:494-506, 1984.
29. Torbeck RL: Diagnostic ultrasound in equine reproduction. Vet Clin North Am [Equine Pract] 2:227-252, 1986.
30. Villahoz MD, Iuliano MF, Squires EL: The use of real-time ultrasound for pregnancy detection in embryo transfer mares. Theriogenology 19:149, 1983.
31. Vogelsang MM, Vogelsang SG, Lindsey BR, et al: Reproductive performance in mares subjected to examination by diagnostic ultrasound. Theriogenology 32:95-103, 1989.
32. Curran S, Ginther OJ: Ultrasonic diagnosis of equine fetal sex by location of the genital tubercle. Equine Vet Sci 9:77-83, 1989.
33. Adams-Brendemuehl CS, Pipers FS: Antepartum evaluations of the equine fetus. J Reprod Fert Suppl 35:565-573, 1987.
34. Adams-Brendemuehl CS: Fetal assessment. *In* Koterba AM, Drummond WH, Kosch PC: Equine Clinical Neonatology. Philadelphia, Lea & Febiger, 1990, pp 16-33.
35. Pipers FS, Adams-Brendemuehl CS: Techniques and applications of transabdominal ultrasonography in the pregnant mare. J Am Vet Med Assoc 185:766-771, 1984.
36. Reef VB, Vaala WE, Worth LT, et al: Transabdominal ultrasonographic evaluation of the fetus and intrauterine environment in healthy mares during late gestation. Vet Radiol Ultrasound 36:533-541, 1995.
37. Reef VB, Vaala WE, Worth LT, et al: Ultrasonographic assessment of fetal well-being during late gestation: A preliminary report on the development of an equine biophysical profile. Equine Vet J 28:200-208, 1995.
38. Chamberlain PF, Manning FA, Morrison I, et al: Ultrasound evaluation of amniotic fluid volume. I. The relationship of marginal and decreased amniotic fluid volumes to the perinatal outcome. Am J Obstet Gynecol 150:245-249, 1984.
39. Chamberlain PF, Manning FA, Morrison I, et al: Ultrasound evaluation of amniotic fluid volume. II. The relationship of increased amniotic fluid volumes to the perinatal outcome. Am J Obstet Gynecol 150:250-254, 1984.
40. Grubb DK, Paul RH: Amniotic fluid index and prolonged antepartum fetal heart rate decelerations. Obstet Gynecol 79:558-560, 1992.
41. Johnson JM, Harman CR, Lange IR, Manning FA: Biophysical profile scoring in the management of the postterm pregnancy: An analysis of 307 patients. Am J Obstet Gynecol 154:269-273, 1986.
42. Manning FA: The fetal biophysical profile score: Current status. Obstet Gynecol Clin North Am 17:147-162, 1990.
43. Manning FA, Harman CR, Menticoglou S, Morrison I: Assessment of fetal well-being with ultrasound. Obstet Gynecol Clin North Am 18:891-905, 1991.
44. Manning FA, Hill LM, Platt LD: Qualitative amniotic fluid volume determination by ultrasound: Antepartum detection of intrauterine growth retardation. Am J Obstet Gynecol 139:254-258, 1981.
45. Manning FA, Morrison I, Lange IR, et al: Fetal assessment based on fetal biophysical profile scoring: Experience in 12,620 referred high-risk pregnancies. I. Perinatal mortality by frequency and etiology. Am J Obstet Gynecol 151:343-350, 1985.
46. Manning FA, Morrison I, Lange IR, et al: Fetal assessment based on fetal biophysical profile scoring: Experience in 19,221 referred high-risk pregnancies. II. An analysis of false-negative fetal deaths. Am J Obstet Gynecol 157:880-884, 1987.
47. Manning FA, Platt LD, Sipos L: Antepartum fetal evaluation: Development of a fetal biophysical profile. Am J Obstet Gynecol 136:787-795, 1980.
48. Patrick J, Fetherston W, Vick H, Voegelin R: Human fetal breathing movements and gross fetal body movements at weeks 34 to 35 of gestation. Am J Obstet Gynecol 130:693-699, 1978.
49. Platt LD, Manning FA, Lemay M, Sipos L: Human fetal breathing: Relationship to fetal condition. Am J Obstet Gynecol 132:514-518, 1978.
50. Vintzileos AM, Campbell WA, Ingardia CJ, Nochimson DJ: The fetal biophysical profile and its predictive value. Obstet Gynecol 62:271-278, 1983.
51. Rantanen NW, Kincaid B: Ultrasound guided fetal cardiac puncture: A method of twin reduction in the mare. Proceedings of the 33rd Annual American Association of Equine Practitioners 33:173-179, 1988.
52. Ball BA, Schlafer DH, Card CE, Yeager AE: Partial re-establishment of villous placentation after reduction of an equine co-twin by foetal cardiac puncture. Equine Vet J 25:336-338, 1993.
53. Allen KA, Stone LR: Equine diagnostic ultrasonography: Equipment selection and use. Compend Contin Educ Pract Vet 12:1307-1311, 1990.
54. Reef VB: Advances in diagnostic ultrasonography. Vet Clinics North Am [Equine Pract] 7:451-466, 1991.
55. Whitwell KE, Jeffcott LB: Morphological studies on the fetal membranes of the normal singleton foal at term. Res Vet Sci 19:44-55, 1975.
56. Jeffcott LB, Rossdale PD: A radiographic study of the fetus in late pregnancy and during foaling. J Reprod Fert Suppl 27:563-569, 1979.
57. Vandeplassche M: The normal and abnormal presentation, position and posture of the foal-fetus during gestation and at parturition. Meded VeeartssSch Rijksuniv Gent 1:36 (Suppl Vlaams Diergeneesk Tijd 1:26), 1957.

58. Yamamoto K, Yasuda J, Too K: Electrocardiographic findings during parturition and blood gas tensions immediately after birth in Thoroughbred foals. Jpn J Vet Res 39:143–157, 1991.
59. Yamamoto K, Yasuda J, Too K: Arrhythmias in newborn Thoroughbred foals. Equine Vet J 23:169–173, 1992.
60. Colles CM, Parkes RD, May CJ: Foetal electrocardiography in the mare. Equine Vet J 10:32–37, 1978.
61. Holmes JR, Darke PGG: Foetal electrocardiography in the mare. Vet Rec 82:651–655, 1968.
62. Hosaka F: Perinatal fetal heart rate changes and neonatal arrhythmias in the horse. Jpn J Vet Res 37:106, 1989.
63. Matsui K, Sugano S, Masuyama I, et al: Alterations in the heart rate of Thoroughbred horse, pony and Holstein cow through pre- and post-natal stages. Jpn J Vet Sci 46:505–509, 1984.
64. Pipers FS, Zent W, Holder R, et al: Ultrasonography as an adjunct to pregnancy assessments in the mare. J Am Vet Med Assoc 184:328–334, 1984.
65. Amada A, Senta T: Proceedings of the 57th Meeting of the Japanese Society of Veterinary Science. Jpn J Vet Sci Suppl 26:431, 1964.
66. Machida N, Yasuda J, Too K: Auscultatory and phonocardiographic studies of the cardiovascular system of the newborn Thoroughbred foal. Jpn J Vet Res 35:235–250, 1987.
67. Kanagawa H, Too K, Kawata K, et al: Fetal electrocardiogram at late gestational stages in horses. Jpn J Vet Res 15:15–19, 1967.
68. Otto C, Platt LD: Fetal growth and development. Obstet Gynecol Clin North Am 18:907–931, 1991.
69. Schifrin BS, Foye G, Amato J, et al: Routine fetal heart rate monitoring in the antepartum period. Obstet Gynecol 54:21–25, 1979.
70. Sertich PL, Reef VB, Oristaglio-Turner RM, et al: Hydrops amnii in a mare. J Am Vet Med Assoc 204:1–2, 1994.
71. De Vore GR, Platt DL: Ultrasound appearance of particulate matter in amniotic cavity: Vernix or meconium? J Clin Ultrasound 14:229–230, 1986.
72. Khaleghain R: Echogenic amniotic fluid in the second trimester: A new sign of fetal distress. J Clin Ultrasound 11:498–501, 1983.
73. Hanson RR, Todhunter RJ: Herniation of the abdominal wall in pregnant mares. J Am Vet Med Assoc 189:790–793, 1986.
74. Meek DG, DeGrofft DL, Schneider EE: Surgical repair of similar parturition-induced midline ventral hernias in two mares: A comparison of results. Vet Med/Small An Clin 72:1066–1074, 1977.
75. Adams SB: Rupture of the prepubic tendon in the horse. Equine Pract 1:17–19, 1979.

CHAPTER

10

Ultrasonography of the Genital Tract of the Stallion

Regina M. Turner, VMD

Since its introduction to veterinary reproduction in the early 1980s, diagnostic ultrasonography has become a commonly used, almost necessary, component of reproductive management of the mare. More recently, the use of ultrasonography has been expanding to include examination of the stallion.[1-7] Although at this time ultrasonography is not used routinely in stallions, it is fast becoming a useful adjunct to the stallion breeding-soundness examination and an important diagnostic tool for examination of reproductive pathology in the stallion.[8-14]

EXAMINATION TECHNIQUE

Patient Preparation — External Genitalia

For examination of the testicles, epididymis, and spermatic cord, the veterinarian is often required to place himself or herself in a potentially dangerous position just in front of the stallion's hind legs. Proper restraint is therefore critical for the safety of all personnel and equipment. If semen is to be collected from the stallion as part of the examination, it is best to perform the ultrasonographic examination after semen collection when the stallion is more relaxed and the testicles more pendulous and easier to manipulate.

Ideally, an experienced stallion handler should restrain the stallion at all times. The handler can back the horse into a corner, with the right side of the horse against a wall. This prevents the stallion from backing or swinging away from the veterinarian and also discourages kicking. The handler stands on the near side of the horse beside the shoulder, out of striking range of the forefeet. The stallion can be discouraged from swinging toward the veterinarian by the handler's right hand on the stallion's shoulder. Most stallions can be safely examined with only a shank over the nose or in the mouth. A twitch or chemical restraint may be used for intractable animals. As an alternative to this set-up, the stallion can be restrained by the handler in stocks with a side panel that can be removed or lowered.

The ultrasound machine should be placed on a cart with wheels to permit quick and easy movement of the apparatus if the stallion misbehaves. An assistant can be very helpful in moving the ultrasound cart into easy view of the veterinarian and out of the way in case of problems. In addition, this person is available for writing notations, thus allowing the veterinarian to proceed without interruptions (Fig. 10-1).

Patient Preparation — Accessory Sex Glands and Aorta

Stallions can be restrained and prepared for examination per rectum similarly to mares (see Chapter 8). For the safety of the veterinarian and the equipment, stocks are preferred, but palpation around a stall door or standing beside the stallion is also acceptable for tractable animals.

Anatomy

External Genitalia

The testicles function in spermatogenesis and hormone production. The normal stallion possesses two scrotal, ellipsoid testicles that are oriented with the long axis horizontal. The spermatic cord is located at the craniodorsal aspect of each testicle and ascends through the inguinal ring. The spermatic cord is covered by the tunica albuginea and contains the testicular artery, pampiniform plexus, and ductus deferens. The testicular artery arborizes over the surface of the testicle. The branches of the testicular artery then extend into the testicular parenchyma. The large central vein of the testicle traverses the center of the testicular parenchyma before emptying into the pampiniform plexus of the spermatic cord (Fig. 10-2*A*). The stallion does not possess a distinct mediastinum testis as is present in men, dogs, boars, and bulls.[15-18]

The epididymis is commonly divided into three areas: the head, the body, and the tail. Sperm leaving the testicle

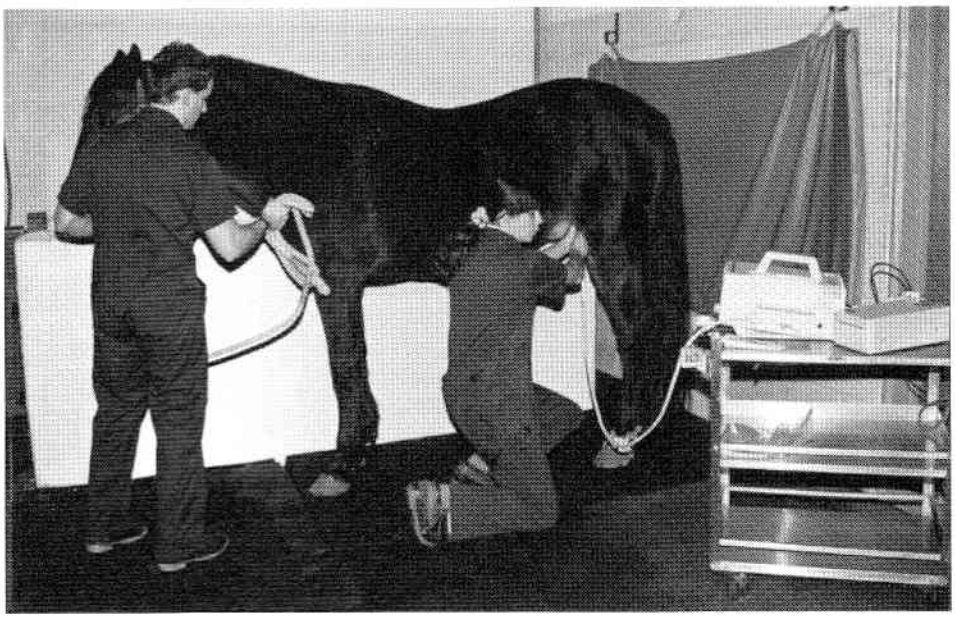

Figure 10-1

Proper restraint of the stallion for testicular examination. Note positions of the stallion, handler, veterinarian, and equipment cart. Ideally, a third person should be available to reposition the cart if needed and to record notes. The pad hanging on the wall behind the stallion is a kick pad to decrease noise and impact should the stallion kick rearward.

travel first through the head, then the body, and then the tail of the epididymis before entering the ductus deferens. In the stallion, the tail of the epididymis is quite prominent and is located at the caudal pole of the testicle. The body of the epididymis courses dorsolaterally along the surface of the testicle, and the head is located craniodorsally, just beside the spermatic cord. The epididymis is composed of a single, highly convoluted duct[19] and functions in sperm storage as well as final sperm maturation. The ductus deferens is a continuation of the duct from the tail of the epididymis.

The tunica albuginea of the testicle is a strong fibrous capsule that is intimately associated with the surface of the testicle and sends connective tissue septa into the testicular parenchyma.[15] The visceral vaginal tunic surrounds and is closely apposed to the tunica albuginea around the testicle, the epididymis, and the spermatic cord. The next outward layer is the parietal vaginal tunic, which is a continuation of the parietal peritoneum. Between the visceral and parietal tunicae is a small space, the vaginal cavity, which is continuous with the peritoneal cavity and normally contains a small amount of peritoneal fluid. The parietal vaginal tunica is loosely connected via fascia to the tunica dartos, and beyond the tunica dartos is the scrotal skin (Fig. 10-2*B*).[20]

Accessory Sex Glands

The normal stallion possesses a full complement of accessory sex glands, including paired ampullae, paired seminal vesicles, a single bilobed prostate, and paired bul-

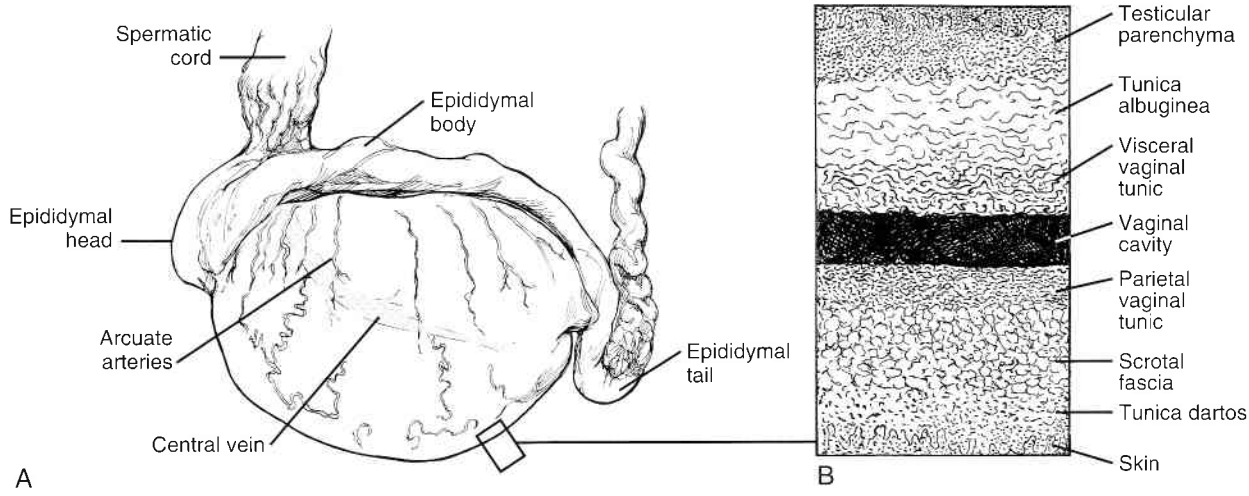

Figure 10-2

A, Anatomy of the testicle, epididymis, and spermatic cord of the stallion. The locations of the central vein and arcuate arteries are shown. *B*, Detail of the tissue layers surrounding the testicle. The tunica albuginea is closely apposed to the testicular surface and sends connective tissue septa into the parenchyma.

bourethral glands. These glands function in adding fluid volume, enzymes, amino acids, and buffers to the ejaculate.[21, 22] The paired ampullae are the most cranial glands and are glandular thickenings of the ducti deferentia proximal to the entry of the ducts into the urethra. The glands are cylindrical and are approximately 15 to 20 cm in length and about 2 cm in diameter.[22] They are palpable per rectum at about wrist depth as two pencil-like structures extending laterally from the midline at approximately a 30-degree angle from the urethra. Just caudal to the ampullae are the paired seminal vesicles. The seminal vesicles are oval bladder-like glands that extend laterally from the midline at approximately a 30-degree angle to the urethra. When empty, the seminal vesicles become flattened (approximately 26 mm in length by 9 mm in height) and when distended with fluid they become roughly oval.[1] In stallions that have not been sexually stimulated, the flattened seminal vesicles are difficult to palpate per rectum. Following sexual stimulation, the seminal vesicles fill with fluid and become more readily detectable by palpation. The seminal vesicles empty into the urethra at the seminal colliculus. The isthmus of the prostate is located on the ventral midline caudal to the seminal vesicles. The right and left lobes of the prostate extend laterally from the isthmus. The prostatic isthmus measures about 6 mm in height, and the lobes measure approximately 23 mm in height by more than 34 mm in width.[1] The prostate gland empties into the urethra through numerous prostatic ducts. The gland may be palpable per rectum if the stallion has been sexually stimulated. The paired bulbourethral glands are roughly circular and are located on either side of the urethra just cranial to the anal sphincter at the ischial arch. These glands are not palpable per rectum owing to their location beneath the urethral musculature. The bulbourethral glands measure approximately 19 mm in width by 32 mm in height (Fig. 10-3).[1] Ultrasonographic size ranges for normal stallion accessory glands vary with the age and breed of the stallion. Normal ranges have been reported for Thoroughbred-type stallions, ponies, miniature horses, and draft horse breeds before and after teasing.[1, 5] Table 10-1 summarizes the reported average normal values for Thoroughbred-type and pony stallions.

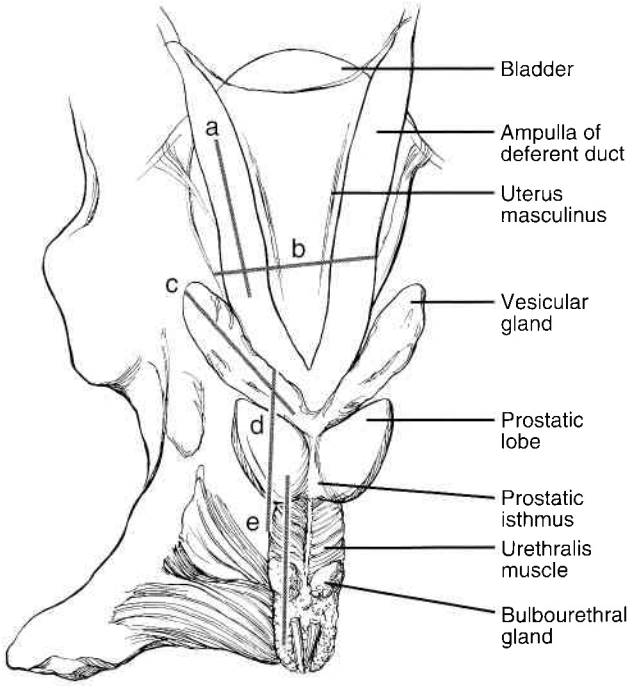

Figure 10-3

Dorsal view of the anatomy of the accessory sex glands of the stallion. Solid lines indicate the proper positions of the transducer. a, Position of the transducer for imaging the left ampulla in sagittal section. b, Position of the transducer for imaging the left and right ampulla in short-axis cross-section. c, Position of the transducer for imaging the left seminal vesicle in sagittal section. d, Position of the transducer for imaging the left lobe of the prostate gland in sagittal section. e, Position of the transducer for imaging the left bulbourethral gland in sagittal section.

Scanning Technique

External Genitalia

Prior to examination with the ultrasound transducer, the testicles, epididymis, spermatic cord, and inguinal region should be examined by palpation and visualization. This allows the stallion to become accustomed to having the area manipulated prior to introducing the transducer and also allows the veterinarian to identify any obvious abnormalities that may warrant further ultrasonographic evaluation.

The veterinarian should approach the horse's left shoulder and, keeping the left side of the body in contact with the stallion, slowly approach the stallion's hindquarters. The right hand can then be used to reach between the hind limbs for palpation. Once the stallion is accustomed to this, ultrasonographic examination can begin.

The ultrasound cart is placed in a location out of reach of the stallion but within sight of the veterinarian (see Fig. 10-1). A coupling gel must be used on the transducer to ensure constant contact between the transducer and the scrotum. Generous amounts of an approved ultrasound coupling gel or a water-soluble gel used for gynecologic examinations can be used. The ideal transducer for examination of the testicles is a linear-array 7.5-MHz transducer. This provides the sharpest detail of the superficially located testicular parenchyma, epididymis, and spermatic cord. In some cases, a 10.0-MHz linear-array transducer may provide enhanced detail of superficial structures (e.g., the epididymis). A wide-bandwidth 6.0-MHz microconvex linear-array transducer provides a wide field of view, with excellent resolution for comparing structures on the right and left sides. A 7.5-MHz transducer with a built-in fluid standoff is also acceptable. Most transducers used for examination of the mare reproductive tract are 5.05 MHz. These transducers are adequate, but some detail is lost. The addition of a standoff pad between a 5.05-MHz transducer and the scrotum can improve resolution but also makes examination more awkward. Sector scanners also can be used, but proper placement of the transducer is more difficult owing to the curved surfaces of the transducer and the testicle.

The stallion is approached as for palpation. Proper

Table 10–1
Mean Dimensions (±SEM) of Accessory Sex Gland Images Measured Prior to and After Sexual Stimulation and After Ejaculation

Ultrasonographic Image	Time of Measurement		
	Before Sexual Preparation	*After Sexual Preparation*	*After Ejaculation*
Bulbourethral gland			
Length (cm)	3.09[a] ± 0.06	3.61[b] ± 0.08	3.16[a] ± 0.08
Width (cm)	1.71[a] ± 0.04	2.13[b] ± 0.06	1.81[a] ± 0.05
Pelvic portion of the urethra			
Diameter (cm)	2.23 ± 0.07	2.29 ± 0.06	2.27 ± 0.06
Ampulla			
Wall diameter (cm)	0.58 ± 0.03	0.58 ± 0.03	0.55 ± 0.02
Luminal diameter (cm)	0.10[a] ± 0.02	0.21[b] ± 0.02	0.07[a] ± 0.01
Total diameter (cm)	1.26[a] ± 0.06	1.37[b] ± 0.06	1.16[c] ± 0.05
Prostate gland			
Lobe thickness (cm)	2.53[a] ± 0.08	3.06[b] ± 0.07	2.41[a] ± 0.08
Isthmus thickness (cm)	0.56[a] ± 0.07	0.73[b] ± 0.06	0.55[a] ± 0.05
Vesicular gland			
Wall diameter (cm)	0.26 ± 0.01	0.26 ± 0.01	0.25 ± 0.01
Luminal diameter (cm)	0.57[a] ± 0.07	0.72[b] ± 0.06	0.44[c] ± 0.06
Total diameter (cm)	1.08[a] ± 0.08	1.24[b] ± 0.07	0.93[c] ± 0.07

[a, b, c]Means with different superscripts within the same row are significantly different ($P < 0.05$).
Adapted from Weber JA, Geary RT, Woods GL: Changes in accessory sex glands of stallions after sexual preparation and ejaculation. J Am Vet Med Assoc 196:1084–1089, 1990.

positioning and visualization of the transducer generally requires that the veterinarian bend or kneel in front of the stallion's hind legs. The left hand is used to push the right testicle up out of the way and hold the left testicle steady to provide a firm contact surface for the transducer. The transducer, with gel applied, is held in the right hand and placed against the lateral surface of the testicle perpendicular to its long axis. The transducer then is slowly moved several times over the entire lateral surface of the testicle to allow proper visualization of the scrotal contents (Fig. 10–4). Sagittal (long-axis) views of the testicular parenchyma can be obtained by moving the transducer over the cranial surface of the testicle and directing the beam caudally or by holding the transducer on the ventral surface of the testicle with the long axis of the transducer parallel to the long axis of the testicle. In most Thoroughbred-type or larger breed stallions, the entire long axis of the testicle is too large to be seen in a single frame of view. The transducer can be moved around as needed to ensure that all areas of the testicular parenchyma have been visualized. The tail of the epididymis can be difficult to image owing to its location on the curved caudal pole of the testicle. The transducer can be placed either directly over the tail or over the testicle just cranial to the tail and the beam directed caudally toward the tail. The latter orientation is usually more satisfactory (Fig. 10–5, position *B*). After examination of the testicles, epididymis, and associated structures, the transducer should be moved farther up into the inguinal region for examination of the spermatic cord. For this examination, the transducer is held in the right hand and positioned over the spermatic cord, parallel to the ground (i.e.,

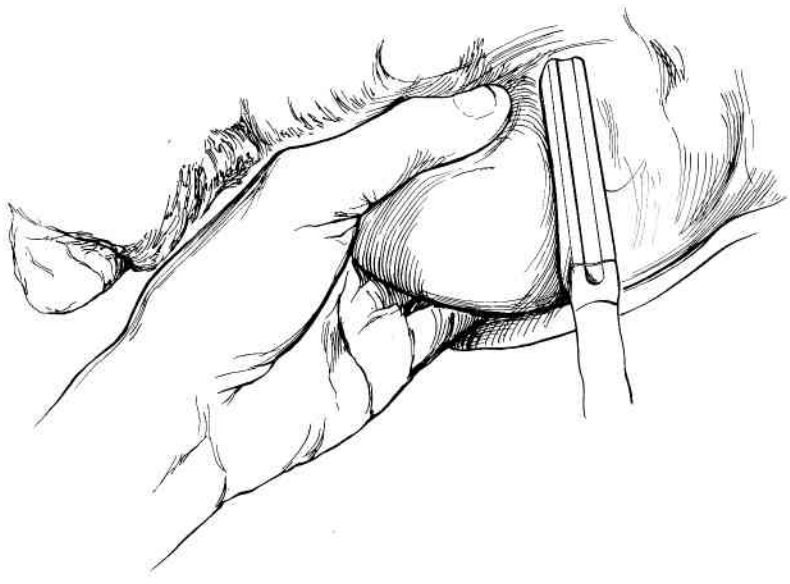

Figure 10-4
Proper position of the transducer for imaging the testicular parenchyma in short-axis cross-section and for measuring testicular width. The left hand applies gentle downward traction on the testicle and pushes the other testicle up out of the scanning plane of the transducer.

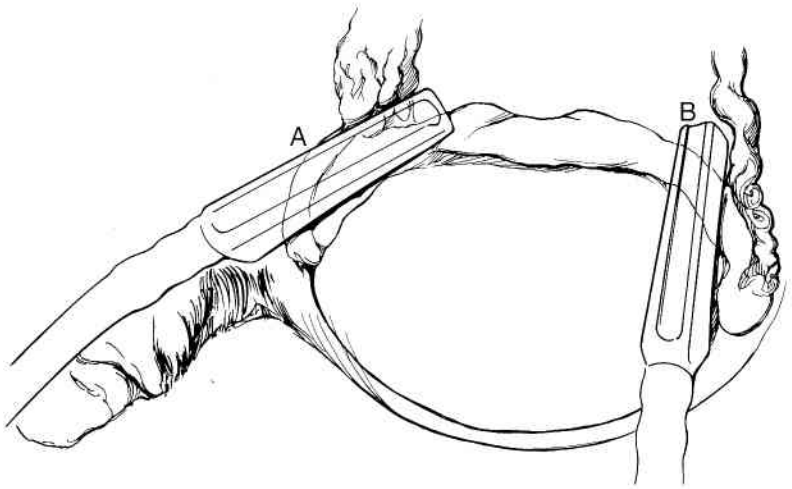

Figure 10-5

Proper positions of the transducer for imaging the epididymal head (A) and tail (B). This illustrates how the epididymal tail can be imaged by placing the transducer over the testicular parenchyma just cranial to the tail and angling the beam caudally. This provides a good contact surface for the transducer. Positioning the transducer directly over the epididymal tail provides poor contact and usually results in an inferior image.

providing short-axis cross-sections of the cord) while the left hand gently but firmly applies downward traction on the testicle (Fig. 10-6). The transducer is slowly moved up and down the spermatic cord as far as it can be safely examined. Long-axis sections of the spermatic cord can also be obtained with a 7.5-MHz transducer by positioning the transducer parallel to the cord. Long-axis views are difficult to obtain with the larger 5.0-MHz transducer because the location of the testicles close to the stallion's body wall may preclude proper positioning of the transducer.

The entire process is then repeated with the right testicle while the left testicle is pushed up out of the way. It may be necessary to rearrange the horse and the equipment to allow examination from the horse's right side.

Accessory Glands

After the stallion is appropriately restrained, the rectum is emptied of feces and the veterinarian should attempt to palpate and identify the ampullae, seminal vesicles, and prostate transrectally. The inguinal rings also should be examined at this time. It may be helpful to use the inguinal rings as landmarks to identify each ductus deferens. The ductus feels like a tense string running out of the internal inguinal ring. Each ductus can be traced caudally from the inguinal rings directly to the ampullae.

Most stallions tolerate this examination surprisingly well, and, once they become used to the presence of the veterinarian's hand, ultrasonographic examination can be safely and efficiently performed. Owing to the superficial location of the accessory glands, a 7.5-MHz linear-array transducer is preferred for this examination. A 7.5-MHz transducer provides excellent detail of the accessory glands and also enhances visualization of smaller structures such as the uterus masculinus (when present) and the seminal colliculus. If a 7.5-MHz transducer is not available, a 5.0-MHz transducer can be used, although some detail is lost. A wide-bandwidth 6.0-MHz microconvex linear-array transducer can be used here also to compare structures on the right and left sides. This transducer is small enough to obtain both long- and short-axis images

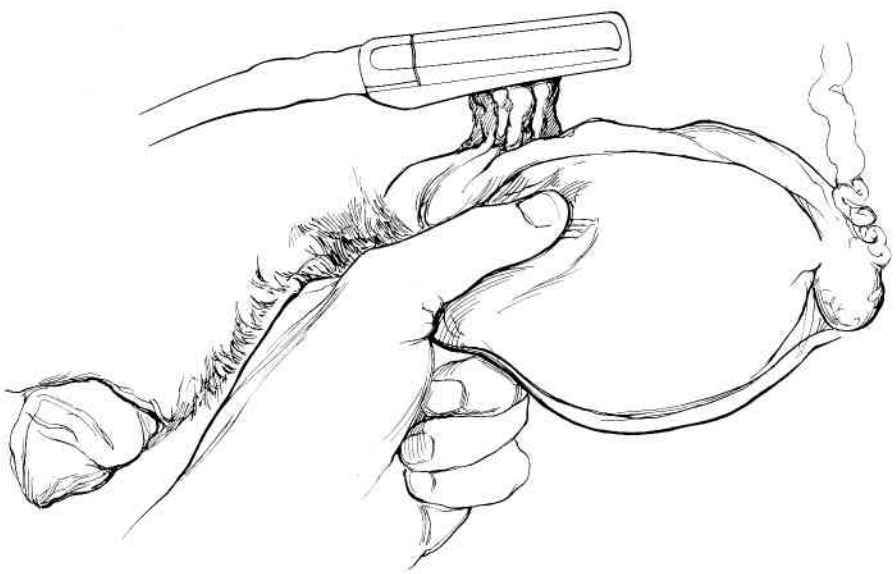

Figure 10-6

Proper position of the transducer for imaging the spermatic cord in short-axis cross-section. Sagittal (long-axis) images of the cord are difficult to obtain with the large 5.0-MHz transducer but may be obtained with a smaller 7.5-MHz transducer.

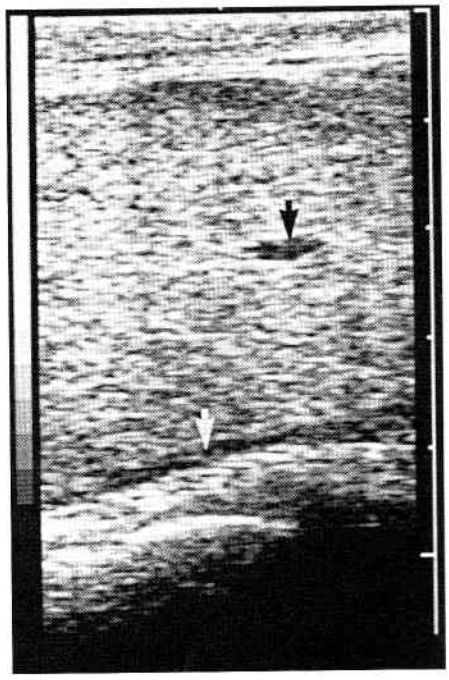

Figure 10-7

Short-axis cross-section ultrasonographic image of normal testicular parenchyma obtained with the transducer held as in Figure 10-4. The central vein appears as an anechoic ellipse within the parenchyma (*black arrow*). In real time, the vein can be traced along its length. Ventral to the parenchyma is normal anechoic fluid in the vaginal cavity (*white arrow*) (7.5-MHz linear-array transducer).

of the internal genitalia. The transducer is held, introduced, and advanced through the rectum as it is for ultrasonography of the mare. If a linear-array transducer is not available, a sector scanner with an off-line beam may suffice. The larger size of the sector scanner can make examination per rectum difficult and may preclude transrectal ultrasonographic examination in ponies or miniature horse stallions.

ULTRASONOGRAPHIC FINDINGS

Normal Findings

Testicle

The testicle to be examined is gently pulled down into the scrotum while the opposite testicle is pushed upward out of the scanning plane. With the transducer held against the lateral surface of the testicle, as described above, a short-axis cross-sectional image of the testicle is obtained. The transducer is then moved across the scrotal surface until the testicular parenchyma has been viewed in its entirety. The ultrasonographic appearance of the normal testicular parenchyma is homogeneous, gray, and granular. A small amount (typically < 5 mm) of anechoic fluid can normally be seen in the vaginal cavity between the visceral and parietal tunicae. The central vein of the testicle is usually visible as an anechoic line traversing the approximate center of the testicular parenchyma. The central vein is widest craniodorsally where it joins the spermatic cord and narrows caudoventrally. Typical width measurements of the central vein vary from 1 to 4 mm depending on which area of the vein is imaged and the angle of the transducer. The parietal vaginal tunic and its associated structures appear as a hyperechoic line outside the vaginal cavity (Figs. 10-7 and 10-8). When the area is scanned with a 7.5-MHz transducer, the small branches of the testicular artery (arcuate arteries) may be seen near the surface of the testicle in the tunica albuginea. These vessels are more difficult to discern when using a 5.0-MHz transducer owing to their location and small (usually < 5 mm in diameter) size (Fig. 10-9).

During the examination of the testicles, the veterinarian should measure length, width, and height of each individual testicle as well as total scrotal width. Because of the anatomic location of the stallion testicles, caliper measurements (especially of testicular height) can be quite difficult. Ultrasonographic measurement is often easier and, if performed correctly, is very accurate.[2] Normal testicular dimensions vary significantly with the age and breed of the stallion and the season of the year. For average, sexually mature Thoroughbred-type stallions, typical testicular length is 80 to 140 mm and width is 50 to 80 mm,[25] with height similar to width. These individual measurements can be valuable in themselves when used as a means of monitoring changes in testicular size over time for an individual stallion. Nonetheless, a stallion should not be labeled abnormal based on a single value outside the normal range. Much more important information is gained by using these values to calculate total testicular volume. Testicular volume can be calculated using the formula for the volume of an ellipsoid, where testicular volume = $4/3\ \pi \times$ height/2 $\times$ width/2 $\times$

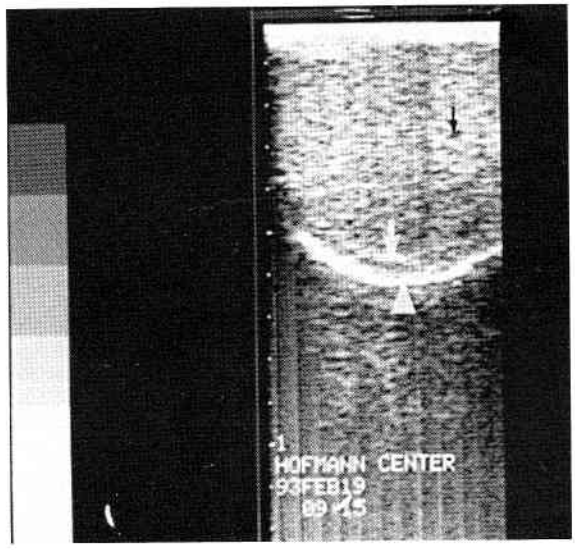

Figure 10-8

Short-axis cross-section ultrasonographic image of normal testicular parenchyma with the transducer held as in Figure 10-4. A small portion of the central vein is visible (*black arrow*), as is a small amount of normal fluid in the vaginal cavity (*white arrow*). The parietal vaginal tunic and its associated structures are clearly visible in this image as a hyperechoic line outside the vaginal cavity (*white arrowhead*) (5.0-MHz linear-array transducer).

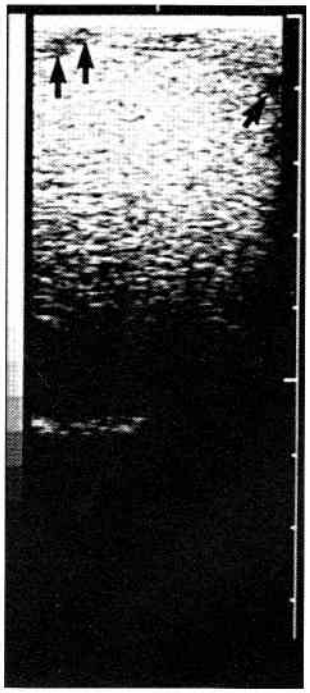

Figure 10-9

Short-axis cross-section ultrasonographic image of normal testicle with the transducer held as in Figure 10-4. Three arcuate arteries are visible as small anechoic regions near the surface of the testicle (*arrows*) (7.5-MHz linear-array transducer).

length/2. Testicular volume can then be used to predict daily sperm output using the graph in Figure 10-10.[2] A stallion is considered to have reached daily sperm output after ejaculating once daily for 1 week.[6] Alternatively, twice-daily ejaculations may allow a stallion to reach daily sperm output within a shorter period of time. Stallions that, at daily sperm output, produce lower sperm numbers than would be expected based on testicular volume should be monitored closely and evaluated for possible testicular degeneration. Another important measurement is total scrotal width. A minimum total scrotal width of 8 cm is required for classification of a stallion as a satisfactory prospective breeder.[24]

For measurement of individual testicular width, the ultrasound transducer should be held on the lateral surface of the testicle, as previously described. Extra care must be taken to ensure that the beam is directed across the widest area of the testicle and perpendicular to its long axis (Fig. 10-11; see also Fig. 10-4). Variations from this position result in artifactual alterations of testicular measurements. Height is measured by placing the transducer on the ventral surface of the testicle and directing the beam dorsally at a 90-degree angle to the long axis of the testicle (Figs. 10-12 and 10-13). Length can be determined by placing the transducer at the cranial aspect of the testicle and aiming the beam caudally. In most stallions, testicular length is too large to fit on the view screen. In these animals, caliper measurements can be substituted. The tail of the epididymis should not be included in either ultrasonographic or caliper measurement of testicular dimensions. Total scrotal width can be measured by gently but firmly holding both testicles extended side by side in the scrotum while placing the transducer perpendicular to the long axis of the testicles and directing the beam across both testicles at their widest point (Figs. 10-14 and 10-15).

In summary, during examination of the testicles the following measurements should be obtained:

- Total scrotal width
- Right and left testicular width
- Right and left testicular height
- Right and left testicular length (may require calipers)

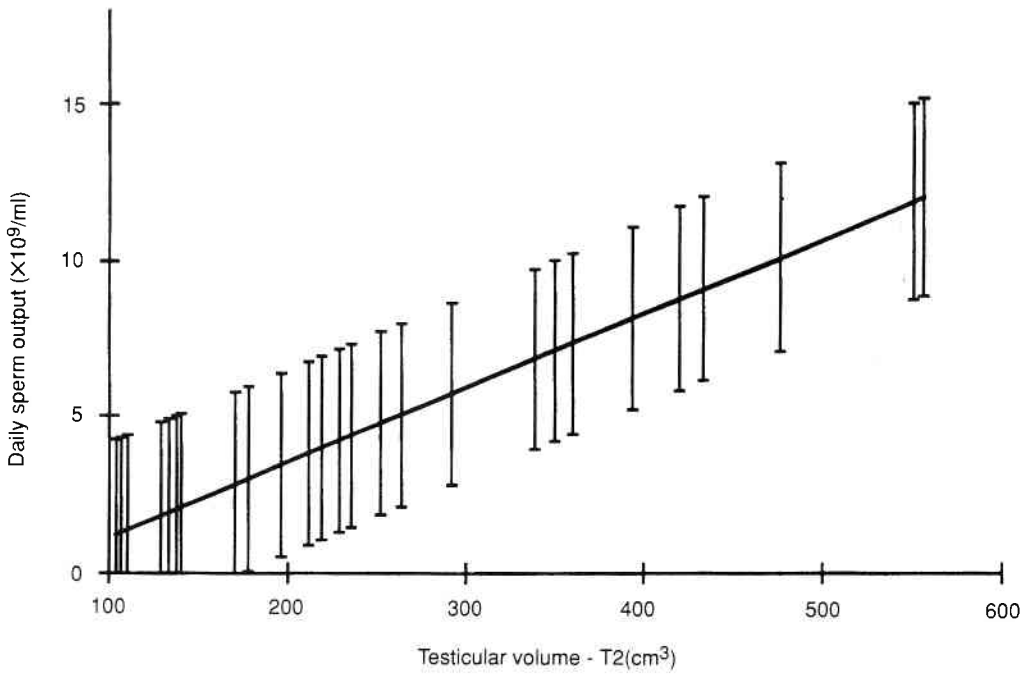

Figure 10-10

Relationship between predicted daily sperm output and testicular volume for 26 stallions. Bars represent 95% confidence interval. Testicular volume was derived using the formula in the text. (From Love CC, Garcia MC, Riera FL, Kenney RM: Evaluation of measurements taken by ultrasonography and caliper to estimate testicular volume and predict daily sperm output in the stallion. J Reprod Fert Suppl 44:99-105, 1991.)

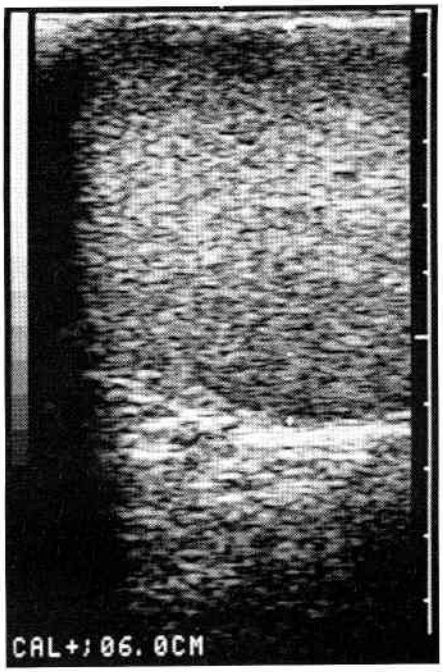

Figure 10-11

Short-axis cross-section ultrasonographic image of normal testicle demonstrating measurement of testicular width with ultrasound calipers. The transducer is held as in Figure 10–4 and the beam is directed across the widest part of the testicle. The calipers delineate the width of the parenchyma (6.0 cm). Note that the parietal tunic and its associated structures are not included in the measurement (5.0-MHz linear-array transducer).

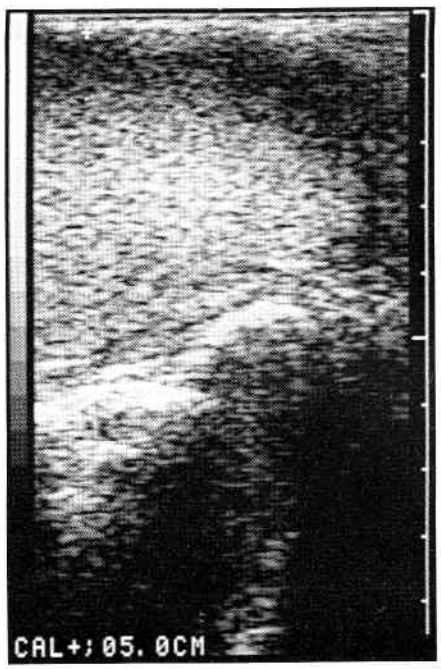

Figure 10-13

Short-axis cross-section ultrasonographic image of normal testicle demonstrating measurement of testicular height with ultrasound calipers. The transducer is held as in Figure 10–12, and the beam is directed across the highest part of the testicle. The calipers delineate the height of the parenchyma (5.0 cm). Note that the parietal tunic and its associated structures are not included in the measurement (5.0-MHz linear-array transducer).

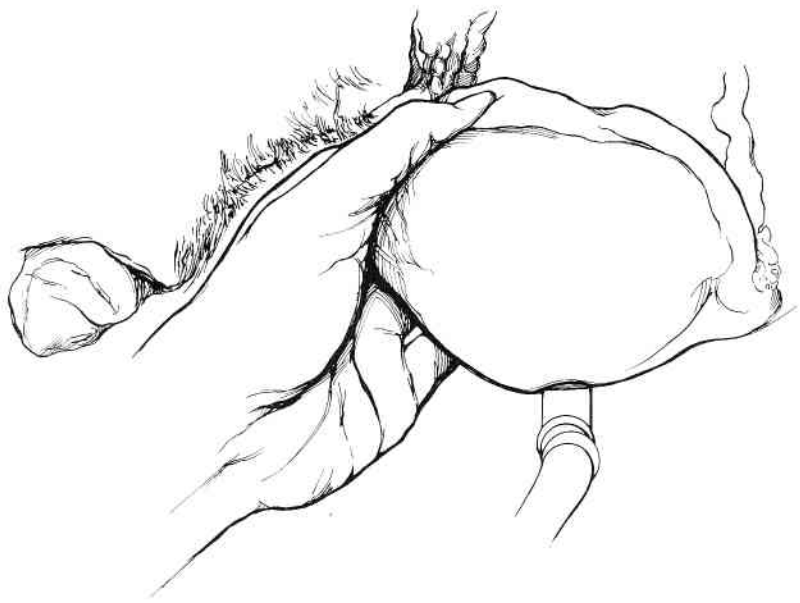

Figure 10-12

Proper positioning of the transducer for measuring testicular height. The beam is directed across the highest part of the testicle.

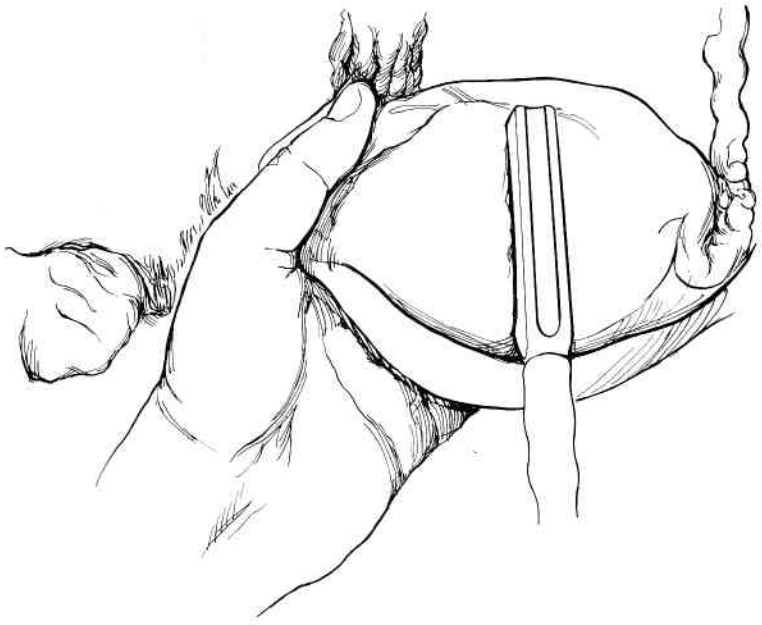

Figure 10-14

Proper positioning of the transducer for measuring total scrotal width. The beam is directed across the widest part of both testicles as the testicles are gently pulled downward and held side by side. The veterinarian's fingers should not be inserted between the testicles, as this could result in errors of measurement and an artifactual increase in total scrotal width.

The last three should be used to calculate testicular volume.

Epididymis

Because the epididymis is composed of a highly convoluted duct, its ultrasonographic appearance is very heterogeneous and gray-black in color (alternating areas of fluid-filled lumen and epididymal wall). The lumen of the epididymal duct is largest in the tail of the epididymis. The epididymal tail is thus distinctly mottled in appearance and is the part of the epididymis most easily visualized.[25] As the lumen becomes narrower in the body and head of the epididymis, the structure becomes more difficult to distinguish from the testicular parenchyma (Figs. 10-16 and 10-17; see also Fig. 10-5).

Spermatic Cord

When visualized in short-axis cross-section, the stallion spermatic cord has a very heterogeneous appearance with distinct anechoic areas surrounded by more hyperechoic areas (Figs. 10-18 and 10-19). This is similar to but more dramatic than the appearance of the epididymal tail. This appearance results from numerous short-axis cross-sections of the lumina of the vessels in the pampiniform plexus and the ductus deferens. In real time, blood flow can be seen within the vessels in most normal stallions.

Accessory Sex Glands

Ampullae

The ampullae are imaged individually in longitudinal sections with the transducer placed directly on top of the gland. In order to obtain a true longitudinal image, the transducer must be angled slightly off midline to parallel the gland (Fig. 10-20*A*; see also Fig. 10-3*A*). The resultant image of the parenchyma is of a narrow gray-white, homogeneous band extending from left to right across the upper edge of the ultrasound screen. Occasionally, the

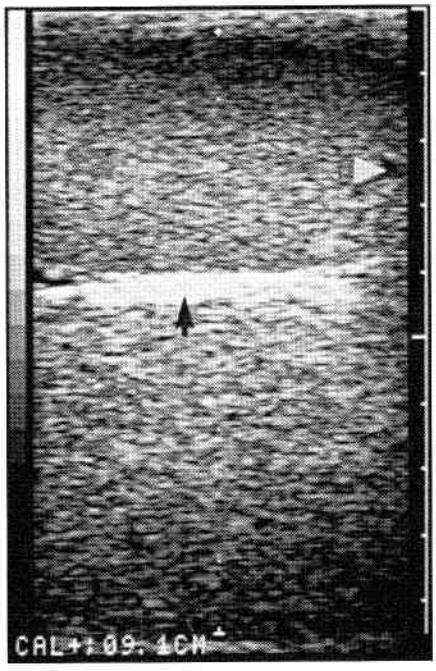

Figure 10-15

Short-axis cross-section ultrasonographic image of normal testicles demonstrating measurement of total scrotal width. The transducer is held as in Figure 10-14, and the beam is directed across the widest part of the adjacent testicles. Measurement is then made across the widest part of the image. Both testicles are clearly visible. The central vein is also apparent in the testicle at the top of the figure (*white arrowhead*). The tunic and associated structures between the two testicles are unavoidably included in the measurement (*black arrow*) (5.0-MHz linear-array transducer).

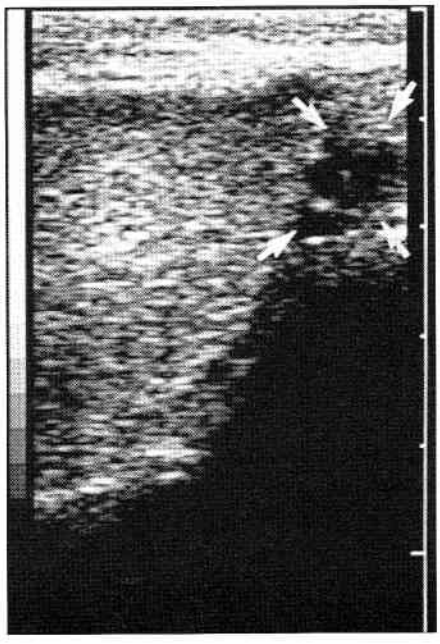

Figure 10-16

Ultrasound image of normal testicular parenchyma and epididymal tail at the caudal pole of the testicle. The epididymal tail is heterogeneous, with anechoic, circular, or oblong areas representing cross-sections of the epididymal lumen. This image was obtained with the transducer held as in Figure 10-5*B*. Arrows surround the epididymal tail (7.5-MHz linear-array transducer).

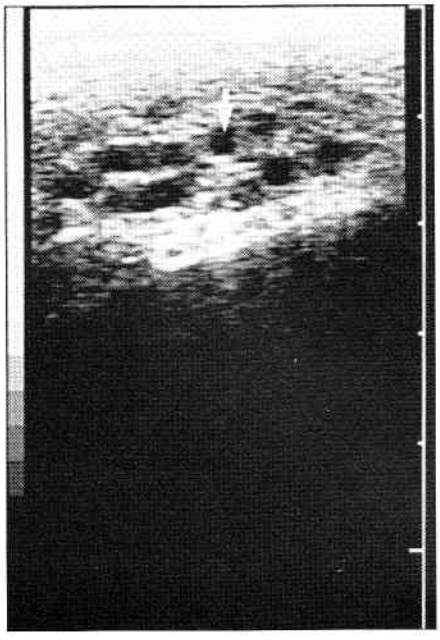

Figure 10-18

Ultrasonographic image of the short-axis cross-section of a normal spermatic cord with the transducer held as in Figure 10-6. Note the numerous anechoic cross-sections of the vessels. In real time, blood flow can be seen within the vessels. Arrow points to one vessel in cross-section (7.5-MHz linear-array transducer).

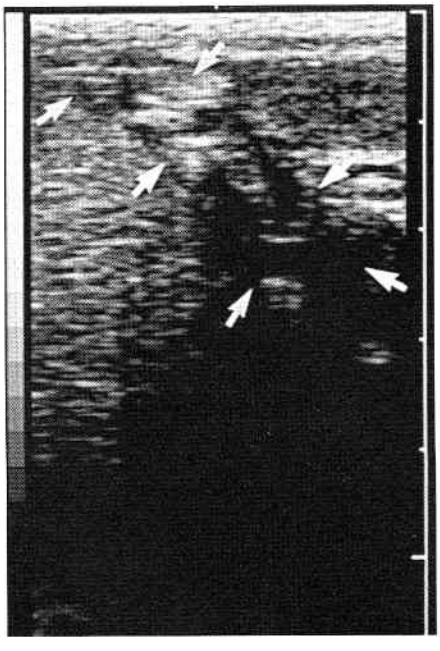

Figure 10-17

Ultrasound image of normal testicular parenchyma and epididymal head and body along the dorsocranial aspect of the testicle with the transducer held as in Figure 10-5*A*. The epididymal head and body are heterogeneous, with anechoic, circular, or oblong areas representing cross-sections of the epididymal lumen. The ultrasonographic architecture of the epididymal head and body is less distinct than that of the tail owing to the small size of the epididymal duct lumen. Arrows surround the epididymal head and body (7.5-MHz linear-array transducer).

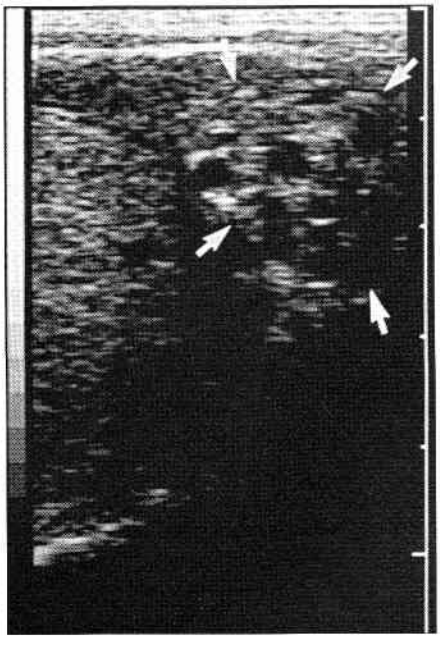

Figure 10-19

Ultrasonographic image of short-axis cross-section of normal spermatic cord adjacent to the normal testicle. This image is obtained as the transducer is moved distally along the spermatic cord toward the testicle. Arrows delineate the spermatic cord (7.5-MHz linear-array transducer).

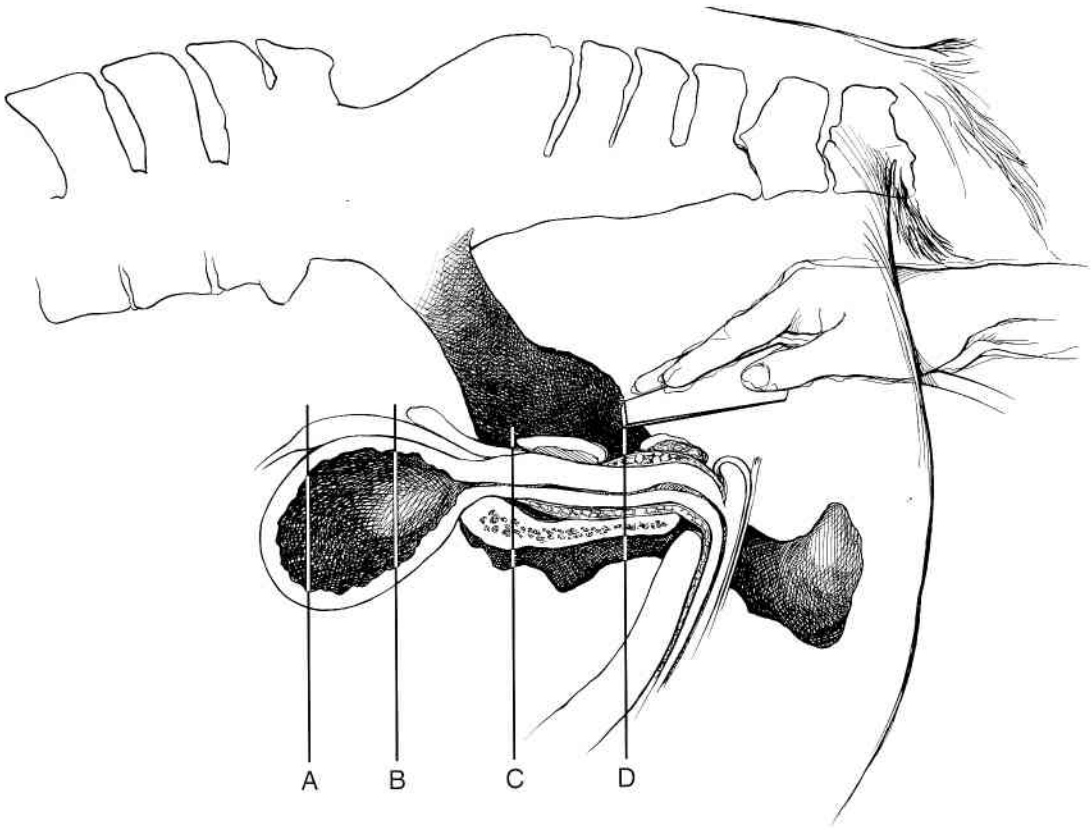

Figure 10-20

Lateral view of the anatomy of the accessory sex glands of the stallion. This diagram illustrates both proper handling and the depth of penetration of the transducer. Solid lines indicate proper location of the cranialmost aspect of the transducer. A, Location of cranialmost aspect of the transducer for imaging the ampullae. B, Location of cranialmost aspect of the transducer for imaging the seminal vesicles. C, Location of cranialmost aspect of the transducer for imaging the prostate. D, Location of cranialmost aspect of the transducer for imaging the bulbourethral glands. Owing to the caudal location of these glands, the palm of the veterinarian's hand must be outside the rectum to properly position the transducer.

lumen of the ampulla is visible as a thin black (fluid) or white (no fluid present) line through the approximate center of the gland (Figs. 10-21 and 10-22). In normal stallions, the lumen and total diameter of the ampulla increase after sexual stimulation and decrease following ejaculation.[7] See Table 10-1 for normal sizes.

The ampullae can also be visualized in cross-section by turning the transducer at a 90-degree angle to the long axis of the gland (see Fig. 10-3*B*). This view is more easily obtained with the smaller 7.5-MHz transducer. With this approach, both ampullae can be seen in short-axis cross-section and followed to their entrance to the urethra (Fig. 10-23).[1] The pelvic urethra becomes visible in short-axis cross-section as the ampullae are followed caudally and approach the midline. If the urethral lumen is empty, it may or may not be visible ultrasonographically as an anechoic spot in the center of the urethra. In some cases, only the urethral wall and its surrounding musculature are visible as a roughly circular gray-white structure medial and ventral to the cross-sections of the ampullae (Fig. 10-24). Following urination, the urethral lumen is often dilated with anechoic fluid and becomes larger and easier to visualize.[26]

When scanning the ampullae of some stallions with a 7.5-MHz transducer, the uterus masculinus, a remnant of the embryologic paramesonephric (müllerian) ducts, may be seen medial to the ampullae just cranial to the prostatic isthmus.[20] Ultrasonographically, the uterus masculinus appears as a thin-walled, oblong structure filled with anechoic fluid.

Seminal Vesicles

The seminal vesicles are imaged by moving the ultrasound transducer slightly caudal and lateral to the ampullae (see Figs. 10-3*C* and 10-20*B*). These glands can be imaged in both longitudinal and short-axis cross-sections, depending upon the positioning of the transducer. At rest, the walls of the seminal vesicles appear gray-white and homogeneous and the entire gland is flattened dorsally to ventrally. Varying amounts of anechoic fluid may be present within the glandular lumen (Fig. 10-25). Following sexual stimulation, the amount of luminal fluid increases and the gland becomes distended and rounded (Fig. 10-26). After ejaculation, the seminal vesicles return to their prestimulation appearance. The decrease in seminal vesicle luminal size after ejaculation is correlated with the amount of gel present in the ejaculate. Seminal vesicle secretions are not always voided at ejaculation, and thus a large lumen prior to ejaculation does not necessarily

Figure 10-21

Ultrasonographic image of longitudinal section of the normal ampulla prior to sexual stimulation with transducer held as in Figures 10-3a and 10-20A. The gland parenchyma is homogeneous (*white arrows*). The lumen is represented by a hyperechoic line (*black arrows*). When ampullary fluid is present, the normal lumen may appear anechoic (7.5-MHz linear-array transrectal transducer).

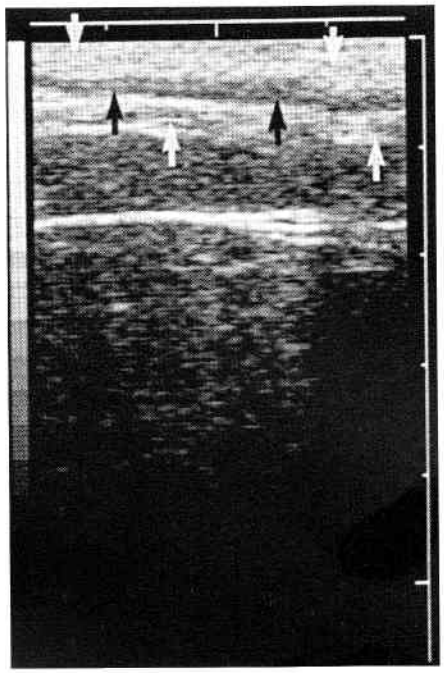

Figure 10-22

Ultrasonographic image of a longitudinal section of normal ampulla after sexual stimulation. The transducer is held as in Figures 10-3a and 10-20A. The lumen has an increased diameter and is filled with normal hypoechoic fluid. White arrows denote glandular tissue. Black arrows point to fluid in the lumen. (5.0-MHz linear-array transrectal transducer).

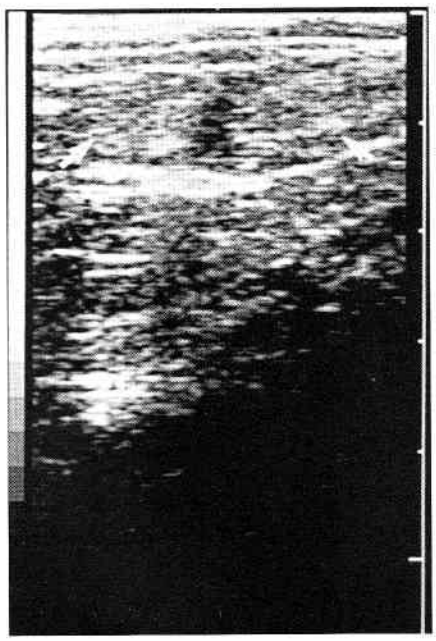

Figure 10-23

Ultrasonographic image of short-axis cross-section of normal paired ampullae. The transducer is held as in Figure 10-3b, with the transducer head turned at a 90-degree angle to the long axis of the ampullae. By moving the transducer cranially to caudally, the glands can be followed in cross-section until they enter the urethra. An arrow points to each gland (7.5-MHz linear-array transrectal transducer).

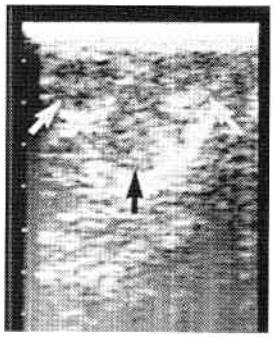

Figure 10-24

Ultrasonographic image of short-axis cross-section of normal paired ampullae dorsal to the normal urethral musculature. The transducer is held as in Figure 10-3b, with the transducer head turned at a 90-degree angle to the long axis of the ampullae. The urethral lumen is not clearly visible. White arrows point to ampullae. Black arrow points to urethral musculature (5.0-MHz linear-array transrectal transducer).

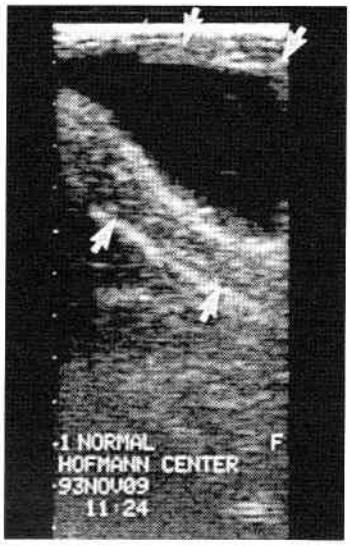

Figure 10-26

Ultrasonographic image of longitudinal section of normal seminal vesicle after extensive teasing. The transducer is held as in Figures 10-3c and 10-20B. The vesicle is rounded and bladderlike, and the lumen is distended with anechoic fluid. Arrows delineate the wall of the gland (5.0-MHz linear-array transrectal transducer).

mean that large amounts of gel will be found in the ejaculate.[7] See Table 10-1 for normal sizes.

Prostatic Isthmus and Prostatic Lobes

The prostatic isthmus is located on the midline just caudal to the neck of the seminal vesicles. The lobes of the prostate extend outward to the right and left of the isthmus. To image the prostatic isthmus, the transducer is moved caudally from the seminal vesicles and kept on the midline parallel to the long axis of the stallion's body. The lobes are viewed by moving the transducer laterally, still parallel to the body's long axis (see Figs. 10-3*D* and 10-20*C*.) In the unaroused stallion, the prostatic parenchyma appears gray-white and heterogeneous, containing multiple anechoic (fluid) spaces (Fig. 10-27). The overall size of the prostate and the size and density of

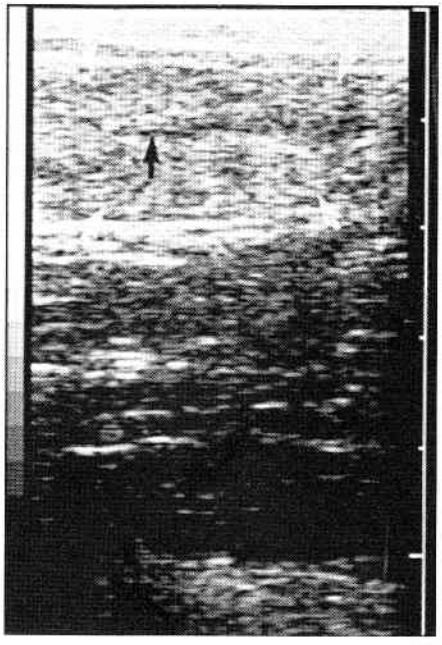

Figure 10-25

Ultrasonographic image of longitudinal section of normal seminal vesicle prior to sexual stimulation. The transducer is held as in Figures 10-3c and 10-20B. The vesicle is flattened dorsally to ventrally. A thin line of seminal vesicular fluid is visible in the center of the gland (*black arrow*). White arrows delineate the wall of the gland (7.5-MHz linear-array transrectal transducer).

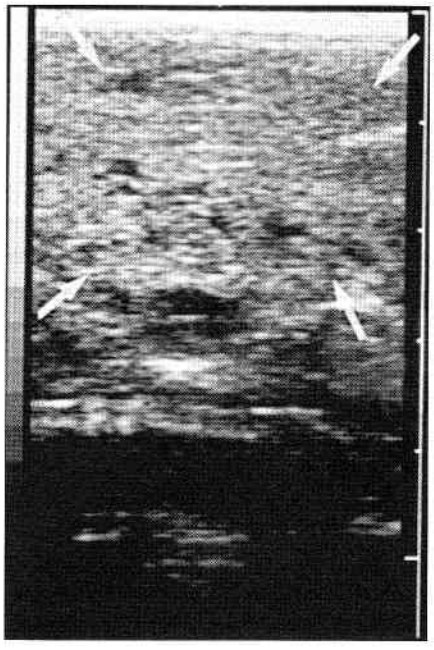

Figure 10-27

Ultrasonographic image of short-axis cross-section of normal prostatic lobe prior to sexual stimulation. The transducer is held as in Figures 10-3d and 10-20C. The parenchyma is heterogeneous gray-white and contains multiple anechoic fluid pockets. Arrows delineate prostatic parenchyma (7.5-MHz linear-array transrectal transducer).

the fluid-filled spaces increase following sexual stimulation. After stimulation, the fluid-filled areas sometimes appear as radiating anechoic spokes (Fig. 10-28). The size of the gland and its fluid-filled spaces decreases following ejaculation.[7] See Table 10-1 for normal sizes.

Bulbourethral Glands

The bulbourethral glands can be imaged to the right and left of the ventral midline and caudal to the prostate. Usually the wrist and palm of the veterinarian's hand must be withdrawn from the rectum, leaving the fingers holding the ultrasound transducer just within the anal sphincter (see Figs. 10-3*E* and 10-20*D*). The bulbourethral glands are circular and, at rest, appear granular gray-white (Fig. 10-29). After sexual stimulation, the glands enlarge and anechoic fluid pockets may be visible within the parenchyma (Fig. 10-30). After ejaculation, the glands return to their prestimulus size and appearance.[7] See Table 10-1 for normal sizes.

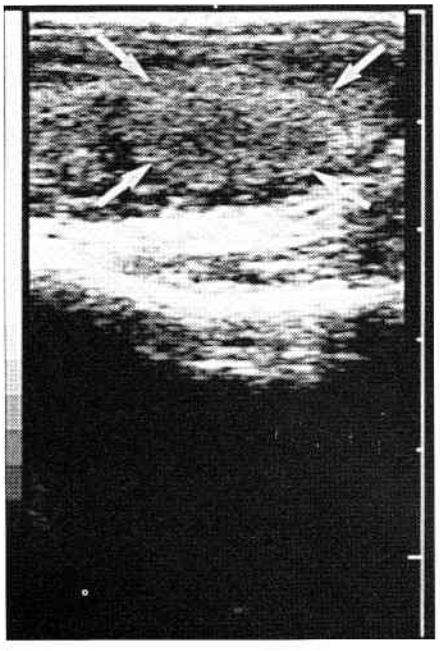

Figure 10-29

Ultrasonographic image of cross-section of normal bulbourethral gland prior to sexual stimulation. The transducer is held as in Figures 10-3e and 10-20D. The gland is roughly circular and homogeneous gray-white. Arrows delineate glandular parenchyma (7.5-MHz linear-array transrectal transducer).

Accessory Sex Glands During Ejaculation

The accessory sex glands have also been visualized during ejaculation in the stallion.[6,7] This technique enabled visualization of the movement of fluid through the glands into the urethra as well as visualization of gland activity during ejaculation. The use of this technique has thus far been reported only in a research situation. The stallion is restrained in a chute and allowed to place his head through a truck tire secured at the stallion's neck level. The veterinarian stands behind and to the left of the stallion, inserts the transducer into the rectum, and holds

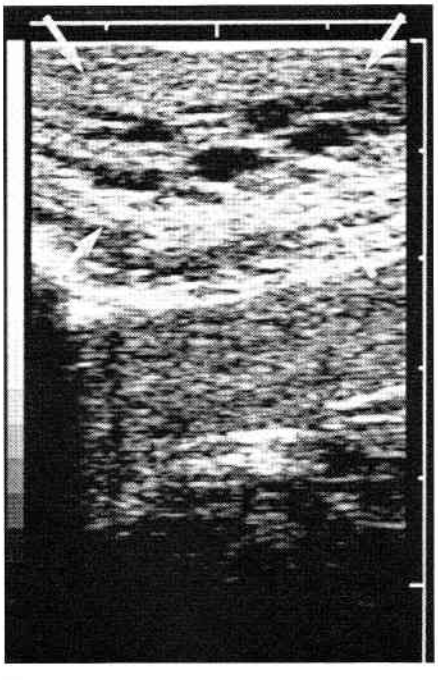

Figure 10-28

Ultrasonographic image of short-axis cross-section of normal prostatic lobe after sexual stimulation. The transducer is held as in Figures 10-3d and 10-20C. The fluid spaces have increased in size, and some appear as radiating spokes. Arrows delineate prostatic parenchyma (7.5-MHz linear-array transrectal transducer).

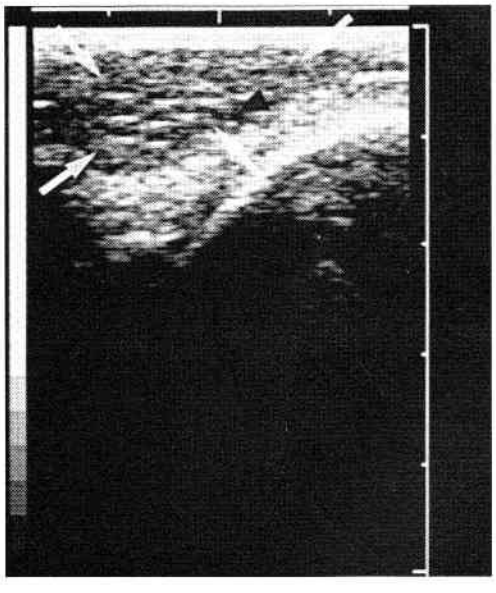

Figure 10-30

Ultrasonographic image of cross-section of bulbourethral gland after teasing. The transducer is held as in Figures 10-3e and 10-20D. Numerous small, anechoic, fluid-filled spaces are now visible scattered throughout the parenchyma. White arrows delineate glandular parenchyma. Black arrowhead points to one fluid-filled space (7.5-MHz linear-array transrectal transducer).

the transducer steadily in position over the desired region during the ensuing ejaculation. An estrous mare is presented to the stallion on the far side of the tire. After the stallion achieves an erection, an assistant places an artificial vagina over the stallion's penis, and semen is collected with the stallion standing on the ground. The chute and tire limit movement of the stallion during thrusting and ejaculation and prevent the stallion from mounting the mare while still allowing him access to her. For more details on this technique, see references 6, 7, and 25.

Abnormal Ultrasonographic Images and Their Interpretation

It is recommended that the practitioner become as familiar as possible with the normal ultrasonographic appearance of the external genitalia and accessory glands. This allows for easier and more accurate detection of abnormalities.

Abnormalities of the Testicles and Scrotal Contents

Cryptorchidism. A cryptorchid horse is one in which one or both testicles have not descended into the scrotum. Male horses can be affected either unilaterally or bilaterally, and the retained testicle may be present either in the inguinal canal or in the abdominal cavity. Normal spermatogenesis does not occur in cryptorchid testicles; however, hormone production is unaffected. Stallions with one cryptorchid testicle and one normal descended testicle are usually fertile. Bilaterally cryptorchid stallions are sterile but continue to exhibit stallion-like behavior. In cases of known or suspected cryptorchidism, ultrasonography can be used to determine the presence and location of a retained testicle. In one report, 11 of 11 retained testicles were accurately identified, located, and measured using a 5-MHz linear-array transducer either transrectally (abdominal testicles) or by scanning externally over the external inguinal ring (inguinal testicles).[13] Scanning over the external inguinal ring is most easily accomplished using a sector scanner. If a sector scanner is not available, a linear-array transducer suffices. The parenchyma of a cryptorchid testicle is generally more hypoechoic than that of a descended testicle but is nonetheless readily identifiable (Figs. 10-31 and 10-32). Identification of a retained testicle by ultrasonography provides valuable information on the testicle's exact location. This can be extremely helpful in cases in which surgical removal is planned.

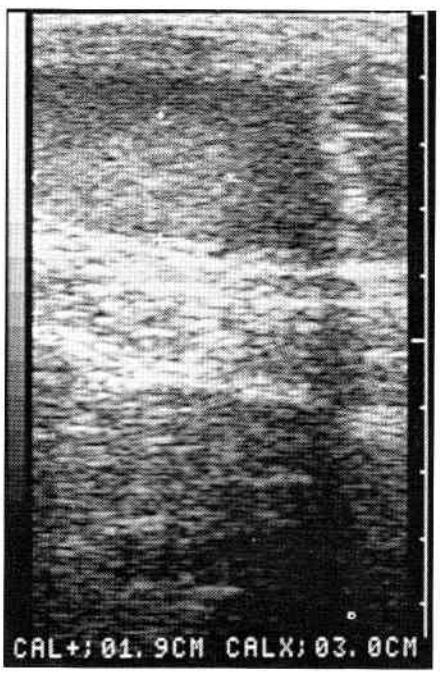

Figure 10-31

Ultrasonographic image of abdominal testicle in a 3-year-old Thoroughbred stallion. This testicle was located adjacent to the left internal inguinal ring. The testicle is small, but the homogeneous testicular parenchyma is readily definable. Calipers delineate the height and length of the testicle (5.0-MHz linear-array transrectal transducer).

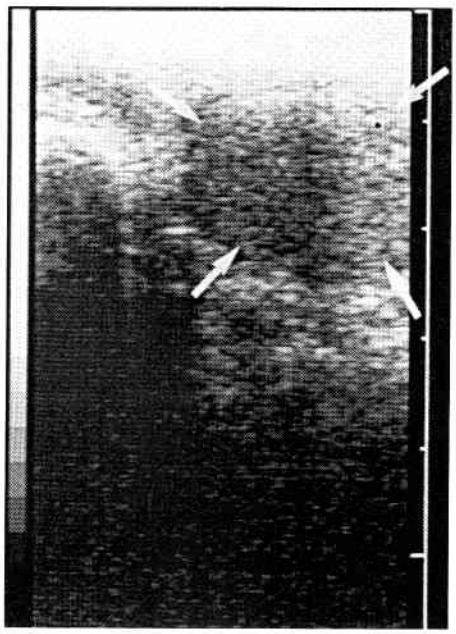

Figure 10-32

Ultrasonographic image of inguinal testicle in a yearling Thoroughbred colt (*arrows*). This image was obtained transcutaneously by pressing the transducer head into the inguinal region over the external inguinal ring. The testicular parenchyma is homogeneous gray-white and is delineated by arrows (5.0-MHz linear-array transducer).

Cryptorchidism should be suspected in any stallion presenting with only one identifiable scrotal testicle or in a supposed gelding with excessively stallion-like behavior. A careful history must be obtained to determine if the missing testicle(s) was surgically removed for reasons unrelated to cryptorchidism. When a retained testicle is suspected, transcutaneous ultrasonographic examination of the inguinal region and transrectal ultrasonography of the abdominal cavity can be performed to confirm the diagnosis. Retained testicles, whether inguinal or abdominal, are generally softer and smaller than are scrotal testicles. Abdominal testicles can be located anywhere from

just caudal to the kidney to within the internal inguinal ring. Most are located in or adjacent to the internal inguinal ring.[22] When searching for an abdominal testicle by palpation or ultrasonography, one of two different approaches can be taken. In the first approach, the ampulla on the side of the missing testicle is located by palpation and followed to the ductus deferens. The ductus, which feels like a tense string transrectally, can then be followed to the testicle. Alternatively, the inguinal ring on the side of the missing testicle is located by palpation. The ring itself and the adjacent areas can then be examined by palpation and ultrasonography until the presence or absence of the testicle is determined. In unusual cases, the testicle may be located near the caudal pole of the kidney (the site of its embryonic origin). This area and the area between the kidney and the inguinal ring should be examined if the testicle is not located in the inguinal region. To search for an inguinal testicle, the horse should be restrained in a manner similar to that described for ultrasonographic examination of the scrotal contents. Copious lubrication should be applied to the skin overlying the external inguinal ring. The head of the transducer is then pressed up into the inguinal region over the external inguinal ring to permit visualization of the inguinal canal. It may be necessary to apply firm pressure to the transducer to ensure good contact with the skin. This may result in slight discomfort to the horse, so caution must be exercised.

In addition or as an alternative to palpation and ultrasonographic diagnosis of cryptorchidism, hormonal assays can be used. The most commonly used assay is the human chorionic gonadotropin (hCG) stimulation test. This assay is useful only in cases in which no scrotal testicle is present. Paired plasma samples are drawn prior to and 30 to 120 minutes after administration of 6,000 to 12,000 IU hCG intravenously. If functional testicular tissue is present, a significant rise in plasma testosterone concentration occurs.[27] This technique is reportedly more than 90% accurate in detecting the presence of testicular tissue.[28] Baseline testosterone concentrations have also been used to diagnose cryptorchidism; however, normal variations in baseline values can make the results ambiguous. Measurement of plasma total conjugated estrogens also has been used to diagnose the presence of a retained testicle.[28] Animals with testicular tissue have significantly higher plasma conjugated estrogens than do geldings. This diagnostic technique is reportedly very successful in differentiating cryptorchid stallions from geldings.

Much debate exists over the heritability of cryptorchidism in the horse. The condition has been reported to be more prevalent in Quarter Horses, Percherons, and American Saddle Horses.[28] As long as sound evidence is lacking to either prove or disprove the heritable nature of cryptorchidism, and because many breed registries consider cryptorchid animals unsound, bilateral castration is strongly recommended.[29] It has also been suggested that cryptorchid testicles may be at an increased risk for neoplasia.[30] Until more information becomes available on the heritability of cryptorchidism, cryptorchid stallions, whether fertile or not, should be classified as unsatisfactory prospective breeders.[24]

Several hormonal treatments have been reported to cause the descent of cryptorchid testicles in humans, with mixed results.[31, 32] To the author's knowledge, these protocols have not been evaluated in horses in controlled studies and are not recommended. Orchiopexy does not result in the return of normal spermatogenesis.[22] Any attempt to either medically or surgically correct a cryptorchid testicle is considered unethical.

Scrotal Enlargement

Scrotal enlargement has many possible causes. Most cases of increased scrotal size are extratesticular in origin (i.e., scrotal hernia, blood, purulent debris, or increased peritoneal fluid in the vaginal cavity). Ultrasonography can be very helpful in determining the cause of scrotal enlargement.

Scrotal Fluid — Hydrocele, Hematocele, and Pyocele. Because the vaginal cavity is continuous with the peritoneal cavity, an increased amount of anechoic fluid (hydrocele) in the vaginal cavity can result from any systemic disease that causes either increased production of peritoneal fluid or decreased drainage of peritoneal fluid from the vaginal space. In addition, trauma, testicular torsion, neoplasia, or systemic disease resulting in dependent edema or pyrexia can result in hydrocele. Hydrocele can also be seen congenitally most often in Shire horses. Congenital hydrocele is usually not detrimental to the stallion.[33] Ultrasonographically, hydrocele is manifested as an increase in anechoic fluid within the vaginal cavity. The increase in fluid volume creates a greater contrast between the spermatic cord and the epididymis and their surrounding structures. A more distinct ultrasonographic outline of the cord and epididymis results (Figs. 10-33 and 10-34).

Blood (hematocele) or purulent fluid (pyocele) can also be visualized ultrasonographically within the scrotum. Clotted blood has an appearance similar to a corpus hemorrhagicum on a mare's ovary (gray-black, mottled, irregular). Hematocele can result from trauma or testicular torsion. The clot gradually increases in echogenicity as it organizes and fibroses. Purulent fluid generally has large amounts of particulate debris floating within it.

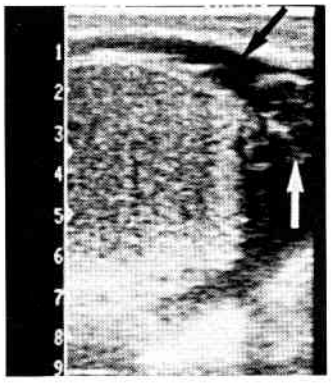

Figure 10-33

Ultrasonographic image of moderate hydrocele. The anechoic fluid (*black arrow*) clearly outlines the testicle and epididymal tail (*white arrow*) (5.0-MHz linear-array transducer).

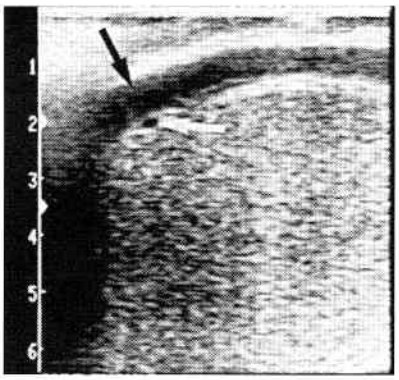

Figure 10-34

Ultrasonographic image of moderate hydrocele. The anechoic fluid (*black arrow*) surrounds the testicle and outlines a cross-section of an arcuate artery (*white arrow*) (5.0-MHz linear-array transsducer).

Pyocele can develop following a penetrating wound, secondary to rupture of an abscess, or as a result of peritonitis. In cases of hematocele and pyocele, fibrin tags may form and may be visible ultrasonographically as grayish structures floating or waving in the surrounding fluid (Fig. 10-35).

The prognosis for stallions with scrotal fluid depends largely on the underlying cause. Any type of fluid can be expected to cause at least transient insulating effects on the testicle and a resultant lowering of semen quality. In cases of hydrocele in which the underlying cause is eliminated and the fluid resolves, semen quality is expected to improve in about one spermatogenic cycle (approximately 60 days). In cases of hematocele or pyocele that develop adhesions or fibrous tissue, the prognosis for return to normal function of the affected testicle(s) is more guarded and depends largely on the extent of the pathology. Small adhesions may have little or no effect on future fertility. Extensive adhesions and fibrous tissue

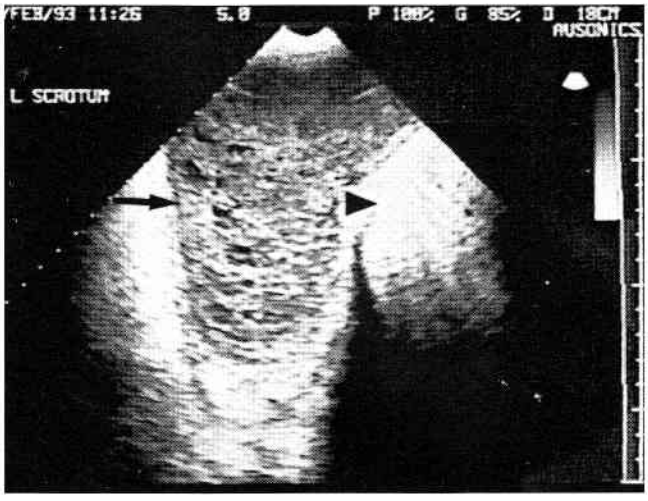

Figure 10-35

Ultrasonographic image of pyocele. Large amounts of purulent debris are distending the vaginal cavity (*arrow*). The fluid is echodense and contains particulate debris that could be seen swirling in real time. The arrowhead points to the testicle (5.0-MHz sector-scanner transducer).

formation may interfere with the normal thermoregulation of the testicles and may cause pressure necrosis of the testicular parenchyma. In bulls with hematocele, the affected testicle is often rendered nonfunctional.[34] Ultrasonography can be a valuable tool for monitoring the progress of affected stallions and is often of prognostic value when used to assess the extent of the pathology. If one testicle is unaffected by the problem, that testicle would be expected to return to normal function once any insulating effects were removed. It has been reported that adhesions between the parietal and visceral vaginal tunics can be found in older stallions, presumably as a result of capillary hemorrhage resulting from trauma to the scrotum incurred during normal activity.[23] Again, the significance of these adhesions depends on their severity.

Treatment of hydrocele depends on the underlying cause. In most instances, systemic anti-inflammatories and cold water hydrotherapy of the scrotum are included as part of the therapeutic plan. Treatment of hematocele resulting from trauma to the scrotum also includes systemic anti-inflammatories and cold hydrotherapy, with the possible addition of systemic broad-spectrum antibiotics. Pyocele is treated similarly to hematocele with the necessary addition of systemic antibiotics, ideally based on culture and sensitivity results (see section on scrotal aspirates, p. 466). In severe cases of hematocele or pyocele resulting in permanent injury to the testicle, unilateral orchiectomy may be considered. In cases of hematocele and pyocele, if one testicle is unaffected by the problem, that testicle is expected to return to normal function once any insulating effects are removed.

Inguinal/Scrotal Hernias. Ultrasonography has been described as a diagnostic aid for detection of congenital inguinal hernias in foals and acquired inguinal and scrotal hernias in horses.[8, 35] An inguinal hernia occurs when a loop of bowel passes into the inguinal canal. A scrotal hernia is a progression of an inguinal hernia in which the bowel loop passes into the scrotum.

Inguinal or scrotal hernias may be congenital or acquired, uncomplicated or complicated. In cases of congenital hernias in foals, the problem typically resolves spontaneously within the first 12 months of age. Congenital hernias typically involve small intestine. The herniated piece is usually viable.

Acquired inguinal and scrotal hernias can occur in geldings or in stallions and may occur with a higher incidence in Standardbreds.[36] Larger inguinal rings may predispose a horse to a hernia.[37] In many cases, acquired inguinal and scrotal hernias are associated with exercise or trauma.[38] Most acquired hernias in horses involve the small intestine. In acquired hernias, bowel loops may be either strangulated or nonstrangulated. Most horses are presented for an enlarged scrotum, colic, or both. Some horses with nonstrangulating inguinal or scrotal hernias do not exhibit any signs of discomfort. When a hernia is suspected, an examination of the internal inguinal ring by transrectal palpation usually confirms the diagnosis. If a hernia is present, loops of bowel can be palpated passing through the inguinal ring into the inguinal canal.

Acquired inguinal and scrotal hernias in horses are most often indirect.[38, 39] In an indirect hernia, an outpouching of the parietal peritoneum occurs through the

inguinal ring. This creates a sac lined by peritoneum that contains abdominal fluid and may or may not contain bowel loops. As the sac enlarges, it descends beside the spermatic cord and eventually into the scrotum. The herniated sac is located outside the tunica albuginea of the testicle. Ultrasonography can greatly aid in the examination of congenital and acquired inguinal or scrotal hernias and in assessing bowel viability. A 7.5- or 5.0-MHz linear-array or sector-scanner transducer can be used to evaluate scrotal contents or can be pressed high into the inguinal region to evaluate the external inguinal ring. When present, bowel loops are usually readily identifiable. In the case of scrotal hernias, variable amounts of free scrotal fluid (hydrocele) may also be detected and the testicle on the affected side may have increased echogenicity (Fig. 10-36).[5, 8] Ultrasonographic hallmarks of viable bowel include peristaltic waves and normal wall thickness. In cases of strangulating hernias, peristaltic waves are reduced or absent and the bowel wall appears thick and edematous. The type of bowel present in the hernia can also be determined using ultrasonography.[40] Small intestine, as is usually present, can be identified by its small diameter and long mesentery. The prognosis for congenital inguinal or scrotal hernia is very good, and most resolve spontaneously with time. In cases of acquired hernia, the most important prognostic indicator is the duration of the hernia. Regardless of whether or not the bowel is strangulated, prognosis is very good for cases in which the hernia is diagnosed and corrected early (<24 hours). Cases in which the hernia is left untreated for a long period of time are associated with a poorer prognosis. Treatment is not generally required for congenital hernias. In some rare protracted cases, surgical correction may be needed. In cases of acquired hernia, treatment is indicated.

In a few cases of uncomplicated acquired inguinal hernia, the hernia may be corrected manually by gentle transrectal traction on the herniated bowel. Bowel viability should be confirmed ultrasonographically before attempting to perform rectal taxis. Regardless of the condition of the bowel, this procedure carries a significant risk of rectal perforation and is not recommended in most cases. Most often, surgical correction of the hernia is required. Any case involving strangulated bowel absolutely requires surgery for resection of the compromised tissue and reduction of the hernia. Generally, the testicle on the side of the hernia is removed at the time of surgery to reduce the chances of recurrence of the hernia. In some cases it may be possible to salvage the testicle, but the owner should be made aware of the possibility of recurrence of the hernia.[39]

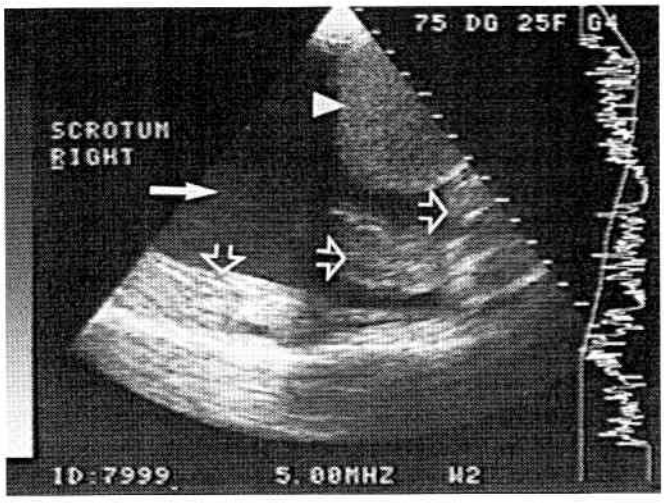

Figure 10-36

Ultrasonographic image of scrotal hernia. Severe hydrocele is present (*white arrow*). The testicular parenchyma is of normal echogenicity (*white arrowhead*). Sagittal sections of bowel loops are visible, and peristaltic waves could be seen in real time (*outlined arrows*) (5.0-MHz sector-scanner transducer).

Testicular Enlargement

Actual enlargement of the testicle itself is uncommon but can be due to orchitis, vascular or lymphatic stasis within the testicle, testicular abscess, testicular hematoma, or, in rare instances, testicular neoplasia. Enlarged testicles usually differ in ultrasonographic appearance from normal testicles. Although some ultrasonographic changes may be fairly subtle, they often become quite apparent if the opposite testicle is normal and its ultrasonographic appearance is compared with that of the affected testicle.

Vascular and Lymphatic Stasis. Chronic vascular stasis or lymphatic stasis, as in cases of chronic spermatic cord torsion, can cause testicular enlargement. If testicular enlargement is a result of spermatic cord torsion, abnormalities of the spermatic cord should also be visible on ultrasound (see section on spermatic cord torsion, p. 467).

Neoplasia. Testicular neoplasia is uncommon in the stallion,[41] and in most cases the testicle is not palpably enlarged. In fact, in many cases of testicular neoplasia, testicular degeneration is also present and the affected testicle is reduced in size. Testicular tumors can arise from either germinal or nongerminal cells. Germinal neoplasms are the most common tumor type found in stallions. Teratomas, seminomas, teratocarcinomas, and embryonic carcinomas are all germinal neoplasms that have been described in stallions.[42] Nongerminal tumors arise from stromal cells and include Sertoli and Leydig cell tumors.[43] A mixed germ cell-sex cord-stromal neoplasia has also been reported.[44] Most testicular tumors in the stallion are benign.

Almost no information is available on the ultrasonographic appearance of different testicular tumors in the stallion, and at this time it is not possible to ultrasonographically differentiate the tumor types. Tentative diagnosis of testicular neoplasia can be made based on ultrasonography; definitive diagnosis requires histopathologic examination. Testicular neoplasia results in a localized heterogeneous appearance to the normally very homogeneous testicular parenchyma. Figures 10-37 to 10-39 show three possible appearances of testicular neoplasia in three stallions.

Treatment for testicular neoplasia is usually orchiectomy of the affected testicle. If the testicle must be salvaged, and because most testicular tumors are benign and small with respect to the surrounding testicular parenchyma, it may be reasonable to refrain from treatment

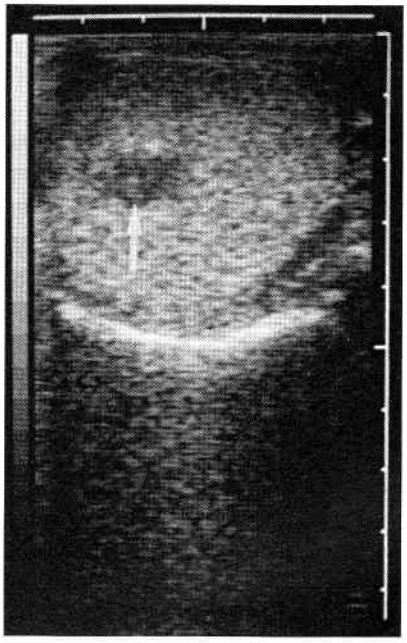

Figure 10-37

Ultrasonographic image of testicular tumor in a stallion. Arrow points to the tumor. The tumor appears as a punched-out lesion in the homogeneous testicular parenchyma (5.0-MHz linear-array transducer).

while continuing to monitor the lesion ultrasonographically for changes in tumor size and in the surrounding parenchyma. It is likely that a portion of the testicle will continue to function and contribute sperm to the ejaculate. In theory, histologic evaluation of an ultrasonographically guided testicular biopsy sample can aid in the decision about removing the testicle. In practice, the additional information gained from a biopsy sample may not be worth the risk of damage to the testicle that may be incurred during procurement of the sample. In humans, testis-sparing surgery for removal of benign testicular tumors has been described.[45] Cryosurgery has been used in one horse in our clinic with a benign testicular tumor. The cryosurgery was intended to halt the growth of the tumor and prevent further pressure

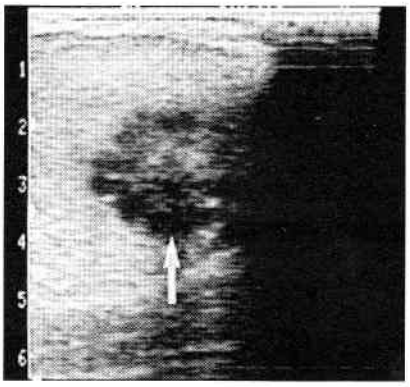

Figure 10-38

Ultrasonographic image consistent with testicular tumor (*arrow*) in an aged stallion. In this case, the lesion is heterogeneous and somewhat lacy compared with the surrounding parenchyma (5.0-MHz linear-array transducer).

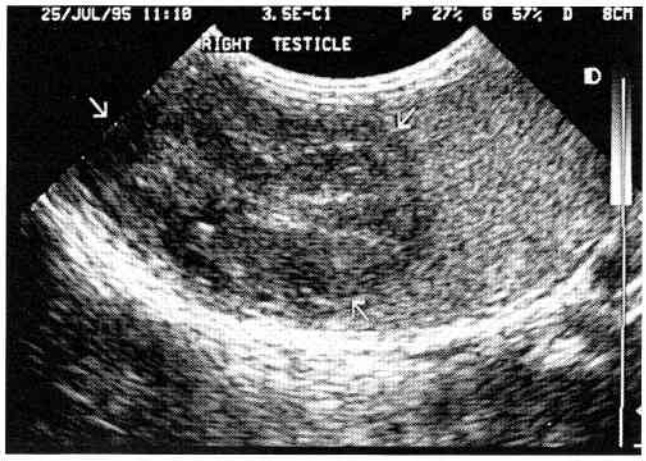

Figure 10-39

Ultrasonographic image of a large seminoma of the testicle in an aged stallion. Arrows delineate the borders of the neoplastic tissue. Normal testicular parenchyma is present to the right of the tumor (3.5-MHz convex linear-array transducer).

necrosis and degeneration of the surrounding testicular parenchyma. Unfortunately, regrowth of the tumor has continued in spite of the surgery.

Orchitis. Orchitis or inflammation of the testicular parenchyma is a rare cause of testicular enlargement in the stallion. Orchitis can arise secondarily to trauma, infection, parasites, or autoimmune disease.[46] The affected testicle is typically enlarged, hot, and painful. Systemic signs such as fever, leukocytosis, and hyperfibrinogenemia may also be present. If semen is collected and evaluated, large numbers of white blood cells are typically found and semen quality is often poor. Cultures of ejaculated semen may aid in identification of the causative organism in cases of infectious orchitis.

The ultrasonographic appearance of orchitis has been described in men and appears to be similar in stallions. In men with orchitis, the affected testicle is edematous and enlarged. Ultrasonographically, the testicular parenchyma usually maintains an overall homogeneously granular appearance but becomes hypoechoic with respect to its normal echogenicity. In some cases, the testicle appears heterogeneous with hypoechoic foci. In cases in which focal lesions are imaged, it may be difficult ultrasonographically to distinguish orchitis from neoplasia. In men, hydrocele, epididymitis, and thickening of the scrotal skin are typically associated with orchitis but not with neoplasia.[47, 48] The ultrasonographic appearance of orchitis in the stallion parallels that in men (Fig. 10-40).

Treatment should be initiated as soon as possible and should include broad-spectrum systemic antibiotics, antiinflammatory drugs, and cold hydrotherapy. If a causative organism is isolated, antibiotic selection should be based on sensitivity results. Alternatively, if the opposite testicle is normal, unilateral orchiectomy can be performed. Orchitis is associated with a guarded prognosis for future fertility.[46] In severe cases in which both testicles are affected, inflammation and increases in local temperature can result in fibrosis and degeneration of the testicular parenchyma. If one testicle is unaffected by the problem,

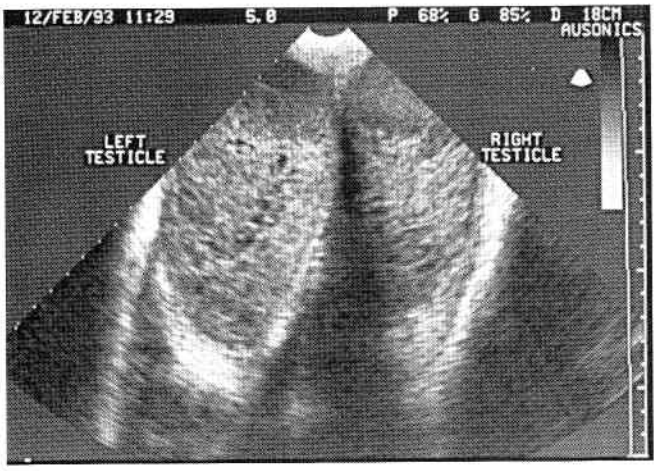

Figure 10-40

Ultrasonographic image of bilateral orchitis. The left testicle appears more severely affected than the right. Note the presence of numerous anechoic foci within the testicular parenchyma. The normal homogenicity of the parenchyma has been lost (5.0-MHz sector-scanner transducer).

the chances for return to normal fertility are greatly improved.

Testicular Abscess. Testicular abscesses can arise as a result of a penetrating wound through the scrotum and testicle, testicular biopsy, a progression of orchitis, a descending infection from the blood stream, or a descending infection from peritonitis. Stallions typically present febrile with a unilaterally enlarged, warm, painful testicle. Evidence of a previous wound or trauma to the scrotum may be found. Testicular abscesses can often be diagnosed with ultrasonography. A well-defined pocket of purulent fluid is generally visible within the testicular parenchyma. Abscess fluid typically contains large amounts of particulate debris that can sometimes be seen swirling in real time. Fibrin tags and adhesions may be visible around the testicle, and hydrocele may be present. If the abscess ruptures, pyocele may result. The ultrasonographic character of the surrounding testicular parenchyma may be altered as a result of pressure from the abscess (Fig. 10-41). Unilateral orchiectomy prior to rupture of the abscess is the treatment of choice in most cases. If the abscess has already ruptured, as evidenced by ultrasonographic appearance of the scrotal contents, the stallion should be treated as for pyocele. Surgery may be indicated to remove the testicle and drain the scrotal contents and so prevent an ascending peritonitis. Following surgical removal, the stallion should be placed on nonsteroidal anti-inflammatory drugs and systemic antibiotics based on culture and sensitivity results. If an attempt is made to salvage the testicle, nonsteroidal anti-inflammatory drugs and systemic antibiotics based on culture and sensitivity results from ejaculated semen or from an ultrasonographically guided aspiration of the abscess should be used. The prognosis for future fertility of an abscessed testicle depends on the size of the abscess and the extent of resulting fibrous tissue formation and pressure necrosis of the surrounding testicular parenchyma. Larger abscesses with extensive fibrous tissue decrease the likelihood that the testicle will return to normal function. If the opposite testicle is normal, the stallion may again be fertile following successful treatment or removal of the abscess. Any disease process that causes pyrexia or insulates the testicle can be expected to cause at least a temporary decrease in semen quality.

Testicular Hematoma. Testicular hematomas usually result from trauma to the testicle. Small hematomas are often seen following testicular biopsy.[49] Hematomas can form within the testicular parenchyma or on the surface of the testicle. Small intratesticular hematomas may not result in any noticeable scrotal enlargement. In the acute stages of a hematoma, the scrotum is enlarged, warm, and painful. The blood clot can often be visualized on ultrasonography. Ultrasonographically, acute testicular hematomas appear similar to a corpus hemorrhagicum on a mare's ovary. Most are distinctly different from normal testicular parenchyma and appear mottled grayish black (Fig. 10-42). If hemorrhage is still occurring, large pockets of relatively hypoechoic unclotted blood may also be seen swirling within the scrotal sac (Fig. 10-43). As the hematoma organizes, its ultrasonographic appearance becomes more echogenic, eventually appearing hyperechoic relative to the surrounding testicle. Fibrin tags and adhesions may also form in the affected area.

Prognosis for future fertility of the affected testicle depends on the size of the hematoma and the degree of fibrous tissue formation. Small hematomas (up to 20 mm in diameter) can be expected to cause only local changes in spermatogenesis, leaving the majority of the testicular parenchyma unaffected or only transiently affected by the temporary increase in temperature. Larger hematomas can be expected to cause more severe effects on fertility. The degree of loss of testicular parenchyma depends on the amount of pressure necrosis and fibrous tissue formation.

If the hematoma is contained, anti-inflammatory drugs, cold hydrotherapy, and stall rest may be the only treatments required. Once the hematoma condenses and the testicular temperature returns to normal, any undamaged testicular parenchyma should once again be able to con-

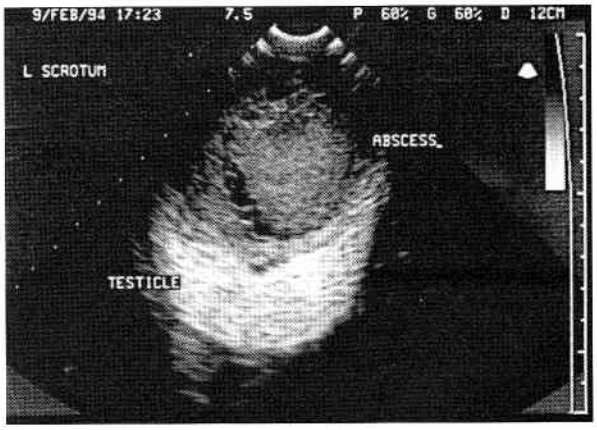

Figure 10-41

Ultrasonographic image of testicular abscess. The abscess contained particulate debris that could be seen swirling on real time. The testicular parenchyma is hyperechoic, possibly owing to compression by the abscess (7.5-MHz sector-scanner transducer).

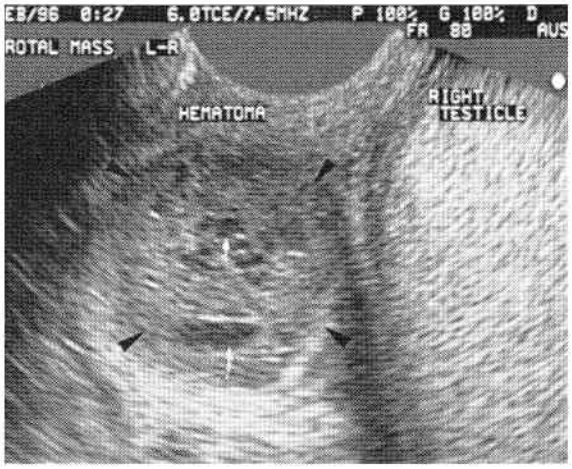

Figure 10-42

Ultrasonographic image of acute testicular hematoma. This hematoma *(black arrowheads)* is adjacent to the testicular parenchyma. The hematoma is mottled gray with several small hypoechoic/anechoic pockets of unclotted blood *(white arrows)*. The ultrasonographic appearances of testicular hematomas, as with any hematoma, can vary significantly depending on the amount of fresh bleeding, the amount of fibrin formation, and compression of the surrounding testicular parenchyma. In this image, the testicular parenchyma (labeled) appears ultrasonographically normal (wide-bandwidth 6.0-MHz microconvex linear-array transducer operating at 7.5 MHz).

tribute sperm to the ejaculate. In cases of extremely large hematomas in which bleeding is not contained, unilateral orchiectomy may be considered.

Other Testicular Abnormalities

Testicular Cyst. We have identified a lesion consistent with a testicular cyst in a fertile resident stallion at our fertility clinic. Ultrasonographically, the lesion is a well-delineated, circular anechoic pocket in the testicular parenchyma. The lesion has been present for at least 4 years with no apparent effect on the stallion's fertility (Fig. 10-44). The ultrasonographic appearance closely resembles that described for simple testicular cysts in humans. In humans, true simple testicular cysts are rare and are considered benign lesions. Ultrasonography can be used to definitively differentiate simple cysts from more aggressive lesions.[50, 51]

Frostbite and Thermal Damage. It has been suggested that ultrasonography may be useful in assessing damage to the testicles from congelation (frostbite) or from insulation or increases in temperature from any cause.[4]

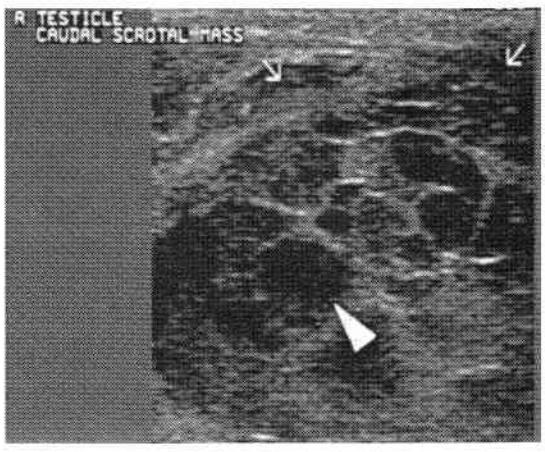

Figure 10-43

Ultrasonographic image of acute testicular hematoma. Note the large anechoic pockets of fresh blood *(white arrowhead)*, which give the image a "lacy" appearance. Thin arrows delineate the edges of the lesion. Testicular parenchyma is not visible (7.5-MHz linear-array transducer).

Testicular Biopsy and Scrotal/Testicular Aspirates

Information obtained from ultrasonographic examination of an abnormally large or small testicle can aid in clinical decisions on further diagnostics, treatment, and prognosis. When the sonogram suggests a localized soft-tissue lesion, such as neoplasia, an ultrasonographically guided testicular biopsy may be indicated to characterize the lesion histologically and determine if orchiectomy should be performed. When indicated, a carefully performed testicular biopsy can cause minimal permanent damage to the testicle. It must be kept in mind, however, that testicular biopsy results in at least some damage to the testicle. In stallions whose fertility is already marginal, biopsy may be contraindicated. The practitioner must carefully weight the diagnostic benefits from a biopsy against the risk of damaging some portion of functional testicular parenchyma. In the author's experience, testicular biopsy is rarely indicated.

A 5.0-MHz linear-array ultrasonography transducer has been used to evaluate localized changes in testicular parenchyma associated with testicular biopsy. Localized (1

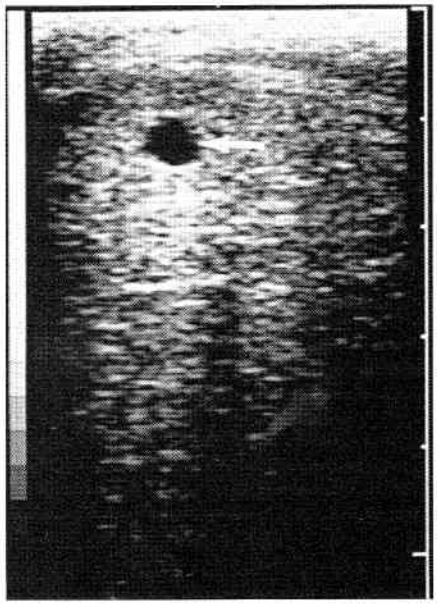

Figure 10-44

Ultrasonographic image consistent with a testicular cyst in a fertile stallion. The lesion is anechoic and appears well delineated *(arrow)* (5.0-MHz linear-array transducer).

to 20 mm) areas of decreased echogenicity were found in four of nine biopsied testicles. These parenchymal changes were associated with granulation tissue formation, fibroplasia, and small vessel infiltration of the parenchyma.[49] Ultrasonography was then used to monitor resolution of the lesions. It is likely that ultrasonographic evaluation will prove useful in detecting granulation tissue formation, fibroplasia, and small vessel infiltrant of the testicular parenchyma regardless of the cause.

When ultrasonographic examination of the scrotal contents indicates the presence of fluid, the ultrasonographic appearance of hydrocele (anechoic), pyocele (purulent debris, fibrin tags, adhesions), hematocele (mottled blood clots, fibrin tags, adhesions), and testicular abscess (localized pocket of purulent debris) may be used to arrive at a diagnosis. In most cases, obtaining an actual sample of the fluid provides little additional information, and physical examination, clinical signs, and ultrasonographic appearance of the fluid provide sufficient information to begin treatment. In cases in which additional information is needed to make a definitive diagnosis, a scrotal or testicular aspirate may be considered. Such aspirates should be avoided when possible owing to the possibility of introducing bacteria into the vaginal cavity or testicular parenchyma. In cases of testicular hematomas or hematocele, additional hemorrhage may result. When a culture and sensitivity testing are required, as in cases of pyocele or testicular abscess, culture of an ejaculate may isolate the inciting organism. An aspirate may be indicated when an organism is not isolated from an ejaculate or when an ejaculate cannot be obtained. Ultrasonography should be used as a guide when obtaining the aspirate, and the procedure should be performed using aseptic technique.

Abnormalities of the Spermatic Cord

Torsion of the Spermatic Cord. Torsion of the spermatic cord causes pathology in the testicle if the torsion results in vascular compromise. Torsions of less than 180 degrees often do not alter blood flow and therefore do not cause any clinical signs. Torsions of greater than 180 degrees can compromise blood flow to the testicle or cause lymphatic and venous stasis. In these cases, clinical signs are usually apparent. Affected stallions present with signs of colic associated with an enlarged and painful testicle, enlarged scrotum, increased scrotal fluid, and an enlarged spermatic cord. When the scrotal contents are evaluated ultrasonographically, abnormalities are readily visible. The lumina of the vessels of the spermatic cord become greatly increased in diameter. The testicular parenchyma may increase or decrease in echogenicity depending on the duration of vascular stasis. Decreased echogenicity may be seen in acute spermatic cord torsion before blood has clotted or in cases of lymphatic stasis. Increased echogenicity is typical in cases of chronic spermatic cord torsion in association with clotted blood or fibrosis. Hydrocele is often present. Ultrasonographic evaluation of the central vein, arcuate arteries, and pampiniform plexus may allow the veterinarian to determine the presence or absence of blood flow to and from the testicle. In some cases, vascular stasis may cause visible enlargement of any or all of these vessels (Figs. 10-45 to 10-49).[3] If Doppler ultrasound equipment is available, it can provide additional information on the presence or absence of blood flow in these vessels. Torsion of the spermatic cord has also been reported in cryptorchid testicles,[30] but no reports are available on the ultrasonographic appearance. The usual treatment for spermatic cord torsion with vascular compromise is castration of the affected testicle. If the torsion and associated inflammation and hydrocele cause an increase in scrotal temperature, a transient decline in semen quality from the contralateral testicle occurs. Once thermoregulation returns to normal, the contralateral testicle should return to normal function within one spermatogenic cycle. In cases of spermatic cord torsion in which the stallion is exhibiting signs of discomfort but the testicle is still viable, surgical correction of the torsion and orchiopexy may be possible to salvage the testicle.[52] Stallions with spermatic cord torsion that does not result in colic signs or vascular compromise require no treat-

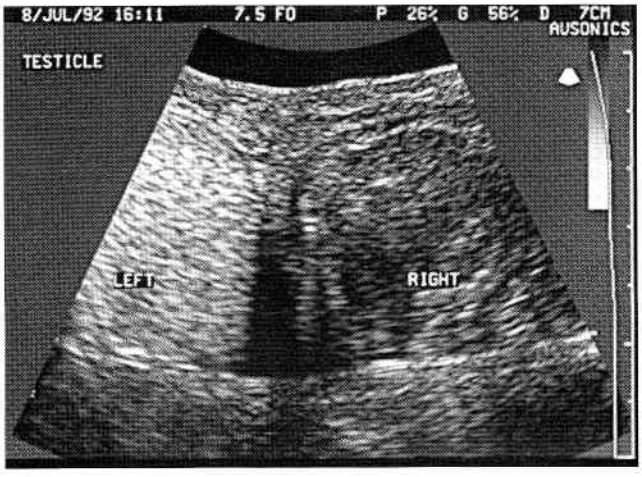

Figure 10-45

Ultrasonographic image of testicle affected by acute spermatic cord torsion. The left testicle is within normal limits. The right testicular parenchyma is hypoechoic owing to vascular and lymphatic stasis (7.5-MHz sector-scanner transducer).

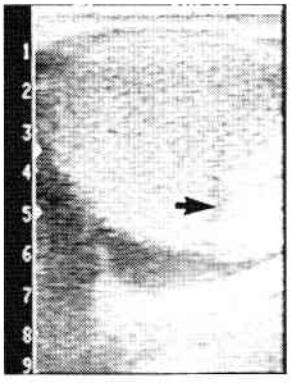

Figure 10-46

Ultrasonographic image of dilated testicular vessel (*arrow*) in a case of spermatic cord torsion in which venous drainage was compromised (5.0-MHz linear-array transducer).

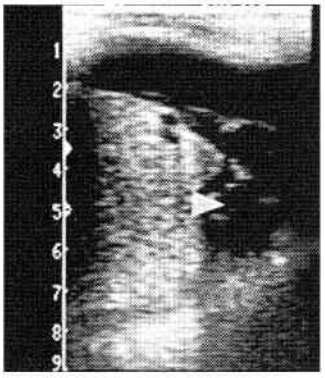

Figure 10-47

Ultrasonographic image of dilated arcuate arteries (*small arrows*) associated with spermatic cord torsion. Hydrocele is also present outlining the epididymal tail (*arrowhead points to tail*) (5.0-MHz linear-array transducer).

ment. In some instances, spermatic cord torsion may be intermittent. Again, if the stallion is asymptomatic and blood flow is not compromised, no treatment is required. Prognosis for stallions with unilateral testicular torsion is very good if prompt and appropriate treatment is provided. If the contralateral testicle was normal prior to the torsion, the stallion should again be fertile once normal thermoregulation is restored.

Varicocele. Varicocele (abnormal dilatation of the veins of the spermatic cord) can be detected ultrasonographically as a well-circumscribed, uniformly anechoic area within the spermatic cord. Varicoceles have been reported in stallions, but their effect on fertility is not known. Some reports suggest that they may cause a slight to moderate decrease in semen quality by interfering with thermoregulation of the testis.[22] A resident stallion at our clinic was determined to have a varicocele of at least 2 years' duration with no apparent effect on fertility (Fig. 10-50).

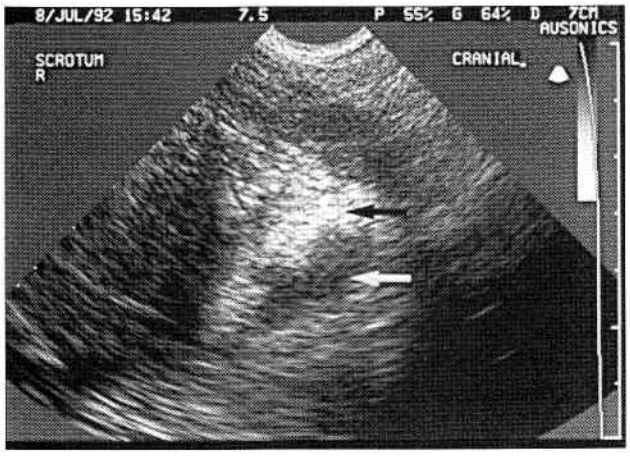

Figure 10-48

Ultrasonographic image of spermatic cord torsion. The cord is enlarged, and the normal architecture of the cord is lost. Areas of increased echogenicity (*black arrow*) are present, as are large hypoechoic fluid pockets (*white arrow*) representing severely dilated vessels and blood stasis (7.5-MHz sector-scanner transducer).

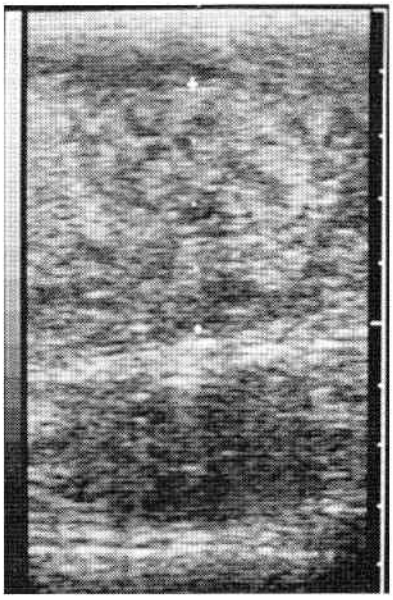

Figure 10-49

Ultrasonographic image of spermatic cord torsion. The affected cord is enlarged (delineated by calipers), and the normal architecture is lost. In this case, the cord appears more echodense owing to clotted blood and fibrin. The normal, unaffected cord is at the bottom of the picture, out of the plane of focus. Note the size relationship (5.0-MHz linear-array transducer).

Abnormalities of the Epididymis

Epididymitis. Although pathology of the epididymis is uncommon, over the last few years there have been multiple reports on the use of ultrasonography to detect epididymal pathology in the stallion.[10–12, 14, 53] As with ultrasonography of abnormal testicles, epididymal pathology usually becomes apparent when the affected epididymis is compared with a normal epididymis.

Ultrasonography can be used to aid in the diagnosis of epididymitis in the stallion. Unilateral epididymitis caused by *Streptococcus zooepidemicus* has been reported in two stallions and bilateral epididymitis caused by *Proteus mirabilis* in one stallion.[11, 53] Ultrasonographic appear-

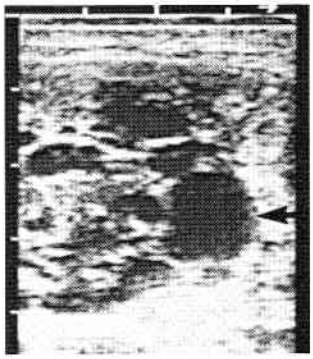

Figure 10-50

Ultrasonographic image of varicocele in a fertile stallion. Note several abnormally dilated, anechoic vessels (*arrow points to largest vessel*). The remainder of the spermatic cord architecture appears normal (7.5-MHz linear-array transducer).

ance of acute epididymitis varies among horses, but generally increased frequency and size of hypoechoic regions within the epididymis are found (presumably associated with accumulation of exudate and abscess formation). In some cases, scattered areas of increased echogenicity are also identified. See Figure 10-51 for one example of the ultrasonographic appearance of acute epididymitis in the stallion. Stallions may present with signs of either colic or lameness. On physical examination, the affected epididymis is enlarged and may be painful. Semen evaluation reveals poor sperm motility and large numbers of neutrophils in the ejaculate. In a report of chronic epididymitis, the appearance of the affected epididymis was again very heterogeneous. Some areas of the epididymis were similar in echogenicity to the testicular parenchyma, whereas others were more hyperechoic, presumably owing to fibrosis. An ejaculate could not be obtained from this horse owing to apparent pain associated with breeding.[14] The ultrasonographic image in Figure 10-52 is consistent with that of chronic epididymitis. When epididymitis is suspected based on physical and ultrasonographic findings, samples for bacterial culture can be obtained from ejaculated semen. Epididymal aspirates should be avoided when possible owing to the theoretic possibility of seeding the vaginal cavity or testicle with the bacteria.

In the reported cases of epididymitis in the stallion, the affected epididymis and testicles were removed by castration. In valuable stallions, systemic antibiotic therapy based on culture and sensitivity results from ejaculated semen, treatment with nonsteroidal anti-inflammatory drugs, and hydrotherapy could be attempted. However, it is difficult to achieve appropriate levels of antibiotics in the epididymis and it is unlikely that the epididymis will be functional even if the infection is cleared. In bulls with moderate or severe unilateral epididymitis, the affected epididymis becomes impatent owing to fibrosis and scar tissue formation, thus rendering the ipsilateral testicle sterile. The unaffected testicle and epididymis continue to function normally. The same is likely to hold true for stallions. Thus, orchioepididymectomy is the most logical course of therapy. In bulls with bilateral epididymitis, the prognosis for future fertility is grave.[22]

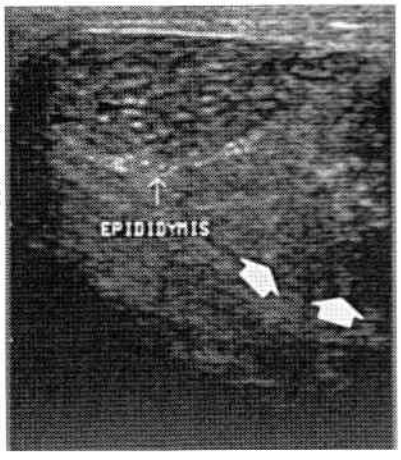

Figure 10-51

Ultrasonographic image of acute epididymitis *(thin arrow)*. This image was obtained over the epididymal body. Note the increase in size of the epididymal body with respect to the testicle and the increase in the number and size of anechoic regions within the epididymis suggestive of a dilated epididymal lumen (e.g., *black arrowheads*) (compare with Fig. 10-17). Some areas of increased echogenicity are also present. Testicular parenchyma is to the right *(large white arrows)*. Acute epididymitis was confirmed histologically following unilateral orchiectomy. The epididymal lumen was distended with large numbers of neutrophils (wide-bandwidth 6.0-MHz microconvex linear-array transducer operating at 10.0 MHz).

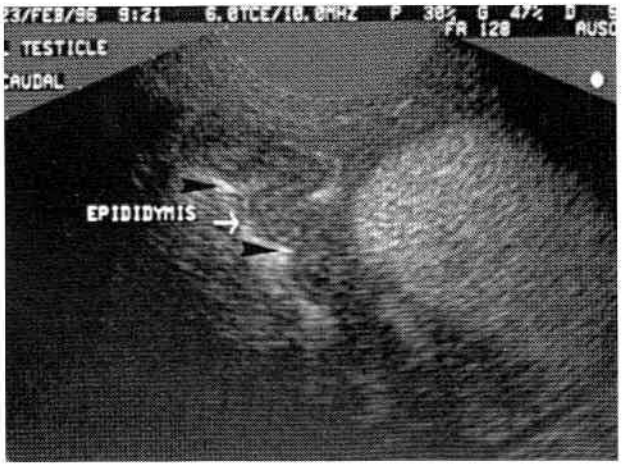

Figure 10-52

Ultrasonographic image of epididymitis *(thin arrow)*. This appearance is more suggestive of a chronic problem but a definitive diagnosis of acute versus chronic epididymitis cannot be made based on the ultrasonographic appearance alone. Note the unusual ribbon-like appearance of the epididymal tail which is distinctly different from the appearance of a normal epididymal tail (Figs. 10-16 and 10-17). A lumen is not obviously visible and the overall appearance is that of solid soft tissue. Areas of increased echogenicity are also present *(black arrowheads)*. Ultrasonographically normal testicular parenchyma is to the right (10.0-MHz sector-scanner transducer).

Sperm Granuloma. The use of ultrasonography to aid in the diagnosis of sperm granuloma in the epididymis has been reported in a stallion.[10] In this case, the epididymis was increased in size. Ultrasonographically, the affected epididymis possessed areas of decreased echogenicity interspersed with regions of increased echogenicity. These changes are compatible with chronic inflammation and are similar to ultrasonographic changes seen in stallions with infectious epididymitis.[14] Ultrasonographically, it is not possible to differentiate this condition from either infectious epididymitis or epididymal neoplasia. A definitive diagnosis of sperm granuloma was made on histopathologic examination of the epididymis following castration. A causative organism was not identified. Epididymal aspirates are not recommended in cases of epididymal pathology owing to the risk of spreading infection in cases of bacterial epididymitis or the risk of introducing infection in the case of sperm granuloma or neoplasia. Because the epididymis is a single duct, biopsies are contraindicated. During procurement of a biopsy sample, the duct could be transected and rendered nonfunctional.

Neoplasia. Ultrasonography was used to aid in the diagnosis of epididymal swelling attributed to lymphosarcoma. In this case, the epididymis had ultrasonographic characteristics similar to those of chronic epididymitis

(heterogeneous appearance of both hypoechoic and hyperechoic areas, sometimes lobulated).[12] In the reported case, the stallion was castrated bilaterally and the final diagnosis was made on histopathologic examination of the epididymis.

Although ultrasonography is helpful in identifying epididymal pathology, it is unlikely that a definitive diagnosis can be made based on ultrasonographic examination alone. In the reported cases, histopathologic examination of the epididymis following castration was required to define the problem definitively. Examination of ejaculated semen may help differentiate infectious epididymitis from sperm granuloma and neoplasia. Bacterial cultures of ejaculated semen are also helpful in antibiotic selection for cases in which medical treatment is attempted. Nonsteroidal anti-inflammatory drugs and cold hydrotherapy are also recommended as part of treatment. The outcome in any of these cases is likely to be an impatent epididymis. Thus, the recommended treatment in all cases is orchiectomy. The prognosis for fertility in stallions with unilateral epididymal pathology is good provided that the opposite testicle is normal. The prognosis is poor for return to normal function of an epididymis affected with any of the above problems.

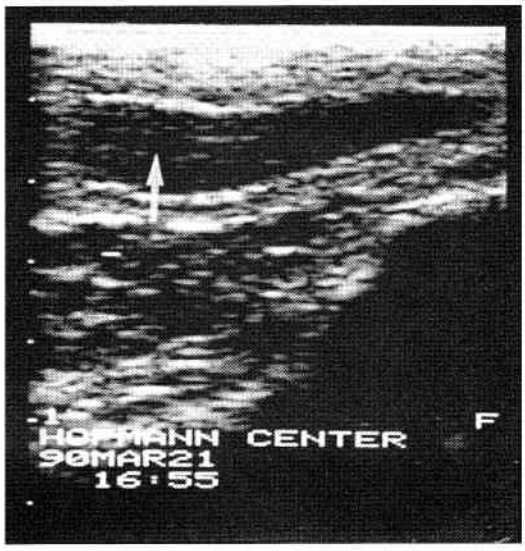

Figure 10-53

Ultrasonographic image of a sperm-occluded ampulla in a stallion. Note the large accumulation of anechoic fluid within the glandular lumen (*arrow*). Compare with Figures 10-21 and 10-22. The ultrasonographic appearance of sperm-occluded ampullae is often not this dramatic. Alternatively, a blockage may appear as a thick echodense line in the center of the gland. Many affected ampullae appear normal on ultrasonography (5.0-MHz linear-array transrectal transducer).

Abnormalities of the Accessory Glands

Pathology of the accessory sex glands of the stallion is rare. Becoming familiar with the normal ultrasonographic appearance of the accessory glands may allow one to identify pathology should it occur. Routine evaluation of the accessory glands has been recommended as part of the stallion fertility evaluation.[24]

Sperm-Occluded Ampullae. Ultrasonography has been used to assist in the diagnosis of sperm-occluded ampullae in the stallion.[54] In affected stallions, the ampullary lumen is often filled by a thick echodense line, probably representing large accumulations of sperm. In addition, the glandular portion of the ampullae may appear more echodense, with hyperechoic spots scattered throughout the parenchyma, again probably representing sperm accumulation. In some affected animals, the sperm blockage results in an accumulation of ampullary fluid. In these cases, the ampullary lumen is distended with abnormally large amounts of anechoic fluid (Fig. 10-53). Treatment for stallions with plugged ampullae involves repeated massage of the blocked ampulla(e) per rectum followed by frequent semen collections to break up and flush out the blockage. When possible, these procedures should be performed two or three times daily and continued until the blockage is resolved. This usually takes at least 1 to 3 days.

Following initial release of the blockage, ejaculates often contain superphysiologic numbers of sperm, with a very high percentage of tail-less heads and poor motility. Semen quality gradually improves with each subsequent ejaculation and eventually returns to normal for the individual as the plugged sperm are flushed out. Generally, a diagnosis of plugged ampullae cannot be made based on ultrasonographic findings alone. In some cases of plugged ampullae, the abnormal gland appears normal on ultrasonography. The ultrasonographic findings must be combined with the history and physical examination findings. Classically, stallions with plugged ampullae were previously fertile. Physical and ultrasonographic examinations reveal normal testicles. When semen is collected and evaluated, azoospermia or asthenospermia is typically present. A high percentage of tail-less heads in ejaculated sperm should also alert the clinician to the possible existence of plugged ampullae. Although the prognosis for stallions with ampullary blockage is good, blockage may recur after periods of sexual rest. It is likely that many cases of unilaterally blocked ampullae go unnoticed.

Seminal Vesiculitis. Seminal vesiculitis is reported uncommonly in stallions.[55-58] Affected animals typically are presented for poor semen quality and/or subfertility. In one instance, signs of colic were attributed to painful seminal vesicles in a stallion with seminal vesiculitis.[55] Affected stallions occasionally experience pain during ejaculation and thus may be presented for ejaculatory failure. Microscopic examination of ejaculated semen may reveal all or any of the following: numerous neutrophils, bacteria (sometimes intracellular), red blood cells, or reduced sperm motility. These findings should prompt further examination of the stallion's genitalia to determine the source of the problem. Palpation per rectum of the glands may reveal no abnormalities, but in some cases affected glands are abnormal on palpation and ultrasonography. In acute cases, the affected gland may be enlarged, painful, and filled with fluid. The fluid can vary from anechoic to relatively hyperechoic, containing particulate debris and fibrin. The lumen of the gland may be irregular rather than oval (Figs. 10-54 and 10-55). It is important to remember that normal seminal vesicles in sexually stimulated stallions can become dramatically enlarged

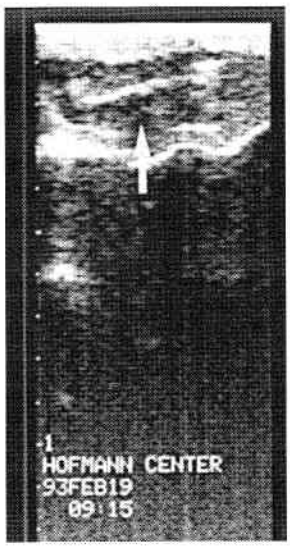

Figure 10-54

Ultrasonographic image of seminal vesiculitis in a draft horse stallion. Fluid in the lumen of the gland is relatively hyperechoic and contains particulate debris (*arrow*). In addition, the lumen is wavy and irregular. Compare with Figures 10-25 and 10-26 (7.5-MHz linear-array transrectal transducer).

and filled with anechoic fluid. Thus, the diagnosis of seminal vesiculitis often cannot be made on the basis of ultrasonographic findings alone. In cases of chronic seminal vesiculitis, affected glands become firm to hard and may contain little or no fluid. Ultrasonography of seminal vesiculitis has been reported more frequently in bulls.[59]

Beta-hemolytic streptococci, *Pseudomonas aeruginosa*, and *Streptococcus equisimilis* have been implicated in causing seminal vesiculitis.[56-58] Bacterial culture and sensitivity of ejaculated semen often isolate the causative organism. Appropriate systemic antibiotic therapy based on sensitivity results can then be instituted. However, treatment of seminal vesiculitis can be frustrating because it is difficult to obtain sustained high concentrations of antibiotics within the gland(s). The course of antibiotic treatment may exceed 4 weeks.[55] Alternatively, a pediatric flexible endoscope can be passed through the urethra and a culture swab advanced directly into the vesicle via the seminal colliculus to culture its contents.[60] This approach can also aid in treatment. A small plastic catheter can be advanced into the gland through the endoscope channel, and the gland can be lavaged and infused with appropriate antibiotics. This should be performed once daily and treatment continued as indicated (generally 1 to 2 weeks). Antibiotic therapy should be combined with regular semen collections with the intent of causing repeated evacuation of the gland. Systemic nonsteroidal anti-inflammatory drugs should also be included in the treatment plan. Evaluation of semen quality and regular ultrasonographic evaluations of affected glands can be used to monitor response to treatment.

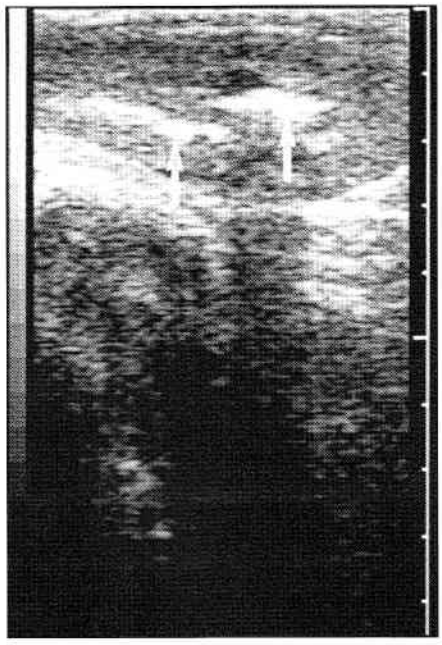

Figure 10-55

Alternative ultrasonographic appearance of seminal vesiculitis. In this case, the gland contains very hyperechoic material (*white arrows*). The general shape of the gland is normal (5.0-MHz linear-array transrectal transducer).

In bulls, intravesicular infusions of sclerosing agents have been used to induce fibrosis in refractory cases of seminal vesiculitis; alternatively, seminal vesiculectomy can be performed. One report of seminal vesiculectomy in a stallion has been published. Surgery was performed via a perineal incision, and the affected seminal vesicle was removed with an emasculator in a manner similar to the technique used in bulls. In this case, surgery was curative.[57] Alternative surgical techniques have also been reported.[60]

The prognosis for stallions with seminal vesiculitis is guarded. Some cases reportedly resolve spontaneously, whereas others remain refractory despite extensive therapy.[56, 58, 60] When treatment is instituted, the cost is often high. Some cases can be effectively cured with persistent and appropriate systemic or intravesicular antibiotics combined with nonsteroidal anti-inflammatory drugs.

Prostatitis. Abnormalities of the prostate have not been reported in stallions. The author is aware of one case of prostatitis that was diagnosed incidentally at necropsy examination.*

Bulbourethral Gland Cysts. Abnormalities of the bulbourethral glands are rare. Cysts of the bulbourethral glands do occur but appear to have no clinical effect on the stallion. Bulbourethral gland cysts may be identified incidentally on ultrasonographic examination of the accessory glands during a breeding-soundness examination. Ultrasonographically, bulbourethral gland cysts appear as localized, circular, anechoic fluid-filled areas within the parenchyma of the bulbourethral glands (Fig. 10-56).

Terminal Aorta and Iliac Arteries

Anatomy, Ultrasonographic Appearance, and Pathology

The termination of the aorta and its branching into the internal and external iliac arteries occur beneath the

* Dr. Patricia L. Sertich, personal communication.

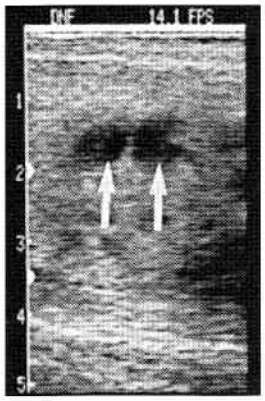

Figure 10-56

Ultrasonographic image of bulbourethral gland cysts. In this case, two cysts are present and appear as paired, anechoic pockets (*arrows*) within the surrounding normal gland tissue (7.5-MHz linear-array transrectal transducer).

sacrum along the dorsal midline. The reader is referred to Chapter 5 for details of ultrasonographic anatomy and technique. During ultrasonographic examination of the accessory sex glands, the terminal aorta and iliac arteries are easily visualized by directing the beam of the transducer dorsally along the midline.

The condition of aortoiliac thrombosis has been reported in horses (see Chapter 5). In stallions, this condition has been associated with ejaculatory failure and weakness in the hind limbs due to vascular compromise, disturbance of innervation, and/or pain.[61] In such cases, ultrasonography was used to aid in diagnosing the condition and forming a prognosis. Ultrasonography allowed visualization and size determination of the thrombus and aided in the assessment of amount of blood flow through the iliac arteries to the hind limbs and penis. The presence of a thrombus typically is easily discernible ultrasonographically. The gray-white thrombus can be seen extending from the wall of the artery into the lumen of the vessel, and the normally smooth flow of blood is interrupted by its presence (see Chapter 5 for normal and abnormal images).

If properly managed, stallions with ejaculatory dysfunction and/or weakness associated with aortoiliac thromboses can return to breeding. Successful management involves pain control with phenylbutazone, extreme sexual stimulation, and controlled exercise to encourage development of blood flow to the extremities. In stallions with good libido that develop an erection, mount, and initiate thrusting but fail to ejaculate, additional stimulation of the penis can be achieved during natural cover or during semen collection into an artificial vagina. This is most often accomplished by applying hot (~50°C) towel compresses to the base of the penis during thrusting. The added stimulation to the penis often induces additional thrusting and results in ejaculation.[61,62] Pharmacologically induced ejaculation can also be attempted.

Metastasis of a transitional cell carcinoma of the bladder to the common iliac artery with resultant iliac thrombus formation has been reported in a neurologic stallion with chronic urospermia.[63] Ultrasonographically, the tumor/thrombus appeared as numerous gray-white soft-tissue masses extending from the wall of the iliac artery and protruding into the iliac lumen (Fig. 10-57). Blood could be seen swirling in an irregular flow pattern as it coursed around the masses. Similar masses were visible extending from the bladder wall into the bladder lumen. It could not be determined whether the tumor was related to the chronic urospermia. The prognosis in cases of metastatic neoplasia is grave. In the case described, the stallion was humanely euthanized.

Penis

Little work has been published on ultrasonographic examination of the stallion penis. The penis can be scanned while fully erect. However, this requires that the stallion stand quietly for examination after teasing and without losing the erection. As an alternative, the stallion can be sedated with xylazine or a similar drug. In many cases, following sedation the penis descends in the flaccid state and can be examined.

Anatomy

The stallion possesses a musculocavernous penis. The penis consists of a base connected by two crura to the ischial arch, a shaft that extends from the base to the glans, and a glans that is the enlarged free end of the penis. The penile urethra is a continuation of the pelvic

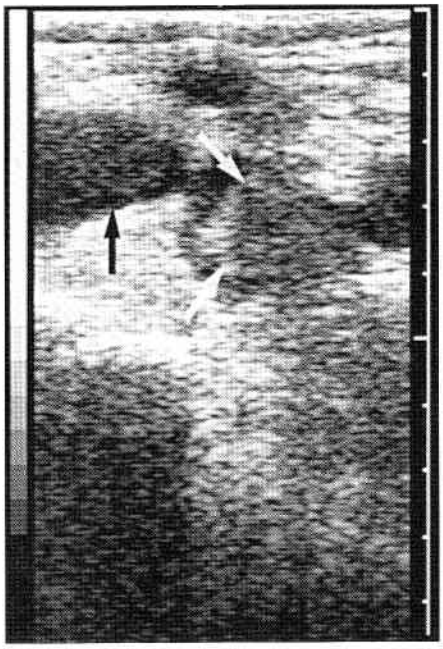

Figure 10-57

Ultrasonographic image of short-axis cross-section of the iliac arteries in a stallion with metastatic transitional cell carcinoma and thrombus formation. The normal artery is indicated by the black arrow. The abnormal artery contains a gray-white mass (*white arrows*) that extends from the wall of the vessel into the lumen. The mass occupied approximately 90% of the vessel lumen and thus severely compromised blood flow (5.0-MHz linear-array transrectal transducer).

urethra. The penile urethra traverses the length of the penile shaft and extends outward from the glans as the urethral process. The urethral fossa is a small invagination of the glans epithelium dorsal to the urethral process (Fig. 10-58*A*).

Erection is caused by engorgement of the cavernous tissues with blood. The corpus cavernosum penis is the larger of the two erectile spaces. It extends along the length of the penile shaft dorsal to the urethra in a roughly crescent shape. The corpus cavernosum penis is surrounded by the tunica albuginea. The corpus spongiosum penis is a smaller area of erectile tissue that extends along the entirety of the penile shaft and surrounds the urethra. It is directly continuous with the erectile tissue of the glans (Fig. 10-58*A*).

Superficial blood vessels are located at irregular intervals around the surface of the penis outside the tunica albuginea (Fig. 10-58*B*). These vessels run parallel to the penile shaft and taper as they course distally toward the glans. In the flaccid state, the penis is completely encased in the prepuce. The prepuce consists of a folded layer of epithelium, the internal preputial fold, and the external preputial fold or sheath. The external fold is a continuation of the skin of the ventral body wall. The internal fold extends from the external fold to the penis. In the erect state, the prepuce unfolds and covers the base of the erect penis, leaving the shaft and glans uncovered.

Patient Preparation

If an appropriate tease mare is available and the stallion is reasonably tractable, he should be teased until a full erection is achieved. The mare can remain within sight of the stallion during the examination to stimulate the stallion to maintain an erection. If the situation is not conducive to this procedure, xylazine or a similar drug can be administered intravenously. In most cases, a dosage that results in moderate sedation (±0.5 mg/kg) causes the penis to descend in the flaccid state. Acepromazine should not be used in stallions owing to its reported association with paraphimosis.[64] Once the penis has descended, the stallion should be restrained as previously described for examination of the testicles. The penis should be cleansed with warm water and dried to provide a smooth surface for examination. A 7.5-MHz linear-array or sector-scanner transducer provides good detail of the penis. A 5.0-MHz transducer is usually adequate if a 7.5-MHz transducer is not available. A standoff pad may be added if a 5.0-MHz transducer is used. An adequate amount of ultrasonographic coupling gel must be used to provide proper transducer contact.

Scanning Technique

The penis is first scanned from the base to the glans, with the linear-array transducer held perpendicular to the long axis of the penis (Fig. 10-59). This provides the veterinarian with short-axis cross-sectional images of the penis. the urethra and its associated musculature, the corpus cavernosum penis, and the corpus spongiosum penis. The transducer should be used to scan both dorsally to ventrally and ventrally to dorsally. The dorsoventral image (Fig. 10-59d) provides the best detail of the corpus cavernosum penis, and the ventrodorsal image (Fig. 10-59c) provides the best detail of the corpus spongiosum penis and the urethra. The penis can also be scanned

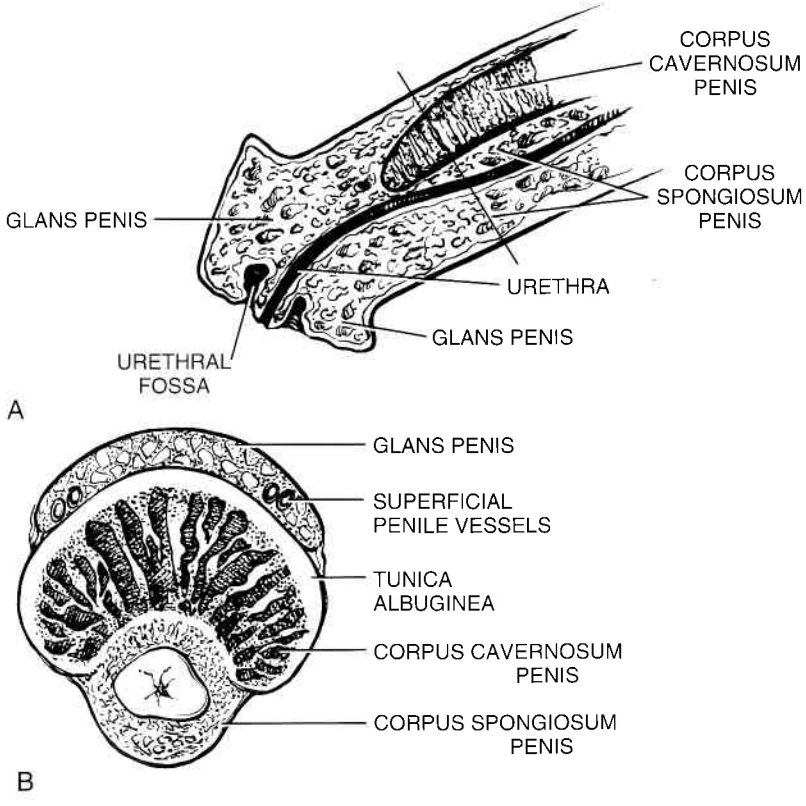

Figure 10-58

A, Sagittal section of a stallion's distal penile shaft and glans, showing the corpus cavernosum penis, corpus spongiosum penis, penile urethra, and erectile tissue of the glans. Notice that the corpus cavernosum penis decreases in size as it proceeds distally along the penile shaft. Also notice that the corpus spongiosum penis is continuous with the erectile tissue of the glans.

B, Short-axis cross-section of the penile shaft of the stallion showing the relative relationships of the various tissues. The positions of the superficial penile vessels can vary. This cross-section is drawn from the area of the solid line in Figure 10-58*A*.

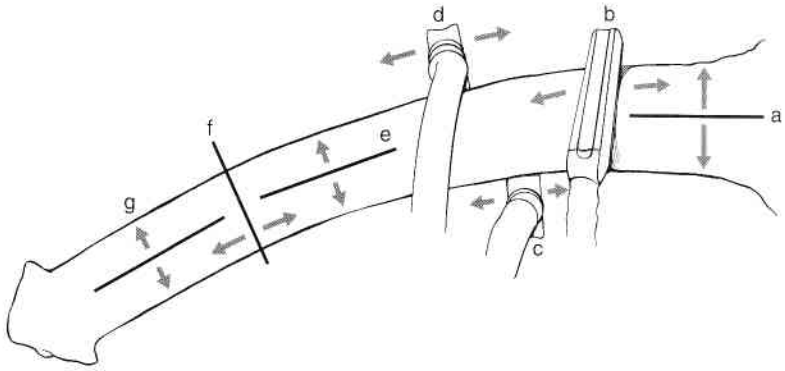

Figure 10-59

Proper positions of the transducer for imaging the stallion penis. Solid lines represent additional transducer positions. a, Position of the transducer to image the penile base in sagittal section. b, Position of the transducer to image the superficial penile vessels in short-axis cross-section. c, Position of the transducer to image the corpus spongiosum penis in short-axis cross-section. d, Position of the transducer to image the corpus cavernosum penis in short-axis cross-section. e, Position of the transducer to image the penile shaft in sagittal section. f, Position of the transducer to image the penile shaft in short-axis cross-section. g, Position of the transducer to image the distal penile shaft and glans section. With the probe in this position, the corpus spongiosum penis can be followed distally as it becomes the erectile tissue of the glans.

in longitudinal section by holding the linear transducer parallel to the long axis of the penis (Fig. 10-59a, e, and g). Oblique short-axis cross-sectional views are best for obtaining images of the superficial penile vessels (Fig. 10-59b).

Normal Images

In short-axis cross-section, the corpus cavernosum penis is crescent-shaped and heterogeneous gray-black. In the erect penis, the blood-filled cavernous spaces of the corpus cavernosum penis can be seen as pinpoint anechoic areas within the surrounding tissue. Hyperechoic trabeculae originating from the tunica albuginea at the ventral aspect of the corpus cavernosum penis may be seen radiating outward through the corpus cavernosum penis (Figs. 10-60 and 10-61). As the transducer is moved distally toward the glans, the crescent-shaped corpus cavernosum penis slowly decreases in size. In long-axis sagittal sections, the corpus cavernosum penis appears as a

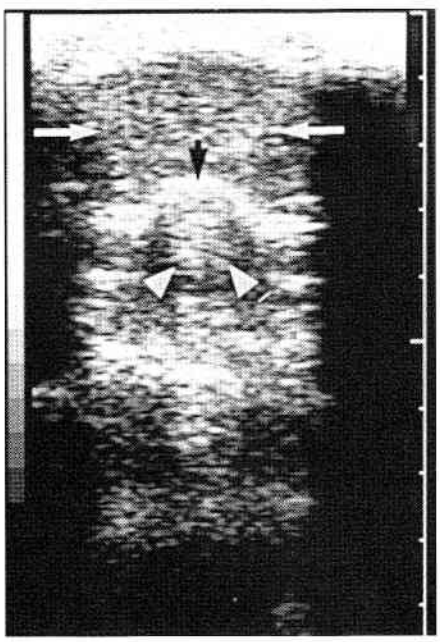

Figure 10-60

Short-axis cross-sectional image of a normal midshaft of an erect penis in a stallion. The transducer is held on the dorsal surface of the penis with the beam directed ventrally as in Figure 10-59d. The corpus cavernosum penis (*white arrows*) is crescent-shaped and heterogeneous gray-white. The tunica albuginea (*black arrow*) surrounds the corpus cavernosum penis. The corpus spongiosum penis (*white arrowheads*) is circular and surrounds the urethra (not visible) (5.0-MHz linear-array transducer).

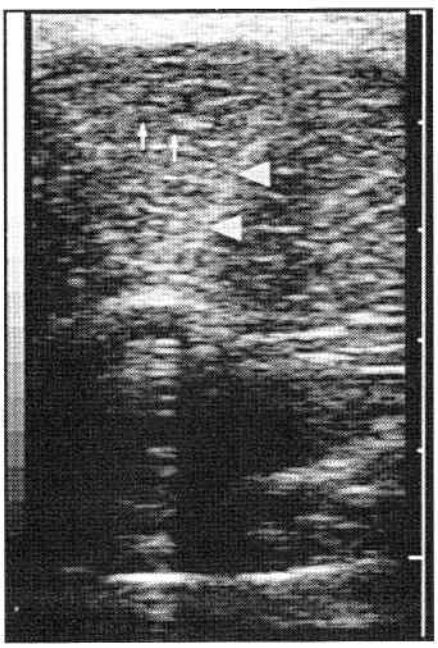

Figure 10-61

Detailed ultrasonographic image of short-axis cross-section of the corpus cavernosum penis in a normal midshaft of an erect stallion penis. This image was obtained with a 7.5-MHz linear-array transducer held as in Figure 10-59d. Blood-filled cavernous spaces can be seen as pinpoint anechoic areas within the corpus cavernosum penis (*white arrows indicate two examples*). Trabeculae are also visible radiating through the corpus cavernosum penis (*white arrowheads delineate one trabeculum*). The corpus spongiosum penis is not clearly visible.

large rectangular area adjacent to the narrower corpus spongiosum penis and urethral musculature. The tunica albuginea is also visible in both short-axis cross-sectional and longitudinal sectional views (Fig. 10-62; see also Fig. 10-60).

Owing to a relative increase in the ratio of cavernous space to tissue, the corpus spongiosum penis has a more lacy appearance than does the corpus cavernosum penis. In short-axis cross-section, the corpus spongiosum penis is doughnut-like and surrounds the urethra and its associated musculature along the entire penile shaft (Fig. 10-63). In long-axis sagittal section, the corpus spongiosum penis is rectangular and much smaller than the corpus cavernosum penis. The corpus spongiosum penis can be seen dorsal and ventral to the urethral musculature (see Fig. 10-62). Near the distalmost aspect of the penile shaft, the corpus spongiosum penis can be followed in long-axis sagittal section as it expands into the erectile tissue of the glans (Fig. 10-64).

The superficial vessels of the penis are best imaged in oblique short-axis cross-section. The exact locations of these vessels may vary in different stallions. Blood flow may be visible in real time (Fig. 10-65). The urethral musculature, and occasionally the urethral lumen, can be visualized ultrasonographically. The urethral musculature is more hyperechoic than the surrounding corpus spongiosum penis. The urethral lumen usually exists as a potential space, and thus the lumen itself is often not clearly visible. If the urethral lumen is distended with fluid, as it may be immediately following urination, it may be visible as an anechoic area within the surrounding muscle.[26] The urethral lumen is more readily defined in longitudinal section than in cross-section (see Fig. 10-62).

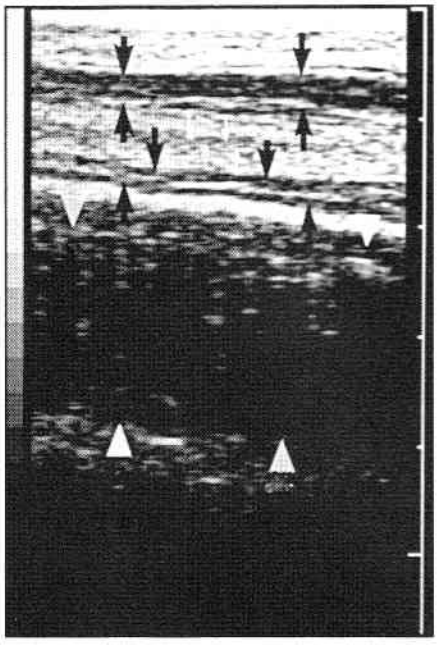

Figure 10-62

Ultrasonographic image of long-axis sagittal section of the midpenile shaft. The transducer is held on the ventral surface of the penis, parallel to the length of the penile shaft, and the beam is directed dorsally. Because it is in the plane of focus for the 7.5-MHz linear-array transducer, the corpus spongiosum penis is seen both above and below the urethra. Black arrows denote the corpus spongiosum penis. The urethra is delineated by small white arrows. The corpus cavernosum penis is beneath the corpus spongiosum penis in this view but is not in the best plane of focus for the transducer (*white arrowheads*). A more detailed image of the corpus cavernosum penis is obtained when the transducer is placed on the dorsal surface of the penis and the beam is directed ventrally.

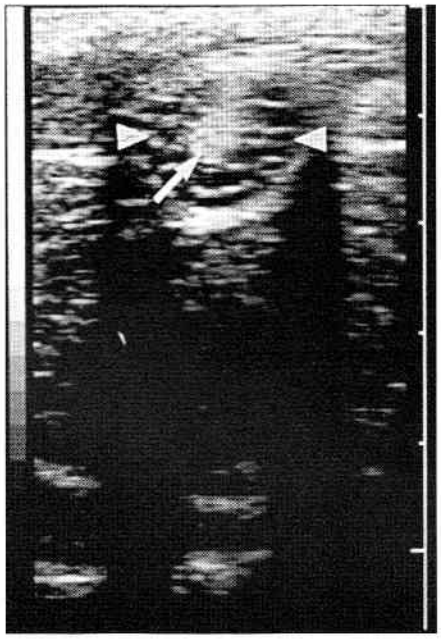

Figure 10-63

Ultrasonographic image of short-axis cross-section of the corpus spongiosum penis and urethral musculature in a normal midshaft of an erect stallion penis. This image was obtained with a 7.5-MHz linear-array transducer held as in Figure 10-59c. The corpus cavernosum penis is not clearly visible. The corpus spongiosum penis (*white arrowheads*) appears lacy and surrounds the more homogeneous, gray-white urethral musculature (*white arrow*). The urethral lumen cannot be seen.

Abnormal Ultrasonographic Findings

Ultrasonographic examination of the penis is indicated in cases of erectile dysfunction, paraphimosis, priapism, or other obvious penile pathology.

Penile Hematoma. Hematomas of the penis are uncommon in stallions and are generally the result of trauma. Typically, the trauma occurs to the erect penis during breeding.[22] Damage to the superficial vessels or to the tunica albuginea resulting in blood leakage from the corpus cavernosum penis has been incriminated in hematoma formation.[65] Hemorrhage from the corpus spongiosum penis resulting in a hematoma has also been reported.[66] The hematoma itself is generally not a serious problem, but if it is large enough it may prevent the stallion from retracting the extended penis. This in turn results in paraphimosis and the development of dependent edema (see section on paraphimosis, p. 476). Ultrasonographic examination of a penile hematoma can provide information on the size and location of any rents in the tunica as well as information on the size of the hematoma. It can also be used to monitor resolution and contraction of the hematoma. Fresh hematomas appear

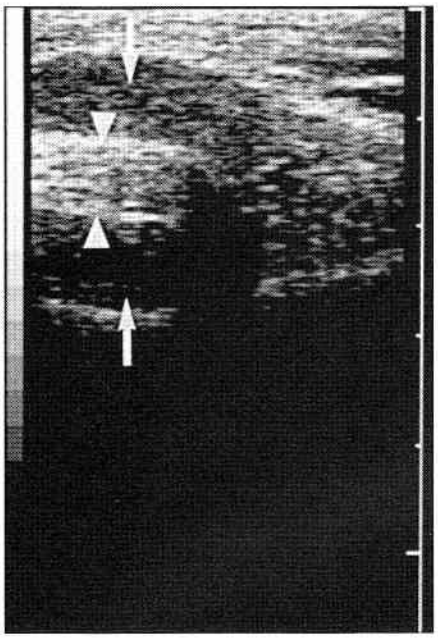

Figure 10-64

Long-axis sagittal section of the distal urethra and erect glans penis in a stallion. In real time, the corpus spongiosum penis can be followed as it expands into the glans. White arrows denote the erectile tissue of the glans. White arrowheads point to the urethral musculature (5.0-MHz linear-array transducer).

mottled gray-black with areas of fluid pockets. As they fibrose and contract, fibrin tags may be seen. The ultrasonographic appearance gradually increases in echogenicity as the clot is replaced by fibrous tissue. Small fibrous scars may persist at the sites of previous hematomas.

In cases of uncomplicated hematomas in which paraphimosis has not occurred, stallions should be treated with anti-inflammatory drugs, cold hydrotherapy, and strict stall rest. They should not be used for breeding or exposed to mares for 3 to 8 weeks following the injury to allow time for the damage to the tunica albuginea to heal.[67] Normal masturbation is difficult to discourage and it is better to allow masturbation than to attempt to prevent it using stallion rings or other devices that may cause further damage to the penis. In bulls with severe penile hematomas resulting in irreducible paraphimosis, efforts have been made to repair the tear in the tunica surgically.[68]

The prognosis for fertility is good in stallions with uncomplicated hematomas. In cases in which secondary paraphimosis develops, the success of treatment depends largely on the ability to correct the paraphimosis.

Paraphimosis. Paraphimosis (inability to retract the penis) can result from traumatic injuries to the penis[69, 70] or debilitation.[71, 72] Administration of phenothiazine tranquilizers has also been implicated as a cause of paraphimosis.[64] Persistent paraphimosis results in dependent edema of the glans and shaft, which increases the size and weight of the penis. A vicious circle results as the penis progressively becomes larger, more dependent, and more difficult to retract. If the condition is allowed to persist, the exposed penis often sustains mechanical injuries or, in cold weather, congelation (frostbite). This results in worsening of the damage and development of granulation tissue.

Examination of affected animals includes physical examination of the penis. Particular attention should be paid to the presence or absence of sensation in the distal penile shaft and glans. Ultrasonographic examination can document the extent of trauma, the degree of edema, the depth of granulation tissue (if present), and the presence or absence of blood flow to the shaft and glans. Penile edema causes a progressive decrease in echogenicity of the affected tissues as fluid accumulates within the tissue. Occasionally, isolated pockets of edema fluid may be visible within the tissue. In one reported case of paraphimosis in a stallion, the corpus cavernosum penis was increased in echogenicity, presumably associated with thrombus formation.[73] In cases of chronic paraphimosis in which severe trauma to the extended penis has occurred, granulation tissue may develop. Ultrasonography can be used to measure the depth of granulation tissue and so can aid in surgical removal of granulation tissue or in monitoring progression or resolution of the problem. Circumcision (reefing operation) may be indicated in stallions with excessive granulation tissue.[74] As with penile hematomas, ultrasonography can be used to define areas of the penis in which blood supply is compromised or absent. When blood supply is absent, flow is not visible in the penile vessels or within the erectile tissue. In cases of thrombus formation, the erectile tissue increases in echogenicity (Fig. 10-66).

Regardless of the external appearance of the penis, the most important prognostic indicator in cases of traumatic

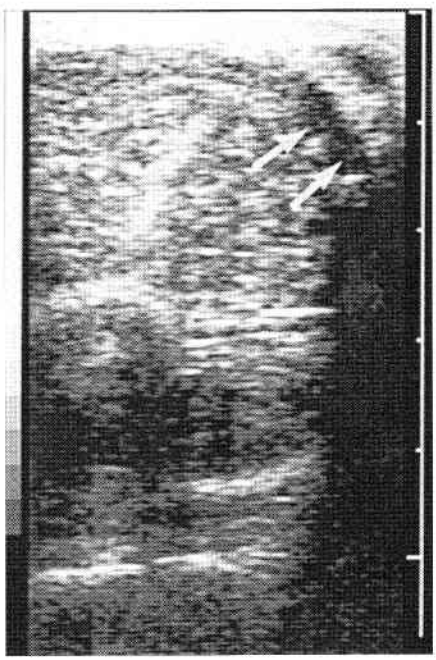

Figure 10-65

Oblique short-axis cross-section of the superficial penile vessels (*white arrows*). In real time, blood flow can usually be seen. The exact location of these vessels can vary slightly from horse to horse. This image also shows the corpus cavernosum penis with one apparent trabeculum, the ventralmost portion of the tunica albuginea, and a poorly detailed corpus spongiosum penis (7.5-MHz linear-array transducer).

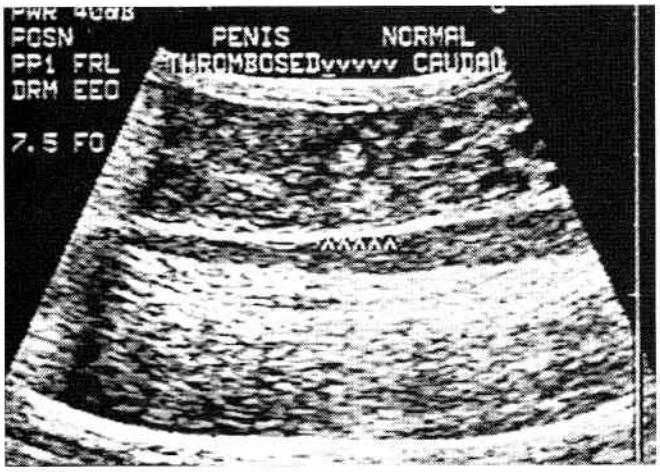

Figure 10-66

Sagittal section of thrombosis of the corpus cavernosum penis in a stallion with chronic paraphimosis. Note the normal, blood-filled cavernous spaces in the unaffected caudal portion of the corpus cavernosum penis. Compare this to the gray-white dense material of the thrombosed portion of the corpus cavernosum penis (*delineated by arrowheads*) (7.5-MHz sector-scanner transducer).

paraphimosis is whether or not the penis can be manually replaced into the sheath. Every effort should be made to replace the penis into the sheath and thus break the cycle of edema/trauma/progressive paraphimosis. Manipulation of the penis may be painful to the stallion, and analgesics and tranquilizers are required. In some cases, general anesthesia may be necessary for the comfort of the stallion and the safety of personnel. Massage and cold hydrotherapy can be used to reduce the size of the penis. In irreducible cases, general anesthesia can be used and the stallion placed in dorsal recumbency. An elastic bandage then can be wrapped tightly around the cleansed penis, starting distally and proceeding proximally. The penis is massaged and the wrapping process is repeated several times. Properly applied, this type of wrap can help compress the edematous penis and reduce its size to allow replacement within the sheath.[75] Once the penis is replaced, an umbilical tape purse-string suture can be placed around the opening of the sheath and tied in a bow. The suture must be tight enough to hold the penis in the sheath but loose enough to allow urination. As much of the suture as possible should be run subcutaneously to reduce contamination and trauma to the penis caused by exposed taut suture. At regular intervals, usually once daily in tractable stallions, the bow can be released and the penis examined. Emollient ointments are applied topically to prevent drying out of the penile skin. The sutures are removed after the stallion is able to retract the penis on his own, typically within 5 days. Nonsteroidal anti-inflammatory drugs and systemic antibiotics should also be administered. Traditionally, diuretics such as furosemide have been used to aid in reducing dependent edema. The efficacy of this treatment is questionable. In refractory cases of paraphimosis, penis retraction using the Bolz technique or amputation of the penis can be performed.[74]

Local edema and swelling are often associated with local increases in temperature. These changes may affect the scrotum and testicles and result in a transient reduction in semen quality. Semen quality is expected to return to normal within 60 days of resolution of the problem. In most cases in which the penis is successfully replaced, normal fertility for the individual is regained.

Paraphimosis related to administration of pharmacologic agents or debilitation also occurs. In these cases, the prognosis for return of normal penile function is more guarded. Normal function may or may not be regained even after replacement into the sheath and retention with purse-string sutures. Such cases can be successfully managed if the owners are willing to perform penile massage at least once daily and regularly replace the penis into the sheath to limit the progression of penile edema. Topical ointments must be applied regularly and care taken to prevent congelation or mechanical trauma. Most affected stallions have been able to establish an erection and to ejaculate, although some have experienced varying degrees of ejaculatory dysfunction. Ultrasonographic examinations can be used to monitor the penis for changes in blood flow, increases or decreases in edema, and development of scar tissue. Some stallions that are unable to establish a normal erection can still return to natural or artificial breeding with proper management.[71-73]

Priapism. Priapism or persistent erection without sexual stimulation is uncommon in horses. When it occurs, it is usually as a result of administration of a phenothiazine-type tranquilizer.[64, 76-78] A case of priapism in a stallion with generalized malignant melanoma also has been reported.[9] Ultrasonographic examination of the penis in horses with priapism can be of prognostic value. Ultrasonography can be used to detect the development of secondary changes associated with prolonged priapism such as thrombosis in and/or fibrosis of the cavernous tissues (Fig. 10-66).[9] Stallions that develop these changes have a poorer prognosis for return to breeding soundness than stallions with uncomplicated priapism.

Acute priapism (<24 hours) can be treated medically with the cholinergic blocking agent benztropine mesylate. Results of treatment have been mixed.[79, 80] Alternatively, in acute cases, a large-bore hypodermic needle can be inserted into the corpus cavernosum penis, which is then flushed with heparinized saline in an attempt to remove sludged blood.[9] This treatment also produces mixed results. Anti-inflammatory drugs, cold water hydrotherapy, topical ointments, massage, and diuretics have all been used in the treatment of priapism. In cases of refractory priapism, surgical correction can be attempted. Creation of a vascular shunt between the corpus cavernosum penis and the corpus spongiosum penis has been described.[79] In the reported case, the shunt resulted in detumescence of the penis over the next several days, but the stallion was unable to retract the penis and also could not achieve an erection. Full recovery can occur in early cases of priapism, whether treated or not, but some cases of priapism have been reported to remain refractory to treatment.

References

1. Little TV, Woods GL: Ultrasound of the accessory sex glands in the stallion. J Reprod Fertil Suppl 35:87-94, 1987.

2. Love CC, Garcia MC, Riera FL, Kenney RM: Evaluation of measurements taken by ultrasonography and caliper to estimate testicular volume and predict daily sperm output in the stallion. J Reprod Fertil Suppl 4:99-105, 1991.
3. Love CC: Ultrasonographic evaluation of the testicles, epididymis, and spermatic cord of the stallion. Vet Clin North Am [Equine Pract] 8:167-182, 1992.
4. Peter AT, Jakovljevic S, Pierson R: Use of real-time ultrasonography in bovine and equine reproduction. Comp Cont Educ Pract Vet 14:1116-1124, 1992.
5. Pozor MA, McDonnell SM: Ultrasonographic measure of accessory sex glands of stallions of various size types. Poster presentation, Society for Theriogenology Annual Meeting, 1994.
6. Weber JA, Geary RT, Woods GL: Changes in accessory sex glands of stallions after sexual preparation and ejaculation. J Am Vet Med Assoc 196:1084-1089, 1990.
7. Weber JA, Woods GL: Transrectal ultrasonography for the evaluation of stallion accessory sex glands. Vet Clin North Am [Equine Pract] 8:183-190, 1992.
8. Blackford JT: Percutaneous ultrasonographic diagnosis of suspected acquired inguinal and scrotal herniation in horses. Proceedings of the 38th Convention of the American Association of Equine Practitioners 1992, pp 357-374.
9. Blanchard TL, Schumacher J, Edwards JF, et al: Priapism in a stallion with generalized malignant melanoma. J Am Vet Med Assoc 198:1043-1044, 1991.
10. Held JP, Prater P, Toal RL, et al: Sperm granuloma in a stallion. J Am Vet Med Assoc 194:267-268, 1989.
11. Held JP, Adair S, McGavin MD, et al: Bacterial epididymitis in two stallions. J Am Vet Med Assoc 197:602-604, 1990.
12. Held JP, McCracken MD, Toal R, et al: Epididymal swelling attributable to generalized lymphosarcoma in a stallion. J Am Vet Med Assoc 201:1913-1915, 1992.
13. Jann HW, Rains JR: Diagnostic ultrasonography for evaluation of cryptorchidism in horses. J Am Vet Med Assoc 196:297-300, 1990.
14. Traub-Dargatz JL, Trotter GW, Kaser-Hotz B, et al: Ultrasonographic detection of chronic epididymitis in a stallion. J Am Vet Med Assoc 198:1417-1420, 1991.
15. Sisson S, Grossman JD: Equine urogenital system. *In* Getty R (ed): The Anatomy of the Domestic Animals. Philadelphia, WB Saunders, 1975, pp 531-535.
16. Cartee RE, Powe TA, Gray BW, et al: Ultrasonographic evaluation of normal boar testicles. Am J Vet Res 47:2543-2548, 1986.
17. Eilts BE, Pechman RD: B-mode ultrasound observations of bull testes during breeding soundness examinations. Theriogenology 30:1168-1175, 1988.
18. Pugh CR, Konde LJ, Park RD: Testicular ultrasound in the normal dog. Vet Radiol 31:195-199, 1990.
19. Nickel RA, Schummer A, Seiferle E, et al: Male genital organs. *In* The Viscera of the Domestic Mammals, 2nd ed. Berlin, Verlag Paul Parey, 1979, p 304.
20. Little TV, Reed Holyoak G: Reproductive anatomy and physiology of the stallion. Vet Clin North Am [Equine Pract] 8:2, 1992.
21. Mann T: Biochemistry of stallion semen. J Reprod Fertil Suppl 23:47-52, 1975.
22. Roberts SJ: Veterinary Obstetrics and Genital Diseases, Woodstock, VT, published by the author, 1986, pp 754-756, 797, 821-823, 828, 843.
23. Amann RP: Functional anatomy of the adult male. *In* McKinnon AO, Voss JL (eds): Equine Reproduction. Philadelphia, Lea & Febiger, 1993, p 646.
24. Kenney RM, Hurtgen J, Pierson R, et al: Theriogenology and the Equine, Part II: The Stallion; Manual for Clinical Fertility Evaluation of the Stallion. Hastings, NE, Society for Theriogenology, 1983, pp 26-29.
25. Weber JA, Woods GL: A technique of transrectal ultrasonography of stallions during ejaculation. Theriogenology 36:831-836, 1991.
26. Schmidt AR: Transrectal ultrasonography of the caudal portion of abdominal and pelvic cavities in horses. J Am Vet Med Assoc 194:365-371, 1989.
27. Vaughen JT: Surgery of the Male Equine Reproductive System. *In* Morrow, D (ed): Current Therapy in Theriogenology. Philadelphia, WB Saunders, 1986, p 750.
28. Threlfall WR: Cryptorchidism in the horse. Proceedings of the Annual Meeting of the Society for Theriogenology, 1991, pp 158-161.
29. Braun WF: Physical examination and genital diseases of the stallion. *In* Morrow D (ed): Current Therapy in Theriogenology. Philadelphia, WB Saunders, 1986, p 649.
30. Hunt RJ, Hay W, Collatos C, Welles E: Testicular seminoma associated with torsion of the spermatic cord in two cryptorchid stallions. J Am Vet Med Assoc 197:1484-1486, 1990.
31. Palmer JM: The undescended testicle. Endocrinol Metab Clin North Am 20:231-240, 1991.
32. Rozanski TA, Bloom DA: The undescended testis: Theory and management. Urol Clin North Am 22:107-118, 1995.
33. Cox JE: Developmental abnormalities of the stallion reproductive tract. *In* McKinnon A, Voss J (eds): Equine Reproduction. Philadelphia, Lea & Febiger, 1993, p 901.
34. Larson L: Examination of the reproductive system of the bull. *In* Morrow D (ed): Current Therapy in Theriogenology. Philadelphia, WB Saunders, 1986, p 110.
35. Reef VB: Ultrasonographic evaluation and diagnosis of foal diseases. *In* Robinson E (ed): Current Therapy in Equine Medicine 3. Philadelphia, WB Saunders, 1992, p 418.
36. Sembrat RF: The acute abdomen in the horse: Epidemiologic considerations. Arch Am Coll Vet Surg 4:34-38, 1975.
37. Ashdown RR: The anatomy of the inguinal canal in the domesticated mammals. Vet Rec 75:1345-1351, 1963.
38. Vasey JR: Simultaneous presence of a direct and an indirect inguinal hernia in a stallion. Aust Vet J 57:418-421, 1981.
39. Schneider RK, Milne DW, Kohn CW: Acquired inguinal hernia in the horse: A review of 27 cases. J Am Vet Med Assoc 180:317-320, 1982.
40. Reef VB: Equine pediatric ultrasonography. Comp Cont Educ Pract Vet 13:1277-1285, 1991.
41. Moulton JE: Tumors of the genital system. *In* Moulton JE (ed): Tumors In Domestic Animals, 2nd ed. Berkeley, Davis Press, 1978, p 309.
42. Ladd PW: The male genital system. *In* Jubb KVF, Kenney PC, Palmer N (eds): Pathology of the Domestic Animals, 3rd ed. New York, Academic Press, 1985, vol 3, pp 409-459.
43. Caron JP, Barber SM, Bailey JV: Equine testicular neoplasia. Comp Cont Ed Pract Vet 7:53-59, 1985.
44. Cullen JM, Whiteside J, Umstead JA, Whitacre M: A mixed germ cell-sex cord-stromal neoplasia of the testis in a stallion. Vet Pathol 24:575-577, 1987.
45. Rushton HG, Belman AB: Testis-sparing surgery for benign lesions of the prepubertal testis. Urol Clin North Am 20:27-37, 1993.
46. DeVries PJ: Diseases of the testes, penis and related structures. *In* McKinnon A, Voss J (eds): Equine Reproduction. Philadelphia, Lea & Febiger, 1993, pp 878-884.
47. Arger PH: Scrotum. *In* Coleman BG (ed): Genitourinary Ultrasonography: A Text/Atlas. Tokyo, Igaku-Shoin, 1988.
48. Scheible W: Scrotal ultrasonography. *In* Reshick MI, Sanders RC (eds): Ultrasound in Urology, 2nd ed. Baltimore/London, Williams & Williams, 1984.
49. Delvento VR, Amann RP, Trotter GW, et al: Ultrasonographic and quantitative histologic assessment of sequelae to testicular biopsy in stallions. Am J Vet Res 53:2094-2101, 1992.
50. Rifkin MD, Jacobs JA: Simple testicular cyst diagnosed preoperatively by ultrasonography. J Urol 129:982-983, 1983.
51. Tosi SE, Richardson JR: Simple cyst of the testis: Case report and review of the literature. J Urol 114:473-475, 1975.
52. Threlfall WR, Carleton CL, Robertson J, et al: Recurrent torsion of the spermatic cord and scrotal testis in a stallion. J Am Vet Med Assoc 196:1641-1643, 1990.
53. Brinsko SP, Varner DD, Blanchard TL, et al: Bilateral infectious epididymitis in a stallion. Equine Vet J 24:325-328, 1992.
54. Love CC, Riera FL, Oristaglio (Turner) RM, Kenney RM: Sperm occluded (plugged) ampullae in the stallion. Proceedings of the Annual Meeting of the Society for Theriogenology, 1992, pp 117-125.
55. Freestone JF, Paccamonti DL, Eilts BE, et al: Seminal vesiculitis as a cause of signs of colic in a stallion. J Am Vet Med Assoc 203:556-557, 1993.
56. Blanchard TL, Varner DD, Hurtgen JP, et al: Bilateral seminal vesiculitis and ampullitis in a stallion. J Am Vet Med Assoc 192:525-526, 1988.
57. Deegan VE, Klug E, Lieske R, et al: Operative Behandlungsmoglichkeit bei einer chronisch-eitrigen Samenblasen-Entzundung beim Pferd. Dtsch Tierarztli Wochenschr 86:140-144, 1979.

58. Van der holst W: Zaadblaasontsteking Bij Twee Dekhengsten. Tijdschr Diergeneeskd 101:375-377, 1976.
59. Mickelson WD, Weber JA, Memon MA: Use of transrectal ultrasonography for the detection of seminal vesiculitis in a bull. Vet Rec 135:14-15, 1994.
60. Varner DD, Taylor TS, Blanchard TL: Seminal vesiculitis. *In* McKinnon AO, Voss JL (eds): Equine Reproduction. Philadelphia, Lea & Febiger, 1993, pp 861-863.
61. McDonnell SM, Love CC, Martin BB, et al: Ejaculatory failure associated with aortic-iliac thrombosis in two stallions. J Am Vet Med Assoc 200:954-957, 1992.
62. Love CC: Semen collection techniques. Vet Clin North Am [Equine Pract] 8:111-128, 1992.
63. Turner RM, Love CC, McDonnell SM, et al: Use of imipramine HCl for treatment of urospermia in a stallion with a dysfunctional bladder. J Am Vet Med Assoc, 207:1602-1606, 1995.
64. Wheat JD: Penile paralysis in stallions given proprioprornazine. J Am Vet Med Assoc 148:405, 1966.
65. Gibbons WJ: Hematoma of the penis. Mod Vet Pract 45:76. 196-i.
66. Firth EC: Dissecting hematoma of corpus spongiosum and urinary bladder rupture in a stallion. J Am Vet Med Assoc 169:800-801. 1976.
67. Bowen JM: Management of the breeding stallion. *In* Morrow D (ed): Current Therapy in Theriogenology. Philadelphia. WB Saunders, 1986, p 643.
68. Musser JMB, St-Jean G, Vestueber JG, Pejsa TG: Penile hematoma in bulls: 60 cases (1979-1990). J Am Vet Med Assoc 201:1416-1418, 1992.
69. Clem MF, DeBowes RM: Paraphimosis in horses—Part I. Comp Cont Educ 11:72-75, 1989.
70. Clem MF, DeBowes RM: Paraphimosis in horses—Part II. Comp Cont Educ 11:184-187, 1989.
71. Carr JP, Hughes JP: Penile paralysis in a Quarter Horse stallion. Calif Vet 5:13-14, 1984.
72. Simmons HA, Cox JE, Edwards GB, et al: Paraphimosis in 7 debilitated horses. Vet Rec 116:126-127, 1985.
73. Love CC, McDonnell SM, Kenney RM: Manually assisted ejaculation in a stallion with erectile dysfunction subsequent to paraphimosis. J Am Vet Med Assoc 200:1357-1359, 1992.
74. Suann CJ, Horney FD: Surgical treatment of paraphimosis in a pony. Can Vet J 24:341-342, 1983.
75. Boero MJ: A simple technique for conservative therapy of acute traumatic paraphimosis in the horse. Proceedings of the American Association of Equine Practitioners, 1990, pp 625-628.
76. Gerring EL: Priapism and ACTP in the horse. Vet Rec 109:64, 1979.
77. Lucke JN, Sansom J: Penile erection in the horse after acepromazine. Vet Rec 105:21-22, 1979.
78. Pearson H, Weaver BM: Priapism after sedation, neuroleptanalgesia and anesthesia in the horse. Eq Vet J 10:85-90, 1978.
79. Schumacher J, Hardin DK: Surgical treatment of priapism in a stallion. Vet Surg 16:193-196, 1987.
80. Sharrock AG: Reversal of drug-induced priapism in a gelding by medication. Aust Vet J 58:39-40, 1982.

CHAPTER

11

Ultrasonographic Evaluation of Small Parts

Sonographic examination of the peripheral lymph nodes, thyroid, parotid salivary gland, trachea, esophagus, and tongue is useful in identifying different disorders affecting these structures.[1-5] Sonographic examination of the mammary gland and of inguinal and scrotal swellings in horses is a useful adjunct to identify abnormalities of these tissues, plan further diagnostic tests, and select appropriate treatment. Sonographic examination of swellings, masses, and draining tracts enables the veterinary clinician to further characterize these lesions and to search for foreign bodies, particularly radiolucent ones in horses.[4-12] Incisional problems can also be evaluated with diagnostic ultrasound, yielding information about the integrity of the incision and other incisional complications such as infection and adhesions.[13-16] Sonographic examination of the eye and orbit yields information about the intraocular structures and retrobulbar space.[6, 17-22] Transpalpebral or transcorneal ultrasonographic examination is extremely helpful in horses with corneal opacities preventing visualization of the deeper intraocular structures. Sonographic examination of the brain has also been performed in foals documenting hydrocephalus.[23, 24] Intraoperative ultrasonography has been used to help the surgeon localize foreign bodies, fracture fragments, important vascular structures, or masses, and to minimize surgical trauma and anesthesia time.[1, 5, 8, 9, 25] This application is likely to expand, as more surgeons become aware of the usefulness of this technique.

EXAMINATION TECHNIQUE

Patient Preparation

Cervical Structures

The skin in the cervical region over the area to be examined should be clipped free of hair with a #40 surgical clipper blade and thoroughly cleaned before applying ultrasound coupling gel. Ultrasound coupling gel should be applied and worked into the skin over the area under investigation.

Thyroid. The skin in the cranial cervical region should be clipped from the caudal edge of the mandible along the jugular groove, beginning at the bifurcation of the jugular vein into linguofacial and external maxillary veins extending distally for approximately 10 cm. The clipped area should extend from the ventral most aspect of the neck to several centimeters dorsal to the jugular vein.

Parotid and Other Salivary Glands. The skin in the proximal cervical region should be clipped free of hair along the caudal edge of the ramus of the mandible over the external maxillary vein from just below the base of the ear extending distally to an area just ventral to the bifurcation of the jugular vein into linguofacial and external maxillary veins. The clipped area should include the entire throatlatch region in the area of the jugular vein bifurcation for a width of approximately 8 to 10 cm. The clipped area should also include the ventral aspect of the jaw from the mandibular symphysis to the second molar, if involvement of the sublingual gland is suspected.

Trachea. The skin over the entire length of the trachea should be clipped free of hair along the ventral aspect of the neck extending around the right and left sides to each jugular groove. The entire trachea from the larynx to the thoracic inlet should be examined.

Esophagus. The skin over the left side of the neck along the left side of the trachea and over the left jugular vein should be clipped free of hair from the caudal aspect of the mandible to the thoracic inlet. The clipped area should be approximately 8 to 10 cm wide and extend to the ventral midline of the neck. The right side of the neck may need to be similarly prepared, as the esophagus is to the right of the trachea in a few normal horses.

Lymph Nodes

The skin over the superficial lymph nodes in question should be clipped free of hair so that the entire lymph node can be examined. The entire throatlatch region from the ventral aspect of the ear to the larynx should be clipped to examine the retropharyngeal lymph nodes. To examine the submandibular lymph nodes the entire

submandibular region between the two sides of the mandible should be clipped from the mandibular symphysis to the larynx. The prefemoral and prescapular lymph nodes should be palpated in their respective locations in the flank fold and along the cranial margin of the scapula, and the region over and around them clipped free of hair.

Tongue

The area between the two rami of the mandible from the mandibular symphysis to the larynx should be clipped free of hair to image the tongue from outside the oral cavity, followed by the application of ultrasound coupling gel. In a cooperative horse, the cranial portion of the tongue can be exteriorized and examined directly.

Mammary Gland

The equine mammary gland is relatively hairless and rarely requires any preparation other than cleaning the skin and the application of ultrasonographic coupling gel.

Inguinal Region and Scrotum

The inguinal region and scrotum are also relatively hairless areas that do not need to be surgically clipped free of hair for sonographic examination. Ultrasound coupling gel should be applied liberally to the area being examined after the skin is cleaned.

Eye and Orbit

The eyelids rarely require clipping for transpalpebral examination of the eye and orbit, as the hair on the eyelid is very short and fine. However, the supraorbital space often requires clipping the area free of hair to examine the retrobulbar space from this window. The entire supraorbital space should be clipped to its bony margins and the skin cleaned. Ultrasound coupling gel can then be carefully applied to the eyelid and supraorbital space. Sterile coupling gel is often recommended to minimize the chance of corneal or conjunctival irritation. Direct application of the ultrasound transducer onto the cornea usually requires topical anesthesia of the eye. An auriculopalpebral nerve block may be needed in horses with severe ocular pain or blepharospasms. Sterile coupling gel is recommended for transcorneal examinations.

Brain and Spinal Cord

The hair on the skin over the cranium should be clipped over the open fontanelle or any palpable defect in the cranium followed by the application of ultrasound coupling gel. If there is no defect in the cranium or vertebral column, a surgical defect must be created to image the brain or the spinal cord, respectively, with diagnostic ultrasound.

Anatomy

Cervical Structures

Thyroid. The thyroid gland, located in the proximal cervical region caudal to the larynx, is an oval structure lying on both sides of the proximal trachea just caudal to the larynx at the level of the first three to four tracheal cartilages. The thyroid gland is approximately 1.5 to 2.5 cm thick, 4 to 6 cm long, and 2 to 3 cm wide in most horses. The two thyroid gland lobes are usually connected by a narrow fibrous isthmus at the caudal aspect of the gland. The ventral angle of the parotid salivary gland covers the cranial aspect of the thyroid gland. The parathyroid glands are located on the dorsal medial edge of the thyroid gland.

Parotid and Other Salivary Glands. The parotid salivary gland is located in the cranial cervical region extending proximally along the ramus of the mandible adjacent to the external maxillary artery. The parotid salivary gland is located between the vertical ramus of the mandible and the wing of the atlas, extending distally to the linguofacial vein. This gland is approximately 20 to 25 cm long and 2 cm thick. Its medial surface is adjacent to the guttural pouches and the retropharyngeal lymph nodes. The parotid salivary gland is composed of multiple lobules of glandular tissue enclosed in a fascial capsule. The parotid salivary duct originates at the ventral aspect of the gland, dorsal to the linguofacial vein, and follows the linguofacial vein to the third cheek tooth, where it enters the mouth through the parotid papilla opposite the last upper premolar. The mandibular salivary gland is medial to the parotid salivary gland and lateral to the guttural pouch. The mandibular salivary duct opens into the mouth along the lateral aspect of the sublingual caruncle. The sublingual gland lies between the tongue and the mandible underneath the sublingual fold and extends from the mandibular symphysis to the second molar. The sublingual ducts are small pores in the sublingual recess.

Trachea. The trachea is composed of multiple cartilaginous rings interconnected by a tough flexible membrane. The cervical trachea originates at the larynx and terminates at the thoracic inlet. The trachea is dorsal to the esophagus in the cranial portion of the neck and dorsomedial to the esophagus in the mid-cervical region and medial to the esophagus in the distal third of the neck. The tracheal rings or plates are composed of hyaline cartilage forming nearly circular rings in the cranial cervical region with a diameter of approximately 5 to 6 cm and flattening out distally to a transverse diameter of 7 cm or more. The trachea has a fibrous outer adventitia, the musculocartilaginous layer, a submucosa, and a mucosal surface.

Esophagus. The esophagus originates from its pharyngeal opening at the dorsal left side of the larynx and courses distally in the neck to its position along the left side of the trachea. In a small percentage of horses the esophagus crosses the midline, ventral to the trachea, and proceeds to the thoracic inlet along the right side of the trachea. The esophagus has a mucosal lining, a submucosa, a muscular wall composed of striated muscle

in the cervical region, and a serosal surface or fibrous sheath around the muscular layer. The esophagus is usually collapsed, unless fluids or ingesta are passing through the lumen.

Lymph Nodes

The superficial lymph nodes in the horse are usually small and include the submandibular, prescapular, and prefemoral lymph nodes. The submandibular lymph nodes are located between the two rami of the mandible ventral to the tongue. These lymph nodes may be as large as 10 to 16 cm long and 2 to 2.5 cm wide, and are narrowest rostrally. The prescapular lymph nodes are located cranial to the shoulder joint at the cranial border of the cleidoscapularis pectoralis. The prefemoral lymph nodes are located at the craniomedial aspect of the tensor fascia latae muscle midway between the patella and tuber coxae. The inguinal (or mammary) lymph nodes are located on the ventral portion of the abdominal musculature cranial and caudal to the spermatic cord in the male and between the ventral abdomen and the udder in the female. The lateral retropharyngeal lymph nodes are located along the lateral side of the guttural pouch, ventral to the parotid salivary gland. The medial retropharyngeal lymph nodes are located on the dorsolateral aspect of the pharynx and may extend to the lateral aspect of the guttural pouch. The cervical lymph nodes may be found along the trachea, with the largest accumulation in the caudal cervical region at the thoracic inlet. The inguinal, retropharyngeal, and cervical lymph nodes are accessible sonographically in the horse, particularly when they are enlarged.

Tongue

The tongue is located between the two rami of the mandible, with a large frenulum present in the horse. The root of the tongue is attached to the hyoid bone, the soft palate, and the pharynx. The upper surface of the caudal portion of the tongue slopes caudally and ventrally. The body of the tongue has a slightly rounded dorsal surface and flat lateral surfaces. The tip of the tongue is free and somewhat spatula-shaped with a flat upper and lower surface and rounded lateral edges.

Mammary Gland

The two mammary glands, located on either side of the midline in the prepubic region, are attached to the ventral abdomen by loose areolar tissue containing a venous plexus, fat, and lymph nodes. The medial surface of the gland is flattened, whereas the lateral surface is convex. The gland has a fibroelastic capsule containing glandular tissue and fat. The lactiferous sinuses at the apex of the gland empty into the teat, which is usually 2.5 to 5.0 cm long.

Inguinal Region and Scrotum

The scrotum in the gelding is composed only of the skin and underlying subcutaneous tissues remaining following castration. The remnant of the spermatic cord may remain in the dorsal portion of the scrotum external to the external inguinal ring in some geldings. The anatomy of the scrotum and inguinal region in the stallion has been thoroughly covered in Chapter 9 and is similar in the gelding with the exception of the testicles, epididymis, and distal portion of the spermatic cord, which are removed at castration.

Eye and Orbit

The equine orbit is a complete bony orbit made up of the frontal, lacrimal, zygomatic, temporal, sphenoid, palatine, and maxillary bones. The eye is positioned in the orbit with the seven extraocular muscles, which originate from the bony orbit or adjacent bony structures and insert on the sclera. The normal globe in the adult horse ranges from 40 to 44 mm long in postmortem measurements, but the plane of measurement has not been mentioned.[19] A large retrobulbar fat pad surrounds the optic nerve behind the globe. The anterior chamber is the space between the cornea and iris. The posterior chamber is a small space between the iris and the anterior capsule of the lens. The vitreous chamber lies between the posterior capsule of the lens and the retina.

Brain and Spinal Cord

The brain is housed in the cranium and is usually inaccessible for sonographic imaging unless there is a defect in the cranium or an open fontanelle. Similarly the spinal cord is encased in the bony vertebrae with little opportunity for sonographic imaging other than in the intervertebral spaces.

Scanning Technique

Cervical Structures—Thyroid Gland, Parotid and Other Salivary Glands, Trachea, and Esophagus

The structures in the proximal cervical region (thyroid, salivary glands, trachea, and esophagus) are imaged with a high-frequency transducer (6.0 to 10.0 MHz) and a displayed depth of 4 to 8 cm. A transducer containing a built-in fluid offset or using a hand-held standoff pad is ideal to obtain optimal image quality of the these superficial structures. A transducer with a large footprint facilitates optimal imaging of the thyroid and parotid salivary gland.

Lymph Nodes

The superficial lymph nodes are imaged with a high-frequency transducer (6.0 to 10.0 MHz) and a displayed

depth of 4 to 8 cm. A transducer containing a built-in fluid offset or using a hand-held standoff pad is ideal to obtain optimal image quality of the superficial lymph nodes.

Foreign Bodies and Draining Tracts

Locate the tract at its point of drainage and follow it for as long as possible.[7] Although one author recommends the instillation of sterile saline or antibiotic solution into the draining tract to aid the clinician in examining the tract,[7] this introduces air and should be avoided if at all possible, unless a careful initial sonographic examination fails to determine the source of the drainage. The introduction of air with the fluid is more likely to obscure the deeper tissues to which the tract may be leading because air is a nearly perfect reflector of ultrasound. If a hyperechoic structure is imaged it should be examined in as many planes as possible to determine if acoustic shadowing is occurring from the surface of this structure.[7] The strength, depth, and type of acoustic shadow should be determined.

Tongue

Sonographic examination of the tongue in horses has been described from a submental approach.[5] A 5.0-MHz transducer was used in this report, and the examination was performed from the ventral aspect of the jaw with the animal in a standing position with the head in a neutral or extended position. The transducer was moved from the left to the right horizontal ramus of the mandible and from the mandibular symphysis to the thyroid cartilage. The wide acoustic shadows generated by the mandible preclude assessment of the rostral portion of the tongue from the submental window, particularly if a transducer with a wide footprint is used. The placement of a higher-frequency transducer (6.0 to 10.0 MHz) directly on the tongue in horses will enable successful imaging of the rostral portions of the tongue. With many higher-frequency transducers the tongue can be successfully examined from the submental approach, as previously described. The use of a higher-frequency transducer with a smaller footprint will also enable successful imaging of the sublingual muscles in horses.

Mammary Gland

The sonographic examination of the mammary gland is performed with a high-frequency (6.0 to 10.0 MHz) transducer at a displayed depth of 6 to 12 cm. A transducer with a built-in fluid offset or with a hand-held standoff pad and a wide footprint or a large field of view is helpful in obtaining high-quality images of this gland, particularly of the teat. The sonographer should stand next to the mare's foreleg and reach caudally to examine the mammary gland from this position.

Scrotum and Inguinal Region

The sonographic examination of the scrotum and inguinal region in the gelding is performed with a high-frequency (6.0 to 10.0 MHz) transducer containing a built-in fluid offset or using a hand-held standoff pad as the structures are immediately underneath the skin surface. A small transducer with a small footprint is usually needed to evaluate the inguinal canal from the external inguinal ring. The sonographer should stand next to the gelding's foreleg and reach caudally to examine the scrotum and inguinal region safely. The sonographic examination of the stallion's scrotum and inguinal region is described in Chapter 9.

Eye and Orbit

A high-frequency (6.0 to 10.0 MHz) transducer is recommended to scan the equine eye adequately. The examination can be performed with the transducer placed on the patient's eyelid (transpalpebral) or directly on the patient's cornea (transcorneal). Transpalpebral scanning of the eye creates more artifacts owing to the presence of the eyelid and the interface between the eyelid and the cornea. Transpalpebral scanning is indicated in horses in which corneal perforation is imminent. Transcorneal imaging yields the best-quality images and is therefore ideal if tolerated by the horse. The use of a standoff pad is important for optimal imaging of the cornea and other superficial structures. The cornea will be lost in the transducer artifact if a standoff pad is not used with transcorneal ultrasonography.[20] Topical anesthesia of the eye is necessary if the ultrasound transducer is placed directly on the horse's cornea. Blocking the horse's eyelids with an auriculopalpebral nerve block may also be helpful, particularly if the horse has severe blepharospasm. Sedation may also be necessary if the horse is uncooperative during ocular ultrasonography. Ideally, sterile nonirritating ultrasound gel should be used if the transducer or standoff pad is placed directly on the horse's cornea.[20] However, nonsterile ultrasound coupling gel has been used on the equine cornea without problems.[19] The eye should be thoroughly rinsed of coupling gel following the sonographic examination if gel is placed directly on the cornea.[19] Standard ultrasound coupling gel can be used if transpalpebral scanning is being performed.

Sonographic examination of the retrobulbar space can be performed through the eye or through the supraorbital fossa. Examination through the supraorbital fossa may yield superior sonographic images in some horses, owing to the lack of artifacts caused by the orbital fat when scanning through the cornea and the shorter distance to the retrobulbar mass.[22] The use of this window to the retrobulbar space may simplify ultrasonographically guided aspiration of the retrobulbar mass.[22]

Brain and Spinal Cord

Sonographic examination of the brain can be performed in the equine neonate with a high-frequency transducer

(7.5 MHz) and a displayed depth of 6 to 12 cm. These images must be obtained through an open fontanelle present in the foal at birth, so a transducer with a small footprint is ideal for this examination. Sonographic examination of the brain in the adult horse can be performed only through a persistent fontanelle or through a defect in the cranium, either of which could serve as an acoustic window. A "windshield wiper" technique has been described for sonographic examination of the neonatal brain in the dog.[26] With this technique the transducer is placed in the open fontanelle and the transducer is rocked rostrally and caudally to obtain transverse images and side-to-side for parasagittal images. Sonographic examination of the brain can also be performed intraoperatively through a craniotomy. The equine spinal cord can be examined with diagnostic ultrasound intraoperatively during a hemilaminectomy. In the normal horse the vertebrae prevent successful imaging of the spinal cord.

ULTRASONOGRAPHIC FINDINGS

Normal Structures

Cervical Structures

Many small structures are intimately related to one another in the cranial cervical region. The relationship among the trachea, esophagus, carotid artery, and jugular vein is easily demonstrated sonographically (Fig. 11-1). The thyroid gland is adjacent to these structures in the proximal cervical region. The relationship of the parotid salivary gland to the jugular vein, external maxillary vein, linguofacial vein, and guttural pouch is important in evaluating this salivary gland. The retropharyngeal lymph nodes are also in close association with the parotid salivary gland.

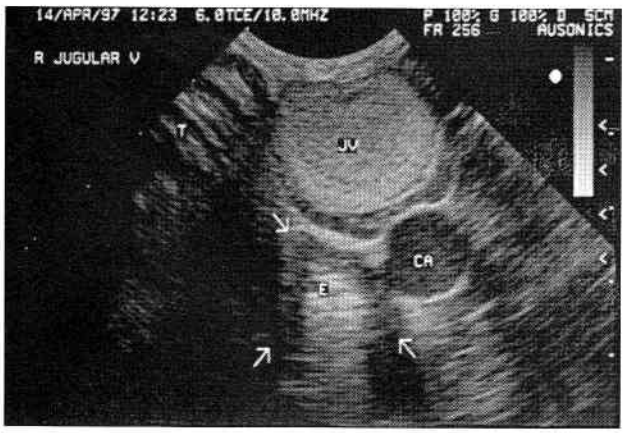

Figure 11–1

Sonogram of the right cranial cervical region, obtained from a 10-year-old Thoroughbred mare. The jugular vein (JV) was being occluded in the distal cervical region, accounting for the jugular venous distention and the echogenic blood swirling within the vein. The carotid artery (CA) is immediately deep to the jugular vein and slightly dorsal to it. The blood in the carotid artery has the typical anechoic to hypoechoic appearance. Ventral to the jugular vein is the trachea (T) with its cartilaginous rings. Deep to the jugular vein, dorsal to the trachea, and ventral to the carotid artery is the esophagus (E). In most horses the esophagus is on the left side of the trachea, but in some normal horses, like this mare, it is located to the right of the trachea. Notice the hypoechoic esophageal wall and its hyperechoic lumen, associated with gas and mucus in the lumen of the esophagus *(arrows)*. This sonogram was obtained with a wide-bandwidth 6.0-MHz microconvex linear-array transducer operating at 10.0 MHz at a displayed depth of 5 cm. The right side of this sonogram is dorsal and the left side is ventral.

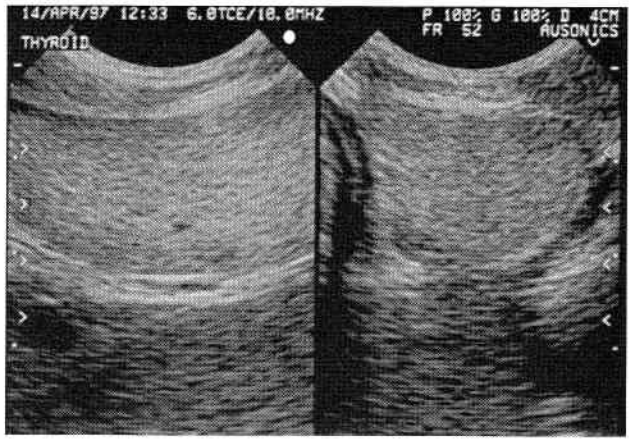

Figure 11–2

Sonograms of the right thyroid gland obtained from a 10-year-old Thoroughbred mare (same as in Figure 11-1). Notice the homogeneous echogenic appearance of the thyroid, which is approximately 2 cm thick and 4 cm long. These sonograms were obtained with a wide-bandwidth 6.0-MHz microconvex linear-array transducer operating at 10.0 MHz at a displayed depth of 4 cm. The right side of the right image is dorsal and the left side is ventral. The right side of the left image is cranial and the left side is caudal.

Thyroid. The equine thyroid gland is an oval structure with a homogeneous echogenic appearance (Fig. 11-2), with a thickness of approximately 1.5 to 2.5 cm, a width of 2 to 3 cm, and a length of 4 to 6 cm. The thyroid gland is more echogenic than the adjacent cervical musculature. The thyroid gland in human beings is described as a homogeneous gland of medium to high echogenicity, similar to that found in the horse.[27]

Salivary Glands. The parotid salivary gland is a well-demarcated, oval, multilobulated structure with an echogenic capsule and septae and hypoechoic parenchyma (Fig. 11-3). The parotid salivary gland is approximately 2 cm thick and 20 to 25 cm long. The mandibular salivary gland is more difficult to recognize, as it lies deep to the parotid salivary gland and the guttural pouch but has a sonographic appearance similar to that of the parotid salivary gland. The salivary ducts are not normally detected.

Trachea. The trachea is composed of multiple hypoechoic circular rings, representing the tracheal cartilage, and hyperechoic areas between the tracheal rings, representing gas along the tracheal mucosal surface (Fig. 11-4). The trachea is approximately 5 cm wide in the cranial cervical region and becomes slightly wider near the thoracic inlet.

Esophagus. The esophagus is a tubular hypoechoic structure with an echogenic serosal surface and a hyperechoic irregular to star-shaped lumen associated with gas and mucus along the mucosal folds of the collapsed esophagus (Fig. 11-5). The wall of the esophagus is relatively thin, measuring 3 to 4 mm thick in the col-

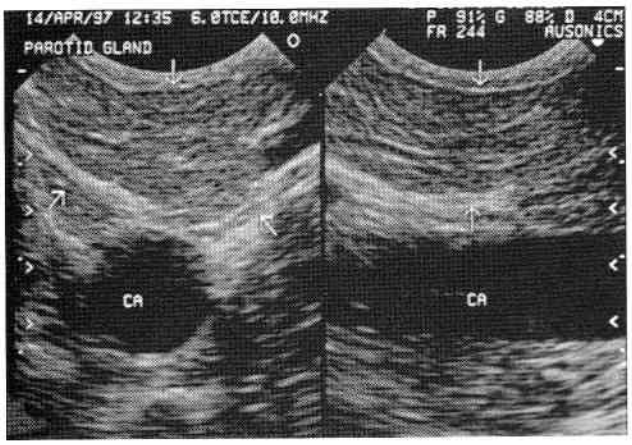

Figure 11–3

Sonograms of the right parotid salivary gland obtained from a 10-year-old Thoroughbred mare (same as in Figures 11-1 and 11-2). Notice the anechoic to hypoechoic glandular parenchyma with hyperechoic septae throughout the gland *(arrows)*. The gland is located in the proximal cervical region superficial to the carotid artery (CA), immediately underneath the skin. These sonograms were obtained with a wide-bandwidth 6.0-MHz microconvex linear-array transducer operating at 10.0 MHz at a displayed depth of 4 cm. The right side of the left image is cranial and the left side is caudal. The right side of the right image is proximal and the left side is distal.

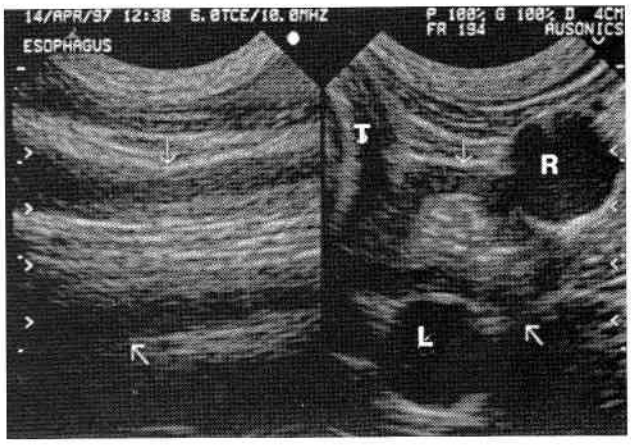

Figure 11–5

Sonograms of the esophagus obtained from a 10-year-old Thoroughbred mare (same as in Figures 11-1 through 11-4). The mucosal folds of the esophagus are clearly visualized in the long axis scan *(left image)* as echogenic linear folds alternating with hyperechoic folds. The esophageal wall *(arrows)* appears relatively hypoechoic with an echogenicity similar to the adjacent cervical musculature. The esophagus *(arrows)* is imaged in short axis section *(right image)* adjacent to the trachea (T) between the left (L) and right (R) carotid arteries. The echogenic-to-hyperechoic appearance of the esophagus is caused by gas and mucus along the mucosal surface. These sonograms were obtained with a wide-bandwidth 6.0-MHz microconvex linear-array transducer operating at 10.0 MHz at a displayed depth of 4 cm. The right side of the left image is proximal and the left side is distal. The right side of the right image (R) is dorsal and the left side (L) is ventral.

lapsed esophagus. The esophagus is several centimeters in diameter when without ingesta. When the horse swallows, the esophagus is readily identified, as a wave of saliva, fluid, or ingesta passes through the esophageal lumen.

Tongue and Associated Structures. The genioglossus muscle is readily identified as several parallel echogenic lines overlying the root of the tongue when the oral cavity is imaged from the ventral aspect of the jaw.[5] The body of the tongue has a homogeneous hypoechoic appearance (Fig. 11-6), as does the tip of the tongue. The interface between the tongue and the air in the oropharynx is imaged as a hyperechoic line dorsal to the tongue. This interface is more distinct between the tongue and the hard palate than in the caudal pharynx in

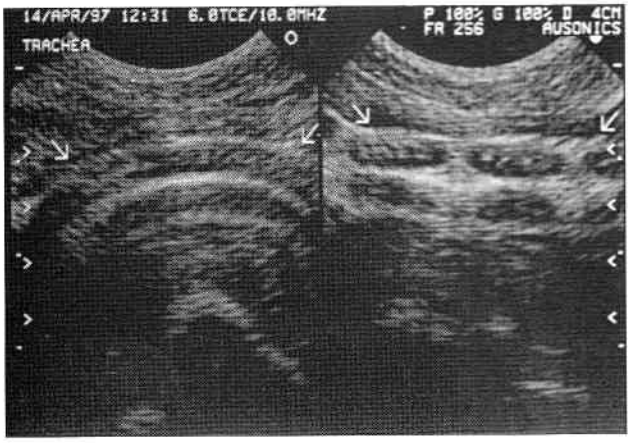

Figure 11–4

Sonograms of the trachea obtained from a 10-year-old Thoroughbred mare (same as in Figures 11-1 through 11-3). The tracheal rings are hypoechoic and the intervening mucosal surface is hyperechoic due to the gas within the tracheal lumen. The arrows point to the ventral aspect of the trachea. The multiple concentric ring construction of the trachea is easily visualized. The air-filled trachea casts multiple reverberation artifacts from the imaged surface. These sonograms were obtained with a wide-bandwidth 6.0-MHz microconvex linear-array transducer operating at 10.0 MHz at a displayed depth of 4 cm. The right side of the left image is the left side of the trachea. The right side of the right image is proximal and the left side is distal.

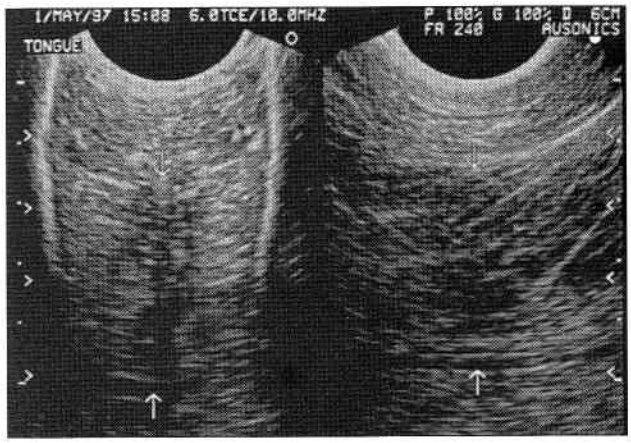

Figure 11–6

Sonograms of the tongue obtained from a normal 14-year-old Thoroughbred gelding. The up arrows are on the oral (dorsal) side of the tongue and the down arrows delineate the ventral aspect of the tongue. These sonograms were obtained with a wide-bandwidth 6.0-MHz microconvex linear-array transducer operating at 10.0 MHz at a displayed depth of 6 cm. The right side of the right image is cranial and the left side is caudal. The right side of the left image is toward the left side of the mandible.

the region of the soft palate, possibly because of the similar acoustic impedance between the tongue and the soft palate. However, air in the oropharynx creates a hyperechoic line along the dorsal aspect of the tongue, which usually casts a dirty shadow. Fluid in the form of saliva may also be imaged between the tongue and the hard and soft palates.

Lymph Nodes

The lymph nodes are well-demarcated structures with an echogenic capsule and homogeneous hypoechoic tissue within (Fig. 11-7). There may be an echogenic center associated with the hilus of the lymph node or several echogenic septae in lymph node aggregates.

Eye and Orbit

The cornea, iris, ciliary body, anterior lens capsule, posterior lens capsule, and posterior tunics of the eye appear relatively echogenic, whereas the aqueous humor, lens, and vitreous humor appear relatively anechoic (Fig. 11-8).[19, 20] The cornea appears as a thin hypoechoic or echoic convex curved structure immediately beneath the fluid offset.[19, 28] The anterior capsule of the lens appears as a convex echogenic line, whereas the posterior capsule of the lens is a concave echogenic line.[19] The echoic tissue imaged abaxially at the equator of the lens is the iris and ciliary body. The iris and ciliary body are irregular structures located posterior to the anterior chamber and anterior to the lens and extend centrally from the margins of the globe.[28] No clear separation is imaged in the extirpated equine eyes between the iris and ciliary body. The ciliary body is measured as an irregular hyperechoic structure posterior to the iris in these eyes.[28] The granula

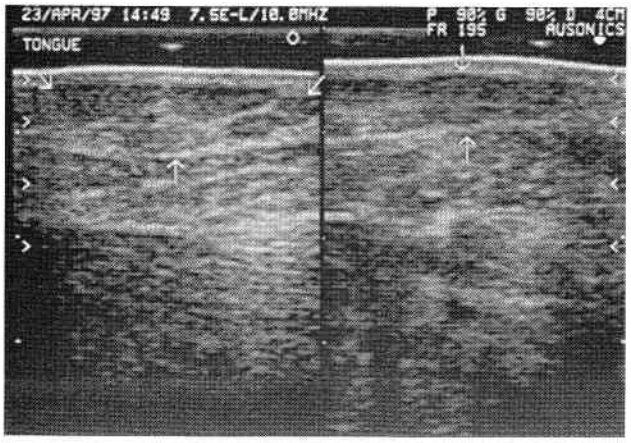

Figure 11–7

Sonograms of the submandibular lymph nodes obtained from a 12-year-old Thoroughbred gelding. The submandibular lymph nodes are small and homogeneously hypoechoic within a discrete echogenic capsule. These sonograms were obtained with a wide-bandwidth 7.5-MHz linear-array transducer operating at 10.0 MHz using a hand-held standoff pad at a displayed depth of 4 cm. The right side of the left image is cranial and the left side is caudal. The right side of the right image is toward the left side of the mandible.

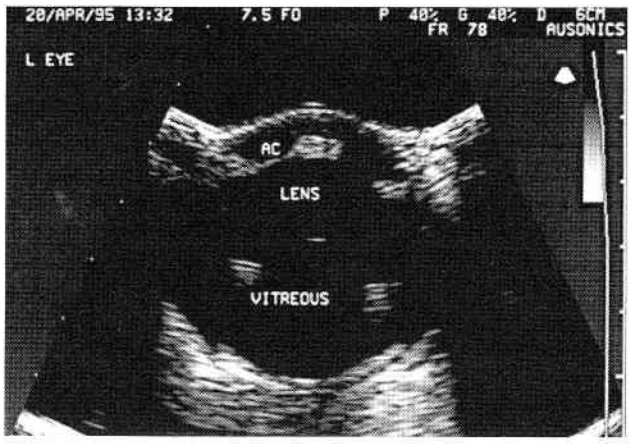

Figure 11–8

Sonogram of a normal left eye obtained from a 25-year-old crossbred gelding. The cornea is represented by a thin line directly under the transducer artifact, which is difficult to see. The anterior chamber (AC) is small, and the echogenic mass in the anterior chamber is part of the corpora nigra. The lens is anechoic with an echogenic anterior capsule and posterior capsule. The vitreous chamber is also anechoic. The two sets of multiple linear echoes in the vitreous are artifacts. This sonogram was obtained with the transducer placed directly on the cornea with a 7.5-MHz sector-scanner transducer containing a built-in fluid offset at a displayed depth of 6 cm. The right side of this sonogram is lateral and the left side is medial.

iridica or corpora nigra is imaged as a hyperechoic mass on the anterior surface of the iris at the margin of the pupil.[28] The retina-choroid and scleral reflection is an echogenic line that curves toward the transducer.[19] These layers cannot normally be differentiated ultrasonographically. In the extirpated equine eye the retina is interpreted to be a concave hypoechoic structure composing the inner walls of the posterior globe, but in reality the hyperechoic area seen probably represents the retina and the choroid.[28] The head of the optic nerve usually casts acoustic shadows from its margins. The retrobulbar fat is hypoechoic to echogenic and somewhat heterogeneous (Fig. 11-9), and the retrobulbar muscles have the normal hypoechoic speckled appearance of normal striated muscle (Fig. 11-9). The extraocular muscles originate from the equator of the globe and extend toward the opening in the orbit through which the optic nerve passes.[19] The retrobulbar fat pads allow visualization of the anechoic optic nerve and the extraocular muscles.[19] The bony orbit is imaged as a hyperechoic structure casting acoustic shadows.

Sonographically obtained measurements of the normal extirpated equine eye have been reported.[28] The mean diameter of the equine eye obtained at the axis bulbi from 95 normal equine eyes is 39.4 ± 2.3 mm.[28] The equine eye measures slightly larger in the dorsal-to-ventral scan plane (42.5 ± 3.6 mm).[28] Dorsal-ventral axis measurement (compared with that of the axis bulbi) was larger in all equine eyes studied. The mean corneal thickness measured 2.33 ± 0.39 mm in these horses, with an anterior chamber of 4.22 ± 1.29 mm deep (mean), a mean lens thickness of 11.93 ± 1.1 mm, a mean vitreous depth of 17.37 ± 1.98 mm, and a mean retinal thickness of 2.2 ± 0.48 mm.[28] No posterior chamber was detected

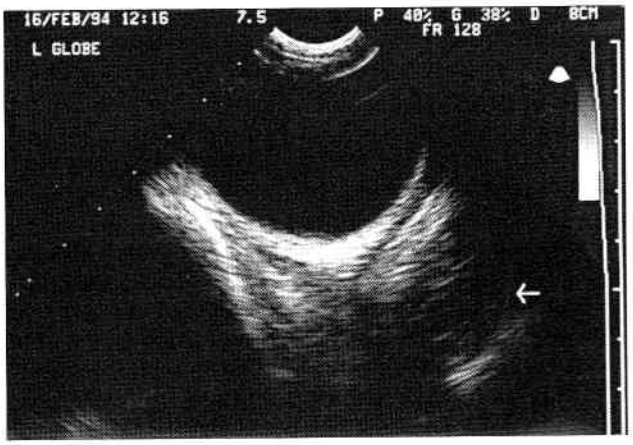

Figure 11–9

Sonogram of the retrobulbar space obtained from a 15-year-old Thoroughbred gelding with a bulging supraorbital space and prominent eyes. A large mass located dorsally in the retrobulbar space *(arrow)* appears relatively homogeneous and hypoechoic and is consistent with a large retrobulbar fat pad. The retrobulbar muscles appear more echogenic than the retrobulbar fat and have a speckled striated appearance. This sonogram was obtained with a 7.5-MHz sector-scanner transducer at a displayed depth of 8 cm. The right side of this sonogram is dorsal and the left side is ventral.

sonographically in the extirpated equine eyes or in eyes of normal live horses. It was detected sonographically, however, in one equine eye 2 hours after surgical enucleation of the eye but had not been detected sonographically prior to enucleation.[28] The mean thickness of the iris and ciliary body were 2.5 ± 0.66 mm and 3.99 ± 1.13 mm, respectively.[28] In this study the sonographically derived corneal measurements and dorsal-ventral axis measurements of the eyes were larger than the physical measurements. Also the dorsal-ventral axis measurements obtained sonographically or physically from male horses were smaller than those obtained from female horses.[28]

Brain and Spinal Cord

The lateral ventricles should appear as anechoic curved fluid-filled structures. The height of the lateral ventricles in normal foals has not been determined, nor has the ventricle-mantle ratio (the ratio of the lateral ventricular height to the distance between the roof of the lateral ventricle and the brain surface) or the ventricle-hemisphere ratio (the ratio of the lateral ventricular height to the hemispheric width).

Sonographic examination of the normal neonatal canine brain has been described[26, 29] using the bregmatic fontanelle as the acoustic window into the cranium for 3 to 4 weeks after birth. The ultrasonographic anatomy of the normal canine spinal cord has also been described, but a hemilaminectomy must be performed to create a sonographic window through which to image the spinal cord.[30]

Abnormal Structures

Thyroid Gland

Abnormalities of the thyroid gland function are rare in horses. Goiter or thyroid gland enlargement can occur with hypothyroidism, hyperthyroidism, or euthyroidism. Both hypothyroidism and hyperthyroidism are rare in adult horses. Equine thyroid enlargement has been detected in some normal horses having no clinical signs of thyroid disease (Fig. 11–10). Marked enlargement of the thyroid gland and hypothyroidism have occurred in foals with excessive dietary iodine intake.[31, 32] Hypothyroidism of unknown etiology associated with a hyperplastic thyroid gland has been shown in some foals.[33, 34] In some foals with thyroid hormone inadequacy, a hypometabolic state has been reported.[35] These foals are incoordinated, have poor sucking and righting reflexes, and are hypothermic. Developmental lesions have also occurred in foals with normal thyroid levels, indicating possible thyroid deprivation during gestation.[35] Foals with this syndrome, which appears to be limited to western Canada, have incompletely ossified cuboidal bones, mandibular prognathia, flexural deformities in the forelimbs, and rupture extensor tendons. The thyroid gland in these foals may be normal or mildly enlarged.

Marked enlargement of the ventral aspect of the neck was seen in one older mare who presented with a gradually enlarging mass in the throatlatch region. Sonographic examination of this mass revealed a very small amount of thyroid tissue (approximately 1.5 cm long and 1 cm wide). The remainder of the thyroid gland was replaced with heterogeneous hypoechoic tissue with small irregular anechoic areas (Fig. 11–11). Histopathologic examination of this tissue revealed an organizing hematoma with no evidence of neoplasia. Thyroid adenomas are common incidental findings in older horses. Thyroid gland carcinomas, characterized by very vascular and aggressive tumors, have been reported as rapidly enlarging masses in the cervical region of horses.[36–39]

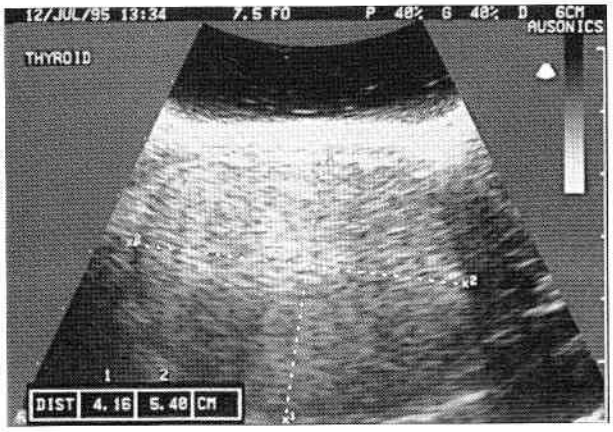

Figure 11–10

Sonogram of the left lobe of the thyroid gland obtained from a 3-year-old Thoroughbred cross gelding. The left lobe of the thyroid gland was enlarged, measuring 5.4 cm long (x^2), 4.16 cm wide (x^1), and 3.4 cm thick. The right lobe of the thyroid gland was significantly smaller, measuring 5.4 cm long, 2.7 cm wide, and 1.7 cm thick. The left lobe of the thyroid gland has normal-appearing glandular architecture, but the proximal and deeper portions of the gland are more hypoechoic. Benign thyroid hyperplasia was diagnosed on biopsy of this gland. This sonogram was obtained with a 7.5-MHz sector-scanner transducer containing a built-in fluid offset at a displayed depth of 6 cm. The right side of this sonogram is proximal and the left side is distal.

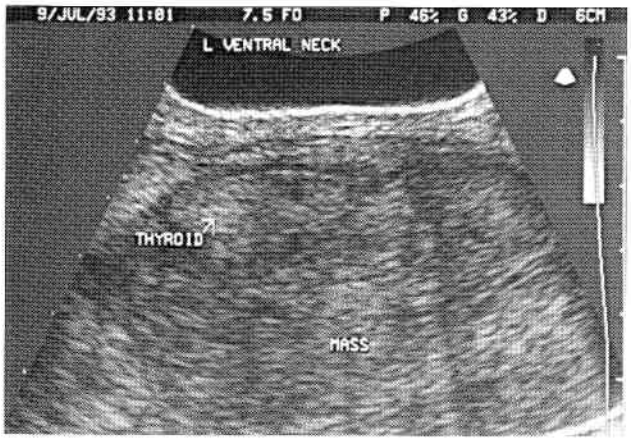

Figure 11–11

Sonogram of the ventral neck region obtained from a 30-year-old pony gelding. This mass measured 8.81 cm by 8.01 cm in diameter and appeared heterogeneous. It was only slightly less echogenic than the adjacent thyroid gland, which appeared to be involved with this mass, as the borders of the thyroid gland could not be distinguished from those of the mass. An ultrasound-guided aspirate of the mass revealed hemorrhagic tissue, and the biopsy was consistent with fibrovascular proliferation and hemorrhage. The heterogeneous appearance of the mass was associated with the large amount of organizing hemorrhage and fibrovascular proliferation. This sonogram was obtained with a 7.5-MHz sector-scanner transducer containing a built-in fluid offset at a displayed depth of 6 cm. The right side of this sonogram is dorsal and the left side is ventral.

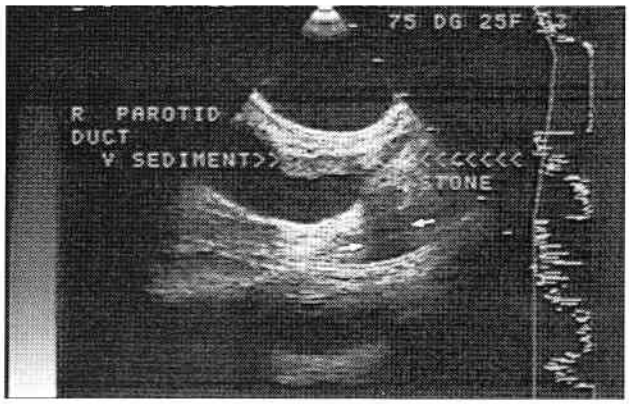

Figure 11–12

Sonogram of an enlarged right parotid salivary duct obtained from a 4-year-old Thoroughbred gelding with a sialolith and salivary gland obstruction. The right salivary duct is dilated (2 cm), filled with hypoechoic sediment along its ventral margin *(left arrowheads)* and is obstructed by an echogenic sialolith or salivary stone *(right arrowheads)* casting an acoustic shadow *(small arrows)*. The acoustic shadow originates from the far side of the sialolith, suggesting a large proteinaceous component. This sonogram was obtained with a 7.5-MHz sector-scanner transducer obtaining a built-in fluid offset at a displayed depth of 9 cm. The right side of this sonogram is cranial and the left side is caudal.

Parotid and Other Salivary Glands

Abnormalities of the salivary glands are uncommon and occur primarily in the parotid salivary gland. Obstruction of the parotid salivary gland has been seen in horses, usually associated with obstruction of the parotid duct by a sialolith,[40] which may form around cellular debris or vegetable foreign material that entered the salivary papilla. The parotid duct is enlarged, nonpainful, and freely movable along the cheek. The enlarged mandibular salivary duct is freely movable and nonpainful along the ventral aspect of the masseter muscle. Occasionally the parotid salivary gland is also enlarged. The parotid salivary duct may be lacerated in horses with facial trauma that have leakage of saliva from the wound. Bacterial sialoadenitis associated with an ascending infection may occur in horses (most likely in those with parotid duct obstruction, hematogenous infection, or trauma). Neoplasia of the salivary gland is uncommon, except for melanomas that have a predilection for the parotid salivary gland.[41, 42]

The obstructed parotid salivary duct is imaged as a large tortuous anechoic tubular structure coursing along the cheek before entering the oral cavity (Fig. 11-12). The sialolith appears as a hyperechoic structure casting an acoustic shadow typical of a mineral concretion. Echogenic debris may accumulate caudal to the obstruction, which may represent a mixture of saliva, mucus, and inflammatory cells. Obstruction of the salivary gland with a sialolith has been imaged in one horse with obstruction of the mandibular salivary duct. Enlargement of the salivary gland can be imaged in horses with obstructive sialolithiasis, parotitis, abscessation of the salivary gland, or neoplastic infiltration of the parotid salivary gland. An abscess in the parotid salivary gland appears similar to abscesses elsewhere, with a cavitation within the gland containing hypoechoic material. Neoplastic infiltration of the salivary gland is common in horses with melanomas.[41, 42] The neoplastic infiltration of the salivary gland in horses with melanomas usually appears sonographically as discrete homogeneous masses that are nearly isoechoic with the normal parotid glandular tissue (Fig. 11-13).

Enlargement of the salivary gland is common in human beings with parotitis, with the parotid gland retaining a

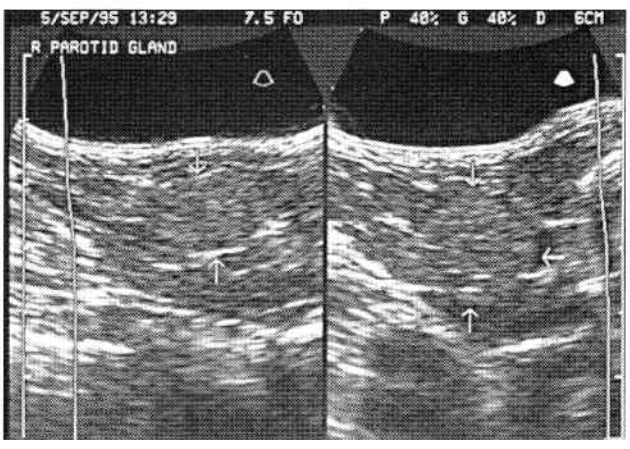

Figure 11–13

Sonograms of the right parotid gland obtained from a 9-year-old grey Thoroughbred gelding with melanomas. Notice the homogeneous mass *(arrows)* invading the parotid salivary gland, which is only slightly more echogenic than the adjacent salivary gland tissue. These sonograms were obtained with a 7.5-MHz sector-scanner transducer containing a built-in fluid offset at a displayed depth of 6 cm. The right side of the left image is proximal and the left side distal. The right side of the right image is cranial and the left side is caudal.

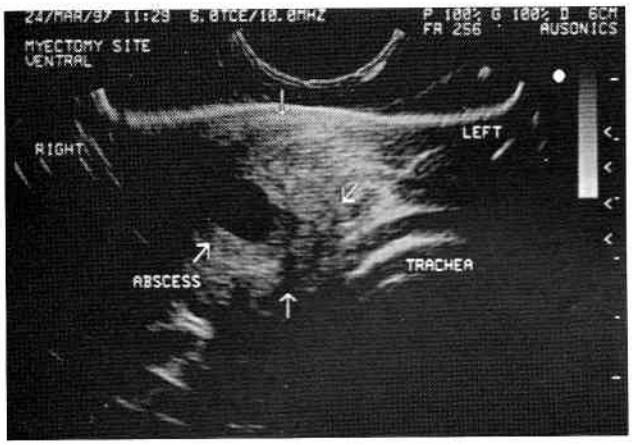

Figure 11–14

Sonogram of a peritracheal abscess following a transtracheal aspirate obtained from a 5-year-old Thoroughbred gelding. The abscess *(arrows)* is thick walled and contains anechoic fluid. The abscess is primarily to the right side of the midline, adjacent to the trachea, and does not extend superficially to the skin surface. This sonogram was obtained with a wide-bandwidth 6.0-MHz microconvex linear-array transducer operating at 10.0 MHz using a hand-held standoff pad at a displayed depth of 6 cm. The right side of the sonogram is to the left side of the ventral cervical region.

uniform and hypoechoic echotexture.[43] Sialectasis may or may not be present in these patients. With chronic forms of parotitis, multiple lucencies may be detected within the parotid salivary gland, associated with nonobstructive cystic sialectasis and or foci of reactive lymphoid aggregates.[45] The vascularity is also increased in human beings with parotitis.[43]

Tracheal Diseases

Abnormalities of the trachea are not frequently recognized in horses. Tracheal trauma may result in tracheal fracture, with the horse presenting with subcutaneous emphysema and diffuse soft tissue swelling in the region of the ventral neck. Congenital cysts associated with the trachea are rare. Abscesses from transtracheal aspirates are probably the most common cause of swelling around the trachea. These abscesses, if large, may compress the trachea and cause the horse to make a respiratory noise or cause respiratory distress.[44] Soft tissue masses in the peritracheal tissues may be large enough or positioned in such a way to compress the trachea; neoplasia would be likely in this situation. Intratracheal soft tissue masses have been infrequently detected in horses and are usually associated with neoplasia. Tracheal collapse is rare in horses but can occur as a congenital or acquired abnormality. Inspiratory and expiratory distress may occur if the tracheal collapse is severe. Exercise intolerance, respiratory stridor, and tachypnea may be present.

Peritracheal abscesses usually contain hypoechoic fluid (Fig. 11-14) and may also contain hyperechoic echoes consistent with free gas (Fig. 11-15). Abscesses involving the trachea causing tracheal deformities (Fig. 11-16) may be imaged sonographically. Soft tissue masses may also impinge on the trachea (Fig. 11-17). Deformities in the tracheal cartilage are easily recognized ultrasonographically by the misshapen appearance of the trachea. Sonographic examination of the cervical trachea reveals a collapsed oval or elongated shape to the normally circular trachea in horses with tracheal collapse. Intratracheal soft tissue masses with a complex pattern of echogenicity have also been imaged in horses with bronchial neoplasia.

Esophageal Diseases

Horses experience a wide variety of esophageal disorders, the most common of which is esophageal obstruction. Esophagitis, esophageal stricture, or esophageal

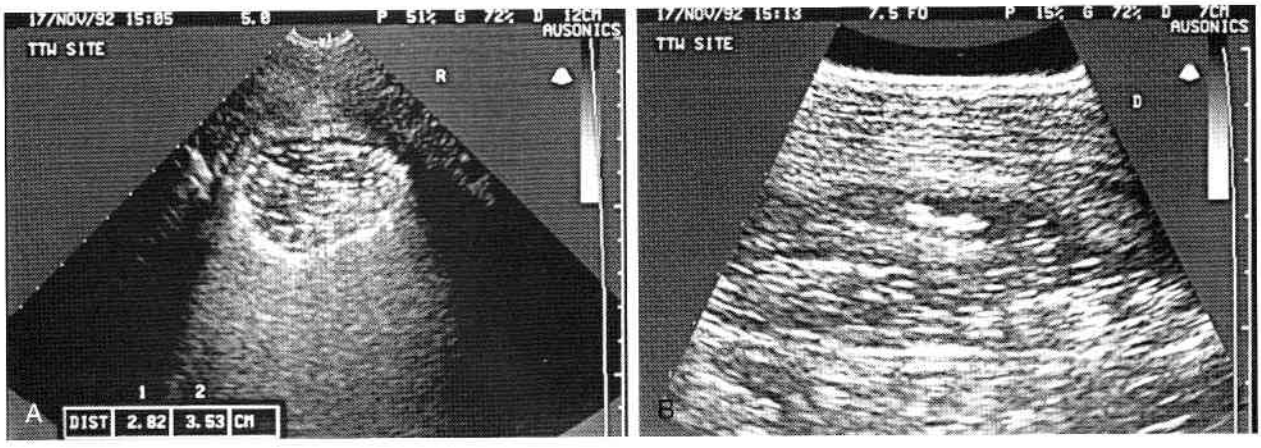

Figure 11–15

Sonograms of a large peritracheal abscess secondary to a transtracheal wash obtained from a 2-year-old Thoroughbred gelding. There are multiple hyperechoic echoes swirling in the hypoechoic fluid contained within a somewhat circular cavitation, consistent with an anaerobic abscess.

A, The abscess is located 2.82 cm from the ventral surface of the neck (x^1) and has a diameter of 3.53 cm (x^2). The large amount of gas within the abscess shadows the deeper structures (dirty shadows) making it impossible to identify the trachea in this view. The right side of this image is the left side of the trachea. This sonogram was obtained with a 5.0-MHz sector-scanner transducer at a displayed depth of 12 cm.

B, The abscess margins are less well defined but can be distinctly separated from the surrounding musculature. This sonogram was obtained with a 7.5-MHz sector-scanner transducer containing a built-in fluid offset. The right side of this sonogram is proximal and the left side is distal.

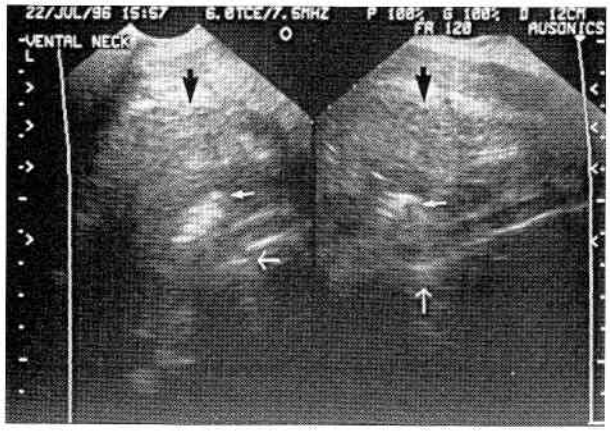

Figure 11–16

Sonograms of a slightly deformed trachea secondary to a peritracheal abscess following a transtracheal aspirate obtained from a 4-year-old Standardbred stallion. The abscess involves the wall of the trachea *(larger arrows)* resulting in the slight step imaged in the transverse view (left image) and the bulging into the tracheal lumen in the sagittal view (right image). There is a dorsal clump of hyperechoic echoes casting a weak acoustic shadow *(smaller arrows)* consistent with free gas. There is extensive thickening of the tissues adjacent to the abscess consistent with a surrounding area of cellulitis and muscle necrosis walling off the local infection *(black arrows)*. The abscess cavitation is deep (approximately 5 cm from the skin surface). These sonograms were obtained with a wide-bandwidth 6.0-MHz microconvex linear-array transducer operating at 7.5 MHz at a displayed depth of 12 cm. The right side of the right image is proximal and the left side is distal. The right side of the left image is toward the left side of the neck.

dilitation occur most often following esophageal obstruction. Trauma to the cervical region may lead to esophageal rupture or the formation of an esophageal diverticulum. Esophageal duplication cysts, persistent right aortic arch, megaesophagus, and esophageal atresia have also been reported in horses. Neoplasms involving the equine esophagus are extremely rare.

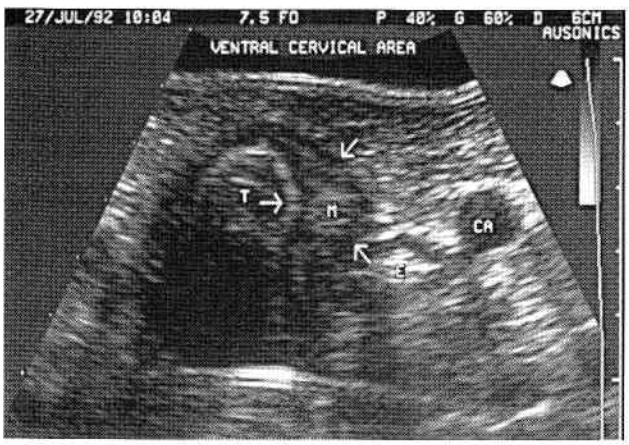

Figure 11–17

Sonogram of a peritracheal mass *(arrows)* obtained from a 22-year-old Welsh pony mare. The mass (M) is hypoechoic and is compressing the left side of the trachea (T). The mass is between the trachea and esophagus (E) but appears to originate from the esophagus. This sonogram was obtained with a 7.5-MHz sector-scanner transducer containing a built-in fluid offset at a displayed depth of 6 cm. The right side of this sonogram is the left side of the pony's neck. CA, Carotid artery.

Esophageal Obstruction. Feed impaction is a common cause of esophageal obstruction in horses.[45] Beet pulp and poorly masticated carrots and apples have also been associated with esophageal obstruction.[45] Fragments of nasogastric tubes have been reported as esophageal foreign bodies causing esophageal obstruction in two horses and an intact nasogastric tube caused esophageal obstruction in one horse.[46, 47] Antibiotic boluses, wood, wood chips, and a riding crop have also been reported to cause esophageal obstruction in horses.[45, 48, 49] Squamous cell carcinoma, the most commonly reported esophageal tumor in the horse, may also cause esophageal obstruction.[50, 51]

Feed impactions of the esophagus are recognized as heterogeneous echogenic masses within the esophageal lumen causing esophageal dilitation. The nasogastric tube has a distinct sonographic appearance and is imaged as a double-walled tubular structure. The antibiotic boluses, wood, wood chips, and riding crop obstructing the esophagus in the cervical region should also be visible sonographically. Antibiotic boluses should appear as echogenic to hyperechoic oval structures in the esophageal lumen. Wooden foreign bodies should be hyperechoic and cast a strong acoustic shadow from the surface of the wood. Wood chips are likely to cast multiple weak shadows from the multiple reflecting surfaces of the impacted chips.

Esophageal Stricture. Esophageal strictures have been reported more frequently in young horses (median age of 1.5 years in one study).[45] External cervical trauma (kick), nasogastric intubation, and dietary indiscretion were predisposing causes in several affected horses.[45] Sonographic examination of an esophageal stricture is possible if the lesion involves the cervical esophagus. A narrowing of the esophagus with loss of the normal esophageal motility and possible periesophageal abnormalities may be detected sonographically. Echogenic periesophageal tissue may be imaged associated with periesophageal scar tissue and defects in the adjacent cervical musculature associated with previous external trauma are the most frequent periesophageal findings.

Esophageal Cysts and Diverticula. Esophageal duplication cysts and intramural esophageal cysts have been shown to cause esophageal obstruction in the horse.[52–54] Esophageal diverticula have been reported, causing esophageal obstruction and a cervical mass that enlarged or was detected after eating.[45, 55, 56] In the horses with an esophageal diverticulum, trauma to the cervical region preceded the development of the esophageal diverticulum.

A phytobezoar in a horse, which had probably formed in an esophageal diverticulum and subsequently become dislodged, caused esophageal obstruction in the distal cervical esophagus.[57] Sonographic examination of the ventral aspect of the neck, immediately cranial to the thoracic inlet, would have revealed feed material within the esophageal diverticulum or the obstructing mass within the lumen of the esophagus in the horse with the phytobezoar. Visualization of the esophageal diverticulum should have been possible sonographically. The accumulation of saliva, fluid, and food material within the diver-

ticulum would have facilitated its sonographic recognition. Collapse of the esophageal diverticulum after passage of the phytobezoar may have limited sonographic visualization of the esophageal diverticulum. A pulsion esophageal diverticulum is thought to form secondary to external trauma, impacted feedstuffs, and fluctuations in esophageal pressure.[55-57] In this horse, a fractured tracheal ring that had apparently subsequently healed was detected in the adjacent cervical region. The fractured tracheal ring was the probable etiology of the esophageal diverticulum in this horse. This type of tracheal ring abnormality can also be detected sonographically.

Megaesophagus. Megaesophagus occurs in horses as a congenital or acquired condition, the latter being most common.[58, 59] Esophageal dilitation occurs most frequently secondary to chronic esophageal obstruction with the megaesophagus occurring in the portion of the esophagus proximal to the obstruction or stricture. Esophageal dilitation may also result from previous esophageal trauma. Central or peripheral nervous system disorders affecting esophageal motility can lead to esophageal dilitation, as can muscular disorders affecting the esophagus. Clinical signs of megaesophagus include dysphagia, ptyalism, swelling in the cervical region, and nasal reflux. Affected horses may also have aspiration pneumonia.

The enlarged dilated esophagus is easily demonstrated sonographically if the cervical portion of the esophagus is affected (Fig. 11-18). The markedly dilated esophageal lumen is imaged with the normal gas and mucus-covered luminal surface, creating a hyperechoic appearance on the esophageal mucosa. Poor esophageal motility may be imaged during a real-time examination while the horse swallows.

Esophageal Rupture. Rupture of the pharynx or esophagus is most common secondary to trauma, which may be iatrogenic or associated with a kick or other external trauma in this region.[45, 60, 61] Esophageal rupture in horses has been reported following nasogastric intubation.[45, 61] Iatrogenic esophageal trauma and subsequent rupture are more common in miniature horses and in horses with colic.[61] Prolonged intubation has also been implicated as a cause of esophageal rupture.[61, 62] Esophageal perforation has also been reported in horses secondary to prior feed impaction and retropharyngeal abscesses.[45] Clinical signs of horses with esophageal or pharyngeal trauma include esophageal spasm, ptyalism, dysphagia, and coughing.[45, 61] Fever and signs of toxemia are seen in horses with esophageal or pharyngeal rupture and severe cellulitis. The esophageal perforations are usually found in the cervical region.[45]

Ultrasonographic examination of the cervical and retropharyngeal regions can identify the cellulitis and its relationship to the esophagus and other surrounding structures. Actual perforation of the esophageal wall is not likely to be visualized owing to the severe cellulitis at the site. Bright hyperechoic echoes in the inflamed subcutaneous tissues represent free gas, a common finding in cervical cellulitis associated with esophageal rupture (Fig. 11-19). The large amounts of gas in the soft tissues may prevent visualization of some of the adjacent structures.

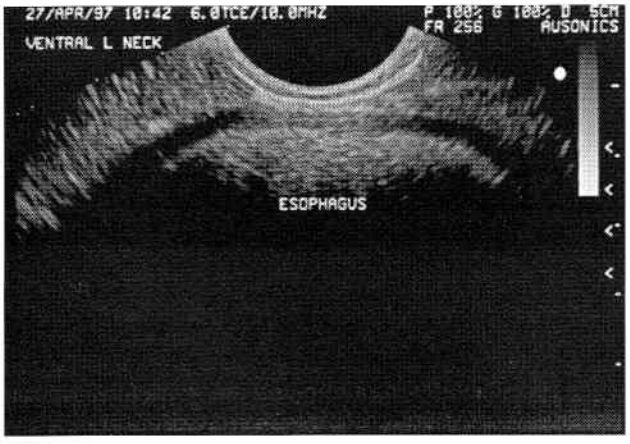

Figure 11–18

Sonogram of megaesophagus secondary to a kick in the ventral neck region obtained from a 5-year-old Thoroughbred gelding. The esophagus is greater than 6.5 cm in diameter just cranial to the thoracic inlet. The wall thickness of the esophagus is normal, but the normal esophageal mucosal folds are not imaged. This sonogram was obtained with a wide-bandwidth 6.0-MHz microconvex linear-array transducer operating at 10.0 MHz at a displayed depth of 5 cm. The right side of this sonogram is the left side of the neck.

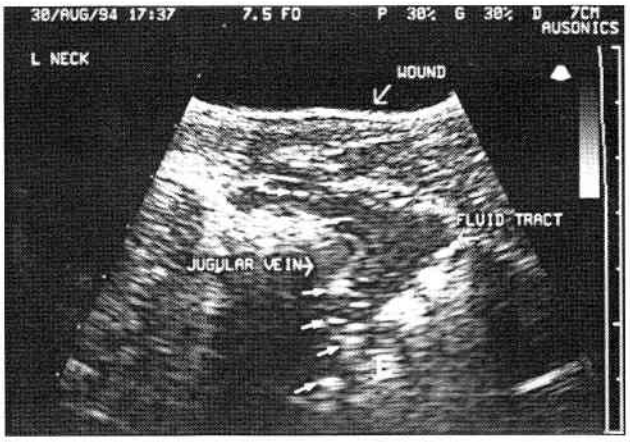

Figure 11–19

Sonogram of the left side of the neck obtained from a 19-year-old Thoroughbred gelding with a kick wound to the neck and a ruptured esophagus. The skin wound *(arrow)* extends through the subcutaneous tissues, around the jugular vein to the deeper tissues. A large amount of hyperechoic echoes associated with free gas in the tract are imaged in the deeper portions of this tract *(small arrows)*. The esophagus (E) is imaged surrounded by the greatest amount of fluid and gas. Although a defect in the esophageal wall is not imaged owing to the superimposed gas, the gas echoes appear to be originating from this area. This sonogram was obtained with a 7.5-MHz sector-scanner transducer containing a built-in fluid offset at a displayed depth of 7 cm. The right side of this sonogram is dorsal and the left side is ventral.

Swellings and Masses

Cysts. Cysts occur infrequently in horses. Cervical cysts, reported primarily in young horses, develop in the retropharyngeal or cranial cervical area.[63-65] These types of cysts are associated with salivary mucoceles,[63] branchial cysts,[64-66] thyroglossal cysts,[53, 67, 68] or paralar-

yngeal accessory bronchial cysts.[69] Cervical cysts cause swelling in the throatlatch region, which is usually bilaterally symmetrical and nonpainful to palpation. The guttural pouches may be displaced cranially and the trachea ventrally in some affected horses.[65] Dorsal compression of the trachea was reported in affected horses.[63-65] These cysts can become so large that they may result in respiratory stridor.

Pharyngeal cysts usually occur in young horses that present with respiratory stridor or dysphagia.[67, 68] Cysts in the subepiglottic location are thought to be remnants of the thyroglossal duct, whereas dorsal pharyngeal cysts are probably remnants of the cranial pharyngeal duct.[67] Cystic structures within the guttural pouches have been reported in horses and may be associated with retention of the first branchial arches.[65] Intramural esophageal inclusion cysts have also been reported in horses. These horses present with bilateral nasal discharge, choke, and may have an enlarging neck mass.[2, 52, 53] Compression of the esophagus was present in all affected horses. One foal with swelling in the right caudal portion of the jugular groove had a combined esophageal and tracheal duplication cyst with no signs of esophageal obstruction.[3]

Sonographic examination of these cysts reveal them to contain anechoic fluid and to be either unilocular or multilocular (Fig. 11-20). Fibrinous loculations and echogenic clot associated with hemorrhage in the cyst has been imaged in some horses (Fig. 11-21). In one weanling a peritracheal mass located at the thoracic inlet was imaged with a gelatinous spongy consistency, having hypoechoic areas and anechoic areas within the mass (Fig. 11-22). The mass lay on the ventral surface of the trachea and displaced it dorsally. Excisional biopsy of this mass revealed it to be most consistent with an embryologic remnant.

A branchial cyst that was imaged in a 10-month-old Belgian filly contained anechoic fluid within a hyperechoic capsule with small hyperechoic fimbriae moving freely within the fluid.[1] Ultrasound was used to identify the source of the cyst (esophagus) and demonstrate the location of the intramural esophageal cysts relative to the important surrounding structures (trachea, jugular vein, and carotid artery).[2] A hypoechoic fluid-filled mass surrounded by a hyperechoic capsule was imaged adjacent to the esophagus in two horses with esophageal intramu-

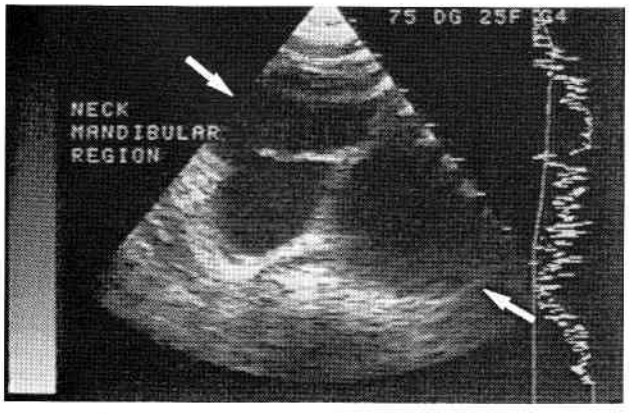

Figure 11–20

Sonogram of a large ultimobranchial cyst in the ventral throatlatch region obtained from a 5-year-old Quarter Horse gelding. The cyst is multiloculated and filled with anechoic fluid, measuring 5.5 cm long by 7.2 cm wide. Notice the acoustic enhancement of the far wall of the cyst indicating that this structure is fluid filled. This sonogram was obtained with a 5.0-MHz sector-scanner transducer at a displayed depth of 9 cm. The right side of this sonogram is cranial and the left side is caudal.

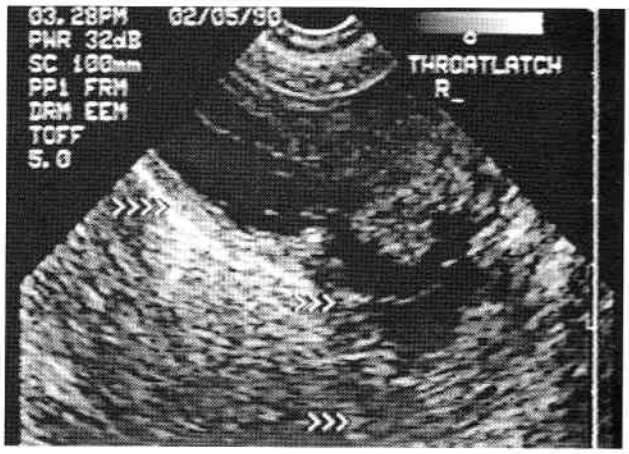

Figure 11–21

Sonogram of a large multiloculated cystic structure in the right throatlatch region of an 18-year-old Morgan mare. There was homogeneous echogenic tissue within the large multiloculated cystic mass which appeared to resemble normal thyroid tissue. Fibrinous loculations were also imaged throughout the cystic mass. No other identifiable thyroid tissue was imaged in the right side of the neck, although the parotid gland, jugular vein, and carotid artery were imaged adjacent to this mass. This sonogram was obtained with a 5.0-MHz sector-scanner transducer at a displayed depth of 10 cm. The right side of this sonogram is proximal and the left side is distal.

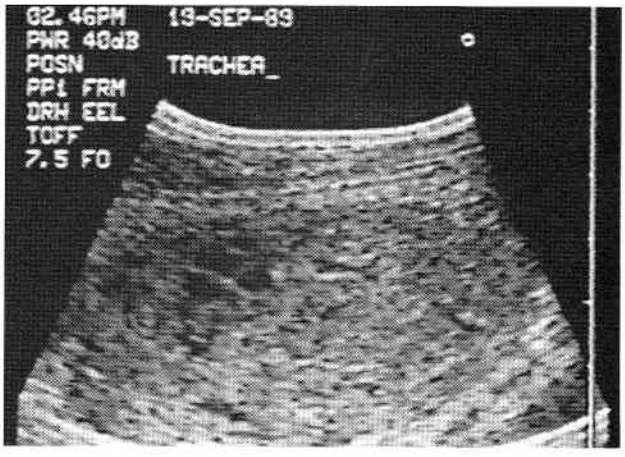

Figure 11–22

Sonogram of a large oval peritracheal mass in the thoracic inlet region obtained from a 5-month-old Morgan filly with respiratory tract obstruction. The mass had a spongy gelatinous heterogeneous appearance with hypoechoic to anechoic areas within. The mass measured 3.8 cm thick by 7.1 cm long and extended around both sides of the trachea, displacing it dorsally but not invading the trachea. The final histopathologic diagnosis on the mass removed by an excisional biopsy was a cystic embryologic remnant of unknown origin. This sonogram was obtained with a 7.5-MHz sector-scanner transducer containing a built-in fluid offset at a displayed depth of 7.5 cm. The right side of this sonogram is cranial and the left side is caudal.

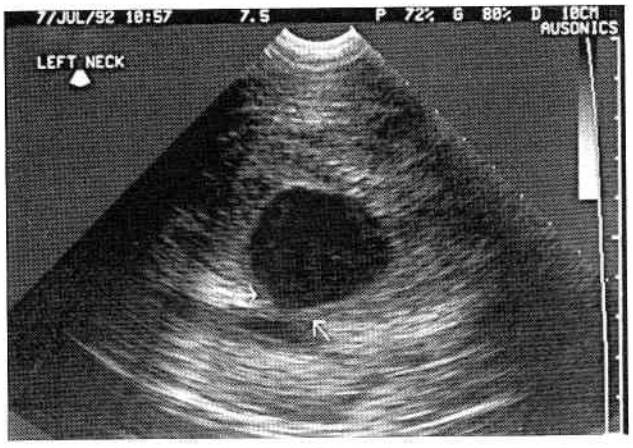

Figure 11–23

Sonogram of the left cervical region obtained from a 2-year-old Thoroughbred colt with a neck abscess. The abscess is anechoic, has discrete margins, measures 2.98 cm by 3.55 cm in diameter, and connects through a small opening to a small deeper portion between the fascial planes *(arrows)*. The surrounding musculature has lost its normal striated muscle pattern and has a more homogeneous hypoechoic appearance. A hematoma or cyst should also be considered for this mass, owing to the anechoic appearance of this fluid collection. However, the lack of fibrinous loculations makes a hematoma less likely, and the small opening connecting to the fascial planes makes a cyst less likely. Cysts have not been reported in this area, and the area was warm and painful to the touch. This sonogram was obtained with a 7.5-MHz sector-scanner transducer at a displayed depth of 10 cm. The right side of this sonogram is caudal and the left side is cranial.

ral inclusion cysts.[2] Multiple small hyperechoic foci were imaged in the cyst fluid in one horse. In one horse with an intramural esophageal inclusion cyst the mass appeared hyperechoic and homogeneous and was also imaged adjacent to the esophagus.[2] An ultrasound examination of the swelling in the filly with the combined esophageal and tracheal duplication cyst revealed the mass to appear fairly uniformly echogenic with a slightly more hypoechoic center, not involving the adjacent jugular vein, carotid artery, or sternocephalicus muscle.[3]

Dentigerous Cysts. A dentigerous cyst is an odontogenic cyst surrounding the crown of a tooth, caused by incomplete closure of the first branchial cleft. The supernumerary tooth has been associated with the temporal bone (most common), mandible, frontal bone, or bones of the skull.[70, 71] Dentigerous cysts are frequently associated with a firm swelling and intermittent serous or seropurulent drainage from the cyst.

Sonographic examination of the draining tract can be used to follow the drainage to the source (the dentigerous cyst). This cyst, in contrast to other cysts found in the horse, should have a composite sonographic appearance with hyperechoic areas casting acoustic shadows detected within the cyst associated with the tooth.

Abscesses. Abscesses are common in horses associated with a penetrating wound through the skin or an iatrogenic injection. Often the inciting incident is unknown; the horse presents with a warm, painful swelling and is reluctant to move the affected area. The swelling is usually firm, but a soft spot may be palpable if the abscess is close to breaking out to the skin surface.

Trauma to the pharynx associated with passage of the nasogastric tube may result in the development of a cervical or pharyngeal abscess.[72] Large pharyngeal masses often are accessible to sonographic examination from the retropharyngeal area. The large pharyngeal abscesses reported in horses would have been amenable to sonographic examination had an ultrasound examination been performed.[72, 73] Inspiratory respiratory distress indicates an obstruction located within the upper airway or cervical trachea.[44] Caudal cervical lymph node abscess formation causes respiratory distress with tracheal compression in the caudal cervical trachea.[44] Sonographic examination of the thoracic inlet in this colt may have helped identify the cause of the respiratory distress and monitor the colt's response to treatment.[44]

Sonographic examination of abscesses reveals a fluid-filled cavitated area in the affected tissues. The normal tissue architecture in the region of the abscess is absent, replaced by the cavitating area containing exudate.[6] The fluid may be anechoic (Fig. 11-23) or hypoechoic (Fig. 11-24) to echogenic, depending primarily on the cellularity of the abscess fluid.[6] Pinpoint hyperechoic echoes may be detected sonographically, consistent with gas production within the abscess by anaerobic bacteria, or a dorsal hyperechoic layer or "gas cap" may be detected (Fig. 11-25). Hyperechoic free gas echoes have appeared sonographically in an abscess in the cervical musculature. This was associated with anaerobic bacteria.[6] The abscess fluid may have a composite appearance with hypoechoic to echogenic strands of fibrin within (Fig. 11-25). Necrotic tissue is also often present within the abscess and may appear anechoic initially, with early tissue necrosis.

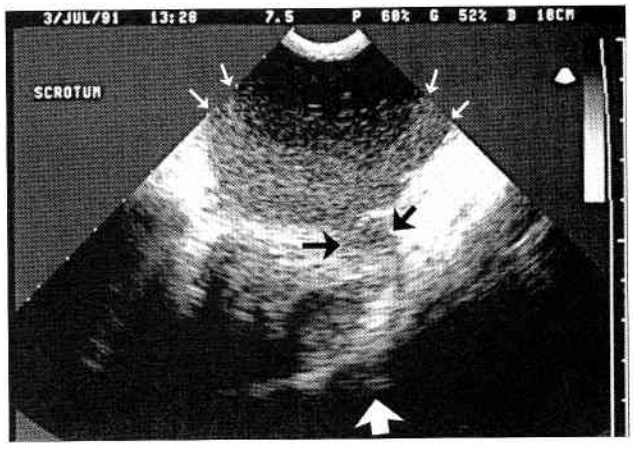

Figure 11–24

Sonogram of large scrotal abscess obtained from a 16-year-old Morgan gelding castrated as a yearling. A large, composite fluid-filled mass ventrally in the scrotum *(small arrows)* communicates through a small tract *(larger arrows)* to a composite fluid and soft tissue structure near the left external inguinal ring. The scrotal abscess *(small arrows)* is anechoic ventrally with flocculent material imaged within the fluid. The more hypoechoic fluid is dorsal and is similar to the hypoechoic fluid imaged in the tract. Anechoic and hypoechoic fluids are imaged adjacent to a somewhat heterogeneous echogenic mass near the inguinal ring *(wide arrow)*. A scirrhous cord causing the scrotal abscess was found during surgery. Neoplastic infiltration of the remnant of the spermatic cord with secondary abscessation should also be considered in the differential diagnosis for this sonographic appearance. This sonogram was obtained with a 7.5-MHz sector-scanner transducer at a displayed depth of 10 cm. The right side of this sonogram is towards the left side of the scrotum.

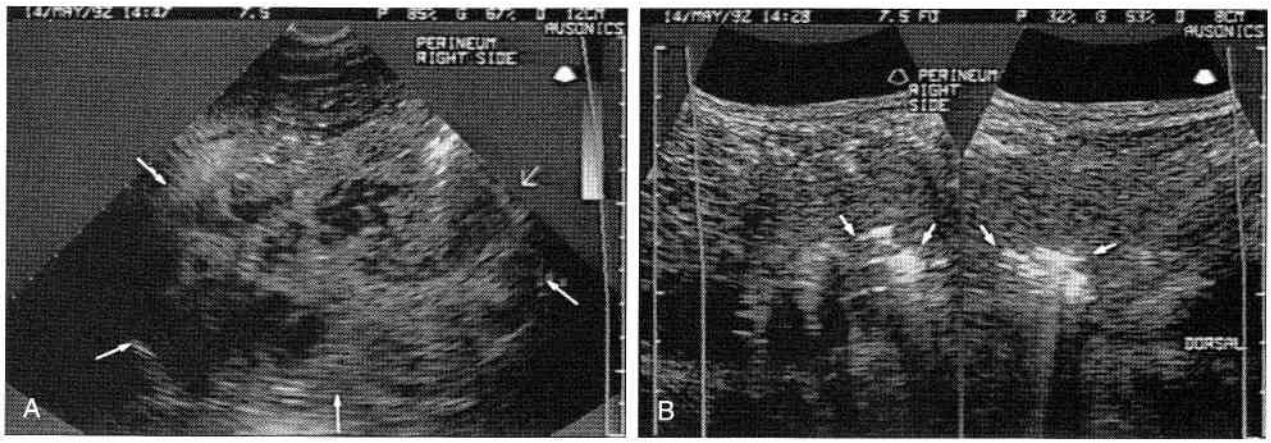

Figure 11–25

Sonograms of the right perineal region obtained from a 1-year-old Thoroughbred gelding with a large perineal abscess. These sonograms were obtained with a 7.5-MHz sector-scanner transducer *(A)* and a 7.5-MHz sector-scanner transducer containing a built-in fluid offset *(B)* at a displayed depth of 12 cm *(A)* and 8 cm *(B)*.

A, The abscess *(arrows)* is cavitated and loculated with anechoic, hypoechoic, and hyperechoic areas within. The small hyperechoic areas represent free gas in the tissues, which is consistent with an anaerobic infection. The abscess has completely destroyed the normal musculature in this region. The right side of this sonogram is dorsal.

B, A large collection of hyperechoic echoes *(arrows)* casts dirty shadows associated with free gas in the more dorsal portion of this abscess. The right side of the right image is dorsal and the left side is ventral. The right side of the left image is toward the midline.

However, most necrotic tissue within an abscess is echogenic to hyperechoic and surrounded by less echogenic fluid (Fig. 11-26). This necrotic tissue may often act as a foreign body. Although the abscess may have irregular margins initially, it usually develops better-defined margins once the abscess has started to organize and is more chronic. A discrete capsule is usually not detected unless the abscess is very long standing. The abscess capsule is usually echogenic because of its fibrous composition.

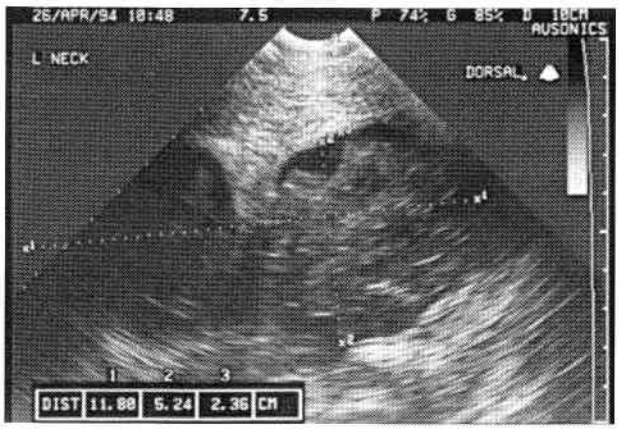

Figure 11–26

Sonogram of the left cervical region obtained from a 3-year-old Thoroughbred gelding with a neck abscess. The abscess is very large and well defined from the adjacent cervical musculature which has increased echogenicity associated with inflammatory infiltrate in the adjacent musculature. The abscess has two major compartments: the dorsal one, which appears to contain primarily echogenic necrotic material, and the ventral area, which has more anechoic fluid. The abscess was located 2.36 cm deep to the skin surface (x^4) and was more than 11.8 cm long (x^1). The dorsal compartment was 5.24 cm thick (x^2) and 8.66 cm wide. The small hyperechoic echoes in the dorsal compartment of the abscess may represent free gas echoes, and an anaerobic culture should also be performed on fluid obtained from an aspirate of this abscess. This sonogram was obtained with a 7.5-MHz sector-scanner transducer at a displayed depth of 10 cm. The right side of this sonogram is dorsal and the left side is ventral.

Corynebacterium Pseudotuberculosis Abscesses. Large external abscesses, also called "pigeon fever," have been reported in horses with *Corynebacterium pseudotuberculosis* infection.[74, 75] These abscesses are most common in horses in the western United States, particularly California, and in Brazil.[75] In California this disease is most common during the fall and early winter months.[74, 75] Most horses (75%) have a single abscess detected in the pectoral, axillary, ventral abdominal, or inguinal region.[75] Recurrence of the abscess is uncommon. Internal abscesses also occur in horses with *Corynebacterium pseudotuberculosis* infection. Clinical signs in horses with external abscesses usually include diffuse or local swellings, fever, lameness, edema, and nonhealing wounds.[74, 75]

Sonographic examination of horses with *Corynebacterium pseudotuberculosis* abscesses should reveal large echogenic fluid-filled masses, which, in some horses, may be surrounded by a thick echogenic capsule. The exudate contained within the abscess should appear echogenic owing to the thick and caseous nature of the purulent material contained in these abscesses.

Perirectal Abscesses. Horses with perirectal abscesses frequently have signs of intermittent colic and depression. Anorexia, lack of fecal production, tenesmus, and fever have frequently been reported.[76] A history of intramuscular injections in the gluteal region was present in 33% of horses with perirectal abscesses, in one review.[76] One mare had experienced a dystocia 1 month before presenting with a perirectal abscess. Perivaginal masses, which may be hematomas or abscesses, are common following parturition. Rectal trauma may also be associated with the development of a perirectal abscess. Anorectal lymph nodes may become secondarily infected in this region, causing perirectal abscesses. Rectal palpa-

tion is useful in localizing the abscess around the rectum, but in some horses, the complete extent of the abscess cannot be determined rectally owing to the severity of the resultant rectal obstruction. Perirectal abscesses can also be seen in horses associated with perirectal neoplasia. A perirectal abscess was reported associated with a perianal squamous cell carcinoma in a mare.[77] Sonographic examination of the perineum and rectum in this mare could have revealed the extent of neoplastic involvement of the perirectal tissues and the perirectal abscess.

Sonographic examination of the perirectal or perivaginal abscess can help the clinician differentiate between an abscess and a hematoma (Fig. 11-27) or soft tissue mass, determine the extent of the abscess and the involvement of other perirectal structures, and select the surgical approach for successful drainage of the abscess. Most perirectal or perivaginal abscesses contain a large amount of gas, owing to the production of gas within the abscess by anaerobic organisms (Fig. 11-27).

Granuloma. Subcutaneous and/or skin granulomas can present with swelling in the skin and subcutaneous tissues or with or without ulceration of the overlying skin. Fungal and parasitic granulomas are uncommon in horses. Habronemiasisis is the most common parasitic granuloma involving the skin and subcutaneous tissues. *Halicephalobus deletrix* (previously *Micronema deletrix*) granulomas have also been reported in horses. These granulomas most frequently involve the maxilla, although a nasal granuloma has been reported in a horse with *Halicephalobus deletrix* infection.[78-81]

Sonographic examination of the mandible in one horse with a *Halicephalobus deletrix* granuloma revealed a heterogeneous soft tissue mass with hypoechoic tracts leading to the mandible (Fig. 11-28). The bony surface of the mandible was irregular, with periosteal lytic and proliferative changes and a fluid layer adjacent to the bone, consistent with osteomyelitis. Sonographic examination of a large oval retropharyngeal mass in another horse revealed an outer homogeneous mass with a hyperechoic center surrounded by several anechoic areas suggesting central necrosis (Fig. 11-29). Excisional biopsy of this mass revealed a granulomatous lymph node infected with *Mycobacterium avium.*

A subcutaneous granuloma associated with *Cryptococcus neoformans* has been reported in the skin and subcutaneous tissues of the left side of a horse's thorax.[82] This mass began as a small subcutaneous swelling that enlarged and developed two draining tracts discharging purulent material. Sonographic examination revealed a multilobulated mass with dense echogenic areas and hypoechoic pockets with tracts leading into the hypoechoic areas.[82] Areas of mineralization were imaged in the tenth and eleventh intercostal spaces. An ultrasound-guided biopsy yielded the diagnosis of cryptococcal infection.[82]

Cellulitis. Cellulitis is characterized by a diffuse soft tissue swelling that is hot and painful and is associated with a suppurative process that dissects tissue planes. The initial clinical signs are fever, swelling, and lameness, if a limb is involved. Staphylococcal organisms (usually *Staphylococcus aureus*) has been involved in several cases of cellulitis involving the distal limbs of Thoroughbred racehorses.[83] Clostridial species have also been involved with cellulitis, particularly those that develop secondary to intramuscular injections.[84-88] When cellulitis is detected in the cervical region in horses, esophageal or pharyngeal rupture should be suspected.

The subcutaneous tissues are usually markedly thickened and have increased echogenicity (Fig. 11-30). Numerous vessels may be imaged in the affected area and the vessels adjacent to the area of cellulitis are often markedly enlarged. Hypoechoic or anechoic fluid pockets may be imaged in a large area of cellulitis as the infection starts to organize (Fig. 11-31).

Thickening and increased echogenicity of the skin and subcutaneous tissues is detected in human beings with

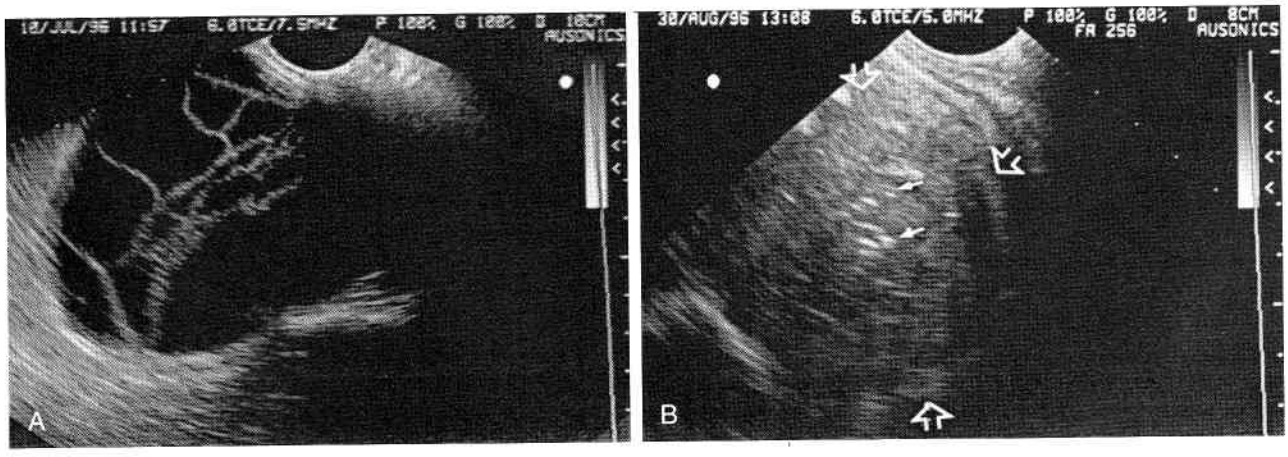

Figure 11-27

Sonograms of a large perivaginal and perirectal mass obtained from a 5-year-old Thoroughbred mare. These sonograms were obtained with a wide-bandwidth 6.0-MHz microconvex linear-array transducer operating at 7.5 MHz (A) and 5.0 MHz (B) at a displayed depth of 10 cm (A) and 8 cm (B). The right side of these sonograms is dorsal and the left side is ventral.

A, A large anechoic loculated mass was imaged consistent with a hematoma. It extended cranially adjacent to the cervix.

B, The character of the mass was very different 6 weeks later. Drainage of the hematoma resulted in a secondary infection of the hematoma. The mass now contains hypoechoic fluid and hyperechoic free gas echoes *(arrows),* consistent with anaerobic infection, and now has a thicker capsule with extensive thickening of the tissues surrounding the mass *(open arrows).*

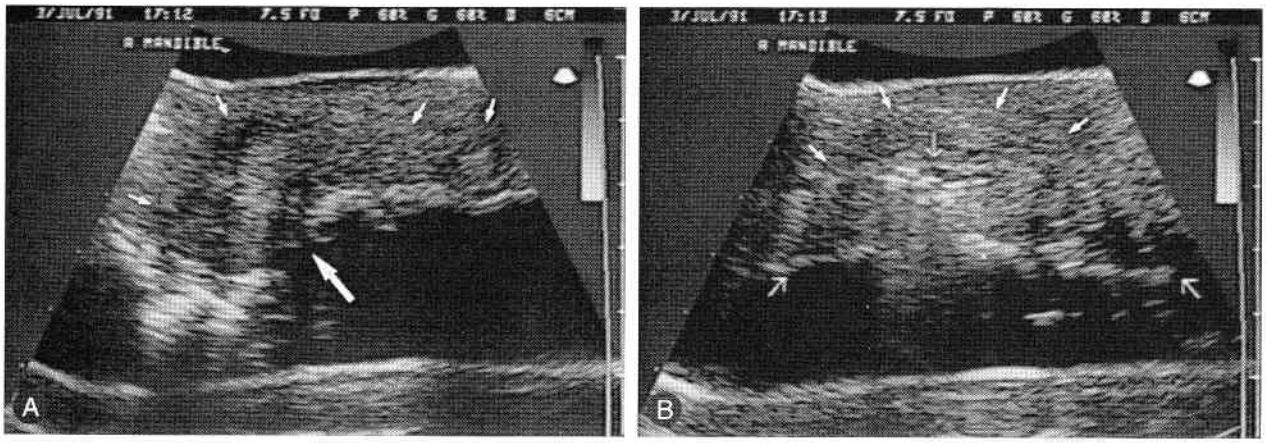

Figure 11–28

Sonograms of the right side of the mandible obtained from a 13-year-old Palomino Quarter Horse gelding with *Halicephalobus deletrix* granulomas involving the soft tissues, masseter muscle, and mandible. There is a mass of complex echogenicity *(small arrows)* involving the mandible, resulting in an irregular bony surface echo. The bony surface echo is thicker than normal, with lytic and proliferative areas. Excisional biopsy of this mass revealed the *Halicephalobus deletrix* organism. These sonograms were obtained with a 7.5-MHz sector-scanner transducer containing a built-in fluid offset at a displayed depth of 6 cm. The right side of these sonograms is rostral and the left side is caudal.

A, The mass *(small arrows)* appears to involve the bone as well as the surrounding soft tissues and a defect in the bone *(large arrow)* is present in the center of the mass. The complex echogenicity of the mass and the bony involvement are most consistent with a neoplasm.

B, This portion of the mass appears encapsulated *(small arrows)*. There is a fluid layer along the irregular bone *(right diagonal arrow)* consistent with a diagnosis of osteomyelitis. There are small hyperechoic echoes casting dirty shadows consistent with free gas within the mass *(down arrow)*. These free gas echoes could be consistent with concurrent anaerobic infection of the mass or may indicate a communication with the oral cavity or the skin surface if these air echoes can be followed along a tract.

cellulitis.[43] Increased numbers of vessels are imaged in the subcutaneous tissues with color Doppler ultrasound, and pulsed-wave Doppler spectral analysis demonstrates lower resistance flows in the area of cellulitis than in the adjacent normal areas.[43]

Lymphangitis. Lymphangitis usually affects the lymphatics in the limbs and results in local infection, with swelling, edema, and pain. Ulcerative lymphangitis is the most common form of this condition and is associated with *Corynebacterium pseudotuberculosis,* which causes severe lymphangitis and cellulitis in affected horses.[74, 75] Multiple nodular swellings are usually detected along the medial aspect of the limb, associated with small abscesses along the lymphatics. Other bacteria (*Pseudomonas aeruginosa, Staphylococcus* sp. and *Streptococcus* sp.) have

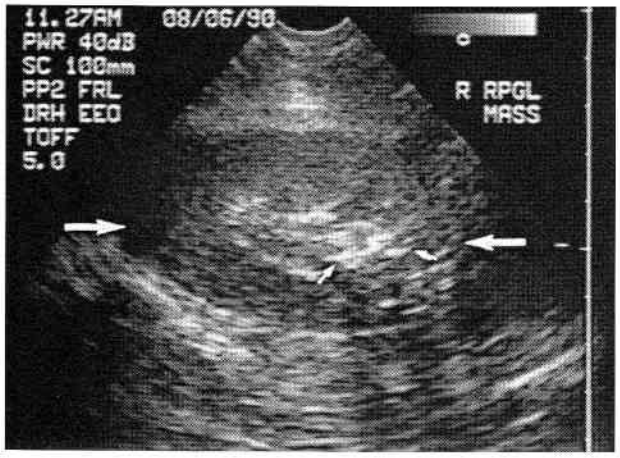

Figure 11–29

Sonogram of a large retropharyngeal mass obtained from a 15-year-old Quarter Horse mare with multiple *Mycobacterium avium* granulomas. The retropharyngeal mass *(large arrows),* located in the retropharyngeal lymph node, is a large oval mass measuring 4.7 cm wide, 10 cm long, and 7 cm thick. The mass had a hypoechoic, more homogeneous outer rim with a central hyperechoic area casting multiple acoustic shadows *(small arrows)* consistent with early calcification. The area around the hyperechoic center is slightly less echogenic than the outer rim, consistent with tissue necrosis. This sonogram was obtained with a 5.0-MHz sector-scanner transducer at a displayed depth of 10 cm. The right side of this sonogram is cranial and the left side is caudal.

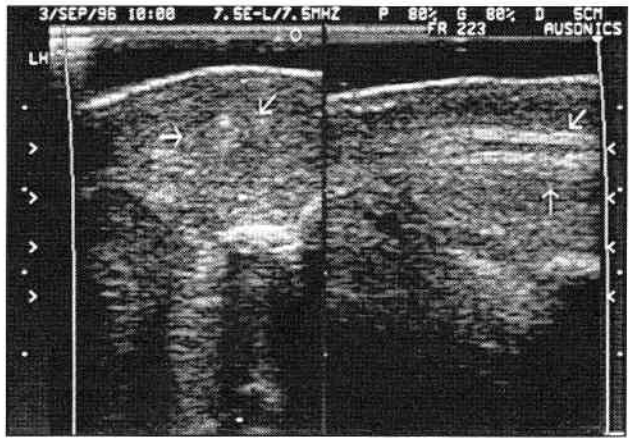

Figure 11–30

Sonograms of the right hind leg obtained from a 3-year-old Thoroughbred colt with massive cellulitis. The subcutaneous tissues are markedly thickened and have a generalized increased echogenicity. There is a small thrombosed artery *(arrows)* in the area of the cellulitis. These sonograms were obtained from the medial side of the distal metatarsal region with a wide-bandwidth 7.5-MHz linear-array transducer operating at 7.5 MHz using a hand-held standoff pad at a displayed depth of 5 cm. The right side of the right image is proximal and the left side is distal. The right side of the left image is dorsal and the left side is plantar.

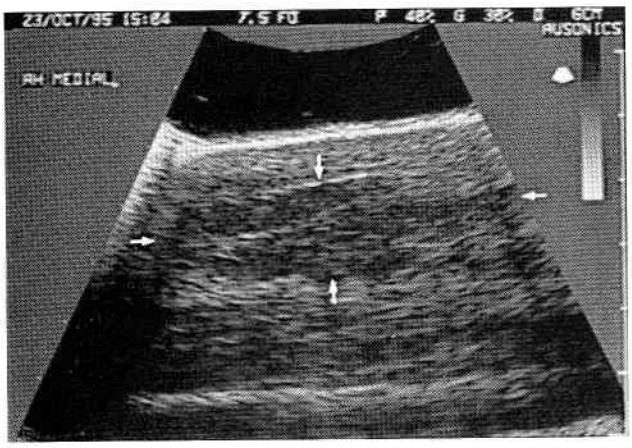

Figure 11–31

Sonogram of the right hind leg obtained from a 2-year-old Thoroughbred colt with severe diffuse cellulitis. The infection is beginning to localize adjacent to the medial aspect of the metatarsus where a poorly defined accumulation of hypoechoic fluid *(arrows)* is imaged. This sonogram was obtained with a 7.5-MHz sector-scanner transducer containing a built-in fluid offset at a displayed depth of 6 cm. The right side of this sonogram is proximal and the left side is distal.

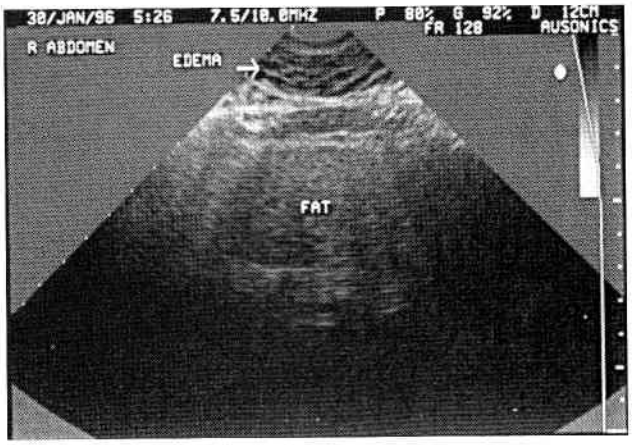

Figure 11–32

Sonogram of the right side of the ventral abdomen obtained from a 3-year-old Standardbred mare with ventral edema. Notice the plaque of anechoic loculated fluid in the subcutaneous space *(arrow)*, superficial to the ventral abdominal musculature. Dorsal to the abdominal musculature is a large layer of hypoechoic to echogenic tissue, consistent with intraabdominal fat. This sonogram was obtained with a wide-bandwidth 7.5-MHz sector-scanner transducer operating at 10.0 MHz at a displayed depth of 12 cm. The right side of this sonogram is cranial and the left side is caudal.

also been demonstrated to cause ulcerative lymphangitis. Sporotrichosis, caused by *Sporothrix schenckii*, also causes cording of the lymphatics and nodular eruptions.

Sonographic examination of horses with lymphangitis often reveals a diffuse subcutaneous swelling that is also more echogenic than normal. Small tortuous fluid-filled tubular structures representing the dilated lymphatic vessels are often imaged in affected horses if a high-frequency transducer is used. Small abscesses may be imaged in conjunction with the lymphatic distention in horses with ulcerative lymphangitis or sporotrichosis.

Edema. Edema is a cool diffuse swelling that pits on pressure and is found usually in the more ventral tissues. Anechoic septated fluid in the subcutaneous tissues is typical of edema. This fluid is usually easily deformed or "pitted" with the pressure of the ultrasound transducer. Anechoic septated edema fluid is frequently found along the ventral abdomen (Fig. 11-32) and the distal limbs (Fig. 11-33) in horses that are "stocking up" or have a swelling or mass in the more proximal portion of the limb, occluding venous return.

Hematomas. Large fluctuant swellings are the most common clinical presentation of hematomas in affected horses. These swellings may be painful if the trauma causing the hematoma is recent; however, long-standing hematomas are usually nonpainful. The hematomas may be associated with ruptured blood vessels, fractures, muscle tears, or other types of local trauma.

The sonographic appearance of the hematoma varies with the stage of the hematoma (how recently the bleeding occurred), the tissues into which the bleeding occurred, and the involvement of adjacent structures. If the hemorrhage into the tissues is recent, the area may have a homogeneous echogenic appearance similar to that detected in jugular vein obstruction and when observing red blood cells settle in an occluded vein. However, the typical sonographic appearance of a hematoma is that of an anechoic fluid-filled structure containing fibrinous loculations.[6] The hematoma may be small and localized (Fig. 11-34) or very extensive (Fig. 11-35). Hypoechoic to echogenic masses may be imaged within hematomas associated with organizing clot (Fig. 11-36).[6] In long-standing hematomas, the clot may become so organized that it has a homogeneous hyperechoic appearance, often casting an acoustic shadow from the far surface of the clot (Fig. 11-37). The organized hematoma may appear encapsulated by a thick echogenic capsule, but the contents remain echogenic and loculated.[6] Occasionally fibrinous loculations are not present within the hematoma and only anechoic fluid is found (Fig. 11-38).

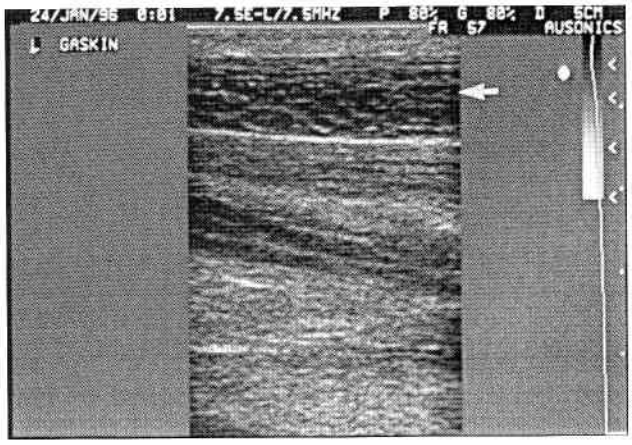

Figure 11–33

Sonogram over the left gaskin region obtained from a 3-year-old Thoroughbred gelding with subcutaneous edema. The anechoic lacy loculated fluid in the subcutaneous space *(arrow)* represents edema in these tissues. This sonogram was obtained with a wide-bandwidth 7.5-MHz linear-array transducer operating at 7.5 MHz at a displayed depth of 5 cm. The right side of this sonogram is proximal and the left side is distal.

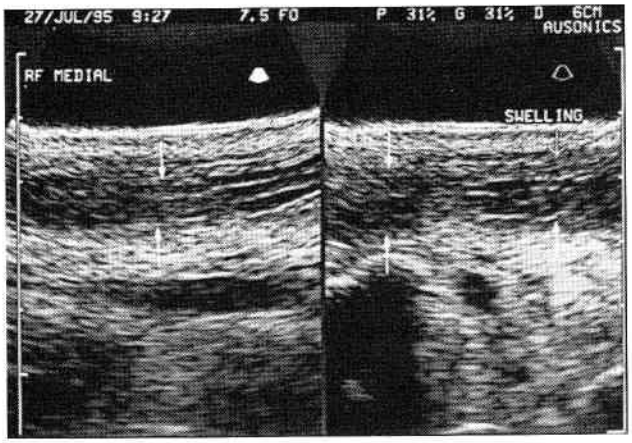

Figure 11–34

Sonograms of the medial aspect of the right foreleg obtained from a 3-year-old Standardbred gelding with a fluctuant swelling over the second metacarpal bone. The anechoic loculated swelling is consistent with a hematoma in the subcutaneous tissues *(arrows)*. This hematoma is approximately 4 cm long, 4 cm wide, and 1 cm thick. The anechoic tubular structure deep to the hematoma is the median artery. These sonograms were obtained with a 7.5-MHz sector-scanner transducer containing a built-in fluid offset at a displayed depth of 6 cm. The right side of the left image is proximal and the left side is distal. The right side of the right image is dorsal and the left side is palmar.

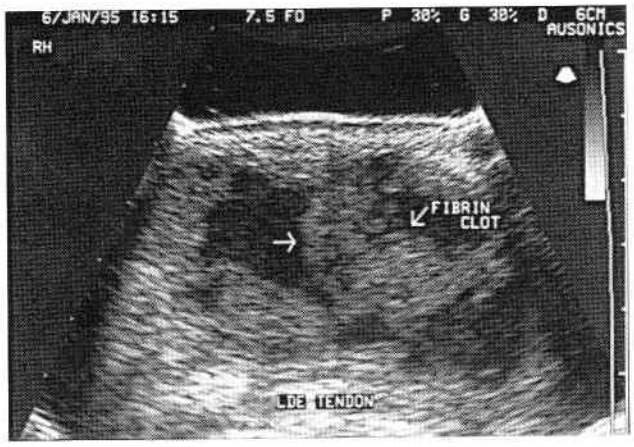

Figure 11–36

Sonogram of the dorsal aspect of the right metatarsophalangeal joint obtained from a 9-year-old Thoroughbred gelding with a large diffuse swelling over the dorsal aspect of the distal metatarsus and metatarsophalangeal joint. A large anechoic fluid collection contains numerous irregular hypoechoic masses floating within the fluid *(arrows)*, consistent with organizing fibrin (fibrin clot). The swelling overlies the long digital extensor tendon (LDE), but does not involve this tendon. This sonogram was obtained with a 7.5-MHz sector-scanner transducer containing a built-in fluid offset at a displayed depth of 6 cm. The right side of this sonogram is lateral and the left side is medial.

Seromas. The sonographic appearance of a seroma is indistinguishable from that of a hematoma in most instances. The history of recent surgery at the site of the seroma makes this differential more likely, particularly in areas with considerable dead space. In such cases, seromas are anechoic fluid-filled structures containing fibrinous loculations at the site of the surgical incision (Fig. 11-39).

Soft Tissue Masses

Sarcoids. Sarcoids are the most prevalent equine neoplasm and the most common of all skin tumors in horses.[89] Sarcoids can present in one of four ways: verrucous, fibroblastic, mixed verrucous, and fibroblastic and flat. Sarcoids may appear as movable subcutaneous masses with intact overlying skin.[89] More commonly, however, the epidermis overlying sarcoids is thick,

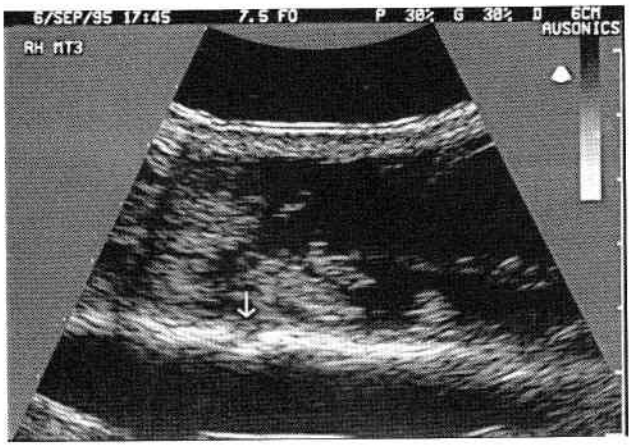

Figure 11–35

Sonogram of the dorsal aspect of the right hind leg obtained from a 9-year-old Thoroughbred gelding with "timber shins." The subcutaneous tissues are filled with anechoic fluid containing fibrinous loculations and fibrin clumps, extending the entire length of the dorsal, medial, and lateral aspects of the third metatarsal bone and surrounding the metatarsophalangeal joint. There is an irregular underlying bony surface *(arrow)* with depressions consistent with lysis and raised areas consistent with proliferative change, suggesting repeated trauma to this region. This sonogram was obtained with a 7.5-MHz sector-scanner transducer containing a built-in fluid offset at a displayed depth of 6 cm. The right side of this sonogram is proximal and the left side is distal.

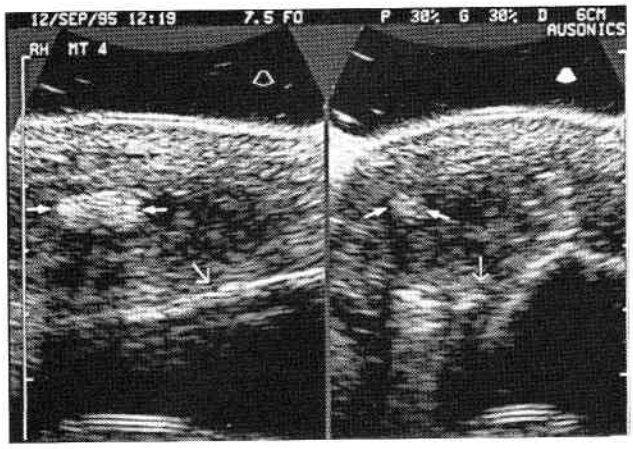

Figure 11–37

Sonograms of the right hind leg obtained from a 10-year-old Holsteiner mare with a large resolving hematoma. The large echogenic oval mass *(small arrows)* casts an acoustic shadow from its far surface, representing an organized clot. A hairline fracture *(larger arrows)* is detected in the fourth metatarsal bone, suggested by the slight irregularity in the bony surface echo from the fourth metatarsal bone. This fracture was confirmed with routine radiography. These sonograms were obtained with a 7.5-MHz sector-scanner transducer containing a built-in fluid offset at a displayed depth of 6 cm. The right side of the left image is proximal and the left side is distal. The right side of the right image is dorsal and the left side is plantar.

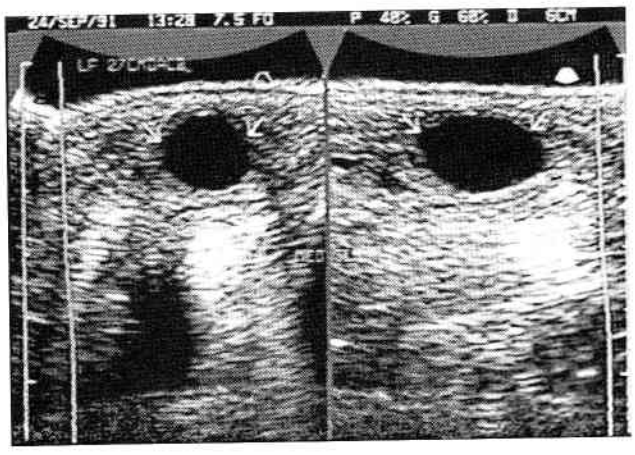

Figure 11–38

Sonograms of the medial aspect of the distal metacarpus obtained from a 9-year-old Thoroughbred gelding with a hematoma. Notice the anechoic fluid swelling in the subcutaneous space *(arrows)* overlying the medial branch of the suspensory ligament (MED SL) but not involving the suspensory ligament. Immediately adjacent to this swelling was a fracture of the second metacarpal bone. This discrete anechoic swelling is consistent with a hematoma, cyst, or abscess. The presence of the adjacent fractured second metatarsal bone is consistent with this swelling being a hematoma, although the lack of loculations in the hematoma is an atypical sonographic appearance for a hematoma. A cyst in this location would be unlikely and most abscesses would contain some internal echoes within the abscess cavity. This sonogram was obtained with a 7.5-MHz sector-scanner transducer containing a built-in fluid offset at a displayed depth of 6 cm. The right side of the left image is dorsal and the left side is palmar. The right side of the right image is proximal and the left side is distal.

rough, and hyperkeratotic or ulcerated. Sarcoids are often locally invasive, occurring primarily on the head, legs, and ventral abdomen. Sonographic examination of the typical sarcoid is not usually performed. Mildly invasive fibrosarcomas can be detected in horses with sarcoids that involve the skin and subcutaneous tissues (Fig. 11–40).

Lipomas. Lipomas involving the musculoskeletal system are rare in horses.[90] In reported cases, horses developed large fluctuant nonpainful masses in the subcutaneous tissues and musculature.[90–92] Sonographic examination of these masses was not performed in these horses but would have been useful in characterizing the invasiveness of the tumor prior to surgery. The lipoma should have a somewhat heterogeneous appearance in the subcutaneous tissues or when invading the musculature.

Hemangiomas, Hamartomas, Hemangiosarcomas, Lymphangiomas. Vascular neoplasms involving the skin of horses are uncommon. However, vascular skin neoplasms have been reported from all areas of the horse, most frequently involving the limbs.[93, 96]

Hemangiomas are more common and have been reported most frequently in young horses.[93] Many hemangiomas and hemangioendotheliomas in horses are congenital and are present in affected foals at birth.[93, 94] Malignant vascular tumors (hemangiosarcomas) are more common in older horses.[93, 95] Horses with this disorder present with superficial, fluctuant to nodular masses that vary in size from 1.5 to 31 cm or larger.[93] Often there is a history of gradually enlarging masses in the skin or subcutaneous tissues. The vascular masses frequently ulcerate, and bleeding from the areas of ulceration may occur, especially following superficial trauma.[93]

Vascular malformations such as hamartomas have also been reported and are considered to be an excessive overgrowth of normal mature cells. The distinction between hemangiomas and hamartomas, however, is difficult, although the cells in hemangiomas are more proliferative and immature.[93, 96]

Lymphangiomas occur infrequently in horses and have

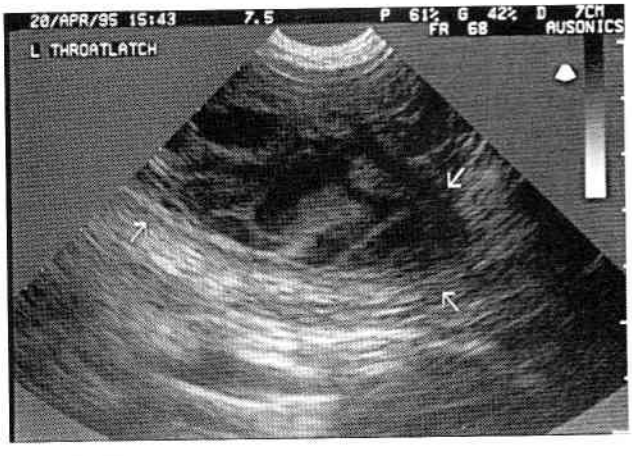

Figure 11–39

Sonogram of the left throatlatch region obtained from a 10-year-old Thoroughbred gelding following surgical placement of a laryngeal prosthesis. There is a large collection of anechoic loculated fluid at the surgery site, most consistent with a postoperative seroma. There is a large amount of fibrinous loculations, but the surrounding fluid appears very anechoic, suggesting low cellularity. This sonogram was obtained with a 7.5-MHz sector-scanner transducer at a displayed depth of 7 cm. The right side of this sonogram is dorsal and the left side is ventral.

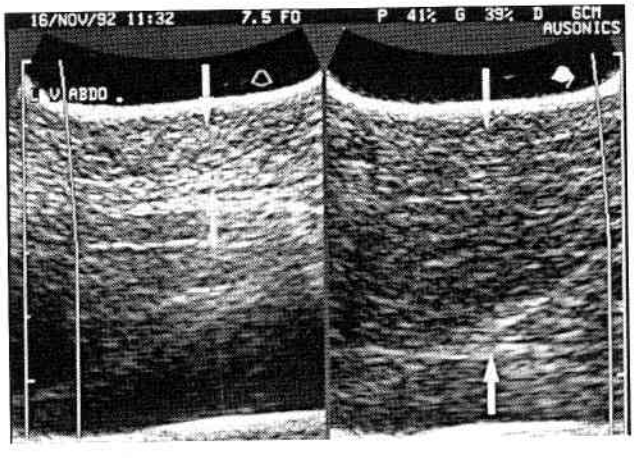

Figure 11–40

Sonograms of two ventral abdominal masses obtained from a 9-year-old Thoroughbred cross gelding. The smaller mass (left image) is relatively homogeneous and involves only the skin and subcutaneous tissues *(arrows)*. The larger mass (right image) is more hypoechoic but also involves only the skin and subcutaneous tissues and does not extend into the adjacent musculature *(arrows)*. An excisional biopsy of one of these masses revealed a low-grade fibrosarcoma. These sonograms were obtained with a 7.5-MHz sector-scanner transducer containing a built-in fluid offset at a displayed depth of 6 cm. The right side of these sonograms is toward the left side of the horse.

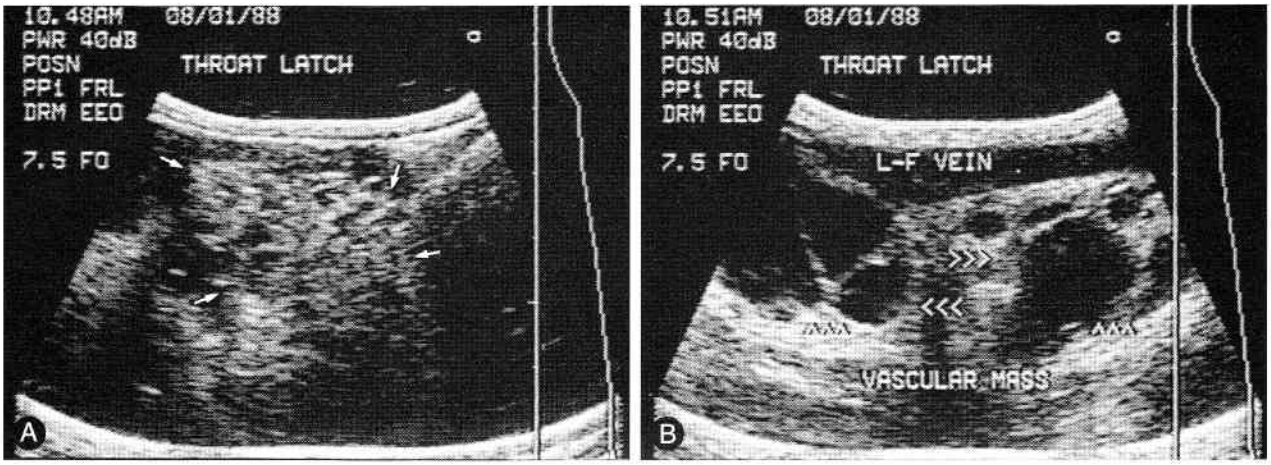

Figure 11–41

Sonograms of a large cutaneous vascular mass in the throatlatch region obtained from a 2-year-old Thoroughbred filly with a hemangioma. The mass has a more solid, but very vascular, component *(A)* with a network of very large vessels extending rostrally along the linguofacial vein *(B)*. These sonograms were obtained with a 7.5-MHz sector-scanner transducer containing a built-in fluid offset at a displayed depth of 7.5 cm.

A, The mass is adjacent to the mandible. It has a very vascular appearance, with echogenic tissue interspersed with a network of small anechoic vessels and vascular spaces *(arrows)*. The right side of this sonogram is dorsal and the left side is ventral.

B, Adjacent to the more solid portion of the mass is this extensive network of markedly dilated vessels *(arrowheads)* running rostrally alongside the linguofacial (L-F) vein. The right side of this sonogram is rostral and the left side is caudal.

been reported in the hind limb, abdomen, and retroperitoneum of one colt.[97] This colt presented with multiple nodular masses in the left inguinal region and preputial masses. The masses progressively enlarged and invaded the surrounding tissues in this colt, leading to his humane destruction.

Sonographic evaluation of these masses reveal fluid-filled masses in the skin and subcutaneous tissues with echogenic septae (Fig. 11-41). Large areas of hypoechoic tissue with a spongelike appearance may be imaged in some affected horses, associated with the proliferation of small vessels and endothelial tissue (Fig. 11-42). Sonographically, more benign vascular neoplasms may appear similar to homogeneous hypoechoic granulation tissue. Many blood vessels may be detected within or associated with this mass (Fig. 11-43). Arteriovenous communications may be detected within the vascular mass. Echogenic soft tissue masses with small anechoic cavitations

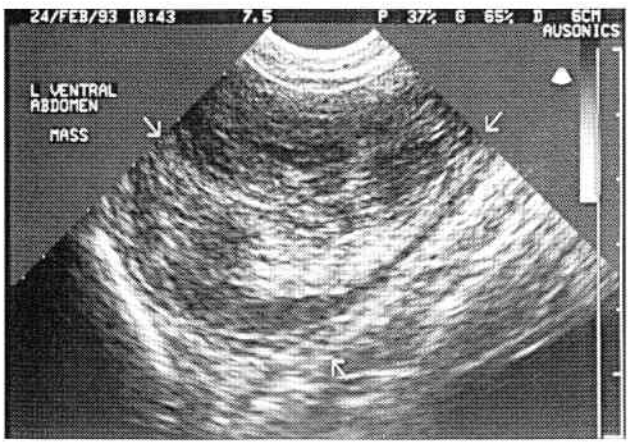

Figure 11–42

Sonogram of a diffuse ventral abdominal swelling obtained from a 16-year-old Tennessee Walking Horse gelding. This image was obtained from the center of the mass. The swelling is diffuse and heterogeneous with poorly defined margins in the subcutaneous tissues *(arrows)*. The mass has a fine multiloculated appearance similar to that of a sponge. At the edge of the mass the subcutaneous tissues remain thickened but are more echogenic and less finely loculated. The finely loculated appearance of this mass suggested a neoplasm of vascular or lymphatic origin. No blood flow could be detected in the loculated space in this mass with Doppler ultrasound. An ultrasound-guided biopsy of the mass revealed a lymphangioma. This sonogram was obtained with a 7.5-MHz sector-scanner transducer at a displayed depth of 6 cm. The right side of this sonogram is cranial and the left side is caudal.

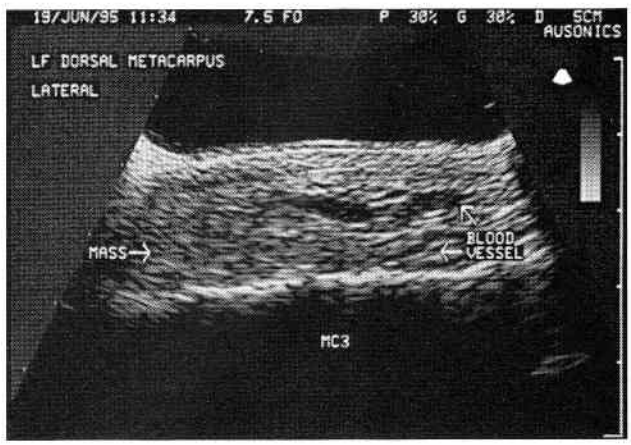

Figure 11–43

Sonogram of the left dorsal metacarpal region obtained from a 9-year-old Morgan gelding with a vascular hamartoma. The mass has an overall heterogeneous hypoechoic appearance, similar to that of granulation tissue but was laden with small and larger blood vessels. The mass was causing some reaction in the underlying metacarpus detected as irregularities in the bony surface echo. Excisional biopsy of this mass revealed it to be a vascular hamartoma. This sonogram was obtained with a 7.5-MHz sector-scanner transducer containing a built-in fluid offset at a displayed depth of 5 cm. The right side of this sonogram is proximal and the left side is distal.

have been imaged in several horses with hemangiosarcomas (Fig. 11-44); these masses may involve primarily the subcutaneous tissues (Fig. 11-45), fascia (Fig. 11-45), or skeletal muscle (Figs. 11-44 and 11-45). The extension of these echogenic masses into differing but adjacent tissues is consistent with a hemangiosarcoma, as well as with other malignant neoplasms. Hemangiosarcoma also frequently involves the pleura, and a hemothorax may be detected concurrently in some horses with superficial hemangiosarcomas, suggesting widespread metastases (Fig. 11-46).

Involvement of the adjacent flexor tendons, synovial sheaths, or muscle have been reported in horses with hemangiosarcomas.[95, 96, 98] Although muscle involvement was not detected clinically in several horses with metastatic hemangiosarcomas, it could have been detected ultrasonographically.[95, 99] These areas are characterized by large areas of muscle fiber disruption and fluid accumulation (see Chapter 3). Involvement of the surrounding structures indicates a more invasive mass and a malignant neoplasm should be considered.[96, 98, 99]

Melanocytomas, Melanomas. Melanocytomas (benign melanomas) are benign tumors that occur most frequently in young horses.[100] These tumors occur in horses of a variety of coat colors, and ulceration of the overlying epidermis is common. Melanocytomas are solitary tumors, usually localized on the legs or the trunks of horses. In contrast to melanomas in older horses, melanocytomas are not found in a perineal location.[100] These tumors arise from melanin-producing cells at the epidermal-dermal junction.[100]

Melanomas have a high incidence in older grey horses, are often multiple, and involve the perineal region, the vulva, and the underside of the tail.[42, 101] Other predilection sites include the parotid salivary gland, the head below the entrance to the pinna, and the margin of the ear.[41, 42, 101] Melanomas in older horses can be hard or soft and may be single or multiple. These tumors are usually slowly enlarging dermal masses, typically covered by intact epidermis. Over time, some melanomas can become ulcerated and infected,[41] but these types of tumors usually grow slowly over years without metastasis.[41, 42, 101] The benign growth may, after many years, suddenly assume malignant characteristics and metastasize.[41, 42, 101] A few melanocytic tumors are malignant from their first appearance and readily metastasize, usually to the lungs, spleen, and liver.[41, 42, 101] A foal with a congenital malignant melanoma has been reported.[102]

Malignant melanomas and melanosarcomas have been reported in the muscles of horses presenting with lame-

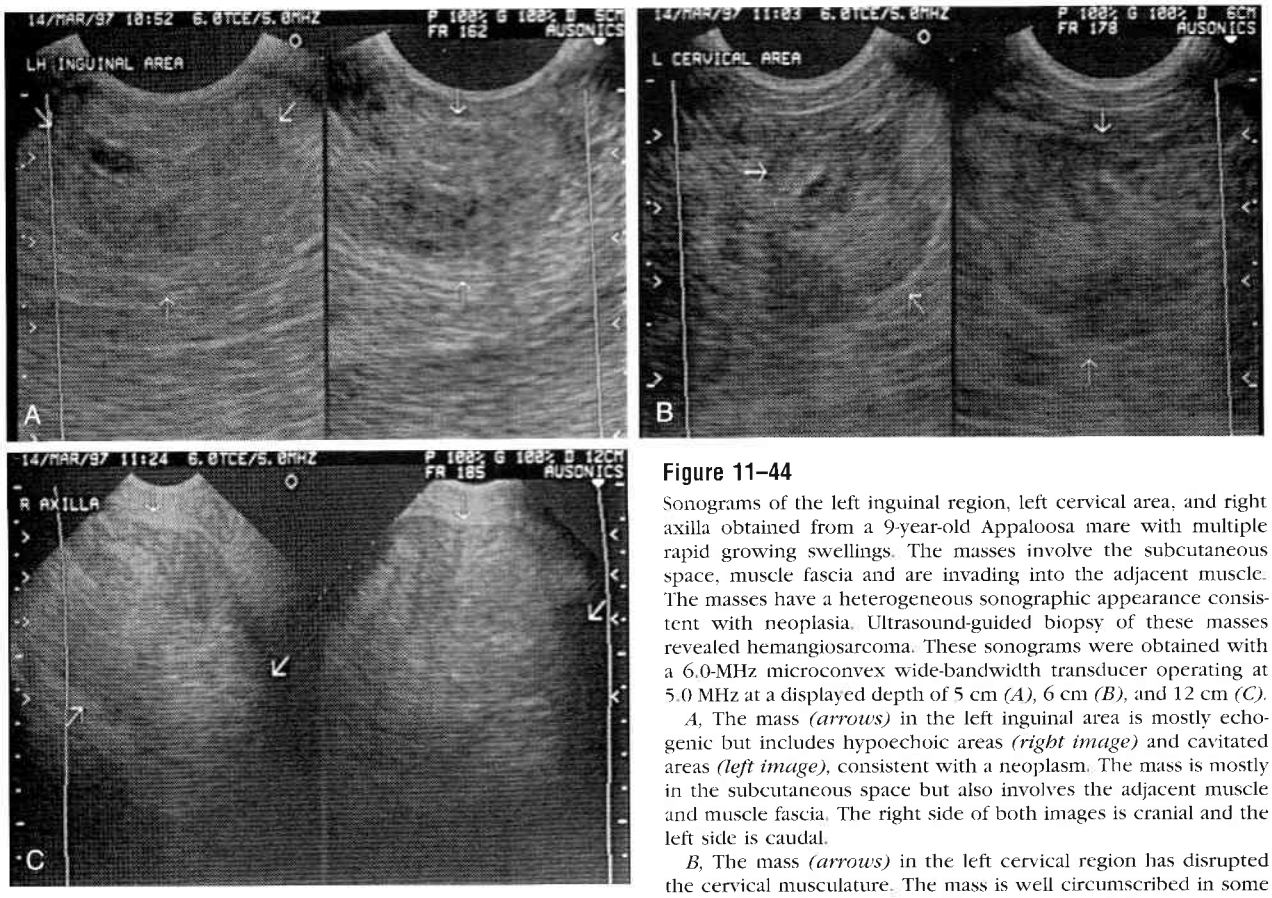

Figure 11–44

Sonograms of the left inguinal region, left cervical area, and right axilla obtained from a 9-year-old Appaloosa mare with multiple rapid growing swellings. The masses involve the subcutaneous space, muscle fascia and are invading into the adjacent muscle. The masses have a heterogeneous sonographic appearance consistent with neoplasia. Ultrasound-guided biopsy of these masses revealed hemangiosarcoma. These sonograms were obtained with a 6.0-MHz microconvex wide-bandwidth transducer operating at 5.0 MHz at a displayed depth of 5 cm *(A)*, 6 cm *(B)*, and 12 cm *(C)*.

A, The mass *(arrows)* in the left inguinal area is mostly echogenic but includes hypoechoic areas *(right image)* and cavitated areas *(left image)*, consistent with a neoplasm. The mass is mostly in the subcutaneous space but also involves the adjacent muscle and muscle fascia. The right side of both images is cranial and the left side is caudal.

B, The mass *(arrows)* in the left cervical region has disrupted the cervical musculature. The mass is well circumscribed in some areas but has poorly defined margins in other areas. A small area of cavitation is imaged in the center of this mass. The right side of the left image is dorsal and the left side is ventral. The right side of the right image is cranial and the left side is caudal.

C, The mass *(arrows)* in the right axilla is very echogenic and has disrupted the regional musculature. The mass again has a heterogeneous sonographic appearance consistent with neoplasia. The right side of the left image is toward the right and the left side is toward midline. The right side of the right image is cranial and the left side is caudal.

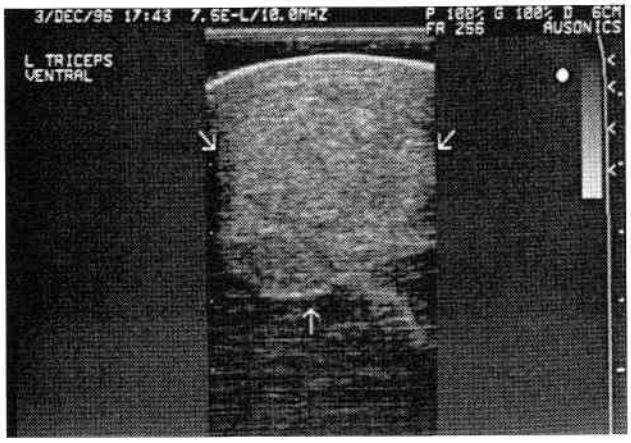

Figure 11–45

Sonogram of an echogenic slightly heterogeneous mass *(arrows)* in the region of the left triceps muscle obtained from a 3-year-old Thoroughbred filly. This mass is located in the subcutaneous space but has invaded the adjacent triceps musculature. The mass has a multiobulated appearance and is a soft tissue mass, most consistent with a neoplasm. Ultrasound-guided biopsy of this mass revealed a hemangiosarcoma. This sonogram was obtained with a wide-bandwidth 7.5-MHz linear-array transducer operating at 10.0 MHz with a hand-held standoff pad at a displayed depth of 6 cm. The right side of this sonogram is dorsal and the left side is ventral.

ness.[103-105] Melanomas have occurred in conjunction with malignant lymphoma in one older grey stallion.[106]

Most benign melanomas in older grey horses have a homogeneous echogenic sonographic appearance and distinct borders (Fig. 11–47). A somewhat more heterogeneous appearance is seen with the more invasive melanomas, which involve skeletal muscle (Fig. 11–48). Lysis of the underlying bone may also be detected with more aggressive melanomas (Fig. 11–49). The more aggressive malignant melanomas have a more complex sonographic appearance and irregular borders (Fig. 11–50). Malignant melanomas usually invade adjacent tissues and destroy the normal architecture of that tissue.

Cutaneous Lymphosarcoma. Cutaneous lymphosarcoma is a tumor of the skin and subcutaneous tissues that is infrequently reported in horses. These lesions may appear suddenly but usually enlarge slowly. Affected horses usually have multiple subcutaneous nodules that vary in size from < 1 to 20 cm in diameter. The masses can be found in the skin and subcutaneous tissues all over the body, possibly involving peripheral lymph nodes and internal organs also.[107-109] The mass associated with cutaneous lymphosarcoma typically appears homogeneous sonographically and may be discrete or coalescing (Fig. 11–51).

Squamous Cell Carcinoma. Squamous cell carcinoma is the most common oral or pharyngeal tumor reported in horses.[110] The external male genitalia is the most common reported site of squamous cell carcinoma (44.8%), followed by the head, eye, and ocular adnexa (43.1%) and the female genitalia (12%).[111, 112] Squamous cell carcinoma also often develops at the site of a previous scar[113] or burn. The mean age of affected horses in one large study was 12.4 years.[111] Squamous cell carcinoma often presents as nodular ulcerating masses involving the aforementioned structures. These masses usually have a composite sonographic appearance, but a homogeneous sonographic appearance may also be imaged, often in the more slowly growing tumors.

Other Neoplasms. A wide variety of other neoplasms may occur in the skin, subcutaneous tissues, or superficial muscles or superficial structures, causing visible swellings or masses. These masses may have a homoge-

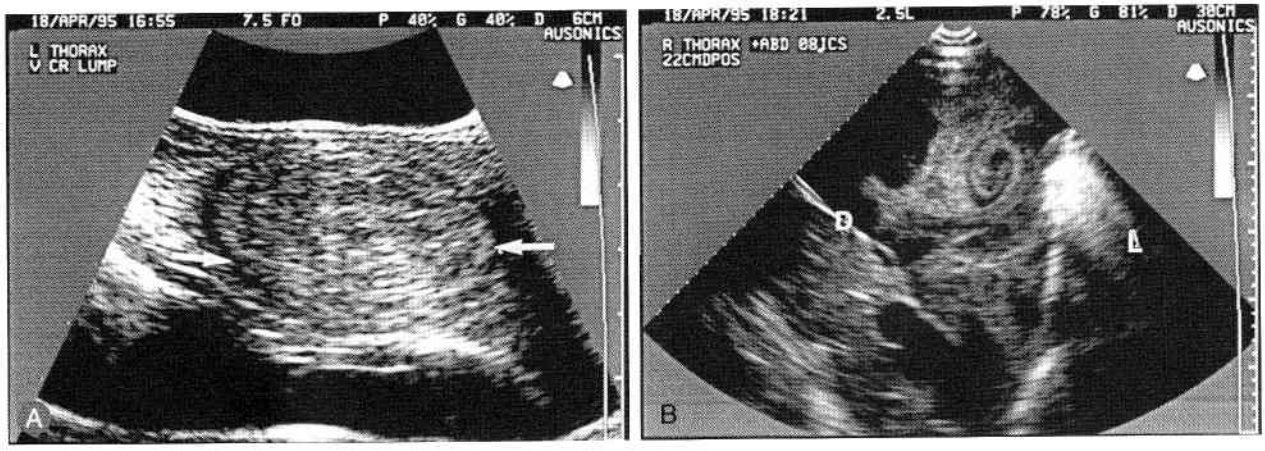

Figure 11–46

Sonograms of a mass on the left thorax *(A)* and of the right side of the thorax and abdomen *(B)* obtained from a 5-year-old Thoroughbred filly with hemangiosarcoma. This filly presented for hind limb lameness and was anemic at the time of presentation. These sonograms were obtained with a 7.5-MHz sector-scanner transducer containing a built-in fluid offset *(A)* and a 2.5-MHz sector-scanner transducer *(B)* at a displayed depth of 6 cm *(A)* and 30 cm *(B)*.

A, The well-encapsulated heterogeneous oval mass *(arrows)* overlying the ventral aspect of the left seventh rib measured 4.65 cm wide and 2.69 cm thick. The somewhat heterogeneous mass involves the subcutaneous tissues overlying the rib and some of the adjacent intercostal musculature. The mass appears to have concentric rings of tissue, creating its oval shape. The right side of this sonogram is cranial and the left side is caudal.

B, The lung (L) is imaged in the dorsalmost portion of the right side of the thorax with the echogenic swirling pattern consistent with hemothorax detected filling the pleural cavity to a line 22 cm dorsal to a line level with the point of the shoulder. The diaphragm (D), liver, and colon are imaged in the abdominal cavity. The right side of this sonogram is dorsal and the left side is ventral.

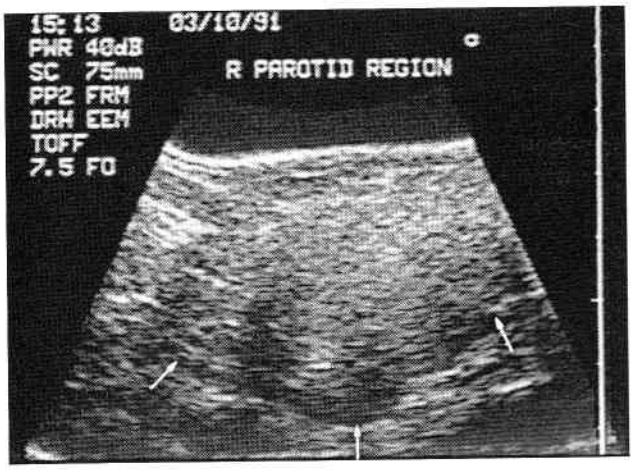

Figure 11–47

Sonogram of a melanoma in the right parotid region obtained from an 11-year-old Thoroughbred gelding. The mass *(arrows)* appears relatively homogeneous and echogenic and involves the subcutaneous tissues in the region of the parotid salivary gland. This sonogram was obtained with a 7.5-MHz sector-scanner transducer containing a built-in fluid offset at a displayed depth of 7.5 cm. The right side of this sonogram is cranial and the left side is caudal.

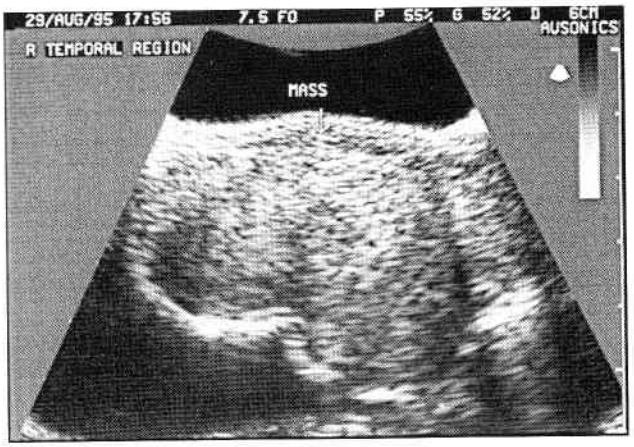

Figure 11–49

Sonogram of a mass in the right temporal region obtained from a 9-year-old grey Thoroughbred gelding (same as in Figure 11-13). This mass is echogenic to hyperechoic and heterogeneous, overlying the right temporal bone and resulting in an abnormal bony surface echo, consistent with a malignant melanoma. This sonogram was obtained with a 7.5-MHz sector-scanner transducer containing a built-in fluid offset at a displayed depth of 6 cm. The right side of this sonogram is dorsal and the left side is ventral.

neous or composite sonographic appearance. Masses may be well demarcated (Figs. 11-52 and 11-53) or have irregular margins (Fig. 11-54). Masses with a complex or composite sonographic appearance are more likely to be malignant, as are masses with irregular margins and those that invade surrounding tissues, disrupting their normal architecture. Anechoic areas within soft tissue masses are consistent with tumor necrosis. Ultrasound-guided biopsy or excisional biopsy of these masses is necessary to diagnose the tumor type definitively.

Ameloblastomas are tumors of the oral cavity in horses, usually involving the mandible; they are locally invasive but rarely metastasize.[115, 116] These tumors are most frequently reported in older horses and result in marked cortical thinning, with areas of cortical disruption. Ameloblastomas can be imaged through the thin or disrupted

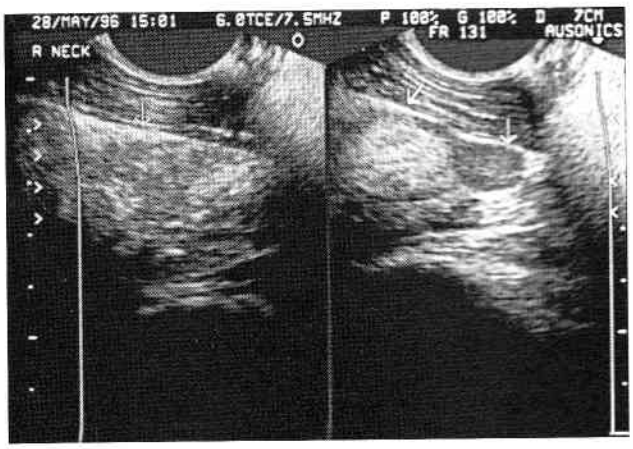

Figure 11–48

Sonograms of the right side of the neck obtained from a grey 6-year-old Trakhener gelding with melanoma. The large multiobulated mass *(arrows)* with a complex pattern of echogenicity completely disrupted the cervical musculature and extended deep to the cervical vertebrae. This mass measured 30 cm long, 12 cm in a dorsal to ventral direction and 8 cm deep. The caudalmost aspect of the mass contained more homogeneous masses *(right image)* that were hypoechoic or echogenic, which may represent a more benign component of the mass. The remainder of the mass *(left image)* appeared very heterogeneous with hyperechoic areas casting acoustic shadows consistent with areas of calcification. This complex pattern of echogenicity is consistent with an aggressive neoplasm. These sonograms were obtained with a wide-bandwidth 6.0-MHz microconvex linear-array transducer operating at 7.5 MHz at a displayed depth of 7 cm. The right side of these sonograms is dorsal and the left side is ventral.

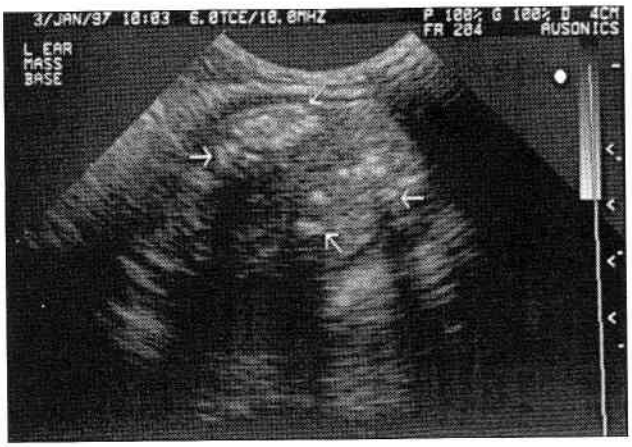

Figure 11–50

Sonogram of a mass at the base of the left ear obtained from a 19-year-old Quarter Horse mare with an invasive recurring melanoma. The mass has a complex sonographic appearance with hyperechoic areas casting acoustic shadows *(arrows)*, echogenic area, and hypoechoic areas. The hyperechoic areas represent areas of calcification. The location of this mass and its heterogeneous appearance containing areas of calcification or bone are consistent with a neoplasm. This sonogram was obtained with a wide-bandwidth 6.0-MHz microconvex linear-array transducer operating at 10.0 MHz at a displayed depth of 4 cm. The right side of the sonogram is cranial and the left side is caudal.

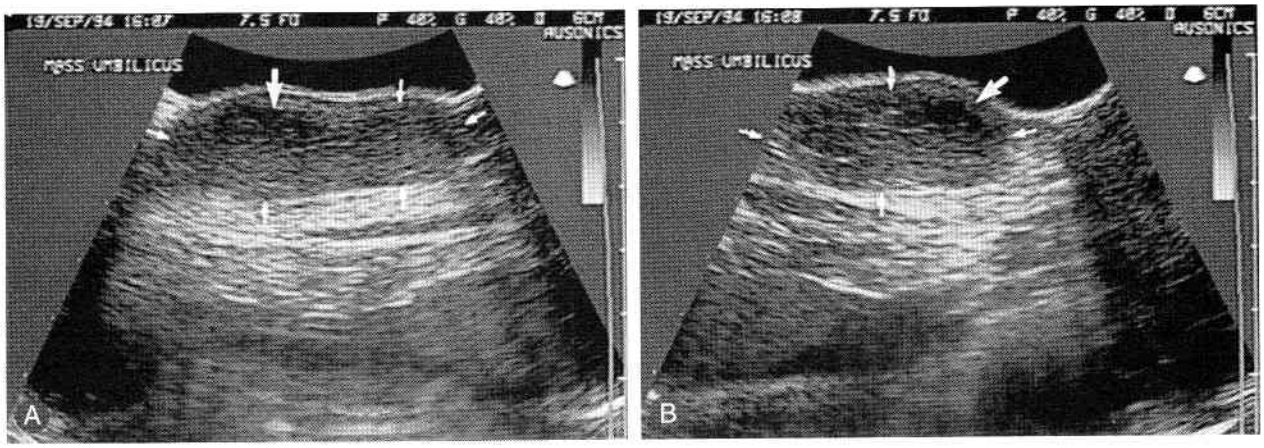

Figure 11–51

Sonograms of multiple masses along the ventral abdomen obtained from a 15-year-old Thoroughbred mare with cutaneous lymphosarcoma. These masses were relatively discrete and well demarcated from the surrounding tissues and were hypoechoic relative to the surrounding tissues. A biopsy of these masses revealed cutaneous lymphosarcoma. These sonograms were obtained with a 7.5-MHz sector-scanner transducer containing a built-in fluid offset at a displayed depth of 6 cm.

A, These masses *(small arrows)* have a relatively homogeneous echogenicity with the exception of the most superficial portion of the left mass, which is more anechoic at the skin edge *(larger arrow)*. The right side of this sonogram is the left side of the horse.

B, This mass *(small arrows)* has a more heterogeneous sonographic appearance with a larger anechoic area near the skin *(larger arrow)* and slight variations in parenchymal echogenicity and texture throughout the mass. These anechoic areas are consistent with areas of necrosis. The right side of this sonogram is the right side of the abdomen.

cortical bone and typically have a complex sonographic appearance. Cystic spaces may be imaged within the mass.

Osteomas are most frequently reported in the mandible of horses and may have areas of lysis through which a portion of the mass can also be imaged. A complex pattern of echogenicity is usually present in osteomas and osteosarcomas.

An ossifying fibroma associated with the right side of the mandible was imaged in one 2-year-old filly and was successfully removed surgically without recurrence (Fig. 11-54). A fibrosarcoma in the subcutaneous tissues of the right flank of another horse had widespread metastases to the skeletal muscles, lymph nodes, internal organs, and vertebral column.[117] A fibrosarcoma has also been reported associated with burn scars in a horse.[114]

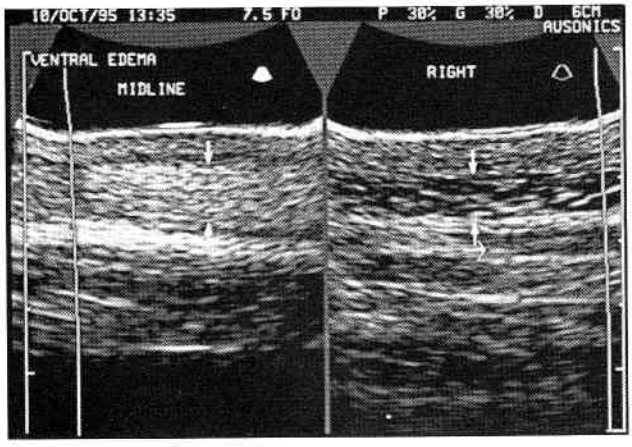

Figure 11–52

Sonograms of the ventral abdomen obtained from a 9-year-old Thoroughbred gelding with recurring ventral edema and subcutaneous masses along the ventral abdomen. The oval echogenic subcutaneous mass *(small arrows)* in the left image is located along the ventral midline and appeared well demarcated from the surrounding tissues. To the right of midline in the right image lies a layer of anechoic septated subcutaneous tissue consistent with edema *(small arrows)*. The horizontal arrow points to the superficial abdominal musculature. The right side of the right image is to the right of the abdomen and the left side is toward the midline. The right side of the left image is cranial and the left side is caudal.

A rhabdomyosarcoma in the deep digital flexor muscle of a horse occurred as a small cutaneous mass on the medial aspect of the hock. The mass had grown in the several months prior to presentation and was sensitive on palpation; the horse was also lame in this limb.[11] Sonographic examination of this mass revealed it to appear as homogeneous soft tissue surrounding the deep digital flexor tendon. No comment was made on the sonographic appearance of the deep digital flexor muscle, which was completely replaced by disorganized tissue in its distal half at postmortem examination. This disorganized tissue should also have been detectable sonographically.

An anaplastic sarcoma was reported in the caudal thigh of one horse,[118] and another horse had a carcinoma in the adductor muscle, which had metastasized, primarily to the lungs.[119] Both masses should have been detected as large composite soft tissue-density masses disrupting the musculature of the thigh, had sonographic examinations of these areas been performed. Central necrosis of these large tumors usually appears as a hypoechoic to anechoic area, which may occasionally appear loculated.

In one horse, a keratoma was imaged as a soft tissue-density mass between the hoof and the second and third phalanges. Radiographs of the area had been inconclusive.[120]

Puncture Wounds, Draining Tracts, and Foreign Bodies

Puncture wounds occur frequently in horses, and the penetration of vital structures is often difficult for the veterinarian to determine. Ultrasonographic examination

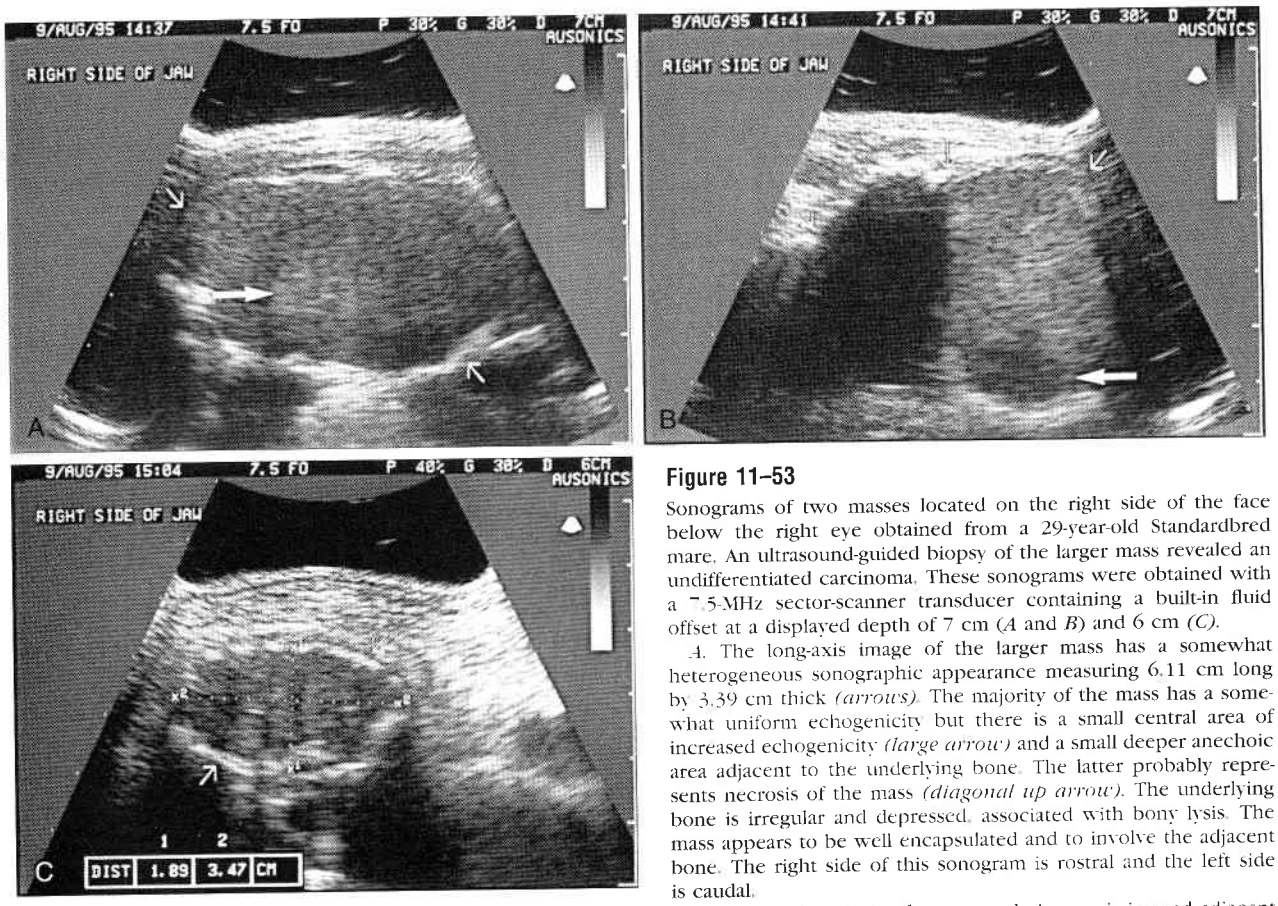

Figure 11–53

Sonograms of two masses located on the right side of the face below the right eye obtained from a 29-year-old Standardbred mare. An ultrasound-guided biopsy of the larger mass revealed an undifferentiated carcinoma. These sonograms were obtained with a 7.5-MHz sector-scanner transducer containing a built-in fluid offset at a displayed depth of 7 cm (*A* and *B*) and 6 cm (*C*).

A, The long-axis image of the larger mass has a somewhat heterogeneous sonographic appearance measuring 6.11 cm long by 3.39 cm thick *(arrows)*. The majority of the mass has a somewhat uniform echogenicity but there is a small central area of increased echogenicity *(large arrow)* and a small deeper anechoic area adjacent to the underlying bone. The latter probably represents necrosis of the mass *(diagonal up arrow)*. The underlying bone is irregular and depressed, associated with bony lysis. The mass appears to be well encapsulated and to involve the adjacent bone. The right side of this sonogram is rostral and the left side is caudal.

B, The short-axis image of the larger mass reveals it to be fairly homogeneous, although the deeper anechoic area is imaged adjacent to the deep bony echo consistent with tissue necrosis *(large arrow)*. The mass appears to originate from the bone in this image as more normal bony surface echoes are imaged on either side of the mass *(arrows)*. The right side of this sonogram is dorsal and the left side is ventral.

C, The smaller mass *(arrows)* is also somewhat well encapsulated and somewhat heterogeneous sonographically with a hyperechoic rim and small hyperechoic areas within. This mass measured 1.89 cm deep (x^1) by 3.47 cm long (x^2). The right side of this sonogram is rostral and the left side is caudal.

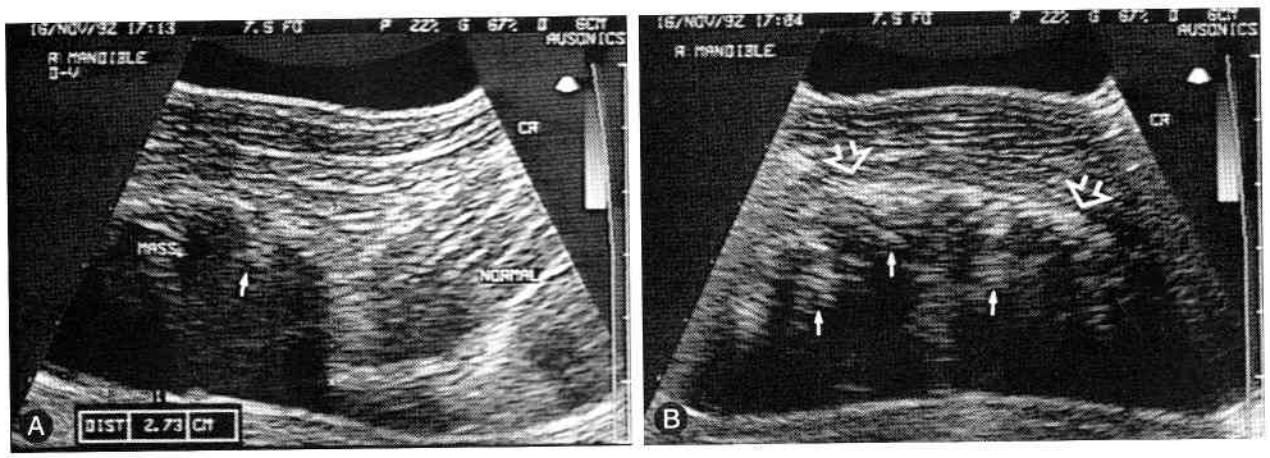

Figure 11–54

Sonograms of a mass associated with the right side of the mandible obtained from a 2-year-old Thoroughbred filly with an ossifying fibroma. This mass was primarily hyperechoic, consistent with calcification of the mass with a few echogenic areas scattered near the periphery of the mass *(small arrows)*. These sonograms were obtained with a 7.5-MHz sector-scanner transducer containing a built-in fluid offset at a displayed depth of 6 cm. The right side of these sonograms is rostral and the left side is caudal.

A, The mass protruded from the right side of the mandible 2.73 cm (x^1) and displaced the overlying musculature. The mass, which is oval with a slightly irregular border, is well delineated from the adjacent structures, other than the mandible.

B, The mass *(open arrows)* has several echogenic areas *(small arrows)* that are not calcified and that allow transmission of the ultrasound beam for a short distance into the parenchyma of the mass consistent with dense soft tissue or fibrous tissue. The mass is approximately 8 cm long and 6 cm wide.

of the puncture wound enables the veterinarian to rapidly determine the path of the penetrating object and which structures were damaged in the process, simplifying the diagnostics needed to make an appropriate treatment decision.

The echogenicity of the tract the penetrating object has made through the tissue varies, ranging from anechoic to hyperechoic, depending on the degree of hemorrhage, whether an air-filled structure was penetrated, if there is a sucking wound, and the time that has lapsed since the injury occurred. If the thoracic cavity or lung is punctured, a hyperechoic tract is produced through the deeper thoracic musculature (Fig. 11-55). If the underlying bone is involved, a hypoechoic to anechoic bony defect should be detected at the site of bone puncture (Fig. 11-56). The involvement of a synovial structure such as the joint (Figs. 11-57 and 11-58) or tendon sheath (Fig. 11-59) can be determined, so that appropriate aggressive treatment of these contaminated structures may begin promptly, improving the prognosis. If the puncture wound is more long-standing, marked soft tissue swelling is often seen in the injured tissues and the original tract into the tendon sheath (Fig. 11-59) or joint (see Fig. 11-58) is clearly imaged. The tract associated with the original injury can be imaged for weeks or even months after the skin wound has healed over and should be carefully screened for foreign material that may have been deposited along the tract as a result of the puncture. The presence of foreign material along the tract is common with puncture wounds associated with wood (Figs. 11-59 and 11-60) or pitchforks (see Fig. 11-56).

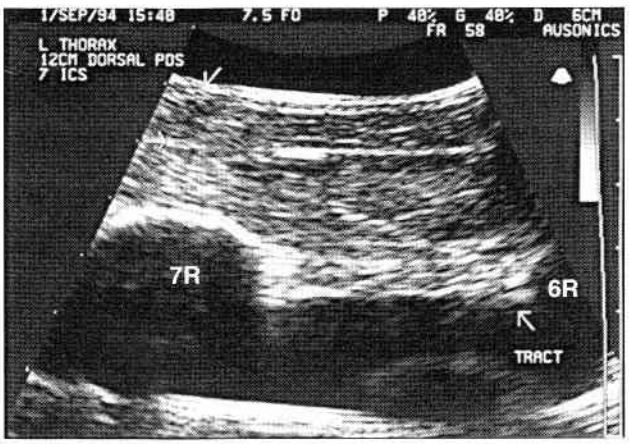

Figure 11–55

Sonogram of a tract in the intercostal musculature associated with a puncture wound to the thoracic cavity sustained 3 hours earlier when this 3-year-old Thoroughbred filly fell into the guardrail at the track, puncturing her side with the broken rail. The entrance wound at the skin was clearly visible 2 hours later *(diagonal down arrow)* and the tract was imaged, extending toward the 7th rib (7R), where it was deflected cranially *(horizontal arrow)* through the intercostal musculature into the thoracic cavity *(diagonal up arrow)*. The path that the penetrating object took was clearly visible 2 hours later, demonstrating that the thoracic cavity was penetrated by the break in the echo from the parietal pleura immediately caudal to the 6th rib (6R). The tract is hypoechoic near the skin surface and hyperechoic near the thoracic cavity: the former is a result of hemorrhage along the penetrating wound and the latter is probably a result of gas in the tract from the adjacent lung and its perforation. The adjacent lung was perforated because a sonographic examination of the pleural cavity revealed a dorsal pneumothorax and ventral hemothorax. This sonogram was obtained with a 7.5-MHz sector-scanner transducer containing a built-in fluid offset at a displayed depth of 6 cm. The right side of this sonogram is cranial and the left side is caudal.

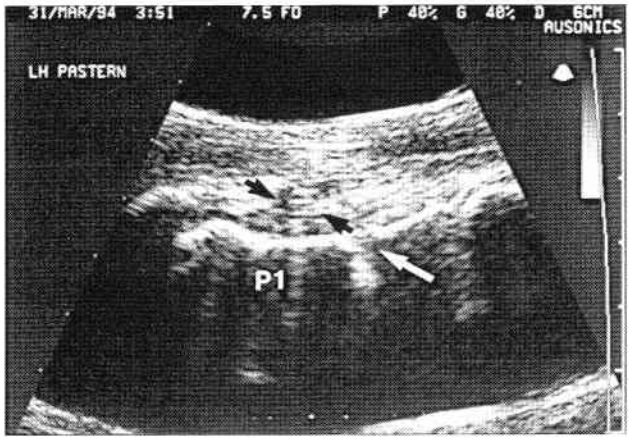

Figure 11–56

Sonogram of the plantar aspect of the left hind pastern obtained from a 2-day-old Thoroughbred cross filly. This filly had a history of having been accidentally stabbed by a pitchfork 2 hours earlier. The tine of the pitchfork was stuck in the bone and had to be forcibly extracted. This image reveals that metallic foreign material *(vertical arrow)* was left in the limb dorsal to the deep digital flexor tendon and plantar to the straight distal sesamoidean ligament. The foreign material is probably metallic (rust flaked off the pitchfork) because it casts a reverberation artifact. The straight distal sesamoidean ligament appears disrupted as its longitudinal fibers *(black arrows)* are not visible parallel to the fibers of the deep digital flexor tendon. The pitchfork was clearly stuck in the bone of the first phalanx because there is a hypoechoic defect *(large arrow)* in the bony surface echo of the plantar aspect of the first phalanx (P1) where the pitchfork penetrated the cortex, allowing the ultrasound beam to penetrate the cortical surface of the bone. This sonogram was obtained with a 7.5-MHz sector-scanner transducer containing a built-in fluid offset at a displayed depth of 6 cm. The right side of this sonogram is proximal and the left side is distal.

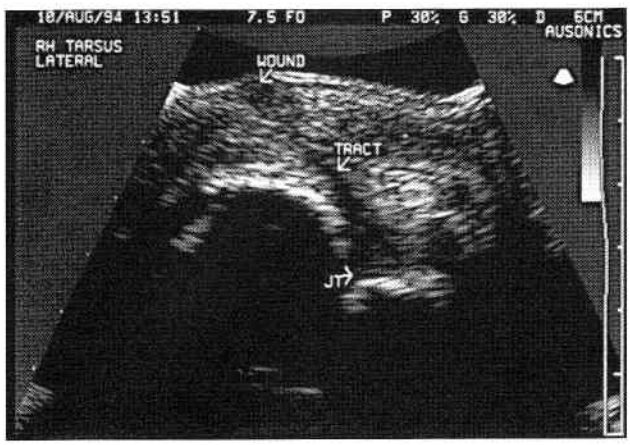

Figure 11–57

Sonogram of the right tarsus obtained from a 6-year-old Thoroughbred gelding with a penetrating wound into the lateral aspect of the tarsocrural joint (JT). The hypoechoic tract extends directly from the wound at the skin surface through the subcutaneous tissues into the joint which contains a small amount of hypoechoic fluid. This sonogram was obtained with a 7.5-MHz sector-scanner transducer containing a built-in fluid offset at a displayed depth of 6 cm. The right side of this sonogram is proximal and the left side is distal.

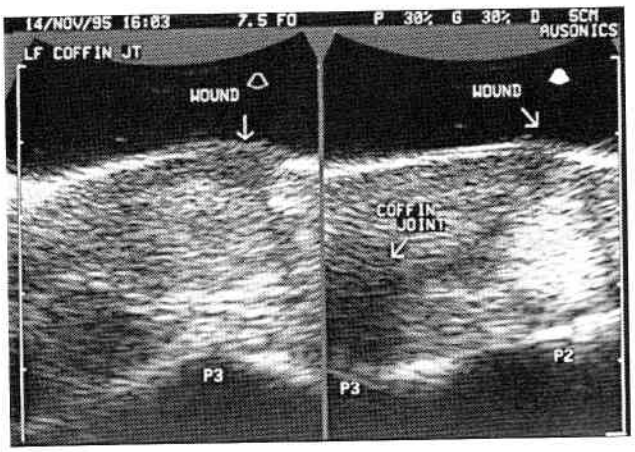

Figure 11–58

Sonograms of the left fore distal interphalangeal joint obtained from a 10-year-old Quarter Horse gelding with a puncture wound to the dorsal aspect of the distal pastern. A hypoechoic tract is imaged extending from the skin wound distally into the distended coffin joint, documenting that penetration of the coffin joint occurred. These sonograms were obtained with a 7.5-MHz sector-scanner transducer containing a built-in fluid offset at a displayed depth of 5 cm. The right side of the right image is proximal and the left side is distal. The right side of the left image is lateral and the right side is medial. P2 = second phalanx. P3 = third phalanx.

Draining tracts are common problems in horses and the detection of the source of the drainage, prior to the advent of ultrasonography, was sometimes a daunting task for the veterinary clinician. Contrast radiography was often used to follow the draining tract to its source.[121] In one horse, a draining tract was located cranial to the scapula following puncture of this region with a wooden rail 4 months earlier.[122] In this report the authors were able to locate the foreign bodies with fistulography while the horse was under general anesthesia. Sonographic examination of the area immediately caudal to the dorsal border of the scapula would have revealed the foreign bodies, facilitating their surgical removal. Sonographic examination of the area underneath the scapula would have been necessary under anesthesia to attempt to determine if additional foreign bodies were present in this location. Draining tracts were followed to screws in the mandibular symphysis with a fistulogram in a horse whose lingual foreign body had to be removed via a mandibular symphysiotomy.[123] Sonographic examination of these draining tracts would have revealed the infection of the implant and osteomyelitis of the mandible (see Chapter 3).

Draining tracts in horses have been associated with tooth roots, foreign bodies, sequestrae, osteomyelitis, necrotic tissue, and abscesses. The tract is more hypoechoic than the surrounding tissues and is followed sonographically to its end. The end of the tract may be a local abscess secondary to a previous cellulitis (Fig. 11-61) that is still draining, associated with residual infection or necrotic tissue in the abscess. If the draining tract is confined to the soft tissues, a thorough examination of the entire tract or tracts should be performed to rule out the presence of a foreign body or necrotic devitalized tissue acting as a foreign body. It is critical for all tracts to be followed carefully to their end to be sure that no other source of the drainage is present. The draining tract may end at a bone with a hypoechoic or anechoic fluid layer, consistent with a diagnosis of osteomyelitis (Fig. 11-62). A bony sequestrum may also be imaged at this site as a separate hyperechoic structure pulled slightly away from the parent surface of the bone in both short- and long-axis planes, surrounded by hypoechoic to anechoic fluid (Fig. 11-63). Because bony sequestrae are usually necrotic pieces of bone, any acoustic shadow that

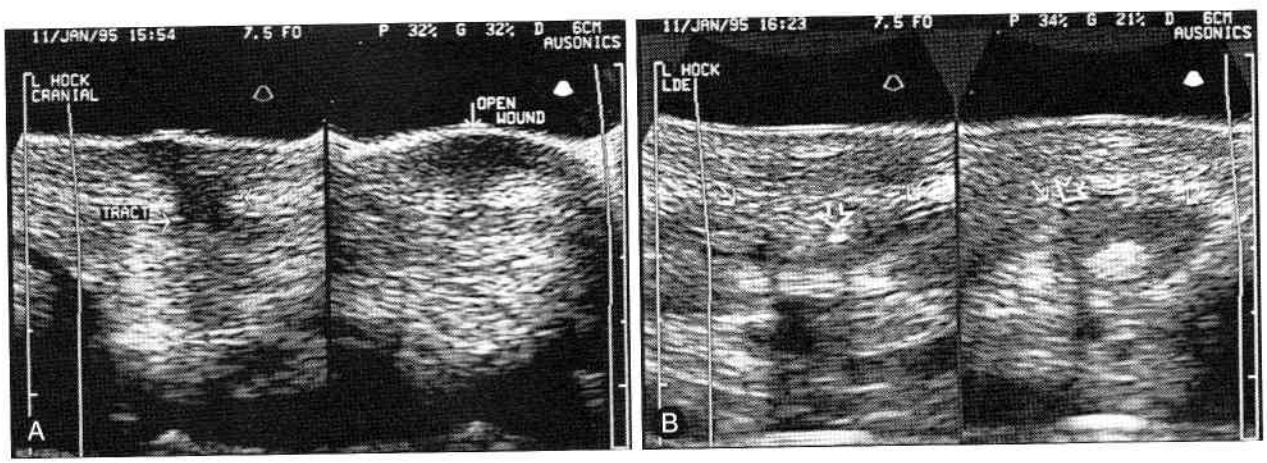

Figure 11–59

Sonograms of the dorsal aspect of the left hock demonstrating a hypoechoic tract into the soft tissues and long digital extensor tendon sheath (LDE) obtained from a 4-year-old Thoroughbred filly. These sonograms were obtained with a 7.5-MHz sector-scanner transducer containing a built-in fluid offset at a displayed depth of 6 cm.

A, The skin wound is open and draining *(vertical arrow)* and the anechoic to hypoechoic tract is readily imaged extending into the swollen echogenic soft tissues *(horizontal arrows)*. The right side of the short-axis view *(right image)* is lateral and the left side is medial. The right side of the long-axis view *(left image)* is proximal and the left side is distal.

B, The tract could be followed to the long digital extensor tendon sheath, which it penetrated. The long digital extensor tendon sheath is distended with hypoechoic fluid *(arrows)* and a small hyperechoic foreign body casting a acoustic shadow *(open arrows)* is best imaged within the tendon sheath in the long axis view *(left image)*, consistent with a piece of wood. The right side of the short-axis view *(right image)* is lateral and the left side is medial. The right side of the long-axis view is proximal and the left side is distal.

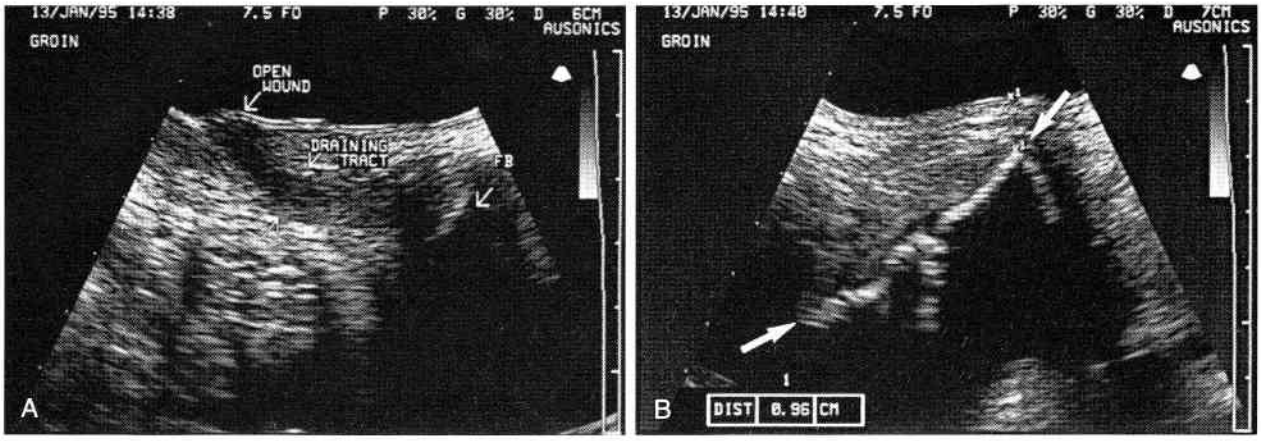

Figure 11–60

Sonograms of the prepuce obtained from a 14-year-old Thoroughbred cross gelding with a draining tract associated with wooden foreign bodies in the wound. These sonograms were obtained with a 7.5-MHz sector-scanner transducer containing a built-in fluid offset at a displayed depth of 6 cm (A) and 7 cm (B). The right side of these sonograms is cranial and the left side is caudal.

A, The anechoic tract *(arrows)* along the caudal aspect of the prepuce is followed from the open wound cranially to a hyperechoic structure surrounded by fluid representing a foreign body (FB).

B, Centering the image over the foreign body reveals multiple hyperechoic structures casting strong acoustic shadows consistent with wood *(arrows).* The wood is 0.96 cm (x[1]) from the skin surface at this location.

is produced usually originates from the far side of the bony fragment, rather than the near side, as occurs with new bone fragments. A tooth root may also be the source of purulent drainage (Fig. 11-64). In these horses the hypoechoic tract extends to the root of the affected tooth.

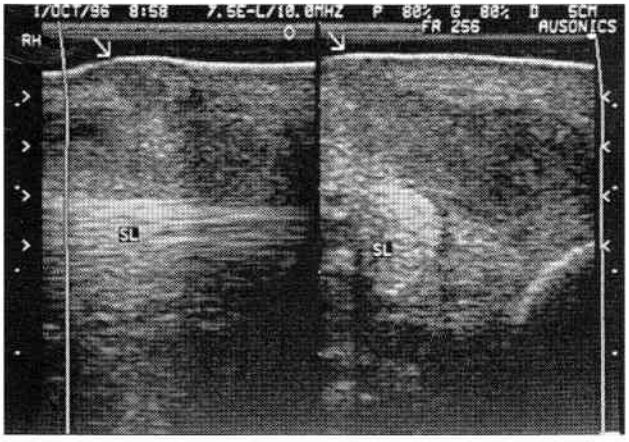

Figure 11–61

Sonograms of the right hind leg obtained from a 16-year-old Thoroughbred mare with a draining tract from the medial aspect of the right hind leg. This mare originally presented for cellulitis in this limb, which, after several weeks of systemic antimicrobial therapy and local poulticing and hosing of the limb, localized to the medial aspect of the distal metatarsus. Surgical drainage and debridement of this area resulted in a persistent draining tract, prompting this sonographic examination. The hypoechoic tract is imaged at the skin surface *(arrows)* extending into the deeper tissues but did not involve the suspensory ligament (SL), digital sheath, metatarsal bones or metatarsophalangeal joint. No foreign body was detected. The tract contained hypoechoic to echogenic tissue consistent with chronic inflammatory tissue. An additional 2 weeks of systemic antimicrobial therapy, based on the original results of culture and sensitivity testing of the fluid from the abscess, resulted in resolution of the drainage and local abscess. These sonograms were obtained with a wide-bandwidth 7.5-MHz linear-array transducer operating at 10.0 MHz with a hand-held standoff pad at a displayed depth of 5 cm. The right side of the transverse view *(right image)* is dorsal and the left side is plantar. The right side of the sagittal view is proximal and the left side is distal.

Wood, some types of graphite, and plastic are radiolucent foreign bodies, whereas wire, metal, glass, bullets, other types of graphite, and rock are radiopaque.[124] Ultrasonography can identify all different types of foreign bodies in soft tissue. In one study a nail, wire, and BB pellets all produced a distinct linear trail of echoes that extended beyond the thickness of the tissue specimen—a typical metallic reverberation artifact.[124] Sonographic examination of a nail in a chicken breast resulted in the detection of a "comet tail" artifact that began at the nail and extended beyond the limits of the chicken breast.[125] This "comet tail" artifact appears as a hyperechoic trace immediately distal to the metal piece resulting from the reverberations inside the metallic body itself.[126] This type of artifact is nearly always present with metallic foreign bodies, provided that the reflector lies within the focal zone of the transducer.[126] Both glass and gravel produced a strong echo from the near surface of the foreign body and a strong acoustic shadow.[124, 125] Glass in a chicken breast was imaged as a linear series of bright echoes along the path of the foreign body, whereas wood produced a discrete acoustic shadow.[125] In one study, wood and graphite produced only moderate to good surface echoes compared with those of glass and gravel.[124] Graphite produced only moderate shadowing deep to the surface echoes, whereas wood, glass, and gravel produced strong acoustic shadows.[124] Bone fragments (sequestrae) and wood often appear similar sonographically with a hyperechoic structure casting a strong acoustic shadow.[7] Both cast an acoustic shadow in a piece of muscle obscuring the echo from the bottom of the water bath and originating at the near surface of the hyperechoic structure.[7] The only difference was that the echo from the piece of wood was described as less well defined than the bone fragments in the muscle preparation.[7] The acoustic shadow cast from a foreign body varies with the type of

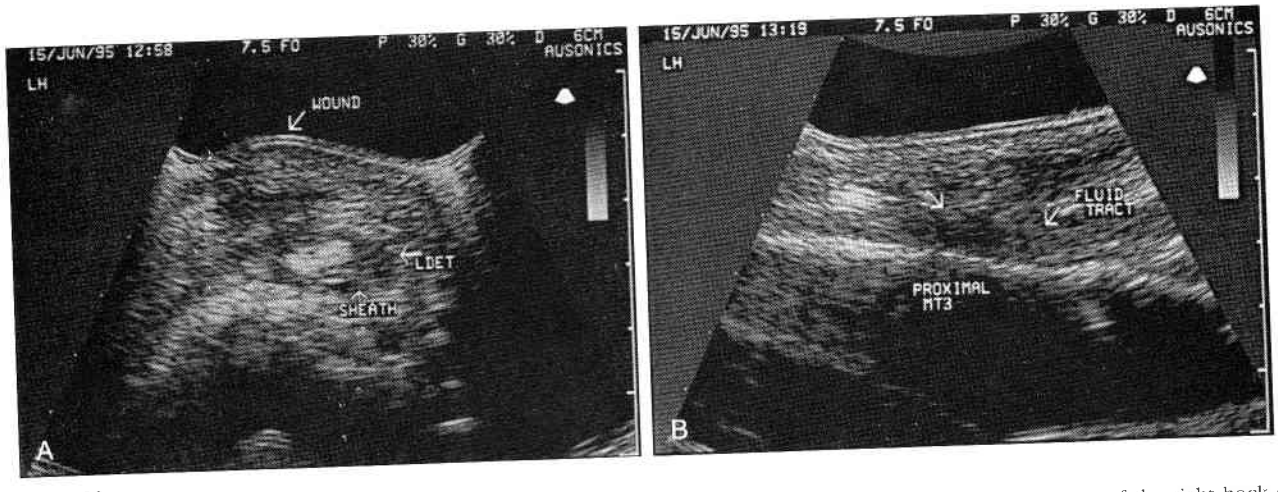

Figure 11–62

Sonograms of the left hind leg from a 10-year-old Quarter Horse mare with a penetrating wound over the dorsal aspect of the right hock and a draining tract. These sonograms were obtained with a 7.5-MHz sector-scanner transducer containing a built-in fluid offset at a displayed depth of 6 cm.

A, The tract can be followed from the wound at the skin surface into the long digital extensor tendon sheath. Hypoechoic fluid is imaged surrounding the long digital extensor tendon (LDET) and along the length of the tract. The right side of this sonogram is lateral and the left side is medial.

B, The tract continues to the dorsal surface of the third metatarsal bone, where a fluid layer is imaged immediately overlying the bone. The bony surface echo from the dorsal surface of the third metatarsal bone is thin and hypoechoic, consistent with bone necrosis and osteomyelitis. Along the proximal surface of the bone a proliferative change is imaged, where soft tissue once again covers the bone. The right side of this sonogram is proximal and the left side is distal.

the foreign body and the position of the ultrasound beam relative to the foreign body.[7] Wood casts the strongest acoustic shadow when detected in muscle in the dog.[12] No echoes should be detected within the hyperechoic structure if it is composed of bone or wood.[7] If an echogenic or hyperechoic structure is imaged that does not cast an acoustic shadow in any plane but is surrounded by fluid, necrotic tissue or fibrous tissue should be considered. If no acoustic shadow is detected and only low-amplitude echoes are detected, an abscess filled with cellular debris should be suspected.[7]

Foreign bodies have been found in many locations in

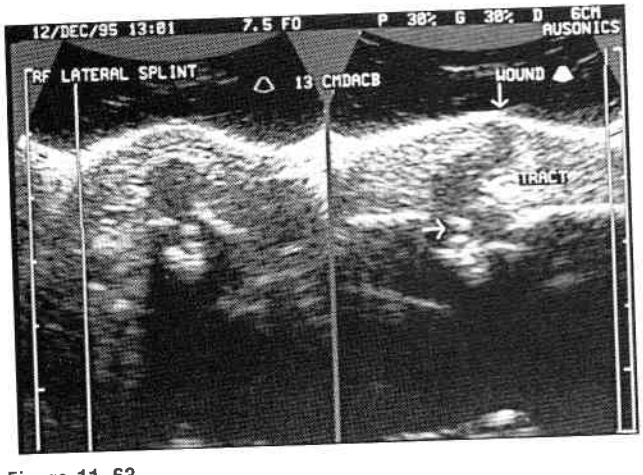

Figure 11–63

Sonograms of the right foreleg obtained from a 6-year-old Arabian mare with a draining tract at the skin surface associated with a bony sequestrum involving the fourth metacarpal bone. The hypoechoic fluid tract is imaged going directly to the bone in the long-axis scan of the tract *(right image),* where a large lytic area (defect) in the fourth metacarpal bone is imaged. This area contains hypoechoic fluid and two hyperechoic pieces consistent with sequestrae *(horizontal arrow).* In the short axis scan of the sequestrum the large lytic lesion in the fourth metacarpal bone is imaged containing a hyperechoic piece of bone surrounded by hypoechoic fluid. Only one of the sequestered pieces of bone is imaged in this view. These sonograms were obtained with a 7.5-MHz sector-scanner transducer containing a built-in fluid offset at a displayed depth of 6 cm. The right side of the right image is proximal and the left side is distal. The right side of the left image is dorsal and the right side is palmar.

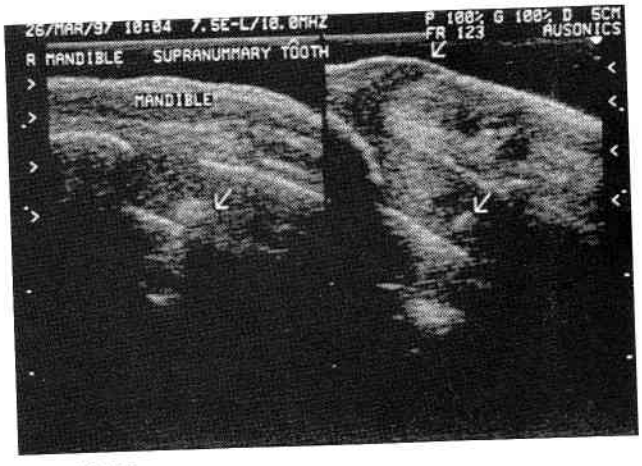

Figure 11–64

Sonograms of the right side of the mandible obtained from a 4-year-old Thoroughbred gelding with a draining tract from a supranummery tooth. The tract is hypoechoic. The entire tract from the skin surface *(upper arrow)* to the root of the tooth *(lower arrow)* is clearly visible in the right image (a long-axis scan of the tract). In the short-axis scan of the draining tract *(left image)* a defect in the mandible is imaged which is approximately 1 cm in diameter and the root of the tooth is imaged at the end of the draining tract *(angled arrow).* These sonograms were obtained with a wide-bandwidth 7.5-MHz linear-array transducer operating at 10.0 MHz with a hand-held standoff pad at a displayed depth of 5 cm. The right side of the long-axis image is dorsal and the left side is ventral. The right side of the short-axis image is rostral and the left side is caudal.

horses, many of which are inaccessible radiographically. Sonographic examination of a swelling or draining tract can be extremely useful in localizing a foreign body within the mass or at the end of the draining tract. In many instances ultrasonography facilitates the surgical approach to foreign body removal by identifying the precise location of the foreign body and its relationship to adjacent structures. One horse examined by the author had a 4-month history of a draining tract over the left point of the shoulder following an encounter with a wooden fence. The tract was followed sonographically to the thoracic inlet region, where it coursed between the two carotid arteries and then dove medially between the right scapula and the right chest wall. Preoperatively, sonographic examination of the axillary region was performed under general anesthesia with the right foreleg abducted. In this position the tract was again identified and followed to a linear hyperechoic structure casting a strong acoustic shadow lying immediately dorsal to the brachial plexus, consistent with a piece of wood. Surgical removal of the embedded piece of wood resulted in successful resolution of the drainage and horse's return to racing. Some areas underneath the scapula are not amenable to sonographic examination, however, even under general anesthesia.

Most foreign bodies are lodged in muscle, which appears heterogeneous with hyperechoic speckling. A foreign body is recognized ultrasonographically when an echogenic or hyperechoic structure is identified surrounded by anechoic to hyperechoic fluid or walled off in the surrounding soft tissues (Fig. 11-65). A strong hyperechoic linear structure casting reverberation artifacts is consistent with a metallic foreign body (Fig. 11-66). Bullet fragments or lead may appear hyperechoic and may not cast a distinct acoustic shadow or reverberation artifact, depending on the position of the bullet fragment or lead within the soft tissue, the shape of the projectile, and the direction of the ultrasound beam (Fig. 11-67). Wooden foreign bodies normally cast a strong acoustic shadow from a hyperechoic linear surface (Fig. 11-68). Glass also normally appears hyperechoic and casts a

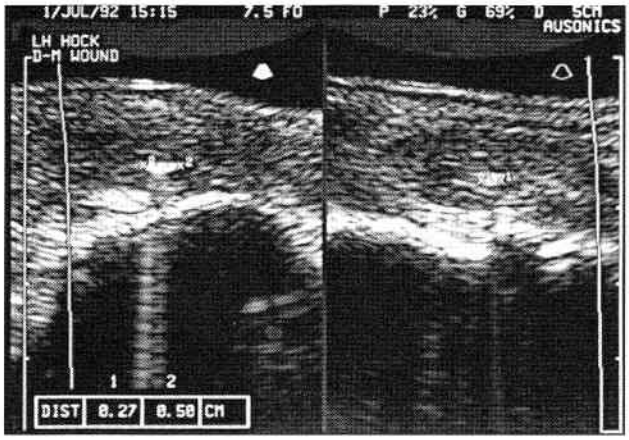

Figure 11–66

Sonograms obtained of a foreign body in the dorsal medial aspect of the left hock obtained from a 13-year-old Thoroughbred mare. The foreign body was located slightly proximal to the opening of the draining tract at the skin surface. The foreign body measured 0.27 cm (x^1) by 0.50 cm (x^2) and was extra-articular. The multiple hyperechoic reverberation artifacts from the foreign body when imaged in its long axis suggest that this foreign body is metallic. The hyperechoic linear foreign body is surrounded by hypoechoic fluid, the typical reaction found surrounding a foreign body. These sonograms were obtained with a 7.5-MHz sector-scanner transducer containing a built-in fluid offset at a displayed depth of 5 cm. The right side of the left image is cranial and the left side is caudal. The right side of the right image is proximal and the left side is distal.

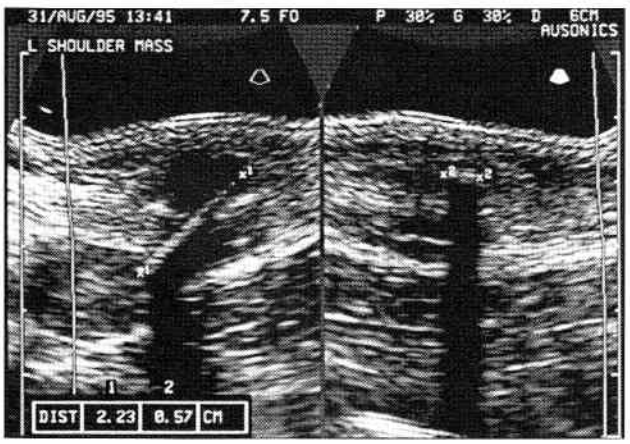

Figure 11–65

Sonograms of a soft tissue swelling over the lateral aspect of the left shoulder obtained from a 12-year-old Quarter horse gelding. A long (2.23-cm) hyperechoic linear foreign body (x^1) casting a strong acoustic shadow consistent with wood is detected in the left image, surrounded by anechoic fluid. The short-axis view of the wooden foreign body reveals it to be 0.57 cm wide (x^2) and to cast a strong acoustic shadow from its surface. The wooden foreign body is near the skin surface, but a draining tract has not formed. These sonograms were obtained with a 7.5-MHz sector-scanner transducer containing a built-in fluid offset at a displayed depth of 6 cm. The right side of the right image is dorsal and the left side is ventral. The right side of the left image is cranial and the left side is caudal.

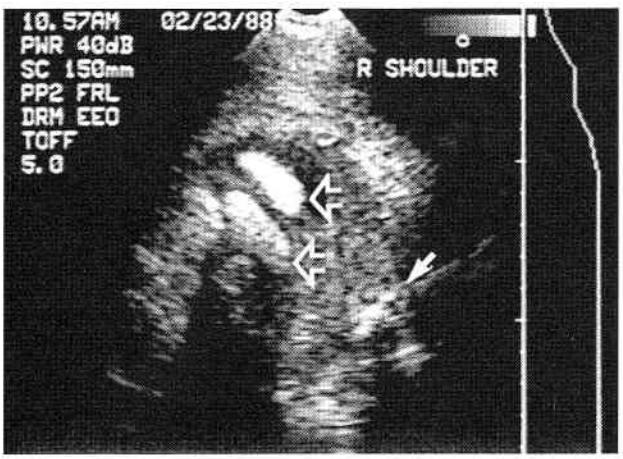

Figure 11–67

Sonogram of the left shoulder obtained from a 4-year-old Standardbred stallion with gunshot wounds in his left shoulder region. Multiple hyperechoic oval lead fragments cast varying acoustic shadows *(open arrows)*, and smaller irregular hyperechoic fragments cast acoustic shadows associated with fragments of the fractured scapula *(small arrow)*. This sonogram was obtained with a 5.0-MHz sector-scanner transducer at a displayed depth of 15 cm. The right side of this sonogram is cranial and the left side is caudal.

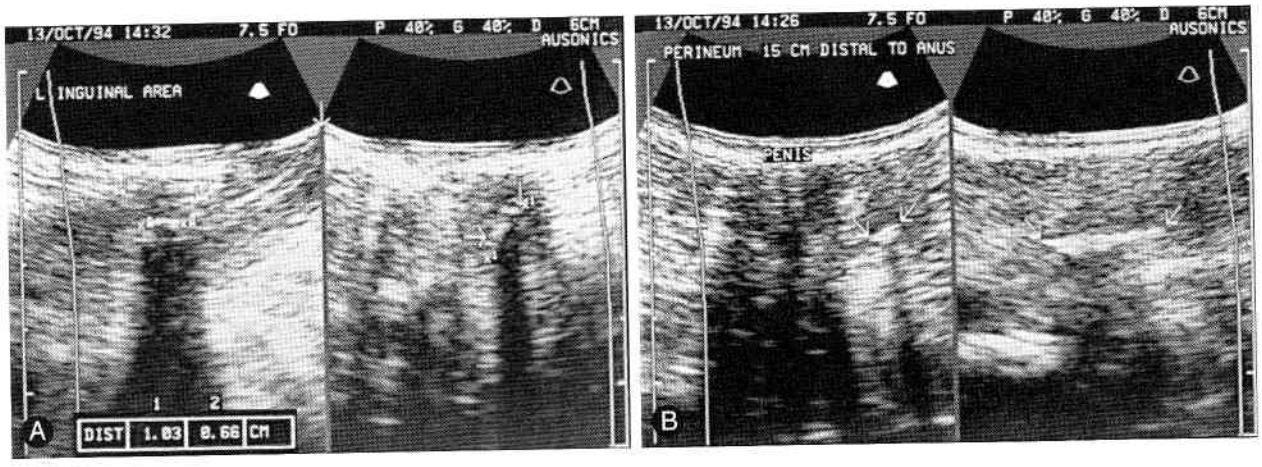

Figure 11–68

Sonograms of the inguinal and perineal regions, from a 10-year-old Welsh pony gelding with a draining tract. These sonograms were obtained with a 7.5-MHz sector-scanner transducer containing a built-in fluid offset at a displayed depth of 6 cm.

A, Sonograms of the draining tract in the left inguinal region demonstrating the tract at the skin surface *(left image)*, leading to a hyperechoic linear foreign body casting a strong acoustic shadow. This sonographic appearance is consistent with a piece of wood. The linear foreign body measures 0.66 cm (x^2) by 1.03 cm (x^1) in two mutually perpendicular planes. The tract is easiest to follow in its short axis *(right image)*, keeping the hypoechoic tract centered in the image. The tract is slightly hypoechoic and extends to the skin surface *(down arrow)* with hyperechoic margins along the edges of the tract. The tract does not end at this foreign body. Hypoechoic material is imaged deep to the hyperechoic linear foreign body in the long-axis view of the tract *(left image)*. This indicates an additional source of drainage (most likely another foreign body) and this hypoechoic tract should be followed to its source. The right side of the left image is cranial and the left side is caudal. The right side of the right image is toward the left side of the horse.

B, The hypoechoic tract was followed to the perineal region to a point 15 cm distal to the anus, where another hyperechoic linear foreign body casting an acoustic shadow *(arrows)* was imaged to the left of the penis. The acoustic shadow from this foreign body is not as strong, suggesting that this foreign body may be more decomposed, but this sonographic appearance is still consistent with a piece of wood. The angle at which the ultrasound beam hits the foreign body and the flatness of the surface of the foreign body also determine the type of acoustic shadow that is cast from the foreign body. In the short-axis sonogram of the perineal region and the tract *(left image)*, the hypoechoic circular penis with an anechoic urethra is imaged with the hyperechoic foreign body *(arrows)* located immediately adjacent to the penis. The right side of this image is the left side of the perineal region. The corresponding long-axis view of the foreign body *(arrows)* is seen in the right image. The hypoechoic tract ended at this foreign body. The right side of this sonogram is dorsal and the left side is ventral.

strong acoustic shadow. The shadow normally arises from the near surface of the hyperechoic structure in each of these situations. Tubular hyperechoic structures that cast weak acoustic shadows may represent a piece of hoof within the soft tissues associated with the drainage (Fig. 11-69). If the acoustic shadow arises from the far surface of the structure, a dense soft tissue structure such as necrotic muscle acting as a foreign body should be considered. A foreign body can be present in the muscle or soft tissues and cause little reaction, but this is not the norm (Fig. 11-70). Iatrogenically implanted foreign bodies impregnated with antimicrobials can be imaged at the site of implantation (Fig. 11-71). These reportedly cause a foreign body reaction once the antibiotics have eluted from the polymethyl methacrylate beads and require surgical removal at that time.

Needles that have accidentally broken off in the tissues can be located sonographically to facilitate their surgical removal (Fig. 11-72). The needle should cast a reverberation artifact when intercepted by the ultrasound beam. The characteristic metallic reverberation artifact may not be produced, however, owing to the smooth, rounded surface of the needle. The soft tissue reaction associated with a broken needle depends on the conditions under which the needle was inserted. If the skin was surgically prepared prior to the injection, the reaction around the broken needle may be minimal (Fig. 11-72).

Ultrasound was used in a study of 22 horses with gunshot wounds to help localize the site of the projectile fragments and determine the extent of damage to soft tissues or to vital structures along the path of the projectile.[12] In a colt with a diffuse swelling in the left side of the neck and a history of a previous puncture wound in this region after running into a wooden fence, ultrasound was used to identify foreign bodies in the cervical region adjacent to the internal carotid artery and jugular vein.[9] The foreign bodies were hyperechoic and as a group cast a strong acoustic shadow consistent with that of wood. Surgical removal at this time was believed to be too risky because of the close association of the foreign body with the adjacent vital structures. Two months later the colt presented with esophageal obstruction, and a fluid-filled pocket causing esophageal obstruction was identified around the foreign body with ultrasonography.[9] Intraoperative ultrasonography was used to identify the cervical foreign body in this horse and facilitate its surgical removal, as the location of the foreign bodies and abscess was not evident after surgical exposure. The use of intraoperative ultrasonography avoided extensive surgical exploration and potential damage to the carotid artery, vagosympathetic trunk, and recurrent laryngeal nerve.[9] Preoperative ultrasonic examination of a draining tract from the pectoral region in one yearling revealed a hyperechoic foreign body casting an acoustic shadow consistent with a piece of wood, subsequently removed at surgery.[6] Ultrasonography was used in another horse to identify a foreign body over the dorsal aspect of the carpus between the common digital exten-

sor tendon and the long digital extensor tendon.[4] The foreign body appeared hyperechoic and was a discrete linear structure casting a strong acoustic shadow surrounded by an ill-defined, poorly echoic area, consistent with a piece of wood. Intraoperative ultrasonography was used to guide a needle so that it was in contact with the foreign body guiding the surgical approach and removal of the wooden foreign body.[4]

The use of ultrasonography is important to identify and remove radiolucent foreign bodies, as well as to localize foreign bodies that are seen on survey radiographs but are difficult to locate.[123] Ultrasound is superior to survey radiographs in the precise localization of the foreign body.[124] Ultrasonography used to detect foreign bodies can prevent complications such as infection and osteomyelitis by enabling the veterinary clinician to remove the foreign body promptly.[124] The precise localization of the foreign body with ultrasound minimizes surgical time, the size of the surgical incision, and the amount of tissue dissection.[124] Precise localization of suspected foreign bodies for surgical removal, especially in the extremities, is the biggest advantage of sonographic examination of human patients.[125, 128]

Draining tracts have been frequently seen postoperatively in horses following ventral midline celiotomy. Sonographic examination of the incision reveals hypoechoic to anechoic tracts from the skin surface to the underlying sutures, which are often surrounded by fluid-forming suture sinuses (Fig. 11-73). The suture material appears hyperechoic and often casts an acoustic shadow through the deeper tissues (Fig. 11-74). Multiple sutures are usually involved and a hypoechoic fluid tract can often be followed along a portion of the length of the incision, or in some cases, along the entire incision. The hypoechoic tracts should be followed to their deepest extent, as the incisional infection can extend throughout the entire thickness of the incision to the peritoneum (Fig. 11-75)

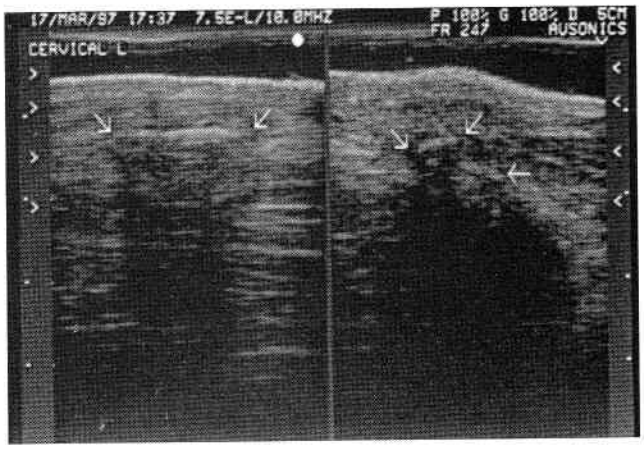

Figure 11–70

Sonograms of the left cervical region obtained from a 14-year-old Thoroughbred gelding with an embedded wooden foreign body from an encounter with a fence 4 years earlier. Notice the hyperechoic linear structures *(arrows)* casting an acoustic shadow consistent with pieces of wood. In the short-axis view *(right image)*, two foreign body fragments are imaged; the foreign body closest to the skin surface is the one imaged in the long-axis view *(left image)*. The foreign body at an angle *(horizontal arrow)* is not seen in the long-axis scan, as it is in a different scan plane. The foreign bodies are encapsulated by thick (3–4 mm) echogenic tissue (fibrous capsule) and little fluid is shown surrounding the foreign bodies, indicating little reaction to their presence. This sonogram was obtained with a wide-bandwidth 7.5-MHz linear-array transducer operating at 10.0 MHz with a hand-held standoff pad at a displayed depth of 5 cm.

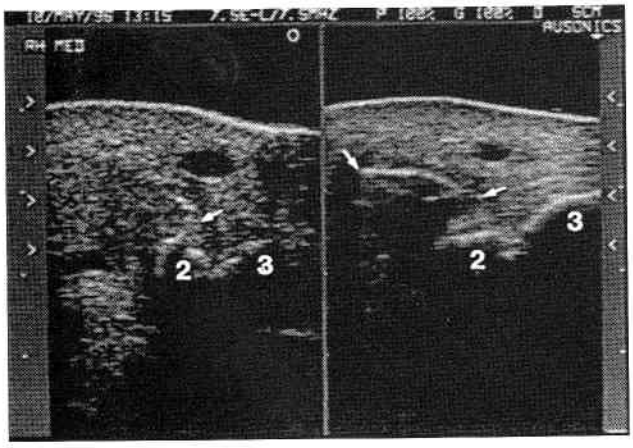

Figure 11–69

Sonograms of the medial aspect of the right hind leg obtained from a 10-year-old Appaloosa gelding with a history of a draining tract for 4 months following a kick. Notice the hyperechoic double-walled structure *(small arrows)* in the right image, casting an acoustic shadow. The double-walled appearance is reminiscent of a piece of hoof which is the embedded foreign body surrounded by a small amount of hypoechoic fluid. The hoof was imbedded adjacent to the second (2) and third (3) metatarsal bones. The edge of the hoof fragment *(small arrow)* is imaged in the left image with the hypoechoic fluid layer extending deeper to the second (2) and third (3) metatarsal bones. The fluid layer adjacent to the bones and the roughening of the bony surface echoes is consistent with a local osteomyelitis. These sonograms were obtained with a wide-bandwidth 7.5-MHz linear-array transducer with a hand-held standoff pad operating at 7.5 MHz at a displayed depth of 5 cm. The right side of these sonograms is dorsal and the left side is plantar.

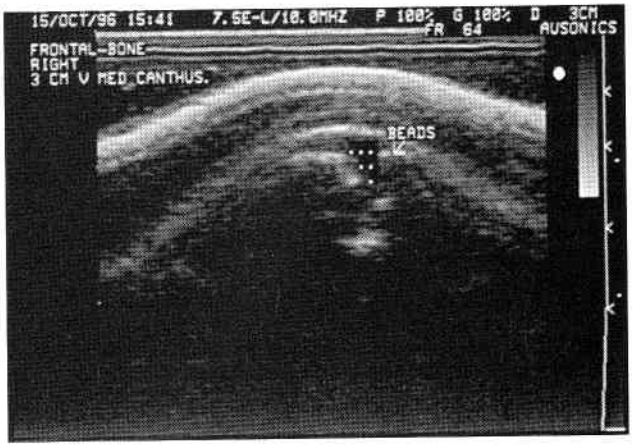

Figure 11–71

Sonogram of amikacin-impregnated polymethyl methacrylate beads implanted in a bony defect in the frontal bone obtained from a 12-year-old Appaloosa gelding with chronic osteomyelitis. The beads appear as hyperechoic dots in anechoic triangular structure and were implanted 3 cm ventral to the medial canthus of the right eye. This sonogram was obtained with a wide bandwidth 7.5 MHz linear-array transducer operating at 10.0 MHz with a hand-held standoff pad at a displayed depth of 3 cm. The right side of the sonogram is toward the midline and the left side is toward the right side of the horse.

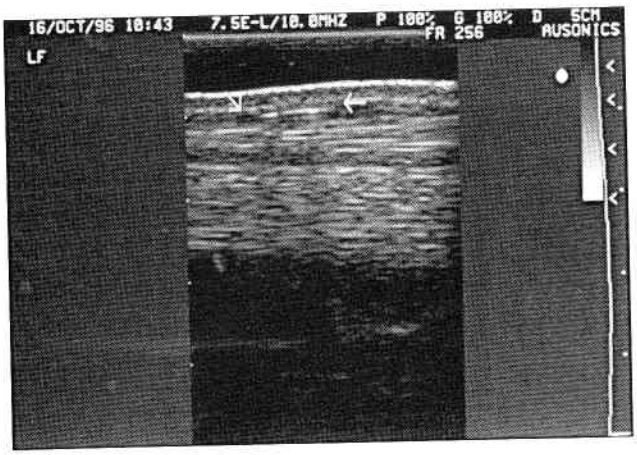

Figure 11–72

Sonogram obtained from a 5-year-old Thoroughbred gelding imaging part of a 25-gauge needle that broke off in the left fore leg during an injection. The thin linear hyperechoic structure *(arrows)* lies in the subcutaneous tissues immediately adjacent to the superficial digital flexor tendon. Dirty acoustic shadows are cast from the ends of the needle. This sonogram was obtained with a wide-bandwidth 7.5-MHz linear-array transducer operating at 10.0 MHz with a hand-held standoff pad at a displayed depth of 5 cm. The right side of this sonogram is proximal and the left side is distal.

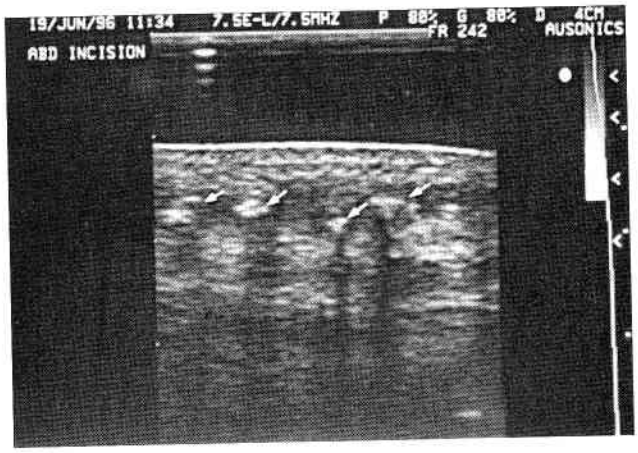

Figure 11–74

Sonogram of the ventral midline incision obtained from a weanling Quarter horse colt following a ventral midline celiotomy. Notice the hyperechoic sutures *(arrows)* casting acoustic shadows. The sutures are surrounded by hypoechoic fluid consistent with suture sinuses. This sonogram was obtained with a wide-bandwidth 7.5-MHz linear-array transducer operating at 7.5 MHz with a hand-held standoff pad at a displayed depth of 4 cm. The right side of this sonogram is cranial and the left side is caudal.

and, in some cases, into the peritoneal cavity (Fig. 11-76). Similarly, draining tracts associated with suture sinuses can be followed from the skin to the offending suture material at other surgical sites (Fig. 11-77), especially in horses in which the surgical site was infected or contaminated before surgery.

Peri-incisional edema, a common postoperative complication following ventral midline celiotomy, was detected ultrasonographically in nearly all ponies 1 week after surgery.[13] The peri-incisional edema was described as a hypoechoic area extending 5 to 10 cm on either side of the incision line. The sutures in the linea alba were described as focal hyperechoic structures approximately 1 to 2 mm in diameter with distal acoustic shadowing.[13] Small suture sinuses imaged as 1 to 2 mm hypoechoic to anechoic areas around the sutures were present in 71%

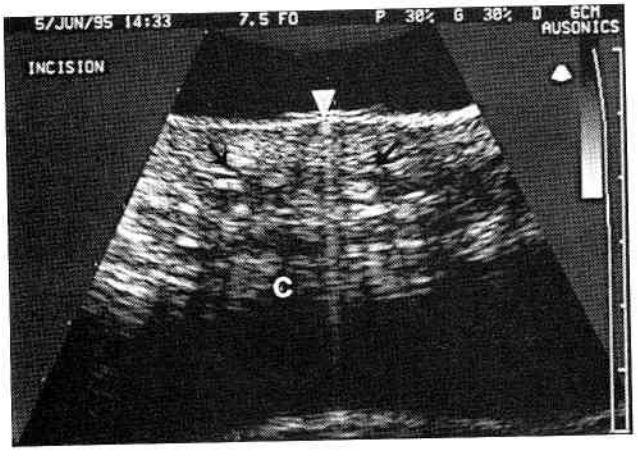

Figure 11–73

Sonogram of suture sinuses in a ventral midline incision obtained from an 8-year-old Thoroughbred mare following a ventral midline celiotomy. There is slightly hypoechoic fluid surrounding sutures in the middle of the abdominal incision *(arrows)*. These suture sinuses are not associated with a draining tract at this time and do not extend down to the peritoneum. The large colon (C) was moving freely against the peritoneum. A metallic reverberation artifact is present from one of the staples in the skin *(arrowhead)*. This sonogram was obtained with a 7.5-MHz sector-scanner transducer containing a built-in fluid offset at a displayed depth of 6 cm. The right side of the sonogram is cranial and the left side is caudal.

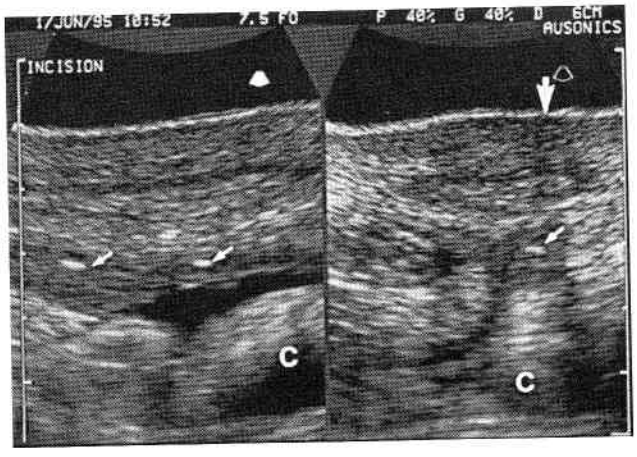

Figure 11–75

Sonograms of the ventral midline incision obtained from an 11-year-old Thoroughbred mare following a ventral midline celiotomy. Hypoechoic tracts are imaged from the skin surface *(large arrow)* in the transverse (right) image extending to the peritoneum, where this material surrounds a suture *(small arrow)*. Multiple sutures *(small arrows)* are affected, which can be appreciated in the sagittal (left) image extending to the peritoneum. The large colon (C) was moving freely against the abdominal incision with no evidence of adhesions. These sonograms were obtained with a 7.5-MHz sector-scanner transducer containing a built-in fluid offset at a displayed depth of 6 cm. The right side of the transverse (right) image is the left side of the incision. The right side of the sagittal (left) image is cranial and the left side is caudal.

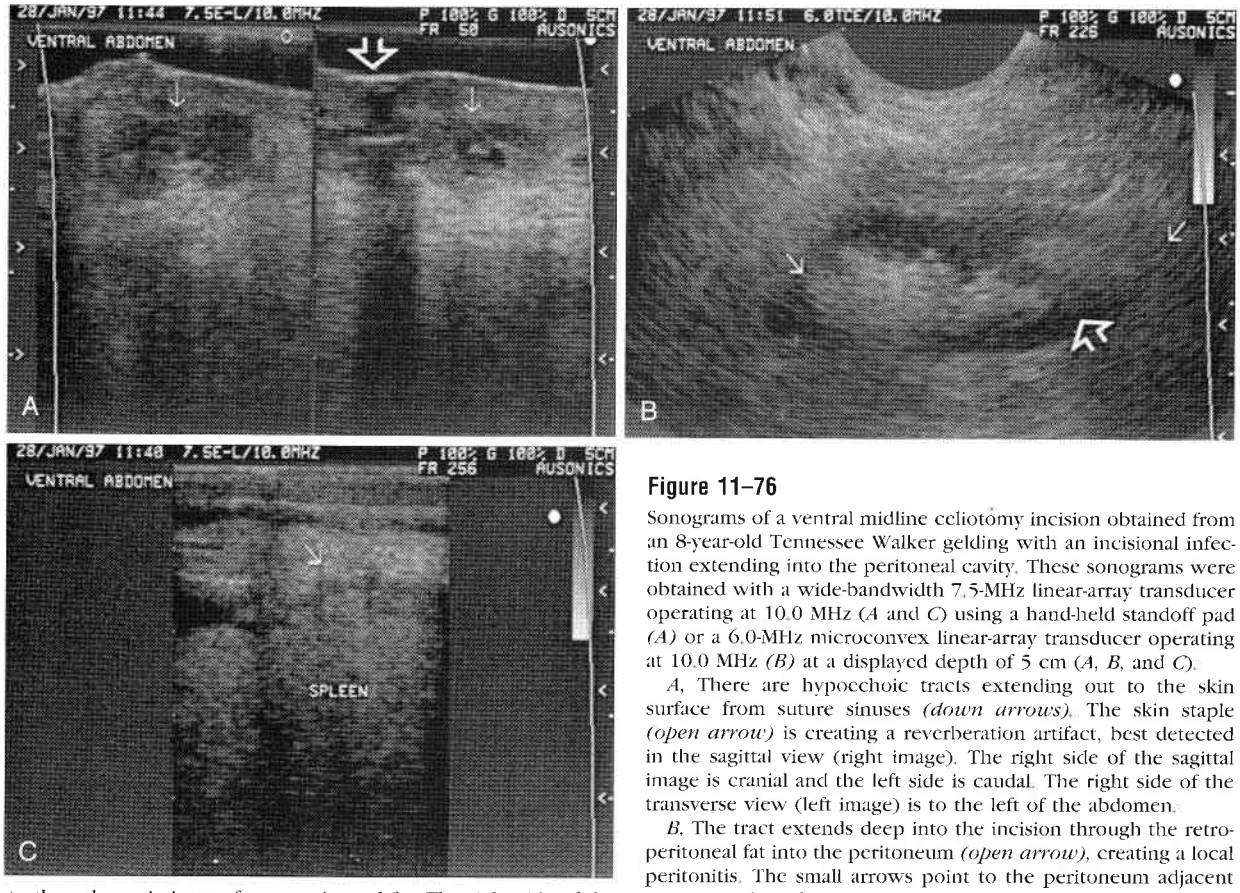

Figure 11–76

Sonograms of a ventral midline celiotomy incision obtained from an 8-year-old Tennessee Walker gelding with an incisional infection extending into the peritoneal cavity. These sonograms were obtained with a wide-bandwidth 7.5-MHz linear-array transducer operating at 10.0 MHz (*A* and *C*) using a hand-held standoff pad *(A)* or a 6.0-MHz microconvex linear-array transducer operating at 10.0 MHz *(B)* at a displayed depth of 5 cm (*A*, *B*, and *C*).

A, There are hypoechoic tracts extending out to the skin surface from suture sinuses *(down arrows)*. The skin staple *(open arrow)* is creating a reverberation artifact, best detected in the sagittal view (right image). The right side of the sagittal image is cranial and the left side is caudal. The right side of the transverse view (left image) is to the left of the abdomen.

B, The tract extends deep into the incision through the retroperitoneal fat into the peritoneum *(open arrow)*, creating a local peritonitis. The small arrows point to the peritoneum adjacent to the echogenic layer of retroperitoneal fat. The right side of this sonogram is the left side of the abdomen.

C, There are fibrinous adhesions *(arrow)* between the spleen and the peritoneum on the edge of the local area of peritonitis. The arrow is superimposed on the layer of retroperitoneal fat. The right side of this sonogram is cranial and the left side is caudal.

of ponies 1 week postoperatively; these usually resolved in 3 to 4 weeks.[13] Sonographic monitoring of incisional swelling or drainage with ultrasound is recommended to identify pockets that should be drained or sutures that should be removed.[15]

Closure of ventral midline incisions with polypropylene has been associated with suture sinus formation in horses.[14] Sonographic examination of the ventral midline incision was performed in two horses, revealing the suture abscesses and the draining tracts extending from the sutures. The suture abscesses appeared as a region of heterogeneous echogenicity surrounding a hypoechoic region (presumed to be fluid) containing a small focal hyperechoic area thought to represent suture material. The near-far-far-near pattern of incisional closure has been associated with a higher incidence of incisional complications in horses.[14, 129] In one of three horses studied, cultures of the fluid surrounding the sutures yielded bacterial growth. The use of braided or multifilament suture material is associated with a higher incidence of suture sinus formation.[130] Contamination at the time of suture placement and excessive tension on the suture material may contribute to suture sinus formation.[14]

A ventral midline incisional hernia is diagnosed with the detection of a swollen or pendulous region along the previous incision and palpation of defects in the body wall. Incisional hernias occur after all types of surgery, usually as a result of a failure of the incision to heal, rather than from suture failure.[15] The incidence of ventral hernias following ventral midline celiotomies in horses ranges from 11 to 16% in horses followed for 4 months postoperatively.[13, 131] Hernias developed in most horses within 12 weeks of surgery.[131] Incisional hernias developed in horses that were significantly older than in horses that did not develop a postoperative ventral midline incisional hernia.[131] Horses operated on for intestinal problems are at a higher risk for the development of postoperative incisional hernias than those having abdominal surgery for problems other than intestinal disease.[13] Incisional drainage also increases the risk for incisional hernia formation.[15] Purulent incisional discharge or severe periincisional edema was present in 84% of horses preceding the development of a ventral midline hernia.[16] As many as 97% of hernias develop after incisional complications.[131] Horses with incisional drainage were 17.8 times as likely to develop an incisional hernia following ventral midline celiotomy than were those without incisional drainage.[131] These incisional complications are usually noticed by 9 days after surgery.[16, 129] Other investigators have reported that 10 to 25% of ventral midline incisions develop subcutaneous infections.[129, 132]

Sonographic examination of a ventral midline hernia reveals the thinner-than-normal abdominal wall with varying amounts of abdominal musculature along the edges

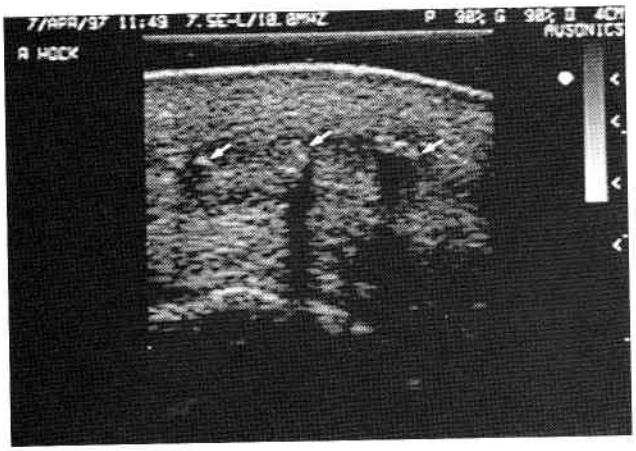

Figure 11–77

Sonogram of suture sinuses obtained from a 10-year-old Thoroughbred gelding with a diffuse cellulitis surrounding the hock and a septic calcaneal bursitis. The sutures *(arrows)* are hyperechoic, cast acoustic shadows and are surrounded by hypoechoic fluid consistent with suture sinuses. This sonogram was obtained 2 months after surgical treatment of septic calcaneal bursitis and debridement of a draining tract associated with a previous puncture wound. This sonogram was obtained with a wide-bandwidth 7.5-MHz linear-array transducer operating at 10.0 MHz with a hand-held standoff pad at a displayed depth of 4 cm. The right side of this sonogram is proximal and the left side is distal.

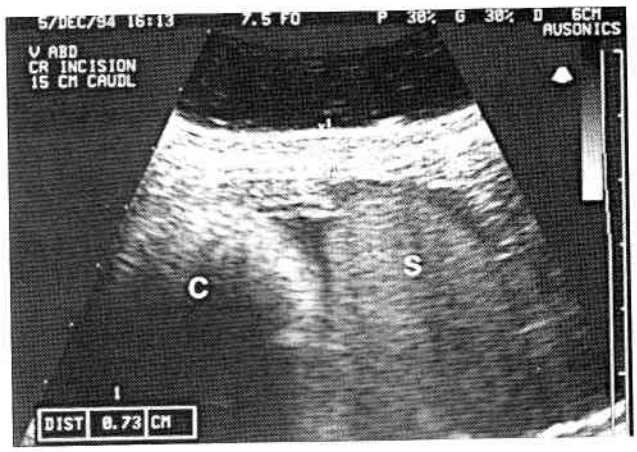

Figure 11–78

Sonogram of a ventral midline hernia obtained from an 8-year-old Thoroughbred mare. The skin and a small amount of subcutaneous tissues measuring 0.73 cm (x^1) are all that contain the large colon (C) and spleen (S). This sonogram was obtained with a 7.5-MHz sector-scanner transducer containing a built-in fluid offset at a displayed depth of 6 cm. The right side of this sonogram is the left side of the abdomen.

of the hernia. The ventral midline hernia may be full thickness with only the skin containing the abdominal contents (Fig. 11–78) or be partial thickness with some muscle layers intact and some disrupted (Fig. 11–79). In most horses with abdominal hernias following ventral midline celiotomy, areas of both partial-thickness and full-thickness herniation are detected along the length of the incision. The hernial repair can be followed sonographically to monitor wound healing. Sonographic examination of a hernia repaired with mesh can also be performed, although only the edges of the hernial repair and the tissues superficial to the mesh can be evaluated because the mesh is hyperechoic and casts a strong acoustic shadow (Fig. 11–80). However, problems with incisional drainage can be traced to the mesh in some horses indicating infection of the implant (Fig. 11–81).

Ultrasonographic examination of ventral midline incisions can be useful in predicting herniation in horses with compromised incisions and in confirming the herniation and its extent, once herniation has occurred.[13] The incisional hernias had reduced tissue thickness along the

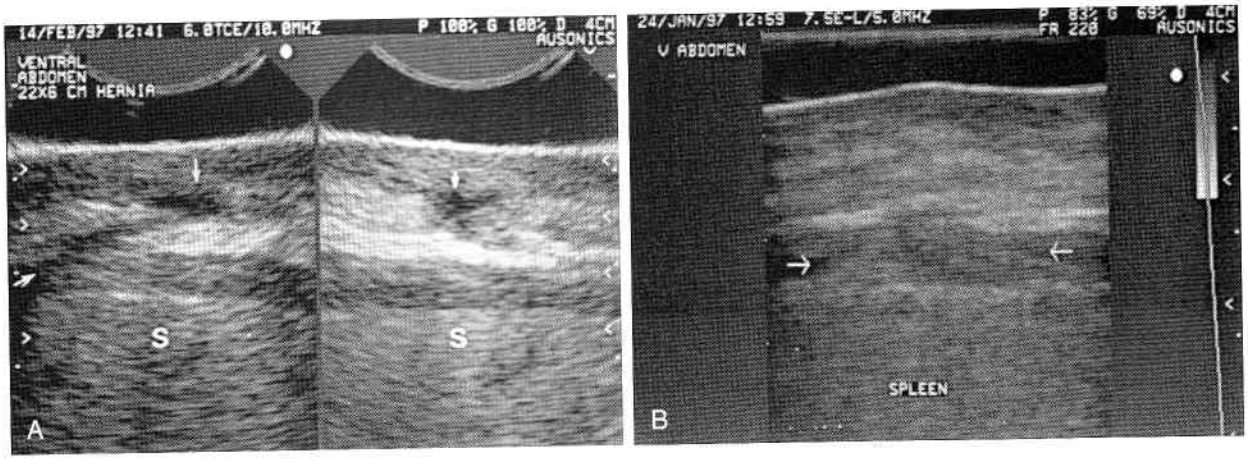

Figure 11–79

Sonograms of a ventral midline celiotomy incision in a 16-year-old Thoroughbred gelding with an incisional infection that extends into the peritoneal cavity and a developing ventral abdominal hernia.

A, A hypoechoic to anechoic tract *(small arrows)* is imaged in the abdominal wall extending into the peritoneal cavity with the spleen (S) adhered to the incision at this point. This sonogram was obtained 3 weeks after the image in *B*. The thinning of the ventral abdominal musculature is becoming evident as the hernia develops secondary to the incisional infection. These sonograms were obtained with a wide bandwidth 6.0 MHz microconvex linear array transducer operating at 10.0 MHz with a hand-held standoff pad at a displayed depth of 4 cm. The right side of the right image is cranial and the left side is caudal. The right side of the left image is the left side of the abdomen.

B, The spleen is adhered to the peritoneum adjacent to and at the incision with hypoechoic fibrin *(arrows)*. This sonogram was obtained with a wide-bandwidth 7.5-MHz linear-array transducer operating at 5.0 MHz with a hand-held standoff pad at a displayed depth of 4 cm. The right side of this sonogram is cranial and the left side is caudal.

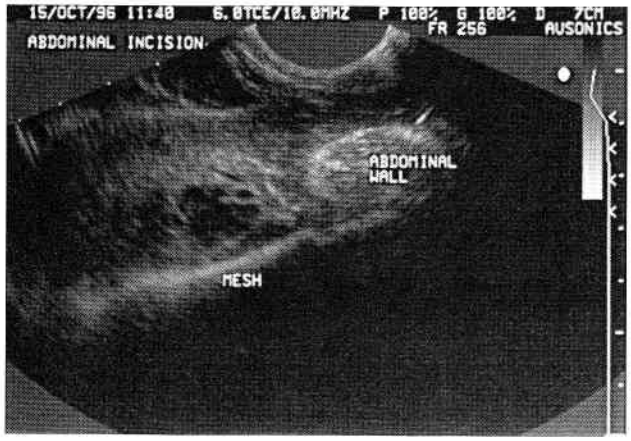

Figure 11–80

Sonogram of a mesh implant used to repair a large ventral midline hernia that developed following a previous ventral midline celiotomy obtained from a 15-year-old American Saddlebred mare. A large fluctuant swelling developed ventral to the mesh following hernia repair. The edge of the left abdominal wall is imaged to the right of the sonogram and the hyperechoic mesh casting an acoustic shadow is imaged dorsal to the left ventral abdominal wall. Ventral to the mesh is a hypoechoic loculated fluid collection which represents a postoperative seroma. This sonogram was obtained with a wide-bandwidth 6.0-MHz microconvex linear-array transducer operating at 10.0 MHz at a displayed depth of 7 cm.

linea alba and an increased distance between the apposing rectus abdominus muscles.[13] Sonographic examination of the hernia is also useful in alerting the surgeon to the presence of adhesions which might result in extended surgical time and possible additional intestinal surgery at the time of hernia repair.[16]

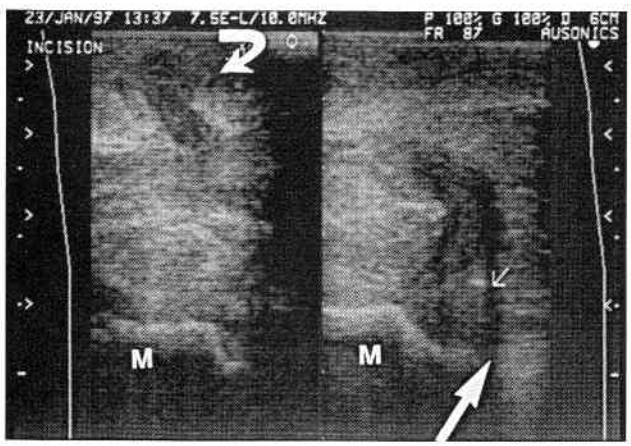

Figure 11–81

Sonogram of an infected mesh implant (M) obtained from a 15-year-old American Saddlebred mare (same as in Fig. 11-80) 3 months following hernia repair with a mesh implant. There is extensive swelling of the ventral abdomen (4–5 cm thick) with hypoechoic to echogenic tissue representing chronic inflammatory tissue. Hypoechoic tracts extend from the skin *(curved arrow)* along the ventral abdominal incision (left image) down to the edge of the mesh implant (M) and its junction *(large arrow)* with the ventral abdominal wall (right image). A small hyperechoic structure consistent with a suture is present near the mesh implant and its junction with the lateral body wall *(small arrow)*. These sonograms were obtained with a wide-bandwidth 7.5-MHz linear-array transducer operating at 10.0 MHz at a displayed depth of 6 cm. The right side of these sonograms is the left side of the mesh implant.

Abdominal wall hernias can occur secondary to abdominal trauma or can be associated with parturition or excessive edema of the abdominal wall. Severe soft tissue swelling and edema is usually present acutely in horses with naturally occurring abdominal wall hernias. The area is often painful to palpation, and abdominal discomfort may be detected. In horses with acute abdominal trauma, palpation of the body wall is difficult and the severity of the muscle damage is difficult to detect. A defect may be detected in the abdominal wall but it is often difficult to determine on palpation if the defect is full thickness. If the caudal dorsal abdominal wall is involved, a defect may be detected on rectal palpation.

Hernias can be fortuitously detected sonographically before clinical signs are present. The detection of a lateral ventral abdominal hernia involving the peritoneum, retroperitoneal fat, and inner abdominal muscle layer was detected in one late gestation mare during routine sonographic examination of the fetus and uterus because of a previous history of placentitis. Sonographic examination of the abdominal swelling can determine the extent of the defect in the abdominal wall and the muscle layers affected. The contents of the hernia are usually easily assessed. However, in horses with older hernias of the abdominal wall, the viscera entrapped in the hernial sac may be mistaken for large bowel if the small intestine has been entrapped for a prolonged period of time and become markedly distended and somewhat sacculated in appearance. Adhesions between the abdominal wall hernia and the adjacent viscera can also be determined (Fig. 11-82). Although ultrasonographic examination of the swelling can determine the extent of the hernia and its contents, the viability of the abdominal musculature around the edges of the hernia is difficult to assess, particularly in the horse with an acute abdominal wall hernia.[130]

Inguinal hernias are most frequently detected in stal-

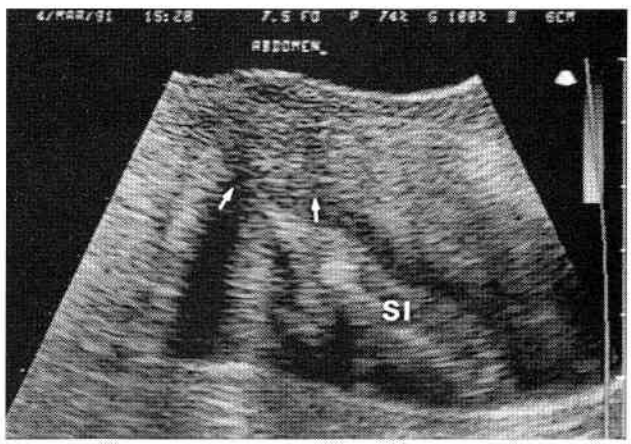

Figure 11–82

Sonogram of a healing ventral abdominal wall hernia obtained from an 18-month-old Thoroughbred cross filly with adhesions of small intestine (SI) to the defect in the ventral abdominal wall *(arrows)*. The hypoechoic tissue between the ventral abdominal musculature extends ventrally to the skin surface which is interrupted by an area of granulation tissue. This sonogram was obtained with a 7.5-MHz sector-scanner transducer containing a built-in fluid offset. The right side of this sonogram is to the left of the abdomen.

lions but have been reported in geldings.[133] Acquired inguinal hernias have been associated with events that increase abdominal pressure in the horse, as well as with breeding, strenuous exercise, and abdominal trauma.[132] Scrotal swelling is usually present, and the horse may exhibit signs of mild discomfort or severe abdominal pain (see Chapter 9).[132]

The sonographic detection of small intestine in the scrotum is diagnostic of an inguinal hernia (see Chapter 9). The small intestine is recognized by its small tubular shape (circular on short-axis cross section) and relatively long mesentery (jejunum). The entrapped small intestine is usually surrounded by anechoic fluid and may exhibit normal peristaltic activity, if strangulation of the entrapped bowel has not occurred (Fig. 11-83). Inguinal hernias can also be detected sonographically in geldings following castration (Fig. 11-84). With intestinal strangulation, the wall of the affected small intestine will become markedly thickened, the lumen of the bowel will be filled with anechoic fluid, and the bowel will appear turgid, hypomotile, or amotile in real-time imaging (see Chapter 6).

Disorders of the Lymph Nodes

Enlargement of the lymph nodes is detected in horses with lymphadenitis with a decrease in the normal parenchymal echogenicity (Fig. 11-85). Areas of cavitation within the lymph node are consistent with areas of infection and may be anechoic (Fig. 11-86), hypoechoic (Fig. 11-87), or have a complex sonographic appearance with anechoic to echogenic areas (Fig. 11-88). The entire architecture of the lymph node may be completely disrupted with a large abscess (Fig. 11-89). Echogenic to hyperechoic masses may be imaged within the abscessed lymph node associated with necrotic tissue. Lymph nodes abscesses often break to the outside and a draining tract is detected sonographically connecting with the necrotic area in the abscessed lymph node (Fig. 11-90). Less frequently, the lymph node may break internally into an adjacent structure such as the guttural pouch (see Fig. 11-88). The tissues surrounding the abscessed or infected lymph node are usually swollen and more echogenic than normal when associated with a local cellulitis.

Enlarged rounded lymph nodes are commonly imaged

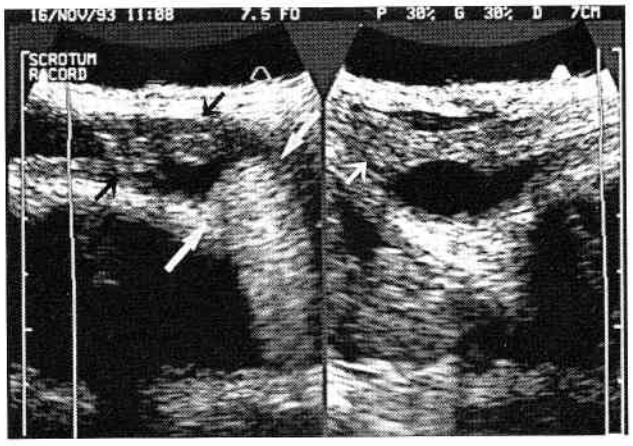

Figure 11–84

Sonograms of the right side of the scrotum obtained from a 2-year-old Thoroughbred gelding with scrotal swelling. There is anechoic fluid in the right side of the scrotum with hypoechoic heterogeneous tissue most consistent with omentum, floating in the fluid *(arrows)*. A loop of small intestine *(large arrows)* is imaged adjacent to the omentum in the short-axis view *(left image)*. The detection of omentum and small intestine in the scrotum is consistent with an inguinal hernia. These sonograms were obtained with a 7.5-MHz sector-scanner transducer containing a built-in fluid offset. The right side of the right image is proximal and the left side is distal. The right side of the left image is cranial and the left side is caudal.

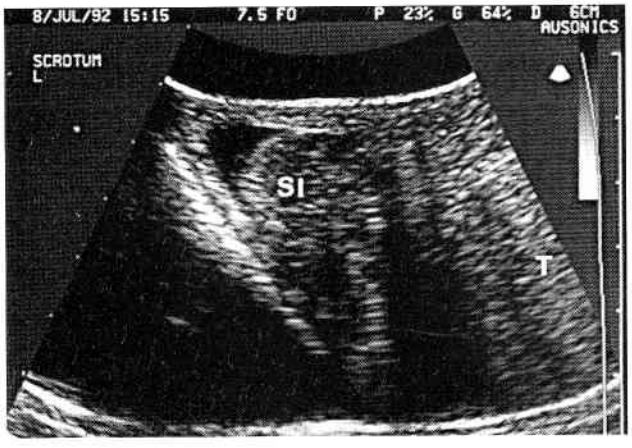

Figure 11–83

Sonogram of the left side of the scrotum obtained from a 2-year-old Standardbred colt with an inguinal hernia. There is a loop of jejunum (SI) in the scrotum adjacent to the left testicle (T) surrounded by a small amount of anechoic fluid. This sonogram was obtained with a 7.5-MHz sector-scanner transducer containing a built-in fluid offset at a displayed depth of 6 cm. The right side of this sonogram is cranial and the left side is caudal.

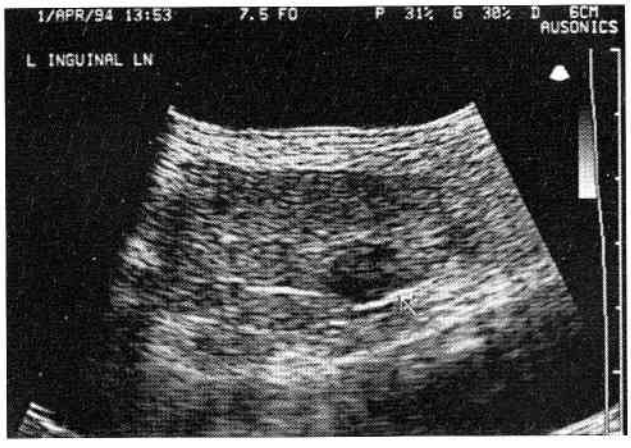

Figure 11–85

Sonogram of the left inguinal lymph node obtained from a yearling Thoroughbred colt with an enlarged inguinal lymph node and cellulitis of the left hind leg. There is an anechoic area within the lymph node consistent with lymphadenitis. The fluid within this area is relatively anechoic, but infection of the node must still be considered. An ultrasound-guided aspirate of this node was performed and a sample obtained for culture and sensitivity testing, which yielded no growth. This sonogram was obtained with a 7.5-MHz sector-scanner transducer containing a built-in fluid offset at a displayed depth of 6 cm. The right side of this sonogram is cranial and the left side is caudal.

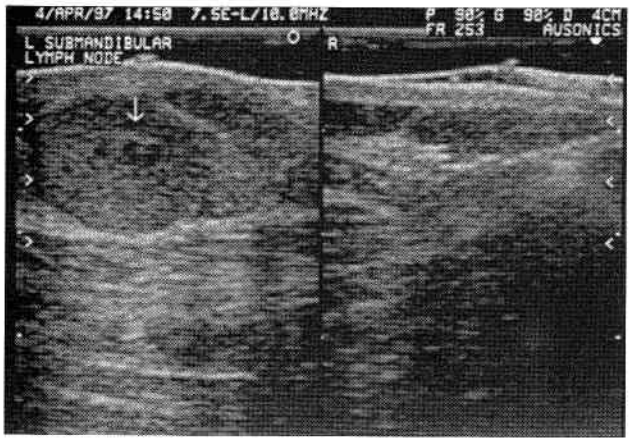

Figure 11–86

Sonogram of the submandibular lymph nodes obtained from a 4-year-old Thoroughbred colt with lymphadenitis. The normal right side mandibular lymph node is depicted in the right image and the enlarged left submandibular lymph node is depicted in the left image. Notice the loculated center of the left submandibular lymph node *(arrow)*. An ultrasound-guided aspirate of this area was positive for *Actinomyces* sp. These sonograms were obtained with a wide-bandwidth 7.5-MHz linear-array transducer operating at 10.0 MHz with a hand-held standoff pad at a displayed depth of 4 cm. The right side of these sonograms is cranial and the left side is caudal.

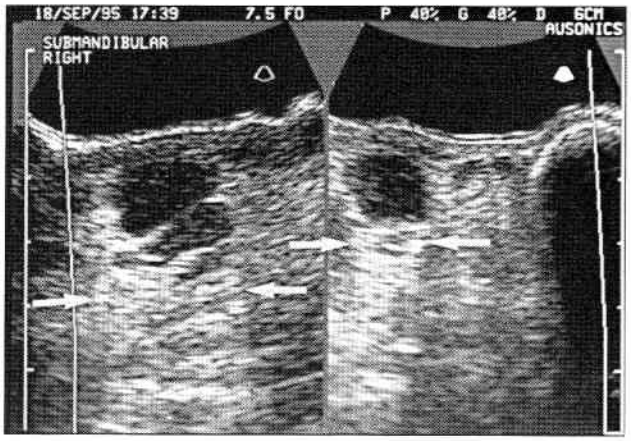

Figure 11–87

Sonograms of an abscessed right submandibular lymph node obtained from a 6-year-old Standardbred mare. There is a large hypoechoic cavitated mass with some loculations disrupting the normal lymph node architecture. There is acoustic enhancement of the far wall of the abscess cavity *(arrows)*, confirming that this structure is fluid-filled. These sonograms were obtained with a 7.5-MHz sector-scanner transducer containing a built-in fluid offset at a displayed depth of 6 cm. The right side of the left image is rostral and the left side is caudal. The right side of the right image is the right side of the mandible.

in human beings with acute lymphadenitis.[35] The cortex of the affected lymph node is usually uniformly thickened and more sonographically lucent than normal; the normally echogenic hilum is compressed, displaced, or completely obliterated.[43] The surrounding connective tissues may be edematous or appear more echogenic than normal, if associated with a local cellulitis. Increased blood flow is present, particularly within the hilar areas, which is detected as high-velocity, low-resistance arterial flow.[35] Sonographic examination of the cervical lymph nodes in dogs revealed one dog with a pyogranulomatous lymphadenitis and two with reactive lymph nodes.[134] The lymph nodes in these dogs were enlarged, round to oval, moderately well marginated, and hypoechoic.

Replacement of the normal lymph node tissue with a diffuse infiltration with neoplastic cells or discrete metastases is common in horses with neoplasia. Lymphosarcoma is the most common neoplasm involving the lymph nodes in horses.[135] Involvement of the submandibular, retropharyngeal, and cervical lymph nodes is frequently detected in horses with multicentric lymphosarcoma. The other peripheral lymph nodes may also be affected. Metastases to the local draining lymph nodes may also be

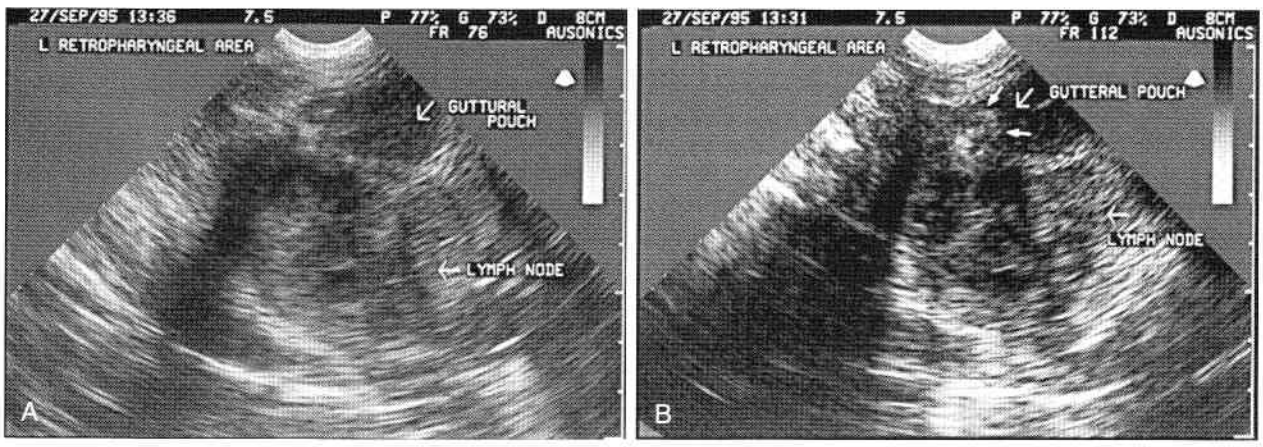

Figure 11–88

Sonograms of an abscessed left retropharyngeal lymph node obtained from a yearling Thoroughbred filly. The retropharyngeal lymph node is enlarged and cavitated with hypoechoic fluid filling the areas of cavitation, consistent with abscessation. Hypoechoic material is also imaged within the left guttural pouch consistent with empyema of the left guttural pouch. These sonograms were obtained with a 7.5-MHz sector-scanner transducer at a displayed depth of 8 cm.

A, The enlarged cavitated left retropharyngeal lymph node measured 4.1 cm by 4.88 cm. The right side of this sonogram is dorsal and the left side is ventral.

B, There is a heterogeneous small nodular mass *(small arrows)* pushing in the ventral and medial walls of the left guttural pouch. This nodular mass appears to originate from the retropharyngeal abscess. The right side of this sonogram is cranial and the left side is caudal.

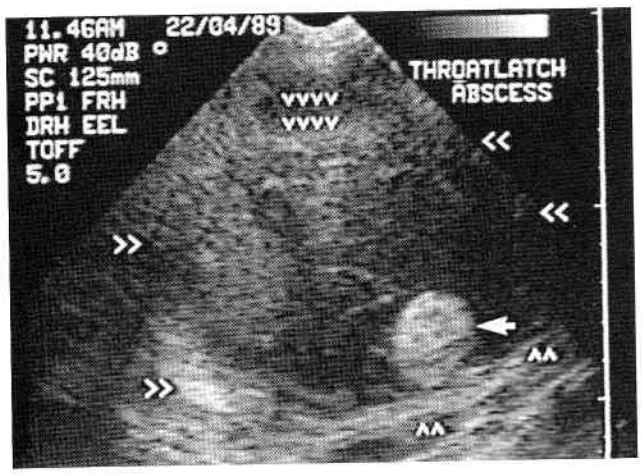

Figure 11–89

Sonogram of the throatlatch region obtained from a 3-year-old Thoroughbred gelding with an abscessed retropharyngeal lymph node. The lymph node architecture was completely destroyed and measured 7–8 cm in diameter. The abscess *(arrowheads)* contained anechoic to echogenic fluid and a hyperechoic to echogenic mass of tissue *(arrow)* consistent with necrotic tissue. This sonogram was obtained with a 5.0-MHz sector-scanner transducer containing a built-in fluid offset. The right side of this sonogram is dorsal and the left side is ventral.

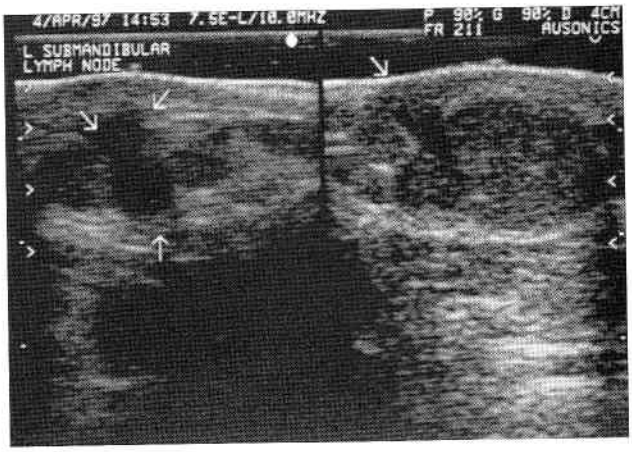

Figure 11–90

Sonograms obtained from a 4-year-old Thoroughbred colt with a draining tract from the left submandibular lymph node. The draining tract could be followed into the caudal aspect of the lymph node as a slightly more hypoechoic area adjacent to an anechoic area. No foreign bodies were imaged. The tract from the skin surface *(arrow)* is shown in the right image (sagittal image) leading to the caudal aspect of the lymph node. The more anechoic region containing fluid *(arrows)* was imaged just caudal to the tract and is shown in transverse section *(left image)*. These sonograms were obtained with a wide-bandwidth 7.5-MHz linear-array transducer operating at 10.0 MHz with a hand-held standoff pad at a displayed depth of 4 cm. The right side of the sagittal image is cranial and the left side is caudal. The right side of the transverse image is toward the left side of the mandible and the right side is toward midline.

present in horses with other types of neoplasia. The lymph nodes draining an area with a suspected neoplasm should be carefully examined for spread of the tumor to the adjacent lymph nodes.

Sonographic examination of affected lymph nodes in horses with multicentric lymphosarcoma reveals complete destruction of the lymph node architecture (Fig. 11–91). In some horses with lymphosarcoma the affected lymph nodes are homogeneously infiltrated with tissue of increased echogenicity (Fig. 11–92). With the more aggressive malignant tumors, the lymph node is replaced with tissue of composite echogenicity. Central hypo-

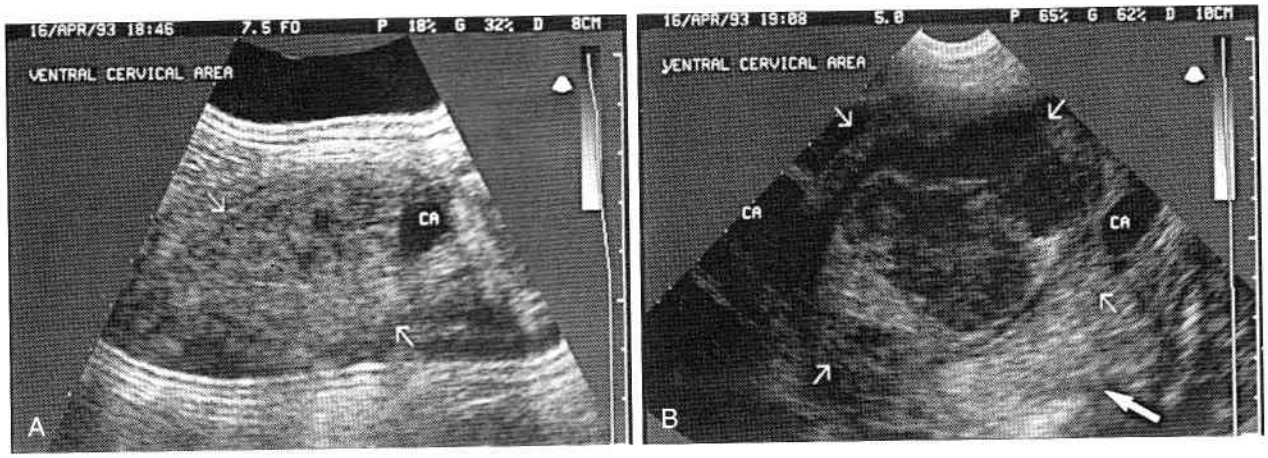

Figure 11–91

Sonograms of the ventral cervical region at the thoracic inlet obtained from a 20-year-old Clydesdale mare with multicentric lymphosarcoma. There is a large multilobulated mass in the ventral cervical region with ill defined borders and a complex pattern of echogenicity. An ultrasound-guided biopsy of these masses confirmed the diagnosis of lymphosarcoma. These sonograms were obtained from with a 7.5-MHz sector-scanner transducer containing a built-in fluid offset *(A)* and a 5.0-MHz sector-scanner transducer *(B)* at a displayed depth of 8 cm *(A)* and 10 cm *(B)*.

A, This portion of the mass *(arrows)* has a complex sonographic appearance, although there are few anechoic areas. The mass is compressing the carotid artery and is surrounding it from the dorsal, medial, and lateral sides. The left carotid artery (CA) appears somewhat irregular in transverse section, owing to the compression of the artery by the surrounding mass. The right side of this sonogram is toward the left side of the horse and the right side is toward the midline.

B, This mass *(arrows)* has a cavitated appearance with large anechoic to hypoechoic areas and few echogenic areas. These anechoic to hypoechoic areas represent areas of tissue necrosis within the mass and possible secondary abscess formation. This mass is located between the carotid arteries (CA). Below the left carotid artery there is a more homogeneous echogenic mass *(large arrow)*, more typical of lymphosarcoma. The left carotid artery is on the right side of the sonogram and the right carotid artery is to the left of the image.

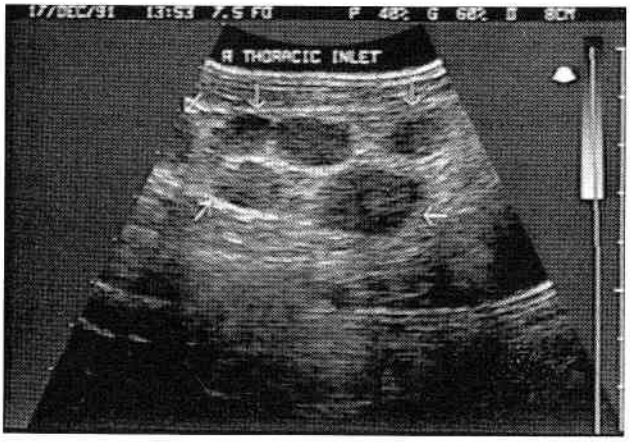

Figure 11–92

Sonogram of infiltrated cervical lymph nodes obtained from a 10-year-old Arabian mare with multicentric lymphosarcoma. The ventral cervical lymph nodes are homogeneously enlarged and hypoechoic, appearing in grapelike clusters along the ventral aspect of the neck and at the thoracic inlet. This sonogram was obtained with a 7.5-MHz sector- scanner transducer containing a built-in fluid offset at a displayed depth of 8 cm. The right side of this sonogram is cranial and the left side is caudal.

echoic or anechoic areas are commonly detected if the tumor is growing rapidly, associated with tumor necrosis (see Fig. 11-91).

Involvement of the supramammary lymph nodes has been reported in one horse with squamous cell carcinoma involving the mammary gland.[112] Ileal, inguinal, and sublumbar lymph node infiltration is common in horses with neoplasia of the tissues drained by these lymph nodes. In three dogs with lymphoma the lymph nodes were enlarged, mildly heterogeneous, and hypoechoic with fair to good margination.[134] In human beings with confirmed head and neck malignancy, ultrasound has a 90% sensitivity for the detection of metastatic lymph nodes.[136, 137]

Tongue and Oral Cavity

Abscesses in the tongue and oral cavity are uncommon in the horse and are most frequently secondary to oral trauma. Sonographic examination of the tongue or oral cavity reveals a fluid-filled mass in the tongue or tissues of the oral cavity. The echogenicity of the fluid contained within the abscess varies, and small hyperechoic echoes associated with gas in the abscess are commonly seen, as anaerobic infection is not uncommon with oral contamination of the initial wound (Fig. 11-93). A large anechoic loculated mass in the tongue of one horse was consistent with an initial hematoma (Fig. 11-94). This area was adjacent to but separate from a cavitated hypoechoic area containing hyperechoic echoes consistent with free gas and a hyperechoic linear foreign body (Fig. 11-94). The initial lingual trauma may have caused the lingual hematoma adjacent to the area punctured by the foreign body, creating this sonographic appearance. Anechoic fluid-filled masses have been reported in the tongue of one horse with a penetrating lingual foreign body.[5]

Dysphagia, ptyalism, halitosis, nasal discharge, a change in phonation, stertorous breathing and intermandibular, submandibular, or retropharyngeal swelling have been reported in horses with oral or pharyngeal foreign bodies.[8, 123, 138, 139] A draining tract may also be present, associated with a foreign body.[122, 123] Metallic foreign bodies have been detected radiographically in several horses,[123, 138, 139] although their surgical removal without sonographic guidance is difficult.

Ultrasonography can be extremely helpful in the location and successful surgical removal of foreign bodies in the oral cavity, just as it is elsewhere. Sonographic examination of the oral cavity enables the clinician to identify radiolucent foreign bodies (Fig. 11-94) but is also useful in further localizing radiopaque foreign bodies (Fig. 11-95). The general location of the radiopaque foreign body can be determined using routine radiography. Precise localization of the foreign body can be obtained ultrasonographically, localizing the foreign body in the surrounding tissues and determining the relationship of the foreign body to adjacent vital structures. This information is invaluable in planning the optimal surgical approach for foreign body removal. Intraoperative ultrasonography is also very useful in further localizing the foreign body at the time of surgery, minimizing surgical trauma.

Diagnostic ultrasound was used in conjunction with radiography to localize a metallic foreign body in the lingual parenchyma in one horse and dorsal to the larynx and ventral to the guttural pouches in another horse.[4, 5] Sonographic examination of the tongue in the horse with the lingual foreign body revealed several well-defined anechoic areas within the tongue that represented fluid pockets (abscesses), adjacent to the hyperechoic linear foreign body casting reverberation artifacts typical of those seen associated with metallic objects.[5] Intraopera-

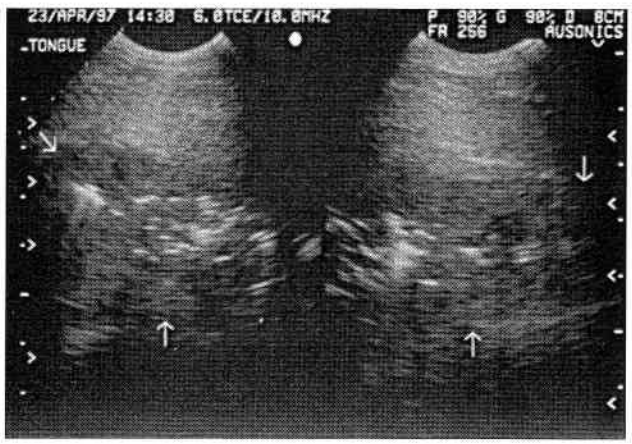

Figure 11–93

Sonograms obtained from a 13-year-old Thoroughbred gelding with a lingual abscess. The tongue *(arrows)* has hyperechoic echoes within its center, consistent with free gas echoes, suggesting anaerobic infection and small anechoic cavitated areas. The right image is the cranial portion of the tongue and the left image is the adjacent caudal portion. These images were obtained from a submental window with a wide-bandwidth 6.0-MHz microconvex linear-array transducer operating at 10.0 MHz at a displayed depth of 8 cm. The right side of both images is rostral and the left side is caudal.

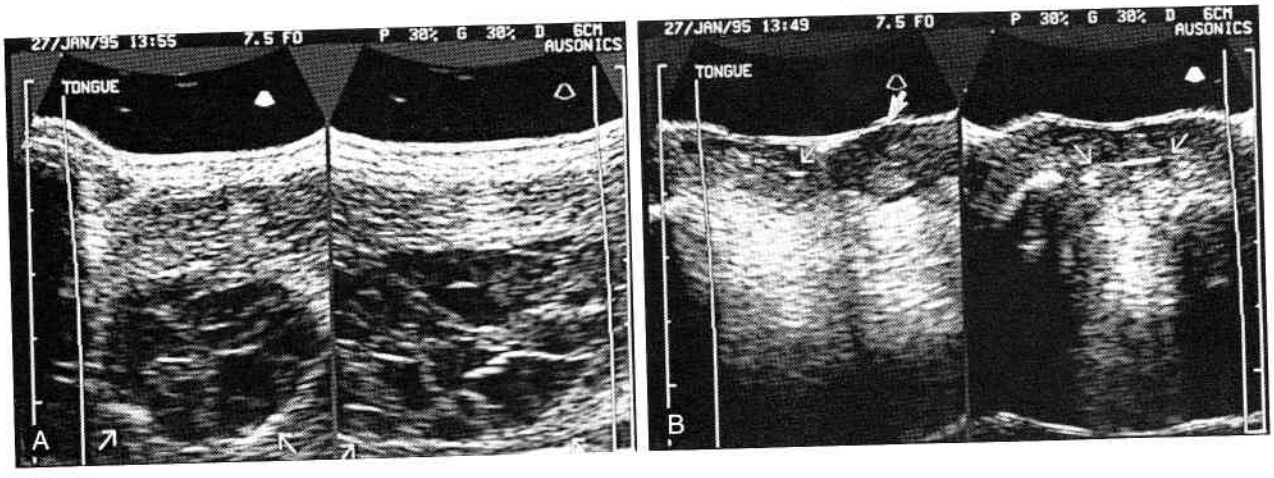

Figure 11–94

Sonograms of the tongue obtained from an 8-year-old Thoroughbred stallion with a lingual abscess. These sonogram were obtained with a 7.5-MHz sector-scanner transducer containing a built-in fluid offset at a displayed depth of 6 cm.

A, Sonograms of the tongue obtained through the intermandibular space demonstrating a large loculated fluid filled mass *(arrows)* in the tongue, most consistent with a hematoma. The mass measured 2.5 cm deep, 3.5 cm wide, and 6 cm long. This mass appeared to originate from a swelling in the cranial portion of the frenulum of the tongue. The right side of the transverse view *(left image)* is the left side of the mandible. The right side of the sagittal view *(right image)* is rostral and the left side caudal.

B, A hyperechoic linear structure *(arrows)* measuring 2 mm by 8 mm was imaged in the rostral portion of the lingual frenulum. It was surrounded by hypoechoic fluid. Cranial to the hyperechoic linear structure in the parasagittal view *(left image)* a nearly anechoic tract *(large arrow)* was imaged extending to the ventral aspect of the frenulum where it appeared likely that the abscess would break and drain. Immediately dorsal to this foreign body and the surrounding hypoechoic tissue was hyperechoic tissue with pinpoint hyperechoic echoes consistent with possible gas in the tissues, suggesting anaerobic infection. The right side of the parasagittal view is rostral and the left side is caudal. The right side of the transverse view *(right image)* is the left side of the mandible.

tive ultrasound was then used to help localize both foreign bodies during their surgical removal.[4, 5] Sonographic examination of the tongue and intermandibular space in one horse was unsuccessful in locating the metallic foreign body because the ultrasound could not penetrate deep enough into the tissues to image the foreign body.[123] Use of a lower-frequency transducer should have resulted in the successful imaging of the foreign body in this horse.

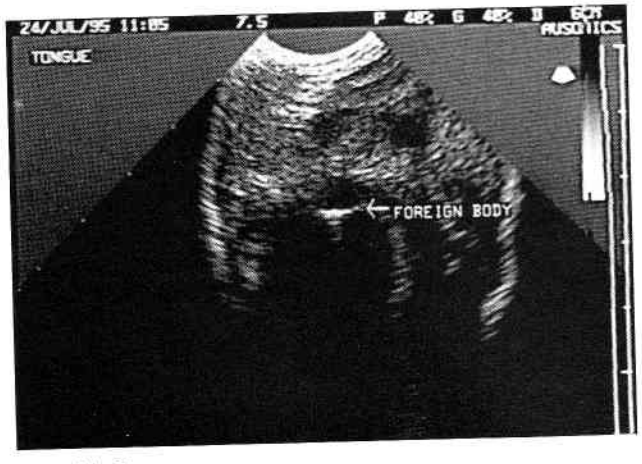

Figure 11–95

Sonogram of the tongue obtained from a 10-year-old Quarter Horse gelding with a tongue abscess associated with a metallic foreign body. The foreign body was 2.36 cm from the ventral skin surface and measured 0.48 cm wide by 2 cm long. Anechoic fluid surrounded the foreign body in the tongue. This sonogram was obtained from the submental window with a 7.5-MHz sector-scanner transducer at a displayed depth of 6 cm. The right side of this sonogram is the left side of the mandible.

Oral and lingual neoplasms are uncommon in horses.[110, 140] Squamous cell carcinoma and lymphosarcoma are the most likely tumors of this area, but a rhabdomyosarcoma of the tongue has been reported in a horse.[110, 140] Sonographic examination of the tongue in a horse with an oral or lingual neoplasm is likely to reveal a heterogeneous mass with composite echogenicity in the case of squamous cell carcinoma or rhabdomyosarcoma. Lymphosarcoma involving the oral cavity is more likely to have a homogeneous sonographic appearance, but a complex pattern of echogenicity is also possible. Oral or lingual neoplasms should be readily distinguished from abscesses. Most abscesses involving the oral cavity are cavitated and contain fluid and free gas echoes, whereas neoplasms are primarily soft tissue masses that may contain areas of cavitation associated with tissue necrosis.

Ultrasonographic examination of the tongue has been useful in small animals for characterizing the architecture, size, and extent of the lingual mass.[5] Previously undetected portions of the tumor mass were detected in some of these patients. Malignant and inflammatory lesions usually appear as hypoechoic masses and may occasionally be cystic in both small animals and human beings.[5, 141, 142] Hyperechoic areas in the lingual parenchyma of human beings are most likely fibrotic areas.[142] However, a hyperechoic lingual mass in a cat was diagnosed as squamous cell carcinoma, as was a mostly hyperechoic lingual mass with a complex echo texture in another cat.[5] Sonographic evaluation of the type of lingual or oral mass (discrete or diffuse), its sonographic characteristics, and the involvement of adjacent structures can aid the clinician in determining the appropriate course of action for diagnosis and treatment of the lingual or oral mass.

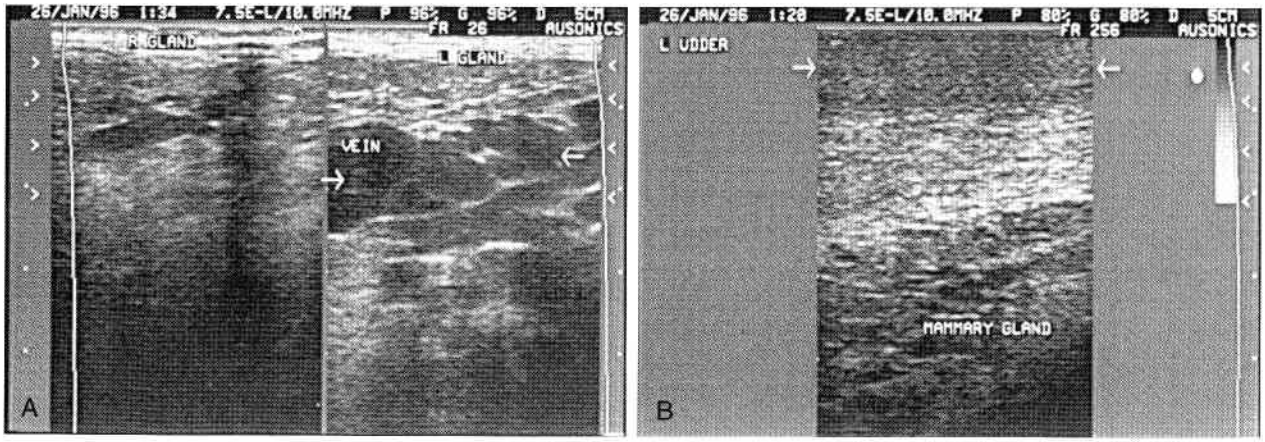

Figure 11–96

Sonograms of the mammary gland obtained from a 3-year-old Thoroughbred filly with swelling of the left mammary gland and lymphangiectasia. These sonograms were obtained with a wide-bandwidth 7.5-MHz linear-array transducer operating at 10.0 MHz at a displayed depth of 5 cm. The right side of these sonograms is cranial and the left side is caudal.

A, A markedly enlarged venous plexus *(arrows)* was imaged, comparing the left mammary gland *(right image)* with the right *(left image)*, consistent with venous occlusion. The site of the venous occlusion was not found.

B, Diffuse thickening of the subcutaneous tissues of the left mammary gland *(arrows)*, probably associated with the vascular occlusion that appears to be present, resulting in venous obstruction. The sonographic appearance of this diffuse soft tissue thickening is more consistent with cellulitis or diffuse soft tissue infiltrate than with edema.

Disorders of the Mammary Gland

Disorders of the mammary gland are uncommon in horses. Swelling of the mammary gland can occur with diffuse edema or cellulitis of the ventral abdomen. Swelling of one mammary gland has been seen in a horse with local lymphangiectasia. Enlargement of the mammary gland may also be detected in horses with mastitis, mammary gland abscesses, fibrosis, and neoplasia. Mammary tumors are uncommon in horses but have occasionally been reported. Squamous cell carcinoma was reported in one mare with hyperparathyroidism that involved the vulva, perineum, mammary gland, and associated lymph nodes.[1,12] More than half of the mammary tissue was replaced by firm nodules, many of which contained thick caseous material.

Sonographic appearance of mammary gland lymphangiectasia included markedly enlarged venous plexus associated with the affected mammary gland and diffuse edema of the affected gland (Fig. 11-96). Enlargement of the mammary gland with cystic or cavitated spaces in the mammary gland is most consistent with mastitis but may also be a sequela to chronic infection of the gland (Fig. 11-97). Echogenic to hyperechoic areas in the mam-

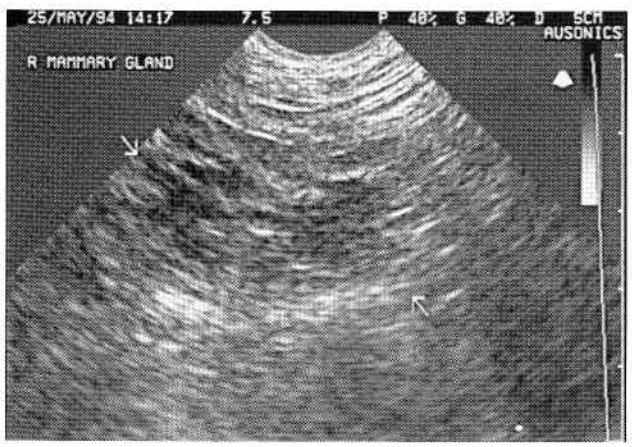

Figure 11–97

Sonogram of a mass in the right mammary gland obtained from a 26-year-old Morgan mare. The mammary gland is enlarged and the mass *(arrows)* has a heterogeneous appearance with loculated fluid filled spaces, most consistent with chronic infection. This sonogram was obtained with a 7.5-MHz sector-scanner transducer at a displayed depth of 5 cm. The right side of this sonogram is proximal and the left side is distal.

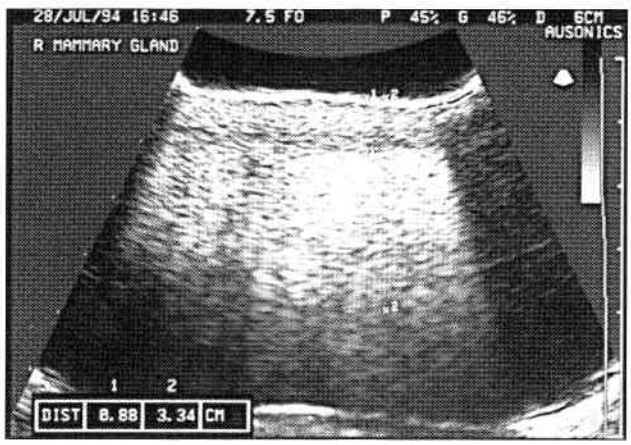

Figure 11–98

Sonogram of the enlarged right mammary gland obtained from a 6-year-old Standardbred mare. The ventralmost aspect of the right mammary gland is hyperechoic measuring 3.34 cm thick (x^2), consistent with a cellular infiltrate in this portion of the gland, most likely fibrosis. This firm area was located in the glandular parenchyma just underneath the skin surface (x^1 = 0.88 cm). Normal glandular parenchyma was imaged dorsal to this diffuse area of increased parenchymal echogenicity. This sonogram was obtained with a 7.5-MHz sector-scanner transducer containing a built-in fluid offset at a displayed depth of 6 cm. The right side of this sonogram is proximal and the left side is distal.

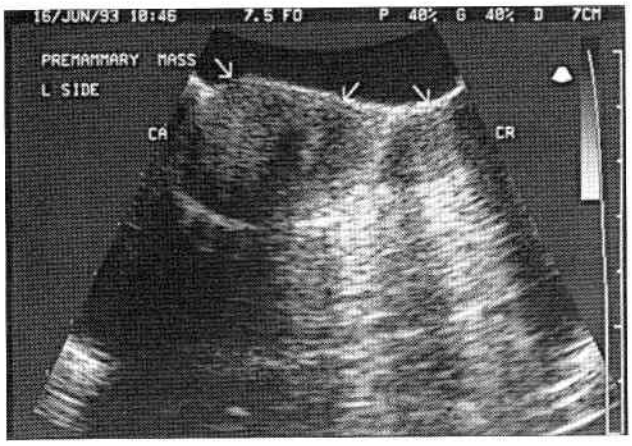

Figure 11–99

Sonogram of two masses adjacent to the left mammary gland obtained from a 9-year-old Welsh pony mare with sarcoids. The smaller cranial (CR) mass *(right arrow)* is hypoechoic and homogeneous. The larger caudal (CA) mass *(left and center arrows)* is mostly hypoechoic with a cavitated area in the cranial portion of this mass *(central arrow)* containing an echogenic center. These masses are soft tissue masses, most consistent with neoplasia. Excisional biopsy of these masses revealed sarcoids. This sonogram was obtained with a 7.5-MHz sector-scanner transducer containing a built-in fluid offset at a displayed depth of 7 cm. The right side of this sonogram is cranial and the left side is caudal.

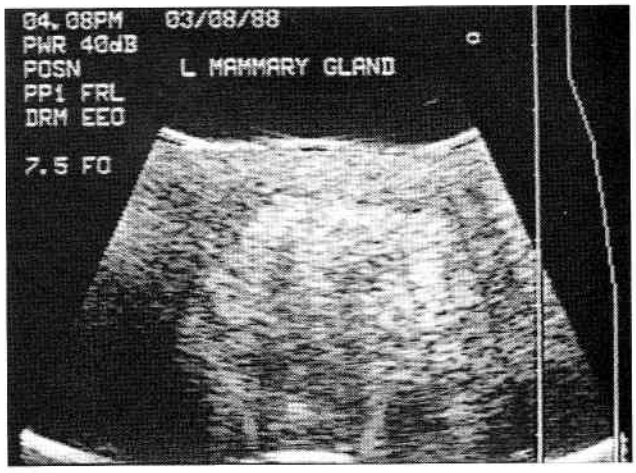

Figure 11–101

Sonogram of the left mammary gland obtained from a 22-year-old Thoroughbred mare with mammary gland carcinoma. The masses in this gland are hyperechoic and replaced most of the normal glandular tissue. This sonogram was obtained with a 7.5-MHz sector-scanner transducer containing a built-in fluid offset at a displayed depth of 7.5 cm. The right side of this sonogram is dorsal and the left side is ventral.

mary gland parenchyma are most consistent with dense cellular infiltrate, usually fibrosis (Fig. 11-98). This dense sonographic appearance is also usually a sequela to chronic mastitis. Hypoechoic homogeneous to heterogeneous cavitating masses have been identified from the mammary glands of horses with cutaneous and subcutaneous tumors such as melanomas and sarcoids (Fig. 11-99). Sonographic examination of the mammary gland in horses with mammary gland carcinoma has revealed multiple discrete hypoechoic (Fig. 11-100), echogenic, or hyperechoic (Fig. 11-101) masses scattered throughout the gland or coalescing masses throughout the gland with composite echogenicity (Fig. 11-102). In both forms, marked destruction of the glandular parenchyma has occurred with little or no normal mammary parenchyma remaining. The replacement of the mammary gland with heterogeneous composite masses and diffuse cellular infiltrate is consistent with mammary neoplasia.

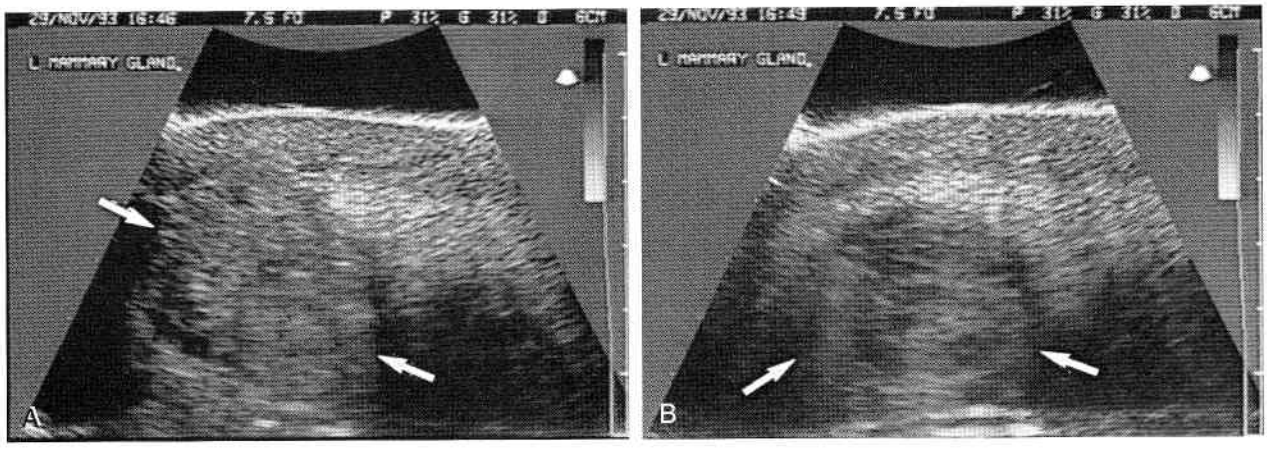

Figure 11–100

Sonograms of an enlarged left mammary gland obtained from a 20-year-old Thoroughbred mare with mammary gland carcinoma. The gland has multiple round to oval masses with a heterogeneous sonographic appearance scattered throughout. Some of these masses were draining into the teat cistern, which was filled with hypoechoic material. No normal glandular tissue was imaged in this gland. These sonograms were obtained with a 7.5-MHz sector-scanner transducer containing a built-in fluid offset at a displayed depth of 6 cm. The right side of these sonograms is dorsal and the left side is ventral.

A, This mass *(arrows)* is heterogeneous but appears relatively solid with a primarily echogenic sonographic appearance with a few anechoic and hyperechoic areas.

B, This mass *(arrows)* is more cavitated with large anechoic areas in an echogenic to hypoechoic parenchyma. These cavitated anechoic areas are consistent with tumor necrosis.

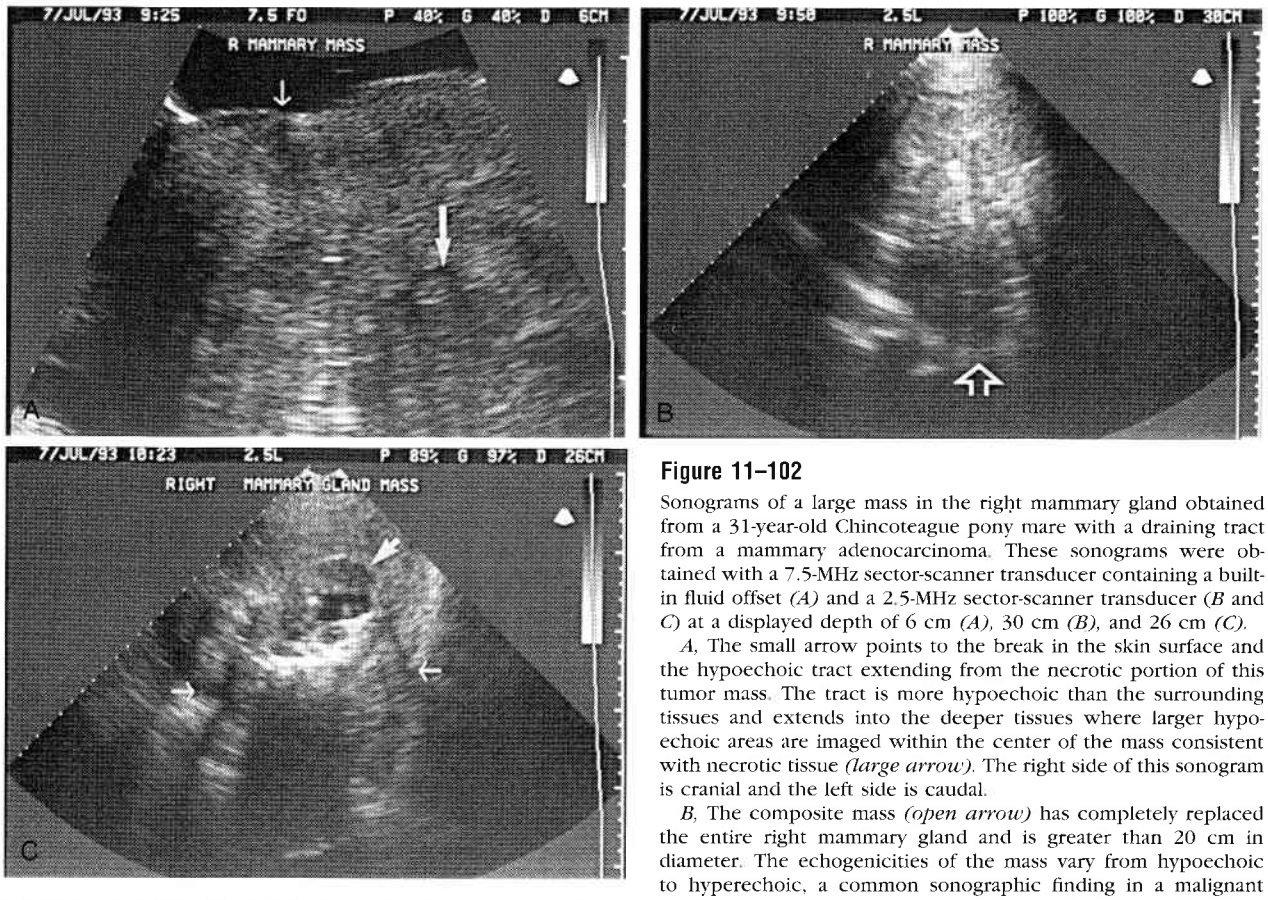

Figure 11–102

Sonograms of a large mass in the right mammary gland obtained from a 31-year-old Chincoteague pony mare with a draining tract from a mammary adenocarcinoma. These sonograms were obtained with a 7.5-MHz sector-scanner transducer containing a built-in fluid offset *(A)* and a 2.5-MHz sector-scanner transducer (*B* and *C*) at a displayed depth of 6 cm *(A)*, 30 cm *(B)*, and 26 cm *(C)*.

A, The small arrow points to the break in the skin surface and the hypoechoic tract extending from the necrotic portion of this tumor mass. The tract is more hypoechoic than the surrounding tissues and extends into the deeper tissues where larger hypoechoic areas are imaged within the center of the mass consistent with necrotic tissue *(large arrow)*. The right side of this sonogram is cranial and the left side is caudal.

B, The composite mass *(open arrow)* has completely replaced the entire right mammary gland and is greater than 20 cm in diameter. The echogenicities of the mass vary from hypoechoic to hyperechoic, a common sonographic finding in a malignant neoplasm. The right side of this sonogram is dorsal and the left side is ventral.

C, The complex sonographic appearance of the mass *(thin arrows)* is evident. The central portion of the mass is anechoic *(short arrow)*, surrounded by more homogeneous hypoechoic tissue. Deep to the cavitated area is a hyperechoic area within the mass, casting acoustic shadows consistent with calcification of this portion of the mass. The right side of this sonogram is dorsal and the left side is ventral.

Scirrhous Cord

Infection of the spermatic cord occurs most frequently in the days following castration, but reports of inguinal and scrotal swellings associated with an infected spermatic cord have been reported in geldings that had been castrated several years previously.[143, 144] The scrotal or inguinal mass is usually associated with lameness in horses with chronic infection of the spermatic cord.[143, 144] Purulent drainage from the mass may be detected, and the horse often has a history of improvement with antimicrobial treatment. Pain and heat may also be detected associated with the mass. Rectal examination of the internal inguinal ring usually reveals no abnormalities, although extension of the infection into the abdominal cavity along the spermatic cord is possible. The scirrhous cord has been described as a hard, thickened, chronically infected cord associated with a low-grade infection, usually staphylococcal. Multiple small areas of abscessation, discharging sinuses, and exuberant granulation tissue are frequently detected in horses with scirrhous cord. Scrotal abscesses also occur in horses following castration. These horses usually have markedly enlarged scrotums with scrotal heat and sensitivity. Neoplastic infiltration of the spermatic cord and of the scrotal and inguinal areas is rare in geldings but can occur in horses, probably most frequently in those with squamous cell carcinoma of the penis.

Sonographic evaluation of the scrotal or inguinal mass usually reveals a fluid-filled structure (Fig. 11-103) with enlargement and involvement of the spermatic cord (Fig. 11-104). The hypoechoic to echogenic material is imaged emanating from the distalmost end of the spermatic cord and may be imaged ascending into the inguinal ring along the remnant of the spermatic cord. The spermatic cord is usually echogenic with a heterogeneous appearance associated with chronic inflammatory, granulomatous, or fibrotic infiltrate secondary to the chronic infection. A large scrotum filled with hypoechoic fluid is usually found in horses with scrotal abscesses (Fig. 11-105). Fibrinous loculations are often seen in the fluid collection (see Fig. 11-105). Echogenic to hyperechoic tissue is also frequently detected, associated with necrotic tissue. Neoplastic infiltration of the remnant of the spermatic cord and surrounding tissues has been detected in horses with squamous cell carcinoma of the penis (Fig. 11-106).

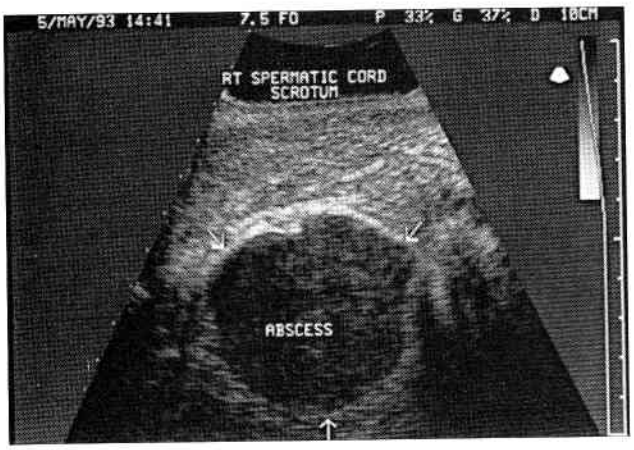

Figure 11–103

Sonogram of the right inguinal region obtained from a 2-year-old Thoroughbred gelding with scrotal and inguinal swelling. A large hypoechoic fluid filled mass *(arrows)* is associated with the right spermatic cord. The more echogenic tissue adjacent to the abscess is inflammatory tissue surrounding the abscess at the end of the enlarged spermatic cord. This sonogram was obtained with a 7.5-MHz sector-scanner transducer containing a built-in fluid offset at a displayed depth of 10 cm. The right side of this sonogram is cranial and the left side is caudal.

Ocular Diseases

When direct visualization of the eye is not possible, ultrasonography can provide the clinician with important diagnostic and prognostic information.[6, 19] Indications for ocular ultrasonography include eyelid or third eyelid swellings or masses that prevent ocular examination; opacities of the cornea, aqueous, lens, or vitreous preventing a complete intraocular examination; exophthalmos; and a suspected increase or decrease in the size of the globe.[20] Suspected ocular trauma should also prompt a careful ophthalmologic examination and sonographic examination of the eye and retrobulbar structures. Ultrasonographic examination of the eye can be useful in horses with corneal edema in which standard ophthalmologic examination techniques cannot be applied.

Corneal Ulcer. Sonographic examination of the equine eye is not routinely indicated in horses with corneal ulcers. However, transpalpebral examination of the eye can be useful in horses with marked eyelid swelling, preventing visualization or examination of the cornea. The cornea has a pitted appearance associated with the areas of ulceration that can be detected sonographically (Fig. 11-107). High-frequency ultrasound (10.0 MHz or higher) can obtain some impression of the depth of corneal ulceration.

Corneal Stromal Abscesses. Corneal stromal abscesses result from a penetrating injury with entrapment of an organism[145, 146] or foreign material[147] in the stroma and in association with recurrent uveitis.[148] Corneal stromal abscesses are usually associated with small corneal puncture wounds and abrasions that become infected, rather than with large corneal ulcers.[145] The topical application of antibiotic-corticosteroid-containing preparations to the eye in horses with corneal ulcers has also been implicated in the pathogenesis of corneal stromal abscesses.[145] The horse presents with an opaque, yellow-white stromal infiltrate involving most or all of the corneal stroma.[145] Most horses have a miotic pupil and some evidence of ocular pain, more common with the more severe corneal stromal abscesses.[149] The more severe corneal lesions may be accompanied by anterior uveitis and endophthalmitis.[149] Glaucoma has also been reported in horses with corneal stromal abscesses.[147, 149] A descemetocele and corneal rupture resulting in iris prolapse has

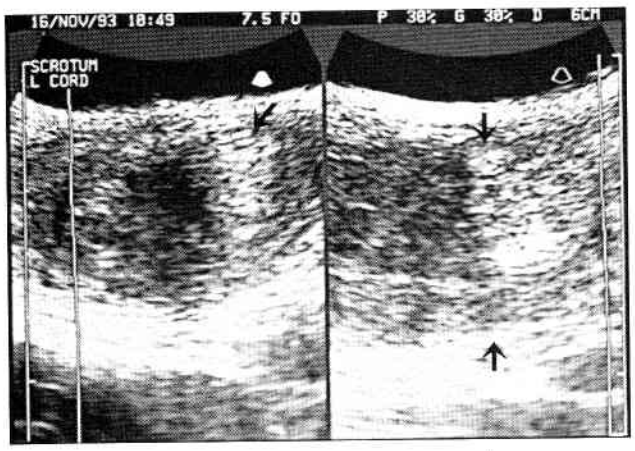

Figure 11–104

Sonograms of the left spermatic cord obtained from a 2-year-old Thoroughbred gelding with scrotal swelling. The spermatic cord is markedly thickened *(arrows)* and contains hypoechoic loculated fluid at the distal end of the cord consistent with infection and a scirrhous cord. These sonograms were obtained with a 7.5-MHz sector-scanner transducer containing a built-in fluid offset at a displayed depth of 6 cm. The right image is a long-axis image of the spermatic cord, with the right side of the image being proximal and the left side distal. The left image is a short-axis image of the spermatic cord, with the right side being cranial and the left side caudal.

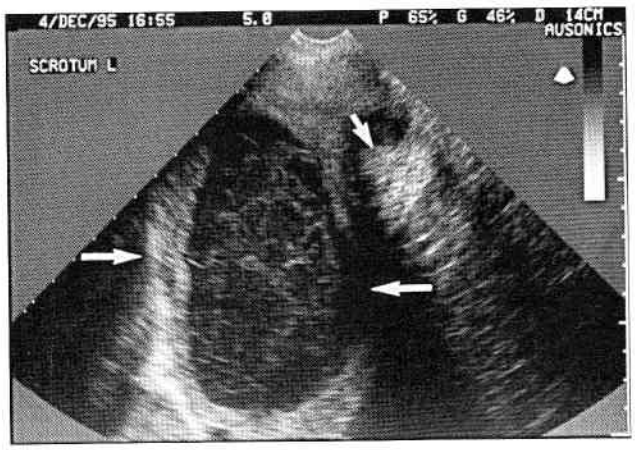

Figure 11–105

Sonogram of the left side of the scrotum obtained from a 1-year-old Thoroughbred gelding with a scrotal abscess following castration. Notice the large loculated structure containing hypoechoic fluid in the left side of the scrotum *(large arrows)*. This sonographic appearance is most consistent with a hematoma or seroma, which became secondarily infected. The echogenic structure in the right side of the scrotum *(small arrow)* is the remnant of the right spermatic cord which is surrounded by hypoechoic fluid, consistent with a scirrhous cord. This sonogram was obtained with a 5.0-MHz sector-scanner transducer at a displayed depth of 14 cm. The right side of this sonogram is the right side of the scrotum.

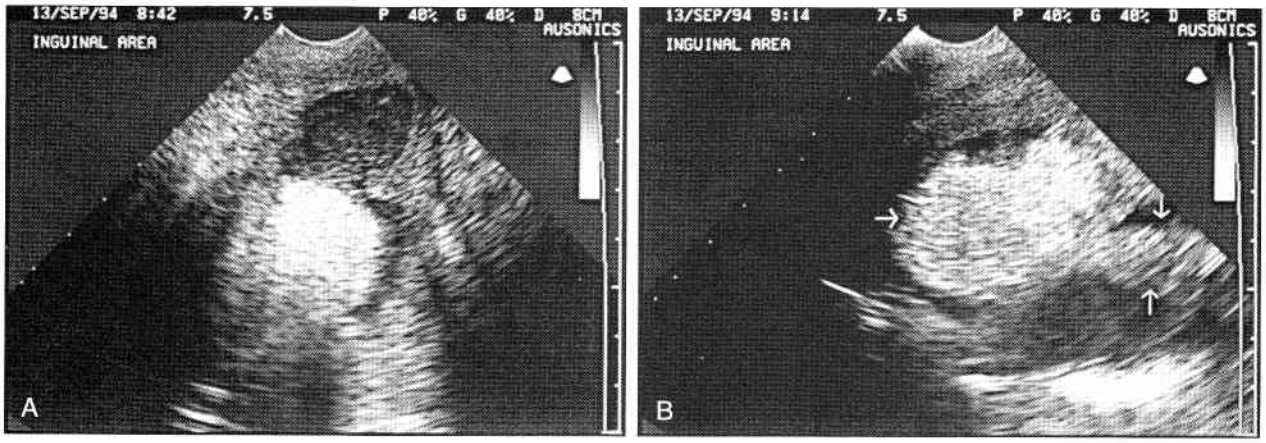

Figure 11–106

Sonograms of the left inguinal area obtained from a 13-year-old Thoroughbred gelding with inguinal swelling. This horse had previously had a reefing operation performed for removal of squamous cell carcinoma of the penis. These sonograms were obtained with a 7.5-MHz sector-scanner transducer at a displayed depth of 8 cm.

A, The ventral aspect of this mass was hypoechoic and flocculent, consistent with an abscess. Dorsally a hyperechoic mass was imaged extending up toward the left inguinal ring. This sonogram was obtained with the transducer placed on the ventralmost aspect of the swelling and aiming dorsally. The right side of this sonogram is cranial and the left side is caudal.

B, This mass *(horizontal arrow)* is heterogeneous and hyperechoic and appears to be associated with the spermatic cord *(vertical arrow)*, extending up into the external inguinal ring. The heterogeneous appearance of this mass is most consistent with that of neoplasia. The mass is surrounded by hypoechoic fluid, consistent with inflammatory cells. An excisional biopsy of this mass revealed squamous cell carcinoma. This sonogram was obtained with the transducer placed on the left side of the swelling and aiming across the swelling. The right side of this sonogram is dorsal and the left side is ventral.

also been reported in horses with corneal stromal abscesses.[149]

The corneal opacity seen in horses with corneal stromal abscesses may prevent visualization of the intraocular structures. In these horses sonographic examination of the eye reveals the corneal abscess, the intraocular structures, and any associated pathology. The corneal abscess should be examined with the highest-frequency ultrasound available (10.0 MHz or higher) and a hand-held standoff pad or using a transducer containing a built-in fluid offset to determine if foreign material is present within the abscess.[6] A small echogenic linear foreign body was detected ultrasonographically in a horse with a nonhealing stromal abscess (Fig. 11–108). Surgical exploration of this stromal abscess revealed the foreign body to be an embedded eyelash hair.

Foreign Bodies. Ocular foreign bodies may be successfully imaged ultrasonographically and usually appear as echogenic or hyperechoic structures, the latter usually

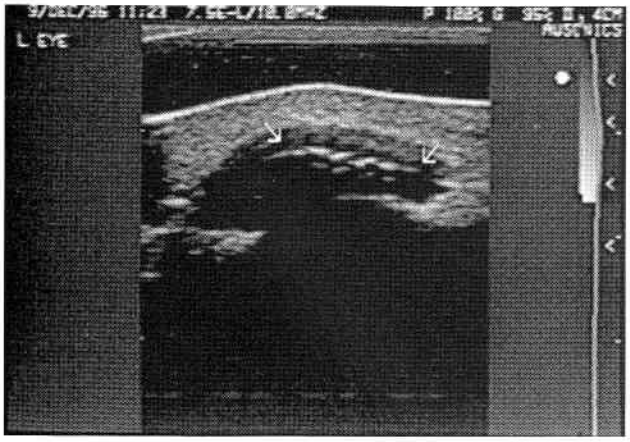

Figure 11–107

Transpalpebral sonogram of the left eye obtained from a 4-year-old Thoroughbred filly with a corneal ulcer. The cornea is severely ulcerated with pitting of the cornea *(arrows)* extending deep through the cornea. The eyelid is very swollen, making visualization of the cornea impossible. This sonogram was obtained with a wide-bandwidth 7.5-MHz linear-array transducer operating with a hand-held standoff pad at a frequency of 10.0 MHz at a displayed depth of 4 cm. The right side of this sonogram is lateral and the left side is medial.

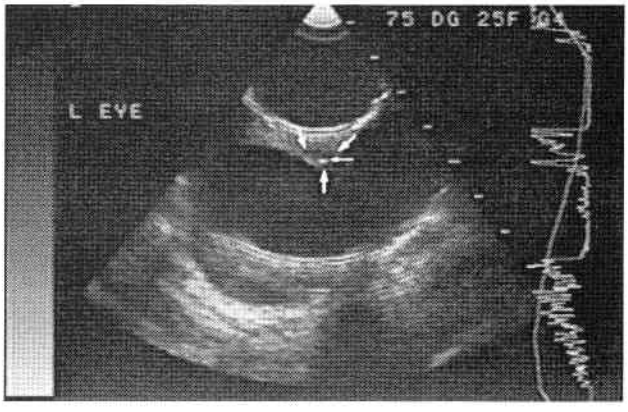

Figure 11–108

Sonogram of the left eye obtained from a 10-year-old Thoroughbred mare with a nonhealing corneal stromal abscess. The sonogram reveals a small hyperechoic foreign body *(horizontal small arrow)* in the cornea surrounded by an accumulation of hypoechoic material *(larger arrows)* creating the corneal stromal abscess. This foreign body was an eyelash hair that was surgically removed with a partial-thickness keratectomy. This sonogram was obtained with a 7.5-MHz sector-scanner transducer containing a built-in fluid offset at a displayed depth of 9 cm. The right side of this sonogram is dorsal and the left side is ventral.

casting an acoustic shadow typical of a wooden foreign body. Fractures of the bony orbit may be located in the retrobulbar or periorbital space and could be mistaken for a foreign body because fracture fragments also appear hyperechoic and cast a strong acoustic shadow. In horses with suspected trauma the orbit should be carefully scanned for the presence of fracture fragments or foreign bodies.

Panophthalmitis. Sonographic examination of the equine eye can provide useful information in horses with panophthalmitis. Panophthalmitis in horses is usually associated with sepsis and hematogeneous spread of the infection to the eye.[150, 151] Multiple organ system involvement may be present.[150] In horses with panophthalmitis the eye is likely to be enlarged, with corneal edema and hypopyon (Fig. 11-109).

Glaucoma. Glaucoma occurs infrequently in horses despite the species' relatively high frequency of ocular trauma, corneal perforation, and severe uveitis, which are predisposing conditions for the development of glaucoma in other animals.[152] Ocular trauma may be the initiating event in many horses with glaucoma.[152] and glaucoma may be more common in older horses.[153] Complete anterior synechiae associated with transcorneal scars have been reported in two horses, a ruptured lens with a perilenticular fibrovascular membrane that traversed the lens and covered the pectinate ligament was reported in one horse and in one horse, a growth of corneal epithelium covering the anterior face of the iris with an abnormally deep anterior chamber and posterior recession of the filtration angle was detected consistent with postcontusion glaucoma. Glaucoma can also occur in horses secondary to chronic intraocular inflammation, extensive anterior and posterior synechiae, and recurrent uveitis.[147, 152, 154, 155] Glaucoma was reported as a sequela to iris prolapse and its subsequent repair in horses.[156] Maldevelopment of the filtration angles should also be considered, particularly in young horses with other congenital ocular anomalies.[152, 152] Hypoplasia of the iris and microphthalmia were found in one foal with glaucoma.[152] There is no age, breed, or sex predilection in horses with glaucoma.[152]

Unilateral corneal cloudiness is the initial symptom in most horses with glaucoma.[152, 153] The corneal edema may clear temporarily with the application of topical corticosteroids.[152, 153] Corneal edema, corneal striae, and pupillary dilation are early signs of glaucoma that should prompt tonometric and sonographic examination of the eye. Chronic corneal edema, subtle corneal vascularization, corneal striae (deep stromal corneal opacities), obvious enlargement of the globe, fixed and dilated pupils, and blindness in the affected eye are present in most horses with glaucoma.[152, 153] Corneal ulcers or corneal stromal abscesses may also be present because corneal trauma is more likely in a horse with a blind buphthalmic eye.[20, 147] Enlargement of the globe is seen with chronic glaucoma and may develop over several months or years.[152, 153] Ocular pain is infrequently detected in horses with glaucoma.[152, 153]

The diagnosis of glaucoma is usually made by tonometry or histopathologic examination of the eye. Ultrasonographic measurement of the size of the globe in horses with suspected glaucoma can aid in the diagnosis of this disease (Fig. 11-110). Ultrasonographic examination of the filtration angle may also reveal this angle to be narrowed. Buphthalmos has been reported diagnosed sonographically in horses with glaucoma that was subsequently confirmed with applanation tonometry.[20] In horses with unilateral glaucoma, enlargement of the affected eye, with diameters of 40.7 and 43.3 mm, has been obtained sonographically, compared with ocular diameters of 37.3 and 40.3 mm in the unaffected normal eye.[20] Anterior lens displacement and abnormally echogenic posterior segment structures suggestive of hemorrhage or vitreal degeneration were detected in one of these horses with glaucoma.[20] Collapse of the iridocorneal drainage angle was detected in this horse on histopathologic examination of the eye.

Iris Prolapse. Both sharp perforating corneal injuries and blunt trauma causing rupture of the cornea, limbus, and/or sclera are common causes of iris prolapse in the horse.[157-159] Perforated corneal ulcers in horses are also a common cause of iris prolapse (47%)[160] and were as common as full-thickness corneal lacerations (47%) in one study of 32 horses.[156] Corneal stromal abscesses are an uncommon cause of iris prolapse.[149, 156, 161] Moderate to severe aqueous flare and fibrin were detected in the eyes of all horses with iris prolapse at initial ophthalmologic examination, regardless of the cause of the iris prolapse. Hypopyon was present in 82% of eyes in horses with ulcerative iris prolapse, whereas hyphema was detected in 4 of 15 horses with traumatic iris prolapse.[156] Total hyphema preventing anterior segment examination was present in 75% of horses with traumatic iris prolapse,

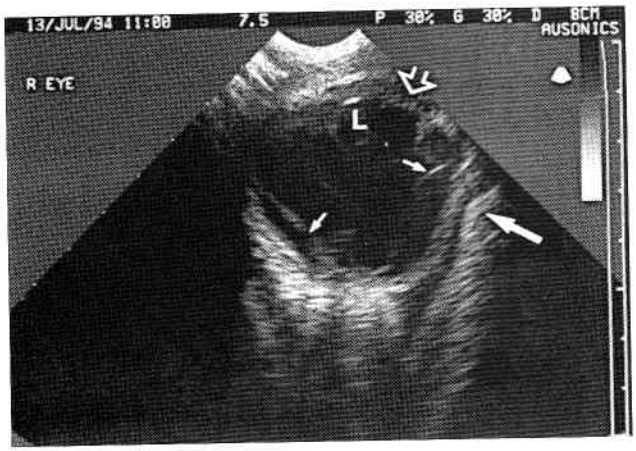

Figure 11-109

Transpalpebral sonogram of the right eye obtained from a 12-year-old Quarter Horse gelding with severe uveitis and panophthalmitis. The eyelids are swollen shut, preventing routine examination of the eye. The anterior chamber is collapsed and the lens (L) is adjacent to the thickened edematous cornea *(open arrow)*. Hypopyon was imaged within the globe as filmy hypoechoic strands floating within the eye. The eye is enlarged and lacks its normal circular shape as it bulges around the orbital rim. Retinal detachment is imaged with the hypoechoic membranes of the retina *(small arrows)* slightly pulled away from the underlying choroid and the back of the globe. The lateral margin of the bony orbit is impinging on the globe *(large arrow)*. This sonogram was obtained with a 7.5-MHz sector-scanner transducer at a displayed depth of 8 cm. The right side of this sonogram is lateral and the left side is medial.

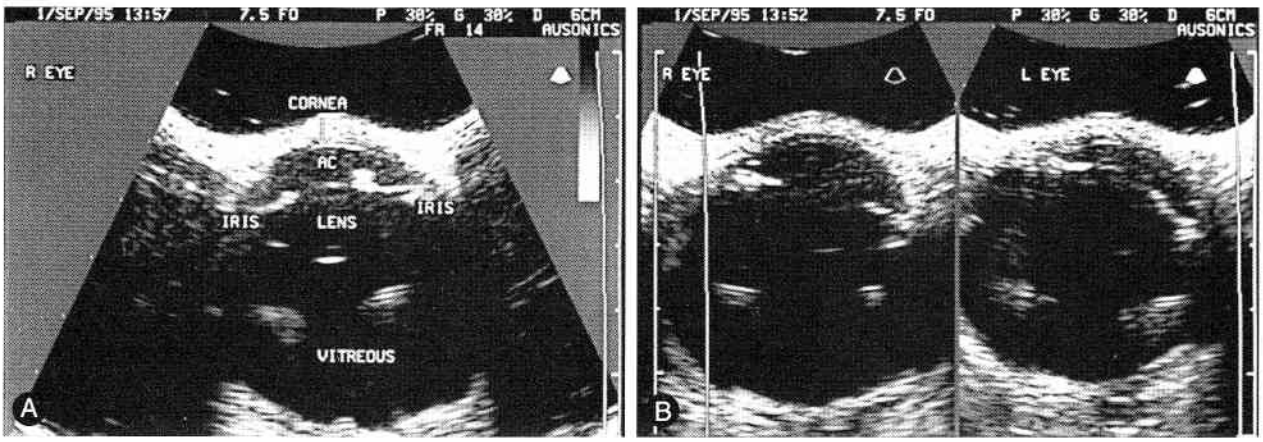

Figure 11–110

Transpalpebral sonograms of the right and left eye obtained from a 15-year-old Appaloosa mare with glaucoma. These sonograms were obtained with a 7.5-MHz sector-scanner transducer containing a built-in fluid offset at a displayed depth of 6 cm. The right side of these sonograms is lateral and the left side is medial.

A, The thin echogenic line representing the cornea is barely visible adjacent to the eyelid. The anterior chamber (AC) is imaged with the echogenic masses protruding from the iris, representing the corpora nigra. The anterior and posterior capsules of the lens are imaged as echogenic linear echoes. The globe appears enlarged and bulging.

B, Comparison of the size of the right *(left image)* and left *(right image)* eye demonstrates the enlargement of the right eye and the turgid bulging appearance of the anterior and vitreous chambers. The multiple linear echoes imaged within the vitreous are artifacts.

and posterior segment examinations could not be performed in any horse initially because of significant anterior segment disorganization, inflammation, and/or miosis.

Careful transpalpebral sonographic examination of horses with iris prolapse would reveal the pathology in the portions of the eye not visible on routine ophthalmologic examination.[156] Extreme care must be used in performing sonographic examination of the eye in a horse with acute iris prolapse, as any pressure on the globe may increase the severity of the prolapse. In horses with iris prolapse and collapse of the anterior chamber, the iris is imaged protruding through the cornea. Hyphema is usually present in the eye with acute trauma, and damage to other intraocular structures can be assessed (Fig. 11–111). In horses that have previously experienced iris prolapse, anterior synechia is imaged. In some horses the tract of the previous penetrating object into the intraocular structures can be imaged (Fig. 11–112).

Abnormalities of the Lens. Cataracts in horses may be congenital or acquired.[162] Congenital cataracts have been reported in Belgian[163] and Morgan horses.[164, 165] The development of cataracts in horses with iris prolapse caused blindness.[156] A cataract was reported in 1 of 10 horses with retinal detachment.[21] A cataract was reported secondary to an intraocular melanoma in one horse.[166] Routine ophthalmologic examination can reveal cataracts as opacities in the lens if the lens is not obstructed from view.

In horses with corneal clouding or other opacities preventing visualization of the lens, ultrasonographic examination of the eye can be useful in detecting cataracts within the lens.

Cataracts appear as echogenic to hyperechoic areas within the normally anechoic lens (Fig. 11–113). Hypermature cataracts have a hyperechoic lens and/or lens capsule with wrinkling of the capsular surface of the lens (Fig. 11–114). The axial diameter of the lens may be smaller in horses with cataracts. Sonographic examination of the eye is also useful in horses with cataracts prior to cataract surgery to evaluate the posterior segment of the eye when a complete ophthalmologic examination is not possible owing to opacity of the anterior segment. After cataract surgery, sonographic examination of the eye can also be performed if the entire globe is not visible on routine ophthalmologic examination. The lens capsule is still visible after aspiration of the lens (Fig. 11–115), a treatment for horses with cataracts.

In dogs with cataracts examined ultrasonographically prior to cataract surgery, 23% of eyes had vitreous degeneration and 11% had retinal detachment.[167] These findings

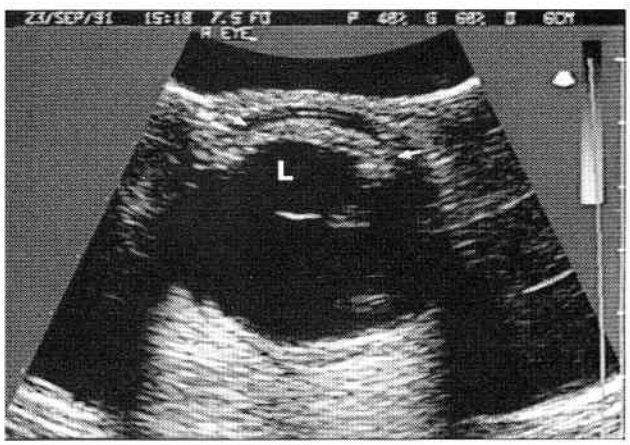

Figure 11–111

Sonogram of the right eye obtained from a 3-year-old Thoroughbred gelding with hyphema. A hypoechoic layer of clot *(arrows)* overlies the anterior capsule of the lens (L), filling most of the anterior chamber. This sonogram was obtained with a 7.5-MHz sector-scanner transducer containing a built-in fluid offset at a displayed depth of 6 cm. The right side of this sonogram is lateral and the left side is medial.

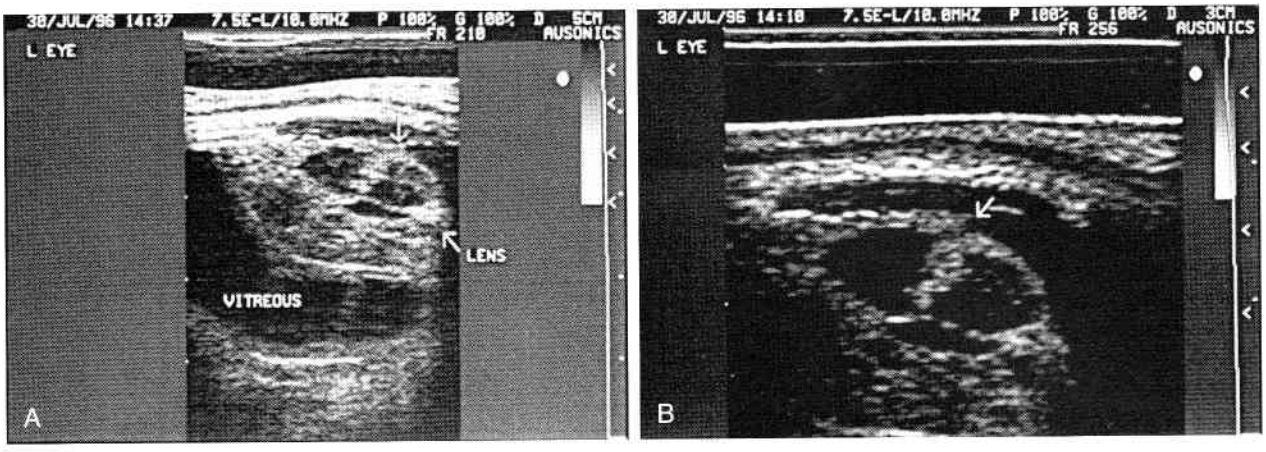

Figure 11–112

Sonograms of the left eye obtained from a 2-year-old Holsteiner filly with previous ocular trauma. The filly had sustained a penetrating injury to the globe, resulting in the development of a phthisical globe. These sonograms were obtained with a wide-bandwidth 7.5-MHz linear-array transducer operating at 10.0 MHz with a hand-held standoff pad at displayed depths of 5 cm *(A)* and 3 cm *(B)*. The right side of these sonograms is lateral and the left side is medial.

A, The path of the penetrating wound is still visible *(arrow)* as it extends through the lens. An echogenic linear tract extends through the center of the lens, representing the path of the penetrating object, rupturing the lens. The echogenic material imaged behind the lens is organized fibrin and lens material, which appears to be contained in the retrolenticular space. The thin echogenic strand attached to the anterior capsule of the lens at the site of the entrance of the penetrating foreign body represents fibrin and anterior synechiae. The additional linear echoes within the lens are secondary to hemorrhage from the original trauma. The vitreous chamber is smaller than normal and also contains fibrin strands.

B, The break in the anterior capsule of the lens is clearly visible *(arrow)*, and the tract through the lens is visible. The anterior synechiae is attached to the break in the anterior capsule of the lens and to the cornea.

in the posterior segment of the eye were detected most frequently in dogs with hypermature cataracts.[167] Hypermature cataracts are those with visible evidence of lens resorption on biomicroscopy, with mineralization within the lens or wrinkling of the anterior lens capsule.[167] A significant association between the classification of the cataract and retinal detachment was reported.[167] The axial diameter of the lens varied between the right and left eyes in dogs with cataracts, with the eye associated with the hypermature cataract usually having the smaller axial diameter.[167] During vitreous degeneration, the vitreous liquifies to varying degrees, resulting in the presence of tissues of differing acoustic impedances within the vitreous.[167] These areas of different acoustic impedances result in areas or lines of differing (increased) echogenicities within the vitreous.[167] Vitreous degeneration is easier to detect if the far-field gain is increased, making subtle differences in echogenicities easier to detect.[167]

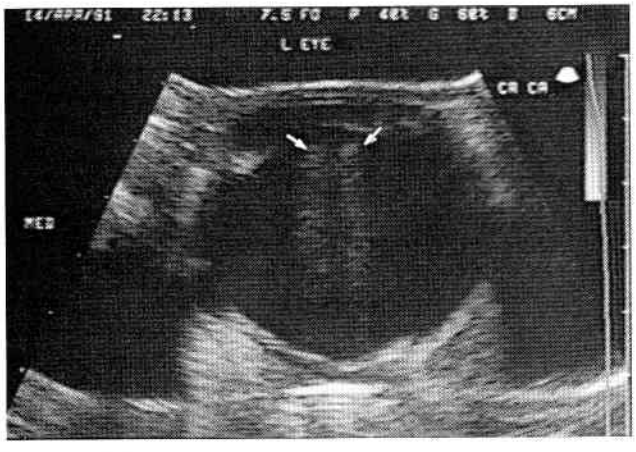

Figure 11–113

Sonogram of the right eye obtained from an 18-year-old Quarter Horse mare with cataracts. Echogenic areas within the lens *(arrows)* cast shadows consistent with cataracts. This sonogram was obtained with a 7.5-MHz sector-scanner transducer containing a built-in fluid offset at a displayed depth of 6 cm. The right side of this sonogram is lateral and the left side is medial.

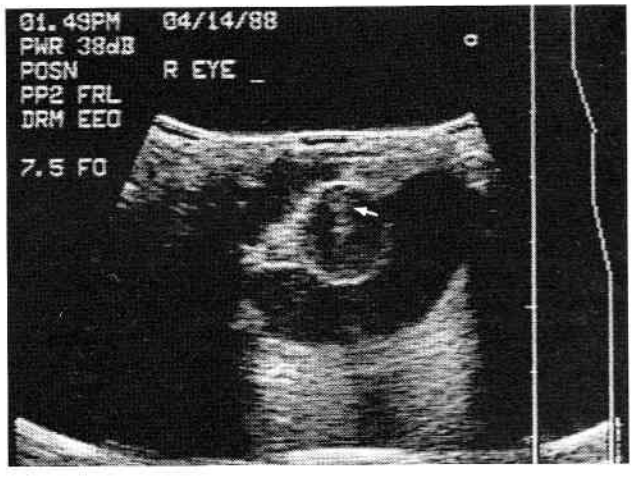

Figure 11–114

Sonogram of the right eye obtained from a 14-year-old Trakhener mare with a phthisical eye and hypermature cataracts. The lens is rounder than normal and contains echogenic areas *(arrow)* which are shadowing slightly, consistent with cataracts. The anterior capsule of the lens appears slightly irregular and wrinkled. The anterior lens capsule appears thickened and hyperechoic and in some views casts a weak acoustic shadow. The globe is significantly smaller than normal. This sonogram was obtained with a 7.5-MHz sector-scanner transducer containing a built-in fluid offset at a displayed depth of 7.5 cm. The right side of this sonogram is lateral and the left side is medial.

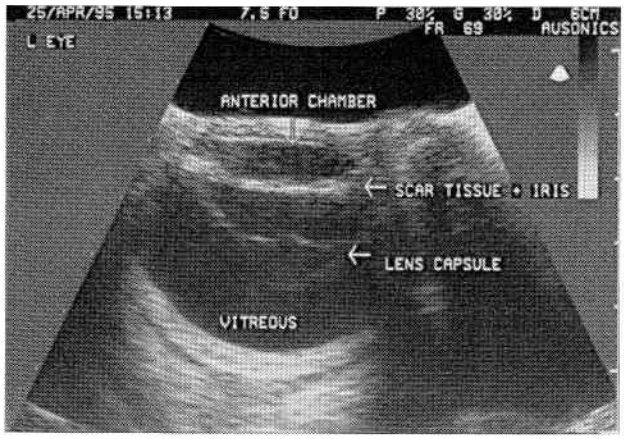

Figure 11–115

Transpalpebral sonogram of the left eye obtained from a 10-year-old Thoroughbred gelding with a history of recurrent uveitis and cataract removal. The lens is absent but the anterior and posterior capsules of the lens are imaged midway between the scarred iris and the retina. The pupil was completely obscured by scar tissue covering the pupillary margins. The anterior chamber is enlarged (0.66 cm deep). This sonogram was obtained with a 7.5-MHz sector-scanner transducer containing a built-in fluid offset at a displayed depth of 6 cm. The right side of this sonogram is dorsal and the left side is ventral.

Luxation of the lens occurs most frequently secondary to ocular trauma. Luxations of the lens has been seen in horses with ocular trauma and iris prolapse[156] or retinal detachment.[21] Penetrating scleral wounds often result in lens displacement.[19] Prolapse of the lens has been reported in two horses with iris prolapse.[156] Both of these horses also had vitreous prolapse and one of them also had concurrent retinal prolapse.

Rupture of the lens occurs infrequently associated with ocular trauma (see Fig. 11-112). In horses with a ruptured lens, a defect or tract is imaged into the anterior or posterior lens capsule, or both. The lens may appear collapsed with hypoechoic fibrin strands imaged in the anterior and/or vitreous chambers or the lens may appear enlarged and more echogenic than normal, associated with hemorrhage within the lens capsule.

Sonographic diagnosis of lens luxation should be made when the lens is detected in an abnormal position anterior or posterior to its normal location (Fig. 11-116). Luxation of the lens has been diagnosed sonographically in the horse.[6] Intraocular hemorrhage is frequently detected in horses with traumatic lens luxations. Intravitreal hemorrhage may be difficult to detect immediately following the ocular trauma and is more apparent once the hemorrhage begins to clot.[19] Echogenic masses and loculations have been imaged in the vitreous in a horse with ocular trauma and intravitreal hemorrhage.[19] Injury to the lens itself can be imaged as an echogenic line in horses with a history of a penetrating injury to the globe (see Fig. 11-112).

Retinal Detachment. Retinal detachment occurs infrequently in horses but has been reported with trauma,[157, 158] nonspecific intraocular infection,[161] intraocular neoplasia,[168] and as a complication of equine recurrent uveitis.[169, 170] It may be congenital[21, 171] or idiopathic.[21, 172] Acute or chronic chorioiditis or recurrent uveitis is the most common cause of retinal separation.[21] Trauma to the globe was the cause of retinal detachment in 2 of 10 horses in one study, with one horse having congenital retinal detachment associated with microphthalmia.[21] Many different types of retinal detachment have been described in horses.[21] Retinal detachment can be unilateral or bilateral, with the retina partially or completely detached from the underlying pigment epithelium.[171] Trauma usually causes unilateral retinal detachment, whereas retinal detachment associated with chronic uveitis can be unilateral or bilateral.[21, 171] In 10 horses with retinal detachment, bilateral retinal detachment was present in 30% of the horses.[21] In 12 of 13 eyes the retinal detachment was complete. The partially detached retina was detected as small tissue folds adjacent to the optic papilla.[21]

In many horses, retinal detachment cannot be diagnosed with only routine ophthalmologic examination. Only 3 of 10 horses in one study had total retinal detachment detected ophthalmoscopically.[21] The retina was adhered only at the margins of the optic disc and was seen as a free-floating, undulating, milky-opaque veil overlying the optic disc. Extensive retrolental membranes, intraocular tissue masses, fibrin-rich exudate, lens opacities, and synechia hid the retinal detachment from view in these horses. Slight to moderate bulbous atrophy was also present in these horses. Multiple congenital abnormalities in foals with congenital retinal detachments may also present visualization of the retina.[171]

Retinal detachment is easily diagnosed ultrasonographically.[6] Sonographic examination of the eye is particularly important in horses when the deeper structures in the

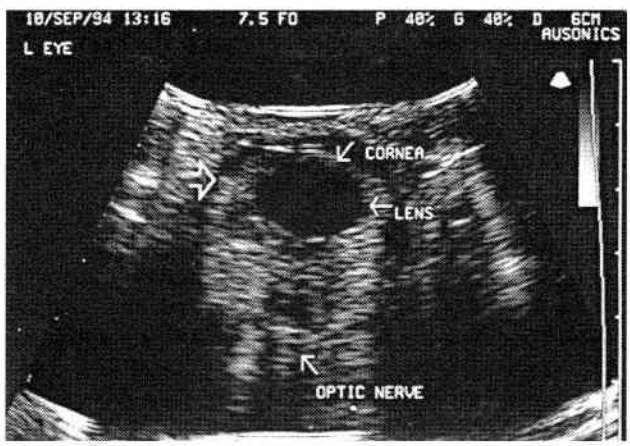

Figure 11–116

Transpalpebral sonogram of the left eye obtained from a 15-year-old Thoroughbred Quarter Horse cross mare with recent ocular trauma. The globe is very small and phthisical and measured 2.81 cm in diameter compared with the normal right eye, which measured 3.55 cm. The anterior chamber is collapsed and the cornea is adjacent to the anterior capsule of the lens. The posterior chamber is filled with echogenic material consistent with blood (hyphema). The lens appears luxated relative to the medial portion of the iris and ciliary body *(open arrow)*. Retinal detachment around the optic disc is also evidenced, as there is no hemorrhage in the vitreous in this region and a hypoechoic membrane is imaged between the hemorrhage and the more anechoic fluid. This sonogram was obtained with a 7.5-MHz sector-scanner transducer containing a built-in fluid offset at a displayed depth of 6 cm. The right side of this sonogram is lateral and the left side is medial.

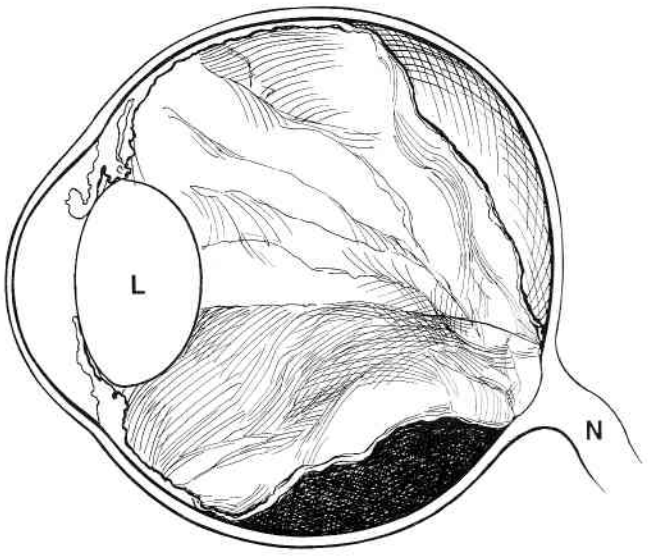

Figure 11–117

Diagram of a detached retina in the equine eye. Notice the funnel-shaped appearance of the retina as it is pulled away from the globe, only attached at the optic disc and ora serrata. L = lens, N = optic nerve.

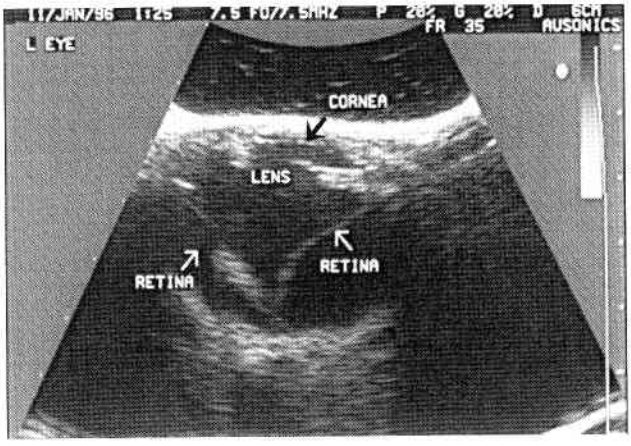

Figure 11–118

Transpalpebral sonogram of the left eye obtained from a 4-year-old Thoroughbred colt with a phthisical eye and retinal detachment. The retina is completely detached *(up arrows)* and pulled away from the back of the globe from the optic disc to the ciliary body. The anterior and posterior chambers are smaller than normal, and the lens also appears smaller than normal, although this image does not bisect the lens through its center. The cornea is visualized as an echogenic line just beneath the eyelid *(diagonal down arrow)*. This sonogram was obtained with a wide-bandwidth 7.5-MHz sector-scanner transducer containing a built-in fluid offset operating at 7.5 MHz at a displayed depth of 6 cm. The right side of this sonogram is lateral and the left side is medial.

eye are obscured from view. The detection of retinal detachment is extremely important when assessing the eye for possibility of future vision. Retinal detachment may be complete or partial. With complete retinal detachment the retina may have a funnel-shaped sonographic appearance where the entire retina is pulled away from the back of the globe, attached only at the optic disc and ora serrata (Figs. 11-117 and 11-118). The detached retina may appear as a membrane lifted off all or part of the back of the globe (see Figs. 11-109: Figs. 11-118 and 11-119). In acute retinal detachment, hemorrhage may be associated with the detachment and may be detected in the vitreous chamber or may be associated with the ciliary body (Fig. 11-119).

Ultrasonographic examination enables the clinician to demonstrate the extent of retinal detachment.[21] Ultrasonographic examination of the equine eye can be used

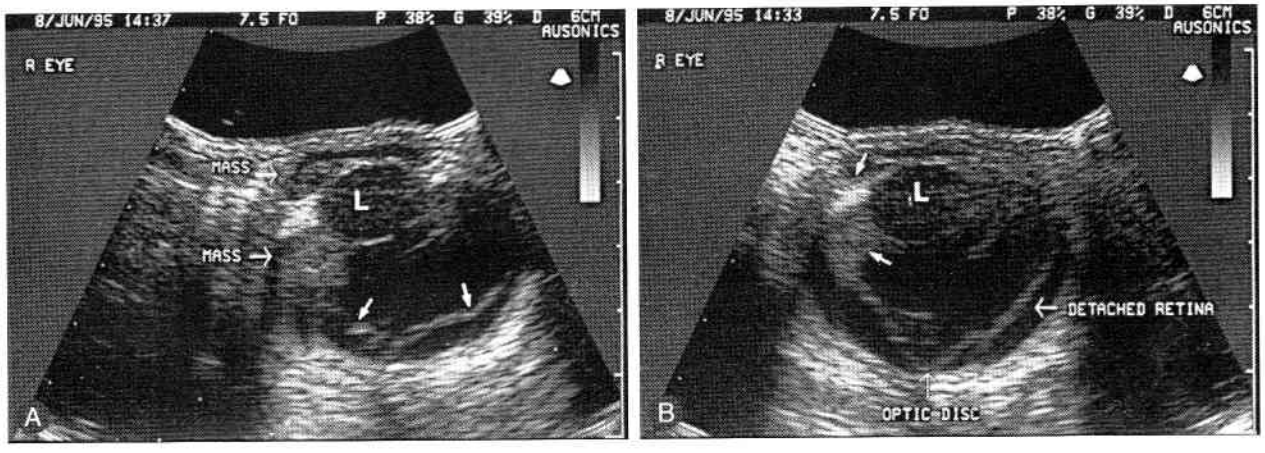

Figure 11–119

Sonograms of the right eye obtained from a 10-year-old Appaloosa gelding with intraocular masses and retinal detachment. These sonograms were obtained with a 7.5-MHz sector-scanner transducer containing a built-in fluid offset at a displayed depth of 6 cm. The right side of these sonograms is medial and the left side is lateral. L = lens.

A, Two relatively homogeneous masses are imaged in the medial aspect of the eye: one small mass in the anterior chamber and a larger mass in the vitreous chamber. Both masses appear to be associated with the medial ciliary body. These masses are homogeneous and hypoechoic and were thought to represent organizing clot associated with the ciliary body. The retinal detachment is imaged as the hypoechoic membranes pulled away from the back of the globe *(small arrows)*.

B, The detached retina is seen more clearly in this sonogram, with the hypoechoic membranes representing the retina pulled away from the back of the globe. The retinal detachment on the medial side of the globe appears to involve the larger mass which is imaged deep to the ciliary body and the lens *(small up arrow)*. A small portion of the smaller mass is imaged in the anterior chamber adjacent to the medial ciliary body *(small down arrow)*.

in conjunction with electroretinography to evaluate the equine retina for accurate assessment of structural (ultrasonography) and functional (electroretinography) abnormalities of the equine retina.[21] Retinal detachments have been imaged sonographically in horses.[19] The funnel-shaped appearance of detached retinas was described in one horse with bilateral retinal detachments. The funnel shape is caused by the retina remaining attached at the optic nerve head and the ora serrata (see Fig. 11-117).[19] Appearance of retinal detachments range from bulbous elevations of the retina to complete disinsertions of the retina.[19] Dystrophic calcification may occur with long-standing retinal detachments.[19]

Ocular Neoplasia

Epibulbar Neoplasia. This is the most common neoplasia associated with the equine eye and occurs most frequently with sarcoids and squamous cell carcinoma. Squamous cell carcinoma is a common equine tumor that frequently involves the lateral limbus in older horses.[173-175] Draft breeds (Belgian, Clydesdale, and Shire) and Appaloosas have a greater prevalence of ocular/adnexal squamous cell carcinoma than do Quarter horses.[173, 174] Geldings have a significantly greater likelihood of having ocular/adnexal squamous cell carcinoma than do sexually intact males or females.[174] The prevalence of ocular/adnexal squamous cell carcinoma was significantly greater for all hair coat colors when compared with bay, brown, or black.[174] Horses kept in areas of high solar radiation are predisposed to the development of ocular squamous cell carcinoma.[176] The mass often appears as a pink, lobulated, vascularized, raised mass involving the conjunctiva and cornea, usually originating near the lateral canthus of the eye. The nictitating membrane, nasal canthus, or both (28.1%); the bulbar conjunctiva, cornea (limbus), or both (27.5%); and the eyelid (22.8%) were the most common locations for ocular/adnexal squamous cell carcinoma.[176] Epibulbar melanocytoma has been reported in a location common to that of squamous cell carcinoma—the limbus.[177] This mass was mobile over the sclera, except at the lateral limbus. Ocular hemangioma has been reported in a horse that presented with a highly vascular irregularly shaped mass that initially occupied the ventral 40% of the cornea but did not appear to involve deeper structures within the eye.[178] At the time of enucleation the mass involved 80% of the cornea, and visualization of the deeper ocular structures was difficult. Sonographic examination of the eye would have revealed corneal involvement only in this horse. Ocular angiosarcoma (hemangiosarcoma and lymphangiosarcoma) has been reported in several horses with corneal thickening, conjunctival masses, masses involving the nictitating membrane.[179]

Sonographic findings in horses with squamous cell carcinoma involving the adnexa include an irregular hypoechoic mass invading the conjunctiva, extending out toward the cornea, usually at the lateral canthus of the eye (Fig. 11-120). The nictitating membrane and eyelid may also be involved.[6] As the tumor progresses, the mass may extend out over and invade the cornea or other intraocular structures (Fig. 11-121). A melanocytoma could have the more common homogeneous hypoechoic sonographic appearance or may be heterogeneous with echogenic and hyperechoic areas casting acoustic shadows associated with calcification. The masses associated with hemangiomas or angiosarcomas would probably have a hypoechoic vascular appearance, similar to the sonographic appearance of these tumors in subcutaneous tissues.

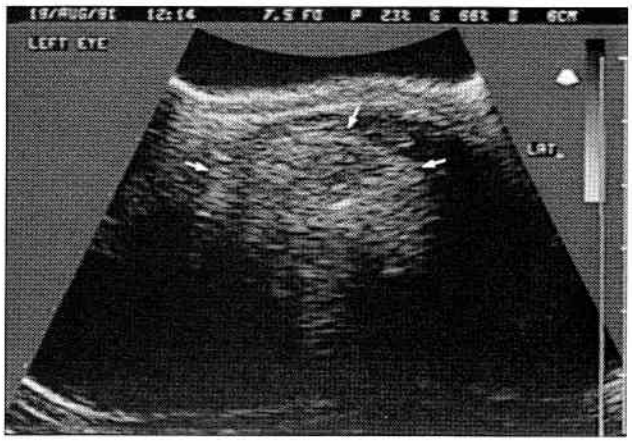

Figure 11-120

Sonogram of the left adnexa obtained from a 20-year-old Paint gelding with squamous cell carcinoma. There is a slightly heterogeneous soft tissue density mass *(arrows)* at the left limbus involving the conjunctiva. This sonogram was obtained with a 7.5-MHz sector-scanner transducer containing a built-in fluid offset at a displayed depth of 6 cm. The right side of this sonogram is lateral and dorsal.

Intraocular Neoplasia. Intraocular neoplasia is uncommon in horses.[166] Intraocular melanomas have been reported in the equine eye.[166, 168, 180] An intraocular melanoma appears as a dark-pigmented mass, usually associated with the iris or ciliary body and pigmented particles in the aqueous or vitreous.[166, 168] Aqueous flare, cataractous changes in the lens, posterior synechia, an indistinct retina, and low intraocular pressure were reported in one horse with ocular melanoma.

The sonographic appearance of intraocular neoplasia is that of a mass detected within the eye. The mass may be associated with the cornea, iris (Fig. 11-122), ciliary body, or optic nerve. Other intraocular structures are less frequently involved. The mass in horses with intraocular melanoma is usually found in the iris or ciliary body (Figs. 11-123 and 11-124). An intraocular melanoma may have a relatively homogeneous hypoechoic or echogenic sonographic appearance or may have a composite heterogeneous appearance with hyperechoic areas within the mass casting acoustic shadows, consistent with areas of calcification (Fig. 11-124).

Other tumors have also been reported in the equine eye. A neuroepithelial tumor of the optic nerve was reported in a horse with severe exophthalmos and a large mass visualized in the vitreous cavity.[181] Medulloepitheliomas and a malignant teratoid medulloepithelioma have also been reported in the equine eye.[182-184] These tumors are congenital tumors of nonpigmented epithelial tissue and usually arise from the ciliary body, ciliary process, and posterior surface of the iris, but they have the potential to form other cell types.[181] The intraocular structures could not be imaged in one severely affected horse be-

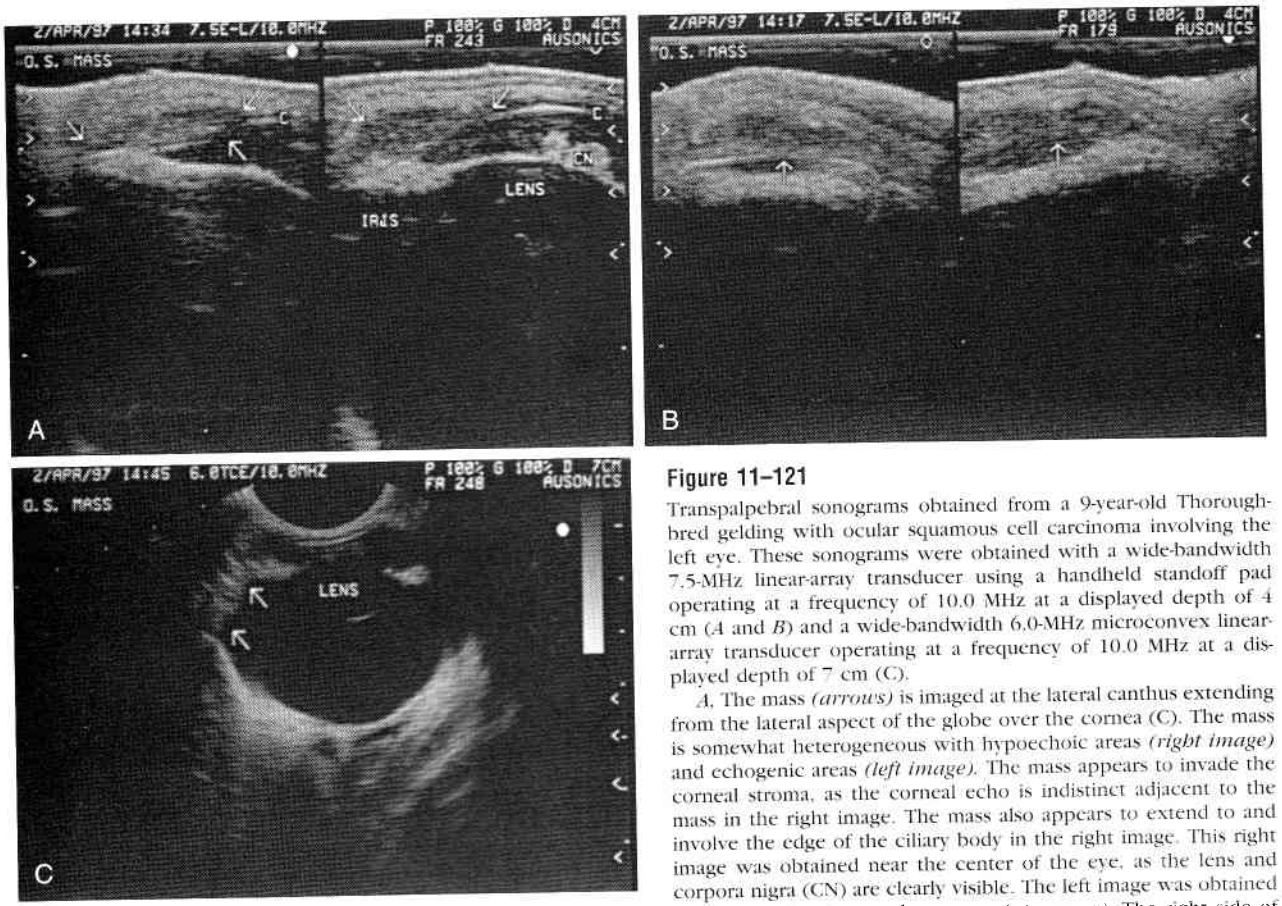

Figure 11–121

Transpalpebral sonograms obtained from a 9-year-old Thoroughbred gelding with ocular squamous cell carcinoma involving the left eye. These sonograms were obtained with a wide-bandwidth 7.5-MHz linear-array transducer using a handheld standoff pad operating at a frequency of 10.0 MHz at a displayed depth of 4 cm (*A* and *B*) and a wide-bandwidth 6.0-MHz microconvex linear-array transducer operating at a frequency of 10.0 MHz at a displayed depth of 7 cm (C).

A, The mass *(arrows)* is imaged at the lateral canthus extending from the lateral aspect of the globe over the cornea (C). The mass is somewhat heterogeneous with hypoechoic areas *(right image)* and echogenic areas *(left image)*. The mass appears to invade the corneal stroma, as the corneal echo is indistinct adjacent to the mass in the right image. The mass also appears to extend to and involve the edge of the ciliary body in the right image. This right image was obtained near the center of the eye, as the lens and corpora nigra (CN) are clearly visible. The left image was obtained more ventrally, where the mass appears to be separate from the cornea *(C)* but is indenting the cornea *(up arrow)*. The right side of these sonograms is medial and the left side is lateral.

B, The mass *(arrows)* is imaged along the lateral and ventral aspects of the globe, where it again appears to invade the cornea just before its junction with the sclera. The corneal echo *(up arrow)* is visible in the left image but appears invaded by the mass; whereas in the right image, immediately dorsal to the left image, the corneal echo *(up arrow)* is lost and the mass appears to invade the cornea. The right side of these sonograms is medial and the left side is lateral.

C, The echogenic, somewhat heterogeneous mass *(arrows)* appears to be invading the globe from its lateral aspect at the level of the ciliary body and deep to the ciliary body. The right side of this sonogram is medial and the left side is lateral.

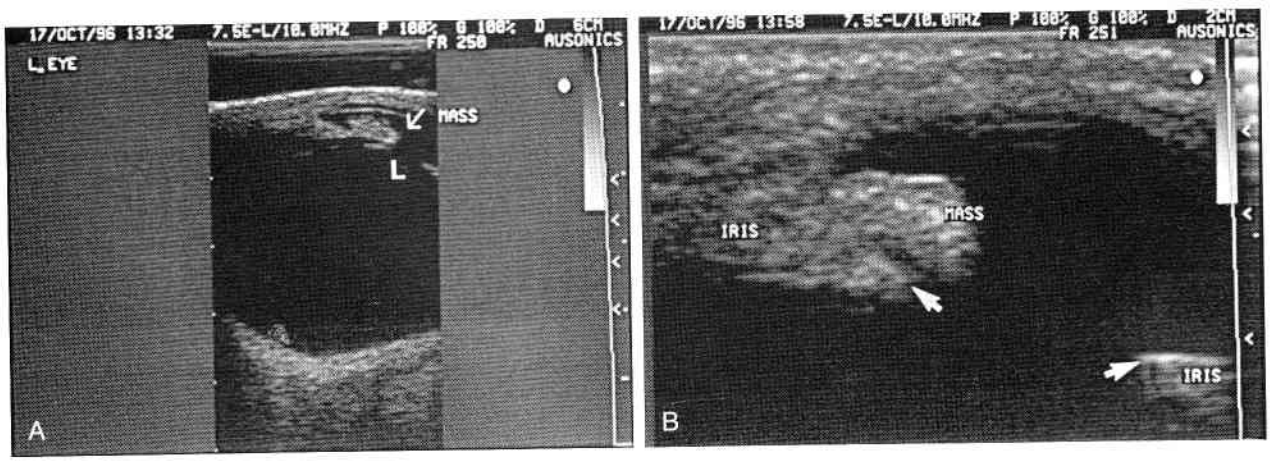

Figure 11–122

Transpalpebral sonograms of the left eye obtained from a 3-year-old Thoroughbred gelding with an intraocular mass. The mass originates from the iris at the pupillary margin and is growing over the pupillary opening. These sonograms were obtained with a wide-bandwidth 7.5-MHz linear-array transducer operating at a frequency of 10.0 MHz using a handheld standoff pad (A) at a displayed depth of 6 cm *(A)* and 2 cm *(B)*. The right side of these sonograms is dorsal and the left side is ventral.

A, The mass has an echogenicity similar to that of the iris and is imaged extending over the anterior capsule of the lens (L) obscuring part of the pupil.

B, The mass is imaged originating from the iris and then proliferating toward the pupillary margins *(arrows)*. In this view the mass appears to be slightly heterogeneous with echogenic areas within the hypoechoic mass.

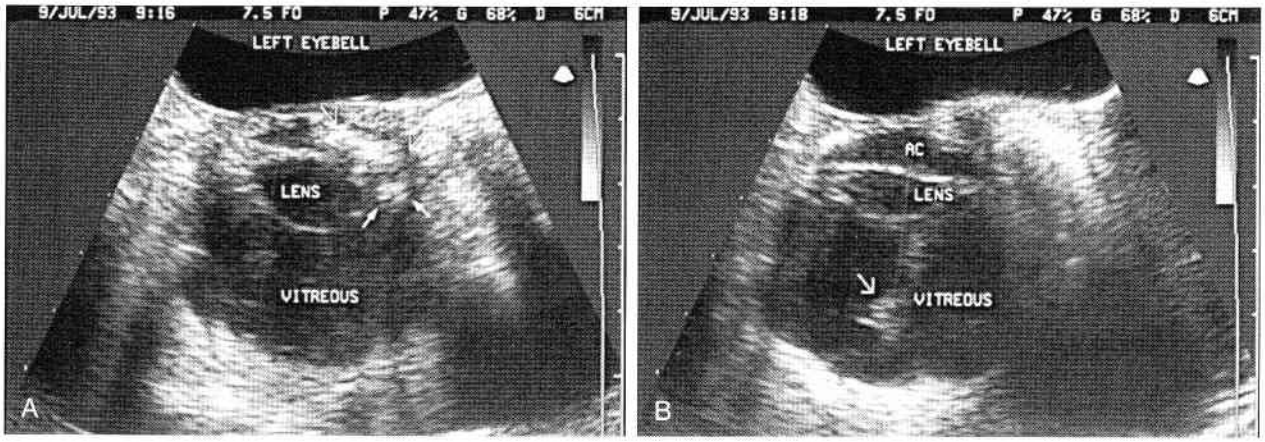

Figure 11–123

Sonograms of the left eye obtained from an 11-year-old Quarter Horse mare with an intraocular melanoma. These sonograms were obtained with a 7.5-MHz sector-scanner transducer containing a built-in fluid offset at a displayed depth of 6 cm.

A, The largest portion of the mass involved the temporal lateral portion of the anterior chamber *(larger arrows).* The mass appeared to involve the lateral ciliary body and the temporal lateral portion of the posterior chamber *(smaller arrows).* The mass is hyperechoic and casting weak acoustic shadows indicating calcification within the mass. The right side of this sonogram is lateral and the left side is medial.

B, The echogenic material in the vitreous *(arrow)* is hypopyon. The globe also has a somewhat irregular shape. The right side of this sonogram is dorsal and the left side is ventral.

cause of an opaque, densely vascularized cornea.[184] Sonographic examination of the eye would have revealed a large soft tissue mass with composite echogenicity in the anterior and posterior chambers that extended into the vitreous, and displacement of the lens that was cataractous in the horse with the malignant teratoid medulloepithelioma.[184] The heterogeneous sonographic appearance of the tumor is created by the multiple tissue types present within this type of tumor.

Retrobulbar Masses

Sonographic evaluation of the equine eye and orbit enables the clinician to obtain precise information about the presence of a retrobulbar mass, as well as its location, extent, character, and relationship to the intraorbital structures.[6, 22] The retrobulbar mass may be discrete, a common finding in horses with retrobulbar abscesses and some neoplasms, or diffuse, usually imaged in horses with ocular trauma and retrobulbar hemorrhage, retrobulbar cellulitis, and some retrobulbar tumors.

Retrobulbar Hemorrhage. Trauma to the equine eye or skull usually results in retrobulbar hemorrhage, rather than hemorrhage in the retina or choroid.[171] Exophthalmos and swelling in the supraorbital region have been reported in horses with retrobulbar hemorrhage.[22] Fractures of the bony orbit, particularly of the zygomatic process of the frontal bone, may also cause exophthalmus

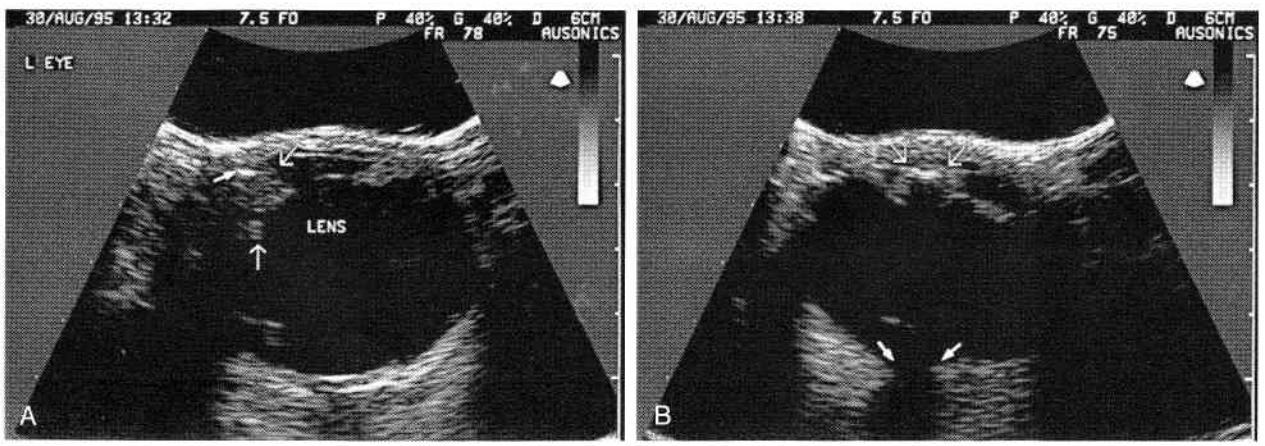

Figure 11–124

Sonograms of the left eye obtained from an 8-year-old Paso Fino gelding with an intraocular melanoma. The mass *(larger arrows)* is associated with the lateral aspect of the iris and the lateral ciliary body and extends from the anterior chamber to the posterior capsule of the lens. The mass has a hyperechoic center which casts an acoustic shadow. The composite sonographic appearance of this mass is most consistent with a neoplasm. These sonograms were obtained with a 7.5-MHz sector-scanner transducer containing a built-in fluid offset at a displayed depth of 6 cm.

A, The hyperechoic area *(small horizontal arrow)* is on the temporal lateral edge of the mass and is just barely imaged in this view. The right side of this sonogram is medial and the left side is lateral.

B, This sonogram is obtained directly over the hyperechoic portion of the mass, demonstrating the acoustic shadow cast *(small arrows at the back of the globe),* consistent with calcification within the mass. The right side of this sonogram is medial and the left side is lateral.

and be imaged as hyperechoic structures casting acoustic shadows.[185] These fractures are likely to be associated with periorbital hemorrhage.

Ultrasonographic examination of the eye and swollen supraorbital fossa revealed a large anechoic to hypoechoic well-circumscribed mass posterior to the eye in the dorsal medial confines of the orbit.[22] Scanning this retrobulbar mass through the supraorbital fossa revealed it to appear more anechoic than when imaged through the globe. A small hyperechoic structure located ventrally within the mass cast an acoustic shadow.[22] Although this was interpreted at the time of the sonogram to represent local calcification of a foreign body, an organizing clot should also be considered for this sonographic appearance, as the hyperechoic mass was imaged in its entirety before an acoustic shadow was cast from its far surface. With calcification and most foreign bodies, the acoustic shadow is cast from the near surface of the hyperechoic structure. An ultrasound-guided aspirate of this retrobulbar mass revealed it to be a hematoma.[22]

Abscesses and Foreign Bodies. Exophthalmos is common in horses with retrobulbar masses and abscesses. Abscesses are most frequently extraocular, with the abscess creating exophthalmos. Orbital cellulitis also occurs in horses and may result in exophthalmos. *Cryptococcal neoformans* infection of the frontal sinus that subsequently extends into the orbital region may also cause exophthalmos.[186]

The retrobulbar abscess usually contains hypoechoic fluid, displacing the globe within the orbit. Layering of the fluid within the abscess may be detected in some horses with retrobulbar abscesses (Fig. 11-125). The abscess often bulges out in the supraorbital space. The abscess is usually contained within a well-defined capsule, whereas the retrobulbar swelling is more diffuse and echogenic in horses with retrobulbar cellulitis. Small cavitating areas may be imaged in horses with retrobulbar cellulitis as the infection organizes to form an abscess. Abscesses may be associated with foreign bodies, which typically appear as echogenic or hyperechoic structures, often casting an acoustic shadow, surrounded by hypoechoic to anechoic fluid. Wooden foreign bodies should be considered when hyperechoic foreign bodies that cast a strong acoustic shadow are imaged.

Intraorbital abscesses and foreign bodies are common structures that can be diagnosed sonographically. Intraorbital abscesses have been detected sonographically and have been imaged impinging on the globe. The abscess may be encapsulated with a clearly defined echogenic wall surrounding the anechoic to hypoechoic fluid or may be poorly defined in the periocular tissues.[19]

Retrobulbar Neoplasia. Orbital neoplasia is uncommon in horses but is associated with exophthalmos, blindness, strabismus, anisocoria, and neurologic or behavioral abnormalities. Retrobulbar neoplasia is a common cause of exophthalmus in horses. The various neoplasms that have been reported in the retrobulbar space in horses include melanoma,[187] granulocytic sarcoma,[188] hemangioma,[189] multilobular osteoma,[190] lipoma,[191] adenocarcinoma,[191] microglioma,[192] neuroepithelioma of the optic nerve, and lymphosarcoma. Retrobulbar melanoma in one horse was associated with progressive exophthalmos and a prolapsed nictitating membrane.[187] A gradually enlarging retrobulbar mass was detected in the horse with the multilobular osteoma, resulting in a firm palpable mass in the supraorbital fossa. Sonographic examination of this mass would have revealed multiple, small hyperechoic areas within the mass associated with the mineralization seen radiographically; an ultrasound-guided biopsy could also have been performed.[190]

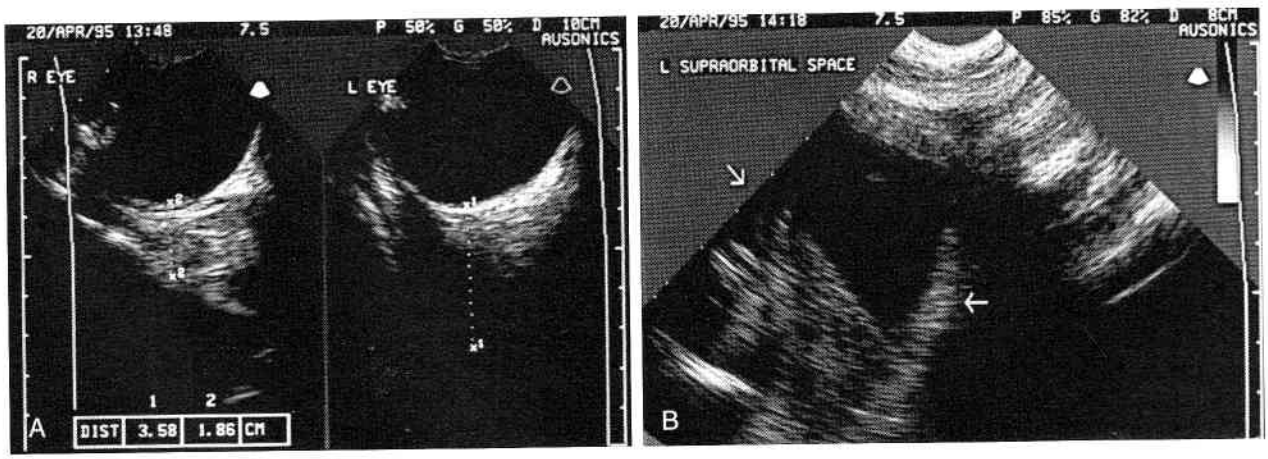

Figure 11-125

Sonograms of the retrobulbar space obtained from a 25-year-old crossbred gelding with a retrobulbar abscess and a pituitary adenoma. These sonograms were obtained with a 7.5-MHz sector-scanner transducer at a displayed depth of 10 cm *(A)* and 8 cm *(B)*.

A, Sonograms of the left retrobulbar space (right image) obtained through the globe, compared with the normal right retrobulbar space *(left image)*. The space between the back of the globe and the bony orbit is markedly enlarged on the left side (3.58 cm) compared with the normal right side (1.86 cm). The right side of these sonograms is dorsal and the left side is ventral.

B, Sonogram of the left retrobulbar space obtained from the left supraorbital space. Notice the large abscess *(arrows)* bulging dorsally in the supraorbital space from the retrobulbar space. The abscess is layered with the dorsal anechoic fluid component *(right horizontal arrow)* and the ventral cellular component *(left diagonal arrow)*. The interface between the cellular component and fluid component is angled because of the position of the horse's head. An ultrasound-guided aspirate of the mass through the supraorbital space confirmed the diagnosis of a retrobulbar abscess. The right side of this sonogram is cranial and the left side is caudal.

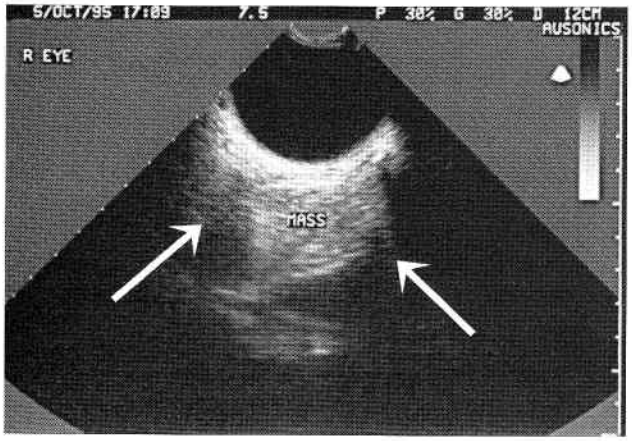

Figure 11–126

Sonogram of the retrobulbar space obtained from a 16-year-old Trakhener mare with retrobulbar lymphosarcoma and glaucoma. The heterogeneous mass depicted in the retrobulbar space *(arrows)* measures 3.79 × 2.73 cm and is the cause of the mare's exophthalmos. This sonogram was obtained with a 7.5-MHz sector-scanner transducer at a displayed depth of 12 cm. The right side of this sonogram is lateral and the left side is medial.

Sonographic examination of the retrobulbar area reveals a space-occupying mass in the retrobulbar space.[6] The mass may have a homogeneous appearance, most typical of lymphosarcoma (Fig. 11–126), or a more composite appearance (Fig. 11–127), as is seen with more aggressive neoplasms. Recognition of the extraocular muscles may be difficult if the tumor has infiltrated the entire retrobulbar area. Hyperechoic echoes casting acoustic shadows may be imaged within the mass associated with calcification of the mass or bony tissue in the mass. Involvement of the surrounding bony orbit may be detected.

Retrobulbar Cyst. A retrobulbar hydatid cyst was reported in a horse, causing exophthalmos and blindness.[189]

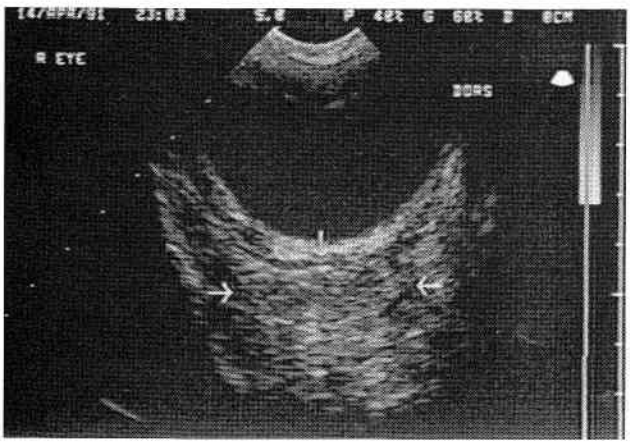

Figure 11–127

Sonogram of a large retrobulbar mass obtained from a 20-year-old Quarter Horse mare with marked exophthalmos and retrobulbar lymphosarcoma. The mass *(arrows)* has a hypoechoic, somewhat heterogenous, appearance and has more irregular margins. This sonogram was obtained with a 5.0-MHz sector-scanner transducer at a displayed depth of 8 cm. The right side of this sonogram is dorsal and the left side is ventral.

A large firm fluid-filled cyst was present on the floor of the orbit near the optic nerve that would have been detected with sonographic examination of the retrobulbar area. Sonographic examination of the eye and orbit in this horse would have revealed a large anechoic cystic structure in the orbit adjacent to the optic nerve. Although hydatid cyst disease is common in the United Kingdom, ophthalmologic involvement is rare.[189, 193]

Palpebral Swelling or Masses

Swelling of the eyelid is common in horses with most ocular diseases and usually responds to treatment of the primary ocular problem. In horses with acute ocular trauma, hemorrhage in the surrounding structures is a common cause of eyelid swelling. Abscesses in the eyelid have been detected sonographically in horses, particularly secondary to the placement of indwelling subpalpebral treatment catheters (Fig. 11–128). Tumors involving the ocular adnexa, such as squamous cell carcinoma, often involve the eyelid as well.

Neurologic Diseases

In a newborn Miniature Horse colt a thin cerebral mantle (< 1 cm) was detected, consistent with hydrocephalus. Both lateral ventricles in this foal were 5 cm high. Although normal values for these structures have not been obtained in Miniature Horse foals, hydrocephalus was suspected in this foal based on the ultrasonographic findings and a larger-than-normal cranium found on skull radiographs.[23] A dilated cranial vault with a very thin soft tissue shadow surrounding anechoic fluid and two echogenic structures (one in the frontal lobe area and

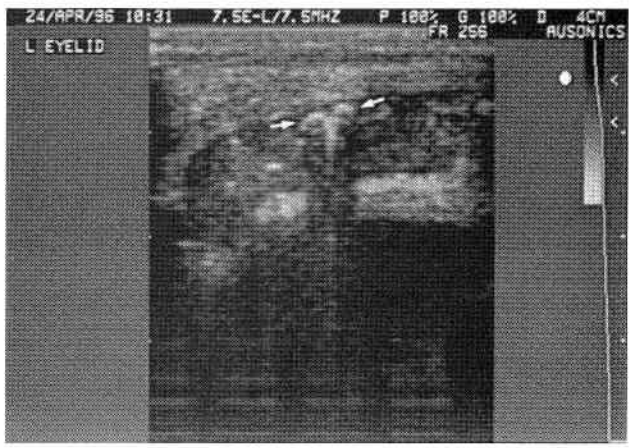

Figure 11–128

Sonogram of the left upper eyelid obtained from a 23-year-old Thoroughbred mare with an abscess within the left eyelid. The hypoechoic fluid swelling in the eyelid is consistent with purulent fluid; the hyperechoic echoes within this fluid cast dirty shadows *(arrows)* consistent with gas, mostly likely associated with infection of the eyelid with anaerobic organisms. No foreign body was imaged. This sonogram was obtained with a wide-bandwidth 7.5-MHz linear-array transducer operating at 7.5 MHz at a displayed depth of 4 cm. The right side of this sonogram is dorsal and the left side is ventral.

one in the area of the cerebellum) were all that could be imaged of the brain in a Quarter Horse foal with severe hydrocephalus.[24] These images of the brain were obtained through a defect in the foal's skull over the left eye. Sonograms obtained following a surgical attempt to drain the excess cerebrospinal fluid continuously revealed homogeneous ovoid echogenic masses with a soft parenchymal texture consistent with blood clots floating within the cerebrospinal fluid and an irregular linear echogenic structure pulled away from the skull, believed to be collapsed cerebral cortex.

Intraoperative Ultrasonography

The major benefits of intraoperative ultrasonography are the decreased radiation exposure to operating room personnel and the horse and the decreased amount of tissue dissection and operative time.[4–6, 8, 9] The need for intraoperative radiography is reduced or eliminated when intraoperative ultrasound is used. The structure of interest and important adjacent structures to be avoided can be identified in the surgical approach. Intraoperative ultrasonography is extremely helpful in removal of foreign bodies, particularly radiolucent ones such as wood. The site of the initial surgical incision is selected based on the location of the foreign body and its relationship to other surrounding vital structures. This technique is equally important in rapidly locating radiopaque foreign bodies at the time of surgical removal. The area can also be examined after foreign body removal and prior to closure to ascertain that all foreign body fragments have been removed. The use of intraoperative ultrasound will ensure that the surgeon follows all the tracts in the tissue to their source, removing all infected material possible. In many instances the localization of the foreign body with traditional surgical techniques such as the use of new methylene blue or fistulography is unrewarding, as the foreign body may be in a place inaccessible to radiography or cannot be safely reached surgically by following a tract of new methylene blue.

The sonographic examination of soft tissue masses or abscesses in areas with limited surgical access in the operating room can also aid the surgeon in determining the best surgical approach to avoid the adjacent vital structures. In many instances this type of examination is facilitated by having the patient anesthetized and positioned appropriately for surgery; it may also provide the surgeon with information different from that taken during the awake preoperative ultrasound examination with the horse standing. Small bony fragments that are often difficult to find at the time of surgery can also be located in the operating room, thus shortening the length of surgery and the time the horse spends under general anesthesia.

The use of ultrasound in the preoperative or intraoperative evaluation of lacerations can determine the extent of these horses' tendon and ligament injury. The surgeon's observation of the amount of tendon and/or ligament damage in these horses may be inaccurate because internal tendon or ligament damage can occur at the time of the laceration without disruption of the paratenon or the external tendon or ligament fibers. Puncture of the tendon or ligament may also occur without obvious tendon or ligament rupture. This puncture wound into the tendon or ligament may be missed at the time of surgery, causing the surgeon to leave foreign material in the tendon or ligament and/or causing sepsis to be introduced into these structures. The treatment of horses with tendon and ligament puncture should be more aggressive and the prognosis may be poorer, depending on the extent of tendinous or ligamentous damage.

The inclusion of intraoperative ultrasound in the operating room is becoming more frequent in equine practice, particularly among surgeons with significant experience in interpreting sonographic images.

Intraoperative ultrasonography has been used successfully in three horses to guide the surgeon to the location of intra-articular bone fragments.[4] The localization of foreign bodies with ultrasonography is much more precise than that obtainable with survey radiographs.[122] Intraoperative ultrasonography has been used successfully to remove foreign bodies in the tongue, carpus, retropharyngeal region, and cervical area of horses.[4, 5, 8] It has also been used to aid in the placement of a transvenous pacing wire in a horse with complete heart block.[25] In the horses with intra-articular bone fragments, the intra-articular or extra-articular location of the bone fragments could not be definitively determined radiographically.[4]

PATIENT MANAGEMENT AND PROGNOSIS

Cervical Structures

Abnormalities of the thyroid, parotid salivary gland, and surrounding the trachea most frequently involve masses in or around these structures. Ultrasound-guided aspirates or biopsies of these masses should be performed with samples submitted for cytologic evaluation, culture, and sensitivity testing, or histopathologic examination, and then treated accordingly.

Thyroid Gland Disorders

On farms where animals have excess dietary iodine intake the elimination of this dietary excess will eliminate new cases of goiter; in addition, thyroid enlargement in affected animals will gradually decrease. Analysis of the ration for excess iodine should be performed if dietary excess is a possible cause of goiter. An ultrasound-guided aspirate or biopsy is indicated with cytologic or histopathologic evaluation of the specimen obtained to diagnose the abnormality causing thyroid enlargement. If thyroid hormone levels are low, a thyroid stimulation test is indicated. If thyroid hormone levels are low in foals with clinical signs of hypothyroidism, thyroid supplementation is indicated.[45] Thyroid adenomas are benign and do not require surgical resection. Careful resection of thyroid carcinomas is indicated owing to their highly vascular and aggressive nature.[38]

Salivary Gland Disorders

Removal of a sialolith can occasionally be performed by massaging the sialolith through the parotid papilla into the oral cavity. An oral (preferable) or transcutaneous sialolithotomy can be performed with good success. Lacerations of the salivary ducts should be cleaned and debrided and closed primarily if possible, to minimize the formation of a salivary fistula. If an enlarged, inflamed salivary gland is detected, the horse should be carefully examined for partial obstruction of a salivary duct or damage to the duct resulting in secondary infection of this gland. Broad-spectrum antimicrobials should be administered if salivary gland infection is suspected.

Tracheal Disorders

Masses impinging on the trachea should be surgically removed or drained as appropriate, to prevent respiratory distress from developing or worsening. Peritracheal abscesses should also be treated with broad-spectrum antimicrobials until the results of culture and sensitivity testing of an aspirate from the abscess is available. If free gas echoes are imaged, anaerobic as well as aerobic coverage is important. Fractures of the tracheal cartilage with the leakage of subcutaneous air is usually managed with the application of a pressure bandage and conservative management with stall rest and restricted exercise until the tracheal defect has healed and air no longer leaks subcutaneously.

Esophageal Disorders

Esophageal Obstruction, Stricture, and Diverticuli. Sonographic evaluation of the cervical region may be useful in localizing the obstruction and in the detection of a foreign body or esophageal diverticulum or stricture. Cervical radiographs and endoscopic examination are also helpful in diagnosing the esophageal obstruction and planning the appropriate treatment. However, endoscopy is not helpful in differentiating simple obstructions from anatomic disorders until the feed impaction is resolved.[45] Contrast radiography was helpful in one study in outlining the mucosal lesions in the distal esophagus that could not be visualized endoscopically.[45]

Relief of the esophageal obstruction should be performed as quickly as possible to prevent the subsequent development of esophageal stricture. Feed impaction is usually successfully resolved by hydropropulsion and lavage via nasogastric intubation while the horse is sedated.[45] Survival of horses with esophageal impactions is good, with a short-term survival of 78% and a long-term survival of 49%.[45] Chronic obstruction at home was reported in 37% of the horses that survived long term.

Short-term survival of horses with esophageal strictures was poor; that of horses with acute strictures of less than 2 weeks' duration was better. Long-term survival was better in horses treated surgically for esophageal stricture than it was for those treated medically; their survival was no different than for horses with esophageal impactions.[45] The use of soft diets and nonsteroidal anti-inflammatory drugs has also been successful in the management of horses with acute esophageal stricture.[194]

The prognosis for long-term survival for horses with an esophageal diverticulum is excellent.[45] All horses treated surgically or nonsurgically for an esophageal diverticulum survived long term. Successful repair of esophageal diverticula has been reported in horses with either inversion of the esophageal mucosa or diverticulectomy.[45, 55, 56] However, inversion of the redundant mucosa is preferred over diverticulectomy to minimize postoperative infection.[45]

Esophageal foreign bodies have been successfully removed surgically with an esophagotomy if necessary.[46] Aspiration pneumonia and pleuritis were common complications in horses with esophageal disorders, and the long-term survival was significantly lower in horses with these complications.[45] Persistent respiratory disease that necessitated exercise modifications was detected in 21% of horses surviving long term following esophageal impactions. Periesophageal infection occurred in 53% of horses with surgical treatment for esophageal disease and was more common with surgical procedures entering the esophageal lumen. Postoperative mortality was higher in horses in which the surgeon entered the esophageal lumen.[45]

Esophageal Rupture. Surgical treatment of traumatic esophageal rupture has been reported.[45, 60] Surgical correction of esophageal perforation resulted in better long-term survival than in horses treated medically. Continuous intubation with a soft tube for feeding a slurry diet is indicated to allow the esophagus and surrounding tissues to heal without additional feed material being deposited in the adjacent soft tissues. An esophagostomy distal to the area of rupture may be indicated in some horses. Periesophageal drainage of the cellulitis associated with esophageal rupture is often indicated. Sonographic examination of the periesophageal tissues can be useful in monitoring the resolution of the cellulitis and the involvement of periesophageal structures. Sonographic examination of the thoracic inlet and cranial mediastinum can also be performed to monitor the horse for development of mediastinitis.

Swellings and Masses

Cysts

Cervical cysts should be removed surgically using a ventral pharyngotomy approach,[53, 68] a ventral laryngotomy approach,[67] or a modified Whitehouse approach.[63-65, 69] Prognosis for horses with pharyngeal and cervical cysts is usually good with surgical removal.[67, 68] Intramural esophageal cysts in horses have been treated with surgical removal of the cyst and marsupialization of the cyst.[2, 53] If complete removal of the cyst is not possible, all of the mucosal lining should be removed to prevent recurrence of the cyst.[52] Marsupialization of the intramural esophageal cyst appears to be the preferable surgical

technique for removal of these cysts.[2, 52] Dentigerous cysts should also be surgically removed once diagnosed.

Abscesses

Abscesses should be aspirated and a sample submitted for cytologic examination and culture and sensitivity testing, or be surgically drained if large or impinging on vital structures. Antimicrobial therapy should be based on the sonographic characteristics of the abscess and the most likely organisms to be involved. Anaerobic coverage should be included when free gas echoes are imaged and a sample should be submitted for anaerobic, as well as aerobic culture. Ultrasonography is the method of choice for determining how to drain abscesses and to monitor the response of abscesses to treatment.[5] Ultrasound-guided percutaneous drainage of deep cervical abscesses has been used successfully in human beings to minimize the risks associated with more invasive surgical drainage.[195]

***Corynebacterium pseudotuberculosis* Abscesses.** Sonographic examination of the swellings in horses with *Corynebacterium pseudotuberculosis* abscesses will help determine the location of the abscess, the involvement of adjacent structures, and the optimal site for surgical drainage if the abscess is mature enough to allow for surgical drainage. In most horses with *Corynebacterium pseudotuberculosis* infection, the abscess should be managed conservatively initially, until it is organized and close to the skin surface. In one study, ultrasonographic examination helped localize the deeper abscesses requiring surgical incision and drainage in affected horses. Abscesses resolved within 18 days once surgical drainage was established.[75] The use of systemic antimicrobials in horses with external abscesses associated with *Corynebacterium pseudotuberculosis* infection is controversial and may prolong the course of the disease.[74, 75] An elevated synergistic hemolysis inhibition (SHI) titer $\geq$ 512 is useful for the diagnosis of internal abscesses in horses with *Corynebacterium pseudotuberculosis* infection but is not reliable for the diagnosis of external abscesses. The prognosis for horses with external abscesses is excellent with a survival rate of 99.2%, compared with a survival rate of 59.5% for horses with internal abscesses.[75] The development of a marked or prolonged fever was associated with a poorer prognosis in one study, with 92% of these horses developing complications. The most favorable prognosis was for horses with pectoral and inguinal abscesses.[74]

Perirectal or Perivaginal Abscesses. Sonographic examination of perirectal abscesses should be performed both transrectally and from the perianal window to determine the possibility of perianal drainage. In mares with a ventral perirectal abscess, perivaginal sonographic examination is indicated to discover whether perivaginal drainage is feasible. The complete extent of the abscess should be determined to be sure that the abscess does not extend cranially into the peritoneal cavity. If the cranialmost extent of the abscess is not detectable transrectally or from the perianal or perivaginal approach, sonographic examination of the caudal abdomen should be performed to determine if an abdominal component of the abscess is visible. An ultrasound-guided aspirate can be performed from the perianal or perivaginal window if cytologic confirmation of the abscess is needed before surgical drainage of the mass.

Streptococcus zooepidemicus and/or *Escherichia coli* were cultured from five horses with perirectal abscesses.[76] It is not clear whether anaerobic cultures were performed on the fluid obtained from these perirectal abscesses. Initial broad-spectrum antimicrobial treatment can be guided by the sonographic appearance of the abscess until the culture and sensitivity testing results of the abscess fluid are obtained. Antimicrobial therapy should include anaerobic coverage if gas echoes are imaged in the abscess cavity. The perirectal abscess should be lavaged with dilute povidone-iodine solutions only in those horses in which the abscess does not extend cranially into the peritoneal cavity. Bran mashes or mineral oil may be needed to keep the horse's feces soft until the abscess resolves. A warm water enema is also occasionally needed in affected horses. Sonographic monitoring of the resolution of the abscess is helpful in following the horse's response to treatment. Prognosis for affected horses is good if surgical drainage was effective, unless the abscess extends into the peritoneal cavity.[76]

Granuloma

Prognosis for horses with granulomatous disease is usually poor. Fungal cultures and histopathologic examination of the affected tissues should be performed to diagnose the etiology of the granuloma and plan a course of treatment based on these results.

Cellulitis, Lymphangitis, and Edema

Sonographic examination of a horse with cellulitis or lymphangitis helps determine whether there is a localized area of fluid accumulation within the infected tissues. If a hypoechoic or anechoic pocket of fluid is imaged, an aspirate of this area should be obtained aseptically for cytologic evaluation and culture and sensitivity testing of the fluid. Broad-spectrum antibiotics should be selected until the culture and sensitivity testing results become available. If cellulitis is imaged surrounding a synovial structure, aspirate of the synovial structure through this thickened echogenic tissue is contraindicated because of the risk of introducing infection into the synovial structure. The sonographic detection of edema should prompt a search for the underlying causes of the edema, if the cause is not clinically apparent. If the distal limbs are involved, a support wrap should be applied to help minimize tissue swelling. Cold water hosing of the limbs may also be helpful in horses with cellulitis and lymphangitis.

Hematomas

Hematomas are often best left to resolve on their own, except when they are large and limit function of the affected area. The tissues surrounding the hematoma

should be carefully examined for muscle trauma or fractures, which may be associated with the hemorrhage. Radiographs of the area should be obtained if bony trauma is likely or detected sonographically. The sonographic appearance of a hematoma is so characteristic that an ultrasound-guided aspirate is unnecessary for diagnosis unless the sonographic appearance of the hematoma is atypical or the clinical signs indicate another likely differential diagnosis. An ultrasound-guided aspirate of the area should be performed to confirm that the atypical mass is a hematoma. Strict aseptic procedures should be followed, to minimize the risk of introducing bacteria into the hematoma. The hematoma should be drained surgically only when absolutely necessary, as secondary infection of the hematoma may occur if surgical drainage is inadequate, creating a large abscess in the area. A hemangioma or hemangiosarcoma may occasionally present with a sonographic appearance similar to that of a hematoma, especially when the skeletal muscle is involved. If the hematoma appears atypical, an ultrasound-guided biopsy should be submitted for histopathologic evaluation.

Seromas

Postoperative seromas should be allowed to resolve on their own in most instances, unless a secondary infection is suspected. Strict asepsis should be used when obtaining a sample for cytology and culture and sensitivity testing, to prevent accidental contamination of the seroma with bacteria.

Soft Tissue Masses

An ultrasound-guided excisional biopsy of these masses should be performed to definitively determine the tissue type associated with the soft tissue mass and to select appropriate treatment. Sonographic examination of these masses is important prior to excisional biopsy or the surgical removal of larger masses to delineate the extent of the mass, its relationship to surrounding tissues and vital structures, and its local invasiveness.

Sarcoids. Numerous treatments for sarcoids have been proposed including surgical excision, cryotherapy, carbon dioxide laser surgery, immunotherapy with bacille Calmette-Guérin (BCG), interstitial brachytherapy, hyperthermia, and chemotherapy. Surgical treatment alone appears to be less effective than other forms of treatment. The choice of treatment is often dictated by the anatomic location of the lesions.[89]

Lipomas. Surgical resection of lipomas in affected horses has been difficult; however, because the recurrence of these tumors is low in affected horses surgical resection is often recommended.[90-92]

Hemangiomas, Hamartomas, Hemangiosarcomas. The distinction among hamartomas, hemangiomas, and hemangiosarcomas is difficult to make on biopsy in many cases.[96] If biopsy precedes surgical excision of the mass, sonographic selection of the site for biopsy is indicated to avoid larger vessels associated with the vascular neoplasm, which may result in excessive bleeding if biopsied. Surgical resection of hemangiomas has been successfully performed in horses with a low incidence of recurrence of the vascular neoplasms.[93] Although hemangiomas may regress spontaneously in human beings, spontaneous regression has not been reported in the horse to the author's knowledge. Two of three horses with hemangiosarcomas were free of recurrence following surgical removal of the masses, but the other horse had rapid and extensive recurrence of the tumor, which resulted in the humane destruction of the horse.[93] Because rapid metastases of hemangiosarcomas throughout the skeletal muscles and internal organs occur in horses, surgical treatment is indicated only if a single discrete resectable mass is detected.[93] Chemotherapy is an option for horses with vascular neoplasia, but it is very expensive and therefore rarely used.

Melanocytomas, Melanomas. Early excisional biopsies of melanocytic tumors is recommended as not all of these tumors are benign in young horses.[100, 102] Chemotherapy, radiotherapy, and BCG have been of little clinical value in the treatment of equine melanomas.[41, 42] Recurrences after surgical incision and cryonecrosis are common. Wide surgical excision, an accepted form of treatment, is recommended for tumors that are small to medium-sized (< 3 cm in diameter), are not numerous (<15), and are located in surgically accessible regions.[42] Cryonecrosis is recommended for treatment of tumors when the size of the mass precludes surgical excision and primary closure. The mass should be debulked as much as possible before cryonecrosis. Treatment of melanomas with oral cimetadine has been successful, particularly in horses with melanomas that are actively increasing in size and number.[41, 42] Both a decrease in tumor diameter (by approximately 50%) and a regression of the numbers of tumors (half) have been reported.[41] Intralesional injection of cisplatin may also be beneficial after tumor debulking.[42]

Other Neoplasms. Surgical excision of single neoplasms is usually recommended and can be performed as an excisional biopsy if the mass is small or following a biopsy confirmation of the neoplasm. Intratumoral administration of cisplatin is a safe and effective treatment of sarcoid and squamous cell carcinoma/papilloma in horses with tumor regression occurring in all treated horses and minimal cisplatin-related local toxicosis. The horses selected for this treatment were those in which other previous treatments had failed or the mass was not amenable to conventional treatment. The mean relapse-free interval was 21.6 months for horses with sarcoids and 14 months for those with squamous cell carcinoma/papilloma.[196] When intratumoral administration of cisplatin was combined with cytoreductive surgery in horses with macroscopic evidence of residual tumor within the wound, the mean relapse-free interval was 41 +/−3.7 months.[197] Wound healing was not compromised and local cisplatin-related toxicosis was minimal. The treated tumors included sarcoids, squamous cell carcinomas, and one hamartoma.[197]

Foreign Bodies and Draining Tracts

Ultrasonography is the method of choice for determining how to remove the foreign body, drain the abscesses

associated with it, and monitor the response of abscesses to treatment.[5] The foreign body should be precisely localized sonographically and the surgical approach selected. All tracts should be followed back to their source, as more than one foreign body may be present or a foreign body may be present in association with a sequestrum or necrotic tissue, which should also be removed at the time of surgery. A draining tract associated with osteomyelitis should be followed to the affected bone, which should be surgically debrided if surgical treatment is selected. In cases of osteomyelitis when medical treatment is selected, an ultrasound-guided aspirate of the fluid overlying the bone is indicated to evaluate cytologically and to submit for culture and sensitivity testing. The prognosis for most horses with draining tracts is good if the tracts can be followed to their source or sources and the cause of the drainage removed or treated successfully with antimicrobials.

Prognosis for horses with gunshot wounds is good if only skeletal muscle and skin are involved. Minimal debridement, lavage, and establishment of drainage usually result in an excellent outcome in these affected horses.[12] If the gunshot wound penetrates vital structures such as the abdomen or thorax, the horse's prognosis is guarded to grave, depending on the structures involved and the severity of the initial damage. Long-term survival was poorest for horses with abdominal injuries and best for those with ocular injuries.[12]

If sonographic examination of a postoperative incision indicates suture sinus formation and infection or draining tracts are detected associated with the incision, an ultrasound-guided sample should be obtained for cytologic evaluation and culture and sensitivity testing. Broad-spectrum antimicrobials should be administered initially until the results of culture and sensitivity tests are available. Offending sutures should be removed, if possible, to enable the incision to drain to the outside. A support wrap should be placed on ventral abdominal incisions to support the incision in the event that herniation may occur. Antimicrobials should be continued until the suture sinuses and tracts through the incision have resolved.

If the hernia is small the defect may be possible to close without the use of an implant. However, large defects usually require implantation of a synthetic mesh to completely close the ventral hernia.[198] After hernia repair, the incision should be monitored by palpation and ultrasound to determine when increased activity of the horse is possible without potential risk of reherniation.[15]

Disorders of the Lymph Nodes

An ultrasound-guided aspirate should be obtained from any lymph node with an area of cavitation for cytologic evaluation and culture and sensitivity testing. If bacteria other than *Streptococcus equi* is obtained the horse should be treated with antimicrobials based on the results of culture and sensitivity testing. If *Streptococcus equi* is obtained the reader is referred to a current text on equine internal medicine for the appropriate management of horses with this infection. If the lymph node appears enlarged and diffusely infiltrated, an ultrasound-guided biopsy of the affected area or node should be performed to determine if it is neoplastic. Fungal or parasitic infection of the affected lymph node should be considered if the lymph node has an unusual sonographic appearance or there is evidence of systemic granulomatous disease.

Tongue and Oral Cavity

Lingual and Oral Abscesses

The abscess should be carefully scanned for a possible foreign body, as metallic foreign bodies are common in horses with lingual abscesses. If a foreign body is suspected but not confirmed sonographically a radiograph should be obtained because most oral foreign bodies are radiopague. The prognosis for lingual and oral abscesses is usually good if surgical drainage can be achieved. If surgery is not an option the abscess should be cultured under sonographic guidance and a sensitivity pattern established for the organisms recovered. Because most lingual and oral abscesses contain gas echoes produced by anaerobic bacteria within the abscess, broad-spectrum antimicrobial coverage should be used in addition to drugs effective against anaerobic organisms.

Oral Foreign Bodies

Sonographic examination of the tongue and oral cavity should be performed in all horses presenting with dysphagia and ptyalism if a lingual laceration or other cause of the clinical signs is not found. Surgical removal of oral foreign bodies is usually indicated under sonographic guidance. Intraoperative use of ultrasonography is extremely useful in locating the foreign body and minimizing the surgical trauma required for its removal. Intraoperative ultrasonographic examination of the tongue was used to guide foreign body removal from the tongue of one horse.[4, 5] However, in one report of a horse with a metallic foreign body at the base of the tongue, the clinical signs resolved without surgical removal of the foreign body.[123]

Oral Masses

Oral neoplasms are uncommon but if detected should be excised in toto or a biopsy obtained under sonographic guidance for histopathologic evaluation. Treatment depends on the type of neoplasia detected histopathologically.

Mammary Diseases

If the sonographic findings are consistent with mastitis a sterile culture of fluid stripped from the affected mammary gland should be submitted for cytologic evaluation and culture and sensitivity testing. An ultrasound-guided biopsy of mammary masses should be performed whenever possible and submitted for histopathologic evalua-

tion, if excisional biopsy is not an option initially because of the size or location of the mass. Resection of mammary tumors should be performed in horses in which mammary adenocarcinoma has been confirmed on histopathologic examination of a biopsy specimen, once metastatic neoplasia has been ruled out.

Infection of the Spermatic Cord

Definitive treatment for scirrhous cord or chronic funiculitis is excision of the infected cord.[143, 144] These tissues should be submitted for culture and sensitivity testing. Histopathologic examination of the excised tissues should also be performed if the etiology of the scirrhous cord is unclear (e.g., horse has not been recently castrated) to rule out neoplastic involvement and secondary abscessation. Sonographic examination of the scrotal or inguinal swelling is indicated prior to surgical incision to characterize the extent of the spermatic cord involvement. Rectal examination of the affected inguinal ring should also be performed before surgery to rule out extension of the infection into the peritoneal cavity. If any enlargement of the spermatic cord is detected rectally the internal inguinal ring and the cord should be examined sonographically.

Ocular Diseases

Treatment indicated for a horse with ocular disease depends on the ocular lesion detected. Readers are referred to an ophthalmology or equine internal medicine text for treatment of corneal ulcers and other ophthalmologic disorders not covered in this section or for a more in-depth coverage of patient management.

Corneal Stromal Abscess

The placement of a subpalpebral lavage system with frequent treatment of the eye with topical antimicrobials, antifungals, acetylcysteine, and atropine in conjunction with systemic nonsteroidal anti-inflammatory drugs (flunixin meglumine) and daily scraping of the corneal abscess to denude the corneal epithelium, has been successful in the treatment of corneal stromal abscesses in horses.[148] Surgical treatment, in conjunction with medical treatment, is recommended when corneal rupture is imminent, the iridocyclitis is intractable, a foreign body is suspected, or there is minimal response to intensive medical therapy.[149] Keratectomy has been recommended and used successfully by some investigators, as well as a conjunctival flap used when greater than one half of the thickness of the corneal was surgically removed.[146, 149] Although some investigators have discouraged surgical treatment for corneal stromal abscesses because of the frequency of deep corneal abscesses,[145] only 20% of horses required penetrating keratectomies and frozen corneal grafts in a more recent study.[146] Transpalpebral or transcorneal ultrasound examination can be used to evaluate the extent of the corneal involvement and to monitor healing, especially in horses in which a conjunctival flap has been used. The prognosis for vision in the treated eye is good for horses with corneal stromal abscesses; all nine horses treated medically and 14 of 15 horses treated medically and surgically retained vision in the affected eye (one horse's eye was enucleated owing to an iris prolapse at presentation).[149]

Foreign Bodies

Surgical removal of foreign bodies is indicated when detected in the eye or adnexal structures. A careful sonographic examination should be performed prior to surgery or ultrasound used intraoperatively to minimize tissue trauma and to be sure that all foreign material is surgically removed.

Panophthalmitis

Panophthalmitis usually carries a poor prognosis for vision, as it is usually associated with disseminated sepsis. Uveitis and stromal abscess formation with eventual enucleation and death have been reported in affected horses with panophthalmitis associated with *Streptococcus equi* infection.[150, 151]

Glaucoma

Glaucoma in the horse usually has a poor to grave prognosis for vision in the affected eye, as early diagnosis is rare. Acute glaucoma is rarely identified because the early ocular signs are subtle and missed by most horse owners and trainers. Most veterinarians also lack the tonometric instrumentation to measure increased intraocular pressure in horses. Recognition of the early clinical signs of glaucoma may improve the prognosis for affected horses since the appropriate medical and/or surgical treatment can be instituted before the eye has reached end-stage status.[152, 153] Topical and systemic anti-inflammatory drugs in combination with topical atropine are helpful in horses with glaucoma associated with uveitis.[153] Although atropine is contraindicated in patients with glaucoma in which aqueous drainage is primarily iridocorneal, in horses uveoscleral aqueous drainage appears to be more important.[20, 199] Atropine may increase uveoscleral drainage of aqueous humor and may be beneficial in horses with glaucoma.[20] However, in many horses the disease is so advanced by the time glaucoma is diagnosed that anti-inflammatory treatment and atropine are not successful.[20] Cryosurgical treatment of glaucoma in a horse was successful.[200] Cyclocryotherapy can decrease aqueous humor production in experimental and clinical situations, decreasing both the intraocular pressure and the size of the glaucomatous eye.[200] Enucleation is often the treatment of choice for the affected horse if the glaucoma is unilateral and the disease is advanced and nonresponsive to treatment or if other abnormalities affecting vision are present. Enucleation of the affected eye has been performed successfully in horses with glaucoma, and a

marked improvement in attitude has been reported following enucleation in affected horses, suggesting that the condition may be more painful than was initially appreciated.[20]

Iris Prolapse

Surgical repair of corneal lacerations was performed primarily in 21 of 24 horses with iris prolapse and subsequently covered with a conjunctival graft in 13 horses. Perioperative antibiotics and nonsteroidal anti-inflammatory drugs are recommended. The use of systemic nonsteroidal anti-inflammatory drugs is critical for successful management of the profound iridocyclitis and endophthalmitis in horses with iris prolapse. Ocular survival following combined medical and surgical therapy in horses with corneal lacerations was 80% in 15 horses, with horses having corneal lacerations less than 15 mm long tending to have a favorable visual outcome. Vision was retained in 71% of horses with corneal wounds ≤ 15 mm and in 80% of horses with lacerations confined to the cornea alone.[156] Similar findings correlating corneal wound length and final outcome have been reported by other investigators.[159] Longer corneal lacerations; lacerations that extended to, along, or beyond the limbus; and hyphema adversely affected visual outcome. All horses presenting with hyphema involving more than 10% of the anterior chamber developed blindness or phthisis bulbi or underwent enucleation of the affected eye. Blindness, phthisis bulbi, or enucleation was the outcome of all horses with corneal lacerations longer than 15 mm. Vision was lost in all horses with limbal rupture, and two of three eyes were enucleated.[156] Vision was lost, the eye became phthisical or was enucleated in 86% of horses with limbal ruptures or corneal lacerations extending into the limbus or sclera.[154] Iridectomy did not adversely affect visual outcome and may facilitate postoperative mydriasis and prevent septic endophthalmitis. Initial routine ophthalmologic examination coupled with a careful transpalpebral examination of the eye may help the clinician determine the appropriate course of treatment. Primary enucleation should be considered in horses with hyphema, trauma to the posterior segment, and corneal lacerations longer than 15 mm that extend to, along, or beyond the limbus.[156] Transpalpebral sonographic examination of the horses with conjunctival grafts would be helpful in monitoring corneal and ocular healing.

The prognosis for vision with perforating corneal ulcers is guarded and depends on the size of the ulcer, its location, and the mechanism of injury.[156, 157] Culture and sensitivity testing of a corneal scraping is recommended in all affected horses. Antimicrobial or antifungal treatment should be based on the results of the cytologic evaluation of the corneal scraping and the results of the culture and sensitivity testing. Ocular survival following combined medical and surgical therapy was 67% in 15 horses with ulcerative keratitis. Horses with a history of ulcerative keratitis of more than 15 days' duration tended to have a poorer visual outcome, as did horses with keratomalacia.[156]

Abnormalities of the Lens

Surgical aspiration of cataracts may be performed in some horses to improve their visual outcome. Surgery is most successful when the cataracts are not the result of uveitis or severe ocular trauma. If the back of the globe is not visible during routine ophthalmologic examination, sonographic examination of the eye should be performed to evaluate the retina for possible detachment and look for other ocular abnormalities that might affect the visual outcome of the eye. This should be performed with extreme care if the horse has experienced recent ocular trauma. The prognosis for successful repair of traumatized eyes is poor in cases of luxation of the lens or lenticular injury.[19] Because rupture of the lens leads to chronic uveitis, an enucleation should be considered for all horses with traumatic injury to the globe and lens rupture.

Retinal Detachment

Early recognition and immediate therapy is crucial to have any hope of retinal reattachment. Severe atrophy of the photoreceptors was found in horses with retinal detachment as well as atrophy of all the neuronal retinal structures. The photoreceptors are the retinal elements most susceptible to any disruption between the photoreceptor and the pigment epithelium. Progressive retinal atrophy leads to total destruction of the retinal architecture, and at this stage reattachment and regeneration of the retina are probably impossible.[21]

Ocular Neoplasia

The prognosis for horses with ocular squamous cell carcinoma depends on the extent of corneal involvement at the time of the original diagnosis and on the treatment chosen. The prognosis for horses with ocular/adnexal squamous cell carcinoma also depends on the location of the tumor, the tumor stage, and the history of recurrence.[176] In one review of ocular/adnexal squamous cell carcinoma, however, tumor location had no relationship to outcome.[171] Horses with squamous cell carcinoma involving the eyelid or orbit had the poorest prognosis. There was an inverse relationship between tumor stage (maximal dimension) and survival. Recurrences of squamous cell carcinoma markedly reduced the chances of survival. In this study there was no relationship found between treatment prior to referral, the presence of a single or multiple tumors or the treatment modality used.[176] Recurrences of ocular/adnexal squamous cell carcinoma has ranged from 30.4%[176] to 42.4%.[175] Superficial keratectomy of the lesion, in conjunction with strontium-90 beta-radiation, cryosurgery, radiofrequency hyperthermia, interstitial radiotherapy (cesium-137, cobalt-60, gold-198, iridium-192, or radon-222), immunotherapy, carbon dioxide laser ablation, intralesional matrix chemotherapy, or exenteration of the orbit or penetrating keratoplasty with a fresh equine corneal graft have been recom-

mended for treatment of equine ocular squamous cell carcinoma.[176] The decision between superficial or penetrating keratectomy or enucleation of the eye and surgical removal of any surrounding affected periocular tissues depends on the degree of corneal involvement and involvement of the extraocular structures with the neoplasm.[175]

The prognosis for horses with ocular angiosarcoma is poor, with recurrence and metastases of the tumor occurring frequently.[179] Intraocular melanoma appears to have a somewhat better prognosis with enucleation of the affected eye.[163, 166] One horse with a epibulbar melanocytoma had no recurrence of the mass during the 2-year follow-up period after surgical excision of the epibulbar mass.[177] The biologic behavior of medulloepitheliomas is unknown, as long-term follow-up of affected horses has not been reported.[184] A primitive neuroepithelial tumor of the optic nerve spread rapidly in one horse following enucleation, resulting in the demise of the horse.[182]

Retrobulbar Masses

Sonographic examination of a retrobulbar mass should prompt an ultrasound-guided aspirate or biopsy with cytopathologic or histopathologic examination of the specimen obtained. The supraorbital area and the periorbital region should be scanned to determine the best approach for ultrasound-guided aspiration of the mass.

Retrobulbar Hematoma. Treatment for a retrobulbar hematoma or drainage of the hematoma is indicated only for severe exophthalmus, risking loss of vision in the affected eye, or if there are associated fractures of the orbit that require repair. In most horses with retrobulbar hemorrhage, conservative treatment with anti-inflammatory drugs as indicated and careful clinical and sonographic monitoring of the eye and retrobulbar space is chosen, with gradual resolution of the retrobulbar hemorrhage occurring.

Retrobulbar Abscess. Drainage of the retrobulbar abscess is usually indicated in conjunction with antimicrobial therapy based on the results of cytologic examination and culture and sensitivity testing of the fluid obtained from the ultrasound-guided aspirate. The abscess should be carefully scanned to rule out the presence of a concurrent foreign body.

Retrobulbar Neoplasia. Once an ultrasound-guided biopsy of the retrobulbar mass has been performed and retrobulbar neoplasia confirmed, enucleation of the eye is the treatment of choice. Surgical resection of retrobulbar tumors is indicated unless central nervous system signs are already present.[149] The detection of neuroendocrine tumors originating from the nasal cavity and maxillary sinus extending into the retrobulbar space is associated with a poor prognosis.[201] Retrobulbar melanoma has a variable prognosis and one horse with this tumor survived for more than 26 months with progressive exophthalmos and prolapse of the nictitating membrane but no other clinical signs.[187] One horse with multilobular osteoma was treated successfully with surgical removal of the retrobulbar mass and return of the horse to full athletic function.[190]

Brain and Spinal Cord

The prognosis for foals with hydrocephalus is grave. Although the placement of a catheter to drain the excess cerebrospinal fluid in a foal has been attempted,[24] the practicality of this treatment and the severity of the hydrocephalus in many affected foals precludes its use as a widespread salvage procedure in affected foals.

References

1. Hance SR, Robertson JT, Wicks JR. Branchial cyst in a filly. Equine Vet J 1992;24:329-331.
2. Sams AE, Weldon AD, Rakestraw P. Surgical treatment of intramural esophageal inclusion cysts in three horses. Vet Surg 1993;22:135-139.
3. Peek SF, DeLahunta A, Hackett RP. Combined oesophageal and tracheal duplication cyst in an Arabian filly. Equine Vet J 1995;27:475-478.
4. Rose PL, Penninck D. Use of intraoperative ultrasonography in six horses. Vet Surg 1995;24:396-401.
5. Solano M, Penninck D. Ultrasonography of the canine, feline and equine tongue: Normal findings and case history reports. Vet Radiol Ultrasound 1996;37:206-213.
6. Reef VB. The use of diagnostic ultrasound in the horse. Ultrasound Q 1991;9:1-33.
7. Cartee RE, Rumph PF. Ultrasonographic detection of fistulous tracts and foreign objects in muscles of horses. J Am Vet Med Assoc 1984;184:1127-1132.
8. French DA, Pharr JW, Fretz PB. Removal of a retropharyngeal foreign body in a horse, with the aid of ultrasonography during surgery. J Am Vet Med Assoc 1989;194:1315-1316.
9. Adams R, Nixon A, Hager D. Use of intraoperative ultrasonography to identify a cervical foreign body: A case report. Vet Surg 1987;16:384-388.
10. Chandna VK, Morris E, Gliatto JM, Paradis MR. Localized subcutaneous cryptococcal granuloma in a horse. Equine Vet J 1992;25:166-168.
11. Clegg PD, Coumbe A. Alveolar rhabdomyosarcoma: An unusual cause of lameness in a pony. Equine Vet J 1993;25:547-549.
12. Vatistas NJ, Meagher DM, Gillis CL, Neves JW. Gunshot injuries in horses: 22 cases (1971-1993). J Am Vet Med Assoc 1995;207:1198-1200.
13. Wilson DA, Badertscher II RR, Boero MJ, et al. Ultrasonographic evaluation of the healing of ventral midline abdominal incisions in the horse. Equine Vet J (Suppl) 1989;7:107-110.
14. Trostle SS, Hendrickson DA. Suture sinus formation following closure of ventral midline incisions with polypropylene in three horses. J Am Vet Med Assoc 1995;207:742-745.
15. White NA. Incisional hernia after abdominal surgery in the horse. Equine Vet Educ 1996;8:308-312.
16. Cook G, Bowman KF, Bristol DG, Tate LP. Ventral midline herniorrhaphy following colic surgery in the horse. Equine Vet Educ 1996;8:304-307.
17. Byars TD, Halley J. Uses of ultrasound in equine internal medicine. Vet Clin North Am (Equine Pract) 1986;2:253-258.
18. Freestone JF, Glaze MB, Pechman R, McClure JR. Ultrasonic identification of an orbital tumor in a horse. Equine Vet J 1989;21:135-136.
19. Miller WW. Diagnostic ultrasound in equine ophthalmology. Proc Am Assoc Equine Pract 1991;36:559-565.
20. Read RA, Barnett KC. Equine glaucoma diagnosed with the aid of ultrasonography. Equine Vet Educ 1995;7:225-228.
21. Mätz-Rensing K, Drommer W, Kaup F-J, Gerhards H. Retinal detachment in horses. Equine Vet J 1996;28:111-116.
22. Boroffka SAEB, van den Belt AJM. CU/Ultrasound diagnosis—

retrobulbar hematoma in a horse. Vet Radiol Ultrasound 1996; 37:441-443.
23. Rivas LJ, Hinchcliff KW, Robertson JT. Cervical meningomyelocele associated with spina bifida in a hydrocephalic miniature colt. J Am Vet Med Assoc 1996;209:950-953.
24. Foreman JH, Reed SM, Rantanen NW, et al. Congenital internal hydrocephalus in a Quarter horse foal. J Equine Vet Sci 1984;3:154-164.
25. Reef VB, Clark S, Oliver JA, et al. Implantation of a permanent transvenous pacing catheter in a horse with complete heart block and syncope. J Am Vet Med Assoc 1986;189:449-452.
26. Hudson JA, Simpson ST, Cox NR, et al. Ultrasonographic examination of the normal canine neonatal brain. Vet Radiol 1991;32:50-59.
27. Simeone JF, Daniels GH, Mueller PR, et al. High-resolution real-time sonography of the thyroid. Radiology 1982;145:431-435.
28. Rogers M, Cartee RE, Miller W, Ibrahim AK. Evaluation of the extirpated equine eye using B-mode ultrasonography. Vet Radiol 1986;27:24-29.
29. Spaulding KA, Sharp NJH. Ultrasonographic imaging of the lateral cerebral ventricles in the dog. Vet Radiol 1990;31:59-64.
30. Finn-Bodner ST, Hudson JA, Coates JR, et al. Ultrasonographic anatomy of the normal canine spinal cord and correlation with histopathology after induced spinal cord trauma. Vet Radiol Ultrasound 1995;35:39-48.
31. Baker HJ, Lindsey JR. Equine goiter due to excess dietary iodide. J Am Vet Med Assoc 1968;153:1618-1630.
32. Drew B, Barber WP, Williams DG. The effect of excess dietary iodine on pregnant mares and foals. Vet Rec 1975;97:93.
33. Shaver JR, Fretz PB, Doige CE, Williams DM. Skeletal manifestations of suspected hypothyroidism in two foals. J Equine Med Surg 1979;3:269-275.
34. McLaughlin B, Doige C. A study of ossification of carpal and tarsal bones in normal and hypothyroid foals. Can Vet J 1982;23:164-168.
35. Irvine C. Hypothyroidism in the foal. Equine Vet J 1984;16:302-302.
36. Held J, Patten C, Toal R, et al. Work intolerance in a horses with thyroid carcinoma. J Am Vet Med Assoc 1985;187:1044-1045.
37. Hillidge C, Sanecki R, Theordorakis M. Thyroid carcinoma in a horse. J Am Vet Med Assoc 1982;181:711-714.
38. van der Velden MA, Meulenaar H. Medullary thyroid carcinoma in a horse. Vet Pathol 1986;23:622-624.
39. Lucke VM, Lane JG. C-cell tumors of the thyroid in the horse. Equine Vet J 1984;16:28-30.
40. Bouayad H, Lahoussine O, Johnson DW, et al. Sialoliths in the horse. Equine Pract 1991;13:25-27.
41. Goetz TE, Ogilvie GK, Keegan KG, et al. Cimetidine for treatment of melanomas in three horses. J Am Vet Med Assoc 1990;196:449-452.
42. Goetz TE, Long MT. Treatment of melanomas in horses. Compend Contin Educ Pract Vet 1993;15:608-610.
43. Stavros AT, Rapp CL, Thickman D. Sonography of inflammatory conditions. Ultrasound Q 1995;13:1-26.
44. Tessier GJ, Neuwirth LA, Merritt AM. Peritracheal abscess as the cause of tracheal compression and severe respiratory distress in a horse. Equine Vet Educ 1996;8:127-130.
45. Craig DR, Shivy DR, Pankowski RL, et al. Esophageal disorders in 61 horses. Results of nonsurgical and surgical management. Vet Surg 1989;18:432-438.
46. Baird AN, True CK. Fragments of nasogastric tubes as esophageal foreign bodies in two horses. J Am Vet Med Assoc 1989;194:1068-1070.
47. Traver DS, Egger E, Moore JN. Retrieval of an esophageal foreign body in a horse. Vet Med/Small Anim Clin 1978;73:783-785.
48. DeBowes RM, Grant BD, Sande RD. Esophageal obstruction by antibiotic boluses in a Thoroughbred filly: A case report. J Equine Vet Sci 1982;2:23-26.
49. Harris JM. Esophageal obstruction by a wood bolus. Mod Vet Pract 1981;14:163-164.
50. Roberts MC, Kelly WR. Squamous cell carcinoma of the lower cervical esophagus in a pony. Equine Vet J 1979;11:199-201.
51. Moore JN, Kintner LD. Recurrent esophageal obstruction due to squamous cell carcinoma in a horse. Cornell Vet 1976;66:589-596.
52. Orsini JA, Sepsey L, Donawick WJ, McDevitt D. Esophageal duplication cyst as a cause of choke in the horse. J Am Vet Med Assoc 1988;193:474-476.
53. Scott EA, Snoy P, Prasse KW, Hoffman PE, Thrall DE. Intramural esophageal cyst in a horse. J Am Vet Med Assoc 1977;171:652-654.
54. Sams AE, Weldon AD, Rakestraw P. Surgical treatment of intramural esophageal inclusion cysts in three horses. Vet Surg 1993;22:135-139.
55. Hackett RP, Dyer RM, Hoffer RE. Surgical correction of esophageal diverticulum in a horse. J Am Vet Med Assoc 1978;173:998-1000.
56. Frauenfelder HC, Adams SB. Esophageal diverticulectomy in a horse. J Am Vet Med Assoc 1982;180:771-772.
57. MacDonald MH, Richardson DW, Morse CC. Esophageal phytobezoar in a horse. J Am Vet Med Assoc 1987;191:1455-1456.
58. Bowman KF, Vaughn JT, Quick CB, et al. Megaesophagus in a colt. J Am Vet Med Assoc 1978;172:334-337.
59. Rohrbach BW, Rooney JR. Congenital esophageal ectasia in a thoroughbred foal. J Am Vet Med Assoc 1980;177:65-67.
60. DeMoor A, Wouters L, Mouens Y, et al. Surgical treatment of a traumatic esophageal rupture in a foal. Equine Vet J 1979;11:265-266.
61. Hardy J, Stewart RH, Beard WL, Yvorchuk-St-Jean K. Complications of nasogastric intubation in horses: Nine cases (1987-1989). J Am Vet Med Assoc 1992;201:483-486.
62. MacHarg MA, Foerner JJ, Phillips TN, et al. Bypass surgery for the treatment of small intestinal ileus in the horse. A report of three cases. Vet Surg 1988;17:15-17.
63. Mayhew IG, Lumsden JH. A cervical cyst in a horse. Can Vet J 1973;14:46-49.
64. Field JR, Trout D, Physick-Sheard PW. Ablation of a congenital neck mass in a foal. Can Vet J 1990;31:643-644.
65. Hance SR, Robertson JT, Bukowiecki CF. Cystic structures within the guttural pouch (auditory tube diverticulum) in two horses. J Am Vet Med Assoc 1992;200:1981-1983.
66. Gordon LR. The cytology and histology of epidermal inclusion cysts in the horse. J Equine Med Surg 1978;2:371-374.
67. Koch DB, Tate LP. Pharyngeal cysts in horses. J Am Vet Med Assoc 1978;173:860-862.
68. Spiers VC, Smyth GB, Moffatt R. Pharyngeal growth as a cause of abnormal respiratory sounds and dysphagia in horses. J Equine Med Surg 1979;33:473-478.
69. Baxter GM, Allen D, Farrell RL. Paralaryngeal accessory branchial cyst as a cause of laryngeal haemiplegia in a horse. Equine Vet J 1992;24:67-69.
70. Lane JG, Gibbs C, Meynink SE, Steele FC. Radiographic examination of the facial, nasal and paranasal sinus regions of the horse: I. indications and procedures in 235 cases. Equine Vet J 1987;19:466-473.
71. Fessler JF. Heterotopic polyodontia in horses: Nine cases (1969-1986). J Am Vet Med Assoc 1988;192:535-538.
72. Scott EA. Cervical abscess and pharyngeal fistula in a horse. J Am Vet Med Assoc 1975;166:775-777.
73. Sweeney CR, Sweeney RW, Raker CW, Freeman DE. Upper respiratory tract obstruction caused by a pharyngeal abscess in a filly. J Am Vet Med Assoc 1985;187:268-270.
74. Miers KC, Ley WB. *Corynebacterium pseudotuberculosis* infection in the horse: Study of 117 clinical cases and consideration of etiopathogenesis. J Am Vet Med 1980;177:250-253.
75. Aleman M, Spier SJ, Wilson D, Doherr M. *Corynebacterium pseudotuberculosis* infection in horses: 538 cases (1982-1993). J Am Vet Med Assoc 1996;209:804-809.
76. Sanders-Shamis M. Perirectal abscesses in six horses. J Am Vet Med Assoc 1985;187:499-500.
77. Wilson DA. Management of perianal squamous cell carcinoma with permanent colostomy in a mare. J Am Vet Med Assoc 1994;205:1430-1431.
78. Anderson RV, Bemrick WJ. *Micronema deletrix* n. sp.: a saprophagous nematode inhabiting a nasal tumor of the horse. Proc Helminth Soc Wash 1965;32:74-75.
79. Johnson KH, Johnson DW. Granulomas associated with *Micronema deletrix* in the maxillae of a horse. J Am Vet Med Assoc 1966;149:155-159.
80. Keg PR, Mirck MH, Dik KJ, Vos JH. *Micronema deletrix* infection in a Shetland pony stallion. Equine Vet J 1984;16:471-475.
81. Ruggles AJ, Beech J, Gilette DE, Midla L, Reef VB, Freeman DE.

Disseminated *Halicephalobus deletrix* infection in a horse. J Am Vet Med Assoc 1993;203:550–552.
82. Chandna VK, Morris E, Gliatto JM, Paradis MR. Localized subcutaneous cryptococcal granuloma in a horse. Equine Vet J 1992;25:166–168.
83. Markel MD, Wheat JD, Spenser SJ. Cellulitis associated with coagulase-positive staphylococci in racehorses: Nine cases (1975–1984). J Am Vet Med Assoc 1986;189:166–1604.
84. Reef VB. *Clostridium perfringens* cellulitis and immune-mediated hemolytic anemia in a horse. J Am Vet Med Assoc 1983;182:251–254.
85. Hagemoser WA, Hoffman LJ, Lundvall RL. *Clostridium chauvoei* infection in a horse. J Am Vet Med Assoc 1980;176:631–633.
86. Murphy DB. *Clostridium chauvoei* as the cause of malignant edema in a horse. Vet Med/Small Animal Clin 1980;75:1152–1154.
87. Westman CW, Traub JL, Schroeder WG. Clostridial infection in a horse. J Am Vet Med Assoc 1979;174:725–726.
88. Rehbun WC, Shin SJ, Kurg JM, et al. Malignant edema in horses. J Am Vet Med Assoc 1985;187:732–736.
89. Marti E, Lazary S, Antczak DF, Gerber H. Report of the first international workshop on equine sarcoid. Equine Vet J 1993;25:397–407.
90. Bristol DG, Fubini SL. External lipomas in three horses. J Am Vet Med Assoc 1984;185:791–792.
91. Blackwell JG. Unusual adipose tissue growth in a colt. J Am Vet Med Assoc 1972;161:1141–1142.
92. Pascoe RR, Summers PM. Clinical surgery of tumors and tumor-like lesions in horses in southeast Queensland. Equine Vet J 1981;13:235–239.
93. Hargis AM, McElwain. Vascular neoplasia in the skin of horses. J Am Vet Med Assoc 1984;184:1121–1124.
94. Sartin EA, Hodge TG. Congenital dermal hemangioendothelioma in two foals. Vet Pathol 1982;19:569–571.
95. Waugh SL, Long GG, Uriah L, Grant B. Metastatic hemangiosarcoma in the equine: Report of 2 cases. J Equine Med Surg 1977;1:311–315.
96. Johnstone AC. Congenital vascular tumours in the skin of horses. J Comp Pathol 1987;97:365–368.
97. Turk JR, Gallina AM, Liu IM, et al. Cystic lymphangioma in a colt. J Am Vet Med Assoc 1979;174:1228–1230.
98. Van Pelt RW, Langham RF, Gill HE. Multiple hemangiosarcomas in the tarsal synovial sheath of a horse. J Am Vet Med Assoc 1972;161:49–52.
99. Valentine EA, Ross CE, Bump JL, Eng VM. Intramuscular hemangiosarcoma with pulmonary metastasis in a horse. J Am Vet Med Assoc 1986;188:628–629.
100. Foley GL, Valentine BA, Kincaid AL. Congenital and acquired melanocytomas (benign melanomas) in eighteen young horses. Vet Pathol 1991;28:363–369.
101. Levene A. Equine melanotic disease. Tumori 1971;57:133–168.
102. Hamilton DP, Byerly CS. Congenital malignant melanoma in a foal. J Am Vet Med Assoc 1989;164:1040–1041.
103. Kirker-Head CA, Loeffler D, Held J-P. Pelvic limb lameness due to malignant melanoma in a horse. J Am Vet Med Assoc 1985;186:1215–1217.
104. Kunze DJ, Monticello TM, Jacob TP, Crane S. Malignant melanoma of the coronary band in the horse. J Am Vet Med Assoc 1986;188:297–298.
105. Grant B, Lincoln S. Melanosarcoma as a cause of lameness in a horse. Vet Med/Small Anim Clin 1972;67:995–998.
106. Conboy HS, Powers RD. Equine malignant lymphoma. J Am Vet Med Assoc 1971;159:53–54.
107. Gupta BN, Keahey KK, Ellis DJ. Cutaneous involvement of malignant lymphoma in a horse. Cornell Vet 1972;62:205–215.
108. Neufeld JL. Lymphosarcoma in the horse: A review. Can Vet J 1973;14:129–135.
109. Sheahan BJ, Atkins GJ, Russell RJ, O'Connor JP. Histiolymphocytic lymphosarcoma in the subcutis of two horses. Vet Pathol 1980;17:123–133.
110. Dorn CR, Priester WA. Epidemiologic analysis of oral and pharyngeal cancer in dogs, cats, horses and cattle. J Am Vet Med Assoc 1976;169:1202–1205.
111. Strafuss AC. Squamous cell carcinoma in horses. J Am Vet Med Assoc 1976;168:61–62.
112. Karcher LF, LeNet J-L, Turner BF, Reimers TJ, Tennant BC. Pseudohyperparathyroidism in a mare associated with squamous cell carcinoma of the vulva. Cornell Vet 1990;80:153–162.
113. Baird AN, Frelier PF. Squamous cell carcinoma originating from an epithelial scar in a horse. J Am Vet Med Assoc 1990;196:1999–2000.
114. Schumacher J, Watkins JP, Wilson SR, et al. Burn-induced neoplasia in two horses. Equine Vet J 1986;18:410–412.
115. Gardner DG. Ameloblastomas in the horse: a critical review and report of an additional example. J Oral Pathol Med 1994;23:41–44.
116. Rosol TJ, Nagode LA, Robertson JT, Leeth B, et al. Humoral hypercalcemia of malignancy associated with ameloblastoma in a horse. J Am Vet Med Assoc 1994;204:1930–1933.
117. Reinertson EL. Fibrosarcoma in a horse. Cornell Vet 1974;64:617–621.
118. Danton CAS, Peacock PJ, May SA, Kelly DF. Anaplastic sarcoma in the caudal thigh of a horse. Vet Rec 1992;131:188–190.
119. Cook G, Divers TJ, Rowland PH. Hypercalcaemia and erythrocytosis in a mare associated with a metastatic carcinoma. Equine Vet J 1995;27:316–318.
120. Seahorn TL, Sams AE, Honnas CM, et al. Ultrasonographic imaging of a keratoma in a horse. J Am Vet Med Assoc 1992;200:1973–1974.
121. May SA, Wyn-Jones G. Contrast radiography in the investigation of sinus tracts and abscess cavities in the horse. Equine Vet J 1987;19:218–222.
122. Barber SM. An unusual location of foreign body in the horse. Can Vet J 1983;24:63–66.
123. Engelbert TA, Tate LP. Penetrating lingual foreign bodies in three horses. Cornell Vet 1993;83:31–38.
124. Shah ZR, Crass JR, Oravec DC, Bellon EM. Ultrasonographic detection of foreign bodies in soft tissues using turkey muscle as a model. Vet Radiol Ultrasound 1992;33:94–100.
125. Gooding GAW, Hardiman T, Sumers M, Stess R, et al. Sonography of the hand and foot in foreign body detection. J Ultrasound Med 1987;6:441–447.
126. Fornage B. Preoperative sonographic localization of a migrated transosseous stabilizing wire in the hand. J Ultrasound Med 1987;6:471–473.
127. Little CM, Parker MG, Callowich MC, Sartori JC. The ultrasonic detection of soft tissue foreign bodies. Invest Radiol 1986;21:275–277.
128. Fornage B, Schernberg FL. Sonographic diagnosis of foreign bodies of the distal extremities: Case report. AJR 1986;147:567–569.
129. Kobluck CN, Ducharme NG, Lumdsen JH, et al. Factors affecting incisional complication rates associated with colic surgery in horses: incidence and predisposing factors. J Am Vet Med Assoc 1989;195:639–642.
130. Smeak DD, Wendelburg KL. Choosing suture materials for use in contaminated or infected wounds. Compend Contin Educ Pract Vet 1989;11:467–475.
131. Gibson KT, Curtis CR, Turner AS, et al. Incisional hernias in the horse—incidence and predisposing factors. Vet Surg 1989;18:360–366.
132. Hance S, DeBowes RM, Clem MF, Welsh RD. Umbilical, inguinal, and ventral hernias in horses. Compend Contin Educ Pract Vet 1990;12:862–871.
133. Boussauw B, Wilderjans H. Inguinal herniation 12 days after a unilateral castration with primary wound closure. Equine Vet Educ 1996;8:248–250.
134. Wisner ER, Nyland TG, Mattoon JS. Ultrasonographic examination of cervical masses in the dog and cat. Vet Radiol and Ultrasound 1994;35:310–315.
135. Rehbun WC, Bertone A. Equine lymphosarcoma. J Am Vet Med Assoc 1984;184:720–721.
136. Bruneton JN, Roux P, Carmella E, et al. Nose and throat cancer: Ultrasonic diagnosis of metastases to the cervical lymph nodes. Radiology 1984;152:771–773.
137. Gooding GAW. Gray scale ultrasound of the parotid gland. *AJR* 1980;134:469–472.
138. Kiper ML, Wrigley R, Traub-Dargatz J, Bennett D. Metallic foreign bodies in the mouth or pharynx of horses: seven cases (1983–1989). J Am Vet Med Assoc 1992;200:91–93.
139. Baum KH, Halpern NE, Banish LD, Modransky PD. Dysphagia in horses: the differential diagnosis - part II. Compend Contin Educ Pract Vet 1992;200:91–93.

140. Hanson PD, Frisbie DD, Dubielzig RR, Markel MD. Rhabdomyosarcoma of the tongue in a horse. J Am Vet Med Assoc 1993;202:1281–1284.
141. Neuhold A, Fruhwald F, Balogh B, Wicke L. Sonography of the tongue and the floor of the mouth. Part I: Anatomy. Eur J Radiol 1986;6:103–107.
142. Fruhwald F, Neuhold A, Seidl G, Pavelka R. Sonography of the tongue and the floor of the mouth. Part II: neoplasia of the tongue. Eur J Radiol 1986;6:108–112.
143. Wright JG. The surgery of the inguinal canal in animals. Vet Rec 1963;75:1352–1367.
144. Fitch G, Schumacher J. Infection of the spermatic cord of a pony gelding. Equine Vet Educ 1996;8:251–252.
145. Rehbun WC. Corneal stromal abscess in the horse. J Am Vet Med Assoc 1982;181:677–680.
146. Hamilton HL, McLaughlin SA, Whitley EM, Gilger BC, Whitley RD. Histological findings in corneal stromal abscesses of 11 horses: correlation with cultures and cytology. Equine Vet J 1994;26:448–453.
147. Gilger BC, McLaughlin SA. Glaucoma and corneal stroma abscess in a horse treated by an intraocular silicone prosthesis and a conjunctival flap. Equine Pract 1993;15:10–15.
148. Sweeney CR, Sweeney RW, Roby KAW, Irby N. Corneal stromal abscesses in two horses. Compend Contin Educ Pract Vet 1984;6:595–601.
149. Hendrix DVH, Brooks DE, Smith PJ, et al. Corneal stromal abscesses in the horse: A review of 24 cases. Equine Vet J 1995;27:440–447.
150. Kaplan NA, Moore BR. *Streptococcus equi* endocarditis, meningitis and panophthalmitis in a mature horse. Equine Vet Educ 1996;8:313–316.
151. Barrett-Boyes SM, Young RL, Canton DD, Mohr FC. *Streptococcus equi* infection as a cause of panophthalmitis in a horse. Equine Vet Sci 1991;11:229–231.
152. Wilcock BP, Brooks DE, Latimer CA. Glaucoma in horses. Vet Pathol 1991;28:74–78.
153. Pickett JP, Ryan J. Equine glaucoma: a retrospective study of 11 cases from 1988 to 1993. Vet Med 1993;88:756–763.
154. Barnett KC, Paterson BW, Ricketts SW. Buphthalmos in a Thoroughbred foal. Equine Vet J 1988;20:132–135.
155. Cook CS, Peiffer RL, Harling DE. Equine recurrent uveitis. Equine Vet J 1983;Suppl 2:57–60.
156. Chmielewski NT, Brooks DE, Smith PJ, Hendrix DVH, Whittaker C, Gelatt KN. Visual outcome and ocular survival following iris prolapse in the horse: A review of 32 cases. Equine Vet J 1997;29:31–39.
157. Brooks DE, Wolf ED. Ocular trauma in the horse. Equine Vet J 1983;Suppl 2:141–146.
158. Turner LM, Whitley RD, Hager D. Management of ocular trauma in horses. Part 2. Orbit, eyelids, uvea, lens, retina and optic nerve. Mod Vet Pract 1986;67:341–347.
159. Whitley RD, Turner LM. Management of ocular trauma in horses. Part I: Cornea and sclera. Mod Vet Pract 1986;67:233–238.
160. McLaughlin SA, Gilger BC, Whitley RD. Infectious keratitis in horses: Evaluation and management. Compend Contin Educ Pract Vet 1992;14:372–379.
161. Rebhun WC. Diagnosis and treatment of equine uveitis. J Am Vet Med Assoc 1979;175:803–808.
162. Gelatt KN, Myers VS Jr, McClure JR Jr. Aspiration of congenital and soft cataracts in foals and young horses. J Am Vet Med Assoc 1974;165:611–615.
163. Eriksson K. Hereditary aniridia with secondary cataract in horses. Nord Vet Med 1955;7:733–793.
164. Beech J, Aguirre G, Gross S. Congenital nuclear cataracts in the Morgan horse. J Am Vet Med Assoc 19984;184:1363–1365.
165. Beech J, Irby N. Inherited nuclear cataracts in the Morgan horse. J Heredity 1985;76:371–371.
166. Neumann SM. Intraocular melanoma in a horse. Mod Vet Pract 1985;66:559–560.
167. van der Woerdt A, Wilkie DA, Myer CW. Ultrasonographic abnormalities in the eyes of dogs with cataracts: 147 cases (1986–1992). J Am Vet Med Assoc 1993;203:838–841.
168. Murphy J, Young S. Intraocular melanoma in a horse. Vet Pathol 1979;16:539–542.
169. Jones TC. Equine periodic ophthalmia. Am J Vet Res 1942;3:45–71.
170. Walde I. Differential diagnostische and therapeutische Aspekte bei der "Mondblindheit" des Pferdes. Pferdeheilkunde 1986;2:67–78.
171. Rebhun WC. Equine retinal lesions and retinal detachments. Equine Vet J 1983;Suppl 2:86–90.
172. Joyce JR. Detached retina in a colt. Vet Med Small Anim Clin 1972;67:399–400.
173. Schwink K. Factors influencing morbidity and outcome of equine ocular squamous cell carcinoma. Equine Vet J 1987;19:198–200.
174. Dugan SJ, Curtis CR, Roberts SM, et al. Epidemiologic study of ocular/adnexal squamous cell carcinoma in horses. J Am Vet Med Assoc 1991;198:251–256.
175. van der Woerdt A, Gilger BC, Wilkie DA. Penetrating keratoplasty for treatment of recurrent squamous cell carcinoma of the cornea in a horse. J Am Vet Med Assoc 1996;208:1692–1694.
176. Dugan SJ, Roberts SM, Curtis CR, et al. Prognostic factors and survival of horses with ocular/adnexal squamous cell carcinoma: 147 cases (1978–1988). J Am Vet Med Assoc 1991;198:298–303.
177. Hirst LW, Jabs DA, Stoskopf M, et al. Benign epibulbar melanocytoma in a horse. J Am Vet Med Assoc 1983;183:333–334.
178. Crawley GR, Bryan GM, Gogolewski RP. Ocular hemangioma in a horse. Equine Pract 1987;9:11–14.
179. Hacker DV, Moore PF, Buyckmihci NC. Ocular angiosarcoma in four horses. J Am Vet Med Assoc 1986;189:200–203.
180. Ramadan RO. Primary ocular melanoma in a young horse. Equine Vet J 1975;7:49–50.
181. Bistner S, Campbel RJ, Shaw D, et al. Neuroepithelial tumor of the optic nerve in a horse. Cornell Vet 1983;73:30–40.
182. Bistner SI. Medulloepithelioma of the iris and ciliary body in a horse. Cornell Vet 1974;64:588–595.
183. Eagle RC, Font RL, Swerczek TW. Malignant epithelioma of the optic nerve in a horse. Vet Pathol 1978;72:1039–1057.
184. Szymandki CM. Malignant teratoid medulloepithelioma in a horse. J Am Vet Med Assoc 1987;190:301–302.
185. Caron JP, Barber SM, Bailey JV, et al. Periorbital skull fractures in five horses. J Am Vet Med Assoc 1986;188:280–284.
186. Scott EA, Duncan JR, McCormack JE. Cryptococcosis involving the postorbital area and frontal sinus in a horse. J Am Vet Med Assoc 1974;165:626–627.
187. Sweeney CR, Beech J. Retrobulbar melanoma in a horse. Equine Vet J 1983;Suppl 2:123–124.
188. Koch DB, Leitch M, Beech J. Orbital surgery in 2 horses. Vet Surg 1980;9:61–65.
189. Barnett KC, Cottrell B, Rest JR. Retrobulbar hydatid cyst in the horse. Equine Vet J 1988;20:136–138.
190. Richardson DW, Acland HM. Multilobular osteoma (chondroma rodens) in a horse. J Am Vet Med Assoc 1983;182:289–290.
191. Lavach JD, Severin GA. Neoplasia of the equine eye, adnexa, and orbit: A review of 68 cases. J Am Vet Med Assoc 1977;170:202–203.
192. Finn JP, Tennant BC. A cerebral and ocular tumor of reticular tissue in a horse. Vet Pathol 1971;8:458–466.
193. Cranley JJ. Survey of equine hydatidosis in Great Britain. Equine Vet J 1982;14:153–157.
194. Todhunter RJ, Stick JA, Trotter GW, Boles C. Medical management of esophageal stricture in 7 horses. J Am Vet Med Assoc 1984;185:784–787.
195. Baatenburg De Jong RJ, Rongen RJ, Laméris JS, et al. Ultrasound-guided percutaneous drainage of deep neck abscesses. Clin Otolaryngol 1990;15:159–166.
196. Théon AP, Pascoe JR, Carlson GP, et al. Intratumoral chemotherapy with cisplatin in oily emulsion in horses. J Am Vet Med Assoc 1993;202:261–267.
197. Théon AP, Pascoe JR, Meagher DM. Perioperative intratumoral administration of cisplatin for treatment of cutaneous tumors in Equidae. J Am Vet Med Assoc 1994;205:1170–1176.
198. Tulleners EP, Fretz PB. Prosthetic repair of large abdominal wall defects in horses and food animals. J Am Vet Med Assoc 1983;182:258–262.
199. Smith PJ, Samualson DA, Brooks DE, Whiteley RD. Unconventional aqueous humor outflow of microspheres perfused into the equine eye. Am J Vet Res 1986;47:2445–2453.
200. Frauenfelder HC, Vestre WA. Cryosurgical treatment of glaucoma in a horse. Vet Med Small Anim Clin 1981;76:183–186.
201. van Maanen C, Klein WR, Dik KJ, et al. Three cases of carcinoid in the equine nasal cavity and maxillary sinuses: histologic and immunohistochemical features. Vet Pathol 1996;33:92–95.

ISBN 0-7216-5023-6

SAUNDERS
An Imprint of Elsevier Science

www.elsevierhealth.com